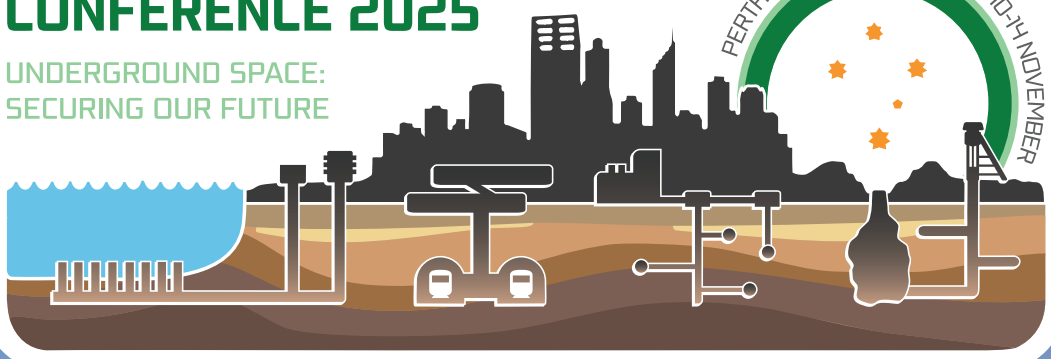
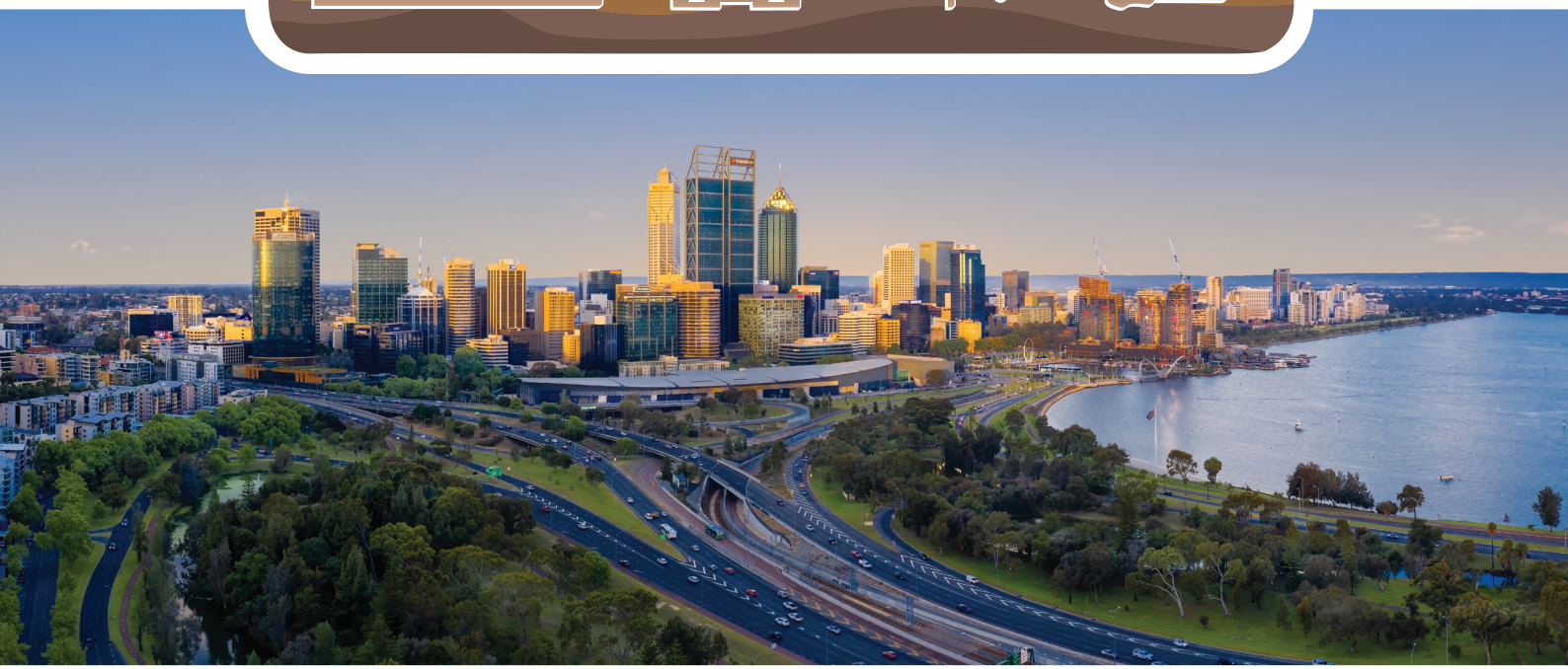
AUSTRALASIAN TUNNELLING CONFERENCE 2025

UNDERGROUND SPACE:
SECURING OUR FUTURE





Hugo E. Acosta-Martínez,
Doug Stewart &
Eric Hudson-Smith

Editors

Proceedings of the

19th Australasian Tunnelling Conference

Perth, Western Australia | 10-14 November 2025

ENGINEERS AUSTRALIA

AUSTRALIAN TUNNELLING SOCIETY

THIS PAGE INTENTIONALLY LEFT BLANK

19th AUSTRALASIAN TUNNELLING CONFERENCE

THIS PAGE INTENTIONALLY LEFT BLANK

PROCEEDINGS OF THE NINETEENTH AUSTRALASIAN TUNNELLING CONFERENCE, PERTH, WESTERN AUSTRALIA, AUSTRALIA, 10-14 NOVEMBER 2025

19th Australasian Tunnelling Conference

Editors
Hugo E. Acosta-Martínez
WSP, Perth, Australia

Doug Stewart
FSG Geotechnics + Foundations, Perth, Australia

Eric Hudson-Smith
Geosite Pty Ltd, Perth, Australia

AUSTRALIAN TUNNELLING SOCIETY
ENGINEERS AUSTRALIA

© 2025 Australian Tunnelling Society, Canberra, Australia

All rights reserved. No part of this publication or the information contained herein may be reproduced, stored in a retrieval system, or transmitted in any form or by any means, electronic, mechanical, by photocopying, recording or otherwise, without written prior permission from the publishers.

Although all care is taken to ensure integrity and the quality of this publication and the information herein, no responsibility is assumed by the publisher nor the author for any damage to the property or persons as a result of operation or use of this publication and/or the information contained herein.

Published by: Australian Tunnelling Society
e-mail: ats@engineersaustralia.org.au
www.australiantunnellingsociety.com.au

ISBN 978-0-85825-002-4

Table of contents

Introduction XIII

Reviewers XV

Theme 1. Linings and TBMs 1

Efficient design in the Alkimos intake and outfall tunnels 3
K. Katpakanathan, A. Harding, J. Cockerall & M. David

Design challenges on Western Harbour Tunnel mega TBM segment and cross passages 11
S.F. Chau, H. Asche, J. Shepherd & C. D'Hondt

Autonomous tunnel boring machines in action 23
M.H. Kamal Arifin, A. Francis & D. Boylan

Design of deep undrained tunnels for groundwater pressure using Australian Standards 31
H. Alaedini, H. Asche & T. Peglas

Comparative analysis of crack width calculation methods for tunnel lining design 39
N. Shafiei, J. Ho & C. Ng

A comparative study on 2D numerical modelling methods for tunnel junctions 47
L.Y. Chan, W.S. Tsui & M.C. Hui

Shallow urban tunnelling method in complex geological conditions; case study: Naghsh-e-Jahan station-line 2 metro of Esfahan 55
A. Moghbeli, H. Samadi, S. Tarigh Azali & F. Suorineni

TBM launch temporary works: Melbourne North East Link 65
J. Zeneli & D. Kubik

North East Link segmental lining lessons learnt - from design to construction 73
J. Zeneli, M. Behrens & R. Shi

Sydney Metro West - Eastern tunnelling project - TBM temporary works 81
E. Adcock & D. Kubik

Repurposing Roma Street station's temporary access adit as an emergency egress adit 89
M. Lecina, S.J. Clarke & J. Vallino

Impact of construction phase on the interaction between lining and rock mass in pressure tunnel and shafts 99
M. Zoorabadi

Insights into the load transfer mechanisms of grouted rock bolts under tension 105
A. Emadi & A. RA Gomes

Design and implementation of a precast lining system for mined tunnels in Sydney Metro West 113
N. Lewis, J. Nethercott, A. Golshani & A. Mirzayee

Robofactory: the future of large-scale TBM segments production 121
G. Faini, D. Sirtori & G. K. Pini

Breaking ground with umbilical and flying launch systems: innovations to manage space constraints in Australia's Suburban Rail Loop Project Tunnels South 129
V. Tata & J. Mackell

Spoil reconciliation in slurry TBM tunnelling: A literature review and framework designed for application on Melbourne's Suburban Rail Loop East – Tunnels South 137
M. Taneja & M. Terenzi

Assessing the geotechnical feasibility of shallow TBM launch in India's urban landscape: a focused case study 145
M. Gowtham Sri Sai, Vignesh R, Visakan R & Doraswamy Raju G
Research on composite rock breaking tests and efficiency evaluation of cutter disk hobs for TBM with large taper face 153
J.B. Li, Y.Q. Lu, Y. Zhu, C.X. Cao & Y.H. Wei
TBM excavation in poor squeezing ground condition. The LPFZ crossing in Snowy 2.0 163
M. Franceschi, F. Lazzarin, D. Evans & S. Loasses
Design considerations and criteria for underground structures – structural verifications of waterway concrete linings in pumped storage power plants 171
F. Cippà & M. Cadenelli
Real-time geological prediction technology based on TBM rock-breaking seismic source HSP method and engineering practice 179
T. Gu, S. Lu, L. Meng, X. Wang & K. Wu
The use of optical televiewer and endoscope imaging methods in TBM tunnels to predict ground conditions 187
R. A. Susilo, F. Alvarado, B. Requiliani, F. Stroppa & K. Stariha
To jamb or not to jamb: Evaluating cross passage permanent support systems 195
V. Balakumarasingham
Artificial ground freezing for cross passage construction 203
C.K. Tsang, Tong Sia & Frank Li
Comparison of the effects of new and existing building developments on large tunnels 211
D. Duorina, A. Bennett & N. Makin
Automatic and real-time positioning of vault and full round tunnel shutters based on camera sensor units 221
M. Jarvis, S. Wojtkowiak & N. Mattburger

Theme 2. Temporary Support 229

Designing canopy tubes for tunnel stability in weak ground: A comparison of analytical and 3D numerical approaches 231
A. Sarathchandran & S. Yao
Effect of recycled fine waste glass powder on workability performance in sustainable backfill 239
Sumedha Koul, Mehdi Serati, Niki Jackson & Ian van Wijk
The mined tunnels of the Sydney Metro West – Western Tunnelling Package: Narrow pillars and heritage sewers 247
J. Nethercott & A. Mirzayee
Primary support installation for the Albert Street Station cavern and main station entry shaft intersection, Cross River Rail, Brisbane 255
R.Elliott, D.Keating & B.Shen
Numerical analysis and design of an SEM tunnel through jet-grouted Coode Island Silt 263
A. Shafee, E. Kaese & M. Behrens
Mechanical Analysis of Shotcrete Support Based on Rock-Shotcrete Composite Effect 271
Y. Deng
Stability Analysis of a Nozzle Headwall considering interaction with adjacent piles: Insights from Sydney Metro West 279
Ivy Zhang & Ali Golshani

Theme 3. Sprayed Concrete and Ground Support 287

Shrinkage cracking in slender shotcrete tunnel linings 289
E.S. Bernard
High temperature bond behavior of Spray Applied Waterproof Membranes (SAWMs) 305
M. Reinhold & G. Bhatta
Practical shotcrete design approach based on full-scale load-deflection tests using numerical analysis 313
J. Oh & T. Moon
Evaluating the setting behaviour of shotcrete with crushed waste glass as sand replacement 321
M. Serati, X. Zhu, M. J. Luana & M. Booy
Optimizing artificial ground freezing design for cross passage construction: Construction and practical considerations 329
C.F. Tsang, D. Devrnja, M. Gresz & G. Quigg
Laboratory test methods and results for double shear performance of Australian CT bolts in simulated strata 339
S. Worrall, R. Walker & D. W. Evans
Characterization of fiber-reinforced concretes activated at very early ages 347
N. Leclere & B. De Rivaz
Investigation of composite shell lining interface behavior of rock tunnel 355
W. Shuyi, D. Yisan, W. Ning & Y. Xiangjun
Evaluation of rockbolt performance using field testing 363
S. Soni & P. Clark

Theme 4. Caverns 373

Design and construction of the AS1 shaft within the Albert Street Cavern, Cross River Rail, Brisbane 375
A.C. Rogan, B. Swinn, S.J. Clarke & J. Ahn
Design and construction challenges for the TBM traverse through Brisbane's partially excavated Albert Street Station cavern 389
M.A. Habte, A.G. Smith & S.J. Clarke
Design and testing of BA anchors for temporary support of reinforcement in cavern linings, Cross River Rail, Brisbane 397
S.J. Clarke, F. Cerone & P. Liebrich
Design and construction of the Woolloongabba station caverns for Brisbane's Cross River Rail project 407
M. Habte, B. Shen, M. Kobler & A.C. Rogan
Investigations for tunnels and storage caverns 415
I. Gray & J.H. Wood
Snowy 2.0 down stream surge shaft chamber geological/geotechnical hazards and design challenges 425
A. Palomo, J. Sotomayor, S. Nosrati & D. Hughes
Observational method for the deep powerhouse cavern construction of Snowy 2.0 project 433
I. Ching, M. Diederichs, B. Chapman, K. Thermann & K. Acharya
Temporary slender pillar design in low strength sandstone: A theoretical study on enhancing stability of temporary deep caverns 441
S. Salari, H. De Silva, M. Narayana & C. Xu
Ground response for construction of 15 caverns in diverse ground conditions in Sydney – Part 1: Ground support 449
Y. Bai, M. Trim, T. Bentley, M. Salcher & R. Stocker
Ground response for construction of 15 caverns in diverse ground conditions in Sydney – Part 2: Construction sequence and ground response 461
Y. Bai, M. Trim, T. Bentley, M. Salcher & R. Stocker
Innovations in strand anchor design as part of the support system for a deep underground cavern 471
S.van Ameijde, A. Dunleavy, A. Tarrant & J. Laukner

Modelling the impact of blasting on excavation perimeters 479
P.C. Dare-Bryan & E. Dixon

Theme 5. Underground Mining 487

Using mature and proven technology for mechanized excavation of tunnels and shafts for hydropower schemes to provide sustainable clean energy 489
K. Bäppler
Integrative Feedback Loops: Optimised tunnelling with digital platforms to improve efficiency, safety, and sustainability through a paperless Permit-To-Tunnel process 497
K. Macintosh, R. Hawkey, J. Walton & P. Gaylard
Influence of strain-softening behaviour of fissured clays on deep shaft excavations 505
A. Purwodihardjo, A. Lesmana & P. Booth
A cutting pick for tunneling roadheaders to improve sustainability 513
W. Roach
Assessment of real-time seismic wave velocity in underground mining using laboratory simulations and optimized fuzzy systems 521
H. Samadi & F. Suorineni
Effects of in-situ principal stress magnitudes on unloading strength 531
A. Rooz & B. Sainsbury

Theme 6. Shafts and Cut & Cover 539

Optimized operational and structural solution for a TBM service shaft – Design and construction 541
L. Facibeni, G. Turinetti, V. Besharat & L. Yogasuthan
Multi-criteria analysis of construction methodologies and lining options for deep bored shaft excavations 549
A. Purwodihardjo & P. Booth
Geotechnical design and performance of a rock excavation under a cut and cover tunnel structure in Sydney 557
D. Zografou, V. Tandjiria & M. Mo
Westmead metro station excavation: Design challenges and ground performance 565
Y.H. Toi, E. Chang, C.W. Boon & M.A. Khoo
Ground anchor design and installation challenges within saturated Sydney basin alluvium: A case study for Sydney Metro - The Bays station 575
F. Ceballos Martinez, S. Monroe, S. Mohammadi & D. Jacob
Impact of deep underground station excavation on existing assets in Sydney, Australia 583
S. Manoj, B. Okumusoglu & P. Kozak
Large temporary secant-piled peanut-shaped shaft constructed for the Alkimos desalination plant in Perth: Design and construction 591
J.R. Bombin Saiz, A. Gabarron Duran, S. Jimenez Perez and C. Sancho Perez
Melbourne's Metro Tunnel – City Square rock pillar replacement wall 601
A.L. Watson

Theme 7. Tunnelling Systems 611

Low-pressure ventilation system for road tunnel normal operations – West Gate Tunnel 613
C. Biotto, C. Sahayanathan, C. Jasper & J. Wee
Ventilation challenges and opportunities at tunnelling construction operation – Snowy 2.0 Powerhouse Complex 621
M. J. Jamieson & C. Giordano
A study of mitigation strategies against excessive trackway depressurisation in stations with full-height platform screen doors 629
K. Oguz, O. Ceylan & A. E. Patniotis
Global Navigation Satellite System (GNSS) repeater trial 637
N. Casey & S. Subenthiran
Thermal properties of the Triassic rock formations across the Sydney region for the use in tunnel ventilation design 645
J. W. Davidson, D. Saunsbury, A. Bidarmaghz & D.J. Och
Muck discharge technology and application through slurry circulation system on the EPB TBM 653
Z.G. Zhang, L. Yang, Y.F. Yin, P.Y. Pang, K.P. Chen, K.J. Li & Y.L. Bai
Advanced spoil management in Gotthard Lot 111: Integrated solutions for a challenging alpine tunnel project 659
P.A. Scherwey
Validation of plume dispersion modelling for approval/acceptance against CASA requirements 669
M. Beyer, C. Stacey & A. Gálffy
Physical reasoning behind the critical velocity equation development 681
C. Stacey & M. Beyer
Enhancing operator enclosure air quality in tunnelling operations: addressing silica dust exposure and compliance through AS/ISO 23875 687
J.L. Moredock & K. Cole
Challenges implementing AS61508 on infrastructure projects 693
P. Kroon

Theme 8. Geotechnics 701

Tunnel and marine nearshore ground investigation for Alkimos seawater desalination plant, Western Australia 703
T. Gourlay, T. Whitnall, J. O'Donovan & C. Nash
Engineering geotechnical model and geotechnical interpretation, intake and outfall tunnels, Alkimos seawater desalination plant, Western Australia 711
T. Gourlay, T. Whitnall, J. O'Donovan & C. Nash
Seawater intake riser and brine linear outfall diffuser pile design and impacts from tunnel construction 723
P. Retsos, T. Gourlay & K. Liew
A study on the monitoring technology for the second Jiaozhou Bay subsea tunnel project 731
Zhang Wenbo & He Rongguo
Evaluating deterministic and probabilistic seismic hazard assessments for the tunnel design in Sydney: Insights and comparisons 739
C. Dai
Vibration impacts due to roadheader excavations in Hawkesbury Sandstone on underground structures 747
A. Goldsmith, M. Sheffield, Y. Dong, G. Alvarado, S.X. Poo & N. Lyons
Towards reliable UCS inputs for tunnel design: Learnings from Snowy 2.0 757
A. Chen, M. Zoorabadi & K. Stariha

Dyke encounters in the Sydney basin: Insights from 30 km of mined tunnel excavations 765
N. Lyons & T. Nash
Tunnels and the geologist – are we using geologists effectively? Thoughts and case studies from a 20 year career. 773
H. Baxter-Crawford
Hydrothermally altered Silurian bedrock in Melbourne's North-East Link Tunnel 781
H. Hughes -Adams, D. Tepavac, B. Carnes, C. Hunt & J. Martin
Reducing cost and carbon emissions through rapid design optimisation during construction 791
T.P. Roper, L. Gelonch, C. de Santos, M. Ali & J. Karlovšek
Effect of moving train load on tunnel deformation and track-tunnel interaction 801
H. Farooq, S. Nimbalkar & D. Sheng

Theme 9. Groundwater Control 809

Using the Lugeon test in tunnelling groundwater control - analysis and interpretation 811
H.R. Asche
Waterproofing system selection for tunnel linings 819
U. Pelz & Dr. J. Karlovšek
Exploring innovative groundwater control methods and waterproofing techniques in Sydney tunnels 827
A. Talos & Q. Kenny
Optimum pressure for rockmass grouting between TBM segmental linings of a twin tunnel 835
I. PH. Yim & J. H. Raymer
Water ingress into UECP-2A TBM tunnel – its mitigation and control 841
D.J. Lees, J.L. Sanchez, C. Yi, I. Wanigasekara & S. Banda
Groundwater control in tunnelling using injected polymer barriers 849
R. Colman, A. Osborne, N. Grobler & D. Van Dyk
Numerical modeling of the water pressure influence on the mechanical behaviour of lining 857
N. Wang & X. Yang

Theme 10. Pipe Jacking and Trenchless Technology 863

XXL Pipe Jacking: Technological aspects of large-diameter and long-distance drives 865
B. Hayes
Mechanized cross passage construction 873
M. Bischoff & P. Schmäh
Gold Coast Light Rail: An example of capitalising on underground space to deliver above ground infrastructure 879
A. Edney, D. Keating & A. Browne

Theme 11. Planning, Procurement and Risk Management 885

Important considerations when assessing options to manage ground risk on tunnelling and underground works 887
S.V.L. Barrett
Methodology for comparing dangerous goods risks in road tunnels to those on alternative routes 895
N. Casey, C. Stacey, G. Zaunrith, B. Kohl & A. Dix
A robust approach to major tunnelling fire safety during the construction phase 903
A. Bruce, C. Hiscock, E. Wright, L. Haines & T. Sandum

Selection of different arch shapes rock mass opening for underground space development – Considering rock support pressure requirements and spatial utilisation efficiency 911
K.W.K. Kong & J. Karlovsek
Evaluating Progress: Trends in respirable crystalline silica exposure in tunnel construction 919
K. Cole & T. Driscoll
Importance of risk mitigation for a live tunnel refurbishment project 927
A. Chang, C. Biotto & R. Fernando
Using AI agents for research - a case study the Lane Cove tunnel collapse 935
T. Nye

Theme 12. Asset Management 943

Durability design for tunnels and approaches 945
F. Papworth
Advanced engineering methods to extend and expand the use of reclaim tunnels at Pilbara mine sites 955
J. W. Lee, G. R. Pandey, D. Yau & P. Cutter
Application of geospatial data and artificial intelligence in underground infrastructure development near existing structures 963
H. Wang, A. Rawlinson, J. Sanderson & W. Y. Soo
Challenges in electrical and mechanical asset renewal in established road tunnels 971
J. Cadena Gomez & R. Lau

Theme 13. Digital Engineering 977

Automated extraction of geotechnical data from core photography for tunnelling projects using artificial intelligence 979
S. Johnson & L. D'Andrea
Applying convolutional and artificial neural networks for image-based numerical modelling analysis in tunnelling 987
N. Mirsepassi & A. Mastan
Use of photogrammetry to quantify tunnel overbreak 995
S. Zafari & M. Smith
Digital engineering - lessons learnt from a major Sydney tunnel project 1003
M. G. Sheffield, C. E. Williams & A. L. Tarua
Advancing geotechnical construction phase workflows: leveraging digital tools for improved construction outcomes 1011
H. Buchanan & R. Brehaut
The hidden engine of project success: Best practices for managing large 3D models and 2D documentation in infrastructure projects 1021
E. Saminfar, C. Holt, J. Bateman & E. Westergren
Automation of tunnel modelling for enhanced project efficiency 1029
P. Bueno Leal, F. Calle Lamelas & F. Ceballos Martinez
How I learned to stop worrying and manage the digital - Hard-earned lessons from a major Sydney tunnelling project 1037
A. Monemvasioti Kappos
Enhancing tunnel design and construction through Building Information Modeling (BIM): A case study approach 1045
A. Rajesh & M. Mohandas

Theme 14. Case Histories 1055

Design of the Sydney Metro West turnback tunnels 1057
S.J. Clarke, A. Merritt, D. Tran, D. Wang & M. Lecina
Tawhai tunnel lining recovery 1067
S.F. Chau, T. Cheung, R. Ballen & I. Duncan
Design of the Te Ara O Te Ata – Mt Messenger Bypass project tunnel 1075
J.Q. Cooper, M. Hashim, K. Howard & J. Lim
The Blue Mountains Route Clearance Project – tunnel lining modifications for the Ten Tunnels Deviation 1083
C.K. Bodner & R.M. Gibson
Research and application of key technologies of 15 m super-large diameter single shield TBM in complex geological highway tunnel 1093
Z.G. Zhang, F. He, Y.Q. Lu, S.X Yuan, Z.F. Liu, W.H. Yin, E.J Peng, B. Zheng & H. Liu
Delivering Watercare's Central Interceptor project, Auckland New Zealand 1101
J.B. Sickling
Southern tunnel works – A case history 1109
N Mackintosh, T Bentley & K Teruya
Surface settlement monitoring of the urban canyon - a case study from Brisbane metro 1117
A.J Coulthard, L.W Walsh, P Mathers & S. Keen

Authors index 1125

Introduction

The 19th Australasian Tunnelling Conference was organised by the Australian Tunnelling Society (ATS) and held in Perth, Western Australia, at the Perth Convention and Exhibition Centre between 10 and 14 November 2025. The theme of the conference was Underground Space: Securing our Future.

The intent of the event was to bring together leading professionals, engineers, and innovators in tunnelling and underground infrastructure from across the Australasian region and beyond.

254 abstracts were submitted to the conference, resulting in 130 papers that are included in this volume of proceedings. The papers were prepared by tunnelling practitioners from Australia, New Zealand and nine other countries from Asia and Europe. The papers were grouped thematically into subjects, namely:

1. Linings and TBMs;
2. Temporary support;
3. Sprayed concrete and ground support;
4. Caverns;
5. Underground mining;
6. Shafts and cut and cover;
7. Tunnelling systems;
8. Geotechnics;
9. Groundwater control;
10. Pipe jacking and trenchless technology;
11. Planning, procurement and risk management;
12. Asset management;
13. Digital engineering, and;
14. Case histories.

The editors would like to thank all the general authors and volunteer experts involved in the peer-review of the papers. We would like to thank the local Organising Committee for their support during preparation of this volume. Robin Lehane assisted with final formatting of papers and Major Graphics Printers Pty Ltd completed the pre-press for the electronic volume.

The support of all major sponsors is gratefully acknowledged.

Hugo E. Acosta-Martínez
WSP Australia

Doug Stewart
FSG Geotechnics + Foundations, Australia

Eric Hudson-Smith
Geosite Pty Ltd

THIS PAGE INTENTIONALLY LEFT BLANK

Reviewers

All technical papers in this volume were peer-reviewed. The volunteer reviewers are acknowledged and listed below.

Giovanny Alvarado
Andrew de Ambrosis
Edmund Ang
Justin Arifin
Harry Asche
Ed Ayre
Sam Azari

Blake Bambridge
Paul Barraclough
Stephen Barrett
Helen Baxter-Crawford
Ewan Bennett
Erik Bernard
Robert Bertuzzi
Vahab Besharat
Cristian Biotto
Christian Bodner
John C. Braybrooke

Andrew Campbell
Fernando Ceballos-Martinez
Marlisio O. Cecilio Jr.
Geoffrey Chan
He-in Cheong
Strath Clarke
Ben Coombes
Matthew Cowan
Stuart Cowan

Benjamin Day
Stephen Duffield

Derek Edwards

Hannah Farrant

Peter Gaylard
Soroush Ghaderi
Robert Gibson
Darius Golmadi
Ali Golshani

David Hake
Ivan Haryono
Erik van der Horst
Ian Hosking
Katerina Howard

Craig Johnson
Gwyn Jones
Sam Jones

Jurij Karlovsek
Andrew Kindred
Gencer Koc
Sabrina Kost
Alagesan Ramesh Kumar

Adam Lander
David Lees

Kaylah Macintosh
Ritesh Mahajan
Alex Makaronas
Hossein Masoumi
Andrew Merritt
Nick Mirsepassi
Mojtaba Mohammadnejad

Amit Narsey
Jason Nitz
Ted Nye

Wataru Okada

Roy Bautista Pablo
Stephen Parrish
Ulrike Pelz
Guillermo Andres Peman
Charita Pin

Tony Rechsteiner
Thomas Roper

David Sainsbury
Hanan Samadi
Elnaz Saminfar
Mark Sheffield
Arjun Raja Shivasami
Subhash Soni
Andrew Sorrie
Conrad Stacey
Kevin Stewart
Tim Swavley

Edmund Geoffrey Taylor
Gary Tang
Massimiliano Terenzi
Mark Trim
Chin Fung Tsang

Alessandra Vecchiarelli

Roland Walker
John Wiley
Mahdi Zoorabadi

THIS PAGE INTENTIONALLY LEFT BLANK

We would like to thank our PARTNERS and SPONSORS

Platinum Partner

acciona

Gold Partners

HERRENKNECHT Tunnelling Systems

TUNPROTEC®

Silver Partners

AUS TUNNEL

Bekaert

CREG Underground Solutions

WIRTH

SANDVIK

UNITED SAFETY & SURVIVABILITY CORPORATION

fire protection TECHNOLOGIES

Bronze Partners

FAMA HIGH INTENSITY OF INNOVATION

GS E&C Australia Grow Sustainably

JOHN HOLLAND

Leviat A CRH COMPANY

MONITEL

WHITTENS

Major Conference Supporter

DYWIDAG

Conference Dinner Partner

CPB CONTRACTORS

Welcome Reception Partner

AUS TUNNEL

Barista Sponsors

aurecon

Jacobs

Lanyard Sponsor

AUS TUNNEL

Technical Stream Host (Caverns)

Jacobs

Conference Supporter

ARX SMART MINDS

Official Airline Partner

QANTAS Spirit of Australia

THIS PAGE INTENTIONALLY LEFT BLANK

Building an underwater motorway without harming marine life?

Now it's possible.

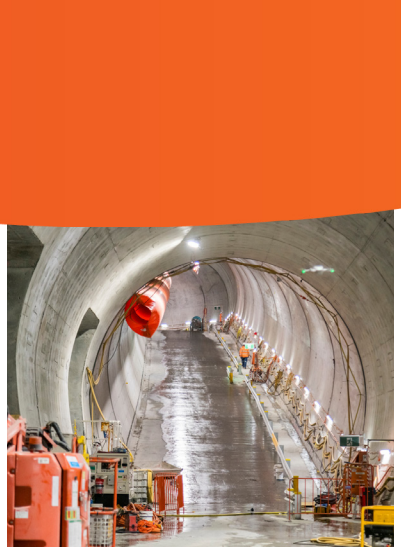


Scan the QR code to learn more

acciona

BUSINESS AS UNUSUAL







Breaking through to a better tomorrow

Global tunnelling expertise, driven by safety, innovation and sustainability.



gsenc.com.au

GS E&C Australia
Grow Sustainably

Constructing our future together

CPB Contractors, Australia's specialist tunnelling contractor, is delivering next generation projects that are reshaping urban transportation and better connecting people and communities.

Working across the roads, mining, rail and utilities sectors for more than 90 years, we've undertaken some of the region's largest tunnelling projects, including:

- the original Snowy Mountains Scheme,
- The Sydney Harbour Tunnel,
- Brisbane Airport Link,
- Epping to Chatswood Rail Link,
- WestConnex M4, M8, Rozelle Interchange,
- Sydney Metro Western Sydney Airport - Station Boxes and Tunnels and Sydney Metro City and Southwest, Northwest Rail Link and,
- Singapore's T-09 Deep Tunnel Sewerage.

Combining the construction track record and expertise formerly delivered by Thiess and Leighton Contractors, our Tunnelling team continues to deliver vital, long-term infrastructure, including:

- Sydney Metro West - Eastern Tunnelling Package,
- Melbourne's West Gate Tunnel, North East Link and Suburban Rail Loop Tunnels,
- Brisbane's Cross River Rail.

DID YOU KNOW?

CPB Contractors is a leader in front-end engineering studies that help our clients effectively deliver their projects. Get in touch now to find out how we can help you.

For more information, scan the QR code

www.cpbcon.com.au | glyn.edwards@cpbcon.com.au

A MEMBER OF THE CIMIC GROUP



HERRENKNECHT DOWN UNDER

WESTERN AUSTRALIA'S SOLUTION FOR WATER SUSTAINABILITY

ALKIMOS SEAWATER DESALINATION PLANT PROJECT, AUSTRALIA
- Client: Water Corporation
- Contractor: Alkimos Seawater Alliance
- Tunnelling length: 4,060 m, 2,600 m
- Machine type: 2 × Mixshield
- Diameter: 2 × 4,125 mm

PIONEERING UNDERGROUND TOGETHER

Visit us at ATC in Perth booth #54 / 55 / 57

TUNPROTEC®

Provided by VID FIREKILL® LOW PRESSURE WATERMIST

Supported by LPGFIRE AUSTRALIA

Infrastructure Fire Protection

NFPA cen

Eco-Friendly System · Sustainable solution · Water saving · Energy efficient

Heysen Tunnel:
first water mist system in tunnel in Australia.

vidfirekill.com lpgfire.com.au

AUS TUNNEL









WE KNOW THE DRILL

By leveraging advanced technologies and a customer-focused approach, Austunnel delivers tailored solutions that meet the unique needs of each project, ensuring timely and cost-effective completion. Austunnel provides reliable, cutting-edge, services and equipment for all tunnelling needs. Partner with Austunnel and experience the dedication and excellence that have established us as a trusted name in the tunnelling and mining sectors.
At Austunnel, We Know The Drill.
austunnel.com.au

Steel fibre concrete reinforcement

Dramix®

No rebar, steel fibre only



David Clague
David.Clague@bekaert.com
M +61 455 052 025

Bekaert

PROTECTING PEOPLE, ASSETS, AND OPERATIONS

SY-KLONE POSITIVE PRESSURE HEPA CAB FILTRATION

- Exceed ISO AS 23875
- Reduce silica dust exposure
- Protect operators' lungs and long-term health



CLEANER AIR. SAFER OPERATORS

FOGMAKER & QTEC MOBILE FIRE SUPPRESSION

- Designed for tunneling and heavy equipment
- Rapid detection & suppression
- Reliable protection where it matters most



STOP FIRES BEFORE THEY SPREAD

fire protection TECHNOLOGIES

TUNNEL FIRE SOLUTIONS

- Fibre Optic Linear Heat Detection
- FireDos® Proportioning Systems
- Watermist Technology
- Video Imaging Detection Systems



ADVANCED TECHNOLOGY, ENGINEERED FOR TUNNELS

E: SALES@USSC.COM.AU | USSC.COM.AU | P: 02 4040 3537

UNITED SAFETY & SURVIVABILITY CORPORATION™

CREG WIRTH

ROAD TUNNEL

CREG 15.7m DIAMETER SLURRY TBM COMPLETES FAT

The super-large diameter slurry TBM "CREC 1459" has an excavation diameter of 15.7m.With a total length of approximately 113m (excluding the rear platform trailers), the TBM is integrated with a number of intelligent technologies, including **the cutter flushing robot, disc cutter changing robot, disc cutters monitoring system, grout proving system, automatic segment hoisting system and spacer grabbing robot.** These intelligent technologies can effectively reduce exposure to high operational hazards and improve the overall construction efficiency through increased use of artificial intelligence and automation.



UNDERGROUND SOLUTIONS PROVIDER

www.crectbm.com E-mail: info_intl@crectbm.com

DYWIDAG

Ground support driven by safety and reliability

Ground Support | Anchors | Soil Nails

- Durable strength
- Customised solutions
- Trusted performance
- Expert guidance



Get in touch

DYWIDAG Australia

sales.au@dywidag.com

17 Nelson Road,
Cardiff NSW 2285

dywidag.com/contact

SANDVIK

mining.sandvik/groundsupport

Reinforcing Australia's future beneath the surface

Sandvik is at the heart of Australia's tunnelling and construction industry. From complex infrastructure to everyday safety, our ground support solutions deliver proven results across a wide range of underground projects.

Safety First – Protecting the people who make progress possible
Reliable Performance – Trusted to keep projects on track
Technical Expertise – Advancing tunnels efficiently for communities
Customer Focused – Solutions that make a real difference

We keep people safe.



Theme 1. Linings and TBMs

THIS PAGE INTENTIONALLY LEFT BLANK

19th Australasian Tunnelling Conference – Acosta-Martínez, Stewart and Hudson-Smith (Eds.)
© 2025 Australian Tunnelling Society, ISBN 978-0-85825-002-4

Efficient design in the Alkimos intake and outfall tunnels

K. Katpakanathan, A. Harding & J. Cockerall
Jacobs Australia, Australia

M. David
Acciona, Perth, Western Australia, Australia

ABSTRACT: For the first time in Perth segmentally lined intake and outfall tunnels have been adopted for a desalination plant: the Alkimos Seawater Desalination Plant, which is currently under construction. These tunnels are also the first segmentally lined desalination intake and outfall tunnels in Australia to be predominately in soft soils. The segmental linings posed a number of design challenges that involved design, construction, and operational considerations. These included setting a diameter and selecting an appropriate alignment. These decisions were constrained by a need to provide sufficient space for tunnel logistics and safety as well as hydraulic requirements, balancing minimum cover with a need to minimise intervention pressures, as well as the design challenges of managing significant internal pressures and significant future regrading and development on the land above the tunnel. The design also had to support a tight procurement schedule that saw the first tunnel being launched just over a year after contract signing. This paper describes some of the constraints that led to segmentally lined tunnels being selected and then describes how the design and construction teams worked together to address the challenges and provide a robust, economical, constructible and safe design.

1 INTRODUCTION

1.1 *Project Overview*

The Alkimos Seawater Desalination Plant (ASDP) Project (The Project) will contribute significantly to the Government of Western Australia's vision for Perth as a liveable, waterwise city and respond to several water supply and demand drivers, including:

- A continuing and long-running declining rainfall trend
- A reduction of inflow volume to Integrated Water Supply Scheme (IWSS) dam network
- A 30GL/a reduction in groundwater allocation from the Gnangara Mound in 2028
- A projected 1.3 million population increase and an estimated 125 billion liters per year increase in potable water demand by 2035.

Located in the high growth area of Alkimos to the North of Perth, the Project includes the design, construction, operation, and maintenance of a new desalination plant equipped for 158ML/d (50GL/a) during stage 1, and future proofing for an additional 158ML/d (50GL/a) during stage 2. The scheme also includes the Eglington Groundwater Scheme (GWS), providing an additional 4.9GL/a, or 18ML/d.

The Alkimos Seawater Alliance (ASWA) has been commissioned to undertake the design and construction (D&C) works for the ASDP. The ASDP is proposed to have the following offshore and onshore elements for the seawater intake and brine outtake structures.

- 2.5 km seawater intake tunnel with vertical risers and intake structures on the sea floor.
- 4 km brine outfall tunnel with vertical risers and outfall diffuser structures on the sea floor.

– Seawater Intake Pumping Station shaft (SWIPS), comprising Onshore Intake, Outfall and Pumping Shaft/ combined into a single structure. This shaft/s will serve to launch the TBMs and be the permanent water intake, outfall, and pumping shafts.
– Main Onshore Desalination Plant.

Both tunnels will be installed as segmentally lined sub-sea tunnels using slurry TBMs. Pipe jacking was not considered feasible for the required length. Trenching was rejected due to significant terrestrial and marine environmental impacts, as well as poor previous local experience installing trenched pipe in the challenging local sea state.

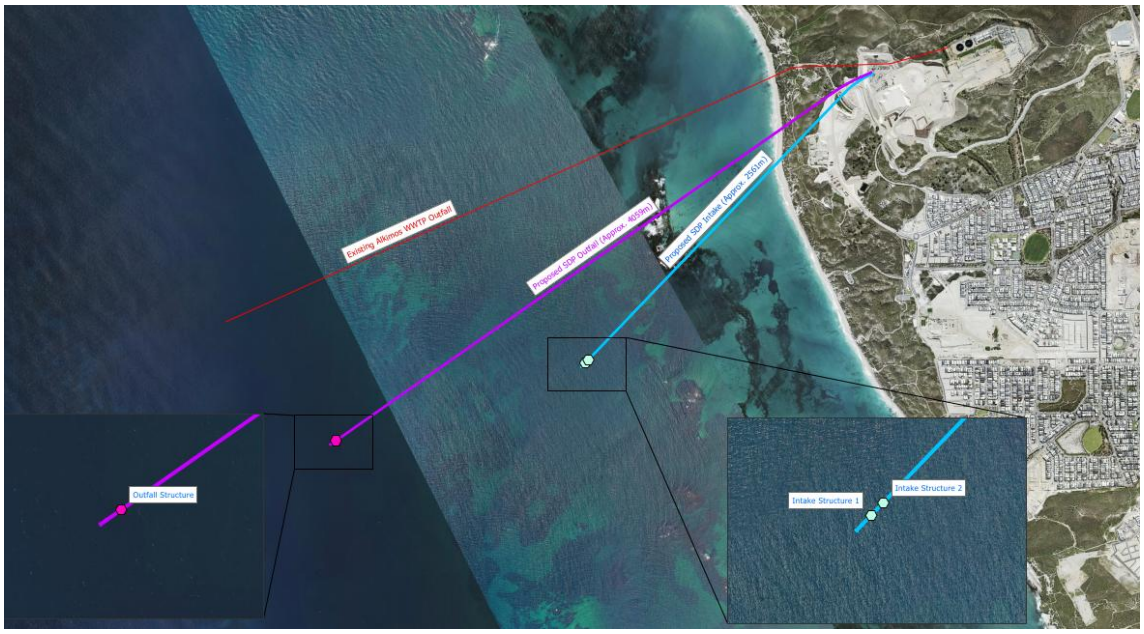


Figure 1. Location of Alkimos Seawater Desalination Plant

1.2 *Functional Requirements*

The TBM tunnel internal diameter (ID) 3.505m is driven by construction stages and space proofing rather than overall hydraulic performance, considering the system hydraulics could manage with a tunnel internal diameter of approximately 2.8m. The key driving construction considerations are.

– To provide the access necessary for the TBM operation and provide sufficient space to run the tunnel trains safely and efficiently.
– Space proofing to dictate the internal diameter of the tunnel for safe access/egress and construction, including ventilation and lighting requirements and to comply with current legislation.
– Providing sufficient space for two trains to pass in the tunnel, and for a train to pass the slurry booster pumps

1.3 *Outfall (Brine Diffusers) System and Requirements*

The brine system primarily consists of the outfall shaft, the tunnel, the riser and the brine diffuser. The brine diffuser is designed with multiple ports to diffuse the brine into the surrounding seawater to meet a salinity of within 0.8 ppt above ambient salinity at a maximum of 100m from the dis-charge point.

Internal water pressure in the outfall tunnel is higher than the ambient seawater pressure due to hydraulic energy losses in the diffuser, riser and tunnel. The majority of the energy losses in the brine system occur at the brine diffuser itself due to the jet velocities required to achieve minimum

dilution rates. Thus, diffuser design and configuration have a significant impact on the internal tunnel pressures.

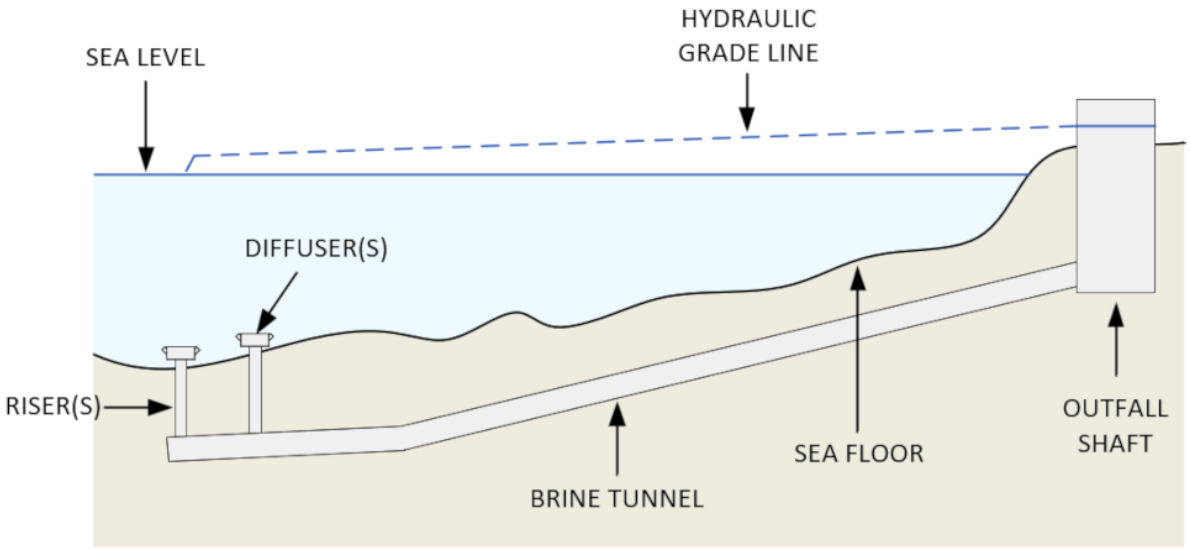


Figure 2. Brine outfall system arrangement

2 DESIGN CHALLENGES

2.1 *Ground Conditions*

The primary engineering geological units encountered along a tunnel face including Tamala Limestone, Ascot Formation, and TQ Sands.

- The Tamala Limestone is of Quaternary geological age underlying the Marine Sediments, three sub-units relating to the degree of leaching and engineering properties varied from Fresh to Residual Soil.
- The Ascot Formation is of Tertiary geological age underlying the Marine Sediments and Limestone. Four sub-units have been determined: Mostly rock strength and cemented materials, mostly soils but with some cemented layers, Variable sand layers and Silt / Siltstone materials.
- The TQ Sands are of Tertiary geological age and only encountered at the outfall tunnel, underlying the Ascot Formation. The unit comprises of predominantly coarse grained (i.e. non-cohesive) materials.

Generally, the Intake Tunnel and the Outfall Tunnel pass underneath Alkimos beach and vegetated sand dunes onshore, and thereafter underneath marine sediments, coral reefs, and ocean water. Both tunnels will traverse the Tamala Limestone early in the drive and pass into the Ascot Formation, which is expected to have lower permeabilities and fewer solution features. From CH2025, the outfall tunnel will pass through mixed ground conditions comprising of the Ascot Formation within the upper portion of the tunnel, and the TQ Sands within the lower portion. Figure 6 presents the geological section along the outfall tunnel alignment.

2.2 *Internal Water Pressure*

One of the unusual challenges of outfall tunnels is the need to design for internal water pressures that exceed the external pressures. In this scenario the tunnel risks going into tension, which requires special features to resist tension such as those described in Harding et al (2014) and Aradas et al. (2016):

- Resist net tension forces by relying on the dowels as illustrated in Figure 3
- Actively resist the tension with permanent bolts and conventional reinforcement

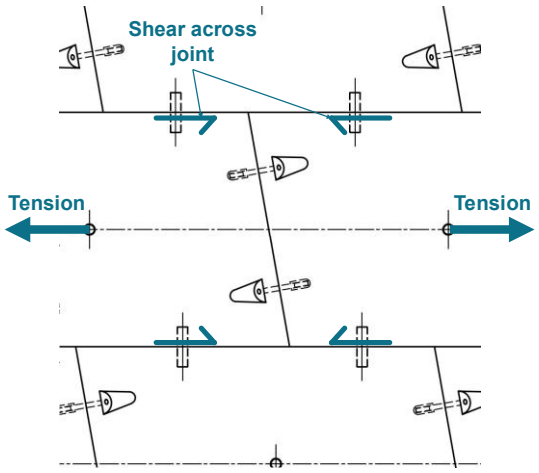


Figure 3. Dowels in the lining acting as a tension transfer mechanism

Using the dowels for the Alkimos project was considered appropriate for resisting tension movements and preventing collapse in an accidental situation where nozzles were blocked and the pressure in the tunnel high, as this scenario was unlikely to occur over the life of the project. However, for normal operation the pressure could change from net tension to net compression several times a day, resulting in the joints opening and closing around 100,000 times over the design life of the project. Under this number of cycles it was possible that the grout/soil/joint interface would deteriorate, leading to loss of structural integrity. Actively resisting the tension by structural means would be difficult due to the aggressive brine conditions in the outfall tunnel. It would also be costly due to the complexities of the connection system and additional thickness required to accommodate two layers of conventional reinforcement.

Therefore, the most efficient design would rely on the effective ground pressures acting on the tunnel to provide additional pressure to resist the tension. Estimating this ground pressure can be difficult because most analytical methods for establishing the ground loads on the tunnel tend to overestimate the ground loads, as this results in higher hoop loads and bending moments and a more conservative design. However, for outfall tunnels this can lead to unconservative designs: where the analysis overestimates the load and indicates there is sufficient effective stress to resist the ground loads but in reality there is not.

To ensure that the load was not over-estimated, analysis was undertaken to establish the minimum ground load on the lining using a Plaxis 3D model that simulates the TBM face pressure, annulus pressure and grout pressure to establish the loads in the lining following TBM construction. Ground loads were expressed as a proportion of the surplus effective stress above face pressure defined as:

$$Restrained\ relaxation = \frac{effective\ pressure - face\ pressure}{insitu\ pressure - face\ pressure}$$

Expressing the relaxation this way allowed a more accurate lining load to be obtained in Plaxis 2D by applying the face pressure as an all round pressure to the excavated annulus and then relaxing the lining by the required percentage. This approach was validated by comparing the 2D models to 3D, for critical sections and load scenarios, while allowing a large number of other scenarios and sections to be evaluated, including a comprehensive sensitivity analysis.

As a result of the analysis the minimum effective load on the lining was 48 kN/m under the worst operational load, providing just enough axial force to maintain gasket pressure and prevent the joint opening.

2.3 Brine Diffuser Configuration

2.3.1 *Type of Diffusers*

Brine diffuser ports may be arranged along a linear diffuser or clustered radially around one or more rosette diffusers. These potential configurations are shown visually in Figure 4. There are examples of each type of diffuser in Australia – Sydney, Melbourne and Adelaide's desalination plants use rosette diffusers and Perth's other desalination plant uses a linear diffuser.

Research by Abessi and Roberts (2014) shows that for both linear and rosette diffusers, the ports and risers should be adequately spaced to avoid individual jet merging. If jet merging occurs, the effective dilution is reduced. Where jet merging cannot be avoided, Roberts proposes dilution reduction factors to account for the reduction in dilution as a result of jet merging. For rosette diffusers, it has been found by Abessi et al. (2016) that there is some jet merging for all rosette diffusers tested, so a dilution reduction factor is recommended to be applied to rosette diffusers depending on the number of ports – from a 27% reduction for 4 ports to 50% reduction for 12 ports (Roberts, 2018). As a result, higher port velocities and higher energy losses are required for rosette diffusers to meet the same dilution criteria compared to a linear diffuser with adequately spaced ports.

2.3.2 Rosette vs linear diffuser outcomes for the Alkimos Desalination Project

The tender design for the Alkimos Desalination Project proposed two rosette diffusers each with 7 ports. Subsequently, during design development, a linear diffuser was investigated for its ability to achieve improved dilution at lower port velocities. The two designs are compared in Table 1 below.

Design flow case results for internal tunnel differential pressure for both the linear and rosette diffuser designs are shown in Figure 5 below. The rosette diffuser design resulted in significantly higher port differential pressures than the linear diffuser design. This is primarily due to the required application of a dilution reduction factor of 0.64 for a 7-port rosette design, which means that smaller ports with higher velocities are required to achieve the same dilution.

For the rosette diffuser design, several flow cases resulted in differential pressures exceeding the maximum for the tunnel lining of 2.7m (27 kPa net internal pressure). Additionally, higher port velocities have been associated with shear mortality of marine micro-organisms (Roberts, 2018), so the lower velocities from the linear diffuser present an environmental benefit.

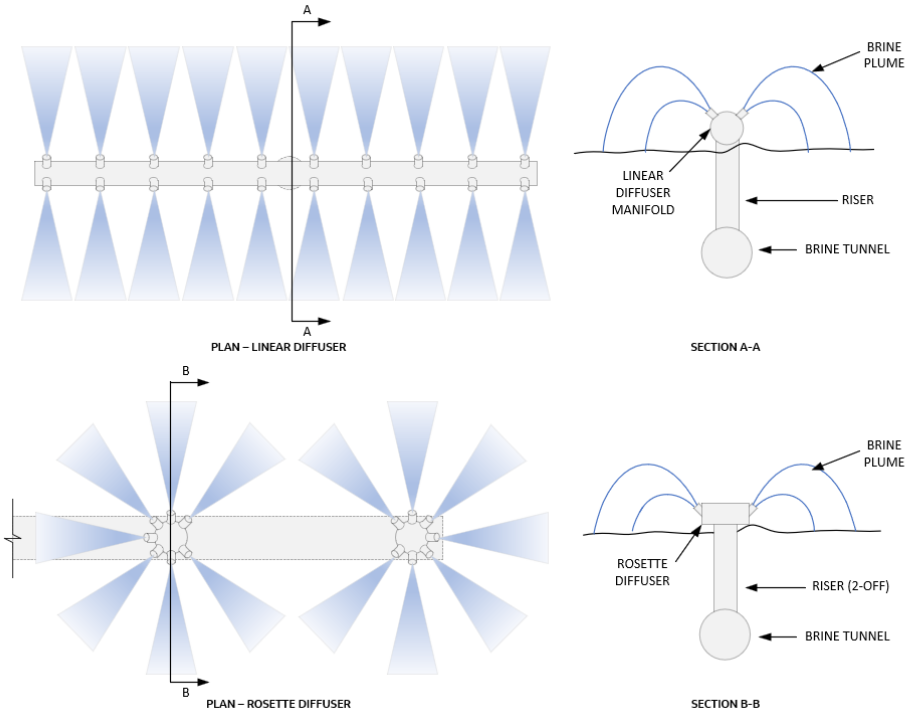


Figure 4. Type of Brine Diffusers

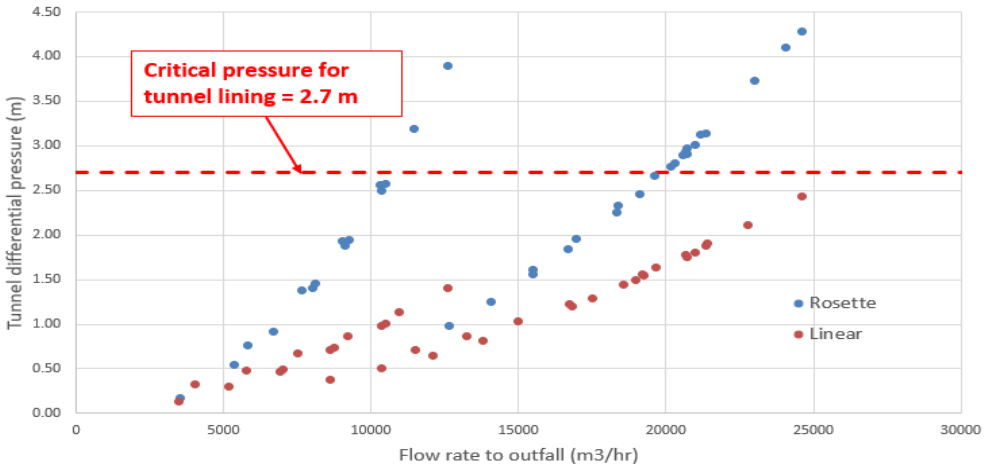


Figure 5. Tunnel differential pressure for rosette and linear diffuser designs

Table 1. Rosette vs liner diffuser design parameters

Parameter	Rosette diffuser design value	Liner diffuser design value	Unit
Number of ports	14	20	Nos.
Port internal diameter	270	308	mm
Port angle from horizontal	40	45	degrees

3 ALIGNMENT AND TBM SELECTION

The alignment was selected to provide the best possible conditions for productive operation of the TBM, while minimising maintenance. The main criteria were:

- Avoid the Tamala limestone as far as possible due to the risk of high permeability/voids that could make interventions very difficult
- Avoid the potentially contaminated soil in the Osborne formation as far as possible
- Provide sufficient cover to prevent blowout
- Avoid local low points if possible

The TBMs launch into the Tamala Limestone, so to minimise the length of tunnel in this deposit the TBMs immediately decline into the Ascot formation. Once in the Ascot formation they follow a very shallow grade (0.35%) to the intake or outfall location, maintaining sufficient cover to prevent blowout.

When subject to internal pressures it can be tempting to make the alignment deeper to secure more axial load and improve tension resistance. However, for Alkimos this would result in very deep tunnels (over four bar water pressure), making interventions longer and more hazardous due to the increased pressures. Furthermore, Aradas (2016) showed that deeper alignments can actually result in lower effective ground pressures on the tunnel due to higher ground strengths. The same was found with the Alkimos alignment, where one of the critical sections was in a full face of limestone where the ground was largely self-supporting. Therefore taking the TBM below the Ascot formation was ruled out. The alignment of the outfall tunnel is outlined in Figure 6.

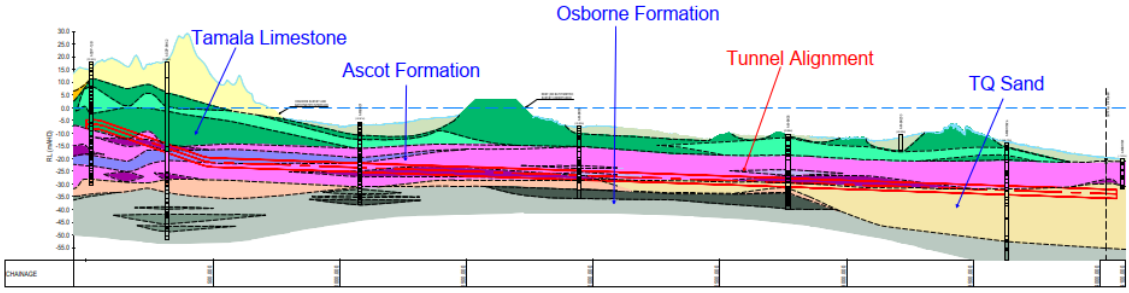


Figure 6. Outfall tunnel alignment (Intake tunnel is similar but shorter)

4 DESIGN SOLUTIONS

4.1 *Ring Configuration*

A tapered universal ring type with internal diameter of 3505mm and external diameter of 3905 mm with lining thickness 200mm and a nominal ring length of 1300mm was adopted. There are a total of 6 segments of each ring. The circumferential joints are connected by 12 Nos of dowels, distributed in an alternating pattern of 28° and 32° which repeats every 60°. This differs from the traditional uniform 30° pitch and it only permits 6 build positions, spaced at 60°.By placing the 28° gap in the middle of the segment on the trailing edge and between the joints on the leading edge, the joints must be placed between the dowels of the previous ring as illustrated in Figure 3. Building the ring with the joints in the same location is not physically possible as the dowel recesses do not align as shown in Figure 8. This ensures the dowels can assist in resisting the tension required, as described in Section 2.2.

The radial/longitudinal joints are connected by 2 Nos of bolts, distributed equally. The radial and circumferential joints are flat joints. The taper was designed as +/- 10 mm based on minimum horizontal radius of 600m and corresponding theoretical design radius of 254m. The segments are equipped with a gasket groove for an elastomeric waterproofing gasket on the extrados side of the joint contact face. Figure 7 below presents the ring configuration viewed from the trailing edge.

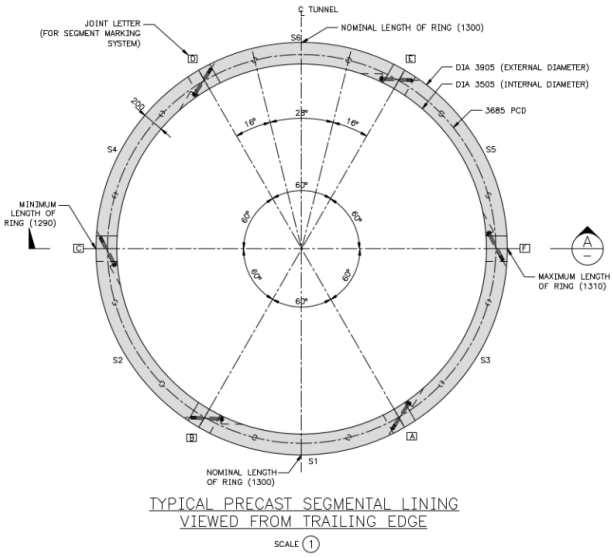


Figure 7. Ring configuration

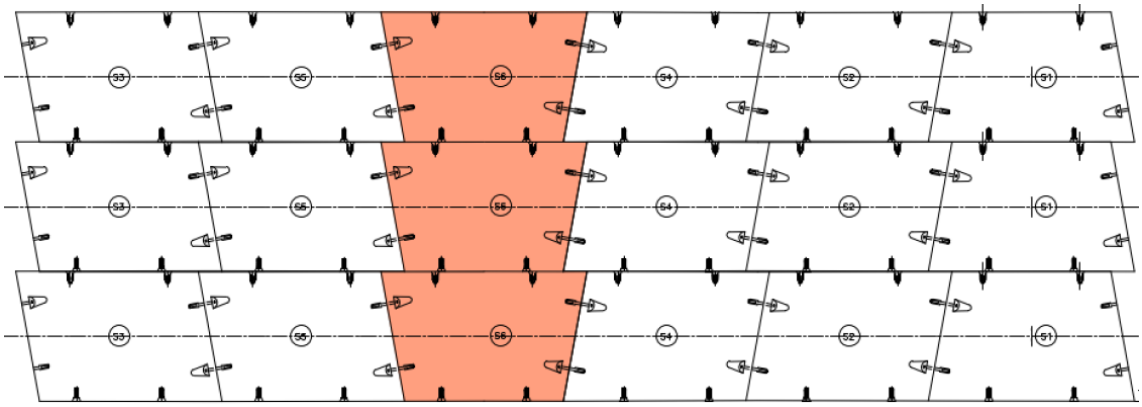


Figure 8. Segment built to the same orientation: dowel locations do not match (not physically buildable)

4.2 *Lining design*

The 2D and 3D models mentioned in the sections above on internal pressure were also used to calculate the moments and axial forces in the lining. Some sections subject to significant cut and fill post tunnel construction to facilitate future development. This generated significant moments and made it necessary to place restrictions on the amount of cut and fill in some locations.

The joint strengths in the deepest sections were at the limit of fibre reinforced joint capacity. In order to prove the joint capacity a novel method for calculating joint eccentricity accounting for both ground loads and build tolerances as described by Harding et al. (2025) was used.

5 CONSTRUCTION CONSIDERATIONS

The intake and outfall bored tunnel construction activities are on or near the critical path and need to be executed productively with minimum associated risks along the entire alignment and the interfaces with other underground structures. A shallow alignment improves risers, tunnel, and shaft constructability. The supports the efficient erection of the lining while still meeting the stringent requirements on accuracy of build as follows:

- Use of a six-segment trapezoid/parallelogram ring, which is proven to build quickly and accurately due to the inclined joints and evenly sized segments.
- Use of dowels on the circumferential joint, which help align the rings while eliminating the need for bolts and the time required to install them, as well as being configured to render undesirable ring build combinations unbuildable.
- The placement of ferrules evenly around the rings provides fixing points for tunnel services, eliminating the need for drilling into the concrete and associated health hazards.

6 CONCLUSION

The design of the segmental lining for the Alkimos intake and outfall tunnels offers an economical solution as summarized below:

- The outfall tunnel is subjected to tension as the internal water pressure acting on the lining exceeds the external pressure. The most efficient design approach was considered by applying minimum face and grout pressure to ensure effective pressures, and then minimizing the pressure losses in the outfall system to minimize net internal water pressures.
- Estimating the ground loads using analytical methods overestimates the ground loads and leads to unconservative design, matching previous research.
- Distributing circumferential dowels in an alternating pattern of 28° and 32° which repeats every 60° can restrict building the rings with joints in the same locations, ensuring the dowels can assist in resisting the tension required in the accidental case.

7 REFERENCES

Abessi, O., Roberts, P., & Gandhi, V. 2016. Rosette Diffusers for Dense Effluents. Journal of Hydraulic Engineering, Volume 143, Issue 4.

Abessi, O., & Roberts, P. 2014. Multiport Diffusers for Dense Discharges. Journal of Hydraulic Engineering, Volume 140, Issue 8.

Aradas, R. D., Fernandez, J. M., Harding A. & Tsingas, D. 2016. Challenges in the design of segmentally lined tunnel for combined sewer outfalls. World Tunnel Congress 2016 (WTC 2016). San Francisco, U.S.

Harding, A; Zernich, B; Wone, M. 2014. Clean Design in Dirty Water: The Blue Plains Tunnel Segmental Lining. North American Tunnelling Conference, Los Angeles, 22-25 June 2014, pp. 464-473, Society for Mining, Metallurgy & Exploration, Englewood, CO, USA.

Harding, A., Boye, B., Katpakanathan, C. Practical design of segmental lining joints for the impact of joint tolerances. World Tunnel Congress. 2025. 8-15 June 2025, Stockholm, Sweden

Roberts, P. 2018. Brine Diffusers and Shear Mortality. Atlanta: Eastern Research Group.

19th Australasian Tunnelling Conference – Acosta-Martínez, Stewart and Hudson-Smith (Eds.)
© 2025 Australian Tunnelling Society, ISBN 978-0-85825-002-4

Design challenges on western harbour tunnel mega TBM segment and cross passages

S.F. Chau & H. Asche
Aurecon, Auckland, New Zealand

J. Shepherd & C. D'Hondt
Acciona, Sydney, Australia

ABSTRACT: The Western Harbour Tunnel project in Sydney consists of twin three-lane tunnels driven under Sydney Harbour by tunnel boring machines (TBMs), which provide design challenges that smaller tunnels do not face. These include increased thrust forces applied to relatively thinner linings. The project tunnels will be the largest diameter TBM tunnels in the southern hemisphere and the largest diameter TBM tunnels with Steel Fibre Reinforced Concrete (SFRC) only segmental lining worldwide. Solutions for cross passage opening design include cored shear keys to transfer loads around the segment opening, including a cast-in bond-breaker to minimise damage. The collar structure of the cross passage is configured to maximise the opening width. This paper describes the design philosophy, engineering challenges and the associated engineering solutions for the segment and cross passages design for this mega TBM tunnel project.

1 INTRODUCTION

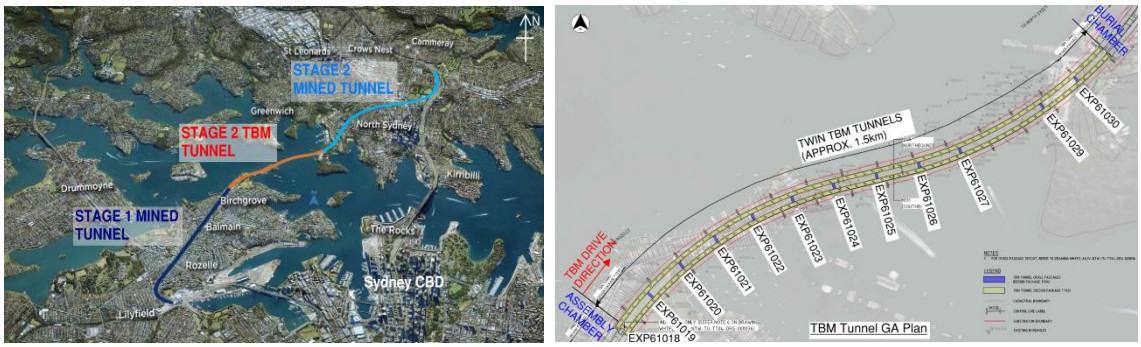
With the needs of urban road network development and development of the tunnelling technique, the use of mega tunnel boring machines (TBMs) with a cut diameter of more than 14 metre rapidly increases. Up until 2024, more than 40 tunnelling projects worldwide have used a mega TBM. The segmental linings for most of these mega TBM tunnels have traditional steel rebar reinforcement (FHWA2020). However, the mega TBM tunnels recently completed or being constructed in Australia and New Zealand, including Auckland's Waterview Tunnels, Melbourne's West Gate Tunnels (WGT) and North East Link (NEL), and Sydney's Western Harbour Tunnel (WHT), are constructed/ lined with Steel Fibre Reinforced Concrete (SFRC) lining (Chau et al. 2024).

WGT and NEL linings are the largest diameter SFRC-only TBM lining without rebar ever completed (WGT tunnel excavation and lining completed in mid-2023, NEL tunnel excavation and lining partially completed 2025 – due for completion mid-2026). WHT is being constructed and will, upon completion, be the largest diameter TBM tunnel with SFRC-only segmental lining in the world.

This paper focuses on the engineering challenges on the mega TBM tunnel segment and cross passage design of the WHT Project.

2 PROJECT BACKGROUND

2.1 *General*



a) WHT overview (image from https://caportal.com.au/rms/wht/)

b) WHT TBM tunnel and cross passage layout plan

Figure 1. WHT overview and TBM tunnel layout plan

Western Harbour Tunnel (WHT) is a new crossing under Sydney Harbour, linking Rozelle Interchange to the Warringah Freeway in Sydney, Australia. The twin 6.5-kilometre motorway tunnel will have three lanes in each direction and will create a western bypass of the Sydney CBD, taking pressure off the Sydney Harbour Bridge, The Sydney Harbour Tunnel, Anzac Bridge and Western Distributor corridors. WHT is being delivered in two stages (Figure 1a). Stage 2 of the project is being delivered by ACCIONA for Transport for NSW, with the designer AECOM AURECON Joint Venture (JV). Stage 2 will use several roadheaders to excavate the northern section and two TBMs to construct the southern section. The 1.5 kilometre long twin TBM tunnels are located between Birchgrove and Waverton and pass beneath Sydney Harbour. Figure 1b shows the TBM tunnel and cross-passage layout plan.

2.2 *Geology and Hydrogeology*

The inferred geology along the alignment of the TBM tunnels is shown in Figure 2. The TBM tunnels will be excavated mostly in Hawkesbury Sandstone, except for a short 180m section of soft ground (alluvial soil of Pleistocene age), where the tunnels cross a paleochannel under the harbour. Marine boreholes have identified geological features, including laminite beds, dykes, open joints and thrust faults in Hawkesbury sandstone, due to stress relief from valley bulging in the eroded paleovalley.

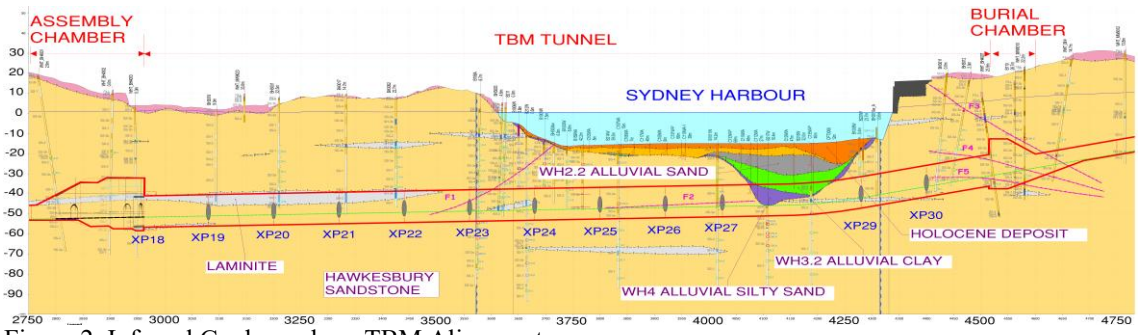


Figure 2. Inferred Geology along TBM Alignment

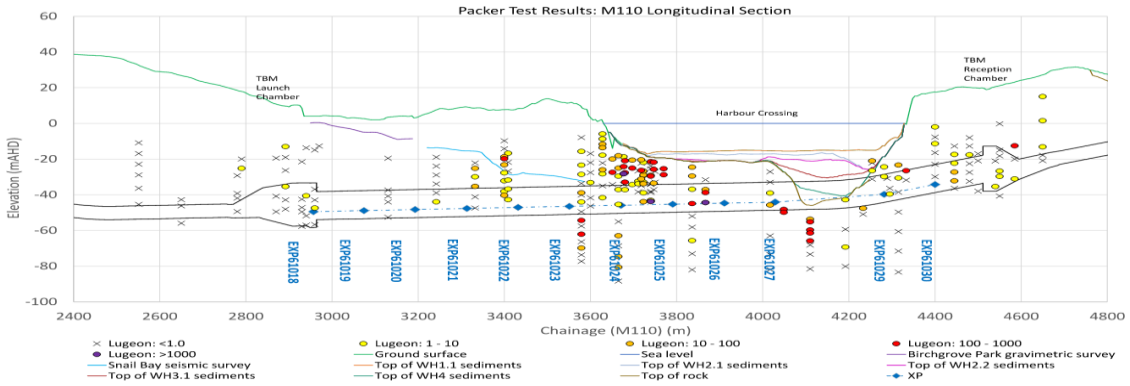


Figure 3. Packer test results along TBM Alignment

The groundwater head to tunnel crown ranges from 35m to 45m (40m to 50m to cross passage crown). Hawkesbury Sandstone is a dual porosity aquifer where groundwater flow potential is dominated by secondary features, such as joints, fractures, faults and bedding planes, whilst the intact Hawkesbury sandstone is mainly impermeable.

Figure 3 illustrates the magnitude and variability of rock mass permeability along the tunnel alignment. Rock mass permeability is higher around the valley that forms the Harbour, where the rock has experienced stress relief and valley bulging (>100 Lugeons). In these areas, existing open discontinuities and rock joints developed at the harbour valley-sides increase the defect aperture, potentially increasing groundwater flow.

2.3 *TBM Tunnels and Cross Passages*

The TBM tunnels have an ID of 14.15 metres and lining thickness of 500 millimetres and will be constructed by two 15.7 metre mixshield (slurry) machines, both advancing from the assembly caverns at the south and will be entombed in reception chambers at the north. It accommodates a three-lane traffic envelope, with a box culvert for facilitating tunnel construction logistics, future-proofing and subgrade backfill to the road level. Figure 4 shows the TBM tunnel and cross passage cross-section.

The TBM section has eleven cross passages with a typical spacing of 120 metres (Figure 1b). Cross passages in road tunnels are for emergency pedestrian movement from the incident tunnel to the non-incident tunnel. The spaceproofing of the cross passages provides the following elements:

– Civil/ Structural: segment opening and collar, emergency egress, comms pit, wall elements, fire-rated doors, internal structures, and drainage.
– MEP (Mechanical, Electrical and Plumbing): Deluge main, Deluge manifold, electrical equipment room (EER), mechanical ventilation equipment, ITS, and lighting.

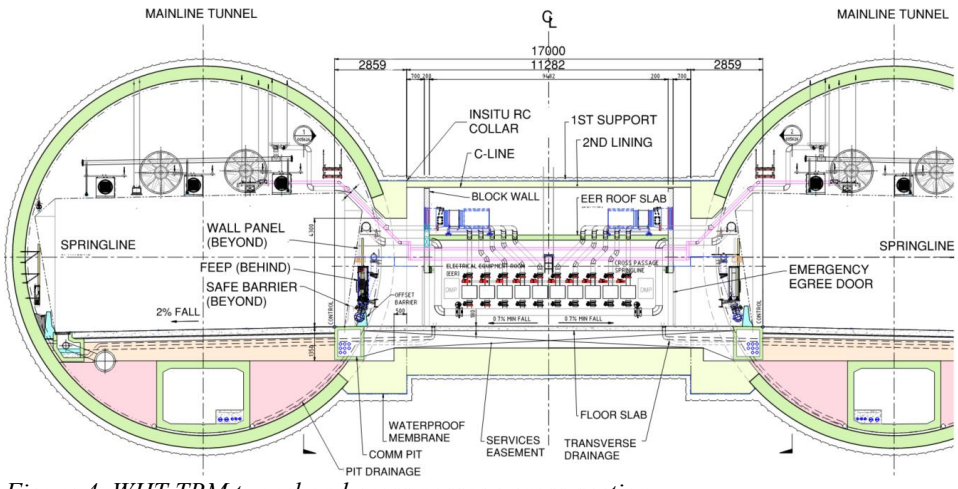


Figure 4. WHT TBM tunnel and cross passage cross-section

3 UNDERSEA TBM TUNNEL STABILITY CHALLENGES

The reference design construction method for the WHT harbour crossing section was immersed tube tunnel (IMT). According to Brown 2023, one of the reasons was to reduce the risk of deep tunnelling (e.g. TBM) through the expected poor geology under Sydney Harbour. Confirming the closed face slurry TBM tunnels altering the IMT for constructing the WHT harbour crossing, there were many other concerns on the environment, construction risks, programme and cost associated with the IMT and cofferdams. However, a crucial technical challenge for TBM tunnel feasibility is understanding the soil/ ground cover to achieve subaqueous tunnel stability regarding structural integrity, tunnel flotation resistance and construction phase blowout prevention.

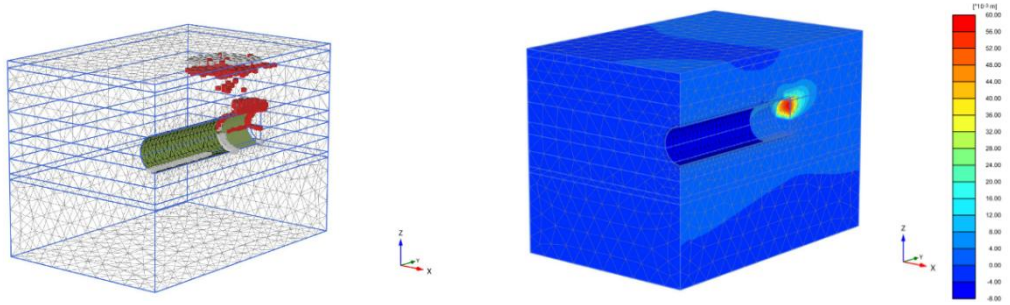
3.1 *Tunnel Flotation, Face Pressure and Blowout*

The minimum soil cover to tunnel crown at soft ground section is approximately 19 metres. Chau et al 2024 has described the methodology and analysis for flotation and blowout checking, including:

- Adopting the model and formulas from Lo et al. 2012 for flotation check, with partial factors derived from PAS 8810:2016 Table 11 and 12 (Limit State UPL).
- Using DAUB 2016 guide to determine the lower face pressure limit to prevent tunnel face cave-in failure and the upper face pressure limit to avoid blowout of the support medium.
- Alternatively, developing a limit equilibrium model including soil shear strength as suggested by Lo et al. 2012 to estimate the maximum face pressure against blowout.
- Undertaking 3D numerical analysis to verify the minimum and maximum face pressure.

3.2 *Annulus Grout Pressure*

Effective annulus grouting of the rings is essential to achieve tunnel safety and ring quality, as well as preventing slurry leaking through the tail shield seals. To achieve this, the primary grout pressure is set to be two bars above the hydrostatic pressure. The tunnel lining has been designed for a maximum annulus grout pressure of two bars plus hydrostatic pressure from the highest water table. The TBM tunnels will be excavated mostly in rock, which is stable for the grout pressure. However, the tunnel and ground stability challenge remain at the soft ground section, at which the maximum grout pressure should be calculated to avoid blowout failure. The maximum grout pressure can be verified same as the maximum face pressure, as checked by Lo et al. 2012 and is 1.2 times the proposed grout pressure. The numerical analysis by 3D Plaxis (Figure 5) has demonstrated this limit with a factor of safety (i.e. phi/c' reduction) of 1.072 against the stability.



a) Plastic points (indicated in Red zones) b) Ground movement shading (heave of 3mm at seabed)

Figure 5. 3D face pressure model results (ultimate face pressure = 2 bars plus hydrostatic pressure)

3.3 *Cutterhead Intervention*

Compressed air pressure for cutterhead intervention is calculated for planning purposes according to the GEO249 guide (GEO 2009). The construction strategy is to carry out interventions in rock

geology under atmospheric or low-pressure hyperbaric conditions. It is planned to avoid undertaking interventions in soft/mixed ground zone, a cutterhead inspection and tool re-dress will be carried out before entering this zone, and a similar exercise will be undertaken approximately 180-200m later when the TBM is back within the full face of rock.

Following the groundwater inflow monitoring, compressed air pressure is set as low as possible without compromising the excavation face stability. Should high-pressure hyperbaric interventions be required, suitably trained hyperbaric workers and supervisors, including mixed gas trained/certified personnel, will undertake the work.

4 SEGMENT DESIGN CHALLENGES

Mega TBM tunnels are always associated with huge hoop forces and TBM ram thrust forces and linings are normally RC segments or SFRC segments with joint reinforcement. In WHT, more challenges for SFRC segment design include high groundwater pressure and a section of soft ground under Sydney Harbour. This required consideration of appropriate design codes, SFRC properties specification, using different empirical and numerical analyses on segment joint design to overcome the design challenges and to confirm the SFRC only lining design.

4.1 *SFRC Segments*

The WHT segmental lining design follows a similar design philosophy to WGT (Ireland et al. 2019, Chau et al. 2020) with project-specified considerations, to overcome the technical challenges to verify the SFRC segment capacity. It mainly includes:

- Adopting PAS8810 code for lining design.
- Using FIP Model Code 2010 for SFRC behaviour.
- Undertaking FEM models to model plastic behaviour of SFRC – validated empirical formulae derived from joint test results for segment joints design.
- Specifying material and segment testing to verify the design approach and assumptions.

WHT adopts SFRC-only segments for the tunnel alignment, except for RC segments at cross-passage opening locations. Upon completion, the WHT tunnel will be the world's largest diameter SFRC-only segmental lined tunnel. The design compressive strength of the concrete segment is 65 MPa. The design characteristic residual flexural tensile strengths of the SFRC are fR1 of 4.0 MPa and fR4 of 4.0 MPa. The characteristic splitting strength is 6.0 MPa. All the design parameters for the SFRC are to be verified by testing.

4.2 *Ring Configuration and Rhomboidal Segment*

The mega TBM tunnels in recent years mostly adopt ring configuration of 9-12 numbers segments with equal subtended angles. WHT tunnels have 10 segments in a ring at an even 36-degree angle subtended by rhomboidal segments (8 nos.) and two trapezoidal segments, the key and the counter key. The nominal length of a ring is 2400 millimetres. The radial joint angle for the rhomboidal segments is 5 degrees, and the radial joint angle for the key and adjacent segments is 10 degrees, with a key segment insert variant angle of 7.5 degrees to achieve a workable key draw distance. The segment ring is a universal taper ring with a taper of 60mm (+/-30mm) so that the key can be built in all 20 possible locations. The schematic developed plan view of the ring arrangement and segment joint arrangement is shown in Figure 6.

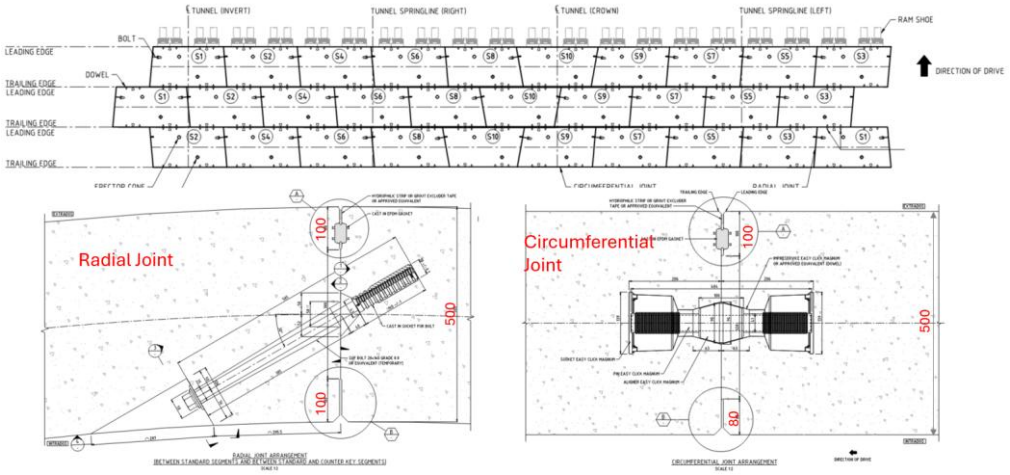


Figure 6. Ring configuration and segment joint arrangement

Based on the available information, the segments of mega TBM tunnels are more commonly rectangular, including the WGT, NEL and Waterview tunnels. For WHT, the preferred ring configuration was to use rhomboidal segments together with circumferential joint dowels to improve the precision of the ring build and to lessen the potential for leakages through the lining joints under high water pressures. WHT is the second largest TBM tunnel with a rhomboidal segment ring arrangement, after the Santa Lucia Tunnel in Italy. A detailed study has been undertaken to compare the rectangular and rhomboidal segment arrangements regarding ring stiffness and bursting stresses at circumferential joints. Chat et al. 2024 have described the details and results, which are summarized below:

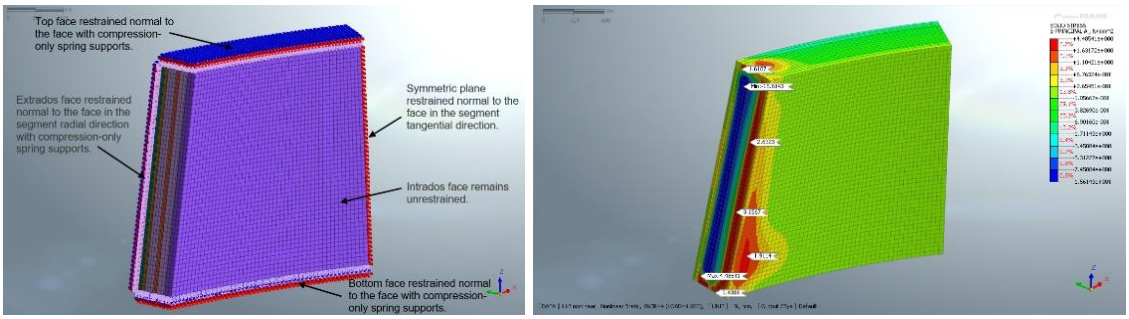
- Rhomboidal segment has a slanted joint, the axial force acting perpendicular to the joint is slightly less than a flat joint, as a result, the slanted joint reduces the maximum moment and therefore, the equivalent rotational stiffness is slightly reduced.
- Ram load impact analysis by Midas (non-linear model FEM software) and ATENA (concrete specialist software) indicates that both rhomboidal and rectangular segments are within acceptable limits for estimated cracking.

4.3 *Segment Joints*

The WHT tunnel radial and circumferential joint design has eliminated the joint steel ladder/ reinforcement requirement. Figure 6 shows the joint details. The WHT Mega TBM lining is subject to bursting stress from high hoop loads and ovalisation on the radial joint and high TBM ram forces on the circumferential joint, compared to metro size tunnels. The gasket groove is long enough to accommodate the larger gasket size and hydrophilic strip or grout excluder tape and to resist concrete corner failure due to gasket compression force. Caulking groove in radial joints is designed to avoid segment intrados corner contact damage due to ring ovalisation. In circumferential joints, the larger the joint contact area, the higher joint capacity is to resist TBM ram load.

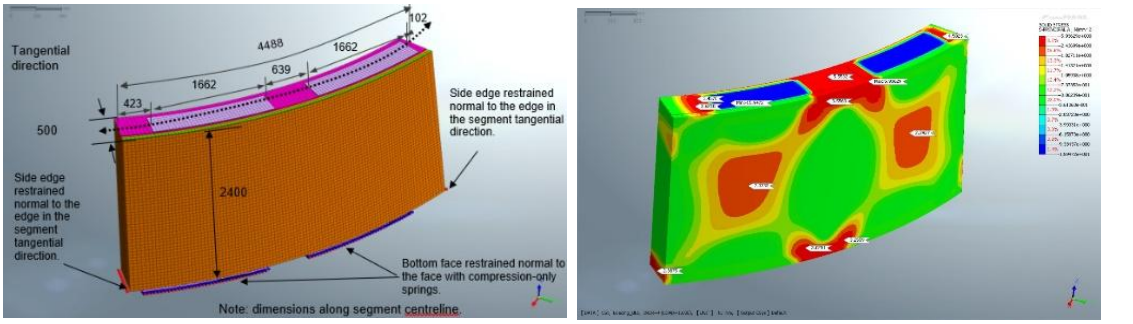
The WHT radial and circumferential joints design and analysis has followed the approach developed from the WGT projects (Chau et al. 2020, Ireland & Chau 2025), which mainly includes:

- Use of empirical Curtis equations to calculate splitting forces crushing resistance etc.
- Elastic analysis by Guyon 1972 method – this has been developed for post-stressed concrete structures and deals with the transmission of high forces through the surface of an elastic body – to check that cracking (SLS) does not occur.
- FEM analysis by Midas - A non-linear analysis is performed with elasto-plastic behaviour for compressive (crushing) and tensile (cracking) of the SFRC material. These models run for both SLS case to determine crack widths and ULS case to confirm structural capacity. Figure 7 and Figure 8 show the 3D analysis for radial joint and circumference joint respectively.

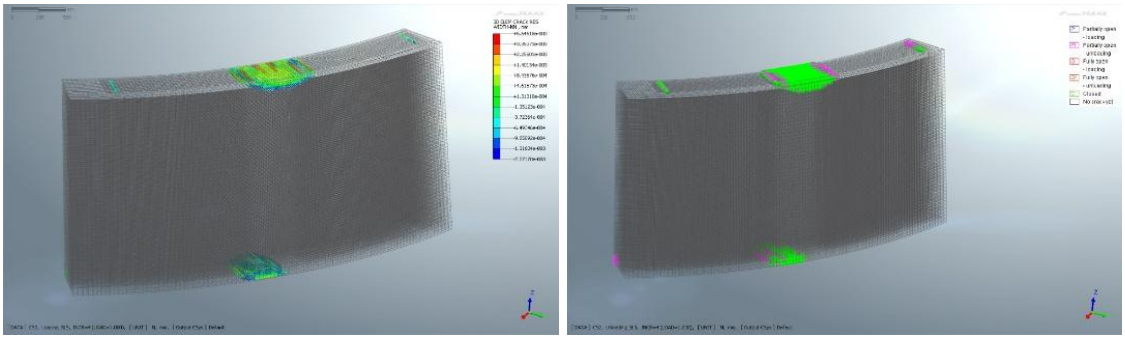


a) Radial joint model input b) Calculated bursting stresses

Figure 7 3D Midas radial joint model



a) Circumferential joint model input b) Principal tensile stress



c) Calculated cracking pattern (colour shading = cracks with RAM load but within crack limits) d) Calculated cracking pattern (green areas = cracks closed after removing RAM load)

Figure 8. 3D Midas ram load and circumferential joint model

5 CROSS PASSAGE DESIGN CHALLENGES

5.1 *Segment Opening and Shear Keys*

Cored and grouted heavy shear keys are described in Della Valle et al 2014, Walter 2019 and Chau et al 2023. Figure 9 shows the shear keys in relation to the opening in the ring arrangements. Bicones are also shown in the joints of the opening sets; four bicones per segment, as well as shear dowels, two per segment.

The action of breaking out the core may lead to damage to the gasket joint. Under Sydney Harbour, this damage would be difficult to repair with potentially five bar of water pressure behind it. To avoid such damage, a solution has been chosen to install a semi-circular bond-breaker in all segments in the opening set and post-core only at the required locations. Site trials of this concept have demonstrated that this approach works; the core to the remaining segment is removed easily without damage (Figure 10).

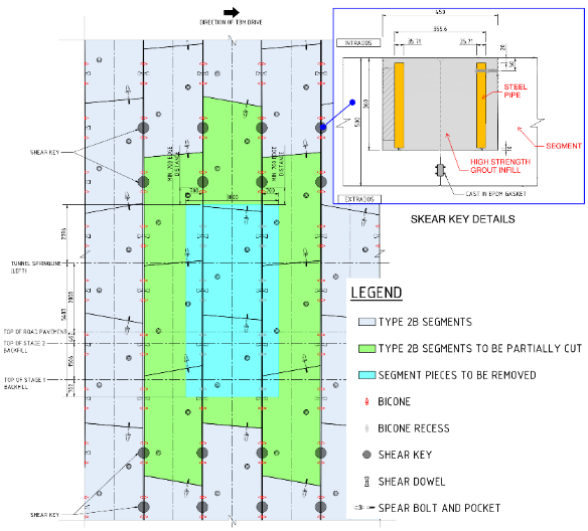
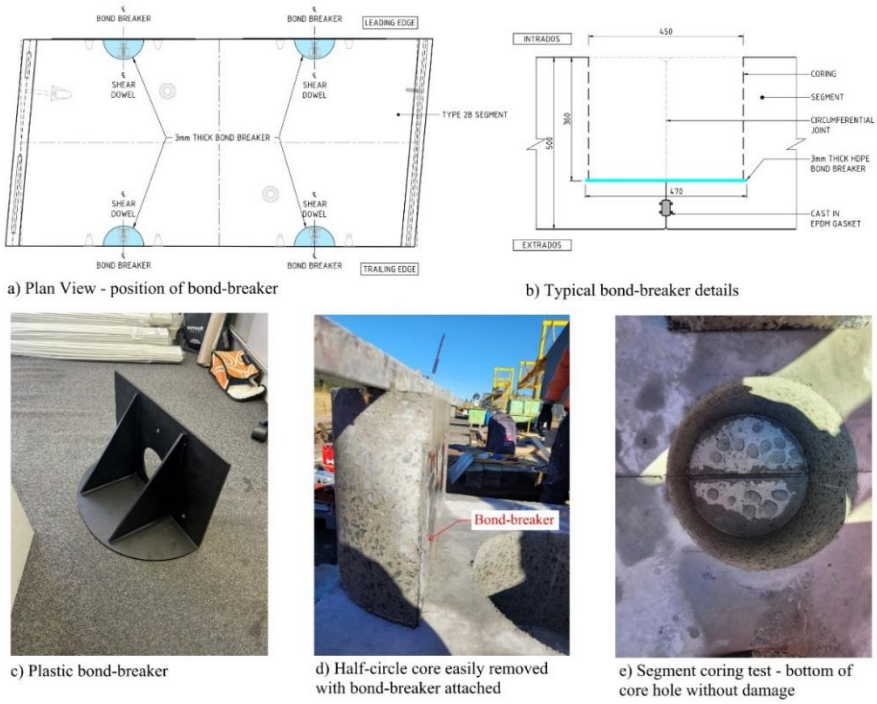


Figure 9. Shear keys and bi-cones arrangement in the segment opening



a) Plan View - position of bond-breaker

b) Typical bond-breaker details

c) Plastic bond-breaker

d) Half-circle core easily removed with bond-breaker attached

e) Segment coring test - bottom of core hole without damage

Figure 10. Shear key/ bond-breaker arrangement and bond-breaker installed for cored shear keys

For the cross passage opening rings, traditional reinforced concrete (RC) segments are adopted to resist the high lining hoop forces from tunnel lining opening that is transferred through the opening ring shear keys. The steel bars around the shear key areas have been arranged to avoid clashing with the bond-breaker.

The analysis of the opening set adopts the conservative consideration that, while the area in front of the opening has the water pressure relieved, the pre-grouting has been effective in limiting water movement and the full water pressure remains around the segment away from the opening. Due to the possibility of intersecting with a high-volume water bearing fissure, pre-drainage around the cross passage has not been considered to be feasible. The segment opening support system had been designed for unbalanced water pressure, full at crown and non-opening side and 5 rings away from opening and varying to zero at opening.

5.2 *Cross Passage Lining and Collar Structure*

The cross passages are in rock, generally Hawkesbury sandstone, or in some locations, also intersect a shale band. Probing and grouting are designed to control water to minimise construction impacts, except at some of the cross passages where areas with high ground permeability will still require a high level of water control. Excavation of cross passages will be by rock hammer. The primary support includes pattern rockbolts and shotcrete.

The secondary lining is designed to be undrained to carry the full external water pressure; this load predominates. The shape of the secondary lining has been chosen to minimise the bending moment generated by the water loading, and the invert and bases of the walls are reinforced with conventional bar reinforcement. In contrast the walls and crown of the lining are SFRC-only.

The collar structure carries the proportion of the permanent load imposed on the cross passage opening after construction is completed; the segments and shear keys carry some of the permanent loads. To maximise the opening space, the lintel beam carries the load in torsion and bending behind the segments to the jamb member located behind the segments (Figure 11). The load distribution on the collar structure in the permanent case is three-dimensional and is primarily influenced by the change in water pressure as the water table returns to its original level post-construction. Structural analysis for the construction stages, with the permanent collar introduced after the temporary opening stage and disregarding the temporary bi-cones and shear dowels (Figure 9), has been undertaken to determine the degree of load sharing between segments, shear keys and collars in the permanent case.

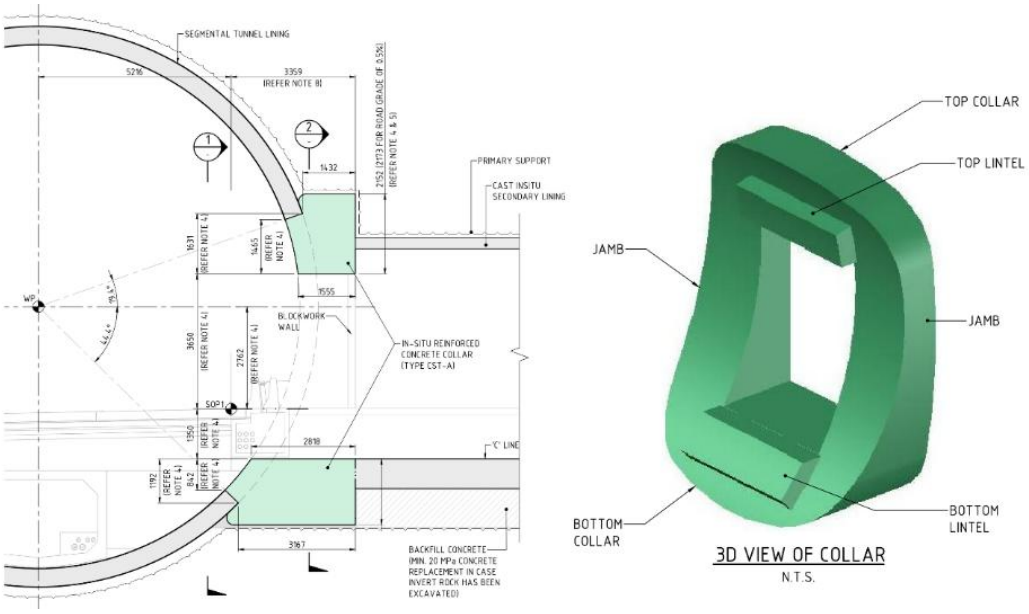


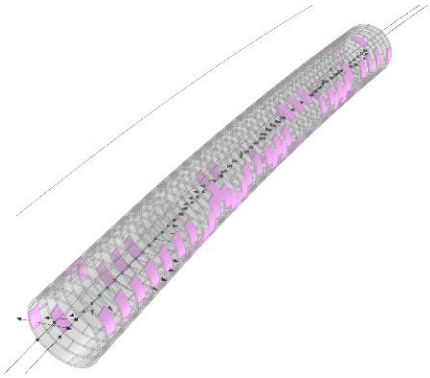
Figure 11. Collar structure showing jamb behind the segments

6 DIGITAL TUNNEL DESIGN

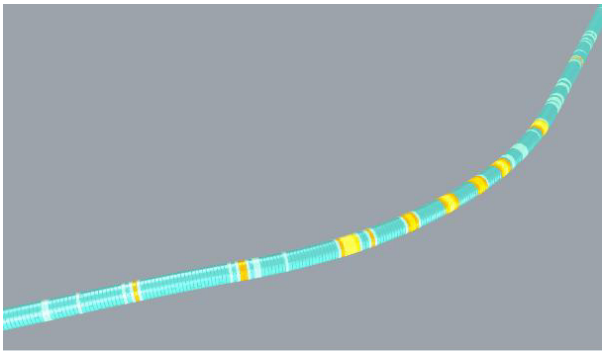
There are a few geometrical complexities in road alignment and cross passage design. The road alignment of the TBM tunnel is generally an "S" shape consisting of two (~960m) curves. However, TBM launch starter rings need to be straight. At cross passages the opening set rings follow the curved road alignment with limited allowable ring build positions, due to an undesirable key segment steeper angle in relation to the opening. Segment creep/ shrinkage normally happens in mega TBM tunnels that affect the actual cross passage locations.

Digital tunnel design (Figure 12) has been carried out to check and verify the above geometrical challenges. A ring model with all segment configuration is created and all 20 ring build positions are defined. The proposed ring build positions at TBM starter rings (for straight alignment) and at cross passages locations (to follow road alignment) based on opening support requirements are

assigned. The digital platform automatically selects the optimum ring build positions to meet the tunnel alignment curve and calculate the ring build position tolerance, with colour coding output. Although there had been many trial runs on different proposed ring build positions, the digital design were efficient and confirmed the allowable ring build positions for TBM launching and at cross passages, which also facilitated the construction planning.



a) Ring build position optimization



b) Colour coding indicating ring build position tolerance amount

Figure 12. Digital tunnel design

7 CONCLUSION

This paper describes the main design challenges associated with Western Harbour Tunnel's mega TBM segments and cross passages. A comprehensive analysis of the stability of the TBM tunnel undersea has demonstrated the feasibility of TBM tunnelling through the soft ground conditions under Sydney Harbour. The segment design has used different empirical and numerical analyses to overcome many design challenges and confirmed the SFRC lining design for the tunnel alignment. Segment opening is designed to be supported by cored shear keys to transit the opening forces, with a bond-breaker at the base of the cored hole to minimise segment damage. Staged construction 3D modelling for segment opening and collar structure allows structural optimisation so that the jambs of collar structure are located behind the segment opening to maximise the opening size while keeping a line of thrust within the cut segments. Digital engineering tools are also used to facilitate tunnel design and construction planning.

8 ACKNOWLEDGMENTS

The paper is published with permission from Transport for NSW, which the authors would like to gratefully acknowledge. The views and opinions expressed in this paper are the authors' and may not represent those of Transport for NSW.

9 REFERENCES

Asche, H., Chau, S.F., Shepherd, J., & D'Hondt, C. 2025. Managing Design Risks for Large TBM Cross Passages, *Proceedings of the World Tunnel Congress 2025*, 9-15 May 2025. Stockholm, Sweden

Brown, T. 2023. A Major Change at the Last Minute for a Major Tunnel Project… Surely Not!, *Proc. of 18th Australasian Tunnelling Conference 2023*, 247-258. 6-8 October, Auckland, New Zealand.

Chau, S.F., Ireland, T., Asche H, Muir, J., & Clarke, B. 2020, SFRC Linings of Mega TBMs, *Proc. of 17th Australasian Tunnelling Conference 2020+1*, 319-331. 10-13 May, Melbourne, Australia.

Chau, S.F., Ireland, T., Lu, L., Gauffre, J., & Cole-Hawthorne, C. 2023. Design and Construction of Segment Opening on Mega TBM Tunnel, *Proc. of 18th Australasian Tunnelling Conference 2023*, 1066-1082. 6-8 October, Auckland, New Zealand.

Chau, S.F., Asche, H., Oliveira, D., Shepherd, J., & D'Hondt, C. 2024. Segment Design for Australia's Largest Diameter TBM Tunnel, *Proceedings of the World Tunnel Congress 2024*, 19-25 April 2024. Shenzhen, China

Curtis DJ. 1976. Discussion of paper by Muir-Wood. *Géotechnique*, Vol 26, No 1.
DAUB. 2016. *Recommendations for Face Support Pressure Calculations for Shield Tunnelling in Soft Ground*. 2016, Deutscher Ausschuss für unterirdisches Bauen e. V. (DAUB)
Della Valle, N., Salas Monge, R., & Savin, E. 2014. Adoption of shear keys to provide stability to TBM tunnels segmental lining during cross passages construction: The example of Aked tunnel. *Proceedings of World Tunnel Congress 2014*. Foz do Iguaçu, Brazil.
FHWA. 2020. *Precast Concrete Segmental Liners for Large Diameter Road Tunnels Literature Survey and Synthesis*, U.S. Department of Transportation Federal Highway Administration, FHWA-HIF-20-035, September 2020
GEO (Golder Associates). 2009. *Ground control for slurry TBM tunnelling*, Geotechnical Engineering Office (GEO) Report No 249, 2009, Golder Associates HK.
Guyon, Y. 1972. *Limit-State Design of Prestressed concrete*, Applied Science Publishers Ltd. London
Ireland, T., Chau, S.F., Asche, H., Muir, J. & Clarke, B. 2019. Steel Fiber Segmental Linings for Mega TBMs, Proc. of the Rapid Excavation and Tunneling Conference 2019, 16-19 Jun, Chicago, US
Ireland, T. & Chau, S.F. 2025. Innovations in Segmental Lining Joint Design for Mega TBMs, Proc. of the Rapid Excavation and Tunneling Conference 2025, 8-11 Jun, Dallas, US
Lo, J., Frew, R., Tsang, C.K., Wong, J., and Choi, K. 2012. Discussion on Soil Cover for a Subaqueous Bored Tunnel, *ITA-AITES World Tunnel Congress 2012*, Bangkok, Thailand.
FIB. 2010. *Model Code for Concrete Structures*. FIB bulletin No. 65. (Sections 5.6 and 7.7 only)
PAS 8810:2016. *Tunnel Design – Design of concrete segmental tunnel linings – Code of practice*. British Tunnelling Society
Walter, A., Mihaylov, V., & Wagner, H. 2019. Development of a guideline for cross passage junctions in segmental lined tunnels. *Geomechanik und Tunnelbau*, 12, 19-32.

THIS PAGE INTENTIONALLY LEFT BLANK

19th Australasian Tunnelling Conference – Acosta-Martínez, Stewart and Hudson-Smith (Eds.)
© 2025 Australian Tunnelling Society, ISBN 978-0-85825-002-4

Autonomous tunnel boring machines in action

M.H. Kamal Arifin, A. Francis & D. Boylan
Gamuda Australia, Sydney, NSW, Australia

ABSTRACT: The application of an Autonomous Tunnel Boring Machine (A-TBM) has demonstrated significant potential in enhancing the precision and efficiency of tunnelling operations. This study evaluates the performance of an AI-driven autonomous system during the construction of the Sydney Metro West – Western Tunnelling Package. Real-time operational data was analysed to compare the alignment accuracy, cutter disc wear and energy consumption of a autonomous and a manually operated Tunnel Boring Machine under similar geological conditions. The results show that the autonomous system reduced alignment deviations, minimised cutter disc replacements and optimised energy usage. These findings highlight the capability of A-TBM's to optimise large scale tunnelling projects effectively.

1 INTRODUCTIONS

1.1 *Objective*

This study aims to conduct a thorough comparative analysis of the performance of automated and manual Tunnel Boring Machine (TBM) operations. By selecting key performance indicators (KPIs), we intend to quantitatively evaluate the benefits of each operating mode and compare their performance across these metrics.

1.2 *Background*

A-TBM's is an advancement in mechanised tunneling, developed to reduce reliance on skilled human operators and improve the overall performance and efficiency of TBM operations. The system uses control algorithms to automate key TBM functions such as steering, advance and excavation control. It was successfully implemented on the Klang Valley MRT Line 2 in Malaysia, where it was initially deployed resulting in improved accuracy, consistency, and safety in tunnelling processes (*J. Lim Ji Xiong et al., 2020*).

2 METHODOLOGY

2.1 *Experimental Location Settings and Timeframe*

The experiment conducted a comparative analysis of two 7.0m diameter Hard Rock Double Shield Gripper TBM's operating on a section of the Sydney Metro West – Western Tunnelling Package in Sydney, Australia. A 560m test section of the tube alignment was selected for the trial with one TBM operating wholly in autonomous mode, while the other operated wholly in manual

mode. The first TBM excavated the test section in autonomous mode from February to March 2024 and was followed by the second TBM operating in manual mode from March to April 2024. The two test alignments were separated by 13 meters in horizontal distance only, following almost identical horizontal and vertical alignments and encountered almost identical geotechnical conditions.

2.2 *Geological conditions*

The tunnelling alignment through which the trial was carried out lies within a geological zone composed of sedimentary shale and sandstone from the Permian and Triassic periods. For the test alignment, the TBM's progressed through a shale-sandstone interface to a full face of sandstone, before completing the trial section in a similar transition zone of sandstone to shale as shown in Figure 1. This trial area ensured that both TBMs encountered a varied range of geological conditions, allowing for a comparative analysis of their performance under differing ground lithologies in autonomous and manual operation.

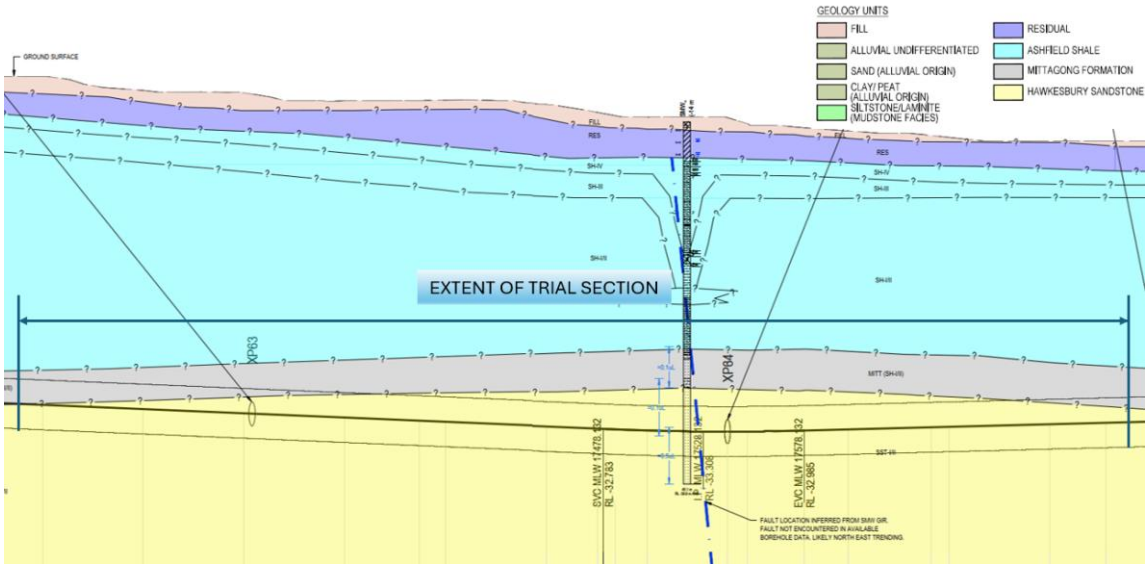


Figure 1. geological conditions during experimental section.

3 KEY PERFORMANCE INDICATORS ANALYSED

3.1 *Steering Data Analysis*

Steering data encompasses several critical elements that can be analyzed to compare the performance of autonomous and manual operation modes. The navigation system of the TBM captures the live positional data, which is then retrieved by a data acquisition program and uploaded to cloud storage. The data examined in this paper was the Front Shield Deviations (Horizontal and Vertical) which refers to the horizontal and vertical displacement of the midpoint of the TBM's front shield in relation to the design tunnel alignment. It indicates the extent to which the current position of the front of the TBM shield diverges from the design tunnel alignment as the TBM progresses.

3.2 *Advance parameter data analysis*

Three significant Advance Parameter variables were selected for analysis in order to compare performance between autonomous and manual modes. The three variables analysed were:

– Penetration: This variable measures the depth of advance achieved by the TBM with each revolution of the cutterhead. It is crucial as it directly reflects the volume of material excavated per revolution of the TBM cutterhead. A consistent penetration rate indicates optimal TBM

operation and is influenced by various factors, including the encountered geological conditions, the TBM thrust force applied, the rotational speed of the cutterhead, and the wear condition of the cutting tools.

- TBM Thrust Force: This is the axial force exerted by hydraulic cylinders at the rear of the shield, propelling the cutterhead and shield forward. Thrust force must be dynamically adjusted by either the autonomous system or the manual operator in order to respond to changes in ground conditions. Improper application of thrust can reduce excavation efficiency, lead to over-excavation, and accelerate wear on the cutting tools.
- Cutterhead Torque: This refers to the rotational force applied to the TBM cutterhead, allowing it to cut and break the ground at the tunnel face. Deviations from the optimal cutterhead torque can signal poor excavation efficiency, increased power consumption, and heightened wear on the cutting tools.

During TBM operation, these three variables have set maximum limits that define the optimal operating conditions for the machine. The closer the TBM operates to these setpoint limits, without exceeding them, the more efficient its performance. In this report, the values presented in the results tables below represent the ratio of the actual recorded average values to the setpoint limits. Additionally, scatterplots have been included to illustrate the spread & maximum instantaneous values in each mode.

3.3 *Cutter Replacement Data*

The rate of cutting tool replacement is a key factor that directly impacts the efficiency of TBM operations. Individual cutting tools represent a significant expense, and the downtime incurred during tool changes delay the TBM's progress. Therefore, optimising cutting tool replacement rates is essential for improving TBM operational efficiency. Achieving the right balance between either excessive or insufficient tool replacements is vital for maximizing the average advance rate during a tunnel drive.

3.4 *Energy consumption data*

Energy readings are collected from the TBM Power Monitoring Device (Sentron PAC3220), which tracks cumulative energy consumption in kilowatt-hours (kWh) for each TBM. This data then undergoes filtering and processing to determine the energy consumption per advance. These results are sumarised in table 7 below for each TBM mode during the test period.

4 RESULTS

4.1 *Summary Tables and Scatter Plots Analysis*

Steering and advance parameter data from the experiment were analysed to directly compare the performance of Autonomous and Manual TBM modes. For advance parameters, performance was evaluated using the ratio of actual values to their setpoint limits, measuring how closely each mode operated to the defined setpoints. The results are assessed using the following statistical metrics:

- Median – Indicating the central value of the dataset, representing typical system behaviour. A value closer to target reflects better control.
- Width / Interquartile Range – Measures the spread between the 25th and 75th percentiles. A smaller width implies more consistent and stable performance.
- Maximum (Max) / Minimum (Min) – Captures the range of extreme values, helping to identify outliers and operational anomalies.

In addition to the statistical summaries, scatter plots have been used to visualise the maximum values of key advance parameters such as penetration rate, thrust force, and cutterhead torque for each advance. These plots help illustrate the frequency and magnitude of values exceeding the set operational limits, providing further insight into control behaviour between Autonomous and Manual operating modes.

4.2 *Front shield deviations*

Table 1 demonstrates that the Autonomous mode allows the TBM to follow the horizontal tunnel alignment more accurately than Manual mode, as indicated by a lower median deviation of 0 mm in Autonomous mode. In contrast, the Manual mode shows a median deviation of -2 mm.

Table 1. horizontal and vertical front shield deviations

Axis (Mode)	Median	Width	Max	Min
	mm	mm	mm	mm
Horizontal (Autonomous)	0	4	+29	-26
Horizontal (Manual)	-2	8	+35	-48
Vertical (Autonomous)	+4	3	+26	-12
Vertical (Manual)	+8	2	+33	-3

In addition to the median, the width reflects how consistent the data is. Autonomous mode shows better consistency in horizontal alignment, with a narrower interquartile range (IQR) of 4 mm, compared to 8 mm in Manual mode.

In the vertical plane it can also be seen that Autonomous mode keeps the vertical alignment closer to the tunnel design, with a median deviation of 4 mm, while Manual mode recorded a higher value of 8 mm. However, it is interesting to note that Autonomous mode did have a higher rate of vertical deviation above and below the design alignment resulting in a wider interquartile range of 3 mm compared to 2mm for Manual mode.

Figure 2 provides an alternative visualisation of Front Shield Deviations using a scatter plot format to represent tunnel alignment. Each marker corresponds to one TBM advance, with average deviations plotted along the horizontal and vertical axes. Overlaid ovals highlight the general clustering of data points for both Autonomous and Manual modes. In Manual mode, the horizontal deviations tend to cluster further to the left (negative side) compared to Autonomous mode. This pattern reflects a common operator behaviour — manually steering the TBM toward the inside of curves. As the majority of the test alignment section comprised of a left-hand curve, this steering tendency results in a consistent leftward bias, contributing to a more negative median deviation. Further to this the clustering of results in manual mode above the design tunnel alignment also displays a common trait of manual operation with operators tending to always guide the TBM higher to prevent the falling below the design which can be more difficult to recover in some situations.

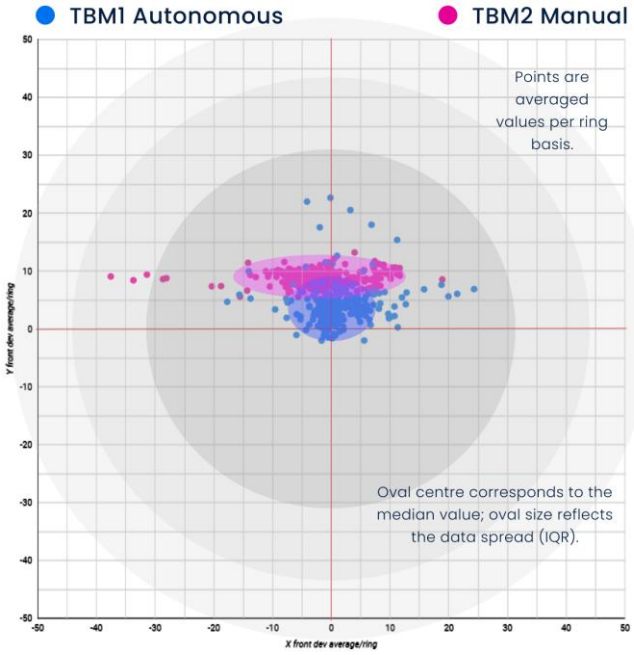


Figure 2. front shield deviations autonomous and manual (tunnel alignment visualisation)

4.3 *Penetration*

Table 2 and the scatterplot below presents the data collected for cutterhead penetration and it shows that Autonomous mode maintains penetration rate consistently below the set upper penetration limit, in contrast to Manual mode which had more occurrences exceeding the penetration limit. In Manual mode, the maximum penetration ratio reached nearly 100% over the setpoint value at 1.99, whereas in Autonomous mode, it was significantly better controlled with a maximum value only 5% over the setpoint value at 1.05.

Table 2. autonomous and manual comparisons for penetration: limit ratio

Mode	Median	Width	Max
Autonomous	0.62	0.11	1.05
Manual	0.65	0.09	1.99

In terms of consistency both Autonomous and Manual modes showed comparable results with widths of 0.11 & 0.09 respectively.

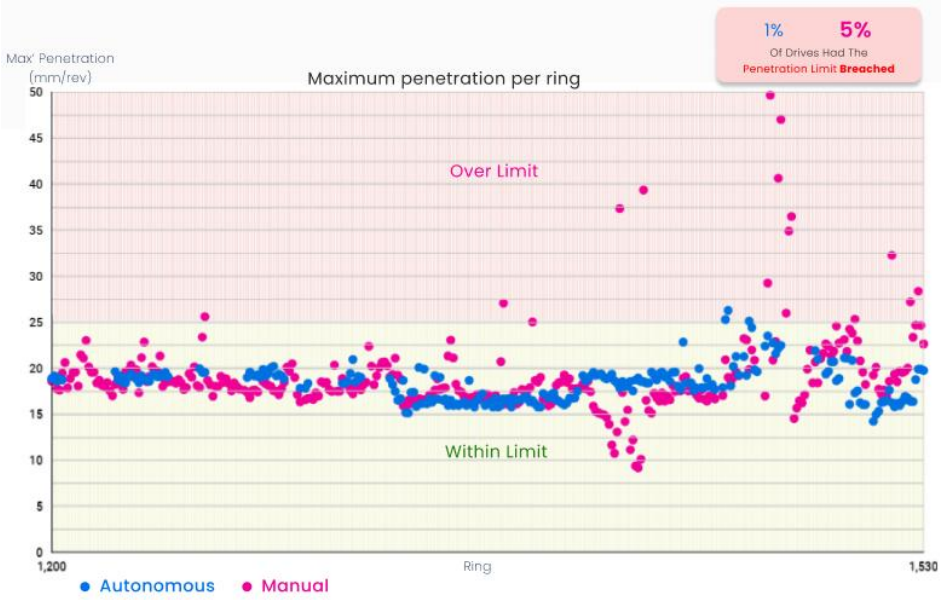


Figure 3. scatter plot of maximum penetration values from ring number 1200-1530

Figure 3 above presents a scatter plot of maximum penetration values, showing that approximately 5% of the advances in Manual mode exceeded the set limit, compared to only 1% in Autonomous mode. This demonstrates how Autonomous mode effectively regulates penetration to stay within the required thresholds more efficiently than manual mode.

4.4 *Thrust force*

Table 3 illustrates that Autonomous mode maintains thrust force below but closer to the set maximum limit than manual with median values of 0.78 and 0.76 for Autonomous and Manual modes respectively. In terms of consistency, Autonomous mode shows a narrower width (Interquartile Range) of 0.10, compared to 0.13 in Manual mode, indicating more stable control. This suggests that Autonomous mode was able to regulate thrust force closer to the set limit resulting in more controlled and predictable operation of the TBM.

Table 3. autonomous and manual comparisons for thrust force: limit ratio

Mode	Median	Width	Max
Autonomous	0.78	0.10	1.02
Manual	0.76	0.13	1.09

Referring to Figure 4 below, which presents a scatter plot of maximum thrust force values, shows that 3% of the recorded values in Manual mode breached the limit, while no exceedances

were observed in Autonomous mode. Additionally, in Manual mode, several points show unusually low maximum thrust values indicating erratic application of TBM thrust as the manual operator may over adjust TBM thrust according to their perceived "feel" of the ground conditions being encountered.



Figure 4. scatter plot of maximum thrust force values from ring number 1200-1530

4.5 *Cutterhead torque*

Table 4 shows that Autonomous mode consistently maintains cutterhead torque levels below the defined limit, whereas Manual mode displays exceedances, with a maximum value reaching 2.21—nearly twice the set limit. Additionally, Autonomous mode demonstrates greater consistency, as indicated by a narrower width (Interquartile Range) of 0.11, compared to 0.32 in Manual mode.

As illustrated in Figure 5, the scatter plot of maximum torque values reveals a stark contrast between the two modes: approximately 59% of advances in Manual mode recorded torque levels exceeding the defined limit, while in Autonomous mode, only 2% of advances breached the same threshold. This significant difference highlights the effectiveness of Autonomous mode in actively regulating cutterhead torque, ensuring operations remain within safe and controlled parameters.

Table 4. autonomous and manual comparisons for cutterhead torque: limit ratio

Mode	Median	Width	Max
Autonomous	0.46	0.11	0.84
Manual	0.77	0.32	2.21

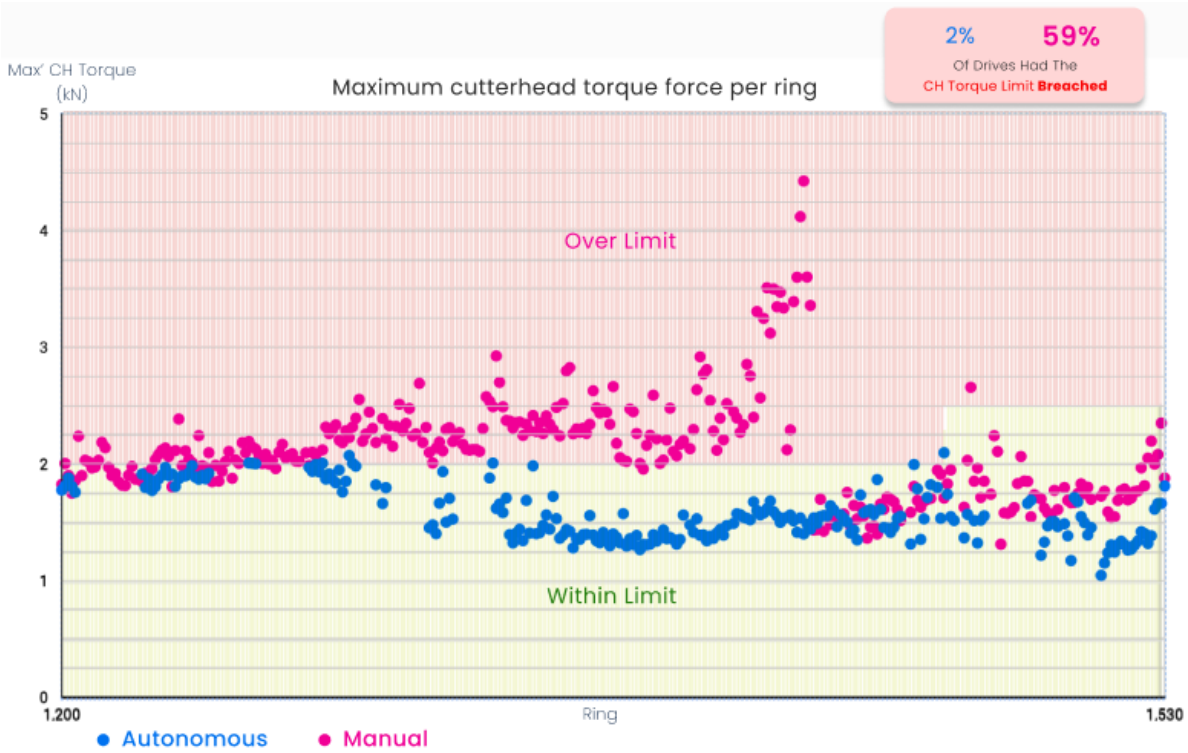


Figure 5. scatter plot of maximum torque values from ring number 1200-1530

4.6 *Cutterhead disc replacement comparisons*

The total number of cutter discs replaced for each TBM during the experimental period is summarised in Table 5 below. TBM 1 operating in Autonomous mode required only one cutter disc change while TBM 2 operating in manual mode required six cutter discs to be changed over the 560m experimental period.

A similar trend was observed throughout the complete length of these two 4.5km drives. Outside of the experimental period, the operating mode of the TBM was not strictly enforced and was left to the discretion of the individual operators subject to the ground conditions encountered. TBM 1 operated in Autonomous mode significantly more than TBM 2 and required a total of 16 cutter disc changes while TBM 2, with a higher percentage of operation in manual mode, required 35 cutter discs.

Table 5. autonomous and manual comparisons for disc replacements

Mode	Test Period	Total 4.5km Drive
Autonomous	1	16
Manual	6	35

4.7 *Energy consumption comparisons*

The energy consumption data over the test period for both TBM's is summarised in Table 6 below. The results show that Autonomous mode consumed less energy during the Advance phase, with an average energy usage of 403 kWh, whereas Manual mode had an average energy use of 467 kWh per advance, 64 kWh higher than Autonomous.

Additionally, Autonomous mode demonstrated greater consistency, reflected by a narrower interquartile range (IQR) of 31 kWh, compared to a significantly wider 80 kWh in Manual mode, more than twice the variation, indicating more stable and efficient energy usage under autonomous control.

Table 6. autonomous and manual energy comparisons during advance

Mode	Average	Width	Max	Min
	kWh	kWh	kWh	kWh
Auto	403	31	524	320
Manual	467	80	714	363

Moreover, the outlier values further support the improved performance of Autonomous mode. The minimum energy consumption recorded in Autonomous mode was 320 kWh, which is 43 kWh lower than that of Manual mode. Similarly, the maximum energy consumption in Autonomous mode was 524 kWh, compared to 714 kWh in Manual mode. This significant difference on maximum side is due to the excessive torque that has been observed in Figure 5. These findings suggest that with effective control of Advance parameters, Autonomous mode not only reduces average energy use but also avoids energy spikes, resulting in a more efficient and stable tunneling operation.

5 CONCLUSIONS

The above experiment set out to test under a structured framework key TBM performance indicators, including steering accuracy, advance parameter control and overall energy efficiency of the autonomous TBM compared to traditional manually controlled TBM operation. Under controlled conditions the autonomous TBM used on the Sydney Metro West - Western Tunnelling Package demonstrated measurable improvements in these areas when compared to manual operation.

Specifically, it achieved better alignment control with reduced front shield deviation from the design alignment. Also, the TBM maintained advance parameters within acceptable limits more consistently than manual operation leading to fewer cutting tool replacements overall reducing total maintenance downtime. Furthermore, the autonomous TBM demonstrated more efficient energy consumption compared to manual operation during the experimental period. These improvements contribute to lower operational costs and more efficient TBM operations.

In conclusion, the findings from this experiment underscore the potential of autonomous tunnelling technology to improve tunnelling operations. By enhancing precision, reducing maintenance, and improving energy efficiency, autonomous TBMs can lead to more sustainable and cost-effective tunnelling solutions.

6 REFERENCES

Lim Ji Xiong, J., Liew Kit Shen, S., Jon Batty, R. and Chin Jing Ho, J., 2020. The Pursuit of an Autonomous Tunnel Boring Machine. In: International Tunnelling and Underground Space Association. Available at: https://library.ita-aites.org/wtc/1885-the-pursuit-of-an-autonomous-tunnel-boring-machine.html

19th Australasian Tunnelling Conference – Acosta-Martínez, Stewart and Hudson-Smith (Eds.)
© 2025 Australian Tunnelling Society, ISBN 978-0-85825-002-4

Design of deep undrained tunnels for groundwater pressure using Australian Standards

H. Alaedini, H, Asche & T. Peglas
Aurecon, Brisbane, Australia

ABSTRACT: As urban areas expand, tunnels are increasingly constructed at greater depths to avoid existing infrastructure and water bodies. Deep tunnels are sometimes designed as undrained (tanked) to reduce environmental impact, lower operational costs, and minimise settlement risks. In the case of segmental linings installed by Tunnel Boring Machines (TBMs), the PAS 8810/EC2/Fib Model Code combination provides a coherent method of design for such tunnels. No such method exists for non-TBM (mined) tunnels. In Australia, the AS 5100 Bridge Standard set is commonly cited for major public projects. AS5100 has been written to provide bridge and associated infrastructure with a 100-year design life. However, applying AS 5100 to tunnels presents challenges, particularly regarding deep tanked tunnels. These challenges relate to design approaches for tunnels. This paper examines these challenges and proposes recommendations for design approaches and the application of load factors in the design of deep, undrained tunnels using the AS 5100 series, where groundwater is the dominant case and governs the structural response.

1 INTRODUCTION

As urban areas grow, the demand for tunnelled infrastructure increases. In Sydney alone, over 80 km of road and rail tunnels have been constructed in the last two decades. These tunnels often avoid existing or planned infrastructure, and tunnel alignments that were traditionally shallower are now being constructed at greater depths. At the same time, some clients have called for running tunnels to be tanked, citing operational and environmental requirements.

For tunnels constructed using TBMs with precast segmental linings, PAS 8810 is commonly used as the overarching document providing the design approach and the load factors. This is then used with compatible codes for conventionally reinforced or fibre reinforced segments, being Eurocode 2, and the Fib Model Code, respectively. PAS 8810, is specifically written for segmentally lined tunnels and contains a coherent workflow.

For mined tunnels, no such document exists. Australian delivery authorities commonly reference the AS 5100 Bridge Design series as the preferred design standard. Developed for bridges, and intended to deliver infrastructure with a 100 year design life, AS 5100 sets out requirements for the design, assessment, strengthening, and rehabilitation of existing bridges, as well as the design of related structures.

Intended to clarify this matter, the latest revision of AS5100.3 states that the AS5100 series is not intended for the design of driven tunnels. However, it notes that the approach for soil-supported structures may be adopted for driven tunnels, together with the guidance described in the ATS Tunnel Design Guideline (ATS, 2024).

This paper presents the authors' observations on the application of Australian Standards, particularly AS 5100, in tunnel design, based on their experience with major tunnel infrastructure

projects across Australia. It provides recommendations for the application of load factoring approaches and effective use of AS 5100, with a focus on deep, undrained tunnels subjected to sustained groundwater pressure, where groundwater is the dominant case and governs the structural response.

2 DRAINED VS UNDRAINED TUNNEL SYSTEMS

Tunnels and other underground structures can be designed with a full-perimeter groundwater control system to prevent groundwater ingress. This approach requires the tunnel structure to withstand the full hydrostatic pressure and its fluctuations over the typical 100-year design life. A full-perimeter groundwater control system is implemented using sealing accessories such as gaskets (for segments) or using a waterproofing membrane for mined tunnels.

In contrast, drained tunnels allow full or partial ingress of groundwater, which is then controlled and redirected through designed drainage elements, typically located around the tunnel perimeter or at the invert. For example, some tunnels feature a waterproofing membrane at the crown to reduce ingress and prevent dripping, while the walls and invert remain unsealed.

Undrained tunnels generally require a more robust structural design than drained tunnels, due to the need to resist groundwater pressure. If this pressure is at all significant the lining will involve a lining all around the tunnel and thick reinforced concrete sections.

3 GROUNDWATER LOAD IN UNDRAINED TUNNELS

3.1 *General*

In undrained tunnel designs, groundwater is often a significant, if not the dominant, load case. As an external load on the tunnel lining, groundwater exhibits several unique characteristics:

- It is a sustained load, continuously present over the tunnel's design life, unlike transient loads which may be intense but short in duration.
- It follows the lining as it deflects without diminishing its intensity, unlike ground loads which tend to diminish with deformation.
- Its pressure increases with depth, typically resulting in the highest load at the invert.
- It can induce flotation, leading to uplift forces and potential gap formation at the invert, subjecting it to bending stresses.
- Groundwater load variability depends on site-specific hydrological conditions, including:
  - In some locations, the groundwater table lies close to the surface. Provided flooding does not occur, the groundwater may rise only to ground level, resulting in limited variability between typical and extreme conditions.
  - In urban environments, groundwater levels are often suppressed by nearby infrastructure such as basements, sewer systems, or stormwater drains, leading to significant variation between typical and extreme levels
  - Where surface flooding can occur and is hydraulically connected to the groundwater; flood levels must be considered in the assessment of load variability.

Figure 1 shows the typical situation. In Figure 1(a), the loading is shown, with a larger magnitude of load on the invert than on the crown (Archimedes principle). In Figure 1(b), the deformation due to this load is shown, with deformation in the crown restrained by the ground, but a gap in the invert allowing deformation. In Figure 1(c), the bending moment is shown. Bending moment is proportional to the second derivative of deflection. In the crown, where deflection is restrained, bending moment is negligible. In the invert, large bending moments can occur.

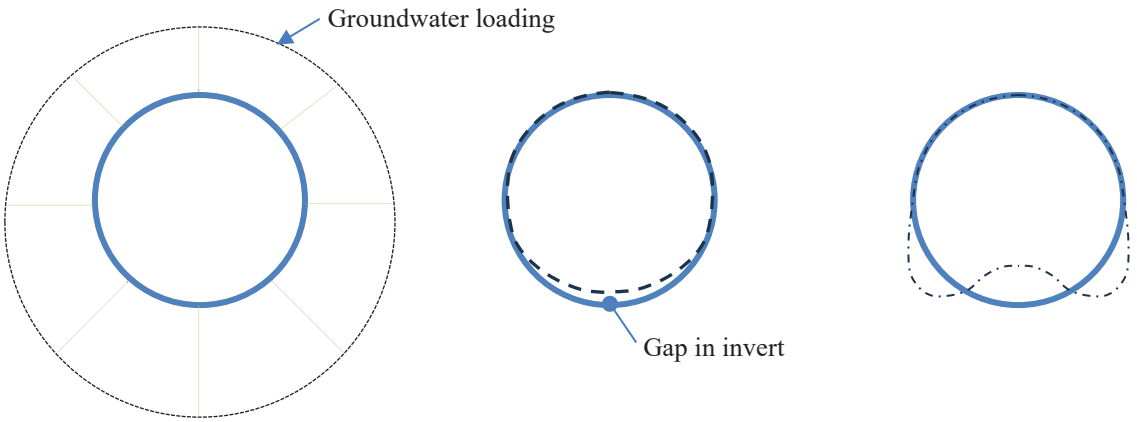


Figure 1 (a) loading due to groundwater, (b) deflection, (c) bending moment

3.2 *TBM tunnels versus mined tanked tunnels*

There is a difference between TBM tunnels with gasketed segmental linings and mined tunnels that are constructed undrained. The following discussion compares a single shield TBM driven with a closed face and some face pressure, with a mined tunnel, however the degree of difference will be less if the TBM is a double shield without face pressure.

In the case of the TBM, the excavation boundary is pressurised to a proportion of the insitu stress, often not to the full extent of the insitu stress, but a significant fraction. The slurry will maintain the pressure around the shield until the backfill grouting; the backfill grouting itself will be injected at a fraction of the insitu stress. The distance behind the face where the lining is installed will depend on the shield geometry, which, in general, tends to be in inverse proportion to the diameter of the tunnel. Thus, due to these three factors, face and shield pressure, backfill grout pressure, and closeness to the face, the segments will be installed without complete release of the insitu ground pressure. In terms of shrinkage of the segments, much of this will have occurred before the segment is installed. As far as the groundwater is concerned, the lining is prestressed by the process, and a gap may not form.

In the case of a mined tanked tunnel, the situation is completely different. The face will be far away from where the lining is installed, and the lining is installed unstressed. The lining will now shrink away from the ground. When the groundwater begins to recover, the lining will tend to float, and the final outcome is that there will be a significant gap between the lining extrados and the ground, in the invert. This gap allows for bending to occur in the invert; this is usually the design case requiring the most reinforcement.

4 LIMIT STATE DESIGN FRAMEWORK FOR TUNNELS

4.1 *Probabilistic Basis and Load Factoring Principles*

The following principles are from the Probabilistic Model Code (JCSS, 2001):
"Structures and structural elements shall be designed, constructed and maintained in such a way that they are suited for their use during the design working life and in an economic way.
In particular they shall, with appropriate levels of reliability, fulfil the following requirements:

- They shall remain fit for the use for which they are required (serviceability limit state requirement)
- They shall withstand extreme and/or frequently repeated actions during their construction and anticipated use (ultimate limit state requirement)
- They shall not be damaged by accidental events like fire, explosions, impact or consequences of human errors, to an extent disproportionate to the triggering event (robustness requirement)."

These statements are carefully worded. The phrase "*with appropriate levels of reliability*" lead in this code, to tables of maximum values of the probability of failure. These values are very low, reflecting societal intolerance for loss of life resulting from structural failure. The use of probabilistic methods in practice is limited, because they require high levels of expertise in a range of mathematical techniques. Nevertheless, interest in and the adoption of these methods are increasing (Low, 2022).

Most current structural design codes have not fully adopted probabilistic methods. Instead, they employ a simplified approach using partial safety factors, known as the Load and Resistance Factor Design (LRFD) method. This method treats loads and resistances as separate and independent probability distributions, and partial factors are chosen to reduce the probability of the load exceeding the resistance to a sufficiently small value.

In reality, load and resistance distributions are not known. At the time of introducing the limit state methods in Australia, Pham and others studied statistical models for loads and resistances, and calculated the probability of failure given by the existing working stress method (Pham 1985). Partial factors for limit state design were chosen for the various dead load, live load, wind load and for materials such as steel and concrete. Pham noted the arbitrary nature of the split between strength and load factors. For example, a load factor of 1.4 combined with a capacity reduction factor of 0.6 has the same result as a load factor of 2.8 with a capacity reduction factor of 1.2. Pham proposed the following criteria for selecting partial factors:

- The strength factor and load factors should reflect, in their relative values, the respective uncertainties associated with the resistance and load effects.
- The strength factor should be kept sufficiently low to allow for potential future increases without exceeding the value of 1.0.
- The combination of factors should provide results consistent with full probabilistic design.

Load factors assigned by code writers can occasionally result in apparent anomalies. An example is given in Day (2001). Day considers a beam supporting an open water tank. Since any excess water simply overflows, the load can be considered to be very certain in its magnitude. However, Day demonstrates that using a partial load factor of 1.0 in this case leads to underdesign. This is because the capacity reduction factors in the normal codes have been chosen to be compatible with load factors for uncertain loads (such as dead and live loads) which the code authors have selected to give "sensible" numerical values. For this reason, AS 1170 assigns a load factor of 1.2 for liquid loads, even though it is physically impossible for the hydrostatic load to reach 1.2 times its nominal value, so as to achieve an acceptable probability of failure for all structures and all load cases.

This example is analogous to a misconception sometimes encountered in the design of undrained tunnels subject to groundwater pressure. Designers argue that when the design groundwater level multiplied by the relevant load factor exceeds the ground surface, the result is physically unrealistic and therefore overly conservative. On this basis, they may justify applying a lower factor of safety. However, this approach overlooks the probabilistic foundations underpinning limit state design. The intent of applying a load factor, even if it leads to seemingly implausible conditions, is to achieve an overall acceptable probability of failure when combined with the relevant capacity reduction factors. Arbitrarily reducing these factors based on perceived physical limitations compromises the limit state approach and may lead to unsafe designs.

In summary:

- The use of partial factors is based on the assumption that load and resistance probability distributions are independent.
- Partial factors are arbitrary and interrelated. Load factors from one standard should not be used with capacity reduction factors from an unrelated standard.
- Partial factors are not independent from each other. Individual load factors relate to corresponding capacity reduction factors and to other load factors.

4.2 *Application of Limit State Design to Tunnel Engineering*

The application of LRFD to geotechnical design has long been controversial.

- In geotechnical engineering, the distinction between "load" and "resistance" is often blurred, as geotechnical materials can function as both, complicating the assignment of partial factors. As a result, geotechnical LRFD codes provide specific design methods for different structures in which individual partial factors are applied differently, depending upon the structure type.
- The strength of geotechnical materials often do not follow a normal distribution; this means that the common definition of the “characteristic value” based on standard deviations from the mean can lead to unreasonable values. In geotechnical design “the characteristic value of a geotechnical value should be a conservatively assessed value” (AS5100.3), noting that AS5100 recommends “engineering judgement” and “geotechnical engineering advice”.

Tunnel design presents further complexity, as the ground and groundwater simultaneously serve as both the load and a high proportion of the resistance. Schweiger (2017) considers alternative Design Approaches (DA) within Eurocode 7 to address this issue. There is considerable complexity around this issue, however both PAS 8810 and, as will be described below, AS5100.3 recommend that the approach should be followed such that the analysis is carried out without assigning partial factors either to loads or materials, with checks of capacity occurring after analysis.

5 USE OF AS 5100 FOR TUNNEL DESIGN

5.1 *General*

The AS 5100 Bridge Design codes set comprises nine parts covering the design, assessment, rehabilitation, and strengthening of bridges. Part 1 describes the overall principles for the set. Part 2 describes load cases and load factors. Part 3 describes geotechnical design. Part 5 describes concrete and Part 6 describes steel structures.

The design life for structures under AS 5100 is 100 years. Ultimate and serviceability design actions are defined with a 5% probability of exceedance, either over the design life for ultimate limit states (corresponding to a 2000-year return period), or per year for serviceability limit states (corresponding to a 20-year return period).

For non-geotechnical structures, where loads and resistances are clearly independent, design is based on considering load cases using Part 2 for guidance, and then providing suitable capacity using Part 5 for concrete structures, and Part 6 for steel structures. Specifically for ultimate limit states, load factors are applied to individual loads from Part 2 before deriving actions such as thrust and bending moment, which are checked using the appropriate capacity reduction factors from Parts 5 or 6.

In the case of geotechnical structures; footings, piles, retaining walls, buried structures, Part 3 is to be used. Each of these types of structure are assigned different design methods. For example, for soil-supporting structures, the analysis is carried out with all loads unfactored. At the completion of the analysis, the action effects (thrust, shear, bending moments) are factored by a global factor of 1.5. Structures are then checked using the appropriate capacity reduction factors from Parts 5 or 6.

5.2 *Tunnel design in general*

AS5100.3 Section 1.2 Application, describes how to use this code set in tunnel design.

“The AS5100 series is not intended to be used for the design of driven tunnels. If approved by the relevant authority, temporary and permanent concrete/shotcrete tunnel linings may be designed using the provisions in this Standard for soil-supporting structures, in particular Clause 2.3.3(e), together with the guidance described in the ATS Tunnel Design Guideline.”

This is very clear. Clause 2.3.3 specifically describes the procedure of analysing with all loads unfactored. At the completion of the analysis, the action effects (thrust, shear, bending moments) are factored by a global factor.

The words above also mention the ATS Tunnel Design Guideline as a source of guidance. This is because the global load factor approach does not account for the variability or probability of groundwater levels, which can fluctuate significantly over the 100-year design life. Applying a fixed factor of 1.5 does not reflect the probabilistic nature of groundwater loading and may result in either unconservative or overly conservative designs depending on the assumed design level.

6 APPLICATION OF THE ATS TUNNEL DESIGN GUIDELINE TO GROUNDWATER LOADING

The ATS Tunnel Design Guideline (ATS, 2024) provides supplementary design guidance specific to Australian conditions and tunnel practices. Sections 5.4.8 and 5.4.11 provide key insights into groundwater loading, with Section 5.4.11 particularly relevant to deep, undrained tunnels subject to sustained hydrostatic pressure, where groundwater is the dominant case and governs the structural response.

The guideline stresses the importance of appropriately assessing groundwater pressures acting on tunnel linings, particularly in undrained configurations where the permanent lining must withstand constant and unrelenting hydrostatic pressures throughout the design life. Unlike many other loads, groundwater pressure is independent of the tunnel lining behaviour. Groundwater levels should not be considered static. The design should account for a full range of possible scenarios, including climate change impacts, flooding, tidal fluctuations, and post-construction groundwater recovery.

The guideline recommends that groundwater loads for both Ultimate Limit State (ULS) and Serviceability Limit State (SLS) be derived from comprehensive hydrogeological investigations, that consider the most adverse groundwater conditions likely to occur during both construction and operation.

Suggested categorisation of groundwater levels are as follows:

- Initial or Monitored groundwater level: The observed level during investigations.
- Normal or Usual groundwater level: Reflecting seasonal variation, long-term trends, and climate change.
- Unusual groundwater level: Significant deviation from Normal or Usual levels.
- Extreme groundwater level: Associated with rare events such as groundwater levels influenced by the Probable Maximum Flood (PMF), where applicable.

Load factors and load combinations are discussed and direction is provided on reconciling conflicting guidance across different Australian Standards. For ULS design, the guideline recommends applying a different load factor ranging from 1.0 to 1.5, depending on the groundwater level category. The selected load factor should reflect the required factor of safety, the probability of groundwater level occurrence, and the level of confidence in the groundwater level estimates.

In summary, the ATS Tunnel Design Guideline provides guidance for incorporating groundwater loads into undrained tunnel design. It acknowledges the limitations of standard LRFD approaches for geotechnical structures and supports alignment with AS5100.3 methodologies. Importantly, it highlights the importance of considering multiple groundwater scenarios and selecting appropriate load factors, informed by the overall factor of safety requirements, probability of occurrence, and confidence in groundwater level predictions.

7 RISK-BASED METHODOLOGY FOR GROUNDWATER LOAD CLASSIFICATION AND FACTOR SELECTION

Building on the recommendations presented in the ATS Tunnel Design Guideline (ATS, 2024), the following risk-based methodology is proposed for classifying groundwater loading scenarios and assigning appropriate load factors for use with the AS5100.3 approach. This approach is intended to support the design of undrained tunnels subject to sustained groundwater pressures, where groundwater is the dominant case and governs the structural response, allowing engineers to consider load factors based on available data, risk profile, and design objectives.

Table 1. Risk-based approach for assigning groundwater load factor

Step 1	Establish the baseline groundwater level through geotechnical investigations conducted prior to tunnel excavation.
Step 2	Assess groundwater level variability due to seasonal fluctuations, temporary drawdown during construction, permanent drawdown or recharge over the design life of the tunnel, impacts to hydrostatic pressures due to surface flooding (consider return periods from 1:50 to 1:2000, and PMF if applicable), and climate change effects.
Step 3	Classify each groundwater level (load case), in alignment with the ATS Tunnel Design Guideline: - Normal/Usual cases: Observed or seasonally adjusted groundwater levels, including trends and long-term effects such as recharge or climate change. If surface flooding may affect groundwater levels or result in external water pressure on the tunnel lining, consider a 1:100 AEP event. - Unusual cases: Elevated groundwater levels beyond the Normal/Usual range. For cases involving surface flooding that could influence groundwater level or static water pressure acting on the tunnel lining, consider a 1:2000 AEP event. - Extreme cases: Rare events beyond the Unusual category, including PMF or 1:10,000 AEP flooding, where such conditions influence groundwater or induce static pressure on the tunnel lining. These scenarios are unlikely for most urban tunnels, and their applicability should be carefully evaluated based on consequence, infrastructure criticality, and design credibility.
Step 4	Apply groundwater load factors considering the ranges below to achieve the suitable factor of safety, (refer recommended factors of safety in Section 6 of this paper), based on confidence in the groundwater data: - Normal/Usual cases: Load factor 1.25–1.35. Use the lower end if groundwater level reliability is high or variation is <10% of the existing hydraulic head; otherwise, use the higher value. Use a still higher value if the uncertainty surrounding groundwater levels is significant. - Unusual cases: Load factor 1.1–1.25. Apply criteria as above depending on reliability of the data and extent of variation. - Extreme cases: Load factor 1.0–1.1. Use the lower end only if groundwater predictions are well-supported and variation remains low; otherwise, adopt the higher value.
Step 5	- Compare the criticality of groundwater-dominant cases with other load combinations. Remove groundwater to assess whether it governs structural response. - Where groundwater pressure is applied symmetrically, high compressive forces may develop in the lining, increasing apparent moment capacity when assessed using interaction diagrams. These compressive effects may not be uniform throughout the tunnel, particularly in dry sections or areas with low permeability. Therefore, such forces should not be relied upon to unrealistically enhance structural capacity or safety margins.

Engineering judgement is essential in applying this methodology. Designers must consider multiple groundwater scenarios, select appropriate load factors based on the required factor of safety, and account for both the probability of groundwater level occurrence and the confidence in available data. This approach supports a balanced, risk-informed design that reflects the inherent uncertainties in groundwater behaviour over the design life of a tunnel.

The factors proposed above can be compared with the PAS 8810/Eurocode design for segmentally lined tunnels. PAS 8810 considers groundwater load as a Permanent load. In this code, such a load is assigned a partial load factor of 1.35. However, this load factor cannot be considered in the absence of consideration of its relationship to the partial load factors for materials (see discussion in Section 4.1 above). Eurocode 2 assigns, for concrete in bending with limited axial load, a partial factor of 1.5. The equivalent factor in AS5100.5 is a capacity reduction factor of 0.6 (or 1/1.67). A simple comparison between these two cases would suggest a partial load factor of 1.22 in conjunction with AS5100.5. However, as discussed above in Section 3.2, there is a difference between segmental linings and tanked mined tunnels so we recommend a larger number.

8 CONCLUSION

Designing deep, undrained tunnels subjected to sustained groundwater pressure introduces additional challenges not fully addressed by current Australian Standards.

AS 5100.3, although not originally intended for driven tunnels, offers a suitable framework when applied with engineering discretion and in conjunction with the guidance described in the ATS Tunnel Design Guideline.

The ATS Guideline provides a more practical basis for assessing groundwater pressures in tunnel design, recommending a scenario-based approach that categorises groundwater conditions as Usual/Normal, Unusual, or Extreme. Building on this, the paper proposes a risk-based methodology for selecting appropriate groundwater load factors, informed by site-specific conditions, expected variability, and confidence in available data.

Ultimately, the design of deep undrained tunnels should adopt a probabilistic, scenario-based approach that reflects the full range of groundwater conditions likely to be encountered over the tunnel's design life. Load factors, informed by the overall factor of safety requirements, should be selected to suit each scenario, accounting for the probability of occurrence and the reliability of groundwater level predictions.

9 REFERENCES

ATS. 2024. Tunnel Design Guideline. 2nd ed. Australian Tunnelling Society / Engineers Australia.

BSI, 2016. PAS 8810.

Day, R. 1997. Structural limits states design procedures in geomechanics. Sydney, G.J.Chirgwin, pp. 275-286.

Day, R. 2001. Factored material properties and limit state loads - Unlikely extreme or impossible pretense. Proceedings ICE Geotechnical Engineering, October, pp. 209-210.

JCSS. 2001. JCSS Probabilistic Model Code. Joint Committee on Structural Safety.

Low, B. 2022. Correlated sensitivities in reliability analysis and probabilistic Burland-and-Burbidge method. Georisk: Assessment and Management of Risk for Engineered Systems and Geohazards, 16(3), pp. 397-412.

Pham, L. 1985. Load combinations and probabilistic load models for limit state codes. Transactions of the Institution of Engineers, Australia. Civil engineering, 27(1), pp. 62-67.

Schweiger, H.P. & Paternesi, A. & Tschuchnigg, F. 2017. Eurocode 7-based design of SCL tunnels by means of numerical analyses. Géotechnique, 67(9), pp. 837-844.

AS 5100. 2017, Bridge Design series.

19th Australasian Tunnelling Conference – Acosta-Martínez, Stewart and Hudson-Smith (Eds.)
© 2025 Australian Tunnelling Society, ISBN 978-0-85825-002-4

Comparative analysis of crack width calculation methods for tunnel lining design

N. Shafiei, J. Ho & C. Ng
Delve Underground, Sydney, Australia

ABSTRACT: Crack width assessment is a critical component of the serviceability limit state (SLS) design check for the reinforced concrete tunnel linings, as it impacts the long-term performance and serviceability of the structures throughout the design lives. A comprehensive understanding of crack width design improves the serviceability and durability of concrete structures and reduces both material usage and maintenance cost. Various design approaches documented in Codes and Standards regarding flexural crack width calculation and assessment are suggested, depending on the specific project requirements. In this paper, three principal methods outlined in Australian Bridge Design Code, Australian Standard for Concrete Structures and Eurocode 2 with regards to flexural crack width design are compared. A SLS axial force-bending moment (N-M) interaction diagram is developed in accordance with approaches in the Standards, and the application of N-M interaction diagram for lining design is demonstrated. Additionally, the influence of as-built excess concrete cover is investigated.

1 INTRODUCTION

Crack width calculation is a critical component of the serviceability limit state (SLS) design check for permanent reinforced concrete (RC) lining in tunnels, as it directly impacts the long-term performance and serviceability of tunnel structures throughout their design lives. Compliance with crack width limits and requirements stated in standards and codes (standards hereafter) are conventionally the fundamental design consideration for permanent tunnel reinforced concrete linings. For the majority of underground tunnel design projects in Australia, the crack width limit for the permanent reinforced concrete lining is typically required to be calculated on the basis of the relevant Australian Standards (AS), and incorporating standards of other countries based on the specific project requirements, including the widely used European Standard, Eurocode 2: Design of Concrete Structures (EN 1992-1-1).

For the design of reinforced concrete, numerous factors influence the crack width design, including steel reinforcement diameter, concrete compressive strength, concrete durability cover, bond characteristics and reinforcement quantity, orientation and distribution across and near the potential crack. However, flexural crack width calculation essentially correlates crack spacing and strain differences between steel reinforcement and concrete strains. The flexural crack width estimation is mainly influenced by the crack spacing parameter.

Australian Bridge Design Code (AS 5100.5), Australian Standard for Concrete Structures (AS 3600) and Eurocode 2 (EN 1992-1-1) are the widely used standards in Australian tunnel projects for SLS crack width design of reinforced concrete structures. The approaches regarding crack width design in reinforced concrete structure design using these standards and the associated similarities and differences amongst the standards are investigated in the sections below.

The essential and principal crack width formulation in these standards is based on Formula 1.

$$\omega = S\,(\varepsilon_{sm} - \varepsilon_{cm}) \quad (1)$$

where, ω is the crack width; S is the maximum spacing between cracks; and ε_{sm} and ε_{cm} are the mean steel and concrete strains over length or spacing between cracks, respectively.

For crack control of reinforced concrete, a minimum area of reinforcement, $A_{s.min}$ is typically required in standards.

In this paper, the SLS axial force-bending moment (N-M) interaction diagram has been developed according to Australian Standards and Eurocode 2 for crack width calculations, and comparisons between envelopes using various design parameters, conditions and considerations are provided.

2 SERVICEABILITY LIMIT STATES AXIAL FORCE-BENDING MOMENT INTERACTION DIAGRAM WITH SPECIFIED CRACK WIDTH LIMIT

Tunnel linings are predominantly flexural-compression structural members (rather than pure flexural members), and the beneficial effects of the compression force must be considered for efficient design. The paper considers the influence of the axial force on the crack width limit design.

Figure 1 illustrates the reinforced concrete SLS axial force-bending moment limit envelope, known as the RC SLS N-M interaction diagram, for the reinforced concrete section defined in Figure 2, with the short- or long-term crack width limited to 0.2 mm, 0.3 mm and 0.4 mm, and uncracked condition. These values are commonly documented in Australian standards and Eurocode for varying structure environmental exposure categories and are discussed in Section 3. Moreover, the maximum concrete compressive stress in the SLS is limited to 0.6 f_c' according to EN 1992-1-1, Clause 7.2 in Figure 1, where f_c' is the characteristic concrete compressive strength.

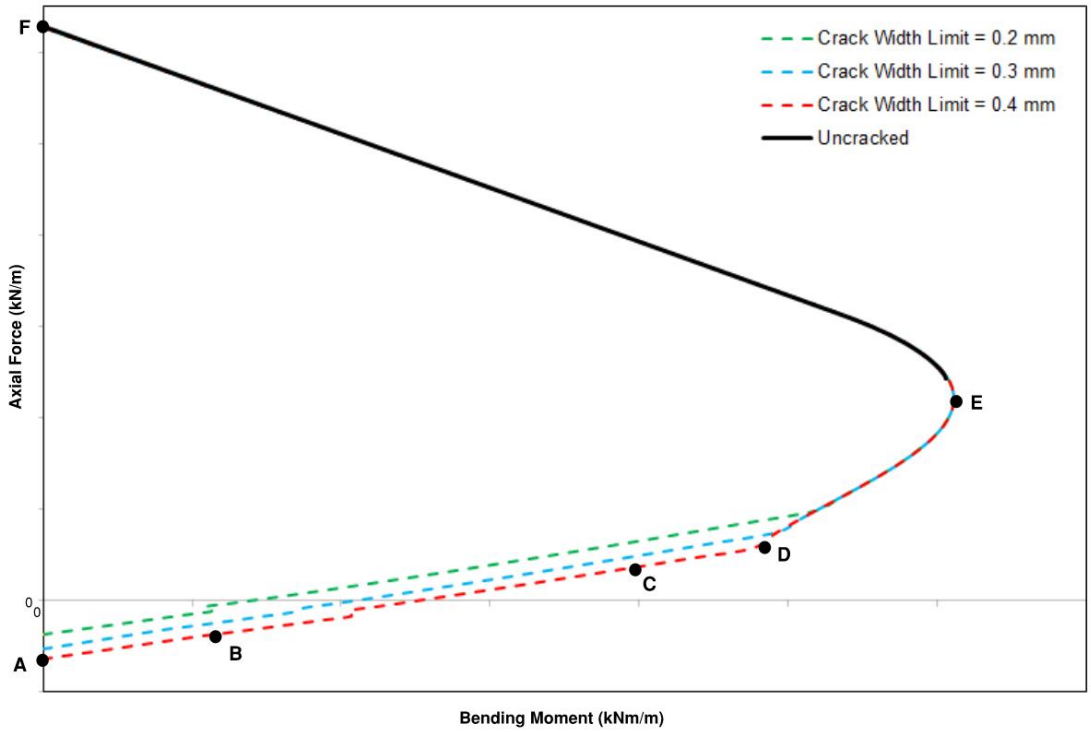
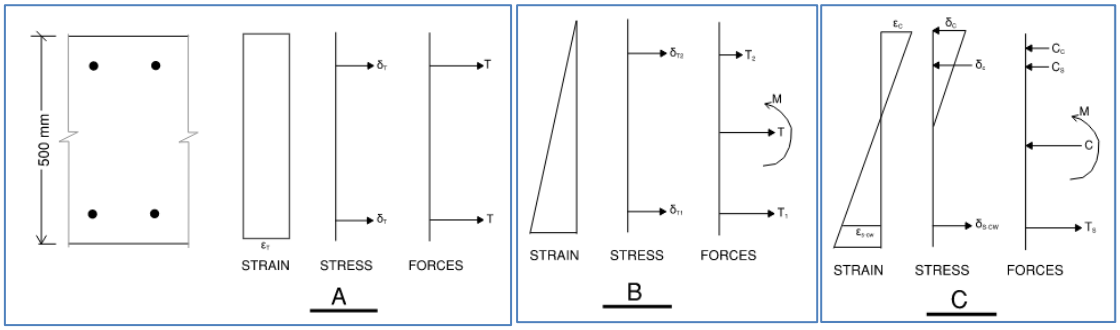
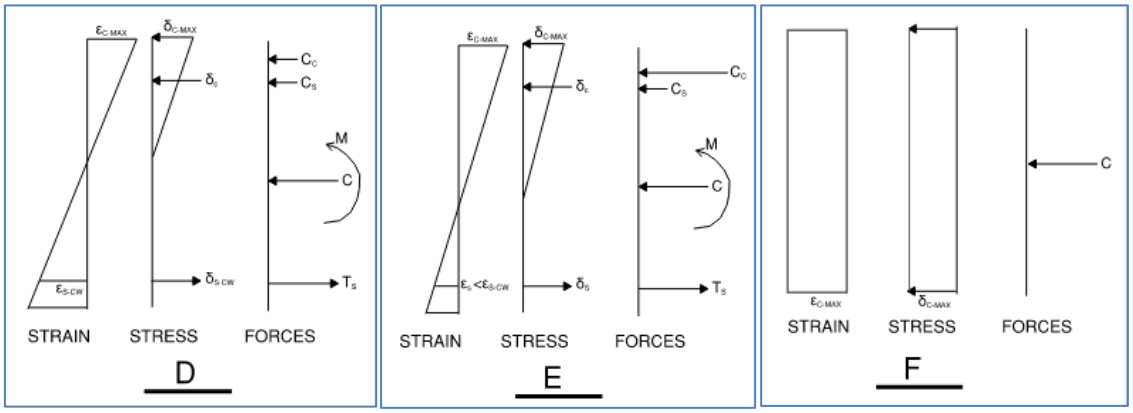


Figure 1. Cracked reinforced concrete N-M interaction diagram with crack width limits of 0.2, 0.3 and 0.4 mm, and uncracked condition.

The SLS N-M limit diagram shown in Figure 1 represents the cracked and uncracked reinforced concrete section behavior under the SLS design limits, namely limited by the maximum concrete compressive stress and the maximum steel tensile stress corresponding to the specified crack width limit.



(a) Point A: Pure axial tension condition; Point B: Transition from pure tension to flexural tension condition; and Point C: Flexural compression condition.



(b) Point D: Balanced condition; Point E: Maximum bending moment under axial compression condition; and Point F: Pure compression condition.

Figure 2. Stress-strain diagrams under various types of design behaviors (a) and (b) of RC section.

The SLS N-M interaction envelope is defined by points A to F.

– Point A represents the pure tension condition, which is governed by the steel stress associated with the specified crack width limit under the design condition of pure axial tension.

– Point B corresponds to the condition where the neutral axis is located at the top of the section. It is the transition between the types of reinforced concrete design behavior from pure tension to flexural tension, as defined in AS 5100.5, Clause 8.6.1. A linear transition is assumed between points A and B in accordance with relevant standards.

– Point C is an intermediate condition between B and D, where the concrete compressive stress remains below the SLS limit, and the steel tensile stress meets the limit for the specified crack width.

– Point D is the balanced condition, where the neutral axis depth results in both the concrete reaching its SLS compressive stress limit and the reinforcement reaching the steel stress limit associated with the specified crack width. This point also marks the transition from primarily flexural to compressive behavior.

– Point E represents the condition with maximum bending moment for the section under axial compression. Here, the neutral axis is located below the balanced condition depth, the concrete compressive stress is at the SLS limit and the steel stress is less than the stress associated with the

crack width limit. The increase in bending moment from point C to point E is attributed to the eccentricity of the increasing axial compression force.
– Point F represents the pure compression condition, governed solely by the compressive stress limit for the reinforced concrete.

The SLS limit envelope between points A and D is generally governed by the steel tensile stress limit. The envelope between points D and F is generally governed by concrete compressive stress limit. The sudden change in the SLS N-M interaction envelope between points B and C is due to the transition of the neutral axis across the top reinforcement shown in Figure 2, which changes the function of the reinforcement from tension to compression bars; consequently, there is a notable reduction in the bending moment limit.

For crack width design calculation, AS 5100.5 prescribes a fixed steel stress approach. However, both AS 3600 and EN 1992-1-1 do not prescribe a fixed steel stress limit across the entire interaction envelope for direct crack width calculation. Instead, steel stress varies to comply with the design crack width criteria to calculate the points defining the interaction envelope. Three interdependent variables in the strain diagram for the reinforced concrete section are required to be simultaneously resolved, which involves iterative calculations. These parameters are (1) the concrete compressive stress and strain, (2) the depth of the neutral axis and (3) the steel stress and strain corresponding to the specified crack width limit. As a result, AS 3600 and Eurocode 2 standards require iteration processes to determine the limit envelope between points B and D.

3 FLEXURAL CRACK WIDTH APPROACHES IN DESIGN STANDARDS

The three fundamental and commonly applicable standards in Australian underground tunnel projects are Australian Bridge Design Code, AS 5100.5; Australian Standard for Concrete Structures, AS 3600; and European Standard, Eurocode 2: Design of Concrete Structures, EN 1992-1-1. This section interprets the approaches regarding crack width design in reinforced concrete structure design.

3.1 *Flexural crack width approach in Australian Bridge Design Code, AS 5100.5*

In AS 5100.5, Clause 8.6 and Clause 9.4, no crack width formulations or calculation methods are suggested. However, from Clause 8.6.1(c) it requires two load effect cases to be considered and assessed for the purpose of crack control in reinforced concrete structure design, including SLS load combinations (Case I) and SLS permanent effects for structures within the exposure environment classifications B2, C1, C2 and U (Case II), where exposure classifications are defined in Clause 4.3.

3.2 *Flexural crack width approach in Australian Standard for Concrete Structures, AS 3600*

The crack width formulation given in AS 3600, Clause 8.6.2.3, is the same as Formula 1 and is applicable to both beam and slab design. Moreover, AS 3600 Supplement 1 Clause C8.6.2.3 states that the calculation of crack width in AS 3600 is a modified version of the design calculation approach and procedure documented in EN 1992-1-1. The influence of shrinkage and creep in reinforced concrete is recommended in AS 3600 and in the N-M interaction diagram for the crack width design.

3.3 *Flexural crack width approach in European Standard, Eurocode 2: Design of Concrete Structures, EN 1992-1-1*

In accordance with EN 1992-1-1, Clause 2.3.2.2, the significant impact of shrinkage and creep shall be taken into account for verification in SLS design and only considered at ultimate limit states (ULS) design while age-related effects are significant. The crack width formula given in EN 1992-1-1, Clause 7.3.4 is the same as Formula 1.

4 COMPARISONS OF DESIGN STANDARDS FLEXURAL CRACK WIDTH APPROACHES FOR TUNNEL LINING DESIGN

A case study has been conducted and is discussed in this section with regards to typical underground tunnel permanent linings in Australia and the application of the SLS reinforced concrete N-M interaction diagram to the lining design.

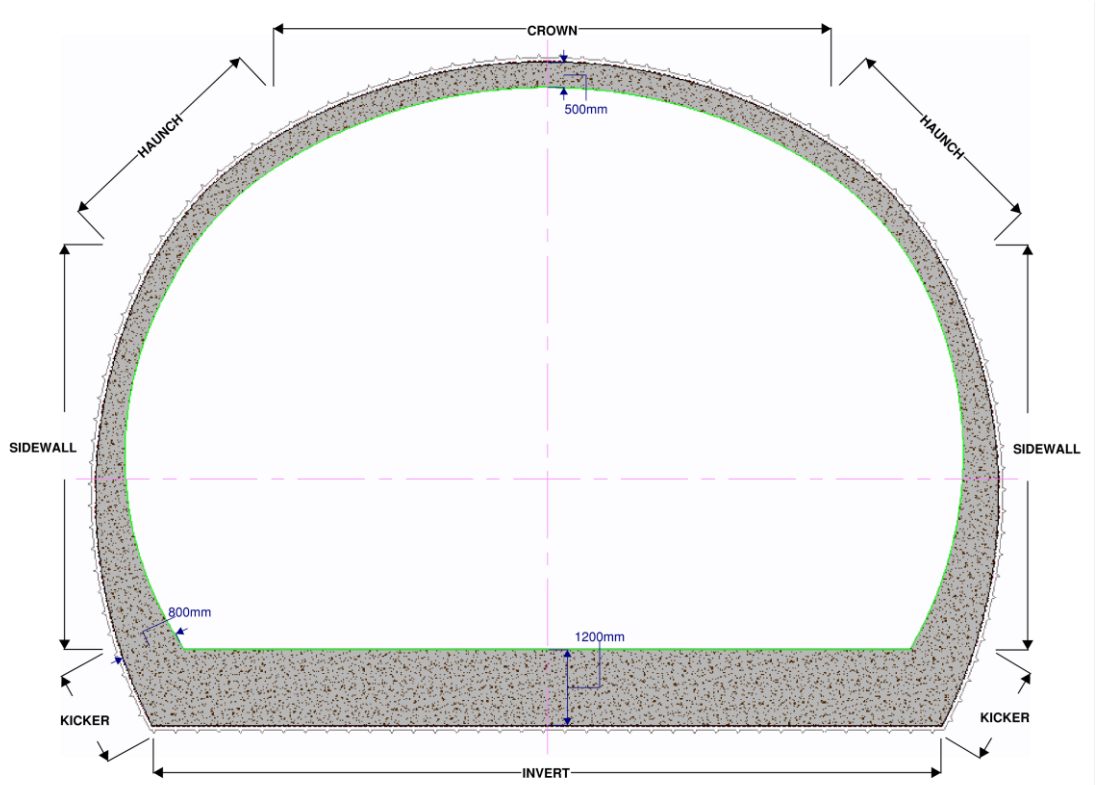


Figure 3. Typical permanent lining nomenclature with indicative thicknesses for 16.0 m wide by 11.5 m high cross-section.

Figure 3 illustrates a typical underground tunnel profile. The representative profile includes the following components–crown (roof slab), haunches, sidewalls, kickers and invert (base slab)–where the thicknesses are assumed as 500 mm, 800 mm and 1,200 mm, respectively, as indicated in Figure 3. In this study, the characteristic compressive concrete strength (f'_c) is 40 MPa. In this tunnel lining design instance, the crack width requirement of reinforced concrete sections under the SLS design is 0.3 mm, with 50 mm of durability concrete cover, and the concrete compressive stress limit is 0.6 f_c', which is 24 MPa.

Per AS 5100.5, AS 3600 and EN 1992-1-1, four SLS N-M interaction envelopes were developed for the 800 mm thick reinforced concrete kicker section in the permanent tunnel lining and are overlain in Figure 4. The AS 5100.5 interaction envelopes were developed for Case I and Case II–details are discussed in Section 3.3. A typical lining SLS compressive force is adopted to determine the bending moment (cracking) limit for the kicker to these standards. The reinforcement arrangements in this tunnel lining example are described in Table 1 and the adopted intrados and extrados bar sizes and spacings are the same.

The crown, kicker and invert sections in the tunnel lining example, with typical reinforcement were evaluated for crack limited bending moment assuming an axial compression force of 1000 kN/m and the results are shown in Table 1. In Figure 4 and Table 1, the AS 3600 N-M limit envelope was developed considering a tunnel lining near the end of its 100-year design life, incorporating time-dependent effects of shrinkage and creep in the calculations. Consequently,

the AS 3600 N-M interaction envelope demonstrates the lowest bending moment limit amongst all standards in Figure 4. This is because of the explicit consideration of age-related effects on the crack width calculation.

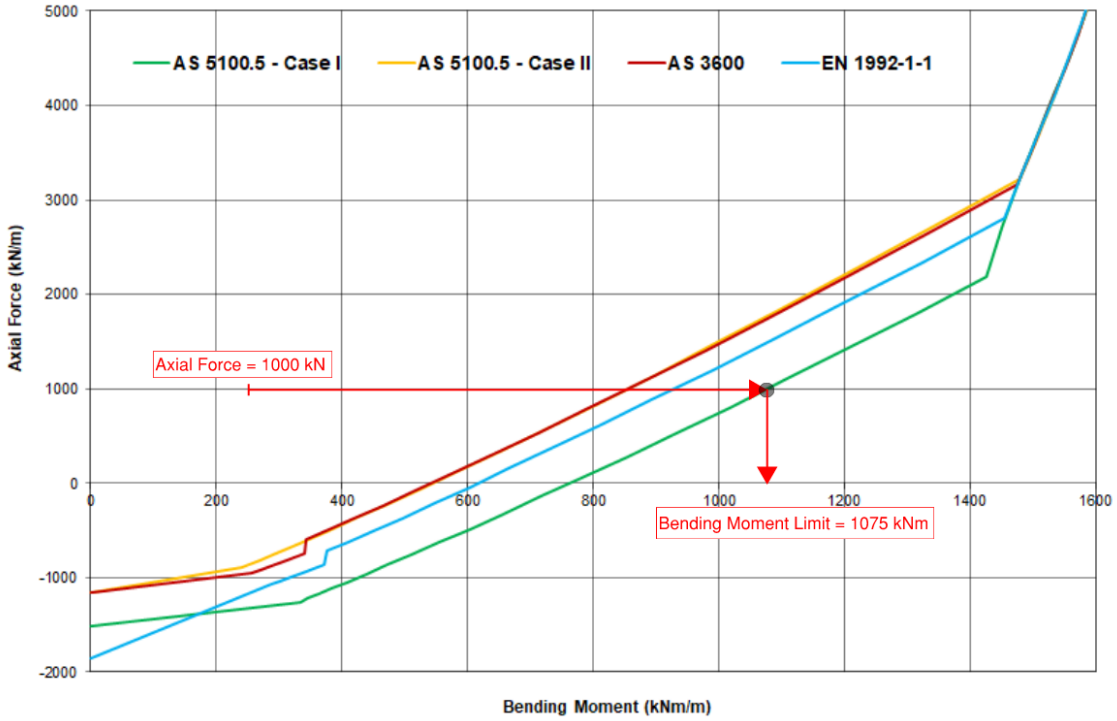


Figure 4. 800 mm thick RC SLS N-M interaction diagram with f_c' of 40 MPa, reinforcement of N28-150 and crack width limit of 0.3 mm.

Table 1. SLS bending moment limit with f_c' of 40 MPa, axial force of 1000 kN, crack width limit of 0.3 mm and durability cover of 50 mm.

Locations	Section Thickness (mm)	Reinforcement[a]	SLS Bending Moment Limit			
			EN 1992-1-1 (kNm)	AS 3600[b] (kNm)	AS 5100.5 Case I[c] (kNm)	Case II[d] (kNm)
Crown, Haunches & Sidewalls	500	N24-150	475	440	516	420
Kickers	800	N28-150	928	851	1075	851
Invert	1200	N32-150	1715	1572	2048	1595

(a) Intrados and extrados reinforcements are identical in each section along the permanent lining. N24-150: Ductility class N steel reinforcement in accordance with AS 5100.5, 24 mm bar, and spacing of 150 mm.
(b) The influence of shrinkage and creep on the N-M interaction diagram of the reinforced concrete crack width design is included in accordance with AS 3600.
(c) Case I: SLS load combinations, from AS 5100.5 Clause 8.6.1(c).
(d) Case II: SLS permanent effects for structure within the exposure classifications of B2, C1, C2 and U, from AS 5100.5 Clause 8.6.1(c).

Moreover, in Figure 4 and Table 1, the N-M interaction envelopes developed on the bases of AS 5100.5 case II and AS 3600 align closely. This indicates that the influences of long-term concrete aging, namely shrinkage and creep are considered in the AS 5100.5 crack width

formulation when evaluating the permanent effects in concrete lining response for extreme exposure classes. As presented in Table 1, the variations amongst SLS bending moment limits developed from various standards are significant for the thicker reinforced concrete sections.

5 INFLUENCE OF "EXCESS" COVER IN REINFORCED CONCRETE FLEXURAL CRACK WIDTH DESIGN

Excess concrete cover in the as-built reinforced concrete underground structure, particularly tunnel linings, is common. Excess cover is a relative term and for this discussion is assumed to be a concrete cover to reinforcement greater than required for durability with the highest environmental exposure class plus a positive construction tolerance. As the tunnel linings are predominantly flexural-compression structural members (rather than pure flexural members), the influence of excess concrete cover on the SLS N-M interaction envelope of reinforced concrete structure in the compression zone is investigated in this section. The influence of excess concrete cover in the RC section is demonstrated in Figure 5. The paper considers the influence of the axial force on the crack width limit design. An 800 mm thick RC section with reinforcement of N28-150 or N36-150 is examined to determine the effect of excess cover. In this study, three scenarios of concrete covers are investigated, including zero excess cover, which is the base case and ideal design condition, and 50 mm or 100 mm excess concrete cover, assuming 50mm durability cover and ignoring reinforcement placement tolerances.

The excess cover is considered to be located exclusively on the tensile face of the RC section. The results, when adopting the EN 1992-1-1 formulation and assuming 40 MPa concrete, showed that for a RC section in the regions in the compression zone of the N-M interaction diagram, the increase of concrete cover enhances the magnitude of the SLS bending moment limit at the durability cover depth because of increased section thickness. As the durability-related concrete cover requirement for the structural element has been achieved and exceeded, it is reasonable to consider and calculate what the crack width may be below the concrete surface at durability cover depth from the reinforcement. While the concrete surface crack width may be visible and easily measurable post-construction, the structure design life is generally related to protection of steel bar reinforcement against corrosion and SLS crack widths at durability cover are the primary design approach achieving the intended design life.

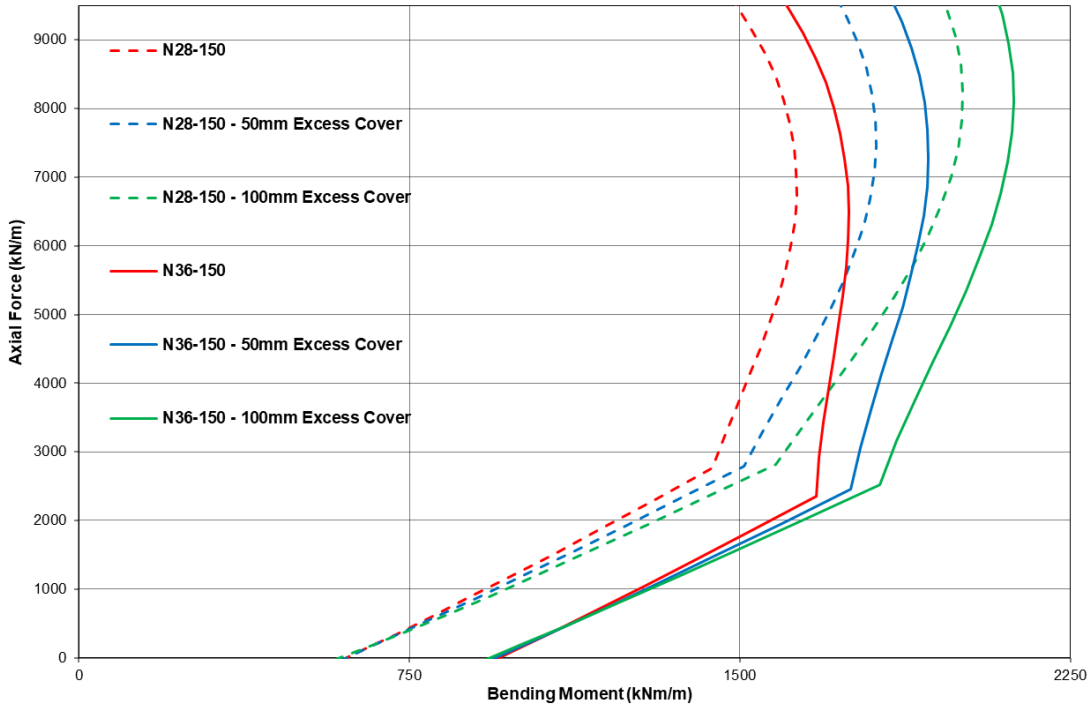


Figure 5. 800 mm thick RC SLS N-M interaction diagram with various excess covers.

6 CONCLUSION

Specific project requirements for permanent lining design for most Australian underground tunnel projects—especially metro tunnel projects—widely adopt the SLS crack width design criteria for reinforced concrete elements. The SLS crack width design typically governs the design.

AS 5100.5, AS 3600 and EN 1992-1-1 are the three essential, and applicable standards adopted for Australian underground tunnel project design. The formulae for calculation of design SLS crack widths in reinforced concrete structures documented in AS 3600 and EN 1992-1-1 adopt the same technical approach. The age-related material effects, shrinkage and creep, to be considered in SLS design according to AS 3600. Their incorporation understandably results in bending moment limit reductions in the N-M interaction diagram compared with the EN 1992-1-1 approach.

In accordance with AS 5100.5, two load effects cases are required in SLS crack width design, namely case I–SLS load combinations and case II–SLS permanent effects.

For the tunnel lining SLS structural design, the critical design cases, with respect to crack width limit, are when the load case combinations result in low axial compression force in the lining. In this scenario, the N-M interaction diagram based on the AS 5100.5 case I approach gives the largest bending moment limit at the adopted crack width compared with the other standards. The AS 5100.5 case II envelope gives similar, but slightly beneficial limits, as the AS 3600 approach envelope which gives the lowest bending moment limit. The limit developed according to EN 1992-1-1 falls near the middle of the three AS limits.

The influence of excess concrete cover, after lining construction, on the bending moment limit associated crack width at durability cover depth in the compression zone was investigated. The study results, with the EN 1992-1-1 approach, demonstrated that the effect of excess cover in concrete section under axial compression force zone, the bending moment limit increases due to increase of section thickness. It is recommended that, in the case of as-built excess concrete cover to reinforcement, design crack widths should be always confirmed at durability cover depth from reinforcement rather than at concrete surface.

ACKNOWLEDGEMENTS

The authors are grateful to Delve Underground for supporting this paper. The authors wish to express deep appreciation and gratitude to our colleague Michael Behrens for his critical suggestions and valuable review.

7 REFERENCES

Council of Standards Australia. 2018. AS 3600:2018 Concrete Structures. Standards Australia Limited.

Council of Standards Australia. 2022. AS 3600:2018 Sup 1:2022 Concrete Structures – Commentary (Supplement 1 to AS 3600:2018). Standards Australia Limited.

Council of Standards Australia. 2017. AS 5100.5:2017 (Incorporating Amendments up to and including No.2) Bridge Design Part 5: Concrete. Standards Australia Limited.

European Committee for Standardization. 2018. Eurocode 2: Design of Concrete Structures – Part 1-1: General Rules and Rules for Buildings. EN 1992-1-1:2004 +A1:2014.

Warner, R. F., Rangan B. V., Hall A. S., & Faulkes, K.A. 1998. Concrete Structures. Addison Wesley Longman Australia Pty. Ltd. South Melbourne. Australia.

19th Australasian Tunnelling Conference – Acosta-Martínez, Stewart and Hudson-Smith (Eds.)
© 2025 Australian Tunnelling Society, ISBN 978-0-85825-002-4

A comparative study on 2D numerical modelling methods for tunnel junctions

L.Y. Chan
Sener Group, Brisbane, QLD, Australia
W.S. Tsui & M.C. Hui
Aurecon Hong Kong Ltd, Hong Kong

ABSTRACT: Tunnel junction effects in underground engineering challenge accurate prediction of displacement and liner reaction. While 3D models offer higher accuracy, 2D models are often preferred in design for efficiency. However, limited guidance exists on assessing inherently 3D tunnel junction problems in 2D. This paper compares two 2D numerical modelling approaches for tunnel junctions: the Diagonal Span Method, representing the junction as an ellipse with width equal to its 45° diagonal span, and the Weakened Ground Method, simulating the junction by tripling the surrounding ground's j_n value. Their performance is evaluated against 3D model results to examine how effectively they capture the complex interactions within tunnel junctions, highlighting each method's strengths and limitations.

1 INTRODUCTION

In recent years, authors have contributed to studying the behaviour of rock mass and supports within or around an underground junction. For instance, Hsiao et al (2009) has pointed out that the rock mass strength/stress ratio plays an important role in junction roof settlement. Chortis & Kavvadas (2021) performed a series of 3D models with Abaqus code, studying the junction effect under a wide range of factors including construction sequence, rock mass strength, field stress, lateral stress and deconfinement. His work not only proved the relevance of these parameters to junction settlement and stress behaviour, but also proposed a design chart for junction zone design normalising tangential axial force under "modified geotechnical conditions". Gkikas & Nomikos (2021) proposed equations and tables to estimate the additional displacement and changes in hoop axial force to the main tunnel lining induced by the formation of junction, the predictions were compared with FLAC3D models with good agreement.

Despite the numerous efforts made in studying junction zones and proving the capabilities of three-dimensional numerical models in simulating junction behaviour, up to this date, less than enough spotlight has been put on linking two-dimensional numerical modelling methods with its three-dimensional counterparts, considering the comparatively excessive computing time and effort often needed to perform three-dimensional analyses. Cohen et al (2023) has made effort in studying the correlation between 3D and 2D modelling results for horseshoe shaped T-junctions under simplified conditions. The established methodology and findings have laid good foundation for further study into the topic that has encouraged this research.

2 MODELLING METHODOLOGY

2.1 *Modelling parameters*

In this study, series of 2D and 3D finite element models have been computed with Plaxis 2D and 3D. All models are circular openings with elastic liners, set in dry and elastic grounds with varying

parameters , including Young's modulus, main tunnel – cross adit span ratios (only varying in main tunnel sizes and keeping the cross adit size constant) and in-situ stress as represented by overburden ground stress and Coefficient of earth pressure at rest (K_0), which are the important factors to junction behaviour as identified by Hsiao et al. (2009) and Chortis & Kavvadas (2021). Each varying parameter was assigned four discrete values, with the resulting combinations forming the basis of the analysis. The varying model parameters used are summarised in Table 1. The rock strength parameters with relevance to the Q values adopted, with reference being made to Hong Kong Granite rock mass strength data from past projects, is presented in Table 2.

Table 1. Model Parameters

Fixed Parameters				
Cross Adit Radius (m)	4			
Intersection Angle (deg.)	90			
Coefficient of earth pressure at rest , K_0	1			
Poisson's ratio, *v*	0.3			
Hoek–Brown material constant (slope of the failure envelope), mi	32			
Proposed Alternating Variables				
Main Tunnel Radius (m)	4.4	4.8	6	8
NGI Q System Rock Mass Quality Index, Q	0.1	0.3	1	3
Initial In-situ Stress, P_0 (MPa)	2.6	4.4	7.5	13

Table 2. Rock Strength Parameters of Hong Kong Granite from Past Projects.

NGI Q System Rock Mass Quality Index (Q)	Geological Strength Index (GSI)	Uniaxial Compressive Strength of Intact Rock (σ_{ci})	Young's Modulus of Intact Rock (Ei)	mi*	Disturbance Factor (D*)	mb #*	s #*	a #*	Deformation Modulus of Rock Mass (E_{rm})	Rock Mass Uniaxial Compressive Strength (σ_{cm})
		MPa	GPa						MPa	MPa
0.1	23.3	40	16	32	0	2.07	0.0002	0.535	870	6.7
0.3	33.2	75	30	32	0	2.94	0.0006	0.518	3013	16.2
1	44	100	40	32	0	4.33	0.0020	0.509	8372	27.2
3	53.9	120	48	32	0	6.17	0.0060	0.504	18471	39.8

* mi, mb#, s# and a# are the Hoek-Brown material constants for slope of failure envelope, fractured rock, rock mass strength and non-linearity of rock mass strength respectively.

2.2 *Model set-up*

A simple geometric set-up inspired by Cohen et al. (2023) is adopted. Although horseshoe shaped tunnels are the most common in real life projects, circular openings that are just as common are adopted in this study. As the focus will be on the liner displacement and stress reaction at tunnel crown and springline, considering that horseshoe shaped and circular shaped tunnel have comparable geometries above springline, the results are also argued to be comparable for both types of tunnels, while circular tunnels provide sufficiently more computation efficiency. The tunnel intersection angles are also kept at 90 degrees, as this has been proven by numerous studies to be the most critical intersection angle in terms of junction zone deformation and support reaction.
Two commonly adopted modelling techniques were used and compared for the 2D models, namely (i) the Diagonal Span Method, which models a tunnel junction with an ellipse of width equivalent to the diagonal span of the junction at 45 degrees; and (ii) the Weakened Ground Method, which models a tunnel junction by weakening the surrounding ground with a tripled Jn value. The model geometries of the 2D models are shown in Figure 1 and 2. As presented in the figures, the 2D models are set with a boundary of minimum 10x main tunnel span, to ensure that boundary effects would be negligible. Tunnel linings (blue line) and interface between lining and

ground (green line) are applied. The overburden load from ground material above tunnel opening is modelled by directly applying a vertical line load on top, for numerical modelling calculation efficiency and simplicity. The green (Y) and red (X) arrows shown indicate the axis of plane that the plane-strain model lays on.

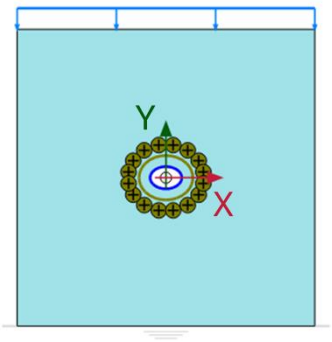


Figure 1. Example setup of Diagonal Span Method Model in Plaxis 2D, with an elliptical opening.

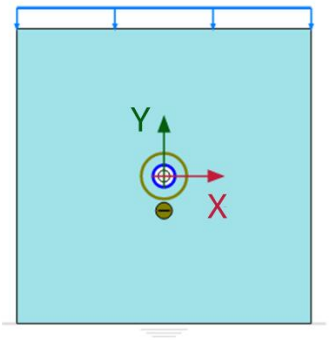


Figure 2. Example setup of Weakened Ground Method Model, with a circular opening.

The 2D models contain three stages:
(i) Initial stage before excavation
(ii) Main Tunnel excavation and liner installation
(iii) Cross adit excavation

The model setups for both methods in stages (i) and (ii) are identical. They only vary in stage (iii) where the Diagonal Span Method represents the action of cross adit excavation by enlarging the circular excavation to an ellipse equivalent to the diagonal span of the junction. The Weakened Ground Method would perform such action by weakening the surrounding ground strength parameters.

For the 3D models, the model geometry is illustrated in Figure 3. They have an almost identical staging as the 2D models. In stage (iii), an adit would be excavated up to a conservative 5x adit radius without support to model the effect of junction opening before any support is installed at the newly formed adit, which is usually considered to be one of the most critical steps in junction construction.

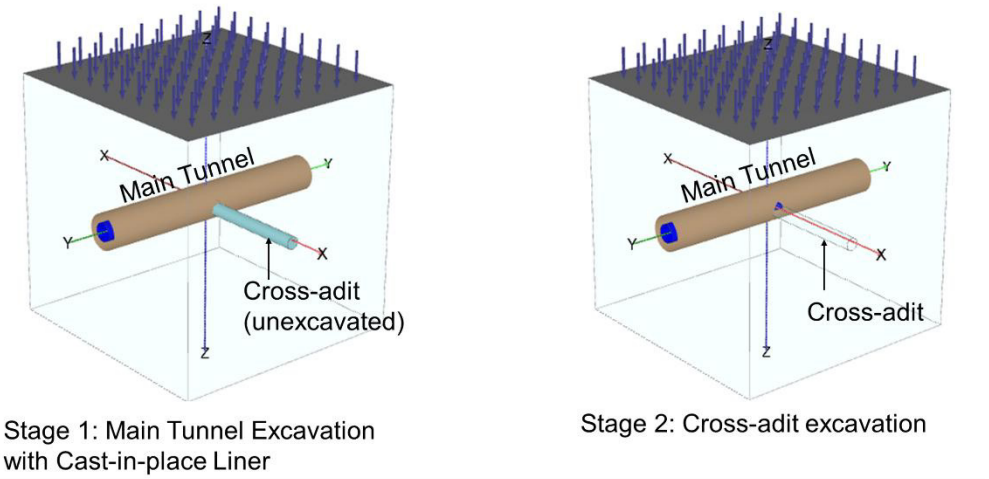


Figure 3. Setup of staged 3D model.

3 RESULTS AND INTERPRETATION

3.1 *Data extraction and analysis method*

A total of 64 sets of models were computed and analysed. Data was extracted from the monitoring points in the 2D and 3D models as illustrated in Figures 4 and 5. In Figure 4,

- Section 1 is in the middle of the junction.
- Section 2 is located at one cross adit radius from middle of junction.
- Section 3 is at one main tunnel radius from middle of junction.
- Section 4 is at 3 main tunnel radius from middle of junction.

Data will be collected from all 4 sections for the 3D models; Figure 5 shows that 3 data points on the crown (point a) and two sides of the springline (point b and c) of the main tunnel are referenced to for both 3D and 2D models.

To assess the accuracy between the 2D predictions and 3D model results, the coefficient of determination (R^2) values were calculated. This metric measures how well the 2D predictions match the 3D model results, with a score of 1.0 representing a perfect match (where all data points fall exactly on the y=x line. Linear fitted lines are also proposed to help diagnose systematic bias where the fit's R^2 (R_{fit}^2) measures linearity, and its slope and intercept quantify scaling and offset biases. To evaluate the relationship between model parameters and the accuracy of 2D predictions relative to 3D results, Pearson correlation coefficients were calculated between each parameter and the mean absolute error (MAE) of the 2D results. A modified geotechnical condition ratio $(\sigma_{cm} / P_o)^{0.55}$(Overburden Height/Tunnel Diameter)$^{0.45}$ proposed by Chortis & Kavvadas (2021), which represents the incorporated effect of overburden height ratio on geotechnical conditions ratio, is also included in the analysis as a proven relating parameter to junction effects.

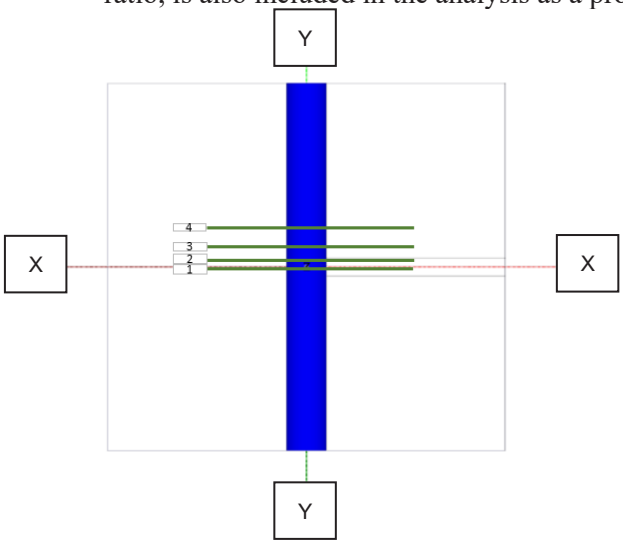


Figure 4. Illustration of sections where data points are on located in 3D models.

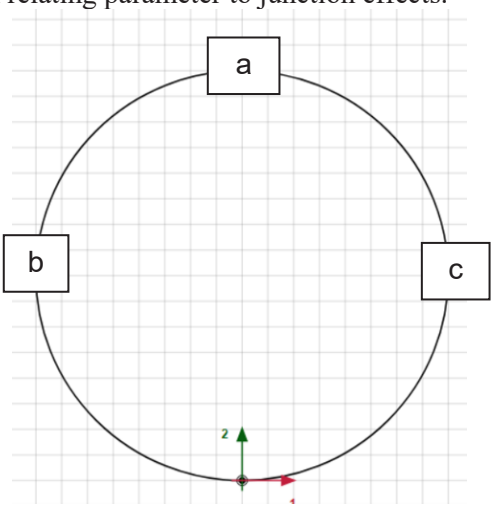


Figure 5. Illustration of data point locations on a cross section of the main tunnel.

3.2 *Comparative Accuracy of 2D vs. 3D Results at Tunnel Crown (Location a)*

To evaluate the reliability of simplified 2D approaches in capturing the structural response of the tunnel junction, a detailed comparison was conducted between the 2D Diagonal Span and Weakened Ground methods and the 3D model results at Location a (crown), across four representative cross-sections at the Cross Adit stage.

The vertical displacement (Uy) demonstrated strong linear correlation between the 2D prediction and 3D model results for both methods, with R_{fit}^2 close to 1.0. The Diagonal Span method showed excellent agreement ($R^2 = 0.99$) with the 3D results, only slightly overestimating the Uy magnitude. The Weakened Ground method showed poorer accuracy ($R^2 = 0.56$) and tends to overestimate Uy magnitude by roughly 50%. Both methods show poor agreement with horizontal displacement (Ux), with R^2 below 0, from the extremely limited horizontal movement at tunnel

crowns across all sections in 3D models compared to 2D results, while in theory the Ux at crown in 2D models should be extremely close to 0, the noticeable Ux recorded is possibly due to modelling artifact like mesh bias.

In terms of axial force (Nx2D), both methods exhibited strong linear correlation with the 3D model data ($R_{fit}^2 > 0.96$). The Diagonal Span method produced estimates that are slightly underpredicted in magnitude while maintaining a considerable extent of agreement ($R^2 = 0.88$). The Weakened Ground method gives a higher degree of accuracy ($R^2 = 0.91$). For this method, it is observed that 3D model data from section 4 are the closest to the y=x line, while the section 1 data lies above both the y=x line and linear fit line, indicating that it gives slight overpredictions to the axial force magnitude in the middle of junction.

Predictions for shear force (Q2D) and bending moment (M2D) were notably less reliable in both methods. The Diagonal Span method produced highly variable Q2D results, with errors ranging from moderate underestimation to extreme overestimation for all sections ($R^2 < 0$) with poor linear correlation ($R_{fit}^2 = 0.35$). Under the same method, the M2D predicted had limited accuracy ($R^2 < 0$) and poor linear correlation ($R_{fit}^2 = 0.23$), suggesting a curve may be a better fit. While the Weakened method tended to significantly underestimate shear response with poor agreement ($R^2 < 0$), for M2D results, the agreement was also poor with R^2 below 0 but the linear fitted line achieves a considerable prediction accuracy of $R_{fit}^2 = 0.87$ with the tendency to overpredict.

These findings underscore that the Diagonal Span method gives the most accurate approximation of vertical displacements at the tunnel crown during junction excavation, while the Weakened Ground method offers robust estimations for axial and bending load. However, simplified 2D models remain limited in capturing stress redistributions associated with complex 3D effects such as shear, particularly in geometrically discontinuous regions like tunnel intersections.

A correlation analysis was conducted to evaluate the influence of key geomechanical and geometric parameters on the accuracy of 2D model results relative to 3D outcomes at the tunnel crown (Location a). The analysis focused on mean absolute error (MAE) across all five key response variables (Ux, Uy, Nx2D, Q2D, M2D), calculated for each model configuration.

For the 2D Diagonal Span method, strong negative correlations were observed between MAE and several rock mass strength indicators, including σ_{cm}/P_o (-0.63), σ_{cm} (-0.57), GSI (-0.57), and Erm (-0.54). This suggests that the Diagonal Span method performs more accurately in stronger, more competent ground conditions, where simplifications inherent to 2D modelling have reduced impact. The most substantial positive correlation was observed with P_0 (+0.64), indicating that models with higher initial in-situ stress are associated with increased 2D-3D discrepancies.

The Weakened Ground method showed similar trends but generally weaker correlations, with top contributors including Q, σ_{cm}/P_0, and E_{rm} (correlation coefficients around -0.6). These findings reinforce that both 2D methods are sensitive to ground condition strength, but the Diagonal Span method is more strongly influenced by parameter variation.

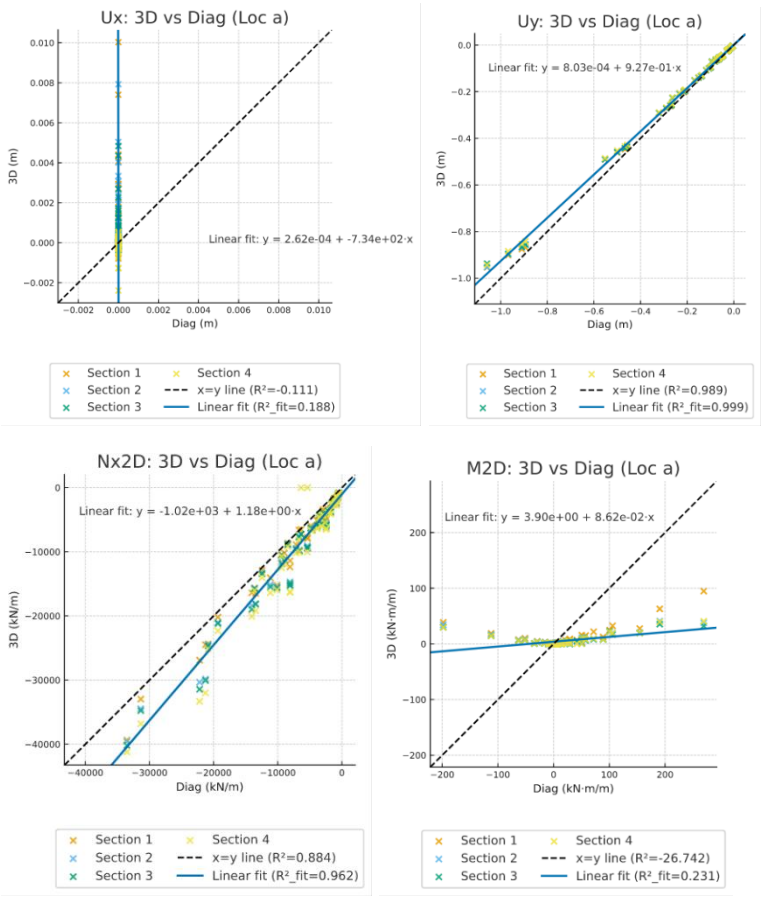


Figure 6 (Diagonal Span Method) Comparison between 2D and 3D model results at the tunnel crown (Location a) during the Cross Adit excavation stage, Plot of Ux, Uy, Nx2D and M2D shown.

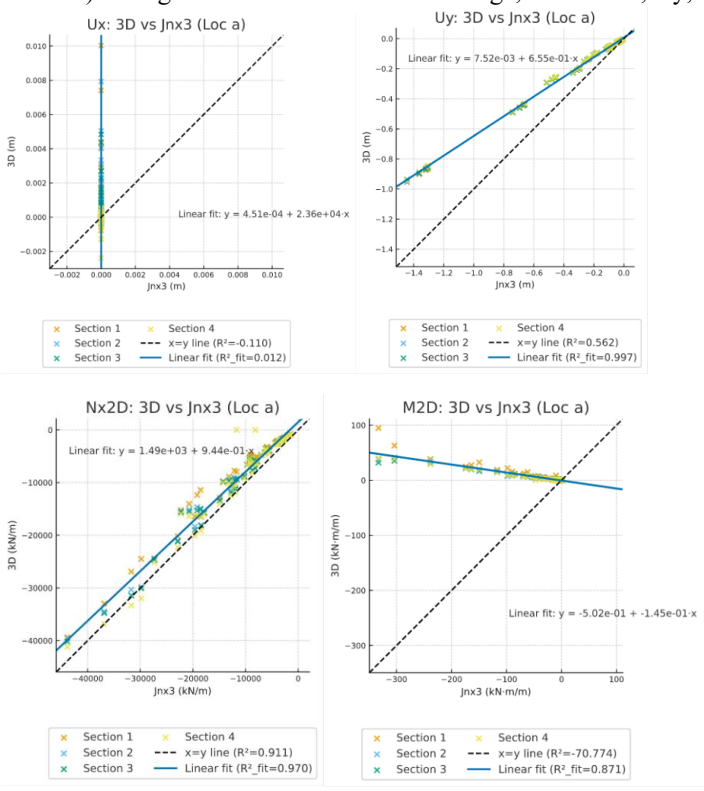


Figure 7 (Weakened Ground Method) Comparison between 2D and 3D model results at the tunnel crown (Location a) during the Cross Adit excavation stage, Plot of Ux, Uy, Nx2D and M2D shown.

3.3 *Comparative Accuracy of 2D vs. 3D Results at Tunnel Springline (Location b & c)*

Across both springline locations, the Diagonal Span method closely matched 3D results for displacements and axial force but poorly predicted shear force (Q2D) and bending moment (M2D). At Location b, vertical displacement (Uy) showed near-perfect agreement (R^2 close to 1). Lateral displacement (Ux) showed low direct agreement ($R^2<0$), while axial force (Nx2D) showed considerable accuracy ($R^2=0.90$). The results were affected by varying degrees of systematic over-prediction, although both Ux and Nx2D still maintained a high linear correlation ($R_{fit}^2 > 0.89$) between the 2D and 3D data. However, the Q2D and M2D predictions were highly unreliable ($R^2< 0$ and R_{fit}^2 close to 0). Location c, excluding Section 1 due to adit excavation, showed similar trends: Uy and Nx2D showed considerable accuracy and linearity ($R^2 > 0.84$ and $R_{fit}^2 > 0.85$) while Q2D, and especially M2D, had poor agreement and linear correlation. Similar to location a, an exponential curve would serve better M2D predictions. Correlation analysis of mean absolute error versus geotechnical parameters highlighted how model accuracy varies with rock mass strength, stiffness, and stress state. At Locations b and c, the errors of the 2D Diagonal Span method showed strong negative correlation with parameters such as σ_{cm} /Po (-0.55 to -0.63), GSI (-0.58 to -0.59) and Erm (-0.51 to -0.53). These results indicate that the Diagonal Span method performs best in stronger, more competent rock masses. A strong positive correlation was observed with in-situ stress Po (+0.5 to +0.61), suggesting that high stress magnitudes reduce 2D-3D agreement.

In contrast, the Weakened Ground method provides stronger Ux estimations (R^2 ranges from 0.44 to 0.66, and $R_{fit}^2 >0.83$). For Nx2D, it gives slightly less accurate yet still reliable results with $R^2 >0.7$ and $R_{fit}^2>0.78$. Similar to location a, the Q2D at locations b and c are highly dispersed, while the M2D at location b shows good linearity but poor agreement ($R^2< 0$ and $R_{fit}^2 =0.98$). However, at the side of adit opening location c, the M2D predicted have both poor agreement and linearity. At locations b and c, the mean absolute errors of the Weakened Ground method showed moderately negative correlations with Q, GSI, and Modified Geotechnical Condition Ratio (-0.38 to -0.67 range), while demonstrating strong positive correlation with Po at location b (+0.81) and moderately strong at location c (+0.50), revealing similar trends as that of the Diagonal Span method.

3.4 *Summary*

The results from all three observation points - Location a (crown), Location b (left springline), and Location c (right springline) - reveal consistent trends in the reliability and limitations of simplified 2D numerical modelling in tunnel junction scenarios. Across all locations, the 2D Diagonal Span method consistently demonstrated strong agreement with the 3D model results in reflecting vertical displacement and axial load, while the Weakened Ground method gives reliable predictions to axial load at all locations.

In contrast, both 2D methods exhibited poor performance in estimating shear force (Q2D), with large relative errors often >1000% and weak agreement ($R^2 < 0$).

The Weakened Ground method followed similar trends but generally showed larger deviations and weaker R^2 values than the Diagonal Span method, particularly in vertical displacement and axial force prediction. Correlation analysis between 2D-3D error and model parameters revealed that 2D model accuracy improves significantly in stronger, stiffer ground conditions, and degrades under high in-situ stress. It is concluded that the key influencing parameters (highest correlations with reduced error) includes σ_{cm} /P_o, E_{rm}, σ_{cm}, GSI, Q, and the modified geotechnical condition ratio.

The overall findings are summarized as follows:

- The 2D Diagonal Span method provides reliable estimates for vertical displacement and axial load across all junction locations, especially in competent rock masses under moderate stress.
- The Weakened Ground Method provides good estimation for axial responses at crown, and its estimate for horizontal displacement at the springline is better than that of the Diagonal Span method.

- Shear behaviors cannot be confidently captured by 2D simplifications and require full 3D modelling for critical analysis.
- The Diagonal Span method is more sensitive to parameter changes than the Weakened Ground method, making it more responsive but also more vulnerable to deviation under poor ground conditions.

4 CONCLUSION

In effort of investigating the relationship and comparability between two- and three-dimensional numerical modelling results of a junction zone, an extensive study was undertaken involving a series of Plaxis 2D and 3D models. In this study, it is concluded that the Diagonal Span method generates closer results to the 3D models in terms of crown settlement, along with consistent accuracy in predicting axial load in liners, while the Weakened Ground method yields better predictions on springline horizontal displacements. These findings would justify using 2D models as a first pass analysis in early stage designs, though it shows potential at current stage of studies, more in-depth research would need to be undertaken for 2D models to act as a replacement for 3D modelling. Further studies are recommended to better understand and develop two-dimensional modelling methods that can produce comparable predictions with its three-dimensional counterparts, for example, different main tunnel and adit shapes can be included, and K0 values not limited to 1 can also be used.

5 REFERENCES

Chortis, F., & Kavvadas, M. (2020). Three-Dimensional numerical analyses of perpendicular tunnel intersections. *Geotechnical and Geological Engineering, 39(3), 1771–1793*. https://doi.org/10.1007/s10706-020-01587-w

Cohen, S., Mitelman, A., & Elmo, D. (2023). A methodology for the analysis of tunnel intersections using two-dimensional numerical modeling. *IOP Conference Series Earth and Environmental Science, 1124(1), 012069*. https://doi.org/10.1088/1755-1315/1124/1/012069

Gkikas, V. I., & Nomikos, P. P. (2021). Primary support design for sequentially excavated tunnel junctions in Strain-Softening Hoek–Brown Rock Mass. *Geotechnical and Geological Engineering, 39(3), 1997–2018*. https://doi.org/10.1007/s10706-020-01602-0

Hsiao, F., Wang, C., & Chern, J. (2009). Numerical simulation of rock deformation for support design in tunnel intersection area. *Tunnelling and Underground Space Technology, 24(1), 14–21.* https://doi.org/10.1016/j.tust.2008.01.003

19th Australasian Tunnelling Conference – Acosta-Martínez, Stewart and Hudson-Smith (Eds.)
© 2025 Australian Tunnelling Society, ISBN 978-0-85825-002-4

Shallow urban tunnelling method in complex geological conditions; case study: Naghsh-e-Jahan station-line 2 metro of Esfahan

A. Moghbeli
RahsazTarh (RST) Consulting Engineers Co., Tehran, Iran

H. Samadi
School of Mining and Geosciences, Nazarbayev University, Astana, Kazakhstan
Underground Structures Engineering Research Group Institute (USERG), Tehran, Iran

S. Tarigh Azali
RahsazTarh (RST) Consulting Engineers Co., Tehran, Iran
Underground Structures Engineering Research Group Institute (USERG), Tehran, Iran

F. Suorineni
School of Mining and Geosciences, Nazarbayev University, Astana, Kazakhstan

ABSTRACT: The paper investigates a case study of metro station construction in urban areas using the New Austrian Tunnelling Method - Shallow Tunnelling Method (NATM-STM). Naghsh-e-Jahan metro station, located on Line 2 of the Esfahan metro, was constructed using an underground approach and a combined method that included the NATM with STM, with low overburden in the upper part of the platform level and supported lateral piles in the lower part of the platform level. The choice of the underground construction method was due to the requirements imposed by the location of the station in the historic fabric of Esfahan, which has a high sensitivity to settlement, and the high groundwater level that rules out systematic dewatering. This article systematically shows the potential use of combined methods and the application of STM in the construction of urban shallow underground spaces, despite the complex geological and geotechnical conditions. The findings of the study can be used for future tunnelling projects under the same conditions.

1 INTRODUCTION

Tunnelling and metro systems play a vital role in modern urban infrastructure, particularly in densely populated cities where surface transportation options are limited. As urban areas expand and encounter increasing population density, the demand for underground transportation networks has risen significantly (Cui et al., 2017). The evolution of tunnelling techniques underwent a major transformation in the mid-20th century with the introduction of the new Austrian tunnelling method (NATM), which became widely adopted due to its flexibility under various geological conditions. However, debates exist regarding its applicability in soft ground. In response to challenges posed by soft ground, the Institution of Civil Engineers (ICE) introduced the concept of sprayed concrete lining (SCL) (ICE, 1996). Soft soils present unique challenges that may not align with conventional NATM theories; thus, the development of SCL aimed to address these issues and offer a more effective solution for tunnelling in such geological conditions. Continuous monitoring and control during the use of SCL in soft ground are essential to ensure tunnel safety (Brown, 1981).

Subsequently, the shallow tunnelling method (STM) emerged as a valuable technique for tunnel construction at shallow depths, particularly in densely populated urban areas with soft ground conditions (Moghbeli et al. 2025b). Key characteristics of STM include shallow overburden (requiring careful control of surface ground movements), the sensitivity of soft soils to deformation and instability, and the need to minimize surface movements to protect infrastructures (Moghbeli et al. 2025c). The development of pre-reinforcement techniques has significantly enhanced the stability and safety of shallow tunnels in challenging geological environments. Drawing from successful experiences with NATM and adapting them to shallow tunnelling conditions, engineers can continue to improve the efficiency and effectiveness of STM projects (Cui et al., 2017,

Moghbeli et al. 2025a). Fang et al. (2012) showed the effectiveness of STM for tunnelling in soft ground with shallow depth. Amiri and Dehghan (2022) reported that STM significantly reduced surface settlement compared to the pile and rib method (PRM), with a maximum settlement of approximately 6 cm. According to Liu et al. (2022), STM is commonly applied to shallow tunnels in soft soils in China, particularly in metro projects. Zhang et al. (2020) proposed a complex construction plan for shallow urban tunnels in silty soils, a case study in Fuzhou, Fujian Province.

The present paper investigates a case study (Naghsh-e-Jahan station-line 2 metro of Esfahan) of underground metro station construction in urban areas using the NATM-STM. It provides a detailed analysis of the design of an underground station, including construction method, structural design, and architecture, in complex geotechnical and geological conditions in the historic fabric of Esfahan city.

2 PROJECT DESCRIPTION

2.1 Project characteristics and geological settings

The project's alignment depth at this station is 17.10 meters below the ground surface, with an overburden of approximately 8 meters. The central core structure of the station, designed at a depth of 16.4 meters below the ground level, has a length of 105 meters and comprises a single level (the station platform). This core includes the ticket hall and side structures extending over a length of 65 meters. A connecting gallery, linking the side structures, is located at a depth of approximately 11.40 meters and extends about 20 meters in length. The general layout of the station, including the central core and its side structures, is presented in Figure 1.

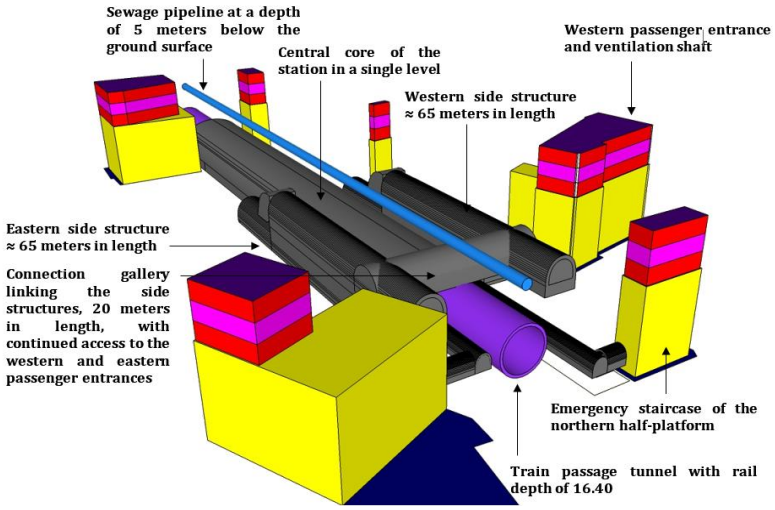


Figure 1. General layout of the Naghsh-e-Jahan station-line 2 metro of Esfahan.

The construction method used for this station is a combination of NATM and STM. Excavation was carried out in two main parts, upper and lower, each subdivided into three drifts (two side drifts and one central drift). The cross-sectional area of the NATM segment is approximately 100 square meters, while the total excavation cross-sectional area of the station is 180 square meters. The internal height of the excavation section is 12 meters, and the width is 17 meters. A cross-sectional view of the station, showing the excavation subdivisions considering the geological layout, is presented in Figure 2.

Table 1-A presents the physical and mechanical properties of the project site. The first major challenge of the project is the relatively shallow overburden of the tunnel compared to the ground surface, which increases the risk of ground settlement sensitivity. The second challenge arises from the station's location at an intersection surrounded by deteriorating urban infrastructure and historically significant cultural buildings. Additionally, the presence of the Zayandeh Rood River,

which flows through the central area of Isfahan, results in a high groundwater level. The station is constructed in clayey soil with coarse-grained interlayers, exhibiting hydrodynamic characteristics such as high transmissivity and permeability coefficients. Consequently, dewatering and pumping operations have not been effective in lowering the groundwater level. The main geological and physical challenges of the project are summarized in Table 1-B.

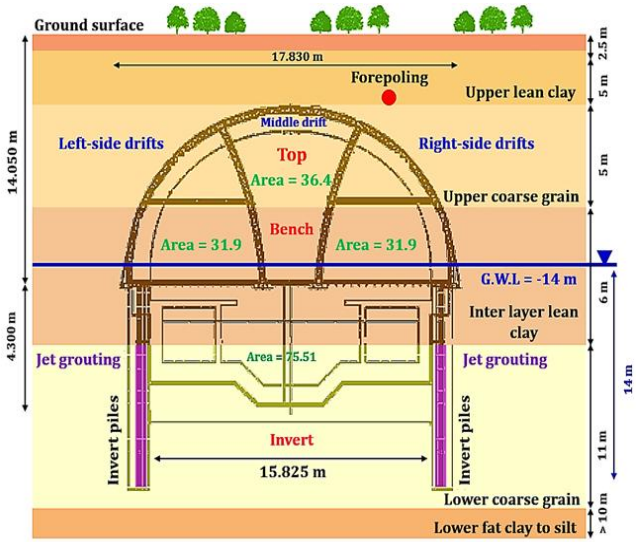


Figure 2. Schematic design of the Naghsh-e-Jahan station-line 2 metro of Esfahan, considering the geological layout (Moghbeli et al. 2025d).

Table 1. (a) Key characteristics of the project, (b) Main challenges of the project.

Part A		Part B	
Parameters	Descriptions	Challenges/Limitations	Descriptions
Tunnel length	105 m	Congestion and traffic	Yes
Excavation method	NATM-STM	Uncompacted and fine-grained soil	Yes
Tunnel diameter	12 m	Sensitive railway tracks	No
Overburden	8 m	High groundwater level	Yes
Overburden/diameter ratio	0.66	Historical buildings	Yes
Geological unit	Clayey soil with coarse-grained interlayers	Sensitive and deteriorated infrastructures	Yes

2.2 Engineering geological and geotechnical investigation

The Naghsh-e-Jahan station-line 2 metro of Esfahan project is situated within the Qm sedimentary unit. Engineering geological and geotechnical specifications were defined using pre-construction laboratory testing and in-situ field investigations, as well as sampling during station construction. Table 2 presents the geotechnical properties of materials along the project alignment, which were utilized in the design phase of the construction.

Table 2. Geotechnical characteristics of materials along the project.

Geotechnical factors	Unit	Man fill	Upper lean clay	Upper coarse-grained	Inter-layer lean clay	Lower coarse-grained	Lower fat clay to silt
Depth	m	0-2.5	2.5-7.5	7.5-12.6	12.6-18	18-29	29-40
Elastic modulus	Kg/cm^2	100	170	270	156	330	140
Poisson	-	0.3	0.35	0.3	0.35	0.3	0.35
Friction angle	degree	15	26.7	36.5	29	34.3	26.7
Cohesion	Kg/cm^2	0.1	0.25	0.06	0.24	0.04	0.24

Wet density	gr/cm^3	2.05	1.98	2.07	2.01	2.08	1.85
Dry density	gr/cm^3	2.0	1.9	2.05	1.95	2.1	1.81
Permeability	cm/s	-	$1.0*10^{-6}$	$1.0*10^{-4}$	$5.36*10^{-6}$	$2.6*10^{-4}$	$1.0*10^{-6}$

2 PROPOSED TUNNELLING METHOD

The Naghsh-e Jahan Station is constructed underground, on a single level, using a combined NATM-STM method along with braced piling. The choice of an underground construction method was necessitated by the proximity of deteriorated and historical buildings, which made surface-level construction operations unfeasible. Moreover, due to the high groundwater level, the station was designed and constructed as a single-level structure to reduce exposure to groundwater-related challenges. Access to the station's central core was designed through a shaft approximately 9 by 18 meters in size, extending to the platform level, along with an access gallery at the platform elevation. Excavation of the upper part of the platform (divided into three sections: two side drifts and one central drift) was carried out using the NATM technique, while the lower part was executed using braced piling. The upper structure of the station's central core consists of 35 cm-thick shotcretes, reinforced with mesh and rebar. To ensure structural integrity, the design calculations were based on the early-cured age compressive strength of shotcrete (160 kg/cm^2). In the lower part of the platform, piles with a diameter of 0.9 meters and a spacing of 2.5 meters were used. The construction stages associated with the application of the combined NATM-STM with braced piling method for this station are presented in Figure 3.

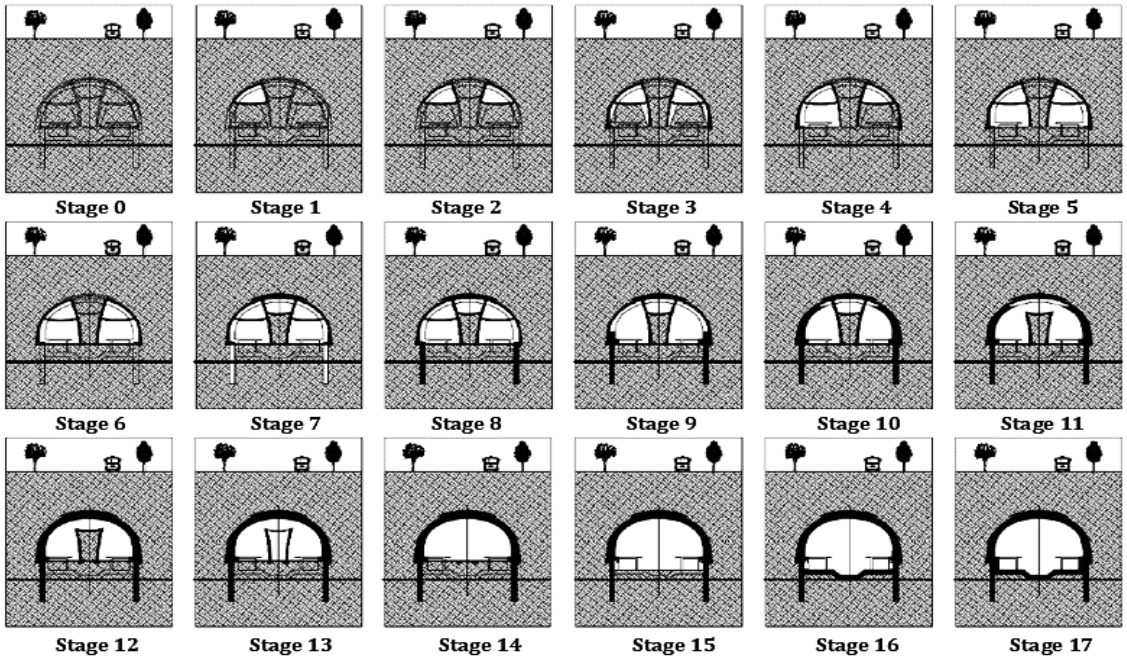
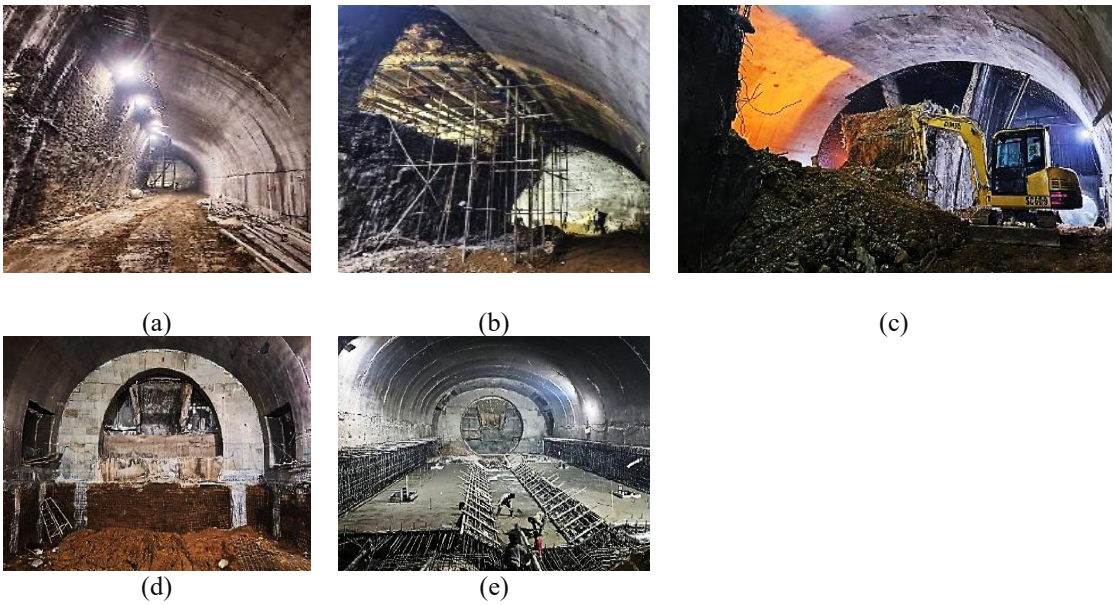


Figure 3. Step-by-step construction stages of the stations' central core using NATM-STM and braced piling methods.

It is worth noting that in the initial design, before the removal of the temporary central lattice girders, the use of a forepoling pre-reinforcement system was planned for the upper section. However, its implementation proved unsuitable due to the poor groutability of the upper soil layer above the crown. Consequently, a new construction approach was adopted, involving the installation of side arch walls (within the side drift zones) supported on a deep foundation system (the same lateral piles initially intended for the excavation beneath the platform), before the removal of the central temporary lattice girders. To achieve this, pile cap beams were first constructed atop the side piles. Then, the arch walls were executed from those beams, extending as far as feasible

into the stable zones (Figure 4a). Following the construction of these walls, the upper portion of the central lattice girders was removed (Figure 4b), and the stabilizing side arch walls were connected by completing the remaining portion of the arched roof. Ultimately, the remaining parts of the central drift were removed (Figure 4c), and excavation of the lower section was carried out (Figure 4d), thereby completing the final profile of the station cross-section (Figure 4e).



(a) (b) (c)

(d) (e)

Figure 4. The construction sequence in the southern section of Naghsh-e Jahan Station, (a) construction of side arch walls, (b) removal of the lattice girder in the central drift, (c) complete removal of the central drift, (d) excavation of the lower section, (e) completion of the central core cross-section through foundation construction.

3 MONITORING

Instrumentation and monitoring systems were used concurrently with the construction activities as a mandatory requirement for the execution of underground spaces in urban environments. A total of 288 instruments were employed in the project, including 8 deep settlement gauges, 100 ground surface settlement gauges, 60 building settlement gauges, 14 convergence measurement sections, 42 crack meters, and 64 surveying targets. Among the approximately 100 ground surface settlement gauges and 60 building settlement gauges installed within the station area, the maximum recorded ground surface settlement reached 109.4 millimeters at ground settlement gauge G02-E, while the maximum building settlement reached 43 millimeters at building settlement gauge SW206.

According to the monitoring results, the excavation sequence of the upper section of the central core in a portion of the station was modified. Assuming the intersection point between the access ramp and the central core as the boundary between the northern and southern sections of the station, the instrumentation data indicated that the settlement values in the northern section were consistent with predictions, whereas in the southern section, the observed settlements exceeded the values anticipated by the design calculations.

Since the additional surface settlement in the southern section occurred after the excavation and stabilization of the side drifts and before the removal of the central drift, continuing construction stages—including completion of the central drift and removal of the temporary lattice girders—would have led to excessive surface settlement beyond the permissible limits and posed a risk of damage to the adjacent deteriorated structures within the excavation's impact zone. Therefore, a change in the construction method and implementation of additional settlement control measures became necessary.

An example of ground surface settlement measurements in the southern section of the station is presented in Figure 5. As seen in the graph, on 4 October 2023, corresponding to the completion of the side drift removals, the ground surface settlement reached approximately 8 centimeters. Subsequently, the side arch walls were constructed, and the temporary central lattice girders were removed. As a result, the ground settlement increased by only 0.5 millimeters up to 4 June 2024, indicating the effectiveness of the side arch walls in controlling surface settlement following the completion of the upper section excavation of the station core. Following this phase, excavation of the lower section of the station platform was carried out and completed by 4 December 2024. This phase resulted in an additional settlement of only 1.5 centimeters, confirming overall settlement control throughout the station construction.

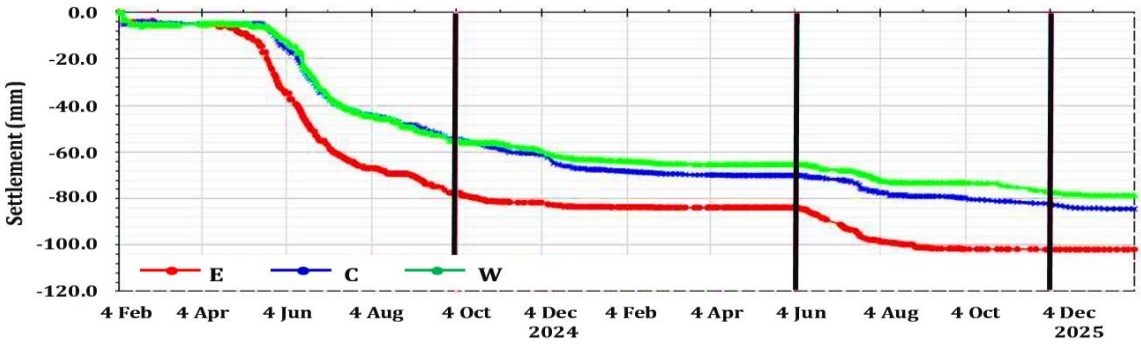


Figure 5. Monitoring results obtained from the three-point settlement gauge G06 in the southern section of Naghsh-e Jahan Station.

4 NUMERICAL MODELLING

A two-dimensional model of the central core of Naghsh-e Jahan Station was developed using Plaxis 2D v21 before construction, including soil–structure interaction. This model was subsequently updated using data obtained from instrumentation and monitoring during construction. Ground surface settlement was controlled throughout all construction stages, and the maximum settlement in the upper section constructed using the NATM-STM was recorded at various stages, as illustrated in Figures 6 to 9. According to the results, the maximum surface settlement increased from approximately 7.6 cm (following the removal of side drifts) to about 10.2 cm after the full completion of the cross-section. This corresponds closely with the monitored data obtained during construction, demonstrating a strong agreement between the numerical model and field observations.

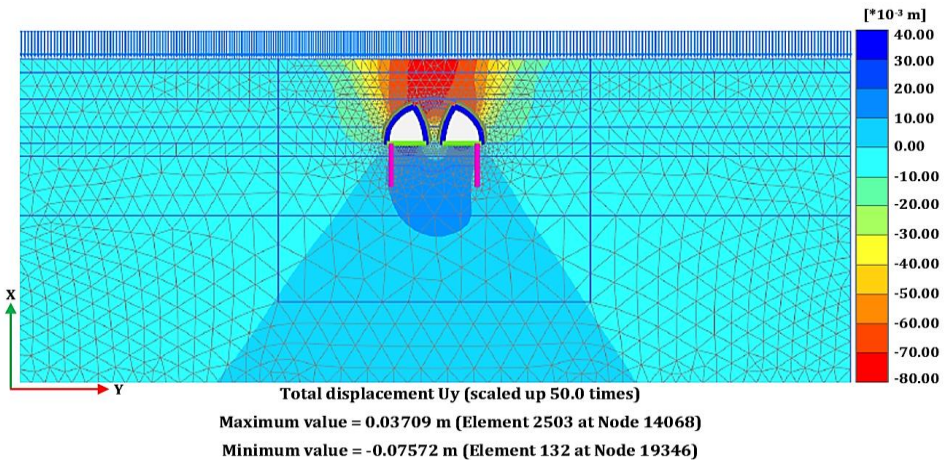


Figure 6. Settlement of Naghsh-e Jahan station after the removal of the side drifts based on the results of 2D modelling with Plaxis.

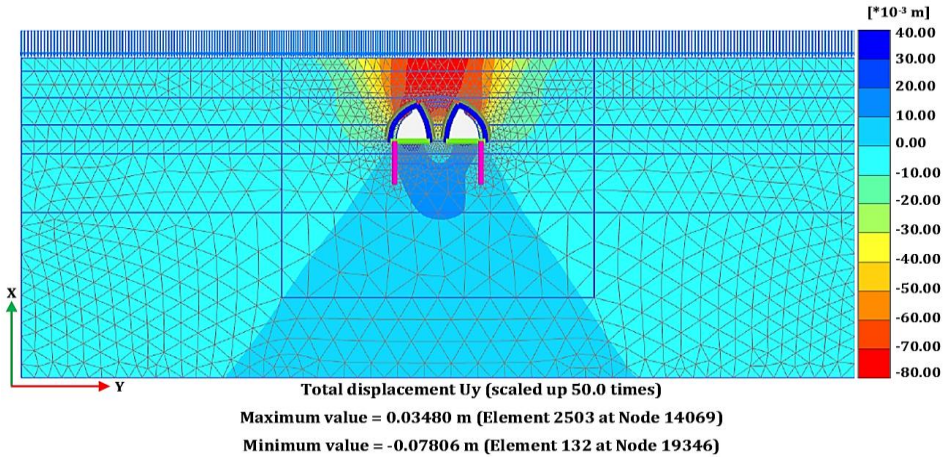


Figure 7. Settlement of Naghsh-e Jahan station after the construction of the arch walls based on the results of 2D modelling with Plaxis.

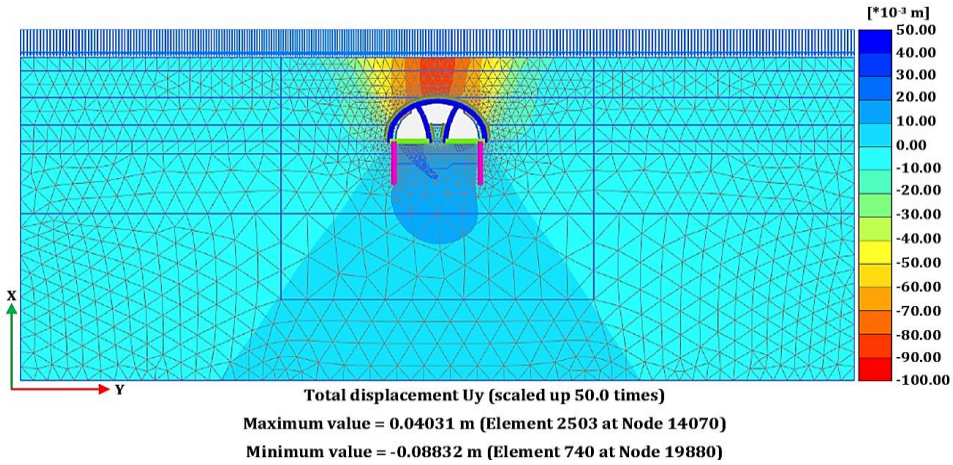


Figure 8. Settlement of Naghsh-e Jahan station after the removal of the upper part of the central drift based on the results of 2D modelling with Plaxis.

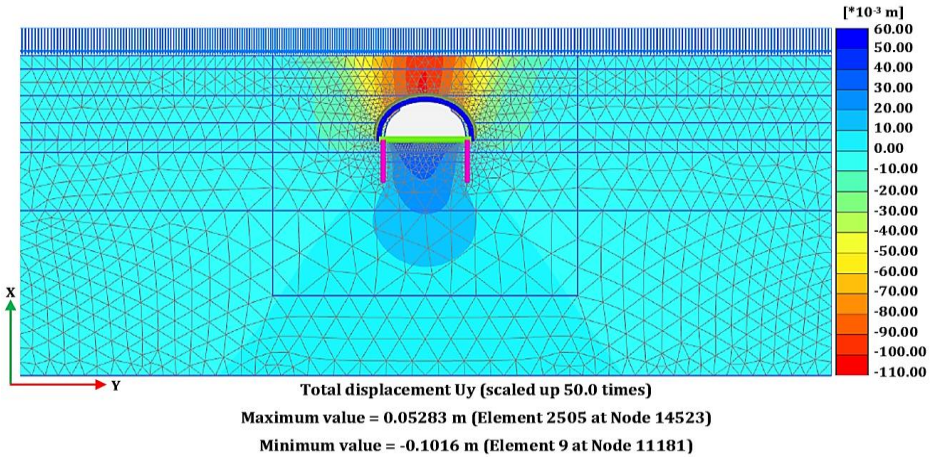


Figure 9. Settlement of Naghsh-e Jahan station after the complete removal of the central drift and connection of the arch walls based on the results of 2D modelling with Plaxis.

5 CONCLUSIONS

This paper examines the construction approach of the Naghsh-e Jahan metro station in Isfahan, utilizing the NATM-STM method in urban areas. This study presents the overall station layout, geometric design, challenges encountered during the design and construction phases, and proposed solutions to overcome these obstacles in the project. The successful construction of such metro stations, particularly those located near significant historical landmarks, existing infrastructure, or below the groundwater table, necessitates the application of the NATM-STM method alongside precise monitoring. The case study detailed in this paper shows how the geometric design of such stations is critical to their successful implementation in complex urban environments. By highlighting the strategic application of NATM-STM techniques in this project, the paper aims to provide a comprehensive understanding of the method's effectiveness in both theoretical and practical contexts. The outcomes emphasize the importance of adapting design approaches to specific geological and environmental conditions. The insights gained from this project offer guidance for future projects in similar geotechnical settings, illustrating the capability of NATM-STM to address complex construction challenges effectively.

6 ACKNOWLEDGMENT

The authors wish to extend their heartfelt appreciation to RahSaz Tarh (RST) Consulting Engineers Co. and Underground Structures Engineering Research Group Institute (USERG) for generously providing valuable information to conduct the present study. The authors also acknowledge the support of the Nazarbayev University Faculty Development Competitive Research Grant Program number 201223FD8835.

7 REFERENCES

Amiri, S. & Dehghan, A.N., 2022. Comparison of shallow tunneling method with pile and rib method for construction of subway station in soft ground. *Frontiers of Structural and Civil Engineering*, 16(6), pp.704-717. https://doi.org/10.1007/s11709-021-0746-4

Brown, E.T., 1981. Putting the NATM into perspective. *Tunnels & Tunnelling International*, 13(10). http://worldcat.org/issn/0041414X

Cui, Y., Kishida, K. & Kimura, M., 2017. Prevention of the ground subsidence by using the foot reinforcement side pile during the shallow overburden tunnel excavation in unconsolidated ground. *Tunnelling and Underground Space Technology*, 63, pp.194-204. https://doi.org/10.1016/j.tust.2016.12.014

Design, I.C.E., 1996. *Practice Guides: Sprayed concrete linings (NATM) for tunnels in soft ground*. Institution of Civil Engineers, London.

Fang, Q., Zhang, D. & Wong, L.N.Y., 2012. Shallow tunnelling method (STM) for subway station construction in soft ground. *Tunnelling and Underground Space Technology*, 29, pp.10-30. https://doi.org/10.1016/j.tust.2011.12.007

Liu, S., Liu, S., Lu, S., Ma, F. & Pei, G., 2022. Seismic behaviour of shallow tunnelling method tunnels accounting for primary lining effects. *Buildings*, 13(1), p.20. https://doi.org/10.3390/buildings13010020

Moghbeli, A., Samadi, H., Tarigh Azali, S., Hassanpour, J. & Rostami, J., 2025a. Introducing an innovative tunneling method to construct underground subway station underground water level. In book: *Tunnelling into a Sustainable Future – Methods and Technologies*. https://doi.org/10.1201/9781003559047-39

Moghbeli, A., Samadi, H., Tarigh Azali, S., Hassanpour, J., Roodbari, A.A. & Suorineni, F., 2025b. Shallow tunneling method (STM) for underpass construction in soft ground; a case study: Galoobandak underpass project. American Rock Mechanics Association, ARMA 2025, Santa Fe, USA.

Moghbeli, A., Samadi, H., Tarigh Azali, S., Hassanpour, J., Roodbari, A.A. & Suorineni, F., 2025c. NATM-STM application for tunnel construction underneath the operating railway, case study: Azadegan depot link tunnel of Tehran metro line 3. American Rock Mechanics Association, ARMA 2025, Santa Fe, USA.

Moghbeli, A., Samadi, H., Tarigh Azali, S., Rostami, J. & Hassanpour, J., 2025d. Shallow tunneling method for subway station construction in challenging projects. In book: *Tunnelling into a Sustainable Future – Methods and Technologies*. https://doi.org/10.1201/9781003559047-294

Zhang, S., He, S., Qiu, J., Xu, W., Garnes, R.S. & Wang, L., 2020. Displacement characteristics of an urban tunnel in silty soil by the shallow tunnelling method. *Advances in Civil Engineering*, 2020(1), p.3975745. https://doi.org/10.1155/2020/3975745

THIS PAGE INTENTIONALLY LEFT BLANK

19th Australasian Tunnelling Conference – Acosta-Martínez, Stewart and Hudson-Smith (Eds.)
© 2025 Australian Tunnelling Society, ISBN 978-0-85825-002-4

TBM launch temporary works: Melbourne North East Link

J. Zeneli
Webuild, Melbourne, Australia

D. Kubik
Delve Underground, Melbourne, Australia

ABSTRACT: North East Link freeway is a 10km long portion of Melbourne's northeast transport network. The Spark consortium has been contracted by North East Link to complete the missing link in Melbourne's orbital freeway between an upgraded Eastern Freeway and the M80 Ring Road. Spark is responsible for delivering the Primary Package under a public-private partnership (PPP) framework encompassing the design, financing, construction and commissioning of the Works, including 6.5km twin three-lane tunnels, with interchanges at Manningham and Lower Plenty Roads and upgrades to Greensborough and Bulleen Roads. To complete the 6.5km twin 14.1m internal diameter tunnels, two tunnel boring machines (TBM) were assembled and launched from the Watsonia trench site. The TBMs will arrive, traverse and relaunch at the Lower Plenty Road cut and cover structure and will finish at the Manningham cut and cover structure. Delve Underground, in close collaboration with Spark, designed the TBM assembly gantry crane foundations, launch frame, cradles, false ring support and launch seals. This paper discusses the design of the above elements, providing insight into key design decisions and the structural behaviour of the temporary works versus the modelled predictions.

1 INTRODUCTION

North East Link (NEL) freeway is a 10km long portion of Melbourne's northeast transport network. The project includes Victoria's longest and largest twin road tunnels from Watsonia to Bulleen. The segmentally lined tunnels are 14.1m internal diameter (ID) designed and constructed along most of the alignment using the latest industry practice.

Two tunnel boring machines (TBM1 and TBM2) were assembled and initially launched from the Watsonia trench site. This paper aims to share lessons learnt from the NEL project TBM assembly and launch. A number of integrated elements of temporary works are required to safely assemble, launch and service the TBMs. A general overview of the Watsonia trench site is shown in Figure 1 below, which includes the following Temporary Works design scope:

- Temporary runway beams and columns located on top of the Watsonia permanent piled walls for the support of the TBM assembly gantry crane.
- Temporary foundation beams and retaining wall behind the Watsonia piled headwall for the support of the TBM assembly gantry crane.
- TBM launch frame, ground anchor hold-downs and foundations to support the TBM thrust loadings during launch and initial excavation.
- Temporary eye seal for TBM launch fixed with ground anchors into rock to provide confinement of annulus grouting during initial permanent segment installation.
- TBM launch cradle and TBM backup gantry trench to enable the assembly and support of the TBM equipment during assembly and launch.
- Temporary frames to support the temporary false concrete tunnel segments. This supports the false rings which transfer the TBM thrust loads to the launch frame.

This paper concentrates on the TBM launch frame and gantry crane temporary runway beams and columns.

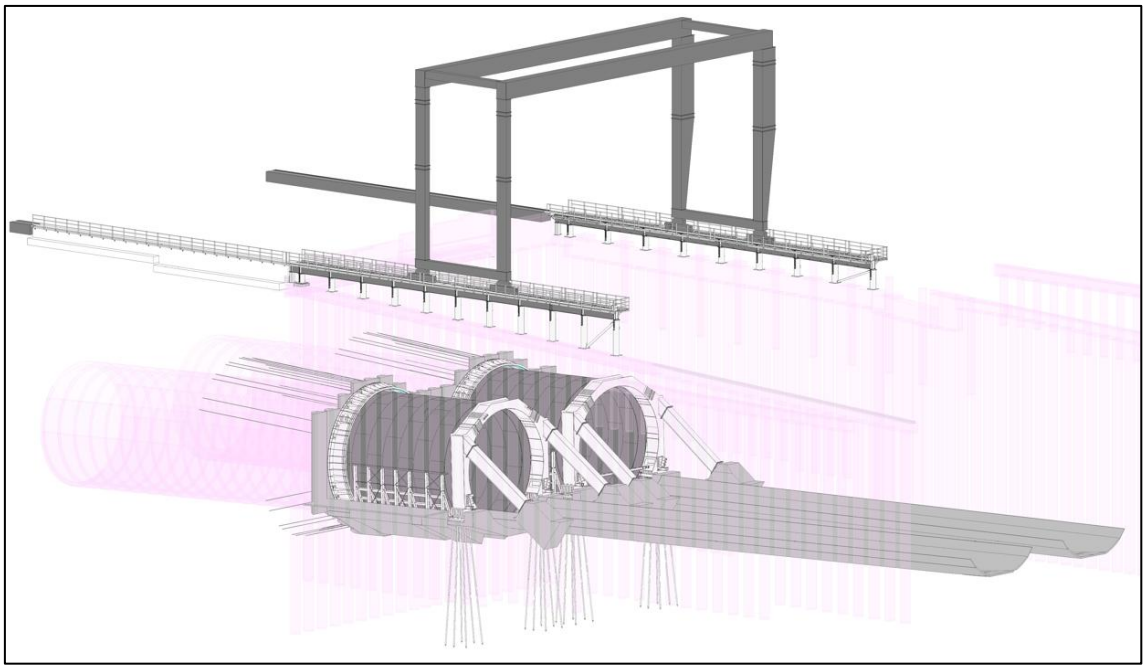


Figure 1. TBM temporary works at the Watsonia trench site

2 DESIGN DEVELOPMENT

The Watsonia TBM Temporary Works package was risk assessed and identified as a critical design package, and as such, was delivered using the same design management plan as the Permanent Works. The design was delivered in a staged manner: Preliminary Design, Draft Certified Design and Certified Design. Throughout the design stages, workshops were held with the constructor to identify key issues and decide on the best strategy to overcome them. This section details key changes implemented over the design stages for key elements of the Temporary Works design package.

2.1 TBM launch frame

To construct the 14.1m ID segmentally lined tunnel, a 15.55m TBM with a bore diameter of 15.61m was procured. The TBM consists of a 2500tonne, 13.5m long shield and three trailing backup gantries. The total length and weight of the TBM with backup gantries is 90m long and 4000tonne respectively. At the Watsonia trench launch site, the ground conditions were predominantly in moderately weathered siltstone which provided a relatively strong sub-grade for the temporary foundations to bear onto.

The design TBM launch thrust load at Watsonia trench site was 38,000kN, applied via 20 thrust jack pairs evenly arranged around a 14.6m diameter circle. The thrust jacks are used to advance the TBM shield forward as it mines through soil and rock; initially pushing on the launch frame, then temporary false rings, and then the typical case of pushing onto the permanent tunnel rings. Both the temporary and permanent tunnel rings are 500mm thick. The thrust jack positions are shown on the left-hand side of Figure 2, below.

The custom fabricated box beams that are typically used for added stability on large TBM launch frames have an inherently high torsional capacity which allows for flexibility in the location of the web and stiffener plates in relation to the TBM thrust jack positions. To simplify the installation of the frame and reduce the amount of site splices, the inherent torsional stability of the box beams made possible for the adoption of a horseshoe arrangement for the main launch

frame. The horseshoe arrangement resulted in the upper splice connection between the top and side members requiring less manipulation during installation due to the splice plates being on an angle. The top member could be directly lowered into the space between the two side members more efficiently compared to a more traditional launch frame which would be composed of a horizontal top member and angled corner members resulting in two vertically oriented splice plates on each side of the traditionally framed top member. The front frame was designed to be lifted in separate pieces or one large module. This improved the installation and removal for the initial use at Watsonia trench site and for re-use at Lower Plenty Road cut and cover structure.

Adopting the horseshoe arrangement, however, resulted in a more complex loading arrangement than a traditional frame's top member. The combined structural actions of bending, shear, and torsion in the top member of the horseshoe had to be carefully considered. To accurately model the structure, a full 3D finite element (FE) model was utilized as shown in Figure 2, below. The higher stressed regions in the upper web of the top shoulders of the horseshoe-shaped frame required a thicker web plate to resist the additional shearing stress due to torsion in the member.

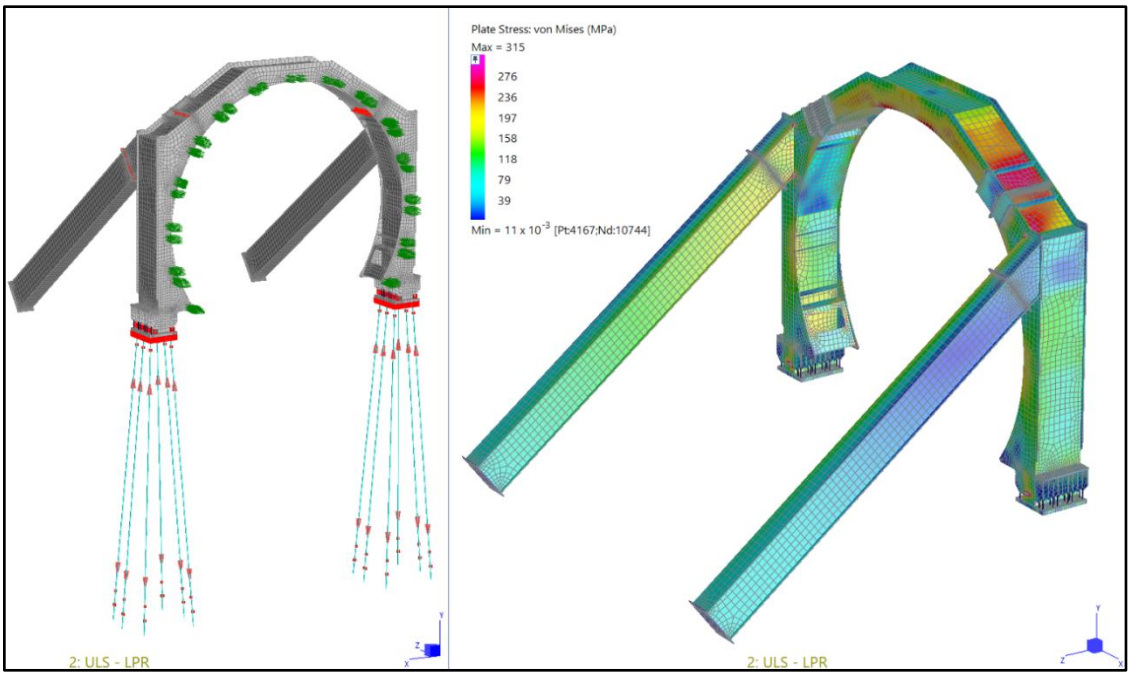


Figure 2. TBM launch frame FE model

Tensioned ground anchors were used to resist the upwards force created by the rear strut angle, shown on the left-hand side of Figure 2, above. The tensioned ground anchors were connected to the side members via thick steel adapter plates. Using adapter plates with oversized holes for the ground anchors provides more installation tolerance than cast-in threaded anchors. After the ground anchors were installed through oversized holes in the concrete foundation, the thick steel adapter plates were lowered over the top of the ground anchor tendons into position, then flood-grouted underneath. The ground anchors were then proof-loaded and locked off, with the specified lock-off load based on the expected working load in the anchors, ensuring a small amount of stretch in the anchors. This ensured a pinned rather than a fixed-end connection, thereby equalizing the load in the stress bars that connected the side members to the adapter plate. Steel packing behind the bottom of the launch frame side members transfers the horizontal shear load into the concrete invert foundation. This arrangement is shown in Figure 3, below.

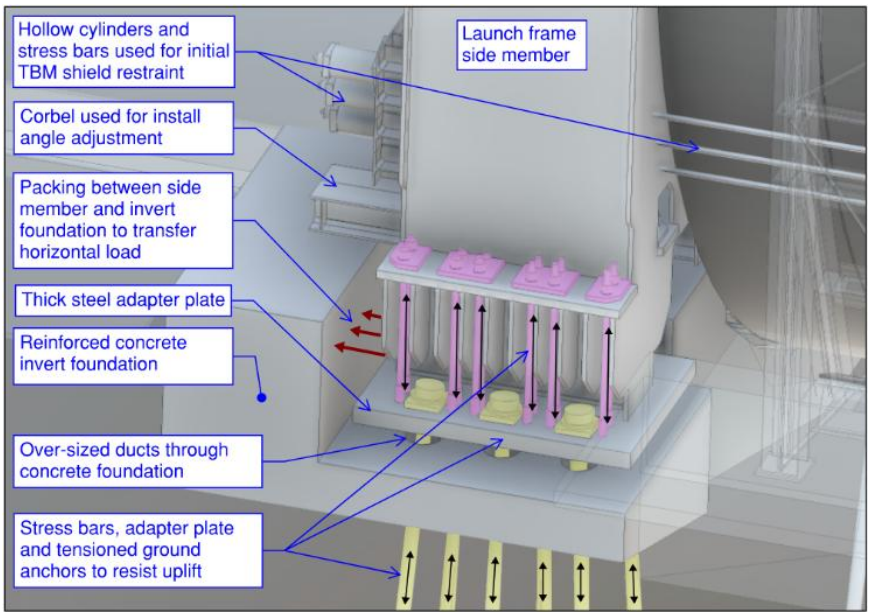
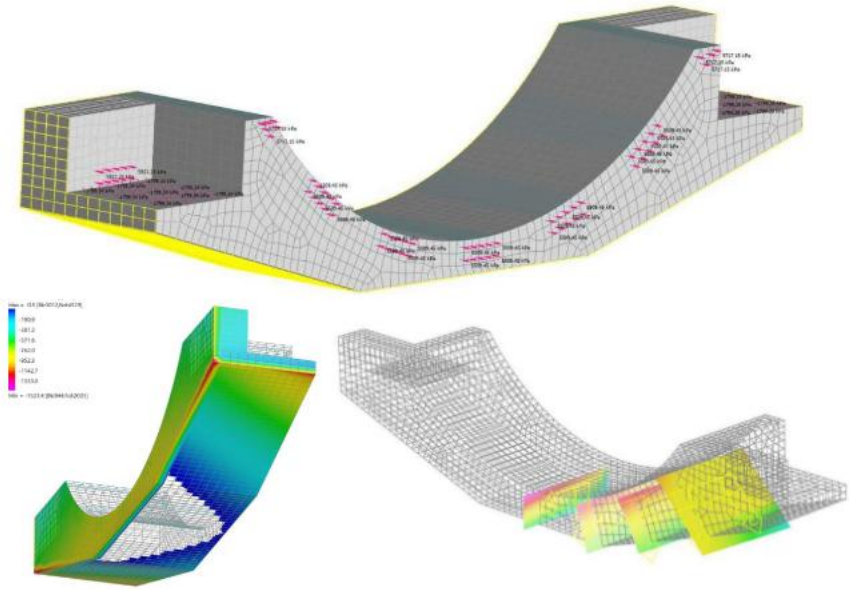


Figure 3. Launch frame side member load paths

Another simplification made to the launch frame was the omission of a steel bottom member and instead, using a reinforced concrete invert foundation. The concrete invert foundation transferred the loading directly from the lower TBM thrust jacks and each launch frame side member into the vertical face of the excavated siltstone cut face. To accurately model the complex shape and loadings, a 3D soil structure interaction (SSI) brick model was used to assess the design actions for the design of the concrete and reinforcement, as shown in Figure 4, below.


Figure 4. TBM launch frame reinforced concrete invert FE brick model

Certain steel elements in the launch frame required relatively thick steel plates. The risks and effects of lamellar tearing were assessed, from both the fabrication sequence and the loaded state, and the joints were detailed accordingly to mitigate the through plate tension stresses. Examples of this detailing are the launch frame hold-down connections and the upper frame to side member connection are also shown in Figure 5 below. For critical connections in tension, under head bolt loads were transferred in bearing and compression into stiffeners with long fillet welds along the

stiffener edges working in shear rather than a direct end plate to flange butt weld. For plates greater than 32mm thickness, plate with improved through thickness properties (Z-grade) and/or weld pre-heating were specified.

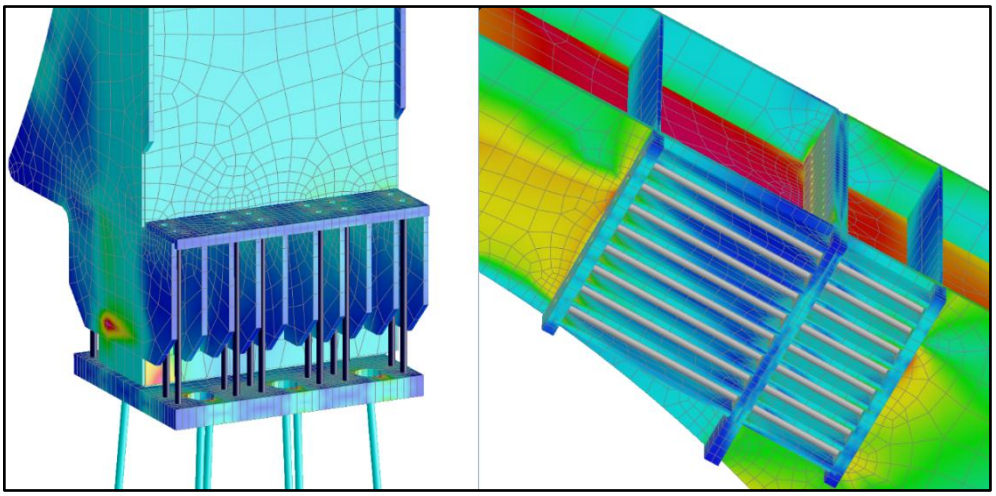


Figure 5. TBM launch frame hold-down and upper shoulder connection detailing

2.2 Gantry crane support structure

To assemble both TBMs in the Watsonia trench, a 550t capacity gantry crane was proposed. At the initial concept design stage, two 21m span gantry cranes were planned, which would have required a central temporary steel runway beam supported on temporary columns between the two TBMs. As shown in Figure 6 below, the clearance between the two TBMs was quite limited. Having a central crane beam on columns would have greatly reduced the already tight access and reduced the overall structural redundancy in the system, should the columns ever be subjected to collision loads by plant or lifted loads. Other design considerations regarding the relative stiffness between the central temporary columns and the reinforced concrete piled permanent trench walls, and how to effectively brace the central crane beam without creating additional lifting hazards would also have needed to be addressed.

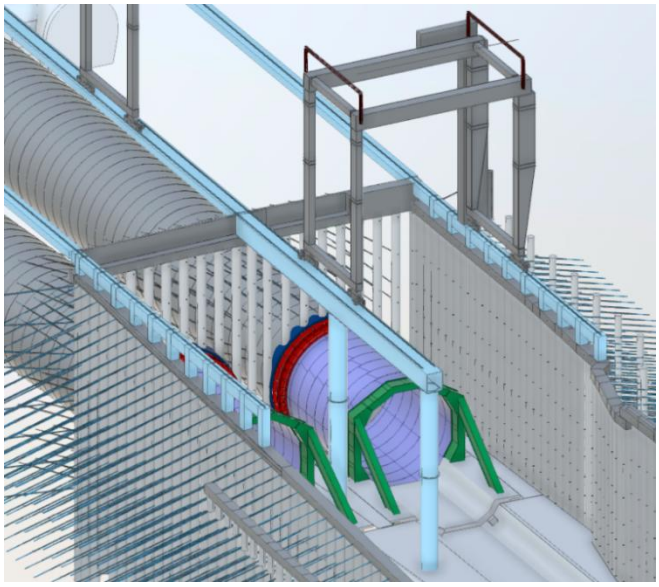


Figure 6. TBM assembly gantry crane original concept with central beam supported on columns

Considering the issues previously discussed, the decision was made to procure a larger 47m span gantry crane and omit the central beam on columns. This resulted in a safer and more structurally sound solution. In the assembly yard, the gantry crane rails ran on top of concrete cast in-

place ground beams. Over the trench, the crane rails ran on top of steel box beams, which were supported by temporary steel columns on top of the permanent structures retaining walls, as shown in Figure 7.

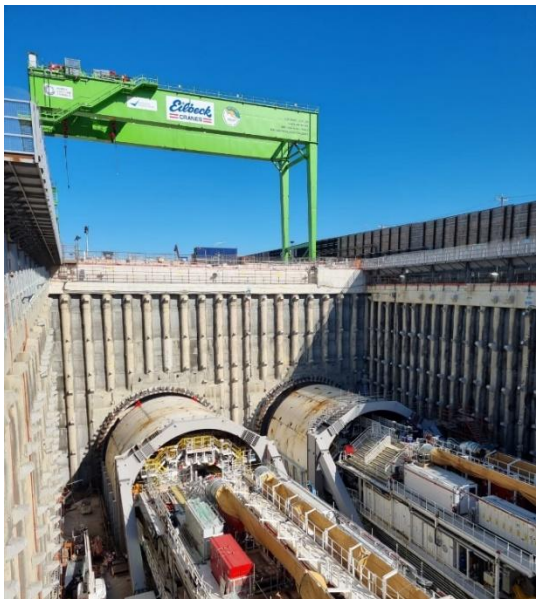


Figure 7. 550t capacity, 47m span gantry crane

Careful design and detailing of the temporary structure were required to keep the loadings centralized, prevent unwanted eccentricities and provide a solution that was simple to install and deconstruct at the top of the trench wall. Structural detailing of the beam-to-column connection is shown in Figure 8, below.

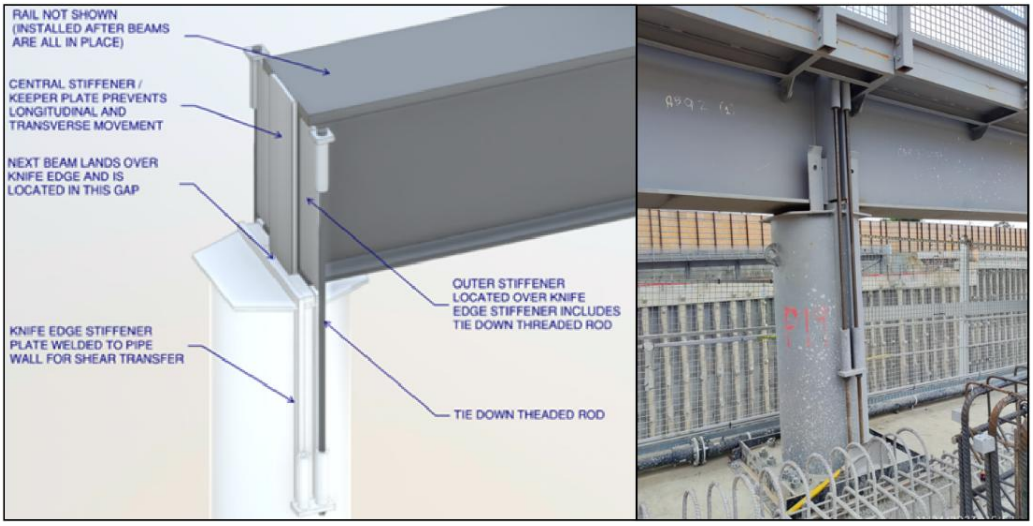


Figure 8. Gantry crane support beam connection detailing

3 CONSTRUCTION MONITORING

3.1 TBM launch frame

Launch frame displacement was monitored daily (at 8-hour intervals) during the initial TBM launch. Survey prisms were mounted on the top member to record the parallel displacement, as shown in Figure 9, below.

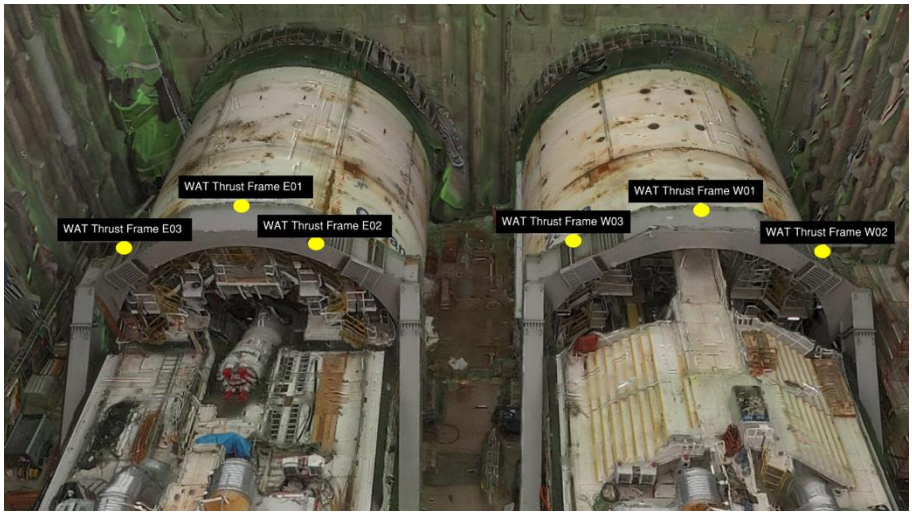


Figure 9. TBM launch frame monitoring prism locations (in yellow)

In Figure 10 below, a plot of the recorded parallel displacements of the launch frame top member is shown. For TBM1, the peak displacements were measured between 14/08/2024 and 16/08/2024, when the TBM cutterhead was excavating through the GRP-reinforced piles and the first 15m of rock. The thrust load at this stage of the initial TBM launch ranged from 24,000kN to 34,800kN. Displacements typically reduced after commencement of tail skin grouting, with the exception of minor increases in displacement when thrust forces were increased. Displacements stabilised until TBM1 launch frame was removed on 15/09/2024. Negative thrust frame movement recoded on 21/08/2024 was due to survey control, which required a review of the survey data and re-baselining. Similar trends were observed for the TBM2 launch.

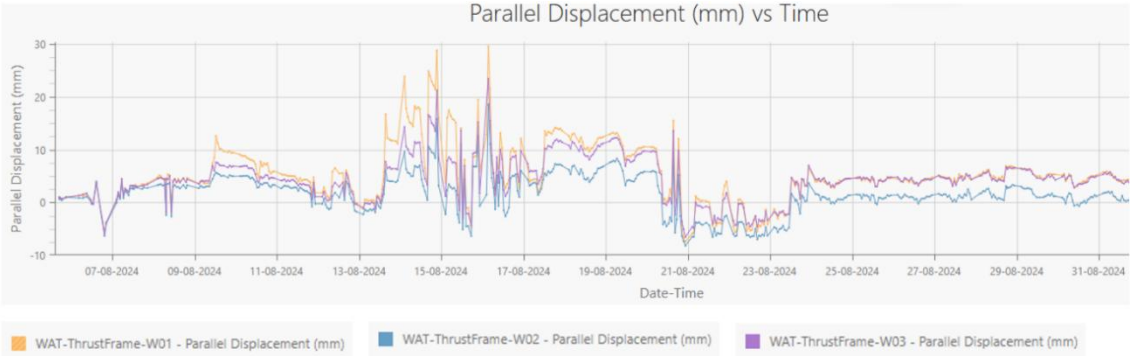


Figure 10. TBM1 launch frame monitoring results

The measured maximum displacement of 30mm at 30,000kN during initial TBM launch was backchecked by inputting this thrust load into the FE model. The FE model was in close agreement with a predicted 32mm of displacement in the top member.

3.2 Gantry crane support structure

Gantry crane beams and columns were monitored continuously during operation with increased frequency for lifts greater than 250t. Monitoring points were installed at the top of all columns and at mid-span points for the runway beams. The estimated mid-span vertical deflection was

9mm for a 550t lift (crane leg load of 4650kN), and 4mm for a 250t lift. The estimated maximum lateral displacement when operating at the maximum allowable loading conditions was approximately 5mm.

In Figure 11 below, a typical example of the monitoring plots reported daily for the gantry crane runway beams and columns is shown. Lifts between 250t to 520t showed noticeable displacements on both the gantry crane beams and columns, while lifts below 200t showed negligible movement. It is worth noting that certain lifts, such as the tail skin, required the load to be suspended until welding was completed, which could take several shifts over a period of days. Lifts that occurred over a longer period required further collaboration with the gantry crane supplier to develop additional load cases and reaction loads for specific lifts, considering various wind speeds over the lift period. Outliers in the data below represent days over which lighter loads, such as the tail skin, were suspended over a period of days, and higher winds than expected (that were still within safety margins) were experienced. This led to the Amber monitoring trigger level being exceeded. In turn, the frequency of monitoring and inspection of the monitoring data were increased over the period.

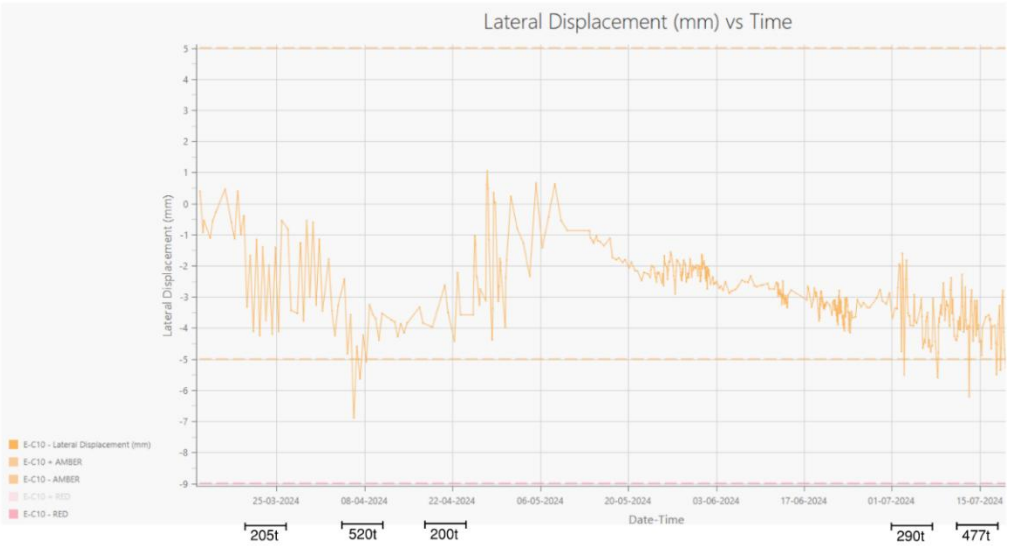


Figure 11. Gantry crane lateral displacement with corresponding key lifts for TBM2

4 CONCLUSION

This paper presents valuable insight into the design development and construction monitoring of large-scale Temporary Works designs on the North East Link Project. Optimized designs were effectively implemented through close collaboration between the contractor, design engineer and crane supplier.

Generally, the structural models closely matched real-world deflections and displacements. However, the installation of the TBM tail skin highlighted a loading condition that at first did not appear to be critical, due to the tail skin's relatively light weight, but did cause an exceedance of trigger levels due to the extended period the load was suspended. This highlights the requirement for detailed consideration of gantry crane skewing loads and closer consideration of the consequences of wind loading being higher than anticipated when loads need to be suspended over a period of days.

5 ACKNOWLEDGEMENTS

The authors would like to thank North East Link Project Authority, Spark, Webuild and Delve Underground for providing the necessary resources and collaboration that contributed to the successful completion of this project.

19th Australasian Tunnelling Conference – Acosta-Martínez, Stewart and Hudson-Smith (Eds.)
© 2025 Australian Tunnelling Society, ISBN 978-0-85825-002-4

North East Link segmental lining lessons learnt - from design to construction

J. Zeneli
Webuild, Melbourne, Australia

M. Behrens, R. Shi
Delve Underground, Melbourne, Australia

ABSTRACT: Major tunnelling projects, ranging from metro-sized tunnels to large diameter road tunnels, have boomed in Australia in recent years. Unfortunately, due to the lack of comprehensive guidance within existing Australian or international standards specifically for tunnels, let alone large diameter tunnels, some of the typically adopted design targets may not be practically achievable in construction. Some unsuitable requirements can lead to excessive compliance effort during the construction phase. This paper aims to share some lessons learnt from North East Link segmentally lined tunnels and provide an objective review on current segmental lining design and construction processes.

1 INTRODUCTION

North East Link (NEL) is the biggest ever infrastructure investment in Melbourne's northeast. The project includes Victoria's longest and largest twin road tunnels from Watsonia to Bulleen, and a segmentally lined tunnel with a 14.1m internal diameter (ID) was designed and constructed along the majority of the alignment using the latest industry practice.

The current approach for segmental lining design in Australia is to adopt the AS 5100 Bridge Design code and various Eurocodes (building codes). The British Tunnelling Society Specification for Tunnelling (BTSS) and local state authority specifications such as VicRoads Standard Specifications are commonly required by clients for segmental lining production and installation. It is recognised there is a lack of comprehensive guidance within existing Australian or international standards specifically for tunnels, let alone large diameter tunnels. The tunnel size and precast element size can have a large influence on the lining component for production and installation, and some of the typically adopted design targets may not be practically achievable in construction. Many experienced tunnellers know a few 'tricks' to work around impractical requirements, but some unsuitable requirements can lead to excessive compliance effort during the construction phase.

This paper aims to share lessons learnt from NEL segmentally lined tunnels, focusing on the recurring issues during construction phase which can be mitigated through more reasonable design practice and specification targets. Some sections of the paper might seem disjointed due to the nature of the content. Rather than telling a single story, the paper addresses multiple key challenges that are unrelated to each other, yet each contributes to the overall puzzle. The authors hope this paper will initiate critical thinking within the industry. Instead of merely replicating past practices, some of which are commonly associated with above-ground structures, the industry should critically examine existing issues and unsuitable practices and begin considering ways for improvement.

The key discussion points in this paper include the suitability of the BTSS specified segment tolerances for large diameter tunnels and the necessity and applicability of certain concrete

segment production tests. Ways to improve construction efficiency via design, and in-depth discussions on common lining installation-related issues are also considered.

2 DESIGN OVERVIEW

The segmental lining for NEL has an internal diameter (ID) of 14.1 m. The majority of the 5.0 km twin TBM tunnel alignment is supported by steel fibre reinforced concrete (SFRC) segments. Steel bar reinforced segments are utilised at various locations, primarily at cross passages, ventilation adits and ventilation shaft connections.

As shown in Figure 1, each ring consists of ten segments: seven rectangular segments, two trapezoidal counter key and one key segments. The segments are 500 mm thick and 2400 mm wide. Each longitudinal joint edge contains a guide rod and two spear bolts. Each circumferential joint edge contains two spear bolts and four shear bicone recesses, with shear bicones being installed in steel bar reinforced segments only.

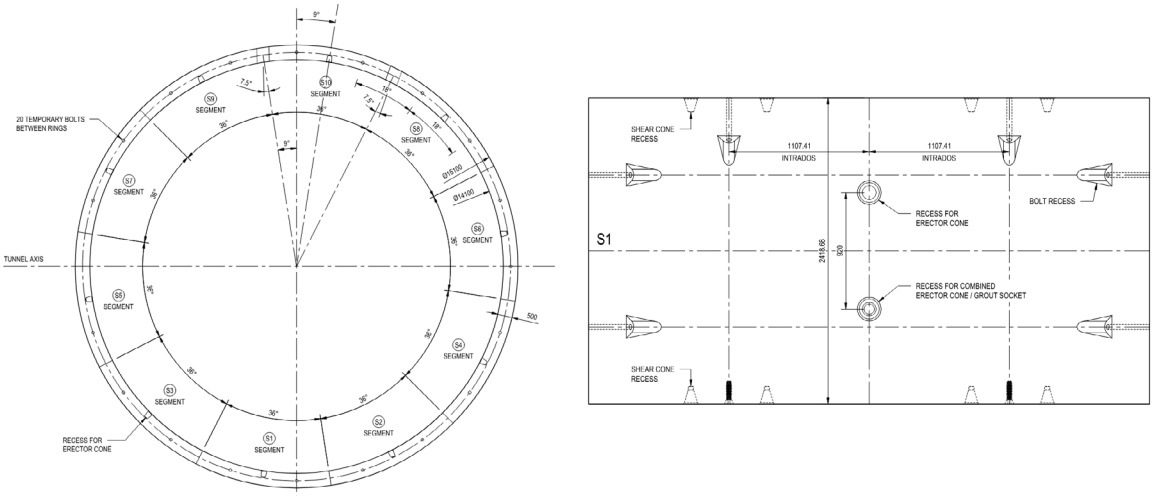


Figure 1. Elevation of erected ring (left) and developed view for a typical segment (right).

3 SEGMENT PRODUCTION

3.1 *Segment production tolerance*

Segment production tolerances refer to the allowable geometrical deviations of any segment dimension from its theoretical size. Stringent tolerance requirements are imposed on segments for quality assurance and installation accuracy to ensure lining structural and functional system consistency. Exceedance of the allowable tolerances leads to rigorous investigations into the usability of the segments. Therefore, it is important to set realistic targets for segment production tolerances.

The segmental lining for NEL is required to comply with the production tolerances in BTSS which does not make allowance for tunnel size. In fact, BTSS tolerance requirements are more suitable for metropolitan train size tunnels up to ~8m ID. NEL is one of the largest segmental lining tunnels in Australia, and all of the BTSS tolerance requirements are not practically achievable. As a result, a large number of Non-Conformance Requests (NCRs) were received during segment production. The parameter with the highest number of dimensional nonconformances is segment width. BTSS tolerance for segment width is ±1mm whilst the nonconforming segments show a shortening up to 3mm which has a significant impact on the lining circumferential joint watertightness.

The segment dimensional measurements were undertaken by 3D laser scanning. Out of 1746 measurements taken during the 2023 to 2024 production period, 41% were out of tolerance. Among these, 39% show a segment shortening of 1 to 2 mm, and 2% show a segment shortening of 2 to 3 mm. The measurements were taken when segments were a few days to a few

months old. A review of the mould dimension conformances and concrete shrinkage measurement trends suggests the segment shortening is likely to be associated with drying shrinkage and thermal effects (Victoria can have large daytime temperature variations throughout the parts of the year that could contribute the dimensional non-compliance). However, the maximum drying shrinkage test result for the segments is 640 με, well within the allowable limit of 750 με based on VicRoads Specification 610. How can segments have out-of-tolerance shortening when they meet the relevant performance goals?

Table 1 presents a summary of the segment theoretical shortening for both design shrinkage and maximum test result drying shrinkage, assuming a temperature differential of 10ºC. The result shows, due to the segment size, even if segments meet the performance requirement for drying shrinkage, it is not theoretically possible for them to also meet the BTSS width tolerance requirement of ±1 mm.

Table 1. Summary of segment theoretical shortening across segment width (2.4 m).

Drying Shrinkage (με)	750	640
Shrinkage Shortening* (mm)	1.80	1.56
Temperature Differential (ºC)	10	10
Thermal Length Change** (mm)	0.24	0.24
Anticipated Total Shortening (mm)	2.04	1.80

* Strain variation of ±20% not considered
** Thermal variation of ±20% not considered

There is a need to understand the technical basis and limitations for dimensional tolerances in existing tunnel specifications as all may not be appropriate for large precast segments / diameter tunnels. Interestingly, a literature review of international published tolerance guidance was undertaken, including ITA Working Group 2 Guidelines (2019), and no specifications consider segments of this size. The author recommends that a project-specific assessment of tolerances considering concrete shrinkage and temperature differences, at a minimum, be completed for tunnel linings > 10 m diameter to minimise exaggerated demands for segment accuracy and increases in production costs. The guidance provided by ÖVBB (2011) and Kolić and Mayerhofer (2009) should be considered both for design and production verification purposes.

3.2 *Dimensional check frequency*

The segment dimensional compliance checks are typically carried out pre-production to ensure each fabricated segment mould can produce segments conforming to the specified dimensions and tolerances. During production, routine segment dimensional checks are also carried out as part of production control. The checks can be undertaken for individual segments or a combination of moulds and segments. There are no standards or guidelines in the industry for segment dimensional check frequency, and it is often left to the engineer's discretion in setting a reasonable dimensional measurement frequency and mitigation plans in the event of non-compliant results. Since the dimensional checks can be disruptive to precast production, it is in construction team's interest to reduce the checking frequency.

The authors' opinion is that more regular dimensional checks on both moulds and individual segments should be performed at the start of production for an extended period of time. The number of the checks completed needs to be sufficient for engineers to gain confidence in the adopted casting scheme, concrete mix and production controls. Relationships between dimensionally acceptable segments and other factors also need to be established. The checking frequency can be revisited after there is a consistent record of segments meeting the specified tolerances.

During the initial phase of NEL segment production, the moulds were measured twice per month for over six months, and segments produced over more than six months were also measured. Upon reviewing the whole data set, the designers observed strong correlation between acceptable segment dimensions, compliant mould dimensions and concrete drying shrinkage test results. This provided the basis for the decision to stop post-pour segment dimensional measurement, provided that:

– Mould measurements were carried out twice per month and show dimensional compliance; and
– Concrete drying shrinkage tests were carried out once per month and show compliant results.

As a mitigation plan for gross dimensional non-compliance, a representative number of samples are required to be guaranteed to be available for segment dimensional checks in the event of a concrete drying shrinkage NCR. The authors note this concession is only acceptable due to the large amount of data collected at the start of the production.

3.3 *Production tests*

3.3.1 *Fibre washout test*

One of the more frequently received CRFIs relates to low steel fibre content in SFRC segment test samples. Steel fibre content is often considered an important measurement for SFRC segments as low steel fibre content could be an indication of insufficient residual flexural tensile strengths. However, based on the test data collected, a clear relationship between fibre content and residual flexural tensile strengths is not always evident.

Figure 2 shows the available fibre content test results from March 2023 to July 2024. A few test results do not meet the target fibre contents (shown as straight lines) with Sample NP1-1153 showing the lowest average fibre content of 21.1 kg/m^3, 26% lower than the target value (28.5 kg/m^3). It is reasonable to assume the segment represented by Sample NP1-1153 would have unsatisfactory residual flexural tensile strengths.

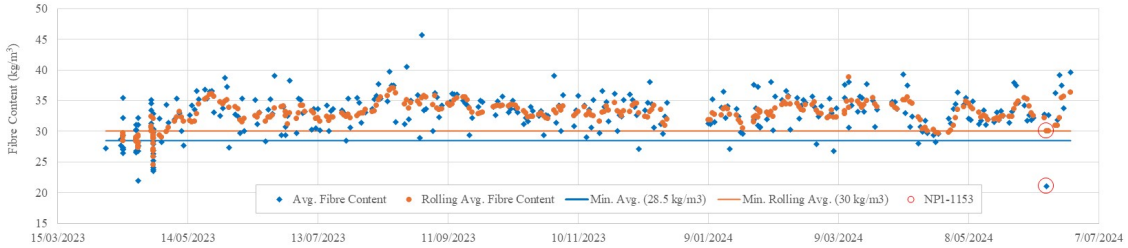


Figure 2. Fibre content test results from March 2023 to July 2024

However, the available residual flexural tensile beam test results (tested to BS EN 14651) from March 2023 to July 2024, shown in Figure 3, suggests a different story. The residual flexural strengths result for Sample NP1-1153 is relatively high within the data set, and no clear correlation is observed between fibre content and flexural tensile strengths. Note some samples exhibit strain hardening behaviour (i.e. $f_{R3} > f_{R1}$). This is beneficial for capacity as the design has conservatively assumed SFRC has strain softening behaviour which leads to lower theoretical strength. At the time of testing, the samples had reached and exceeded the 28-day compressive strength requirement of 50 MPa.

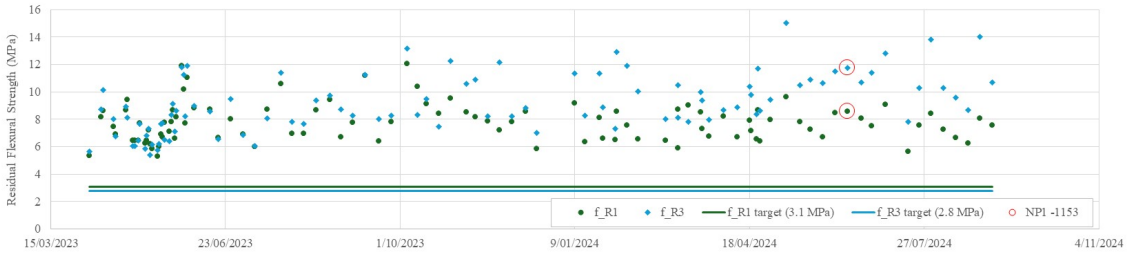


Figure 3. Available residual flexural tensile beam test results from March 2023 to July 2024.

To investigate this further, the steel fibre distribution for Sample NP1-1153, shown in Figure 4, was inspected and compared to the number of fibres protruding from both failure surfaces for available samples over an eight month period.

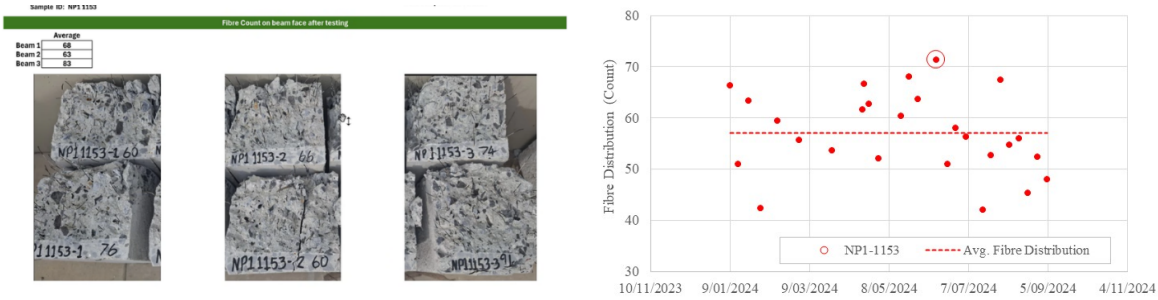


Figure 4. Fibre distribution count for Sample NP1-1153 and available fibre count results from March 2023 to July 2024.

Figure 4 shows Sample NP1-1153, with the lowest average fibre content, has the highest average fibre count amongst the available results, which is consistent with the residual flexural tensile strength test results. This suggests the potential causes of some low test results might be measurement error, sampling error or poor fibre distribution within the concrete mix.

The fibre content is measured using VicRoad Test Method RC377.01 – Determination of the fibre content of fresh concrete (wash-out method). The 3 washout samples (approx. 5 L sample volume/test) were theoretically taken near the beginning, middle and end of the pour. In comparison, BS EN 12350-1:2000 Testing fresh concrete – Sampling, which is the basis for BS EN 14651 residual flexural tensile beam manufacture/testing, says to take at least 1.5 x quantity required for fibre content tests. BS EN 14651 needs approximately 38 L concrete to make 3 beams, so approximately 56 L concrete is sampled for fibre content test. This is a significantly larger sample volume compared to the adopted washout test method and would give a more accurate concrete material behaviour compared to fibre count. The small fibre count sample size amplifies human errors in sampling, potentially selecting samples that are not representative of the batch.

In terms of the impact of uneven fibre distribution within mix, a plot of the available fibre count results versus residual flexural tensile strengths, f_{R1} and f_{R3}, in Figure 5 shows the residual flexural tensile strengths can vary significantly with the same fibre count, and even with a fibre count as low as 35, the residual strengths are well above the target performance criteria. Therefore, segments with pockets of poor fibre distribution can still exceed the target residual flexural tensile strengths.

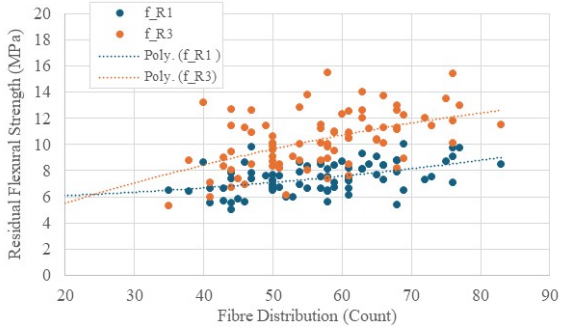


Figure 5. Available fibre count versus residual flexural strength plot from March 2023 to July 2024.

It is suggested that fibre content testing may not be necessary as a routine test as low fibre content does not always have strong association with low residual flexural strengths. The fibre content testing may potentially be replaced with the adoption of automatic batching. It is more important to ensure the steel fibres are well distributed within the concrete mix.

3.3.2 *Water penetration test target*

Water penetration testing to BS EN 12390-8 was carried out during concrete mix trials/pre-production (3 tests per mix design) and during production (3 tests per month). The Water Pene-

tration criteria was set to 10 mm max. at 28 days testing in the project specification. Although pre-production trials demonstrated the mix achieved the strict limit of 10 mm, it is known to be difficult to measure the penetration accurately with reasonable repeatability and exceedances of the penetration limits are to be expected. It was found that the high water penetration values were confined to local areas on the sample surface which was not consistent with lower water penetration over the rest of the sample. This area of higher water penetration is likely due to poorer surface preparation and compaction around aggregate particles on the surface of the sample as illustrated in Figure 8. Water penetration testing is not specified in project requirement or referenced documents, however, has been typically introduced due to previous precedence in Victoria on recent major projects. In the authors' opinion, the requirement for water penetration testing during production should be assessed for each project by the Durability Engineer, as there are typically other forms of durability/quality testing during the trial mix stage which may produce more repeatable/reliable results.



Figure 6. High water penetration result impacted by sample preparation and presence of aggregate.

3.4 *Standardised reinforcement cage*

Steel bar reinforcement cages are generally tailored for each individual segment. The cage construction is both labour intensive and time consuming. One way to improve fabrication efficiency is to use a standardised steel reinforcement cage for segments with similar geometry.

One of the main obstacles to standardising reinforcement cages is the maximum concrete cover requirement from AS 5100.5. The code requires reinforcement provided for structural reasons to be located within 80 mm of the face for crack control. Figure 7 shows the developed layout (intrados) for Segment 1 (S1) and Segment 7 (S7). The two segments are identical except for the width due to ring taper. The difference in width is less than 30mm on one side and 17mm on the other side. Since the design cover for NEL segments is 60mm, if the reinforcement cage for S7 is to be used for S1, the theoretical cover for S1 is 75mm. The decision was made not to standardise the cage for S1 and S7 due to the concern on maximum allowable cover exceedance with construction tolerances.

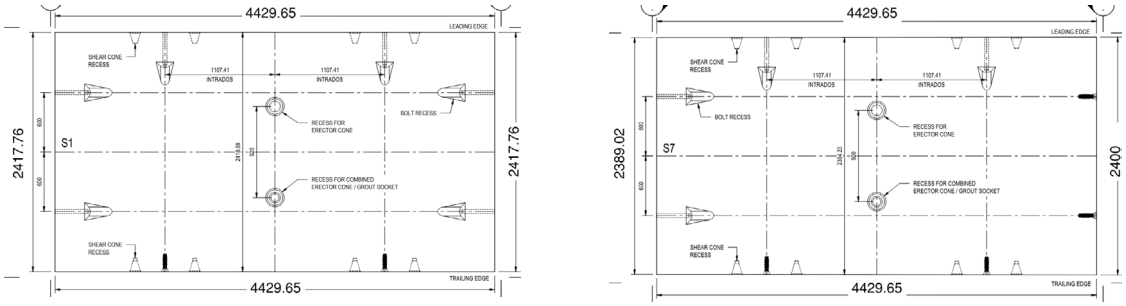


Figure 7. Segment developed layout (Intrados) for S1 (left) and S7 (right).

From a structural perspective, segments are primarily compression members and the edges of the segments are not subject to high bending moments which induce cracking. Instead of adopting a fixed value for maximum cover, it might be more appropriate to determine required cover based on strength and crack width calculations. Another consideration is the location of peak bursting stress for joint design. The bursting reinforcement is most effective when installed before or at the peak bursting stress depth from the joint face which is typically about 0.1 to 0.5 * segment thickness (d) as shown in Figure 8.

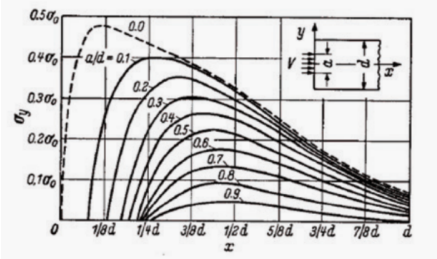


Figure 8. Tensile stress distribution at segment joints (Leonhardt,1964).

The authors' view is that standardising reinforcement cages for multiple segments is feasible as long as the appropriate analyses are undertaken to ensure adequate structural performance.

4 SEGMENTAL LINING INSTALLATION

4.1 *Ovalisation*

Deformations of the lining system are assumed to occur from two main sources: ring build deformations (including all build tolerances) and additional deformations caused by all permanent, construction and accidental loading conditions. The former is typically set to be within 0.5% of the theoretical design diameter of the ring measured on completion of ring build and grouting. The latter is based on design assumptions and calculations. A combination of these two sources of deformation results in a total maximum ring deformation/distortion for radial joint design and spaceproofing purposes. The total ring ovalisation shall not exceed 1% of the theoretical ring design diameter per the BTSS.

The current practice is to verify the ring build deformation using wriggle survey. The wriggle survey of segmental lining is typically carried out after the TBM back-up gantries have cleared the area (a minimum distance of 100 m behind the cutter head). At this time, the annulus grout has already hardened, and the segmental lining is subject to external loads from the ground and potentially via groundwater recovery. As a result, in addition to the ring build deformation, the measured ring ovalisation also includes the induced deformation from external loading, either partial or in their entirety.

To measure the ring build deformation only, the measurement should be taken when the rings are still within the TBM shield - which cannot be achieved in practice to the required accuracy. The authors' opinion is that applying the 0.5% ovalisation criteria to the wriggle survey data is conservative and will raise non-conformances which are not necessarily defects. Potentially adopting an intermediate ovalisation criteria through the approved Design Documentation would be beneficial during the construction phase. Segmental lining design for NEL adopted an ovalisation up to 0.79% for wriggle survey validation through careful considerations of ground conditions, groundwater levels and gasket performances due to joint opening.

4.2 *Segment joint steps and lips*

The out-of-tolerance step and lips for the Southbound TBM tunnel from Ring 1 to Ring 650 are plotted in Figure 9. Whilst the data shows general improvement of ring-build accuracy with time, a number of segment joints still have steps and lips in the 5-15 mm range, exceeding the BTSS requirement of 5 mm.

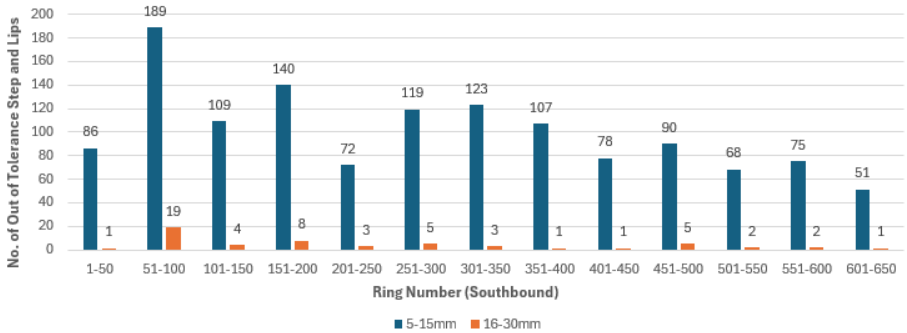


Figure 9. Example of out-of-tolerance segment joint steps and lips for Southbound TBM tunnel.

Segment steps and lips impact the as-built gasket offset which is one of the key parameters for determining gasket watertightness capacity. The gasket design for NEL requires the gasket to maintain watertightness at a test pressure of 8 bar at 6.5 mm joint opening gap with a 10 mm offset. The adopted product, Datwyler M80103 “West Gate”, has the capacity to resist 8 bar pressure at 6.5 mm opening with a 15 mm offset. Therefore, segment joints with a step or lip up to 15 mm are considered to have low risk of leakage. For segment joints with a step and lip of 16-30 mm, location specific assessments were carried out considering gasket gap and groundwater level at the particular ring build location, and feedback was sought from the manufacturer.

The authors’ view is that applying the 5 mm step and lip tolerance is conservative and raises non-conformances which are not necessarily defects. The step and lip criteria should be based on the specific gasket performance for the required design water pressure, and a more refined criteria through the approved Design Documentation would be beneficial during the construction phase.

5 CONCLUSION

This paper presents valuable construction and test data for NEL segmental lining. It critiques certain unreasonable design and impractical construction requirements for large diameter tunnels and suggests alternative targets. Additionally, the paper addresses recurring NCRs and CRFIs encountered during construction and offers recommendations for design improvements.

6 ACKNOWLEDGEMENTS

The authors would like to thank North East Link Project (NELP) Authority, Spark and Delve Underground for providing the necessary resources and collaboration that contributes to the successful completion of this project. Special gratitude to our colleagues, Sam Swartz and Dean Treweek for their expert guidance and unwavering support throughout the project.

7 REFERENCES

International Tunnelling and Underground Space Association (ITA), Working Group 2, Report n°22 - Guidelines for the Design of Segmental Tunnel Linings, April 2019.

Kolić D., Mayerhofer A, Segmental Lining Tolerances and Imperfections, ITA WTC 2009 Symposium, Budapest, May 23-28, 2009, pp.8

Leonhardt, F., Pre-stressed concrete: design and construction. W. Ernst, 1964.

ÖVBB, Guideline for concrete segmental lining systems, Austrian Society for Concrete and Construction Technology (ÖVBB), 2011.

19th Australasian Tunnelling Conference – Acosta-Martínez, Stewart and Hudson-Smith (Eds.)
© 2025 Australian Tunnelling Society, ISBN 978-0-85825-002-4

Sydney metro west—eastern tunnelling project—TBM temporary works

E. Adcock
John Holland CPB Contractors Ghella JV, Sydney, Australia

D. Kubik
Delve Underground, Sydney, Australia

ABSTRACT: The Eastern Tunnelling Package section of Sydney Metro West includes twin 3.5-kilometre tunnels with tunnel boring machine (TBM) drives, starting from The Bays Station box, traversing through Pyrmont Station cavern, and finishing at Hunter Street Station. Delve Underground, working in close collaboration with the John Holland CPB Contractors Ghella Joints Venture (JV), designed the TBM launch frame, steel temporary rings, steel cradles and launch seals. Notable elements include an oversized launch frame that enabled partial assembly before the TBM shield traverses through it, and the use of steel rails with a travelling jacking dolly for the traverse of Pyrmont Station using the TBM thrust jacks. This paper discusses the design of the TBM temporary works and presents key feedback from the contractor on the design.

1 INTRODUCTION

Sydney Metro is Australia's biggest public transport project, with the vision "to transform Sydney with a world-class metro." In 2030, Sydney will have four metro lines, 46 stations and a 113-kilometre standalone metro railway system, revolutionising the way Australia's biggest city travels. Sydney Metro West (SMW) is a new 24-kilometre metro line with nine new stations confirmed at Westmead, Parramatta, Sydney Olympic Park, North Strathfield, Burwood North, Five Dock, The Bays, Pyrmont, and Hunter Street in the Sydney central business district.

For the Eastern Tunnelling Package (ETP) section of the works, two tunnel boring machines (TBM1 and TBM2) were assembled and initially launched from The Bays Station; received, traversed through and re-launched at Pyrmont Station; and then retrieved at Hunter Street Station.

The following temporary works (TW) design elements were delivered as a design package:

- TBM launch, retrieval and traverse alignments
- TBM shield cradle and jacking dolly*
- TBM backup gantry rails and supports*
- TBM launch frame and foundations*
- Temporary steel ring segments and steel fuses*
- TBM launch seal*
- Temporary backfill and concrete slabs

This paper will concentrate on key innovations for the items noted with an asterisk above, and key monitoring results and feedback from the constructor.

2 DESIGN DEVELOPMENT

The TBM TW design package was identified as a High-Risk package, thereby requiring an independent proof engineer (peer review). Throughout the design stages, workshops were held with the constructor to identify key issues and decide on the best strategy to overcome them. This section details the key design features that were implemented as a result of the close collaboration

between the constructor and the designer. One of the main high-risk elements was the travers and relaunch of the TBMs inside a Sequentially Excavated (SEM) station at Pyrmont with no overhead access.

2.1 *TBM shield cradle and jacking dolly*

The TBM shield cradle supports the shield using two rails—in this case, with a 56-degree inclusive angle—and is designed to transmit the shield into the foundation. The normal load (applied radially) to the shield cradle rails is supported on steel stools with a steel tension tie between the stools which prevents them from splitting apart as shown in Figure 1, below. The use of a tension tie reduces the required number of fixing anchors into the foundation slab.

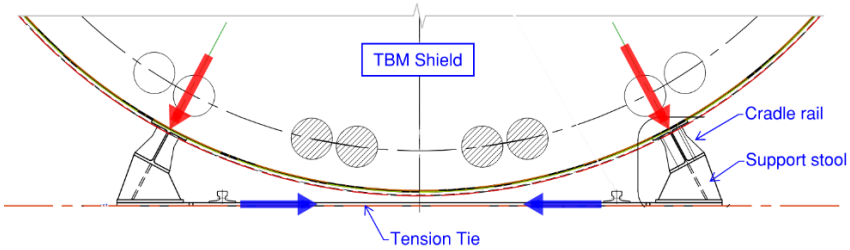


Figure 1. TBM shield cradle tension tie load path

The support stools were set at 1.7m spacings to match the length of the permanent tunnel segment rings. This spacing was adopted as it simplified the jacking dolly and jacking packer arrangement, described in detail below and shown in Figure 2, below. Cradle modules of 11.9m and 3.4m were adopted with each module consisting of a pair of rails with welded support stools and loose tension ties. Each rail has hollow bars welded in centrally at 1.7m spacings over the support stools. The hollow bars act as keepers for the steel pins used to transfer load from the jacking dolly into the cradle rails. The long modules are used for straight alignment sections and the short modules are used for curved alignment sections. For traversing each station, three different horizontal curves were designed for; 500m, 355m and 165m. To install the cradles at the required the horizontal curves, different length web splice plates between the short modules were specified.

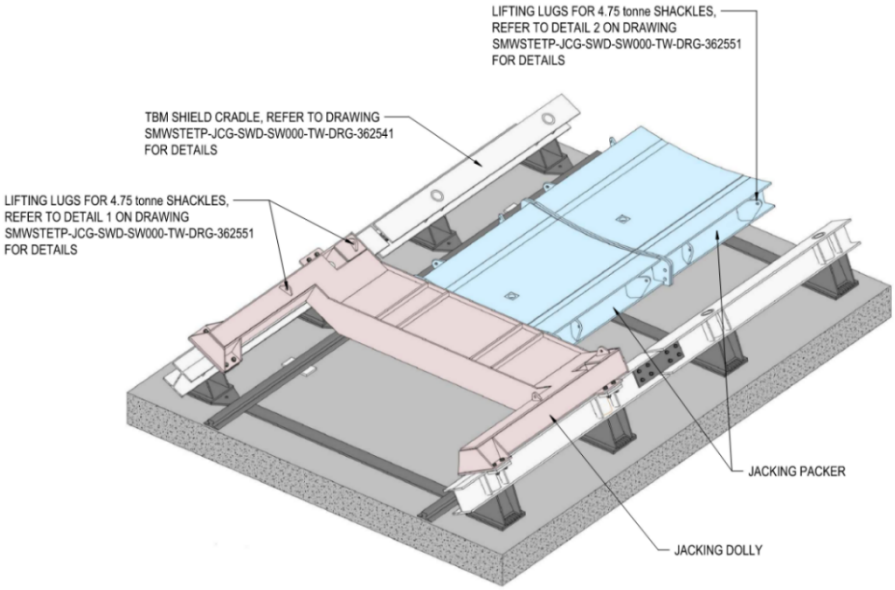


Figure 2. TBM shield cradle and jacking dolly

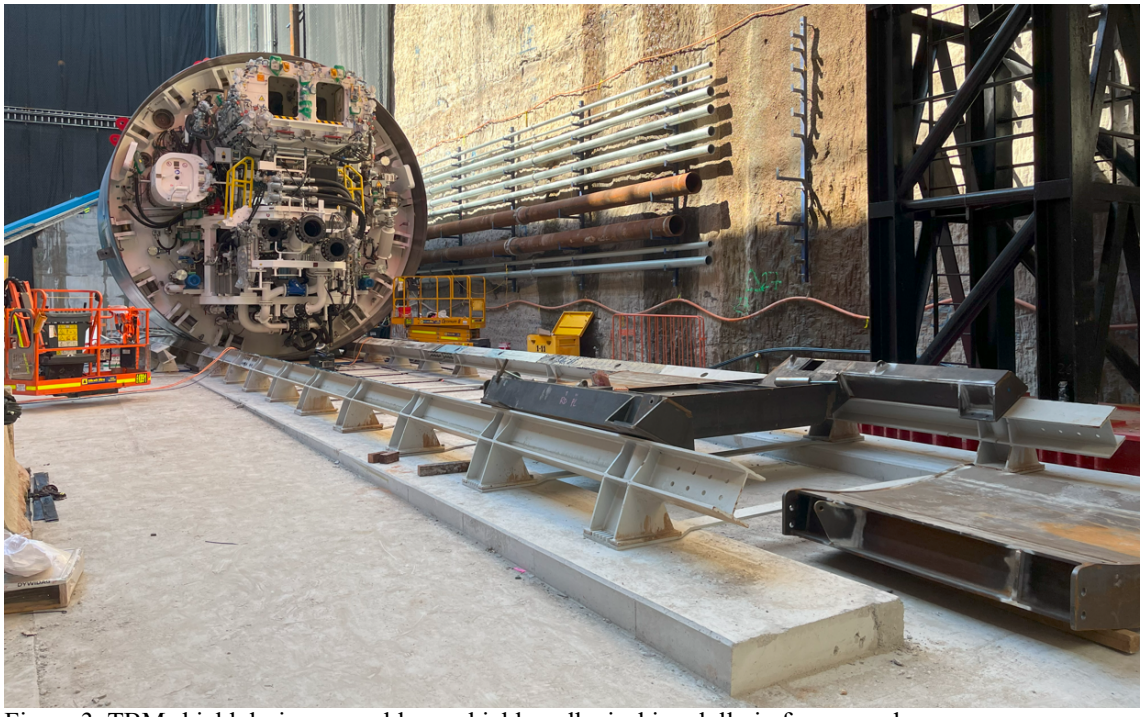


Figure 3. TBM shield during assembly on shield cradle, jacking dolly in foreground

The jacking dolly is used to advance the shield and backup gantries forward when outside of the ground while traversing through stations. At The Bays Station, the TBM shield was assembled approximately 50m back from the headwall. Once the TBM shield was assembled, the jacking packers were installed inside the TBM tail skin / ring build area. The jacking dolly was then fixed onto the TBM shield cradle behind the TBM shield by means of large steel pins on each side that are lowered into the holes in the TBM shield cradle rails. The bottom two thrust jack pads then pushed against the jacking packers and jacking dolly causing the TBM shield (and TBM backup gantries when connected) to advance. As the TBM shield is pushed forward, the tension force created by friction between the TBM shield and the rail surface is resolved by the shear load transferred into the cradle rails via the jacking dolly pins behind the shield as shown in Figure 4, below.

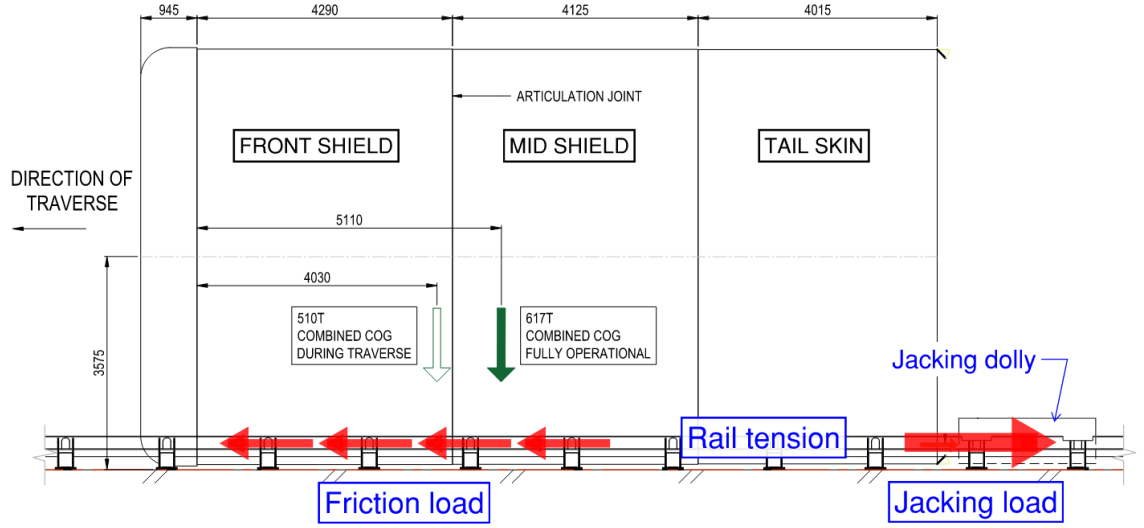


Figure 4. Balance of TBM jacking force in cradle rails

2.2 *TBM trailing backup gantry cradles*

During typical station traversing, the backup gantries travel on vertical legs with steel wheels on steel rails. This reduces the amount of steelwork required for traversing the backup gantries. However, when the backup gantries are operational and inside the tunnel rings, the gantries ride on angled bogies. This meant short gantry cradles to support the angled bogies were required for both the TBM launch and TBM retrieval. The arrangement is shown in Figure 5, below. The higher cradle rails are used for Gantry 1 bogies with an inclusive angle of 110°. The lower cradle rails are used for the typical gantry bogies with an inclusive angle of 70°. Various design options for the angled support legs were provided to cater for the varied site requirements.

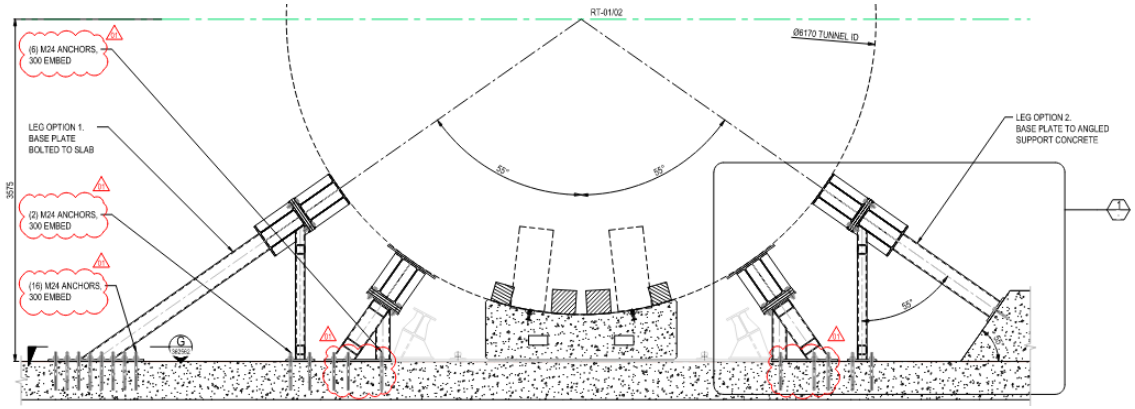


Figure 5. TBM trailing backup gantry transition cradles

2.3 *TBM launch frame*

To construct the 6.17m internal diameter (ID) segmentally lined tunnels, two 6.97m TBMs with bore diameters of 7.02m were procured. Each TBM consists of a 620-tonne, 13.38m-long TBM shield, eight trailing gantries and a bridge gantry section between trailing backup gantry one and two. The total length of each TBM with trailing backup gantries is 126.5m. At The Bays Station launch site, the ground conditions were predominantly in Unweathered Class I/II sandstone rock, which provided a relatively strong base for the temporary foundations to bear onto.

The design TBM launch load at The Bays Station box was 15,500kN, applied via 18 thrust jack pairs, evenly arranged around a 6.43m-diameter circle. The thrust jacks are used to advance the TBM shield forward as it mines through soil and rock; initially pushing on the launch frame, then temporary false rings, and then the typical case of pushing onto the permanent tunnel rings.

Early in the concept design phase, the decision was made to adopt a “drive-through” type frame arrangement. This consists of an oversized external frame with rear struts that the TBM shield can still pass through when the frame is erected first. This external frame included the foundation and load transfer elements. Once the TBM shield has traversed through the main outer frame and rear struts, smaller members, sized to be installed by chain hoist, are installed inside the main outer frame. This offers both time savings and a reduced risk. The risk of lifting large members inside a confined space that typically exists inside sequential excavation method (SEM) station box caverns is reduced because the lifted items are smaller and lighter. It is also very hard, if not impossible, to install the TBM side member that is between the TBM and the cavern side wall once the backup gantries are in the way. The use of an oversized “drive-through” frame avoids this issue. The TBM launch frame main frame is shown in Figure 6, below. The green shaded main side members and rear struts are installed first. The remaining members shown in various shades of pink/purple are installed after the TBM shield passes through the outer frame members and rear struts. An overview showing the entire temporary works in place just prior to TBM launching is shown in Figure 7, below.

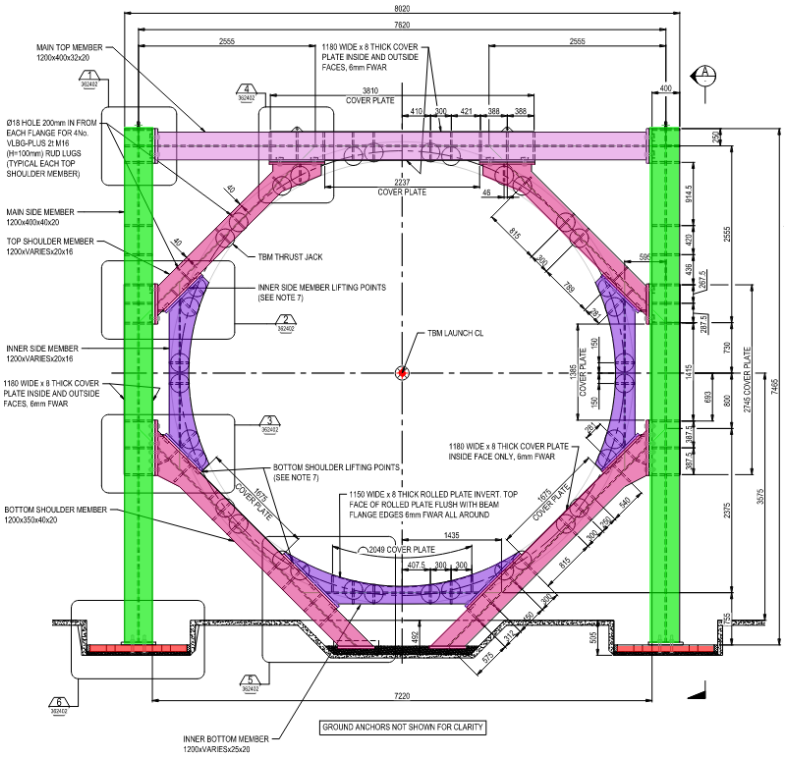
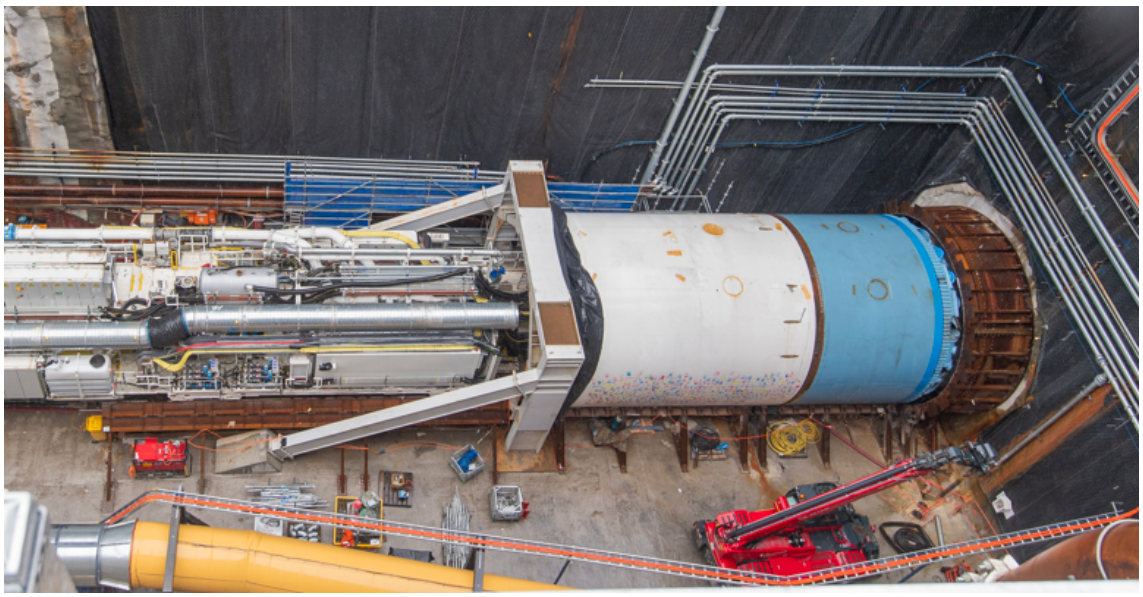


Figure 6. TBM over-sized "drive-through" launch frame


Figure 7. TBM backup gantry cradle, launch frame, temporary ring cradle and launch seal at the headwall

Tensioned ground anchors were used to resist the upwards force created by the rear strut angle. The tensioned ground anchors were connected to the side members via thick steel adapter plates. Using adapter plates with oversized holes for the ground anchors provides more installation tolerance than cast-in threaded anchors. After the ground anchors were installed through oversized holes in the concrete foundation, the thick steel adapter plates were lowered over the top of the ground anchor tendons into position, then flood-grouted underneath. The ground anchors were then proof-loaded and locked off, with the specified lock-off load based on the expected working load in the anchors, ensuring a small amount of stretch in the anchors. This provided a pinned rather than a fixed-end connection, thereby equalizing the load in the stress bars that connected the side members to the adapter plate. Steel packing behind the bottom of the launch frame side

members transfers the horizontal shear load into the concrete invert foundation. This arrangement is shown in Figure 8, below.

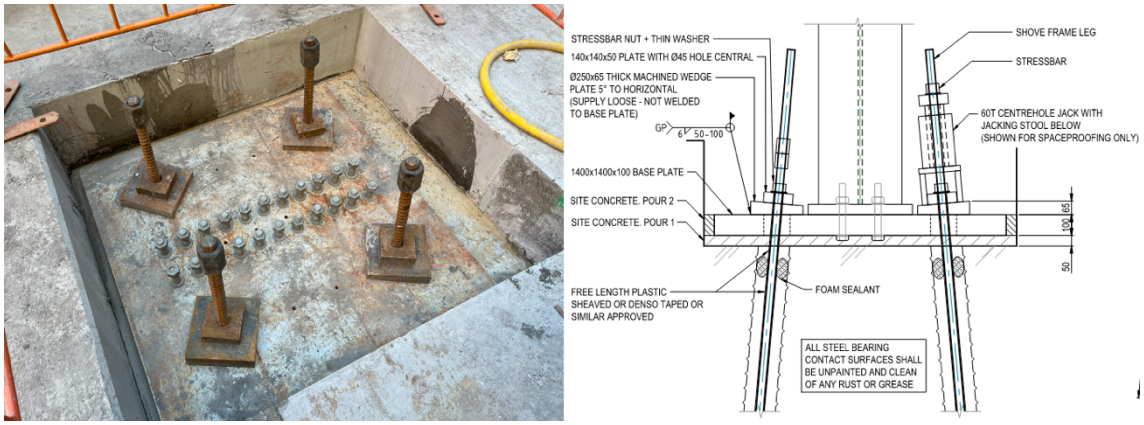


Figure 8. TBM launch frame ground anchor hold down detail

2.4 *Temporary steel rings*

To simplify installation, removal and re-use, temporary steel rings were used rather than reinforced concrete. An advantage of using steel rings is that segment side restraint frames are not required because the steel rings are lighter than concrete rings and the radial joints between the segments are designed to resist ring self-weight ovalisation. Removal of the steel rings is generally less disruptive during removal to other works at the tunnel portal when compared to concrete temporary rings (which are typically demolished). The temporary steel rings have greater flexibility in removal as well as they are designed to be lifted out as either one full ring, separate rings, or individual segments.

2.5 *TBM launch seal*

The launch seal provides containment for the TBM slurry and TBM annulus grouting. The launch seal steel can length is set to allow the TBM cutterhead to be pushed completely past the two rubber lip seals prior to the TBM being launched. Once the cutterhead advances past both lip seals, the TBM head chamber can be pressurised with slurry. As the TBM shield advances completely through the launch seal, the inflatable seal is pressurised with grout to seal the larger gap between the launch seal and the extrados of the last temporary steel ring. A launch seal design section and site photo of both launch seals are shown in Figure 9 and Figure 10 respectively.

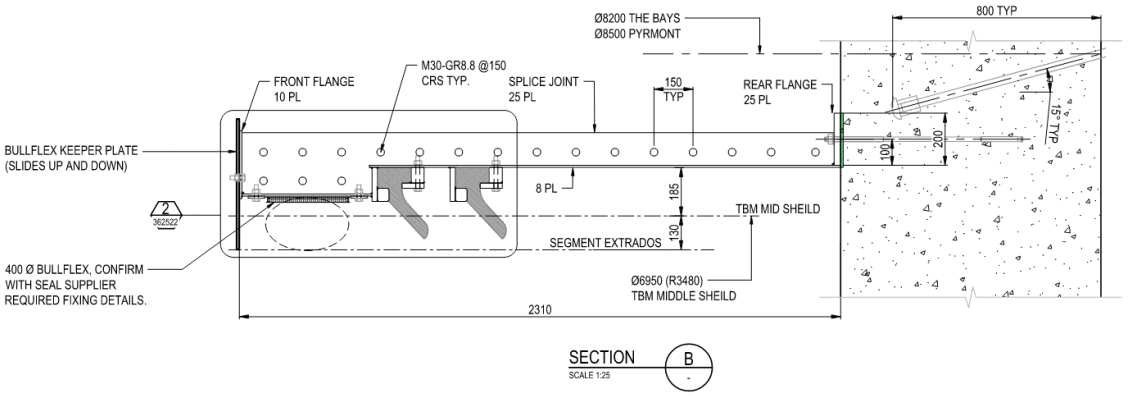


Figure 9. TBM launch seal section



Figure 10. TBM launch seals at The Bays Station

The launch seal is designed as a bolted steel tension shell loaded primarily in hoop tension from the pressurized slurry initially, inflatable seal pressure, and then finally the external anulus grouting. A load path for the TBM shield weight is provided with legs underneath the launch seal which have levelling nuts to help with installation. The outwards force from the internal fluid pressure is transferred through the shell into the headwall via bolts and then into the ground using ground anchors splayed outwards away from the TBM alignment.

After completion of the TBM launch at The Bays, the launch seals were removed for re-use at Pyrmont Station.

2.6 *Design process*

The design process for the launch of a TBMs within the Bays station box was a critical phase in the ETP project as it needed to ensure a safe, efficient, and timely commencement of tunnelling operations. Early integration between the JCG JV construction team and the Delve Underground design team played a pivotal role in optimizing this process. By collaborating from the initial planning stages, both parties were able to align design proposals with practical construction methodologies, leading to significant cost savings and improved efficiency. This early engagement allowed for the identification and mitigation of potential risks, streamlined the approval process for temporary works, which included Proof Engineering, and enabled the reuse of steelwork and other components where possible.

As a result, the TBM launch was executed smoothly, with minimized delays and enhanced safety, demonstrating the tangible benefits of early and continuous collaboration.

2.7 *Construction benefits of the design*

The final design for the TBM temporary works has the following benefits to the construction team:

- The ability of the steel rings to be re-used in subsequent launches of the TBMs, instead of casting additional concrete segments (and demolishing them).
- The jacking dolly not being permanently fixed, and instead utilizing pins, offered several key benefits during the TBM launch at The Bays Station. Mainly, its removable design allowed for greater flexibility during assembly and launch operations, enabling it to be easily repositioned once the TBM shield had advanced.
- For the launch frame, the oversized external frame allowed the TBM shield to pass through before the full frame assembly was complete, offering considerable time savings and

flexibility in the construction sequence. By enabling the installation of the smaller internal members after the TBM had traversed the main frame, the design minimized the need for lifting large structural components in the confined environment of the station box. Components of the launch frame were also to be re-used for the second TBM launch from the Pyrmont station towards the new Hunter Street station.
- Tension ties which connected the stools of the TBM shield cradles reduced the amount of fixings into the slab, providing both time and cost benefits.

In summary, it was key for the JCG JV construction team to launch the TBMs within The Bays Station box on time and therefore any programme savings resulting from efficient and simple temporary works designs provided considerable benefits for the project. Minimizing the fixing anchors, minimising the quantity of steelwork and reducing the amount of steel connections within the design ensured the programme savings were achieved.

2.8 *Lessons learnt*

Overall, the design was efficient and cost effective for the construction team. However, the following items at The Bays Station launch were identified as potential improvements:
- It would be beneficial to reduce the amount of fixings between the eye seal and the concrete headwall, as it was difficult to line the launch seal up with the protruding bolts. Having larger oversized holes through the rear flange of the launch seal would also improve installation tolerance.
- For the upcoming Pyrmont Station launch, which reuses the temporary works, the site is more confined than The Bays Station box and therefore creates greater constructability issues. A better understanding of the constraints at Pyrmont Station from the construction team at the time of detailed design may have allowed for more provisions incorporated into the launch design for Pyrmont Station.

3 CONCLUSION

This paper presents valuable insight into the design development and construction monitoring of large-scale Temporary Works designs on the Eastern Tunnelling Package section of the Sydney Metro West project. Optimized designs were effectively implemented through close collaboration between the contractor and design engineer.

4 ACKNOWLEDGEMENTS

The authors would like to thank Sydney Metro West, John Holland CPB Ghella Joint Venture, and Delve Underground for providing the necessary resources and collaboration that contributed to the successful completion of this project.

19th Australasian Tunnelling Conference – Acosta-Martínez, Stewart and Hudson-Smith (Eds.)
© 2025 Australian Tunnelling Society, ISBN 978-0-85825-002-4

Repurposing Roma Street station's temporary access adit as an emergency egress adit

M. Lecina & S.J. Clarke
PSM, Sydney

J. Vallino
CBGU JV, Brisbane

ABSTRACT: Brisbane's Cross River Rail project includes the excavation and construction of four new underground stations, including the large and geometrically complex underground station beneath the existing railway station at Roma Street. A temporary adit was excavated to provide construction access to the cavern, and was sized for excavation plant, tunnel ventilation, and worker access. Upon the completion of construction, the temporary adit is being repurposed as a permanent emergency egress tunnel for rail passengers. The small permanent tunnel was constructed within the larger temporary adit with the void around the tunnel lining backfilled. Key performance requirements were targeted by the backfill specification, in particular durability, strength and deformation properties. The permanent adits comprise precast concrete units on a cast in situ concrete invert slab. This paper presents the design and construction challenges and unique solutions developed to meet the site constraints and project requirements.

1 INTRODUCTION

Cross River Rail (CRR) is a new 10.2 km long metro rail line in Brisbane extending between Dutton Park in the south and Bowen Hills to the north, which includes 5.9 km long twin tunnels below the Brisbane River and CBD.

The project is being constructed by a joint venture of CPB Contractors, BAM International Australia, Ghella and UGL (CBGU JV) as part of Cross River Rail's Tunnel, Stations and Development (TSD) package.

The TSD component includes construction of twin Tunnel Boring Machine (TBM) excavated tunnels and mined running tunnels; four new underground stations at Boggo Road, Woolloongabba, Albert Street and Roma Street; and dive structures at each end of the running tunnels. The Pulse consortium (including the CBGU JV) was awarded the contract to design and construct the TSD works.

A temporary adit (RTA1) excavated to provide construction access to the Roma Street cavern from the Gallipoli Shaft was subsequently repurposed as a permanent emergency egress adit (Figure 1). Given that the adits's permanent function is limited to passenger evacuation, the required internal envelope was substantially smaller than that of the original RTA1 excavation.

Options considered for the permanent adit included lining the overly large temporary adit or construction of a smaller adit within the temporary adit and backfilling the void around the permanent adit lining. The second option was adopted because it was more cost effective.

2 TEMPORARY CONSTRUCTION ACCESS ADIT RTA1

The temporary adit (RTA1) was required to provide construction access from the Gallipoli shaft to the Roma Street Station cavern, with an overall length of approximately 100 m (Figure 1).

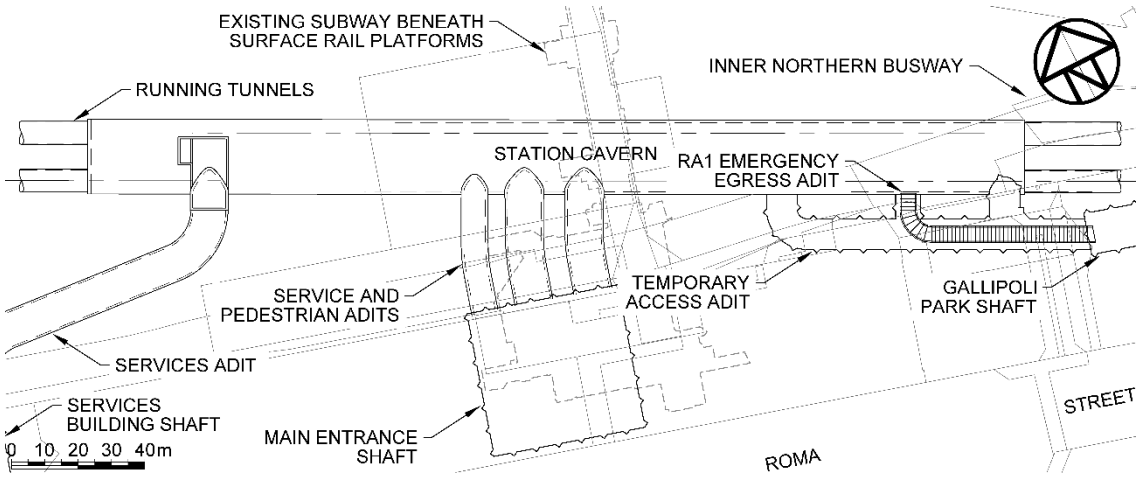


Figure 1. Roma Street station layout showing temporary access adit and emergency egress adit.

The invert level of the temporary access adit drops from RL -3.6 m at the base of the Gallipoli shaft down to RL -14.5 m where it connects to the invert level of the station cavern.

The adit initially provided construction access to the heading level at the east end of the cavern. It was subsequently extended to create access for the permanent adit to the mezzanine level of the cavern and then extended again down to the invert level of the cavern.

The temporary adit was sized for excavation plant, tunnel ventilation ducts, and safe worker access with a span of 9 m and a maximum height of up to 12 m (Figure 2).

3 PERMANENT EMERGENCY EGRESS ADIT RA1

3.1 *Lining geometry*

The RA1 permanent adit was constructed within the RTA1 temporary adit, extending from the Roma Street Station cavern to the Gallipoli Park shaft with an overall length of approximately 65 m (Figure 1). This length included a 90° sweep bend, with a gentle slope of 26.6H:1V in the vertical alignment between the upper horizontal landing near the base of the Gallipoli shaft and the lower landing level at the bend adjacent to the connection to the cavern.

The minimum clear opening (MCO) required for the egress adit comprised a clear span of 4.2 m and a height of 3 m.

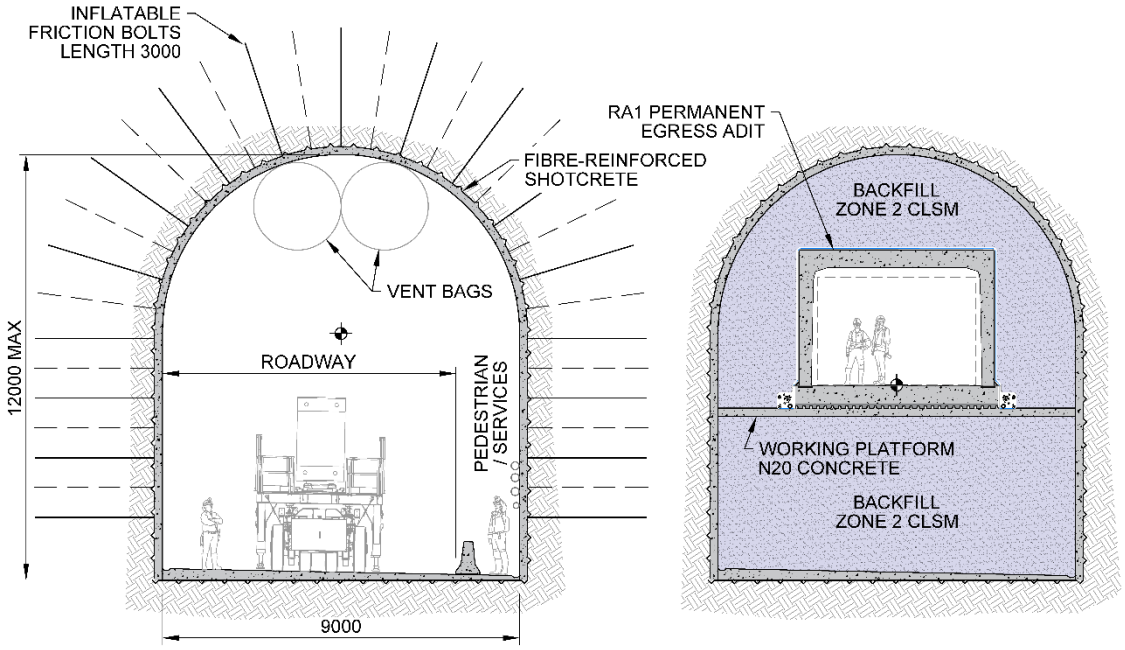
PSM designed the permanent lining for all the underground mined tunnel structures for the CRR project, including the emergency egress adit RA1. As the emergency egress adit was constructed within an existing void, the use of conventional intrados in-situ formwork for the permanent lining was not possible. To address this and improve construction efficiency, the RA1 permanent lining comprised a cast in-situ concrete slab and prefabricated concrete units, offering a more cost- and time-effective solution.

Given that the required MCO was a rectangular envelope, the use of modified precast culvert units - similar to those typically used for road drainage - offered a relatively simple design solution. A standard 1.2 m long precast box culvert in accordance with AS 1597.2 was proposed, as this satisfied the MCO requirements.

The design considered input from CBGU's preferred precast box culvert supplier to develop the geometrical design of the non-standard units required to accommodate the 90° change in direction and the variation in vertical alignment adjacent to the horizontal landings.

3.2 *Permanent lining design*

Rather than undertaking a full in-house design of the precast units, it was considered more efficient to develop a comprehensive culvert specification that defined the project-specific requirements for geometry, materials, durability, waterproofing, lifting, and fixings. The specification also provided details of the applicable loads and load combinations to be considered.



(a) Temporary construction access adit (b) Permanent emergency egress adit

Figure 2. Cross section of the adit at differing stages of the project.

In addition to the typical ground and groundwater loads relevant to standard drainage culverts, the units were also required to be designed for load cases associated with tunnel permanent lining design, such as blast and fire. The design for these loads was carried out in-house and translated into the minimum unit thickness and concrete cover requirements, making compliance with the blast and fire design requirements straightforward to implement.

External design loads applied to the precast box units included vertical and horizontal ground loads and groundwater pressures (Figure 3). The ground loads applied to the culvert units within the RTA1 temporary adit considered rock loads, backfill weight, and the Brisbane Live future development loads. Brisbane Live comprises a proposed stadium located above the station cavern (Shen *et al*, 2022). For the units within the Gallipoli Park shaft excavation footprint, future development and rock loads were not applicable, though the weight applied by a depth of approximately 15 m of CLSM fill within the shaft was substantial.

Tolerances complied with relevant Australian Standards for standard drainage precast box culverts, as well as the requirements in CBGU's specification for the fabrication of the units. The standards specified a length tolerance of ±15 mm, while the project specification required a verticality tolerance of side and end faces within ±20 mm over the full height, a maximum deviation from straightness of 6 mm when measured with a 1 m straight-edge, and end faces square within ±4 mm. The adoption of these tolerances proved to be problematic and led to gaps between the units larger than 10 mm and alignment issues with station cavern interface (see Section 5).

The permanent adit drainage system included a Cavidrain S60 sheet drainage layer installed beneath the invert slab. This product is manufactured from high density polyethylene and comprises square cuspates of 60 mm depth which, when backfilled with mortar, form a load-bearing layer which is crisscrossed by closely-spaced drainage channels.

Corrugated slotted pipes of 100 mm diameter fitted with filter socks were installed either side of the invert slab. These pipes were embedded within a shallow trench of 20 mm gravel aggregate which abutted the Cavidran (Figure 4). The gravel was wrapped in geotextile fabric and membrane to ensure that it was not clogged during placement of the CLSM backfill.

Drainage was directed towards the station cavern, with the slotted pipes draining into the Cavidrain system near the opening. Flushing-points were provided at the top of the culverts within the Gallipoli shaft structure.

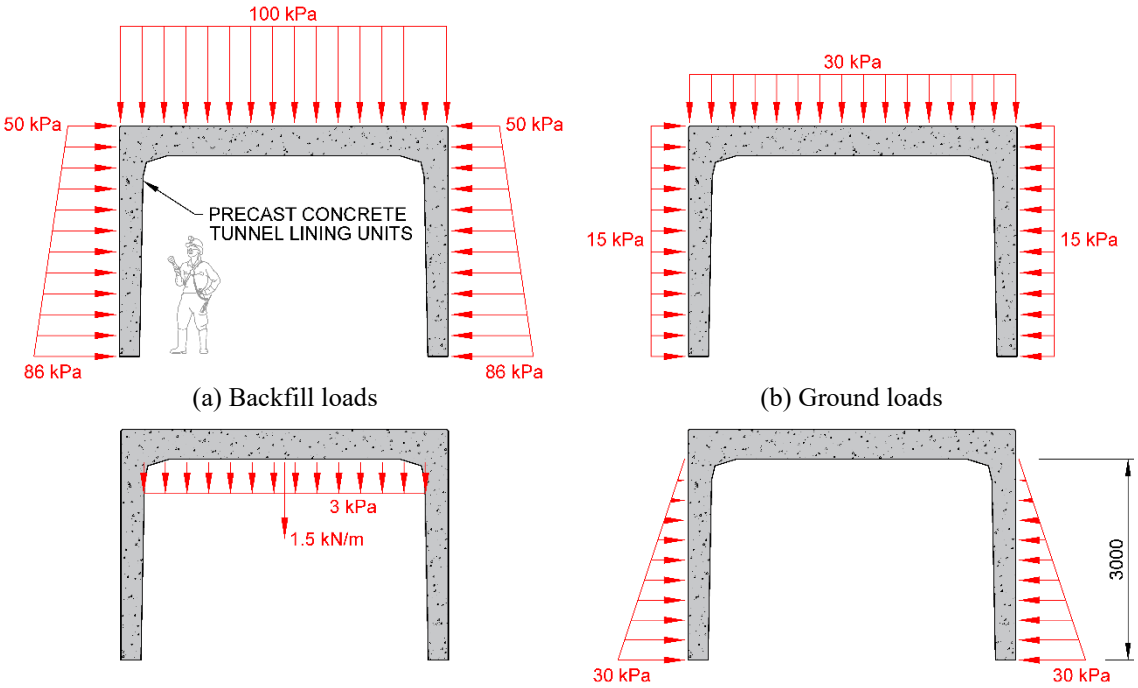


Figure 3. Key design load cases for the precast culvert units.

A waterproofing membrane was installed over the top and sides of the culvert units, with a protective geotextile placed between the units and the membrane. Rearguard PVC waterstops were provided at vulnerable connections located at each end of the culverts.

In addition to the membrane, hydrophilic waterstops were required to be installed at the key joints provided between culvert units. These measures were detailed to satisfy the project's long-term watertightness and durability requirements.

4 CONTROLLED LOW STRENGTH MATERIAL (CLSM)

4.1 *Overview*

Controlled Low Strength Material (CLSM), or flowable fill, comprises a cementitious fill with flowable consistency at the time of placement and achieves limited compressive strength when fully cured. These characteristics makes it well-suited for backfilling trenches that may require future excavation or complex-geometry voids where its flowability ensures complete filling, while accelerating the construction program, as CLSM can be mixed, transported, and placed using standard ready-mix concrete methods.

The strength of CLSM varies widely, depending on its application, from soil strength up to low strength concrete.

CLSM typically comprises a mixture of cement, water, fine aggregate, and supplementary cementitious materials such as fly ash or slag. The high slump of the CLSM significantly reduced placement time and equipment requirements, leading to lower labour and machinery costs. Its flowable consistency allows it to be placed quickly and uniformly, even in confined or irregular spaces, minimising the risk of voids and potential subsidence.

CLSM was originally intended to be utilised to backfill the totality of the void around the RA1 permanent adit lining. Two distinct CLSM mixes were developed following a review of relevant Australian and international guidelines and technical literature to suit different design and construction purposes.

The first mix (referred as Zone 1 – Backfill) was designed for general backfilling applications, where ease of placement and flowability were the primary considerations.

The second mix (referred as Zone 2 Fill – Structural fill) was specifically designed for placement beneath the permanent invert slab of the RA1 adit and either side of the precast units.

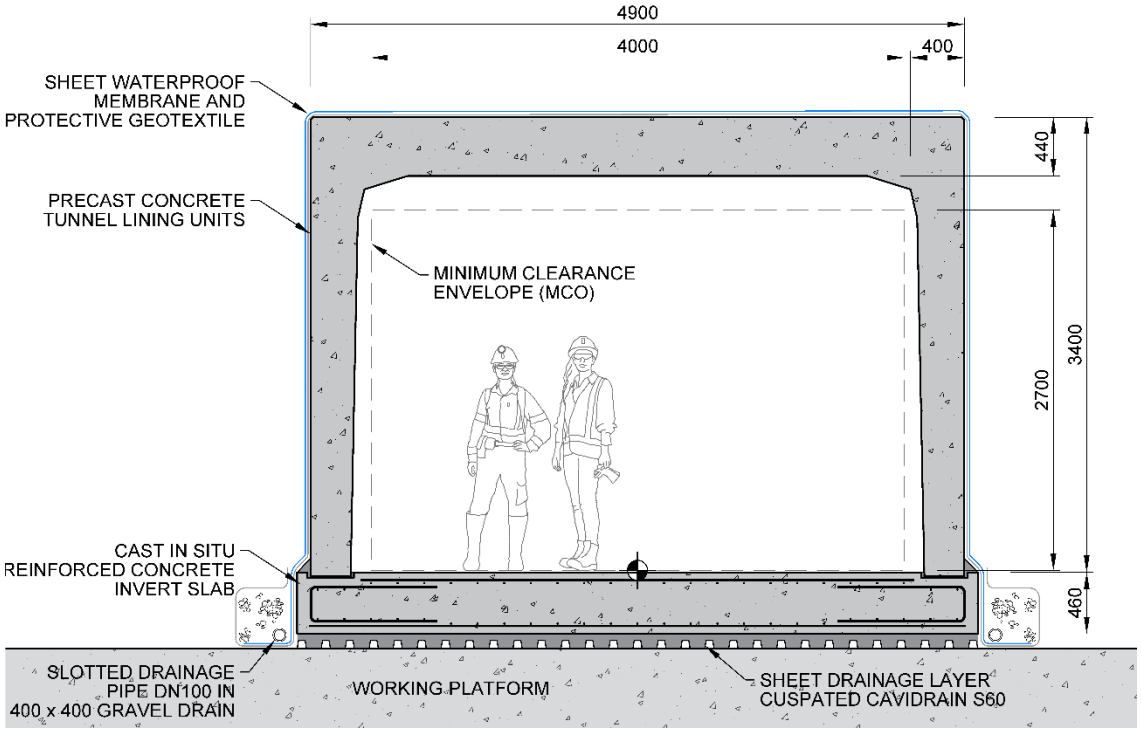


Figure 4. Detailed section of the emergency egress adit.

This mix was subject to stricter performance criteria, the objective being to minimise post-construction settlement and provide an adequate foundation for the invert slab of the permanent adit. Unlike the Zone 1 mix, the function of the Zone 2 mix was that of a controlled engineered fill.

Due to cost and program constraints, the construction team opted to place a 200 mm thick N20 concrete working platform immediately beneath the RA1 invert slab to allow trafficking of the slab at an earlier age than would have been possible with Zone 2 fill.

A total volume of 5940 m^3 of CLSM was required to backfill around the egress adit within the RTA1 adit (i.e. excluding backfilling of the Gallipoli shaft).

4.2 *Zone 1 Fill – Specification requirements*

The Zone 1 Fill mix was provided as a low-cost backfill material for use in areas where structural performance was not required. It was designed to be self-levelling, with sufficient flowability to fill voids without the need for mechanical compaction.

Key performance requirements included a maximum density of 2000 kg/m^3 to limit loads on the culvert units, and a minimum slump of 200 mm to achieve the required flow characteristics. A nominal minimum compressive strength of 0.5 MPa at 28 days was specified for quality control purposes. No specific limits were imposed on modulus, creep, or bleed, as these properties were not relevant.

Controls on aggregate size, fines content, plasticity, and chloride levels were adopted to promote uniformity and durability of the mix in accordance with the project requirements.

4.3 *Zone 2 Fill – Specification requirements*

The Zone 2 Fill mix was required for use beneath and either side of the culvert units, and thus required structural properties regarding strength, deformation, and durability.

The mix was specified with a maximum density of 2300 kg/m^3, consistent with the higher strength requirements for this application. A maximum slump of 150 mm was adopted to accommodate the formation of the RA1 permanent adit ramp, which has a gradient of approximately 1V:26.6H, while ensuring adequate workability without excessive flow.

Table 1. Adopted CLSM Specification

Properties	Test method	Zone 1 Backfill	Zone 2 Structural fill	Purpose
Compressive strength (3 hrs)	AS 1012.18	-	> 0.1 MPa	Provide worker access
Compressive strength (28 days)	AS 1012.9	> 0.5 MPa	> 2.0 MPa	Long term load capacity
Modulus (28 days)	AS 4133.4.3.2	-	> 4.0 GPa	Control settlement and provide support for cavern sidewall
Slump	AS 1012.3.1	> 200 mm	< 150 mm	Ensure self-levelling (Zone 1) and allow formation of 26.6H:1V slope (Zone 2)
Density	AS 1012.12	< 2000 kg/m^3	< 2300 kg/m^3	Adopted in load assessment
Creep strain (100 years)	Bespoke *	-	< 0.0005	Control settlement
Aggregate size	AS 1141.11.1	< 19 mm		Facilitate flowability
Fines content (< 75 mm)	AS 1141.12	< 20%		Ensure homogeneity
Plasticity index	AS 1289.3.3.1	< 15%		Ensure homogeneity and limit shrinkage
Chloride content	AS 1012.20.1	< 0.1%		Durability

* Test methodology modified from concept in ASTM C1181-00, with a test period of 3 months with a test stress equivalent to 40% of the required 28-day compressive strength. Refer to Figure 5 and test description in Section 4.3 for further details.

Early age strength requirements included a minimum compressive strength of 0.1 MPa at 3 hours to provide sufficient bearing capacity for early worker access and allow preparation for subsequent lift placements. A minimum 28-day compressive strength of 2.0 MPa was adopted to provide adequate bearing capacity both upon completion of backfilling above the culvert units and when the units were subject to long-term ground loads.

A key property for the specification of the Zone 2 Fill was deformation. The required modulus at 28 days was determined based on the need to provide sufficient stiffness and adequate support to the permanent station cavern sidewalls upon backfilling of the construction adit.

Time-dependent creep behaviour was also a critical design consideration, with the intent of limiting the total post-construction settlement of the adit to less than 10 mm. Creep testing was required to ensure that the proposed CLSM mix was suitable, though selection of the test method was difficult due to the relatively short period of time available to do the testing and the fact that the standard methods were not intended for testing CLSM. The AS 1012.16 method involves the stacking of several cylinders and a test period of one year and was thus deemed unsuitable.

An alternate method, ASTM C1181-00 “Compressive creep of chemical-resistant polymer machinery grouts” was proposed by Boral testing laboratories. This is a clever test configuration, using prestressed springs to apply a constant load over a long period of time. The basic concept was adopted, then modified to suit the CLSM cylinder samples (Figure 5).

A key change to the ASTM method was the use of more flexible springs (k = 159 N/mm), rather than the stiff springs nominated in the ASTM standard (k = 6700 N/mm). The use of the more flexible springs means that the load changes by only 0.2% at the allowable creep deflection of 0.06 mm over 90 days, whereas the use of the stiffer springs results in a theoretical load change of 8.5%.

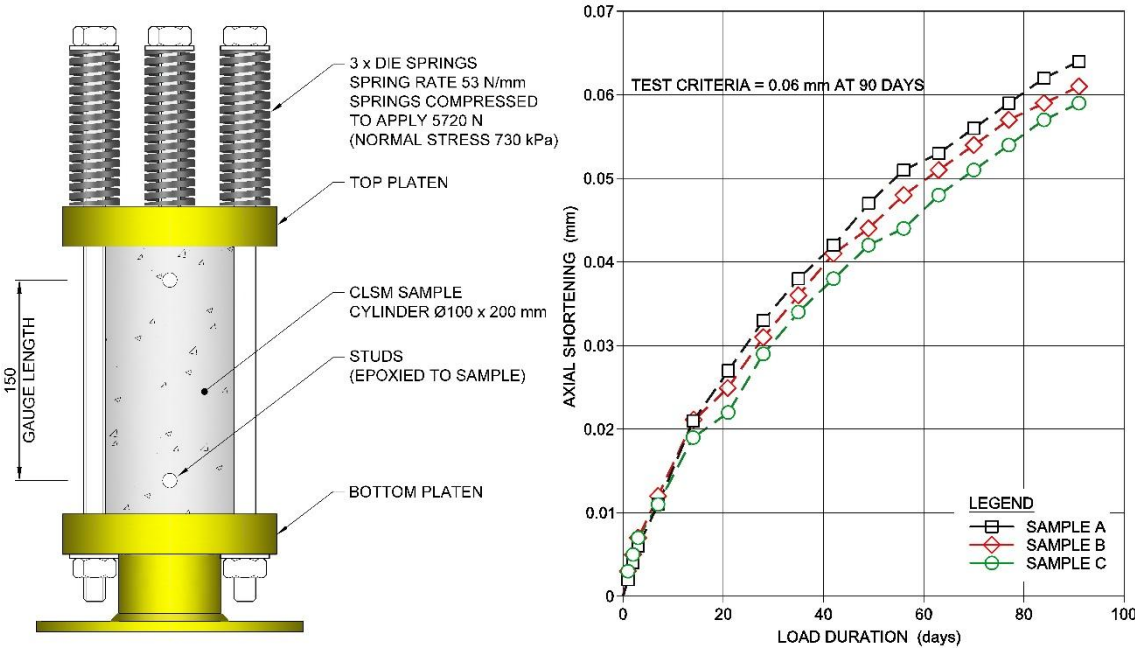


Figure 5. Creep test configuration and test results (After Shen *et al*, 2022) of 0.06 mm over 90 days.

4.4 *Departures from proposed mixes*

The Zone 2 Fill was proposed for the plug at the cavern sidewall opening and for backfilling a large proportion of the temporary adit beneath the RA1 permanent invert slab (Figure 6a), making it well suited for mass backfilling. This led to the decision not to use the lower specification Zone 1 Fill material in the area below the permanent adit.

The design also nominated the use of the non-structural Zone 1 Fill for backfilling above the culvert units and within the Gallipoli Shaft. However, it was found that the cost to supply the Zone 1 Fill was more than that of the higher performance Zone 2 Fill. As a result, only the Zone 2 Fill mix (hereafter referred to as CLSM) was used for backfilling the void around the RA1 permanent lining and the Gallipoli shaft structure (Figure 6b).

The CLSM mix used to backfill above the culverts was modified to achieve a lower density to limit the load applied to the top of the culvert units.

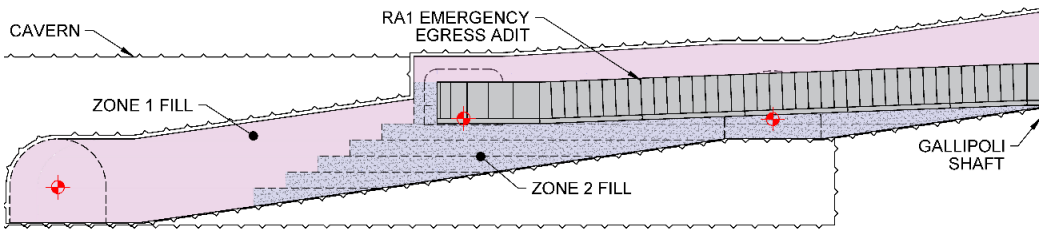
4.5 *CLSM – Test results*

Different testing frequencies and methodologies were nominated for various backfilling areas within the temporary adit to confirm the mix design requirements. An initial intensive testing regime was implemented to confirm the performance of the CLSM mix and establish a reliable correlation between the cylinder and cube compressive strength testing. Due to the high rate of backfilling, the frequency of 28 days compressive strength testing was reduced, while additional 7 day tests were undertaken as early indicators of potential non-compliance. Further production testing, including modulus and creep strain, was specified for the CLSM placed within 5 m beneath the RA1 invert slab to ensure the mix met the performance requirements.

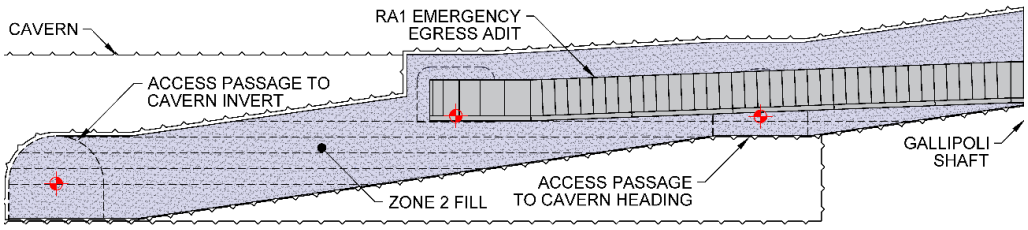
5 CONSTRUCTION

5.1 *Sequence*

Once the RTA1 temporary adit was no longer required for construction access to the cavern, the sidewall opening in the cavern lining was closed. Formwork was erected on the cavern side to create a pour face for the CLSM to be pumped into the temporary adit to complete the plug and backfill. After formwork removal, a protective geotextile and PVC waterproof membrane was installed and integrated with the cavern waterproofing.



(a) Originally proposed application of the CLSM mixes.



(b) As-built extent of CLSM.

Figure 6. Long section through the RTA1 temporary adit and RA1 permanent egress adit.

The structural fill was placed using a line pump and hoses, which were moved manually or with a Dieci telehandler to implement the backfilling sequence. Care was required during the placement of the CLSM at the cavern plug and near the crown of RTA1 to avoid air entrapment.

The last layer of CLSM beneath the culvert invert slab in the original design was replaced with a 200 mm thick working platform, with the finished surface screeded to support the Cavidrain system. N20 concrete mix was used instead of the CLSM mix to achieve faster strength gain, allowing earlier access for the 12 tonne Dieci telehandler used for steel and material delivery required for the invert slab works. The design of the working platform's thickness and characteristic strength accounted for two key scenarios: during the early age when the platform was loaded by the telehandler, and after the platform had attained its full strength, when the RA1 permanent invert slab was constructed and the culvert transporter, carrying the heaviest precast box culvert unit, trafficked on the invert slab.

A total of fifty-two precast box culvert units, ranging in weight from 10.8 tonnes to 22.3 tonnes, were lifted by gantry crane to the base of the Gallipoli shaft, then rotated and placed onto a self-propelled modular transporter (SPMT). The SPMT is of modular construction, with the one used to move the culverts comprising 16 wheels arranged on four axle lines, with each axle line rated at 40 tonnes. Wheels are grouped in pairs, with the direction, speed, and height of each pair remotely controlled by the plant operator to provide precise movement control in every direction. A power pack containing the engine and hydraulic pumps hangs from the back of the SPMT.

The transporter has a nominal bed level of 1.5 m above ground level, with a movement range of ±0.3 m, and thus required addition of a support frame to enable it to reach up to the underside of the culvert units (Figure 7). The transporter then moved the precast units to their final positions, the first unit being placed adjacent to the cavern and progressing eastward towards the shaft.

CLSM was placed adjacent to the culvert legs in 300 mm to 500 mm thick layers to maintain safe worker access to the precast units.

5.2 *Productivity*

Prior to commencing the backfilling of the adit, a series of trials were undertaken to improve the construction team's understanding of the CLSM material, particularly key differences with concrete.

The relationship between slump and strength and flowability was investigated to ensure that the CLSM could be placed efficiently without compromising the specified engineering properties. The trials were also important for the batch plant so that they could become familiar with the production of the mix. The capacity of the agitators delivering the mix to site as well as the achievable pumping rates were established to permit accurate scheduling of the works program.

Table 2. Summary of available test results performed on Zone 2 Fill

Property	Number of tests	Unit	Measured Values		
			Min.	Median	Max
Compressive strength (7 days)	37 (25)	MPa	1.4 (1.9)	1.6 (2.3)	2.5 (3.1)
Compressive strength (28 days)	106 (88)	MPa	1.5 (2.2)	4.6 (6.0)	8.3 (11)
Modulus (28 days)	2	GPa	13.3	13.5	13.7
Density (28 days)	106 (88)	kg/m³	1920 (1940)	2040 (2050)	2160 (2260)
Creep deflection (91 days)	3	mm	0.059	0.061	0.064

* Values in brackets represent results from tests conducted on cube samples.

The placement rate of CLSM within the temporary adit varied depending on the proximity to RA1 culvert units and the RTA1 crown. During mass backfilling of open areas, placement progressed at approximately 30 m³/h. However, this rate was significantly less when backfilling adjacent to the culvert units to prevent unbalanced lateral loads.

5.3 *Lessons learnt*

The main lessons learnt were related to the varying geometric tolerances of the cavern lining, culvert units, and permanent egress structure within the Gallipoli shaft.

Construction of the collar around the RA1 opening in the cavern sidewall was subject to the adopted tunnel lining tolerances for the project, which included a generous -0 mm/+150 mm excavation tolerance for the extrados surface. The culvert units were required to butt up against the collar, though these tolerances permitted the collar surface to vary significantly from vertical, such that an additional lightly reinforced concrete collar section was required to be built to provide a better-matching planar surface.

As noted in Section 3.2, the culvert design adopted the standard drainage culvert geometric specification. The culverts had been constructed then stored outside for about a year prior to being

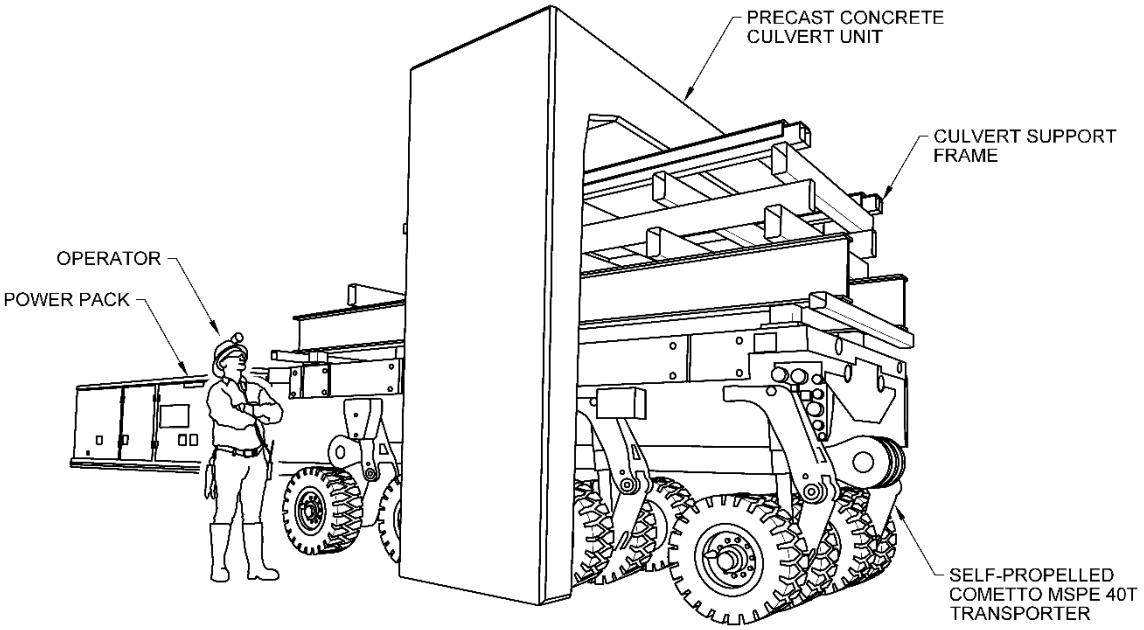


Figure 7. Cometto four axle self-propelled modular transporter used to place culvert units.

installed. They were found to be bowed/distorted such that the crown of the adjoining culvert faces were not square/aligned resulting in gaps of up to 15 mm. This wider gap had the potential to compromise the effectiveness of the hydrophilic waterstop. In some locations it proved necessary to repack the bases to decrease the gap and maintain the design crown alignment. In locations where the gap was greater than 10 mm the waterproof membrane was reinforced by a second layer at the joint location.

A further challenge was the exposed edge risks due to the necessity to work from the top of the culverts. This resulted in changes to the staging of waterproofing, drainage and backfilling around the culverts. When backfilling either side of the adit the waterproofing layers on the top were initially left off to avoid damage. The crown waterproofing was subsequently installed then protected by a 100 mm to 200 mm layer of CLSM.

The final challenge was connecting the culverts to the egress shaft structure. Due to the inability to adjust the overall length of the culverts the final culvert could not be positioned at the nominated design interface location with the shaft, and this resulted in modification to the shaft structure.

Some of the challenges with the culvert tolerances may have been managed by further changes to the standard culvert joint detail. A stepped/lapped detail such as employed in spigot and socketed concrete pipes could have provided the means to adjust the position of the culvert units.

6 CONCLUSIONS

The construction of the RA1 permanent emergency egress adit within the existing RTA1 temporary access adit provided an efficient and cost-effective solution to repurpose the excavation. Bespoke precast culvert units, designed to meet stringent project-specific requirements, ensured the required structural performance and durability, despite the challenges posed by dimensional tolerances and structural interfaces.

The application of CLSM for backfilling the void around the permanent lining proved advantageous, as its flowability made it easier to place in complex areas and helped maintain the construction schedule.

ACKNOWLEDGEMENTS

The authors would like to acknowledge the Pulse consortium and CPB Contractors, BAM International Australia, Ghella and UGL Joint Venture for their permission to publish this paper. The authors also express their thanks to Alexander Rogan and Wendy Luo who provided PSM's site presence during the building of the adit. Finally, the authors express their appreciation to the CBGU construction team for their professionalism in building this unusual design solution.

REFERENCES

Shen, B., Clarke, S.J., Rogan, A., and McCormack, P. 2022. Design and construction of Roma Street station cavern, Cross River Rail, Brisbane, *Australian Geomechanics*, Vol. 57, No. 4, pp 115-128.

Cammack, R., Bertuzzi, R., Smith, A. and Brehaut, R. 2022. Rock Mass Parameters for the Brisbane CBD. *Australian Geomechanics*, Vol. 57: No. 4, pp. 47 – 72.

ACI Committee 229. 1994. Controlled low-strength materials (CLSM). *Concrete International* 16(7): pp. 55–64

Department of Transport and Main Roads (Queensland) 2019. Technical Note TN187: Controlled Low-Strength Material for Pipe Installation. Brisbane: Department of Transport and Main Roads

VicRoads 2008. Technical Note TN 007: Flowable Fill. Melbourne: VicRoads.

Cement Concrete & Aggregates Australia (CCAA), 2008. Controlled Low-Strength Material datasheet.

Standards Australia/Standards New Zealand, 2007. *AS/NZS 3725*: Design for installation of buried concrete pipes – Appendix A Controlled Low Strength Material (CLSM).

National Clay Pipe Institute (NCPI), n.d. Guidelines for Controlled Low Strength Material (CLSM): Mix Design, Placement and Testing for Use as a Bedding Material for Vitrified Clay Pipe.

Darafill, n.d. Controlled Low Strength Material (CLSM): Technical Bulletin 1104.

19th Australasian Tunnelling Conference – Acosta-Martínez, Stewart and Hudson-Smith (Eds.)
© 2025 Australian Tunnelling Society, ISBN 978-0-85825-002-4

Impact of construction phase on the interaction between lining and rock mass in pressure tunnel and shafts

M. Zoorabadi
SMEC Australia, Melbourne, UNSW, Sydney

ABSTRACT: Designing the lining of pressure tunnels is a complex engineering task, requiring careful consideration of both hydraulic and mechanical factors and the complex reaction between the lining and the surrounding rock mass. The design must minimise head losses, prevent excessive leakage, eliminate the risk of hydraulic fracturing or displacement of the rock, and ensure long-term structural integrity during filling, commissioning, operation, and de-watering phases. In reinforced concrete-lined pressure tunnels or shafts, when the internal water pressure exceeds the external groundwater pressure, the differential pressure in distributed between the lining and the surrounding rock mass. The load distribution depends on the stiffness and hydraulic conductivity of both the undisturbed and disturbed rock mass zones, as well as the properties and behaviour of the lining. Commonly used analytical methods, such those proposed by Fernandez (1994) and Schleiss (1986, 1997), assume that the water pressure on the extrados of the lining just before first filling is equal to the height of the existing groundwater level. However, this assumption does not accurately reflect the actual changes in groundwater pressure caused by tunnel excavation. In reality, the water pressure on the extrados of the lining can be significantly lower than the initial groundwater pressure. This discrepancy between the real groundwater pressure and the assumed value in these analytical methods can lead to unsafe lining design for pressure tunnels.

1 INTRODUCTION

Hydropower and pumped hydro projects are a highly relevant sources of renewable energy and play a crucial role in the provision of sustainable energy supply and storage. The design of pressure tunnels is one of the most critical technical challenges of this type of projects.
If the intrados of a pressure tunnel has higher water pressure compared to the extrados, the support of the differential water pressure will be split between the lining and the surrounding rock mass. The distribution of the load between the lining and the rock mass depends on the stiffness and hydraulic conductivity of both. Structural cracking of the lining occurs when the stresses in the concrete exceed its tensile strength. In general, stiffer rock masses will absorb a larger portion of the differential water pressure, reducing the likelihood of lining cracks. When designing a reinforced lining, the primary objective is to determine the most economic thickness of the lining and the density of reinforcement, while also ensuring that the width of cracks caused by differential water pressure remains within a specified limit.

Commonly used analytical methods, such those proposed by Fernandez (1994) and Schleiss (1986, 1997), assume that the water pressure on the extrados of the lining just before first filling is equal to the height of the existing groundwater level. However, this assumption does not accurately reflect the actual changes in groundwater pressure caused by tunnel excavation. In reality, the water pressure on the extrados of the lining can be significantly lower than the initial groundwater pressure due to active drainage during the construction. Therefore, the differential pressure between intrados and extrados of the lining can be higher than the assumption made in the analytical methods. This paper examines this issue in greater detail using a numerical model of a typical pressure tunnel. The findings offer additional insights into the safe design of reinforced concrete linings for pressure tunnels and shafts.

2 ANALYTICAL FORMULATIONS

Jaeger (1979) used thick elastic cylinder theory to calculate the magnitude of the stress transmitted from the concrete lining to the rock surface (P_{fa}) due to the water pressure (p_i) acting to the intrados of a pressure tunnel/shaft (Figure 1).

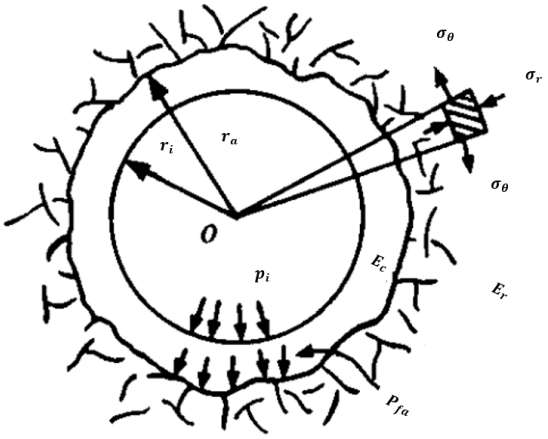


Figure 1. Schematic of boundary conditions considered in Jaeger's (1979) formulation.

Legend:
- r_i…internal tunnel radius
- r_a…external tunnel radius
- E_c and E_r …elastic modulus of the concrete lining and the rock
- m_c and m_r…the inverse of Poisson ratio for the concrete lining (ν_c) and rock (ν_r)
- λ …ratio of the transmitted stress to the internal water pressure.
- p_i…internal pressure inside the tunnel

The formula to calculate the stress transmitted from the concrete lining to the rock surface, applicable for a pressure tunnel/shaft below the groundwater (wet rock) with no consideration of a disturbed zone around the tunnel is presented in Equation (1).

$$P_{fa} = \lambda p_i = \frac{\frac{2r_i^2}{E_c(r_a^2-r_i^2)}}{\frac{m_r+1}{m_r E_r}+\frac{(m_c-1)r_a^2+(m_c+1)r_i^2}{m_c E_c(r_a^2-r_i^2)}}(p_i - P_a) \quad (1)$$

where p_a is the groundwater pressure acting on the extrados of lining which is assumed to be equal with the original groundwater pressure. Jaeger (1979) also proposed the following equation to calculate the tensile stress developed in the lining:

$$\sigma_t = -\frac{r_a^2+r_i^2-2\lambda r_a^2}{r_a^2-r_i^2}(p_i - P_a) \quad (2)$$

Fernandez (1994) developed his method by establishing analytical formulations to determine the pore pressure changes in the rock mass due to the water pressure difference ($\Delta p_w = p_i - p_a$) between intrados and extrados (caused initially by the existing groundwater head) of the concrete lining as follows:

$$P_{fa} = \lambda \Delta P_w = \frac{\Delta P_w}{1+\frac{E_c t_c}{E_r (r_i+{}^{t_c}/_2)}(1+\nu_r)} \quad (3)$$

The design method proposed by Fernandez (1994) relies on the tensile strain developed in the lining. Following formulation can be developed to calculate the induced tensile stress by combining the formulation presented in Fernandez (1994) and stress-strain relationships in cylindrical coordinate.

$$\sigma_t = E_C * \left[\frac{\Delta P_w}{\left(1+\frac{E_c}{E_r}*\frac{t_c}{(r_i+{}^{t_c}/_2)}(1+\vartheta_c)\right)} \frac{(1+\vartheta_r)}{E_r} \right] + \vartheta_c \Delta P_w \quad (4)$$

Schleiss (1986, 1997) used the porous thick elastic cylinder theory to formulate the magnitude of stress transmitted to the rock surface. Schleiss assumed that the internal hydrostatic pressure (p_i) generates an excessive pore pressure at the lining extrados and in the rock mass and proposed the following equation to calculate the transmitted stress to the rock surface.

$$P_{fa} = \frac{\{(p_i - p_a)[\frac{2(2-\vartheta_c)}{\left({r_a}/{r_i}\right)^2 - 1} + \frac{1-2\vartheta_c}{1-{r_i}/{r_a}}] - 3\left(\frac{E_c(1+\vartheta_c)}{E_r(1+\vartheta_c)}\right)p_a\}}{3[\frac{2(1-\vartheta_c)}{\left({r_a}/{r_i}\right)^2 - 1} + \frac{E_c(1+\vartheta_r)}{E_r(1+\vartheta_c)} + 1 - 2\vartheta_c]} \quad (5)$$

Schleiss (1997) also proposed the following formulation to calculate the magnitude of tensile stress developed in the lining:

$$\sigma_t = \frac{(p_a - p_i)(2-\upsilon_c)}{3(1-\upsilon_c)}\left[\frac{1+\frac{r_a^2}{r_i^2}}{\frac{r_a^2}{r_i^2}-1} + \frac{1-\frac{r_i(1+\upsilon_c)}{r_a(2-\upsilon_c)}}{1-\frac{r_i}{r_a}}\right] + \frac{2P_{fa}}{1-\frac{r_i^2}{r_a^2}} \quad (6)$$

It should be noted that in Equation (6), the term (p_i) denotes the differential water pressure between the intrados and extrados of the lining, which is equal to $(p_i - p_a)$.

All the analytical methods mentioned above assume that, just prior to the first filling, the groundwater pressure (p_a) acting on the extrados of the lining remains equal to the pre-excavation groundwater pressure and is unaffected by the construction process.

3 DEPRESSURISATION OF GROUNDWATER DURING CONSTRUCTION

In the most cases, the pressure tunnels and shafts are constructed by drained excavation techniques. In drained tunnelling, the groundwater pressure at the excavation boundary drops to atmospheric pressure, creating a hydraulic gradient toward the tunnel and extending groundwater depressurisation beyond the excavation boundary.

The following equation is derived by rearranging the formulation proposed by Fernandez (1994) to calculate the groundwater pressure distribution (depressurisation) along the springline of a circular tunnel lined with concrete, assuming a lining hydraulic conductivity of K_c ($K_c = 1e-9\ m/s$ was used in this paper based on Fernandez, 1994) and atmospheric pressure at the intrados:

$$P_w(r) = h_0 - [(h_0 - h_l) * \frac{Ln\left(1+\frac{L^2}{r^2}\right)}{Ln\left(1+\frac{L^2}{r_a^2}\right)}] \quad (7)$$

where r is the radial distance from the tunnel center, h_0 is the initial groundwater pressure at the tunnel boundary prior to excavation, and h_l represents the groundwater pressure immediately behind the lining, resulting from head loss through the lining. This pressure is a function of the hydraulic conductivities of both the lining and the surrounding rock mass (K_r), as expressed below:

$$h_l = \frac{h_0}{1+\left(\frac{Ln\left(\frac{2*h_0}{r_i}\right)}{Ln\left(\frac{r_a}{r_i}\right)}\right)*\left(\frac{K_c}{K_r}\right)} \quad (8)$$

Equations (7) and (8) were used to calculate the groundwater pressure gradient behind the lining just prior to the first filling (Figure 2) for a tunnel with an intrados radius of 4.93 m and a lining thickness of 0.42 m (resulting in an excavation radius of 5.35 m). It is important to note that the analysis assumes all drainage holes are closed, allowing groundwater pressure to build up behind the lining prior to the filling. In addition to the results from the analytical equations, the plot (Figure 2) also presents results from a simplified numerical model using RS2 (Rocscience©). In this analysis and modelling, the hydraulic conductivity of the rock mass is assumed to be 1e-8 m/s, with an initial groundwater head of 584 m at tunnel level prior to excavation.

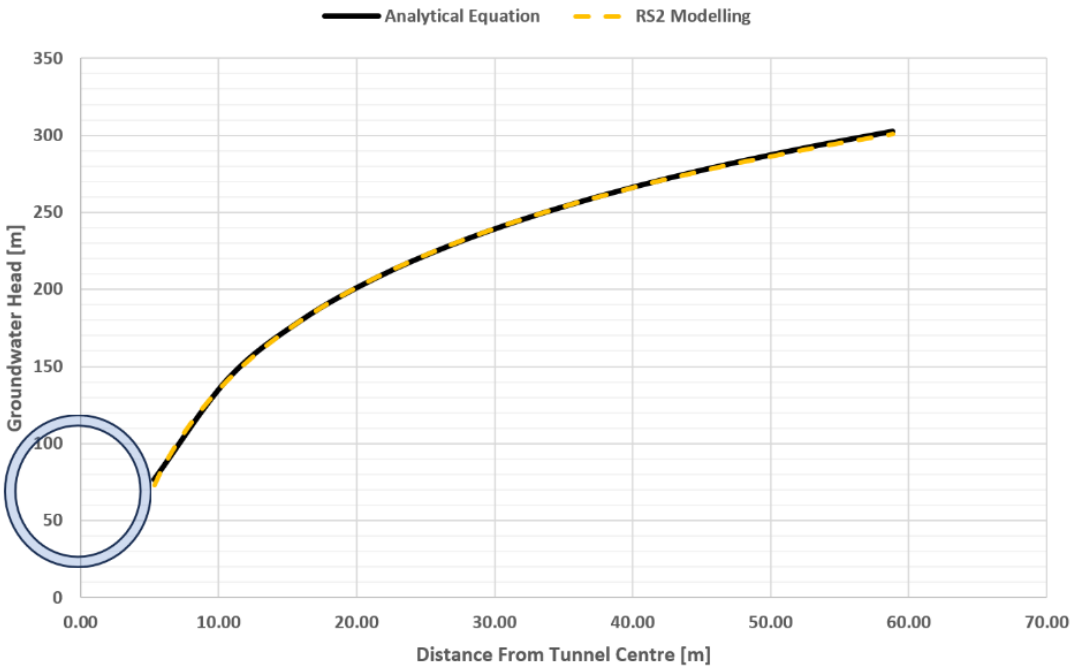


Figure 2. Groundwater pressure distribution behind the lining before first filling

As shown in Figure 2, there is excellent agreement between the results of the analytical equation and the numerical modelling. The results indicate that, when the drainage holes are closed prior to the first filling, groundwater pressure behind the lining reaches approximately 76 m and gradually increases with distance from the tunnel boundary into the surrounding rock mass.

4 INDUCED TENSILE STRESS IN LINING

As previously mentioned, when the internal water pressure in the pressure tunnel or shaft increases during filling and exceeds the external pressure acting on the lining extrados, the resulting differential pressure is distributed between the rock mass and the lining, depending on their relative stiffness and hydraulic conductivity. The commonly used analytical framework for designing linings in pressure tunnels and shafts (Equations 1 to 6) does not account for groundwater depressurisation caused by excavation. To evaluate the impact of this depressurisation on the induced resulting tensile stresses in the lining, numerical modelling was employed. The model considered both the rock mass and the lining as a continuum elastic material with uniform and isotropic properties. Figure 3 illustrates the geometry of the numerical models employed in the comparative investigation presented in this paper. It is important to notice that the consideration of an elastic constitutive model for the rock mass is a conservative approach for the assessment of cracking pressure of linings in pressure tunnels. For the purposes of this study, the rock mass is assumed to have a deformability modulus of 13 GPa ($E_r = 13\,GPa$) and a relatively low hydraulic conductivity of 1×10−8 m/s ($K_r = 1e-8\,m/s$). The initial groundwater head is 584 m, while the hydrostatic water head inside the tunnel at the end of filling is assumed to be 668 m.

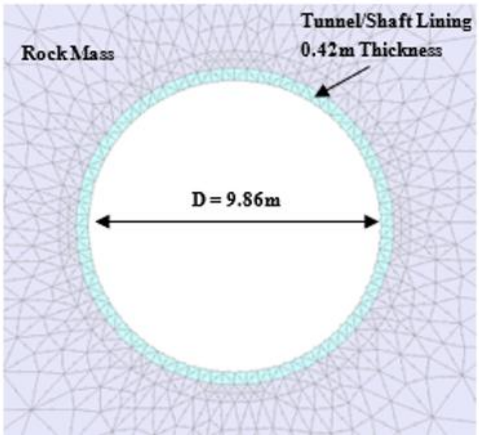


Figure 3. RS2 model used for a typical pressure tunnel.

It should be noted that the filling rate for each pressure tunnel or shaft is determined based on the critical requirement of avoiding significant differential water pressure acting on the lining. This consideration is especially important in lower-quality rock masses, where lower stiffness and higher hydraulic conductivity increase the risk of significant cracking. Consequently, monitoring groundwater pressure in the rock mass behind the lining is essential for designing a safe first-filling strategy, including appropriate filling rates and pauses. Assessing the impact of the filling rate requires more advanced numerical modelling, including an elastic-plastic constitutive model and simulation of the evolution of the lining's hydraulic conductivity. As such, the effect of filling rate is not evaluated in this study. A filling rate of 2 m/h which is common in commissioning of most pressure tunnels was used in this study to avoid unreasonable boundary conditions.

Table 1 presents the results from analytical methods assuming groundwater depressurisation prior to filling. Numerical modelling was used to evaluate both boundary conditions: with and without groundwater depressurisation.

Table 1. Comparison between analytical formulation and RS2 model for full groundwater head acting to the extrados of lining.

Parameter	Without depressurisation				With de-pressurisation
	Method				
	Jaeger (1979)	Fernandez (1994)	Schleiss (1997)	RS2 Model	RS2 Model
Tensile stress in lining [MPa]	-2.13	-2.18	-2.74	-2.3	-6.2

As shown in Table 1, there is a relatively close agreement between the results from the RS2 model and all analytical formulations when the full initial groundwater pressure is assumed to act on the extrados of the lining. Similar consistency between analytical and numerical results was also reported by Zoorabadi et al. (2023).

The induced tensile stress obtained from the numerical model that accounts for groundwater depressurisation prior to filling is approximately three times greater than that from the model which neglects the depressurisation effect. In real cases, when the induced tensile stress exceeds the tensile strength of the lining, cracks may form, leading to an increase in the lining's hydraulic conductivity and allowing greater water leakage. This leakage raises the groundwater pressure at the interface between the rock and the lining. If the pore pressure at this interface exceeds the mechanical pressure transferred to the rock, separation can occur, creating a void that allows pressure equalisation between the intrados and extrados of the lining. This mechanism helps to limit the development of further excessive tensile stress in the lining. Therefore, the induced tensile

stress value presented in the last column of Table 1 should be viewed as illustrative only and are unlikely to develop in the lining under real-world conditions.

5 DISCUSSIONS AND CONCLUSIONS

The primary design philosophy for linings in pressure tunnels and shafts is not to prevent cracking altogether, but to control crack width through appropriate reinforcement design. Therefore, it is important to assess the initial cracking stress with adequate accuracy. Tensile stress develops when the internal water pressure exceeds the groundwater pressure acting on the extrados of the lining. Depressurisation caused by water inflow during excavation lowers the groundwater pressure near the tunnel boundary and, in highly permeable rock masses, can even reduce the regional groundwater level. Despite the dynamic nature of groundwater pressure around pressure tunnels, existing analytical design methods for tunnel and shaft linings do not account for the effects of depressurisation. This oversight effectively assumes that the lining acts as an impermeable barrier, which is not accurate. This paper presents an illustrative numerical model to highlight this limitation in existing analytical formulations, aiming to prevent unsafe design of linings for pressure tunnels.

An analytical formulation based on the method proposed by Fernandez (1994) was first developed to calculate the depressurisation profile resulting from drained excavation. The results from this formulation showed excellent agreement with those obtained from seepage analysis using RS2.

Subsequently, the numerical model was extended to evaluate the induced tensile stress in the lining for an illustrative case. While there was strong agreement between the numerical model and the analytical methods proposed by Jaeger (1997), Fernandez (1994), and Schleiss (1997) under conditions without groundwater depressurisation, a significant difference in tensile stress was observed when the effect of groundwater depressurisation was included. These results underscore that neglecting excavation-induced groundwater depressurisation can lead to unsafe designs of concrete linings for pressure tunnels and shafts.

Further investigation into the effects of filling rate, the evolution of the lining's hydraulic conductivity, and potential gap formation during filling requires more advanced coupled hydro-mechanical numerical modelling. This will be the focus of the author's ongoing research and will be presented in future publications.

6 REFERENCES

Fernandez G. 1994. Behaviour of pressure tunnels and guidelines for liner design. Journal of Geotechnical Engineering. Vol. 120, No. 10. Pp. 1768-1791.

Jaeger C. 1979. Rock mechanics and engineering, 2th Edition. Cambridge University Press.

Rocscience, 2022. RS2 Finite Element Analysis, https://www.rocscience.com/software/rs2

Schleiss A. 1986. Dimensioning of pressure tunnels, Part II: Influence of seepage flow in concrete lining and rock, mechanical-hydraulic interactions, design criteria. PhD Thesis, Laboratory of hydraulic engineering, hydrology and glaciology at ETH Zurich, Switzerland.

Schleiss A. 1997. Design of reinforced concrete lining of pressure tunnels and shafts. The international Journal on Hydropower & Dams. Issue 3. Vol. 4.

Zoorabadi M, Gomes ARA, Kost S, Satici A. 2023. Comparative assessment of analytical and numerical methods to evaluate the cracking pressure of concrete lining in pressure tunnels. Australasian Tunnelling Conference, Auckland, New Zealand.

19th Australasian Tunnelling Conference – Acosta-Martínez, Stewart and Hudson-Smith (Eds.)
© 2025 Australian Tunnelling Society, ISBN 978-0-85825-002-4

Insights into the load transfer mechanisms of grouted rock bolts under tension

A. Emadi
SMEC, Australia

A. RA Gomes
Tunnels and Underground Engineering, SMEC, Australia

ABSTRACT: This study investigates load transfer mechanisms among bolt, grout and rock in fully-grouted rock bolts subjected to axial tension, both before and after bolt yielding. For that, a three-dimensional ABAQUS finite-element model is used to explicitly simulate bolt ribs, incorporating an elasto-plastic material model for steel, Concrete Damage Plasticity for grout, and interface interactions defined by hard contact in the normal direction and tangential behavior using the penalty method with friction. After validating the model against published pull-out tests, parametric analyses are conducted to assess the impact of rib height and spacing in the system behavior. Results show that load is progressively transferred from steel to grout, with peak stresses becoming nearly uniform along the anchorage at maximum load. Failure occurs through a coupled mechanism: grout cracking initiates at rib corners and propagates diagonally to form a conical shear band, accompanied by localized bolt yielding. Increasing rib height improves peak capacity and post-yield ductility up to ≈1 mm, beyond which benefits taper off. Conversely, excessively tight or wide rib spacing reduces energy absorption or strength. It has also been demonstrated that standard bond-slip models calibrated for reinforcing bars underestimate peak load and soften prematurely, as they neglect interlock and confinement effects.
These findings offer a micromechanical basis to refine simplified design models and optimize rib geometry for balanced strength and ductility in underground reinforcement systems.

1 LITERATURE REVIEW

Efficient load transfer in fully-grouted rock bolts hinges on the coupled response of steel, grout, and rock, with shear strength at the bolt–grout and grout–rock interfaces controlling system stability. Three-dimensional FE studies in Abaqus (e.g., Ho et al., 2019) model this behavior, typically combining an elasto-plastic steel law with Concrete Damage Plasticity for grout to capture cracking, plastic flow, and stiffness loss validated against pull-out tests.

Once slip initiates, strain incompatibility at the steel–concrete interface reduces axial stiffness and increases bolt displacement. To represent this bond–slip behavior, several studies have introduced equivalent interface models—most notably those proposed in FIB Bulle-tin 70 (2014)—that employ simplified traction–separation laws or cohesive elements. Parametric analyses (Cao et al., 2014; others) show that rib spacing, height, shape, and in-situ confinement dictate peak bond strength, post-peak softening, and the sequence of load-transfer stages.

Together, the literature underscores a complex interplay among material properties, rib design, and geology; capturing these interactions, especially beyond bolt yielding, is vital for reliable underground reinforcement.

2 VERIFICATION PROCEDURE

As a first step, the numerical model is verified against experimental results to ensure that its mechanical behavior and modelling assumptions accurately reflect test conditions. For this study, the pull-out tests conducted by Benmokrane et al. (1995) are simulated in Abaqus. The model reproduces the actual geometry - including bolt ribs - and boundary conditions. As shown in Figure 1a, the concrete cylinder has a diameter of 200mm and a height of 340 mm; a 38 mm-diameter borehole is drilled at its center. A deformed bolt with a core diameter of d = 15.8 mm and a rib height of h_a = 1.1 mm is grouted into the borehole using hardened cement paste at various embedment lengths. A steel plate placed at the top of the specimen prevents axial displacement of both grout and concrete during testing.

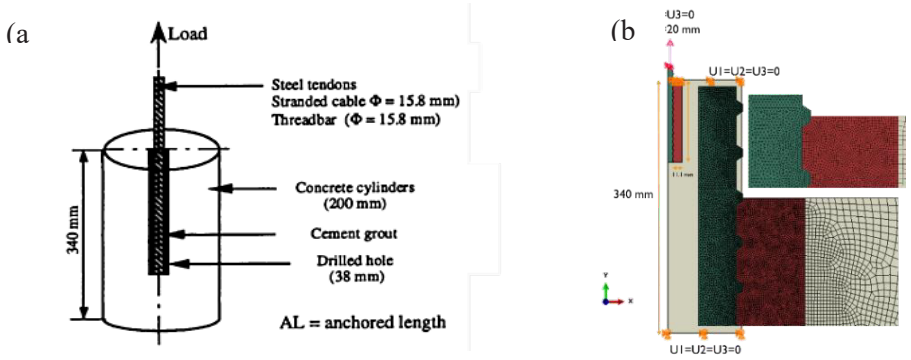


Figure 1. a) Schematic of the concrete cylinder test setup (Benmokrane et al. (1995)); b) Axisymmetric numerical model of pull-out tests conducted by Benmokrane et al., with a zoomed- in view of the discretized elements and boundary condition.

The key material properties of the steel bolt are: Young's modulus = 210 GPa and a Poisson's ratio=0.3. The grout is modelled using the Concrete Damage Plasticity (CDP) model, where, after initial debonding, the bolt-grout interface is represented by a frictional coefficient of μ=0.4. Figure 1b shows the axisymmetric finite-element model and the discretization details.

Figure 2 compares the load-displacement response obtained from the numerical model with the experimental model curve. The close agreement between the two confirms the accuracy and reliability of the modelling methodology.

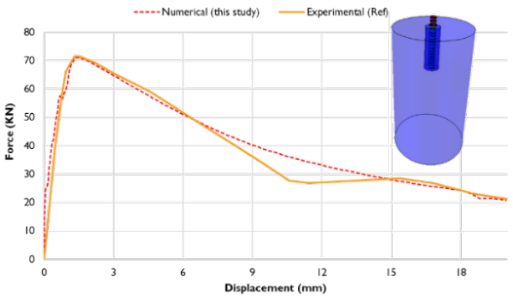


Figure 2. Comparison of the numerical model and experimental load-displacement curves.

3 PARAMETRIC STUDY

After model validation, parametric analyses were conducted varying rib height (0.5, 1.0, 2.0 mm) and spacing (7.25, 14.5, 29 mm). The simulations tracked stress evolution at different pull-out test stages to assess the impact of rib arrangement and the validity of equivalent models, such as the bond-slip model proposed by FIB and empirical formulas.

3.1 *Geometry and material properties*

Based on the actual shape of the threaded steel rock bolt, the transverse rib plays a crucial role in the load transfer mechanism and can influence the bolt's failure mode. To establish a realistic reference model for subsequent parametric studies, the numerical model includes a bolt rod with a 20 mm diameter, featuring a 1.5 mm × 1 mm spline and spiral ribs with dimensions of 1 mm (height) × 1.5 mm (width) × 14.5 mm (spacing). The ribs are inclined at a 54-degree angle relative to the rod axis (Figure 3a). The borehole diameter is 44 mm, creating a grout annulus of 12 mm. The surrounding rock cylinder has a 100 mm diameter and a 500 mm length, while the bolt length is 300 mm. The overall geometry of the numerical model is shown in Figure 3b.

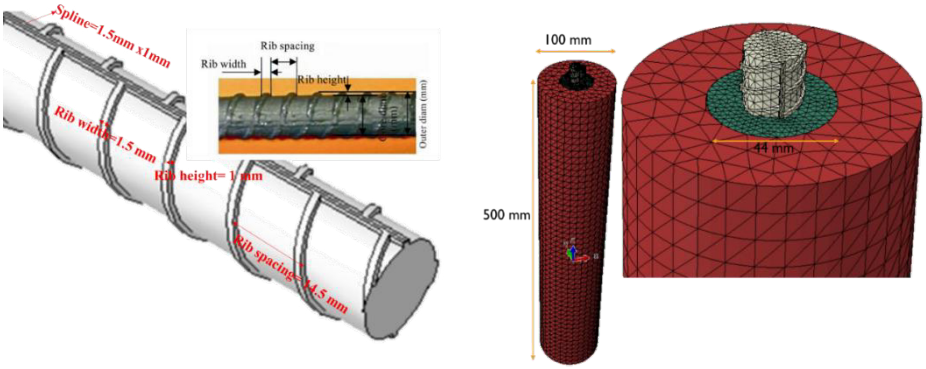


Figure 3. a) Geometric configuration of the rock bolt, D=20 mm. b) Geometry of the numerical model with a zoomed-in view of the discretized elements.

The steel bolt is modelled as an elasto-plastic material with strain hardening. Its key material properties include a Young's modulus of 210 GPa, a Poisson's ratio of 0.3, and a yield stress of 450 Mpa. The grout parameters considered in the CDP model are presented in Table 1, where E is the Young's modulus, v is the Poisson's ratio, fc Is the uniaxial compressive strength, f_t is the tensile strength, ψ is the angle of dilatancy and e is the eccentricity. The ratio fb/fc0, represents the biaxial-to-uniaxial compressive strength, defined as per ABAQUS CDP recommendations. The grout and steel bolt parameters considered in this study are representative of typical values found in common engineering practice, ensuring the relevance of the findings to real-world application.

Table 1.Grout parameters used in the CDP model

Parameter	E (GPa)	Density(Kn/m3)	ν	fc (MPa)	f_t (MPa)	e	K	ψ (°)	fb/fc_0
Value	25.8	23	0.15	51.8	4.2	0.1	1.12	30	1.12

In Abaqus, the parametric model incorporates surface interaction defined by normal behavior using hard contact, and tangential behavior modeled with the penalty method and a friction coefficient of 0.4. The rock is modeled using the Mohr-Coulomb failure criterion. Its mechanical properties consist of a Young's modulus of 6000 MPa, a Poisson's ratio of 0.25, a density of 24 kN/m³, a friction angle of 50°and cohesion of 500 kPa. In the model, a fixed boundary condition is applied to the outer surface of the rock cylinder, fully constraining all degrees of freedom.

3.2 *Analysis of Pull-Out Test Results and Stress Distribution*

Figure 4 presents the results of the pull-out test. The initial portion of the curve shows a steep, nearly linear increase in force from 0 to approximately 150 kN over a displacement of about 1 mm, indicating elastic deformation, where the rock bolt resists the applied load with minimal strain.

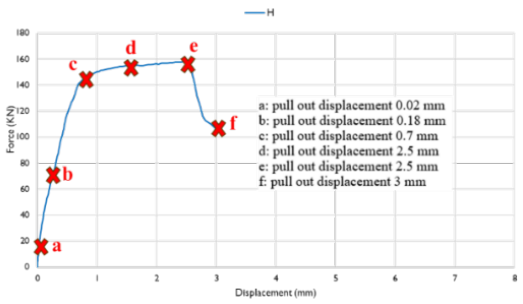


Figure 4. Load–displacement curve from reference pull-out test

Beyond this point, the curve begins to flatten, marking the onset of plastic deformation or yielding, with the force peaking at approximately 159 kN at a displacement of 2.5 mm. A sharp drop follows, with the force decreasing to around 100 kN at 3 mm displacement, likely indicating bond failure at the bolt-grout or grout-rock interface. After this stage, the curve stabilises around 100 kN, suggesting the presence of residual strength as the rock bolt continues to slide and deform.

Figure 5 illustrates the longitudinal normal and tangential stress distribution at the steel/grout interface during different loading stages: before peak load (P_1 = 50 kN), at peak load (P_2 = 159 kN), and after peak load (t_3, P_3 = 120 kN). The stress profiles exhibit fluctuations that correspond to the bolt's rib spacing (14mm). As axial displacement increases, the influence of the ribs on the stress distribution becomes more pronounced, highlighting the role of bolt geometry in the bolt-grout interaction. Prior to peak load, the tangential stress (Figure 5b) gradually mobilizes from the bolt head along the interface. At peak load, although the tangential stress reaches its maximum and is mobilized over a greater length, localized fluctuations remain significant due to the mechanical interlocking between the ribs and the grout. Therefore, while the global trend of stress distribution becomes broader and more mobilized, the stress does not become completely uniform along the interface.

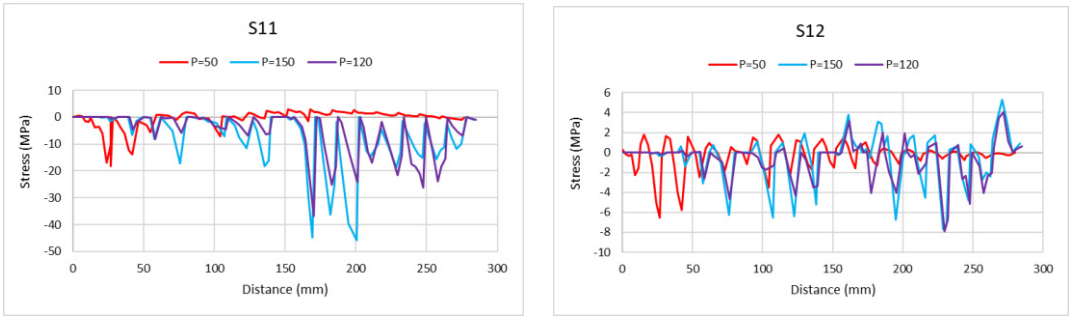


Figure 5. Longitudinal distribution of stresses (a) Normal stress s11 (b) Tangential stress s12.

Figures 6 and 7 illustrate the progressive failure mechanisms during a simulated pull-out test, as captured by the evolution of Plastic Strain Equivalent (PEEQ) and Tensile Damage (DAMAGE-T) across six distinct stages (a–f), revealing a coupled failure mechanism involving both grout cracking and bolt yielding. It should be noted PEEQ is a non-negative scalar that indicates the accumulated plastic strain and is used to identify regions of plastic deformation.

In the initial stages of displacement (Figures 7a–b and 8a–b), the rock bolt remains elastic while tensile cracks nucleate at rib corners near the loaded end and grow longitudinally as load transfers from steel to grout.

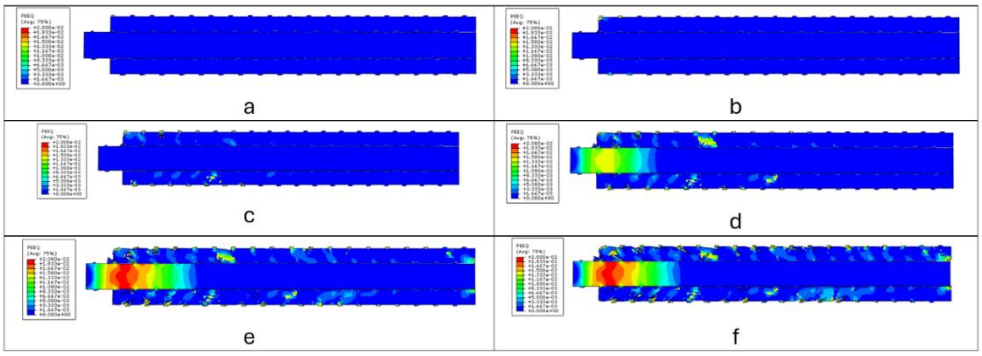


Figure 6. evolution of plastic strain equivalent (PEEQ) in the rock bolt model.

During the subsequent stages (Figures 7c–e and 8c–e), tensile damage extends progressively along the anchorage length. A distinct fracture path initiates at an angle of approximately 60° to the bolt axis (stage b), which gradually evolves into a conical shear failure inclined at roughly 45°. This transition reflects the influence of compressive stress concentrations at the rib angles, guiding crack propagation in alignment with orientations of maximum tensile stress. At the same time, plastic strain in the bolt increases, indicating the onset of local steel yielding.

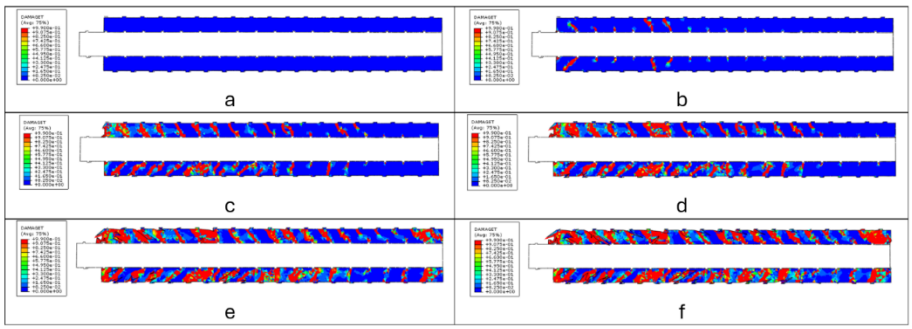


Figure 7. Evolution of the tensile damage (DAMAGE-T) of grout in the rock bolt model.

In the final stage (Figures 7f and 8f), extensive damage is observed in the grout, which coalesces into a shear band. This leads to the complete loss of load transfer and eventual pull-out of the rock bolt. The initiation of cracks at the rib corners and subsequent diagonal propagation confirm that transverse ribs play a critical role in dictating the failure paths. It is important to note that the failure observed in this model arises from the combined effects of grout degradation and bolt yielding, rather than either mechanism acting independently.

3.3 *Rib height and space*

A numerical simulation study was conducted with rib height and rib spacing as key variables. The modeling process considered three rib heights (0.5 mm, 1 mm, and 2 mm) and three rib spacings (7.25 mm, 14.5 mm, and 29 mm). Table 2 presents the analyses cases along with the corresponding rib height and rib spacing.

Table 2. Analyses cases with corresponding rib heights and rib spacings

Analyses case	Rib height (mm)	Rib Spacing (mm)
H or S	1	14.5
0.5H	0.5	14.5
2H	2	14.5
0.5S	1	7.25
2S	1	29

Figure 8 illustrates the equivalent plastic damage observed under different transverse rib heights and spacings. When the transverse rib height is 0.5 mm, cracks extend fully along the rock bolt, leading to complete bond failure and bolt disengagement. At greater rib heights, the failure mechanism changes significantly: the rock bolt remains more securely anchored and does not pull out. Instead, yielding occurs at the front end, with cracks appearing at the interface near the transverse ribs. As rib height increases, the mechanical coupling effect at the interface is enhanced, shifting the failure mode from abrasion, expansion, and rib sliding to rib body shearing and interface crack propagation. When rib spacing is too large, the number of transverse ribs along the bolt decreases, limiting their reinforcing effect and preventing full stress mobilization. Conversely, excessively small rib spacing can lead to cracks in the grout forming too closely together, which reduces the anchoring efficiency of the ribs.

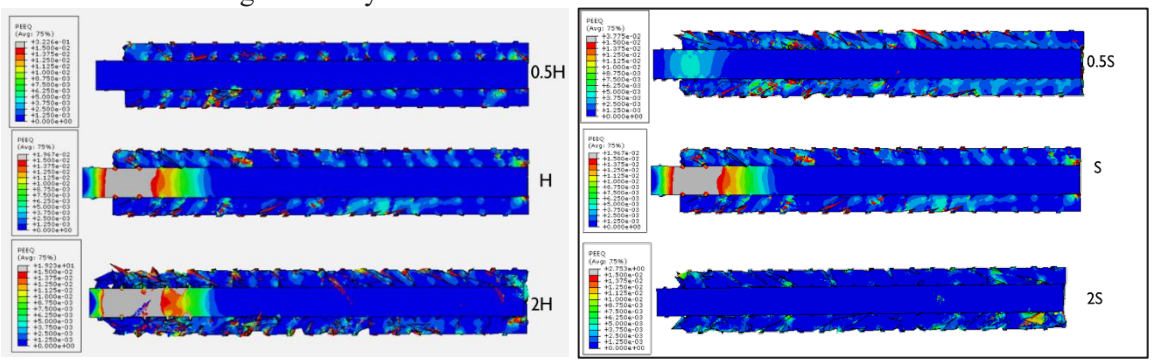


Figure 8. equivalent plastic strain under different transverse rib heights and spacings all subfigures use the same contour range with a maximum displayed value of 0.015; values exceeding this are shown in gray.

Figure 9 presents the load–displacement curves for rock bolts with varying transverse rib heights and spacings. The results show that for rib heights of 0.5 mm, 1mm, and 2.0 mm, the ultimate anchorage-bearing capacities are 136kN, 159kN, and 162kN, respectively. Increasing rib height from 0.5 mm to 1 mm, yields a 15% improvement in bearing capacity. However, as rib height increases further, the rate of improvement gradually diminishes.

It is also observed that as rib height increases, failure occurs at a later stage under tensile loading, indicating enhanced post-yield performance and improved load transfer capacity. This occurs because smaller ribs offer less mechanical interlocking and reduced frictional resistance at the interface, weakening the interface's ability to resist shear failure. These findings confirm that mechanical engagement and frictional resistance are critical to the load-bearing capacity of the transverse ribs. As displacement increases, smaller ribs are less effective at maintaining interlock, resulting in weaker anchorage performance of the rock bolt.

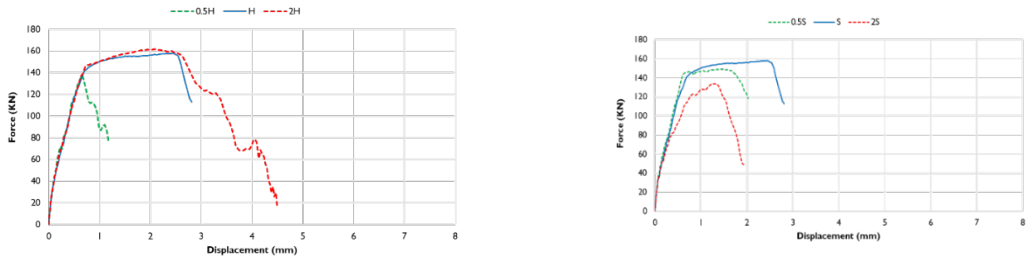


Figure 9. Load–displacement curve for different rock bolt transverse rib heights (left) and spacings (right).

The results indicate that for rib spacings of 7.25 mm, 14.5 mm, and 29 mm, the ultimate bearing capacities are 149 kN, 159 kN, and 132 kN, respectively. The load–displacement curves show that as transverse rib spacing increases, the peak load gradually decreases. While the three curves exhibit similar peak capacities, the improvement with reduced spacing become marginal beyond a certain density (e.g., below 15 mm). This suggests that increasing rib density beyond a threshold does not significantly increase the peak bond strength.

The 7.5 mm spacing (green), although achieving a peak load similar to reference model, shows a steeper post-peak drop, indicating lower energy absorption and a more brittle failure mode. When ribs are too closely spaced (e.g., 7.5 mm), the grout between ribs becomes too thin, and interlocking zones begin to interfere with each other. This results in premature shear failure of the thin grout layers, limiting the system's ability to develop distributed slip and plastic deformation.

The outcome is localized shear damage, loss of confinement, and reduced overall ductility of the rock bolt system.

3.4 *Empirical methods (equivalent interface models)*

Three different modeling approaches were considered to simulate the interaction between bolt and grout:

a) the base model with explicit rib geometry (blue solid line),
b) the FIB-based bond-slip model (red dashed line), and;
c) the equivalent bond-slip model with modified parameters and mesh (gray solid line).

To simulate the interaction between bolt and grout, bond-link elements are employed. These elements have no physical dimensions and connect two coincident nodes via nonlinear springs (Figure 10). By assigning appropriate force–displacement relationships to these springs, the bond–slip behavior at the concrete–rebar interface can be accurately captured. Initially the parameters used for bond-slip relationship are defined using the equation provided in Table 6.1.1 of the FIB Model Code, corresponding to confined concrete under favorable bond conditions.



Figure 10. Schematic representation of bond-link elements modeling the rebar–grout interface using four dimensionless nonlinear springs per interval

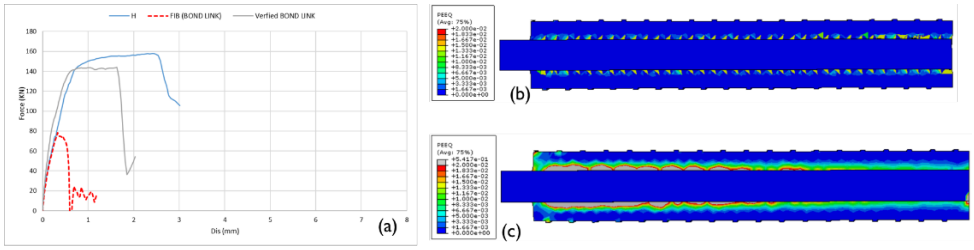


Figure 11. a) Comparison of load-displacement curves for base model (explicit rib geometry), FIB-based bond-slip model, and modified bond-slip model b) PEEQ distribution in FIB-based bond-slip model showing minimal grout plasticity with no steel plasticity c) PEEQ distribution in modified bond-slip model showing distributed grout plasticity but no steel plasticity

Figure 11 presents the load-displacement curves for each one of the modelling approaches. The FIB-based model shows a peak load of approximately 80 kN, substantially lower than the 160 kN achieved with the explicit base model. The peak load capacity of the modified bond-slip model is in the same order of magnitude of the based model, though with slightly different post-peak behavior. The plastic equivalent strain (PEEQ) distributions reveal fundamental differences in failure mechanisms between the modeling approaches. The base model shows concentrated plastic deformation in both the grout around the bolt ribs and in the steel bolt itself, indicating a combined failure mechanism involving both materials. In contrast, both bond-slip models (Figure 11) show plastic deformation exclusively in the grout, with no plasticity observed in the steel bolt component. The FIB-based bond-slip model exhibits minimal plastic deformation, with damage primarily concentrated at the grout-bolt interface in discrete bands. The modified bond-slip model shows more distributed plastic deformation throughout the grout volume but still fails to capture the steel

plasticity observed in the reference model. These results demonstrate that while bond-slip models can be calibrated to match the overall load-carrying capacity, they fail to accurately capture the complex failure mechanisms associated with ribbed rock bolts in grout. Although the bond–slip model is based on standard formulations, such as those in the FIB Model Code for reinforcing bars in concrete, it fails to capture the mechanical interlock and confinement effects induced by the rib geometry of rock bolts embedded in grout. It is important to emphasize that the FIB Model Code is primarily calibrated for reinforcing rebars in concrete structures and may not accurately capture the behaviour of rock bolts in grout.

4 SCOPE AND LIMITATION

The findings presented in this study are based on the specific geometric and material parameters of the reference model. Variations in bolt and rib geometry, grout properties, confinement conditions, or loading rates may result in different load transfer behaviors and failure patterns.

5 CONCLUSIONS

Based on the analyses conducted, the following key findings can be highlighted:

- Stress distribution: FE analysis shows that rib geometry significantly influences stress along the bolt–grout interface, producing periodic fluctuations. Although the overall mobilization of tangential stress increases at peak load, the stress distribution remains locally non-uniform.
- Failure mechanism: Cracking initiates at rib corners, then propagates diagonally through the grout, forming shear bands controlled by rib geometry and local confinement condition; failure is a coupled mechanism involving both grout cracking and bolt yielding.
- Rib height: Increasing rib height enhances bond strength and post-yield performance; however, improvements diminish beyond 1 mm. Taller ribs tend to shift the failure mechanism from rib abrasion or sliding to rib body shearing and interface cracking. In contrast, ribs with 0.5h height showed lower bond capacity due to reduced mechanical interlock and frictional resistance compared to the baseline and larger rib cases.
- Rib spacing: Very tight spacing (≈ 7.25 mm) produces brittle, localized shear due to thin grout layers and overlapping interlock zones, while wide spacing (≈ 29 mm) lowers capacity by reducing the number of effective ribs. Below ~15 mm, extra ribs offer little additional peak strength.
- Load–displacement response: Rib geometry governs both peak capacity and ductility; optimal spacing and height balance strength with energy absorption.
- Bond–slip models: Bond-slip models, while computationally efficient, demonstrate significant limitations in capturing the complex failure mechanisms of ribbed rock bolts in grout.
- Design implication: Detailed micromechanical modelling might be recommended to inform design decisions of high-performance rock bolt systems, especially in complex conditions.
- Scope: Findings apply to the reference model; other parameter variations may yield different load transfer behaviors and failure patterns.

6 REFERENCES

Benmokrane, B., Chennouf, A. and Mitri, H.S., 1995, October. Laboratory evaluation of cement-based grouts and grouted rock anchors. In International journal of rock mechanics and mining sciences & geomechanics abstracts (Vol. 32, No. 7, pp. 633-642). Pergamon.

Cao, C., Ren, T., Cook, C. and Cao, Y., 2014. Analytical approach in optimising selection of rebar bolts in preventing rock bolting failure. *International Journal of Rock Mechanics and Mining Sciences*, *72*, pp.16-25.

Ho, D.A., Bost, M. and Rajot, J.P., 2019. Numerical study of the bolt-grout interface for fully grouted rockbolt under different confining conditions. *International Journal of Rock Mechanics and Mining Sciences*, *119*, pp.168-179.

19th Australasian Tunnelling Conference – Acosta-Martínez, Stewart and Hudson-Smith (Eds.)
© 2025 Australian Tunnelling Society, ISBN 978-0-85825-002-4

Use of precast lining within the mined spurs on Western tunnelling package, Sydney metro west

N. Lewis
Tunnelling Solutions, Melbourne, Australia

J. Nethercott
Gamuda Australia, Sydney, Australia

A. Golshani
SMEC, Sydney, Australia

A. Mirzayee
GHD, Sydney, Australia

ABSTRACT: The Gamuda Laing O'Rourke consortium on the Western Tunnelling Package of Sydney Metro West opted for a precast lining for the two, altogether 1.5km spur tunnels connecting the dive structure to the underground junction caverns at Clyde. This selection was influenced by the length of the spur tunnels, tight alignment curves, and the desire to provide a ring similar to the mainline tunnels. The mined horseshoe-shaped spur tunnels, reinforced with rock bolts and a shotcrete primary lining, presented unique challenges for the design of the permanent lining. The precast lining consisted of three trapezoidal steel-fibre reinforced segments for the sidewalls and crown, along with a steel-reinforced concrete flat invert segment. The Lining Erection Machine (LEM) was designed and built in collaboration with Herrenknecht to efficiently erect these precast concrete segments. This paper discusses the selection and design of the precast lining, the development of the complete system and process, the machine itself, and the on-site experiences throughout the project delivery.

1 INTRODUCTION

Traditionally, mined tunnels are tanked using waterproof membranes and large arch formwork. For the 1.5 km Roadheader-driven spur tunnels, GLC challenged this approach by proposing a segmental precast lining system—leveraging existing TBM lining expertise and in-house precast production at Eastern Creek.

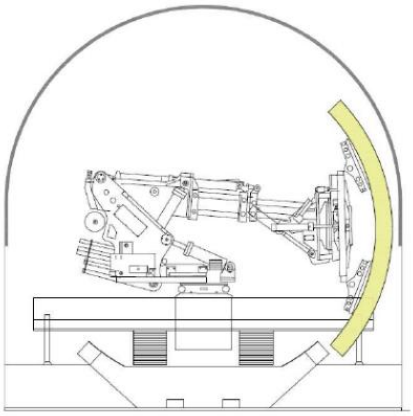


Figure 1. Original concept

The initial methodology involved segment placement using a spider grab, delivery via MSV, and staged backfilling with pea gravel and grout. This streamlined approach eliminated membrane installation and formwork, significantly improving safety and productivity. See Figure 1.

Key safety benefits included reduced work at height, lower manual handling risks, fewer tunnel interactions, and a shift to controlled off-site fabrication—leading to a 4–5x productivity increase. Additional advantages included improved finish quality and alignment with TBM tunnel standards.

This innovation introduced new challenges, particularly the use of gasketed segment joints to achieve water tightness—a rare application in mined tunnels with limited precedent or design guidance.

2 DESIGN INNOVATION

2.1 *Design integration and delivery*

To align with the construction sequence, the design was split into two coordinated packages:

- Primary Lining – excavation profile, bolting, and shotcrete support.
- Permanent Lining – precast segments, LEM interface, and backfill design.

Success relied on early integration between both packages—critical in a D&C environment where late changes would impact constructability, cost, and program. For example, the tunnel size was reduced to control backfill volume, which constrained excavation efficiency and plant access.

Figure *2* below provides the general arrangement of the two mined tunnels.

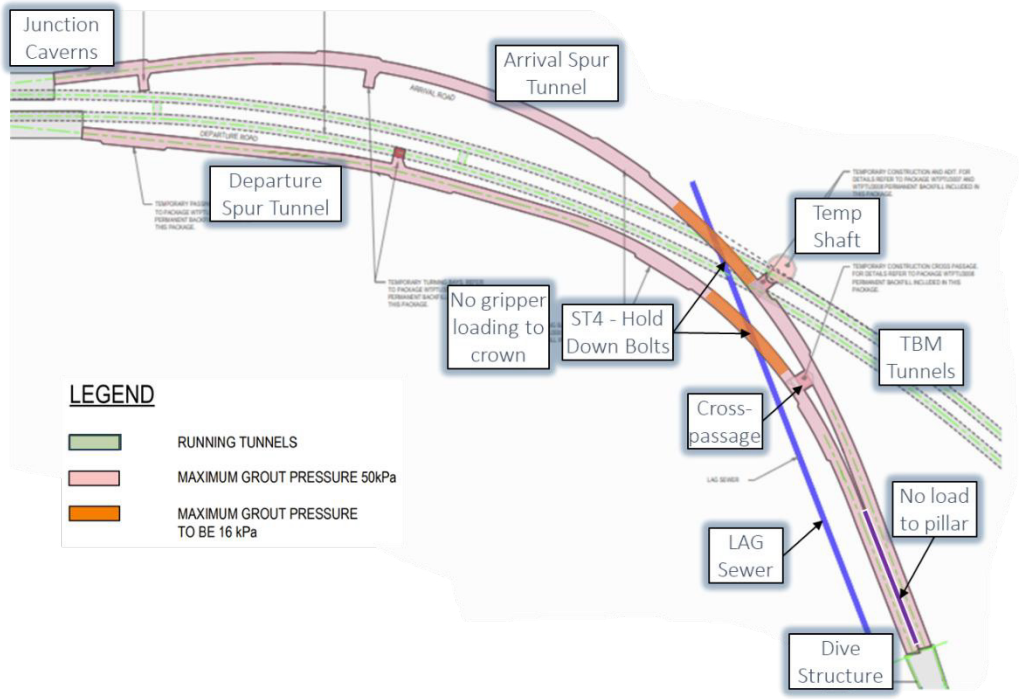


Figure 2. General arrangement

The primary lining also had to accommodate the LEM's core functions: segment placement, gasket compression, and advancement. The backfill process was later integrated into the LEM, further reinforcing the need for close design coordination.

Many key decisions during the design process needed to be made "at risk" to meet procurement and offsite manufacturing timelines, these included:

- The excavation profile and construction tolerances
- Segment size, shape and geometry, gasket and fittings

If we were to do it all again, we would be far better equipped to establish the timeline for key decisions, bring in the necessary partners at the right time and implement the key learnings from WTP into the design process.

2.2 *Permanent lining*

The permanent lining comprised three trapezoidal SFRC segments for the crown and sidewalls, and a flat invert segment with conventional reinforcement. The LEM, developed with Herrenknecht, was purpose-built to install these segments efficiently in a mined environment.

Unlike TBM tunnels, where grouting is simultaneous with ring building, this approach required several rings to be built first, followed by gravity-based backfill grouting from invert to crown—without pressure. This sequence introduced key design considerations:

- Ring Stability: Rings had to support their own weight prior to grouting.
- Buoyancy: Grout rising around unfilled voids could lift segments. This was mitigated by fully grouting the invert before installing side segments.
- Staging: Grouting was done in two stages—up to the axis, then to the crown—with a minimum compressive strength required before the second stage.
- Tolerances: The segment geometry required tight control of ring build tolerances to ensure structural integrity and alignment.

The LEM ring consists of four segments: an 8-ton flat invert (S1), two 6-ton trapezoidal SFRC side segments (S2 & S3), and a 6-ton rhomboid crown (S4). A 60 mm taper, in line with ITA guidelines, was adopted to accommodate horizontal curves. Vertical alignment was managed through packing.

Figure *3* below provides a 3-dimensional view and the left and right ring geometry.

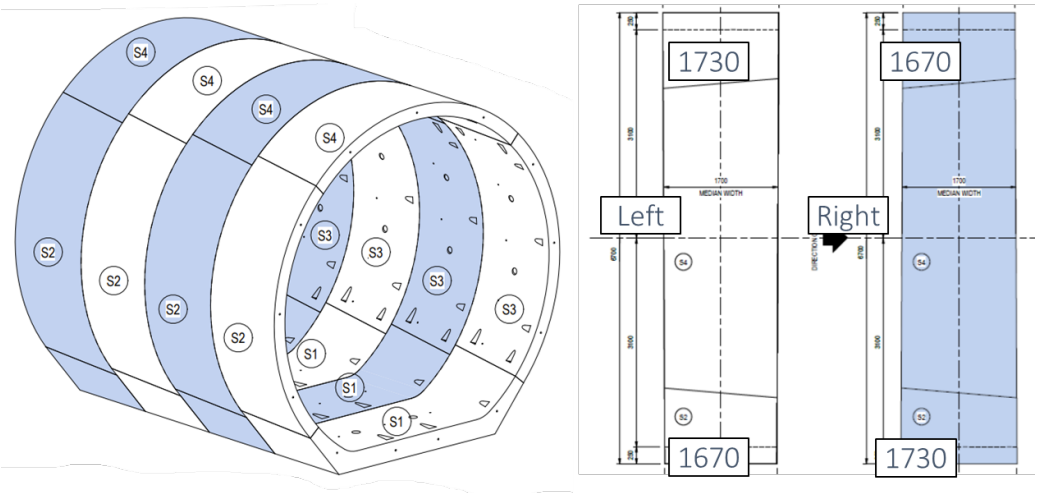


Figure 3. Ring design

2.3 *The solution taken into delivery*

The final design solution was the result of the efforts of the integrated design, manufacturing and construction. There were 3 main components:

- Temporary works / pre-work ahead of the LEM
- Ring building / gasket compression
- Backfill

Figure 4 and Figure 5 below show the complete solution developed for the LEM process

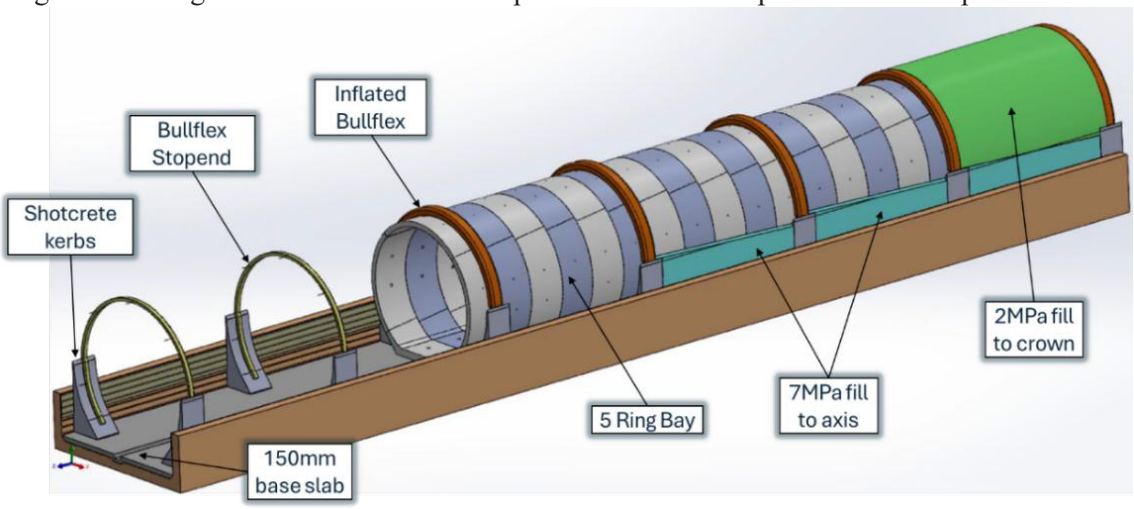


Figure 4. Segmental lining process overview

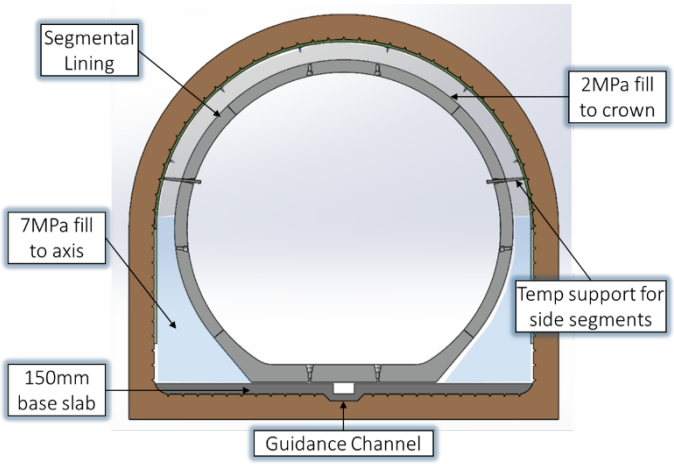


Figure 5. Segmental lining cross-section

2.3.1 *Temporary works / pre-work ahead of the LEM*

Three key elements were required to prepare the tunnel for LEM operation: the base slab, Bullflex stop-ends, and kerbs construction.

The base slab, developed in early design workshops with Herrenknecht, served multiple purposes: providing a level running surface for the 200-ton LEM, supporting the segment rings with 20 mm HDPE packers, resisting gripper forces, and guiding the machine via a cast-in channel. Alternatives such as steel rails were explored but proved costly and less effective under combined load and alignment constraints. The final concrete solution was cost-effective, quick to install, and allowed precise LEM steering via dual chassis.

Bullflex bags provided ring support during gasket compression and served as stop-ends for staged backfilling. Chosen for their proven performance in TBM launch applications, the bags were custom designed to span the tunnel arch. A full-scale tunnel trial validated their suitability.

Shotcrete kerbs were installed to form a consistent profile for Bullflex seating. After considering slipform, precast, and in-situ options, a ply-formed, mesh-reinforced shotcrete solution was adopted for its simplicity, adaptability, and integration with other ongoing works—despite some challenges with ventilation and work sequencing.



Figure 4. Temporary works ahead of LEM

2.3.2 *Ring building / gasket compression*

The LEM was developed with Herrenknecht to perform three core functions – to build the segmental ring, compress the gaskets and advance to the next position.

The LEM was purpose-built to install gasketed precast segments within the confined geometry of a mined tunnel. Its design integrated several systems to manage segment handling, alignment, gasket compression, and machine propulsion with precision and reliability.

The segment handling system comprised three main components. Segments were first transferred from the Multi-Service Vehicles (MSVs) by a segment crane, which rotated and positioned them onto the segment feeder. The feeder then advanced each segment into position for the segment erector, which lifted, placed, and manipulated the segments to construct a precise and watertight ring.

Crown-mounted hydraulic grippers provided the necessary reaction force to stabilise the machine during ring assembly. These grippers anchored the LEM to the primary lining, allowing controlled application of internal forces during segment placement and gasket compression.

Gasket compression was achieved using four pairs of hydraulic cylinders strategically positioned around the ring. These applied the necessary force to compress the circumferential and radial gaskets, ensuring watertightness at the joints. The two invert-mounted cylinders served a dual function, also acting as propulsion units to advance the LEM to the next build location once a ring was complete.

Together, these systems enabled the LEM to operate efficiently within the constraints of a mined tunnel environment while achieving the precision required for gasketed segmental lining.

Figure *5* and Figure *6* below provide an overview of the key components of the LEM.

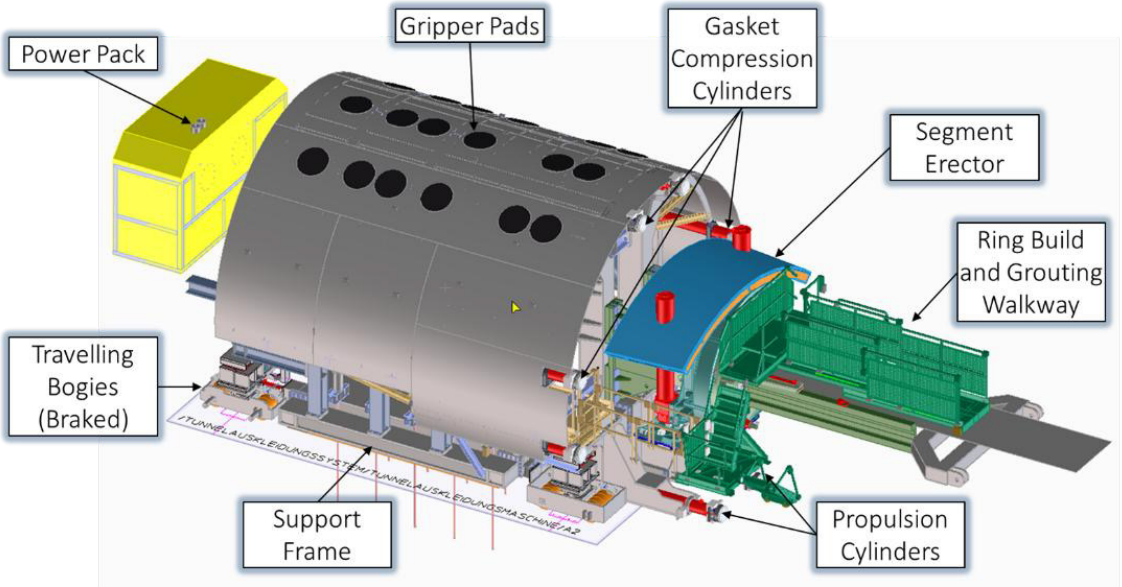


Figure 5. LEM sheild

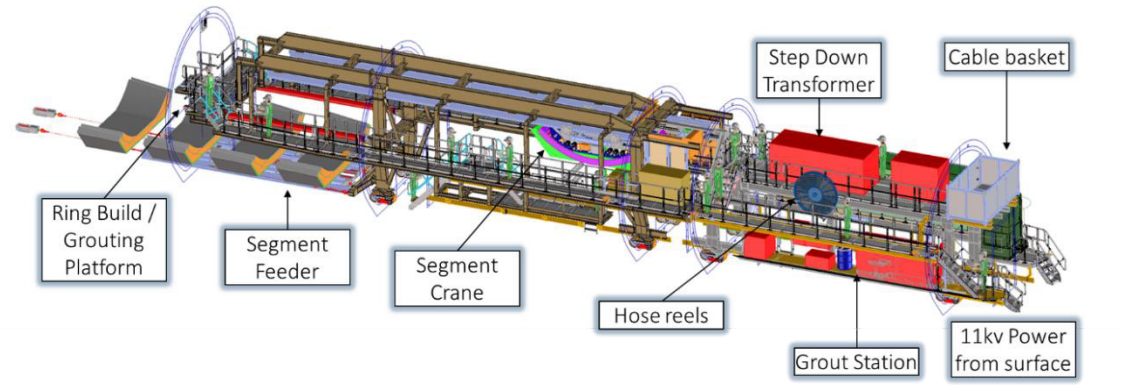


Figure 6. LEM gantries

2.3.3 *Backfill / grouting operations*

The ideal scenario was to identify a single grout product that could meet all the performance requirements for the LEM's operations. However, due to the differing functional demands, this was refined to two grout types covering three key applications:

- Invert Grout required high early strength (20 MPa), shrink compensation, and high flowability to provide a stable base for ring building and accommodating early loading. The selected solution was Masteroc MG01, which offered the necessary strength and placement characteristics soon after mixing.
- Bullflex Grout needed to be pressure-stable, high strength, and shrink-resistant to ensure reliable sealing at the stop ends. A blended grout supplied by a commercial partner was used, based on a standard base mix without retarder, enhanced with additives to stabilise flow, control shrinkage, and improve pressure response.
- Backfill Grout targeted 7 MPa compressive strength, with low shrinkage and bleed characteristics. The same blended grout base was used, this time with a retarder added to delay hydration, ensuring controlled placement behind the segment rings. Sodium silicate was introduced as a secondary component to accelerate setting and gel the grout in situ.

To support these operations, Gantry 2 of the LEM was developed specifically for grouting. It housed grout tanks, pumps, pig catchers, control panels, and a fully integrated system for storing, dosing, and delivering chemical additives. This configuration enabled continuous and controlled

grouting in parallel with ring building, improving productivity and overall construction efficiency.

3 CONSTRUCTION PERFORMANCE

Construction of the segmentally lined spur tunnels presented several unique challenges that required adaptation and continuous improvement throughout the works. Although the LEM ring build shared some similarities with traditional TBM methods, the absence of a tail can, the flat invert, and the tapered geometry introduced new complexities. Building accurate, tight rings required precision in placement and sequencing, particularly in managing gasket compression and ring alignment within the mined tunnel profile. Achieving consistency in ring construction was a steep learning curve, especially in the early phases.

Flowable grout, used for backfilling, initially caused segment movement and leaks through minor imperfections. These performance issues led to the adoption of sodium silicate dosing, which enabled the grout to gel rapidly after placement, reducing the potential for leakage and helping to stabilise the rings.

Another challenge was the variability in the pre-mixed grout supplied from the batching plant. Inconsistent mix properties were observed, which affected both productivity and quality control. In response, a remixing system was established on site to improve uniformity and reliability. This gave the project team greater control over grout consistency, particularly when managing additives and maintaining performance tolerances.

Despite these challenges, the project successfully delivered 1.5 km of segmentally lined tunnel. The use of precast segments offered several advantages over conventional in-situ concrete: improved safety by shifting labour off-site, enhanced finish quality, and faster installation with reduced curing delays.

The LEM was designed to construct six rings per 24-hour period, a target achieved in the latter stages of the first drive. At the time of writing, early results from the second drive indicate that production rates are on track to exceed this benchmark.

4 CONCLUSION AND LESSONS LEARNT

The completion of the segmentally lined mined tunnels on the Western Tunnelling Package represents a significant achievement. Delivering this outcome required sustained effort, continuous innovation, and close attention to detail. The project team navigated numerous technical and logistical challenges to implement a first-of-its-kind precast lining system in a mined horseshoe tunnel. The result is a high-quality, durable, and watertight tunnel structure that demonstrates the viability of this approach in complex underground environments.

Three common questions arise when reflecting on the LEM and the segmental lining system: Was it worth it? Would we do it again? And what would we do differently? Despite operating under the constraints of a fixed-price D&C contract where innovation is often limited the project team succeeded in delivering a cost-effective system. The development and deployment of a gasketed precast lining within an excavated tunnel set a new benchmark for mined tunnel construction. Its successful implementation opens the door for similar solutions on future projects with comparable conditions.

The experience gained on this project positions the team well for future rollouts. Having refined the methodology and improved productivity over the course of the works, the system now presents a compelling alternative to conventional cast-in-place solutions. With early integration of lessons learned particularly in planning and design the approach has the potential to deliver both time and cost savings on other projects.

Looking ahead, two key areas have been identified for improvement: ring geometry and grout supply. The 60 mm left/right taper and flat invert created alignment challenges, particularly on tight curves, and strict adherence to ITA guidance proved unsuitable in this context. A more flexible approach to ring geometry linked to tunnel alignment should be explored earlier in future projects. Additionally, self-performing grout mixing on site proved invaluable for ensuring quality and maintaining production. Controlling this process from within the team allowed greater

responsiveness to changing conditions and should be considered a core component of future deployments

The completed tunnel is shown Figure *7* below.



Figure 7. Completed segmentally lined tunnel

19th Australasian Tunnelling Conference – Acosta-Martínez, Stewart and Hudson-Smith (Eds.)
© 2025 Australian Tunnelling Society, ISBN 978-0-85825-002-4

Robofactory: the future of large-scale TBM segments production

G. Faini
Digitalnology, Via Como 3/5, Nova Milanese, Italy

D. Sirtori, G. K. Pini
CPT Group, Via Como 3/5, Nova Milanese, Italy

ABSTRACT: Making precast concrete segments is a critical activity for contractors involved in tunnel construction using Tunnel Boring Machine (TBM) technology. However, the global shortage of skilled personnel poses a growing challenge, making it increasingly difficult to maintain the required production capacity and ensure high product quality.

Robofactory addresses this issue by introducing an innovative precast plant where robots and automated systems collaborate with operators to enhance efficiency in a modernised working environment. This approach significantly reduces the risk of injuries while optimising production workflows.

Over the past two years, Robofactory plants have been successfully implemented in Italy, the UK and France, setting a new paradigm for precast production. Robots handle tasks such as mould opening and closing, cleaning and oiling, with the potential to extend their functionality across various stages of the segment production cycle.

By transferring workers from physically demanding tasks to supervisory and control roles, these automated plants improve working conditions while at the same time, significantly boosting efficiency. Current production data indicates a 30% increase in daily output, along with a substantial reduction in segment defects and workplace injuries, thereby enhancing overall production effectiveness.

The precast plant becomes digitally integrated through tracking software monitoring the production schedule, product quality, component stock levels, and logistics management, from initial storage to the installation of segments in the tunnel.

1 INTRODUCTION

The world becoming progressively more urbanised comes with a rising demand for underground transport systems, which are absolutely vital to global connectivity. The invention and implementation of the Tunnel Boring Machine (TBM) has revolutionised mechanised tunnel construction by boosting the excavation of tunnels. In this field, however, a valuable component of the process remains to this day susceptible to production bottlenecks, which can cause significant delays: the manufacture of precast concrete segments. As the TBM advances, it installs the tunnel lining, which is composed of high-precision precast concrete segments. These segments need to be produced rapidly, precisely and safely, a challenging undertaking to achieve in an era where we are subjected to skilled labour shortages and rising quality demands.

Traditional precast production methods, which are considerably reliant on manual labour, have struggled to keep up with the ever-growing demand and associated standards. This has increased general interest in automation and its endless possibilities. In this context, Robofactory proves itself to be a fresh, novel approach to precast production, reimagining production plants as hybrid environments where the human workforce and robotic applications can work together to enhance efficiency and quality.

The production of these concrete blocks offers the chance to provide the tunnelling industry with recent innovations, shifting this part of the project from a construction site to an industrial plant, thereby enhancing safety standards, the quality of the process and the digitalisation of information.

This paper examines the Robofactory model and its implementation in several European contexts. It explores how automation can enhance not only productivity but also workplace safety and product consistency. It will aim to lay out the lessons and information learnt from this technology-driven alteration in the precast segment industry in Europe in view of a future application on Australian projects.

2 THE VERY FIRST APPROACH: STATIONARY PRODUCTION

2.1 *General overview*

The production of TBM segments has been performed using traditional methods since the 60s. As a matter of fact, for decades, the only production concept in use was made up of stationary moulds.

This type of production plant, as seen in Figure 1, involves having the different moulds fixed on the ground, with the different operations needed for the production being performed at every station. This means that the production crew move from one mould to the other while repeating the following steps:

1. Mould preparation (spraying of release agent, installation of gasket, cast-in items and rebar)
2. Pouring and vibration
3. Extrados smoothing
4. Mould covering for proper curing
5. Mould opening
6. Segment demoulding
7. Mould cleaning and closing

The same process has to be applied for all the moulds in the factory, relying on a concrete truck for the discharge of concrete and on an overhead crane for the demoulding of the segments.



Figure 1. Stationary plant.

2.2 *Recurring issues*

There are some commonly encountered issues experienced by contractors and factory workers when adopting a stationary production, some of which we will take a look at below.

It can sometimes be difficult to find manpower for the production. Segment production plants are often located in rural areas. Moreover, it’s a demanding job and isn’t always appealing to the workforce, who are often drawn towards other opportunities.

Different tasks in the segment production process are performed manually and can be source of injuries. This can be seen through the bolting and unbolting of moulds’ locking screws as they are performed by using heavy bolting guns, which transmit heavy stress and vibrations to the arms of the workers. Extensive use of these tools can cause a whole range of long-term, irreversible and debilitating effects on their health, thereby preventing them from performing their job properly and affecting their overall quality of life.

The opening of the moulds is done manually and pulling down the heavy side panels of the mould poses the risk of being hit by a metal panel weighing 600 kg. Lid opening is also a manual-based task that involves pulling and pushing a 500 kg metal panel. Performing a repetitive task such as this one, eight hours a day, can lead to back pain and strain injuries. Segments are stored in stacks, where these concrete pieces are separated using timber dunnage. As the positioning of the timber blocks is done manually, lifting these 20 or so kilogramme, heavy components over multiple hours can also lead to injuries.

It should also be said that, seeing as though many tasks are performed manually, there are few guarantees on the quality of the segment. In fact, they often need to be adjusted after being demoulded to correct any eventual defects.

The production capacity is constrained to the layout of the plant as only two pours per day can be done, due to the length of the curing cycle. Higher demands of segments cannot be fulfilled if not planned at the beginning of the project. Logistics must be carefully planned, as concrete trucks and lifting equipment need to be able to access every mould. Dedicated lanes must be foreseen for the passage of vehicles and clear paths for suspended loads.

3 A STEP FORWARD: CAROUSEL PLANTS

3.1 *General overview*

Thanks to the ever-increasing use of TBMs as a main excavation method for medium-long tunnels, and to the rise of industrial plants in other sectors, the so-called carousel plants started to appear in specific markets.

A carousel plant is a sort of automated production line, in which the plant is divided into two main areas:

- A working line, where all the production activities are performed
- A curing chamber, where poured segments are cured for several hours to reach the requested strength.

In these factories, it's no longer up to the production team to move from one mould to another to perform the different tasks, but instead, it is the moulds that move along the production line, like in an assembly line.

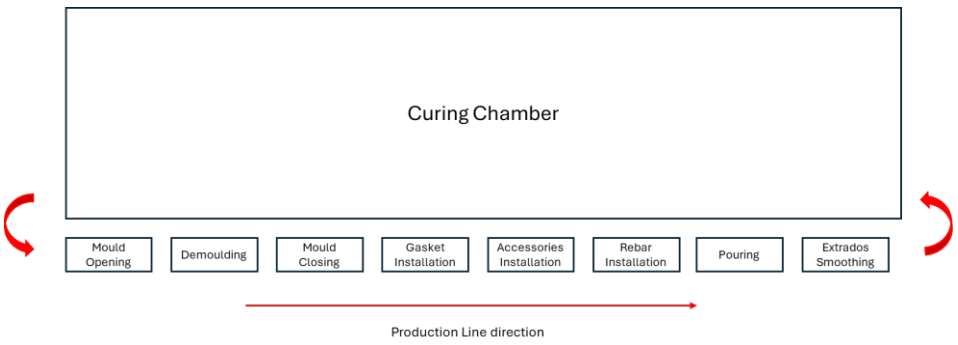


Figure 2. Carousel plant schematic layout.

3.2 *Advantages vs. recurring issues*

Compared to stationary plants, implementing a carousel allows for an optimisation of logistics, the flow of raw materials, vehicles, finished production as well as the required workforce. Production capacity is not bound anymore by the number of moulds in the factory, which encourages flexibility and facilitates managing demand peaks. Furthermore, by being responsible for specific tasks, operators can focus on single activities, thus increasing the quality of the production process. Carousel plants demonstrate an increase in productivity over time of around 30%, thereby reducing cycle times. This means that one segment is usually produced every 7 to 10 minutes. The quality of the segments also turns out better as there are fewer parameters in play

that could jeopardise it. There is also less need for manual workforce which could lead to possible cost savings. As the moulds are in an isolated chamber during the pouring process, overall noise levels in the plant are lessened. This is advantageous not only from a technical standpoint, but also in terms of creating a safer working environment and reducing the risk of accidents and injuries among workers.

That being said, carousel plants can still be far from the safety standards and quality processes applied in other sectors, such as automotive or food production factories. More specifically, we will look at some aspects of this production method that could be improved. Although the number of workers needed is lower compared to stationary plants, in some areas, manpower can be difficult to find, especially for plants which must run on night shifts. Some quality aspects remain aleatory; by this, it's meant that they still rely on human workers. Examples can be tightening moulds at the correct torque, segment defects identification, release agent spraying, etc.

Being an automated production line comes with the limitation that the fault of a single component affects the overall production cycle. This can cause delays and further problems when trying to resolve the initial one.

Compared to other sectors where automated plants have represented the basic production concept for decades, the precast industry is still behind in that matter, with contractors sometimes opting for a direct production of segments, thus venturing outside their core business and having to set up new factories as well as rapidly gain skills. This leads to a neglect of running costs with the only focus being on the investment cost, as the key objective is to produce segments at the right pace, rather than slowing down the TBM.

Focusing on repetitive tasks such as the ones presented in Figure 2 can be alienating, leading to high staff turnover. Despite many improvements from previous production plant types, fatigue-intensive and incident-prone activities are still present in the production process. Accidents may also happen due to moving machines and insufficient safety standards.

4 ROBOFACTORY: THE NEW PRODUCTION PARADIGM

4.1 *Robotics and automation implementation*

Stemming from the need of different precast plants and construction sites all around the world, CP Technology has spent the last few years developing a new and innovative carousel plant concept: Robofactory, as depicted in Figure 3. This concept involves robots, digital solutions and automated equipment working alongside operators.

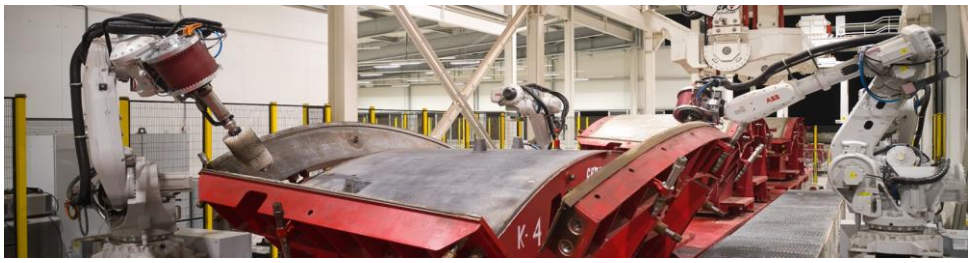


Figure 3. Robofactory in Italy.

While the production sequences remain the same as those of a carousel plant, some stations have been improved by adding robotic solutions in order to bring benefits to both the people working in the plant and the quality of the process.

Concerning mould opening, robots are responsible for unbolting the locking screw by applying the correct torque. The moulds are opened and closed automatically by a hydraulic system. Similarly, when preparing to close the moulds, robots are responsible for cleaning the internal surfaces of the moulds by using specific brushes. They are also in charge of spraying the release agent before the moulds exit from the robotic enclosed area.

When demoulding the segment from the mould, an automated machine as seen in Figure 4 is used to demould, turn the segments as shown in Figure 4(a) and move them towards the storage location. While the segment is being flipped, safety bars that can also be seen in Figure 4(a) are

used to “catch” the segment in case of any kind of slipping malfunction. This way, it acts as a sort of safety net for the precast elements. The demoulding machine itself uses friction to keep the segment in place, reducing the stress on the segment extrados compared to the traditional vacuum solution. The contact pads that hold on to the segment can be seen in Figure 4(b). This equipment is particularly useful as it limits the different handling phases and the quantity of manpower needed for these operations.



(a) Device holding a concrete segment. (b) Empty device with exposed contact pads.

Figure 4. Demoulding and tilting machine in France.

Once the concrete starts being poured in the mould, load cells and automation work as support for the workers when controlling concrete pouring. Another improvement is the adoption of electrical vibrators instead of the traditional pneumatic vibrators used in stationary plants and in most carousel plants. This is advantageous as there is the possibility of adjusting the sequence and the frequency of each vibrator, while the pneumatic ones only work on an on/off basis. Vibration processes can be memorised based on the type of mould or the type of concrete which contributes to improving overall simplicity and efficiency within the casting chamber.

When exiting the casting station, the segments’ extrados usually needs to be smoothed out. For this particular step, robots can likewise be used to optimise the finishing of segments, without the need for operators. Robotic arms can also be used for the positioning of dunnage on the segments before stacking them in storage and in printing traceability labels that can be stuck on the segment in order to keep track of its specificities and whereabouts.

The utilisation of robots and automated technologies has resulted in a transition of workers from manual and repetitive tasks to roles involving control and supervision. This pushes the workforce towards more value-added tasks, and it can lead to the formation of new and useful competences. These skills can be applicable to different sectors, seeing as though in some areas, a tunnelling project or segment production may just be a temporary venture. Additional improvements have been made to the production process that don’t involve robotics but other kinds of equipment and tools.

4.2 *Other improvements of the Robofactory*

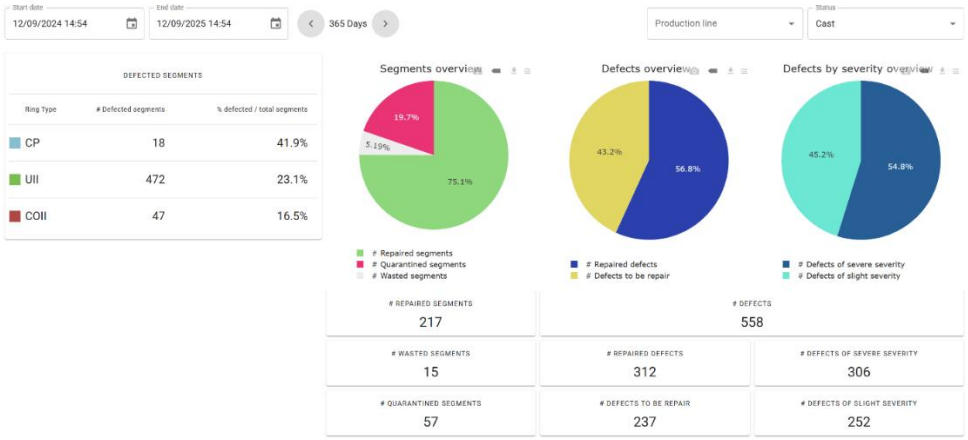
Production surveillance using traceability methods is a smarter way to track segments and related equipment. Thanks to self-developed software, production managers have access to a real-time dashboard, as seen in Figure 5(a), to control the status and the performance of the production. This includes information like the number of segments produced, an overview of the production trend, the percentage of different types of segments cast, etc. Other dashboard interfaces can contain indications of the defects rate, as shown in Figure 5(b), of the bottlenecks and of the storage yard mapping, as shown in Figure 5(c), with the aim of always optimising the production process and pouring time.

All the data regarding the production of the segments is collected in a smart and digitalised way, without the need to compare delivery notes, dispatching bills and serial numbers. Gaskets, rebar, cast-in items and concrete batches are scanned before the installation, such as to link their production lot to the specific segment being poured. This also considers all the process-related

parameters (such as pouring time, demoulding time, etc) with the goal of providing a complete record of information that is crucial for the owner of the tunnel for the future maintenance.



(a) Display of production performance.



(b) Defects overview.



(c) Storage yard layout representation.

Figure 5. Example of dashboard interface.

Special temperature probes based on a Long Range (LoRa) connection are installed on the moulds' erector cones in order to measure the temperature at the centre of the segments. By doing so, it is possible to correlate the temperature of the concrete to its maturity, with the aim of spotting in advance if a segment has not yet reached the necessary strength for demoulding. Each mould

inside the curing chamber is represented digitally and the temperature is visible to the plant operators.

A set of sensors, paired with a connection between the Robofactory's different pieces of equipment, allows the operating parameters of the machines to be monitored. The aim is to reduce power consumption if it is not necessary for production while also offering a general overview and the ability to control equipment consumption levels. For instance, the curing system power can be adjusted using temperature probes placed inside the curing chamber, which modulate the curing system if temperature increases aren't required.

The vapour control system enables the operator to adjust the vapour's temperature and humidity using a proportional-integral-derivative (PID) control system, thereby optimising response time, stability and adaptability. This system controls the valves for each of the curing chamber zones individually. It automatically keeps track of the curing environment. It also provides a user-friendly interface, giving operators all the necessary data. This display allows them to measure, control and record the different phases of a complete curing cycle. The temperature shows up at the bottom of the screen, providing an easy overview of the conditions to which the concrete elements are being subjected.

To assist electricians and fitters, specific maintenance scheduling and routines can be drafted to minimise the downtime of the equipment. Real-time data monitoring can also allow us to spot unexpected behaviours or changes of running parameters, suggesting preventive maintenance interventions.

In order to promote a safer working environment, alarmed gates and fences as well as 3D laser scanners are just a few examples of new-generation safety devices that are adopted in Robofactories to verify the absence of workers from hazardous areas and contribute to the reduction of injuries. 3D laser scanners are easily programmable and adjustable to survey specific areas and differentiate between relevant disturbances, such as those caused by the light reflected by people, or non-relevant ones, like ones by light reflected by dust. They have a detection range of up to 8.4 metres with a scanning area of 190°. Entering an area when the carousel is about to move or already in motion automatically stops the carousel and the Programmable Logic Controller (PLC) will generate an alert. The various information related to the event is recorded, such as the position, when it occurred and how long it lasted. This way, there's a possibility to check the logs for any past detection history, with up to 500 events that can be saved. This is useful in determining why a specific machine encountered a stop.

These developments aren't limited to process improvements. In fact, new spacers made of recycled plastic have been developed by CP Technology, under the name Green Spacers. Not only is their durability greater than timber spacers, but their weight is one fourth of the previously used timber ones. This tremendously benefits the people whose job it is to lift them every day as part of their tasks on precast sites.

5 CASE STUDIES

5.1 *Implementation in Europe*

Robofactories from CP Technology have been operating for 3 years in Europe, with plants serving the following projects:

- Messina-Catania Railway (Catania, Italy)
- Naples-Bari, Hirpinia-Orsara & Orsara-Bovino High-Speed Railway (Foggia, Italy)
- Turin-Lyon Tunnel (La Chapelle, France)
- HS2 – Northolt Tunnel East & Euston Tunnel High-Speed Railway (Hartlepool, UK)

5.2 *Plant overall efficiency*

The main improvements that have been achieved thanks to the adoption of Robofactories are the following:

- 50% reduction of manpower needed by going from 12 to 15 workers, like on a traditional carousel plant, down to 7 workers
- 30% reduction of cycle times by going from ten minutes per segment like on a traditional carousel plant to 6 to 7 minutes per segment, with a potential production of up to 170 segments

per day
– 40% decrease in segment defects.

Let's refer to Figure 6 and Table 1 to take the example of a carousel in Australia and a Robofactory in Italy. Based on data extracted from the production tracking system over the course of two months, it's clear that the Naples-Bari production plant showed better results, with an overall production increase of around 18% and a daily production increase of around 31% in comparison with the carousel plant.

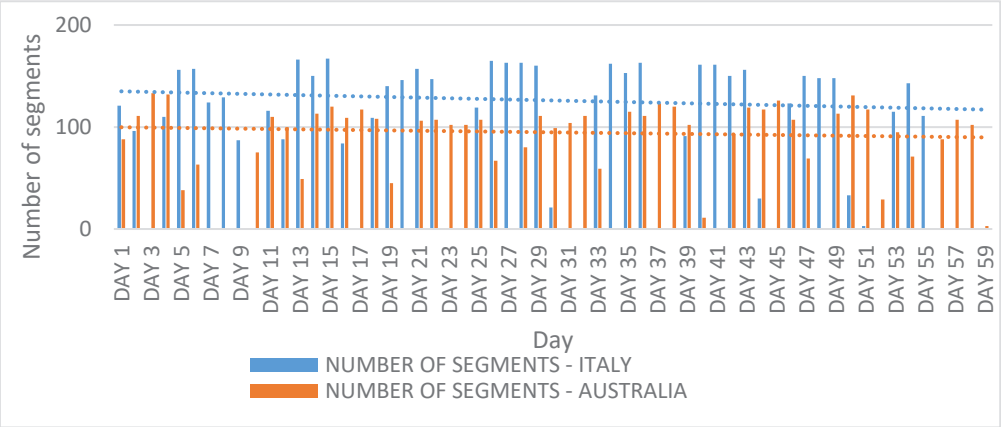


Figure 6. Graph comparing segment production in Italy and Australia

Table 1. Australia and Italy production comparison.

Country	Daily average production	Lowest daily production	Highest daily production	Total production
Australia	96.57	3	133	4732
Italy	126.66	3	167	5573

5.3 Conditions and suggestions for the Robofactory

Although the Robofactory is crucial to cut the operating costs of segment production, the initial investment is higher than a traditional carousel. For this reason, they are more often suggested when the following conditions are met:
– High cost of local manpower
– Long tunnels to be excavated, meaning large-scale and/or rapid segment production
– Universal factory, with the ability to produce segments for different projects over the years.

Analysis conducted with our clients shows the break-even is reached for tunnels of 10 km in length in Italy and tunnels of 5 km in length in Australia.

6 CONCLUSIONS

Long-standing challenges related to workforce shortages, workplace safety concerns, and production inefficiencies are in dire need of being addressed and worked on.

By integrating robotics, automation, and digital monitoring systems, the innovative Robofactory plant model is a revolutionary development in TBM segment production, which enhances operational reliability, reduces the need for manual labour, and significantly lowers defect rates. Its effectiveness is highlighted by the results observed across various European infrastructure projects, such as increased output, improved quality, and safer working environments, which truly highlight its effectiveness.

Although the initial investment is greater than that required for traditional carousel systems, the long-term benefits in terms of cost savings, scalability and sustainability make the Robofactory a compelling solution for modern tunnelling projects, particularly those with high production demands and strict quality requirements. This renders it a compelling option that should not be overlooked for future tunnelling projects in Australia.

19th Australasian Tunnelling Conference – Acosta-Martínez, Stewart and Hudson-Smith (Eds.)
© 2025 Australian Tunnelling Society, ISBN 978-0-85825-002-4

Breaking ground with umbilical and flying launch systems: innovations to manage space constraints in Australia's Suburban Rail Loop Project Tunnels South

V. Tata & J. Mackell
Suburban Connect (CPB, Acciona, Ghella Joint Venture), Melbourne, Australia

ABSTRACT: The flying launch method, widely used internationally, will be implemented for the first time in Australia on the Suburban Rail Loop project. This launch technique is ideal for constrained sites where full TBM assembly and conventional thrust frames are not feasible. In such cases, an umbilical launch is used, involving the partial assembly of the TBM within a shaft and the use of hoses and cables—called umbilicals—to supply services from the surface. When a thrust frame cannot be installed due to spatial limitations, a flying launch is adopted. It positions a reaction frame near the headwall, with the TBM advanced via hollow jacks and stress bars connected through a star compression ring. At the Clarinda site, four TBMs will be launched using this combined umbilical and flying launch method, each with a tailored approach. This paper explores the design, implementation, and challenges of this innovative launch strategy.

1 INTRODUCTION

Suburban Rail Loop (SRL) is a significant transport infrastructure project in Australia's fastest growing city, Melbourne. SRL is an orbital rail line that will connect the existent major railway lines from Cheltenham in the Southeastern suburbs to Werribee in the west, passing through Tullamarine Airport. The project is divided into four major sections: East, North, Airport and West. SRL East is the first phase of multi-decade project. Now into delivery, SRL East will span 26 kilometres of twin tunnels connecting six new underground stations between Cheltenham and Box Hill across Melbourne's middle suburbs.

Four TBMs will construct the tunnels between Cheltenham and Glen Waverley for the Suburban Rail Loop East's, Tunnels South. The project involves twin tunnels, each approximately 16 kilometres in length. All four TBMs will be launched from the Clarinda site, employing umbilical systems combined with the flying launch technique.

This paper explores and evaluates the various launch methods available and explains the rationale for selecting the flying launch for this project. The advantages and drawbacks of each approach are assessed and, the technical aspects of the flying launch are discussed, including design and assembly. An evaluation of the alternative solutions considered prior to finalizing the implementation strategy on site is also presented.

The Clarinda launch site, located in the south-east of Melbourne, is being prepared to accommodate all necessary equipment for tunnel construction. In addition, a shaft will be excavated and set up exclusively for the TBM launches. The shaft is divided into two sections: East and West. Each section will launch two TBMs—those in the East will tunnel towards Glen Waverley, passing through Clayton and Monash stations, whilst the West TBMs will head towards Cheltenham, passing the South Stabling Yard. Due to space limitations on site, the launch shafts cannot accommodate the full assembly of the TBMs. Traditional launch methods involving a thrust frame are also not feasible. After extensive analysis and consideration of various options to ensure an effective launch, the flying launch method, combined with umbilicals, has been selected.

The flying launch method has been developed by Hochtief Infrastructure Gmbh and was first implemented in 2006 on the North-South Urban Light Railway Project in Cologne, Germany (Assenmacher, 2007, p. 23). Since then, it has been utilised on several projects throughout Europe and Asia including Deep Tunnel Sewerage System Project Phase 2 (DTSS 2) in Singapore and Central Interceptor Project in New Zealand. The methodology has never been used in Australia.

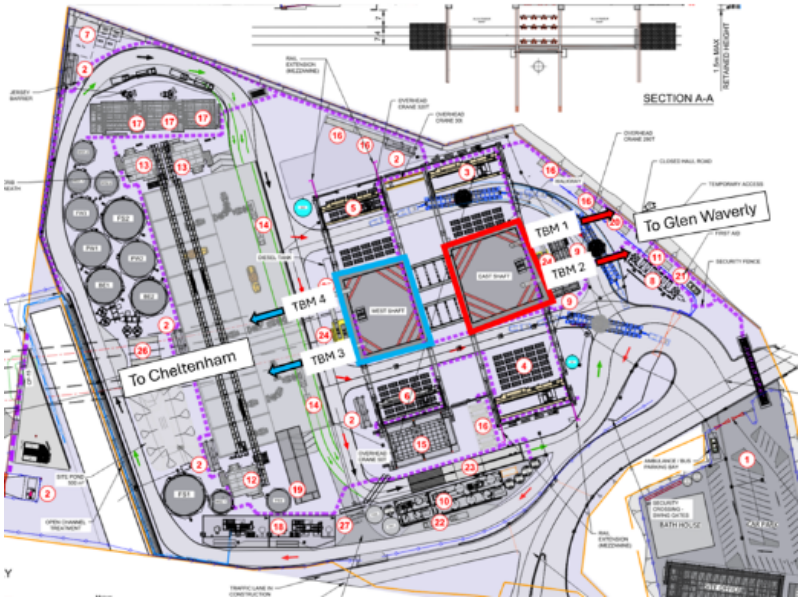


Figure 1. Alex Fraser launch site layout

2 TBM LAUNCH METHODOLOGIES

There are various methods and techniques available for launching TBMs. Typically, the TBM is fully assembled, including the shield and gantries, and launched using a thrust frame in combination with blind rings. However, in areas with limited space, the flying launch technique can be employed.

2.1 *Conventional launch*

Conventionally, a TBM launch employs a thrust frame which enables the TBM to build rings and push into the ground. The machine is positioned at the headwall, and the thrust frame is assembled behind the shield, specifically behind the tail skin. Thrust frames can vary in design and assembly methods, but they are generally portal-shaped and connected to the machine via a steel ring that is installed in the tail skin and pushed against the frame.

The steel ring is then secured to the thrust frame using welding or bolting. The TBM is pushed into the ground by thrust cylinders acting against the steel ring. After each push, which depends on the extension of the cylinders, a new precast ring is added. The thrust frame is designed to absorb the force from the cylinders and continues to hold its position in the launch area until the grouted rings in the ground can support the push. To ensure stability during the pushing phase, the frame is typically anchored to the ground or base slab with ground anchors.



Figure 2. Conventional thrust frame.

2.2 *Flying Launch*

Unlike the conventional launch, the flying launch is primarily used to pull the TBM into the ground. This method involves several key components: a reaction frame, a star compression ring, hollow jacks, and stress bars to facilitate the pulling of the TBM.

In some cases, instead of using a reaction frame, the system can be jacked from the headwall, provided the design of the headwall can support the pulling forces of the machine. The TBM shield is first assembled at the launch site, and the reaction frame is then constructed around the shield, positioned near the headwall. Similar to the thrust frame, the reaction frame is anchored to the ground to absorb all pulling forces.

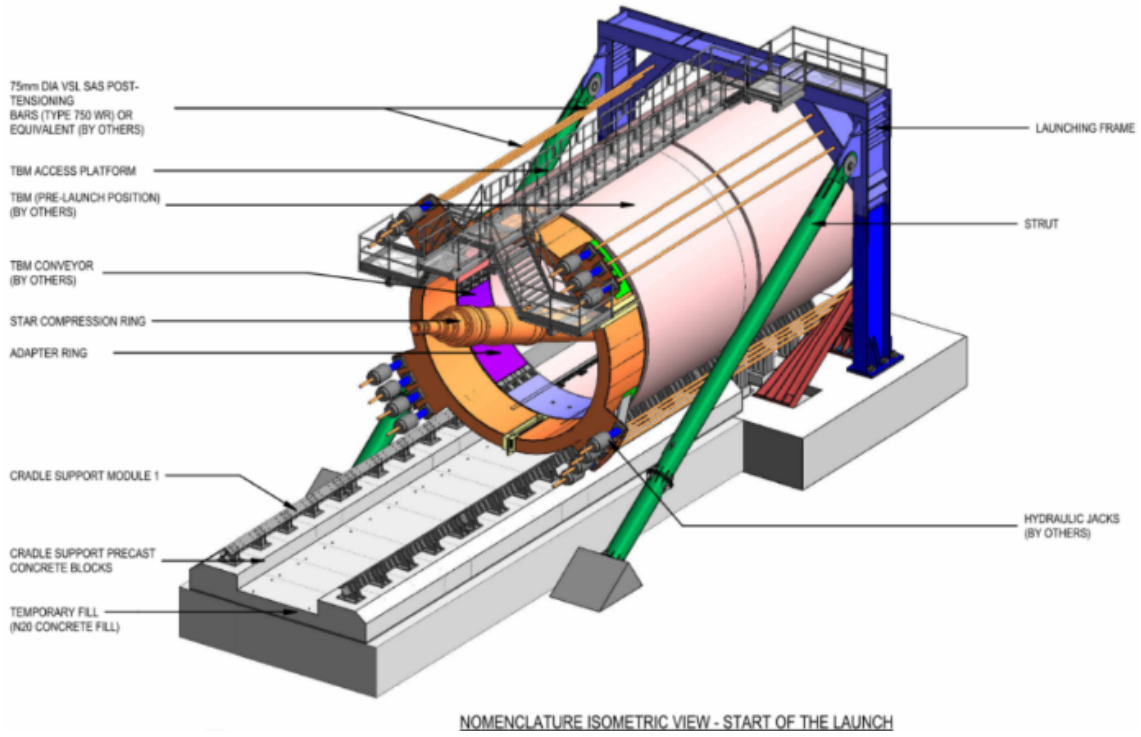


Figure 3. Flying launch assembly.

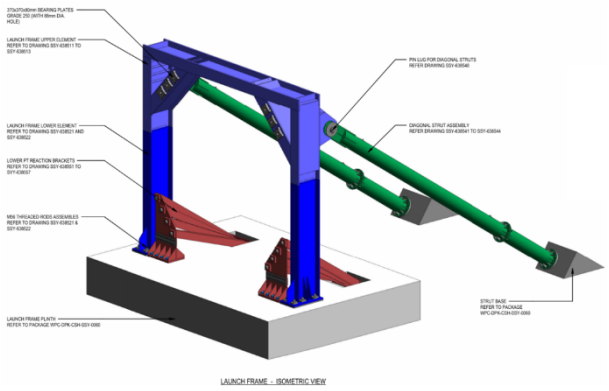


Figure 4. Flying launch reaction frame.

A steel ring is installed in the tail skin of the TBM, which is connected to the star compression ring positioned behind the tail skin. The steel ring is pressed against the star compression ring and fixed in place by welding or bolting. At this stage, hollow cylinders are positioned against the star compression ring, through which stress bars are inserted. The stress bars are secured with nuts and washer plates, connecting the hollow cylinders to the reaction frame. Additionally, a fixation point on the star compression ring helps maintain its position as the hollow cylinders are readjusted after each stroke.

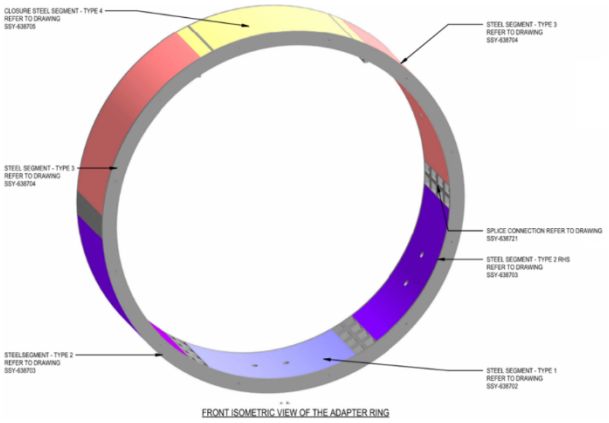


Figure 5. Adapter ring.

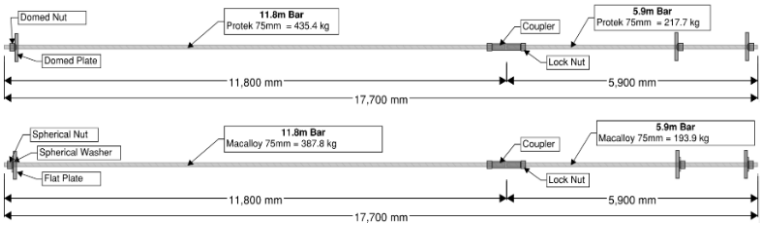


Figure 6. Stress bar assembly

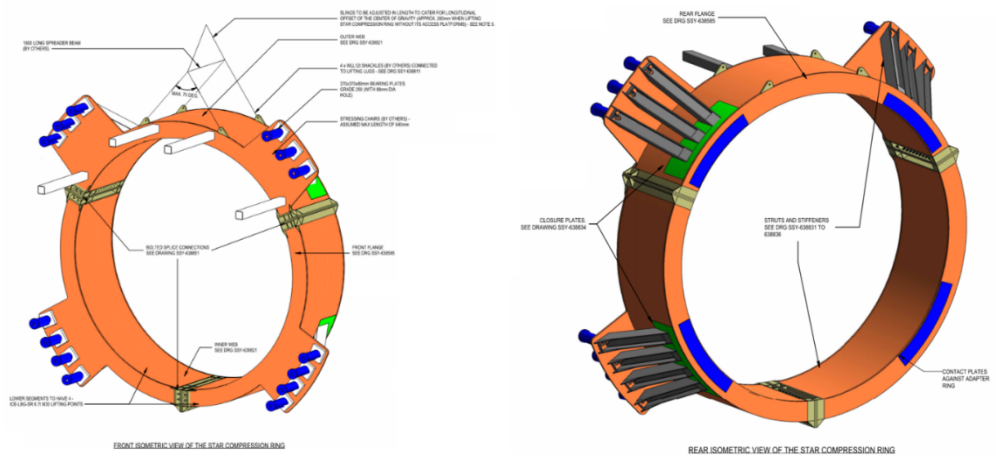


Figure 7. Star compression ring front and back view

Once the entire system is assembled, with all bars in place, the hollow cylinders are hydraulically and electrically connected to a power pack. When activated, the hollow cylinders start pulling on the stress bars, causing the TBM shield to move towards the headwall. The hollow cylinders generally have a shorter extension compared to the TBM's thrust cylinders, requiring re-adjustment after each stroke. The thrust cylinders are powered by an erector emergency pump, remaining at a fixed extension and pressure to keep the steel ring in place. As the hollow cylinders retract, the star compression ring is held in position by the fixed nuts and washer plates. The TBM, along with the star compression ring and steel ring, is then pulled until the steel ring reaches the headwall. At this point, concrete rings are installed and grouted to the ground. The star compression ring, stress bars, and hollow cylinders remain in place until the grouted rings can support the excavation.

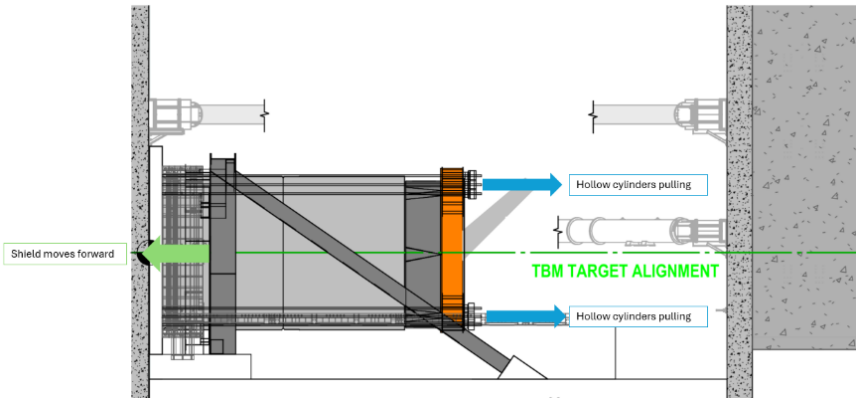


Figure 8. Initial flying launch configuration

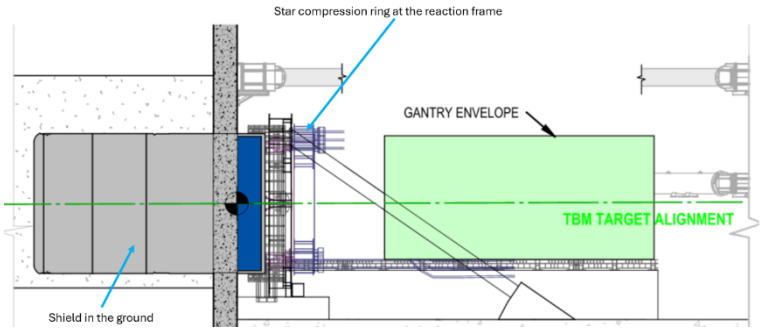


Figure 9. Final flying launch configuration

The primary difference between these two launch methods is the way the TBM is moved. The traditional thrust frame operates by pushing the TBM toward the headwall, whereas the flying launch pulls the TBM forward. The thrust frame remains stationary, and new rings are progressively installed to push the TBM. In contrast, the flying launch system moves with the TBM until it reaches the headwall. With the thrust frame, the TBM's thrust cylinders perform the pushing action, while in the flying launch, the TBM's thrust cylinders are locked in terms of pressure and extension, and the hollow cylinders handle the pulling.

The key distinction lies in the use of space: the thrust frame must be positioned a certain distance from the headwall to allow the installation of multiple blind rings to push the TBM forward and into the ground. In contrast, the reaction frame for the flying launch is placed very close to the headwall, with the star compression ring positioned at the back of the shield, making the space confined to the size of the TBM shield. This is the primary reason that the flying launch is a valuable solution in situations where space constraints prevent the construction of a thrust frame.

However, there are also some disadvantages to the flying launch. It requires additional components, such as the star compression ring, stress bars, and hollow cylinders, which increase the overall cost and extend the installation process. Furthermore, since the hollow cylinders need to be re-adjusted after each stroke, launch time is typically longer and requires additional personnel to manage the operation.

3 FLYING LAUNCH DESIGN FOR SUBURBAN RAIL LOOP

3.1 *Overview*

The design of the flying launch accounts for a maximum thrust force of 17,500 kN, as well as the design of the TBM and concrete segment rings. All associated equipment has been selected and designed to accommodate this force.

The design selected for the Suburban Rail Loop project includes the following components:

- 14 stress bars;
- 14 hollow cylinders;
- 1 reaction frame;
- 1 star compression ring;
- 1 steel ring.

Specifically for the stress bars, the system includes six bars positioned at the top and eight bars positioned at the bottom, evenly distributed between the left and right. Each stress bar is approximately 18 meters in length with a diameter of 75 mm and is designed to withstand the pulling force. 40% of the load is exerted on the top bar and 60% on the bottom.

The hollow cylinders required for this application are specifically chosen to handle the pulling force and the dimensions of the stress bars. The cylinders have a stroke of approximately 240mm and have an opening for the stress bars of 110mm.

The reaction frame consists of three main components: the portal, the reaction struts, and the reaction brackets at the bottom as shown in Figure 4. All three components are anchored to the ground to effectively transfer the forces. The portal is divided in three main sections: two columns and one cross structure that connects the columns, all of which are bolted together. The central structure holds the top stress bars. The struts are diagonal members that are connected through a bolt to the portal. The reaction brackets are not linked to the main portal. It instead consists of a diagonal member welded to a vertical column. Through the vertical column, the bottom stress bars are installed.

The star compression ring, shown in Figure 7, is designed to accommodate the pulling forces, the dimensions of the stress bars, and the size of the TBM shield, which in turn determines the size of the steel ring. It is made of three sections that are pre-assembled and fixed on surface before being lowered into the shaft.

The steel ring shown in Figure 5 is engineered to withstand both the thrust and pulling forces, as well as the concrete rings installed during the TBM's excavation. Six segments constitute the steel ring over a length of two metres, which allows the ring to reach the star compression ring without fully extending the TBM thrust cylinder.

3.2 *System installation*

The process begins with positioning the columns of the reaction frame in the shaft. Once that is in place, the TBM shield is lowered in the shaft. After the shield is set, the top part of the reaction frame and the struts are installed and secured. Next, the star compression ring is lowered into position, initially on support legs. The support legs provide stability for the star compression ring before the installation of the stress bars and hollow cylinders. Once the star compression ring is supported, the stress bars are installed and secured with a washer plate and nut system at the dead end (reaction frame) and life end (hollow cylinder). At the star compression ring side, the locking system is provided by using a counter washer plate and a nut. The hollow cylinders are installed after the stress bars are positioned and secured. The star compression ring is then fixed to the steel ring, which the TBM's thrust cylinders push against. Finally, the system is connected to the power pack through hoses and cables, making it ready for operation.

Upon activation, the hollow cylinders pull the stress bars, allowing the star compression ring to move and push the TBM forward toward the headwall. After each stroke (approximately 240 mm), the star compression ring is locked into position using the counter washer and nut, and the hollow cylinders are retracted and secured again with the washer plate and nut. The pulling process then resumes, continuing until the first concrete ring is installed. At this stage, the position of the flying launch remains fixed, and the system only serves to support the excavation. Once the grouted concrete rings can support the excavation, the flying launch system is disassembled and can be reused for the next launch.

3.3 *Umbilicals*

Given the limited space within the shaft, the back-up gantries will be installed on the surface. This unique challenge requires all services supporting the shield to be managed. The services will be managed in four different ways:

- Short support gantry: a small temporary gantry will be launched with the machine. This will follow the machine until a point it can be reconfigured to a full machine. The gantry will house the below services:
    - 2MVA transformer
    - drive motor MCC's
    - grease drums and pumps
    - grout A and B tanks and pumps
- Festoon system: an electric hoist-controlled festoon system with sufficient capacity to support machine until reconfiguration. It will contain all hydraulics to support shield.
- Cable reeler: borrowed from the back up gantries, the reelers that are usually utilised for pipe extension within the tunnel will be installed within the shaft. These will feed:
    - compressed air
    - water
    - grout A
- Cable basket: Given that the HV transformer is installed on the short support gantry, only comms and HV cables will need to be run from the shaft to the machine. These two cables will be strapped together and installed in a "figure 8" configuration into a basket which will be fed out as the machine advances.

The preferred approach for all services is to minimize / eliminate the need to break services for extensions from within the tunnel. This means all planned extensions occur within the shaft, making management of spillage easier resulting in a safer working environment within the tunnel.

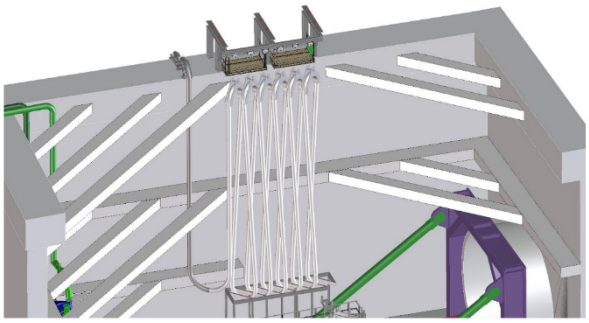


Figure 10. Umbilical festoon system

3.4 *Expected challenges and limitations*

Various challenges and lessons will need to be managed during the launch process, given that this project will employ the flying launch system for the first time in Australia. A common challenge will be to ensure consistent distribution of forces according to the design, maintaining the 40/60 thrust load ratio between the top and bottom stress bars as accurately as possible. The primary ongoing challenge that is expected, however, is maintaining TBM alignment ensuring that the cylinders extend uniformly with each stroke. This will be managed using a power pack located at the bottom of the shaft, connected to all hollow cylinders. The power pack will be equipped with a PLC system that monitors and provides data on cylinder extension and the applied pressure. This requires precise coordination among all system components.

Due to the use of umbilicals instead of the full set of gantries behind the shield, the TBM's productivity will be affected, resulting in a reduced advance rate but offset by the overall increased efficiency.

3.5 *Benefits*

The benefits of the flying launch and the reason this method was selected are:

- Reaction frame positioned at headwall rather than several metres back.
    - Increased launch efficiency due to increased shaft space.
    - Safer access to tunnel for personnel
- Reduced shaft requirements.
    - Time and cost saving in reduced shaft excavation.
- Eliminates need for high-risk false ring disassembly.

4 CONCLUSIONS

The flying launch concept offers several benefits to a conventional launch where sites have space limitations, or shafts are being constructed exclusively for launch, such as on Suburban Rail Loop's, Tunnel South. The additional time and cost associated with the more complicated launch process are easily and comprehensively offset by savings in reduced shaft excavation and by eliminating the need to install and remove false rings.

5 REFERENCES

Assenmacher, S, 2007. "Flying Shield Start-Up": Innovative Start-Up Method for Shield-driven Tunnels, in Tunnel 03/2007, p. 23

Suburban Rail Loop Authority, 1 May 2025. https://bigbuild.vic.gov.au/projects/suburban-rail-loop/srl-east

19th Australasian Tunnelling Conference – Acosta-Martínez, Stewart and Hudson-Smith (Eds.)
© 2025 Australian Tunnelling Society, ISBN 978-0-85825-002-4

Spoil Reconciliation in Slurry TBM Tunnelling: A literature review and framework designed for application on Melbourne's Suburban Rail Loop East – Tunnels South

M. Taneja
Suburban Connect, Melbourne, Victoria, Australia
M. Terenzi
Suburban Connect, Melbourne, Victoria, Australia

ABSTRACT: Accurate muck reconciliation is critical for efficient slurry TBM operations, ensuring alignment between theoretical and actual excavation volumes. This paper reviews methodologies for TBM dry mass calculation, volume measurement, and slurry treatment plant (STP) reconciliation, analysing challenges including sensor inaccuracies and geological variability. A novel risk-aware framework is developed to guide method integration, demonstrating how hybrid approaches reduce errors. The framework will be applied on Melbourne's Suburban Rail Loop (SRL) East – Tunnels South (delivered by Suburban Connect JV: CPB Contractors, Acciona and Ghella) to support reconciliation in mixed-ground conditions.

1 INTRODUCTION

The slurry shield, pioneered in the UK during the 1970s, addressed excavation control in challenging ground, initially targeting submerged sand/gravel without face instability. Recent decades have seen global adoption for long-distance tunnelling in complex geology due to technical feasibility and automation. Projects like the Channel Tunnel Rail Link (UK), Shanghai Yangtze River Tunnel (China), and Singapore's Deep Tunnel Sewerage System (DTSS) exemplify its application in variable strata under high water pressures (Shirlaw et al., 2003; Thewes & Hollmann, 2016). Similar methodologies are implemented in Sydney's Eastern Tunnelling Package (ETP).

1.1 *Slurry System*

Face support is provided by bentonite/polymer-water slurry counterpressure, forming a filter cake or impregnated zone to transfer pressure and mitigate collapse risks (Maidl et al., 2012; Hochart et al., 2021). Excavated material is transported to surface STPs for separation and bentonite recycling (Herrenknecht, 2020). Advanced software standardises dry mass/volume calculations for real-time efficiency monitoring (EFNARC, 2005; Peila & Picchio, 2020).

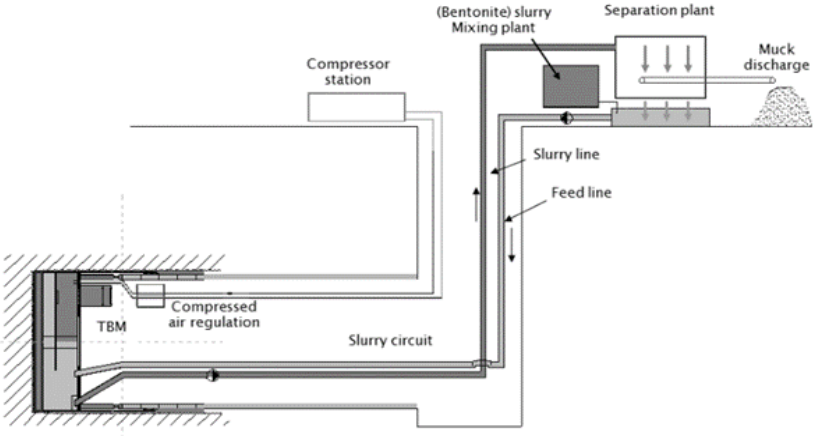


Figure 1 - Slurry circuit (Duhme et al., 2016)

1.2 *Need for three distinct reconciliation approaches*

Three distinct reconciliation approaches - TBM dry mass calculation, TBM volume measurement, and slurry treatment plant (STP) muck reconciliation - are critical to address uncertainties in excavation management, particularly in scenarios involving over-excavation (Tang et al., 2021).

The need for distinct approaches has been also extensively discussed in recent literature, emphasising the accuracy of mass and volume-based reconciliation techniques (Gravemeijer & Peila, 2022)

1.2.1 *Scenario 1: Over-Excavation with Unfilled Void:*

When over-excavation occurs, and the resulting void remains unfilled, excess soil volume is transported through the discharge line. This leads to a measurable discrepancy between the theoretical and actual volumes, directly indicating the over-excavation volume. Volume-based measurements alone, however, may fail to detect localised ground loss or slurry infiltration into adjacent strata, necessitating complementary mass-based calculations (Connors, 2017).

1.2.2 *Scenario 2: Over-Excavation with Void Filled by Slurry*

In this case, the void created by over-excavation is filled with slurry, masking the volume discrepancy. While the measured volume aligns with theoretical expectations, the dry mass of excavated material will exceed projections due to the additional soil removed. This highlights the necessity of integrating mass reconciliation to identify hidden over-excavation risks, as volume measurements alone become insufficient (Herrenknecht, 2020).

1.2.3 *Why Three Approaches Are Required*

1. TBM Dry Mass Calculation: Determines the actual excavated soil mass by accounting for slurry density, flow rates, and solids content. This method detects over-excavation even when voids are slurry-filled, as mass discrepancies persist despite normalized volumes (EFNARC, 2005).
2. TBM Volume Measurement: Monitors real-time slurry inflow/outflow volumes to identify unfilled voids. However, it cannot distinguish between soil displacement and slurry infiltration, requiring cross-verification with mass data (Tang et al., 2021).
3. STP Muck Reconciliation: Validates excavated material quantities post-separation at the slurry treatment plant. By comparing STP outputs with TBM data, this approach identifies systemic errors (e.g., sensor drift, slurry loss) and ensures alignment between theoretical and actual excavation (Underground Singapore, 2018).

The integration of these methods mitigates risks such as ground subsidence, face instability, and project cost overruns. For instance, STP reconciliation at Singapore's Thomson-East Coast line revealed inconsistencies in fine particle retention within the slurry circuit, which were undetectable via TBM sensors alone (Underground Singapore, 2018). Similarly, the Sutong GIL Chang Jiang Tunnel project demonstrated that traditional volume-based systems underestimated over-excavation by 12–18% in permeable sandy ground, necessitating improved mass-balance models (Tang et al., 2021).

An approach grounded in the same principles is also being applied on other major tunnelling projects delivered by the same joint venture partners. For example, the Eastern Tunnelling Package (ETP) in Sydney, is implementing a spoil reconciliation methodology aligned with slurry TBM operations frameworks.

2 BASIC CONCEPT OF SOIL AND ROCK COMPOSITION

To understand the theory of the excavation management system, it is necessary to refer to the basic soil structure (Figure 2), which consists of three primary phases: solid particles, water, and air (Terzaghi et al., 1996). In geotechnical engineering, soil behaviour under excavation depends on the interaction of these phases, particularly in saturated or partially saturated conditions. For

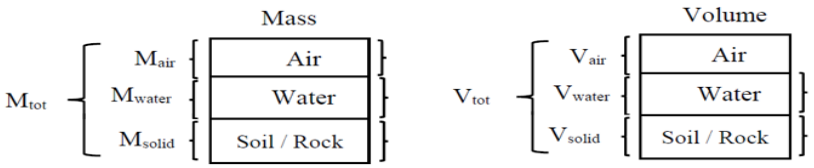


Figure 2 - Basic soil structure.

fully saturated in situ soil or rock, the mass and volume of air (M_{air}, V_{air}) are negligible and can be assumed as zero, as voids are entirely filled with water (Das & Sobhan, 2018).

2.1 *Soil/Rock Properties and Variables*

The following variables are essential for quantifying soil/rock behaviour and ensuring accurate excavation management:

1. M_{air}: Mass of air (equal to zero)
2. V_{air}: Volume of air (negligible in saturated conditions)
3. M_{water}: Mass of water
4. V_{water}: Volume of water, linked to porosity ($n = V_{water} / V_{tot}$).
5. M_{solid}: Mass of solid particles
6. V_{solid}: Volume of solid particles
7. M_{tot}: Total mass of soil or rock ($M_{solid} + M_{water}$)
8. V_{tot}: Total volume of soil or rock ($V_{solid} + V_{water} + V_{air}$)
9. ρ_{water}: Density of water (M_{water} / V_{water})
10. ρ_{solid}: Density of solid particles (M_{solid} / V_{solid})
11. μ: Moisture content (M_{water} / M_{solid})

These parameters underpin calculations for dry density ($\rho_{dry} = M_{solid} / V_{tot}$), void ratio ($e = V_{void} / V_{solid}$) and degree of saturation ($S = V_{water} / V_{void}$), which are pivotal in slurry shield TBM operations to balance excavation pressures and avoid ground collapse (Maidl et al., 2012).

2.2 *Application to Excavation Management*

In slurry shield tunnelling, deviations in moisture content (μ) or void ratio (e) directly impact the stability of the excavation face. For instance, fully saturated soils (S = 100%) require precise slurry pressure to counteract hydrostatic forces, while partially saturated soils (S < 100%) demand adjustments to account for air compressibility (Herrenknecht, 2020). Modern TBMs integrate sensors to monitor ρ_{solid}, μ, and V_{tot} in real time, enabling dynamic adjustments to slurry density and flow rates (EFNARC, 2005).

3 THEORETICAL EXCAVATION VOLUME

The theoretical excavation volume depends on the TBM cutting diameter and the theoretical length of advance, calculated as in equation 1 below:

$$V_{theo} = \frac{\pi d_T^2}{4} L_{advance} \tag{1}$$

where d_T is the cutting diameter of the TBM in meters and $L_{advance}$ is the length of advancement in meters.

This formula assumes a perfectly cylindrical excavation profile, which is critical for benchmarking against actual excavated volumes to detect over- or under-excavation (Maidl et al., 2012).

3.1 *Theoretical Dry Volume and Dry Mass*

The dry mass is derived from the equivalence of total mass and phase relationships:

$$M_{tot} = M_{solid} + M_{water} \tag{2}$$

which can be expressed as:

$$V_{tot}\rho_{in\,situ} = V_{solid}\rho_{solid} + V_{water}\rho_{water} \tag{3}$$

The volume of water is expressed as:

$$V_{water} = V_{tot} - V_{solid} - V_{air} \tag{4}$$

For the fully saturated soil the volume of air is equal to zero, therefore:

$$V_{water} = V_{tot} - V_{solid} \tag{5}$$

And substituting:

$$V_{tot}\rho_{in\,situ} = V_{solid}\rho_{solid} + (V_{tot} - V_{solid})\rho_{water} \tag{6}$$

Further elaborating the formula:

$$V_{tot}\rho_{in\,situ} = V_{solid}\rho_{solid} + V_{tot}\rho_{water} - V_{solidt}\rho_{water} \tag{7}$$

$$V_{tot}\rho_{in\,situ} - V_{tot}\rho_{water} = V_{solid}\rho_{solid} - V_{solidt}\rho_{water} \tag{8}$$

$$V_{tot}(\rho_{in\,situ} - \rho_{water}) = V_{solid}(\rho_{solid} - \rho_{water}) \quad (9)$$

The volume of solids is equivalent to the Dry Volume; therefore, the formula can be expressed as:

$$V_{dry} = V_{tot}\left(\frac{\rho_{in\,situ} - \rho_{water}}{\rho_{soild} - \rho_{water}}\right) \quad (10)$$

The dry soil mass can be then calculated as:

$$M_{dry} = V_{tot}\left(\frac{\rho_{in\,situ} - \rho_{water}}{\rho_{soild} - \rho_{water}}\right)\rho_{solid} \quad (11)$$

This derivation ensures accurate reconciliation between in situ soil properties and excavated material, particularly in saturated conditions where pore water pressure significantly impacts stability (Mitchell & Soga, 2005; Das & Sobhan, 2018).

3.2 *Practical Implications*

Over-Excavation Detection: Deviations between V_{theo} and actual volumes signal potential ground loss or slurry infiltration, necessitating adjustments in slurry pressure (Herrenknecht, 2020). Moisture Content Sensitivity: Errors in μ (moisture content) measurements can lead to overestimation of M_{dry}, affecting spoil disposal and slurry recycling efficiency (EFNARC, 2005).

4 MEASUREMENT OF ACTUAL EXCAVATION VOLUME

During tunnelling operations, excavated materials are conveyed into the slurry discharge line through the excavation chamber. This process increases the discharge flow rate (Q_{out}) proportionally to the material ingress rate, while the feed flow rate (Q_{in}) supplies fresh slurry to maintain face support (Herrenknecht, 2020) (Figure 3).

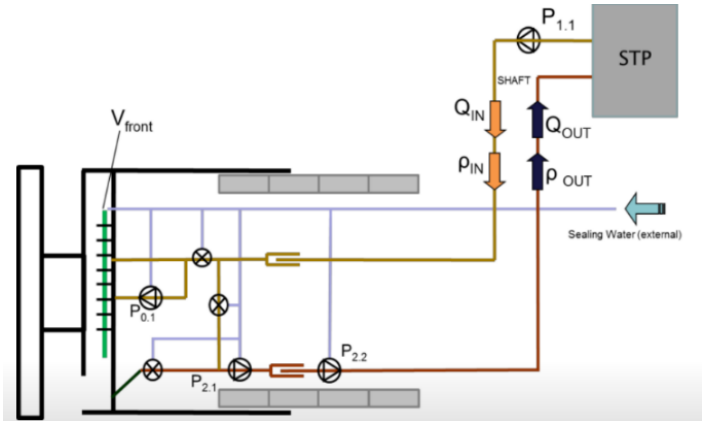


Figure 3 - Slurry flow schematic diagram.

4.1 *Schematic for Actual Excavation Volume Determination*

The actual excavation volume V_{tot} is calculated by integrating the discharge and feed flow rates over time, adjusted for changes in the excavation chamber volume $\triangle V_{chamber}$:

$$V_{tot} = \int Q_{out}\,d_t - \int Q_{in}\,d_t + \triangle V_{chamber} \quad (12)$$

Where:

- Q_{in}: Feed flow rate (m³/hr), supplying slurry to the excavation chamber.
- Q_{out}: Discharge flow rate (m³/hr), transporting excavated material to the surface.
- $\triangle V_{chamber}$: Net volume change in the excavation chamber from TBM advancement or slurry compression (Maidl et al., 2012), monitored in real-time via wire rope level sensors detecting slurry level variations in the chamber.

5 ACTUAL MEASUREMENT OF EXCAVATED SOLIDS (DRY MASS AND DRY VOLUME)

For fully saturated soil, the dry volume formula (Equation 13) is applied, assuming no air entrapment in feed/discharge pipelines (Mitchell & Soga, 2005):

$$V_{dry} = V_{tot}\left(\frac{\rho_{insitu}-\rho_{water}}{\rho_{soild}-\rho_{water}}\right) \quad (13)$$

The total discharge dry volume can be calculated by considering the total volume of slurry passing through the discharge flow meter at the recorded density of ρ_{out}.

$$V_{tot(out)} = Q_{out}\Delta_t \quad (14)$$

$$V_{dry(out)} = Q_{out}\Delta_t \left(\frac{\rho_{out}-\rho_{water}}{\rho_{soild}-\rho_{water}}\right) \quad (15)$$

The total feed Dry Volume can be calculated considering the total volume of slurry (Q_{feed} $\triangle$t) passing through the discharge flow meter at recorded density of ρ_{feed}.

$$V_{tot(in)} = Q_{in}\Delta_t \quad (16)$$

$$V_{dry(in)} = Q_{in}\Delta_t \left(\frac{\rho_{in}-\rho_{water}}{\rho_{soild}-\rho_{water}}\right) \quad (17)$$

The total Dry Volume is the difference of dry volumes in the feed and discharge over time and can be therefore expressed as:

$$V_{dry(solid)} = \int Q_{out}\left(\frac{\rho_{out}-\rho_{water}}{\rho_{soild}-\rho_{water}}\right) d_t - \int Q_{in}\left(\frac{\rho_{in}-\rho_{water}}{\rho_{soild}-\rho_{water}}\right) d_t \quad (18)$$

The above can also be calculated as dry mass considering the equation:

$$M_{dry(soil)} = \int Q_{out}\left(\frac{\rho_{out}-\rho_{water}}{\rho_{soild}-\rho_{water}}\right)\rho_{soild} d_t - \int Q_{in}\left(\frac{\rho_{in}-\rho_{water}}{\rho_{soild}-\rho_{water}}\right)\rho_{soild} d_t \quad (19)$$

This method ensures real-time reconciliation of excavated solids, critical for detecting ground loss or slurry infiltration (Herrenknecht, 2020).

6 INFLUENCE OF EXTERNAL FACTORS ON THEORETICAL AND ACTUAL MEASUREMENTS

6.1 *Key Factors Affecting Accuracy*

Mis-calibration: Sensor drift in flowmeters or densitometers skews Q_{in}, Q_{out}, and ρ_{out} values (Connors, 2017).

Sealing Water: Injected sealing water from rotary pumps increases V_{tot} but does not alter M_{dry} and V_{dry}.

Time Influence: Prolonged excavation cycles cause particle settling in slurry pipelines, skewing density readings. Time-lagged sensor responses may also distort real-time Q_{out} integration (Herrenknecht, 2020).

Leakages: Slurry leakage from fractured pipelines or faulty joints reduces Q_{out} which can falsely indicate under-excavation. Conversely, groundwater ingress inflates Q_{in}, masking over-excavation (Shirlaw et al., 2020).

Interventions: Manual interventions (e.g., cutterhead inspections) halt slurry circulation, allowing solids to settle. Post-intervention restarts require purging to avoid biased ρ_{out} measurements (Maidl et al., 2012).

Pipe Extension: Adding segments to the discharge pipeline introduces air pockets, temporarily disrupting Q_{out} stability (Tang et al., 2021).

Slurry Travel Time: For long tunnels, transit delays between TBM and STP sensors complicate data reconciliation. Installing intermediate density/flow meters along the pipeline mitigates synchronization errors by enabling sectional monitoring.

Bubble Chamber Variations (Mix Shield TBMs): For double-chamber TBMs equipped with a bubble chamber, it is essential to account for variations in slurry volume and mass within the bubble chamber. The slurry level in the chamber, measurable via sensors, is then correlated to the corresponding volume variation.

While the variation in volume in the chamber is straight forward, the variation in solids particles should be calculated as a dry volume or dry mass:

$$Chamber_{dry\ soil} = \triangle V_{chamber}\left(\frac{\rho_{out}-\rho_{water}}{\rho_{soild}-\rho_{water}}\right) \quad (20)$$

The measured dry mass formula considering variation in bubble chamber would then be:

$$M_{dry(soil)} = \int Q_{out}\left(\frac{\rho_{out}-\rho_{water}}{\rho_{soild}-\rho_{water}}\right)\rho_{soild} d_t - \int Q_{in}\left(\frac{\rho_{in}-\rho_{water}}{\rho_{soild}-\rho_{water}}\right)\rho_{soild} d_t + \triangle V_{chamber} \quad (21)$$

Sensor-based slurry level monitoring in the bubble chamber is essential to track $\triangle V_{chamber}$ (Maidl et al., 2012).

In-Situ Density Variability: Fluctuations in $\rho_{in\ situ}$ (e.g., due to heterogeneous strata) directly impact both theoretical and measured dry mass, requiring probabilistic models for error margins (Tang et al., 2021).

7 SECONDARY MEASUREMENT AT THE SLURRY TREATMENT PLANT AND MUCK PIT

Secondary reconciliation measurements at the STP rely on belt weighers installed between the STP and muck pit. However, these systems capture only coarse particles (gravel/sand) separated by sieves and cyclones, excluding fines below the STP's separation threshold. The total excavated dry mass is derived by combining measured coarse solids with estimated fines.

7.1 *Fines Calculation in Slurry Systems*

7.1.1 *Initial Fines Mass (Pre-Excavation):*

Measured before mining starts: Slurry density ρ_{slurry} is measured using density meters in the regulating tank.

$$M_{dry\ fines,\ before} = (V_a + V_b + V_c)\left(\frac{\rho_{slurry} - \rho_{water}}{\rho_{soild} - \rho_{water}}\right)\rho_{solid} \quad (22)$$

Where:

- V_a = Volume of active tank (tank placed on the surface in line with the circuit)
- V_b = Volume of slurry pipes
- V_c = Volume of excavation chamber

7.1.2 *Final Fines Mass (Post-Excavation):*

Measured after mining completes: Slurry density is rechecked at the same locations, typically showing increased values due to fines accumulation during excavation.

$$M_{dryfines,after} = (V_a + V_b + V_c)\left(\frac{\rho_{slurry} - \rho_{water}}{\rho_{soild} - \rho_{water}}\right)\rho_{solid} \quad (23)$$

7.1.3 *Net Fines Retained:*

Represents fines excavated during mining**, calculated from the density-driven mass difference.

$$M_{dry,fines} = M_{fines,after} - M_{fines,before} \quad (24)$$

7.1.4 *Adjustments for Slurry Disposal/Addition*

Slurry Disposal:

In the event that slurry is disposed of from the active tank during mining operations, the mass of fines (M_{fines}) for the disposed slurry must be accounted for and added to the calculations. For disposal of slurry during the mining, the corresponding dry mass of fines is calculated as follows:

$$M_{dryslurry\ disposed} = V_{slurry\ disposed}\left(\frac{\rho_{slurry\ disposed} - \rho_{water}}{\rho_{solid} - \rho_{water}}\right)\rho_{solid} \quad (25)$$

Bentonite Addition:

Dry mass of bentonite powder could be taken directly from record of fresh bentonite or calculated using fresh bentonite density as:

$$M_{dryslurry\ added} = V_{slurry\ added}\left(\frac{\rho_{fresh\ bentonite} - \rho_{water}}{\rho_{bentonite} - \rho_{water}}\right)\rho_{bentonite} \quad (26)$$

Revised Fines Mass:

To account for the fines in the system, it is required to add back the solids being disposed and subtract the slurry being added:

$$M_{dry,fines} = (M_{fines,after} - M_{fines,before}) + (M_{dry\ slurry\ disp.} - M_{dry\ slurry\ added}) \quad (27)$$

7.2 *Dry Mass Calculation Methods at STP*

7.2.1 *Method 1: Moisture Content-Based*

Starting from the total mass composition formula:

$$M_{tot} = M_{solid} + M_{water} \quad (28)$$

On both side of equation, we divide by M_{solid}:

$$\frac{M_{tot}}{M_{solid}} = 1 + \frac{M_{water}}{M_{solid}} = 1 + \mu \quad (29)$$

Isolating the solid mass we obtain:

$$M_{solid} = \frac{M_{tot}}{1 + \mu} \quad (30)$$

Weight shown by the belt weight measurement from pre-screen equates to the total weight of gravel: $M_{tot\ gravel}$.

$$Dry\ mass\ of\ gravel\ M_{gravel\ dry} = \frac{M_{tot\ gravel}}{(1+ \mu_{gravel})} \quad (31)$$

Weight shown by the belt weight measurement from cyclones equates to the total weight of soil: $M_{tot\ soil}$.

$$Dry\ mass\ of\ Soil\ M_{soil\ dry} = \frac{M_{tot\ soil}}{(1+ \mu_{soil})} \quad (32)$$

Total fines remaining in the system is the dry mass of fines $M_{fines\ dry} = M_{fines\ after\ mining} - M_{fines\ before\ mining}$.

$$M_{fines\ dry} = V_{tot} \left(\frac{\rho_{in\ situ} - \rho_{water}}{\rho_{soild} - \rho_{water}}\right) \rho_{solid} \quad (33)$$

$$\textbf{Total Dry Mass from STP} = M_{gravel\ dry} + M_{soil\ dry} + M_{fines\ dry} \quad (34)$$

7.2.2 *Method 2: Density-Based*

$$M_{dry} = V_{tot} \left(\frac{\rho_{in\ situ} - \rho_{water}}{\rho_{soild} - \rho_{water}}\right) \rho_{solid} \quad (35)$$

Divide both sides of the equation by $\rho_{in\ situ}$:

$$\frac{M_{dry}}{\rho_{in\ situ}} = V_{tot} \left(\frac{\rho_{in\ situ} - \rho_{water}}{\rho_{soild} - \rho_{water}}\right) \frac{\rho_{solid}}{\rho_{in\ situ}} \quad (36)$$

Further elaborating the formula:

$$M_{dry} = V_{tot} \rho_{in\ situ} \left(\frac{\rho_{in\ situ} - \rho_{water}}{\rho_{soild} - \rho_{water}}\right) \frac{\rho_{solid}}{\rho_{in\ situ}} \quad (37)$$

$$M_{dry} = M_{tot} \left(\frac{\rho_{in\ situ} - \rho_{water}}{\rho_{soild} - \rho_{water}}\right) \frac{\rho_{solid}}{\rho_{in\ situ}} \quad (38)$$

$$M_{dry\ gravel} = M_{tot\ gravel} \left(\frac{\rho_{in\ situ} - \rho_{water}}{\rho_{soild} - \rho_{water}}\right) \frac{\rho_{solid}}{\rho_{in\ situ}} \quad (39)$$

$$M_{dry\ soil} = M_{tot\ soil} \left(\frac{\rho_{in\ situ} - \rho_{water}}{\rho_{soild} - \rho_{water}}\right) \frac{\rho_{solid}}{\rho_{in\ situ}} \quad (40)$$

8 COMPARISON OF DRY MASS BY DIFFERENT METHODS

All data for comparing TBM dry mass calculations were sourced from the Deep Tunnel Sewerage System 2 (DTSS2) Project, Contract T-09, in Singapore, executed by Leighton Contractors (Asia) Limited (Singapore Branch) and CPB Contractors Tunnelling Business Unit.

The graphs in Figure 4 compare:

- Theoretical Dry Mass: Derived from in situ soil properties and TBM advance metrics (Equation 10).
- Actual TBM Dry Mass: Calculated via the Automated Excavation Management (AEM) system using real-time slurry density and flow data.
- STP Dry Mass:
  - Method 1: Moisture content-adjusted calculations (Equations 31–32).
  - Method 2: Density-based reconciliation (Equations 39–40).

Notable sharp reductions in dry mass values occurred at:

- Ring 0: Incomplete sensor commissioning during initial TBM launch
- Ring 90: Chamber interventions (e.g., cutterhead inspections)
- Rings 950 & 1470: TBM recommissioning after crossing intermediate shafts

These deviations highlight how operational resets affect sensor calibration but do not invalidate the overall reconciliation methodology. The consistency across methods elsewhere provides a reliable cross-check when one approach shows discrepancies.

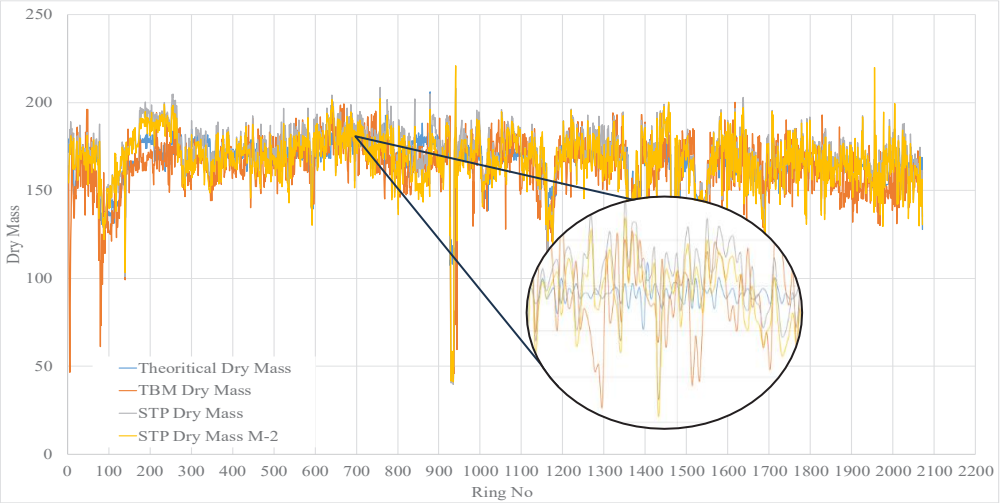


Figure 4 - Methods comparison graph.

9 CONCLUSION

The integrated framework—combining TBM dry mass, volume, and STP reconciliation—overcomes volumetric limitations in slurry-filled void scenarios. Field application on SRL East – Tunnels South (Suburban Connect JV, TBM launch 2026) will demonstrate real-time implementation in Melbourne's mixed-ground conditions, enhancing face stability control in urban environments.

10 REFERENCES

Connors, D. 2017. *Clogging mechanisms in slurry shield TBMs*. Journal of Geotechnical Engineering 143(8).

Das, B.M. & Sobhan, K. 2018. *Principles of Geotechnical Engineering* (9th ed.). Boston: Cengage Learning.

EFNARC 2005. *Specifications and Guidelines for the Use of Specialist Products for Mechanized Tunnelling (TBM) in Soft Ground and Hard Rock.* Farnham: EFNARC.

Gravemeijer, R., & Peila, D. 2022**.** *Managing TBM tunnelling in variable ground conditions: lessons from urban mega-projects*. Tunnelling and Underground Space Technology 129: 105033.

Herrenknecht AG 2020. *Slurry Technology: Efficient Tunnelling in Challenging Ground Conditions.* Schwanau: Herrenknecht AG.

Hochart, A. and Vialle, D. (2021), *Innovative slurry solutions for demanding TBM drives through soil with high permeability in a dense urban area.* Geomechanics and Tunnelling, 14: 489-500.

Maidl, B., Schmid, L., Ritz, W. & Collmann, M. 2012. *Hardrock Tunnel Boring Machines*. Berlin: Ernst & Sohn.

Mitchell, J.K. & Soga, K. 2005. *Fundamentals of Soil Behavior* (3rd ed.). New York: Wiley.

Peila, D., & Picchio, A. 2020. *Slurry TBM excavation in heterogeneous grounds: A review of key operational parameters*. Geotechnical and Geological Engineering 38(3): 2805–2821.

Shirlaw, J.N., Richards, D.P., Ramond, P. & Longchamp, P. 2003. *Recent applications of slurry shield tunnel boring machines*. Tunnelling and Underground Space Technology 18(4): 353–367.

Shirlaw, J.N., Tiong, R.L.K., Wong, K.Y. & Zhao, J. 2020. *Ground response and TBM performance in glacial deposits: Seattle SR99 case study*. Tunnelling and Underground Space Technology 103: 103456.

Tang, S.H., Zhang, X.P., Liu, Q.S., Li, J. & Chen, R. 2021. *Improved calculation method for excavation management in permeable sandy ground*. Tunnelling and Underground Space Technology 116: 104103.

Thewes, M. & Hollmann, F. 2016. *Assessment of face support pressure for slurry shield tunnelling*. Geomechanics and Tunnelling 9(5): 462–475.

Underground Singapore 2018. *Theory and Application of Excavation Management System for Slurry TBM in Singapore*. Singapore: Underground Singapore.

19th Australasian Tunnelling Conference – Acosta-Martínez, Stewart and Hudson-Smith (Eds.)
© 2025 Australian Tunnelling Society, ISBN 978-0-85825-002-4

Assessing the geotechnical feasibility of shallow TBM launch in India's urban landscape: a focused case study

M. Gowtham Sri Sai, Vignesh R, Visakan R & Doraswamy Raju G
L and T Construction, Manapakkam, Chennai, India

ABSTRACT: This study evaluates the feasibility of using shallow tunnel boring machine (TBM) launches for underground tunneling in Mumbai, focusing on adapting a standard shallow TBM launch section to the city's unique geotechnical conditions. Mumbai's soil profile, characterized by soft clays, silts, and weathered tuff, presents challenges for conventional tunneling methods, which are constrained by high costs, long construction timelines, and the need for minimal disruption in densely populated areas. With over 23.15 million people in the Mumbai metropolitan region, projected to increase by 30 million by 2050, there is a pressing need for efficient, cost-effective tunneling solutions. Conventional methods are often impractical due to space limitations and prolonged construction periods, making shallow TBM launches a promising alternative. These launches offer reduced surface disruption and faster construction. Numerical analysis is conducted to assess the structural safety and performance of shallow TBM launches in Mumbai's challenging geology, with results confirming satisfactory performance.

1 INTRODUCTION

Urban tunneling projects in rapidly developing cities such as Mumbai are increasingly relying on Tunnel Boring Machines (TBMs) for underground construction. Shallow TBM launches, where the tunnel is launched at depths less than one time the tunnel diameter, presents a unique set of challenges. These challenges primarily arise from the limited overburden, which can lead to significant ground movement, including surface settlement, deformation of surrounding infrastructure, and reduced support for the tunnel face. While traditional TBM launches generally occur at greater depths, shallow launches require specialized engineering solutions to ensure stability and minimize disruption to the surface and existing structures.

Mumbai's geological profile, characterized by a complex and highly variable combination of soft clays, silts, weathered tuff, and basalt, presents significant challenges for tunneling operations. Conventional tunneling techniques, such as shaft box construction, typically require extensive excavation and are associated with prolonged construction timelines of 18-24 months, often leading to substantial surface disruption. In contrast, the application of shallow Tunnel Boring Machine (TBM) launches offers a more efficient alternative, significantly reducing both excavation duration and surface impact. This paper investigates the feasibility of implementing shallow TBM launches in Mumbai, considering the city's diverse geotechnical conditions and outlining the necessary engineering approaches to ensure successful deployment in such a complex urban environment.

2 METHODOLOGY

2.1 Site selection: Mumbai's subsoil conditions

Mumbai was selected for this study due to its diverse and varied subsoil conditions, which present distinct challenges for Tunnel Boring Machines (TBMs), coupled with the city's rapid

urbanization, making it an ideal candidate for evaluating tunneling technologies. The geological profile of the region is dominated by Deccan basalts, associated with pyroclastic and plutonic rocks from the Upper Cretaceous to Palaeogene age, forming the Sahyadri Group (Sethna, 1999). The Deccan volcanic terrain, covering nearly 500,000 km² of the Indian subcontinent, has a thickness of up to 1.6 km above mean sea level. The Deccan basalt in Mumbai is of Eocene age (Subbarao, 1988). The geology of the region also includes ultrabasic, basic, and acidic volcanic formations with intertrappean beds, agglomerates, and tuffs. Basalt flows in the area are categorized into compound (pahoehoe type), simple, and unclassified flows (Jain et al., 2011; Singh et al., 2009). These diverse geological conditions, coupled with a high-water table, result in challenging ground behavior that significantly influences TBM performance. Mumbai's dense urban environment further necessitates the use of shallow TBM launches, as they minimize surface disruption and avoid extensive excavation pits. The city's geological profile includes soft clays, silts, weathered tuff, and basalt, with significant variability across short distances.

2.2 Geotechnical conditions at the TBM launch area

A detailed geotechnical analysis was performed to assess the properties of the strata encountered during tunneling operations. Laboratory tests, field investigations, and geotechnical models were utilized to simulate ground behavior and optimize TBM performance. The table below summarizes the key geotechnical parameters, including Uniaxial Compressive Strength (UCS), Geological Strength Index (GSI), Rock Quality Designation (RQD), Modulus of Elasticity (Ei), and Rock Mass Modulus (Erm), crucial for designing and optimizing TBM operations. The Hoek-Brown failure criterion was applied to rock layers (tuff and basalt), while the Mohr-Coulomb failure model was used for soil layers

Table 1. Geotechnical Properties of Subsurface Strata at the TBM Launch Site

Geological Profile	Depth of stratum Top (m)	Unit Weight (kN/m^3)	Poisson's Ratio	TCR (%)	RQD (%)	UCS, (MPa)	GSI	Ei, (GPa)	Erm, (MPa)
Marine Clay	0	17	0.45	-	-	-	-	-	-
Grade V Tuff	5	20	0.25	30	0	1.4	22.5	0.28	14.56
Grade III to II Tuff	6.5	21	0.22	83	51	7.4	52.5	2.94	1046.22
Grade IV Tuff	11	21	0.22	33	3	1.4	28.5	0.28	20.71
Grade IV Tuff with shale	20	21	0.22	46	13	2.9	30.5	0.58	48.75
Grade V Tuff	27.5	23	0.22	48	0	1.4	27	0.28	18.88
Grade III Tuff	32	27	0.22	66	42	15	48	5.99	1625.97
Grade II Basalt	33.5	27	0.2	89	80	55.4	67	17.95	12097.0
Grade II Tuff	36.5	27	0.22	89	59	56.6	56.5	22.6	9969.29
Grade I Basalt	38	27	0.2	96	90	37.4	72	16.83	12934

The data presented in Table 1 and Figures 1 and 2 below depict the variation of critical geotechnical parameters, including UCS, RQD, and core recovery, with depth at the TBM launch site. This data is crucial for a comprehensive understanding of the subsurface conditions and plays a pivotal role in optimizing TBM design and tunneling strategies, tailored to the unique geological challenges presented by Mumbai's complex geology.

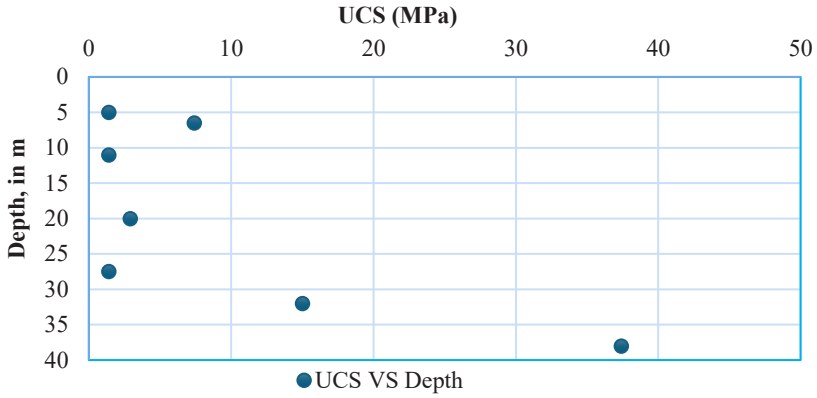


Figure 1. Variation of (Depth vs UCS)

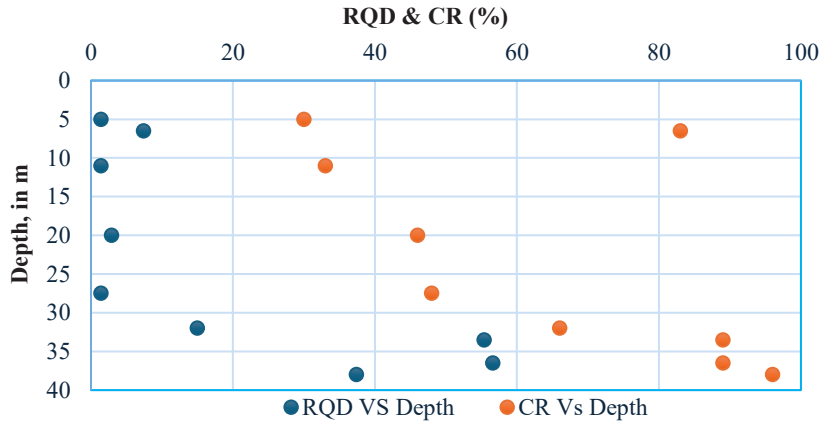


Figure 2. Variation of (Depth vs RQD & CR)

2.3 Shallow TBM launch section design for Indian geological condition

The analysis utilizes a shallow TBM launch section to assess its applicability to Indian geological conditions. The reference design includes a reinforced concrete protective slab with a thickness of 1.5 meters, a secant pile wall that is 1.0 meter thick and 7.5 meters long, with a 5-meter embedment into rock, and a tunnel with an internal diameter of 5.8 meters (outer diameter 6.35 meters). Numerical analysis was performed to evaluate the structural and geotechnical performance of this design. The system is designed to support the TBM launch while maintaining the alignment gradient until a safe geological section is reached. The protective structure includes the reinforced concrete slab, which ensures stability and prevents collapse during the TBM launch. Additionally, an unreinforced concrete slab provides temporary protection to mitigate subsidence risks during the TBM's progress, with both slabs length and specifications adjusted based on design requirements and local conditions.

A Secant pile wall serves as a temporary protective structure, stabilizing the surrounding area and preventing lateral ground movements. The wall is designed with a 5-meter embedment in rock to ensure its stability under load. For the numerical analysis, the geotechnical design parameters for the clay within the improved zone were exclusively considered. Prior to improvement, the clay exhibited a cohesion (c) of 15 kPa and a Young's Modulus (E) of 2700 kPa. Following ground treatment, these parameters were enhanced to a cohesion (c) of 50 kPa and a Young's Modulus (E) of 9000 kPa, reflecting the increased strength and stiffness achieved through the ground improvement process. These measures are critical for providing optimal steering control of TBM. The support systems, including the reinforced slab and Secant pile wall, remain in place until the TBM reaches more homogeneous material, allowing the necessary soil

arching to occur above the TBM and ensuring its stability and safe passage. The Numerical model for this design is shown below.

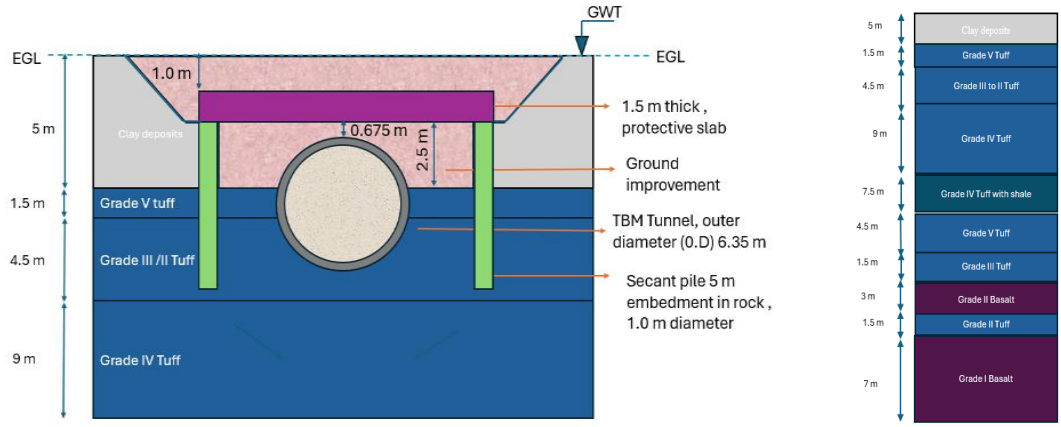


Figure 3. Cross-section utilized for numerical analysis at the shallow TBM launch

3 NUMERICAL ANALYSIS AND CONSTRUCTION METHODOLOGY

The construction of the Tunnel Boring Machine (TBM) launch site is a complex process that requires careful planning and execution to ensure safety, stability, and efficient tunneling operations. The process begins with a comprehensive initial phase, which includes site surveying, geotechnical investigations, infrastructure setup, and implementation of safety protocols. These initial steps lay the foundation for the subsequent excavation work. Excavation begins at the surface level, Initial excavation proceeds with a temporary sloped cut from the surface, reaching a design depth of 2.5 meters. Following the completion of this initial excavation, the secant pile wall is meticulously constructed, subsequently providing critical shoring and effectively stabilizing the excavated profile for the ensuing TBM launch operations.

Dewatering measures, including well-point systems, are employed to manage groundwater levels and prevent hydrostatic pressures that could destabilize the excavation site. In the next phase, ground improvement techniques such as soil replacement or stabilizing agent injection are used to enhance the clay layers up to a depth of 5 meters. A protection slab is placed to distribute loads and maintain stability during the excavation. Once these preparatory steps are complete, the TBM is prepared for launch. Tail void grout is applied to fill any gaps between the TBM and the final tunnel lining, ensuring water ingress is prevented. A contraction factor is incorporated to account for any potential conicity during TBM operation.

Once TBM is activated, continuous monitoring of ground movement, Secant pile-wall deflection, and surface settlement is conducted to ensure the stability of the TBM and surrounding infrastructure. Grout pressure at the TBM tail is closely monitored to ensure tunnel integrity and minimize void formation. After the tunneling operations are completed, a final assessment is carried out to evaluate the effectiveness of the excavation. Shear forces, bending moments, and deformations in the Secant pile wall are analyzed, and surface heaves and Secant pile wall deflection are checked to ensure they are within acceptable limits. The effectiveness of the void grouting process is also assessed to guarantee the long-term stability of the tunnel.

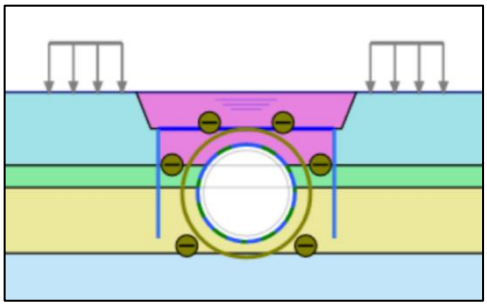


Figure 4. Numerical model at final stage after installation of tunnel lining

4. RESULTS AND DISCUSSIONS

4.1 Numerical simulation output

The analysis of the shallow TBM launch section yielded critical data on the geotechnical and structural performance of the design. Through numerical simulations, the performance of key structural elements such as the Secant pile wall and surrounding soils was assessed in detail. The results of these simulations provide insights into the behavior of the system during tunneling and the effectiveness of geotechnical measures to control surface settlement and lateral deflection.
The analysis of specific settlement characteristics reveals that surface settlements primarily occurred due to the tunneling operations.

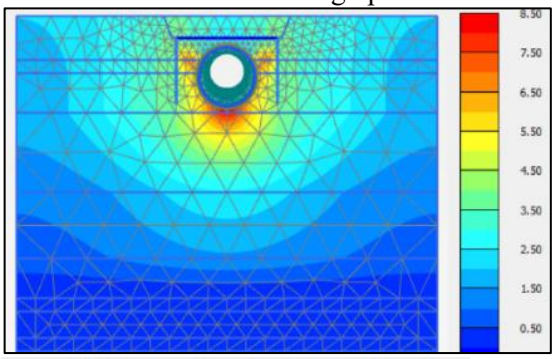


Figure 5. Deformations at final stage after installation of tunnel lining

Figure 5 shows the detailed deformations at the final face of the tunnel after the installation of the TBM lining. This figure underscores the localized effects of tunneling on surface stability.
Settlement analysis showed a maximum settlement of 9 mm, which is within the expected range for tunneling in Mumbai's soft soil conditions. This result is significant as it suggests that the shallow TBM launch design can be safely implemented in urban environments without causing excessive settlement or disruption to surface infrastructure. The uniform distribution of settlement along the alignment indicates that the system effectively minimizes localized surface displacement.

The lateral deflection of the Secant pile wall was observed to be minimal. This confirms that the Secant pile wall performs as intended under the imposed loads from the TBM. The wall provides the necessary lateral resistance, ensuring the integrity of the tunnel during excavation. The lateral deflection profile further supports the adequacy of the wall design for the specific geotechnical conditions encountered.

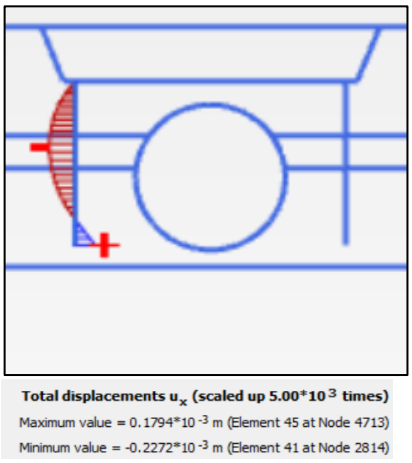


Figure 6. Deformations of secant pile wall at final stage after installation of tunnel lining

This figure illustrates the calculated lateral deflections of the Secant pile wall at the final stage of installation. This figure is integral for assessing the performance of the Secant pile-wall under dynamic loads imposed by the TBM operations.

The results suggest that while the shallow TBM launch method is effective for the given geotechnical conditions, further design optimization may be necessary. Additional geotechnical measures, such as soil improvement techniques, should be considered to reduce risks associated with localized instabilities and ensure the long-term safety of the project.

The analysis of the bending moment variation along the tunnel lining, with a maximum value of 47.94 kN/m, is crucial for assessing the tunnel's structural integrity under dynamic loads. This data helps optimize the tunnel lining design, ensuring it can withstand both construction and long-term operational conditions. Including this analysis in the paper ensures the safety, durability, and efficient use of materials in the tunnel's construction, providing confidence in its performance. throughout its service life.

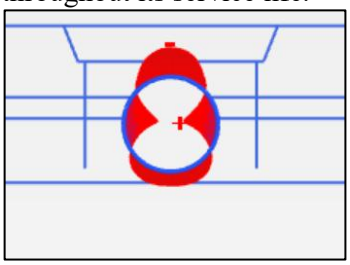


Figure 7. Bending moment distribution at the final stage of tunnel lining installation.

This figure illustrates the variation in bending moments along the tunnel lining, highlighting critical stress points that ensure the tunnel's structural integrity under operational loads.

4 CONCLUSIONS

Feasibility of Shallow TBM Launches: The feasibility of shallow TBM launches in urban environments is primarily determined by the local geological conditions. According to Numerical analysis, the expected settlement is minimal (9 mm), and the deformations of the secant pile remain within the permissible limits as outlined in the reference. This ensures that tunneling can be carried out safely, with negligible impact on adjacent structures.

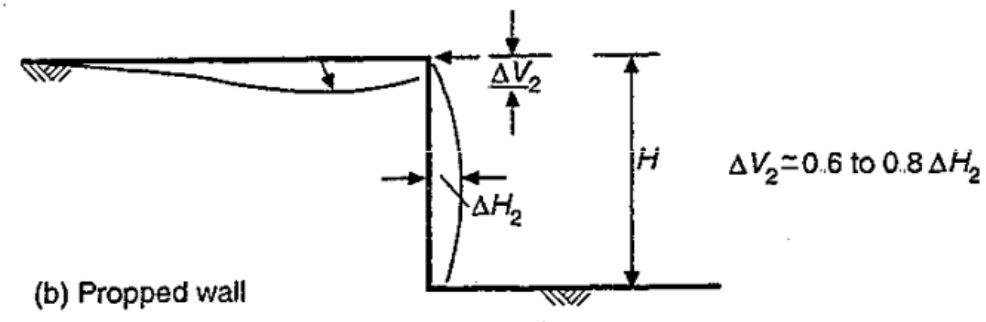


Figure 8. Comparative wall and ground movements after Burland et al. (Ciria C517)

Structural Integrity: The adopted design and construction methods effectively control ground movement and structural deflection, maintaining safety within permissible limits.

Continuous Monitoring: Real-time monitoring using advanced instrumentation (e.g., inclinometers, piezometers) is crucial for detecting and mitigating potential risks during tunneling.

Ground Improvement: Pre-excavation ground improvement techniques, such as grouting and soil stabilization, are recommended to enhance soil stability and minimize settlement and deflection risks.

Shallow TBM Launch Viability and Future Work**:** Shallow TBM technology, when implemented with comprehensive geotechnical assessments, continuous monitoring systems, and robust risk management strategies, offers significant advantages such as reduced noise pollution, a smaller carbon footprint, and minimal environmental impact. Its adaptability to various geological conditions contributes to efficient urban infrastructure development. Continued innovation in TBM methods and geotechnical practices will be crucial for enhancing safety, operational efficiency, and the overall success of underground construction in future projects.

5 REFERENCES

Angerer, W., Haimoni, A.M., Ozturk, A. & Tellioglu, V. 2019. Shallow TBM launch: An alternative to cut and cover. In: Peila, V., Viggiani, G. & Celestino, R. (eds), Tunnels and Underground Cities: Engineering and Innovation Meet Archaeology, Architecture and Art. London: Taylor & Francis Group. https://doi.org/10.1201/9781003031659-7Taylor & Francis

Bhanage, V., Lee, H.S., Gedam, S. & Latha, R. 2022. Impacts of future urbanization on urban microclimate and thermal comfort over the Mumbai metropolitan region, India. Sustainable Cities and Society, 79: 103703. https://doi.org/10.1016/j.scs.2022.103703

Bentley Systems 2023. PLAXIS 2D 2024.1 Material Models Manual 2D. Bentley Advancing Infrastructure.

Bentley Systems 2023. PLAXIS 2D – Reference Manual. Bentley Advancing Infrastructure.

Bieniawski, Z.T. 1989. Engineering Rock Mass Classification. New York: Wiley Interscience.

Bowles, J.E. 1997. Foundation Analysis and Design (5th ed.). New York: McGraw-Hill.

Castellví, H., Torelló, X., Rogala, T. & Doulkas, G. 2020. Shallow TBM launch of the Northolt Tunnel West TBMs at West Ruislip. HS2 Learning Legacy. https://learninglegacy.hs2.org.uk/document/shallow-tbm-launch-of-the-northolt-tunnel-west-tbms-at-west-ruislip-hs2-lot-s2/HS2 Learning Legacy+1majorprojects.org+1

CIRIA 1995. The Standard Penetration Test (SPT): Methods and Use. CIRIA Report 143. London: CIRIA.

Hoek, E., Carranza-Torres, C. & Corkum, B. 2002. Hoek-Brown criterion – 2002 edition. In: Proceedings of NARMS-TAC Conference, Toronto.

Hoek, E., Carter, T.G. & Diederichs, M.S. 2013. Quantification of the Geological Strength Index chart. In: 47th US Rock Mechanics/Geomechanics Symposium. American Rock Mechanics Association.

Indian Standards 1998 (Reaffirmed 2019). IS 8764: Method of Determination of Point Load Strength Index of Rocks. New Delhi: Bureau of Indian Standards.

Oldenhave, A.H. 2014. Starting a large diameter TBM from surface: Feasibility study for the Netherlands. MSc Thesis, Delft University of Technology. https://repository.tudelft.nl/record/uuid%3A172ab959-402c-46ec-912f-a01ed7d2cf61TU Delft Repository

Tomlinson, M.J. 2001. Foundation Design and Construction (7th ed.). Harlow: Longman Scientific and Technical.

Zhang, D.D., Zhou, J.F., Zhang, W.G., Zhu, C.B., Sun, R.R., Ji, L.J. & Wu, Z.X. 2011. The finite element analysis of the excavation on adjacent buildings based on Mohr-Coulomb model. Advanced Materials Research, 374–377: 2171–2175. https://doi.org/10.4028/www.scientific.net/AMR.374-377.217

19th Australasian Tunnelling Conference – Acosta-Martínez, Stewart and Hudson-Smith (Eds.)
© 2025 Australian Tunnelling Society, ISBN 978-0-85825-002-4

Research on composite rock breaking tests and efficiency evaluation of cutter disk hobs for TBM with large taper face

J.B. Li, Y.Q. Lu, Y. Zhu, C.X. Cao, Y.H. Wei
China Railway Engineering Equipment Group Co., Ltd., Zhengzhou, Henan, China

ABSTRACT: The conical cutterhead is a highly feasible rock-breaking method in composite rock fragmentation with free faces, characterized by a shear-tension failure mechanism. Notably, this failure mode becomes more pronounced with increasing taper, where a taper of 30°-45° is typically defined as large-taper. To thoroughly investigate the rock-breaking mechanism of large-taper conical cutterheads in Tunnel Boring Machines (TBMs), this paper takes the action of the large-taper conical cutterhead on high-strength amphibolite as the research object, carries out rock-breaking tests, and performs numerical simulations using LS-DYNA. The results demonstrate that large-taper conical cutterheads exhibit excellent adaptability in hard rock formations. Compared with flat cutterheads, the large-taper conical cutterheads require lower average thrust forces, generate rock debris with higher roughness indices, and achieve superior rock-breaking efficiency. The results of this study can provide both theoretical and practical foundations for the structural design of large-taper conical cutterheads.

1 INTRODUCTION

As a critical equipment in underground engineering construction, tunnel boring machines (TBMs) have diverse cutterhead structural forms. In domestic and international engineering applications and research, common cutterhead types include flat cutterheads, spherical cutterheads, conical cutterheads, etc (Zhao et al., 2016), as shown in Figure.1.

The flat cutterhead has become a widely used structural type due to its advantages such as excellent geological adaptability, simple manufacturing process, and high thrust utilization. Compared to flat cutterheads, other structural forms are less frequently applied in engineering practice. However, these cutterheads also possess unique strengths. For example, conical and spherical cutterheads exhibit superior structural strength and stiffness, with outstanding auxiliary rock-breaking effects under free-face conditions (Zhang 2003).

Current research on composite rock-breaking with free face is primarily divided into mechanical multi-stage rock-breaking and high-pressure water jet composite rock-breaking. Mechanical multi-stage rock-breaking focuses on improving cutterhead structures, where preceding cutters prepare free faces for subsequent cutters to enhance efficiency. Examples include conical cutterheads (Figure 1b) and spherical cutterheads (Figure 1c). Ramezanzadeh & Hood (2010) reported the CMM-type boom-type roadheader developed by German company AKER-WIRTH, which utilizes undercutting-mode cutters to fully exploit free-face effects, thereby enhancing rock-breaking efficiency. Geng et al. (2014, 2015, 2016, 2021) proposed a multi-stage TBM cutterhead design (Figure 2b), systematically exploring the preparation of free faces by front-stage cutterheads for rear-stage cutterheads, as well as the dynamic evolutionary mechanisms of free-face groups, which provides a theoretical basis for designing free-face height and spacing. Building on this, Experimental and numerical studies have been conducted to investigate the influence of

parameters such as rock type, free-face height, and spacing on rock-breaking load, efficiency, and failure modes (Zhang et al., 2018; Zhang et al., 2022; Wang, 2020).



(a) (b) (c)

Figure 1. Type of cutterhead for tunnel boring machine. (a) Flat cutterhead (Rostami, 2008). (b) Conical cutterhead (Rostami & Chang, 2017). (c) Spherical cutterhead (Wang, 1980).

High-pressure water jet composite rock-breaking enhances the efficiency of disc cutters by forming free faces through water jet grooving. Research approaches include laboratory tests, numerical simulations, and field trials. Laboratory tests show: Fenn et al. (1998) found that a 40 MPa water jet can reduce the force on disc cutters by 40%; Ciccu & Grosso (2014) demonstrated that water jets doubled the penetration rate and increased the rock-breaking volume to 3.8 times; Cheng et al. (2020) revealed significant specific energy reduction with slot depth increase; He et al. (2023) suggested optimizing the jet cutting capability and reducing the blade width and slot spacing to enhance the rock-breaking effect. The water-jet-equipped TBM "Longyan Hao" has undergone field trials in Fujian's Wan'anxi Project (Li, 2020).

These studies demonstrate that rational free-face arrangements facilitate crack propagation toward free faces, forming rock fragments and reducing rock-breaking loads while improving efficiency. The high-pressure water jet composite rock-breaking technology faces challenges such as complex equipment systems and low energy utilization efficiency, and has not yet achieved widespread adoption (Wei et al., 2024). Currently, the conical cutterhead, as a representative of mechanical multi-stage rock-breaking, is recognized as the most feasible rock-breaking approach based on composite rock-breaking with free face. TBM cutterheads are generally defined into three categories based on taper angles: small taper (0° to 15°), medium taper (15° to 30°), and large taper (30° to 45°). The larger the taper, the more fully the composite rock-breaking with free face is utilized. Existing studies on conical cutterheads focuses on structural stiffness, cone angles, and stability during the tunneling process. However, these studies remain confined to the theoretical level, with a lack of research on the rock-breaking mechanism of conical cutterheads and full-scale rock-breaking experiments (Zhang et al., 2020; Zhang et al., 2018; Liu, 2003; Zhang & Zhang, 2007).

To further explore the effect of composite rock-breaking with free face, this study investigates the rock-breaking mechanisms of large-taper conical cutterheads. First, rock-breaking experiments under forward thrust and swing modes were conducted on high-strength amphibolite. Second, a finite element model using LS-DYNA was developed to analyze cutter load distribution patterns. The findings provide theoretical and practical guidance for the structural design of large-taper conical cutterheads.

2 ANALYSIS OF ROCK-BREAKING MECHANISM FOR DISC CUTTERS

2.1 *Analysis of the compressive rock-breaking mechanism of disc cutters*

The rock breaking mechanism diagram of the cutter is shown in Figure 3. Under the combined action of normal force and rolling force, the cutter gradually cuts into the rock mass. This process triggers multiple stress effects such as shear, tension and compression in the rock, forming a broken area under the cutter, which is transformed into a hemispherical dense core by compaction. With the continuous pressure of the disc cutter, the dense core produces a radial extrusion effect, which transfers the stress to the surrounding rock mass, promotes the germination of microcracks inside the rock mass, and extends to both ends and deep part of the disc cutter. When the distance between adjacent disc cutters is appropriate, the lateral tensile cracks are connected to each other,

and the broken rock mass is formed between the disc cutters and the parent body is peeled off, and finally the rock mass is broken.



(a) (b) (c)

Figure 2. Composite rock-breaking with free face. (a) CMM-type boom-type roadheader with under-cutting rock-breaking system (Ramezanzadeh & Hood, 2010). (b) Multi-stage cutterhead (Geng et al., 2016). (c) High-pressure water jet composite rock-breaking (Li, 2020).

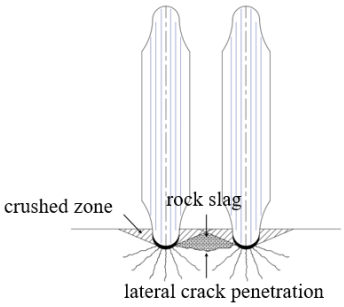


Figure 3. Schematic diagram of the rock fragmentation process by a disc cutter.

2.2 *Mechanism analysis of composite rock-breaking with free face*

In the process of large-taper conical cutterhead penetrating into the rock, the main disc cutter array penetrates into the rock at the same time. Due to the installation height difference of disc cutters in the tapered area, each cutter penetrates successively, and the previously penetrated cutter can create a free face for the subsequent ones. It can be seen from Figure.4 that the positive disc cutter group A can prepare the free face for the cone disc cutter b, and the cone disc cutter b can prepare the free face for the cone disc cutter c. The rock breaking mechanism of the large-taper conical cutterhead is 'shear-tension failure'. The ' shear-tension failure' is a comprehensive failure mode under the combined action of shear and tension. The shear stress dominates the crack initiation, and the tensile stress dominates the crack propagation. Specifically, the shear force is generated in the contact area between the disc cutter and the rock in the cone area, resulting in the formation of initial microcracks in the rock. With the repeated extrusion of the disc cutter in the cone area, the tensile stress is generated in the rock mass, which promotes the microcracks to penetrate rapidly to the free face. Therefore, compared with the flat cutterhead, the large-taper conical cutterheads make full use of the composite rock breaking with free face, and its ' shear-tension failure ' mode is more efficient than the traditional extrusion failure mode.

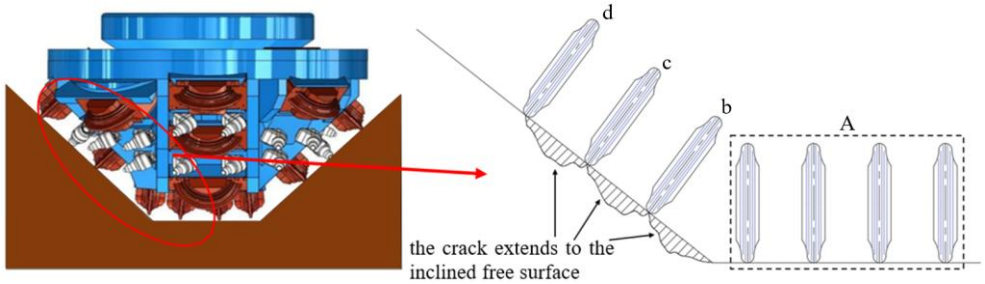


Figure 4. The composite rock-breaking mechanism of a large-taper conical cutterhead.

3 ROCK BREAKING TEST OF LARGE-TAPER CONICAL CUTTERHEAD

3.1 *The main technical parameters*

This experimental study takes the CTR450 cantilever roadheader with an excavation section size of 9.3m×8.2m as the carrier object to carry out relevant tests. This cantilever TBM is equipped with a 45° conical cutterhead (Figure 5). The single excavation area of the cutterhead reaches 76 m^2, and the rock-breaking capacity of its hard rock cutterhead is designed to range from 80 to 120Mpa. The main design parameters of the cutterhead are shown in Table 1.

Table 1. Main design parameters of conical cutterhead.

Parameter	value
Excavation capacity (Mpa)	80-120
Excavation diameter (mm)	1800
Structure form of cutterhead	45° conical shape
Number of cutters	13
Total weight (t)	5.6
Drive power (kW)	450

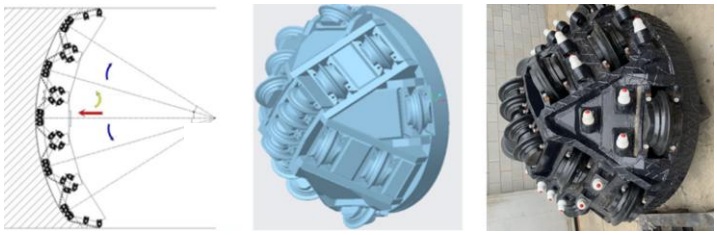


Figure 5. 45-degree conical hard-rock cutterhead.

3.2 *Rock-breaking test procedure*

To verify the rock-breaking effect of the large-taper conical cutterhead, the processing and manufacturing of the conical face cutterhead were completed based on the above design parameters. Physical model tests were carried out under laboratory conditions. For amphibolite (with a compressive strength of 108.3MPa, tensile strength of 7.2MPa, Young 's modulus 75.6GPa, and Poisson 's ratio of 0.25), rock-breaking tests were conducted in four operation modes: forward push, downward swing, left swing and right swing (Figure 6).



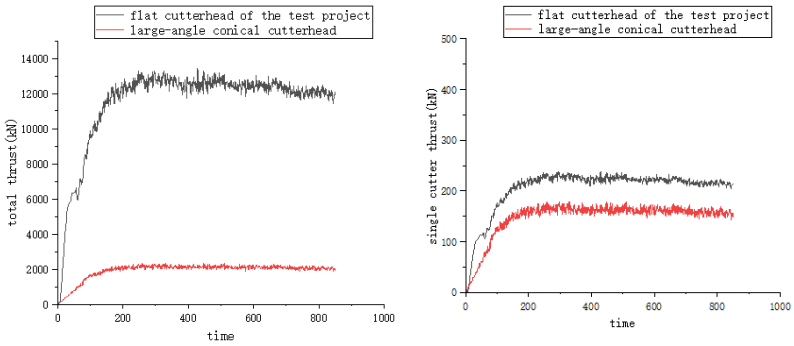
Figure 6. Large-taper conical cutterhead rock-breaking test.

3.3 *Comparative analysis of thrust force*

A comparative analysis is conducted on the rock-breaking thrust force between the large-taper conical cutterhead and the flat cutterhead used in the test project, with the relevant data shown in Figure 7. Among them, the total number of cutters equipped on the flat cutterhead is 56, while the total number of cutters on the large-taper conical cutterhead is 13. From the variation trend of the

rock-breaking thrust, both types of cutterheads show the characteristic of rising first and then gradually stabilizing.

It can be clearly observed from Figure 7a that due to the significant difference in the number of cutters, the total thrust of the flat cutterhead is much larger than that of the large-taper conical cutterhead. In order to compare the performance of the two types of cutterheads more fairly, the total thrust of each is divided by the number of cutters, thereby obtaining the thrust value of a single cutter. Through comparison, it is found that when the rock-breaking thrust reaches the stable stage, the average thrust of a single cutter of the flat cutterhead is 222.08kN, while that of a single cutter of the large-taper conical cutterhead is 161.71kN. This indicates that the average thrust of a single cutter of the large-taper conical cutterhead is 27.18% lower than that of the flat cutterhead, and the total thrust of the large-taper conical cutterhead is smaller when the number of cutters is the same.



(a) (b)

Figure 7. (a) Comparison of total thrust. (b) Comparison of single disc cutter thrust.

3.4 *Particle size analysis of rock debris*

The particle size roughness of rock debris serves as a critical indicator for evaluating rock-breaking efficiency, with higher proportions of large fragments correlating to greater efficiency (Yan et al., 2020). Due to rock joints and the complexity of rock breaking, the rock debris generated during the rock-breaking process of a large-taper conical cutterhead takes various forms. (Figure 8). By screening 703.74 kg of rock debris, data for nine particle size grades were obtained. (Table 2).



Figure 8. Pictures of rock debris at various grade.

Table 2. Particle size distribution of rock debris.

Particle size of rock debris (mm)	mass(kg)	mass fraction
≥60	120.62	17.45%
40-60	58.32	8.44%
20-40	89.00	12.88%
10-20	65.54	9.48%
5-10	49.14	7.11%
2-5	62.61	9.06%
1-2	25.66	3.71%
0.5-1	101.64	14.71%
≤0.5	118.51	17.16%

The roughness index of rock debris is obtained by adding up the cumulative residue rates of each screen after sieving. Its mathematical expression (Roxborough & Rispin, 1973) is:

$$X_i = \frac{W_i}{W_t} \times 100\% \quad (1)$$

$$I_C = \sum X_i \quad (2)$$

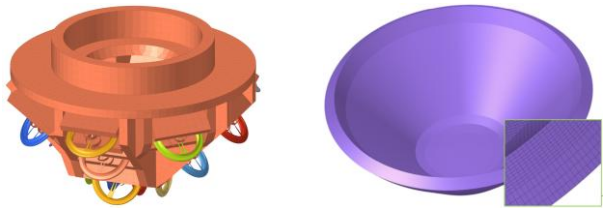
Where W_t = total mass of rock debris; W_i = total mass of rock debris larger than a certain particle size; X_i = residual screening rate of rock debris larger than a certain particle size; I_C = roughness index of rock debris.

Substituting the total mass of rock debris at all grades shown in Table 2 into Equations (1) and (2), it is calculated that the roughness index of rock debris obtained from the rock breaking test with the large-taper conical cutterhead is 508. Comparing the rock debris roughness index of 320-450 during the construction of a double-shield TBM in a Lanzhou tunnel, it is demonstrated that cantilever TBMs equipped with large-taper conical cutterheads exhibit higher rock debris roughness indices in hard rock formations, thereby achieving superior rock-breaking efficiency. Moreover, the rock debris produced is mostly flat and flaky, which reduces cutter wear and further verifies that the conical cutterhead has a significant advantage over the traditional extruded rock breaking, and it is a more suitable structural form for tunnel boring in hard rock tunnels.

4 SIMULATION ANALYSIS FOR COMPOSITE ROCK BREAKING OF LARGE-TAPER CONICAL CUTTERHEAD

4.1 *The composite rock breaking model for the large-taper conical cutterhead*

In this paper, the numerical model of rock breaking of large-taper conical cutterhead is constructed by using LS-DYNA finite element software. (Figure 9). In the modeling process, in order to realize the simplification and efficient solution of the model, the shell element is used to model the cutterhead structure. For the cutter model, it is simplified into an annular structure composed of shell elements. As for the cutter ring, only the cutting edge that comes into contact with the rock is retained. Revolute joint connections were established between the cutter rings and shafts to enable self-rotation functionality. Since the stiffness of rock material is significantly lower than that of the cutter, and the focus of this study does not involve the internal stress state of the cutter, the cutter is therefore simplified as a rigid body. For the rock mass model, the tunnel face is simplified as a conical rock mass block, and local mesh refinement is performed on the contact area between the cutter and the rock mass.



(a) (b)

Figure 9. (a) Finite element model of cutterhead. (b) Finite element model of tunnel face.

4.2 *Load analysis of cutters on the large-taper conical cutterhead*

The trajectory of the disc cutters is shown in Figure 10. Numbers 1 to 4 are the center disc cutters, and the installation angle of each disc cutter is 5°, Numbers 5 to 13 refer to the positive cutters, among which the No. 5 cutter is in the transition area, and its installation angle is 25°. The installation angle of positive disc cutters numbered from 6 to 12 is 45°, the installation angle of the No.13 disc cutter is 59.8°.

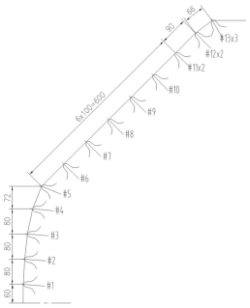


Figure 10. Schematic diagram of disc cutter trajectory.

Taking the No.8 cutter as an example, its load is shown in Figure 11. During 0-0.01 s, the cutterhead advances along the Y-axis to achieve target penetration depth, causing the vertical force to rapidly increase to its peak value. After 0.01 seconds, the cutterhead rotates uniformly around the Y-axis. The rock continuously fractures, and the failed elements are deleted. The load on the cutter oscillates around a mean value over time. The vertical force of the cutter is much greater than the lateral force and rolling force, and the lateral force fluctuates around zero.

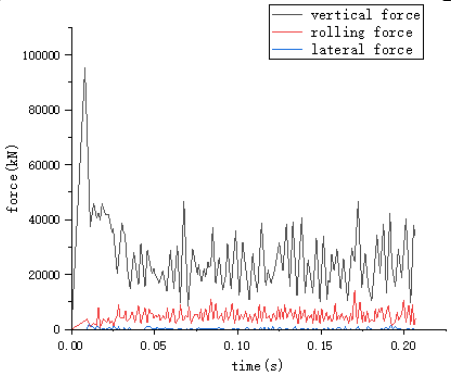


Figure 11. Load of the 8th disc cutter.

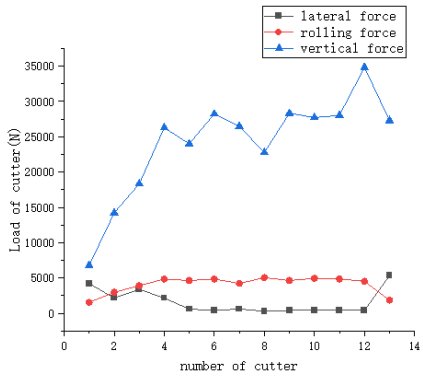


Figure 12. Load of each disc cutter.

To mitigate the influence of the initial penetration of the disc cutter into the rock, the average load during the stable contact phase between the disc cutter and the rock (0.04-0.2 seconds) was adopted as the cutter load, with the results presented in Figure 12.

From Figure 12, it can be seen that overall, the vertical force of the cutter is much greater than both the rolling force and the lateral force, and the rolling force is also greater than the lateral force. The vertical force of the disc cutter increases rapidly to a stable and slight fluctuation with the increase of the disc cutter number. The rolling force increases slightly to a stable state and then decreases slightly. The lateral force of the disc cutter first decreases to a stable value and then increases.

Through the comparative analysis of the mechanical properties of the disc cutters in each area of the cutterhead, it is found that the vertical force increases gradually from No.1 to No.4 cutter, and then tends to be stable. Simulation data indicate that the average vertical force of conical cutters(No.5-13 cutters) reaches 27,623N, 1.67 times higher than the 16,504N average of central

cutters(No.1-4 cutters). This demonstrates that conical cutters exert greater vertical forces during rock fragmentation, resulting in superior rock-breaking efficiency.

5 CONCLUSION

In this paper, the rock breaking test is carried out by using the large-taper conical cutterhead of TBM acting on high-strength amphibolite, and the rock breaking efficiency is analyzed. Based on the field test, the finite element model for composite rock breaking of a large-taper conical cutterhead was constructed to investigate the load distribution pattern of disc cutters. The following conclusions provide theoretical guidance for the design of large-taper conical cutterheads:

1) The composite rock-breaking mechanism of the large-taper conical cutterhead follows a "shear-tension failure" pattern. The shear stress dominates the crack initiation, and the tensile stress dominates the crack propagation. Compared with the flat cutterhead, the large-taper conical cutterheads make full use of the composite rock breaking with free face, and its ' shear-tension failure ' mode is more efficient than the extrusion failure mode of most flat cutterheads breaking hard rock.

2) Experimental studies on large-taper conical cutterheads reveal that compared with the flat cutterhead, the large-taper conical cutterhead has a smaller average thrust per cutter, produces rock fragments with a higher roughness index, and the fragments are mostly thick, flat flakes. Therefore, the large-taper conical cutterhead exhibits higher rock-breaking efficiency.

3) Simulation results of large-taper conical cutterheads indicate that the vertical force of the conical cutter is significantly greater than that of the central cutter, so the conical cutter has better rock breaking efficiency than the central cutter.

4) The conical cutterhead has a composite rock breaking function, which is far superior to the flat cutterhead in terms of rock breaking efficiency. It is expected that the conical cutterhead will gradually become the main structural form in the future. The greater the compressive strength of the rock, the more prominent the effect will be.

6 REFERENCES

[1] Zhao, K.T., Zheng T.K., Li N. and Ma C.C. 2016. Analysis on Static Mechanical Performances of TBM Cutterhead with Different Geometries. *Tunnel Construction* 36(1): 102-107.

[2] Rostami, J. 2008. Hard rock TBM cutterhead modeling for design and performance prediction. *Geomechanik und Tunnelbau: Geomechanik und Tunnelbau* 1(1): 18-28.

[3] Rostami, J. and Chang, S.H. 2017. A closer look at the design of cutterheads for hard rock tunnel-boring machines. *Engineering* 3(6): 892-904.

[4] Wang, J.L. 1980. Discussion on Foreign Rock Tunnel Boring Machines Part 1- Prototype Design. *Power Generation Technology* (2): 1-13.

[5] Zhang, Z.H. 2003. Side-slip Analysis of Disc Cutter on All Kinds of Cutterheads of Full Face Rock Tunnel Boring Machine. *Modern Electric Power* 20(2): 16-18.

[6] Ramezanzadeh, A. and Hood, M. 2010. A State-of-the-art Review of Mechanical Rock Excavation Technologies. *International Journal of Mining and Environmental Issues* 1(1):29-39.

[7] Geng, Q., Wei, Z.Y., Meng, H., Macias, F.J. and Bruland, A. 2016. Free-face-Assisted Rock Breaking Method Based on the Multi-stage Tunnel Boring Machine(TBM)Cutterhead. *Rock Mech Rock Engineering* 49: 4459-4472.

[8] Geng, Q., Wei, Z., Meng, H. 2014. Numerical and experimental method for determining the boring diameters of the two-stage TBM cutter head to prevent rockburst. *Journal of Mechanical Science and Tecnology* 28(11): 4613-4620.

[9] Geng, Q., Ye, M., Lu, Z.Y., Liu, X.H. and Wang, X.B. 2021. Numerical Study on Free Face-Assisted Rock Fragmentation Induced by a TBM Disk Cutter. *11th Conference of Asian Rock Mechanics Society* (861): 032082.

[10] Geng, Q., Wei, Z.Y., He, F. and Meng, H. 2015. Comparison of the mechanical performance between two-stage and flat-face cutter head for the rock tunnel boring machine (TBM). *Journal of Mechanical Science and Technology* 29(5): 2047-2058.

[11] Zhang, X.H., Xia, Y.M., Zeng, G.Y., Tan, Q. and Guo, B. 2018. Numerical and experimental investigation of rock breaking method under free surface by TBM disc cutter. *Journal of Central South University* 25(9): 2107-2118.

[12] Zhang, X.H., Hu, D.B., Liao, Y.S., Xia, Y.M. and Sun, X.J. 2022. Comparative Study on Cutting Red Sandstone by TBM Hob under Free Face and Normal Working Conditions. *Journal of Basic Science and Engineering* 4: 1-11.
[13] Wang, K. 2020. Numerical Simulation Research on the Rock Fracturing by a TBM Disc Cutter Assisted by Free Faces. *Journal of Railway Engineering Society* 37(10): 96-102.
[14] Fenn, O., Protheroe, B.E. and Joughin, N.C. 1998. Enhancement of roller cutting by means of water jets. *Rapid Excavation and Tunneling Conference* 341-356.
[15] Ciccu, R. and Grosso, B. 2014. Improvement of Disc Cutter Performance by Water Jet Assistance. *Rock Mechanics and Rock Engineering* 47(2): 733-744.
[16] Cheng, J.L., Jiang, Z.H., Han, W.F., Li, M.L. and Wang, Y.X. 2020. Breakage mechanism of hard-rock penetration by TBM disc cutter after high pressure water jet precutting. *Engineering Fracture Mechanics* 240(3): 107320.
[17] He, F., Zhang, J.L., Lu, Y.Q., Luo, X.C. and Xia, Y.M. 2023. Experimental and simulation study on cutting extremely hard granite by disc cutter-high velocity waterjet coupling. *Journal of Central South University(Science and Technology)* 54(3): 1187-1203.
[18] Li, J.B. 2020. *Future technology of tunneling machine*. China: China Communications Press.
[19] Wei, J.P., Cai, Y.B., Liu, Y., Yu, D.Y., Huang, Y., Li, X. and Gao, M.Y. 2024. Progress and trends in non-tool rock breaking theory and technology. *Journal of China Coal Society* 49(2): 801-832.
[20] Zhang, Z.H., Chai, C.Q. and Zhao, H. 2020. Research on cutterhead structural design of TBM. *Heavy Machinery* (4): 69-76.
[21] Zhang, Z.H., Li, Z. and Song, C.N. 2018. Development and challenge on structural design of cutterhead of full-face rock TBM. *Mining & Processing Equipment* 46(9): 1-7.
[22] Liu, Y.Y. 2003. Determination of Models and Main Parameters of Full Section Rock Tunneller. *Construction Machinery and Equipment* 34(1): 11-15.
[23] Zhang, H.X. and Zhang N.C. 2007. Brief Discussion on Cutter Head Vibration of Type 803E TBM. *Tunnel Construction* 27(6): 76-78+111.
[24] Yan, C.B, Fan, M.H., Chen, K., Yang, Y.D., Zhang, B. and Yang, J.H. 2020. Analysis on TBM cutter consumption based on the particle size distribution of rock debris. *Journal of China Coal Society* 45(12): 4216-4227.
[25] Roxborough, F.F. and Rispin, A. 1973. The mechanical cutting characteristics of the lower chalk. *Tunnels* (5): 45-67.

THIS PAGE INTENTIONALLY LEFT BLANK

19th Australasian Tunnelling Conference – Acosta-Martínez, Stewart and Hudson-Smith (Eds.)
© 2025 Australian Tunnelling Society, ISBN 978-0-85825-002-4

TBM excavation in poor squeezing ground condition. The LPFZ crossing in Snowy 2.0

M. Franceschi, F. Lazzarin
Future Generation Joint Venture, Cooma, Australia

D. Evans
Snowy Hydro Limited, Cooma, Australia

S. Loasses
Webuild Group, Italy

ABSTRACT: The "Long Plain Fault zone" (LPFZ) is a challenging stretch of the Headrace Tunnel with highly squeezing and fractured ground, faults up to 50% frequency, and fault zones thicknesses up to 40m. A recent geological investigation revealed the original plan to use TBM#1 generates unacceptable risks of prolonged shields jamming. It was therefore decided to adopt a different and innovative technology and methodology that foresees the use of new and different type of machine, TBM#4, a trial-mode Open/EPB/Variable density TBM capable of applying up to 8 bar active support pressure and to cope with the different criticalities expected along the drive. Additionally, the design and implementation of a complex drainage system to reduce the pore water pressure in weathered shear zones, thereby increasing effective soil stress and stabilizing the surrounding ground.

1 INTRODUCTION

This paper presents the innovative solution developed by Future Generation Joint Venture (FGJV, led by Webuild) for excavating a tunnel section with extremely poor, highly convergent ground conditions (the LPFZ) using a Tunnel Boring Machine (TBM). In Australia, where experience with such geology is limited, conventional excavation would have posed greater risks and complexity. The TBM approach supports project schedule requirements. The solution was developed collaboratively by FGJV, the design joint venture (DJV) including Lombardi Group, TBM supplier Herrenknecht (HKN), technical teams from Webuild and Snowy Hydro Ltd. (SHL), and independent consultants such as ARX. Excavation of the LPFZ is set to begin in June 2026.

2 SNOWY 2.0 PROJECT

Snowy 2.0 is one of the world's largest pumped hydro schemes, highlighting the Snowy Scheme's critical role in the National Electricity Market (NEM). It will add 2,200MW of generation capacity and provide around 350,000MW/h of energy storage. The project includes intake and outlet structures at Tantangara and Talbingo Reservoirs in Kosciuszko National Park, 27km of concrete-lined tunnels between the reservoirs, 20km of supporting tunnels, and an underground power station nearly 1km deep. FGJV—formed by Webuild, Clough, and Lane—was established to deliver integrated engineering, procurement, and construction management services, drawing on extensive global infrastructure expertise.

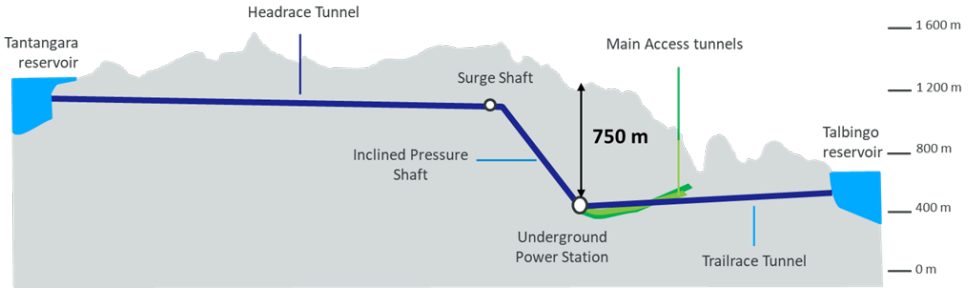


Figure 1. Snowy 2.0 Project Alignment

3 GEOLOGICAL AND GEOMECHANICAL CONTEXT

From the geotechnical point of view one of the most challenging sections of the entire project is the excavation of the Headrace Tunnel, running from the Tantangara Reservoir to the Upstream surge shaft. This is a 17,3km long "wet tunnel" with an inner diameter of 9,9mt. As per the tender scheme it was expected to be excavated entirely using two TBMs. The geotechnical baseline report was indicating a very variable ground across the entire length of the drive, with soft and hard rocks, several possible faults, risk of asbestos fibers, and a long stretch of poor material of approx.1650m known as the Long Plain Fault Zone (LPFZ), which required a specific further investigation campaign, after the project start date. Two additional directional boreholes drilled from the surface and parallel to the entire LPFZ were executed between the end of 2023 and early 2024 (BH5401 and BH5402/BH5402W1). They showed a more extensive section of very poor rock mass properties compared to the previous profile.

The LPFZ is falling into the Ravine Bed East formation (RBE), which comprises interlaminated siltstone and sandstone with occasional thicker beds of each of these lithologies. The rock mass is highly fractured, typically spaced at 60 to 200 mm, and crushed zones and sheared seams are often observed. This unit has a steeply dipping foliation with dips of 45-60° towards the E-SE, with a slaty cleavage appearance and common quartz veining and less common intrusive dykes described as volcanics and ignimbrites/tuffs of rhyodacitic, basaltic and andesitic composition. Rather than a well-defined fault, the LPFZ is a wider zone in which sections of highly disturbed rock mass (faults and fractured rock mass) alternate with section of relatively undisturbed rock mass. After the last geotechnical investigations, over a total LPFZ length of approx. 1650mt, it has been identified a stretch of approx. 815mt with a higher frequency of faults between 30% and 50% and thickness up to 40m. The most relevant update of the last campaign is represented by the description of the LPFZ structure, by defining three different typical rock mass conditions classified by colours on the basis of the Fault frequency:

1- Green zones, where fault frequency is less than 10% and the FZ thickness is generally less than 1m. The rock mass presents relatively good conditions. These conditions are expected in the external portions of the LPFZ;

2- Yellow zones where fault frequency is less than 30% and the FZ thickness is less than 5m. These rock-mass conditions, intermediate between green and orange zones, represent the transition zone from the external part (Green stretch) towards the central part of the LPFZ where the shear is more pervasive;

3- Orange zones, where the fault frequency is up to 50% and the FZ thickness up to 30-40m. It is expected in the central part of the LPFZ and it represents the worst rockmass conditions along the HRT. The high heterogeneity of the ground is here defined by the alternation of good quality rock layers and layers of fault with gouge and/or fault breccia. The presence of high intensity faults in the Orange zone, often containing gouge in variable proportions, required an in-depth analysis of the factors predisposing a risk of TBM jamming. The thicknesses of the prevailing gouge represent the most severe conditions identified for jamming risk, which have been assessed also considering the scale of the tunnel, and the contribution of the adjacent materials, represented by breccias and fractured rock masses, whose deformability generates a lower risk of jamming.

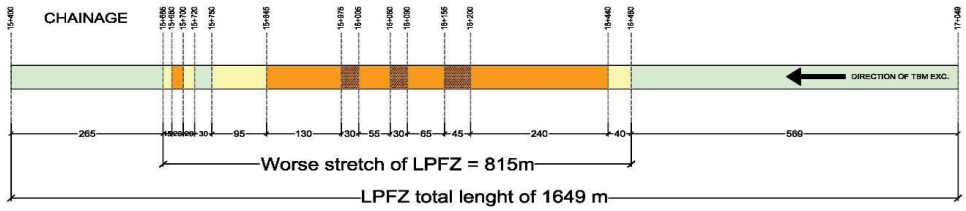


Figure 2. LPFZ different rockmass condition and distribution.

A critical factor for the evaluation of the excavation method was also the permeability value (k). The permeability observed in packers and DST tests. The Fault Zone was defined with a low permeability of $4*10^{-8}$ m/s to $1.2*10^{-9}$ m/s, while for the *prevalent gouge*, given that the fine-grained nature of the material, a single permeability of $1.2*10^{-9}$ m/s was selected. Unfortunately, with the available information it was not possible to determine the exact distribution of the permeability across the worst stretch of the LPFZ. What is known is that higher range permeability in the orange zones represent the more complex scenario to be considered, with a high convergency risk of more than 5%.

4 RISK OF ENTRAPMENT OF TBM#1 ALREADY MOBILIZED IN THE PROJECT

The TBM#1 jamming risk was evaluated by Lombardi Group by means of an axisymmetric model (3D cylinder) that simulates the TBM advance along the central axis with fully coupled analyses (mechanical and hydrogeological equilibrium are managed simultaneously). Starting from a predefined pressure on the excavation boundary (i.e. the maximum pressure that can be assumed according to TBM#1 data), a calculation of the ground displacement along the tunnel axis and a comparison between this displacement profile with the TBM#1 geometry has been assessed. A sensitivity study with several combinations of parameters has been performed with the Software FLAC developed by Itasca Consulting Group Inc., USA. Below are reported the most relevant two cases that essentially shows the great influence of the ground permeability on the TBM#1 jamming risk.

							TBM jamming (excessive displacement for the shields)					Face stability		
Case	φ	c	k	P_F	P_{10m}	P_{rad}	TBM#1 - Standstill time					TBM#1 standstill time		
	[°]	[kPa]	[m/s]	[kPa]	[kPa]	[kPa]	0 h	12 h	2 days	4 days		12 h	2 days	4 days
14	30	10	1.20E-09	200	1000	2000	✓	✓	✓	~		✓	✓	~
16	35	300	1.20E-08	200	1000	2500	×	×	×	×		✓	~	×

× TBM jamming expected
~ Possible risk of TBM jamming
✓ Low risk of TBM jamming

× Extrusion > 30 cm
~ Extrusion = 15-30 cm
✓ Extrusion < 15 cm

Figure 3. TBM jamming risk analysis for 2 load cases, considering radial convergencies and face extrusion.

Case 14 shows the results of a simulation with poor geotechnical parameters (friction angle of 30° and cohesion c of 10 kPa) and a ground permeability of 1.2E-9 m/s. Under such conditions, the TBM#1 could withstand a standstill of up to 2 days since the convergence profile is compatible with its geometry. However, it must be noted that the required TBM-thrust force during excavation is about 120 MN, which corresponds to the total thrust at max. operating pressure, while during standstill the required TBM-thrust force increases to approx. 200 MN, slightly above the total exceptional thrust of TBM#1. Therefore, the analysis is really at the limit.

Case 16 shows the results of a simulation with better geotechnical parameters than case 14 (friction angle of 35° and cohesion c of 300 kPa). However, since a higher ground permeability has been considered (k = 1.2E-8 m/s), the results show that under such conditions the jamming of TBM#1 is expected since the convergence profile is not compatible with its geometry.

The result of the analysis indicated high jamming risk of the TBM#1 along the poorest geological stretch of the LPZF (the so called “orange zone”). The main parameter governing this risk are the geometry of the TBM#1 and the assumed ground properties, especially the permeability (higher permeability leads to a higher jamming risk).

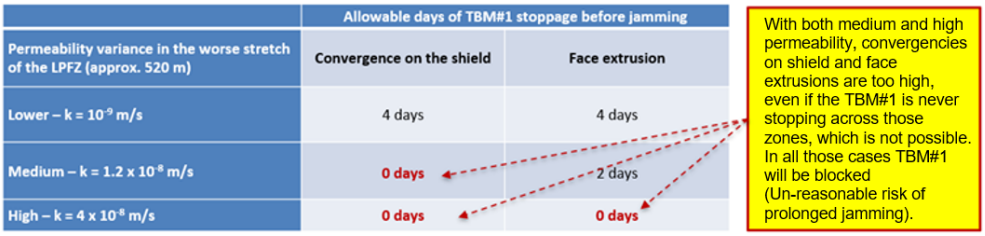


Figure 4. Influence of permeability (k) in TBM#1 jamming risk and allowable standstill time.

5 TBM#4 SPECIAL DESIGN

TBM#4, employed in the Snowy project, was specifically designed to address the challenges posed by the LPFZ, mainly the high convergences of the ground and its pressure on the TBM shield. As such, it integrates a range of technical solutions that make it unique in its class. The fundamental geotechnical risks when planning tunnel projects, which are relatively high within the LPFZ, especially in the current case for snowy 2.0, can be largely compensated for by choosing the most suitable TBM type, in accordance with DJV recommendations. By considering the worse possible ground behavior, Lombardi Group indicates the following main characteristics:

a) Total shield length reduced to 11,2 m, with consequent reduction of the ring length;
b) Shield conicity of 85mm, with additional overcutting capacity up to 130 mm on radius
c) Tail shield able to resist up to 20 bar of ground pressure
d) Exceptional total thrust of 250.000 KN, nominal of 157.000 KN
e) Active operative face support pressure of 6bar, nominal of 8bar.

TBM shall provide the possibility of applying active support pressure to pass through the LPFZ, as the tunnel face is expected to be unstable in some sections and the strong weathering/shearing of the rock means that a classic hard-rock cutterhead reaches its limits when it comes to soil excavation or mucking. The muck channels or the openings for the buckets of the cutterhead would quickly become blocked and the feasibility of the TBM would even be called into question. Therefore, the two TBM types EPB or Slurry were basically the only recommended for tunnelling through the LPFZ, or a combination of both. A technical comparison was made between Slurry and EPB TBM, particularly focusing on the capability to operate in pressurized mode with large conicities and extreme overcutting.

A Slurry TBM can operate at higher pressures and uses a low-density slurry to pressurize the face and to transport the muck along the tunnel through a pipeline. But in this specific case due to the large gap between the excavation profile and the shield and the potential high risk of over excavation at the crown of the tunnel due to the poor ground conditions, it would be difficult if not impossible to keep the low-density slurry confined under pressure at the face; it will rather flow away in an uncontrolled manner through the large gap between the shield and the excavation profile and through the overbreak's in the tunnel crown.

On the contrary an EPB TBM uses a very dense paste to pressurize the face. This paste, formed by the excavated material mixed with conditioning agents, being very dense will fill the gap between the excavation and the shield without flowing away. At the same time the dense EPB paste that fills the gap between the excavation and the shield and provides good confinement and support to the TBM body, facilitating the steering of the machine.

Since the mucking system of the EPB TBM at the end of the screw conveyor is usually an open atmospheric one, the application area of the EPB technology is limited by the maximum possible support pressure that must be degraded along the screw conveyor to ensure safe advance. As a rule, this is a maximum of around 3-4 bar, provided that the muck is sufficiently cohesive or plastic to form a kind of soil-plug in the screw. With higher support pressures like in this case (6-8bar), the option was to foresee an extended screw conveyor, whereby the mucking could continue by means of an existing conveyor belt. This arrangement has been used in several TBMs in the last 40 years, including the Channel Tunnel TBM and more recently in Cepav 2 project in Italy. A further measure to extend the application area of a classical EPB TBM would be attaching a so-called slurryfier-box to the screw outlet (Figure 5), which acts as a kind of mechanical plug, but requires a slurry circuit with all the necessary components (pumps, separation, etc.). The

mucking would then be enclosed within the slurry-pipe system, which means that it could compensate for the risk of unexpectedly extremely high support pressures, but also, very important for the snowy 2.0 projects, serving as a protection in case of encountering asbestos.

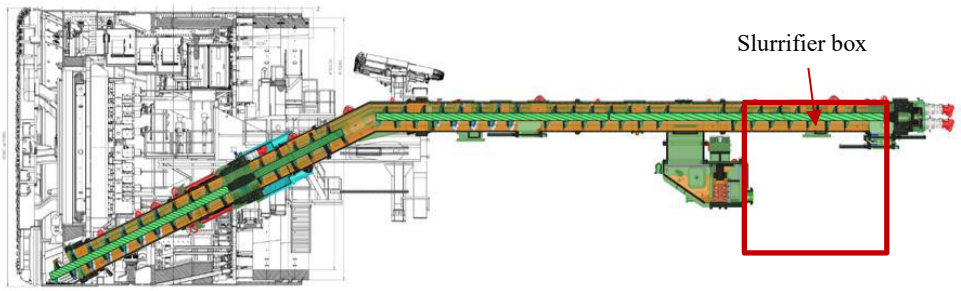


Figure 5. TBM#4 circuits, extended screw conveyor and slurrifier box

If the bentonite-slurry is only added to the slurryfier box at the end of the screw, mining can run as a classic EPB advance and foam can also be added to the muck to reduce the risk of clogging.

For the reasons stated above, an EPB TBM with additional screw conveyor section and a slurryfier box was considered as the best option. The selected TBM#4 can also operate in full open mode with reduced overcutting while excavating the Marica Adit, before to enter the LPFZ, giving an extraordinary wide range of flexibility depending on the different ground conditions (Figure 6).

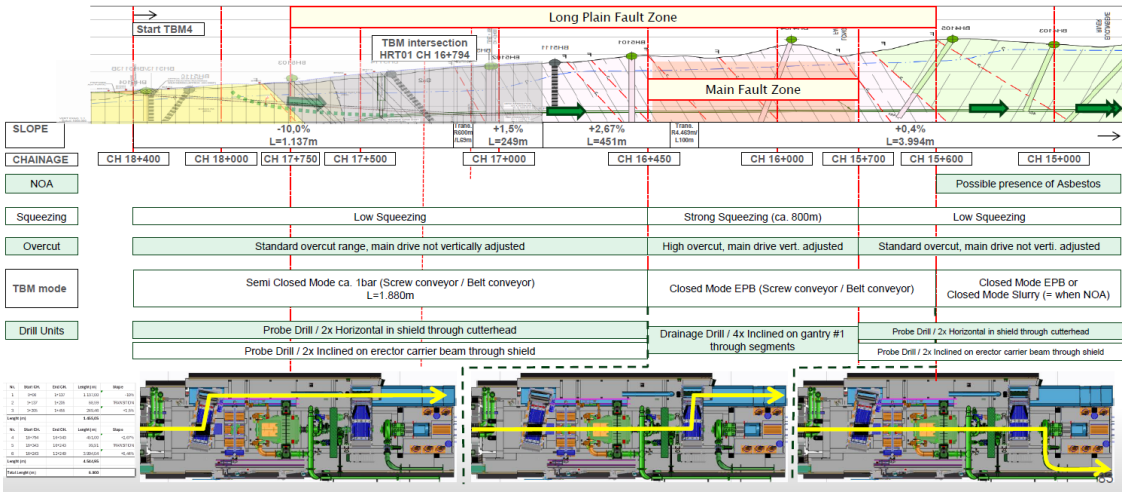


Figure 6. TBM#4 different operating modes across the LPFZ excavation.

Other advanced features have been implemented in the TBM#4 to minimize the risk associated with crossing the LPFZ:

- Integrated hydrodemolition systems, both static and "on-the-go", mounted on the shields. Based on the records of the COCIV Project (Italy), where Hydrodemolition system was installed in two EPB TBMs, activation of the Hydrodemolition on the go can reduce the TBM thrust up to 40%. Moreover, the Hydrodemolition “static” is effective in case of major events or very long TBM stand by time;
- Front active articulation, to improve the steering capability;
- Possibility to disassemble the machine within the tunnel without the need for a dismantling chamber, thanks to the presence of a sacrificial shield which ensures safe operations. This feature is particularly important in case the TBM will need to be disassembled within the LPFZ or in the following region, where there is a risk of asbestos presence.
- In-operation maintenance; a redundant number of filters has been installed, allowing replacements to be carried out without halting TBM operations.

- Special attention to design of the cutterhead, including selection of excavation tools and wear protections. The cutterhead structure was reinforced compared to previous designs;
- Real-time monitoring systems for ground convergence and shield contact pressures;
- Enhanced face conditioning system, to lubricate excavated material and minimize the risk of clogging and bentonite shield lubrication system to reduce friction with the ground and avoid blocking of TBM;
- High-powered main drive with a two-stage reduction system, enabling high speeds to operate in hard rock and very high torque at low cutterhead rotation speeds to operate into the fault zone;
- Back-up system designed to allow the opening of a bypass tunnel, if necessary, without disconnecting or dismantling the back-up structure.

6 DESIGN OF A COMBINED DRAINAGE SYSTEM

As demonstrated by Lombardi Group's analyses conducted and further confirmed by independent assessments carried out by ARX, in areas of moderate/high permeability, the TBM's characteristics—exceptional—would not be sufficient on their own to ensure a restart after prolonged standstills. The face extrusion induced by hydrostatic loads would be excessive after 12hours of TBM stop. Then, a complex drainage system was discussed and introduced as a further remedial action to reduce ground pressures on the TBM both at the tunnel face and along the TBM shield. The main effect of drainage is a reduction of the hydraulic head within the region of the tunnel. Timely installation of drains with respect to TBM advance rate translates in lower water pressures and smaller seepage forces within the rock mass, resulting in smaller total pressures on the machine. The key objective was to identify an execution method that could be implemented with minimal risk of interference with the TBM's advance. As demonstrated by the numerical model, the only reliable condition for successfully overcoming the LPFZ is to maintain as much as possible continuous and uninterrupted TBM progress. Therefore, introducing additional operations (such as the installation of drains) during the progress by stopping excavation was inherently contradictory to this principle. Consequently, a dual-system approach was adopted.

6.1 *Longitudinal drillings from the surface.*

From one side, two 1500mt long drainages performed from the surface by controlled guided drilling and parallel to the tunnel alignment, at a distance of approx 6m from the lining, can be drilled in advance of TBM excavation. They will be activated by means of additional short drills performed from the tunnel, in a second stage, through the segmental lining before crossing the fault zone area.

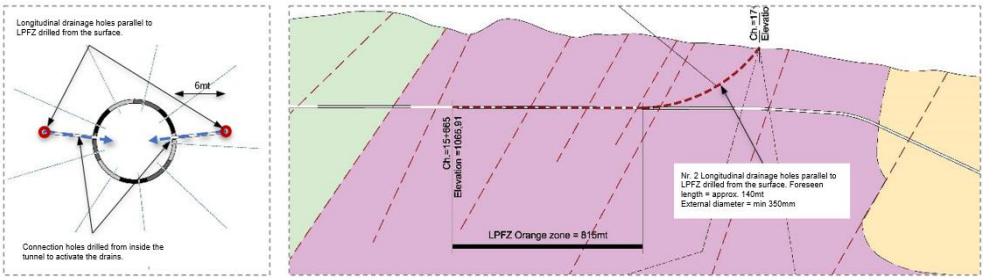


Figure 7. Longitudinal drainages from the surface. Connection scheme with the tunnel for their activation.

Clear beneficial effects have been predicted for this configuration by DJV (face extrusion reduced to more workable values) and ARX (both reduction of face pressure and thrust required after one week stop still lower than maximum machine thrust). The detailed results in terms of jamming risk/required thrust and tunnel face extrusion are recalled in the Figure 9 below (case A) comparing the convergencies with/without the two long drains. Although non-negligible face extrusions still develop after few days of stop, the comparison with the maximum pressure on the machine head in case of constrained extrusion show large pressure reductions compared to the

base case. Constrained extrusions could be dealt by means of a limited retraction of the excavation head (e.g. not greater than 10cm), combined with excavation of the tunnel face with no TBM advance. In this sense, overall constrained extrusions in the order of 20cm appear realistic and the relevant face pressure that is obtained appears to be compatible with the TBM exceptional thrust. The innovative and challenging method adopted for the execution of these long drains was developed based on successful experiences in the oil & gas sector—practices that are less commonly applied in the construction industry. However, this is the first time it will be implemented in conjunction with a TBM excavation. If successful, it could pave the way for new approaches to mechanized tunneling in poor ground conditions.

6.2 *Radial drillings from the machine, without stopping TBM#4 excavation*

On the other side, 2 x additional 80mt long radial drainages to be executed from the machine itself, every approx. 20mt of advance are foreseen during excavation. To prevent TBM stoppages the drilling rigs are installed on special sleeves which allow drilling two drains in parallel while the TBM is moving. Because of the overlapping, the effect of combining this setup with the 2 longitudinal drains @ 20 m will permit to have always at least 4 drains from the TBM and the 2 longitudinal ones, for a total of 6 active drains at every tunnel meter, active for more than 5-7 days. This system would also require special segment rings. A special triplet of rings is foreseen every 20 mt to permit the radial drillings in 4 identified fixed location not interfering with any of the multiple TBM equipments. The rings of each triplet are composed by 9 special precast segments already prepared with holes, so to avoid the risk to damage the reinforcement during the perforation. Special reo cages are assembled around the holes to compensate the altered stress distribution. Each of the ring of the triplet is different from the other two.

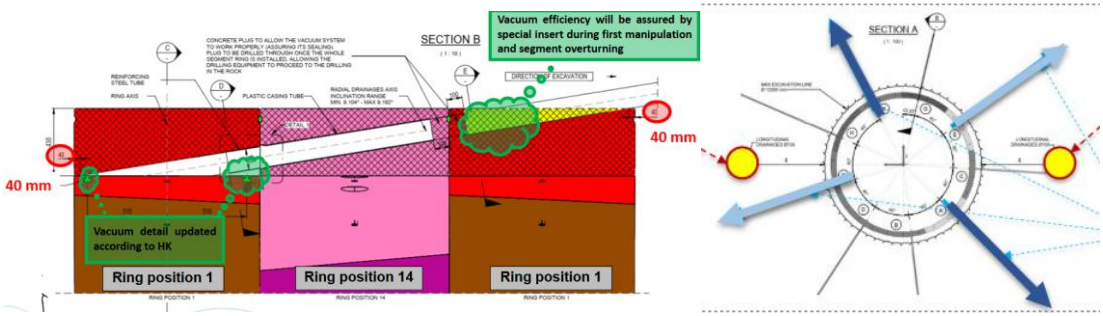


Figure 8. Special ring triplet detail for radial drillings and section view of the 4 selected drill locations.

Figure below shows how the required advance thrust is reduced markedly after drains installation, which is a key condition to allow for machine restart, which would otherwise prove non-feasible in the absence of drains. A comparison with the latest HKN nominal thrust (157MN) shows that additional drains would be required besides the pair of longitudinal drains to allow for normal operation of the TBM, also for continuous advance.

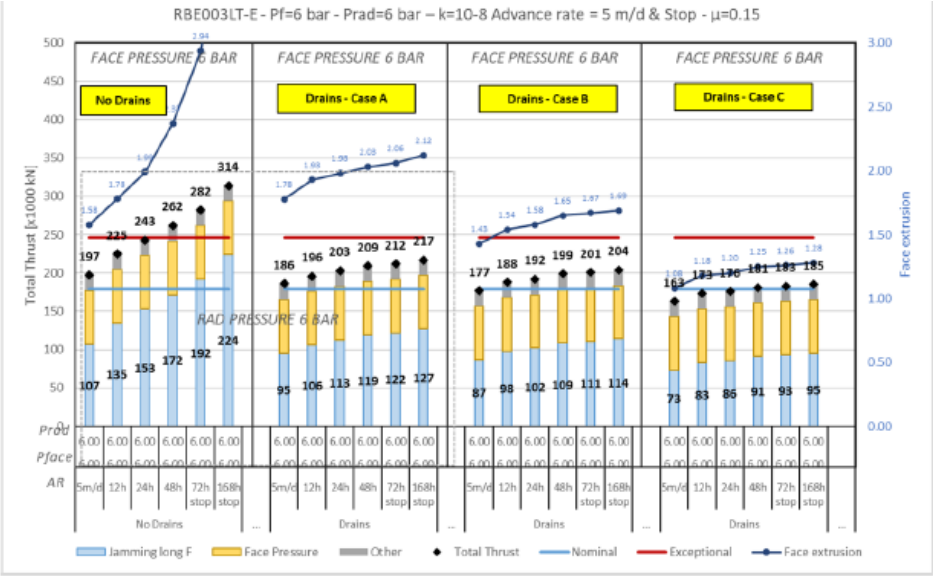


Figure 9. Summary of the results with/without drains. Assuming TBM advance 5mt/day, permeability k=1*10-8m/sec, pressure 6bar. Case 0= no drains Case A= long drains only Case C = long + radial drains.

It is worth remembering all results recalled so far are relevant to a case among the most challenging within the LPFZ, which is the result of an unfavourable combination of permeability and strength rock mass properties. For various other sections of the LPFZ, TBM operation is expected to be less problematic, for example for the excavation in rock masses with lower permeability (e.g. lower than approx. 5x10-9m/s), where the pair of longitudinal drains is expected to be sufficient. The adoption of a mechanised excavation approach could then be combined with a procedure to guide the definition at site of the most appropriate drains set-up, in particular the number of drains to be installed from the TBM in addition to the pair of longitudinal drains. Local ground conditions, known on the basis of the recent additional boreholes, probe holes and the drilling records from previous drainage installation would be the input data needed for this scope.

7 CONCLUSION

The excavation of the LPFZ using a TBM represents a highly challenging operation, whose success relies on three key actions, as outlined in this presentation: first, achieving the most detailed possible understanding of the geological conditions, which in this case was made possible by two directional boreholes drilled parallel to the entire critical section of the LPFZ; second, the design of a TBM specifically tailored to these conditions, involving top-tier international suppliers and equipped with the most advanced available technologies; and third, the implementation of an innovative associated drainage system, capable of reducing pressure on the shields, thereby extending the allowable machine standstill time under worst-case conditions to approximately one week—before pressures exceed the TBM's thrust capacity. Furthermore, the use of mechanized excavation under such extreme conditions contributes to increase the safety on site and represents a further advancement in the application of TBM technology, while simultaneously reducing both construction time and costs.

19th Australasian Tunnelling Conference – Acosta-Martínez, Stewart and Hudson-Smith (Eds.)
© 2025 Australian Tunnelling Society, ISBN 978-0-85825-002-4

Design considerations and criteria for underground structures – structural verifications of waterway concrete linings in pumped storage power plants

F. Cippà & M. Cadenelli
Lombardi SA Ingegneri Consulenti, Giubiasco, Switzerland

1 INTRODUCTION

Final linings of hydraulic pressure tunnels and shafts are designed following several different practices. As this can lead to significant differences in the results, the question of the most suitable methods for analysis and design is of utmost importance and is approached in this article for some typical hydraulic underground works.

This is even more crucial for pumped storage powerplants (PSP) as rapid start/stop manoeuvres and fast transitions between generation and pumping modes create more frequent and generally higher peaks of hydraulic dynamic pressures than traditional hydropower plants.

2 HYDRAULIC VS. NON-HYDRAULIC UNDERGROUND WORKS AND GEOTECHNICAL VS. STRUCTURAL MODELS

Hydraulic pressure tunnels and shafts mainly differ from other underground facilities by the water contained by the lining during normal operation. This persistent internal pressure acting on the lining during most operating conditions is a missing load case for many other underground structures such as road and railway tunnels. For these dry structures, the final lining design is normally controlled by load combinations with external geotechnical actions covering a vast variety of occurrences, from moderate wedge pressures to high pressures given, for example, by squeezing or swelling rock masses. The advances in numerical analysis have allowed increasingly comprehensive modelling of most geotechnical load cases, including the time-dependent rock mass behaviour typically associated with tunnel and shaft excavation. By means of stress fields, thrust forces, bending moments, deformations, and other results, they provide a sufficient output for the design of most non-hydraulic underground structures. As the geotechnical actions are determinant for the lining design of these structures, the analysis assumptions are normally aimed at maximizing their effects, seeking for the most unfavourable lining demand. However, in hydraulic tunnels and shafts, the effects of external geotechnical actions are often opposite to those of internal water pressure.

Therefore, designing a hydraulic tunnel or shaft like a non-hydraulic structure by adding the internal water pressure as an additional step of a sequential, time-dependent geotechnical analysis is often misleading, given that the internal water pressure is likely to release the effects of the geotechnical actions, possibly not showing the hazards related to internal pressure load cases.

Instead, the designer of any hydraulic tunnel or shaft is advised to carefully question whether the external geotechnical actions can be reliably accounted for when designing the final lining under internal pressure conditions. Higher mechanical properties of the rock mass than conservatively assumed for the geotechnical design, more favourable characteristics of the rock mass discontinuities, as well as variations of the time-dependent rock mass behaviour, are typical issues able to significantly reduce the effects of geotechnical actions on the lining. In fact, in many cases, the geotechnical actions are finally deemed so unpredictable that the internal pressures are dealt with in a separate design where geotechnical actions are fully neglected or are applied only locally to induce some unfavourable additional bending in the lining. Therefore, the further considerations in this article refer to analyses performed on structural models rather than geotechnical models.

3 LINING PERMEABILITY

The structural behaviour and the design of hydraulic tunnel and shaft linings depend on their permeability, where three options are distinguished. In case of the first option, measures are deliberately taken to establish a high lining permeability (drains through the lining, unsealed construction joints, etc.), thus speaking of a drained lining. The second option does not include watertight layers to assure the lining impermeability, but permeability is lowered as far as possible (low-permeability lining). The third option is impervious, for example by the use of a continuous steel lining or of an embedded or exposed waterproofing membrane.

An impervious lining is typically needed when the ratio between rock cover and internal pressure is below the necessary minimum for safety against hydrofracturing as well as in case of water-sensible rock masses, as indicated by Deere-Lombardi (1988).

If an impervious lining is not necessary, a choice is needed between a drained and a low-permeability lining. The drained lining is typically more cost-effective because of the reduced structural capacity compared to the low-permeability lining. In fact, the primary objective of drains lies in balancing the pressures in the tunnel and in the rock mass to reduce the lining demand imposed by hydraulic loads. However, the execution of drained tunnels and shafts is subject to a number of conditions and limitations, listed below, requiring a proper evaluation before the drained lining solution is adopted:

- The rock mass permeability should be controlled by a system of widespread, interconnected and differently oriented discontinuities, highly likely to be intercepted by drains.
- The rock mass, including the fill material in faults and cracks, should not be prone to be washed out by water or, at least, it should be possible to control the risk by filters and similar provisions in the drains.
- Drained linings are mostly used in waterway sections not affected by frequent and intense water pressure variations. In this way, on the one hand, excessive stress on the drains is avoided (a particularly important aspect in modern highly flexible pumped storage schemes); on the other hand, drains subject to severe water hammer can hardly be so effective as to prevent transient hydraulic loads on the lining, thus not attaining the goal of a thin and cost-effective lining.
- To prevent excessive water losses from the waterways, the groundwater pressure in the rock mass surrounding a drained lining should be higher than the internal pressure.
- The effects of a drained tunnel or shaft on the local hydrogeological conditions should be evaluated. Drained works in permeable formations can cause groundwater levels to decline and springs to dry up.
- Surface settlements induced by the construction of underground works should be assessed, considering that settlements tend to be greater if the works are drained.

4 HYDRAULIC LOADS ACTING ON THE LINING

In the case of the third option (impervious lining), the internal water pressure and the external water pressure (groundwater pressure) are independent actions and the relieving effect of an external water pressure in the internal pressure design shall only be considered after careful evaluation. In many cases, despite a possible location below the groundwater table, the external pressure is neglected, either due to technical reasons (for example, in low permeability rock masses, the rock mass can be locally dry even below the groundwater table) or if the reference design codes require to do so.

In the case of the first and second option (drained lining and low-permeability lining) the internal water pressure and the water pressure on the outer lining surface are interacting through the drains or through lining seepage given, for example, by primary concrete permeability or, more likely, by cracks in the lining concrete. Internal and external pressures on the lining are thus no longer independent. While the internal water pressure is still given by the hydraulic operating conditions of the waterways (static head, head losses, transient effects), the water pressure on the outer lining surface depends on a series of parameters:

– In the case of the first option (drained lining), the pressure on the outer lining surface is normally assumed to be equal to the permanent component of the internal water pressure.
– In the case of the second option (low-permeability lining), the pressure on the outer lining surface depends on the relative permeability of the lining and of the rock mass, as well as on the groundwater level in the rock mass.

In both cases the variable or dynamic component of the internal water pressure is normally assumed not to affect the water pressure on the outer lining surface, as it is unlikely that the system has enough time to react to such a short-term load variation. However, extreme loading conditions may require novel constructive solutions where the drains are designed to provide such an intense effect as to compensate, at least to some extent, also the variable component of the internal water pressure, with the inclined shaft of the Snowy 2.0 PSP in New South Wales being an outstanding example.

So, the permanent component of water pressures – the main actions in most hydraulic tunnels and shafts – can be seen as "conventional" mechanical loads only in the case of impervious linings, whereas in all other cases the water load magnitude on the lining results from a seepage flow through the lining and the surrounding rock and depends on the permeability of the system components, as indicated by Schleiss (1986). For the variable or dynamic component of water pressures (water hammer or surge events in the waterways, for example), the inertia necessary for the seepage flow to develop must be additionally considered, meaning that these actions are typically modelled as mechanical loads, especially when they are affected by sudden variations.

A summary of hydraulic loads acting on tunnel linings is given in Table 1, including also the load case of tunnel dewatering for inspection and maintenance. For this last case, the effect of drains is significant as they allow the rock mass to release water, decreasing the external pressure on the lining.

Table 1: Hydraulic load acting on the lining as a function of lining permeability and type of hydraulic load.

			Lining permeability			
			Option 3	Option 2	Option 1	
			Impervious lining	Low permeability lining	Conventionally drained lining	Intensely drained lining
Hydraulic loads	Load cases with resulting internal pressure	Permanent loads	Entire permanent load	Partial permanent pressure given by seepage model	Almost no load	No load
		Variable loads	Total variable load	Total variable load	Total variable load	Partial variable load given by hydraulic model
	Dewatering (load case with resulting external pressure)		Entire external pressure	Partial external pressure given by seepage model	Highly reduced external pressure given by seepage model or minimum loading according to good practices	

5 LINING STIFFNESS

Once the internal water pressure and the pressure on the outer lining surface are known, the system comprising the lining and the surrounding rock mass can be calculated. This structural analysis yields the necessary values for the lining design, with the analysis results depending upon the relative stiffness of the lining and of the rock mass. It is noted that the lining is typically subject to circumferential tension and the stiffness is therefore affected by cracking. Furthermore, the analysis should consider the effect of the outer pressure on the rock mass and a contact non-linearity at the lining-ground interface, given that a structural interaction of both elements is

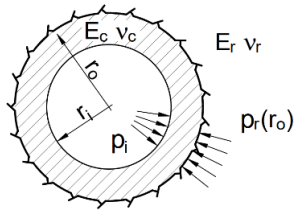
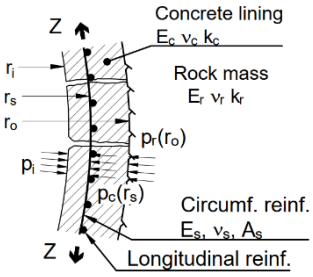
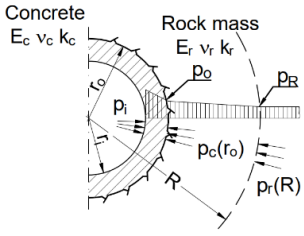
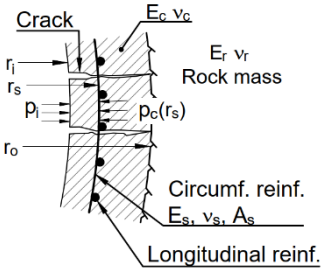
normally only admitted over effective compressive stresses, whereas tensile stresses can't be taken into account as the tensile strength at the interface is neglected for design purposes.

6 MODELLING OPTIONS FOR NON-LINEARITIES

It has been shown in the two previous sections that the effects of the water pressure acting on the lining of hydraulic tunnels and shafts depend on the relative permeability of lining and rock mass and on their relative stiffness. Material non-linearity affects the lining stiffness in tension, whereas a contact non-linearity should be introduced at the lining-ground interface. The non-linear behaviour of the system is enhanced by the interrelationships between some of the material characteristics: the permeability of a reinforced concrete lining, for example, strongly depends on its stiffness, given that open cracks cause a significant permeability increase.

Depending on the extent to which these points are considered, a set of possible modelling options is obtained as shown in Table 2 for low-permeability linings.

Table 2: Summary of main modelling options for reinforced concrete linings of tunnels and shafts, adapted from Schleiss (1986). r_i, r_o = inner and outer lining radius; r_s = steel reinforcement radius; R = radius of the rock mass portion affected by the tunnel; E_c, $E_{c,uncracked}$, E_r, E_{lining}, E_s = modulus of concrete, uncracked concrete, rock mass, lining, reinforcement steel; ν_c, ν_r, ν_s = Poisson's ratio of concrete, ; k_c, k_r = permeability of concrete, rock mass; p_i = internal water pressure; p_o = water pressure acting at the lining-rock mass interface; p_s = water pressure acting at $r = r_s$; p_R = water pressure acting at $r = R$; A_s = area of circumferential steel reinforcement.

		Lining stiffness		
		Uncracked concrete	Preset value for cracked concrete	Lining stiffness adjusted based on expected structural behaviour
Model for water pressure distribution	Impervious pipe model	Model A.1 	Model A.2 The same as Case A.1, but with reduced concrete modulus (for example E_{lining} = 1/3 $E_{c\ uncraked}$)	Model A.3 
	Pervious pipe model	Model B.1 	Model B.2 The same as Case B.1, but with reduced concrete modulus (for example E_{lining} = 1/3 $E_{c\ uncraked}$)	Model B.3 

The first main variable is the model used for the water pressure distribution inside the system. In the upper row of the table (Models A.1 to A.3) the resulting water load, i.e. the internal pressure

minus the external pressure, is modelled as a mechanical load applied to the internal lining surface.

Concrete and rock experience this load through changes in their total stresses, while it is assumed that no changes occur in the pore pressures (except for some pore over- and under-pressures).

In the lower row (Models B.1 to B.3), on the contrary, the water loads are the result of a seepage flow through the system, with effects on both the total and the effective stresses.

The expected structural behaviour is:

- Models B for permanent (static) water loads
- Models A or B for dynamic or transient water loads, depending on the application rate:
  - Models A for impulsive, short-term loads
  - Models B or intermediate between A and B for slowly applied loads.

The second main variable is the assumed lining stiffness. In the left column (Models A.1 and B.1), the uncracked lining stiffness is used. In the right column (Models A.3 and B.3), the stiffness results from an in-depth calculation based on the lining loadings, providing the most accurate description of the lining behaviour. However, it has to be kept in mind that this calculation depends on several parameters like the concrete tensile strength and the number of pre-existing cracks (including cracks due to shrinkage and thermal effects), which are subject to a natural variability, thus limiting the reliability of the results. A practical way to overcome these limits and make calculations more straightforward is given in the mid columns (Models A.2 and B.2), consisting in the use a preset value for the lining modulus smaller the uncracked modulus but conservatively greater than that resulting from Models A.3 and B.3. A sound value can often be assumed equal to $E_{lining} = 1/3\ E_{c,uncracked}$.

Please note that all models shown in Table 2 can be used to design low-permeability linings, which are likely to be cracked to some extent. In other words, it should not be understood that Models A.1 and B.1 are intended for uncracked linings, whereas the other models are associated to cracked and consequently more permeable linings.

At this point, three aspects appear to be of interest:

- How much do non-linearities and model selection practically affect the system behaviour and the structural analysis results?
- How can such a complex behaviour be reasonably modelled for design purposes, i.e. putting aside the scientific aim of a precise behaviour description and instead focusing on a safe and efficient design?
- How much freedom is allowed by Australian and international design codes for such methods of analysis and design?

These aspects are treated in the following sections.

7 MODEL IMPACT ON STRUCTURAL ANALYSIS RESULTS

To visualize the modelling significance on the analysis results, an example of a vertical shaft is shown. The main geometric characteristics are 25.0 m inner diameter, 0.80 m lining thickness, 2 reinforcement layers d24 spaced 200 mm (A_s = 4,524 mm^2/m). The concrete properties are $E_{c,uncracked}$ = 32,800 MPa, Poisson's ratio $\nu_c = 0.20$, permeability $k_{c,uncracked} = 10^{-9}$ m/s. The rock mass properties are E_r = 7000 MPa, Poisson's ratio $\nu_r = 0.25$, permeability $k_r = 10^{-7}$ m/s. The calculated load case is an increase in the internal water pressure by 60 m, i.e. 600 kN/m^2.

The corresponding increase $\Delta\sigma_s$ in the reinforcement tension stress in shown in Table 3 for the six modelling options previously presented in Table 2. The results greatly vary between the extreme cases represented by Model A.1 and Model B.3. While the value $\Delta\sigma_s$ = 550 MPa for Model A.1 exceeds the tensile strength of conventional reinforcement and calls for a substantial reinforcement increase, the values according to other models are well below and compatible with the declared reinforcement.

Table 3: Summary of main modelling options for reinforced concrete linings of tunnels and shafts.

	Lining stiffness		
	Uncracked concrete	Preset value for cracked concrete	Lining stiffness adjusted based on expected structural behaviour
Impervious pipe model	Model A.1 $\Delta\sigma_s$ = 550 MPa	Model A.2 $\Delta\sigma_s$ = 274 MPa	Model A.3 $\Delta\sigma_s$ = 247 MPa
Pervious pipe model	Model B.1 $\Delta\sigma_s$ = 476 MPa	Model B.2 $\Delta\sigma_s$ = 191 MPa	Model B.3 $\Delta\sigma_s$ = 148 MPa

The example confirms that model selection plays a key role in the structural design of concrete linings for hydraulic tunnels and shafts. In fact, the modelling relevance can be so significant that other typical design inputs like load factors, maximum surge oscillations, and groundwater levels, which are often treated more in depth than modelling assumptions, may seem to become secondary. The designer of hydraulic tunnels and shafts should be aware of how much the design results for concrete linings are affected by modelling and support the corresponding assumptions with experienced judgement to ensure the structure can fulfil all structural and durability requirements during its design working life.

8 REAL STRUCTURAL BEHAVIOUR VS. DESIGN MODEL

The accurate modelling of the system behaviour is decidedly complex, with the most targeted approach likely being the monotonic loading increase proposed by Stucchi (2024). The procedure requires modelling of the progressive lining cracking, updating of the permeability calculation after each loading step as a function of the estimated number of cracks and by considering the corresponding stress redistribution given that, as mentioned above, the tensional state also depends on the permeability of the lining and the rock mass. Beside hydraulic pressure, the analysis should include thermal and concrete shrinkage effects that are likely to produce cracks in the lining even before the first waterway filling.

The natural variability of analysis parameters like the concrete strength and deformation properties, as well as the difficulty in predicting the effectiveness of contact and consolidation grouting and its effects on the system permeability, are examples of issues that even the most sophisticated deterministic model can hardly control. Therefore, for design purposes, the use of simplified models may be preferred, e.g. referring to Model B.2 in Table 2 instead of Model B.3 or paying attention to the assumed preset value of lining stiffness in order to not underestimate the lining demand.

9 DESIGN CODE PRESCRIPTIONS

The Australian standard AS 3600 for concrete structures supports non-linear analysis as the basis for design, requiring that “the calculations shall be undertaken using the mean values of all relevant material properties […], such as concrete strength, initial elastic moduli, and yield stress and yield strength of the steel reinforcement”. Furthermore, “additional analysis shall be considered using other values of material properties to allow for variability” and “checks shall be made to investigate the sensitivity of the results of non-linear stress analysis to variations in input data and modelling parameters”. For concrete linings of hydraulic tunnels and shafts, this typically means that the permeability of the cracked lining, determined with models based on number and width of the cracks and on assumptions for the seepage characteristics through the cracks, should

be set conservatively low. The concrete tensile strength should instead be assumed conservatively high (at least equal to the mean tensile strength of the used concrete), as the number of longitudinal cracks induced by the internal water pressure will be less with increasing tensile strength, thus causing the lining to be stiffer.

No specific rules are included in AS 3600 for partial coefficients to be used for design based on non-linear analysis, meaning that the same partial coefficients shall be used as for conventional linear analysis.

The recently issued second generation Eurocodes (EN 1990:2023 with the basis of structural and geotechnical design, and EN 1992-1-1:2023 for the design of concrete structures) include similar rules, calling for sensitivity analysis with respect to significant material characteristics like concrete strength. With regards to the partial coefficients, the Eurocodes confirm those for actions as used for linear analysis, while the option of using different safety formats to determine the design value of the structural resistance is introduced. Similar safety formats are included in the FIB Model Code 2010, discussed in technical literature and deemed generally capable of yielding a less conservative design.

10 CONCLUSIONS

The evaluation of the hydraulic boundary conditions, lining and rock mass permeabilities, and lining stiffness, as well as the consequent adoption of a proper structural resistance model of the linings, require careful attention by the designer when performing the structural verifications of the concrete linings.

Overestimating the actual forces acting on the linings could lead to unnecessarily high costs or even render the project unfeasible. On the other hand, uncertainty of the hydraulic boundary conditions (and effective lining permeability) and of the linings stiffness, if underestimated, may result in underestimating the loads in the linings, and consequently result in an unsafe design.

The model selection for water pressure distribution and stiffness plays a key role in the structural design of concrete linings for hydraulic tunnels and shafts. Other typical design inputs, like load amplification factors, maximum/minimum surge oscillations, and groundwater design levels, which are often treated more in depth than modelling assumptions, may become secondary. The designer of hydraulic tunnels and shafts should be aware to what degree the concrete lining design results are affected by modelling and support the corresponding assumptions with experienced judgement to make sure that the structure can fulfil all structural and durability requirements during its design working life.

For design purpose, the expected structural behaviour of low-permeability linings is:

- Models B (pervious pipe model) for permanent (static) water loads; e.g. operation steady conditions
- Models A (impervious pipe model) or B for dynamic or transient water loads, depending on the application rate:
  - Models A for impulsive, short-term loads, e.g. water hammers and surge
  - Models B or intermediate between A and B for slowly applied loads, e.g. during dewatering operations

The use of simplified models may be preferred, e.g. referring to Model B.2 in Table 2 instead of Model B.3, while paying attention to the assumed preset value of lining stiffness. If the less conservative Model B.3 is used, parameters subjected to a natural variability should be selected cautiously in order not to underestimate the stresses in the lining.

11 REFERENCES

AS 3600:2018 *Concrete structures*

Deere D.U., Lombardi G. 1988, Lining of pressure tunnels and hydrofracturing potential, in *De Mello Volume*, Edgar Blücher Ltd

EN 1990:2023 Eurocode – *Basis of structural and geotechnical design*

EN 1992-1-1:2023 Eurocode 2 – *Design of concrete structures – Part 1-1: General rules and rules for buildings, bridges and civil engineering structures*

International Federation for Structural Concrete (FIB), *Model Code 2010*, 2012

Schleiss A. 1986, Bemessung von Druckstollen – Teil II: Einfluss der Sickerströmung in Betonauskleidung und Fels*, Mechanisch-hydraulische Wechselwirkungen, Bemessungskriterien*, VAW-Mitteilung 86, ETHZ

Stucchi R. 2024, Hydro-mechanical behaviour of reinforced concrete linings in hydraulic tunnels: steady state, in *Proceedings of the Institution of Civil Engineers – Engineering and Computational Mechanics*. Emerald. https://doi.org/10.1680/jencm.24.00020

19th Australasian Tunnelling Conference – Acosta-Martínez, Stewart and Hudson-Smith (Eds.)
© 2025 Australian Tunnelling Society, ISBN 978-0-85825-002-4

Real-time geological prediction technology based on TBM rock-breaking seismic source HSP method and engineering practice

T. Gu & S. Lu & L. Meng & X. Wang & K. Wu

China Railway Academy Group Co., Ltd., Chengdu, Sichuan, China

China Railway Southwest Research Institute Co., Ltd., Chengdu, Sichuan, China

ABSTRACT: In order to overcome the geological adaptability challenges encountered in TBM construction and avoid blind tunneling through unfavorable geological conditions that were not clearly identified beforehand, the implementation and innovation of geological detection methods during the construction phase are particularly critical. It has become a consensus to fully utilize TBM to carry out advanced geological prediction techniques suitable for TBM construction. This paper focuses on the real-time geological prediction technology based on the TBM rock-breaking seismic source HSP method, which involves mounting the HSP forecasting equipment on the TBM to complete the processes of rock-breaking vibration, acoustic wave information collection, data processing, anomaly identification, and interpretation. This results in automatic information collection, intelligent data processing, intelligent anomaly recognition, and real-time interpretation of the results. As TBM excavation progresses and the thickness of the geotechnical layer decreases, a data processing technology based on multiple forecast result iterations is proposed to improve accuracy.

1 INTRODUCTION

With the rapid development of major infrastructure projects in China, the number of long, deeply buried tunnels crossing rivers and seas steadily increases. The safe, efficient, and environmentally friendly TBM (tunnel boring machine) method is increasingly applied in tunnel construction due to its advantages in tunneling speed, minimal disturbance to surrounding rock, and enhanced tunnel construction quality.

However, the TBM construction method necessitates a TBM structure that occupies substantial tunnel space, resulting in a weak response capability or low treatment efficiency when facing unknown unfavorable geological bodies. Once unfavorable geological bodies are encountered, the safety of personnel, machinery, tools, and construction progress are at significantly greater risk compared to the drilling and blasting method.

Given the spatial characteristics of TBMs and the interference factors—such as vibrations, metal bodies, and electromagnetism—that affect geophysical prediction signal sources, researching appropriate and effective geological exploration technologies has become a key focus area for scholars. Focusing on the differences in the physical characteristics of unfavorable geological conditions, such as speed, density, electrical properties, and rock temperature, the geophysical prediction prediction technologies specifically dedicated to or suitable for TBM tunnels include elastic wave reflection methods for non-blasting seismic sources, such as HSP (horizontal sonic/seismic profiling)[1], ISP(integrated seismic prediction) [2], SAP (seismic ahead prospecting)[3], TST(tunnel seismic tomography) [4], and TSWD (tunnel seismic while drilling)[5]; electrical (magnetic) methods, such as BEAM(bore-tunneling electrical ahead monitoring) [6], TEAM(tunneling electrical ahead monitoring) [7], TIP (time increased probability)[8], and CFC(complex frequency conductivity) [9]; and the RTP(rock-mass temperature probing) method [10]. This paper elaborates on the real-time geological prediction technology based on the TBM rock-breaking seismic source HSP method and highlights its application in the Xianglushan TBM Tunnel of Water Diversion Project in Central Yunnan, and the Daliangshan TBM tunnel on the Leshan–Xichang Expressway. These insights can serve as a reference for advanced geological prediction in similar projects.

2 DIFFICULT ISSUES AND METHOD SELECTION FOR GEOLOGICAL PREDICTION IN TBM CONSTRUCTION

2.1 *Analysis of Geological Risks of TBM Tunnels*

Long tunnels increases the risk for TBMs of encountering geological hazards like water or mud inrushes and collapses, which can potentially lead to jamming or trapping accidents and even casualties. Many typical disasters and accidents have been reported in China and other countries. In mild cases, TBM jamming or mechanical damage may occur, while in severe instances, the entire TBM may need to be scrapped, leading to serious consequences such as abandonment of the TBM construction and even casualties.

2.2 *Characteristics of TBM Construction and Difficult Issues for Geological Prediction*

The characteristics of TBM construction technology and its unique spatial structure impose restrictions on the application of various traditional prediction methods. The main reasons include:

(1) The TBM fully occupies the working face, restricting the visibility of working face conditions to portions only observable through the cutter holes and reserved manholes. Consequently, traditional methods such as GPR (ground penetrating radar) and transient electromagnetic methods, which require measuring lines to be positioned on the working face, cannot be implemented;

(2) Due to the narrow space, for the prediction method that requires drilling holes for receiving sensors and field source excitation, hole drilling is not only time-consuming but also inconvenient, and it often causes significant noise interference;

(3) Among seismic wave methods, the prediction method that utilizes explosive blasting vibrations as the seismic source carries the risk of damaging the TBM. Additionally, the process is time-consuming and generates dust, which can adversely affect the construction environment;

(4) The direct current method is constrained by spatial limitations, and the detection equipment can restrict the detection distance. As a result, it often facilitates only short-distance detection, which does not align with the rapid tunneling requirements of TBM operations. Consequently, this method is typically utilized as a supplementary detection technique in critical risk areas;

(5) The current suction effect of the TBM's metal body can impact both the detection distance and effectiveness of electrical methods. Furthermore, the required contact electrodes may be hindered by the supporting structure, making their arrangement inconvenient or even impossible. It is essential to implement integrated installation and targeted design to complete the detection;

(6) The TBM construction procedures are closely interconnected, and the tunneling is fast, necessitating that the geological prediction is completed in a short timeframe, with results submitted timely.

When selecting geological detection methods for TBM construction, it's essential to consider the effectiveness of the method, the feasibility of implementation, the convenience of operation, and the timeliness of results. The purpose is to determine the optimal prediction method that aligns with the specific construction environment and engineering requirements.

2.3 *Selection of Prediction Method*

The selection of a geophysical prediction method for advanced geological prediction in tunnels focuses on the physical characteristics of unfavorable geology, the required prediction distance, and the tunnel environmental characteristics to identify the most suitable method. An analysis is provided below in several aspects:

(1) Analysis of field source type and excitation form

The field source types typically utilized in geological prediction during tunnel construction include the elastic wave field, electric field, electromagnetic field, and temperature field. Given the characteristics of the TBM body and the space, the elastic wave field and electric field are two types of field sources that are well suited for the TBM environment.

The excitation modes of the elastic wave field encompass both active and passive sources. Active sources include explosive seismic sources and various forms of hammering, such as manual, hydraulic, electric, and pneumatic hammering. Passive sources include cutter rock-breaking seismic sources and environmental noise seismic sources. The excitation modes of the electric

field include both DC (direct current) and AC (alternating current) power supplies. Due to the low resistivity of the TBM metal, power is typically supplied primarily through contact electrodes.

(2) Analysis of integration mode of prediction equipment

A key technology for enhancing intelligent prediction is the automatic acquisition of physical field sensing information. The integration of prediction equipment with TBMs is essential for establishing a pathway for this automatic acquisition. The HSP method for TBM construction employs vibration signals generated during the rock mass shearing by the cutterhead and cutters as the seismic source. The detection equipment is installed within the TBM chamber and is controlled via an upper computer, allowing for effective detection. These methods introduced innovations in equipment arrangement, field source acquisition, equipment adaptability, and data processing algorithms. By mounting the equipment or sensors onto the TBM, they enhance intelligent prediction in the TBM construction environment.

(3) Analysis of prediction length and result timeliness

It is clear that the accuracy and effective application of prediction results are critical factors in evaluating the prediction quality. For efficient TBM construction, the prediction length and timeliness of results should be fully considered when selecting the prediction method. Therefore, the long-distance prediction or short-distance real-time (or quick result acquisition) prediction method will be more suitable for TBM construction.

Based on the aforementioned three considerations, this paper will elaborate on the HSP method, which employs TBM rock-breaking vibrations as the seismic source. The equipment utilized in this method is mounted on the TBM, enabling real-time prediction without requiring any shutdowns. The characteristics of this method and its application in several key TBM projects in China will be discussed below.

3 REAL-TIME GEOLOGICAL PREDICTION TECHNOLOGY BASED ON ROCK-BREAKING SEISMIC SOURCE HSP METHOD

3.1 *Theoretical Framework*

(1) Seismic wave reflection theory

The HSP method is grounded in the theory of seismic wave reflection, which is utilized to detect unfavorable geological bodies characterized by differences in seismic wave impedance within the media. As indicated by Formula (1), when there is a disparity in the product of density and longitudinal wave speed between an unfavorable geological body and the surrounding rock, a reflection phenomenon will occur. A greater disparity results in more pronounced reflection characteristics. Common types of unfavorable geology include fault structural zones, densely jointed zones, and karst strata. They exhibit differences in seismic wave impedance. Through reflection wave imaging, the locations, scales, and filling properties of unfavorable geological bodies can be effectively detected.

$$R_{12} = \frac{\rho_2 v_2 - \rho_1 v_1}{\rho_2 v_2 + \rho_1 v_1} \tag{1}$$

where, R_{12} denotes the reflection coefficient, ρ represents the strata density, and v is the longitudinal wave speed of the strata.

(2) Seismic interferometric imaging technology

According to the reciprocity theory of Green's function [11], seismic data collected from any two receiving points can be utilized for deconvolution processing to derive their Green's function.

For receiving points in the same domain, the convolution formula in the frequency domain is given below:

$$u(r_a, s, w) = W(s, w)G(r_a, s, w) \tag{2}$$

where: G is the Green's function and W is the frequency domain source function. The cross-correlation is performed for seismic information collected at the two points. Then, their frequency domain formula is as follows:

$$C_{ab} = |W(s)|^2 G(r_a, s)G * (r_b, s) \tag{3}$$

where, $|W(s)|^2$ is the influence factor of the seismic source, which varies with the changes in seismic source s, and the asterisk indicates the conjugate. According to the equation, the cross-

correlation C_{ab} is influenced by the energy spectrum $W(s)$. The frequency domain formula for the deconvolution of receiving points a and b is given below:

$$D_{ab} = \frac{u(r_a,s)}{u(r_b,s)} = \frac{G(r_a,s)G*(r_b,s)}{|G(r_b,s)|^2} \quad (4)$$

Information $u(r_a, s)$ and $u(r_b, s)$ is recorded at points a and b, and cross-correlation is performed for seismic information collected at the two points. The influence of source function characteristics on the processing results is eliminated through deconvolution. The extracted seismic signals consist of the causal part, the non-causal part, and the impulse response.

Thus, if the seismic signals recorded by two different free geophones are cross-correlated, a new seismic signal can be generated, incorporating the causal part, the non-causal part, and the impulse response. The causal part corresponds to that of seismic waves recorded by an observation system utilizing one geophone as the virtual source and the other as the geophone. Consequently, wave field separation and speed imaging can be achieved without prior knowledge of the seismic source characteristics.

3.2 *Technical Scheme for Real-time Prediction*

Based on theoretical analysis and considering the requirements for TBM construction, spatial characteristics, and geological prediction, an HSP real-time prediction technology is proposed, which utilizes the rock-breaking vibrations from TBMs as the seismic source. The detection scheme is illustrated in Fig. 1.

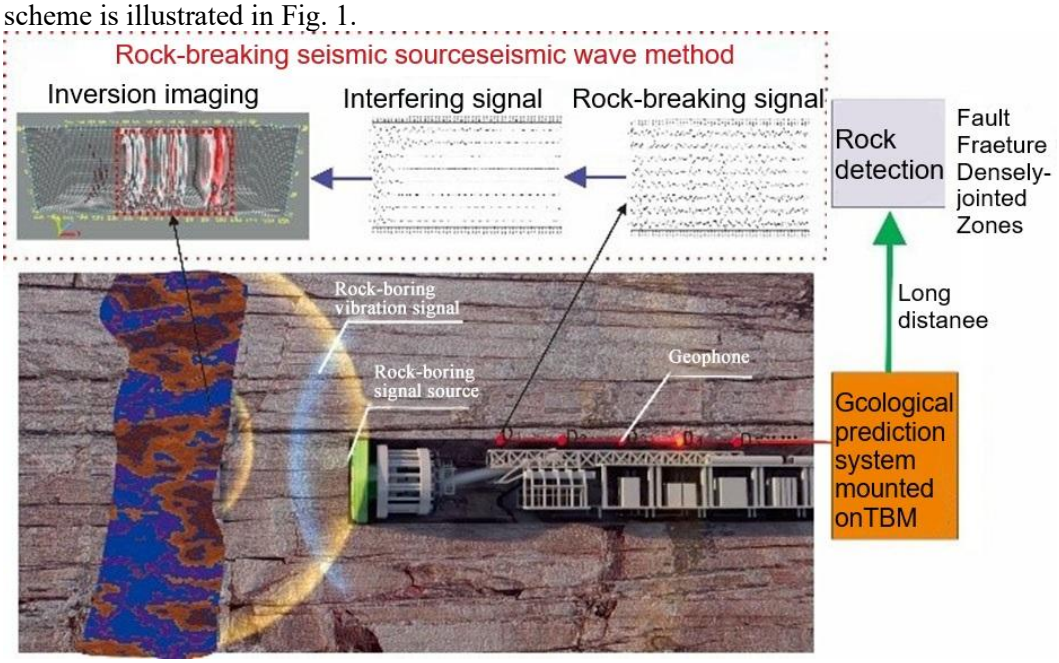


Fig.1 Schematic diagram of HSP detection layout

This technical scheme effectively utilizes the rock-breaking seismic source to implement real-time predictions of unfavorable geological bodies up to 100 meters ahead. Its real-time performance is primarily enabled through the following aspects:

(1) The TBM continues tunneling without interruption during the detection process;

(2) The HSP equipment is mounted on the TBM, allowing for the automatic interaction of basic data such as mileage, tunnel diameter, and coordinates;

(3) After the geophone layout and automatic parameter settings are completed, detection can be initiated with a single click. The system automatically acquires data for a minimum of 8 minutes, followed by data processing, virtual source establishment, ellipsoid imaging, anomaly picking, and result display, all according to the built-in processing workflow, with the entire process taking approximately 10 to 12 minutes.

(4) The resulting data is automatically stored in a database, enabling iterative analysis of adjacent detection results through human-computer interaction.

Field signal acquisition involves using 6 signal receiving geophones installed along the tunnel profile and 1 noise receiving geophone mounted on the TBM body (structural beam) to continuously gather a sufficient amount of vibration information (typically no less than 8 minutes, with more than 1000 data recording channels per test) while the TBM is fully advancing. Furthermore, the signal data undergoes various analyses, including time-domain waveform analysis, spectral analysis, filtering, correlation interference analysis, reflection imaging, time-depth conversion, extraction of anomalies from geophysical prediction, and geological interpretation. From the installation of geophones to the output of results, the entire process takes approximately 20 to 25 minutes, allowing for preliminary results to be obtained on the TBM construction site.

By pre-setting acquisition parameters (sampling rate, acquisition duration, etc.), equipment parameters (spatial coordinates of geophones), data processing (filtering parameters, interferometric data channels, etc.), and inversion parameters (initial wave velocity, anomaly picking threshold, etc.), functions such as automatic data acquisition, immediate processing, and intelligent identification of rock-breaking signals are executed. Data processing encompasses spectral analysis and filtering, the establishment of a virtual seismic source, 3D imaging, and anomaly picking and interpretation, which collectively yield preliminary results for geological predictions. If geophysical prediction images reveal a significant unfavorable geological body, manual intervention is invoked for precise processing, ultimately enabling the detection of the location, scale, and nature of the unfavorable geological body ahead of the working face, thereby guiding safe TBM operations.

3.3 *Key Technologies of Data Processing*

During TBM tunneling, rock-breaking vibration signals are generated and captured by receiving geophones amidst the interference from cutters and the filtering effects of the strata. The unfavorable geological body ahead of the working face can be detected through effective signal selection and preprocessing, correlation interferometry, virtual source extraction, and focused imaging. The key processing technologies are described below.

(1) Signal selection and preprocessing

Multi-source interferometry continuously collects a substantial amount of data during TBM tunneling, which inevitably introduces construction noise.

By analyzing time and frequency domain signals, the system deletes abnormal high-amplitude data. Additionally, it removes high-frequency and low-frequency interference through frequency domain filtering. It is important to clarify that during the data processing, it is neither feasible nor realistic to pursue complete noise filtering and removal. Maximum efforts should be made to ensure that reasonably effective time-frequency domain signals are not filtered out; occasional noises can be mitigated through techniques such as focusing and iteration.

(2) Virtual source extraction

Seismic interferometry is employed to perform interferometric processing on the selected filtered signals received along the tunnel profile. The data will contain reflection information. By applying speed analysis and focused imaging, stratigraphic distribution information can be derived.

(3) Focused imaging

The core concept of focusing is to maximize energy. Based on the principle that the sum of distances from two focal points of an ellipsoid to any point on its surface is constant, the reflected wave fields are spatially superimposed at different speeds. This results in the optimal speed, where the reflection energy spectrum in the anomalous area focuses most strongly. Consequently, a final 3D spatial reflection energy spectrogram of the strata is formed.

(4) Automatic anomaly identification

Through focused imaging and calculation, the spatial position of the point with the maximum focused energy can be identified during the iteration process. By analyzing the area covered by the energy group, the spatial position and scale of the anomaly can be determined. Leveraging experience and prior geological information, the anomalous areas are clustered and diminished to facilitate the automatic identification of anomalies, leading to preliminary prediction conclusions.

4 ENGINEERING APPLICATION

4.1 *Xianglushan TBM Tunnel of Water Diversion Project in Central Yunnan*

(1) Project overview and geological conditions

The Xianglushan Tunnel is located in the Hengduan Mountains of northwestern Yunnan, with a total length of 62.596 km. It represents the most typical key and challenging components of the Water Diversion Project in Central Yunnan. In the tunnel area, the exposed geology primarily consists of sandstone and mud shale interbedded with coal streaks from the Permian basalt and Heinishao formations.

(2) Case analysis

Real-time advanced geological prediction was conducted using the HSP method, focusing on fault structural zones encountered by the TBM. Geophones were arranged along the upper tunnel profile of the operation platform, positioned between the gripper and the main equipment chamber. Three geophones were placed on each side—left and right—to continuously collect rock-breaking signals for over 10 minutes while the TBM was fully advancing. The prediction mileage ranges from DLI54+000 to DLI53+631, resulting in a prediction distance of 369 meters (average of 4 detection results). For the prediction results, TBM tunneling parameters, and revealed conditions, please refer to Fig. 2.

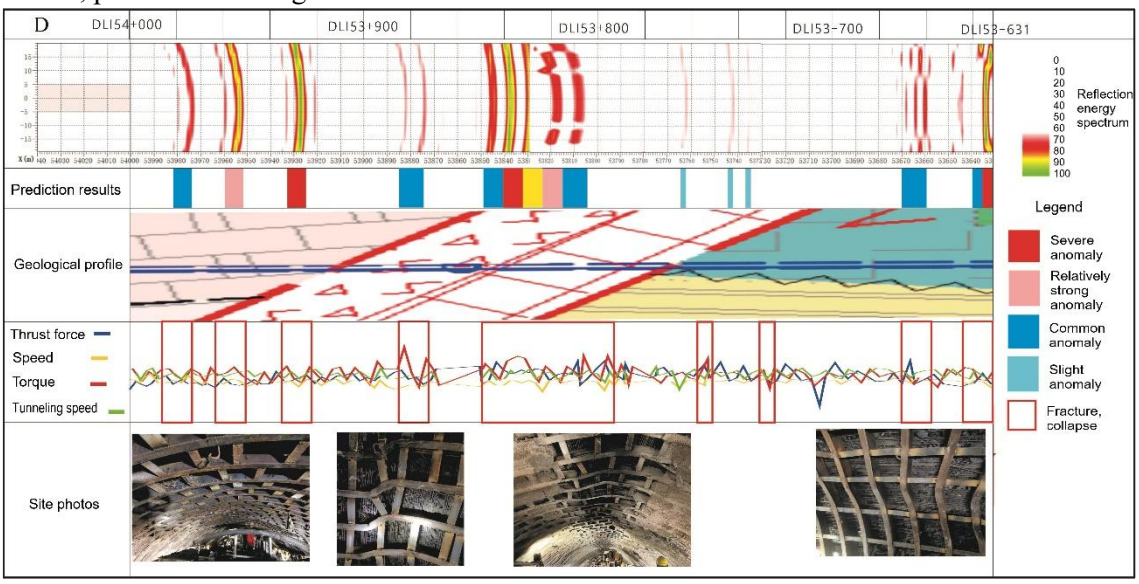


Fig.2 Statistical Analysis of Prediction Results

From the figure, it is evident that there are several strong reflection zones in this test area, characterized by high reflection energy spectrum values (relative). Notably, in the section from DLI53+850 to DLI53+800, there are continuous anomalous areas, indicating risks of spalling or collapse.

(3) Verification after excavation

After excavation, the analysis of tunneling parameters—such as thrust force, speed, and torque—along with the interaction of on-site support structures, indicates a significant influence from the F12 fault. This influence is evidenced by abnormal fluctuations in tunneling parameters and severe deformation of the support structures. The affected area aligns closely with the predicted anomalous area. In particular, within the section from DLI53+850 to DLI53+800, the amplitude of the reflection energy spectrum exceeds 70% of the specified value, with the core exhibiting values approaching the specified maximum. During tunneling and crossing, the tunneling parameters exhibit abnormal fluctuations, and the deformation of the supporting structures is pronounced. However, the length of the predicted anomalous area is shorter than the affected area indicated in the geological profile. The geological conditions of the tunnel are further detailed through prediction.

4.2 *Daliangshan No. 1 TBM Tunnel on Leshan–Xichang Expressway*

(1) Project overview and geological conditions

The Daliangshan No. 1 Tunnel, the dominant works of the Leshan–Xichang Expressway, is situated in the transitional zone between the Yunnan–Guizhou Plateau and the southwestern Sichuan mountainous region, bordering the Sichuan Basin to the northeast. The main tunnel is approximately 15.3 km long and features a cross-sectional layout of one main tunnel plus one parallel adit. The parallel adit was constructed using the TBM method. The tunnel traverses eight geological formations, including Jialingjiang, Leikoupo, and Xujiahe. It encounters several unfavorable geological conditions, such as karst strata, rock bursts, water inrush, significant deformation, and gas presence. The tunnel crosses through limestone and basalt water-rich sections and intersects F1 and F2 faults multiple times, which posed a substantial risk of water inrush.

(2) Case analysis

The focus was placed on the detection of the section from DK87+680 to DK87+220, covering a length of 460 m (average of 5 detection results). Geophones were arranged on both sides along the upper tunnel profile of the operation platform, positioned between the gripper and the main equipment chamber. In this case, the TBM will traverse basalt primarily classified as Grade III and IV.

Fig. 3 clearly shows several strong reflection zones in this test area, characterized by high reflection energy spectrum values (relative). There are extensive anomalous areas in the sections from DK87+680 to DK87+620 and from DK87+520 to DK87+500, where the prediction indicates risks of spalling or collapse. Additionally, several smaller anomalous areas are present, where the prediction suggests that they are local fracture areas. There is a possibility of local collapse.

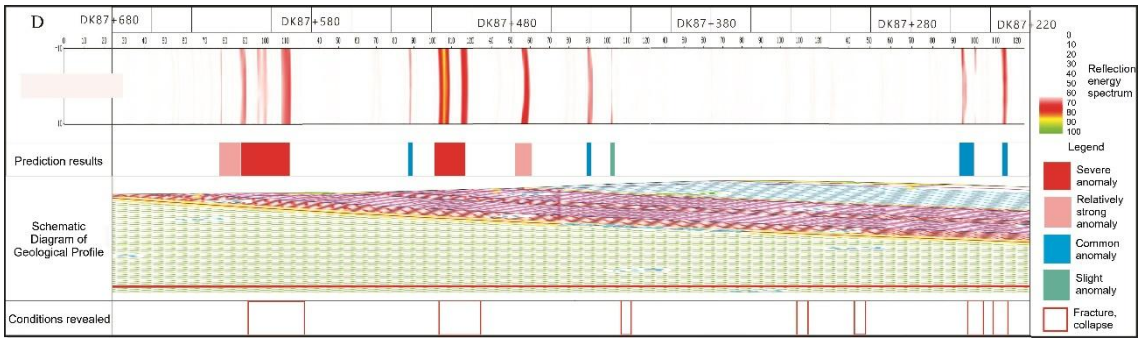


Fig.3 Statistical Analysis of Prediction Results

(3) Verification after excavation

According to the verification conducted after excavation, the construction of sections from DK87+635 to DK87+580 and from DK87+520 to DK87+495 encountered fractured rock masses and developed groundwater. This resulted in crown collapse and the formation of cavities of a significant scale in the surrounding rock. The results generally align with the anomalous sections identified by the prediction, though there is a slight discrepancy in position, attributed to the differences between stratigraphic anisotropy and the speed inversion model. Nevertheless, this long-distance prediction effectively identifies unfavorable geological bodies that could cause disasters.

4.3 *Summary of Application*

The HSP method, which utilizes vibration signals generated from rock mass shearing by the TBM cutterhead and disc cutters as the excitation source, exhibits the following characteristics:

(1) It enables convenient field tests without the need for blasting or hammering. Additionally, it does not require TBM shutdown, ensuring that construction is not affected.

(2) The deployment of detection points is highly adaptable, allowing for their arrangement at any position along the tunnel profile.

(3) It achieves a short on-site test duration. Geophones can be installed in approximately 10 minutes. Once in place, they can continuously collect rock-breaking signals for no less than 8 minutes.

(4) The object under detection meets the requirements of the long-distance seismic wave method, with an effective detection distance of up to 100 m. Unfavorable geological bodies, including karst strata, weak interbeds, fractured strata, faults, densely jointed zones, water-rich structural zones, boulders, and bedrock relief, can be effectively detected.

(5) The equipment can be installed without the need to modify the TBM. It is suitable for various types of TBMs, including open-type TBMs and those with single or double shields.

5 CONCLUSION

It has become a consensus to fully utilize TBMs to implement advanced geological prediction technology. Previous studies have devised solutions through geophysical prediction methods, such as electrical methods and elastic wave methods, by analyzing the characteristics of TBM construction technology and the structure of the TBM body. In light of the key and difficult issues in TBM geological prediction, this study examines the critical factors of geophysical prediction methods, including the field source type and excitation form, the integration mode of prediction equipment, and the prediction length and result timeliness. Additionally, it celebrates the theory and key technologies of real-time geological prediction based on the TBM rock-breaking seismic source HSP method. This method has led to key technical breakthroughs, including automatic information collection, intelligent data processing, intelligent anomaly identification, and real-time result interpretation. The technology has been successfully implemented in the TBM construction of several projects such as the Xianglushan Tunnel of Water Diversion Project in Central Yunnan and the Daliangshan No. 1 Tunnel on the Leshan–Xichang Expressway. It has produced positive results and has played a significant role in enhancing the efficiency of TBM construction, underscoring its considerable importance.

REFERENCES

[1] LU Song, LI Cangsong, WU Fengshou, et al. Application of HSP (Horizontal Sonic Profiling) Sound Wave Reflection Method to Geological Prediction of TBM Tunnel of Hanjiang River Weihe River Water Diversion Project[J]. Tunnel Construction, 2017, 37(2): 236.

[2] LV Erchao. ISP Geological Prediction System Applied in the TBM Construction of the Hanjiang to Weihe Project[J], Railway Construction Technology, 2016(6) :52.

[3] DENG Mingjiang, XU Zhenhao, LIU Bin. Establishment and application of “1km + 100m+ 50m” geological prediction system for extra-long 'TBM tunnels: a case study on water supply project ll in Xinjiang, China[J]. Tunnel Construction2021.41(9):1433.

[4] ZHAO Yonggui, JIANG Hui, etc. Tunnel seismic tomography method for geological prediction and its application, Applied Geophysics, 2006 , 3(2):69.

[5] PETRONIO L, POLETTO F. Seismic-while-drilling by using tunnel boring machine noise[J]. Geophysics, 2002, 67 (6): 1798.

[6] Kaus A, Boening W. BEAM-Geoelectrical Ahead onitoring for TBM-Drives[J]. Geomechanik and Tunnelbau, 2008, 1(5):442.

[7] WEI Xiaolong, ZHENG Junxiang, LIN Fulong, et al. A geological prediction system for shield construction based on focusing frequency IP method [J]. Chinese Journal of Underground Space and Engineering, 2022, 18(1): 290.

[8] Nie L, Song Z, Li Z, et al. Ground-tunnel geological prospecting and treatment methods of small-diameter TBM crossing shallow buried water-rich tunnel: A case study[J]. Tunnelling and Underground Space Technology, 2024, 153: 106024.

[9] CHEN Fangming, XIE Mian, JIANG Hui. Application of complex frequency conductance technique in the advanced water exploration in tunnel, Yangtze River, 2015， 46(21), 50.

[10]HE Faliang, GUO Rujun, LI Cangsong, et al. The temperature of rock tunnel construction ahead of tunnel water inflow prediction, Cheng Du: Southwest Jiaotong University Press,2009:22.

[11]Ivan V R. Interferometry by deconvolution, Part l- Theory for acoustic waves and numerical examples[J]. Geophysics, 2008, 73(3):115.

19th Australasian Tunnelling Conference – Acosta-Martínez, Stewart and Hudson-Smith (Eds.)
© 2025 Australian Tunnelling Society, ISBN 978-0-85825-002-4

The use of optical televiewer and endoscope imaging methods in TBM tunnels to predict ground conditions

R. A. Susilo
Snowy Hydro Limited, Cooma, Australia

K. Stariha
SMEC Australia Pty Ltd, Melbourne, Australia

B. Requiliani & F. Stroppa
Webuild, Australia

F. Alvarado
Future Generation Joint Venture, Cooma, Australia

ABSTRACT: Snowy 2.0 is a 2.2 GW pumped hydro project currently under construction in the Snowy Mountains, New South Wales, Australia. Four shielded TBMs are being used to progress approximately 31.4 km of tunnels through complex alpine ground conditions. Due to the nature of shielded TBMs, obtaining information on ground conditions is extremely challenging compared to D&B tunnelling. Information from probe holes in advance of the TBM is therefore key in risk mitigation; predicting ground conditions and features of concern in advance of the excavation and allowing them to be dealt with appropriately. This paper explores the use of imagery in percussion drilled probe holes ahead of TBM excavation to forecast ground conditions. A comparison between Optical Televiewer (OTV) and Endoscope imaging methods is made, including the observed key benefits and challenges of each method, the outcomes of each method such as key outputs, image quality, time and cost efficiency

1 INTRODUCTION

The Snowy 2.0 Pumped Storage Project (S2.0), currently under construction, represents a significant expansion to the renowned Snowy Mountains Hydroelectric Scheme. The original Scheme, located in New South Wales, Australia, was constructed between 1948 and 1974. It is recognized as one of the world's most impressive civil engineering feats, with a capacity of 4.1 GW, 16 dams, 9 power stations, and a network of 145 km of tunnels. S2.0 will enhance the existing scheme by adding 2.2 GW of power generation capacity with 350,000 MWh of storage, providing deep energy storage to support the growth of Australia's renewable energy generation. S2.0 involves substantial and complex underground works including ~31.4 km of TBM-driven tunnels, ~10 km of drill-and-blast tunnels, three shafts, and a power station complex located ~750 m below surface. This paper will focus on the TBM driven power waterway tunnels, excavated by 4 single-shield TBMs.

Snowy Hydro Limited, the owner, has engaged Future Generation as Principal Contractor for civil works - a consortium comprising Webuild, Clough, and Lane. The design joint venture includes Lombardi, Tractebel, and Coffey, whilst SMEC are engaged to provide technical engineering support to the owner.

The project is situated in a complex alpine geological setting, with 7 geological formations and over 40 lithologies (Figure 1). Rigorous site investigations have been undertaken in many stages throughout the project to date. However, due to the long, linear and deep nature of the project, the complex geological setting, and access limitations from the project sitting within a remote and pristine national park, it was not practically possible to fully define ground conditions along the entire alignment prior to excavation. This is particularly true for the long TBM driven power waterway tunnels, with some sections having up to 2.5 km between boreholes. The tunnels' segmental lining (and the TBM's themselves) are designed to cover the full range of ground condi-

tions considered possible along the alignment. However, understanding when to implement support classes, pre-treatment, or TBM excavation modes requires good understanding of ground conditions directly ahead of the TBM excavation. This can be challenging in a shielded TBM due to minimal opportunities and accessibility to directly view ground conditions.

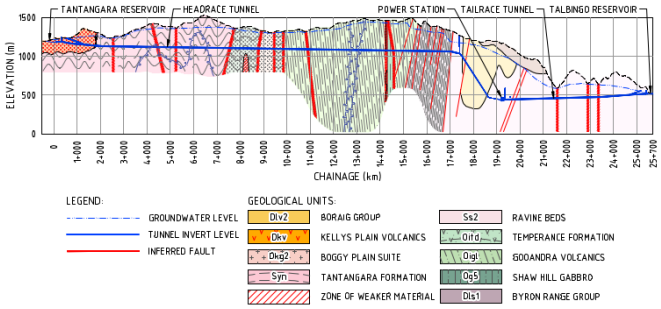


Figure 1. Geological long section of the S2.0 Power Waterways tunnels

To ensure sufficient notice is given on ground conditions directly ahead, each TBM is equipped with a minimum of two drill rigs capable of both percussive and rotary drilling (Figure 2). Percussively drilled probe holes are undertaken in an overlapping fashion. These provide information on conditions ahead through the return of small rock chips, measurements of groundwater inflow, drilling parameters, and, the subject of this paper - imagery in the form of Optical Televiewers (OTV) and Endoscopes. Face mapping is undertaken daily together with photogrammetry, and is combined with information from probing and TBM parameters to assess ground conditions, verify design assumptions, assess whether pre-treatment is required, and select the correct segment support class for installation. This paper will focus on the use of imagery in percussively drilled probe holes, and will discuss what information can be obtained from each imagery type, the advantages and limitations of each and key observations.

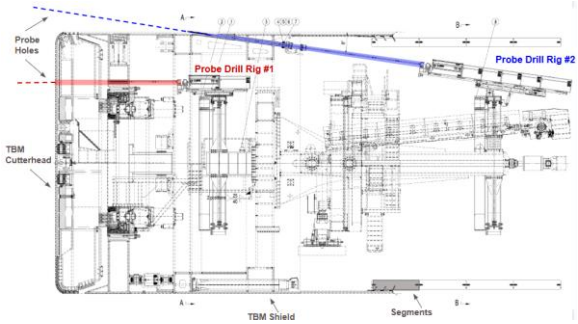


Figure 2. Positioning of drill rigs and probing locations from TBMs

2 METHODOLOGY

Ground conditions ahead of the TBM are defined based on information from multiple sources, including probe drilling, face mapping, and photogrammetry. While geological mapping and photogrammetry is typically undertaken daily, this provides only single spatial snapshot of conditions at the excavation face, and not beyond. To collect information in advance of the excavation and continuously along the drive, probe holes are progressed 60-100 m ahead of the face.

On S2.0, all TBMs are equipped with drills capable of both percussive and rotary drilling. Drilling cored holes from within the TBM is possible and is advantageous in terms of sample recovery. However, depending on hole length and ground conditions, this may take up to several days to complete and is therefore not a time-efficient option as construction is halted during these activities. In contrast, a percussively drilled probe hole of the same length can be progressed in a

fraction of the time - as little as a few hours. This provides rock chip return, an assessment of groundwater conditions, drilling parameters, and an opportunity to insert cameras into the hole. However, percussively drilled probe holes can present certain limitations. Sample return is often challenging, as rock chips often become trapped between the rock and the TBM shield. Drilling parameters can be highly variable for reasons other than ground conditions, including factors like drilling technique, machine performance and equipment condition, and are therefore difficult to reliably assess.

OTV and endoscope recordings prove to be extremely valuable in providing direct visual confirmation and aiding in the interpretation of subsurface conditions. This provides key information on lithology, defect spacing, and some aspects of defect condition, whilst taking only two hours.

After completion of drilling and flushing of the hole, the geologists perform the image inspection. Depending on observations during drilling, the geologist on site has the authority to decide if it is necessary to do a preliminary inspection of the hole with the endoscope (to assess the hole condition) or proceed directly with OTV inspection. This is done to minimize risk of damaging the OTV tool, as it is more costly and fragile. The process ends with a groundwater inflow measurement, inserting a packer at 4m depth. Finally, all observations from the endoscopes and OTV, are reported in the probe hole geological assessments, which compiles assessments from all datasets including drilling parameters, cuttings description and water inflow measurements. These are assessed against design assumptions.

2.1 *Optical Televiewer (OTV)*

2.1.1 *Tool*

The OTV QL40 probe line is designed to capture high-resolution, magnetically oriented colour images of borehole walls, enabling detailed logging of rock types and structures. The tool uses a digital camera paired with a conical mirror to produce continuous 360-degree images in both air- and water-filled boreholes.

OTV tools are designed primarily for use in vertical holes and have fragile glass housing for cameras. Scenarios like steeply inclined boreholes, with non-curvilinear geometries, or the presence of residual materials within the borehole that cannot be adequately cleaned, therefore render OTV usage challenging. To mitigate this, on S2.0, a light perspex housing is applied overlying the glass, to reduce glass fractures and/or waterlogging the camera.

2.1.2 *Procedure*

The following outlines the steps of executing imagery using the OTV tool:

- Instrumentation Setup: Connect the OTV, datalogger, and winch to the power source; configure recording and image acquisition settings.
- Tool Insertion: Insert the tool into the probe hole (PH) and set the 0-meter depth reference and start the preliminary record. Push the instrumentation into the PH using 32 mm PVC tubing and maintain a maximum speed of 5m/min to avoid tool crashing. During the pushing in of the tool, the images are checked for quality and equipment setup.
- Tool Retrieval: Upon reaching the end of the hole, stop recording. Begin a new recording during retrieval setting the winch at a maximum of 3 m/min for best image quality. Operators detach PVC tubes as they exit the hole, reducing the speed during this process to avoid interference with the winch and image quality.

2.1.3 *Data Analysis*

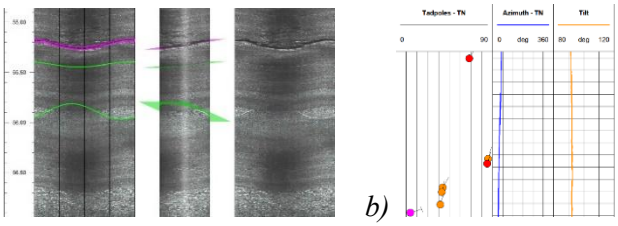
WellCAD is a software by RocScience used for the import, processing, interpretation, and visualization of geophysical and geological data collected in boreholes with OTV. The software allows analysis of geological structures including location, type, and orientation of defects, as well as aperture, infilling, and to some extent waviness.

Images are processed by splitting them along a reference azimuth (typically north), then unrolling and flattening them into a 2D log for interpretation, and borehole irregularities such as breakouts or washouts can be identified. This method transforms raw image data into a precise structural map of the borehole.

Within the S2.0 project, two distinct reports are developed. A preliminary report is produced

immediately after drilling and presents an image of the borehole accompanied by azimuth and inclination data of the hole. This provides a quick but effective preview of the status of the rock mass, and permits a quick visualization of whether critical zones are present. Subsequently, the final report is produced, elaborated with WellCAD, involving picking of the geostructures. This report displays the image of the borehole in two forms: an unwrapped 2D image and a 3D core-like view. It presents an overlay of the structure on the borehole image, hole survey information (Figure 3a) and tadpoles illustrating the corrected orientation of the structures, along with azimuth and tilt charts (Figure 3b). It is worth noting that in the TBM environment, the method is limited in Azimuth (TN) accuracy for the first 10m to 15m due to magnetic interference from the shield.

Defect information such as type, orientation, and aperture, and other information such as hole survey, temperature, magnetic field can be easily exported (a sample of extracted defect attributes from WellCAD shown in Figure 4) and used to analyse the rock mass properties in excel sheets and 3D modelling software such as Leapfrog Work, Vulcan and Rhino.



a) *b)*

Figure 3. a) Visual modules in an OTV report and b) tadpoles of structures and hole survey in an OTV report

Depth	Dip	Azimuth	Type	Aperture	Infilling	Shape
m	deg	deg		mm		
0.37	78.74	231.53	JT	0	N	PL
0.43	13.97	123.88	PT	1.27	N	PL
0.79	78.38	289.47	JT	2.49	N	PL
1.26	79.4	216.25	JT	0	N	PL
1.4	82.96	224.85	JT	1.45	N	PL
1.53	21.91	39.3	PT	0	N	PL
1.88	35.98	23.11	JT	0	N	PL
2.06	15.18	102.94	PT	0	N	PL
2.12	86.72	27.58	JT	0	N	PL
2.53	13.39	66.01	PT	0	N	PL
2.74	52.55	200.42	VO	0	H	CU
3.75	44.72	19.22	JT	0	N	CU
3.98	70.11	24.79	JT	0	N	CU
4.2	84.73	109.08	JT	0	N	CU
4.49	49.55	12.38	JT	0	N	CU
4.96	81.31	202.77	JT	7.94	N	UN

Figure 4. Example of extracted information of picked structures from WellCAD

2.2 *Endoscope*

2.2.1 *Tool*

On the S2.0 project, two types of endoscope cameras are used. The DGRT Wireline Digital Camera 360 View provides very good resolution and accurate images, however has similar limitations to the OTV due to its dimensions (1m length and 40mm diameter), weight, and equipment set up requiring a winch. The Ridgid Seesnake is simpler to use due to the 35mm diameter and 42mm length camera, equipped with 11mm push cable and powered by battery.

Both provide a practical and effective method for examining geologic structures and discontinuities in real time. The Ridgid camera has certain limitations, such as a lower resolution and accuracy than the DGRT camera, but is typically sufficient in providing preliminary information for the scale of the tunnels. The Ridgid camera is the preferred method for collecting the endoscope images in S2.0.

The endoscope is an invaluable tool in specific project scenarios where the use of an OTV is hindered by technical challenges, as mentioned in Section 2.1.1. In such cases, the endoscope proves its worth by enabling the acquisition of visual data, playing a crucial role in ensuring that probe hole imagery can still be captured, maintaining the continuity and reliability of the data

collection process.

2.2.2 *Procedure*

The following outlines the steps of executing imagery using the endoscope tool:

- Instrumentation Setup: configure recording and image acquisition settings.
- Tool Insertion: Insert the tool into the probe hole (PH) using the self pushing cable (Ridgid) or PVC pipe (DGRT). Set the 0-meter depth reference and start recording.
- During: Real time footage is monitored via screen, with operators targeting certain sections of interest with slower speed if needed, or stop the pushing if the hole is obstructed.
- Footage is captured both inwards and outwards through the hole, giving different quality of images depending on the water flow condition of the hole.

2.2.3 *Data Analysis*

For endoscopic imagery, the first analysis is undertaken simply by watching the video screen as the tool is inserted into the hole. This provides an immediate assessment of conditions, and checks whether it is safe to proceed with the OTV record. Then, the geologists again watch and analyse the endoscope video, where more detailed observations and notes of ground conditions and any potential geohazards are taken and reported in the probe hole geological assessment.

3 RESULTS

3.1 *Geotechnical features interpretation*

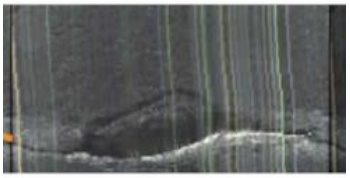
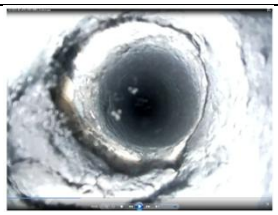
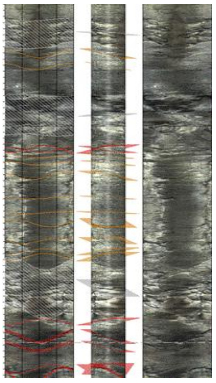
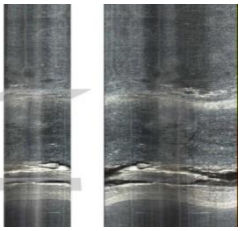
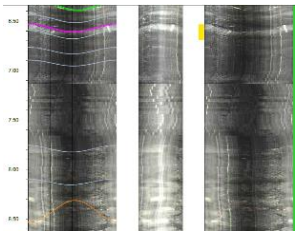
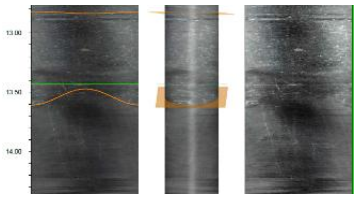
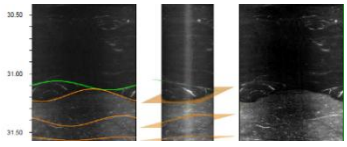
Side-by-side comparison of OTV and endoscope data from the same borehole illustrates the unique perspectives each tool provides for geostructural and geotechnical feature analysis. Table 1 presents examples where OTV and Endoscope imagery was useful in understanding specific geological conditions, and the key differences of OTV and endoscopes in these situations.

Extracts and screenshots from images produced by the OTV and endoscope quickly show that by nature of the camera lens, features typically appear larger in endoscopes, whilst OTV provides a less biased view of the aperture of a feature, see Observation 1 in Table 1. In Observation 2, the high quality image allowed good visibility of the sheared features of concern and ability to easily assess geotechnical attributes which led to timely decision-making by the designer in regards to the suitable excavation support class in that section.

Observation 3 in Table 1 shows endoscope imagery of a geological feature where water flow was observed. This confirmed the exact location of water inflow and visual assessment of the rate and behavior of inflow, which could not be captured precisely either from an OTV or the standard inflow test. On the other hand, OTV provided high-quality images and strong quantitative data of the feature such as defect type, defect orientation, defect location, planarity, infilling and aperture. In addition to the outputs from each tool, the combination of the two sources of information provided complementary benefits and better understanding of the situation.

Changes of geological formations are also effectively presented by the OTV reports in Observation 4 and Observation 5. Notably in Observation 5, the contact is not easily distinguishable in the endoscope videos. In combination with the accurate depth tracking, ability to pick dip and dip direction, planarity and correction based on hole survey, a confirmation of the precise location and direction of the contact was obtained.

Table 1. Key observation findings.

Key Observations	Extract from OTV reports, depth scale of 1:20m	Screenshots from Endoscope videos
Observation 1: Sheared feature observed in a probe hole showing typical ground conditions in Ravine Beds West. Endoscope allows slightly more visibility of defect coating due to the nature of the camera lens.		
Observation 2: Observed sheared features in OTV, excavation support class change was recommended by the designer. The mapping performed on this area later confirmed the presence of these sheared zones.		No endoscope is available for this probe hole.
Observation 3: Geological feature from where water flow was observed in Endoscope video. OTV image does not capture water flow but provides high-quality image of the defect.		
Observation 4: Geological formation Ravine Beds West to Boraig Group, clearly observed in OTV. In the endoscopic image, the contact is not easily distinguishable.		
Observation 5: Intercalated contacts between Kelly's Plain Volcanics Formation and Peppercorn Formation at 13.0m depth and 31.0m depth. Also, a change in TBM parameters and lack of rhyodacite in the cuttings has confirmed that the excavation has passed through the contact.	 	No endoscope is available for this probe hole.

4 DISCUSSION

Table 2 below summarizes key outputs available, and advantages and disadvantages of the two imaging tools.

Overall, whilst OTV generally provides a more technically rigorous output and its information is powerful in assisting design assumptions confirmation, the simplicity and cost advantages of endoscopes spotlight the tool's beneficial practicalities while typically still being able to provide sufficient information to clear that no geological hazards are present along the hole.

Noting the prominent time saving between progressing percussively drilled holes vs. cored holes, the ability to capture imagery in percussive holes allows a similar level of information to be obtained at an overall fraction of the time, offering a significant production advantage with still great information return.

It is important to note that in cases of very poor ground conditions where the drilled hole is collapsing, or where there is a high groundwater inflow at high pressures, the use of either tool would not be physically feasible, and in this case, assessment will rely on drilling parameters and coring, it is also noted that the knowledge that the hole was collapsing is in itself noteworthy and to be considered in the evaluation.

Table 2. Summary of available outputs, pros and cons of OTV and Endoscope

	OTV	Endoscope
Outputs	– Output format as image, or pdf – Quantitative data (defect type, defect orientation, defect location, planarity, infilling, aperture) via WellCAD – Qualitative (observation of grain size, change in lithology, weathering) – High quality imagery – Survey data (orientation of probe hole in the form of Tilt and Azimuth)	– Output format as video – Qualitative assessment (defect relative orientation, estimated defect location, planarity, infilling, aperture, observation of grain size, change in lithology, weathering) – Location of the water sources and estimation of the water inflow observed
Pros	– Accurate quantitative geotechnical parameters obtainable, high quality imagery allowing detailed assessment – Corrected dip/dip direction of picked features based on hole survey – Easy extraction of information allowing straightforward inputs to geological models, and/or calculations – Image output easily accessible and shareable – The ability to adjust the depth scale during viewing and printing	– Local providers with stock available – Specialist software to interpret data is not required – Tool is typically lower cost – Allows observations of water inflow – Versatility due to the small diameter and strong camera – Battery powered
Cons	– Tool is typically higher cost and more fragile – It does not provide images in front of the tool, risking its integrity when it needs to be pushed into the hole – Power connection is required – Cannot easily show locations of water inflow	– Video formats can be inconvenient for sharing/communication or storage consuming, especially in larger scale projects – Geotechnical parameters such as dip/dip direction of the structures can only be inferred from video – Observations both qualitative only and less accurate – Assessment may be more time-consuming due to video format

4.1 *Role of OTV and Endoscope in Clarification of Design Assumptions and Risk Management*

As discussed, the project sits within a complex alpine geological setting, with limited information available along some portions of the alignment, particularly the long TBM driven power waterways. Although there are several predicted areas of higher geological risk, there remains potential

for additional unexpected geological hazards to be present in other areas. Unlike a smaller metropolitan project where the ground conditions are heavily investigated and understood, on long, deep and remote alpine projects it is not possible to pre-prescribe support to a certain area. The design is rigorous in being able to cover the full range of conditions which may be encountered. However, there remains a level of uncertainty as to precisely where along the alignment any particular hazard may be encountered, and therefore where a certain pre-treatment, support class, or even TBM excavation mode may be required. Being able to understand the conditions directly ahead of the TBM excavation is therefore vital for risk mitigation, to highlight any hazards present ahead and to act accordingly. This allows the TBM to proceed with confidence, understanding that the risk of encountering unexpected features without advance warning is reduced.

Imagery acts to enhance the information available from percussively drilled holes, which is in particular useful for validating and, if needed, modifying design assumptions. Segmental lining design uses Geological Strength Index (GSI) as one of the key parameters. The use of OTV allows for the estimation of GSI, by providing information on defect spacing/RQD and many properties required to assess defect condition (aperture, infilling, weathering, and to some extent, waviness). This allows for the validation of design assumptions and the appropriate selection of support for installation. Similarly, where larger features (such as shear zones) are encountered, imagery from both OTV and Endoscope can provide more information on the nature and extent of the feature than simple drilling parameters. This provides the designers with the information required to assess whether a feature falls within or outside of design assumptions, and whether any pre- or post-treatment may be required. Should more detailed information be required, the TBMs are equipped with coring capability which can be used to target areas of concern highlighted by the percussive probing and imagery.

5 CONCLUSION

The use of downhole imagery has proven to be exceedingly useful on S2.0, offering an advantage over standard percussively drilled holes, which are more heavily reliant on simple drilling parameters and chip collection. It allows geological information gathered to rival that obtained during core drilling, but at a fraction of the drilling time.

Having these instruments as part of the contractors' toolbox increases the capability to react to encountered conditions quickly and mitigate the always present risks and uncertainties during tunnelling. Observations from S2.0 discussed in this paper have demonstrated the value of advance information from probing, amplified by downhole imagery and the unique benefits that each tool brings, with a specific focus on changes in lithology and geological formation, groundwater inflow, and understanding features of concerns. Both OTV and Endoscopes are useful tools with advantageous practicalities that play an important role in risk mitigation, predicting ground conditions in advance of the TBM excavation and allowing them to be dealt with appropriately and safely.

19th Australasian Tunnelling Conference – Acosta-Martínez, Stewart and Hudson-Smith (Eds.)
© 2025 Australian Tunnelling Society, ISBN 978-0-85825-002-4

To jamb or not to jamb: Evaluating cross passage permanent support systems

V. Balakumarasingham
Aurecon (formerly Link Alliance & Tonkin and Taylor), Auckland, New Zealand

ABSTRACT: This paper explores design considerations for cross passage permanent support systems, comparing the use of jambs versus lintels. Focusing on the City Rail Link in Auckland, which employs jambs, the study examines the associated benefits, such as enhanced structural support and improved load distribution. However, the incorporation of jambs introduces challenges, including installation complexities, maintenance issues, and potential access restrictions within the tunnel system. The paper highlights specific design and execution challenges faced during the City Rail Link project. It also discusses the advantages of lintel designs, which may offer improved flexibility and simplified construction, while emphasising the need for structural stability and safety. Through an analysis of the trade-offs between jamb and lintel designs, the findings aim to inform best practices for future urban tunnelling projects, contribute to discussions on optimal design strategies that enhance operational efficiency and construction safety in the future.

1 INTRODUCTION

1.1 *Project Background*

The City Rail Link (CRL) is the largest transport infrastructure project ever to be constructed in New Zealand's. CRL is a 3.45km twin-tunnel underground rail link up to 42 metres below the city centre. It will transform the downtown Waitematā Station (Britomart) into a two-way through-station that better connects the city's rail network.

It includes a redeveloped Maungawhau Station, where CRL connects with the North Auckland (Western Line) and new underground stations - one midtown underneath Albert Street called Te Waihorotiu Station and Karanga-a-Hape Station just off Karangahape Road with entrances at both Mercury Lane and Beresford Square.

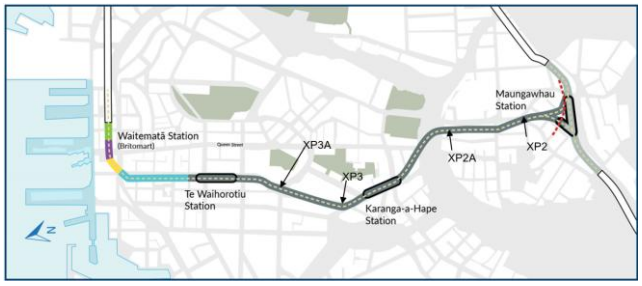


Figure1. City Rail Link Contract C3 Alignment and Station Location Plan

The Link Alliance is delivering the main works including three new stations, twin tunnels, rail systems and work at the existing Waitemata Station (Britomart) to accommodate the new rail connection. Link Alliance comprises City Rail Link Limited, Vinci Construction Grands Projets, Downer NZ Ltd, Soletanche Bachy International NZ Limited, WSP (NZ) Limited, AECOM New Zealand Limited and Tonkin + Taylor Limited[i].

There are two bored tunnel cross passages between each of the stations. The cross passages between Maungawhau Station and Karanga-a-Hape Station were labelled XP2 & XP2A and the cross passages between Karanga-a-Hape Station and Te Waihorotiu Station were labelled XP3 & XP3A in Figure 1. The spacing between the cross passages was determined following a fire life safety assessment which is beyond the scope of this paper. All cross passages on CRL were constructed with jambs.

1.2 *Definitions*

The elements that form cross passage permanent support are lintels, jambs, collar and side walls (Figure 2). These elements are defined as:

- Lintels: These are horizontal structural elements that span the openings above cross passages. They bear the load from the tunnel segments and help distribute it evenly across the support system.
- Jambs: The vertical supports that frame the sides of the lintels. Jambs effectively act as columns and carry vertical loads and bending.
- Collar: The section immediately behind the segments that receives the load from the lintel and transfer loads to the side walls
- Side walls: The elements that support the collar.

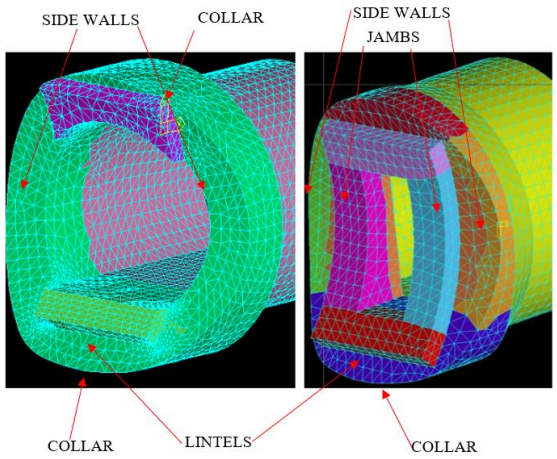


Figure 2. Cross passage permanent support definitions

2 A REVIEW OF THE BASICS

2.1 *Load transfer mechanisms*

The vertical load from the segments must ultimately be transferred into the side walls of the collar to find an equilibrating reaction from the bottom segment load or the ground (Figure 3). The load from the segments is usually considered to be uniform at the top and bottom of the opening so the most direct load path is provided by the jamb system.

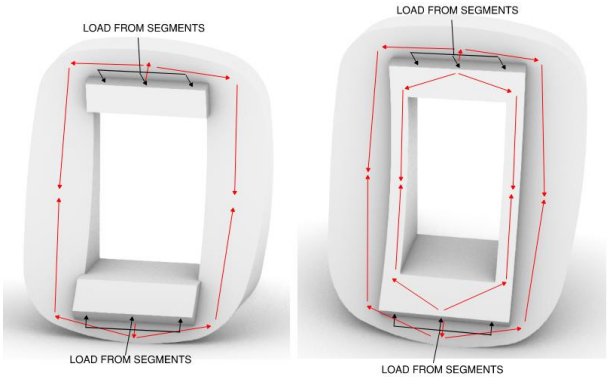


Figure 3. Load transfer mechanisms with no-jamb and jamb systems

For lintel only systems, given typical span and depth ratios, it can be designed using a strut and tie approach, with the primary design action being the axial load from the segments (Figure 4). The vertical load is subsequently transferred back to the collar along with the associated torsion. These actions are in turn is transferred to the side walls. Both systems require ground loads to be considered on the collar and side walls.

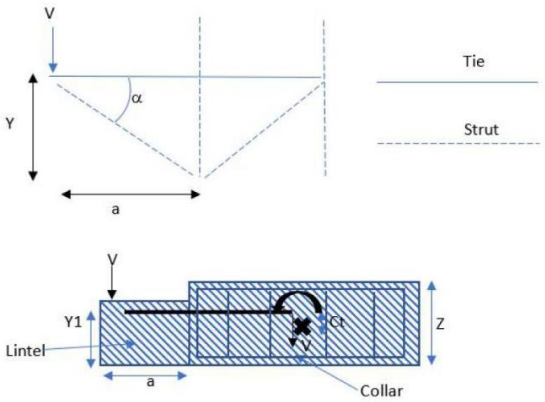


Figure 4. Strut and tie model and lintel collar transfer mechanism

2.2 Global Behaviour

The global behaviour of the permanent support systems is more readily comprehensible in the absence of jambs. In a no-jamb configuration, the segments exhibit a squeezing action that induces a tendency to close in towards the opening. This phenomenon results in the collar flexing and moving in both vertical and horizontal planes (Figure *5*). Consequently, the ground must effectively resist these movements unless the cross passage lining is explicitly designed to provide additional restraint to the collar. If the ground cannot restrain the movements or there isn't a suitable movement joint between the collar and the cross passage lining, the dynamics of movement may compromise the structural integrity and stability of the cross passage.

In contrast, when a jamb system is implemented, movements are better accommodated and restrained due to the presence of a stiffer support structure surrounding the opening. This stiffness contributes to a more direct load path, which efficiently transfers the forces from the segments into the jambs. As a result, the design enhances the overall stability of the support system by mitigating lateral and vertical displacements.

In essence, a no-jamb system presents challenges that necessitate careful consideration of ground resistance and the adequacy of the cross passage lining. However, these risks are not insurmountable especially in favourable ground conditions. The incorporation of jambs leads to a

more secure and resilient structural solution. This distinction is critical for designers when determining which support system best meets the demands of the project in question.

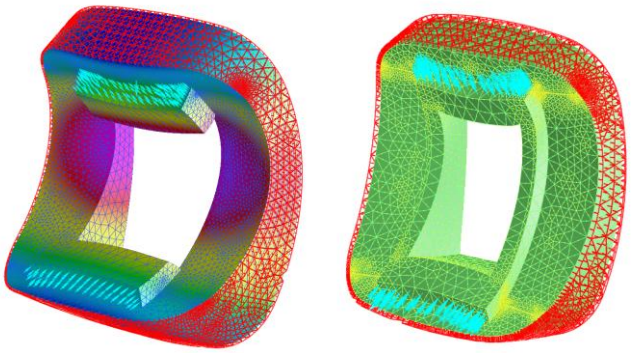


Figure 5. Global behaviour of a no-jamb system and jamb systems

4 DDITIONAL PERMANENT SUPPORT OPTIONS

4.1 *Shear keys*

Shear keys facilitate load transfer, improve stability, and alleviate potential movement between the segments. They have been used successfully in temporary support to facilitate the construction of openings in the segmental linings of large diameter TBM tunnels (Chau et al., 2023).

Shear keys act as mechanical interlocks between adjacent segments, and they help to distribute the axial forces in the segments around the opening. When used in conjunction with either of the jamb or no jamb systems, they would act to reduce the load taken by the lintels and jambs.

However, when incorporating steel shear keys into the design of a permanent support system, several factors would have to be assessed. These include but are not limited to:

1. The long-term durability of the shear key. Steel is commonly used due to its acceptable mechanical properties Protective coatings may need be applied to enhance corrosion resistance, particularly in moist or chemically aggressive environments.
2. Construction tolerances and ring roll if the shear keys are cast into the segments
3. Coring and reinforcement clashes as well construction logistics challenges associated with installation after the ring build.

Given these factors and the relatively low magnitude of the axial forces in a metro tunnel compared to a road tunnel shear keys were not adopted on CRL.

4.2 *First stage concrete (FSC)*

The track bed first stage concrete was used as a flexible strut both in the temporary and permanent case on CRL. This resulted in no temporary lintel having to be lifted and fixed in place before the opening of the segments (Figure 6). Moreover, it resulted in a more rigid permanent support system for the cross passages and additional load sharing between the segments either side of the opening and the collar.

On CRL analysing the effect of the first stage concrete in the permanent case involved carrying out a construction stage analysis calculation where temporary support elements (bicones in this case) are ‘switched off’ and the permanent support is wished into place. The analysis is then rerun, and sections were cut through each of the structural elements (1.2) to determine the design actions.

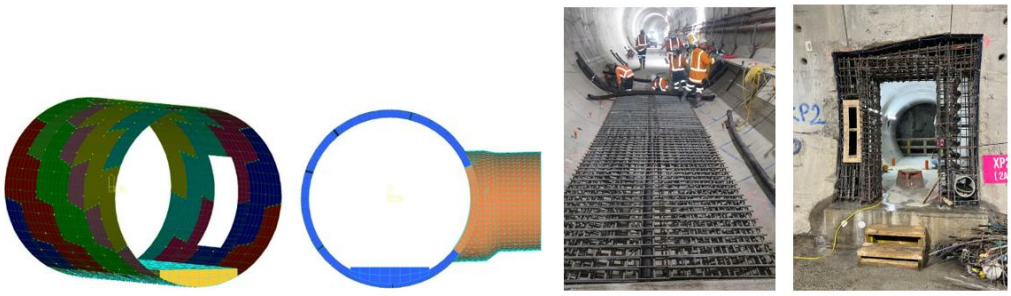


Figure 6. FSC Analysis models, FSC installed reinforcement, Segment opening without temporary lintels

5 CONSTRUCTABILITY

5.1 *Formwork and Reinforcement Detailing at Element Transitions*

Regardless of the chosen structural system, the formwork will likely need to be bespoke; in CRL's case, Liando formwork was utilized (Figure 7). Careful consideration must be given to the reinforcement detailing at the transitions between elements. Initially, the plan for CRL was to construct the permanent structure in a single pour; however, this strategy was adjusted to require two separate pours. Consequently, the introduction of couplers was necessary to effectively connect the flat invert with the curved sections, ensuring the integrity and continuity of the reinforcement across the junction (Figure 8). Non-contact laps were used to ensure continuity with the curved bars above the construction joint. In this instance the choice of a jamb system was beneficial as the side walls are generally lighter in reinforcement than no-jamb systems. Proper detailing at these transition points is critical for maintaining structural performance and durability requirements.

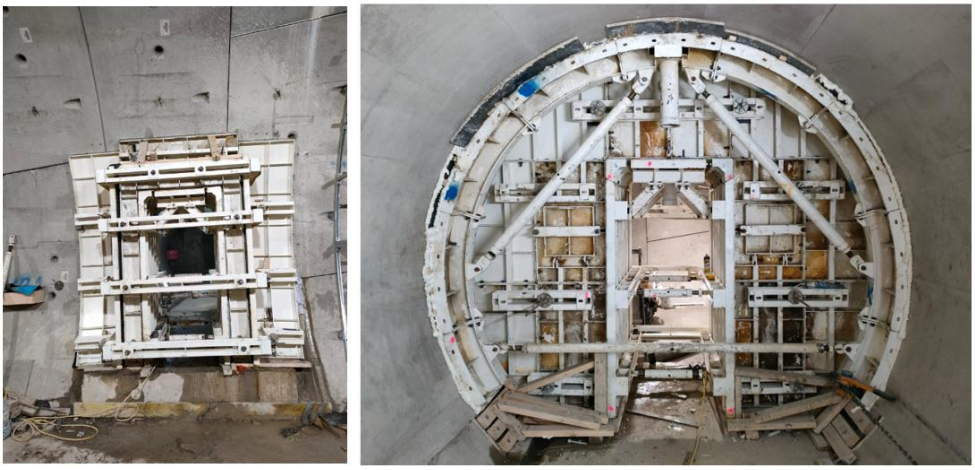


Figure 7. Liando formwork for the cross passage permanent support on CRL

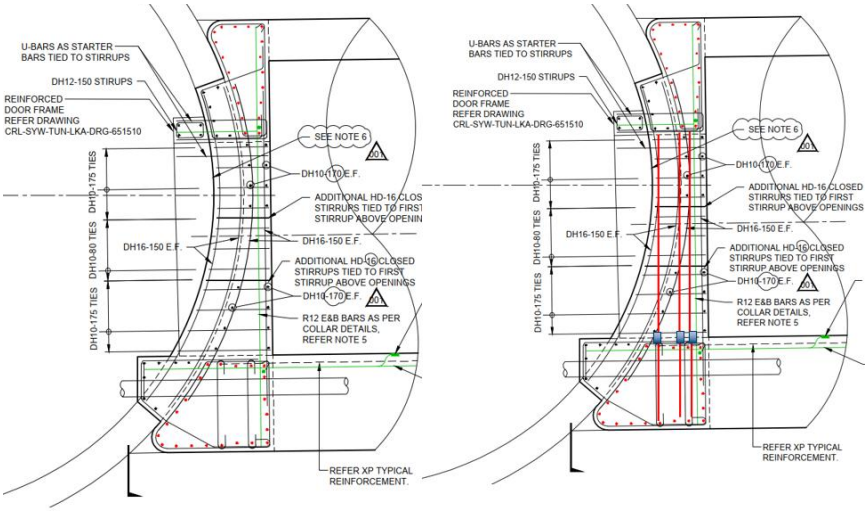


Figure 8. Original Reinforcement arrangement without couplers (left) and construction phase red-line mark up of couplers and starter bars

5.2 *Alliance considerations*

CRL was delivered through an alliance model, which enabled early contractor involvement and fostered enhanced collaboration among the alliance team. This approach facilitated informed decision-making that aligned with the project's objectives. A key result of this collaboration was the selection of jambs in conjunction with the first-stage concrete for the permanent support system. This choice led to a significant reduction in reinforcement requirements. This reduction not only improved structural efficiency but also lowered material costs. Additionally, the use of jambs simplified construction logistics throughout the lifecycle of both the temporary and permanent works. The clearer task delineation associated with implementing jambs and first-stage concrete enabled more efficient scheduling and resource allocation. Overall, the alliance delivery model contributed to a more effective design solution while enhancing the project's constructability.

The permanent support design decisions did lead to some additional logistical challenges for the construction team. Firstly, the pours needed to be co-ordinated with a separate team within the Alliance. Additionally, the integration of services through the jambs required specific design checks on site to ensure the type and number of ducts were suitable to house the services (Figure 9).



Figure 9: Cross passage reinforcement and concrete after striking

5.3 *No jambs*

Eliminating the need for jambs can offer advantages in terms of constructability and access, particularly when addressing the secondary lining section between the collars. Without jambs, there is the potential for greater manoeuvrability of formwork through the temporary opening and potential for an additional service path for plant. In some instances, this may improve cycle times for cross passage construction. Additionally, not having jambs means that ducting does not need to be routed through the reinforcement, simplifying the reinforcement detailing

6 MAINTENANCE

The maintenance considerations are broadly similar for both systems with the lintel only system having fewer elements to maintain. In the case of CRL the permanent support was designed with minimal maintenance requirements during the 120-year design life.

7 CONCLUSIONS

7.1 *Summary*

This paper evaluates the design considerations for cross passage permanent support systems, focusing on CRL in Auckland, which employs jambs. It discusses the benefits of jambs, such as enhanced structural support and improved load distribution, but also highlights challenges including installation complexities and potential access restrictions. The analysis contrasts jamb and lintel designs, noting that jambs can lead to significant reductions in reinforcement requirements, improving material efficiency and lowering costs. Additionally, the paper emphasizes the advantages of not using jambs, including increased constructability, greater manoeuvrability for formwork, and simplified ducting without interference with reinforcement. Ultimately, the findings aim to inform best practices in urban tunnelling projects by weighing the trade-offs between structural robustness and construction efficiency.

7.2 *Selection of jambs on CRL*

Jambs were chosen on CRL primarily because they provide enhanced structural support and a more direct vertical load path, improving load distribution and increasing the overall robustness of the permanent support system. This approach reduces the reliance on the collar alone, resulting in better tunnel stability by accommodating movements and minimizing displacements. Additionally, the use of jambs allowed for a significant reduction in reinforcement requirements, improving material efficiency and lowering costs. Despite adding some construction complexity, jambs integrated well with the first-stage concrete and the alliance delivery model, simplifying construction logistics through early contractor involvement and effective collaboration.

7.3 *Comparison*

Aspect	No Jambs	Jambs
Load Path	Horizontal spanning + distributed hoop stress through collar.	Combined vertical (through jambs) and horizontal spanning + collar action.
Load Transfer	Lintel to collar- collar to side walls – side walls to ground (or equilibrating force from bottom lintel)	Loading split between lintel to jambs and lintel to collar.
Structural Redundancy	Moderate — relies on collar and tunnel lining integrity.	High — jambs provide an independent, direct vertical load path alongside collar support.
Tunnel Stability	Good, but more sensitive to deformation if collar installation or material behaviour is imperfect.	Very robust — tunnel lining integrity is well maintained through multiple load paths.

Construction Complexity	Simpler — fewer structural elements to install (no jambs).	More complex — requires precise jamb installation plus collar and lintel works.
Maintenance / Inspection	Easier — fewer elements; collar inspection is important.	Slightly more challenging — multiple elements must be inspected and maintained.
Access Impact (Tunnel Operations)	Better — no vertical elements (jambs) obstructing passageway.	Reduced — jambs may slightly restrict space inside cross passage.
Best Use Cases	In good ground, where construction speed, flexibility, and minimal intrusion are priorities.	Where maximum long-term structural robustness and reduced deformation are critical.

ACKNOWLEDGEMENTS

The author would like to thank City Rail Link Ltd for permitting the publication of this paper and Brandon Wang of Aurecon for his help with model generation.

8 REFERENCES

[i] https://www.cityraillink.co.nz/

2 Design and Construction of Segment Opening on Mega TBM Tunnel *Shu Fan Chau, Tom Ireland, Luke Lu, Jonathan Gauffre, Clara Cole-Hawthorne, ATC 2023 Conference Proceedings, Trends and Transitions in Tunnelling.*

19th Australasian Tunnelling Conference – Acosta-Martínez, Stewart and Hudson-Smith (Eds.)
© 2025 Australian Tunnelling Society, ISBN 978-0-85825-002-4

Artificial Ground Freezing for Cross Passage Construction

C.K.Tsang, Tong Sia and Frank Li

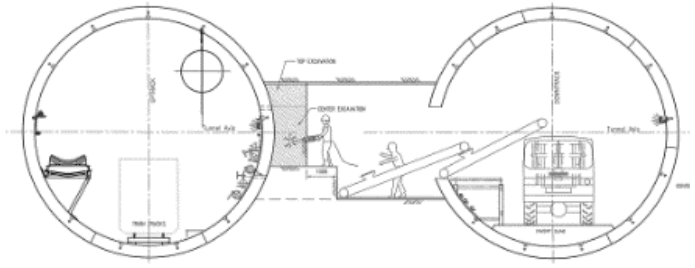
SMEC Australia Pty Ltd

ABSTRACT: Artificial ground freezing (AGF) is a soil improvement method carried out by continuously refrigerating the soil and converts pore water to ice. The effectiveness of freezing depends on the presence of pore water to create ice, cementing the particles and increasing the strength of the ground to achieve the design strength. The AGF freezing technique has been successfully applied for cross passage (CP) construction in soft ground between twine bored TBM tunnels. The method involves installation of freezing pipes around the cross passage opening. Freezing is then achieved by circulated a cooling fluid into freezing pipes and heat is removed from the soil in a cylindrical pattern around freeze pipes. This process produces a column of frozen soil for each tube. The columns continue to expand until they intersect with each other creating a solid ring of frozen ground. The formed ice ring will be virtually impermeable and the soil/ice structure will have greatly enhanced strength so that excavation work can proceed safely in dry condition. The major objective of this paper is to describe the key considerations for design and construction of AGF applied for cross passage construction. Discussion on the importance of instrumentation monitoring to check the development of ice ring will be provided.

1 INTRODUCTION

1.1 *Construction of cross passage (CP) between twin bored TBM tunnel*

The construction of CP, especially in soft ground, between the twin bored TBM tunnel is one of the most high-risk construction activities for tunnelling projects. The CP is generally constructed using traditional mining techniques to create a link between two tunnels, as shown in Figure 1. Depending on the ground conditions, different ground treatment methods can be implemented.



- Carry our ground treatment works
- Open main tunnel segmental lining
- Excavation of CP by mined method
- Shotcrete the excavated roof and walls to acts as a temporary support
- Continue excavation and shotcrete, stage by stage, until reaching the receiving end
- Apply smoothing concrete before the installation of waterproofing membrane
- Spray permanent shotcrete or cast in-situ concrete to form the CP permanent structure
- Construction of collar structure between the CP and main tunnel

Figure 1. Typical construction of cross passage.

1.2 *Application of AGF for cross passage excavation*

When ground treatment cannot be carried out from the ground surface due to site constraints or environmental concerns, AGF is generally considered one of the best ground treatment methods

to be adopted from inside the tunnel for cross passage excavation in soil. The ground freezing method is very reliable in achieving design strength and watertightness. The principle of AGF is where refrigeration of the ground converts pore water to ice, binding together the soil particles as a form of improvement. The method involves a system of pipes consisting of an outer pipe and concentric inner feedpipes. Freezing is then achieved by circulating a cooling fluid into the inner pipe and back up the outer pipe. During the process, heat is removed from the soil in a cylindrical pattern around freeze pipes. This process produces a column of frozen soil for each tube. The columns continue to expand until they intersect with each other. From here, the frozen mass will expand outwards creating a wall or solid ring of frozen soil. The formed ice ring will be virtually impermeable, and the soil/ice structure will have greatly enhanced strength.

2 KEY DESIGN CONSIDERATIONS FOR GROUND FREEZING WORKS

2.1 *General*

Site characterization is always the most important element for successful implementation of all underground engineering projects, including AGF projects. The type of soil encountered and the ground water condition must be accurately investigated to ensure an appropriate design. In particular, for AGF projects, the thermal properties of encountered soils and their mechanical properties after frozen should be tested. A high groundwater velocity (i.e. > 2 m/day, Harries 1995) may erode the ice ring at the same time it is being formed, yielding discontinuities of ice ring and hence longer active freezing period. High salinity sites would cause degradation of freezing temperature and lower frozen strengths. However, as salinity increases, frost heave, thaw settlement, and heaving force will decrease.

2.2 *Types of cooling agent*

Brine freezing is typically used for large, longer-term applications. Brine temperatures of -25°C or less are typically sufficient for most projects. The corresponding freezing pipe is a double concentric pipe system for circulation of brine. The outer pipe has a closed end while the inner pipe has an open end. The brine is pumped into the inner pipe from the freezing units and circulated back at the open end of the inner pipes. On its way back through the annulus between inner and outer pipes, the brine absorbed the heat from the ground.

Liquid nitrogen freezing acts more quickly than the brine system and has been used effectively for short interventions and emergency use. Liquid nitrogen boils at a temperature of -196°C and may be used in the place of a generic coolant. Due to the extremely low temperature of liquid nitrogen, freezing soil in contact with liquid nitrogen occurs much more quickly. Therefore, complete freezing can be accomplished much faster.

3 DESIGN OF AGF FOR CROSS PASSAGE CONSTRUCTION

3.1 *Ground freezing design*

The ground freezing design is an iterative procedure. An initial arrangement of freezing pipes is estimated based on previous experience as the initial trial. With this arrangement, both thermal analysis and structural analysis are carried out. The flow chart of ground freezing design is shown in Figure 2.

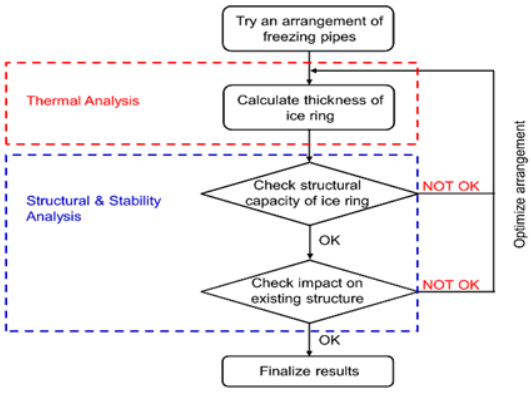


Figure 2. Proposed procedure of ground freezing design

3.2 *Thermal analysis*

The thermal analysis can be carried out by finite element software, such as ABAQUS, ANSYS and TEMP/W. This analysis aims to determine the ice ring thickness against time with the predetermined arrangement of the ground freezing pipes. The analysis algorithm is based on the heat balance equation from the principle of conservation of energy.

The input data for thermal analysis include geometry, thermal properties of surrounding soil and boundary conditions. The initial temperature and temperature at boundary of the model should be set as the ambient temperature. On the other hand, the temperature at the locations of the freezing pipes is reduced progressively from ambient temperature to -28°C for brine and -196°C for liquid nitrogen.

The thickness of freeze wall will be one of the input data for structural analysis. Generally, it is usually defined as the distance between two -10°C or -15°C isotherms. The other important output is the active freezing period which should be tally with the construction program. In order to tackle some emergency issues, a 24-hour stoppage time is suggested to be considered in the model so that the thickness of freeze ring could be determined conservatively and adverse impact due to breakdown of plants could be minimized.

3.3 *Structural analysis*

The structural analysis could also be conducted by finite element software, such as ABAQUS, ANSYS and PLAXIS. The structural capacity of the freeze ring determined in the thermal analysis will be assessed. The analysis should also consider the characteristic behavior of frozen soil, including frost heave and thawing settlement. To consider the effect of frost heave, usually a positive volume strain is assigned to the frozen zone to model the expansion effect caused by formation of ice lenses. On the contrary, a negative volume strain is thus assigned to the frozen zone to simulate the thaw consolidation.

The structural analysis could also provide the internal forces of temporary support (i.e. temporary steel ribs), if any, for the subsequent structural design. In addition, the impact of ground freezing works on adjacent existing structures and utilities could also be investigated.

3.4 *Typical ground freezing design and arrangement of the ground freezing pipes*

Based on the design approach as described in the previous sections, a typical ground freezing design with consideration on the dimensions of cross passage opening and main tunnel diameter is shown in Figure 3.

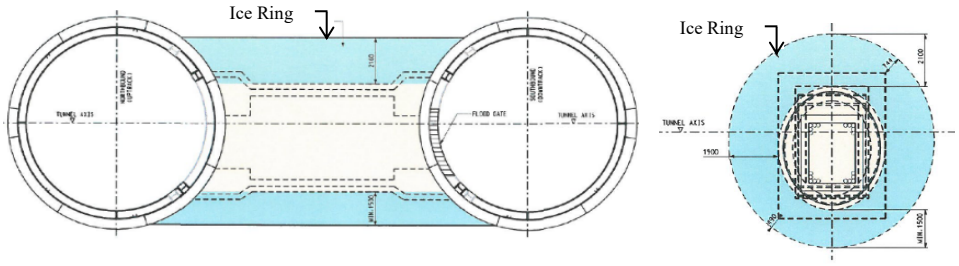


Figure 3. Design of ice ring

The key design of ice ring is summarized below:

- The design thickness of ice ring is 2.1m (top) / 1.9m (side) / 1.5m (bottom)
- The design temperature at the boundary of defining the ice ring thickness is -10°C.
- Strength of ice ring: the minimum and maximum compressive strength of ice ring is1.5MPa and 3MPa respectively.
- 48 numbers of freezing holes are designed around the cross passage opening to form the ice ring.

The arrangement of ground freezing pipes to form the required ice ring is shown in Figure 4.

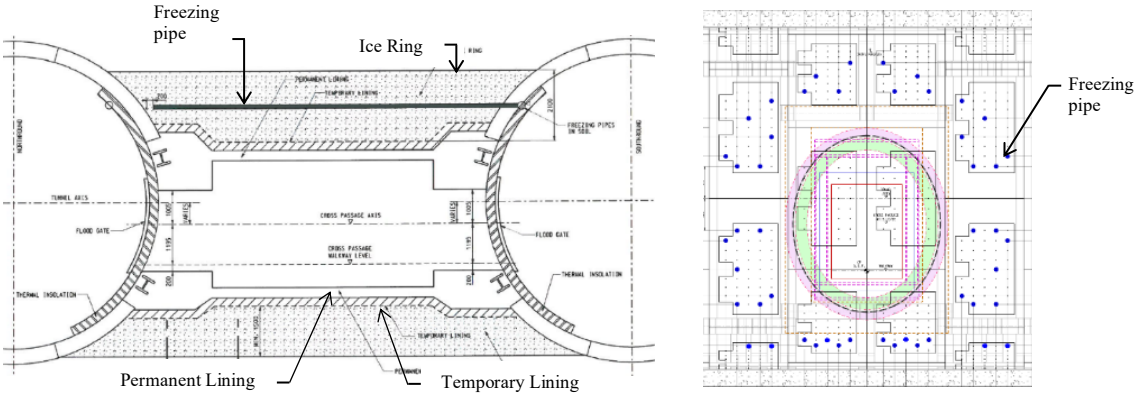


Figure 4. Arrangement of freezing hole on tunnel segment

4 CONSTRUCTION OF AGF WORKS

4.1 *General arrangement*

The construction of AFG works is described by a project with 6 cross passages (CP1-CP5 and CP8) for AGF works between the up-track and down-tack tunnels. To achieve a safe and fast track construction, the 6 cross passages are divided in to two groups for AGF such that the works for each group can be carried out simultaneously in a streamlined manner. The construction arrangement is illustrated in Figure 5.

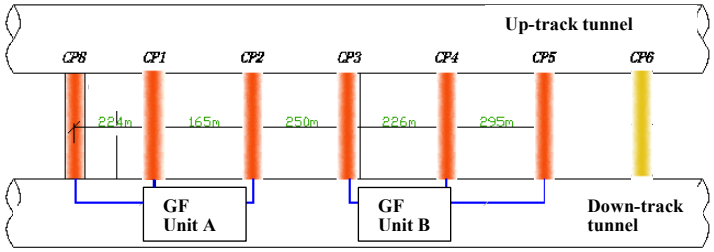


Figure 5. Layout plan for the grouping of cross passage

4.2 *Construction methodology*

The first step is to drill holes for installing freezing pipes and thermometers in the freezing zone of cross passage. At the same time, cooling stations are installed. Once the freezing pipes and cooling stations are installed, freezing works can be started to strengthen the soil. After the design freezing time, the ground freezing is verified by instrumentation monitoring to check if the performance requirements of ground freezing works are achieved. Subsequently, the tunnel segmental lining can be removed and excavation of cross passage can be carried out stage by stage with installation of temporary support. Upon excavation of the entire cross passage is completed, a waterproofing layer will be laid against the temporary lining. Finally permanent lining will be cast.

4.3 *Construction of freezing hole and installation of freezing pipes*

The drilling of freezing holes is carried out according to the below steps:

(1) Setting up of the drilling rig and equipped with the grouting pump.
(2) Special type ϕ89 drill rods equipped with guiding function drill bit and oblique sensor are used with recirculate water flush rotary drilling.
(3) Measurement of the drilling direction is carried out at 2m interval using Gyro inclinometer. Adjustment of the drill bit direction is carried out according to the measured inclination. Measurement of derivation is checked again when the design depth of drilling is reached.

(4) When drilling the freezing pipe reach to the design depth, pull back the drill rod and filling the hole with grout is carried out concurrently until the whole drill rod is retrieved out. Close the blow out preventor to prevent leakage of grouting.

The installation of the freezing pipes is carried out as below:

(1) The freezing pipes is connected by using of threading, when the casing is threaded tightly, the pipe joint is weld manually to ensure concentricity and strength.
(2) Install freezing pipe on drill rig and carry out drilling. Connect the freezing pipe one by one until drilling depth is reached.
(3) Install the liquid supply tube inside the freezing pipe, then weld the freezing pipes end cap, return liquid steel tube and the final connection hose.

4.4 *Installation of the colling stations*

Cooling station is installed in the tunnel between CP1 and CP2 to support the freezing works of CP1, CP2 and CP8, another cooling station is installed in the tunnel between CP3 and CP4 to support the freezing works of CP3, CP4 and CP5. The general arrangement of the cooling system is shown in Figure 6.

Due to poor ventilation inside the tunnel, cooling water circulation system of the cooling station include cooling tower, water pump and water tank are be installed at the ground near TBM launching shaft. The circulation system of the cooling station including cooling pumps, brine water pump and brine water tank are installed inside the tunnel as shown in Figure 7.

Cooling station platforms are set up at one side of tunnel, the width and length of the platform is approximately 2.8m and 40m respectively. The main equipment to be installed at the cooling station platform include cooling plan, brine water tank, brine water pump, power distribution cabinets and cables.

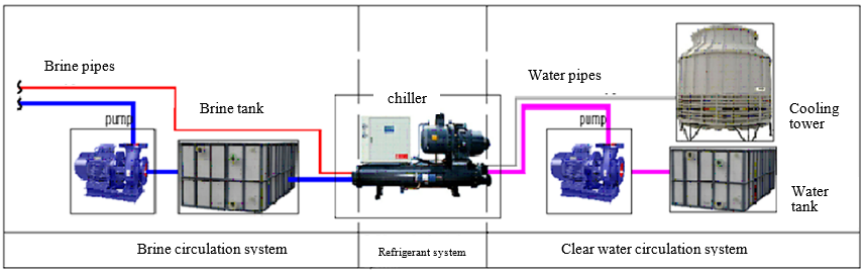


Figure 6. Illustration of cooling system

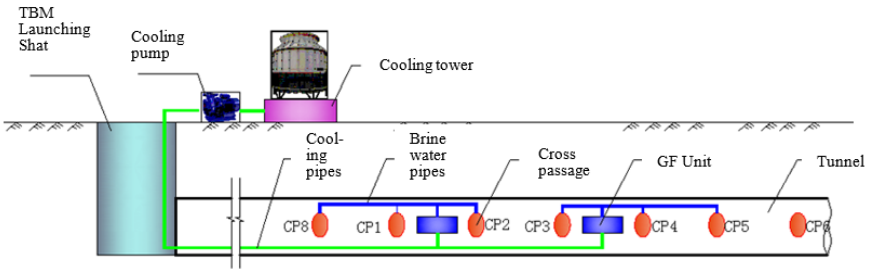


Figure 7. On-site arrangement of cooling stations

4.5 *Piping system installation*

(1) The pipes are connected with flange connection and the brine water pipes inside the tunnel are support by the steel bracket installed on the segment in order not to affect tunnel access.
(2) Testing equipments such as pipeline valves, pressure gauges and thermometer are required to be set up on the brine water and cooling water pipes.
(3) Once brine water pipes are installed, water tightness test is carried out for maintaining testing pressure of 0.6MPa for 15 minutes.
(4) The connection between the brine water feeding pipe and the freezing pipe are provided by high pressure rubber house. Valves are installed at both inlet and outlet of feeding pipe at each to control the flow.

4.6 *Insulation works*

(1) The evaporation parts of cooling station and low temperature pipe are insulated. Brine water tank and brine water pipes are insulated with 50mm thick insulation material. Brine water pipe insulation material are wrapped by plastic film.
(2) Insulation on tunnel segments at both sides of cross passage: Since the heat loss on concrete tunnel segments surface is relative easier than soil layer, in order to enhance the effectiveness of ice ring at the tunnel segment, insulation measures are provided at the surface of segments at both ends of cross passage to reduce heat loss.
(3) The insulation layer are provided at the tunnel segments surface affecting the ground freezing works.
(4) For area where end of freezing pipes are in touch with tunnel segments, additional freezing pipes are provided at surface of tunnel segments. Insulation layer are provided at the surface of tunnel segment at the ice ring development area to reduce heat loss.

4.7 *Freezing operation*

(A) Freeze System Testing

Testing and commissioning are carried out after all equipments are installed. During testing, pressure, temperature and other operation parameters are adjusted to suit the technical requirements of equipment. After testing and commissioning, the system can be operated for active freezing.

(B) Active Freezing Stage

This stage is the formation of ice ring period. During the active freezing stage, instrumentation monitoring is carried out to check if the ice ring is closed and achieve the design thickness. The main technical specifications are as follow:

(1) Brine water temperature during the active freezing stage ranging from -25 °C ~ -30 °C.
(2) The flow rate of single freezing hole shall not less than $5m^3/h$;
(3) The temperature of brine water for 7 days of active freezing should dropped below -18 °C. The temperature of brine water for 15 days of active freezing should dropped below -24 °C. The temperature of brine water to drop to -30 °C before excavation.
(4) The temperature difference between feeding pipe line and return pipe line of brine water shall be less than 2^oC.
(5) The design freezing time is about 45 ~ 50 days, if brine water temperature and flow rate do not meet the design requirements, active freezing time should be extended.

(C) Maintenance Freezing Stage

Maintenance freezing stage is maintenance period of ice ring. When the ice ring meeted the design requirements, it can be changed to maintenance freezing stage.
The temperature of maintenance freezing stage is about -28 °C ~ -23 °C. The freezing time is based on progress of cross passage excavation and construction of permanent structure.

4.8 *Excavation and installation of primary support*

Before commencement for opening the tunnel segments, information on monitoring data of thermal sensors, prizometer and probe holes are reviewed. Table 1 showed the technical requirements to be met before excavation.

Table 1. Technical requirements for commencement of excavation

Item	Requirement	Method
Ice Ring Thickness	Design Values	Using mapping method
Ice Ring Temperature	-10°C	Thermocouple temperature monitoring
Brine Water Temperature	-28～-23°C	Monitored with thermometer, thermocouple
Brine loop temperature different	Within 5°C	Monitored with thermometer, thermocouple

Temperature difference between feeding and return pipes	Within 2°C	Monitored with thermometer, thermocouple
Piezometer	0.15MPa increment of water pressure	According to reading of pressure gauges, no water and mud outflow

Excavation work can be started after confirmation with the result of instrumentation monitoring and probe holes drilling. The tunnel segment can be cut and removed, excavation of CP is carried out by top heading and benching method. Temporary support of steel ribs and shotcrete are applied.

In view of relatively high strength of the frozen soil and strong ice ring formed by ground freezing method, the excavation advance can be carried out between 0.5 ~ 0.8m. The condition of ground freezing is reviewed with the exposed ground during excavation and instrumentation monitoring. The excavation advance and temporary support can be adjusted to suit the actual ground condition to ensure safety of works.

4.9 *Waterproofing installation and construction of permanent structure*

Hydrophilic strip and embedded re-injectable grout pipe are provided at the interface between the tunnel segment and cross passage permanent support. After the excavation and temporary support for enlarged section at tunnel segment are completed, waterproofing membrane from tunnel crown, along the side walls and connected with membrane at the floor to form a closed waterproofing layer.

Permanent support in form of in-situ reinforced concrete are provided at cross passages. In order to minimize the number of construction joints, continuous casting of concrete are carried out after cross passage excavation and temporary support is completed. To improve the quality of concrete, concreting works are carried out in batches, grouting machine are used to fill up the voids in the concrete if necessary. Embedded water-stop are provided at the construction joints.

4.10 *Thawing and compensation grouting*

During the natural thawing, monitoring control system is performed to monitor soil temperature, settlement. Compensation grout is used to control ground settlement. Reserve grout holes in the concrete segment are provided in the mainline tunnels. Reserve grout holes at cross passage lining is arranged with 4 grout holes installed at 2m interval at each cross passage. The grout holes are staggered into two types as shown in the Figure 8. The acceptance of grouting works shall be based on the monitoring data of ground settlement and whether thawing is completed. Under the condition where thawing is completed with grouting not carried out, if the record settlement is less than 0.5mm in half-month period for continuous monitoring for a month. Compensation grouting can be stopped.

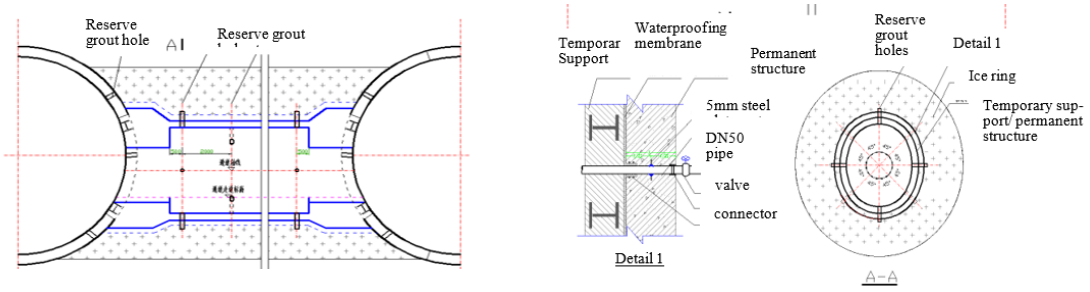


Figure 8. Grout holes installation and details

4.11 *Monitoring and control*

Temperature monitoring is carried out by installation of thermal couples, constantan wire is connected for transmitting signal. Thermal couples are located at the interface between ice ring and segmental lining, with typical spacing of 2m c/c.

Perforated pipes with staggered slots are applied as piezometer as pressure relief tubes. Pressuremeter is installed at the end of the tube with cables connecting to the data logger. Pressure

vale is provided at the head of piezometer, in case the internal soil pressure excesses the corresponding hydraulic pressure by 0.1MPa, the pressure relief valve is then be opened for pressure relieving purpose. The general layout of the instrumentation monitoring is shown in Figure 9.

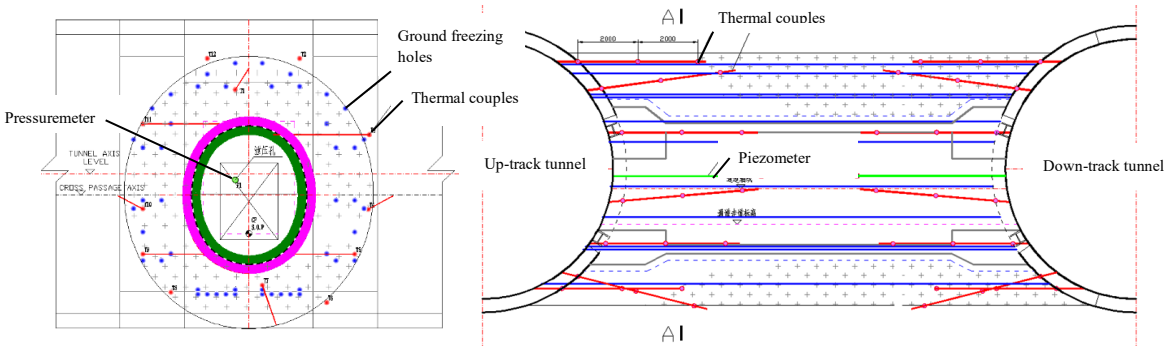


Figure 9. General layout of instrumentation monitoring

5 CONCLUSION

The construction of cross passage is one of the high-risk activities for tunnel construction. The AGF freezing technique has been successfully applied as ground improvement method for cross passage construction in soft ground between twine bored TBM tunnels. The key considerations for design and construction of AGF works for cross passages are presented in this paper. The ground freezing method is very reliable in achieving design strength and watertightness with careful planning, design and instrumentation monitoring of ice ring development.

6 REFERENCES

Andersland, O. & Ladanyi, B. 2004. *Frozen Ground Engineering (2nd ed.)*. Wiley and Sons, Hoboken, NJ.

Harris, J.S. 1995. *Ground Freezing in Practice*. Thomas Telford.

Martin, O., Storry, R., Harris, D. & Pegon, J.L. 2005. Ground Freezing in Hong Kong for Mining Cross-passages under Sensitive Ecological Area. *Underground Construction – 2005 Conference and Exhibition, 26 to 27 October*, London.

Pakianathan, L. J., Kwong, A., McLearie, D. D. and Chan, W.L. 2002. Pipe Jacking: Case Study on Overcoming Ground Difficulties in Hong Kong SAR Harbour Area Treatment Scheme. *Proceedings of Trenchless Asia 2002, 12-14 November 2002*, Hong Kong, UK Society for Trenchless Technology.

Polycarpe, S., Ng, P.L. and Barrett, T.N.D.R. 2012. Construction Risk Mitigation of the Tunnel to Station Connection Using Artificial Ground Freezing in the MTRCL West Island Line Contract 703. *Proceedings of HKIE Geotechnical Division Annual Seminar, 25 May 2012*: 137-146.

Tsang, L., Cheung, A., Leung, C. and Chan, W.L. 2012. Artificial ground freezing for TBM break-through – Construction. *Proceedings of HKIE Geotechnical Division Annual Seminar, 25 May 2012*: 125-130.

Tsang, L., Cheung, A., Leung, C. and Chan, W. L. 2012. Mined tunnel construction using artificial ground freezing technique for HATS 2A Project. *Proceedings of HKIE Geotechnical Division Annual Seminar, 25 May 2012*: 131-132.

Tsang, C.K., H.Z. Yu, C.S. Kong and Alan Hu 2019. Artificial Ground Freezing Application for Tunnelling Works in Hong Kong. *Proceeding of 13th Australia New Zealand Conference on Geomechanics, 1-3 April 2019.*

19th Australasian Tunnelling Conference – Acosta-Martínez, Stewart and Hudson-Smith (Eds.)
© 2025 Australian Tunnelling Society, ISBN 978-0-85825-002-4

Comparison of the effects of new and existing building developments on large tunnels

D. Duorina, A. Bennett & N. Makin
Aurecon Australia Pty Ltd

ABSTRACT: Assessing the interactions with nearby buildings is a key consideration during tunnel lining design, more so with the increase of tunnelling in developed urban areas where tunnelled infrastructure is intended as a catalyst for growth and densification. The interactions between tunnels and building developments will be varied, not only because of the buildings themselves, but also because the effects depend on the relative timing of the building and tunnel construction, even where the building is the same.

This paper compares the interactions between large tunnels such as metro tunnels and existing and future building construction. It presents an analysis of a hypothetical tunnel to demonstrate potential differences in the effects on the tunnel design due to building loading or unloading. It also discusses consideration of clearances between the building and the tunnel, and the potential impacts on tunnel constructability.

1 INTRODUCTION

In high-density urban environments, tunnelling serves as a strategic catalyst for sustainable growth and controlled densification, optimising land use while minimising disruption at ground surface. As urban development continues to intensify, large tunnels, such as those used for metro systems and roadways, will be increasingly constructed near or beneath existing or future buildings. This proximity will bring interactions between tunnel structures and adjacent buildings, making it essential to evaluate how these interactions influence tunnel design and construction.

These interactions between tunnels and buildings vary, not only influenced by the structures themselves, but also by the relative sequencing of construction activities. Even with identical structural configurations, variations in construction sequences can lead to different impacts on tunnels.

Therefore, this paper compares the interactions between a hypothetical tunnel (with an internal diameter of 6.4 m which is typical of rail and metro projects) and both existing and future buildings as they relate to three major aspects: effects on the tunnel design due to building loading or unloading, effects due to clearances between the building and the tunnel, and the potential impacts on tunnel constructability. It highlights how different construction sequences between tunnels and buildings influence requirements for tunnel lining design, proposes mitigation measures to minimise risks and associated adverse effects, and notes the importance of the project team understanding these differences, at least in principle, for assessments of acceptability of adjacent developments.

As there is a large number of permutations of tunnel, ground, and adjacent developments, this paper aims to provide an indicative comparison of such impacts due to different construction sequences. By adopting this illustrative perspective, the study seeks to identify and summarise impacts and potential risks that can inform planning and mitigation strategies and design works in future projects.

2 PURPOSE AND METHODOLOGY

The primary objective of this comparison is to demonstrate how the relative construction sequence of buildings and tunnels influence tunnel lining performance. To this end, a set of typical development allowances has been adopted. Reference has been made to tunnel design requirements for Future Development Loads (FDL) in published documents for recent major tunnel projects such as Melbourne Metro Project (Bennett 2018), West Gate Tunnel, North East Link, and Suburban Rail Loop (Suburban Rail Loop Authority 2025). Based on a combination of project experience, technical guidelines, and engineering judgement, three interactions of developments with tunnels were considered to evaluate their potential effects on the design of a tunnel and its construction. These were:

- Application of additional loadings to simulate buildings above tunnels
- Application of unloading effects to simulate bulk excavation above tunnels and deep excavation adjacent to tunnels
- Consideration of the implications of the clearances between tunnels and a development, particularly deep foundations, such as piling works.

In each scenario, different construction sequences have been considered to assess tunnel lining performance. Scenarios where tunnels are constructed before or after buildings have been compared separately against a baseline scenario without any buildings. This approach helps to separate and clearly demonstrate the impact of construction sequence on tunnel behaviour. Effects due to loading or unloading on tunnel lining, effects due to the clearances between the building and the tunnel, and the potential impacts on tunnel constructability are discussed in Section 3, Section 4, and Section 5 respectively and illustrate the significance of the loading sequence used to assess the risk to tunnels and tunnelling from adjacent buildings.

3 EFFECTS OF LOADING/UNLOADING ON TUNNEL LINING

The effects of loading and unloading on a tunnel lining are influenced not only by the quantum of the building loads, but also by the timing of the construction sequences of the tunnel and buildings. The timing of construction can lead to different load distributions applied on the tunnel lining, affecting its structural performance. Details of the analyses and comparison of the results are provided in Section 3.1 and Section 3.2 respectively.

3.1 *Analysis of tunnel lining*

For the purposes of the modelling, the following parameters were adopted for the hypothetical tunnel lining:

- Tunnel internal diameter: 6.4 m
- Lining thickness: 300 mm
- Concrete stiffness: 34,800 MPa for short term and 17,400 MPa for long term
- Ground parameters: Unit weight 21 kN/m3; effective cohesion 2 kPa; friction angle 36^{o}; drained modulus 80 MPa; unload/reload modulus 240 MPa; Poisson's ratio 0.3 and at rest earth pressure coefficient 0.7.

As a starting point, the hypothetical tunnel lining without any development was modelled in Plaxis 2D as a baseline. The impacts on the tunnel lining in this scenario, for comparison with the building load cases, are indicated in Figure 2.

To illustrate the influence of construction sequence on tunnel performance, the following loading and unloading cases were modelled using Plaxis 2D as shown in Figure 1.

- A 50 kPa vertical loading, representing effects from building developments near the surface above the tunnel
- A vertical unloading condition, modelled as a 7 m depth bulk excavation above the tunnel with 7 m of ground remaining between the excavation and the tunnel
- An adjacent deep excavation down to tunnel level, modelled as a limited lateral release of 20 mm at 5 m horizontally from the tunnel

Each of the building load cases was activated either before or after the tunnel lining construction in the Plaxis model with a ground relaxation factor of 20% applied, and the resulting impacts

on tunnel lining can be compared with those from a baseline case involving a tunnel without any developments. The results illustrate the trends under the various scenarios and show, in Figure 2 and Figure 3, that, in some cases, the MN results shift closer to the capacity boundary of the MN interaction diagram when external development is conducted after tunnel construction.

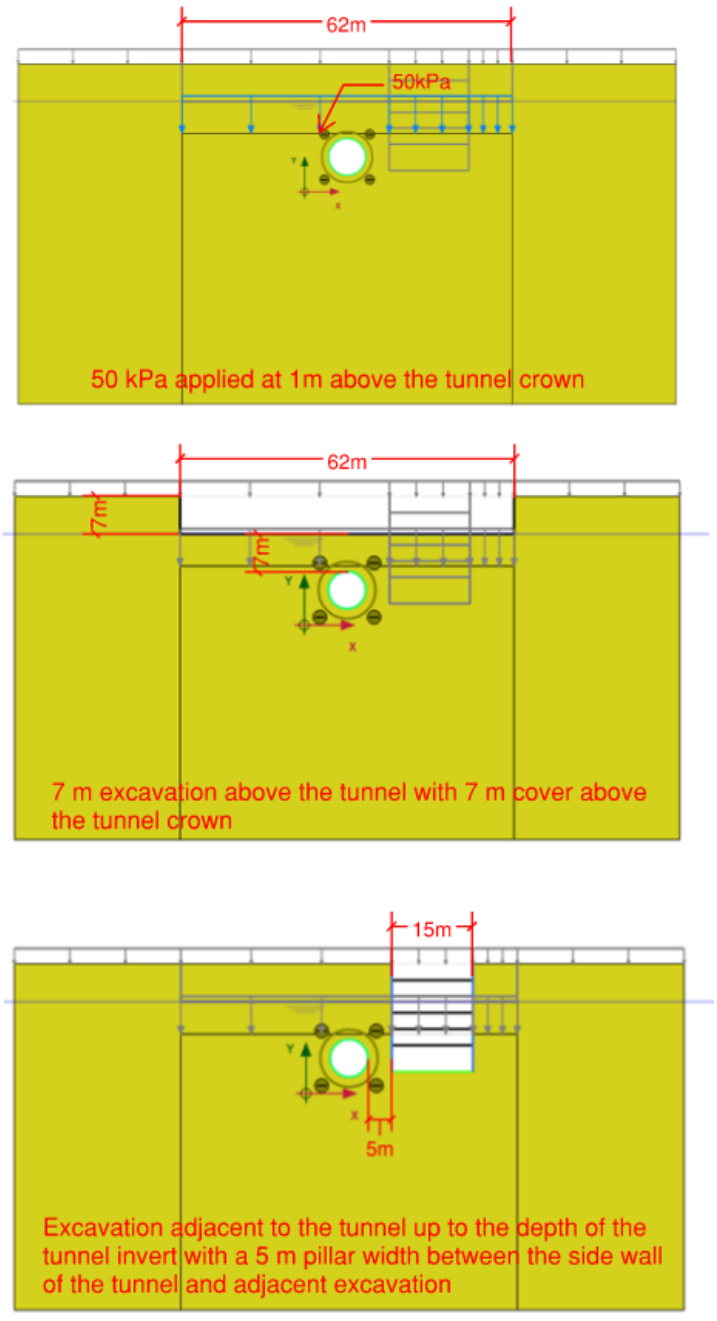


Figure 1. Plaxis model to simulate loading and unloading cases. For comparison purposes, soil parameters and material properties in each model are the same.

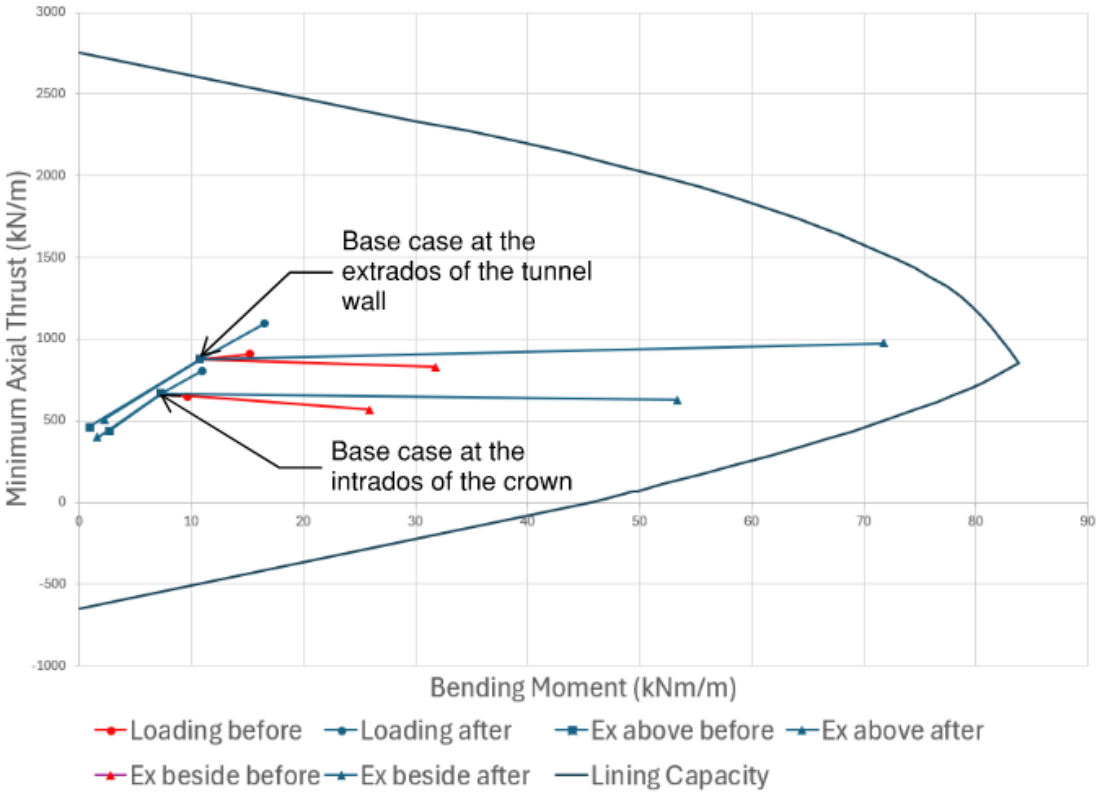


Figure 2. Comparison of the outputs of the Plaxis models.

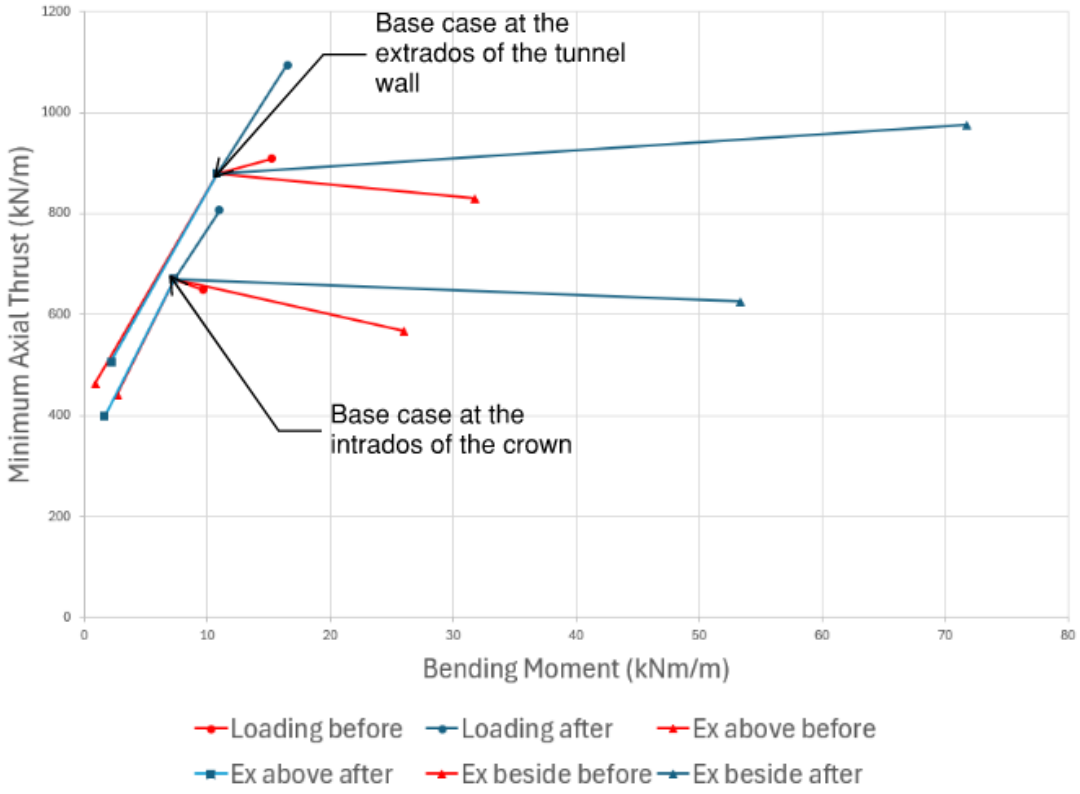


Figure 3. Detail of the outputs of the Plaxis models.

3.2 *Loading effects on tunnel lining*

The results plotted in Figure 2, indicate loading effects experienced by the tunnel lining with different construction timing in relation to a development for the following scenarios. For easy comparison, resulting stresses calculated on an uncracked section are shown in Table 1.

Table 1. Stress from Plaxis results calculated on a monolithic section.

	Minimum stress (difference from baseline)* (MPa)	Maximum stress (difference from baseline)* (MPa)	Comment
Base Case	1.7	3.7	
50 kPa before tunnel	1.5 (-0.2)	4.0 (+0.3)	Increased average stress across the lining section. Small difference on tensile side from responses to Ko and n effects. In-crease in peak compression.
50 kPa after tunnel	2.0 (+0.3)	4.7 (+1.0)	
7 m excavation before tunnel	1.3 (-0.4)	1.6 (-1.1)	Reduced average stress across section. Reduction in peak compressive stress
7 m excavation after tunnel	1.2 (-0.5)	1.7# (-1.1)	
Side excavation before tunnel	0.2 (-1.5)	1.8 (-1.9)	Tensile changes on tensile side and compressive changes on peak compresion due to moment increases.
Side excavation after tunnel	-1.5 (-3.2) -1.5# (-3.7)	4.9 (+1.2)	

*Calculated on a monolithic section.
#Peak value changed position and shown below

In the hypothetical case analysed, the positions of the critical stress cases remained in the same areas in most cases, with the most tensile cases at the intrados of the crown, and the most compressive stresses at the extrados of the tunnel wall. However, the two results marked with a hash tag show where the minimum or maximum stress changed position from the wall to the crown, or vice versa. However, in both cases, the stress values at the original positions were within 10% of the listed values.

– Loading scenario (50 kPa load applied above the tunnel)

Applying development loads after the tunnel has been constructed causes higher axial force and bending moments when compared with the same building loading in place before the tunnel was constructed. The structural configuration of the lining and the ratio of moments to axial forces would be used to determine whether this was critical for the design of the lining, but in any case, it would need to be assessed for the tunnel design in areas where this loading might arise.

– Unloading (7 m ground cover above tunnel)

When excavation is carried out above the tunnels, the modelling indicated only a relatively small difference in the tunnel axial forces and moments, but still requiring assessment during design as the changes bring the loadings slightly closer to the structural capacity of the tunnel lining. The modelling also indicated, as would be expected, that the ground heave associated with an excavation would affect the vertical alignment of an existing tunnel but would not be expected to affect a tunnel driven after the excavation in most circumstances. Reduced axial loading across joints in a segmental lining would also need to be checked for its effects on joint seals.

– Adjacent excavation (5 m distance to tunnel)

Compared with a deep development excavation before tunnelling, excavation after tunnelling clearly leads, in our example, to an obvious increase in bending moments for the tunnel design resulting from the lateral ground movement and stress release. In this case, this could be the critical design loading for design.

These results demonstrate that loading effects on tunnels are generally more larger when buildings are constructed after tunnels, which matches both the authors' experience over a number of

projects and assessments, and experienced industry expectation. Therefore, considering that the timing of future developments can be uncertain, understanding the potential sequence of nearby developments and incorporating potential future development effects into the tunnel design are important factors both during the design of tunnels, and assessing the acceptability of proposed adjacent developments.

These findings are consistent with the anticipated interactions. When a building has been constructed, its loadings are already added to the stress field through which a tunnel is driven. Only a portion of the ground stress is applied to the tunnel lining. Conversely, when a tunnel lining is already in place, it experiences the full magnitude of the changes in the ground stress field. If the lining is stiffer than the surrounding ground, it can attract an even higher proportion of the general ground loading to itself.

4 EFFECTS OF CLEARANCE ON TUNNEL LINING

Effects of clearance on tunnels primarily concern the structural and geotechnical impacts arising from minimal distances between building foundations and tunnels. The clearance which may affect the tunnel design and construction include ground cover above a tunnel, the proximity of deep excavations, piles to tunnels, relative base levels of adjacent excavations, and pile toe levels surrounding tunnels. Whether the tunnel is constructed either before or after the surrounding buildings, the various consequences of these clearances must be considered in the tunnel design and construction and also the protection of tunnels after they are in place.

4.1 Clearance effects from existing building on future tunnels

When a building has been constructed before the tunnelling works, it might require management of ground movement effects during tunnel construction to protect the existing structures in their proximity. The ground movements caused by tunnelling not only include settlement and heave at ground surface but also vertical and lateral soil displacements on deep foundations or adjacent retention systems. These movements might have impacts on the existing building's stability and serviceability, such as potentially inducing differential settlement on the ground surface, increased bending moments in piles, or additional loading on retaining structures.

When deep piles are installed prior to tunnel construction, their presence may change the initial stress in the ground, thus, altering ground conditions that need to be considered in the tunnel boring process. Potential pile-induced ground stiffening or the transfer of concentrated stresses near the pile shafts also need to be accommodated in the tunnel lining design. These interactions can result in complex stress redistributions around the tunnel and may require enhanced lining sections or, in cases where practically feasible, modified alignment to avoid conflict with foundation clearance zones.

4.2 Clearance effects from future developments on existing tunnels

When the tunnel is already in place before a building is constructed, the future construction of deep foundations and excavation activities can pose potential risks to the tunnel. Close proximity might lead to not only stress concentrations but also mechanical interference on the lining. To avoid potential risks to the existing tunnel lining, building construction in the vicinity of an existing tunnel with minimal clearances needs to be reviewed from the following perspectives.

– "Out of Tolerance" intrusions into the ground

When a building is constructed close to an existing tunnel, there is a risk that excavation, ground retention, or foundation work may unintentionally extend into the protected zone around the tunnel. This can happen during piling, deep excavation, or even utilities installation. If these intrusions go beyond the limits of no-go buffer zones (i.e., "out of tolerance"), they may physically damage the tunnel lining. Also, loads transferred from piling works may alter the surrounding soil support conditions, increasing the tunnel's stress or displacement.

– Impact on redundant ground support systems of the tunnel

During mined tunnel construction, ground support systems (such as rock bolts, dowels or cables) might be installed as temporary works and could be redundant depending on the tunnel

design and site condition. However, the proposed building works nearby, especially involving deep foundation installation, could potentially interfere with these support elements and cause damage to the tunnel lining itself or of the waterproofing system.

– Local disturbance of the ground around the tunnel lining

Even without direct physical contact, nearby construction can disturb the ground surrounding the tunnel. This can happen due to the interruption of ground arching actions, vibration from piling works, or changes in groundwater levels. Such disturbances may lead to ground settlement or heave, which can impose forces on the tunnel lining beyond those that were designed for. As time passes by, this can lead to cracking, joint displacement, leakage at seals, or misalignment of the tunnel.

– Local loading and unloading from piles

The presence of deep foundations, particularly large-diameter piles, can induce significant local loading changes on tunnel linings and these effects from future piles are generally larger than those from existing piles. When piles, especially larger diameter piles, are installed in close proximity to tunnels, the concentrated loads imposed on the surrounding ground, both by skin friction and end bearing, can lead to localised increases in pressures on the tunnel lining. These effects arise from the additional stresses transmitted through the ground to the tunnel structure during both installation and service stages of pile foundations. Conversely, excavation of these piles, particularly for large piles, can cause temporary unloading of the ground above or adjacent to the existing tunnel. This unloading may lead to stress redistribution, ground relaxation, and even movements of the tunnel lining. Risks for piling adjacent to a tunnel lining need to be identified and managed.

5 IMPACT ON TUNNEL CONSTRUCTABILITY

An existing building might influence the construction methodology of a new tunnel. To maintain the minimum required clearance between existing buildings and tunnels, very precise tunnel direction control is essential.

In addition, strict vibration and settlement limits on the building development may require adjustments in tunnelling methods, such as altering advance rates and face pressures.

This constraint might also limit the availability of suitable construction sites and access routes for tunnel works if the development is in the vicinity of a tunnel launch site or its main access routes. Limited surface access due to known and approved developments may constrain construction programs, spoil removal routes, or site setups.

Moreover, the need to protect the tunnel against known future ground disturbance may lead to the early implementation of enhanced waterproofing systems, more conservative ground support systems and ground improvement works during tunnel construction. Early and continuing coordination among all interested parties is essential to anticipate and resolve these construction challenges.

Further complexities arise when tunnelling and building construction occurs concurrently. Close coordination becomes critical to mitigate risks where surface and underground space works influence each other, to prevent construction delays, and to ensure overall safety. Tunnel construction must be carefully planned and executed to account for nearby building works and avoid adverse effects from simultaneous excavation or piling. For instance, deep excavation adjacent to a tunnel might cause unexpected ground movements that destabilise partially completed linings, while vibrations from piling could affect tunnel works. Additionally, real-time monitoring systems and adaptable construction planning may be needed to ensure that both tunnel and building works proceed smoothly without any disruption. It should also be recognised that concurrent works would make understanding the sources of observed measurements more difficult.

6 MITIGATION MEASURES

While existing or future buildings near tunnels present challenges, potential adverse effects on tunnels can be effectively mitigated by integrating appropriate design and construction measures, and also maintaining close collaboration among all interested parties throughout planning, design

and construction stages. Some practical measures have already been briefly discussed in other sections, and more measures applied on tunnels and buildings can be implemented collectively to ensure the safe coexistence of buildings and tunnels.

6.1 Measures applied on buildings

If the magnitude of loading/unloading and the limits of ground movement are of concern, they can be mitigated by optimising foundation design, adjusting construction stages, or using light-weight structures directly above the tunnel. These are some examples of measures that could be considered during a building's design and construction stages.

- One of the key contributors to tunnel deformation is the unloading of ground leading to reduced pressure on a tunnel lining during basement excavations. To mitigate this, if an issue, excavation works can be staged to control the magnitude of unloading. Temporary support systems such as struts or ground anchors can also help to maintain stability and minimise ground movement near the tunnel alignment.
- Where developments are proposed directly above tunnels and additional loading on the tunnel lining is an issue, structural bridging systems can be incorporated into the building design. These systems transfer loads across the tunnel clearance zone without applying unacceptable additional stresses onto the tunnel itself. Common solutions include transfer beams, deep slabs, or portal frames designed to span over the tunnel.
- For deeper foundations, building loads can be transferred to below the tunnel stratum using sleeved piles, which are designed to prevent load transferring into the ground until the pile sockets into deeper, more competent ground. This approach helps avoid stress concentrations or ground movements around the tunnel, particularly in soft soils, thereby reducing potential impacts on the tunnel structure.
- The clearance between buildings and tunnels could also be controlled by relocating pile positions, using shallow foundations, or adjusting excavation depths at the early design stage. If proposed clearances are less than the allowances included in the design, it must be demonstrated that the risk to the tunnel can be maintained at acceptable levels with proper engineering control and design refinement.

6.2 Measures applied on tunnels

Tunnel design and alignment should proactively accommodate the loadings and locations of existing and known and approved future developments or could be adjusted as necessary to avoid potential detrimental effects and conflicts with building foundations.

- To accommodate additional loading beyond the initial design requirements, design changes could be proposed for tunnel lining such as thicker linings, higher-strength materials, or reinforced segments in zones with additional loadings. While these changes increase initial costs, they significantly reduce constraints on future developments and lower the potential risk on the tunnel structure.
- To mitigate adverse effects on buildings and tunnels, the ground movement impact could be controlled through refined tunnel construction methods (e.g., earth pressure balance (EPB) or slurry TBMs), controlling face pressure and advance rates, or implementing ground improvement techniques such as jet grouting or freezing to stabilize ground conditions.
- Additionally, continuous monitoring of ground and tunnel conditions during construction is essential. Instrumentation systems (e.g., strain gauges, settlement markers, piezometers) could provide real-time feedback, allowing for rapid intervention if site conditions exceed predetermined thresholds.

For future unknown developments, current tunnelling projects in Victoria incorporate additional design loading allowances to provide some capacity for future works in the vicinity of the tunnels. While not accommodating all possible developments, these allowances allow some flexibility for feasible and safe construction of future works.

Besides the mitigation measures discussed above, allowances of clearances and loadings from both existing and future buildings should be clearly identified in the tunnel design requirements. Moreover, clear allocation of responsibilities between stakeholders, such as who is involved in determining acceptability of a development, and detailed risk assessments also plays a key role to

mitigate potential risks on tunnels. A successful application of these measures relies on early planning, thoughtful design, good communication and efficient coordination at both design and construction stages.

7 SPECIAL CONSIDERATIONS ARISING FROM AUTHORS' EXPERIENCE

The period between the commitment to tunnelling and the construction of the tunnels' permanent lining is a phase in the timing of the interactions that requires careful consideration. This is because both the designers and the assessors of developments need to understand that there are a number of possible sequences which could change both the types and magnitudes of the interaction effects.

It has been typical practice that when a proposed development has been approved by the appropriate authorities, it is treated by the tunnel project as a given loading, with the allowance for future development loadings (FDL) also applied as an additional loading. Given the lead time for tunnelling between commitment and construction, the expectation is that the approved development will be in place by the time that tunnels are driven past. However, this is not a certainty, and the possibility that the development's changes could occur after tunnelling should be a design case.

A similar situation arises during the early periods of a tunnelling project when new developments are proposed after the commitment is made for a tunnel project. In these cases, the effects of a development must be accommodated within the FDL allowances to avoid varying the projects specified loading requirements. It would normally be expected that the critical load cases for the tunnel would be when the development occurs after tunnelling. However, recognising the different time scales usually involved, the implications of all relative timings should be considered. It is also vital that the details of any developments approved during this phase are provided to the project's construction team.

The reviews and assessments of proposed developments for recent tunnel projects are conducted within the framework of applications for planning permits, where the application is referred to the project authority in response to a planning overlay. As the overlays are established for the protection of the tunnels over their lifespan, the referral triggers are related to the more critical cases, usually the tunnels being in place. The assessment of a proposed development is usually conducted by a multidisciplinary team that integrates the planning framework with geotechnical, structural, and construction expertise. Within this setting, it is critical for tunnelling engineers to be able to clearly articulate design assumptions, potential risks, and their implications to other disciplines and stakeholders. Effective communication and collaboration across the project team are essential to ensure alignment on design methodologies and to support informed decision-making throughout both the design, construction, and assessment phases.

8 CONCLUSION

The different effects on tunnels from existing and future buildings have been compared from loading, clearance and construction aspects and summarised below.

- Loading: Tunnels are generally more sensitive to loading/unloading effects from future developments compared with those due to existing buildings. When buildings are constructed before tunnels, the tunnel design should comprise the ground conditions and loadings altered by the existing building foundations. When buildings are constructed after tunnels, significant loading/unloading effects due to future excavations and deep foundations need to be considered in the tunnel design. Local stress redistributions and disturbance of existing ground condition also need to be incorporated in the tunnel design.
- Clearances: When buildings precede tunnel construction, management of ground movement effects caused by a nearby tunnel construction is required to protect existing buildings. Depending on the clearance between foundations and tunnels, additional loading and changed ground conditions induced by existing buildings may need to be considered in the tunnel design. In contrast, when tunnels are in place first, subsequent building works, especially deep excavation and piling, will pose potential threats to tunnel integrity due to stress concentration,

interference with ground support systems, or disturbance to surrounding ground. Effective clearance management and construction tolerances are vital to ensure safety of tunnels.

– Constructability: Existing buildings may constrain available surface access and underground space for tunnel construction, demand strict control of tunnel alignments, or require adjustments in tunnelling methods to manage vibration and settlement limits. Future developments, even when considered in tunnel design, may still bring uncertainties because of unknown foundation details and construction activities. When tunnels and buildings are constructed concurrently, careful coordination of excavation, foundation, and tunnelling activities must be carried out to avoid potential disruptive interference between the two projects. Real-time monitoring, flexible construction planning, and early engagement with stakeholders are also critical so that these constructability challenges could be managed effectively.

By integrating the mitigation measures discussed in Section 6 and maintaining close collaboration among all interested parties, the safe coexistence of tunnels and buildings can be achieved and provide strong support for sustainable developments of urban areas and transportation systems.

9 REFERENCES

Bennett, A. 2018. Future Development Loading Report to Support GC82. https://bigbuild.vic.gov.au/__data/assets/pdf_file/0006/229965/MT-Amendment-G-Future-Loading-Development-Report.PDF. Melbourne Metro Rail Project: Melbourne Metro Rail Authority.

Suburban Rail Loop Authority. 2025. Future Development Loading – Summary. https://bigbuild.vic.gov.au/__data/assets/pdf_file/0011/934517/Future-Development-Loading-Summary.pdf. Suburban Rail Loop Project.

19th Australasian Tunnelling Conference – Acosta-Martínez, Stewart and Hudson-Smith (Eds.)
© 2025 Australian Tunnelling Society, ISBN 978-0-85825-002-4

Automatic and real-time positioning of vault and full round tunnel shutters based on camera sensor units

M. Jarvis
VMT Tunnel Guidance, Melbourne, VIC, Australia

S.Wojtkowiak & N. Mattburger
VMT GmbH, Bruchsal, Baden-Württemberg, Germany

ABSTRACT: Traveller Formwork Gantries or Shutters are used for the secondary lining in both conventional and mechanised tunnelling, but current processes involve low levels of digitalisation and automation. Shutter positioning relies on conventional surveying with Total Stations, often causing delays. Setup and concrete pouring are typically documented on paper, later digitised in the office, which limits productivity and performance analysis. This paper presents the development of an automated measuring system designed to speed up shutter setup and reduce labour demands. Prototype systems have been trialled on vault and 360° shutters in Germany, Poland, England, and Australia to evaluate site acceptance and assess time and labour savings. While surveying teams have responded positively, end-user feedback is mixed. Additionally, discussions are underway regarding real-time onsite data capture, aiming to eliminate paper reporting, reduce redundant data entry, improve data collection efficiency, and streamline verification and evaluation processes for better site management.

1 INTRODUCTION

Traveller Formwork Gantries, also known as Arch Forms or Shutters are essential for the secondary lining phase in both conventional and mechanised tunnelling projects. This phase involves constructing the final tunnel lining, which requires high geometric precision and structural integrity. In recent years, the positioning and alignment of shutters have been conducted using conventional surveying techniques, primarily manual procedures such as block axis nail calibration or use of Total Stations. While reliable, these methods are time-consuming and iterative, often leading to significant waiting times for the production team and reducing overall workflow efficiency.

Accurate setout and calibration are critical, as the shutter must be precisely positioned to meet strict design tolerances. This includes both the alignment along the tunnel axis and control of roll (rotational positioning), vertical height, and potentially lateral offset. Achieving this correct spatial configuration is essential to ensure formwork is ready for the next concreting cycle and meets quality standards.

Work processes including shutter positioning, alignment verification, and concrete pour status are typically documented manually with pen & paper. These records are then transcribed into digital formats at a later stage in the site office. This approach introduces delays, data redundancy, and the risk of transcription errors, while also limiting the availability of real-time performance metrics. Furthermore, systematic tools for evaluating productivity, cycle times, and construction progress are scarce, restricting opportunities for process optimization.

Improving these workflows is both a technical challenge and an opportunity to innovate within the tunnelling industry. Despite the critical role of the inner lining in achieving a durable and safe

tunnel structure, the complexity and importance of this stage are often underestimated in comparison to tunnel excavation. Emerging technologies and automation strategies now aim to modernize this area – enhancing precision and efficiency of formwork positioning while improving safety, reducing manual labour demands, and enabling better decision-making through real-time data acquisition and analysis.

2 TRADITION MEETS NOVEL APPROACH

The standard work cycle of a Traveller Formwork Shutter includes the steps of installing reinforcement, shutter advance, positioning of the shutter, concrete pour and concrete curing / hardening. When the curing process is fulfilled, the shutter may relocate and advance to the next block. Relocation and setup require support of a Surveyor to controls the position of the shutter.

In former times, a Surveyor would stakeout and install block axis nails on the floor along the planned axis and determine "asbuilt" coordinates. Work processes were recorded with pen and paper, the Surveyor handwriting within their field book. The height of each installed nail was compared to design and a delta height manually calculated.

A plumb-bob or plumb-line would hang down from the formwork carriage. To locate the shutter the plumb line would be orientated about the block axis nail. This comes along with a waiting time until the pendulum effect of the plumb line is complete. To control roll of the shutter, two block axis nails may be staked out at similar lateral offset from the centre of the shutter axis.

If the shutter must be positioned within the "gap" between two blocks, plumb lines are also required on the backside of the formwork traveller. As the shutter is iteratively positioned to account for roll, vertical or horizontal, the pendulum effect of the plumb line must be allowed to finish.

A more recent approach is an iterative measurement by a Surveyor via Total Station and prisms. Reference points are welded on the steel frame of the traveller, with adapters used to mount prisms. Total Station orientation is determined via free stationing using coordinates of the tunnel survey network. Two prisms left and right sided remain to local coordinates in the shutter coordination system. The Total Station measures e.g. the left prism to locate the coordinates. For the roll the prism on the other side is measured too. The shutter is moved according to the results and the iteration of measuring the prisms until the right position of the shutter is verified. Handwritten notes may be replaced by a tablet or controller with software to import data such as a coordinate file. The controller may be wirelessly linked to the Total Station via Bluetooth. The Foreman or Leading Hand references the tablet for shutter positioning and moves the shutter iteratively according to the data output.

The modern approach seeks to improve setup time of the shutter for a faster advance in the tunnel. A sensor unit is used to determine the forward position of the shutter. Each unit consists of two measuring cameras and one dual-axis inclinometer. The sensor unit is firmly mounted on the steel frame of the traveller as high as feasible, close to the upper formwork cap. Based on two incoming camera images and the roll values of the inclinometer, software used photogrammetric intersection to determine the traveller shutter axis in relation to the theoretical block axis.

At the beginning of the project a comprehensive machine measurement is needed to calculate the traveller axis and local coordinate system, plus the relative position of the formwork shutter and cap. Reference points are welded to the steel traveller to enable faster positioning during system commissioning. After installation, a calibration measurement is used to determine the position of each camera relative to the traveller coordinate system, values known as "assembly dimensions".

In preparation, the Surveyor must stakeout block axis holes to represent design alignment of the secondary lining. Each location is defined by a hole drilled into the base concrete slab and a standard Survey "spigot" screwed within. These locations supersede the previously used block axis nails. Important to note, these Survey setout works may be completed off the critical path, at a time convenient for tunnel operations.

Each location is signalled via one visual bracket called a Ringed and Automatically Detected Marker. RAD-Markers are essentially a target (white with black imprints) designed so the measuring cameras can precisely detect their centre point. RAD-Markers are housed within an aluminium bracket, which screws down into the Survey spigot.

System data is transferred to the industrial computer within the Central Box and software calculates the spatial position of the shutter by means of image detection and transformations. The position relative to design is represented numerically in the positioning module and shows the operator which direction to move the shutter. The operator may choose between indicated corrections or deviations of the shutter axis in relation to the designed block axis. As soon as the cameras detect the RAD-Marker in the field of view, software calculates the deviations of the shutter from the desired position in three dimensions: chainage, horizontal to block axis and elevation). The dual-axis inclinometer ensures the roll of the shutter is determined and software visualization shows the deviation in roll. The calculated differences for chainage, horizontal and vertical deviation as well as roll are represented in the software in a numerical and graphical manner.

During concreting and curing, the position may be automatically recorded by user defined intervals. The position and deviations are continuously indicated to the operator. Due to the use of a tablet on which a visualization of the positioning system is running, the operator is not tied to a certain place and may set up the shutter in a remote-controlled manner.

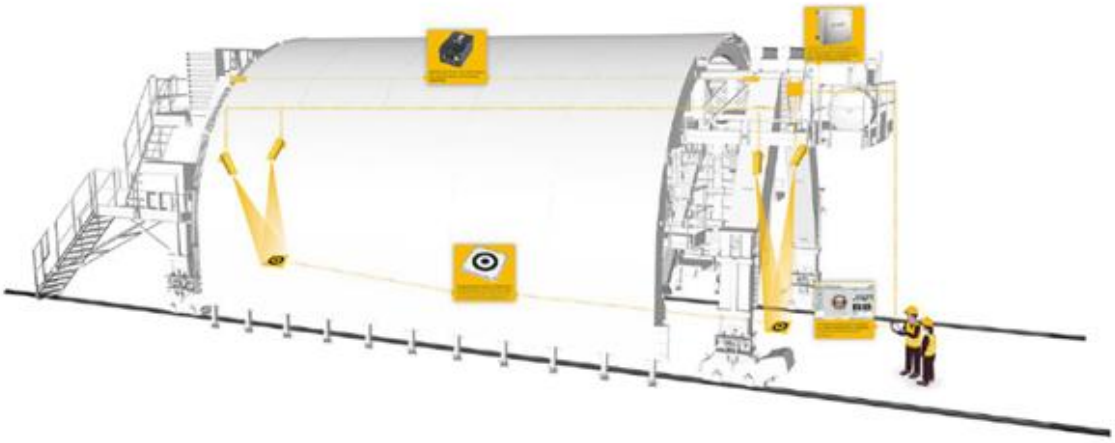


Figure 1. Overview of positioning system hardware and concept

3 TIME, COST & WORK FLOW

To assess validity and implications of the novel method, we compare both methods from various perspectives.

Table 1 provides a simplified comparison of the methods and some of their key parameters.

Table 1. Comparison of total station positioning method and novel method.

	Total Station Method	Novel Method
Quick and fast setup	Install prisms and setup Total Station	Once installed no further set up time/ RAD markers are relocated each block
Position determination	Using Total Station and prism – iterative procedure	Using camera-based sensor units / as backup system transferable to Total Station
Monitoring function during the processes	Manual process by Surveyor	Automated monitoring function via camera-based system configured in different intervals as needed
Use of specialized labour	Surveyor involved in set up phase and pre-pour check	Tunnel personal such as Foreman trained to manage system.

		Surveyor on call and for pre-pour check only
Time needed for setup	Up to one hour	Approximately 8-10 minutes
Digitalization and database handling	Handwritten and converted in office	Automated data upload from shutter position for automated Reports
Quality of the inner lining	No values	Monitoring improves quality process

Considering the roll of the shutters, the traditional setout of the shutter may have taken up to one hour and required a Surveyor with specialized equipment including Total Station and prisms. When the traditional method was employed, user must consider significant waiting time regarding the pendulum effect of the plumb-bob over each block axis nail. This must be considered after each iterative traveller movement. Where a dedicated Surveyor and Total Station are employed, each traveller movement requires new prism measurements and subsequent calculation are required until the shutter setup is completed.

The novel method demonstrates a reduction of setup time and supplements a full-time Survey team by enabling other personal to complete the process. Surveyors are required only to prepare the block axis position for markers and conduct a final pre-pour check for quality control. When RAD-Markers are repositioned, they are screwed in the pre-drilled holes and the camera detection recognizes the input of the software. As the shutter approaches the block joint and cameras visualise the RAD-Markets, all required correction values are calculated and displayed on the tablet. Thus, the shutter can be setup for a new cycle in minutes. Waiting time for the production team is mitigated and the Surveying team may focus on critical path tasks.

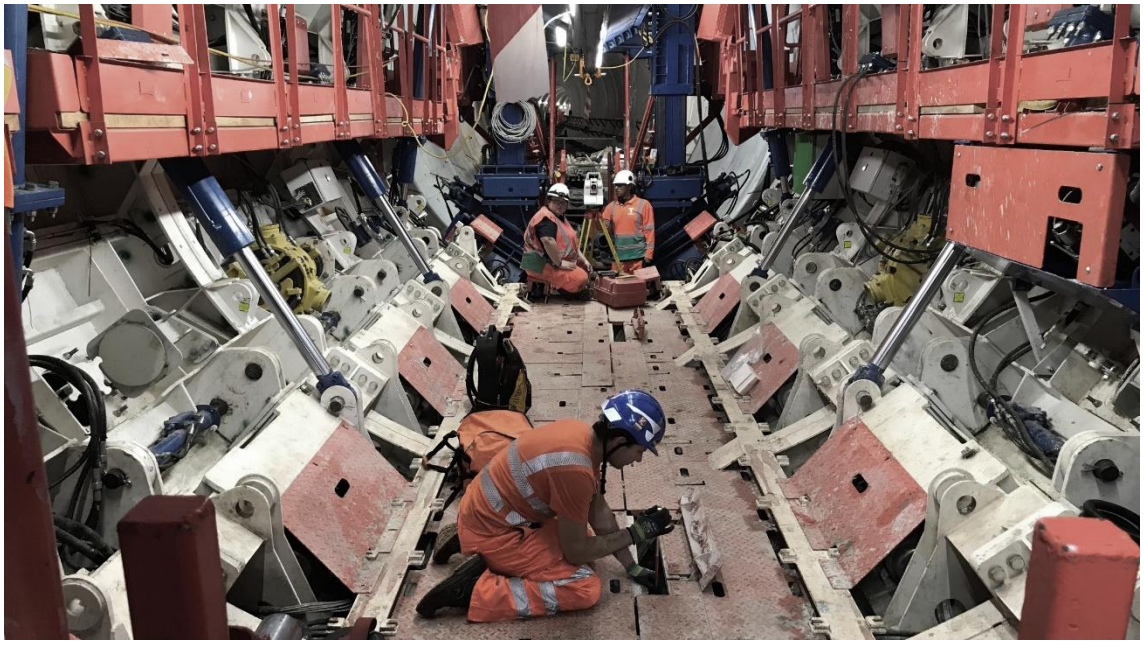


Figure 2. Survey personnel employ iterative total station positioning method

4 INNOVATION & DIGITIZATION

The traditional set up of the shutter does not include live positioning values. Once the shutter is setup, concrete cured and the shutter advanced, the cycle starts again. The novel method determines the current position of the shutter compared to the designed block axis in real-time. To achieve this, the system uses camera sensor units installed at within the steel traveller frame, connected to the shutter cap at the crown. Position and roll are continuously displayed to the operator. This allows an exact vertical and horizontal setup with relation to the design block axis that can be precisely controlled. The current chainage, block number and roll of the shutter complete the information that is important for the operator. The operator may select position display as either horizontal and vertical corrections, or deviations in relation to the block axis. Camera images are live streamed into the main system view, enabling errors to be recognized directly. The operator is in optimal control of necessary steering movements. The status of all system components is monitored live. Green status means all is normal, while warning colours yellow and red indicate system issues for immediate action.



Figure 3. Positioning main screen from operators view during setup phase of a shutter

Traditionally the Foreman or Leading Hand would note production information on paper in the field and record in the construction office at the end of shift. This process allows limited options for analyzing productivity and construction progress.

The novel monitoring method of the shutter position during the concreting process and acquisition of the position during the concreted blocks can be actualized in intervals for the recordings and for saving them in the database. Values are set by the user in the system configuration and may be written into the PLC of the machine manufacturer to enable automatic positioning of the shutter. The system provides full documentation of the positioning in a database and is the basis for reports, data exports (CSV, XLSX) or other analyses. It has the potential to mitigate or replace manual recording in the field and rework in the office.

The system software runs on a Windows-based industrial PC. The module and function access are controlled by robust user management. The high information content of the displayed data ensures an optimal control of the machine position to achieve uniform positioning of the shutter with small deviations from the block axis. The final shutter position is stored in the database and reported digitally for quality management.

Reference points welded into the shutter, with known coordinates in the shutter system, can be used to independently determine the shutter position through an independent measurement by means of the Total Station as well as with prisms and subsequent transformation in the software module.

5 LABOUR & PERSONNEL

The conventional method requires a Survey team to be involved in all processes along the tunnel network and shutter setting modes. Positioning the shutter requires personal and waiting times for the team until the final positioning is done by the Surveyors.
With the novel method Survey may prepare their works off the critical path, at a time convenient for tunnel operations. Their primary task is setout of block axis locations which represent design alignment of the secondary lining. Each location is defined by a standard Survey "spigot" screwed into a hole drilled into the base concrete slab. Surveyors prepare a coordinate file and upload on the tablet. These locations supersede the previously used block axis nails.
As the shutter advances to the next block, one of the production team must simply relocate a single RAD-Marker by screwing into the spigot. Surveyors are largely released from shutter setout and must only conduct a final pre-pour check for quality control. Waiting time for the production team is mitigated and the Surveying team may focus on critical path tasks.

To improve health and safety of site personnel the remote-controlled manner of the positioning system ensures that the operator is not tied to a certain place to complete the work. The operator may reference the positioning system from a safe and comfortable location. Support personnel are not required to climbing around the shutter gantry during setup to visually assess the position. Use of a Total Station and tripod is mitigated improving access along the tunnel alignment for personnel and plant.



Figure 4. Production personnel screw in a RAD-marker to pre-coordinated survey "spigot"

6 PROTOTYPE ANALYSIS & FUTURE WORKS

Prototype systems were evaluated on vault and 360° shutters in Germany, Poland, England and Australia. The goal was to gather experience on benefits with respect to time and labour efficiency, safety of personnel, plus listen to key users regarding potential improvements. Prototype systems were assessed in parallel to the standard setup cycle and reviewed against previously stated perspectives. Key improvements on the operational side include reduction of total setup time and the number of specialized personnel required. It was generally accepted that the camera-based sensor unit system improves most key parameters.

As there is naturally a cost to procure and commission such a system, some sites noted a greater benefit where more blocks were poured. Where 25 or fewer blocks were poured, the overall cost-

benefit was reduced. As the total number of blocks increased above 30, the overall cost-benefit was significant.

As of 2025, manufacturers of Tunnel Boring Machines (TBM) use technologies that enable automated data acquisition and position determination of future advances. The secondary lining processes of conventional tunnelling are far behind.

Soon, comparable technologies will be available for conventional inner lining processes that are done by shutters, such as data acquisition and digital shift management reporting.

Positioning values may be written into the machine PLC and systems will support and integrated and automatic positioning of the shutter throughout the setup phase. This will apply to vault, arched and full-round shutters.

Data Management and Documentation will be streamline through automated documentation of the position, block reports, shift data management and an asbuilt of the shutter position prior to stripping formwork – all available in automated reports stored in the cloud.

The camera-based sensor unit enables a monitoring process to provide information regarding movement of the formwork during concrete pouring and curing. Additional sensors will deliver information regarding concrete temperature, pressure and load. Industry should anticipate that each positioning task will be automated to ensure each process is faster, safer and of higher quality.

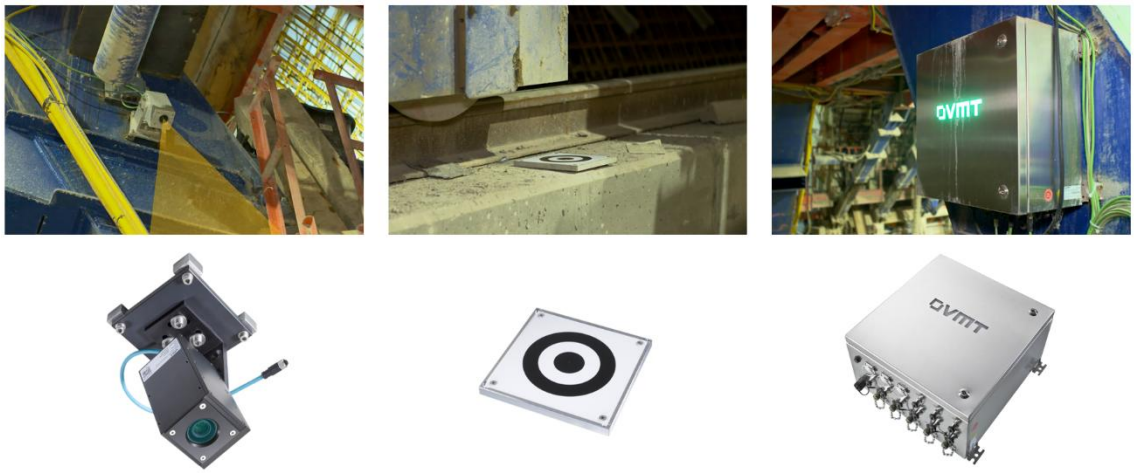


Figure 5. Sensor technology enables advances in automation, data management and reporting.

Each year the civil tunnelling industry aspires for greater implementation of 3D modelling and BIM technology to follow each process via a digital twin. The modern conventional construction site cannot be tracked in the same high standard as a the TBM method. While TBM construction sites have tools in the cloud to view the status of production in real time, the work of the inner lining with shutters may be loosely analysed via handwritten notes. To leverage technology currently utilized in TBM tunnelling, tenders for secondary lining must be modernized. Such topics should consider navigation support of shutter formwork, data integration with machine PLC's, automated reporting and shift data. Quality assurance and documentation topics should be supported by asbuilt block reports, concrete batch traceability, monitoring of concrete temperature, pressure and load during both concrete pouring and curing.

7 CONCLUSION

This paper has looked at the role of Traveller Formwork Shutters as used for secondary lining of conventional and mechanised tunnelling. We examined the task of positioning shutters by traditional methods and compared to a modern novel method with sensor units. By comparing both methods, this paper established the novel method enhances speed, safety, efficiency and cost-savings, plus greater possibilities around data acquisition and reporting. Furthermore, prototype testing on construction sites around the world have shown the waiting time in the positioning phase of the shutter can be mitigated, and the Survey team is released from critical path activities.

During the early years of underground tunnel excavation, works were performed with the simplest methods, rudimentary position control and a large workforce. Tunnel Boring Machines have embraced technology and evolved through more complex and automated methods. By contrast the secondary lining processes can be greatly enhanced. In the coming decades, one focus of tunnel construction will be the automation of the processes to increase the safety and efficiency. We seek to eliminate paper reports and redundant data entry, enhance data collection efficiency, enabling better evaluation, and streamlining the verification process for site management. In this context the camera-based positioning system is a development step which brings more automation and a reduction of personnel needed and makes an important contribution to this evolution.

8 REFERENCES

[1] Baubetrieb und Bauverfahren im Tunnelbau, 13.4 chapter Accessed 10 April 2024; https://books.google.de/books?id=ENQqhrjb1m0C&lpg=PT224&ots=KSrEQ2HzHz&dq=positionierung%20von%20schalwagen&hl=de&pg=PT233#v=onepage&q=positionierung%20von%20schalwagen&f=false

[2] Daniele Cappelletti (Kern Tunneltechnik SA); https://www.kern-tunneltechnik.com/en/progetto/62/thames-tideway-east-grect

Theme 2. Temporary Support

THIS PAGE INTENTIONALLY LEFT BLANK

19th Australasian Tunnelling Conference – Acosta-Martínez, Stewart and Hudson-Smith (Eds.)
© 2025 Australian Tunnelling Society, ISBN 978-0-85825-002-4

Designing canopy tubes for tunnel stability in weak ground: A comparison of analytical and 3D numerical approaches

A.Sarathchandran & S.Yao
AECOM, Sydney, Australia

ABSTRACT: The use of canopy tubes as pre-support in weak ground is a widely adopted method to control deformation in tunnelling. By redistributing ground loads radially and longitudinally, canopy tubes enhance tunnel stability and reduce the risk of collapse. Many analytical and semi-empirical methods have been proposed. Three-dimensional numerical modelling typically remains impractical for routine design due to computational demands. As a result, designs often rely on simplified approaches. This paper reviews available methods, focusing on two representative analytical models: a simplified beam-on-elastic-foundation method by John & Mattle (2002) and a more refined Pasternak foundation model by Wang et al. (2009). These are benchmarked against finite element modelling results for underground conditions representative of Sydney sandstone and shale. The study assesses the analytical methods in conjunction with equivalent finite element models, highlighting their capabilities and limitations, and explores the implications for practical canopy tube design.

1 INTRODUCTION

Canopy tubes (pipe umbrellas) are a well-established pre-support method for tunnelling in weak ground. By redistributing loads radially and longitudinally, they improve roof stability and reduce the risk of deformation or collapse, supporting ground between the installed lining and the tunnel face.

Although their benefits are clear, the load transfer mechanisms are complex. Full 3-Dimensional (3D) numerical modelling can capture these mechanisms in detail but is rarely practical for routine design due to its computational cost. As a result, design typically relies on simplified analytical or semi-empirical methods, which provide conservative estimates based on assumed boundary conditions and input parameters.

This paper reviews selected analytical and semi-empirical methods for canopy tube design, focusing on two: the simplified beam model of John & Mattle (2002) and the beam-on-elastic-foundation model of Wang & Jia (2008) and Wang et al. (2009). Their predictions are benchmarked against 3D finite element modelling for Sydney sandstone and shale conditions, highlighting the influence of modelling assumptions, boundary conditions, and the capabilities and limitations of each approach.

2 LITERATURE REVIEW

Various analytical and semi-empirical methods have been developed to analyse canopy tube design actions in weak ground conditions. Oke et al. (2016) provides an excellent overview of the various semi-analytical methods that are available. Oke et al. (2016) broadly classifies the semi-analytical solutions available into two categories: simplified beam models (Harazaki et al., 1998;

John and Mattle, 2002) and elastic foundation models (Wang & Jia, 2008; Yuan et al., 2013; Song et al., 2013).

2.1 *Simplified beam models*

Simplified beam models idealise the canopy tubes as isolated beams subjected to external loads, neglecting the interaction between the ground and the structure. Harazaki et al. (1998), as cited by Oke et al. (2016), employed such a model based on field observations from the Maiko Tunnel in Kobe, Japan. Their analysis, which involved a simplified beam model to capture the moment profile of the canopy tube, interpreted the observed bending moment behaviour of the steel pipes in the field data as being similar to that of a beam simply supported on two pivots and subjected to a distributed load. John & Mattle (2002) used a similar approach, with relatively simple boundary conditions that incorporate the ground support without explicitly modelling soil stiffness, which is elaborated further in Section 2.3.1.

2.2 *Elastic foundation models*

Elastic foundation models conceptualise canopy tubes as beams resting on a continuous elastic medium, incorporating ground parameters to estimate spring stiffness and thereby more realistically represent ground-structure interaction. Song et al. (2013) developed a simplified theoretical beam-spring structural analysis model based on elastic foundation theory to calculate bending moment and shear forces. Their findings show that the factor of safety (FOS) against bending is generally lower than the FOS against shear, suggesting that pipes are more susceptible to failure in bending than in shear. Similarly, Yuan et al. (2013) modelled the pipe roof as a beam on an elastic foundation to examine how excavation-induced loads are redistributed by the pipe roof to the supporting structure and the unexcavated soil ahead of the tunnel face. Wang & Jia (2008), Wang et al. (2009), proposed an enhancement to the Winkler Spring model by adopting the Pasternak elastic foundation model, which incorporates the shear interaction between adjacent springs and can potentially yield improved predictions of ground deformation. Although analytically more complex, these models offer a more realistic representation of the load transfer mechanism in front of the tunnel face.

2.3 *Analytical methods for canopy tube design*

Among the various available methods, this paper focuses on two representative analytical approaches: the simplified beam model described by John & Mattle (2002) and the Pasternak elastic foundation model developed by Wang & Jia (2008), Wang et al. (2009). Sections 2.3.1 and 2.3.2 review these methods in detail and are subsequently evaluated against 3D numerical modelling results to assess their practical relevance and applicability in tunnel support design.

2.3.1 *John & Mattle (2002)*

This paper presents a simplified structural analysis method for the analysis of canopy tubes, modelling them as longitudinal beams supported at one end by the tunnel lining and embedded at the other end in the ground ahead of the tunnel face. A series of numerical analyses were conducted using the Finite Element Method (FEM) with an axisymmetric model. The results indicated that the bending moment distribution resembled that of a beam on elastic support, showing smaller negative and positive values near the supported end and larger values closer to the unsupported region. This was idealised in a simplified structural model as an equivalent beam hinged at the tunnel lining and fixed at the face, as shown in Figure 1a. The effective length of this equivalent beam was taken as 1.5 times the unsupported length based on consideration of a number of case studies. Bending moments calculated using this simplified model showed good agreement with the bending moments from the FEM analysis. Additionally, the study found that the ground loads estimated through FEM were in good agreement with those calculated using Terzaghi's silo theory.

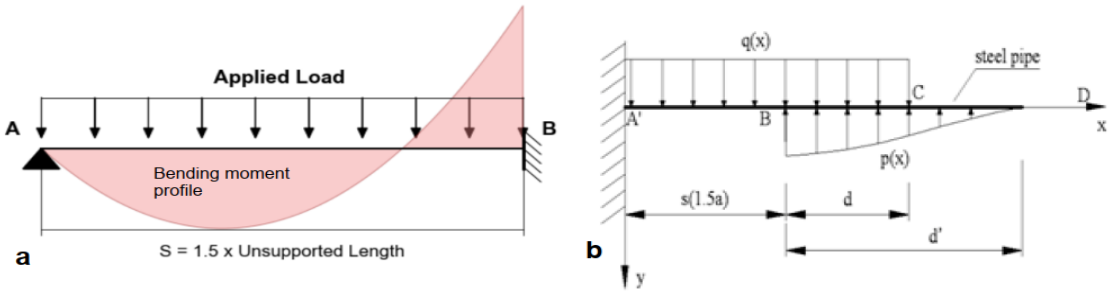


Figure 1. a). Analytical model proposed by John & Mattle (2002) b). Mechanical model of pipe roof reinforcement during tunnel excavation (Wang & Jia. 2008)

2.3.2 *Wang & Jia (2008)*

Wang and Jia (2008) developed an analytical model to assess pipe roof reinforcement ahead of tunnel faces. The model uses the Pasternak elastic foundation beam theory, which includes shear interaction, an improvement over the Winkler model. The model assumes a semi-infinite beam on a Pasternak elastic foundation, fixed at one end to represent the tunnel lining. The fixed end has prescribed vertical displacement (to simulate staged excavation) and no rotation. The free end, positioned ahead of the tunnel face and beyond the failure zone, is assumed to have negligible movement or rotation.

Geometry and Load Definition (see Figure 1b):

- Pipe is fixed at Point A′, located 0.5 longitudinal spans behind the leading edge of the initial shotcrete support.
- Pipe extends to Point B, with a total span of:
    - s=1.5× unsupported excavation length
- The active failure zone ahead of tunnel face is assumed to extend for a length, d = h·tan(45°−ϕ/2), where ϕ is soil friction angle. Overburden pressure q(x) is assumed to act up to this distance, indicated as C in Figure 1b.
- Length of pipe ahead of the face, d′ will be greater than d.

The pipe carries downward overburden pressure *q(x)* and upward subgrade reaction *p(x)* from the ground ahead of the face. Wang et al. (2008) combined beam theory with a Pasternak elastic foundation to derive a fourth-order equation for vertical deformation ω(x), from which bending moments are calculated. Both Wang & Jia (2008) and John & Mattle (2002) estimate loads using Terzaghi's silo theory but differ in boundary conditions: Wang & Jia assume full fixity at the lining, while John & Mattle place it at the unexcavated face.

In practice, abutment conditions vary, so both models use conservative simplifications:

- Simplified beam: Rigid face support, hinged support 0.5 spans behind the lining; tube spans 1.5× unsupported length.
- Elastic foundation: Elastic support beyond the face, fixed support 0.5 spans behind the lining; fixed in rotation but allowed vertical deflection.

Both assume one (elastic) or two (simplified) rigid/near-rigid abutments, acknowledging that face and lining support are rarely fully effective, consistent with case histories.

3 COMPARATIVE ASSESSMENT

This section compares the two analytical approaches by comparing their predictions against results from three-dimensional finite element analysis (FEA) using PLAXIS 3D version 2024.2 software. The analysis methods used are presented in Table 1. Bending moments were extracted from each method to evaluate canopy tube behaviour under varying tunnel and ground conditions. A series of tunnel configurations were analysed, varying by:

- Ground conditions: Sydney Sandstone Class V and Shale Class V
- Tunnel Heading heights: 7 m and 8.5 m
- Overburden depths: 5 m, 10 m, 15 m and 20m.

Table 1. Analysis methods used for comparative assessment

Comparative Assessment performed		Objective
Section 4.1 Comparison of Analytical models	Simplified Beam Model vs. Beam on Elastic Foundation	Compare analytical methods and plot moment distribution profiles under identical conditions using full overburden load. Assess the impact of boundary conditions and ground stiffness ahead of tunnel on bending moment predictions.
	Beam on Elastic Foundation: Impact of Heading height	Assess the influence of tunnel heading height on bending moment predictions using beam on elastic foundation.
	Ground Load using Terzaghi's Silo theory for various overburdens	Quantify the sensitivity of maximum bending moment to overburden depth using Terzhaghi's silo loads. Compare the moment profiles with full overburden loads
Section 4.2 Idealised FEA models	Beam on Elastic Foundation vs. FEA Validation Model (PLAXIS 3D)	Validate analytical predictions using FEA model with same assumptions (such as full overburden load, elastic foundation). Compare moment profiles and identify limitations of analytical model if any.
Section 4.3 Soil Structure interaction models	Analytical vs. Soil-Structure Interaction FEA Model	Compare the moment distribution of beam on elastic foundation models with 3D FEA models.
	FEA Model – Variation of Tunnel Heading Height (7 m vs. 8.5 m)	Assess the influence of tunnel heading height on bending moment predictions using FEA models.

Initially, the analytical methods were evaluated against each other for identical tunnel advance length and uniform full overburden load, for two ground types, relatively stiff Class V sandstone and a weaker Class V shale. A tube spacing of 350mm centre to centre was assumed for all calculations. The rock mass properties adopted are detailed in subsequent sections. The full overburden load was directly applied, thereby eliminating the influence of rock mass properties typically required for calculating silo pressure. Rock mass properties also do not affect the boundary conditions for simplified beam models with fixed or simply supported boundaries. However, they are critical in beam-on-elastic-foundation models, where deformation depends on foundation stiffness.

Following this, a validation model was developed using PLAXIS 3D FEA software, as shown in Figure 2a. This model replicates the assumptions of Wang & Jia (2008) and allows for direct comparison of results between the analytical beam on elastic foundation model and the finite element model under identical conditions with full overburden load imposed.

The impact of varying the applied loads was explored for both analytical methods, and a simplified ground-structure finite element model, simulating a single tunnel advance as shown in Figure 2b was developed. The following assumptions were made for the finite element model:

- A stiff shotcrete liner as shown in blue in Figure 2b was assumed to support the canopy tubes over the excavated region. Similar to the analytical models, the edge of the liner terminates 1.5 times the unsupported length away from the face of the tunnel (i.e. behind the actual leading edge of the installed support).
- Model simulations are based on Mohr-Coulomb parameters. The equivalent Mohr-Coulomb parameters are derived from the Hoek-Brown criterion, calibrated for the low confining stresses as shown in Table 2.
- The adopted cohesion values, particularly for Class V Shale, were low, which contributed to face instability in preliminary analyses. To achieve model convergence, cohesion values were increased ahead of the tunnel face to induce a more elastic response, while maintaining low stiffness. This approach enabled controlled deformation towards the tunnel face without

triggering model failure. Detailed analyses involving support systems such as dowel bars or shotcrete for tunnel face stability are not included in this study.

– Embedded beam elements in PLAXIS 3D are utilised to model individual canopy tubes as circular hollow tubes.

The outcomes of these comparisons, along with the key differences identified, are discussed in detail in the following sections.

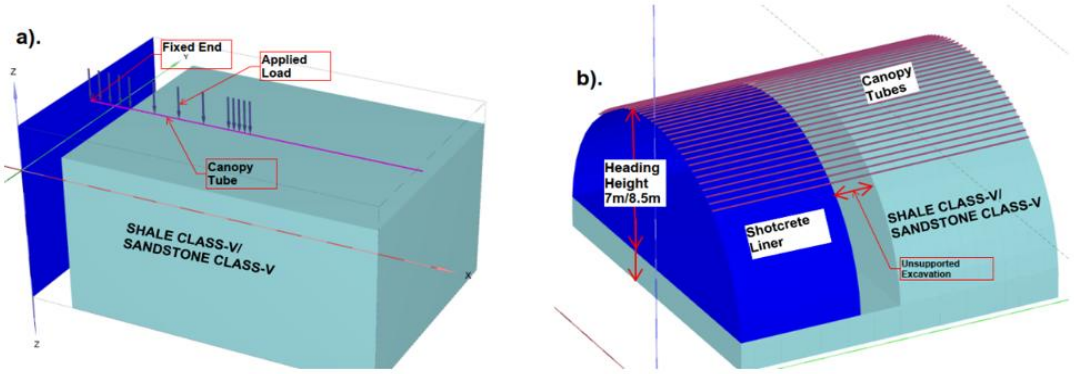


Figure 2. a). Validation model developed in FEA software b). Soil structure interaction model in FEA software

3.1 *Rock mass and pipe reinforcement properties*

Sydney Sandstone parameters are based on Bertuzzi (2014) classifications commonly used in local tunnel design. Class V Sandstone and Class V Shale were chosen to represent poor ground where canopy tubes are typically applied. Rock mass properties (Table 2) use Mohr–Coulomb parameters for both analytical load calculations and FEA. The canopy tube model is elastic, 114 mm OD, 6.3 mm wall, 15 m length, 210 GPa modulus, axial skin resistance 5000, set high to avoid local ground failure in unsupported spans.

Table 2. Rock parameters adopted in 3D FEM analysis

Geotechnical Parameters			Ashfield Shale Class V(SH-V)	Sandstone Class V(SS-V)
Intact Rock Parameters	Uniaxial compressive strength (MPa)		1	5
	Poisson's Ratio		0.3	0.3
	Material constant (m_i)		8	12
	Unit Weight (kN/m^3)		24	
Continuum parameters	GSI		20	35
	Rock Mass Modulus E_{mass} (MPa)		15	100
	Mohr-Coulomb(*)	c' (kPa)	9	26
		ϕ'(°)	30	38

*Confining stress range of 0.05 to 0.25MPa assumed based on tunnel overburden depth.

4 ASSESSMENT RESULTS

The following section presents the results obtained from both analytical and FEA simulations. Trends in bending moments are compared with respect to variations in ground conditions, tunnel geometry, and applied loading scenarios.

4.1 *Comparison of analytical models*

Figure 3a presents bending moment distributions for a canopy tube under 10 m overburden using John & Mattle (2002) and Wang & Jia (2008). Both methods produce broadly comparable peak magnitudes (within ~10–15%) but differ in profile. The John & Mattle simplified beam model, independent of ground stiffness and based solely on the applied load, does not compute moments ahead of the tunnel face, giving identical results across ground conditions. In contrast, the beam-on-elastic-foundation model provides a profile extending ahead of the face. In weaker ground, such as Class V Shale, reduced stiffness increases the effective span, producing higher peak moments than the simplified beam approach. In both methods, maximum moments occur at rigid boundaries—the face for the simplified beam model and the leading edge of the initial support for the elastic foundation model.

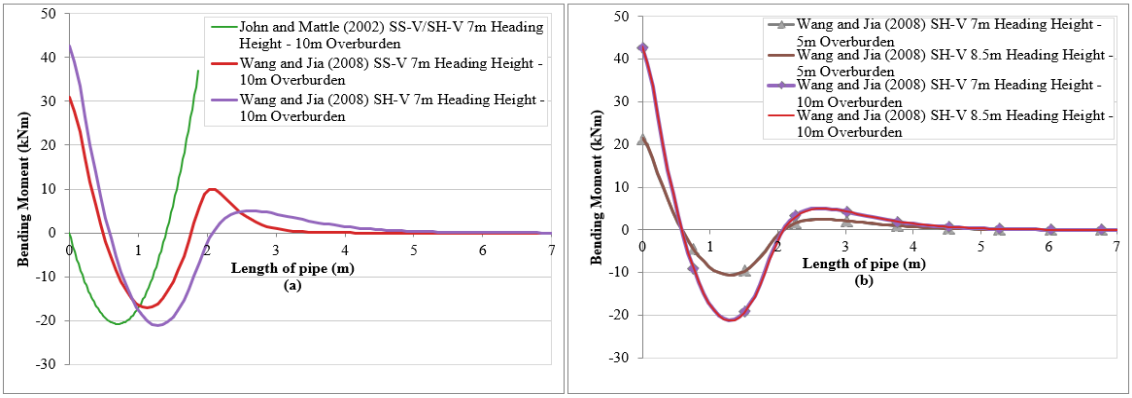


Figure 3. a). Predicted bending moment profile along the canopy tube based on John & Mattle(2002 and Wang & Jia (2008) b). Bending moment profile for tunnel heading heights 7m and 8.5m (plots are overlapping on top of each other) for various overburdens.

Wang & Jia (2008) suggests that the failure zone ahead of the tunnel is dependent on the tunnel heading height ('d' as shown in Figure 1b. To assess the influence of heading height two tunnel heading heights were analysed, 7m and 8.5m. The results (Figure 3b) show that increasing the heading height had no impact on the predicted bending moments.

The comparison presented in Figure 3b assumes full overburden loading. In Figure 4b, ground loads for Class V Shale were recalculated for tunnel overburdens of 5m, 10m, and 15m using Terzaghi's silo theory Wang & Jia (2008), Wang et al. (2009), and John & Mattle (2002). The results show a substantial reduction in maximum bending moments of about 50% for shallow tunnels. This corresponds directly to a reduction in vertical ground pressure, which decreases by approximately 50% for shallow tunnels and up to 75% for deeper tunnels. However, for shallow tunnels, the typical design practice is to consider full overburden pressure to account for ground variability. In line with the premise of the silo-theory, there is no significant increase in load beyond a certain depth.

4.2 *Idealised FEA model*

The analytical model (Figure 1b) was compared with an idealised FEA beam-on-elastic-foundation model (Figure 2a). John & Mattle (2002) was excluded, as its propped cantilever behaviour and profiles are already well understood. Figure 4a compares bending moment profiles from FEA and elastic foundation models for Class V Shale and Sandstone under 5 m and 10 m overburden. Agreement is generally good, but discrepancies appear near the fixed end. These are attributed to the central difference method used in the analytical model, which estimates moments from deflections using data points beyond the beam's physical limits, introducing larger boundary errors.

4.3 *Soil structure interaction model*

In this section, the results from a FEA soil structure interaction model using PLAXIS3D 2024.2 (Figure 2b) are presented. The model explicitly models individual canopy tube elements supported on the leading edge of the stiff tunnel liner with a free end embedded ahead of the tunnel face. To reduce computational demands, the staged excavation process was not modelled; instead, overburden pressures were applied in a single load step. Figure 5a presents the results of this analysis for the weaker ground condition (Class V Shale).

FEA and analytical results (using Terzaghi's silo load) yield similar peak bending magnitudes but differ in distribution. In weak ground, FEA shows peaks near the tunnel face, reflecting face extrusion effects not captured in the analytical models, which predict peaks at the fixed end. In competent sandstone, FEA results match Wang & Jia (2008), with peaks near the lining. Increasing heading height raises structural demand, an effect modelled in Wang & Jia's deeper failure plane but absent in the analytical results.

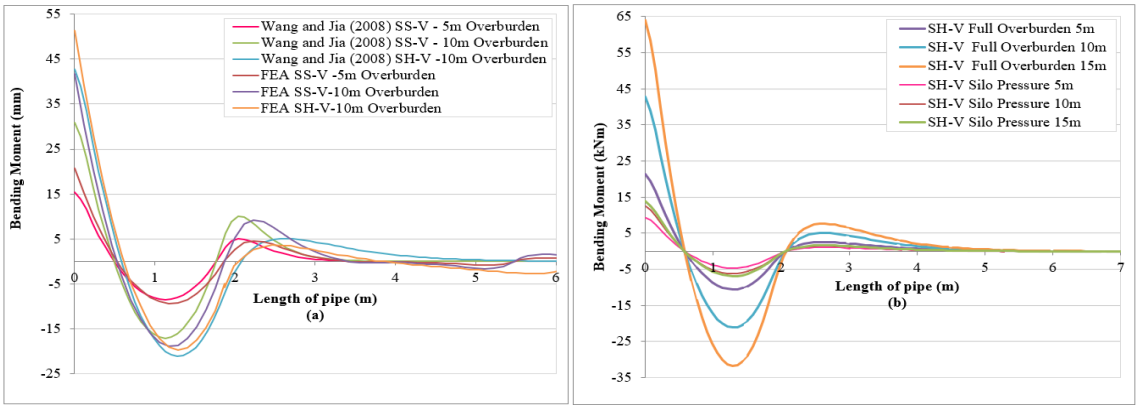


Figure 4. a). Idealised PLAXIS3D model vs. elastic foundation model predictions (Class V Shale and Sandstone) b). Moment profile generated using Wang & Jia (2008) for full overburden pressure vs silo theory-based pressures

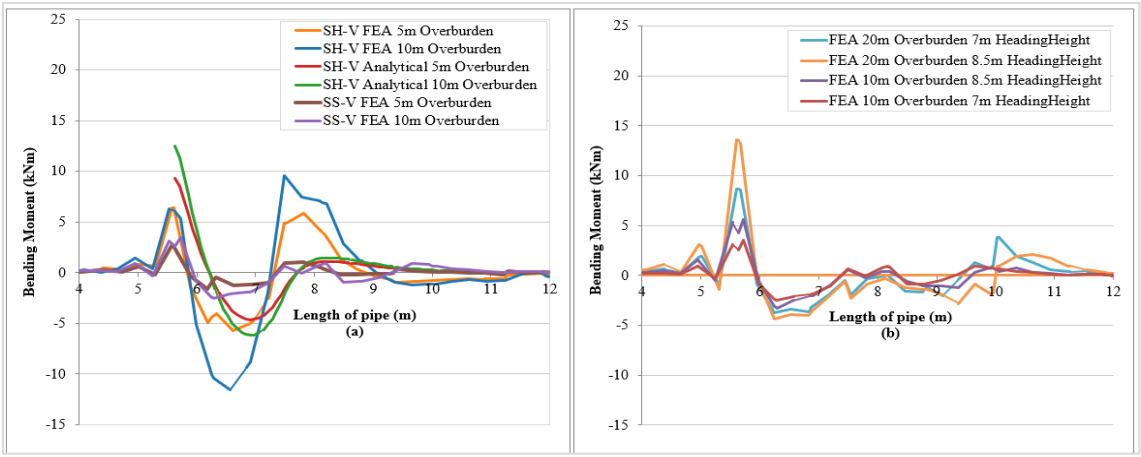


Figure 5. a) Results from the idealised FEA model compared to those of the elastic beam foundation model with Terzaghi's silo pressure load for Class V Shale, b). FEA model for Class V Sandstone comparing the results of 7 & 8.5m Heading height

5 CONCLUSION

Two analytical methods are evaluated alongside an equivalent numerical model representative of typical Sydney geology. The results of the analyses and review suggest the following.

- The applied load is a critical factor influencing the structural actions of canopy tubes; however, it may be challenging to estimate it accurately. Modelling suggests that Terzaghi's silo theory provides a reasonable approximation.
- Both analytical methods were effective at predicting peak bending moments reasonably well, though they differ in assumed boundary conditions and load transfer mechanisms. The method proposed by Wang & Jia (2008) showed closer agreement with FEA results, for weaker ground conditions ahead of the tunnel face.
- Pre-support systems implicitly rely on the face as a means of supporting the ground loads associated with potentially unstable ground ahead of the installed supports. Hence, maintenance of face stability is crucial.
- The assumption of fixed boundaries in both analytical approaches leads to a conservative estimate of maximum moment. It is acknowledged, and the FEA results show, that in effect each abutment of the pre-support system is in fact soft to some degree, with flexure of the lining (and also importantly early age strengths) and deformation of the ground at the face leading to lesser moments than predicted by the analytical methods.
- An increase in tunnel heading height may lead to higher face instability, face deformation leading to higher structural actions in canopy tube, this effect is not directly captured by analytical methods.

In summary, the comparison between analytical methods and FEA demonstrates that analytical approaches can offer a robust estimation of bending moments. Adequate support of the tubes via the initial lining and tunnel face is vital, often the face stability being the critical factor. Designs must adhere to applicable national standards and consider key elements such as tube connections, overlap with subsequent arrays, and ensuring that structural response remains within the elastic range to achieve a safe and robust solution

6 ACKNOWLEDGEMENT

Writing and researching have been invaluable learning experiences. We would like to sincerely thank our colleagues at AECOM, Geoff Charlesworth and Sajjad Anwar, for their valuable ideas and support throughout the development of this paper. We have enjoyed the opportunity to collaborate, reflect, and explore new perspectives, and we look forward to continuing our journey of research and contribution within the tunnelling discipline.

7 REFERENCES

Bertuzzi, R. 2014. Sydney sandstone and shale parameters for tunnel design. Australian Geomechanics Journal, 49(1), 95–104.

Harazaki, I., Anon, H., Matsuda, A., Aoki, T., Hakoishi, Y. 1998. Field observation of large supported by umbrella method: case of Maiko Tunnel in Kobe, Japan. In: Tunnelling and Metropolises, Proceedings of the World Tunnelling Congress, pp. 1009–1014.

John, M., & Mattle, B. 2002. Design of tube umbrella. Magazine of the Czech Tunnelling Committee and Slovak Tunnelling Association.

Oke, J., Vlachopoulos, N., & Diederichs, M. S. 2016. Semi-analytical model for umbrella arch systems employed in squeezing ground conditions. Tunnelling and Underground Space Technology, 56, 136–156.

Song, K.I., Cho, G.C., Chang, S.B., Lee, I.M. 2013. Beam-spring structural analysis for the design of a tunnel pre-reinforcement support system. Int. J. Rock Mech. Min. Sci. 59, 139–150.

Wang, H., & Jia, J. 2008. Analytical method for mechanical behaviours of pipe roof reinforcement. In 2008 International Conference on Information Management, Innovation Management and Industrial Engineering.

Wang H, Jia J & Kang H . Analytical approach and field monitoring for mechanical behaviors of pipe roof reinforcement. Journal of Central South University of Technology. 2009. 16(5):827-834. doi:10.1007/s11771-009-0137-9.

Yuan, X., Zhou, S., & Gong, Q. 2013. Three-Dimensional Analysis of Excavating Face Stability Supported by Pipe Roof. Applied Mechanics and Materials, 275-277, 1257-1263. doi:10.4028/www.scientific.net/AMM.275-277.1257.

19th Australasian Tunnelling Conference – Acosta-Martínez, Stewart and Hudson-Smith (Eds.)
© 2025 Australian Tunnelling Society, ISBN 978-0-85825-002-4

Effect of recycled fine waste glass powder on workability performance in sustainable backfill

Sumedha Koul, Mehdi Serati
University of Queensland, Brisbane, Queensland, Australia

Niki Jackson
Sustainable Future by Design, Central Coast, New South Wales, Australia

Ian van Wijk
FSG Geotechnics and Foundations, Brisbane, Queensland, Australia

ABSTRACT: One of the common problems in tunnel construction is ensuring efficient and low-cost backfilling of the void areas found behind the excavation contour. Paste backfill is a widely used backfill technique globally, which typically contains cementitious material, sand, and water. As per several reports, Australia consumes around 1.3 megatons of glass per annum, of which around 56% end up in landfills. Since glass has been successfully used as a sand replacement in pavement and concrete, the present study aims to substitute sand with fine waste glass powder to enhance sustainability in backfilling while reducing costs. The current study experimentally examines how the workability, yield stress, compressive strength, and tensile strength are impacted when sand is partially replaced with recycled waste glass powder. The obtained results indicate that 25% replacement improves the performance of the paste while increasing sustainability and reducing costs.

1 INTRODUCTION

Backfilling is the process of placing materials into an excavation to provide temporary or permanent support in order to help prevent ground subsidence and enhance strength and stability. It is widely used in both structural and non-structural civil and geotechnical engineering applications, including conduit bedding, mining, tunnelling, bridge abutments, and retaining walls, among others.

In the context of tunnel construction, we often encounter void areas located behind the excavation contour. These can arise from various causes, including the collapse of the overburden, large area overbreak, or due to the presence of karst caves within the geological formation (Zhang et al., 2022). If left unfilled, these voids can compromise the stability of the surrounding ground, pose safety risks, and significantly increase construction costs. Consequently, backfilling these voids is a critical and indispensable aspect of the overall tunnel engineering process. In particular, backfilling contributes to the stabilisation of soft soils near tunnel portals and facilitates the plugging of unused cross-passages or temporary connections, thereby preventing ground movement and mitigating potential hazards. Additionally, in tunnel boring machine (TBM) excavations, annular gap grouting requires the use of a self-levelling material that demands minimal compaction to ensure that the space between the excavated ground and the segmental linings is filled, which is essential for minimising settlement risks and maintaining the structural integrity of the tunnel lining (Das, 2021). Beyond TBM applications, backfilling also plays a vital role in redundant or abandoned tunnels, shafts, and utility trenches by providing long-term stabilisation and support. Moreover, it is an integral component in the design of tunnel foundation layers, where it ensures adequate support for the overlying structural courses, maintains overall stability, and facilitates efficient load transfer by being in direct contact with the rock base or with the permanent concrete lining, thereby enhancing both safety and durability of the tunnel structure (Riviera et al., 2019).

Cemented paste backfill (CPB) was proposed in the 1980s and is one of the most popularly used methods these days. Typically, the mix design consists of 70-80% solid content (sand), 1-

10% binder content by weight, and a 25-35% water-to-cement ratio (Behera et al., 2021, Sheshpari, 2015, Sivakugan et al., 2015), costing around 25-50 AUD/m^3.

1.1 *Recycled fine waste glass powder as a sand replacement*

Numerous reports suggest that Australia consumes around 1.3 million tonnes of glass annually (He et al., 2024, Kazmi et al., 2021, Kazmi et al., 2019, Serati et al., 2022, Serati et al., 2017). While efforts have been taken to reuse glass to manufacture other glass products, it is extremely challenging as glass pieces need to be separated based on their colour to maintain the quality of the manufactured products. Moreover, several sectors resort to crushing glass to minimise freight costs, thereby making recycling glass more challenging. As a result, around 56% of the consumed glass ends up in landfills, and since glass is an inert material, it remains in landfills for about 4,000 years. Figure 1 shows the glass waste flow in Australia as per the data from the report of the Department of Environment and Energy in 2019 (DEE, 2019).

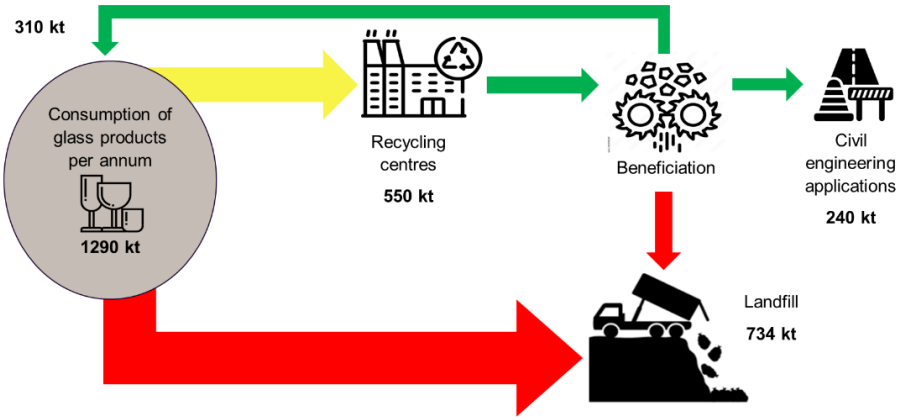


Figure 1. Glass waste flow diagram in Australia.

Recently, various studies have focused on reusing waste glass as a construction material in several civil engineering applications, such as pavement construction, drainage blankets, filter media, ultra-high-performance concrete, and mortar (Sankh et al., 2014, Tamanna et al., 2020). This study aims to partially replace sand with recycled fine waste glass powder in cement paste backfills and assess its impact on slurry and hardened-stage properties like yield stress, workability, compressive strength, and tensile strength. The potential advantages of using glass include reducing backfill costs, as sand costs around 55 AUD/tonne while fine glass costs 45 AUD/tonne. Additionally, it lessens the burden on landfills, decreases sand usage, and since glass is inert, it doesn't pollute the water table or release greenhouse gases (Disfani et al., 2011).

2 EXPERIMENTAL METHODS

The experimental program consists of slurry and hardened-stage testing of two mix designs, namely, the reference mix design and the 25% replacement mix design. The former tests include measuring the yield stress, slump, and spread, while the latter includes UCS and Brazilian tensile strength testing. The experimental set-up and methods followed are highlighted in the following section.

2.1 *Sample preparation*

The cement paste backfill (CPB) samples for the reference mix design were made by mixing general purpose portland cement conforming to AS 3972, mine tailings sourced from a mine in Australia as the solid material and tap water. For the 25% replacement mix, the same materials were used, except that 25% of the mine tails were replaced with recycled crushed waste glass sourced from a local supplier. The quantities of raw materials mixed for both the mix designs are

shown in Table 1. Trials were conducted to optimise the water content in the 25% replacement mix design. Since glass doesn't absorb any water, the water content is reduced to regulate the segregation and bleed.

Table 1. Mix design details for the present study.

Raw materials	Reference mix design	25% replacement mix design
GP cement	98 kg/m^3	98 kg/m^3
Mine tailings	1530 kg/m^3	1,147.5 kg/m^3
Waste glass	0 kg/m^3	382.5 kg/m^3
Water	390 kg/m^3	385 kg/m^3

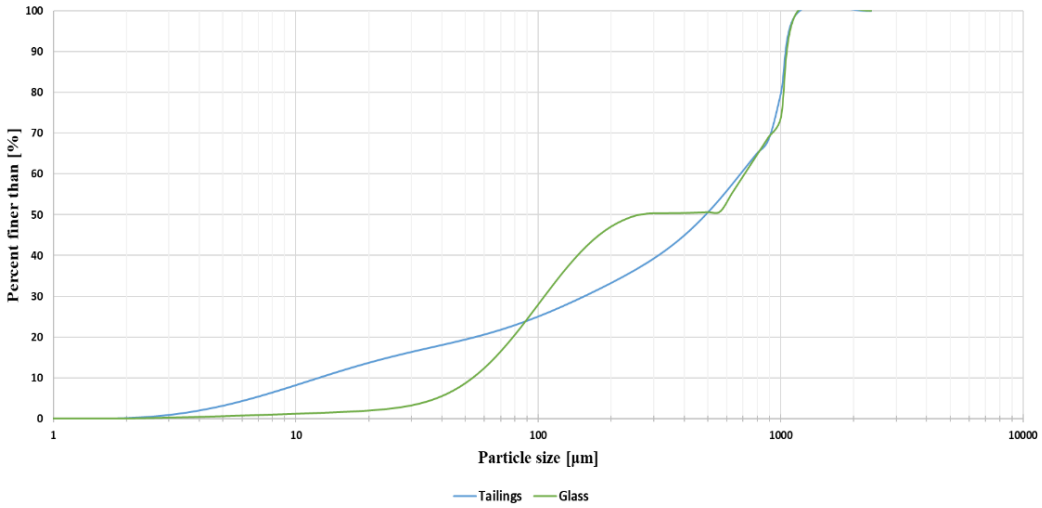


Figure 2. Particle size distribution of tails and glass used.

The mixing process involved dry mixing the solid materials for 3 minutes to break any lumps, post which cement was added and mixed for 1 minute. Lastly, water was added, and the mixture was mixed for 3 minutes (Sheshpari, 2015). The particle size distribution of the tailings and glass used is shown in Figure 2.

2.2 *Experimental set-up and methods*

Table 2 shows the list of tests conducted for both the mix designs, with their acceptable values and the test methods followed. In order to study the evolution of compressive strength with the curing duration, UCS testing was carried out on specimens with curing ages of day 1, 3, 7, and 28 on cylindrical samples with a diameter of 50 mm and a length of 100 mm. While the indirect Brazilian test was carried out for the curing age of 28 days to check the tensile strength on cylindrical samples with a diameter of 100 mm and a length of 200 mm. Since there are no standard procedures mentioned in the literature for the yield stress measurements, trials were conducted using the AntonPAAR MCR 102e rotational rheometer. The fluid was subjected to various low shear rate values for different durations to minimise the influence of instrument inertia and viscous resistance (Dzuy and Boger, 1985) and to check which speed gave the most suitable results. It was seen that subjecting the backfill slurry to a shear rate of 1s^{-1} for a duration of 150 seconds yielded the most appropriate results.

Table 2. Tests on CPB samples.

Tests	Acceptable results	Standards
Slump (Cao et al., 2021)	235 - 275 mm	AS 1012.3.5
Yield Stress (Li et al., 2020)	200 - 250 Pa	-
Compressive Strength (Feng et al., 2023)	0.4 - 4 MPa	AS 5101.4
Tensile Strength (Feng et al., 2023)	0.04 - 0.4 MPa	AS 1012.10

3 RESULTS AND DISCUSSION

3.1 *Workability*

Figure 3 (a) and (b) show the J-ring slump test results obtained for the reference mix design, measured immediately after mixing and after a one-hour retention period, respectively. Similarly, Figure 3 (c) and (d) show the results obtained for the 25% replacement mix design, measured immediately after mixing and after a one-hour retention period, respectively. It can be seen that the slump and spread results are comparable for both mixes when measured immediately. However, the reference mix design wasn't flowable after a one-hour retention period, while the 25% replacement mix design still flowed well. The values obtained for the slump, spread, J-ring passing ability difference, and flow rate are shown in Table 3. The J_r and T_{500} values are also similar for the mixes, indicating that they are flowable and resistant to segregation.

Table 3. Workability results for reference and 25% replacement mix design.

Values	Reference mix	25% replacement mix
T_{500} [s]	0.65	0.75
Jr [mm] – immediate	6	6
Slump [mm] – immediate	280	270
Spread [mm] – immediate	760	690
Jr [mm] – 1 hour	–	11
Slump [mm] – 1 hour	130	240
Spread [mm] – 1 hour	–	570

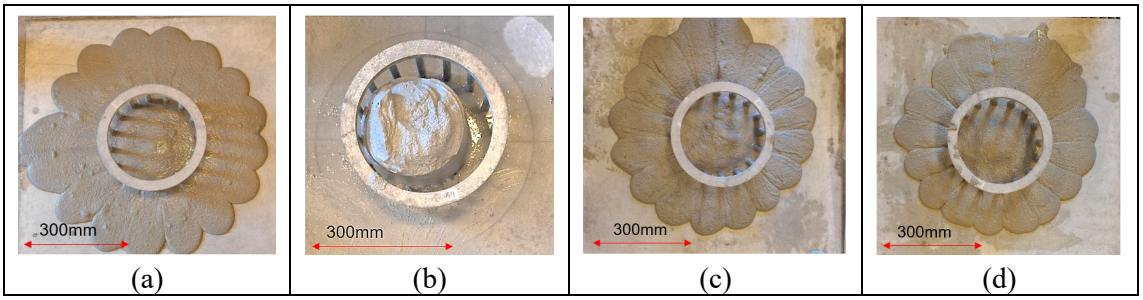


Figure 3. J-ring slump test results for reference mix (a) immediately, (b) 1 hour after mix and 25% replacement mix (c) immediately, (d) 1 hour after mix.

3.2 *Yield stress*

In order to determine the yield stress of the mixes, a vane rotor of diameter 14 mm and length 28 mm was used along with the cup holder with an inner diameter of 28.9 mm. All the tests performed on a sample were repeated at least two times to ensure repeatability and their average was taken. Figure 4 shows the yield stress of the reference and 25% replacement mix design. It can be seen that the yield stress of the reference mix design is 670 Pa, while that of the 25% replacement mix design is 175 Pa, which is significantly lower than the reference. A lower value of yield stress,

despite a higher solid percentage and a lower water-to-cement ratio, is favourable since it ensures better filling of voids and reduces the risk of pipe blockages, which are often associated with significant financial consequences as the progress of the project gets delayed and the operating costs increase. Additionally, lower yield stress facilitates easier and more efficient pumping, which can lead to a reduction in the pumping costs (Haiqiang et al., 2016).

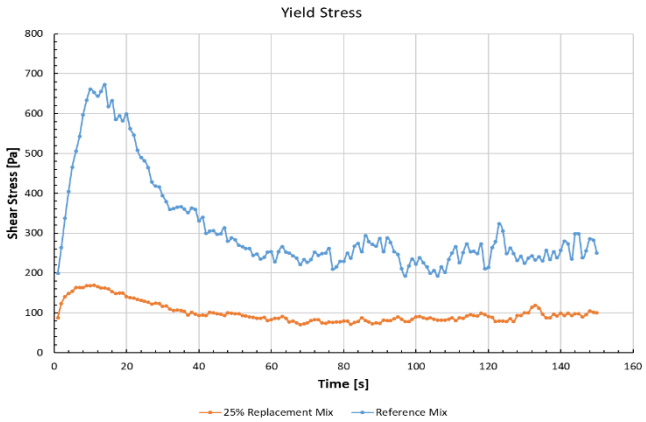


Figure 4. Yield stress results for the reference mix and the 25% replacement mix.

3.3 *Compressive strength*

Figure 5 (a) illustrates the UCS results obtained for the reference and 25% replacement mix for different curing ages of 1d, 3d, 7d, and 28d. It can be seen that the 25% replacement mix is overall stronger than the reference mix. The difference keeps getting more pronounced as the curing age increases, with the compressive strength of the 25% replacement mix samples on day 28 being around 1.5 times the strength of the reference mix sample. Figure 5 (b) and (c) present the photographs of the failure pattern observed in the 28-day samples for the reference and 25% replacement mix design, respectively.

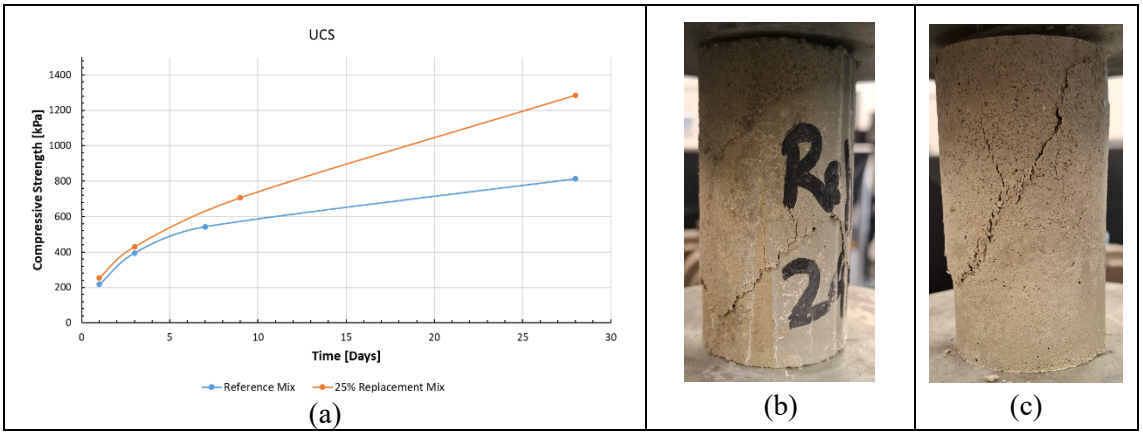


Figure 5. (a) Graph comparing UCS results for the reference mix and the 25% replacement mix (b) photograph of 28-day sample for the reference mix (c) photograph of 28-day sample for the 25% replacement mix.

3.4 *Tensile strength*

In addition to the assessment of the compressive strength, it is also essential to evaluate the tensile strength of CPB. As per several studies, typically, the tensile strength of a CPB sample is around 10% of its compressive strength (Behera et al., 2023). Using the indirect Brazilian test, the tensile strength of the reference mix was 175 kPa, while that of the 25% replacement mix was 235 kPa. Similar to the UCS, the replacement mix was significantly stronger in tension as well. Figure 6 (a) and (b) show the Brazilian test samples for the reference and replacement mix, respectively.

As expected, the failure plane is located along the vertical plane passing through the disk's centre, perpendicular to the applied load for both the samples.



(a) (b)

Figure 6. Brazilian test samples for (a) reference and (b) 25% replacement mix.

4 CONCLUSIONS

One of the most commonly encountered problems in tunnel construction is ensuring efficient and low-cost backfilling of the void areas found behind the excavation contour, which can be caused by the collapse of the overburden, large area overbreak, or by encountering karst caves. Paste backfilling is a widely used technique to overcome this problem, which typically consists of sand, cementitious material, and water. The present study studies how the partial replacement of sand with recycled crushed waste powdered glass impacts the strength parameters – UCS and tensile strength, and fluid behaviour parameters – workability and yield stress. To do so, two mix designs were prepared, namely, the reference mix design and the 25% replacement mix design and tested for the following properties.

The workability results were similar for both the mixes when tested immediately after mixing, however, the 25% replacement mix was flowable after one hour retention, while the reference mix design was not flowable. There was a significant reduction in the yield stress for the replacement mix design, which is favourable since it ensures better filling of voids and reduces the risk of pipe blockages, while facilitating easier and more efficient pumping, which can lead to a reduction in the pumping costs. The 25% replacement mix design exhibited higher compressive and tensile strengths compared to the reference mix, making it more favourable in terms of hardened stage properties as well. Hence, these results indicate that the partial replacement of sand with glass not only enhances the sustainability and cost-effectiveness of backfilling but also improves its fresh and hardened properties.

5 REFERENCES

BEHERA, S., MISHRA, D., SINGH, P., MISHRA, K., MANDAL, S. K., GHOSH, C., KUMAR, R. & MANDAL, P. K. 2021. Utilization of mill tailings, fly ash and slag as mine paste backfill material: Review and future perspective. *Construction and Building Materials,* 309**,** 125120.

BEHERA, S. K., MISHRA, D. P., SINGH, P., GODUGU, A., MISHRA, K., MANDAL, P. K., MANDAL, S. K. & MISHRA, A. K. 2023. Tensile strength of cemented paste backfill for lead–zinc mill tailings: lab and in situ scenarios. *Arabian Journal of Geosciences,* 16**,** 451.

CAO, S., XUE, G., YILMAZ, E. & YIN, Z. 2021. Assessment of rheological and sedimentation characteristics of fresh cemented tailings backfill slurry. *International Journal of Mining, Reclamation and Environment,* 35**,** 319-335.

DAS, S. 2021. *Performance enhancement of controlled low-strength grout material (CLSM) For annulus voids of sliplined culverts.* The University of Akron.

DEE 2019. Assessment of Australian recycling infrastructure-Glass packaging update. *In:* ENERGY, D. O. E. A. (ed.).

DISFANI, M., ARULRAJAH, A., ALI, M. & BO, M. 2011. Fine recycled glass: a sustainable alternative to natural aggregates. *International Journal of Geotechnical Engineering,* 5**,** 255-266.

DZUY, N. Q. & BOGER, D. V. 1985. Direct yield stress measurement with the vane method. *Journal of rheology,* 29**,** 335-347.
FENG, Y., QI, W., ZHAO, Q., HUANG, Y., REN, Q., QI, W. & KONG, F. 2023. Synthesis and characterization of cemented paste backfill: Reuse of multiple solid wastes. *Journal of Cleaner Production,* 383**,** 135376.
HAIQIANG, J., FALL, M. & CUI, L. 2016. Yield stress of cemented paste backfill in sub-zero environments: experimental results. *Minerals Engineering,* 92**,** 141-150.
HE, J., SERATI, M., VEIDT, M. & ALWIS, A. 2024. Determining rock crack stress thresholds using ultrasonic through-transmission measurements. *International Journal of Coal Science & Technology,* 11.
KAZMI, D., SERATI, M., WILLIAMS, D. J., QASIM, S. & CHENG, Y. P. 2021. The potential use of crushed waste glass as a sustainable alternative to natural and manufactured sand in geotechnical applications. *Journal of Cleaner Production,* 284**,** 124762.
KAZMI, D., WILLIAMS, D. & SERATI, M. 2019. Waste glass in civil engineering applications—A review. *International Journal of Applied Ceramic Technology,* 17.
LI, W., GUO, L., LIU, G., PAN, A. & ZHANG, T. 2020. Analytical and experimental investigation of the relationship between spread and yield stress in the mini-cone test for cemented tailings backfill. *Construction and Building Materials,* 260**,** 119770.
RIVIERA, P. P., BERTAGNOLI, G., CHOORACKAL, E. & SANTAGATA, E. 2019. Controlled low-strength materials for pavement foundations in road tunnels: feasibility study and recommendations. *Materials and Structures,* 52**,** 72.
SANKH, A. C., BIRADAR, P. M., NAGHATHAN, S. & ISHWARGOL, M. B. Recent trends in replacement of natural sand with different alternatives. Proceedings of the international conference on advances in engineering and technology, 2014. 59-66.
SERATI, M., JAKSON, N., ASCHE, H., BASIREDDY, S. & MALGOTRA, G. 2022. Sustainable shotcrete production with waste glass aggregates. *SN Applied Sciences,* 4**,** 82.
SERATI, M., MASOUMI, H., WILLIAMS, D. & ALEHOSSEIN, H. 2017. *Modified Brazilian Test for Indirect Measurement of Tensile Strength of Brittle Materials*.
SHESHPARI, M. 2015. A review of underground mine backfilling methods with emphasis on cemented paste backfill. *Electronic Journal of Geotechnical Engineering,* 20**,** 5183-5208.
SIVAKUGAN, N., VEENSTRA, R. & NAGULESWARAN, N. 2015. Underground Mine Backfilling in Australia Using Paste Fills and Hydraulic Fills. *International Journal of Geosynthetics and Ground Engineering,* 1**,** 18.
TAMANNA, N., TULADHAR, R. & SIVAKUGAN, N. 2020. Performance of recycled waste glass sand as partial replacement of sand in concrete. *Construction and Building Materials,* 239**,** 117804.
ZHANG, C., YANG, J., XIE, Y., FU, J., WANG, S. & YIN, J. 2022. Utilization of tunnel spoils as a lightweight filling material for the voids behind tunnel excavation contour. *Journal of Cleaner Production,* 372**,** 133559.

THIS PAGE INTENTIONALLY LEFT BLANK

19th Australasian Tunnelling Conference – Acosta-Martínez, Stewart and Hudson-Smith (Eds.)
© 2025 Australian Tunnelling Society, ISBN 978-0-85825-002-4

The mined tunnels of the Sydney Metro West – Western Tunnelling Package: Narrow pillars and heritage sewers

J. Nethercott
Gamuda Australia, Sydney, NSW, Australia
A. Mirzayee
GHD Australia, Sydney, NSW, Australia

ABSTRACT: The scope for the Gamuda Laing O'Rourke Consortium (GLC) on the Sydney Metro West – Western Tunnelling Package (WTP) consisted of more than twin TBM tunnels. GLC delivered a significant amount of mined tunnel scope with multiple challenges. The mined tunnel scope was split between Clyde and Westmead. The scope at Clyde included twin 750m long spur tunnels from the surface of the Clyde stabling facility, joining twin junction caverns intersecting the TBM tunnels. This paper explores some of the associated technical challenges, the solutions developed and the results of those efforts through delivery. Some of the notable challenges included: excavating below the heritage-listed Lidcombe Auburn Granville (LAG) sewer tunnel including temporary support, instrumentation and monitoring in live sewer conditions; creating a less than 1 m thick shale pillar between tunnels; intersection of adverse geological features, including dykes; and reduced rock cover at the tunnel portal.

1 INTRODUCTION

The Sydney Metro West project involves a 24 km metro rail line between Westmead and the Sydney CBD.

The Clyde caverns were accessed from the Clyde Dive site, located beside James Ruse Drive and Rosehill Gardens Racecourse as part of the WTP project. This site links the Maintenance and Service Facility (MSF) to the mainline running tunnels via a cut and cover dive structure and two spur tunnels. The horseshoe-shaped spur tunnels are 7 m wide and 8 m high, converging upon each other to a minimum distance of 900mm at the tunnel portal. They are vertically offset by 1.5m to maximise cover to tunnel under the LAG sewer.

This paper discusses the engineering challenges of excavating the tunnels in close proximity to each other as well as below the active LAG sewer. Figure 1 shows the arrangement of Spur tunnels and location of Heritage Sewer and narrow pillar zone.

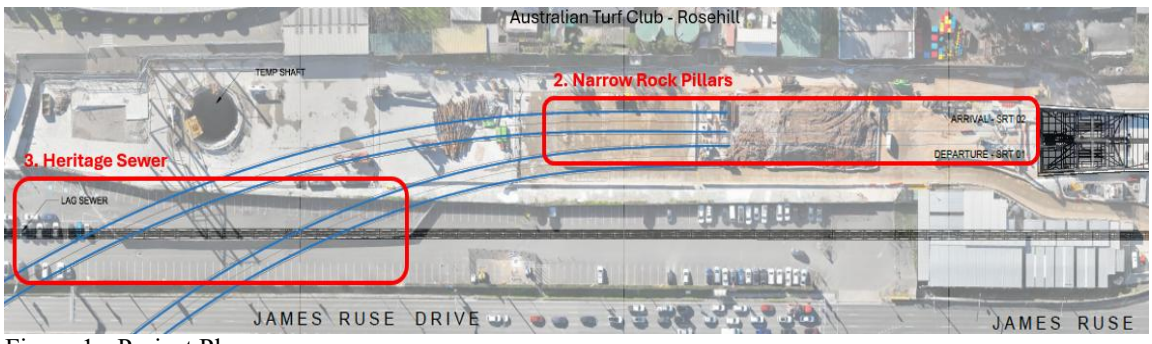


Figure 1 - Project Plan

2 NARROW ROCK PILLARS

As the spur tunnels connected to the dive structure, GLC and Sydney Metro (SM) revised the design by extending the tunnels 40 metres and shortening the dive structure. A cost-benefit analysis showed this approach was more economical, sustainable, and quicker to construct. However, it introduced new challenges. The converging tunnel alignments became more complex, and ground conditions near the portals worsened. While majority of the tunnel alignment was excavated through stable Class 2 Sandstone (SS-II) with over 20 m cover, the new alignment reduced cover to 5 m, transitioning into weaker alluvium and weathered shale posing increased risks for stability and requiring more robust support and excavation techniques. Figure 2 demonstrates the ground conditions at the narrow pillar zone including the dyke encountered during excavation of the Spur tunnels.

The initial risk mitigation strategy for the converging pillar comprising of alluvium and weathered shale between the two spur tunnels involved the excavation of a pilot drift, which was subsequently backfilled with mass concrete, to provide temporary structural integrity and control unravelling of any weathered material as shown in the light green colour in Figure 3. However, this method proved to be neither environmentally sustainable nor efficient in terms of construction time. It required the removal of a significant volume of rock, only to replace it with concrete that would eventually be re-mined once the two spur tunnels were fully excavated.

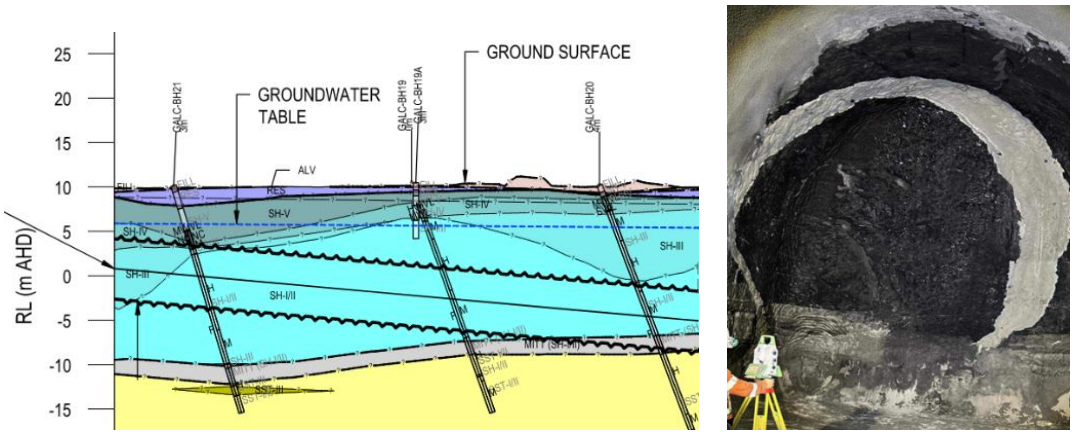


Figure 2 – Left: Geological long section of tunnel at the narrow rock pillar, Right: Geological feature (Dyke)

As excavation of the dive portal progressed and greater confidence was gained in the geotechnical data and rock mass quality, GLC revisited the design with the aim of optimizing the approach. Rather than removing and replacing the reducing pillar, efforts shifted toward retaining and reinforcing the in-situ rock. The Spur tunnels were subsequently divided into five distinct support categories, ST7A, ST7B, ST7C, ST7D, and a specialized portal support system tailored to varying ground conditions. Figure 4 shows the distribution of the varying support systems utilised to reinforce the rock pillar.

To assess the feasibility of preserving the rock pillar, stability analyses were conducted along the 160 m tunnel extent using both empirical methods and numerical modelling. Preliminary findings indicated that in zones where the rock mass was classified as Class 3 Shale (SH-III) or poorer, the in-situ material lacked the necessary strength to ensure stability. In these critical sections particularly where Class 3 Shale (SH-III) was anticipated the initial strategy of removal and replacement with reinforced concrete remained necessary to maintain structural integrity.

The conventional pillar stability checks showed that the Class 2 Shale (SH-II) rockmass had adequate capacity to withstand the ground loads as a rock pillar. These approaches considered the rockmass as a continuous material and the mode of failure is the intact rock yielding assuming that the discontinuities are supported with additional measures such as temporary stitching bolts. Conventional stitching methods were used where the rock pillar was greater than 2.5 m in width. This type of stitching bolt could be installed post excavation of both tunnels after the excavation face had passed.

Where the remaining rock pillar between the tunnels was less than 2.5 m, the assumption that the remaining rock is self-supported and stable may not be feasible. Additionally, the consequences of a local rock wedge failure may end up in losing a major portion of resisting rock material which will significantly increase the risk of pillar collapse. Considering these elements, an innovative inclined temporary stitching bolt (sidewall forepoling) has been designed for the narrow pillar zone within the Spur tunnels. The inclined stitching bolt was installed after excavation and support of the first tunnel, SPT-ST7B, Figure 4. All stitching bolts were temporary until the secondary lining was installed.

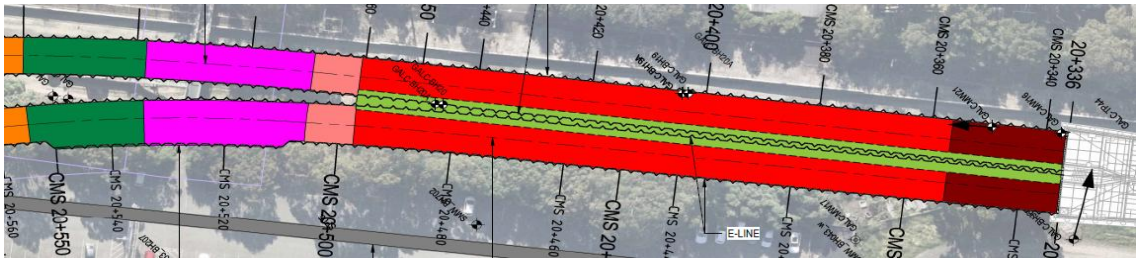


Figure 3 – Initial design

The intention of the inclined stitching bolt was to ensure installation before the excavation of the second tunnel i.e. before the rock pillar is formed. In this approach the newly formed rock pillar in each excavation advance of the second tunnel, is pre-supported by GRP bolts which is bonded into rock mass at the face of the excavation. The following parameters were considered in geometrical design of inclined stitching bolts:

- Excavation advances in second tunnel: An excavation advance of 1.4 m was adopted for the second tunnel. Inclined stitching bolts were designed in order to ensure sufficient bond length was present within every 1.4 m of excavation advance.
- For a bolt length of 6 m, three different inclinations were designed to optimise the utilisation of the inclined stitching bolts.
- Arrangement of discontinuities: Typical Class 2 Shale (SH-II) discontinuities including systematic beddings and subvertical defects were considered in the design. The presence of fault zones was not allowed within the pillar zone.

The inclined stitching bolts were designed for the narrow pillar zone considering that the first tunnel will be completely excavated and supported and the encountered ground condition at the rock pillar zone can be verified before excavation of the second tunnel.

The revised design, which allowed for the retention and reinforcement of a significant portion of the rock pillar, marked a major success in optimizing both construction methodology and structural stability. Due to design constraints requiring a 20 m longitudinal offset between the excavation faces of the adjacent tunnels, only a single roadheader was needed for this section of the works.

Excavation began with the departure spur tunnel in accordance with the design requirement to prioritize the excavation of the lower tunnel first. This sequence was essential for enabling the effective stitching of the pillar between the two tunnels. The use of a temporary active support system, consisting of CT bolts and shotcrete, allowed the initial drive to progress quickly through to breakthrough. Following breakthrough, the installation of the passive support (pillar stitching bolts with additional mesh and shotcrete), were carried out off the critical path ahead of the adjacent tunnel drive.

The success of this staged approach relied on ensuring that the passive support in the Departure tunnel reached its full design strength at least 20 m in advance of the advancing face of the Arrival tunnel. This was crucial to maintaining the stability of the shared pillar during the sequential excavation process. Due to the deterioration of the rock class to Class 3/4 Shale (SHIII/IV) within the final 20 m of the pillar zone, removal and replacement became necessary. A combination of pillar replacement and canopy tubes at tunnel crown were adopted at the tunnel portal zone. Steel set arches embedded in shotcrete were constructed under the canopy tubes at tunnel portal before the tunnel breakthrough, SPT-ST7C/D.

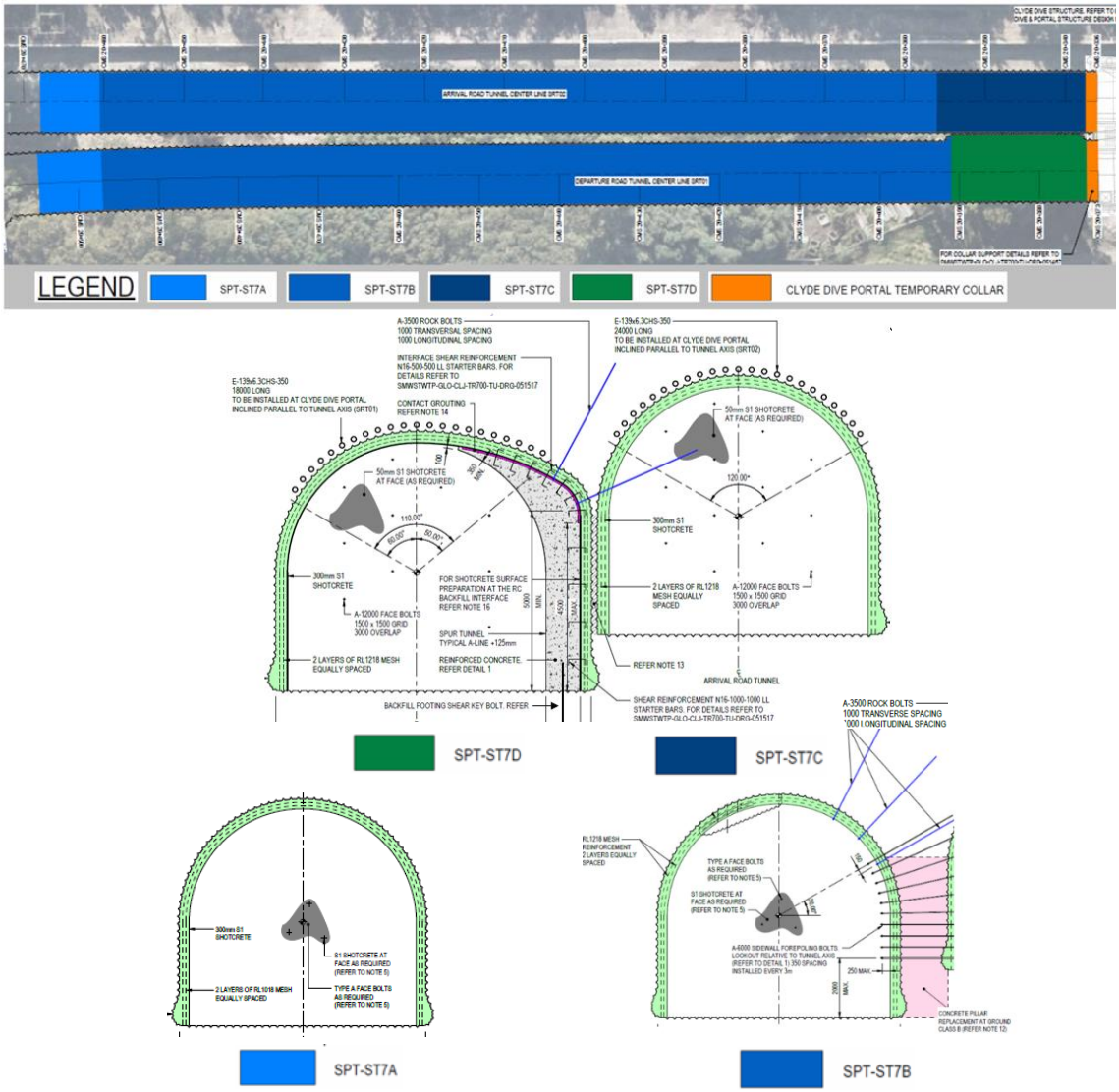


Figure 4 – (Top) Revised support categories to reinforce pillar, (Middle) ST7C/D Primary Support, (Bottom) ST7A and ST7B Primary Support.

The tunnel excavation and ground support operations effectively validated the initial design assumptions and analytical predictions. Predominantly, the geological conditions encountered during the first tunnel drive comprised Class 2 Shale (SH-II), with the rock pillar zone exhibiting overall structural integrity. A single, discrete geological anomaly (identified as a dyke with a thickness of less than 1 m) was observed within the rock pillar zone, Figure 2. Excavation proceeded through this zone, and a supplementary design verification was undertaken to assess the structural adequacy of the inclined stitching bolts in accommodating this feature. Targeted core sampling of the dyke material was conducted, resulting a minimum of 8MPa uniaxial compressive strength, confirming compatibility with the support design parameters. The material within the dyke zone was identified as medium to high-strength rock. After completion of the first tunnel and prior to the advance of the second, it was concluded that the inclined stitching bolts were adequate to maintain the rock pillar through the dyke zone.

The design outputs show that the excavation of the second tunnel would have some impacts on the primary support of the first tunnel, the additional loads due to further ground relaxation was considered in the design capacity of the lining of the first tunnel. The numerical modelling results showed a potential movement of up to 5 mm in the first tunnel due to excavation of the second tunnel depending on the in-situ stress in rock mass.

The primary support of the first tunnel was monitored at every 10m length of the tunnel during the excavation of the second tunnel, Figure 5. This additional monitoring aimed to address the residual risks due to unknown ground conditions, so that if any trend of movement is observed in the first tunnel ahead or at the location of the newly formed rock pillar, the excavation advance of the first tunnel will be adjusted.

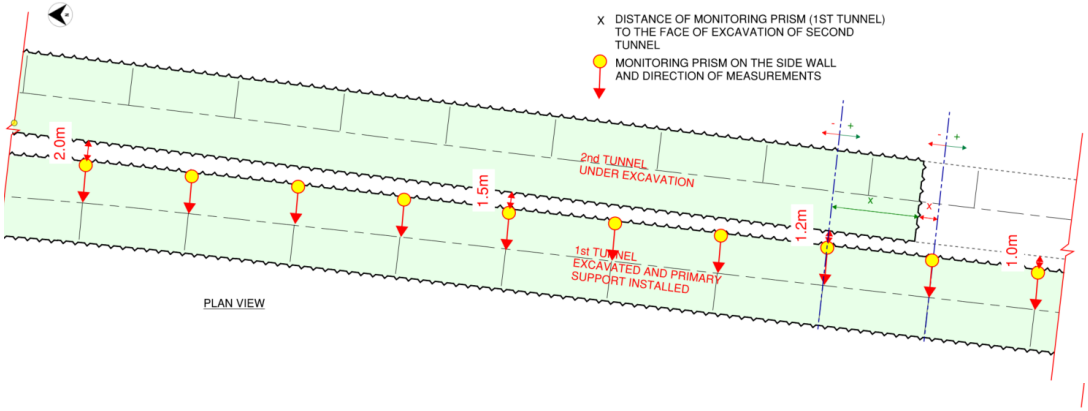


Figure 5 – Location of additional monitoring targets on the 1st tunnel sidewall

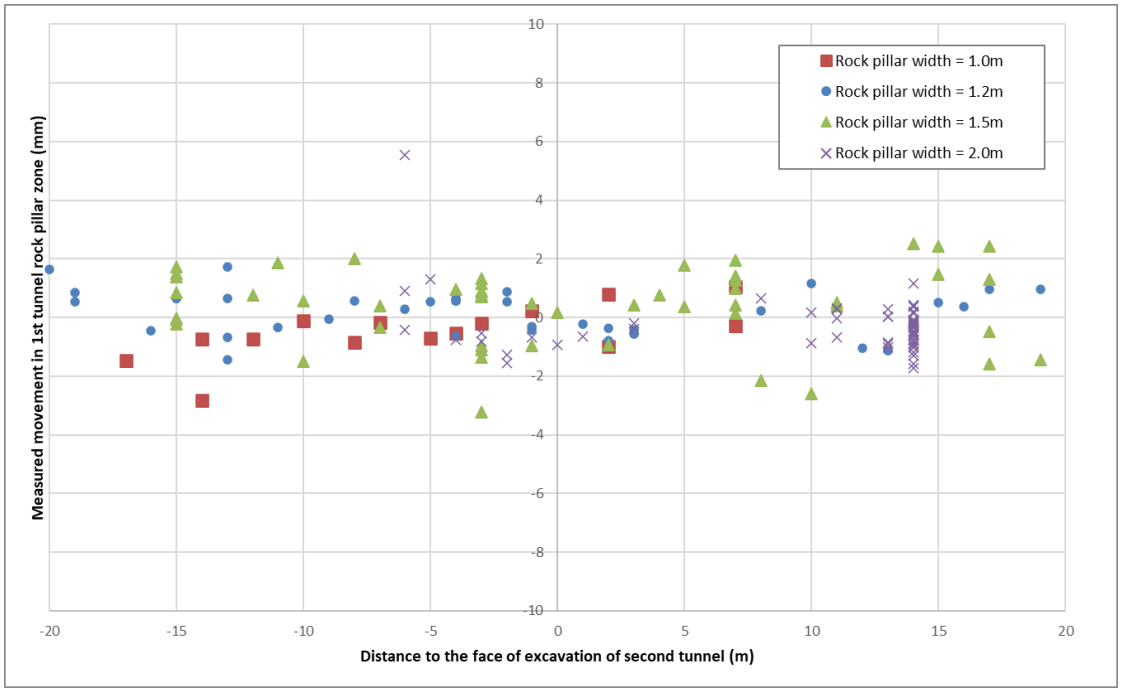


Figure 6 – Measured ground movement at rock pillar zone (different colours show different pillar width)

The measured ground movement in the first tunnel, resulting from the excavation of 2nd tunnel, was less than 3 mm in average without showing any specific trend of movement, Figure 6. As no significant overbreak was observed on the rock pillar side during the second tunnel's excavation, it was concluded that the installed stitching bolts effectively supported the rock blocks, preserving the structural integrity of the rock pillar. The monitoring data aligned more closely with the lower bound of rock mass in-situ stresses investigated in numerical modelling. This outcome was considered reasonable, given that the rock pillar was in a shallow section of the tunnel, with an overburden depth ranging from 15 m to 5 m.

3 HERITAGE SEWER

The original spur tunnel design at Clyde Dive was limited by surface service banks, restricting the ability to commence diving the rail alignment early enough for sufficient cover beneath the LAG sewer including a 4.5% maximum rail gradient. An early concept involved rerouting the LAG sewer using four shafts and micro-TBMs, but this posed tunnelling and long-term service-ability challenges due to the sewer already being at minimum grade.

SM and GLC re-evaluated the alignment, reducing proximity to the service banks and max-imising cover to the sewer. Factors such as land resumption, mainline gradients, junction location, and spur tunnel length was also considered. A final alignment was achieved with 1.3 m to 2.4 m of rock cover between the sewer and primary support, Figure 7. Both tunnels crossed below the sewer line acutely therefore the length of tunnel impacting the sewer was 51m in both drives.

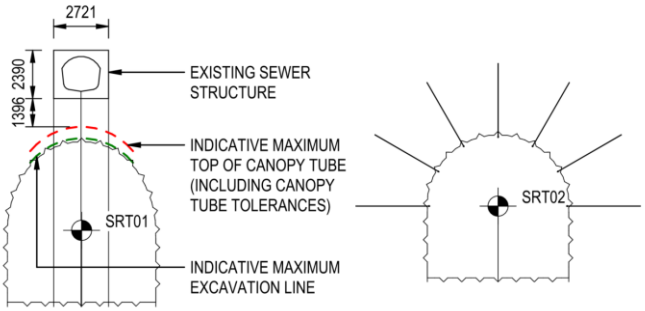


Figure 7 – Sewer minimum clearance to Spur tunnels.

The LAG Submain was constructed around 1925 with internal dimensions of 1727mm high × 1752 mm wide with a grade of 1 in 2280. Works As Executed (WAE) drawings show a timber frame (Oregon) as shoring of the tunnel excavation, Figure 8. Oregon timber is a softwood and is unlikely to have lasted for the nominally 100-year exposure period in the sewer tunnel which was evident during coring of the sewer walls. The most likely excavation technique in this ground type back in 1925 would have been drill and blast techniques fracturing the rock between the invert of sewer and tunnel crown. The excavation was then lined with an unreinforced concrete lining.

In June 2021, SASTTI completed a dilapidation survey of the sewer which indicated that the sewer is in reasonably good condition for its age with only minor seepage shown at isolated con-struction joints with no significant structural defects worth noting.

As the tunnel alignment through the LAG sewer zone of influence was situated in Class 2 Sandstone (SS-II), the typical approach would be to design an active support utilising bolts and shotcrete. With the reduced cover and uncertainty on rock completeness, GLC and the Design Joint Venture (DJV) consisting of GHD and SMEC designed a passive support of canopy tubes and shotcrete with small excavation advances. The primary focus being the implementation of support as quick as possible post excavation to reduce convergence and settlement. The final design consisted of 140 mm diameter canopy tubes at 9 m length with 3 m overlap and 250 mm shotcrete.

The DJV assessment and modelling indicated that the predicted displacements of the LAG Submain remained less than 5 mm with the proposed sequential excavation techniques as men-tioned above. The assessed maximum increases in tensile strain of the LAG Submain among all of the Sensitivity Analysis cases ranged from 38μm to 90μm with the base Case predicted value of 65μm.

It was calculated that during the construction of the unreinforced concrete lining with progres-sive construction joints, the initial shrinkage in the concrete would equate to 44μm based on 10MPa concrete. Structural assessment of a further 65μm increase in the tensile strain would equate to cracks of 0.08 mm which can be considered as self-healing and is well less than the 150-190μm range of 10MPa concrete. Further investigations works would later prove that the concrete unconfined compressive strength (UCS) was much greater than the assumed 10MPa, increasing the actual tensile strain limit of the LAG concrete to greater than the calculated 190μm limit.

As part of the initial investigation works to confirm initial design assumptions, manned access to the sewer under controlled conditions were undertaken to measure wall thickness, check compressive strength of concrete and endoscope the annulus between rock and sewer. The compressive strength results of the concrete were tested with results ranging from 21-25MPa with a consistent wall thickness resembling the work as executed drawings. Endoscopes showed running groundwater in an annulus packed with rock spalls creating further engineering concerns.

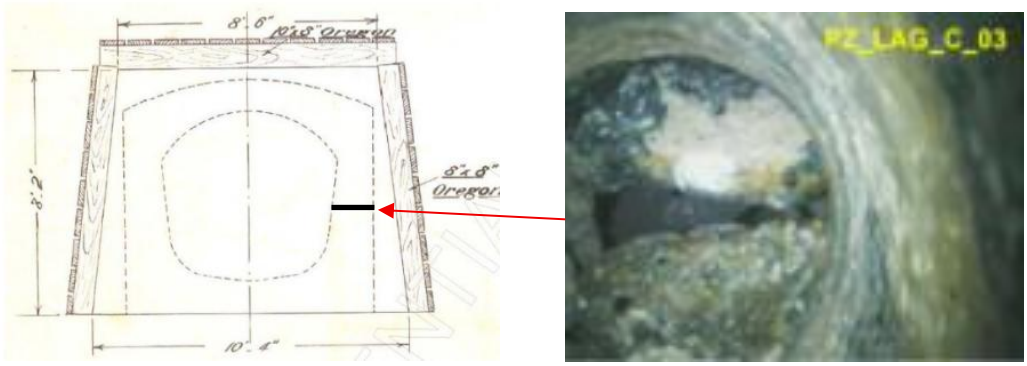


Figure 8 – Left: Work as executed (LAG Sewer 1920); Right: Endoscopes through sewer wall

The side wall endoscopes showed that gravel / rock spalls to the sides of LAG appears to be well packed providing confinement to a bottom construction joint between invert and wall against failure, Figure 8. The crown endoscope probe additionally showed gravel / rock spalls above the crown of the LAG. However, it was unable to be seen from the imaging whether the rock spalls were continuous for the full annulus. This would be consistent with any settlement that may have occurred over the past 100 years.

Due to the inability to conclusively confirm full confinement at the top of the structure, combined with localised groundwater drawdown resulting from the spur tunnel excavation below, it became evident that the sewer system could be subject to internal pressurisation. This pressurisation may exceed the available external confinement, particularly during significant rainfall events. In this event a weak point may exist between the construction joint of the walls and crown of the sewer. This joint may be exposed to a failure mechanism where the crown could lift with the walls collapsing into the sewer void with the sewer crown collapsing into the invert of the sewer main post rain event.

To mitigate this failure mechanism, steel strapping was designed and installed to tie the crown of the sewer to the walls prior to groundwater drawdown to overcome a pressure differential of 53kPa. The straps were installed at 1.2m centres and anchored with stainless steel chemical anchors, Figure 9.

Although the design solution was technically functional, it did not meet Sydney Water's standards in three specific criteria. Following the Specialist Engineering assessment (SEA) conducted by the DJV, a Deviation from Specification was prepared for these three items and submitted to Sydney Water for approval. The deviations were as follows:

- Approval to encroach within nominated Exclusion zone of SW asset of a new structure.
- Approval to increase limit of maximum tensile strain from 20 to 150µm and reduce the minimum incremental radius of curvature from 60km to 8km.
- Approval to adopt revised vibration limits set out in BS 7385 Part 2-1993 "Evaluation and measurement for vibration in buildings Part 2", due to current SW standard nominating a limit of 3mm/s for buried unreinforced structures in a typical soil trench.

All proposed changes were endorsed during workshops with Sydney Water and documented in the SEA report. The first two deviations were theoretical and required no further monitoring once approved. The third required vibration monitoring within the sewer to confirm compliance with revised limits. Recorded vibration stayed well below these limits. Additional sewer lining monitoring included piezometers, as well as flow and vibration sensors Figure 9.

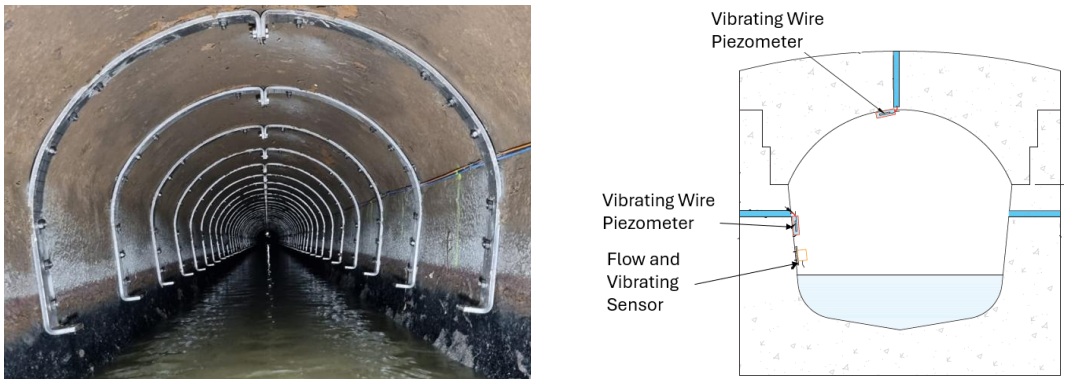


Figure 9 – Left: Sewer Strapping, Right: Sewer Lining I&M arrangement

4 CONCLUSION

At Clyde, extending the spur tunnels and shortening the dive structure improved cost, schedule, and sustainability. However, it created challenges near the portals, where ground cover was low and geology weakened to weathered shale and alluvium. A key issue was the stability of the rock pillar between tunnels. Inclined stitching bolts were used to pre-support the pillar before excavating the second tunnel, reducing risk. Monitoring confirmed the support system's effectiveness, with minimal movement observed during adjacent tunnel excavation.

In addition to the converging pillar design the spur tunnels had further design and construction challenges where the alignments crossed under the 100-year-old LAG sewer with limited rock cover and unknown structural reliability. Rerouting the sewer was not beneficial due to its shallow gradient and proximity to other infrastructure. Instead, the tunnel alignment was optimised to maintain a safe rock cover of 1.3 m to 2.4 m below the sewer. Due to uncertain rock conditions, a passive support system was adopted using canopy tubes, shotcrete, and small excavation steps to minimise ground movement. Detailed modelling showed sewer movement would stay below 5mm, expected strain levels were well within the concrete's safe limits and vibration was negligible.

19th Australasian Tunnelling Conference – Acosta-Martínez, Stewart and Hudson-Smith (Eds.)
© 2025 Australian Tunnelling Society, ISBN 978-0-85825-002-4

Primary support installation for the Albert Street Station cavern and main station entry shaft intersection, Cross River Rail, Brisbane

R.Elliott, D.Keating
SYSTRA ANZ, Brisbane, Australia

B.Shen
PSM, Brisbane, Australia

ABSTRACT: As part of the Cross River Rail (CRR) project in Brisbane, the Albert St Station mined cavern was one of the most technically complex underground structures. Constructed beneath the city's central business district (CBD), the cavern featured a critical junction that connected two pedestrian adits and a services adit directly to the main station entry shaft. Excavation and support activities were constrained by limited site access, proximity to adjacent basements, and the requirement to maintain ground stability in challenging geotechnical conditions. This paper outlines the primary ground support design, construction staging and highlights key lessons learnt.

1 INTRODUCTION

Albert St Station was constructed as part of the Cross River Rail (CRR) project, and the station cavern was one of the most technically challenging structures of the underground works. Located beneath Brisbane's CBD, Albert Street Station comprises of a 290m-long cavern with two entrances along its alignment, referred to as the main station entry shaft and northern entry shaft. The cavern is connected to the main station entry shaft by two pedestrian adits (AA5 and AA7) and one services adit (AA4) with as little as 5m of separation between the cavern and the shaft (Figure 1).

The complexity of this 45m long junction lies in its location within low-cover, faulted rock mass conditions and the need for concurrent excavation adjacent to a 45m wide by 50m deep shaft. The interaction of multiple excavation fronts, proximity to high-rise buildings, stringent monitoring requirements, and the presence of a temporary access adit (ATA1) necessitated a highly tailored ground support solution.

This paper outlines the geological context and structural design behind the primary support system, as well as the deviation from the IFC (Issued for Construction) assumptions that occurred during construction. By comparing the original design intent with the actual methodologies adopted on site, and analysing the technical and logistical challenges encountered, this paper aims to share practical insights into managing construction of junctions.

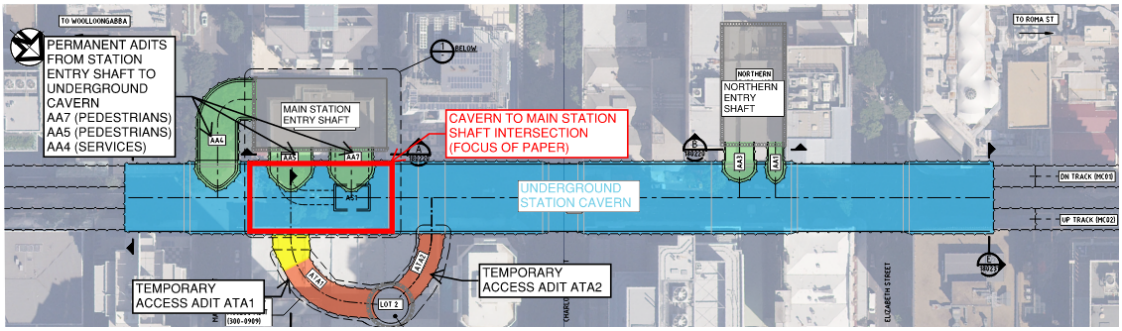


Figure 1. Albert St Station general arrangement

2 DESIGN

2.1 *Geological setting*

The ground at Albert St Station is underlain by rock mass of the Neranleigh-Fernvale Group (NFG) with rock mass units as described in Cammack et al. (2022). The Albert St Station cavern was excavated predominantly within NFG1/2 (typical UCS of 50 MPa) with low rock cover. At the cavern junction, the top heading encountered NFG2, and the geotechnical investigations indicated approximately 2m of NFG2 above the crown, overlain by a south-to-north dipping NFG3 unit between 1 to 3m thick, 1m of NFG4/5, followed by around 10m of alluvium and fill. Borehole data suggested the presence of a significant low angle fault at the location of the junction between the cavern and the main station entry shaft.

2.2 *Primary support design*

The cavern was excavated in a triple heading sequence with the primary support implemented in two stages:
Stage 1 – Initial support comprising of 5.4m long inflatable friction bolts or cement grouted CT bolts and 100mm thick synthetic fiber reinforced shotcrete (SFRS)
Stage 2 –Intersection support comprising an 800mm thick bar and mesh reinforced shotcrete passive shell lining supported on 1800mm wide elephant's footings.

A heavy primary support was required due to the concurrent excavation of the adjacent main station entry shaft. An additional design consideration was the interaction with a temporary adit (ATA1), which connects to the cavern at invert level on the eastern side of the cavern. A key constraint was that the ATA1 concrete collar had to achieve a compressive strength of 20MPa before excavation of the heading directly above the access adit could proceed. Figure 2 below shows typical cavern primary lining design cross sections.

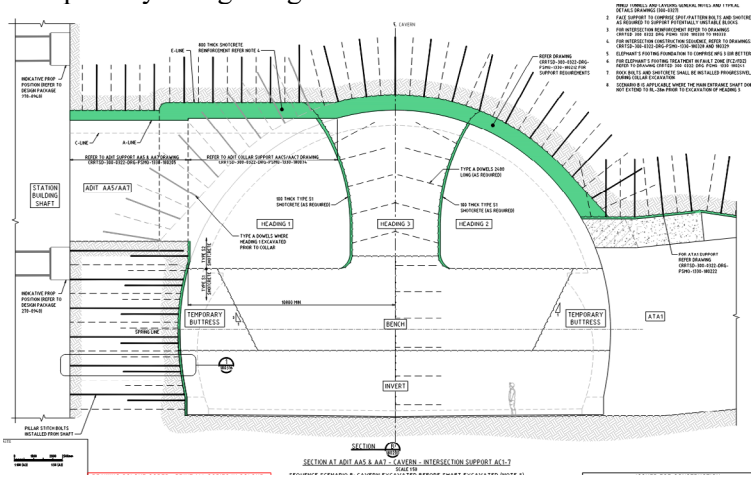


Figure 2. Primary support for cavern junction

2.3 *Other design considerations*

The rock pillar between adits AA5 and AA7 was designed to be excavated out and replaced with mass infill concrete as the rock mass at the pillar was not suitable to be left in place. The rock pillar was excavated as a split heading using rock bolts and 100 mm thick SFRS as temporary support. The design stipulated that the pillar replacement had to be constructed prior to allowing the cavern to be excavated to the full span in the junction area.

Due to the potential presence of a fault dipping through the rock mass between the cavern and station box, stitch bolts were mandated in the design to reinforce this rock pillar. The stitch bolts comprised cement grouted Dywidag WR36 bars stressed to 500kN, installed at 1200mm to 1800mm spacing from the cavern side and shaft side, with recessed anchor plates and a dome nut.

3 CONSTRUCTION

3.1 *Key safety and quality considerations during construction*

Safety measures on site included controlling unsupported ground with signage and barriers to inform personnel of hazardous areas. A typical signage and barrier set up is shown below in Figure 3. Ventilation and dust control were managed using three dust scrubbers in the Albert St cavern, with one servicing the south and two servicing the north. To ensure safe people-plant interaction, dedicated personnel walkways were delineated from tunnel plant using crowd control barriers, and no personnel were allowed in front of the rear jacks of the bolting rig. The delivery team maintained safety through weekly safety task observations and inspections. Quality control measures included rock bolt pull testing and shotcrete testing using cylinders and sprayed panels. A challenge faced was ensuring that the panels remained in an area free of potential damage for at least 24 hours.



Figure 3. Typical signage and barrier set up in cavern

3.2 *Key equipment*

Main equipment utilised to construct the junction primary support was a road header for excavation, Robodrill for installation of rock bolts and a MEYCO Potenza for shotcreting.

3.3 *Design assumed construction methodology*

The assumed construction sequence for the junction triple top heading involved: excavating and supporting top heading 1 (TH1) to full length, followed by the excavation and support of top heading 2 (TH2) to full length. Stage 2 primary support would then be installed in both TH1 and TH2. Once this was completed, the central pillar would be excavated with Stage 1 support installed, followed by the completion of the Stage 2 primary support.

3.4 *Actual construction methodology*

The actual adopted construction method varied considerably from the approach assumed in design as a split heading sequence was approved prior to commencing the junction excavation. The adopted methodology is summarised in Figure 4. The yellow hatch in Figure 4 represents excavation in that stage, grey represents top heading rock to be excavated.

In summary, 8190 bank cubic meters (BCM) of rock was excavated, approximately 900 bolts were installed and 1600m^3 of shotcrete sprayed to provide the primary support for the junction area. Works were conducted on a 24/7 operation. Overall duration to complete the works associated with the cavern junction was approximately 6 months.

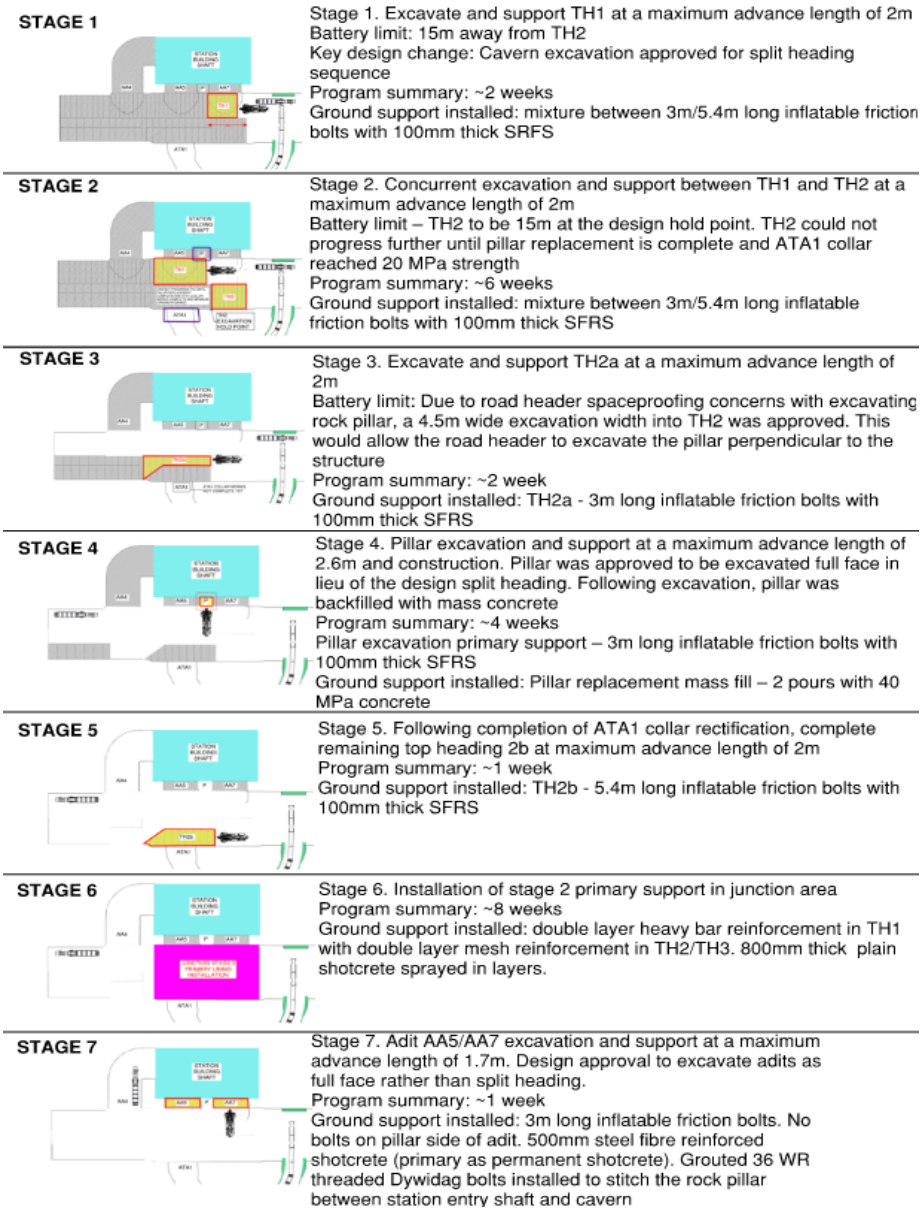


Figure 4. Actual construction methodology for main station entry junction

A photo during construction of the junction top heading is provided in Figure 5 below.



Figure 5. Photo during construction of Albert St Station main entry shaft junction

4 KEY CHALLENGES

4.1 *Key challenge 1 – interaction with station building main entry shaft*

Initially, the design assumed that the adjacent main entry shaft excavation would progress further than the cavern, leading to the adoption of a triple heading sequence. However, the triple heading design posed constructability issues, such as the road header's inability to reach the deep elephant's foot profile and clashes with the ventilation ducting. As construction progressed, the cavern's top heading advanced faster than the main station entry shaft excavation, prompting the tunnelling contractor to adopt a split heading sequence with specific constraints, including requiring a minimum rock cover of 3m of NFG2 overlain by 3m of NFG3. The constraint on the adjacent shaft excavation was that the shaft could not progress below RL -12m prior to the cavern junction primary lining reaching a minimum strength gain of 20MPa. Additionally, there was a potential clash between the cavern heading rock bolts and the main station entry shaft pile anchors. Refer to Figure 6 below. Initially, 5.4m bolts were installed in the cavern heading directly adjacent to the shaft, but a clash with the adjacent shaft anchors occurred, leading to a revised bolting arrangement using a combination of 3m and 5.4m long bolts to ensure cavern temporary support was not comprised. To mitigate this issue, the contractor re-bolted a section of the junction with 3m long bolts.

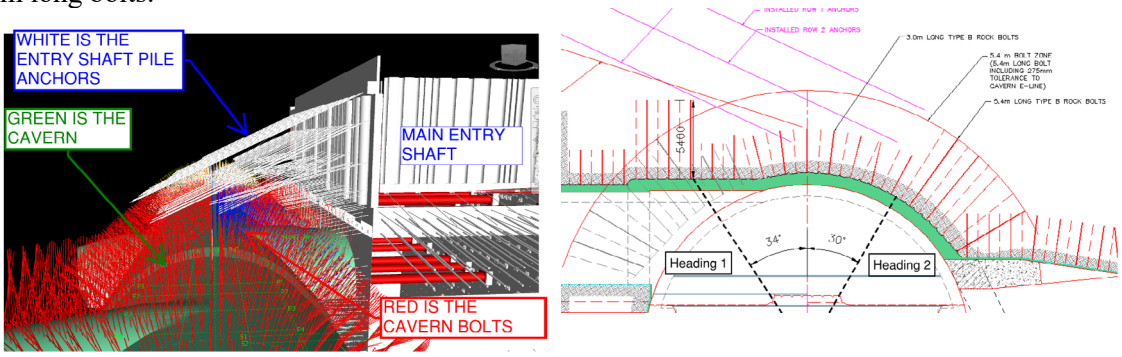
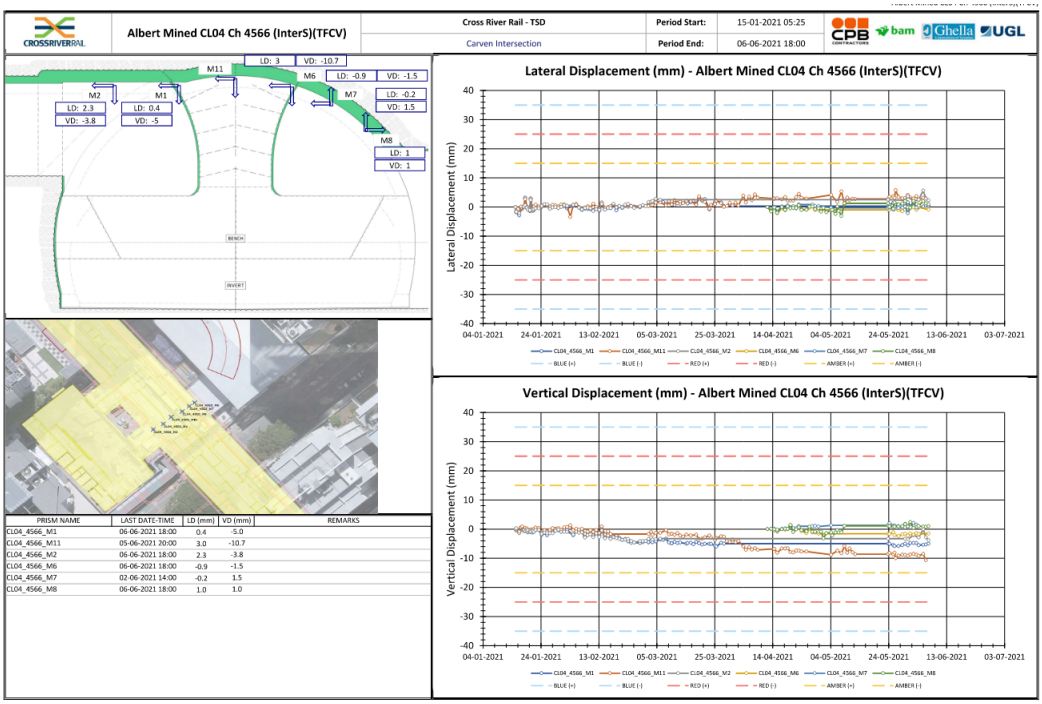


Figure 6. Cavern rock bolt clashes with main station entry shaft anchors

4.2 *Key challenge 2 – strict monitoring requirements during construction*

Due to the location of the Albert St Station cavern, it was determined that a daily permit to tunnel (PTT) would be employed to ensure a comprehensive review of the previous 24 hours of excavation activities. This meeting would assess and interpret ground monitoring data and instrumentation results, confirm alignment with design predictions and allowable limits, and determine and agree on the excavation and ground support for the next 24 hours. Key areas of monitoring included the Albert St footpath between Mary St and Charlotte St for surface settlement, the Sebel Hotel and Festival Towers, which were neighboring high-rise buildings to the junction construction, monitored for displacement and tilt, and in-tunnel monitoring where survey targets were required to be installed in arrays every 10 metres through this junction area as per the design. The design drawings stipulated trigger levels for each type of monitoring instrument depending on location and support type. An example monitoring graphs that were reviewed daily in the PTT are given in Figure 7 below.

If the trigger action levels were breached, a Management Action Team or 'MAT' meeting was called. In total, 40 MAT meetings were held during the full cavern construction program, with 9 occurring during the period of the junction top heading construction. Of these, 3 were due to surface settlement alarms on the Albert St footpath above, with a maximum settlement of 12mm recorded during this time. Tiltmeters on Festival Towers caused a red alarm during this period, but it was concluded that there were no major issues as the tiltmeter sensors were very sensitive to rain events. The construction of the junction top heading took place in summer, a season characterized by frequent rain in Brisbane. In summary, the design predictions on ground, tunnel, and building movement were all within design expectations.



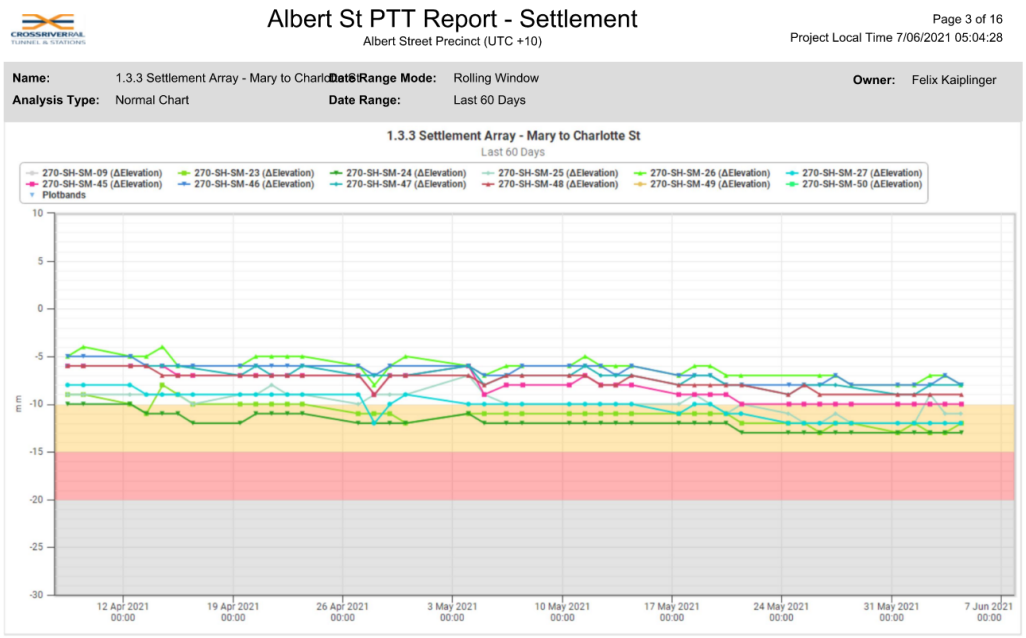


Figure 7. Example monitoring data reviewed during Albert St tunnel permit to tunnel meetings

4.3 *Key challenge 3 – ATA1 collar rectifications*

Following pillar construction, excavation of the final section of the junction was delayed due to an unforeseen construction issue involving the concrete collar constructed at temporary access adit ATA1, associated with Stage 5 of the referenced construction methodology. While the specifics of this issue are beyond the scope of this paper, rectification involved the road header sumping a window into the remaining rock mass (labelled TH2b in the Stage 5 schematic) and drilling from the cavern junction to the ATA1 collar to facilitate grouting of the affected area. Although this issue impacted the junction excavation sequence, the overall effect on cavern progress was minimal, as the road header was able to continue excavation in other areas.

4.4 *Key challenge 4 – Stage 2 junction primary lining*

Due to the major design constraint of the adjacent main station entry shaft, after completing the cavern top heading excavation and Stage 1 primary support, it was necessary to install extrados and intrados layers of reinforcement, with shotcrete layers applied to encapsulate the reinforcement. Rebar was utilised in TH1 with top and bottom mesh to be installed in TH2 and in the central heading. Stremaform (a stay-in-place formwork) was installed at the intersection of the headings to create a construction joint. The sequence of works to complete the junction reinforcement followed these steps: preparing the scaffold area, erecting the scaffold, installing anchors for dummy bars, setting dummy bars, installing and tying extrados reinforcement, removing the scaffold and storing it underground, applying shotcrete to the passive lining, re-erecting the scaffold, installing and tying intrados reinforcement, removing the scaffold, and finally, shotcreting the remaining passive lining. The main purpose of utilizing a scaffold instead of scissor lifts for the rebar installation was due to several reasons: it enabled a stable working platform, productivity was assumed to be quicker than with a scissor lift, and it minimised the potential for slips and trips. Refer to Figure 8 for as built photo of the scaffold. Interface management was crucial during this stage, as the adjacent AA4 adit was to be excavated simultaneously with the reinforcement installation. Therefore, the scaffold structure had to be protected from plant interaction, which was achieved by using pinned-down concrete barriers directly next to the scaffold structure.



Figure 8. Scaffold erection in constrained top heading

4.5 *Key challenge 5 – shotcrete voids*

Following completion of the stage 2 junction primary lining, shotcrete inspections were undertaken to investigate potential voids in the junction primary lining. This included hammer tests, coring work and endoscope inspections. The inspections identified an extensive number of voids within various locations across the junction as shown in the “heat map” presented in Figure 9.

The methodology adopted for the lining remediation involved pressure grouting via injection. The grouting was conducted from south to north, focusing on voids around the adit collars before moving out towards the center of the cavern crown. The process began with setting up a grout pump and securing the work area, followed by installing inlet plates and pressure gauges. Grout was batched at a specified water-cement ratio, tested for fluidity, and pumped through inlet valves

with breather valves open. Once grout was visible at breather holes, they were sealed, and pumping resumed until a maximum pressure of 50kPa was reached. The pressure was held and monitored; if stable, the line was shut and bled. Grout samples were collected, and the injected section was left to cure. The process was repeated for each void, and once grout reached 2MPa strength, secondary inspection holes were cored and examined via endoscopes with the CPS team. Remediation of the junction lining became critical as bench blasting and excavation could not continue until the lining remediation was completed.



Figure 9. Identified shotcrete voids in junction area

5 LESSONS LEARNT

5.1 *Location of temporary access adit*

A key lesson learnt is to avoid locating a temporary access adit at an already complex junction area in future projects. The presence of ATA1 introduced significant construction constraints, including delays to Stage 2 primary support works in the junction. Specifically, excavation of the top heading above ATA1 could not proceed until the concrete collar had achieved 20MPa strength. Early planning should carefully consider adit location to avoid interference with major structural elements and staging of primary support works.

5.2 *Reinforced primary lining*

The primary lining on the adit side of the top heading comprised two layers of N32 bars and 800mm thick shotcrete. Given the bar size, spacing and two layers of the reinforcement, application of shotcrete proved to be more difficult than anticipated. Remediation of the voids in the lining necessitated an extensive injection grouting campaign, which in turn constrained subsequent bench blasting activities. The following alternatives were considered:

- Hand spraying: This was considered to not be feasible due to the large volume of shotcrete required (1400m3).
- Cable bolt support: This was considered but deemed unviable due to low rock cover, risk of clashes with adjacent shaft anchors and also due to the loading from the main station building shaft.

An additional key lesson was the importance of thoroughly reviewing shotcrete mix designs during the planning phase. An alternate mix may have reduced the risk of void formation.

6 REFERENCES

Cammack, R., Bertuzzi, R., Smith, A. and Brehaut, R. 2022. Rock Mass Parameters for the Brisbane CBD. Australian Geomechanics, Vol. 57: No. 4, pp. 47 – 72.

19th Australasian Tunnelling Conference – Acosta-Martínez, Stewart and Hudson-Smith (Eds.)
© 2025 Australian Tunnelling Society, ISBN 978-0-85825-002-4

Numerical analysis and design of an SEM tunnel through jet-grouted Coode Island Silt

A. Shafee, E. Kaese
Delve Underground, Sydney, New South Wales, Australia

M. Behrens
Delve Underground, Melbourne, Victoria, Australia

ABSTRACT: Hobsons Bay Main Yarra Crossing Duplication Project is a major project for Melbourne Water involving the construction of a new duplicate sewer and rehabilitation of the existing sewer, currently conveying approximately 30 percent of Melbourne's wastewater. As part of the project, a new tunnel, between the new junction manhole and new siphon inlet shaft, was constructed in very soft to soft, saturated Coode Island Silt. Jet grout columns, including inclined columns around an abandoned sewer overpassing the tunnel, were installed to form a stabilized grouted mass in the tunnelling zone. The project represents a successful integration of soft soil ground improvement and open-face tunnelling through treated ground. It is among the first projects to combine the two in Victoria's tunnelling history. This paper presents a three-dimensional numerical analysis of encountered ground conditions to gain insights into excavation and support performance through fully and partially jet-grouted silt.

1 INTRODUCTION

1.1 *Project background*

The current Hobsons Bay Main sewer siphon, which is a pivotal component of the sewer network for the city of Melbourne, transfers about 30 percent of the city's wastewater to the Western Treatment Plant. It was constructed under the Yarra River between Port Melbourne and Spotswood in the 1960s, replacing the original 1895 tunnel when Spotswood Pumping Station was decommissioned, and is nearing the end of its service life. In September 2021, a project was initiated to construct a duplicate conduit that diverted sewage flows during rehabilitation works of the existing sewer. The duplication component of the overall project was delivered by John Holland for Melbourne Water and was completed in December 2024.

With the existing sewer being relined in 2025, the new duplication and the refurbished siphon will provide greater wastewater flow transfer capacity in parallel and are designed to accommodate flows projected for the year 2071.

1.2 *Project components*

The project works consist of a 678 m long siphon tunnel beneath the Yarra River between the siphon inlet and outlet structures on each riverbank. On the east bank, a new upstream connection structure (UCS) intercepts the original sewer system, isolating and diverting the flow to the new siphon inlet structure (SIS) via a connection tunnel. On the Yarra River's west bank, the siphon

tunnel links to the new siphon outlet structure, then to the new downstream connection structure on the existing North Yarra main sewer.

On the east bank, installation of the UCS and SIS structures began with circular shaft construction using secant piles. Secant piles were selected over soldier piles to minimise the risk of the groundwater table lowering during construction, which would induce excessive long-term ground settlement due to depressurisation consolidation in silty ground. Following piling, the tunnelling zone between the UCS and SIS was ground treated. After excavation of the shafts, the connection tunnel was constructed via the sequential excavation method (SEM) between August and September 2023.

1.3 *Ground conditions in tunnelling and shaft base zones*

The project area is located within an estuary consisting of very soft, saturated soils on the east riverbank near the current junction of the Yarra River with Port Philip Bay. The project Geotechnical Interpretive Report (GIR) (WSP Australia 2022) describes the east bank geology as a layer of fill at the ground surface overlying a sequence of Quaternary sediment deposits. One near-surface sediment unit is Coode Island Silt, a dark grey to black, very soft to soft, normally to slightly overconsolidated silty clay expected and encountered at tunnelling depth for the SEM connection tunnel. An extensive site investigation and laboratory testing program provided geotechnical properties for this ground type, suggestive of a very soft and yielding material with undrained shear strength values of only 20 to 50 kPa, negligible effective cohesion, an effective friction angle of 26 degrees, and a drained elastic modulus between 4 and 9 MPa.

The shafts on the east bank were expected to be founded in cohesive Fishermens Bend Silt. The laboratory testing program determined that this material had an undrained shear strength varying between 40 and 125 kPa and a drained elastic modulus of approximately 17 MPa.

2 CONTROL OF EXCAVATION RISKS

2.1 *Concept design*

Coode Island Silt has very little to no stand-up time from a tunnelling time perspective. This does not allow SEM tunnel passive support systems adequate time to gain sufficient strength and stiffness and to abate soil movements caused by the excavation without robust control of groundwater and ground collapse risks. Risks of consolidation of the silt layer due to groundwater table drawdown, potential excessive groundwater ingress into the tunnel excavation, and large tunnel deformations were all serious concerns. During the design phase, these risks were mitigated by adopting a relatively new option in Victorian tunnelling history (Vincent et al. 2020): jet grouting ground improvement in the tunnelling zone preceding SEM excavation. Delve Underground completed the concept and tender designs for the ground improvement and related project specifications packages.

While not as yielding as Coode Island Silt, Fishermens Bend Silt is a low-strength material. Shaft excavations the size of the UCS and SIS shafts were expected to induce considerable strain and deformation in the material, leading to the potential for hydraulic fracturing of the shaft base and instability. As this was a significant construction risk, a jet-grouted base plug of 3.5 to 4.5 m thick was incorporated in the design of both east bank shafts.

2.2 *Detailed design*

Menard Oceania was appointed by the principal contractor, John Holland, to carry out the detailed design and construction of the ground improvement works—namely, the grout plugs at the base of the UCS and SIS shafts and a treated ground block along the tunnel alignment with dimensions of 7 m high by 7 m wide by 23 m long. The jet grouting specifications required a maximum 1.0×10^{-7} m/s hydraulic conductivity, minimum 1.5 MPa unconfined compressive strength at 28 days, and minimum 250 MPa elastic modulus be achieved (Menard Oceania 2022).

The treated ground block was planned to be constructed by overlapping 1.9 m nominal diameter vertical jet grout columns. However, an abandoned diversion sewer traversing over the connection tunnel at less than 1.5 m clearance to the excavation line introduced significant complication and risk to the design and construction of the treated ground block. For the ground improvement works to maximise the extent of treated ground at the underside of the diversion sewer, 2.4 m nominal diameter inclined jet grout columns were adopted. While the risk of a small, potentially untreated soil zone in the tunnel crown area remained, as shown in Figure 1, this construction approach minimised the risk.

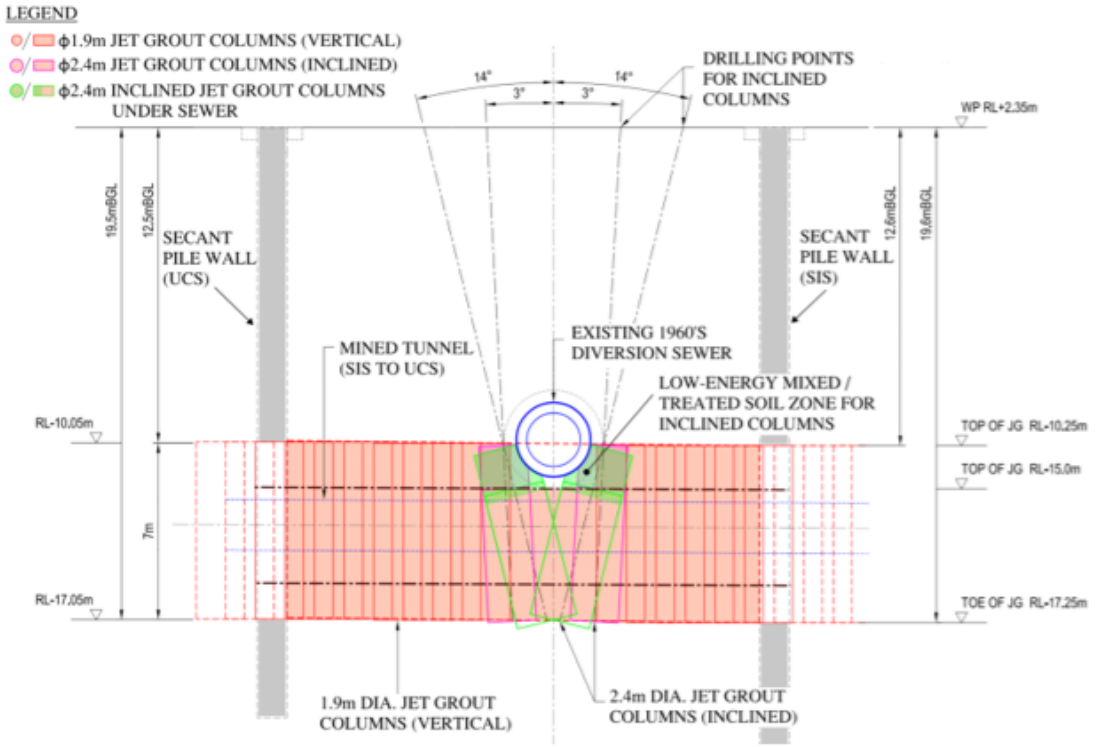


Figure 1. SEM tunnel ground treatment block with inclined jet grout columns (from Menard Oceania 2022).

Consequently, Delve Underground's SEM tunnel temporary support design accounted for two scenarios: (1) fully treated ground and (2) major zones of partially or untreated ground. Design calculations demonstrated that the fully grouted ground mass was generally self-supporting, and only a 100 mm layer of shotcrete, designated support type I, was needed for kinematic support of potential ground wedges. Conversely, the partially treated ground mass retained, to a lesser degree, the risks associated with excavation in soft soil, and accordingly, support type II addressed these risks with pre-support in the form of 6.0 m long steel face dowels at 750 mm spacing, or 6.0 m long hollow steel spiles at 200 mm spacing, with a passive support system of steel sets at 1.0 m spacing with a 200 mm layer of shotcrete. During the construction phase, the contractor added an option where light gauge steel channel-section lagging could be added above the steel sets in support type II to control any potential running ground.

2.3 *Construction*

Because of the uncertainty in the ground improvement achieved under the sewer, the project's success relied on the observational method, in which the relevant support type to be installed in the next excavation advance is selected from a predesigned toolkit of engineered support systems that address the possible geotechnical risks (Peck 1969). Hence, the support type selection (e.g. I-II) is based on observations of the ground conditions encountered during probing and excavation.

Production of jet grout columns began following a test program to adjust equipment and material parameters (e.g. nozzle pressure, water/binder ratio, etc.), which provided evidence of achieving design parameters and initial quality control requirements. Jet grout columns were installed in an overlapping hexagonal pattern. SEM tunnel excavation, with continual forward probing, began from the SIS shaft. Support type I was installed between chainages 0–4.5 m and 8.0–21.0 m measured from the SIS breakout, whereas support type II was installed between chainages 4.5–8.0 m. Further details of construction methods and observations can be found in Kaese and Shafee (2024) and Hubaut et al. (2024).

3 TUNNEL DESIGN

3.1 *Soil-structure interaction analyses*

Given the complexity of the design problem, a three-dimensional (3D) soil-structure interaction numerical analysis was created using FLAC3D to better understand tunnel excavation and support behaviour through the jet-grouted block and the potential for non-treated or partially treated ground underneath the abandoned sewer. The UCS and SIS shafts, abandoned sewer, and connection tunnel were incorporated in the 3D analysis, with the general construction sequence of constructing the abandoned sewer, followed by resetting the displacements to zero, installing secant piles and jet grout for shaft base plugs and SEM tunnel treated zone block, excavating both shafts, breaking out from the SIS shaft, and constructing the SEM tunnel through to break in at the UCS shaft. Figure 2 shows the 3D analysis components as well as the 7 m x 7 m x 23 m jet-grouted block (created by vertical jet grouting columns) for the connection tunnel and a potentially untreated or partially treated zone.

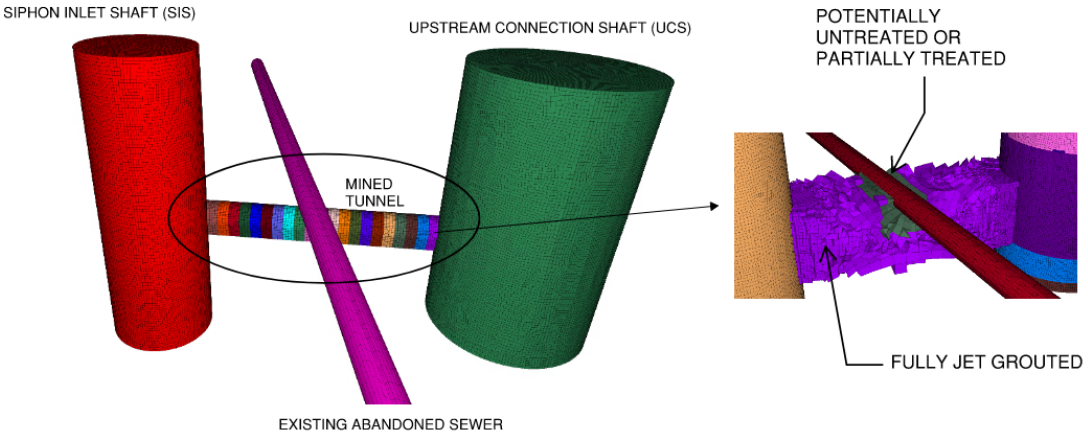


Figure 2. FLAC3D analyses with anticipated ground conditions around the connection tunnel.

Initial analysis was carried out assuming an untreated Coode Island Silt zone around and beneath the abandoned sewer extending to about 1.0 m from the abandoned sewer extrados (see Figure 2). An elastic constitutive model with 150 MPa drained modulus (conservatively assumed to be less than jet grout design value) was assigned to fully treated jet grout block, and a plastic-hardening model with Mohr-Coulomb failure criterion was assigned to Coode Island Silt zone (see Section 1.3 for recommended geotechnical design parameters). Results from the initial analysis indicated tunnel instability with very large ground strains and deformations around the excavated opening beneath the abandoned sewer. This was expected, given that Coode Island Silt does not have sufficient shear strength to be self-supporting, even temporarily. Thus, inclined jet grout columns were recommended and included in the jet grouting program (see Section 2.2) to treat any material in the vicinity of the abandoned sewer.

In an updated analysis, it was assumed that Coode Island Silt zone around and beneath the abandoned sewer is partially treated via the addition of inclined jet grout columns. A conservative approach was adopted in predicting geotechnical design parameters for the partially treated Coode Island Silt by assuming that the stiffness of the natural soil is unchanged, a cohesion increase of 30 kPa and a 15% friction angle increase. This assumption was to be verified by observation and monitoring during the construction of the tunnel. This numerical analysis was performed adopting support type I in the fully treated zone and support type II in the anticipated partially treated zone, as shown in Figure 3.

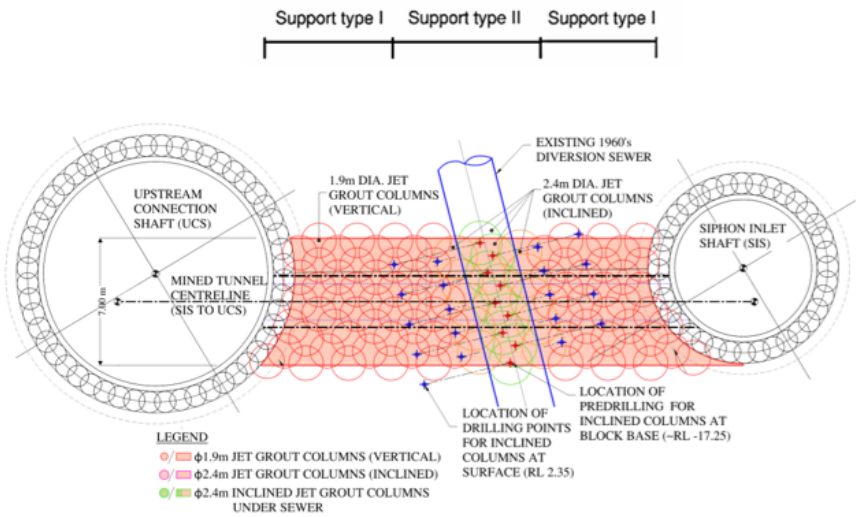


Figure 3. Different support types incorporated in the FLAC3D analysis.

3.2 *Analysis results and field observations*

Numerical analyses suggested that in the support type I fully treated zone (with vertical columns), tunnel deformations would be negligible and maximum principal stresses would be less than the factored unconfined compressive strength of the jet-grouted material. However, the analyses predicted that in the support type II partially treated zone (with inclined columns), despite the passive steel sets and shotcrete being within capacity, approximately 20 mm of tunnel convergence could be expected at the crown beneath the abandoned sewer. Therefore, these were the most critical tunnel advance cuts and were to be monitored carefully during construction. Figure 4 shows the predicted vertical deformation at the final stage of SEM tunnel construction, with the lower bound assumption of a partially treated zone extending 1.0 m beyond the abandoned sewer extrados.

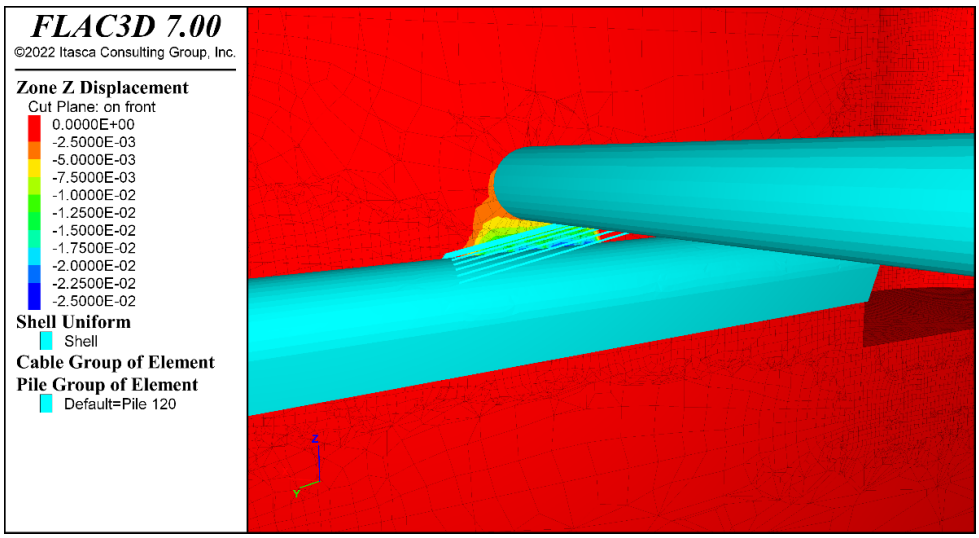


Figure 4. Vertical deformation contours (metres) after SEM tunnel construction.

During construction, it was observed that the ground zones beyond the abandoned sewer (support type I zones shown in Figure 3) were fully treated, with only minor (less than 5 percent of the exposed face) untreated Coode Island Silt inclusions being noted. Tunnel construction in this zone was completed with smooth cut profiles, negligible overbreak, and no notable challenges. This observation correlated well with design analyses results. However, an interesting on-site observation was that the ground treatment around the sewer was successful: the extent of the partially treated zone around and beneath the abandoned sewer was notably less than the 1.0 m extent design assumption affecting about four to five 1.0 m advances. The semi-treated zone was limited to the two cuts directly beneath the sewer centreline. Field observations at these cuts showed that about 15 to 20 percent of the exposed face was composed of untreated inclusions, primarily concentrated in the crown. Figure 5 shows examples of two tunnel face conditions for each support type.

In-tunnel convergence monitoring was not conducted during construction due to space limitations and confidence in design. However, surface movements were monitored above the tunnel during construction and marginal (near zero) settlement was recorded, which was in line with numerical analysis results.



Figure 5. Example of tunnel face conditions from (a) support type II zone and (b) support type I zone.

3.3 *Numerical analysis of actual partially treated zone*

A post-construction numerical analysis was performed with a modified extent of partially treated zone, limited to a V-shaped area just beneath the sewer based on field observations, as shown in Figure 6. Analysis results suggested lesser deformations in the partially treated zone and lower structural demands on the support elements, as seen in Figure 7. Unfortunately, a detailed numerical analysis was not possible to estimate equivalent shear strength properties of the partially treated zone due to a lack of deformation monitoring while excavating underneath the sewer.

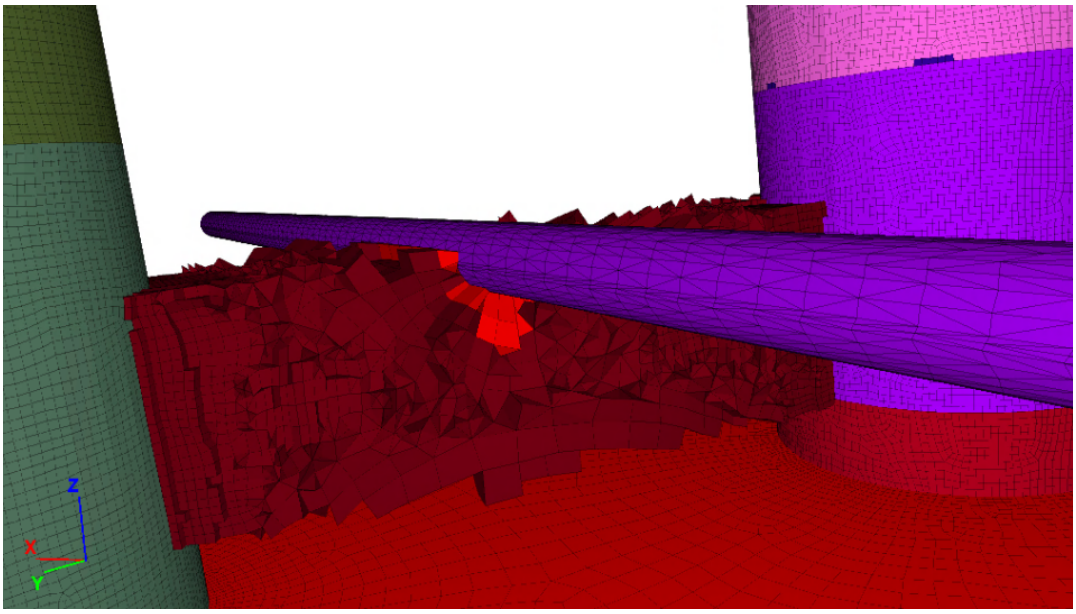


Figure 6. Numerical analysis of SEM tunnel construction with observed partially treated zone during construction.

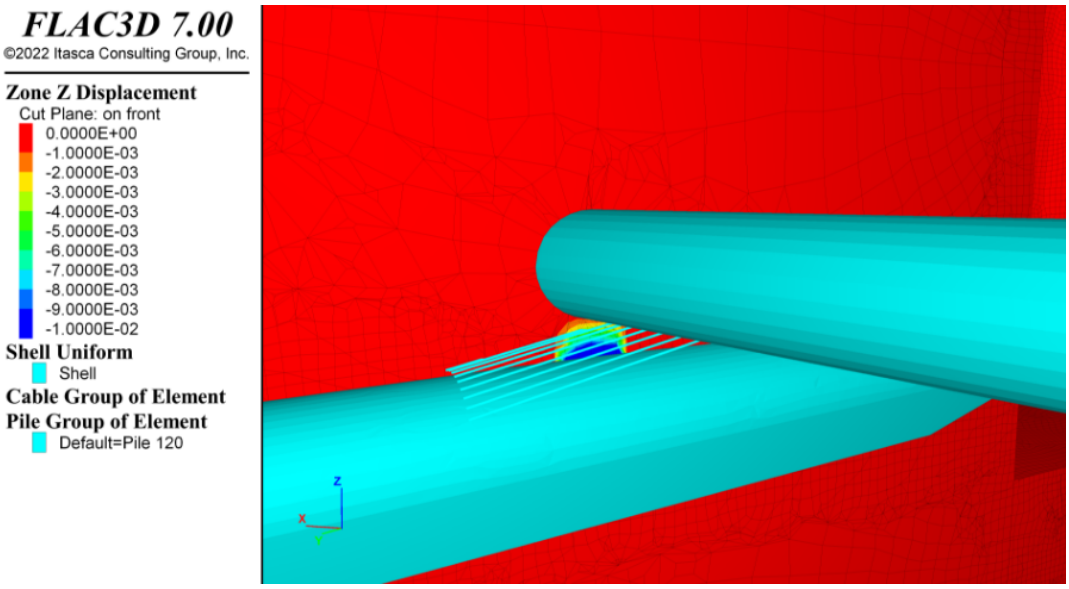


Figure 7. Vertical deformation contours (metres) after SEM tunnel construction with observed partially treated zone during construction.

4 CONCLUSION

The Hobsons Bay Main Duplication upstream connection tunnel stands as one of the pioneering projects in Victoria, successfully combining soft soil ground improvement using jet grouting with subsequent SEM tunnelling through the treated ground. Numerical analyses during the design phase and construction observations confirmed that the ground improvement works significantly reduce the risks of tunnelling through saturated, highly compressible soils, even when passing just 1.5 m beneath an existing sewer through partially treated ground. While observational methods adopted in this project successfully managed potential geotechnical risks, the project could

have benefited by adding extra support types to the design, assuming a variety of scenarios for the partially treated zone and potentially reducing the project's tunnel cost.

5 REFERENCES

Hubaut, A. et al. (2024) 'Case study: Deep mixing ground treatment for Hobsons Bay Main sewer upgrade in Australia', Japanese Geotechnical Society and International Society of Soil Mechanics and Geotechnical Engineering, *Proceedings of the 2024 Deep Soil Mixing Conference*, Yokohama, Japan, December 2024: 1–6.

Itasca Consulting Group. (2019) FLAC3D (*Fast Lagrangian Analysis of Continua in Three Dimensions*), Version 7.0. Minneapolis, MN: Itasca.

Kaese, E. and Shafee, A. (2024) 'Jet grouting campaign to minimise tunnelling risks in Coode Island Silt', Australian Geomechanics Society and New Zealand Geotechnical Society, *Proceedings of the 15th Young Geotechnical Professionals Conference*, Adelaide, Australia, November 2024: 1–6.

Menard Oceania. (2022) *Hobsons Bay Main Sewer - Yarra River Duplication Project, Ground treatment design and construction method report*.

Peck, R. (1969) 'Advantages and limitations of the observational method in applied soil mechanics'. *Géotechnique*, 19(2): 171–187.

Vincent, P., Hubaut, A., Chan, S.P. and Auvergne, S. (2020) 'Cross passage ground treatment for Melbourne Metro tunnel project'. Australian Geomechanics Society, *Proceedings of the 2020 Australian Geomechanics Society Sydney Chapter Symposium*, November 2020: 17–30.

WSP Australia. (2022) *Hobsons Bay Main Sewer - Yarra River Duplication Project, Geotechnical Interpretive Report*.

19th Australasian Tunnelling Conference – Acosta-Martínez, Stewart and Hudson-Smith (Eds.)
© 2025 Australian Tunnelling Society, ISBN 978-0-85825-002-4

Research on the mechanism of shotcrete support based on the combined effect of rock-shotcrete

Y. Deng
China Railway Academy Group Co., Ltd., Chengdu, China

ABSTRACT: The most significant feature of shotcrete is its ability to tightly adhere to the surrounding rock, thereby forming a load-bearing composite structure between shotcrete and loose rock blocks. To quantitatively analyze this complex mechanism, we derived the theoretical bearing capacity by analyzing the cross-sectional stress-strain relationship of the composite structure composed of shotcrete and loose rock blocks. By adopting the principle of equivalent fracture energy, we fitted post-peak test data of bond stress at the rock-shotcrete interface and established an interface mechanical model. Based on this model, the discontinuous deformation analysis (DDA) method was employed to simulate the composite structure. The research demonstrates that shotcrete significantly enhances the bearing capacity of the rock-shotcrete composite through interfacial bonding. Furthermore, the mechanical properties of the rock-shotcrete interface directly influence the failure mode of the composite structure.

1 INTRODUCTION

In tunnel engineering with severe structural cutting, there is a possibility of local loosening and collapse of multiple rock blocks. After the application of shotcrete, the relative sliding and loosening of the rock blocks can be prevented by the bonding force between the shotcrete and the rock blocks, resulting in a certain range of shotcrete and block rock forming a whole that can bear pressure. Therefore, the key to analyzing the shotcrete support for multiple rock blocks is to clarify how its interfacial bonding effect mobilizes the joint bearing capacity of the rock blocks. In response to this, scholars have conducted research from different directions. For example, Bernard, E.S. et al. summarized the important role of rock-shotcrete bonding performance in the support of fiber shotcrete [1], Zhang, P. et al. studied the interaction between rock mass and shotcrete through numerical simulation [2], Dong, W. and Dong, X. et al. studied the mechanical properties of the rock-shotcrete interface through DIC technology and numerical simulation [3, 4], Sjölander, A. et al. studied the influence of rock-shotcrete bonding strength and shotcrete thickness on the support effect [5, 6], and Chang, Y. et al. studied the support effect of rock-shotcrete interface bonding performance on a single moving rock mass[7]. On the basis of the above research, this article quantitatively analyzes the supporting mechanism of the overall load-bearing structure formed by the bonding between shotcrete and rock blocks, and verifies it through simulation using discontinuous deformation method.

2 MECHANICAL ANALYSIS OF SHOTCRETE SUPPORT BASED ON ROCK-SHOTCRETE COMPOSITE EFFECT

If the bonding effect between shotcrete and rock is not considered in the research, and it is only regarded as a simple resistance structure, and loose rock blocks are completely regarded as loads,

then the stress analysis of shotcrete is to regard it as a bending thin plate under uniformly distributed loads. When the tensile stress on the lower side of the thin plate reaches the ultimate tensile strength of the material, the support cracks and fails. Therefore, the flexural bearing capacity M_{R1} of shotcrete support without considering interface bonding can be obtained by the following equation:

$$M_{R1} = f_{pt} \times t^2/6 \tag{1}$$

In the equation, f_{pt} is the tensile strength of shotcrete material, and t is the thickness of the shotcrete layer.

But if the bonding effect between shotcrete and rock is considered, and shotcrete and rock blocks are regarded as a whole structure composed of bonding effect, then the thickness of the structure can be equivalent to the sum of the height of the rock block and the thickness of the shotcrete, as shown in Figure 1.

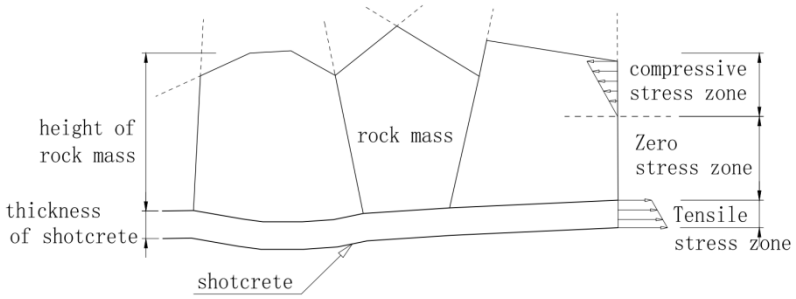


Figure 1. A shared load-bearing structure composed of shotcrete and multiple rock blocks

In this structure, compressive stress can be transmitted between rock blocks, but tensile stress cannot be transmitted. The tensile stress is borne by the shotcrete adhered to the bottom surface of the rock blocks. At the same time, the entire structure is still considered to satisfy the assumption of a plane section during the analysis process.

According to the assumption of a flat section and the axial force balance equation of the section, the height x of the compressive stress zone can be calculated as:

$$x = -\lambda \cdot t + \sqrt{\lambda^2 \cdot t^2 + 2\lambda \cdot t \cdot (b + t/2)} \tag{2}$$

In the equation, b is the height of the rock mass jointly carried by the shotcrete, t is the thickness of the shotcrete, $\lambda = E_p/E_c$, E_c is the elastic modulus of the rock, and E_p is the elastic modulus of the shotcrete.

When the overall structural bearing capacity is controlled by the strength of the shotcrete material at the lower edge of the section, the flexural bearing capacity M_{R2} of the support considering interface bonding can be obtained by the following equation:

$$M_{R2} = f_{pt} \cdot \left(1 + \frac{b-x}{b-x+t}\right) \cdot \frac{t}{2} \cdot \left[\left(b - x + \frac{t}{2}\right) + \frac{2x}{3}\right] \tag{3}$$

When the overall structural bearing capacity is controlled by the bonding strength of the rock-shotcrete interface, the bending bearing capacity M_{R3} of the support considering the interface bonding can be obtained by the following equation:

$$M_{R3} = f_{lt} \cdot \left(1 + \frac{b-x+t}{b-x}\right) \cdot \frac{t}{2} \cdot \left[\left(b - x + \frac{t}{2}\right) + \frac{2x}{3}\right] \tag{4}$$

In the equation, flt represents the strength of the rock-shotcrete interface.

Given the significant impact of the bonding performance of the rock-shotcrete interface on the support effect of shotcrete in the above mechanical analysis, it is necessary to establish a mechanical model for the interface between shotcrete and rock in order to quantitatively calculate the

support capacity of shotcrete.

3 MECHANICAL MODEL OF THE INTERFACE BETWEEN SHOTCRETE AND ROCK

Due to the complex factors such as physical interlocking and chemical bonding involved in the composition of rock-shotcrete interface performance, it is not possible to simply describe it using concepts from elastic mechanics. Therefore, it is necessary to construct corresponding models for crack initiation and damage evolution for analysis. Therefore, based on the damage bonding model as the mechanical model for the interface performance of rock-shotcrete, the interface failure is divided into two stages. In the initial stage of tension, the interface is in an elastic state, and the bond stress and interface opening displacement are linearly related, with the ratio being the elastic bond stiffness; When the bonding stress reaches its peak, the interface transitions to the plastic softening stage, and the degree of damage to the bonding stiffness is defined by the damage factor ω, which is a single value function of the opening displacement. The specific mechanical model concept is shown in Figure 2, and the mechanical model function is shown in equation (5).

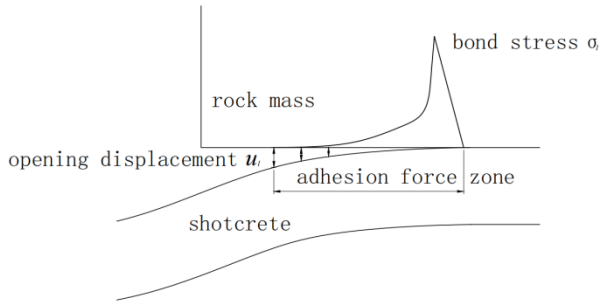


Figure 2. Conceptual diagram of the rock-shotcrete interfacial damage bonding model

$$\sigma_l(u_l)=\begin{cases}k\cdot u_l & u_l \le u_{l0}\\ k(1-\omega)\cdot u_l & u_l > u_{l0}\end{cases} \tag{5}$$

In the equation, σ_l is the bond stress, u_l is the opening displacement, k is the elastic bond stiffness, ω is the damage factor, and u_{l0} is the opening displacement corresponding to the peak bond stress.

According to the tensile test of the bond between shotcrete and rock, the natural exponential function is used to fit the post peak curve, and the stress opening displacement function relationship can be expressed as follows:

$$\sigma_l(u_l)=\sigma_{lf}\cdot e^{-\left(\frac{u_l-u_{l0}}{u_{lf}-u_{l0}}\right)} \qquad u_l > u_{l0} \tag{6}$$

In the equation, σ_{lf} is the peak value of bond stress, u_{lf} is the characteristic value of post peak opening displacement defined, and its product with the peak value of bond stress σ_{lf} is equal to the post peak fracture energy of the test. The definition of Ulf is shown in Figure 3, where G'_{lf} represents the post peak fracture energy.

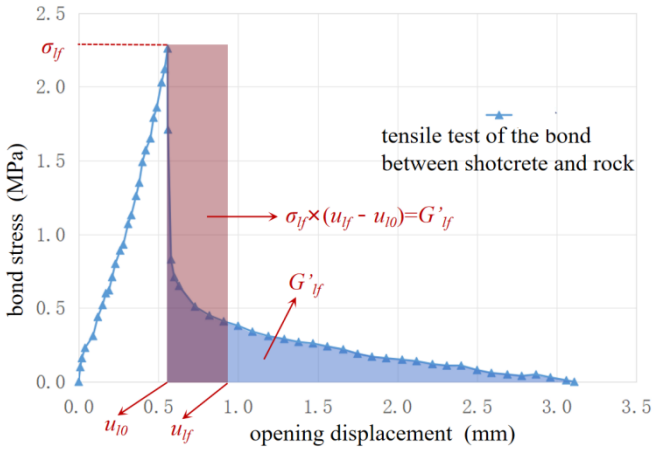


Figure 3. Definition of characteristic post-peak opening displacement based on the principle of equivalent fracture energy

By solving equations (1) and (2) together, the damage factor ω can be obtained as:

$$\omega(u_l)=1-\frac{u_{l0}}{u_l}\cdot e^{-\left(\frac{u_l-u_{l0}}{u_{lf}-u_{l0}}\right)} \qquad u_l>u_{l0} \tag{7}$$

4 SIMULATION ANALYSIS OF SHOTCRETE SUPPORT CONSIDERING ROCK-SHOTCRETE INTERFACE BONDING

To further analyze the impact of interface bonding failure on the effectiveness of shotcrete support, the discontinuous deformation analysis method (DDA) was used to simulate the process of shotcrete support failure under the action of a single rock block. In DDA simulation calculations, the previously fitted rock-shotcrete interface mechanics model equation (5) is used as the interface bonding constitutive model. The parameters of the rock mass and shotcrete materials are shown in Tables 1 and 2:

Table 1. Material parameters for simulation of rock block and rock-shotcrete interface

Project		Parameter value	Unit
rock mass	compressive strength	40	MPa
	tensile strength	2.4	MPa
	deformation modulus	40	GPa
	Poisson's ratio	0.2	/
	density	2.2	t/m^3

Table 2. Material parameters for shotcrete simulation

Project		Grade of Shotcrete					
		C40	C60	C80	UC100	UC120	UC160
shot-crete	compressive strength	40MPa	60MPa	80MPa	100MPa	120MPa	160MPa
	tensile strength	2.39MPa	2.85MPa	3.11MPa	5MPa	7MPa	9MPa
	elastic modulus	32.5GPa	36.5GPa	38GPa	40GPa	40GPa	45GPa
	Poisson's ratio	0.2	0.19	0.18	0.17	0.16	0.15

The model consists of shotcrete and multiple rock blocks, with a span of 4m and a height of 0.5m. The shotcrete layer tightly adhered below is 0.08m thick. The boundary conditions at both ends of the model are contact boundaries, simulating the surrounding intact rock mass wrapping. Apply uniformly distributed load on the top of the rock block and gradually increase it in the calculation. The specific calculation model is shown in Figure 4.

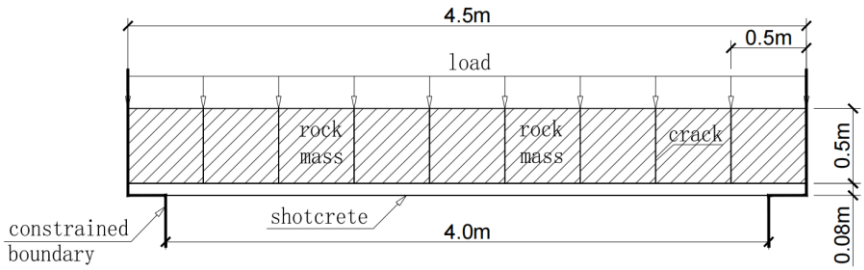
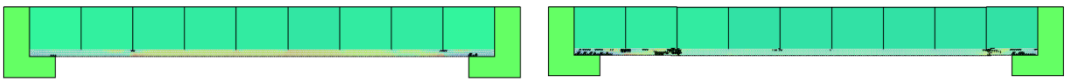


Figure 4. DDA simulation model of joint support of shotcrete and rock blocks

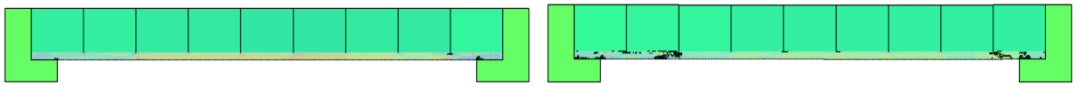
When using C40 shotcrete to support rock masses, the failure first occurs at the top of the shotcrete layer, as shown in Figure 5 (a). At this time, there is no obvious debonding at the rock-shotcrete interface, and the initial failure is the shear failure starting from the top of the shotcrete. As the load increases, the number of damage locations on the top of the shotcrete increases, and the cracks gradually extend from top to bottom until the load cannot continue to increase, as shown in Figure 5 (b). Therefore, under this calculation model, the failure of C40 shotcrete material occurs before the failure of the rock-shotcrete interface, and increasing the shotcrete grade is an effective means of enhancing support.



(a) Initial strength failure of shotcrete (b) Expansion of strength failure range of shotcrete

Figure 5. Simulation analysis of C40 shotcrete and rock block combination

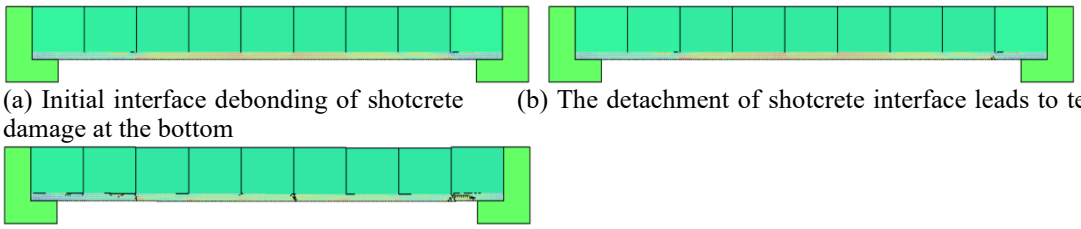
When using C60 shotcrete to support rock masses, the initial failure is also shear failure starting from the top of the shotcrete, with cracks extending from top to bottom. The failure mode is basically the same as C40 shotcrete support, as shown in Figure 6.



(a) Initial strength failure of shotcrete (b) Expansion of strength failure range of shotcrete

Figure 6. Simulation analysis of C60 shotcrete and rock block combination

When using C80 shotcrete to support rock masses, the first failure that occurs is the debonding of the rock-shotcrete interface. At this time, the shotcrete material has not yet undergone significant damage, as shown in Figure 7 (a). As the load increases, interface debonding occurs, leading to tensile failure at the bottom, as shown in Figure 7 (b). As the load continues to increase, the number and range of interface debonding locations increase, and the cracks gradually penetrate the support section from below to above, as shown in Figure 7 (c). Therefore, under this calculation model, the rock-shotcrete interface failure has already occurred before the C80 shotcrete material failure.

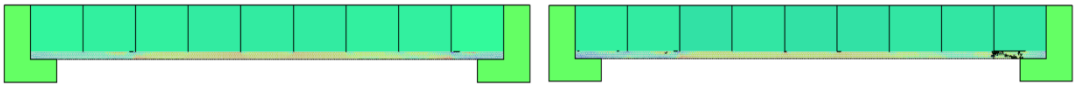


(a) Initial interface debonding of shotcrete (b) The detachment of shotcrete interface leads to tensile damage at the bottom

(c) Interface debonding and expansion of tensile failure range of shotcrete

Figure 7. Simulation analysis of C80 shotcrete and rock block combination

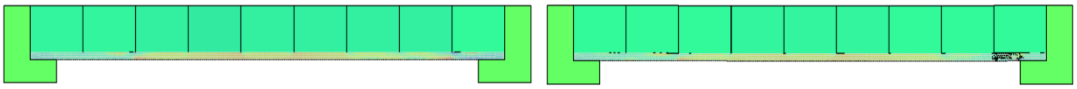
When using UC100 shotcrete to support rock masses, the failure mode is entirely governed by the rock-shotcrete interfacial failure. When the interface debonding range has extended to a larger range, the shotcrete will cause tensile damage to the bottom, as shown in Figure 8.



(a) Initial interface debonding of shotcrete (b) Interface debonding and expansion of tensile failure range of shotcrete

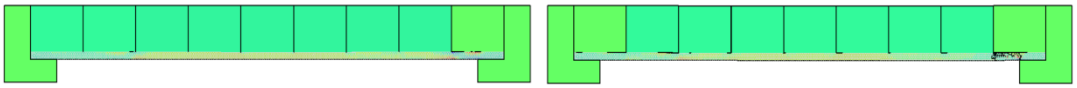
Figure 8. Simulation analysis of UC100 shotcrete and rock block combination

When using UC120 shotcrete or even stronger UC160 to support rock masses, the form and position of support failure are basically the same as those of UC100, as shown in Figures 9 and 10. At this time, the bonding strength of the rock-shotcrete interface is the controlling factor for failure, and the high performance of the material itself is not fully utilized.



(a) Initial interface debonding of shotcrete (b) Interface debonding and expansion of tensile failure range of shotcrete

Figure 9. Simulation analysis of UC120 shotcrete and rock block combination



(a) Initial interface debonding of shotcrete (b) Interface debonding and expansion of tensile failure range of shotcrete

Figure 10. Simulation analysis of UC160 shotcrete and rock block combination

Figure 11 shows the load displacement curve of shotcrete and rock mass simulation analysis. It can be seen from the figure that when the shotcrete grade is lower than C80, the support failure is controlled by the material strength. Therefore, the higher the grade, the stronger the support bearing capacity. When the shotcrete grade is higher than UC100, the support failure is controlled by the bonding strength of the rock-shotcrete interface. Continuing to increase the shotcrete grade has limited effect on enhancing the support. The load displacement curves of UC100, UC120, and UC160 shotcrete supports are basically the same.

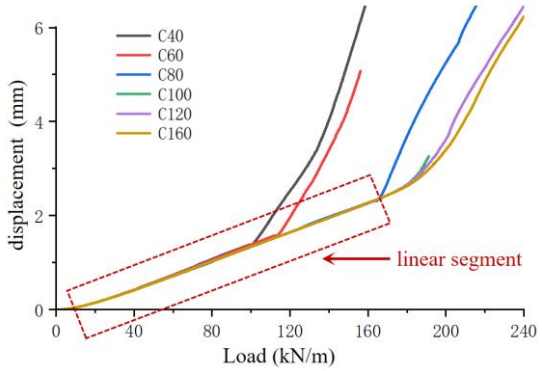


Figure 11. Load displacement curve of shotcrete and rock mass simulation analysis

In Section 1, the theoretical flexural bearing capacity expressed by equations (3) and (4) was obtained through cross-sectional analysis of a joint load-bearing structure composed of shotcrete and rock masses. Therefore, the linear segment bearing capacity calculated by DDA simulation (as shown in Figure 11, the maximum load of each labeled shotcrete linear segment) was converted into the bearing capacity of a 4m span simply supported beam and compared with the theoretical value to verify the results of the two analysis methods, as shown in Figure 12.

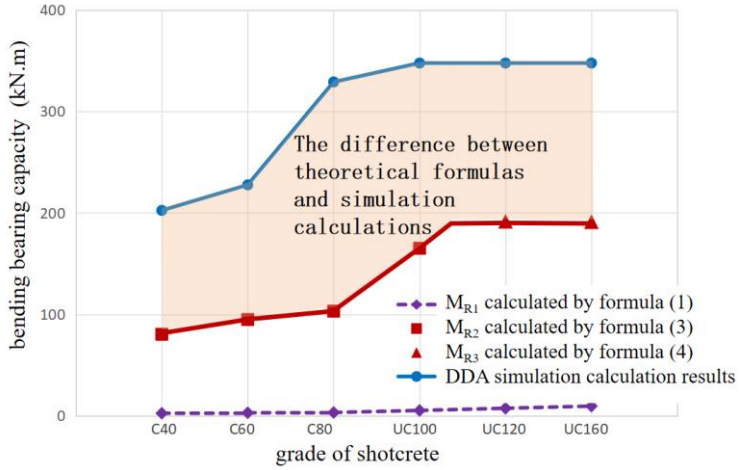


Figure 12. Flexural bearing capacity of shotcrete support with different grades

As shown in Figure 12, the theoretical equations and simulation calculations demonstrate that the failure modes of each grade of concrete support are basically the same, and the trend of change is consistent. A support model that only considers the resistance of shotcrete itself will seriously underestimate the support effect of shotcrete; When the shear strength of the rock-shotcrete interface remains unchanged, the flexural bearing capacity of the overall rock-shotcrete structure begins to be controlled by the interface strength after the shotcrete grade is increased to UC100. Increasing the strength of the shotcrete material has limited impact on the support effect; Only by increasing the strength of strong shotcrete materials without damaging the rock-shotcrete interface can the thickness of shotcrete be effectively reduced. At the same time, in the simulation calculation, the two sides of the loose rock block are constrained by the simulated intact rock mass, further improving the bearing capacity of the rock block combination, namely the Voussoir Beam effect. Therefore, the simulated bending bearing capacity is significantly higher than the theoretical equation, and the degree of improvement of each label is basically the same.

5 CONCLUSIONS

This article studies the mechanism of shotcrete support based on rock-shotcrete combination effect through theoretical analysis and numerical simulation. The main conclusions are as follows:

1) The damage bonding model established based on the principle of equivalent fracture energy through rock-shotcrete interface tests can better reflect the mechanical properties of the interface from cracking to debonding, providing a basis for quantitative analysis of rock-shotcrete composite structures.
2) The mechanical properties of the rock-shotcrete interface not only determine the failure mode of shotcrete support, but also affect the resistance performance of shotcrete materials. When the adhesion force is maintained, the failure of shotcrete will be controlled by its shear resistance. Only when shotcrete first peels off from the rock and loses its adhesion force, bending failure becomes possible.
3) A support model that only considers the resistance of shotcrete itself will seriously underestimate the support effect of shotcrete. In addition to its own material resistance, shotcrete can prevent relative sliding and loosening of rock blocks through its bonding force with the contact surface, resulting in the formation of a load-bearing whole between shotcrete and block shaped rock mass within a certain range. Due to the improvement of integrity, the Voussoir Beam effect of rock blocks becomes more significant compared to the unsupported condition.
4) Comparing the results of discontinuous deformation simulation analysis (DDA) and theoretical equation calculation of the bearing capacity of rock-shotcrete composite structures, it can be seen that the failure modes of each grade of concrete support obtained by the two methods are basically the same, and the trend of bending bearing capacity changes of the two methods is consistent, which can mutually confirm the mechanism of shotcrete support based on the rock-shotcrete composite effect.

6 REFERENCES

Bernard, E.S., Thomas, A.H. 2020. Fibre reinforced shotcrete for ground support. *Tunnelling and Underground Space Technology* 99: 103302.

Chang, Y., Höök, C. 2024. Shotcrete structural behaviours as tunnel support in hard jointed rocks-Swedish state of the art. *In Proceedings of the World Tunnel Congress 2024*, 450-465.

Dong, W., Wu, Z.M. et al. 2017. An experimental study on crack propagation at rock-shotcrete interface using digital image correlation technique. *Engineering Fracture Mechanics* 171: 50-63.

Dong, X., Karrech, A. et al. 2020. 3D bolted cohesive element for the modelling of bolt-reinforced rough rockshotcrete interfaces. *Computers and Geotechnics* 125: 103659.

Sjölander, A., Hellgren, R. et al. 2020. Verification of failure mechanisms and design philosophy for a bolt-anchored and fibre-reinforced shotcrete lining. *Engineering Failure Analysis* 116: 104741.

Sjölander, A., Ansell, A. et al. 2021. Variations in rock support capacity due to local variations in bond strength and shotcrete thickness. *Engineering Failure Analysis* 128: 105612.

Zhang, P., Nordlund, E. 2021. A 3DEC Numerical Analysis of the Interaction Between an Uneven Rock Surface and Shotcrete Lining. *Rock Mechanics and Rock Engineering* 54(1): 2267-2289.

19th Australasian Tunnelling Conference – Acosta-Martínez, Stewart and Hudson-Smith (Eds.)
© 2025 Australian Tunnelling Society, ISBN 978-0-85825-002-4

Stability Analysis of a Nozzle Headwall considering interaction with adjacent piles: Insights from Sydney Metro West

Ivy Zhang
Senior Engineer, SMEC, Australia

Ali Golshani
Principal Engineer, SMEC, Australia

ABSTRACT: The Sydney Metro West Western Tunnelling Package (WTP) consists of 9 km of twin TBM tunnels linking Sydney Olympic Park and Westmead. At eastern end of Parramatta station box, 16 m-long nozzles connect the station box to future TBM tunnels.

A critical challenge involves excavating nozzles within 4.6 meters of a commercial building's pile foundations, necessitating tunnel-pile interaction analysis to verify headwall stability and primary support adequacy.

This study applies 2D and 3D Finite Element Modellings (FEM) to assess these interactions, incorporating geological conditions, structural geometry, and construction sequencing. Analytical verification methods and numerical modelling results were compared, evaluating their applicability for the site's multi-layered geology, bolt lengths and shear resistance.

Findings highlight 3D FEM's superiority in capturing spatial complexities, while affirming the applicability and conservatism of analytical approaches. The research offers practical guidance on integrating analytical and numerical techniques to enhance design accuracy and risk management in tunnel engineering.

1 INTRODUCTION

The plan view of the Parramatta (PTA) nozzle enlargement mined tunnel is shown in Figure 1 (a). Nozzle enlargement tunnels will be excavated from within the Parramatta station. The total length of the nozzles is 16m with the RT01 nozzle located on the southern side and the RT02 located on the northern side.

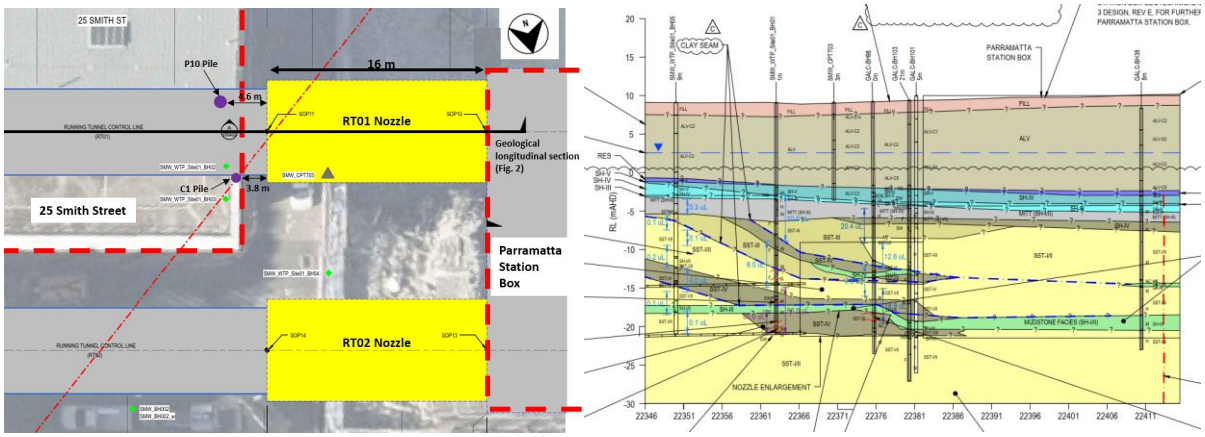
Building No. 25 Smith Street is located to the south-east of the nozzles and is marked out on the top left corner of Figure 1. The P10 pile—which carries the highest ultimate pile load—and the C1 pile are the two closest foundation elements to the nozzle headwall. Given their proximity, they are considered the most critical analyses cases regarding interaction between piles and headwall.

This paper analyses the stability of the nozzle headwall and the adequacy of headwall primary support prior to TBM running tunnel breakthrough, with particular focus on the influence of piles. An analytical approach, along with 2D and 3D FEM were undertaken, and the results were compared.

This analytical method, based on Pells (2001), was refined to place greater emphasis on rock bolt capacity. This capacity was evaluated in detailed considering rock properties, bolt type and bolt spacing, grouting strength, and most importantly, the length of the bolts embedded within the potential rock failure wedge. The method for determining the rock bolt capacity within a failure wedge followed the approach proposed by Anagnostou (2014). In addition, the shear resistance provided by rock bolt 'dowel action' was also considered, using the methodology proposed by Pells (2002).

The 2D and 3D FEM models undertaken using RS2 and RS3 programs considering the anticipated local geology. In the 2D model, a support pressure (derived from calibration of monitoring data) was applied on the nozzle crown and headwall to simulate the effect of the supporting system. In the 3D model, the ground support system was installed as per design and the excavation of nozzles were modelled following the proposed construction sequence. Stability conditions of the nozzle headwall

obtained from 2D and 3D models were compared with results from the analytical method. Results and findings are presented in Section 6 of this paper.



(a) (b)

Figure 1. (a) Parramatta nozzle enlargement plan view; (b) Parramatta station box and nozzle enlargement – RT01 control line geological longitudinal section.

2 SITE GEOLOGY

The geological longitudinal section of the PTA nozzle enlargement tunnels aligned along the RT01 nozzle control line is presented in Figure 1 (b). PTA nozzle enlargement tunnels are underlain by a thick layer of Alluvium (around 10 m thick) followed by Ashfield Shale Class IV to Class I/II located on top of the nozzle crown. Nozzle headwall mainly intersects with declined Sydney Sandstone Class IV – II dipping towards the nozzle opening.

3 ANALYTICAL DESIGN METHOD

3.1 *Headwall stability*

The headwall stability analysis was carried out applying the limit state design principle. The proposed support system is deemed acceptable if the following principal equation is satisfied:

$$FoS = R/D. \tag{1}$$

where R is the total resistance force acting on the failure surface; D is the total driving force happened on the surface; FoS is the resulting factor of safety. The typical failure mechanism of a headwall is presented in Figure 2 (a).

R represents the total resisting force, comprising the headwall support force F_s provided by rock bolts; the shear and friction resistance at the base of the wedge and the additional shear resistance R_b mobilized by rock bolts intersecting the failure surface where the "dowel action" takes place.

D represents the total driving force, comprising the self-weight of the wedge G; the full overburden load from upper underground material above the tunnel crown V_s and the pile load V_{pile}.

$$R = \left[G \cdot cos\alpha + F_s \cdot sin\alpha + (V_s + V_{pile}) \cdot cos\alpha\right] \cdot tan\Phi + F_s \cdot cos\alpha + c \cdot H/sin\alpha \cdot w + R_b \tag{2}$$

$$D = G \cdot sin\alpha + (V_s + V_{pile}) \cdot sin\alpha \tag{3}$$

where α = failure angle between failure surface and horizontal level; Φ = internal friction angle on the failure surface; c is cohesion on the failure surface; H is tunnel height; w is tunnel width.

3.2 *Headwall support force F_s*

The headwall support force F_s is determined by the total capacity of all rock bolts installed in the headwall.

Generally, the support force provided by each bolt depends on the following factors:

- The bolt's factored tensile capacity (F_t),
- The diameters of the grouted borehole (d) and the bolt (d_b),
- The bond strength between the soil and grout interface (τ_m),

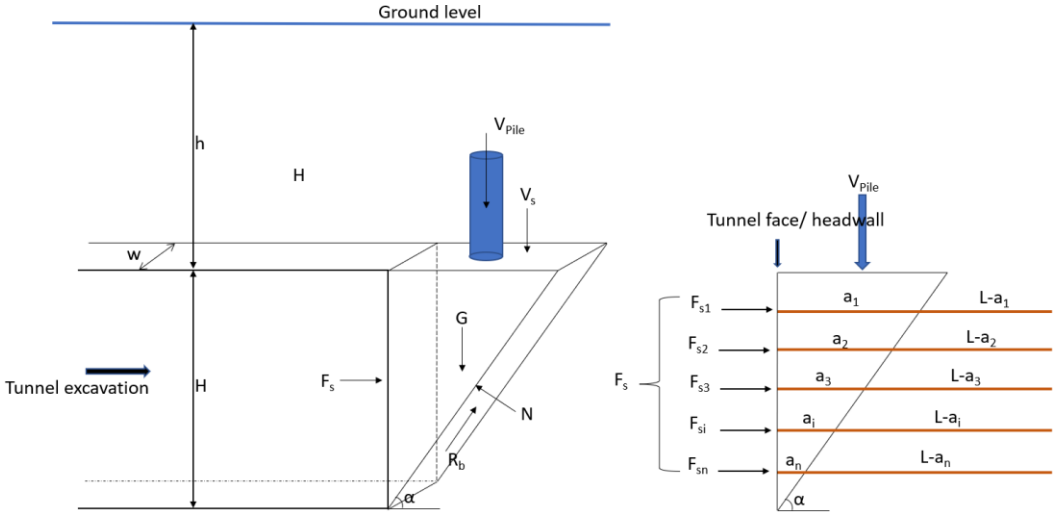
- The bond strength between the grout and bolt interface (τ_g),
- The anchorage length within the failure wedge (a) and
- The anchorage length ($L-a$) in the bedrock ahead of the inclined failure surface ($L-a$) as shown in Figure 2 (b).

The surface reinforcement equation introduced by Anagnostou (2014) is given as:

$$F_s = N \cdot \min\left[F_t, \max\left(\min\left(d\tau_m, d_b\tau_g\right)\pi a, F_p\right), \min\left(d\tau_m, d_b\tau_g\right)\pi(L-a)\right]. \quad (4)$$

This equation accounts for the factored rock bolt tensile capacity (F_t), the failure of the anchor face plates (F_p) and the shear failure at the bolt-grout-rock interface both inside the failure wedge (2nd term) and outside of the failure wedge (3rd term). The support force (F_s) provided by each rock bolt is determined by the minimum of these three terms.

For a given bolt length (L) installed in a specific rock layer with a determined bolt spacing, once the failure surface angle α is known, a_i and $L-a_i$ can be calculated at each row of rock bolts. Using Equation (4), the minimum of these three terms can be determined and the total support force (F_s) is the sum of the capacities of each individual rock bolt.



(a) (b)

Figure 2. (a) Headwall failure mechanism; (b) rock bolt support force F_s distribution on tunnel headwall.

3.3 *Rockbolt additional shear resistance* R_b

In wedge stability analysis, grouted rock bolts provide a 'dowel action' that is activated by the movement of the wedge. This dowel action only becomes active once the wedge begins to move, offering an additional resisting force along the potential sliding plane, thereby enhancing the overall stability of the system.

Research published by Pells (2002) specifically addressed the contribution of rock bolt to the 'cohesive' strength of the joint, and the contribution of tension mobilized in the bolt to the frictional resistance developed on the joint plane.

Pells (2002) suggests that the presence of a reinforcing bolt or cable increases the shearing resistance of the joint by the following mechanisms:

1. An increase in shear resistance due to the lateral resistance developed by the bolt via 'dowel action' – force R_1,
2. An increase in normal stress as a result of prestressing of the bolt – force R_2,
3. An increase in normal stress as a result of axial force developed in the bolt from dilatancy of the joint – force R_3, and
4. An increase in normal stress as a result of axial force developed in the bolt from lateral extension – force R_4.

R1 can be considered as increasing the cohesion of the joint, while R2, R3 and R4 contribute to increasing the frictional component of the interface strength by increasing the effective normal stress on the interface. Therefore, the force acting normal to the joint plane is given by:

$$N = R_2 + R_3 + R_4 \quad (5)$$

So that the additional shearing resistance generated by each rock bolt intersecting with the failure surface R_b is given by:

$$R_b = R_1 + N \cdot tan\Phi_j \quad (6)$$

where Φ_j is the friction angle of the rock wedge failure surface. Detailed calculation steps for R_1, R_2, R_3 and R_4 were presented in Pells (2002). In this paper, shear displacement = 1 mm was adopted in the failure surface to calculate the additional shear resistance.

4 2D FINITE ELEMENT MODELLING

4.1 *Ground model*

The longitudinal cross section of the RT01 control line was developed using Rocscience RS2 program and is presented in Figure 3 (a). The model followed the geological long section shown in Figure 1 (b). As this paper focuses on the nozzle headwall stability, the excavation of Parramatta station box and the future RT01 TBM running tunnel were not incorporated in the model.

Support pressure applied on the nozzle crown and headwall simulated the effect of the installed supporting system. The pressure magnitude was calibrated to match the displacement values observed in real-time monitoring.

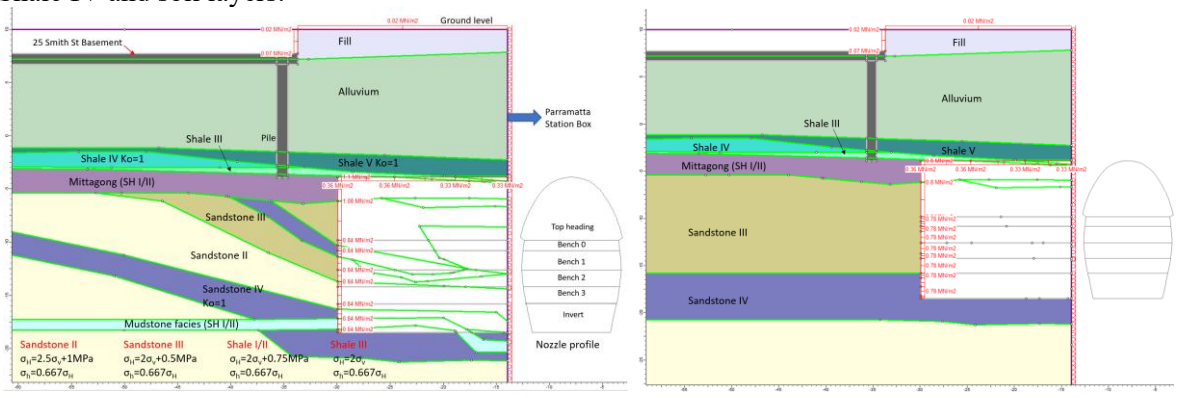
A total ultimate pile load of 10.3 MN was applied. This approach was adopted to represent a conservative (worst-case) loading condition.

The nozzle long section shown in Figure 3 (a) was modelled following the proposed construction stages as outlined below:

- Initialization stage
- Application of ground floor surcharge
- Excavation of the basement and pile, followed by concrete placement.
- Application of ultimate pile load of 10.3 MN
- Excavation of the nozzle top heading and application of support pressure
- Excavation of the remaining benches and invert, with support pressure applied.

Based on the project's geotechnical interpretive report (GIR) and the actual nozzle alignment orientation, the major in-situ stress (σ_H) was applied out-of-plane and the minor in-situ stress (σ_h) was applied in-the-plane (as shown in Figure 3 (a)).

Rock mass parameters were based on Project's GIR and are presented in Table 1. In this analysis, tunnel scale parameters were used. Hoek-Brown failure criterion was adopted for Sandstone Class II & III, Mittagong (Shale I/II) and Shale III. More-Coulomb failure criterion was adopted in Sandstone IV, Shale IV and soil layers.



(a) (b)

Figure 3 (a) RS2 model RT01 longitudinal cross section and nozzle cross section; (b) RS2 sensitivity case.

Table 1 – Characteristic rock mass parameters

Design approach	Parameter	SST II	SST III	SST IV	SH II	SH III	SH IV	SH V
Substance	Intact UCS (MPa)	25	15	10	15	8	4	1
	Poisson's ratio, ν	0.25	0.25	0.25	0.25	0.25	0.25	0.3
Tunnel scale rock mass	Mass modulus (MPa)	2000	1000	500	1000	300	110	15
	GSI	65	55	45	50	40	30	20
	m_b	3.438	2.406	-	1.341	0.939	-	-

Hoek-Brown[1]	s	0.0205	0.0067	-	0.0039	0.0013	-	-
	a	0.502	0.504	-	0.506	0.511	-	-
Mohr-Coulomb[2]	C' (kPa)	-	-	200	-	-	90	40
	Φ (°)	-	-	40	-	-	25	15
	T (kPa)	-	-	10	-	-	0	0

Notes:

1. Damage parameter 'D' of 0, assumes minimal disturbance to rock mass surrounding tunnel.
2. Normal stress range of 0 to 2 MPa assumed.

4.2 *Shear strength reduction approach*

The Shear Strength Reduction (SSR) option in RS2 can automatically perform a finite element slope stability analysis and compute a critical strength reduction factor for the model. The critical strength reduction factor (SRF) is equivalent to the "safety factor".

SSR analysis was conducted in RS2 model to evaluate the headwall stability and determine the critical strength reduction factor of the nozzle headwall. Three typical excavation stages (top heading, bench 0 and full-face excavation) were considered. For each stage, the headwall toe displacement was plotted against the corresponding SRF. The point at which the displacement curve begins to increase noticeably is interpreted as the onset of failure, with the corresponding SRF taken as the Factor of Safety (FoS) for the headwall. Detailed RS2 analysis results are summarised in Table 3.

5 3D FINITE ELEMENT MODELLING

5.1 *Ground model*

A 3D model was developed, incorporating the geology, nozzle excavation, and the basement and piles of the 25 Smith Street building. As in RS2 model, the Paramatta station box and the future TBM running tunnels were not incorporated in the model. The high in-situ stress major direction was assigned along the nozzle transverse direction. Ultimate pile pressures were applied at the pile toes as shown in Figure 4 (a). The material properties used in the model are presented in Table 1.

The proposed nozzle supporting system was incorporated in accordance with the anticipated ground conditions (Figure 4 (b)):

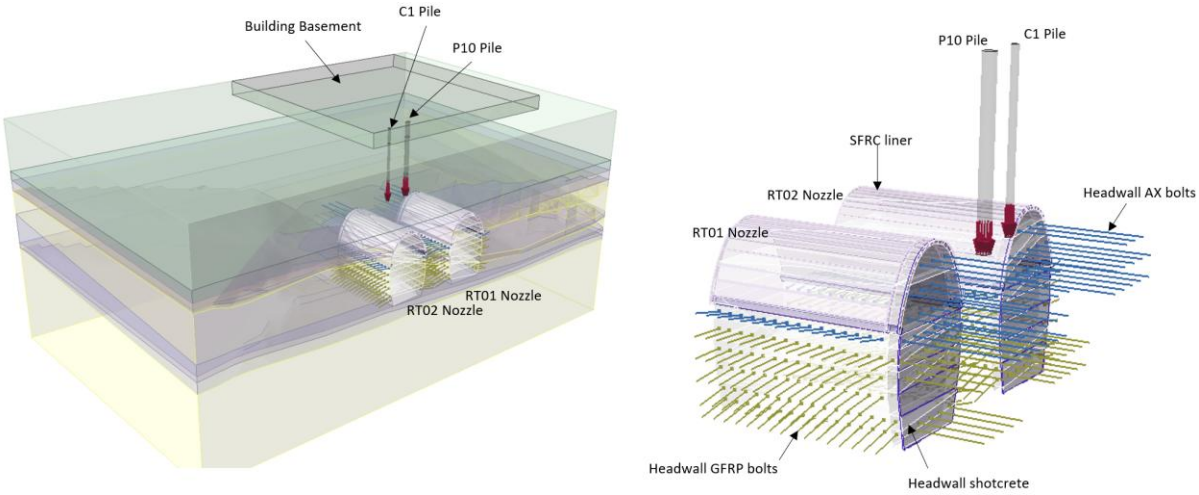
- Nozzle crown: 300 mm steel fiber reinforced shotcrete (SFRS).
- Nozzle sidewalls:
  - Bench 0: 4m long CT bolts on pillar side and 3 m long on the non-pillar side;
  - Bench 1/2/3 and invert: 4m long GFRP bolts on pillar side and 3 m long on the non-pillar side;
- Nozzle RT01 headwall: 9m long CT bolts on the top heading area; 6m long GFRP bolts on the benches and invert. 100 mm steel fiber reinforce shotcrete (SFRS) on the headwall.
- Nozzle RT02 headwall: 4m long CT bolts on the top heading area; 4m long GFRP bolts on the benches and invert. 100 mm SFRS on the headwall.

The stages considered in the RS3 modelling were the following:

- Initialization stage
- Excavation of basement and piles, followed by concrete application
- Application of piles ultimate pressure at pile toe
- Excavation of RT02 nozzle and installation of support in a single stage
- Excavation of RT01 nozzle top heading, with shotcrete application and installation of headwall rock bolts
- Excavation of RT01 Benches and Invert and installation of the corresponding rock bolts and shotcrete on the sidewall and headwall at each excavation stage

5.2 *Shear strength reduction approach in RS3*

Shear strength reduction analysis was also performed in RS3 to assess the stability of the RT01 headwall. After the nozzle excavation was completed, the headwall toe displacement was plotted against the strength reduction factor. When the displacement curve begins to noticeably increase, the headwall failure is considered to have occurred, and the corresponding SRF is taken as the factor of safety for the RT01 headwall in the 3D condition.



(a) (b)

Figure 4 (a) RS3 model overview; (b) RS3 model two nozzles with supporting system.

6 ANALYTICAL METHOD AND FEM MODELLING RESULTS

The FoS obtained for the nozzle headwall, determined using both the RS2 shear strength reduction analysis and the analytical method, is summarized in Table 2.

The FoS from RS2 modelling was determined by plotting the headwall toe total displacement against SRF. The SRF at the point where the total displacement curve begins to noticeably increase was selected as the headwall FoS.

The analytical method was calculated using the SMEC in-house spreadsheet. The detailed calculation process is presented in Section 3. By inputting specific parameters such as geological layer thickness, bolt spacing, bolt length, and bolt design capacity, the FoS for a potential wedge failure at any failure angle α can be calculated. The failure angle α must fall within a specific range that considers the pile load (as shown in Figure 2 (b)). Thus, the headwall FoS is the minimum value within this α range.

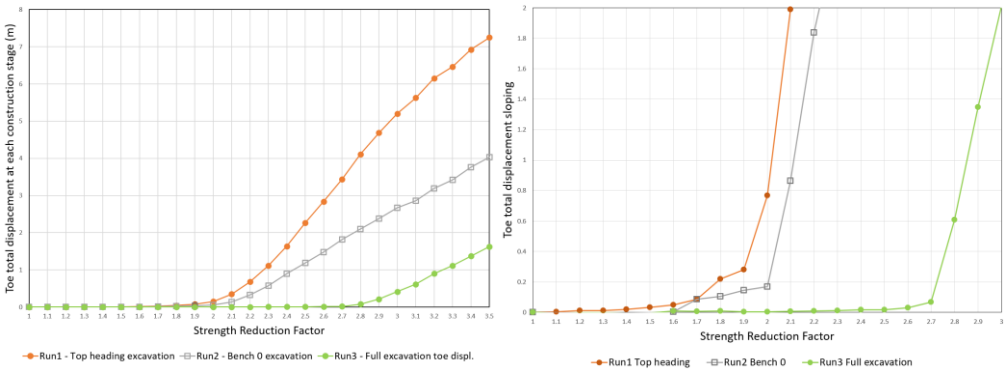
Table 2. Analytical method and FEM modelling results

Run ID	Modelling scenario	FoS from RS2	FoS from RS3	Analytical method FoS without/ with additional shear resistance (as a counter check to FEM)
Run1	Excavate till top heading level	2.0	2.3	1.8 / 2.0
Run2	Excavate till Bench 0 level	2.0	2.3	1.7 / 1.8
Run3	Nozzle fully excavate	2.7	2.9	1.6 / 1.9

The RS2 headwall toe displacement versus SRF is shown in Figure 5 (a), while the toe displacement increment sloping versus SRF is plotted in Figure 5 (b). An example of that can be seen in Figure 6 where RS3 Run1 and Run 3 results are shown.

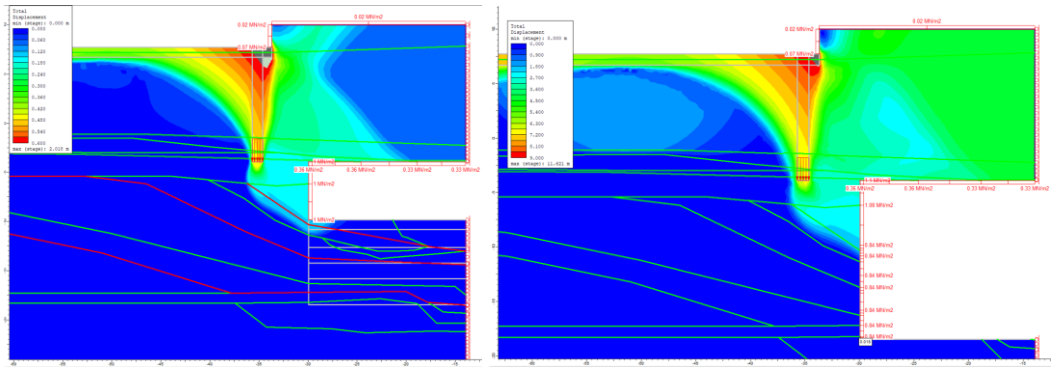
Figure 5 (b) shows that in Runs 1, 2 and 3, total toe displacements experience significant increments at SRF values of 2.0, 2.0 and 2.7, respectively, which correspond to their respective FoS. The total displacement contour for RS2 Run 1 (Figure 6 (a)) indicates a failure surface passing from pile toe to the top heading toe at SRF=2.0. In RS2 Run4 (Figure 6 (b)), although a large toe displacement increment is observed at SRF=2.7, the total displacement contour doesn't show an obvious failure surface. This is primarily due to the geological conditions behind the headwall. As shown in Figure 3 (a), a wedge of Sandstone Class III and a declined strip of Sandstone Class IV are located behind the top heading, causing the rock to fail along this material boundary.

The RS3 model results for the toe displacement of top heading, bench 0 excavation and full-face excavation and their corresponding rate of increment (sloping) are presented in Figure 7 (a). A noticeable increase in toe displacement for top heading, bench 0 level and full-face excavation occurs at SRF=2.3, 2.3 and 2.9. Thus, FoS for top heading, bench 0 level and full-face in RS3 model were determined. RT01 nozzle full-face rock displacement passing through the RT01 control line at SRF=2.9 was presented in Figure 7 (b).



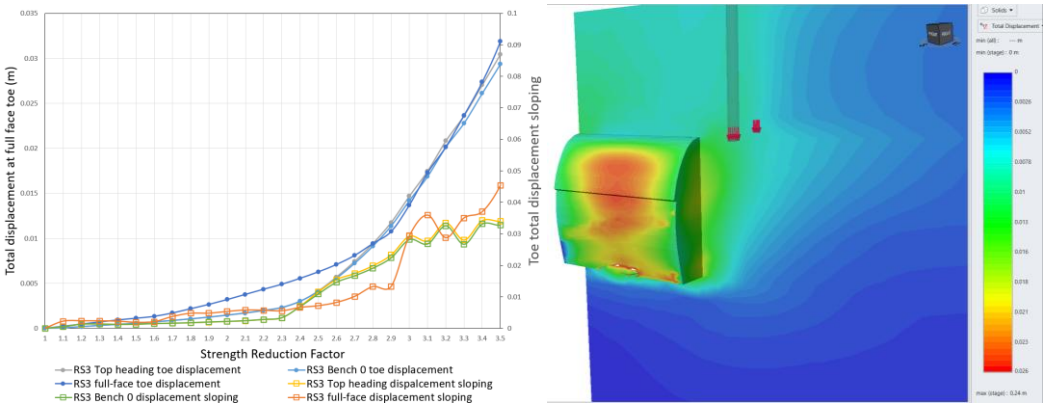
(a) (b)

Figure 5. (a) RS2 headwall toe displacement versus SRF; (b) Toe displacement sloping versus SRF.



(a) (b)

Figure 6. (a) RS2 Run1 top heading displacement contour at SRF=2.0; (b) RS2 Run3 full face displacement contour at SRF=2.7.

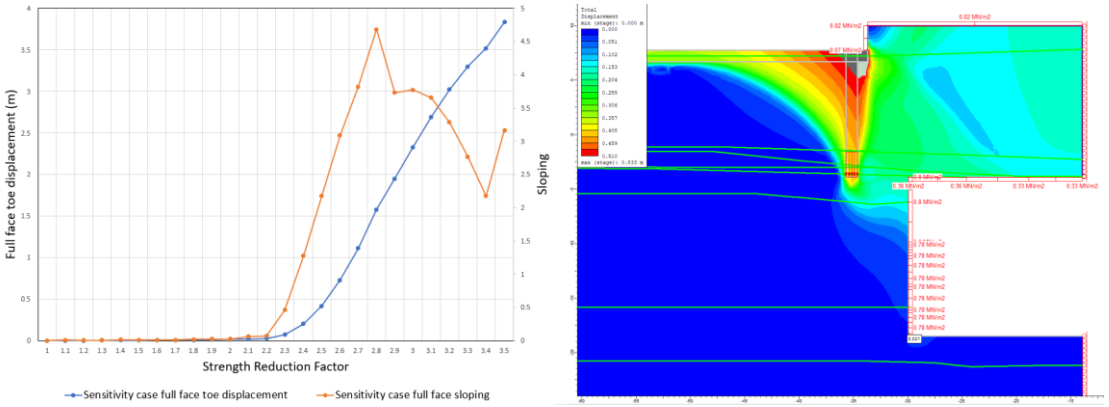


(a) (b)

Figure 7. (a) RS3 full face toe displacement and increment sloping versus SRF; (b) RS3 RT01 full face rock displacement contour at SRF = 2.9.

To assess the influence of geological geometry on headwall stability, a sensitivity analysis was conducted by modelling the ground stratification to be horizonal, instead of being inclined, as shown in Figure 3 (b). In this sensitivity case, the geology above headwall level remained unchanged, while the boundaries between Mittagong formation (SH I/II), Sandstone Class III and Sandstone Class IV were assumed to be horizontal. Sensitivity analysis results are presented in Table 3 and Figure 8. The headwall FoS under this geological configuration was determined to be 2.1. The corresponding FoS from the analytical method for the same geological setup was 1.6/1.8.

The sensitivity analysis highlights the significant role that geological shape plays in headwall stability. When the material boundary behind the headwall is horizontal, the analytical method aligns more closely with the RS2 results, although both remain slightly conservative.



(a) (b)

Figure 8. (a) RS2 sensitivity case full face toe displacement and increment sloping versus SRF; (b) sensitivity case full face toe contour at SRF=2.2.

Table 3. RS2 sensitivity analysis results

Run ID	Modelling scenario	FoS from RS2	Analytical method FoS without/ with additional shear resistance (as a counter check to FEM)
Sensitivity case	Nozzle fully excavate	2.2	1.6/ 1.8

7 FINDINGS AND CONCLUSION

The paper compares the 2D and 3D finite element modelling with an analytical approach to assess the stability of nozzle headwalls under the load of adjacent piles.

In this paper, ground support was modelled in RS2 by applying support pressure based on back-calculations from monitoring data. This is because a longitudinal 2D model cannot accurately represent the arching effect in the tunnel transverse direction. Using the same input parameters (including pile depth, pile pressure, and geology), the RS3 model produced a similar headwall FoS to RS2 and the headwall displacement closely matched the observed displacement monitoring data, validating the RS3 modelling approach. The analytical approach is always conservative as it excludes several factors such as geological stratigraphy, in-situ stress conditions, pile shaft friction and face shotcrete. In this study, the contribution of rock bolt dowel action was incorporated when a failure surface is formed. The results indicate that accounting for this dowel action leads to an increase in the headwall FoS by approximately 0.2 to 0.5.

When geology consists of moderate to weak strength material and is inclined towards the tunnel opening, the failure surface is more likely to develop along the material boundary, regardless of the tunnel opening size. To assess the influence of geological geometry on headwall stability, a sensitivity analysis was carried out using RS2, where the geological layers were adjusted to a horizontal configuration. Under this scenario, the analytical results aligned more closely with the RS2 result but remained conservative. This highlights the importance of considering the actual geological profile and applying sound engineering judgement when evaluating failure surfaces. A larger tunnel opening does not necessarily imply a lower FoS.

8 REFERENCES

G. Anagnostou, P. Perazzelli. Analysis method and design charts for bolt reinforcement of the tunnel face in cohesive-frictional soils.

Pells, P. J. N. Development in the design of tunnels and caverns in the Triassic rocks of the Sydney region. International Journal of Rock Mechanics and Mining Sciences, Vol 39, pp 569 -587 2002.

Pells, P.J.N. A Note on Rockbolt Design for Load Supporting Ledges in Hawkesbury Sandstone. Aust. Geomechanics, Dec 2001.

Theme 3. Sprayed Concrete and Ground Support

THIS PAGE INTENTIONALLY LEFT BLANK

19th Australasian Tunnelling Conference – Acosta-Martínez, Stewart and Hudson-Smith (Eds.)
© 2025 Australian Tunnelling Society, ISBN 978-0-85825-002-4

Shrinkage Cracking in Slender Shotcrete Tunnel Linings

E.S. Bernard
Victoria University, Melbourne, Australia

ABSTRACT: Drying shrinkage cracks in shotcrete linings are widely assumed to be benign and are often dismissed as inconsequential to the performance of shotcrete linings. However, recent experience in Australian tunnels constructed with slender shotcrete linings indicates that this type of cracking presents a significant maintenance issue due to the frequent leakage of groundwater into the tunnel space through these cracks. This paper examines the formation and consequences of drying shrinkage cracks in slender shotcrete tunnel linings and discusses measures developed to treat the durability and maintenance problems that arise as a result of water leakage though shrinkage cracks.

1 INTRODUCTION

In recent years there has been a move toward more slender shotcrete linings in tunnel excavations, particularly in hard ground that is relatively stable and amenable to support based primarily on bolting. This trend was originally driven by economic considerations but has more recently been supplemented by 'carbon minimisation' concerns. The result has been slender final linings constructed using shotcrete of only 50-125 mm thickness, often with no primary lining. For example, the Eastern Distributor (Pells, 2002), Norfolk tunnels (Clarke et al, 2014), Lane Cove Tunnel (Maconachie et al, 2005), M5 East tunnel (Adams et al, 2001; Hanke et al, 2001), Cross City Tunnel (Asche and Bernard, 2004), and WestConnex tunnels (Aitchison et al, 2018; Barry et al, 2021) all included slender shotcrete linings in at least a portion of their length. These linings usually form part of a 'drained canopy' approach to management of water ingress in which numerous drainage elements are placed on the rock (or 50 mm initial lining) surface before spraying the final layer, thereby facilitating transfer of groundwater to drains at the sides of the tunnel space. While these slender linings may satisfy structural requirements for support of self-weight and occasional loose ground, they have tended to experience a significant amount of cracking due to drying shrinkage, as well as other problems (Kost et al, 2021).

1.1 *Background*

The extent of drying shrinkage cracking experienced by recently completed shotcrete linings has varied both within and between projects. Many linings have zones within them in which drying shrinkage cracks are infrequent, but the same linings have suffered severely from shrinkage cracking in nearby areas. The incidence of cracking does not appear to be related locally to thickness, but thin linings (<75 mm) have generally been observed to suffer more widespread drying shrinkage cracking than thicker linings (>150 mm).

Assessments of cracks in recently constructed tunnel linings have indicated that the majority of cracks have been caused by drying shrinkage (as opposed to ground movement) and the majority of these cracks pass all the way through the lining rather than being blind cracks. This has resulted in frequent uncontrolled seepage of groundwater through the linings, although this varies

with the availability of groundwater which changes both spatially and temporally. It also indicates that no net compressive action exists in these linings. Very few of the cracks exhibit continuous ingress of running groundwater; the majority exhibit slow and intermittent seepage leading to evaporation of moisture on the drying surface of the lining leaving salts such as halite (NaCl), mirabilite ($Na_2SO_4 \cdot 10H_2O$), epsomite ($MgSO_4 \cdot 7H_2O$), and copiapite ($Fe^{2+}Fe^{3+}_4(SO_4)_6(OH)_2 \cdot 20H_2O$) to accumulate in and around the crack. While the concentrations of these minerals in the nearby groundwater are seldom of concern (Hunter, 2025), their steady accumulation by evaporation in and around drying shrinkage cracks can lead to elevated concentrations that potentially pose a threat to both the steel fibres and concrete matrix that comprise most shotcrete tunnel linings.

The spacing between observed drying shrinkage cracks appears to be related to the thickness. For shotcrete sprayed onto rock of relatively even geometry, the ratio of spacing/thickness has typically been observed to range from 10-20, although occasionally it is as low as 6. For shotcrete sprayed onto waterproof membranes, the ratio of spacing/thickness has been observed to range from 20-40. Drying shrinkage cracks have often been observed to coincide with discontinuities in the underlying rock strata, particularly joints and steps in rock strata, and with covered drainage features such as strip drains. This may have some bearing on why the observed range of crack spacing appears to be so broad. Nevertheless, observations of typical drying shrinkage crack spacings in shotcrete linings are much greater than the characteristic spacing between flexural cracks, which is commonly approximated as equal to the thickness of a member (DBV, 2002; *fib*, 2022). Taking the drying shrinkage spacing to be equal to the thickness of the lining will result in a gross under-estimate of crack width, since width is calculated on the basis of the factored accumulation of shrinkage strain between cracks.

Drying shrinkage cracks are typically difficult to find on a gun-finish shotcrete surface unless they are revealed by seepage of moisture and/or accumulation of calcite and salts. This suggests a bias is likely in observed distribution because their occurrence will appear to be more frequent in areas with ample groundwater. Since most shotcrete linings in Australia are drained structures, in which the lining forms a canopy that is part of a drainage system incorporating strip drains and mats immediately behind or within the lining, it is not surprising that groundwater will find its way through cracks in the lining. Indeed, it appears irrational to assume that a lining which is known to suffer shrinkage cracking is capable of fully diverting groundwater to the sides of a tunnel space without leaking.

According to industry specifications such as B82 Shotcrete Work (TfNSW, 2022), the maximum permissible unrestrained drying shrinkage strain for shotcrete at 56 days is 800 με (based on AS1012.13). Taking the exposed perimeter of the lining into account (in accordance with AS5100.5) to calculate the hypothetical drying thickness (equal to twice the actual thickness), a realistic design drying shrinkage strain lies somewhere between 480 and 800 με for a 75 mm thick lining depending on the relative humidity. For an elastic modulus of 15-25 GPa (depending on the age of the shotcrete), this implies a shrinkage-induced tensile stress far in excess of the typical tensile strength of shotcrete. In the opinion of the author, it is inevitable that a lining made of such a material will suffer drying shrinkage cracking. Indeed, the design for many recently constructed tunnel linings anticipated that drying shrinkage cracks would occur in the shotcrete lining and limits were therefore set on maximum allowable crack widths. The problem for the operators of the tunnels has been the very large number of drying shrinkage cracks that occur, and the ongoing challenge of managing the impacts associated with these cracks.

Tunnels are usually required to be at least free of dripping water. For transport tunnels, drips are not permitted onto trafficable surfaces such as roadways due to concerns about vehicle slippage. Moreover, drips are not permitted on equipment such as catenary in rail tunnels or M&E due to corrosion concerns. As described above, it is difficult to produce an entirely 'waterproof' lining so measures need to be taken to prevent or intercept the dripping groundwater. One approach is to include a water-proofing membrane within the lining, but this approach may not be entirely effective. A second approach is to intercept drips using strip drains and drainage mats that are usually installed when and where dripping is observed. However, this has also been found to be only partially effective. A third approach is to drill weep holes into the surrounding rock, intercepting geological features such as bedding planes to provide alternative routes for the groundwater to drain before it contacts the shotcrete lining. Each of these methods has its own

advantages and disadvantages, but all have been developed in response to the fact that drying shrinkage cracks are ubiquitous in slender shotcrete linings and lead to leaks and seeps.

2 EFFECT OF SHRINKAGE CRACKS ON LINING DURABILITY

The design exposure environment prevailing for shotcrete linings in tunnels within Australia is usually taken to be governed by the requirements of AS5100.5. Unfortunately, this document was never intended to be applied to tunnel linings and remains inadequate to the task as it does not take into account the unique micro-environments prevailing in most tunnels. Tunnels are dynamic environments through which groundwater and air move at a much more rapid rate than other underground structures such as piles and foundations. Exposure classifications based on stationary contact with non-flowing groundwater are inappropriate to the assessment of the potential deterioration mechanisms unique to tunnel linings. Moreover, evaporation of groundwater at drying surfaces (particularly around cracks, Figure 1) has been observed to be significant in Australian tunnels: this process increases the ionic strength of contaminants in the groundwater that remains at points of evaporation on the lining surface leading to a more aggressive exposure condition than is suggested by the concentration of contaminants in groundwater within the surrounding rock.

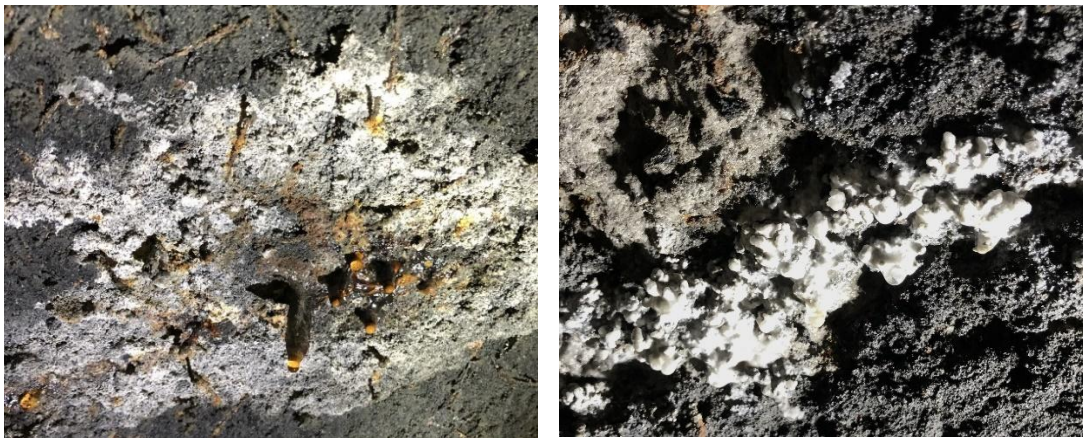


Figure 1. Examples of calcite precipitation in the form of a crust at a drying surface adjacent to slowly leaking cracks in a shotcrete lining.

Conventional thinking posits that calcite, generated by reactions between calcium hydroxide in the shotcrete and carbonic acid in percolating groundwater, will precipitate within and seal cracks that occur in a shotcrete lining. However, the presence of metallic ions in groundwater, such as magnesium and ferrous ions, increases the solubility of calcite thereby preventing precipitation of calcite in cracks (Katz et al, 1993; Nielsen et al, 2013). This process will often preclude autogenous sealing of cracks that occur through concrete linings in underground environments due to the ubiquitous occurrence of metallic ions in groundwater (Edvardsen, 2022). The failure of calcite precipitation to seal cracks is evidenced by the clear absence of calcite in through-thickness cracks observed in cores drilled through some tunnel linings. Instead, when the groundwater (ladened with dissolved calcite) emerges from a crack into the tunnel space and contacts air, the ferrous ions are precipitated out as iron oxide which then allows the calcite to precipitate as a crust at the mouth of cracks (Figure 1). The absence of precipitated calcite within the cracks means that steel fibres bridging the cracks are not protected from corrosion.

Evaporation of groundwater at drying surfaces in and around cracks leads to an accumulation of salts such as sodium chloride and magnesium sulphate which subsequently precipitate within the crust at the mouth of the crack (Figure 2). Given that the solubility of sodium chloride is 386 g/L, and that of magnesium sulphate is 186 g/L (at 20°C), the concentration of these salts must reach extreme levels in water within the crack for precipitation to occur. Relatively high concentrations of solid chloride- and sulphate-rich salts within the calcite-dominated efflorescence at the crack mouth act as a buffer to maintain elevated concentrations of these ions in the water within

the crack during periods of near zero flow. Moreover, during periods of drying the surface meniscus of the water within a crack will steadily recede into the crack: this process will draw salt-rich water from the crack mouth deep into the crack thereby further promoting corrosion of the steel fibres (Figure 2).

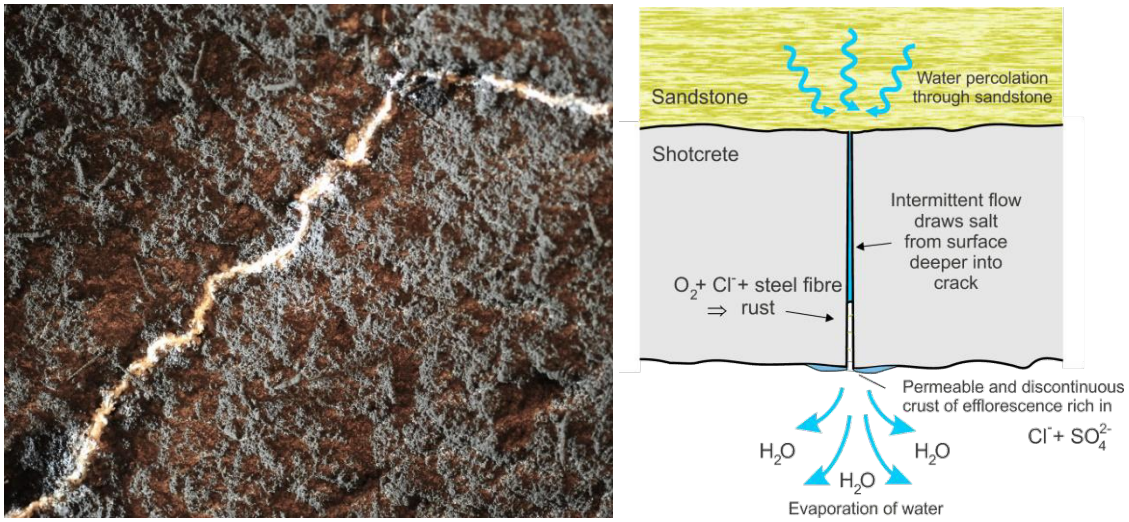


Figure 2. Percolation of groundwater through shrinkage cracks in a shotcrete lining lead to accumulation of calcite and salt at the drying surface.

Since cycles of wetting and drying occur regularly within most tunnels this process will result in a steady penetration of elevated concentrations of chloride and sulphate ions into cracks, despite the fact that gravity usually acts to drive water in the opposite direction (out of the crack) during periods of higher groundwater flow. The nett outcome is that chloride ions become concentrated in the small amount of water remaining within and around the crack, leading to rapid corrosion of steel fibres (Marcos-Meson et al, 2018) and sulphate ions become concentrated to levels at which they are more likely to attack the concrete (Romer, 2003; Hagelia, 2011, 2018; see Figure 3). Use of macro-synthetic fibres eliminates the problem of corrosion (Chernov et al, 2006) but will not prevent sulphate attack of the concrete matrix.

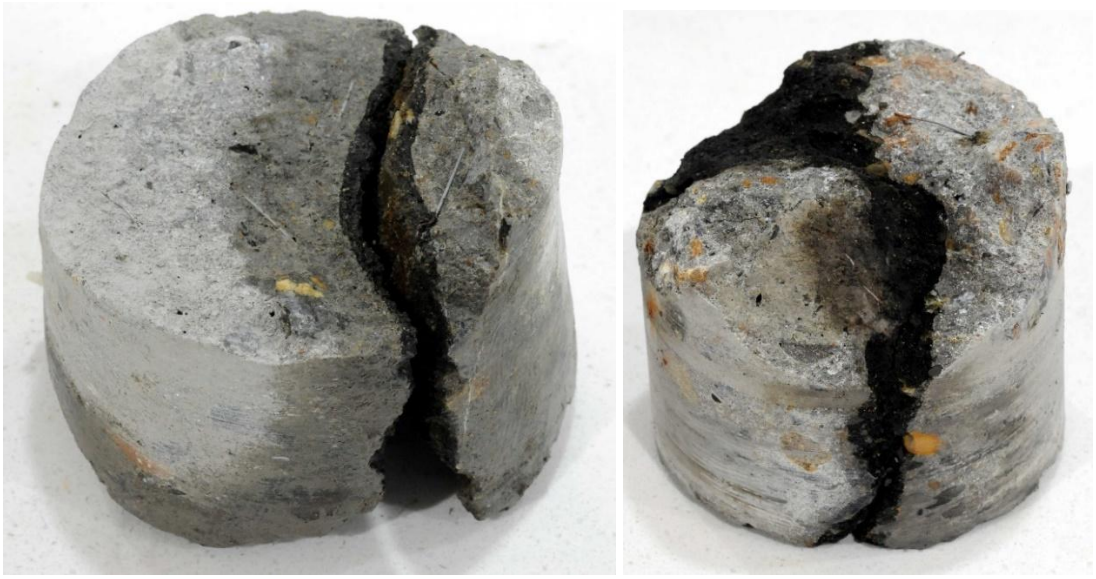


Figure 3. Examples of sulphate attack in shrinkage cracks through a shotcrete lining in a tunnel due to accumulation of sulphate ions through evaporation. Soft dark zone is depleted of calcium and enriched in magnesium and ferrous iron compared to adjacent un-altered shotcrete. The dark colour is caused by accumulation of ferrous oxide in degraded shotcrete.

The rate of corrosion of steel fibres is also governed by availability of oxygen, thus corrosion is more active near the atmospheric end of each through-crack and is relatively limited in the deeper recesses. Observations of corroded steel fibres in shrinkage cracks through shotcrete linings indicate that the 'oxidation depth' is about 50 mm for cracks 0.15 mm or greater in width. For this reason, shrinkage cracks through thin linings (< 150 mm) are likely to suffer more complete corrosion of steel fibres than would occur in shrinkage cracks (of equal width) through thick linings (> 150 mm).

3 EFFECT OF SHRINKAGE CRACKS ON STRUCTURAL CAPACITY

The most common method of designing slender shotcrete linings on hard rock is the method by Barrett and McCreath (1995). This method posits that the two main modes of lining failure are flexural and shear-based (see Figure 4). If the bond to the ground is poor or non-existent, a flexural mode of failure will govern the local load resistance of most linings. If the lining is well bonded to the ground the flexural resistance of the lining/rock composite (which tends to act like a beam) will most likely exceed the shear resistance of the lining so shear tends to govern capacity. The flexural and shear resistance of a lining are therefore estimated and compared to the load actions developed as a result of ground instability.

The presence of shrinkage cracks through a shotcrete lining can reduce the structural resistance of the lining for both flexural and shear modes of failure. Corrosion of steel reinforcement and fibres bridging a crack can locally eliminate both the tensile and flexural resistance. This is more likely to occur as the width of shrinkage cracks increases. If wider than about 0.3 mm, shrinkage cracks will also largely eliminate shear resistance. Thus, the existence of shrinkage cracks (especially wider than 0.3 mm) can locally diminish, or eliminate, the two principal mechanisms of load resistance described by Barrett and McCreath (1995). However, the extent to which this occurs will also depend on the thickness of the lining and density of local cracking.

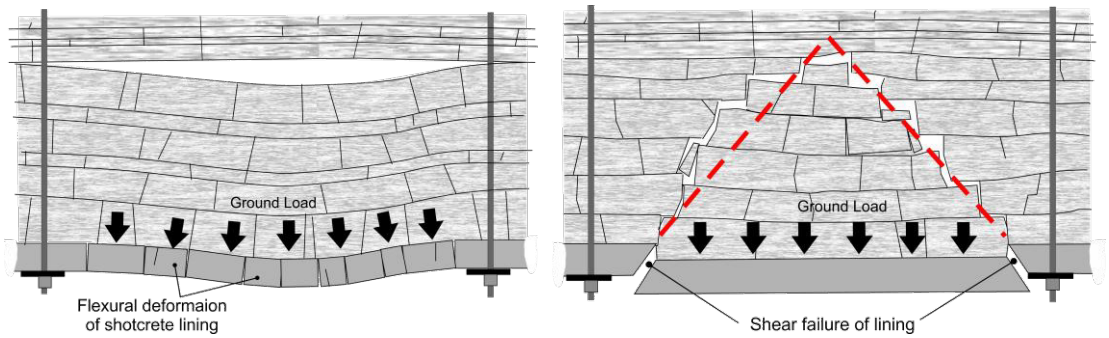


Figure 4. a) Flexural, and b) shear failure modes for slender shotcrete linings (based on Barrett and McCreath, 1995).

Many linings exhibit much greater load resistance than is suggested by pure flexural or shear action alone, largely due to Compressive Membrane Action (CMA, Reid and Bernard, 2024). This mechanism of load resistance is strongly dependent on the degree of in-plane restraint available within a shotcrete membrane, which, in turn, is diminished by the presence of shrinkage cracks. The presence of a discontinuity such as a through-thickness shrinkage crack reduces the in-plane stiffness of a lining and increases the magnitude of deformation in the flexural failure zone required before CMA is achieved (Figure 5). For example, through-thickness cracks of about 0.3-0.4 mm width can largely eliminate the potential for CMA in a slender lining of 50 mm thickness (when assessed using the method by Reid and Bernard, 2024). This is particularly significant for de-bonded regions of lining between widely spaced points of support. Elimination of CMA will reduce the load resistance of a slender lining to a level based on pure bending or shear, but as mentioned earlier, shrinkage cracking and corrosion of steel fibres can also diminish or eliminate load resistance associated with these simpler modes of resistance.

Given the significant effect that shrinkage cracking and deterioration within these cracks can have on water ingress and load resistance, it is prudent to examine what can be done to prevent the high incidence of shrinkage cracking observed in many tunnels or repair the cracks that already exist. Strategies for managing shrinkage cracks are described in the following pages.


Figure 5. Drying shrinkage cracks through the thickness of shotcrete linings. These cracks diminish in-plane stiffness and, as a result, reduce the effectiveness of CMA.

4 SEALING OF CRACKS

Surveys of cracks in shotcrete linings in Australia have identified that the majority arise as a result of drying shrinkage rather than thermal shrinkage or ground movement. This is particularly true of areas exhibiting extensive inter-connected cracking in which polygonal 'plates' form between the cracks (Figure 6a). In other areas, the shrinkage-based nature of cracking has been confirmed by surveys which have demonstrated an absence of convergence or localised ground movement.


Figure 6. a) Polygonal drying shrinkage cracks in a shotcrete lining, and b) secondary cracking of an epoxy repair membrane caused by on-going shrinkage of the lining.

In the absence of groundwater, shrinkage cracks are seldom noticed. However, groundwater often finds and leaks through these cracks leading to dripping and durability problems. When this happens, tunnel operators are usually required to 'manage' the leak in a manner that conforms with operational requirements to limit water ingress onto road surfaces, rail infra-structure, and mechanical equipment.

One solution often proposed to the problem of 'managing' drying shrinkage cracks that drip groundwater is to seal them with resin or grout as they occur. There are several problems with this approach:

1. Sealing a crack does not reduce shrinkage strains in the surrounding lining and therefore does not diminish the incidence of these cracks,
2. Sealing merely prevents water leakage and does not reinstate the structural performance of a lining,

3. Sealing of a crack in the lining diverts the groundwater and very likely promotes leakage somewhere else,
4. Drying shrinkage clearly occurs over an extended period of time (evidenced both by measurements in the lab and survey evidence of steady crack width increase over time in tunnels). Sealing them when they first appear therefore leads to the necessity to re-seal them as they suffer secondary cracking due to continued drying shrinkage (Figure 6b). If they are left to progressively widen until they reach a stable long-term width (which can take several years), leakage of groundwater and accumulation of aggressive ions at the drying surface can damage the lining and reinforcement in the vicinity of the crack before sealing is implemented,
5. Drying shrinkage cracks often induce curling and de-bonding of a lining on each side of the crack (Malmgren et al, 2005). The pressure required to inject grout into a crack to effect proper filling may therefore 'jack' the lining off the substrate which can lead to more serious long-term problems than dripping (Figure 7).

Further to the curling issue listed above, the problem of lining curl on either side of cracks has been extensively examined by Malmgren et al (2005), Carlswärd (2009), and Sjölander and Ansell (2017) who all concluded that de-bonding of a lining in the vicinity of a crack is inevitable because the tensile stress generated at the substrate boundary far exceeds the tensile strength of concrete (Silfwerbrand, 1997). Once initiated, the de-bonding extends to a width equal to about three times the thickness on either side of a crack (Figure 7a). Injecting grout or resin under pressure into a crack with de-bonded edges could therefore induce peeling at the adjacent boundary between lining and ground (Figure 7b). Peeling can result in a very low effective bond strength between lining and ground, as evidenced in tests conducted by Fernandez-Delgrado et al (1975), leading to the enlargement of de-bonded regions around a crack. Peeling action was described as 'adhesive failure' by Barrett and McCreath (1995) and was recognised as a significant mode of lining failure by Hahn and Holmgren (1979).

The potential for effective crack sealing is better for narrow cracks compared to wide cracks, thus any measure that reduces crack widths will improve the likelihood of successful sealing. Reinforcement may provide some control on the width of drying shrinkage cracks once they occur (Granju, 1997), but the beneficial influence of fibres is relatively limited at the dosage rates typically used in shotcrete linings. Post-crack creep through pull-out of both steel and macro-synthetic fibres, especially at early ages (Larive et al, 2016; Boshoff and Nieuwoudt, 2017; Babafemi et al, 2018), can limit the effectiveness of fibres in controlling drying shrinkage crack widths. Corrosion of steel fibres will also diminish or eliminate the likelihood that this type of fibre will restrain the widening of shrinkage cracks. All the shotcrete linings observed by the author to suffer drying shrinkage cracks (with average widths of 0.3-0.4 mm) were reinforced with between 30 and 45 kg/m^3 of hooked-end steel fibres, thus the presence of steel fibre reinforcement clearly failed to prevent the development of unacceptably wide shrinkage cracks in linings constructed to date.

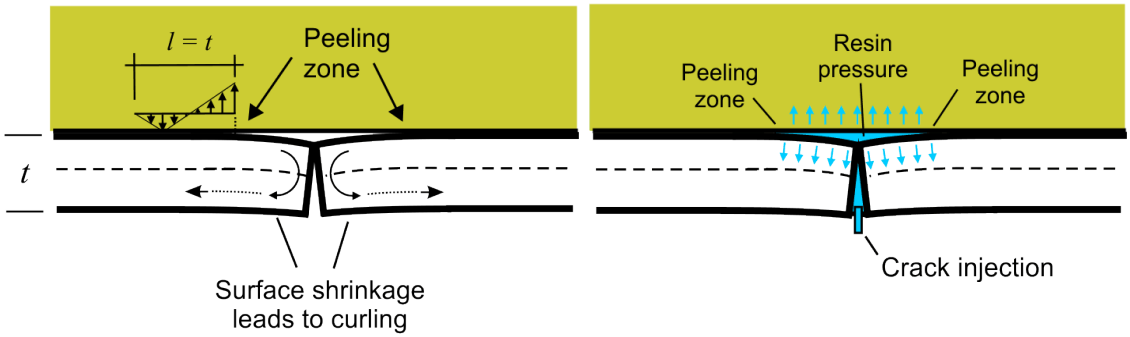


Figure 7. a) Curling and de-bonding of a shotcrete lining from the substrate at a crack due to differential shrinkage strains between exterior and interior regions of the lining (Reid and Bernard, 2019), and b) enlargement of de-bonded zone by resin injection.

The widespread incidence of drying shrinkage cracks in shotcrete linings observed both in Australia and internationally indicates that the common analytical approach of modelling shrinkage strains using 'thermal equivalence' does not result in a realistic estimate of lining behaviour. Instead, drying shrinkage causes a slender lining to break into plates bounded by cracks that, as a result of corrosion, creep, and other processes, lack sufficient tensile capacity across the cracks to

induce a uniform tensile stress field throughout a lining. The presence of cracks disrupts the distribution of stress thereby undermining the models used to assess long-term behaviour (Bodner, 2022). An improved means of modelling drying shrinkage in shotcrete linings that takes account of the presence of cracks is clearly needed.

5 THE EFFECTS OF WIND, HUMIDITY, AND TEMPERATURE

Shotcrete tunnel linings tend to be quite thick in most countries, and shotcrete-based final linings are still relatively rare. Australia has been a pioneer in the use of slender single-pass shotcrete linings, but they are also used in Scandinavia and to a lesser degree in Chile. It is therefore instructive to examine the in-service performance of shotcrete linings in these countries in relation to drying shrinkage cracking.

The Norwegian practice for construction of shotcrete linings in road tunnels has been to apply a minimum thickness of 50 mm in stable hard-rock conditions, which was increased to 80 mm in 2020 (Holter et al, 2021). Further increases in thickness can be introduced to allow for degraded stability (NTS, 2010). Examination of these linings after 15-20 years of service has revealed a relatively low incidence of drying shrinkage cracking in some areas (Manquehual et al, 2022), but a high incidence in others (Holter, 2015). The incidence of cracking appears to be related to the average relative humidity in Norwegian tunnels, with some very humid coastal tunnels experiencing low levels of cracking.

Temperature variations can have a significant influence on existing crack widths. Mapping of cracks and measurement of crack widths in a shotcrete lining in Norway by Holter (2015) over a period of a year indicated that the width of cracks varied seasonally. For a 110 mm thick lining sprayed over a spray-on waterproof membrane base (which itself covered a primary lining sprayed onto a drill and blast rock surface) the mean spacing between drying shrinkage cracks was 700-1000 mm. The width of the drying shrinkage cracks varied by about 0.2 mm between winter and summer, with maximum crack widths occurring in winter and minimums in summer (for a mean seasonal temperature change in the lining of 6°C). This implies that injection sealing should be done in winter but also suggests that sealing is unlikely to be completely effective due to the combined effects of creep and seasonal thermal straining.

Low temperatures can also have a direct effect on drying shrinkage cracking of young shotcrete by limiting the development of tensile strength during the first few days of hydration. In cool and dry conditions, the likelihood of shrinkage cracking is increased because the development of tensile stress in the young lining as a result of drying shrinkage may exceed the rate of tensile strength increase. Warm humid conditions with minimal air flow represent the ideal environment for curing young shotcrete.

Investigations of drying shrinkage cracks over drain mats in Swedish tunnels (Ansell and Bryne, 2015) have indicated crack widths can average as much as 1.2 mm when shotcrete is sprayed onto a substrate providing low restraint. Since most fibre reinforced shotcrete is strain softening in direct tension, only one crack tends to form over a drain and all the accumulated drying shrinkage in the adjacent lining tends to manifest as widening of the initial crack. This was observed to occur even when curing conditions were good.

Australian tunnels generally suffer from low ambient humidity made worse by forced ventilation. Of particular concern is the Relative Humidity of air forced into tunnels during nights, especially in winter. Cool external air moving into a warm tunnel space tends to warm up upon contact with tunnel surfaces. Given that the total moisture content of the air remains relatively constant, this leads to a fall in Relative Humidity. For example, using the method of RH estimation described by Korotcenkov (2018), external air at 10°C and 60% RH entering a tunnel and rising in temperature to 20°C will experience a fall in RH to 45%. Heating of air in the tunnel also occurs due to vehicle operation, further exacerbating the problem. These processes cause the tunnel environment to be more arid than the nearby external environment. A more arid environment will lead to increased drying shrinkage.

The effect of a reduction in humidity on shrinkage strains can be assessed as follows. Using Figure 6.1.7.2 of AS5100.5 one can estimate that the long-term drying shrinkage strain will increase by 30% if the exposure environment changes from ‘temperate’ to ‘arid’. Alternatively, Model Code 2010 considers of the effect of Relative Humidity on drying shrinkage via Eqn. 5.1-

77, which includes a relative humidity factor β_{RH} (in which RH is expressed in percent) applied to the total design drying shrinkage:

$$\beta_{RH} = 1.55\left[1 - \left(\frac{RH}{100}\right)^3\right] \quad (1)$$

This equation implies that drying shrinkage in hardened concrete will increase by 16% with a fall in RH from 60 to 45%. This function also appears in ACI 209.2R, but an alternative factor equal to $\beta_{RH} = (1 - (RH/100)^4)$ is available within this guideline that implies a change of only 10% in drying shrinkage.

Another factor to consider is that an increase in ambient humidity may cause concrete to absorb moisture from the air and swell (Neville, 1996). The magnitude of this swelling will depend on the Relative Humidity, temperature, and age of the concrete, but can be as great as 300 με. Successive cycles of wetting and drying may cause a shotcrete lining to experience cyclic changes in surface strain and crack widths similar to the effects induced by thermal changes.

The effect of wind (including ventilation) over the surface of a young shotcrete lining draws moisture out of the surface of the lining and increases drying shrinkage. It has been known for a long time that effective curing measures such as ponding or application of curing compounds are required to prevent loss of moisture from the surface of young concrete (Hover, 2006). However, neither ponding nor curing compounds are practical in tunnel construction where shotcrete layers tend to be built up in multiple layers. Relative Humidity, temperature, and wind speed relative to the surface of the concrete all contribute to moisture loss which adversely affects hydration and especially shrinkage strains. The absence of bleed and the roughness of most shotcrete linings exacerbates the problem for tunnel linings. Zhang et al (2020) demonstrated that wind speeds of 0.5-1.5 m/s over the surface of young cement paste can substantially increase drying shrinkage strains (by up to 100%) over the first few days of hydration, compared to samples in still air. The necessity of ventilating tunnels during construction increases the amount of drying shrinkage the lining is likely to experience compared to the 'temperate' conditions assumed in AS5100.5, with the worst shrinkage likely to occur in the most heavily ventilated areas such as near the excavation face.

The damaging effect of wind is another reason why thin shotcrete linings tend to suffer worse drying shrinkage cracking than thicker linings: the outer layer of shotcrete suffers the most severe dehydration but also protects the underlying shotcrete from water loss. As thickness is increased, a larger proportion of the total shotcrete thickness is protected from moisture loss by the outermost layer.

5.1 *Effect of Set Accelerators on Drying Shrinkage*

Like all accelerators, Aluminium Sulphate-based set accelerators are known to increase drying shrinkage (Goodier et al, 2007; Lagerblad et al, 2010; Yang et al, 2022). They do this by changing the chemistry of the hydration reactions in sprayed shotcrete compared to shotcrete lacking an accelerator. The magnitude of the effect varies with the type of accelerator and dosage rate used. Due to the difficulty of producing unrestrained shrinkage specimens using set accelerated shotcrete, the typical magnitude of unrestrained drying shrinkage strain likely to occur in Australian shotcrete mixtures has seldom been examined.

To address this shortcoming, two trials were undertaken in which the dosage rate of SA160 set accelerator was varied from 0 to 4% by weight of cement (bwc). One mix included 30 kg/m^3 of Dramix RC35/65 3D fibres, while the other had 6 kg/m^3 of Barchip BC48 macro-synthetic fibres. Both sets of specimens were made with the same shotcrete mixture dosed with differing types of fibre (Table 1). This mix was a commercial shotcrete mix supplied by a local ready-mixed concrete supplier. Unrestrained drying shrinkage specimens were produced by spraying accelerated and non-accelerated shotcrete into beamlet moulds and screeding the surface level immediately after spraying. All specimens were wet-cured for only one day and AS1012.13 shrinkage measurements out to 5 years were based on the initial beamlet length measured at one day's age.

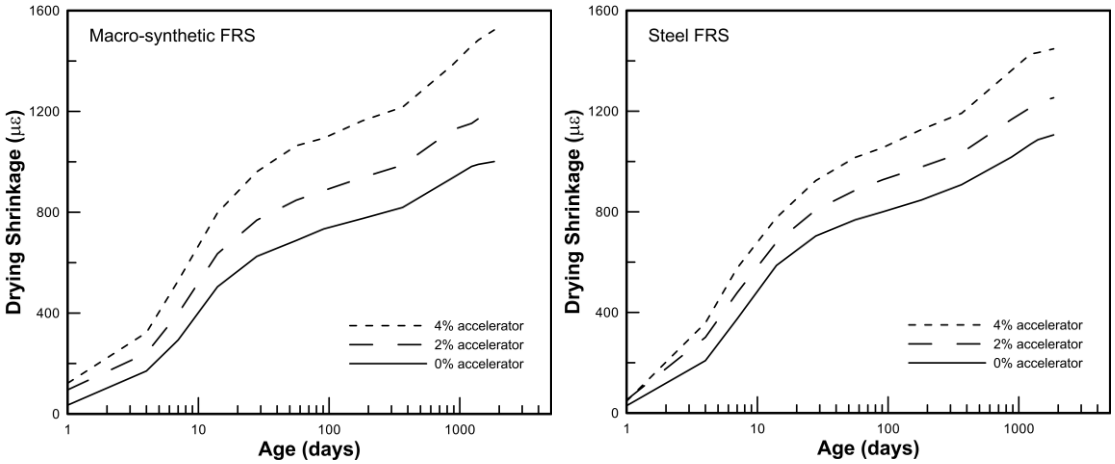


Figure 8. Drying shrinkage to 5 years for sprayed shotcrete reinforced with a) macro synthetic fibres (L), and b) steel fibres (R), for varying dosages of set accelerator (bwc).

The results indicated that addition of 2% bwc SA160 set accelerator increased the drying shrinkage by an average 17% compared to the non-accelerated sprayed mix, and addition of 4% bwc SA160 increased the drying shrinkage by an average 41% at 5 years (Figure 8). The mean 5 year drying shrinkage strain was 1485 με for the 4% mixes compared to 1050 με for the non-accelerated mix and 1226 με for the 2% mixes. However, in these trials the as-delivered shotcrete included some inadvertent entrained air, which was expelled upon spraying and caused the as-delivered cast shrinkage specimens to exhibit a 5 year drying shrinkage strain similar to the sprayed specimens with 2% set accelerator. The 28 day UCS was 34 MPa and 365 day UCS was 53 MPa. These results are consistent with shrinkage data obtained by Goodier et al (2007) for shotcrete sprayed with and without set accelerator tested to an age of three years.

When assessing the significance of measured unrestrained drying shrinkage according to AS1012.13, it should also be noted that these tests (even when based on only one day of curing) do not include autogenous shrinkage, which is largely related to the strength of the concrete and is independent of drying effects. For a 40-50 MPa shotcrete mixture the typical magnitude of autogenous shrinkage is about 50 με at an age of one day. Autogenous shrinkage is unavoidable in situ and therefore must be added to the drying shrinkage values measured using tests such as AS1012.13 to arrive at the total expected unrestrained shrinkage.

The results of the trial described above indicate that measurements of cast non-accelerated unrestrained drying shrinkage obtained at 56 days under-estimates the long-term drying shrinkage likely to occur in shotcrete sprayed with realistic dosages of set accelerator. This needs to be taken into account in estimating the long-term potential for shrinkage cracking. The results also confirm that the type of fibre used in the mix has a minimal effect on unrestrained drying shrinkage at the dosage rates typical of shotcrete (Zhang and Li, 2001). This data indicates that limits on the maximum allowable dosage rate of set accelerator should not be based solely on the potentially damaging effect these admixtures can have on long-term strength and durability but should also be based on their potentially deleterious effect on drying shrinkage.

Table 1. Mix design for shotcrete used to assess effect of set accelerator on drying shrinkage

Ingredient	Quantity
Coarse aggregate (10/7 mm basalt)	610
Coarse sand (Clarence sand)	350
Fine sand (beach sand)	680
Cement (Gladstone SL)	345
Fly Ash (Gladstone)	100
Undensified Silica Fume	10
PCE Super (L/m^3)	1.0
Slump (mm)	150

6 PREVENTION OF SHRINKAGE CRACKING

The conclusion from the discussion and test data presented above is that drying shrinkage cracking is a problem that cannot easily be remedied in arrears but is best addressed by prevention. The available methods of achieving this are most likely restricted to only three options: development of a more effective means of curing, development of low-shrinkage shotcrete mixtures, or imposition of stricter limits on dosage rates of set accelerator.

6.1 *Surface Curing*

In the absence of water-based curing, using, for example, misting or regular hosing, curing membranes could be applied as soon as the final layer of shotcrete is completed. This could possibly be combined with the black paint that is normally applied to shotcrete linings. However, surface curing may not be effective if the final lining is applied weeks or months after the initial layer. Moreover, a surface layer will interfere with bond between the lining and any supplementary shotcrete that might be applied at a later date, say, in the event of large cracks occurring in the lining or construction damage. Constructors are therefore reluctant to use surface-curing compounds on shotcrete linings.

6.2 *Internal Curing Compounds*

Internal curing compounds (ICC) have often been cited as a possible solution to the problem of drying shrinkage cracking of tunnel linings, but evidence from comparative trials (using shotcrete dosed with and without ICC, Bernard, 2006) has shown that these additives have a minor effect on unrestrained drying shrinkage strains (Figure 9). The mean reduction in 56 day drying shrinkage for shotcrete dosed with the recommended dosage of ICC was only 5% compared to plain controls in dry cure (DC) conditions (one day of wet cure followed by continuous atmospheric cure at 50% RH and 23°C). As expected, shrinkage in continuous wet-cure conditions was negligible. The control contained 50 kg/m^3 of steel fibres, 420 kg/m^3 of cementitious material, and had a 28 day UCS of 32 MPa.

In the absence of any evidence to the contrary, internal curing compounds do not appear to reduce drying shrinkage strains by a meaningful amount compared to plain shotcrete, so they are not going to be effective in controlling drying shrinkage cracks in shotcrete linings.

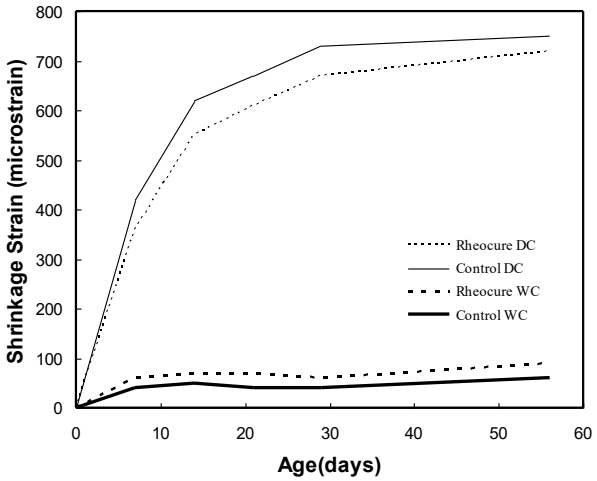


Figure 9. Unrestrained drying shrinkage strain results for Rheocure 736 ICC (Bernard, 2006).

Greater success was observed with the inclusion of Shrinkage Reduction Agents (SRA) in shotcrete (Bernard, 2006; Holter et al, 2023). This type of admixture was found to reduce drying shrinkage by about 20% compared to a plain control when used at the recommended dosage rate. Although their effects on other properties of shotcrete remain to be examined, this type of admix-

ture may prove useful in limiting the extent of drying shrinkage cracking especially if used together with other measures. Other materials, such as Crack Reduction Admixtures and Type K cement, also present opportunities for drying shrinkage reduction.

6.3 *Low Shrinkage Shotcrete*

An alternative approach to controlling drying shrinkage cracking is to develop mix designs that exhibit inherently lower levels of drying shrinkage. There are several possible approaches to achieving low shrinkage: either use a geo-polymer or produce a very dense conventional mix with a very low water/binder ratio. Such a mix can be developed within the context of the B82 Base Mix evaluation requirements for the development of a mix conforming with the B82 Shotcrete Work specification (TfNSW, 2022), but with an emphasis on minimising drying shrinkage to values less than the presently permitted 800 με at 56 days. However, the B82 guideline primarily focuses on the development of a base mix produced in a batch plant so additional consideration must be made to the effect of accelerators.

7 COMPLICATING FACTORS

The main factor that is not accounted for in most design estimates of in situ drying shrinkage strains and crack widths for shotcrete linings is the influence of the restraint provided by the rock or underlying primary shotcrete lining. A stiff high-friction substrate will limit the magnitude of shrinkage strain experienced locally within a bonded lining. That is why membranes such as FRS linings, which almost always exhibit post-crack strain-softening behaviour in direct tension, experience distributed cracking rather than one large crack in response to shrinkage. As outlined in CIRIA C766D (Bamforth, 2018) and described by Raoufi et al (2011), shrinkage crack spacing (and consequently crack widths) will depend on the stiffness and coefficient of friction with restraining surfaces that are in contact with the shrinking concrete member. For the case of shotcrete sprayed on hard rock, the stiffness of the rock substrate is largely fixed, but the coefficient of friction will depend on roughness, cleanliness, and other factors. Additionally, the presence of a water-proofing membrane will reduce the effective stiffness of the substrate as a result of the time-dependent shear characteristics of the materials typically comprising the membrane. Finally, the stiffness of a thin lining is lower than that of a thick lining hence the substrate will induce a higher relative degree of substrate restraint for a thin lining than a thick lining (Destrée et al, 2016).

A problem will arise if bond between the lining and substrate is lost with the passage of time. An unbonded lining will be subject to less restraint against shrinkage than a fully bonded lining, with the likely outcome that cracks are fewer in number but greater in width. However, given the uncertainty that exists regarding the rate and pattern of bond loss that a lining may experience, it is difficult to quantify precisely how bond loss is likely to affect crack widths. Moreover, no agreed method of analysis exists to estimate drying shrinkage crack spacing for a strain-softening bonded lining so this critical aspect of lining design for serviceability and durability is difficult to implement.

Tensile creep is another phenomenon that tends to mitigate the damaging effect of shrinkage but only if restraint against shrinkage exists. The most common manifestation of the effect of tensile creep is the advantage provided by high levels of tensile reinforcement across cracks (Granju, 1997). Reinforcement will not prevent the occurrence of cracks but may act to limit crack widths even for a strain-softening material. It does this by inducing tension in the surrounding shotcrete, which leads to tensile creep in the uncracked material, thereby reducing the total tensile strain that is manifested at the crack (Destrée et al, 2016). However, the effect of creep and time-dependent slip at the fibre-paste boundary, which occurs for both steel and macro-synthetic fibres (Boshoff and Nieuwoudt, 2017; Babafemi et al, 2018), reduces the restraint provided by fibres in relation to crack widening (Bernard and Amin, 2023). Unfortunately, this aspect of shotcrete behaviour is very complex to model and remains within the realm of research and is ignored in most designs.

7.1 *"Thicker is Better" for Drying Shrinkage*

Apart from the protection against drying that the outermost exposed layer of shotcrete provides to shotcrete located deeper within a newly sprayed lining, two other factors combine to reduce the degree of drying shrinkage a thick lining will experience compared to a thin lining of similar composition.

The in situ drying shrinkage exhibited by a slender lining will be affected by rebound during spraying. Internal restraint against drying shrinkage of the shotcrete is strongly affected by the amount of coarse aggregate present in the mix (all other factors being equal). Rebound of coarse aggregate is generally highest as the first 15-20 mm of shotcrete is sprayed onto a hard surface (Armelin and Banthia, 1998). As the thickness of the lining increases, the surface becomes relatively soft and sticky and thus the rebound of coarse aggregate decreases. This means that thin shotcrete linings (say, of 50 mm thickness) are relatively devoid of coarse aggregate particles compared to thicker linings (of 100-150 mm thickness) even if the same mixture is used to spray both. The result is a higher degree of potential drying shrinkage in thin linings.

Thin linings also have a smaller reservoir of embodied moisture available to supplement evaporation at the drying surface of a freshly sprayed surface than thick linings. This increases the risk of desiccation in the event of rapid evaporation from a freshly sprayed surface and generally reduces the degree of hydration achieved in the surface regions of a thin lining in the event of poor curing. The result is that thin linings are more sensitive to poor curing practices than thick linings and may potentially exhibit higher levels of drying shrinkage cracking in the event of sub-optimal curing.

8 SUMMARY

Drying shrinkage of shotcrete used in tunnel linings is significant compared to other forms of concrete and continues well beyond the normal 56-day period of specification and measurement. The result in recently constructed tunnels in Australia is a high incidence of shrinkage cracks. Shrinkage cracks in shotcrete linings are not benign as they can have a detrimental effect on both the durability and the structural capacity of a lining in addition to facilitating water ingress. For this reason, they must be addressed seriously during the design, construction, and service of shotcrete linings.

The present paper describes several mechanisms of lining deterioration observed to occur in some Australian tunnel linings and discusses the merits of alternative approaches to the prevention of shrinkage crack formation such as low shrinkage mix development, lower maximum allowable accelerator content, better wet curing practices (including misting), and reduced reliance on thin linings for long term support. It also addresses the problem of managing existing cracks, with particular attention given to the difficulties associated with water ingress and durability when numerous leaking shrinkage cracks arise and widen over a protracted period of time.

9 REFERENCES

Adams, D.N., Lechner, M.K. and Lamb, I., 2001. M5 East Tunnels: A Flat Roofed, Bolt and Shotcrete-Lined Highway, *Rapid Excavation and Tunneling Conference 2001*, Society for Mining, Metallurgy & Exploration, pp501-512.

Aitchison, B., Oliveira, D, Backhouse, D. and Netterfield, R., 2018. Design and Construction of a Shallow Cover Tunnel Junction Using Sprayed Concrete, Sydney, Australia, *Eight Int. Symposium on Sprayed Concrete - Modern Use of Wet Mix Sprayed Concrete for Underground Support*, Trondheim, Norway, 11-14, June 2018, pp9-23.

Ansell, A. and Bryne, L.E. 2015. In situ Observations and Laboratory Testing of Shrinkage Cracking in Shotcrete on Soft Drains. *Spritzbeton-Tagung 2015*, Alpbach, Austria, pp1-14.

Armelin, H.S. and Banthia, N., 1998. Mechanics of aggregate rebound in shotcrete (Part I), *Materials and Structures,* Vol. 31, No. 2, pp. 91–98.

Asche, H.R. and Bernard, E.S., 2004. Shotcrete design and specification for the Cross City Tunnel, Sydney, *Shotcrete: More Engineering Developments*, Bernard (ed.), pp 27-38, Taylor & Francis, London.

Babafemi, A.J., du Plessis, A. and Boshoff, W.P., 2018. Pull-out creep mechanism of synthetic macro fibres under a sustained load, *Construction and Building Materials*, Vol. 174, pp. 466-473.
Bamforth, P., 2018. Control of cracking caused by restrained deformation in concrete, *Report C766D*, Construction Industry Research and Information Association (CIRIA), London.
Barrett, S. & McCreath, D.R., 1995. Shotcrete Support Design in Blocky Ground - Towards a Deterministic Approach, *Tunnels and Deep Space*, 10(1), pp79-88.
Barry, J.S., Bodner, C., and Bedford, N., 2021. Hanging linings – a new approach to permanent lining design, *17th Australasian Tunnelling Conference 2020+1*, 10–13 May 2021, Melbourne, pp12-22.
Bernard, E.S., 2006. The Influence of Curing on the Mechanical Performance of Fibre Reinforced Shotcrete, *ECI Conference on Shotcrete for Underground Support X*, (Ed. Morgan & Parker), Whistler, Canada, September 12-16, 2006, pp176-193.
Bernard, E.S. and Amin, A., 2023. Creep Relaxation of Fibre Reinforced Shotcrete in the ASTM C1550 Panel Test, *FRC2023: Fiber Reinforced Concrete: from Design to Structural Applications*, Joint ACI-fib-RILEM International Workshop, Tempe, Arizona, September 18, 2023.
Bodner, C., 2022. How can shrinkage affect the performance of permanent linings in tunnels?, *Shotcrete Developments*, Australian Shotcrete Society Seminar, Sydney November 16-17, 2022.
Boshoff, W.P, and Nieuwoudt, P.D., 2017. Tensile creep of cracked steel fibre reinforced concrete: Mechanisms on the single fibre and at the macro level, *Proceedings of the International RILEM Workshop FRC-Creep 2016*, (Ed. Serna et al), Valencia, p63-75.
Carlswärd, J., 2006. Shrinkage cracking of steel fibre reinforced self compacting concrete overlays: Test methods and theoretical modelling, *Doctoral Thesis*, Luleå University of Technology, ISBN: 978-91-85685-04-2
Chernov, V., Zlotnikov, H., & Shandalov, M. 2006, Structural synthetic fiber reinforced concrete: experience with marine applications, *Concrete International*, ACI, Vol. 28, No. 8, pp56-61.
Clarke, S.J., de Ambrosis, A.L., Bertuzzi, R., and Redelinghuys, J., 2014. Design and Construction of the Widening of M2 Norfolk Twin Tunnels, *15th Australasian Tunnelling Conference*, Sydney, 17-19 September 2014, pp591-601.
DBV, 2002. *Recommendation Design Principles of Steel Fibre Reinforced Concrete for Tunnelling Works*, Deutscher Beton-Verein.
Destrée, X, Yao, Y., and Mobasher, B., 2016. Sequential Cracking and Their Openings in Steel-Fiber-Reinforced Joint-Free Concrete Slabs, *Journal of Materials in Civil Engineering*, ASCE, Vol. 28, No. 4: 04015158
Edvardsen, C., 2022. On the autogenous Healing of Cracks in waterproof Concrete Structures – Experiences in the Field and Conclusions drawn, *GeoResources Journal*, 4, 2022, pp21-26.
Fernandez-Delgrado, G., Mahar, J.W., and Parker, H.W., 1975. Structural Behavior of Thin Shotcrete Liners Obtained from Large Scale Tests, *Shotcrete for Underground Support*, Proceedings of the Engineering Foundation Conference, Tidewater Inn, Easton, Maryland, USA, October 4 - 8, 1975, ACI Publication SP-54. pp399-442.
fib, 2022. Bulletin 105, *Fibre Reinforced Concrete: State of the Art Report*, November 2022, fédération internationale du béton.
Goodier, C.I., Austin, S.A. and Robins, P.J., 2007. Low-volume wet-process sprayed concrete: hardened properties. *Materials and Structures*, 41(1), pp. 99-111.
Granju, J-L., 1997. Thin bonded overlays: About the role of fiber reinforcement on the limitation of their de-bonding, *Advanced Cement Based Materials*, Vol. 4, No. 1, pp21-27.
Hagelia, P., 2011. Deterioration Mechanisms and Durability of Sprayed Concrete for Rock Support in Tunnels, *Doctoral Thesis*, TU Delft.
Hagelia, P., 2018. Durability of sprayed concrete for rock support – A tale from the tunnels, *8th International Symposium on Sprayed Concrete – Modern Use of Wet Mix Sprayed Concrete for Underground Support*, Trondheim, Norway, 11 – 14 June 2018, pp167-182.
Hahn, T. and Holmgren, J. 1979, Adhesion of Shotcrete to various types of Rock Surfaces, in *Proceedings of the 4th International Congress on Rock Mechanics*, Montreux, pp421-429.
Hanke, S.A., Collis, A., and Bernard, E.S., 2001. The M5 motorway: an education in Quality Assurance for fibre reinforced shotcrete, *Shotcrete: Engineering Developments*, Bernard (ed.), pp 145-156, Swets & Zeitlinger, Lisse.
Holter, K.G., 2015. Performance of EVA-Based Membranes for SCL in Hard Rock, *Rock Mechanics and Rock Engineering*, DOI 10.1007/s00603-015-0844-5
Holter, K.G., Strømsvik, H, and Grøv, E. 2021. Materials Technology and Spray Application Development for Waterproof and Durable Sprayed Concrete Linings: Goals and Background for the Supercon Research Project, Norway. *Spritzbeton-Tagung 2021*, Alpbach, Austria, pp112-130.
Holter, K.G., Hammer, T.A.M., and Trussell, M.H., 2023. New development of sprayed concrete with improved waterproofing, durability and sustainability performance, *Expanding Underground. Knowledge*

and Passion to Make a Positive Impact on the World, (Eds. Anagnostou, Benardos & Marinos), Taylor and Francis.
Hover, K.C., 2006. Evaporation of Water from Concrete Surfaces, *ACI Materials Journal*, V. 103, No. 5, pp384-389.
Hunter, A., 2025. Management of Acid Sulfate Rock in a Sydney Road Tunnel, *Australian Geomechanics Journal,* Vol. 60, No. 1, pp37-58.
Katz, J.L., Reick, M.R., Herzog, R.E., and Parsiegla, K.I., 1993. Calcite Growth Inhibition by Iron, *Langmuir*, 9, pp1423-1430.
Korotcenkov, G., 2018. *Handbook of Humidity Measurement: Methods, Materials and Technologies*, CRC Press.
Kost, S., Ching, I., and Gomes, A.R.A., 2021. Tunnel design – recent experiences from design and certification of major tunnel projects in Sydney, *Australasian Tunnelling Conference, ATS 2020+1*, Melbourne, Victoria, 10–13 May 2021.
Lagerblad, B., Fjallberg, L. and Vogt, C., 2010. Shrinkage and durability of shotcrete, in *Shotcrete: Elements of a System* (Ed. Bernard), Taylor & Francis, London.
Larive, C., Rogat, D., Chamoley, D., Regnard, A., Pannetier, T., Thuaud, C., 2016. Influence of fibres on the creep behaviour of reinforced sprayed concrete. Pro*ceedings of ITA World Tunnel Congress WTC 2016*, April 22-28, San Francisco, United States.
Maconachie, D J, Loganathan, N and Bertuzzi, R., 2005. Design of the Lane Cove Tunnel, *12th Australian Tunnelling Conference*. AUCTA, AusIMM and Engineers Australia, Brisbane.
Malmgren, L., Nordlund, E. and Rolund, S., 2005. Adhesion strength and shrinkage of shotcrete, *Tunnelling and Underground Space Technology*, 20, pp33–48
Manquehual, C.J., Jakobsen, P.D., Holter, K.G., De Weerdt, K., Danner, T. and Bruland, A., 2022. Comparison of the condition of steel fiber-reinforced shotcrete with water-glass and alkali-free activators after more than 20 years of service in a subsea road tunnel, *Construction and Building Materials*, Vol. 328, 2022, 127090.
Marcos-Meson, V., Michel, A, Solgaard, A, Fischer, G., Edvardsen, C., Skovhus, T.L., 2018. Corrosion resistance of steel fibre reinforced concrete - A literature review, *Cement and Concrete Research*, V. 103, January, pp1-20.
Neville, A.M., 1996. *Properties of Concrete*, 4th ed, Longman.
Nielsen, L.C., De Yoreo, J.J., and De Paolo, D.J., 2013. General model for calcite growth kinetics in the presence of impurity ions, *Geochimia et Cosmochimica Acta*, 115, pp100-114.
Norwegian Tunnelling Society, 2010. *Rock Support in Norwegian Tunnelling*, Publication No. 19, pp89, 2010.
Pells, P.J.N., 2002. Developments in the design of tunnels and caverns in the Triassic rocks of the Sydney region, *International Journal of Rock Mechanics & Mining Sciences*, 39, pp569–587
Raoufi, K., Pour-Ghaz, M., Poursaee, A., and Weiss, J., 2011. Restrained Shrinkage Cracking in Concrete Elements: Role of Substrate Bond on Crack Development, *Journal of Materials in Civil Engineering*, 2011, Vol. 23, No. 6, pp895-902.
Reid, S.G. and Bernard, E.S., 2019. De-bonding of Shotcrete Linings at the Substrate Boundary, *World Tunneling Congress 2019*, Naples, May 3-8.
Reid, S.G. and Bernard, E.S., 2024. Wedging Model of Compressive Membrane Action for a Conical-Fan Failure Mode in a Reinforced Concrete Plate with In-Plane Restraint, *Journal of Structural Engineering*, ASCE, Volume 150, Number 11, Sept. 11, 2024.
Romer, M., 2003. Detachment of Shotcrete Linings due to Long Term Interaction with Ground Water, *International Seminar on the Thaumasite Form of Sulfate Attack on Concrete*, June 24, 2003, Sheffield, UK.
Sjölander, A. and Ansell, A., 2017. Numerical Simulations of Restrained Shrinkage Cracking in Glass Fibre Reinforced Shotcrete Slabs, *Advances in Civil Engineering*, Vol. 2017, Article ID 8987626, pp11, https://doi.org/10.1155/2017/8987626.
Silfwerbrand, J., 1997. Stresses and strains in composite concrete beams subject to differential shrinkage, *ACI Structural Journal*, Vol. 94, No. 4, pp347-353.
TfNSW, 2022. *Shotcrete Work*, Transport for New South Wales, Sydney.
Yang, R., He, T., Guan, M., Xu, Y., Ma, X., Lin, Y., Gui, M., and Ke Y., 2022. Experimental study on sulfate resistance of shotcrete with different liquid accelerators, *Case Studies in Construction Materials*, 16, e01100
Zhang, J. and Li, V.C., 2001. Influences of fibers on drying shrinkage of fiber-reinforced cementitious composite, *Journal of Engineering Mechanics*, ASCE, Vol. 127, No. 1, pp37-44.
Zhang, L., Qian, X., Lai, J., Qian, K. and Fang, M., 2020. Effect of different wind speeds and sealed curing time on early-age shrinkage of cement paste, *Construction and Building Materials*, 255 (2020), 119366

THIS PAGE INTENTIONALLY LEFT BLANK

19th Australasian Tunnelling Conference – Acosta-Martínez, Stewart and Hudson-Smith (Eds.)
© 2025 Australian Tunnelling Society, ISBN 978-0-85825-002-4

High temperature bond behavior of Spray Applied Waterproof Membranes (SAWMs)

M. Reinhold & G. Bhatta
Normet Asia- Pacific Pty Ltd, Adelaide, Australia

ABSTRACT: Unlike self-supporting linings like cast in situ linings with sheet membranes, composite shell or permanent concrete linings need extra support. These systems rely on the waterproofing membrane's double bonding ability to hold the sprayed membrane and inner surface of fire protection layer in place. A bond strength of 0.5 MPa at both membrane interfaces was established as the minimum industry standard (e.g. ITAtech Guidelines for SAWMs). The paper discusses the load bearing and bond behavior of three SAWMs based on ethylene-vinyl acetate copolymer (EVA) and Styrene Butadiene Rubber (SBR) technology which becomes critical in case of fire events to ensure safe access to - and structural soundness of - underground structures during and after fire events. Experimental setups were developed based on the relevant industry standards and the bond and behavior of the membranes were tested at elevated temperatures and thereafter, when the membranes were cooled back down to room temperature.

1 INTRODUCTION

Underground construction is growing worldwide because it reduces surface space consumption and keeps infrastructure protected from the various threats they might be exposed to. Whether it is for tunnels, caverns, basements or underground stations, it is essential to keep these underground structures watertight. One of the most effective ways to achieve this is the use of SAWMs, which are sprayed directly onto the surface to create a waterproof barrier.

SAWMs are popular because they are easy to apply, especially in tunnels and structures with complex shapes. The double bonding properties of SAWMs allows them to adhere to both primary and secondary linings eliminating the need for traditional cast in-situ concrete as secondary lining, which typically requires large shutters and additional manpower. This not only simplifies construction in complex tunnel geometries but enhances efficiency by using the same equipment and personnel already available on site (Dimmock, Haig & Su 2011).

Due to the confined nature of underground structures and the limitations on escape ways fire safety is always a major concern in underground structures. In double bonded systems the membrane is part of the load bearing system or even just the substrate for fire protecting layers and hence it is essential that the cohesive and adhesive strength of the SAWM is not compromised during or after underground fire events to the extent that parts of the structure de-bond and pose threats to first responders or during rehabilitation work. In the event of fire, temperatures can reach very high levels which, due to their polymeric nature, can weaken the membrane and its bond to neighboring layers of the structure.

According to ITAtech guidelines, a minimum bond strength of 0.5MPa is recommended for both membrane interfaces to ensure structural soundness, safety and durability, (ITAtech Activity Group lining and waterproofing 2013). The ISO 834 fire curve is a widely used standard for

structural fire testing, representing temperature development under severe fire conditions (International Organization for Standardization, 2025). In real tunnel environments, sprayed waterproofing membranes are not directly exposed to fire. They are typically embedded between concrete layers, and the use of fire protective layer which is common industry practice further reduces the thermal exposure. As a result, the temperature experienced by the membrane is significantly lower than the surface temperature during a fire. A large-scale fire test by Duan et al. (2021) showed that at depths of approximately 30 mm and 60 mm within concrete, temperatures after 120 minutes of fire exposure ranged from 100 °C to 160 °C, depending on the location across the tunnel section (Duan et al., 2021). This indicates that the membrane experiences much lower temperatures than the temperature mentioned in the ISO 834 curve. In practice, a 50 mm concrete protective layer is commonly applied over the membrane. Based on all this information, in this study the performance of three different SAWM products were assessed under heat exposure of 100°C and 160°C.

Membranes 1 and 3 are powdered products based on EVA polymers and membrane 2 is a liquid SAWM based on SBR technology. The study aimed to evaluate the properties such as load bearing behavior, bond and cohesive strength of spray applied waterproofing membranes under elevated temperature conditions as well as its form stability when sandwiched in between two concrete layers.

2 OBJECTIVES

The main objectives of this study are:

1. The evaluation of the bond strength of three different spray-applied waterproofing membranes under elevated temperature conditions.
2. The assessment of stability and performance of the SAWMs in a sandwiched, confined application, embedded between two layers of concrete under elevated temperature conditions.

3 METHODS

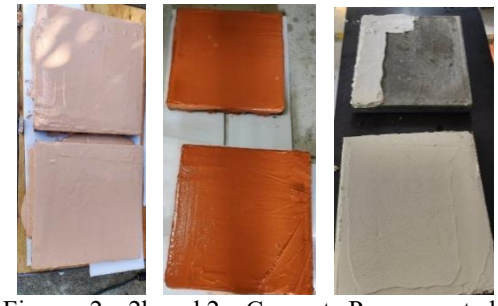
3.1 *Double-bond strength evaluation under elevated temperatures.*

To address the first objective, a modified version of ASTM C1583/C1583M was developed (ASTM International,2020). The method described in the standard presents two major practical challenges: Firstly, core drilling through the secondary lining and the membrane bears the danger of breaking the bond between concrete and membrane due to vibration, and secondly, glue failure (cohesive or adhesive) is a quite regular occurrence, especially when applied onto water-based membranes. For the here determined high-temperature application this issue is particularly prominent in addition to the property changes of the glue at higher temperatures.
To overcome these limitations, a following tailored test setup was devised:

- Substrate Preparation: Commercially available concrete pavers (l x w x h: 400 mm x 400 mm x 40 mm) were used as the substrate. Each paver was coated with two or more layers of membrane, adding up to a 3 mm dry film thickness.
- In figure 2, membrane 1 (left) and membrane 3 (right) are powdered materials and EVA based whereas membrane 2 (middle) is a liquid SBR polymer-based product.



Figure 1. Concrete Pavers.



Figures 2a, 2b and 2c. Concrete Pavers coated with 3mm thick membranes 1, 2 and 3.

– Casting individual pull-off specimens onto the membranes: Cylindrical cement mortar specimens (50 mm diameter, 50 mm height) were cast directly onto the membrane surfaces, eliminating the need for core extraction. Thermocouples and M10 threaded bolts were embedded within the mortar during casting.



Figure 3. Cylinder mold with thermo- couple



Figure 4. Threated bolt centralized in casting lid



Figure 5. Cylindrical specimens cast and covered for curing

– Load application system: The bolt served as a mechanical anchor for a custom-fabricated dolly, enabling the direct connection to the pull off tester without the use of adhesives.



Figure 6: Load Application System



Figure 7. Sample slabs inside the oven

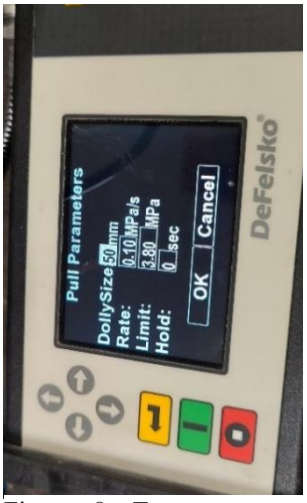


Figure 8. Test parameters, displayed on pull-off tester screen

– Temperature control and monitoring: Prior to testing, the samples assembled were subjected to elevated temperatures (100°C and 160°C) in a laboratory oven. Thermocouples embedded in the cement mortar measured internal temperature and overnight heating continued until a stable temperature was reached.
– Testing: The membrane was cut around the cast specimens. Pull off tests were conducted at room temperature on some specimens to verify the test method and set the reference. The membrane and specimen carrying concrete slabs were placed inside an electric oven and heated overnight. After heating to the desired temperatures, the concrete slabs were taken out of the oven and specimens were immediately pulled off, recording the actual pull-off temperature and bond-strength. Finally, the samples were cooled back down to room temperature and the remaining specimens were pulled off recording the bond strength after the simulated fire events.

3.2 *Performance evaluation under confined / sandwiched conditions*

The second objective was an additional test resulting from an observation during experimental campaign one. During the first stage of experiments the formulation of bubbles underneath the membrane was observed in areas where it was exposed directly without any mortar cast onto it. In order to address this experimental artifact and to simulate confined site conditions during a fire event, specimens were prepared where the membrane was sandwiched between two concrete layers and heat exposure occurred from only one side.



Figure 9: Thermocouple 1, 2 and 3 placed from corner to center of paver



Figure 10: Thermocouple 4 elevated and placed in center of mortar layer



Figure 11: Sprayed membrane sandwiched between concrete paver and cement mortar layer

In actual underground fires, the heat typically flows from the interior side, affecting the protective layer first, while the outer surface which is in contact with the surrounding ground remains at a lower temperature.

To simulate this scenario, a wooden frame was constructed in the shape of the oven door. This setup allowed the protective mortar layer of the specimen to be placed inside the oven, while the concrete paver side remained outside at room temperature. The experiment setup created a one directional heat flow, replicating the thermal conditions that may occur during underground fires. For all three membranes the temperature of the oven was set at 210°C and the oven was turned off when at least two of the thermocouples reached around 160°C.



Figure 12: appr. 50mm thick mortar layer on membrane

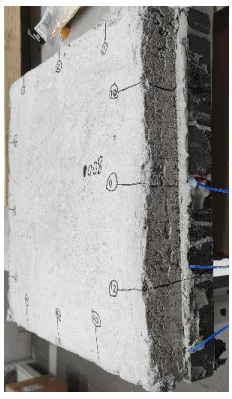


Figure 13: sandwiched membrane

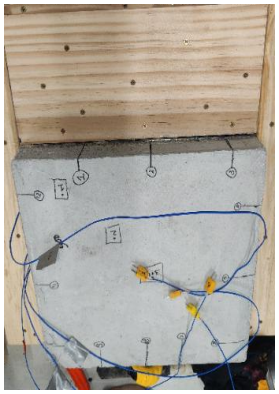


Figure 14: specimen prepared for heat exposure



Figure 15: specimen placed for heat exposure

After the specimens cooled down to room temperature the thickness change of the sandwich structure was measured to determine the volume stability of the membrane under heat exposure.

Also, cores were drilled from the surface using diamond core drill through the previously thermally stressed membrane into the substrate and double bonding performance on the sandwich structure was determined by means of pull-off testing.

4 RESULTS

4.1 *Bond strength results at elevated temperatures*

Initial tests were conducted at room temperature to verify the effectiveness of the modified pull off test setup and set the bond strength baseline for all three SAWMs. All three materials demonstrated pull off strengths exceeding the minimum industry benchmark of 0.5 MPa. This confirmed that the test method was valid for further evaluation at elevated temperatures.
Subsequently, pull off tests were conducted at two elevated temperatures: 100°C and 160°C. After each thermal exposure, the specimens were cooled back to room temperature, and the pull off tests were repeated to assess bond strength. Thermocouples embedded in the mortar confirmed the internal temperature of the specimen during each test.

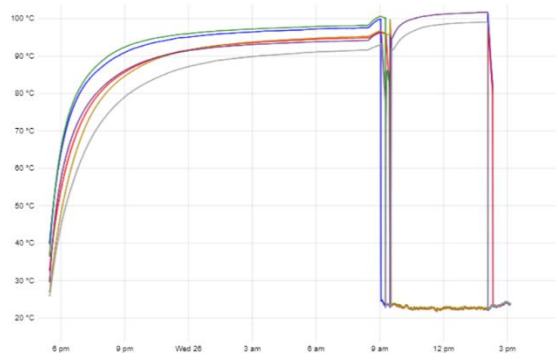


Figure 16. Temperatures recorded within specimens during heat exposure at 100 ° C

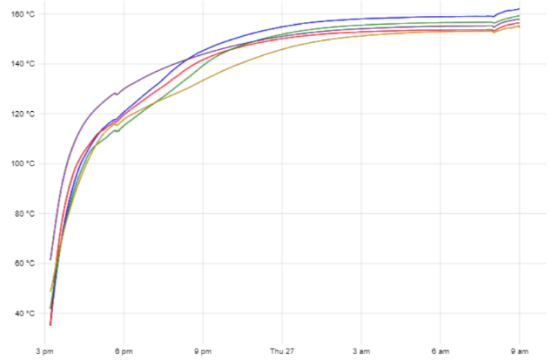


Figure 17. Temperatures recorded within specimens during heat exposure at 160 ° C

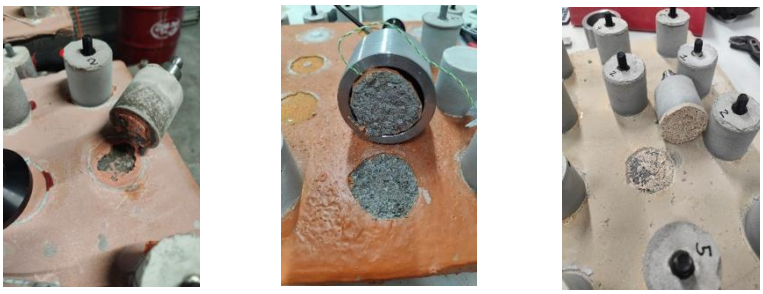


Figure 18 a-c: all possible failure modes were observed while pulling off the specimens from the membranes (cohesive failure in substrate, membrane or cast on mortar specimens, adhesive failure at interface either side of the membranes as well as mixed failure modes)

Table 1. Pull-off test results for membrane 1 (EVA)

Test Condition	Average bond Strength (MPa)	Average Specimen Temperature at Pull-Off (°C)
Reference test at 23°C	1.02	23
Exposure to 100°C	0.28	90
After exposure to 100°C	1.07	23
Exposure to 160°C	0.04	147
After exposure to 160°C	0.45	22

The EVA based membrane 1 exhibited a strong bond at room temperature during the virgin reference test as well as after exposure to 100ºC and 160ºC. Expectedly the bond strength dropped significantly while heated, especially at 160°C as the elongation behavior of EVA polymers increases with temperature. The heat exposure of the substrate resulted however in water vapor developing which created partial de-bonding of the membrane. The low results for exposure to 160ºC and afterwards can also be partially attributed to this effect.

Table 2. Pull-off test results for membrane 2 (SBR)

Test Condition	Average Bond Strength (MPa)	Average Specimen Temperature at Pull-Off (°C)
Reference test at 23°C	1.34	23
Exposure to 100°C	0.38	90
After exposure to 100°C	1.05	20
Exposure to 160°C	0.14	134
After exposure to 160°C	1.37	22

Membrane 2 showed good thermal resistance, maintaining relatively high pull off strength values across all stages. The bond strength at elevated temperatures is lower than 0.5 MPa but still within a range to prevent secondary lining dropouts. After cooling from 160°C, the bond strength slightly increased compared to initial reference value which may indicate the hardening of the membrane or simply increased bonding forces between the membrane and both concrete layers.

Table 3. Pull-off test results for membrane 3 (EVA)

Test Condition	Average Bond Strength (MPa)	Average Specimen Temperature at Pull-Off (°C)
Reference test at 23°C	0.94	23
Exposure to 100°C	0.21	91
After exposure to 100°C	0.83	23
Exposure to 160°C	0.26	149
After cooling from 160°C	1.20	22

Similar to membrane 2, membrane 3 also showed a reduction in bond strength during heating phases but recovered well after cooling. The post cooling pull-off strength values were close to or higher than the virgin reference.

4.2 *Results on sandwich system*

For the second test setup, the thickness of the sandwich structure was measured at 12 marked points using a vernier caliper before heating. After thermal exposure, thickness was measured again at the same points to access for any deformation. Across all three membranes, minor surface cracks were observed around the membrane area, but no visible blistering occurred. The overall sandwich structure remained intact, and the protective layer and concrete paver stayed well bonded to the membrane.

Table 4: Thickness change after exposure to 160°C

Description	Membrane 1 (EVA)	Membrane 2(SBR)	Membrane 3(EVA)
Average thickness before test (mm)	94.0	88.6	93.9
Average thickness change (mm)	1.2	1.0	0.7

Even though the membrane thickness was not measured exactly, it must be stated that with a thickness increase of around 1 mm over an average membrane thickness of around 3 mm indicates that some sort of change must have happened within the membrane or the concrete-membrane interfaces.

After the samples were cooled from 160°C to room temperature, cores were drilled through the cement mortar, simulating the secondary lining and through the membrane into the concrete paver. Dollies were glued onto the core surface and pull off tests were conducted.



Figure 19: Pull off test – adhesion failure to secondary lining



Figure 20: Sandwich specimen after heating at 160°C



Figure 21: Pull-off tests

Table 5: Average pull-off double-bond strength after exposure to 160ºC

Description	Membrane 1(EVA)	Membrane 2 (SBR)	Membrane 3(EVA)
Number of cores	3	3	3
Failure mode	Adhesion to cement mortar	Adhesion to cement mortar	Adhesion to cement mortar
Average pull-off strength (MPa)	0.27	0.38	0.27

It must be stated that the pull off strength results stated in table 5 were considerably lower as compared to results from the first test campaign (method 3.1). This may be due to the use of a diamond core drill during sample preparation. The high-speed drilling, associated vibrations may have caused damage to the bonded surface, raising concerns about drilling method and its potential impact on bond strength. The observed failure mode, for all cores to fail at the interface membrane – cement mortar (secondary lining) is strongly supporting this theory.

In order to determine whether the low bond strength recorded is indeed an artifact of sample preparation or is credited to thermal damage to the bonding ability, further testing is recommended avoiding core drilling after thermal exposure.

5 CONCLUSION

Based on the findings of the study it can be concluded that the tested EVA and SBR polymer based SAWM products remain mechanically intact during and after underground fire events for assumed membrane temperatures of 100ºC and 160ºC. Other properties such as water tightness or durability after fire events were not considered.

For the duration of the increased membrane temperature its load bearing behavior is reduced and after the cool down period returns to its original or even increased values. This reduced load

bearing ability remains at all times at a level where no dropouts from secondary lining or fire protecting layers based on membrane failure would be expected. Based on these findings, the use of the tested products does not add any additional risk to first responders or during remedial work.

6 RECOMMENDATION

Full scale fire testing may be required based on specific project conditions and the positioning of the membrane, as performance can vary depending on design factors. Furthermore, the apparent increase in bond strength observed in membrane 2 after cooling warrants further investigation to understand its nature and effects. For sandwich system, it is also recommended to employ testing methods that eliminate the need for drilling after thermal exposure, as drilling may compromise the accuracy of bond strength measurements.

7 REFERENCES

American Society for Testing and Materials [ASTM]. 2020. *ASTM C1583: Standard Test Method for Tensile Strength of Concrete Surfaces and the Bond Strength or Tensile Strength of Concrete Repair and Overlay Materials by Direct Tension (Pull-off Method)*. West Conshohocken, PA: ASTM International.

Dimmock, R., Haig, B. and Su, J. 2011. Spray applied waterproofing membranes–key success factors and development of efficient sprayed concrete tunnel linings. In *Sixth International Symposium on Sprayed Concrete, Tromso, Norway* (pp. 110-124).

Duan, J., Dong, Y., Xiao, J., Zhang, D., Zheng, W. and Zhang, S. 2021. A large-scale fire test of an immersed tunnel under the protection of fire resistive coating. *Tunnelling and Underground Space Technology*, *111*, p.103844.

International Organization for Standardization. 2025. *ISO 834-1:2025 Fire-resistance tests — Elements of building construction — Part 1: General requirements*. 2nd edn. Geneva: ISO.

ITAtech Activity Group. 2013. *ITAtech Report n°2 – Design guidance for spray applied waterproofing membranes*. April 2013. Lausanne: International Tunnelling and Underground Space Association. ISBN 978-2-9700858-1-2.

19th Australasian Tunnelling Conference – Acosta-Martínez, Stewart and Hudson-Smith (Eds.)
© 2025 Australian Tunnelling Society, ISBN 978-0-85825-002-4

Practical shotcrete design approach based on full-scale load-deflection tests using numerical analysis

J. Oh
School of Minerals and Energy Resources Engineering, UNSW Sydney, NSW, Australia

T. Moon
HNTB Corp, New York, NY, USA

ABSTRACT: This study investigates the performance and failure mechanisms of shotcrete in underground construction using numerical analyses by replicating full-scale load-deflection tests based on field test data. A series of parametric studies examined the interaction between support elements such as bolt spacing, shotcrete thickness, and shotcrete bonding under various loading conditions. The analysis results reveal that the ultimate capacity of the shotcrete panel is primarily governed by flexural tensile failure mode after the major bonding failure. The residual bonding area along the periphery of the shotcrete panel plays an important role in reducing the effective moment arm, thereby enhancing the ultimate flexural resistance. In addition, the negative bending moment induced by the interaction between the rock bolt/plate and the shotcrete panel can significantly reduce the positive bending moment at the midspan of the shotcrete panel. Based on these findings, a practical shotcrete design approach using the concept of the bending moment coefficient has been proposed in conjunction with the Q-system.

1 INTRODUCTION

Shotcrete is a crucial method of a ground-support system that is pneumatically sprayed, typically onto the exposed surface of an excavation face, resulting in a compacted, self-supporting, and load-bearing layer. Shotcrete serves as both an essential component of an initial ground support system and the permanent structure, providing a cost-effective application to a variety of civil construction and mining applications. The primary role of shotcrete liners in underground mining or tunnel excavation is to prevent the dilation of loose blocks and ravelling, thereby facilitating the rock fragments to interact with each other (Kaiser & Tannant, 2001).

In general, tensile-flexural failure on a shotcrete liner occurs when the rock fractures and bulges behind the shotcrete layer (Kaiser & Tannant, 2001). Many researchers have devoted considerable efforts to gaining a comprehensive understanding of the various facets of shotcrete failure mechanism and performance. Barrett and McCreath (1995) have attempted to provide shotcrete failure modes for blocky ground conditions, as shown in Figure 1, and postulated a two-step failure process, initially dominated by the loss of adhesion to the rock and followed by flexural failure, and further emphasised that the adhesion is of critical importance in maximising the peak ground support capacity of the shotcrete, whereas flexural strength and toughness play a crucial role in the post-peak behaviour.

The following equations give the proposed design shear and flexural capacity of the shotcrete (Barrett & McCreath, 1995).

$$C_{ds} = 4\tau_{ds}t \quad \text{[kN/m]} \quad \text{For direct shear capacity} \tag{1}$$

$$Mo = \frac{1}{8}w(s-c)^2 \quad \text{[kN-m/m]} \quad \text{For design peak moment} \tag{2}$$

$$C_{flex} = \sigma_{flex}\frac{t^2}{6} \quad \text{[kN-m/m]} \quad \text{For flexural capacity} \tag{3}$$

where t_{ds} is the shear strength of the shotcrete, s is the nominal bolt spacing, t is the thickness of the panel, w is the magnitude of uniformly distributed load, and c is the width of face plates.

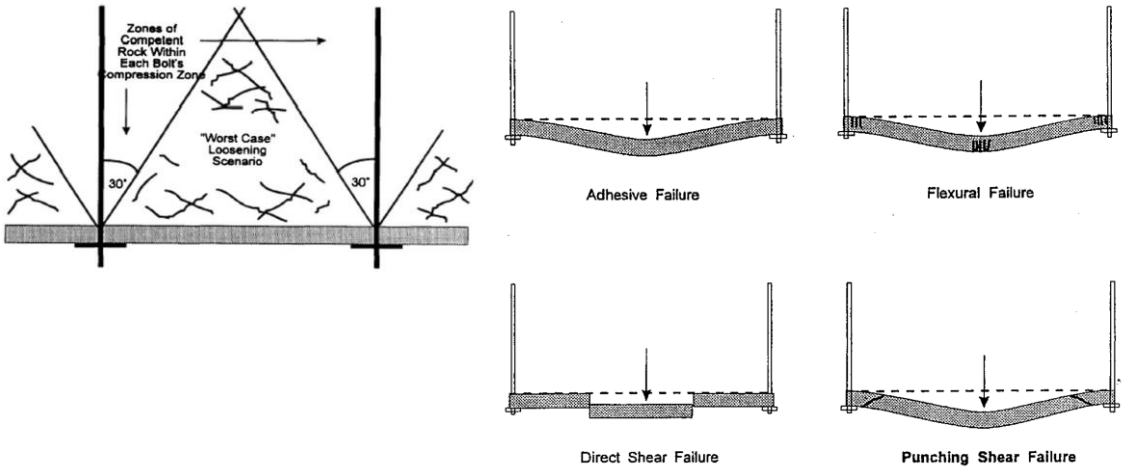


Figure 1. Typical shotcrete failure modes (Barrett & McCreath, 1995)

Although many researchers have elucidated the performance and failure mechanism of the shotcrete liner, unknowns and misinterpretations still remain on the failure process of FRS, such as the interactions between shotcrete and rock bolt configuration, the effect of the shotcrete adhesion, and the effect of in-plane confining loading conditions on the shotcrete liner, etc. These factors are essential in understanding and developing a more practical and suitable shotcrete lining design. Thus, the main objective of the paper is to 1) investigate the influence of those key factors that could affect the performance and the failure mechanism of the FRS using a full-scale load-deflection numerical analysis, 2) identify the influences of bolt spacing and thickness of shotcrete on FRS comparing with the full-scale field tests performed by Forrest (2019) and Bernard et al, 2022, and 3) propose a practical shotcrete design approach based on the findings above.

2 FE MODEL SETUP AND CONFIGURATION

To assess the performance and failure process of the shotcrete panel, a series of numerical analyses have been performed using LS-DYNA, a non-linear three-dimensional numerical software developed by LSTC (2019). The shotcrete panel was modelled with a concrete constitutive model known as the Continuous Surface Cap Constitutive Model (CSCM) (Murray, 2007). This model allows for capturing both the pre- and post-failure behaviour of shotcrete. The influence of fibre reinforcements has been calibrated with tensile fracture energy or strain energy release rate, G_c in the CSCM. The elastic behaviour of the CSCM is governed by the bulk and shear modulus until the yield surface of the CSCM is reached. The yield surface is formulated with three stress invariants and uses a multiplicative formulation to combine a shear failure surface with a hardening compaction cap surface that is smooth and continuous.

The formula of the yield surface shown in Equation (5) is a function of the first, second, and third stress invariants of the deviatoric stress tensor (i.e., J_1, J'_2 and J'_3, respectively), as shown in Equation (4).

$$J_1 = 3P^*, J'_2 = \frac{S_{ij}S_{ij}}{2}, J'_3 = \frac{S_{ij}S_{ik}S_{ki}}{3} \tag{4}$$

$$Y(J_1, J'_2, J'_3, k) = J'_2 - \Re^2 F_f^2 F_c \tag{5}$$

where k is the hardening cap parameter at the intersection of the cap and shear surface, F_f is the shear failure surface, S_{ij} is the deviatoric stress tensor, P^* is pressure, F_c is the hardening cap, and $\Re$ is the Rubin third-invariant factor. The shear failure surface is defined as:

$$F_f(J_1) = \alpha - le^{-\beta J_1} + \theta J_1 \tag{6}$$

where α, β, λ and θ are determined by fitting the model surface to a triaxial compression test for concrete cylinder specimens. The cap hardening surface is defined as:

$$F_c = \begin{cases} 1 - \frac{(J_1 - L(k))^2}{(X(k) - L(k))^2} & for\ J_1 \geq L(k) \\ 1 & for\ J_1 < L(k) \end{cases} \quad (7)$$

$$L(k) = \begin{cases} k & k \geq k_0 \\ k_0 & k \leq k_0 \end{cases}$$

$$X(k) = L(k) + R^* F_f(J_1)$$

Equation 7 describes the cap for the failure surface that occurs when J_1 is greater than or equal to $L(k)$. The value of J_1 at which the shear surface initially intersects with the cap surface is k_0. An increase in $X(k)$ and k signifies the expansion of the cap surface when compaction occurs, while a decrease in $X(k)$ and k signifies a contraction of the cap surface when dilation occurs. This intersection depends upon the cap ellipticity ratio, R^*, which represents the ratio of its major to minor axes. In this manner, compression, shear, and tensile failures are represented and consolidated for post-processing by means of a single damage variable as:

$$\varepsilon_v^P = W\left(1 - e^{D_1(X - X_0) - D_2(X - X_0)^2}\right) \quad (8)$$

where ε_v^P is the plastic volume strain, W is the maximum plastic volume strain, and X_0, R, D_1, and D_2 are model input parameters obtained from the best-fit to pressure-volumetric strain curves in uniaxial compressive strength test. Note that in this study, those input parameters were obtained using the pre-determined default values as a function of compressive strength, shear modulus, and bulk modulus (LSTC, 2019).

To simulate the fracture or crushing of shotcrete in the numerical model, the erosion algorithm, based on Equation (8), is implemented. When the material response in an element reaches a critical value of the plastic strain, the element is immediately deleted. The deletion process is irreversible, meaning that the deleted material will not be able to offer further resistance even when the applied load is reversed. For the sake of the FE model stability, the steel wire mesh embedded in the shotcrete panel was modelled with beam elements based on the elastic constitutive model. In addition, the substrate material in contact with the shotcrete panel was modelled with solid elements using the elastic constitutive model. In this study, coal material was assumed to be the substrate bedrock material, consistent with field test conditions done by Forest (2019). The FE model configuration is shown in Figure 2, and the material properties used in the FE analysis are summarised in Table 1.

The interface between the shotcrete panel and substrate is modelled with the "Surface to Surface Mortar Contact Model" in LS-DYNA. The mortal contact is a penalty-based segment-to-segment contact that incorporates finite element consistent coupling between the non-matching discretisation of the two sliding surfaces (Puso & Laursen, 2004a, b). The contact material properties in this study are assigned with the adhesion strength of 1 MPa and static and dynamic friction coefficients of 0.6 and 0.5, respectively.

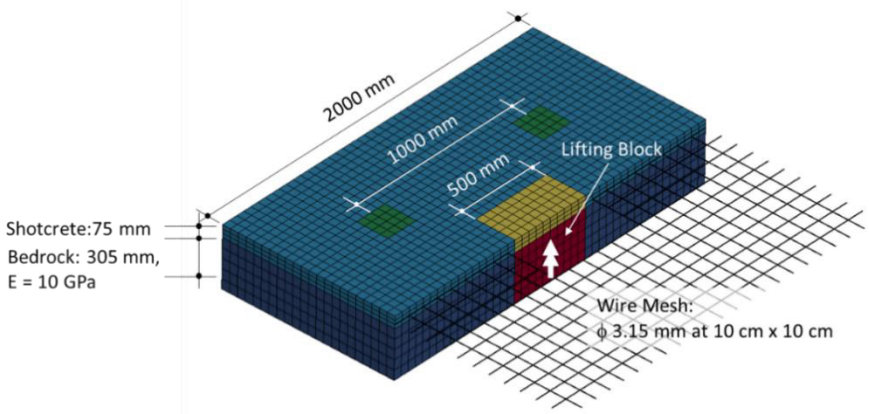


Figure 2. FE model configuration of the full-scale uniformly distributed load-deflection test, spacing-1000 mm, thickness-75 mm.

Table 1. Material properties used in FE analysis

Type	Unit weight (kg/m^3)	Poisson's ratio	f'$_c$ (MPa)	E (GPa)
Shotcrete	2400	0.2	40	30
Steel Wire Mesh	7850	0.3	N/A	215
Substrate rock (Coal)	1500	0.35	N/A	10

2.1 *FE Model calibration*

Before conducting the full-scale load-deflection test, the FE material properties of the shotcrete panel were calibrated based on Uniaxial Compressive Strength (UCS) and Round Panel Tests (RPT) in comparison with the laboratory tests and literature resources (Forrest, 2019, Bernard et al. 2022). It is known that the fibre reinforcements in the shotcrete contribute to an increase in the tensile fracture energy or strain energy release rate, Gc. To calibrate this, various values of Gc were tested, ranging from 75 N-m/m2 to 126 N-m/m2.

The results of UCS tests indicate that despite some minor variation after the peak loads, the maximum UCS of 40 MPa and the Elastic Young's modulus of 30 GPa were found to be constant across the different strain energy release rates. This is attributed to the strain energy release rate, mainly affecting tensile strength.

The RPT has been performed to estimate bending capacity based on ASTM 1550. The FE model configuration of the RPT panel consists of a radius, *R* of 400 mm, thickness, *t* of 75 mm, and the distance between the centre of the support and the centre of the panel, *r*, of 375 mm. The panel is point-supported at the perimeter with a spacing of 120^{o} ° and is loaded by a hemispherical piston at its centre (Bernard & Pircher, 2001). The diameter of the hemispherical loading piston is 50 mm. The loading piston advances at a constant rate of 4.0 mm/min. The interface between the shotcrete panel and the transfer plate is set up with a penalty-based "Surface to Surface Contact Model" in LS-Dyna, while the bottom of the transfer plates is supported by a fixed boundary condition. Table 2 shows the summary of material properties obtained from the laboratory tests and numerical analysis.

Table 2. Material properties obtained from the laboratory tests and numerical analysis

	UCS (MPa)	Adhesive Strength (MPa)	Peak Load of RPT (kN)	Flexural Strength (MPa)
Laboratory Test	44.0	1.0	-	-
Laboratory Test (Forrest, 2019)	44.4	-	23.2 (avg.)	4.5 (avg.)
LS-DYNA (Case 3)	40.0	1.0	22.0	4.2

3 FULL-SCALE LOAD-DEFLECTION TESTS

This section presents the full-scale load-deflection test using numerical analysis, compared with the field test results. A series of sensitivity analyses were performed under various loading conditions to evaluate the influence of shotcrete bonding, shotcrete thickness, and bolt spacing.

3.1 *Full-scale load-deflection field tests*

The full-scale load-deflection field test was conducted in an underground cross-passage in a longwall mine in Australia. The test involved the use of two types of lifting bags, named HLB31 (approximately bag sizes of 500 mm x 500 mm) and V68 (bag size of 1000 mm x 1000 mm), having a maximum load capacity of peak load capacity of 310 kN and 677 kN for HLB31 and V68, respectively. These lifting bags were pre-installed prior to spraying shotcrete. To evaluate

the influence of rock bolt supports, the various spaced M24 JX bolts, Jennmar with the cover plates, were installed, ranging from 1 meter to 2 meters. The length of the bolt is 1.5 meters. After curing the shotcrete liner for around three months, these bags were pressurised with water. Additional details on the field test configuration and procedures can be found in Forrest's thesis (Forest, 2019) and Bernard et al. 2022.

3.2 *Evaluation of shotcrete bonding effect*

The effect of the shotcrete bonding has been investigated using an adhesive strength of 1 MPa obtained from the laboratory tests (Table 2). Due to the lack of information on the adhesion stiffness of the shotcrete, a sensitivity analysis has been performed based on the literature sources (Bae, et al. 2004, Chu & Kwan, 2019, Dong et al. 2016, Saiang et al. 2005). These studies found that the normal bond stiffnesses varied significantly, ranging from 50 GPa/m and 900 GPa/m, depending on the strength of the substrate, roughness of the surface, and adhesion strength, etc.

After conducting a series of trials with various bond stiffnesses, ranging from 54 GPa/m to 540 GPa/m, using the shotcrete sample with 1 meter bolt spacing and a thickness of 75 mm, it has been found that the stiffness of 136 GPa/m is well comparable with the field test results, i.e., maximum bond failure of 106 kN and ultimate load of 210 kN, respectively, as illustrated in Figure 3. In all cases, the first peak loads relating to the initial bonding failure are observed. Afterwards, the resisting loads gradually increase as the deflection increases.

3.3 *Effects of shotcrete bolt spacing and thickness*

The effect of bolt spacings was investigated using 1 m, 1.5 m, and 2 m spacings with a uniform panel thickness of 75 mm. To eliminate the influence of shotcrete bonding, the panel is simply supported by the bolt plates only. Figure 4 illustrates the development of damage/cracking on the shotcrete panel in terms of the load increments. At stage 1, minor damage is initiated at the front face of the panel along the footprint of the push block area, which is likely induced by the flexural damage and/or local shear damage, and other damage at the bottom face is observed near the support plates, which could be associated with the negative bending moment and/or local shear failure induced by the interaction of the bolt plates.

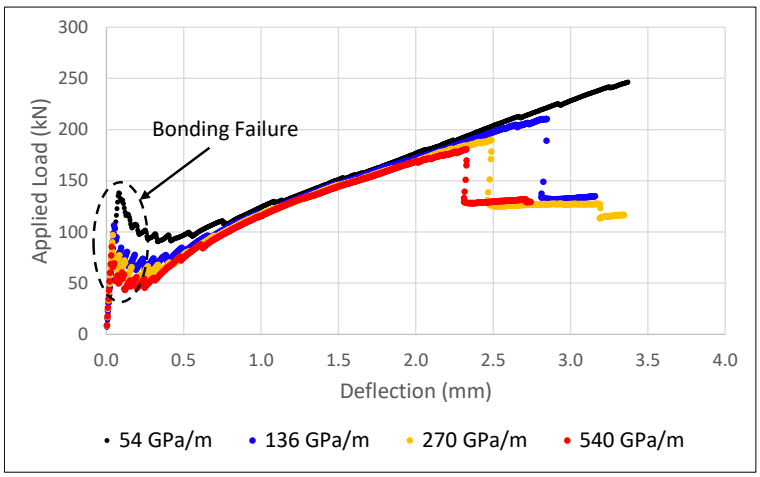


Figure 3. Load-deflection charts estimated from field tests using the scaled peak load in terms of 75 mm thickness.

After this point (a), the deflection is slightly levelled off. As the load increases at stage 2, the damage on the front face of the panel is diagonally extended and propagated, as shown in Figure 4 (b), while the local damage shown on the bottom face extends and interconnects with a round shape. At stage 3, Figure 4 (c), the damage zone further extends, and one of the diagonal damages shown on the right-hand side of the front face asymmetrically propagates further, leading to the panel collapse at Stage 4 (d). Table 5 summarises the analysis results for bolt spacing effects.

Table 2. Summary of analysis results for bolt spacing effects

Bolt Spacing (m)	Panel Thickness (mm)	Max. Deflection (mm)	Max. Resisting Force (kN)
1	75	2.8	169
1.5	75	7.8	135
2	75	12.5	140

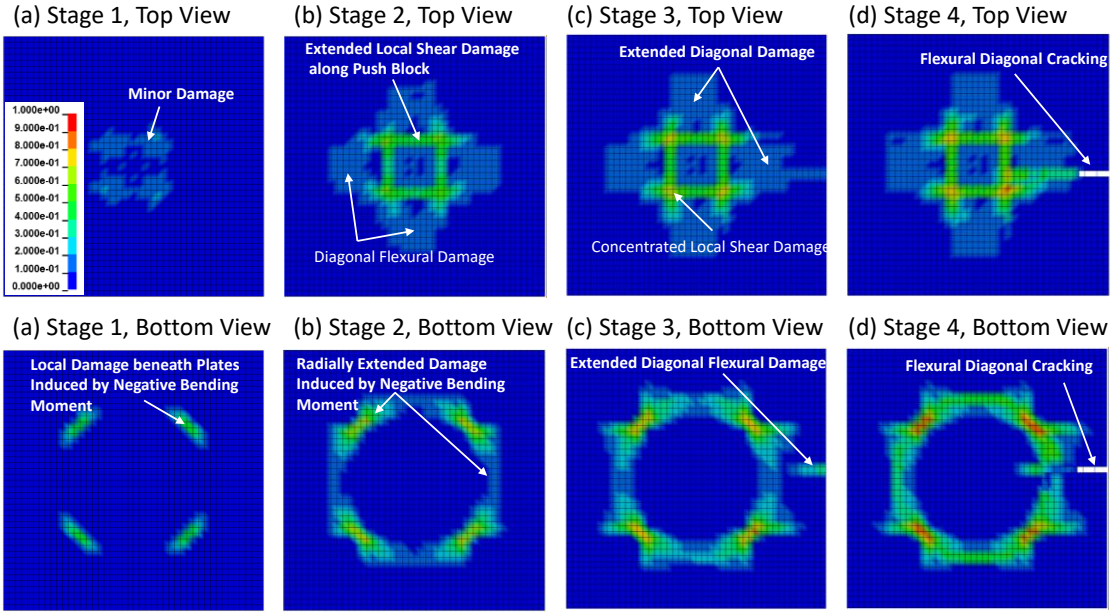


Figure 4. Development of damage distributions and cracking for 1 m bolt spacing without bonding condition.

3.4 *Moment coefficients for shotcrete flexural capacity*

The moment ratio and the corresponding moment coefficient values for all field tests and LS-DYNA analysis results are presented in Figure 5. The field test results for HLB31 and V68, having the shotcrete bonding effect, show a moment ratio of 0.16 and a moment coefficient of 0.02.

A similar result is observed in the LS-DYNA analysis for the shotcrete bond models. These relatively low moment ratio and coefficient values are likely attributed to the bonding effect, which enhances flexural strength. However, in cases where bonding was not considered, the analysis predominantly yielded a moment ratio of 0.2 and a moment coefficient of 0.025. Thus, the ultimate moment induced, M^* representing the ultimate flexural failure of the shotcrete panel, is calculated by the multiplication of M_o and a shown in Equations (9) and (10).

$$M^* = \alpha\left(\frac{1}{8}w(s-c)^2\right) \approx \alpha\frac{P}{8}\ [kN-m/m]$$

$$M^* = 0.16\frac{P}{8} = 0.02P\ [kN-m/m] \quad \text{for bonding condition} \tag{9}$$

$$M^* = 0.2\frac{P}{8} = 0.025P\ [kN-m/m] \quad \text{for no-bonding condition} \tag{10}$$

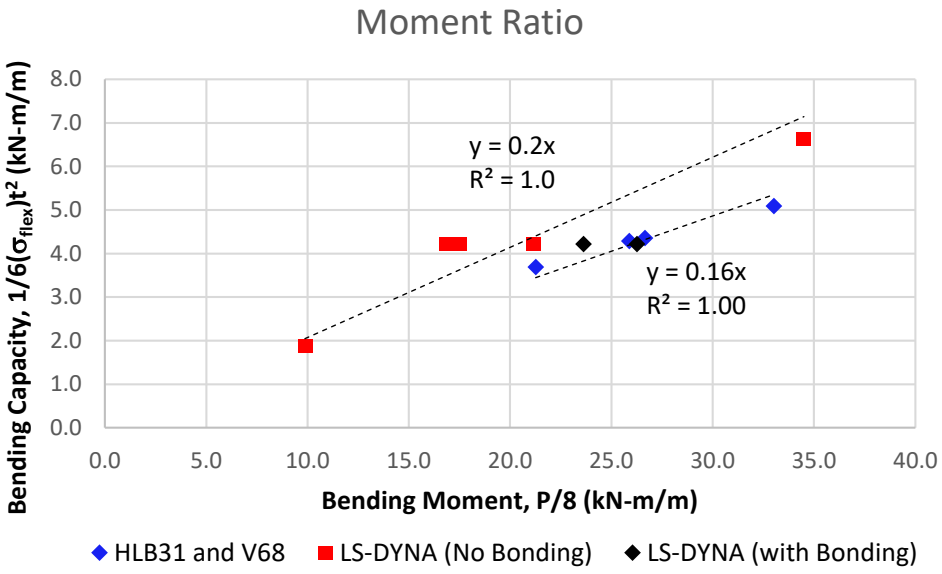


Figure 5. Bending Moment ratios obtained from field tests and LS-DYNA analyses.

4 APPLICATIONS OF SHOTCRETE SUPPORT DESIGN

Using the concept of the moment coefficient mentioned in Section 3.4, a practical shotcrete design approach is proposed in conjunction with the Q-system (Barton et al. 1974). In this shotcrete design approach, the shotcrete adhesion effect is conservatively ignored to take into account the long-term stability and reliable shotcrete design. The critical bending moment acting on the shotcrete panel corresponds to approximately 20 % of the simple span bending moment as formulated in Equation (10).

The ground support pressure, *w* is determined using Eqs 3 and 10, as a function of bolt spacing and shotcrete thickness shown in Equation (11).

$$w = 6.7\sigma_{flex}\left(\frac{t}{s}\right)^2 \quad \text{or} \quad t = 0.39s\sqrt{\frac{w}{\sigma_{flex}}} \tag{11}$$

Subsequently, the ground support pressure is integrated with the Q-system through a generic ground load form, as shown in Equation (12).

$$w = a_1 B\gamma_{rock} Q^{a_2} \tag{12}$$

where a_1 and a_2 represent coefficients, B denotes the tunnel span or height.

The input data points, including tunnel span or height, shotcrete thickness, bolt spacing, and Q values, are retrieved from the Q-system chart (Grimstad & Barton, 1993). For this study, the flexural strength of the shotcrete and rock unit weight are assumed to be 4.5 MPa and 27 kN/m^3, respectively, with the Excavation Support Ratio (ESR) of 1, which represents typical values of design input parameters. The regression analysis yielded the coefficients, a_1 and a_2, of 0.28 and -0.7, respectively, as presented in Equation (13).

$$w = 0.28B\gamma_{rock} Q^{-0.7} \tag{13}$$

For a given bolt spacing, the required shotcrete thickness can be determined using Equations (11) and (13), as follows:

$$t = 0.2s\sqrt{\frac{B\gamma_{rock}Q^{-0.7}}{\sigma_{flex}}} \tag{14}$$

5 CONCLUSION

The main conclusions of this study can be summarised as follows:

- The flexural tensile failure mode predominantly governs the ultimate capacity of the shotcrete liner.
- The effect of shotcrete thickness was evaluated using numerical analysis. The result of the analysis revealed that the maximum resisting loads appear to be a square relation with shotcrete thickness.
- There was a constant ratio between the bending moment capacity, C_{flex} and the estimated bending moment, M_o based on the simple span formula, approximately 0.2 for the "no-bonding condition" and 0.16 for the "bonding condition", respectively.
- A practical shotcrete design method has been proposed based on the moment ratio of 0.2 presented in Equation (11) or Equation (14).

6 REFERENCES

Bae, G.-J., Chang, S.-H., Lee, S.-W., Park, H.-G. (2004). Evaluation of interfacial properties between rock mass and shotcrete. Int. J. Rock Mech. Mining sci. 41, 106-112.

Barrett, S.V.L., McCreath, D.R., 1995, Shotcrete Support Design in Blocky Ground: towards a Deterministic Approach. Tunn. Undergr. space Technol. 10(1), pp. 79-89.

Barton, N., Lien, R., Lunde, J., 1974. Engineering classification of rock masses for the design of tunnel support. NGI Publication No. 106, Oslo, 48.

Bernard, E.S., Oliveira, D.A.F, Forrest, B.H., 2022. In situ flexural failure of unbonded fibre reinforced shotcrete linings in response to point loading, Tunn. Undergr. space Technol. 119, 104235

Bernard, E.S., Pircher, M., 2001, The influence of thickness on performance of fibre-reinforced concrete in a round determinate panel test. Cement, Conc. Aggreg. CCAGDP, 23(1), pp. 23-33.

Chu, S.H., Kwan, A.K.H. (2019). A new bond model for reinforcing bars in steel fibre reinforced concrete. Cement and Concrete Composites, 104, 103405.

Dong, W., Wu, Z., Zhou, X., 2016., Fracture Mechanisms of Rock-Concrete Interface: Experimental and Numerical, 142(7), 1-11.

Forrest, B., 2019. Load capacity of fibre reinforced shotcrete in coal. Master's thesis, UNSW Sydney.

Grimstad, E., Barton, N. 1993. Updating of the Q-system for NMT. Proc. Int. Sym. Sprayed Concrete, Fagerner, Oslo, 22-26, 1993, pp 46-66.

Kaiser, P.K., Tannant, D.D., 2001. The Role of Shotcrete in Hard-Rock Mines. Underground Mining Methods, Engineering Fundamentals and International Case Studies, Hustrulid & Bullock (eds.), Society for Mining, Metallurgy and Engineering Inc., Litteton, CO, pp. 579-592.

LS-DYNA User's Manual Ver R11, 2019. Livermore Software Tech. Corp. Livermore, California.

Murray, Y. 2007, User manual for LS-DYNA concrete material model 159, FHWA-HRT-05-062.

Puso, M.A., Laursen, T.A., 2004a. A mortar segment-to-segment contact method for large deformation solid mechanics. Comput. Methods Appl. Mech. Engrg. 193, pp. 601-629.

Puso, M.A.. Laursen, T.A., 2004b. A mortar segment-to-segment frictional contact method for large deformations, Comput. Methods Appl. Mech. Engrg. 193, pp. 4891-4913.

Saiang, D., Malmgren, L., Nordlund, E. (2005). Laboratory Tests on Shotcrete-Rock Joints in Direct Shear, Tension and Compression. Rock Mech. Rock Eng. 38(4), 275-297.

19th Australasian Tunnelling Conference – Acosta-Martínez, Stewart and Hudson-Smith (Eds.)
© 2025 Australian Tunnelling Society, ISBN 978-0-85825-002-4

Evaluating the setting behaviour of shotcrete with crushed waste glass as sand replacement

M. Serati, X. Zhu & M. J. Luana
University of Queensland, Brisbane, Australia

M. Booy
Heidelberg Materials Australia, Brisbane, Australia

ABSTRACT: The increasing demand for shotcrete, driven by the expansion of underground construction, has intensified concerns on its supply chain over natural sand depletion. This issue is particularly pressing as shotcrete typically requires an over-sanded mix, further straining finite resources and posing environmental and economic challenges. To address this, a novel approach was proposed using crushed waste glass (CWG) as a partial replacement for natural sand. Given the importance of early-age strength in shotcrete, especially when used with accelerators, this study focused on the influence of CWG on setting behaviour. A series of tests using thermocouple-embedded cube moulds were conducted across CWG replacement levels from 0% to 50%. Findings revealed the overall comparable setting dynamics across different mixes, while it was observed that CWG inclusion caused a slight increase in peak temperature and a minor delay in setting initiation, which requires careful consideration in developing shotcrete mix design.

1 INTRODUCTION

With rapid urbanisation and growing demand for construction, tunnelling has become essential not only for transportation, but also for resource and energy sectors, including shaft construction and pumped hydro for sustainable energy storage (Blakers et al., 2021). As the tunnelling projects increase, so does the demand for shotcrete. It is a specialised form of concrete applied pneumatically through a nozzle, offering notable advantages in flexibility and efficiency (Australian Shotcrete Society, 2020). Shotcrete application provides immediate support to the rock mass after excavation, making it especially valuable in most tunnelling methods, such as drill and blast. It can serve as both a temporary and final rock support system. Unlike conventional concrete, shotcrete does not require traditional formwork, thereby reducing both construction time and cost.

To meet application demands, shotcrete must exhibit high flowability in its base mix (without accelerator) and minimise rebound during application (Armelin & Banthia, 1998). Achieving these properties requires modifications to conventional concrete mix designs. In addition to chemical admixtures such as accelerators, superplasticisers and retarders, shotcrete uses smaller aggregates, typically up to 10 mm, and a significantly higher proportion of fine aggregates. Natural sand is the most commonly used fine aggregate due to its wide availability and reliable performance history.

However, natural sand is now the second most consumable resource globally. Its annual consumption exceeds 50 billion tons, with a growth rate of 5% per year (Kazmi et al., 2020). Despite the economic impact of the increasing market price, over-excavation of natural sand has also led to environmental degradation, such as deforestation and riverbank corrosion. Given the over-sanded mix design of shotcrete, such depletion presents a critical supply chain concern for the shotcrete industry.

In response, the industry is actively seeking alternatives to natural sand. The author group has explored the use of synthetic fine aggregates derived from solid waste for shotcrete production, with crushed waste glass (CWG) emerging as a promising option (Kazmi et al., 2021; Kazmi et al., 2020; Zhu et al., 2025; Zhu et al., 2023). As a material originally manufactured from natural sand, CWG shares a similar chemical composition, primarily composed of silica (SiO_2). It is also advantageous due to its non-biodegradability and inert nature.

The reuse of waste glass, particularly from packaging such as bottles and jars, which are difficult to recycle due to variations in colour and composition, also addresses landfill reduction and sustainability goals. Industrial glass (e.g., windows) is more easily recycled, while packaging glass often ends up as waste due to the higher energy cost of sorting and reprocessing (Costa & Meillon, 2022).

To advance sustainable practices in shotcrete production, the author group has conducted a series of investigations on CWG at multiple scales, ranging from grain-level characterisation to laboratory batch testing and progressing toward field trials. In the first laboratory-scale study, the incorporation of CWG as a partial replacement for natural sand (up to 50%) was shown to maintain comparable mechanical strength and fresh properties, demonstrating its feasibility for structural applications (Serati et al., 2022). Recognising the critical role of early-age strength in ensuring safe site access after shotcrete application, a subsequent study focused specifically on the interaction between CWG content and accelerator dosage, which is currently under publication process (Zhu et al., 2025). This second investigation examined the early-age strength development of shotcrete mixes with varying CWG replacement levels (0%, 10%, 25%, and 50%) while maintaining a constant accelerator dosage of 3%. The results, summarised in a forthcoming conference proceeding, revealed that CWG-containing mixes exhibited reduced strength at 3 hours based on end-beam tests. However, as hydration progressed, strength levels improved and approached those of conventional mixes, indicating a distinct early-age behaviour influenced by the presence of CWG.

These findings align with previous literatures working on CWG replacing natural sand in concrete materials, where unconfined compressive strength (UCS) demonstrated similar trends, with initial strength reductions attributed to weaker interfacial transition zone (ITZ) (Shao et al., 2000; Tamanna et al., 2020; Tan & Du, 2013). However, the presence of amorphous silica in fine glass particles can lead to pozzolanic activity, enhancing strength at later ages. In accelerated shotcrete, though, pozzolanic reactions are unlikely to significantly contribute within short timeframes. Instead, the early-age strength reduction may be linked to delayed cement hydration caused by the glass aggregates, which is an area requiring further research.

This gap in understanding underscores the need for deeper investigation into the setting behaviour of shotcrete containing CWG. One effective method for evaluating setting behaviour is thermal characterisation. Cement hydration is an exothermic process, and temperature monitoring provides insight into setting dynamics. While prior studies have used isothermal calorimetry to evaluate hydration rates in glass-containing cementitious materials, such tests are limited to small samples (e.g., pastes or mortars) and do not fully represent shotcrete behaviour (Jochem et al., 2021; Liu et al., 2015; Mirzahosseini & Riding, 2014).

To address this, Poutos et al. (2008) have measured temperature changes using thermocouples embedded in a 200 mm concrete cube with 100% aggregate replacement by various types of crushed glass. The study revealed significant differences in temperature profiles, indicating variations in setting behaviour. Building on this foundation, the present study improves upon previous studies by accounting for practical shotcrete mix conditions, including chemical admixtures, adjusted water-to-cement ratios and increased thermocouple distribution to capture localised effects on cement hydration.

This study investigates four shotcrete mixes with 0%, 10%, 25%, and 50% replacement of natural sand by CWG, with a focus on early-age setting behaviour. By adopting the same mix design as previous studies, this work aims to provide deeper insight into the influence of CWG on early hydration and setting dynamics.

2 EXPERIMENTAL PROGRAM

2.1 *Materials*

The shotcrete mix used in this study was specifically designed for tunnelling applications and has been successfully implemented in actual tunnel construction projects. The constituent materials, including fine sand, medium sand, coarse aggregates, cement, fly ash, and the reference mix design, were supplied by Wagners, a collaborating concrete supplier, with raw materials sourced from local quarries and cement plants. Chemical admixtures were provided by GCP Applied Technologies and included Tytro WR172 (water reducer), Tytro HC270 (hydration stabiliser), and ALSET 13 (accelerator).

The crushed waste glass originated from landfilled glass waste, primarily consisting of beverage bottles in various colours. The raw glass underwent heat treatment to remove paper labels and contaminants, followed by crushing into multiple size fractions. For this study, different CWG sizes were blended to closely match the particle size distribution of the medium sand they replaced. This approach ensured that the combined aggregate gradation remained consistent across all CWG-containing mixes.

Table 1. Shotcrete mix design per m^3 with different CWG replacement ratios.

Materials	0%	10%	25%	50%
7mm Aggregate (kg)	450	450	450	450
Medium Sand (kg)	1,016	914	762	508
Crushed Waste Glass (kg)	0	102	254	508
Fine Sand (kg)	153	153	153	153
Cement (kg)	345	345	345	345
Fly Ash (kg)	115	115	115	115
Tytro WR172 (kg)	3.71	3.64	3.64	3.49
Tytro HC270 (kg)	1.1	1.1	1.1	1.1
Water (L)	245	245	245	245

The mix designs, summarised in Table 1, were developed through iterative adjustments to the water reducer (Tytro WR172) and water content, with the goal of achieving slump values comparable to the reference mix. Optimised shotcrete mixes reached target slump values in the range of 230–250 mm. Notably, mixes incorporating CWG required reduced dosages of both water and water reducer, likely due to the hydrophobic nature of glass. This observation aligns with findings reported by Serati et al. (2022) and Zhu et al. (2023).

2.2 *Experimental Process*

The experimental tests were performed using 200 mm concrete cube moulds as shown in Figure 1a. Each mould was instrumented with five thermocouples, positioned vertically and equally spaced, with the alignment displayed in Figures 1b and 1h. Type T thermocouples with 0.5 mm diameter, supplied by TC Measurement & Control, were used in the setup. The thermocouple used in this study is made from copper, allowing measurement up to 125°C with a tolerance of +/- 0.5°C. Thermocouple junctions were formed by twisting and connecting both wires, and the extension cables were made from the same thermocouple wire, fitted with thermocouple connectors (both socket and plug in Figs 1d, e). Data acquisition was managed using a Keysight 34980A system, which supports up to 40 simultaneous inputs and operates within the environmental parameters specified for the test.

The experimental process was divided into two phases: mixing (in Fig. 1f) and conditioning (in Fig. 1g), with temperature continuously recorded throughout by the data logger. All four mixes were prepared on the same day. Aggregates and binders were pre-weighed, dried, and dry-mixed before adding water and admixtures. Each batch was mixed for no longer than 10 minutes and immediately cast into moulds. Since mixed order can influence temperature development, two separate trials were conducted to account for this variable. In Trial 1, mixes were prepared in the

order of 50%, 25%, 10%, and 0% CWG replacement; in Trial 2, the order was reversed. This allowed for normalisation of temperature profiles by averaging the data from both trials to establish a consistent baseline.

To ensure consistent curing conditions, the conditioning phase was conducted in the Concrete Creep Room at the University of Queensland's Civil Engineering Laboratory. This facility maintains a stable environment of 23.5°C and 50% relative humidity, minimising the influence of external temperature fluctuations. The transition from mixing to conditioning took approximately one minute, during which data logging was temporarily paused.

Temperature was recorded continuously at a frequency of 1 Hz throughout the test. For post-processing and analysis, the data were averaged at 15-minute intervals to reduce noise and improve clarity of the temperature profiles.

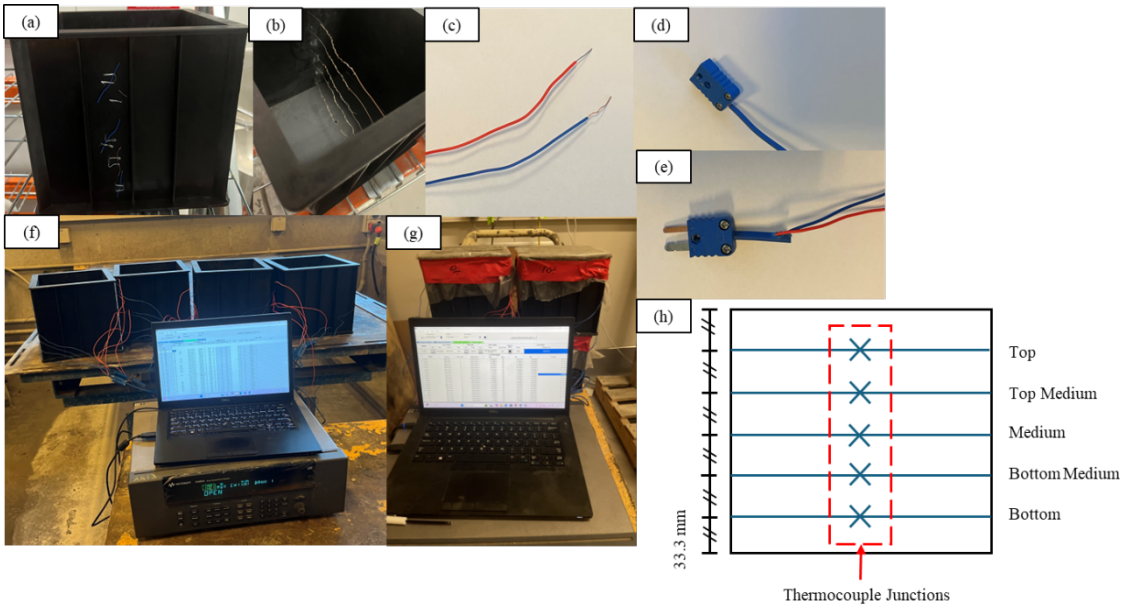


Figure 1. Experimental test setup: (a) 200 mm cube mould, (b) thermocouples installed in mould, (c) Type T thermocouples, (d) thermocouple socket connector, (e) thermocouple plug connector, (f) measurement setup in mixing phase, (g) measurement setup in conditioning phase and (h) thermocouple installation alignment.

3 RESULT DISCUSSION

Figure 2 presents the averaged temperature profiles of all four shotcrete mixes, compiled from both experimental trials. The results demonstrated minimal variation among thermocouple positions. While the bottom thermocouple occasionally displayed slight deviations from the general trend, which is likely due to proximity to the mould boundary and heightened sensitivity to ambient temperature, these differences were minor and did not significantly affect the overall analysis. The consistency across thermocouple readings indicates that cement hydration occurred uniformly throughout the shotcrete matrix, with no evidence of localised hotspots. This spatial uniformity enabled the use of averaged temperature values across all ten thermocouples (two trials, five per mould) for each mix.

These average profiles are plotted in Figure 3a. To further interpret the hydration kinetics, the rate of temperature change was analysed and presented in Figure 3b. This was calculated as the slope between successive 15-minute intervals, providing an estimate of the instantaneous rate of temperature increase or decrease.

In the first 7 hours following mixing, temperature variation largely reflected external influences - namely, the transition from ambient mixing conditions to the controlled environment of

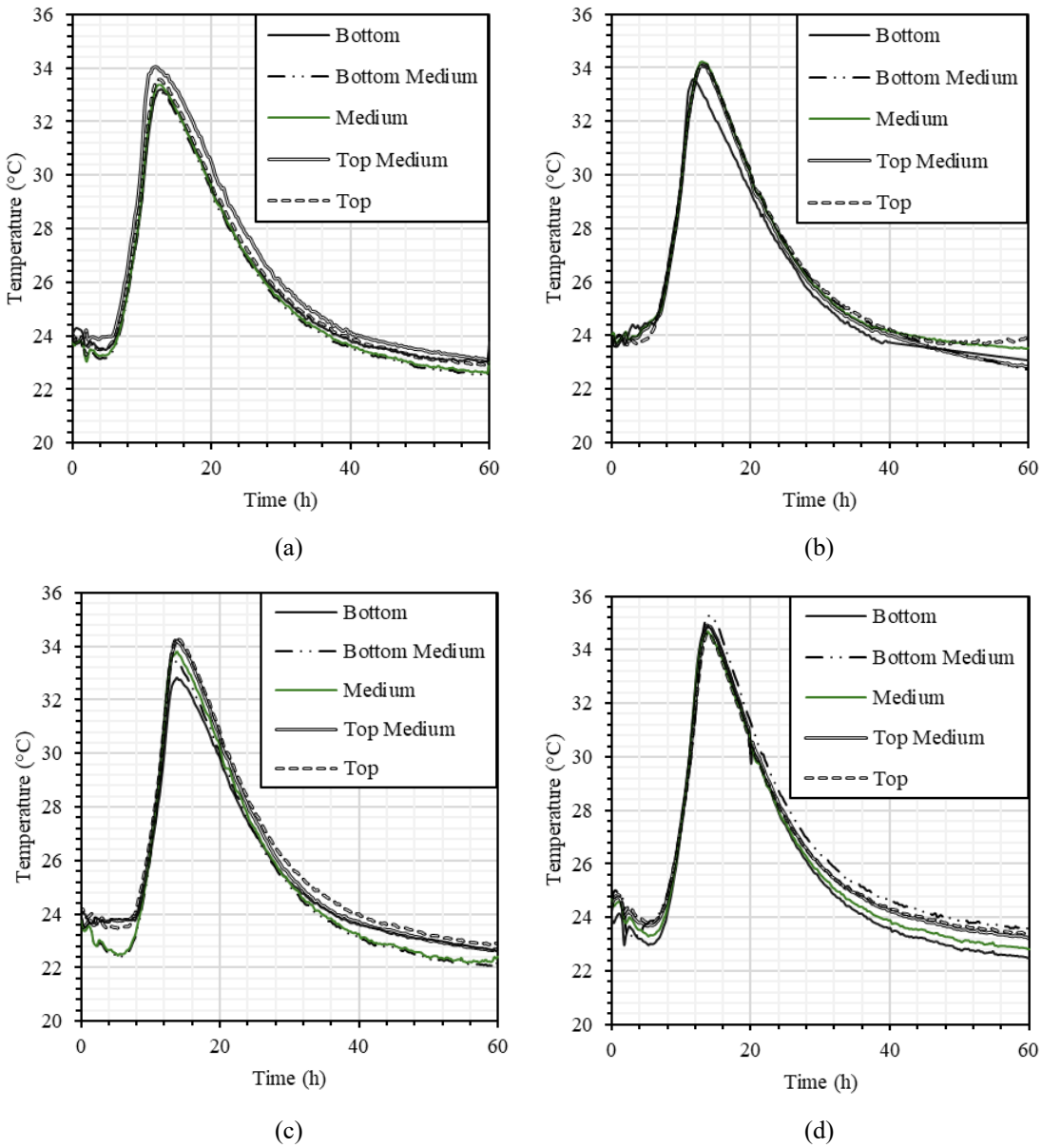
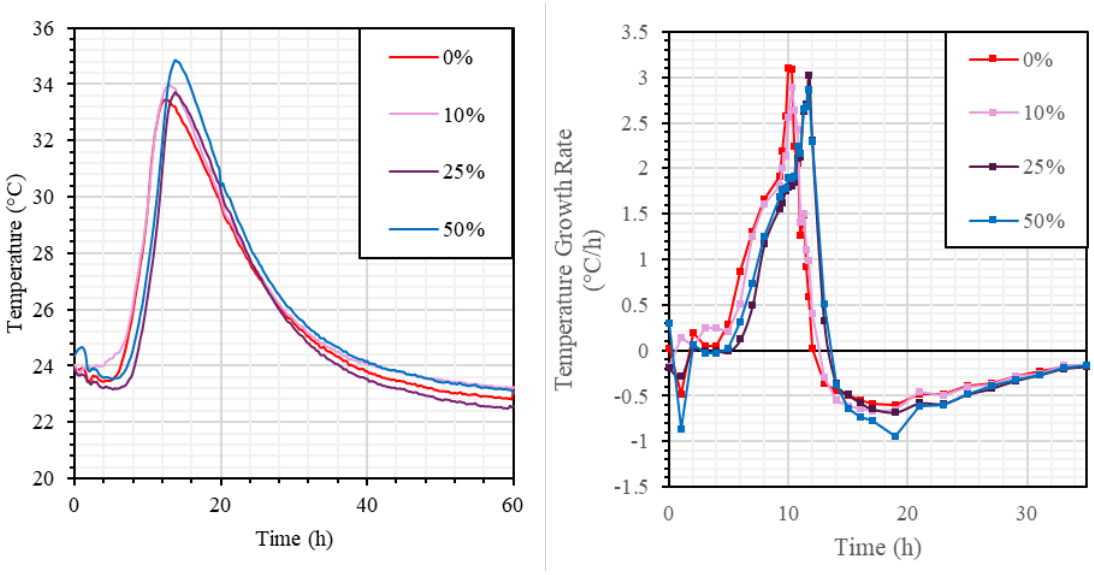


Figure 2. Average temperature profile from shotcrete mixes based on two trials: (a) 0% CWG mix, (b) 10% CWG mix, (c) 25% CWG mix and (d) 50% CWG mix.

the conditioning room. Additionally, the mixing process itself may have slightly elevated temperatures due to mechanical energy input; however, given the controlled slump across all mixes, flow-related differences were considered negligible.

Overall, the inclusion of CWG did not significantly alter the thermal profile of cement hydration. Maximum recorded temperatures ranged from 34°C to 36°C, comparable reported temperature rise in the literature for cementitious materials due to cement hydration (Poutos et al., 2008; Schackow et al., 2016; Wade et al., 2010). Figure 3a shows a slight increasing trend in peak temperature with higher CWG replacement. Notably, the mix with 50% CWG exhibited a temperature approximately 2°C higher than the reference mix. An additional observation was a modest delay in setting initiation for mixes with higher CWG content, with onset delayed by approximately 1 hour. To address the key findings from this study, the outcomes may be explained by the following mechanisms related to CWG properties:

– Unlike natural sand, which is predominantly composed of crystalline silica, glass is made of amorphous silica. The disordered atomic structure of amorphous silica results in lower thermal conductivity, slowing heat transfer (Zhou et al., 2020). Consequently, heat generated during hydration is retained longer, potentially elevating peak temperatures.



(a) (b)

Figure 3. Analysed temperature profiles for four mixes: (a) temperature variation and (b) temperature growth rate.

- Fine CWG particles with high specific surface area can act as pozzolanic reactants. The reaction between amorphous silica in glass and calcium hydroxide (portlandite), a hydration by-product, forms secondary C-S-H gel (Shao et al., 2000; Tamanna et al., 2020). Although pozzolanic reactions typically occur after initial cement hydration, their exothermic nature may contribute to slightly higher temperatures observed at later stages.
- Glass particles are smoother and more hydrophobic than natural sand, as confirmed in Zhu et al. (2023). This can hinder water absorption, reduce paste-aggregate bonding, and slow hydration. Despite the consistent dosage of hydration stabiliser, the hydrophobic nature of CWG may contribute to delayed setting through retention of free water in the mix.
- The CWG used in this study was sourced from recycled beverage containers. The treatment process involved only thermal cleaning without washing, likely leaving residual sugar from contents such as honey and soft drinks. Previous research has proven that sugar contamination can retard the setting of cementitious materials, which may further explain the observed delay in hydration onset (Khan & Baradan, 2002; Wang et al., 2022).

4 CONCLUSION

This study explored the influence of crushed waste glass (CWG) as a partial replacement for natural sand in shotcrete applications, with a focus on its effects on early-age temperature development and setting behaviour. The experimental approach involved full-scale batching of shotcrete mixes incorporating CWG at varying replacement levels (0%, 10%, 25%, and 50%), followed by detailed thermal monitoring using embedded thermocouples under controlled environmental conditions. Key findings are as follows:

- Temperature profiles obtained from multiple thermocouple positions confirmed that cement hydration occurred uniformly throughout the shotcrete matrix, allowing reliable analysis based on averaged temperature data.
- Across all mixes, peak hydration temperatures ranged from 34°C to 36°C, with a slight upward trend observed as CWG content increased. The increase, although modest, suggests that the presence of CWG may contribute to improved thermal retention within the matrix.
- Higher CWG replacement ratios were associated with a delay in the initiation of cement setting by approximately one hour. This delay is attributed to several interrelated factors, including thermal conductivity, potential pozzolanic activity, unique surface characteristics and sugar contamination.

Overall, the inclusion of CWG up to 50% did not negatively impact the thermal signature of cement hydration, and in fact, exhibited slightly elevated peak temperatures with minimal disruption to setting kinetics. These findings support the feasibility of CWG as a sustainable alternative to natural sand in shotcrete, with manageable effects on early-age behaviour. The study also provided an explanation for previous findings in the early-age strength pattern of CWG-incorporated shotcrete with accelerator dosage. This finding suggested the potential to adjust the accelerator dosage or reduce the retarder content to enhance the early-age performance of shotcrete with high CWG replacement ratios.

5 ACKNOWLEDGEMENT

The project team wishes to acknowledge the financial support from the Queensland Government (Australia) under the Advanced Queensland Industry Research Fellowships program (No. CTS 20355/21), awarded to Dr Mehdi Serati. We also appreciate the support from industry partners Aurecon, Heidelberg Materials Australia, GCP Applied Technology, GHD and Sustainable Future by Design. Additionally, the project team thanks Mr Shane Walker and Dr Sergio Zarate Orrego for their assistance with the experimental stage.

6 REFERENCE

Armelin, H. S., & Banthia, N. 1998. Mechanics of aggregate rebound in shotcrete—(Part I). *Materials and structures*, *31*, 91-98.

Australian Shotcrete Society (Ed.). 2020. *Recommended Practice - Shotcreting in Australia* (Third ed.). TechMedia Publishing Pty Ltd.

Blakers, A., Stocks, M., Lu, B., & Cheng, C. 2021. A review of pumped hydro energy storage. *Progress in Energy*, *3*(2), 022003.

Costa, S., & Meillon, M. 2022. *Improving Australia's glass recycling*. Retrieved January 5th from https://www.csiro.au/en/news/all/articles/2022/august/glass-recycling

Jochem, L. F., Casagrande, C. A., Onghero, L., Venancio, C., & Gleize, P. J. 2021. Effect of partial replacement of the cement by glass waste on cementitious pastes. *Construction and Building Materials*, *273*, 121704.

Kazmi, D., Serati, M., Williams, D. J., Qasim, S., & Cheng, Y. P. 2021. The potential use of crushed waste glass as a sustainable alternative to natural and manufactured sand in geotechnical applications. *Journal of Cleaner Production*, *284*, 124762.

Kazmi, D., Williams, D. J., & Serati, M. 2020. Waste glass in civil engineering applications—A review. *International Journal of Applied Ceramic Technology*, *17*(2), 529-554.

Khan, B., & Baradan, B. 2002. The effect of sugar on setting-time of various types of cements. *Sci. Vis*, *8*(1), 71-78.

Liu, S., Xie, G., & Wang, S. 2015. Effect of curing temperature on hydration properties of waste glass powder in cement-based materials. *Journal of Thermal Analysis and Calorimetry*, *119*, 47-55.

Mirzahosseini, M., & Riding, K. A. 2014. Effect of curing temperature and glass type on the pozzolanic reactivity of glass powder. *Cement and concrete research*, *58*, 103-111.

Poutos, K., Alani, A., Walden, P., & Sangha, C. 2008. Relative temperature changes within concrete made with recycled glass aggregate. *Construction and Building Materials*, *22*(4), 557-565.

Schackow, A., Effting, C., Gomes, I. R., Patruni, I. Z., Vicenzi, F., & Kramel, C. 2016. Temperature variation in concrete samples due to cement hydration. *Applied thermal engineering*, *103*, 1362-1369.

Serati, M., Jakson, N., Asche, H., Basireddy, S., & Malgotra, G. 2022. Sustainable shotcrete production with waste glass aggregates. *SN Applied Sciences*, *4*(3), 1-14.

Shao, Y., Lefort, T., Moras, S., & Rodriguez, D. 2000. Studies on concrete containing ground waste glass. *Cement and concrete research*, *30*(1), 91-100.

Tamanna, N., Tuladhar, R., & Sivakugan, N. 2020. Performance of recycled waste glass sand as partial replacement of sand in concrete. *Construction and Building Materials*, *239*, 117804.

Tan, K. H., & Du, H. 2013. Use of waste glass as sand in mortar: Part I–Fresh, mechanical and durability properties. *Cement and Concrete Composites*, *35*(1), 109-117.

Wade, S. A., Nixon, J. M., Schindler, A. K., & Barnes, R. W. 2010. Effect of temperature on the setting behavior of concrete. *Journal of Materials in Civil Engineering*, *22*(3), 214-222.

Wang, T., San Nicolas, R., Kashani, A., & Ngo, T. 2022. Sustainable utilisation of low-grade and contaminated waste glass fines as a partial sand replacement in structural concrete. *Case Studies in Construction Materials*, *16*, e00794.

Zhou, W. X., Cheng, Y., Chen, K. Q., Xie, G., Wang, T., & Zhang, G. 2020. Thermal conductivity of amorphous materials. *Advanced Functional Materials*, *30*(8), 1903829.

Zhu, X., Serati, M., Asche, H., Booy, M., & van Wijk, I. 2025. Characteristics of Shotcrete with Crushed Waste Glass as Fine Aggregates. *Construction and Building Materials*, *490*, 142216. https://doi.org/https://doi.org/10.1016/j.conbuildmat.2025.142216

Zhu, X., Serati, M., Asche, H., Yang, X., & Gayler, A. 2023. Solid waste characterisation for use in shotcrete production. ATC 2023: Australian Tunnelling Conference: Conference Proceedings: Trends and Transitions in Tunnelling,

19th Australasian Tunnelling Conference – Acosta-Martínez, Stewart and Hudson-Smith (Eds.)
© 2025 Australian Tunnelling Society, ISBN 978-0-85825-002-4

Optimizing artificial ground freezing design for cross passage construction: Construction and practical considerations

C.F. Tsang, D. Devrnja, M. Gresz & G. Quigg
CPB Contractors Pty Ltd, Australia

ABSTRACT: Artificial Ground Freezing (AGF) is a favoured method for temporary ground support in cross passage construction between tunnels in soft soils, noted for its structural stability and water tightness. This paper addresses a notable gap in AGF optimization from a construction perspective, by delineating critical design considerations. The design of AGF's configurations range from dual-sided with standard collars to minimal collar, each influencing pipe length, number, and installation angles. Reducing collar height optimizes these variables, decreasing both material costs and project duration. Lining type selection is crucial, with considerations extending to spatial constraints posed by traditional reinforced concrete segments. Steel linings can be proposed as an alternative, facilitating improved load transfer and minimizing internal temporary support for spaceproofing. The use of nitrogen as a freezing agent, offering substantial reductions in freezing time compared to brine, is evaluated against safety risks and cost. The goal of this paper is to present a comprehensive framework for integrating design considerations for AGF, and discuss their practical implications in a construction context.

1 INTRODUCTION

Artificial Ground Freezing (AGF), a technique pioneered in Germany, has become a versatile solution for ground stabilization in various engineering projects. The core principle of AGF involves extracting heat from the soil, lowering its temperature below the freezing point of interstitial water. As this moisture freezes, it acts as a binding agent, effectively cementing soil particles together and creating a robust structural network within the soil mass.

The AGF process is implemented through a system of freezing pipes strategically installed in the target area and circulate a cryogenic liquid through these pipes. This process creates cylindrical frozen zones around each pipe, which gradually expand and merge to form a continuous, self-supporting, and impermeable frozen body.

While significant research exists on the thermal and structural behaviour of AGF, there is limited guidance on optimizing its design during construction. Existing studies primarily focus on freeze wall development and frozen soil strength. However, the design optimization for pipe arrangements and interdisciplinary collaboration remains underexplored. These gaps can result in conservative and cost-inefficient designs. This paper aims to address the gap in the literature by presenting an integrated design framework for AGF in cross passage construction. The focus is on practical considerations that influence geometry and time optimization, including freezing pipe arrangements and lining design. The objectives are to propose a design framework for AGF that balances safety, cost, and construction time and provide a decision-making framework that integrates multidisciplinary inputs for AGF design optimization.

2 CROSS PASSAGE CONSTRUCTION WITH ARTIFICIAL GROUND FREEZING

AGF plays a crucial role in the construction of cross passages between bored tunnels, particularly in challenging subsurface conditions. Cross passages are essential safety features in modern twin tunnel designs, providing emergency escape routes between tunnels (Murray & Eskesen 1997). There are different methods for cross passage construction. The paper focuses on developing an integrated design framework for a Sprayed Concrete Lining (SCL), also known as shotcrete primary lining with a sheet membrane for waterproofing, followed by cast-in situ reinforced concrete secondary lining.

AGF offers an effective solution by creating a stable, impermeable frozen soil mass between tunnels, enabling safe cross passage excavation. The construction of a cross passage using AGF typically involves five stages (Figure 1 - left).

The soil freezing process for cross passage construction involves placing freezing pipes in a strategic pattern between tunnels. Temperature sensors are installed to monitor the growth of the frozen body. Depending on inter-tunnel distance, pipes may be inserted through the segment lining from one or both tunnels (Figure 1 - right). The freezing process begins with the formation of frozen columns around each pipe, which eventually merge into a continuous freeze wall (Figure 1c - left). This method allows for controlled soil stabilization, enabling safe excavation of the cross passage.

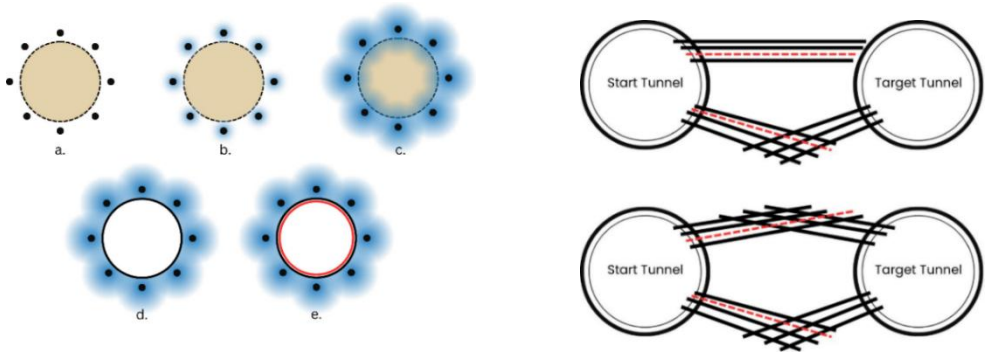


Figure 1. (left) Schematic view of artificial ground freezing stages during cross passage construction. a. Installation of the freeze pipes b. Growing of the columns around the freeze pipes c. Closing of freeze wall d. Excavation of the cross passage and apply primary lining e. Installation of the secondary lining; (right) Possible freeze pipe configurations.

3 SITE ASSESSMENT

A comprehensive site assessment is imperative before implementing AGF in construction projects. This assessment entails a detailed evaluation of the site's geological and hydrological conditions. Accurate characterization of soil and rock, including permeability, thermal conductivity, and moisture content, is crucial for designing the freezing system. Soils with low permeability require extended freezing times, while low thermal conductivity soils demand more intensive freezing efforts. Groundwater flow velocity is critical, as flowing water increases heat transfer, potentially undermining freeze wall integrity.

Lab tests provide essential data on soil behavior under freezing conditions. Tests on thermal conductivity, uniaxial compression, and creep behavior are conducted at temperatures between -10°C and -20°C. Groundwater analysis identifies salinity, chemical composition, and flow rates, as these factors can lower the freezing point and affect freeze wall formation. A list of typical tests for AGF generally include moisture content, dry density and specific gravity, Atterberg limits, grain size analysis, triaxial compression test (CU), uniaxial compression test (frozen), triaxial compression test (frozen), uniaxial creep test (frozen), frost heave, frost pressure and salinity.

4 PROJECT REQUIREMENTS AND CONSTRAINTS

The effective implementation of AGF for cross passage construction requires a thorough understanding of specific project requirements and constraints. These considerations encompass geometric constraints and interfaces, specified tolerances, and clearly defined target properties for the frozen body.

A critical geometric constraint is the diameter of the Tunnel Boring Machine (TBM) tunnel, which determines the available space for installing freezing equipment and influences the design of the freeze wall. Additionally, the timing of the cross passage construction whether it occurs during or after the mainline TBM tunnelling, impacts the sequencing of operations and resource allocation. Space constraints due to operational utilities, such as ventilation ducts, further limit the area available for freezing pipe installation and must be carefully considered.

Specifying tolerances is vital to ensure the accuracy and effectiveness of the freezing process. Freezing pipe drilling tolerances must be strictly adhered to, as deviations can lead to discontinuities in the freeze wall. The effect of tolerances on AGF design will be discussed in details under section 6.3.

Defining target properties for the frozen body is essential to achieve the desired ground stabilization and impermeability. The following are example criteria that needs to be established for the frozen body: i) thickness of the frozen body is $\geq$ 1.5 m, ii) temperature of the frozen wall boundary is $\leq$ –2 °C, iii) average temperature within the ring is $\leq$ –10 °C and iv) temperature at the core of the frozen body is $\leq$ –15 °C. These parameters ensure that the frozen body provides sufficient structural support and watertightness. A freeze wall thickness of at least 1.5 m is required to maintain stability, measured outward from the excavation line.

5 SEGMENTAL LINING DESIGN AND MATERIAL CONSIDERATIONS

Selecting appropriate segmental lining materials is crucial for both structural performance and construction efficiency. Reinforced concrete segments are commonly used but may not be suitable in certain situations. They often require internal temporary supports during installation, which can cause space constraints within the tunnel. This space proofing issue can interfere with equipment placement and construction activities inside the tunnel.

To address these challenges, steel linings may be considered as an alternative. However, the use of steel segments introduces other considerations. The steel lining details, such as whether an open pan design, post-fixed panels, or concrete-filled configurations are used, can significantly influence the freeze program. For instance, an open pan steel lining may lack sufficient thermal insulation at the interface of the frozen ground and the segmental lining, leading to increased freeze times.

Steel linings with pre-defined drill ports offer advantages in terms of reduced collar thickness and, consequently, reduced freeze time. However, this option has limitations. The drilling pattern must be pre-defined and account for all anticipated tolerances for each cross passage. This requirement demands precise planning and may limit flexibility during construction.

6 GEOMETRY OPTIMIZATION

Geometry optimization for freezing pipe layout is crucial for project scheduling and cost management in cross passage construction using AGF. Optimized freezing pipe layout can result in reduction of freezing pipes and freezing time. Factors influencing geometry include the primary and secondary lining design, and construction tolerances.

6.1 *Primary lining design*

The primary lining must interact effectively with the frozen ground, accommodating loads from the frozen soil and any movements that occur during thawing. Thickness optimization is necessary to balance structural requirements with material costs and installation feasibility. Two scenarios are typically considered for primary lining design. In the first scenario, the freezing system is

switched off after the primary lining has been installed but prior to the installation of the waterproofing membrane. This approach requires the primary lining to withstand all loads during thawing, including groundwater pressures, potentially increasing thickness and reinforcement needs. In the second scenario, the freezing system is maintained until after the secondary lining has been installed, allowing the primary lining to be thinner since the secondary lining provides full support. A critical consideration is the interaction of the frozen ground with the primary support. The frozen ground and primary lining must provide temporary support during excavation.

6.1.1 *Excavation line*

To accurately determine the required locations for the start and end points of each freezing pipe in the crown and along the sides of the cross passage collars, a design line is employed. This design line is positioned in relation to the Excavation Line (E-Line)**,** from which the freeze wall must be dimensioned outward to ensure the necessary structural integrity and watertightness.

Given that the targeted freeze wall thickness is 1.5 m, the design line is established at a distance approximately equal to half of this required thickness from the E-Line. This positioning allows for the development of the freeze wall to the full required thickness while accommodating construction tolerances and ensuring that the frozen body fully encompasses the excavation area.

By extending the freezing pipes beyond the design line, the design ensures that any potential deviations or tolerances in drilling and excavation do not compromise the minimum required freeze wall thickness.

6.2 *Secondary lining design*

The secondary lining is integral to the long-term structural integrity and durability of cross passages constructed using AGF. Its design must accommodate the complex interactions between the frozen ground and primary support structures. A critical component of the secondary lining is the collar, whose size and geometry significantly influence the placement of freezing pipes.

6.2.1 *Collar design*

The collar's dimensions control the location of freezing pipes by defining the excavation limits and the necessary freeze wall thickness. Specifically, the targeted freeze wall thickness of 1.5 m is measured from the E-Line of the collar. Therefore, optimizing the collar size is essential not only for structural considerations but also for enhancing the efficiency of the freezing process.

Collaboration between the secondary lining designer and the primary lining designer is essential to achieve an optimal collar design. The secondary lining designer must ensure that the collar provides sufficient structural integrity for the cross passage opening, while the primary lining designer must determine an appropriate shotcrete thickness that offers adequate support during excavation. By jointly refining the collar dimensions and shotcrete thickness, it is possible to reduce the number of freezing pipes required, thereby streamlining construction and reducing costs.

6.2.2 *Freezing pipe pattern*

Optimizing the geometry of freezing pipe arrangements is crucial for efficient cross passage construction. The overall pipe arrangement broadly comprises two components: 1) The configuration of each pipe in relation to the 'start' and 'target' tunnel and 2) the pipe layout around the cross passage. The pipe configuration needs to be considered with respect to the tunnel geometric constraints and construction-related logistical considerations. An example of four different configurations is presented in Table 1, each with distinct characteristics:

Table 1. Freezing pipe configurations

Pattern	Configuration	Collar Design
1	Two-sided from crown and invert	Standard size collar
2	One-sided from crown and invert	Standard size collar
3	Two-sided at tunnel crown and one-sided at invert	No collar or smaller collar
4	One-sided at tunnel crown and two-sided at invert	No collar or smaller collar

The design of the pipe layout and spacing surrounding the cross passage opening is also critical for achieving uniform freezing, with pipes typically installed in a grid pattern and should be considered in conjunction with the pipe configuration. Pipe spacing is determined by the required freezing radius and the ground's thermal conductivity, ensuring the entire area receives adequate cooling to form a continuous frozen mass. Collaboration with the cross passage designer to improve the structural form of the opening set enables placement of freezing pipes as close to the excavation area as possible.

Collar geometry plays a vital role; reducing collar height allows for a lower freezing pipe angle, decreasing both the number and length of pipes needed. Patterns 3 and 4, featuring reduced or no collar, potentially reducing the total number of required pipes, thereby enhancing efficiency and potentially reducing costs and construction time. Operational constraints within the tunnels, such as TBM operation, must be considered when determining the freezing timeline. Precise installation of freezing pipes is essential to avoid gaps or overlaps that could lead to ineffective freezing, underscoring the importance of careful planning and execution in freezing pipe arrangement optimization.

6.3 *Tolerances management*

AGF design needs to integrate all geometric constraints, interfaces, and anticipated construction tolerances to facilitate the formation of a freeze wall meeting the required target properties. Freezing pipe design is influenced by several expected construction tolerances. These tolerances include: i) Freezing pipe drilling tolerances, ii) cross passage excavation and primary lining tolerances and iii) bored tunnel driving tolerances.

6.3.1 *Freezing pipe drilling tolerances*

During the drilling of designed freezing pipe boreholes, deviations along the length of the drilling are expected. The design accounts for a maximum drilling tolerance of the drilling length for the freezing pipes. The drilling tolerance must be defined by the designers or contractors depending on the cross passage length or drilling length.

6.3.2 *Cross passage excavation and primary lining tolerances*

In developing the freeze wall, it is essential to consider that the excavation of the cross passage may overlap with the surrounding frozen ground, leading to a reduction in the available freeze wall thickness. By definition, the interior surface of the primary lining corresponds to the exterior surface of the permanent lining. To determine the distance of the E-Line from the outside of the permanent lining, the cross passage excavation and primary lining tolerances need to be considered. The tolerances that need to be considered are shown in Figure 2.

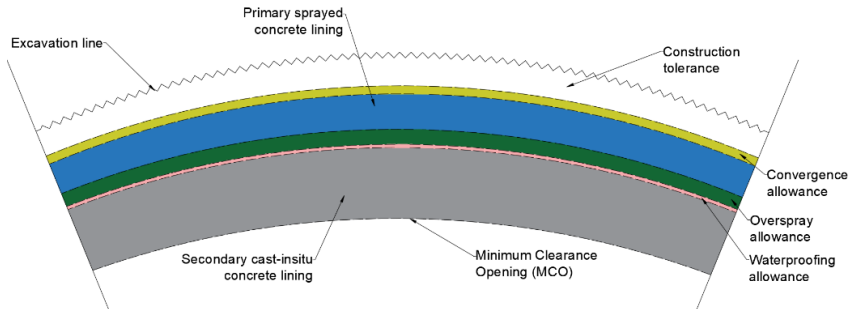


Figure 2. Cross passage excavation and primary lining tolerances

6.3.3 *Bored tunnel driving tolerances*

AGF with a reinforced concrete lining in the bored tunnels is typically unaffected by potential vertical and horizontal shifts, ring roll, and skew of the tunnel from which they are drilled. On the

other hand, AGF with steel lining requires consideration of bored tunnel driving tolerances as the freezing pipe drillings are conducted through pre-determined drilling ports located within the steel lining.

For steel linings the following bored tunnel driving tolerances are considered: i) vertical tolerances, ii) horizontal tolerances, iii) ring roll and iv) skew.

These bored tunnel driving tolerances should be integral to the development of the preliminary freezing pipe drilling design. By combining the tolerances of individual cases, various scenarios can be modelled and investigated. For each case, the freezing pipe drilling design should be adjusted to ensure that, regardless of the tolerances encountered, the required freeze wall could be established. This involved applying and combining the maximum tolerances to the relevant elements of the model, checking for potential object collisions, and ensuring minimum required distances between freezing pipes and the tunnel extrados.

7 TIME OPTIMIZATION

Optimizing the freezing duration is pivotal for project scheduling and cost management in cross passage construction using AGF. Factors influencing freezing time include the choice of cooling systems, the impact of lining materials, and the excavation sequence.

7.1 *Cooling system*

AGF employs two main cooling systems: closed brine systems and open liquid nitrogen systems, each with distinct benefits and limitations.

Brine system is a closed-loop system using calcium chloride ($CaCl_2$) brine cooled to approximately -32°C. The brine circulates through freezing pipes, absorbing heat from the surrounding soil before being re-cooled and recirculated. This system is cost-effective for long-term use and safer in enclosed spaces, as it eliminates the risk of gas leakage. However, it has slower freeze times and is less effective in soils with water flow velocities above 2 m/day (Mira-Catto & Roberti 2018). Liquid nitrogen is an open-loop system where liquid nitrogen at -196°C is injected into the pipes. The extreme cold rapidly freezes the soil and creates a more rigid frozen body, effective in high groundwater flow conditions (up to 10 m/day). However, the system is costly due to continuous nitrogen consumption and poses safety risks in confined spaces due to potential oxygen displacement. Each system has distinct characteristics, advantages, and limitations that influence their suitability for different project conditions. Brine systems are preferred for long-term, lower-flow projects, while nitrogen is used for rapid freezing or in high-flow conditions. Balancing cost, efficiency, and safety is critical in AGF system selection.

7.2 *Excavation sequence*

Once the freeze wall has been established and its watertightness verified, construction of the cross passage can proceed. The construction sequence includes the following steps in order: i) door opening in segmental lining, ii) excavation of frozen ground, iii) application of primary lining (shotcrete), iv) placement of waterproof membrane and v) secondary lining (cast-in situ reinforced concrete). Optimizing the excavation sequence is critical for enhancing both the advance rate and overall project efficiency. One of the primary considerations is the behaviour of the frozen ground itself. The properties of the frozen soil, including its strength and ability to support itself (stand-up time), dictate the rate at which excavation can proceed. Generally, a single cross passage can be excavated within two weeks, with an average excavation rate of approximately 1 to 1.6 m/ day. However, this rate is subject to the specific conditions of the frozen ground and must be closely monitored to ensure stability throughout the excavation process.

Another critical factor is the thickness of the shotcrete used for the primary lining. The thickness must be carefully calibrated to provide adequate temporary support during the excavation phase while minimizing the impact on the excavation rate. The design team must balance the need for rapid excavation with the requirements for stability and safety during the transition from the primary to the secondary lining.

Successful excavation sequence optimization requires close collaboration between the ground freezing designer and the primary lining designer. The ground freezing designer must provide accurate and detailed information regarding the properties of the frozen ground. The primary lining designer, in turn, must use this information to determine the excavation advance rate.

8 CONSTRUCTION AND PRACTICAL CONSIDERATIONS

8.1 *Excavation methodology and sequencing*

Excavation of the cross passages proceeds with advance lengths appropriate for the project conditions, with extended lengths in the enlarged collar areas. Excavated material and shotcrete are transported to the cross passage face via dumper and mixer trucks. It is anticipated that the heat generated from the application of shotcrete may cause the frozen body to thaw, leading to a lack of adhesion during spraying operations and resulting in material wastage.

Initially, the excavation face may be sealed in the first few advances, as is common in shotcrete works; however, to enhance stability and reduce heat generation, this requirement might be removed based on site conditions. Shotcrete will be applied in multiple passes to ensure proper adhesion to the frozen ground. In unfavourable ground conditions, the initial application may be restricted to 50 mm in the crown and shoulders, allowing for initial adhesion before topping up to the full design thickness as work advances (Hamad et al. 2024).

8.2 *Tunnel logistics and waterproofing*

Simultaneously with cross passage construction, various activities occur within the Upline and Downline tunnels. These include operations involving MSVs, TBM passenger service vehicles (PSVs), construction of tunnel invert concrete, subcontractor logistics, and tasks such as extending tunnel conveyor belts and cables. AGF design needs to consider the spaceproofing within the mainline tunnel, in which temporary supports should be minimized.

Temperature fluctuations during the freezing and thawing processes can affect gasket materials used in the tunnel lining, potentially leading to leakage paths. Selecting gaskets that can accommodate thermal expansion and contraction is essential for maintaining long-term tunnel integrity.

8.3 *Monitoring and instrumentation practices*

Temperature monitoring is required to assess the freeze wall growth during construction and confirm minimum design requirements are met and maintained. Temperature measurement pipes need to be designed alongside with freezing pipes to target critical areas of freeze wall development as determined during design. Thermocouples are installed at regular intervals internally within the pipes to monitor soil temperatures at varying distances from freezing pipes, enabling precise assessment of freeze wall development. Additional thermocouples need to be strategically installed at the opposite tunnel, where fewer freezing pipes are installed, to ensure sufficient sealing at the target tunnel extrados. Placement of these sensors targets potential weak or critical zones identified by thermal design.

Furthermore, pore water pressure is also required to be monitored inside the frozen body using drainage pipes equipped with valves and pressure gauges. As the freeze wall forms and confines the enclosed water, there is a sharp increase in pore water pressure inside the frozen body, indicating that cut-off of groundwater by the frozen body has been achieved. These measurements provide real-time data to assess freeze wall integrity, with excess water pressure measured at inside the cross passages barrel. This instrumentation strategy ensures robust monitoring, enabling informed decisions during construction. Monitoring is a key element for AGF design and this will be further discussed in future publications.

9 INTEGRATED DESIGN FRAMEWORK

An integrated design framework for AGF in cross passage construction involves a holistic approach that considers feasibility, geometry, time, cost, and safety is presented in Figure 3. This framework is a summary of the design considerations mentioned hereinbefore.

10 CONCLUSIONS

This paper presents an integrated approach to optimizing AGF for cross passage construction in tunnelling projects. By addressing practical design considerations, including freezing pipe arrangements, freezing durations, lining material selection, and tolerance management. The paper bridges the gap in the literature concerning the application of AGF in construction settings. The proposed framework emphasizes the importance of multidisciplinary collaboration, integrating geotechnical, structural, thermal, and construction expertise to develop efficient and safe designs. The consideration of tolerances in drilling, excavation, and tunnel driving is critical to ensuring the integrity of the freeze wall. This comprehensive approach aims to improve the efficacy of AGF in cross passage construction, contributing valuable insights to the field of underground engineering.

11 REFERENCES

Hamad, A., Terry, D., Himmelsbach, S., Allvey, P. and Dimmock, R. 2024. Innovative cross passage design & construction using sprayed concrete and ground freezing between two HS2 TBM-driven tunnels. In Proceedings of the 9th Symposium on Sprayed Concrete. Pp. 89-99.

Mira-Catto, F. and Roberti, P. 2018. Ground freezing as temporary excavation support: a sustainable geotechnical technique in Tunnelling & Trenchless Conference (TT2018), Canada.

Murray, M.J., and Eskesen, S.D. 1997. Design and construction of cross passages at the Storebælt Eastern Railway Tunnel. In Proceedings of the Tunnelling 97 Conference, pp. 463–479.

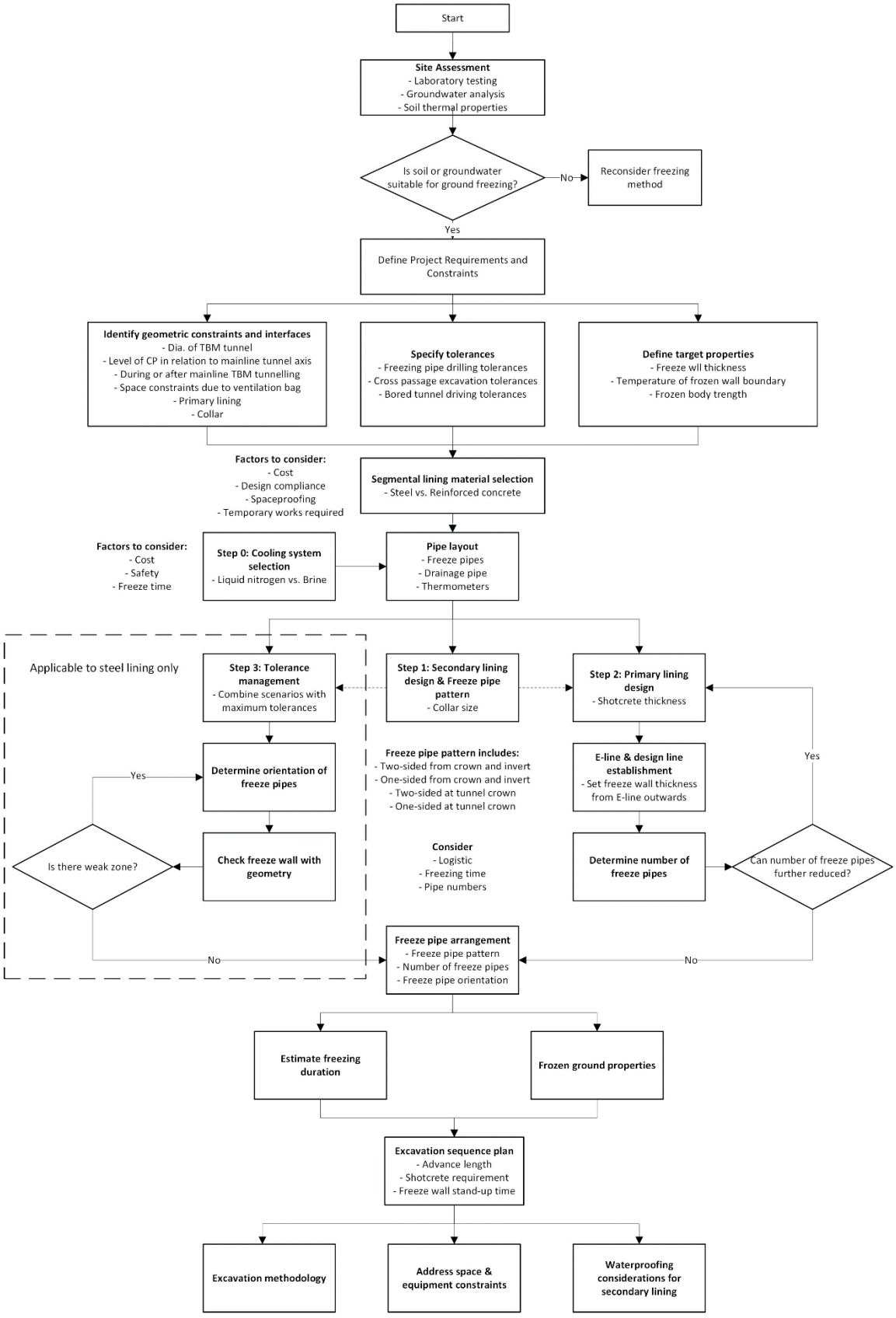


Figure 3. Integrated design framework for AGF in cross passage construction

THIS PAGE INTENTIONALLY LEFT BLANK

19th Australasian Tunnelling Conference – Acosta-Martínez, Stewart and Hudson-Smith (Eds.)
© 2025 Australian Tunnelling Society, ISBN 978-0-85825-002-4

Laboratory test methods and results for double shear performance of Australian CT bolts in simulated strata

S. R. Worrall, R. Walker, D. W. Evans
Sandvik Ground Support Division, Newcastle, New South Wales, Australia

ABSTRACT: Australian CT Bolts are a strata support system used in major Australian tunnelling projects, engineered for a 100-year lifespan using the Double Corrosion Protection (DCP) system. Sandvik Ground Support (formerly DSI Underground Australia) has undertaken a series of comprehensive test programs on the Australian CT Bolts in collaboration with tunnel designers and construction companies. A major component of this work has been laboratory double shear tests, providing critical information on the deformation limits of the bolt for combined shear and tension. This paper discusses a program of laboratory double shear testing that was conducted on three types of Australian CT Bolts: the 310kN solid steel rebar, a 579kN solid steel rebar, and a 573kN steel strand cable bolt. The results from this test program provide evidence for a practical shear displacement limit for the Australian CT Bolt design.

1 INTRODUCTION

The Australian CT bolt product family is widely used within civil tunneling applications for permanent and primary ground support. During the construction and service life of the tunnel, the shear displacement of strata is a common geotechnical concern that impacts upon the lifespan of strata control elements (Bertuzzi 2004) and (Pells & Bertuzzi 1999). Due to the redistribution of rock stresses arising from tunnelling excavations, it is common for the strata to move with a shearing motion (Roper et al. 2021) – and this shear can cause installed rock bolts to bend and permanently deform. For sheathed bolts, the impact of shear deformation on the outer plastic sheathing is important to evaluate, as this sheath forms a primary protective layer against the ingress of water. If the sheathing is punctured, water ingress may initiate corrosion of the steel tendon, compromising the lifespan of the installed bolt. In addition to corrosion, mechanical shear damage to the internal steel tendon is also important to assess as this is the structural element of the bolt.

Three bolt types are discussed within this paper; the CT Corrosion Protected Mechanical Bolt (abbreviated hereafter as CT bolt), the CT High Strength Corrosion Protected Mechanical Bolt (abbreviated hereafter as CT26WR bolt) and the Double Corrosion Protected Cable Bolt (abbreviated hereafter as DCPCB) – the three bolt types are shown for comparison in Figure 1. For clarity, note that these bolt types are products of Sandvik Ground Support Australia. The internal steel tendon is the primary difference between each bolt type, each tendon having different mechanical properties; the CT bolt is a 310kN solid bar with a 21.7mm diameter high tensile steel rebar, the CT26WR bolt is a 579kN continuously threaded high tensile solid steel bar with 26.5mm diameter thread and the DCPCB contains a 573kN 21.8mm diameter nineteen wire steel strand cable bolt. The CT bolt uses a nominal 35mm diameter plastic sheath, while the CT26WR and DCPCB both use a nominal 45mm diameter plastic sheath.



Figure 1. From left to right - DCPCB, CT26WR, and CT bolt

Over the past decade, Sandvik Ground Support (DSI Underground Australia) has undertaken a total of nine in-house test programs for the shear testing of CT Bolts (product group), at the request of and in co-operation with tunnel designers and construction companies. The initial test method was developed with the direct input of clientele, as well as in reference to previously published techniques (Aziz & Jalalifar 2007). Prior to the first test program, only limited information existed concerning the shear performance of double corrosion protected bolts and specifically the outer plastic sheath. Given the complex and time-consuming nature of both sample preparation and the test technique, each program was typically limited to three tests in total, of the same bolt type and the same rock block type. Additional test programs were progressively requested by clientele, to investigate further test variables and different bolt types. The test method was subsequently refined and improved, evaluating different shear block types, test fixture modifications and improved post load analysis of the test samples.

Presented and discussed in this paper is the shear test method, results of the test programs, and results to provide evidence for a practical shear displacement limit for the Australian CT Bolt design.

2 DOUBLE SHEAR TEST METHOD

2.1 *Double shear test overview*

The shear strength of a material is determined by applying opposed forces between two parallel planes to induce shear stress within the test specimen. Although shear displacement within strata will typically occur between a single pair of shear planes, it is a common laboratory technique to simultaneously place load across two pairs of parallel shear planes within the same specimen. This technique is known as the double shear method, which permits the balance of overall forces within the test sample and the test equipment. The two shear planes are positioned well apart in the test jig design, so that there is negligible stress influence between the two shear planes during the test.

A double shear test method was used to apply a specific, pre-determined shear displacement across the rockbolt, as installed within the shear blocks. Full sized rockbolts were used for the testwork, along with shear blocks of strength and properties comparable to common strata conditions encountered within the relevant underground environment. A steel framework was used to house the shear block segments, allowing for accurate control and progressive measurement of shear displacement during each test. Shear forces were applied to the test samples using a calibrated universal test machine. After each test, the blocks were dissected and samples analysed to find the effects of shearing on the rockbolt. Figure 2 shows both a photo and graphic images of a test arrangement prior to shear loading.

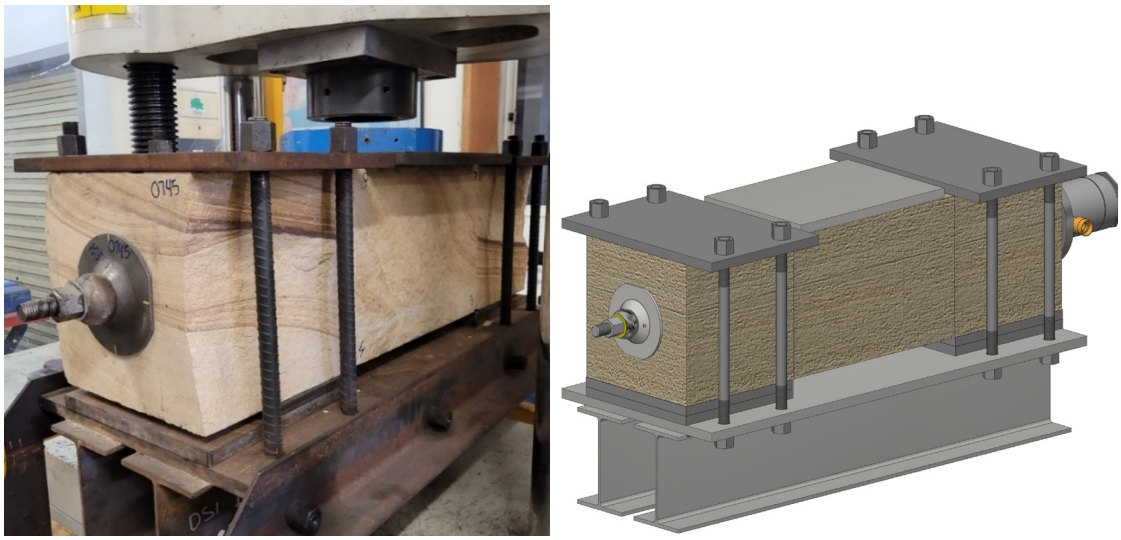


Figure 2. The left image shows test frame and machine prior to load testing, at the Sandvik ground support laboratory at Newcastle. The right image shows a graphic representation of the test sample and apparatus.

2.2 *Shear displacement measurement*

Across all test programs, the primary aim was to determine the durability limit of the plastic sheathing, given a specific shear displacement. The established test method permitted excellent control of the block shear displacement and could be directly correlated to sheathing durability, providing clear test outcomes. Displacement measurements were recorded from the change in crosshead position on the universal test machine. The zero point (or first measurement) for displacement initiates at a load of 2kN applied to the test sample.

Note that it is only possible to observe the sheathing condition following the completion of each test and after sectioning of the block sample. For this reason, a pre-determined shear displacement value was set for each test – and across the majority of the test programs, this targeted value was set by the tunnel designers, being the clientele of the test program. Due to the cost and complexity of testing, initial test programs only had a limited number of test samples available to determine the durability limits of the sheathing. Hence, the initial test programs targeted lower and more conservative shear displacements, with later test programs focusing on achieving higher displacement values.

A further focus area of the test work was to measure the performance of the steel tendon. During shear testing, the axial loads induced on the steel tendon were recorded using a load cell located at the distal end of the tendon and seated against the outer block face. This enabled measurement of the axial force induced onto the steel tendon during shear displacement of the centre test block. Following test completion, the permanent bend displacement and damage of the steel tendon was measured to provide a subjective indication of bolt strength.

2.3 *Exclusion of shear force measurements*

While the true shear strength of the installed bolt assembly (including grout, plastic sheath, and steel tendon) is of interest, it is problematic to measure with any degree of accuracy. The predominant influence is the frictional forces generated between the contact faces of the test block shear planes. Frictional forces are induced initially during axial bolt pre-tensioning and progressive increase of axial bolt loading during loading. Normal stresses induced through initial pre-tensioning and the continuous anchorage of the bolt within the surrounding rock mass are also known to have a significant effect on the shear forces during loading (Aziz & Jalalifar 2007). Subsequently the interaction of the forces between the bolt assembly and the rock blocks cannot be isolated.

The shear force results applied to the test samples were recorded, however they are not presented within this paper and were not used to determine sheathing durability. Instead, the shear

displacement applied to the block was used as a far more reliable test measurement, reflecting the primary aim across the test programs.

2.4 *Test samples and apparatus*

The size, shape, and materials used for the test samples were selected to accurately replicate the mechanics of a full sized rockbolt. Each test sample and blocks were used only once and consisted of the following:

- 1500mm long rockbolt (plastic sheathing, steel tendon, bolt specific fasteners).
- Two 'end position' rock blocks, each with dimensions of 300 x 300 x 300mm long.
- One 'centre position' rock block, with dimensions of 300 x 300 x 450mm long.
- A bore hole drilled through the centre of the three blocks with diameter to suit each bolt type.
- 50kN of pre-tension applied with fasteners typical to each bolt type.
- Cementitious grout pumped into the rockbolt and bore hole. Typical grout strength of 40MPa UCS. Unconfined compression testing was conducted for each test sample to determine grout strength.
- Each sample contained either homogeneous sandstone or concrete blocks containing no reinforcing elements. Sandstone blocks were sourced pre-cut from a quarry and concrete blocks were cast in the laboratory.

A mechanical test frame was developed to house the three blocks (and installed test bolt) to permit the use of a universal test machine. The test frame consisted of a rigid solid steel frame, with packing plates and tensioning bolts to restrain the two end blocks while providing clearance for movement of centre block (see Figure 2).

Note that one set of tests for the CT26WR bolts, requiring displacements of 20 and 30mm, included further confinement of the centre block, using an additional four horizontal tensioning bolts and steel side plates. This additional support was required due to the high compressive strength and more brittle properties of the concrete blocks that were used for this specific test.

2.5 *Sample analysis*

Post-test sectioning of the test samples was required to determine the level of damage to the plastic sheathing. This was undertaken in a series of sequenced steps as the different layers of the test sample were progressively exposed. The stages of sample analysis included:

- The test blocks were cut using a concrete saw through to the centre grout and bolt element – see Figure 3. The conditions of the outer grout layer and the overall condition were subsequently documented.
- The bolt was then extracted from the blocks and the external sheath surface was inspected and photographed. Any suspected damage or perforations of the sheath were subsequently documented.
- Two 250mm long sections of the sheath were then removed from the bolt, one from each of the two shear plane regions. Removal of the sheath enabled visual inspection of grout coverage within the inner annulus and was photographed at each location (see Figure 4 as an example).
- The cut-away sheath sections were then cleaned and placed above a light source to enable clear visual inspection for any perforations, with photographed records being maintained. Where indicated by the backlighting, each individual perforation was measured using digital vernier calipres to calculate the area of that opening (in mm^2). Figure 5 shows an example of the sheath section before and after removal from the bolt. Typically, holes were irregular in shape and measurements for area were completed using a rectangular size estimation – for example, a 1mm by 0.2mm measurement yielding a $0.2mm^2$ area.
- The final stage was to measure the steel tendon for bending. Measurements of the axial offset of the tendon centre portion were taken using a rule and square. An example of this axial offset is shown in Figure 6.



Figure 3. Initial sectioning of a CT26WR shear test sample after 20mm of shear. The centre block has been halved and opened, with the outer grout annulus remaining intact (lower left section), also revealing the bolt and sheathing (upper right section).



Figure 4. Sectioning of a tested CT26WR bolt sample at the shear plane, following 20mm of shear displacement. The inner annulus of cement grout has substantively held together during deformation of the bolt at the shear plane.

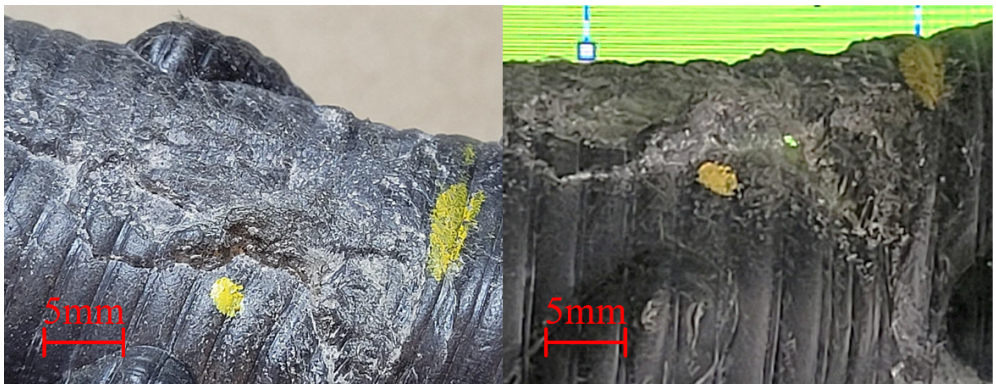


Figure 5. Example of a small perforation revealed under back-light inspection, the left image shows before the sheath was removed from the bolt and the right image shows the sheathing under back-light inspection.



Figure 6. An example of a bolt, taken at the shear plane, following loading to 20mm shear displacement test.

3 RESULTS

The results in this paper are drawn from nine different test programs that were conducted between 2016 and 2022. Acknowledging that minor improvements in methodology were made across the test programs, the overall procedure and technique offered consistency to provide a full set of aggregated data. In total there were 27 individual double shear tests completed. A summary of the results is provided in Figure 7 and Table 1.

Each test was completed at, or marginally above, a pre-determined shear displacement, with measurements of force and displacement recorded during the test. Visual analysis of the test sample after block sectioning consistently revealed compressive fracture of the block material and the outer grouted annulus (external to the sheathing) at each of the two shear planes. All samples consistently displayed full grout encapsulation of the inner and outer annulus. During inspection of the bolt, before the sheath was removed from the bolt, it was not possible to see perforations in the sheath smaller than the order of 5mm². Upon sectioning of the sheathing, the internal grout annulus typically displayed only minor compression fractures within each shear plane region, as exampled in Figure 4. Bolt bend measurements were taken for both the CT and CT26WR bolt types across the axial offset, as exampled in Figure 6. In all test samples, the internal steel tendon had no cracks or ruptures – only bending and minor elongation modes being witnessed. As indicated by the lack of change in the distance between the ribs of the steel tendon, there was no evidence of high levels of permanent tensile elongation. Deformation results could not be taken for the DCPCB bolt, as the internal steel cable would elastically return to its original shape after release from load testing.

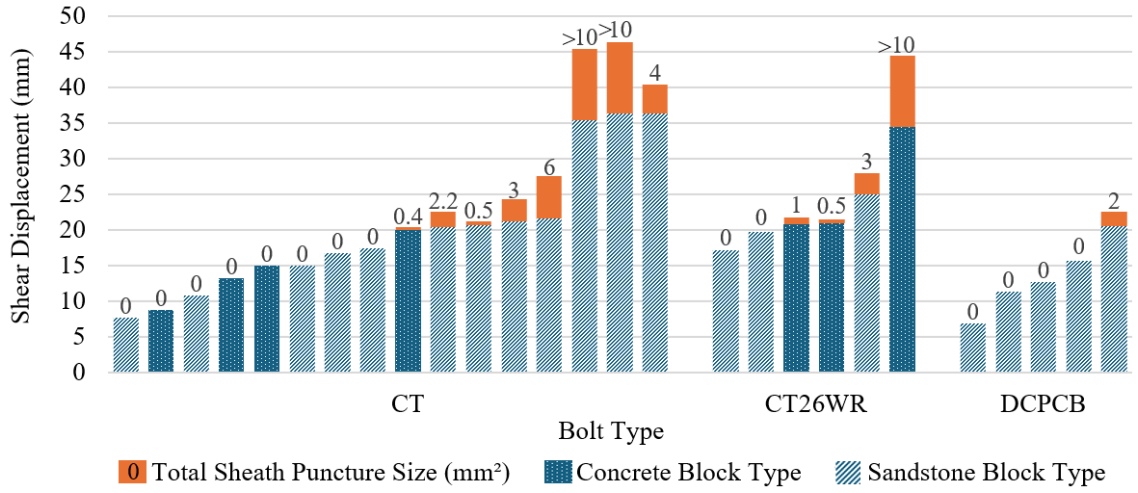


Figure 7. Shear displacement values for all test results, with bolt type, sheath puncture area and block type used.

Table 1. Summary table of individual test results across all test programs.

Bolt Type	Shear Displac-ment (mm)	Shear Block Material	Block Strength UCS (MPa)	Total Sheath Puncture Area (mm²)*	Bolt Bend Measurement (mm)**	Peak Load at Bolt End (kN)**
CT	7.8	Sandstone	35	0	-	18
CT	8.8	Concrete	26.5	0	1.5	0
CT	10.8	Sandstone	35	0	-	0
CT	13.3	Concrete	41.5	0	4	0
CT	15	Concrete	41.5	0	5	13
CT	15	Sandstone	35	0	-	6
CT	16.75	Sandstone	35	0	-	6
CT	17.5	Sandstone	35	0	-	6
CT	20	Concrete	41.5	0.4	7	18
CT	20.4	Sandstone	35	2.25	9.5	15
CT	20.7	Sandstone	35	0.5	10	5
CT	21.3	Sandstone	35	3	8	-
CT	21.6	Sandstone	35	6	8	5
CT	35.4	Sandstone	35	>10	22.5	25
CT	36.4	Sandstone	35	>10	23	25
CT	36.4	Sandstone	35	4	24	15
CT26WR	17.14	Sandstone	35	0	-	-
CT26WR	19.78	Sandstone	35	0	-	-
CT26WR	20.8	Concrete	60	1	9	3
CT26WR	21	Concrete	60	0.5	7.25	18
CT26WR	24.99	Sandstone	35	3	-	-
CT26WR	34.5	Concrete	60	>10	16.5	60
DCPCB	7	Sandstone	35	0	-	-
DCPCB	11.4	Sandstone	35	0	-	-
DCPCB	12.7	Sandstone	35	0	-	-
DCPCB	15.7	Sandstone	35	0	-	-
DCPCB	20.6	Sandstone	35	2	-	-

*Figures shown are the total sum of area for all holes in a test sample – and includes the two shear planes within this summation.
** Some test results for bolt bending and bolt end load were not recorded, indicated with a "-" symbol.

4 DISCUSSION

As each test program was completed over time, a clear understanding emerged regarding the performance and trends of CT bolt sheathing durability. At around 20mm shear displacement, any holes observed in the sheath were typically sub-millimeter in size. Above 20mm, the hole area increased in line with increasing displacement. A general observation across test samples is that the sheathing could withstand large amounts of plastic deformation damage before puncture.

Holes were rarely circular and would range in shape from thin slits to irregular polygonal shapes. Grout would typically be lodged within the area where holes occurred and careful effort was required to remove the grout before a hole could be seen. However, the possibility existed that the grout removal process may have initiated a hole, or caused further damage to an existing hole within the sheath sample – particularly given the fine nature of the required technique to measure hole area.

Damage to the steel tendon from shear testing was less severe than anticipated. The permanent bend within the steel tendon would increase proportionately with shear displacement, with the 35mm shear displacement tests showing the highest amount of bend. The amount of permanent elongation for all steel tendon types suggested the shear stress applied to the tendon was well below its ultimate strain and material strength. For both the CT and CT26WR bolt tests, the final displacement of the steel tendon sample did not match shear blocks test displacement. The strongest evidence for the difference in observations is due to the compressive fracture of the block and grout material at the shear planes. Compression of the block and grout caused shear forces to disperse across the steel tendon and resulted in the S-shaped bend within the tendon.

The lack of damage to both internal and external grout annulus in the regions near the shear planes are a match to the low axial loads witnessed at the bolt ends during shear loading. This is an indicator that the axial load placed on the steel tendon during the test were predominantly restrained by load transfer within the fully grouted bore hole.

There was minimal evidence arising from the overall test program to suggest that the durability performance of the sheath was affected by the shear block type and strength used. Beyond the block material type differences, the three tests with centre block confinement and higher UCS block material did not indicate a difference in sheathing durability. However, further test data would be required to explore these parameters more fully.

5 CONCLUSION

Double shear tests, conducted on the Australian CT Bolt product family across nine test programs and 27 individual tests, clearly show the durability limits of the plastic sheathing with a reasonable confidence level. A number of parameters were explored throughout these programs; shear block material, sheathing diameter and steel tendon type – with the durability limit of the plastic sheathing under shear returning similar values across these programs.

6 REFERENCES

Aziz, N I, Jalalifar, H 2007. Experimental and numerical study of double shearing of bolt under confinement. *Proceedings of the 26th international conference on ground control in mining, Morgantown, WV, USA*: 242–249

Bertuzzi, R. 2004. 100 – Year design life of rock bolts and shotcrete. *Ground Support in Mining and underground construction – Villaescusa and Potvin*: 425-429

Pells, P & Bertuzzi, R. 1999. Permanent rockbolts - the problems are in the detail. *Tenth Australian Tunnelling Conference 1999*: 255-259.

Roper, T, Calbrix, L-P, Gonzalez, M, Kabbaj, R, and Forbes, B 2021. High stress tunnelling in Sydney a design and construction case study. *17th Australasian Tunnelling Conference*, [online] pp.180–190.

19th Australasian Tunnelling Conference – Acosta-Martínez, Stewart and Hudson-Smith (Eds.)
© 2025 Australian Tunnelling Society, ISBN 978-0-85825-002-4

Characterization of fiber-reinforced concretes activated at very early ages

N. Leclere
Sigma Béton, Isle d'Abeau, France

B. De Rivaz
Bekaert Underground Solutions, Zwevegem, Belgium

ABSTRACT: Tunnels can be excavated using traditional explosives. A temporary fiber-reinforced shotcrete lining could be used to ensure wall stability. These fibers absorb post-cracking forces and limit crack propagation. This study focuses on the early-age mechanical behavior of chemically activated wet-mix shotcretes. A new preparation and characterization protocol was developed based on NF EN 14488-5 and NF EN 14488-3 method B standards. The influence of fiber spacing on the granular skeleton was considered. For the studied formulations, performance was evaluated at 7.5 hours, 24 hours, and 28 days at ambient temperatures between 20°C and 25°C. Prospect includes optimizing the granular-fiber skeleton ratio, assessing the impact of admixture concentration and concrete consistency on mechanical properties, and studying the effect of ambient temperature on strength development.

1 INTRODUCTION

In France and Europe, the use of wet-sprayed fiber-reinforced concrete for the support of tunnel walls during excavation work is governed by the NF EN 14487-1 standard. This standard specifies compliance requirements to ensure the safety of people working in tunnels, particularly by preventing the fall of rock elements. Sprayed concrete also ensures the stability of the walls after excavation, pending the implementation of the final lining. The vaulted geometry of tunnels requires rapid strength development to guarantee the integrity of the structure from the very first moments, whether by the concrete's own weight or by the stress of the surrounding terrain.

Short-term performance, defined as the period less than 24 hours after spraying, is evaluated according to the NF EN 14488-2 standard. During suitability tests, companies define their requirements in terms of early-age strength class (J1, J2, J3) based on the required performance, to ensure safety. Evaluating the evolution of ductility at the early age of fiber-reinforced sprayed concrete, according to the NF EN 14488-3 method B or by measuring energy absorption capacity according to the NF EN 14488-5 standard, is particularly complex. The fragility of test specimens makes their transport from the site to the laboratory delicate, risking compromising their integrity. However, it is crucial to understand the evolution of concrete behavior and the contribution of fibers to its structural reinforcement from the very first moments.

These pre-qualification tests aim to provide insights into the performance of activated concretes, allowing rapid optimization of fiber-formulation parameters and adapting the recipe without systematically requiring on-site spraying tests. A new methodology for the laboratory fabrication and characterization of activated concrete samples to approximate correct implementation by spraying. The ductility of a typical fiber-reinforced sprayed concrete formula was evaluated at an early age and at a normative curing duration. The characterized concrete formulas consider the impact of fibers on the loosening of the granular skeleton.

This research project received financial support from Bekaert, who also supplied the steel fibers used in the experimental campaign.

2 EXPERIMENTAL PROGRAMME

The formulation, machine settings, and spraying techniques influence the performance of sprayed fiber-reinforced concrete. However, due to the logistics required for these very early age tests, the effect of spraying has not been studied. All test specimens were made in the laboratory.

The experimental program is based on:

- Compressive strength measurements (NF EN 12390-3 standard) at 7.5 hours, 24 hours, and 28 days on activated fiber-reinforced concrete cylinders (11x22 cm);
- Residual flexural strength measurements (NF EN 14488-3 method B standard) at 7.5 hours, 24 hours, and 28 days on activated fiber-reinforced concrete notched panels (60x60x10 cm);
- Residual energy absorption measurements by punching (NF EN 14488-5 standard) at 7.5 hours, 24 hours, and 28 days on activated fiber-reinforced concrete panels (60x60x10 cm). The performance of the concrete was evaluated according to the classification specified in the fib Model Code 2010;
- Continuous temperature evolution measurements for 24 hours on activated fiber-reinforced concrete for 24 hours.

3 MATERIALS AND MIX DESIGNS

The concrete was formulated based on materials used in experimental sprayed fiber-reinforced concrete projects in France. Two fibers were characterized. The first is metallic (Dramix® 4D 65/35 BG) with dosages of 25 kg/m³ and 40 kg/m³. The second is synthetic (Synmix® HP 55) with dosages of 5 kg/m³ and 8 kg/m³. These fibers differ in their composition, morphology, and mechanical properties. Table 1 summarizes the characteristics of fibers.

Table 1. Characteristics of the fibers.

Designation	Dramix® 4D 65/35 BG	Synmix® HP 55
Length (mm)	35	55
Diameter (mm)	0,55	0,64
Aspect ratio (mm)	65	86
Tensil strength (MPa)	1850	510

A compactness analysis was conducted following a protocol inspired by ([1] De Larrard, 2000). This method relies on experimental compactness measurements of the granular cuts, completed with the proportion of fibers in the concrete to recreate the loosening effect of the larger elements, as shown in Figure 1.

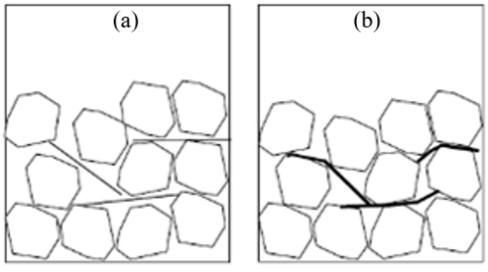


Figure 1. Diagrams illustrating the loosening effect of gravel in the presence of rigid fibers (case a), or in the presence of flexible fibers such as synthetic fibers (case b); excerpt from (De Larrard, 2000).

The cement matrix was adapted to increase compressive strength and reduce porosity. A water-to-cement ratio (W/C) of 0.40 was applied. Silica fume was also added to improve the pumpability of the concrete. The granular curve was adjusted with a sand-to-gravel ratio (S/G) of 0.5. The goal is to increase the sand content in anticipation of potential spraying tests, to improve pumpability, following these initial pre-characterization tests in the laboratory.

Figure 2 shows the granular packing curve of the formula compared to the granulometric range for a Dmax 10mm cut according to the NF P 95-102-1 standard (2023), based on ASQUAPRO recommendations.

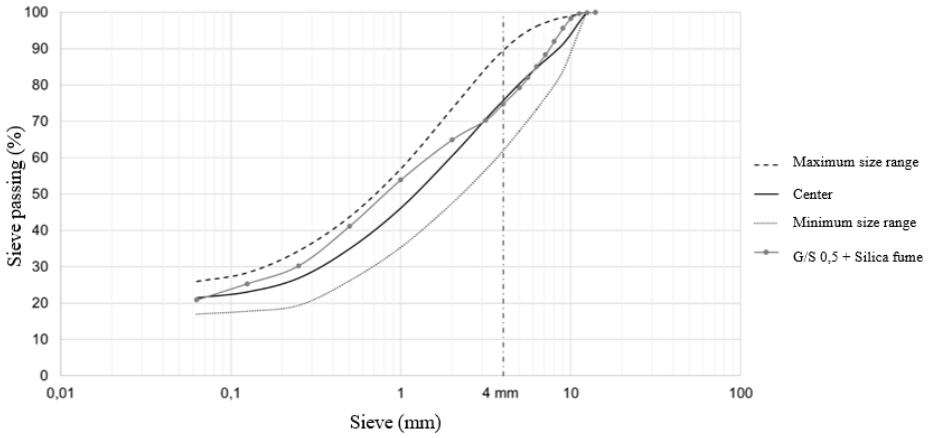


Figure 2. Granular skeleton envelopes (aggregates – hydraulic binders – additions) of the study concrete with a G/S ratio of 0.5 (NF P95-102-1 (2023) Annex E).

The concrete mix designs used in the experimental program are given in Table 2 below.

Table 2. Composition of the four mix designs.

Materials	Formula Dramix® 4D 65/35 BG	Formula Synmix® HP 55
Gravel / Sand	0,5	0,5
CEM I 52,5 N SR3 CE PM-CP2 NF (kg/m^3)	450	450
Silica fume (kg/m^3)	25	25
Dramix® 4D 65/35 BG (Bekaert) (kg/m^3)	25 40	0
Synmix® HP 55 (Bekaert) (kg/m^3)	0	5 8
Admixture 1 (%weight of powder)	0,3	0,3
Admixture 2 (%weight of powder)	1,2	1,2
Activator (%weight of cement)	4	4
Efficient water (kg/m^3)	178	178
Efficient water / Cement	0,40	0,40
Efficient water / Powder (< 63 µm)	0,37	0,37

Regarding the consistency of wet-sprayed concrete, the recommendations of Asquapro's fascicle 4 indicate that to achieve optimal pumpability, the concrete consistency should follow a class S3 to S4 [3].

To facilitate the preparation of test specimens and achieve an optimal matrix, the activator dosage was set at 4% of the cement mass. The dosages typically encountered on-site range between 6% and 8%. A lower concentration avoids concrete setting prematurely in the mixer and gives enough time to manufacture test specimens. This value strikes a balance to achieve the minimum performance necessary for the press detection thresholds.

The nature and dosage of fibers influence the workability of concrete by impacting the granular arrangement and stiffening the cement matrix, known as the tightening effect. The workability of fiber-reinforced concretes can usually be improved by adding superplasticizer and rheology extender admixtures. In this study, the admixtures dosage parameter had been fixed.

For better readability of the results, the formula coding is annotated as follows: Fiber type Dosage / Test deadline in hours or days, such as:

- Dramix® 4D 65/35 BG : M25/7,5 hours - M25/24 hours - M25/28 days;
- Dramix® 4D 65/35 BG : M40/7,5 hours – M40/24 hours – M40/28 days;
- Synmix® HP 55: S5/7,5 hours - S5/24 hours - S5/28 days;
- Synmix® HP 55: S8/7,5 hours – S8/24 hours – S8/28 days.

4 MATERIALS AND METHODS FOR PRODUCING TEST SPECIMENTS

The testing press used for flexural and punching tests is a universal testing machine (UTM). Its measurement range varies from 1 kN to 100 kN, compliant with class 0.5 over this range. The method for preparing and activating the concretes is summarized in Figure 3.

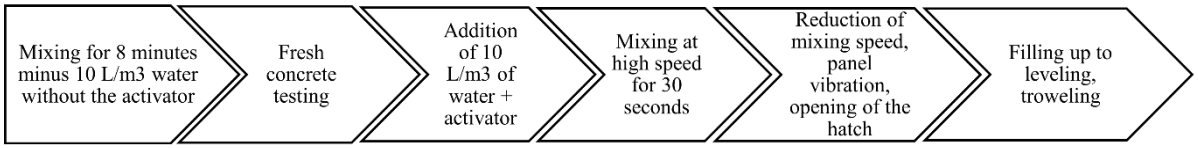


Figure 3. Steps for preparing test specimens.

Each panel was produced individually by 50 L batches. Activator was first pre-mixed with an equivalent of 10 L/m³ of water before being introduced into the concrete. All tests were carried out at ambient temperatures between 20°C and 25°C. Up to 24 hours, the specimens were also kept in their molds under polyethylene sheeting at a temperature between 20°C and 25°C. For the 28-day curing period, the specimens were stored in humid conditions (relative humidity > 95%) at a temperature between 20°C and 25°C.

5 RESULTS

5.1 *Visual aspect of test specimens*

Slumps have been measured before adding the premixed activator and additional water. The average slump values are between 30 – 50 mm. Despite the firm consistency obtained, the method used to prepare the 60 × 60 × 10 cm panels on a vibrating table proved suitable for producing sound specimens with no surface defects. The observation of the rupture faces of the panels did not show defects such as fiber nests or compaction issues, regarding cylinders for compressive strength, compaction defects were observed (Fig. 4). The fabrication methodology should be adapted for further tests.

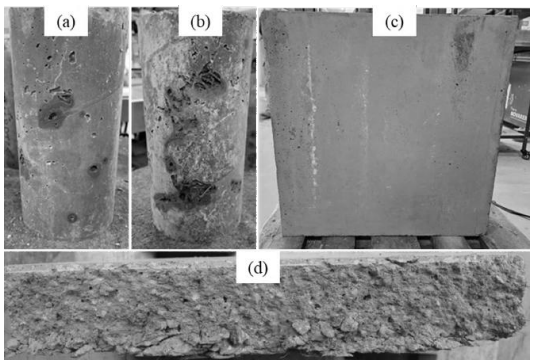


Figure 4. Example of test specimens: cylinder type (a), (b), panel (c), and observation of a rupture face on one panel (d).

5.2 *Compressive strength according to NF EN 12390-3*

The average compressive strengths of the active fiber-reinforced concretes were measured at different intervals on 9 cylinders of 11x22 cm (Fig. 5).

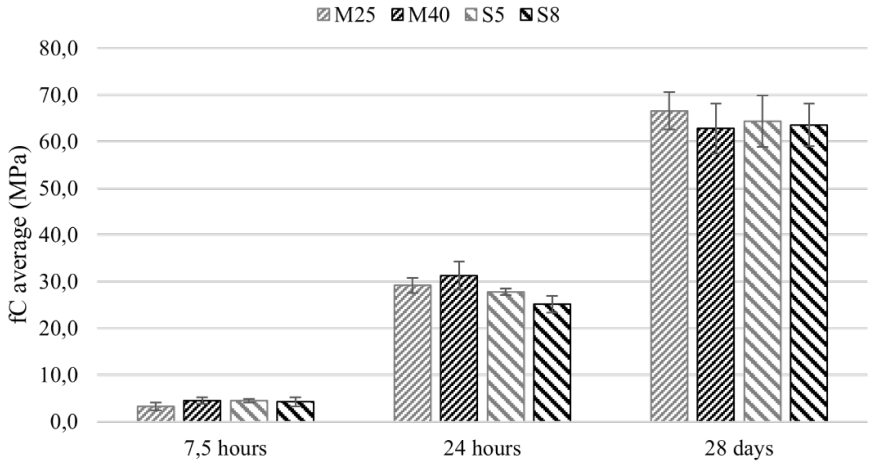


Figure 5. Compressive average and characteristic strengths at 7.5 hours, 24 hours, 28 days.

The modification of the dosage and the nature of the fibers has little impact on the compressive strengths. The tests at 7.5 hours required sulfur capping, with average strengths ranging from 3.2 MPa to 4.5 MPa. The four tested formulas show equivalent strength developments. At 28 days, the average strengths vary between 62.8 MPa and 66.6 MPa. At 24 hours and 28 days, the standard deviations range from 1 MPa to 5 MPa. The compaction defects of the specimens could explain this variability. The characteristic strengths allow the concrete to be classified as at least C50/55.

5.3 *Absorption energy according to NF EN 14488-5*

The average absorption energies measured at a deflection of 25 mm are presented for each formula in Figure 6.

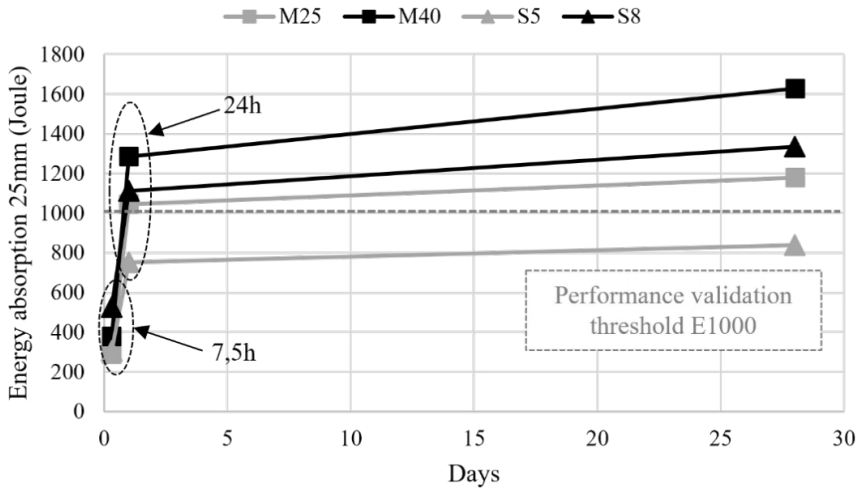


Figure 6. Energy absorption at 25 mm according to NF EN 14488-5 at 7.5 hours, 24 hours, 28 days.

For this experimental campaign, the reference threshold at 28 days is 1000 Joules (E1000). This threshold may be required for terrains needing support materials with high absorption capacity to compensate for lack of cohesion or to withstand high stress.

At 7.5 hours, none of the concretes provide a fiber reinforcement combined with sufficient hardening to reach a performance threshold of E600. At 24 hours, the formulas show a similar trend in performance gain. The formulas M25, M40, and S8 already reach the E1000 threshold targeted at 28 days. Only the concrete S5 does not have a sufficient fiber-matrix combination to allow optimal grip during the punching duration, significant enough to achieve the performance.

At 24 hours after activation, the desired performances of the concretes at 28 days are achieved for three concrete configurations. The performances of the concretes continue to increase. It is noted that for this test, the performances of the synthetic solution dosed at 8 kg/m³ are almost equivalent to those of the metallic fiber formula dosed at 25 kg/m³. Only the concrete S5 does not reach the threshold of 1000 Joules.

5.4 *Residual flexural strength according to NF EN 14488-3 method B*

5.4.1 *Dramix® 4D 65/35 BG*

The performance of concretes reinforced with 25 kg/m³ and 40 kg/m³ of steel fibers is summarized in the Table 3. The performances are classified according to the 2010 model code of the *fib* [2].

Table 3. Dramix® 4D 65/35 BG– Flexural tensile strength classes.

Formula	Testing age	Fr1s	Fr3s	Model Code 2010 classification
M25	7.5 hours	0.18 MPa	0.27 MPa	0 e
	24 hours	1.42 MPa	1.68 MPa	1 d
	28 days	2.81 MPa	2.93 MPa	2.5 c
M40	7.5 hours	1.34 MPa	1.44 MPa	1 c
	24 hours	2.56 MPa	2.80 MPa	2.5 c
	28 days	3.87 MPa	3.82 MPa	3 c

The average and characteristic flexural strengths of each formula are given in Figure 7.

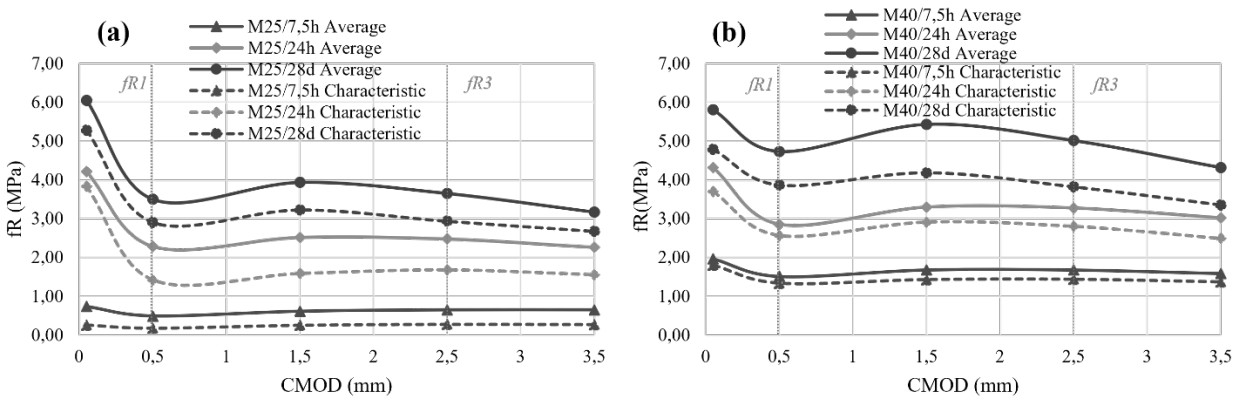


Figure 7. Dramix® 4D 65/35 BG - Average and characteristic residual flexural strengths for mixes through time – (a) 25 kg/m³ and (b) 40 kg/m³.

5.4.2 *Synmix® HP 55*

The performance of concretes reinforced with 5 kg/m³ and 8 kg/m³ of steel fibers is summarized in the table 4. The performances are classified according to the 2010 model code of the *fib* [2].

Table 4. Synmix® HP 55 – Flexural tensile strength classes.

Formula	Testing age	Fr1s	Fr3s	Model Code 2010 classification
S5	7.5 hours	0.58 MPa	0.57 MPa	0 c
	24 hours	1.03 MPa	1.11MPa	1 c
	28 days	1.29 MPa	1.29 MPa	1 d
S8	7.5 hours	0.66 Mpa	0.65 Mpa	0 c
	24 hours	1.75 Mpa	2.04 Mpa	1.5 c
	28 days	1.86 MPa	2.46 MPa	1.5 e

The average and characteristic flexural strengths of each formula are given in Figure 8.

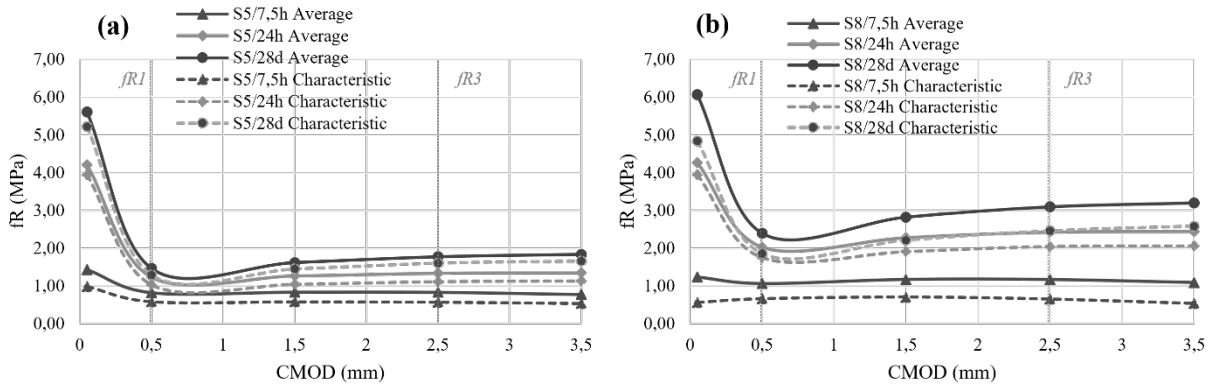


Figure 8. Synmix® HP 55 - Average and characteristic residual flexural strengths for mixes through time - (a) 5 kg/m³ and (b) 8 kg/m³.

6 CONCLUSION AND PROSPECTS

A new method for characterizing early-age performances of wet spray activated concrete at a laboratory level has been developed. It enables a pre-selection of fiber types and content and more globally of concrete formulations as an upstream phase of shotcrete test.

The concrete mix was adapted to consider the spacing of the granular skeleton generated by the synthetic or metallic fibers. In general, it would be relevant for study phases to consider this approach to correct paste defects. Adjusting the compactness would also improve fiber grip in the matrix and concrete pumpability. The rheological and tribological behavior of these concretes could be studied additionally.

The experimental campaign was conducted using a single activator incorporated at a dosage of 4% by cement mass. This value was chosen as a compromise between workability and setting time to make the test specimens. For future studies, higher levels of activator as well as other types could provide a more representative basis for prequalifying concrete regarding the need of the structure.

Concrete consistency should be more fluid and closer to those on-site, at least 160 mm according to the formulation. The effect of activation on rheology should also be considered. Despite the firm consistency, no fiber defects were observed in the test panels.

The performance of activated concrete at a very early age is influenced by the external temperature, the material temperature, and the concrete temperature after activation. To compare the performances of concrete at a very early age, it is essential to control the initial temperature of the concrete and the ambient environment. The specimens can be instrumented to verify that the tests were conducted under the same conditions.

Compressive strength was measured. The type and dosage of fibers did not influence the results: all the concretes exhibited the same strength development over time. The required mechanical class C50/55 is reached

Flexural and punching performances of activated concretes were measured at an early age, i.e., less than 24 hours. Only two very early age intervals were studied. Other measurement intervals could be conducted for a finer analysis of activated concrete behavior. The method assesses the influence of different fiber types on the targeted performance characteristics. At 28 days, metallic fibers continue to improve tensile strength. Performances of 2c and 3c are obtained respectively for dosages of 25 kg/m³ and 40 kg/m³. The improvement of post-cracking strength behavior at 28 days is more significant with the metallic fiber than the synthetic fiber.

Due to the current state of the art, EN 14 488-3 method b would be the reference standard for spray concrete material characterization [4] [5] [6] [7] [8] [9] [10] [11].

Absorption energies were measured. For synthetic fibers, only the formulation containing 8 kg/m³ met the threshold of 1000 J.

A correlation between laboratory tests and on-site shotcrete tests should be established to confirm this observation. Optimization could be carried out using these concentrations by testing intermediate fiber dosages.

7 REFERENCES

F. De Larrard 1999, “Concrete Mixture-Proportionning – A Scientific Approach”, *Modern Concrete Technology Serie, N°9, E & FN SPON*, London.

fib, 2013, fib Model Code for Concrete Structures 2010, Weinheim, Germany: Wiley-VCH Verlag GmbH & Co. KGaA. DOI: 10.1002/9783433604090.

ASQUAPRO 2010, Fascicule 4 – Formulation des bétons projetés, France

Carlesso, D.M., Leporace-Guimil, B., Aguado, A., de la Fuente, A. & de Rivaz, B., 2025. Sprayed steel fiber reinforced concrete: strength classes obtained through EN 14488-3 Method B. In: *Tunnelling into a Sustainable Future – Methods and Technologies. CRC Press*. DOI: https://doi.org/10.1201/9781003559047-37.

Larive, C., Chalencon, F., Leclere, N., De Rivaz, B., Tolka, N., Bonjour, T., Mestari, A., Zghondi, J. & Bouteille, S. 2025. New experiments to improve sprayed concrete performances for final support and lining. In: *Tunnelling into a Sustainable Future – Methods and Technologies. CRC Press*. DOI: https://doi.org/10.1201/9781003559047-287.

PEASTON C., DE RIVAZ B., EN 14488-3 notched panel versus EN 14651 notched beam testing for preconstruction trial conformance testing of Sprayed Concrete Linings (SCL), *Tunnelling for a Better Life* - Yan, Celestino, Thewes & Eberhardt (Eds), ISBN 978-1-032-80042-4

Peaston C., De Rivaz, B., 17-20 June 2024, Notched beam and panel test alternatives for conformance testing of sprayed concrete linings consistent with limit state design, *9th International Symposium on sprayed concrete*, Sandefjord, Norway

Zenebe Gezahegn, M., Tiberti, G., Trabucchi, I. & Plizzari, G.A. . Post-cracking performance criteria for fibre-reinforced sprayed concrete in permanent tunnel linings. *Spray Concrete Symposium*.

Laval University 2021. Three point bending test on square panel with notch on sprayed specimens (3PBT on square panel) – Dramix 4D 65/35 BG. Laval University report, Mat 2021.

Meda, A. 2018. Comparison between EN14651 EFNARC three point bending test. University Tor Vergata Roma, Report April 2018.

AFTES 2023. Wet-Mix Sprayed Concrete for Permanent Application in Underground Structures: *Principles and Specification*. Guide 2023.

19th Australasian Tunnelling Conference – Acosta-Martínez, Stewart and Hudson-Smith (Eds.)
© 2025 Australian Tunnelling Society, ISBN 978-0-85825-002-4

Investigation of composite shell lining interface behavior of rock tunnel

W. Shuyi, D. Yisan, W. Ning & Y. Xiangjun
China Railway Academy Group Co., Ltd.,,Chengdu,China

ABSTRACT: The utilization of sprayed membranes facilitates the creation of a composite effect between shotcrete and sprayed membranes within tunnel linings. Nevertheless, the mechanism governing the composite shell lining remains indistinct. Through the employment of laboratory testing methodologies, shear compression tests were executed on specimens featuring varying core angles and sprayed membranes to ascertain the adhesive strength, internal friction angle, and shear stiffness of the sprayed membranes. The ultimate tensile compressive shear strength envelope was subsequently generated, serving as the threshold for the interfacial anti-slip strength. Furthermore, the normal stress and shear stress at each point along the interface were derived via numerical simulation, and an assessment was conducted to determine if each stress surpassed the strength envelope line, thereby establishing whether the interface experienced misalignment.

1 GENERAL INTRODUCTION

Upon the application of spray waterproofing featuring high double-sided bonding strength, in conjunction with the utilization of permanent shotcrete as the initial and subsequent layers of shotcrete, the synergistic interaction between these layers allows for the conceptualization of the first and second layers of shotcrete as a unified composite structure, namely a composite shell lining [1].

Despite the issuance of the "ITAtech Design Guidance For Spray Applied Waterproofing Membranes"[2] by the International Tunneling Association in 2013, intended to provide guidance and standardization for the application of this technology, it did not offer a definitive calculation methodology for the stress exerted upon the lining structure, nor did it include empirical parameter data. Reference [3] delves into the stress state and potential failure mechanisms of spray membrane interfaces, as well as methodologies for membrane testing. Additionally, various scholars have embarked on explorations using numerical simulation techniques. In recent years, research endeavors have included experimental examinations of simulated tunnel lining structures incorporating spray membranes. References [4-5] detail the collaborative efforts of the UK-based Aecom Corporation and Warwick University, which executed spray panel tests on composite shell linings within soft soil conditions, and conducted cyclic tensile and shear tests on the core for analytical purposes. References [6,7] present laboratory tests on sandwich beams, yielding load-deflection curves that substantiate a significant composite effect at the spray membrane interface. The University of Cambridge has engineered a compression bending test beam featuring a spray membrane layer, and has scrutinized the stress and strain variations of the specimens' sections throughout the loading process, initiating a preliminary investigation into the mechanical properties of the specimens [8]. Chinese scholars have also pursued research into the load-bearing mechanism, material characteristics, and structural design of the technology. Zhou Ping [9] employed experimental methodologies to dissect the stress characteristics of multi-layer lining structures under the influence of interlayer action. Previous research has indicated that each layer of multi-layer

shotcrete exhibits a radial anti-slip effect, and when combined, they can constitute an integrated load-bearing structure. Jiang Yajun et al. [10] formulated numerical calculation models for double shell lining, composite shell lining, and single shell lining, grounded in the mechanical and interface parameters of the sprayed membrane derived from experimental measurements, and conducted an internal force analysis of the composite lining. Jiang Yajun et al. [11] explored the shear failure mechanism and mechanical properties of the interlayer interface within the double-sided bonded tunnel lining structure, procuring pertinent parameters based on the Mohr Coulomb constitutive model, which can be utilized as a foundation for assessing the failure of the contact surface within the double-sided bonded tunnel spray membrane lining. Deng Yisan [12] quantitatively assessed the integrity of structures with robust interlayer bonding, yet did not establish a mechanical correlation between the external load and the various composite layers.

This study employs laboratory experimentation to evaluate specimens featuring sprayed membrane at varying core angles. Through these tests, the adhesion force, internal friction angle, and shear stiffness of the sprayed membrane are determined. Subsequently, an ultimate tensile compressive shear strength envelope is constructed, serving as the threshold for the interface's resistance to slippage.

2 LABORATORY TEST

2.1 *Test Purpose*

In the elastic phase, the interface performance of the composite shell lining significantly impacts the overall stiffness and load-bearing capacity of the composite structure. Therefore, a quantitative analysis of the composite shell lining requires the precise measurement and comprehensive understanding of the mechanical properties of the interface.

The actual contact surface, comprising shotcrete and a sprayed membrane, is distinguished by its roughness and irregularity, presenting challenges for the mechanical performance analysis conducted on this surface. As a result, the paper posits the hypothesis of an interface layer.

The interface layer encompasses sprayed membrane and shotcrete that is in direct contact with it. Owing to the irregularity of the actual contact surface, contiguous media do not perpetuate a uniform deformation as a cohesive unit. Consequently, shear failure does not invariably transpire on the material's contact surface, but is more probable to emerge in the media layer encircling the contact surface, resulting in a shear dislocation layer proximate to the contact surface. The stress and deformation characteristics within this displacement layer are markedly distinct from those of the encompassing shotcrete. Hence, within the composite structure model of the waterproof single-layer lining, the sprayed waterproof material and the shotcrete at the interface are designated as a singular material interface layer, and it is presumed that its contact surface with the surrounding shotcrete is linear, as depicted in Figure 1.

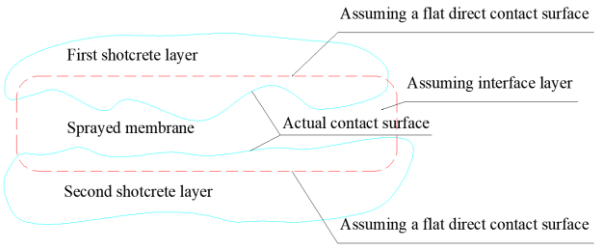


Figure 1. Schematic diagram of interface layer composition

The ultimate strength envelope of the interface layer, as delineated by the Mohr-Coulomb criterion, can be determined through shear compression and uniaxial tensile tests. By employing this

envelope, the strength parameters of the interface layer can be obtained for simulation computations, thereby enabling precise determinations of interface failure occurrences within composite structures.

2.2 *Shear compression test on interface layer*

2.2.1 Test method

Given the intimate adherence of the contact surface between shotcrete and sprayed membrane to the irregularities of the tunnel excavation surface, the interface layer and the orientation of the ground load manifest varying inclinations. Consequently, the ultimate stress of the interface layer is ascertained through shear compression tests conducted on shotcrete core samples at differing interface inclinations. Standards such as ASTM 1583/C 1583M (Pull-off Method), EN ISO 4624 (utilizing a 50mm dolly), EN 1542, and JGJ372-2016 specify the fabrication of cylindrical specimens with a diameter of 50mm and a length of 100mm. However, the production of specimens with a diameter of 100mm and superior core quality is more feasible. Thus, a cylindrical specimen with a diameter of 100mm and a length of 200mm was crafted from a large plate test block.

A direct shear test requires repeated tests under several axial loads (typically three to five) to determine friction angle and cohesion. In contrast, an inclined/tilt shear test applies normal stress through the sample's inclination angle, allowing direct measurement of sliding angle in a single test—no complex loading apparatus or multiple test runs needed.The inclined shear test loads along a pre-existing discontinuity without artificially creating a flat base, thus more accurately capturing natural friction, block interlocking, and surface roughness effects. While direct shear testing is easier to perform, its imposed flat shear plane can lead to less realistic results.The tilt angle inherently includes both the material's internal friction and its surface roughness. Direct shear tests, by contrast, yield a linear envelope and often require multiple normal stress levels to estimate friction angle—but can't separately quantify roughness effects.A waterproof layer with varying inclination angles was interposed within the column, employing Sika lastic-245 as the waterproof material. The test specimen is depicted in Figure 2. A press machine was utilized to apply continuous loading to the specimen at a rate of 0.1Mpa/min until failure ensued.The test number, interface inclination angle and sprayed membrane thickness are shown in Table 1.



Figure 2. Test specimen before interface layer shear test

Table 1. Interface layer shear compressive test

No.	Specimen number	Interface inclination angle°	Interface finish (substrate roughness)	Membrane thickness mm
1	∠20°-1	20	As sprayed panel	2.3
2	∠20°-2		As sprayed panel	2.1
3	∠24°-1	24	As sprayed panel	2.2
4	∠25°-1	25	As sprayed panel	2.2
5	∠40°-1	40	As sprayed panel	2.1
6	∠40°-2		As sprayed panel	2.2
7	∠40°-3		As sprayed panel	2.1
8	∠45°-1	45	As sprayed panel	2.4
9	∠45°-2		As sprayed panel	2.2
10	∠45°-3		As sprayed panel	2.2
11	∠46°-1	46	As sprayed panel	2.3

2.2.2 *Result analysis*

Utilizing the experimental methodology delineated in the preceding section, the shear compression test was executed. The subsequent failure analysis is depicted in Figure 3, while the graphical representations of the test load and vertical displacement are presented in Figure 4.



(a)Destructive specimens after testing (b)The failure state of specimens at different angles

Figure 3. The failure state of the test specimen in the interface layer shear test

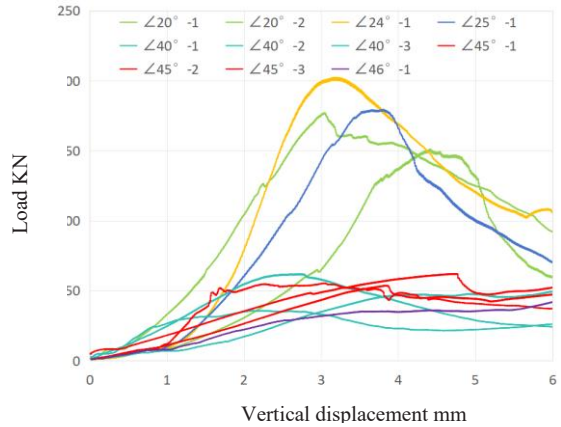


Figure 4. Load-displacement curve of interface layer shear test

As depicted in Figures 3 and 4, the shear compression failure of the interface layer is representative of a post-peak stress softening pattern. When the inclination angle of the interface layer is small, the normal stress at the interface significantly exceeds the tangential stress. Concurrently with the interface failure, the concrete substrate undergoes substantial compressive failure, and the peak value as well as the slope of the load displacement curve are notably high; Conversely, when the inclination angle of the interface layer is large, the disparity between the normal stress and tangential stress at the interface diminishes, and the failure is predominantly due to interface shear slip. The damage to the concrete substrate is minimal, and the peak value of the load displacement curve is also diminished, characterized by a relatively flat curve.

As depicted in Figure 4, the load displacement curve of the specimen serves as a comprehensive representation of the failure of the interface layer and the degradation of the concrete substrate, exhibiting no discernible linear segment. Consequently, this investigation employs the initial significant slope alteration point on the curve to compute the normal and tangential shear stresses of the interface layer, designating it as the inception of interface layer failure. The outcomes are delineated in Table 2.

Table 2. Results of interface layer shear test

Specimen number	Interface inclination angle°	Load kN	vertical displacement mm	Normal stress Mpa	shearing stress Mpa
∠20°-1	20	168.2	2.9	18.91	6.88
∠20°-2		128.2	3.7	14.41	5.24
∠24°-1	24	186.0	2.8	19.76	8.79
∠25°-1	25	173.7	3.5	18.16	8.47
∠40°-1	40	44.6	3.9	3.33	2.79
∠40°-2		36.2	2.1	2.70	2.26
∠40°-3		57.8	2.2	4.31	3.62
∠45°-1	45	62.0	4.7	3.94	3.94
∠45°-2		50.1	1.7	3.18	3.18
∠45°-3		53.4	3.8	3.39	3.39
∠46°-1	46	28.8	2.6	1.76	1.83

Upon linearly correlating the normal stress and shear stress of the interface layer within the stress domain, the Mohr-Coulomb shear compression strength envelope for the interface layer is derived, as depicted in Figure 5. From the fitting line equation y=0.3106x+1.9355 presented in the figure, the shear strength parameters of the interface layer are determined to be: cohesion of 1.9355 MPa, and an internal friction angle of arctan(0.3106), which equates to 17.3 degrees.

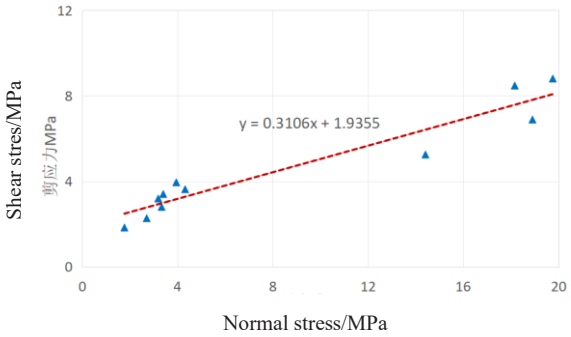


Figure 5. Envelope line of shear test strength of interface layer

2.3 *Uniaxial tensile test on interface layer*

2.3.*1 Test method*

In order to enhance the envelope of the interface layer within the tensile quadrant of the stress space, axial tensile tests were executed to ascertain its tensile characteristics. The experimental procedure also encompassed the fabrication of cylindrical specimens, each with a diameter of 100mm and a length of 200mm, derived from extensive plate test blocks. The composition of the specimens was identical to that utilized in the shear compression test.Due to the difficulty of coring at various inclined angles—particularly those less than 45 degrees—this tensile test uses sprayed membrane that is laid horizontally. The specimen is shown in Figure 6. A tensile machine was employed to apply a continuous load at a rate of 0.1 Mpa/min until the specimen succumbed to failure, with the locus of failure being significant at the interface layer.



Figure 6. Interface layer uniaxial tensile specimen

2.3.2 Result analysis

The specimen's predominant mode of failure is characterized by interfacial adhesion failure, specifically the detachment of the sprayed membrane from the mortar specimens at the interface subsequent to tensile stress application. The tensile test was executed in accordance with the methodology delineated in the preceding section. The maximum stress attained during the tensile process represents the peeling strength of the adhesive material, the test outcomes detailed in Table 3.

Table 3. Results of axial tensile test on the interface layer

Specimen number	ZL-1	ZL-2	ZL-3	ZL-4	ZL-5	ZL-6	ZL-7	ZL-8	ZL-9	ZL-10
Loa/kN	4.79	2.12	4.79	3.53	3.14	10.28	8.63	7.3	10.36	11.54
Axial tensile stress/Mpa	0.61	0.27	0.61	0.45	0.40	1.31	1.10	0.93	1.32	1.47

Throughout the stretching procedure, the initial phase exhibits a relatively slow rate of change in stress values, succeeded by a swift escalation of stress within a matter of seconds. Upon achieving bond strength, the waterproof membrane detaches from the mortar specimen in an almost instantaneous manner. In certain specimens, subsequent to the stress value attaining the bond strength, the stress diminishes incrementally until the membrane separates from the mortar block, signifying a gradual failure of the interface during the stretching process. For specimens characterized by immediate detachment of the membrane, the membrane completely separates from the mortar block, preserving its integrity post-separation of the bond surface. For specimens experiencing a gradual failure, both the interface separation and the destruction of the waterproof membrane transpire concurrently,the post-test failure analysis is depicted in Figure 7,



Figure 7. The failure state of the interface layer

Upon examining the outcomes of the axial tensile test, a tensile stress circle is delineated within the stress space. This tensile stress circle is subsequently linked to the shear compression envelope via an involute curve, culminating in the formation of the comprehensive tensile shear compression envelope, as depicted in Figure 8. The involute methodology is illustrated in Figure 9.

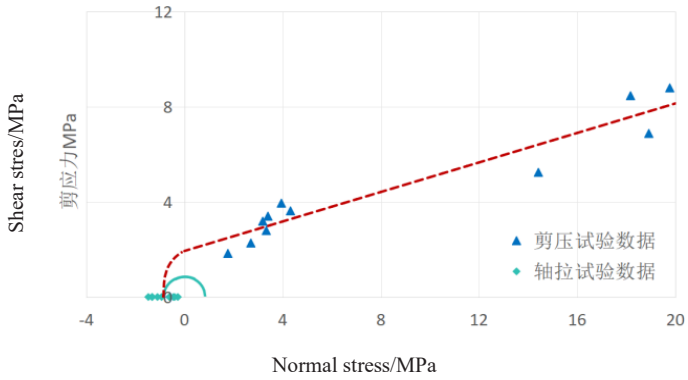


Figure 8. Envelope line of tensile, shear and compression test strength at the interface layer

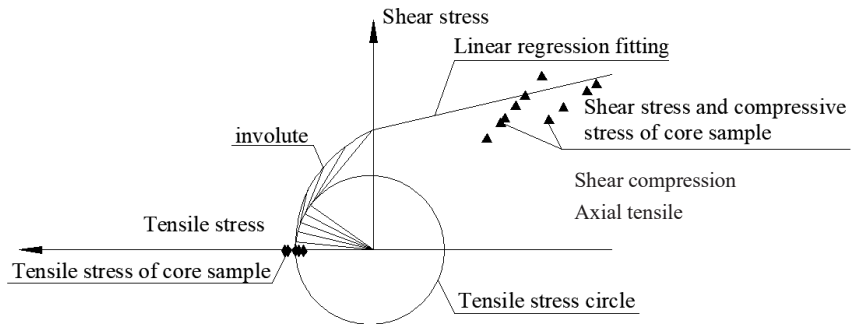


Figure 9. Illustration of the drawing of a gradual line

3 CONCLUSIONS

This study undertakes a comprehensive examination of the mechanical characteristics of the interface of a composite lining with an applied sprayed waterproof layer, employing laboratory-based testing methodologies. The investigation encompasses an interface layer shear compression test and a uniaxial tensile test, with the objective of ascertaining the interface layer's ultimate strength envelope in accordance with the Mohr Coulomb criterion.

(1) The shear compression test was executed on core samples of sprayed concrete at varying interface angles. The outcomes indicated that the shear compression failure of the interface layer exhibited a characteristic post-peak stress softening behavior, with the failure modality being influenced by the interface angle. The Mohr Coulomb shear compression strength envelope of the interface layer was derived via linear regression, and the shear strength parameters of the interface layer were obtained.

(2) The uniaxial tensile test quantified the tensile characteristics of the interfacial layer, revealing that the effective failure mode of the specimens was interfacial bonding failure. The standard bonding strength value can be considered as 0.5 MPa. Utilizing the outcomes of the axial tensile test, a tensile stress circle was delineated and integrated with the shear compression envelope to establish a comprehensive tensile shear compression envelope.

4 REFERENCES

Alun Thomas.Sprayed Concrete Lined Tunnels Second Edition.2022.

ITAtech Activity Group Lining and Waterproofing. ITA tech design guidance for spray-applied waterproofing membranes[R]. Geneva: ITA, 2013.

Su J . Stress status of sprayed waterproofing membrane under groundwater pressure within composite SCL tunnels[J]. Expanding Underground, 2023, 3(2):1003-1011

Su J , Bloodworth A G , Haig B . Experimental investigation into the interface properties of composite concrete lined structures[C]// World Tunnel Congress. 2013.

Jiang, Bloodworth, Alan. Interface parameters of composite sprayed concrete linings in soft ground with spray-applied waterproofing.[J]. Tunneling & Underground Space Technology, 2016, 59:170-182.

Su J , Bloodworth A . Experimental and numerical investigation of composite action in composite shell linings[C]// 7th International Symposium on Sprayed Concrete. 2014.

Su J , Bloodworth A .Numerical calibration of mechanical behaviour of composite shell tunnel linings[J].Tunnelling and Underground Space Technology, 2018, 76(JUN.):107-120.

Nakashima M, Hammreb Al, Thewes M,etal. Mechanical behaviour of a sprayed concrete liningisolated by a sprayed waterproofing membrane [J].Tunnelling and Underground Space Technology, 2015,47: 143.

Zhou Ping, Wang Zhijie, Lei Feiya, etc.Experimental study on the stress characteristics model of single-layer lining of steel fiber reinforced concrete tunnel considering interlayer effect[J].China Civil Engineering Journal, 2019.

Jiang Yajun, He Bin, Zhao Jumei, etc.Study on the mechanical properties of tunnel spray film waterproof lining structure[J].Modern Tunnelling Technology, 2022(001):059.

Jiang Yajun, Zhao Jumei, He Yudi, etc.Mechanical Characteristics of Interface Between Layers of Double-Sided Adhesive Spray-Applied Membrane Waterproof Tunnel Lining[J].Tunnel Construction（chinese and english）, 2023.

Deng San, Li Gang, Zhang Jianwei, etc. Study on composite surface of waterproof single-layer lining by tests[J]. Journal of Railway Science and Engineering, 2022(003):019.

19th Australasian Tunnelling Conference – Acosta-Martínez, Stewart and Hudson-Smith (Eds.)
© 2025 Australian Tunnelling Society, ISBN 978-0-85825-002-4

Evaluation of rockbolt performance using field testing

S. Soni & P. Clark
Infrastructure Projects and Engineering, Transport for New South Wales, Sydney, Australia.

ABSTRACT: Permanent rockbolts are essential components of tunnel ground support systems, providing structural stability and controlling ground movement. Their design must account for axial and shear loading capacity, effective load transfer along the bolt length, and compatibility with expected rock mass conditions and ground behaviour. The stiffness characteristics of rockbolts are critical in determining how effectively load will be distributed and transferred along the bolt length. Pull-out testing is routinely conducted to validate design parameters and assess installation quality. This study presents a detailed analysis of production pull-out testing data from 1306 tests recently undertaken on Sydney Road tunnel projects, supplemented with published research, to assess the influence of rockbolt type, length, and grout bond strength on rockbolt performance. Findings show that rockbolt tests provide concordant stiffness and displacement control in most conditions, while cable bolts deliver higher stiffness but display greater variability in weak or fractured rock masses. The study proposes improved testing strategies to improve design validation, predictive modelling, and tunnel safety.

1 INTRODUCTION

Rockbolts are essential structural elements used extensively in tunnel ground support systems to stabilise excavations and mitigate ground movement in challenging geological environments. The stiffness characteristics (load-displacement relationship) of rockbolts play a crucial role in determining their load-bearing capacity and effectiveness in transferring forces along the bolt length. Additionally, stiffness is a key input parameter for all finite element (FE) modelling, influencing the accuracy and reliability of simulations used to assess tunnel support performance. The most common types used and investigated for this study are cement grouted double corrosion protected (DCP) combination bolts commonly referred to as DCP CT bolts and DCP cable bolts. This paper presents an evaluation of the performance of these rockbolts using extensive field-testing data collected from multiple Sydney tunnel projects in different ground conditions. Findings from this study contribute to the improvement of existing validation and design practices for rockbolts and provide practical recommendations for performance-based ground support design.

2 BACKGROUND – ROCK REINFORCEMENT SYSTEM

2.1 *Rock Reinforcement System*

The rock reinforcement system consists of a steel bar (CT bolt) or steel cable (cable bolt) pre-fitted with an expansion shell and a corrugated polyethylene sheath. This arrangement allows the bolt to provide immediate mechanical anchorage via the expansion shell while facilitating complete grout encapsulation for long-term bond integrity and corrosion protection. Typical mechanical characteristics of CT bolts and cable bolts, including tensile strength, stiffness, and elongation

capacity, are summarised in Table 1 (Bluey, 2016; Bluey, 2025; DSI, 2025). Cement grout used is a standard formulation with low shrinkage characteristics, specific gravity greater than 1.95, compressive strength greater than 40 MPa, and high early strength exceeding 10 MPa at 24 hours.

Table 1. Typical characteristics of steel elements within bolt types (Bluey 2016, Bluey, 2023, DSI,2025)

Property	Unit	CT Bolt (DSI)	Cable bolt (BlueGeo CF 22)
Diameter	mm	21.7 / 23.2	21.8 (19 Wires)
Area	mm^2	370	312.9
At Yield (@ proof 0.2% strain)	MPa	600 MPa (220kN)	525 kN
Tensile Strength	MPa	840 MPa (310kN)	590 kN
Young Modulus	MPa	200 GPa	189.5 GPa
Elongation	%	13%	Min 3.5% / Typical 6-7%

2.2 *Design Considerations*

Axial performance of rockbolts needs to be assessed in both elastic and plastic domains. The elastic limit is typically defined by the yield strength of the bar or cable, and design loads are usually limited to less than 80% of the yield strength to avoid permanent deformation under expected service loads. However, when rockbolts are provided as a system (e.g. pattern), yielding of discrete rockbolts may be acceptable as loads are distributed to adjacent rockbolts. If this occurs however, adjacent bolts may also yield, leading to a potential for progressive collapse occurring. For bolts designed to behave plastically, the design must demonstrate stable post-yield behaviour without sudden rupture or progressive failure.

Shear loading on rockbolts arises from rock mass movements in stratified or jointed rock because of stress relief or creep movement, as well as from ground movement due to tunnel excavation. These shear forces may act independently or concurrently with axial loads. Shear performance is particularly critical for sheathed bolts, where protecting the integrity of the sheath is essential to maintain long-term durability. According to Pellet & Egger (1996), combined axial (P_u) and shear (V_u) loading can be assessed using an elliptical failure criterion:

$$\left(\frac{P}{P_u}\right)^2 + \left(\frac{V}{V_u}\right)^2 \leq 1$$

2.3 *Stiffness and Bond Characteristics*

Stiffness characteristics of fully grouted rockbolts are predominantly governed by the bond behaviour at the bolt-grout interface. There are a number of design approaches that model stiffness behaviour, including Clarke (2012) (bilinear stiffness behaviour), Blanco-Martín et al. (2013) (trilinear bond-slip model), Nemcik et al. (2014) (non-linear bond-slip constitutive law) and Aghchai et al. (2020) (modelling the bolt as an elastic-plastic continuum). The assessment by Aghchai et al. (2020) demonstrates that upon yielding of the bolt, shear resistance at the bolt-grout interface diminishes rapidly, leading to progressive debonding and ineffective load transfer. This approach also identifies that bond strength is underestimated if plastic deformation is ignored. Plastic behaviour studied by Yu et al. (2019) observed that even with increased embedment length and grout strength, the bond interface cannot sustain load transfer once bolts yield, resulting in crack propagation in grout as well as interface and bond failure.

2.4 *Rockbolt Verification and Validation Testing*

Typical rock reinforcement specifications require performance-based validation of ground support elements. Verification and validation procedures include pre-production acceptance testing and quality assurance production testing. Pre-production pull out tests are conducted to validate the load transfer mechanism, bond strength and identify any installation-induced issues. Assessments of pre-production testing exist, e.g. Salcher & Bertuzzi (2018), but production testing assessments such as this paper are rare.

Production testing validates bolt performance consistency during construction. Pull-out tests are performed incrementally, with load steps in the expected elastic state (~70% of yield) only held for specified durations and movements recorded. Typical acceptance criteria require bolts to sustain designated loads with minimal displacement and stability for at least 10 minutes. Typical initial testing frequencies are 5% of installed bolts in each rock mass type, reducing to 1% following successful validation. Should failures occur, testing may revert to a higher frequency, and adjacent bolts are subjected to additional verification to ensure local stability.

Full-scale pre-production shear testing of sheathed bolts is also specified, evaluating sheath integrity and bolt response under imposed displacements of 10 mm to 25 mm, with shearing limits for durability typically set at 10mm and higher limits permitted for safety.

3 PERFORMANCE ASSESSMENT AND DATA ANALYSIS

3.1 *Overview and Rock Mass Conditions*

This study analysed a comprehensive dataset comprising 1,306 production pull-out tests conducted across multiple tunnels in the Sydney region. The unfiltered dataset includes a total of 1,306 pull-out production tests, of which 32 tests (2.4%) resulted in failure. Out of the total tests, 251 were conducted on cable bolts and 1,055 on CT bolts (Figure 1).

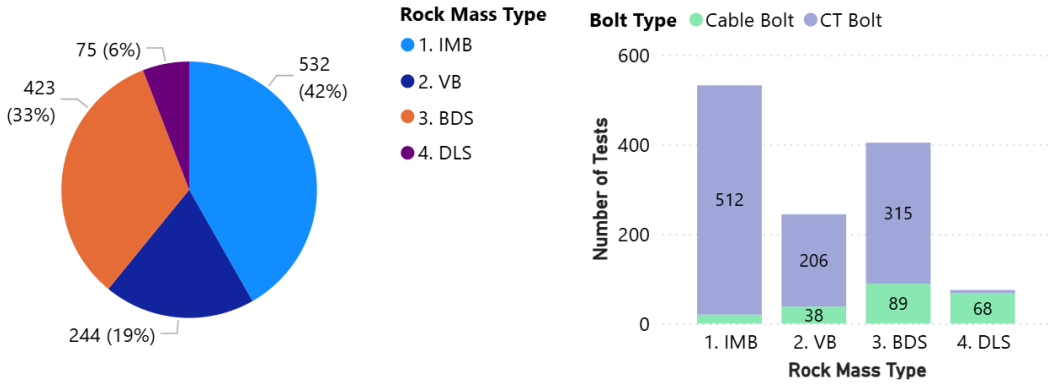


Figure 1. Production pull-out test data summary.

For analytical purposes, rock mass conditions encountered during tunnel excavation were categorised into four distinct classes, broadly equivalent to rock mass classes described in the GSI system (Marinos and Hoek, 2000) and the Sydney Rock Mass Classification (SRMC) system (Pells et al. 1998), and broadly corelated as described in Bertuzzi (2014) and Bertuzzi et al. (2016):

1) Intact or Massive to Blocky (IMB)- Intact, massive or undisturbed rock masses with minimal defects (broadly equivalent to SRMC Class I/ II Sandstone).
2) Very Blocky (VB) - Rock masses exhibiting multiple defect sets, weak bedding planes, or occasional minor clay seams, where defects regularly impact local stability (broadly equivalent to SRMC Class III-V Sandstone and Class I/II Shale).
3) Blocky/Disturbed/Seamy (BDS) - Rock masses surrounding major geological structures (e.g., faults and dykes) or a disturbed rock fabric and sheared defect surfaces broadly equivalent to Class III/IV shale and damage zones that surround fault as described in Kim, et al. (2004).
4) Disintegrated, Laminated or Sheared (DLS) - Zones of significantly fractured, crushed or sheared rock masses, often with clay fault gouge. Typically associated with fault zones or high to extreme weathering (broadly equivalent to SRMC Class V Shale and fault zones as described in Childs, et al. (2009).

Raw data from the pull-out test results were assessed for potential errors. Since most production tests were conducted on hardened shotcrete, a stable and consistent base was assumed, minimising the risk of inaccuracies in baseline displacement readings. As a result, errors related to initial

readings were limited to only a few tests. In cases where anomalies were identified, base corrections were applied during the assessment of net cumulative displacement at each load increment. This ensured that the derived load–displacement curves shown below accurately reflects the true performance of the rock bolts under in-situ conditions.

3.2 *Impact of Rock Reinforcement Length*

Analysis of the pull-out test data revealed significant variations in bolt deformation patterns depending on bolt type and rock mass type. Figure 2 presents cumulative displacement (loading stage) trends for CT bolts (less than 7.5m long) and cable bolts (greater than 6.5m long), emphasising the differing responses of these systems to applied loads.

Box and whisker plots are used as an effective graphical method to summarise data distribution. The boxes in the following plots represent the interquartile range (IQR), capturing the central 50% of the data. The whiskers extend to the 5th and 95th percentiles, providing a representation of characteristic lower and upper bounds, while identifying potential outliers beyond these limits.

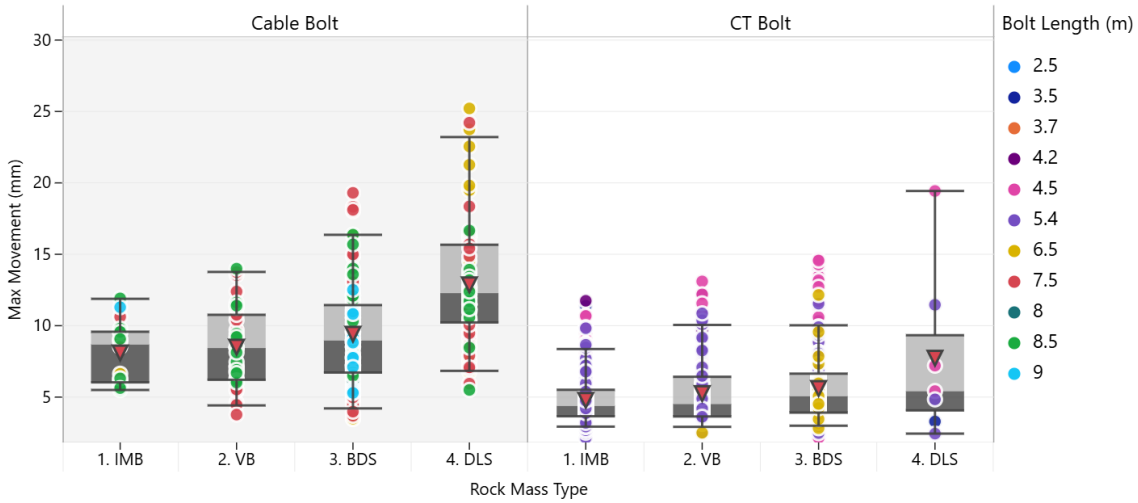


Figure 2. Distribution of cumulative displacement for CT and cable bolts

Key observations in Figure 2 include cable bolts show greater variability in poorer quality rock masses, CT bolts have consistent performance across all rock mass types, no clear correlation between bolt length and movement for either bolt type. These observations highlight CT bolts superior capability to limit ground movement, particularly under challenging conditions and suggests that initial bonded segments govern the bolt load–displacement response, with total installed length having a limited influence on the measured displacement range.

3.3 Evaluation of bolt stiffness

To estimate stiffness at various stress levels for CT and cable bolts the following formula is used:

$$Stiffness, k\ (\ kN/mm) = \frac{\Delta Load\ (kN)}{\Delta Displacement\ (mm)}$$

Bolt stiffness was evaluated using two complementary approaches:

1. Individual Test Stiffness Estimation:
   The Stiffness (secant) value was calculated for each individual pull test by determining the slope of the load–displacement curve. These values were then subjected to statistical assessment for various rock mass types to identify trends and consistency in bolt behaviour.

2. Displacement-based Stiffness Estimation:
   Rockbolt displacement values at key load levels were statistically analysed to assess deformation patterns. Stiffness (secant) was then estimated from the incremental changes in load and displacement, providing a load specific understanding of bolt response.

3.3.1 *Individual Test Stiffness Estimation*

The box and whisker plot comparison of cable bolts and CT bolts for the four rock mass types is shown in Figure 3.

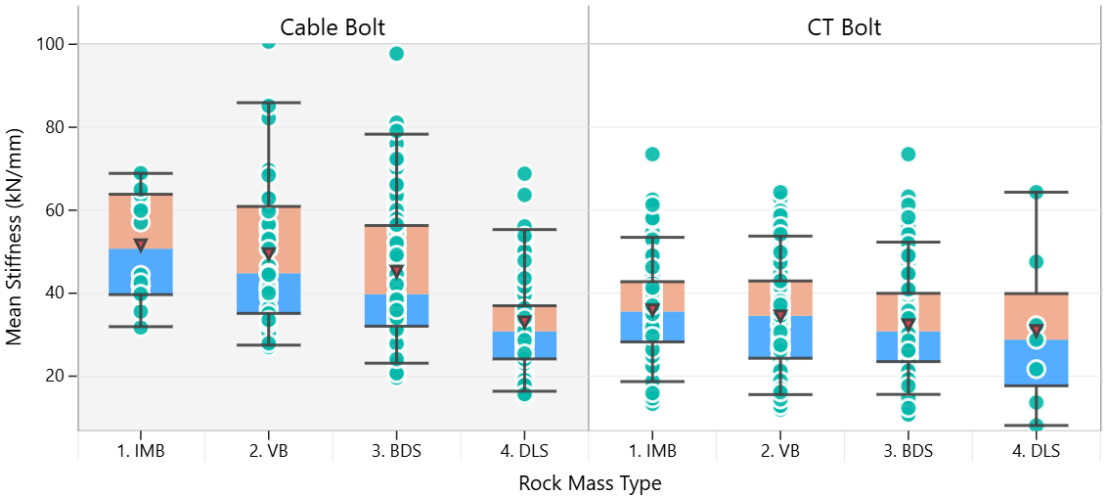


Figure 3. Statistical distribution of rockbolt stiffness value from individual test stiffness estimation

For cable bolts, median stiffness remains relatively high for all rock mass types. The highest median stiffness is observed in IMB rock masses, with a relatively narrow interquartile range, indicating consistent performance in relatively good quality rock masses. In VB and BDS rock masses, cable bolts continue to perform well but with greater variability. Notably, BDS and DLS rock masses show significant data dispersion. This high variability in poor quality rock masses suggests that while cable bolts can offer high stiffness, their performance becomes more dependent on installation quality and local anchorage conditions.

In contrast, CT bolts exhibit lower mean stiffness across all rock mass types, with stiffness values tightly clustered (narrow IQR), indicating greater consistency and predictability even in poor geological conditions. CT bolts exhibit lower stiffness variability across rock mass types, justifying their suitability for applications requiring uniform response and controlled deformation.

3.3.2 Displacement-based Stiffness Estimation

Rockbolt displacement distribution at various loading levels are statistically analysed for the four types of rock masses and bolt types. Figure 4 shows the actual load displacement profiles from the field production pull out tests. Bolt stiffness is then estimated by averaging values for each rock mass type. The distribution of displacement data is shown in Figure 4 and stiffness values for various loads and rock mass types are assessed in Figure 4 using the formula provided in Section 3.3.

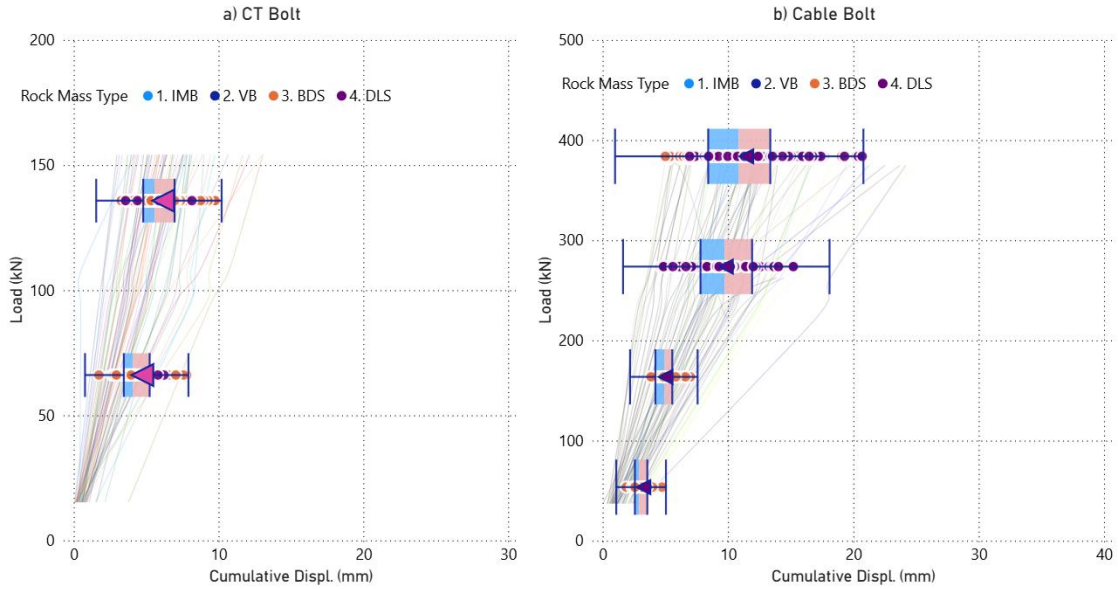


Figure 4. Statistical distribution of rock bolt displacement used in displacement-based stiffness estimation.

The predicted load-displacement behaviour of CT and cable bolts (Fig. 5), demonstrates clear trends between the four rock mass types. IMB rock masses exhibit comparable stiffness value of for both bolt types, reflecting stable and predictable performance. However, as rock mass conditions deteriorate, disparities in behaviour become evident. In VB and BDS rock masses, cable bolts maintain higher stiffness values, whereas CT bolts show a significant reduction, particularly in VB rock masses. Overall, this assessment suggests that cable bolts provide enhanced resistance to displacement and maintain better load transfer in weak or fractured rock masses.

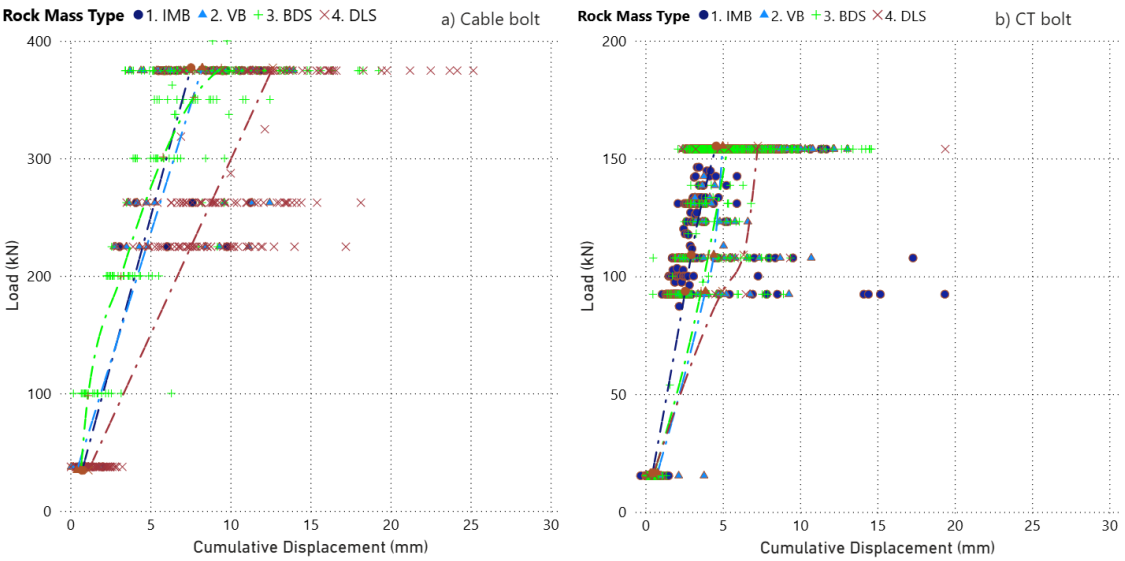


Figure 5. Predicted stiffness using displacement-based estimation, Lines indicate mean value at load.

3.3.3 Comparison of Stiffness

The stiffness comparison of CT and cable bolts for the four rock mass types are summarised in Table 2 for both individual test estimation and displacement methods. This table provides mean values as well as upper and lower bound characteristic values for use in design.

Table 2. Summary of estimated stiffness from individual test estimation and displacement method estimation. Mean value is provided along with 5% and 95% characteristic values in brackets

Rock Mass Type	Individual Test Stiffness (kN/mm)		Displacement-based Stiffness (kN/mm)	
	CT Bolt	Cable Bolt	CT Bolt	Cable Bolt
1. IMB	35 [18 - 53]	~50 [31 - 69]	36 [21 - >100]	36 [25 - >100]
2. VB	35 [15 - 54]	~50 [27 - 86]	26 [13 - 79]	43 [24 - >100]
3. BDS	32 [15 - 52]	~45 [23 - 78]	27 [15 - 106]	47 [32 - 78]
4. DLS	~30 [8 - 64]	33 [16 - 55]	25 [15 - 50]	28 [17 - 65]

Individual test estimation, where stiffness is calculated from each bolt's load–displacement values tend to produce a tighter and more consistent distribution. This is because each test captures the full load history and progressive deformation of a single bolt, reflecting gradual ground-bolt interaction. In contrast, displacement-based stiffness methods rely on averaging ground movement at fixed load levels across multiple bolts. This introduces variability due to differences in installation quality, ground heterogeneity, and local conditions, but consequently, is more representative of actual bolt performance.

The comparison of both individual test estimation and displacement-based stiffness estimation methods shows similar trends for all four rock mass types, with displacement-based values generally being slightly lower. This assessment is consistent with Clarke (2012) that showed a bilinear stiffness pattern for short bolts and noting that stiffness in the early phase is mainly controlled by the initial bonded segment.

The comparison of stiffness values for CT and cable bolts across different rock mass types reveals clear performance trends. In IMB rock masses, both bolts perform well, with cable bolts showing slightly higher stiffness. However, as rock mass conditions deteriorate from VB rock masses through to DLS rock masses, cable bolts consistently maintain higher stiffness and more stable performance than CT bolts. This indicates that cable bolts are better able to adapt to variable rock masses, potentially because of their flexible, multi-strand structure. In contrast, CT bolts show a noticeable decline in stiffness in weaker rock masses, reflecting their more rigid response and greater sensitivity to bond degradation. Overall, cable bolts demonstrate superior stiffness retention in challenging conditions, while CT bolts offer more predictable performance in stable rock masses.

4 DISCUSSION AND RECOMMENDATIONS

The analysis of production testing shows distinct performance differences between cable and CT bolts. CT bolts exhibit more concordant stiffness and displacement control across all rock masses. In contrast, cable bolts showed higher stiffness in IMB rock masses and VB rock masses, but their performance is more variable in BDS and DLS rock masses, albeit still maintaining higher stiffness than CT bolts. These trends align with the bilinear stiffness model presented in Clarke (2012).

The analysis also revealed that although the overall failure rate of rock bolts was 2.4%, only around 1% of installed bolts are typically subjected to pull-out testing. This suggests that current testing frequencies may be insufficient to detect and address performance variability, especially in critical or complex geological settings. Given the essential role of rock bolts in maintaining tunnel stability, the current production testing frequency warrants revising.

A robust evaluation of rockbolt performance must distinctly address two critical mechanisms, namely, bond interface behaviour and steel yield capacity. It is important to note that pull-out testing only assesses behaviour within the elastic limit of the bolt, meaning the steel component in a rockbolt remained un-yielded during testing. The current practice of using elastic-state assumptions for bond failure testing results in a limitation of how bond degradation interacts with plastic deformation of the steel element in a rockbolt. This represents a significant limitation, as real tunnel loading scenarios, particularly in highly deformable or faulted rock masses, may induce strains that exceed the yield point of the reinforcement. Without understanding the bond behaviour post yielding, the interaction between steel and grout, and between the grout and rock,

remains uncertain for design cases that predict yielding and current production testing will not validate post yielding performance.

To improve current practice, the following recommendations are suggested:

1) Where plastic deformations are permitted, establish performance-based criteria for plastic deformation for rockbolts and pre-production suitability test methods to verify the criteria.
2) Undertake suitable design assessments and ensure parametric or sensitivity assessments are undertaken for the range of likely performance of rockbolts. Appropriate characteristic ranges for bolt stiffness values are provided in this paper.
3) Ensure production testing protocols include post-yield performance for all rock mass types.
4) Adopt combined axial-shear interaction envelopes (e.g., Pellet & Egger method) as standard practice for rockbolt design evaluation and validation.
5) Production testing frequencies be increased, especially in poorer ground conditions where installation quality and bond performance are more variable. For example, in BDS and DLS, a testing rate of at least 10% may be more appropriate to confirm system reliability.

5 CONCLUSIONS

This study has provided a comprehensive evaluation of rockbolt performance in Sydney tunnels through the analysis of an extensive dataset of pull-out test data. The results confirm that CT bolts deliver consistent stiffness and displacement control across most conditions, making them suitable for most rock mass conditions. In contrast, cable bolts demonstrated higher stiffness and greater adaptability in poor quality rock masses, although with increased variability in poorer quality rock masses.

A critical limitation of the current testing practices is the focus on elastic-state behaviour only. The lack of testing beyond yield strain means that the interaction between the bolt, grout, and rock under post-yield conditions remains poorly understood. This is especially critical in rock masses affected by major geological structures such as faults and dykes and other highly deformable ground where plastic deformation is possible.

To enhance ground support reliability, it is recommended that design and design validation methods be expanded to include post-yield bolt performance and combined axial-shear interaction assessments. This approach will ensure greater reliability for performance-based design approaches in relatively complex geological settings.

ACKNOWLEDGEMENTS

The authors would like to acknowledge the support and feedback from reviewers both internal and external. The authors also gratefully acknowledge the support of Transport for New South Wales in the preparation of this paper. The views and opinions expressed in this paper are the authors and do not necessarily represent those of Transport for New South Wales.

6 REFERENCES

Aghchai, M.H., Maarefvand, P. & Salari Rad, H. 2020. Analytically determining bond shear strength of fully grouted rockbolt based on pullout test results. In Periodica Polytechnica Civil Engineering, 64(2): 371–378. Budapest: Budapest University of Technology and Economics.

Bertuzzi, R., 2014. Sydney sandstone and shale parameters for tunnel design. Australian Geomechanics Journal 49, 95–104.

Bertuzzi, R, Douglas, K, Mostyn, G. 2016. Comparison of quantified and chart GSI for four rock masses. In Engineering Geology 202, 24-35.

Blanco-Martín, L., Tijani, M., Hadj-Hassen, F. & Noiret, A. 2013. Assessment of the bolt-grout interface behaviour of fully grouted rockbolts from laboratory experiments under axial loads. In International Journal of Rock Mechanics and Mining Sciences, 63: 50–61. Amsterdam: Elsevier.

Bluey. 2016. BluGeo CF Rockbolt – Technical Report rv3. Sydney: Bluey Technologies Pty Ltd.
Bluey. 2023. BluGeo CF Rockbolt – Technical Data Sheet R01/2023. Available at: https://www.bluey.com.au/wp-content/uploads/2016/07/BluGeo-CF-Rock-Bolt-TDS-R012023.pdf (accessed 16 May 2025).
Childs, C., Manzocchi, T, Walsh, J.J, Bonson, C.G., Nicol, A., Schopfer, M.P.J. 2009. A geometric model of fault zone and fault rock thickness variations. In Journal of Structural Geology 31 117-127.
Clarke, S.J. 2012. Interpretation of pull test results of grouted rockbolts. In Proceedings of the 11th Australia & New Zealand Conference on Geomechanics, Melbourne, 15-18 July 2012: 89–95. Melbourne: Institution of Engineers, Australia.
DSI. 2025. CT Corrosion Protected Mechanical Bolt. Available at: https://www.dsiunderground.com.au/fileadmin/downloads/dsi-underground-com.au/products/CT_-_CT_Corosion_Protected_Mechanical_Bolt.pdf (accessed 16 May 2025).
Kim, Y.S, Peacock, D.C.P, Sanderson, D.J. 2004. Fault Damage Zones. In Journal of Structural Geology 26, 503-517
Marinos, P, Hoek, E. 2000. GSI – A geologically friendly tool for rock mass strength estimation. Proceedings of GeoEng 2000, International conference on geotechnical and geological engineering, Melbourne Australia, P 1422-40
Nemcik, J., Aziz, N., Ren, T. & Geng, X.Y. 2014. Numerical modelling of failure propagation in fully grouted rockbolts subjected to tensile load. In International Journal of Rock Mechanics and Mining Sciences, 71: 237–245. Amsterdam: Elsevier.
Pellet, F. & Egger, P. 1996. Analytical model for the mechanical behaviour of bolted rock joints subjected to shearing. In Rock Mechanics and Rock Engineering, 29(2): 73–97. Vienna: Springer.
Pells, P.J.N., Mostyn, G.R., Walker, B.F., 1998. Foundations on sandstone and shale in the Sydney region. Australian. Geomechanics Journal. 33, 17–29.
Salchar, M. & Bertuzzi, R. 2018. Results of pull tests of rockbolts and cable bolts in Sydney sandstone and shale. In Tunnelling and Underground Space Technology, 74: 60–70. Amsterdam: Elsevier.
Yu, S., Zhu, W., Niu, L., Zhou, S. & Kang, P. 2019. Experimental and numerical analysis of fully grouted long rockbolt load-transfer behavior. In Tunnelling and Underground Space Technology, 85: 56–66. Amsterdam: Elsevier.

THIS PAGE INTENTIONALLY LEFT BLANK

Theme 4. Caverns

THIS PAGE INTENTIONALLY LEFT BLANK

19th Australasian Tunnelling Conference – Acosta-Martínez, Stewart and Hudson-Smith (Eds.)
© 2025 Australian Tunnelling Society, ISBN 978-0-85825-002-4

Design and construction of the AS1 Shaft within the Albert Street Cavern, Cross River Rail, Brisbane

A.C. Rogan
PSM, Brisbane

B. Swinn
Systra & CBGU JV, Brisbane

S.J. Clarke
PSM, Sydney

J. Ahn
RocScience, Brisbane

ABSTRACT: Albert Street Station is one of the new Cross River Rail project underground stations in Brisbane's CBD. It is being constructed by the CPB Contractors, BAM International Australia, Ghella and UGL (CBGU) Joint Venture, with PSM designing the primary support and permanent cavern lining. To link the cavern under platform ventilation and services with the nearby 50 m deep Main Access Shaft, the AS1 shaft was excavated 12 m below the cavern invert level, with two adits connecting the two shafts. The AS1 shaft geometry, design constraints, interfaces, and construction sequence introduced unique challenges to its design and construction. The shaft was excavated from the cavern invert level via pre-blasting of the bedrock, with a substantial shaft capping beam constructed prior to removal of the blasted rock. The Kicker Beam (i.e. western capping beam) was undercut by the excavation, spanning 12 m across the AS1 shaft, and was subsequently subject to several significant temporary load cases. These included a temporary steel deck and plant loads, formwork loads associated with the largest cavern lining pour for the project, as well as acting, in conjunction with a capping slab, as the permanent 'bridge' to span the shaft and support the overlying track slab and train loads. Long-term ground load associated with AS1 included those from the narrow rock pillar remaining between the cavern and the Main Access Shaft. This paper presents the design and construction challenges for the AS1 shaft primary support and permanent lining, as well as the experiences and learnings gained throughout the project.

1 INTRODUCTION

Cross River Rail (CRR) is a new 10.2 km long metro rail line in Brisbane between Dutton Park in the south and Bowen Hills to the north, which includes 5.9 km long twin tunnels which pass below the Brisbane River and CBD. The Tunnel, Stations and Development (TSD) component of the project includes construction of twin Tunnel Boring Machine (TBM) excavated and mined running tunnels; four new underground stations at Boggo Road, Woolloongabba, Albert Street and Roma Street; and dive structures at each end of the running tunnels.

The Pulse consortium (including the CBGU JV) was awarded the contract to design and construct the TSD works.

Albert Street Station, located in the CBD of Brisbane, is constrained and surrounded by existing infrastructure. The 290 m long station cavern runs parallel to the alignment of the overlying Albert Street, with access to the station to be facilitated by the adjacent Lot 1 (i.e. Main Access) and Lot 3 shafts via adits linking to the mezzanine level of the station cavern. The cavern is the largest mined station on the project, with an excavation span of 22.6 m and excavated height of 16.7 m. PSM provided the design for the excavation primary support as well as the permanent lining, with Robert Bird Group (RBG) designing the internal structures within the cavern and AS1 shaft.

With the entire station developed as an underground structure, the pedestrian, maintenance and mechanical and electrical access is all facilitated via adits linking the cavern to the adjacent shafts. A total of seven adits are utilised, five linking to the 50 m deep Main Access Shaft and two to the Lot 3 Shaft. Of the adits linking to the Main Access Shaft, three link to the cavern mezzanine level, whereas the other two (AA2 and AA6) are located below the cavern invert level, linking with the AS1 Shaft, which is excavated 12 m below the cavern level for under platform ventilation and services. The Main Access Shaft and the AS1 shaft are some of the deepest excavations within the Brisbane CBD.

The geometry, interfaces, and construction sequence of the AS1 shaft introduced numerous unique design and construction challenges, the key ones of which are presented below.

2 SHAFT GEOMETRY AND GEOTECHNICAL CONDITIONS

Figure 1 shows a cross-section of the AS1 Shaft and key interactions with the station cavern and Main Access Shaft. The AS1 Shaft is 15.3 m by 12.1 m in plan, extending approximately 12 m below the cavern invert level, with a capping beam surrounding the top of the shaft, and the AA2 and AA6 adits extending out from the shaft southern and western sidewalls respectively.

On the western side of the shaft, the 'capping beam' is undercut by the AS1 Shaft (and AA6 adit), with this beam (referred to as the 'Kicker Beam') required to span the length of the shaft and support the overlying cavern permanent lining sidewall, as well as the permanent rail track slab (via a capping slab). A series of internal walls sub-divide the shaft into sectors for the under-platform ventilation, as well as providing support for the overlying platform units. The rock pillar that separates the AS1 Shaft and cavern from the Main Access Shaft is approximately 5.7 m wide.

Albert Street is underlain by the Neranleigh-Fernvale Group (NFG) rock mass. The NFG rock mass comprises weakly metamorphosed sandstone (meta-greywacke and arenite), phyllite and subordinate quartzite and meta-basalt. Meta-greywacke and arenite were typically high strength,

whilst the phyllite was typically weaker. The foliation in the NFG dipped 40° to 50° to the north-east (i.e. dipping towards the cavern), with a 14° shallow angle, 0.3 m thick, contact fault (separating the phyllite and meta-greywacke), dipping to the east and cross-cutting through the rock pillar separating the cavern and Main Access Shaft above the level of the Kicker Beam.

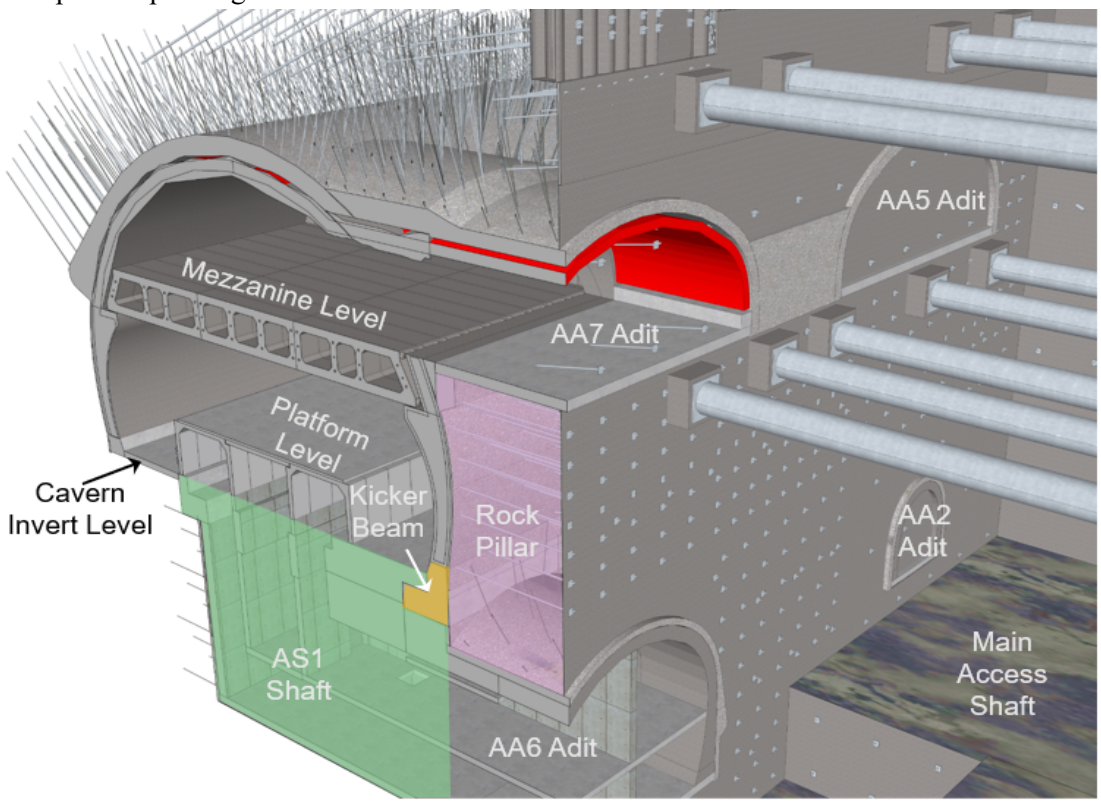


Figure 1. AS1 Shaft arrangement.

The geotechnical rock mass conditions within the AS1 shaft were typically mapped as NFG2 or NFG1, as per the definitions given in Cammack *et al.* (2022).

3 PROJECT SCOPE AND TECHNICAL REQUIREMENTS AND LOAD CASES

The Project Scope and Technical Requirements (PSTR) included key requirements related to the AS1 Shaft:

- Design in accordance with the Australia Standard (AS) 5100 series (2017).
- Minimum B2 exposure classification with crack widths estimated via the approach given in EN1992-1-1 and a crack width limit of 0.3 mm.
- Design life of 100 years for the permanent lining.
- Benefit of primary excavation active support (e.g. rock bolts) to be ignored in the design of the permanent lining.

The cavern (and AS1 Shaft) were designed as a drained tunnel, with Cavidrain S60 sheet drainage installed beneath the cavern invert slab and the AS1 Shaft invert (which collects groundwater inflows and conveys them to a sump in the Main Access Shaft), and a polyvinyl chloride (PVC) sheet waterproof membrane installed around the cavern and adit crowns and sidewalls and the AS1 shaft walls. This waterproof membrane was required to lap underneath the AS1 Shaft capping beam, resulting in a key design and construction challenge (refer Section 6.4).

The unfavourable foliation orientation (dipping to the north-east), thin rock pillar and the presence of faulted ground created adverse geotechnical conditions for the western cavern sidewall, AS1 Shaft walls and Kicker Beam foundation. These conditions were further complicated by the presence of the AA7 adit at the cavern mezzanine level, resulting in a complex and highly three-dimensional arrangement for the estimation of ground loads. Additionally, at the time of design, uncertainty in the excavation staging of the Main Access Shaft relative to the cavern and AS1 Shaft required sensitivity testing to ensure a robust design that could facilitate the range of potential construction sequences. For example, the existing Mantra building, on the western side of the Main Access Shaft has the potential to drive a large scale wedge sliding mechanism towards the shaft along the NFG foliation. During excavation, this wedge was supported by pre-stressed ground anchors, however, these were required to be considered as sequentially de-stressed as the permanent shaft structure was constructed from the bottom up, with load transferring through the Main Access Shaft structure, onto the rock pillar linking to the cavern, ultimately creating ground load for the cavern and AS1 Shaft permanent linings to resist. This scenario, in particular, resulted in complex load cases for the AS1 Kicker Beam.

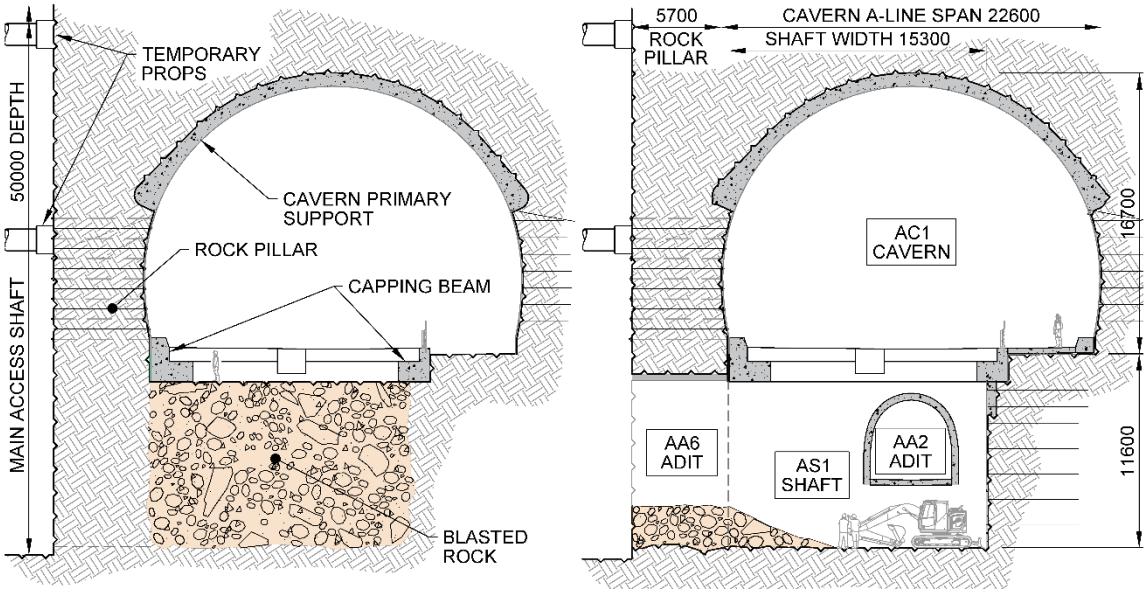
As shown in Figure 1, the AS1 Shaft underlies the rail track slab on the western side of the cavern. The Kicker Beam, capping slab (and underlying AA6 ‘headwall’ lining), were required to act as a ‘bridge’ to support the track slab and associated live rail loads as well as a portion of the platform loads. In the final state, the internal shaft walls (designed by RBG) provided a degree of ‘propping’ to the shaft walls.

As a result of the construction sequence (as further discussed in Section 4), there were also several key construction cases loading the capping beam, shaft walls and Kicker Beam, including:

- Equipment loads on the cavern invert, adjacent to the shaft, creating lateral ground loads on the AS1 Shaft walls.
- A temporary steel deck, supported on the capping beam, that spanned the shaft and was required to support several construction load cases.
- The formwork for the cavern and AA7 intersection pour above the AS1 shaft was supported on the western side by the Kicker Beam, with this comprising the largest single pour in the mined tunnel packages.

4 PRIMARY AND PERMANENT SUPPORT

The construction sequence was complicated by the need to construct portions of the permanent tunnel lining structures as the shaft was being excavated (Figure 2).



(a) Blast shaft and partially excavate to construct capping beam.

(b) Excavate shaft, underpin capping beam then excavate and support adit AA2 and heading of AA6.

Figure 2. Abbreviated summary of shaft excavation sequence.

Due to the very high bedrock strength and that roadheader shaft excavation was impractical, the rock within the shaft was first blasted to permit excavation by hydraulic excavator.

The AS1 shaft was then excavated to a depth of a few metres to permit installation of the upper level of shaft waterproofing, followed by construction of the capping beam and cavern sidewall Kicker Beam. Excavation of the shaft continued, with the progressive installation of sidewall rock bolts and underpinning bolts beneath portions of the capping beam.

Once the excavation reached the invert level of adit AA2, the adit was excavated by drill and blast methods and primary support installed. The heading of AA6 was also excavated and supported prior to completion of the shaft excavation. Swinn *et al.* (2023) discusses challenges encountered during the excavation of AA2, and some damage caused to the overlying cavern invert slab that ultimately required remediation.

Due to critical program drivers for construction works occurring overhead in the mainline cavern, a temporary 100 tonne steel deck was erected across the shaft and supported by the capping beam and Kicker Beam. Construction of the AA6 adit permanent lining 'headwall' under the Kicker Beam span was also on the critical path, as it was required to withstand the largest load case associated with the formwork for pouring the overlying cavern permanent lining.

The shaft waterproofing was next installed and the permanent lining of the adits constructed, as well as shaft walls, headwalls, and internal shaft walls.

The shaft works were completed when the temporary deck was removed, capping slab constructed and contact grouting performed (see Section 4.2), precast station platform units installed, and track slab constructed.

4.1 *Excavation and primary support*

During cavern excavation and prior to blasting the AS1 Shaft, stitching of the approximately 5.7 m wide rock pillar located between the cavern and the Main Access Shaft was undertaken to improve the faulted rock bearing capacity. The stitch bolts comprised DN36 GEWI threadbars fitted with 300 x 300 x 50 mm anchors plates (Figure 1), prestressed to 500 kN prior to grouting. The stitch bolts were spaced at 1.2 m centres vertically, and between 1.2 m and 1.8 m horizontally.

Primary support for the shaft walls comprised 5.4 m long steel rock bolts spaced at 1.5 m centres with a thin shotcrete facing. Glass fibre reinforced polymer (GRP) rock dowels were available for the face support of the adits, however not required during excavation.

Underpinning of the capping beam was undertaken where the beam was required to resist substantial temporary construction loads. The underpinning bolts comprised 6 m long Dwyidag

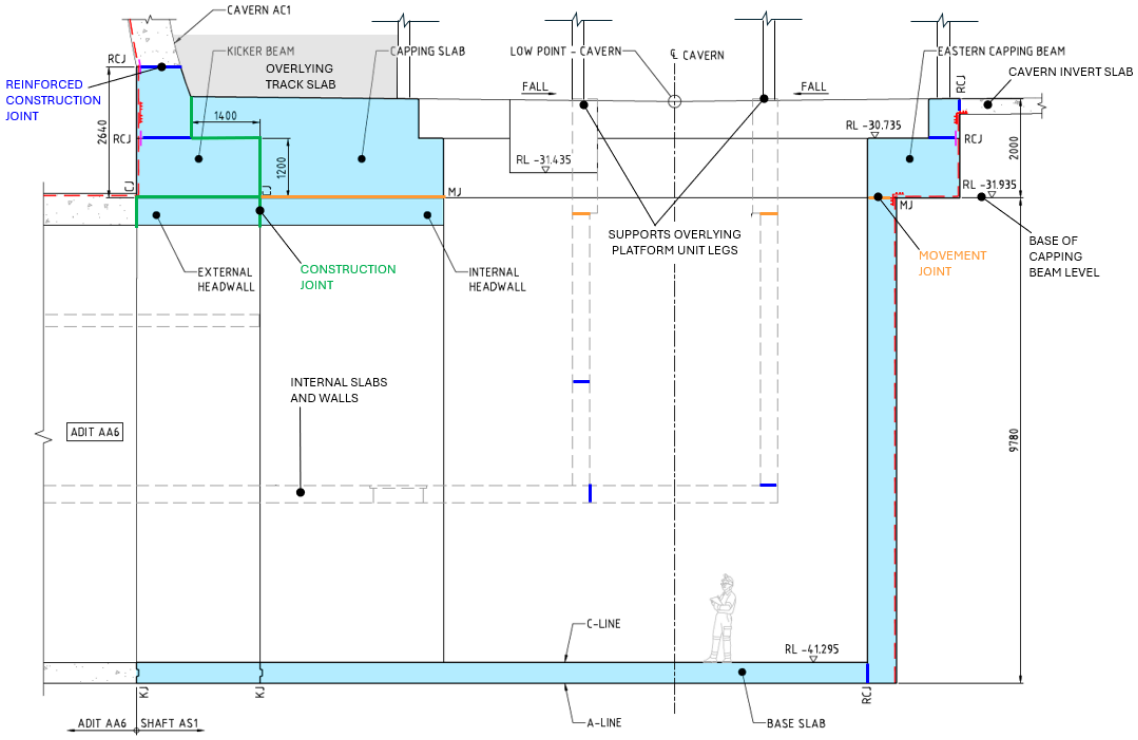


Figure 3. AS1 shaft permanent lining and movement joint locations.

WR36 threadbars with a 3 m free length and prestressed to 500 kN. An increased shotcrete thickness of 600 mm was adopted at the underpinned areas.

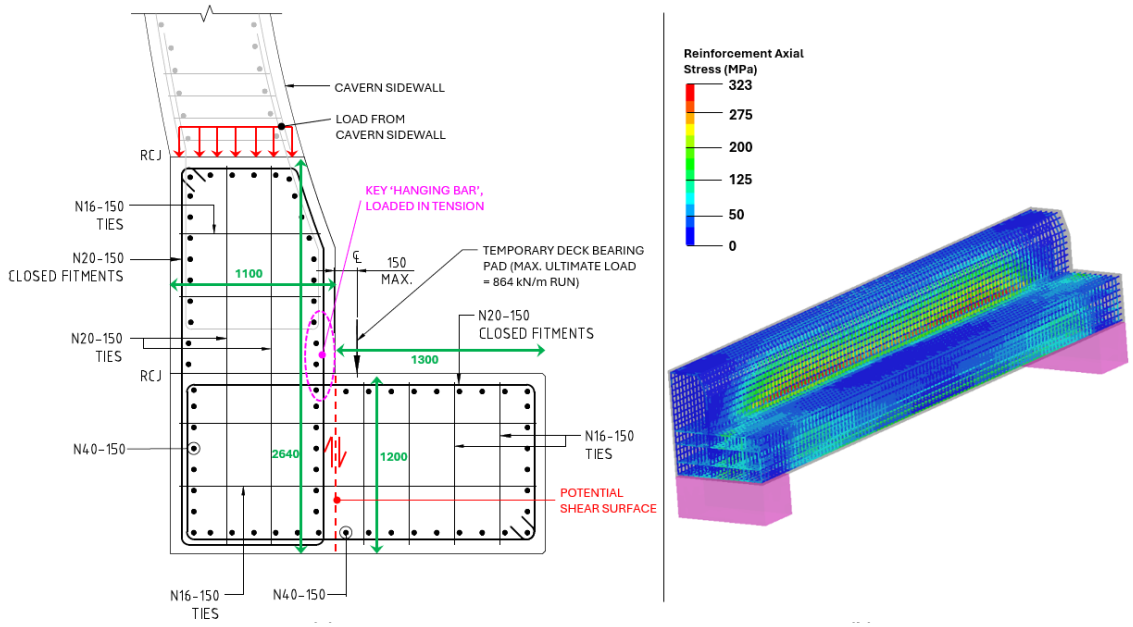
Primary support of the two adits leading from the shaft comprised a passive shotcrete lining with a design thickness of 400 mm.

4.2 *Permanent support*

The AS1 shaft walls were designed as 500 mm thick bar reinforced concrete with a characteristic compressive strength of 40 MPa. The capping and Kicker Beams have a thickness up to 2.4 m, partially to facilitate bearing pads for loading from the temporary steel deck during construction. The capping beams connected into the 300 mm thick cavern invert slab, which was a continuous slab along the length of the cavern with bar and steel fibre reinforcement. As shown in Figure 3, a reinforced concrete construction joint was utilised to connect the cavern invert slab to the capping beam. At the interface between the capping slab and the (north and south) capping beams, a series of ANCON DSD130 shear connectors were used to limit vertical and lateral (east/west) movements and help control deflections of the overlying structures and track slab.

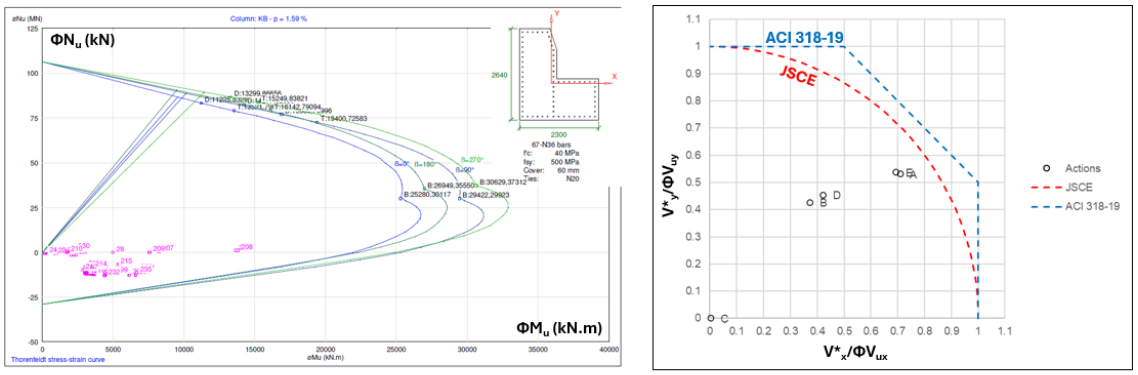
The construction of the permanent lining was highly sequenced, in line with the excavation and primary support sequence. The Kicker Beam and capping beams were constructed first, with the AS1 shaft walls and invert and capping slab constructed last, with a sequence of excavation stages in between. To help facilitate this sequence, a Movement Joint (MJ) was incorporated at the base of capping beam level (as shown in Figure 3), effectively separating the cavern invert and capping beam support system from the AS1 shaft walls and invert slab. A similar MJ was adopted in the internal shaft walls. A consequence of this was that the Kicker Beam and capping beam support and the AS1 shaft wall and invert support systems were designed to act independently.

In areas such as the Kicker Beam and the capping slab, the underlying ‘AA6 headwall’ ultimately provided additional support through an unreinforced construction joint interface. Given the requirement for the capping slab to support the overlying track slab, and be subjected to cyclical loading associated with the metro trains, a grid of grout tubes were installed through the capping slab to allow grouting of this joint interface following the critical initial concrete shrinkage stages to fill gaps that may have formed.



(a) geometry and reinforcement (b) flac3d analysis outputs.

Figure 4. Kicker beam geometry, reinforcement details and structural analysis.



(a) Bi-axial bending (b) Bi-axial shear.

Figure 5. Kicker beam analysis outputs

Following the completion of excavation, the waterproofing of the AS1 shaft was installed and connected to the waterproofing at the base of capping beam level (which had been installed prior to shaft excavation). Damage to the membrane at the base of capping beam level necessitated a remedial solution, as further discussed in Section 6.4. The AA6 headwalls were then constructed, followed by the shaft invert slab and the shaft external and internal walls, constructed in a series of bottom up jump form lifts. The capping slab was then constructed as a final 'puddle pour'.

4.3 *Other design interfaces*

The design of the internal shaft walls and slabs were undertaken by RBG, with the 50 MPa characteristic compressive strength internal structures connected to the external shaft walls, invert slab and capping beams via reinforced constructed joints. The internal structures consequentially provided a degree of 'propping' to the shaft and load transfer between the external permanent lining and internal structures. This degree of interaction was highly complex and was managed by both designers by developing and utilising a shared Strand7 structural design model to estimate design actions. For the design of the external walls, bookend scenarios for the stiffness of the internal

walls (i.e. ‘pre’ and ‘post’ creep, estimated as 41.8 GPa and 13.9 GPa respectively) were accounted for to understand the potential range of load transfer under the spectrum of conditions that could occur over the design life of the structure.

5 KICKER BEAM

The Kicker Beam is a critical structure within the AS1 Shaft permanent lining, effectively acting as the foundation to the overlying cavern arch lining and part of the permanent support for the track slab. The range of load cases (including several critical temporary construction load cases), geometry of the Kicker Beam and variation in the surrounding support during construction resulted in a number of design and construction challenges.

5.1 *Design approach*

The design approach of the Kicker Beam needed to account for several key stages. During the excavation of the AS1 shaft, the Kicker Beam effectively acted as a ‘bridge’, spanning across the length of the shaft, and the temporary steel deck loading the ‘lower flange’ as a ‘corbel’ via a bearing pad. During this stage, the Kicker Beam was essentially ‘simply supported’ at the northern and southern abutments.

At later stages, the Kicker Beam became supported along its length by the underlying AA6 headwalls, and was subjected to loads from the capping beam, track slab (and trains) as well as long term ground loads associated with the cavern crown (transferred via the cavern sidewall) and lateral load applied by the ‘rock pillar’ between the cavern sidewall and the Main Access Shaft.

The differing loading combinations and support combinations resulted in numerous potential failure mechanisms and combinations of design actions. Two main design approaches were utilised to inform the design, namely:

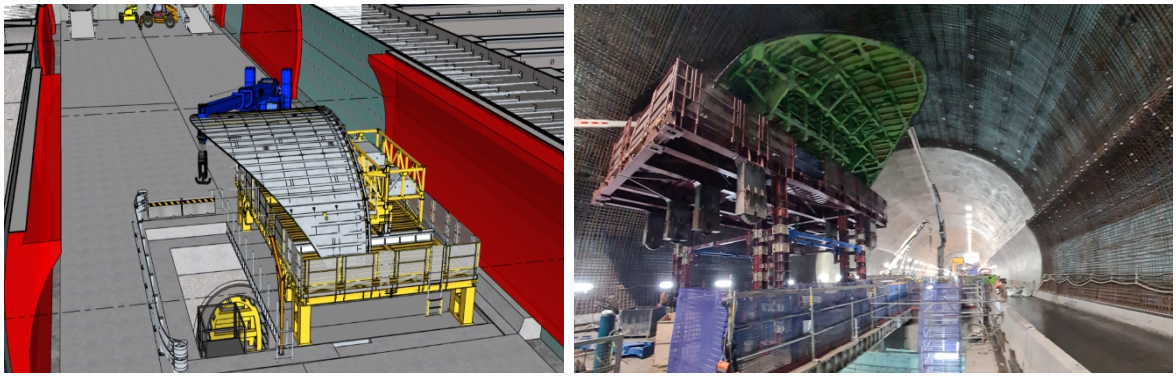
- Linear-elastic analysis for key cross-sections along the Kicker Beam, with calculated actions extracted from the Strand7 structural model
- Non-linear elastic analysis, complying with AS5100.5 Clause 2.3.6, undertaken with FLAC3D for critical load cases, with reinforcing bars discretely modelled.

Discussion of the above two approaches is outlined for the critical temporary construction load case, where the Kicker Beam was acting as a ‘bridge’, the temporary deck was supported by the lower flange and was carrying loads associated with the overlying cavern form, resulting in a total ultimate load of 864 kN/m run on the Kicker Beam.

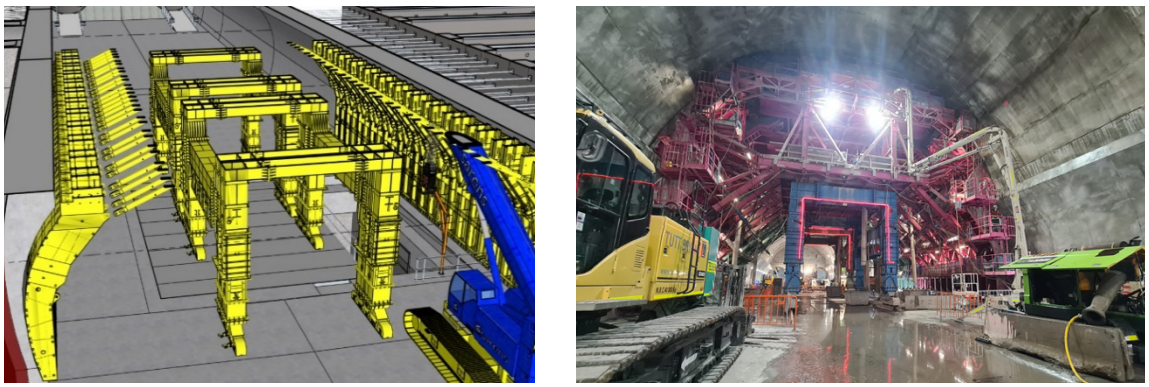
As shown in Figure 4(a), this generated potential mechanisms for bearing failure (where the bearing pad rested on the flange), shear failure of the flange from the web, generation of bi-axial bending forces and loading of the web intrados bar as ‘hanging reinforcement’ with significant tensile stresses. Local bearing failure was assessed using Clause 2.3.3 of AS5100.5, whilst the flange shear failure was assessed using a shear-friction capacity assessment, in line with Clause 8.4.3 of AS5100.5. The reinforcement design was assessed via a strut-and-tie check for the ‘hanging bar’, as well as by elastic analysis.

Within the Strand7 model, the Kicker Beam was modelled using plate elements, and equivalent beam actions were calculated at five cross-sections along the Kicker Beam. The eccentricity of the bearing pad, asymmetrical cross-section and support conditions resulted in significant bi-axial bending and shear actions being generated. Bi-axial bending capacity was assessed in line with AS5100.5 Clause 10.6.4 (as shown in Figure 5(a)) along with beam clauses for the combined effects of uniaxial shear and torsion. However, for bi-axial shear, as no methods were outlined within AS5100.5, interaction diagrams from ACI 318-19 Clause 22.5.1.10 and 11, and JSCE guidelines (2007) Clause C9.2.1 were utilised for the section checks (as shown in Figure 5(b)).

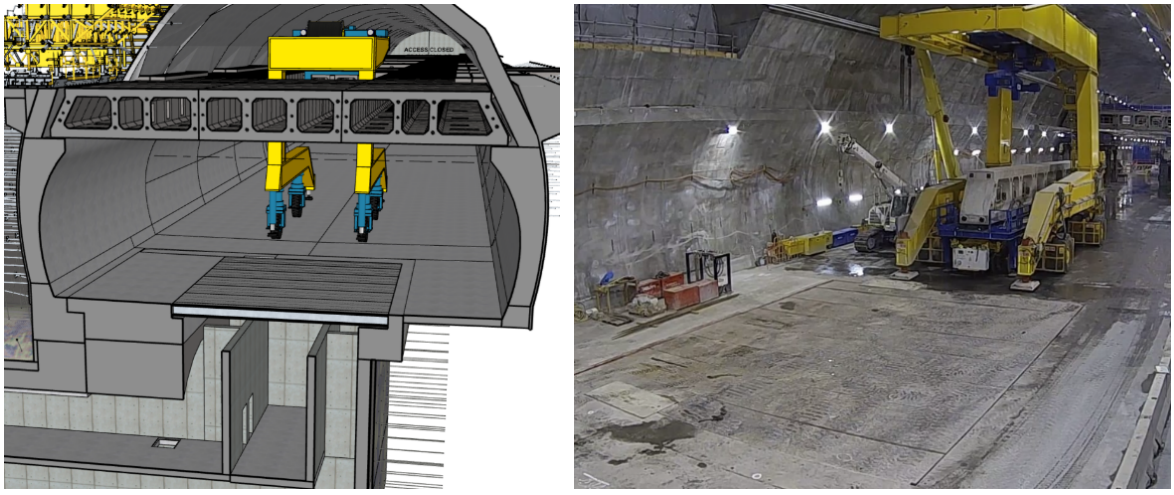
Following initial sizing of the reinforcement by the above approaches, a 3D model of the design reinforcement was created within the software package FLAC3D in combination with a constitutive concrete model to undertake non-linear elastic analysis. An example of the estimated bar stresses is shown in Figure 4(b). The method was undertaken consistent with the approach outlined in Tran *et al.* (2025), with results providing validation of the design.



(a) Upper Adit AA7 Stampella formwork



(b) Permanent Cavern Lining formwork system over the AS1 shaft



(c) Mezzanine loader traversing the AS1 shaft

Figure 6. Selected examples of stages required for the AS1 platform deck installation.

For the Serviceability Limit State (SLS) crack width estimation, section analysis was undertaken using the *RC Column* program, which implements the crack width estimation method outlined in AS3600 (2018). Due to the parameter differences, for typical sections and conditions, crack widths estimated via EN1992-1-1 (as required by the PSTR) typically estimate a crack-width 15% larger than those estimated via AS3600. Consequently, to allow for this, the 0.3 mm crack width limit was reduced to 0.26 mm when comparing against the *RC Column* outputs. Further crack width validation was provided by comparing SLS steel bar stresses against the maximum steel stress limit of 280 MPa, given in Table 8.6.1(B) of AS5100.5.

An SLS deflection limit of 1/640 of the span was adopted, in line with AS5100.2 Clause 9.10. The resulting final reinforcement configuration is shown in Figure 4(a).

5.2 *Temporary construction load cases*

The AS1 temporary steel deck was critical to de-couple critical path activities in the mainline cavern from the permanent lining activities in the AS1 shaft and adits below. The steel deck was designed and manufactured to be utilised in different positions over the shaft, moving from east to west multiple times (Figure 6), to facilitate mainline cavern works. These activities included:

- Working at heights access to waterproof the mainline cavern, and steel fixing cavern lining.
- Stampella formwork for the upper AA7 adit (Figure 6(a)).
- Ability to traverse the two (2) rolling TFI cavern formwork systems across the shaft under dynamic loading through the rails placed on the cavern invert (Figure 6(b)).
- Formwork and concrete loadings for the mainline cavern arch pour.
- Mezzanine loader for both traverse and static installation setups (Figure 6(c)).

The temporary load cases varied for 22 different construction scenarios, all being transferred through the main steel deck centre beam to a bearing plate on the east and western (i.e. Kicker) beams. These loads on the deck ranged from 682 kN point loads from the mezzanine loader, to 270 kPa track loads from a crawler crane. Careful permit systems and signage were implemented to manage loads and stacked activities on the platform deck during construction.

6 OTHER KEY DESIGN AND CONSTRUCTION CHALLENGES

6.1 *Capping slab*

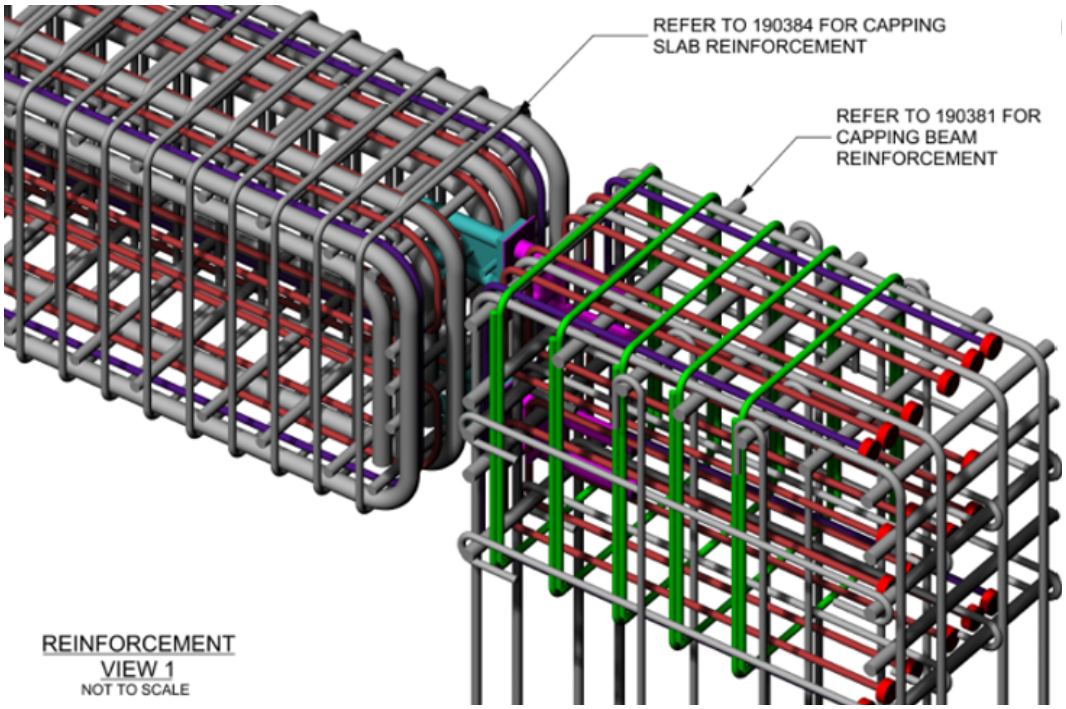
The capping slab is supported by the Kicker Beam flange on the western side and otherwise sits on the AA6 headwall, with the track slab constructed on top. Shear dowels were installed between the capping beam and capping slab to minimise differential displacements between the two structures for the overlying internal structures. As the capping slab supports the rail track, it is subject to cyclic rail loading and was designed for fatigue as per AS5100.2 and AS5100.5.

The design of the 2 m thick capping slab incorporates zones with closed shear ligatures (required to resist torsional actions) as well as shear ligatures cogged at each end. An acceptable alternative detail to closed shear ligatures from ACI 318-19 Figure R9.7.7.1 was utilised in some locations to aid constructability.

The overlying track slab supports the rail tracks, which have a ±5 mm maintenance tolerance for both horizontal and vertical directions. Partly due to the restriction from the PSTR that the rock anchors in the rock pillar between the Main Access Shaft and the cavern sidewall could not be relied upon, there was the potential for horizontal ground loads to develop against the extrados of the cavern sidewall. To help mitigate this, a 30 mm to 40 mm layer of Class L / SL Polystyrene (EPS) to AS1366.3 (1992) was installed at the vertical interface between the Kicker Beam / cavern sidewall and the track slab, allowing horizontal movement of the cavern sidewall in response to the ground load prior to loading the track slab.



Figure 7. Kicker and capping beam assembled reinforcement



(a) Reinforcement 3D model

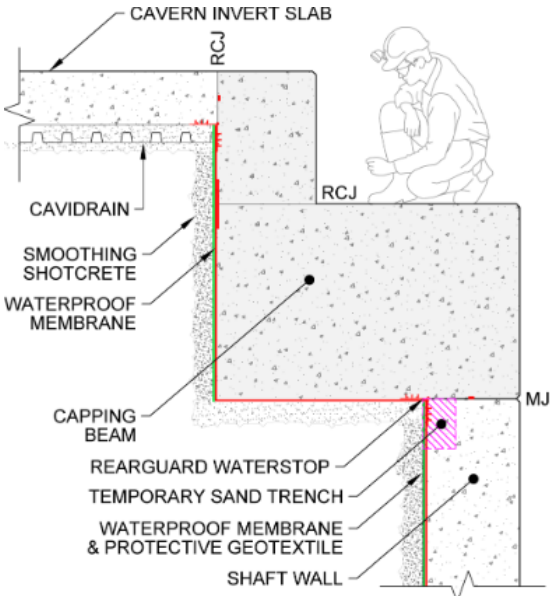


Figure 8. Capping Beam reinforcement details.

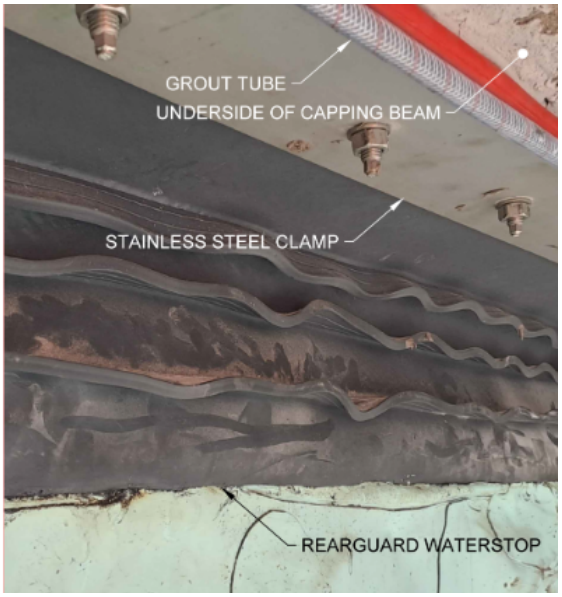
6.2 *Steel-fixing construction challenges*

Due to the depth and geometry of the large Kicker Beam, and the large diameter bars inducing longer lap lengths, the steel-fixing required careful planning to successfully schedule and assemble the reinforcement in line with the design requirements. The steel reinforcing cages for the corners were prefabricated, weighing approximately 6 tonnes each, and landed into the waterproofed excavation.

As the capping beam and Kicker Beam was a single sided form (i.e. cast against the primary lining) access was only available from the front face (Figure 7), further emphasising the need for planning and progressive inspections.



(a) Sand trenches and sawcut protection



(b) Remedial rearguard waterstop

Figure 9. AS1 Waterproofing

6.3 *Capping beam reinforcement congestion*

Sixteen ANCON DSD130 shear dowels were installed at the interface between the northern and southern capping beams and the capping slab. The required shear dowel local reinforcement and the capping beam web upstand geometry resulted in significant reinforcement congestion.

During the design phase, this was managed by discussing opportunities with ANCON to utilise some of the capping slab global reinforcement as part of the required local reinforcement (where possible), as well as developing a detailed 3D model of the reinforcement to identify clashes.

For some of the local reinforcement, shown in red and purple in Figure 8(a), there was insufficient length in the capping beam upstand to provide an effective development length, or sufficient space to cog the bars. Shear studs were utilised for these bars to provide adequate anchorage.

Despite the 3D clash detection model an additional reinforcement congestion issue was encountered during construction. The cavern invert slab longitudinal bars required anchorage (via an L-bar attached to a coupler) within the capping beam upstand. As the cavern invert slab was constructed ahead of the capping beam, the coupler positions for the L-bars where effectively set, and in several areas created complications for the installation of the shear dowels and associated capping beam reinforcement. To overcome the clashes in these areas and provide gaps between the bars for concrete placement and access for probe vibrators, a few of the cavern invert L-bars where cut and welded to adjacent bars as a welded splice (still providing development length), but improving steel congestion.

Figure 8(b) shows the final reinforcement positions in the capping beam upstand prior to pouring. Despite the dense reinforcement, the capping beam was successfully poured, which would have been extremely difficult without the clash detection modelling during design.

6.4 *Waterproofing*

As part of the MJ detail at the base of the capping beam, an allowance for vertical movement was required for the waterproofing, with half of the rearguard waterstop at the MJ required to be cast into the base of the capping beam at the initial excavation stage, 18 months prior to the other half being cast into the rear face of the shaft walls. This required significant efforts to protect the membrane and waterstop during the various construction activities.

The protection method involved excavating a trench to cast half of the rearguard waterstop into the capping beam initially and protect the membrane within a temporary sand trench during the concrete pour (Figure 9(a)). Once shaft excavation began, the rearguard was ‘released’ from the sand and suspended under the capping beam overhang until ultimately being cast in the wall pour.

Despite the efforts some sections of the rearguard were damaged during the excavation of the remainder of the shaft, with the waterproofing subcontractor performing repairs where possible. In some areas, an extra remedial solution was required to provide an acceptable waterproofing solution for the 100 year design life, which incorporated a fresh rearguard waterstop to be cast into the shaft walls, which was then pinned to the underside of the capping beam via a clamping detail (M12 stainless fasteners at 200 mm spacing) and welded onto the remaining waterproofing under the capping beam, a re-injectable grout tube was also included to add additional redundancy and accommodate the expected joint movement range (Figure 9(b)).

7 CONCLUSIONS

The AS1 Shaft is a complex structure, which provided numerous design and construction challenges. These challenges included construction sequencing, impacts of temporary loads, ground loads and interactions with the nearby Main Access Shaft, impacts from cyclical train loads, waterproofing and components of the shaft designed by different designers.

A suite of design stage and construction phase measures were implemented to manage risks associated with the above challenges. These measures included utilising movement joints to facilitate the construction sequence, protection of earlier constructed elements against impacts from the subsequent excavation of the shaft, sensitivity testing at the time of the design to de-risk Main Access Shaft construction timeline interactions, detailed clash detection modelling of

congested reinforcement areas, use of a shared structural analysis model between designers and detailed assessment of ground loads.

Despite the numerous challenges, the AS1 Shaft was successfully constructed.

8 ACKNOWLEDGEMENTS

The authors would like to acknowledge the Pulse consortium together with CPB Contractors, BAM International Australia, Ghella and UGL Joint Venture for granting permission to publish this paper. The authors also wish to express their appreciation of the professionalism and technical expertise provided by colleagues at PSM in the development of a practical design solution and the CBGU construction team for implementing the complex design to a high standard.

9 REFERENCES

American Concrete Institute. 2019. Building Code Requirements for Structural Concrete (ACI 318-19), Commentary on Building Code Requirements for Structural Concrete (ACI 318R-19).

Cammack, R., Bertuzzi, R., Smith, A. and Brehaut, R. 2022. Rock Mass Parameters for the Brisbane CBD. *Australian Geomechanics*, Vol. 57: No. 4, pp. 47 – 72.

European Standard. 2004. Eurocode 2: Design of concrete structures – Part 1-1: General rules and rules for buildings.

Japan Society of Civil Engineers. 2007. JSCE Guidelines for Concrete No. 15, Standard Specifications for Concrete Structures – 2007 "Design".

Standards Australia. 2018. AS 3600 – Concrete Structures.

Standards Australia. 2017. AS 5100 – Bridge Design.

Swinn, B., Osterman, R., Alt, D., McNicol, J. and Zappelli, L. 2023. Cross River Rail – Blasting AA2 Tunnel under Cavern. Proceedings of the 18th Australasian Tunnelling Conference, Auckland, New Zealand.

Tran, D., Clarke, S. and Afshar, P. 2025. Numerical analysis and design of complex bar reinforced concrete tunnel structures with FLAC3D. Proceedings of the 32nd Biennial Concrete Institute of Australia national conference, Adelaide.

THIS PAGE INTENTIONALLY LEFT BLANK

19th Australasian Tunnelling Conference – Acosta-Martínez, Stewart and Hudson-Smith (Eds.)
© 2025 Australian Tunnelling Society, ISBN 978-0-85825-002-4

Design and construction challenges for the TBM traverse through Brisbane's partially excavated Albert Street Station cavern

M.A. Habte, A.G. Smith, S.J. Clarke
PSM, Sydney, Australia

ABSTRACT: Albert Street Station is one of four underground stations currently under construction as part of Brisbane's Cross River Rail project. The station comprises an underground cavern, entry shafts and a series of adits connecting the entry shafts with the cavern.

The original cavern construction sequence included excavation of the cavern prior to receiving the Tunnel Boring Machines (TBMs) used to excavate the running tunnels. Due to favourable excavation conditions for the TBMs and delays to cavern construction, the TBMs arrived prior to commencement of the cavern bench excavation. Since halting the TBM operation had significant cost and scheduling implications, the construction team opted to continue TBM excavation through the partially excavated cavern.

This paper presents design and construction approaches to address the impact of this changed approach to the stability of the already constructed adits, cavern sidewalls and rock pillar between the cavern and shaft.

These measures resulted in a successful traverse of TBM through the cavern and significant savings to construction time and cost.

1 INTRODUCTION

Cross River Rail (CRR) is a new 10.2 km long metro rail line in Brisbane between Dutton Park in the south and Bowen Hills to the north, which includes 5.9 km long twin tunnels that pass under the Brisbane River and the CBD. A joint venture of CPB Contractors, BAM International Australia, Ghella and UGL (CBGU JV) is building the tunnels.

The Pulse consortium (including the CBGU JV) was awarded the contract to design and construct the Tunnel and Station Development (TSD) works which includes construction of twin Tunnel Boring Machine (TBM) excavated running tunnels and mined running tunnels; four new underground stations at Boggo Road, Woolloongabba, Albert Street and Roma Street; and dive structures at each end of the running tunnels.

Albert Street Station is the central station on the CRR alignment and is connected by twin TBM tunnels to Woolloongabba Station to the south and Roma Street Station to the north. Significant infrastructure including essential utilities and high-rise buildings with deep basements are located within close proximity to the station excavations.

The underground excavations for the station include a 290 m long cavern, two entry shafts, a construction access shaft, seven pedestrian/service/egress adits, an internal services shaft and two temporary access adits (Figure 1).

Five of the seven pedestrian/service/egress adits connect from the two entry shafts into the station cavern at mezzanine level, whereas the other two adits connect the main entry shaft with the cavern via an internal service shaft excavated below the cavern invert (Rogan et al, 2025)

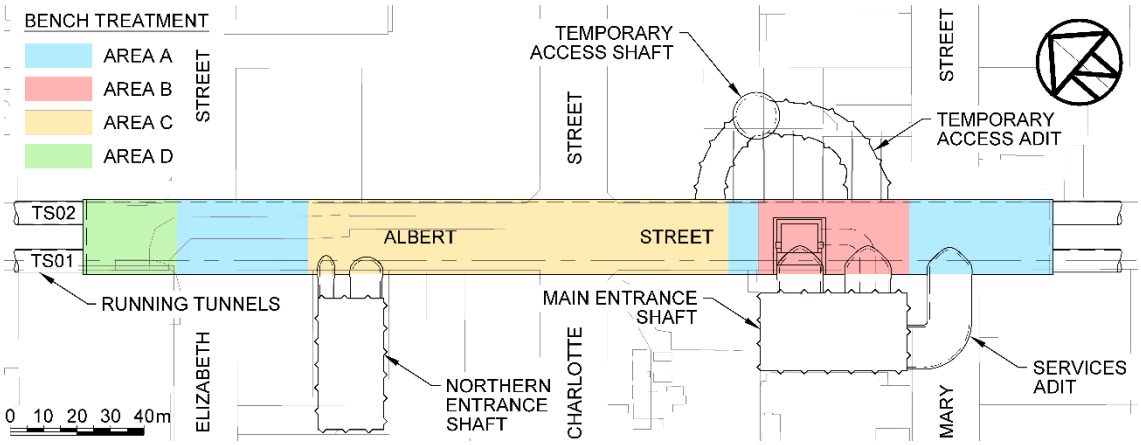


Figure 1. Albert Street Station configuration (Area A to Area D refer to the bench treatment excavation sequence zones discussed in Section 5 and Section 6).

The excavated span of the cavern is up to 25 m with an excavated height of up to 17 m. The excavated spans of the adits range from 5 m to 14 m and their excavated heights range from 5 m to 10 m. The Main Entrance shaft which provides the main vertical transport access for the station is about 24 m wide and 44 m long with a depth of up to 50 m.

The station is in a highly developed urban environment with a significant number of adjacent multi-storey structures resulting in relatively tight movement tolerances.

2 GROUND CONDITIONS

The ground conditions at Albert Street Station comprise fill, alluvium and residual soils underlain by bedrock of the Neranleigh Fernvale Group (NFG). The total depth from the ground surface to top of the station cavern ranges from 18 m to 21 m. Thickness of competent rock cover above the cavern crown is about 6 m to 14 m.

The NFG comprises weakly metamorphosed sandstone (meta-greywacke and arenite), phyllite and subordinate quartzite and meta-basalt. Meta-greywacke and arenite are typically high strength, while phyllite (metamorphosed mud rocks or argillite) is typically weaker. The NFG rock mass is sub divided into five classes based on rock mass quality, with Class 1 (i.e. NFG1) being the most competent and Class 5 (i.e. NFG5) being the poorest quality (Cammack et al, 2022).

Borehole data in the vicinity of the station shows strongly developed foliation and fabric with a series of moderately dipping fault zones (dipping approximately 50° towards the north-east). In addition, a low-angle contact fault dipping into the cavern was encountered within the rock pillar separating the cavern from the main entry shaft.

The ground level at Albert Street is at approximately RL 4 m and previously comprised swampy terrain. The interpreted groundwater levels prior to tunnelling varied between RL -5 m and RL -9 m.

3 CONSTRUCTION SEQUENCE

The Albert Street cavern excavation commenced from a breakout chamber located at the intersection of the cavern with the temporary access adit on the northern side of the construction access shaft. Once the breakout chamber was completed, excavation of the top heading of the cavern progressed to the north and south using a staggered three heading sequence comprising two side drifts and a central pillar.

A staggered two heading sequence was also adopted in favourable ground conditions with bolted support. The excavation of the station cavern and adits was carried out predominately using

road headers with some adits excavated by drill and blast methods. Section 6 describes the cavern bench excavation sequence undertaken with drill and blast methods.



Figure 2. Breakthrough into the segmental lining showing the nominal cover over the crown (16 December, 2021)

The primary (temporary) support for the cavern and adits typically comprises rock bolts and thin shotcrete or a passive thick shotcrete lining at intersections and/or where low rock cover or fault disturbed ground occurs.

The construction sequence for the bolted support was essentially cut, bolt, and spray shotcrete.

The sequence for the passive shotcrete lining adopted the same sequence as the bolted support types for the initial side headings but with full thickness of the passive shotcrete lining constructed in the two side headings prior to excavation of the central heading. The full span passive shotcrete lining was completed as excavation of the central heading was advanced. Structural continuity of the passive shotcrete lining was achieved using a 'Stremaform' sacrificial formwork detail in the longitudinal construction joint between the side headings and the central heading. The 'Stremaform' formwork system implemented in the Albert Street Station cavern is similar to the system described in Shen et al (2022) for the Roma Street station cavern lining.

The adit excavations were generally undertaken as full span headings, and where required, bench excavation was undertaken.

4 TBM TRAVERSE

The original construction program for the TBM traverse through the station was based on sliding the TBM along skids erected on the invert of the fully excavated cavern. However, the excavation rate for the top heading of the cavern was much slower than anticipated due to the extremely high strength massive Metagreywacke rock encountered in the northern section of the cavern (Keating and Swinn, 2023).

Due to favourable excavation conditions for the TBM and the delayed cavern excavation, the TBMs arrived at the station before commencement of the cavern bench excavation.

The two program sequencing options considered by the construction team were either to delay the TBM traverse until completion of the cavern bench or else facilitate TBM tunnelling through the cavern bench and complete the cavern excavation after the TBM traverse.

Since halting the TBM operation until completion of the cavern excavation had significant cost and scheduling implications, the construction team chose to continue TBM tunnelling through the partially excavated cavern (Keating and Swinn, 2023).

The first TBM (TS01) arrived at the southern end of the cavern in the second week of June 2021 and continued traversing towards the northern end while the second TBM (TS02) arrived at in the first week of July 2021. Both TBM's required about four weeks to traverse the length of the cavern.

Survey of the floor levels in the excavated top heading indicated the thickness of rock between the heading floor and top of the TBM segmental lining ranged from about 0.3 m in the northern section to about 0.5 m in the southern section (Figure 2). Rock cover was absent in the central section and the segments were exposed to a depth of up to 0.4 m.

Construction plant exclusion zones were set-up directly above the TBM tunnels due to the minimal rock cover. Operation of construction plant was allowed within the exclusion zone by placing additional backfill material above the segmental linings. The required thickness of backfill material ranged from 0.3 m for general construction plant up to 1.5 m for road headers.

Because the segmental lining within the cavern was only required temporarily, CBGU were able to use segments that were structurally adequate but unsuited for use within the permanent tunnel linings, such as due to minor damage or imperfections.

5 SIDEWALL SUPPORT

5.1 *Sidewall underpinning*

The proposed bench excavation methodology involved blasting over the full depth of the central bench and invert. This resulted in a reduction of the available lateral support to the cavern sidewall due to the loss of confinement provided by the insitu rock and the presence of the excavated TBM tunnels. This mechanism had the potential to compromise the stability of the elephants footing of the passive shotcrete arch lining and also the stability of the narrow rock pillar between the cavern and main entrance shaft.

The risk of deformation or instability to the elephant's footing was addressed by underpinning the footing with additional sidewall bolts installed from the top heading prior to blasting of the central bench. The underpinning sidewall bolts for bench treatment Area C and Area D (Figure 4a) comprised 3 m long rock bolts installed at a nominal inclination of 10° below horizontal and at a longitudinal spacing of 1.5 m, while a reduced spacing of 1.0 m was implemented within bench treatment Area B.

Temporary underpinning bolts were also installed within the rock pillar zone for bench treatment Area B. The temporary underpinning installed on the shaft side of Area B comprises pairs of 40 mm diameter glass-fibre reinforced polymer (GRP) bolts installed at a nominal inclination of 20° to 30° and a longitudinal spacing of 1.2 m.

5.2 *Rock pillar stitching*

One of the design challenges for the TBM traverse through the cavern bench was the potential for excessive ground loads acting on the TBM tunnel segmental lining due to a large-scale rock wedge formed by the contact fault encountered in the rock pillar between the cavern and the main entry shaft excavation. The risk of instability due to the wedge was minimised by installing pillar stich bolts from the already excavated main entry shaft (Figure 3).

The pillar stitch bolts comprise 36 mm diameter high strength threaded GEWI bars installed in 100 mm diameter holes with bolt heads secured using 220 mm wide square anchor plates and dome nuts. The stich bolts were sleeved to provide a 3 m free length while the remaining portion of the stich bolts was grouted to in the bond zone. The net bonded length for the stich bolts installed from the shaft ranged from about 2.7 m to 4.6 m. The pillar stitch bolts were pre-stressed

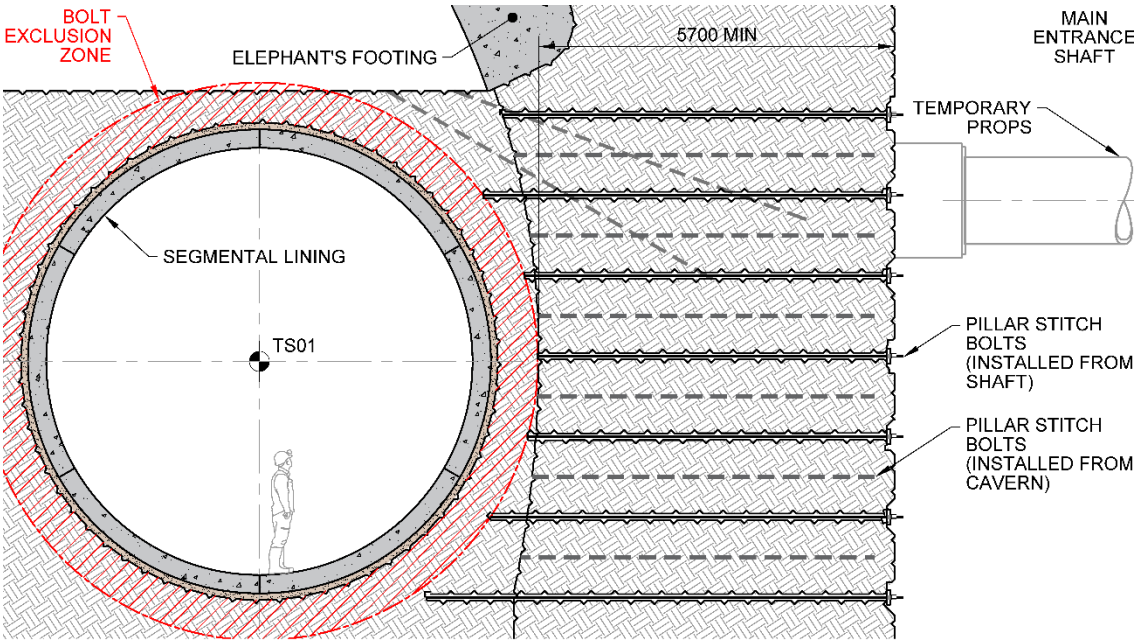


Figure 3. Details of pillar stitch bolts.

to a nominal load of 500 kN to increase the strength of the rock pillar and reduce potential deformation by providing lateral confinement. Complete confinement of the rock pillar between the cavern and the main entry shaft was achieved by installing additional stich bolts of the same specification from the cavern side during cavern bench excavation (Figures 3 and 5b).

5.3 *Shaft temporary props*

The design incorporated a total of 12 large props installed in two rows within the main entry shaft for the purposes of limiting deformation and providing support particularly on the cavern side of the shaft. Six props were installed at cavern crown level and six props were installed near the top level of the cavern bench. The props were installed prior to the TBM traverse and were manually adjusted with hydraulic jacks to provide the required compressive pre-load and limit deformations. The prop loads were controlled with a minimum loading of 10 MN but also a maximum load limit of 15 MN to prevent the props inducing load and deformation into the TBM excavation and cavern during the various excavation and support stages.

6 BENCH AND INVERT EXCAVATION

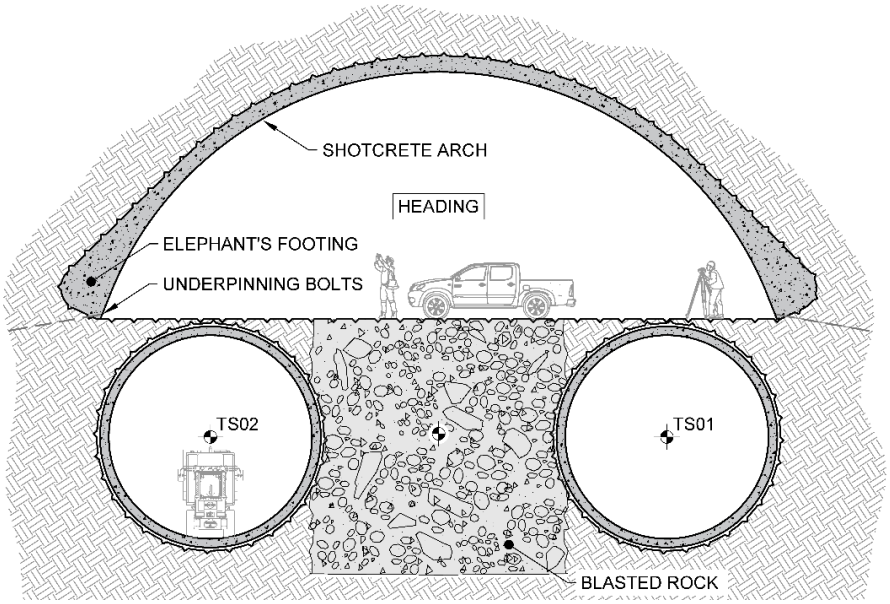
6.1 *Bench treatment zones*

Excavation of the cavern bench and invert was undertaken after completion of the TBM traverse. The original bench excavation sequence was to excavate full width benches while leaving a 1.5 m minimum width temporary buttress immediately beneath the elephant's footing. The buttress was to be excavated in 4 m to 6 m advances and 1 m to 1.5 m lifts with sidewall support installed at each excavation lift.

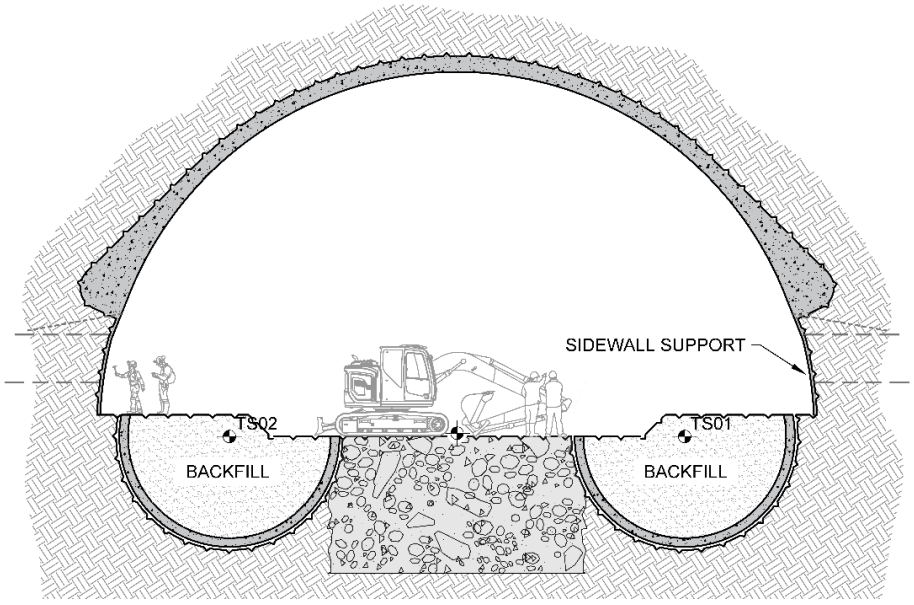
The adopted method of excavation for the changed sequence involved blasting of the central bench between the two TBM tunnels followed by demolition of TBM lining, then trimming of sidewalls and installation of sidewall support.

The bench excavation sequence was grouped into four treatment areas (Figure 1), mainly governed by the cavern sidewall support constraints:

– Area A: Bolted support was implemented in the cavern crown and additional bench treatment was not required.



(a) Blasting over the full depth of bench and invert.



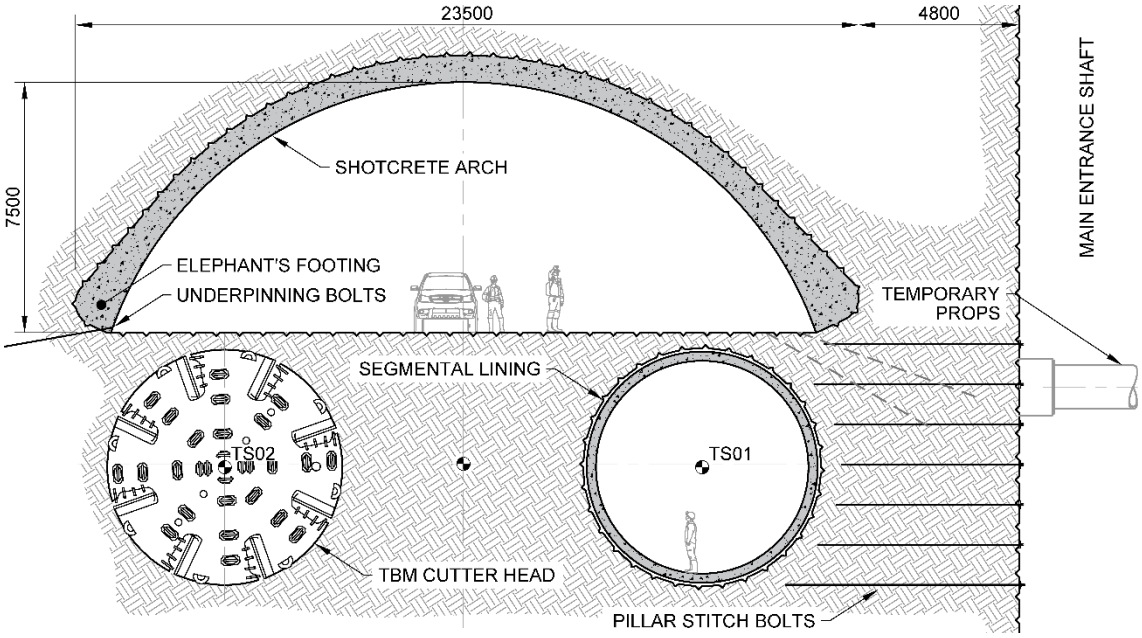
(b) Backfilling of TBM tunnels and installation of sidewall support.

Figure 4. Bench and invert excavation sequence for Areas A, C and D

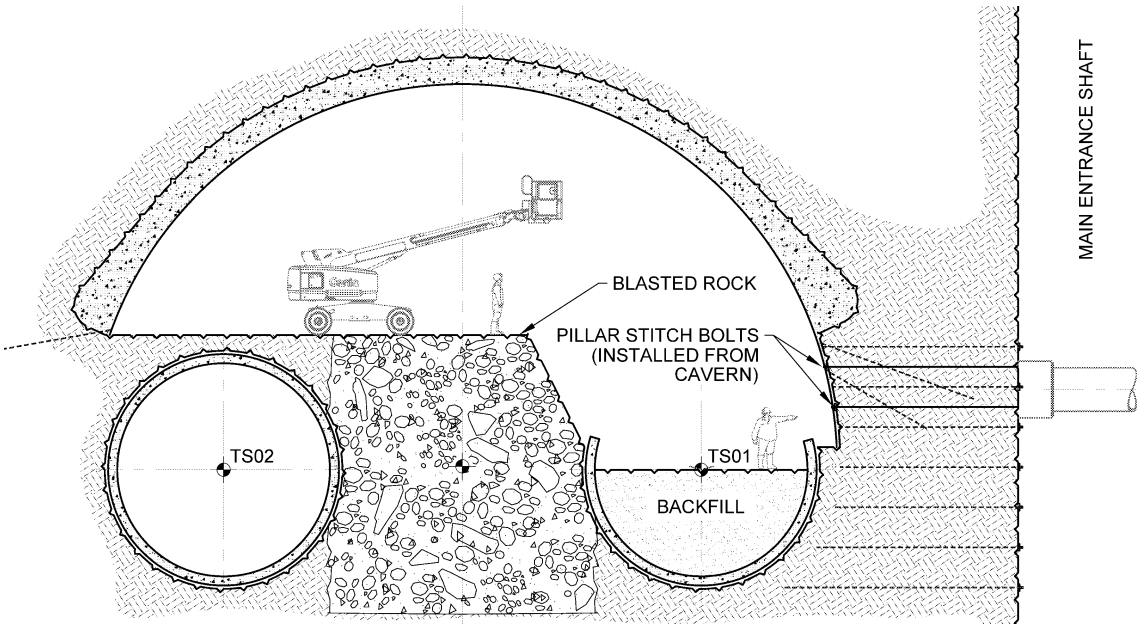
- Area B: Adjacent to the main entry shaft where a passive shotcrete arch lining was constructed to support the cavern crown. This area was the most critical due to the requirement to install pillar stich bolts progressively prior to completion of the bench excavation.
- Area C: Passive shotcrete arch lining was installed in the cavern crown and additional sidewall bolts were required to underpin the elephant's footing.
- Area D: Northern end of the cavern where the cavern top heading was not excavated prior to the TBM traverse. Passive shotcrete arch lining was installed and additional sidewall bolts were required to underpin the elephant's footing . The elephant's footing was constructed at a raised level to provide a minimum rock cover of 1.5 m above the TBM segmental lining.

The bench excavation sequence adopted in bench treatment Area A, Area C and Area D included (Figure 4):

- Blast the full height of bench and invert (Figure 4a).
- Demolish top segments in both TBM tunnels.
- Backfill both TBM tunnels to create a working platform (Figure 4b).



(a) TBM traverse through bench of cavern.



(b) Blasting of rock between tunnels and installation of pillar stitch bolts.

Figure 5. Bench and invert excavation sequence adjacent to the main entry shaft (Area B).

- Trim the sidewall in 1.5 m lifts and install sidewall support (Figure 4b).
- Demolish the remaining TBM lining and complete invert excavation, trim the sidewalls and install support at each lift.

6.2 *Modified sequence*

Controlling the risk of pillar instability in Area B required the installation of pillar stich bolts from the cavern bench side prior to blasting the bench (Section 5.2). The adopted construction sequence for the excavation of the cavern bench and invert in this area included (Figure 5):

- Demolish top segments in TBM tunnel TS01.
- Backfill TBM tunnel TS01 tunnel to create a working platform (Figure 5b).
- Trim the sidewall in 1.2 m lifts and install pillar stich bolts from the cavern side (Figure 5b).

- Continue to demolish TBM rings, trim sidewalls and install stitch bolts in 1.2 m increments down to the TBM springline level (Figure 5b).
- Blast the full height of the central bench and invert (Figure 5b).
- Demolish top of the segmental lining in TBM tunnel TS02.
- Partially backfill TBM tunnel TS02 tunnel to create a working platform.
- Trim sidewall in 1.0 m lifts and instal sidewall support
- Demolish the remaining TBM lining and complete invert excavation, trim the sidewalls and install support at each lift.

7 CONCLUSIONS

Construction of Brisbane's Cross River Rail project encountered a critical construction program challenge due to early arrival of the tunnel boring machines prior to the completion of the excavation of the Albert Street station cavern.

Cost and program implications from this unforeseen scenario necessitated the TBMs to traverse through the partially excavated cavern. As a result, it was necessary to develop an alternative approach for the excavation of the cavern bench and invert.

The adopted approach involved underpinning the elephant footing, TBM tunnelling through the cavern bench, drill and blast excavation of the central bench, demolition of the TBM tunnel segmental lining, installation of pillar stich bolts, staged trimming of the cavern sidewalls and installation of sidewall support.

Potential risks of deformation and instability of the cavern, adits and main entry shaft due to the changed construction sequence were managed via a coordinated effort between the designers of the cavern primary lining, cavern construction team, main entry shaft construction team, designers of the entry shafts, and designers of the TBM segmental lining.

The adopted design approaches and construction methodology resulted in a successful traverse of the TBM through the cavern with deformations well within acceptable margins and resulted in significant savings to construction time and cost.

ACKNOWLEDGEMENTS

The authors would like to acknowledge the Pulse consortium together with CPB Contractors, BAM International Australia, Ghella and UGL (CBGU) Joint Venture for granting permission to publish this paper.

The authors also wish to express their appreciation of the high level of professionalism and technical expertise provided by colleagues at PSM in the development of a practical design solution and the CBGU construction team for implementing the design.

8 REFERENCES

Cammack, R., Bertuzzi, R., Smith, A. and Brehaut, R. 2022. Rock Mass Parameters for the Brisbane CBD. Australian Geomechanics, Vol. 57: No. 4, pp. 47 – 72.

Keating, D. and Swinn, B. 2023. Underground Cavern Blasting – Post TBM Traverse. 18th Australasian Tunnelling Conference, Sydney, Australia, pp. 152- 159.

Rogan, A.C., Swinn, B., Clarke, S. J. and Ahn, J. 2025. Design and construction of the AS1 Shaft within the Albert Street Cavern, Cross River Rail, Brisbane. 19th Australasian Tunnelling Conference, Perth, Australia, 2025.

Shen, B., Clarke, S.J., Rogan, A.C. and McCormack, P. 2022. Design and Construction of Roma Street Station Cavern, Cross River Rail, Brisbane. Australian Geomechanics, Vol. 57: No. 4, pp. 115 – 128

19th Australasian Tunnelling Conference – Acosta-Martínez, Stewart and Hudson-Smith (Eds.)
© 2025 Australian Tunnelling Society, ISBN 978-0-85825-002-4

Design and testing of BA anchors for temporary support of reinforcement in cavern linings, Cross River Rail, Brisbane

S.J. Clarke
PSM, Sydney, Australia

F. Cerone
Bluey Technologies, Brisbane, Australia

P. Liebrich
Queensland Hydro, Brisbane, Australia

ABSTRACT: BA anchors were used extensively to provide temporary support for steel bar reinforcement in the Cross River Rail caverns and adits prior to pouring the permanent concrete linings. The load capacity of BA anchors is uncertain due to their short length and use of a plastic sleeve to transfer load between the threaded bar and founding stratum. The arched profile of the caverns and adits means that the anchor threaded rods are often subject to combined bending and axial loads. This introduces uncertainty in the design and application of BA anchors since threaded bars are not intended for use in bending.

A series of load tests were conducted to measure the axial tensile capacity of the anchors as well as confirm the combined bending and axial capacity of the threadbar. These tests enabled the validation of the design load capacity and adoption of a more efficient support design. This paper discusses failure mechanisms associated with BA anchors and proposes design methods which were validated by load testing. The maximum capacity of the BA anchors was found to be well in excess of values often assumed in design.

Thousands of BA anchors were installed across the project. Increasing the anchor spacing through robust design and testing achieved meaningful schedule and cost benefits.

1 INTRODUCTION

Cross River Rail (CRR) is a new 10.2 km long underground metro rail line in Brisbane extending from Dutton Park in the south and Bowen Hills in the north. It includes 5.9 km long twin tunnels below the Brisbane River and CBD. The Tunnel, Stations and Development (TSD) component of the project involves construction of twin Tunnel Boring Machine excavated and roadheader mined running tunnels; four new underground stations at Boggo Road, Woolloongabba, Albert Street and Roma Street; and dive structures at each end of the running tunnels.

The underground stations, running tunnels between Woolloongabba and Dutton Park, and all adits and cross passages were mined and utilised permanent cast-in-place concrete linings. Sheet waterproofing membrane was installed across the crown and sidewalls of the mined tunnels.

BA anchors were used in the crown and sidewalls of the tunnels where bar reinforcement was required (Figure 1). BA refers to “breakthrough anchor”, in which an anchorage point for steel fixing is provided with the anchor extending beyond the waterproof membrane and bonded within the external substrate, but without compromising the continuity or integrity of the waterproofing system. These anchors have a temporary function of supporting the reinforcement prior to placement of concrete to form the permanent tunnel linings.

Due to the highly manual nature of erecting reinforcing steel the consequences of anchor failure have the potential to result in injury to personnel.

The focus of this paper are the crown anchors in the station caverns as these are required to support the dead load of the reinforcement, whereas the sidewall reinforcement is typically self-supporting and only utilises anchors to prevent toppling of the reinforcing cage.

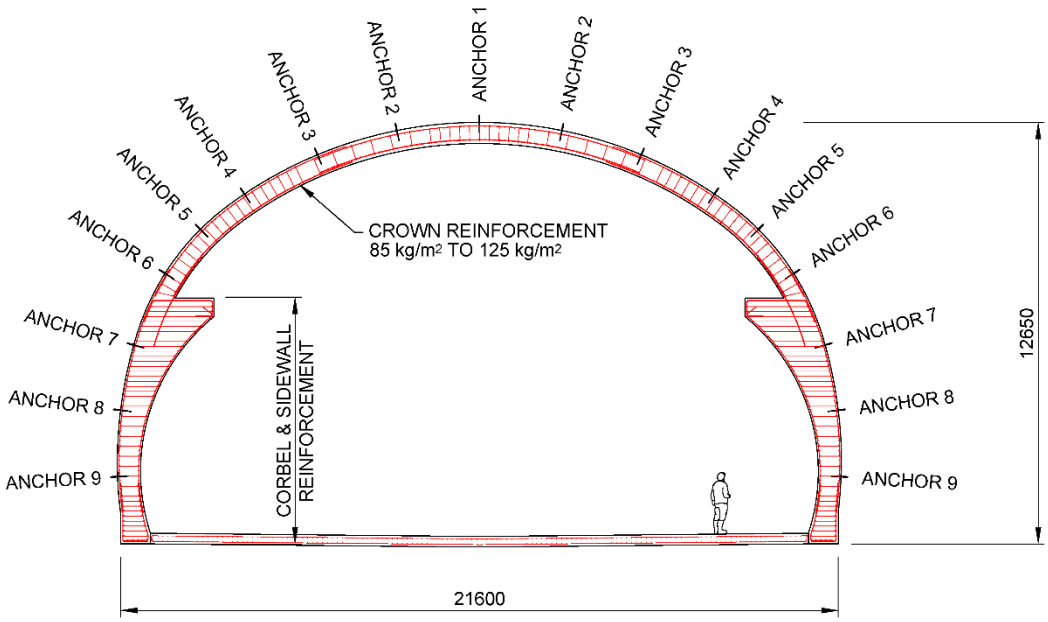


Figure 1. Boggo Road Station cavern lining reinforcement and adopted BA anchor layout.

BA anchors were used extensively across the project with thousands installed. Increasing the spacing of BA anchors through robust design and appropriate testing represented meaningful schedule and cost benefits to the project.

2 BA ANCHORS

2.1 *Description*

BA anchors are understood to have been first used in the Cohlfirst tunnels in Switzerland which was completed in 1996.

They consist of a rigid polyethylene (PE) or polyvinyl chloride (PVC) sleeve and flange, into which an M16 x 2.0 threaded steel rod is inserted (Figure 2). The embedment length of the anchors considered in this paper is less than 200 mm though the authors are aware that similar longer anchors are also available. The sleeve has an outer diameter of 28 mm and incorporates a coarse external thread to facilitate a high strength bond with the epoxy resin used to secure the anchor to the substrate.

A flexible membrane disc of approximately 300 mm diameter is factory-welded to the flange, which ensures a high quality weld and watertight seal. The membrane can be manufactured in either very low-density polyethylene (VLDPE) or PVC to achieve compatibility with the tunnel waterproofing membrane being installed.

2.2 *Applications*

Traditionally BA anchors are used to facilitate the installation of reinforcing steel bars without compromising the waterproofing membrane (Figure 3). Dummy bars are not part of the design reinforcement but are used to support the design reinforcing bars. The dummy bars are attached to the threadbar of the BA anchor via welding or use of a clamp. For CRR a simple clamp detail was developed which comprised two short lengths of unequal angle (UEA) held in place by nuts on either side. This detail can hold two dummy bars of up to N24 size.

Other common applications for these anchors are for anchoring scaffolding, and hanging of services such as ventilation bags, electrical cables and temporary lighting after the waterproofing membrane has been installed. The use of eye bolts threaded into the anchor is often employed in hanging services.

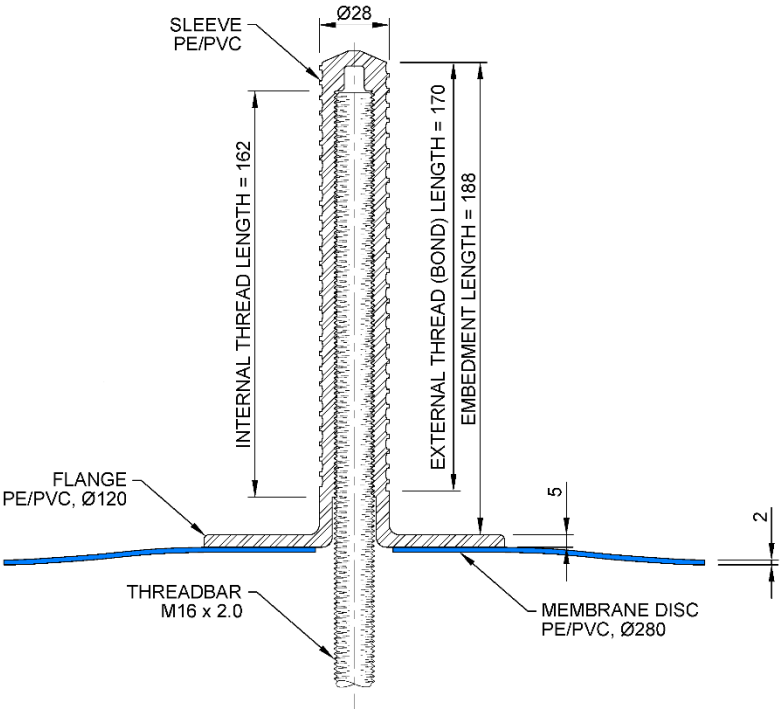


Figure 2. Sectional elevation of a BA anchor used on the CRR project.

2.3 *Load capacity*

There are many variables which can affect the load capacity of BA anchors. It is therefore difficult to determine a single reliable load capacity for a BA anchor. These variables include, but are not limited to:

- Thickness and strength of shotcrete substrate (where present).
- Rock substrate condition.
- Strength and extent of defects.
- Moisture condition in the drilled hole.
- Type of epoxy resin or grout.

As a conservative guide, an axial load capacity of 20 kN and shear load rating of 10 kN are often quoted by suppliers and manufacturers with the proviso that it is important to undertake pull-out tests of production anchors on site.

Section 3 and Section 5 of this paper discuss anchor failure mechanisms and production testing regimes as they apply to load capacity.

2.4 *Installation and QA procedures*

The typical installation procedure for BA anchors is as follows:

1. Mark out anchor installation locations, which may require surveyors for irregular or complex arrays.
2. Drill 32 mm diameter holes through the waterproofing membrane and into the substrate, to a depth of 200 mm, using a depth stop to ensure that the correct depth is achieved.
3. Blow out hole to remove debris and dust using a manual or powered blower until no more dust is produced.
4. Inject the specified epoxy resin from the back of the hole. The correct volume shall fill the hole once the anchor is installed, but not to the extent that excess epoxy is ejected. The epoxy must be suited to overhead application (i.e. sufficiently high viscosity that it remains in the drill hole).
5. Inspect each anchor prior to installation to ensure that there is no damage or manufacturing defects present.

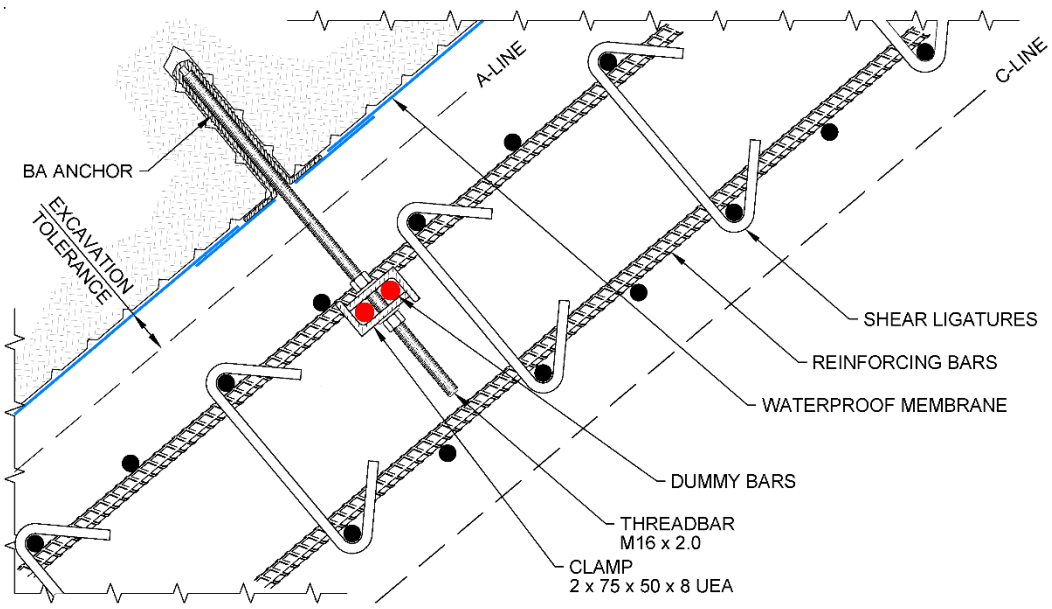


Figure 3. Typical BA anchor application used to support bar reinforcement prior to and during placement of concrete to form the permanent tunnel lining.

6. Install the anchor by pushing and twisting into the hole to ensure proper encapsulation of the external thread.
7. Screw threadbar of the required length and strength grade into the BA anchor sleeve using a depth mark to ensure that the bar reaches the base of the anchor but does not punch through the bottom and compromise the waterproofing function of the sleeve.
8. Weld the full circumference of the BA anchor membrane to the waterproofing membrane.
9. Test the weld using the needle or vacuum test methods.
10. Pull test anchors at the frequency and to the methodology required by the design.

3 FAILURE MECHANISMS

3.1 *Overview*

Figure 4 presents a graphic summary of failure mechanisms applicable to BA anchors. Since that since these anchors are very short and employ a plastic sleeve around the steel bar additional mechanisms are relevant in comparison to that of simple rock anchors. Figure 4 is arranged in four rows with each row addressing a different category of failure:

– Threadbar overload.
– Piston pullout.
– Substrate failure.
– Installation issues.

3.2 *Threadbar overload*

Axial loading of the anchor has the potential to rupture the threadbar in pure tension (Figure 4(a)). This failure mode is considered the least likely of those considered due to the relatively high axial tensile strength of threadbar (Table 1). It is noted that nuts and washers and other components need to be proportioned and specified such that they do not compromise the strength of the system.

Threaded bar is not an ideal structural member because the threads act as notches and, when subject to bending (Figure 4(b)), material failure can occur at a lower load than that for a smooth bar due to stress concentrations associated with the roots of the threads [Ref. 1]. To the authors' knowledge, the bending capacity of bolts or threaded bar is not addressed by structural standards, though BA anchors are commonly subject to this type of loading.

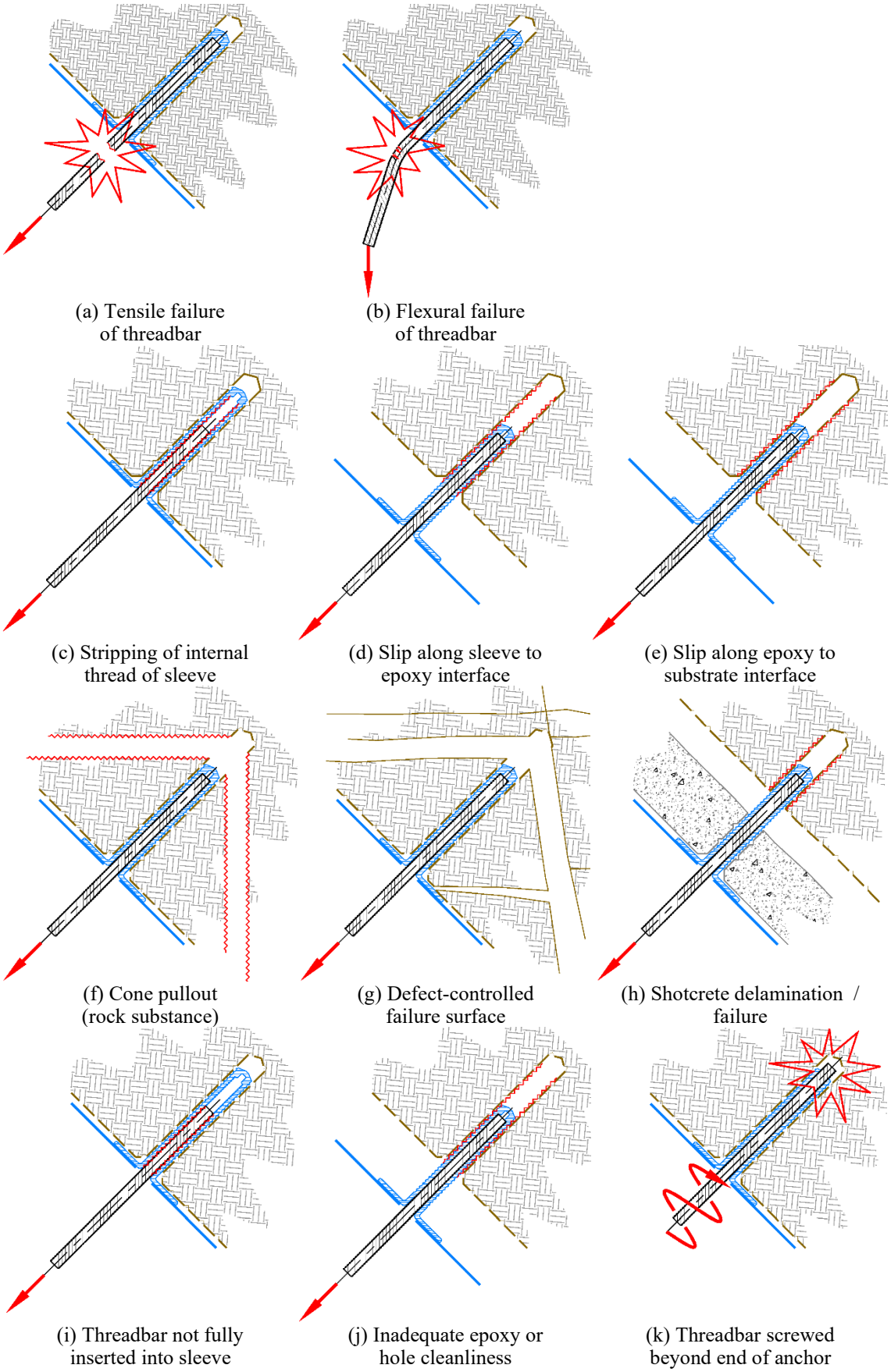


Figure 4. Potential failure mechanisms for BA anchors.

Table 1. Design threadbar strengths

Bolt grade	Minimum tensile strength (1.)	Nominal yield strength (2.)	Design capacity (3.)		
			Shear (4.)	Tension (5.)	Bending (6.)
	f_{uf} (MPa)	f_y (MPa)	ϕV_f (kN)	ϕN_{tf} (kN)	ϕM_s (kNm)
4.6	400	240	27.0	50.2	0.08
8.8	800	640	54.0	100.5	0.21
10.9	1040	940	58.2	130.6	0.31

Notes:
1. Values given for M16 x 2.0 threadbar.
2. Nominal yield strength as per Table 1 of AS 4291-2015 (applied to calculation of design bending capacity only).
3. Capacity factor of 0.8 adopted as per Table 3.4 of AS 4100-2020.
4. Adopted minor diameter area 136 mm^2 as per Table 3.3 of AS 1275-1985.
5. Tensile stress area for M16 x 2.0 thread is 157 mm^2 as per Table 3.3 of AS 1275-1985.
6. Nominal section capacity moment calculated for a compact section as per Clause 5.2.3 of AS 4100-2020 with an effective section modulus calculated assuming a circular bar of diameter equivalent to the tensile stress area, i.e. d = 14.1 mm.

Table 1 presents calculated design bending capacities based on assumptions outlined in the table notes. Validating the veracity of these assumptions was the focus of the testing undertaken as described in subsequent sections.

Section 8 of AS 4100 provides approaches to assess the adequacy of members subject to combined actions. Where the design axial force is a small proportion of the design capacity (say, < 10%) then the bending capacity is reduced by no less than 90%.

3.3 *Piston pullout*

Figure 4(c) to Figure 4(e) illustrate failure mechanisms characterised by "piston pullout" which relates to failure along a cylindrical surface coinciding with the interface between different materials. These include:

- Stripping of the internal plastic thread inside the anchor sleeve as shown in (Figure 4(c)). This was originally considered a vulnerable failure mode and was a key reason for performing the axial load tests described in Section 4.1.
- Slip through the epoxy resin (or grout) as shown in Figure 4(d). This failure mode is primarily dependant on the strength of the epoxy employed, as well as the mechanical interlock provided by the external thread of the sleeve.
- Shear failure along the substrate to epoxy resin interface as shown in Figure 4(e). The strength of this interface is influenced by the characteristics of the substrate (e.g. shotcrete or rock), the roughness of the drilled hole, as well as the cleanliness and moisture condition of the hole upon application of the epoxy.

The above piston pullout failure mechanisms were investigated and strengths of the various interfaces quantified by the axial loading tests described in Section 4.1.

3.4 *Rock / substrate failure*

Figure 4(f) to Figure 4(h) illustrate mechanisms characterised by failure of the substrate, whether that be shotcrete or bedrock, or a combination of the two materials.

Failure through a homogenous material such as shotcrete or bedrock (without defects) is shown in Figure 4(f). This mechanism is typically associated with conical failure surfaces, with the failure load governed by the depth of anchor embedment and the strength of the substrate. The Hilti technical literature for chemical anchors can be used to provide an initial estimate of the likely failure load in concrete and shotcrete.

Figure 4(g) comprises a failure governed by pre-existing defects in the rock mass such as joints, bedding planes, shears etc. Depending on the frequency and orientation of the defects the failure

load could be very low. The very short embedment length of BA anchors also means that any rock bolts installed nearby are unlikely to improve the load capacity of the anchor.

The final sketch in this series comprises thin shotcrete sprayed onto bedrock (Figure 4(h)). The failure mechanism is complicated by the interaction between the shotcrete and rock, and the relatively low strength of thin shotcrete to resist concentrated loads. The bond strength between shotcrete and rock is also a source of uncertainty, with adhesion rarely relied upon by tunnel designers. Unless the shotcrete has been specifically designed for the BA anchor loads, it is the authors' opinions that relying upon shotcrete without suitable testing is to be avoided.

3.5 Installation issues

Figure 4(i) to Figure 4(k) illustrate failure mechanisms associated with installation issues.

Where the threadbar is not fully screwed into the anchor sleeve the bond length is reduced and thus also the load capacity. This issue can be managed by marking bars prior to insertion to provide a visual check as to whether they have achieved full depth or not.

Inadequate placement of epoxy resin is addressed in Figure 4(j), and includes inadequate cleaning of the hole, excessive moisture or water present prior to injecting the epoxy, and incomplete filling of the hole with epoxy. Failure to apply epoxy at all is also possible and may not be detected until the anchor is first loaded.

Figure 4(k) involves screwing the threadbar too far into the sleeve, such that it punches through the base of the sleeve. This is unlikely to affect the strength of the anchor but rather results in compromising the continuity and thus integrity of the tunnel waterproofing system.

Additionally there other challenges associated with installation, such as those mentioned previously in Section 2.4. However, these are considered manageable by use of appropriately trained and motivated installers, and implementation of an effective QA system.

4 TESTING PROGRAM

4.1 *Axial capacity*

A series of three axial load tests were performed to investigate the piston pullout failure mechanisms (Figure 5). These tests were performed in ideal conditions and are considered to represent the maximum strengths which can be achieved for this type of anchor.

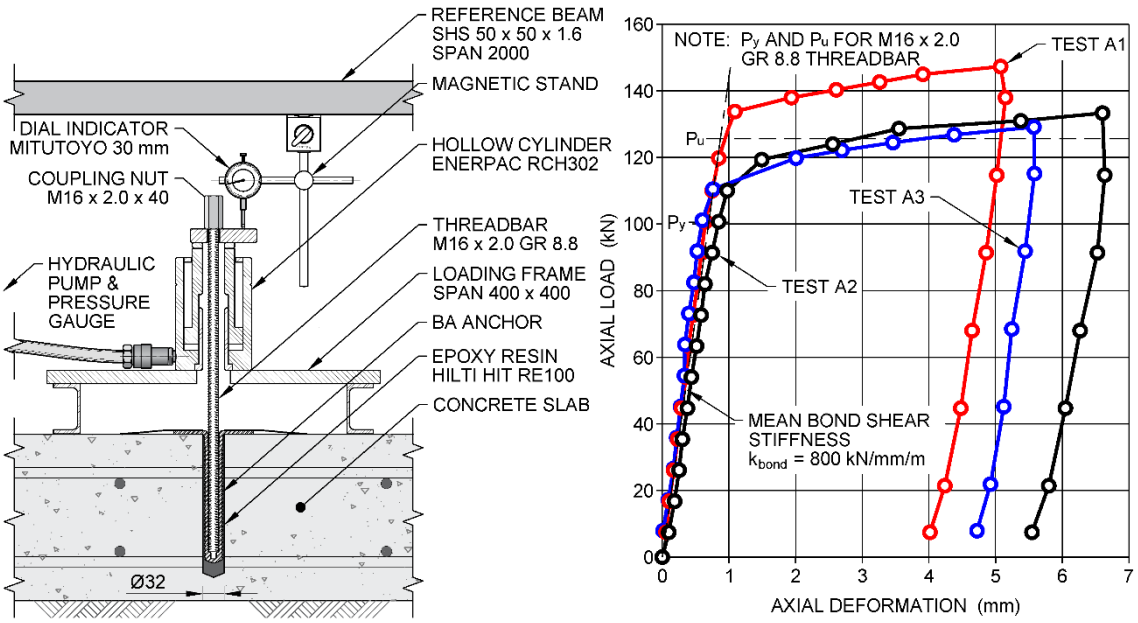


Figure 5. Axial pull test arrangement and summary results.

All three tests were governed by yielding of the steel threadbar rather than other failure mechanisms. It is noted that the yield load and ultimate loads measured were about 10% higher that the strength grade would suggest. This was borne out by the test reports and certificates obtained for the relevant manufacturing lots which indicated ultimate tensile strengths 113% to 115% of the requirement for Grade 8.8 threadbar, and 105% to 106% of the requirement for Grade 10.9 threadbar.

The minimum ultimate load from the three tests was 130 kN. Based on the lengths of the various interfaces indicated by Figure 2, the following interface strengths were calculated:

– Threadbar to sleeve, $f_s > 18.1$ MPa.
– Sleeve to epoxy, $f_s > 8.8$ MPa.
– Epoxy to concrete, $f_s > 6.9$ MPa.

For comparison, the Hilti technical datasheet (TDS) for HIT-RE 100 Injection Mortar gives a characteristic resistance of 183 kN for an M27 anchor installed in a 30 mm diameter hole with an embedment depth of 240 mm [Ref. 2]. This capacity corresponds to an interface strength, $f_s = 8.1$ MPa between the epoxy resin and concrete, which accords well with the above test results.

Bond shear stiffness was also calculated from these tests, as shown in Figure 5, noting that this parameter is not required for the design of BA anchors, and is provided purely for comparison with other rock bolt and anchor systems.

4.2 *Combined axial and bending capacity*

A further testing program was undertaken to investigate the load capacity of BA anchors when subject to combined bending and axial loading, such as occurs for most anchors installed to support bar reinforcement within the crown of a tunnel (Figure 1). A bespoke test configuration was designed in which a dead load was applied to the end of threadbar, with the angle of the threadbar able to be adjusted (Figure 6). The test regime was based on Section 17.4 of AS 4100, which relates to proof load testing of prototype specimens as a valid design approach, and includes the following key requirements:

– Applied test load is representative of limit state being assessed.
– Prototype shall be representative of production works.
– Period of loading no less than 15 minutes.
– Load factor of 1.2 applied where 10 prototype samples are tested (Table 17.5.2).

Four tests configurations were investigated, with proof loads applied to each of 10 samples for each configuration:

– Test B1, Grade 8.8 threadbar, applied load = 2.61 kN, anchor angle = 46°.
– Test B2, Grade 10.9 threadbar, applied load = 3.51 kN, anchor angle = 46°.
– Test B3, Grade 8.8 threadbar, applied load = 4.88 kN, anchor angle = 67°.
– Test B4, Grade 10.9 threadbar, applied load = 5.76 kN, anchor angle = 65°.

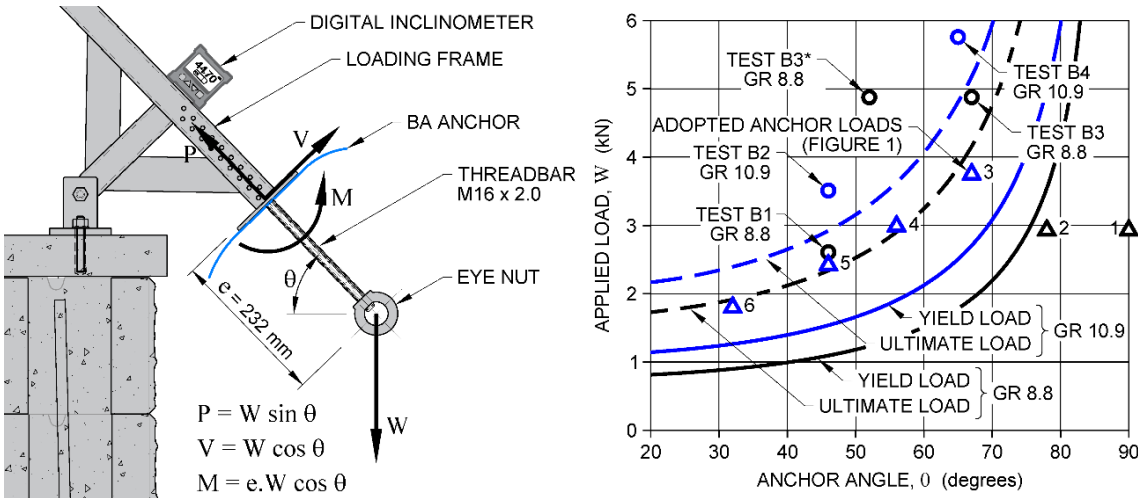


Figure 6. Bending proof load test configuration and summary results.

Table 2. Summary of pull test methods for production BA anchors

Failure mode		Capabilities of each test method		
		Simple pull test	Pull test with load frame	Proof load
Threadbar overload	Tensile failure of threadbar	✓	✓	✓
	Flexural failure of threadbar	×	×	✓
Piston pullout	Stripping of internal thread of sleeve	✓	✓	✓
	Slip along sleeve to epoxy interface	✓	✓	✓
	Slip along epoxy to substrate interface	✓	✓	✓
Substrate failure	Cone pullout (rock substance)	×	✓	✓
	Defect-controlled failure surface	×	✓	✓
	Shotcrete delamination / failure	×	✓	✓
Installation issues	Threadbar not fully inserted	✓	✓	✓
	Inadequate epoxy or hole cleanliness	✓	✓	✓
	Threadbar screwed beyond end of anchor	×	×	×

In addition, a single sample was the subject of Test B3*, in which the anchor angle was reduced to 52° to increase the bending moment applied to the bar.

All the tests satisfied the proof load testing requirements of AS 4100, with noticeable bending of the bars observed upon application of the proof load. Some of this deformation was recoverable and some permanent. Permanent deformation of all threadbars was observed, with the bars typically bent by 1° to 3.5°, and Test B3* recording over 7°.

The proof load tests show that the loads carried by the anchors exceeded the theoretical ultimate load capacity for each of the stress grades considered. This apparent inconsistency is attributable to two factors; the strength of the bars exceeded the requirements of the stress grades (refer to Section 4.1), and the significant bending of the bars during the test resulted in a reduction in the eccentricity of the applied load and thus the bending moment experienced by the bars.

Figure 6 also shows the anchor installation angles and calculated loads for each of the crown anchors indicated in Figure 1. Two strength grades were adopted as indicated by the colours of the symbols (i.e. black corresponds to Grade 8.8 and blue to Grade 10.9). The graph also demonstrates that the adopted anchor loads are consistent with the proof load test results.

5 DESIGN AND TESTING RECOMMENDATIONS

The use of higher stress grades provides a simple method to address bars which are required to resist flexural loading. Structural design checks for bending based on a plain circular bar of diameter consistent with the effective stress area were found to provide a reasonable assessment of capacity as verified by the test results. Because bending performance is sensitive to the adopted lever arm, over-excavation (see Figure 3 for excavation tolerances) can result in flexural overload and thus survey of the as-built membrane surface is recommended to allow calculation of the actual lever arm associated with the design loads.

Reliance on manufacturer's lot certificates which indicate bar strengths greater than those required for the different stress grades is not recommended since these vary lot by lot.

Piston pullout modes of failure can be checked based on the results of the axial load tests reported in this paper.

Failure of the substrate is a key limitation of BA anchors due to their very short length. An exception to this generalisation is where the substrate comprises a thick passive shotcrete lining, or similar, where the material conditions and uniformity are known with a high degree of

confidence. Pull testing of anchors is essential where the substrate comprises fractured bedrock or thin shotcrete.

A number of anchor pull test methods are available:

1. Simple pull test, where the anchor is pulled by a hydraulic cylinder, and the load frame bears against the substrate immediately adjacent to the anchor. This method does not permit the various substrate failure mechanisms to occur, nor apply flexural loads to the bar.
2. Pull test with a loading frame, similar to the simple test method but a loading frame is used such that the area within, say no less than 300 mm, of the anchor bar remains unloaded by the frame. This allows checking of the substrate failure mechanisms but does not apply flexural loads to the bar.
3. Proof load test, in which a dead load is suspended from the end of the anchor to properly simulate the vertical gravity load applied by the bar reinforcement.

The capabilities and limitations of each pull test method are summarised in Table 2.

Checking the adequacy of the installation may be addressed by specification of experienced and qualified contractors, adoption of effective quality assurance procedures, and adoption of an appropriate test method and test frequency.

Redundancy in design is an important consideration in the frequency of testing of production anchors. For an anchor layout which provides a significant degree of redundancy, testing of no less than 10% of anchors is recommended. Where failure of a single anchor could result in progressive failure and collapse of the entire reinforcing steel then testing of a very high proportion of anchors is appropriate. A higher rate would also apply where higher loads are applied, there is uncertainty in the substrate conditions or installation standard, or where inadequate performance is identified by initial test results.

6 CONCLUSIONS

BA anchors are widely used in the construction of bar reinforced concrete structures which employ a sheet waterproof membrane. Due to the unique features of this type of anchor they are susceptible to a larger range of potential failure mechanisms compared to simpler anchor types. This paper considers each of these failure mechanisms and proposes design approaches to address them. The test results presented in the paper reduce the uncertainty in the load capacity of the plastic sleeve employed in the anchor and demonstrate that much larger axial load capacity is possible compared to load capacities often quoted by manufacturers and suppliers. The bending capacity of the threadbar employed in the anchor is identified as a basic limitation of this type of anchor, and methods to perform structural checks are proposed and validated by full scale testing.

The design and testing approaches presented in this paper were applied in the Cross River Rail project and permitted optimisation of the spacing of BA anchors employed in the construction of the permanent tunnel linings and provided meaningful schedule and cost benefits to the project.

ACKNOWLEDGEMENTS

The authors would like to acknowledge the Pulse consortium together with the CPB Contractors, BAM International Australia, Ghella and UGL Joint Venture for granting permission to publish this paper. The authors also wish to express their appreciation to the CBGU construction team for their constructive inputs during the optimisation of the BA anchor design for the Boggo Road Station cavern.

7 REFERENCES

Fernando, S., Specification of threaded bar in structural applications, Steel Construction, Journal of the Australian Steel Institute, Vol 47, No. 1, July 2014, pp. 2 - 15.

Hilti Technical Datasheet, HIT-RE 100 Injection Mortar, Jan 2023.

AS 4100 Steel structures, Standards Australia, 2020.

19th Australasian Tunnelling Conference – Acosta-Martínez, Stewart and Hudson-Smith (Eds.)
© 2025 Australian Tunnelling Society, ISBN 978-0-85825-002-4

Design and construction of the Woolloongabba station caverns for Brisbane's Cross River Rail project

M. Habte, B. Shen, M. Kobler, A.C. Rogan
PSM, Brisbane, Australia

ABSTRACT: The Woolloongabba Station for Brisbane's Cross River Rail project comprises two caverns separated by a station building shaft. The caverns are D-shaped arched excavations of up to 25 m wide and 16 m high. The ground surface is approximately 8 to 16 m above the cavern crown. The site geology comprises Brisbane Tuff, overlying the Aspley Tingalpa formation, overlying the basement Neranleigh-Fernvale Group (NFG) beds. The presence of deep weathering profiles and tectonic deformation added further complexity to the ground conditions at the site. The initial primary support of the cavern comprised rock bolts and a thin shotcrete lining for the South Cavern and a passive arch lining for the North Cavern. The cavern permanent lining consisted of a steel fibre reinforced concrete crown, bar reinforced concrete sidewall with corbel and headwalls at either end of the cavern. This paper presents key challenges for the design and construction of the primary and permanent supports, adopted support solutions, the as-encountered ground conditions, and comparison of design predictions with measured monitoring data.

1 INTRODUCTION

Cross River Rail (CRR) is a new 10.2 km long metro rail line in Brisbane between Dutton Park in the south and Bowen Hills to the north, which includes 5.9 km long twin tunnels that traverse under the Brisbane River and the CBD. The Pulse consortium (including the CPB Contractors, BAM International Australia, Ghella and UGL Joint Venture, CBGU JV) was awarded the contract to design and construct the Tunnels, Stations and Development (TSD) works which includes construction of twin Tunnel Boring Machine (TBM) excavated and mined running tunnels; four new underground stations at Boggo Road, Woolloongabba, Albert Street and Roma Street; and dive structures at each end of the running tunnels.

2 WOOLLOONGABBA STATION

The new underground Woolloongabba Station is situated to the southeast of the Brisbane CBD and at the heart of a precinct undergoing major urban regeneration. The station will be at the new urban core which will be a destination and focal point of Brisbane's inner south as a place to live, work, play and learn.

The station comprises of a 33 m deep main station building shaft and two caverns, one to the north and one to the south. The caverns are 90 m (North Cavern) and 106 m (South Cavern) long respectively, with an excavation span of up to 25 m and excavated height of 16 m (Figure 1)

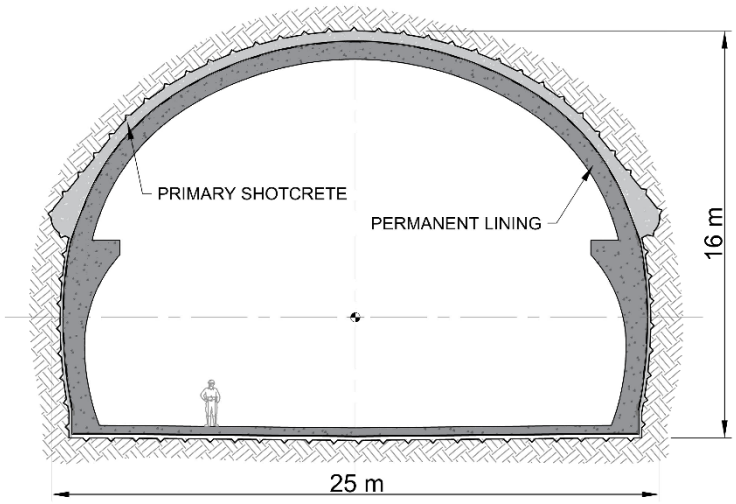


Figure 1. Station Cavern Profile

3 ENCOUNTERED GEOTECHNICAL CONDITIONS

The geotechnical conditions at the Woolloongabba site are complex with multiple rock lithologies that have undergone deformation associated with the Normanby Fault Zone (NFZ).

For design and construction, each of the lithologies encountered at Woolloongabba were classified into five rock mass classes ranging from class 1 (high to very high strength blocky rock mass) to class 5 (soil to very low strength disintegrated to disturbed rock mass). A sub-class of NFG 2 (denoted as NFG 2A) was included in the rock mass classification to represent a blockier rock mass due to fault disturbance in the NFG while the fault zone was sub-divided into a fault disturbed zone (FDZ) and fault crush zone (FCZ) (Cammack et al., 2022).

The mapped rock mass classes and key faults are presented in Figure 2 (North Cavern) and Figure 3 (South Cavern). The typical profile from surface down includes:

- Soil, including up to 4 m of Fill overlying 1.5 m of Alluvium.
- Brisbane Tuff (Tuff). A typical weathering profile was encountered, grading from Tuff 5 to Tuff 1 with depth. A horizon of variably deformed Tuff (jointed, sheared and variable strength) was encountered at the base of the unit. This horizon comprises Tuff 1 to Tuff 3 and the width is variable along the alignment.
- Unconformity zone 1 (UZ-1). A 300 mm (approx.) wide zone comprised of very low to low strength Tuff overlying a 50-100 mm thick medium strength sandstone bed. Clay seams (<100 mm thick) parallel to the UZ-1 are common both within the UZ-1 and several metres either side of the zone. Shearing is evident along some seams, and a paleosol origin is also possible. The overall shape of the UZ-1 is sub-horizontal.
- Aspley Tingalpa Formation (Aspley) – Sandstone and Siltstone (SD). SD 1 and SD 2.
- Aspley – Conglomerate and Sandstone (CD). CD 1 and CD 2.
- Unconformity zone 2 (UZ-2). This zone ranges from healed/intact, clean open defect, up to 50 mm clay (unclear if paleosol or sheared), and localised Tuffaceous beds.
- Neranleigh-Fernvale Group (NFG). The NFG encountered at Woolloongabba is significantly different to the NFG typically encountered in the Brisbane CBD. It is pale and dark grey, high to very high strength, foliated, weakly metamorphosed sandstone and phyllite. At Woolloongabba, two distinct NFG lithological types were encountered:
  - NFG “brecciated”. This is a re-healed chaotic breccia with significant red and green alteration, likely re-healed fault gouge associated with the NFZ. Foliation is present in some areas, is highly variable in orientation and persistent only over several metres. The rock class is typically NFG 1 and NFG 2.
  - NFG “foliated”. This is a foliated rock mass with foliation persistent on the cavern scale. Significant deformation and alteration have resulted in a beige and dark grey rock mass,

with pockets of quartzite. Foliation is orientated steeply towards the north-east. The rock class is typically NFG 1 and NFG 2.

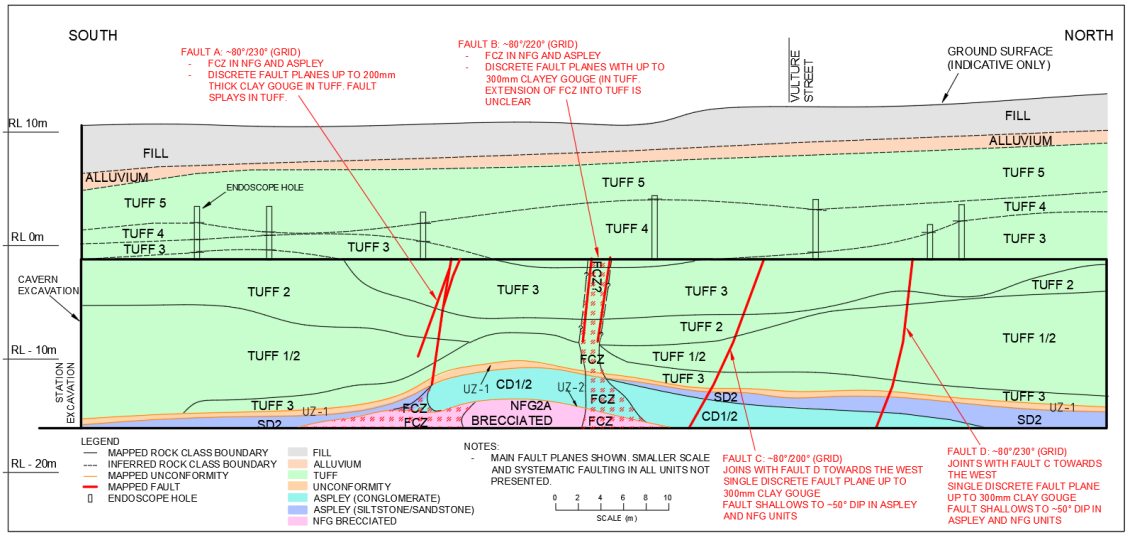


Figure 2. Mapped North Cavern Geotechnical Conditions

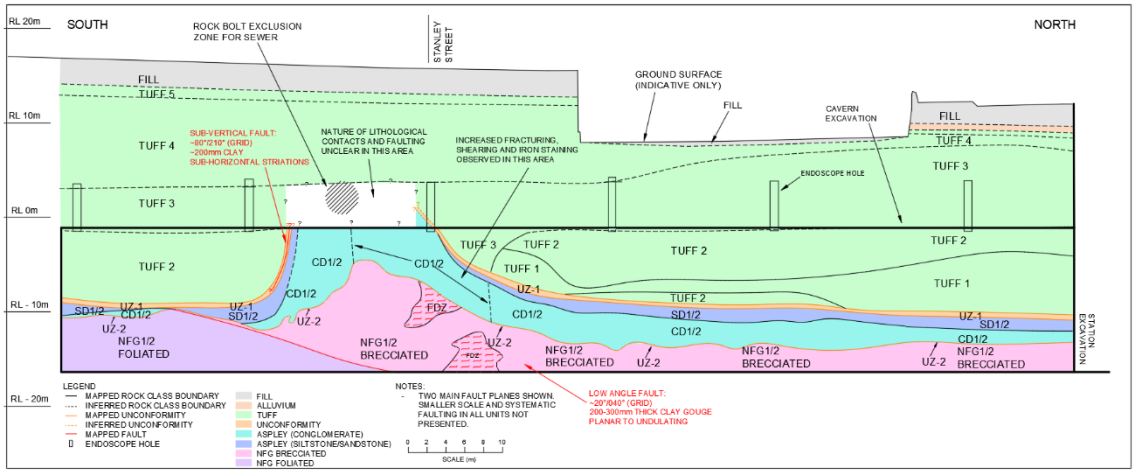


Figure 3. Mapped South Cavern Geotechnical Conditions

The Normanby Fault Zone (NFZ) is a major northwest-southeast (NW-SE) striking fault zone encountered in several CBD projects which can be traced from Normanby in the north, along the western edge of the CBD parallel to the Brisbane River, to Woolloongabba in the south. The NFZ has experienced numerous phases of deformation in its complex geological history. It has the characteristics of both a thrust and strike slip fault, but may have developed as a regional normal fault early in its existence. It is expressed as a wide "structural zone", where variably faulted rock could occur (Cammack et al., 2023). Deformation associated with the NFZ at the Woolloongabba site is detailed below.

A sub-vertical fault zone strikes NE-SW through the North Cavern and extends through the Tuff, Aspley and NFG units. The overall zone is approximately 50 m wide, and the rock class boundaries deepen in proximity to the fault zone with increased jointing, shearing and weathering. In the Tuff, there are distinct fault planes with up to 300 mm clay gouge that persist across the cavern scale and splay. The rock mass between the fault planes is variably damaged. The UZ-1 forms a domed shape, and it is unclear if this is a result of faulting or deposition. Limited vertical offset (<0.5 m) along the distinct fault planes is observed. The fault presents as zones of FCZ in the Aspley and NFG. The rock mass between the FCZ is variably deformed, including NFG 1,

NFG 2 and NFG 2A. Evidence of normal, reverse and strike-slip faulting is observed on slickensides within the fault zone, however the overall sense of movement is interpreted as strike-slip.

A complex fault zone was encountered in the South Cavern, with evidence of multiple phases of deformation and re-healing of the rock mass. Two discrete geotechnical faults (i.e. weak planes) were mapped; a low angle fault and a sub-vertical fault. A zone of increased deformation is observed for approximately 25 m to the north of these two faults, with pockets of FDZ in the NFG, increased weathering, jointing and shearing in the CD unit, and a deeper Tuff 3 profile. The domed and uneven lithological boundaries is likely due to a combination of deposition and faulting. The low angle fault is a discrete fault plane oriented ~20°/040° (grid) with 200-300 mm clay gouge present in the NFG and Aspley units. The fault appears to terminate in the Aspley. Reverse movement is inferred, and the scale of movement is larger than the cavern scale. NFG "foliated" is present on the south side of the fault (footwall), and NFG "brecciated" is present on the north side of the fault (hanging wall) all the way through the station box and North Cavern. The sub-vertical fault is observed in the Tuff above the low-angle fault. It is a discrete plane oriented ~80°/210° (grid) with ~200 mm thick clay. The fault terminates within the Tuff, and the exact termination was not mapped. Sub-horizontal striations were observed, indicative of strike-slip movement.

4 PRIMARY SUPPORT

In good ground conditions, the primary support for the cavern comprises inflatable friction rock bolts and a thin synthetic fibre-reinforced shotcrete (SFRS) while a passive shotcrete arched lining was implemented where poorer ground conditions were encountered due to deep weathering within the Tuff (Figure 4). Table 1 presents a summary of the primary support types designed to cater for the range of expected ground conditions.

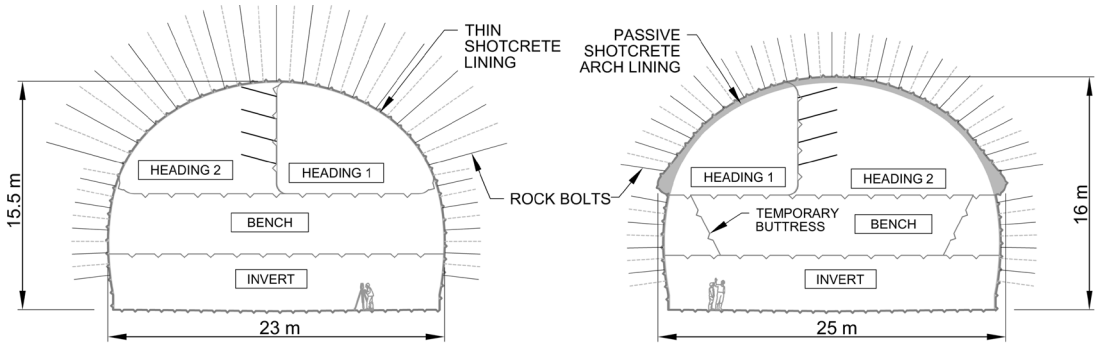
Table 1. Summary of primary support types.

Support type	Bolt length (m)	Bolt spacing (m)	Shotcrete thickness (mm)	Applicable ground conditions
Type 1	5.4	1.75	50	Tuff 1/2 or NFG 1/2
Type 2	5.4	1.5	75	Tuff 3 or NFG 3 or CD 1/2 or SD 1/2
Type 3	5.4	1.25	100	Tuff 1/2/3 or NFG 1/2/3 or CD 1/2 or SD 1/2 with adversely oriented faults and shears
Type 4	3.0	1.5	300	Tuff 4
Type 5	3.0	1.5	400	Tuff 5

The design calculations undertaken to demonstrate the suitability of the proposed tunnel support design included preliminary assessments using empirical and precedence-based approaches followed by detailed assessments which included kinematic assessment of rock blocks, 2D and 3D wedge stability analyses, 2D and 3D finite element stress-deformation analyses. The analyses were undertaken for representative ground conditions along the alignment of the South and North Caverns.

The geotechnical assessments indicated the dominant failure mechanism for the South Cavern and the northern end of the North Cavern was structurally controlled rock block movement and falls (including wedge failures and sliding blocks). The primary support for this mode of failure is pattern bolting with thin shotcrete (Support types 1 to 3). Ravelling ground and crown failure are expected to be the dominant failure mechanisms for the southern half of the North Cavern. The primary support for this failure mechanism is a thick shotcrete passive lining (Support types 4 and 5).

The construction sequence for the bolted support types (Support types 1 to 3) is to advance the tunnel face to suit the encountered geotechnical conditions, install rock bolts and then spray shotcrete. The sequence for the passive shotcrete lining (Support types 4 to 5) adopts the same sequence as the bolted support type for the lead heading. The design provides an option for full thickness of passive linings to be constructed for the full span of the cavern such that lining connections are not required.



(a) Bolted Support Type (b) Passive Arch Lining Support Type

Figure 4. Primary Support Details

The two caverns were excavated using road headers from the central shaft towards the north and south directions. The cavern excavation for both the bolted and passive support types adopted a split top heading sequence where the trial heading is staggered from the lead heading by a minimum offset distance to suit the ground conditions. Following completion of the top heading, full width benches were excavated to invert level.

The main challenge for the design and construction of the primary support included risks associated with the presence of complex adverse ground conditions (Section 3) which included complex faulting due to tectonic deformation associated with the NFZ, deep weathering within the Tuff unit, and highly variable unconformity zone at the contact between the Tuff and Aspley unit. To manage the risks due to highly variable ground conditions, several sensitivity analyses were undertaken during the design stage to confirm survivability of the design under adverse ground conditions. In addition, the design included provision for additional stitch bolts where there is a potential to encounter a large scale adversely oriented structure. The construction stage measures implemented to manage the risks associated with complex adverse ground conditions included additional borehole drilling, logging of anchor drill holes for the shaft support, inspection of endoscope holes above the cavern crown and longitudinal probe holes drilled from the lead heading. The additional information from these investigations were used to identify location and characteristics fault zones, unconformity zones and other adverse ground conditions.

The design and construction of the primary support for the Woolloongabba station caverns was also constrained due to the presence of settlement sensitive critical infrastructure located directly above the cavern. These included a 600 mm diameter cast iron cement lined (CICL) water main and a 1500 mm diameter micro-tunnelled sewer trunk. Settlement risks at the CICL water main and the micro-tunnelled sewer were managed by limiting the excavation advance length when tunnelling directly below this sensitive infrastructure. The cavern primary support at the location of the sewer main required modification to avoid clashes with the bolt exclusion zone around the sewer. The modified support at this location comprises 300 mm thick shotcrete, 2.4 m long crown bolts inclined forward to avoid clashes with the sewer and 5.4 m long bolts on the shoulders away from the sewer exclusion zone (Figure 5).

The primary support design for Woolloongabba station caverns involved an iterative process with settlement analysis and predicted effects assessments to ensure the predicted effects are within acceptable limits for all the infrastructure within the influence zone of the cavern excavation. In addition, surface settlement monitoring was undertaken to enable review of the actual ground movements from the cavern excavation relative to the design predictions. Overall, review of the monitoring data indicated the measured ground movements were within the design predictions. The maximum surface settlement above the Woolloongabba caverns for the design cases was predicted to be up to 40 mm above the North Cavern, whereas the measured maximum surface settlement above the North Cavern was 35 mm. Figure 6 shows a good comparison between the measured and predicted surface settlement through a cavern section at the CICL water main.

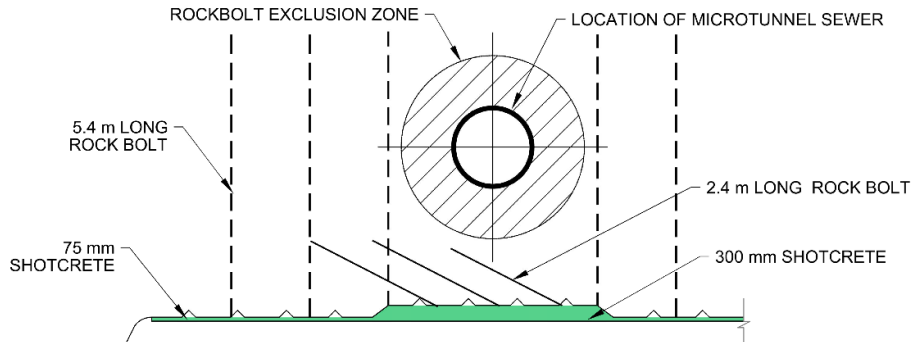


Figure 5. Longitudinal section showing the modified cavern primary support below the sewer trunk

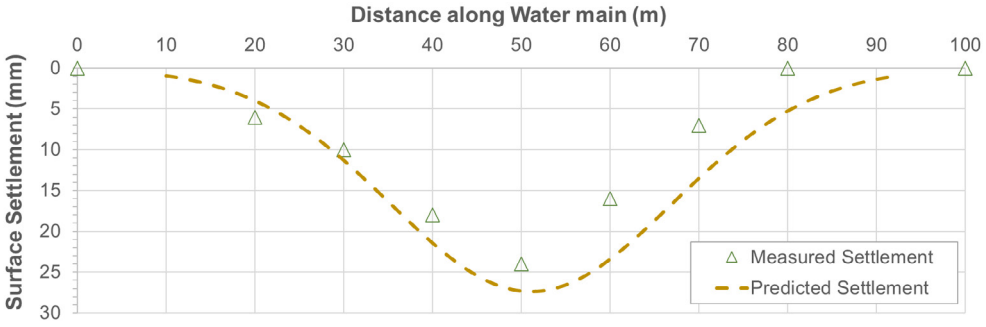


Figure 6. Comparison of measured and predicted settlements at the CICL water main

5 PERMANENT LINING

The permanent lining of the two caverns comprised bar reinforced concrete sidewalls with a Steel Fibre Reinforced Concrete (SFRC) crown. The sidewalls also incorporated a large corbel to support a concrete mezzanine slab, which spans across the cavern, imposing a working line load of up to 640 kN/m run. The cavern invert slabs were designed accounting for both bar and steel fibre reinforcement, with a thickness of 300 mm, based on the Contractor's preference to minimise material quantities. Bar reinforced concrete headwalls, 1 m thick, were located at either end of the cavern, with openings for the TBM tunnels at the northern end and the mined running tunnels at the southern end. Waterproofing, comprising sheet membrane and protective geotextile, was employed around the cavern sidewalls, crown and headwalls, with Cavidrain S60 installed under the cavern invert to facilitate a drained tunnel. Rearguard and hydrophilic waterstops were utilised at construction joints, which in conjunction with the membrane helped mitigate the risk of water leakage into the tunnel via the construction joints.

The thickness of the SFRC cavern crown varied depending on the geotechnical conditions, and corresponding ground loads for the permanent lining. The method to assess the design ground load was consistent with that outlined in Shen et al. (2022). As discussed in Section 4, the South Cavern utilised a bolted support type, whereas the poorer geotechnical conditions in the North Cavern required a passive shotcrete arch lining. The passive arch shotcrete was designed in accordance with the RMS B82 shotcrete specification to achieve a 100-year design life for the compressive strength of the shotcrete, allowing for a 'primary as permanent' approach where the ground load was shared between the primary lining (with degraded stiffness) and the permanent concrete lining.

The design vertical ground load for the cavern crown was estimated to be 80 kPa for the South Cavern, and 110 kPa for the North Cavern, with the horizontal ground loads (mostly associated with loosening rock wedges) for the cavern sidewalls and headwalls ranging from 10 to 25 kPa for the Tuff, NFG and Aspley units. A minimum SFRC thickness in the cavern crown of 600 mm and 700 mm was adopted for the South and North Caverns respectively.

Design of the SFRC lining was undertaken consistent with approaches outlined in AS5100.5 (2017) and the DAfStb Guideline (2015). Excavation of the cavern often resulted in localised areas of over-excavation, with the permanent lining over-poured to 'make-up' the difference, resulting in an irregular extrados profile and variable lining thickness. Finite element structural analysis within ATENA was undertaken accounting for the as-excavated primary lining face position to assess the risk of stress localisation causing undesired crack widths in the permanent lining prior to pouring. An example of such analysis is presented in Liu et al. (2025).

Poor geotechnical conditions were encountered in a number of areas of the cavern foundation, with FDZ, NFG 2A and SD 3 materials encountered. The combination of the mezzanine internal structure load and external ground loads resulted in an equivalent working load of approximately 2.9 MN/m run acting on the foundation below the cavern sidewall kicker. A tight tolerance for differential settlement of the internal structures (less than 3 mm) necessitated foundation treatment in most of the areas that poorer geotechnical conditions were encountered. Accounting for access and timeframe limitations, a 'remove and replace' foundation treatment solution was adopted as the preferred approach. The depth of removal was tailored to the encountered geotechnical conditions and the overlying load (which was less away from the cavern kickers), with 40 MPa concrete poured as the replacement material. Detailed geotechnical mapping of the invert during the cavern excavation as well as plate load testing of representative areas of poorer materials were undertaken to decide on foundation treatment requirements, with zones with an estimated Young's modulus of 700 MPa identified via the plate load testing. The foundation treatment varied between removal depths of up to 1.25 to 2 m under the cavern sidewall kickers and up to 0.75 m under the cavern invert, with an example of the design analysis approach undertaken presented in Shen et al. (2022).

Construction of the cavern headwalls was undertaken prior to the pouring of the adjacent cavern arch lining, which meant, that in combination with the thin 300 mm invert slab there was minimal passive resistance against overturning during construction of the headwall (which was constructed in a series of 'bottom up' horizontal pour lifts). In particular, during the higher lifts, the wet concrete hydrostatic forces generated significant overturning forces, that required additional temporary support to resist and enable construction. The South Cavern headwall was constructed using a significant A-frame to prop the lower portions of the headwall, with ground anchors installed through the invert slab to resist the A-frame uplift forces. The North Cavern headwall utilised a grid of 75 kN 'BA Anchors' with a minimum embedment of 500 mm into rock to support the formwork walers and resist the overturning forces. To achieve the 75 kN pull out capacity (which was verified via pull testing), a different system to the traditional BA Anchor was utilised, where a M20 steel bar was grouted into a hole drilled into the rock with HILTI RE-500. The bar was then integrated into the waterproofing system using a Bluey 'trumpet' system that 'sealed' onto the bar and then could be welded onto the waterproof membrane.

At the interface between the caverns and the station box shaft (located between the two caverns), a waterproofing detail was required between the cavern sheet membrane and the extrados of the shaft concrete lining, as shown in Figure 7. Over-excavation of the shaft however resulted in a zone of over-pour for the shaft walls, that the interface rearguard waterstop would tie into. There was a concern that over the design life, cracking could develop in this overpour concrete if it was unreinforced, effectively allowing seepage to bypass the waterproofing measures. To counteract this, a zone of localised reinforcement was installed in the 'over-pour' zone of the shaft walls, as shown in Figure 7, to mitigate the risk of cracking developing adjacent to the interface rearguard waterstop.

6 CONCLUSIONS

The primary and permanent ground support for Woolloongabba station caverns presented design and construction challenges due to highly variable and complex ground conditions and the presence of settlement sensitive critical infrastructures in close proximity to the cavern excavation, a zone for which details regarding its location and characteristics were limited prior to construction. A suite of design stage and construction phase measures were implemented to manage risks associated with geotechnical uncertainties without hindering the construction program. These

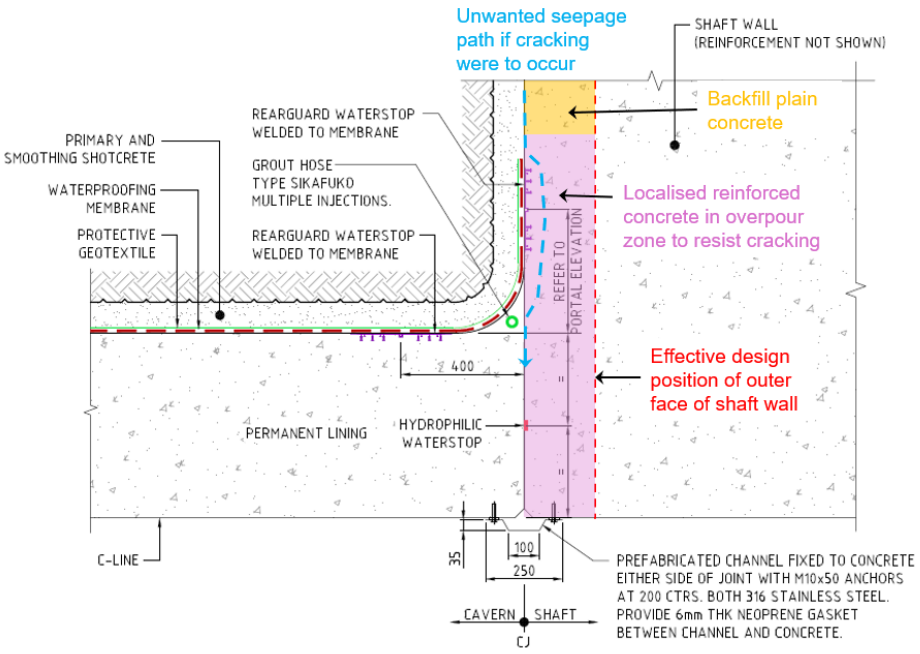


Figure 7. Cavern to Station Shaft waterproofing detail (long section)

measures included a range of support types to account for variable ground conditions, construction stage probing to identify adverse ground conditions, construction sequencing to suit ground conditions, and construction stage monitoring of ground movements to verify design assumptions.

The cavern excavation and primary support were completed on time to meet the construction program requirements for launching the TBMs from the North Cavern and commencing excavation of the mined running tunnels from the South Cavern.

ACKNOWLEDGEMENTS

The authors would like to acknowledge the Pulse consortium together with the CBGU JV for granting permission to publish this paper. The authors also wish to express their appreciation of the high level of professionalism and technical expertise provided by colleagues at PSM in the development of a practical design solution and the CBGU JV construction team for implementing the design to an exceptional standard.

We would also like to acknowledge our friends and colleagues no longer with us, in particular, vale Patrick McCormack, who was integral in the design of the CRR tunnel permanent linings, including Woolloongabba Station.

7 REFERENCES

Cammack, R., Bertuzzi, R., Smith, A. and Brehaut, R. 2022. Rock Mass Parameters for the Brisbane CBD. Australian Geomechanics, Vol. 57: No. 4, pp. 47 – 72.

Cammack, R, Shen, B., Kobler, M. 2023. Geotechnical Characterisation of the Normanby Fault Zone for Roma Street Station Cavern Design, Cross River Rail, Brisbane. Proceedings of the 18th Australasian Tunnelling Conference, November 2023, Auckland, New Zealand, pp 141-151.

German Committee for Structural Concrete. 2015. Commentary on the DAfStb Guideline 'Steel fibre Reinforced Concrete'. Berlin.

Liu, L., Tran, D., Rogan, A. and Clarke, S. 2025. Optimisation of the design of steel fibre reinforced concrete tunnel linings with the ATENA software package. Proceedings of the 32nd Biennial Concrete Institute of Australia national conference, Adelaide.

Shen, B., Clarke, S., Rogan, A. and McCormack, P. 2022. Design and Construction of Roma Street Station Cavern, Cross River Rail, Brisbane. Australian Geomechanics, Vol. 57: No. 4, pp. 115 – 128.

Standards Australia. 2017. AS 5100 – Bridge Design.

19th Australasian Tunnelling Conference – Acosta-Martínez, Stewart and Hudson-Smith (Eds.)
© 2025 Australian Tunnelling Society, ISBN 978-0-85825-002-4

Investigations for tunnels and storage caverns

I. Gray & J.H. Wood
Sigra Pty Ltd, Brisbane, Australia

ABSTRACT: This paper describes the methods that have been used in exploration for mines, tunnels and storage caverns. This exploration can be conducted from surface and from underground. The techniques include core drilling: core orientation and logging; rock stress measurement; fluid pressure and permeability testing: geophysical logging and some alternative rock testing methods that are particularly useful in anisotropic rock. The paper also considers the use of open hole drilling as a cost effective way to get a lot of information quickly and at a lower cost than coring. This particularly applies to long directional drilled boreholes which are ideally suited to many tunnel exploration cases.

1 INTRODUCTION

Sigra have been involved in the geotechnical and geofluid investigations for mines, tunnels and underground caverns in rock for 31 years. During this period a number of important lessons have been learned and new techniques developed.

The first and most important lesson is that it is not possible to produce an good design without a thorough understanding of the geology. The extent of understanding must extend beyond the construction areas as potential regional effects must also be characterised and quantified.

The simplest geology is normally associated with sedimentary sequences, but these have their complications. The strata will thin, thicken, have gradational changes and disappear. There are also unconformities to consider.

Igneous rocks may be massive plutonic batholiths, which are often made up of several injection phases. They may be dykes and sills or extrusive events that cover the surface in lava or ash flows.

Metamorphic rocks are often complex as they are frequently made up of varying original material which has been heated, squeezed and recrystalised. They may be subsequently altered.

The complications continue as the stresses will have changed in the rock mass leading to various phases of faulting and jointing. The presence of dykes and faults is an indication of the stress state at the time of their placement. They may be thought of as giant hydrofracture events. The effects of cooling may destress the rock mass substantially. Tectonic events may lead to major regional stress changes while local folds lead to local ones.

Ground fluids may be water that flows freely or is trapped and connate. The groundwater chemistry may vary widely and be acidic, saline or fresh. The fluid in the ground may not be water, but rather gas or oil. In the former case it may be held by sorption within the carbonaceous matter in the rock mass as well as in pore or fracture space. Gas is a major hazard in coal mining and can also be to tunnelling. The storage of most fluid in rock is within pore space, which can be solution cavities, or in fractures. How ground fluids flow will depend on the rock, the fluid and the fluid potential gradient which comprises pressure and gravitation terms.

It is the job of the site investigation or exploration operation to determine all of these factors which may be summarised as regional geology, lithology, structural geology, rock properties,

rock stresses, fluid type, fluid pressure, fluid storage, fluid type and the permeabilities. To what extent each of these factors is important is dependent on the nature of the underground construction and its depth. The requirements for pressurised gas storage are very different from those for a drainage tunnel.

2 DRILLING

Following an initial investigation which should include pre-existing geological information, an examination of surficial features, aerial photographic interpretation and satellite imagery the most common approach to ground exploration is by drilling.

The orientation of the drilling needs to be such that lithology changes and structural features are intersected. In flat lying sedimentary ground vertical holes will be best to pick up lithological change but may miss a dyke or a normal fault. In more complex geologies the lithological change may require angled drilling. Drilling along a tunnel alignment has appeal as it provides direct information.

In short holes conventional coring may be used but as the holes get longer wireline coring takes over as the most economical method. This can be used in all orientations, though up hole drilling requires care as does drilling in gassy formations as the risk of having a core barrel ejected by gas exists.

Core drilling is normally undertaken in vertical or angled holes from surface. When it is used at flatter angles the power requirements of the drill rig increase significantly due to friction opposing the rotation of the drill string in the hole. As holes get longer the time involved in retrieving the inner core barrel with the core become higher largely due to hydraulic issues around the drill string and core barrel. These effects combined with the time to make drill bit changes limit the economic length of a horizontal core hole to about 1 km, depending on the drill and the drilling conditions. Directional coring is possible but the core size is small and the process is slow. Typical wireline coring rates lie in the range of 10 to 40 m per day.

On option, where long holes are required, is to consider open hole drilling. If the rock is suitable this can be undertaken using polycrystalline diamond cutter bits (PCDs or PDCs in the oilfield) and drilling can proceed at rates of 100 to 400 m per day. This is an order of magnitude quicker than coring. Virtually all sedimentary rock, some metamorphic and fewer igneous rocks are amenable to the use of this kind of drill bit. Where the rock is very hard and the risk of excessive cutter damage to the PCD bit exists then recourse needs to be made to tricone roller bits but with a substantial reduction in penetration rate. Another advantage of open hole drilling is the ease at which directional control can be achieved. This can be by the use of down hole mud motors or by rotary steering systems.

Downhole mud motors are motors on the end of the drill string that rotate the drill bit and are operated by the drilling fluid that is pumped through the drill string. To be used in directional drilling they are fitted with a bend which is either located between the motor and the bit or behind the motor. In this configuration they never drill straight and the borehole trajectory will be made up of multiple arcs as the drill string is slid forward and its orientation changed. When the drill string is rotated these systems tend to drill increasingly downwards. This can be a severe limitation as the rotation of the drill string is very important in clearing cuttings in flatter trajectories.

Rotary steering systems use the rotation of the drill string to turn the drill bit. This rotation improves cuttings clearance. Directional control is achieved by having pads that push outwards from the drill string. These pads are usually mounted on a non rotating sleeve and their operation is controlled electronically. Such systems have been widely used in oil and gas drilling and have significant potential in tunnel investigation. Hybrid systems that lie between the two methods are being developed.

Under the right conditions it is possible to drill several kilometres horizontally using open hole drilling systems.

The prime limitation on drilling long holes near surface is the drilling fluid pressure gradient required to transport cuttings back up the annulus of the borehole. The longer the hole the higher the pressure gets. This can lead to the hydrofracture of the ground.

Drilling into high fluid pressures always requires the use of a properly cemented standpipe with adequate well control features to permit the withdrawal of the drill string and bit out of the hole

and to control outflow. The outlet pressure at the standpipe may need to be controlled so that the drilling fluid acts to support the hole but does not increase to the extent that hydrofracture of jointed rock or liquefaction of soft ground occurs.

3 THE CORE

Engineers and geologists like to see and retain core and it does provide the best samples. Core orientation is essential. Orientation of the core may be gained by using an orientation tool that fits at the top of the inner tube and records its down side. This can only function in non vertical holes. Alternatively, core orientation can be achieved by subsequently logging the hole with an acoustic televiewer (ATV) or optical televiewer (OTV) and matching the structural features logged in the core with those observed on the borehole wall.

The process of logging core should be taken in several stages. The first is to measure the core and determine whether the full length has been retrieved or whether some is lost or gained from the last core run. The second stage is to log the core for its lithology. The third stage is to log the structural features on the core without disturbing them so that their orientation may be determined relative to either the core orientation tool, or some arbitrary line on the core if the approach of using an ATV or OTV image for orientation is to be taken. The fourth stage is to open any joints in the core and to examine them for any infill and their roughness. The final stage is to sample the core for geotechnical testing. This requires the sampler to be competent. It is not a job for the junior person on the site. To sample sensibly requires an understanding of the underground structure to be created along with a concept of the stresses that will be imposed on the structure and that will exist within the rock mass along with the likely failure modes. It is no good taking multiple samples for uniaxial testing if the likely failure mode involves shear on a foliation or bedding plane which is approximately orthogonal to the core. The types of tests that are appropriate are discussed later.

Oriented core provides the basis for analysing structural features usually in the form of stereoplots and joint frequency measurements with orientations. These are a basis for design, not simple numbers from RQD measurements.

4 ROCK TESTING

The standard tests that are applied to rock core are uniaxial compressive testing for strength and sometimes to provide values of axial Young's modulus and Poisson's ratio. Triaxial testing is used for shear strength behaviour but suffers the same limitations in that the test result is highly influenced by the relative orientation of the core to foliation, bedding or any other plane of weakness. The tensile strength of the rock is occasionally measured using the indirect Brazilian test. Very occasionally a joint may be tested for its shear behaviour. It is unusual for testing to properly deal with anisotropy, though so much rock is anisotropic, both in its pre-failure and its failure characteristics.

4.1 Cyclic uniaxial testing

The purpose of conducting cyclic uniaxial testing is to determine at what stress the rock may start to behave in a plastic manner. This is achieved by loading to an initial stress and then unloading and checking whether there was any permanent axial or circumferential offset. This is repeated in a number of increasing load cycles. The test therefore serves to indicate the plastic offset with stress, the axial Young's modulus and the associated Poisson's ratio. The latter two may be highly nonlinear. This test is described in more detail in Gray (2020).

4.2 Triaxial testing for Young's moduli and Poisson's ratios

To be able to interpret the results of the overcore stress measurements it is essential to know the Young's moduli and Poisson's ratios of the frequently anisotropic rock. The method used to derive the different rock moduli involves step loading of a core with first an axial increase in load

followed by a confining load increase. This sequence is repeated. After the peak load is reached the sample is then unloaded in decrements. Strain gauges are used to measure strains on the surface of the core. The process enables the determination of the Young's modulus in the axial and transverse directions with the associated Poisson's ratios. (Gray, Zhao and Liu, 2018).

It is quite normal for sedimentary rocks to be significantly stiffer in the direction of bedding compared to across it, though this is not always the case. A similar effect has been observed in altered gneissic rocks where the Young's modulus was five times higher in the plane of foliation than across it. This particular specimen also showed auxetic behaviour, meaning the Poisson's ratio was negative under some stress states. Sedimentary and to a lesser extent metamorphic rocks frequently exhibit significant nonlinearity of their elastic behaviour.

While the need to determine rock properties came from the need to analyse stress from overcores the information from these tests should be incorporated into the models that are used for design. Too often numerical models have very simple isotropic linear rock properties to failure. These bear no relation to the real rock behaviour.

4.3 Shear testing

Most uniaxial and triaxial test specimens will fail in shear but unless by fortuitous circumstances of alignment the shear failure will not be on the plane of greatest weakness. The process of taking a sample and casting it in a test jig and then shearing it is time consuming and expensive. What is required is a quick shear test that will enable the rock to be tested. Gray (2020) has described two tests to do this. Both tests are reliant on the weakest plane being orthogonal to the axis of the core. This is well suited to cores from vertical holes and horizontally bedded strata. The first test is one of simple shear transverse to the core in an arrangement by which the core is supported in two lower saddles and is sheared by the action of an upper saddle pushing downwards. The core invariably breaks at one end and the shear stress readily calculated. The second test was adapted from the Russian GOST standards. It involves placing the core in a holder that is a split cylinder that can be oriented at various angles within a universal test machine. The orientation determines the ratio between normal and shear stress on loading. This test device can be readily used to measure the shear behaviour on the basis of a Mohr-Coulomb envelope. These tests are described in Gray (2020).

4.4 Tensile testing

The indirect Brazilian test to measure tensile strength relies on the core being isotropic and linearly elastic to failure. The tensile stress generated is a function of the line loading of the core and its cylindrical shape. In any rock that does not behave linearly or is anisotropic will complicate the interpretation of the Brazilian test.

The alternative is direct tensile testing. This is more expensive to perform but allows the tensile strength to be directly measured. In bedded or foliated rocks it is particularly useful in measuring the tensile strengths across and along the structural features. If the core is drilled approximately perpendicular to the foliation then it is easy to glue ends on the core and pull directly on these to find the tensile strength. The tensile strength along the bedding may be obtained by cutting a biscuit shaped specimens along the foliations and glueing this into end plates and then pulling the core apart through load on these. Laminated siltstones may show a tensile strength of 6 MPa in the direction of the foliation and 0.1 MPa transverse to it. While civil engineers like to think that they do not rely on the tensile strength of rock most or at least many of their designs in rock would fall down without it. Therefore measuring tensile strength properly matters.

4.5 Point load testing

Point loading imposes a complex loading on to the specimen being tested with crushing, shear and tensile components. The tensile or splitting strength of the rock is most important. While point load testing is often regarded as a lower cost method to obtain an equivalent uniaxial compressive strength this is probably the least useful way to use the test method. While the correlation between uniaxial compressive strength and point load test value is valid for most homogeneous elastic rocks it is not valid when the rock is nonlinear or anisotropic. Point load testing is valuable

in determining the anisotropy of the rock. The standard approach to point load testing is described by Ulusay and Hudson (2007). For isotropic rock it recommends testing along the axis and across the diameter of the rock. It recognises that anisotropic rock exists and recommends that in the case of foliated rock testing should be conducted along and perpendicular to the foliation.

Where a stronger foliated rock is of sufficient strength that breaking a sample along a foliation specifically for testing is not practical the alternative is to first test across the sample and parallel with the foliation. Secondly to test in similar material across the core diameter and perpendicular to the test made in line with the foliation.

In foliated rock a number of point load tests are typically regarded as invalid, according to the recommendations of Ulusay and Hudson (2007), because the fracture caused by point loading did not pass through the entire length or diameter of the core sample. This deficiency can be rectified by amending the fracture area to that which really exists and converting this to an equivalent diameter. Taking this approach enables a lot of tests on anisotropic rock to be used where breakage occurs along a foliation and daylights in the core ends.

5 DOWN HOLE GEOPHYSICS

5.1 Deployment method

The question of how to get geophysical sondes up near horizontal holes hundreds of metres long for logging without risking them in the event of local hole collapse has been solved by running the wireline (HRQ) drill pipe back down the hole with a special shoe and latching sub at the inner end. The geophysical sonde is then pumped down the drill pipe towing with it a disposable cable. When it has reached the end of the drill pipe it latched in place with the required portion of the sonde protruding from the end of the shoe. Logging is then achieved by pulling back rod by rod and cutting off the disposable cable and reconnecting each time. Once the system had been developed this is a relatively quick process and recently a 460 m hole was logged easily in two 12 hour shifts. The sonde location is monitored by measuring the position of the drill pipe and reconnecting the monitor after each rod was removed.

If the boreholes are slightly down dip then the problem of keeping the hole water filled does not occur. If they are up dip holes it is possible to keep them water filled if they do not leak. This does require the use of a standpipe and it complicates the process considerably.

5.2 Full wave sonic log

Experience with a sonic log in metamorphic rock has shown a remarkably good comparison between the Young's modulus and Poisson's ratio derived from the compressional and shear waves on and isotropic basis and those derived from laboratory testing. Zones of fracturing and weaker material are shown very clearly by the full wave sonic log.

5.3 Acoustic televiewer

The key to the operation of the acoustic televiewer (ATV) is to have it mounted centrally in the borehole during the logging process. This can be achieved to within 3 mm in a 96 mm diameter borehole. One of the key reasons for the use the acoustic televiewer is for the orientation of structures within the hole so as to enable these to be compared with those measured in core. An acoustic televiewer log can also be used to check on the core orientation sub at the back of the inner tube of the core barrel. The only real problems encountered by the use of an acoustic televiewer in a horizontal hole have been caused by the presence of sand (cuttings) on the base of the hole. These holes had clearly not been flushed out properly despite the rotation of the drill string whilst circulating and withdrawing it. Flushing is extremely important for a range of tests including the acoustic televiewer. Better results could be achieved with a higher flushing rate.

6 ROCK STRESS MEASUREMENT

6.1 Methodologies

Rock stress measurement may be accomplished in a number of ways depending on the rock conditions. The one method by which the full strain tensor can be obtained is by overcoring. However, it can only be used in elastic rock without failure occurring on the hole wall. Hydrofracture can be used but it gives a limited two dimensional picture of stress orthogonal to the hole. Where the larger stress is required it is necessary to have a linearly elastic rock in which the initial hydrofracture closes perfectly before reopening. Hydrojacking may be used on pre-existing joints and provides the stress normal to the joint. This is of direct relevance to pressurised conduits in the rock mass. Borehole breakout observations from an ATV image provide an incomplete picture of stress orthogonal to the hole but provide a direction and may be used with other measurements to get a picture of stress. Core ovality measurement offers the prospect of enabling the determination of the difference between the stresses orthogonal to the hole. Its use requires a core barrel that is running true and has a drill bit that has an internal taper to avoid regrinding the core. It also requires a rock that is sufficiently stressed and with a low enough modulus that the readings from it are big enough to be measured. Overall, the most combinations of stress measurement that can be brought to bear are required. Good point measurements are of limited use if it is impossible to interpolate between them. Interpolation may require the use of lesser accuracy systems to fill in the gaps. Gray (2023) describes these methods in further detail.

6.2 The IST3D overcore tool

The Sigra IST3D is a three dimensional overcore tool that has been operated in vertical holes to 800 m depth and in horizontal ones to 421 m length. The process used for stress measurement is to retrieve the last core run by wireline and then to pump in a countersink bit to grind the core stump. This is then pulled on wireline and a pilot hole-cone drilling assembly is pumped into the core barrel. It is used to prepare the end of the hole for the stress measurement cell. This system is pulled by wireline. The electronics with the cell containing 21 strain gauges are then mounted in the setting tool which is pumped into the cone-pilot hole and glued in place. When the glue has set the setting tool is retrieved and the drill string is pulled back 6 m so that the electronics may record the magnetic field data for orientation purposes. The inner tube assembly is then pumped down the hole and the cell is overcored. During this time strain data is recorded in the electronics. The electronics tool, cell and core are retrieved by wireline. The data is downloaded and the assembly is then placed in a hydrostatic test cylinder to reload the core. This provides a check on the function of the strain gauges. It also provides a basis for determining the Young's moduli of the core, provided that a mean value of Poisson's ratio may be estimated. Figure 1 shows the operation of the tool.

Obtaining the correct rock properties is extremely important. Firstly, any plastic effects must be detected as they may render the test invalid, secondly the rock's properties must be determined with appropriate orientation, hence the test methodology described in section 4.2. Using these core tests results it is possible to calculate the rock stress.

The tool is available in variants to work with PQ, HQ and NQ wireline coring operations. The NQ variant is of particular importance as so much underground exploration drilling is undertaken using this size of hole. Gray and Keloth (2025) describe results of the use of the tool and its predecessor, the IST2D tool, in a mining situation.

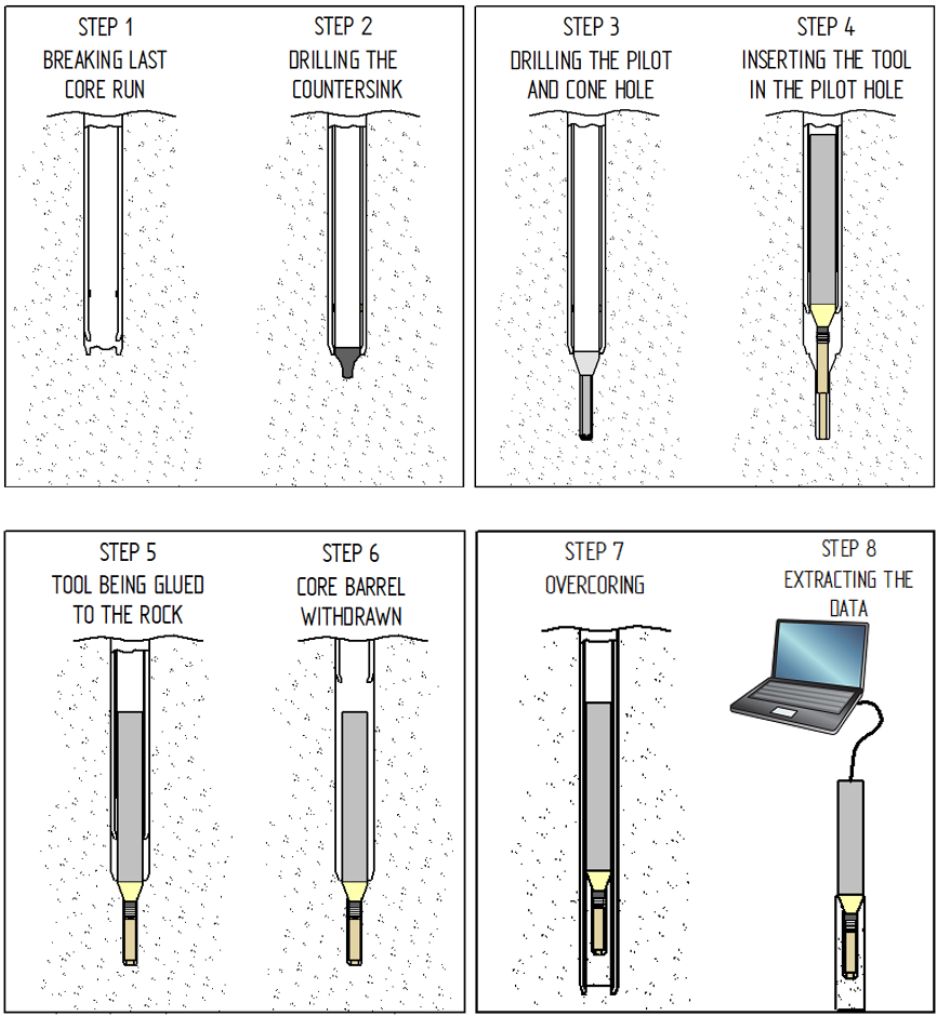


Figure 1. Operation of the IST3D overcore stress measurement system.

6.3 Examining the results

The results of stress measurement in rock are seldom without some surprises. The simplest case of flat lying of sedimentary rocks can be thought of as being under the effect of overburden weight acting in a zero lateral strain environment. To this may be added tectonic strains that load the rock laterally (Gray, 2000). There are multiple exceptions to this simple model due to faulting, folding and erosion but mostly it works, especially on the eastern side of Australia. When stress measurements are made in igneous or metamorphic rocks no such simple model may be applied. The loadings and the strains which have created them are complex

7 PERMEABILITY AND FLUID PRESSURE TESTING

7.1 Test methodology

The two key fluid related parameters that are required for the design of an underground openings are the permeability and the natural fluid pressure within the ground. These enable the determination of fluid influx and efflux during mining and operation.

To obtain these parameters by investigation from a borehole it is necessary to seal a test section and to wait as long as possible for stabilisation of pressure. The test section should then have a flow induced into or withdrawn from it. The test section should then be sealed again and the pressure allowed to recover. The analysis of such a test is based on knowing the flow rates with time and the pressure change following shut in when there is no flow. The analysis is of the

transient pressure recovery is with respect to a function of time and flow. This is standard petroleum practice and has many advantages. The most important of these is that the effects of local variations in permeability near the borehole are eliminated from the analysis and static fluid pressure may be estimated. The basis of this is the work by Horner (1951) extended by superposition to the multi flow rate situation. Analysis by type curves (Bourdet, Ayoub & Pirard, 1989) can be used but tend to be less fruitful in a fractured rock situation.

Sigra has recently conducted some testing in 450 m horizontal holes drilled from underground. Two packers were run in hole to test depth on the end of an HRQ drill string with a 29.4 m straddle. The choice of new HRQ rods was made because these can be readily and reliably sealed with thread tape wound on and over the end of their pin thread. Achieving this level of sealing requires extreme cleanliness on assembly. Above the straddle was a main valve which was fully balanced, meaning that changes in pressure in the test zone, or in the rods above the test zone, did not cause it to open or shut. The main valve was opened, connecting the test zone with the drill pipe, by pulling the drill string toward the hole collar and closed by pushing the drill string into the hole. A pump in head that contained pressure transducers and electronics was then pumped to latch on to a spear connection above the valve trailing a geophysical tool wireline. The top of the drill pipe was then sealed around the wireline with a side port for injection or outflow from the drill string. The geophysical wireline carried digital signal information from the transducers monitoring the test zone, packer and in-pipe pressures and a temperature sensor in the downhole tool to a display on a laptop at the collar of the hole.

The test zone was then flushed and the drill string slid into the hole to shut the main valve. The packers were then inflated to by pressurising the drill string. The effect of packer inflation could be immediately seen on screen at the collar of the hole. It manifested as a pressure rise in the test zone between the packers if the tests zone was tight. The pressure rise and the rate at which it dissipated was a good indication of near well bore permeability before full testing started.

The pressure must be allowed to settle in the test zone before the main test. Depending on this pressure, two types of tests were conducted. If the test zone pressure was less than half hydrostatic a decision was made to inject water into the test zone at a pressure to near hydrostatic. If the stable pressure was above half hydrostatic the hole was permitted to flow and the outflow was measured.

Flow monitoring is best accomplished by positive displacement flow meters. Obtaining these can be difficult particularly as the flow rates are usually not known prior to a test. Sigra built one for its own operations that is accurate to 10 ml in 3 litres and can measure flows up to 3.5 litres/second.

At the end of pressure recovery from each test the packers are depressurised and the geophysical cable withdrawn with the pump in instrumentation head. The drill pipe is then shifted to cover the next test interval. The process was then repeated. In new equipment the need to recover the geophysical cable is avoided and a sacrificial cable is used instead. This speeds the process.

7.2 Testing characteristics

The system works well and has been used to measure permeability measurements down to 1×10^{-18} $m^{2.}$, the equivalent of 1.3×10^{-11} m/s with water at 33ºC. It could be used to measure permeabilities six orders of magnitude higher if the high permeability zone could be isolated and the operation at the drill rig were not inundated. The main constraint on low permeability measurement is time. It takes time to achieve pressure stabilisation before flow and though the flow period can be short it takes time to achieve an analysable recovery.

A complication is the time a horizontal hole takes to be drilled. This may allow significant depressurisation. The consequence of this is that full stabilisation is not achieved on shut in before flow. If the flow is by injection the draw down following shut in occurs rapidly but with longer times the pressure starts to rise as the test section starts to recover to the original ground fluid pressure. This can compromise the analysis. It may be best to test sections of a hole at each core bit change so as to avoid depressurisation problems. These are not generally as severe in vertical holes as drilling fluid pressure is frequently similar to the stabilised pressure in the test zone.

It is important to consider how much ground has been tested so as to gain an understanding of the applicability of the measurements. By assuming a porosity-compressibility product it is possible to arrive at a mean effective radius of investigation for each test.

8 CONCLUSIONS

The methods described in this paper may be readily and reliably used with HQ core drilling to beyond 1 km. This means that rock stress may be measured, geophysical sondes run and permeability and fluid pressure determined. The option of drilling directional open holes is discussed as an economic option. This can be used with torque and thrust sensor located behind the drill bit and with a drilling rate sensor on the drill. In this form can provide information at the hole collar on the rock being drilled. Open holes may be geophysically logged to provide important geotechnical information and where uncertainty exists it is quite possible to cut a branch off the main hole and then core the area of uncertainty. Not all situations are suitable for such long hole directional exploration drilling.

The testing of rock core has been discussed with a view trying to get the right measurements being made. This requires careful thought about the underground structure and the modes of loading it may endure. The rock test method needs to be tailored to suit this and the characteristics of the rock which are frequently anisotropic, non-linear and may also behave plastically. Tests which can extract the relevant information are outlined and include cyclic uniaxial, triaxial, shear, tensile and point load testing. The methods suggested are a little different from current practice. Choosing what needs to be tested and how it is tested is not however a job for the inexperienced.

Overall, the paper tries to present a short space the philosophy and technology developed by Sigra as to how obtain the right information for the design for projects in the ground.

9 REFERENCES

Bourdet, D. Ayoub, J.A. & Pirard, Y.M. 1989. Use of pressure derivative in well test interpretation. *SPE Formation Evaluation, vol. 4, no. 02,* 293–302. https://doi.org/10.2118/12777-PA

Gray, I. 2000.The measurement and interpretation of stress. In J.W. Beeston (ed.), *Bowen Basin Symposium 2000: The new millennium – Geology.* Proc conf. Rockhampton, Qld, 22-24 October 2000. Bowen Basin Geologists Group and the Geological Society of Australia. Coal Geology Group.

Gray, I. Zhao, X & Lui, L. 2018. The determination of anisotropic and nonlinear properties of rock through triaxial and hydrostatic testing. *Asian rock mechanics (ARMS 10)* Proc, intern conf. Singapore, 29 October to 3 November, ISRM.

Gray, I. 2020. Rock property determination. In J Wesseloo (ed). *Underground mining technology*. Perth, 3–4 November 2020: Australian Centre for Geomechanics. ISBN 978-0-9876389-9-1.

Gray, I. 2023. The fundamentals of stress measurement in rock. *Proc. 14th Australia and New Zealand conf. on* geomechanics. Cairns Queensland, Australia. 2-6 July 2023.

Gray, I. & Keloth, R. 2025. Stresses within the area of a longwall in massive strata. *Resource Operators Conference. Proc. Conf., Brisbane, 6-7 February 2025.* https://doi.org/10.71747/uow-r3gk326m.c.7651142.v1

Horner, D.R. 1951. Pressure build up in wells. *Proceedings of the Third World Petroleum Congress*.

Ulusay, R. & Hudson, J.A. 2007. Suggested method for determining point load strength. *ISRM point load test. Suggested methods prepared by the commission on testing methods.* ISRM Turkish national group. Ankara, Turkey.

19th Australasian Tunnelling Conference – Acosta-Martínez, Stewart and Hudson-Smith (Eds.)
© 2025 Australian Tunnelling Society, ISBN 978-0-85825-002-4

Snowy 2.0 Down Stream Surge Shaft Chamber Geological/Geotechnical Hazards and Design Challenges

A. Palomo, J. Sotomayor, S. Nosrati
Snowy 2.0 Design Joint Venture, Lombardi Engineering PTY. LTD., Cooma, NWS, Australia

D. Hughes
Snowy Hydro, SMEC Dams and Hydro, Canberra, ACT, Australia

ABSTRACT: The Snowy 2.0 Down Stream Surge Shaft Chamber (DSSC), with approximately 37 m in width, is one of the world's widest chambers ever built in hydropower projects, if not the widest. Once construction is completed, the chamber will provide sufficient underground space to accommodate the equipment for excavating the downstream surge shaft with a 28 m excavation diameter and 200 m depth using raise boring and shaft sinking methods. Considering the size of the DSS chamber, the geological and geotechnical conditions become even more prominent and critical to ensure the safe design and work environment during the shaft excavation considering the 150 years of project life during the operational phase. The detailed design of the DSS chamber was completed in 2024, followed by construction, which will be completed in the first quarter of 2025. This paper presents the geological and geotechnical hazards and associated risks identified during the ground investigation stage, the foreseen ground behaviours and the challenges the designers faced during the design stage, involving solutions and design decisions made by the Design Joint Venture (DJV). This paper also provides information on adopted construction sequences and methodologies, limitations, and preliminary design verification by the use of the observational method, which assesses geological and geomechanical conditions, geotechnical monitoring, and instrumentation data acquired during the construction phase.

1 INTRODUCTION

1.1 *General Layout*

The Snowy 2.0 Pumped Storage Power Plant (PSPP - Snowy 2.0) is a major pumped-hydro expansion of the existing Snowy Scheme, located in the Kosciuszko National Park (New South Wales, Australia). The project aims to increase the scheme's generation capacity by 2,200 MW and will connect the existing reservoirs impounded by the Tantangara and Talbingo dams, via approximately 27 km of power waterway tunnels and an 800 m underground power station.

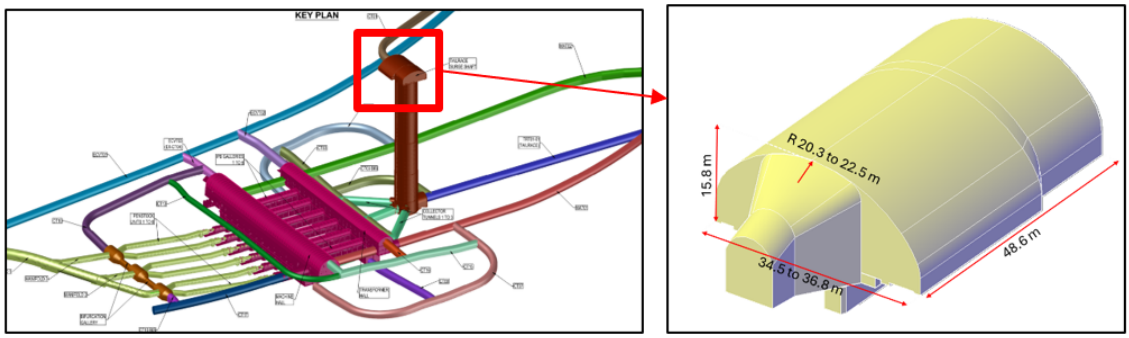


Figure 1. General layout of the Power Station Complex (PSC, left): Geometry of the upper chamber (right).

As part of the powerhouse complex, the downstream surge shaft is an equilibrium chimney with a chamber located at the top. The chamber is connected to the CT01connection tunnel via a transition zone and extends 48.6 meters in length. The cross-section is asymmetrical for the first 33.1 meters due to a lateral egress path, totalling 36.8 m in width. Beyond the egress path, the cross-section becomes symmetrical, with an overall width of 34.5 meters to accommodate the downstream surge shaft collar, excavation equipment and a gantry crane. The maximum height of the cavern is 15.8 meters for both asymmetrical and symmetrical sections (Fig.1). With its significant dimensions, the upper surge shaft chamber is the widest underground structure in the Snowy 2.0 project and one of the widest in the world.

1.2 *Geomechanical Inputs*

The DSS is entirely placed within the interbedded and interlayered siltstones and sandstones of the Ravine Beds West Formation (RBW). The rock mass is of good quality, with generally high RQD and GSI values. The initial geological and geotechnical assessment outcomes revealed the unlikelihood of certain ground conditions and, subsequently, ground behaviours and ground response to the drill and blast excavation associated with soft ground, groundwater, and high induced stress conditions. Therefore, the focus for the detailed design analyses remained on the discontinuity-driven and stress-related behaviour of the rock mass. Analyses revealed that there are no significant risks associated with the in-situ and induced stress behaviours, or with the influence of water.

The rock mass parameters and discontinuities used in the design were based on the evaluation of geotechnical investigations conducted in the area, including geological face mapping data obtained during the excavation of the CT01 inclined connection tunnel (Tables 1 and 3).

Table 1. Geomechanical properties assumed in the design

H [m]	K [-]	g [kN/m^3]	σ_{Ci} [MPa]	m_i [-]	D [-]	E_i [MPa]	GSI [-]	ν [-]	E_{rm} [MPa]	c [MPa]	φ [°]
540	1.7	27	55	7	0	45000	67	0.1	30327	2.288	39.0

2 DESIGN

2.1 *Excavation Sequence and Support*

Validated through the use of numerical models, the designed support system of the upper chamber primarily caters to discontinuity-driven behaviour and consists of primary and secondary arrangements. The design approach prioritises rock bolts as the primary element of the support system, providing sufficient and safe resistance loads against the possible formation of wedges and blocks. The chamber shotcrete lining was designed to serve two main functions: providing continuity and uniformity for the support system and securing minor wedges and blocks that may occur between rock bolts [10], thereby enhancing the overall shear resistance of the support system.

The chamber primary support system was designed to provide adequate and safe resistance to the likely probable wedges formed during multi-stage excavation. It includes 25 cm thick reinforced shotcrete (SFR40) with wire mesh (SL81) and 8 m long rock bolts (CT26WR) in a 1.90 x 1.90 m pattern.

The secondary support system was designed to provide long-term and safe conditions by supporting the probable largest wedges formed, considering the full span of the chamber. This includes an additional 15 cm thick reinforced shotcrete layer and wire mesh (SL81), as well as 11.8 m long rock bolts (CT26WR) in a 1.90 x 1.90 m pattern.

Due to the span of the chamber, the method designed for the surge shaft chamber excavation follows the multiple stages drill & blast approach. After each advance of excavation within several stages, the installation of the support system is to be completed as per the following sequence (Figure 2):

- Stage 1: CENTRAL TUNNEL: Excavation of the central top heading pilot tunnel and installation of the primary support;

- Stage 2: CENTRAL TUNNEL: Bench excavation of the central top heading floor by 2.5 m; installation of the secondary support, 11.80 m long CT-Bolts;
- Stage 3: EAST: Side slashing in 3.80 m advances and installation of the primary support, followed by secondary support. When completing 12 m of fully supported excavation at the east side, the west side slash excavation can be started (See figure 2.b);
- Stage 4: WEST: Excavation of the side slashing in 3.80 m advances and installation of primary support, followed by secondary support; and
- Stage 5: Excavation of the final bench and installation of primary and secondary support.

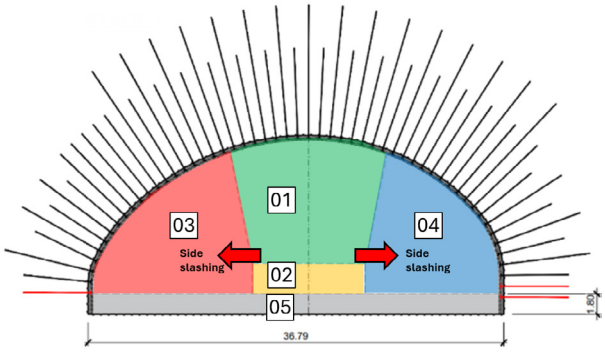


Figure 2. Cross section excavation stages and side slashing for stages 3 and 4.

2.2 *Numerical modelling*

Considering the chamber's favourable ground conditions and based on the outcomes of the initial geotechnical assessment, the ground behaviours associated with the in-situ and induced stresses are not foreseen. The numerical analysis results still provided valuable information and helped validate the earlier findings.

Both 2D and 3D-FDM FLAC numerical models were used to analyse the behaviour of the rock mass related to the stresses during the excavation stages. The main purpose of the models is to verify and confirm the feasibility of the chosen chamber geometry and excavation sequences in terms of total displacements and distribution of plastic zones; and to determine the behaviour of the rock bolts.

A strain-softening behaviour method is shown in Table 2, utilising friction angle and cohesion parameter reductions as functions of plastic shear strain, was employed. Each element of the model, until reaching the first plasticisation, the strength parameters considered are the peak values. Once this limit is exceeded, plastic shear strain begins to occur, initiating a linear reduction in the strength parameters until reaching post-peak values at a plastic shear strain of 2%, which remains constant.

Table 2. Parameters of the strain-softening model used

TYPE	OVERBURDEN	γ	ν	E_{rm}	c	φ	$K_{0,H}$	$K_{0,h}$	ψ
	[m]	[kN/m^3]	[-]	[MPa]	[MPa]	[°]	[-]	[-]	[°]
Peak	540	27	0.1	20200	2.29	39.0	2.1	1.3	5
Post-peak	540	27	0.1	20200	1.64	29.4	2.1	1.3	5

For the analysis of the three-dimensional behaviour of the cavern, and in particular, the excavation sequence effect and the interaction with the shaft's excavation, a 3D model has been performed. The analysis of the induced stress distribution and ground deformation in response to the excavation around the DSS was done without including the support system (Figure 3).

The results provided by the 2D and 3D continuous models are consistent and completely aligned. Limited by the modelling of the shaft excavation, the 2D model results adequately present the behaviour of the ground in response to the chamber excavation.

Figure 3 shows the analysis outcomes indicated a maximum total displacement of 3.5 cm, an extension of the plastic zone of 11 m in the crown, and a plastic shear strain of less than 1.5%.

Rock bolts showed good behaviour with limited plastic zones and axial displacement within the acceptable range.

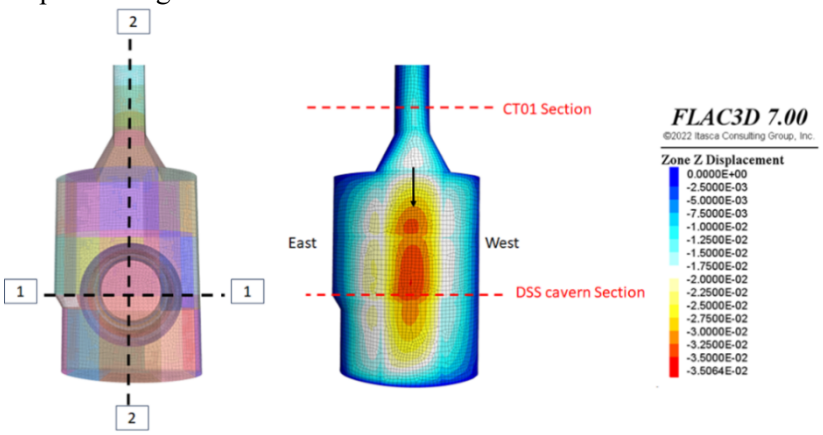


Figure 3. 3D numerical model for the DSS chamber showing stress distribution and estimated displacement.

The maximum representative rock wedge is defined by combining both the limit equilibrium method analysis (purely discontinuum rock mass model) with stress-strain modelling (purely equivalent-continuum rock mass model). In fact, within the cavern's plastic radius and according to plastic shear strain concentration, the development of new fractures contributes to free rock volumes whose shapes and dimensions cannot be predicted solely by the geo-structural conditions of the rock mass.

2.3 *Discontinuous analysis (Wedges)*

Unwedge analyses have been carried out using the discontinuities defined by the geomechanical model, applying load factors to the acting forces, reduction factors to the resisting forces, and imposing a global safety factor of 1.
Different load combinations are considered in the calculations, where load and reduction factors have been applied according to AS-1170 [12], the reduction factor for shotcrete shear strength according to AS-3600 [13], and the reduction factor for the resistance of rock bolts according to AS-5100.3 [14].

2.4 *Maximum wedge over the crown*

The dimensioning rock volume weight is assessed by considering all the key controlling geological and geomechanical features, which include geo-structural discontinuities and the geotechnical properties, as well as the plastic behaviour of the rock mass around the excavation. For the latter, different rock volume shapes and dimensions are considered. The proposed analytical approach considers the maximum triangular wedge geometrically possible at the cavern roof.

The resulting wedge shape is not strictly related to the orientation of existing natural discontinuities in the rock mass. The orientation of the planes delimiting the wedge is defined by considering the most unfavourable conditions. Figure 4 presents that the dimensioning wedge does not depend on actual rock mass quality or discontinuities orientation, but on the shear strength of the rock joints and external acting forces.

When the opening of the wedge is more than double the friction angle (φ), the wedge is unstable and requires support pressure to avoid failure. On the other hand, the wedge is considered stable if the opening is less than two times the friction angle because the sub-horizontal forces acting on

the lateral faces tend to lock the wedge in place. Therefore, the friction angle of the discontinuities defines the maximum opening and depth of the potentially unstable wedge.

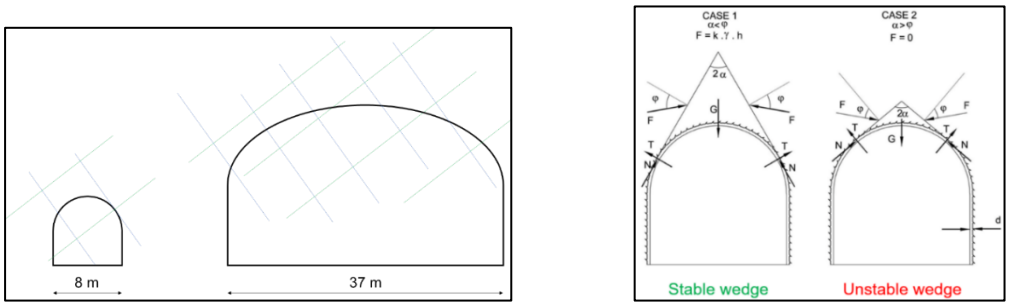


Figure 4. Maximum wedge dimensioning by shear strength of the joints and external acting forces (left) and wedge stability according to shear strength of the joints and external acting forces (right).

3 DESIGN VERIFICATION USING THE OBSERVATIONAL METHOD

Throughout the excavation and after the completion of Stage 1 and the initial advances of Stage 3, the verification of the geomechanical model, the likelihood of unfavourable wedges forming, evaluation of the design support, confirmation, and characterisation of the encountered geology and geological structures were carried out using the observational method. Further assessments are to be carried out using the same principle for the subsequent excavation phases of the chamber, based on data collection from probe holes, monitoring, and site information, among other sources.

3.1 *Geological Conditions of the Central Tunnel*

Excavations of the Central Tunnel confirmed the presence of well-defined interbedded siltstone and sandstone of the Ravine Beds West, identified as being in fair to good quality, dry conditions, with few joint sets. No signs of overstressing were observed on Stage 1 to initial advances of Stage 3.

Consistent with a GSI value of 67 assumed in the design, the rock mass is characterised by an average RMR of 66 GSI, ranging from 65 to 75, with an average of 66 as shown in figure 5 (based on a 10-point rating assigned during face mapping).

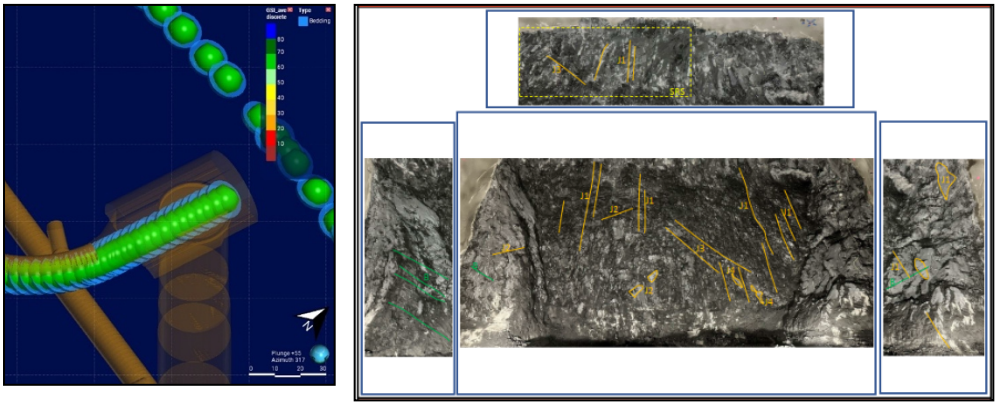
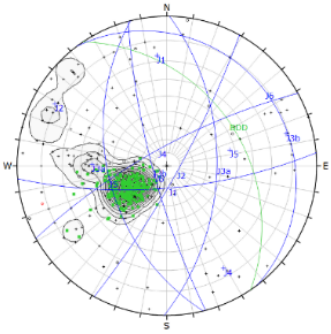
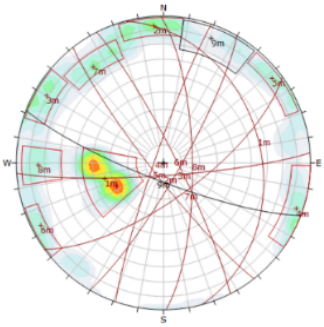


Figure 5. Distribution of RMR and GSI for the DSSC Stage 1 to initial advances of Stage 3.

The identified dominant joint during excavations aligned with those defined in the design. Additionally, the sets (table 3) indicate minor rotations in dip and the direction of dip. The rock mass proved to be of good (favourable) quality, with only one healed sheared feature was identified during the key cuts of the initial advances of the Stage 3 excavation. In general, the sets had a persistence of less than 3 m, undulated, slightly rough, and with apertures less than 1 mm and hard infill

Table 3. Discontinuity sets identified in the Central Tunnel and considered in the design.

Set	DSS STAGE 1 Dip/Direction of Dip		DESIGN Dip/Direction of Dip	
Bedding	35/056		34/075	
J1	71/163		83/176 (J1)	
J2	80/111		81/120 (J2)	
J3A	53/090		83/063 (J5)	
J3B	79/255		83/232 (J4)	
J4	77/335		85/289 (J3)	
J5	44/256		-	
J6	11/053		70/144 (J6)	
J7	-		74/089 (J7)	
J8	-		80/201 (J8)	

3.2 *Geotechnical Monitoring and Ground-Support System Evaluation*

In accordance with the design, the ground-support system and the identification of potential large-dimension wedges are evaluated through geotechnical monitoring of multiple sections along the excavation. Geotechnical monitoring presented in figure 6, included total displacement monitoring points, multiple rod extensometers, anchor load cells, laser scans, systematic and non-systematic shear displacement monitoring, and transversal probe hole investigation.

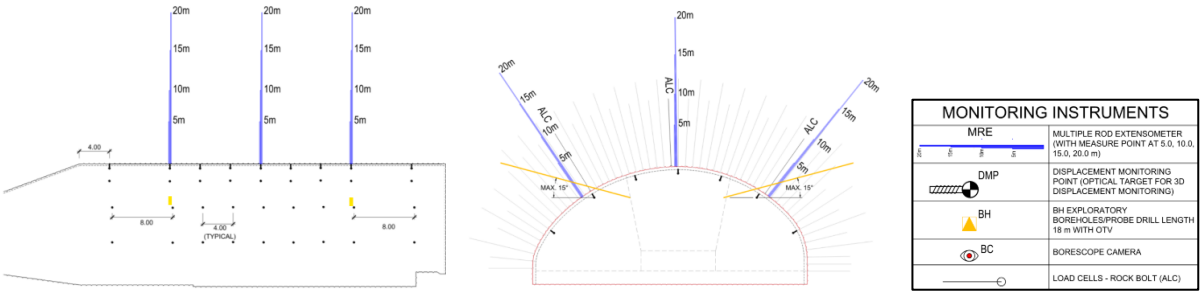


Figure 6. Geotechnical monitoring of the DSS chamber with the location of DMP's, MRE's. ALC's.

The total displacements recorded at the monitored sections during Stage 1 excavations remained stable, with values of less than 13 mm. Rock bolt load cells recorded less than 5 kN, and extensometers recorded less than 1.7 mm (Table 4).

The systematic shear displacement monitoring carried out on the designed 89 mm and 10 m long drainage holes, using an endoscope, showed a dry, very homogeneous rock mass where sheared features were not detected. OTV inspections of the four executed transversal probe holes, drilled towards Stage 3 and 4, also did not confirm the presence of sheared surfaces.

Table 4. Geotechnical monitoring results of the DSS during Stage 1 excavations

SECT. TYPE	INTSTR., QUANT.[2]	DIST. OF APPL.	CHAINAGE, MAXIMUM VALUE[1]								
			0+004	0+012	0+016	0+020	0+024	0+028	0+032	0+036	0+044
SU1	DMP, 7	Ea. 4 m	< 9.3		< 10.1	< 10.4	< 10.0	< 9.8	< 10.9		< 10.7
SU2	DMP, 7 MRE, 3 ALC, 3	Ea. 20 m		< 8.0 -0.6 < 5			1.7 < 5			< 12.5 -0.6 < 5	
SU3	DMP, 5	At Sheared Plane	No sheared features were identified during the excavations of Stage 1.								

[1] DMP (displacement monitoring point, total in mm), MRE (multi rod extensometers, mm), ALC (anchor load cells, kN).

[2] Quantity of instruments is detailed for full excavation span.

Non-systematic shear displacement monitoring was carried out for the single shear identified on the face mappings of Stage 3 initial cuts via endoscopic inspection of the drainage hole in proximity to the identified feature. The presence of sheared features was not confirmed.

Shotcrete deterioration, such as cracks, spalling, or deformation indications on the support, including rock bolts, during the excavation activities of Stage 1 until the initial advances of Stage 3, was not reported.

3.3 *Ocurrence of overbreaks and support verification*

The most critical overbreaks of the Stage 1 excavation were identified at chainage 0+001 and 0+021, with lengths of 0.63 m and 0.77 m, respectively. A trend of overprofiling and construction-related overbreaks towards the crown and right-side walls can be attributed to the presence of bedding planes in combination with sub-vertical sets (J2 and J3b).

The primary support was verified in both the temporary and permanent phases using Unwedge (figure 7), considering the discontinuities identified in the face mappings. The assessment confirmed, aligning to the design, that the potential wedges have a FoS greater than 1.

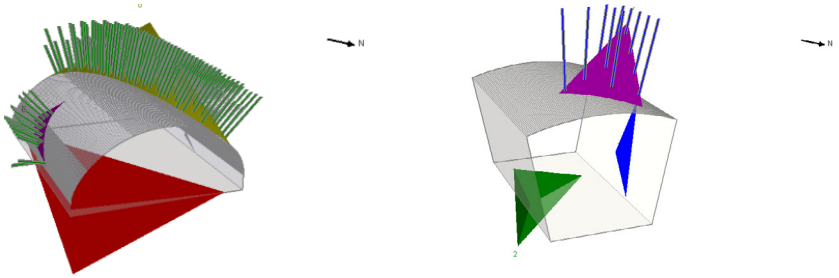


Figure 7. Discontinuous Unwedge analysis for design (left) and stage 1 central tunnel temporary phase (right).

4 GEOTECHNICAL RISK MANAGEMENT AND DESIGN OPTIMISATION

For the mitigation of any geotechnical risks associated with the design of such wide excavations, as is the downstream surge shaft excavation, the potential formation of the largest possible wedges on the full span of the excavation was evaluated and detailed.

This risk was then translated into the execution of the excavation by performing transversal probe holes and shear displacement monitoring to identify any possible shear features. Systematic and non-systematic shear displacement monitoring was also prescribed in the design and later executed during excavation activities.

The multi-staged excavation sequence was halted at defined locations and excavation phases by the execution of different hold points. Hold points consisted of evaluating the design assumptions against the actual conditions before allowing the continuation of new stages of excavation. The confirmation of the design assumptions according to the encountered conditions permitted for design optimisations on the sequence of execution of the chamber.

5 DISCUSSION AND CONCLUSIONS

The downstream surge shaft of the Snowy 2.0 Pumped Storage Power Plant, one of the widest in the world and currently under construction, is an equilibrium chimney with a chamber localized at the top.

The detailed design was undertaken based on the available geotechnical investigations and face maps of the connecting tunnel structure to the chamber. The primary support is designed to hold the possible wedges during the multi-stage excavation, while the secondary support is designed to hold the largest wedges that may form across its full span. The design was evaluated using 2D and 3D numerical modelling for the analysis of rock mass behaviour and rock bolts during excavation, considering strain-softening behaviour. Both the 2D and 3D models aligned, adequately

reproducing the behaviour of the excavation, including the displacement, dimension of the plastic zone, and plastic shear strain. The representative wedges formed were defined with limit equilibrium analyses with a discontinuum rock mass model and a stress-strain modelling for an equivalent-continuum model. Discontinuum analysis used different combinations of acting forces, loads, and reduction factors for the resisting forces to achieve a global safety factor of 1.

The verification of the geomechanical model used in the design was conducted using the observational method, which involved assessing the characterised geology, geologic structures, the formation of potential wedges, and stability evaluation. For this purpose, geological face mappings, probe hole data with OTV, laboratory test results, overbreak reports, shear displacement monitoring and geotechnical monitoring data were used.

The analysis confirmed that the rock mass parameters have similar values to those assumed in the design. The very few shears identified during excavation were not confirmed during shear displacement monitoring and transversal probe holes. Therefore, the presence of sheared features that could potentially form a large wedge encompassing the full span of the excavation was not confirmed. The analysis of the reported overbreaks and actual conditions permitted the validation of the support. The installed support has not presented any indication of deformation or deterioration.

6 ACKNOWLEDGEMENTS

This document was supported by Lombardi Engineering PTY LTD as part of the design resident team at the Snowy 2.0 Pumped Storage Power Plant. Snowy Hydro Limited is acknowledged for permission to publish this document. The support of the colleagues and team members of Future Generation Joint Venture, Snowy Hydro Limited and Lombardi Engineering PTY LTD is greatly appreciated.

7 REFERENCES

[1] Amberg A., Lombardi G. 1974. An elasto-plastic analysis of the stress-strain state around an underground opening. 3rd International Congress of Rock Mechanics, Denver.
[2] Bieniawski, Z.T. 1989. Engineering rock mass classifications. New York: Wiley.
[3] Cai M., Kaiser P.K., Uno H., Tasaka Y. and Minami M. 2004. Estimation of Rock Mass Deformation Modulus and Strength of Jointed Hard Rock Masses using the GSI system. International Journal of Rock Mechanics and Mining Sciences n.41, pp.3-19.
[4] Cai M., Kaiser P.K. et Al. 2007. Determination of the residual strength parameters of jointed rock masses using the GSI system.
[5] Hoek E., Carranza-Torres C., Corkum B. 2002. Hoek-Brown failure criterion-2002 Edition. Proc. North American Rock Mechanics Society.
[6] Hoek E., Diederichs M.S. 2006. Empirical estimation of rock mass modulus. International Journal of Rock Mechanics & Mining Sciences 43, pp. 203-215.
[7] Hoek E., Marinos V., Marinos P. 2005. The geological strength index: applications and limitations. Bull. Eng. Geol. Environ., 64.
[8] Hoek, E. – Brown E.T. 1982. Underground excavation in rock. The institution of Mining and Metallurgy, London.
[9] Lunardi, P. 2000. Design and constructing tunnels - ADECO-RS approach. T&T International special supplement
[10] S.V.L Barrett, D.R. McCreath. 1999. Shotcrete support design in blocky ground: towards a deterministic approach
[11] Walton G., Labrie D. et Al. 2019. "On the residual strength of rock and rock masses" – Rock Mechanics and Rock Engineering.
[12] AS/NZS 1170.0:2002 – Structural design actions – Part 0: General principles – Standards. Australia Ltd.
[13] AS 3600:2018 – Concrete Structures AS 5100.3:2017: Bridge design -Foundation and soil-supporting structures

19th Australasian Tunnelling Conference – Acosta-Martínez, Stewart and Hudson-Smith (Eds.)
© 2025 Australian Tunnelling Society, ISBN 978-0-85825-002-4

Observational method for the deep powerhouse cavern construction of Snowy 2.0 project

I. Ching
SMEC Pty. Ltd., Sydney, NSW, Australia

M. Diederichs
Queen's University, Kingston, Ontario, Canada

B. Chapman
Snowy hydro Limited, Cooma, Australia

K. Thermann
Tractebel Engineering, Germany

K. Acharya
Future Generation Joint Venture, Cooma, NSW, Australia

ABSTRACT: The Observational Approach for geotechnical design and construction was discussed by Bjerrum and Terzaghi in the early 1960's as a means to cope with the uncertainty of working with Earth materials. In 1999, CIRIA R185 suggested "The Observational Method in ground engineering is a continuous, managed, integrated, process of design, construction control, monitoring and review…" This paper highlights the application of observational method for the design and construction of the deep powerhouse caverns of Snowy 2.0 project which is a 2200MW pumped storage expansion to the existing Snowy Hydroelectric Scheme. From establishing the design assumptions and acceptance criteria; to support performance prediction and construction control monitoring; and finally, the review and back-analysis based on the observed ground responses and ground conditions, the complete cycle of observational method with design, monitoring, re-analysis and response has been demonstrated.

1 BACKGROUND

The Observational Approach for geotechnical design and construction was discussed by Bjerrum and Terzaghi in the early 1960's as a means to cope with the uncertainty of working with Earth materials. Rather than defining, a priori, all underground conditions, the project team conducts exploration to define the nature, pattern and range of properties, assess the most probable deviation from these conditions, establish a design based on most probable condition, with a toolbox of modifications to the design should there be a foreseeable deviation. Measurable quantities during construction are to be determined and monitored. The as-built design is then verified or modified to suit actual conditions. Similarly, CIRIA R185 "Broadly speaking, the Observational Method (OM) is a process in which acceptable limits of structural and geotechnical behavior are established. In addition, performance predictions, monitoring, review and modification plans, and emergency plans, are fully prepared." This method served geotechnical engineering well, but as Peck observes, ""It is essential that the quantities to be observed should reflect the phenomena that will actually govern the behavior of the works to be constructed....A mistaken preconception of the nature of the problem may lead to omission of observations of types that would have disclosed the real reasons for concern." Rather than utilizing a codified classification scheme for conditions, or relying on standard measurements such as closure, conditions to be recorded, quantities to be observed, and triggers for response, must be relevant to the instability mechanisms anticipated. The application of OM for the powerhouse cavern construction of Snowy 2.0 project has been agreed in the early stage of the project due to its complexity. Both ground conditions as well as ground performance are integrated into an observational design cycle with design, monitoring, re-analysis and response tailored to specific deformation and instability modes identified during investigation and pre-construction modelling.

2 SNOWY 2.0 PROJECT

Snowy 2.0 is a major renewable energy infrastructure project located in the Kosciusko National Park (KNP) in southern NSW Australia, currently under construction. Upon completion, the project will increase the generating capacity of the existing Snowy Hydroelectric Scheme by 2200 MW. The project links two existing reservoirs, Tantangara (elevation 1231 m) and Talbingo (elevation 546 m), through 27 km of waterway tunnels and an underground power station equipped with 6 Francis pump-turbine units. The project also includes more than 10 km of access tunnels. The project is owned and operated by the Snowy Hydro Limited (SHL). The design and build contract has been awarded in 2019 to the principal contractor Future Generation Joint Venture (FGJV) and a Design Joint Venture (DJV) has been appointed by the contractor to carry out the engineering design for civil and mechanical and electrical works. The project has introduced new contract arrangements following a major project reset in 2023.

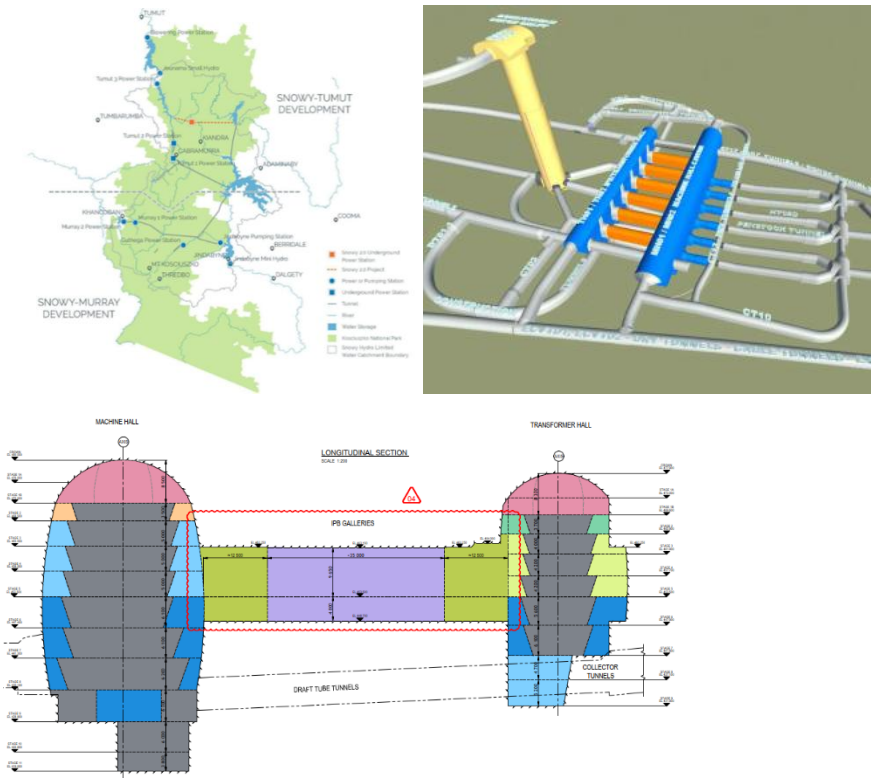


Figure 1. Snowy 2.0 project location (top left); Power station complex isometric view (top right); Cross-section of PSC and excavation stages (bottom)

3 THE POWERHOUSE CAVERNS

The Power Station Complex (PSC) is within the Ravine Beds West (RBW) formation at about 750m below ground in sedimentary rocks (predominated by interlaminated and interbedded siltstone and sandstone) with two main caverns, the Machine Hall (MH) and the Transformer Hall (TH) connected by the axillary tunnels. The 251m long, 32m wide and 52m height Machine Hall will host six units of pump-turbines, motor-generators, main in-let valves. The TH where the six main transformers, draft tube valves and cooling water equipment are located, is 217m long, 20m wide and 46m height. The distance between the two main caverns is 60m. There are two Main Access Tunnels (MAT and ECVT) and six Isolated Phase Busbar (IPB) tunnels which house the electrical equipment required between the motor-generators and the main transformers. The IPB tunnels are 10m wide and 14.5m high. The pillar width between IPB tunnels are 18m to 19m. The

caverns have been excavated by conventional Drill and Blast (D&B) method with heading, benching and side-slashing excavation sequence. The design has considered 11 and 9 stages excavation for the MH and TH respectively (Refer to Figure 1).

4 DEFINITION OF ACCEPTANCE CRITERIA

4.1 *Global stability criteria*

According to the Employer's Requirements (ER) of the project, the general design criteria of PSC must achieve functionality, stability, and safety along the entire design life of the Project. The design shall ensure safety during construction and operation, considering uncertainties known and unknown (local variability of rock behavior and unexpected conditions). For the functionality requirement, the design must fulfill the space proofing requirement to host the facilities in the IPB gallery tunnels connecting the generators in the MH to the transformers in the TH, as well as various other important electrical equipment related to the reversible pump-turbines units. Stability was referring to the design must provide a sufficient margin against the state of failure without excessive deformation and/or progressive failure over the design life.

The design requirement of rock pillars between IPB was the critical criteria for the global stability of the caverns. It also affected the overall PSC layout and excavation volume, and eventually had the cost and programme impact. One of the challenges of the design was due to the significancy of the in-situ stress resulted in a relative low ratio of the sigma_ci/sigma_1 such that the rock mass could reach post-yield state upon excavation.

To develop the acceptance criteria for the IPB rock pillar performance with optimized pillar sizes, rock pillar stability assessment using different design approaches were performed and investigated. Empirical approach using Lunder and Pakalnis plot was performed to determine the rock pillar size ratio W/H (width/Height) at a specific average pillar vertical stress and the intact strength of rock mass. The W/H ratio provided an indication of the pillar stability based on the statistic of historical database mainly from mining industry with interpreted trend. The database and trend lines were reviewed and modified to exclude the data from irrelevant ground condition or ground behavior to improve the estimation.

Numerical approach was adopted to determine the spare capacity/margin (Factor-Of-Safety) of the pillars. This margin was important to cover uncertainties related to material, long term behavior, design modelling. The assessment using both Shear Strength Reduction (SSR) and Strength/stress method (SSM) methods were performed. The SSR method was the measure of the reduction of rock mass capacity (shear strength) until full pillar plasticized in the model occurs. This was equivalent to decreasing the failure envelope in a similar fashion until the rock mass softening happens. The FOS was the ratio between the actual strength of the material to the minimum required strength to prevent the full plasticity of pillars.

The SSM applied vertical displacement to the pillars in the model at the end of caverns excavation stage to increase the rock pillars stress. Considering the central 1/3 area of the pillar cross section as the central core which to be loaded until yielding (softening occurred) to determine the pillar strength. The pillar stress was the pillar core stress at caverns excavation completion. The FOS was defined as the pillar strength divided by the pillar stress (Strength/Stress). Both assessments provided a similar result achieving FOS=1.3 with an elastic core surrounded by different degree of yielded rock mass.

4.2 *Rock reinforcement acceptance criteria*

The Double Corrosion Protection (DCP) rock bolts were used for the cavern excavations. Based on the predicted failure mechanisms and durability requirements of the rock reinforcement at different stage of the project, acceptance criteria were established and verified by specific pre-production testing. Under the action of shear displacement of rock defects, the protective sheathing of the installed DCP bolts could be compromised. In order to quantify and correlate the shear displacement of the rock discontinuity to the damage of rock bolts, double shear tests were carried to confirm the bolt performance under the acceptance criteria of 20mm and 35mm shear displace-

ment for durability and structural integrity respectively. Besides, a strain-based acceptance criteria was established based on the result from the design analysis to reflect the combined action of pull and shear on the bolt section across the sheared features. Double embedment elongation tests were carried out to confirm the performance of bolts under the 1.5% and 2.5% bolt strain limits for secondary and primary bolts respectively. Figure 2 below presents the shear test setup and the results from the three tests (DSI CT26WR).



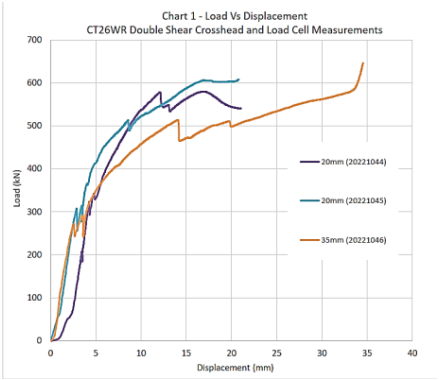




Figure 2. Double shear test of bolt (left); Load-displacement curves of CT26WR double shear tests for 20mm and 35mm limits (right); CT26WR after 35mm shear displacement (bottom)

5 PREDICTED GROUND BEHAVIOUR AND SUPPORT PERFORMANCE

5.1 *Predicted rock mass behavior*

The ground behavior assessment for the PSC excavation corresponded to an evaluation of potential failure mechanisms that would control the behavior of the unsupported excavation. The assessment considered relevant influencing factors, such as ground type (geotechnical units and ground parameters), excavation profile and span, in situ stress, over-burden, etc. According to the GBR, the potential controlling failure mechanisms for underground excavations could be categorized as per Table 1 below.

Table 1. Major controlling failure mechanism

Failure mechanism	Description
Discontinuities and Gravity	Failure controlled by the rock mass discontinuities, including overbreak, fall of wedges or blocks, friable ground, up to unravelling ground and chimney failure conditions. Ground majorly in elastic domain and/or with lack of confinement.
Ground Overstress	Failure controlled mainly by rock mass overstress, which can occur with or without association with existing ground structures. Ground damage in form of shear and brittle (tensile) failure with increasing depths of damage into the surrounding rock mass. When rock is massive and hard, rock failure will tend to be controlled by brittle (extension)

	failure, whereas shear tends be dominant in weak and fractured ground. Combination of both type of failures occurs over a broad range of conditions.
Groundwater	Rock mass deterioration and instability due to groundwater presence, flow or pressure. Hazards includes wash of fines flowing ground or slaking/swelling phenomena.
Frequently Changing Conditions	This overarching category is meant to capture the situation where ground conditions are very complex and frequently changing. This includes highly heterogeneous and anisotropic rock mass with frequently changing strength and deformation conditions.

The strength and deformability of rock mass depended on the strength and deformability of the intact rock, the discontinuities, and the geo-environmental conditions such as natural stresses and hydrogeological conditions. The primary criteria for the determination of the ground behavior included: the rock mass fabric expressed with the parameter Geological Strength Index (GSI); the compressive strength of intact rock (UCS) and of rock mass; and the initial stress state and maximum stress around the excavation opening. Based on the strength and stress parameters obtained from the SI, it was estimated that the failure mechanism of the excavation could be controlled by plastic behaviors at locations with stress concentration such as the IPB rock pillars. Wedge instability or geological overbreak, resulting from deconfinement and the presence of structural discontinuities within the cavern crown and sidewalls, could represent the predominant mechanism. This mechanism could be enhanced by the blasting activities. At locations where main sheared features were encountered, shear displacement mechanism was expected.

5.2 *Predicted support performance*

Following the predicted ground behavior, a dedicated flexible support system comprising rock bolts and shotcrete lining (Figure 3) was designed to address the failure mechanisms and design life requirement. The support system allowed the ground to deform as per prediction and provided necessary confinement to maintain the local and global stability during construction and the design life. The long-term global stability was maintained by the systematic secondary rock bolts to from a reinforced rock arch around the excavation. The primary rock bolts were installed after each round of excavation to maintain the stability during excavation and provided a "supported" ground for personnel entry. The shotcrete lining was designed to hold the rock mass (any damage/plastic zone) between rock bolts. The use of stainless-steel wire mesh within the shotcrete was to increase the lining ductility to meet the ground deformation and durability requirement. Due to the depth of the caverns and the observed pre-sheared features within the rock mass, it was expected that the combination of the elevated in-situ stress and the shear displacement failure mechanism of rock reinforcement could be the main driver of potential instability in the caverns. The displacement of rock blocks along sheared joints due to ground deformation could yield a grouted bolt locally where it crossed the rock joints. The bolt could be loaded by a combined action of tensile and shear forces induced by the shear displacement. The ultimate load depended on the inclination of the rock bolt crossing the rock joint. To assess the interaction between the rock blocks and the bolts, discrete element analysis (Figure 3) coupling the interaction between the rock discontinuities and the rock bolt structural elements was performed to allow quantitative assessment of this failure mechanism.

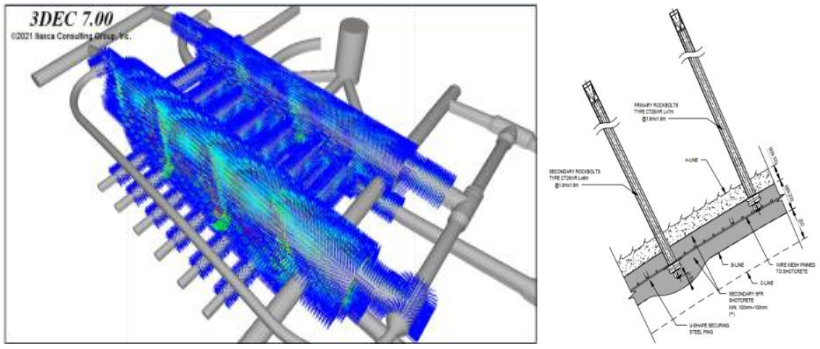


Figure 3. 3DEC analysis with rock bolt and sheared features modelled explicitly (left); PSC cavern rock support system (right)

6 CONSTRUCTION CONTROL AND MONITORING

Under the Employer's Requirements and the framework of Geotechnical Baseline Report (GBR), major construction control activities were developed to fulfill the requirement, such as Geological data acquisition plan; PSC caverns geotechnical instrumentation and monitoring plan; Excavation performance review process etc. The geotechnical information and monitoring data collected during construction were processed and reviewed in the regular meeting such as the daily geotechnical monitoring meetings and weekly geo-hazard meetings. The outcomes from these meetings such as the confirmation of ground behavior and ground support were conveyed to the frontline of construction for execution via the Permit-To-Tunnel (PTT) process where the details and requirements for the next round cavern excavation such as supports and monitoring, advance length and sequencing were confirmed.

The construction control activities also formed a linkage between the design assumed conditions and the actual conditions encountered. The probe hole drilling estimated the rock mass quality and the groundwater inflow rate ahead the excavation face. The geological face mapping assessed the actual rock mass classification GSI/RMR and identified the defects of the exposed ground. Other construction requirements such as blast control underneath the support of crane beam for stage 3 (Figure 4) excavation. With the construction control activities in place, the design assumptions and limits could be confirmed and validated. Contingency measures shall be applied when the encountered conditions outside the design limits or predictions. The instrumentation and monitoring plan was developed, and the instrument adopted could be classified as two groups: 1) ground response monitoring such as Displacement Measuring Point (DMP); Multi-Rod Extensometers (MRE); and Piezometer. 2) support performance monitoring such as shear monitoring holes; load cells; and strain gauges. The monitoring strategy has provided sufficient information for the intended purposes.



Figure 4. Stage 3 excavation of TH (left); Stage 3 excavation of MH (right)

7 REVIEW AND BACK-ANALYSIS

In general, the review and back-analysis is a process of using observed or measured data during construction to refine and calibrate the initial design assumptions, models, or parameters bridging the gap between theoretical design and actual performance, ensuring safer and more efficient construction activities. In the PSC cavern construction, this continuous review process has been formalized by adopting design hold points (HPs) and witness points (WPs) system. HPs or WPs have been established for each critical stage of construction, such as:

- HP0: End of central heading excavation prior to side slashing, to confirm the wedge analysis.
- HP1: End of cavern crown (stage 1) excavation, to confirm the pre-sheared features in the crown.
- HP1a: End of central heading excavation, to confirm the design for the intersection between the cavern and the MAT01 TBM tunnel underneath.
- HP2: End of stage 3 excavation, to confirm the design for IPB tunnels and intersections.
- HP3/HP4: End of IPB excavation and end of caverns excavation respectively, to confirm the rock pillars behavior and support performance.
- WP1/WP2: End of stage 2 and stage 5 respectively, to review and update the design with obtained data.

The sheared features/surfaces were identified by geological mapping and the data from 3D Lidar scans after the Stage 1 excavation of the crowns. These features were then confirmed by drilling of dedicated shear monitoring holes with endoscope inspection to record the details of the shear features. Endoscope inspections in systematic drainage also played an important role to confirm the extent of the sheared features and determine the "critical zones" for shear displacement monitoring. The baseline condition of each shear holes was established and compared with subsequent inspection. The endoscope inspection was a direct and quantitative measurement for shear displacement. A combination of qualitative monitoring measures was adopted to monitor the "critical zones" identified. Figure 5 presents the identified sheared features at the crowns of MH and TH with the endoscope images of the targeted features.

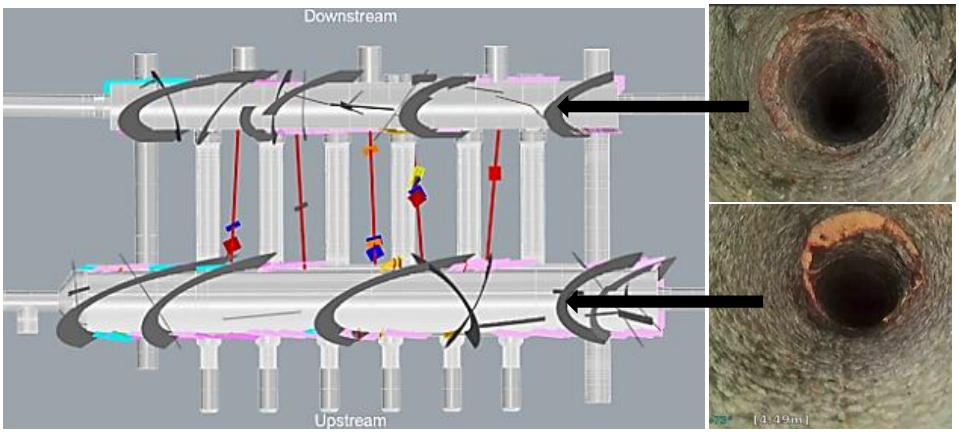


Figure 5. Plan view of 3D geological model with sheared features identified at the crowns of cavern (left); endoscope images of targeted features (right).

The back-analysis was conducted utilizing the 3DEC discontinuum analysis. A critical input for this analysis was the interpreted ground structural model, as illustrated in Figure 5. Other essential rock mass parameters, such as a GSI of 72 and a UCS of 58, were derived from actual ground conditions identified through comprehensive mapping data. The 3D geological model underwent significant refinement, incorporating the actual main sheared features identified within the crowns of the excavations. This update was further supplemented by initial findings from five inclined boreholes drilled specifically for pillar investigation. Subsequently, this refined 3D geological model was imported into the 3DEC numerical model to simulate the excavation and support installation sequence. The performance of the rock support, encompassing both primary and secondary bolts, was then assessed based on the numerical analysis results and corroborated with site monitoring data to determine any triggers for re-bolting. The numerical analysis was calibrated against actual ground response data obtained from field monitoring. Figure 6 shows the comparison between the measured MRE readings (at 2m, 5m, 10m, 15m, and 20m anchor lengths) and the corresponding output from the 3DEC model at Chainage 0+116 of the MH. Displacements from the extensometer initiated during Stage 1 excavation, exhibiting a notable increase upon the side-slashing (full span) was opened. During the Stage 2 excavation, a general increasing trend with a relatively mild slope was observed. After the entire span of Stage 2 was opened, the displacements increased, stabilizing at a final cumulative displacement of approximately 13mm. This observation aligns with the result from the 3DEC model.

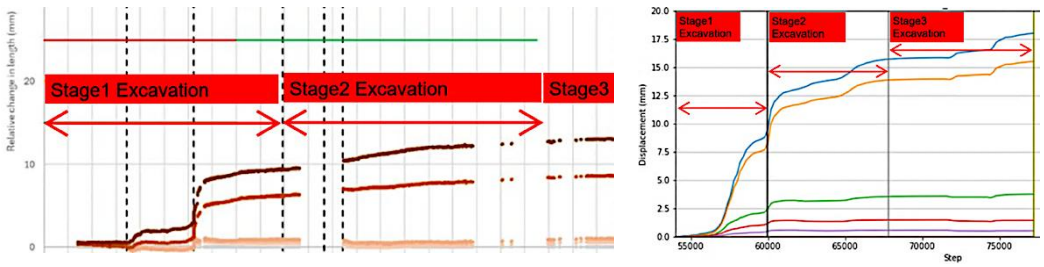


Figure 6. the measured MRE readings (at 2m, 5m, 10m, 15m, and 20m anchor lengths) at Chainage 0+116 of the MH crown (left); The corresponding output from the 3dec model (right).

8 CONCLUSION

The implementation of the observational method for the construction of the Snowy 2.0 powerhouse caverns has effectively mitigated the complexities associated with geological uncertainties. By establishing predefined acceptable limits derived from design predictions, performance was systematically measured and evaluated through construction control procedures. The primary instability mechanism was identified based on anticipated ground behavior, informing the development and application of targeted monitoring strategies and trigger values during construction. The actual conditions and site data observed throughout construction were integrated into a continuous review process, enabling iterative design updates and modifications to accommodate actual conditions. This comprehensive application of the observational method has yielded tangible benefits in terms of risk mitigation and optimization opportunities.

9 ACKNOWLEDGEMENTS

The authors acknowledge the permission granted by SHL to publish this paper. The authors also acknowledge the joint effort and the contribution of the colleagues from SHL, FGJV, Design Joint Venture (Lombardi, Tractebel and Coffey) and SMEC on the project.

10 REFERENCES

Chapman B. Yee M., Gomes A.R.A. 2019. Engineering challenges of the Snowy 2.0 pumped storage project. ITA-AITES World Tunnel Congress WTC2019, Naples, Italy - Tunnels and Underground Cities: Engineering and Innovation meet Archaeology, Architecture and Art – Peila, Viggiani & Celestino (Eds), Taylor & Francis Group

Ching, I., Diederichs, M., Chapman, B. & Cardone G. 2024. Deep powerhouse caverns design development and challenges – Snowy 2.0 experience. ITA-AITES World Tunnel Congress WTC2024, Shenzhen, China - Tunnelling for a Better Life – Yan, Celestino, Thewes & Eberhardt (Eds), Taylor & Francis Group

Diederichs, M., Miller, D., Chapman, B., Ching, I. & Gomes, A. 2022. Snowy 2.0 Pumped Storage Scheme: Rock Engineering Challenges in Tunnelling and Cavern Construction, Proceedings of the 2022 Tunnelling Association of Canada Conference, Vancouver, B.C., Canada

Gomes, A.R.A, Chapman, B., Diederichs, M. & Ching, I. 2023. Conceptual Framework of the Snowy 2.0 Pumped Storage Project (PSP) Geotechnical Baseline Report (GBR) for underground works. ITA-AITES World Tunnel Congress WTC2023, Athens, Greece - Expanding Underground - Knowledge and Passion to Make a Positive Impact on the World – Anagnostou, Benardos & Marinos (Eds), Taylor & Francis Group

Gomes, A.R.A, Chapman, B., Chapman N. and Cortes, F. 2021. Development of the Geotechnical Baseline Report for the Snowy 2.0 Pumped Storage Project, ATS 2020+1 Tunnel conference, Melbourne.

Hoek, E. 2006. Practical rock engineering.

Nicholson, D., TSE, C. & Penny, C. 1999. The observational method in ground engineering – principles and applications. Report 185. CIRIA. London. 214p.

19th Australasian Tunnelling Conference – Acosta-Martínez, Stewart and Hudson-Smith (Eds.)
© 2025 Australian Tunnelling Society, ISBN 978-0-85825-002-4

Temporary slender pillar design in low strength sandstone: A theoretical study on enhancing stability of temporary deep caverns

S. Salari, H. De Silva, M. Narayana, C. Xu
WSP, Australia

ABSTRACT: This paper presents the design and analysis of a yielding slender temporary pillar in massive sandstone at a depth of 100 metres, forming part of a temporary cavern at the base of a shaft footprint. Traditional empirical methods often result in conservative pillar designs that are unsuitable in rockmasses such as sub-horizontal bedded sandstone. To address this, the study explores the use of rock bolt reinforcement to delay brittle failure, improve energy dissipation, and change the mode of failure. Two slender temporary pillars supporting a large-span cavern were assessed using a combination of empirical design and numerical modelling. The design utilised reinforcement as a means to enhance temporary pillar confinement. This integrated design approach offers a practical alternative to conventional methods, enabling safe and efficient slender pillar construction in sub-horizontal bedded sandstone formations. The findings have implications for optimising temporary pillar dimensions and improving constructability in confined underground projects.

1 INTRODUCTION

The stability of temporary caverns in underground excavations is a critical concern for civil engineering and mining projects. This study focuses on designing ground support systems for a temporary cavern excavation, located at a depth of 100 m in sub-horizontal bedded sandstone formation. The theorised cavern, measuring 22.7 m in length, 13.6 m in width, and 7.5 m in height, is intended for spoil removal from upper levels and will be operational for 2 to 3 years before transitioning to a permanent shaft structure. Traditional empirical pillar designs, developed for mining in fractured rockmasses, often result in oversized pillars that are impractical for massive, sub-horizontal bedded sandstone formations, leading to inefficiencies in space utilization and increased construction costs.

This paper adapts the yielding pillar concept, which allows pillars to undergo controlled plastic deformation, redistributing stresses and preventing sudden inclined shear failure. The ground support system incorporates rock bolts in a pattern arrangement without shotcrete, aimed at enhancing temporary pillar confinement, yielding capacity and optimizing constructability in tight underground spaces, while also allowing the pillar to be observed. The design methodology integrates geotechnical characterization, numerical modeling using 2D finite element (RS2) and 3D finite difference (FLAC3D) methods. The study evaluates the impact of rock bolting on the temporary pillar stability through energy dissipation, delay in brittle failure post-yield, and improvement in progressive failure mode by providing a structured framework for designing temporary slender pillars in space-constrained environments. The remaining parts of this paper are as follows, literature review (section 2), Design methodology (section 3), discussion on temporary pillar stability analysis including empirical approaches and numerical assessment in 2D and 3D (sections 4 and 5), and conclusion on main findings of the current study (section 6).

2 LITERATURE REVIEW: SLENDER PILLARS IN TUNNELLING

The yielding pillar concept, pioneered in room and pillar mining, allows pillars to undergo controlled plastic deformation, absorbing energy and maintaining residual strength to prevent catastrophic failure (Salamon, 1970). This approach enables stress redistribution from the pillar core to surrounding rock, creating a destressed zone that enhances overall excavation stability (Yavuz, 2001). Yielding pillars have been extensively studied in coal and soft rock mining, where they accommodate large deformations without sudden collapse (Esterhuizen et al., 2011) as shown in

Figure 1, unlike the sudden brittle failure shown in Figure 2 (Renani & Martin, 2018). Esterhuizen et al. demonstrated that yielding pillars in coal measures can reduce roof-to-floor convergence by allowing controlled yielding, which is particularly effective in weak rockmasses.

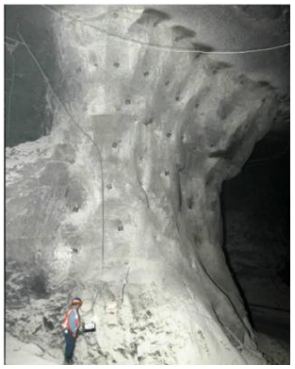


Figure 1: Pillar covered by wiremesh and bolts to prevent sudden brittle failure (Esterhuizen et al., 2011)

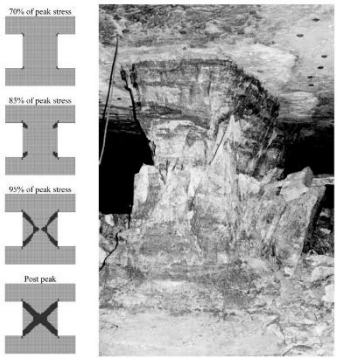


Figure 2: Progressive failure of hard rock pillars (Renani & Martin, 2018)

Martin & Maybee (2000) provided empirical formulas for pillar strength reduction and stability assessment in hard rock mines, which have been widely used in the industry. Their work highlighted the importance of considering the width-to-height ratio and rockmass quality in pillar design. Empirical pillar design methods, such as those by Lunder & Pakalnis (1997), rely on case histories from fractured rockmasses and are often conservative, leading to overdesigned pillars (Martin & Maybee, 2000). These methods underestimate the strength of massive rockmasses, resulting in oversized pillars that reduce usable space and increase construction costs. The application of yielding pillars in civil tunnelling, particularly in massive sandstone, have been recently studied (Thirukumaran & Oliveira, 2023). Employing 3D analysis, slender rock pillars formed in large span road tunnels and cavern Y-junctions in Hawkesbury Sandstone have been studied, combining numerical modeling with empirical methods to ensure pillar stability under high stress conditions. This highlighted the effectiveness of slender pillars in space-constrained environments, supported by rock bolting to enhance ductility. Dressel & Diederichs (2022) investigated the influence of rockmass parameters and yield criterion on pillar design. Their work suggested that 3D numerical modelling can capture the complex interactions between rockmass properties and pillar stability. Hamediazad & Bahrani (2024) evaluated the rock mass strength for hard rock pillar design using bonded block models. Sinha & Walton (2019) conducted numerical analyses of pillar behaviour, varying yield criteria, dilatancy, rock heterogeneity, and length-to-width ratios, to understand the complex interactions that influence pillar stability.

This paper builds upon the yielding pillar framework and adapts it for use in civil tunnelling through massive sandstone. A hybrid design methodology is presented, integrating empirical classification, numerical stress modelling, and practical reinforcement strategies, such as GRP bolts and pattern bolting, to achieve controlled yielding and maintain temporary pillar stability throughout the excavation's operational phase.

3 DESIGN METHODOLOGY

The design methodology adopted in this study integrates empirical and numerical approaches to assess the stability and performance of slender temporary pillars. Furthermore, a numerical pillar compression test was carried out for temporary pillar assessment. Temporary pillar stability in the design of the shaft cavern (a temporary cavern formed at the base of a shaft footprint) has been assessed using the following four methods:

- Pillar strength factor obtained from 2D assessment (RS2)
- Pillar stress assessment in 3D (FLAC 3D)
- Examining of pillar through an empirical approach
- Use of GRP rockbolts to improve failure mode and energy dissipation

3.1 *Ground conditions*

Design parameters for the low strength sandstone rock mass class are listed in Table 1. The groundwater table is significantly below the cavern, eliminating hydrostatic pressure considerations. Bedding and joint set with dip / dip direction of 5°/340° and 85°/220°, respectively was considered.

Table 1: Material properties

Parameter		Value
UCS		12 MPa
Intact Rock Modulus (Ei)		3500 MPa
Unit Weight		23 kN/m^3
Mass Rock Modulus (Em)		3100 MPa
K_0		0.5
Generalised Hoek Brown	mb	8.322
	s	0.108
	a	0.501
Equivalent Mohr Coulomb	ϕ	50°
	C	619 kPa

3.2 *Temporary Cavern and pillar geometry*

The temporary cavern measures 22.7 m in length, 13.6 m in width, and 7.5 m in height, as depicted in Figure 3, with temporary pillar 1 and pillar 2 dimensions as shown in Table 2.

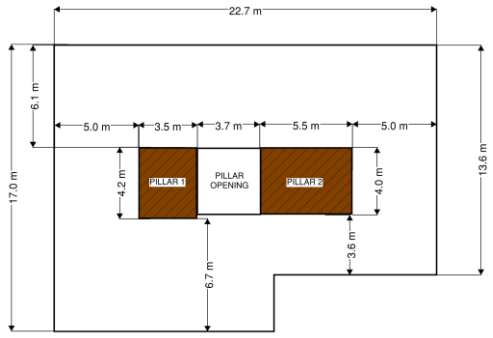


Figure 3: Plan view of Shaft Cavern (Dimensions are in m)

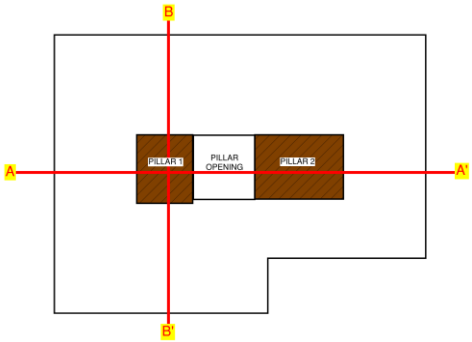


Figure 4 : 2D design analysis sections

Table 2: Temporary pillar dimensions

Pillar No	Pillar Width, W(m)	Pillar Length, L(m)	Pillar Height, H(m)	W/H
1	3.5	4.25	7.5	0.47
2	4.0	5.5	7.5	0.53

3.3 *Modelling approach*

A comprehensive approach was adopted to evaluate the stability of the slender temporary pillars under high-stress conditions. Initially, a two-dimensional finite element analysis was carried out using RS2 software (Rocscience) to further assess the stability of key excavation sections and the effectiveness of proposed support systems. Two critical cross-sections (AA' and BB'), as shown in Figure 4, were selected to analyse the two slender temporary pillars, incorporating staged excavation sequences and rock bolt interaction to accurately reflect construction conditions.

Following the stress analysis from RS2, a three-dimensional numerical model was developed using FLAC3D, which is a finite difference program by Itasca, to simulate temporary pillar stress distribution and identify zones of elevated stress concentrations. Empirical methods based on the work of Martin and Maybee (2000) and Esterhuizen et al. (2011) were then applied to assess the pillar strength, with results indicating a factor of safety slightly below one. Field measurements

of mine pillars have demonstrated that yielding within specific width ranges can potentially enhance pillar strength (Yavuz, 2001), an aspect not considered in the current design where the rock material is limited to elastic behaviour. While yielding may, in certain cases, contribute to the overall strength of the system, this section focuses specifically on the application of pattern bolts to improve the temporary pillar's confinement and post-yield capacity. Further 3D modelling of the pillar in a compression test was undertaken to assess the pillar response to understand the behaviuor of the temporary pillar under the high stress loading conditions.

The geometry and mesh generation of the critical pillar in FLAC3D with the dimension of 4.25 m in length, 3.5 m in width, and 7.5 m in height is described in Figure 5. Furthermore, an elastic-plastic Strain softening Mohr-Coulomb model is introduced employing equivalent Mohr-Coulomb parameters shown in Table 1 with a residual friction angle, $\phi_R = 35^{\circ}$, residual cohesion, $C = 0.0619$ (MPa), and tensile cut-off as $T = 100$ (kPa). The strain softening behaviour is controlled by adopting the parameters provided in Table 3.

Table 3: Mohr-Coulomb Parameters for Strain Softening Model

Strain	0	0.005	0.0051	1
Cohesion (kPa)	619	619	61	61
Friction angle (°)	50	50	35	35
Tensile strength (kPa)	100	100	10	10

For support cases, GRP pattern bolts are installed at the pillar. To capture the post-yield behaviour of the temporary pillar, a displacement-controlled test is conducted using FLAC3D. In this analysis, a total displacement of 35 mm is applied, with increment size of 0.001 mm per step.

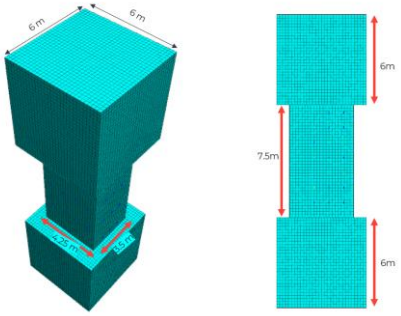


Figure 5: Geometry and Mesh of the Critical Temporary Pillar (Pillar 1)

4 TEMPORARY PILLAR STABILITY ANALYSIS RESULTS

4.1 *Pillar Stress Assessment (FLAC3D)*

The temporary pillar stress distribution in 3D due to high stress loading condition is illustrated in Figure 6. The stress distribution results are analysed across five distinct sections, as defined by the plan illustrated in Figure 7.

Based on the evaluation of stress results in the pillar zone across different sections, it is estimated that high-stress conditions will exist in all sections of the pillar. As shown in Figure 8 and Figure 9, consistently high average stress levels are seen across the entire temporary pillar zone (more than 4 MPa), potentially leading to localized yielding. To address this issue, the initial solution involves the use of pattern bolting to enhance confinement and control brittle deformation, so that yielding of the temporary pillar is controlled. The effectiveness of this approach in enhancing pillar performance is discussed in detail in Section 4.4. For additional safety, impact barriers and a wire mesh around the pillars will be installed. Given the high-stress levels identified in the temporary pillar zones of both Pillar 1 and Pillar 2, the installation of 6-metre-long crown bolts are used to stabilize the cavern under a yielding pillar condition. These bolts are designed to enhance crown stability during temporary pillar yielding by redistributing stresses from the pillar zone to the abutments through the arching action of the compression beam above the crown.

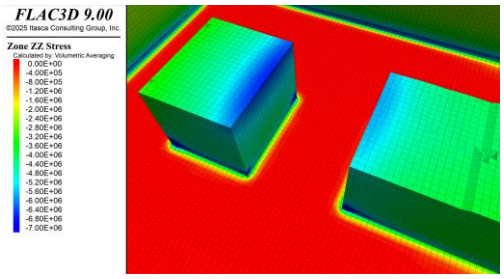


Figure 6: Temporary pillar assessment under stress σ_{zz} (Pa), loading condition in FLAC3D

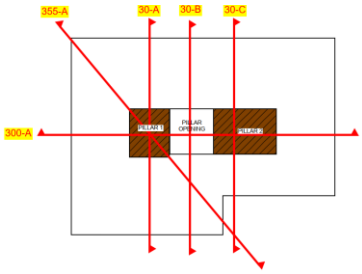


Figure 7: Critical cross sections in FLAC3D model

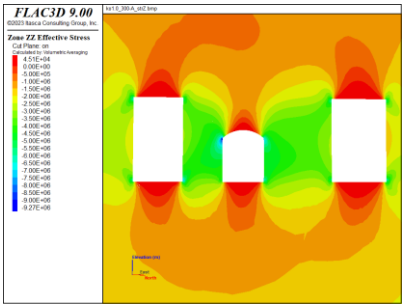


Figure 8: Vertical Stress distribution contour, σ_{zz} (Pa), at pillar zone Section 300-A

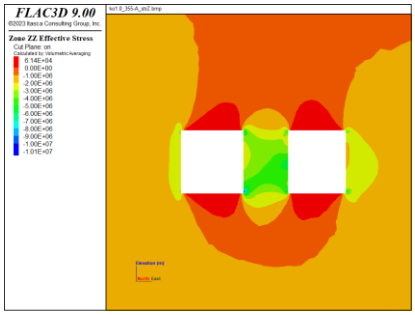


Figure 9: Vertical Stress distribution contour, σ_{zz} (Pa), at pillar zone Section 355-A

4.2 *Temporary Pillar stability – Empirical approach*

Empirical formulas from Martin and Maybee (2000) and Esterhuizen et al. (2011) were used to estimate pillar strength and Factor of Safety (FOS). Pillar stability assessment is typically carried out by estimating the pillar strength and stress and then estimating the margin that exists between the expected pillar strength and stress. The FOS relates the average pillar strength (S) to the average pillar stress (σ_p) as follows,

$$FOS = \frac{S}{\sigma_p} \tag{1}$$

Figure 10 shows a comparison of different empirical formulas used for pillar strength.

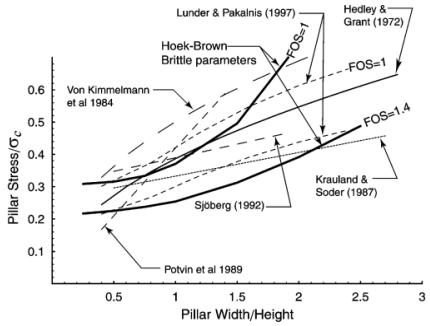


Figure 10: Hard-rock pillar stability and elastic 2D models using Hoek-Brown brittle parameters (Martin & Maybee, 2000).

The average temporary pillar stress (σ_p) is estimated through numerical modelling varies from 4.0 MPa to 4.3 MPa. Table 4 shows the FOS of Pillar 1 and 2 based on the numerical analysis detailed in the FLAC3D elastic model. To verify the outcomes of the pillar strength estimated from the numerical analyses, the relationship developed by Martin and Maybee is also used to estimate the pillar strength (Martin & Maybee, 2000). As can be seen from Table 4 below, the Factor of Safety is less than 1 for the applied stress condition using empirical charts. This indicates the need to increase pillar width.

Table 4:Results of temporary pillar stability assessment

Pillar No	W (m)	H (m)	UCS (MPa)	Average Pillar Stress (MPa) FLAC3D elastic	Martin and Maybee (2000)			Esterhuizen et al. (2011)	
					Reduction factor	Pillar strength, *S* (MPa)	FOS	Pillar strength, *S* (MPa)	FOS
1	3.5	7.5	12	4.3	0.32	3.8	0.90	3.5	0.80
2	4.0	7.5	12	4.0	0.32	3.8	0.95	3.6	0.90

4.3 *RS2 Modelling of Temporary pillar*

A temporary pillar assessment has been undertaken using the design sections shown in Figure 4. The pillar stresses are extracted from the RS2 finite element model (FEM), as shown in Figure 11 and Figure 12. Both temporary pillars, particularly in their lower half, exhibit yielding, requiring: 1- pattern bolting on pillars; 2- longer bolts at the crown; and 3- reinforcement mesh to the bottom section of the pillar sidewalls. As discussed previously, these measures are critical to ensuring stability and mitigating the effects of localized yielding in the pillar zones.

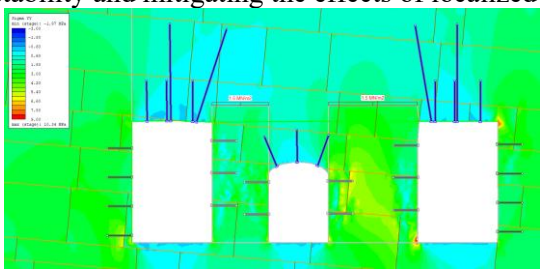


Figure 11: Vertical stress distribution (MPa) in RS2 for section AA': Pillar 1, 2, and opening

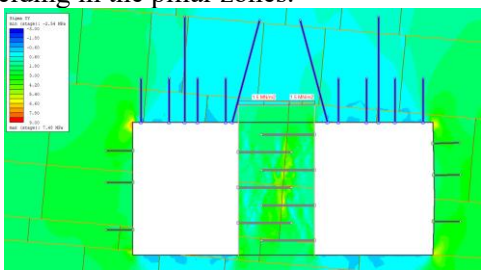


Figure 12: Vertical stress distribution (MPa) in RS2 for section BB': Pillar 1

4.4 *Temporary Pillar bolting- FLAC3D Assessment*

To further understand temporary pillar yielding behavior, a stress-displacement curve has been plotted in Figure 13 to compare the post-yield response and the nature of failure when using GRP bolts. The analysis suggests that the introduction of GRP bolts has improved the failure mode of the temporary pillar, enabling slightly more deformation post yield. It highlights that the temporary pillar with GRP bolt support is provided the benefit of additional displacement before reaching failure. The GRP-reinforced pillar shows a delay in the onset of brittle failure by approximately 3 mm (when comparing plastic portion - refer to Figure 13: (1) Without GRP: 2.5 mm; (2) with GRP: 5.5 mm, which, although small, resulted in measurable energy dissipation.

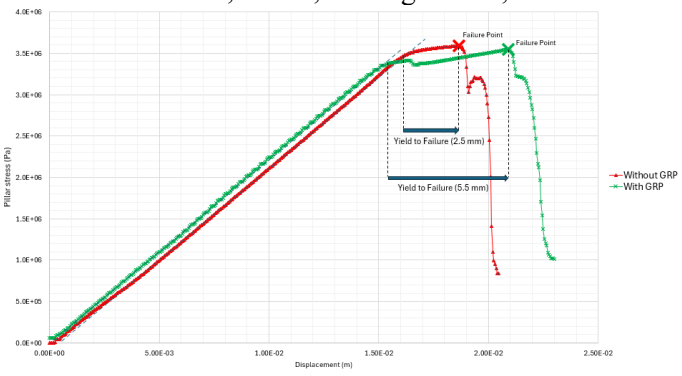


Figure 13: Pillar Strength (Pa) vs Applied Displacement (m), Impact of GRPs on delaying failure

Additionally, relative energy dissipation capacity is increased by approximately 22% before failure due to the inclusion of GRP, referring to the following energy graph in Figure 14.

$$\delta_E = \frac{E_{with\ GRP} - E_{without\ GRP}}{E_{without\ GRP}} \cong 22\% \quad (2)$$

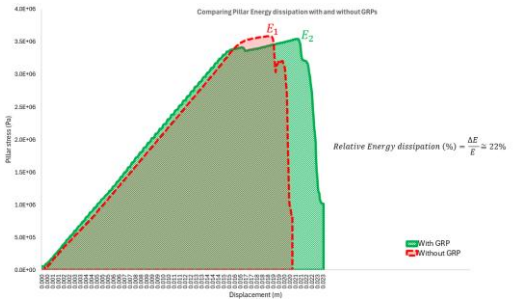


Figure 14: Energy dissipation comparison of the temporary pillar with and without GRPs

Deformation and failure mechanisms of temporary pillar cases, with and without GRP bolts are illustrated in Figure 15 and Figure 16 which shows improvement in post yielding deformation of the temporary pillar while using GRP bolts. The mode of failure using GRP bolts has changed from inclined shear failure to progressive crushing failure, which provides additional time for assessing and monitoring temporary pillar condition at critical stages of excavation.

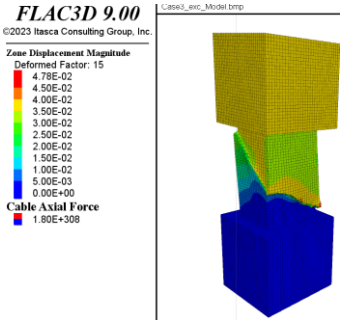


Figure 15: Deformation (m) and Failure Mechanism in Pillar; Case 1- without Support leading to inclined shear failure mode

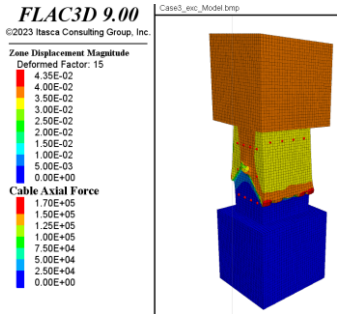


Figure 16: Bolt axial force (N), deformation (m) and Failure Mechanism in Pillar; Case 2- using GRPs leading to progressive crushing failure mode

To examine bolts capacity, the axial force in the GRP bolt pattern is described in Figure 17 and Figure 18 with a maximum value of 170 kN. Maximum principal strain and deformation contours are shown in Figure 17 and Figure 18 respectively. In the current pillar test, the temporary pillar does not exhibit a significant strength gain. However, this limitation is primarily due to the adopted rock mass parameters and adopted strain-softening material model in this experiment, which is more focused on understanding the impact of GRP bolts post-yield behavior. More advanced strain-softening constitutive models can be adopted to better capture the post-peak performance of temporary pillars, as demonstrated in previous studies (e.g., Cammarata et al., 2023; Thirukumaran & Oliveira, 2023). Further assessment, incorporating field mapping, monitoring data and the observed rock mass conditions in massive sandstone, can improve capacity expectations of temporary pillars and forms part of the observational approach in the current design.

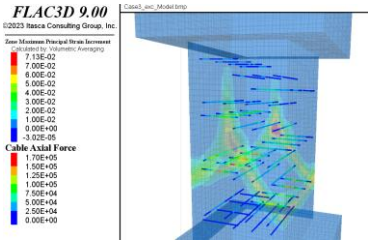


Figure 17: Maximum principal strain and GRP bolt axial force contours (N)

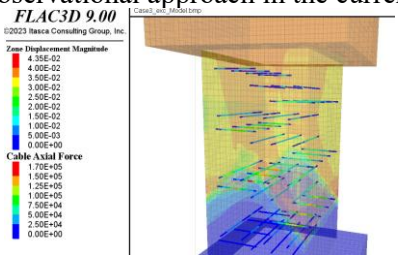


Figure 18: Displacement magnitude (m) and GRP bolt axial force contours (N)

5 SUPPORT STRATEGIES FOR SLENDER TEMPORARY PILLARS

To address the identified yielding and potential instability of slender temporary pillars, a targeted support strategy was implemented. This included GRP bolts, and pattern bolting configured to improve the post yield response and control the mode of failure by adding confinement. The

change from an inclined shear failure to progressive crushing failure provides an additional level of safety by providing the opportunity to observe the effects of overstress and implement mitigation actions. A displacement-controlled FLAC3D analysis demonstrated that GRP bolts delay the onset of failure and enable increased energy dissipation. To account for the risk of brittle failure, 6 m bolts can be proposed at the crown, as a precaution. This allowed the crown to function as a compression arch, redistributing stresses and enhancing global cavern stability in case of yielding. Wire mesh reinforcement could be recommended particularly near the base of the temporary pillars to control rock fall hazards. This provided surface confinement and support against rock spalling.

6 CONCLUSION

This approach developed a structured framework for designing and assessing slender temporary pillars with bolting, aiming to provide more optimised pillar sizes and move away from purely empirical performance-based design. Traditional empirical methods have been developed based on mining in fractured rockmasses and the data is from case histories in the mining industry, leading to large pillars in rockmasses where the methods may yield conservative pillar sizes. The design method adopted in this paper can be employed to optimize temporary pillar dimensions in tight underground areas, where optimal space proofing is crucial for constructability reasons, and risks associated with pillar yielding can be foreseen via the use of numerical modelling tools, and a good understanding of rockmasses where defects are minimal. The use of GRP pattern bolts and mesh wrapping provided essential confinement and energy dissipation, effectively managing the mode of failure transitions from an inclined shear failure to progressive crushing failure in the temporary pillar response. Additionally, the incorporation of longer bolts in the crown facilitated the redistribution of stress away from the pillars, further enhancing cavern stability even in case temporary pillar yields. Progressive failure mode provides additional time to monitor temporary pillar conditions during critical stages of excavation, highlighting the importance of incorporating an instrumentation and monitoring plan into the design phase. For future studies, it is recommended that more advanced constitutive models (e.g., advanced strain-softening or damage-plasticity models) be developed to better capture fracture mechanics, post peak response, and load transfer mechanisms between the rock mass and reinforcement.

7 REFERENCES

Dressel, E.J. and Diederichs, M.S., 2022. A numerical investigation on the influence of rockmass parameters and yield mechanics in pillar design. *The Evolution of Geotech*, p.492. doi:10.1201/9781003188339-62.

Cammarata, G., Elmo, D. and Brasile, S., 2023. Modelling of progressive failure mechanism of mine pillars. *In IOP Conference Series: Earth and Environmental Science* (Vol. 1124, No. 1, p. 012099). IOP Publishing.

Esterhuizen, G.S., Dolinar, D.R. and Ellenberger, J.L., 2011. Pillar strength in underground stone mines in the United States. *International Journal of Rock Mechanics and Mining Sciences*, *48*(1), pp.42-50. https://doi.org/10.1016/j.ijrmms.2010.06.003

Hamediazad, F. and Bahrani, N., 2024. Evaluation of the rock mass strength for hard rock pillar design using bonded block models. *Rock Mechanics and Rock Engineering*, *57*(5), pp.3659-3680.

Martin, C.D. and Maybee, W.G., 2000. The strength of hard-rock pillars. *International Journal of Rock Mechanics and Mining Sciences*, *37*(8), pp.1239-1246. https://doi.org/10.1016/S1365-1609(00)00032-0

Renani, H.R. and Martin, C.D., 2018. Modeling the progressive failure of hard rock pillars. *Tunnelling and Underground Space Technology*, *74*, pp.71-81. https://doi.org/10.1016/j.tust.2018.01.006

Salamon, M.D.G., 1970, November. Stability, instability and design of pillar workings. In *International journal of rock mechanics and mining sciences & geomechanics abstracts* (Vol. 7, No. 6, pp. 613-631). Pergamon. https://doi.org/10.1016/0148-9062(70)90022-7

Sinha, S. and Walton, G., 2019. Numerical analyses of pillar behavior with variation in yield criterion, dilatancy, rock heterogeneity and length to width ratio. *Journal of Rock Mechanics and Geotechnical Engineering*, *11*(1), pp.46-60. https://doi.org/10.1016/j.jrmge.2018.07.003

Thirukumaran, S. and Oliveira, D., 2023. Innovative design of slender rock pillar formed within large span road tunnels and cavern Y-junction in Hawkesbury Sandstone. *Tunnelling and Underground Space Technology*, *141*, p.105376. https://doi.org/10.1016/j.tust.2023.105376

Yavuz, H., 2001, June. Yielding pillar concept and its design. In *17th International mining congress and exhibition of Turkey-MCET* (pp. 397-404).

19th Australasian Tunnelling Conference – Acosta-Martínez, Stewart and Hudson-Smith (Eds.)
© 2025 Australian Tunnelling Society, ISBN 978-0-85825-002-4

Ground response for construction of 15 caverns in diverse ground conditions in Sydney – Part 1: Ground support

Y. Bai & M. Trim
Delve Underground, Sydney, Australia

M. Salcher
Gamuda (formerly PSM), Sydney, Australia

R. Stocker
PSM, Sydney, Australia

T. Bentley
John Holland, Sydney, Australia

ABSTRACT: Eleven road caverns and four ventilation caverns were recently constructed in Sydney as part of the Rozelle Interchange project. The up to 29 m wide road caverns and 24 m high ventilation caverns of the Sydney motorway were excavated in Hawkesbury Sandstone at depths between approximately 17 m and 67 m next to the harbour. The number, size, ground cover and complexity of geological conditions of these large underground excavations are unprecedented in Australia. Three of the 11 road caverns used a concrete replacement pillar. The excavation sequence for each of these caverns was a bespoke design and catered to the varying ground conditions and construction access requirements. Typically, this involved three top headings and a bench, with removal and/or thinning of a central pillar prior to benching. The excavation sequence for the ventilation caverns involved split headings and multiple deep benches to achieve the final height up to 24 m. Temporary and permanent ground support comprised rock bolts and cable bolts in the crown with shotcrete. This part 1 of the paper details the cavern geometry, ground conditions and ground support systems. Part 2 presents the construction sequence and ground response. The ground response is described in terms of in-tunnel convergence, measured using optical survey targets and steel tape extensometers, surface settlement, endoscope hole closure, rock pillar displacement monitored with inclinometers and observations of ground support performance.

1 INTRODUCTION

1.1 *Project description*

The Rozelle Interchange project in Sydney involved the construction of a 23 km long multi-level underground motorway network, including mainlines, caverns, on- and off-ramps, shafts and ventilation tunnels. It provides an underground connection from the M4 and M8 motorways to Iron Cove Bridge on Victoria Road, Anzac Bridge, City West Link and the future Western Harbour Tunnel. At peak tunnelling, 23 roadheaders were used to excavate the tunnels through Hawkesbury Sandstone with regional scale dykes and faults at depths between 5 m and 70 m.

The John Holland Group and CPB Contractors joint venture was awarded the design and construct contract. The joint venture engaged PSM and Delve Underground to design the primary and permanent ground support for the tunnels and caverns. Figure 1 shows a plan of the tunnel network with road caverns and ventilation caverns (also referred to as ventilation facilities) annotated.

This part 1 of the paper details the geology and ground support of the road caverns and ventilation facilities. Part 2 (Salcher, Bai, Stocker, Bentley & Trim, 2025) describes the construction sequence and ground response with particular focus on the rock mass response due to removal of the central temporary pillar and due to deep benching in ventilation facilities.

The paper is written from a construction and construction phase services perspective. It can be considered a companion paper to Bai, Salcher, Fusee, Bentley, Kumar & Trim (2023), which details observations of rock bolt shearing at Rozelle Interchange; and Salcher, Bai, Trim, Bertuzzi & Vidler (2023), which describes the project's Permit to Tunnel (PTT) process.

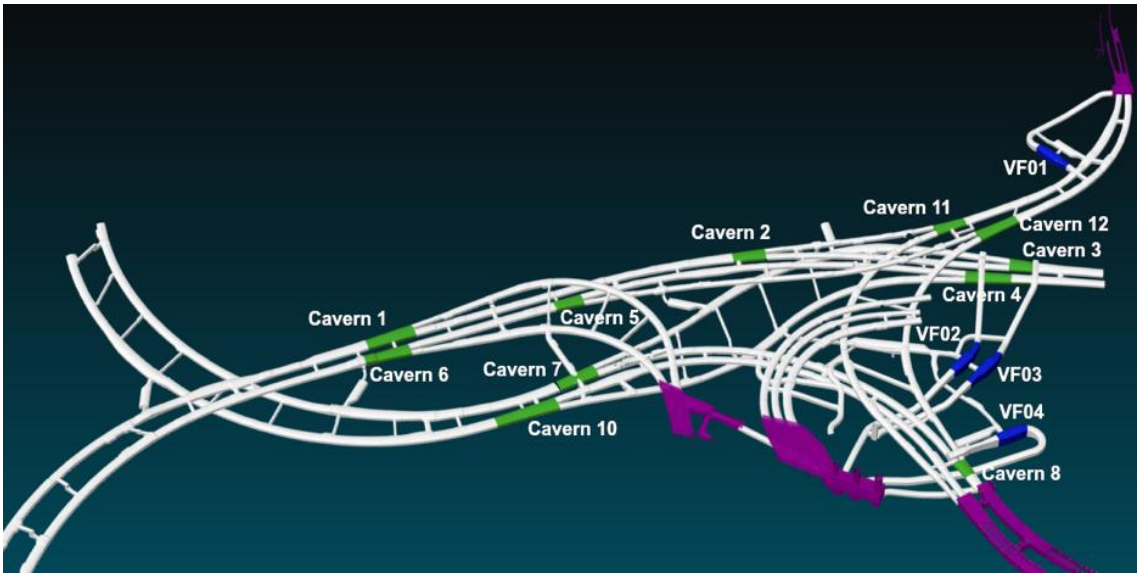


Figure 1. location plan of 11 road caverns (green) and 4 ventilation facilities (blue).Cut-and-cover structures are shown in purple.

1.2 *Cavern geometry*

Table 1 summarizes key geometric details of the road caverns and ventilation facilities.

Table 1. Cavern geometry.

Cavern no.	Type of cavern	Max. span[(1)] (m)	Height[(1)] (m)	Ground cover (m)	Length[(2)] (m)	Cover/span (m/m)
Cavern 1	Road	28.4	9.6	25	120	0.9
Cavern 2	Road	26.0	9.5	49	66	1.9
Cavern 3	Road	28.9	9.9	59	66	2.0
Cavern 4	Road	27.6	10.2	51	86	1.8
Cavern 5	Road	26.1	9.2	29	41	1.1
Cavern 6	Road	26.0	9.2	25	36	1.0
Cavern 7	Road	28.8	9.6	21	77	0.7
Cavern 8	Road	25.2	9.8	17	80	0.7
Cavern 10	Road	28.9	9.6	25	92	0.9
Cavern 11	Road	26.4	10.1	38	24	1.4
Cavern 12	Road	25.9	10.8	30	43	1.2
VF01	Ventilation	18.9	17.2	18	32	1.0
VF02	Ventilation	18.9	21.8	42	35	2.2
VF03	Ventilation	18.9	21.1	43	35	2.3

Cavern no.	Type of cavern	Max. span[(1)] (m)	Height[(1)] (m)	Ground cover (m)	Length[(2)] (m)	Cover/span (m/m)
VF04	Ventilation	18.9	23.5	24	32	1.3

Notes:
1. Span and height represent estimated excavation line (e-line) dimensions.
2. Length is as defined on the design drawings for the cavern profile (i.e., span greater than 21 m for the road caverns).
3. Cavern 9 is not included because it is a cut-and-cover structure.

The road caverns are defined as road tunnels with a span larger than 21.0 m. The span increases from its narrowest at the mainline tunnel interface to its widest at the permanent pillar nose, where the cavern splits into mainline and on/off-ramps. The minimum permanent pillar width varied between approximately 3 m and 4 m. Six of the 15 caverns have a cover-to-span ratio of 1 or less.

A typical plan of the roads caverns is presented in Figure 2, using the example of Caverns 7 and 10. Amongst others, the plan shows the caverns (red hatching), the ramps or mainline tunnels joining or exiting the caverns and the permanent pillar at the end of the caverns between the ramps or mainlines.

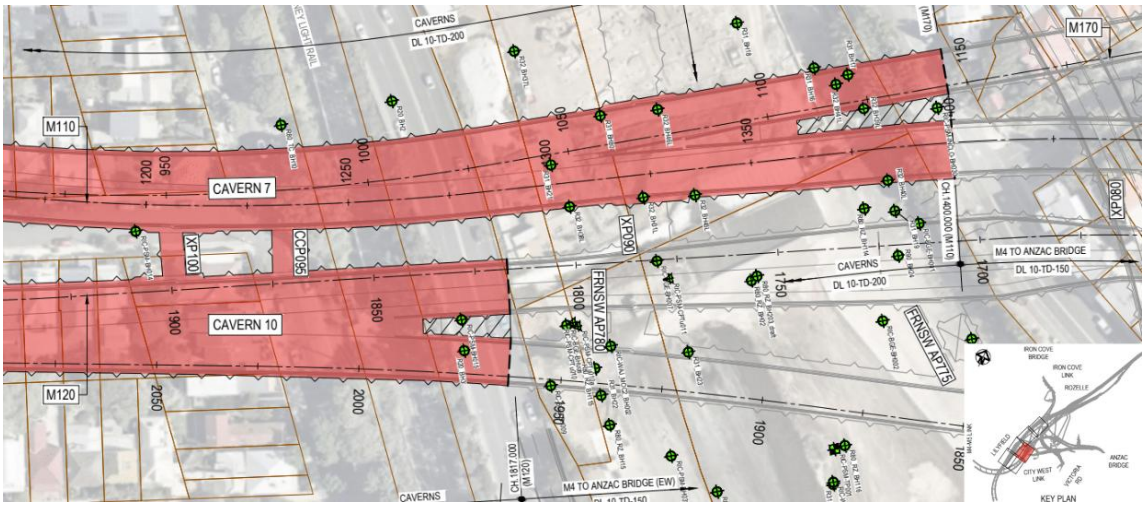


Figure 2. Plan of caverns 7 and 10.

An example of the geometry of the ventilation caverns is given in Figure 3.

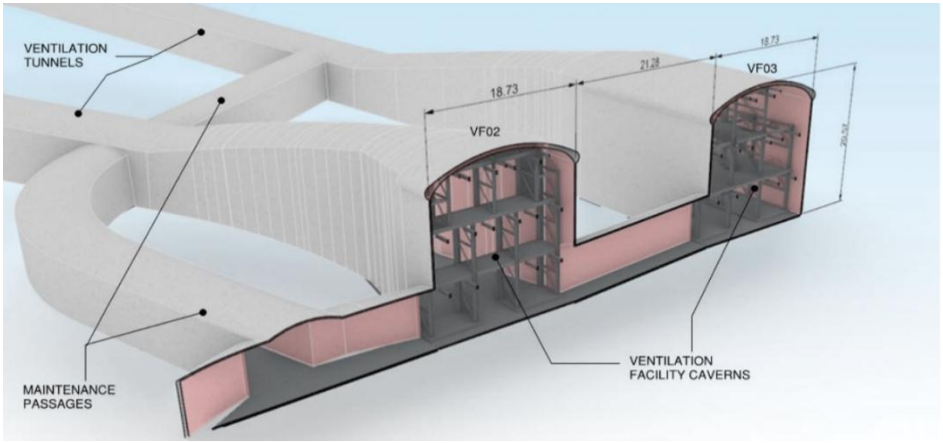


Figure 3. geometry of ventilation facilities VF02 and VF03 (18.9 m wide and 21 m to 22 m high with a 21 m wide pillar between the caverns).

2 GEOLOGICAL AND GEOTECHNICAL CONDITIONS

The Rozelle Interchange tunnels are situated within the Sydney Basin and are located close to the harbour. The tunnels were exclusively excavated through the Lower Triassic–aged flat-lying Hawkesbury Sandstone. Within the Hawkesbury Sandstone, siltstone beds, laminites (interlaminated sandstone and siltstone), and siltstone rip-up clast layers were observed to range in thickness between 0.5 m and 3 m but typically less than 1 m, with varying persistence of less than 10 m to hundreds of meters. The project identified several areas of increased geological structure, including a paleovalley structure, persistent regional scale faults and associated structurally complex zone, and structural corridor. Details are provided by Estrada, Nash, De Ambrosis & Chan (2022).

The main surface drainage in the area is a deep, broad river valley draining from the southwest to the northeast into Rozelle Bay. Over geological time, this river-incised paleovalley was filled to current levels with marine and alluvial soils. Project geotechnical documents indicate geological structures associated with valley bulging. Relief of in situ horizontal stress in the slopes and floor of the infilled river valley and associated geological defects were expected. This included low-angle faults, bedding shears, bedding partings and increased jointing which are typical of areas of stress relief.

Notable regional scale geological structures at Rozelle Interchange include the paleovalley described above, a significant regional scale fault (Fault 1) and a dyke (Dyke B).

Fault 1 is a shallow southeast-to-east-dipping regional-scale fault. It was observed to consist of either a fault core with variable thickness of clay gouge and rock fragments or an intensely sheared and faulted zone. In either case, the fault was typically associated with a damage zone of increased bedding partings, crushed seams, joints and shears. Photographs of two different expressions of Fault 1 are shown in Figure 4 and Figure 5.



Figure 4. Fault 1 encountered in ramp adjacent to concrete replacement pillar of Cavern 5.

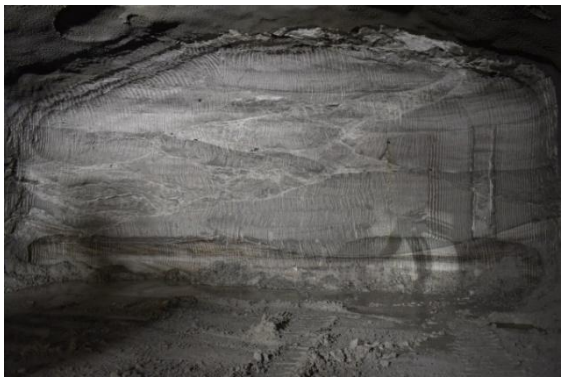


Figure 5. Fault 1 encountered in mainline tunnel.

The other major geological structure observed in the project area was a dyke (Dyke B). It extended through a northwest-southeast-trending structural corridor, characterized by an increase in faults, shears and joints. The subvertical dyke varied between 0.5 m and 3 m wide and consisted of a dolerite intrusion bounded by clayey contacts with the host rock and contact metamorphosed ("baked") sandstone margins. The dyke was associated with a structurally complex zone which

comprised an increase in subhorizontal bedding shears and low-angle shears and faults. The faults observed during tunnelling had clay or rock fragment infilling. The dyke was encountered in nine tunnels throughout the Rozelle Interchange project area, including ventilation facilities and road caverns.

A photograph of Dyke B as encountered in the top heading of ventilation facility VF04 is presented in Figure 6. Figure 7 is a 3D model showing Dyke B and Fault 1 intersecting Caverns 3, 4 and 12.



Figure 6. Dyke B encountered in the top heading of ventilation facility VF04.

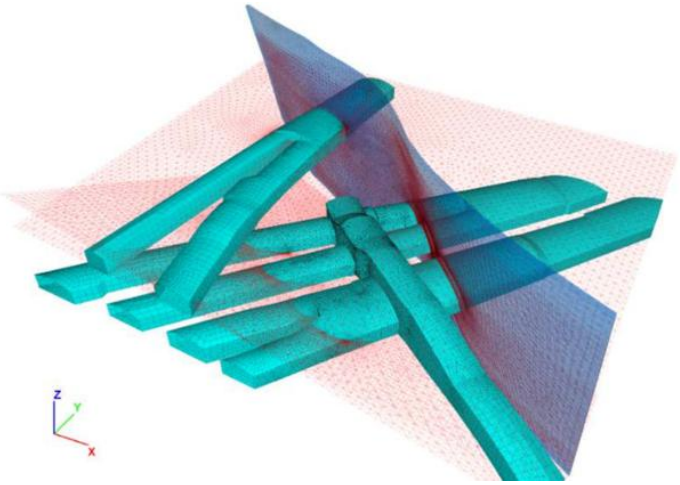


Figure 7. 3D model of Fault 1 (shallow dipping red structure) and Dyke B (near-vertical red structure) intersecting Caverns 3, 4 (lower caverns) and 12 (upper cavern).

High horizontal in situ rock stress was observed at some locations of the project, which resulted in rock bolt shearing during road cavern heading excavation and ventilation facility deep benching. Bai et al (2023) provide a comprehensive summary of rock bolt shearing at Rozelle Interchange, including uphole photographs of 54 shearing events.

Although all 11 road caverns and 4 ventilation caverns were excavated in Hawkesbury Sandstone, ground conditions varied considerably. A summary is provided in

Table 2.

Table 2. Cavern ground conditions as encountered.

Cavern no.	Category	Ground classification[1]	Remarks
Cavern 1	Competent ground	Sandstone Class II	
Cavern 2	Competent ground	Sandstone Class II	
Cavern 3	Poor ground	Sandstone Class II Faults and joints	Structurally complex zone with faulting and jointing encountered; Dyke B intersected in mainlines and ramps beyond permanent pillar
Cavern 4	Poor ground	Dyke Faults and joints	Dyke B (3 m thick dolerite core) and structurally complex zone with faulting and jointing encountered
Cavern 5	Poor ground	Faulted ground	Encountered Fault 1: 3.5m thick fault core equivalent to Sandstone Class IV/V with associated damage zone with increased jointing and faulting
Cavern 6	Intermediate ground	Sandstone Class II Siltstone rip-up clasts	Cavern in proximity to paleovalley; stress-induced rock bolt shearing led to re-bolting
Cavern 7	Intermediate ground	Sandstone Class II Siltstone rip-up clasts Bedding shears	Cavern under paleovalley; increased water inflows and grout takes for rock bolts observed
Cavern 8	Competent ground	Sandstone Class II	Pillar replaced due to its small size
Cavern 10	Competent ground	Sandstone Class II	Cavern under paleovalley
Cavern 11	Intermediate ground	Sandstone Class II Faults and joints	In proximity to Dyke B; structurally complex zone with faulting and jointing encountered
Cavern 12	Poor ground	Dyke Faults and joints	Dyke B (3 m thick dolerite core) and structurally complex zone with faulting and jointing encountered
VF01	Competent ground	Sandstone Class II	
VF02	Competent ground	Sandstone Class II	
VF03	Poor ground	Dyke Faults and joints	Dyke B (3 m thick dolerite core) and structurally complex zone with faulting and jointing encountered
VF04	Poor ground	Dyke Faults and joints	Dyke B (3 m thick dolerite core) and structurally complex zone with faulting and jointing encountered

Notes: 1. Sandstone classification is in accordance with Pells, Mostyn, Bertuzzi & Wong (2019).

3 GROUND SUPPORT DESIGN

The ground support design philosophy for the caverns was largely the same as for the smaller tunnels. As the span increases, convergence is expected to increase, and a greater extent of ground is mobilized that needs to be reinforced. This led to the requirement for longer and higher-capacity crown bolts. Fully grouted rigid rock bolts and cable bolts were installed in combination with sprayed shotcrete. Up to 5.4 m long rock bolts were routinely used for tunnel spans up to approximately 21 m. For cavern profiles with span between 21 m and 29 m, longer and higher-capacity cable bolts were required.

Shotcrete thickness in good ground was unaffected by tunnel span. Shotcrete was designed to span between rock bolts to support small blocks of rock between bolts. When in competent ground, a design thickness of 110 to 130 mm was adopted with a total of 165 mm sprayed locally at bolt heads to provide cover to steel elements. This was the same regardless of tunnel span since the rock bolt spacing in narrower tunnels was equal to that in the caverns. The widest 29 m span cavern was supported with the same thickness of shotcrete as a 6 m wide cross passage.

A typical road cavern ground support cross section (in good ground) is presented in Figure 8. The face is shown split into three headings and a bench. Initial span rock bolts and final span cable bolts are indicated. The left half of the sketch shows the permanent primary shotcrete lining (green) without a waterproofing membrane. The right half of the sketch shows the permanent secondary shotcrete lining (grey) with a waterproofing membrane (red), which was installed if groundwater conditions required it or where project requirements specified membranes to be installed.

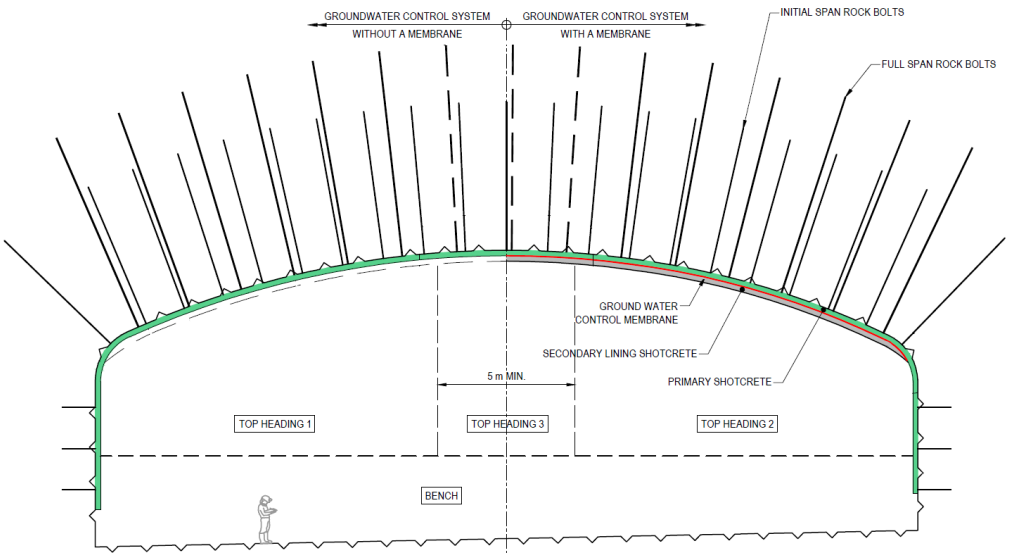


Figure 8. Typical road cavern ground support cross section in good ground.

A different approach to shotcrete was adopted for the high ventilation caverns. Thicker crown shotcrete was considered necessary there due to potential stress-induced fracturing and formation of loose blocks of rock in the crown during deep benching operations.

The construction program was a critical input to support design. Due to plant limitations, it was not possible to install cable bolts at the tunnel face remotely in all instances. Installation of cable bolts by hand under supported ground takes considerable time. Therefore, it was important to adopt an excavation sequence and support design to take installation of cable bolts out of the typical excavation and support cycle.

The sequence adopted involved excavation of three headings with the two side drifts (headings 1 and 2) excavated first and supported with remotely installed rock bolts. Cable bolts in headings 1 and 2 were then installed behind the heading face, off critical path. This enabled construction to pass through the cavern quickly and access other parts of the project. The temporary central pillar (heading 3) was excavated following cable bolt installation in headings 1 and 2.

The ground support installed in headings 1 and 2 before removal of the central pillar is referred to as the initial span support in this paper. The cable bolts installed behind the face prior to excavation of the temporary central pillar and opening up the full span is referred to as the full span support. The initial span rock bolts were considered permanent bolts, which reduced the demand and quantities for the full span cable bolts. Double corrosion-protected (DCP) rock bolts and cable bolts with a protective plastic sheath were used to achieve a 100-year design life.

A photograph showing a Rozelle Interchange motorway cavern under construction with a roadheader in heading 1 and a bolting rig operating in heading 2 is presented in Figure 9.



Figure 9. cavern under construction, showing a roadheader in heading 1 (left) and a bolting rig operating in heading 2 (right). The temporary central pillar (heading 3) is still in place.

Support designs were provided for a range of ground conditions. A selection, referred to here as “favourable” (fav.), “expected” and “adverse”, is presented in Table 3.

Table 3. Selected range of design ground conditions.

Ground conditions	Favourable	Expected	Adverse
UCS	≥ 30 MPa	≥ 25 MPa	≥ 10 to 15 MPa
Defect spacing	≥ 1.5 m	≥ 1.0 m	≥ 1.0 m
Geological structure	Zero to one clay seam in bolted zone above crown	One to two thin clay seams in bolted zone above crown	Two to four clay seams in bolted zone above crown; or joint swarm, thin subvertical fault or thin low angle shear in bolted zone

Notes: 1. The tabulated design ground conditions are simplified for the purpose of this paper. Selection criteria vary across design packages.

Typical support details for the road caverns under these ground conditions are summarised in Table 4 for the various cavern spans. Ventilation cavern support details are included in Table 5.

Table 4. Typical ground support details for road caverns (bolt lengths, types & spacing).

		Initial span		Full span			Shotcrete thickness (mm)	
Ground type	Span (m)	Bolt length and type[1] (m)	Spacing (m) (Trans. x Long.)	Bolt length and type (m)	Bolt length and type (m)	Spacing (m) (Trans. x Long.)	Primary [3]	Secondary [4]
		H1 & H2		H1 & H2	H3[2]			
Fav	22		1.75 x 1.75		-	2.0 x 1.75		
Expected	to		1.50 x 1.50	6.5 R	-	2.0 x 1.50		
Adverse	23		1.25 x 1.25		6.5 R	2.0 x 1.25		
Fav	23		1.75 x 1.75		-	2.0 x 2.5	110	200
Expected	to	5.4 R	1.50 x 1.50	7.5 C	-	2.0 x 2.5		
Adverse	26		1.25 x 1.25		7.5 C	2.25 x 1.75		
Fav	26		1.75 x 1.75			2.50 x 1.75		
Expected	to		1.50 x 1.50	8.5 C	8.5 C	2.50 x 1.50		
Adverse	29		1.25 x 1.25			2.25 x 1.25		

Notes:
1. Rock bolts (R) had ultimate tensile strength of 310 kN. Cable bolts (C) had an ultimate tensile strength of 580 kN.
2. Full span bolts were not required in top heading 3 for favourable and expected ground conditions.
3. At the bolt heads a total of 165 mm of primary shotcrete lining was sprayed locally to provide cover to steel elements.
4. The primary shotcrete lining is a permanent lining. the secondary lining was only installed in areas where a waterproofing membrane was provided. a waterproofing membrane was not required in the majority of the caverns.

For ground conditions poorer than “adverse”, including major faults and dykes, a hybrid support system with rock bolts and a thick (up to 350 mm) structural shotcrete arch was adopted.

A summary of PTT-directed ground support details (refer to Section 4.1) for the 15 road and ventilation caverns is given in Table 5 at their widest span, unless indicated otherwise.

Table 5. Cavern support details per PTT.

Cavern no.	Bolt length and type[2] (m)	Bolt spacing (m)	Primary shotcrete thickness[1] (mm)	Pillar replacement
	Initial span support[3] (Full span support, if applicable[3])			
Cavern 1	5.4 R (8.5 C)	1.5 trans x 1.5 long (2.5 trans x 1.5 long)	110	No
Cavern 2	5.4 R (8.5 C)	1.5 trans x 1.5 long (2.5 trans x 1.5 long)	110	No
Cavern 3	8.5 C	1.25 trans x 1.25 long	175	No
	Cable bolts installed at face without initial span rock bolts			

Cavern no.		Bolt length and type[2] (m)	Bolt spacing (m)	Primary shotcrete thickness[1] (mm)	Pillar replace-ment
Cavern 4	Fault (27.6 m span)	4.5 R (8.5 C)	1.25 trans x 1.25 long (1.0 trans x 1.25 long)	175	No
	Dyke (25.8 m span)	5.4 R (7.5 C)	1.0 trans x 1.25 long (2.0 trans x 1.25 long)	150, passive arch (350, SL81 mesh, passive arch)	N/A
		Concrete strip footing underpinning heading elephant's foot and founded below cavern invert			
Cavern 5		5.4 R (7.5 C)	1.5 trans x 1.5 long (1.0 trans x 1.25 long)	110	Yes
Cavern 6		5.4 R (8.5 C)	1.5 trans x 1.5 long (2.5 trans x 1.5 long)	110	No
Cavern 7		5.4 R (8.5 C)	1.25 trans x 1.25 long (2.25 trans x 1.25 long)	110	No
Cavern 8		5.4 R (7.5 C)	1.5 trans x 1.5 long (2.0 trans x 2.0 long)	175	Yes
Cavern 10		5.4 R (8.5 C)	1.5 trans x 1.5 long (2.5 trans x 1.5 long)	110	No
Cavern 11		5.4 R (7.5 C)	1.25 trans x 1.25 long (2.0 trans x 2.0 long)	175	No
Cavern 12		4.5 (7.5 C)	1.0 trans x 1.25 long (1.5 trans x 1.5 long)	250	Yes
VF01		5.4 R	1.25 trans x 1.25 long, or 1.5 trans x 1.5 long	160	N/A
VF02		5.4 R	1.5 trans x 1.5 long	200	N/A
VF03	Class II SST	5.4 R	1.5 trans x 1.5 long	200	N/A
	Dyke		1.0 trans x 1.25 long		N/A
VF04	Fault	5.4 R	1.0 trans x 1.0 long	250	N/A
	Dyke		1.0 trans x 1.25 long	175, SL81 mesh	N/A

Notes:
1. Unless indicated as a passive arch, shotcrete is designed as a hanging lining, spanning between and pinned by rock bolts.
2. Items outside brackets indicate initial span support elements. Items inside brackets indicate full span support elements. Where no brackets are provided, the initial span ground support was used to support the full span.
3. Bolt lengths outside brackets (initial span) indicate rock bolts with a capacity of 310 kN. bolt lengths in brackets (full span) indicate cable bolts with a capacity of 580 kN.

It is noted that no design changes were made at the PTT. Support directed at the PTT relied on a pre-approved toolbox of support options. Where design changes were made, these followed the approved design changes process. Refer to the paper by Salcher et al (2023) for details on the PTT and design change process adopted at Rozelle Interchange.

A fit-for-conditions groundwater control system was part of the design but is not the subject of this paper. It consisted of a toolbox of groundwater control measures to meet the project inflow requirements, ranging from local flushable strip drains to a waterproofing membrane with a thick secondary lining resting on abutments or hanging off additional rock bolts.

4 ACKNOWLEDGEMENTS

The authors thank the construction joint venture of John Holland and CPB Contractors for permission to publish this material. The authors also gratefully acknowledge the support of Transport for New South Wales in approving this paper. The views and opinions expressed in this paper are the authors and do not necessarily represent those of Transport for New South Wales.

The authors are indebted to the tireless efforts of the many engineers and geologists of the contractors and consultants supporting the project. In particular, we thank Dr. Andrew De Ambrosis for his technical leadership on PSM's road cavern design, Dr. Beatriz Estrada for engineering geological support and Rebecca Fusee for never hesitating to run down the tunnel one more time, ensuring that fault was getting bolted.

We hope that the information presented here will be useful for others planning to construct caverns in Sydney and elsewhere.

5 REFERENCES

Bai, Y., Salcher, M., Fusee, R., Bentley, T., Kumar, A. & Trim, M. (2023). Rock bolt shearing during construction of multi-level tunnels in Sydney. In *Proceedings of the 18th Australasian Tunnelling Conference*, Auckland.

Bai, Y., Salcher, M., Stocker, R., Bentley & Trim, M. (2025). Ground response for construction of 15 caverns in diverse ground conditions in Sydney – Part 2: Construction sequence and ground response. In *Proceedings of the 2025 Australasian Tunnelling Conference*, Perth.

Estrada, B., Nash, T., De Ambrosis, A. and Chan, I. (2022). Characterisation of complex ground conditions for the Rozelle Interchange Project. *Australian Geomechanics*, 57(4).

Pells, P.J.N., Mostyn, G., Bertuzzi, R. & Wong, P. (2019). Classification of sandstones and shales in the Sydney region: A forty year review, *Australian Geomechanics*, 54(2).

Salcher, M., Bai, Y., Trim, M., Bertuzzi, R. & Vidler, B. (2023). The Permit to Tunnel process adopted on Australian infrastructure projects. In *Proceedings of the 18th Australasian Tunnelling Conference*, Auckland.

THIS PAGE INTENTIONALLY LEFT BLANK

19th Australasian Tunnelling Conference – Acosta-Martínez, Stewart and Hudson-Smith (Eds.)
© 2025 Australian Tunnelling Society, ISBN 978-0-85825-002-4

Ground response for construction of 15 caverns in diverse ground conditions in Sydney – Part 2: Construction sequence and ground response

Y. Bai & M. Trim
Delve Underground, Sydney, Australia

M. Salcher
Gamuda (formerly PSM), Sydney, Australia

R. Stocker
PSM, Sydney, Australia

T. Bentley
John Holland, Sydney, Australia

ABSTRACT: Eleven road caverns and four ventilation caverns were recently constructed in Sydney as part of the Rozelle Interchange project. The up to 29 m wide road caverns and 24 m high ventilation caverns of the Sydney motorway were excavated in Hawkesbury Sandstone at depths between approximately 17 m and 67 m next to the harbour. The number, size, ground cover and complexity of geological conditions of these large underground excavations are unprecedented in Australia. Part 1 of this paper details the cavern geometry, ground conditions and ground support systems. This part 2 presents the construction sequence and ground response. The ground response is described in terms of in-tunnel convergence, measured using optical survey targets and steel tape extensometers, surface settlement, endoscope hole closure, rock pillar displacement monitored with inclinometers and observations of ground support performance.

1 INTRODUCTION

Eleven road caverns and four ventilation caverns were recently constructed in Sydney as part of the Rozelle Interchange project. Part 1 of the paper (Salcher, Bai, Stocker, Bentley & Trim, 2025) details the geology and ground support of the road caverns and ventilation facilities. This part 2 describes the construction sequence and ground response, with a focus on the removal of the central temporary pillar in the road caverns and deep benching in the ventilation facilities.

2 CONSTRUCTION SEQUENCE

2.1 *Permit to Tunnel*

All tunnelling on the project was carried out under the Permit to Tunnel (PTT) process. The PTT facilitates a formal review of encountered ground conditions, available monitoring data and observed ground behaviour. It sets out a plan for tunnelling activities for a defined period, location and extent. PTT meetings involving the construction team and the geotechnical construction phase services (CPS) team were held daily. Details on the PTT process adopted on Rozelle Interchange are provided by Salcher, Bai, Trim, Bertuzzi & Vidler (2023).

2.2 *Road caverns*

The construction sequence for the road caverns was primarily driven by the construction program, construction access requirements, ground conditions, ground support requirements and ventilation requirements. The typical construction sequence for a road cavern involved excavation of:

1. Heading 1
   i. On one side of the cavern
   ii. Typically 10 m to 13 m wide
2. Heading 2
   i. On the opposite side of the cavern
   ii. Similar width to heading 1
   iii. A minimum 5 m wide temporary central rock pillar (heading 3) left in place
3. Temporary central rock pillar (heading 3) towards the pillar nose
4. Bench and trench

This sequence is illustrated in Figure 1.

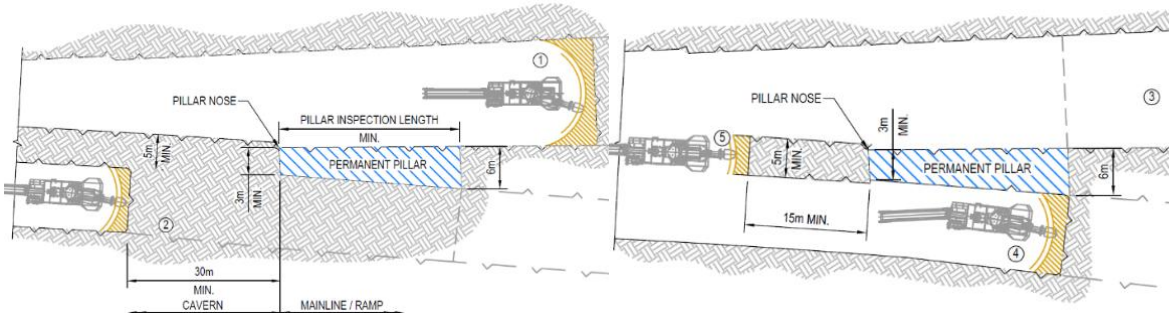


Figure 1. Three heading excavation sequence.

Some considerations associated with the typical steps listed above include:

- Roadheaders were launched into headings 1 and 2 simultaneously. The two headings were sufficiently separated by the minimum 5 m wide temporary rock pillar, allowing both roadheaders to operate at the same time.
- As mentioned in section 3, rock bolts and cable bolts were installed in two stages, referred to as initial span and full span bolts. Cavern 3 is an exception where cable bolts were installed remotely at the face (refer to Table 5 in Bai et al, 2025). The initial span bolts (typically 5.4 m long rock bolts) allowed excavation to progress through headings 1 and 2 with full span bolts (typically up to 8.5 m long cable bolts) installed behind the face off critical path before the removal of the temporary central pillar (heading 3).
- To avoid trimming and thinning of the permanent pillar, as implemented on the M4 East project and described by Salcher, Nash, De Ambrosis & Grabham (2019), strict excavation tolerances were applied to ensure that the minimum permanent pillar width was satisfied.
- At the narrow end of the caverns, headings 1 and 2 converged to transition into a split heading (two headings) at a tunnel span of less than 22 m.

A bespoke construction sequence was applied to a handful of caverns. For example, Caverns 4 and 5 were constructed in difficult ground and required additional considerations, such as replacing the permanent rock pillar with concrete (Cavern 5) or underpinning the heading shotcrete arch during benching (Cavern 4). For more information on Cavern 5, the reader is referred to Stocker, De Ambrosis & Estrada (2023). To facilitate construction access, Caverns 7 and 8 featured an intersecting tunnel cutting the temporary pillar into two portions. This involved a cross-cut through the cavern and installation of full span support before breaking out left and right to form the cavern either side of the cross-cut.

2.3 *Ventilation caverns*

Construction of the tall ventilation facilities was staged as an approximately 7 m high single or split heading followed by multiple deep benches, each 4 m to 5 m high, reaching the total cavern

height of up to 24 m. Given the significant height, it was difficult for construction to reach the crown once one deep bench was removed. The excavation sequence for the ventilation facilities is illustrated in Figure 2 and Figure 3.Figure 4 presents a photograph of a completed ventilation facility. Additional discussion on the construction of the ventilation facilities can be found in Tepavac, Sun, Trim & Kumar (2022).

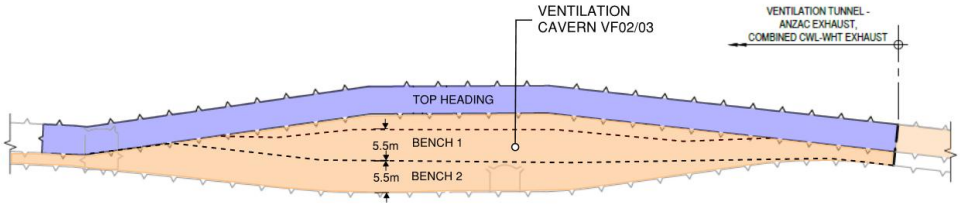


Figure 2. Long section of ventilation facility showing excavation sequence.

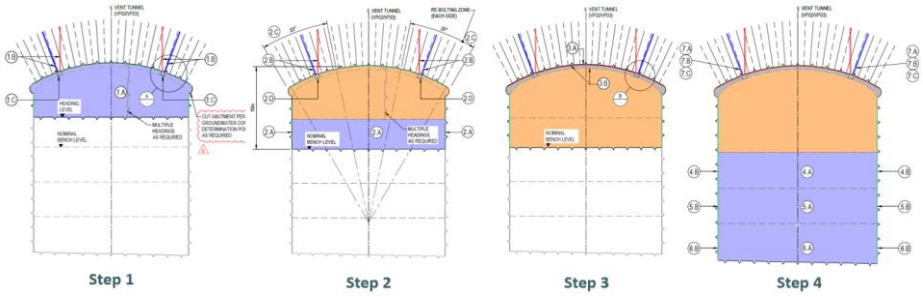


Figure 3. Ventilation facility excavation sequence cross sections.

2.4 *Plant*

Mitsui SLB300 roadheaders with axial cutterheads were employed for cavern heading excavation given their higher reach compared to other roadheaders, thus being able to cut a taller heading. This not only minimised bench excavation volumes but also provided the needed space for installation of long rock bolts and cable bolts. For significant benching activities, such as the deep benches in the high ventilation caverns, Sandvik MT720 roadheaders with a transverse milling head were used. These proved more effective in these types of excavations. Figure 5 presents a photograph of a typical benching operation in a ventilation cavern. In some instances, two roadheaders were used simultaneously side by side to cut a single bench face.



Figure 4. Inspection of endoscope hole for monitoring of rock bolts shearing in crown of completed ventilation cavern.


Figure 5. Sandvik Mt720 roadheader excavating a deep bench in ventilation cavern VF02

Two types of Caterpillar Robodrill rock bolting rigs were used for bolt installation. One was configured with a conventional drifter and was used for installing rigid rock bolts up to 6.5 m long. The other was configured to install cable bolts up to 8.5 m long. Both rigs had the capability to mix and pump grout remotely through the rig after bolt pre-tensioning.

3 GROUND RESPONSE

3.1 *Monitoring methods*

Several methods were used to monitor the response of the rock mass due to removal of heading 3 (temporary central pillar) in the road caverns and deep benching in the ventilation facilities. These methods include in-tunnel optical targets, steel tape extensometer convergence readings, optical surface settlement targets, shear endoscope holes, instrumented rock bolts and inclinometers in the permanent part of the pillar. During cavern constructions, these instruments were read daily. Selected data obtained by these methods are presented in the following sections.

3.2 *Tunnel convergence*

Optical survey targets were installed progressively, approximately every 4 m laterally across the cavern crown, as headings 1, 2 and 3 were excavated. Eye bolts for vertical tape extensometers were installed into the crown and heading floor in headings 1 and 2 on either side of the temporary central pillar (heading 3). Crown optical targets and tape extensometers were installed at a longitudinal spacing of 10 m to 20 m, with a reduced spacing near the large spans.

In-tunnel convergence results are presented in Table 1.

Table 1. Summary of cavern convergence.

Cavern no.	Max. crown sag (optical survey, mm)	Distance of max. crown sag from pillar nose or cavern centre[(1)] (m)	Max. tape extensometer vertical convergence[(2)] (mm)	Max. horizontal convergence (optical survey, mm)
Cavern 1	9	7 (0.2 D)	12	8
Cavern 2	12	12 (0.5 D)	27	15
Cavern 3	44	11 (0.4 D)	86[(3)]	16
Cavern 4	71	48 (1.7 D)	38	20

Cavern no.	Max. crown sag (optical survey, mm)	Distance of max. crown sag from pillar nose or cavern centre[1] (m)	Max. tape extensometer vertical convergence[2] (mm)	Max. horizontal convergence (optical survey, mm)
Cavern 5	11	30 (1.1 D)	52	12
Cavern 6	6	19 (0.7 D)	13	11
Cavern 7	37	33 (1.1 D)	33	11
Cavern 8	22	48 (1.9 D)	-	6
Cavern 10	11	49 (1.7 D)	22	9
Cavern 11	23	62 (2.3 D)	17	9
Cavern 12	26	18 (0.7 D)	50	22
VF01	4	2 (0.1 D)	-	11
VF02	19	3 (0.2 D)	-	26
VF03	31	8 (0.4 D)	-	33
VF04	25	9 (0.5 D)	-	26

Notes:

1. For road caverns (Caverns 1 to 12) value outside the brackets represent the distance in metres of the location of maximum crown sag from the pillar nose. The value in brackets is the same distance as a multiple of the cavern span (D) at the pillar. For ventilation facilities (VF01 to VF04) values outside the brackets represents distance of the location of maximum crown sag to the location of the widest span of the cavern (which coincides approximately with the centre of the cavern along its longitudinal axis). The value in brackets is the same distance as a multiple of the maximum cavern span (D).
2. Where no tape extensometer value is provided, no tape extensometers were installed.
3. Reported Cavern 3 measurement was deemed not reliable by the designer and site team (damage or bench heave suspected). However, tape measurements were still recorded for information only.

Table 1 shows the following:

- In some cases, the tape extensometer readings were significantly higher than crown sag measured by optical survey. This may be explained by floor heave, and in particular by bedding partings below the heading floor "popping up".
- Poorer ground conditions are associated with greater displacements (e.g. Caverns 3, 4, 5 and 12; cf. Table 2 in Bai et al, 2025)
- Maximum crown sag in the road caverns occurs some distance—and often more than one cavern span (D)—from the permanent pillar. This is consistent with observations made by Salcher et al. (2019) for the caverns of the M4 East project.
- Horizontal convergence in the tall ventilation facilities is significant compared to vertical convergence.

Figure 6 shows tape extensometer readings taken during the excavation of the temporary central pillar (top heading 3) in the road caverns. The data is presented in terms of vertical tunnel convergence against distance to the advancing face of the temporary central pillar. Figure 7 shows the same convergence data but plotted against time.

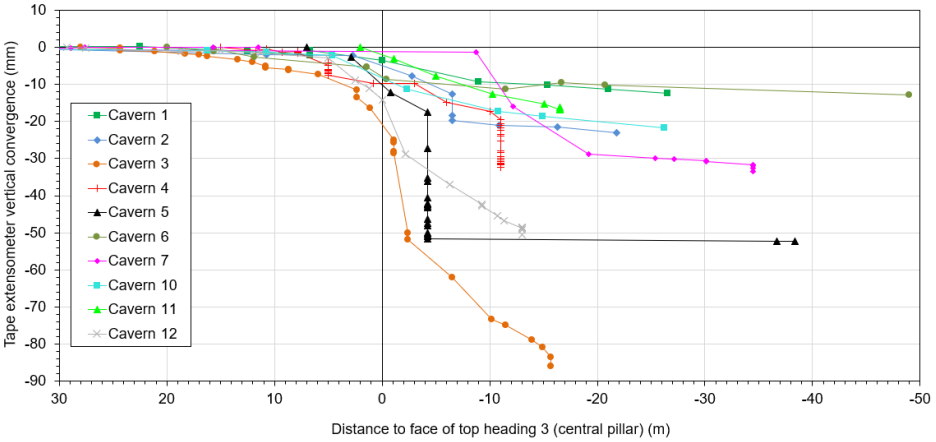


Figure 6. Tape extensometer readings in road caverns during excavation of temporary central pillar (heading 3). Negative convergence values indicate tunnel convergence (i.e. crown sag or invert heave). Negative distance to face values indicate that the tunnel face (i.e. heading 3) has passed the monitoring point.

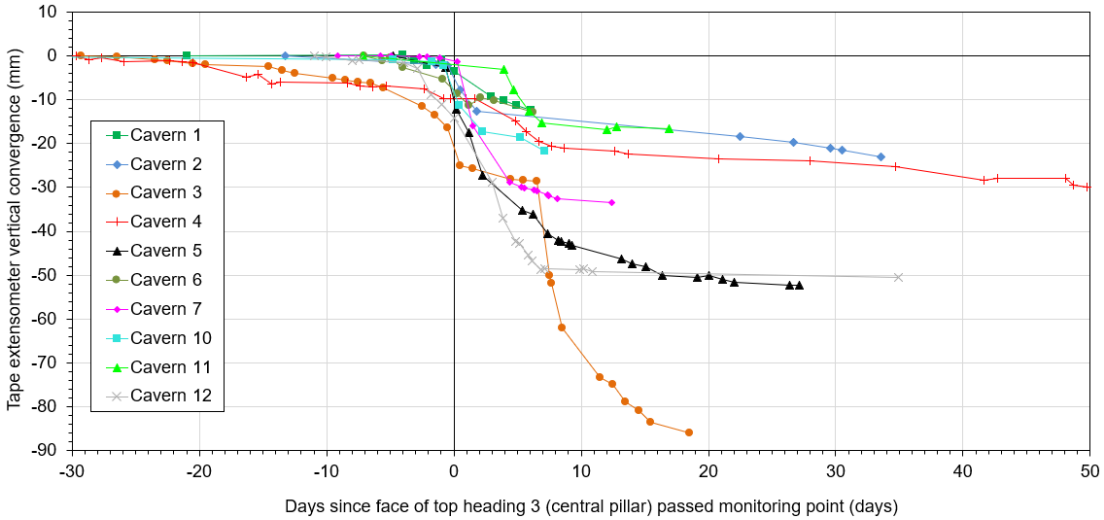


Figure 7. Tape extensometer readings in road caverns during excavation of temporary central pillar (heading 3). Negative convergence values indicate tunnel convergence (i.e. crown sag or invert heave). Positive number of days indicate that the tunnel face (i.e. heading 3) has passed the monitoring point.

Figure 6 and Figure 7 show the following:

- Onset of convergence occurs between 20 m (0.9 D[1]) and 10 m (0.45 D) ahead of the temporary central pillar face
- Convergence increased significantly once the face of the temporary central pillar passed the monitoring point
- Convergence stabilised when the temporary central pillar face had advanced between 10 m (0.45 D) to 20 m (0.9 D) beyond the monitoring point
- In two cases (Cavern 4 and Cavern 5), convergence continued to increase for several weeks even though the excavation of the temporary central pillar had been completed. Both caverns were excavated in poor ground (cf. Table 2 in Bai et al, 2025).

3.3 *Surface settlement*

Optical surface settlement points installed on roads above the caverns were surveyed daily, leading up to, during and for some time after removal of the temporary central pillar. The location of these surface monitoring points focused on publicly accessible areas (e.g., roads, footpaths, bridges, etc.) but also included sensitive privately owned buildings.

Maximum surface settlement recorded by InSAR satellite monitoring was approximately 50 mm. Optical survey of monitoring targets installed on roads and kerbs showed a maximum settlement of 35 mm. Predicted effects and impact assessment demonstrated that with the observed settlement, the risk of structural damage remained within acceptable levels. These maximum values were observed in the area where multiple caverns were excavated in poor ground. A selected settlement plot is presented in Figure 7. Negative values indicate settlement.

[1] *D* represents the 22 m cavern span, which was the limit beyond which a temporary central pillar (i.e. a third heading) was adopted.

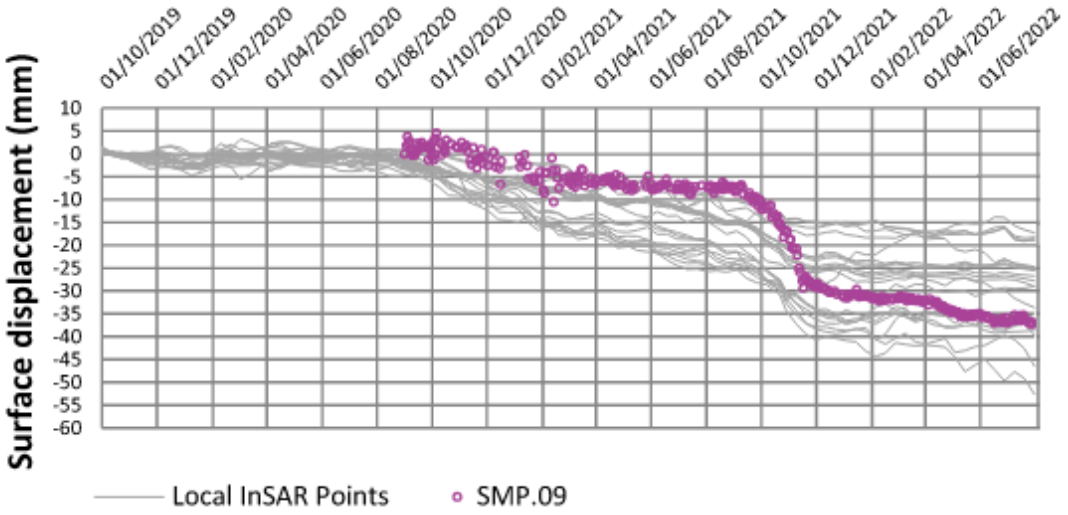


Figure 8. Example surface settlement plot showing InSAR (grey) and optical survey (purple) monitoring data.

It was noted that surface settlement took several days or longer to stabilise following the excavation. This is consistent with observations reported by Salcher et al. (2019) for the construction of the caverns of the M4 East project.

3.4 *Pillar displacement*

Where access was available, inclinometer casing was installed and grouted in boreholes that were drilled from the surface through the permanent pillars of the road caverns. Baseline readings were taken long before the headings on either side of the pillar approached the permanent pillar. During temporary central pillar removal, the inclinometers were read daily.

Figure 9 shows the uncorrected cumulative displacement of the inclinometers installed in Cavern 1. A-axis readings are shown, with the A-axis pointing towards the headings on either side of the pillar. As such, positive and negative readings denote movement towards these headings. The inclinometer response is summarised in Table 2. Photographs showing the pillar ground conditions are presented in Figure 10.

Table 2. Summary of pillar inclinometer readings.

	Cavern 1	Cavern 2	Cavern 7
Inclinometer location	10 m from nose	30 m from nose	37 m from nose
Pillar moved towards	First heading (M150)	First heading (M1D0)	First heading (M170)
Max. displacement	4.3 mm	7.2 mm	6.5 mm
Response to benching	None	None	None
Remarks	Sharp change in movement occurred at siltstone/laminite band at shoulder (see Figure)	No correlation of movement with location of siltstone rip-up clasts in crown)	Ground conditions comprised high-quality sandstone without siltstone bands.

In addition to the remarks in Table 2, the following was observed from the inclinometer readings:

- 0 to 1 mm movement when the tunnel face approached within 5 m of the inclinometer location
- 0.5 to 2.5 mm when the tunnel face was adjacent to the inclinometer location
- 2.5 to 3 mm when the tunnel face was 5 to 10 m past the inclinometer location
- 3 to 5 mm when the tunnel face was approximately 15 to 30 m past the inclinometer location
- Very little to no response to the excavation of the second tunnel
- Very little to no response to excavation of the temporary central pillar

– Very little to no response to excavation of the bench in either tunnel
– Siltstone rip-up clasts did not appear to impact pillar displacement
– Significant movement occurred along siltstone/laminite bands

The observation of the pillar not moving back towards the second tunnel following the excavation of the second tunnel is different from observations made by Salcher et al. (2019) for the caverns of the M4 East project. It is possible that correction of the inclinometer data for systematic errors, such as those described by Mikkelsen (2003), may lead to different conclusions.

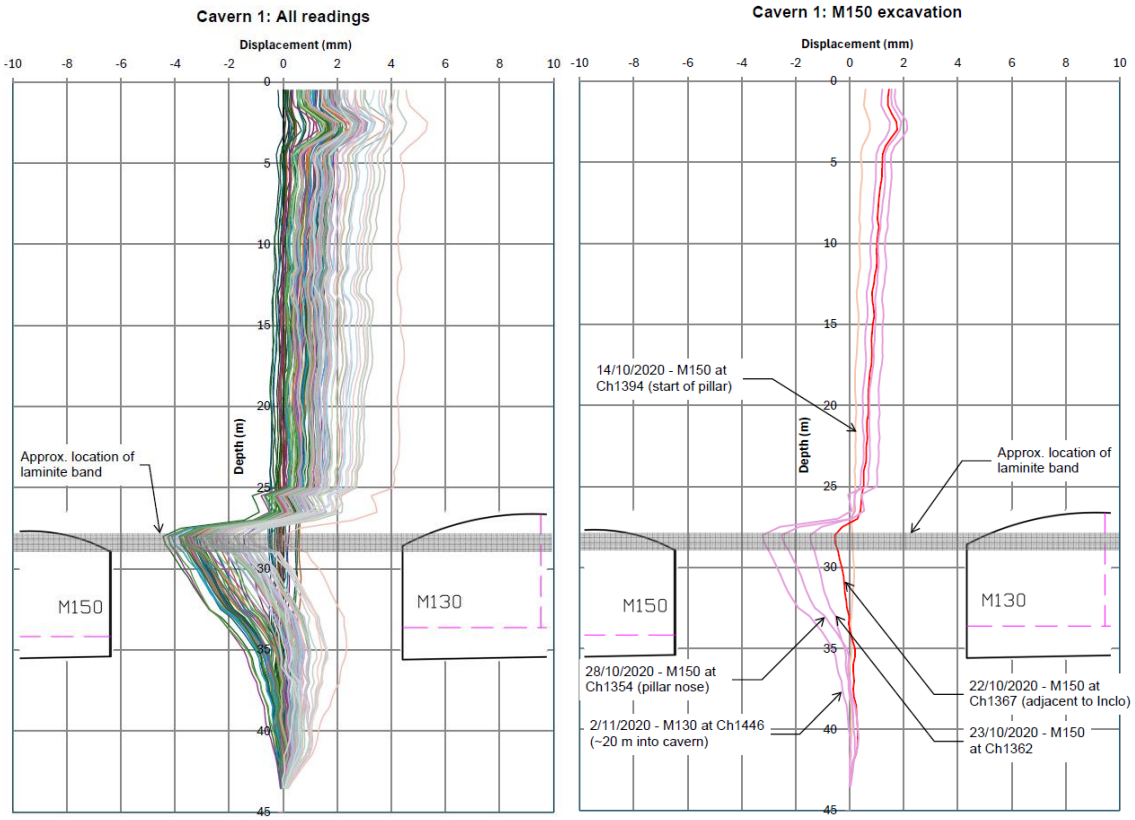


Figure 9. Cavern 1 pillar inclinometer readings. M150 was excavated first.



Figure 10. Laminite band in Cavern 1 temporary pillar (top heading 3) (left) and adjacent M150 ramp (right).

3.5 *Rock bolt shearing*

In the road caverns, endoscope holes were drilled to cable bolt length on both sides of the temporary and permanent pillar to monitor of rock bolt and cable bolt shearing due to bedding plane movements. During central pillar (top heading 3) removal, the holes were inspected daily with an

endoscope camera. Wherever shearing was observed, the magnitude of shear displacement was measured and recorded. The project technical criteria deemed 10 mm of shear displacement as the limit of acceptable deformation of the protective plastic sleeve of rock bolts and cable bolts. The durability of the permanent (100-year design life) bolts was assumed to be compromised for monitoring of rock bolt and cable bolt shearing due to bedding plane movements. For structural bolt deformation, the limit of shear movement set was 20 mm.

During the excavation of top headings 1 and 2 in the road caverns, re-bolting was carried out prior to removal of the central pillar, thus requiring only replacement of the initial span rock bolts and not the full span cable bolts. There were no instances where shearing in the road caverns exceeded the 10 mm limit during or after central pillar removal. As a result, no cable bolts required replacement.

In the tall ventilation facilities, multiple instances of rock bolt shearing were observed. While some shearing occurred during top heading excavation, most instances were observed during the deep benching stages. Shearing was observed in the endoscope holes and confirmed by readings of instrumented rock bolts (i.e., strain gauges attached to rock bolts). A photograph of an endoscope inspection being carried out in the crown of one of the ventilation caverns is provided in Figure 4. A photograph of a typical shearing event, as captured by an endoscope camera looking uphole, is given in Figure 11.



Figure 11: Uphole view of sheared bedding parting in endoscope hole. A rod of known dimension is placed against the shearing plane to assess the shearing magnitude (17 mm in this case). Source: Bai et al (2023).

Maximum rock bolt shear movements measured in the ventilation facilities remained below the 20 mm limit that the project allowed for structural rock bolt deformations (i.e., as opposed to the 10 mm allowable deformation of the plastic sheath for durability purposes). That is, re-bolting was performed before shear displacements could reach this limit.

On some occasions, a fill platform had to be constructed in the ventilation facilities to provide access to the crown for re-bolting, given the significant tunnel height and progress of benching activities at the time of the shearing events. Shearing was almost always associated with cracking of the shotcrete lining in the crown. All instances of shearing of permanent rock bolts and damage to shotcrete were rectified before handover of the tunnels.

Bai, Salcher, Fusee, Bentley, Kumar & Trim (2023) provide more details on rock bolt shearing observed on the Rozelle Interchange project and management of shear movements.

4 CONCLUSION

The scale and number of caverns constructed for the Rozelle Interchange project are unprecedented in Australia. The project involved wide and tall excavations in a variety of ground conditions. Significant dykes and faults were encountered; high quality sandstone came with adverse in situ rock stress conditions. A robust yet efficient design, along with a rigorous monitoring

system, a carefully planned construction sequence, a modern fleet of construction plant and an industry-best Permit to Tunnel system were essential to delivering the project.

The successful completion of the underground works of Rozelle Interchange is an enormous achievement that is best appreciated by walking the seemingly endless kilometres of intersecting and overlapping tunnels, caverns, shafts and passages (Figure 1 in Bai et al, 2025 & Figure 12).



Figure 12. Intersection of road caverns and ventilation tunnels.

5 ACKNOWLEDGEMENTS

The authors thank the construction joint venture of John Holland and CPB Contractors for permission to publish this material. The authors also gratefully acknowledge the support of Transport for New South Wales in approving this paper. The views and opinions expressed in this paper are the authors and do not necessarily represent those of Transport for New South Wales.

The authors are indebted to the tireless efforts of the many engineers and geologists of the contractors and consultants supporting the project. In particular, we thank Dr. Andrew De Ambrosis for his technical leadership on PSM's road cavern design, Dr. Beatriz Estrada for engineering geological support and Rebecca Fusee for never hesitating to run down the tunnel one more time, ensuring that the fault was getting bolted.

We hope that the information presented herein will be useful for others planning to construct caverns in Sydney and elsewhere.

6 REFERENCES

Bai, Y., Salcher, M., Fusee, R., Bentley, T., Kumar, A. & Trim, M. (2023). Rock bolt shearing during construction of multi-level tunnels in Sydney. In *Proceedings of the 18th Australasian Tunnelling Conference*, Auckland.

Bai, Y., Salcher, M., Stocker, R., Bentley & Trim, M. (2025). Ground response for construction of 15 caverns in diverse ground conditions in Sydney – Part 1: Ground support. In *Proceedings of the 2025 Australasian Tunnelling Conference*, Perth.

Mikkelsen, P.E. (2003). Advances in inclinometer data analysis. In *Proceedings of the Symposium on Field Measurements in Geomechanics*, Oslo.

Salcher, M., Bai, Y., Trim, M., Bertuzzi, R. & Vidler, B. (2023). The Permit to Tunnel process adopted on Australian infrastructure projects. In *Proceedings of the 18th Australasian Tunnelling Conference*, Auckland.

Salcher, M., Nash, T., De Ambrosis, A., & Grabham, C. (2019). Ground response due to temporary pillar removal in motorway caverns in Sydney sandstone. In *Proceedings of the 13th ANZ Conference on Geomechanics*, Perth

Stocker, R., De Ambrosis, A. & Estrada, B. (2023). Design and construction of a motorway cavern in faulted Hawkesbury Sandstone, Sydney. In *Proceedings of the 18th Australasian Tunnelling Conference,* Auckland.

Tepavac, D., Sun, Y., Trim, M. & Kumar, A. (2022). Design and construction of large-scale ventilation caverns on WestConnex's Rozelle Interchange project. In *Proceedings of North American Tunneling Conference*, Philadelphia.

19th Australasian Tunnelling Conference – Acosta-Martínez, Stewart and Hudson-Smith (Eds.)
© 2025 Australian Tunnelling Society, ISBN 978-0-85825-002-4

Innovations in strand anchor design as part of the support system for a deep underground cavern

S.van Ameijde, A. Dunleavy & A.Tarrant
DYWIDAG, Newcastle, NSW, Australia

J. Laukner
DYWIDAG, Leipzig, Saxony, Germany

ABSTRACT: Australia is undertaking several nation-building renewable projects involving pumped hydro with large underground caverns which will house power stations providing large-scale storage and on demand energy. During construction the caverns require a temporary crane to be constructed to manoeuvre and position key components of the turbine machinery within the cavern. The large cranes transfer considerable loads, so it is critical that the crane rails are supported within the cavern walls by corbels using multistrand anchors. DYWIDAG has developed an innovative multistrand anchoring system for large capacity loads which overcomes the issues of grouting and stressing in an inclined hole. This system ensures the corbels are supported and connected to the rock while the challenges of the inclined angle during installation are addressed correctly. DYWIDAG's Smart Anchor monitoring system provides 24/7 remote monitoring of the forces in the anchors to ensure they are within the predicted ranges.

1 INTRODUCTION

Australia is undertaking its largest transition in history in the energy sector, shifting to renewable energy. A key part of this transition is a national shift to pumped hydro for the nation's main source of energy. These pumped hydro projects involve linking large reservoirs with long inclined tunnels to large caverns which will form some of the largest and deepest caverns in the world. Given the sheer size of these caverns, the construction sequence and methodology is monitored closely. During the construction phase, a temporary crane is constructed to manoeuvre and position key components of the turbine machinery in the correct locations within the cavern. Due to the considerable loads to be transferred by the large cranes it is critical that the crane rails are supported within the cavern walls by corbels which are installed as the primary support.

DYWIDAG, global systems supplier of ground support for geotechnics and tunnelling has developed, supplied and supervised the installation of an innovative bar and multistrand anchor system for large capacity loads to support corbels in the transformer hall and machine hall caverns. The innovation overcomes the issues of grouting and stressing in an inclined hole ensuring the corbels are supported and connected to the rock while the challenges of the inclined angle during installation are addressed correctly.

1.1 *Challenges*

There are several issues to be considered in the design and installation of the corbels in caverns for pumped hydro:

- High permanent loads in a rock mass with variable quality
- Deep underground anchoring with limited installation space
- Anchor installation in inclination
- Complex grouting requirements

– Design life of a fully permanent system

2 INNOVATION

The key innovations were developed due to the importance of adapting the DYWIDAG multistrand anchor system to the requirements of deep underground caverns in pumped hydro. These caverns require a permanent post tensioning anchor solution for high permanent loads in a rock mass with variable quality. Deep underground anchoring is required in a limited space with complex grouting under an inclined angle. DYWIDAG worked with their partner Anchor Packers Australia, to develop an anchor packer design which assists in overcoming the challenges associated with grouting in challenging geological conditions.

2.1 *Corbel Design*

The corbels supporting the crane are anchored to the rock mass by prestressed multistrand anchors. Due to the high permanent loads in a rock mass with variable quality each corbel was designed with two multistrand anchors installed at inclined angles (13 degrees and 18 degrees) in lengths up to 23m. Extra GEWI® 63.5mm rock bolts were installed for additional support. Working loads were up to 1161kN which indicated it was not possible to achieve these loads with single bar anchors and multistrand anchors were used to anchor deep into the rock mass.

2.2 *Multistrand Anchors*

Most pumped hydro projects require a permanent multistrand solution with 100-year design life. The design life of a fully permanent strand anchor system is not achievable with a DCP strand anchor design while grouting under an inclined angle. Two anchors would be required with a larger bore hole and higher associated costs. DYWIDAG worked collaboratively with the client and partner Anchor Packers Australia (subcontracted by DYWIDAG), to develop an anchor design to accommodate the specific design life requirement of 5 years. The bonded length of the anchor would be protected by a HDPE corrugated sheathing and the grouting procedure would grout both an inner and an outer annulus in one pass.

2.3 *Angled bearing plate*

DYWIDAG worked with the project and design team to refine the multistrand anchor design and develop angle compensating bearing plates tailored for each of the inclined angles to suit the anchors. As a leading global supplier, DYWIDAG leverages extensive technical experience to support clients in adapting multistrand anchor system designs to site requirements. The plates were welded to the corbel to ensure the correct inclination was achieved and to avoid any displacement during the tensioning of the anchor. The bearing plates perform to the specification provided the drillers and welders complete their work as per the QA/QC requirements.

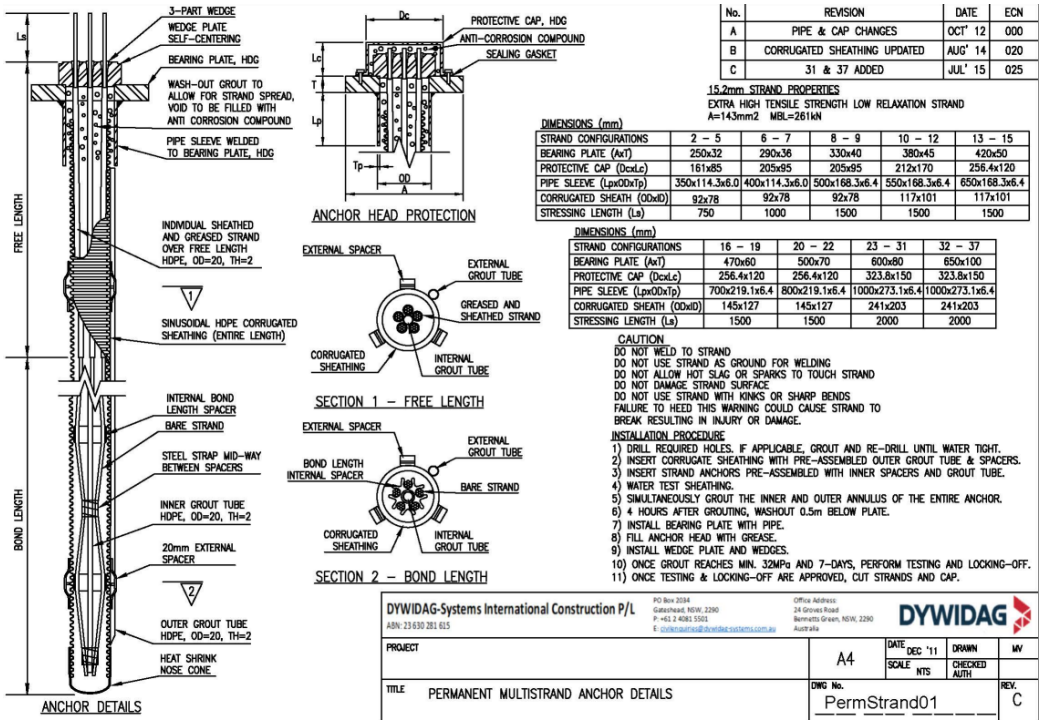


Figure 1. Multistrand anchor detail.



Figure 2. Corbel with bar anchors and angled bearing plate for strands.

2.4 *Anchor installation*

The installation of the post-tensioned anchors was challenging as it requires making an anchor packer that was robust enough to allow the anchor to be pushed into the borehole and withstand potential abrasion and damage from the borehole wall during installation. The packer was installed deep into the hole to separate the bond and free length during grouting procedures.



Figure 3. Anchor Installation.

2.5 *Grouting under an inclined angle*

To overcome the challenges of grouting upwards with two multistrand anchors installed at inclined angles (13 degrees and 18 degrees) DYWIDAG worked with Anchor Packers Australia to develop an innovative packer system designed to ensure that the bond length of the strand anchors could be grouted at the inclined angle. Failure to follow the correct grouting process may result in anchor failure either during testing or at any point during their service life.

In geological formations that are not waterproof, conventional grouting of the bond length may lead to serious issues including grout egress and water ingress. These risks are amplified when aquifers or open fractures within the rock allow:

- Grout to leak out, reducing the integrity of the bond
- Water to enter, decreasing the strength of the grout with the bond length and increasing the corrosion risks

Grouting with the theoretical volume of grout under atmospheric pressure conditions is only acceptable in holes that are proven to be watertight. In any other situation the integrity of the bond length cannot be assured.

2.5.1 *Consequences of compromised grouting*

If the bond length grout is compromised bare strand may become exposed to groundwater leading to:

- Corrosion, especially if the water is acidic or oxygenated
- Decreased bond strength as water weakens the cured grout
- Decreased bond length

Ultimately this may lead to anchor failure in both the short and long term.

The cost of anchor failure may significantly impact a project due to:
- Increased installation costs due to redrilling and regrouting
- Project delays
- OH&S issues
- Decreased client confidence
- Placing a critical piece of the pumped hydro equipment out of service for a prolonged period.

Due to its criticality, the anchor packer design required significant attention with a highly collaborative effort between DYWIDAG and the client. The original packer design included a rubber membrane with an air inflatable packer which is inflated with air to ensure pressure is maintained while grouting and curing is taking place.

While the trials conducted of this system were successful, there was an element of risk identified with the packer design not sufficient to withstand the unexpected water pressures within the cavern. The packer design was modified to a grout inflatable packer which allowed the pressure grouting of anchors to be inflated to a much higher pressure, up to 16 bar (1600kPa). This change ensured the bond length was uncompromised from water ingress during the grout curing time. The anchors grout within the bond length could effectively be guaranteed to be free from defect when grouted as per the specification. This reduced the risks of grout leakage and increased the practicality of the installation in line with available resources onsite at the crew's disposal. The refined packer design included a geo textile bladder which would be inflated with grout and a special sealing arrangement at both ends to hold the grout inside at high pressure. Each anchor would be grouted in two passes. The first pass involving grouted inflation of the packer to form a grout "plug", and the second completes grouting of the bond length after sufficient curing time of the grout packer.

The main challenge with strand anchors being used in this application is that each individual strand which makes up the multistrand anchor requires sealing to maintain sufficient pressure within the packer inflation zone so that it completely blocks the borehole allowing for stage 2 grouting.

Drawing on experience in cable stayed bridges, DYWIDAG developed a sealing system similar to that which is used in cable stayed bridges, comprising compressed rings and at either end of the packer. This refined anchor packer resulted in all anchors being successfully grouted to the required test loads.

3 END TO END QUALITY

DYWIDAG was contracted to supply the complete package of manufacturing the ground anchors, the underground installation supervision, stressing equipment and the digital SMART anchor force monitoring. As well as the innovative strand anchor grout packer which had very specific requirements for this application.

3.1 *Procurement*

The project's highly detailed construction sequence required DYWIDAG's logistics chain to support the project with Just In Time manufacturing and delivery to site of all components. DYWIDAG's bar and multistrand anchor systems hold local and global approvals with full mill certifications provided on all products.

3.2 *Product Quality*

The multistrand system was manufactured under stringent factory conditions in the Australian factory, with the various number of strands required for the project coiled and delivered to site. DYWIDAG's GEWI bar system 12–75mm bar is manufactured in Germany from steel billets produced from scrap metal from the car manufacturing industry using mainly green energy and has ACRS approval against AS4671 and AS4672.

High quality and consistency of product was able to be achieved by producing the anchors in DYWIDAG's factory rather than on site in challenging and uncontrolled conditions with limited space. The factory production of the anchors allowed for:

- Standard and consistent work procedures
- Quality factory manufacturing
- High level safety standards
- Consistent and controlled work environment
- Bespoke equipment
- Experienced production team
- End to end quality registration

3.3 *Stressing Equipment*

The jack is placed on the corbel providing a limitation of diameter of 440mm with the final pre-stressing being carried out from a working platform under the corbel. The working platform proved limitations on the dimensions of the jack and loads on the platform. DYWIDAG was contracted to provide calibrated and maintained stressing equipment for the duration of the stressing works which included 150 tonne and 300 tonne multistrand jacks, pumps and gauges.



Figure 4. Stresing in progress of bar and strand anchors

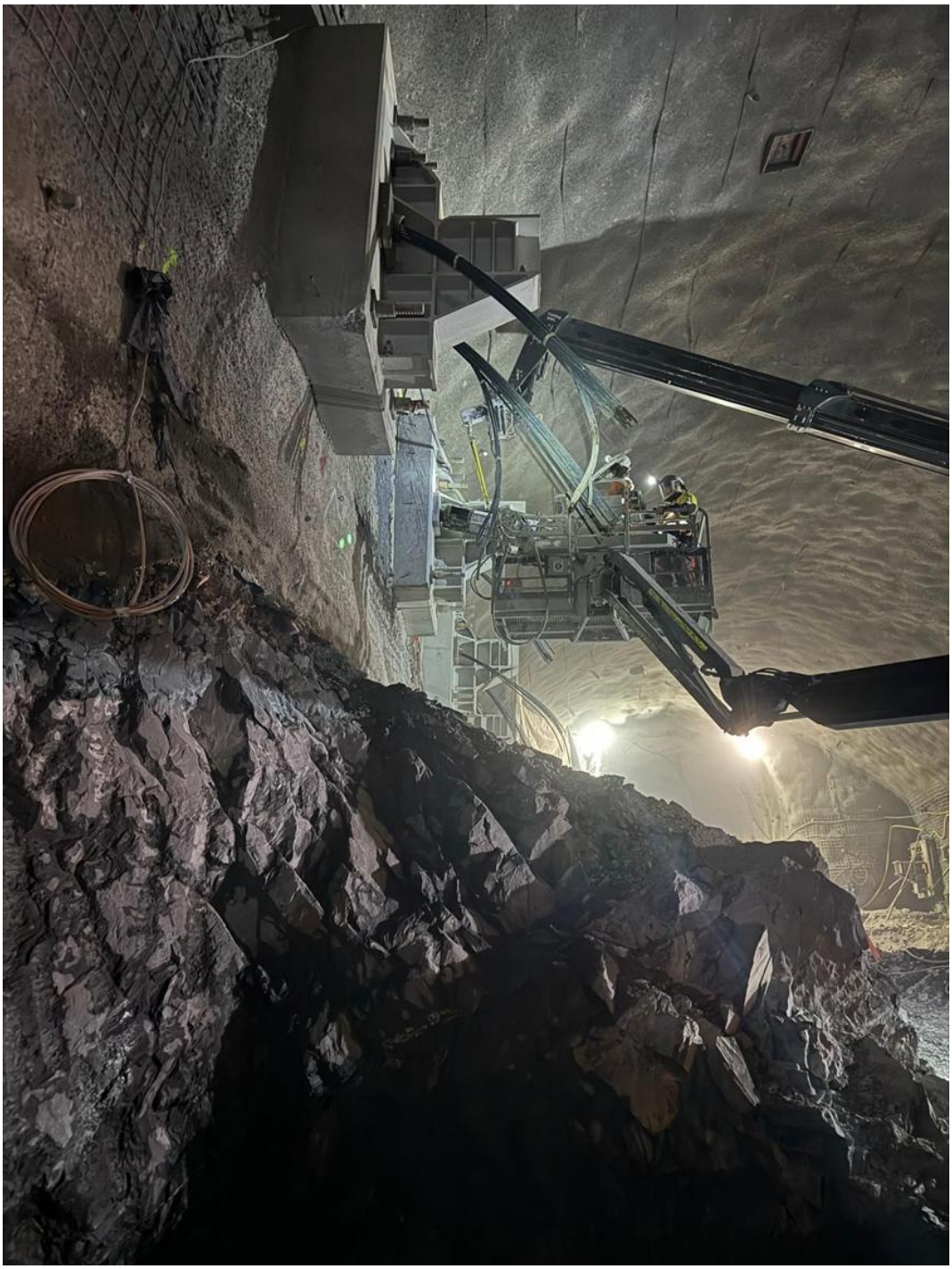


Figure 5. Stresing in progress of bar and strand anchors.

3.4 *Site supervision driving quality*

Due to the criticality of the inclined angle of the anchors, the client required full site supervision to ensure the correct installation of the corbels. DYWIDAG holding TfNSW site supervision approval for the installation of strand and bar anchors, provided around the clock supervision personnel for the entire scope of the installation. This ensured consistency and accuracy of product installation and testing for this highly critical scope of works to ensure consistent quality and fill any knowledge gaps of the main contractor's site crew.

3.5 *Load acceptance and testing*

Each anchor had an acceptance test performed on it to verify it was installed and grouted correctly and was holding the load as per the design requirements.

3.6 *Monitoring challenges and requirements*

Given the challenging and highly loaded anchors and the pivotal role of these anchors in the construction program the decision was made to monitor anchor loads using DYWIDAG Smart Anchors. This state-of-the-art technology is an automated solution that continuously monitors loads in real time to a digital platform with alerts sent to key stakeholders when thresholds are triggered. This eliminated the need for continuous expensive on-site test and provides designers and asset owners with assurance regarding anchor loads. A solution that was previously unavailable.

DYWIDAG's Smart anchor technology is installed on strand anchors at the Te Ara o Te Ata (Mt Messenger Bypass project) and received a merit award at the Ground Engineering Awards in the UK 2024. This advanced monitoring system allows for live data to be observed remotely.

Infrastructure Intelligence features:

- Real time data feed and presentation
- Adjustable trend charts and tabular data
- Alarm management and status reporting
- Data downloads
- Central data/document archive
- 3rd party data feeds
- Tailored display



Figure 6. Smart anchor installed on a strand anchor

4 CONCLUSION

DYWIDAG has been working collaboratively with clients and our partners to provide innovations to the DYWIDAG strand anchor design as part of a support system for deep underground caverns. The innovations address the current site challenges for anchoring with high permanent loads in a rock mass with variable quality, deep underground anchoring with limited installation space, anchor installation in inclination, complex grouting requirements and the design life of a fully permanent system.

19th Australasian Tunnelling Conference – Acosta-Martínez, Stewart and Hudson-Smith (Eds.)
© 2025 Australian Tunnelling Society, ISBN 978-0-85825-002-4

Modelling the impact of blasting on excavation perimeters

P.C. Dare-Bryan and E. Dixon
Orica, Australia

ABSTRACT: In hard rock civil projects blasting is often the preferred option for effective production rates in geometries and rock mass where mechanical excavation is less effective. However, blasting can result in increased damage into the excavation perimeters compared to mechanical excavation techniques. Understanding the impact of blasting within a particular environment is important for the long-term success of a project.

A large civil project in NSW, Australia, was experiencing variability in the conformance of tunnel perimeters after blasting and wanted an improved understanding of the impact of blasting on damage accumulating in the perimeters. Numerical simulations were conducted using a hybrid finite/discrete element program coupled with a non-ideal detonation model. The modelling included a detailed representation of the rock mass including pre-existing jointing and the in-situ stress state. The models assessed the impact of helper and perimeter holes on damage, highlighting the local variation caused by the interaction between explosive energy and jointing.

A subsequent study for a critical cavern excavation within the project assessed the impact of two perimeter designs; smooth wall blasting, which involves charging alternate holes with perimeter bulk product, and close-spaced line drilling of uncharged holes. The modelling indicates that smooth wall design produces greater damage close to the perimeter. However, at distances greater than 0.2 m into the perimeter, there is no significant difference between the two designs in the amount of damage accumulated in the rock mass.

1 INTRODUCTION

In civil tunnelling and cavern excavation removal of the rock mass can be done mechanically or by blasting. Mechanical can be preferred as it does not result in undulations of the perimeter that drill and blast require, allowing the mechanical means to excavate more accurately to the design perimeter. Additionally, mechanical methods limit potential damage accumulated in the rock mass at the perimeter. However, in many hard rock excavations the cost and slow progress rate of mechanical excavation means it is not a viable option for the project. Blasting has been demonstrated time and again to be an effective means of developing a wide range of underground excavations, sometimes in environmentally sensitive areas to very stringent design requirements. However, the success of the technique is highly dependent on an appropriate blast design being carefully applied with the appropriate consideration of the surrounding rock mass and any changes to the rock mass.

A highly complex large scale civil project in NSW, Australia was advancing tunnels in opposite directions and a range of varying rock masses. Inevitably this led to changes in the conformance of the post-blast perimeters. Numerical modelling was conducted to determine the impact of blasting in the least favourable direction with respect to the rock mass structure.

Further modelling work investigated the impact of two different perimeter designs on tunnels leading to a large cavern where the preferred perimeter design will be utilised to excavate the cavern.

2 BLAST MODELLING

The Mechanistic Blasting Model (MBM) is based on Elfen, a large dynamic finite/discrete element code (Owen et al., 1992). MBM simulates the non-ideal explosive loading of the blasthole wall and the subsequent fracturing and bulk motion of the surrounding rock mass due to stress/strain effects and the influence of dynamic gas loading in the blasthole and throughout the fracture network (Minchinton and Lynch, 1996, Dare-Bryan et al., 2012). Fracturing is handled by a strain-rate-dependent softening tensile failure Rankine plasticity model. Under sufficient fracturing, discrete elements are formed as separate, distinct polygonal elements made up of one or more finite elements; as such these discrete elements are fully deformable and can support stress and strain. The detonation of the explosives in the blasthole is modelled using data from a non-ideal detonation model (Kirby et al. 2014) to derive the influence of the rock confinement and blasthole diameter on the resulting velocity of detonation (VoD) and blasthole wall pressure-time profile. The post Chapman-Jouguet (CJ) pressure loading of the rock mass is handled dynamically by a gas flow model.

MBM is limited to two-dimensional geometries and can be run in two configurations:

- Plan view, where a section is taken perpendicular to the axes of the blastholes, to evaluate the interaction of multiple blastholes.
- Axisymmetric, where a section is taken through a single blasthole with the line of symmetry on the axis of the blasthole.

In this study, axisymmetric geometries were built taking a vertical section within the roof, in line with a helper hole and a perimeter hole to determine their impact on the rock mass. While plan view geometries were used to assess the impact of the charged and uncharged holes in smooth wall and line drilling design methodologies.

3 ROCK PROPERTIES

High-fidelity numerical models such as MBM require detailed information on the rock mass. Each rock domain requires data on the:

- Elastic properties: density, P-wave velocity, S-wave velocity, Young's Modulus and Poisson's ratio - these are associated with elastic stress wave propagation through the rock mass.
- Plastic properties: tensile strength, fracture energy - associated with fracture generation and propagation.
- Structural properties: major joint sets and discontinuities (dip angle, dip direction, spacing and persistence) - describes the in-situ rock structure.

The two rock types in this study are defined by the ratios of siltstone and sandstone, where a higher proportion of sandstone produces a more competent rock mass (Table 1). The fracture energy is a required input for the model failure criteria and is calculated from the fracture toughness tensile stress intensity factor (K_{ic}) which is not a parameter that is typically available from operations and so is often derived from literature. The major pre-existing structures within the rock domains are listed in Table 2.

Table 1. Elastic / plastic rock properties.

Rock type	Siltstone / Sandstone	Sandstone / Siltstone
Density (g/cc)	2.75	2.75
Young's Modulus (GPa)	48	58
Poisson's Ratio	0.25	0.25
P-wave velocity (m/s)	4577	5031
S-wave velocity	3411	2905
Unconfined Compressive Strength (MPa)	58	98
Tensile Strength (MPa)	8	11

Fracture Energy (N/m)	100	100
Fracture Toughness K_{ic} (MPa.m$^{1/2}$)*	2.0	2.25

*Derived from literature (Backers, 2005).

Table 2. Rock mass discontinuity data.

Structure	Bedding Plane	Joint Set 1	Joint Set 2
Dip (°)	30	80	80
Dip Direction (°)	050	210	130
Nominal Spacing (m)	0.3	0.3	1.0
Nominal Persistence (m)	5	2	5

4 PERIMETER DAMAGE MODELING

A typical blast design is shown in Figure 1, with the charging for the helper and perimeter holes displayed. All the blastholes are 45 mm in diameter and 3.2 m long. The helper holes are charged with a 0.8 g/cc straight emulsion bulk explosive, Subtek™. The bulk Subtek™ Control in the perimeter holes is a special formulation that is charged at an in-hole density of 0.6 g/cc, essentially over-gassed, the product does not sustain this density during the blast, and collapses down to a density of approximately 0.8 g/cc, this makes the charge partially decoupled from the hole. The air gap reduces the pressure applied to the hole wall, and reduces the confinement of the charge resulting in a lower VoD (and detonation pressures) compared to a fully coupled charge at 0.8 g/cc.

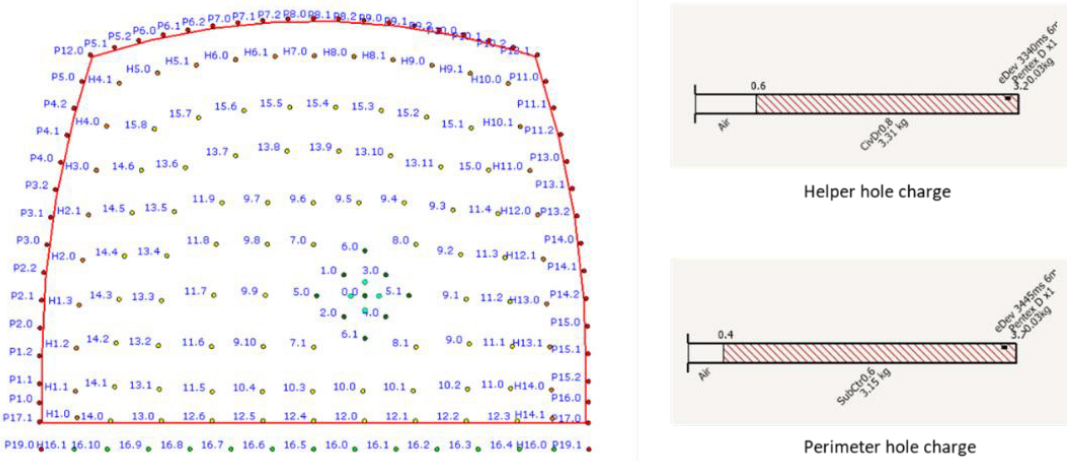


Figure 1. Typical design showing charging for the helper and perimeter holes.

4.1 *Perimeter model geometries*

Separate axisymmetric model geometries were created for a helper and a perimeter hole (Figure 2). The tunnel advance was in a southerly direction which results in the bedding plane (Table 2) cutting through the roof of the tunnel at an unfavourable angle. The helper hole geometry has the hole offset 0.8 m from the tunnel roof. The tunnels are at an approximate depth of 680 m and have in-situ stress conditions with a principal horizontal stress of approximately 30 MPa aligned north-south and a vertical stress of approximately 20 MPa. The red lines in geometries highlight the charged portion of the holes.

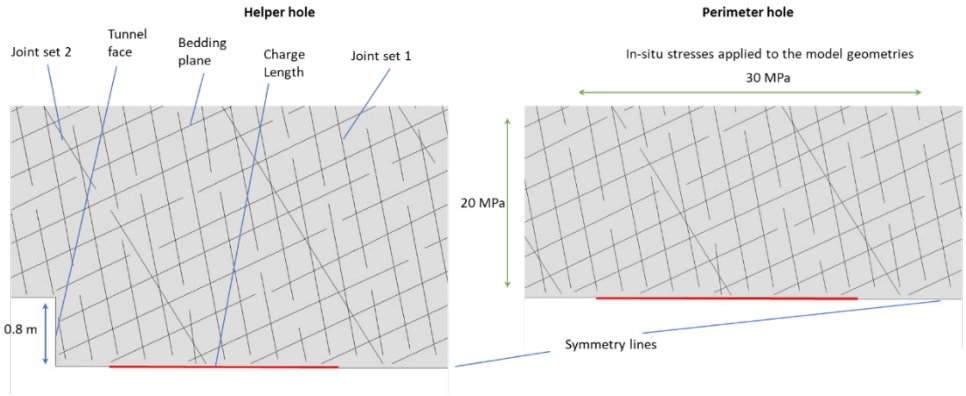


Figure 2. Model geometries for the helper hole (left) and the perimeter hole (right) showing the structures applied as discrete fracture networks and the in-situ stresses.

4.2 *Perimeter in siltstone/sandstone*

The plots of waveform velocity in Figure 3 are captured 0.5 ms after the charges have initiated and highlight the complex wave interaction with the structure in the rock mass, producing local variations in wave amplitude. The broken line through the plots 0.5 m above the perimeter is provided as a reference line. The plots of resulting damage (Figure 4) show minimal damage from the helper hole into the rock mass above the roof line and only limited damage from the perimeter hole into the rock mass above the roof line. The damage from the perimeter hole accumulates principally along the bedding plane discontinuity.

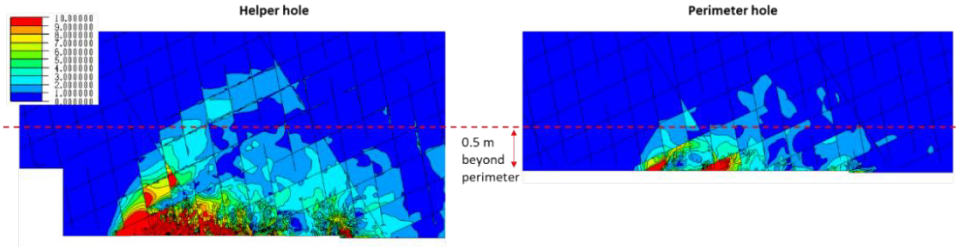


Figure 3. Simulation output for the siltstone/sandstone showing stress waves radiation off the helper (left) and perimeter (right) detonating charges with color contours of resultant velocity (0-10 m/s).

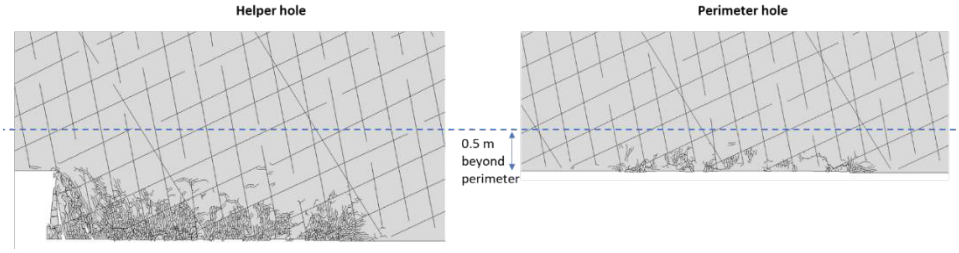


Figure 4. Simulation output for the siltstone/sandstone showing extent of fracturing in the rock mass due to the helper (left) and perimeter (right) charges.

5 COMPARSION OF DAMAGE DUE TO CAVERN PERIMIETER DESIGNS

The two principal perimeter design methodologies applied on the project are smooth wall blasting, which involves charging alternate holes with perimeter bulk product, and close-spaced line drilling of uncharged holes. Numerical modelling has been conducted to evaluate the variation in damage at the perimeter using these two techniques.

Figure 5 shows a typical smooth wall design including the location of the perimeter and easer holes, which are of principal interest due to their proximity to the wall when evaluating damage in the tunnel walls. The combination of charged and uncharged holes in the design requires the modelling of the interaction of multiple holes, therefore, a section of wall will be modelled, as shown within the black broken line. The same section of perimeter will be modelled for the line drilling design (Figure 5). All the holes in the model sections are 45 mm in diameter.

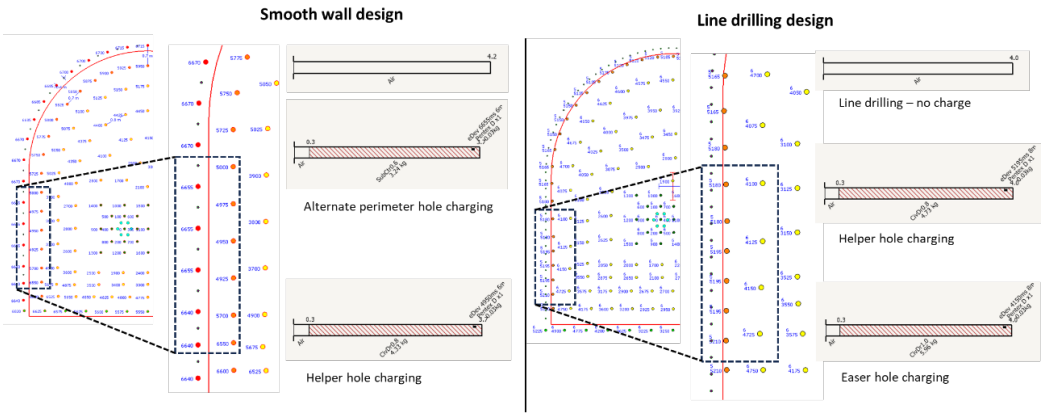


Figure 5. A typical smooth wall design (left), showing a close-up of the perimeter section modelled, and the charging of the perimeter (black and red) and helper holes (orange), and a line drilling design (right) showing a close-up of the wall section modelled, with the line holes (black) and the charging of the helper (orange) and easer holes (yellow).

While the rock mass elastic/plastic properties have remained the same between the two modelling studies, for the carven region the structural data has changed slightly (Table 3). Due to the scale of the perimeter hole designs, with hole spacings in the range 0.3 – 0.4 m, only the Bedding Plane and Joint Set 1 were built into the model geometry as discrete fracture networks. The nominal spacing of 2+ m for Joint Sets 2 and 3 would result in only one or two joints within the model.

Table 3. Rock mass discontinuity data - caverns.

Structure	Bedding Plane	Joint Set 1	Joint Set 2	Joint Set 3
Dip (°)	30	79	81	84
Dip Direction (°)	058	122	053	276
Nominal Spacing (m)	0.3	0.3	2.0	2.0
Nominal Persistence (m)	5	2	5	5

5.1 *Cavern perimeter model geometries*

The cavern orientation and connecting tunnels are approximately northeast-southwest. Therefore, the plane of the model geometry is orientated northwest-southeast within the discontinuities (Table 3).

Figure 6 shows the plane strain model geometries for the two designs. The vertical extent of the model geometries is approximately 3.5 m, with 10 perimeter holes in the smooth wall geometry and 12 line holes in the line drilling design. The model geometry could not support the actual in-situ stresses of 19 MPa vertical and 29 MPa horizontal. Therefore, the models were run with stresses at 10 MPa vertical and 15 MPa horizontal. The reduced stresses will likely result in a marginal overestimation of the damage accumulated in the tunnel wall; however, the relative comparisons between the two designs should not be affected.

The line drilling model included easer and helper holes due to the proximity of the easer holes to the perimeter, and their potential to induce damage further from the holes because of the higher density bulk product (Figures 5 and 6). In contrast, the larger standoff of the easer holes in the smooth wall design would significantly reduce their potential to influence damage in the walls.

Simulations were run with the smooth wall and line drilling designs in the siltstone/sandstone and the more competent sandstone/siltstone.

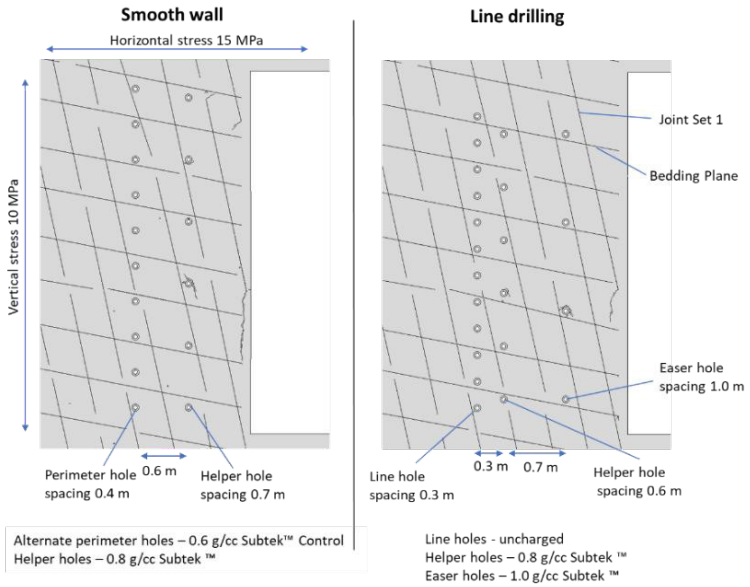


Figure 6. Model geometries for the smooth wall design (left) and the line drilling design (right).

5.2 *Cavern perimeter in siltstone/sandstone*

The simulation outputs for the smooth wall design (Figure 7a and 7b) show that after the helper holes have fired there is little fracturing beyond the perimeter holes. After the perimeter holes have fired, an effective fracture network forms between the holes to define the perimeter. However, there is a variation in the fracture network extending into the wall from the charged perimeter holes due to the influence of the Joint Set 1 structure. If the joint is close to the hole, the fractures are arrested by the joint. However, if the joint is further into the rock mass, fractures can extend further into the rock mass beyond the perimeter.

In the line drilling simulation, there is little damage accumulated at the perimeter after the easer holes have fired (Figure 7c). After the helper holes have fired, there is significant damage up to the location of the line holes (Figure 7d). However, there is not the same network of fractures between the line holes as is present in the smooth wall design (Figure 7b). This indicates that it could be harder to scale back to a clean wall with the line drilling, however, there is less damage in the rock mass at the perimeter with line drilling compared to the smooth wall design.

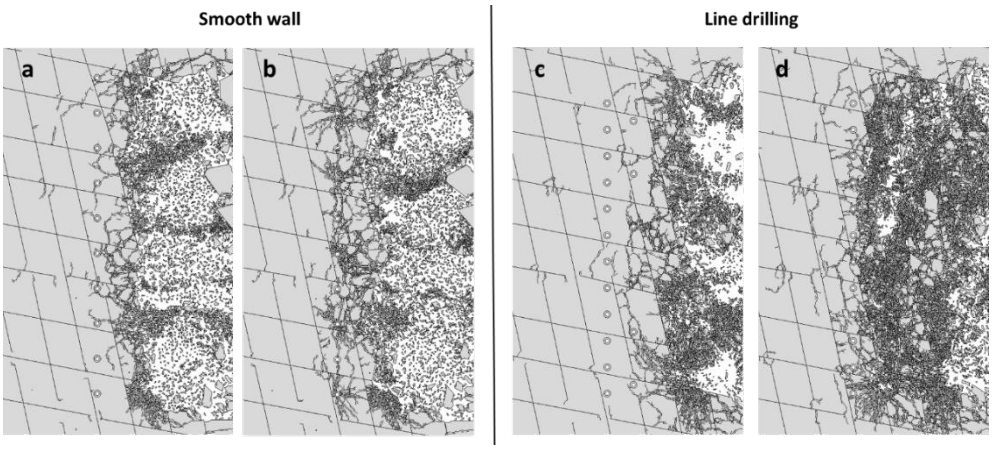


Figure 7. Smooth wall simulation after all the helper holes have fired (a) and after the perimeter holes have fired (b), and the line drilling simulation after all the easer holes have fired (c) and after the helper holes have fired (d) in siltstone/sandstone.

5.3 *Cavern perimeter in sandstone/siltstone*

The smooth wall design in the more competent sandstone/siltstone results in marginally more damage at the perimeter (Figure 8b) compared to the same design in the siltstone/sandstone (Figure 7b). This increase in damage in more competent rock is attributed to the higher strength rock sustaining higher stresses prior to failure, and subsequently undergoing more extensive fracturing as a result of the rock's sensitivity to strain rate. In contrast the line drilling simulation in the sandstone/siltstone (Figure 8d) has produced less damage in the perimeter compared to the same design in the siltstone/sandstone (Figure 7d). However, the overall trend comparing the damage due to the smooth wall design and the line drilling design is maintained across the two rock types.

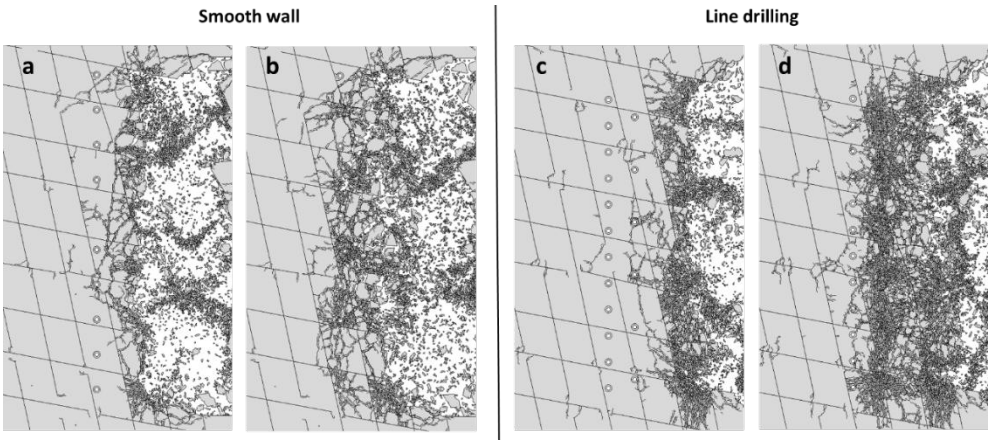


Figure 8. Smooth wall simulation after all the helper holes have fired (a) and after the perimeter holes have fired (b), and the line drilling simulation after all the easer holes have fired (c) and after the helper holes have fired (d) in sandstone/siltstone.

5.4 *Cavern modelling analysis*

The simulation outputs can be analysed to determine the length of new fractures created within a defined area. This enables a quantified assessment of the amount of damage that has been created within the models. Figure 9 shows how the rock mass behind the perimeter was divided into three regions to determine the damage created at the perimeter (0-0.1 m into the rock – blue region), further into the rock mass (0.1-0.2 m – green region), and then further still (0.2-0.5 m – orange region), across the four simulations. Table 4 lists the total new fractures created in the simulations for the three regions. The data shows that in the siltstone/sandstone the smooth wall design produces nearly twice as much damage at the perimeter (blue region) compared to the line drilling, however, further from the wall the amount of damage created is similar. In the sandstone/siltstone there is a larger difference between the damage due to smooth wall and line drilling designs, with the smooth wall design producing greater damage across all three regions.

Overall, the smooth wall design produces greater damage close to the perimeter, however, at distances greater than 0.2 m into the rock there is not a significant difference between the two designs in the amount of damage accumulated in the rock mass. The modelling also indicates that greater than 0.2 m into the perimeter the blast designs induce few new fractures into the rock mass.

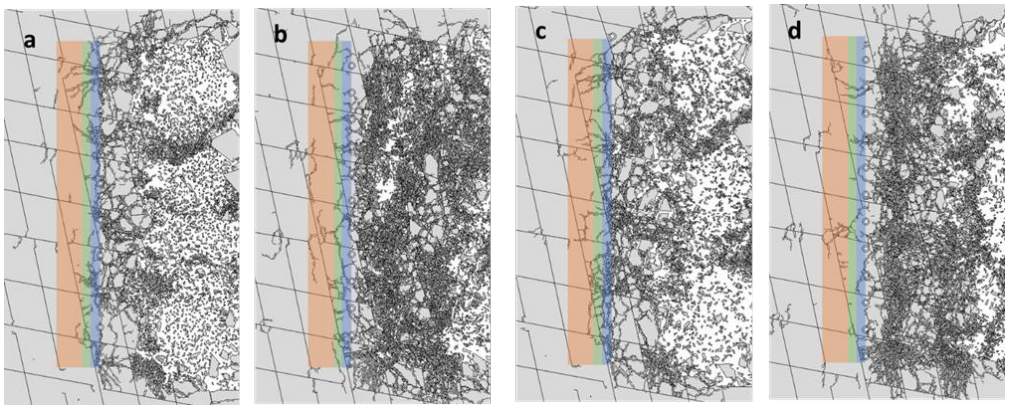


Figure 9. Simulation plots after all the holes have fired, showing the regions behind the wall analysed to calculate the total new fracture length created in the rock mass due to the blast for: siltstone/sandstone smooth wall (a), siltstone/sandstone line drilling (b), sandstone/siltstone smooth wall (c), and sandstone/siltstone line drilling (d).

Table 4. Total new fracture length at different regions away from the tunnel wall.

Rock type	Perimeter design	Fracture length (m) for distances beyond the perimeter		
		0-0.1 m	0.1-0.2 m	0.2-0.5 m
Siltstone/Sandstone	Smooth wall	4.0	1.5	1.3
Siltstone/Sandstone	Line drilling	2.2	1.5	1.8
Sandstone/Siltstone	Smooth wall	5.8	1.9	2.2
Sandstone/Siltstone	Line drilling	1.5	0.7	1.4

6 CONCLUSIONS

High fidelity numerical modelling has been shown to be useful in determining the damage accumulating in the rock mass at the perimeter across a range of blast designs.

In the tunnel round, within the modelled rock mass and stress state, the helper holes have an appropriate standoff from the perimeter to minimize damage beyond the perimeter and the decoupled perimeter charge does not accumulate significant damage in the rock mass.

The comparison of two perimeter designs in the more critical cavern sections of the project highlights the smooth wall design, while requiring less drill meters, accumulates more damage at the perimeter than the line drill design. However, across the two rock types modelled neither design accumulates a significant amount of damage greater than 0.2 m beyond the perimeter.

7 REFERENCES

Backers, T. (2005): Fracture toughness determination and micromechanics of rock under mode I and mode II loading, PhD Thesis, (Scientific Technical Report STR ; 05/05), Potsdam : Deutsches GeoForschungsZentrum GFZ, 95 p.

Dare-Bryan, P.C., Mansfield, S. and Schoeman, S. (2012). Blast optimisation through computer modelling of fragmentation, heave and damage, *Proc. 10th International Symposium on Rock Fragmentation by Blasting*, New Delhi, India, 26-29 November, Rotterdam: Balkema, pp. 95-104.

Kirby, I., Chan, J. and Minchinton, A. (2014). Advances in predicting the effects of non-ideal detonation in blasting, in *Proc. 40th Annual Conference on Explosives and Blasting Techniques*, International Society of Explosives Engineers: Cleveland, pp. 301–314

Minchinton, A. and Lynch, P. M. (1996). Fragmentation and heave modelling using a coupled discrete element gas code, *Proc. 5th. Int. Symp. on Rock Fragmentation by Blasting*, Montreal, Canada, 25-29 Aug, A.A. Balkema, Rotterdam, pp. 71-80.

Owen, D.R.J., Munjiza, A. and Bicanic, N. (1992). A finite element-discrete element approach to the simulation of rock blasting problems, *Proc. 11th Symp. on finite elements in South Africa*, Centre for Research in Computational and Applied Mechanics, Cape Town, 15-17 Jan, pp. 39-58.

Theme 5. Underground Mining

THIS PAGE INTENTIONALLY LEFT BLANK

19th Australasian Tunnelling Conference – Acosta-Martínez, Stewart and Hudson-Smith (Eds.)
© 2025 Australian Tunnelling Society, ISBN 978-0-85825-002-4

Using mature and proven technology for mechanized excavation of tunnels and shafts for hydropower schemes to provide sustainable clean energy

K. Bäppler
Herrenknecht AG, Schwanau, Germany

ABSTRACT: As countries plan for their net zero targets, substantially more long-duration energy storage will be needed to support the integration of intermittent renewable energy sources such as wind or solar. Various storage technologies exist or are being developed, and of particular importance is pumped storage hydropower (PSH), a well-established technology that already provides around 90% of installed electricity storage globally. Hydropower and Pumped Storage Hydropower schemes have a network of tunnels, including pressure tunnels and pressure shafts. This paper focuses on the latest state of mechanized tunnelling technology used to advance the construction of these projects, thereby supporting the clean energy transition.

1 INTRODUCTION

The need for sustainable development and an actionable pathway towards net zero emission are two of the greatest challenges of our time. They are also interlinked; sustainable growth is only truly achievable if it is coupled with a massive upscaling of renewable energy development. As a mature technology, hydropower has played a vital role in enabling the industrial growth of the past, and its unique qualities are highly translatable to the pressing issues of today, such as the need to decarbonize industry and manage our water resources effectively.

Worldwide, there is enormous potential of making use of this technology, which requires the construction of new tunnels and shafts for renewing and upgrading the capacity of existing storage power plants. Environmentally compatible concepts and further development of excavation methods will be important for the economic success of such schemes, quite apart from the development of the worldwide energy market.

Hydropower schemes use the difference in height between the water source at the upper dam source and the turbine to generate electricity as the water flows down under gravity; the greater the height difference, the more power can be generated.

Pumped storage hydropower schemes generate electricity in the same way, but at times of low electrical demand, the excess power available in the grid is used to pump water up to the higher reservoir dam, thus storing power as potential energy. Then, at times of high demand, water can be released back to the lower reservoir through the turbine to generate electricity. Pumped storage hydropower schemes provide almost 90% of the world's energy storage.

Hydropower schemes and pumped storage power plants have a network of tunnels, such as water transfer tunnels, pressure tunnels, pressure shafts, and tailrace tunnels. Conveyance tunnels may be used to transfer additional water to the dams from other catchment areas. The water is then fed from the dam to the hydropower plant through pressure tunnels and pressure shafts. These pressure tunnels may be steeply inclined. After passing through the turbines, the water flows out through tailrace tunnels back to the river or into the lower storage reservoir of the PSH.

Mechanized tunnelling technology plays a vital role in hydropower construction. Tunnel boring machines are used to construct steep pressure tunnels and raise-bore technology supports the ef-

ficient production of vertical shafts. The design of vertical pressure shafts in the waterway systems of pumped storage systems is quite common. The paper highlights the state-of-the-art mechanized technology for tunnel and shaft construction. Applying reused or remanufactured mechanized tunnelling equipment and components can help to reduce the scheme's carbon footprint and improve sustainability performance.

2 MATURE AND PROVEN MECHANIZED TECHNOLOGY FOR TUNNEL AND SHAFT CONSTRUCTION

Hydropower or pumped storage plants are typically located in remote, mountainous, or environmentally sensitive areas.

The majority of the underground hydropower projects are built in rock formations that are suitable for nearly all kinds of mechanized rock excavation technologies. These remote locations present particularly challenging access to the construction sites for assembly and disassembly of TBM excavation equipment and the supply transport logistics.

Hydropower schemes require the excavation of diverse tunnel networks, including inclined tunnels or vertical shafts for access, water transfer and power cables. The latter are typically constructed using raise-bore technology for the efficient production of vertical pressure shafts. If the shaft can be set deeply enough in the rock, thus safeguarding it against hydraulic rock rupture, there is no need for a steel lining in the case of slightly permeable rock formations. This extremely economic concept has already been applied in many hydropower plants.

2.1 *Mechanized technology for tunnel construction*

In recent years, there has been an increased use of TBM technology for the construction of inclined pressure shafts with steep inclines of up to 90%. This paper will highlight some of these lighthouse projects.

For the construction of horizontal or slightly inclined or declined alignments with gradients up to 5% for water transfer, conveyance, headrace, or tailrace tunnels, standard, or close to standard Hard Rock TBMs, such as Gripper or Shielded TBMs, can be applied.

Alignment gradients between 5% and 15% demand adaptations to the TBM handling and supply systems, such as material handling, cranes, and mucking logistics. For declines, special requirements for dewatering must be taken into consideration.

Gradients in the range of 15% and 25% demand a specific TBM and back-up design based on the individual project conditions. These slopes affect not only the material handling and tunnel supply systems but also basic TBM excavation and primary mucking functions, cutter change procedures, maintenance work, the design of working platforms, walkways, segment handling, and process technology such as electrical equipment, hydraulics, lubrication, grout injection and dewatering, to just to name a few.

The steep gradient impacts diverse design aspects and requires a high development effort, both in the design and static calculation of the back-up steel structure and related towing connections.

With tunnel inclinations ≥ 25% the EN16191 demands a safety factor of three for towing connections and, also a redundant secondary towing system in case the back-up systems could move independently due to gravitational force in the event of failure of one towing connection. It also requires the monitoring of the loads carried by the towing connection between the TBM and back-up system.

2.2 *Mechanized technologies for vertical shaft construction*

Some Pumped Hydro Storage (PHS) projects are designed with vertical pressure shafts to carry the water from the dam to the hydropower plant. This involves different mechanized construction technologies for vertical shaft construction.

Typical pressure shafts can be of great depth, up to a couple of hundred meters. These shafts are typically constructed using either conventional drill & blast shaft sinking technology with shaft drilling jumbos or combined technologies using raise bore technology. The type of technol-

ogy used depends on the project conditions or construction sequence. For example, using combined technologies, a vertical shaft is drilled using a raise bore rig, followed by a drilling jumbo to enlarge the raise bore shaft down from the top.

The following chapter will introduce lighthouse projects of pumped storage hydro schemes and applied mechanized construction technology that had to deal with challenges in remote areas and challenging geological conditions.

3 CASE HISTORIES OF INCLINED AND VERTICAL PRESSURE SHAFT CONSTRUCTION USING MECHANIZED TECHNOLOGY SOLUTIONS

This chapter briefly highlights the challenging hydropower projects in terms of their complexity and technical challenges.

3.1 *Pump storage plant Ritom, Switzerland – Tunnel construction under extreme conditions*

The Swiss Federal Railways (German: Schweizerische Bundesbahnen, SBB) SBB Ritom hydroelectric power station in Ticino, built in 1920, is being renovated and expanded to improve the electricity supply for the Gotthard railway line, with its performance being quadrupled. The project is unique due to the geological challenges, including local porous rock layers that are in parts water-bearing and steep gradients of up to 42°, corresponding to an extreme 90% gradient.

The focus in the PSP Ritom project is on the construction of the extremely steep section of the pressure shaft. The construction of the pressure shaft comprised three sections, of which two were constructed using Drill & Blast (D&B) technology. The D&B method was used for the 150m long upper section of the pressure shaft and the 650m long lower section, both being horizontal sections. The main section of the pressure shaft is 1,500m long with an extremely challenging 90% gradient. This inclined shaft was excavated using a specially designed 3.2m diameter Gripper TBM.

Preliminary ground investigations included the drilling of three boreholes along the proposed route of the pressure shaft. The information obtained from the ground investigation program indicated treacherous rock conditions along the lower tunnel section, with porous, permeable, and in parts water-bearing rock layers. The decision was taken to extend this D&B section until good rock conditions were reached so that the inclined shaft section to the upper lake could start in good rock conditions. The shaft had a diameter of 3.20 meters and was excavated by the contractor Marti using a Herrenknecht Shielded Gripper TBM that was specially adapted to the predicted and challenging project conditions with difficult rock and extreme gradient of 90%.

The TBM was launched from a cavern about 650 meters deep in the rock. The 100m long TBM was transported to the cavern on trucks in six sections as shown in the following figure.



Figure 1. Special transport of the TBM Ø3.2m by truck into the shaft base cavern.

The TBM was assembled in the 80m long cavern on a launch ramp having an initial gradient of 26°. During assembly, the TBM was pushed up the launch ramp, and tunnelling could start with a partial installation of the TBM. Temporary arrangements were necessary for muck removal

and material supply for the first few meters of the tunnel until the entire TBM was assembled. The regular advance began when the entire TBM was in the rock. The excavated rock was transported to the starting cavern at the bottom of the inclined shaft by a material channel in the invert. The material slid independently down the inclined shaft with water added to assist the flow. After a 900m long climb at 23° and crossing beneath the River Foss, the TBM then continued its drive for the next 633m with an extreme inclination of 42° corresponding to a 90% gradient. The 100m long and 290-ton machine was reliably prevented from slipping back by the grippers and by means of a specially designed and proven toggle lever device in the safety recoil unit, guaranteeing that the TBM remained securely gripped against the rock at all times. It was decided that, for redundancy and additional safety reasons, a second gripper unit with mechanical clamping function should be implemented. This arrangement always guaranteed that during the excavation cycle, two grippers were braced and at least one gripper with a mechanical self-clamping function was braced.

TBM supply and personnel transport from the starting cavern was managed via a funicular. Supplies were taken to the TBM supply on a just-in-time basis due to the limited storage space available on the 3.2m diameter TBM.

During the construction of the inclined shaft, pipes for cooling water and compressed air were fixed on one side of the tunnel wall, and fresh air and power supply on the opposite tunnel wall. The cable of the funicular was also running on the same side.

The 3.2m diameter TBM was designed with fresh air supply pipes and the slide channels for transportation of the excavated material to the shaft bottom, which were installed underneath the machine. To protect the subsequent work, the tunnel crown was secured with rock bolts and steel mesh, with a specially adapted rock bolting unit directly installed between the front shield and the gripper shield.

The supporting structure and the stairs for the TBM crew were mounted above the muck transport channel in the invert. A material-carrying cableway was installed along all the back-up trailers, and the route had to be kept clear along the entire trailers. Back-up number 1 was located directly behind the safety recoil system and carried an 11KW drill rig and a dust lock for a shotcrete chamber that allowed manual shotcrete application. The air dedusting system and a shotcrete pump were arranged on back-up number 2. The operator’s cabin and the hydraulic power pack with oil tanks were positioned on trailer 3. The other trailers carried transformers, control cabinets and electronics, hose reels for water and compressed air supply, water pumps, fresh air supply and the tunnel funicular station. Periodic track extensions for the funicular and the invert mucking channel were done through mounting holes on trailer 6.

The Ritom TBM was launched at the beginning of 2021 and finished its 1.5km long steep inclined section toward the end of February 2022, having successfully climbed 800 meters in altitude. The focus on safety was of utmost importance throughout the entire construction period and of its project layout.

3.2 *Limberg III pumped storage plant, Austria – Steep TBM challenge*

The Limberg III project is a 480MW pumped storage power project located in Salzburg, Austria. The project will contribute to Austria's goal of covering one hundred percent of its energy needs from renewable sources by 2030. The main challenge in this project was the excavation of the 770m long pressure shaft at a gradient of 42°. The 5.8m diameter Gripper TBM was designed specifically to work at the gradient of 42° with the highest safety standards during construction. The 770m long inclined tunnel is split into a section of 580m for the pressure shaft and a further 190m long section connecting to the surge tank.

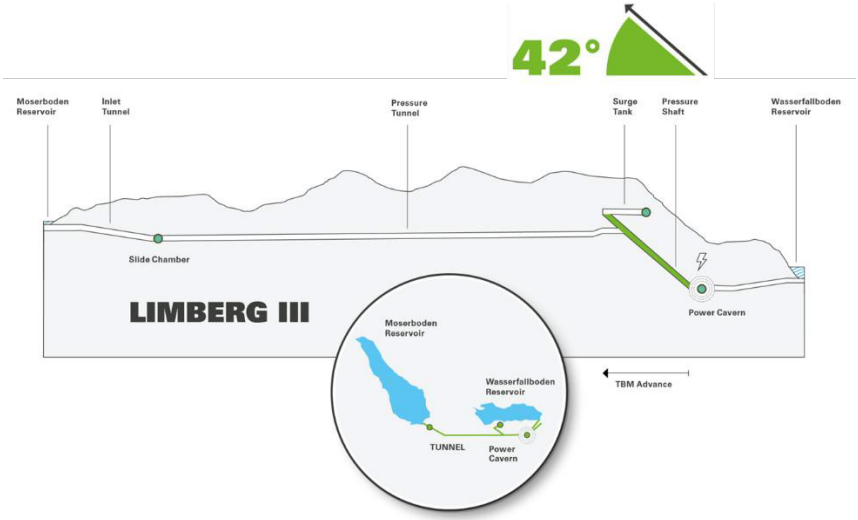


Figure 2. Overview of 770m-long TBM excavated pressure shaft (gradient 42°) at Limberg III.

Predominant rock types are calcareous slates with unconfined compressive rock strengths of 80 to 100MPa and quartz contents of 20 to 30%. The cutterhead was dressed with 17-inch back-loading disc cutters (25x single discs, 4x double discs). Due to the abrasive nature of the rock, the cutterhead was designed with wear protection composed of grillbars, protection wedges and Hardox plates in the face and gauge area of the cutterhead.

The TBM design included three clamping systems that ensured that the machine was always braced on two levels and in all operating conditions, preventing the Gripper TBM from slipping back on this 42° gradient. The first clamping level is the gripper bracing directly behind the cutterhead, followed by a double anti-reverse lock. The anti-reverse locks work mechanically on the principle of a self-locking toggle lever (automatic mechanical wedging), ensuring reliable bracing of the machine against the rock even in the event of a power failure or failure of hydraulic systems.

This double anti-reverse lock was located on the first back-up and had a full backup redundancy of the available bracing levels for the 1,000-ton TBM. It works in the way that while the first anti-reverse lock is rigidly connected to the back-up, the second anti-reverse lock moves along with the TBM advancement in an automated, hydraulic manner so that the back-up moves consistently with the TBM. This results in an operating cycle of TBM advancement, standstill, and re-gripping processes. In all these operating conditions, at least one anti-reverse lock is always securely clamped against the rock. Thus, at least two of three locking systems are independently and safely braced against the rock. This significantly increases the safety for personnel, the machine, and its structure in all operating stages.

For about 85% of the pressure shaft, the rock conditions required support consisting of three anchors at 3m ccs installed on the L1 area immediately behind the TBM and a 50mm shotcrete support in the L2 back-up area. The TBM was designed with two drill rigs that enabled the installation of rock anchors in the L1 area with a 3m anchor length (extendable to 4m) over the upper 180 degrees of the tunnel.

The excavated rock was collected by the cutterhead buckets and the rock chips were transported through an opening in the bottom of the cutterhead to a muck chute and channeled down to an intermediate storage in the starter cavern. The consumable supplies were transported to the TBM

by an overhead monorail. The TBM back-up had intermediate storage locations for consumables, auxiliary, and operating materials.

The TBM was designed and manufactured by Herrenknecht AG in Germany. The assembly of the TBM on site in Kaprun was achieved within two months in a 45m long assembly cavern that was 14m wide and 11.5m high. The assembly started in a horizontal position and during assembly, the TBM was repeatedly moved forward through the starter cavern on steel beams by a pushing system. At the end of the horizontal section, a 40m ramp was built with a vertical radius of 50m through which the TBM was pushed into a profiled 22m long starting tunnel that had a diameter of 5.93m. Launching of the TBM took place with the grippers braced in the profiled starting tunnel and the anti-reverse locks still outside the starting tunnel. The gantries were then pushed into the starting position using the cylinders of the back-up displacement system and an external power pack.



Figure 3. 5.8m diameter Gripper TBM assembled in horizontal position shortly before 50m vertical curve radius.

The Gripper TBM successfully excavated the pressure shaft between May 2022 and October 2022 to help support an essential power bank for a safe, clean, and affordable supply of electricity in Austria.

3.3 *Búrfell Extension hydropower plant in Iceland – Shaft construction using raise boring technology*

The existing Búrfell hydropower plant (270 MW) has an installed capacity of 2,300 GWh per year. The project is located in the south of Iceland, about 130km east of Reykjavik, and has been operating continuously since 1969. A new unit, the Búrfell Extension project, was built to increase the total capacity of the combined Búrfell hydropower stations by 300 GWh per year. This new HPP Búrfell Extension project is located about 2km away from the HPP Búrfell at the foot of the Sámsstaðaklif depression and is one of the main power suppliers for Reykjavik. The nearest port is located some 100km from the site, and the roads leading to the site are part of a well-constructed road network. The area surrounding the site is uninhabited except for the operational personnel at the existing Búrfell Station.

The main structures of this expansion project comprised the construction of a cavern for the powerhouse with an excavation volume of 35,000m^3, various hydro and access tunnels and two vertical shafts with diameters of 4.5m and 6.2m that were constructed using a Herrenknecht VF 400 raise bore rig.



Figure 4. Pressure shaft (steel lined) at Búrfell III excavated by raise bore technology.


Figure 5. Herrenknecht VF 400 raise bore rig in use for the Búrfell II shafts.

All underground structures were constructed using drill & blast, except for the 4.5m diameter cable shaft and the 6.2m diameter pressure shafts that were excavated by raise boring technology.

Marti Tunnel AG executed the access and tailrace tunnels and powerhouse construction and also the raise boring and shaft construction works for the 108.5m deep cable shaft and 96.5m deep pressure shaft in 2017. The main geological structures in the project area consist of basalt with intersections of sedimentary layers. The 96.5m deep vertical pressure shaft was lined with a 5.2m diameter embedded steel liner. It connects the power intake with the turbine unit located in the underground powerhouse cavern. The Medium Voltage (MV) cables are installed in a vertical cable shaft leading to the Transformer building located on the top of the Sámsstaðaklif depression.

The VF 400 raise bore rig, which excavated the 4.5m diameter cable shaft, operated at rates of up to 21.2m per day for the pilot drill between September 3 and 9, 2016.


Figure 6. Herrenknecht VF 400 raise bore rig reamer head used for the cable shaft.

Shaft reaming was completed between October 6 and 18, 2016 at reaming rates of up to 15.9m per day.

The 6.2m diameter pressure shaft pilot was drilled between November 1 and 3, 2016 at rates of up to 44.7m per day and reaming was completed between November 7 and 22, 2016 at rates of up to 10.3m per day. The boreability of the rock was easier than expected and wear and tear was also kept to a minimum.

The raise bores used the Rotary Vertical Drilling System (RVDS) to support reliability and accuracy in drilling.

4 CONCLUSION

The selected hydropower projects are all resilient projects where mechanized tunnelling technology using TBMs and raise bore technology were applied. The highlighted tunnelling technology contributed to renewing and upgrading the capacity of existing storage power plants and thus supporting the supply of sustainable energy generation and storage with a reduced carbon footprint. Financing institutions are already seeking to address climate-related risk by ensuring that projects are planned and operated to be resilient to climate change. The aim is to construct projects safely and reliably to ensure grid stability so that that they can incentivize policy and investment.

5 REFERENCES

Karin Bäppler, Steep TBM challenge for Limberg II pump storage power plant project, RETC 2023 (Rapid Excavation and Tunnelling Conference), Boston, June 2023

2024 World Hydropower Outlook – International Hydropower Association

19th Australasian Tunnelling Conference – Acosta-Martínez, Stewart and Hudson-Smith (Eds.)
© 2025 Australian Tunnelling Society, ISBN 978-0-85825-002-4

Integrative Feedback Loops: Optimised tunnelling with digital platforms to improve efficiency, safety, and sustainability through a paperless Permit-To-Tunnel process.

K. Macintosh
John Holland, New South Wales, Australia

R. Hawkey, J. Walton
Deswik, Queensland, Australia

P. Gaylard

John Holland, Queensland, Australia

ABSTRACT: As the global push for net zero accelerates, hydropower is regaining prominence. The Kidston Pumped Hydro Project in Australia showcases innovation in this space through the Integrative Feedback Loop (IFL), developed by John Holland and Deswik. Originally designed for mining, Deswik's software suite was adapted to civil tunnelling to enhance the Permit-To-Tunnel (PTT) process. The IFL integrates real-time data—geological mapping, convergence monitoring, and as-built survey scans—into a digital, automated platform supporting observational tunnelling. This enables dynamic design optimisation, improves safety, enhances stakeholder communication, and boosts resource efficiency. The system's visual and data-driven approach reflects the industry's shift toward digitisation and sustainability. This case study highlights how combining advanced software with best-practice processes can transform tunnelling operations, offering a model for future hydropower and infrastructure projects.

1 INTRODUCTION

1.1 *Permit to Tunnel (PTT)*

The Permit to Tunnel (PTT) system was developed to manage and document ground conditions, monitoring data and ancillary tunnelling activities. It was introduced in response to major tunnelling incidents in Sydney, Australia, including a fatal rockfall and a tunnel collapse between 2006 and 2008. The PTT ensures compliance with safety regulations by requiring regular inspections and adjustments to ground support methods based on monitoring, inspection and testing data collected during excavation and progressively thereafter. Implemented in Australia, starting with the Airport Link Tunnel in 2009, the PTT helps ensure tunnelling operations adhere to approved designs and allows observational adjustments to tunnelling activities based on ground conditions. It has been utilised in several major projects, such as Sydney's Westconnex and Metro projects, and it has a notable record of avoiding ground support-related fatalities. (Salcher et.al, 2023). This case study considers the application of the PTT process for New Austrian Tunnelling Method (NATM) excavation processes such as Drill and blast, Road header, and other manually excavated tunnelling. It does not consider the application of the PTT to TBM or pipe-jacked tunnelling methods.

Below is a summary of the key Permit to tunnel detail; for further information, refers to Salcher et al., 2023. The PTT process is traditionally conducted as a meeting at set time intervals; a common time domain would be considered permit coverage for a 24-hour period. Whilst often customised to project need the PTT addresses the following outcomes (but not limited to):

- Ground conditions:
  - Projected geological conditions – captured from preconstruction data and validated as excavated geological mapping (in accordance with NATM).
  - Ground support requirements – based on as-excavated geological mapping and other PTT inputs considered holistically.
- Instrumentation & Monitoring (I&M):
  - Convergence and deformation monitoring
  - Project specific instrumentation readings (Surface and/or underground)
- Ground support-related Quality & As-constructed/executed documentation:
  - Excavation reports
  - Rock Bolt/anchor - Pull/proof tests and grout testing
  - Shotcrete thickness reports and adhesion testing
  - Survey control checks to validate alignment.
- Ventilation & Atmospheric Data:
  - Ventilation readings to confirm the excavation extent is adequately ventilated
  - Planned ventilation changes and/or ventilation-related tasks managed through isolated ventilation management procedures.
- Planned works for the permit period:
  - Planned excavation extent (often recorded in chainage)
  - Proactive - Ancillary support tasks to support tunnelling.
  - Reactive – Ancillary tasks to support tunnelling

1.2 *Limitations to the PTT Process*

The PTT process was reviewed, contrasting its evolution from its 2006-2008 needs inception to its application in tunnelling in Australia in 2024. This review was conducted as a workshop with subject matter experts in tunnelling, underground survey, mining, and Geotechnical Engineering. The IFL working group sought to improve data management through PTT; Figure 1 illustrates the improved PTT framework for information and data control as a result of the IFL being implemented. The findings, specifically focused on the PTT process's strengths and limitations, were then summarised into three (3) key limitation themes (LT). The case study sought to solve these limitations themes by introduction of the IFL:

LT1 - Time/resource draw as a result of an increase in tunnelling production rates and scope complexity:

The traditional PTT process is typically documented using conventional word processing files for each permit period and heading. As tunnelling operations scale up, with multiple tunnel headings active concurrently, the manual management of the PTT— including daily data reviews— can become resource-intensive. For example, during the Sydney Rozelle Interchange project, over 20 tunnel headings were active simultaneously, the administrative demands of implementing the PTT procedure were particularly complex. This complexity has led to the establishment of dedicated PTT staff, resulting in increased project resourcing costs.

LT2 - Risk related to human interaction with data and PTT development:

The review and processing of PTT data, often stored in various storage locations and formats, heightens the risk of human error during data consolidation. Transfer errors from data compilers often require reactive corrections during PTT meetings due to manual transfer errors. Additionally, the traditional PTT process re-quires manual data handling for other outcomes, such as quality or safety, resulting in key information being duplicated in other processes, leading to inefficiencies.

LT3 - Transferability of technical information into a format that non-technical personnel can access and understand:

A critical consideration for the PTT process is its communication and accessibility to both the technical audience and the operational workforce. While the PTT is an effective tool for summarizing excavation status, its ability to convey accessible technical information is limited. The data

presented is often in a raw format, which is not easily comprehensible for workforce personnel, thereby impeding its ease of access and utility for individuals who perform non-technical roles.

2 DEVELOPMENT OF THE INTEGRATIVE FEEDBACK LOOP (IFL)

Considering the three limitation themes, the IFL was developed leveraging the Deswik mining solution software platform. The Deswik spatial solution software, together with its Mine Data Management (MDM), Mapping, and other applications, provided adequate customizability and leveraged Deswik's extensive experience in the mining industry to capture learnings with reasonable learnings transferability.

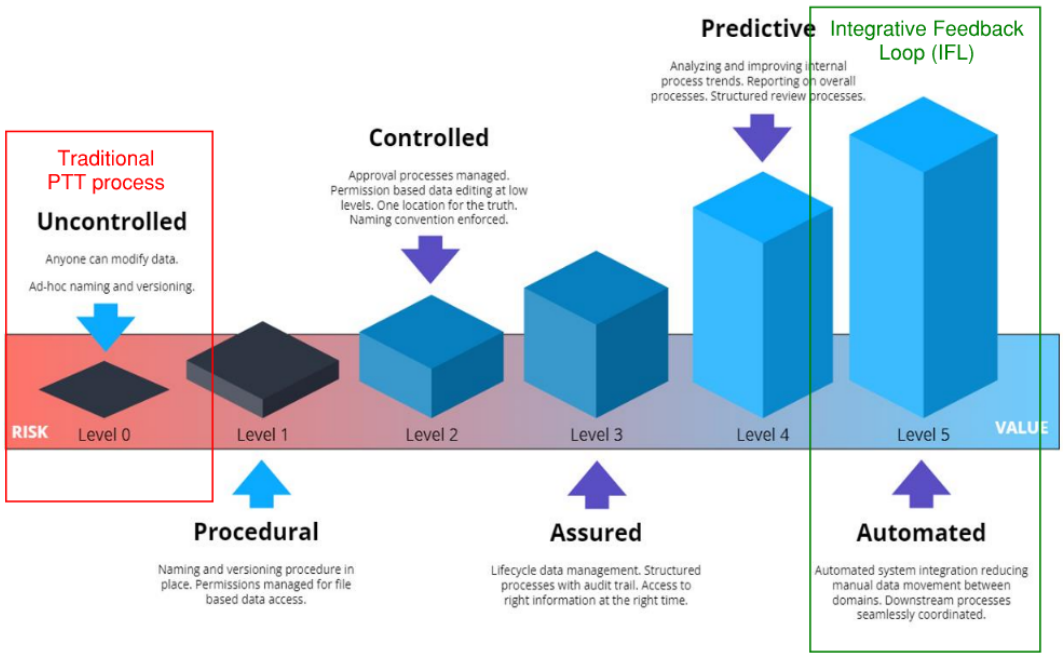


Figure 1. Pre and post implementation of the IFL from the traditional PTT process.

To address LT1 (time and resource draw), the working groups focus was to assess what data inputs were driving PTT outcomes and how handling of the data could be optimized and where possible automated. The table below summarizes the transition from traditional PTT data collection ('Uncontrolled' in Figure 1) to the optimized IFL data storage and collection model (Automated in Figure 1):

Table 1. Comparison of uncontrolled and automated PTT processes

PTT Inputs	Traditional PTT Data collection (Uncontrolled)	Integrative Feedback Loop (Automated)
Ground Conditions	As-Excavated Geological Mapping-Conducted on paper-based mapping form or through a geological mapping application on a tablet or similar.	Integration of the Deswik Mapping tool integrates geological mapping into a live space to review in the IFL model during the PTT. Data is processed in the cloud and automatically uploaded into MDM, digital model and the PTT.
Instrumentation & Monitoring (I&M)	Often taken through manual data reads from equipment or hosted on a cloud platform. I&M applies to both in-tunnel and surface monitoring, depending on the project's needs.	I&M data sets are drawn into the IFL from feed sources stored in the Deswik MDM repository and reported on the PTT through smart process mapping data extraction from the source.
Ground support-related Quality & As-constructed/executed documentation	Collected through either manual recording of data in paper-form or through a survey such as lidar or point-and-shoot collection, saved and attached to quality work lots to demonstrate conformance to design requirements.	Quality data sets are drawn into the IFL from feed sources stored in the Deswik MDM, observable in the model and integrated into the PTT. Any survey files are uploaded by the survey team into MDM where the data/files are integrated into the digital twin model and PTT.
Ventilation & Atmospheric Data	Data is often collected manually and recorded on a word processing document	Ventilation data sets are drawn into the IFL from feed sources stored in the Deswik MDM and reported on the PTT through smart process mapping from the source.
Planned works for the permit period	Completed manually on a word processing document each permit period.	Completed in the digital PTT for each permit period and then workflowed. Once complete, users sign the PTT digitally to approve/acknowledge excavation to proceed. This enables remote users to interact with and monitor the PTT.

Once initiated, the MDM workflow automatically guides users through the tasks relevant to their specific roles. This ensures that all necessary steps of the PTT are completed before the workflow progresses, while also establishing traceability. With the updated IFL data storage and collection model, the redundant processing of data and files used to populate the PTT has been reduced. Responsibility for feeding the PTT is now distributed among different working groups

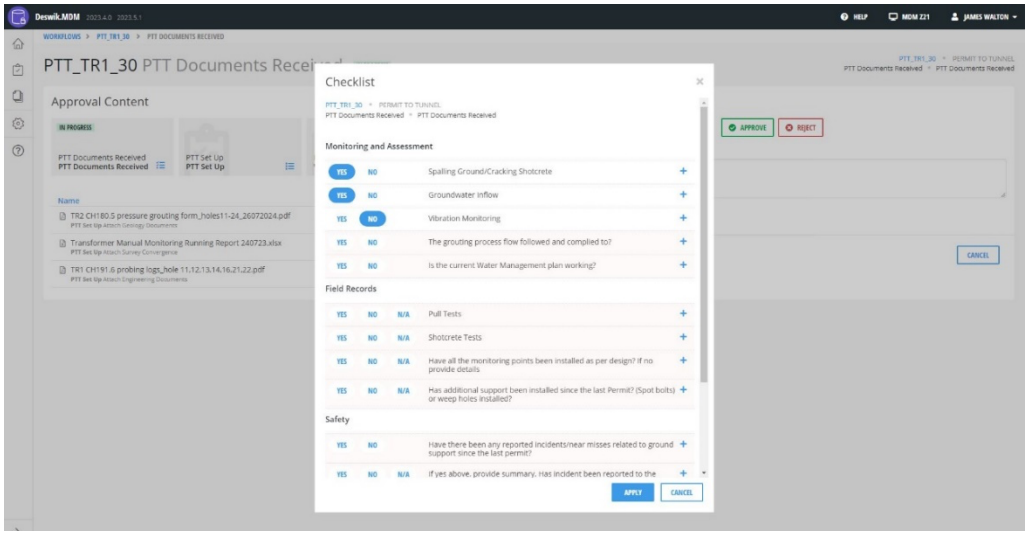


Figure 2. Comparison of uncontrolled and automated PTT processes

(e.g. Survey, geotechnical, Engineering), each contributing the necessary data within a 24-hour period after the previous PTT update. This allows accumulated improvement of the common data model by various subject matter experts, rather than relying on a single resource to compile information from multiple sources. Figure 2 & 3 illustrates the IFL PTT Deswik interface during development and testing.

To address LT2 (Human Error Risk), the same approach as LT1 was used, with a focus on minimizing human interaction with raw data. Raw data is now directly uploaded into the MDM platform and fed into the PTT automatically. For critical information requiring review, the MDM workflow tool allows data to be reviewed and accepted before integration into the PTT. For example, peer review of tunnel mapping or survey/instrumentation data can be done prior to inclusion. Implementing the IFL significantly reduces human handling and processing of raw data by feeding it directly into a digital model, thus lowering the risk of error and data disruption.

In developing the IFL solution for LT3 (Transferability of Technical Information), the working group leveraged the flexibility of Deswik's customizability to improve the visualization of the PTT for both technical staff and the workforce. Each PTT displays the current excavation cut along with key data inputs, providing a comprehensive summary of the excavation as a single source. This enhanced visualization offers non-technical personnel better access to understand the planned work during the permit period and the excavation's current safety status (see Figures 3,4 &5 for an example of a cut summary in the IFL). The 3D model-driven PTT allows interactive discussions during meetings, enhances planning, and enables non-technical staff to export views of the tunnel as excavated, facilitating visually supported communication and instruction to the workforce.

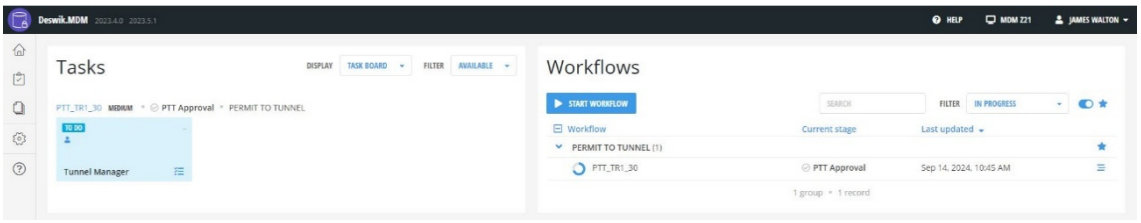


Figure 3. Deswik workflow interface for the PTT.

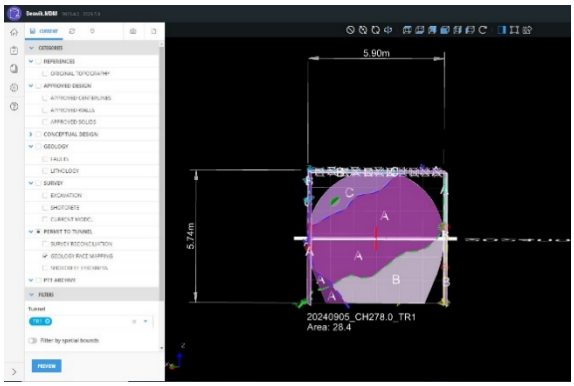


Figure 4. Cross section of geological mapping imported from the deswik mapping tool

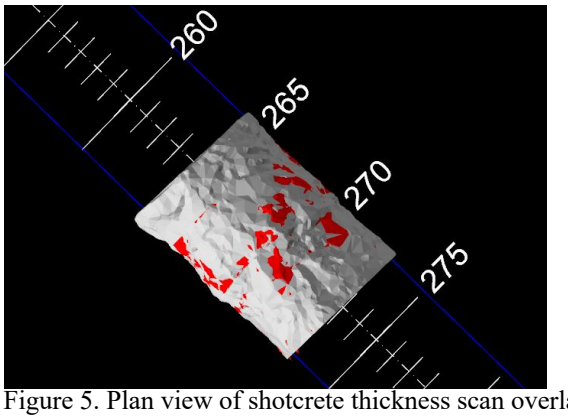


Figure 5. Plan view of shotcrete thickness scan overlay

Live testing of the IFL was conducted on an in-flight pumped hydro project in Australia, successfully validating the effectiveness of the digitalized process. The IFL PTT was tested alongside the traditional PTT process, focusing on a single heading to demonstrate its efficiency, with the expectation that the same approach could be easily adapted for multiple headings within the software. Testing the IFL in parallel resulted in fewer instances of human error during data input and reduced the administration time for PTT end users by distributing input responsibilities across key project teams with implementation automation of data processing.

3 LESSONS LEARNT

The IFL has demonstrated its effectiveness in NATM tunnelling projects where high production rates, complex geometry, or multiple headings are managed under the PTT process. However, its efficacy appears to be limited in projects with single-heading excavations, slow production rates and/or minimal complexity. Further assessment would be needed to evaluate the true time savings and risk control in such cases. An unexpected but valuable outcome from LT3 was the benefit of viewing the model when analyzing the PTT and its interactions with multiple interfacing excavation headings. This allowed the working group to visualize geological features and monitoring information in a holistic manner, considering how each heading might interact geotechnically with the excavation scope. Figures 7 and 8 illustrate the advantages of model visualization when managing multiple headings and their interactions. The transfer of raw data from Deswik MDM to drive the PTT process was largely successful, though further refinement is needed to optimize how raw instrumentation and monitoring data are imported into the platform for improved inputs into the IFL.

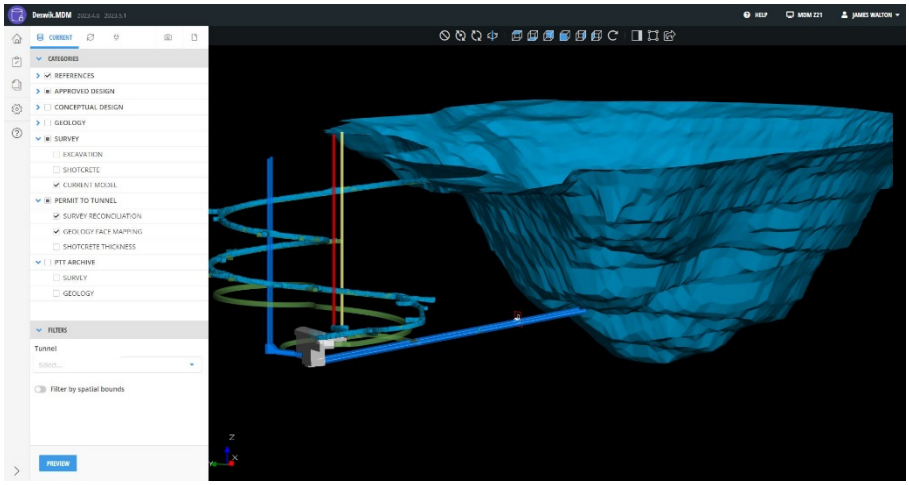


Figure 6. The whole model view showing the ability to review multiple headings in PTT holistically.

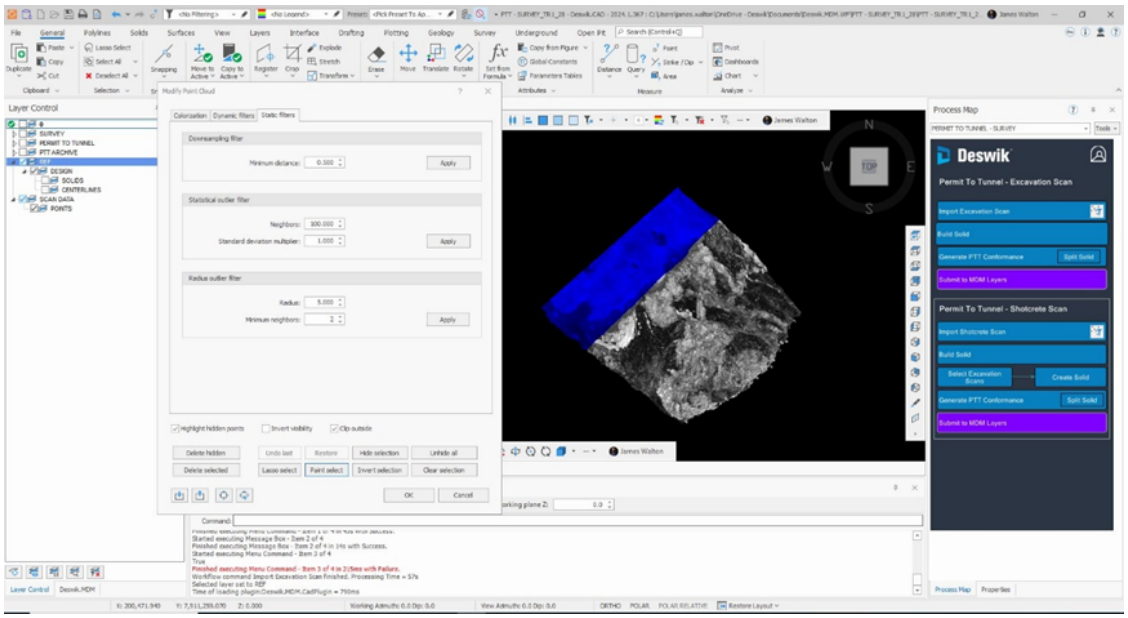


Figure 7. Plan view showing a high-resolution scan of ground conditions being meshed and imported in MDM.

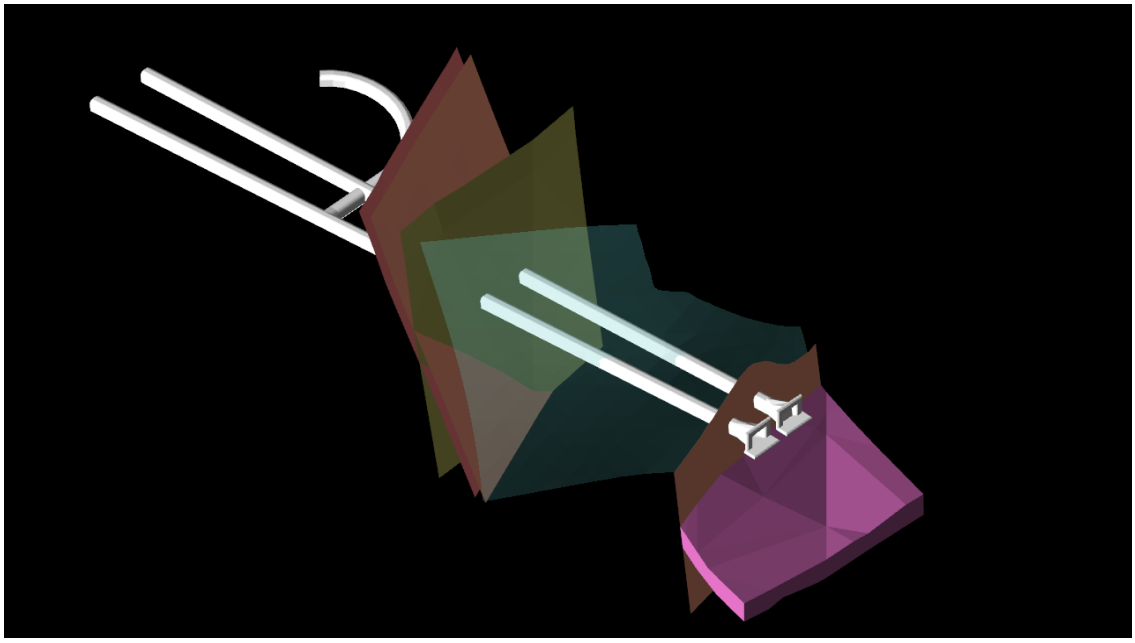


Figure 8. Example of geological model that is validated through the PTT process.

4 CONCLUSION

This case study aimed to review the traditional PTT processes in Australia and explore whether innovative technological approaches could enhance the safety-critical role it serves. As the Australian tunnelling industry evolves, with increasingly complex project scopes, there is a growing need for the PTT process to adapt accordingly. The rise of geometrically complex tunnelling projects, particularly in the re-emerging Pumped Hydro industry, highlights the demand for improved excavation control methods and the integration of technologies from other industries. The implementation of the IFL system represents a significant step towards digitalising key tunnelling processes, including PTT, to align with the industry's rapid growth. The IFL system offers an enhanced user interface and provides several key benefits validated through live testing during this study:

- Increased Efficiency: Rapid access to spatial data and workflow management ensures real-time critical data validation.
- Enhanced Safety: The platform facilitates model-based spatial interaction, reducing the need for human exchange with raw data, and optimises geotechnical assessment tools for safer tunnelling outcomes.
- Sustainable Data Management: The system allows for seamless data transfer between projects and serves as a single source of truth for legacy information, both during and after project completion.

These improvements underscore the need for modernizing tunneling processes to keep pace with the growing technical demands of the industry.

5 REFERENCES

M Salcher, Y Bai, M Trim, R Bertuzzi & B Vidler, 2023, The Permit to Tunnel process adopted on Australian infrastructure Projects, Australasian Tunnelling Conference November 2023, New Zealand

19th Australasian Tunnelling Conference – Acosta-Martínez, Stewart and Hudson-Smith (Eds.)
© 2025 Australian Tunnelling Society, ISBN 978-0-85825-002-4

Influence of Strain-Softening Behaviour of Fissured Clays on Deep Shaft Excavations

A. Purwodihardjo, A. Lesmana and P. Booth
CMW Geosciences Pty Ltd, Brisbane, Australia

ABSTRACT: Deep shaft excavations present significant challenges in fissured clays, which are typically highly plastic and characterised by slickensides and fissures formed through weathering and consolidation. These soils exhibit strain-softening behaviour, where shear strength progressively decreases beyond a critical strain level, increasing the risk of instability. This paper outlines limitations of conventional constitutive models—such as Mohr-Coulomb and plastic hardening soil models—which cannot capture the post-peak strength degradation typical of fissured clays. To address this, an advanced strain-softening model developed by the lead author is introduced, improving accuracy in simulating the complex stress–strain response. Practical implementation is illustrated through a deep shaft project in Queensland, identifying cases where traditional models remain applicable in early design stages and where the advanced model becomes essential under significant softening. The study offers guidance for geotechnical engineers and presents a robust framework for managing strain-softening in deep shaft design and numerical modelling.

1 INTRODUCTION

Castellanos (2014) highlighted the importance of recognising the transitional zone between peak and residual strength in fissured clays, proposing a framework for incorporating strain-softening into practical design. This work serves as a foundation for current efforts in numerical implementation and calibration against field data.

Soft fissured clays present a unique challenge to deep excavation projects due to their complex stress-strain behaviour, particularly the pronounced strain-softening response post-peak strength. Conventional design approaches based on peak or residual strength often fail to capture the transitional degradation of strength mobilised during deformation. This oversight may lead to underestimations of ground movement and structural demands during deep shaft excavations.

Recent advances in numerical modelling have enabled the implementation of strain-softening constitutive laws into finite difference and finite element codes, offering a more realistic simulation of progressive failure mechanisms. This paper builds upon previous research on tunnelling-induced ground movement, including the findings of Purwodihardjo (2003) on the effect of strain-softening on settlement due to tunnelling, and applies a strain-softening soil model to evaluate its influence on deep shaft stability in fissured clays.

This paper first reviews traditional constitutive modelling approaches, including the linear elastic perfectly plastic Mohr-Coulomb model and the plastic hardening soil model. These methods are widely used due to their computational efficiency and simplicity; however, they fall short in capturing the progressive strength degradation and stress–strain complexity typical of fissured clays. To overcome these shortcomings, the paper introduces an advanced strain-softening model, developed by the lead author, specifically tailored to simulate the transitional

stress–strain behaviour observed in such soils. The model incorporates laboratory-derived strength parameters and is implemented in FLAC to simulate the evolving behaviour of deep excavations. This enhanced modelling framework enables more accurate prediction of deformation profiles and support requirements by realistically capturing the transition from peak to residual strength conditions.

The paper also bridges theory with practice by exploring scenarios where traditional constitutive models can still be effectively applied and where the advanced strain-softening model becomes indispensable. A real-world case study of a deep shaft excavation in Queensland is presented, illustrating the practical implementation of these approaches. The case study highlights how traditional models can be utilised in preliminary assessments or for less critical excavation phases, while the advanced model is applied in critical zones to ensure safety and optimise design performance. Construction methodologies, including excavation sequencing and stabilisation techniques, are also detailed to demonstrate the integration of these models in practice.

By evaluating the strengths and limitations of both traditional and advanced modelling approaches, this paper provides valuable insights and guidance for geotechnical engineers in conducting numerical simulations and assessments, offering a balanced framework for managing strain-softening effects in deep shaft excavations.

2 CASE STUDY - FISSURED CLAYS ON DEEP SHAFT EXCAVATIONS

2.1 *Detail of the shaft*

The case study involves the construction of a 350-metre-deep ventilation shaft at an underground coal mine in the Bowen Basin, Central Queensland. The finished internal diameter was 5.0 metres, and excavation was conducted using staged blind boring with a 12 mm thick steel liner installed progressively.

Excavation proceeded in three stages: 7.3 m diameter to 37 m depth (Stage 1), 6.5 m diameter to 58 m depth (Stage 2), and 6.0 m diameter to 350 m depth (Stage 3). Corresponding liner inner diameters were 6.6 m, 6.1 m, and 5.0 m, respectively. The annular gap was backfilled with flowable grout or concrete. Before boring commenced, a 10-metre-deep presink was excavated using open trenching with a 45° batter from 0–2 m depth and 60° batter to the base. A 7.4 m diameter steel pre-collar liner was installed and concreted in place.

Throughout the boring process, drilling fluid (mud) was used to support shaft walls and lift cuttings. Its use was guided by preliminary numerical analysis that indicated instability risks without support. Drilling fluid properties were carefully designed and maintained to match the site-specific ground conditions and ensure excavation stability during boring and liner placement.

2.2 *Geological setting*

The site lies within the Bowen Basin in Central Queensland, a major coal-bearing basin extending approximately 600 km. The geology comprises Quaternary alluvium overlying Tertiary Suttor Formation sediments, which in turn overlie the Permian Fort Cooper and Moranbah Coal Measures.

The Suttor Formation—generally less than 60 m thick however locally up to 150 m—consists of quartz-rich sandstone, conglomerate, sandy and silicified claystone, weathered in places to clay, silt, sand, and gravel. In its eastern extent, it is interbedded with or overlies basalt flows. Prolonged deep weathering of this unit led to a lateritic profile, likely contributing to the development of fissuring in clay-rich layers.

Hyperspectral and XRD analysis (Yu et al.) identified kaolinite as the dominant mineral, although SEM–EDS revealed honeycomb microstructures resembling smectite.

2.3 *Fissured clays*

Fissured clays were primarily encountered within the Tertiary strata, however also in residual soils weathered from Permian rocks. These clays often contain slickensides and fissures formed from differential consolidation and weathering. Residual clays may retain bedding features from the parent rock.

High plasticity fissured clays near the surface or at buried paleo-surfaces display seasonal shrink–swell characteristics. Fissuring tends to increase with higher clay content, liquid limit, and over consolidation ratio.

Triaxial tests from the case study indicate pronounced strain-softening behaviour, marked by significant strength loss beyond a threshold strain, further discussed in Section 3.

2.4 *Interpreted ground conditions*

The cored borehole at the shaft location revealed:
- 0 – 0.2 m: Topsoil
- 0.2 – 10.0 m: Quaternary Alluvium
- 10.0 – 53.0 m: Tertiary Alluvium
- 53.0 – 57.0 m: Extremely weathered Permian sandstone;
- 57.0 – 64.0 m: Highly to Moderately weathered Permian sandstone;
- 64.0 – >64.0 m: Fresh Permian

For the geotechnical analysis, the above stratigraphy was further sub-divided into refined geotechnical units and simplified. The adopted geotechnical units and simplified stratigraphy for geotechnical analysis are presented in Tables 1 and 2 respectively.

Table 1. Adopted geotechnical units

Units	Geological Origin	Sub-Unit	Description
Q	Quaternary Alluvium	Q1C	Stiff Clay/sandy Clay
		Q2A	Very loose to loose Sand/clayey Sand
		Q2B	Medium dense to dense Sand/clayey Sand
T	Tertiary Alluvium	T2	Hard sandy Clay (fissured Clay)
		T3	Hard Clay (fissured Clay)
P	Permian	P1	Highly weathered very low strength Sandstone
		P2	Slightly weathered low to medium strength Sandstone
		P3	Fresh medium to high strength Sandstone

Table 2. Adopted stratigraphy

Layer No.	Unit	Top Depth (m)	Bottom Depth (m)
1	Q2A	0.0	1.5
2	Q1C	1.5	4.0
3	Q2B	4.0	10.0
4	T2	10.0	12.0
5	T3	12.0	14.0
6	T2	14.0	18.0
7	T3	18.0	22.0
8	T2	22.0	24.0
9	T3	24.0	26.0
10	T2	26.0	30.0
11	T3	30.0	48.0
12	T2	48.0	53.0
13	P1	53.0	57.0
14	P2	57.0	64.0
15	P3	64.0	>64.0

Groundwater levels from standpipe readings at the shaft location varied from 46.19m to 46.26m bgl.

3 MODELLING STRAIN-SOFTENING BEHAVIOUR OF FISSURED CLAYS

3.1 *Conventional constitutive model*

Traditional constitutive models widely used in geotechnical analysis include the linear elastic perfectly plastic Mohr-Coulomb model and the plastic Hardening Soil model. These models are

favoured for their simplicity and computational efficiency and are often adequate for early design phases or where deformation is limited. However, both exhibit limitations in capturing the progressive failure mechanisms and post-peak strength degradation characteristic of fissured clays.

The Mohr-Coulomb model assumes constant shear strength parameters (cohesion *c*, friction angle, j) and a linear yield surface. While it can simulate ultimate limit states, it does not account for the reduction of strength with increasing strain. As a result, it cannot replicate strain-softening behaviour or the transition from peak to residual strength that occurs in slickensides, over consolidated clays.

The Hardening Soil model improves on this by introducing stress-dependent stiffness and plastic strain hardening, as well as separate stiffness moduli for loading, unloading, and reloading. However, it still lacks a mechanism to reduce strength once the peak is exceeded and therefore cannot simulate strain-softening behaviour.

To compensate for these shortcomings, one approach is to undertake separate analyses using peak and residual strength parameters to bracket possible system responses. However, this technique does not model the progressive nature of strength degradation. More sophisticated modelling involves applying a strain-softening constitutive model, which progressively reduces strength parameters as a function of plastic shear strain. This approach, adopted in the present study, is detailed in the following section.

3.2 *Advanced strain-softening model*

This model was developed by Purwodihardjo (1999, 2003) based on the main frame of the Mohr-Coulomb model with non-associated shear rule as described earlier. It is formulated within the Mohr-Coulomb framework and employs a non-associated flow rule. Unlike conventional models, it allows key yielding parameters, cohesion, friction angle, dilation angle, and tensile strength, to evolve as a function of accumulated plastic deviatoric strain (εᵖ_dev) after yielding. These parameters may harden or soften, depending on material behaviour.

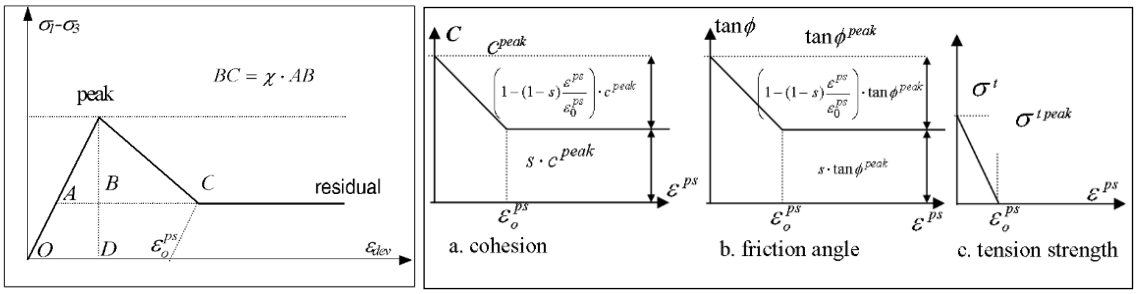
The yield and plastic potential functions are retained from the Mohr-Coulomb model. After the onset of plasticity, strength parameters are modified through a piecewise linear degradation model. This model comprises a softening branch, where parameters reduce from peak to residual, followed by a residual branch with constant values.

Two additional parameters are required: χ (the ratio of post-peak degradation to initial drop) and s (a scaling factor that governs the degradation slope). These are derived from triaxial tests and are key to replicating realistic strain-softening responses.

The model allows the evolution of shear strength and dilation angle to be described as follows:

- For εᵖ_dev = 0 : c = c_peak, φ = φ_peak
- For $0 < \varepsilon^p_dev \leq \varepsilon_0^{ps}$: c and φ reduce linearly to residual values
- For $\varepsilon^p_dev > \varepsilon_0^{ps}$: c = c_res, φ = φ_res

Figures 1(a) and 1(b) illustrate the degradation path and yielding parameter relationships used in the simulations.



(a) (b)

Figure 1. Strain softening model (a) and yielding parameters defined (b)

Parameter identification and validation of this model have been extensively discussed in Purwodihardjo (1999, 2003), including application to axisymmetric triaxial test conditions. The

model has been implemented via FISH scripting in FLAC to dynamically update strength parameters at the element level during plastic loading.

This advanced strain-softening model has been updated on the elastic part by adding a stress-dependent stiffness formulation for the elastic response, as illustrated below:

$$E_{ini} = E_{ini}^{ref}\left(\frac{c \cdot \cot \emptyset - \sigma_3}{c \cdot \cot \phi + p^{ref}}\right)^m \quad (1)$$

Where σ_3 refers to the minor principal stress, often representing the confining pressure in triaxial testing. The reference pressure, p^{ref} , denotes a reference stress, used to normalise the modulus. It is usually taken as 100 kPa.

3.3 *Triaxial Simulation of the Strain-Softening Behaviour of Fissured Clays*

Triaxial laboratory tests on fissured clays from units T2 and T3 were undertaken as part of the shaft geotechnical investigation. While Consolidated Drained (CD) tests are ideal for stiffness determination, Consolidated Isotropically Undrained (CIU) tests with pore pressure correction were used to expedite the programme. Five undisturbed samples were tested to failure under single stage loading as summarised in Table 3.

Table 3. summary of fissured clay samples for CIU triaxial test

Unit	Sample ID	Depth (m bgl)	Test Confining Pressure σ'_3(kPa)
T2	GT019b	10.30	199
	GT082	11.45	460
T3	GT083	19.50	780
	GT045	36.30	1000
	GT051	42.60	361

Test simulations were used to calibrate parameters for both the Plastic Hardening Soil (PHS) and Advanced Strain-Softening (ASS) models. PHS simulations used the PLAXIS 2D Soil Test feature, while the ASS model was implemented in FLAC 2D. The ASS model captured both peak and residual strengths in a single simulation, whereas the PHS model required separate runs for peak and residual envelopes. The assessed design parameters are summarised in Table 4 and Table 5 for PHS and ASS models respectively.

Table 4. Plastic Hardening Parameters (PHS) derived from triaxial test simulation

Unit	E_{50}^{ref} (MPa)	E_{oed}^{ref} (MPa)	E_{ur}^{ref} (MPa)	m	p_{ref} (kPa)	Peak Strength c'(kPa)	φ'(deg)	ψ(deg)	Residual Strength c'(kPa)	φ'(deg)	ψ(deg)	SR*
T2	120	120	360	0.8	100	1	36	0	0.5	32	0	0.85
T3	60	60	180	0.8	100	30	31	0	25	27	0	0.85

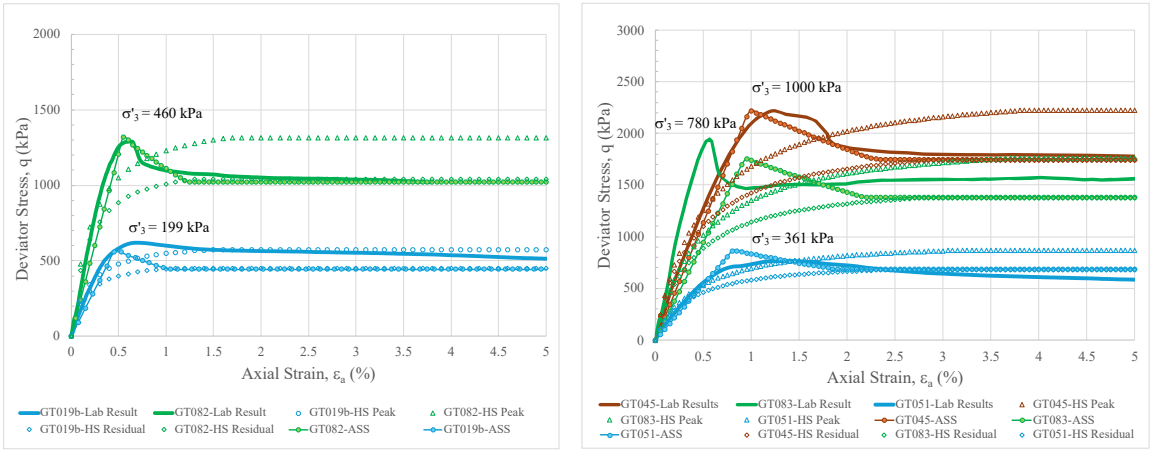
* SR = peak to residual strength reduction factor for both cohesion and internal friction angle (tan j')

Table 5. Advanced Strain Softening (ASS) parameters derived from triaxial test simulation

Unit	E_{ini}^{ref} (MPa)	m	p_{ref} (kPa)	Peak Strength c'(kPa)	φ'(deg)	ψ(deg)	Residual Strength c'(kPa)	φ'(deg)	ψ(deg)	χ	s*
T2	71.7	0.8	100	1	36	0	0.5	32	0	8.0	0.85
T3	48	0.8	100	30	31	0	25	27	0	8.0	0.85

* s = Peak to residual strength reduction factor for both cohesion and internal friction angle (tan j')

The results of the triaxial test simulations are presented in Figures 2 (a) and 2 (b) for fissured clay unit T2 and T3 respectively and the resulting parameters are summarised in Table 4 below.



(a) Unit T2 (b) Unit T3

Figure 2. Triaxial simulation results for Units T2 (a) and T3 (b)

The results confirm that the ASS model more accurately represents laboratory behaviour across the full strain range, particularly in capturing post-peak degradation. Unlike the PHS model—which requires separate analyses for peak and residual conditions—the ASS model simulates progressive strength loss in a single run, making it more suitable for fissured clays where residual strength drives deformation. Strength reduction was more pronounced under higher confining pressures, aligning with laboratory trends. Model parameters were conservatively selected to ensure simulated responses remained within or below observed test envelopes.

4 NUMERICAL ASSESSMENTS OF DEEP SHAFT EXCAVATIONS IN FISSURED CLAYS

Numerical assessments were performed using both PLAXIS 2D and FLAC 2D to leverage their complementary capabilities. The Plastic Hardening Soil (PHS) model, commonly used in practice, was implemented in PLAXIS for its intuitive interface and robust calibration tools. With the model now available in FLAC (since version 8.1), cross-platform consistency was also achieved.

The Advanced Strain-Softening (ASS) model, developed by the lead author, was implemented in FLAC via custom FISH scripting to simulate post-peak strength degradation. While PLAXIS enabled conventional PHS simulations, FLAC allowed advanced modelling tailored to strain-softening behaviour. This dual approach provided both industry-standard benchmarks and detailed insights into the progressive failure mechanisms of fissured clays.

4.1 *Shaft simulation using Plastic Hardening Soil Model - Plaxis*

Axisymmetric shaft excavation simulations through Units T2 and T3 were conducted in PLAXIS 2D to assess the Plastic Hardening Soil (PHS) model's capability in representing fissured clay behaviour. The analysis was limited to a depth of 58 m, capturing the critical zone of weak, strain-softening-prone clays between 10 m and 53 m. Although the full shaft extended to 350 m, the deeper Permian sandstone exhibited greater strength and stiffness, posing minimal deformation risk. The modelling therefore focused on the most vulnerable stratum where post-peak degradation governs performance.

The simulation followed the staged construction methodology applied on site:

- Phase 1: Open-cut excavation to 10 m depth with batter slope of 1V:1.5H.
- Phase 2: Installation of a 7.4 m internal diameter steel pre-collar liner.
- Phase 3: Blind bore excavation to 37 m depth using a 6.6 m diameter (assumed same as liner ID), executed in 4 m increments.

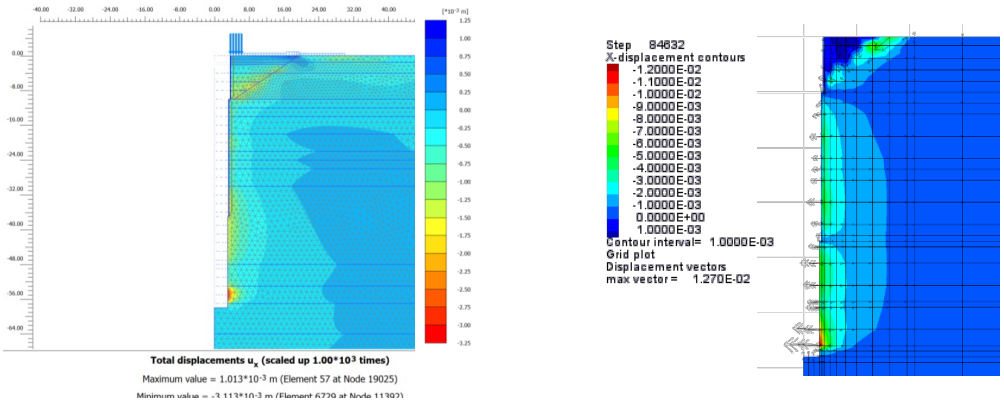
– Phase 4: Installation of 6.6 m ID steel liner.
– Phase 5: Blind bore excavation to 58 m depth using a 6.1 m diameter, also in 4 m increments.

Surcharge loads were applied in Phases 1–5 to replicate operational rig loads and ground surcharges. Uniform surcharge of 25 kPa was applied during the open excavation (Phases 1–2), while staged loadings ranging from 29 to 250 kPa were applied from Phases 3 to 5 to simulate the drilling rig's mass and operational influence near the shaft head.

Initial simulations using peak strength parameters showed instability in unsupported conditions, particularly in Stage 1 where the excavation exceeded 6 m in diameter. Stability was restored by modelling a full-height water column to simulate drilling fluid support, enabling safe progression of the excavation and subsequent sensitivity analyses.

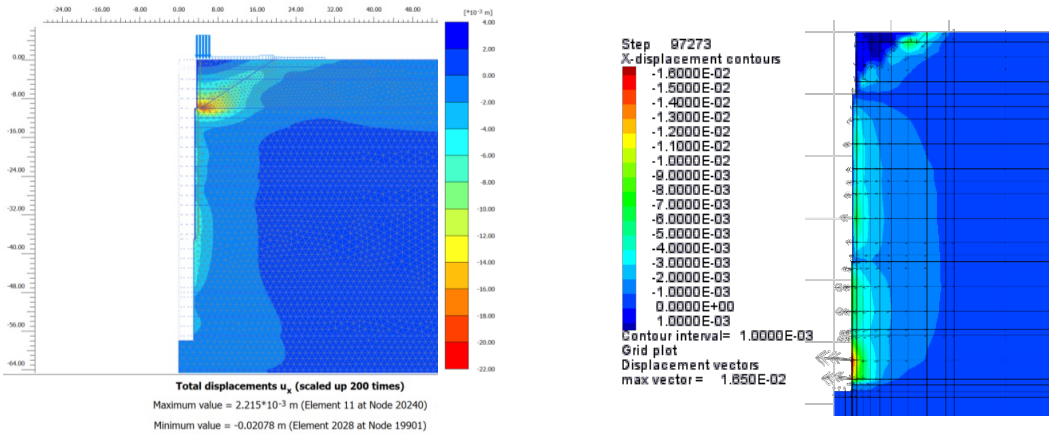
To explore the effect of strain-softening, sensitivity analyses were conducted by varying the strength reduction factor (SR). Values of 0.85, 0.5, 0.4, and 0.3 were applied to represent progressive degradation scenarios. The φ–c reduction method in PLAXIS 2D was then used to compute the Factor of Safety (FoS) for each case. Results show a clear trend: FoS drops from 4.78 (SR = 1.0) to 1.61 (SR = 0.3), indicating the impact of strength degradation on excavation stability.

Results clearly show that FoS decreases as SR lowers, with deformation increasing accordingly. As strain-softening progresses, reduced shear strength leads to ground movement. Figures 3a and 4a illustrates this trend. These outcomes highlight the importance of simulating post-peak behaviour realistically, especially in fissured and weathered clays where strength degradation controls performance.



(a) Plaxis Simulation (b) Flac Simulation

Figure 3. Lateral deformation (in meters) at end of stage 2 blind bore – base case



(a) Plaxis simulation (b) Flac simulation

Figure 4. Lateral deformation (in meters) at end of stage 2 blind bore – sensitivity case 4 (SR = 0.3)

4.2 *Shaft simulation using Advanced Strain-Softening Model - Flac*

FLAC 2D was used to simulate the shaft excavation using the Advanced Strain-Softening (ASS) model, developed by the lead author and implemented via FISH scripting. This custom model captures strength reduction as a function of accumulated plastic strain, allowing continuous transition from peak to residual strength in a single run.

The simulation adopted the same construction sequence and loading conditions outlined in Section 4.1, including staged excavation to 58 m and surcharge loads from 25 to 250 kPa. Model parameters—including peak and residual strengths and softening constants χ and s were derived from triaxial tests and are summarised in Table 5.

Results are shown in Figures 3b and 4b for SR values of 1.0 and 0.3, respectively. Under peak strength conditions, the ASS model yields greater deformation than the PHS model (Figures 3a vs 3b), due to its current limitation of not incorporating rebound stiffness—an important factor in excavation scenarios. However, at SR = 0.3, the ASS model produces less deformation than PHS (Figures 4a vs 4b), as it applies residual strength selectively, only where plasticity has developed, while the PHS model assumes residual strength throughout.

These results highlight the ASS model's ability to realistically simulate post-peak behaviour in fissured clays, offering a more accurate representation of spatially variable strength degradation compared to conventional approaches.

5 CONCLUSION

This study highlights the importance of selecting appropriate constitutive models for deep shaft excavation in fissured clays. The Plastic Hardening Soil (PHS) model, using separate simulations for peak and residual strengths, remains adequate when residual strength does not critically influence stability. However, in cases where strength degradation governs excavation response, this approach can significantly underestimate deformations.

The Advanced Strain-Softening (ASS) model addresses this limitation by capturing progressive strength loss within a single simulation. Results show that the ASS model offers a more realistic representation of post-peak behaviour and spatially variable degradation, making it more reliable in highly fissured and weathered clays.

Despite its strengths, the current ASS implementation lacks rebound stiffness modelling, which may overestimate deformation under peak strength conditions. Future refinement should focus on incorporating stress-dependent elastic recovery.

In practice, a combined modelling approach is recommended: using the PHS model for early-stage assessments and the ASS model for critical design zones. This strategy ensures more accurate prediction of deformation, stability, and support needs in soft ground conditions.

6 REFERENCES

Castellanos, B.A.D. (2014). Evaluation of Strain-Softening Behavior of Soils in Geotechnical Analyses. PhD thesis, University of California, Berkeley.

Hutton, L.J., Grimes, K.G., Law, S.R., & McClennan, T.P.T. (1991). Geology of the Mount Coolon 1:250,000 Sheet Area. Queensland Geological Survey.

Jell, P.A. (2013). Geology of Queensland. Geological Survey of Queensland, Chapter 8.

Purwodihardjo, A. (1999). Numerical Analysis of Tunnelling in Soft Soil with Strain Softening Behaviour. MSc thesis, University of Indonesia and École Centrale de Lyon, France.

Purwodihardjo, A., & Cambou, B. (2003). Effect of Strain-Softening on Settlement due to Tunnelling in Soft Soil. In M.S. Rosenbaum & A.K. Turner (Eds.), Numerical Modelling in Micromechanics via Particle Methods (Lecture Notes in Earth Sciences, Vol. 99, pp. 173–188). Springer-Verlag Berlin Heidelberg.

Yu, T., Cooling, J., Esterle, J., Chadwick, T., & Babaahmadi, A. (2022). "Clay Mineral Composition of the Suttor Formation in the Bowen Basin," Australian Journal of Earth Sciences, 70(1): 1–20.

19th Australasian Tunnelling Conference – Acosta-Martínez, Stewart and Hudson-Smith (Eds.)
© 2025 Australian Tunnelling Society, ISBN 978-0-85825-002-4

A cutting pick for tunneling roadheaders to improve sustainability

W. Roach
Sandvik Mining and Rock Solutions, Heatherbrae, NSW, Australia

ABSTRACT: Cutting picks for Roadheaders are the main consumable when excavating rock and as such will be worn and discarded as part of the rock cutting process.

Through reducing downtime, by eliminating a current maintenance requirement via significant improvements in sleeve wear life and providing a universal one style pick, cutting picks can provide reductions in waste generation.

The collaborative relationships between tunnel operations and the Original Equipment Manufacturer (OEM) consumable provider is key in being able to deliver these benefits. This is achieved through new product trials, providing feedback on new concepts and their ability to make a difference.

This paper will provide an overview of a new universal cutting pick that provides less downtime and maintenance requirements thus improving the overall sustainability for tunneling operations.

1 INTRODUCTION

Roadheaders, refer to Figure 1, when excavating rock to produce a tunnel cannot do so without the use of cutting picks.



Figure 1. Sandvik MT720 Roadheader excavating rock.

The Roadheader and cutting pick market is important to Sandvik, following on from inspirations highlighted during a previous carbide trial there is an opportunity to provide the market with a new style of pick. This pick will increase sleeve life, reduce maintenance downtime, provide easier/safer pick replacement, decrease inventory requirements and promote the benefits of working with an OEM.

1.1 *Cutting Picks*

A typical cutting pick for tunneling is conical in shape and consists of three main components, referring to Figure 2, Roach & Claesson. 2023.:

- The carbide
- The body (Head and Shank)
- The retainer

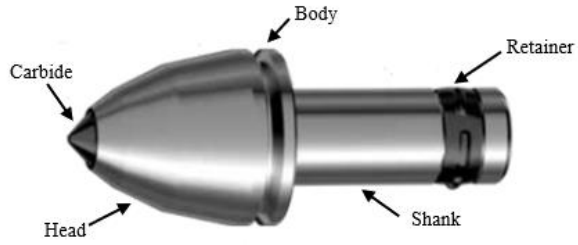


Figure 2. Typical Cutting pick components.

2 DEVELOPMENT AND PROTOTYPING

This new style pick will be categorized as a Full Length Retainer Roadheader (FLRRH) pick. As part of its development the FLRRH pick considered each of the typical cutting pick components.

2.1 *The Carbide*

The carbide for the FLRRH pick development was left to the current tried and proven carbide, which is a Sandvik premium grade (648) used for cutting medium to hard rock, in the form of an NP39 insert, referring Figure 3.



Figure 3. NP39 Carbide Insert.

2.2 *The Body - Head*

The pick head profile was reviewed for its cutting efficiency and body wash characteristics based on the data recorded during a previous carbide trial, Roach & Claesson. 2023. The head profile was reduced in size to allow a sharper cutting profile by removing excess material that also provided no additional benefits in the overall efforts to eliminate body wash, referring Figure 4 versus Figure 5, for the current head profile compared to the proposed new concept.



Figure 4. Current Sandvik Head Profile.



Figure 5. New Concept Head Profile.

2.3 *The Body - Shank*

The pick shank was then assessed for what the effect of reducing its cross sectional area would be to allow the utilisation of a full length retainer. From past history and knowledge, a 15% reduction in cross sectional area was deemed to be acceptable for the initial concept development that would be validated later in proof of concept trials.

The final concept design of the pick shank will need to complement the features of the full length retainer.

2.4 *The Retainer*

The concept of a full length retainer on a pick is not new, they have been employed on small Road Planer picks for some time. Road Planer picks are used to remove the surface layer of a pavement to allow a new surface to be directly overlaid on the existing base layers.

Developing a full length retainer for a Roadheader though would have to encompass a few different considerations:

- The larger size of the pick
- Significant increases in cutting and tangential forces on the pick
- The increase in inertia forces and the variations in force direction
- The environmental effects of cutting fines and slurry

The first design step was trying to understand how different designs would affect the retention ability of the full length retainer. 3D printing was used to check several different design concepts for their retention effectiveness. Four concepts were printed in 3D. The terminology used to describe the various features are noted in Figure 6

To test the retention ability of the 3D printed full length retainer concept designs, they were assembled on a pick shank, then installed in a sleeve and push tested in a Universal Test Machine. A summary of the push test results can be seen in Figure 7.

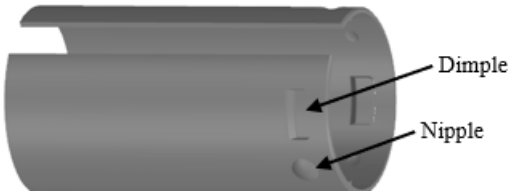


Figure 6. Dimple and Nipple feature designations.

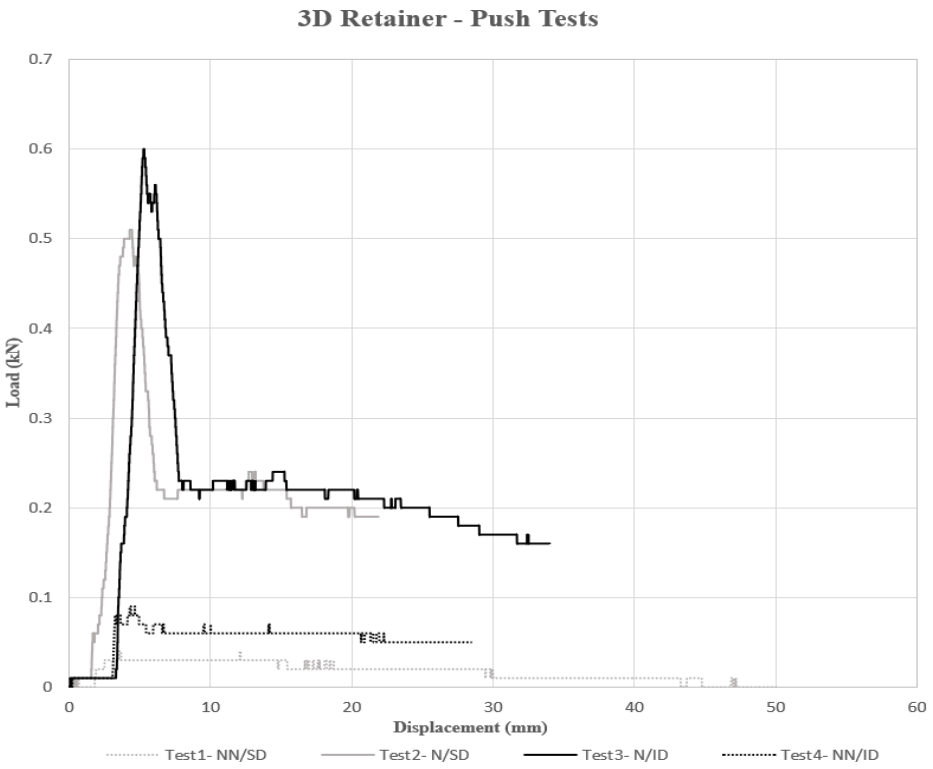


Figure 7. Summary of 3D printed full length retainer push test results.

The testing showed that there was a significant difference in the peak retention load between the full length retainer with a nipple (N) versus the full length retainer without a nipple (NN). The tests also showed that a full length retainer with an increased "at rest" diameter (ID) had a higher retention load versa a Full Length Retainer with a standard diameter (SD).

The next step was to establish what the baseline retention force of a steel version of the full length retainer should be.

The method chosen to determine this was to take the average retention force of the two current 38 mm picks, the P7JU-3885-1962, a friction retainer pick, and the P4AA-3885-3962, a bumped "Dog Collar" retainer pick, referring Figures 8 and 9.



Figure 8. 38 mm - Short Friction Retainer.



Figure 9. 38 mm Bumped "Dog collar" Retainer.

A summary of the test results can be seen in Table 1.

Table 1. Baseline Design Perimeter Determination.

Test Number	Pick/Retainer Sample	Load (N)	Comments
1	P7JU-3885-1962	1560	Short friction retainer
2	P4AA-3885-3962	1630	Bumped "Dog Collar" retainer

The baseline tests showed similar retention loads, closer than predicted, between the two current pick/retention options and set the pass goal, for retention, of the new pick at ≥ 1595 N.

To evaluate the retention performance of steel prototype full length retainer concepts, tests were performed in a Universal Test Machine with a similar set-up to that used before for the 3D printed concepts.

There were five steel prototype concept retention tests conducted in a new sleeve. They were:

- Prototype#1_1 - (SN)*
- Prototype#1_2 - (SN)
- Prototype#2_1 - (SNN)**
- Prototype#2_2 - (SNN)
- Prototype#1_2.2 - (SN)

*SN = Sandvik sleeve, Retainer with nipple.
**SNN = Sandvik sleeve, Retainer with no nipple

A summary of the test results can be seen in Table 2.

Table 2. Prototype#1 retention performance tests in a new sleeve.

Test Number	Pick/Retainer Sample	Load (N)	Comments
1	Prototype#1_1-(SN)	2520	The pick could be started in sleeve by hand but had to be tapped home with a hammer.
2	Prototype#1_2-(SN)	2110	The pick could be started in sleeve by hand but had to be tapped home with a hammer.
3	Prototype#2_1-(SNN)	1080	The pick could be installed in the sleeve by hand.
4	Prototype#2_2-(SNN)	1090	The pick could be installed in the sleeve by hand.
5	Prototype#1_2.2-(SN)	2140	The same pick assembly as used in Test#2 was tested a second time. The pick could be started in sleeve by hand but had to be tapped home with a hammer.

To gain a further understanding of the overall retention performance of the Prototype#1 full length retainer samples, retention tests were also conducted and compared against the retainers currently being utilised, in a worn sleeve. The tests were again performed in the Universal Test Machine with a similar set-up to that used before.

There were four retention tests conducted in a worn sleeve. They were in the form of:

- Prototype#1_1 - (SN)_WS***
- P4AA-3885-3962_WS
- P7JU-3885-1962_WS
- Prototype#1_2 - (SN)_WS

***WS = Worn sleeve

A summary of these test results can be seen in Table 3.

Table 3. Retention performance comparison tests in a worn sleeve.

Test Number	Pick/Retainer Sample	Load (N)	Comments
6	Prototype#1_1-(SN)WS	1510	The pick could be started in the sleeve and then push in by hand, except the last ~15 mm which had to be tapped home with a hammer.
7	P4AA-3885-3962WS	970	The pick could be started in the sleeve and then push in by hand, except the last ~5 mm which had to be tapped home with a hammer.
8	P7JU-3885-1962WS	1270	The pick could be started in the sleeve and then push ~25 mm in by hand, the last ~50 mm had to be tapped home with a hammer.
9	Prototype#1_2-(SN)WS	2030	The pick could be started in the sleeve and then push in by hand, except the last ~ 15 mm which had to be tapped home with a hammer.

The tests showed positive outcomes for the Prototype#1 retainer, achieving the retention baseline of $\geq$ 1595 N and performing well in the worn sleeve, when compared to our current picks.

3 PROOF OF CONCEPTS

To evaluate the system performance of the first production samples of the FLRRH picks in the field a proof of concept trial was conducted at a tunnel project in Sydney, Site 1.

Twelve FLRRH picks were installed in a Sandvik MT720 Road Header, after it had completed its cut cycle, to:

- Check the installation of twelve concept FLRRH picks and, more importantly, the removal of them at the end of the trial.
- Check that the concept FLRRH picks perform as required during operation, i.e.:
  - Are retained and rotate freely in the sleeve
  - Wear evenly

Twelve existing picks were removed from their locations and then the twelve concept FLRRH picks were installed in their place to form a line across each cutter drum.

The Roadheader cut on and off for approximately 10 hours, with an estimated actual cut time of ~7 hours. After the Road Header had completed its cutting cycle, it was trammed back from the face, parked, shutdown and isolated. The cutter head was then washed down, and the condition of the picks/sleeves/drums inspected. The twelve concept FLRRH picks were then removed.

The results showed that the FLRRH picks achieved the desired outcomes of the proof of concept field trials:

- The picks were installed and were removed successfully
- The picks performed functionally to the design requirements
- There were no failures of the pick system or any of its components

4 PRODUCT LIFE MEASUREMENT TRIALS

The goals of the life measuring trial were to:

- Obtain measurements of the bore of the sleeve, over time, to determine the effectiveness of the full length retainer to limit the wear in the bore of the sleeve, i.e. limit the bore wear.
- Continue to monitor the installation and the removal of the FLRRH picks after they have worn
- Check that the FLRRH picks continue to perform as required during operation, i.e.:
  - Rotate freely in the sleeve
  - Are retained in the sleeve
  - The full length retainer lasts beyond the life of the picks
  - Both the carbide and pick body wear evenly during the life of the pick

The initial evaluation was conducted at Site 1, where twelve existing picks were kept in their place to form a line across each cutter drum to act as a baseline, and then FLRRH picks were installed in every other location in each cutter drum. Both cutter drums had been fitted with all new sleeves.

This trial was stopped early though due to some of the full length retainers failing to retain the picks in the sleeves prior to the pick's complete wear life being achieved. This trial also highlighted the significant forces the system needed to cope with that could not be simulated in a laboratory environment.

After investigations the results showed that the FLRRH picks were not that far away from achieving the desired outcomes, so a re-design of the full length retainer was conducted.

An evaluation trial was conducted at Site 1 where twelve FLRRH picks with a re-designed retainer were installed in a line across each cutter drum, and existing picks were installed in every other location in each cutter drum to act as a baseline. Once again, the drums had been fitted with all new sleeves prior to the trial commencing.

This trial ran for 3 weeks and showed very positive results, with the re-designed full length retainer. Unfortunately, the sleeve wear benefits were not able to be quantified during this trial so a further trial would need to be organized to achieve this.

A second tunnel project in Sydney was approached, Site 2, and they were willing to allow a longer life measuring trial to be conducted.

Two complete drums, with new sleeves, were fitted with the latest FLRRH picks. The picks were inspected regularly and when a pick needed replacing the inner bore of the sleeve was measured. The trial was going well with minimal signs of bore wear in the sleeves. After about a month it was reported that some full length retainers were being left behind in the sleeves when the FLRRH picks were being replaced. After investigation and discussions, a tweak was made to the FLRRH pick shank. These latest FLRRH pick samples performed well and all ongoing trial FLRRH picks were made and supplied to this design. These FLRRH picks were then also introduced to a third site, Site 3, to gain more feedback and sleeve wear data. The results from Site 2 and 3 showed that the full length retainers are now lasting beyond the life of the picks.

From a system's life measuring perspective, the bore wear of the sleeves were measured and tracked over a 4 month period at Site 2, on a Sandvik Roadheader, and then at Site 3, on a Sandvik Roadheader for another period of 4 months.



Figure 10. Final FLRRH pick design

The life measuring trial was a success demonstrating the benefits of the FLRRH pick, referring Figure 10, on enhancing the wear life of the bore of the sleeves and eliminating this bore wear as a maintenance consideration in tunnel projects.

A summary of the bore wear per sleeve type can be seen in Table 4.

Table 4. Average bore wear per sleeve type.

Site	Sleeve Type	Bore wear (mm)	Time period (Weeks)	Average wear (mm)	Comments
2	Standard Sandvik	0.01 to 0.3	19	0.1	
3	Standard Sandvik	0.2 to 0.9	10	0.4****	
3	Sandvik Large Head	0.2 to 0.3	11	0.2	
3	Third Party	0.3 to 0.4	7	0.3	

**** Standard "Dog collar" style picks ran in these sleeves for ~ 2 weeks prior to FLRRH picks being installed

The final validation trial was to test the FLRRH pick in a Mitsui Roadheader. The goals of this trial were to:

- Observe the wear/effect on the tail of the FLRRH pick that protrudes from the back of the block and sleeve on the Mitsui Roadheader drum, refer Figure 11
- Monitor the installation and the removal of the FLRRH picks after they have worn
- Check that the FLRRH picks continue to perform as required during operation, i.e.:
  - Rotate freely in the sleeve
  - Are retained in the sleeve
  - The full length retainer lasts beyond the life of the picks
  - Both the carbide and pick body wear evenly during the life of the pick

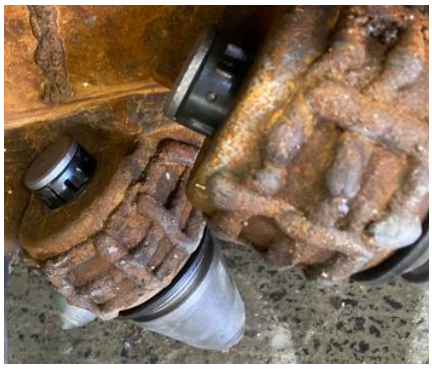


Figure 11. FLRRH picks installed in Mitsui Roadheader drum

The trail was a small initial trial at a tunnel project in Melbourne, Site 4, that involved installing six FLRRH picks in a Mitsui's cutter drum alongside the currently used picks and observing them until the first FLRRH pick needed to be replaced. All six FLRRH picks were then removed for analysis.

The trial was a success with no abnormal wear on the tail of the FLRRH pick observed. The washer on the FLRRH pick protected the block equivalent to that of the large base head on the current picks.

So, in summary the outcome of the trials in the Sandvik and Mitsui Roadheaders were a success. They showed that the FLRRH picks:

- Perform as required during operation in both the Sandvik and Mitsui Roadheaders
- Installed, safely hands free, and were removed easily with either a pick puller or a slide hammer throughout the trials
- Eliminated bore wear in sleeves as a maintenance consideration
- Prevented the wastage of picks being thrown from worn sleeves on Sandvik Roadheaders

5 SUSTAINABILITY IMPROVEMENTS

The sustainability outcomes for the FLRRH pick on a Sandvik Roadheader were:

- Reduced downtime, with respect to changing sleeves, per Roadheader
  = -77 hours/year = 96.25 % less downtown on not having to replace sleeves due to worn bores
- Reduced sleeve consumption per Roadheader
  = 486 less sleeves/year = 96.4 % reduction of the current sleeve usage/year
  Note: Sleeves would only be changed now, using the FLRRH pick, due to the wear on the outside of its head, not its bore
  Savings of 894 kg CO2-eq /year per Roadheader
- Reduced pick wastage per Roadheader
  = 96 less picks/yr = 100 % less of the current pick wastage/year
  Note: No FLRRH picks are lost due to worn sleeve bores
  Savings of 782 kg CO2-eq /year per Roadheader
- Extra sustainability benefits:
  - Weight reduction
    = 15 kg CO2-eq per 120 picks
  - Transport emissions are reduced due to reduced sleeve and pick usage
    = 357 kg CO2-eq per Roadheader
  - End-of-Life emissions are decreased due to reduced sleeve usage and pick wastage
    = 29 kg CO2-eq per Roadheader
  - Circularity - Resource Efficiencies due to less material demand
    = 1347 kg of material/year (Steel and Carbide) per Roadheader

In summary:

- Total annual emission savings
  = 2062 kg CO2-eq /year per Roadheader
- Total annual resource efficiency
  = 1347 kg of material/year (Steel and Carbide)

6 CONCLUSION

This paper has provided an overview of the development of the Sandvik FLRRH pick from its various iterations through the concept and trial stages.

The Sandvik FLRRH pick proved its ability to reduce the wear in the bore of the sleeve to a level that actually eliminates this wear life as a maintenance consideration in tunnel projects, thus providing overall reductions in downtime, sustainability benefits and waste generations reductions.

The effectiveness of the full length retainer to limit the wear in the bore of the sleeve was exceptional and showed that it could also be a true universal, one pick fits all, inventory reducing solution.

7 ACKNOWLEDGEMENTS

During the development of the FLRRH pick and the numerous trials, the work was the joint effort of Weston Doley, Product Line Manager - Cutting, Brad Searle, Parts and Service Sales Representative and Steven Weaver, Global Head of Research and Development from Sandvik. A big thank you to the various tunnel operations and their employees at sites 1, 2, 3 and 4, for their willingness, feedback and patience while this product was developed.

8 REFERENCES

Roach, W, Claesson, B (2023). Roadheader cutting tool developments towards sustainability. *Trends and Transitions in Tunnelling; 18th Australasian Tunnelling Conference*: 525-534.

19th Australasian Tunnelling Conference – Acosta-Martínez, Stewart and Hudson-Smith (Eds.)
© 2025 Australian Tunnelling Society, ISBN 978-0-85825-002-4

Assessment of real-time seismic wave velocity in underground mining using laboratory simulations and optimized fuzzy systems

H. Samadi
School of Mining and Geosciences, Nazarbayev University, Astana, Kazakhstan

F. Suorineni
School of Mining and Geosciences, Nazarbayev University, Astana, Kazakhstan

ABSTRACT: Accurate seismic event source location in underground mines is critical for safety and operational efficiency. Conventional microseismic monitoring systems rely on a single input velocity model, updated periodically, which often results in errors due to ever-changing underground conditions, geological complexity, and evolving mine infrastructure. This study proposes a novel approach using discrete physical models that mimic ever-changing underground mining environments, combined with optimized fuzzy inference systems, to predict real-time input velocities for use in source location algorithms, say SIMPLEX. Laboratory tests involved block samples representing varying ground conditions and the use of acoustic emission techniques (AET) with the SAEU3H system to measure wave velocities. Optimized fuzzy inference systems-learning models, particularly particle swarm optimization-adaptive neuro-fuzzy inference system (PSO-ANFIS), achieved strong performance ($R^2 = 0.97$, NRMSE = 0.001, MAPE = 0.0001). The approach enables more accurate, real-time seismic source location, potentially enhancing the effectiveness of seismic monitoring systems in underground mines.

1 INTRODUCTION

Seismicity in mining involves natural or induced earthquakes, with hazards like rockbursts causing fatalities, losses, and operational challenges (Kebeasy 2017). Predicting rockbursts remains difficult due to settings limitations, though risk zones can be identified (Simser 2019). Microseismic monitoring systems help manage seismic hazards by detecting and locating events, but their accuracy depends on velocity models used. Underground mines feature dynamic rock mass conditions, voids, and varying rock types, making static or layered velocity models inadequate (Trifu and Suorineni 2009). Real-time velocity monitoring is ideal but remains a challenge due to complexity, costs, and constant environmental changes in underground mining.

Real-time seismic wave velocity prediction in mining is vital for improving safety, efficiency, and environmental sustainability (Collins et al. 2014). Research over the past two decades highlights the role of seismic wave velocity in understanding stress conditions, rockburst hazards, and mining-induced seismic events (Trifu and Suorineni 2009, Rebuli 2024). Studies have employed various methods, like passive seismic interferometry (Czarny et al. 2016), in situ measurements (Olivier et al. 2015), numerical modelling (Mukhamedyarova et al. 2023), and ambient noise analysis (Czarny et al. 2019), to track velocity changes and link them to underground stress and structural changes. Findings reveal that velocity drops can indicate stress alterations, and factors like geomechanical properties and ever-changing mining conditions also influence long-term velocity shifts. Advanced models, including empirical and artificial intelligence (AI)-based approaches, have been developed to improve prediction accuracy (Wojtecki et al. 2022). As publications in this area increase, the trend reflects a growing recognition of the need for real-time solutions to predict seismic wave velocity and accurately locate seismic events in underground mines. This study focuses on optimized fuzzy-based learning approaches to meet that need.

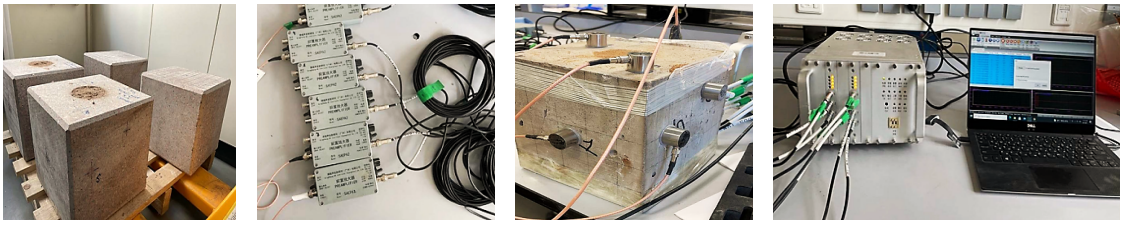
AI-based models, particularly machine learning (ML) algorithms, have shown promise in predicting seismic wave velocity in underground mining, offering improved accuracy over traditional methods (Duan et al. 2021, Wojtecki et al. 2022). However, most rely on field data already affected by errors from static velocity models, limiting their precision. Recent research, including laboratory-based studies like that of Maksut et al. (2022), mimicked real mine conditions to better understand seismic wave behavior. Despite positive outcomes, advanced hybrid learning approaches remain underexplored.

This study aims to predict seismic wave velocity in real time, addressing the limitations of constant velocity models that fail to capture dynamic ground changes from mining activities. A unique laboratory-generated dataset of 675 samples with 54 features was created, including varying block sizes, geomechanical properties, voids and backfill features, and geometrical properties. These controlled laboratory settings mimicked the dynamic conditions of real-case underground mining. To enhance prediction accuracy, optimized fuzzy-based learning algorithms were introduced.

2 DATA ACQUISITION; LABORATORY SETUP- DATA GATHERING

This section presents a laboratory-based approach using discrete physical modelling to simulate underground mine conditions and study seismic wave velocity. Discrete physical modelling captures snapshots of mine degradation over time, replicating the effects of continuous mining activities. Because real underground environments are complex and unpredictable, the researchers developed a controlled laboratory setup to mimic these changes safely (Figure 1). The main objective was to predict seismic wave velocity under varying underground conditions using the acoustic emission technique (AET), which resembles microseismic monitoring in mines. Experiments were conducted using granite and synthetic rock (sand-cement) cubes of different sizes (150–450 mm), some with central holes to simulate excavation. Hole diameters (50-150 mm) increased with block size to represent mining progression. These holes were also backfilled with varying cement-sand mixtures (based on ASTM C-109 C standard, ASTM 2013), ranging from 0% to 20% cement, cured for different periods (8 hours to 28 days).

Static cracking agents were used to simulate rock fracturing, and pulse waves were generated from a source sensor, with seven others recording wave arrival times. The positioning of sensors and source, along with known coordinates, enabled analysis of wave propagation through blocks with different internal conditions. The experimental setup included SAEU3H AE data systems and high-frequency AET sensors (SR150M and SRI150) suitable for different block sizes. Concrete blocks were cast using ASTM standards to ensure consistency, and uniaxial compressive strength (UCS) tests were conducted on samples from the same mixtures for quality control. AET provided insights into the influence of material properties, hole size, backfill composition, and curing age on seismic wave velocity, establishing a foundational database for real-time seismic monitoring tools in underground mining.



(a) (b) (c) (d)

Figure 1. Acoustic emission (AE) testing setup involved concrete cubes designed to mimic underground mining environments, with specific configurations and sensor placements: (a) block specimens both solid and with drilled holes filled with backfill material, (b) external preamplifier units, (c) AE sensors attached to the cube surfaces, and (d) an AE system connected to a laptop for data collection

3 DATA ANALYSIS; DATA PRE-PROCESSING AND PROCESSING

The laboratory tests provided data from three main sources: 839 readings from the base, 269 from cracked G80 sensors, and 674 from fractured blocks using SR150M sensors. These readings were collected from eight different sensors, with Sensor 1 acting as the pulse source. In total, 1782 data records were collected. Each record included details such as the sensor's location (x, y, z), the distance from the source, wave velocity, arrival time, and the block's physical and geomechanical properties (like size, hole diameter, cement content, curing time, backfill strength, and compressive strength). Only the location of the pulse source was recorded for the source sensor. The blocks, both fractured and unfractured, were evaluated using the rock mass rating (RMR) system (Bieniawski 1989), and wave velocities were measured accordingly.

The data gathered from the laboratory experiments included both numerical and non-numerical types. To make the data easier to analyze and more reliable, it was important to organize and clean it properly. The database was formatted to follow a standard structure and included different geomechanical, physical, and geometric properties. Some data entries had a mix of descriptive and numeric values, and others had missing or duplicated data. To fix this, all data formats were converted into a single float type, and descriptive (qualitative) data was changed into a binary format. After cleaning and organizing the raw data, the final database was created using techniques such as one-hot encoding, handling duplicates, filling missing values, and unifying data types (data handling techniques were completely matched with laboratory investigations). This cleaned database had 675 entries and 54 features. From this, 85% (573 entries) were used for training the models, and 15% (102 entries) were set aside for testing. Full details of this database are listed in Table 1.

Table 1. The summarized features of the laboratory simulation-generated database.

Parameters		Unit	Description
Sample		-	Concrete and granite
Block geometrical properties	Block size (BS)	mm	150, 225, 300, 375, 450
	Hole diameter (HD)	mm	50, 75, 100, 125, 150
	Rock mass rating (RMR)	-	58, 59, 62, 65, 67, 69,70, 71, 72, 74
Block geomechanical properties	Uniaxial compressive strength (UCS)	MPa	9.3, 10.4, 10.5, 11.2, 12.9, 14.04, 15.09, 15.7, 15.8, 17.2, 17.7, 18.5, 19.2, 19.3, 19.7, 20.2, 21.6, 22.3, 22.4, 22.7, 23.01, 23.9, 30.4, 32.1, 34.3, 153
	Cement content (CC)	%	5, 10, 15, 20
	Curing time (CT)	days	8 hours, 1 day, 7 days, 14 days, 28 days
Backfill quality	Backfill strength (BST)	MPa	0.245, 0.353, 0.505, 0.573, 0.651, 0.682, 1.006, 1.07, 1.38, 1.61, 1.99, 2.55, 2.26, 3.102, 4.42, 5.245
Sensor parameters	Location coordinats (X, Y, Z)	-	Min X = 0, Max X = 450 Min Y = 0, Max Y = 450 Min Z = 0, Max Z = 240
	Arrival time (AT)	msec	Min= 0, Max = 4735
	Distance (D)	mm	Min = 82.2, Max = 454
	Velocity (V)	m/s	Min = 0, Max = 4532.6

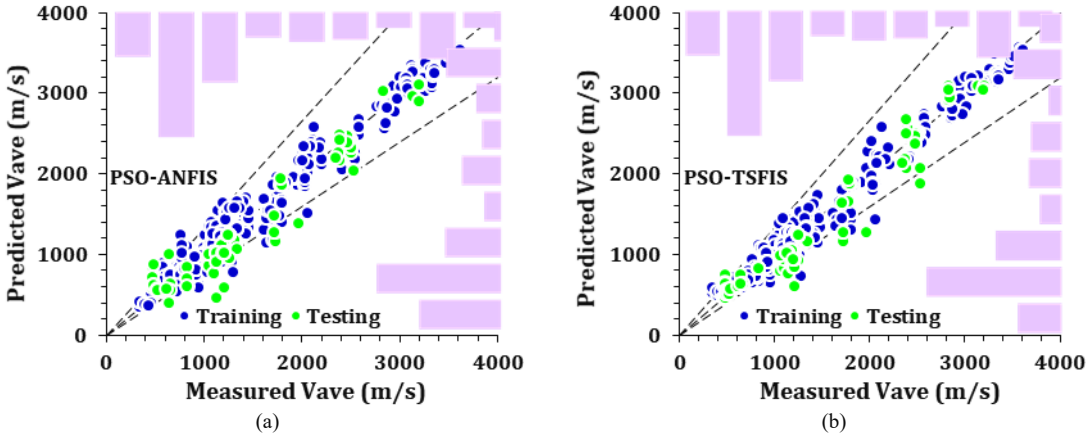
To prepare the numerical data for analysis, a process called scaling was used. This helps ensure that all data values are on a similar scale, especially when they differ in range or units. In this study, the StandardScaler method was used, which adjusts the data so each feature has a mean of 0 and a standard deviation of 1. This method helps to normalize the data and remove bias in the model. The scaled values included block and backfill details, wave velocity output, and sensor readings such as position, distance, velocity, and arrival times.

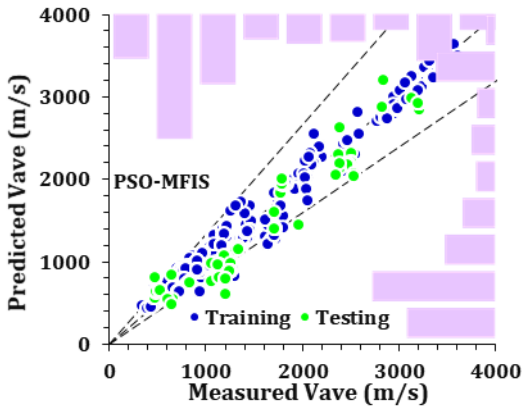
4 RESULTS AND DISCUSSION

This part of the paper presents the results from fuzzy-based learning models and explains how different evaluation methods were used to find the most accurate model for predicting seismic wave velocity. Several advanced fuzzy-based supervised learning models, combined with optimization techniques, were used to estimate seismic wave velocity (V_{ave}). These models include particle swarm optimization- Mamdani fuzzy inference system (PSO-MFIS), particle swarm optimization- Takagi Sugeno fuzzy inference system (PSO-TSFIS), and particle swarm optimization- adaptive neuro fuzzy inference system (PSO-ANFIS). Detailed descriptions of these models have been presented in the literature (Sugeno and Takagi 1983, Walia et al. 2015, Verma et al. 2019), so they are not repeated in this study. To train and test these optimized models, 85% of the total data (573 samples) was used for training, while the remaining 15% (102 samples) was used for testing. Figure 2 shows the relationship between the predicted values (from FIS models) and the actual measured values (from laboratory tests), along with their distribution histograms. The accuracy and performance of the models were measured using several error metrics, such as mean absolute deviation (MAD), normalized root mean square error (NRMSE), relative standard error (RSE), root mean squared logarithmic error (RMSLE), mean absolute percentage error (MAPE), relative absolute error (RAE), root relative squared error (RRSE), relative root mean square error (RRMSE), and the coefficient of determination (R^2). The results of these evaluations are listed in Table 2. While all the models performed well, the PSO-ANFIS model outperformed the rest in both training and testing.

Table 2. The results of loss functions and evaluation metrics for analyzing the outcomes of optimized fuzzy-based models in prediction.

Factors	PSO-MFIS	PSO-ANFIS	PSO-TSFIS
MAPE	0.0001	0.0001	0.0001
MAD	1.7752	1.6103	1.6003
RRMSE	0.2514	0.1142	0.1181
NRMSE	0.0026	0.0012	0.0019
RSE	0.0482	0.0015	0.0015
RRSE	0.2195	0.0385	0.0387
R^2	0.9640	0.9720	0.9780
RAE	0.1940	0.0974	0.2731
RMSLE	0.0431	0.0284	0.0389





(c)

Figure 2. The correlation between the results of optimized fuzzy-based models and findings from laboratory investigations.

To determine the most accurate model, a score ranking analysis was performed using the results from the different loss functions. Since multiple models and loss functions were used, the total number of scores considered was 27 (matrix 9 by 3). Figure 3 shows the results of the score ranking analysis. As seen from the ranking (from 1 to 3) based on each model's performance on the loss functions, the PSO-ANFIS had the highest overall score of 25, making it the top predictor network in this study. In contrast, the PSO-MFIS model ranked the lowest with a score of 10, showing lower accuracy than the other models.

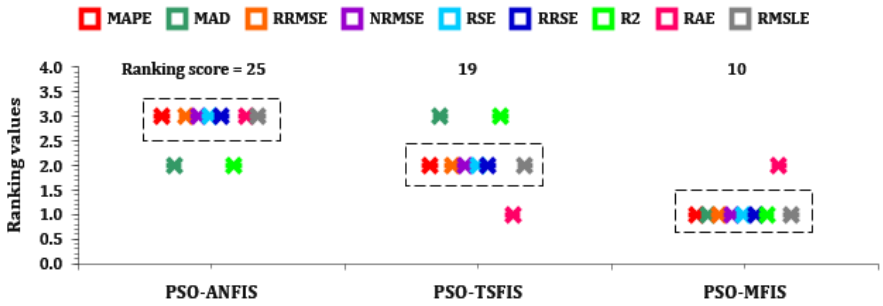
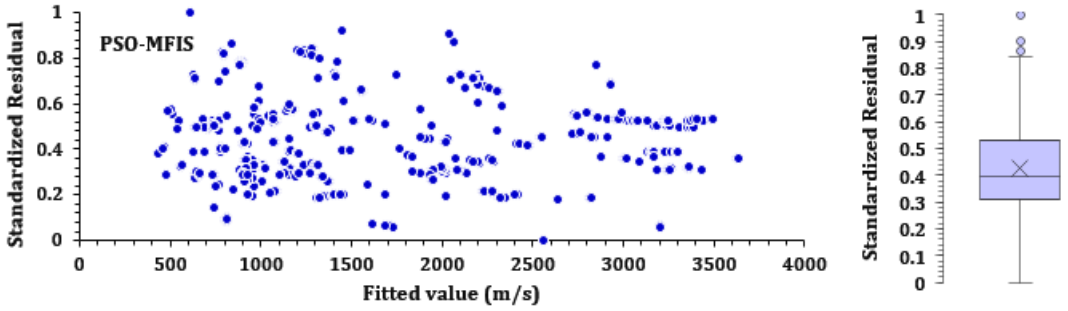


Figure 3. The ranking analysis for optimized fuzzy-based models based on the scores of evaluation metrics.



(a)

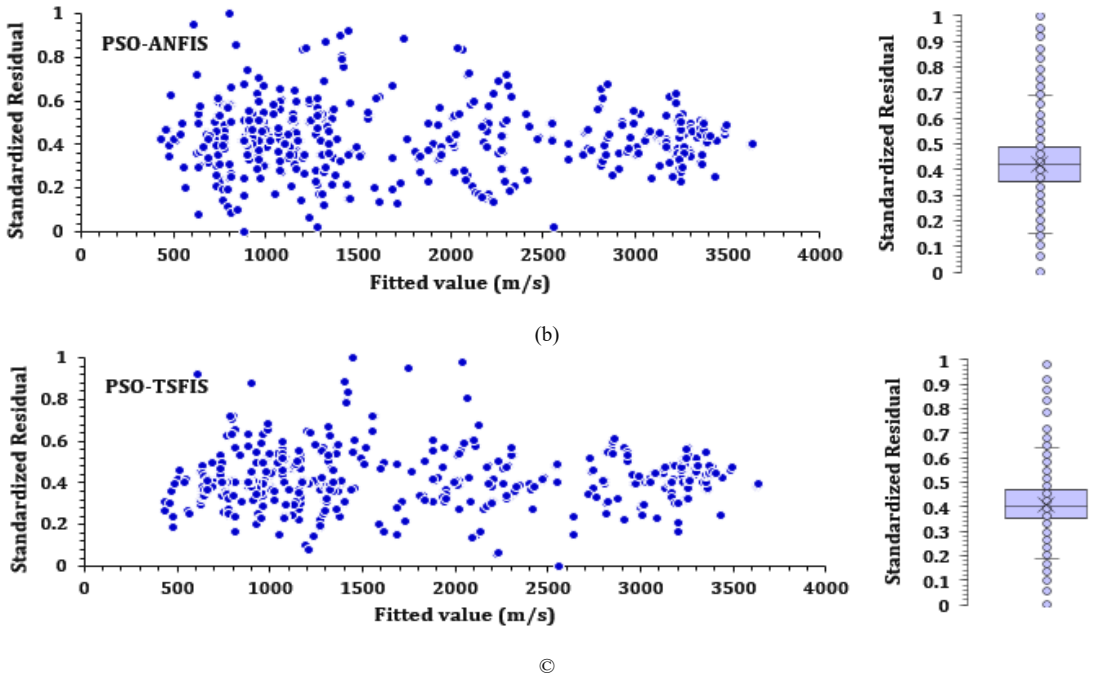


Figure 4. The residual plots for each optimized fuzzy-based model.

The residual plot was considered for evaluation to analyze the model behavior. Residual plots for each model are presented in Figure 4, which shows the acceptable behavior of models in prediction with a high accuracy rate. To better understand how each model performed during training and testing, relative error rates were calculated for each sub-dataset, comparing performance across a range of values. The results shown in Figure 5 indicate that all models had error rates within an acceptable range in both phases. This supports the models' accuracy and reliability in predicting V_{ave}, based on their structures, hyperparameters, data distribution, and chosen optimization method, which was PSO.

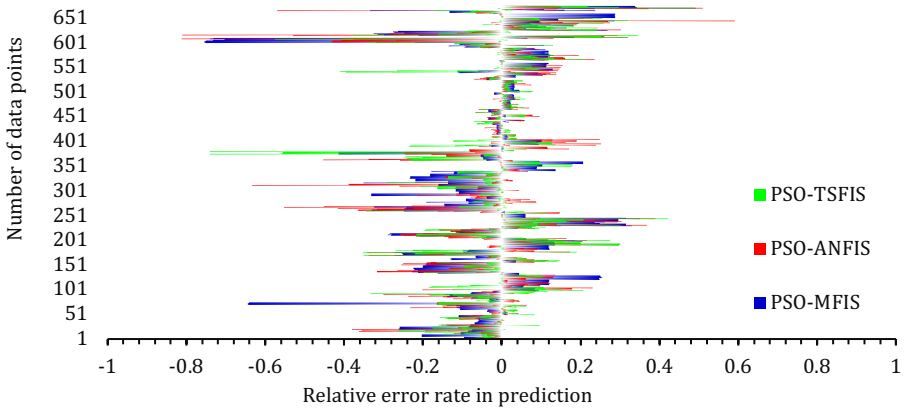


Figure 5. The calculated relative error rate in prediction for each optimized fuzzy-based model.

To compare the performance of models in predicting V_{ave} across different ranges, the predicted and actual values were divided into classes based on the range of V_{ave} values observed. V_{ave} ranged from 335.9 m/s (minimum) to 3206 m/s (maximum) and was divided into seven classes, each with a 500 m/s interval: Class I: 0–500 m/s, Class II: 500–1000 m/s, Class III: 1000–1500 m/s, Class IV: 1500–2000 m/s, Class V: 2000–2500 m/s, Class VI: 2500–3000 m/s, and Class VII: 3000–

3500 m/s. Each class included both measured and predicted values to cover the entire range in the dataset. Based on the laboratory results, the number of data points for each class is: Class I – 30, Class II – 232, Class III – 148, Class IV – 64, Class V – 56, Class VI – 50, and Class VII – 95. A confusion matrix plot (Figure 6) is used to visualize how well each model performed across these classes. The matrix shows that all models were accurate in terms of prediction within each class, with predicted values closely matching the actual ones. This shows that the models had strong prediction performance. The precision rates for each model were: PSO-ANFIS (94%), PSO-TSFIS (90%), and PSO-MFIS (88%).

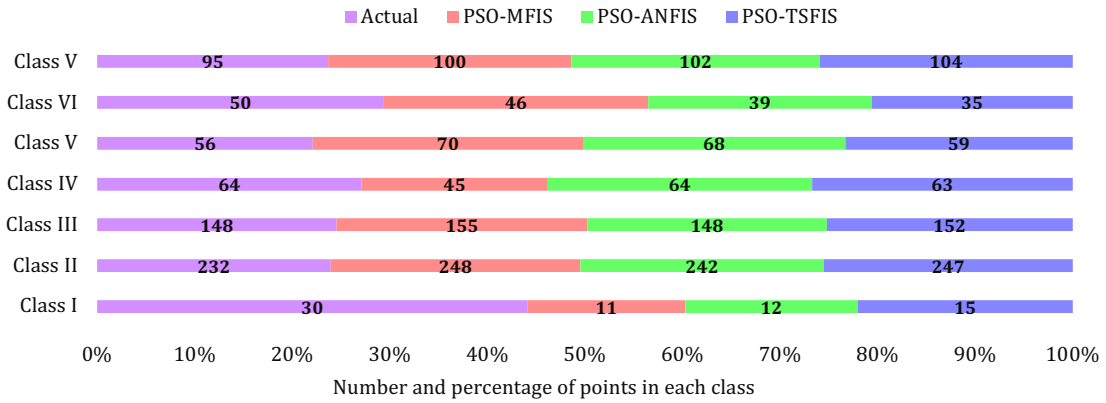
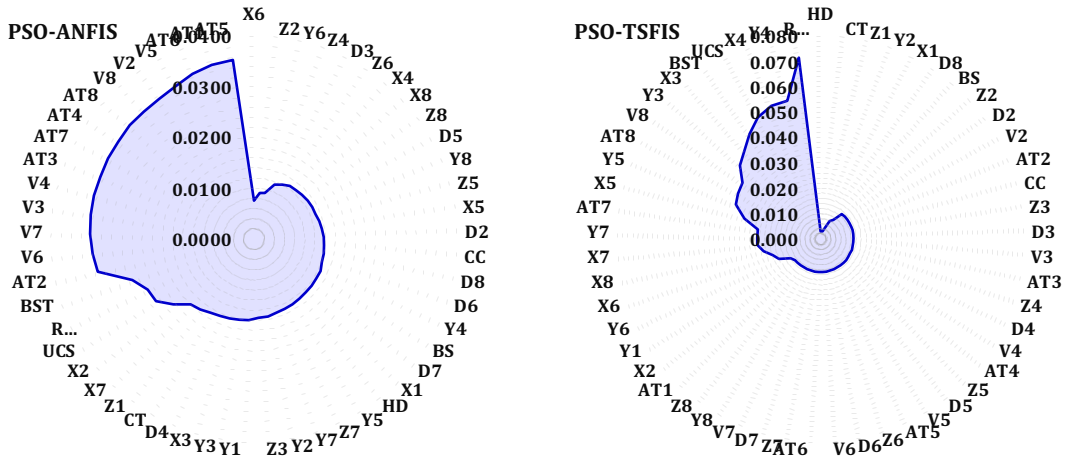
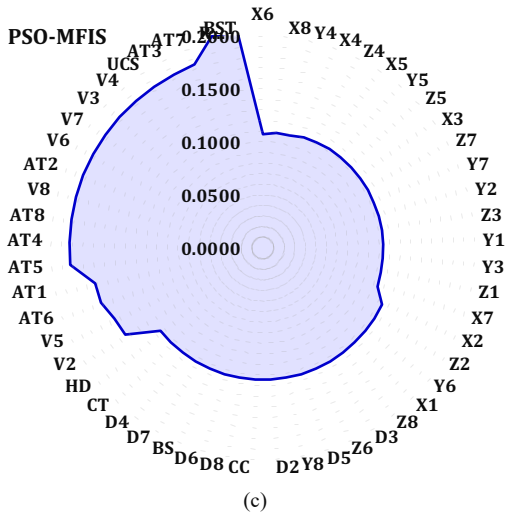


Figure 6. The evaluation of models for each class of V_{ave}- confusion matrix analysis.

To understand how each input factor affects the prediction of the target variable, a sensitivity analysis was done based on optimized fuzzy-based learning models. This analysis shows which inputs have a stronger or weaker effect on predicting V_{ave}. Input factors with higher importance values have more impact on the prediction results, while those with lower values influence the outcome less. Figure 7 presents the results of this sensitivity analysis. The outcomes show that all input factors from the detailed dataset, such as backfill quality, geomechanical features of blocks, block characteristics, location, distance from the source, and arrival time, contribute to predicting V_{ave}. Among them, geomechanical characteristics, backfill quality, and arrival time have a stronger impact. These findings clearly show that using a fixed or constant velocity model is not suitable for locating seismic sources in underground mining, where conditions in the ground change frequently. Instead, a real-time velocity model that adjusts based on current ground conditions is needed to improve the accuracy of seismic event source prediction.



(a) (b)



(c)

Figure 7. The sensitivity analysis based on the performance of optimized fuzzy-based models.

5 CONCLUSIONS

This study focuses on predicting seismic wave velocity under constantly changing ground conditions in underground mining, using laboratory-based simulations that mimic real mining environments. Conventional monitoring systems rely on static single-velocity models and numerical simulations, which are often inadequate due to ever-changing conditions in geomechanical properties, geological structures, and void geometries caused by mining activities. To address these limitations, an extensive laboratory dataset, including 675 samples and 54 features, was collected through well-designed laboratory experiments using acoustic emission techniques (AET) and the SAEU3H system, considering the ASTM C-109 C standard to mimic the real case of constantly changing mining conditions. Optimized fuzzy-based models were employed to predict the wave velocity based on the gathered database. The PSO-ANFIS model achieved the best performance with $R^2 = 0.972$, NRMSE = 0.0012, and MAPE = 0.0001. Feature importance analyses showed that geomechanical properties of blocks and backfills, location coordinates, and arrival time significantly influence seismic wave velocity prediction.

ACKNOWLEDGMENT

This work was supported by Nazarbayev University through the Faculty Development Competitive Grant No. 201223FD8835. Additional support was provided by the Nazarbayev University Collaborative Research Programme (CRP) in the data collection stage. The authors acknowledge the contributions of past undergraduate, graduate and post-graduate students, especially: Zarina Mukhamedyarova, Yerkezhan Modenova, and Kimie Suzuki Morales.

6 PREFERENCES

American Society for Testing and Materials (ASTM). 2013. Committee C-1 on Cement. Standard test method for compressive strength of hydraulic cement mortars (Using 2-in or [50-mm] Cube Specimens). ASTM International.

Bieniawski, Z.T. 1989. Engineering rock mass classifications: a complete manual for engineers and geologists in mining, civil, and petroleum engineering. John Wiley & Sons.

Collins, D.S., Pinnock, I., Toya, Y., Shumila, V. and Trifu, C.I. 2014. Seismic event location and source mechanism accounting for complex block geology and voids. In ARMA US Rock Mechanics/Geomechanics Symposium (pp. ARMA-2014). ARMA.

Czarny, R., Pilecki, Z., Nakata, N., Pilecka, E., Krawiec, K., Harba, P. and Barnaś, M. 2019. 3D S-wave velocity imaging of a subsurface disturbed by mining using ambient seismic noise. Engineering Geology, 251, pp.115-127. https://doi.org/10.1016/j.enggeo.2019.01.017

Czarny, R., Marcak, H., Nakata, N., Pilecki, Z. and Isakow, Z. 2016. Monitoring velocity changes caused by underground coal mining using seismic noise. Pure and Applied Geophysics, 173, pp.1907-1916. https://doi.org/10.1007/s00024-015-1234-3

Duan, Y., Shen, Y., Canbulat, I., Luo, X. and Si, G. 2021. Classification of clustered microseismic events in a coal mine using machine learning. Journal of Rock Mechanics and Geotechnical Engineering, 13(6), pp.1256-1273. https://doi.org/10.1016/j.jrmge.2021.09.002

Kebeasy, R.M. 2017. Seismicity. In The geology of Egypt (pp. 51-59). Routledge.

Maksut, Z., Meiramov, R., Yazici, A. and Suorineni, F. 2022. A Machine Learning-Based Microseismic Event Location and Wave Velocity Prediction. In ARMA US Rock Mechanics/Geomechanics Symposium (pp. ARMA-2022). ARMA. https://doi.org/10.56952/ARMA-2022-0166

Mukhamedyarova, Z., Suzuki Morales, K., Suorineni, F. and Madenova, Y. 2023. Numerical modeling of seismic wave propagation in mimicked underground mine models. In ARMA US Rock Mechanics/Geomechanics Symposium (pp. ARMA-2023). ARMA. https://doi.org/10.56952/ARMA-2023-0111

Olivier, G., Brenguier, F., Campillo, M., Roux, P., Shapiro, N.M. and Lynch, R. 2015. Investigation of coseismic and postseismic processes using in situ measurements of seismic velocity variations in an underground mine. Geophysical Research Letters, 42(21), pp.9261-9269. https://doi.org/10.1002/2015GL065975

Rebuli, D. 2024. Seismic response during a mining stoppage. In Deep Mining 2024: Proceedings of the 10th International Conference on Deep and High Stress Mining (pp. 1051-1062). Australian Centre for Geomechanics. https://doi.org/10.36487/ACGrepo/246567

Simser, B.P. 2019. Rockburst management in Canadian hard rock mines. Journal of Rock Mechanics and Geotechnical Engineering, 11(5), pp.1036-1043. https://doi.org/10.1016/j.jrmge.2019.07.005

Sugeno, M. and Takagi, T., 1983. Multi-dimensional fuzzy reasoning. Fuzzy sets and systems, 9(1-3), pp.313-325.

Trifu, C.I. and Suorineni, F.T. 2009, August. Use of microseismic monitoring for rockburst management at Vale Inco mines. In Proceedings of 7th International Symposium on Rockburst and Seismicity in Mines (RASIM7) (pp. 1105-1114).

Verma, N.K., Singh, V., Rajurkar, S. and Aqib, M. 2019. Fuzzy inference network with mamdani fuzzy inference system. In Computational Intelligence: Theories, Applications and Future Directions-Volume I: ICCI-2017 (pp. 375-388). Springer Singapore. https://doi.org/10.1007/978-981-13-1132-1_29

Wang, J.S. and Lee, C.G. 2002. Self-adaptive neuro-fuzzy inference systems for classification applications. IEEE Transactions on Fuzzy systems, 10(6), pp.790-802.

Wojtecki, Ł., Iwaszenko, S., Apel, D.B., Bukowska, M. and Makowka, J. 2022. Use of machine learning algorithms to assess the state of rockburst hazard in underground coal mine openings. Journal of Rock Mechanics and Geotechnical Engineering, 14(3), pp.703-713. https://doi.org/10.1016/j.jrmge.2021.10.011

THIS PAGE INTENTIONALLY LEFT BLANK

19th Australasian Tunnelling Conference – Acosta-Martínez, Stewart and Hudson-Smith (Eds.)
© 2025 Australian Tunnelling Society, ISBN 978-0-85825-002-4

Effects of in-situ principal stress magnitudes on unloading strength

A. Rooz & B. Sainsbury
School of Engineering, Deakin University, Waurn Ponds, Australia

ABSTRACT: Rock strength is a crucial parameter in underground excavation design, typically assessed under compressional (loading) conditions, termed here as loading strength. However, excavation redistributes in-situ stresses–particularly reducing the minor principal stress–resulting in unloading mechanical behaviour. In this excavation-induced stress regime, the geomechanical response of rock differs from its compressional response and can be referred to as its unloading strength (post-excavation strength). In-situ stress states naturally vary in principal stress magnitude ratios due to geological, structural, and tectonic factors. This study investigates the effect of these stress ratios on unloading strength and compares it to conventional loading strength. Laboratory tests on Adelaide black granite show that unloading strength is consistently lower than loading strength, with the reduction significantly influenced by in-situ principal stress ratios. An empirical relationship is proposed to characterise the unloading strength for the granite and unloading paths tested. The findings demonstrate the importance of incorporating unloading strength to capture softening behaviour in underground excavation design.

1 INTRODUCTION

The safety and stability of underground excavations depend greatly on mechanical properties of the host rock, particularly its strength. The rock mass strength response is strongly influenced by the pre-excavation in-situ stress state and the stress path it undergoes. This response differs significantly between loading (compressional stress path) and unloading (typical eventual excavation-induced stress path). Understanding in-situ stress conditions, typical excavation stress paths, and their influence on rock behaviour is essential for managing and maintaining stability in rock engineering applications (Guo et al. 2024). Typical loading and unloading stress paths are illustrated in Figure 1.

Rock mass near an excavation face will always experience a reduction in the minor principal in-situ stress (σ_3). In more complex cases, the major principal in-situ stress (σ_1) may simultaneously increase, or a series of unloading-loading (complex) combinations may occur.

The magnitude of in-situ stress is influenced by multiple factors, including depth, rock type (lithology), and plate tectonics. Brown & Hoek (1978) analysed 120 stress measurement data points to establish relationships between depth (z, in meter), the stress ratio (k , the ratio of horizontal to vertical stress), and vertical stress (σ_v). Subsequent studies, such as Hudson & Harrison (1997), have shown that localised structurally related stresses can significantly exceed those predicted by gravitational and tectonic components alone. Therefore, incorporating realistic and site-specific stress conditions into experimental design and testing is essential to obtain meaningful predictions of rock mass behaviour.

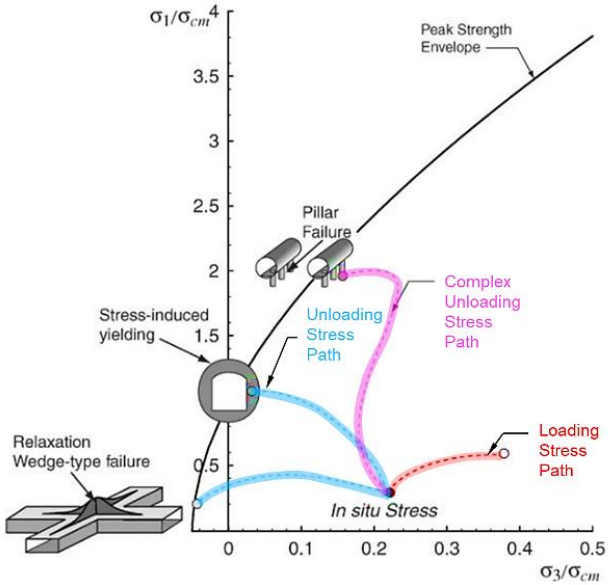


Figure 1. Generalised stress paths during underground excavation (modified after Martin et al. 2003).

In most conventional loading laboratory experiments (e.g., Uniaxial Compressive Strength (UCS) and Triaxial Compressive Strength (TCS) tests), specimens start in a stress-free state (zero confinement), with load applied solely in one direction until failure. In contrast, in-situ rock exists in a state of equilibrium under triaxial stress conditions. During excavation, at least one principal stress component decreases, meaning the stress path in conventional loading tests significantly differs from the actual conditions experienced by the rock. Unloading tests are therefore recommended to better replicate in-situ stress changes and provide more representative rock response data for design (Vervoort 2024).

This study investigates the strength response of Adelaide black granite (ABG) through a series of loading and unloading tests, comparing post-excavation rock strength with conventional compressive strength and evaluating the effect of in-situ principal stress magnitudes. A total of five specimens have been tested for UCS (loading) and nine for TCS (six loading and three unloading).

2 EXPERIMENTAL DESIGN

2.1 *Specimen Preparation and Testing Systems*

A total of 14 cores have been recovered from a slab of ABG and prepared by trimming and grinding both ends to produce standard cylindrical specimens with a diameter-to-height ratio of 1:2 (54 mm × 108 mm), ensuring parallel and perpendicular surfaces. Figure 2 shows the drilled slab and a prepared specimen ready for testing. Full details on sample preparation and characterisation of ABG can be found in Rooz & Sainsbury (2025).

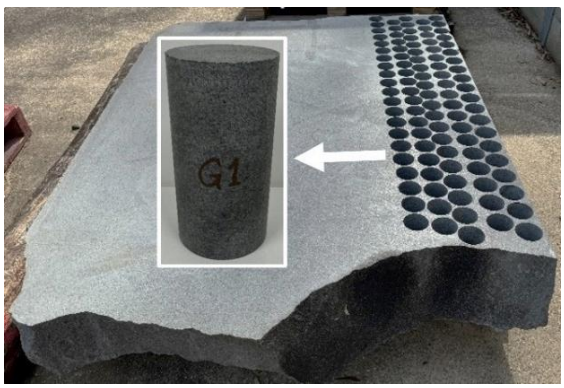


Figure 2. Slab of Adelaide black granite and a representative prepared specimen.

2.2 *Establishment of In-situ Principal Stress Magnitudes*

In lieu of site-specific stress measurements, in-situ stresses can be estimated using Figure 3a, which compiles geostress data from various regions worldwide, including Australia, Canada, USA, Southern Africa, Scandinavia, and others (Brown & Hoek 1978). From these data, a trend line yields the empirical Equation 1 for estimating vertical stress.

$$\sigma_v = 0.027\, z \quad (1)$$

Common excavation depths for underground tunnelling and mining projects range from a few hundred meters to approximately 1500 m, depending on geological conditions and project requirements. For this study, vertical stresses at three depths (z = 500, 1000, and 1500 m) have been considered, giving estimated σ_v values of 14, 28, and 42 MPa, respectively, using Equation 1.

The ratio of in-situ principal stress magnitudes (k-value) can be determined using Equation 2, where σ_h represents horizontal (or lateral) stress.

$$k = \frac{\sigma_h}{\sigma_v} \quad (2)$$

Figure 3b shows the geostress distribution in terms of the k-value. Due to the limitations of the laboratory triaxial system, k-values greater than 1 cannot be reproduced experimentally. As such, k-values of 1, 1/2, and 1/3–corresponding to underground points A, B, and C in Figure 3b–have been selected for testing.

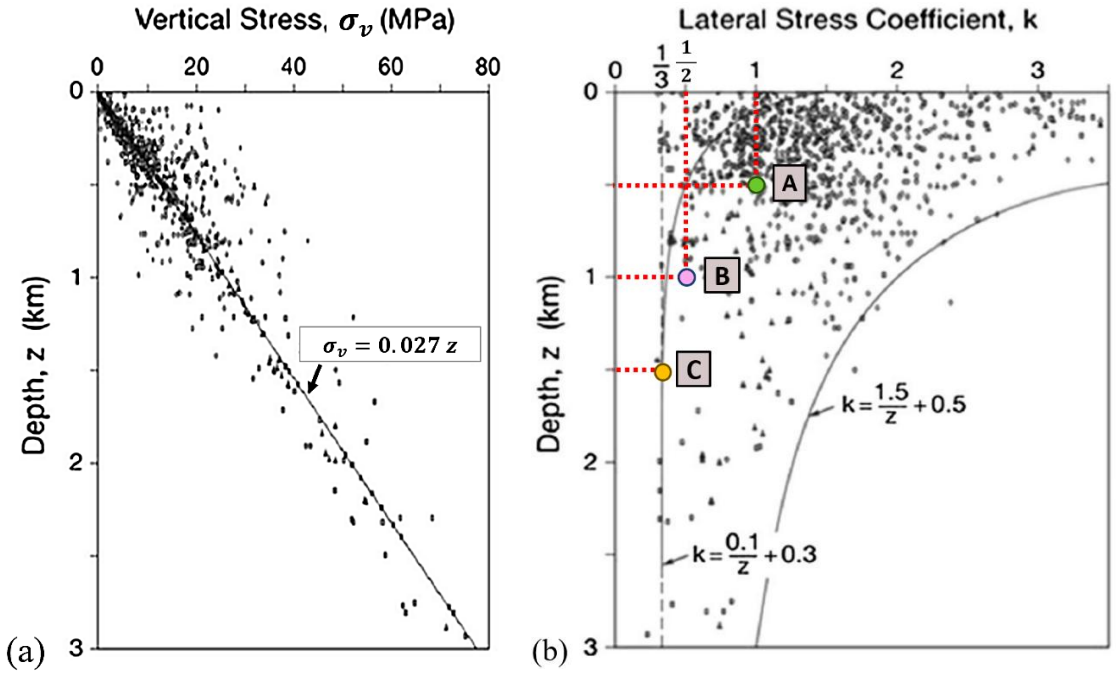


Figure 3. Distribution map of measured geostress data with depth variation: (a) Vertical stress magnitudes; (b) Lateral stress coefficient [modified after Brown & Hoek (1978)].

The horizontal stress has been estimated to be 14 MPa using Equation 2 and kept constant for all tests presented in this study.

2.3 *Testing stress paths*

To determine the conventional strength properties of ABG, two loading stress paths (L1 and L2) have been simulated in the laboratory, as illustrated in Figure 4a. Stress path L1 corresponds to unconfined and zero confining pressure (CP) conditions, while stress path L2 represents triaxial testing with a CP (σ_3) of 14 MPa.

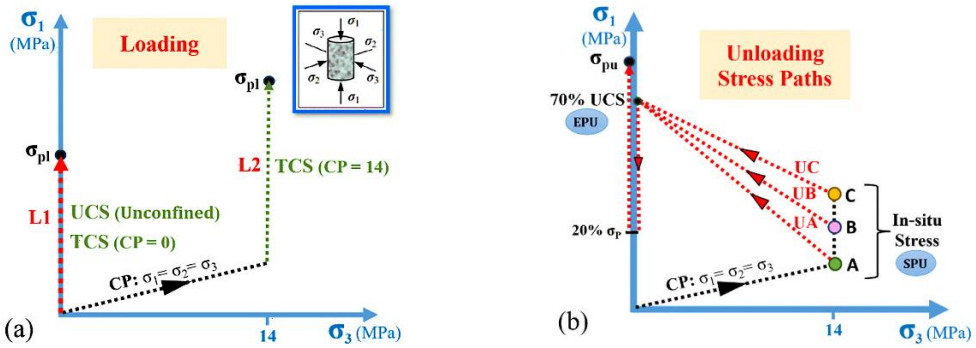


Figure 4. Testing stress paths: (a) Loading in UCS and TCS tests; (b) Unloading, representing excavation-induced stress at depths of A, B, and C.

As shown in Figure 4b, to determine unloading (post-excavation) strength, first the in-situ stresses at points A, B and C (Figure 3b) have been applied, representing the in-situ stress before excavation (pre-excavation stress state). This stress state is referred to as the Starting Point of Unloading (SPU). Once the SPU has been reached, the unloading stress paths of UA, UB or UC have been followed in the triaxial machine to simulate excavation. For each case, the sample reached the same Ending Point of Unloading (EPU) stress, corresponding to 70% of the UCS loading value. This 70% axial stress level has been chosen at the EPU in accordance with previous unloading studies on granite (Alejano et al. 2017, Duan et al. 2019) and represents a value that has exceeded the damage (crack) initiation threshold (Kaiser & Kim, 2015, Bewick 2021), at which spalling failure can be expected (Figure 6). Once zero CP conditions have been reached, the axial stress (σ_1) has been reduced to 20% of the loading strength, representing the lower limit of the elastic zone. Reloading has subsequently been applied until specimen failure to determine the unloading strength and stiffness response (post-excavation strength). Note the stiffness responses are not reported in this study. All tests have been conducted at a constant rate of 0.1 MPa/s.

3 STRENGTH RESULTS AND ANALYSIS

3.1 *Loading strength*

Table 1 presents the average peak loading strength (σ_{pl}) of five completed tests in UCS and three TCS tests conducted at CP = 0 MPa. The triaxial tests have been conducted at 0 MPa CP to confirm the accuracy of the machine and testing procedure, as well as to characterise the volumetric response, which is difficult to capture in a UCS test (Crouch 1970).

Table 1. Loading strength of Adelaide black granite specimens.

Test type	Samples Tested	σ_3 (MPa)	Average σ_{pl} (MPa)
Unconfined Compressive Strength	5	-	246.4
Triaxial Compressive Strength	3	0	244.3
	3	14	414.4

The average loading strength of three tests conducted under stress path L2 (σ_3=14 MPa) has been determined to be 414.4 MPa. The intact compressional response of ABG is represented in Figure 6 as the 'Intact Strength Envelope'.

3.2 *Unloading strength*

Unloading strength refers to the post-excavation strength. Table 2 summarizes the peak unloading strength (σ_{pu}) for each specimen tested. This value represents the stress required to fail the sample

after simulated stress unloading. The loading and unloading strengths are compared in Figure 5, with respect to k-values.

Table 2. Unloading strength of Adelaide black granite specimens at different in-situ principal stress ratios (k-values).

Simulated In-Situ Conditions (SPU)				Simulated Unloaded Conditions (EPU)			Measured σ_{pu} (MPa)
Representative depth (m)	k	σ_1 (MPa)	σ_3 (MPa)	Stress path	σ_1 (MPa)	σ_3 (MPa)	
500	1	14	14	UA	171	0	187.8
1000	1/2	28	14	UB	171	0	220.5
1500	1/3	42	14	UC	171	0	236.6

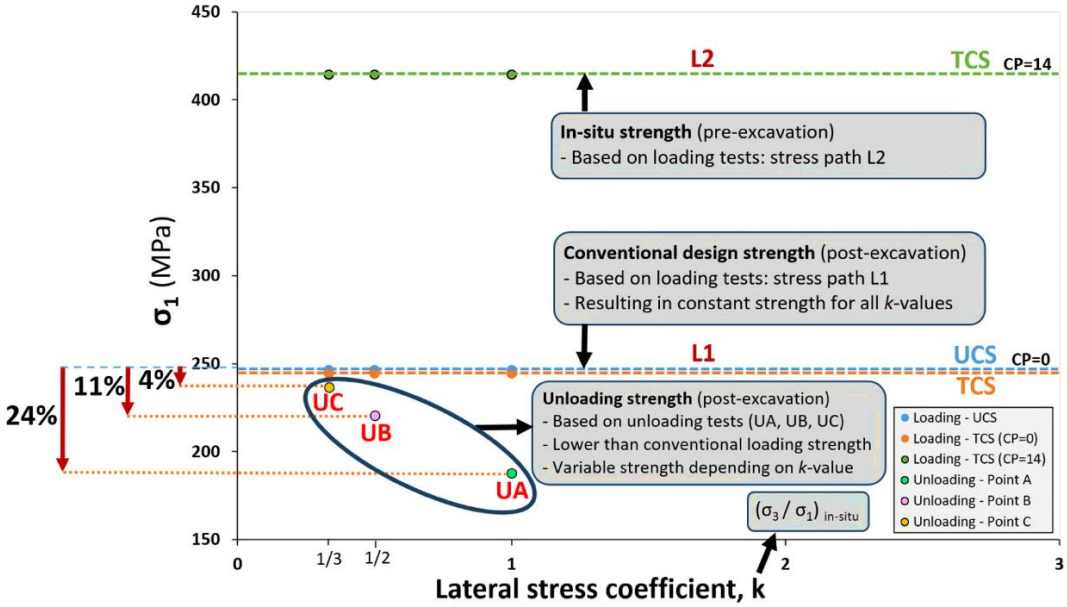


Figure 5. Comparison of loading strengths (points on L1 and L2 dashed lines) and unloading strength magnitudes (UA, UB, UC) of Adelaide black granite specimens at underground locations A, B, and C, with respect to in-situ principal stress ratios (k-values).

The strengths obtained from the unloading tests, shown in Figure 6, are presented with respect to the minor principal stress (σ_3) and compared against the loading strength for intact ABG rock. Their percentage change from their loading response is also presented.

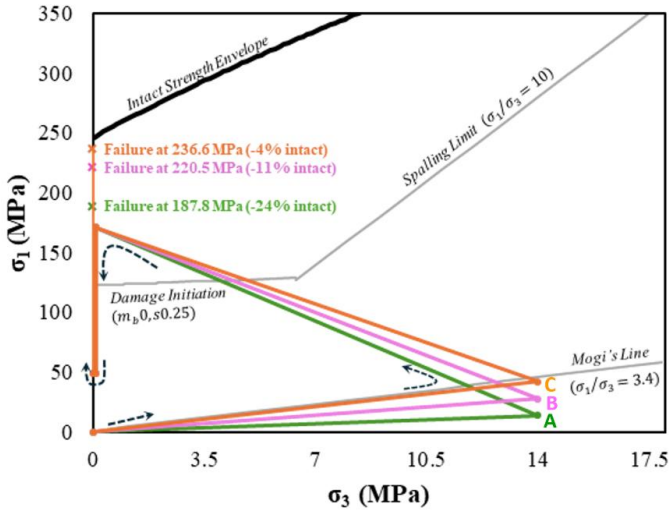


Figure 6. Comparison of unloading strength and loading strength magnitudes of Adelaide black granite specimens at underground locations A, B, and C, with respect to minor principal stress.

From the analysis, the following key conclusions can be drawn.

- All unloading strengths measured are lower than the loading strengths at zero CP. This result suggests that using the loading strength for design overestimates the rock's actual strength in-situ. In practical terms, damage induced on the rock during the unloading process must be considered in the design material strength. This is usually achieved via a strain-softening numerical approach (Rudnicki & Rice 1975).
- The degree of strength deterioration depends on the in-situ stress (pre-excavation) and the unloading stress path. For example, unloading from stress point A, where the principal in-situ stress ratio is greater (k = 1), resulted in significantly lower unloading strength (24% lower than the loading strength). Even unloading from stress point B led to a notable strength reduction (11%). This significant reduction can be attributed to the greater rate of change in σ_1 relative to σ_3 (i.e., the longer unloading path to reach the EPU). This phenomenon has been previously described by Board et al. (2001) related to seismicity.

Figure 7 presents unloading strength ($\sigma_{pu} = \sigma_{p\ (post\text{-}excavation)}$), expressed as a percentage of the loading strength ($\sigma_{pl} = UCS$). This figure relates the ratio of principal stress changes before and after unloading ($\Delta\sigma_1/\Delta\sigma_3$) to the degree of accumulated damage. The 'accumulated damage' (i.e. unloading damage) refers to the percentage reduction in strength from the intact condition (UCS) to the post-excavation condition. This reduction can be quantified using Equation 3:

$$Unloading\ damage\ (\%) = \left(1 - \frac{\sigma_{p\ (post-excavation)}}{UCS}\right) \times 100 \quad (3)$$

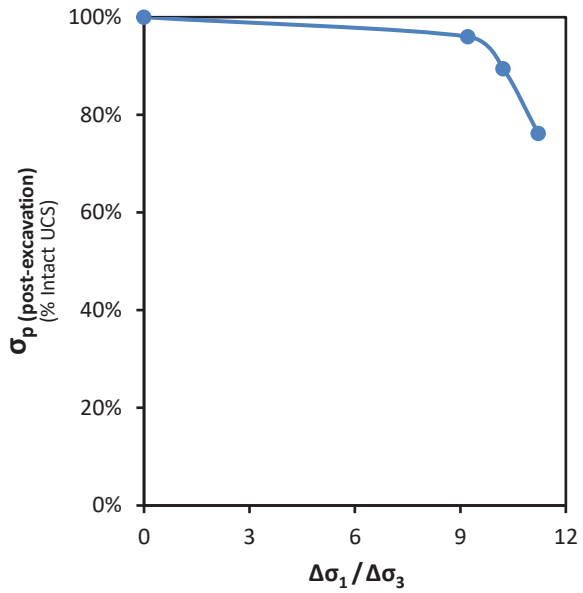


Figure 7. Relationship between changes in principal stress magnitudes from in-situ to final (post-excavation) states ($\delta\sigma_1/\delta\sigma_3$) and post-excavation strength, illustrating accumulated damage.

A relationship can be established to describe the post-excavation design strength (σ_p) in MPa for the stress paths simulated in the ABG, as presented in Equation 4.

$$\sigma_{p\ (post-excavation)} = \frac{UCS}{100}\left[-0.0025\ .\ e^{\left(0.8196 \times \frac{\Delta\sigma_1}{\Delta\sigma_3}\right)} + 100\right] \quad (4)$$

Where *UCS* is measured by the conventional approach (in MPa). $\Delta\sigma_1$ and $\Delta\sigma_3$ represent the differences in principal stresses between EPU ($\sigma_1 = 70\%\ \sigma_p$, $\sigma_3 = 0$) and SPU (in-situ stresses). In the conducted unloading tests, $\sigma_1$increased from 14 (or 28 or 42) to 171 MPa, while σ_3 decreased from 14 to 0 MPa. The values in Equation 4 are adjusted based on Figure 7 to account for percentage damage.

This equation enables estimation of post-excavation (design) strength using only conventional UCS value, without the need to perform unloading tests. However, it has been derived exclusively for ABG and should not be applied to other rock types without further validation.

4 DISCUSSION

Through the application of Equation 3, the problem with conventional techniques used to estimate strength damage in a rock sample are resolved. For instance, the designer no longer needs to estimate plastic strain (Martin & Chandler 1994), complete complex laboratory testing (Guo et al. 2025), or conduct complex simulations (Hajiabdolmajid et al. 2002) in order to quantify the post-excavation strength that should be applied in the design solution. Instead, the strength can be directly estimated based on the UCS and change in in-situ principal stress magnitudes and then applied in analytical design solutions.

However, these outcomes are generalised for Adeliade black granite (a strong and brittle rock) and under a specific loading and unloading stress path. The results should be further explored for a wider range of rock types (sedimentary, metamorphic, and igneous) with varying *UCS* values. Additionally, investigations should consider different stress conditions (in-situ: σ_1 and σ_3), k-value, intact unconfined modulus (E_i), intact confined modulus (E_{ic}), or the modulus ratio ($MR = E_i/UCS$). Future studies should examine the effects of different stress paths (pure unloading only or loading-unloading combinations), unloading rates and anisotropy. A generalized empirical formula incorporating these factors could enhance the characterisation of intact rock softening behaviour under unloading stress conditions.

5 CONCLUSIONS

In underground excavation design, rock strength is a key parameter that engineers rely on. This study investigates rock strength, commonly obtained from UCS test, and compares it with unloading tests that account for excavation effects. For this purpose, Adelaide black granite specimens have been provided and prepared for testing.

The results show that unloading strength is persistently lower than loading strength, particularly at locations with lower major principal in-situ stress magnitudes (or higher k-value). For instance, at point A, representing 500 meters underground, the unloading strength was significantly reduced by 24%. The importance of conducting unloading tests lies in their ability to incorporate in-situ stress conditions, considering factors such as depth, principal in-situ stress ratio, and unloading stress–factors that are often overlooked in conventional loading tests, including UCS (unconfined) and TCS (confined with zero CP).

Although loading tests are significantly simpler and faster approach than unloading tests, they tend to overestimate rock strength after excavation and provide a single strength value for varying underground conditions. Real-world excavation sites may exhibit different in-situ stress conditions (e.g., points A, B, and C). Relying solely on loading strength assumes uniform conditions, which may not accurately represent the actual stress distribution. Unlike conventional loading tests, which do not account for excavation-induced stress changes, unloading tests simulate more realistic stress conditions encountered in underground excavations.

By incorporating triaxial in-situ stress conditions and excavation-induced stress paths, unloading tests provide a more accurate assessment of rock behaviour under actual geological conditions. Therefore, considering unloading effects is crucial for excavation design, underground support, and financial planning in engineering projects.

6 REFERENCES

Alejano, L.R., Arzúa, J., Bozorgzadeh, N. & Harrison, J.P. 2017. Triaxial strength and deformability of intact and increasingly jointed granite samples. *International Journal of Rock Mechanics and Mining Sciences* 95: 87–103.

Bewick, R.P. 2021. The Strength of massive to moderately jointed rock and its application to cave mining. *Rock Mechanics and Rock Engineering* 54(8): 3629–61.

Board, M., Brummer, R. & Seldon, S. 2001. Use of numerical modelling for mine design and evaluation. *Underground Mining Methods: Engineering Fundamentals and International Case Studies; Society for Mining, Metallurgy and Exploration*, Littleton, Colorado, USA, 483–92.

Brown, E.T. & Hoek, E. 1978. Trends in relationships between measured in-situ stresses and depth. *International Journal of Rock Mechanics and Mining Sciences & Geomechanics Abstracts* 15(4) 211–5.

Crouch, S.L. 1970. Experimental determination of volumetric strains in failed rock. *International Journal of Rock Mechanics and Mining Sciences & Geomechanics Abstracts* 7(6): 589–603.
Duan, K., Ji, Y., Wu, W. & Kwok, C.Y. 2019. Unloading-induced failure of brittle rock and implications for excavation-induced strain burst. *Tunnelling and Underground Space Technology* 84: 495–506.
Guo, J., Ma, L., Liu, Z. & Wang, S. 2024. The influence of mining stress paths on rock damage and permeability. *Environmental Earth Sciences* 83(10): Article No. 307.
Guo, S., Qi, S., Zhang, S., Waqar, M.F., Xiong, F., Liang, N., Zheng, B., Ma, X. & Tang, F. 2025. A two-parameter damage-controlled strength model to predict the fracturing of brittle rock mass at great depth. *Case Studies in Construction Materials* 23: Article No. e05028.
Hajiabdolmajid, V., Kaiser, P.K. & Martin, C.D. 2002. Modelling brittle failure of rock. *International Journal of Rock Mechanics and Mining Sciences* 39(6):731-41.
Hudson, J.A. & Harrison, J.P. 1997. *Engineering Rock mechanics An Introduction to the Principles*. Elsevier Science.
Kaiser, P.K. & Kim, B.H. 2015. Characterization of strength of intact brittle rock considering confinement-dependent failure processes. *Rock Mechanics and Rock Engineering* 48(1): 107–19.
Martin, C.D. & Chandler, N.A. 1994. The progressive fracture of Lac du Bonnet granite. *International Journal of Rock Mechanics and Mining Sciences & Geomechanics Abstracts* 31(6): 643–59.
Martin, C.D., Kaiser, P.K. & Christiansson, R. 2003. Stress, instability and design of underground excavations. *International Journal of Rock Mechanics and Mining Sciences* 40(7–8): 1027–47.
Rooz, A.F.H. & Sainsbury, B.A. 2025. Adelaide black granite: geomechanical characterisation for underground design. *Australian Journal of Earth Sciences* 72(2): 233–51.
Rudnicki, J.W. & Rice, J.R. 1975. Conditions for the localization of deformation in pressure-sensitive dilatant materials. *Journal of the Mechanics and Physics of Solids* 23(6): 371–94.
Vervoort, A. 2024. In situ stress paths applied in rock strength characterisation result in a more correct and sustainable design. *Sustainability* 16(11): Article No. 4711.

Theme 6. Shafts and Cut and Cover

THIS PAGE INTENTIONALLY LEFT BLANK

19th Australasian Tunnelling Conference – Acosta-Martínez, Stewart and Hudson-Smith (Eds.)
© 2025 Australian Tunnelling Society, ISBN 978-0-85825-002-4

Optimized operational and structural solution for a TBM service shaft – Design and construction

L. Facibeni & G. Turinetti
ARX (PINI Australia Pty Ltd), Sydney, Australia

V. Besharat
HATCH, Melbourne, Australia

L. Yogasuthan
CPB Contractors and Ghella Joint Venture (CPBGJV), Sydney, Australia

ABSTRACT: The Sydney Metro - Western Sydney Airport project incorporated a Tunnel Boring Machine (TBM) Service Shaft approximately 100 m beyond the Airport Terminal Station. The construction of a large elliptical shaft presented several unique challenges. The initial concept for structural solutions was a rectangular shaft supported by soldier piles and ground anchors. The 26 m deep excavation underwent several engineering design stages aimed to optimize the solution while accommodating the operational space required by the Station Box and Tunnelling (SBT) contractor. The final engineering solution adopted included a self-supporting elliptical shape shaft retained by secant piles. The successful implementation of innovative design resulted in a large strut-free shaft that provided an ideal clear space the smooth operation of two double shield TBMs. This shaft enabled early handover of the excavated station box to the permanent structure contractor and facilitated supply delivery and spoil extraction for the remaining 4.1-kilometer south tunnels excavation.

1 INTRODUCTION

The Sydney Metro - Western Sydney Airport (SM-WSA) is a new 23 km metro line currently under construction. The project is jointly funded by the Commonwealth and NSW Governments and will form the spine for the Greater Western Sydney. The new metro line will commence services from St Marys Station and will travel south through Orchard Hills, Luddenham, connecting to Airport Business Park and Western Sydney (Nancy-Bird Walton) International Airport (WSI) and ends at the new city of Bradfield. Along this alignment, it comprises of twin tunnels, travelling north and south for a total of 9.8 km and a central section at grade including viaducts, bridges and open-cut troughs.

In line with the procurement model adopted for the construction of the SM-WSA the scope was split between two contracts, namely:

- SM-WSA – Station Boxes and Tunnels (SBT) - tasked with design and construction of two sections of twin tunnels from St Marys to Orchard Hills for the North drive and from Airport Business Park Dive structure, underneath the new International Airport, to Aerotropolis for the South drive, the associated dive and portal structures and cross passages and the temporary support and excavation for the four underground stations at St Marys, Orchard Hills, Airport Terminal and Aerotropolis, two intermediate service facility shafts and one TBM service shaft near Airport Terminal station.
- SM-WSA - Stations, Systems, Trains, Operations and Maintenance (SSTOM) which follow on the construction of the permanent station structures the tracks and system along the entire length of the SM-WSA line.

Following a tender process held between April and August 2021, Sydney Metro appointed CPB Contractors and Ghella Joint Venture (CPBG JV) for the design and build of the SBT contract in

December 2021. Detail Design stage commenced in January 2022 and was completed in February 2023 while construction of SBT started in June 2023 and was completed in December 2024.

1.1 *TBM Service Shaft*

The TBM temporary Service Shaft is located 100 m past the Airport Terminal Station to enable an early handover of the excavated station box by the SBT contractor to the SSTOM contractor in charge of the station permanent structures contract and provide a convenient supply and spoils extraction point for the excavation of the remaining 4.1km of the South Tunnels drives. Upon completion of the South tunnel drives and cross passages, the TBM Service Shaft was going to be handed over to SSTOM contractor to build the cross passage permanent structure and backfilling. To this aim, a Design Life was 10 years was required in the project Particular Specification.

Ground conditions at site below the site establishment level around RL 84.5 m comprised of 3 to 4 m of General Fill (Geotechnical Unit S1) overlying 1.5 to 3 m of Residual Clay (S3) and the Bringelly Shale bedrock which was differentiated in extremely and highly weathered Shale V/IV (R1) 1-1.5 m thick, moderately weathered Shale III (R2) from approx. RL 77 m with a thickness varying between 4 and 10 m and slight weathered and fresh Shale II/I (R3) to the Final Excavation Level at approx. RL 58 m. The SLS design groundwater level was RL 78.0 m, approximately at the top of R1 unit.

The Bringelly Shale Formation is a sedimentary rock extensively outcropping in the western part of the Sydney sedimentary basin largely comprising claystone, siltstone with localized layers of higher strength sandstone, typically up to metric thickness. Bedding is typical sub-horizontal with four sets of joints, mainly with dip angle 50-60° and strike ENE-WSW and NNW-SSE. Similarly to the rest of the Sydney basin rocks, the Bringelly Shale has an in-situ horizontal stress higher than the vertical stress: the GIR recommended a major horizontal in-situ stress in the range $(0.3 + 1.3s_v)$ to $(1.1 + 1.3s_v)$ for Shale II/I (R1) and equal to the vertical stress for Shale III (R2).

Table 1. Design parameters for Bringelly Shale Formation rock mass.

Geotechnical Parameters	Unit R3		Unit R2	Unit R1	
	SH-I	SH-II	SH-III	SH-IV	SH-V
Point Load I_{50a} (MPa)	2.2 (1.4 – 3.3)	0.66 (0.5 – 1.2)	0.44 (0.3 – 0.8)	0.2 (0.1 – 0.2)	0.15 (0.06 – 0.17)
UCS (MPa)	20	14	7.1	2.9	1
Poisson's ratio, n		0.25		0.3	
Intact rock Modulus, E (MPa)	5,000	3,500	1,500	510	250
Unit weight, g (kN/m^3)			24		
m_i			8		
GSI	60	60	55	35	25
Rock Mass Modulus, E_m (MPa)	2,600	1,400	500	200	100

Critically for the project, Bringelly Shale was recognized to exhibit swelling potential due to the presence of swelling clay minerals. Testing conducted in 2005 by Williams suggested a rapid swelling process completed in a matter of few weeks whereas in the dedicated testing conducted for the WSA SBT samples were still swelling after a few months. The swelling testing program was fundamental to enable a swelling characterization for use in the UDSM – Swelling Rock model available in the commercial software Plaxis 2D.

1.2 *Reference Design*

The Sydney Metro Reference Design included a 25 m long, 20 m wide rectangular shaft 26 m deep supported by soldier piles 900 mm diameter and restrained by four rows of ground anchors as shown in Figure 1 below. The documentation provided as part of the Reference Design indicated an initial optimization implemented by the owner's Engineer. The TBM Service Shaft was in fact initially located just 20 m past the West headwall of the Airport Terminal Station where it was already serving the purposes indicated above but in the later states of Reference Design was moved to the location of Cross Passage XP-S06, approximately 100 m from the station headwall, so to realize savings in the excavation of one cross passage.

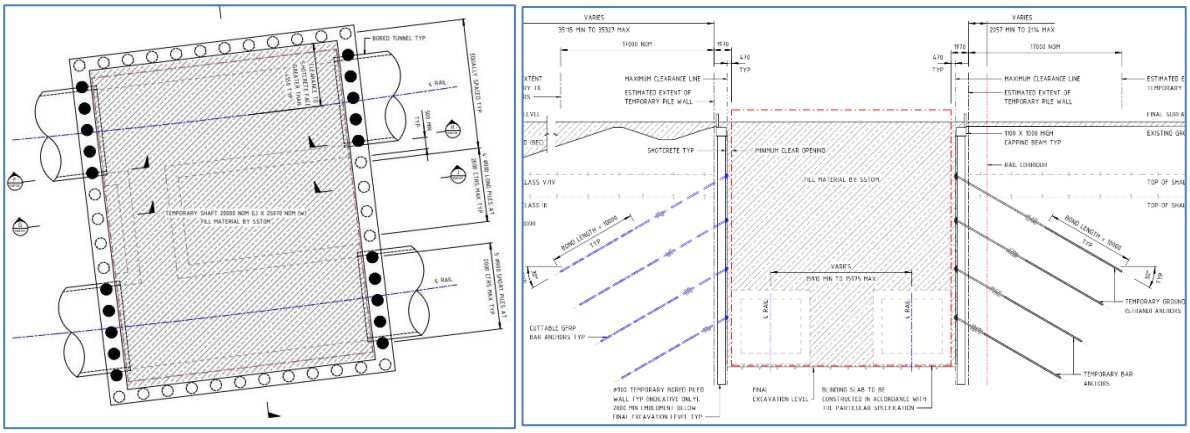


Figure 1. TBM Service Shaft - Reference Design plan and cross section

2 VALUE ENGINEERING

2.1 *Operational requirements driving Tender Design*

Early on during the Tender Design, CPBG JV had already clear ideas on the methodology to extract the material excavated by the two EPB TBMs boring the South drives using an inclined conveyor belt rather than a vertical one. The operational requirements set to the designers included a longitudinal dimension of 48.8 m and an opening in the retaining structure for the inclined conveyor belt 6 m high and 4 m wide immediately below the capping beam.

The required increase in length, doubling up the one in Reference Design, provided a double challenge for the designer: to excavate a larger shaft but reduce the time required for its excavation and support. It appeared clear that this would require to adopt a more structurally efficient curved shape self-supporting retaining structure for the TBM Service Shaft. Early consideration was given to two interlocking shafts – one with diameter of 32 m to encompass the Minimum Clear Opening (MCO) and the second smaller one to achieve the required 48.8 m length. However, this solution required the excavation of unnecessary volume of rock and provided an operational space with the constraint of the limited width and presence of concrete struts at the intersection between the two shafts.

The second idea was to fit an elliptical shaft to encompass the MCO and have the maximum major axis of the required operational length. A suitable ellipse geometry was determined with a major axis measuring 48.8 m and a minor axis of 27.8 m: the resulting eccentricity of 0.80 was still adequate for the hoop force to run all around the elliptical shape as other example in the literature indicated. This configuration allowed for a clear operational space inside the excavation facilitating the construction activities and it was adopted and a concept developed as part of the Tender Design activity.

The shaft structure consisted of a secant pile wall with 900 mm diameter piles, alternated hard-firm, spaced at 600 mm centres, extending to 5 m below the final excavation level. This solution provided a continuous wall with continuity of structural concrete and worked on the principle of arch structure to mostly transfer the external horizontal loads on the wall into axial (hoop) force in the retaining structure. The piled wall was surmounted by a capping beam 1.0 m deep x 2.0 m wide and fitted the 6.0 m by 4.0 m opening at the major axis on the side of TBM relaunch to allow for the passage of the inclined conveyor belt for the removal of the spoil coming from the excavation. For the areas where the TBM break in/out, the design included four concrete wedges - so to provide a planar surface for the machine to restart excavation.

The shaft was designed to remain largely undrained during construction, with drainage limited to that occurring through the base slab: the piled wall was therefore dimensioned to carry both rock and groundwater pressure.

Overall, the changes made at the tender stage reflected a practical response to site constraints, while also considering construction sequencing and TBM requirements.

2.2 *Options considered during Detail Design*

As part of the Detailed Design process, several value engineering options were developed to improve and refine the original tender design. These alternatives were driven by a need to improve constructability, optimize costs, and better align the design with the contractor's planned construction methodology and schedule and included:

- Terminate piles at 14 m below ground level to reach a minimum pile embedment into the Shale III (R2 geotechnical unit). The lower portion of the excavation in R2 and R1 would be now drained supported with conventional rock bolts and shotcrete.
- TBM break-in with short stub tunnels mined in advance and designed to match the TBM space-proofing requirements. This solution increased the operational space at FEL and eliminated the need for a thrust frame for the TBM re-launching operations. However, it also required additional excavation and tunnel lining, which needed to be weighed against the expected time and cost savings.
- Reduced excavated material by leaving unexcavated rock wedges at both TBM break-in and out simplifying the construction process and reducing excavated quantities.

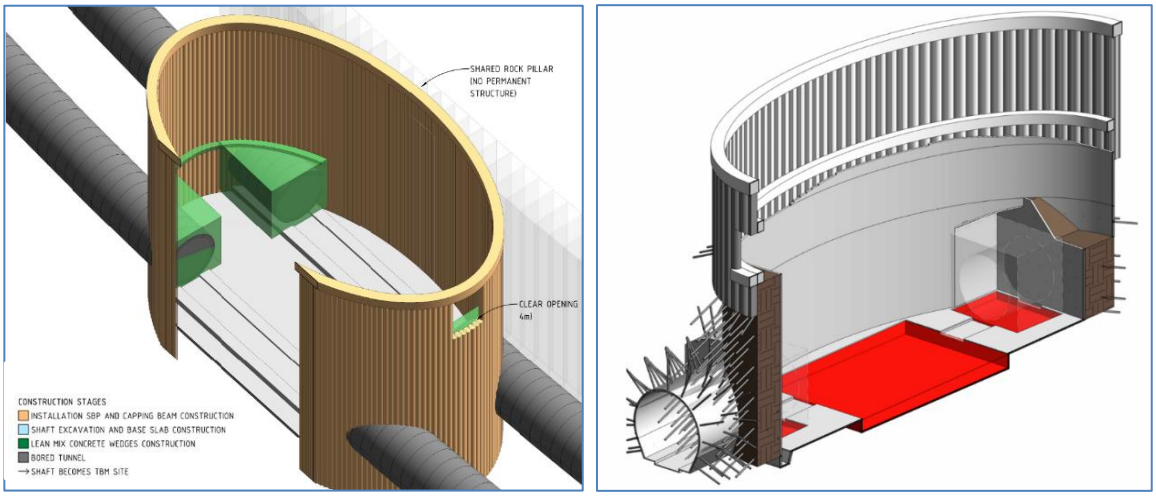


Figure 2. TBM Service Shaft - Tender design 3D view (left) and Detail Design solution (right)

2.3 *Detail Design solution*

The detailed design incorporated most of the value engineering options proposed during the value engineering and brought them even further. The resulting final solution, shown in Figure 2, featured secant piles extending 12 m below ground following the top R2 horizon, and a 1.2 x 1.2 m capping beam. The location of the opening for the TBM conveyor belt was revised and set at 8 m below ground level and required a deep trench to be excavated behind the opening for the conveyor to raise up to ground level. The lower part of the excavation was supported with rock bolts arranged in a 2 x 2 m pattern and 200 mm of shotcrete. The interface with the bored tunnels was revised adopting the two unexcavated rock wedges at the tunnel interface and two 9 m long stub tunnels at the TBM re-launch side, along with four niches on the shaft side wall to facilitate the TBM traverse and the casting of the final lining within the stub.

The detailed design also included a ring beam at RL 75 m to mitigate the risk of pile misalignment reducing the contact area between adjacent piles as well as rock bolts at the toe of the piles to ensure stability of the rock wedge below the toe.

3 DETAIL DESIGN CHALLENGES

The design process incorporated both geotechnical and structural finite element modelling (FEM), alongside UnWedge analyses, to address key challenges. Multiple Plaxis 3D and RS2 models were developed to ensure comprehensive coverage of all design aspects and risks.

3.1 *Axisymmetric Models with Non-axisymmetric Assumptions*

One of the challenges in the design process was the non-axisymmetric nature of various factors, including ground conditions (stratigraphy) across the site, structural openings (for the conveyor), and surface loading patterns (such as crane loads and TBM segment depot). Two main Plaxis 3D models which are illustrated in

Figure 3 were developed cutting along both major and minor axis of the ellipse to ensure that the structural integrity and stability of the openings were thoroughly analysed with the proposed asymmetric surcharge loading patterns, including crane loads and the TBM segment storage. To validate these models, a full model was later developed, and its results were compared with those from the initial stages.

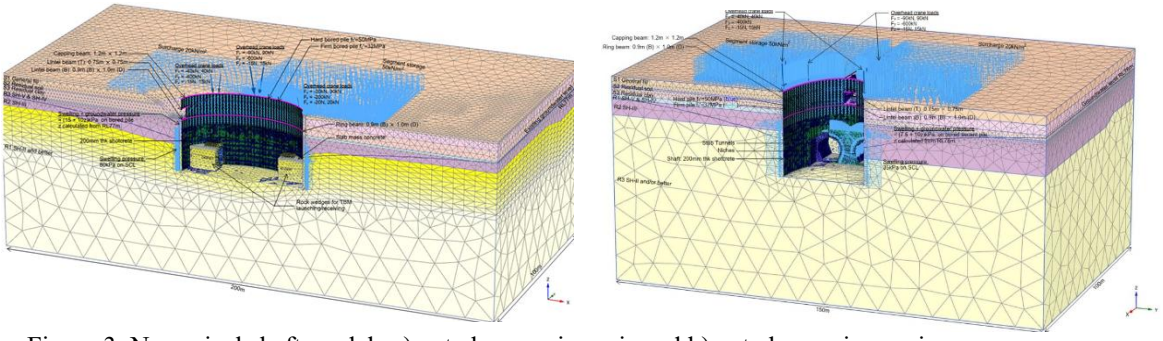


Figure 3. Numerical shaft models a) cut along major axis and b) cut along minor axis

3.2 *Hoop Load Transfer Between Hard and Firm Piles*

Competing requirements of ease of redrilling for the secondary piles and adequate concrete strength to carry the hoop force, resulted in adopting alternate hard (50 MPa) and firm (25 MPa) secant CFA piles. From modelling perspective, each individual pile was modelled as a plate with its own material properties to ensure that all critical interactions between piles were adequately captured, hence each plate was also given an "equivalent thickness" to achieve a realistic axial stiffness. For flexural characteristics, hard and firm piles would experience varying degrees of cracking depending on the design actions experienced which would result in a range of reduced stiffness from the nominal value. In line with the recommendation of Zdravković et al. (2005), the secant piled wall was modelled as anisotropic with reduced axial and bending stiffness of the structural elements in the horizontal direction. Figure 4 (a) and (b) below shows how the plate elements used to model hard pile and firm piles.

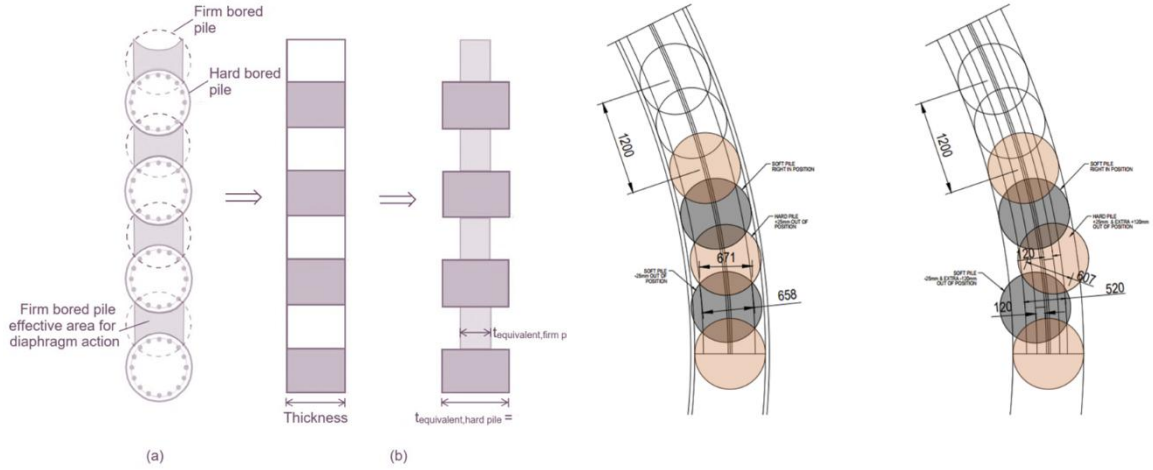


Figure 4. Secant pile wall: (a) as to be constructed; (b) modelled as rectangular slots as plate, (c) nominal pile position and (d) maximum allowed construction tolerance.

3.3 *Construction Tolerances consideration*

Pile construction tolerance of 25 mm position tolerance and 1 in 100 verticality tolerance were stipulated in the design. To account for these construction tolerances, the equivalent thickness for the firm pile elements was adjusted to reflect a further reduction in the width of the connecting section (or "throat") between firm and hard piles. This reduced width, set below the minimum geometric value of 520 mm, resulted in lower axial stiffness for the firm piles and consequently shifts more of the structural load onto the hard piles, which are designed to carry the greater share of demand and was the pinch-point of structural verification. The secant pile position configuration and the allowable construction tolerance is presented in Figure 4 (c) and (d).

3.4 *Composite Beam Behaviour and Flexural Stiffness Adjustments*

In PLAXIS, beam elements are modelled in the same horizontal plane as the pile plate elements. However, the ring and lintel beams will be constructed inside the secant pile wall and connected to the piles using dowel bars. When the secant pile wall undergoes compression in the circumferential direction, it forms a composite "T" beam. This configuration provides a larger effective bending depth and significantly higher flexural stiffness compared to rectangular beams modelled in the same plane as the piles. To accurately represent this increased flexural stiffness, the widths of the rectangular ring and lintel beams were adjusted as illustrated in Figure 5.

3.5 Sensitivity Analyses

In order to confirm robustness of the design solution, comprehensive sensitivity analyses were conducted across three key categories: structural, geotechnical and groundwater level. Each category's sensitivity analyses are detailed in the accompanying tables. In developing the design, a range of stiffness scenarios were considered to account for the likely variations in element stiffness. These scenarios are summarized in

Table 2. Geotechnical sensitivity analyses included the assessment of unbalanced groundwater pressure behind the piles, studied through different models. This approach ensured that all potential uncertainties were thoroughly covered in the design.

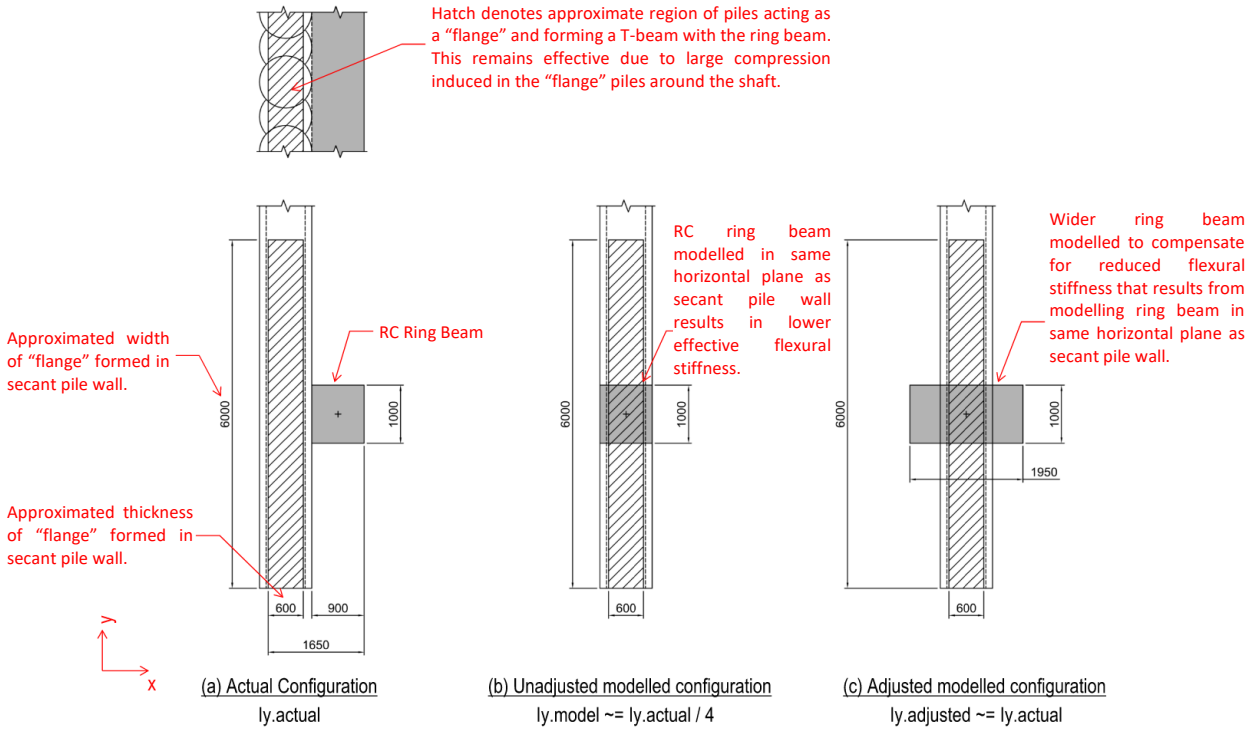


Figure 5. Ring beam showing: (a) Actual configuration; (b) Configuration in model with unadjusted width; and (c) Configuration with artificially increased beam width to achieve correct global bending stiffness.

Table 2. Structural sensitivity stiffnesses cases considered in PLAXIS 3D model and design.

Model	Secant Piles		Capping Beam	Ring, Sill & Lintel Beam
	E1 (ver)	E2 (hor)		
Base Case	70%E	70%E	70%E	70%E
SS 1: (Possibly critical for Capping Beam)	70%E	70%E	100%E	70%E
SS 2: (Possibly critical for Ring & Lintel Beams)	70%E	70%E	40%E	100%E
SS 3: (Possibly critical for Secant Pile Wall)	70%E	20%E	40%E	100%E
SS 4: (Possibly critical for Capping Beam)	50%E	70%E	100%E	40%E
SS 5: (Possibly critical for Ring & Capping)	70%E	20%E	100%E	100%E
SS 6: (Possibly critical for Lintel Beam)	70%E	100%E	70%E	70%E

Table 3. Sensitivity Analyses for Geotechnical parameters and stratigraphy (GS) and Groundwater (GWS)

Model	Description
GS1	Lower bound E module for S3 and R1 adopted; Interface ratio 0.5 applied behind piles.
GS 2	The effect of over-consolidated ratio (OCR) upper value of 3.5 considered in K_0 for S3.
GS 3	Top of R2 layer 1.5 m lower than considered in GIR thus This configuration would increase the soil load and reduce the passive support behind the piles at major axis.
GS 4	Top of R3 layer 1.5 m higher than considered in GIR. High locked-in stress in R3 results in unfavourable bending moment and shear at the bottom of the piles in the SE side.
GWS1	Groundwater at RL 83 m (78+5 m) on one long side and tapering to 0 at symmetry plane
GWS2	Groundwater at RL 83 m (78+5 m) on short side SW, opposite conveyor and reducing to 0

3.6 Design Adaptations for Swelling Pressure in Bringelly Shale

The solution with secant CFA piles only extending to 12 m below ground level already provided a mitigation against this risk as swelling pressure is higher in R2 and R1 when excavated.

Based on the results of swelling testing undertaken for the WSA SBT project, swelling pressure was evaluated using a 2D axisymmetric model that simulated different excavation phases, with the assumption that swelling occurred post-excavation. The swelling pressure acting behind the temporary piles was considered the difference between the pressure recorded at 10 days and the pressure prior to swelling activation and applied as a uniform load distribution.

4 CONSTRUCTION

Operational requirements within the shaft were already indicated as a driving factor for the selection of the elliptical shape of the structure. The activities and installations considered included: (i) most efficient operation of spoil extraction with the inclined conveyor system; (ii) tunnels ventilation ducts; (iii) MSV manoeuvring and loading space; (iv) segment lowering area, (v) portion of permanent cast-in-situ tunnels to be constructed by CPBG up to the MCO of the original Reference Design rectangular MCO; (vi) TBM cradle for retrieval and relaunch.

The 900 mm diameter and 12 m long CFA piles were installed at 600 mm centre-to-centre. Rock excavation was conducted in 1 m lifts, with each lift mapped by a geologist to confirm anticipated ground conditions and propose additional spot bolts, if adverse joint sets were found.

The shaft's structural performance was monitored using survey prisms positioned on both the pile wall and rock face. Permit to Excavate (PTE) meetings are conducted for each lift or weekly (whichever is sooner) to review mapping and monitoring data alongside construction progress, thereby ensuring safe and efficient shaft construction.

4.1 Construction Challenges & Solutions

Constructing a large elliptical shaft posed challenges in pile verticality, pile position, elliptical shape preservation, and accommodating reinforcement bars with varying curve radii for capping and ring beams.

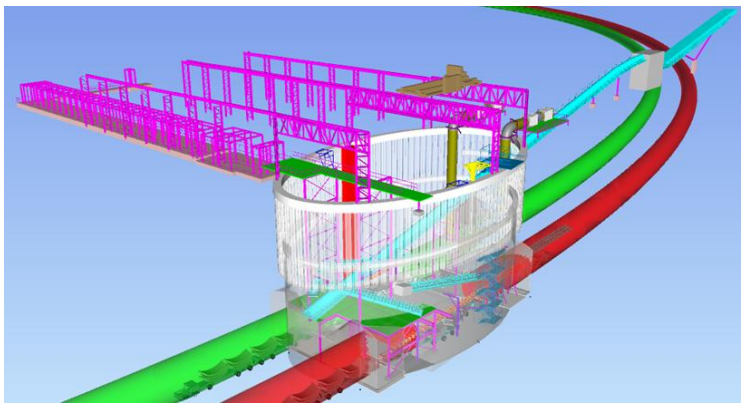


Figure 6. 3D view of the TBM Service Shaft in full operation with gantry crane and conveyor belt

Accurate surveying, guide walls, and maintaining rig verticality (within 1%), CPBG managed to achieve the accurate pile verticality, positioning and preserved the elliptical shape. But hard (secondary) piles' verticality posed difficulties due to drilling through differing material strength (35 MPa concrete firm pile and low strength Bringelly shale < 10 MPa).

Out of 212 piles, 16 exceeded tolerance and all of them are hard piles, primarily due to drilling through mixed materials. These were mitigated by localized minor trimming or filling during shaft excavation without affecting design and project requirements. From this project experience, complete elimination of out-of-tolerance issues in the hard pile is impractical; effective management can be achieved through quality control, regular surveys, and diligent checking of piling machine data to ensure verticality, thereby maintaining the shaft's overall performance and project requirements and/or selecting different piling technique with higher control on verticality such as bored piles. It is recommended that, when constructing complicated curved shafts, a larger verticality tolerance for hard piles may be considered to further reduce this issue.

Due to the elliptically shaped of the shaft, each main bar was required to be bent for varying curvature. This is impossible to do by a factory bar bending machine and required manual bending, and it is also not possible due to safety reasons. Therefore, in collaboration with the designer and reinforcement fabrication subcontractor, CPBG came up with a method for approximating the elliptical beams with a series of circles of constant radii. This allowed safe and effective reinforcement fabrication at the factory. It is recommended that, when designing complicated shape shafts special elliptical shaft, consideration is given to the bar scheduling requirement in the design and allow flexibility for the reinforcement placement to reduce construction RFIs and save time in trial-and-error exercises to come up with a suitable radius that satisfies the design and has less reinforcement placement error.

5 CONCLUSIONS

The paper provided an overview of the entire design development process for the WSA SBT TBM Service Shaft from Reference Design to Issue For Construction (IFC) and through construction highlighting how value engineering driven by contractor’s operational requirements and the need for a more efficient structural solution led to the adoption of an elliptical shaft with optimized support system. To the authors knowledge, while this solution has been used in Australia on mining projects, it is the first application to an infrastructure project.

The design of the elliptical shaft solution provided a number of challenges which were comprehensively addressed to provide a solid design documentation which proved effective at the test of a fast-paced construction. The TBM Service Shaft was a key project element to ensure that the WSA SBT contract was delivered on time to a record 3 years from start of design to completion of the contract works.

19th Australasian Tunnelling Conference – Acosta-Martínez, Stewart and Hudson-Smith (Eds.)
© 2025 Australian Tunnelling Society, ISBN 978-0-85825-002-4

Multi-criteria analysis of construction methodologies and lining options for deep bored shaft excavations

A. Purwodihardjo & P. Booth
CMW Geosciences Pty Ltd, Brisbane, Australia

ABSTRACT: The design and construction of shafts for underground ventilation and access requires a nuanced approach to decision-making, balancing safety, constructability, schedule, resource availability and cost-effectiveness. This study presents a method for Multi-Criteria Analysis (MCA) of construction methodologies and lining options for deep bored shaft excavations. The objective is to evaluate multiple, often conflicting performance criteria to weigh the relative risks and benefits of each option. The goal is to identify which method should be advanced to detailed design. The analysis integrates field data from a real-world ventilation shaft project and offers a practical framework for comparing excavation and lining techniques. It demonstrates how informed decisions can reduce project risks, improve delivery efficiency, and support long-term performance. The MCA process highlights the value of structured stakeholder engagement and transparent risk evaluation in geotechnical design. This approach supports confident, defensible decision-making in complex subsurface environments.

1 INTRODUCTION

The construction of vertical shafts for underground coal mining—particularly for ventilation and access—presents complex engineering and logistical challenges. These stem from heterogeneous ground conditions, fluctuating groundwater regimes, and the high capital cost of shaft infrastructure. Decisions made in early project phases carry substantial implications for safety, schedule, and long-term performance.

To support structured and transparent decision-making under such conditions, Multi-Criteri-Analysis (MCA), also known as Multi-Criteria Decision Analysis (MCDA), offers a robust evaluation framework. MCA allows systematic comparison of alternatives based on multiple, often competing criteria. Its application spans various engineering fields, including infrastructure development and geotechnical design (Saaty, 1980; Dodgson et al., 2009).

The fundamental steps involved in undertaking an MCA process typically include (Dodgson et al., 2009):

- Defining the decision-making problem and its objectives.
- Identifying the potential alternatives.
- Establishing relevant performance criteria.
- Gathering quantitative and qualitative information on each option.
- Assigning preference weightings to the criteria based on their relative importance.
- Evaluating alternatives against these criteria.
- Selecting the most appropriate solution.

This paper presents a case study that demonstrates the application of MCA in the context of a deep bored shaft constructed for a Central Queensland underground coal mine. The purpose of

the MCA was to evaluate excavation and lining options for two key shaft segments—upper and lower—underpinning design decisions that balance geotechnical, operational, and cost-related risks.

One of the principal challenges encountered in MCA application is the inherent subjectivity associated with assigning risk scores and weightings. Variability in expert judgement, incomplete information, and differing stakeholder priorities can lead to bias or reduced transparency. To address this limitation, a structured MCA workshop was convened, engaging representatives from multiple disciplines including geotechnical engineering, construction, mine operations, and cost estimation. The collaborative format enabled collective scrutiny of risks and facilitated alignment of perspectives. As a result, scoring was grounded in site-specific evidence and operational insight, thereby increasing confidence in the robustness and defensibility of the selected solutions.

2 CASE STUDY – LINING OPTIONS FOR DEEP BORED SHAFT EXCAVATIONS

This case study illustrates the practical application of MCA to a real-world shaft excavation project undertaken in the Bowen Basin, Central Queensland. The primary objective of this case study is to evaluate the relative performance of a range of excavation and lining methods for a deep bored shaft, which was required to serve as the primary ventilation and access point for an underground coal mine. The case was selected due to its representative ground conditions, operational complexity, and the need for a structured decision-making framework. By implementing the MCA methodology in a project environment characterised by variable geology, high groundwater potential, and stringent operational timelines, the study demonstrates how multi-criteria assessment can guide the selection of robust, cost-effective and constructible design solutions.

2.1 *The proposed shaft development*

The MCA case study described here focuses on the construction of a bored ventilation shaft for an underground coal mine. The planned final depth of the shaft was 80 m and the planned final internal diameter was 4.5 m.

For the purposes of the geotechnical design and construction, two distinct zones were defined within the shaft, including:

(1) Upper Shaft – (US) – comprising the zone between ground level and the top of moderately weathered Permian rock; and

(2) Lower Shaft – (LS) – the zone below the top of moderately weathered Permian rock.

The MCA approach involved systematically weighing up the relative advantages and disadvantages of a range of prospective shaft excavation and lining method options. It considered the complex interplay between multiple criteria to ensure that decision-making aligned with the project's predefined objectives. The ultimate objective of the MCA was to identify which option or options were to be carried forward to the detailed analysis and design stages of the project, and ultimately be applied in the construction of the shaft.

2.2 *Site Investigation and Ground Model Development*

The project site is located within the Early Permian to Middle Triassic Bowen Basin; a major coal-bearing geological basin that extends for approximately 600 km from Collinsville in the north to Theodore in the south. The site location is underlain by surface deposits of unconsolidated Quaternary alluvium (CLAY, Clayey SAND and Sandy CLAY), which are in turn underlain by poorly lithified Tertiary aged sediments (typically weathered to CLAY and Sandy CLAY). Tertiary aged basalt flows are also known to occur in the area, however these were not encountered at the shaft location. Underlying the Quaternary and Tertiary deposits are the Permian-aged Fort Cooper and Moranbah Coal Measures of the Blackwater Group.

Given the critical role of ground conditions in construction method feasibility and risk management, a detailed understanding of the subsurface profile was essential. Site characterisation involved a phased investigation strategy incorporating regional geological review, surface mapping, and targeted drilling. The centrepiece of this effort was a fully cored geotechnical borehole

extending to 95 m depth, providing high-resolution data on lithology, rock mass quality, weathering profiles, and groundwater conditions. These data were foundational to both preliminary design development and to the MCA framework, ensuring that each construction and lining option could be robustly assessed against realistic subsurface scenarios.

Ground conditions encountered in the fully cored geotechnical borehole drilled to investigate the planned shaft location are summarised in Table 1. These data informed the stratigraphic interpretation and were critical in defining geotechnical boundaries relevant to construction risk and shaft segmentation.

Table 1. Summary of ground conditions.

Stratigraphy	From Depth (m)	To Depth (m)	Thickness (m)	Strength	Weathering
Quaternary Alluvium (CLAY & Sandy CLAY, Clayey SAND)	0	8.8	8.8	VSt-H/ L-MD	N/A
Tertiary Sediments (CLAY & Sandy CLAY)	8.8	12.95	4.15	VSt-H	N/A
Extremely Weathered Permian Interbedded Sandstone & Mudstone	12.95	13.6	0.65	L	XW
Weathered Permian Sandstone	13.6	20.7	11.9	L-M	HW-MW
Fresh Permian Sandstone, Mudstone & Coal	20.7	95	69.5	M-H	SW-FR

2.3 *Shaft zoning and functional requirements*

Based on the stratigraphy, geological sequence, and geotechnical properties revealed by the site investigation, the shaft was subdivided into two distinct functional zones to guide the construction methodology selection:

- Upper Shaft (US): Extending from ground level to the top of moderately weathered Permian rock (~19 m depth), this zone is dominated by weak, highly weathered materials including alluvial soils and Tertiary sediments. The design focus in this zone was on minimising groundwater inflow and ensuring excavation stability.
- Lower Shaft (LS): Commencing at the base of the Upper Shaft and extending to the final shaft depth (80 m), this zone is characterised by more competent Permian rock, including interbedded sandstone, mudstone, and coal seams. Construction in this zone required methods that could accommodate hard rock excavation, potential methane gas emissions, and maintain interface compatibility with underground mine workings.

These zone definitions were critical in framing the MCA, as they required consideration of construction methodologies capable of addressing different ground behaviours, support requirements, and interaction with the mine's operational timeline.

3 CONSTRUCTION AND LINING OPTIONS

Based on the defined shaft zoning and prevailing ground conditions, a set of construction and lining options was developed for both the Upper Shaft and Lower Shaft. Each option was designed to address the unique geotechnical, hydrogeological, and operational challenges associated with its respective shaft segment. The following options were identified and assessed:

3.1 *Upper shaft options*

Four alternative methodologies were considered for the excavation and support of the Upper Shaft:

- US-1: Box Cut with Steel Pre-Sink Collar. Excavation of a box cut to 17.1 m depth, installation of a steel pre-sink collar, and backfilling with stabilised sand. A concrete surface slab would

then be constructed to accommodate the blind bore or raise bore rig.
- US-2: Secant Pile Ring Wall. Installation of a secant pile ring wall to 19 m depth using a guide wall and temporary platform. The piles are integrated with a surface concrete slab and capping beam.
- US-3: Box Cut with Micro-Pile Ring Wall. Combination of box excavation to 14 m depth and vertical micro-pile reinforcement from 14 m to 19 m depth. Stabilised sand backfill and concrete slab construction follow.
- US-4: Contiguous CFA Pile Wall with Shotcrete Support. Construction of a CFA pile wall to 19 m depth with reinforced concrete capping beam at surface level. Excavation inside the pile wall proceeds in stages to 17.1 m depth, with permanent shotcrete lining applied progressively.

3.2 *Lower shaft options*

Four alternatives were considered for the deeper, rock-dominated Lower Shaft:
- LS-1a: Raise Bore with Selective Shotcrete Support. Following pilot hole drilling and raise boring, selective areas of the shaft are stabilised using steel fibre reinforced shotcrete. Target areas for shotcreting are selected based on video inspection.
- LS-1b: Raise Bore with Full Steel Liner. A continuous steel liner is installed following raise boring. The annulus is back-grouted for full contact and corrosion protection.
- LS-2a: Blind Bore with Staged Shotcrete. Blind boring with drilling fluid support, staged dewatering, and sequential application of shotcrete at intermediate and final excavation depths.
- LS-2b: Blind Bore with Full Steel Liner. Full-depth blind boring with drilling fluid support, followed by installation of a steel liner and back-grouting to secure the lining and prevent groundwater ingress.

Each of these construction and lining options formed the basis of the MCA evaluation discussed in the following section.

4 MCA METHODOLOGY

The MCA process was structured to assess the relative merits and risks of each proposed construction and lining option. A two-stage evaluation was implemented:
- Stage 1: Performance Risk Scoring – Each option was scored qualitatively against a predefined set of performance criteria using a scale of 1 to 5, where 1 indicated very low risk and 5 indicated very high risk. A score of 99 denoted a fatal flaw.
- Stage 2: Importance Weighting – Key criteria were assigned weighting factors (1 for neutral importance, 2 for high importance) to reflect their relative impact on project success.

4.1 *Performance criteria*

The following performance criteria were used to evaluate each construction and lining option during the MCA process. These criteria reflect the critical technical, financial, and operational risks relevant to deep shaft excavation in complex ground conditions:
- Geotechnical Risk: Likelihood of instability or deformation of the shaft walls due to varying soil and rock conditions, particularly in zones with weak or weathered materials.
- Groundwater Risk: Risk of water inflow during or after construction, influencing excavation safety, lining integrity, and long-term maintenance requirements.
- Financial Risk of Contingency Measures: Potential cost exposure from unplanned remedial measures required to address unexpected ground behaviour or construction complications.
- Ease of Mobilisation and Set-up: Practical challenges and time requirements associated with assembling equipment, infrastructure, and workforce at the site.
- Impact on Critical Path Activities: Influence on the overall project timeline, particularly on activities that directly control project completion.
- Mine Schedule Alignment: Compatibility with mining operations and sequencing, including whether shaft completion enables or delays key underground development milestones.
- Construction Cost (CapEx): Estimated upfront capital expenditure required for shaft excavation and lining.

- Whole-of-Life Cost: Combined cost of construction, inspection, maintenance, and potential rehabilitation over the shaft's operational life.
- Availability of Qualified Contractors: Market availability and scheduling flexibility of specialist contractors capable of delivering each method to specification.
- Confidence of Successful Implementation: Likelihood that the method will be executed on time, within budget, and without major construction or operational setbacks.
- Impact on Underground Operations: Degree to which shaft construction interferes with existing or planned underground activities, such as requiring access from underground or causing downtime in adjacent mining zones.

To address potential subjectivity in the evaluation process, a structured MCA workshop was conducted involving representatives from geotechnical design, construction planning, mining operations, and commercial management. This multidisciplinary input ensured that scoring and weighting were grounded in both technical knowledge and practical constraints. Discussions during the workshop enabled clarification of assumptions, exploration of risks, and consensus on performance expectations.

The resulting matrix of risk scores and weightings formed the quantitative basis for ranking each construction and lining option.

4.2 *Qualitative risk rating system*

To support the MCA scoring process, a qualitative risk rating system was adopted to ensure consistency and clarity in the assignment of scores. This system defined risk levels across a scale from 1 to 5, with an additional score of 99 used to represent fatal flaws. Each rating corresponds to a general level of concern based on likelihood, severity, and potential impact:

- Rating 1: Very Low Risk – Negligible likelihood or impact; no contingency required.
- Rating 2: Low Risk – Limited likelihood or impact; manageable with routine controls.
- Rating 3: Moderate Risk – Reasonable likelihood and/or moderate impact; mitigation measures required.
- Rating 4: High Risk – High likelihood or impact; significant contingency measures anticipated.
- Rating 5: Very High Risk – Very high likelihood or severe impact; unacceptable without major risk reduction.
- Rating 99: Fatal Flaw – Option is not viable due to prohibitive technical, safety, or operational reasons.

These ratings allowed stakeholders to articulate and quantify risks based on their domain of expertise while preserving a consistent scoring structure across all criteria.

4.3 *Importance Weighting of Performance Criteria*

To reflect their differing levels of criticality, each performance criterion was assigned an importance weighting. This weighting allowed the MCA process to prioritise those criteria deemed most influential in determining the success of the shaft construction. Two weighting levels were adopted:

- Weighting 1 – Neutral Importance: Assigned to criteria considered relevant but not disproportionately influential to the project's outcomes.
- Weighting 2 – High Importance: Assigned to criteria with high impact on project feasibility, safety, operability, or cost.

The weighting structure was agreed upon by consensus during the MCA workshop to ensure balanced representation of technical, commercial, and operational priorities.

4.4 *Key assumptions*

The MCA was developed and applied under a set of defined assumptions that reflect known site conditions, anticipated operational needs, and broader project delivery constraints. These assumptions were agreed upon during the MCA workshop to ensure a common understanding and to avoid scoring discrepancies due to differing expectations. Key assumptions included:

- The shaft would have a finished internal diameter in the range of 4.0 m to 4.5 m.

- The operational life of the shaft would be approximately 10 years.
- The shaft would serve as the primary ventilation conduit for the underground mine, requiring continuous operability.
- Construction of the Upper Shaft would likely coincide with the wet season, implying elevated groundwater levels in near-surface strata.
- Specialist shaft construction contractors and equipment would be available but potentially constrained by procurement lead times.
- The shaft construction program would need to align with the broader mine schedule to avoid delays to critical underground access milestones.

These assumptions informed both the technical evaluation and the practical feasibility assessments of the alternative design and construction options.

5 MCA RESULTS AND DISCCUSSION

The MCA produced a clear ranking of the evaluated construction and lining options based on weighted performance scores. In addition to identifying technically feasible solutions, the process enabled the early exclusion of options carrying unacceptable risk profiles.

One key feature of the methodology involved the use of a 'fatal flaw' rating. Score 99 was assigned to any criterion where an option exhibited a non-negotiable failure risk. This ensured that options presenting insurmountable challenges—such as unacceptable whole-of-life maintenance liabilities or unmanageable groundwater ingress—were systematically removed from consideration. For example, shotcrete lining options were excluded due to concerns around adhesion under wet conditions, risk of degradation over time, and limited ability to safely perform repairs without disrupting mine operations.

Two critical differentiators in the MCA were whole-of-life costs and confidence of success. These provided valuable insight into long-term viability and delivery risk.

Whole-of-life cost considerations extended beyond initial capital expenditure to include recurring inspection, maintenance, and potential rehabilitation demands. Shotcrete-based options were significantly penalised due to anticipated ongoing inspection and remedial requirements—with any video inspections, surveys or remedial shotcrete application activities all necessitating interruptions to the shaft (and therefore mine) operation— posing poor maintainability and high operational risks. In contrast, steel-lined solutions were favoured for their durability and low maintenance profile, reducing total lifecycle costs.

Confidence of success reflected constructability under expected ground conditions, availability of proven construction methodologies, and contractor familiarity. Shotcrete-supported designs scored poorly due to known performance issues in wet environments—related to poor adhesion and washout of the shotcrete—and execution difficulties in deep, confined shafts—related to electrical safety challenges with the operation of the remotely operated shotcreting rig within the potentially explosive gas (methane) environment. Blind bored steel-lined options, in contrast, demonstrated alignment with established techniques, providing greater assurance in delivery.

Table 2 summarises the risk scores and criteria importance weightings derived for each option. The results highlighted significant variability in performance, particularly in relation to lifecycle cost exposure, constructability confidence, and groundwater or geotechnical risk.

Table 2. summary of risk scores by performance criteria.

Performance Criteria	Unweighted Qualitative Ratings				Importance Weighting	Weighted Qualitative Ratings			
Upper Shaft (Ground Level to 17.1 m bgl[1])									
Option Number	US-1	US-2	US-3	US-4	-	US-1	US-2	US-3	US-4
Geotechnical Risk	3	2	3	2	2	6	4	6	4
Groundwater Risk	5	1	5	3	2	10	2	10	6
Financial Risk	4	1	4	3	1	4	1	4	3
Ease of mobilisation	1	3	3	4	1	1	3	3	4
Critical Path Impact	5	3	5	4	2	10	6	10	8
Mine Schedule	1	1	1	1	1	1	1	1	1
Construction Cost	1	4	3	4	2	2	8	6	8
Whole-of-Life Cost	1	1	1	1	1	1	1	1	1
Avail. of Contractors	1	3	2	3	1	1	3	2	3
Conf. of Success	3	1	3	4	1	3	1	3	4
Imp. on Underground	1	1	1	1	1	1	1	1	1
Total Scores:	26	21	31	30	-	40[2]	31	47[3]	43
Lower Shaft (17.1 m to 80 m bgl)									
Option Number	LS-1a	LS-1b	LS-2a	LS-2b	-	LS-1a	LS-1b	LS-2a	LS-2b
Geotechnical Risk	3	3	2	1	2	6	6	4	2
Groundwater Risk	4	3	2	1	2	8	6	4	2
Financial Risk	4	4	2	2	1	4	4	2	2
Ease of mobilisation	4	4	2	2	1	4	4	2	2
Critical Path Impact	3	2	4	3	1	3	2	4	3
Mine Schedule	4	4	1	1	1	4	4	1	1
Construction Cost	3	4	3	4	2	6	8	6	8
Whole-of-Life Cost	99	2	99	2	2	198	4	198	4
Avail. of Contractors	2	2	3	3	1	2	2	3	3
Conf. of Success	99	1	99	1	1	99	1	99	1
Imp. on Underground	5	5	1	1	2	10	10	2	2
Total Scores:	230	34	218	21	-	344[4]	51	325[4]	30

*Notes:

1. m bgl = Metres below ground level.
2. For Upper Shaft Option 1, if the blind bore method were adopted for the Lower Shaft, the Box Cut depth could be reduced to 14 m bgl and the risk score would be ≤40.
3. For Upper Shaft Option 3, if blind bore were adopted for Lower Shaft, the requirement for micro-piles between 14 to 19 m bgl could be eliminated and the risk score would be ≤40.
4. Lower Shaft options incorporating shotcrete support were assigned Fatal Flaw ratings due to: (1) "Whole-of-life costs" and (2) Low "Confidence of Success".

5.1 *Upper shaft results*

Among the Upper Shaft options, US-2 (Secant Pile Wall to 19 m) emerged as the preferred solution. This option offered high confidence in construction success, robust groundwater exclusion, and minimal interface complexity. Other options, such as US-1 and US-3, were associated with higher risks due to reliance on temporary support systems and uncertain ground behaviour in the upper strata.

5.2 *Lower shaft results*

For the Lower Shaft, LS-2b (Blind Bore with Steel Liner) scored significantly better than the alternatives. It offered the highest level of construction reliability, minimal dependence on underground development, and reduced risk of failure due to groundwater or methane ingress. Shotcrete-based options (LS-1a and LS-2a) were penalised for the aforementioned performance issues, execution difficulties, poor maintainability and high operational risks, receiving fatal flaw ratings in several criteria.

5.3 *Lessons Learned from MCA Process*

The structured MCA process enabled comprehensive evaluation of construction and lining options by integrating technical performance, stakeholder input, and implementation risk. The workshop format proved especially valuable, surfacing practical issues that might have been overlooked in a conventional assessment. Incorporating lifecycle and constructability considerations allowed the team to distinguish between options with theoretical merit and those with proven, repeatable execution outcomes.

6 CONCLUSIONS

This study highlights the effectiveness of a structured Multi-Criteria Analysis (MCA) process in guiding complex shaft construction decisions. The framework enabled transparent evaluation of diverse technical and operational options amid uncertainty and competing priorities.

Success relied on active stakeholder engagement through a collaborative workshop, where assumptions were tested, risks clarified, and consensus reached. Key challenges—including subjectivity in scoring, future maintenance uncertainty, and schedule alignment—were openly addressed.

By using agreed performance criteria and importance weighting, the team identified solutions that were both technically feasible and operationally reliable. Lifecycle and constructability considerations were effectively integrated, helping to eliminate options with fatal flaws.

The process provided a shared decision-making foundation and allowed the project to move into detailed design with confidence and alignment across all disciplines.

7 REFERENCES

Dodgson, J., Spackman, M., Pearman, A., & Phillips, L. (2009). Multi-criteria analysis: a manual. Department for Communities and Local Government, London.

Girard, J., & Rotter, B. (2004). Lining Systems for Vertical Shafts in Poor Ground Conditions. In: Shaft Engineering, CIM.

Iannacchione, A.T., Prosser, L.J., & Pariseau, W.G. (2007). Case studies in support of shaft and raise excavation design. NIOSH Mining Publication No. 2007-135.

Saaty, T.L. (1980). The Analytic Hierarchy Process. McGraw-Hill, New York.

19th Australasian Tunnelling Conference – Acosta-Martínez, Stewart and Hudson-Smith (Eds.)
© 2025 Australian Tunnelling Society, ISBN 978-0-85825-002-4

Geotechnical design and performance of a rock excavation under a cut and cover tunnel structure in Sydney

D. Zografou, V. Tandjiria & M. Mo

Jacobs, Sydney, Australia

ABSTRACT: Several major motorway tunnel projects have been completed in Sydney over the last ten years. These projects required complex interfaces and construction staging of main structures including cut and cover tunnel structures. This paper presents the geotechnical design aspects and performance of the top-down rock excavation under a cut and cover tunnel structure, which permanent concrete works were completed as part of an earlier project stage. The excavation works comprised excavation to a maximum depth of 12.5 m in Ashfield Shale. The instrumentation and monitoring data during and after construction have been analysed and are discussed in this paper. A comparison between observed displacements and design predictions is presented, while considering their correlation with the geotechnical design and numerical model assumptions.

1 INTRODUCTION

The project comprised a new major motorway in Sydney which included a cut and cover tunnel structure for the tunnel exit and entry ramps which was designed and constructed in two stages by two different contractors. The Stage 1 project scope included the detailed design of soldier piles, locally with anchors, and headstocks under a new bridge. As part of the Stage 1 work, the excavation progressed to top of bedrock or below the strut beam. Stage 2 project scope comprised the detailed design of the excavation beneath the cut and cover tunnel structure, including excavation rock support, as well as the construction of the motorway to the finished surface level.

This paper presents the geotechnical design of the excavation with a focus on the assessment of lateral displacements. The predicted displacement values are compared with those measured by the instrumentation installed in the excavation.

1.1 *Stage 1 Cut and cover*

The existing cut and cover tunnel structure comprised a roof structure, with super-T girders and a cast in-situ composite deck, which was supported on three rows of soldier piles. A bridge deck with road live traffic was located on top of the cut and cover tunnel structure. A photograph of the existing cut and cover tunnel structure, prior to the rock excavation works, is shown on Figure 1. The general arrangement plan and a typical cross section of the cut and cover tunnel structure are shown on Figure 2 and Figure 3, respectively.

The structure foundations comprised:

- The roof abutments, i.e. the western and eastern retaining walls, and the tunnel portal retaining walls. The soldier piles that formed the retaining walls had a diameter of 900 mm and a spacing of 2.3 m. The portion of the western retaining wall at the deepest north end of the excavation utilised ground anchors for additional lateral support.
- The central pier between the two carriageways, comprised 900 mm diameter piles with a spacing that varied between 2.7 m and 5.5 m.



Figure 1 Existing cut and cover tunnel structure (southern end, photograph taken prior to stage 2 rock excavation works)

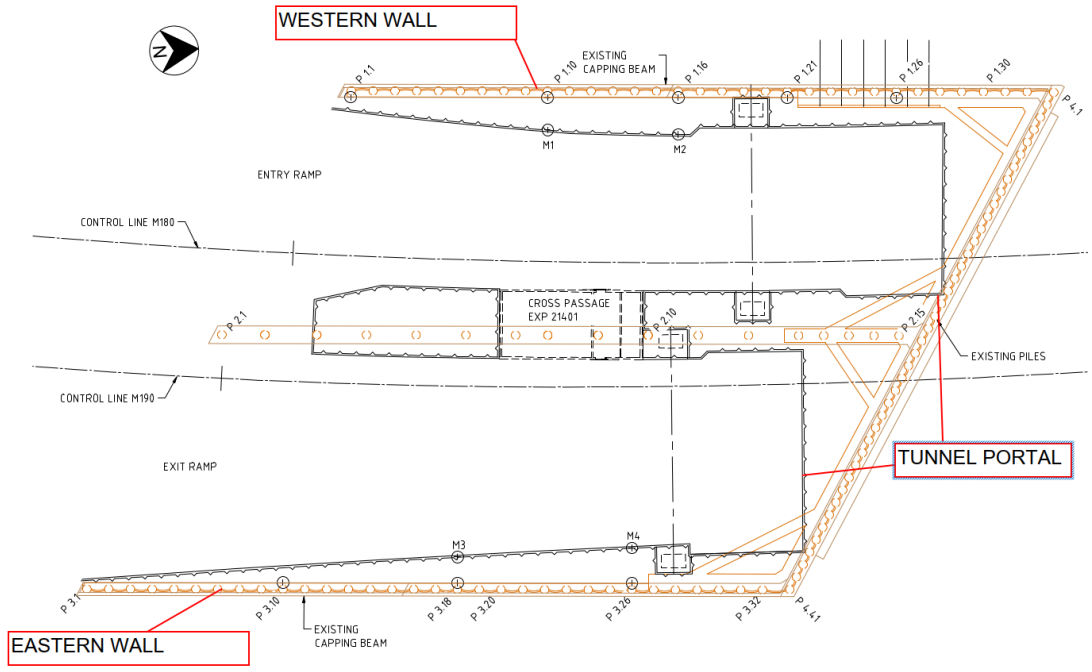


Figure 2 General arrangement plan showing location of survey points

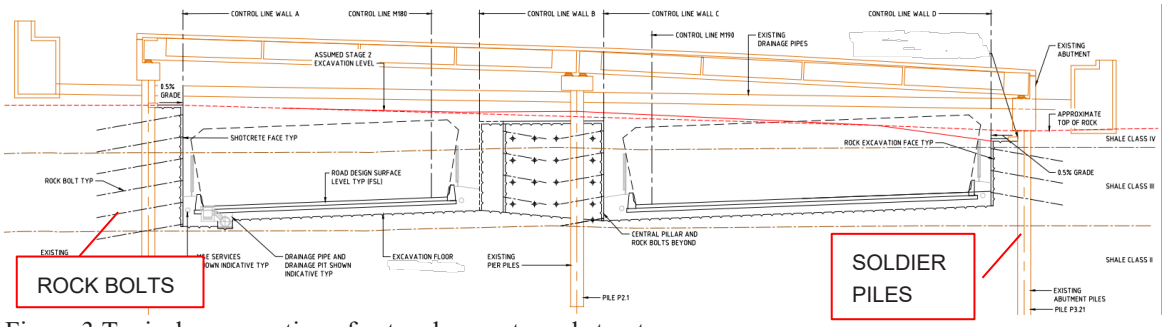


Figure 3 Typical cross section of cut and cover tunnel structure

1.2 *Stage 2 Rock excavation*

The Stage 2 rock excavation works comprised advancement of the excavation works below the top of rock to the underside of the motorway pavement, extending approximately 60 m from the southern end of the cut and cover tunnel structure to the tunnel portals. The detailed design scope comprised the geotechnical design of the rock excavation under the existing structure, and the structural assessment of the elements of the existing structure that were affected by the excavation. The adopted design solution comprised pattern rock bolting and the surface of the excavation walls covered with shotcrete, which is a typical design solution for deep excavations in Ashfield Shale. Pattern rock bolting was specified at the abutment/retaining walls and central pier to ensure stability against a wedge or planar failure case based on regional and site-specific defect data. Rock bolts of 22 mm in diameter were adopted with vertical spacing between 1.0 m and 1.5 m, and horizontal spacing between 0.6 m and 1.7 m.

2 GROUND MODEL AND GROUNDWATER CONDITIONS

The ground model was developed based on ground investigations carried out as part of Stage 1 and Stage 2 designs. The ground conditions comprised uncontrolled fill of up to 2 m thick, overlying a relatively shallow residual soil overlying Ashfield Shale bedrock. The fill and part of the residual soil/extremely weathered material had been excavated as part of the Stage 1 project. The Stage 2 excavation was carried out predominantly in Ashfield Shale. The shale was assessed as highly weathered and of very low to low strength in the upper 2 m (Class IV, Pells 2004). Below this, the weathering of the shale improved with depth to be typically moderately weathered and of medium strength (Class III or better, Pells 2004). The Ashfield Shale geotechnical design parameters are presented in Table 1.

Based on the available groundwater data, perched water pressure at the top of the residual soil was considered in the geotechnical design.

Table 1 Ashfield Shale Geotechnical design parameters for the Stage 2 rock excavation

Parameters	Class IV *	Class III *	Class II *
Unit weight, γ (kN/m3)	23	24	24
Unconfined Compressive Strength, UCS(MPa)	2	6	12
Rockmass Elastic Modulus, E (MPa)	250	500	1,200
mi (Material constant)	8	8	8
GSI (Geological Strength Index)	35	50	60
Poisson's Ratio, ν	0.3	0.25	0.2
Ultimate Bond Stress (kPa)	300	600	900

Parameters	Class IV *	Class III *	Class II *
Horizontal to vertical stress ratio	1.4	1.4	1.4

*Pells (2004)

3 GEOTECHNICAL ANALYSIS

Soil structure analyses were carried out to assess the deformations of the excavation during construction and in the long-term using finite element program Plaxis 2D. The deflections of the retaining walls at the northern end of the abutment piles and at the tunnel portal piles, where retaining walls are restrained by the capping beam and an intermediate strut, were assessed using Plaxis 3D.

Seven representative sections of the eastern and western abutment/retaining walls were analysed using Plaxis 2D. The representative sections, their excavation depth (to underside of pavement) and rock ledge width, are presented in Table 2.

A typical Plaxis 2D model is shown on Figure 4. Analysis was not carried out at the central pier where the piles were predominantly vertically loaded and the excavation did not affect their design loading conditions.

The 3D model is shown on Figure 5. The same construction sequence and assumptions were adopted in the Plaxis 2D and Plaxis 3D analysis.

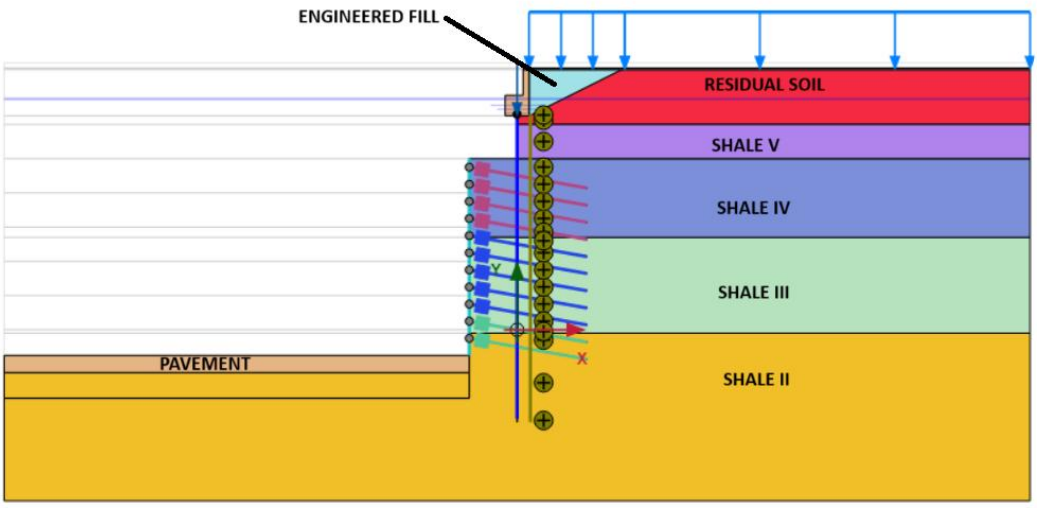


Figure 4 Plaxis 2D model

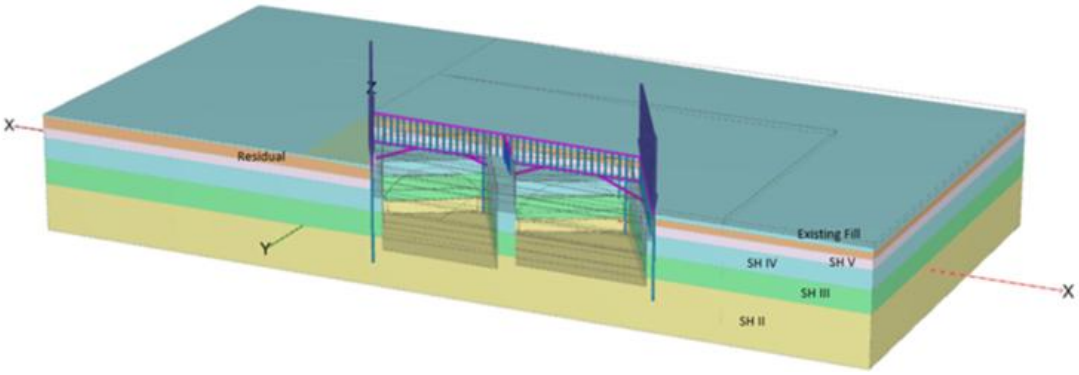


Figure 5 Plaxis 3D model

3.1 *Main inputs and assumptions*

The main inputs and assumptions of the geotechnical analysis are listed below:

- As the deck was simply supported on the abutments/ capping beam, no connection was modelled between the retaining walls and the deck.
- Axial load from the upper structure was applied on the piles based on the values reported on the Stage 1 as constructed drawings.
- Displacements were reset to zero at the end of Stage 1 works so that estimated displacements corresponded to Stage 2 works only.

For the additional Stage 2 excavation works the following construction sequence was adopted:

- Excavation to top of Class IV Shale;
- Excavation from top of Class IV Shale with 2 m deep lifts;
- Application of shotcrete and installation of rock bolts;
- Repetition of the same procedure using 2 m lifts until the final excavation level; and
- Construction of pavement.

3.2 *Predicted deflections*

The predicted pile head deflections based on the geotechnical analysis are presented in Table 2. The predicted values were below the allowable limiting value of 30 mm, taking into account also the Stage 1 deflections that were estimated to vary between 3 mm and 5 mm. The deflections due to the Stage 2 rock excavation varied between 1.1 mm and 2.4 mm per meter of rock excavation. The lower values correspond to a higher percentage of the rock excavation in better quality rock (Class III or better), typically on the eastern abutment. The maximum value of 2.4 mm/m was estimated at pile P1.2. The values of deflections per meter of rock excavation are consistent with the typical ranges reported for deep excavations in Ashfield Shale (e.g. Salcher et al. 2024, Oliveira & Chan 2016, Toh & Mostyn 2015, Walker 2004, Hewitt et al. 1999).

Table 2 Representative sections for geotechnical analysis and predicted and observed deflections

Pile number*	Stage 2 Excavation Depth (m)	Excavated material thickness (m) per rock class**	Rock Ledge Width (m)	Total retained height (m)	Predicted Pile Head Deflection due to Stage 2 excavation		Observed Pile Head Deflection due to Stage 2 excavation	
					(mm)	Ratio of deflection to excavation depth (mm/m)	(mm)	Ratio of deflection to excavation depth (mm/m)
P1.2 (West Abutment)	7.4	3.2/ 4.2/ 0.0	1.2	12.5	18	2.4	7	0.9
P1.9 (Western Abutment)	9.7	3.8/ 5.9/ 0.0	3.2	14.2	18	1.9	12	1.2
P1.16 (Western Abutment)	11.3	4.4/ 5.2/ 1.7	3.7	15.7	16	1.4	NA***	NA***

P1.21 (Western Abutment)	12.5	4.6/ 5.6/ 2.3	2.8	17.8	19	1.5	25	2.0
P3.9 (Eastern Abutment)	5.7	0.8/ 3.2/ 1.7	2.0	9.7	6	1.1	5	0.9
P3.15 (Eastern Abutment)	6.3	1.0/ 3.1/ 2.2	2.8	11.9	10	1.6	8	1.3
P3.26 (Eastern Abutment)	10.7	3.7/ 6.3/ 0.7	3.9	16.0	15	1.4	14	1.3

*Pile locations are shown on Figure 2
**Excavated material thickness (m) per rock class: Ashfield Shale Class IV/ Class III/ Class II
***Not available

4 COMPARISON OF MEASURED AND PREDICTED DEFLECTIONS

Instrumentation for the Stage 2 excavation works comprised optical prisms installed at the pile head ('P') and at the top of rock ledge ('M') at selected sections of the abutment walls. The location of survey points is shown on Figure 2.

The predicted and measured deflections are summarised in Table 2. The measured deflection response during and after excavation is shown at selected monitoring points of the western and eastern abutment on Figure 6 to Figure 8. The excavation works of the western carriageway started first, with a direction south to north, followed by the excavation of the eastern carriageway with a direction north to south. The start and end dates of the excavation for each carriageway are also shown on the figures.

The following observations are made:

- Overall, the maximum measured deflection values are in good agreement with the predicted values. The accuracy of the predicted deflections is typically between 5% and 25% and can be classified based on the prediction quality classification as 'excellent' to 'fair' (Morgenstern, 2000). The main exception is survey point location P1.2 where the measured values may be erroneous.
- At P1.21, deflections exceeded the maximum predicted value but remained within the allowable deflection limit. This is attributed to the position of the pile which was the last pile at the deepest section of the excavation that was not supported by ground anchors. Sudden transitions between anchored and unsupported areas may trigger increased movement. At P1.26, where the piles were supported with ground anchors, the measured deflection is in good agreement with the predicted value.
- At the eastern abutment, the deflections at P3.26 started increasing at the start of the excavation until approximately 20 June. After that, deflections are shown to stabilise prior to the end of the excavation works. This response is attributed to the lateral displacement at P3.26 and at the respective pile (P1.21) on the western abutment closing the abutment gap and causing a propping effect on the top of P3.26.
- Based on the measured deflections of the western abutment, deflections varied between 0.9 mm and 2.0 mm per meter of rock excavation, that is slightly less than the predicted values.

- Where there were survey points placed at the top of rock ledge, the measured deflection response was consistent with that placed on the respective pile behind the rock ledge.

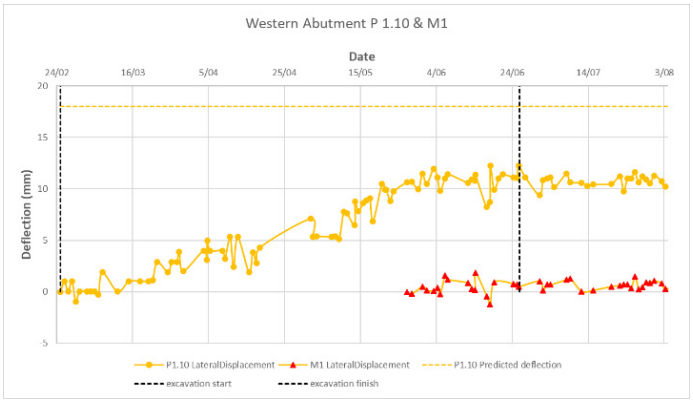


Figure 6 Western Abutment P1.10 measured and predicted lateral displacements

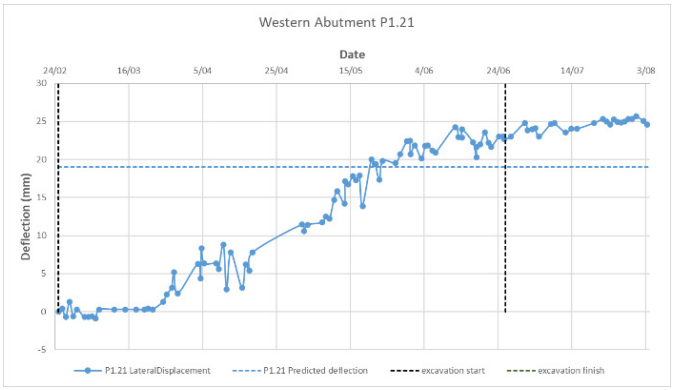


Figure 7 Western Abutment P1.21 measured and predicted lateral displacements

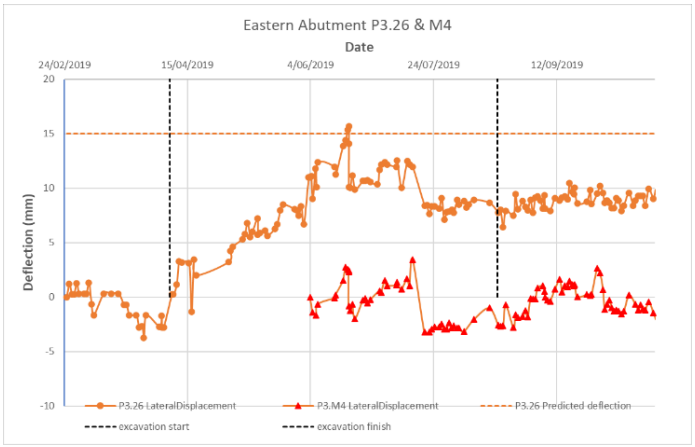


Figure 8 Eastern Abutment P3.26 measured and predicted lateral displacements

5 CONCLUSIONS

The adopted design solution for a deep excavation in Ashfield Shale beneath an existing cut and cover tunnel structure, comprising soldier piles with pattern rock bolting and shotcrete on the wall surface, performed satisfactorily. Deflections stabilised after the end of excavation and remained below the allowable limiting value.

Based on the comparison of the predicted deflection values of the excavation retaining walls with those measured by the instrumentation, the following conclusions were made:

- Deflections are shown to be a function of excavation depth and rock quality (strength and defects).
- The measured deflections varied between 0.9 mm and 2.0 mm per meter of rock excavation, and were slightly lower than the predicted values of 1.1 mm and 2.4 mm per meter. Lower values correspond to higher percentage of the rock excavation in better quality rock (Class III or better).
- Sudden transitions between anchored and unsupported areas of the excavation may have triggered increased deflection at one survey point location compared to that predicted by the 2D finite element geotechnical analysis.
- The accuracy of predictions was generally classified based on the prediction quality classification as 'excellent' to 'fair' (Morgenstern, 2000)

6 REFERENCES

Hewitt, P.B., McQueen, L.B. and Davies, P.R., 1999. Genting Centre, Sydney-Deep Excavation Adjacent to Railway Tunnels. In Australia-New Zealand Conference on Geomechanics (8th: 1999: Hobart, Tas.) 611-617. https://www.issmge.org/uploads/publications/89/88/8ANZ_075.pdf

Morgenstern, N.R., 2000. Performance in geotechnical practice. Hkie Transactions, 7(2), 2-15. https://www.tandfonline.com/doi/abs/10.1080/1023697X.2000.10667819

Pells, P.J.N., 2004. Substance and mass properties for the design of engineering, structures in the Hawkesbury sandstone, Australian Geomechanics journal, 39 https://geomechanics.org.au/admin/wp-content/uploads/2015/03/39_3_1.pdf

Toh, J. and Mostyn, G., 2015. Ground surface deformation adjacent to a deep excavation in shale. Australian Geomechanics journal, 50(2), 57-67. https://www.australiangeomechanics.org/papers/ground-surface-deformation-adjacent-to-a-deep-excavation-in-shale/

Oliveira, D.A.F. and Chan, G., 2017. Ground control for a deep basement excavation in Sydney's GPO fault zone. In Proceedings of the 20th Australian Geomechanics Society Sydney Chapter Symposium, Sydney. https://www.australiangeomechanics.org/papers/ground-control-for-a-deep-basement-excavation-in-sydneys-gpo-fault-zone/

Walker, B.F., 2004. Stress relief on hillsides and hillside excavations. Australian Geomechanics journal,, 39(3), 59-72. https://australiangeomechanics.org/admin/wp-content/uploads/2015/03/39_3_5.pdf

19th Australasian Tunnelling Conference – Acosta-Martínez, Stewart and Hudson-Smith (Eds.)
© 2025 Australian Tunnelling Society, ISBN 978-0-85825-002-4

Westmead metro station excavation: Design challenges and ground performance

Y.H. Toi
SMEC, Brisbane, Queensland, Australia

E. Chang
SMEC, Sydney, New South Wales, Australia

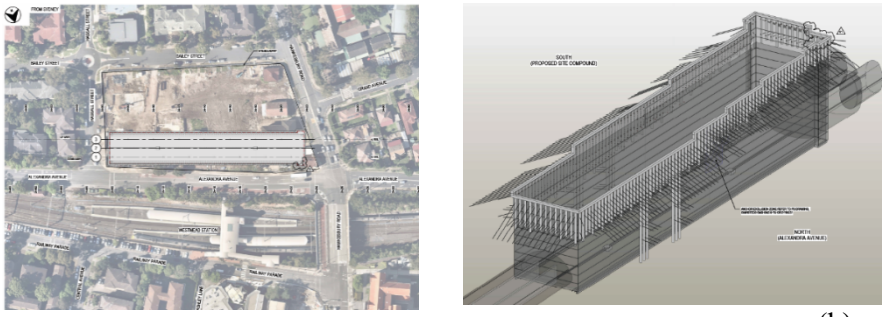
C.W. Boon, M.A. Khoo
Gamuda Australia-Laing O'Rourke Consortium, Sydney, New South Wales, Australia

ABSTRACT: The excavation of Westmead metro station, as part of the Sydney Metro West – Western Tunnelling Package, required careful consideration of complex geological conditions and urban constraints. Risk management relied on robust design strategies, real-time monitoring, and adaptive decision-making. This paper outlines key design considerations, including the retention system, anchor exclusion zone management, and ground stabilisation measures, which were essential to excavation stability and limiting impacts on nearby infrastructure. Observations during excavation, including geological mapping and ground monitoring, provided valuable insights into ground behaviour. Comparing monitoring data with design predictions helped assess excavation performance and informed design adjustments to improve safety and efficiency. This case study highlights the value of robust monitoring systems, adaptive design, and effective collaboration in managing excavation risks. The lessons learnt support best practice development for future underground construction in Australia.

1 INTRODUCTION

Sydney Metro West (SMW) is a new underground railway connecting Greater Parramatta to the Sydney CBD. As part of this project, the Western Tunnelling Package (WTP) involves the construction of 9 km of twin railway tunnels between Sydney Olympic Park and Westmead.
This paper focuses on the excavation of Westmead metro station, highlighting key design considerations and observations made during construction.

The Westmead metro station site has excavation depths varying from approximately 30 m to 38 m. The site is bounded by four roads: Alexandra Avenue and the existing Westmead railway station to the north, Hawkesbury Road to the west, Hassall Street to the east, and Bailey Street to the South. The site features sloping terrain, with a level difference of approximately 12 m from west to east and around 5 m from south to north. The site topography and urban constraints combined with tight project boundaries, presented significant design and construction challenges. The station excavation is adjoining two caverns at its two ends, namely station cavern and crossover cavern respectively (Figure 1). The station is located predominantly within Ashfield Shale.



(a) (b)

Figure 1. Westmead metro station: (a) layout plan, (b) 3-d illustration

2 EXCAVATION DESIGN CONSIDERATIONS

2.1 *Retention system design*

The excavation of the Westmead metro station box required a robust and well-engineered retention structure to address the site's topography, geological and urban constraints. The retention system consists of soldier pile walls (with a pile diameter of 0.75 m) around the perimeter of the station box with the piles installed at a nominal centre-to-centre spacing of 2.0 m and typically socketed 1.5 m into Class I/II Shale (SH-I/II), generally corresponding to the upper third of the excavation (approximately 8–12 m) rather than extending through the full excavation depth. In zones of competent rock mass (e.g., SH-I/II), reinforced shotcrete and patterned rock bolt were provided without soldier piles, as additional support from the piles was not required in these zones. The Ashfield Shale has substantial variation in joint sets with a significant potential for wedge formation during excavation. Hence, a staggered pile toe arrangement with a pile socket of 3.0 m into SH-I/II for every third pile was adopted to mitigate the geological risk.

The retention structure design assessment was carried out using PLAXIS 2D, which accounted for the staged construction of the retention structure and stress relief of the rock strata. The excavation was designed as a drained excavation. The soldier piles were adopted to support both lateral earth pressures within the soils and weaker rock masses, as derived from the PLAXIS 2D analysis, as well as axial loads from ground anchors, an acoustic shed and other construction activities. A shotcrete wall of 200 mm was provided in front of the piles to retain the ground between the piles.

Ground anchors and pile bolts were adopted to provide lateral stability for the soldier pile wall. All elements of the retention system were required to be outside the minimum clear openings (MCO) specified by Sydney Metro. Multiple step levels across the capping beam were required to accommodate the site topography. In critical areas where the piles were required to resist high vertical loads from the acoustic shed or other construction activities, mandatory rock bolts were installed beneath pile toes to provide additional support to the rock mass. Piles supporting gantry systems were designed below the full excavation length (FEL) with minimum 3 m into SH-I/II to resist additional structural loads.

The excavation was predominantly in SH-I/II below the pile toes, where kinematic instability of localised wedges was a key concern. Geotechnical investigation indicated that the typical wedge was a steeply dipping tetrahedral wedge formed by joint intersections between north-northeast (NNE) and east-southeast (ESE) joint sets and random joints. The typical wedge volume was approximately 1 m^3. In addition, a ubiquitous sliding block with a volume of 6.4 m^3 was considered in the design based on the method outlined by Anderson & Pells (2002). The block was assessed to be large with respect to conditions typically encountered in excavations in SH-I/II. Large-scale blocks and wedges associated with persistent geological discontinuities, such as shear zones and faults, were not identified during the design phase—at least none deemed critical to the global stability of the station box retention system. If previously unidentified persistent geological features, such as major faults, were encountered during progressive excavation and face mapping, a formal design review process was implemented. This allowed the contractor to request a

reassessment of required supports by the designers and implement any necessary modifications as required to maintain overall excavation stability.

The assessment of rock wedge / block stability was performed using UnWedge, SWedge, and RocPlane. Pattern rock bolts (with a bolt length of 6.0 m and spacing of 2.40 m horizontal x 1.75 m vertical) and 150 mm steel fibre reinforced shotcrete were adopted to retain the typical wedges and blocks expected in vertical excavations in SH-I/II (see Section 3). Additional spot bolting was provisioned when adverse discontinuities (e.g. faults, joints, etc) were encountered during the excavation. Smaller wedges and blocks formed by tighter defects may not be visible during geological mapping and/or intersected by the pattern bolts. The design intent was to utilise an integrated shotcrete lining to retain the typical wedges that were not intersected by the pattern bolts. Wedges / blocks formed underneath the pile toes carrying significant axial loads were a critical concern. The pile axial loads were also considered in the wedge/block stability assessment, and a rock bolt below the pile toe was provisioned in the design.

A nominal constant groundwater pressure of 10 kPa was considered in both the shotcrete wall in front of the soldier piles and reinforced shotcrete lining analyses to account for localised build-up of groundwater pressure. Mandatory strip drains and/or weep holes (as required) were also installed behind the shotcrete during construction.

2.2 *Anchor exclusion zone*

An anchor exclusion zone of approximately 14 m in length was required along the north wall of the station box, where the ground anchors were prohibited to allow for the future construction of a pedestrian connection to the existing Westmead railway station. A specific design solution was developed for this area, comprising soldier piles supported by two rows of steel walers, which were restrained by ground anchors outside the anchor exclusion zone (Figure 2). Glass fibre reinforced polymer (GFRP) pile bolts were installed through the piles to provide additional support to the retention system. A simplified PLAXIS 3D model was also adopted to study structural interaction between the ground anchors, walers, and retention system within the exclusion zone.

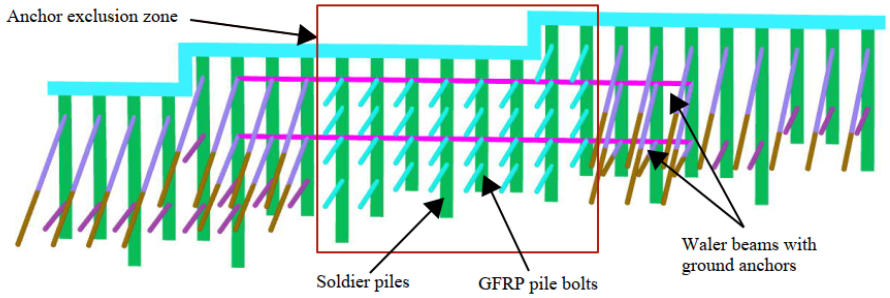


Figure 2. Anchor exclusion zone retention structure

2.3 *Cavern excavation at east wall and west wall*

Excavation of two mined caverns, located along the east and west walls of the station box, was planned to commence from within the box footprint. The design of the soldier piles and ground anchors in these areas was tailored to avoid interference with the future cavern excavation. Modifications included shorter pile toe embedment and ground anchors installed at flatter angles, with bond lengths located in Class III and IV shale. The design also accounted for the effects of cavern excavation on the retention system, resulting in increased design loads for both piles and anchors. GFRP rock bolts were adopted in place of conventional steel bolts to facilitate excavation within the cavern zones.

2.4 *Assessment results – predicted displacement*

Excavation within stressed rock strata, such as Ashfield Shale, can result in ground displacements due to stress relief. Historical data published by Oliveira & Wong (2012) indicate typical cumulative displacements in the range of 0.5–1.5 mm/m of excavation in Sydney region, with rare cases reaching up to 2 mm/m.

For the Westmead metro station excavation, assessment results indicate that predicted horizontal ground movements in soil and weaker rock masses are generally less than 10–15 mm. Within SH-I/II, estimated lateral displacements range from approximately 1.0–1.9 mm per metre of excavation. These estimates are consistent with displacement values recorded in similar geological conditions across Sydney. The predictions were based on lower-bound rock stiffness to account for variability in ground behaviour and to ensure moderately conservative displacement estimate for ground impact assessment. In deep, confined excavations, full stress relief may not develop, which can further reduce observed displacements.

3 OBSERVATIONS DURING EXCAVATION

3.1 *Geological mapping and site conditions*

The station box excavation was expected to be predominantly in Ashfield Shale, only encountering the Mittagong Formation contact towards the base elevation. The Ashfield Shale, distinct from the well-known Sydney sandstone, represents the basal unit of the Wianamatta Group. When fresh, it typically consists of dark grey to black claystones and siltstones, with laminites of fine sandstone. Its formation in low energy lacustrine or brackish marine depositional environments, allowed for the accumulation of fine-grained sediments up to 60 m in thickness. Bedding is invariably horizontal to slightly inclined, with little cross bedding. Sedimentary ‘slump’ structures within the unit, however, are known to influence the presence of joints and faults. A typical Class I/II exposure of Ashfield Shale is shown in Figure 3.

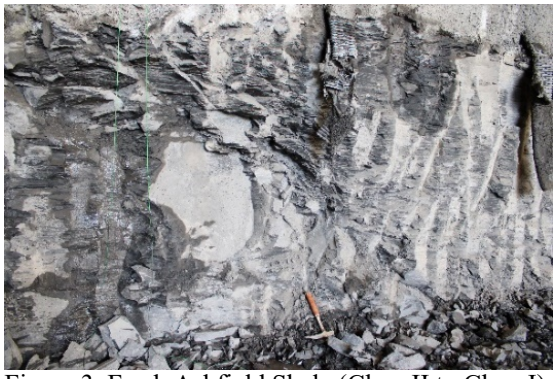


Figure 3. Fresh Ashfield Shale (Class II to Class I) with typical defects

Detailed and extensive field mapping was conducted throughout construction of the Westmead metro station box. The Ashfield Shale excavated at Westmead was mostly fresh to slightly weathered. The residual soil to moderately weathered profile transition comprised the top third of the excavation (i.e. 8–12m on average). The remaining two-thirds of the excavation had consistently fresh to slightly weathered rock mass with UCS values of 6MPa and above. Rock strength was assessed through field tests and limited lab samples. These characteristics remained the same even in areas which were more defect affected. It became clear during construction that Ashfield Shale ground behaviour was defect controlled. Unlike sub-vertical to low-angle horizontal defects in Sydney Sandstone however, these joint and fault defects in shale were predominantly mid-angle. When intersected by horizontal bedding partings, the potential for wedge failure increases. Joints at Westmead were planar, smooth, and clean or clay coated. Although usually of low persistence, these joints still proved challenging due to their random orientations leading to wedge formation such as in Figure 4. Where joints became more persistent – such as in proximity to large-scale fault features, wedge size even approached that of the design wedge, discussed in Section 2. Large moderately dipping faults were also encountered during the Westmead metro station box construction (Figure 5). These persistent features had significant crushed zones of rock fragments and clay, and closely spaced jointing. Other examples can be found in Salcher et al. (2024).

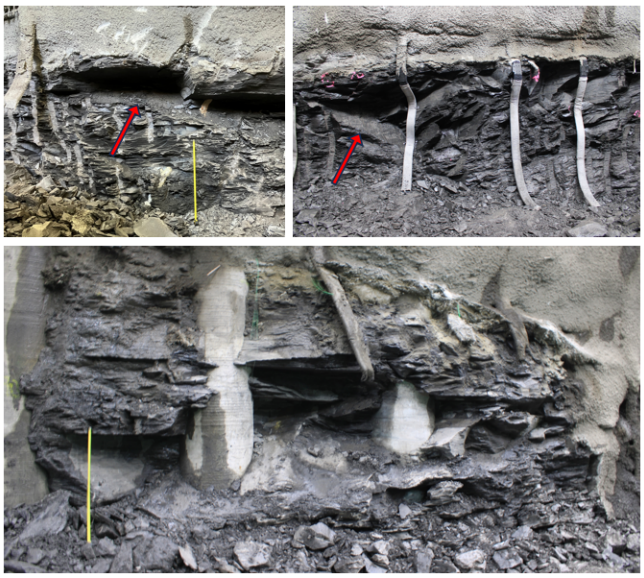


Figure 4. Typical wedges along mid angle defects in Ashfield Shale exposed during excavation. Wedge limited by piles (bottom).

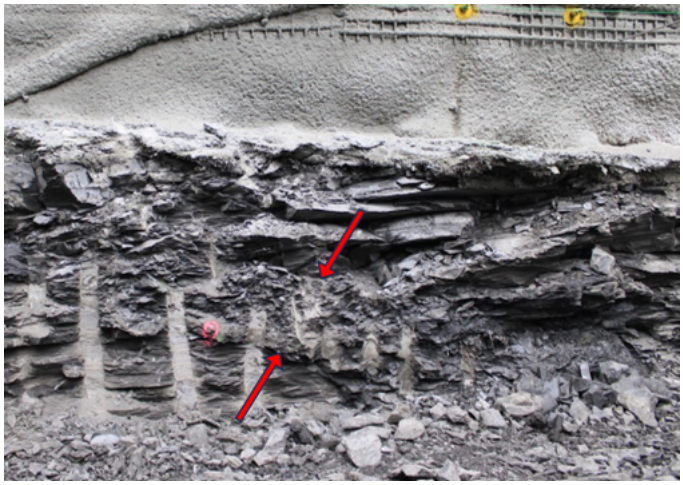


Figure 5. Mid angle fault with crushed zone and rock fragments (red arrows) in Ashfield Shale

3.2 *Comparison of ground monitoring data and design predictions*

The excavation performance of the Westmead metro station box has been comprehensively evaluated through monitoring data from anchor loads and pile displacement surveys, providing critical validation of the original design assumptions while revealing important insights into ground behaviour.

The survey monitoring data demonstrated ground displacement patterns largely consistent with established behaviour for excavations in Sydney's shale formations. Horizontal displacements in the Ashfield Shale ranged between 0.5–1.5 mm/m of excavation. It was observed that monitoring data at pile P126 (anchor exclusion zone) recorded displacements of up to 45 mm (i.e. approximately 1.5 mm/m of excavation), which is higher than the 32–35 mm recorded movements at other sections. While being consistent with design predictions, this larger movement was primarily attributed to the performance of the retention structure with steel waler beams and GFRP pile bolts in this localised anchor exclusion zone, by comparison to active anchors at other locations.

The monitoring data at both east and west wall, where two mined caverns were excavated, provided some insights on the impact of the cavern excavation to the station retention structure. On the east wall, the pile P176 displacement and anchor load were within design expectations, confirming the validity of the original geotechnical assumptions. The monitoring data demonstrates that no noticeable increase of the anchor load was recorded due to the cavern excavation.

However, the ground anchor installed on P85 (west wall) exhibited more than 20% increase in anchor load due to cavern excavation on west wall. The values at the West wall were still within design predictions as the design model was conservative. Nevertheless, the greater increase of anchor load was directly correlating with encountered fault zones and shear planes in this area interfacing with the adjoining mined tunnel excavation (see Figure 6). The station retention system, including the soldier piles and ground anchors, was designed for the potential impact of the cavern excavation to avoid overstressing of the system. Figure 7 illustrates a conceptual approach that was explored, involving the use of multiple instrumentation groups to verify ground performance specific to this scenario. This method, which simulates a desk study using automation tools for identified instruments, highlights a potential to improve efficiency—particularly valuable in projects requiring rapid excavation or mining advance.

The divergence between east and west wall anchor load data highlights how the uniform design assumptions were successfully adapted to address real-world geological heterogeneity. The monitoring data shows that the Ashfield Shale mostly behaved predictably throughout the entire excavation, fault interactions were properly mitigated through the adaptive design and the monitoring protocols effectively identified and managed variance from design conditions. This case study demonstrates how robust numerical modelling, engineering judgements combined with real-time instrumentation can successfully accommodate both expected shale behaviour and unforeseen geology challenges in deep excavations.

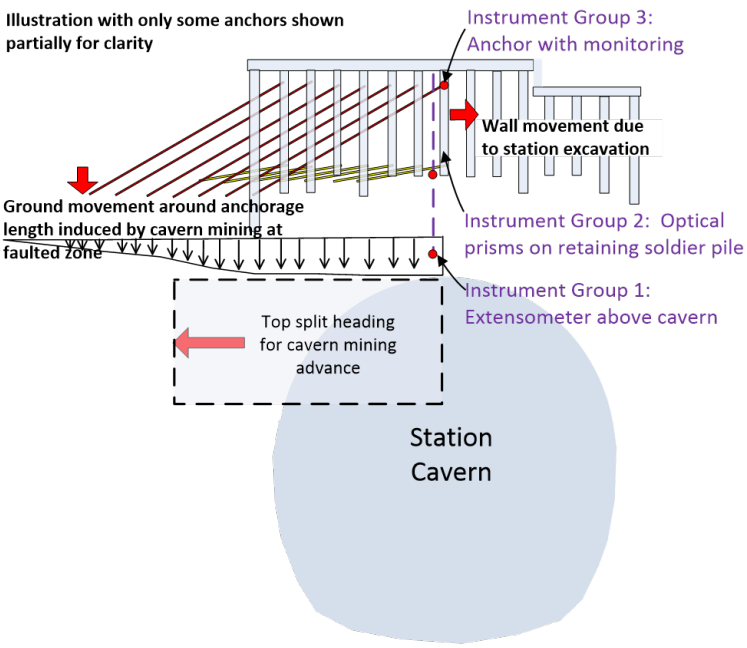


Figure 6. Illustration of interaction between station excavation headwall and cavern excavation

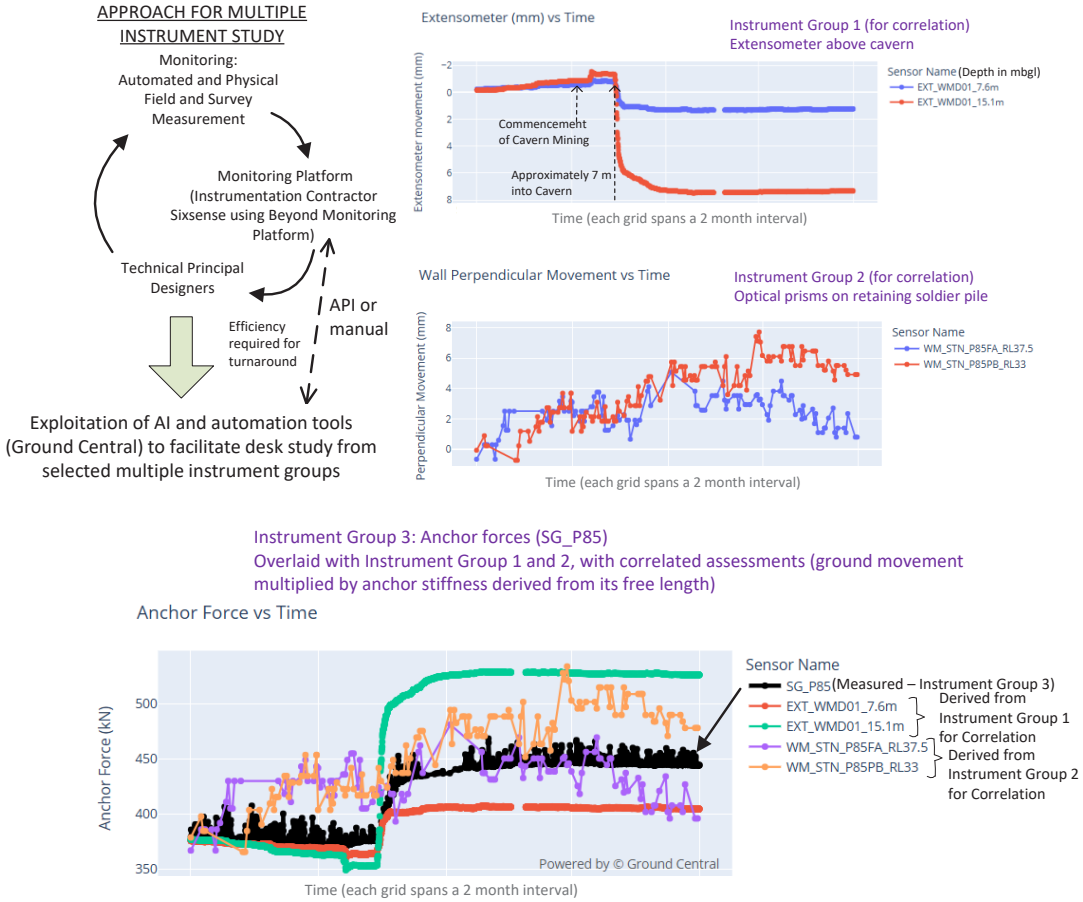


Figure 7. Explored approach using selected multiple instrumentation groups synced in advanced automation dashboards linked to monitoring platform to support desk study objectives aiming at reconciling monitoring performances with technical understanding and confirming trends against expectations

4 ADAPTIVE DESIGN MODIFICATIONS

The excavation of the Westmead metro station box in Ashfield Shale required continuous design adaptations to address the geological variability observed during construction. The initial design assumptions, based on available geotechnical investigation data and developed geotechnical models, were systematically refined through real-time geological mapping and monitoring feedback. This adaptive approach ensured stability while improving construction efficiency.

Detailed and extensive field mapping was conducted throughout construction of the Westmead metro station box to verify the assumed ground conditions. As excavation progressed, detailed geological mapping revealed localised variations in joint frequency, faulting, and rock mass quality. The presence of steeply dipping joint sets necessitated supplementary stabilisation measures beyond the initial pattern bolting design. Where mapping identified critical wedges or unstable blocks, additional spot bolts were installed, often at reduced bolt spacing than originally specified. This proactive approach prevented localised failures from propagating into larger wedge instabilities. In faulted sections, where rock mass behaviour deviated significantly from the design assumptions, pattern bolts were re-designed and adjusted, with bolt lengths extended beyond the potential wedge to ensure adequate load transfer into stable strata. Additional monitoring instruments, e.g. survey prisms, were also installed to mitigate the geotechnical risk.

Instrumentation data played a pivotal role in validating design assumptions and guiding modifications. Anchor load cells and inclinometers successfully captured the impact due to the fault zone and provided early warnings of anomalous behaviour, prompting timely interventions. Displacement trends were compared against predicted thresholds, with exceedances triggering additional bolting or shotcrete reinforcement before instability could develop.

This iterative process—where geological mapping, monitoring data, and numerical modelling continuously informed design adjustments—demonstrated the importance of flexibility in deep excavation projects. By integrating field observations with engineering judgment, the project team successfully mitigated risks while maintaining schedule and safety objectives. The lessons from the Westmead metro station box underscore that in complex geological settings, an adaptive design approach is not merely beneficial but essential for project success.

5 LESSONS LEARNT AND BEST PRACTICES

The construction of the Westmead metro station box within the Ashfield Shale formation provided invaluable insights into the challenges of deep urban excavations in geologically complex environments. The project highlighted critical lessons that can inform future excavations in similar conditions, along with best practices to enhance safety, efficiency, and cost-effectiveness.

5.1 *Geological and geotechnical considerations*

While pre-construction geotechnical investigation data provided a general understanding of site conditions, real-time geological mapping during excavation revealed localised variations—such as unanticipated fault zones and joint concentrations—that required immediate design adjustments. Future projects can consider incorporating higher-density investigations in areas with suspected geological discontinuities.

The behaviour of Ashfield Shale under excavation-induced stress relief also reinforced the importance of robust modelling assumptions. Lower-bound stiffness parameters in numerical models helped accommodate variability, but the project demonstrated that even these could underpredict localised displacements in faulted areas. Adopting probabilistic modelling approaches, which account for geological uncertainty, could further refine predictions.

5.2 *Design and construction adaptions*

The success of the retention system hinged on adaptive design principles, particularly the ability to modify support measures in response to encountered conditions. The use of staggered pile toe embedment proved highly effective in mitigating wedge instability. This strategy should be considered a best practice for excavations in jointed rock masses.

Another key takeaway was the effectiveness of hybrid support systems in constrained areas. The anchor exclusion zone at the north wall necessitated innovative solutions, such as steel walers and GFRP bolts, which provided stability without compromising future construction. Such flexible design approaches should be pre-planned for urban projects where space or functional requirements limit conventional retention methods.

The combination of shotcrete and pattern bolting was critical in the project to secure jointed rock mass. While re-mobilisation of site investigation rigs to verify uncertainty in faulting was commissioned for this site, additional verification via probing was still necessary midway during excavation to verify persistency of discontinuities. The excavation advance depth may need to be improvised depending on the ground conditions encountered.

5.3 *Instrumentation and monitoring*

The project validated the critical role of real-time monitoring in managing excavation risks. Anchor load cells and inclinometers provided early warnings of stress anomalies, enabling proactive interventions. However, the data also revealed that monitoring frequency should increase in faulted or highly jointed zones, where ground behaviour is less predictable.

Establishing predefined response protocols was another best practice. Salcher et al. (2024) provides good recommendations on the instrumentation and monitoring for deep excavations. Clear action thresholds—such as displacement rates exceeding 1.5 mm/m or anchor load deviations beyond 20% of design values—ensured swift decision-making. As demonstrated in this paper, future projects can similarly consider integrating these protocols into automated alert systems and linked to advanced cloud-based dashboards to facilitate desk study beyond display of factual monitoring data for instant team visibility (Figure 7).

6 CONCLUSION

In conclusion, this paper discussed a few design and ground performance challenges in a deep excavation case history sited in Ashfield Shale. The technical challenges and solutions for accommodating an anchor exclusion zone and adjoining cavern excavations were discussed. The collaboration between designers, contractors, and geotechnical specialists was instrumental in addressing these challenges. Contractor design involvement in the earlier design phases facilitated practical solutions, such as the optimised stepped capping beam elevation profile, soldier piling, bolt sequencing and access planning. Automation of review of case specific monitoring data was explored. The benefit of this approach is to increase efficiency of reviews when encountering more complex ground conditions.

7 ACKNOWLEDGEMENTS

Contributions from various teams on the project are fully acknowledged, in particular the GHD-SMEC design team for the station excavation, NOMA design team for the caverns, Sydney Metro, Sixense monitoring contractor, GLC's engineering geologist team, as well as the site team and project manager T. Olorenshaw are acknowledged. Sydney Metro is thanked for providing permission to publish this paper.

8 REFERENCE

Anderson, D. & Pells, P. (2001). An Approach to the Support of Vertical Cuts in Wianamatta Shales. Excavation Retention Symposium, AGM Sydney.

Oliveira, D.A.F & Wong, P.K. (2012). Ground movements associated with deep excavations in Sydney. Australian Geomechanics Journal, 47(4): 87-98.

Salcher, M., Khoo, M., Chan, I. (2024). Observations on the behaviour of surface and underground excavations in the shales of the Sydney region: Geotechnical lessons, Proceedings of the 2024 AGS Sydney Symposium.

THIS PAGE INTENTIONALLY LEFT BLANK

19th Australasian Tunnelling Conference – Acosta-Martínez, Stewart and Hudson-Smith (Eds.)
© 2025 Australian Tunnelling Society, ISBN 978-0-85825-002-4

Ground anchor design and installation challenges within saturated Sydney basin alluvium: A case study for Sydney Metro - The Bays Station

F. Ceballos Martinez & S. Monroe
TYPSA

S. Mohammadi & D. Jacob
Jacobs

ABSTRACT: Excavation and retention of alluvium and sandstone was a significant design component for the construction of The Bays station box for the Sydney Metro West Central Tunnelling Package. The soil in the upper part of the station box comprises of deep saturated estuarine and alluvial sediments, sand, residual soil, and weathered sandstone, with a total thickness up to 22 meters. These soils were designed to be supported by anchored secant pile walls, founded within the sandstone bedrock. In this paper, the design process for the anchors is discussed, from the preliminary design to the testing requirements, as well as the description of different challenges that were encountered during the excavation of the station box in relation to the anchor installation and testing, and the mitigation measures adopted, including specific capacity assessments and installation of additional anchors.

1 INTRODUCTION

1.1 Project Description

The Sydney Metro West project represents a transformative addition to Sydney's public transport network, aiming to enhance connectivity and capacity between the city's central business district (CBD) and Greater Parramatta. Spanning 24 kilometers, this fully underground metro line is designed to double rail capacity along this corridor, offering a target travel time of approximately 20 minutes between the two centers.

A key component of this initiative is the Central Tunnelling Package, comprising 11 kilometers of twin tunnels between The Bays and Sydney Olympic Park, with 5 stations (Sydney Olympic Park, North Strathfield, Burwood North, Five Dock and The Bays). Awarded in July 2021 to a joint venture between ACCIONA Australia and Ferrovial Australia (AFJV), this $1.96 billion contract included the design and construction of these tunnels, with completion anticipated in 2025. The design was carried out by a joint venture between Jacobs Australia and TYPSA (JTJV).



Figure 1. Sydney Metro West – Central Tunnel Package General Layout.

The present paper focuses on the design and construction challenges of the anchored retaining wall constructed at The Bays, where some of the most challenging geological conditions along the project were encountered.

1.2 Geology

The Bays Station at the eastern end of the CTP alignment is located within a low-lying area of reclaimed land, 50m south of the current shoreline of Sydney Harbor (White Bay). Broadly across The Bays area, the geological sequence consists of the following:

- Fill: Uncontrolled anthropogenic fill of unverified origin, with thickness typically ranging from 0.5m to 1.0m.
- Alluvium: Predominantly of Holocene age, comprising interbedded clays and sands. It exhibits high variability and heterogeneity, ranging from soft, loose sands to stiff to very stiff clays, often with interbedded lenses and pockets. The alluvial layer extends to approximately 19 m depth at the western end of the station box.
- Residual Soil / Extremely weathered Sandstone: Soils were predominantly stiff or better clayey soils with variability in thickness that was interbedded with extremely weathered sandstone, that follows the stepped profile of the underlying sandstone bedrock.
- Highly to Slightly Weathered / Fresh Sandstone: Highly weathered sandstone transitioning to slightly weathered to fresh sandstone at depth, with some jointing and bedding planes evident at the upper part.

Additionally, the Great Sydney Dyke crosses the station box diagonally, trending approximately 120°, and intersecting the north and east wall. The dyke is comprised of variably weathered dolerite, with soil properties in its upper part and becoming less weathered and of high to very-high strength with depth, especially in the core. The complexity of this geology, represented in the Leapfrog model that has been included in Figure 2 (left) is described in detail in a separate paper [1].

1.3 Geometrical constraints

The station excavation was designed with a retaining system consisting of secant pile walls, with 1.2m diameter piles, spaced 1.5m between secondary piles, although other solutions (including D-walls and propped options) were explored during the design process. These piles are socketed into fresh sandstone and are laterally supported by active anchors. Due to the complexity of the geotechnical profile described, up to five levels of active anchors are installed in the area with the greatest alluvial thickness, located on the western side of the station box.

The high loads required by the system necessitate anchor lengths of up to 55 meters for the first row of anchors, located at the capping beam, with bond lengths up to 7 meters. Furthermore, geometric constraints imposed by the presence of TBM tunnels at the western wall (where the soil thicknesses reach more than 20m) required precise alignment of the tendon orientations, with adjustments to both vertical and horizontal inclinations to avoid geometric and structural interferences. The use of high-detail 3D geometric models, BIM modeling tools (using Revit, Aecosim and coordination software as Navisworks), and advanced analysis was essential to ensure a correct system design.

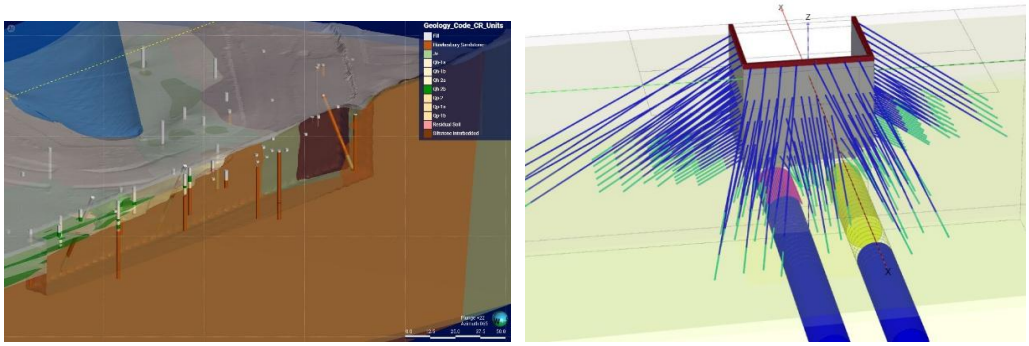


Figure 2- The Bays Station: Leapfrog model (left) and Plaxis 3D of the station box and TBM tunnels (right)

2 ANCHOR DESIGN

Grouted anchors with lengths in excess of 20m are not widely used and their interaction with the surrounding ground and modes of failure have not been extensively researched. The construction of the station box at The Bays for the Sydney Metro West Central Tunneling package comprised the drilling, installation and testing of anchors up to 58m in length, with inclination with the horizontal between 30° and 35° (as shown in Figure 3).The bond length of these anchors were designed for embedment in slightly weathered to fresh sandstone, however, the overburden above the rock head comprises of some man-made fill material but primarily of Holocene and Pleistocene alluvial deposits of non-homogenous clays and silty sands of up to 24m depth. In addition, the northern wall anchors had to pass through the Great Sydney Dyke before reaching competent sandstone.

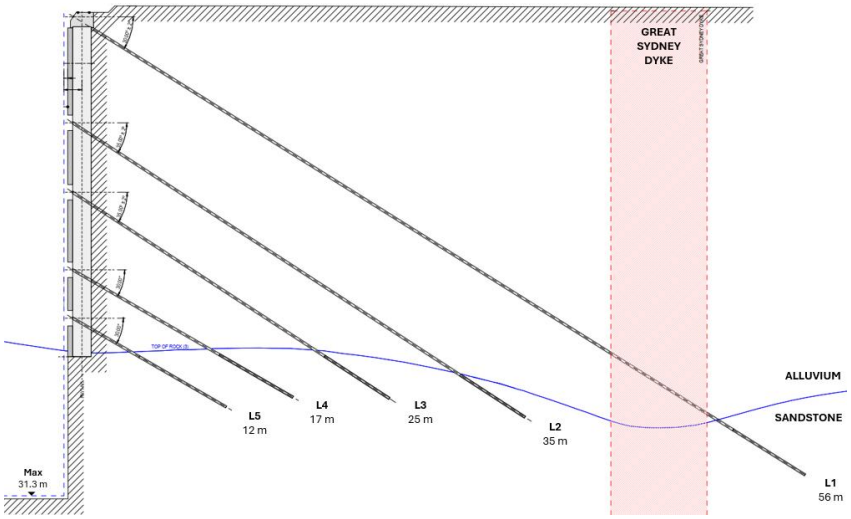


Figure 3. Anchored piled wall – Western part of the station box. Typical section

2.1 Anchored Pile Wall Description

Based on the results of the soil- structure interaction undertaking using FE analyses from which the axial forces experienced by the anchors were determined, active multistrand cable anchors were determined to be suitable for the secant piles. Where localized jointing is observed on the exposed sandstone rock faces where the secant piles do not extend to, passive bar anchors were proposed to be used to resist wedge movements, especially for areas around the dyke and the sandstone interface on the northern wall.

There are certain areas around the station box where geotechnical and geometrical conditions are complex because of the presence of deep-seated alluvium, the presence of the Great Sydney Dyke and the presence of the tunnel nozzles. This is summarized in Figure 4.

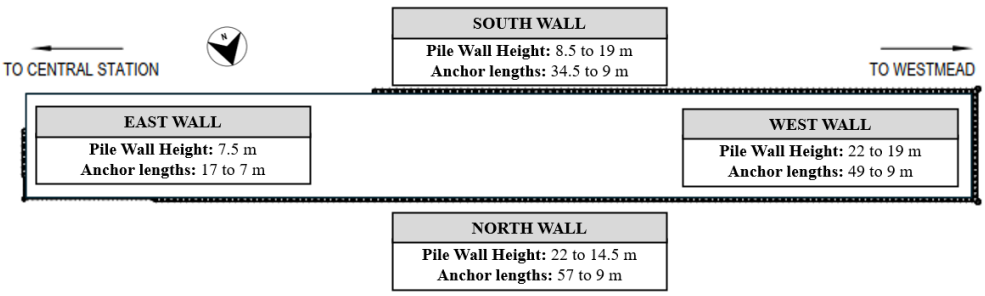


Figure 4. Station layout – Anchor distribution

It is noted that in the design of anchors, the effect of horizontal skewing is understood to increase the load component arising out of load deviation from the normal direction. The corresponding increase in load has been considered in the design of the anchor capacity.

2.2 Design considerations

The modes of failure for grouted anchors [2] working in tension are: failure within the rock mass (1), failure of the steel tendon or cables (2), failure of the rock to grout bond (3) and failure of the grout to tendon bond (4).

The anchor design verification has been undertaken in accordance with AS5100.3 to resist these modes of failures, including a potential gradual long-term deterioration as well [3].

For heavily loaded anchors, that require long bond lengths, it is noted that tests on conventional anchors have shown that the stress distribution along the bond length of an anchor is non uniform [2] [4]. This can cause that, for bonded lengths larger than 6m, a progressive debonding phenomenon (also known as the zipper effect) is noted to occur [5]. The bond stress concentration zone reaches the distal end of the anchor just before failure and this reduces the effective ultimate bond stress for anchors.

Keeping the above in mind, anchor pull tests (proof tests) were undertaken within the vicinity of The Bays Station to better understand the anchor resistance in relation to the ground conditions relevant to design. The undertaking of these tests aimed to provide information on (a) the bond capacity of an anchor at the anchor-grout interface and (b) the bond strength at the grout-rock interface to assess the required resistance for anchor working loads.

Five proof tests were undertaken by a specialist subcontractor. The tests were carried out in accordance with recommendations provided in TfNSW's guideline IC-QA-B114; Tests were carried out for anchors with 12 and with 15 strands and in seven load increments over eight cycles.

The ultimate bond stress values in sandstone and other pertinent anchor design parameters have been summarized in Table 1 below:

Table 1. Rock Mass Parameters for Rock bolts and Anchors

Rock Units	Ultimate Bond Stress* (kPa)	UCS (MPa)	Intact Rock Modulus (GPa)	Unit Weight (kN/m3)	Poisson's Ratio
Sandstone Class I	2000	30	6	24	0.2
Sandstone Class II	2000	20	5	24	0.2
Sandstone Class III	2000+	15	3	24	0.25
Sandstone Class IV	500	8	2	23	0.25
Dykes and Altered rock	250 – 500	8	2	24	0.25

*Failure along grout-steel interface governs in all cases.
+ Optimized from results of pull-out tests.

To account for progressive debonding, an effective bond stress adjusted by an efficiency factor (up to 15%) is often adopted for bond lengths longer than 7m and up to 10m maximum. However, the requirement for an efficiency factor is negated in those cases where bond stress is considered to be mobilized only when shear displacement occurs or in those cases where only residual values of bond stresses were considered for design.

2.2.1 Durability

The required design life for all anchors was a maximum of ten years, as per the requirements of the project's Particular Specification. Although these anchors are subject to the design and testing requirements of TfNSW specification B114, for anchors with a design life of 10 years or less, the corrosion protection requirements of B114 clause 3.2.1 do not apply.

Due to the proximity of the station box to White Bay, generalized or localized corrosion arising as a result of chloride ingress from saline groundwater, acid sulfate attacks and microbially influenced corrosion is anticipated during the design life of all active and passive anchors. Saline intrusion modelling was therefore conducted for the station box piles and anchor elements. The

results of the analysis indicate that seawater is expected to affect the station box excavation within 2 years of construction, with the highest exposure anticipated for the northern wall.

Corrosion protection was therefore provided through close fitting plastic sheaths with corrosion inhibiting grease or lubricant over the free end. Within the bonded end, the tendons were designed to be fully encapsulated with grout, with a minimum grout cover of 20mm.

2.2.2 Category/Reduction factors based on AS5100.3

For serviceability limit state design, the fundamental approach is that all applied loads are increased by a load factor (ψ) to give a design action with a very low probability of occurrence, which the resistances are reduced by a strength factor (φ) to give a design strength (R*) which must be greater than or equal to the design action [6]. Multiplying a design value by a strength or capacity factor implies that the variance of a given parameter will be directly proportional to the characteristic value of that variable and is therefore constant for a wide variety of possible actions and resistances.

Anchor verifications have been undertaken in accordance with AS5100.3, with relevant dispensations made as per requirements provided in the project's Particular Specifications with calculations to ensure that the anchors will not fail under any of the three failure mechanisms identified previously. The design process is summarized in Figure 5.

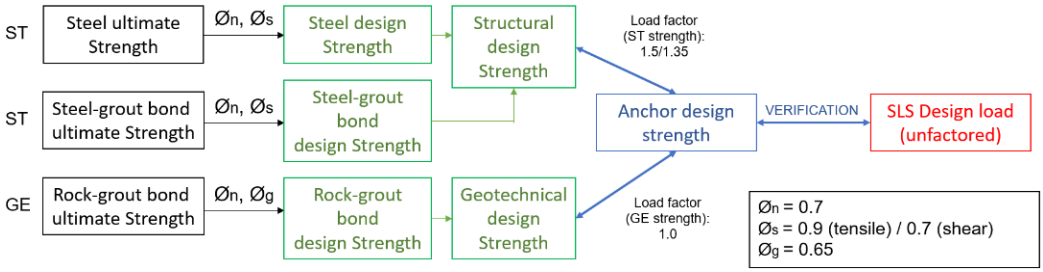


Figure 5. Anchor design flowchart (As per AS5100.3 and project specifications)

3 ANCHOR INSTALLATION

3.1 Anchor installation in alluvium: Challenges

The execution of ground anchors in secant pile walls within heterogeneous alluvial deposits composed of clay and sand, and below the groundwater table, presents notable geotechnical and construction risks.

In saturated sands and loose alluvial materials, the risk of borehole collapse or uncontrolled water inflow during drilling is significant. This can compromise the integrity of the borehole, affect anchor alignment, and may result in loss of ground or the need for additional stabilization measures. Additionally, the migration of soil particles (especially sands) due to the water inflow through the hole created in a watertight structure can cause unexpected settlement and, if ignored, potentially collapse.

During the excavation of The Bays station, excessive settlements were detected in some areas, mainly in the western and southern wall. As shown in Figure 6, the movement was appreciated to accelerate during some periods and stabilize in others (as shown in the settlement markers).

It was determined that the cause of the settlement was due to the soil migration caused by the adopted drilling methodology. This was consistent with some site observations reporting high water inflows through the anchor holes, in some cases accompanied by an influx of some fine-grained soils, and this settlement observations correlated with the timeline of anchor drillings for anchor rows two and three (the two first rows under the groundwater level).

Several Monitoring Action Team (MAT) meetings were held, including representatives from the construction and design team, to analyze the information available and determine the best course of action to correct the drilling methodology and prevent further movements during the excavation of the subsequent rows. Subsequent corrective measures included the adoption of blast

bags to minimize migration of fines during anchor drilling and continuous ground monitoring during anchor drilling and investigations.

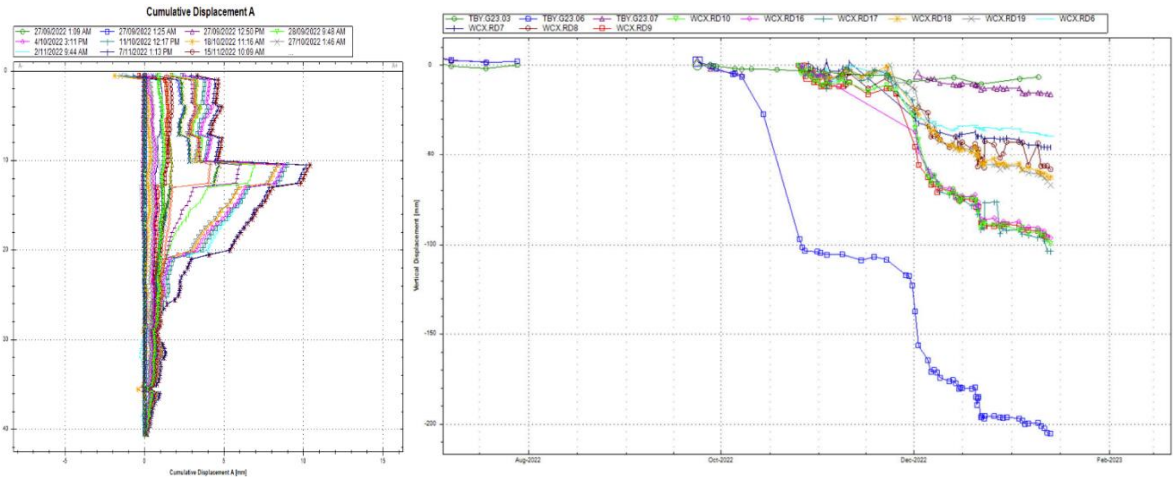


Figure 6. Up–Inclinometer readings (per date) and Settlement marker readings.

3.2 Other challenges during installation

Due to the characteristics of the soil material and the length of the required pilings, several challenges were faced during the execution of the anchors.

- Clash with reinforcement: The design of the pile was contemplated taking several measures into account to avoid reinforcement clashes, including specifically positioning the reinforcement cages with respect to the excavation, and the adoption of one sacrificial bar. In spite of these measures, there were some occurrences of this type of clash, most of which involved the entrapment of anchor drilling bits. Repositioning of anchors and a reassessment of pile capacity was undertaken in these instances.
- Temporary casing retrieval issues: In some instances, the retrieval of the temporary steel casing for piles was hindered due to unknown obstructions encountered in the anthropogenic fill layers. In those instances, the anchor installation and the overall behavior of the pile wall was reanalyzed to assess how the pile capacity reduction due to the temporary casing being in place affected the overall structural design.
- Concrete pouring issues: Due to weather conditions, pile lengths and other variables, some defects were identified during pile integrity testing, or when the station box excavation progressed. The effectiveness of the original anchor design and the structural performance of the pile wall needed to be reanalyzed in some situations.

The presence of the problems described above required different actions from the design perspective, including the relocation of the anchor or a redesign of the wall section considering a different anchor arrangement. The implementation of these measures is described in section 5.

4 ANCHOR TESTING

4.1 Active anchor testing requirements

Proof testing, load testing and acceptance testing were undertaken as per the requirements cited in Annexure B114/L – Testing Procedures for all multistrand anchors and bar anchors (steel and GFRP) for the following requirements:

- Proof tests: Carried out to provide information for the final design (anchor capacity at grout/ground, grout/tendon or duct/grout interfaces). These tests were carried out prior to ground anchor work commencing at the site. Five tests were undertaken.
- Load tests: These were carried out in a similar approach to the Suitability tests presented in TfNSW Specification B114 to verify the performance of represented working anchors, with

a minimum of six load cycles for the 2% of the total number of anchors tested for each distinct anchorage ground condition. Approximately 15 anchors were tested.
- Acceptance tests: These were carried out on all remaining anchors to demonstrate the short-term ability of the anchor to support the proof load with sufficiently low creep rate or load loss, and the efficiency of load transmission to the bonded length.

4.2 Failures during anchor installations

During anchor installation and testing, sixteen instances were noted where acceptance tests failed. These were noted to be either instances where the rate of residual load loss exceeded 1% during acceptance tests or when the strand displacement or elongation was higher than the predicted theoretical extension.

Most of the acceptance test failures were observed at the southern wall of the station box, where anchor lengths were relatively shorter than the northern wall and geological anomalies were not observed. However, the total number of acceptance test failures only made up 2% of the total number of anchors that were installed.

The failures during acceptance testing can likely be attributed to the following factors:

1. Some field tests has shown discrepancies between theoretical and observed extensions in anchor strands occurring due to variations in the Youngs modulus values of steel tendons tested in the laboratory versus when the tests are carried out in field [7] [8] [9]. A possible explanation is that stressing multistrand tendons in the field takes longer than laboratory testing of individual strands, and during this time, plastic deformation occurs in the steel, yielding a larger extension and therefore correspondingly a lower Youngs modulus value.
2. In anchors with long, sheathed tendons enveloped in a protective grout column, friction in the free length of the anchor can be developed around the grip assembly of the anchor head which tends to reduce the measured extension. It is estimated that only about 70 percent of the applied prestress was transmitted along the entire tendon length [10]
3. Over drilling or under drilling the anchor installation borehole is also known to affect the free length extension of the anchor. In cases of under drilling, the strands may experience slack in the boreholes that may be incorrectly logged as excessive elongation.

5 MITIGATION MEASURES ADOPTED

5.1 Anchor capacity assessment

During acceptance testing, in some cases, the strands became damaged or began to extend beyond their theoretical extension limits and the anchor would not load to the test load.

In order to assess the as built conditions, the acceptance test results, the anchor drilling records, and grout compressive reports were reviewed. The acceptance test records provide invaluable information on the available bond length of the anchors; the bond length of the anchors was downgraded when the measured elongation exceeded 110% of the theoretical elongation, as per B114. In addition, the anchor drilling records provided information on where the rock was encountered in comparison to design assumptions.

The review provided information to reassess the remaining capacity of the anchors to support updating the numerical model and reassess the geotechnical capacity of both pile and anchors. The anchors are checked against the three failure mechanisms to ensure no failure will occur upon the changes to anchor forces and strands. Next, the as-built wall section is checked for its structural capacity to sustain the applied forces imposed by the soil and surcharge and satisfy the strength and safety requirements for those sections. If these checks are satisfactory then the anchors can be used as is, otherwise it was advised that an additional anchor was to be installed.

5.2 Additional anchor installation

Where the review of acceptance test results showed the anchor does not have the adequate capacity as required by design, or an unforeseen obstruction was encountered; a replacement anchors with same number of strands and same hole size and orientation as design and same bond length, 0.5m above/below the design level, was used. To not exceed the capacity of the pile or the

maximum capacity of the installed anchors, the maximum excavation level before the installation and stressing of the replacement anchor was limited to 0.5m below the replacement anchor level. In other cases, the relocation of the anchor was required outside the prescribed allowance, requiring a verification of the final situation to check that the loads were within the limits of the pile wall. In all scenarios, the redundant anchor was decommissioned, and the hole was grouted and sealed against the water ingress.

6 CONCLUSIONS

The design and construction of the anchored retaining wall at The Bays Station for the Sydney Metro West project presented significant challenges due to the complex geological conditions and the presence of deep alluvial deposits and the Great Sydney Dyke. Furthermore, the high groundwater table posed further complication to anchor installation leading to occasional sediment and water inflow during drilling of anchors which led to unexpected settlement locally.

The implementation of secant pile walls supported by active anchors required diligent planning and innovative solutions to address issues such as anchor installation difficulties; Digital modeling tools and adjustments to anchor lengths and orientations were adopted to avoid structural interferences such as TBM and anchors.

To ensure the anchor performance, comprehensive proof testing, load testing, and acceptance testing were performed. The test results provided information in identification and mitigation of anchor failures. The mitigation measures included additional anchor installations and/or the remaining capacity assessments of anchors together with assessment of the as built sections to ensure structural integrity remains satisfactory.

Overall, the successful execution of this project highlights the importance of adaptive design strategies and collaborative efforts in overcoming geotechnical challenges using MAT meetings. The lessons learned from this study will contribute to future projects involving similar geological conditions and complex anchor installations.

ACKNOWLEDGMENTS

The authors would like to acknowledge the contributions of the wider Central Tunneling Project team comprising Sydney Metro, Acciona Ferrovial Contractors, Jacobs and Typsa for their valuable input that helped in the completion of this paper. This acknowledgement also extends to the significant collaborative efforts out of which the implementation of this innovative design and construction of The Bays station box was made possible.

7 REFERENCES

C. Parker and J. Raymer. 2025. "Managing challenging ground conditions through targeted rock grouting for the Bays Station Box, Sydney Metro West Project," ATC2025, Perth.

G. Littlejohn and D. Bruce. 1975. "Rock Anchors - State of the Art.," Ground Engineering.

P. Xanthakos. 1991. Ground Anchors and Anchored Structures., Washington D.C.: John Wiley.

G. Vukotic, J. Gonzalez and A. Soriano. 2013. "The influence of bond stress distribution on ground," in 18th International Conference on Soil Mechanics and Geotechnical, Paris.

H. Ostermayer and T. Barley. 2002. "Geotechnical Engineering Handbook, Volume 2: Procedures," in Ernst & Sohn Publications.

R. A. Day, P. K. Wong and H. G. Poulos. 2007. "Fifteen years of geotechnical limit state design in," in Common Ground, Brisbane.

Transport for New South Wales. 2020. "QA Specification B114. Ground Anchors," Transport for New South Wales.

Australia Standard. 2017. "AS5100.3 Bridge Design Part 3: Foundation and Soil Supporting Structures," Australia Standard.

British Standard, "BS8081:2015. Code of Practice for Grouted Anchors," British Standard.

M. Hennquin and H. Cambefort. 1966. " Consolidation du remblai de Malherbe," Revue Generale des.

19th Australasian Tunnelling Conference – Acosta-Martínez, Stewart and Hudson-Smith (Eds.)
© 2025 Australian Tunnelling Society, ISBN 978-0-85825-002-4

Impact of deep underground station excavation on existing assets in Sydney, Australia

S. Manoj
Beca, Australia

B. Okumusoglu
Acciona Geotech, Australia

P. Kozak
Jacobs, Australia

ABSTRACT: Deep excavations and tunnelling have the potential to adversely impact existing assets, and an engineering impact assessment is critical to identify and plan mitigation measures for impacted assets. A targeted geotechnical investigation, detailed analysis using reliable data and design of mitigation measures with well-planned instrumentation and monitoring can help reduce the risk of adverse impacts and failures. This paper discusses the challenges involved and the impact of excavation of a station box and TBM launching, as part of the Central Tunnelling Package of the Sydney Metro Project in Australia. The excavation was near sensitive assets where the presence of loose thick alluvial soil, paleochannel with high ground water table, and presence of The Great Sydney Dyke, presented significant challenges. The paper discusses the challenges and how predicted and acceptable effects were established for the sensitive assets and remediation planned for the successful design and construction of the station box.

1 INTRODUCTION

1.1 *Impact of tunnelling and station excavation on existing assets*

Tunnel construction and associated deep excavation work in urban cities have the potential to significantly impact the existing assets within the influence zone of the construction activities. This can include damage to or failure of impacted assets leading to litigations and/or project delays. Ground water changes caused by drained excavations and drawdown can affect stability of ground or cause contamination and affect water quality. Excessive ground movements and vibrations also can cause damage to sensitive infrastructure. During the planning and design of tunnelling activities it is important to have careful considerations to avoid adverse impact on any assets within the tunnelling influence zone. An assessment identifying the impact of tunnelling and deep excavations on all existing assets including underground utilities within influence zone, is an integral part of any tunnel construction. This includes checking for any adverse impacts and developing mitigation measures and contingency plans.

The challenges involved in the design and construction of retaining system for an underground station excavation at The Bays in Sydney's Inner West, near highly sensitive and heritage structures, are discussed in this paper. The station box was near a heritage structure and several other important assets. The TBM tunnel was to pass through the area with a shallow cover. Presence of The Great Sydney Dyke at this location with thick loose alluvial soils and the presence of a paleochannel with a high ground water table posed major challenges to design and construction. The high permeability of Hawkesbury sandstone in this location allowed depressurisation of overlying alluvial deposits, increasing the risk of ground settlement due to changes in effective stress.

This paper discusses how the design and construction of a robust retaining system was implemented, and the ground movement and ground water drawdown were predicted and its impact on the nearby assets assessed and mitigated, to successfully complete the work without causing any adverse impact on the nearby sensitive assets.

2 THE PROJECT

The Sydney Metro West project is part of Australia's biggest public transport project and will double the rail capacity between Parramatta and the Sydney CBD, transforming Sydney for generations to come. The project includes 24-kilometre twin tunnels excavated using double shield hard rock Tunnel Boring Machines (TBM), excavation and associated civil works for temporary support of the nine deep underground stations, (Figure 1) cross over caverns and access shafts. Acciona Ferrovial Joint Venture (AFJV) was awarded the design and construction of the Central Tunnelling Package (CTP). One of the most challenging aspects of CTP was deep excavation and tunnelling through The Bays station, located between Glebe Island and the White Bay Power Station (WBPS).

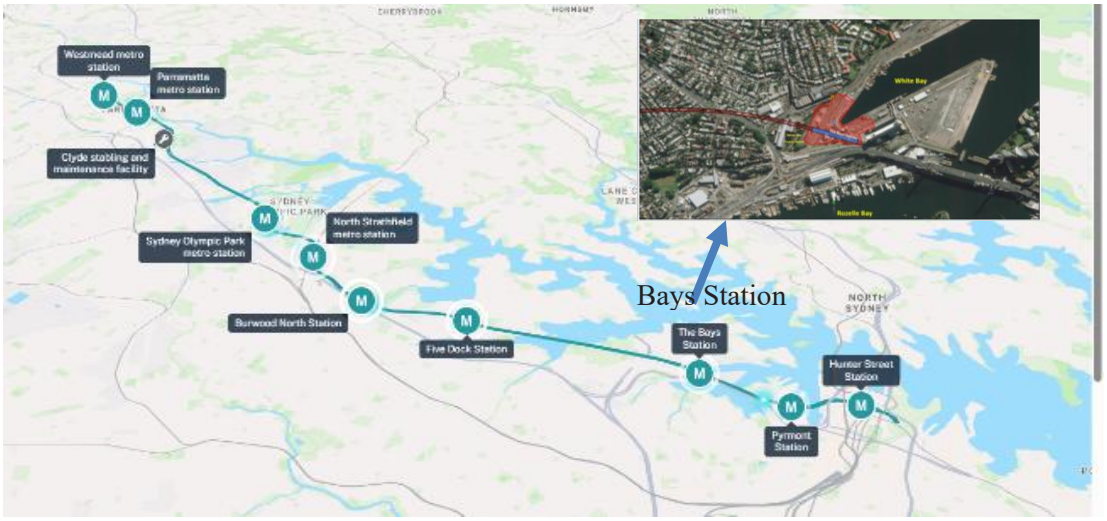


Figure 1. Sydney Metro West 24-kilometre alignment and Station locations

2.1 *The Bays Station*

The Bays station box (Figure 2) has a clear opening of 230m x 24m and 31m depth and is located within the White Bay industrial area, near the White Bay Power Station (WBPS) in an approximate East-West orientation. WBPS is a New South Wales (NSW) state heritage listed building built between 1912 to 1917. The existing ground levels varied between +2.7m to 4.3m AHD. The retaining system consisted of reinforced concrete secant walls embedded into competent rock, and laterally restrained by ground anchors, within the overburden soil. The system was designed with an intended design life of 10 years. Within the rock layers the retention system consisted of spot bolting combined with localized shotcreting below the toe of piles to the depth of excavation, to support and hold potential unfavorable rock wedges or any unstable discontinuities within the rock layer.

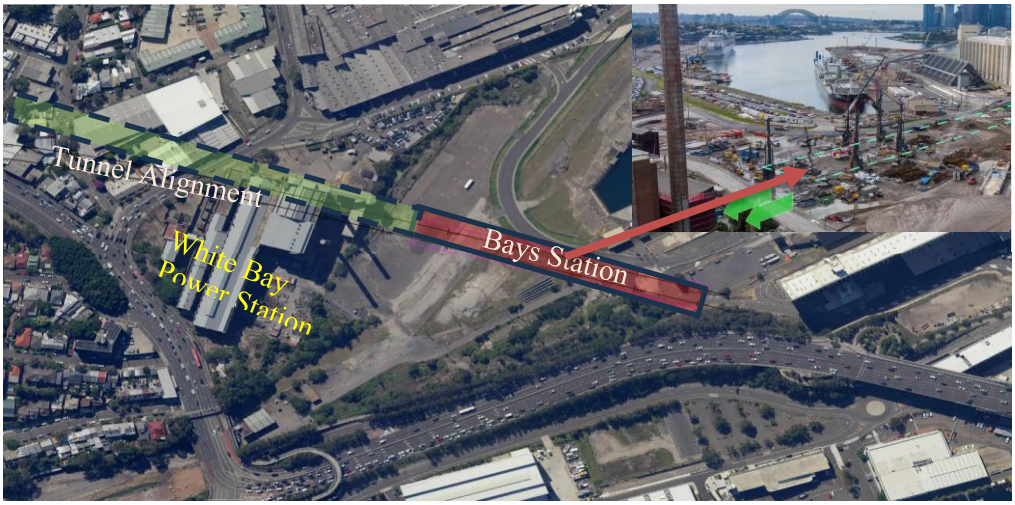


Figure 2. The Bays Station excavation, tunnel alignment and White Bay Power Station location with five piling rigs working simultaneously. The green arrows show the direction of TBM.

2.2 *Typical ground conditions and ground model*

The bedrock geology of The Bays area is characterised by a sub-horizontally lying Permo Triassic sedimentary sequence, approximately 230 million years old. The stratigraphic units expected to be encountered within the area under discussion, is expected to comprise of manmade fill materials followed by quaternary alluvium/estuarine sediments and the Hawkesbury Sandstone formation (Herbert, 1983).

The Great Sydney Dyke which is typically about 6 m wide, extends through the eastern and northern walls of the station box at The Bays Station as shown in Figure 3.

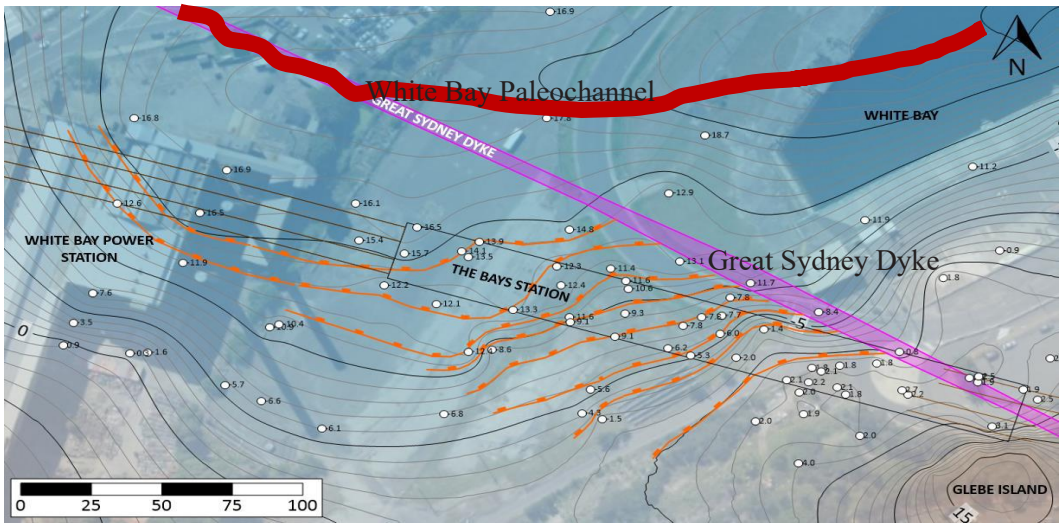


Figure 3. Great Sydney Dyke and the paleochannel

The presence of a palaeochannel in the vicinity near Johnstons Bay is also noted. The floor of the channel is about 36 m below sea level and is infilled with very recent Quaternary, mostly Holocene, and some older underlaying Pleistocene, alluvial deposits comprising rivers, sands, estuarine muds and marine clay deposits. Figure 4 shows the interpreted bedrock contour plan of The Bays area showing the top of highly weathered rock or better, at 1 m interval, based on the investigations done within the station locality.

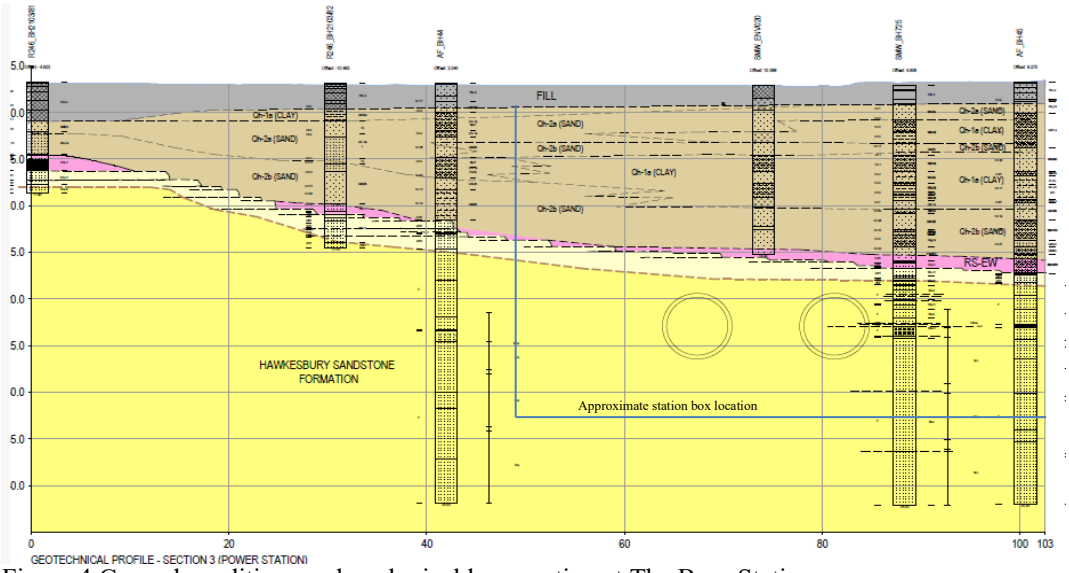


Figure 4 Ground conditions and geological long section at The Bays Station

The geological long section along the station box is shown in Figure 4. The top of rock is shallow at the White Bay Power Station location which indicates that the tunnel would have a thin rock cover above its crown which presents a challenge in terms of the potential impact on the foundations. The ground water table has been established to be between 1.7 m and 3.63 m below ground level (+0.58 and +1.44 m AHD) based on the readings from ground water monitoring wells. The design ground water level has been considered at ground level.

2.3 *Permeability of sandstone*

The station excavation below the rock level is designed to be drained excavation, however, the project specifications required that the inflow into the excavation should be limited to an inflow criteria of less than 5 L/s. Based on the borehole information and water pressure testing in boreholes, the vast majority of the lugeon values for typical Hawkesbury Sandstone was interpreted to be less than 1 uL ($1x10^{-7}$ m/s). However, when the sandstone contains more open defects as a consequence of faulting and shearing or stress relief near the surface or near the paleochannels, higher lugeon values of permeability are possible. Higher values of permeability of > 35 to 100 uL were obtained at few locations within the excavation zone where there were sub horizontal permeable features present. Even in good quality sandstone, the presence of sub horizontal defects could potentially cause large inflows into the excavation.

3 IMPACT ASSESSMENT OF EXISTING ASSETS

The project specifications required that the tunnelling contractors plan and execute their activities in such a way as to cause no adverse and unacceptable impacts on existing assets. There are several buildings, sensitive structures, heritage buildings and utilities within the influence zone of the tunnel and station excavations. As part of the initial design process, an engineering impact assessment was done to establish a zone of influence, (defined as an area within a 5mm settlement contour) by assessing the predicted ground movements due to tunnelling and station excavations (Gaba 2017). A four-stage risk-based approach in accordance with CIRIA PR30 was adopted, where predicted effects due to ground movement and ground water drawn down on existing assets, were compared against a set of established acceptable effects (Burland et.al. 1997, Boscardin and Cording 1989) in the first and second phases, to identify assets requiring detailed assessments. The Phase 3 assessment included identifying mitigation and protection measures and setting alert levels and contingency plans. An instrumentation and monitoring plan was then developed in Phase 4 to follow during the construction stage to monitor the actual impact.

3.1 *Engineering Impact Assessment*

The local geology, depth of cover to the tunnel and soil structure interaction, methods of excavation and type of retaining systems and their installation sequences and ground water conditions can all influence the impact of construction on existing assets. Ground movement resulting from tunnelling, surface excavations and ground water drawdown was estimated to assess the overall impact.

3.1.1 *Tunnelling induced settlements*

The tunnelling work included excavation by Tunnel Boring Machines (TBMs) as well as mined tunnels by road headers for station and ventilation caverns and adits and excavators with impact hammers/drum cutters for cross passages. The tunnel induced settlements were conservatively estimated considering the volume loss (V_L) at the surface with the surface settlement profile simplified as a Gaussian curve in cross section. The width of the settlement trough (k) is influenced by the geology and soil and rock parameters intercepted by the tunnel. Based on contractor experience from previous projects in similar geology, V_L and k values are adopted for the encountered ground conditions, as presented in Table 1 below.

Table 1. Volume loss and trough width parameters adopted for prediction of settlements

Geological Unit	Volume Loss V_L %	Trough Width Constant k
Soil or extremly weathered rock	0.1	0.60
Ashfield Shale (Class IV-V)	0.25	0.50
Ashfield Shale (Class I-III)	0.15	0.35
Hawkesbury Sandstone (Class IV-V)	0.20	0.60
Hawkesbury Sandstone (Class I-III)	0.15	0.60
Ashfield Shale/Hawkesbury Sandstone	0.25	0.40

3.1.2 *Surface excavation induced settlements*

The Bays Station excavation is retained by secant piles within alluvium and within rock with rock stabilisation, and the excavation is progressed from the surface using conventional techniques. Displacement profiles for the retaining walls are calibrated from numerical models, and before calibration the maximum vertical displacement in alluvial soil is assumed to be 70% of the maximum horizontal displacement.

3.1.3 *Groundwater induced settlement*

The tunnel is lined and fitted with a waterproofing gasket and is undrained and not expected to cause significant drawdown. The Bays Station excavation is tanked and retained within alluvium and is drained within rock with controlled drainage. An inflow limit is specified in the project specifications. A detailed hydrogeological model was developed by the consultants and water drawdown induced settlement was calculated as a function of the soil stratification, depth of overburden soil and the water drawdown. The hydrogeological assessment was done for two different scenarios of drawdown predictions. The red contours as shown in Figure 5 indicated the drawdown allowing total inflow to the station box of 5.2 L/s, adopted as Upper Bound scenario for the settlement impact. The hydrological studies predicted significant drawdown based on conservative assumptions and recommended grouting around the power station area thus reducing the ground water inflow into the excavations. A mitigated scenario 2, with rock permeability improved to an average of 1 Lugeon, and inflow to the station box of 3 L/s, is represented by the blue contours. This scenario has the bedrock below the secant pile wall assumed to be grouted around the perimeter of the station box. Grouting reduces the bedrock permeability to 1 Lugeon. This scenario has been adopted as Base Case (most probable) scenario for the settlement impact analysis presented in following section, noting that a third case Green Scenario was analysed as a sensitivity check but not further analysed. An illustration of each drawdown case is shown in Figure 5.

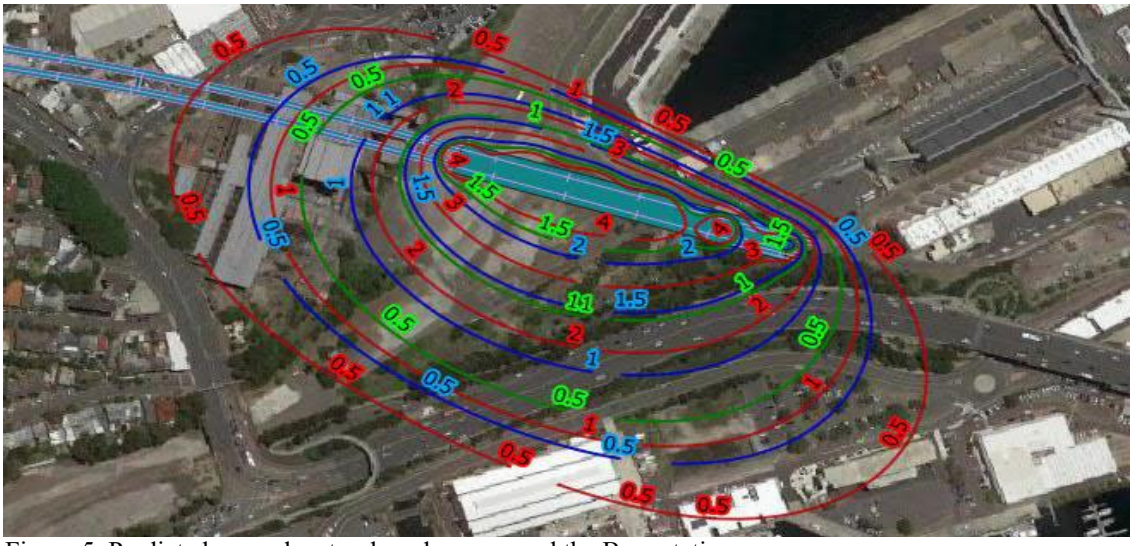


Figure 5. Predicted ground water drawdown around the Bays station area

A sensitivity analysis was performed where the maximum settlement exceeded the established acceptable limits, however, the building slopes and strains were found to be within the acceptable limits. Higher settlement magnitudes near the White Bay Power Station is attributed to the thicker alluvial soft soil deposits of the paleochannel, and water drawdown induced settlements.

3.2 *White Bay Power Station*

The White Bay Power Station is a heritage structure, built between 1912 and 1917. A part of the building is known to be on pile foundations", but more details were unavailable. The northeast corner of the power station is underlain by about 18 to 20 m of surficial fill and saturated alluvial soils over a stepped sandstone cliff profile. The pile foundations are presumed to be round timber piles and floating in the alluvium. The power station and its foundations were reportedly upgraded in 1956 but as-builts are not available. The TBM at the power station has shallow rock cover as shown in Figure 4 and there was concern of the impact on the heritage structure due to the tunnelling and station construction. The chimney of the power station (Figure 6a) has been analysed by advanced finite element modelling, to predict the displacements and stress experienced, based on the impact assessment results (Figure 6b).


Figure 6a. The Chimney of WBPS

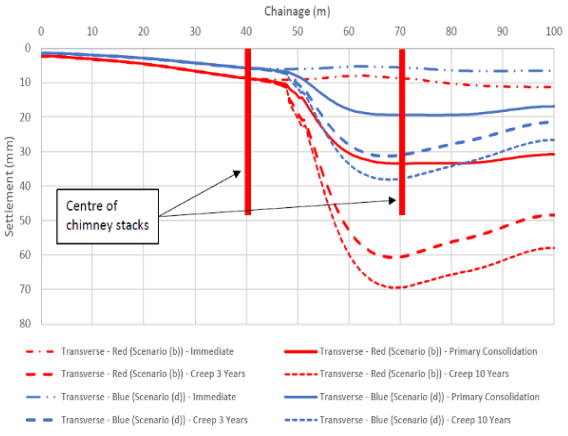


Figure 6b. Predicted settlements at the chimney location

The two chimney stacks are major contributing elements to the visual identity of the White Bay Power Station and needed to be retained in situ and conserved and interpreted as an integral part of the significance of it. Assessment of settlement has been undertaken using Plaxis 2D modelling using Mohr Coulomb material model. A structural 3D finite element modelling was also developed by the consultants, to examine the structure behaviour under predicted settlements. Based on the calculations using the predicted settlements and slopes, the top of chimney was predicted to experience lateral displacement of approximately 51 to 61mm for the two scenarios. Predicted settlements including the primary consolidation settlement, long term creep and immediate elastic settlement were considered in the analysis as shown in Figure 7b.

The results of analysis indicate that the groundwater drawn down without ground treatment results in higher amounts of settlements of the order of 70 to 80 mm at locations where alluvium is thicker. The settlement gradient was also the steepest in this case. It is noteworthy that the coefficient of consolidation of the clay layer varied from 1.6 M2/year to 160 m2 /yr as provided in the Geotechnical reports which resulted in a large variation in the prediction of time period when the predicted settlements will occur. After considering the ground improved by grouting to an average permeability of 1 Lugeon the settlements improved to about 30 to 40 mm. Several contingency plans were developed along with a rigorous instrumentation and monitoring plan, to monitor the ground movements and drawdown affecting the heritage structure and to take necessary action in accordance with the contingency plan if alert levels are exceeded. A watch and act system in a observational approach was adopted where if the ground movements were exceeded then back analysis of the data and installation of mitigation measures were to be immediately applied.

The settlements are predicted conservatively and instrumentation and monitoring along with contingency plans during construction was implemented to monitor and control settlements and trigger action plans if the acceptable settlement limits are exceeded. During construction the actual settlements (Figure 7) at and near the excavation areas were within the acceptable limits established for the structures, thus allowing the construction of the station box and tunnel to be successfully completed.

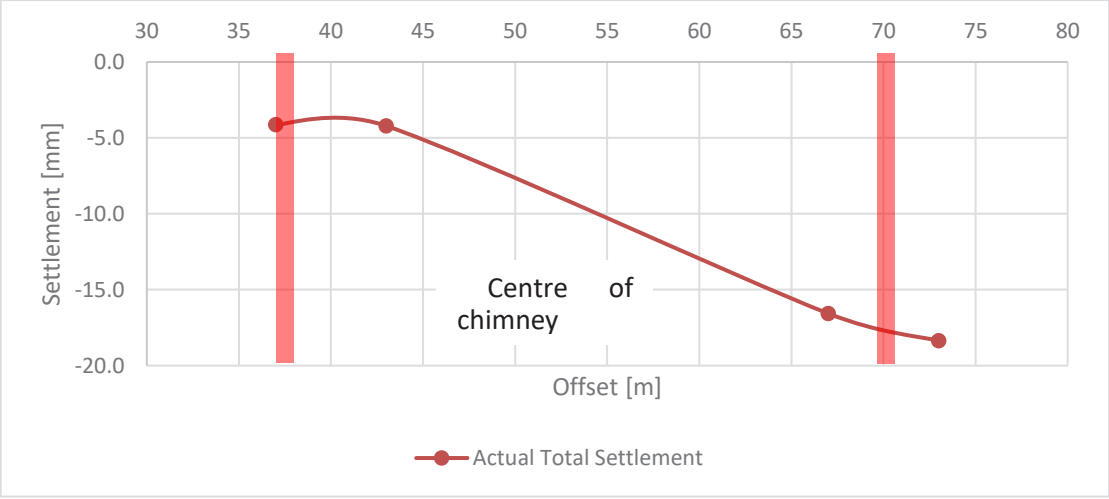


Figure 7. Actual settlements measured at Chimney Stack

4 CONCLUSIONS

The excavation of the Bays Station of SMW included one of the deepest applications of a secant pile wall to date along the shores of Sydney Harbour. The design and construction challenges at this location were overcome by the following approaches to successfully complete the work without causing any adverse impact on the WBPS.

- A reliable and robust ground model incorporating all the subsurface data by a thorough review of historical data and desktop study and a targeted additional geotechnical investigation
- Detailed geotechnical and hydrogeological assessments to establish a range of design parameters including hydraulic conductivity of ground. Geotechnical analysis to predict ground movements, and sensitivity analysis predicting a range of expected ground movements and drawdown for various probable scenarios.
- Establishing acceptable effects for the WBPS which could be compared against the predicted values to confirm that there is no adverse impact on the structure.
- A grouting program with curtain grouting around the box and grouting under the WBPS, targeting the permeability of 1 Lugeon to control the inflows to meet inflow criteria.
- A robust retaining wall design with secant pile walls tanked within the alluvium and rock stabilisation within the rock.

The work was successfully completed without any breach of the alert levels and additional improvement measures in the contingency plan were not warranted during the construction. The successful completion of this project is an example where early understanding of challenging ground conditions by targeted detailed ground investigations and detailed analysis and sensitivity assessments can help overcome such challenges successfully.

ACKNOWLEDGEMENTS

The authors extend their sincere gratitude to Sydney Metro for their support and permission to publish this paper. Additionally, the AFJV site team deserves recognition for their dedicated efforts in executing the challenging works, particularly during heavy rain events encountered during the excavation. The design consultants Typsa Jacobs JV efforts in the design are also thankfully acknowledged. The first author would also like to specially thank her previous employer Mott MacDonald for providing the opportunity to work on this prestigious project.

5 REFERENCES

Sydney Metro West Interactive Portal. https://caportal.com.au/tfnsw/sydmetrowest/map.

Gaba A, Hardy S, Doughty L, PowrieW, Selemetas D. 2017. Guidance on embedded retaining wall design, C760. CIRIA, London

Boscardin, D.M. & Cording, EJ. 1989. Building response to excavation induced settlement. ASCE Journal of Geotechnical Engineering, 115: 1-21.

Burland, J. 1997. Assessment of risk of damage to buildings due to tunnelling and excavation. Earth. Geot. Eng., Balkema, 1189-1201.

Herbert C. 1983. Sydney 1st edition. Geological Survey of New South Wales, Sydney

19th Australasian Tunnelling Conference – Acosta-Martínez, Stewart and Hudson-Smith (Eds.)
© 2025 Australian Tunnelling Society, ISBN 978-0-85825-002-4

Large temporary secant-piled peanut-shaped shaft constructed for the Alkimos desalination plant in Perth: Design and construction

Jose Ramon Bombin Saiz, Alberto Gabarron Duran, Sergio Jimenez Perez and Carla Sancho Perez
Acciona Engineering and Design, Spain

ABSTRACT: Stage 1 of the Alkimos Seawater Desalination Plant (ASDP) is being designed and constructed by the Alkimos Sea Water Alliance (ASWA). The project requires a temporary shaft structure for the intake and outfall tunnels, intake pump station, and outfall chambers. This shaft is crucial for the project as the Tunnel Boring Machine (TBM) launch de-pends on its completion. The shaft features a unique peanut-shaped geometry, combining two intersecting circles of 44.5m and 49.0m in diameter, and is 20m deep. This design minimizes the need for intermediate props, facilitating internal work. The shaft walls are constructed using a secant pile temporary wall (SPW). The paper discusses the complex geotechnical and structural design, challenges faced during construction, and how the design was staged to allow early pile wall construction and how the design sequencing facilitated early construction of the pile wall. The report also details monitoring data collected to ensure construction proceeded safely.

1 INTRODUCTION

For the construction of the Intake Building (within the Alkimos desalination plant complex in Perth, Australia), a temporary earth retaining structure is required to reach the foundation support level of the building, where the tunnel portals will be constructed.

To facilitate these works, this structure must not include struts or bracing struts, leaving the largest open space free of obstacles that could hinder the scheduling and execution of tunnel activities and interfere with the future Intake building.

To achieve this, a peanut-shaped containment shaft is developed. It consists of two intersecting cylinders of 44.50m and 49.0m that fit as closely as possible to the geometry of the Intake building. The earth retaining structure is made up of SPW and a total excavation depth inside the shaft of 20.3m.



Figure 1. Temporary Shaft.

The Intake building located inside receives the intake and discharge tunnels from the sea, which are executed using a TBM. Therefore, once completed, the shaft must be free of any obstructions

that could hinder excavation, storage, and removal of material, as well as the construction of the Intake building in a second phase, facilitating logistics.

This type of structure (peanut-shaped geometry) has often been used in other projects for similar cases, i.e. the need for large spans for the introduction of TBM: Tiete Shaft in Line 6 Metro in Sao Paulo [1] (4 circular secant shaft D=31m and an excavation of 33m). or Shaped Shaft of Silvertown Tunnel Project in London [2] (4 circular secant shaft D=21.2 m and an excavation varies from 20m to 24 m).

2 GEOTECHNICAL INVESTIGATION / PARAMETERS

The desalination plant is located less than 1 km from the coast. It is placed in a dune field. The ground elevation before starting the work was about 10-20 m above sea level. During the preliminary leveling works, the elevation of the desalination plant is between levels +10.50m and +11.00m.

As part of the geotechnical campaign carried out for the design and construction of the Alkimos desalination plant, due to the complexity of this structure, a more intensive geotechnical campaign was developed for this structure. The campaign consisted of the execution of 9 boreholes with lengths from 45 m to 60 m along the peanut shape of the structure. Additionally, due to the particle size distribution of the sandy layer with no cohesion, four pumping tests were conducted to determine the permeability of the materials, as a significant flow of water towards the excavation was expected. Based on the geotechnical campaign carried out, a geotechnical profile was created, which is shown below.

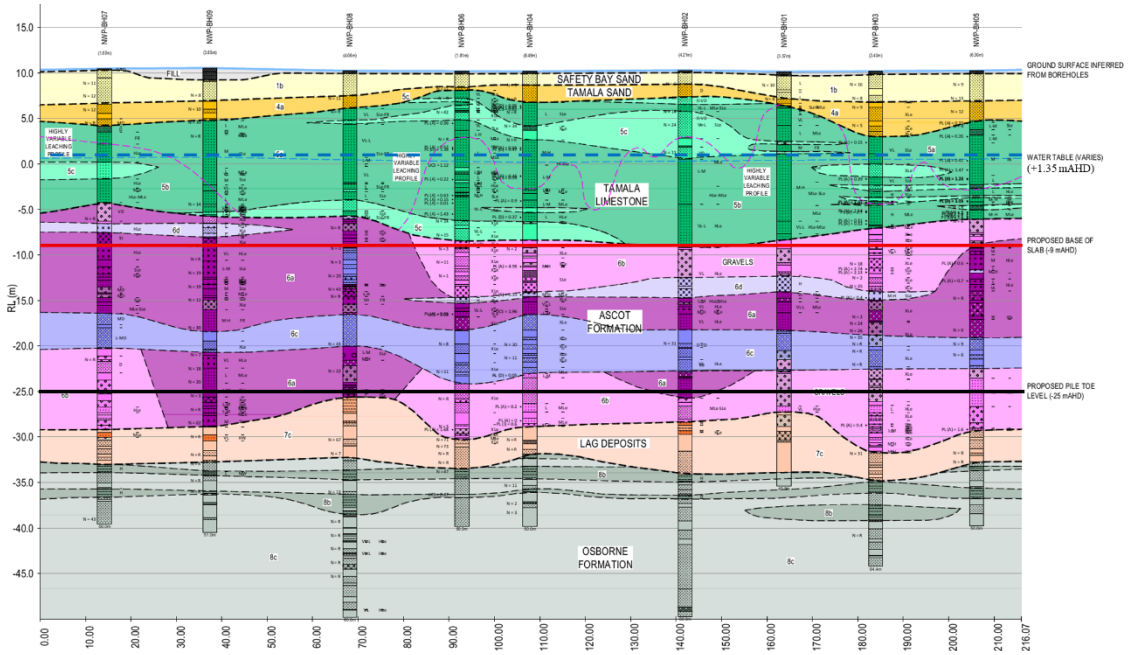


Figure 2. Geotechnical profile

The materials are predominantly granular, with no cohesion. Unit 5a/5b (Tamala Limestone) shows significant cementation, giving it a rocky appearance. However, for design purposes, it has been defined as a granular material with high cohesion, as the boreholes did not ensure continuity in the rock.

A critical factor in the design of this structure is the presence of the groundwater table above the maximum excavation depth. Based on the information from the piezometers and the records of nearby piezometers over several years, the water table level in the shaft area was determined at +1.35 m AHD during the construction process.

The estimated permeability for these levels is high (see table 1). Therefore, detailed assessment of the pumping rate was developed to ensure the excavation stability

The materials are predominantly granular, with no cohesion. Unit 5a/5b (Tamala Limestone) shows significant cementation, giving it a rocky appearance. However, for design purposes, it has been defined as a granular material with high cohesion, as the boreholes did not ensure continuity in the rock.

A critical factor in the design of this structure is the presence of the groundwater table above the maximum excavation depth. Based on the information from the piezometers and the records of nearby piezometers over several years, the water table level in the shaft area was determined at +1.35 m AHD during the construction process.

The estimated permeability for these levels is high (see table 1). Therefore, detailed assessment of the pumping rate was developed to ensure the excavation stability

The following table includes the most significant geotechnical parameters

Table 1: Geotechnical parameters.

Geological Unit		γ_b (kN/m^3)	c' (kPa)	φ' (°)	E_d (MPa)	k_H (m/day)	k_V (m/day)
1b	Safety Bay Sand	17	0	34	25	15	1.5
4a	Tamala Sand	17	0	34	40	20	2.0
5a/5b	Tamala limestone	20	80	30	450	150	15
5c	Tamal residual soils	18	0	36	50	20	2.0
6a/6b	Ascot Formation cemented	22	0	35	100	10	1.0
6c	Ascot Formation Unconsolidated	19	0	35	45	10	1.0
7c	Lag deposits	19	0	40	100	4	2.0
8a/8c	Osborne Formation	19	0	40	90	4	2.0

γ_b = bulk unit weight, c' = effective cohesion, φ' = effective angle of friction, E_d' = effective elastic modulus, k_H = horizontal permeability, k_V = vertical permeability

3 OPTIONEERING AND FINAL SOLUTION

In the Alliance Development phase, the intake and outfall shafts were defined as two independent circular shafts with a diameter of 18 meters. Each shaft was designated as the starting point for the TBM for the construction of the tunnels. This implies the necessity to duplicate many of the elements necessary for the operation of the TBM.

To reduce costs and shorten execution time (the shaft is the critical path of the construction), the project's bidding phase proposed unifying the two shafts as an optimized solution. Initially, a circular shaft encompassing both buildings was proposed, but this design presented significant challenges due to its large diameter.

In a second solution, the two buildings were unified with a D-Wall shaft, which would be part of the permanent structure. However, this solution faced issues with waterproofing, as the joints between wall modules did not provide adequate waterproofing for the 100-year lifespan of the structure, requiring additional treatment. Additionally, straight walls required several levels of intermediate struts to reach the planned excavation level, interfering with necessary openings for the TBM. These struts needed to be substantial, and the reinforcement ratio in the D-walls was very high (more than 300 kg/m³).

As a final solution, a peanut-shaped shaft was analysed, allowing the SWIPS building to be constructed inside. This solution has several advantages:

- Since the SPW was temporary, long-term waterproofing is not necessary.
- The ratio of the shaft excavation area to the building footprint is relatively small.
- The final quality of the SWIPS structure is improved and the leakage risk reduced substantially.
- A cylindrical-shaped retaining wall works mainly under compression, reducing the need of intermediate struts, and, more specifically eliminating them entirely in the launch area, facilitating the associated works.

Various ground retention solutions were evaluated; however, a steel sheet pile wall (SPW) was ultimately selected due to its advantages over alternative methods:

– The presence of rock strata complicates the excavation required for a diaphragm wall (D-Wall), necessitating the use of hydro-milling equipment. This method is significantly more expensive, and the specialized machinery is not readily available.
– The presence of highly permeable soil layers prevents the use of a sequential ring excavation method. Implementing such an approach would require extensive and costly groundwater control treatments to reduce flow and mitigate the risk of piping.

4 DESCRIPTION OF THE FINAL SOLUTION

This structure features a very large peanut-shaped geometry of two partial intersecting circles of 43.3m and 47.8 m in diameter. To support both earth and water pressures, a SPW was constructed as an earth-retaining structure. The wall was constructed using 1200 mm diameter piles, spaced 750 mm apart, and with a length of 35 meters. Unreinforced piles were constructed using 20 MPa concrete, while reinforced piles were made with 40 MPa concrete. A total number of 14 Glass Fiber Reinforced Polymer (GFRP) piles have been installed in the location where the TBM are to be launched.

The piles are located at an elevation of +10.00 m AHD, with the maximum excavation level at -10.30m, resulting in a total excavation depth inside the shaft of 20.3 m. The embedment of the piles below the maximum excavation level was 14.7m.

Three levels of bracing are provided for the SPW, consist of a waler beam section of 0.8x1.0m and props of significant dimensions: 27 meters in length with sections of 2x2m and 2x2.5m. There is an additional bracing, exclusively at the intersection of the cylinders, like a slab supported on the ground with a section of 6 x1.5m.

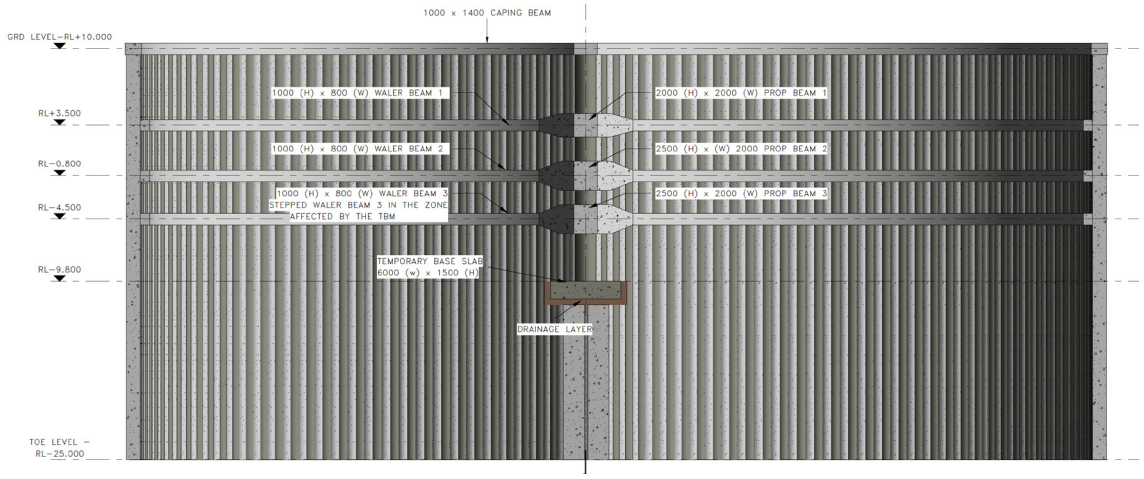


Figure 3. Temporary shaft elevation.

5 CALCULATIONS PERFORMED

5.1 *Plaxis2D/3D modelling*

Due to the complexity of the work, the modelling of the structure and its completion on the ground has been carried out using the Plaxis 2D and Plaxis 3D programs. Multiple analyses have been conducted to adequately understand the behaviour of the structure.

Firstly, an axisymmetric model was created in Plaxis 2D to understand the behaviour of a circular shaft with a diameter of almost 50 meters. This was essential in determining the magnitude of the loads acting on the pile wall. It was observed that the circumferential loads would be much greater than usual for a circular shaft of this diameter. The magnitude of these loads prevented the use of low-strength concrete (<5 MPa) for unreinforced piles. It was found that concrete with a simple compression strength of 20 MPa was necessary for unreinforced piles.

In the Plaxis 2D program, it is common to model walls as "plates" elements, which do not consider the transverse rigidity of the wall for obtaining vertical loads. In a Plaxis 3D model, the

use of isotropic "Plates" results in horizontal loads (bending moments, shear forces) that cannot be developed in a SPW, as there is no transversal reinforcement connecting these elements. Additionally, since this wall is made with piles of two different deformation modules, the behaviour of the whole is not homogeneous.

To determine the deformation module for compression loads in horizontal and vertical directions, a volumetric element modelling of a pile wall in Plaxis 3D with the planned configuration was performed, as shown in figure 4.



Figure 4. Modulization SPW in theorical position (left) and outside the theoretical position (right)

This wall consists of piles with two different deformation moduli, corresponding to concrete strengths of 40 MPa (E = 32,800 MPa) and 20 MPa (E = 24,000 MPa). Simulations also included piles installed within planned tolerances but outside theoretical positions. Results showed that the vertical deformation modulus is primarily controlled by the stiffer, higher-strength piles (around E = 29,800 MPa), both for theoretical and tolerance-based positions. Horizontally, the deformation modulus is closer to that of the 20 MPa piles, with values significantly lower (60 %) when accounting for installation tolerances.

Due to the lack of continuous transverse reinforcement, shear transfer horizontally is limited, so the wall mainly resists stresses along the reinforced piles. This was modelled by reducing transverse shear modulus (G_{12} and G_{23}) near zero, except for vertical shear (G_{13}), kept at 70% of its actual value.

Three SPW types were modelled in Plaxis 2D/3D to assess pile tolerance effects:

- Type 1: Theoretical parameters.
- Type 2: Horizontal stiffness reduced to 10% of theoretical.
- Type 3: Horizontal stiffness at 10% and vertical second moment of area at 33.3% to simulate cracking.

To ensure structural behaviour met design criteria for the large shaft, three perimeter waler beams were proposed at specified levels and modelled as beam elements supporting the SPW plates. These beams reduced vertical loads on piles by acting as stiff “false struts” and absorbed part of circumferential loads, especially in models with lower horizontal stiffness.

Another important element in the design of this shaft is the struts (o props) located at the contact area between the two circular shafts. These elements serve to maintain the continuity of each shaft's circumference. They function to maintain circumferential integrity around each shaft. Given the large loads applied and the ~30 m span between supports, a robust cross-sectional design is required. The connection of these elements with the rest of the structure has been made as a joint, modelled as "node to node" elements in the Plaxis model, as they are only subjected to axial loads in addition to their own weight.

The connection between the SPW and the struts is made through two 1.80 m diameter piles called King Piles, located at the intersection of the two circles that form part of the shaft. Due to the defined characteristics of the SPW, the circumferential load cannot be transferred to the struts through vertical shear at the contact between reinforced and unreinforced piles, as it does not provide sufficient resistance to be considered. Therefore, the only feasible mechanism is through vertical bending of the reinforced piles. This results in very high loads on the king piles, reaching reinforcement quantities of 2.6% steel. This element has been modelled in Plaxis 3D as a beam.

5.2 *Structural elements*

The main structural elements contributing to the arching behaviour of the shaft are the props. There are four props in total. The first three props are beams connected with the waler beam rings,

providing support to the SPW along the peanut shape. The props' dimensions vary from 2.0m to 2.5m in height, 2.0m in width, and 30m in span. The waler beam maintains a constant cross-section of 0.8 m in width and 1.0 m in height, except at the prop connection points where the height is increased to accommodate additional reinforcement. The fourth prop is a slab over the ground, 1.5m thick and 6m wide, mainly supporting the piles at the circle intersection.

Finally, the capping beam at the top of the excavation provides continuity and ensures that all the pile heads displace similarly.

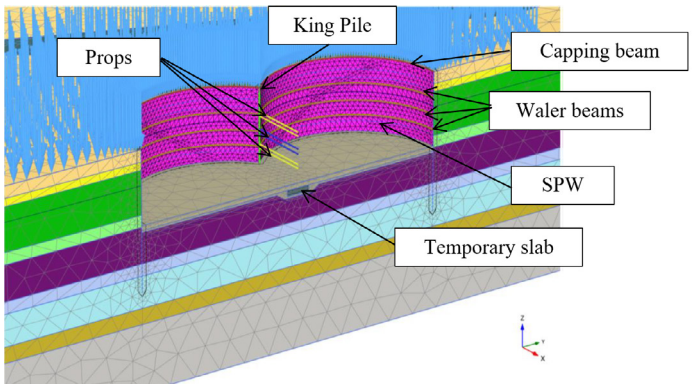


Figure 5. Plaxis 3D Model and structural elements

6 CONSTRUCTION PROCESS

This structure constituted the critical path in the Alkimos project schedule, as tunnelling activities could not commence until the maximum excavation depth was achieved. Consequently, the construction process was executed continuously, without interruptions during weekends or nighttime.

A total of 308 piles were installed, comprising 136 reinforced concrete piles of 1200 mm diameter, 152 unreinforced concrete piles of 1200 mm diameter, 14 GFRP piles of 1200 mm diameter, and two reinforced piles of 1800 mm diameter. The pile installation presented several technical challenges. Given that the unreinforced piles exhibited higher-than-typical strength for a steel sheet pile wall (SPW), it was necessary to formulate a concrete mix with delayed strength gain to minimize resistance during drilling for the installation of the reinforced piles.

As part of the SPW system, strict verticality control was mandatory. Any deviation could generate gaps in the wall, resulting in water ingress and groundwater infiltration into the excavation. Therefore, pile specifications mandated that the first 20 meters be constructed using temporary casing, with a verticality tolerance of less than 5 mm per meter. Beyond this depth, piles were executed without casing, allowing a verticality tolerance of up to 10 mm per meter. These stringent tolerances ensured sufficient pile overlap along the entire length, maintaining the integrity of the wall within the maximum allowable limits.

These rigorous construction requirements necessitated continuous verticality monitoring of the casing for each pile, along with SHAPE testing, which reduced overall construction productivity. During excavation, the correct execution of the piles was confirmed, with only minor water ingress observed at limited pile joints.

Excavation within the shaft was carried out in five phases, each aligned with the installation level of the waler beams. Excavation commenced in early December 2024 and was completed by March 2025. The principal challenge during excavation was the unexpectedly high strength and continuity of the Tamala Limestone layer. Despite prior geotechnical investigations, its resistance exceeded expectations, necessitating the use of hydraulic hammers for rock removal.

The excavation process proceeded in four phases, each advancing to the execution level of the waler beams and props. Excavation was continued until the structural elements reached 80% of their design strength.

Another critical aspect of the construction process was managing water infiltration from the base of the excavation. According to the calculations made and the estimated permeability parameters in the project, a maximum flow rate of 120 l/s was expected. Measurements showed that the maximum pumping flow rate was about 60 l/s.

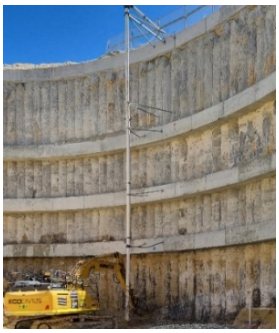

Figure 6. SPW and waler beam


Figure 7. Tamala Limestone rock

7 MONITORING

7.1 *Monitoring plan*

The complexity of the structure implies a monitoring plan for the structure to verify the correct behaviour of the shaft during its construction. A total of 8 inclinometers, settlement control points in the shaft's influence zone, 32 optical prisms on the beams, and over 150 strain gauges inside the beams have been included. All elements are automated, providing real-time excavation data.

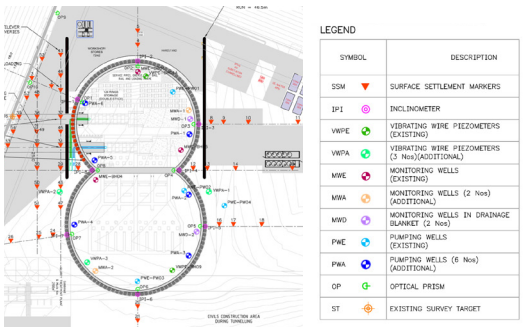


Figure 8. Monitoring plan layout.

7.2 *Monitoring carried out*

Since the start of the excavation works, continuous monitoring of all installed elements has been conducted. As expected, displacements were observed during the excavation phase; however, these movements stabilized once excavation activities ceased and coincided with the concreting stages of the waler beams and struts.

The maximum displacement recorded was minimal—approximately 10 mm—for excavations reaching depths of 20 meters, resulting in negligible ground settlements in the vicinity of the shaft. Compared to the predicted values, displacements were significantly lower below the first waler beam, although slightly higher in the upper sections.

During the dewatering process inside the shaft, a drawdown of approximately two meters was observed in the external groundwater level. This behaviour had been anticipated and was accounted for in the design of the dewatering system.

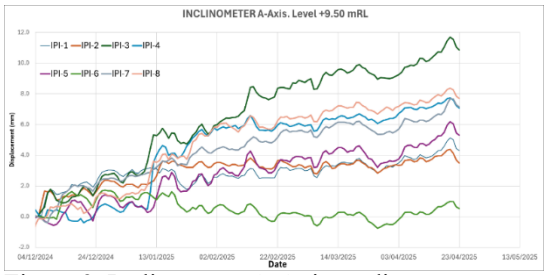


Figure 9. Inclinometer A-Axis readings.

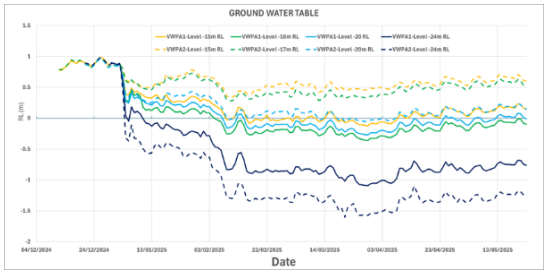


Figure 10. Ground water table outside shaft

After analysing the data, it was concluded that the effect of concrete shrinkage due to temperature drop (the capping beam was executed in summer), along with a 50 m diameter shaft, causes a temperature drop of about 15ºC to produce displacements in the head of the wall of more than 7 mm towards the excavation.

The following graphs show the head displacement of two inclinometers and the ambient temperature. A clear homotheory between the movements and the temperature is observed.

This effect was not accounted for in the design of the WB, as it was not a force specifically dimensioned for the WB structure. However, in the case of the props, the temperature-induced effect necessitated an increase in reinforcement

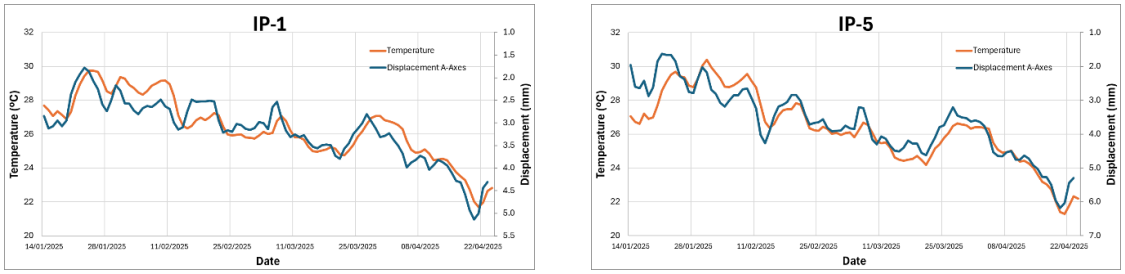


Figure 11. Head displacement at inclinometer 1 and 5 due to temperature variation.

8 CONCLUSION

The design of a peanut-shaped shaft has involved significant challenges due to the following design conditions:

- The requirement to perform an excavation exceeding 20 meters in height and 13 meters below the groundwater table.
- The particle size distribution of the soil leads into a high permeability, resulting in a very high rate of water flow.
- The design required a large interior space, free from bracing elements, for a shaft approximately 50 meters in diameter.
- The novelty of the peanut-shaped geometry for these dimensions.

An interdisciplinary team (geotechnical and structural engineers) carefully analysed the ground and load conditions to develop a robust solution that met all design requirements, while also being developed under a tight timeline due to the project's constrained construction schedule.

Despite these challenges, the construction was completed within the scheduled time, which did not cause any delay in the desalination plant works. The results obtained from the monitoring have proved the validity of the design.

This solution size (50 m diameter) has been adapted for this project based on the geotechnical conditions and the groundwater level position (12 meters). For excavations with a higher groundwater level, the maximum shaft diameter must be adjusted accordingly.

9 ACKNOWLEDGEMENTS

The authors would like to thank the whole Acciona Engineering team that participated in the project. To David Crespo Olazabal, Brad Allpike and John O'Donovan of Acciona Agua and Jacobs. To Michael Murray, Paolo Poggio and Marc Riera of Acciona Construction for their help and support in the execution of the project.

10 REFERENCES

Projeto Executivo do Poço VSE Tietê, Linha 6 (Laranja) do Metropolitano de São Paulo

Vladimir Houst, Luis Armando Frías Cerdáz. *TBM Peanut – Shaped shaft of Silvertown Tunnel Projec*t. ACHE IX Congreso Internacional de estructuras de la Asociación Española de Ingeniera Estructural. 20-27 June 2025 Granada. Spain

THIS PAGE INTENTIONALLY LEFT BLANK

19th Australasian Tunnelling Conference – Acosta-Martínez, Stewart and Hudson-Smith (Eds.)
© 2025 Australian Tunnelling Society, ISBN 978-0-85825-002-4

Melbourne's Metro Tunnel – City Square Rock Pillar Replacement Wall

A.L. Watson
Arcadis/Arup/WSP Design Joint Venture, Melbourne

ABSTRACT: The Metro Tunnel is the biggest transformation of Melbourne's rail network since the City Loop opened in 1982, with twin 9km tunnels passing under Melbourne's CBD and five new underground stations. The City Square shaft is 90m long, 25m wide, 35m deep and runs length-ways against the mined cavern. Geotechnical analysis indicated that the capacity of the residual pillar of rock between the piles and the excavation line of the cavern presented a significant technical and construction risk when supporting the re-distributed stresses generated by excavation of the cavern – if this could not be overcome then the rail alignment and/or cavern width would need to change. An innovative and integrated approach incorporating design and construction thinking was required. The solution was to build a 70m long, 2.5m thick, 10.5m high reinforced concrete wall to replace the rock before the cavern side tunnel was excavated. This paper outlines the analysis, detailing, constructability and methodology considerations to successfully design and build this critical and complex component of the Town Hall Station.

1 INTRODUCTION

The Metro Tunnel connects the Cranbourne/Pakenham and Sunbury Lines, the metropolitan lines that service two of Melbourne's largest growth corridors to the southeast and northwest to create the Sunshine – Dandenong Line, shown in Figure 1. It comprises twin nine-kilometre tunnels and five new underground stations. A key part of the project was the Tunnels and Stations Package delivered by the Cross Yarra Partnership, incorporating John Holland, Lendlease Engineering and Bouygues Construction Australia as the D&C Joint Venture, hereafter described as D&C. Most of the engineering services, including the structures and tunnels were provided by the Arcadis/Arup/WSP (AAW) Design Joint Venture.

Of the five new stations, the greatest anticipated passenger demand is at the Town Hall Station, constructed within Melbourne's Central Business District (CBD), with City Square as its primary entrance. It is located under Swanston Street, extending from Collins Street to Flinders Street. Due to this location, several significant geometric constraints including The Melbourne Town Hall, St Paul's Cathedral, Young and Jackson Hotel and Flinders Street Station – all of which are

heritage listed – a 5-Star hotel and one of the busiest light-rail corridors in the world.

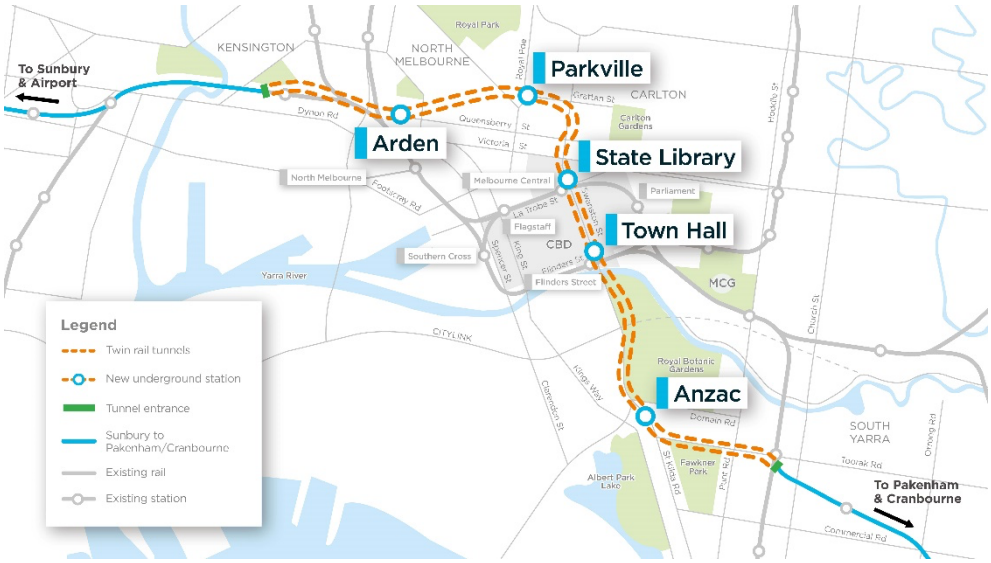


Figure 1. Metro Tunnel Alignment

The combination of these constraints, coupled with the width of the station platform resulted in minimal distance remaining between the cavern extrados and the City Square shaft retention system. The residual rock pillar between these elements was identified as potentially inadequate to support the vertical stresses transferred by the excavation of the tunnels, representing a significant public safety and construction risk. This paper outlines the analysis, detailing, constructability and methodology considerations to replace the rock pillar with a reinforced concrete wall to ensure the overall design could be achieved.

2 TOWN HALL STATION

2.1 *Overall Arrangement*

Town Hall Station comprises a mined trinocular cavern, three entrance shafts, four mined adits and a subterranean link connecting to the existing Campbell Arcade beneath Flinders Street, as shown in Figure 2.

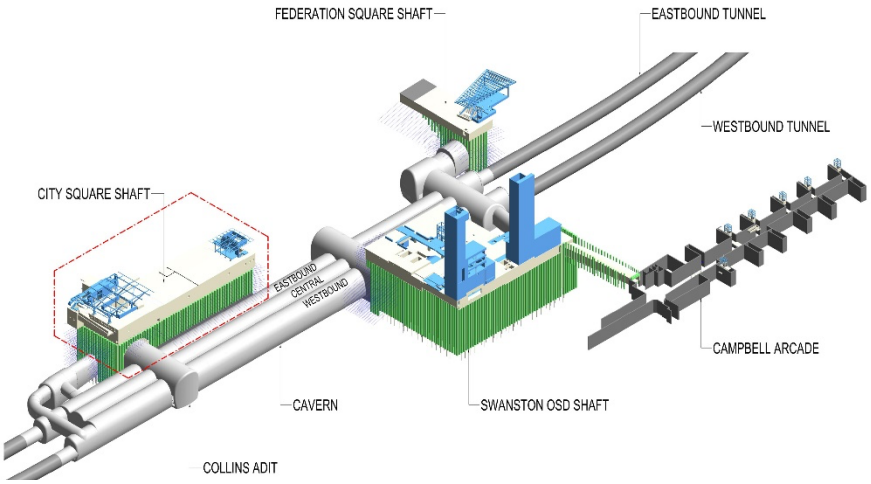


Figure 2. Town Hall Station Arrangement

The 230m long, 14m high, 29m wide cavern containing the platform and track is described as a trinocular due to the arrangement of three overlapping tunnels. It is located 18m below Swanston Street – one of the busiest light-rail corridors in the world. A mined approach was adopted to minimise disruption to the road. The four adits provide horizontal access from the shafts into the

cavern, both during construction and permanently for passengers, services and emergency egress.

The City Square shaft is 90m long, 20-25m wide and 35m deep, with its long axis parallel to the cavern along its western side. It is constructed within a demolished portion of the Westin Hotel basement and abuts the hotel building and remaining basement, as shown in Figure 5. When complete, a new public square will be constructed on top of the station structure. To achieve the required pedestrian flows and services, the plan area of the station was maximised within the existing footprint.

The rail alignment at Town Hall Station was set to maximise separation from Young and Jackson Hotel, which was identified as sensitive to ground movements. This positioning left only 2.5 metres between the cavern excavation-line (E-line) and outer face of the City Square lining wall, which can be seen diagrammatically in Figure 4.

2.2 *Geology*

The geology at the City Square shaft comprises a layer of fill over weathered bedrock described as Melbourne Formation. The Melbourne Formation (also known as Melbourne Mudstone) is an anisotropic rock mass, both in terms of its intact properties and its structural geological features. Based on bore samples, the Melbourne Formation at the Town Hall Station comprises 77% siltstone and 33% sandstone.

The weathering profile of the Melbourne Formation at the Town Hall Station typically ranges from Extremely Weathered (classified as MF4) to Fresh/Slightly Weathered (classified as MF1). At the City Square shaft, the MF2 layer (Moderately Weathered) was anticipated to be encountered at between five and ten metres below surface level. Based on observations during the construction, an additional classification of MF1a was introduced for City Square to account for better than anticipated properties at the deeper portions of the shaft.

The Melbourne Formation is noted as comprising alternating layers of siltstone and sandstone of varying thicknesses, with sandstone typically interbedded within the siltstone. The bedding at Town Hall Station consisted of two distinct sets in at about 22 and 33 degrees, at WNW and NW respectively. It is also noted that joint sets are typically present in the Melbourne Formation. An example of this bedding can be seen in the excavated face shown in Figure 3.

These geological conditions are a key consideration in both the design and construction methodology of the Town Hall Station.



Figure 3. Excavated face of rock at top of wall

2.3 *Construction Sequencing*

The City Square shaft adopted a bottom-up construction methodology. This involved reinforced concrete piles being installed from the surface (within the bounds of the demolished Westin Hotel basement), with lateral retention provided by combination of steel struts and ground anchors in the East-West direction and rock bolts in the North-South direction. These retention elements were progressively removed or destressed during the build-out phase as the permanent walls and slabs were constructed.

Mining of the cavern was undertaken using roadheaders, commencing with the adits from the shafts. Once the heading and necessary benching of the adit was complete, the roadheaders turned 90 degrees and commenced excavation of the central tunnel. Excavation of the platform (side) tunnels could not commence until excavation of the central tunnel was complete, central base slab cast and temporary columns installed to support the transferred vertical load when the platform tunnel heading was excavated, refer to Figure 4.

The overall construction programme required works for the cavern and shafts to be undertaken concurrently with a minimum of constraints.

3 ROCK PILLAR

In simple terms, excavation of a tunnel in rock causes redistribution of stresses from the excavated region into the adjacent un-excavated regions. In the case of the trinocular cavern at CBD South, this redistribution happens twice. First into the rock either side of the central tunnel, then into the temporary columns and rock adjacent the platform tunnel, as represented in Figure 4 by the red arrows. This arrangement results in greatly increased stresses in the rock each side of the cavern. As noted above, there is only 2.5m between the E-line and outer face of the City Square lining wall. When the retention piles are considered, the residual rock pillar between the two structures is reduced to less than 1.5m and would be disturbed by both the piling and mining procedures. Early in the design phase it was identified that the rock pillar would be unlikely to provide reliable support for the transferred stresses and was thus identified as a substantial risk requiring mitigation by design.

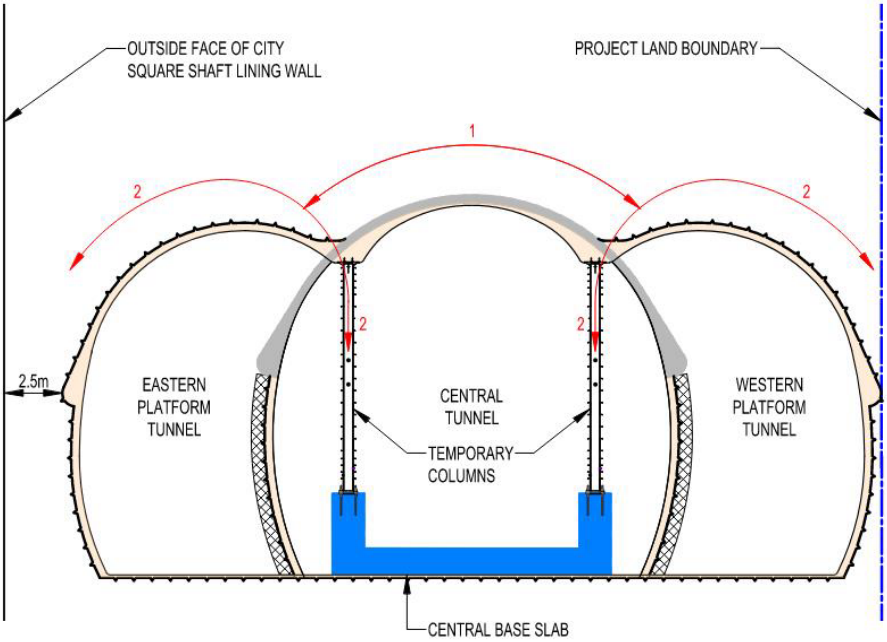


Figure 4. Cavern ground stress transfer sequence

As a reduction in the cavern width or change to the rail alignment were not possible due to constraints and project requirements, the adopted mitigation strategy was the replacement of the rock pillar with reinforced concrete.

Replacement of the rock while excavating the cavern was considered, but discarded for a combination of reasons including:

- Replacement needed to occur prior to excavation of the City Square shaft, introducing a substantial programme constraint as the Collins Adit could not be used to excavate the cavern; and,
- The platform tunnel would need to become wider, creating additional complexities for construction and design of the temporary support.

Therefore, the reinforced concrete pillar would need to be constructed from within the City Square shaft. The full interface between the shaft and cavern needed to be replaced, except at the Collins Adit interface, an extent of approximately 70m. The top of replacement was determined by the cavern geometry, nominally at RL -12.6m and extending to the base of the City Square shaft (which varies between RL -23.1 to -26.6), for a height of up to 14m. The relative position of the City Square shaft to the cavern with the narrow pillar in-between can be seen in Figure 5. Several surrounding constraints are also identified.

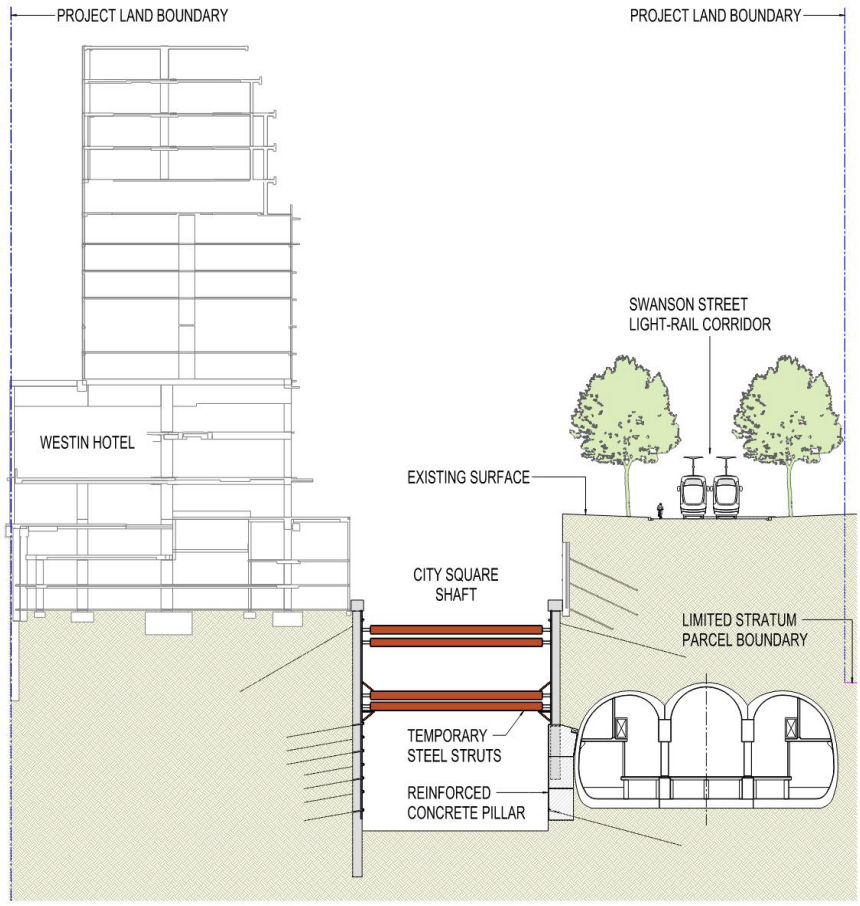


Figure 5. City Square Cross Section

Based on this arrangement, the rock pillar replacement needed to be constructed prior to commencement of excavation of the eastbound platform tunnel so it was in position to support the loads at transfer. This formed a key constraint in the overall construction programme of the Town Hall Station. However, this could be accommodated in the construction programme.

While this arrangement introduced a technical constraint for the platform tunnel excavation, it allowed for concurrent excavation of the central tunnel and the City Square shaft. Once the replacement was completed, it also de-linked excavation/construction of the cavern and shaft primary structure build-out, meaning each could progress independent of the other.

4 DESIGN/CONSTRUCTION METHODOLOGY

Although the overall construction methodology for City Square was bottom-up to allow swifter access for excavation of the adit and cavern, this approach was determined to be inappropriate for the rock pillar replacement wall due to its height and need to undermine the upper retention system to facilitate excavation outside the line of piles (see Figure 3). A bottom-up approach to construction of such an element would have been significantly slower and less safe, especially considering

the 10.5m high vertical rock face which would have been exposed when the piles were demolished.

A top-down construction methodology was adopted for the wall. It was designed with three 3.5m high lifts, which were progressively excavated and constructed with the main shaft excavation.

4.1 *Sequencing*

Due to the depth of the shaft and cavern, the top of the wall is approximately 22.6m below the existing surface. It extends through the line of retention piles and a further 1.5m into the rock. The required excavation undermined the retention piles, compromising their stability and that of the construction deck supported on the capping beam.

To mitigate this issue and ensure vertical support is always provided, a hit-and-miss approach was adopted for each level of the wall. The first step was excavating and constructing the A-blocks – only when they had achieved the minimum required strength could excavation of the B-blocks commence. The final activity on each level was the C-blocks. This arrangement is shown in Figure 6: A-blocks are in red, B-blocks are in yellow, and C-blocks are in green. The Level 1 segments are typically 6.2m long, 3.5m high and 2.5m thick, while the Level 2 and 3 segments are 4.7m long.

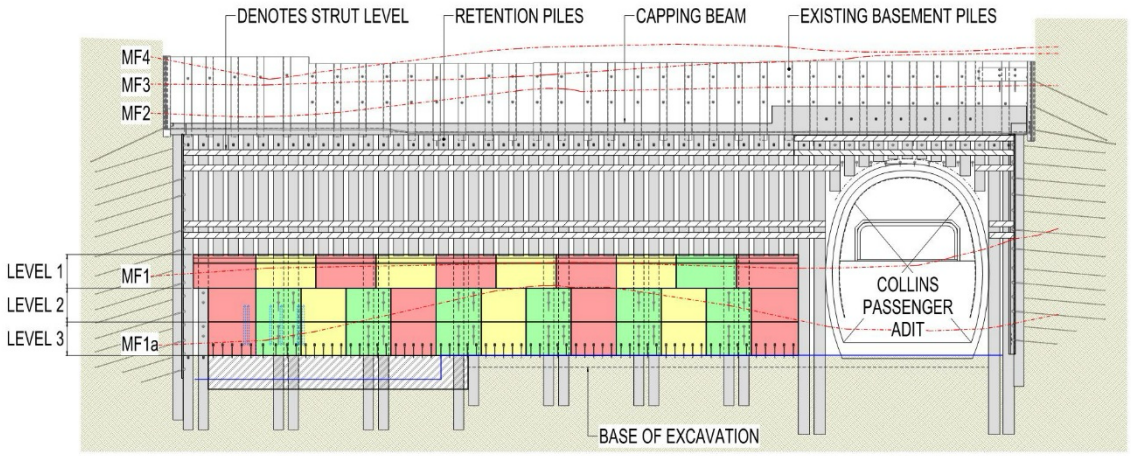


Figure 6. Wall Construction Sequence

This sequence was developed collaboratively by AAW with D&C over multiple workshops and iterations.

4.2 *Design Approach*

The wall was designed for three distinct conditions. A detailed cross-section of the wall can be seen in Figure 7, showing how it is positioned between the City Square primary structure and cavern permanent lining, with the cavern temporary support landing on the corner.

4.2.1 *Stage 1*

The first stage is vertical and horizontal support during excavation of the City Square shaft. During the excavation for Level 1 (excavated arrangement shown in Figure 3) the capping beam was designed to span over the demolished piles, this provided support for the construction deck on the beam, as well as any loads from the piles hanging on the beam.

During excavation for the subsequent levels, vertical support was provided by Level 1 of the wall. This level was designed as a deep beam with continuous horizontal reinforcement (via the use of couplers) and shear ligatures arranged for the vertical condition. Note the top left corner of Level 1 (see Figure 6) is extended onto an additional pile to ensure vertical support is maintained when that end of the wall was undermined. The Level 2 segments are designed to hang off the

underside of Level 1 when they are undermined for the excavation and construction of Level 3.

Horizontal loads were not a significant concern at this stage as the platform tunnel was not being excavated. Restraint was provided by the steel struts against the piles over the wall and friction at the under-side of the wall.

4.2.2 *Stage 2*

The second stage is during excavation of the platform tunnels. This introduces a substantial vertical load on top of the wall with a large lateral component.

The vertical loads are resisted by the wall acting as a pillar, bearing on the rock at the base. The lateral loads are resisted by steel struts against the piles above the wall and regularly spaced stressed ground anchors which were sleeved through the wall at the base, extending beneath the cavern.

The wall was designed to span vertically from top to bottom in this condition.

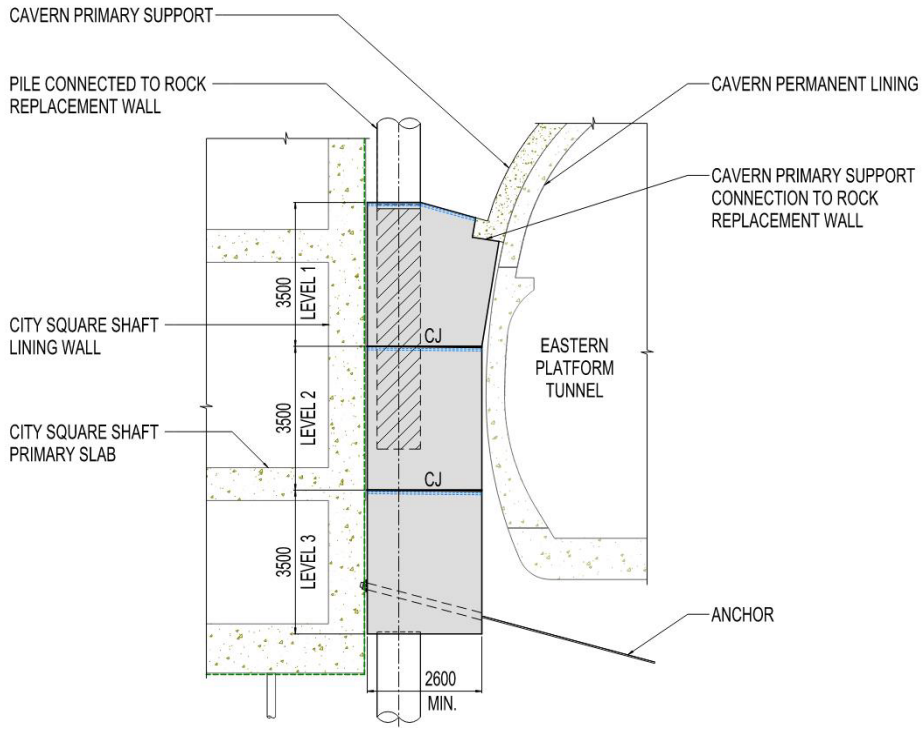


Figure 7. Rock Replacement Wall Section

The piles were installed from the surface with couplers included in the reinforcement cage to facilitate the future connection to the wall. When the piles were demolished to facilitate excavation for the Level 1 segment, the couplers were exposed for the installation of starter bars. The exposed couplers for this connection can be seen in Figure 3. The pile reinforcement for a selection of piles was extended to the toe as they could provide additional robust vertical support for the loads in the temporary condition as the levels were undermined.

Each segment included vertical reinforcement with couplers at the top and bottom to enable the provision of continuous vertical reinforcement. Shear ligatures were provided for the horizontal condition – in Level 1 this was in addition to the shear ligatures for the vertical condition.

Horizontal continuity was not provided between the segments at lower levels, in contrast to Level 1, as it was not necessary for them to span horizontally. They were designed to ‘hang’ from Level 1 when they were undermined. This approach was driven in part by Early Thermal Cracking (ETC) considerations, the omission altered the restraint of the concrete thus significantly reducing the area of reinforcement to limit the crack widths under ETC conditions.

4.3 *Stage 3*

The third stage is the final condition, when the cavern permanent lining and shaft primary structure are completed.

Any vertical and horizontal loads transferred into the wall by the cavern excavation are locked into the reinforced concrete wall, however lateral restraint is provided by the City Square primary structure following removal of the ground anchor and steel struts.

Figure *8* shows the wall on the right-hand side in its final condition, with struts at the top and stressed anchors at the base, before the construction of the shaft primary structure has commenced.



Figure 8. Construction Stage prior to stressing anchors

5 BUILDABILITY

The overall arrangement, dimensions and detailing were carefully developed by AAW in consultation with D&C.

5.1 *Tolerance*

The following considerations were incorporated into the design:

- The front face (against the City Square shaft) was set back from the outer face design line of the lining wall by 20mm to provide additional tolerance;
- The back face (against the cavern) reinforcement was provided with an additional 75mm of cover (150mm in total) to mitigate the risk of damage to reinforcement during excavation of the cavern;
- The connection of the pile to the top of the wall was checked for the potential omission of specific coupled bars to allow for on-site coordination of the circular pile reinforcement with orthogonal wall reinforcement in the event of clashes; and,
- The set-out of vertical reinforcement within the wall was adjusted in the design based on specific detailing feedback.

5.2 *Construction Sequence/Methodology*

The design documentation including construction sequencing drawings developed specifically for the wall segments. These clearly identified the anticipated approach which was considered in the detailing.

This also identified considerations intended to simplify construction, including:

- The use of cement-stabilised sand blinding at the underside of Level 1 and Level 2 for ease of excavation and better identification of the concrete face when excavating the level below;
- Provision of temporary spot bolts for rock face stability during installation of reinforcement;
- Provision of a timber void former at the interface with the cavern primary support for easier identification of the interface; and,
- Localised over-excavation to enable detailed placement of shotcrete to build out to the design face of the wall in a more refined manner.

5.3 *Detailing*

The reinforcement within the segments was detailed to be installed from the cavern side of the segment of the wall towards the shaft, see Figure *9*. This started with a vertical outer-most bar which was a continuation of the bottom reinforcement. This arrangement ensured there were bars against which the horizontal back-face reinforcement could be tied.

The shear ligatures were installed as loose 'candy-canes' at the ends, lapping with straight bars. This did not represent any concerns with detailing requirements to AS5100.5 as the laps were not in the cover zone. The outer 'closed' ligature was made up of individual ligatures with each hooked around a corner bar – this meant the near-face verticals could be one of the last bars installed allowing access to the inside for as long as possible. The horizontally placed shear ligatures were detailed to be inserted from the inside face once all other reinforcement was in place.

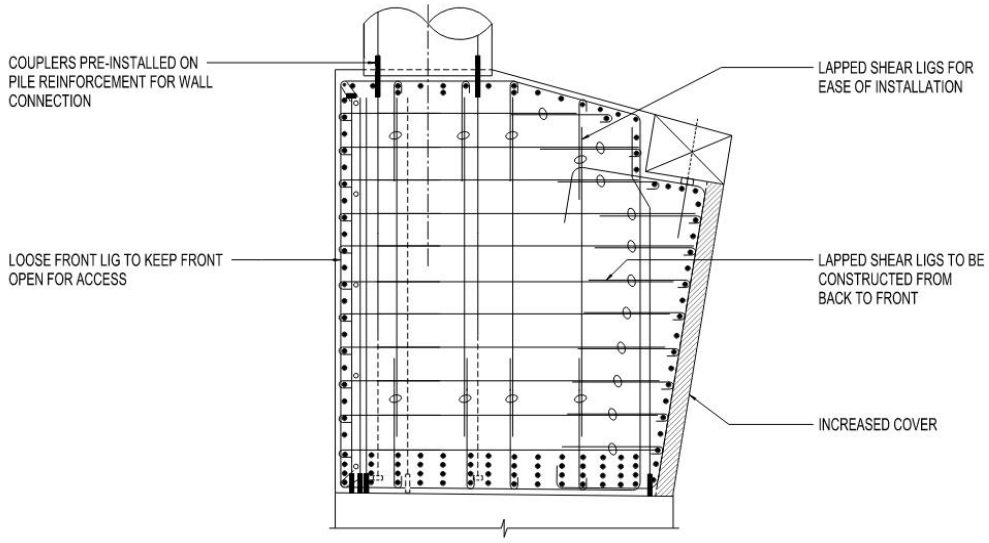


Figure 9. Level 1 Typical Reinforcement

The segment geometry and detailing was modularised as much as possible. This greatly simplified shop detailing, bar bending and installation on site.

5.4 *Shop Detailing*

Given the complexity of the reinforcement to meet design actions, construction methodology, Project Specification requirements and geometry, the shop detailers modelled the reinforcement in three-dimensions, see Figure 10. This model enabled a detailed review of constructability and resolution of clashes prior to fabrication and installation, greatly improving productivity on site.

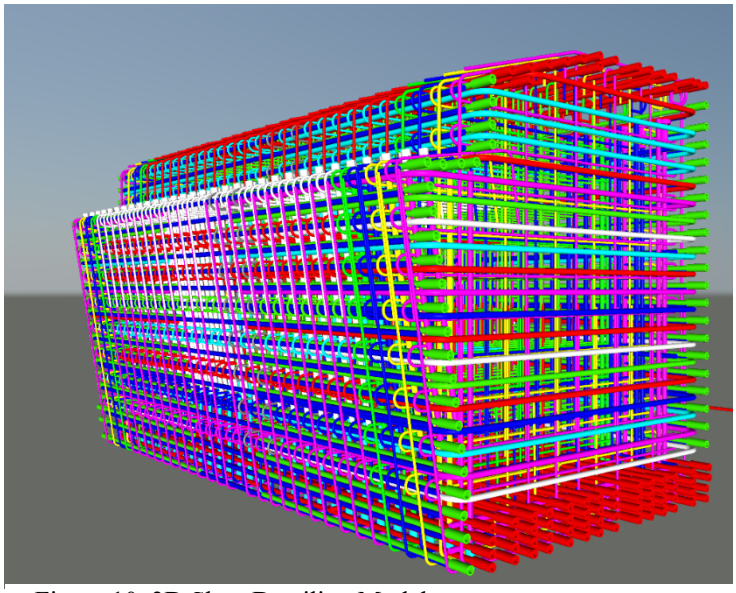


Figure 10. 3D Shop Detailing Model

6 CONCLUSIONS

The Rock Pillar Replacement Wall is an exemplar of how a bespoke design can holistically address major technical, construction, programming and safety challenges.
It highlights the importance of the Design and Construction teams working collaboratively to address a problem. Neither team had the ability to address their respective issues in isolation, it was only through a jointly developed solution for which all parties identified their challenges and constraints that a successful outcome was achieved. Regular workshops and challenge sessions were key to this.

As with all underground and complex structures, understanding the construction sequence is critical. The precise order in which activities can fundamentally change the loading and support conditions. It is important that this is communicated to the Construction team and confirmed as early as possible. The alternate approach would have been to provide a more conservative/expensive design solution which can accommodate multiple different sequences to account for potential challenges at a work front thus mitigating the risk of one problem delaying multiple areas. However, it is inevitable that the design team will not identify all potential construction sequences.

the construction was relatively unhindered as the design detailing carefully considered how each segment would be put together and included measures to enhance buildability and tolerance.

The Rock Pillar Replacement Wall was an ultimately successful solution to a complex problem. Due to attention paid during design and detailing the construction of the segments went smoothly on site, overall stability was maintained, and it was completed in time for excavation of the eastbound platform tunnel.

7 ACKNOWLEDGEMENTS

The author would like to thank the Cross Yarra Partnership Design and Construction Joint Venture and the Metro Tunnel Project Office for granting permission to publish this paper.

Theme 7. Tunnelling Systems

THIS PAGE INTENTIONALLY LEFT BLANK

19th Australasian Tunnelling Conference – Acosta-Martínez, Stewart and Hudson-Smith (Eds.)
© 2025 Australian Tunnelling Society, ISBN 978-0-85825-002-4

Low-pressure ventilation system for road tunnel normal operations – West Gate Tunnel

C. Biotto & C. Sahayanathan
Aurecon, Melbourne, Victoria, Australia

C. Jasper & J. Wee
CPBJH, Melbourne, Victoria, Australia

ABSTRACT: Road tunnel ventilation systems face the dual challenge of managing air quality during standard operations and smoke during fire emergencies, and while longitudinal ventilation systems are often combined with smoke extraction, their requirements differ significantly: normal ventilation must move large volumes of air at low pressure, whereas emergency systems require smaller volumes at much higher pressures. At West Gate Tunnel (WGT), two distinct ventilation systems tailored to these specific operational needs were designed, with large, low-speed, low-pressure fans managing normal and congested traffic conditions, and smaller, high-speed, high-pressure axial fans handling emergency scenarios through a single distributed extraction system; this innovative design is estimated to be significantly more efficient than a single high-pressure fan system and not only enhances ventilation effectiveness but also substantially reduces energy usage, setting a precedent for future tunnel ventilation design in urban environments.

1 ROAD TUNNEL VENTILATION IN AUSTRALIA

Tunnels in Australia require ventilation during normal operations, and in uni-directional tunnels this is often achieved through longitudinal ventilation, where air travels in the direction of traffic due to vehicle movement, as shown in Figure 1; however, Australian requirements often mandate that tunnel air must not exit the portals and instead be extracted prior to the exit via mechanical ventilation.

These extraction facilities exhaust the tunnel air at high level through a ventilation shaft to mix it with atmospheric air and improve air quality at ground level to meet ambient air quality limits as described in Longley (2014), Longley (2018) and Sturm (2019). Furthermore, the operators are required to monitor the air quality along the tunnel and maintain the concentration of pollutants (i.e. CO, NO_2, PM10, PM2.5) below a certain threshold as described in Humphrey (2003).

Tunnel ventilation is also used to manage the spread of smoke in case of a fire in the tunnel and often the two functionalities, i.e. air quality and smoke management, are combined into a single ventilation system which is used for both tasks (e.g. Citylink tunnels, M5 East tunnels).

In some tunnels however, the functionalities are split into two ventilation systems, one for air quality purposes and one for fire emergency purposes (e.g. Airport Link tunnels).

In all Australian tunnel where the tunnel ventilation system is combined, the ventilation requirements are met using high-pressure fans, which are energy inefficient, noisy and heavy. This cannot be avoided in fire ventilation systems (and hence for the combined ventilation systems) as the fans need to overcome a higher resistance to extract air from the tunnel without the help of the cars piston effect, especially where a smoke duct is present (e.g. CityLink tunnels).

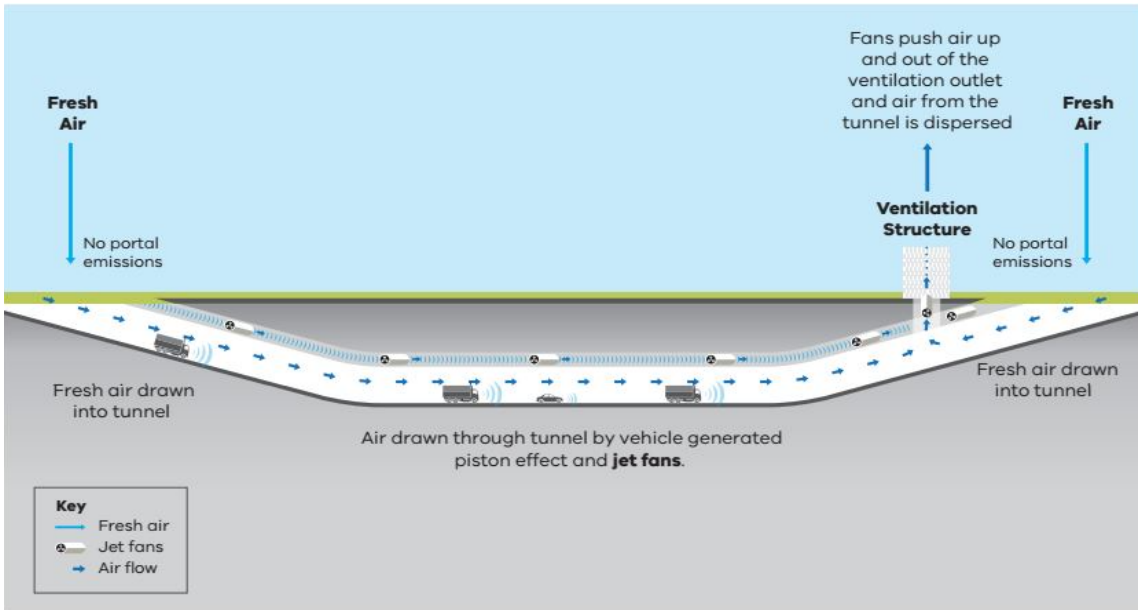


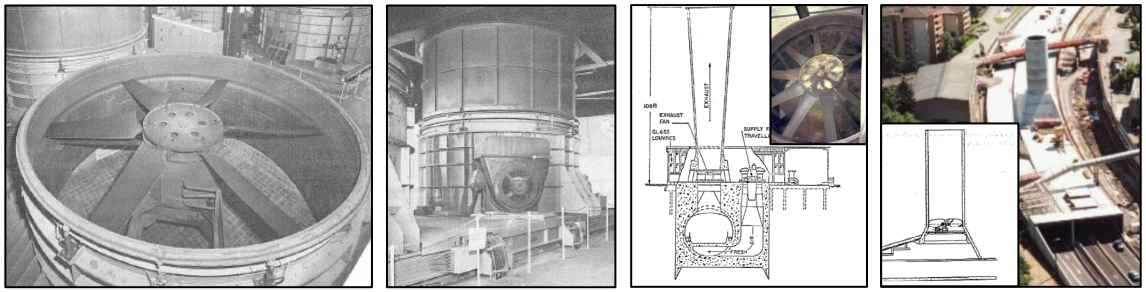
Figure 1. Typical arrangement for longitudinal ventilation with shaft

During most operations, air is naturally pushed along the tunnel to the shafts by the piston effect of moving vehicles, with this flow enhanced by jet fans during slow traffic, the fans only extract air at specific points in the tunnel and push it up the shafts, with the induced flow in the tunnel reducing the required suction-side pressure of the fans. However, the narrow and convoluted air paths in the shafts usually create significant pressure losses, still necessitating high-pressure fans. This limitation was mitigated in WGT and energy efficient, quiet and light low-pressure fans are used for the air quality ventilation system.

2 LOW-PRESSURE FANS IN ROAD TUNNEL VENTILATION

Large low-pressure fans have been historically used in other road tunnels in the world, but not in recent years. Relevant historical examples are:

- Dartford West Tunnel (1963) – 2 fans in 2 shafts, about 175m³/s per fan, as per Kell (1963);
- Dartford East Tunnel (1980) 5 and 6 fans in 2 shafts, about 300m³/s per fan @100Pa, as per Pursall (1982)
- Mersey Kingsway Tunnel (1971) – 4 fans, 6.1m diameter, 108kW, 387m³/s per fan @200Pa, as per Pursall (1973)
- Spier Tunnel (2000) – 1 fan, 6.2m diameter, 87kW, 360m³/s @156Pa as per Van Vemden (2000)
- Ramsgate Tunnel (2000) – 1 fan, 4.0m diameter, 14kW, 100m³/s @95Pa as per Van Vemden (2000)



(a) (b) (c) (d)

Figure 2. Low-pressure fans examples: (a, b) Mersey Kingsway Tunnel, (c) Dartford West Tunnel, (d) Spier Tunnel

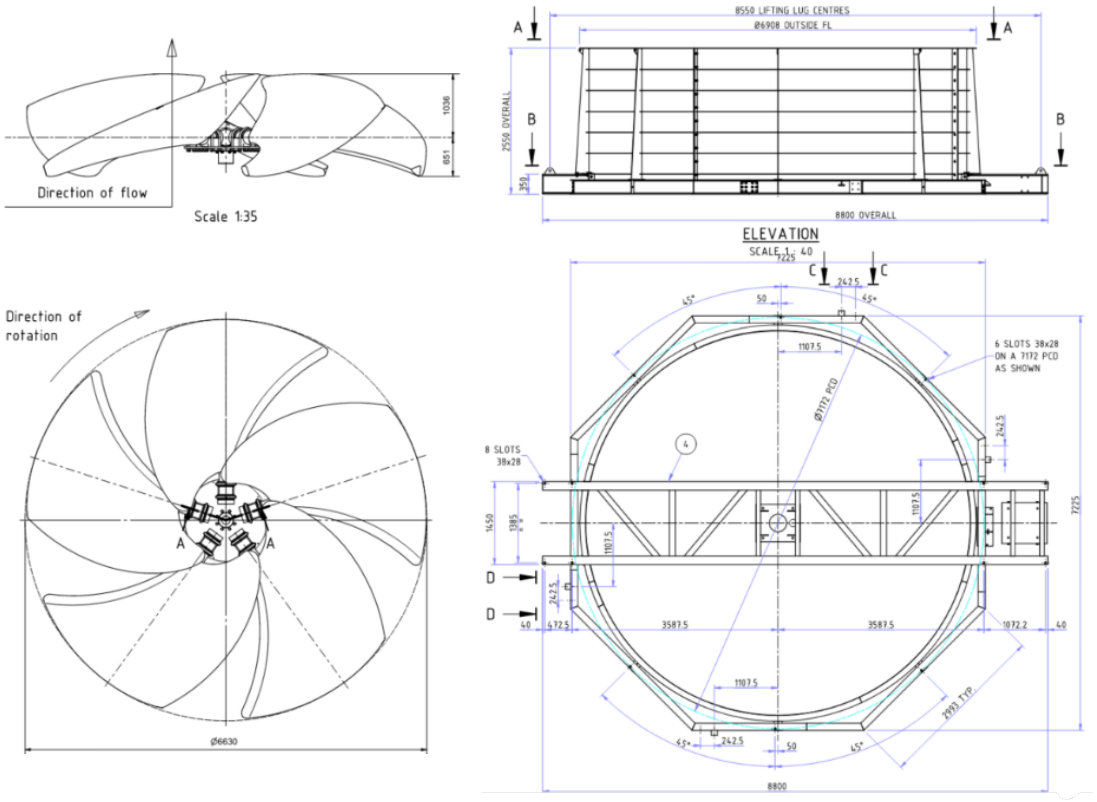


Figure 3. North portal low-pressure fan impeller and casing assemblies

These systems are known for the low noise, long fan life due to lower operating pressures and reduced mechanical strain and low energy consumption. Despite these advantages, low-pressure fan systems have fallen out of favour. Their requirement for large facilities and low-pressure losses poses a challenge, particularly in congested urban areas where road tunnels are often constructed with multiple connections and portals. As a result, more recent projects have opted to combine normal ventilation with high pressure smoke fan systems. However, the recent focus on sustainable infrastructure opens the door for re-evaluating low-pressure fans.

3 AN EFFICIENT VENTILATION SYSTEM FOR THE WEST GATE TUNNEL

3.1 *The West Gate Tunnel project*

The West Gate Tunnel (WGT) Project is a city-shaping project that will deliver a vital alternative to the West Gate Bridge, provide quicker and safer journeys, and remove thousands of trucks off residential streets. The WGT has two separate tunnels: one is 2.79 km long and carries traffic towards Melbourne CBD, known as the Inbound tunnel, the other is a 4.01 km tunnel that carries traffic away from the CBD, known as the Outbound tunnel. Both tunnels share a common civil structure at the northern portal cut and cover (with a full-length dividing wall). Due to their different lengths the two tunnels have separate cut and cover structures at their southern ends, known as the southern portal inbound and southern portal outbound respectively.

3.2 *The air quality ventilation system*

The design team opted for a low-pressure fan system based on several key project requirements. Firstly, the tunnels feature only one entrance and exit for each tube, eliminating slip roads and thereby reducing pressure and airflow losses. Low-pressure fans operate at lower noise levels during regular operations compared to traditional fans, eliminating the need for space and mainte-

nance for sound attenuators. The project requires no emissions at the portals; therefore, the ventilation system is continuously active, pulling large volumes of air through the exit portals. In this respect, low-pressure fans are more energy-efficient than traditional high-pressure alternatives.

Furthermore, the construction programme for the WGT project allowed sufficient time to install the ventilation shafts directly above the cut-and-cover portal, avoiding turns and bends in the airflow path. The use of glass reinformed polymers (GRP) for the low-pressure fans makes them much lighter than steel fans, reducing the static load on the civil infrastructure on the long spans in the portals. The involvement of the operator from the tender design phase focused attention on operational costs, advocating for energy-efficient solutions. Lastly, the WGT shafts were in areas with ample land available to accommodate larger above-ground facilities.

For low-pressure fans at each shaft at the WGT exit portals are Howden SX fans, they are shown in Figure 3 and have the following characteristics:

– North Portal – 4 exhaust fans, 6.63m Ø, 139.6kW, 356m³/s @ 214Pa Static Pressure, 1619kg
– South Portal – 5 exhaust fans, 6.04m Ø, 121.2kW, 267m³/s @ 252Pa Static Pressure, 1502kg

When traffic is travelling above 40km/h the piston effect created by the vehicles, combined with the extraction capabilities of the low-pressure fans, eliminates the need of using jet fans in the tunnel, enhancing the efficiency of the ventilation system with respect to a traditional system.

The project still required a high-pressure fan system for two reasons: the smoke management ventilation has to withstand fire resistance of up to 400°C for two hours, whereas the selected low-pressure fans can only support temperatures up to 250°C, and the project requires a smoke duct for smoke ventilation, leading to high pressure extraction requirements. When in operation, the tunnel ventilation at WGT is estimated to be the most efficient tunnel ventilation in Australia, thanks to this technology, when compared to other main tunnels, as calculated in Biotto (2023).

3.3 *Energy saving benefits*

Fan power is proportional to flow rate and pressure head. Flow rate is fixed by the "no-flow" condition at the portals, leaving little room for reduction through tunnel design. However, optimizing the air path geometry by making it as straight, wide, and short as possible and using quiet fans can reduce pressure losses and lower power. Conservative energy estimates based on the predicted WGT traffic led to a yearly power consumption of 15.5TJ for year 2025 and 16.9TJ for 2031. This is more efficient in comparison to high-pressure fans (420kW for North portal and 300kW for South outbound portal), that would lead to a yearly power consumption of 30.6TJ in 2025 and 33.8TJ in 2031, due to noise attenuation and convoluted air paths. This would require larger electrical facilities and larger infrastructure due to the number of high-speed fans required.

3.4 *Environmental benefits*

Noise generated by low-pressure fans is lower than noise generated by high-pressure fans with the same flowrate, removing the need to install noise attenuator in the system, reducing the pressure losses and minimizing environmental noise. Table 1 compares the noise levels of the air quality low-pressure fans versus the smoke high-pressure fans at WGT.

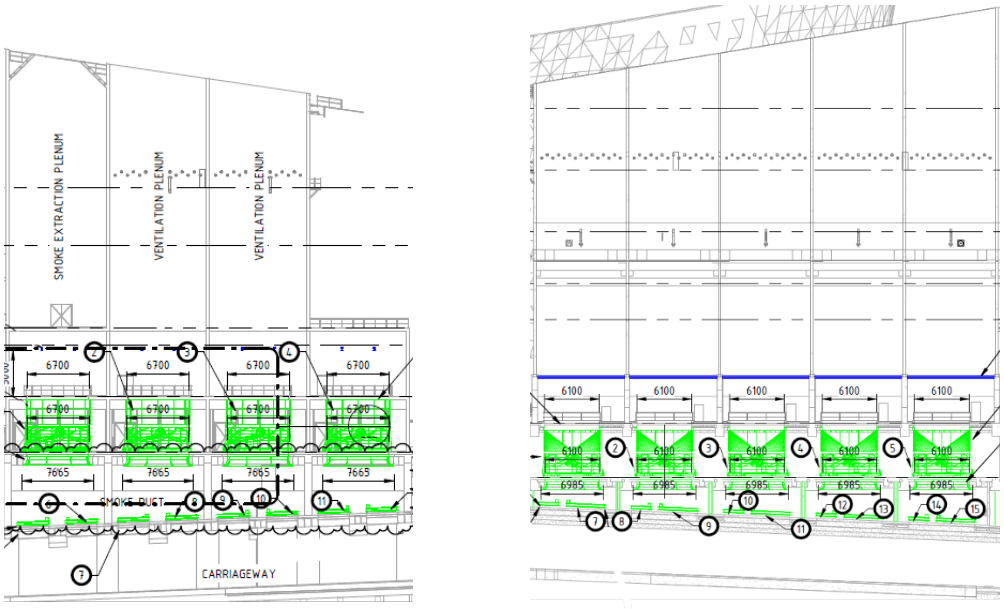
Table 1. Sound power level (dB), installed WGT fans

Fan/f(Hz)	63	125	250	500	1000	2000	4000	8000
Low-pressure	96.3	95.7	92.5	91.0	88.1	83.1	76.3	67.0
High-pressure	107.0	109.0	111.0	119.0	117.0	113.0	109.0	107.0

4 SHAFT LAYOUT AND DESIGN

Fire rated shut off dampers are located below the low-pressure fans and will maintain integrity when exposed to air at 400°C for two hours to act as a barrier between the low-pressure fans and the tunnel, allowing the fans to be mounted directly above the carriageway.

The low-pressure fan units will not be operated during fire incidents and their operational temperature rating remains at the expected tunnel temperature range of -5°C to 55°C.



(a) (b)

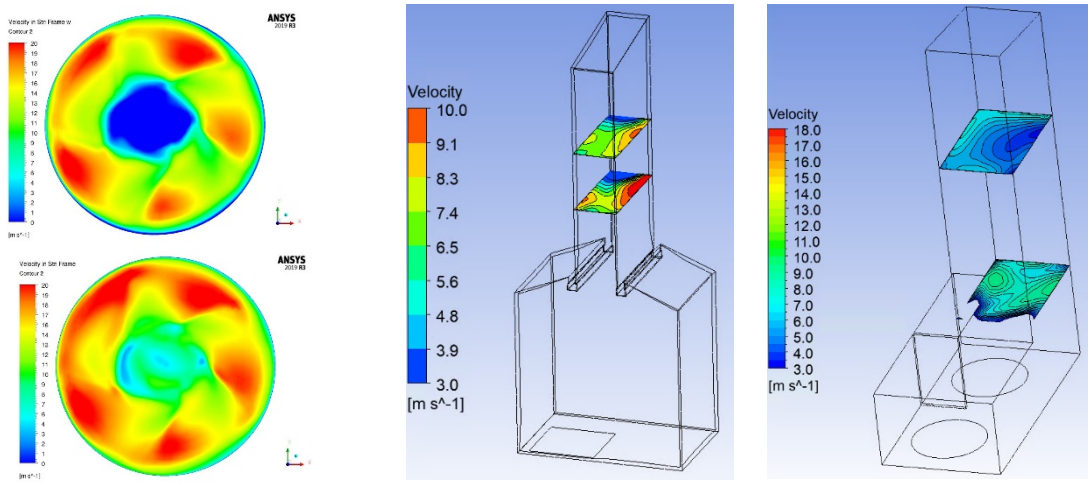
Figure 4. Portal low-pressure fan arrangements: (a) North, (b) South

At the south ventilation facility, each low-pressure fan is installed in its own vertical shaft, while at the north facility, two low-pressure fans service each of the two shafts. All low-pressure fans are mounted on movable skids for easy inspection, maintenance, removal, and reinstallation.

A support bridge holds the fan, motor, and gearbox. At the south site, low-pressure fans are installed at intermediate slab level, which opens directly out to the ground level access road, about 100m from the outbound portal. At the north site, they are positioned at ground level, approximately 100m from the inbound portal.

Tall chambers between the shut-off dampers and low-pressure fans help dissipate pressure waves from tunnel traffic, given a tunnel gradient of about 6% at the portals, the shortest chamber averages 2.5m in height. A bellmouth is installed below each fan slab penetration to reduce pressure losses and ensure uniform airflow, especially at the south portal, where the shafts are 25% offset from the fans, while at the north portal, the shafts are directly above the two central units.

Computational fluid dynamics (CFD) was performed to evaluate pressure between the low-pressure fan and atmosphere, ensuring that AS 4323.1 (1995) required airflow uniformity at the air quality measurement plane in the shaft, was met, as shown in Figure 5.



(a) (b) (c)

Figure 5. (a) Axial velocity and velocity magnitude at the fan exit; (b) South portal typical shaft velocities; (c) North portal typical shaft velocities.

5 FEEDBACK CONTROL AND MONITORING

5.1 *The control system*

The low-pressure fans are monitored with a suite of signals to screen the unit health. This includes bearing vibration (in the motor and the impeller), bearing temperature (in the motor and the impeller), motor winding temperature, gearbox casing vibration (3 axes), air volume flow and fan pressure. The signals from monitoring equipment are sent to the plant monitoring control system (PMCS) and are used by the automatic control system to activate and modulate fan speed, according to traffic and air quality in the tunnel.

During normal operations of the tunnels there are two key sub-systems at work: the first ensures that the in-tunnel air quality is at acceptable levels and the second ensures that, on average, there is always an inflow at all portals, including the exit portals. The following is a brief description of how the ventilation system works to achieve these two requirements.

5.2 *Air quality control*

Vehicles travelling through the tunnel emit various pollutants, with emission levels influenced by factors such as tunnel grade, vehicle speed, vehicle class (passenger car, light commercial vehicle, heavy goods vehicle), and engine type (diesel/petrol).

In-tunnel air quality standards mandate that pollutant concentrations remain within specified limits, both at specific points and averaged over the tunnel. To monitor these levels, groups of three air quality sensors are installed approximately every 400m, operating continuously during both normal and congested conditions.

During normal operations, when vehicles travel at high speeds, the piston effect is generally sufficient to keep pollutant levels within permissible limits, allowing the ventilation system to remain constant. However, in congested conditions with lower speeds, air quality may deteriorate, approaching regulatory limits and jet fans are activated to ventilate in the direction of traffic flow, drawing in fresh air from the tunnel entry portal to dilute pollutant concentrations. Conversely, the number of active jet fans is reduced once air quality improves.

5.3 *Zero portal emissions control*

During normal and congested tunnel operations, the project requires zero portal emissions. At the entry portal the flow is always into the tunnel due to the piston effect of entering vehicles and additional thrust by jet fans during congestion and therefore the design criterion reduces to ensuring air inflow at the exit portals. The tunnel airflow is monitored with air velocity sensors, with three sensors installed at nominally 800-metre intervals.

The key monitoring site is the last set of sensors positioned between the ventilation shaft and the exit portal, ensuring that air inflow velocity remains within the required range: if air inflow at the exit portal drops below the set range, low-pressure fans in the ventilation shaft increase exhaust airflow to boost inflow, equally, if inflow exceeds the set point, these fans reduce airflow, decreasing inflow from the exit portal.

5.4 *Control settings optimisation*

There is a balancing act between the air quality and zero portal emission sub-systems. When pollutants increase due to congested traffic, jet fans activate to ventilate in the direction of traffic, which affects exit portal inflow velocity and causes an increase in low-pressure fan exhaust.

The tunnel control system was modeled during transient scenarios to optimise set points for achieving design criteria during all operations. Key situations assessed include jet fan responsiveness during sudden congestion (when traffic slows from 80 km/h to 20 km/h in 15 minutes) and low-pressure fan responsiveness to maintain zero portal emissions during recovery (when traffic speeds up from 20 km/h to 80 km/h in 15 minutes), as shown in Figure 6.

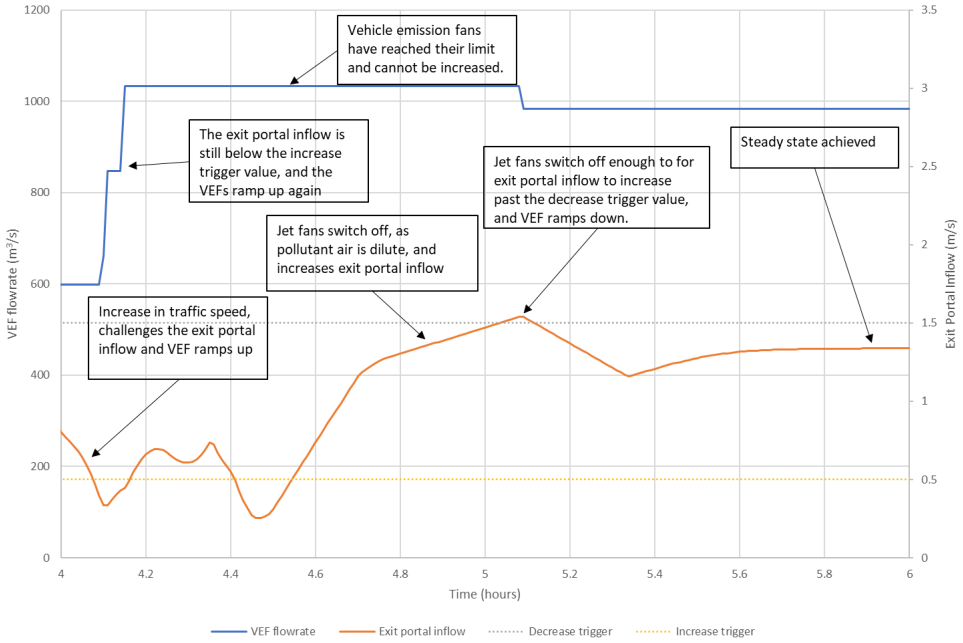


Figure 6. Control performance for morning capacity traffic transition from 20km/h to 80km/h.

6 ASSEMBLY AND INSTALLATION

The installation of large low-pressure fans requires meticulous planning and execution due to their substantial size and complexity. The fan components are procured from multiple suppliers and then assembled on-site; this approach not only facilitates tailored construction to the specific requirements of the installation site but also optimises logistical considerations by reducing transportation challenges associated with fully assembled units.

The construction, and future maintenance, takes place in a designated area adjacent to their final installed position and the pre-assembly of the low-pressure fans involves the following construction steps to ensure that every component is properly aligned and integrated:

- Base frame assembly of the steel fan base frame and partial casing assembly
- Installation of the gearbox, drive shaft, brake, motor and impeller blades
- Completion of the casing elements
- A pre-alignment of the motor, shaft and gearbox out of position
- Setting the blade pitch angle and tip gap checks for the fan

Upon completion of these pre-assembly tasks, the fan is jacked up, and caster wheels are securely mounted to facilitate easy movement. Guide rails are utilised during the relocation process, ensuring precise alignment within the allocated space while a final alignment of the motor, shaft and gearbox is completed in position. Figure 7 shows photos of various installations at the north and south portal at WGT.

7 CONCLUSIONS

This paper has detailed the characteristics of the specific WGT ventilation system, to describe what are the principles behind the low-pressure fans and how they can improve the efficiency of the tunnel ventilation system during normal operations. It also explains what other benefits are related to this system, its limitations and the controls implemented to make the system adapt to traffic and environmental conditions. Even though this specific ventilation concept might not be suitable for other tunnels due to its specific requirements (i.e. low pressure on the suction side,

large footprint at the portals, no-portal emission requirement), its design principles and performance benefits should be considered on similar projects.



(a) (b)

(c) (d)

Figure 7. Low-pressure fans at WGT (a) impeller and bellmouth installed in the north portal shaft; (b) South portal fan casing and transition duct; (c) Pre-assembly yard (d) North portal fan casing.

8 REFERENCES

Longley, I.. 2014. NSW Government Advisory Committee on Tunnel Air Quality, Technical paper TP06: Road tunnel portal emissions.

https://bigbuild.vic.gov.au/projects/west-gate-tunnel-project/construction/tunnel-ventilation-and-air-quality/tunnel-ventilation-system [Last access: 26/07/25].

Longley, I.. 2018. NSW Government Advisory Committee on Tunnel Air Quality, Technical paper TP05: Road tunnel stack emissions.

Humphrey, G. Stricker, J. Holmes, K. Burrell, C. Dix, A. 2003. A perspective of Australian tunnel ventilation - PIARC.

Pursall, B. Powell, E. 1973. The Design and Operation of the ventilation system of the second Mersey (Kingsway) tunnel and duplication, ISAVVT, BHRA.

Pursall, B. & Lowndes, J. 1982. Ventilation system of the 2nd Dartford Tunnel, ISAVVT, BHRA.

Kell, J. 1963. The Dartford Tunnel, Proc. Instn. Civ. Engnrs paper 6671.

Van Vemden, F. 2000. Low Noise GRP fans for tunnel application, ISAVVT, BHRA.

Sturm, P. 2019. NSW Government Advisory Committee on Tunnel Air Quality, TP04.

AS 4323.1. 1995. Stationary source emissions - Selection of sampling positions.

Biotto, C. Belbasis, A. Campbell, A. Ly, H. 2023. Making tunnels think, ATC23.

19th Australasian Tunnelling Conference – Acosta-Martínez, Stewart and Hudson-Smith (Eds.)
© 2025 Australian Tunnelling Society, ISBN 978-0-85825-002-4

Ventilation challenges and opportunities at tunnelling construction operation – Snowy 2.0 Powerhouse Complex Ventilation

M. J. Jamieson
BBE Group, Perth, Australia

C. Giordano
Future Generation JV, Cooma, Australia

ABSTRACT: The Snowy 2.0 project involves linking two existing dams, Tantangara and Talbingo, through 27 km of tunnels and building a new underground power station. Water will be pumped to the upper dam when there will be surplus renewable energy production, and the energy demand will be low and then released back to the lower dam to generate energy when the electricity demand is high. It will provide power while reusing the water in a closed loop and maximise the efficiency of other energy sources to pump water to the higher dam, which will be stored for later use.

This paper focuses on the ventilation challenges, implementation, legislative requirements and planning on one of the sites, taking upfront designs into the execution phase with development and construction taking place before hand-over for long-term use. Lobs Hole consists of the two main tunnels, the Main Access Tunnel (MAT) and the Emergency Cable Ventilation Tunnel (ECVT), both developed by an 11 mØ Tunnel Boring Machine (TBM) that form the access to the two main powerhouse chambers developed by drill and blast techniques. These chambers, or "Halls", will house the electric power station and turbines and will be two of the largest underground chambers in the world (80 m High x 40 m Wide x 250 m Length).

1 INTRODUCTION

Snowy Hydro Ltd is constructing Snowy 2.0 as the next stage in the Snowy Hydro Scheme's Project. It is a renewable energy Project that will provide on-demand energy and large-scale power storage, the largest in Australia. Snowy 2.0 will provide an additional 2 200 megawatts of generating capacity and approximately 350 000 megawatts hours of large-scale storage to the National Electricity Market. This is enough energy to power three million homes over the course of a week (Snowy Hydro Ltd, 2024).

The Project involves linking two existing dams, Tantangara and Talbingo, through 27 km of tunnels and building a new underground power station 800 m below surface. Water will be pumped to the upper dam in a closed circuit when there is surplus renewable energy production utilising excess solar and wind energy when the demand for energy is low. Water will be released back to the lower dam utilising the hydraulic head between the dams to generate energy when electricity demand is high (Figure 1; Snowy Hydro Ltd, 2024).

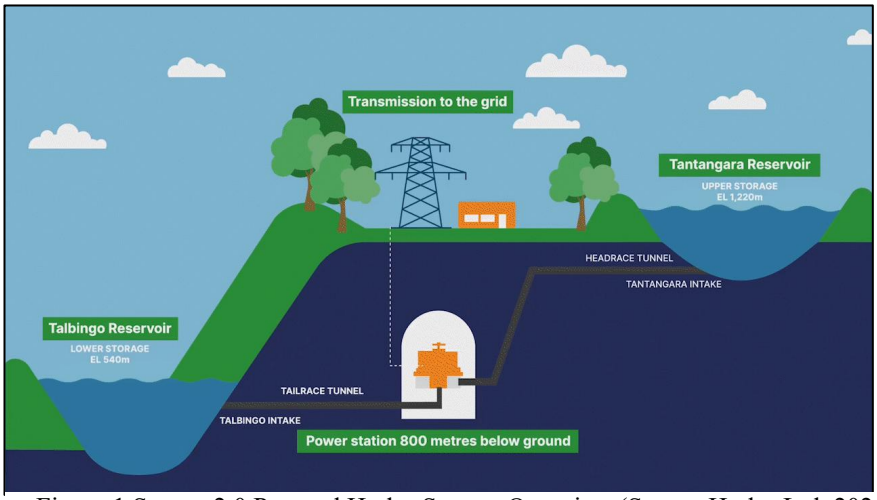


Figure 1 Snowy 2.0 Pumped Hydro System Overview (Snowy Hydro Ltd, 2024)

At the Snowy 2.0, there will be four (4) development sites (Figure 2):

— Talbingo – Tailrace tunnel inlet/outlet
— Lobs Hole – Main Access Tunnel (MAT) and Emergency/Cable/Ventilation Tunnel (ECVT), Tailrace Pressure Shaft and Powerhouse complex
— Marica – Headrace pressure shaft
— Tantangara – Headrace tunnel inlet/outlet.

This paper aims to discuss the challenges and critical solutions employed to change the primary and secondary ventilation circuits at the Lobs Hole site (Figure 2) to adequately ventilate the Transformer and Machine Halls, which will be two of the largest subsurface chambers in the world. The paper will also discuss value-add engineering practices used to conceptualise, design and install ventilation network controls to maintain the legislated level of safety and health for personnel during development and construction.

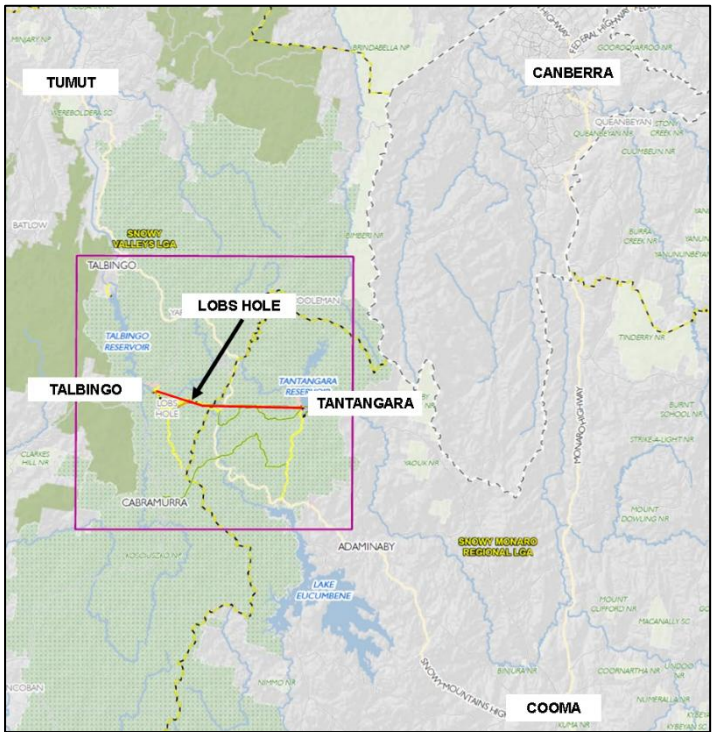


Figure 2. Snowy 2.0 and Lobs Hole Location

2 VENTILATION DESIGN CONSIDERATIONS

Tunnelling guidelines and industry best practice standards for air quality, contaminant dilution and monitoring are discussed in this section. A summary of the ventilation criteria has been provided.

2.1 *Standards*

The Project complies with the SafeWork Australia – Tunnelling Guide and industry-regulated exposure limits, and it is based on the following reference documents:

- SafeWork Australia – Guide for Tunnelling Work (SafeWork Australia, 2013)
- SafeWork Australia – Workplace Exposure Standards (SafeWork Australia, 2024)
- MDG29: Guideline for the management of diesel engine pollutants in underground environments British standard, BS 6164 code of practice for safety in tunnelling in the construction industry (MDG, 2008).

2.2 *Air Quality*

The construction team and ventilation officer must ensure that the air supplied to the ventilation system in the tunnel(s) are obtained from the purest source available (Snowy, 2024; SafeWork Australia, 2013). The recommended minimum standards for sufficient volume, velocity, and quality are:

- 0.3 m/s – with temperature ≤ 25°C wet-bulb
- 0.5 m/s – with temperature ≥ 25°C wet-bulb.
- 2.0 m/s – maximum airflow velocity in work areas together with suitable dust management in place (if in excess, regulated by Risk Assessment).

2.3 *Diesel Equipment and Dilution*

Mine Design Guideline 29 (MDG 29, 2008), 'Management of Diesel Engine Pollutants in Underground Environments', recommends that workers should not be exposed to levels of Diesel Particulate Matter (DPM)—in the form of EC—greater than 0.1 mg/m³. For gaseous emissions (from operating diesel equipment), the minimum ventilation quantity in each place where a diesel engine operates shall be such that a ventilation quantity of not less than:

- 0.067m³/s per rated kW of the maximum capacity of the engine (Australian Tunnelling Guidelines), and by Safe Work Australia standard for diesel particulates at <1.0mg/m³

2.4 *Ventilation System – Monitoring and Testing*

The ventilation management plan (Anon, 2024) should include periodic monitoring and testing of the ventilation system to validate that minimum air velocities and dilution of dust and gases remain within safe limits. This includes developing Trigger Action Response Plans (TARPs) where emissions exceed 50% of the Work Exposure Limit (WEL).

The ventilation management plan should include the following:

- Diesel gas and DPM management plan
- An emergency preparedness management plan
- Specifies the maximum rated diesel engine power that may operate in each tunnel section and how this will be managed
- Radio communication system to alert workers in an emergency
- Welding standard work practices to minimise workers' exposure to welding fumes.

3 THE MAIN FOCUS – VENTILATION REQUIREMENTS AT LOBS HOLE (MAIN ACCESS TUNNELS)

The Lobs Hole site consists of two 11.0 mØ TBM tunnel excavations (MAT and ECVT) concrete segment lined to 9.9 mØ that are ~3.5-4.0 kms each. These tunnels provide connections to the Powerhouse Complex (Transformer and Machine Halls) as shown in Figure 3. Both Halls (red) will be 80 m High x 40 m Wide x 250 m Length and will connect to the penstock (olive) and draft tube tunnels (cyan) to power the turbines. The tunnels established perpendicular off the main TBM tunnels will be an average size of 9 m High x 9 m Wide and will be established by drill and blast techniques.

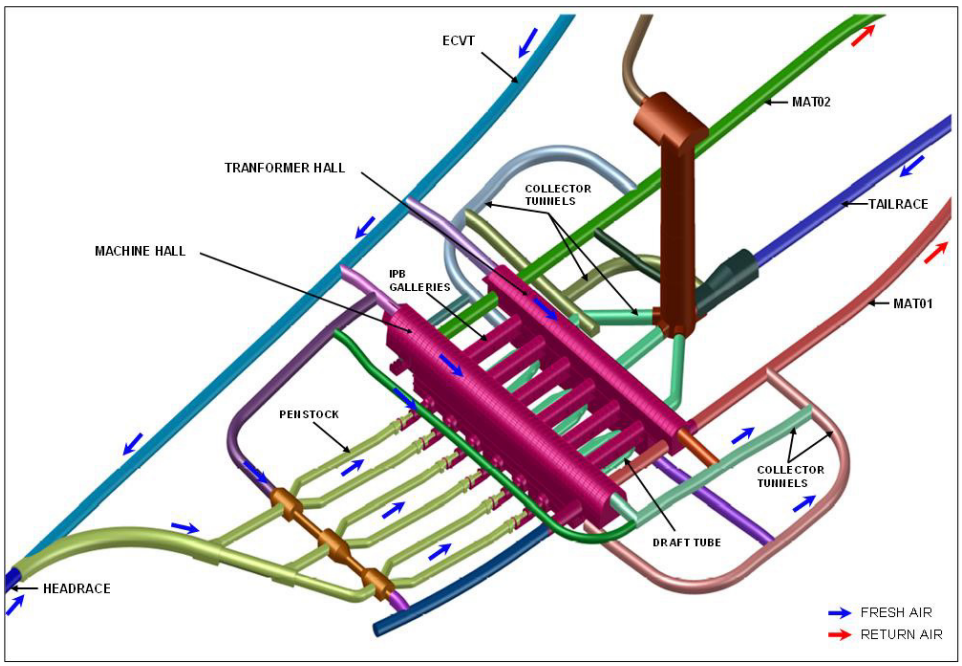


Figure 3 Lobs Hole MAT and ECVT – Powerhouse Complex (isometric view, Fratello and D'Ulisse, 2024)

3.1 *Challenge – Establishing a Primary Ventilation Network During Development*

During the development phase, the ECVT and MAT tunnels will be force-ventilated via two (2) twin-stage 315 kW fans (four fans installed) and one single-stage 500 kW fan from the portals utilising 2.4 mØ and 3.0 mØ ducting. As soon as through-ventilation is established at the Machine and/or Transformer Halls, the ECVT fans will be used as Primary Fans, and the MAT fans will be repurposed as Secondary Development Fans. Air will naturally ventilate to the surface via the MAT tunnel as all ventilation control devices will be commissioned. The ventilation requirement during the development phase is approximately 480 m³/s and will be increased to ~900m³/s to serve the construction phase.

The total airflow of 480 m³/s can serve a total diesel power of 7.2 MW (at 0.067 m³/s per kW) to achieve an average velocity of 1.5 m/s throughout the underground. The total rated power and number of equipment required during the development phase will be 3.26 MW. The fan and ventilation control inventory for underground is indicated in Table 1.

Table 1. Development Phase Infrastructure Requirements

Ventilation Control/Fan	Number of Units
Primary Fans 315 kW	8
Primary Fans 500 kW	1
Auxiliary Fans 55 kW – 160kW	3
Regulated Bulkhead	1
Brattice Wall	1

3.2 *Challenge – Establishing a Primary Ventilation Network During Construction*

The main challenge with establishing minimum ventilation requirements in large, excavated tunnels is that there are no shafts to use as intake or return airways to provide 200 m³/s of fresh air into each of the Machine and Transformer Halls to satisfy the minimum airflow quantity and velocity criteria of 0.3 m/s would be managed on the working floor via strategically placed air-movers. Therefore, it was recommended to use the TBM access tunnels as intake and return in lieu of shafts. Fresh intake air will be supplied via the ECVT tunnel and will be returned via the MAT tunnel creating a primary ventilation circuit (Figure 4).

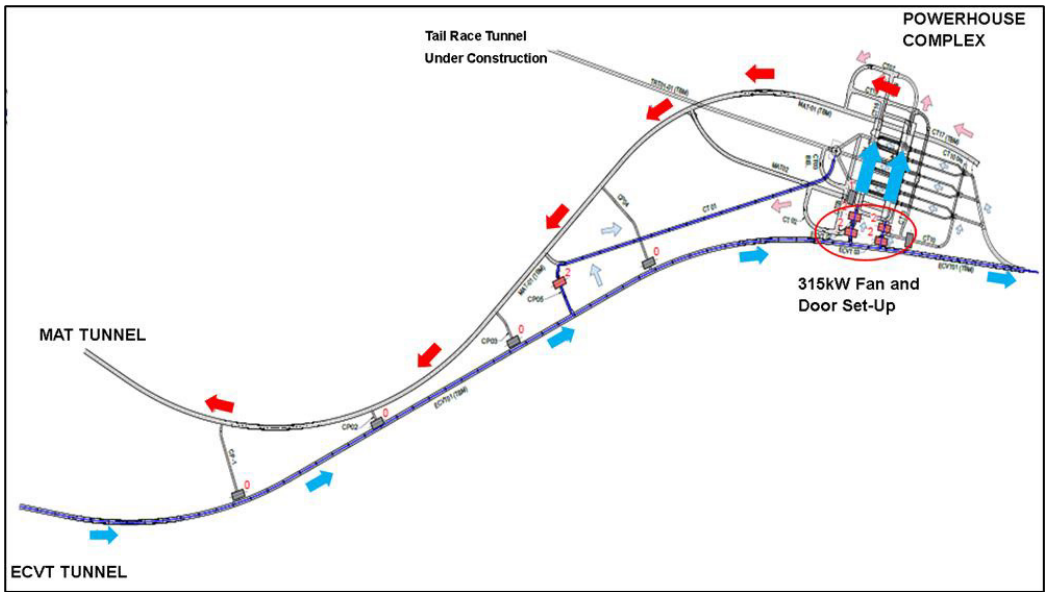


Figure 4. Proposed Primary Ventilation Circuit

This is achieved by installing air lock doors to the access of each hall supported by two single-stage 315 kW fans each (Figure 5). These fans act as the Primary Fans as they are the driving force behind the primary circuit. To minimise contamination, personnel and light vehicles access the complex only via the fresh air intake ECVT. All other heavy vehicles access via the MAT as velocities are expected to reach close to 9.0 m/s towards the surface sections of the MAT.

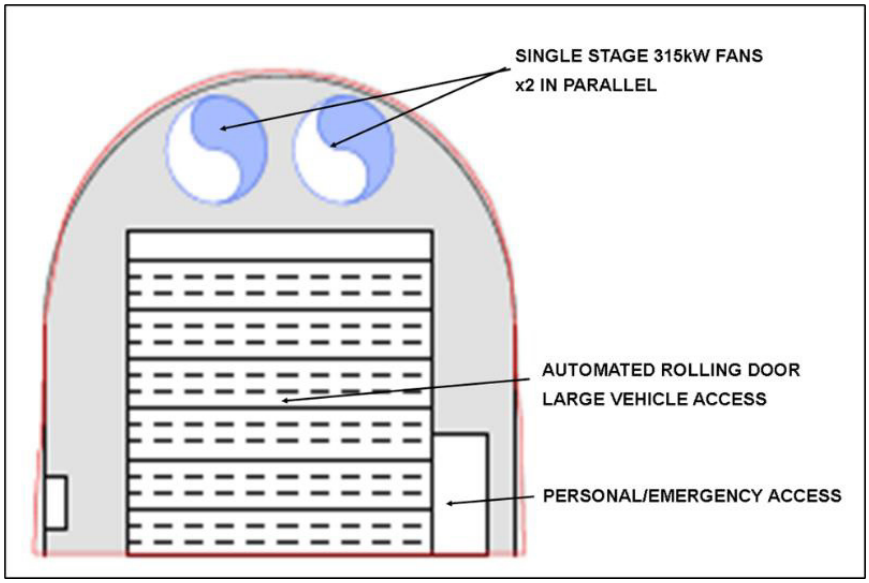


Figure 5. Door/s and Fan Arrangement (Section view, Snowy Hydro Ltd, 2024)

4 VENTILATION OF HALLS DURING DEVELOPMENT AND CONSTRUCTION

Once the primary ventilation circuit is established, the challenge will be to establish a secondary system to adequately ventilate the large halls. Secondary rigid steel ducting teed off from the primary ventilation ducts from the ECVT tunnel will supply air to each of the Halls. Reduced sections of ducts will be installed in each Hall and will be extended vertically down until it reaches each active development level (Figure 6).

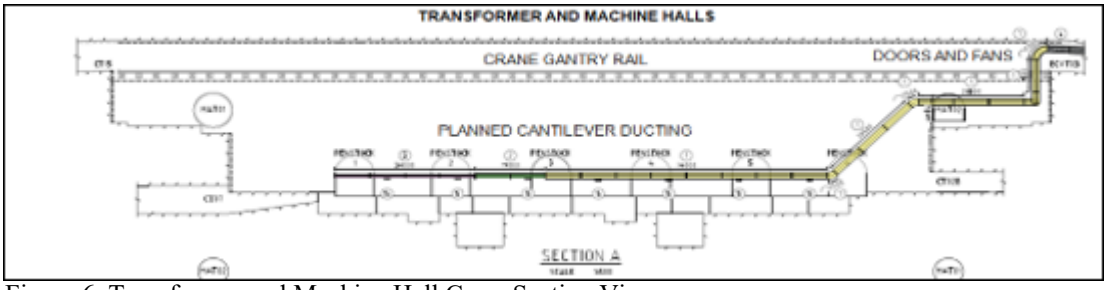


Figure 6. Transformer and Machine Hall Cross Section Views

Ventilation distribution to each Hall will be achieved by using step-down duct sections at strategic locations along the Hall. Modelling and duct calculations were completed to ensure the set-down cantilever duct system is established at the correct locations as indicated in Figure 6. The step-down cantilever duct will comprise flexible ducting to 1.6 mØ, 1.4 mØ and finally 1.2 mØ.

Each section will have two smaller openings to ventilate the development floor as the duct extends. The pressure in the duct is planned be at ~1 500 Pa to 2 000 Pa to ensure equal airflow quantities out of each opening along the length of the steel duct.

With both ducts set up in this configuration in each Hall, the ~200 m³/s can be evenly distributed along the Hall's development floors. The schedule and distribution of works were calculated using diesel fleet loading to create a base to justify predicted contamination dilution rates.

4.1 *Meeting Airflow Requirements*

The quantity at 200 m³/s gives an allowable diesel fleet of 3.0 MW which is ~200% of the planned diesel fleet in a Hall at any one time. Being a large excavation, double the amount of airflow was designed to mitigate dust and heat potential concerns.

Once the ventilation system is set up, the next challenge is achieving the correct velocity to support personnel on the construction floor and meet legislative compliance. With the required quantity in each Hall, the velocity is required to be maintained at no less than 0.3 m/s. This is then achieved via the use of large-scale air movers that will force airflow up to 34 m ahead of its location. Strategically placed fans ensure compliance with regulations and can be easily moved to provide adequate air for active work areas (Figure 7).

Ventilation modelling software was used to evaluate airflow movement, velocity, and heat mapping and to minimise any potential recirculation/re-use of airflow in the Halls. In addition, software is used to ensure air moves from south (ECVT) to north (MAT) through the Halls. This was necessary to identify compliant airflow movement and to ensure the proposed system set-up could meet the optimal working conditions.

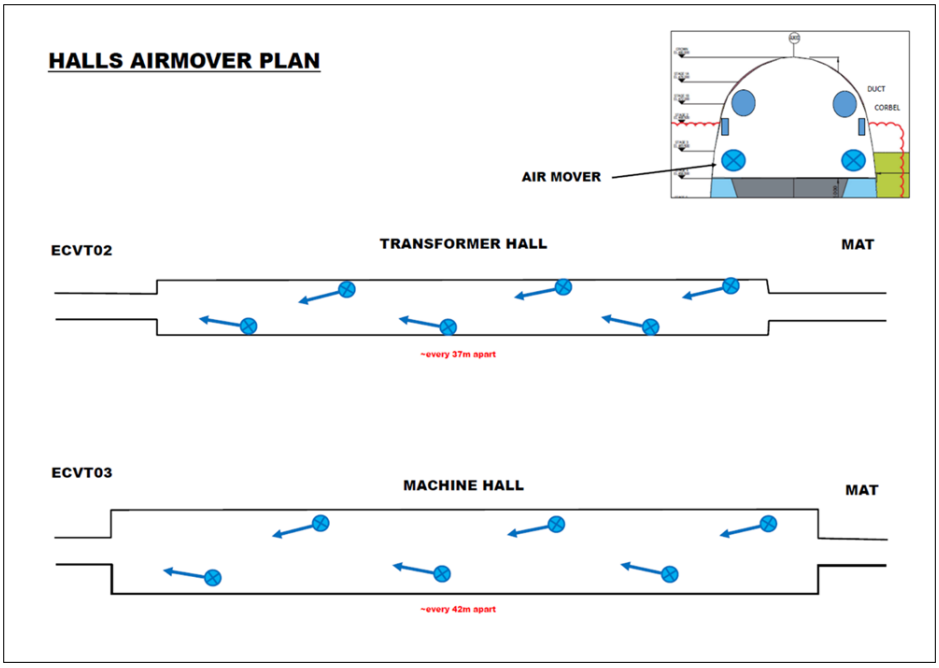


Figure 7. Air Mover Placement in Halls (Top View)

4.2 *Ventilation Controls and System Optimisation*

To achieve the circuit, the main driving force behind the network is the 315 kW force fans from the ECVT portal and the airlock doors at the ECVT side access to each Hall. These are essentially the system's primary fans that deliver the 200 m³/s to the Halls. Figure 5 and Figure 6 shows cross-sectional views of the Transformer and Machine Halls detailing the essential ventilation system requirements and controls to adequately ventilate the halls to acceptable guidelines.

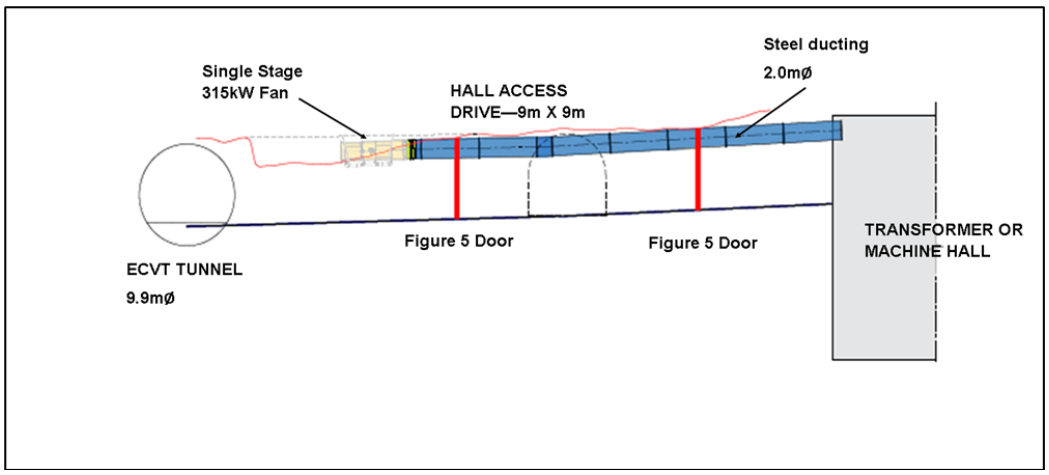


Figure 8. Fan / Door Layout (Snowy Hydro Ltd, 2024)

The pressure ratings for the doors/walls used in this application required an operational design load of ~500 Pa to suit locations with areas up to 100 m² in size. Little to no access will be through these doors as the development profile of the halls have a "drop-off" 20-30 m past them as part of the hall design. All access for personnel and machinery will be via the MAT side. The project was constrained to the extent ventilation controls could be implemented, as nearly all areas required full unrestricted access. Breakthroughs occurred in the halls from the penstock and draft tubes, which made ventilation planning more challenging.

The airlock system for the halls was evaluated for infrastructure movement prior to fabrication and required a temporary engineering design to manage the pressure load of <500 Pa. The doors also needed to be easily installed, maintained and removeable. A set of doors was required at each breakthrough in the halls. They were designed with automation for frequent access and ease of access for large machinery movements (e.g., trucks). These doors were designed to be relocatable, robust in high demand shift changes, operate with high open/close cycles per hour, and withstand easy damage, etc. A robust control system was required to minimise ventilation disruption during operation and provide smooth operation.

5 CONCLUSION

Communication, consultation and engaging all stakeholders were crucial in overcoming the main challenges of increasing airflow and ventilation of two of the largest underground caverns in the world. This ensured the safety and success of the ventilation network and distribution of airflow to the construction work areas. By addressing each stage of ventilation change with development on site and consultants in Torino, Italy, with a systemic and innovative approach, the Lobs Hole site was able to create and implement a primary and secondary ventilation system that supported the project development and construction life and contributed to the overall success of the Snowy 2.0 Project.

By utilising mining, tunnelling and industrial ventilation solutions, the permanent works team were able to successfully identify locations for the ventilation infrastructure with minimal changes as the project progressed, especially with the halls developing deeper.

ACKNOWLEDGEMENTS

The author would like to thank the Snowy Hydro Ltd, Snowy 2.0 and Future Generation JV management teams, for their collaborative and continued support and permission to present this paper. They also acknowledge the assistance and support provided by the various drill and blast and construction managers and engineers.

6 REFERENCES

Anon, 2024. Future Generation JV Ventilation Management Plan, Health and Safety Management Plan.

MDG 29, 2008. Guideline for the management of diesel engine pollutants in underground environments. Available from: *www.dpi.nsw.gov.au/minerals/safety*.

Safe Work Australia, 2013. Australian Guide for Tunnelling Work, Chapter 5. Available from: *www.safeworkaustralia.gov.au/system/files/documents/1702/guide-tunnelling.pdf*

SafeWork Australia, 2024. Workplace exposure standards for airborne contaminants. Available from: *www.safeworkaustralia.gov.au/sites/default/files/2024-01/workplace_exposure_standards_for_airborne_contaminants_-_18_january_2024.pdf.*

Snowy 2.0, 2024. Snowy 2.0 Introduction and Lobs Hole Location. Available from: *www.snowyhydro.com.au/snowy-20/about*.

Snowy Hydro, 2024. Snowy 2.0 documents and drawings. Available from: *www.snowyhydro.com.au/snowy-20/about/, https://www.snowyhydro.com.au/snowy-20/documents*

19th Australasian Tunnelling Conference – Acosta-Martínez, Stewart and Hudson-Smith (Eds.)
© 2025 Australian Tunnelling Society, ISBN 978-0-85825-002-4

A study of mitigation strategies against excessive trackway depressurisation in stations with full-height platform screen doors

K. Oguz
Arup, Melbourne, Australia

O. Ceylan & A.E. Patniotis
Arup, Sydney, Australia

ABSTRACT: Full-height Platform Screen Doors (PSDs) are increasingly used in underground rail systems to enhance safety, reduce energy consumption, and improve the station environment. While their benefits are widely acknowledged, their interaction with Tunnel Ventilation Systems (TVS) requires careful consideration, particularly in emergency scenarios such as fires.

The introduction of full-height PSDs in underground rail stations significantly alters tunnel ventilation dynamics. Under certain scenarios such as a train on fire in the tunnel or at the platform trackway, the tunnel ventilation response can cause excessive negative pressures at the trackway where make-up air paths are not available. This can lead to adverse life safety implications due to the inability to open PSDs and EEDs. This paper aims to draw attention to this issue and reviews various design strategies to mitigate excessive pressures.

1 INTRODUCTION

1.1 *Overview*

The introduction of full-height PSDs significantly alters tunnel ventilation dynamics. The presence of full-height PSDs can influence TVS in several ways including: restricted airflow where PSDs limit the natural exchange of air between the platform and trackway, smoke control challenges in fire scenarios due to limited make-up air paths, and excessive pressure differentials between the platform and trackway which can make it difficult for passengers to open Emergency Escape Doors (EEDs) or PSDs.

Challenges represented by excessive pressure differentials between the platform and trackway have been noted in certain TVS designs particularly during testing and commissioning where EEDs could not be opened during a fire ventilation response. This paper aims to draw attention to this issue which may potentially be overlooked during the TVS design and should be considered.

In TVS designs that consider this challenge, limited mitigation strategies are observed. This includes either the provision of full independent draught relief shafts which consumes valuable underground real estate or oversizing of fans to compensate for at least one draught relief shaft needing to remain open at one end of the station at the expense of a set of fans remaining non-operational. This paper also explores a potential mitigation strategy in the form of a pressure differential reduction mechanism concept to minimise trackway and platform pressure differentials to facilitate safe evacuation.

1.2 *Literature review*

Tunnel and trackway ventilation induced pressures across PSDs during emergency operations and the effects on door opening forces have not been widely documented. Works by the likes of Chun et al. (2004) and Zhou et al. (2021) have been undertaken to study train induced pressures across PSDs, however these are not directly comparable to the considerations in this study. Whilst Zeng

et al. (2023) also analyses train induced pressures on PSDs, it also considers how train induced negative pressures may cause a failure in the proper operation of PSDs.

The use of controllable dampers in platform screen doors to mitigate excessive pressure differentials across PSDs in other works and studies have not been observed by the authors at the time of writing this study. It has been noted however that Yang et al. (2022) have proposed a similar system i.e. adjustable dampers in platform screen doors to provide energy savings to underground rail station Environmental Control Systems (ECS) by utilising the train piston effect for air exchange with the platform during normal train operations. Whilst the function of the platform screen door controllable dampers proposed in this study are different to those by Yang et al. (2022), it brings to light potential benefits outside of those that are the focus of this study.

2 FULL-HEIGHT PLATFORM SCREEN DOORS

2.1 *Overview*

PSDs are used in rail and rapid transit stations to physically separate the platform from the trackway and are a relatively new addition to rapid transit systems with some older stations being retrofitted with PSDs.

PSDs can refer to full-height and part-height barriers with the latter more commonly being referred to as Platform Edge Doors (PEDs). For the purposes of this paper, PSDs refer to full height PSDs which create a complete aerodynamic barrier from floor to ceiling between the platform and the trackway.

PSD assemblies are typically composed of Automatic Sliding Doors (ASDs) that align with train doors. Separate manually operated Emergency Escape Doors (EEDs) can also be provided as part of the PSD assembly to allow evacuation from the tunnel to the platform if the ASDs cannot open such as a train misaligned with the ASDs or a train that is stopped part in tunnel and part at the trackway.

2.2 *Passenger safety*

A key benefit of PSDs is to enhance passenger safety by creating a physical barrier between the platform and trackway which reduces the risk of accidental falls onto the trackway, being near moving trains and uncontrolled access to the trackway.

2.3 *Climate control*

PSDs also improve climate control of the platform by separating the platform from the trackway environment. This allows more efficient heating, ventilation and cooling of the platform and reduces air speeds felt by passengers due to the train induced airflows (piston effect).

2.4 *Impact on tunnel ventilation systems*

The aerodynamic separation provided by PSDs can also benefit the tunnel ventilation system when supplying air by reducing air leakage from the tunnels to the stations through open platforms when PSDs are closed. Conversely, when the tunnel ventilation system is exhausting air, closed PSDs reduce the number of available make-up air paths. In both instances excessive air pressure may become an issue where other relief and make-up air paths are not available.

3 TRANSIT SYSTEM TUNNEL VENTILATION SMOKE CONTROL

3.1 *Overview*

A key function of the tunnel ventilation system for a rail system is to provide smoke control to maintain tenable conditions in the event of a fire scenario. Tunnel ventilation design fire scenarios include fires in tunnels and at the station trackways and should support the fire life safety strategy of the specific project.

Typically, a tunnel ventilation system consists of tunnel ventilation fans that serve the tunnels at either end of an underground station. i.e. supply to or exhaust air from the tunnels. Separate trackway ventilation fans are used to provide trackway ventilation e.g. exhaust from the platform trackways via an Over Track Exhaust Duct (OTE). A typical tunnel ventilation system arrangement schematic for an underground rail station is shown in Figure 1.

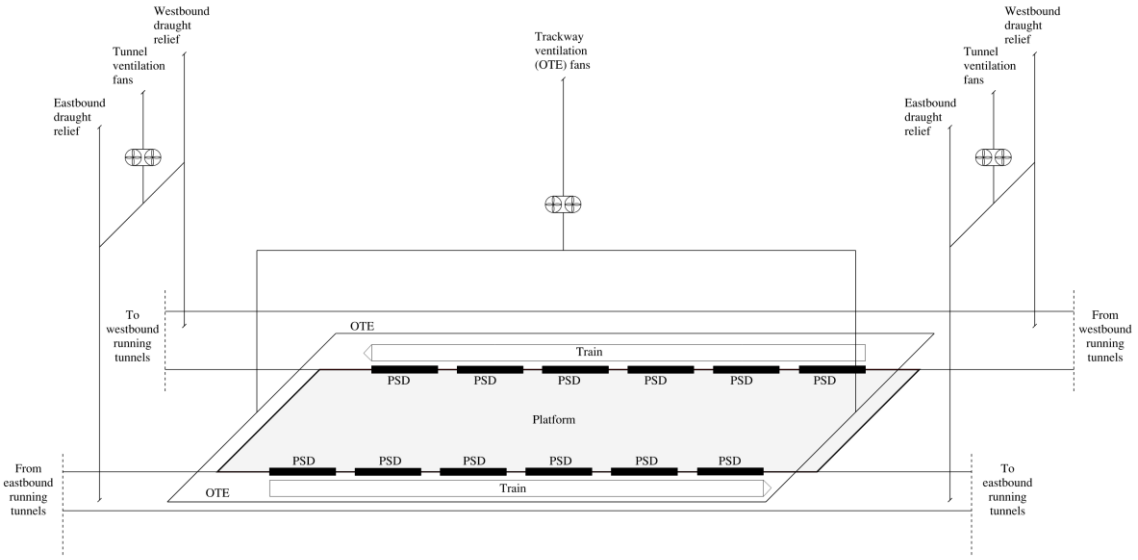


Figure 1. Simplified underground rail station typical tunnel ventilation system arrangement.

3.2 *Smoke control responses*

In the event of a train on fire in a tunnel where the train is not immobilised, the fire life strategy would dictate, where possible, that the train should continue to the next closest station to enable passengers to evacuate through the station. In this situation, typically the tunnel ventilation response would be to initiate a trackway fire response to exhaust air and smoke from the trackway in preparation to or in direct response to the incident train at the platform trackway. Like a tunnel fire response, if the response utilises all available tunnel and trackway fans for optimal use of the available equipment, a typical tunnel ventilation fan arrangement would be left with limited make-up air paths if PSDs and draught relief shafts are closed.

In either of the two situations described, an excessive net negative static pressure difference (trackway static pressure minus platform static pressure) may occur at the trackway leading to high ASD or EED opening forces required for evacuees.

3.3 *Excessive depressurisation and door opening forces*

A range of standards exist that define maximum limits for door opening forces. The Australian National Construction Code (NCC) Part D3 requires that 110N is not exceeded for a door that forms part of a required exit. This generally applies for doors within the station building, however not necessarily the PSDs which generally forms the demarcation between the NCC classified station building and the tunnels. Typically, in Australian underground rail infrastructure projects, the limit identified in NFPA 130 is applied for PSD manual opening forces. This has historically been 220N since the 2007 Edition of NFPA 130. A recent update in the 2023 Edition of NFPA 130 however has reduced this limit to 133N. 220N has been used as the limit for the purposes of this review based on available door opening force to pressure difference limits from past projects. Acceptable pressure differences across doors to maintain door opening forces less than 133N may vary depending on the project and door design.

Where the station tunnel and trackway ventilation fans are exhausting from the trackway generating a net negative static pressure difference between the trackway and the platform, a 'pulling' or 'suction' force is generated on EEDs noting that EED door swings are in the direction of evacuation i.e. open from the trackway to the platform. The pressure difference is exacerbated if make-up air paths are limited as described in Section 3.2.

A static pressure difference between the trackway and the platform can also create additional friction on the sliding door mechanism of ASDs, also making it more difficult to open manually in the event of an emergency.

A direct translation between the 220N door opening force and pressure difference generally depends on the specific door design including its area, weight and opening mechanism. Based on project experience, the pressure difference limit across EEDs have been noted to be circa 200Pa to maintain EED opening forces i.e. less than 220N. Specific pressure difference limits however are subject to the opening force limits and doors to be utilised for a given project.

Typical total tunnel and trackway ventilation fan capacities available for exhaust in an underground rail station trackway can be in the range of hundreds of m^3/s of air. Tunnel and trackway ventilation fan static pressures can range in the thousands of Pa.

The available fan capacities coupled with limited make-up air paths (which may only be made up of long and aerodynamically resistive tunnels connected to trackway) can make it challenging to maintain net negative pressures between the trackway and the platform below 200Pa.

It should be noted that in addition to tunnel ventilation induced pressures, additional transient pressures due to train movements could either positively pressurise or further negatively pressurise the trackway. For the purposes of this study however, it is assumed that train movements in the tunnels during an emergency scenario would be limited and/or stopped minimising transient train induced pressure effects.

3.4 *Mitigation strategies*

The following strategies either currently do or could exist to mitigate the risk of excessive net negative pressure differences across the trackway and the platform:

- Operating the ventilation fans at lower capacities until a confirmed number of EEDs and ASDs are open. This may adversely impact smoke control during the initial phases of evacuation and relies on ASD and/or EED operations.
- Not utilising all available tunnel or trackway ventilation fans to maintain open draught relief shafts. This does not allow for optimal use of available equipment and may lead to oversized equipment and spatial requirements at the station.
- Fully separated draught relief shafts from tunnels to atmosphere. This would typically require additional space at stations both underground and above ground, which is generally prohibitive due to the high value of increasing a station's footprint.
- A concept that includes controllable PSD dampers installed within the bulkhead above the PSD header box which can be opened to reduce the pressure differentials across the PSDs during emergency operations at stations exhausting from the trackway. The controllable PSD dampers could be closed at stations supplying air to minimise leakage air paths. This solution would introduce an opportunity to remove the OTE for smoke control purposes by using TVS fans at both stations for exhaust whilst maintaining make-up air through open controllable PSD dampers. It should be noted that this is only a concept and has not been implemented in any Australian rail infrastructure projects as far as the authors are aware at the time of writing this paper. This solution may be cost prohibitive noting the additional equipment that would be required as part of the PSD assemblies.

4 ANALYSIS DESCRIPTION

4.1 *Overview*

Noting that the proposed pressure differential reduction concept using controllable PSD dampers has not been observed by the authors for the proposed function, a proof-of-concept analysis was completed to evaluate its effectiveness. Three Dimensional (3D) Computational Fluid Dynamics (CFD) was used to compare pressure differential with and without controllable PSD dampers.

The objective was to determine whether open PSD dampers could reduce pressure differentials between the trackway and platform.

Two scenarios were modelled: one without PSD dampers and one with open PSD dampers. A typical underground station geometry was used in the simulations, with the tunnel ventilation system (TVS) and over-track exhaust (OTE) systems configured in exhaust mode. The PSD dampers were modelled as openings located above closed PSDs.

4.2 *Modelling software*

The simulations were carried out using OpenFOAM, an open-source CFD software package. The steady-state solver SimpleFoam was employed to model the airflow within the station environment. Post-processing of the CFD results was conducted using ParaView, enabling analysis of pressure contours and velocity vectors across the station domain.

4.3 *Methodology*

The key focus of this study was to observe the effect that the PSD dampers had on static pressure distribution across the platform and trackway boundary with and without the open PSD dampers. PSDs are closed in all scenarios. Figure 2 illustrates the simplified underground station geometry used and applied boundary conditions (BC).

Two 120m^3/s exhaust flowrate boundary conditions (green) were implemented to simulate a typical exhaust flow rate of a TVS system. Eight 5m^3/s exhaust flow rate boundary conditions (red) were implemented to simulate a typical exhaust flow rate of an OTE system with a total exhaust of 40m^3/s evenly distributed across the eight OTE openings.

A volumetric condition was implemented (blue) which implicitly induces a velocity-dependent pressure loss to simulate realistic aerodynamic drag and frictional losses associated with the resistance to airflow experienced in long tunnel sections either side of the trackway.

Station entrances were defined with boundary conditions set at ambient pressure to represent make-up air inlets. A simplified train was stopped at the station (purple). Seven opening to represent open PSD dampers were evenly distributed along the length of the platform above head height. Each PSD damper opening has a free-flow area of 1m^2, giving a total of 7m^2 area of pressure-relief air path between the platform and the trackway.

The analysis was performed under steady-state conditions to represent a snapshot of the ventilation response during a trackway fire scenario. The numerical CFD simulations were performed using steady-state Reynolds-Averaged Navier-Stokes (RANS) method. For the turbulence model, the k-ω SST model was applied. A structured meshing approach was used to ensure adequate resolution across key flow regions, with increased mesh refinement imposed at the PSD damper opening interfaces.

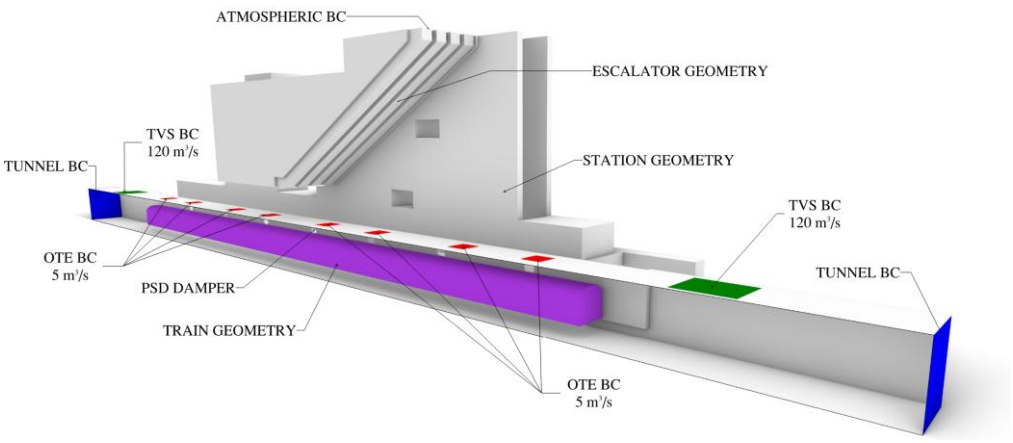


Figure 2. Simplified station geometry used for the 3D CFD study with applied boundary conditions.

5 RESULTS

5.1 *Without PSD dampers*

Results from the base case scenario without PSD dampers and closed PSDs are shown in Figure 3 (plan) and Figure 4 (section). There is minimal pressure variance across the length of the platform on the trackway. Assuming the platforms are at close to ambient pressure, the net static pressure differential between the trackway and the platform is approximately -215Pa. As discussed in Section 3.3, this pressure differential of -215Pa between the trackway and platform is an exceedance of the typical limits to maintain EED opening forces less than 220N.

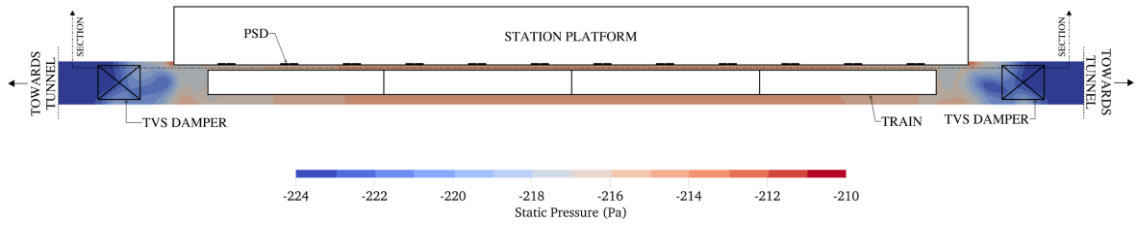


Figure 3. Static pressure profile at 1m above platform floor without PSD dampers – plan view.

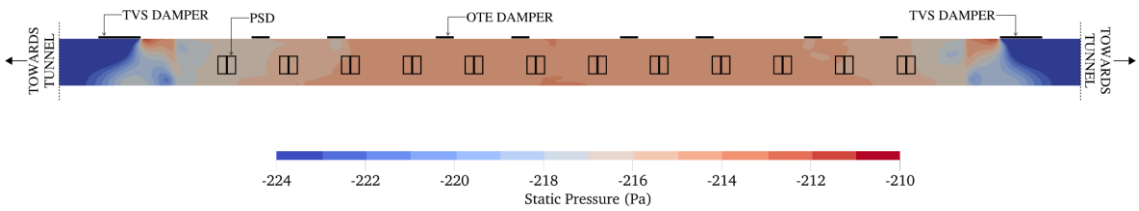


Figure 4. Static pressure profile between train and PSDs without PSD dampers – section view.

5.2 *With PSD dampers*

Results from the case with open PSD dampers are shown in Figure 5 (plan) and Figure 6 (section). There is minimal pressure variance across the length of the platform. Assuming the platforms are at close to ambient pressure, the net static pressure differential between the trackway and the platform is approximately -120Pa. This results in the pressure differential between the trackway and platform being reduced by almost half in comparison to without open PSD dampers and therefore the pressure differential is within typical limits to maintain EED opening forces less than 220N.

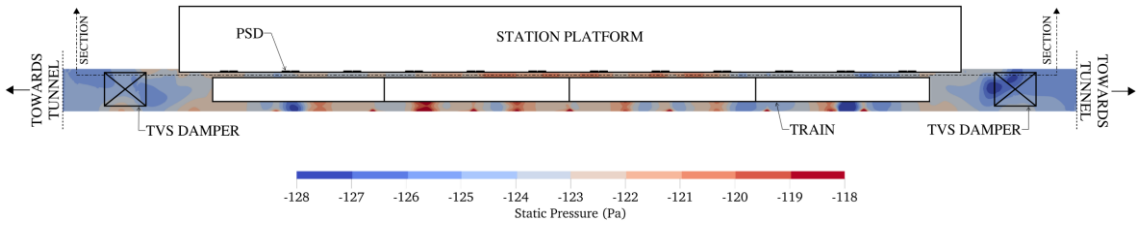


Figure 5. Static pressure profile at 1m above platform floor with open PSD dampers – plan view.

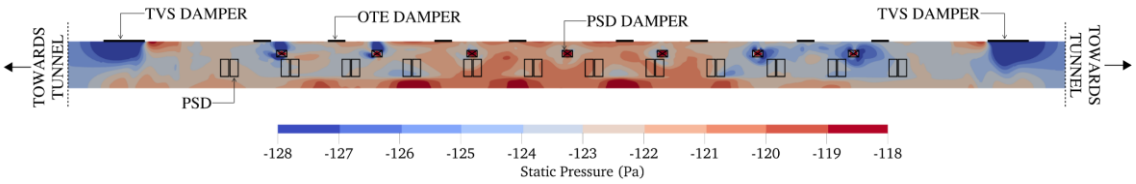


Figure 6. Static pressure profile between train and PSDs with open PSD dampers – section view.

6 CONCLUSION

Consideration should be given to mitigate excessive negative static pressure differences between the trackway and the platform due to the operation of the tunnel ventilation system such that acceptable door opening forces are not exceeded. A range of strategies exist to mitigate this issue.

The concept of using controllable dampers as part of PSD assemblies can also help mitigate excessive negative static pressure differences between the trackway and the platform due to the operation of the tunnel ventilation system. This could present an opportunity to optimise tunnel ventilation systems as it allows the full tunnel ventilation fan capacities at either station end to be utilised with a reduced risk of excessively depressurising the trackway during a tunnel or trackway emergency response when PSDs remain closed.

Example performance of this concept has been demonstrated using 3D CFD analysis. An analysis of the results of an underground rail station experiencing TVS induced air flowrates indicate that the net negative static pressure difference between the trackway and the platform when PSDs are closed can be significantly reduced using PSD dampers facilitating evacuee manual EED operation. Further reductions in the static pressure differences across EEDs could be explored using greater controllable PSD damper free areas e.g. with greater damper opening areas and/or total damper opening numbers. Pressure differences between the trackway and platform with closed PSDs and open controllable PSD dampers will ultimately depend on the specific station geometry, tunnel ventilation system arrangement and response and therefore any controllable PSD damper solution should be uniquely considered for each project.

7 REFERENCES

Australian Building Codes Board. 2022. *National Construction Code.* Canberra: Australian Building Codes Board.

Chun, L.-J.et al. 2004. Pressure Analysis of Platform Screen Door Subjected to a Moving Train in Mass Rapid Transport Underground Station. *Journal of Mechanics,* 20(2), p. 159–166.

National Fire Protection Association. 2007. *Systems, Standard for Fixed Guideway Transit and Passenger Rail.* s.l.:s.n.

National Fire Protection Association. 2023. *Standard for Fixed Guideway Transit and Passenger Rail Systems.* s.l.:National Fire Protection Association.

Yang, J. et al. 2022. Ventilation and energy performance study on platform screen doors with adjustable vents in a subway station. *Tunnelling and Underground Space Technology,* Volume 120, p. 104291.

Zeng, L. et al. 2023. Numerical Study of Train-induced Pressure on Platform Screen Doors of a Subway Station. *Urban Rail Transit,* Volume 9, pp. 179-192.

Zhou, Y., Wang, H., Bi, H. & Wang, J. 2021. Experimental and numerical study of aerodynamic pressures on platform screen doors at the overtaking station of a high-speed subway. *Building and Environment,* Volume 191, p. 107582.

THIS PAGE INTENTIONALLY LEFT BLANK

19th Australasian Tunnelling Conference – Acosta-Martínez, Stewart and Hudson-Smith (Eds.)
© 2025 Australian Tunnelling Society, ISBN 978-0-85825-002-4

Global Navigation Satellite System (GNSS) Repeater Trial

N. Casey & S. Subenthiran
Transport for NSW, Australia

ABSTRACT: A trial of GNSS repeater technology was conducted at the Cooks River Crossing Tunnel to assess whether GNSS repeater technology could provide resilient and accurate location services for several use cases, including public navigation, freight logistics, emergency services response, and facilitating operational and maintenance processes. The GNSS technology configuration selected aimed to provide continuous location coverage for GNSS-enabled devices located in environments with no other coverage, such as road and railway tunnels. At the time of the trial, the technology was configured to capture signals from the Global Positioning System (GPS) constellation only. Analysis of the non-augmented received GNSS signals demonstrated that the technology did not provide sufficiently accurate location services to justify further trials or deployment. Subsequent tests using software-augmented receiver devices resulted in significantly improved accuracy. The paper concludes by summarising the additional work required and the challenges involved in delivering accurate and resilient location services using this technology.

1 INTRODUCTION

1.1 *Need and benefits*

Currently, many systems that rely on GNSS positioning (satellite-based location services) do not work in tunnels. With WestConnex, the M6, and the Western Harbour Tunnel, the busiest integrated road tunnel network in the world will be located in Sydney. This network of tunnels provides the public with over 100 unique journeys (journeys with a unique combination of start and end point) with many possible underground journeys of over 20 km in length. This emphasises the complexity of the network. A large-scale survey of NSW road tunnels users (515 respondees) identified that 93% of road users use electronic navigational aids (i.e. Google Maps) for some journeys. The public therefore has an increasing dependency on this technology, a technology that is not available in tunnels.

The objective of the GNSS repeater trial was to test whether an emerging technology is sufficiently accurate and reliable to benefit location services.

These services include:

- Improved performance of GNSS based navigation devices;
- Improved Emergency Services incident response;
- Ability to more accurately locate workers during maintenance closures; and
- Optimisation of freight logistics tracking in tunnels.

The technology has potential beneficial use cases beyond road tunnels. We are aware the application of GNSS location technology for rural surface level rail in Spain, and believe there are use cases for rail tunnels and rail infrastructure across NSW.

The initial trial was delivered in June 2023. Over 20 test cases were completed over two nights, with tests undertaken by RFI (on behalf of TfNSW), Fire & Rescue NSW, NSW Ambulance and NSW Police Force. The trial was facilitated by Transurban at the Cooks River Crossing tunnel (M5 East Motorway). Further tests were undertaken in December 2023. The trial was funded by the TfNSW Asset Technology Program.

1.2 *Key principles & objectives*

Given the wide range of stakeholders and project participants, an early project strategy was to propose and agree a set of key principles and objectives.

The agreed objectives of the trial were as follows:

1) The trial should aim to assess and optimise the accuracy performance that can be achieved by the technology;
2) The procurement, design and delivery of the trial should aim to maximise the likelihood of success;
3) The trial should focus on the technology that has the greatest chance of satisfying all the identified Use Cases;
4) The trial should engage an independent expert to validate the trial outputs;
5) Demonstrate compliance with ACMA requirements;
6) The successful completion of this trial will not necessarily lead to a decision to undertake a widespread deployment of the technology. There may be other trials required (i.e. system resilience, performance in complex alignments, higher vehicle speeds).

The key principles and objectives were endorsed by the 'GNSS Repeater NSW Working Group' (NSW Telco Authority, FRNSW, NSW Ambulance, NSW Police Force).

1.3 *Market Search*

A number of technology solutions were considered. Most did not offer the potential to meet objective 3 'the greatest chance of satisfying all the identified Use Cases. A 'Market Search' report was produced which identified the range of available technologies and the respective vendors.

The technology solutions include:

- GNSS zone based system;
- Bluetooth based systems;
- Dead Reckoning Technology;
- V2X & WiFi.

This search identified that a 'precision' GNSS Repeater / Simulation product offered by RF Industries / Syntony GNSS offered the solution most likely to satisfy all Use Cases for most users of navigational or location services aids. Therefore, the trial was based on the Syntony GNSS 'precision' solution that is delivered in Australia through RF Industries. This potential solution had the greatest likelihood of satisfying the public navigation use case. The precision system is intended to provide an updated location at each update of the received GPS signal. In contrast a zone system provides one location signal for each geographically defined zone. A zone may be a 100m length of a carriageway.

RF Industries / Syntony GNSS were engaged to assist in the development and final definition of the trial. Trial delivery risks were mitigated by having the technology provider and the experienced systems practitioner engaged in the final definition of the trial.

1.4 *Legislation change*

Prior to undertaking the trial, a transmitter of radiocommunications using the RNSS (GNSS) frequency band was prohibited under the Radiocommunications Act 1992. TfNSW engaged with NSW Telco Authority to lobby the Australian Media and Communications Authority (ACMA) for changes to the legislation that would facilitate the trial.

ACMA released a Radiocommunications (Prohibited Device) (Radio Navigation Satellite Services (RNSS) Jamming Devices) Amendment Declaration in 2020 to facilitate the trials of RNSS repeaters (GNSS repeaters) in road tunnels under short-term scientific licensing. The NSW Telecommunications Authority applied for and received a Scientific Licence from the ACMA to enable the trial to proceed under the guidelines of the amended legislation.

1.5 *Contract arrangements*

RF Industries were engaged through whole of NSW government panel ITS-2573 to undertake the final definition, delivery and post-delivery reporting of the trial. There was no direct contract with Sydney GNSS. The RF Industries work was to focus on delivering trial results for 'public navigation' and also to facilitate tests to be undertaken by Emergency Services.

A formal agreement between TfNSW and WestConnex / Transurban was signed to facilitate the use of the Cooks River Crossing tunnel for the purposes of the trial.

GNSS expert Professor Andrew Dempster of University of NSW was engaged by TfNSW as an 'independent expert'. The purpose of this engagement was to advise TfNSW on the scope of the trial, and to provide independent review of the trial results and outcomes.

2 OUTLINE SYSTEM ARCHITECTURE

Prior to defining the trial system configuration, TfNSW had acquired, through the Swedish Transport Administration (Trafikverket), information relating to the trial of Syntony GNSS 'precision' GNSS Repeater technology in the Southern Link tunnel of Stockholm. The trial results indicate that:

- GNSS accuracy provided by the precision-based solution increases as zone length increases
- Maximum zone lengths are limited by signal decay
- Signal decay is dependent on the specification of existing leaky feeder cables
- Accuracy decreases as vehicle speed decreases
- The longevity of the trial enabled optimisation of the installed system architecture

Based on the above the following principles were to be adopted for the NSW trial:

- The trial should include differing lengths of zone in order to establish the optimal zone length for the leaky feeder cable being used
- At least two zones should form the overall length of the trial installation
- Consideration of whether the trial site can form a 'test bed' for optimisation of the technology

Figure 1 below shows the resultant configuration of the NSW trial. Note in particular:

- The installation of 20 survey marker points along the approach to, within and beyond the exit from the eastbound tube;
- That there are two segments of leaky feeder identified – the system uses the existing leaky feeder communications cable to transmit the repeated GNSS signals;
- The first leaky feeder 'zone' is approximately 120 m, while the second is approximately 280 m;
- Beyond the second leaky feeder there is an approximate 150 m length of tunnel in which the existing leaky feeder cable proved to be inadequate for the purposes of the trial;
- As had been identified in feedback from Trafikverket, the zone length is dependent on the signal decay, which in turn is dependent on the leaky feeder specification;
- The leaky feeder installed from survey point 13 to survey point 16 was unable to sustain the GNSS signal.

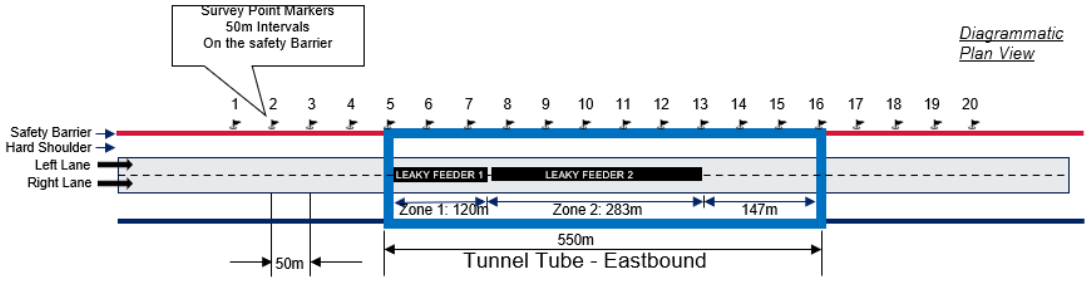


Figure 1. Tunnel illustration showing Cooks River Crossing Tunnel survey points and leaky feeder zones

3 TRIAL LOCATION

3.1 *Selection of trial location*

A number of different trial locations were investigated and an extensive assessment undertaken to gauge the best location. The eastbound tube of the Cooks River Crossing Tunnel was chosen.

The benefits of this location were:

- Regular bi-monthly closures that would allow preparatory and trial works;
- (Seeming) suitability of existing communications systems;
- In Sydney, and hence local to the team delivering the project;
- Minimal further installation required to facilitate the trial;
- Ease of installation (i.e. proximity and access to sub-station for antenna installation);
- Discrete section of roadway;
- At approximately 520 m in length, the tunnel allows testing of entry and exit transitions;
- Engagement with WestConnex / Transurban.

3.2 *Residual issues with trial location*

While initial site inspections were undertaken to confirm the suitability of the tunnel, some aspects of the communications system were only identified once trial installation works were undertaken. In particular, issues with the existing leaky feeder system were identified. The existing system was comprised of two segments – one at the western end of the tunnel (approximately 120 m in length, and the other extending along the remainder of the tunnel. The longer segment was further comprised of three parts, each with different specification. It was found that only the first part of approximately 280 m length was of adequate specification to carry the GNSS signals. While not ideal, this discovery was not deemed to be a 'red flag' but rather would further test the robustness of the system.

The tunnel is also located adjacent to Sydney Airport. Dialogue with the Civil Aviation Safety Authority and Airservices Australia identified a risk of the repeated signal spilling from tunnels entrances and overlapping with and / or affecting aviation equipment at the airport. As a result, a series of controls were put in place during the trial operations.

3.3 *Preparatory works*

3.3.1 *Physical works*

Regular maintenance closures of the M5 motorway facilitated a series of early works. This included:

- Survey, and installation of survey marker points (see Figure 1);
- Survey of existing cable containment and cabling within the tunnel;
- Installation of demultiplexer equipment with the tunnel;
- Installation of GNSS antenna, simulator and de-multiplexer within sub-station 9 (located above the tunnel).

3.3.2 *Trial execution plan*

TfNSW developed a draft 'trial execution plan'. The purpose of this plan was to:

- Define the test cases to be undertaken during the trial;
- Identify the roles and responsibilities required to deliver the trial;
- Identify the equipment needed to delivery the trial;
- Establish that the planned test cases could be delivered in the allotted roadway closure times;
- Establish these aspects as part of a contract document.

RF Industries delivered a final version of the plan as part of their contractual obligations.

3.3.3 *Test case configuration and data analysis plan*

TfNSW developed a draft 'test case configuration and data analysis plan'. The purpose of this plan was to:

- Outline the methodologies to be used for data acquisition during the trial;
- Confirm the data required to be delivered;
- Identify the roles and responsibilities required to deliver the data;
- Identify the equipment needed to delivery the data;
- Establish these aspects as part of a contract document.

RF Industries delivered a final version of the plan as part of their contractual obligations.

4 PARTICIPANTS AND COLLABORATORS

The trial was supported by NSW Emergency Services who were invited to participate. In particular, FRNSW delivered a 'Problem Statement' which identified the communications issues likely to be prevalent across WestConnex without an upgrade of GNSS based systems.

The Emergency Services, FRNSW, NSW Police and NSW Ambulance) developed their own suite of test cases for implementation during the trial. Tests were undertaken on a range of emergency service technologies and vendor products carried within 6 vehicles that were used during the trial.



Figure 2. Emergency services vehicles in the Cooks River Crossing Tunnel during the trial

5 TEST CASES

The following relates foremost to the public navigation use cases. The following test cases were undertaken:

- Quantitative test of accuracy for raw GNSS Received Signal (i.e. Ublox);
- Qualitative test of accuracy for Smartphone signal augmented by mapping application (i.e. Google Maps);
- Qualitative test of accuracy of an in-car factory installed navigation system (including assessment of dead reckoning).

With regard to public navigation the following test cases are proposed:

- ACMA compliance tests;
- Accuracy of the received signal at 0kph;
- Accuracy of the received signal at 20kph;
- Accuracy of the received signal at 80kph;
- Signal capture as the receiver transitions from external to internal;
- Signal capture as the receiver transitions between internal zones;
- Signal capture as the receiver transitions contra flow;
- Signal capture in different lanes;
- Signal capture with repeater system turned off;
- Signal capture as the receiver transitions from internal to external.

5.1 *Success Criteria*

5.1.1 *Navigation*

There are no established acceptance criteria for GNSS system accuracy in underground applications. The following is a draft list of benchmarks that might be used in the evaluation of results from this trial:

- Equivalent accuracy to that provided by GNSS receivers in open sky applications; and
- Required accuracy of Connected and Automated Vehicles.

The use of the UBlox device allowed the accuracy of the repeated GNSS signal to be compared to these benchmarks. This accuracy was assessed both in absolute terms, but also with specific focus on transition areas (i.e. transition from outside to inside the tunnel, transition between internal repeater 'zones'). In addition to the capture of raw data, the trial included qualitative assessment of the accuracy provided by mapping applications on the smartphone device and by mapping applications on an in-car navigation system.

The U-Blox receiver is a tool used to measure and present raw GNSS data. However, most navigational devices intended for general public use, such as smartphones, in-vehicle GPS systems, etc., receive raw GNSS data and process it using augmentation algorithms specific to the device and its intended functionality. These algorithms are designed to collect input data from sensors that monitor factors such as speed, compass direction, steering inputs, etc.; the data are then used to apply correctional factors to the raw GNSS data to improve the accuracy of the positional fix.

5.1.2 *Emergency Response*

The Emergency Services prepared a set of test cases to determine the accuracy and functionality of the received signal. These are not the focus of this paper.

5.1.3 *Spillage of Repeated Signal*

The trial will need to demonstrate that 'spillage' of the repeated signal through the tunnel portal is complaint with requirements set by ACMA.

6 TRIAL RESULTS

6.1 *Initial Tests*

The June 2023 trials only considered the analysis of the performance of the SubWAVE^{TM} GNSS repeater system using the raw GNSS repeated data to compute the position of the test vehicle. A U-Blox receiver was used in all test cases to measure and present the raw captured data. The computed actual position of the test vehicle, relative to a series of pre-existing survey markers whose precise geographical coordinates are known, was then compared to the position given by the measured raw GNSS data to determine the accuracy of the GNSS repeater system solution.

The results obtained in the June trials using the raw GNSS data revealed that the accuracy of the positional fix obtained without the use of augmentation algorithms on the receiving device would not be adequate for public navigation use cases. The repeater solution on its own typically

provides two-dimensional (latitude/longitude) 50th & 95th percentile error bounds of around 30 m and 60 m respectively for dynamic measurements. The tests resulted in varying accuracy depending on whether static or dynamic tests were being undertaken.

A plot showing the results of a 20 kph dynamic measurement through a section of the tunnel during the June trials is shown in Figure 3, where the survey markers in the tunnel are shown in red and the measured test vehicle track markers are shown in blue. The tunnel bores are stylised as the dark yellow traces on the map; the tunnel bore used for the trial is the uppermost eastbound tunnel.

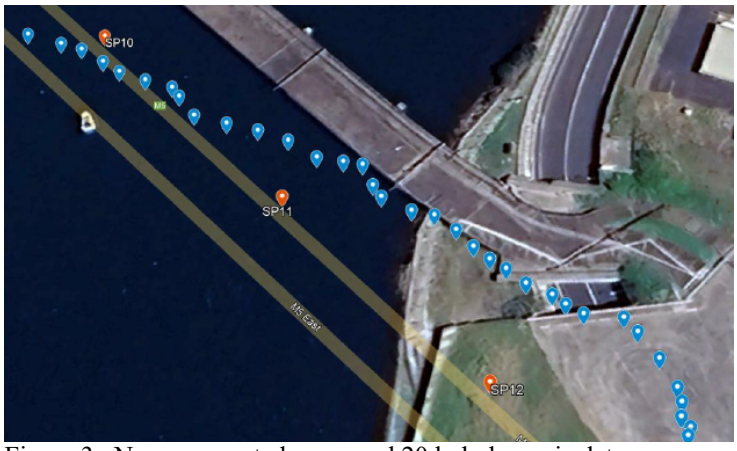


Figure 3. Non-augmented measured 20 kph dynamic data

6.2 *FRNSW Data Analysis*

Results of the Emergency Services test data are not reproduced here. However, analysis undertaken by FRNSW concluded that:

- The trial demonstrated that GNSS simulations can occur in a tunnel environment, although in these trial results the positioning was inaccurate and orientation incorrect.
- As the results displayed large deviations and drift, they did not provide the evidence necessary to support progressing to a broader trial or rollout.

6.3 *Further Tests*

Further public navigation test cases were designed following the analysis of the results obtained during the June trials, and these additional test cases were trialled in December 2023. An Android smartphone was used as the GNSS receiver in all of these test cases (no raw data were collected via UBlox or otherwise). The smartphone had a Syntony (Indoor RTK) application installed which allowed augmentation of the measured raw GNSS broadcasted data to improve the accuracy of the GNSS repeater system solution.

The trial results show very good horizontal accuracy and orientation between the receiver position and the tunnel alignment. This significant improvement was not quantified through raw data so the exact accuracy can not be gauged. Despite these good results, the use of augmented receivers does not achieve the key objectives of that trial namely that ‘the trial should focus on the
technology that has the greatest chance of satisfying all the identified Use Cases’. That receiver augmentation is required to achieve the results, eliminates all who do not have access to the augmentation.



Figure 4. Augmented measured 20 kph dynamic data

7 CONCLUSIONS

The analysis of public navigation test cases undertaken by RF Industries and the separate analysis of FRNSW test cases both concluded that the accuracies obtained did not support an argument to proceed to deployment.

The use of augmented receivers in the December tests showed significantly improved accuracy. However, the use of augmentation does not align with the trial objectives, given that obtaining similar accuracies would require the widespread adoption of such augmentation (assuming such augmentation were available across the wide range of receiver devices).

There was very little difference in the z-axis error percentiles between the June and December tests despite the use of the augmented receiver. The altitude parameter is fixed in the synthesized GNSS signals (it is not computed form the satellite data) and its value depends on the location along the length of the leaky coaxial cable where the measurement is taken.

7.1 *Future considerations*

Beyond the constraints of this trial there are other concerns regarding the performance of the technology. The trials have been in a tunnel devoid of traffic other than the test vehicles. In particular, the signal multipath environment will be quite different with other vehicles travelling in the tunnel with the test vehicle. A variation of performance in the presence of traffic is expected.

The trials have run in a relatively straight, single layered tunnel (no tunnels below or above other tunnels) that does not have exit ramps or turning loops. The elements of scalability may present a number of problems for tunnels of varying geometrical characteristics (long tunnels, curved tunnels, sloping tunnels, overlying or underlying tunnels or parallel tunnels).

The lifetime of any in-tunnel solution will depend on the attention paid at installation to the potential changes to the satellite navigation environment in coming years. For these (spoofing mitigation, multiple GNSS systems on multiple frequencies, receiver authentication signalling, new satellite systems at low earth orbit) there needs to be a solution at installation, or a technology roadmap detailing how these problems will be dealt with in future.

If this general type of technology is deemed worthy of perseverance, any new trials should consider some changes such as a properly instrumented tunnel with no dead zones, a high degree of repetition of the tests, tests with traffic, tunnels with varying geometrical characteristics, and tests with spoofing-resistant receivers.

ACKNOWLEDGEMENT

This paper draws on non-publicly accessible material produced by RF Industries, University of NSW and Fire & Rescue NSW. Their contribution, as well as the contributions of WestConnex / Transurban, NSW Telco Authority, ACMA and colleagues at TfNSW to the trial is gratefully acknowledged.

19th Australasian Tunnelling Conference – Acosta-Martínez, Stewart and Hudson-Smith (Eds.)
© 2025 Australian Tunnelling Society, ISBN 978-0-85825-002-4

Thermal properties of the Triassic rock formations across the Sydney region for the use in tunnel ventilation design

J. W. Davidson & D. Saunsbury
WSP Australia Pty Limited, Sydney, Australia

A. Bidarmaghz
School of Civil and Environmental Engineering, Sydney, Australia

D. J. Och
WSP Australia Pty Limited, Sydney, Australia
School of Biological, Earth and Environmental Sciences, Sydney, Australia

ABSTRACT: The thermal properties of the geological formations that host tunnels are an important parameter in the design of tunnel ventilation systems, particularly for metro and high-speed rail systems. The heat generated in these tunnels is transferred through the tunnel lining and into the geological formations around the tunnels. The rate of heat transfer is influenced by the thermal properties of the ground surrounding the tunnel. The resultant tunnel wall temperatures and air temperatures inside the tunnel are therefore partially dependent on the ground thermal properties. Tunnelling in Sydney Basin region is predominantly in Triassic rock formations of the Narrabeen Group, Hawkesbury Sandstone, transitioning between the Mittagong Formation and Wianamatta Group shales in the central part of the basin. Investigations into thermal properties of the ground across the central and northern parts of the Sydney Basin were conducted for three underground rapid transit projects in Sydney. Testing of borehole samples was undertaken to determine the thermal conductivity and diffusivity of the variable ground conditions around the tunnels. This paper presents the results and analysis of that testing for the purpose of applying to the tunnel ventilation design of current and future tunnel projects. The measured mean thermal conductivity was 2.85 W/m.K and the mean thermal diffusivity was in the range of 1.88×10^{-6} to 1.51×10^{-6} m^2/s.

1 INTRODUCTION

Tunnel ventilation systems are essential components of underground rapid transit infrastructure, designed to manage both emergency scenarios—such as smoke control during fires—and everyday operational conditions, including the regulation of tunnel air temperatures. In high-frequency metro systems, substantial heat is generated from sources such as train braking and acceleration, onboard air conditioning systems, friction, and tunnel-mounted equipment. This heat must be effectively dissipated to maintain safe and comfortable conditions for passengers and equipment, making thermal interaction between tunnel air and the surrounding ground a critical consideration in ventilation system design.

One of the primary mechanisms for heat dissipation is the transfer of thermal energy from the tunnel air to the surrounding ground through the tunnel lining. The effectiveness of this process depends on several factors, including the temperature gradient, the thermal properties of the tunnel lining, and the thermal conductivity of the surrounding geological materials. In regions like the Sydney Basin, where underground rail alignments traverse a variety of sedimentary rock formations, understanding the thermal properties of these materials is vital for accurate thermal modelling and efficient ventilation system design.

Thermal conductivity of geological materials is influenced by a range of internal and external factors. Internally, mineral composition plays a key role—rocks rich in quartz, for example, typically exhibit higher conductivity than those with greater clay content. Pore fluids such as water can enhance conductivity due to the rocks high heat capacity, while rock structure, including

porosity and fracture networks, can impede heat flow by introducing less conductive air pockets. Externally, temperature and pressure also affect conductivity, with higher pressures generally increasing it, particularly in sedimentary rocks. Additionally, mineral grain size, lithology, density, and are all known to correlate with thermal conductivity, further complicating its prediction in heterogeneous rock masses.

However, detailed thermal characterisation of the ground is often overlooked during early design phases due to time and cost constraints. Designers frequently rely on generic reference values (e.g., Robertson, 1988), which may not accurately reflect the heterogeneous and anisotropic nature of local geological formations. This can lead to discrepancies in predicted versus actual tunnel air temperatures, potentially resulting in over- or under-designed ventilation systems.

To address this gap, recent underground rail projects in the Sydney Basin have incorporated targeted geotechnical investigations, including thermal conductivity testing of rock samples obtained from boreholes along proposed tunnel alignments. These tests provided localised thermal property data, enabling more accurate modelling of long-term heat transfer between tunnel air and the surrounding ground.

This paper presents the results of thermal conductivity testing conducted on borehole samples from several corridors across the upper Sydney Basin, including tests previously assessed in Saunsbury et al. (2017). It outlines the geological context of each corridor, details the testing methodology, and analyses the results to inform future tunnel ventilation design.

2 GEOLOGICAL CONDITIONS

The Sydney Basin is a structural and topographic basin extending from Batemans Bay to Lithgow and Raymond Terrace. It was infilled during the Permian and Triassic periods (298–200 million years ago) with thick sedimentary sequences deposited under fluvial and marine conditions (Herbert, 1983).

Minor deformation at the end of the Late Triassic, part of a broader tectonic phase continuing into the Paleogene, contributed to the formation of the Tasman Sea (Herbert & Helby, 1980; Och et al., 2009). This tectonism introduced dominant joints, faults, and igneous intrusions such as dykes and diatremes. Recent studies suggest these features may be influenced by deeper basement structures.

During the Last Glacial Maximum (~120,000 years ago), sea levels were ~100 m lower, shifting the coastline ~20 km eastward. Major rivers, including the Hawkesbury and Parramatta, incised deep valleys into the uplifted eastern margin. Subsequent Pleistocene and Holocene transgressive-regressive cycles led to alternating phases of sedimentation and erosion, producing under-consolidated deposits and complex stratigraphy.

The distribution and composition of these dominant rock formations are summarised to inform this study and guide infrastructure planning for major transport and tunnelling projects in the central Sydney Basin:

2.1 *Ashfield Shale*

The Ashfield Shale, the lowest formation of the Wianamatta Group, becomes increasingly prevalent along tunnel corridors toward Parramatta, where it dips gently westward and reaches thicknesses of up to 50 m. It transitions into the upper Minchinbury Sandstone and Bringelly Shale (excluded from this study) to the west and comprises four stratigraphic members:

- Mulgoa Laminite Member – Dark grey siltstone with light grey sandstone laminations
- Regentville Siltstone Member – Dark grey sideritic-banded siltstone
- Kellyville Laminite Member – Light grey siltstone with fine to medium sandstone laminations
- Rouse Hill Siltstone Member – Dark grey to black claystone-siltstone, slightly carbonaceous

These rocks are anisotropic, with reduced strength parallel to bedding. These rocks are slightly absorbent (avg. moisture ~3%) and contain 3–30% quartz, up to 20% carbonate clasts, and clay cement stained by iron oxides (up to 80%).

2.2 *Mittagong Formation*

Underlying Ashfield Shale, this ~6 m thick formation features alternating shale and sandstone beds, often disturbed by soft sediment deformation and bioturbation. It shares characteristics with Ashfield Shale and Hawkesbury Sandstone but is distinguished by dominant siltstone and finer sandstone facies, respectively.

2.3 *Hawkesbury Sandstone*

The Hawkesbury Sandstone is the predominant rock formation encountered at tunnel depth and is typically characterised as a medium- to coarse-grained sandstone comprising 50–80% quartz with clay (5–40%), secondary silica (up to 20%), and iron carbonate cement (0–15%, occasionally up to 35%). Pore space reaches 5%, and moisture content averages 6.8%. Three facies are identified:

- Massive sandstone facies,
- Cross bedded or sheet facies (well developed or indistinct/poorly developed), and
- Shale/siltstone interbed – Mudstone facies.

2.4 *Narrabeen Group*

Deposited in fluvial to shallow marine settings during the Early to Middle Triassic, this group features variable lithologies including sandstones, siltstones, shales, and claystones. Key formations include Terrigal, Patonga, Tuggerah, and Munmorah, along with Bald Hill Claystone, Newport, and Garie formations.

The Terrigal Formation is notably complex, with interbedded sandstone, siltstone, claystone, and breccia. Petrographic data show 33–67% quartz, 2–12% feldspar, 5–30% lithics, and 5–10% clay matrix, with minor silica or calcite cement. Coarse beds may have up to 6% pore space, while finer beds range from <1% to 3%. The lower Terrigal and upper Tuggerah Formations contain approximately 20% shale members, while the Patonga Claystone includes around 10% sandstone interbeds. These interbedded layers, often more weathered and clay-rich than the Hawkesbury Sandstone, present geotechnical challenges due to strength and the rocks variability.

3 GROUND THERMAL PROPERTIES

3.1 *Legacy values*

Thermal conductivity and thermal diffusivity are the parameters typically used to define ground thermal properties in a tunnel ventilation analysis model. These parameters are direct input for the Subway Environment Simulation (SES) program typically used for rail tunnel ventilation analysis. Legacy values of 1.80 W/m·K for conductivity and 1.15 m^2/s for diffusivity have been used as values for sandstone on several major infrastructure projects in Sydney, for the purpose of designing tunnel ventilation systems.

3.2 *Sample data*

Following a previous study into the sensitivity of tunnel air temperatures to thermal conductivity and diffusivity (Saunsbury et al., 2017), geotechnical borehole testing has been conducted for additional infrastructure projects in Sydney. These tests measured each sample's thermal resistivity (the inverse of conductivity), moisture content, and/or dry density. From this data, it is possible to assess the validity of the legacy values and recommend new values if necessary. For consistency and to ensure the applicability of these values to future projects, only results from the Hawkesbury sandstone samples are presented here.

Three sets of borehole tests were obtained. The first (Dataset 1) includes the sandstone sample results from the previous sensitivity study (Saunsbury et al., 2017). For Datasets 1 and 2, thermal resistivity testing was completed in accordance with IEEE Standard 442, ASTM Standard D5334 and Ausgrid NS130 Appendix K. Tests produced measurements for moisture content, thermal resistivity and density in Table 1 and Table 2. Some details of the Dataset 1 and 2 tests are unknown, such as the condition of the samples prior to testing and whether thermal paste was used to maximise heat transfer at any interface locations.

Dataset 3 was tested at the School of Civil and Environmental Engineering, UNSW, using a C-therm thermal conductivity analyser under ASTM D7984 guidelines. A thin layer of thermal paste was applied to the sensor area and sample surface to minimise the air gaps between the machine and sample. This maximises heat transfer and allows the most accurate measurement possible to be obtained, reproduced in Table 3. Samples were stored to retain as much in situ moisture as possible. Measured values are therefore indicative of the in situ thermal properties.

Table 1. Dataset 1 (Saunsbury et al., 2017).

Test ID	Moisture [% Dry Mass]	Pre-Dry Out Thermal Resistivity [Km/W]	Dry Density [kg/m^3]
01	1.0	0.73	2560
02	6.2	0.72	2200
03	5.9	0.78	2250
04	6.6	0.81	2200

Table 2. Dataset 2.

Test ID	Moisture [% Dry Mass]	Pre-Dry Out Thermal Resistivity [Km/W]	Dry Density [kg/m^3]
05	6.1	0.34	2370
06	3.1	0.54	2525
07	6.0	0.32	2400
08	3.9	0.43	2440
09	6.6	0.29	2290
10	6.0	0.29	2310
11	3.3	0.31	2310
12	6.6	0.40	2240
13	6.7	0.36	2280
14	3.9	0.29	2320
15	4.8	0.27	2320

Table 3. Dataset 3.

Test ID	Moisture [% Dry Mass]	Pre-Dry Out Thermal Resistivity [Km/W]	Dry Density [kg/m^3]
16	-	0.31	-
17	-	0.30	-
18	-	0.39	-
19	-	0.27	-
20	-	0.30	-
21	-	0.36	-
22	-	0.25	-
23	-	0.57	-
24	-	0.47	-
25	-	0.33	-
26	-	0.45	-
27	-	0.19	-
28	-	0.61	-
29	-	0.55	-

3.3 *Sample distribution*

Thermal conductivity was calculated as the inverse of thermal resistance for each sample. Distribution plots for each dataset are presented in Figure 1.

Datasets 2 and 3 feature similar distributions across a similar range of conductivity values, excluding an outlier in the Dataset 3 sample. The maximum Dataset 3 value of 5.19 W/m·K is classified as an outlier because it falls outside the range calculated by the 1.5IQR (interquartile range) method. This is true when Dataset 3 is considered by itself and combined with Dataset 2. It is therefore considered reasonable and conservative to exclude this value from the analysis. The mean of Dataset 2 is 2.98 W/m·K and the mean of Dataset 3 is 2.75 W/m·K, excluding the outlier.

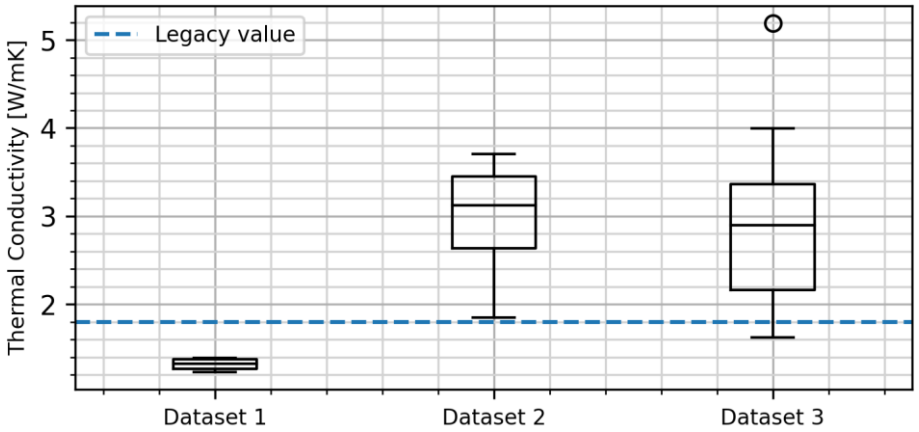


Figure 1. Sample thermal conductivity distributions for each dataset (median indicated by orange line).

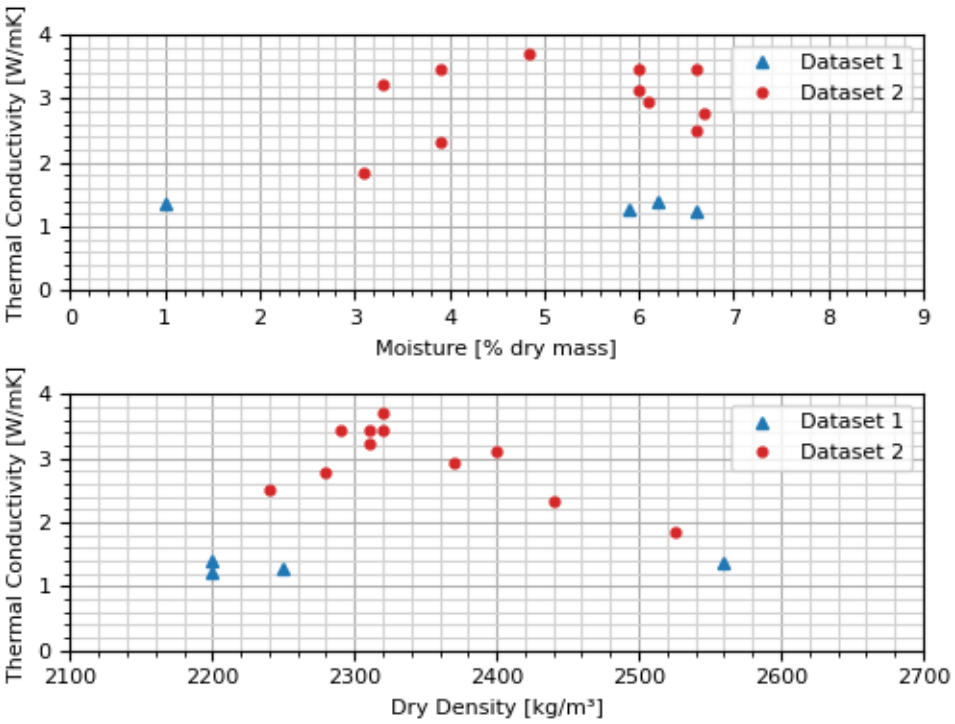


Figure 2. Thermal conductivity plotted against moisture and dry density for Dataset 1 and Dataset 2.

Compared to Datasets 2 and 3, Dataset 1 has significantly smaller conductivity values and a narrower distribution. The consistency between Datasets 2 and 3, and the differences from Dataset 1, suggest an irregularity in Dataset 1.

The available data does not explain the discrepancy between the Dataset 1 and the other datasets. As shown in Figure 2, Datasets 1 and 2 have a similar range of dry density and moisture content values. There is no apparent relationship between these and thermal conductivity in the samples. Differences in these properties between the datasets are therefore not a factor. Dataset 3 cannot be compared to Dataset 1 in this manner, as it does not include moisture or density measurements. Unmeasured parameters may explain the difference, such as gain size or mineralogical composition. Differences in testing conditions, as detailed in Section 3.2, are hypothesised to be more likely explanations for the inconsistency. Dataset 1 had unrecorded sample storage conditions, potentially leading to desiccation and artificially low conductivity.

Based on Dataset 1, which was the only available data at the time, the previous study (Saunsbury et al., 2017) found the sample conductivity values were substantially lower than the legacy value. Relative to Datasets 2 and 3, the legacy value of 1.80 W/m·K is however lower; the minimum value for Dataset 2 is 1.85 W/m·K and the minimum value for Dataset 3 is 1.63 W/m·K.

3.4 *Exploratory data analysis*

A Python script was used to test for any statistically significant differences between the thermal conductivity distributions of Datasets 2 and 3. A Shapiro-Wilk test was first used to test for normality, given the small samples sizes, with a null hypothesis that the datasets are normally distributed and a threshold value of 0.05. The p-values are given in Table 4. The same test was conducted for Dataset 2's moisture and dry density values (Table 5).

Moisture content's p-value is marginally above 0.05, while the others greatly exceed the threshold. All null hypotheses can therefore be accepted. As Dataset 3 does not contain moisture or density data, the same analysis was not performed for these parameters in Dataset 3.

Statistically significant differences in conductivity distribution between Datasets 2 and 3 were tested for. A two-sample t-test and Levene's test were selected. The null hypothesis supposed equal sample mean and variance between the datasets. The p-values are given in Table 6. Again, these exceed 0.05. This confirms the visual observations made in Section 3.3: Datasets 2 and 3 have conductivity normal distributions which are not different to a statistically significant degree.

To derive thermal conductivity and diffusivity values for use in future projects, the two datasets can therefore be considered together.

Table 4. Shapiro-Wilk p-values for Datasets 2 and 3 thermal conductivity values.

Dataset	Shapiro-Wilk p-value
2	0.4619
3	0.5325

Table 5. Shapiro-Wilk p-values for Dataset 2 moisture and dry density values.

Parameter	Shapiro-Wilk p-value
Moisture content	0.0501
Dry density	0.2346

Table 6. T-test and Levene p-values for a comparison of Datasets 2 and 3 thermal conductivity values.

Test	p-value
T-test for equal mean	0.1610
Levene's test for equal variance	0.2551

3.5 *Thermal diffusivity derivation*

As in Saunsbury et al. (2017) estimates of the thermal diffusivity of the samples in situ were calculated using thermal conductivity, wet bulk density, and specific heat capacity.

$$a = \frac{k}{\rho c_p} \quad (1)$$

Where;
a : thermal diffusivity (m^2/s)
k : thermal conductivity (W/m·K)
ρ : density (kg/m^3)
c_p : specific heat capacity (J/kg.K)

In situ wet bulk density was estimated using sample moisture content and dry density. Although thermal diffusivity cannot be directly derived from the sample data, Saunsbury et al. (2017) indicated that tunnel air temperatures are less sensitive to this parameter compared to thermal conductivity. This study adopted the same approach as Saunsbury et al. (2017) for estimating thermal diffusivity for the sensitivity study.

A range of specific heat capacities for sandstone is provided in Konakova et al. (2013) and included below in Table 7. Using the minimum and maximum values in this range, upper and lower estimates for thermal diffusivity were calculated for each sample, respectively.

Thermal diffusivity could not be calculated for the Dataset 3, as sample measurements for moisture and density were unavailable. Dataset 1 was excluded, as discussed previously.

Table 7. Specific heat capacity values from Konakova et al (2013)

Dataset value	Specific heat capacity [J/kgK]
Minimum	645.62
Maximum	801.23

3.6 *Thermal conductivity and diffusivity values to be adopted for future use*

Because the datasets are normally distributed, bell curves were generated using the sample mean and variance (Figure 3). The combined thermal conductivity dataset considered all samples from Datasets 2 and 3, excluding the outlier in Dataset 3. The same was done for thermal diffusivity. Separate curves were produced for the lower and upper estimates. Dataset 1 samples were excluded when generating the distributions. Summary statistics are provided in Table 8.

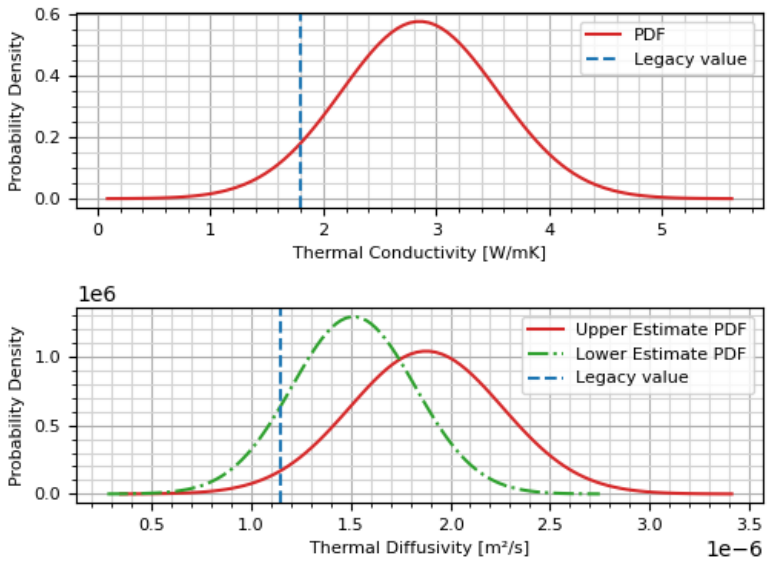


Figure 3. Probability distributions for thermal conductivity and thermal diffusivity.

Table 8. Derived means and 95th percentile values for thermal conductivity and diffusivity.

Parameter	Thermal conductivity [W/m·K]	Thermal diffusivity (upper estimate) [m^2/s]	Thermal diffusivity (lower estimate) [m^2/s]
Mean	2.85	1.88×10^{-6}	1.51×10^{-6}
95th percentile*	1.71	2.50×10^{-6}	2.03×10^{-6}

*For thermal conductivity, "95th percentile" refers to the lower end of the distribution, as this is worse for tunnel air temperatures.

The legacy conductivity value is conservative relative to the borehole sample data. This suggests a higher value may be more appropriate for the design of tunnel ventilation systems which would lead to potentially lower predicted tunnel air temperatures. Conversely, estimated thermal diffusivity values are more conservative relative to the legacy value. However, as found in Saunsbury et al. (2017), tunnel air temperatures are not as sensitive to this parameter.

4 CONCLUSIONS

This study evaluated the thermal properties of different rocks relevant to tunnel ventilation design in the Sydney Basin. Analysis of three datasets revealed that Datasets 2 and 3 produced consistent thermal conductivity values, significantly higher than both Dataset 1 and the legacy value of 1.80 W/m·K. Statistical testing confirmed no significant difference between Datasets 2 and 3, indicating reliability of both datasets. The discrepancy with Dataset 1 likely stems from unaccounted testing conditions or sample characteristics. Consequently, the legacy conductivity value appears conservative, and updated values from Datasets 2 and 3 could be considered more appropriate for future tunnel ventilation design. Thermal diffusivity remains a secondary factor, estimated using established methods.

5 REFERENCES

Herbert, C., 1983. Sydney Basin stratigraphy, Geological Survey of New South Wales, Department of Mineral Resources, Sydney.

Herbert, C. and Helby, R., 1980. A guide to the Sydney Basin, Bulletin 26. Geological Survey of New South Wales, Department of Mineral Resources, Sydney, 603 pp.

Konakova, D., Vejmelkova, E. and Cerny, R., 2013. Thermal properties of selected sandstones. Czech Technical University, Prague.

Och, D.J., Offler, R., Zwingmann, H., Braybrooke, J. and Graham, I.T., 2009. Timing of brittle faulting and thermal events, Sydney region: association with the early stages of extension of East Gondwana. Australian Journal of Earth Sciences, 56(7): 873 - 887.

Robertson, E.C., 1988. Thermal properties of rocks, United States Department of the Interior - Geological Survey, Reston, Virginia.

Saunsbury, D., Fernandes, D. and Och, D.J., 2017. A Preliminary Study on the Thermal Properties of the Ground under Sydney Harbour and the Sensitivity of Tunnel Air Temperatures, 16TH Australasian Tunnelling Conference. ATS, Sydney, pp. 8.

19th Australasian Tunnelling Conference – Acosta-Martínez, Stewart and Hudson-Smith (Eds.)
© 2025 Australian Tunnelling Society, ISBN 978-0-85825-002-4

Muck discharge technology and application through slurry circulation system on the EPB TBM

Z.G. Zhang, L. Yang, Y.F. Yin, P.Y. Pang, K.P. Chen, K.J. Li & Y.L. Bai
China Railway Engineering Equipment Group Co., Ltd., Zhengzhou, China

ABSTRACT: The earth pressure balance tunnel boring machine (EPB TBM) is mainly suitable to cohesive strata, sandy strata and gravel strata with a small amount of groundwater and small permeability coefficient. However, it faces many challenges when tunnelling through water-rich sandy strata with high water pressure, large boulders and high permeability coefficient. The Hamburg's district heating tunnel passes under the Elbe River and mainly goes through gravel, sand, clay, sedimentary limestone strata with local water-rich sandy strata, bringing high construction risks. Based on this project, this paper introduces an EPB TBM innovatively equipped with the slurry circulation system, which can successfully address the tunnelling and muck discharging challenges of the EPB TBM in water-rich sandy strata. It provides a valuable reference for the EPB TBM design in water-rich strata when passing under rivers.

1 INTRODUCTION

With the continuous innovation of the TBM technology, the TBM can be used to bore different types of tunnels, such as metro tunnels, railway tunnels, highway tunnels, municipal tunnels, water diversion tunnels and mine tunnels. Compared with the traditional tunnelling methods, the TBM method can greatly improve the construction efficiency.

In order to adapt to the complex and varied strata and the specific construction requirements, the TBM can be divided into various types including the EPB TBM, slurry TBM, hard rock TBM and multi-mode TBM. Given that the strata are complex and varied strata in China and abroad, a single-mode TBM has relatively higher construction risks while a multi-mode TBM is not cost-effective. For example, the EPB TBM has a major construction risk of muck and water inrush when tunnelling through water-rich sand layer with high water pressure, large boulders and high permeability. Therefore, there is an urgent need to explore a new muck discharge method.

2 PROJECT OVERVIEW

The Hamburg's district heating tunnel in Germany is highly symbolic. With the construction of the TBM method, the tunnel starts from Jachtweg on the south side of the Elbe River, passes beneath the Elbe and finally ends at the Hindenburgpark on the north side. The length is approximately 1,165m with the overburden ranging from 10m to 35m.

This project adopted an EPB TBM with an excavation diameter of 4570mm. The segment ring was 4300 mm in outer diameter, 3700mm in inner diameter and 1200mm in width, which could

precisely meet the project requirements. During tunnelling, the EPB TBM went through gravel, sand, sandy soil, clay, sedimentary limestone and other strata. These strata had significant differences in permeability coefficients, ranging from 5×10^{-3}m/s to 1×10^{-12}m/s. The designed turning radius was 300m and the actual turning radius reached 1,000m during construction, demonstrating the excellent adaptability of the EPB TBM. The geological profile is shown in Figure 1.

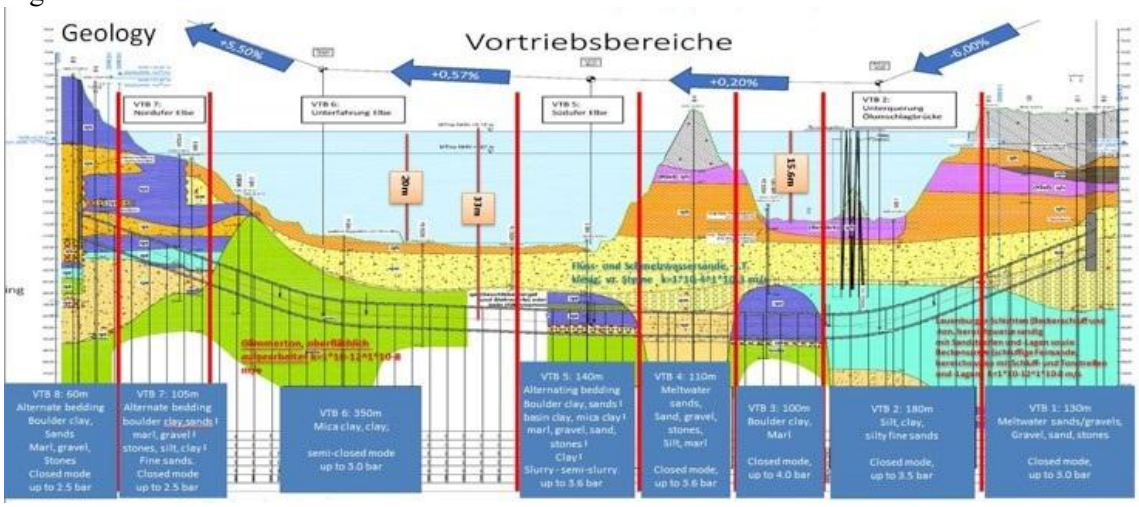


Figure 1. Geological profile of Hamburg's district heating tunnel

3 MUCK DISCHARGE DESIGN THROUGH SLURRY CIRCULATION SYSTEM ON THE EPB TBM

3.1 Principle design of slurry circulation system for muck discharge

The EPB TBM for this project adopts the slurry circulation system to discharge muck. The slurryfier box is connected behind the screw conveyor, followed by a slurry discharge pump. When the muck is discharged by the slurry circulation system, the discharge speed and excavation chamber pressure are controlled by the opening/closing of the discharge gate of the screw conveyor. But at this time, considering the unstable pressure control in the excavation chamber, the AFS system is connected with the slurry feeding pipe to inject the slurry into the excavation chamber by means of pressure compensation, which can realize the control of the excavation chamber pressure and the dilution of the muck in the excavation chamber. Moreover, the foam system and water system can also be used to inject the slurry to the excavation chamber and after the complete mixing with the cutter head, the muck in the excavation chamber is fully diluted. The design principle is shown in Figure 1. After conditioning in the excavation chamber, the muck density is stably maintained between 1.6 and 1.8 t/m³, significantly improving its flowability and transportability. Following further dilution in the slurryfier box, the muck density is reduced to 1.1–1.3 t/m³, making it more suitable for transportation by the slurry discharge pump to the slurry treatment plant. At the slurry treatment plant, the muck and slurry are separated, and the recovered feeding slurry maintains a density of 1.0–1.1 t/m³, which can also meet the requirements for reuse.

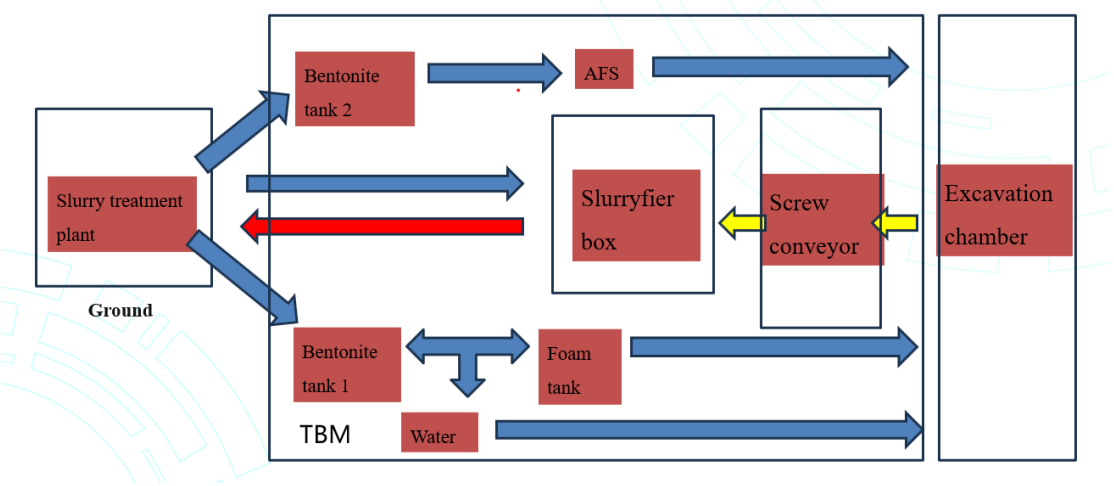


Figure 2. Design principle of the slurry circulation system for muck discharge

3.2 Parameter design of slurry circulation system for muck discharge

One feeding slurry pump is installed on the ground at the launch shaft, with a capacity of 400 m³/h. It delivers the slurry, which has been treated at the slurry treatment plant, to the slurryfier box on the TBM, where it is used to condition and dilute the muck.One discharge slurry pump is installed on a temporary gantry at the rear of the main machine, with a capacity of 400 m³/h. It pumps the muck from the slurryfier box out of the tunnel to the slurry treatment plant. The slurry feeding and discharge pumps are shown in Figure 3.



Figure 3. Slurry feeding and discharge pumps

The slurryfier box is equipped with a built-in jaw crusher and is installed on a temporary gantry at the rear of the main machine. Its front end is connected to the discharge gate of the screw conveyor, while the rear end is connected to the slurry discharge pump. The crusher has a crushing particle size of Φ250mm. The internal grid of the slurryfier box allows particles up to Φ70mm to pass through. The slurryfier box is fitted with four slurry inlet ports with a diameter of Φ100mm and one slurry outlet port with a diameter of Φ200mm. The overall dimensions of the slurryfier box are 2500 × 1300 × 1080 mm, as shown in Figure 4.



Figure 4. Slurryfier box

The slurry treatment plant adopts a three-stage filtration system and is installed on the ground at the launch shaft. Based on the capacity of the slurry circulation system, the treatment capacity of the plant is configured at 450 m³/h, as shown in Figure 5.



Figure 5. Slurry treatment plant

4 PERFORMANCE

The EPB TBM was launched on November 2, 2023, as shown in Figure 6. The construction team adopted the umbilical launch method to start the excavation. During the second launch, the EPB TBM advanced with the cooperation of main machine and temporary gantry. At this time, the muck was excavated by the EPB TBM and discharged by the slurry circulation system.



Figure 6. Official launch

To significantly enhance the muck discharge efficiency during the umbilical launch, a series of effective technical measures were adopted. A crusher is equipped at the discharged gate of the screw conveyor to break down large soil lumps, making them easier for subsequent slurry transportation. Meanwhile, the slurry feeding pump was used to accurately transport slurry into the slurryfier box, where it was thoroughly mixed with the discharged muck to achieve efficient dilution. Afterwards, the slurry discharge pump continuously pumped the diluted slurry from the slurryfier box to the slurry treatment plant on the ground where the separation of soil and slurry was completed.

To maintain the stability of the tunnel face, a foam system and water system were used to inject bentonite into the tunnel face, improving the workability and fluidity of the muck. At the same time, the bentonite system was activated to work in conjunction with the AFS system to maintain stable pressure in the excavation chamber. With this pressure control system, the EPB TBM has achieved continuous tunnelling for 133m and steadily passed through the water-rich sand layers, thus successfully completing the second umbilical launch. The muck discharge process with the slurry circulation system is shown in Figure 7.

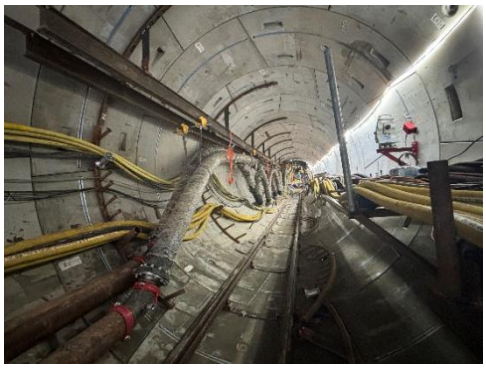


Figure 7. Muck discharge process with the slurry circulation system

During tunnelling through sandy gravel, gravel and water-rich sand strata, the slurry circulation system was adopted for muck discharge. When the TBM advanced by the 77th segment ring, the average thrust speed reached 21.3mm/min, with an average thrust force of 6474.69kN and an average torque of 518.85kN·m. The variations in torque and thrust force are shown in Figure 8.

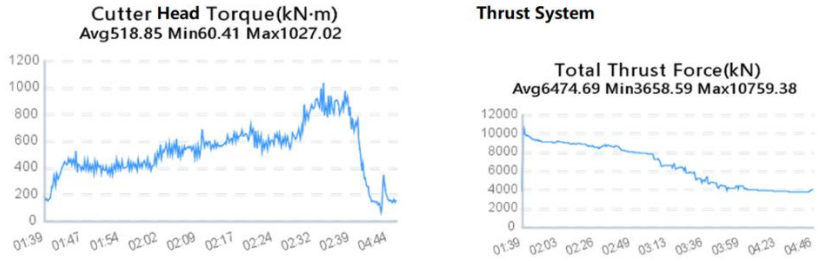


Figure 8. torque and thrust force when tunnelling in sandy gravel, gravel and water-rich sand strata

During tunnelling in clay strata, the belt conveyor of the EPB TBM was adopted for muck discharge. When the TBM advanced by the 717th segment ring, the average thrust speed reached 39.12 mm/min, with an average thrust force of 8012.28 kN and an average torque of 1275.61 kN·m. The variations in torque and thrust force are shown in Figure 9. Since the slurry circulation system was used for muck discharge in sandy gravel, gravel and water-rich sand strata, the friction coefficient of these strata was relatively low, resulting in significantly lower torque and thrust force compared to the clay strata. Moreover, due to the lower water content in clay, the belt conveyor for muck discharge was also relatively faster.

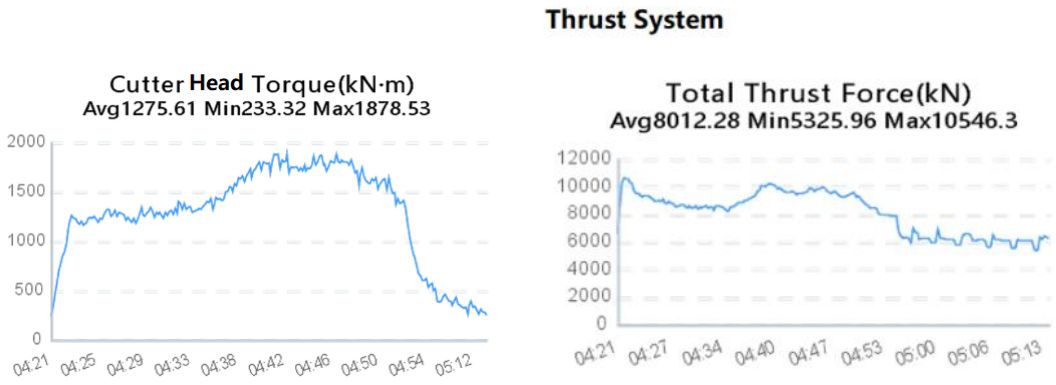


Figure 9. Torque and thrust force when tunnelling in clay strata

Throughout the entire construction process, the innovative EPB TBM with slurry circulation system for muck discharge demonstrated excellent operational performance and was successfully applied. It not only ensured the progress of construction but also showed its strong technical advantages under complex geological conditions, providing a highly valuable practical example for the construction of similar projects in the future.

5 CONCLUSION AND PROSPECT

On December 4, 2024, the Hamburg's district heating tunnel was successfully completed, marking the achievement of another significant engineering milestone. During the construction of this project, the EPB TBM is innovatively designed with a slurry circulation system for muck discharge, successfully overcoming the challenges of tunnelling and muck discharge in water-rich sand layers. This technological breakthrough not only ensured the smooth progress of the Hamburg's district heating tunnel but also provided valuable practical experience and innovative ideas for TBMs in complex geological conditions.

In response to the ongoing expansion of tunnel construction in China and abroad, as well as the increasingly complex construction environments, it is essential to relentlessly strengthen technological innovation. By continuously implementing innovative measures, the growing technological demands in the field of tunnel construction can be met, thus effectively driving the high-quality and sustainable development of the tunnel engineering area.

19th Australasian Tunnelling Conference – Acosta-Martínez, Stewart and Hudson-Smith (Eds.)
© 2025 Australian Tunnelling Society, ISBN 978-0-85825-002-4

Advanced spoil management in Gotthard Lot 111: Integrated solutions for a challenging alpine tunnel project

P.A. Scherwey
Marti Technics, MEA-APAC

ABSTRACT: The construction of the second tube of the Gotthard Road Tunnel, part of a monumental infrastructure upgrade connecting northern and southern Europe, presents significant challenges in material handling and spoil management. Located in a narrow Alpine valley traversed by one of the busiest highways in Europe, the project demands innovative solutions to handle vast quantities of excavation material while ensuring minimal disruption to traffic and the environment. This presentation will provide an in-depth exploration of the large belt conveying systems and processing plants implemented for spoil management in Lot 111, highlighting their role in meeting these challenges

1 INTRODUCTION

The Gotthard Road Tunnel expansion project in Switzerland involves constructing a second tunnel tube parallel to the existing 16.9 km tunnel, which was originally opened in 1980. This initiative aims to enhance safety and facilitate the comprehensive refurbishment of the first tunnel. Construction of the second tube commenced in 2021, with completion anticipated by 2029. Following this, the original tunnel will undergo renovations, and both tunnels are expected to be operational by 2032, each accommodating a single lane of traffic in compliance with Swiss regulations that prohibit increasing traffic capacity across the Alps.

The Gotthard Road Tunnel serves as a vital conduit in the European transport network, linking northern and southern Europe through the Swiss Alps. By providing a year-round, direct route, it facilitates the efficient movement of goods and passengers, thereby enhancing trade and economic integration across the continent. The tunnel's strategic position reduces travel distances and times between key European regions, bolstering connectivity and supporting the broader objectives of the Trans-European Transport Network (TEN-T) in promoting seamless cross-border transportation.

2 PROJECT OVERVIEW AND LOT 111 SCOPE

Lot 111 encompasses the construction and operation of integrated systems for the transport and processing of excavated materials. The scope of works includes the implementation of conveyor belt and rail-based systems to ensure the efficient transfer of spoil from the tunnel face to designated processing or disposal facilities. It further comprises the establishment of specialized plants for the sorting, recycling, and disposal of excavated material, with particular emphasis on compliance with environmental regulations and the optimization of resource utilization. In addition, Lot 111 requires the planning and management of transportation routes and schedules to mitigate potential impacts on local communities and to minimize interference with existing infrastructure (Figure 1).


Figure 1. South spoil management facilities in Airolo

2.1 *Interfaces with Adjacent Lots:*

Interface with Lot 341 (South Portal – Executed by Marti Tunnel AG):

- Lot 341 is responsible for Tunnel Boring Machine (TBM) driven excavation from the Airolo (south) side.
- Lot 111 supports Lot 341 by receiving and processing spoil directly from TBM via conveyor systems.
- The coordination with Lot 341 includes scheduling spoil extraction, monitoring transfer capacities, and ensuring minimal disruption to the southern access routes and processing systems.
- Material from Lot 341's TBM operations is either immediately processed or routed via belt and rail systems for intermediate storage or reuse.

Interface with Lot 342 (North Portal – Executed by Implenia-Frutiger JV):

- Lot 342 manages excavation from the Göschenen (north) side using both conventional methods and a TBM.
- Lot 111 collaborates with Lot 342 by providing continuous spoil removal capacity through belt conveyors connected to processing and logistics hubs.
- Given the constrained northern valley location, spoil management here is especially critical. Lot 111's system prevents excess truck traffic on the A2 motorway, which runs alongside the tunnel portal.
- Interfaces include joint coordination on TBM performance, conveyor throughput rates, and material flow timing to avoid bottlenecks or system overload.

3 TENDERING AND CONTRACT AWARD PROCESS

The Swiss Federal Roads Office (FEDRO/ASTRA) conducted the procurement for the Gotthard Road Tunnel expansion in accordance with national and international public contracting standards. The evaluation of Lot 111 bids was based on a multi-criteria model, where technical and qualitative elements were considered just as important as cost. Key selection criteria included, technical innovation, cost-effectiveness, previous experience, environmental and safety measures. The contract for Lot 111 was ultimately awarded to the Marti Group, a Swiss civil engineering firm with extensive experience in large-scale underground infrastructure, including the Gotthard Base Tunnel.

4 SPOIL MANAGEMENT CHALLENGES AND REQUIREMENTS

4.1 *Estimated total spoil volume*

The construction of the second tunnel tube is expected to generate approximately 7.4 million tons of spoil. This includes material excavated via both TBM and conventional methods (drill-and-blast), depending on geological conditions. All the spoil will be processed, recycled, or disposed. (Figure 2)

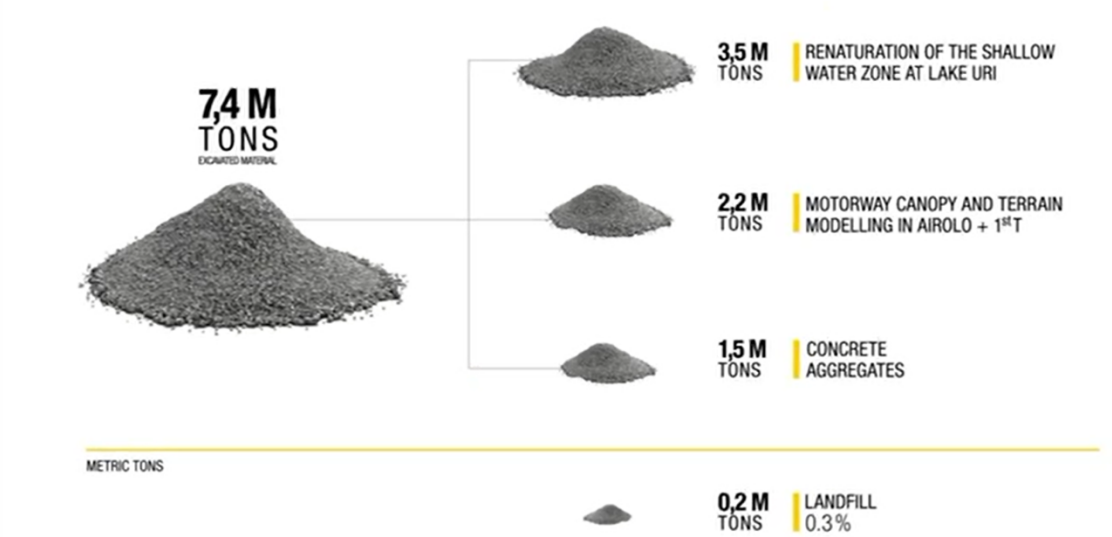


Figure 2. Spoil Bill of Quantity

4.2 *Material classification for spoil management*

To ensure appropriate reuse, recycling, or disposal of excavated material, spoil is classified into three main categories:

- Class A Material
  High-quality excavated rock, typically hard and clean (e.g., granite, gneiss), suitable for reuse in concrete production, tunnel lining segments, or structural backfill. Requires minimal processing.
- Class B Material
  Medium-grade material, such as weathered rock or mixtures with fines. Usable for non-structural applications like road sub-base or general fill, possibly with additional processing.
- Class C Material
  Low-quality or contaminated material (e.g., clay, silt, or chemically unsuitable spoil) that is not fit for reuse. Must be disposed of in accordance with environmental regulations.

4.3 *Spoil flow*

About half of this will be transported by rail to Flüelen, where it will be handed over to a subsequent lot and used for lake infill projects. The remaining A-material will mostly be processed into aggregate for concrete (approximately 1.5-1.7 million tonnes). The rest will be used as fill material, including for the Airolo highway cover. (Figure 3)

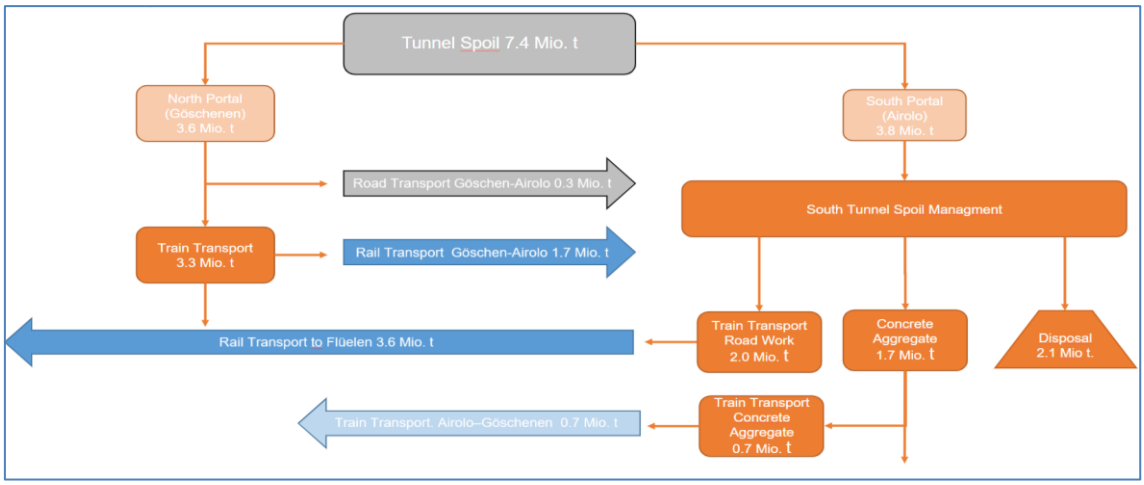


Figure 3. Spoil flow principle

4.4 Environmental sensitivities and compliance requirements

The tunnel portals are located within protected Alpine ecosystems. The project must comply with the Swiss Federal Law, requiring dust suppression systems, noise mitigation barriers, water protection measures. Spoil material is subject to geotechnical and chemical testing to classify it for recycling, reuse or landfill disposal.

5 DESIGN AND TECHNOLOGICAL INNOVATIONS

The key objective is to provide continuous, high-capacity transport and processing of spoil material directly from the tunnel face to treatment or storage areas.

5.1 *Core system components*

The overall solution integrates several sub-systems.

Belt Conveying Systems, including:

– 12km of multi-stage long-distance conveyors, with enclosed belts to minimize dust emissions. Automated loading points from TBM discharge areas, enabling uninterrupted material flow
– Designed for high throughput, with capacities exceeding 1,000 tons/hour in peak operation.

Rail Systems: New logistic facilities include

– a train station with spoil loading facility in Göschenen.
– a train station with spoil loading facility in Airolo.
– and a train station with concrete aggregate loading facility, and a train station with spoil unloading facility in Airolo (Figure 4-5-6-7-8-9).

Rail operations also leverage the existing rail network and the Gotthard Base Tunnel infrastructure to optimize the transfer of materials. This approach avoids reliance on road transport and minimizes disruption to local communities and the surrounding environment.

Material Processing Plants in Stalvedro: The material processing facilities are strategically located near the tunnel portals within secured zones, equipped with noise and dust mitigation barriers to minimize environmental impact. These plants are fitted with:

– Screens and crushers for the breakdown and sorting of excavated spoil.
– Magnetic separators for the extraction of metallic debris.
– Moisture control systems to prevent operational issues associated with slurry handling.

The processed outputs are classified into streams suitable for reuse in tunnel lining segments, backfilling and grading applications, or for external disposal as inert or non-inert waste, in full compliance with environmental standards.

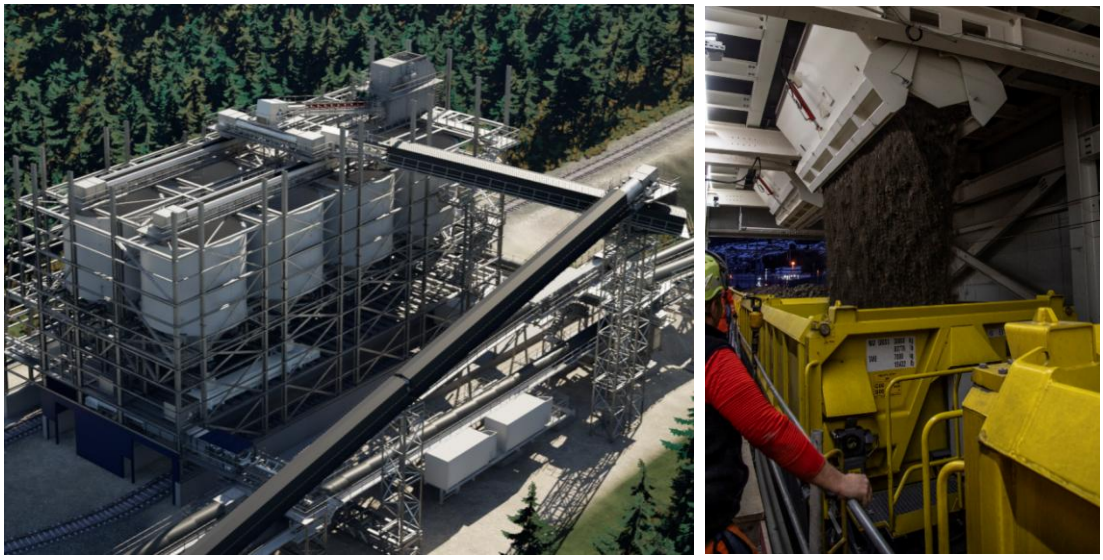
Storage and Recycling Units: Dedicated units are provided for the intermediate storage and recycling of excavated material. These include:

– Covered storage areas designed for temporary buffering of material flows.

- Recycling loops enabling the immediate reuse of suitable spoil in on-site concrete batching plants.
- Environmental protection measures, such as leachate collection systems, dust suppression equipment, and infrastructure designed to allow rapid loading and unloading operations.



Figure 4. Train and train loading/unloading facilities in airolo, south portal


Figure 5. Spoil loading facility


Figures 6. Spoil unloading facility

5.2 *Key design principles*

Continuous Transport and Processing: The continuous transport and processing of excavated material minimizes delays and ensures alignment with excavation rates. A centralized control system oversees key operational parameters, including conveyor speeds, belt loading, equipment status, and environmental compliance, thereby ensuring both efficiency and regulatory adherence.

Environmental and Energy Performance: The system is designed to operate with low emissions, incorporating enclosed conveyor belts, high-efficiency dust filtration units, and energy-efficient drives. These measures significantly reduce noise and airborne pollutants, safeguarding both workforce health and the surrounding environment.

Scalability and Adaptability: The transport infrastructure is based on a modular design, enabling adaptation to varying excavation progress and changes in spoil composition. Custom conveyor alignments have been engineered to traverse confined corridors between valley walls, existing infrastructure, and road networks, thereby minimizing surface disruptions.

Rail Integration: For long-distance spoil removal, the system integrates with the existing rail network, thereby reducing reliance on heavy truck movements through protected Alpine areas and mitigating environmental impact.

Dynamic Load Balancing: Real-time monitoring and control allow material flows to be redirected dynamically, distributing loads based on available capacity at processing stations. This prevents overflows, particularly in sites with limited storage capacity.

Embedded Environmental Monitoring: Sensors installed along the conveyors continuously measure dust concentration, vibration levels, and acoustic emissions. These provide real-time feedback to ensure compliance with strict Alpine environmental regulations.

6 MANUFACTURING, DELIVERY, AND ASSEMBLY

Timeline and Milestones of Component Production:

- Q1–Q2 2022: Finalization of design and technical specifications for key system components, including conveyor structures, drives, rollers, and steel frames.
- Q2–Q4 2022: Fabrication of modular components began at specialized manufacturing facilities in Switzerland and neighboring EU countries.
- Q1 2023: Factory acceptance tests (FAT) were conducted to ensure compliance with mechanical and environmental performance requirements.
- Q2–Q3 2023: Components were staged for delivery in line with excavation milestones at Lots 341 and 342.
- Q1-Q4 2024: Assembly and staggered commissioning
- Q1 2025 2025 Lot 341 interface commissioning

6.1 *Transport logistics to site*

- Due to the narrow access roads and proximity to the A2 motorway, component transport required precise logistics planning.
- Large structural elements (e.g., conveyor gantries, belt supports) were delivered via flatbed trailers during night shifts, avoiding daytime traffic.
- Smaller mechanical and electrical components were delivered in modular crates, optimized for minimal handling and rapid on-site deployment.

6.2 *Assembly strategy*

The system was designed with a modular and staged assembly strategy, suited for confined Alpine spaces and evolving excavation fronts.

Modular Subsystems:

- Conveyor belts, transfer stations, hoppers, and control units were prefabricated in sections and assembled on-site using mobile cranes and specialized lifting platforms. (Figure 10)

– Intermediary storage on site and preassembly area. Large number of components required multiple storage areas. Accurate inventory was kept continuously to not lose components. (Figure 11)

7 COMMISSIONING AND OPERATIONAL SETUP

Once the spoil management infrastructure was assembled and integrated, Lot 111 entered the commissioning and operational phase. This phase was critical to validate the performance of mechanical systems, optimize logistics, and ensure safe, efficient operation in tandem with ongoing excavation work in Lots 341 and 342.

7.1 *Commissioning Process and Testing*

– System Pre-Checks, Dry Run Testing, Integrated Trials, Acceptance and Handover
– Commissioning was completed in phases to match excavation progress and allow early sections of the conveyor system to go live while others were still being installed.


Figure 7. Assembly strategy requiring closure of highway lanes at night


Figure 8. Assembly strategy including temporary storage areas

8 PERFORMANCE AND ENVIRONMENTAL IMPACT

The spoil management system implemented in Lot 111 was designed not only for high operational efficiency but also for strict compliance with Swiss environmental regulations.

Performance metrics and environmental benefits demonstrate the system's value as a benchmark for sustainable tunnelling logistics.

8.1 *Key Performance Indicators (KPIs)*

Material Throughput:

- The belt conveyor system achieves an average capacity of 900–1,200 tons/hour, depending on excavation intensity and material type.
- Peak operational days handles over 20,000 tons of spoil with no system downtime or material backlog.

Reuse and Recycling Rates:

- Approximately 30–40% of excavated material is processed and reused, primarily for Segment production (tunnel lining) and Backfilling and sub-base for infrastructure components. Remaining spoil is classified and transferred via rail to certified disposal sites.

Energy Efficiency.

- The system is designed with high-efficiency motors and regenerative drives, reducing energy consumption by an estimated 20–25% compared to traditional diesel-powered haulage. Automated load balancing further optimized conveyor motor usage during variable throughput periods

8.2 *Environmental performance*

Dust and Noise Reduction: Fully enclosed conveyor belts and drop points, combined with spray and misting systems kept dust emissions well below Swiss thresholds. The conveyor lines is housed in acoustic enclosures where near residential or protected areas, reducing operational noise by over 30 dB(A) compared to truck haulage.

CO_2 Emissions and Climate Impact: By replacing thousands of spoil transport truck trips with belt conveyors and rail wagons, the system prevents an estimated 12,000+ tons of CO_2 emissions over the excavation phase. The use of electricity (with a significant share from Swiss hydroelectric sources) contributed to a low overall carbon footprint.

8.3 *Impact on Road Traffic and Local Community and Community Benefits*

The use of on-site conveyors and rail terminals eliminates the need for spoil trucks on local roads, preventing additional congestion on the A2 motorway, one of Europe's busiest north-south transit routes. This was particularly critical at both tunnel portals, located in narrow Alpine valleys with limited road capacity.

The avoidance of heavy truck movements significantly reduced noise, dust, and road wear for the communities of Airolo (south) and Göschenen (north). The local populations reported minimal disturbance during peak construction activity, and the project received positive feedback from municipal councils and cantonal authorities.

The system's performance contributed to maintaining public trust and political support for the project, reinforcing Switzerland's commitment to environmentally responsible infrastructure development in the Alps.

9 LESSONS LEARNED AND INDUSTRY IMPLICATIONS

9.1 *What worked well*

Seamless Integration with Tunnel Excavation: The alignment between spoil logistics and excavation activities (Lots 341 and 342) ensured that material is removed continuously without disrupting TBM performance or creating bottlenecks.

Use of Belt Conveyors and Rail Transport: The hybrid transport system, combining long-distance belt conveyors with rail freight, was instrumental in eliminating truck movements through sensitive Alpine corridors, significantly reducing noise, emissions, and road wear.

Modular, Scalable Design: The system's modular architecture allowed for staged assembly and adjustment as excavation progressed, improving flexibility and reducing upfront site occupation.

Environmental Compliance and Monitoring: Real-time tracking of emissions, noise, and dust helped maintain compliance with Swiss environmental standards, earning strong support from local communities and regulators.

9.2 *What could be improved in future projects*

- Earlier Integration of specific teams in Planning Phase
- Earlier involvement of the assembly team during the design stage could further optimize Assembly complexity, so reduce the efforts and shorten the Assembly period of time
- Earlier involvement of the operation team during the design stage could further optimize Operation routine
- Automation in Processing Plant. While conveying was highly automated, further automation in material sorting and quality control could improve throughput and reduce labour demands
- AI based operation management. To predict component failures, schedule maintenance before breakdowns occur, generation of reports, providing decision support and action suggestions on dashboard

9.3 *Broader applicability of this system design*

The Lot 111 system provides a highly transferable model for:

- Urban tunnel projects in dense environments with limited space for spoil handling or storage.
- Environmentally sensitive areas, such as mountain passes, coastal zones, or protected ecological regions.
- Multiphase projects where excavation and material processing occur in parallel and require dynamic coordination.

9.4 *Recommendations for similar infrastructure projects*

- Design for Logistics First. Spoil management should be treated as a primary system, not secondary to tunnelling logistics drives excavation efficiency.
- Use Rail and Conveyor Systems Where Possible. These reduce environmental impact, especially in constrained or regulated zones, and can be scaled more sustainably than trucking.
- Invest in Modular, Mobile Units. Mobile processing and sorting plants reduce on-site footprint and can be deployed flexibly based on tunnel advance rates.
- Implement Smart Monitoring Systems. Integrate SCADA or IoT-based systems for real-time operational data and environmental compliance alerts.
- Engage Stakeholders Early. Early communication with local communities, regulators, and utility operators fosters trust and smoother project execution.

10 CONCLUSION

The core objectives of Lot 111 were to:

- Efficiently handle large volumes of excavation spoil
- Minimize environmental and community impact, and
- Integrate seamlessly with tunnel construction operations at both portals

These goals were achieved through the deployment of a high-capacity, modular belt conveying system, advanced material processing facilities, and rail-based logistics—all designed to operate within the strict spatial, environmental, and regulatory constraints of the Alpine setting. Continu-

ous coordination with Lots 341 and 342 ensured that spoil removal supported uninterrupted excavation, while the environmental performance exceeded legal requirements and local expectations.

The solution design:

- Eliminated the need for thousands of spoil truck trips in a sensitive mountain corridor
- Achieved high reuse rates of excavated material,
- Maintained safe, quiet, and clean operations in close proximity to residential and ecological zones
- Operated with reliability, scalability, and resilience over extended construction timelines.

The Lot 111 experience highlights the importance of treating spoil management not as an afterthought, but as a critical, integrated component of tunnel engineering. The system demonstrates that logistics and sustainability can be embedded into core infrastructure delivery, without compromising on performance or budget. From modular system design and automation to environmental monitoring and stakeholder coordination, the solutions developed here set a precedent for future tunnel project in both alpine and urban contexts.

Lot 111 stands as a benchmark for modern spoil management in tunnelling projects and contributes valuable knowledge to the global tunnelling community while reinforcing Switzerland's leadership in sustainable infrastructure innovation. Future projects, whether in mountain regions, urban centres, or environmentally sensitive zones, can look to Lot 111 as a model for balancing efficiency, innovation, and responsibility.

11 REFERENCES

FEDRO/ASTRA – Project documentation for the Gotthard Road Tunnel second tube. - Swiss Federal Roads Office. Marti Group – Belt conveyor system and logistics design references for Lot 111.

https://www.marti.com - Academic or Industry Publications. ITA-AITES (International Tunneling and Underground Space Association). – Guidelines on material handling and spoil management.

https://about.ita-aites.org/files/WG14-15-ITA-REPORT-MudHandling.pdf. - Transweb / Mineta Transportation Institute – Report on spoil volumes and logistics strategies in long tunnel projects.

https://transweb.sjsu.edu/sites/default/files/1429-long-tunnels-trend-analysis.pdf. - Tunnel Magazine – Project overview and updates on Gotthard second tube construction.

https://www.tunnel-online.info - Environmental and Project Regulatory Documents. Swiss Federal Environmental Protection Act (USG) – National framework for dust, noise, emissions, and groundwater protection.

https://www.fedlex.admin.ch/eli/cc/1985/241_241_241/en . Alpine Convention / Alpine Initiative – Frameworks limiting traffic growth and enforcing sustainability in Alpine transit corridors.

https://www.alpconv.org - Cantonal environmental offices of Uri and Ticino – Environmental impact assessments and construction permits related to Lot 111 operations. - Marti Technik AG Tech News, Juni 2023

19th Australasian Tunnelling Conference – Acosta-Martínez, Stewart and Hudson-Smith (Eds.)
© 2025 Australian Tunnelling Society, ISBN 978-0-85825-002-4

Validation of plume dispersion modelling for approval/acceptance against CASA requirements

M. Beyer & C. Stacey
Stacey Agnew Pty Ltd, Darra, Australia

A. Gálffy
Turbulence Solutions GmbH, Vienna, Austria

ABSTRACT: The impact of road tunnel portals and stacks on aircraft safety has not been well treated by the tunnel building industry but an example from the power industry provides support for an effective approach. The Tallawarra B power station was constructed with a plume dispersion device (PDD) on top of the exhaust stack to mitigate updraft velocities that could affect aircraft safety. The resulting plume velocity profile is a non-Gaussian characteristics and therefore a 3D CFD (computational fluid dynamics) analysis was seen to be appropriate to assess the detailed plume behaviour and updraft velocity. The CFD modelling approach and results were accepted by the planning department following review by the Civil Aviation Safety Authority (CASA) and the stack operation with the PDD was approved, with the proviso that the updrafts be measured in operation. The CFD results are compared to on-site measurements of the exhaust plume after project completion. Within the slight variation of meteorological conditions between the model and the measurements, the shape of the plume and the magnitude of the updraft velocities resulting from the model compare reasonably well with the measured values, justifying our approach to assessing the simpler case of road tunnel stack impacts on aircraft safety.

1 INTRODUCTION

In unidirectional urban road tunnels with high traffic, the vehicle piston effect can induce high portal outflows with temperatures considerably above the ambient temperature. That buoyant plume, either released via the portal or partly via stacks, could lead to updraft velocities affecting aircraft at relevant flight protection surfaces in the proximity of the portals or stacks. Therefore, appropriate modelling should be done to inform project decisions at early stages.

The impact of road tunnel portals and stacks on aircraft safety has not been well treated by the tunnel building industry. All recent Australian road tunnel stacks (up to 2023) where aircraft upset is relevant have been designed and sized by project managers, who relieved engineers of the task. That is; the designs were based on grossly conservative rules of thumb, that could get procedural approval without further attention. No cost comparisons have been done, but the cost for such portal plants is tens of millions of dollars, and in many cases, the majority of that could have been saved by engineers applying their professional skills, with no greater approval risk.

Stack plumes causing flight interference are not unique to road tunnels. More detailed work has been conducted by the power industry where plume buoyancy and vertical velocities can be significantly greater. Recent work associated with the Tallawarra B power station provides a useful and instructive case study of a CFD modelling approach and plume measurement that is relevant to road tunnels and portals.

Tallawarra B power plant near Shellharbour City in New South Wales operates an open-cycle gas turbine (OCGT). The gas turbine is designed for fast-start and can attain full load within 30 minutes, to supply power to the grid once there is high demand in the National Electricity

Market (NEM). The OCGT unit produces a large flow of hot exhaust gas, that rises quickly into the atmosphere, generating updraughts with potentially high vertical velocities and turbulence up to elevations that are likely to adversely affect aircraft flying in the vicinity of the exhaust stack. To reduce the vertical velocity and buoyancy of the plume, a plume dispersion device (PDD) was mounted on top of the stack, splitting the exhaust into twelve equal parts, each discharging nearly horizontally and in different directions from a central point. Since the PDD emits the 'plumelets' nearly horizontally, the initial vertical plume momentum is eliminated. In addition, the entrainment of ambient air into the twelve parts of the plume is enhanced. This greatly reduces overall plume acceleration, resulting in reduced vertical plume velocity.

The plume behaviour initiated by the PDD is complex and cannot be characterised accurately by a Gaussian plume model or other screening model. Instead, a CFD analysis was seen to be appropriate to assess the detailed plume behaviour and height-dependent updraft velocities during the design and approval stages of the power station's development.

After completion and commissioning of the Tallawarra B power station, on-site measurements of the detailed plume characteristics and updraft velocities were conducted with a high wing Cessna 172 equipped with inertial sensors and a tailored differential pressure sensor probe mounted on the strut. The on-site measurements were compared with the CFD model results to evaluate the appropriateness of the model assumptions and to confirm that the power station's approval condition, as defined by the Civil Aviation Safety Authority (CASA), regarding updraft velocities, is met.

2 CASA'S PLUME RISE ASSESSMENT AND CRITERION

2.1 *Overview of assessment process*

CASA's Advisory Circular (Civil Aviation Safety Authority, 2023) provides information about assessing the potential impacts of exhaust plumes on aircraft safety. If the stack exit velocity exceeds 4.3 m/s, several exhaust plume rise assessment steps are required. According to (Civil Aviation Safety Authority, 2023), that velocity criterion relates to a level of turbulence in the plume that may be capable of affecting normal flight.

CASA via (Civil Aviation Safety Authority, 2023) describes the plume rise assessment process, which firstly requires a proponent of a new activity that may generate an exhaust plume to submit details of the exhaust plume to CASA if the exit vertical velocity exceeds 4.3 m/s. If the stack exit velocity is higher than 4.3 m/s, CASA uses these details to conduct a screening assessment. If that screening assessment confirms that the plume velocity will exceed 4.3 m/s at or above a flight protection surface, the impact of the exhaust plume is to be further examined by CASA using the Exhaust Plume Analyzer (EPA). The EPA is a model developed by MITRE in the US (Gouldey, et al., 2012).

If the exhaust plume violates certain assumptions related to the EPA model (e.g., non-identical stacks with non-aligned and non-uniform spacing, stacks with engineered modifications such as the use of a PDD), CASA via (Civil Aviation Safety Authority, 2023) suggests using CFD modelling or scale modelling to assess the plume behaviour. While this all sounds like risky/complicated work, and therefore may frighten project managers, seeking to avoid it by limiting efflux velocity to 4.3 m/s not only gives bad project outcomes, but also does not guarantee that the updraft velocity stays below 4.3 m/s due to the usual expected buoyancy of the plume once the exhaust left the stack (see next Section).

2.2 *Critique of vertical velocity criterion*

The application of the vertical velocity criterion of 4.3 m/s at stack exit does not necessarily ensure that the vertical velocity induced by the plume remains below 4.3 m/s at higher elevations. A plume with stack exit velocity at or below 4.3 m/s, can accelerate if the initial buoyancy of the plume, together with the meteorological conditions (ambient temperature, wind speed and atmospheric stability) causes a density deficit and consequently results in a buoyancy head that is higher than the dynamic head of the stack exit velocity. Thus, looking only at a low stack exit velocity is not appropriate, as it does not provide sufficient information on whether the updraft velocities might affect normal flight.

As an example, vehicle 'piston' effects in a three-lane unidirectional road tunnel can generate a mass flow rate of up to 1000 kg/s with a portal exit temperature of up to 20°C above ambient. The flow coming out of that tunnel portal would have a thermal power, relative to ambient, of approximately 20 MW. Such tunnel portal flows with almost zero initial vertical velocity would bend upwards and generate updraft velocities with peak values that have the potential to exceed CASA criteria. Releasing part of the tunnel flow via portal exhaust stacks with an average exit velocity of 4.3 m/s and an exit temperature of 20°C above ambient has also been found to generate averaged updraft velocities in the plume that may affect aircraft safety.

A plume rise velocity criterion in general is also not sufficient, as the shape of the vertical velocity profile (velocity gradients across the plume) and the aircraft characteristics (wingspan, weight, speed, etc.) are the essential parameters to understand potential impacts on aircraft. The problem is not as simple as any vertical velocity measure. It is recommended that the plume characteristics be analysed and then used to simulate/calculate the aircraft response (for site-typical aircraft types) based on the plume data at relevant elevations.

2.3 *MITRE Exhaust Plume Analyzer (EPA)*

For typical tunnel stack applications, once the initial assessment and the screening tool indicates that the plume velocity will exceed 4.3 m/s at or above a flight protection surface, CASA will conduct a detailed assessment using MITRE's EPA (Civil Aviation Safety Authority, 2023). However, there are several limitations and problems with the EPA by MITRE (Gouldey, et al., 2012). Firstly, the mean flow behaviour of the plume is estimated by the Spillane model. The Spillane model has no ability to calculate the Zone of Flow Establishment (ZOFE). The ZOFE is from stack outlet up to 6.25 times the stack diameter if there is no cross wind. Flow calculations in the Spillane model start above that zone. Flow within that zone is relevant if the flight protection surface is close to the stack outlet (e.g. for a stack diameter of 8 m the ZOFE is 50 m high).

In addition to predicting potential aircraft upset conditions, the MITRE EPA outputs the probability of G-loads occurring for different aircraft types depending on the stack flow parameters and a set of meteorological conditions. The probability calculation is mainly driven by a gust probability function but besides that, it depends only on the meteorological data (probabilities of stack operation, of aircraft flying directly over the plume etc. are not considered). The gust probability function applies an additional updraft velocity component on the mean updraft centreline velocity obtained from the Spillane model, which should account for turbulence related velocity fluctuations.

This is an improper assumption as the velocity fluctuations assumed in the MITRE EPA relate to small scale turbulent fluctuations obtained from measurements (Papanicolaou & List, 1988) and not to large scale atmospheric turbulence that may affect aircraft. The small-scale turbulent gusts considered in MITRE's EPA have negligible / no impact on flight dynamics, as they are small in scale, and get averaged along the wingspan. As the applied gust probability function in MITRE's EPA significantly increases the updraft velocity (factor of 1.75 or more (Gouldey, et al., 2012)), the method grossly overestimates the potential aircraft impact and resulting G-force. This, in combination with simplifications in the calculation of the maximum load factor (e.g., neglecting pitch response, neglecting lateral wing averaging effects etc.) leads to an overall load factor overestimation by a factor of around two. Consequently, the MITRE EPA can lead to incorrect predictions of non-compliant turbulence intensities and G-forces (see tables and description in (Civil Aviation Safety Authority, 2023) for further details on turbulence intensity probabilities and their acceptance). Even if the plume rise velocity drops below 4.3 m/s MITRE's EPA would conclude non-compliant turbulence intensities. That is seen to be a contradiction, as CASA's Advisory Circular states that for velocities at and below 4.3 m/s, no further assessment steps are required. The MITRE EPA includes a cutoff mean velocity, normally set at 4.3 m/s in Australia, below which the results are truncated and ignored. This appears to be a fix for the contradiction caused by the EPA model indicating unacceptable impacts at well below that velocity level. Such a truncation is seen to be necessary due to the underlying formulation issues and subsequent overestimation of the G-force probability. The alternative would be accepting the MITRE EPA results with no cutoff, and then very low updraft velocities could still lead to suggestion of unacceptable impacts. Applying a cutoff velocity to restrain the EPA prediction to be consistent with CASA's lower limit of concern (CASA are not concerned below 4.3 m/s) is hard

to justify. If it is accepted that there is no problem below 4.3 m/s then the MITRE EPA should not be predicting high aircraft upset probability at much lower velocities, so a fix of the underlying formulation issues should be sought. For all stack applications including tunnel applications, it is recommended that a detailed assessment be performed as explained in Section 3 and suggested in Section 6. For some minor circular stacks, a Gaussian plume analysis might be sufficient for predicting updraft velocities. A simple method for large stack flows (e.g. cooling towers) or complex stack geometries does not currently exist.

2.4 *Criterion for CFD plume modelling*

For the Tallawarra B power station with PDD, CFD modelling was seen to be appropriate for assessing the vertical velocity of the exhaust plume. While assessing the detailed plume characteristics and the resulting aircraft response is more realistic and informative than either the EPA or Gaussian models, the criterion for plume modelling according to (Civil Aviation Safety Authority, 2023), and the Tallawarra project's requirement, was to not exceed an average plume velocity (top hat profile velocity) of 6.1 m/s (CASA's criterion for CFD assessments) at and above the relevant flight protection surface.

If the vertical velocity profile has a Gaussian distribution, the average plume rise velocity ('top hat' profile velocity) would be half of the maximum plume rise velocity (peak plume rise velocity). However, the velocity profile of a plume released by a PDD does not have a Gaussian distribution. As the real velocity profile differs from a Gaussian distribution, the equivalent top hat velocity will no longer necessarily be half of the maximum velocity. The averaging area is also uncertain, with the plume edges being indistinct. Notwithstanding this, CASA stated in the context of Tallawarra B, that it will accept half of the maximum CFD-derived plume rise velocity as the average plume velocity at the flight protection surface (700 ft above mean sea level), for the purpose of comparison with CASA's criterion of 6.1 m/s. Consequently, in the context of the peak plume rise velocity determined using a CFD model for Tallawarra B power station, CASA's criterion is effectively a peak velocity of 12.2 m/s at 700 ft.

3 CFD PLUME MODELLING OF TALLAWARRA B POWER STATION

Tallawarra B Power Station plume modelling was carried out using the CFD-software ANSYS Fluent (Release 2020 R1). The overall domain size that was adopted was, in plan, 3,700 x 3,700 m, with a height of up to 3,000 m, to capture the entire plume flow without adverse influences from the domain boundaries. The stack was positioned approximately in the middle of the domain. The PDD is mounted on top of the stack and has in total 12 openings all at the same level evenly distributed around the circumference to release the exhaust jets alternately horizontally and slightly downward.

Two wind cases were adopted for the CFD modelling as depicted by Figure 1. Firstly, wind conditions were generated by Katestone using The Air Pollution Model (TAPM), covering a 5-year period. The specific conditions that resulted in the 99.9th percentile plume average vertical velocity at 700 ft were selected during the design phase as the first wind case for CFD modelling. Following completion and commissioning of the power station and following collection of the on-site measurements, a further wind case that was obtained during the measurements was also used for the purpose of detailed model validation (see Section 5).

The stack flow parameters that were used in the design phase CFD modelling (760.9 kg/s and 639.3°C) are slightly different to those recorded by the Tallawarra B control team during the on-site measurements (756.35 kg/s and 644.2°C). The design stack flow parameters were used for the initial CFD model and the measured data were used for the post measurement validation case.

The buoyant plume behaviour was found to be transient and to be quite sensitive to ambient conditions. After establishing the flow field and refining the initial mesh to the desired final mesh resolution, the flow field was finally simulated with a transient solver and the transient behaviour was monitored during the simulation over a period of about 25 real minutes. To capture the worst conditions, the detailed plume parameters were then analysed at a time when the highest vertical plume velocity arose at the monitored elevations. The initial CFD modelling showed that the

PDD effectively disperses the plume, so that the updraft velocity was close to, but below, CASA's Critical Plume Velocity.

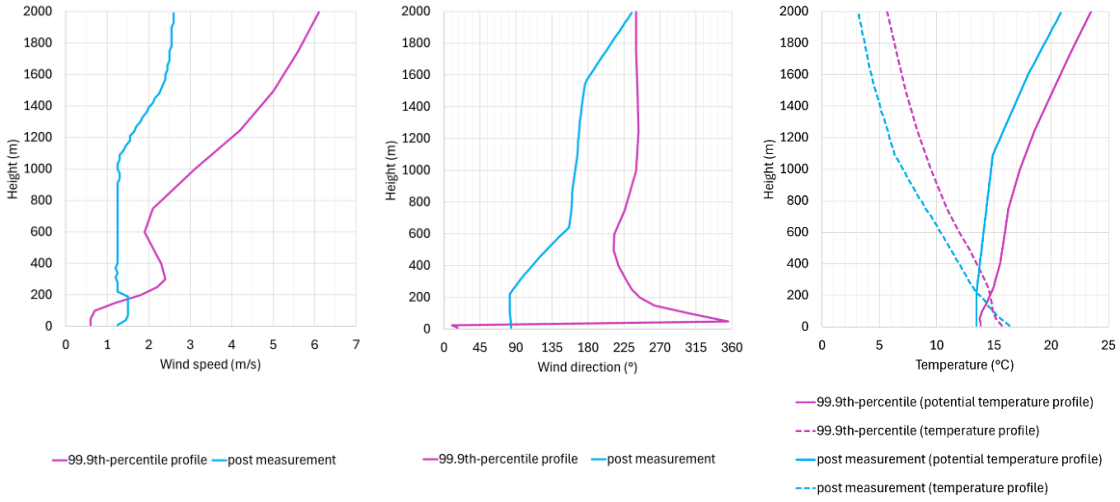


Figure 1. Profiles of wind speed (left), wind direction (middle) and temperature (right) provided by Katestone and used for the assessment.

4 ON-SITE PLUME MEASUREMENTS

The applied measuring principles and the detailed plume velocity measurement techniques were developed and performed by the Austrian company Turbulence Solutions GmbH[1]. The measurement campaign was a complex undertaking that required the expertise and assistance of different disciplines and experts and was accompanied and supported by Stacey Agnew[2], Airspeed Aviation[3], Katestone[4], Aviation Projects[5], as well as the Tallawarra B operating and project teams from Energy Australia[6]. The success of the measurement program is down to the innovative technology and expertise provided by Turbulence Solutions and the highly professional collaboration, initiative and input of the project team and all parties involved.

4.1 *Measurement principle and program*

A Cessna 172 hired by Energy Australia and operated by Airspeed Aviation was equipped with a self-contained measurement probe mounted on the strut (see Figure 2) and inertial sensors mounted in the cockpit at the centre of gravity. The flow sensor probe measured the flow field based on differential pitot pressures in three different directions, while the flight dynamics impact was measured by the inertial sensors in the cockpit as well as by acceleration and gyroscope sensors in the probe mounted on the strut. Barometric pressure and GPS signals were also logged by sensors in the cockpit. By measuring the motion of the aircraft in combination with the flow

[1] Turbulence Solutions is developing an innovative aircraft stability product to limit turbulence effects on aircraft and, in doing so, has world-leading expertise in the measurement of atmospheric turbulence, and the effect that turbulence has on aircraft.
[2] Stacey Agnew accompanied and coordinated the measurement program in detail
[3] Airspeed Aviation operated Cessna 172 and provided pilots with experience in flight instruction and aerobatics.
[4] Katestone provided expertise and processed meteorological data and forecasts from Meteomatics.
[5] Aviation Projects accompanied and coordinated measurement program from aviation safety perspective (selecting aircraft operator, organising Temporary Danger Area, NOTAM preparation, liaise with aviation authorities and local pilots etc.).
[6] Energy Australia initiated the project and coordinated overall project, companies, teams and people involved.

field and the sensor motion, it is possible, via deconvolution, to extract the flow impact on the measurement probe due to the aircraft motion, and account for that to obtain the flow field and turbulence in the atmosphere, or in this case the exhaust plume. The probe samples data at 500 Hz and the cockpit logger at 200 Hz. The result is a high-rate sampling of the flow the aircraft is flying through (500 Hz, one measurement every 2 ms, which is equivalent to 0.1 m sampling at a flight speed of 50 m/s). Further information on the measuring principle and the flow sensor can be found in (Gálffy, et al., 2021).



Figure 2. Self-contained flow sensor probe mounted on the strut (left and middle picture) and inertial sensors mounted in the cockpit (right picture)



Figure 3. Photos taken during the plume surveys on 5th of Aug. 2024 (left) and 7th of August 2024 (right)

To limit the risk to the measurement team and the experienced pilots, the expected aircraft response was assessed based on flight dynamics simulations of a Cessna 172 using the flow field obtained from the CFD simulations. This pre-assessment confirmed that the expected G-load impact and roll response were within the range of normal and safe aircraft operation. Further precautions were undertaken to reduce traffic interactions with measurement flights by arranging a Temporary Danger Area (TDFA) and a Notice to Airmen (NOTAM) issued on each day prior to test flights commencing.

An hourly average weather forecast for the local project area out to 7 days was provided four times a day by Katestone, with model data from Meteomatics[7]. The local weather forecast allowed the project team to prepare test flights and plant operations to coincide with upcoming weather conditions that were conducive to elevated vertical plume velocities (low temperature, low wind speeds, stable/neutral atmosphere and comply with Visual Meteorological Conditions minima).

In total, it was possible to conduct 2 hours and 45 minutes of calibration flights and 8 hours and 35 minutes of exhaust plume survey flights, with approximately 430 individual plume fly-throughs at different elevations (from 500 ft up to 2,600 ft) as depicted in Figure 4. Figure 3 shows photos from the aircraft flying over the stack while it is taking measurements.

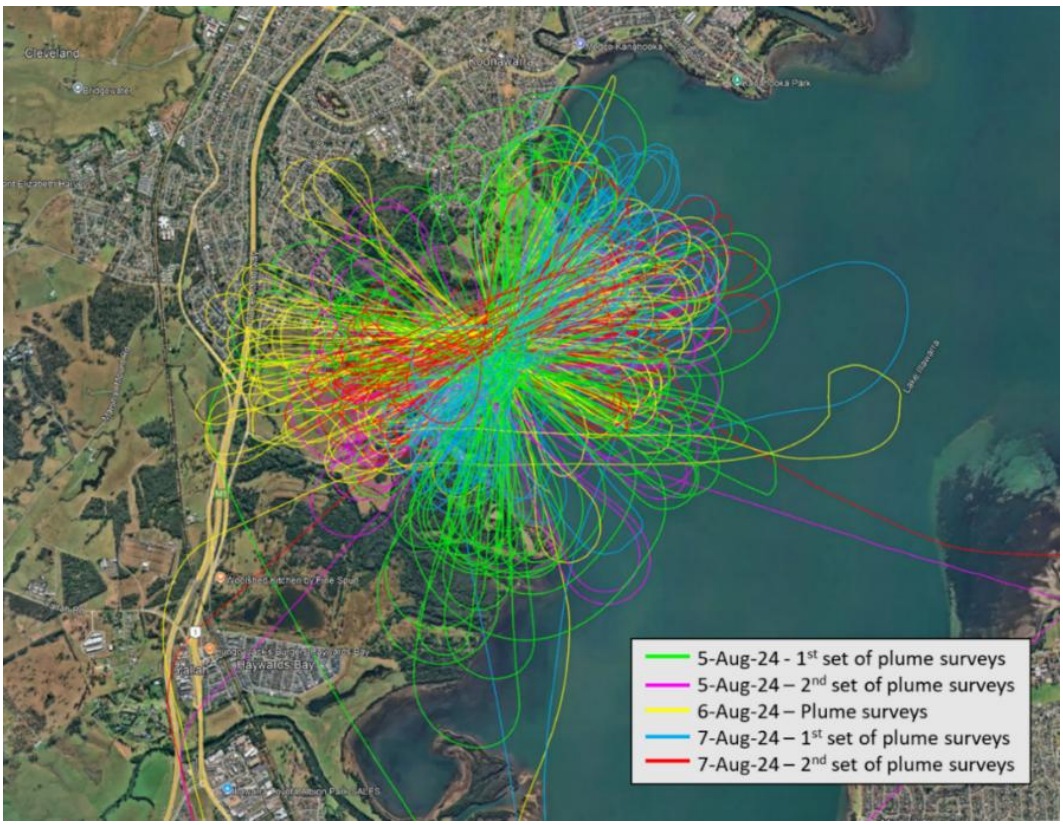


Figure 4. Figure-eight manouvres and tracks through the exhaust plume based on recorded GPS data for the individual test days and plume surveys.

4.2 *Measurement results*

Compared to the simulation results, the maximum peak plume rise velocity was slightly higher (orange squares), which is likely related to the slight differences in the meteorological conditions between simulation and observed during that test day. Of particular note, on 7-Aug-2024 between 9 am and 10 am, the wind direction changed from the west with a speed of about 1.5 m/s to from the east with a speed of about 1.9 m/s. During this wind direction change, the wind speed approached values close to zero, whereas the wind speed in the CFD model (99.9-percentile wind case) was always above 0.5 m/s.

[7] Enhanced downscaled model data based on the European Center for Medium-Range Weather Forecasts' (ECMWF) Integrated forecasting System (IFS),. The downscaling improves the coarse grid native representation down to a resolution of 90 m. This is achieved by applying high-resolution land usage data, soil, terrain data, astronomical computations & other sources.

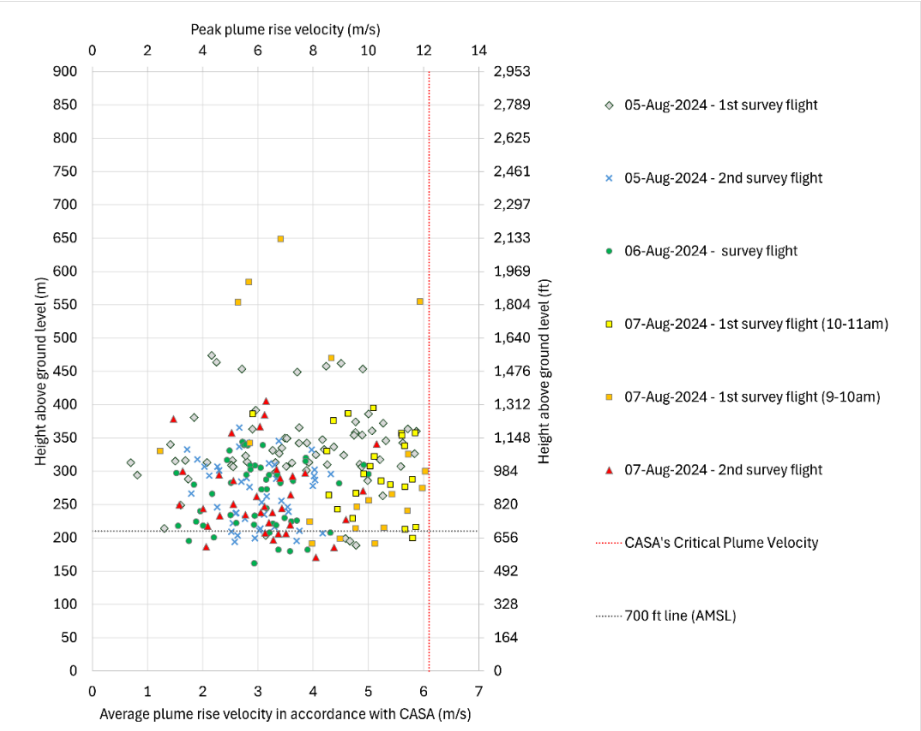


Figure 5. Highest recorded plume rise velocity per fly-through and elevation for the individual test periods. The primary x-axis at the bottom is the average plume rise velocity in accordance with CASA's criterion which is half of the peak plume rise velocity shown on the secondary x-axis at the top of the plot.

5 CFD PLUME MODEL VALIDATION

As noted in Section 3, the initial CFD model with the design wind case (99.9th percentile case) was run again with a representative wind case as obtained during the measurement campaign, to confirm observations and to validate the model assumptions and technique. For that, the profile with the lowest wind speed, was taken as new input, in combination with the lowest temperature observed during the plume surveys. Accordingly, the values of the two profiles 7-Aug-2024 at 10 am and 7-Aug-2024 at 11 am were averaged to obtain representative conditions over that measurement period. Stack flow parameters as discussed in Section 3 were also adjusted to reflect the post construction site conditions.

After establishing the flow field and refining the initial mesh to the desired final mesh resolution, the flow field was finally simulated with a transient solver over a period of 25 real minutes. Even at constant meteorological conditions, the buoyant plume showed a transient behaviour with a peak updraft velocity variation of about 3 m/s at one elevation. However, the wind conditions usually vary with time and do not remain constant for long periods. That leads to a much bigger variation in the real plume shape and exhaust plume velocities, compared to the simulation with the constant meteorological conditions. This circumstance makes it hard to compare the shape and peak of velocity profiles of individual plume passes with the simulation results. Further, the meteorological data are supported by weather stations but are based on weather modelling to obtain the local prevailing weather conditions during the measurement period. The modelled weather data are based on hourly averaged values and, therefore, detailed information about the meteorological conditions between any two hourly averaged datasets is not available. During the relevant plume survey flight (7th of August 2024, 1st survey flight between 10 am and 11 am), the wind conditions will have been changing and so, even if both measurements and simulations were 'perfect', the results from the measurement may not compare perfectly with the simulation results where the wind conditions were constant.

To evaluate the CFD plume profile at different elevations and time steps in an effective and uniform way, virtual flight trajectories were placed through the centre of the stack and were rotated in 5° intervals as illustrated by the contour plot in Figure 6.

The plot in Figure 6 compares the plume shapes obtained from the CFD simulation at stack-centred trajectories (blue lines) with the plume shapes obtained from the comparable measurement fly-throughs (red lines) at similar elevation. Measured plume profiles with an elevation close to the evaluated elevation have been bundled together in one plot.

In general, the maximum plume rise velocities obtained during the relevant test flights are about 1 m/s higher than from the CFD results with the 'post measurement' wind condition. During the plume survey on the 7th of August between 10 am and 11 am (red lines in Figure 6), the wind speed changed from 0.8 to 1.9 m/s below 400 m whereases the averaged wind speed applied in the CFD model was about 1.5 m/s below 400 m. This difference in the low-level wind speed could be the reason for the slightly lower maximum peak plume rise velocities predicted by the CFD.

Considering uncertainties in the applied modelling and measurement methodologies, as well as in the exact meteorological conditions during a plume pass, the simulation results correlate well with the measurement results and give confidence that the applied CFD modelling methodology can be used for estimating/assessing exhaust plume rise velocities with sufficient accuracy.

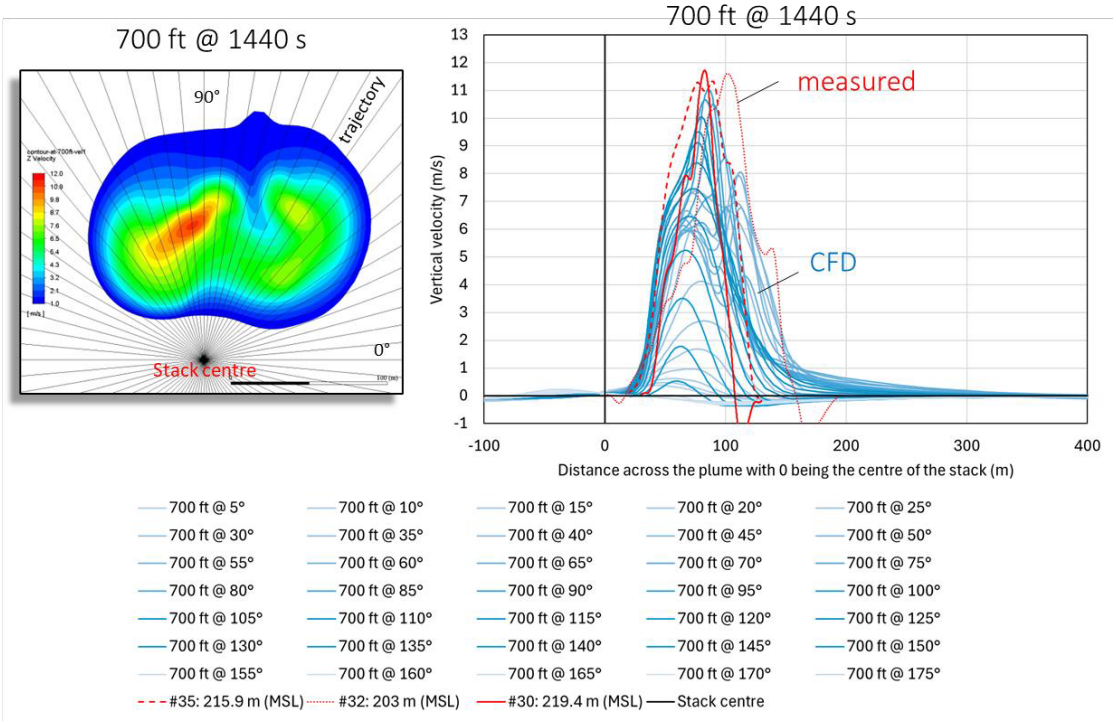


Figure 6. Trajectories through the plume in 5° intervals with the stack centre being the origin shown on a contour plot at 700 ft at a simulation time of 1440 s (colour depicts the updraft velocity and is clipped to 1 m/s). Plot on the right shows plume profiles obtained from the CFD simulations at 1440 s based on the stack-centred trajectories (blue) compared to the measured plume profiles as sampled on the 7th of August 2024 during the first plume survey flight between 10 am and 11 am at around 700 ft (red).

6 ROAD TUNNEL APPLICATIONS

Managing portal emissions of polluted air from road tunnels by exhausting parts or all of it via stacks can lead to a buoyant plume that potentially affects aircraft during normal flight. Even if the average stack exit velocity is below 4.3 m/s and passes the CASA criterion for not undertaking further assessments (Civil Aviation Safety Authority, 2023), the density deficit in the plume can cause an updraft velocity that exceeds the initial average stack exit velocity, and may exceed

CASA criteria. In such cases, it is recommended that a detailed CFD analysis be undertaken based on the methodology proposed in Section 3, followed by simulation/calculation of the aircraft response based on the plume data obtained from the CFD at relevant elevations. A detailed CFD assessment should be preferred, as flaws in the MITRE EPA lead to an overestimation of the impact/G-force (see Section 2.3). Initial plume assessments and analysis of resulting aircraft response is seen as essential to inform the early stages of tunnel projects with portals near airfields, in establishing and planning for appropriately economical mitigation measures and to reduce the project risk to stakeholders.

Given below is an example of a unidirectional 3-lane road with a tunnel air/exhaust mass flow rate of approximately 1000 kg/s (induced by the vehicle piston effect) and a temperature of approximately 20°C above the ambient temperature outside the tunnel.

By using the same model methodology as noted in Section 3, Figure 7 shows an example of a plume generated by a 100% portal flow out of a unidirectional tunnel (left) and generated from four stacks capturing 80% of that portal flow (middle). Both simulations were carried out in still air (no wind), which is the worst-case scenario in terms of maximum updraft velocities. The right plot in the figure shows the maximum updraft velocities as a function of height for the two example cases. Even if the stack exit velocity is already high (around 10 m/s) the plume further accelerates due to the density deficit and resulting buoyancy force, up to a peak updraft velocity of approximately 12 m/s. If the exit velocity were lower (e.g. 4 m/s) the final peak updraft velocity would end up at a similarly high value. In case of the 100% portal flow, the peak updraft velocity reaches approximately 4 m/s, with the potential to be higher if the exit gallery geometry did not cause the plume to be split into two parts (causing higher entrainment and lower buoyancy).

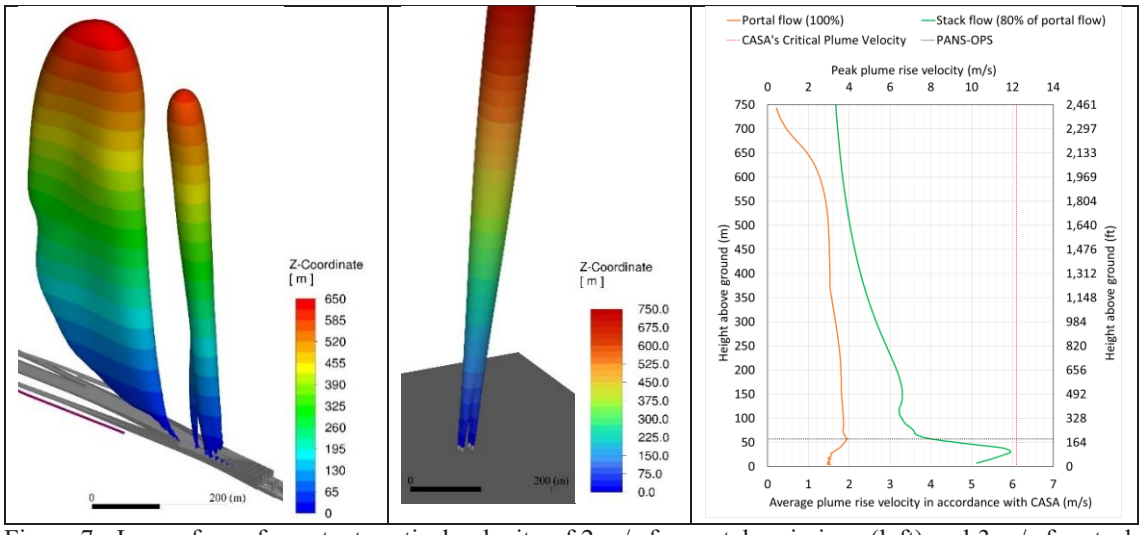


Figure 7. Iso-surface of constant vertical velocity of 2 m/s for portal emissions (left) and 3 m/s for stack emissions (middle). The plot on the right shows the maximum plume rise velocity as a function of height for the two example cases (left: 100% portal flow, middle: 80% of portal flow extracted via stacks). Colouring of the envelopes depicts the plume height.

Figure 8 shows the velocity profile generated by the four stacks at the PANS-OPS surface with the worst flight paths for the load factor impact (blue) and roll angle impact (red). Putting aside MITRE's EPA due to the flawed turbulence modelling, but using the aircraft parameters contemplated by the MITRE EPA model (weight of 1,250 kg, 10.2 m wind span and aircraft speed of 37 m/s), the resulting G-load and roll response is 0.5 g and 29°, respectively, when flying through the example plume generated by the stacks at PANS-OPS (about 50 m above ground level). To put that impact in context, CASA's Advisory Circular (Civil Aviation Safety Authority, 2023) provides a table with expected G-loads depending on the turbulence intensity and defines a G-load between 0.15 and 0.49 as light, between 0.5 and 0.99 as moderate and between 1.0 and 1.99 as severe turbulence intensity. Depending on the flight protection surface definition, the threshold is to not to encounter moderate turbulence intensity more often than once per 10^5 operations. With

the probability covered by considering worst case flight path calculations, and the G-load still within the moderate band, in this example, the CASA criterion would be met.

Using aircraft parameters of the smallest aircraft that can be expected on airports (weight of 750 kg, 8 m wind span and aircraft speed of 50 m/s to 30 m/s) the resulting G-load and roll response would be 0.85 g and 40°, respectively. This result is in CASA's moderate turbulence range and so more work would need to be done on probability for such very light aircraft.

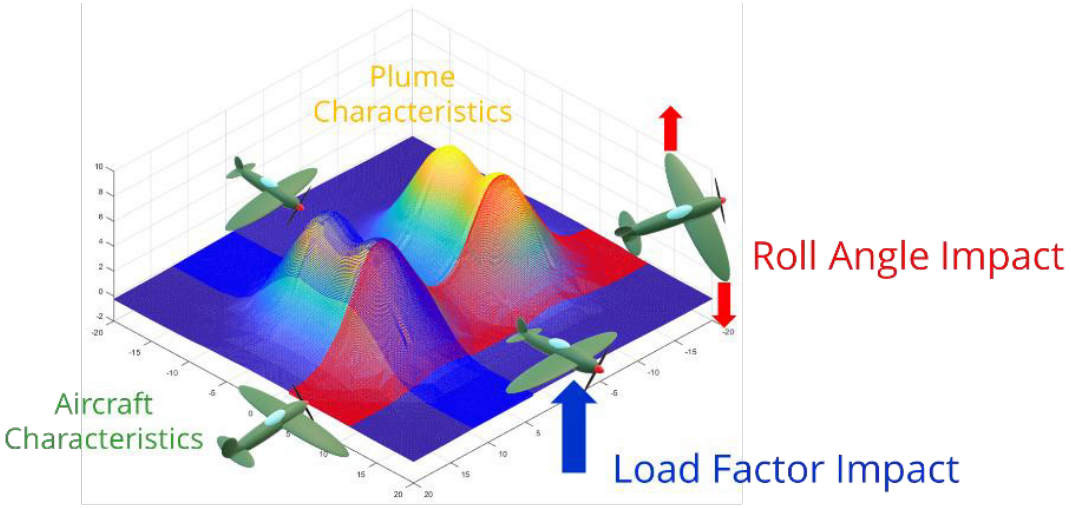


Figure 8. Velocity profile generated by the four stacks at the PANS-OPS surface with the worst flight paths for the load factor impact (blue) and roll angle impact (red). The vertical axis is the plume rise velocity (in m/s) and the horizontal axes are the horizontal distances in the x- and y-directions (in m).

ACKNOWLEDGEMENT

The authors express their gratitude to EnergyAustralia (EA) Tallawarra Project for their invaluable support and contribution to this paper. The development and operation of the Tallawarra B Power station, the subject of this study, was made possible through the dedication and commitment of EA, with significant support and funding provided by the New South Wales Government. Their professional collaboration and transparency have been critical in facilitating the research and analysis presented herein. We acknowledge the meteorological input that was essential to the project, and paper review comments, by Simon Welchman and Frank Quintarelli of Katestone Environmental, noting that we have different views on some of the content. We also acknowledge the crucial contribution of Airspeed Aviation and Aviation Projects. Their expertise and involvement were instrumental in successfully carrying out key aspects of the project, and their highly professional collaboration was greatly appreciated throughout the process.

REFERENCES

Civil Aviation Safety Authority. 2023. *Advisory Circular AC 139.E-02v1.0 - Plume rise assessments.* s.l.:Australian Government Civil Aviation Safety Authority, https://www.casa.gov.au/sites/default/files/2023-03/advisory-circular-139e-02-plume-rise-assessments.PDF.

Gálffy, A. et al. 2021. Turbulence load prediction for manned and unmanned aircraft by means of anticipating differential pressure measurements. *CEAS Aeronautical Journal,* Volume 12, https://link.springer.com/article/10.1007/s13272-021-00512-y.

Gouldey, D., Hopper, J. & Schwalbe, J. 2012. *MITRE - Expanded Model for Determining the Effects of Vertical Plumes on Aviation Safety,* s.l.: MITRE, http://www.ctcombustion.com/oxc/20130730-FAA-FOIA-Response/MITRE/September%20Plume%20Report%20Final%5B1%5D.pdf.

Papanicolaou, P. N. & List, E. J. 1988. Investigations of round vertical turbulent buoyant jets. *J. Fluid Mech.,* Volume 195, pp. 341-391, https://doi.org/10.1017/S0022112088002447.

THIS PAGE INTENTIONALLY LEFT BLANK

19th Australasian Tunnelling Conference – Acosta-Martínez, Stewart and Hudson-Smith (Eds.)
© 2025 Australian Tunnelling Society, ISBN 978-0-85825-002-4

Physical reasoning behind the critical velocity equation development

C. Stacey & M. Beyer
Stacey Agnew Pty Ltd, Darra, Australia

ABSTRACT: This paper provides additional background on the development of the Beyer Stacey Brenn equation for estimating critical velocity in tunnel fires. Building on the need for a more physically consistent model, it focuses on how the critical velocity problem was approached and explains and illustrates the underlying principles that formed the revised critical velocity model. The role of CFD validation and full-scale test data in shaping the model is highlighted, along with key design considerations that may clarify the intent behind the simplified model adopted in NFPA 502 (2026 edition).

1 BACKGROUND

Critical velocity, the air speed needed to stop smoke spreading upstream in a tunnel fire, is a familiar design parameter in our industry, especially in the US, Australia, Asia, Africa and the Middle East. For many practitioners, it's seen as settled science, supported by decades of testing, modelling, and international standards. It has not been that simple. The go-to reference for road tunnel critical velocity calculation has long been an annex to the US standard NFPA 502. The 2014 edition (NFPA 502, 2014) and prior editions referenced an equation proposed by (Danzinger & Kennedy, 1982) and (Kennedy, 1996). That equation followed a 1/3 power of the heat release rate, which is now known to be over-simplified, but it gave reasonable results compared to the Memorial Tunnel tests (MTFVTP, 1995a), (MTFVTP, 1995b) at around 50 MW or so, and consequently it had reasonable utility for road tunnel design.

The equations were adjusted in the 2017 edition of the NFPA 502 (NFPA 502, 2017) to better represent small-scale test results published by (Li, et al., 2010), (Li & Ingason, 2018) and were fully replaced in the 2020 edition (NFPA 502, 2020) by Li et al.'s proposed formula (Li, et al., 2010), (Li & Ingason, 2017), (Li & Ingason, 2019). These changes moved progressively further from values that were known and accepted. The adjustments in the 2017 edition increased ventilation requirements considerably for typical tunnels. In the 2020 edition, which was public late in 2019, the critical velocity values went up again, by around 40% over the 2014 values at 50 MW HRR (by using the Memorial Tunnel as example).

Based on the investigation by (Stacey & Beyer, 2020a), (Stacey & Beyer, 2020b) for the Graz conference in 2020, it has been made clear that the work by (Li, et al., 2010), (Li & Ingason, 2017), (Li & Ingason, 2019) and (Li & Ingason, 2018) overpredicts the critical velocity. That was because it used the critical velocity values recorded during the Memorial Tunnel data but 'corrected' them for backlayering which was neither there nor recorded in the test notes, and adjusted them using a tunnel height different from the one required by the formula the authors were supposedly using, as demonstrated in (Stacey & Beyer, 2020a), (Stacey & Beyer, 2020b), (Beyer, et al., 2021), (Li, et al., 2024). That fully explains why Kennedy (Kennedy, 1996) and Li et al. (Li, et al., 2010) could both claim support from Memorial Tunnel data for very different

critical velocity values. The representation of the Memorial Tunnel data by (Kennedy, 1996) was correct. Based on these findings, Annex D of the 2020 version of the standard NFPA 502 was retracted in 2021 (NFPA 502, 2020).

The subsequent revision of Annex D in the 2023 edition of NFPA 502 (NFPA 502, 2023) re-instated equations from the 2014 and 2017 editions of NFPA 502 (except that the definitions of the tunnel height and tunnel area parameter had been changed). Having two equations with one of them (2017 edition) still connected to the 2020 edition did not achieve the required clarity. The investigations by (Shi, et al., 2022) and (Shi, et al., 2023) further revealed the connections to the 2020 edition and the 'limitations' of the equations in the 2017 edition. That led to work on a new Annex D for the 2026 edition (NFPA 502, 2026) and eventually to the adoption of the Beyer Stacey Brenn equation (Beyer, et al., 2024).

The paper explains how the critical velocity problem was approached and how mathematical modeling helped to understand and confirm observations from full-scale tests, which finally led to the physical model proposed by Beyer, Stacey & Brenn (Beyer, et al., 2024).

2 HOW TO APPROACH THE PROBLEM

The fundamentals about smoke movement in tunnels had already been established by Thomas in 1958 (Thomas, 1958), (Thomas, 1968), who concluded that the upstream spread of hot smoke in tunnel fires can be described by the ratio between the inertial and the buoyancy forces. The buoyancy force is of course related generally to the fire heat release rate (HRR), but more specifically to the density deficit. So, it appeared to be crucial to describe the density deficit in a way that is more relevant for the upstream smoke propagation (than just using HRR). To obtain equilibrium between the inertial and the buoyancy force in relation to upstream smoke propagation, the inertial force (velocity head) needs to be increased once the buoyancy force (density deficit) increases. Equipped with that understanding, further observations were made.

An observation was that all the analysed small-scale test data showed similar characteristics where the critical velocity increases with the HRR and then stays constant above a specific HRR (Oka & Atkinson, 1995), (Wu & Bakar, 2000) and (Li, et al., 2010). The Memorial Tunnel data in contrast showed that the critical velocity stays pretty much the same over a wide range of HRR (from a nominal HRR of 10 MW to 100 MW) (MTFVTP, 1995a) and (MTFVTP, 1995b). A further observation was that all the analysed small-scale tests used propane burners with a fixed diameter/area and increased the HRR by increasing the fuel flow (Oka & Atkinson, 1995), (Wu & Bakar, 2000) and (Li, et al., 2010) while the Memorial Tunnel tests had fuel pans (constantly re-filled with fuel-oil) where the HRR was increased by increasing the pool area (by adding fuel pans in longitudinal direction) (MTFVTP, 1995a) and (MTFVTP, 1995b). If the geometric tunnel parameters and ambient conditions stay the same for individual tests sequences, the only parameter that distinctly influences critical velocity is the density deficit relevant for the upstream smoke spread. For tunnel fires, a measure for the local density deficit (local temperature) is the heat release rate per unit area (HRRPUA or fire intensity). By putting the fundamentals and the observations together, it became clear that increasing the HRR by increasing the pool area in the longitudinal direction does not change the heat release rate per unit area (density deficit or fire intensity) and therefore does not change the critical velocity. In contrast, increasing the HRR (by increasing an LPG fuel flow) and keeping the burner area the same increases the heat release rate per unit area (density deficit or fire intensity) and so the critical velocity changes with HRR.

There is also a physical limit on the HRRPUA. If too much gaseous fuel gets injected (or evaporated) into a small area, some of it gets advected and burned downstream as also observed and confirmed by (Wu & Bakar, 2000). That extends the effective area of combustion downstream, keeping the fire intensity at the front of the fire nearly constant. This is believed to be the reason for the kink in the critical velocity plots, and the velocity becoming independent of further rise in the total HRR in the trend lines derived from small-scale tests. It appears that the characteristics of the trend lines are a result of the burner types used in the very confined space of small-scale tunnels, and therefore are not seen to be so relevant for real tunnel fires. However, they have contributed by confirming the relevance of fire intensity.

Based on the observations, it became evident that the fire intensity is probably the most important parameter for estimating critical velocity once the fire is large, but there was then a task

to find out how much of the fire extent contributes to the plume dynamics and the density deficit relevant for building a smoke backlayer. There was that thought experiment regarding a petrol soaked mooring rope that may burn at 20 kW/m for 2500 m down the tunnel to give 50 MW total (Stacey & Beyer, 2020a). The last bit of the mooring rope 2.5 km away clearly does not contribute to the most upstream part of the fire or any backlayering. Especially for fires considerably extended in the longitudinal direction, the most upstream part of the fire will have the most influence on backlayering, with subsequent parts being progressively less influential.

The extent of the fire is of course directly connected to the HRR and fire intensity. The fire intensity depends on the fuel type (heat of combustion) and the burning rate (fuel to mix and burn before being advected downstream). For a given fuel type and burning rate, the HRR is proportional to the fire extent. With a fixed or maximum fire width, to increase HRR, the fire needs to extend in the longitudinal direction, and so critical velocity becomes more and more independent of the HRR.

A further parameter that was believed to be relevant for the local density deficit (local temperature) was the amount of air that gets mixed with the plume. Much of the air arriving along the tunnel may bypass the plume front, especially if the fire is narrow (relative to the tunnel width) or the ratio of tunnel width to tunnel height is high.

All these observations and considerations needed to be implemented in a physical model with the aim of estimating critical velocity from both small-scale tests and full-scale tests, with a priority on the full-scale tests as being the most relevant. This approach ensured that the geometrical dependencies were adequately taken into account.

To confirm certain dependencies (e.g. grade factor, width of the fire) there was also a need for a validated CFD model. Despite earlier gravity-related research, grade was not so readily adjustable in the Memorial Tunnel. So, one of the first tasks was to build a CFD model and establish a methodology that was able to appropriately reproduce the Memorial Tunnel full-scale test data over a wide range of HRR (10 MW to 100 MW). More details about the validation of the CFD model can be found in (Beyer, et al., 2024) and (Beyer & Stacey, 2022).

As demonstrated in the noted references, the CFD model methodology used could represent the smoke propagation and temperature distribution of the Memorial Tunnel tests with sufficient accuracy for the three different fire sizes. With that confidence in the model methodology, the relative change of critical velocity between a sloped tunnel and a flat tunnel based on the Memorial Tunnel geometry and fire characteristics was analysed for different tunnel slopes. This was done for a nominal fire size of 50 MW, as, based on tunnel design practice, it is perhaps the most relevant fire scenario for road tunnels. As noted in (Beyer, et al., 2024), it was concluded that for most design purposes, the grade factor can be ignored for the critical velocity problem (when there is no smoke propagation upstream of the fire front).

However, as discussed in a different study by (Beyer & Stacey, 2024), the tunnel slope affects the backlayer dynamics if upstream smoke propagation is controlled to a certain maximum smoke backlayer distance ('confinement velocity'). It is shown that in some circumstances, the backlayer distance is lower for downgrade tunnels at the same airspeed.

The derived equations indicated that there might be a dependency of critical velocity on the width of the fire. The Memorial Tunnel tests had the same fire width throughout all tests and the small-scale results (Oka & Atkinson, 1995), (Wu & Bakar, 2000) and (Li, et al., 2010) were not sufficient to fully understand the trend between fire width and critical velocity (e.g. change in fire intensity, insufficient datapoints, use of water spray, lack of systematic parameter change). The most economical way to find an answer was to use the validated CFD model based on the Memorial Tunnel geometry and change the fire width systematically, keeping everything else the same (e.g. length of the fire pan, fire intensity, tunnel profile etc.). The CFD results showed that the critical velocity decreases if the fire width increases. The observed behaviour can be explained by considering that the frontal area of the rising plume represents an obstacle for the flow past the fire. If the fire is wide and spans almost across the tunnel width, there is not much space for the oncoming air to go around the plume. Therefore, the plume becomes more deflected by the upstream flow, and more mixing into the plume occurs, so that the upstream velocity required to prevent backlayering goes down. This finding on fire width was not new, as Oka & Atkinson made similar observations in small scale tests (Oka & Atkinson, 1995). An appropriate correlation that describes the behavior was found and implemented via the function K_F (see (Beyer, et al., 2024)).

For the full development and for the holistic set of the Beyer Stacey Brenn equation, limitations and parameter description, please refer to the original source (Beyer, et al., 2024), https://doi.org/10.1007/s10694-024-01607-8.

2.1 *Validation and checking behaviour of equations*

If the relevant physical factors that influence critical velocity are captured, then the equations should be able to reproduce results from full-scale as well as small-scale tests. The empirical constants in the equations were adjusted to match both full-scale and small-scale test results, keeping the empirical constants the same throughout the comparison with different test results (trying to capture the variety of the different tests such as tunnel geometry, fire geometry, fire intensity, HRR etc. with one set of empirical constants). That process was assisted by the validated CFD model, where different parameters were systematically varied (e.g. fire intensity, fire length, fire width, tunnel profile) to increase the variety of the data and confirm that the derived empirical constants were appropriately calibrated. The CFD allowed trends for individual parameters to be explored, before seeking an overall 'best fit' with all test datasets considered. The derived empirical factors and constants can be found in (Beyer, et al., 2024).

3 CONSIDERATIONS FOR DESIGN

The full set of equations, providing adjustment for all sorts of scenario parameters, are good for comparison against specific tests. However, for practical design, many of those parameters cannot be known or assumed, as a design fire is usually defined by a HRR and not a particular fire scenario. A tunnel design needs to address reasonably foreseeable fires (so far as is reasonably practicable) that can lead to the design fire HRR (e.g. most onerous possible fire scenario such as pool fire). Designers will not know the width or length or intensity of a 'design' fire, or the height of the fire seat. Appropriate values need to be assumed, taking a conservative view within reasonable bounds. A set of such assumptions led to a simplified equation (as presented in Section 6.3 in Beyer, Stacey & Brenn (Beyer, et al., 2024)) that is sufficient for most design purposes. The assumptions are summarised below but for the set of simplified equations and their limitations please refer to (Beyer, et al., 2024).

The greatest critical velocity from a fire relates to the fire seat being on the roadway with a high heat release rate per unit area, such as a pool fire. It is reasonable that some fuel load may spill down to the roadway as a result of collision or the fire, so the fire plume height will be taken as the tunnel height (from floor to highest point at the ceiling). With the fire width dependence discussed in Section 0 and using the Memorial Tunnel parameters as an example, it turns out that for road tunnels with similar geometrical characteristics, critical velocity is about at a maximum for fire seats about 2.5 m wide. As this is the same as the width of a truck and is a potential spill width (Beyer, et al., 2024), it was a realistic but conservative figure to adopt for design. With tunnels typically much wider than 2.5 m ($A > H(2.5\ [m] + 0.35 \cdot H)$), that makes the minimum function noted in the denominator of ΔT_p in Equation (36) of (Beyer, et al., 2024) redundant. Most tunnel designs need to address fires much larger than 10 MW (for tunnel height $H < 9\ m$), so the minimum function noted in the numerator of ΔT_p in Equation (36) of (Beyer, et al., 2024) can also be discarded. Hydrocarbon pool fires are about as intense as fires come, so the fire intensity can reasonably be taken from a pool fire value (on the roadway).

The Beyer Stacey Brenn equation presented in (Beyer, et al., 2024) are not derived or validated for fires with considerable blockage. The blockage would have additional effects on the plume and would require an appropriate implementation in the equations. However, as a tunnel design can't rely on a considerable blockage once a fire occurs, such a scenario was not seen to be important for the study.

The several years in which the design guidance from NFPA 502 (NFPA 502, 2017), (NFPA 502, 2020), and (NFPA 502, 2023) lost its way has been the driver for improving the science of critical velocity estimation, with the improved critical velocity model now serving that purpose, including within NFPA 502 2026 edition (NFPA 502, 2026).

After establishing a sensible critical velocity value for a proposed tunnel, the ventilation power and equipment to achieve that can be determined and designed. Whether critical velocity is the

appropriate operational target for any particular fire scenario is a different matter, for another discussion.

4 REFERENCES

BEYER, M. & STACEY, C., 2022. *CFD VALIDATION FOR TUNNEL SMOKE CONTROL DESIGN.* GRAZ, ITNA-REPORTS VOLUME 105.

Beyer, M. & Stacey, C., 2024. *Confinement Velocity for Smoke in Tunnels – How to Poke a Stick at it.* Graz, s.n.

Beyer, M., Stacey, C. & Brenn, G., 2024. A Mixed Convection Model for Estimating the Critical Velocity to Prevent Smoke Backlayering in Tunnels. *Fire Technol, https://doi.org/10.1007/s10694-024-01607-8,* Volume 61, pp. 295-342.

Beyer, M., Stacey, C. & Dix, A., 2021. Critical velocity and the significance of the imminent retraction of 2020 NFPA 502's Annex D critical velocity equations part one. *Australian Tunnelling Society,* Issue https://www.ats.org.au/2021/03/11/critical-velocity-a-cautionary-note-to-practitioners/.

Danzinger, N. & Kennedy, W., 1982. *Longitudinal Ventilation Analysis for the Glenwood Canyon.* York, UK, 23-25 March 1982, s.n., pp. 169-186.

Kennedy, W., 1996. Critical velocity: Past, Present and Future. *Seminar of Smoke and Critical Velocity in Tunnels,* 9-11 March.pp. 305-322.

Li, Y. & Ingason, H., 2017. Effect of cross section on critical velocity in longitudinally ventilated tunnel fires. *Fire Safety Journal,* Issue 91, pp. 303-311.

Li, Y. & Ingason, H., 2018. Discussions on critical velocity and critical Froude number for smoke control in tunnels with longitudinal ventilation. *Fire Safety Journal,* Issue 99, pp. 22-26.

Li, Y. & Ingason, H., 2019. Corrigendum to "Effect of cross section on critical velocity in longitudinally venti-lated tunnel fires" [Fire Saf. J. 91 (2017) 303-311]. *Fire Safety Journal,* Issue 110.

Li, Y., Lei, B. & Ingason, H., 2010. Study of critical velocity and backlayering length in longitudinally ventilated tunnel fires. *Fire Safety Journal,* Issue 45, pp. 361-370.

Li, Z., Lei, B. & Ingason, H., 2024. Clarification to 2010 paper "Study of critical velocity and backlayering length in longitudinally ventilated tunnel fires", by Li, Lei, and Ingason. *Fire Safety Journal,* Volume 144.

MTFVTP, 1995a. *Memorial Tunnel Fire Ventilation Test Program - Comprehensive Test Report,* Boston: Bechtel/Parsons Brinckerhoff.

MTFVTP, 1995b. *Memorial Tunnel Fire Ventilation Test Program - Memorial Tunnel Test Data Report incl. 9 discs of raw data,* Boston: Bechtel/Parsons Brinckerhoff.

NFPA 502, 2014. *Standard for Road Tunnels, Bridges, and Other Limited Access Highways,* s.l.: NFPA 502.

NFPA 502, 2017. *Standard for Road Tunnels, Bridges, and Other Limited Access Highways,* s.l.: NFPA 502.

NFPA 502, 2020. *Standard for Road Tunnels, Bridges, and Other Limited Access Highways,* s.l.: NFPA 502.

NFPA 502, 2020. *Tentative Interim Amendment (TIA), TIA 20-1, Reference: Annex D, 11.3, A.11.4.2, Annex O, 26th August 2021,.* [Online]
Available at: https://docinfofiles.nfpa.org/files/AboutTheCodes/502/TIA_502_20_1.pdf

NFPA 502, 2023. *Standard for Road Tunnels, Bridges, and Other Limited Access Highways,* US: The National Fire Protection Association.

NFPA 502, 2026. *Standard for Road Tunnels, Bridges, and Other Limited Access Highways,* s.l.: NFPA 502.

Oka, Y. & Atkinson, G. T., 1995. Control of Smoke Flow in Tunnel Fires. *Fire Safety Journal,* Issue 25, pp. 305-322.

Shi, Y. S. et al., 2023. *NFPA 502 Critical velocity calculation methodologies and dimensionless heat release rate.* Stavanger, s.n., pp. 513-525.

Shi, Y. S., De Los Rios, N. & Lopez, K., 2022. *The critical penalty.* Brighton, UK, s.n.

Stacey, C. & Beyer, M., 2020a. *Critical of critical velocity - An industry practioner's perspective.* Graz, s.n., pp. 220-235.

Stacey, C. & Beyer, M., 2020b. *Recorded talk on Critical of Critical Velocity - An Industry Practitioner's Perspective.* Graz, Austria, 1st to 3rd of December 2020, s.n.

Thomas, P., 1958. The Movement of Buoyant Fluid Against a Stream and the Venting of Under-ground Fires. *Fire Research Station,* Issue Fire Research Note No 351.

Thomas, P., 1968. The Movement of Smoke in Horizontal Passages Against an Air Flow. *Fire Research Station,* Issue Fire Research Note No 723.

Wu, Y. & Bakar, M. Z. A., 2000. Control of smoke flow in tunnel fires using longitudinal ventilation system – a study of the critical velocity. *Fire Safety Journal,* Issue 35, pp. 363-390.

19th Australasian Tunnelling Conference – Acosta-Martínez, Stewart and Hudson-Smith (Eds.)
© 2025 Australian Tunnelling Society, ISBN 978-0-85825-002-4

Enhancing operator enclosure air quality in tunnelling operations: addressing silica dust exposure and compliance through AS/ISO 23875

J.L. Moredock
Sy-Klone International, Jacksonville, FL, USA
International Society of Environmental Enclosure Engineers, Jacksonville, FL, USA

K. Cole
Cole Health Pty Ltd, NSW, Australia

ABSTRACT: Tunnelling operations pose many occupational health hazards, primarily due to exposure to airborne contaminants such as respirable crystalline silica (RCS). This exposure is linked to serious health conditions such as silicosis, chronic respiratory diseases, and increased mortality rates. This white paper explores the health risks associated with tunnelling operations and highlights the critical importance of effective air quality management. It discusses the role of AS/ISO 23875 in mitigating these hazards, outlining how its implementation can safeguard operator health by improving enclosure air quality, ensuring compliance, and reducing health risks for contractors and equipment suppliers.

1 INTRODUCTION

Tunnelling operations inherently generate fine particulate dust, much of which contains crystalline silica, a byproduct of drilling, blasting, and mechanical excavation of rock. Long-term exposure to this dust, even at low concentrations, can result in severe health conditions: silicosis, chronic obstructive pulmonary disease, lung cancer, and an increased risk of tuberculosis and kidney disease [1]. Despite advancements in machinery and ventilation, operator enclosures can still be vulnerable to contamination due to inadequate filtration systems, poor sealing, and a lack of ongoing air quality performance monitoring. Operator cabs, typically seen as passive protective spaces, require robust systems that needs to be validated on an ongoing basis to ensure their effectiveness in safeguarding operator health.

In response to the hazards posed by dust exposure, the international standard ISO 23875: Operator Enclosures – Air Quality Control Systems and Performance Testing was first developed by the ISO Technical Committee 82 – Mining in 2021 and was subsequently adopted in Australia in 2023.

The implementation of AS/ISO 23875 fosters a culture of safety and sustainability, leading to safer working environments, reduced health risks, and improved operational efficiency [2]. The standard provides a comprehensive, performance-based framework designed to ensure machine operators, particularly in dust-heavy environments such as tunnelling, are consistently protected from harmful airborne particles. AS/ISO 23875 prioritises system simplicity and clarity, making it applicable for both original equipment manufacturers (OEMs) and retrofit scenarios. The standard encourages stakeholder collaboration and places a strong emphasis on practical, field-based performance testing to ensure air quality systems perform effectively under actual operational conditions.

1.1 *System components*

The effective implementation of AS/ISO 23875 relies on the integration of multiple interdependent system components that function synergistically to maintain safe air quality within operator

enclosures. The key elements include the performance and control of the HVAC system, which must reliably supply clean, conditioned air while effectively removing airborne contaminants. This is achieved through both intake and recirculation filtration systems, which play a critical role in capturing respirable dust particles such as crystalline silica.

Maintaining positive cabin pressure is essential to prevent the infiltration of contaminated air, and this is only effective when coupled with robust cabin seal integrity, ensuring that unfiltered air does not bypass the system. Real-time air quality monitoring is also a vital component, providing continuous assessment of internal cabin conditions and enabling immediate intervention if parameters deviate from established safety thresholds. The combined functionality of these components is essential for protecting worker health in high-risk environments such as tunnelling operations.

2 CASE STUDY

AS/ISO 23875 requires field-based performance validation to verify that the components are functioning correctly. Performance metrics such as carbon dioxide (CO_2) concentration, pressure differential, dust ingress rates, and airflow capacity are used to assess the overall effectiveness of the air quality control system. These tests are conducted on-site to ensure that the systems operate effectively in real-world conditions, as opposed to controlled lab environments.

A case study is presented to illustrate the critical role of air exchange combined with high-efficiency intake and recirculation air filtration and continuous cab pressurization, in significantly reducing particulate decay times [3].

A drill rig working in an open-pit gold mine was retrofitted to the requirements specified in AS/ISO 23875. The tested machine operated under challenging environmental conditions, including temperatures as low as −29°C with strong winds with a three-machine drilling configuration producing substantial quantities of visible airborne dust. With three operators present, the cab door was opened over thirty times, as was typical for the working shift.

Figure 1 demonstrates the results of the particulate monitor which was located inside the drill rig cabin. The monitor measured PM_{10} concentrations each minute of operation. Figure 1 shows many elevated spikes in dust concentrations, which corresponded to the door being opened and closed. PM_{10} concentrations reached 1708 µg/m³ and reduced to <22 µg/m³ within 3 minutes. Throughout the test, continuous cab pressurisation was maintained at 200 Pa and the rapid air exchange effectively reduced these dust concentrations, maintaining an average PM_{10} concentration within the cab below 10 µg/m³ over the period of 2 hours

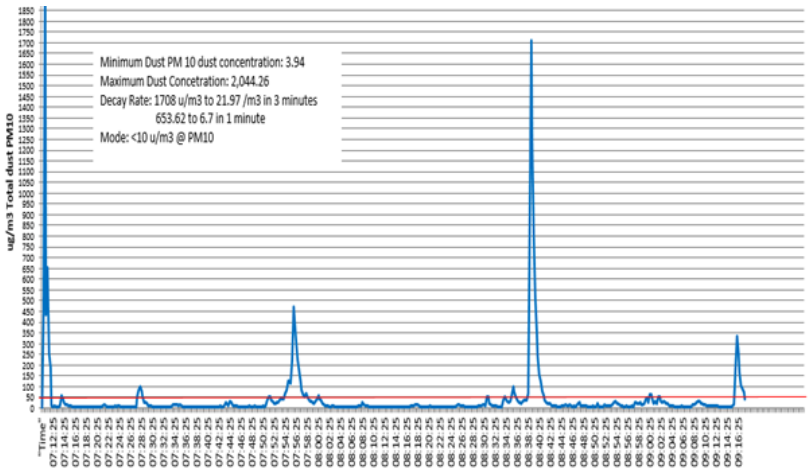


Figure 1. Particulate matter PM_{10} concentrations in operator cab during multi-machine drilling operations showing peak exposures and rapid decay following the operator leaving and reentering the drill cab.

To evaluate the effectiveness of the installed system, multi-day testing was performed using both static (area) and personal monitoring for RCS. Both personal and static samples were collected on the same day, with area samples situated in the air space within the cabin, and personal samples collected from drill operators. NIOSH test method 7500 was used for sampling and analysis for a total test time of approximately 9.5 hours, which reflected the drill operator's duration of exposure. Sampling took place over 6 different days between March 10, 2015 and October 20, 2015.

Figure 2 presents the results obtained during the multi-day testing. On average, personal exposure to RCS concentrations decreased by 87% when the system was installed, compared to when it was not. In-cabin concentrations, based on static sampling, were reduced by 56% under the same conditions.

A Wilcoxon rank sum test confirmed a statistically significant difference in RCS concentrations between conditions with and without the system installed, with lower concentrations observed when the system was in use.

This real-world example highlights how the performance requirements specified by AS/ISO 23875 can be effectively met in typical drilling operations, underscoring the practical value and applicability of the AS/ISO 23875 performance tests. Despite the harsh environmental conditions, the engineering controls specified by AS/ISO 23875 were able to effectively maintain good air quality within the enclosure.

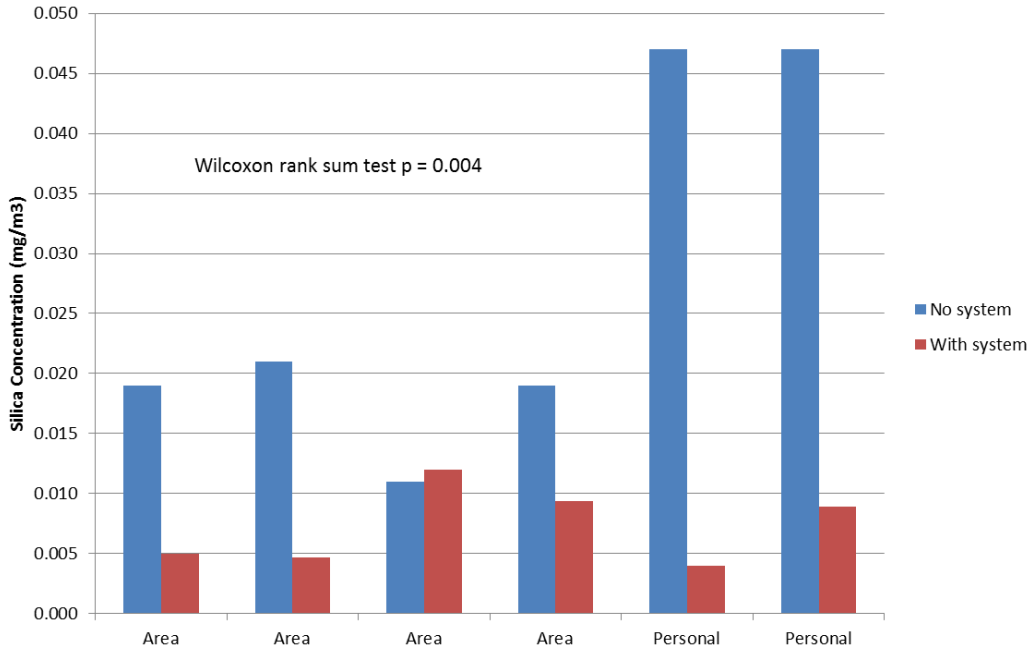


Figure 2. RCS concentrations (in milligrams per cubic meter) with and without a ISO 23875 system installed.

3 DISCUSSION

Tunnel construction can present challenges for managing RCS exposure, particularly among heavy equipment operators who spend extended periods inside enclosed cabins. The workplace exposure standard (WES) for respirable crystalline silica (RCS) is 0.05 mg/m³, based on an eight-hour time-weighted average. In tunnel construction, heavy plant operators such as those who operate excavators, dozers, articulated haul trucks, and drill rigs spend a significant amount of time inside enclosed cabins. These workers often complete extended shifts of up to twelve hours, requiring the WES to be adjusted to lower levels, such as approximately 0.03 mg/m³, to account for the longer exposure period.

Air monitoring for RCS is routinely undertaken in tunnel construction projects. Since 1 September 2024, notification to the WHS Regulator has been mandatory for any results that exceed the adjusted WES. Analysis of reported exceedances in New South Wales indicates that more than half originate from the tunnelling sector [4], with a proportion associated with operators of heavy plant and machinery [5][6]. In circumstances where RCS concentrations exceed the WES, respiratory protective equipment is typically used. However, reliance on personal protective equipment alone is not a sustainable solution, given that it represents the final and least effective layer of the hierarchy of controls.

Engineering interventions, such as the installation of AS/ISO 23875 compliant systems, offer a more effective means of protecting workers by reducing airborne contaminant levels within operator cabins. By significantly lowering personal exposure levels, these systems help reduce dependence on respiratory protection, decrease the incidence of regulatory exceedances, and enhance overall worker safety outcomes.

Effective implementation of AS/ISO 23875 requires a structured program of training and education that reaches all levels of an organisation. The International Society of Environmental Engineers (ISEEE) supports adoption by developing technical resources and training materials designed for operators, maintenance personnel, supervisors, safety professionals, and senior management. Training initiatives, such as the "Application of ISO 23875 in Operator Cab Air Filtration, Pressurization, and Certification," provide practical guidance on achieving and maintaining compliance. Through comprehensive education and broad engagement, tunnelling operations can embed air quality management practices into daily operations and foster a strong culture of occupational health and safety.

Beyond the health benefits, the adoption of AS/ISO 23875 offers economic advantages. Efficient operation of HVAC and filtration systems reduces maintenance costs and extends equipment lifespan. Improved system performance also enhances machine reliability and uptime, minimising costly production interruptions. Furthermore, reducing reliance on respiratory protection leads to better health outcomes, supporting workforce stability and productivity. Compliance with internationally recognised standards strengthens a company's reputation and improves its competitiveness in attracting and retaining skilled workers in a tight labour market.

In the context of increasing litigation related to occupational dust exposure, the ability to better protect workers is crucial. Adoption of AS/ISO 23875 provides a robust framework for documenting system performance, establishing continuous air quality monitoring, and evidencing preventative measures to protect worker health. This strengthens compliance efforts while reinforcing an organization’s commitment to safeguarding employees.

The tunnelling industry has started to adopt AS/ISO 23875 compliant cabins across several projects in Australia. To further enhance understanding of the practical benefits of AS/ISO 23875 in tunnelling environments, additional case studies are being sought. Tunnelling contractors and project teams are invited to participate in future trials. Contributions from industry participants will help build a broader evidence base, support ongoing improvements in air quality management, and drive better health outcomes for workers across the sector.

4 CONCLUSIONS

Tunnelling remains a high-risk industry, with exposure to RCS being a risk that must be proactively managed. AS/ISO 23875 presents a practical, flexible, and effective standard that ensures operator enclosures meet the highest air quality standards. By adopting this standard, tunnelling stakeholders can shift to a proactive approach, ensuring ongoing and long-term protection for operators. The widespread adoption of this standard will help the tunnelling industry offer a safer, healthier, and more sustainable future for both its workforce and the broader tunnelling sector.

5 REFERENCES

Guha, N., K. Straif, and L. Benbrahim-Tallaa, *The IARC Monographs on the carcinogenicity of crystalline silica.* La Medicina del lavoro, 2011. 102(4): p. 310–320.

Moredock, J., B. Dutta, and A. Chatterjee, *The Case for ISO 23875:2021 W/Amendment 1: 2022 as the Path to Hemm Protection from Respirable Crystalline Silica (Rcs)*. 2023. p. 345–354.

Morin, K., Lachapelle, G., & Hon, C.-Y, *Pilot evaluation of novel engineering control to reduce airborne exposure to particulates inside drilling cabs.* Canadian Institute of Mining Journal, 2016. 8(2)(12).

SafeWork NSW. *Silica dashboard*. 2024 30 April]; Available from: https://www.nsw.gov.au/departments-and-agencies/customer-service/publications-and-reports/silica-dashboard.

Parliament of New South Wales, *Return to Order (Public) - "Respirable crystalline silica air monitoring" dated 18 December 2024, together with an indexed list of documents.* 2024.

Parliament of New South Wales, *Return to Order (Public) - "Respirable crystalline silica air monitoring" dated 21 February 2025, together with an indexed list of documents.* 2025.

THIS PAGE INTENTIONALLY LEFT BLANK

19th Australasian Tunnelling Conference – Acosta-Martínez, Stewart and Hudson-Smith (Eds.)
© 2025 Australian Tunnelling Society, ISBN 978-0-85825-002-4

Challenges implementing AS61508 on infrastructure projects

P. Kroon
Kroon Technology, Adelaide, Australia

ABSTRACT: Functional safety, as defined in AS61508 [1], provides a robust framework for the delivery of safety related systems. It has been a common requirement in infrastructure projects for over 2 decades. The objectives for its inclusion, and thus how it has been specified, have varied between projects. This has created confusion over what a compliant process may be. In all cases though, the core objective has been to deliver safer and more reliable systems.

In this paper the author aims to identify many of the common challenges encountered in projects in delivering safety related systems intended to be compliant with AS61508 [1] in infrastructure projects. Looking at some common challenges in delivering AS61508 [1] across the lifecycle from identification of hazards, selecting appropriate Safety Integrity Levels (SILs), delivering compliant solutions, and maintaining their performance in an operational context.

1 INTRODUCTION

Infrastructure projects are increasingly relying on complex control systems to enhance safety and efficiency resulting in more value from the investment. Whilst complex control systems can provide tangible benefits in these areas, they can also be a source of new risks and inefficiencies if not implemented effectively. As a result, it has become common practice to include reference to AS61508 [1] in infrastructure projects to support the development of complex control systems. AS61508 [1] provides guidance on functional safety of electrical, electronic and programmable electronic safety related systems. It covers the entire lifecycle for a system from concept through to decommissioning.

Whilst AS61508 [1] is routinely specified in infrastructure projects, the scope of its application varies between projects creating confusion in industry on how to achieve compliance. In many cases, the focus is on software development with the hardware aspects of AS61508 [1] disregarded to the detriment of the level of safety achieved. An understanding of some key hardware concepts considered in AS61508 [1] including Systematic Capability (SC), energise to trip, proof testing, and useful life, can benefit not only functional safety but good control system engineering.

2 SYSTEMATIC CAPABILITY

A logical consideration in the selection of components for safety applications is having confidence the component will work reliably when required. Whilst there is typically lot of focus on quantifying the effect of random hardware failures, commonly referred to as calculating the PFD (probability of dangerous failure on demand), little consideration is given to systematic failures. Components that form part of a safety function need to be selected with the goal of minimising systematic faults. AS61508.2 [3] sets out two options for demonstrating the appropriate selection of components based on hardware, Route 1_S and Route 2_S.

2.1 Route 1_S

Route 1_S, relies on a component being engineered in accordance with the relevant techniques and measure to ensure the likelihood of systematic faults being present is sufficiently low. AS61508.2 [3] includes several requirements and tables detailing techniques and measures to be used in the engineering of a component. The level effort and effectiveness in the implementation of these techniques and measures is also specified with the aim being to achieve a level of rigour commensurate with the target Safety Integrity Level (SIL).

It is impractical for integrators and end users to determine whether a device has been engineered in accordance with the relevant techniques and measures set out in AS61508.2 [3].

Therefore, in practice, Route 1_S relies on the concept of independent certification, where a third party attests that a claim of compliance with the relevant parts of AS61508 [1] made by the manufacturer is true based on the provision of objective evidence.

There are four levels of Systematic Capability SC1, SC2, SC3, and SC4. The required SC is aligned with the target SIL, for example a minimum of SC1 is required for a SIL1 application. Another example, a component that certified as SC3 is suitable for use in safety functions allocated SIL1, SIL2, or SIL3. In practice, integrators and end users can select a certified component with the appropriate SC, confident that the component is sufficiently free from systematic faults relative to the SIL for the safety function they are implementing.

This is the simplest approach to demonstrating systematic capability, but it may not be practical for some specialist components, or where a well proven component is preferred rather than using a new certified component that is untried in an application.

2.2 Route 2_S

AS61508 [1] does not require the use of certified components. It is an option but is not mandatory. If a component can be demonstrated to work effectively in a given application with a suitably low failure rate, then it may prove to be a better option over an untested certified component. This is known as proven in use.

AS61508.2 [3][2] route 2_S includes the requirements to be satisfied in order to demonstrate a proven in use argument to justify using a device in a given application.

Using the proven in use approach, there must be objective evidence available that demonstrates the component has worked reliably in similar applications, thus proving through operational experience that the component is sufficiently free from systematic faults to be trusted for use in a safety application.

3 ENERGISE TO TRIP

In many industries, it is typical practice to design safety functions so they remove energy to achieve a safe state, commonly referred to as a deenergise to trip function. In infrastructure projects, it is typical for safety function to need energy to perform their function. This could be to power jet fans or pumps to achieve or maintain a safe state. For these types of applications a loss of power would present a dangerous failure, as no power would compromise the safety function. These types of safety functions are typically referred to as energise to trip, as they require energy when there is a demand on the safety function. Energise to trip functions present a few challenges, in particular:

- Most safety PLCs are only suitable for deenergise to trip; and
- The energy source must be considered in the quantification of random hardware failures.

3.1 Safety PLC limitation

Most safety PLCs are only certified for deenergise to trip functions. Safety PLCs have very high levels of diagnostics and are designed to revert to a safe state when a fault is detected. The safe state for safety PLCs designed for deenergise to trip functions is to turn off its outputs.

In a deenergise to trip function, this would be the equivalent to the safety function activating and thus revert the system to a safe state. However, this behaviour would prevent an energise

to trip safety function from operating and thus compromise the ability for the safety function to respond when there is a demand.

Careful consideration needs to be given to whether a safety function is energise to trip and if the control system is suitable for use for energise to trip functions.

As an example a popular architecture for infrastructure projects is to use Rockwell ControlLogix PLCs which Rockwell Automation state are suitable for SIL1 or SIL2 applications. Rockwell Automation provides a reference manual for the use of ControlLogix for SIL 2 applications [6]. In the manual it states, "*If the application cannot tolerate an output that fails open (de-energized), then an external means such as a manual override or output must be wired in parallel*". The manual goes on to provide an example architecture, that is shown in Figure 1, along with a method of operation.

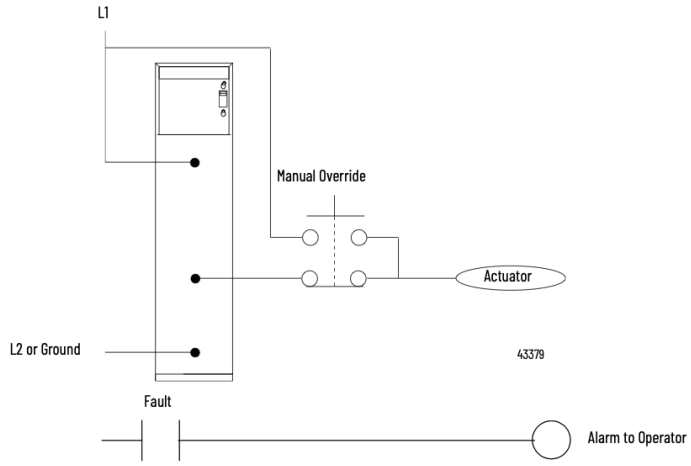


Figure 1. Example provided in Rockwell publication for energise to trip function

The proposed method indicates that in the event that a fault is detected by the PLC, an alarm should be provided to the operator who then uses a manual override to achieve the safety function, essentially manually turning on the device. In practice, for infrastructure projects manual overrides to compensate for PLC degradation would be impractical to implement as they are remotely operated and have the potential to exacerbate a hazardous event with incorrect or uncoordinated operations.

PLCs designed for energise to trip functions such as the HIMA HiMax [7], will continue to function in a degraded state, enabling safety functions to be preserved in the presence of a fault. Another popular PLC for infrastructure is the Siemens S7 1500 series PLC, as noted in associated functional safety certification [9] "*on condition that the "0 state" (closed-circuit principle) is defined as the safe state for the binary inputs and outputs*". This indicates that the PLC platform is only suitable for deenergise to trip applications.

3.2 Consideration of energy source in PFD calculations

For energise to trip functions to operate, they need energy/power. Therefore, in accordance with AS61508.2 [3], consideration of the energy/power source must be made in the PFD calculations, as a loss of power would result in the safety function failing to operate if there were a demand. Failure to consider the reliability of the energy/power source would completely negate the PFD calculations.

4 PROOF TESTING

It is typical to design safety functions so that they place or maintain a system in a safe state if certain conditions are present, or when initiated by an operator as opposed to continuous control. These types of functions are defined as demand mode safety functions, as they are

safety functions that only perform on demand. If a safety function fails when there is a demand, it is reasonable to conclude, one or more components implementing the function must have:

- Failed in a manner that compromised its operation, as it did not operate when required.
- The presence of the failure was unknown, otherwise appropriate actions would have been taken to remedy the failure.

These types of failures are defined in AS61508 [1] as dangerous undetected failures. Other common terms include, dangerous dormant failures, dangerous hidden failures; and unrevealed failures.These failures present the biggest risk to safe operation, as they prevent a safety function operating on demand. As a consequence, AS61508 [1] requires proof testing to be undertaken to reveal dangerous undetected failures. AS61508.4 [4] clause 3.8.5 defines a proof test as a "*periodic test performed to detect dangerous hidden failures in a safety-related system so that, if necessary, a repair can restore the system to an "as new" condition or as close as practical to this condition*". Various issues have been observed in relation to proof testing in the infrastructure sector, including:

- impractical proof testing intervals;
- assuming perfect proof test coverage;
- failure to define appropriate proof tests;
- failure to undertake suitable proof tests at the specified interval

Each of these issues compromise any safety argument, either through creating an overly optimistic predicted of random failure rate (e.g. PFD) or adversely affecting the capacity to reveal dangerous undetected failures in practice.

4.1 Impractical proof testing intervals

The proof test interval has a direct effect on predicting the random failure rate of a safety function which is required by AS61508.2 [3] clause 7.4.5. The average probability of dangerous failure on demand (PFD_{avg}) of a single component can be calculated by the following equation based on the PDS Method Handbook [8].

$$PFD_{avg1oo1} = \frac{\lambda_{DU}\, TI}{2}$$

Where λ_{DU} = rate of dangerous undetected failures; TI = proof test interval.

As shown by this equation, the proof test interval is directly proportional to the PFD_{avg}. As observed on one project, the PFD_{avg} was reduced from 1 year (8760 hours) to 8 hours for jet fan proof testing. This had the effect of reducing the PFD_{avg} by 3 orders of magnitude or approximately 1000 times lower having a profound effect on the PFD_{avg}. However, it was impractical to implement and Imposes significant obligations on the operators and maintainers.

As a proof test for a component is intended to reveal all dangerous undetected failures, it typically requires a visual inspection and function testing, which is not practical every 8 hours. Further, it is unlikely that the contribution of a single jet fan to the tunnel air velocity can be effectively evaluated with the instrumentation installed in the tunnel, thus the proof test coverage (PTC) would be in question, the impact of which is discussed later.

It is critical that specified proof test intervals are achievable. Preferably minimum proof test intervals based on access and maintenance resource levels are specified in the contract documents.

4.2 Assuming perfect proof test coverage

Many PFD calculations encountered for infrastructure projects assume 100% PTC, that is, they assume all dangerous undetected failures will be revealed. In practice, this is very unlikely to be achieved. To be compliant with AS61508 [1], manufacturers are required to supply a safety manual that includes a proof test procedure and the associated PTC. Typically the PTC for transmitters is around 90 to 95% for devices intended for safety applications.

Figure 2 highlights the impact of imperfect proof testing, it is based on AS61508.6 [5] Table B.9. It shows that a reduction from 100% to 90% PTC doubles the PFD. This example

highlights that failure to consider PTC in calculating the PFD results in overly optimist results.

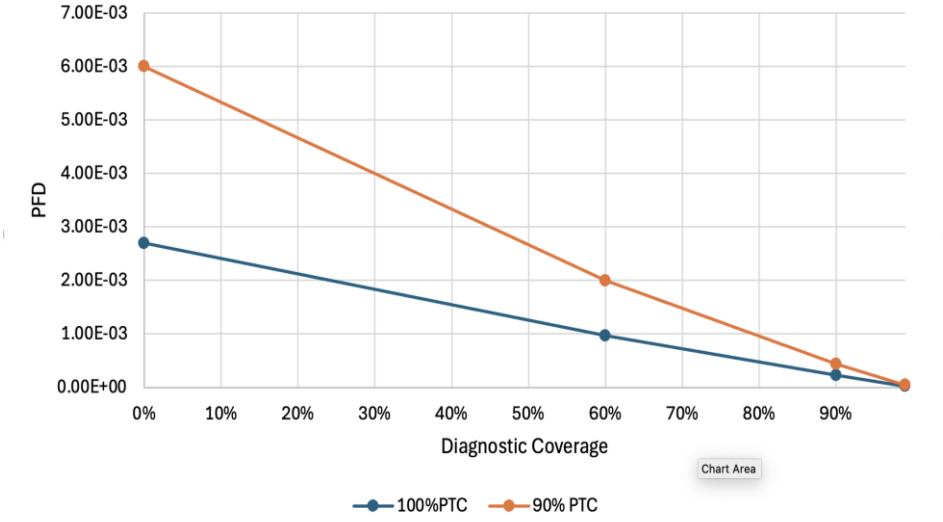


Figure 2. Impact of non-perfect proof test

4.3 Failure to define appropriate proof tests

It is typical to review operation and maintenance manuals, only to find no or very generic information in relation to proof test procedures. Proof test procedures must be developed and provided that provide clear guidance on how to inspect and test a device with the aim of revealing all dangerous undetected faults. The procedure should be step by step and repeatable by any technician, ensuring a consistent repeatable activity. Failure to provide this critical information or failure by operators and maintainers to follow the proof test procedures will compromise the integrity of the safety function.

4.4 Failure to undertake suitable proof tests at the specified interval

As noted in section 4.1, the PTI has a direct effect on the PFD. As unreliability is the complement of reliability it can be concluded that over time the likelihood of the device failing increases. This concept is shown in Figure 3, which shows the probability of failure increases over time in line with a natural decay curve.

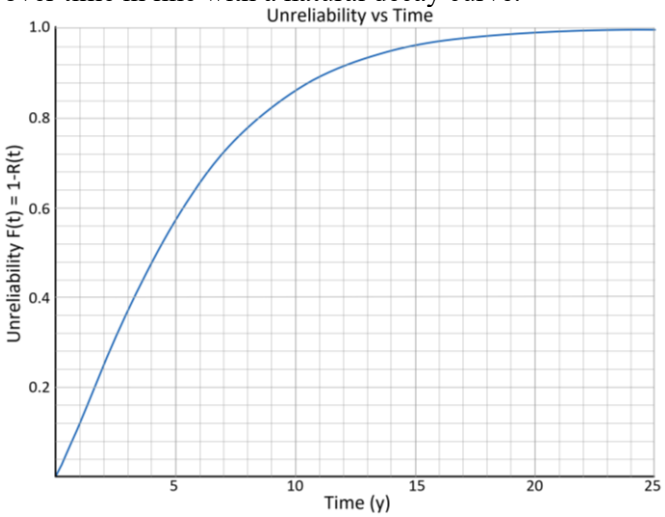


Figure 3. Unreliability versus time

If after a defined period, a device is proof tested following a procedure with a 100% PTC and any faults present fixed, restoring the device to as new condition, then the likelihood of a dangerous undetected fault being present reverts back to zero. The average of this period can

then be derived. If the proof test interval is consistent then the average for one period is the average for the useful life of the device. This is shown in Figure 4.

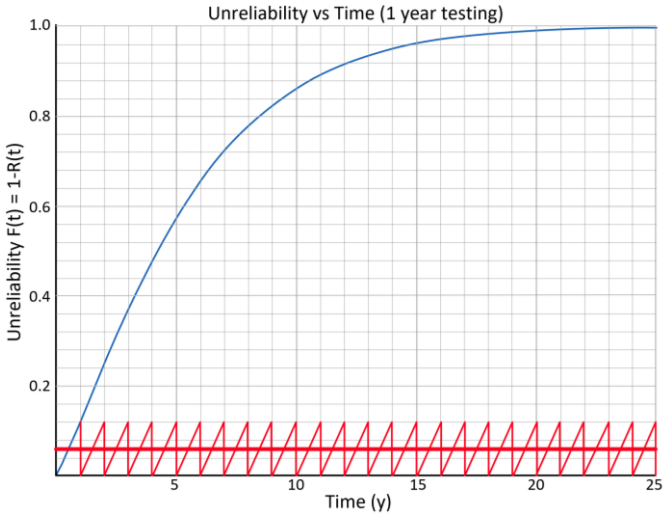


Figure 4. PFD instantaneous and PFD average, 1 year proof test interval

If the proof test interval is extended to 5 yearly for operational reasons, then the PFD average will increase proportionally, as shown in Figure 5.

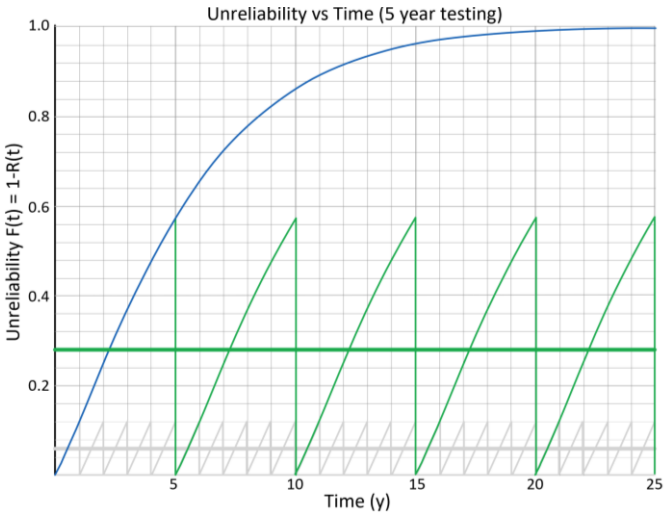


Figure 5. PFD instantaneous and PFD average, 5-year proof test interval

Where proof testing either is not undertaken at all or the proof testing is delayed to align with other operational considerations then the PFD increases. In practical terms, this means a safety function is more likely to fail due to a random hardware failure when it is called upon.

In the design phase it is important to ensure the proof test intervals used in the PFD calculations are practical and the testing can be completed at the nominated interval. In the operational phase it is critical suitable proof tests are undertaken within the intervals used in the PFD calculations.

5 USEFUL LIFE

A key assumption for the PFD calculations to be valid, is that components have a consistent failure rate. To achieve this, components forming part of a safety function must be replaced prior to the device reaching the end of its useful life.

A classic concept in reliability theory is the bathtub curve. The bathtub curve suggests there

are three distinct phases, wear in, useful life, wear out. During wear in there is a higher failure rate which rapidly diminishes. This is also commonly referred to as burn in. There is then a period with a constant failure rate which is considered to be the useful life. Then there will be a rapid rise in the failure rate as the component moves into the wear out phase. This concept is illustrated in Figure 6. In Figure 6, the x axis is time, however the useful life of a component could be determined as a function of time, hours of operation, or number of cycles.

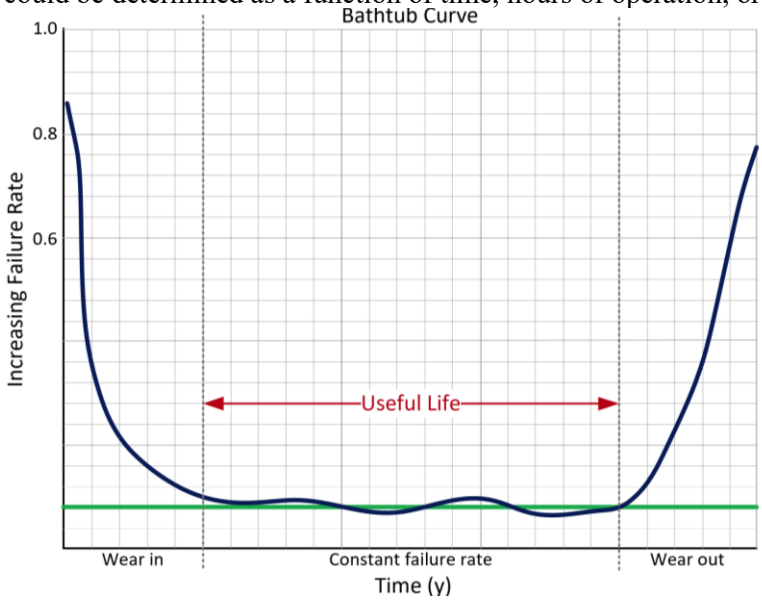


Figure 6. Reliability bathtub curve

If components are left in service until failure, then the likelihood of a component being in a failed state when there is a demand on the safety function becomes almost inevitable. It simply becomes a case of a failure being revealed through a failure of a safety function during a demand or periodic testing.

Even if components are being replaced periodically, if they are left in service after reaching the wear out phase then the likelihood of failure starts increasing exponentially and thus the likelihood of a failure of the safety function also increases rapidly, negating the PFD calculations and the integrity of the safety function. In practice, for every component used in a safety function:

- the useful life must be specified in an appropriate manner, i.e. time in service, hours run, or number of cycles;
- the current life of each component must be tracked;
- Components need to be replaced prior to reaching wear out;
- Component failure data collected; and
- Useful life assumptions periodically verified.

6 CONCLUSION

There are a number of concepts defined in AS61508 [1] that are crucial for ensuring the integrity of control system. Failure to address any of the key hardware concepts discussed, increases the likelihood of a safety function not working when there is a demand with potentially tragic consequences.

These same concepts can be used for other control systems to enhance their integrity improving the performance of the systems they support.

Whilst some projects have utilised AS61508 [1] to provide a framework for the delivery of robust software, without a systems thinking approach and suitable hardware the potential benefit offered by adopting AS61508 [1] will not be realised.

The guidance provided in AS61508 [1] represents good engineering practice, providing a framework for implementing an engineering process with rigour. Experience in other

industries has shown that once the concepts are understood for deploying safety related systems, the knowledge permeates into the development of other control systems. This results in an improvement in the performance of those control systems and thus an improvement in the performance and safety of the systems of interest they are intended to control and monitor.

7 REFERENCES

[1] AS61508 2011. *Functional safety of electrical/electronic/programmable electronic safety-related systems Parts 1 to 7.* Standards Australia

[2] AS61508.1 2011. *Functional safety of electrical/electronic/programmable electronic safety-related systems Part 1: General requirements.* Standards Australia

[3] AS61508.2 2011. *Functional safety of electrical/electronic/programmable electronic safety-related systems Part 1: Requirements for electrical/electronic/programmable electronic safety-related systems.* Standards Australia

[4] AS61508.4 2011. *Functional safety of electrical/electronic/programmable electronic safety-related systems Part 4: Definitions and abbreviations.* Standards Australia

[5] AS61508.6 2011. *Functional safety of electrical/electronic/programmable electronic safety-related systems Part 6: Guidelines on the application of IEC 61508-2 and IEC 61508-3*. Standards Australia

[6] 1756-RM001U-EN-P-March2025. *ControlLogix SIL 2 Applications.* Rockwell Automation Publications

[7] HI 801 001 E Rev. 3.00 (0944). *HIMax System Manual*. HIMA Paul Hildebrandt GmbH +Co KG

[8] PDS method handbook. 2010 *Reliability prediction method for safety instrumented systems*. SINTEF

[9] Z10 067803 0020 Rev.00. *Report to certificate Safety-related Programmable System Simatic Safety System.* TÜV SÜD Product Service

Theme 8. Geotechnics

THIS PAGE INTENTIONALLY LEFT BLANK

19th Australasian Tunnelling Conference – Acosta-Martínez, Stewart and Hudson-Smith (Eds.)
© 2025 Australian Tunnelling Society, ISBN 978-0-85825-002-4

Tunnel and marine nearshore ground investigation for Alkimos seawater desalination plant, Western Australia

T. Gourlay, T. Whitnall, J. O'Donovan & C. Nash
Jacobs, Australia

ABSTRACT: The Alkimos SeaWater Alliance (ASWA) is designing and constructing Stage 1 of the Alkimos Seawater Desalination Plant (ASDP). This paper describes the 2024 nearshore geotechnical investigation for ASDP Stage 1 and three historical campaigns (2021-2023). It details the groundbreaking methods and marine surveys used for assessing the seabed and underlying geology for the nearshore tunnel alignments. This paper also reviews and compares the success of the geotechnical investigation methods adopted in terms of defining the subsurface geology and interfaces between geological units, obtaining representative samples for laboratory testing, identifying geotechnical risks associated with tunnel design and construction. Challenges unique to nearshore investigations are discussed, including sea state, weather, tides, ecology, and vessel operations. The paper also addresses the complexities of designing a nearshore investigation scope while balancing value for money and comprehensive data collection.

1 INTRODUCTION

The ASDP, located 40 km north of Perth, will deliver 50 GL of drinking water annually in Stage 1, with Stage 2 adding another 50 GL. The nearshore components include the Seawater Intake Tunnel (SIT), Brine Outfall Tunnel (BOT), two Seawater Intake Riser (SIR) structures, and a Brine Linear Outfall Diffuser (BLOD) structure (subject to state environmental approval). This paper focuses on the tunnels.

2 NEARSHORE STRUCTURES

2.1 *Intake and Outfall Tunnels*

The SIT and BOT are 2.6 km and 4.1 km long respectively (see Figure 1) and will be excavated using slurry Tunnel Boring Machines (TBMs) with a 4.185 m excavation diameter. Excavations will start from onshore at the temporary TBM access shaft, progressing seaward. The tunnels will be lined with steel fibre reinforced concrete segments (3.505 m Inside Diameter (ID), 3.905 m Outside Diameter (OD)). TBM shields will be sacrificed at drive completion. For the onshore section of the tunnel, it will be constructed between approximately 4.7 m and 20.6 m below the water table. For the offshore section of the tunnel, it will be constructed below the seabed where water depths below sea level range from 20.6 m to 32.2 m.

2.2 *Seawater Intake Risers and Brine Linear Outfall Diffuser*

Two SIR structures will convey seawater into the SIT. The proposed foundation system for each structure consists of four driven steel tubular piles (1050 mm OD, 40 mm Wall Thickness (WT)) with 8.95 m spacing. These piles extend above the seabed and connect to the SIR structure's head. A driven steel circular liner (3074 mm OD, 37 mm WT) will provide ground support for

an1800mm ID Glass Reinforced Plastic (GRP) riser connecting to the SIT. Figure 2 illustrates this foundation system.

The BLOD diffuser expels brine from the BOT into the ocean. It consists of a 135 m long horizontal High-Density Polyethylene (HDPE) pipe supported by twelve driven steel tubular piles (1050 mm OD, 40 mm WT) spaced 10.0-10.5 m apart. Precast reinforced concrete ballast blocks are placed along the BLOD. A steel circular liner (3074 mm OD, 37 mm WT) provides ground support for an 1800 mm ID Glass Reinforced Plastic (GRP) riser connecting to the BOT and supports the precast outfall head joining the HDPE pipe sections. Figure 2 illustrates this foundation system.



Figure 1. Plan layout of Outfall and Intake Tunnel.

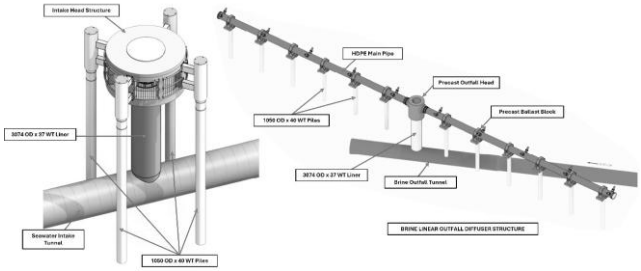


Figure 2. Intake Riser and Outfall Diffuser Structure.

3 GEOLOGY

The Alkimos site's surface geology is characterised by the Holocene Safety Bay Sand onshore, forming dunes up to 40 m AHD and 25 m thick, and Marine Sediments offshore, a variable layer of shelly sand and gravel up to 9.7 m thick. Both units are relatively recent formations, with the Safety Bay Sand continuing to develop today and the Marine Sediments subject to ongoing wave and current action.

Underlying these surface layers is the late Pleistocene Tamala Limestone, a widespread formation that creates the Spearwood Dune System and offshore reefs. This variably cemented carbonate rock mass, interlayered with uncemented sand bodies, is found beneath the Safety Bay Sand onshore and the Marine Sediments offshore, sometimes exposed as reefs.

The Tertiary Ascot Formation underlies the Tamala Limestone. It consists of carbonate calcareous materials with variable properties, likely representing shallow marine to lagoonal environments. Below this, along the outer part of the Outfall Tunnel alignment lies the informal late Tertiary 'TQ-Sand' unit (possible Rockingham Formation), situated between the Ascot Formation and the underlying Cretaceous Osborne Formation.

4 SEABED CONDITIONS

The marine area features discontinuous shallow reef networks parallel to the coastline, separated by deepening lagoons offshore. Reefs range from several metres above sea level to 18 m below

sea level on parts of the outer reef, while inter-reef depressions reach depths of 25 m below sea level.

5 HISTORICAL NEARSHORE INVESTIGATIONS

5.1 *Phase 1 & 2 (2021)*

The Phase 1 and 2 marine investigations included both geotechnical investigations and geophysical surveys. The geotechnical investigation involved drilling six boreholes between 0.3 km to 2.0 km offshore in water depths of 3 m to 12 m. The boreholes were drilled to depths of 28.5 m to 37.7 m using a drilling rig mounted on a four-legged Jack-Up Barge (JUB). The investigation included soil and rock laboratory testing for material classification, strength/stiffness properties, Acid Sulfate Soil (ASS) and palynological assessment.

Geotechnical investigations were undertaken between 12 November 2018 and 8 March 2019. The boreholes were drilled using rotary mud-flush drilling rig. Borehole collars were established on the seabed with PW 140mm casing to stabilise the primary drill string against currents and waves. PW casing was also reamed downhole to stabilise boreholes at depth if required. Boreholes were advanced using PQ3 triple-tube diamond coring to retrieve soil and rock core samples for geological logging and laboratory testing.

The geotechnical investigation experienced logistical challenges due to operating the JUB in open-ocean swells and wind driven seas which resulted in substantial weather downtime.

Swell conditions resulted in standby events due to limitations associated with barge towing even though the investigation occurred during the Summer where swell conditions in Perth are typically smallest. Problematic swell conditions commonly persisted for days to weeks and impacted mobilisation, demobilisation, and transfer of the JUB to borehole locations. The variable bathymetry, shallow reef systems are thought to have increased swell conditions (wave height and steepness) associated with the Perth Metropolitan coastline.

Wind or wind-driven sea states also resulted in standby events again due to limitations of barge towing, however these were typically short durations in comparison to the problematic swell conditions. Wind conditions in the Alkimos project area were commonly associated with the 'typical summer wind patterns' experienced along the Perth metropolitan coastline, comprising offshore winds in the morning followed by strong onshore winds (sea-breezes) and increasing sea-states in the afternoon. As such, minimising the impact of wind was able to be managed more effectively than the impact of swell, with daily operations commencing at dawn to maximise the potential working hours available prior to the onset of coastal sea breezes.

The geophysical survey employed various techniques including Multibeam Echosounder (MBES), Side Scan Sonar (SSS), Sub-bottom Profiler (SBP), seismic refraction, electrical resistivity, and magnetometer survey covering an area from the coastline to 5.5 km offshore. MBES and SSS covered an area of about 8 km^2 with the remaining geophysical surveys covering about 30 km and 112 km along linear lines. The geophysical survey involved liaison with the Department of Primary Industries and Regional Development to coordinate with active lobster research. The study area is a marine habitat to the Western Rock Lobster with lobster pots present during the geophysical surveys.

5.2 *Phase 3 (2023)*

Phase 3 comprised a geotechnical investigation to address data gaps with the investigation focusing on acquiring geotechnical data along the proposed outfall tunnel alignment, 2.0 km to 3.5 km offshore, and at the outfall riser locations. Three boreholes were drilled, two near the proposed outfall riser location (3.5 km offshore) and one about 2.5 km offshore. Borehole depths ranged from 5.9 m to 26.4 m. Laboratory tests were carried out on the samples recovered and included classification tests, rock tests and ASS testing.

An assessment of alternative methodologies was carried out to identify drilling methods that were less susceptible to unfavourable weather and sea state. Methods assessed were a heave-compensated drillship, subsea drilling rig operated remotely from a support vessel (PROD) and subsea drilling rig operated by divers with support from the surface. Considering commercial, technical and logistical factors the subsea diver-operated drilling option was chosen. Initially a

floating barge (TAMS9) was used to support operations, however the local metocean conditions and sea-state characteristics were found to be very challenging for operating the barge. The floating barge was demobilised, and a DP1-class supply vessel (Offshore Supplier) was used to support operations and with significantly improved operability in the metocean conditions.

Boreholes were drilled by TAMS utilising a subsea mud-flush drilling rig operated by commercial divers. Diving and drilling operations were supported from the barge TAMS9 and Offshore Supplier.

Drilling conditions were found to be very challenging most notably in the thick TQ-Sand deposits where borehole collapse, bogging/binding of the drill string and sand 'rushing-up the drilling rods' resulted in mechanical issues and slow progress. The geotechnical investigation was terminated early due to the slow progress (approx. 4m per day) and vessel availability.

5.3 *Phase 4 (2023)*

Phase 4 included both geotechnical investigation and geophysical surveys. The geotechnical investigation was carried out using a Portable Remote Operated Drill (PROD) for borehole drilling and Cone Penetration Testing (CPT) at three locations 2.6 km to 3.4 km offshore. Five boreholes were attempted, reaching depths of 11.9 to 46.03 m. The Normand Ranger, a 91 m long vessel with a draft exceeding 7.9 m, supported operations in wave heights up to 2.5 m and wind strengths of 25 knots.

The PROD involved remote operation from the vessel, with telemetry, power, and drilling fluids supplied via umbilical lines. Drilling techniques included wash boring, piston sampling, rotary coring, and CPT, adapted to ground conditions.

Geophysical surveys utilised Multi-Phase Echo Sounder (MPES) bathymetry, sidescan sonar, boomer SBP, Continuous Marine Seismic Refraction (CMSR), and Multi-channel Seismic Refraction (MCSR) profiles. Comparison with Phase 1 data showed relatively stable seabed conditions, with most areas showing less than 0.5 m variance. Rocky areas remained stable, while sandy areas exhibited some deposition or scour.

Boomer SBP and MCSR were moderately effective in correlating with certain geological formations, though distinguishing between Tamala Limestone and Ascot Formation proved challenging due to similar seismic characteristics and variability in material strength with depth, thus not providing sufficient resolution and reliability. CMSR provided potential correlations with in situ strength through p-wave velocity measurements, but once again the resolution was not always reliable.

6 DETAILED GEOTECHNICAL INVESTIGATIONS

6.1 *Phase 5 Investigations (2024)*

ASWA conducted a gap analysis to identify what further geotechnical investigations were required to inform detailed design. Detailed investigations were carried out to address data gaps, improve understanding of ground conditions, refine geological and geotechnical models, enable additional sampling and testing, support derivation of site-specific characteristic design parameters, and reduce geotechnical risk. The planning of the investigations considered the time of year where sea conditions were favourable, completed boreholes out of sequence targeting the critical intake and outtake structures and the commissioning of a JUB with variable leg length which suited a range of water depths.

6.1.1 *Method of Investigations*

6.1.1.1 Nearshore Boreholes

The geotechnical investigation was carried out from April 3 to May 16, employing an Edson 3000 rig mounted on a four-legged JUB. Nine boreholes were drilled to depths ranging from 26 m to 30 m below the seabed using PQ3 coring equipment. Adverse weather conditions led to the cancellation of two planned boreholes.

JUB positioning involved tow vessels to push the barge into position followed by lowering the JUB legs. The barge and drill rig's position were verified using onboard Differential Global Positioning System to ensure placement within 10 meters of the proposed coordinates. The barge was then jacked up to an operational height determined by the Barge Master, allowing sufficient air gap below the pontoons to accommodate anticipated tidal cycles and wave heights.

The drilling process began with lowering the casing just above the seabed and taking a deck-to-seabed measurement. Once the casing reached the seabed, PQ coring commenced using mud flush recovery. The boreholes were cased over the full depth of drilling.

Laboratory testing included classification tests, chemical tests, and rock testing (point load strength index, Uniaxial Compressive Strength (UCS), Cerchar abrasion, Brazilian indirect tensile strength).



Figure 3. JUB.

6.1.1.2 Geophysical Survey

The geophysical survey included MBES for bathymetry, SBP using a pinger, CMSR, and MCSR surveys. Additionally, a focused MBES and SSS survey was performed within a 200 m radius of the proposed riser locations.

7 INVESTIGATION OUTCOMES

7.1 *Boreholes*

The outcomes for the boreholes drilled as part of the 5 phases of investigations are described in the subsections below.

7.1.1 *Operational Challenges*

The ASDP intake and outfall tunnel drilling investigation faced significant challenges due to sea state, water depth variations, and presence of reef structures. The detailed investigation succeeded despite these obstacles, attributed to favourable sea state conditions, appropriate plant and equipment selection, effective team communication, and strategic flexible borehole planning. When the weather and sea state was poor, boreholes closest to shore were drilled within shallow water depths. When the weather and sea state were favourable, boreholes farthest from the shore were drilled in deeper water.

7.1.2 *Poor Sample Recovery*

Poor sample recovery was observed in several boreholes, particularly in the Ascot Formation, due to incompatibility between the rotary core drilling method and material properties. In both historical and detailed investigations, much of the Ascot Formation was recovered as carbonate/calcareous rock gravel, with possible matrix washout during drilling. This resulted in uncertain cementation levels and unreliable Rock Quality Designation (RQD) values, especially in poorly recovered zones. For the detailed investigations, where possible, materials in the Ascot Formation were assigned Duricrust Mass Grades as per AS1726:2017.

A high-level assessment of sample recovery across the five investigations is presented in Table 1, showing meters drilled and associated core loss. The use of a Jack-Up Barge (JUB) with a conventional drilling rig provided the lowest percentage of core loss (17% to 23%), while the Diver Operated Rig and Portable Remote Operated Drill (PROD) resulted in higher percentages of core loss (25% to 40%). The Phase 1 and 5 drilling investigation included casing each borehole over its full depth, which improved mud drilling returns and is the likely reason for less core loss.

Table 1. Marine Investigations Core Loss Assessment.

Year	Phase	Methodology	Total Drilled (m)	Core loss (m)	Core Loss (%)
2021	1	JUB & Conventional Drilling Rig	188	44	23
2023	3	Diver Operated Rig	55	14	25
2023	4	PROD	179	71	40
2024	5	JUB & Conventional Drilling Rig	255	43	17

7.1.3 *Quality of Data Recovered*

The investigation provided sufficient data for the development of the Engineering Geological Model. The team balanced the cost of additional drilling against obtaining further insights into the subsurface conditions, considering the high variability within each geological unit. While the broad distribution of relevant geologies was established, finer sub-unit distribution remained variable.

ASWA determined that the developed Engineering Geological Model was suitable for detailed design, despite the investigation's scope being more limited compared to investigations typically conducted for tunneling projects of this nature. For example, boreholes for tunnel infrastructure are typically spaced between 50 m and 150m. Eurocode 7 (BS EN 1997-2) provides guidance on the spacing of exploratory holes for long linear infrastructure (roads, railways, pipelines, or tunnels) advising on spacings ranging from 20 m – 200 m. For this project, the borehole spacing ranged from 50 m to 600m with 50m spacing at the critical SIR and BLOD structures and the 600m spacing along the tunnel alignment between the shore and 1km offshore in the reef area.

7.2 *Cone Penetration Testing*

CPTs were conducted from the PROD. Due to the variable strength of the subsurface material with depth, CPTs often refused after short depths of penetration. Following refusal, the CPT was removed, the hard layer drilled out and the CPT attempted again. The CPT data, whilst sparse, was useful for interpreting material parameters in units comprising loose to dense granular units or uncemented layers within rock strength units.

7.3 *Geophysical Survey*

7.3.1 *Multibeam echo sounder (MBES) for bathymetry*

The 2019 bathymetric data was unsuitable for the assessment of seabed features and seabed types because the data had been provided at a low-resolution cell size of 1 m and the overall poor quality of the dataset. The 2022 bathymetry contains strong motion artifacts in the order of 7cm total amplitude (+/- 3.5 cm) along the nadir (directly below the MBES transducer), and 30 cm (+/- 15 cm) along the outer beams, however, this data was fit for the purpose of levelling the associated geophysical interpretation to AHD. The 2022 bathymetry data was supplied at 50 cm cell size and

provided a useful comparison with the Surrich 2024 data, showing close agreement with the ripple seabed structures observed indicating this ripple structure is invariant over time.

7.3.2 *Side Scan Sonar (SSS)*

The SSS mosaics over the intake and outfall risers provided in the order of 200% to 300% coverage within the 200m radius boundaries. The data had some distortion due to wave motion; however good coverage was achieved (>200%) meaning there were > 2 swaths available for inspection which provided ability to interpretate Seabed Features.

7.3.3 *Sub-bottom profiling (SBP) using a pinger*

Pinger SBP is a seismic reflection technique similar to Multichannel Seismic Reflection (MCSR). The key distinction lies in the pinger-type source, which offers higher resolution, but lower penetration compared to Boomer or Sparker sources used in MCSR. Pinger SBP lines were conducted typically at 12.5 m spacing with a higher density of 5 m coverage over the riser sites. This tighter line spacing aimed to detect potential hazards for jack-up barge operations during riser construction.

The Pinger SBP chosen was an Innomar Medium instrument and is a single transducer with heave correction and provides tolerance to turns and swell conditions. However, acquisition was particularly difficult in the area southwest of the reef on the intake alignment, where 2.2 m swells and breaking waves were encountered. Depth of penetration was primarily limited by the presence of cemented material or coarse sediments, such as gravels or thick beach sands exceeding 5 m in thickness. These geological factors, combined with the challenging sea conditions, influenced the overall effectiveness and depth of the Pinger SBP survey, and therefore limited the usefulness of the data obtained.

7.3.4 *Continuous Marine Seismic Refraction (CMSR)*

CMSR is a technique which measures the velocity “Vp” of a wavefront along a streamer towed behind an airgun. CMSR data could not be acquired across the shallow reef, and the sections were broken at this location. The CMSR method requires at least 100 m of travel at the start of the line, with the streamer at operational altitude above the seabed, and the vessel on-line, to establish good streamer geometry before the data is fit for use. To minimise lost data between the beach and the shallow reef, each line was run in both directions and the data merged before calculation of the Vp section.

7.3.5 *Multi-channel Seismic Reflection (MCSR)*

Multichannel Seismic Reflection (MCSR) is a seismic reflection technique similar to Pinger SBP. The pinger-type source offers higher resolution, but lower penetration compared to Boomer or Sparker sources. The multi-channel processing approach was chosen over traditional single-channel SBP for its ability to suppress artifacts, thereby improving interpretation quality. The processed datasets comprised five parallel lines at 12.5 m spacing along the alignments, with an additional five perpendicular lines over the riser sites.

Initial work utilised a boomer source at low speed to leverage its high-quality wavelet using the latest seismograph and streamer technology. Data was acquired along center lines using both shallow and deeper streamer tow depths. Analysis revealed good subsurface imaging in deeper seabed areas below -10m AHD; however, minimal penetration was achieved in shallow water, particularly where Tamala Limestone was exposed at the seabed. Subsequently, a sparker source was trialed, achieving deeper imaging in challenging conditions, including shallow water and extensive rock seabed.

Data acquisition was conducted at low vessel speed, with the vessel traveling into the seas to maintain optimal streamer geometry. However, during sea state trials, low vessel speed resulted in compromised streamer geometry due to periodic surging and stalling on overtaking swells.

7.4 *Geotechnical Risks*

Geotechnical investigations identified geotechnical risks including rod drops indicating potential small karsts, loss of drilling fluids indicating potential karsts or high permeability materials and mixed face conditions in the Tamala Limestone and Ascot Formation. The mixed face conditions

pose risks to TBM operations in terms of controlling face pressures and stability of formations. No significant rod drops were recorded during the investigation with one record noting an 80 mm rod drop (the maximum recorded) during the investigation confirming potential small cavities.

The loss of drilling fluids was a regular occurrence during drilling in the Tamala Limestone and Ascot Formation which confirms the potential for encountering high permeability materials during the TBM operations. Drilling fluid losses appeared to be contained within the respective geological formations.

8 CONCLUSION

The ASDP project has undergone extensive nearshore geotechnical investigations through five phases from 2021 to 2024. These investigations have been crucial in developing a sound understanding of the complex geological conditions along the intake and outfall tunnel alignments.

The investigations employed a variety of methods, including borehole drilling from a JUB, diver-operated seabed rigs, PROD, cone penetration tests (CPTs), and multiple geophysical survey techniques. Each method contributed relevant data, despite challenges such as poor sample recovery in some formations and operational difficulties due to sea state, bathymetry, and water depths. Fully cased boreholes drilled from a jack-up barge using coring techniques and mud flush return resulted in the least amount of core loss and most reliable data for defining subsurface conditions and interfaces between units. The geophysical data, namely the seismic reflection and seismic refraction data, typically had poor resolution due to variable strength materials with depth and was therefore the least reliable in defining subsurface conditions and interfaces between units.

The phased approach to investigations allowed for iterative refinement of the geotechnical model, addressing data gaps and reducing uncertainties. While budget constraints limited the scope of investigations compared to typical tunneling projects, the data collected was deemed sufficient for developing an Engineering Geological Model suitable for detailed design.

Key challenges encountered included poor sample recovery in the Ascot Formation, variable strength of subsurface materials affecting CPT performance, and operational difficulties due to environmental conditions. Despite these challenges, the investigations provided valuable information on subsurface stratigraphy, material properties, and potential geotechnical risks.

The combination of borehole data, CPT results, and some geophysical data has provided a sound understanding of the nearshore geology, including the identification of key geological units and interfaces between the Tamala Limestone and Ascot Formation. This information has been essential for the design and construction of the intake and outfall tunnels and associated marine structures.

ACKNOWLEDGEMENTS

The authors want to thank Water Corporation for allowing this paper to be published and also want to thank the wider design and construction team for their support in delivery of this project.

9 REFERENCES

Australian Standard, AS1726:2017 Geotechnical site investigation.

Australian Standard, AS1289.6.3.1-2004 Methods of testing soils for engineering purposes, Method 6.3.1: Soil strength and consolidation tests – Determination of the penetration resistance of a soil – Standard penetration test (SPT).

19th Australasian Tunnelling Conference – Acosta-Martínez, Stewart and Hudson-Smith (Eds.)
© 2025 Australian Tunnelling Society, ISBN 978-0-85825-002-4

Engineering geotechnical model and geotechnical interpretation, intake and outfall tunnels, Alkimos seawater desalination plant, Western Australia

T. Gourlay, T. Whitnall, J. O'Donovan & C. Nash
Jacobs, Australia

ABSTRACT: The Alkimos SeaWater Alliance (ASWA) is designing and constructing Stage 1 of the Alkimos Seawater Desalination Plant (ASDP). This paper outlines the development of an engineering geotechnical model (EGM) for a 2.6 km intake tunnel and 4.1 km outfall tunnel. The EGM considers the variable subsurface conditions along the tunnel alignment, with particular focus on the Tamala Limestone, Ascot, and Rockingham Formations through which the tunnel will be constructed. This paper also describes the interpretation of the characteristic geotechnical and hydrogeological parameters used for design, taking into consideration identified geotechnical risks, limited groundbreaking and non-invasive investigations, in situ testing, pumping and injection well tests, laboratory analysis, published correlations, and comparisons with parameters assessed for the onshore works and local projects that encountered similar ground and groundwater conditions.

1 INTRODUCTION

The Alkimos Seawater Desalination Plant (ASDP), located 40 km north of Perth, will deliver 50 GL of drinking water annually in Stage 1, with Stage 2 adding another 50 GL. The nearshore components include the Seawater Intake Tunnel (SIT), Brine Outfall Tunnel (BOT), two Seawater Intake Riser (SIR) structures, and a Brine Linear Outfall Diffuser (BLOD) structure (subject to state environmental approval). This paper focuses on the tunnels. A site layout plan is shown in Figure 1.



Figure 1 Plan layout of Outfall and Intake Tunnel

2 INTAKE AND OUTFALL TUNNELS

The SIT and BOT are 2.6 km and 4.1 km respectively and will be excavated using slurry Tunnel Boring Machines (TBMs) with a 4.185 m excavation diameter. Excavations will start from onshore at the temporary TBM access shaft, progressing seaward. The tunnels will be lined with steel fibre reinforced concrete segments (3.505 m ID, 3.905 m OD). TBM shields will be sacrificed at drive completion. The tunnels are relatively shallow with tunnel crown depths varying from a minimum of approximately 12.3 m (intake tunnel) to a maximum of approximately 46.1m below surface or seabed level (outfall tunnel). For the onshore section of the tunnel, it will be constructed between approximately 4.7 m and 20.6 m below the water table. For the offshore section of the tunnel, it will be constructed below the seabed where water depths below sea level range from 20.6 m to 32.2 m.

3 GEOLOGY

The Alkimos site's surface geology is characterised by the Holocene Safety Bay Sand onshore, forming dunes up to 40 m AHD and 25 m thick, and Marine Sediments offshore, a variable layer of shelly sand and gravel up to 9.7 m thick. Both units are relatively recent formations, with the Safety Bay Sand continuing to develop today and the Marine Sediments subject to ongoing wave and current action.

Underlying these surface layers is the late Pleistocene Tamala Limestone, a widespread formation that creates the Spearwood Dune System and offshore reefs. This variably cemented carbonate rock mass, interlayered with uncemented sand bodies, is found beneath the Safety Bay Sand onshore and the Marine Sediments offshore, sometimes exposed as reefs. The Tertiary Ascot Formation underlies the Tamala Limestone. It consists of carbonate calcareous materials with variable properties, likely representing shallow marine to lagoonal environments. Below this, along the outer part of the Outfall Tunnel alignment lies the informal late Tertiary 'TQ-Sand' unit (possibly the Rockingham Formation), situated between the Ascot Formation and the underlying Cretaceous Osborne Formation.

4 HYDROGEOLOGY

Historically, groundwater levels onshore in the area typically ranged between RL 0.7 m AHD and RL 1.0 m AHD. Tidal ranges of approximately 0.1 m to 0.8 m have been observed in near-coastal

groundwater. Away from the coast, seasonal groundwater fluctuations along the tunnel alignment typically range from RL 0.6 m AHD (seasonal low) to RL 0.9-1.0 m AHD (seasonal high). For the design of the onshore tunnel sections, recommend groundwater levels, considering a 1 in 100 Year ARI event and accounting for potential climate influences based on published state government data range from a minimum of 0.5 m AHD to 0.25m AHD to a maximum of 1.65m AHD to 2.3 m AHD.

5 SEA LEVEL

The offshore mean sea level (MSL) at Alkimos is 0 m AHD, with a Lowest Astronomical Tide (LAT) of -0.51 m AHD and Highest Astronomical Tide (HAT) of 0.63 m AHD. Sea levels are used in tunnel design for assessing groundwater pressures on the tunnel lining.

6 GEOTECHNICAL INVESTIGATIONS

6.1 *Geotechnical Risks*

Key risks for TBM tunnels given the existing ground and groundwater conditions at the ASDP included variable earth pressure coefficients, karsts, highly permeable zones, mixed face tunnelling conditions and ground settlements within the onshore section of the tunnel.

6.2 *Fieldworks*

6.2.1 *Historical Investigations*

ASWA conducted a gap analysis to assess what additional onshore and nearshore geotechnical investigations were needed to supplement historical data for detailed design. Existing data included 24 boreholes, 11 Cone Penetration Tests (CPTs). The historical boreholes were drilled to depths of 5.9 m to 46.3 using a variety of methods conventional drilling using Jack-Up Barge (JUB), diver operated drilling rig and Portable Remote Operated Drill (PROD) for drilling and CPTs. The geophysical surveys consisted of 8 km^2 Multibeam Echo Sounder (MBES), 8 km^2 Sidescan Sonar (SSS), 105 km of seismic reflection, 54 km of seismic refraction, 30 km of electrical resistivity, and 112 km of magnetometer, and geotechnical soil, rock, geochemical and chemical laboratory testing.

6.2.2 *Detailed Investigations*

Detailed investigations aimed to address geotechnical risks and data gaps to improve understanding of ground and groundwater conditions. These investigations comprised 6 onshore boreholes, 9 nearshore boreholes, 12 groundwater monitoring wells, 5 pumping wells, 6 injection tests, groundwater tests, and overwater geophysical surveys (approximately 0.75 km^2 MBES, 30.8 km continuous marine seismic refraction (CMSR), 32.5 km multi-channel seismic reflection (MCSR), and 37.6 km Pinger SBP).

The onshore boreholes were drilled using a Hydropower Scout V track-mounted drilling rig. Boreholes terminated at depths ranging from 43.73 m to 55.50 m below ground level. The borehole drilling utilised PQ triple barrel coring equipment (PQ3). Boreholes were logged in accordance with AS1726:2017 with SPTs carried out in accordance with AS1289.6.3.1-2004. The nearshore geotechnical investigation used an Edson 3000 rig mounted on a four-legged JUB. Boreholes were drilled (fully cased) to depths ranging from 26 m to 30 m below the seabed using PQ3 coring equipment. The groundwater boreholes were drilled using a Hydropower Scout V track mounted drill rig. Boreholes were terminated at depths ranging from 30.0 m to 40.5 m below ground level. The boreholes were drilled using mud rotary equipment to advance them.

6.3 *Laboratory Testing*

Comprehensive laboratory testing was conducted as part of the historical and detailed investigations. Testing included soil classification tests, density tests, permeability tests, chemical tests

(ASS Testing), rock tests (point load strength index, Uniaxial Compressive Strength (UCS), Cerchar abrasion, Brazilian indirect tensile strength) and advanced analyses (palynology, X-Ray Diffractometer, Scanning Electron Microscope). These tests aimed to refine geological and geotechnical models and derive site-specific characteristic design parameters.

7 ENGINEERING GEOLOGICAL MODEL

7.1 *Development of Model*

The EGM incorporated data from various sources throughout the project's lifecycle, including reinterpretation of information from historical investigations. It was structured by dividing observed materials into Units sharing similar characteristics and distinguishable from adjacent Units. While Units generally aligned with geological stratigraphy, some were merged or split based on engineering behaviour similarities or differences and their relevance to the project. The resulting model (see Table 1), based on intrusive investigations, in situ and laboratory testing, approximates actual site conditions. Use of the geophysical data obtained from CMSR, and MCSR to inform the EGM was limited due to issues with the resolution and reliability of the results, however it was correlated with the borehole data where possible. In particular, where strong limestone outcropped at the seabed (reef structures) or was found at shallow depth, the resolution of the seismic refraction and reflection with depth was impeded. The lesson learnt is that the benefit of conducting geophysics in such nearshore environments should be carefully considered in terms of the usefulness and limitations of the data that can be retrieved at depth.

Table 1. Developed Engineering Geological Model for the nearshore tunnel alignments

Project Unit	Project Unit Name	Approximate Geological Age	Project Sub-Unit	Description
2	Marine Sediments	Recent to Quaternary	2c	Coarse grained (i.e., materials of a non-cohesive nature) soils
5	Tamala Limestone	Quaternary	5a	Fresh to Moderately Leached limestone / carbonate sandstone in the Unit
			5b	Moderately to Highly Leached limestone / carbonate sandstone in the Unit
			5c	Extremely Leached Limestone to Residual Soils. Possibly a range of relic paleosols, solution feature infill, or carbonate depleted layers within the Tamala Limestone
6	Ascot Formation	Tertiary	6a	Variably cemented silty sands with variable quantities of authogenic nodules (recovered as gravels during investigation). Local layers cemented to rock generally varying from very low to medium strength. Typically varying from type D1 duricrust to type D3 duricrust according to AS1726:2017. Sub-Unit 6a consists of mostly rock strength and cemented materials
			6b	Sub-Unit 6b consisting mostly of soil strength materials but with some cemented layers
			6c	Unconsolidated sand layers within the Ascot Formation
			6d	Silt / Siltstone layers within the Ascot Formation
8	Osborne Formation	Cretaceous	8a	Variably cemented glauconitic sandstones and fine-grained materials. Including very low strength rocks, claystones, and sandstones
			8b	Fine grained (i.e., materials of a cohesive nature) soils
			8c	Coarse grained (i.e., materials of a non-cohesive nature) soils
9*	TQ Sands	Tertiary	9a	Marine sands underlying the Ascot Formation

*It should be noted that Unit 9 (TQ Sands) is numerically out of sequence due to project phasing from onshore to nearshore. Chronologically Unit 9 should sit above Unit 8.

Extracts from the geological sections for both the intake and outfall tunnel alignments are presented in Figure 2 (outfall tunnel) and Figure 3 (intake tunnel) with the vertical tunnel alignment shown in red.

7.2 *Complexity*

The project site's complexity stems from variable properties of Tamala Limestone and Ascot Formation in the tunnel alignment. These carbonate units show diverse characteristics due to carbonate enrichment and leaching processes. This variability was captured in the EGM by dividing these units into sub-units. Tamala Limestone is a cemented sand dune sequence with carbonate variations and karstic features. The Ascot Formation, more advanced at Alkimos than at Perth Airport, represents a transition between carbonate soil and rock. Poor sample recovery during drilling, especially in the Ascot Formation, led to uncertainties in determining cementation and Rock Quality Designation (RQD) values. The EGM aimed to provide a reasonable interpretation of materials likely encountered, considering these complexities.

7.3 *Tamala Limestone*

Tamala Limestone in the project area exhibits wide-ranging engineering properties, from well-cemented, high-strength rock to very weakly cemented, low-strength rock. These variations are associated with post-depositional processes like cementation and dissolution. The EGM divides Tamala Limestone into three Sub-Units, Fresh to Moderately Leached Limestone; Moderately to Highly Leached Limestone; Extremely Leached Limestone, and Void infill. Geotechnical conditions vary significantly throughout the project area, with material types ranging from loose sand to variable strength rock, including high-strength calcrete or 'limestone caprock'. This variability occurs over short lateral and vertical distances due to differences in cementation, solution weathering, and the presence of features like pinnacles and subvertical solution cavities.

7.4 *Ascot Formation*

Underlying the Tamala Limestone and overlying Osborne Formation, Ascot Formation shows highly variable properties from soil to rock. Predominantly carbonate calcareous materials, it varies due to dissolution and re-precipitation processes. Authigenic cementation resulted in a spectrum of uncemented soil to fully cemented carbonate rock. Sample recovery challenges led to uncertainties in material properties across the site.

7.5 *TQ Sand*

'TQ-Sand', not formally recognised in the Perth Basin, is a typically very dense, quartz sand unit between the Ascot and Osborne Formation along the outer Outfall Tunnel alignment. Presumed to be late Tertiary deposits, possibly Rockingham Formation, though previously thought not to extend north of Perth. The Unit is dominated by coarse grained soil materials. Approximately 70.5 % of the sampled material was soil, with 29.5 % of core loss also noted, which implies a higher soil fraction.

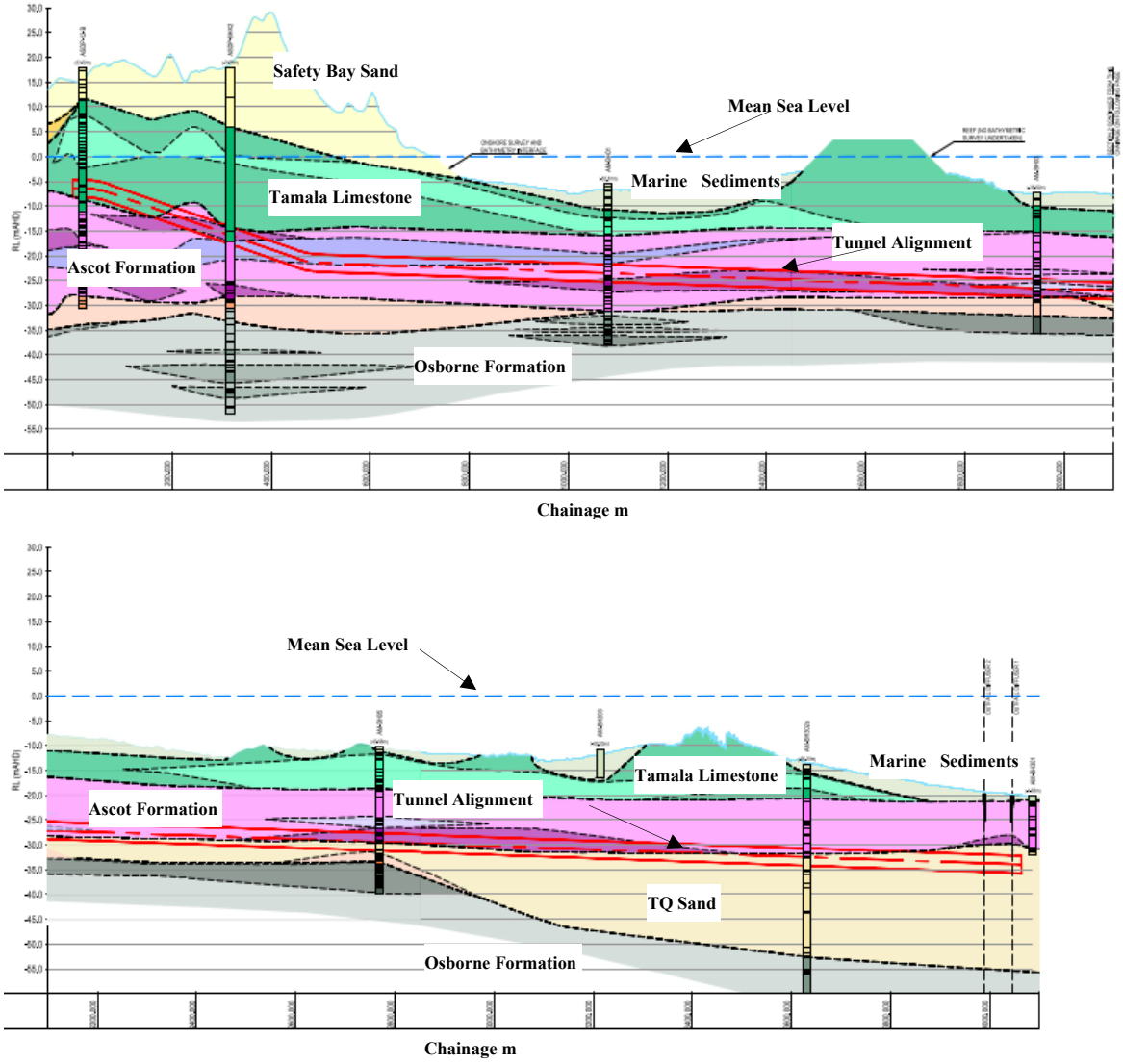


Figure 2. Outfall tunnel geological section

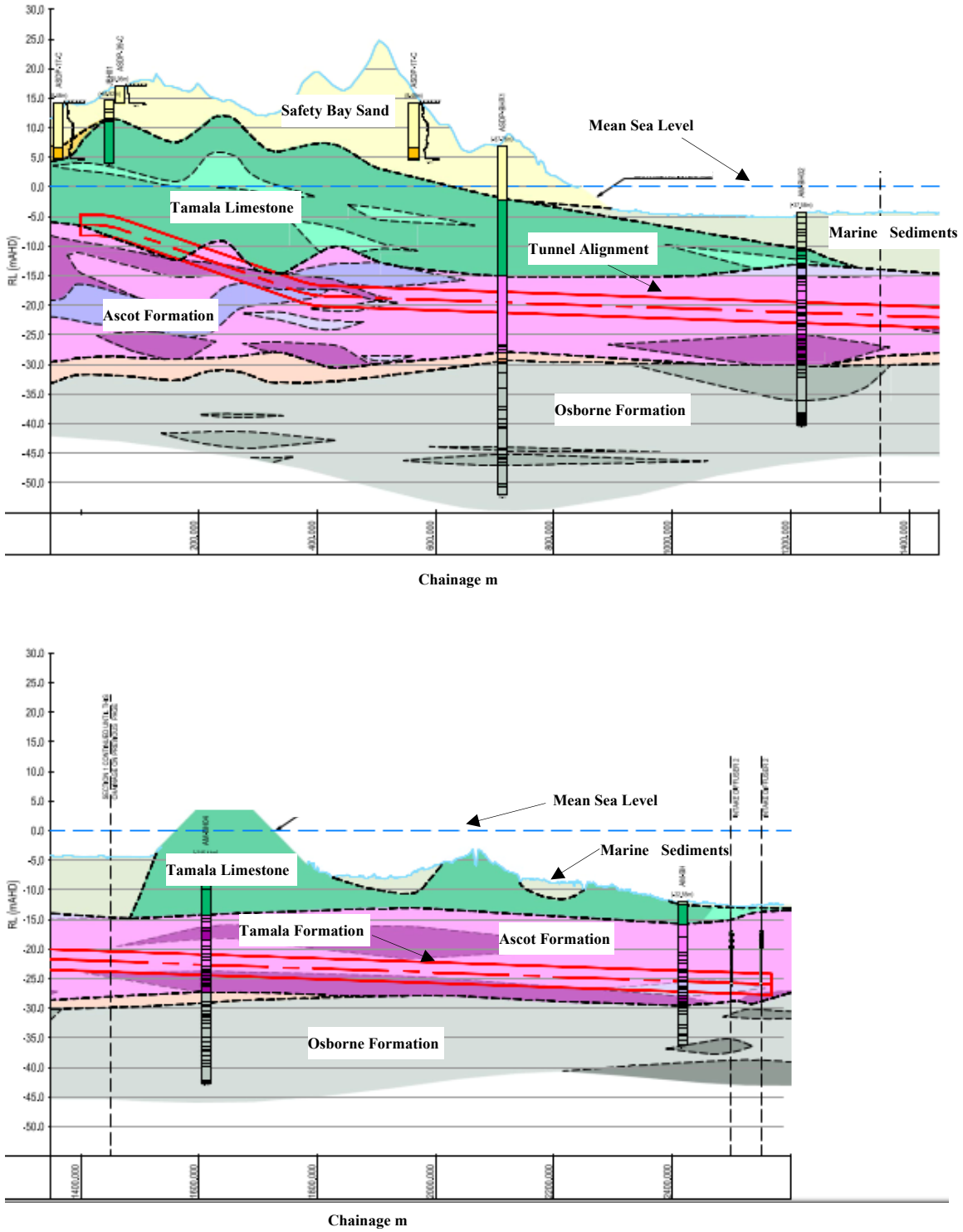


Figure 3: Intake tunnel geological section

8 INTERPRETATION

8.1 *Geotechnical Parameters*

Material properties for nearshore geotechnical units were derived from borehole logs, CPT traces, geophysical survey data, and in situ and laboratory test results. Rock mass parameters considered rock mass structure, discontinuities, and Geological Strength Index (GSI). Nearshore and onshore parameters for the same units were compared.

Effective friction angles for coarse-grained soils were estimated using SPT N values (Schmertmann, 1975) and CPT tip resistance data (Robertson, 2012). For fine-grained soils, correlations with plasticity index were employed (BS8002; Kenney, 1959; Parry, 1960; Zhu and Yin, 2000; Sorensen, 2013). Young's modulus was estimated from SPT N values (Decourt, 1995) CPT data for soils (Robertson, 2012) and published correlations for rock (Tomlinson, 2001; Deere and Miller, 1966; Hoek & Diederichs, 2006). Stress history and earth pressure coefficients were derived using CPT and DMT data (Kulhawy and Mayne, 1990).

8.2 *Hydrogeological Parameters*

Vertical and horizontal permeability were assessed for relevant geotechnical units using Particle Size Distribution test data (Hazen, 1911), falling head permeability tests (Cedergren, 1977) onshore monitoring wells, and onshore pumping and injection well test results. Interpreted parameters were compared to Alkimos Wastewater Treatment Plant data, local and regional published data, and estimates from nearby Perth-based projects.

The aquifer pumping test results were interpreted based on two conceptualisations: unconfined (Neuman, 1974) and leaky confined (Hantush, 1960) aquifers. The high permeability of the aquifers caused a rapid response in nearby observation bores, potentially indicating a partially confined response. While the Tamala Limestone is primarily considered an unconfined water table aquifer, the lower part of the limestone exhibited confined behavior due to the pumping well screen placement and possible layering. The unconfined model was therefore deemed more appropriate based on the absence of significant low permeability layers and better curve matching the test data. The Neuman curve more closely followed the observed data slope compared to the Hantush curve, which deviated in the latter half of the final step of the pumping test.

The injection test results were analysed using Aqtesolv. The unconfined (Neuman) solution with 20% specific yield best represented the test results. For injection tests conducted in wells with screens in the Tamala Limestone, results generally aligned with pumping test results, except for a single well which showed lower hydraulic conductivity (100 m/day vs. 175 m/day). Two injection well tests yielded slightly higher results, while one injection test matched the pumping tests. The injection tests produced a narrower hydraulic conductivity range of 100-150 m/day for Tamala Limestone. However, due to the longer duration of the pump out tests and absence of significantly larger impressed heads induced during injection, the pumping test results were considered to be more reliable for determining hydraulic properties.

8.3 *Characteristic Design Parameters*

A summary of the geotechnical and hydrogeological design parameters recommended for tunnel design is presented in Table 2. Design ranges are presented along with the recommended characteristic values. Where geotechnical units comprised both soil and rock materials and could behave as a combined material, unified material parameters (i.e., composite soil and rock parameters) were developed to simplify analysis for design. Unified parameters were developed by assessing an average Geological Strength Index (GSI) for a combined soil and rock within a unit and then the GSI used to assess lower bound rock mass design properties using published correlations. An example of the rock laboratory test results (point load strength index and UCS tests) carried out along the outfall tunnel alignment are shown in Figure 4 and 5 at the end of this section.

Table 2: Characteristic Design Parameters

Unit	Material	UCS	g'	c'	f'	n'	E'	E_m	OCR	K_0	K_h / K_v
-	-	MPa	kN/m^3	kPa	(°)	-	MPa	MPa	-	-	m/day
2	Soil	-	18 (15-19)	0	35 (34-38)	0.3	30 (20-50)	-	1-2	0.52 (0.41-0.62)	-
5a	Rock	4.0 (3.8-5.0)	20	See note 4	See note 4	0.3	-	800 (400-1200)	-	0.80-1.20	
	Soil	-	18 (16-20)	0	36 (34-38)	0.3	60 (30-90)	-	1-3	0.62 (0.41-0.79)	
5b	Rock	2.0 (1.0-3.5)	19	-	-	0.3	-	-	-	0.80–1.20	100-200 / 50-100
	Unified	-	19	See note 4	See note 4	-	-	250 (100-500)	-	0.40-1.20	
5c	Soil	-	19 (18-20)	0	36 (32-38)	0.3	50 (30-90)	-	1-3	0.62 (0.41-0.79)	
	Soil	-	20 (19-21)	0	38 (34-40)	0.3	60 (30-100)	-	1-4	0.68 (0.38-0.90)	
6a	Rock	2.0 (1.0-2.5)	22	-	-	0.3	-	-	-	0.50–2.00	
	Unified	-	21	See note 4	See note 4	-	-	200(100-400)	-	0.40-2.00	30-40 / 3-4
6b	Soil	-	19 (18-20)	0	36 (34-39)	0.3	50 (30-75)	-	1-4	0.71 (0.41-0.93)	
6c	Soil	-	19 (18-20)	0	36 (34-39)	0.3	50 (30-75)	-	1-4	0.71 (0.41-0.93)	
6d	Soil	-	19 (18-21)	0	30 (28-32)	0.3	35 (25-45)	-	1-4	0.79 (0.50-1.00)	
9a	Soil	-	20 (19-21)	0	39 (38-40)	0.3	90 (80-120)	-	1-6	0.82 (0.37-1.15)	10-60 / 1-6

1. γ' = bulk unit weight, c' = effective cohesion, φ' = effective angle of friction, ν' = Poisson's ratio, E' = effective elastic modulus, OCR = overconsolidation ratio, K_0 = at-rest earth pressure coefficient, K_h = horizontal permeability, K_v = vertical permeability.
2. Alluvium can contain interbedded material of variable consistency and relative density. Design parameters are considered representative of soil mass. Location specific parameters were considered in geotechnical design.
3. Range provided and parameter adopted for design selected based on location specific geotechnical investigation data with reference to soil and rock constituents.
4. Mohr-Coulomb parameters assessed utilising RocScience RSData (v1.005) utilising a Generalised Hoek-Brown failure criterion to define c' and φ' for a given depth, relative to the element under assessment

Published correlations used for assessing characteristic parameters appeared to provide parameters that were similar to or of the same order as parameters recommended for local projects which encountered similar ground conditions.

Comparison of the above characteristic parameters for the nearshore works with those of the onshore works indicate the onshore subsurface materials comprise more competent rock, particularly within the Tamala Limestone and Ascot Formation.

8.4 *Karsts*

Tamala Limestone, formed from windblown dunes and cemented through non-marine processes, exhibits karstic characteristics throughout its formation. Observed features include surface pinnacles, subvertical tube structures, minor voids, and pockets of uncemented material within competent layers.

The limestone showed varied leaching states, indicating carbonate depleted and enriched zones. Drilling observations revealed zones of flush loss, possibly due to planar features like relict bedding or historical water tables. Larger uncemented zones (Unit 5c) may have resulted from carbonate depletion or represent relic uncemented areas.

While the risk of large voids or cavities below the water table was considered low based on drilling investigations (drilling fluid loss, small rod drops) and geophysical survey data, their presence could not be completely discounted.

The Ascot Formation presented a low risk of karst development based on the drilling and geophysical results, with the potential for minor cavities. This formation can be characterised as a soil that has undergone authigenic cementation processes, but in most instances, the cementation has not progressed sufficiently to develop a massive rock texture. Any cavities present could possibly be the result of soil material being washed out from within a skeletal cemented matrix, as well as the dissolution of carbonates typically associated with karst formation.

8.5 *Mixed Face Tunnelling Conditions*

The Tamala Limestone and Ascot Formation will likely present challenging tunnelling conditions due to their highly variable rock strength and structure. Mixed face conditions, including uncemented sand bodies and interbedded layers of soft clay and loose sand, are likely to be encountered based on the EGM developed for the tunnels. These formations can range from very low to medium strength, with occasional high-strength intervals, and often consist of fractured rock masses with high-strength fragments in a sandy or clayey matrix. These mixed face conditions, which may also occur at the interfaces between the Tamala Limestone, Ascot Formation and TQ-Sand, could potentially impact TBM operations.

The varying permeability and strength of materials could lead to preferential excavation difficulties in maintaining face pressures. Careful design and control of TBM operations will be crucial to mitigate these challenges and prevent adverse impacts on performance, productivity, and ground movements. Ground movements are of risk for the onshore portion of the tunnels which will be constructed below existing onshore structures and therefore instrumentation and monitoring will be installed to monitor ground movements. Environmental issues with regards to the use of bentonite slurry in the TBM operations in permeable ground is considered to be a very low risk based on the pumping tests conducted onshore within the Tamala Limestone and Ascot Formation.

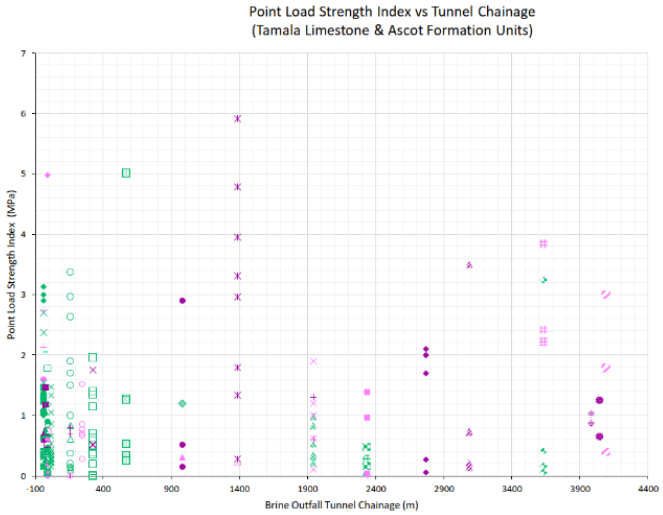


Figure 4 PLT (MPa) vs. BOT Chainage (m)

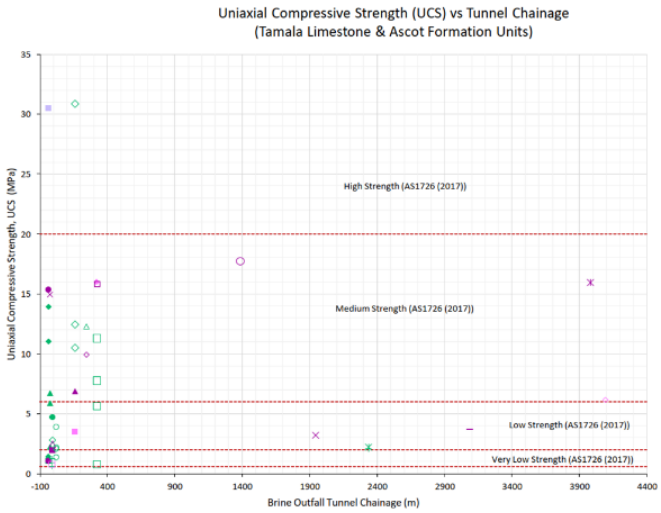


Figure 5 UCS (MPa) vs. BOT Chainage (m)

9 CONCLUSIONS

The project site presents complex geotechnical and hydrogeological conditions, primarily due to the variable properties of the Tamala Limestone and Ascot Formation. While the risk of large voids in the Tamala Limestone is considered low, smaller karstic features are likely present, which could potentially impact tunneling operations.

Pumping and injection well tests below the water table yielded permeability results consistent with published data and local projects, indicating the potential presence of small karstic voids. The Ascot Formation poses challenges in accurate characterisation due to its variable nature and poor sample recovery during drilling investigations. An EGM has been developed to convey the area's complex geological and engineering characteristics. Nearshore geotechnical and hydrogeological design parameters have been recommended for each unit, considering material property variability and uncertainty. These parameters are in good agreement with the onshore parameters and compare well with published data and parameters adopted on other local projects with similar ground and groundwater conditions.

The project will require careful planning, continuous monitoring, and adaptable design approaches to address the challenges posed by these complex geological and hydrogeological conditions.

10 ACKNOWLEDGEMENTS

The authors wish to thank Water Corporation for allowing this paper to be published and wish to thank the wider design and construction team for their support in the delivery of this project.

11 REFERENCES

BSI Standards Publication BS 8002:2015: Code of practice for earth retaining structures.
Cedergren, H.R. 1977. Seepage, drainage, and flow nets. John Wiley & Sons (Second Edition).
Decourt, L. 1995. Prediction of load-settlement relationships for foundations on the basis of the SPT. Proc. of the Conf. in Honor of Leonardo Zeevaert, Mexico City, Oct. 28-Nov. 6, pp. 87-103.
Deere, D. U. and Miller, R. 1966. Engineering classification and index properties for intact rock, Technical Report AFWL-TR-65-116, Department of Civil Engineering, University of Illinois, Urbana Illinois.
Hantush, M.S. 1960. Modification of the theory of leaky aquifers, Jour. of Geophys. Res., vol. 65, no. 11, pp. 3713-3725.
Hazen, A. 1911. Discussion: dams on sand foundations. Trans Am Soc Civ Eng. 1911; 73:199–203.
Hoek, E. and Diederichs, M.S. (2006) Empirical estimation of rock mass modulus. International journal of rock mechanics and mining sciences 43, 203-215.
Kenney, T. C. 1959. Discussion, Journal of Soil Mechanics, and Foundation Division, A.S.C.E., 85(SM3):

67-79.
Kulhawy, F.H. and Mayne, P.W. 1990. Manual on Estimating Soil Properties for Foundation Design. Electric Power Research Institute EL-6800, Project 1493-6, Electric Power Research Institute, Palo Alto, California.
Neuman, S.P. 1974. Effect of partial penetration on flow in unconfined aquifers considering delayed gravity response, Water Resources Research, vol. 10, no. 2, pp. 303-312.
Parry, R. H. G. 1960. Triaxial Compression and Extension Tests on Remoulded Saturated Clay, Geotechnique, Vol 10, p.166.
Robertson. 2012. Interpretation of in-situ tests, Proceedings of ISC 4, Recife, Brazil, September 2012.
Schmertmann, J.H. 1975. Measurement of In-Situ Shear Strength. Proceedings of ASCE Spec. Conference on In-Situ Measurement of Soil Properties, Raleigh, NC, Vol. 2, 57-138.
Sorensen, K. K. 2013. Correlation between drained shear strength and plasticity index of undisturbed overconsolidated clays. Proceedings of the 18th International Conference on Soil Mechanics and Geotechnical Engineering, Paris 2013.
Tomlinson, M. J. 2001. Foundation Design and Construction, Seventh Edition, Prentice Hall.
Zhu G.F. and Yin J.-H. 2000. Elastic visco-plastic finite element consolidation modelling of Berthierville test embankment. International Journal of Numeric and Analytical Methods in Geomechanics, 24: 491–508.

19th Australasian Tunnelling Conference – Acosta-Martínez, Stewart and Hudson-Smith (Eds.)
© 2025 Australian Tunnelling Society, ISBN 978-0-85825-002-4

Seawater intake riser and brine linear outfall diffuser pile design and impacts from tunnel construction

P. Retsos, T. Gourlay, K. Liew
Jacobs Australia

ABSTRACT: Stage 1 of the Alkimos Seawater Desalination Plant (ASDP) is currently being designed and constructed by the Alkimos SeaWater Alliance (ASWA). This paper provides an overview of the geotechnical interpretation for analysis and design of the piled foundations for the Seawater Intake Riser (SIR) and Brine Linear Outfall Diffuser (BLOD) structures, and the potential impact from Tunnel Boring Machine (TBM) excavations from tunnels. Piled foundations comprise driven steel tubes through calcareous soil deposits, which pose known issues and challenges for geotechnical pile design and tunnelling works. The potential impact of the TBM tunnel excavation works on the SIR and BLOD structures was assessed using 2D finite element analyses to assess soil movements and structural effects. Risk mitigation measures such as monitoring the tunnelling excavation volume during construction, grouting works, groundwater control and other measures have been considered to prevent the risk of excessive movements.

1 INTRODUCTION

Stage 1 of the Alkimos Seawater Desalination Plant (ASDP) is currently being designed and constructed by the Alkimos SeaWater Alliance (ASWA). The ASDP is located within the high growth area of Alkimos about 40 km to the north of Perth, is less than about 1 km from the coast and located to the west of the existing Alkimos Wastewater Treatment Plant (AWWTP). When commissioned, Stage 1 of the ASDP will deliver 50 GL per annum of drinking water to the northern suburbs of Perth for commercial and residential use. Stage 2 of the ASDP (planned for future expansion) will provide an additional 50 GL per year.

Nearshore components of the ASDP include the Seawater Intake Tunnel (SIT), Brine Outfall Tunnel (BOT), two Seawater Intake Riser (SIR) structures and a Brine Linear Outfall Diffuser (BLOD) structure.

2 NEARSHORE STRUCTURES

The SIT and BOT have a total length of about 2.6 km and 4.1 km respectively and will be excavated separately using slurry TBMs with a 4.185 m excavation diameter. Excavation will begin on land from a temporary access shaft in the north-western corner of the onshore ASDP site, progressing outward to the ocean. The two TBM shields will be sacrificed at the end of the drives. Both tunnels will have reinforced concrete segmental linings with a design internal diameter (ID) of 3.505 m and a design outer diameter (OD) of 3.905 m.

Two SIR structures will convey seawater into the SIT. The proposed foundation system for each SIR structure comprises of four driven steel circular tube piles with an OD of 1050 mm and

wall thickness (WT) of 40 mm (1050 OD x 40 WT) with a pile spacing of 8.95 m. The piles extend above the seabed level and are structurally connected to the head of the SIR structure. A driven steel circular liner (casing) with an OD of 3074 mm and WT of 37 mm (3074 OD x 37 WT) shall be placed to provide ground support for construction of an 1800 mm internal diameter (ID) Glass Fibre Reinforced Plastic (GRP) riser that connects into the SIT. Figure 1 illustrates the proposed foundation system for a SIR structure.

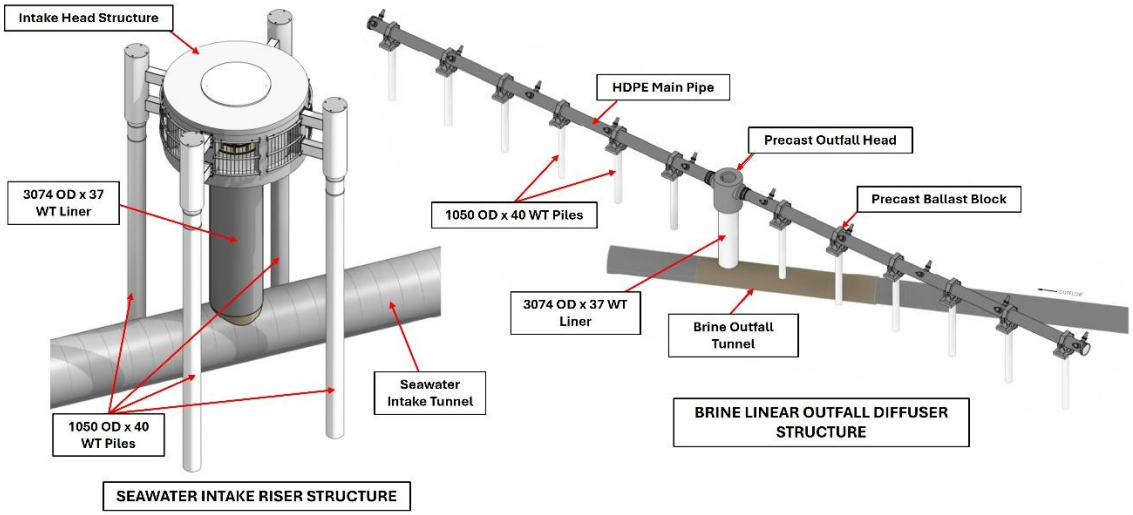


Figure 1. Proposed foundation system for the Seawater Intake Riser (left image) and Brine Linear Outfall Diffuser (right image) structures.

The BLOD diffuser will expel brine coming from the BOT into the ocean. The BLOD comprises of a horizontal High-Density Polyethylene (HDPE) pipe supported by pile foundations and has a total length of about 135 m. Precast reinforced concrete ballast blocks are placed along the BLOD and are supported by twelve driven steel circular tube piles with an OD of 1050 mm and WT of 40 mm (1050 OD x 40 WT). Centre to centre pile spacings are 10.0 m to 10.5 m. A driven steel circular liner (casing) with an OD of 3074 mm and WT of 37 mm (3074 OD x 37 WT) shall be placed to provide ground support for construction of an 1800 mm ID GRP riser that connects into the BOT and to support the precast outfall head which connects the two HDPE pipe sections together. Figure 1 illustrates the proposed foundation system for the BLOD structure.

3 GEOLOGICAL MODEL

A comprehensive assessment of site investigation information led to the development of an Engineering Geological Model (EGM) for the ASDP. The primary engineering geological units encountered at nearshore structures included the Marine Sediments (Unit 2), Tamala Limestone (Unit 5), Ascot Formation (Unit 6), Osborne Formation (Unit 8) and the TQ Sands (Unit 9).

The Marine Sediments are the youngest unit being of recent to Quaternary age deposits. They primarily comprise of coarse grained (i.e. non-cohesive) soils, and ascribed sub-unit 2c. They are present along the ocean seabed at both the SIR and BLOD structures.

The Tamala Limestone is of Quaternary geological age and only encountered at the SIR structures, underlying the Marine Sediments. Three sub-units relating to the degree of leaching and engineering properties of the Tamala Limestone have been ascribed: Unit 5a Fresh to Moderately Leached; Unit 5b Moderately to Highly Leached; Unit 5c Extremely Leached to Residual Soil.

The Ascot Formation is of Tertiary geological age, underlying the Tamala Limestone at the SIR structures and underlying the Marine Sediments at the BLOD structure. Four sub-units have been determined: Unit 6a Mostly rock strength and cemented materials with soil, rock strengths varying from very low to medium, and typically varying from type D1 to type D3 duricrust according to AS1726:2017; Unit 6b Mostly soils but with some cemented layers; Unit 6c Variable sand layers; Unit 6d Silt / Siltstone materials.

The Osborne Formation is of Cretaceous geological age, underlying the Ascot Formation at the SIR structures and underlying the TQ Sands at the BLOD structure. Three sub-units have been determined: Unit 8a Variably cemented fine-grained material and weathered sandstones, claystones; Unit 8b Fine grained (i.e. cohesive) materials; Unit 8c Coarse grained (i.e. non-cohesive) materials.

The TQ Sands are of Tertiary geological age and only encountered at the BLOD structure, underlying the Ascot Formation and above the Osborne Formation. The unit comprises of predominantly coarse grained (i.e. non-cohesive) materials, and ascribed sub-unit 9a.

Calcareous deposits typically consist of carbonate materials from marine life debris. Unlike silica soils, calcareous soils are primarily composed of calcium carbonate, which has a lower hardness compared to quartz. This makes them more susceptible to crushing under relatively low stresses. Calcareous soils typically have high porosity (and void ratio), resulting in low density and high compressibility. They are also prone to post-deposition alterations by biological and physiochemical processes under normal pressure and temperature conditions, forming irregular cemented layers that significantly impact their mechanical behavior.

The Marine Sediments (Unit 2), Tamala Limestone (Unit 5) and Ascot Formation (Unit 6) projects units have been treated as calcareous soil deposits for the purposes of pile foundation design at both the SIR and BLOD structures.

4 GEOTECHNICAL INTERPRETATION

The interpreted geotechnical design ground models for the SIR and BLOD structures are illustrated in Figure 2.

Table 1 presents characteristic geotechnical design parameters for project units at nearshore structures. Whilst these values represent each unit, variability within units is expected. Upper and lower bound parameters were also assessed using available site data and considered in design where necessary, though not reported here.

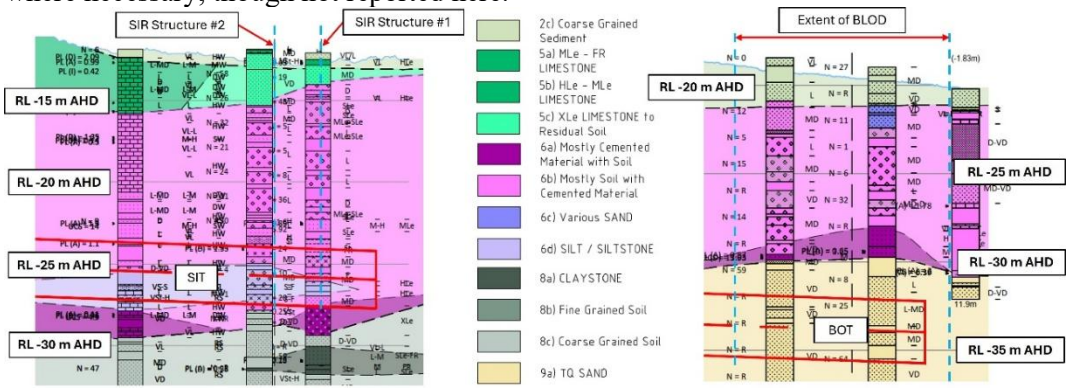


Figure 2. Interpreted ground models for the nearshore structures.

Table 1. Characteristic geotechnical design parameters.

Project Unit	Unit Weight, γ (kN/m^3)	Effective Cohesion, c' (kPa)	Effective Friction Angle, φ' (degrees)	Poisson's Ratio	Drained Elastic Modulus (MPa)	OCR	At-rest Earth Pressure Coefficient, K0
2c	18	0	35	0.3	30	1	0.52
5c	19	0	36	0.3	50	2	0.62
6a	20	0	38	0.3	60	3	0.68
6b	19	0	36	0.3	50	2	0.71
6d	19	0	30	0.3	35	2	0.79
8c	20	0	38	0.3	90	3	0.82
9a	20	0	39	0.3	90	3	0.82

5 PILE DESIGN

5.1 *Design standards and codes*

Pile design was primarily undertaken in accordance with the AS/NZS 1170 series and AS2159:2009 – Piling Design and Installation. Several other international design standards and codes were referred to and used to inform design.

5.2 *Design loading*

The predominant loading type on the structures is wave and current induced. A combination of dead loads and wave induced loads was assessed as the critical load combination with appropriate partial factors applied for Serviceability Limit State (SLS) and Ultimate Limit State (ULS) design combinations. SLS wave loads considered a 1:1 Average Recurrence Interval (ARI) event whilst ULS was loads considered a 1:2000 ARI event. Pile and liner design loads were provided at the design seabed and scour levels for geotechnical assessment. The design scour depths (below design seabed levels) at the SIR and BLOD structures was 4.0m and 4.5 m respectively.

5.3 *Ultimate limit state design*

A geotechnical strength reduction factor (φ_g) of 0.75 has been adopted for axial compression loading in accordance with Clause 4.3 of AS 2159:2009. High-strain dynamic pile load testing has been nominated at pile locations at both the SIR and BLOD structures.

The ultimate skin friction (f_s) for piles in non-cohesive (i.e. sand and gravel) materials has been calculated in terms of effective stress using $f_s = K \tan \delta \, \sigma'_v$, where K = coefficient of lateral pressure; δ = pile-soil interface friction angle; σ'_v = effective vertical stress. A K/K0 value of 1.0 and a δ/φ' value of 0.6 have been used for geotechnical design.

The ultimate end bearing (f_b) pressure under compression for non-cohesive materials has been calculated using $f_b = \sigma'_t \, Nq$, where σ'_t = effective vertical stress at the pile tip (toe); Nq = bearing capacity factor. The bearing capacity factor (Nq) has been assessed based on the effective friction angle (φ') with reference to the works by Berezantzev et al. (1961). The effective friction angles at the pile tip were adjusted according to Poulos and Davis (1980) to account for pile installation.

Geotechnical pile design has incorporated findings from previous offshore investigations and studies, accounting for the calcareous nature of certain project units. This approach included selecting appropriate limiting skin friction values, end bearing pressures, a low pile-soil interface friction angle (δ) for driven piles in sand, and a suitable K/K0 value.

Lateral pressure-displacement (p-y) curves were developed to account for the nonlinear behaviour of soil. Three different methods of calculating p-y curves have been considered to investigate the behaviour of piled foundations under lateral loading. These methods are documented in Poulos and Ameratunga (2022), the American Petroleum Institute (API) RP 2A (2010), and Dyson and Randolph (2001).

A geotechnical strength reduction factor of 0.4 was considered when assessing pile lateral stability under ULS loading with and without consideration of scour. The lateral deflection and structural responses in piles (i.e. induced bending moment and shear force) due to ULS design loads have been assessed using LPILE.

5.4 *Serviceability limit state design*

Pile vertical settlements under SLS design loads were assessed using PLAXIS3D. Laterally loaded piles under SLS design loads have been assessed using LPILE. The assessed SLS vertical settlements and lateral displacements were provided to the ASWA Marine Structural Design Team for consideration of serviceability performance requirements.

The PLAXIS3D models, using the Mohr-Coulomb soil material model, were also used to compare the pile behaviour (i.e. the calculated shape of shear force and bending moment diagrams along the pile) and results under SLS loads with those from the three p-y curve methods used in LPILE. Pile design loads were applied at the design seabed and / or scour level.

5.5 *Other considerations*

Other notable considerations included:

- Cyclic Effects: the predominant loading on the SIR and BLOD structures is due to wave loading which can be considered as cyclic loading. It was shown that cyclic loading would have an insignificant impact on pile axial design requirements. The lateral pressure-displacement relationship from API RP 2A (2010) can cater for cyclic loading, by further reducing the soil lateral resistance for cyclic load effects. This has been considered in pile designs.
- Liquefaction: Borehole and laboratory test data was used to inform liquefaction assessments at nearshore structure locations. The outcome of the liquefaction assessment indicated that the risk of soils liquefying below the ground water table at the SIR and BLOD structures is low and therefore unlikely.
- Earthquake Loading: AS2159:2009 states that the effects of earthquake loading on both the design axial and lateral ultimate geotechnical capacities (strengths) are to be considered. The assessment of both the inertial and kinematic effects was undertaken but noted that earthquake loading was not a governing load case, and that wave loading on the structures provides the most adverse loading conditions for design.
- Pile Driveability: Thorough pile drivability assessments have been undertaken considering the proposed hammer and driving setup, drop heights, and plugged versus unplugged base soil conditions. There is also the potential for driven piles and liners to refuse on dense to very dense sand layers (within the Ascot Formation, Osborne Formations and TQ-Sand) and / or weathered bedrock (e.g. Tamala Limestone) and / or cemented zones (e.g. within Unit 6a from the Ascot Formation). A 'drill and drive' method may be required to overcome this to reach design pile toe founding levels.

6 IMPACT FROM TUNNELS

PLAXIS2D finite element analyses assessed the potential impact of TBM tunnel excavation on SIR and BLOD pile foundations. The assessment aimed to determine additional pile movements, shear forces, and bending moments resulting from tunneling.

The PLAXIS2D models incorporated construction tolerances for TBM alignment, excavation, grout support, and pile positioning. A single steel tube pile was modeled as an embedded beam element, with half of the 4.185 m circular excavation diameter modeled for both tunnels. SLS design loads were considered without scour, assuming unlikely ULS loading during the brief tunneling period.

The TBM and segmental lining were modeled as plate elements, with a 2% volume loss applied as a line contraction. Annulus grouting was simulated using radial pressures of 280 kPa (SIT) and 490 kPa (BOT) as advised by the ASWA Tunnel Design Team. The Hardening Soil material model was used for all project units. A typical 2D finite element model is shown in Figure 3.

An additional assessment of ground movement was assessed without pile loads to develop a lateral soil movement profile due to TBM tunneling for use in LPILE with SLS and ULS loads.

Figure 3 shows horizontal pile movements from TBM tunnel excavation at SIR structure #2, with similar results at SIR structure #1 and slightly lower displacements at the BLOD. The lateral soil (free field) movement on the piles resulting from TBM tunnel excavation and without SLS design loads was similar. The additional vertical settlement of the piles due to TBM tunnel excavation was also assessed.

The lateral soil movement profiles were applied in LPILE with SLS and ULS design loads in both the same and opposite directions. The results from the API RP 2A (2010) method with consideration of cyclic load effects were used to compare findings of the effects on piles with and without TBM tunnel excavation. For the SIR structures there was a notable increase in the calculated shear force and bending moment values in the piles adjacent to the SIT whilst for the BLOD there was an insignificant increase. Maximum calculated shear force and bending moment values at all structure locations were less than the design ultimate structural capacities on the piles.

TBM tunnel excavation induces additional down drag axial force on piles due to negative skin friction from downward soil movement, as illustrated in Figure 4. These forces were assessed for each structure and provided to the ASWA Marine Structural Design Team. Per AS2159:2009

Clause 3.3.2 (b), this down drag force must be multiplied by 1.2 and added to design axial actions for structural design.

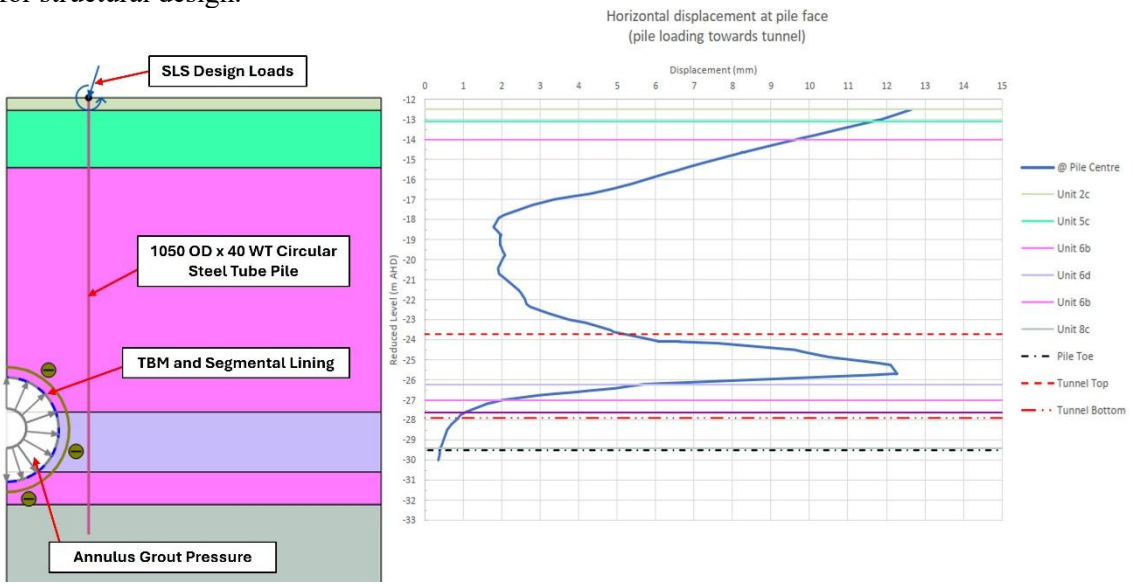


Figure 3. Example of 2D finite element model in PLAXIS2D (left image). Example of calculated horizontal movement on pile due to tunnel excavation (right image)

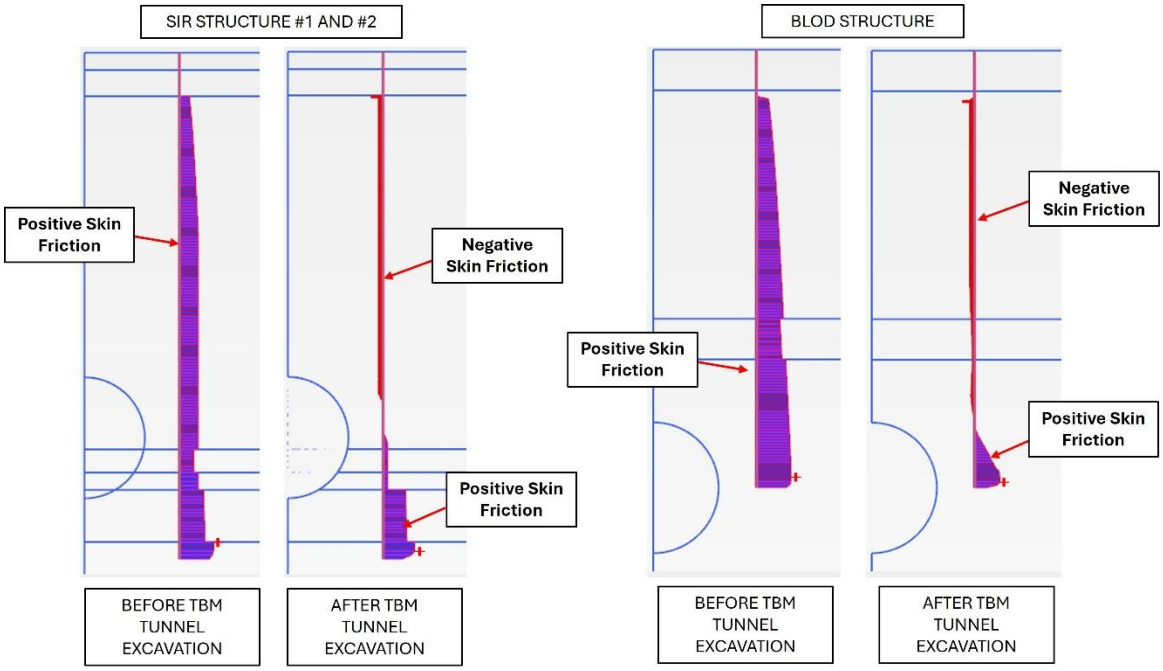


Figure 4. Development of down drag axial force on pile resulting from TBM tunnel excavation.

7 RISK MITIGATION MEASURES

Due to the highly variable geological, geotechnical and hydrogeological properties of the encountered project units there is the potential for complications associated with controlling face pressures, stability of the formations, limiting ground / volume loss and minimising groundwater ingress during TBM tunnelling. Grouting in front of the TBM face may be required to help alleviate some of these concerns. Grouting will also likely be required to infill the annulus between the tunnel concrete lining segments and the surrounding soil / rock behind the TBM shield. Grouting

conducted in these zones must consider the possible presence of high permeability material (Tamala Limestone, Ascot Formation, TQ Sands) which may result in grout loss or loss of grout pressure during the grouting process. In this case it may be necessary to carry out additional grouting during construction.

The volume loss is a key factor in assessing ground movements resulting from tunnelling. Grout pressures may need to be adjusted (that is increased) to minimise the potential for significant ground / volume loss to occur which could adversely impact pile foundations. Furthermore, appropriate TBM operating procedures including consideration given to speed of excavation, type of cutting tool, slurry support mix and maintenance intervals should be allowed for. Convergence monitoring of installed segmental lining segments is also a useful way to investigate ground movements following tunnel excavation.

Sophisticated and state of the art monitoring and global position systems are available and are understood to have been included with the TBM's for the ASDP Project that will allow for meticulous excavation control along the tunnel alignments, limiting deviations and over-excavation to in the order of 100 mm. A bigger challenge is the location and positioning of the piles and liners from a jack-up barge. A temporary pile driving steel template, that can be lowered and placed on the seabed, has been recommended to assist with locating the plan position of the piles and liners.

8 CONCLUSIONS

The susceptibility to crushing of the grains and the random cementation extent have generally been understood to be key features which distinguish calcareous sediments apart other sediments. Given their unique and intricate composition, they deserve special consideration when assessing them for design and construction purposes. Sufficient, targeted and specialised geotechnical in-situ and laboratory testing should be undertaken to assist with determining critical design parameters and to better inform their challenging engineering behaviour. Field tests and trials are encouraged to be considered in complex and difficult geological environments where anisotropic conditions and a high degree of material variability are anticipated.

Appropriate risk mitigation measures should also be developed to prevent or minimse the risk of excessive ground movements resulting from TBM tunnelling and to not adversely impact pile foundations. Some of these measures include grouting ahead of the TBM, maintaining slurry and grout pressures during segmental lining installation, convergence monitoring and onboard real time monitoring of TBM excavations.

9 ACKNOWLEDGEMENTS

The authors of this paper would like to thank Water Corporation for allowing them to publish this paper which presents an overview of the approach and findings from the ASDP nearshore structures pile design. The project is on-going and construction well underway.

10 REFERENCES

American Petroleum Institute. 2010. Recommended practice for planning, designing and constructing fixed offshore platforms – working stress design, *API RP 2A-WSD*, 21st edition, Errata and Supplement.

Andersen, K.H., Puech, A.A., Jardine, R.J. 2013. Cyclic resistant geotechnical design and parameter selection for offshore engineering and other applications. *Proceedings from ISSMGE TC 209 Workshop – Design for cyclic loading: piles and other foundations,* Paris, France, 4 September 2013: pp.9-44.

Berezantzev, V.C., V. Khristoforov and V. Golubkov. 1961. Load bearing capacity and deformation of piled foundations. *Proceedings from the 5th International Conference, ISSMFE,* Paris, Vol. 2, 1961: pp. 11–15.

BS EN ISO 19901-4:2016 Petroleum and natural gas industries – Specific requirements for offshore structures – Part 4: Geotechnical design considerations (ISO 19901-4:2016).

Dyson, G.J. and Randolph, M.F. 2001. Monotonic lateral loading of piles in calcareous sediments. *Journal of the Geotechnical Engineering, ASCE,* Volume 127, Issue 4: pp.346-352.

Fleming, K., Weltman, A., Randolph, M., Elson, K. 2009. Piling Engineering – Third Edition, London and New York: Taylor and Francis.
Green, R. A., and Ziotopoulou, K. 2015. Overview of screening criteria for liquefaction triggering susceptibility. *Proceedings of the Tenth Pacific Conference on Earthquake Engineering Building an Earthquake-Resilient Pacific, 6-8 November 2015, Sydney Australia*.
Idriss, I.M., and Boulanger, R. W. 2004. Semi-empirical procedure for evaluating liquefaction potential during earthquakes. *Proceedings of the 11th ICSDEE and 3rd ICEGE, January 7-9, 2004*: pp.32-56.
Jardine, R., Chow, F., Overy, R., Standing, J. 2005. ICP design methods for driven piles in sands and clays. London: Thomas Telford.
Jardine, R.J., Standing, J.R. 2012. Field axial cyclic loading experiments on piles driven in sand. *Soils and Foundations,* Volume 52, Issue 4, September 2012: pp.723-736.
Kulhawy, F. H., Trautman, C. H., Beech, J. F., O'Rourke, T. D, McGuire, W. 1983. Transmission line structure foundations for uplift-compression loading. *Report No. EL-2870, Electric Power Research Institute*. Palo Alto, California.
LPILE v2022 Technical Manual – A program for the analysis of deep foundations under lateral loading. Ensoft Inc., February 2022.
Maurer B.W., Green R.A., and Taylor O.S. 2015. Moving towards an improved index for assessing liquefaction hazard: lessons from historical data. *Soils and Foundations,* Volume 55, Issue 4, July 2015: pp.778-787.
Mayne, P.W., and Kulhawy, F.H. 1982. K0-OCR relationships in soil. *Journal of the Geotechnical Engineering Division, ASCE,* Volume 108, No. GT6, June 1982: pp.851-869.
Nauroy, J-F., Brucy, F., Le Tirant, P., Kervadec, J-P. 1986. Design and installation of piles in calcareous formations. *Proceedings from the 3rd Internation Conference on Numerical Methods in Offshore Piling, Nantes, France*: pp.461-481.
OuYang, H., Dai, G., Gong, W. 2024. Analysis of influencing factors of penetration mechanism and vertical bearing characteristics of monopile in calcareous sand: Laboratory model testing and in-situ testing. *Soil Dynamics and Earthquake Engineering,* Volume 180, May 2024.
Poulos, H.G. and Davis, E.H. 1980. Pile Foundation Analysis and Design. John Wiley and Sons, New York.
Poulos, H.G. 1988. Cyclic stability diagram for axially loaded piles. *Journal of Geotechnical Engineering,* Volume 114, No. 8, August 1988. pp.877-893.
Poulos, H.G. 1988. The mechanics of calcareous sediments. *Proceedings from the 5th Australia – New Zealand Conference on Geomechanics, 1988, Sydney*.
Poulos, H., G. 2018. Rational assessment of modulus of subgrade reaction. *Geotechnical Engineering Journal of the SEAGS & AGSSEA*, Volume 49, No.1, March 2018: pp.1-7.
Poulos, H. G. Ameratunga, J. 2022. A practical approach to bridge foundation design. *Australian Geomechanics*, Volume 57, Issue 2, June 2022: pp.71-92.
prEN1997-3:2022 Eurocode 7 – Geotechnical Design – Part 3: Geotechnical structures.
Puech, A., Benzaria, O., Thorel, L., Garnier, J., Foray, P., Silva, M., Jardine, R. 2013. Cyclic stability diagrams for piles in sands. *Proceedings from ISSMGE TC 209 Workshop – Design for cyclic loading: piles and other foundations*, 4 September 2013, Paris, France: pp.85-88.
Randolph, M.F., Dolwin, J., Beck, J. 1994. Design of driven piles in sand. *Geotechnique*, Volume 44, No. 3: pp.427-448.
Randolph, M.F. and Gourvenec, S. 2011. Offshore Geotechnical Engineering. New York: Spon Press.
Stas, C.V., and Kulhawy, F. H. 1984. Critical evaluation of design methods for foundations under axial uplift and compression loading. *Report for EPRI*, No. EL-3771, Cornell University.
Tandjiria, V. 2022. Practical reliability-based approach for liquefaction vulnerability. *Proceedings from the 20th International Conference on Soil Mechanics and Geotechnical Engineering*, *Sydney 2022*.
The Overseas Coastal Area Development Institute of Japan, 2020*, Technical Standards and Commentaries for Port and Harbour Facilities in Japan*.
Tomlinson, M.J. 1994. Pile Design and Construction Practice – Fourth Edition, London: E & FN Spon.
Tsuha, C.H.C., Foray, P.Y., Jardine, R.J., Yang, Z.X., Silva, M., Rimoy, S. 2012. Behaviour of displacement piles in sand under cyclic axial loading. *Soils and Foundations*, Volume 52, Issue 3, June 2012: pp.393-410.

19th Australasian Tunnelling Conference – Acosta-Martínez, Stewart and Hudson-Smith (Eds.)
© 2025 Australian Tunnelling Society, ISBN 978-0-85825-002-4

A Study on the Monitoring Technology for the Second Jiaozhou Bay Subsea Tunnel Project

Zhang Wenbo & He Rongguo
China Railway Academy Co., Ltd.,Chengdu , Sichuan , China

ABSTRACT: The Second Jiaozhou Bay Subsea Tunnel (hereinafter referred to as "JBSST") in Qingdao is currently the largest-scale and longest subsea road tunnel in Asia. The tunnel was constructed using a combination of drill-and-blast (D&B) and tunnel boring machine (TBM) methods. Due to numerous hazards such as subsea fault zones, deep weathering troughs, and weak fractured zones, the project faces extremely high risks and challenges. This paper systematically investigates the overall tunnel monitoring implementation scheme including the scope of instrumentation and measurement, intelligent blast vibration monitoring, the integration of construction-phase and operation-phase monitoring, and the development of a digital monitoring platform, by taking into account the risks and challenges faced in the tunnel. The results from the project implementation validate the effectiveness and applicability of the proposed scheme.

1 INSTRUCTION

The JBSST is Asia's longest subsea road tunnel project. It employs a construction method that combines D&B and TBM. The tunnel is 17.5 km long, with the maximum overburden of approximately 115 m below sea level as shown in Figure 1 (Xiao et al. 2023, Qu et al. 2024). The JBSST passes through various geological units and will inevitably encounter adverse geological bodies such as subsea fracture zones, faults, weathered deep troughs, and weak fractured zones, giving rise to a multitude of significant geohazard risks (Qu et al. 2024, Li et al. 2024). Twenty-two structural zones have been identified in which the rock mass is fractured, making it highly susceptible to tunnel lining dislocation, structural fractures, and potential collapses, as well as water and mud inrush disasters (Wu et al. 2023). The geological longitudinal profile of the JBSST is shown in Figure 2. The D&B sections of the tunnel are situated near densely populated residential areas within the urban built-up zone. The offshore section constructed using the D&B method on the Huangdao side underpasses a "100,000-ton" crude oil transfer terminal, which is highly sensitive to potential ground vibrations and noise from construction activities (Chen et al. 2024). The complex geological conditions and sensitive surrounding environment present world-class challenges for the monitoring tasks.To address these risks and challenges, a monitoring scheme during the tunnelling and operation is developed. This paper investigates major technologies employed in the scheme.



Figure 1. Location map of the JBSST

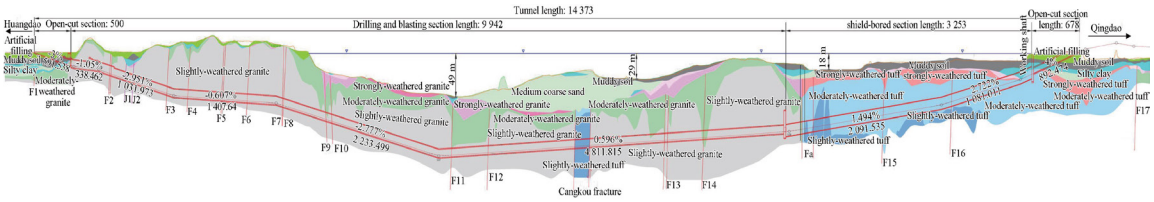


Figure 2. Longitudinal geological profile showing the major fault zones traversed by the JBSST

2 MONITORING TECHNOLOGY

2.1 Overall Monitoring Scheme

The monitoring scheme for the JBSST has been designed with the principles of "precision, comprehensiveness, reliability, and cost-effectiveness" in mind. In conjunction with the construction methods and geological risks, a specified monitoring system has been established. For the D&B sections, crown settlement, clearance convergence, and peak particle velocity (PPV, the maximum value in three orthogonal directions) are the core indicators. These are supplemented by monitoring items such as internal displacement of the surrounding rock, surrounding rock pressure, support structure stress, and water pressure, focusing on the assessment of surrounding rock stability and blast impact. For the TBM sections, segment displacement (vertical displacement, horizontal convergence) is the core indicator, supplemented by segment stress, bolt stress, surrounding rock pressure, and water pressure, focusing on the synergistic monitoring of structural forces and ground deformation. Guided by the principle of "highlighting key points while ensuring comprehensive coverage", the entire monitoring system targets critical risks such as surrounding rock stability and blast impact in the D&B sections, and segment structural forces in TBM sections. Monitoring points are densified at critical locations like subsea fault zones, covering the entire cycle from construction to operation. Millimetre-level precision control is achieved through automated monitoring. The arrangement of monitoring sections in the D&B tunnel is shown in Figure 3, and the layout of displacement monitoring points in the TBM sections is shown in Figure 4.

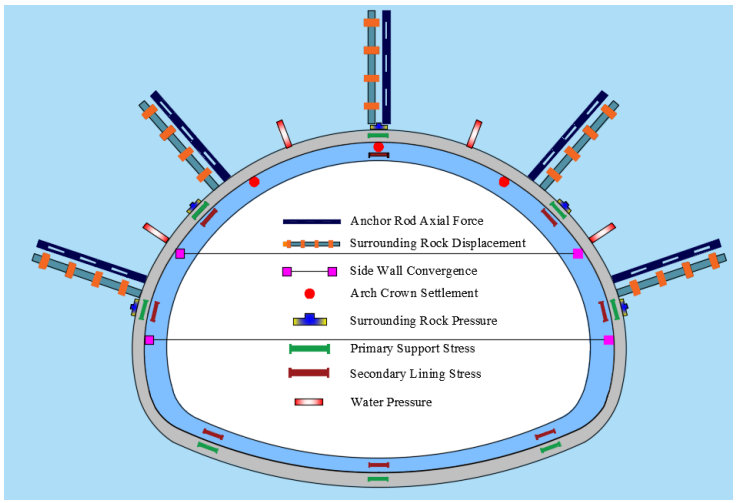


Figure 3. Setup of Monitoring Items for D&B Tunnels

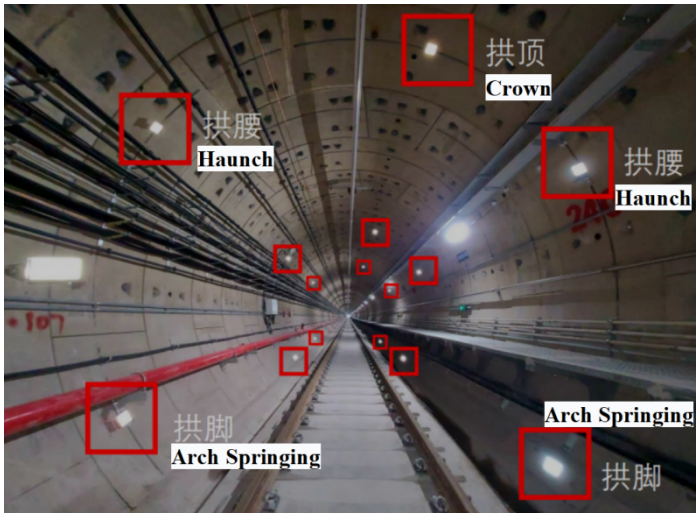


Figure 4. Layout of Displacement Monitoring Points for TBM Tunnels

2.2 Intelligent PPV Monitoring

To address the challenge of vibration control for blasting construction near sensitive environments, an automated monitoring system based on the Internet of Things (IoT) was developed, forming an integrated "perception-transmission-analysis-decision" solution as shown in Figure 5. In terms of hardware architecture, high-precision vibrating wire triaxial sensor arrays are employed to achieve precise acquisition of PPV vector data. A hybrid communication network solves the data transmission challenges in complex environments. At the software level, a BIM visualization module and an intelligent analysis platform were developed and integrated. This constructs a multi-source dataset incorporating blasting parameters, geological characteristics, and vibration responses, establishing a vibration velocity prediction model. This enables early warning of PPV and back-analysis for optimizing construction parameters, enhancing the timeliness and decision-support value of monitoring results. Comparison with traditional technology is shown in Table 1. The innovations of this monitoring scheme are:

– Achieving "real-time spatial distribution reconstruction - time-series trend prediction - dynamic risk level assessment" of PPV effects through automated data acquisition, intelligent noise filtering algorithms, and a 3D visualization analysis platform.

– The intelligent early warning model, incorporating engineering geological features and blasting techniques, improves warning accuracy by 30% compared to traditional single-threshold methods.
– Lightweight sensor integration technology enables the rapid deployment of miniaturized equipment in complex tunnel environments, increasing installation efficiency by 50%.

Table 1. Performance Comparison of Intelligent PPV Monitoring

Comparison Content	Traditional PPV Monitoring	Intelligent PPV Monitoring
Overlimit Times / Monitoring Times	33/275	3/202
Data Calculation and Analysis Time (s)	220	120
Sensor Installation and Layout Time (min)	20	10
Data Source.	The Inclined Shaft of the JBSST (Jul-Oct 2021).	The North Line Tunnel of the JBSST(Jun-Aug 2023)

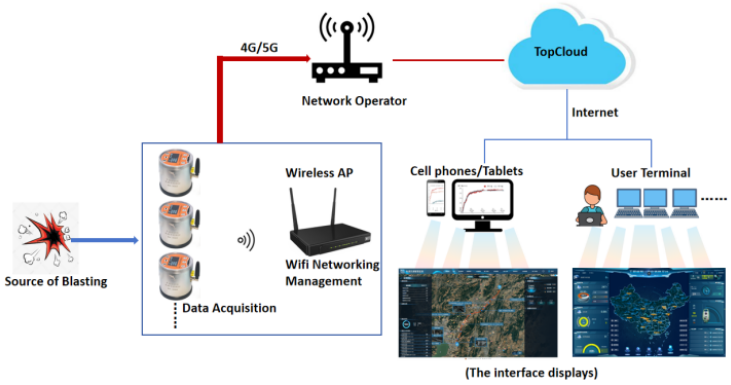


Figure 5. Intelligent Monitoring of PPV

2.3 Integrated Construction-Operation Phase Monitoring

Given the technical limitations of traditional monitoring, which is often characterized by phased implementation and data discontinuity, the concept of tunnel monitoring is elevated from ensuring construction-phase safety to guarantee the entire lifecycle (hereinafter referred to as "EL") safety and an Integrated Construction-Operation Phase Health Monitoring System is established. By pre-embedding lifecycle sensors and integrating intelligent monitoring technologies, the continuity and traceability of monitoring data at key risk locations is ensured, to solve the traditional issue of the "separation between construction and operation phases. The sensor design adopts an integrated approach such that operation-phase monitoring elements are pre-embedded during the construction phase. This approach prevents secondary damage to the structure from retrofitting sensors later and reduces the EL monitoring cost by over 30%, the comparison of monitoring costs is shown in Table 2. The monitoring section for the EL is shown in Figure 6. In the D&B tunnels, vibrating wire pressure cells and fiber Bragg grating (FBG) strain gauges are pre-embedded between the primary support and secondary lining in fault fracture zones and weak surrounding rock sections to monitor changes in surrounding rock pressure and lining stress. FBG displacement meters and bolt stress gauges are pre-embedded at segment joints and sections traversing fracture zones, with bolt stress gauges embedded within segment connecting bolts. During construction, segment convergence and bolt forces are monitored. During operation in the D&B tunnels, structural deformation is scanned in real-time via a distributed optical fiber network. A "segment-surrounding rock synergistic monitoring" mode is adopted. Earth pressure cells and pore water pressure gauges are simultaneously installed behind the TBM cutterhead. During construction, this setup assesses the disturbance of surrounding soil caused by TBM advancement. During operation, it monitors the impact of long-term ground creep on the structure.The layout of TBM tunnel monitoring sensors is shown in Figure 7.

Table 2. Comparison of Monitoring Costs

Comparison Content	Traditional Monitoring	Integrated Construction-Operation Phase Monitoring
Construction Monitoring Cost	CNY 2.0 M	CNY 6.0 M
Operational Monitoring Cost	CNY 6.8 M	
Data Source	Costs for 12 monitoring sections of a tunnel in Southern China.	Costs for 12 monitoring sections of the JBSST.

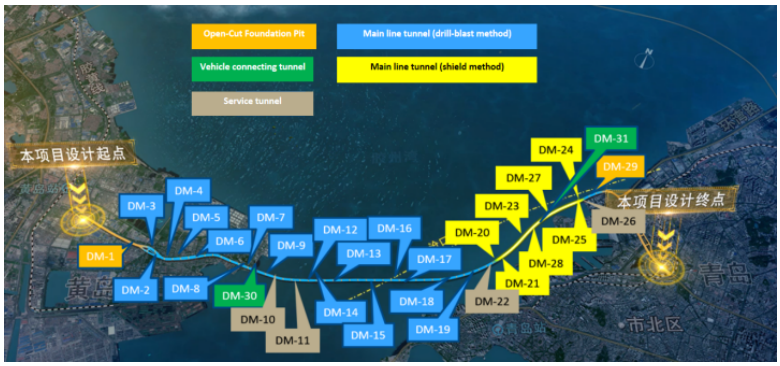


Figure 6. Integrated Monitoring Sections for Construction and Operation Phases

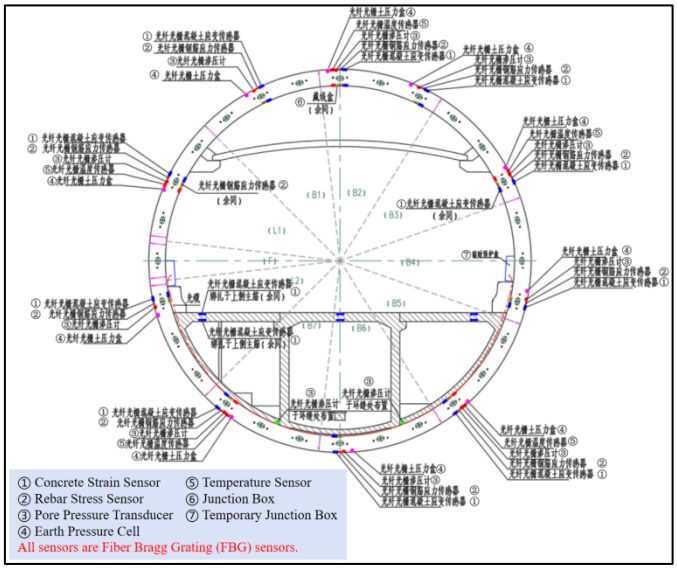


Figure 7. Sensor Layout for Health Monitoring of the TBM Sections

2.4 Construction of the Digital Monitoring Platform

For the JBSST project, a dedicated digital monitoring platform is constructed to meet the project's complex monitoring demands, as shown in Figure 8. The platform utilizes BIM+GIS technology as its core framework and integrates key information such as structural segments, fault zones, and on-site monitoring point positions. The platform then integrates IoT devices, big data modules for processing real-time monitoring data, and intelligent algorithms to establish a monitoring system characterized by "the digitalization of the entire process and EL integration". The schematic of the early warning display interface is shown in Figure 9. Here, "full-process digitalization" covers

the whole workflow from on-site data collection to automated calculation and online report output, while "EL integration" links construction-phase monitoring with operation-phase health tracking. Its technical features and innovations are reflected in:

- Automated Multi-source Data Acquisition and Fusion. Employing a "24-hour automated acquisition as primary + human-machine collaboration as auxiliary" model, it integrates diverse devices such as vibrating wire sensors, FBG sensors, and LiDAR.
- Intelligent and Visualized Risk Prevention and Control. Establishing an "intelligent early warning - dynamic back-analysis - closed-loop management" system. Based on a BP(Back Propagation) neural network model, it predicts trends in monitoring data, improving warning accuracy by 40% compared to traditional threshold methods. For instance, when monitoring data exceeds limits, the system automatically triggers an alarm, synchronously pushes information to all stakeholders, and highlights the risk area in the linked BIM model, achieving a "monitoring-analysis-handling" response within 10 minutes (down from 90 minutes).
- Full Coverage of Construction Methods and System Synergy. Developing dedicated subsystems for different construction methods like D&B and TBM. These subsystems communicate with the platform through standardized data interfaces, solving the "data silo" problem inherent in traditional isolated multi-system operations.
- Digital Reconstruction of Management Processes. Implementing the entire process of monitoring data acquisition, calculation, and warning online.

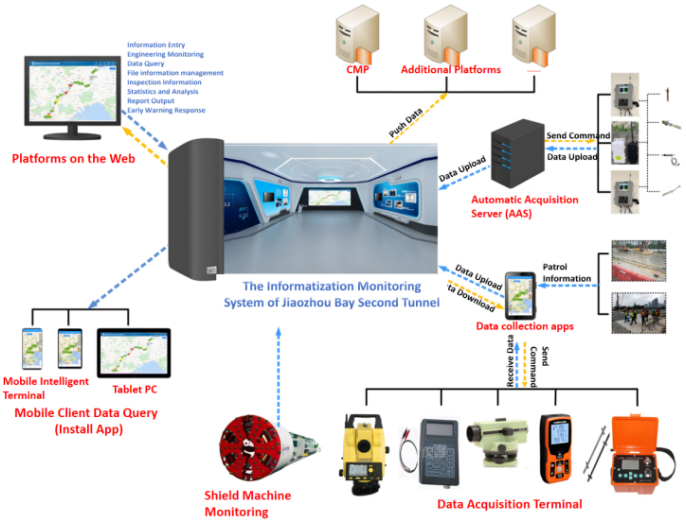


Figure 8. Information-based Monitoring Platform

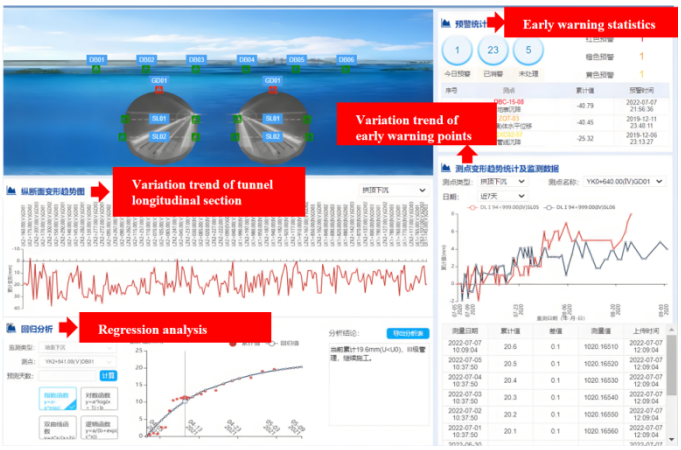


Figure 9. Structural Deformation Early Warning on the Display Interface

3 CONCLUSIONS

From this study, the conclusions can be drawn as follows:

(1) Effectiveness of the Monitoring Technology System. The information-based and automated integrated instrumentation and measurement technology system established has effectively controlled safety risks during the construction phase of the subsea tunnel, the warning response efficiency is nine times as high as that of traditional systems. Particularly under complex conditions such as traversing 22 structural zones and high-water-pressure and water-rich strata, it has achieved 234 early warnings, innovations in EL Monitoring, and dynamic control of disasters like structural deformation.

(2) Pioneering the "Integrated Construction-Operation Phase Monitoring System," continuous EL data acquisition is achieved through sensor pre-embedding technology. This overcomes the technical bottleneck of traditional monitoring, characterized by "phased implementation and data discontinuity," reduces EL monitoring costs by over 30%, offers foundational data support for the long-term health assessment of the tunnel, and ensures seamless integration of the "construction-operation" monitoring system for the subsea tunnel.

(3) Effectiveness of Intelligent PPV Monitoring. This solution has reduced the rate of PPV velocity exceeding limits from 12% to 1.5%, and improved monitoring data processing efficiency by 80%. It offers comprehensive technical support for tunnel blasting construction near sensitive targets, encompassing "real-time monitoring - intelligent analysis - active control," thereby promoting the shift from empirical to digital and intelligent PPV control.

4 REFERENCES

Xiao M.Q. et al. 2023. Study on general design of second Jiaozhou Bay subsea tunnel. *Tunnel Construction*43(2):199.

Qu L.Q. et al. 2024. Research on smart design and innovation of Jiaozhou Bay Second Tunnel.*WTC2024*.

Qu L.Q. et al. 2024. Challenges and technological innovations in the Jiaozhou Bay Second Submarine Tunnel project. *Modern Tunnelling Technology*61(2): 223-231.

Li Z.Q. et al. 2025. Primary unfavorable geology and construction risks of the Second Subsea Tunnel of Jiaozhou Bay in Qingdao City.*Journal of Engineering Geology*33(1): 302-314.

Wu Z.S. et al. 2023. Antidislocation structure design of Jiaozhou Bay Second Subsea Tunnel crossing an active fault. *Tunnel Construction* 43(5): 826.

Chen L.B. et al. 2024.Comparative study on construction methods for the Second Subsea Tunnel of Jiaozhou Bay crossing the building-dense area in the Huangdao Land section .*CHINA ROCK 2024*: 448-453.

THIS PAGE INTENTIONALLY LEFT BLANK

19th Australasian Tunnelling Conference – Acosta-Martínez, Stewart and Hudson-Smith (Eds.)
© 2025 Australian Tunnelling Society, ISBN 978-0-85825-002-4

Evaluating deterministic and probabilistic seismic hazard assessments for the tunnel design in Sydney: Insights and comparisons

C. Dai

Tetra Tech Coffey, Sydney, Australia

ABSTRACT: This paper evaluates the application of Deterministic Seismic Hazard Analysis (DSHA) for tunnel design in the low-seismic context of Sydney and compares its outcomes with National Probabilistic Seismic Hazard Assessments (NSHA18 and NSHA23) and the AS1170.4 design standard. While DSHA is valuable in regions with recognised active faults, its use in Sydney—where no active faults have been identified—can significantly overstate hazard levels.

The study shows that PSHA-derived ground motions are substantially lower than those from DSHA and AS1170.4, indicating that AS1170.4 provides a conservative basis for design in this region. In particular, DSHA scenarios involving the Lapstone Structural Complex produce unrealistically high ground motions, despite the fault being classified as inactive under international and ANCOLD guidelines.

The findings support the use of PSHA informed by NSHA23, which, when paired with appropriately selected deterministic scenarios and the conservative provisions of AS1170.4, offers a more realistic and economically justifiable approach to infrastructure design in Sydney's low-seismicity environment.

1 INTRODUCTION

Section 6.4 in Austroads Guide to Road Tunnels (2021) (AGRT) has those definitions for different seismic design events based on performance-based design principles:

- After the design return period event (sometimes referred to in other countries as maximum design earthquake MDE), the tunnel should be usable by emergency traffic, although damage may have occurred, and some temporary repairs may be required. Permanent repair to reinstate the design capacities for both static and seismic loading should be feasible.
- After an event with a return period significantly less than the design value (sometimes referred to in other countries as operating design earthquake ODE), damage should be minor, and there should be no disruption to traffic.
- After an event with a return period significantly greater than the design return period event (the maximum considered earthquake MCE), the tunnel should not collapse, although damage may be extensive. It should be usable by emergency traffic after temporary repairs and should be capable of permanent repair, although a reduced capacity for further seismic events may be acceptable, given this is a highly infrequent event.

The definitions for ODE, MDE, and MCE are adapted from international practices, particularly from countries where maintaining tunnel operability post-earthquake is critical due to realistic threats such as aftershocks, emergency response, and commuter demands. These definitions are applicable across all seismic regions, with their relevance becoming more pronounced in areas of moderate to high seismicity, such as New Zealand, where the magnitude and frequency of seismic events are greater.

While Sydney is located in a low-seismicity region where seismic loading may not typically govern tunnel design, this does not preclude the application of AGRT. The definitions of MDE, ODE, and MCE remain valid and are determined by return periods, regardless of seismicity level. However, in such regions, the differences between return period events are relatively small, and the probability of a disruptive earthquake is low. As a result, designing for post-earthquake operability, such as continued emergency traffic use, may be considered overly conservative or economically disproportionate to the actual risk. Of course, this depends on the availability of the application of the probability of exceedance.

However, AGRT does not define the design earthquakes in terms of probability of exceedance or return periods.

In this paper, the author conducts a Deterministic Seismic Hazard Analysis (DSHA) for the Sydney region, using the ground motion model developed by Somerville et al. (2009) for the Sydney Basin. The results are compared with those from the National Seismic Hazard Assessments (NSHA) 2018 and 2023, alongside the requirements outlined in AS 1170.4, which is applicable to all structures, including tunnels. The active faults in the Sydney area are identified for the DSHA application or selection. The probability of exceedance or return periods has been discussed and recommended.

2 PSHA HAZARD CURVE AND COMPARISON WITH AS1170.4

Following the release of the 2018 Probabilistic Seismic Hazard Assessment (PSHA18), Geoscience Australia, in collaboration with the broader Australian seismology community, developed the 2023 National Seismic Hazard Assessment (NSHA23). This updated assessment is intended for incorporation into the upcoming 2024 edition of Standards Australia's Structural design actions, Part 4: Earthquake actions in Australia (AS 1170.4–2024).

Seismic hazard curves provide the annual probability of exceeding a given ground motion level. Hazard curves calculated on AS1170.4 Site Class Be are calculated for the localities listed in Table 3.2 of the AS1170.4–2024 (Standards Australia, 2024), and additional sites.

Figure 1 summarises a comparison of mean seismic hazard curves for the NSHA18 and the NSHA23, and shows the annual probability of exceedance against Peak Ground Acceleration (PGA) for Sydney. The annual probability of exceeding a given PGA level (in g) for Sydney on AS1170.4 Site Class Be (equivalent to VS30 = 760 m/s). The plots compare the mean NSHA18 and NSHA23 hazard curves. The 5th - 95th percentile curves are shown for the NSHA23, while the AS1170.4 - 2024 Z value is plotted together with the hazard floor value of 0.08g as used in the AS1170.4 - 2024. The rationale for the changes in hazard between the NSHA18 and NSHA23 is discussed in (Allen et al., 2023).

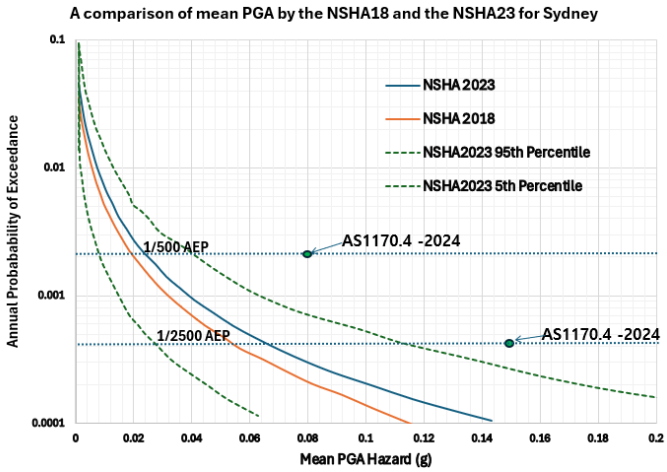


Figure 1 Comparison: mean PGA by NSHA18 and NSHA23

As can be seen in Figure *1*. The PGA obtained by either PSHA18 or PSHA23 is much lower than the PGA obtained by AS1170.4 (2024) for the Sydney region.

Table 1 below compares PGAs using different models.

Table 1. The difference in PGA by different models

AEP	PGA (g)		
	NSHA18	NSHA23	AS1170.4
1/475	0.021	0.026	0.08
1/2475	0.056	0.07	0.144

To evaluate the conservatism of each model, a Deterministic Seismic Hazard Analysis (DSHA) based on the ground motion model by Somerville et al. (2009) is conducted for further comparison and comment purposes. For DSHA purposes, we need to review the seismic scenarios in the Sydney Basin.

3 EARTHQUAKE SCENARIOS IN SYDNEY

The Sydney Basin is underlain by a thick sequence of sedimentary rocks deposited during the Permian to Triassic periods, roughly between 290 and 200 million years ago. Situated well within the stable interior of the Australian tectonic plate, the basin typically experiences low levels of seismic activity, especially in comparison to areas located near active plate boundaries. Nevertheless, seismicity within the basin is not evenly distributed, with relatively higher activity observed in its southern and western regions.

Allen et al. (2011) published the geographical distribution of past earthquake events within the basin. The Geoscience Australia recorded earthquake activity shows:

1. No earthquakes greater than magnitude three have been recorded within 20 km of Sydney's Tunnels.
2. The strongest earthquake ever recorded in the Sydney Basin had a magnitude of 5.6.

Paleo-seismic research by Clark (2010) indicates that the LSC is capable of producing earthquakes with moment magnitudes (Mw) of up to 7.5, although such events are expected to recur only every 1 to 2 million years.

In addition to the LSC, other fault systems within the Sydney Basin may also exhibit seismic activity. Berryman et al. (2009), using geological and seismological data gathered from regional mining and tunnelling projects, assessed the likelihood of moderate-magnitude earthquakes occurring along these faults. Their analysis suggests that individual faults could generate events ranging from Moment Magnitude (M_w) 5.0 to 6.0, with recurrence intervals spanning several million years. Collectively, these findings indicate that the overall seismic hazard for tunnels in the Sydney region is low, due to the region's low seismicity and limited potential for strong ground shaking. Nevertheless, a higher moment M_w is conservatively assumed in the following DSHA to account for uncertainties and ensure robustness in the design approach.

For deterministic seismic hazard assessment (DSHA) in tunnel design, two representative earthquake scenarios are commonly considered:

- A M_w 7.5 event originating from the LSC, situated 20–50 km from the Sydney CBD.
- A hypothetical Mw 5.5 earthquake occurring 20 km from the city.

Although these scenarios represent extreme cases, they are treated as maximum credible earthquakes (MCE) within current seismic hazard frameworks (Clark, 2010; Berryman et al., 2009).

4 DSHA MODEL AND COMPARISON

The two scenarios in the above section involved DSHA. The analyses are based on the model of Somerville et al. (2009). The 5%-damped uniform hazard horizontal acceleration response spectra for Class B – Rock (Vs30 = 760m/s) are shown in Figure 2 also compares the uniform hazard

spectra within the DSHA results for M_w of 5.5 and 7, PSHA23, and AS1170.4. As we can see, the DSHA spectra for M_w of 7.5 are significantly higher than those for M_w of 5.5 and AS1170.4.

Table 2 gives the PGA comparison. M_w=5.5 DSHA obtains a PGA of 0.06, and for M_w=7.5, DSHA gets the PGA of 0.2. Compared with AS1170.4, PGA is 0.08 for the case of the 10% in 50 years (AEP of 1/475 - Probability factor kp of 1). PGA is 0.144 for the case of the AEP of 1/2475 (Probability factor kp of 1.8). AS1170.4 does not explicitly include seismic magnitude in its assessment.As a scenario-based DSHA, the results by DSHA are governed by magnitude (Mw) selection. Through the comparison in

Table 2, PGA by DSHA for M_w of 7.5 is much higher than the minimum PGA value in AS1170.4 (2024). Is the DSHA overestimating the seismic hazard in the Sydney region? Or should the selected seismic with an M_w of 7.5 not be included in the Sydney Basin seismic analysis? As we know, the DSHA does not apply to the inactive faults. DSHA only applies to active faults because it assumes a fault can generate a future earthquake of maximum credible magnitude. Inactive or ancient faults are excluded because they are not expected to rupture again within relevant engineering timescales. Now, we face the question: What is an Active Fault? Or what is the criterion for determining whether faults are active?

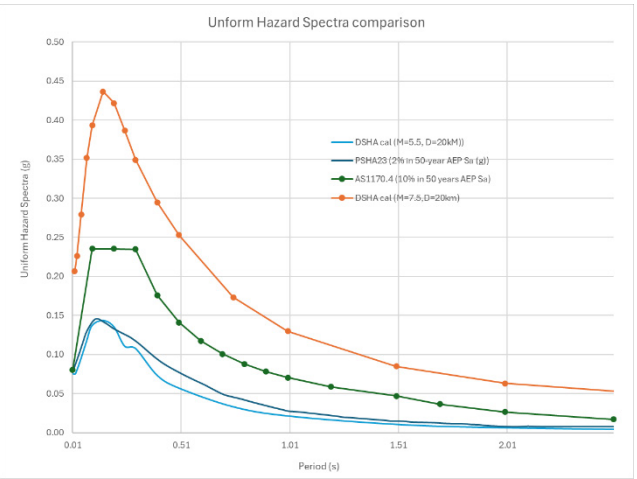


Figure 2. Uniform Hazard Spectra comparison

Table 2. Deterministic Seismic Hazard Analysis for Sydney

PGA (g)			
DSHA		AS1170.4	
		AEP=1/475	AEP=1/2475
Mv=5.5	0.078	0.08	0.144
Mv=7.5	0.2		

5 WHAT IS AN ACTIVE FAULT?

The terminology is from the Australian National Committee on Large Dams (ANCOLD) Guidelines for Design of Dams and Appurtenant Structures for Earthquake, which is adapted from the International Commission on Large Dams (ICOLD - 2016):

– An active fault is defined as a fault, reasonably identified and located, known to have produced historical earthquakes or showing evidence of movements in Holocene time (i.e. in the last 11,000 years) and large faults that have moved in the latest Pleistocene time (i.e. between 11,000 and 35,000 years ago).

– A Neotectonic fault is a fault, not active as defined above, that experienced displacement under conditions imposed in the current crustal stress regime, and hence may move again in the future.

In the ANCOLD commentary, the very long faults that have moved repeatedly in Quaternary time (the last 1.8 million years) are not included as active faults, as they would be too conservative for use in the deterministic analysis approach. However, these faults are included in PSHA as Neotectonic faults.

These are both active faulting areas along plate tectonic boundaries, whereas most of continental Australia apart from the north adjacent to PNG, is a tectonically inactive craton/plate that is far removed from subduction zones.

Based on the NZ definition (Litchfield et al., 2013), a fault zone is classified as active if there is evidence, or inferred evidence, for ground surface displacement in the past 125,000 years (Late Pleistocene, i.e. since the peak high stand of the last interglacial period, marine isotope stage 5e).

In the USA, the California Department of Water Resources, Division of Safety Dams

(DSOD) oversees more than 1,200 existing dams. Fraser and Chief (2001) provide fault activity descriptions used by DSOD for their dam safety assessments:

– Active: Faults with proven displacement in the last 35,000 years.
– Inactive: Faults with confidently located traces that are consistently overlain by unbroken geologic materials 35,000 years or older.
– Conditionally Active: A fault that has been active in Quaternary time (about the last 2.6 million years), but its displacement history during the last 35,000 years is not known well enough to determine its activity or inactivity. Conditionally active seismic sources are considered active for dam safety evaluations. Following the definitions above, the author conservatively considers an active fault as a fault that has moved in the past 125,000 years.

6 DETERMINE THE DSHA RESULT IN THE LOW SEISMIC ACTIVITY ZONE OF SYDNEY

The seismic scenario described in Section 3 occurred within the thick sedimentary sequence of the Sydney Basin, composed of Permian–Triassic aged rocks (approximately 290–200 million years old). As outlined in Section 4, DSHA is typically applied to active faults, which are assumed to be capable of rupturing at any time. In this context, a fault is generally considered active if there is evidence of movement within the past 125,000 years. Based on the assessment results in Section 5, faults with no evidence of movement within this timeframe may be treated as inactive for design purposes, given the low likelihood of reactivation within a typical infrastructure design life of 100 to 150 years.

However, this does not imply that faults with long recurrence intervals are disregarded. For the purpose of this DSHA, and in the absence of definitive evidence confirming inactivity, these faults are conservatively treated as “active” to ensure that potential seismic hazards are not underestimated in the subsequent analysis.

Including these “active” faults by DSHA would skew engineering design and economic feasibility, leading to unnecessarily conservative outcomes.

As discussed in scenario 2 of Section 3. The LSC is approximately maximum earthquake magnitudes ~M_w7.5 might occur on the LSC with an average frequency of between 1 and 2 million years. It can be treated as an inactive fault. DSHA in Sydney should exclude the magnitudes of M_w 7.5.

In the region of very low to low seismic activity, our knowledge of faults and their activity is derived from NSHA23, and there are no active faults in the Sydney basin. Therefore, we selected a DSHA check for a reasonable nearby earthquake (Mw = 5.5 and D = 20km) for AS1170.4 Site Class Be, as shown in Table *3* below. The results show that the 84th percentile of DSHA is similar to PSHA at 2,475 years return. Refer to Figure *2* above, where hazard values are calculated to Sa (3.01 s), but are truncated to Sa (2.5 s) for plotting clarity.

Table 3. Selected DSHA output in Sydney (Mv=5.5, D=20km)

	Baseline: 5% Damping			
T (s)	PSa Median for 5% damping	PSa Median + 1.σ for 5% damping	PSa Median - 1.σ for 5% damping	Sd Median for 5% damping
0.01	0.07803	0.15306	0.03978	0.00019
0.02	0.07495	0.14730	0.03814	0.00074
0.03	0.08035	0.15950	0.04048	0.00180
0.05	0.09613	0.19479	0.04744	0.00597
0.075	0.11794	0.24367	0.05709	0.01647
0.1	0.13753	0.28592	0.06615	0.03414
0.15	0.14377	0.29726	0.06953	0.08030
0.2	0.13576	0.27865	0.06615	0.13481
0.25	0.11072	0.22647	0.05413	0.17179
0.3	0.10793	0.22170	0.05255	0.24114
0.4	0.07340	0.15174	0.03550	0.29152
0.5	0.05720	0.11949	0.02738	0.35498
0.75	0.03330	0.07084	0.01565	0.46496
1	0.02162	0.04622	0.01011	0.53671
1.5	0.01081	0.02309	0.00506	0.60394
2	0.00649	0.01386	0.00304	0.64469
3	0.00306	0.00655	0.00143	0.68375
4	0.00180	0.00381	0.00085	0.71431
5	0.00118	0.00250	0.00056	0.73228
7.5	0.00049	0.00103	0.00023	0.68216
10	0.00026	0.00055	0.00013	0.65576

7 CONCLUSIONS

This paper has examined the application of Deterministic Seismic Hazard Analysis (DSHA) in the low-seismicity context of the Sydney region and compared its outcomes with those from National Probabilistic Seismic Hazard Analyses (NSHA18 and NSHA23) and the current design standard AS1170.4 (2024). While DSHA offers valuable insights for regions with well-defined, active faults, its application in areas with low seismicity, such as Sydney, must be approached with caution.

The comparative analysis shows that PGA values derived from NSHA (both 2018 and 2023 updates) are significantly lower than those stipulated in AS1170.4, suggesting that the current standard may be conservative for Sydney's seismic environment. Moreover, the DSHA results, particularly for the Mw of 7.5 scenario sourced from the Lapstone Structural Complex (LSC), produced ground motions exceeding those from both AS1170.4 and PSHA. However, considering that the LSC has an estimated recurrence interval of 1 - 2 million years and lacks evidence of movement within the past 125,000 years, it should be classified as an inactive fault under international and ANCOLD guidelines. Including such a scenario in DSHA overstates the actual seismic hazard and may lead to overly conservative designs.

Furthermore, the assessment confirms that no active faults have been identified within or near the Sydney Basin according to modern criteria. The DSHA scenario based on the Mw of 5.5 event at 20 km distance aligns reasonably with the upper-bound results from PSHA at the 2,475-year return period. This supports the view that for the Sydney region, where there are no currently recognised active faults, AS1170.4 provides a reasonable conservative solution for seismic design.

In conclusion, while DSHA remains a useful tool in regions with recognised active faults, its application in low-seismicity areas like Sydney, where no active faults have been identified, should be limited. For infrastructure such as road tunnels in the Sydney Basin, seismic design based on PSHA, informed by the latest NSHA23 data and consistent with the conservative approach of AS1170.4, provides a more realistic, reliable, and economically justifiable solution.

8 ACKNOWLEDGEMENT

This paper is in memory of our deceased colleague, geologist Richmond Beetham, in New Zealand. He undertook the geological part of the PSHA work for this project. The author recognised and appreciated his contribution to the project.

9 REFERENCES

Austroads. 2022. Guide to Road Tunnels Part 2: Planning, Design and Commissioning.

Australian Standard AS1170.4 – 2024 (2024) Structural Design Actions, Part 4: Earthquake Actions in Australia. Standards Australia.

Allen, T. I., J. D. Griffin, D. J. Clark, P. R. Cummins, H. Ghasemi, and R. Ebrahimi. 2023. The 2023 National Seismic Hazard Assessment for Australia: model overview, Geoscience Australia Record 2023/53, pp, doi: 10.26186/148969

Allen, T., J. Griffin, and D. Clark. 2018. The 2018 National Seismic Hazard Assessment for Australia: model input files, Geoscience Australia Record 2018/32, Canberra, pp 32, doi: 10.11636/Record.2018.032

Allen, T., Leonard, M. and Collins, C. 2011. The 2012 Australian Seismic Hazard Map – Catalogue and Ground Motion Prediction Equations. AEES 2011

ANCOLD. 2019. Guidelines for the design of dams and appurtenant structures for earthquake, May 2019. ed.

Clark, D. 2010. Large earthquake recurrence in New South Wales: implications for earthquake hazard. Australian Geomechanics Society Sydney Symposium October 2010. Pp. 27-36

ICLOD, Selecting seismic parameters for large dams: Guidelines, Bulletin 148, 2016 Revision

Gibson, G. 2005. Seismicity of the Sydney Basin Region. Potential Geological Sources of Seismic Hazard in the Sydney Basin. Proceedings of the Seismic Hazard in Sydney Workshop. Geoscience Australia Record 2009/11

Jeff Bayless, Paul Somerville, Hong Kie Thio, María Elisa Ramos-Sepúlveda. 2023. Updates to the Somerville et al. (2009) Ground Motion Model for Australia Using Broadband Ground-Motion Simulations, 2023 National Conference, 23-25 November 2023.

Somerville, P., Graves, R., Collins, N., Song, S. G., Ni, S., & Cummins, P. 2009. Source and ground motion models for Australian earthquakes. In Proceedings of the 2009 Australian Earthquake Engineering Society Conference (pp. 11-13).

19th Australasian Tunnelling Conference – Acosta-Martínez, Stewart and Hudson-Smith (Eds.)
© 2025 Australian Tunnelling Society, ISBN 978-0-85825-002-4

Vibration impacts due to roadheader excavations in Hawkesbury Sandstone on underground structures

A. Goldsmith
Acciona Construction, Australia

M. Sheffield, Y. Dong
Aurecon, Australia

G. Alvarado, S.X. Poo
AECOM, Australia

N. Lyons
John Holland Group, Australia (Formerly Acciona Construction)

ABSTRACT: Over the past decade, Sydney's tunnel construction boom has relied heavily on continuous miners and roadheaders. A key challenge has been understanding and managing vibration risks to underground infrastructure during excavation. Historically, predictions relied on international case studies, such as those from Hiller (2011), which focused on hydraulic hammers rather than roadheaders, while Hackney (2002) provided Sydney-specific sandstone data from rock hammers. Neither used real roadheader data in Hawkesbury Sandstone. This paper presents measured vibration data from two Sydney tunnel projects, monitoring vibration on underground pipelines, basements, and mass-transit tunnels. Our findings provide insight into actual vibration levels experienced by these assets during roadheader excavation for improved risk management.

1 INTRODUCTION

1.1 Background

Mined tunnel construction typically involving roadheaders has raised questions for asset owners regarding the extent to which vibration propagates through a rock mass and affects nearby underground assets. While tunnel excavation has the potential to be disruptive, the challenge lies in understanding if the vibration generated is significant enough to pose a risk to sensitive infrastructure.

Vibration generated by tunnel excavation presents a key concern for both underground asset owners and designers, especially where works are in close proximity to assets. In many cases, conservative vibration criteria, such as the commonly adopted 1.5 to 20 - 25 mm/s Peak Particle Velocity (PPV) limits, are applied to protect existing assets and infrastructure. As a result, questions often arise regarding the appropriateness of vibration limits, the validity of predictive models, and the need for mitigation measures. In many cases these limits are applied from international literature developed in ground conditions different to Sydney conditions. Criteria have commonly not been developed and sourced from a response to excavation in local Sydney conditions.

An assessment of vibration caused by mined tunnel construction in moderate to high strength, fresh Hawkesbury Sandstone, has been undertaken using vibration monitoring data collected from two major tunnelling projects in Sydney. These were the Project A tunnels which passed above an existing water supply tunnel and were constructed using roadheaders. Data was also collected from Project B, which was constructed in similar ground conditions using similar techniques and machinery, passed over mass-transit tunnels and under existing buildings.

2 LITERATURE REVIEW

Various vibration case studies from the UK were presented in the paper by Hiller 0. His plots have shown that when tunnelling in rock, disregarding blasting (which is rare in Sydney), the largest vibration source is associated with hydraulic impact hammers, in comparison to TBMs and roadheaders. For this study, the hydraulic hammer data from Hiller 0 has been replaced with the data provided by Hackney 0, which is more relevant to our case studies in Class I/II Sydney sandstones, refer to Figure 1.

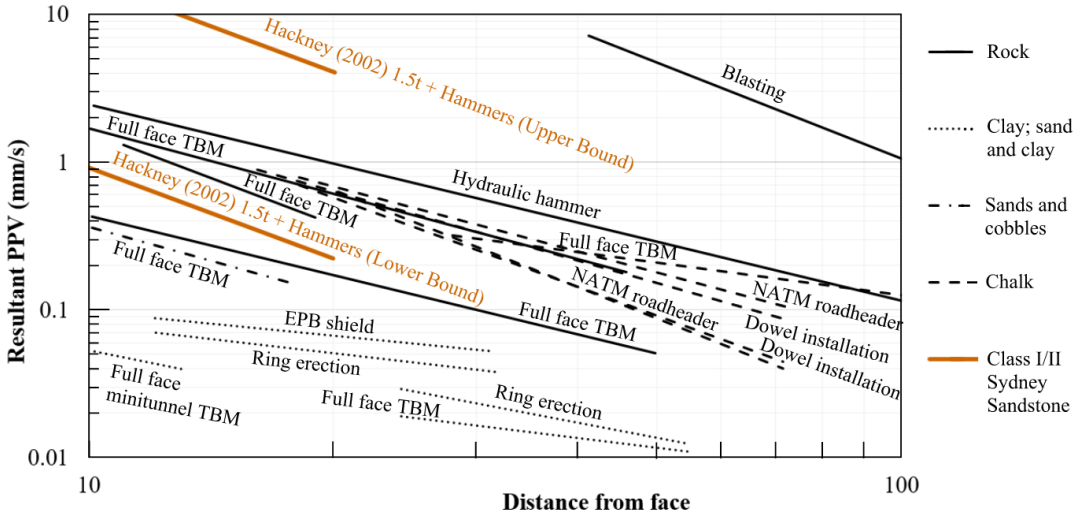


Figure 1. Tunnelling vibration data classified according to geology and equipment based on Hiller 0 & Hackney 0 (amended).

3 TYPICAL VIBRATION THRESHOLD LIMITS

Vibration threshold limits vary considerably and are dependent on a number of factors such as the type, age, condition and sensitivity of an asset, together with the duration of vibrations. Typical values which are often applied by key Sydney asset owners are listed below.

3.1 Water Supply Tunnels

The threshold vibration limits for buried assets in reasonable condition, as defined by the asset owner 0 are outlined in Table *1*.

3.2 Mass-transit & Rail Tunnels

As shown in Table *1* & Figure *2*, there are a number of guidelines and standards which define vibration threshold limits. Maximum peak particle velocity limits for mass-transit tunnels 0 and rail tunnels 0 in Sydney, depending on the structure type, are typically in a range from 15 mm/s to 20 mm/s. However, for buildings and structures, as illustrated in Figure *2* there are numerous guidelines and international standards for conditions different to those encountered in Sydney.

Table 1. Vibration criteria for tunnel linings.

Type of Asset		Threshold / Maximum PPV mm/s
Water Tunnel/ Pipes	Brittle Pipe assets – RC, VC/ EW, CICL	Intermittent - 10, Continuous - 5
	Ductile Pipe assets – SCL, DI, PVC, PE, PP, GRP	Intermittent - 20, Continuous - 10
	Masonry	3
	Unreinforced concrete	3
Tunnel Linings	Brick or mass concrete in good condition	15
	Cast iron, steel, or concrete segments	20

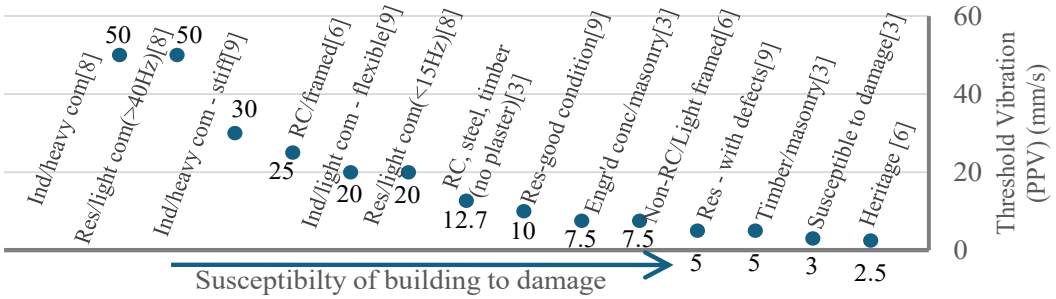


Figure 2. Threshold vibration limit PPV vs Susceptibility of building to damage.

4 FIELD MONITORING INFORMATION

4.1 Vibration sensor / geophone – type & accuracy

There are a number of vibration monitoring devices available on the market and selection of the appropriate type is dependent on factors such as the accessibility of an asset for both installation, maintenance and also regular collection of data from the device. Vibration monitors selected typically have a reading frequency which can be sourced on an interval as closely spaced as every second, with frequencies selected for the sensitivity of the asset. In all cases frequency of readings are at least every five minutes over the life of the logger until decommissioning. This has provided a unique and extensive dataset for the monitoring of these assets during the construction phase



a) Geophones b) Building monitoring device

Figure 3. Vibration monitoring devices.

For the two projects which form the basis of this paper, the following types of devices were used:

– Project A Tunnels. Access to the water supply tunnels was not possible, hence geophones were installed in the base of boreholes adjacent to the water tunnel and at the same elevation. The type of device is shown in Figure *3*(a).
– Project B Tunnels. In contrast to Project A, access to the assets adjacent to the mined tunnels was possible. Surface mounted monitoring devices were used as shown in Figure *3*(b). Wireless devices were used which avoided the need to provide and an external power source which was challenging because of restrictions around the timing of access to the assets. In addition, use of wireless devices significantly obviated the need for access to download data and provided real-time feedback during tunnel construction.

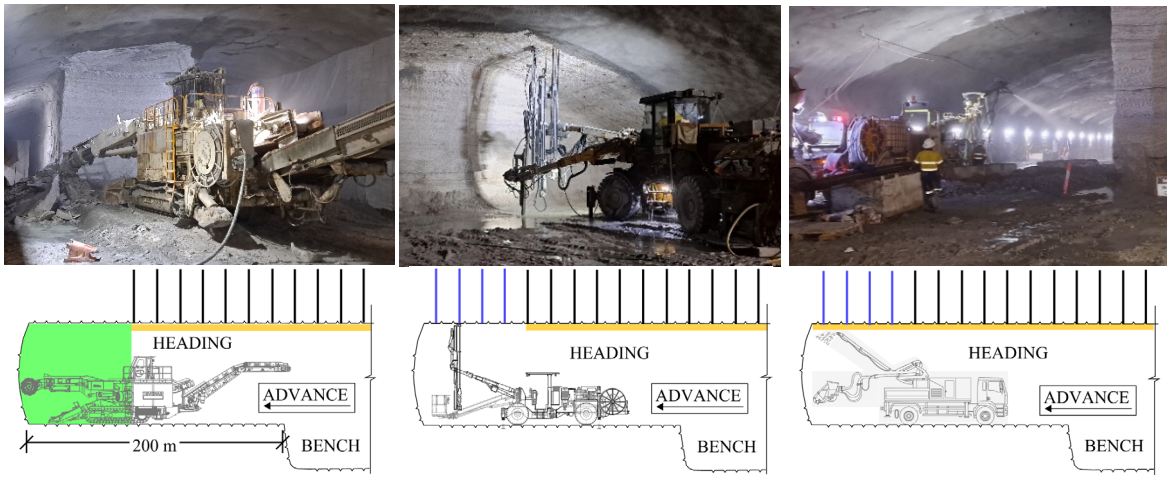
5 MINED TUNNEL CONSTRUCTION IN HAWKESBURY SANDSTONE

The ground conditions in Sydney are unique and ideally suited to underground construction. The medium to high-strength Hawkesbury Sandstone has been proven to perform well in a range of excavation sizes and shapes which has allowed significant and complex underground development in close proximity to existing underground assets.

Extensive development into the use of permanent rock bolts was undertaken by designers, constructors, asset owners and material suppliers in the 1990s to achieve a support system that achieved a 100-year design life.

This development resulted in the use of rock bolts comprising a double corrosion protection system and changed the approach to the construction of tunnels in Sydney. Thin permanent shotcrete (sprayed concrete) primary linings and associated permanent rock bolts could be installed as part of the excavation and support cycle. It was no longer necessary to install thick concrete secondary linings.

Thus, a sequential excavation sequence comprises an excavation phase followed by the installation of rock support comprising rock bolts and shotcrete. The heading is typically advanced between 1 m and 6 m subject to the ground conditions and achieving supported ground requirements. A typical sequential excavation sequence is shown in Figure 4.



(a) Excavation (b) Installation of rockbolts (c) Application of shotcrete

Figure 4. Typical mined tunnel construction sequence.

6 PROJECT A TUNNELS - WATER SUPPLY TUNNEL CROSSING

Twin mainline tunnels located within the Hawkesbury Sandstone passed over the water supply tunnel with approximately 7.4 m clearance. The mined tunnels were approximately 20 m wide, which enabled the heading to be divided into a smaller lead and trail and they were constructed as described in Section 5 and Figure *7*.

A number of borehole-triaxial-geophones were installed to measure peak particle velocity (PPV) within the rock adjacent to the water supply tunnels. The geophones were installed in boreholes, which considered surface restrictions such as roads, cadastral boundaries and the exclusion zones around the water tunnels, within the Hawkesbury Sandstone near the crossings of the mined tunnels before any construction in the area.

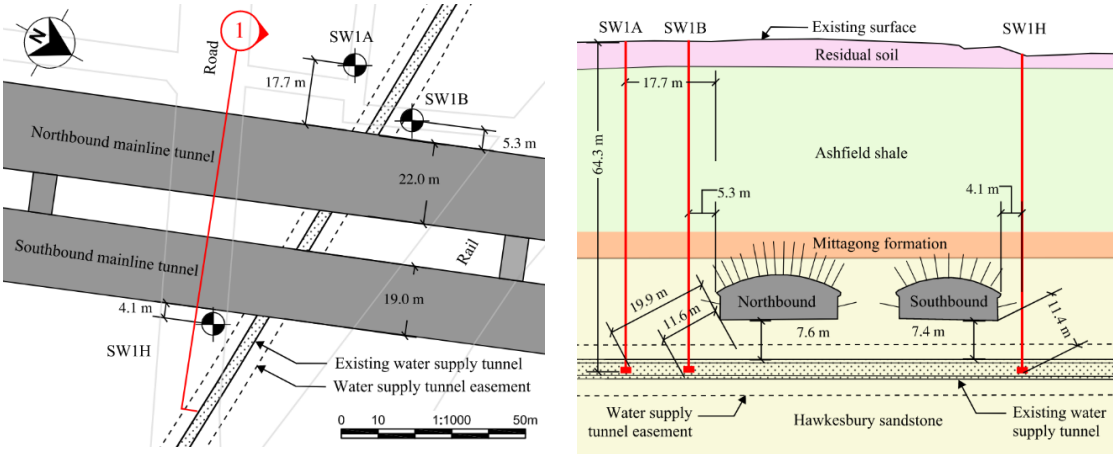


Figure 5. Location (plan and section) of geophones near Water Supply Tunnel.

7 PROJECT B TUNNELS - CROSSING UNDERNEATH EXISTING BUILDINGS

As shown in Figure 6, the Project B tunnels, which comprised twin mainline tunnels which were 13.5 m to 20 m wide and a 12 m wide exit ramp tunnel are located within fresh, medium to high strength Hawkesbury Sandstone. The tunnels passed over the mass-transit tunnels and under the basement of an existing building. The respective clearances varied from 6.8 m to 14 m. The ramp tunnel was advanced in an east-west direction commencing at the tunnel portal several months ahead of the mainlines. As shown in Figure 7, a typical sequential excavation sequence was adopted which comprised a lead and trail heading.

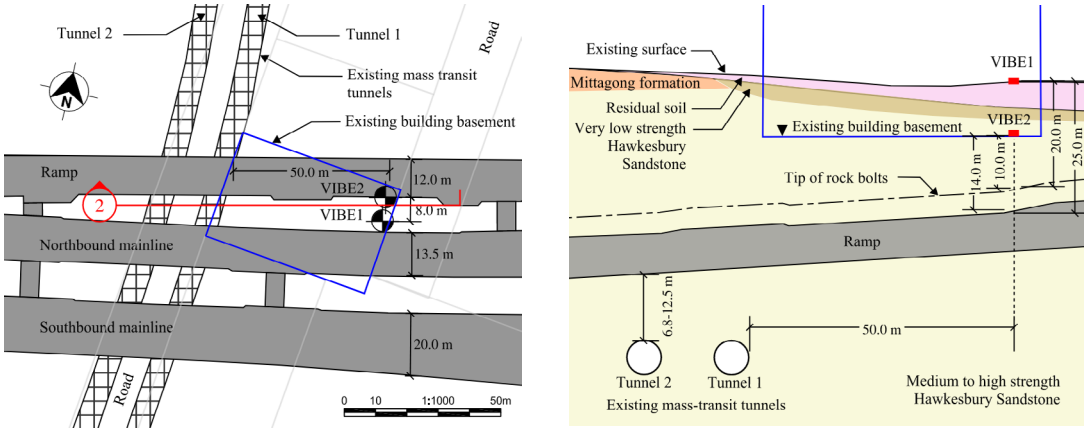


Figure 6. Location (plan and section) of vibration monitoring devices near existing buildings.

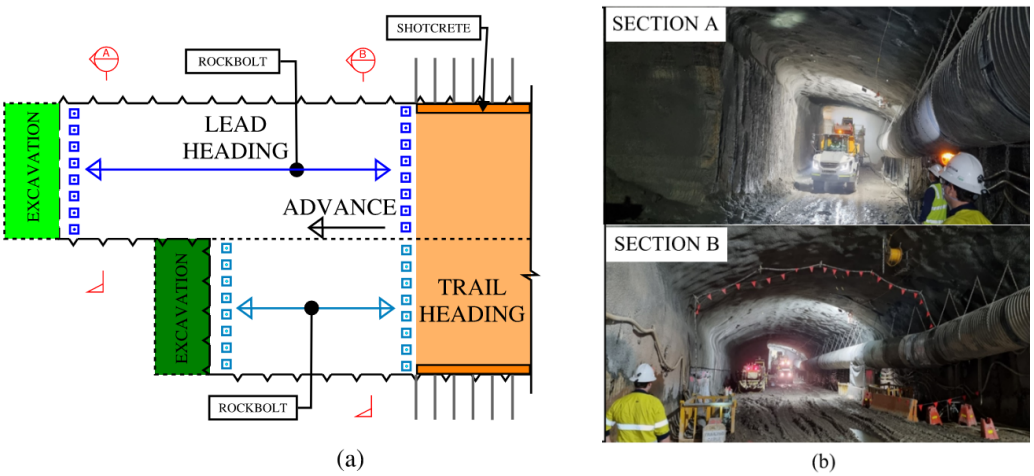


Figure 7. Project B (a) Plan showing typical sequential excavation sequence. (b) Lead and trail headings.

Wireless vibration monitoring units (refer to Figure 3) were placed in two locations within and adjacent to an existing school because of access restrictions during term time. One device (VIBE 1) was placed just below the ground surface (at RL 84 m) adjacent to a school building and the other within a pool basement plantroom (VIBE 2) (at RL 73.4 m), 10 m below ground surface. These devices were located 25 and 14 m respectively above the ramp tunnel. Regular monitoring commenced when tunnel headings were approximately 150 m away from the units.

It is important to note that the data collected and presented within this paper is from the construction of the ramp tunnel only. This drive has been selected as the crown level is the shallowest and hence excavation was closest to the vibration loggers. Furthermore, the data collected includes the monitoring device within the building, i.e. there is a direct correlation between the vibration source (the construction plant) and the vibration experienced within the building. Whereas the data presented from Project A tunnels was from the monitoring devices adjacent to an asset, i.e. there is an inference that the vibration experienced by the asset would be similar to that experienced by the surrounding ground.

8 ANALYSIS OF FIELD MONITORING DATA

8.1 Project A Tunnels

The vibration readings from the construction of the mainline tunnels adjacent to the crossing of the water tunnel, with an interval of one minute, measured in three directions. For the geophones SW1A, SW1B and SW1H, the highest velocities recorded during the tunnelling activity before approaching the geophones were 0.19 mm/s, 0.29 mm/s and 0.30 mm/s for the distances of 19 m, 11.5 m and 11.5 m respectively. The combined daily average vibration data from the three geophones from Project A and 2 devices from Project B has been presented in Figure 8. This figure illustrates how vibration levels change as the distance from the geophone to the excavated face varies.

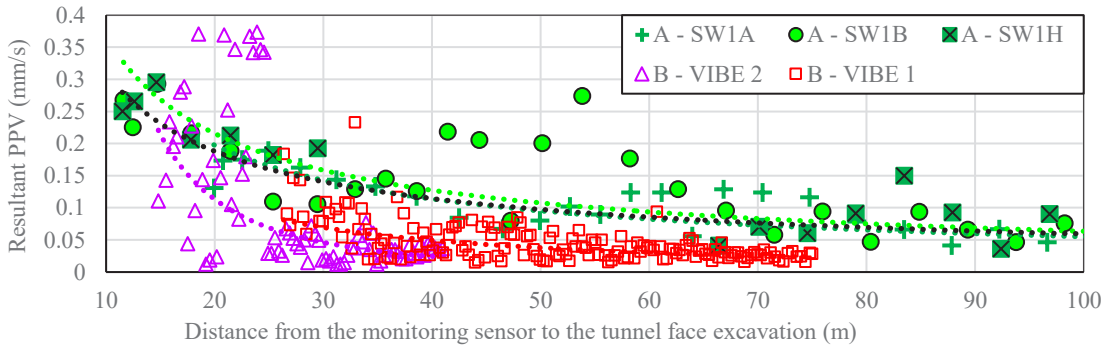


Figure 8. Major tunnel projects - PPV vs distance (combined lead and trail heading excavation, daily average)

8.2 Project B Tunnels

The vibration readings from the construction of the ramp tunnel were collected from Tunnel crossing just below the ground level and basement level, measured in three directions. The highest daily average velocities recorded by the geophone during the tunnelling activity was less than 0.35 and 0.4 mm/s for the distances of 25 and 14 m, respectively refer to Figure *8*.

8.2.1 Analysis of Sequential Excavation Sequence

An analysis of the excavation and support cycle was undertaken in order to confirm which activity causes the greatest vibrations. Construction reports were analysed and compared against the vibration data from the monitoring devices (VIBE 1 & VIBE 2).

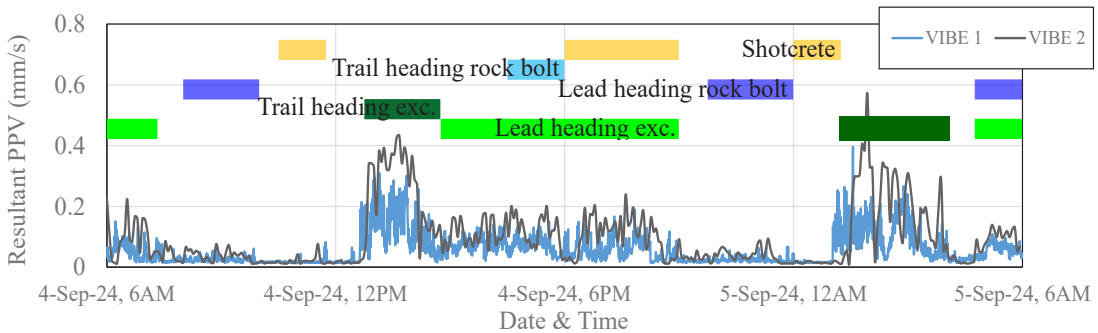
The resultant PPV and construction activity has been plotted against time was assessed over a three-week period during which the excavation passed by the location of the geophone shown in Figure 6. An example of the assessment is shown in Figure 9.

The vibration levels are initially low due to the large distance between the excavation face and the monitoring device, but they gradually increase as the tunnel advances, and the separation reduces.

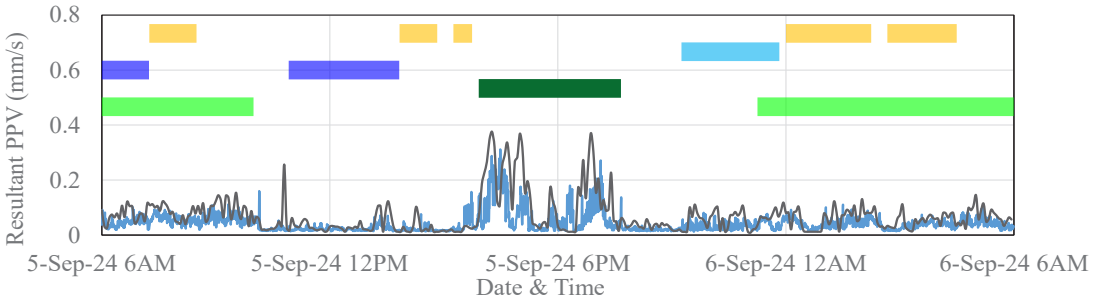
The vibration induced by trail heading ranges from approximately 0.15 mm/s to 0.6 mm/s, whereas the lead heading generates vibrations between 0.15 mm/s and 0.2 mm/s. This is expected because the trail heading is closer to the monitoring device than the lead heading. Furthermore, as the heading moves away from the monitoring device, vibrations are generally lower because distance is increasing but this would also be attributable to the removal of rock as the medium through which vibrations propagate.

When the excavation face was closest to the monitoring device, the vibration due to rock bolt installation varied from approximately 0.025 mm/s to 0.1 mm/s since the activity typically occurred 2 to 3 m back from the tunnel face, i.e. lower than excavation. In addition, when excavation and rock bolt installation occur simultaneously, there was no discernible increase in vibration.

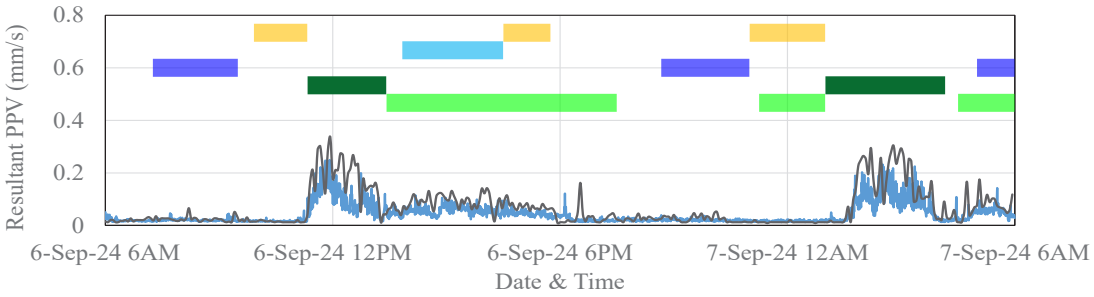
Furthermore, the vibrations due to the application of shotcrete were lower than either of the other activities because there is no impact on the surrounding rock mass.



(a) Vibration data just before trail heading reaches the sensors



(b) Vibration data when trail heading reaches the sensors



(c) Vibration data just after trail heading passes the sensors

Figure 9. Vibration (PPV) and Construction Activity vs Time.

8.3 Combined Monitoring Data

To enable a comparison with the data presented by Hiller 0 and Hackney 0 and demonstrate how sequential excavation using roadheaders compares with construction activities in a similar vibration range, data from Project A and B has been plotted against distance on Figure *10*.

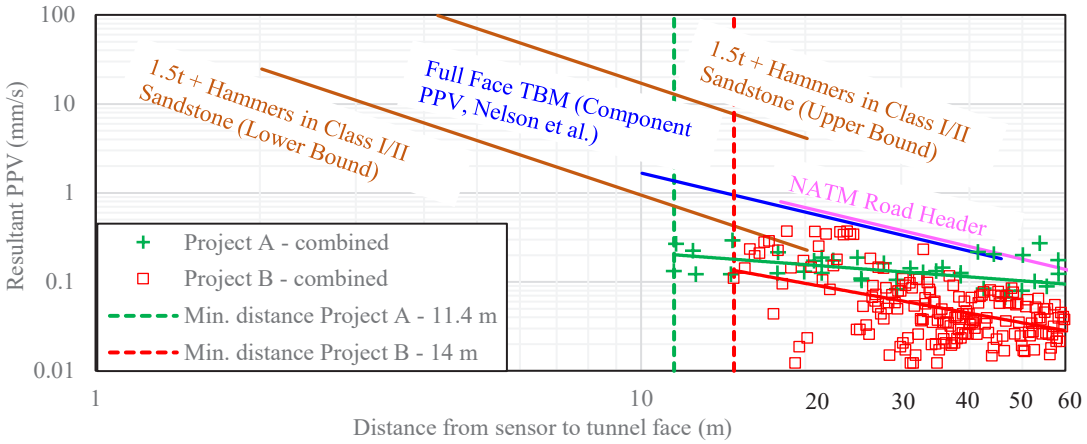


Figure 10. Vibration (PPV) vs distance for various construction activities.

Data from each monitoring device for each project has been combined and presented as the two series shown. Furthermore, each data set has been curtailed 60 m from the monitoring device because as shown in Figure 8, at greater distances, vibration reduces to background levels (0.05 mm/s). Trendlines indicate that vibrations associated with the use of roadheaders in Hawkesbury Sandstone are lower than the other construction techniques plotted by Hiller 0 and Hackney 0.

8.4 Background Vibration

Vibration sensors (refer to Figure 3) were fixed to the surface of the tunnel linings within the existing operational mass-transit tunnels, where trains were passing at intervals of 3 to 5 minutes and the highest vibrations recorded were 4 mm/s (Refer to Figure *11*). The vibration due to tunnel construction has been overlaid from VIBE 1. During the period between 12 pm and 2.30 pm on 5th Sept 2024, when no construction activities were occurring and the trains were running, the vibration levels were similar to the background levels (less than 0.05 mm/s), i.e. no vibration within the building was attributable to the operating trains.

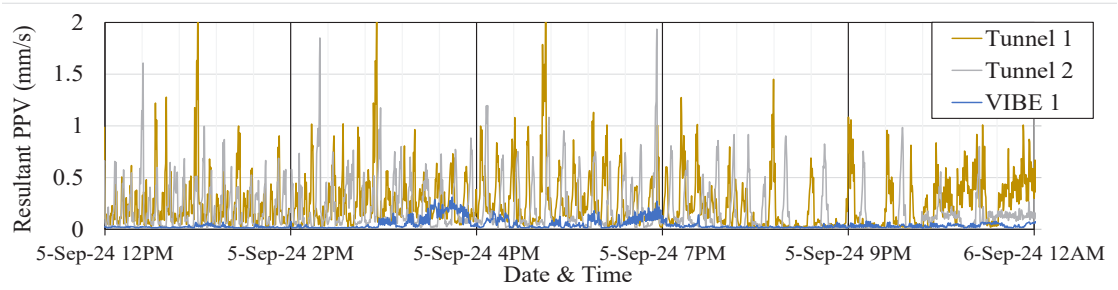


Figure 11. Vibration (PPV) vs time within the mass-transit tunnels.

9 CONCLUSIONS

Vibration monitoring was undertaken at multiple existing underground assets. The results show that in competent rock such as fresh, medium to high strength Hawkesbury Sandstone, vibration levels generated by roadheader excavation are typically well within threshold limits and do not pose a significant risk to most underground infrastructure. Results also suggest that vibration levels generated as close as 15 m to underground infrastructure results in vibration levels significantly lower than the most stringent vibration alarm criteria.

Based on the monitoring results presented in Figure 10, it is estimated that the vibration impact due to the construction of the tunnels using roadheaders will be less than an average of 0.4 mm/s, within a distance of 12m, which is insignificant in comparison to the threshold limits for water supply / train tunnels (3 to 20 mm/s), and structures / buildings (1.5 to 25 mm/s). The magnitude of vibrations associated with mined tunnel construction is also insignificant compared with the vibrations imposed on a tunnel lining due to the operation of mass-transit trains (4 mm/s). It was also observed that vibration greater than 60 m away from a monitoring device is insignificant.

10 REFERENCES

Hackney, G.A. 2002. Excavation induced vibrations in Sydney sandstones. *Proceedings 5th Australian New Zealand Young Geotechnical Professional Conference, Australian Geomechanics Society, NZ.*

Hiller, D. 2011. The prediction and mitigation of vibration impacts of tunnelling. *Proceedings of the Acoustics—Breaking New Ground, pp.2-3.*

Federal Transit Administration. 2018. Transit noise and vibration impact assessment manual. *US Department of Transportation, John A. Volpe National Transportation Systems Center.*

Sydney Water. 2001. Specialist engineering assessment procedure.

Sydney Metro. 2021. Sydney Metro Underground Corridor Protection Technical Guidelines.

Sydney Metro City & Southwest. 2017. Construction Noise and Vibration Strategy.

TfNSW. 2018. Development Near Rail Tunnel Version 2.0. *Transport for New South Wales Standards.*

BS7385:2 1995. Evaluation and measurement for vibration in buildings.

BS5228:4 1992. Code of practice for noise and vibration control applicable to piling operations.

19th Australasian Tunnelling Conference – Acosta-Martínez, Stewart and Hudson-Smith (Eds.)
© 2025 Australian Tunnelling Society, ISBN 978-0-85825-002-4

Towards reliable UCS inputs for tunnel design: Learnings from Snowy 2.0

A. Chen & M. Zoorabadi
SMEC, Australia

K. Stariha
Snowy Hydro Limited, Australia

ABSTRACT: UCS is a critical parameter in underground tunnel design, serving as a fundamental input for numerical modelling. However, current practices in tunnel design often face challenges due to reliance on UCS results obtained during the geotechnical investigation stage, where limited borehole coverage may lead to a biased estimation. Variations in UCS results across laboratories can introduce inconsistencies due to differences in apparatus, interpretation methods and descriptions of failure mode. This paper addresses these gaps by leveraging the extensive UCS testing conducted for Snowy 2.0 project, particularly in its power station caverns. The project not only incorporated a wide range of UCS but also executed a proficiency test across labs using identically prepared grout samples. The study features a statistical analysis, a failure type screening and a discussion of using UCS in Hoek-Brown's criterion. This work underscores the importance of UCS data processing and its critical role in bridging gaps in current geotechnical practices

1 INTRODUCTION

Uniaxial Compressive Strength (UCS) and Young's Modulus (E) are fundamental parameters in the design and construction of underground works. UCS provides a direct measure of the peak compressive strength of intact rock under unconfined conditions, while E quantifies the elastic stiffness of the rock, governing its deformation response under applied stress. Accurate determination of both parameters is essential for numerical modeling, support design, and predicting ground behavior during and after excavation. Although there are other more advanced laboratory and in-situ tests available for characterizing rock strength and deformation properties, the UCS test remains widely used in the industry due to its simplicity and cost-effectiveness. Both UCS and E can be derived from a single test procedure, making it highly efficient in terms of sample usage and testing time. The straightforward setup and minimal equipment requirements, make the test a practical choice for site investigations, however there are limitations inherent in the test process itself which are not always accounted for in practice. Geological variability, laboratory practices, and data interpretation methods can significantly affect the derived inputs. This paper will utilize the UCS test data obtained from the geotechnical investigations conducted as part of the Snowy 2.0 project. The extensive database from this large-scale infrastructure development provides a valuable opportunity to examine the reliability, variability, and practical interpretation of UCS and E modulus results in the context of real-world engineering applications. The study will focus on UCS and E as design inputs only and will not comment further on other inputs for rock mass strength estimation.

2 PROJECT OVERVIEW AND SCOPE OF THE STUDY

Snowy 2.0 is a major pumped hydro expansion of the Snowy Mountains Hydroelectric Scheme in New South Wales, Australia, aimed at providing large-scale energy storage and grid stability to support the nation's transition to renewable energy. The Power Station Complex (PSC) is a major feature of Snowy 2.0, consisting of a Machine Hall and a Transformer Hall, with a maximum span of 33m and overburden of 600-750m (Figure 1).

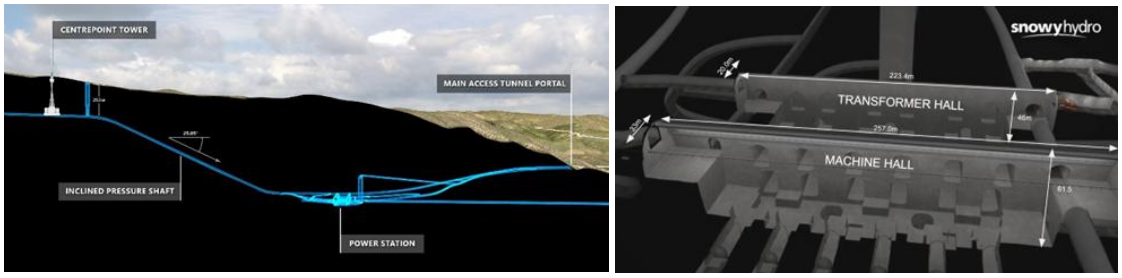
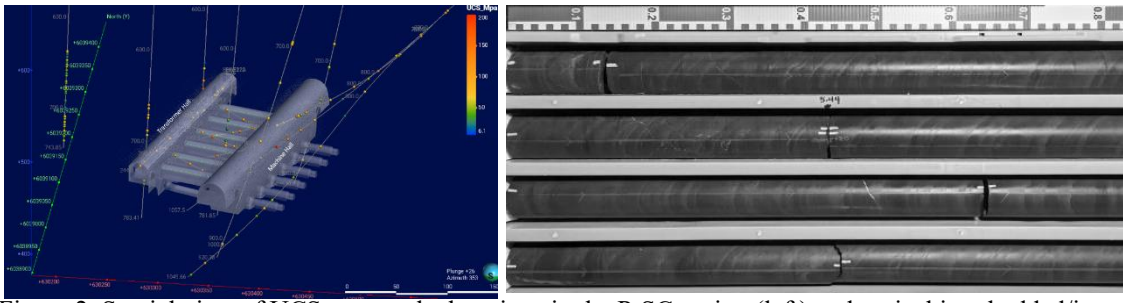


Figure 1. General location and layout of the PSC.

A total of 247 UCS test results were compiled, incorporating data from cored holes undertaken both pre-construction from the surface and during construction, into the PSC area from adjacent construction tunnels (Figure 2). The majority of UCS tests were performed in accordance with AS 4133.4.3.1 and AS 4133.4.3.2, which also outline deformability-related parameters such as Secant (E_s) and Tangent (E_t) Young's Modulus and Poisson's Ratio (v). Results have been used to inform the intact rock strength during the design phase, as well as to support design verification throughout the construction phase. This study will focus on the examination of the two principal parameters derived from this testing - UCS and E_s values of 69.1 MPa and 45.1 GPa respectively, with standard deviations of 35.7 MPa and 13.2 GPa.


Figure 2. Spatial view of UCS test results locations in the P SC region (left) and typical interbedded/interlaminated sandstone & siltstone in RBW formation (Right).

The PSC area is set in the Silurian age Ravine Bed West Formation (RBW), which comprises interbedded to interlaminated metasiltstone and metasandstone, with minor conglomerate. Due to the involvement of several laboratories over a period of 7 years, the lithological descriptions and break types recorded during UCS testing were not consistent across all datasets. To address this, the project owner's geology team re-assessed the lithology and break types of all tested samples, ensuring greater consistency and accuracy in classification. As a result of the re-assessment of lithology, the 247 samples were classified as follows: 233 samples as interbedded or interlaminated sandstone and siltstone, 6 samples as conglomerate, 5 samples as interbedded conglomerate and sandstone, and 3 samples as sandstone. Since the influence of grain size variation in sedimentary rocks on UCS and E_s is well documented/ and observed (UCS for 3 sandstone samples vary from 182-270 MPa, significantly larger than global mean), and most of the samples (233 out of 247) are classified as interbedded or interlaminated sandstone and siltstone, the subject of this study is limited to this lithological group.

3 ASSESSMENT OF FAILURE MODE ON UCS AND YOUNG'S MODULUS

3.1 *Re-assessment of failure mode: Intact vs Discontinuity-controlled*

An overview of the data and laboratory reports indicates that both UCS and E_s exhibit high variability. In addition, many samples show failure modes influenced by natural defects, suggesting that these results are not fully representative of intact rock properties. Variations in failure mode descriptions, even within the same laboratory, further complicate the differentiation between intact and discontinuity-controlled failures. To address this, the owner's engineering team re-assessed the failure modes using a project-specific guideline developed based on the work of Basu et al. (2013) and Chakraboty et al (2019). The failure mode classifications are summarized in Table 1, along with a pie chart illustrating the distribution following re-assessment. Representative core samples for each typical failure mode are presented in Figure 3. Spalling failure mode is excluded from assessment since it is considered as a premature and therefore invalid mode.

The distributions of UCS and E_s are presented in Figure 4, showing both histograms categorized by failure mode and normalized probability distribution curves. Key statistical results are summarized in Table 2. For UCS, samples exhibiting Joint/Vein failure modes display significantly lower strength, with a mean value of 37.7 MPa compared to the overall mean of 65.8 MPa. In contrast, samples with Shattered failure modes show substantially higher UCS values, with a mean of 100.2 MPa. Other failure types exhibit mean UCS values relatively close to the global mean. A similar trend is observed for E_s; however, the variance between failure modes is considerably smaller, suggesting that E_s is less sensitive to failure mode differences compared to UCS.

Table 1. Failure modes and description assigned by Owner's Engineering team

	Description	Summary
Shear	Break along single or multiple shear plane	Intact rock failure
Split	Axial splitting / Tensile dominated	Intact rock failure
Shatter	Shattered	Intact rock failure
Bedding	Break along foliation, bedding or cleavage	Discontinuity induced failure
Joint/Vein	Break along natural defect (joint, vein)	Discontinuity induced failure
Mixed mode	Break along multiple axial planes	Combination of intact and discontinuity failure
Spall	Minor break	Intact rock failure (premature, invalid)

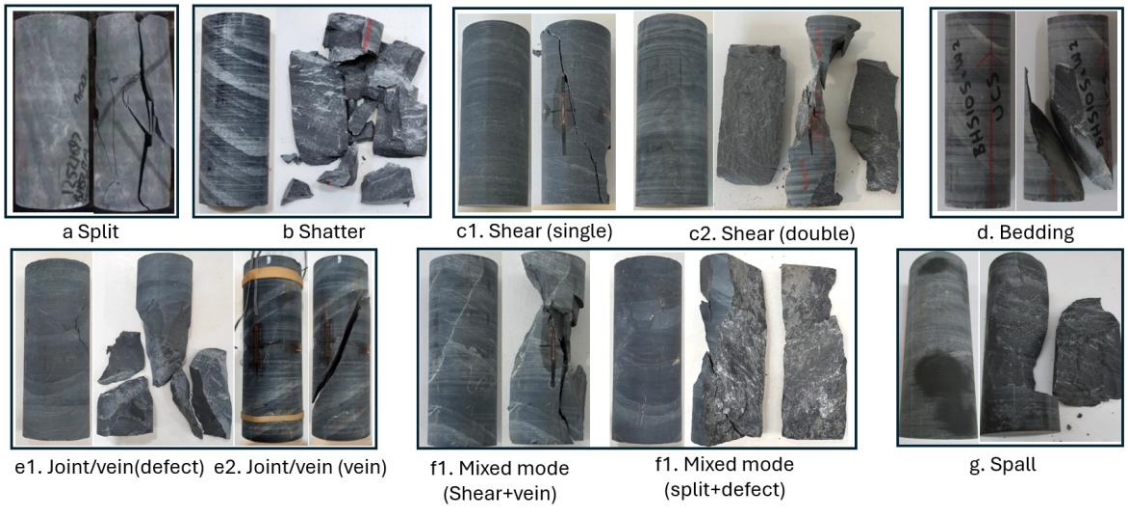


Figure 3. Examples of typical assigned failure modes, with samples before test at the left.

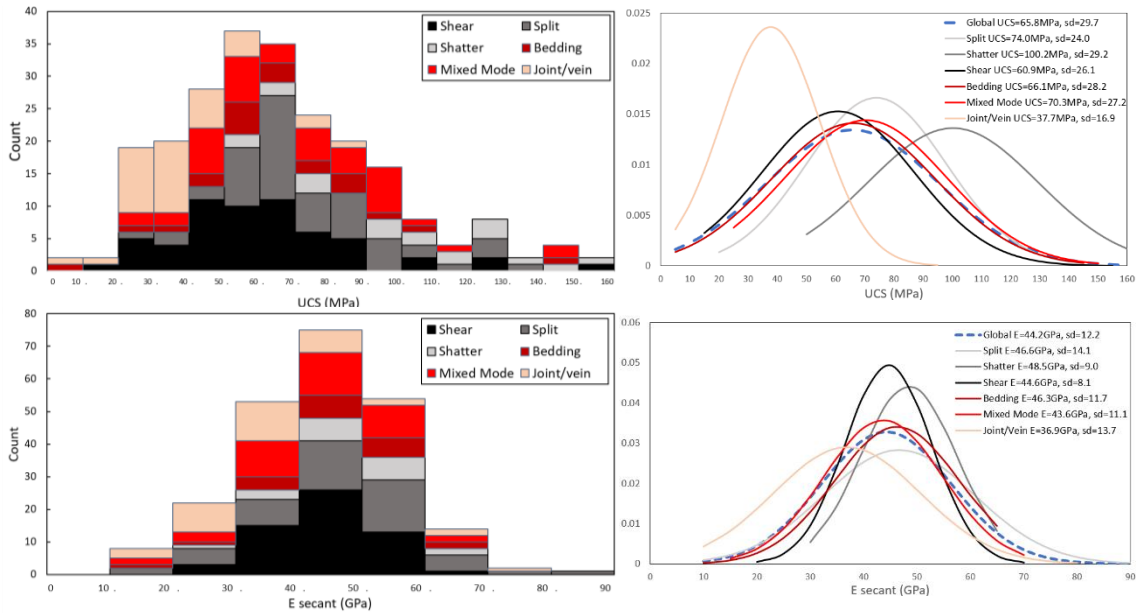


Figure 4. UCS (top) and E_s (bottom) distribution for different failure modes, presented by histogram (left) and normalized probability curve (right).

Table 2. Summary of statistical analysis results for UCS and E_s with different failure modes

		UCS			E_s		
Failure Mode	Count	Mean	Median	Mode	Mean	Median	Mode
Split	55	74.0	68.4	60-70	46.6	48.8	50-60
Shatter	20	100.2	100.2	N.A.*	48.5	48.9	40-50,50-60
Shear	58	60.9	58.4	50-60	44.6	45.8	40-50
Bedding	21	66.1	64.5	50-60	46.3	47.9	40-50
Mixed Mode	41	70.3	66.4	N.A.*	43.6	45.4	40-50
Joint/Vein	36	37.7	33.2	30-40	36.9	35.6	40-40
Global	233	65.8	64.4	50-60	44.2	64.4	40-50

*Modes for Shatter and Mixed mode is not defined due to 3 or more bins with the same count, which also indicates the UCS for these two are non-normally distributed. Refer to Histogram in Figure 4 for explicit data.

It should be noted that, as the reassessment relied primarily on photographs provided in laboratory reports (which were often unclear), substantial weight was still placed on the original laboratory descriptions. Additionally, the term "Mixed Mode" can be ambiguous when differentiating between intact and discontinuity-controlled failures: while some Mixed Mode cases involve combinations of intact failure mechanisms, others clearly involve discontinuity-driven behaviour. This mixed nature also explains why the average UCS and E_s values for Mixed Mode samples are relatively close to the global mean, reflecting the contribution of both stronger intact failures and weaker discontinuity-controlled failures within this group. To maintain a conservative approach, for this study all Mixed Mode failures were classified as discontinuity controlled.

3.2 *Further discussion on Veins and Beddings controlled failure*

In the failure modes described in 3.1, “Joint/Vein” failure mode is assigned if a failure plane occurs along visible surface veins. Within the RBW formation, veins are often present (Figure 2 and Figure 3), however the nature of veins varies in orientation (random or parallel with bedding), aperture and mineralogy – all of which may affect the UCS. Furthermore, micro-veins may be present which are not easily visible. This may trigger initial cracking at a lower strength, mislabeling the failure type to intact modes. The influence of veins on UCS has been discussed extensively in the literature (Everall 2019, Martin 2022, Rudderham 2023, Wang 2025), the author does not intend to elaborate further but wishes to emphasize the importance of identifying and

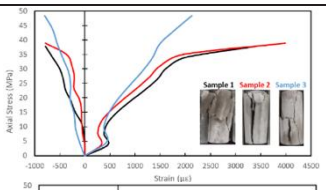
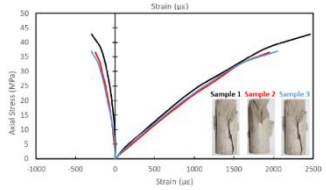
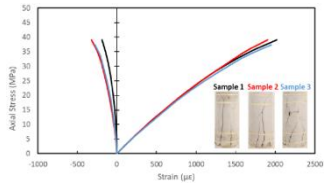
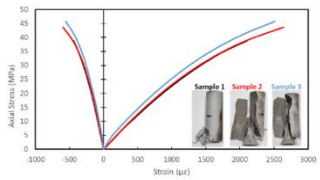
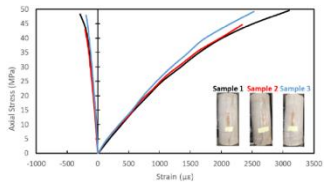
recording vein features during construction, as they can have a significant impact on the assessment of intact rock strength.

The "Bedding" failure mode (occurring along sandstone–siltstone bedding / laminations) presents similar challenges. Only a small proportion of samples failed in this mode. Both very low and very high UCS results were observed within this category, and in some cases intact failures had lower results than bedding failures. The impact of bedding on UCS has been studied by researchers like Davarpanah et al (2020), however as this topic involves complex geological and mechanical interactions, the author does not intend to elaborate further but notes its significance for interpretation.

4 EFFECTS FROM LABORATORY PRACTICES FACTORS

While analysing the data, the owner's engineering team observed that laboratory practices themselves may contribute to variation within the dataset. To further investigate this, a "proficiency test" was conducted. Theoretically identical grout specimens were sent to five laboratories 4 contracted to Snowy 2.0 and one external, labelled A, B, C, D, E. Each laboratory tested three samples followed the procedures outlined in AS 4133.4.3.2, while one (Lab E) followed the ISRM Suggested Methods. Unlike typical laboratory reporting, raw data files were also made available for independent interpretation by the engineering team. The key results of the proficiency test are summarized in Table 3, along with stress–strain curves re-generated from the raw data.

Table 3. Key results from the internal proficiency tests, with max. & min. values underlined.

LAB	ID	UCS (MPa)	E_s (GPa)	v	Failure Mode	Stress vs Strain plot
A	A1	38.0	28	0.27	shear	
	A2	39.0	30	0.18	shear	
	A3	48.0	25	0.29	shear+split	
B	B1	42.8	23.3	0.06	shear+split	
	B2	36.6	22.2	0.10	shear	
	B3	37.0	22.5	0.11	shear	
C	C1	39.0	24	0.05	split	
	C2	39.0	24	0.12	shear+split	
	C3	37.0	24	0.10	shear+split	
D	D1	38.9	23.2	0.20	spalling	
	D2	43.6	23.3	0.20	shear	
	D3	45.7	24.5	0.20	shear	
E	E1	49.7	24.1	0.16	split	
	E2	44.7	25	0.13	split	
	E3	49.3	23.7	0.12	split	

Despite the use of theoretically identical specimens and four (A, B, C, D) laboratories following the same AS 4133.4.3.2 standard, noticeable variation is observed. UCS values range from 36.6 MPa to 48 MPa, showing a spread of around ±15%, while E_s values are more consistent, clustering between 22 GPa and 30 GPa. Failure mode classification shows greater inconsistency. For Lab A, a constant loading rate was not achieved, making its higher E_s questionable. The variation observed, even under common testing standards, highlights that laboratory practice and control (rather than methodology differences) are key contributors to data variability, emphasizing the need for stricter procedural enforcement to ensure reliable results.

4.1 *Further discussion on effects of loading rate*

For the proficiency test described above, Laboratory E followed ISRM Suggested Methods rather than AS 4133.4.3.2. The primary difference between the two standards lies in the loading rate requirements: AS 4133.4.3.2 specifies a displacement rate of ≤ 0.1 mm/min, whereas ISRM requires a constant stress rate of 0.5–1.0 MPa/s. This difference appeared to directly contribute to higher UCS results for Laboratory E. To further investigate this effect, graphs of loading rate and test duration versus UCS have been plotted in Figure 5, using both the proficiency test data and the Snowy 2.0 PSC SI sample results. Clear correlations between loading rate, test duration, and UCS are evident. No such trend was observed for E_s; therefore, it is not presented.

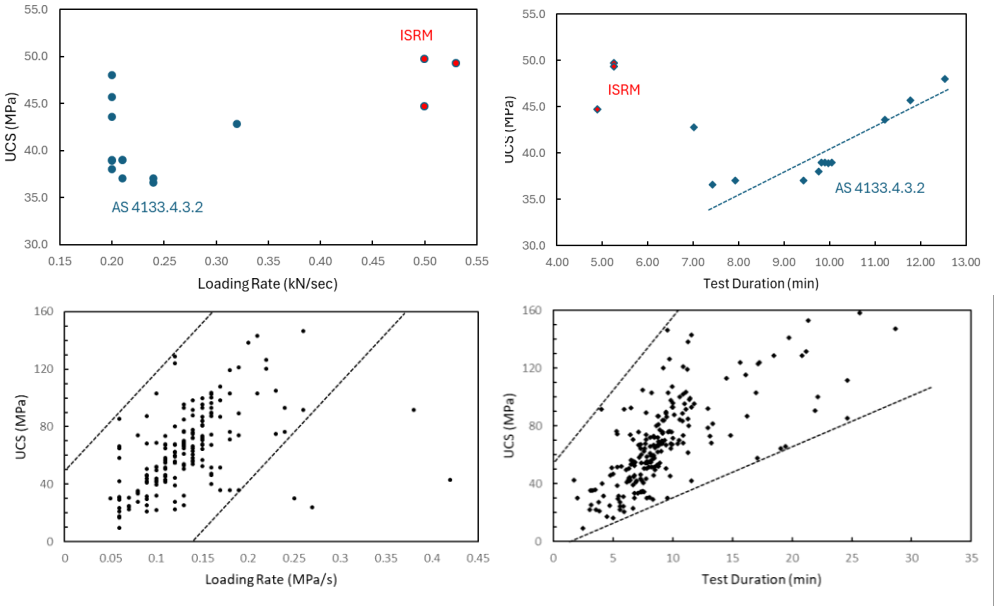


Figure 5. Plots of Loading Rate (left) and Test Duration against UCS. Results from top are from the proficiency test and bottom are from Snowy 2.0's site investigation UCS tests.

The effect of loading rate on UCS is a well-known and extensively discussed topic, encompassing aspects such as ductile versus brittle behavior, energy dissipation mechanisms, strain rate sensitivity, and crack propagation dynamics (Cao 2019, Závacký 2019). As these discussions are highly scientific and outside the intended scope of this study, the author instead highlights two key practical observations: (1) Loading rate requirements vary significantly across different codes and standards, as shown in Table 4. The bias introduced by different loading controls can be substantial. For example, in the Snowy 2.0 PSC dataset, all tests with recorded loading rates were below 0.4 MPa/s, which is below the minimum specified in EN 1926:2006 and the ISRM Suggested Methods (2) Among the standards considered, AS 4133 is the only one that differentiates loading rate requirements based on rock strength. While this appears to be a reasonable approach, it has introduced complications where the sample strength is close to the boundary between methods. E.g., in the Snowy 2.0 PSC dataset 29% of samples lie between 40-60 MPa. This raises the

question of whether the appropriate standard procedures were consistently applied for UCS values in these cases.

Table 4. Requirement on loading rates from different standards & codes

Standard	Loading Rate Requirement
AS 4133.4.3.1:2009 (UCS ≥ 50 MPa)	Load continuously at a constant stress rate so that failure occurs within 5–15 minutes.
AS 4133.4.3.2:2022 (UCS < 50 MPa)	Load continuously without shock; achieve a displacement rate ≤ 0.1 mm/min.
EN 1926:2006 (2006)	Load continuously at a constant stress rate of (1 ± 0.5) MPa/s.
ASTM D2938-95 (2017)	Load continuously without shock. Maintain a constant stress or strain rate to produce failure between 2–15 minutes. Stress/strain rate must not deviate by more than ±10%.
ISRM Suggested Methods (2018)	Load continuously at a constant stress rate of 0.5–1.0 MPa/s, aiming for failure within 5–10 minutes.

5 DISSCUSSION ON USING OF UCS RESULTS IN HOEK-BROWN CRITERION

In rock-mass parameter interpretation, the GSI–Hoek-Brown system is typically combined with the Hoek–Diederichs modulus equation to build the constitutive model. The Hoek-Brown formulation treats the intact unconfined compressive strength (σ_{ci}) and intact material constant (m_i) as baseline inputs that are subsequently reduced by GSI and disturbance factors to give rock-mass parameters. Hoek & Brown (1968, 1983, 2018, 2023) have consistently highlighted the preference for triaxial testing over UCS testing in the derivation of σ_{ci}, noting that many UCS specimens fail by axial splitting or mixed tensile mechanisms, whereas the criterion is intended to describe shear failure. Bewick et al. (2015, 2019) likewise advise excluding UCS results from σ_{ci} determination unless failure-mode screening is performed to include only specimens that show a clear shear break. Snowy 2.0 PSC samples were tested with a complete, high-quality triaxial programme that satisfies the original Hoek (1983) requirements σ_{ci} has been derived directly from triaxial data using the recommended regression procedure (Table 5). The derived σ_{ci} is 97.5 MPa, significantly larger than the global UCS (65.8 MPa) and the suggested shear-mode failure UCS (60.9 MPa), but interestingly close to the shatter-mode failure UCS (100.2 MPa). This warrants additional investigation together with the consideration of effects from loading rates & microstructures, as discussed earlier.

Table 5. σ_{ci} and m_i from Snowy 2.0 triaxial results, calculated following Hoek (1983).

Test ID	Rupture angle	R^2	σ_{ci} (MPa)	*mi*
1a	75	0.96	59.9	5.08
1b	70	0.88	97.3	5.64
2a	50	0.99	104	7.15
2b	60	0.99	98.2	8.13
4a	45	0.90	99.8	6.65
4b	60	0.96	119	9.37
5a	70	0.94	89.1	7.74
5b	70	0.98	112	7.54
Mean	62.5	0.95	97.5	7.16

6 CONCLUSION AND RECOMMENDATION

This paper investigated the processing and reliability of UCS data based on the extensive Snowy 2.0 database. A project-specific re-assessment of lithology and failure modes significantly enhanced the clarity of the dataset and demonstrated the value of targeted re-screening in improving

the interpretation of UCS. Two key sources of variability were identified: (i) laboratory practices, and (ii) the broad and often loosely defined loading-rate requirements across existing standards, particularly the impracticality of the 50 MPa boundary specified in the AS 4133.4.3.1 and AS 4133.4.3.2. Noting the difficulties in such a task, an industry-wide discussion is recommended on the specification of loading rates in testing standards. Alternately, major projects could consider adopting a project-specific loading-rate specification after achieving a good understanding of the fundamental geotechnical conditions. It is worth highlighting the importance of supervising, reviewing, and providing feedback to laboratories to ensure the ongoing reliability of test results. Additionally, comparison between UCS-derived inputs and industry-standard Hoek-Brown rock mass estimation methods revealed that UCS results tended to underestimate the intact compressive strength (σ_{ci}) relative to triaxial regression. These findings highlight the importance of a rigorous, site-specific approach to selecting design parameters for numerical modelling and empirical assessments.

Snowy 2.0's unusually large, fully documented dataset offers a rare benchmark for deeper study of loading-rate effects, laboratory reproducibility and intact-to-rock-mass conversions. Continued scientific analysis of this material is strongly encouraged to refine test standards and to anchor empirical design methods in more defensible, project-specific evidence.

7 REFERENCES

ASTM International (2017). ASTM D2938–95: Standard Test Method for Unconfined Compressive Strength of Intact Rock Core Specimens.

Basu A, Mishra A, Roychowdhury K (2013) Rock failure mode sunder uniaxial compression, Brazilian, and point load tests. Bull Eng Geol Environ 72:457–475.

Bewick, R. P.et al. (2015). Interpretation of UCS Test Results for Engineering Design. Proceedings 13th International Congress of Rock Mechanics - ISRM Congress 2015, Montreal, 1-14.

Bewick, R. P.et al. (2019). Strength of massive to moderately jointed hard rock masses. Journal of Rock Mechanics and Geotechnical Engineering, 11, 562-575.

Cao, S. et al. (2019). Loading rate effect on uniaxial compressive strength behavior and acoustic emission properties of cemented tailings backfill. *Construction and Building Materials* 213 (2019) 313–324.

Chakraboty, S. et al (2019). Failure Modes of Rocks under Uniaxial Compression Tests: An Experimental Approach. Volume 2, Issue 3. Journal of Advances in Geotechnical Engineering.

Davarpanah, S.M. et al. (2020). Technical Note: Determination of Young's Modulus and Poisson's Ratio for Intact Stratified Rocks and their Relationship with Uniaxial Compressive Strength. *AUSTRALIAN GEOMECHANICS VOLUME* 55: NO.4.

European Committee for Standardization (CEN) (2006). EN 1926:2006: Natural Stone Test Methods – Determination of Uniaxial Compressive Strength.

Everall, T.J. et al. (2018) The Influence of Pre-Existing Deformation and Alteration Textures on Rock Strength, Failure Modes and Shear Strength Parameters. *Geosciences* 2018, 8(4), 124.

Hoek, E (1968). Brittle Fracture of Rock. Rock Mechanics in Engineering Practice.

Hoek, E (1983). Strength of jointed rock masses. Lecture notes. Geotechnique, Vol.23, No.3, 1983, pp. 187-223.

Hoek, E & Brown, E.T (2019). The Hoek-Brown failure criterion; and GSI – 2018 edition. Journal of Rock Mechanics and Geotechnical Engineering 11 (2019) pp. 445-463.

Hoek, E. (2023). *Practical Rock Engineering*, Chapter 3: Intact Rock Strength. Toronto: Rocscience Inc., 34 pp. Available at: https://www.rocscience.com/learning/practical-rock-engineering.

International Society for Rock Mechanics (ISRM) (2018). Suggested Methods for Determining the Uniaxial Compressive Strength and Deformability of Rock Materials.

Martin, L et al. (2022). Relationship between fissility, composition, rock fabric and reservoir properties in Vaca Muerta Formation (Neuquén Basin, Argentina): from outcrop to subsurface core data. *Andean Geology* 49(3).

Rudderham, G.A. & Day, J.J. (2023). Veined Rock Performance under Uniaxial and Triaxial Compression Using Calibrated Finite Element Numerical Models. *Geotechnics* 2023, 3(4), 1219-1250.

Standards Australia (2009). AS 4133.4.3.1–2009: Method 4.3.1: Rock Strength Tests – Determination of Deformability of Rock Materials in Uniaxial Compression – Strengths of 50 MPa and Greater.

Standards Australia (2022). AS 4133.4.3.2–2022: Method 4.3.2: Rock Strength Tests – Determination of the Deformability of Rock Materials and Uniaxial Compressive Strength – Rock Strength Less Than 50 MPa.

Wang, H. et al. (2025). An Investigation of the Effect of Fissure Inclination on Specimen Deformation and the Damage Mechanism Based on the DIC Method. Buildings 2025, 15, 71.

Závacký, M & Stefanak, J (2019). Strains of Rock During Uniaxial Compression Test. Article No. 32, The Civil Engineering Journal 3-2019.

19th Australasian Tunnelling Conference – Acosta-Martínez, Stewart and Hudson-Smith (Eds.)
© 2025 Australian Tunnelling Society, ISBN 978-0-85825-002-4

Dyke encounters in the Sydney basin: Insights from 30 km of mined tunnel excavations

N. Lyons
John Holland Group, Australia

T. Nash
PSM, Australia

ABSTRACT: This paper presents observations from 66 intersections of dykes encountered across more than 30 km of mined tunnels in the Sydney Basin, primarily within Hawkesbury Sandstone. The data, collected from six major tunnelling projects including WestConnex and NorthConnex, focus on dyke geometry, material and mass characteristics, host rock mass condition, and groundwater behavior.

Dykes were found to be generally steeply dipping and aligned with regional joint sets, with two-thirds being less than 2 m thick and half less than 1 m. Intact strength estimates suggest a real trend of increasing strength with depth, attributed to reduced weathering and stress relief in deeper settings. While most dykes had good rock mass conditions, a small subset had significant clay seams and jointing. Host rock mass conditions reverted to background conditions typically within 5 m of the dyke margin and was generally greater at shallow depths. Groundwater seepage from dykes or the surrounding host rock was observed in under half the cases, with notable inflows limited to depths less than 50 m.

The findings suggest commonly a localized and occasionally significant impact of dykes on the host rock mass.

1 INTRODUCTION

This paper presents observations and geotechnical characteristics of volcanic dykes and adjacent rock mass conditions encountered during recent tunnelling projects across the Sydney metropolitan area. The study is based on data from six mined tunnel projects: all stages of the WestConnex development (including the M8, M4-M5 Link, M4 East, Rozelle Interchange, and Western Harbour Tunnel) and the NorthConnex project. Collectively, these projects represent over 30 km of tunnel excavation, predominantly within Hawkesbury Sandstone. Excavation was primarily undertaken using roadheaders, in either full-face or split-face configurations, with typical ground support comprising rock bolts and shotcrete in drained conditions.

Across these projects, 66 volcanic dyke intersections were mapped, some at depths of cover of up to 90 m. The focus of this paper is on characterizing the dykes and their immediate host rock in terms of material and mass properties. Mapping was undertaken during the excavation cycle, prior to shotcrete application, and from safe working distances. As a result, tactile field tests were generally not possible, and the data are largely qualitative. It also relies on visual interpretation by multiple mappers of varying backgrounds and experience.

1.1 Background

Sydney Basin is generally considered to have uniform geological conditions particularly for tunnelling, dominated by the Hawkesbury Sandstone, Mittagong Formation, and Ashfield Shale. These units have been extensively studied and are well understood in the context of tunnel design

and performance (e.g. Pells et. al., 1998; Bertuzzi, 2014). In contrast, volcanic dykes represent discrete zones of geological heterogeneity and introduce local complexity into an otherwise mostly predictable stratigraphy. These intrusions must be explicitly considered in tunnel design and construction due to their variable geometry, material strength, and hydrogeological behavior.

Doleritic and basaltic dykes typically occur as steeply dipping to vertical, sheet-like bodies that intruded along pre-existing discontinuities such as joints, faults, and shears within the sedimentary sequence. It remains uncertain to what extent the host rock conditions we observe today are a result of pre-existing weaknesses, the intrusion process itself, or subsequent weathering and stress relief. In some cases, the rock mass adjacent to dykes shows pronounced fracturing and degradation; in others, there appears to be little to no departure from background conditions.

Thermal alteration effects are occasionally observed at dyke margins, likely caused by the high emplacement temperatures of the intrusive material. In rare cases, this has resulted in localised contact metamorphism of sandstone to quartzite (e.g., the Bondi columnar sandstones; Morrison, 1904). Observations from the tunnel mapping show a spectrum of host rock responses from unaltered to highly fractured and weathered depending on lithology, proximity to the dyke, and depth.

2 DYKE OCCURRENCES

Of the 66 dyke intersections, 12 were mapped in tunnels comprising Ashfield Shale and 54 were mapped in tunnels in sandstone. This equates to a dyke intersected roughly every 500 m of tunnel excavation.

The orientation of the dykes intersected is presented in Figure 1. This shows the dykes follow the broad and well-established basin wide joint patterns of sub vertical dip (i.e. > 70°) with two or more set orientations being approximately northwest-southeast and northeast-southwest.

From the mapping data, eight key characteristics have been inferred as detailed in Table 1.

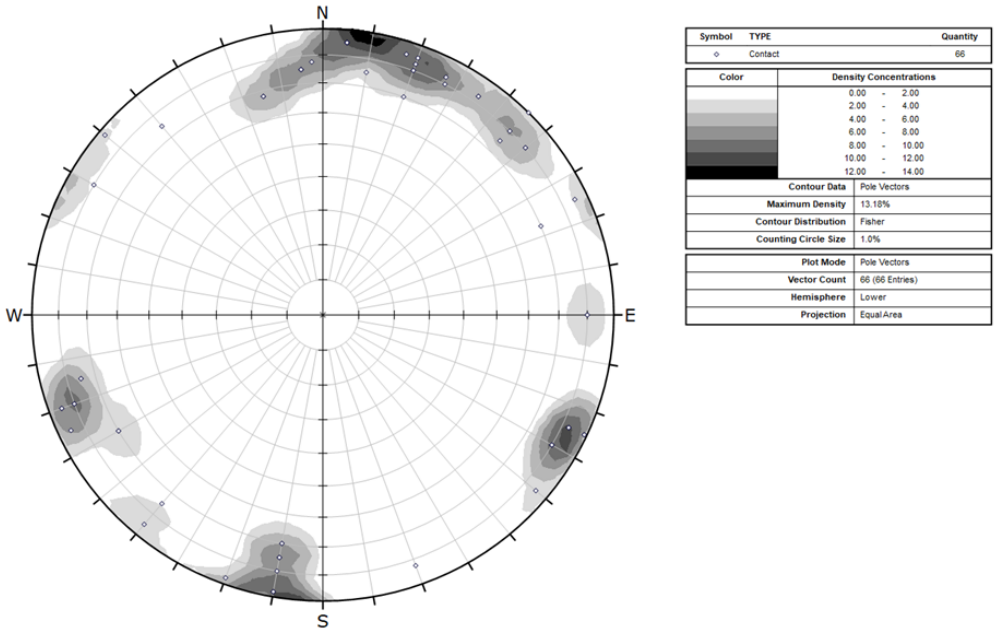


Figure 1: Stereonet Plot showing 66 dyke intersections mapped and their orientations

Table 1: Key physical characteristics recorded in the database

Characteristics	Detail
Host lithology	Rock type that the dyke has intruded into. Mittagong Formation has been grouped with Ashfield Shale
Depth of cover	Distance between tunnel crown and the ground surface at the dyke contact
Dyke rock material and mass conditions	Inferred intact and mass characteristics of the dyke intrusion itself including GSI estimates
Dyke thickness	The true thickness of the dyke
Contact between dyke and host rock	Inferred nature and characteristics of the contact between dyke and host rock
Host lithology rock mass and material conditions	Inferred conditions of the host rock including substance strength, jointing, faulting or infilling of discontinuities adjacent to the dyke
Zone of disturbance in host rock	The distance from the dyke where the host rock mass and material conditions revert to background conditions
Groundwater ingress at dykes	Estimation of the groundwater inflow in the tunnel adjacent to the dyke at the time of mapping

3 RESULTS

Figure 2 presents the data on dyke thickness and Figure 3 shows this as a function of depth of cover.

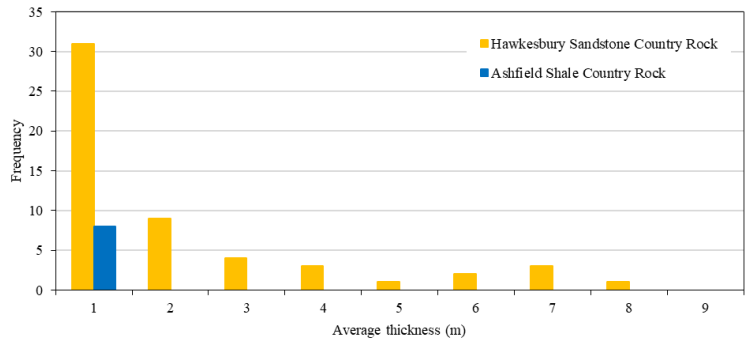


Figure 2: Dyke thicknesses

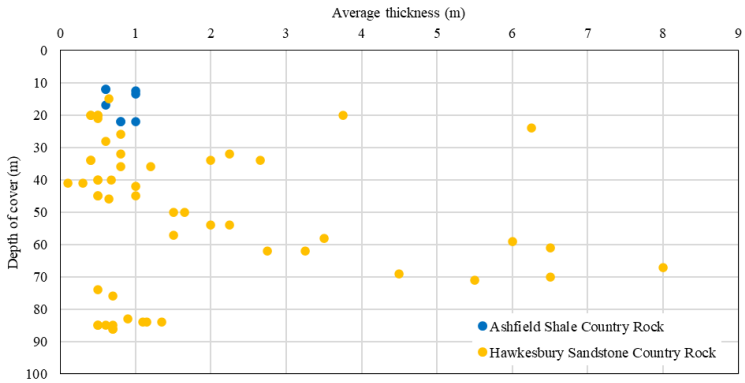


Figure 3: Dyke thickness as a function of depth of cover.

Table 2 presents data for dyke field estimated intact strength and GSI from mapping for each host rock lithology.

Figure 4 shows dyke field estimated intact UCS versus depth of cover.

Table 2: Dyke characteristics

	Dyke characteristics							
	Ashfield Shale Country Rock				Hawkesbury Sandstone Country Rock			
	Count	Av.	Range	SD	Count	Av.	Range	SD
UCS (MPa)	11	13	2-40	10	19	26	7-40	10
GSI	5	62	40-90	26	27	89	70-92	6

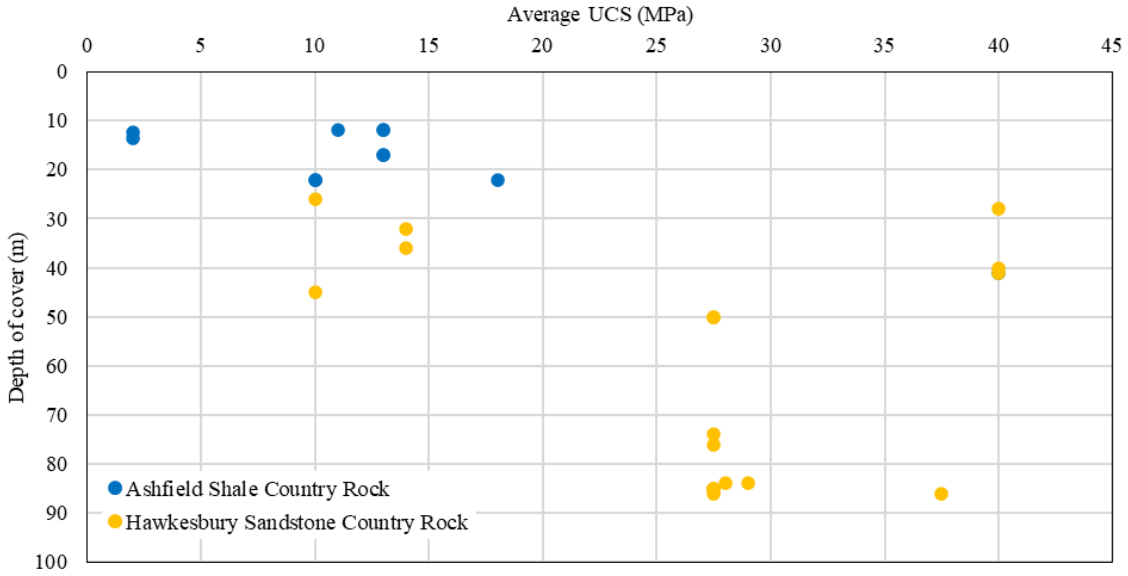


Figure 4: Dyke intact strength as a function of depth of cover.

Descriptions of the general rock mass conditions of the dykes and country rock have been categorized into fields to represent the observations, Figures 5 to 8. Groundwater inflow observations from the dykes or country rock are shown in Figure 9.

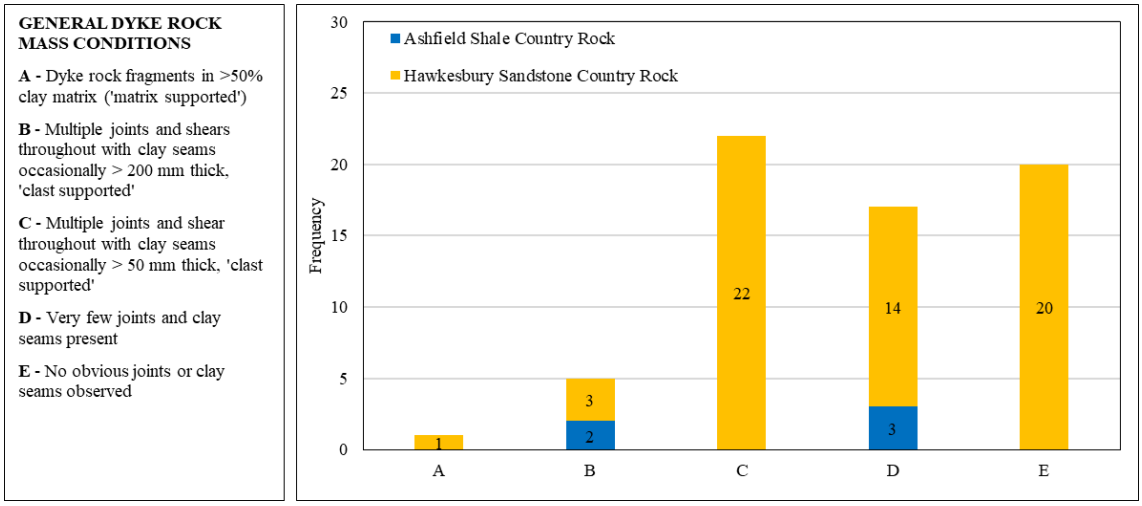


Figure 5: General dyke rock mass conditions in different country rock.

CONTACT BETWEEN DYKE AND COUNTRY ROCK

A - Multiple contacts infilled with clay and/or rock fragments >100 mm thick

B - Multiple contacts infilled with clay and/or rock fragments between 20 mm and 100 mm thick

C - Single contact infilled with clay or rock fragments <20 mm thick

D - Single tight contact with no evidence of infill

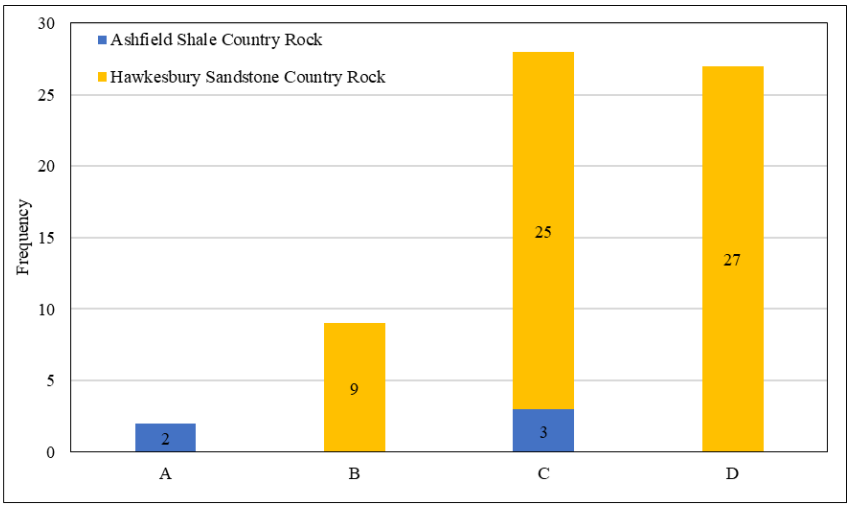


Figure 6: Contact between dyke and country rock condition.

HOST ROCK GENERAL MATERIAL AND MASS CONDITIONS

A - Highly fractured rock with obvious clay infilling or open defects

B - Highly fractured rock, multiple open defect orientations, some with occasional clay infilling observed

C - Multiple closely spaced tight to open defects (0-10 mm aperture), some clay filled parallel to dyke and inclined bedding partings

D - Single to multiple, wide spaced defects either parallel to dyke, inclined or horizontal (bedding partings) with aperture tight to 10 mm.

E - Single tight discontinuity parallel to dyke.

F - Rock mass appears unchanged from background conditions

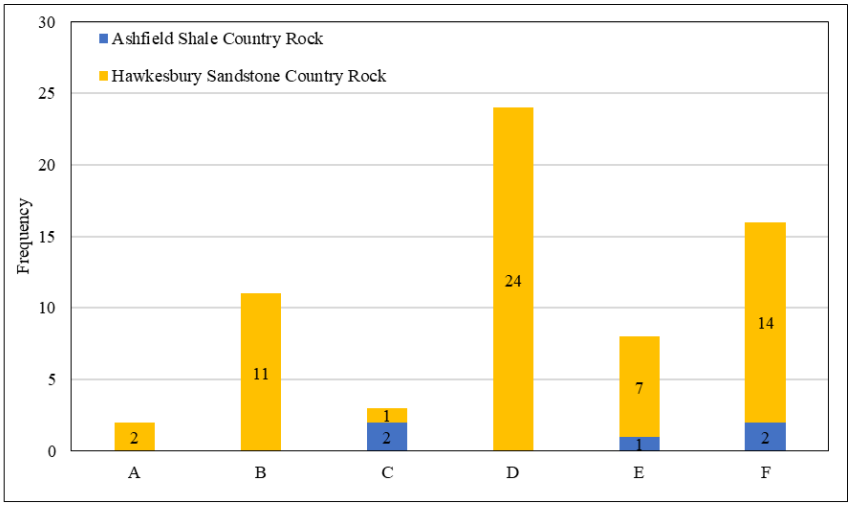


Figure 7: Host rock general material and mass condition.

ZONE OF DISTURBANCE IN HOST ROCK

A - >10 m

B - 5-10 m

C - 3-5 m

D - 1-3 m

E - <1 m

F - 0 m

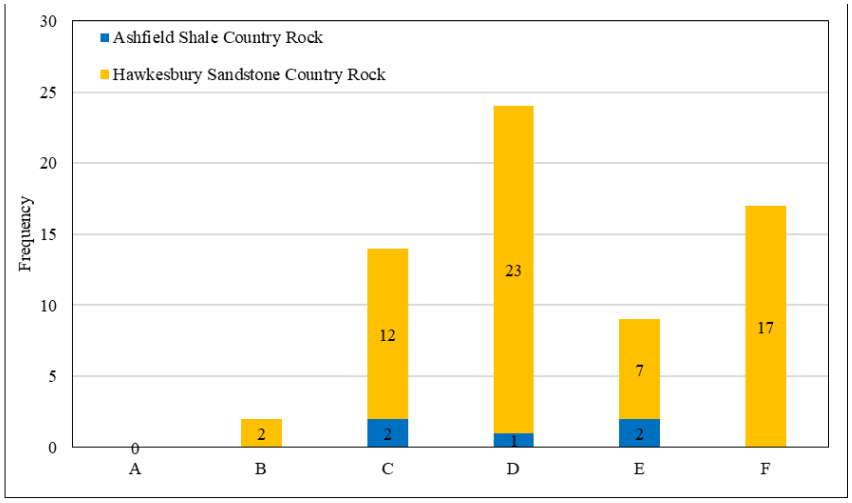


Figure 8: Zone of disturbance in host rock.

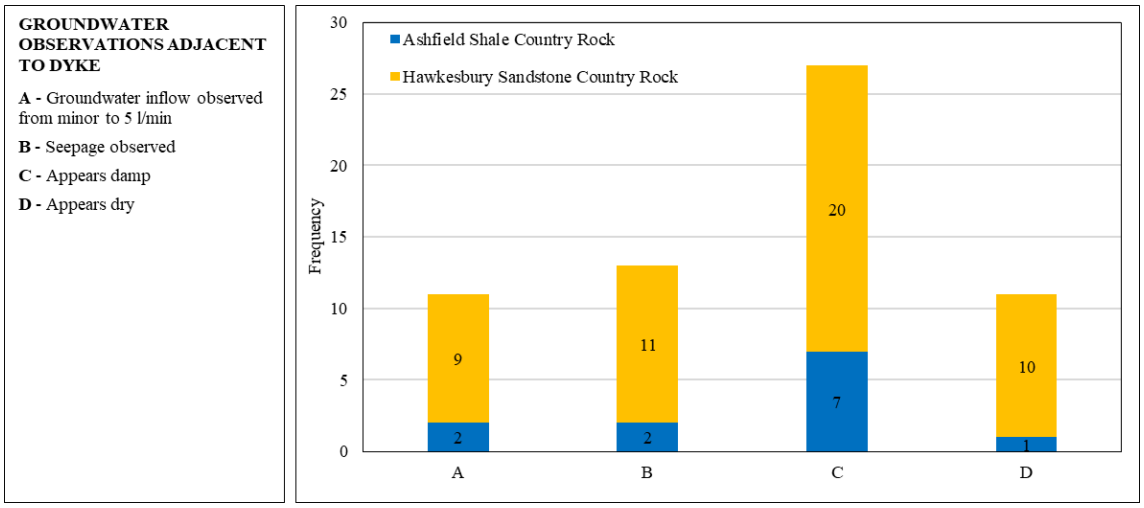


Figure 9: Groundwater observations adjacent to dykes.

These general dyke rock mass conditions and groundwater observations for all lithologies are plotted with depth of cover in Figure 10.

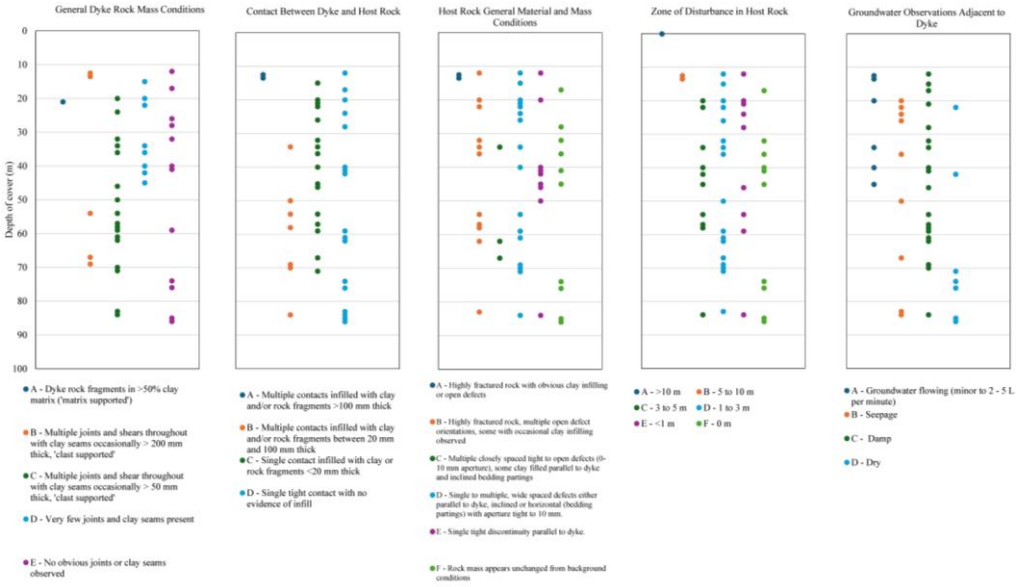


Figure 10: Summary characteristics plotted with depth of cover.

4 DISCUSSION

4.1 *Dyke termination, orientation and thickness*

There is limited evidence regarding the termination of dykes on geological features such as bedding planes, lithological boundaries, or other structural discontinuities. However, the authors have observed one instance where a dyke in the Hawkesbury Sandstone terminated in the overlying Ashfield Shale. This suggests that structures into which the dykes were emplaced are regional or at least persistent enough to extend across multiple lithologies.

Dyke orientations in this study closely reflect the regional joint set patterns described by Bertuzzi (2014), with dominant trends sub-vertical towards approximately NE–SW and NW–SE. This alignment supports the hypothesis that dykes were emplaced along pre-existing joint sets or structural weaknesses.

In terms of thickness, two-thirds of all dykes recorded had thicknesses less than 2 m, with half of them being less than 1 m. Notably, all dykes observed within Ashfield Shale were less than 1 m thick, although this is likely due to the limited sample size.

Two third of the dykes recorded had a thickness of < 2 m, with 50% being < 1 m thick. All dykes emplaced in shale had a thickness < 1 m, but this is likely to be due to the small sample size. The data suggests a general trend of increasing dyke thickness with depth in Hawkesbury Sandstone. However, thin dykes are also observed at all depths, and the apparent correlation between thickness and depth lacks a clear geological basis for the Sydney Basin. The trend is therefore considered coincidental.

4.2 *Dyke intact and mass characteristics*

Dyke intact strength estimates show a trend of increasing with depth. Below approximately 30–40 m from surface, uniaxial compressive strengths (UCS) are typically high (>20 MPa). At depths less than this, dykes are typically medium strength (UCS 6–20 MPa). This is likely due to reduced weathering and alteration at greater depths, where dykes retain more of their original mechanical properties. In contrast, shallower dykes appear more susceptible to degradation through stress relief and weathering processes.

Approximately half of the dykes had very few to no joints or seams and about one-third showed multiple joints or shears, some with clay infill up to 50 mm thick. This means that nearly 90% of mapped dykes could be classified as having 'reasonably good' rock mass conditions. The remaining 10% were assessed as poor, with pervasive clay seams and shearing. No consistent correlation was found between rock mass quality and depth of cover.

Dyke-host rock contacts were either tight and clean (40%) or had minor infill with clay or rock fragments (40%). These conditions were observed across the full depth range from 10 m to 90 m. The remaining 20% of cases had infill thicknesses up to or exceeding 100 mm, again with no clear depth dependence.

4.3 *Host lithology rock mass characteristics*

Poor host rock mass conditions characterized by highly jointed or faulted ground with clay-infilled defects were only recorded at shallow depths (<20 m cover). In contrast, more competent host rock masses (Categories D to F: from widely spaced defects to no observable change from background) made up approximately 75% of the dataset and occurred across the entire depth range.

For the zone of disturbance in the host rock, 95% of records showed a return to background conditions within 5 m, and a quarter of all cases showed no noticeable disturbance at all. Only two instances showed zones of disturbance extending beyond 5 m, both of which occurred at cover depths <20 m. This suggests that the influence of dykes on the surrounding rock mass is typically localised.

4.4 *Groundwater*

Groundwater seepage from dyke contacts or adjacent host rock defects was observed in just under half of the records. Category A inflows (2–5 L/min) were only documented at shallow depths (<50 m), supporting the findings of Hewitt (2004) and others that dykes can influence groundwater storage and movement, particularly in shallower, stress-relieved rock masses dykes. These findings also suggested the likely increase the permeability of the Hawkesbury Sandstone because dyke features are typically accompanied by defects (bedding plane shears and joints) dipping towards the dykes which often create transmissive zones.

Despite this, many observations recorded dry or damp conditions in both the dyke and host rock suggesting that they are not consistent sources of groundwater inflow across all conditions or depths.

4.5 *Sandstone versus shale host rock*

It is hard to draw many conclusions for dykes in shale owing to the small number of them encountered in tunnels. There are a few reasons for the smaller dataset, the main one being most tunnelling targets the sandstone as it is a better tunnelling medium. If there was shale overlying sandstone along an alignment, the ramp and mainline tunnels vertical alignments were designed to dive through the shale as much as the gradient allowed thus limiting exposure. Notwithstanding, there are no records of no influence (category F, Figure 8) of a dyke on the rock mass when in shale, this could potentially suggest that dykes have the potential to have a more severe influence of Shale rock mass characteristics rather than sandstone.

5 CONCLUSIONS

A review of the mapping data of 66 dyke intersections across six Sydney tunnel projects provides some insights into the rock and groundwater characteristics:

- Dyke orientation aligns closely with regional joint sets, supporting the interpretation that dykes exploit pre-existing structural weaknesses.
- Two-thirds of dykes had a thicknesses < 2 m, the maximum recorded was 8 m. An apparent trend of increasing thickness with depth was not considered geologically valid.
- Dyke substance strength has a consistent trend of increasing with depth. This is likely due to reduced weathering and stress relief effects in deeper zones.
- Rock mass conditions within dykes were generally considered good, with only a small proportion showing extensive jointing or clay seams. No clear depth dependency was observed.
- Host rock response was typically localised, with most disturbance zones reverting to background conditions within 5 m of the dyke.
- Groundwater inflows were observed in fewer than half the cases, with higher inflow rates restricted to depths <50 m, perhaps consistent with the stress relief patterns in the Sydney Basin.

Overall, while volcanic dykes introduce geological complexity into an otherwise uniform sedimentary rock sequence, their influence on tunnelling is often localised. Recognising their likley presence and understanding their variability should be a consideration for tunnel design and construction.

6 REFERENCES

Bertuzzi, R., 2014. Sydney sandstone and shale parameters for tunnel design. Australian Geomechanics, 49(1), pp.1-39.

Estrada B, Nash TJ, De Ambrosis A (2023), characterization of complex ground conditions for the rozelle interchange projects

Hewitt, P. & Smirnoff, T. (2005). Groundwater Control for Sydney Tunnels. Proceedings of the Society for Mining, Metallurgy & Exploration.

Nash, Et al. 2021, Mined tunnel ground behavior with faults and dykes in Sydney sandstones and shales Australasian tunneling conference 2020+1

Pells, P.J.N., Mostyn, G., Bertuzzi, R. and Wong, P.K., 2019. Classification of sandstones and shales in the Sydney region: a forty year review. *Australian Geomechanics*, *54*(2), pp.29-55.

Pells, P.J.N. (2004). Substance and Mass Properties for the Design of Engineering Structures in the Hawkesbury Sandstone. Australian Geomechanics Vol 39 No 3.

19th Australasian Tunnelling Conference – Acosta-Martínez, Stewart and Hudson-Smith (Eds.)
© 2025 Australian Tunnelling Society, ISBN 978-0-85825-002-4

Tunnels and the geologist – are we using geologists effectively? Thoughts and case studies from a 20 year career.

H. Baxter-Crawford
SMEC, Australia

ABSTRACT: Geologists are a fundamental part of the tunnelling workforce through all stages – site investigation, design and construction. How their skills have been used since the turn of the century has changed, fundamentally as a consequence of mandated changes in tunnel support requirements to improve tunnel safety. This paper discusses case studies demonstrating effective contributions by geologists beyond the requirements of Standards and classification systems. It presents observations as to how the geologists role has changed and the impacts that has on tunnelling in Australia, with particular commentary on whether or not we are using geologists effectively on projects at present. The paper discusses whether these changes have been for the better or to the detriment of the industry and whether the push for the use of technology and reduced facetime, guised as improvements to safety, are truly making for a safe workplace.

1 INTRODUCTION

Specialist trained geologists are fundamental when it comes to investigation and design of tunnels, but even more so at the construction stage. While their role encompasses a multitude of tasks, the key roles of the geologist at each stage are:

- Investigation Stage:
  - Collect soil and rock geotechnical data to the relevant standard of the time (presently to AS1726-2017).
  - Advise / supervise / delegate the necessary testing (field and laboratory) that will allow for characterisation of the soil or rock mass and the geological structure/s.
  - Collate and report the factual information that is reliable and consistently catalogued into the Geotechnical Factual Report (GFR).
- Design Stage:
  - Classify borehole data using stratigraphy specific engineering classification schemes.
  - Develop the engineering geological model (EGM) and complete associated reporting.
  - Advise geotechnical strength parameters for geological structures, defects and rock mass.
  - Advise possible geohazards.
  - Advise tunnel optimisation that could improve the ratio of tunnelling in good ground conditions to poor conditions, optimal tunnelling directions to avoid crown spalling or delamination, optimal orientation of caverns to minimise influence of stress etc.
  - Develop the Geotechnical Interpretive Report (GIR) (potentially as key input to the Geotechnical Baseline Report (GBR)).
- Construction Stage:
  - Collect geological data at prescribed cycles such that the entirety of the excavation is documented.
  - Collate the as-built geological data and compare to the predicted.

- Advise where conditions are deviating from predicted.
- Update the model and predictions based on the newly acquired construction data to allow for an update the design or support recommendations.
- Document the completed as-built record, preferably with the development of a geological digital twin 3D model.

There is consistency in the approach and associated tasks required to be completed by the geologist across all tunnelling projects, but, as with anything in nature, there is significant variability in the complexity and level of data collection required to document a site. As such, it is reasonable to assume the size and abilities of the geological workforce used should only be influenced by the geological complexity of a site and physical scale of a project. However, we have seen a different pattern emerge since the early 2000s, particularly influenced by the contractual deadlines enforced on construction programs.

This is not a smite on the engineer - they most definitely have their role to play. The commentary on this paper is a reflection on how geologists are used and are being gradually replaced from project roles despite the apparent increase in numbers being used on projects.

This paper compares the single-heading scale, road-header excavation components of two projects completed within the Sydney Basin's Hawkesbury Sandstone, and discusses how the use of the geologist has changed over the last twenty years, despite the stratigraphy, lithology and basics of design remaining the same. The paper provides commentary on the impacts changes in safety regulations have had on the required workforce (and project costs) in response to tunnel instability incidents, and how the changes implemented may result in a hidden danger. It foreshadows potential issues related to increased use of technology at the expense of the observational method of tunnel data collection and design validation and the implications this may have if underground face-time of the geologist is further reduced.

Further, the paper discusses how a requirement of geotechnical site investigation standards is to inform the stratigraphy (Standards Australia, 2017), yet tunnel design is reliant on inputs more related to lithology-based classification schemes than stratigraphy and where refinements to the unit demarcation are made, significant improvements to a design can be obtained through understanding lithological variations as opposed to stratigraphy.

2 CHANGES OBSERVED IN INDUSTRY PRACTICE FOR THE GEOLOGISTS CONSTRUCTION PHASE ROLES

The Hawkesbury Sandstone stratigraphic unit provides a sound basis for assessing how industry practice has changed since the turn of the century. The unit has long been recognised for its engineering properties, reusability and limited need for excavation support, dating back to the convict excavation of the Argyle Cut in the Rocks area of Sydney – an excavation that commenced in 1842 by hand, progressing to explosive use in 1859, with minimal to no support (Rocks Discovery Museum, 2025), Figure 1.

The authors first underground experience came with the Epping to Chatswood Rail Line – a combination of road header excavation station caverns and tunnel boring machine (TBM) rail lines. The project included five stations, each with a single geologist completing mapping during daily road header maintenance shutdowns, with one dedicated TBM geologist. Support consisted of pattern bolting of various spacing/lengths for each of the ground types and support classes. The entirety of the crown remained visible until project fit outs and mapping could be revisited and double checked at any time.

Fast-forward 15 years to the WestConnex megaprojects and excavation was 24/7, with a team of geologists covering multiple excavation faces under simultaneous development. Geologist coverage was also 24/7, on call to map faces upon exposure, immediately prior to the application of shotcrete as a support (on top of whatever bolting pattern is assessed as appropriate in the design and approved for installation at excavation). That drastic increase in staffing also notably saw geotechnical engineers positioned as mappers due to a shortage in engineering geologists. While these geotechnical engineers were trained for their daily duties, there is an inherent limitation to their understanding of geology and ability to recognise the implications of changing geological situations that is a project risk. We, as an industry have to recognise that we function best when using the most appropriately trained persons for each task.

A comparison between the road-header single-heading excavation progress between the projects is presented in Table 1. The single-heading excavations were of approximately the same size dimensions, completed by similar machinery. This shows two key differences between the heading excavation rates for the projects – the overall daily meterage has reduced per road header heading excavation while the number of staff has dramatically increased. A less obvious difference is the excavation exposures are covered by shotcrete in the more recent projects preventing any rechecks or validation of the mapping data collected.

What has caused this change in support requirements in the same stratigraphy, same excavation scale and tunnelling conditions? A notable fatality in the Cross-City Tunnel in August 2004 in which, as documented by Burman, Kotze and Chan (2018) resulted in a change to industry policy that "mandated one round of pattern bolting must be installed as part of every single excavation sequence irrespective of span and ground conditions", together with use of structural shotcrete. It is noted that the Cross-City Tunnel incident occurred in excavation within the Ashfield Shale stratigraphic unit, but the changes to industry practise have been implemented across all stratigraphic units, in civil tunnels Australia-wide, such that no work is conducted under "unsupported ground", which in all subsequent projects now includes the use of structural shotcrete to satisfy project specifications. Pells (2008) states: "The basic principle behind the design of shotcrete, in the loosening pressure environment, is to support and contain the rock between the rockbolts", however, a result of this is the time required to spray and cure the shotcrete impacts excavation schedule and further reduces the geologists face-time to complete the observational method of mapping, while also excluding the possibility of reviewing or checking the data collection. This further highlights the criticality of using an experienced engineering geologist for the task such that if anything untoward is apparent, it is more likely that it will be captured, documented and advised and actioned appropriately.



Figure 1. Historic photograph of the Argyle Cut, the Rocks, Sydney, showing the excavated spoil and unsupported slopes. (Rocks Discovery Museum, 2025)

Some projects are adopting the use of LiDAR scanning technology to capture the face conditions. This is fantastic for record keeping, providing a 3D output of the excavation profile and defect orientation assessments, but is pushing further tasks onto an already stretched work-force, resulting in further use of lesser experienced or appropriate personnel. Additionally, the skills required to "map" from LiDAR are deeply rooted in the skills obtained by mapping in person. It's the observations you learn to make through mapping in real life that allows you to

recognise the key features observable from a point cloud. Just being able to load the point cloud into a 3D modelling program does not upskill you enough to process the data.

Table 1. Comparison between road-header heading excavation progress of projects in Hawkesbury Sandstone pre and post the Cross-City Tunnel fatality in 2004

Project	Epping to Chatswood Rail Line	WestConnex New M5 (M8)
Era	2002-2008[1]	2017-2020
Excavation area	Single heading road-header cutting within station cavern	Single heading road-header cutting within mainline
Typical road header progress rates for each heading/machine	10-15m per day (15 to 20m per day for benching)	5-8m per day (15 to 20m per day for benching)
Geologist schedule	1 geologist per station (each covering 2 active headings)	2 to 8 geologists per base site (each covering up to 4 active headings)
	Mapping during daily 4 hr maintenance	24/7 on call coverage
	5 days per week, no weekends	7 days per week
	10hr shifts, days only	8 to 12 hr shifts, including overnight
Peak geologists count	4	24
Support used	Pattern bolts, spot bolts, localised mesh	Pattern bolts with mandatory shotcrete

[1] Roadheader component completed by end of 2003.

Key issues for the geological workforce that have arisen with the mandated changes are:

- Doubling of personnel (as a minimum) to provide 24-hour coverage. In reality, fatigue management usually means this needs to be three persons on eight hour shifts or teams of four with rotating day and night shift combinations. Result: cost increase three to four times.
- Further, replacement or gap filling of geological personnel with geotechnical engineers as part of the pool of face mapping staff to ensure adequate bodies are provided, but who have limited geological background.
- Lesser time to complete their maps, increasing the risk that something is missed.
- Safety push preventing any actual mapping of the face. Geological compasses can no longer be used to measure the in situ orientation of defects in a face exposure as this is considered “unsupported ground” despite being at a distance of less than one bolt pattern array from “supported ground”. This means defect orientations are estimated via line of sight and may be erroneous.
- Safety and “innovation” push to use LiDAR scanning of faces rather than field personnel. This work is being delegated to survey workforce but any delay in data delivery results in delay of information to a “desk geologist” and limits real observations.
- The risk in itself of the shotcrete – both hiding geological features and as a spalling hazard. The author has observed significantly more spalling of shotcrete from the crown than rock spalling as a hazard when working underground.

3 STRATIGRAPHY – IS THIS NEEDED AS A REQUIRED PART OF LOGGING?

A required component of any geotechnical borehole log to comply with AS1726-2017 is to assign the stratigraphy. However, the state-run Geological Surveys have struggled to keep up to date with mapping to accurately reflect the stratigraphic distribution of units, particularly at the 1:100,000 scale. The Sydney 1:100,000 geological map dates back to 1983 (Geological Survey of New South Wales, 1983) - its older than many of the staff presently working in the engineering geology sector in NSW. The adjacent Penrith (1991) and Wollongong-Port Hacking (1985) sheets are of comparable vintage. These have been digitised on the Seamless Geology platform, however, there appears to be little, if any updating of the data. Known variations in the stratigraphy of the Sydney Basin from the significant infrastructure works completed (and much of it published) by the wider government or private sectors has not been incorporated into the maps.

Taking a further example from Sydney, the main stratigraphic unit present (and which comprises much of the tunnelling completed) is the Hawkesbury Sandstone, a unit that is some 300 m thick. The Hawkesbury Sandstone is a fluvial sequence that comprises sheet (cross-bedded) facies, massive facies and siltstone or shale facies, Figure 2, each of variable thickness and continuity, formed through variations in the dynamics of fluvial action at the time of deposition. The continuity and persistence of each facies band is then further complicated by post-lithification faulting and folding.

Presently, the majority of excavations in the Hawkesbury Sandstone have centred around Sydney in the upper portion of the unit, underlying the contact with the Mittagong Formation. We are fortuitous that there has been enough data collected and laboratory testing completed that the material property parameters in this upper portion are well understood. However, a negative impact of that advanced knowledge base is that project specific laboratory testing programs have been observed to be reduced as a means of cost cutting. As tunnels extend further from Sydney, with the fast rail services presently being considered, the risk becomes that a change in the relative position within the 300 m sequence is not appropriately recognised and future project workers adopt limited laboratory testing as that has been their personal "recent experience". The full 300 m sequence took over 5 million years to deposit which would suggest there must be an inherent variation to its composition and testing of the Hawkesbury Sandstones geochemical make-up varies across the Sydney Basin would support this, with laboratory assessments of quartz to feldspar ratio varying from 7:1 to 400:1 (Swanson, Ward, & Franklin, 2002), a characteristic attributable to the variation in performance of the material as a building façade stone. It is not unreasonable to assume there could be an inherent difference in the geotechnical properties of the unit over its 300 m thickness either.

Engineers have modified the original Pells Classification Scheme developed for foundation design in Sydney of Pells, Mostyn and Walker (1998) for sandstone to be used in tunnel design which simplifies the rock mass into five classes defined by strength, defect spacing and allowable seams (Pells P. , 2002). This allows for design of tunnel support systems commensurate to each class and simplifies the design and support process. Geologists can contribute further to design improvements by understanding the intricacies of the Hawkesbury Sandstone lithology and assessing the facies distribution. The ground behaviour and response to tunnel excavations is different depending on the facies encountered and the required support also varies accordingly. A tunnel crown in massive sandstone is desirable, as it is more favourable to self-supporting arch action and therefore require less installed artificial support, while cross-bedded sandstone may delaminate in the crown, and require local increased support. Shale/siltstone horizons may act as focus for shoulder convergence, spalling of the crown, or heave of the invert. As such, the geologist can contribute significantly to a tunnel design by undertaking facies analysis. Which begs the question, why then, do the standards focus on stratigraphy?



Figure 2. Examples of sheet, massive and siltstone/shale facies in the Hawkesbury Sandstone

Similarly, if stratigraphy is such a key field, it must be included in all factual borehole logs, why is the geotechnical characterisation of the Mittagong Formation so contentious? The Mittagong Formation is typically less than 10 m thick and comprises interbedded to interlaminated siltstone and sandstone. Various adjacent projects have considered it a shale class (adopting the Pells scheme for shale), others a sandstone class, based on relative (local) variation as to which lithology dominated.

As we move even further afield, to greenfield locations being targeted for pumped hydro schemes, not only are we not confident the geological survey mapping accurately reflects the stratigraphy, we know even less about the lithology and we don't have the vast testing databases

to help with design. The inclusion of stratigraphy on logs in these situations, becomes more interpretive than factual and defeats the intent of the standard.

4.1 *Facies Differentiation Completed Case Study*

Design for the dual tunnel M8 alignment from Kingsgrove to St Peter's involved assessment of lithological conditions in Hawkesbury Sandstone for much of the 8km alignment with both tunnel exits in Ashfield Shale. Drilling at close spacing along the alignment was not economic or warranted. As such, along the mainline tunnels, the drill spacing was 300 to 1000m with a higher density of drilling around the Bexley and Arncliffe tunnel access areas where there were junctions of adits and shafts into the mainline tunnels. A facies model, attempting to align the distribution of cross-bedded sandstone layers and massive sandstone layers and identify any areas of persistent siltstone was developed by the design geological team. This model helped in two key ways:

1. By cross-checking lineaments observed in the surface topography against the facies distribution either side of the lineament, the geologists could advise whether there was any indication of displacement of material either side of the lineament (suggestive of faulting) and advise if further site investigation was warranted and
2. The tunnel profile could be assessed to identify areas of tunnel that may have less than ideal rock material in the crown (cross-bedded sandstone or siltstone lenses), and allow the geologists to advise options for changes to tunnel crown elevation that could be assessed by engineers to optimise the design.

Within the Arncliffe area of the tunnels, such an optimisation was possible. Geologists recognised a persistent, 5m thick massive sandstone bed occurred a few metres above the original proposed tunnel crown. With this information in hand, engineers were able to redesign the tunnels to align the crown with the more favourable rock. This shifted this section of tunnel from a class III support to a class I/II support, reducing support costs and improving excavation rates.

4.2 *Facies Differentiation Not Completed Case Study*

For the Macquarie University Station of the Epping to Chatswood Rail Line, there was no facies differentiation completed. The crown of the station was expected to be in the projects rock classification type II, a robust material type with 1.5m bolt spacing and spot bolts as required. However, one portion of the crown intersected distinctly cross-bedded sandstone and at an angle of intersection and excavation direction for a most undesirable result – daylighting cross-beds that delaminated in the crown. The support was locally increased to a type IV mesh and bolt combination – no requirement for shotcrete. While this project predates use of televiewer for defect orientation, oriented core was available to provide understanding of the unfavourable excavation direction for this portion of crown and excavation from the opposite direction was in fact possible.

5 DISCUSSION AND CONCLUSIONS

The paper is not suggesting there is a need for an increase in overall geology-specific inputs to a tunnel design/construction – the geologists provision of GFR, GIR and inputs to GBR are appropriate for design and the use of geologists for mapping is appropriate for construction. However, the inherent knowledge base of the geologist is needed to flag atypical ground conditions bespoke to a geology type and when unusual or deteriorating geological conditions are occurring during construction. To quote Fookes, Lee and Gilligan (2005) "Problems have to be identified before they can be solved" and that is where the geologist provides the most to a project.

So how do we keep the right personnel doing the tasks they are specifically trained for in a stretched workforce to maintain quality in our projects? Is it possible for the industry to take a collective breath and revert back to 20 hour excavation and maintenance shifts? Are there ground types that do not gain from the addition of shotcrete that we can leave visible? Can we think outside the box and develop skills for newer graduates via training centres to have them at the

faces mapping so the mid-levels are available to action rigorous review both data and alternate data collection methods? These are all things we can think about.

In a lot of ways, the safety culture has changed for the better, particularly in regard to respiratory protection. But the mandate for shotcrete as a means of temporary support on all exposed stratigraphies has resulted in a balancing act between allowing the geologists the necessary time to map the exposures, while maintaining excavation performance rates. This balance is often tipped to be unfavourable to the geologist. This should be cause for alarm – if the time to map appropriately is not given, we run the risk that something critical will be missed. The mandated application of shotcrete on all rock classes, prevents later checks or capture of this information.

6 REFERENCES

Burman, B., Kotze, G., & Chan, L. 2018. *www.researchgate.net/publication/329739655_Lane_Cove_Tunnel_collapse_and_sinkhole_a_forensic_review_-_1_The_collapse.* Retrieved from www.researchgate.net: https://www.researchgate.net/publication/329739655_Lane_Cove_Tunnel_collapse_and_sinkhole_a_forensic_review_-_1_The_collapse

Fookes, P., Lee, E., & Gilligan, G. 2005. *Geomorphology for Engineers.*

Geological Survey of New South Wales. 1983. Sydney 9130 1:100000 Geological Sheet.

Geological Survey of New South Wales. 1985. Wollongong-Port Hacking 9029-9129 1:100000 Geological Sheet.

Geological Survey of New South Wales. 1991. Penrith 9035 1:100000 Geological Sheet.

Pells, P. (2002). Developments in the design of tunnels and caverns in the Triassic rocks of the Sydney region. *International Journal of Rock Mechanics and Mining Sciences*.

Pells, P. 2008. What happened to the mechanics in rock mechanics and the geology in engineering geology . *The Journal of The Southern African Institute of Mining and Metallurgy VOLUME 108*.

Pells, P., Mostyn, G., & Walker, B. 1998. Foundations on Sandstone and Shale in the Sydney Region. *Australian Geomechanics*.

Rocks Discovery Museum. 2025. *https://rocksdiscoverymuseum.com/stories/creating-the-argyle-cut.*

Standards Australia. 2017. *Geotechnical Site Investigations AS1726.*

Swanson, J., Ward, C., & Franklin, B. 2002. Mineralogy of Sydney building sandstones in relation to geotechnical properties - 1: relation of quantitative xray diffraction data to other chemical and petrographic indicators. *Australian Geomechanics*.

19th Australasian Tunnelling Conference – Acosta-Martínez, Stewart and Hudson-Smith (Eds.)
© 2025 Australian Tunnelling Society, ISBN 978-0-85825-002-4

Hydrothermally altered Silurian bedrock in Melbourne's North-East Link Tunnel

H. Hughes-Adams, D. Tepavac, B. Carnes
Delve Underground Ltd, Melbourne, Australia

C. Hunt
Delve Underground Ltd, Vancouver, Canada

J. Martin
Spark Consortium, North East Link, Melbourne, Australia

ABSTRACT: The North East Link Project is a 26-kilometre tolled motorway scheme in Melbourne, Australia, which includes a 6.5 km tunnel that was constructed using both sequential excavation methods (SEM) and a tunnel boring machine (TBM). The 450 m section of SEM tunnel encountered hydrothermally altered rock in the excavation of the top heading. The altered rock derivate presented as a "soil like" material formed from the Silurian sedimentary parent rock. The hydrothermally altered siltstone is nearly indiscernible from the fresh and unaltered Silurian siltstone by visual inspection, yet it may bear vastly different geotechnical and geomechanical properties, as well as tunnelling conditions. In the presence of minor water inflow, the altered siltstone slakes, disintegrates and may create a "running ground" condition, a significant potential risk to the safety of the works. This paper focuses on Silurian-age siltstone and sandstones and how the unique characteristics of the hydrothermally altered derivates present unique risks to tunnel excavation and support implementation. The paper also explores the experiences of encountering hydrothermally altered siltstone on the North East Link tunnels and sets out a series of design and construction risk mitigation measures adopted on the project. These measures are not unique to the North East Link project but form the basis of a proposed set of good practices with respect to underground excavation in hydrothermally altered rock.

1 INTRODUCTION

This paper aims to present the experiences of the design and construction of SEM tunnelling in rock mass conditions that contain hydrothermally altered rock within Silurian siltstone and sandstone. The paper presents the geological background and mechanism of hydrothermal alteration. Additionally, recovered samples were tested and reviewed in order to determine engineering design parameters and comparison with pre-construction parameters was made. The knowledge gained from the experience is summarized herewith; the risks of tunnelling in these conditions are presented with the ultimate solutions and outcomes highlighted.

2 GEOLOGICAL BACKGROUND OF PROJECT

The North East Link (NEL) project area is founded on the Anderson Creek and Melbourne formation. Both formations are sufficiently similar that throughout the project they have been referred to as the "Silurian formation". This bedded sedimentary formation, consisting of mostly siltstone with some sandstone, was deposited in a deep marine environment during the Silurian era, approximately 420 to 440 million years ago (mya). In the middle Devonian (approximately 380 mya), this formation underwent an orogenic deformation event, which resulted in folding and faulting of the bedrock into a series of synclines and anticlines trending NE to SW. In the late Devonian, this bedrock was intruded by a series of plutonic rocks in the granite family. These

intrusions have weathered into soft white clay inferred to consist largely of kaolinite. The bedrock was subsequently incised by the Yarra River and its tributaries, and then later infilled with Quaternary sediments.

During the tectonic movement of the Devonian period, the Silurian bedrock underwent another period of deformation, which included hydrothermal alteration. This hydrothermal alteration occurred in discontinuous and seemingly random locations and is therefore difficult to predict in the project area. The mineralogy of the altered formation indicated the presence of chlorite and sericite (Golder, 2023a), giving the altered rock a slight greenish hue, though this largely remained similar to fresh rock. The strength of the hydrothermally altered siltstone was inferred to vary based on intensity of alteration and ranges between a clay-like consistency and rock with low hardness (Golder, 2023a).

The four primary units within the Silurian bedrock have been classified based on strength and weathering grade, and have been numbered S1, S2, S3 and S4, with increased numbers corresponding to higher weathering grade and decreased strength. S1 is classified as fresh bedrock.

3 HYDROTHERMAL ALTERATION

Hydrothermal alteration can be defined as a very complex process involving mineralogical, chemical and textural changes resulting from the interaction of hot aqueous fluids with the rocks through which they pass, under evolving physicochemical conditions (Pirajno, 1992). It is considered that as part of Devonian tectonic deformation and metamorphism, hot aqueous fluids circulated through the defections and pores in rocks, dissolving and depositing minerals, leading to changes in the rock's composition and structure. The altered areas often surround intrusions or fault zones, indicating the source and path of the hydrothermal fluids.

One critical observation regarding the on-site assessment of hydrothermal alteration was that there is often no obvious visual difference between rock inferred to have been hydrothermally altered and the surrounding unaltered rock mass. However, the behaviour of the ground as a result of excavation and potential for groundwater-induced erosion upon excavation (running ground conditions) were vastly different, as is discussed further below.

4 DESIGN STAGE RISK MINIMIZATION MEASURES

Fundamentally, one of the greatest sources of risk with tunnelling projects in rock mass conditions containing hydrothermally altered rock is twofold. First, identifying the altered siltstone material in advance of the tunnel heading based on visual inspection or interpretation of the preconstruction site investigation is extremely difficult. Second, the altered siltstone is highly variable in terms of strength and stiffness, as well as in size and extent.

During the preconstruction stage, one intention of the geotechnical interpretation was to highlight the risk of the material but was unable to quantify its extent and location given the practical limitation of using boreholes. Where the altered siltstone was inferred to be encountered during geotechnical drilling (see Figure 1) it was visually very similar to the surrounding fresh rock, as discussed above.

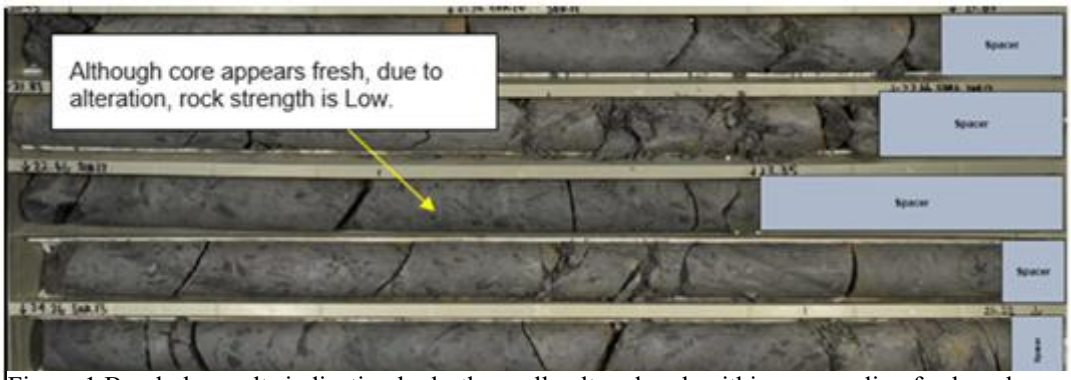


Figure 1 Borehole results indicating hydrothermally altered rock within surrounding fresh rock.

Nevertheless, the geotechnical interpretation was able to provide estimated rock mass characteristics and expected behaviour and parameters of the hydrothermally altered siltstone, which enabled the designers to develop support and sequence in anticipation of encountering the conditions. The design support concept focused on managing expected ground behaviour by providing pre-support elements like spiles, face support bolts, and thicker heading crown shotcrete with optional mesh reinforcement and a tighter bolt pattern.

Addressing the next challenge of identifying the material ahead of the tunnel face was attempted to be mitigated via systematic forward probing. The foundational risk mitigation measure developed at the detailed design phase was forward probing for geotechnical features such as altered siltstone and groundwater inflow. The intention for the requirements for probe cuttings to be inspected, monitoring of penetration rates, groundwater inflow rates and endoscopic inspection during design was to identify hydrothermally altered ground.

5 ENCOUNTERING HYDROTHERMAL ALTERATION

Hydrothermal alteration was first inferred to have been encountered on the project during excavation of the cut-and-cover box adjacent to the mainline portal at the Trinity site (Bulleen End) and throughout the excavation of the top heading.

During excavation in the lower levels of the Trinity cut-and-cover box adjacent to the northbound mainline drive, a section of medium-strength clay was encountered by the geotechnical team at a similar elevation to the tunnel crown. This clay was greenish in hue and surrounded by S4 rock, as predicted by the geotechnical interpretation (Golder, 2023a). Due to the greenish coloration of the clay, it was inferred to be hydrothermally altered S4 rock. Due to entry and space restrictions, this material was not sampled. An image of the inferred hydrothermally altered siltstone is shown below in Figure 2.



Figure 2. Inferred hydrothermally altered rock with clay-like strength in the northbound portal excavation (left). Inferred hydrothermally altered rock with decreased strength from surrounding rock in heading excavation denoted by red circles (right).

Delve Underground's Construction Phase Service (CPS) team also inferred the presence of hydrothermally altered S1 siltstone in several tunnel heading advances. In the mainline excavation, hydrothermal alteration typically appeared in discrete zones within the headings and was typically presented in relatively localized areas, 2 to 5 metres in width and length, and adjacent or in proximity to faulting and inclusions. Some areas presented as a greenish-grey colouring, appearing slightly weathered to fresh rock, but would "delaminate" and peel away from surrounding rock in the form of thin wedges, or larger wedges where the outer bounds of the altered siltstone interacted with steeply dipping bedding partings. The failure surfaces that remained irregular and had no clear joint orientations or discernible bedding fabric. In some instances, the altered siltstone appeared as dark grey and similar to that of fresh rock. However, the bedding fabric would be difficult to discern, and the affected rock would typically slake when washed with water, disintegrating into a soil-like material.

In all cases, the stand-up time of the material was the biggest risk with respect to profile control and face stability. As the colour of the rock was not a reliable indicator of the presence of alteration, the behaviour and lack of bedding of the altered siltstone was largely used to discern where the rock was likely to be hydrothermally altered. Most of the hydrothermally altered rock encountered on the project was identified in the tunnel face, and less commonly identified in the sidewalls and crown. In some cases, however, where the hydrothermally altered siltstone was found in the crown or sidewalls, overbreak was common. Large areas of increased intensity could potentially have more serious impacts on tunnel stability and stand-up time of the excavated faces.

Groundwater inflows in the tunnel were generally minimal, with minor seepage commonly observed in the lower half the top heading excavation. High groundwater inflows should be considered a high risk in tunnel projects where hydrothermal alteration is present based on the observations of this material to slake and swell when in contact with water.

6 LAB TESTING

The geotechnical interpretation (Golder, 2023a) used on the project provided anticipated geomechanical properties for the hydrothermally altered siltstone; however, these values were derived largely from regional experience and engineering estimates. As part of this publication and post-construction, Delve Underground, with support by the Project, commissioned laboratory testing on the hydrothermally altered siltstone that was recovered in the mainline of the SEM tunnel to review and analyze the design parameters of the encountered material. It should be noted the recovered material was not representative of the inferred hydrothermally altered clay-like material that was observed and mapped at the tunnel portal.

6.1 *Sampling methodology*

Hand samples of hydrothermally altered siltstone were extracted after completion of an excavation with hydrothermally altered siltstone present. In preparation for laboratory testing, all samples were field strength tested and visually inspected in order to confirm them as typical S1 or hydrothermally altered rock before being air dried, photographed and sent to the lab for testing, as demonstrated in Figure 3.



Figure 3. Fresh unaltered Silurian rock s1 sample (left). Inferred hydrothermally altered sample (right).

6.2 *Lab testing*

The intent of the lab testing regime was to better understand the geomechanical properties of the hydrothermally altered siltstone, including uniaxial compressive strength (UCS), cohesion and friction angle. Three unaltered samples and three hydrothermally altered samples underwent point load tests (PLTs) to characterize the changes in strength due to alteration. The hydrothermally altered siltstone was collected from S1 rock mass for comparison.

Additionally, two hydrothermally altered samples were saturated in water for 24 hours and then point load tested to investigate the effect of moisture content on the strength of the rock. A three-stage triaxial test was completed on the largest sample of altered siltstone, which was saturated prior to testing in order to yield conservative results. Due to the irregular shape and limited size of the samples, however, most of the testing completed was irregular lump point load testing.

6.3 *Lab results*

The PLT results returned indicated a clear difference in point load strength index ($I_{s(50)}$) between the air-dried hydrothermal samples and the air-dried unaltered samples. Please see Table 1 below, which compares unaltered sample strength to altered samples. The arithmetic mean unaltered sample $I_{s(50)}$ strength was 2.43 MPa, compared to the arithmetic mean hydrothermally altered siltstone strength of 0.34 MPa.

Table 1. Air-dried point load testing results

Sample #	Point Load Strength Index ($I_{s(50)}$) MPa
Sample 1 (unaltered)	1.40
Sample 2 (unaltered)	1.70
Sample 3 (unaltered)	4.20
Sample 4 (hydrothermally altered)	0.77
Sample 5 (hydrothermally altered)	0.08
Sample 7 (hydrothermally altered)	0.16

Table 2 below, shows the point load testing results from the two saturated samples. The results appeared consistent with other hydrothermally altered samples but did not indicate that strength results were discernibly lower than air-dried samples. During excavation, the hydrothermally altered siltstone in the tunnel excavation would typically disintegrate, slake and create shallow raveling failure upon contact with water. However, the point load testing results of saturated hydrothermally altered samples did not present a discernible decrease in strength compared to the air-dried samples. The arithmetic mean strength of the saturated samples was 0.33 MPa.

Table 2. Saturated point load testing results for hydrothermally altered samples

Sample #	Point Load Strength Index ($I_{s(50)}$) MPa
Sample 2 (hydrothermally altered)	0.22
Sample 3 (hydrothermally altered)	0.45

All PLT samples failed as a fracture through the rock substance and did not appear to be influenced by weak planes such as bedding partings. The largest hydrothermally altered sample was cored to a length of 115.8 mm and a diameter of 48.5 mm, then saturated in water for 24 hours. A three-stage triaxial test was completed, yielding the results shown in Table 3 and Figure 4, below. The deduced uniaxial strength was achieved by using a Mohr-Coulomb failure linear approximation on the test results presented in Figure 4. Minor vs major principal stress from triaxial testing.

Table 3. Results from three-stage triaxial test.

Property	Result	Unit
Rock density	2531	kg/m^3
Peak confining pressure	6.00	MPa
Peak failure stress	27.8	MPa
Failure load	48.5	ken
Deduced cohesion	1.60	MPa
Peak angle of shearing resistance, φ_p	32.6	MPa
Residual angle of shearing resistance, φr	31.6	MPa
Deduced UCS (peak)	5.70	MPa
Residual UCS (residual)	4.80	MPa
m_i	3.34	-

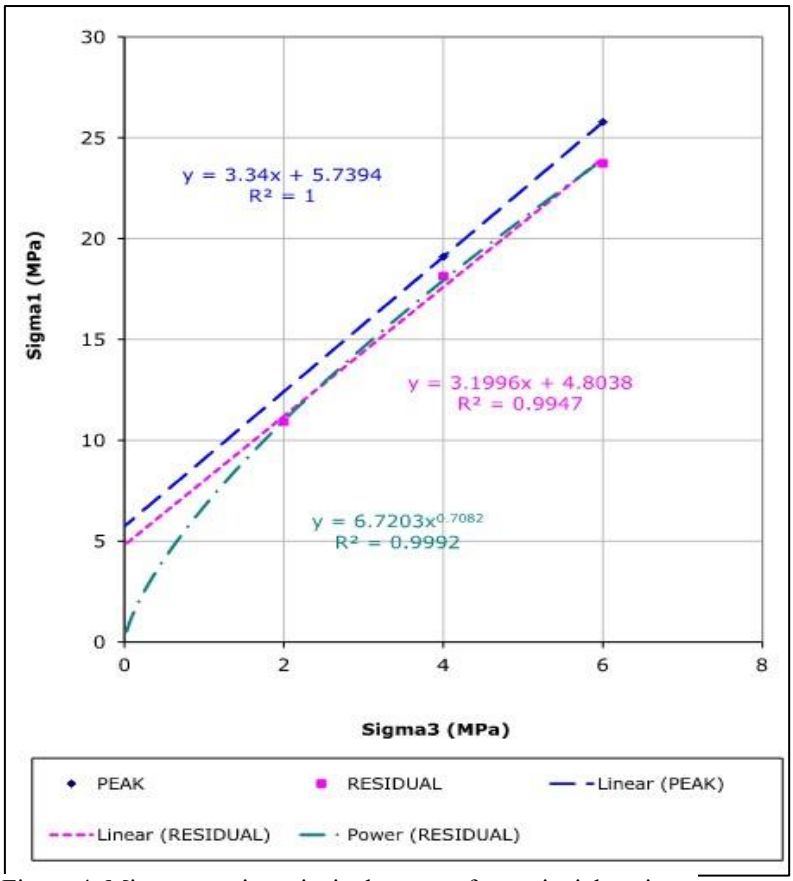


Figure 4. Minor vs major principal stresses from triaxial testing.

6.4 *Results analysis*

While there are many empirical methods that exist to correlate PLT to UCS strength based on rock type, there are few methods that may account for hydrothermal alteration. Complications further arise when considering the strength of the altered rock can vary greatly depending on the intensity of the alteration and therefore multiple correlations would be required depending on inferred alteration intensity.

The 2002 Hoek-Brown failure criterion was used to relate the results to the inferred Geological Strength Index (GSI) observed on site. Following the original guidance by Hoek (1994), Delve Underground CPS staff estimated the GSI through qualitative field assessments of the rock structure and discontinuity conditions within the zone of hydrothermally altered siltstone. Noting the limitations of GSI and based on geological judgment, the GSI adopted for this method was 30 and a disturbance factor D of 0, given the survey-guidance controlled excavation with the roadheader (Hoek, 2002).

The corrected value for "tunnel scale" cohesion becomes $c' = 0.31\ MPa$; and the corrected friction angle becomes $\varphi' = 9.7°$. Compared to the preconstruction geotechnical interpretation, the calculated results differ from the strength parameters suggested during the design phase, which were $c' = 0.13\ MPa$ and $\varphi' = 45°$; however, due to inherent limitations and uncertainties of lab testing, more data is needed to verify these results.

7 FIELD SOLUTIONS AND CONSIDERATIONS

As discussed in Section 4, the preconstruction geotechnical interpretation was unable to provide a design case for hydrothermally altered siltstone, nor was it able to predict any expected locations within the tunnelling works. Due to the random and localized nature of the altered rock mass, it

was difficult to intersect during forward probing investigations. Should it have been encountered during probing, the apparent lack of weathering as described above made it difficult to differentiate from fresh rock, and the localized nature of the softer material was unlikely to have a noticeable impact on the overall drill rate of the 30 to 40 m long probe holes. Hence, hydrothermally altered rock was difficult to predict and was primarily identified during geotechnical mapping works. When encountered, the CPS team raised a construction request for information to the designer for the Design team to confirm support and sequencing requirements for the observed conditions. The outcomes of that design guidance is provided below.

7.1 *Spile bars and GRP CT bolts*

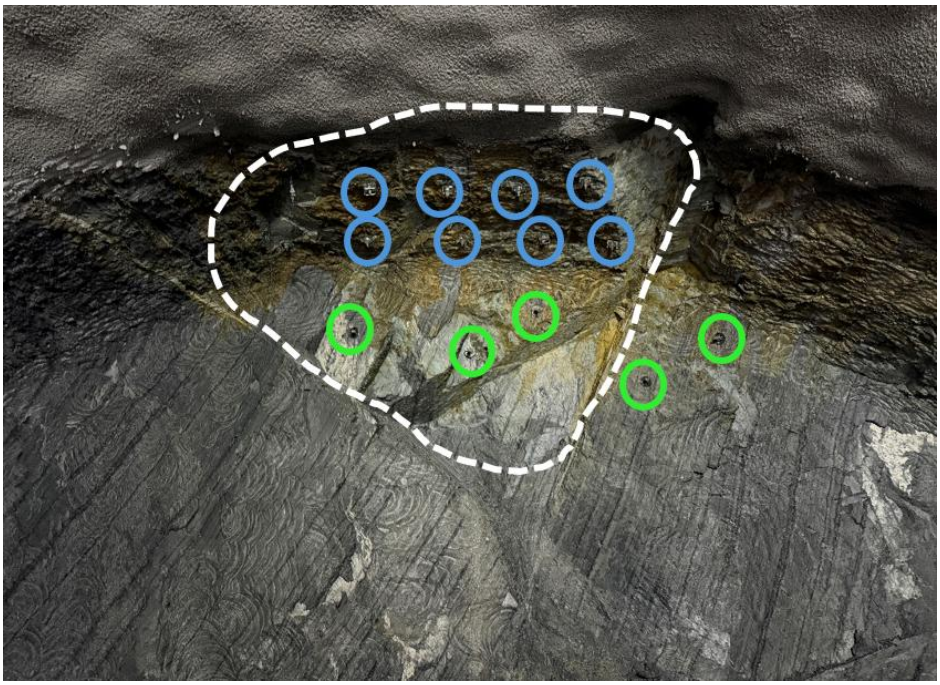
Where the local stability and/or integrity of the tunnel profile was a concern, localized spiling, in the form of GRP (glass-reinforced polymer) CT bolts was the solution implemented to support and confine the hydrothermally altered rock mass and allow the surrounding ground to redistribute stresses around the affected localized zone of altered siltstone. This was inferred to significantly reduce the overbreak in the tunnel profile. GRP CT rock bolts allowed for remote installation and grouting, which ensured that personnel were not entering unsupported ground These GRP CT bolts were installed at a low angle within the tunnel face as close as practical to the tunnel excavation profile. GRP bolts were also cuttable and hence removed the need for a "sawtooth" support profile. This allowed for the maintenance of tunnel profile control during the subsequent excavations, as excavation times could span multiple hours.

Face support was also a critical consideration when tunnelling in hydrothermally altered siltstone. Where required, pattern or spot GRP CT rock bolts with a minimum 2.0 m overlap were deployed when the altered siltstone was identified. Face support pattern geometry extents and timing relative to advance were all determined by the Delve Underground CPS team and supported by design guidance.

7.2 *Support installation sequencing*

Typically, the tunnel support installation construction cycle during the SEM mainline excavation was to first excavate, then install tunnel crown and sidewall rock bolts, then install the fibre-reinforced shotcrete. In some instances, the presence of altered siltstone in the tunnel face and in the crown presented a stability risk during excavation. In these cases, a geotechnical inspection was requested by the operator mid-excavation. The CPS team and the tunnel designers occasionally opted to alter the sequencing.

Occasionally, reducing the tunnel/heading advance length to a "half cut" was specified to reduce the tunnel support cycle time and therefore mitigate the stand-up time limitations of the material. In another case, direction was made to temporarily pause excavation and install localized support in the affected rock mass area (see Figure 5). The excavation cycle was then resumed per normal operation. Finally, in one instance, the direction was given to install the initial layer of shotcrete before beginning the bolting cycle. As previously mentioned in this paper, the material occasionally presented as local raveling ground when the face was washed with water. When this behaviour was encountered within the tunnel profile during geotechnical mapping, rock bolting was not deemed a viable solution for temporary support in order to mitigate the stand-up time limits. Therefore, the initial layer of shotcrete was installed to immediately provide confinement and reduce atmospheric exposure of the hydrothermally altered siltstone.


Figure 5. Pattern CT rock bolts (blue) and GRP face dowels (green) installed mid-excavation with inferred altered rock denoted (white).

7.3 *Mechanical and hydro scaling*

The altered siltstone typically presented in localized areas in the tunnel face at minimal depth, often less than one tunnel advance (1.25 to 3.0 m) length. In these cases, the primary risk was tunnel localized face stability and the loosening of rock sliding off the face and rolling beyond the excavation exclusion zone. In these instances, and after a thorough risk assessment, tThe CPS team would request that the loose rock be mechanically scaled off the face using the excavator bucket during the "muck out" of the excavated spoil. If an excavator was not available at the time of inspection, the bolting arm of the Robodrill was also used to scale off the weaker material.

Finally, the remaining loose material would be scaled using the high-pressure hydroscaler on the shotcrete rig prior to shotcrete application. Given the volatility of the altered rock when interacting with water, this would only be carried out following an assessment of the overall stability of the tunnel excavation and extent of the altered siltstone.

All three methods of scaling were performed remotely by operators within cabins and/or under supported ground at a safe distance away from the exclusion zone to avoid interaction with loosened material.

8 CONCLUSION AND RECOMMENDATIONS

The experience of completing the construction of the SEM mainline tunnels and having successfully managed the risks of hydrothermally altered rock in Silurian siltstone and sandstone have resulted in several recommendations for future design and construction in similar conditions. These include the following:

- Hydrothermally altered material can have highly variable strength and is likely spatially unpredictable. The intensity of alteration and its extent in conjunction with groundwater presence can influence the stand-up time and stability of an underground excavation, and in some cases may even require a passive support solution.
- On projects where hydrothermally altered material may be present, risk minimization measures to be developed during the design phase. If a design case cannot be accurately established, risk controls should be developed based on the difficulties of identifying the material strength and extent in advance of tunnel excavation. The primary risk control method

based on the NEL experience is to develop a toolbox of support items, which include face support and pre-support, such as utilizing cuttable dowels, reduced heading/tunnel advance and increased shotcrete thickness. The toolbox selection criteria should be prescriptive and well-defined.
- During the site investigation stage, hydrothermally altered material should be tested and characterized if encountered. Attempts to establish a design case including location and extent should be pursued as far as reasonably practical.
- Forward probing for geotechnical features such as hydrothermally altered material is a reasonable base case design mitigation measure; however, guidance should be provided that it is not an all-encompassing measure, and probing may miss the zone of hydrothermally altered material or prove to be ineffective for identification. The probing regime should be carefully considered for each case.
- Hydrothermally altered material has highly variable strength. The extent and location, although loosely associated with faulting, is also variable. While sampling and testing of altered material encountered behind the tunnel portal was not recovered, qualitative observations identified that the material was very low strength and behaved as clay, which likely contained significant deviation in strength from the surrounding rocks. Had the highly altered clay-like material been encountered during mainline excavation, a fully passive support solution would likely have been required.
- Further research should be completed to understand the effect of hydrothermal alteration on underground projects.

9 REFERENCES

Golder Associates. 2023a. *Geotechnical Interpretative Report – All Zones*. Prepared by D. Paul, reviewed by R. Buckingham. Internal project report prepared for the multi-national consortium SPARK.

Golder Associates. 2023b. *Geotechnical Interpretative Report – SEM Tunnel*. Prepared by D. Paul, reviewed by R. Buckingham. Internal project report prepared for the multi-national consortium SPARK.

Hoek, E. 1994. 'Strength of rock and rock masses', *ISRM News Journal*, 2(2), pp. 4–16.

Hoek, E., Kaiser, P.K. and Bawden, W.F. 1995. *Support of Underground Excavations in Hard Rock*. Rotterdam: Balkema.

Hoek, E., Carranza-Torres, C. & CHR S. 2002. Hoek-Brown failure criterion – 2002 edition. In: Proc. NARMS-TAC Conference, Toronto, 2002, 1, pp. 267–273. Available at: https://www.rocscience.com/assets/resources/learning/hoek/Hoek-Brown-Failure-Criterion-2002.pdf.

Pirajno, F. 1992. 'Hydrothermal Alteration', In: Hydrothermal Mineral Deposits. Springer, Berlin, Heidelberg.

Powell, C. McA., Baillie, P. W., and Vanberg, A.H.M. 2003. 'Silurian to mid-Devonian basin development of the Melbourne Zone, Lachlan Fold Belt, southeastern Australia', *Tectonophysics,* 375, pp. 9–36.

19th Australasian Tunnelling Conference – Acosta-Martínez, Stewart and Hudson-Smith (Eds.)
© 2025 Australian Tunnelling Society, ISBN 978-0-85825-002-4

Reducing cost and carbon emissions through rapid design optimisation during construction.

T.P. Roper
Acciona Construction Australia, NSW, Australia

L. Gelonch & C. de Santos
SAALG Geomechanics, Barcelona, Spain

M.Ali
Acciona Construction Australia, NSW, Australia

J. Karlovšek
The University of Queensland, School of Civil Engineering, QLD, Australia

ABSTRACT: Major excavations are often designed in the face of considerable geotechnical uncertainty. During the design phase, limited site data and conservative assumptions on the expected geology and geotechnical parameters are typically used to manage this uncertainty. However, as construction progresses and site conditions are observed, much of this uncertainty is reduced. The Observational Method (OM) is a structured framework that takes advantage of this evolving understanding by enabling real-time design optimisation based on actual performance. This paper presents a retrospective case study using machine learning back-analysis platform DAARWIN to investigate how the OM could have optimised ground support for a deep station box excavation. By integrating monitoring data with automated model calibration, the study captures how the evolving understanding of the geological conditions could have enabled design optimisation in real time. Estimated benefits include ~$8 million in cost savings, ~2 weeks in program acceleration, and 120 tonnes of CO_2 avoided. These represent the opportunity cost of not implementing an observation-led approach. The paper concludes by addressing institutional barriers to broader OM adoption.

1 INTRODUCTION

The Observational Method (OM) is widely recognised as a tool for managing geotechnical uncertainty, yet its full potential remains underutilised in modern infrastructure delivery, particularly in its full framework. While contingency-based triggers are commonly employed to address adverse outcomes, the opportunity to optimise designs through progressive modification is seldom realised. This paper explores what could have been achieved had the OM been fully implemented during the excavation of The Bays Station Box, a structure within the Sydney Metro West project. Using DAARWIN, a cloud-based back-analysis platform, we conducted a retrospective analysis of construction-phase monitoring data to identify missed opportunities for design refinement. The aim is not to critique past decisions, but to illustrate how real-time digital tools can enable performance-driven optimisation, improving cost, carbon, and program outcomes. In doing so, we highlight the practical, institutional, and contractual barriers that currently limit OM adoption—and point to a pathway forward.

2 OBSERVATIONAL METHOD

2.1 *Background*

Designing deep excavations in urban environments often involves limited geological information, requiring conservative assumptions about stratigraphy, strength parameters, and hydrogeology. However, knowledge gained during construction provides an opportunity to refine this understanding based on direct and indirect geological observations. The OM is a structured process for managing uncertainty by integrating prediction, monitoring, and adaptive decision-making during construction. Originally formalised by Karl Terzaghi and Ralph Peck (Peck 1969) and later adopted into guidance such as CIRIA 185 (Nicholson et al., 1999) and Eurocode 7 (CEN, 2004),

the OM provides a feedback loop between design and observed performance. Rather than relying solely on conservative assumptions, it involves establishing a working design based on moderately conservative conditions, defining acceptable limits of behaviour, and preparing pre-agreed design modifications that can be triggered in response to monitored ground and structural behaviour. The intent is not to design by improvisation, but to enable data-driven refinement in real time—enhancing safety, efficiency, and confidence as the project progresses.

2.2 *On why the observational method remains underused*

Despite its reputation as one of the most elegant frameworks for managing geotechnical uncertainty, the OM remains underutilised in contemporary practice. This underuse is not due to a lack of theoretical support, indeed, the OM has been celebrated by generations of engineers, as much as it is due to a confluence of practical, institutional, and psychological barriers.

First, contractual, and procedural rigidity prevents flexible design updates during construction. Public projects require certified designs before construction begins, and any changes must pass through formal approval gates. The design change process is lengthy and slow (weeks to months) for modest changes. This structure is fundamentally at odds with OM's core requirement: the ability to adapt the design based on monitored performance.

Second, the OM suffers from misconceptions. It is often misunderstood as a reactive or improvised method, used only when a project has gone wrong (Liew et al 2023). This leads to resistance from stakeholders who perceive it as less rigorous than conventional design. There is also an unfair association between the OM and higher levels of risk (Powderham 2002).

Third, there is a strong desire for certainty, particularly among client organisations. As discussed by Machiels et al. (2021) and Powderham and O'Brien (2020) uncertainty avoidance is a deeply rooted behavioural bias. Kahneman and Tversky's (1974) Prospect Theory explains why individuals prefer fixed, deterministic designs, even when flexible alternatives may offer better outcomes. In this context, OM's adaptive nature is often seen as a risk rather than an advantage.

Finally, there is a perception that OM relies on engineering judgement more than conventional design, which some view as subjective or fallible (HSE, 1996). This discomfort, coupled with a lack of clear guidance on when and how OM should be applied, often leads to its exclusion from the design process altogether. Together, these factors create a systemic bias against the OM, not because it is ineffective, but because it challenges entrenched norms in project delivery.

2.3 *Progressive modification*

Progressive modification refers to making design improvements, typically by relaxing initial conservatism, as uncertainty is reduced through observations. As shown in Figure 1, current practice often involves setting traffic-light style thresholds to detect when behaviour deviates from expectations, enabling intervention via contingency actions. However, the reverse is rarely performed: when monitored behaviour confirms conditions to be better than the conservative assumptions, the design is seldom adjusted to be more efficient. This is a missed opportunity for economic optimisation, noting that early applications of progressive modification can lead to safe, staged relaxation of support schemes during construction based on actual performance.

2.4 *The impact on structural safety*

A central challenge in applying the OM is how to transparently demonstrate its impact on structural safety. How does the 'factor of safety' or probability of failure of a structure change during an application of the OM? Recent research has explored this question through the lens of reliability-based design, with contributions from Johansson et al. (2016), Spross and Johansson (2017), Bjureland et al. (2017), and Spross and Gasch (2019). In geotechnical engineering, as in other structural domains, design adequacy is typically justified through the inclusion of safety margins, usually quantified via deterministic approaches. However, as noted by Lacasse and Nadim (1998), and Duncan and Sleep (2015), when uncertainty is significant, deterministic methods can obscure the actual level of safety being achieved, making them a poor medium for communicating risk.

As demonstrated in Roper et al (2024) when framed probabilistically, sceptics might incorrectly interpret the OM as narrowing the margin between load and capacity, thereby increasing the probability of failure (Figure 2A). OM enhances safety through two distinct mechanisms.

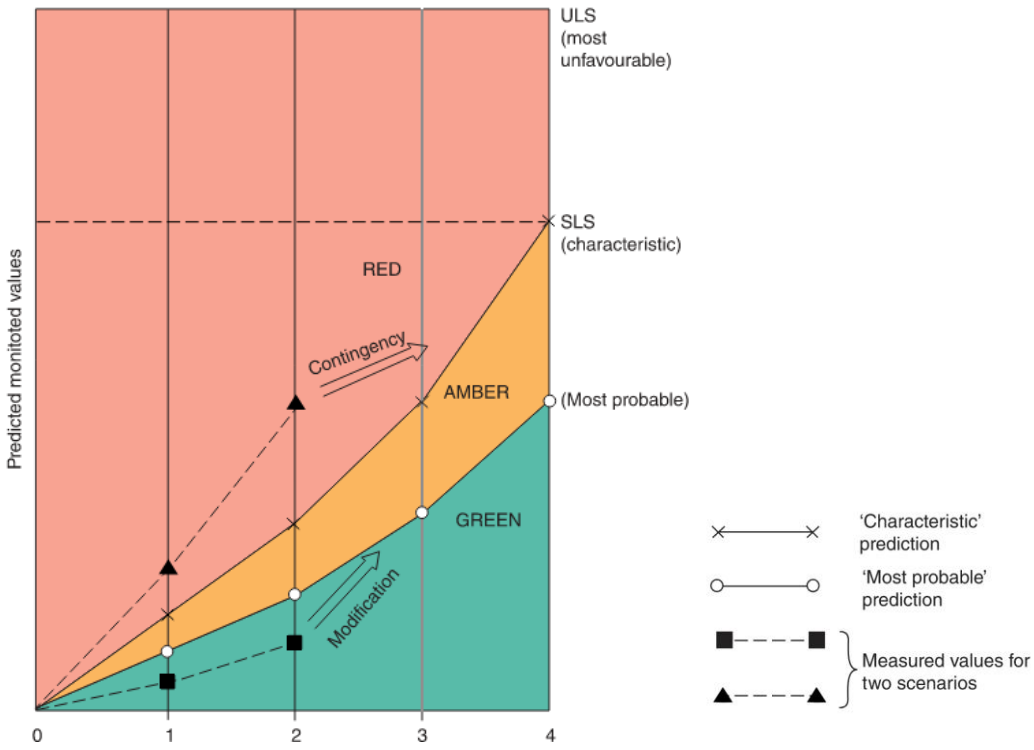


Figure 1 Multi-stage construction trigger values and modification (after Patel 2023)

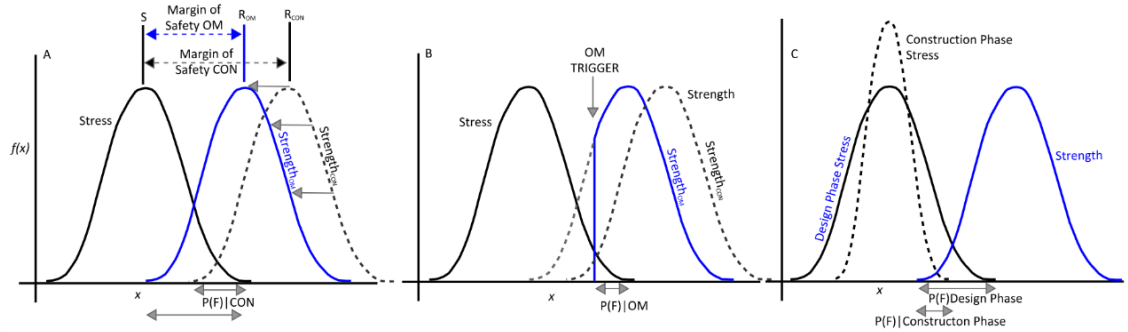


Figure 2 The impact of the observational method using strength-stress-interference (after Roper et al., 2024) where CON= Conventional approach, OM = Observational method approach.

First, the use of monitoring 'triggers' introduces predefined interventions (Figure 2B), which effectively remove the lower tail of possible outcomes by activating contingency measures as needed. Second, uncertainty itself is progressively reduced during construction, as field observations and monitoring refine the understanding of geotechnical conditions (Figure 2C).

2.5 *Aim of this paper*

Construction in Australia has a productivity crisis and geotechnical engineers must explore new strategies to help address this challenge. Unlocking the potential of the OM is one such strategy, but doing so requires more than sound design. It demands appropriate contractual frameworks, a clear communication of its impact on structural safety, cultural shifts within the industry, and tools that enable rapid, evidence-based decision-making. This article contributes to this challenge by demonstrating how modern digital technologies, specifically DAARWIN, can enable timely design optimisation as uncertainty is progressively reduced. A recently constructed station box on the Sydney Metro West project is used as the vehicle for this investigation, specifically, the analysis focuses on the progressive modification of the design (Fig 1), taking advantage of the reduced uncertainty through construction phase data.

3 RETROSPECTIVE CASE STUDY

3.1 *Geological and design context*

The retrospective case study presented in this paper is based on the excavation of The Bays Station Box, one of five new metro stations constructed as part of the Sydney Metro West – Central Tunnelling Package. The excavation is substantial in both scale and complexity, measuring approximately 230 metres long, 25 metres wide, and 32 metres deep (Figure 3). The site is in a low-lying area approximately 4 to 5 metres above sea level, with challenging geological and hydrogeological conditions. The ground profile consists of approximately 4 metres of reclaimed landfill, underlain by up to 20 metres of Holocene and Pleistocene alluvium, comprising interbedded clays and sands. Beneath this, the excavation intercepts Hawkesbury Sandstone.



Figure 3 The Bays Station Box looking west.

In the original design, characteristic soil parameters were selected to conservatively represent the ground conditions, typically corresponding to the lower bound of tested values—around the 80-90th percentile for strength and stiffness. This approach is standard practice in geotechnical engineering to manage uncertainty during early design phases.

The high groundwater table imposed significant hydrostatic loading on the excavation support system, necessitating robust structural and waterproofing measures. The temporary retention system adopted was an anchored secant pile wall (SPW) with toe embedment into the underlying sandstone. The SPW was supported by multiple rows of active ground anchors, ranging from five rows at the deeper western end to two rows at the shallower eastern extent. At the western end, the anchors comprised 19-strand post-tensioned systems, with the longest anchors extending up to 60 metres in length to achieve the required rock embedment. Detailed design description can be found in Okumusoglu and Sentry (2025). The wall was monitored with inclinometers, wells, survey prisms, and load cells on select anchors.

Following installation of the piles, capping beam, and the first row of anchors, excavation progressed in stages, pausing at each level to install the next anchor row. This staged approach (excavate > install > repeat with continuous monitoring) provided natural intervals to compare observed behaviour against design expectations (Figure 4).

3.2 *DAARWIN as tool for progressive modification during construction*

DAARWIN is a cloud-based geotechnical back analysis platform that automates the inverse modelling process by combining high-performance computing with machine learning optimisation.

Specifically, it integrates field monitoring data (e.g., inclinometers, strain gauges, prisms) with numerical simulations in Plaxis to iteratively calibrate soil parameters through genetic algorithms. The core of the process is the minimisation of an objective function, defined as the discrepancy between predicted and observed ground behaviour. By systematically adjusting parameters such as stiffness modulus, cohesion, friction angle etc, DAARWIN identifies best-fit soil models that replicate site behaviour with high fidelity. A complete description of the methodology can be found in de Santos (2015).

Each back analysis run deploys up to 200 parallel simulations in a cloud environment, enabling the rapid evaluation of thousands of models in a fraction of the time traditional methods require. This functionality enables the OM to be applied proactively during construction, supporting real-time decisions and progressive optimisation of design. This approach that has been successfully demonstrated in deep excavation case studies; Cordoni et al (2024) and Liew et al (2023).

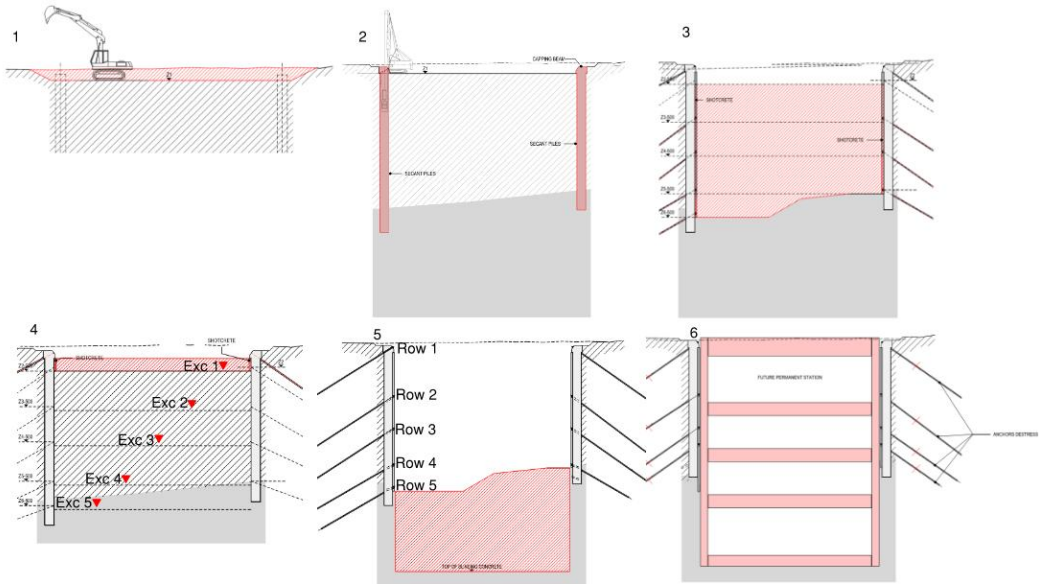


Figure 4 The Bays Station Box construction sequence.

3.3 *Methodology - Implementation of Back-Analysis Framework*

The methodology was as follows,

1. Construction and monitoring: Following the excavation down to anchor row 3, prior to installation of the anchors, inclinometer data are used to show the response of the retaining wall. We then simulate how the OM could have been used to optimise the following rows of anchors.
2. Data selection and model calibration: Using monitoring data from inclinometers at excavation stage 3, we performed a back-analysis of soil behaviour. Thousands of Plaxis models were generated in DAARWIN and soil parameters calibrated to match observation.
3. Design parameter testing: Using the best-matching calibrated model, key design variables (anchor stiffness and spacing) were systematically adjusted to assess the feasibility and impact of progressive optimisation. A simplified design criteria was selected, max horizontal deflection ($U_{x,max}$) of 40mm to ensure the outcome does not exceed that of the original design.
4. Quantification of outcomes: Translate the design optimisation in to cost, program, and carbon savings.

The analysis centred on a back analysis of monitoring data collected during excavation Stage 3. Figure 5A shows the difference between the original design model outcome for horizontal deflection and the inclinometer data. Over 3,000 Plaxis models were generated in parallel across cloud computing environments to iteratively calibrate soil parameters—including stiffness modulus (E') and cohesion (c')—to best match the observed ground movements.

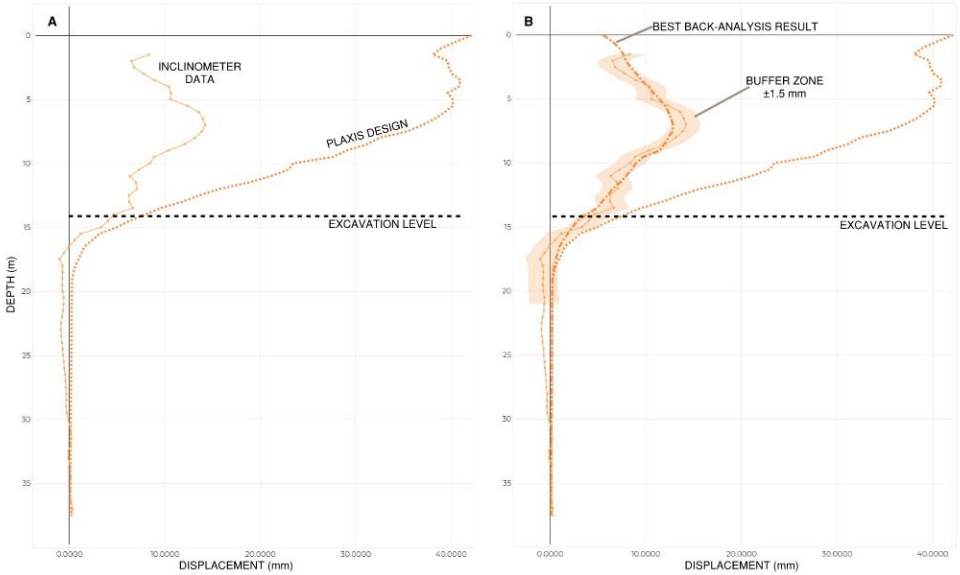


Figure 5 – Inclinometer data versus design. Figure 5A shows the comparison between the inclinometer data (solid line with points) and the original Plaxis model response (dashed line) at Excavation 3. Figure 5B shows the best individual model iteration (dashed line with points) can match the inclinometer data. The buffer indicates the data selected for the analysis. In this case, we defined the buffer width as ±1.5 mm around the monitoring data. The buffer width defines the "good" simulated cases, that is, simulations that match at least 80% of their response within the buffer.

The back-analysis confirmed that the original soil parameters adopted in the design could be improved with the benefit of new information. Specifically, the clayey sand layers, which had been modelled as loose to medium dense, were found through inverse analysis to behave as medium dense to dense granular materials, exhibiting significantly higher stiffness moduli (E') than previously assumed. Similarly, the loose clayey sand layers, initially assumed to be cohesionless, displayed behaviour consistent with dense, partially cemented sands, with apparent cohesion values reaching up to 30 kPa. The back-analysis, calibrated using monitoring data within DAARWIN, provided a more representative picture of actual ground behaviour, revealing that the soils were denser and stiffer than assumed. This refined understanding offers clear justification for design optimisation, where parameters can be updated during construction as uncertainty is progressively reduced. The implications of these adjustments are explored in the sensitivity analysis shown in Figure 6.

Following calibration, we conducted a sensitivity analysis to evaluate the influence of different anchor design parameters on wall displacements, with particular focus on row 3 (S3) and row 4 (S4) anchors as these were significant for consumable quantities. Design variables tested included anchor stiffness and spacing. The model used for this assessment was based on averaged parameters from the top 20 best-matching simulations. Only one parameter was modified at a time to preserve clarity around its individual influence. The results are shown in Figure 6.

3.4 *Results and implementation of optimisation*

The back-analysis conducted using DAARWIN identified several feasible optimisation opportunities for the ground anchor system in The Bays Station Box, without compromising the original deflection performance criteria. The scenarios explored were:

- Reducing anchor capacity in either Row 3 or Row 4 by lowering the number of strands per anchor.
- Doubling the anchor spacing in Row 3 from 1.5 m to 3 m.

In contrast, increasing the anchor spacing in Row 4 was found to have a significant negative impact on wall deflection and was therefore deemed non-viable (Figure 6D). Row 3 presented the greatest opportunity for optimisation. With over 200 anchors, each up to 30m long and originally designed with 15 strands, even modest changes led to substantial material, cost, program, and carbon saving. These scenarios, optimisation options, are summarised below. Table 1 presents a summary of the outcomes, including material savings, carbon emissions, and direct/indirect costs.

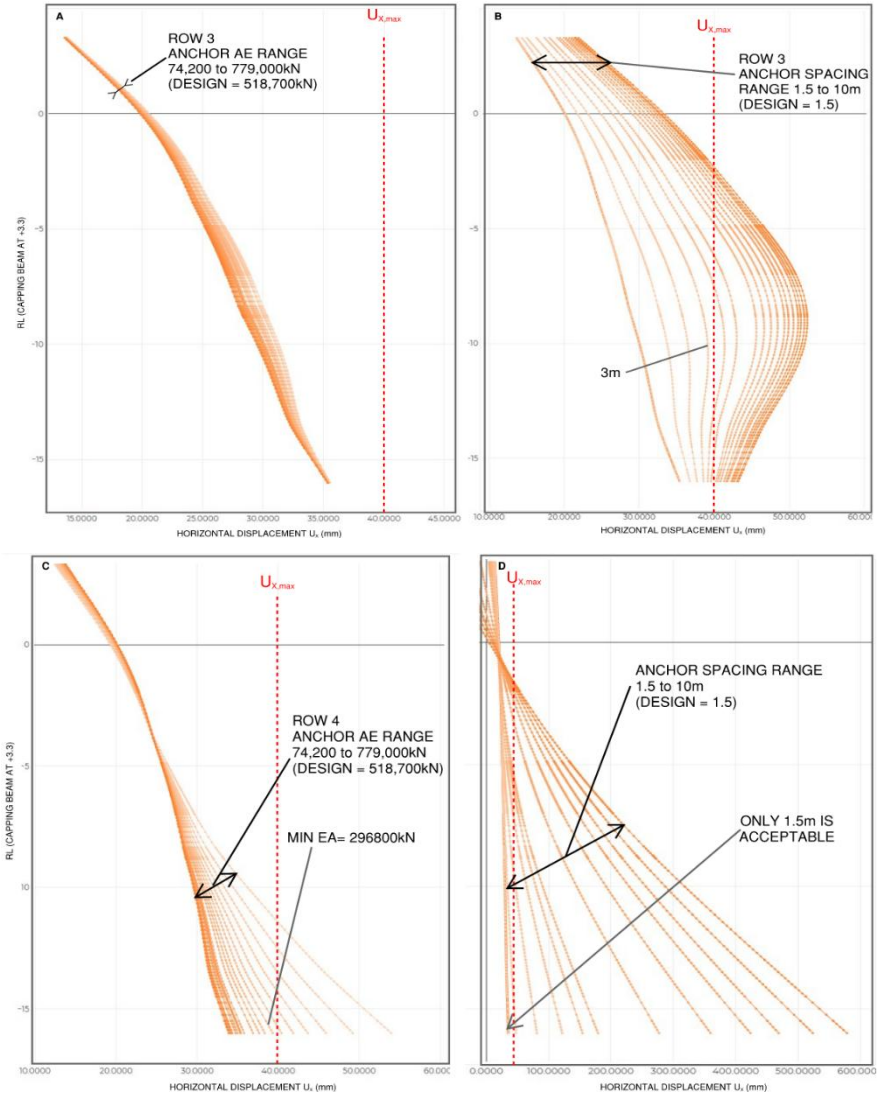


Figure 6 Horizontal displacement of the retaining wall at the final excavation stage, showing results from a sensitivity analysis of ground anchor parameters. Each plot illustrates the influence of a single variable on wall performance, with the red dashed line indicating the design displacement limit ($U_{x,max}$), set at 40mm. (A) Variation in axial stiffness (EA) of Row 3 anchors. (B) Variation in spacing of Row 3 anchors, demonstrating that up to 3 m spacing remains acceptable. (C) Variation in axial stiffness (EA) of Row 4 anchors, with a feasible minimum of 296,800kN (~10 strands). (D) Variation in spacing of Row 4 anchors, showing that only the original 1.5 m spacing satisfies deflection criteria.

1. Row 3 – Strand Reduction: Anchors reduced from 15 to 4 strands, leading to smaller drill holes (from Ø150 mm to Ø90 mm) and reduced bond length in rock (from 5 m to 3 m).
2. Row 4 – Strand Reduction: Anchors reduced from 19 to 10 strands, with drill hole diameter reduced to Ø130 mm and bond length to 4 m.
3. Row 3 – Spacing Increase: Anchor spacing increased from 1.5 m to 3 m (while keeping strand count constant), halving the total number of anchors.

Table 1 Ground anchor quantities in the original design and revised design and the impact of cost, carbon, and program.

OPTION	ROW	NO. ANCHORS	SUM OF TOTAL STRAND LENGTH (KM)	TOTAL STEEL (T)	GROUT (T)	CO_2 SAVING (T)*	DIRECT COST SAVING **	INDIRECT COST**	PROGRAM
1	3	213	65.7 → 14.5 **(Δ = -51.2)**	91 → 20 **(Δ = -71)**	49 → 16 **(Δ = -33)**	120	~$0.35 M	~$1.7 M	~3-4 days
2	4	162	32.6 → 15.2 **(Δ = -17.4)**	44 → 20 **(Δ = -24)**	20 → 14 **(Δ = -6)**	41.4	~$0.15 M	~0.6 M	~2 days
3	3	**213 → 107 (Δ = -106)**	65.7 → 33.3 **(Δ = -32.7)**	91 → 45.5 **(Δ = -45.5)**	49 → 24 **(Δ = -25)**	79.9	$~1.3 M	> 6.5 M	~2 weeks

*CO_2 savings calculated using emission factors of 1.7 tCO_2/t steel and 0.1 tCO_2/t grout.

** The cost figures ($AUD 2024) are indicative only and were developed with input from industry professionals.

While the material cost of post-tensioned strand is modest (~$3.30/m), the most significant benefits of optimisation stem from indirect efficiencies. Lighter and shorter anchors are easier to handle, allowing multiple units to be transported on a single reel and installed with less manual effort. Smaller drill holes reduce grout consumption and spoil volumes, while faster drilling and grouting cycles improve installation productivity. Collectively, these improvements help to streamline construction sequencing and reduce the likelihood of delays caused by bottlenecks in anchor installation.

Option 3, doubling the spacing of Row 3 anchors, offers the most substantial potential savings across all metrics ($1.3M direct + $6.5M indirect). However, this scenario would require more extensive structural verification. Reducing the number of ground anchors places greater reliance on the stiffness and capacity of the secant pile wall, which may necessitate supplementary support such as temporary walers. While walers are quicker to install than long ground anchors, the trade-off between material costs, installation speed, and constructability would need to be evaluated.

From a delivery perspective, program gains are particularly valuable. On major public infrastructure projects, delays can attract liquidated damages in the order of AUD$1 million per day. A modest reduction in ground anchors can translate into 1–2 weeks of program savings, representing a significant financial benefit well beyond the material cost savings alone. Moreover, the embedded carbon savings are meaningful, 120t with option 1 is an outcome to be proud of.

4 DISCUSSION AND CONCLUSIONS

Limitations of the study: It is important to acknowledge that the modelling conducted for this study is deliberately limited in scope. For example, changes to anchor capacity were assessed within the bounds of the Plaxis model only and were not followed by detailed structural checks on pile behaviour, reinforcement design, or load redistribution.

Practical considerations and constraints: Chief among the practical considerations is the sequencing of construction and procurement activities. For example, ground anchors are typically pre-ordered with long lead times, sometimes weeks in advance, even in major cities where local production may be available. Practitioners must weigh these practical ‘nuisance costs’ (as defined in Roper and Karlovšek, 2023) specific to their project when deciding whether and how to implement the OM.

The economics of the OM: One of the prerequisites when deciding to use the OM is that there must be a business case (Powderham and O’Brien 2020). Roper and Karlovšek (2023) and Roper et al. (2024) explore the nuance of this economical decision and proposed a structured decision-making framework grounded in Expected Utility (EU) theory, which provides a rational economic basis for adopting the OM before construction begins. Crucially, this economic framing enables stakeholder to understand the benefit of the OM: it allows for estimation of potential savings under different ground conditions before construction starts. Instead of hoping that value will emerge reactively, the framework enables design teams to assess—ex ante—the expected value

of adaptability. This not only strengthens the business case for OM but also provides a means of navigating contractual discussions, where value engineering or early contractor involvement mechanisms might be needed to realise shared benefits. By embedding the OM within a rational economic model, engineers can better align it with project goals, client preferences, and broader sustainability objectives.

5 REFERENCES

Bjureland, W., Spross, J., Johansson, F., Prästings, A. and Larsson, S., 2017. Reliability aspects of rock tunnel design with the observational method. International Journal of Rock Mechanics and Mining Sciences, 98, pp.102–110.

Cordoni, V.I., Gelonch, L., Solà, B., de Santos, C. and Ledesma, A., 2024. *Back-analysis of deep excavations supported by strutted retaining walls*. In: Proceedings of the XVIII European Conference on Soil Mechanics and Geotechnical Engineering (ECSMGE 2024)

Comite Europeen de Normalisation (CEN. (2004). Eurocode 7: Geotechnical Design - Part 1: General Rules
(EN 1997-1:2004). *Brussels: European Committee for Standardisation.*

DAARWIN cloud-based platform. Accessed on 01 March 2023.

De Santos, C., 2015. Backanalysis Methodology Based on Multiple Optimization Techniques for Geotechnical Problems. Ph.D. thesis. Universitat Politècnica de Catalunya – BarcelonaTECH.

Duncan, M.J. and Sleep, M.D., 2015. Evaluating reliability in geotechnical engineering. In: Risk and Reliability in Geotechnical Engineering. Boca Raton, FL: CRC Press.

Health and Safety Executive (HSE), 1996. Safety of New Austrian Tunnelling Method (NATM) tunnels: A review of sprayed concrete lined tunnels with particular reference to London clay. Suffolk, England: HSE Books.

Johansson, F., Bjureland, W. and Spross, J., 2016. Application of reliability-based design methods to underground excavation in rock. BeFo Report, 155.

Kahneman, D. and Tversky, A., 1979. Prospect theory: An analysis of decision under risk. Econometrica, 47(2), pp.263–292.

Lacasse, S. and Nadim, F., 1998. Risk and reliability in geotechnical engineering. In: International Conference on Case Histories in Geotechnical Engineering.

Liew, K.L., De Santos, C., Gelonch, L. and O'Brien, A., 2023. Enhancing the observational method through digital innovation. HS2 Learning Legacy. Available at: https://learninglegacy.hs2.org.uk/document/enhancing-the-observational-method-through-digital-innovation/ [Accessed 30 Mar. 2025].

Machiels, T., Compernolle, T. and Coppens, T., 2021. Explaining uncertainty avoidance in megaprojects: Resource constraints, strategic behaviour, or institutions? Planning Theory & Practice, 22(4), pp.537–555.

Nicholson, D., Tse, C.M. and Penny, C., 1999. The observational method in ground engineering: Principles and applications. London: CIRIA (CIRIA Report 185).

Okumusoglu, B. and Sentry, M., 2025. Support of 30-m-deep excavation for TBM launch and future underground station of Sydney Metro West. In: C. Rujikiatkamjorn, J. Xue and B. Indraratna, eds. Proceedings of the 5th International Conference on Transportation Geotechnics (ICTG) 2024, Volume 3. Lecture Notes in Civil Engineering, 404. Singapore: Springer, pp.199–208.

Peck, R. B. (1969). Advantages and limitations of the observational method in applied soil mechanics.
Géotechnique, 19(2), 171–87.

Patel D. (2012). *Observational method* in Burland, J. B., Chapman, T., Skinner, H., Brown, M. J., & Institution of Civil Engineers. (2012). ICE manual of geotechnical engineering volume II: geotechnical design, construction and verification. ICE Publishing.

Powderham, A.J., 2002. The observational method—learning from projects. Proceedings of the Institution of Civil Engineers - Geotechnical Engineering, 155(2), pp.59–69.

Powderham, A.J. and O'Brien, F., 2020. The observational method in civil engineering: Minimising risk, maximising value. Boca Raton, FL: CRC Press, Taylor & Francis Group.

Roper, T.P. and Karlovšek, J., 2023. A framework to assess the expected utility of the observational method. In: Proceedings of the ITA-AITES World Tunnel Congress 2023 (WTC 2023), 12–18 May 2023, Athens, Greece.

Roper, T.P., Bertuzzi, R., Oliveira, D. and Karlovšek, J., 2024. A framework to demonstrate the utility and safety of the observational method. Geomechanics and Tunnelling. https://doi.org/10.1002/geot.202300041.

Spross, J. and Gasch, T., 2019. Reliability-based alarm thresholds for structures analysed with the finite element method. Structural Safety, 76, pp.174–183.

Spross, J. and Johansson, F., 2017. When is the observational method in geotechnical engineering favourable? Structural Safety, 66, pp.17–26.

Tversky, A. and Kahneman, D. (1974) Judgment under uncertainty: Heuristics and biases. *Science, 185(4157), pp. 1124-1131.* DOI: 10.1126/science.185.4157.1124

THIS PAGE INTENTIONALLY LEFT BLANK

19th Australasian Tunnelling Conference – Acosta-Martínez, Stewart and Hudson-Smith (Eds.)
© 2025 Australian Tunnelling Society, ISBN 978-0-85825-002-4

Effect of Moving Train Load on Tunnel Deformation and Track-Tunnel Interaction

H. Farooq, S. Nimbalkar and D. Sheng
University of Technology Sydney, Sydney, NSW 2007, Australia

ABSTRACT: Underground railway transportation systems offer a sustainable solution to urban space constraints. However, the construction of such structures presents significant challenges, including ensuring a stable environment for a smooth train transition and balanced interaction between the tunnel and the surrounding soil. This study investigates the influence of moving train load on the concrete inlay and soft rock formations adjacent to the tunnel. A viscoelastoplastic model is developed considering Hooke's, Newton's and St. Venant's elements. An integrated interaction of track and tunnel systems is considered to assess the behaviour of the integrated track-tunnel system and to understand the long-term stability of tunnels in soft rock formations.

1 INTRODUCTION

In view of the ever-growing demand for space in urban environments, constructing underground railway systems offers a practical and sustainable solution. This approach not only saves land use but also contributes to sustainability by minimising noise pollution, reducing disruption to the natural landscape, and ultimately improving the quality of life. Nevertheless, building underground transport networks is complex and requires careful design, which considers all factors essential for feasibility and long-term performance. While modern tunnel construction increasingly favours non-ballasted systems such as fixed or floating slab tracks due to their lower maintenance demands and geometric stability (Gala et al., 2020), a significant number of existing and new railway tunnels still utilise conventional ballasted tracks. These ballasted systems present unique and complex challenges, particularly concerning the time-dependent deformation of the granular ballast and the long-term creep settlement of the surrounding ground, which is the specific focus of this investigation.

The engineering challenges and dominant deformation mechanisms in tunnelling are fundamentally dictated by the geological setting. In hard rock, stability is primarily governed by structural discontinuities, and time-dependent deformation is often negligible, with design focused on controlling block falls or rock bursts (Hoek & Marinos, 2000). Conversely, in soft ground, the critical challenges are low strength and high compressibility, where long-term settlement is mainly driven by consolidation processes (Zhang et al., 2021b). However, soft rock formations are prone to significant time-dependent creep settlement under sustained train (Kovačević et al., 2021).

Effective design and maintenance planning for underground railways necessitate a comprehensive understanding of the railway track, the tunnel structure, and the surrounding ground. Several methods exist for analysing such systems, including empirical approaches, numerical simulations, and rheological modelling. Empirical equations rely on experience and have a limited scope for complex designs, and numerical simulations are time-consuming and expensive. In contrast, rheological modelling provides a more robust way to assess underground responses (Zhang et al., 2021b).

Previous research has primarily focused on evaluating ground movements under instantaneous conditions. However, assessing the time-dependent stability is crucial for ensuring the safety and stability of underground structures (Zhang et al., 2021a). Time-dependent stability issues include deformations of the tunnel lining and the surrounding soil (Hu et al., 2024). Some researchers, such as Hu et al. (2024), employed the rheological model following the Kelvin-Voigt theory to address these issues in the ground surrounding the tunnels. Zhang et al. (2021a) investigated the time-dependent behaviour of ground movements in tunnel soil using a Boltzmann viscoelastic model.

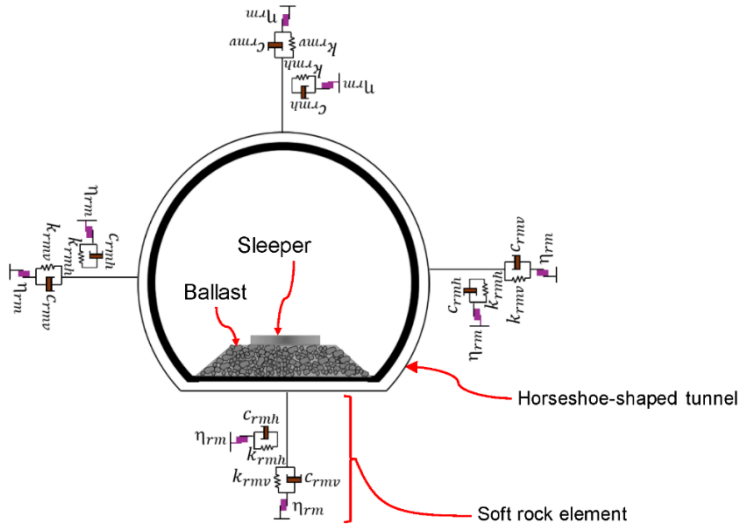
For a well-designed railway tunnel, the surrounding ground must be stable, ensuring minimal deformation occurs during train operations. For such complex structures, ground settlements are often overlooked in their design. However, this assumption is fallacious when the tunnel is situated in soft rock, as these rocks are prone to time-dependent creep settlement (Kovačević et al., 2021). Past studies have also focused on the assessment of time-dependent behaviour using viscoelastic and viscoplastic approaches. For example, Yang et al. (2020) evaluated tunnel safety in argillaceous sandstone by studying its permeability characteristics, Kovačević et al. (2021) and Li et al. (2023) studied the soft rock surrounding the tunnel using Burger's model, while Zaheri and Ranjbarnia (2024) analysed the time-dependent behaviour of pressurised circular tunnels. These studies evaluate the time-dependent response due to overburden and surcharge pressures, using viscoelastic or viscoplastic models. A more complete understanding requires investigating the integrated interaction of track and tunnel systems, encompassing both elastic and plastic responses. This can be achieved using a viscoelastoplastic model, by incorporating both immediate elastic deformation and time-dependent plastic flow, allowing for a more accurate assessment of overall tunnel stability. In addition, most prior research using rheological models has focused on circular tunnels, while the horseshoe shape is more commonly used in practice.

To address these limitations, this study presents a computational methodology for analysing the dynamic effects of moving train loads on an integrated tunnel-track system. The approach employs a novel viscoelastoplastic model that simulates the behaviour using a combination of Hooke's, Newton's, and St. Venant's elements. The model represents a ballasted track with a ballast layer resting on a concrete inlay, treated as a rigid base behaving like a continuous beam. The tunnel is horseshoe-shaped. To simulate the interaction with the surrounding weak rock in the rheological model, Hooke's and Newton's elements are integrated at the concrete inlay interface to represent stiffness and damping, while St. Venant's elements are included to specifically model the plasticity of the soft rock. The accuracy and reliability of the model have been demonstrated by validating against results from past investigations.

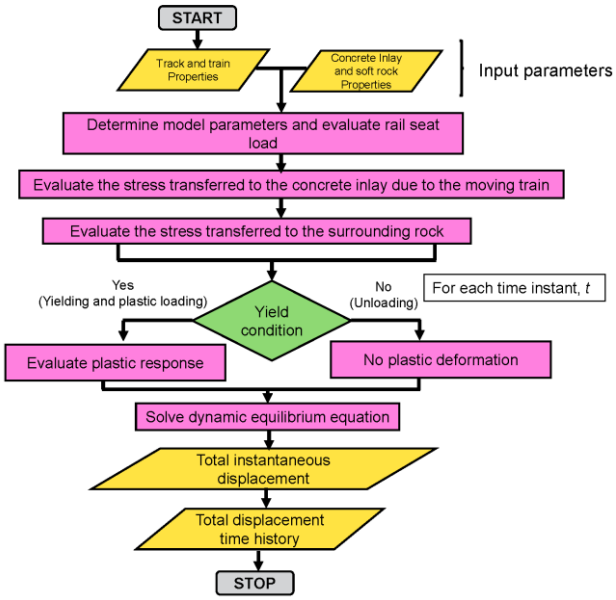
2 MODEL DEVELOPMENT

This study proposes a viscoelastoplastic rheological model for an integrated tunnel-track system. The system consists of a ballasted railway track positioned on a concrete inlay, which is treated as a rigid beam, surrounded by soft rock. The soft rock is the karstic rock, which is prone to creep and settlement. Figure 1 (a) shows the viscoelastoplastic model of the integrated tunnel track surrounded by karstic rock and Figure 1 (b) includes a flowchart to represent the plastic strain accumulation process for each time step. The model incorporates Hooke's (elastic), Newton's (viscous), and St. Venant's (plastic) elements for both the ballasted track and the surrounding rock mass.

For determining the response of the tunnel and the surrounding rock under a moving train load, the dynamic response is first evaluated. The resulting stresses transferred from the track to the inlay are then treated as internal pressure to predict the deformation of the surrounding weak rock. Plasticity in the ballast is based on the Nor-Sand model (Jefferies, 1993), employing a non-associated flow rule (Oka and Kimoto, 2017). For the weak rock, the Hoek-Brown strength criterion is utilised to define its yield behaviour, capturing the time-dependent deformations (Hoek & Brown, 2019).



(a)



(b)

Figure 1 (a) Viscoelastoplastic model of a horseshoe-shaped tunnel surrounded by soft rock (b) flowchart for determining response

The Nor-Sand model developed is based on critical state theory and captures the track response under various conditions. A non-associated flow rule is applied to the granular ballast to depict the realistic material behaviour. The yield surface (f) was defined by Jefferies and Been (2015) using the following equation:

$$f = {}^{\eta}/_{M_i} + ln\left({}^{p}/_{p_i}\right) - 1 \quad (1)$$

where M is the critical stress ratio; subscript i represents image state condition; η is the ratio of deviatoric (q) to mean effective stress (p), defined using the following equations:

$$p = \sigma_{kk}/3 \quad (2)$$

$$q = \sqrt{\frac{3}{2}\sigma_{ij} - p\delta_{ij}} \tag{3}$$

where σ_{ij} is the stress tensor and δ_{ij} is the Kronecker delta.

The non-associated flow rule accounts for both the yield function (*f*) and plastic potential function (g) as distinct terms in this study. The plastic potential function is defined using the following equation:

$$g = \frac{\eta}{M_g} + \ln\left(\frac{p}{p_i}\right) - 1 \tag{4}$$

where M_g is the dilatancy-modified stress ratio; p_i is the mean effective stress in the image state condition. The stress-dilatancy relationship for the non-associated was given by Oka and Kimoto (2017) and is expressed as:

$$D_{ij} = \frac{1}{N} \times \frac{d\varepsilon_v^p}{d\varepsilon_q^p} \tag{5}$$

where D_{ij} is the plastic dilatancy; $d\varepsilon_v^p$ and $d\varepsilon_q^p$ are the plastic volumetric and deviatoric strain increments; N is the non-associativity parameter ($0 < N < 1$). Table 1 includes the input parameters used in this study for evaluation of elastic and plastic deformation of the track.

For evaluating the plasticity of the surrounding rock, the Hoek-Brown criterion is utilised, which is based on three essential parameters: uniaxial compressive strength (σ_c), a constant m_i and geological strength index (GSI) (Hoek & Marinos, 2000). In this study, σ_c values were adopted from the triaxial tests utilised in the study of Kovačević et al. (2021), m_i and GSI were determined either from qualitative rock description outlined by Hoek and Brown (1997). The generalised expression for this criterion is defined using the following equation:

$$\sigma'_1 = \sigma'_3 + \sigma_c\left({m_b}^r \frac{\sigma'_3}{\sigma_c} + s^r\right)^a \tag{6}$$

where σ'_1 and σ'_3 are the major and minor principal stresses (MPa); σ_c is uniaxial compressive strength; ${m_b}^r$, s^r and a are rock mass constants, expressed as follows:

$${m_b}^r = m_i \times e^{\left[\frac{GSI-100}{28-14D_f}\right]} \tag{7}$$

$$s^r = e^{\left[\frac{GSI-100}{9-3D_f}\right]} \tag{8}$$

$$a = 0.5 + 0.17\left(e^{-GSI/15} - e^{-20/3}\right) \tag{9}$$

where m_i is a material constant; D_f is the disturbance factor signifying damage, which is influenced by the dilation caused in the rocks due to excavations in the surroundings. The various input parameters used in this study are included in Tables 1, 2 and 3.

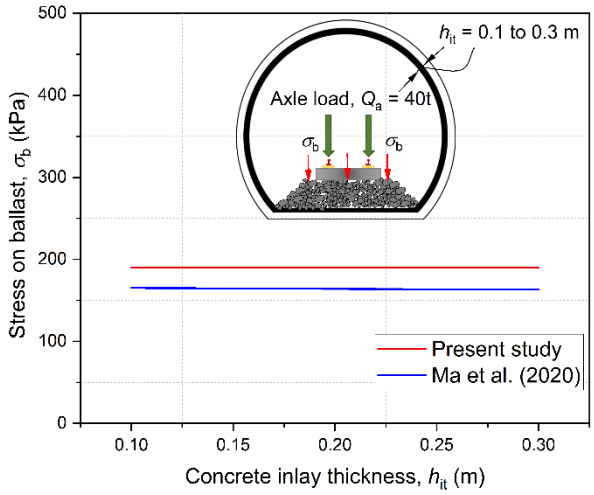


Figure 2 Comparison of stress on ballast calculated using present study and results of Ma et al. (2020)

Table 1 Input parameters for the railway ballast

Parameters	Symbol	Unit	Value
Young's modulus of ballast	E_b	MPa	276
Poisson's ratio of ballast	ν_b	-	0.3
Density of ballast	ρ_b	kg/m^3	1760
Thickness of ballast	h_b	m	0.3
Shear stiffness of ballast	k_b^s	MN/m	78.4
Shear damping of ballast	c_b^s	kNs/m	80
Critical stress ratio	M_{tc}	-	1.25
Slope of critical state line	λ	-	0.05
Hardening parameter	H	-	50-250
Cyclic hardening parameter	a_h	-	0.9
Volumetric coupling coefficient	N_v	-	0.2
Non-associativity parameter	N	-	0.5
Maximum dilatancy	χ_i	-	3

3 MODEL VALIDATION

To validate the model, results were compared against a previous study by Ma et al. (2020), who developed a model of a single-track ballasted tunnel in rock to investigate damage and fatigue under a heavy 40t axle load simulated with an excitation force function. Figure 2 presents this comparison, specifically showing the vertical stress on the ballast top as the thickness of the inlay varies, as calculated by both Ma et al. (2020) and the present study. The close agreement between the results suggests that the present model is capable of accurately simulating track-tunnel behaviour. This comparison demonstrates the ability of the model to capture and predict key stress distributions within the tunnel structure, highlighting its potential value for assessing and reducing damage risks associated with ballasted tunnel operations.

Table 2 Input parameter values for concrete inlay and sleeper

Parameters	Symbol	Unit	Value
Concrete inlay:			
Young's modulus	E_{it}	MPa	0.0033
Poisson's ratio	ν_{it}	-	0.3
Thickness	h_{it}	m	0.02
Damping	c_{it}	kNs/m	100
Stiffness	k_{it}	kN/m	1.7×104
Density of sleeper	ρ_s	kg/m^3	2500
Width of sleeper	b_s	m	0.3
Length of sleeper	l_s	m	2.6
Sleeper spacing	s	m	6.5

Table 3 Input parameter values for soft rock

Parameters	Symbol	Unit	Value
Poisson's ratio	ν_{rm}	-	0.25
Internal friction angle	φ	°	25
Density	ρ_{rm}	kg/m3	2450
Geological strength index	GSI	-	29
Material constant	m_i	-	7
Young's modulus	E_r	MPa	20000
Rock mass constants	s^r	-	0.001
	a	-	0.5
Disturbance constant	D_f	-	0.1

4 RESULTS AND DISCUSSION

In an integrated tunnel-track system, concrete inlay thickness, h_{it} is a critical factor that influences the structural behaviour and load capacity of the system. To assess its impact, h_{it} was systematically increased from 0.02 to 0.1 m. This investigation revealed that increasing the inlay led to a roughly proportional increase of approximately 50% in both inlay deflection, d_{it} and reaction force, f_{it}. However, the rate of this increase was highest for smaller thickness increments, i.e., a 25.9% rise between 0.02 and 0.05m, and decreased significantly for greater thicknesses, i.e., only 6.3% from 0.075 to 0.1m. This indicates that the effectiveness of increasing inlay thickness diminishes at higher values. This behaviour is consistent with findings from Ma et al. (2020), who noted that increased h_{it} improved stress distribution on the inlay, likely due to enhanced stiffness and reduced stress concentration. Figure 3 demonstrates how h_{it} affects the overall structural response.

Evaluating the impact of repetitive train loads on soft rock settlement, S_r was conducted for the tunnel embankment for a depth of 30 m. The tunnel is located at 20 m depth from the ground surface, z. Figure 4 presents these findings, showing that S_r varied non-linearly with z. For a 25t axle load at 150 km/h, the highest S_r of 1.3 mm was recorded at the tunnel base, decreasing sharply to become almost negligible (99% reduction) at the ground surface. This pattern indicates that the influence of train loads on rock settlement is concentrated near the tunnel, having minimal impact closer to the surface.

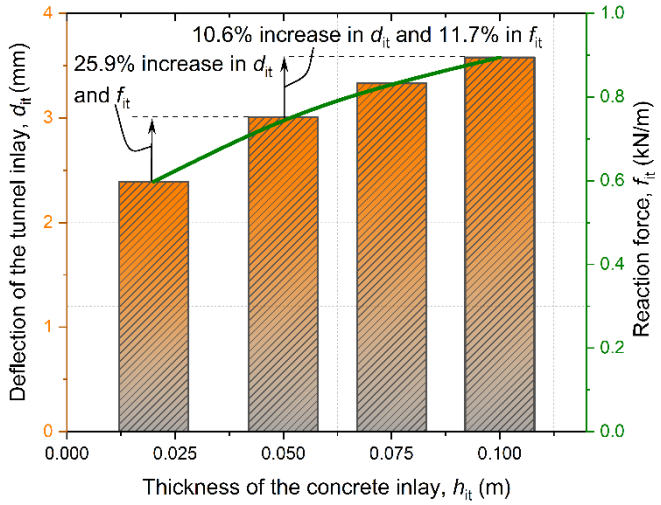


Figure 3 Deflection and reaction force on the concrete inlay due to increasing thickness of the concrete inlay

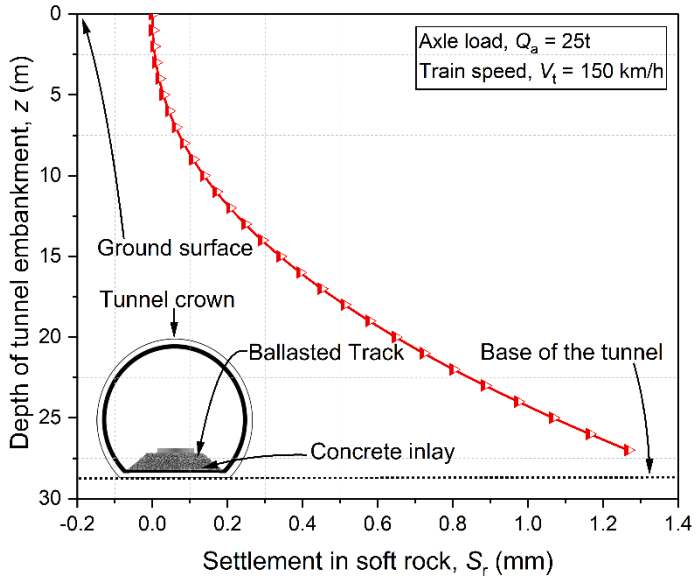


Figure 4 Settlement in the soft rock due to train passage

5 CONCLUSIONS

Construction of underground railways in soft rock poses severe challenges, particularly concerning time-dependent stability under dynamic train loads. In order to address gaps in previous literature, this study presents a novel viscoelastoplastic model for the integrated tunnel-track and the surrounding soft rock. The model is validated against past studies. The model simulates complex material behaviour using Hooke's, Newton's, and St. Venant's elements, incorporating the Nor-Sand and Hoek-Brown criteria. The dynamic track-inlay response and resulting ground (soft rock) settlement are evaluated. Key findings illustrate the increased deflection of the concrete inlay with an increase in concrete inlay thickness. The results from the present study reveal that train-induced rock settlement is primarily localised near the tunnel base. This research provides practising engineers with a valuable computational tool for assessing the long-term structural response of integrated tunnel-track systems in challenging soft rock formations.

While the presented viscoelastoplastic model effectively captures the cumulative ground settlement resulting from repeated train loads through a time-dependent creep mechanism, it does not explicitly account for the potential fatigue degradation of the rock intrinsic strength and stiffness. Incorporating this represents a valuable and complex avenue for future work, which would allow for an even more comprehensive assessment of the long-term integrity and service life of the integrated tunnel-track system under operational loading.

6 REFERENCES

Gala, M., Sestakova, J., & Dvorak, T. (2020). State of the art of slab track systems. In MATEC Web of Conferences (Vol. 310, p. 00004). EDP Sciences.

Hoek, E., & Brown, E. T. (1997). Practical estimates of rock mass strength. International journal of rock mechanics and mining sciences, 34(8), 1165-1186.

Hoek, E. & Brown, E. T. (2019). The Hoek–Brown failure criterion and GSI–2018 edition. *Journal of Rock Mechanics and Geotechnical Engineering*, *11*(3), 445-463.

Hoek, E. & Marinos, P. (2000). Predicting tunnel squeezing problems in weak heterogeneous rock masses. *Tunnels and tunnelling international*, *32*(11), 45-51.

Hu, A., Xie, S., Xiao, Z., Hu, Wang, M., Chen, Y. & Chen, Y. (2024). Analytical solution for consolidation of saturated viscoelastic soils around tunnels with general Voigt model. *Computers and Geotechnics*, *166*, 105926.

Jefferies, M. G. (1993). Nor-Sand: a simle critical state model for sand. *Géotechnique*, *43*(1), 91-103

Jefferies, M. G. & Been, K. (2015). *Soil liquefaction: a critical state approach*. CRC press.

Oka, F., & Kimoto, S. (2017). Effect of the non-associativity of plasticity model on the cyclic behavior of geomaterials. Key Engineering Materials, 725, 322-327.

Kovačević, M. S., Bačić, M., Gavin, K., & Stipanović, I. (2021). Assessment of long-term deformation of a tunnel in soft rock by utilizing particle swarm optimized neural network. Tunnelling and underground space technology, 110, 103838.

Li, X., Liu, X., Tan, Y., Chen, A., Wang, H., Wang, X., & Yang, S. (2023). Rheological mechanical properties and its constitutive relation of soft rock considering influence of clay mineral composition and content. International Journal of Coal Science & Technology, 10(1), 48.

Ma, W. B., Chai, J. F., Han, Z. L., Ma, Z. G., Guo, X. X., Zou, W. H., ... & Niu, Y. B. (2020). Research on Design Parameters and Fatigue Life of Tunnel Bottom Structure of Single-Track Ballasted Heavy-Haul Railway Tunnel with 40-Ton Axle Load. Mathematical Problems in Engineering, 2020(1), 3181480.

Yang, F., Zhou, H., Zhang, C., Lu, J., Lu, X., & Geng, Y. (2020). An analysis method for evaluating the safety of pressure water conveyance tunnel in argillaceous sandstone under water-weakening conditions. Tunnelling and Underground Space Technology, 97, 103264.

Zaheri, M., & Ranjbarnia, M. (2024). An analytical–numerical method for the hydraulic–mechanical coupling analysis of time-dependent behavior of pressurized tunnels: Impact of an excavation damaged zone. Computers and Geotechnics, 170, 106299.

Zhang, Z., Huang, M., Pan, Y., Jiang, K., Li, Z., Ma, S., & Zhang, Y. (2021). Analytical prediction of time-dependent behavior for tunneling-induced ground movements and stresses subjected to surcharge loading based on rheological mechanics. Computers and Geotechnics, 129, 103858.

Zhang, Z., Zhang, M., Pan, Y., Li, Z., Shen, A., & Zhao, Q. (2021). Mathematical modelling for ground consolidation settlements induced by lining leakage of shield tunnel under train loading in viscoelastic porous soils. Applied Mathematical Modelling, 98, 537-562.

Theme 9. Groundwater Control

THIS PAGE INTENTIONALLY LEFT BLANK

19th Australasian Tunnelling Conference – Acosta-Martínez, Stewart and Hudson-Smith (Eds.)
© 2025 Australian Tunnelling Society, ISBN 978-0-85825-002-4

Using the Lugeon test in tunnelling groundwater control - analysis and interpretation

H.R. Asche
Design Director, Aurecon, Brisbane Australia

ABSTRACT: Groundwater control in tunnelling projects is one of the critical elements in tunnel design and construction. This aspect can often drive the entire tunnel concept. The Lugeon or packer test is commonly used to characterise the potential for groundwater inflow into rock tunnels and it is an essential part of geotechnical investigations for tunnel projects. However, the specification, documentation and interpretation of this seemingly simple test has many pitfalls. The paper describes key aspects of Lugeon testing for tunnel projects and provides recommendations for carrying them out. The paper also describes interpretation of these tests and their use in designing groundwater control for tunnel projects.

1 DISCONTINUITIES AND GROUNDWATER FLOW IN A ROCK MASS

1.1 *Types of discontinuities*

Discontinuities (the generic term) can be classified into the categories of bedding, foliation and fractures based on the origin of the discontinuity. Bedding occurs during the sedimentation process while foliation is caused by recrystallisation under heat and pressure, generally normal to the major principal stress at the time of the metamorphism. Fractures are caused by applies stress exceeding the rock strength, either due to tension or shear.

While the processes described above may lead one to suspect that discontinuity spacing is quasi-regular, the conclusions of Priest and Hudson (1976) and Priest (1993) is that the distribution of total discontinuity spacings is modelled by the negative exponential probability density distribution for many situations.

1.2 *Groundwater flow in the rock mass*

Most fractured rocks have very low primary porosity and groundwater is contained within, and moves through, secondary features such as joints and fractures. Krásný and Sharp (2007) provide a comprehensive overview of general subject of groundwater in fractured rocks. Other important general references for fractured rock aquifers include Priest (1993), Cook (2003), Singhal and Gupta (2010), Gustafson (2012) and Sharp (2014).

1.3 *Groundwater flow in an individual discontinuity*

In theory, the transmissivity of a discontinuity is described by the well-known cubic law for the idealised situation of flow in an aperture of smooth parallel walls is:

$$T = \frac{\rho g}{12\mu} \cdot b^3 \qquad (1)$$

where b is the aperture, ρ and μ are the density and dynamic viscosity of water and g is the acceleration due to gravity. Transmissivity has units m^2/s.

Figure 1 shows a series of water-bearing bedding planes daylighting on a slope.



Figure 1. Limestone with bedding planes, Dolomites, Italy.

Each of the beds of limestone are supported on the bed below; there is transmission of vertical force across the bedding planes. However, each of the planes is also transmitting water sub-horizontally. The only way that these two processes can occur simultaneously is if elements of contact and elements of separation occur in the planes (Lombardi 2003). Refer Figure 2.

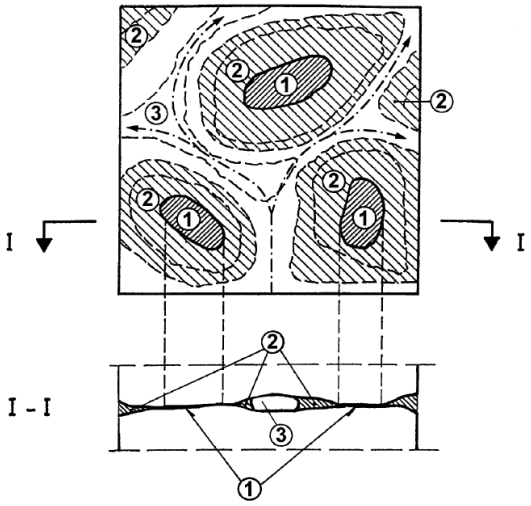


Figure 2. Lombardi conceptual model of a discontinuity (Lombardi 2003). ① full contact areas, ② areas with bound water and ③ areas where water can flow.

2 DATA AND DATA ANALYSIS

2.1 *Preliminaries*

An excellent introduction to data analysis is included in Kitanidis (1997) – Chapter 2. The pre-requisites for data analysis should be obvious:

- The data is drawn from a single population, so that the analysis can provide a useful prediction within that population. For example, if the tunnel passes through completely different materials, it makes little sense to mix data from each material; the analysis will be of low value.
- Similarly, even if within a single geotechnical domain, it makes little sense that the results of different tests are mixed.
- Finally, the data should be a random sample, rather than a "selected" sample. (In some cases this is inevitable; UCS tests cannot be performed on broken or crushed rock core – UCS test are inevitably skewed towards the stronger end of rock strength.

A common practice in geotechnical investigations of the past has been to review the core to locate a few of the largest and apparently wettest fractures in the borehole and then to adjust the packer positions to the least fractured area to avoid packer leakage. A dataset of tests selected in this manner will not be amenable to data analytical methods, for two reasons:

- Obviously, this process of selection is strongly skewed to sample only the high end of the population.
- Less obviously, but still important, different lengths of packer test are in fact different tests, because the length of a packer test is associated with the variability; short packer tests will vary more than long tests – the long test tends to average out the results.

2.2 *Censored data sets*

It is common for data sets to have missing values for various reasons:

- Measurement techniques may fail or may not be accurate at very low values. In the particular case of the packer test, flow meters may not register or be accurate at very low values of flow, or the flow may be indistingushable from leakage.
- Measurement techniques may fail or may not be accurate at very high values. In the particular case of the packer test, it may not be possible to provide sufficient flow down a hose down the borehole.

In both cases described above, the tests have meaning, even if they do not have a defined value. For example, each test with very low flow indicates tight rock, whereas each test with very high flow indicates the opposite. Techniques exist for dealing with censored data which respects the existence and meaning of the tests although the values are unknown.

2.3 *Quantities with and without finite variance*

There are many quantities in nature and engineering in which the values cluster around a mean value. While the individual quantity in question may not necessarily be normally distributed, the Central Limit Theorem says that larger samples (usually larger than 30) of randomly chosen values will be normally distributed. Most undergraduate courses in statistics describe methods for quantities where the Central Limit Theorem holds. If the sample size is not large enough, special techniques are used (Student's "t" distribution is substituted for the normal distribution).

There are some quantities in nature and engineering for which the Central Limit Theorem does not apply. Mathematically, this is where the population variance is not finite.

Taleb (2007) provides an example showing the difference between these cases. An example where the Central Limit Theorem applies is that of human weight. Assume a stadium is full of (say) 100,000 people and the mean weight of the spectators is measured as (say) 75 kg. Pick a person at random and remove them, replacing with the heaviest person in the world and then recalculate the mean. According to Wikipedia, the heaviest person who ever lived was was 635 kg, so the mean weight of the stadium will increase by 5.6 grammes, a negligible amount. However, substituting for the finanicial worth of the spectators, let's assume that the mean turns out to be (say) $750K. Replacing a person at random with one of the multi-billionaires of our time (say $500B), the mean increases by $5M, a very significant increase. The distribution of net worth is well described by a power law, as famously proposed by Pareto. Taleb warns against using techniques, developed where the Central Limit Theorem applies, to situations where it does not apply.

From Adamic and Huberman (2002): "Many man made and naturally occurring phenomena, including city sizes, incomes, word frequencies, and earthquake magnitudes, are distributed accroding to a power-law distribution. A power-law implies that small occurrences are extermely common, whereas large instances are extremely rare."

2.4 *Distributions for discontinuity characteristics*

Table 1 shows distributions proposed for various characteristics associated with discontinuities

Table 1. Distributions proposed for discontinuity characteristics

Characteristic	Distribution	Reference
Transmissivity of individual discontinuities	Pareto distribution	Gustafson and Fransson (2005)
Spacing of discontinuities	Negative exponential distribution	Priest and Hudson (1976)
Number of discontinuities between packers	Negative binomial distribution	Kozubowski et al (2008)
Packer test results	Log-normal distribution	Raymer (2001), Raymer and Maerz (2014)

There are several practical conclusions that arise from Table 1:

- The Pareto distribution is an implementation of the power law. If a packer test is the sum of the transmissivities of a number of discontinuities, the Pareto distribution means that most of the transmissivity is coming from only a very few of them, most likely from one only.
- The Central Limit Theorem does not apply to sums of transmissivities – if it did, the distribution of packer tests would be normally distributed. However, if the sum includes enough samples (in this case discontinuity transmissivities), the analogy of the Central Limit Theorem for the power law suggests the log-normal ditribution.
- Kozubowski et al (2008) study packer tests simulated by combining the Pareto distribution for individual transmissivities with the negative binomial distribution for the number of discontinuities, and show that the log-normal distribution fits the results better when the packer tests are longer, i.e. there are enough fracures in the packer test length for the log-normal distribution.

3 THE PACKER (OR LUGEON) TEST

3.1 *History and general usage*

Lugeon (1932) is credited with the test for water absorption in a borehole. His paper of 1932 includes a diagram of test results for the planning of curtain grouting for the Sarrans dam. Figure 3 shows the diagram in full and a magnified snip of the legend. Note that the tests are all of the same length and not "selected"; rather they are sequentially located.

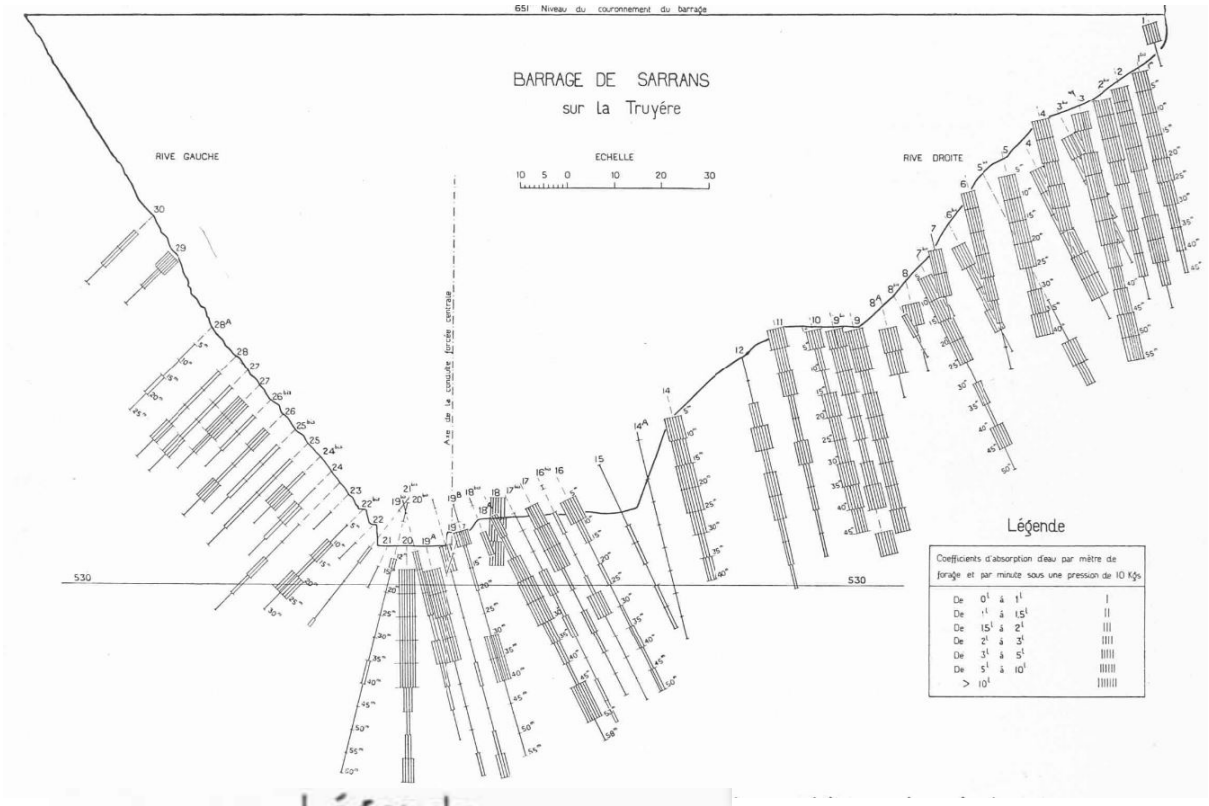
Translating the legend in Figure 1 loosely, the units of the test are "absorption of water per metre of borehole in litres per minute for an overpressure of 10 kg/cm^2." Modern sources substitute the overpressure as 1 MPa = 10 bar, which is approximately equal to 10 kg/cm^2.

Modern standards for running the test include ASTM D4630-96, ISO 22282-3:2012(E), and the ISRM suggested method by Vaskou et al. (2019). Papers describing the theory and practice of the test include Houlsby (1976 and 1990), Pearson and Money (1977), and Quiñones-Rozo (2010). Vaskou et al. (2019) describe the history of the test in detail and make the important point that, while other hydrogeological tests are designed for ground with a primary porosity, the packer test is more specifically used for fractured rock masses.

The ISO standard defines the test unit to be "Lugeon". Vaskou et al propose "LU". (The ASTM standard does not refer to the Lugeon unit at all.) For this paper, the nomenclature of "Lugeon" will be used, or in abbreviation, "Lu".

If the 1 MPa pressure is converted to 100 m of water head, the possibility exists of a direct conversion to m/s, with 1 Lugeon = 10^{-3} m^3 / (60 s x 100 m x 1 m) = 1.667 x 10^{-7} m/s. This paper argues against adopting this conversion for two reasons:

- There are many methods for converting Lugeon test results to hydraulic conductivity with results in units of m/s but with factors different to the value above. There is a significant possibility of confusion.
- As will be argued further, it makes little sense in converting individual packer tests to a hydraulic conductivity as if the local fractured rock mass was an isotropic Darcy media.



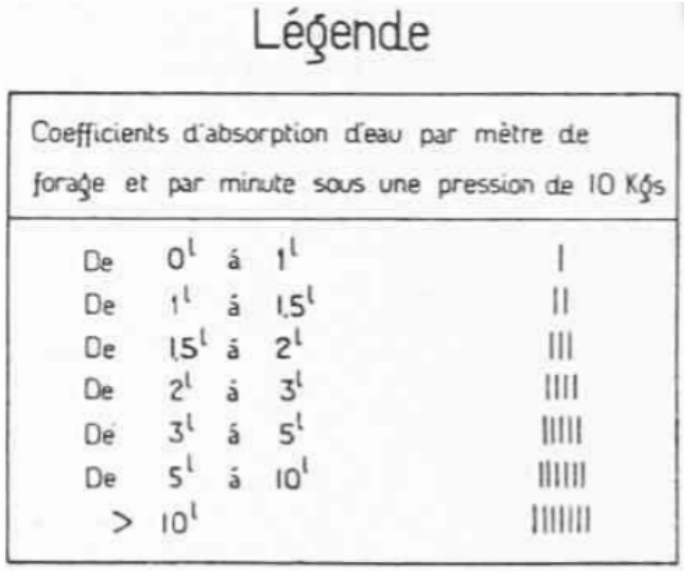


Figure 3. Diagram in Lugeon (1932), with detail enlarged.

The Lugeon test has remained in use because it is closely aligned to practical uses. Speaking generally for both tunnels and dam foundations, values around 1 Lugeon represent tight rock, which in most cases will not require treatment in that local area. Values above 10 Lugeon almost certainly will require treatment. The Lugeon test is also relatively cheap to conduct in conjunction with cored boreholes.

The Lugeon test is usually carried out in five stages, starting and ending with a lower pressure, and then progressing up and down again in pressure. In perfect theoretical conditions, there should be a linear relationship between the flows measured at the pressures. Houlsby (1976) describes the interpretation of the results when the linear relationship is not seen.

3.2 *Quantitation limits*

While water absorption in a borehole can vary over many orders of magnitude, there are practical limitations on the accuracy of the test over a subset of this range.

As described above, at the lower end of the test range, small flows cannot be measured accurately and may be indistinguishable from leakage in the system. At the upper end of the test range, there are practical limitations on the delivery of large flows of water to the test. Raymer (2001) calls these limits the Lower and Upper Quantitation Limits (LQL) and (UQL). Understanding that these limits exist is key to understanding the packer test.

Raymer suggests typical values for these, with recommended values:

– LQL = 0.1 Lugeon
– UQL = 50 Lugeon

As will be seen below, the analysis method proposed by Raymer (2001) is not sensitive to these values; the user may vary these values and return similar results. Note that in Figure 3, Lugeon implicitly adopts an LQL and UQL.

3.3 *Direct conversion to hydraulic conductivity?*

Many authors, including the international standards, suggest various formulae or methods for directly converting a packer test result to a hydraulic conductivity. A commonly quoted formula is from Moye (1967) which assumes cylindrical flow in an isotropic Darcy material and derives the following for the equivalent hydraulic conductivity K:

$$K = \frac{Q}{2\pi \cdot L \cdot \Delta h} \cdot \left[1 + \ln\left(\frac{L}{2 \cdot r_w}\right)\right] \quad (2)$$

with flow Q in a borehole radius r_w, length between packers L and overpressure (expressed as a head) of Δh.

Gustafson (2012) provides an alternative formula:

$$K = \frac{Q}{2\pi \cdot L \cdot \Delta h} \cdot \ln\left(\frac{L}{r_w}\right) \quad (3)$$

As discussed below, the correct viewpoint is to consider individual packer tests as part of a statistical population with an effective hydraulic conductivity resulting from analysis of all of the tests.

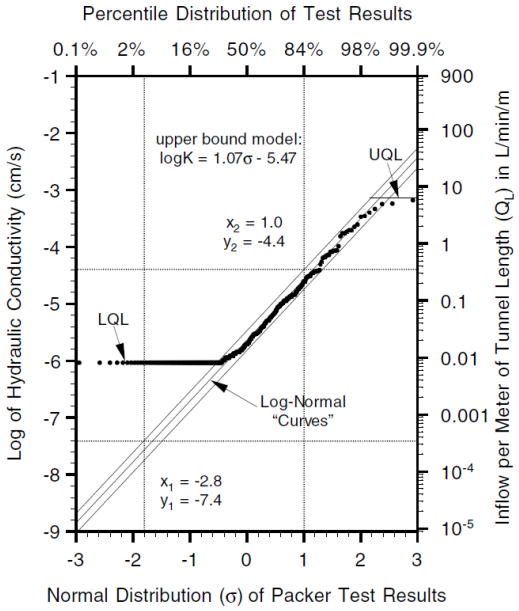


Figure 4. Raymer plot for a set of packer results (from Raymer 2001)

3.4 *Raymer analysis*

Raymer (2001) describes a graphical technique for fitting censored data to the log-normal distribution. The procedure is to consider all tests, including those where the result is expressed as

either “no flow” or “flow too small to measure” (which are assigned the value of the LQL).

Figure 4 shows the Raymer plot of a typical set of packer tests (from Raymer 2001). It can be seen from Figure 4 that the result is insensitive to the choice of LQL and UQL. The fitted line is to a log-normal distribution, with an intercept and slope. Due to the use of the base 10 log, the parameters estimated for the log-normal distribution need to be adjusted as follows:

$\mu = ln(10) \cdot intercept$ (4)

$\sigma = ln(10) \cdot slope$ (5)

Note that the parameters (μ, σ) are not the mean and standard deviations, but are the parameters of the log-normal distribution:

$$p_x(x) = \frac{1}{\sqrt{2\pi} \cdot \sigma \cdot x} \cdot \exp\left[-\frac{(\ln(x)-\mu)^2}{2 \cdot \sigma^2}\right] \quad (6)$$

4 PRESENTATION AND USAGE OF DATA

4.1 *Presentation of the data*

From the parameters μ and σ, the following can be calculated:

- arithmetic mean: $\exp\left(\mu + \frac{\sigma^2}{2}\right)$
- median (= geometric mean): $\exp(\mu)$
- mode: $\exp(\mu - \sigma^2)$
- variance: $[exp(\sigma^2) - 1] \cdot \exp(2\mu + \sigma^2)$

What does not make any sense, but is frequently seen, is to calculate the mean and standard deviation using the arithmetic. The conventional calculation of the mean and variance of log-normal data, even when the data is not censored, is known to be highly unstable, because the data sets are dominated arithmetically by the highest values.

When the data is censored, there is no excuse to attempt to calculate the mean and standard deviation using the conventional formulae – the results must be meaningless.

4.2 *Use of the analysis*

Estimation of the effective hydraulic conductivity of the rock mass: Parsons and Raymer (2024) provide a comprehensive discussion of this topic, based on the parameters (μ, σ) derived from a Raymer analysis.

Estimation of apertures: If the number of fractures is recorded with the packer test results, it is possible using Fransson’s method (Fransson 2002) to estimate the parameters of the Pareto distribution, and therefore to estimate the ditribution of the aperture values.

Probing and grouting: Asche and Smith (2013) provide a method for calculating the probability that probe triggers are exceeded during probing and pre-excavation grouting for tunnels.

5 CONCUSIONS AND RECOMMENDATIONS

The following recommendations are provided:

1. Packer tests should be randomly selected, or what is effectively similar, to conduct tests head-to-tail sequentially up the borehole,
2. Packer tests should all be the same length,
3. The proposed constant length is 5 m so that the packer test represents the sum of enough transmissivities that the log-normal distribution is a reasonable fit.
4. The fracture count between the packers is routinely recorded with the packer test result
5. The Packer test result is retained in Lugeon values rather than attempting to ascribe a fictitious hydraulic conductivity value to individual test results
6. The tests are analysed by the Raymer (2001) or similar method which correctly accounts for censored data
7. The results are reported as the parameters μ and σ with further calculations based on those values. Arithmetic methods should never be used on the raw data.

6 REFERENCES

Adamic LA 2002. Zipf, Power-laws, and Pareto - a ranking tutorial. Internet Ecologies area, Xerox Palo Alto Research Center, Palo Alto, CA 94304 (http://ginger.hpl.hp.com/shl/papers/ranking.html)

Asche HR, and Smith PS, 2013. Probing and Grouting Predictions for Rock Tunnels. Rapid Excavation and Tunneling Conference, Washington.

Cook, PG, 2003. A Guide to Regional Groundwater Flow in Fractured Rock Aquifers, CSIRO, Seaview Press.

Fransson Å, 2002. Nonparametric method for transmissivity distributions along boreholes. Ground Water 40(2):201–204

Gustafson, G, 2012. Hydrogeology for Rock Engineers, BeFo - Rock Engineering Research Foundation Stockholm, www.befoonline.org.

Gustafson, G., & Fransson, Å. 2006. The use of the Pareto distribution for fracture transmissivity assessment. Hydrogeology Journal, 14, 15-20.

Houlsby, AC 1976. Routine interpretation of the Lugeon water-test. Quarterly journal of engineering geology and hydrogeology, 9(4), 303-313. doi:10.1144/GSL.QJEG.1976.009.04.03

Houlsby, AC, 1990. Construction and Design of Cement Grouting: A Guide to Grouting in Rock Foundations. Wiley Series of Practical Construction Guides, John Wiley and Sons Inc.

Kitanidis PK, 1997. Itroduction to Geostatistics, Applications in Hydrogeology, Cambridge University Press

Krásný, J, and Sharp JM Jr, 2007. Hydrogeology of fractured rocks from particular fractures to regional approaches: State-of-the-art and future challenges. In Groundwater in Fractured Rocks, IAH Selected Papers on Hydrogeology 9, Taylor and Francis/Balkema, Leiden.

Kozubowski TJ, Meerschaert MM and Gustafson G, 2008. A new stochastic model for fracture transmissivity assessment. Water Resources Research 44: W02435 doi:10.1029/2007WR006053, 2008

Lee, CH, and Farmer, I, 1993. Fluid Flow in Discontinuous Rocks. Chapman and Hall.

Lombardi G, 2003. Grouting of Rock Masses. Invited key note lecture at the 3rd International Conference on Grouting and Ground Treatment, New Orleans, edited by Lawrence F. Johnsen; Donald A. Bruce; and Michael J. Byle

Lugeon, M, 1932. Barrages et géologie., Bulletin Technique de la Suisse Romande, Vol 58, Nos 19 and 20, pp225-240, 17 Sept and 1 Oct 1932.

Moye, DG, 1967. Diamond Drilling for Foundation Exploration. Civil Engineering Transactions Inst. Eng. Australia, April 1967, pp 95-100.

Parsons S and Raymer J 2024. Determining the effective hydraulic conductivity for tunnel design and impact. 2024 Australasian Tunnelling Conference Auckland.

Pearson R, Money MS 1977. Improvements in the Lugeon or packer permeability test. Q J Eng Geol 10(3):221–239

Priest SD and Hudson JA, 1976. Discontinuity Spacing in Rock, International Journal of Rock Mechanics and Mining Sciences & Geomechanics, Volume 13, Issue 5 May 1976.

Priest, SD, 1993. Discontinuity Analysis for Rock Engineering, Chapman and Hall.

Quiñones-Rozo, C. 2010. Lugeon test interpretation, revisited. Paper presented at the Collaborative management of integrated watersheds, US Society of Dams, 30th annual conference.

Raymer, J. 2001. Predicting groundwater inflow into hard-rock tunnels: Estimating the high-end of the permeability distribution. Paper presented at the 2001 Rapid Excavation and Tunneling Conference.

Raymer, J., & Maerz, N. H. 2014. Effect of variability on average rock-mass permeability. Paper presented at the 48th US Rock Mechanics/Geomechanics Symposium.

Singhal, BBS, and Gupta, RP, 2010. Applied Hydrogeology of Fractured Rocks, 2e, Springer.

Sharp JM Jr (Ed), 2014. Fractured Rock Hydrogeology, International Association of Hydrogeologists Selected Papers on Hydrogeology 20, CRC Press/Balkema, Leiden.

Taleb NN, 2007. The Black Swan, The Impact of the Highly Improbable, Penguin Books

Vaskou P, de Quadros EF, Kanji MA, Johnson T, Ekmekci M, 2019. ISRM Suggested Method for the Lugeon Test.

19th Australasian Tunnelling Conference – Acosta-Martínez, Stewart and Hudson-Smith (Eds.)
© 2025 Australian Tunnelling Society, ISBN 978-0-85825-002-4

Waterproofing system selection for tunnel linings

U. Pelz
GHD Pty Ltd, Brisbane, Australia & University of Queensland (UQ), Brisbane, Australia

Dr. J. Karlovšek
University of Queensland (UQ), Brisbane, Australia

ABSTRACT: The selection of appropriate waterproofing systems for mined tunnel linings is critical to ensure the structural integrity and longevity of underground structures. This paper explores various waterproofing techniques, including sheet membrane systems, spray applied waterproofing membranes and waterproofing using admixtures, evaluating their effectiveness in different geological and environmental conditions. Key factors influencing the selection process, such as water pressure, geology as well as preparatory works and installation requirements which impact on time and cost of the project are reflected on. Implications of the choice of waterproofing systems on the design are also discussed. Published case studies of experiences with different systems are used to illustrate best practices and innovative solutions. The findings aim to guide engineers in making informed decisions to enhance the quality of installation, durability and performance of tunnel waterproofing and linings.

1 INTRODUCTION

There are several waterproofing systems for tunnel linings on the market. The traditional approach with sheet membranes is well known with respect to its limitations and advantages, but other systems have gained increasing popularity in tunnel construction due to their seemingly easier and seamless application, flexibility, and potential cost savings. However, selecting an appropriate membrane system requires a thorough understanding of material properties, in-situ conditions, and project requirements. This paper outlines considerations for a structured selection process based on key performance criteria, project-specific considerations, and industry experiences.

2 WATERPROOFING APPROACHES

Several waterproofing approaches can be applied for the waterproofing of tunnels. The selection depends on the following main factors which will be further reflected on in this paper and often not holistically considered in the decision making:

- Contractual requirements
- Geology / Ground Conditions
- Hydrogeology
- Water pressure – Drained or Tanked Tunnel
- Environmental conditions / Contamination / Ground Water chemistry
- Constructability considerations
- Other project specific requirements and considerations

2.1 *Sheet membranes*

Traditional sheet membranes as they are used for tunnel waterproofing are applied between the primary and secondary tunnel linings without bond to the secondary lining. They are often made from materials such as PVC, EPDM, HDPE or VLDPE. They can be used for drained tunnels, in the crown only, or for tanked tunnels, covering the entire tunnel circumference. The membranes often have a thin coloured protection layer on the tunnel facing side, which allows for visual identification of scratches or damage. Such membranes offer high durability and resistance to mechanical damage as well as a strong waterproofing performance under high hydrostatic pressure

These membranes are often installed against a smoothing layer. At a minimum a geotextile layer is installed as a protective layer between the concrete surface and the waterproof membrane. This acts to protect the membrane from damage from substrate roughness and acts as a water path behind the membrane. The geotextile is fixed to the underlying shotcrete lining using shot nails which also pin membrane rondels to the geotextile and are spaced at regular intervals. The sheet membrane is installed over the geotextile by welding to the membrane rondels and the separate sheets are likewise welded to together. Single or double welded seems can be carried out depending on the water pressures. Water bars welded to the membrane are used for tanked tunnels to compartmentalise the membrane, usually at joint locations. If water inflow is experienced, the leak location is most likely in the compartment where the water ingress is observed. As the membrane is not bonded to the secondary lining, without compartmentalisation, water can flow between the membrane and the lining if damage to the membrane occurs and may find a way through joints or cracks into the tunnel at a location potentially far away from the actual membrane damage.

As shotcrete does not bond to these types of membranes, its application against such membranes requires reinforcement, is time-consuming and relies on excellent quality of workmanship. Concrete linings cast with a lining formwork are commonly constructed as final tunnel linings with this type of membrane. While not always the case, often the primary lining is deemed to be temporary in this scenario. Construction joints as the weak spots in the system should membrane leakage occur, are often fitted with secondary waterproofing measures. To avoid membrane penetrations, the secondary tunnel lining should be designed to take the loads from all in-tunnel equipment to avoid the need to anchor back into the ground. To fix support bars for the installation of a reinforcement cage for the secondary lining, BA-bolts are applied.

Water ingress between the membrane and the permanent lining during construction needs to be avoided, as this water can travel in the system and find the path of least resistance into the structure. Double layer membranes for high water pressures or bonded membranes, which bond with the concrete cast against them and thus prevent a water path between membrane and lining, might be applied in special cases.

2.2 *Spray applied membranes*

Spray-applied membranes are typically used as intermediate waterproofing layers between the primary and secondary tunnel linings. The material bonds to the linings and as such forms a partially composite lining (ITAtech Activity Group, 2013). The most used materials include Ethyl Vinyl Acetate (EVA), Styrene-Butadiene Rubber (SBR), Methyl-Methacrylate (MMA), Polyurethane (PU), and Polyurea (PUA). Each of these materials has distinct performance characteristics affecting their suitability for different tunnel environments and material parameters of products differ even within the same material group (Lemke and Moran, 2015). Thus, the material selection needs to be given adequate consideration.

The installation of spray applied membranes itself is simple, they are sprayed onto the substrate like shotcrete. While there are one-pass systems on the market, often two thin membrane coats of different colours area applied, as the continuity check is for most materials except for non-conductive, resin-based membranes, purely visual. Due to the limited continuity testing options, very high-quality control during application is required. While it is often stated that due to the lack of water path between membrane and lining, the area where water is observed on the tunnel intrados is the location of membrane damage, this has not been confirmed in practical applications

as the water will find the way of least resistance through the lining, which may not always be the location of membrane damage.

2.3 *Pore blocking admixtures*

Pore-blocking waterproofing technologies are hydrophilic additives that utilize a chemical reaction that creates microscopic crystals to seal pores and voids within the concrete or shotcrete matrix. These crystalline admixtures enhance the concrete's resistance to water ingress by reacting with moisture and non-hydrated cement particles to form insoluble crystals within the capillaries and microcracks. These technologies have various advantages and limitations when applied to tunnel linings (Guðmundsson,2008). Some of the benefits of these products are:

- Easily applied as they are just added to the concrete or shotcrete mix, reducing labour and construction time.
- Provide integral waterproofing and become part of the concrete, eliminating the need for external membranes and reducing installation complexity.
- They have self-healing properties as they can seal microcracks through continuous crystallization when exposed to water.
- Durable and provide long-term resistance to water.

On the other hand, they have their limitations compared to other waterproofing systems. They:

- Are not a continuous physical barrier and do not prevent water inflow into concrete but limit permeability.
- Are not immediately effective as they have a certain reaction time. Crystal growth can take days to weeks to fully block pores.
- May show varying performance depending on concrete mix design, the batching process, curing conditions, and tunnel groundwater conditions.
- They are difficult to repair if not performing to the requirements.
- May not be compatible with repair materials or prevent bonding of concrete coatings.

3 WATERPROOFING SELECTION CONSIDERATIONS

3.1 *Contractual requirements*

The starting point for the selection of any material or approach is to ensure it complies with the relevant standards, guidelines, contractual requirements and technical specifications, including the allowable inflow, wetness criteria, hydrogeological impacts, and other factors which may exclude particular solutions from the onset. The requirements will also be driven based on tunnel type and function.

3.2 *Location and environmental conditions*

The actual conditions under which the waterproofing measure is installed need to be fully understood for the design life of the tunnel. Some examples of conditions are:

- Hydrostatic Pressure: High water pressure conditions require robust and flexible membranes.
- Compatibility with groundwater chemistry is crucial. Some chemicals may degrade or weaken certain membrane types over time. Material selection may need to involve chemical resistance testing under project-specific conditions.
- Soil and Rock Conditions: Aggressive ground conditions necessitate chemically resistant materials.
- Seismic Activity: Flexible systems perform better in seismic-prone areas to accommodate ground movements. Membranes with tensile strengths exceeding 1.5 MPa and elongation capacities over 150% perform well in dynamic environments.
- Groundwater Chemistry: High salinity or acidic water necessitates chemically resistant waterproofing solutions.

- Application temperature and humidity requirements must align with site conditions. EVA-based membranes require temperatures above 5°C and humidity below 90% for optimal performance. Some membranes may not cure properly in cold or humid conditions, leading to adhesion failure. Long-term exposure to extreme temperatures including freeze-thaw cycles should be assessed.
- Curing conditions: Spray-applied membranes require a dust free environment with good ventilation.

3.3 *Hydrogeology and inflow conditions*

The hydrogeological conditions during construction and in the long term are one of the most important factors for the right choice of waterproofing system. The question if the tunnel is drained or tanked, the permeability of the ground and how much water inflow is expected during construction. For spray-applied membranes which need to be installed on a dry surface, the effort of preventing inflow during curing can potentially far outweigh any benefits. This could be grouting, water channelling, piping, strip drains on rock or installing a temporarily waterproof primer to name a few

3.4 *Installation requirements*

For sprayed membranes, a smooth surface is also important as the preparation of the substrate does affect the membrane performance (Dimmock et al., 2011) and will help to control material usage. The underlying shotcrete and substrate age is also a consideration for spray applied membrane application as the outgassing hydration heat can cause damage to the not fully cured membrane (Ballantyne, 2016). The membrane curing time needs to align with project scheduling to prevent delays. The age of the membrane at the application of the second membrane layer and the secondary lining are also to be considered for the overall construction program.

The membrane thickness criterion is to be selected carefully. Thicker membranes have better crack bridging faculties but are more prone to rupture and impact on the composite action and the design parameters (Su and Bloodworth 2016). Creep, shrinkage, temperature differences and other factors contributing to the movement of the lining needs to be evaluated. The thickness, as well as other installation factors have an impact on the design and need to be decided on early on.

Penetrations of bolts or bars through the lining can be achieved by covering the shafts of the penetrating items with membrane. Under water pressure, this measure may not be sufficient to achieve water tightness and further measures may be required (Wille and Lehr, 2005).

Comprehensive pre-production testing for spray-applied membranes under project conditions is recommended for all the above-mentioned aspects to understand the best application method for an individual project.

3.5 *Design implications*

The lining design for different waterproofing systems will fundamentally differ and this is an important understanding the operational teams do not always fully comprehend. Even without a waterproofing membrane, a permanent shotcrete lining comes with its own challenges. Delamination and even lining failure have been reported on Sydney Projects, due to loss of adhesion (Reid and Bernard 2019) or environmental conditions (Hunter 2025). While hanging linings (Barry, et al. 2021) and other mitigation measures have been proposed for redundancy and reliability (Haider, et al. 2023), shotcrete linings remain far more condition and implementation reliant than cast in-situ linings.

As a spray applied membrane bonds to the primary and secondary linings, a partial composite lining system is established and the degree of composite action which can be realised depends on the bond of the membrane to the linings. Short-term and long-term bond strength to the shotcrete linings may differ (Holter and Geving, 2016). The designer needs to undertake a sensitivity analysis, covering all conditions. The design will also need to consider any drainage system within the lining, the location of the membrane within the composite structure, the thickness of the membrane and accordant material parameters.

To avoid stress spikes and the potential of damage, it is important that the lining is constructed within the given tolerance to the required geometry (Pickett and Thomas, 2013) including waviness and ovalisation criteria, which can prove challenging to construct and can have a detrimental effect on long-term lining performance if not achieved.

3.6 *Material properties*

Any membrane material needs to meet the project requirements in view of:
- Durability and Longevity: Materials must resist aging and mechanical stress.
- Flexibility and Crack Bridging: Essential in dynamic and high-stress environments.
- Chemical Resistance: Required in aggressive underground environments.

For spray-applied membranes, different materials have different properties and as there is no clear regulation, different products within the same material group can exhibit different behaviour. Manufacture's advice and data need to be reviewed and followed, and project specific testing may be required to confirm the suitability of a material.

For sheet membranes, the material selection depends predominantly on the flexibility required as well as the hydrostatic pressure to be resisted. A very-low-density polyethylene liner material is lighter and much more flexible than a high-density polyethylene liner of the same thickness. VLDPE is stiffer and less flexible but may be more robust under high hydrostatic pressures and specific conditions.

3.7 *Testing and quality control*

Sheet membranes are welded together, and the weld seams which are inherently the weak spots can be tested via vacuum testing using a vacuum bell and pump. For this test a soap solution is spread over the seams and a vacuum bell is firmly pressed over the seam applying a vacuum. If there are any leaks in the weld, the soap solution bubbles under the vacuum. For double seams, air pressure can be applied between the two welds to test for leaks.

For spray applied membranes, in-situ testing is quite limited. The suppliers typically provide laboratory testing of the tensile strength, elongation, and chemical resistance as well as any other constraint against environmental conditions for the specific product. On-site the adhesion can be tested using a dolly and wet thickness by dipping a gauge. The dry thickness can be verified by cutting out squares from the membrane. The membrane is typically installed in two layers of 2-3 mm thickness and different colour. The two colours are used because for most materials the coverage continuity can only be tested by visual inspection. For membrane materials which are electrically conductive, continuity testing, also known as holiday testing, can be applied, which is a non-destructive method to detect pinholes and gaps in the coat. It involves using an electrical circuit, current flow is an indication of a discontinuity.

3.8 *Construction impact*

Sheet membranes require for larger tunnel sizes typically a travelling working platform or scaffold to apply the membrane. The installation is labour intensive, and the final cast in-situ concrete lining requires formwork.

A spray applied membrane in comparison is much easier and faster to apply (Saraiva et al., 2014). But the effort water management, substrate preparation and smoothing layer, sealing of penetrations, geometrical compliance of the lining in excavation and shotcrete application can take significant effort and if not carried out correctly, can lead to extensive re-work and maintenance tasks.

3.9 *Cost and life-cycle considerations*

The cost of membrane materials, installation, and potential repairs should be evaluated. This needs to be realistic and based on pre-production testing to understand all implications and what a high-quality installation takes. Furthermore, long-term maintenance and durability assessments should be included in decision-making.

A comparative analysis of initial costs vs. lifecycle costs can determine the most cost-effective option. Higher-quality membrane systems with better durability and less sensitivity to errors may justify higher initial investment by reducing long-term repair expenses. Availability and Supply Chain should be considered as readily available materials reduce lead times. Sustainable and environmentally friendly options are preferred for modern infrastructure projects. And regulatory compliance needs to be ensured as reflected on in the next section.

4 CASE STUDIES

Sheet membranes are well established and have been satisfactorily used all over the world. Membranes that have been exposed and tested after several decades of usage, e.g. by the FH Münster (Tunnel, 01/2018) show that the membranes exhibit good durability and long-term performance. Likewise, there are reports of very successful usage of spray applied membranes ((Verani and Aldrian, 2010), (Naylor et al., 2011)) but it needs to be reiterated that the application is not simple.

At the Crossrail Project in London, spray applied membranes have been employed for the tanked station structures which were fully excavated in London clay, based on the low permeability of clay and minimal expected water inflow. In some areas, where the clay interfaced with the Lambeth Group, excessive water inflow with subsequent blistering of the membrane was experienced. The spray-applied membrane in the invert was substituted with sheet membrane in these areas (Diez, 2018). This highlights the necessity to understand the conditions which may be encountered and to have planned for mitigation measures of some sort, to be able to react to the circumstances present. Some stations on the same project were waterproofed using sheet membranes whereas others utilised spray-applied membrane, depending on the ground conditions and expected inflows. A comparison of the efficiency of both approaches has been published, including the membrane application itself as well as the final lining being constructed from cast in-situ concrete in the first case versus the use of shotcrete in the latter. For the membrane application, it was found that the sheet membrane installation was faster than the sprayed membrane (Batty et al., 2016). This was due to groundwater ingress through the outer lining in areas where sprayed membrane was designated, leading to additional effort for water management and repair of damaged sections. However, in a dry tunnel the effectiveness of the spray applied membrane would have certainly outperformed the sheet membrane installation.

On some Australian projects, the experience has likewise been that the effort of cutting the correct profile, installing the lining to the correct geometry and preparing the surface for membrane installation was cost and time-wise inferior to a cast in-situ lining. It cannot be emphasised enough that the success of the application process for sprayed membranes is far more dependent on the conditions encountered the workmanship and the full comprehension of the design approach as realised by the wider industry. There is a level of risk associated with this method which does not exist in the same way for sheet membranes.

Larive et al. (2020) attempted a cost and time comparison of traditional sheet membranes and cast in-situ lining with sprayed membranes in combination with shotcrete linings. Their assessment is based on many assumptions which need to be evaluated for each individual project. Their cost analysis is based on the material costs for the membrane materials, shotcrete or concrete, formwork for the cast in-situ option and labour. Based on this assessment, under the assumed rates, they determined that for a shorter tunnel a spray applied membrane is the more cost-effective option but with increased tunnel length, the formwork cost is amortised against the higher cost of the spray applied membrane. From a program perspective, the comparison makes the spray applied membrane appearing advantageous. However, neither water management, nor surface preparation and smoothing layer works have been taken into consideration in this example.

4.1 *Project-specific selection strategy*

The following steps in addition to the inflow flowchart given in the ITA guideline or the slight alteration by (Pelz and Karlovšek 2023) is recommended to be used for selecting a tunnel membrane:

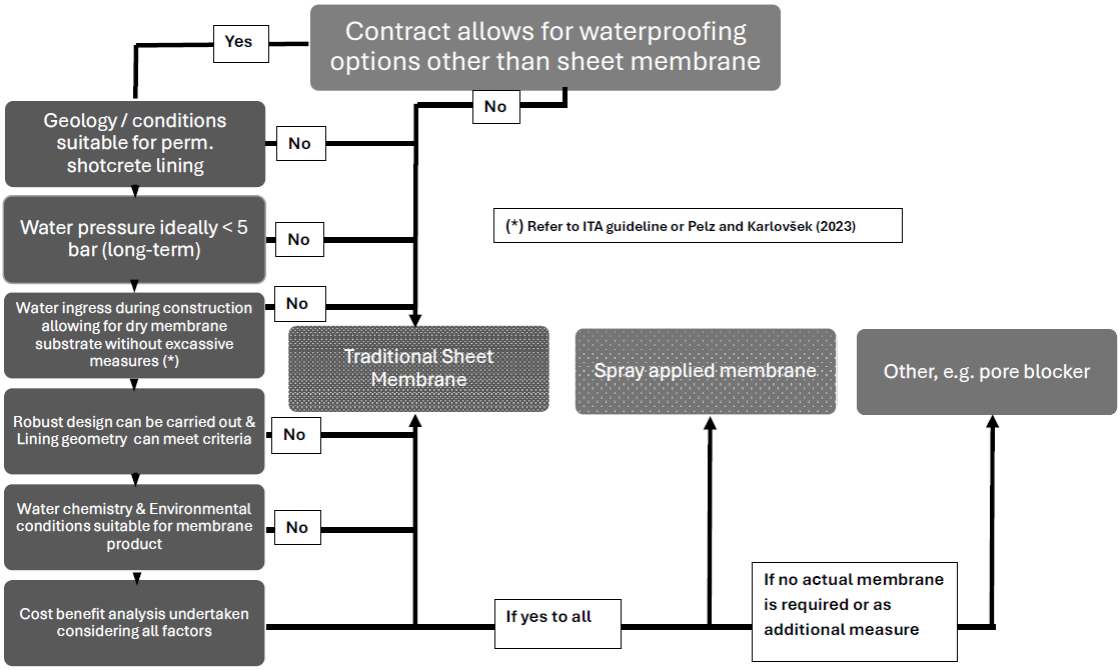


Figure 1. Membrane selection guidance

5 CONCLUSIONS

Selecting the appropriate waterproofing system for tunnel linings is a multifaceted process that requires careful consideration of various factors, including material properties, site conditions, application requirements, and industry standards. While no single system is perfect, a structured evaluation process can help project stakeholders achieve optimal waterproofing performance, cost-effectiveness, and long-term durability.

Sheet membranes, though labour-intensive, offer well-known performance outcomes, while spray-applied membranes provide faster installation but require meticulous execution and environmental considerations. Pore-blocking admixtures serve as effective supplementary solutions, particularly in environments with high hydrostatic pressure or structural movement, often in conjunction with other systems for comprehensive protection.

A comprehensive evaluation of environmental, functional, material, and economic factors is essential for making an informed choice that enhances structural integrity and ensures long-term performance. Future research should focus on long-term field performance data and the dissemination of project successes and failures to improve material selection methodologies and industry awareness.

By following these guidelines, stakeholders can minimize maintenance costs and operational disruptions, ensuring the longevity and reliability of tunnel structures.

6 REFERENCES

Ballantyne, B., 2016. Impervious Infrastructure, *Tunnels & Tunnelling International*.

Barry, J.S., Bodner, C. & Bedford, N. 2021. Hanging linings – a new approach to permanent lining design.

Batty, E., Bond, N., Kentish, E., Skarda, A. & Webber, S. 2016. Comparison between sprayed and cast in-situ concrete secondary linings at Bond Street and Farringdon Stations.

BTS, T.B.T.S., 2010. Specification for tunnelling - third edition.

Diez, R. 2018. Crossrails SCL Design. *Tunnels & Tunnelling International March 2018*.

Dimmock, R., Haig, B. & Su, J. 2011. Spray Applied Waterproofing Membranes - Key Success Factors and Development of Efficient Sprayed Concrete Tunnel Linings.

Guðmundsson, G. 2008, Waterproofing of Shotcrete with XYPEX Admix.
Haider, S., Clark, P. & Douglas, K. 2023. Reliability Approach to Shotcrete Design in Sydney Tunnels.
Holter, K. & Geving, S. 2016. Moisture Transport Through Sprayed Concrete Tunnel Linings. *Rock Mechanics and Rock Engineering 49, 243-272.*
Hunter, A. 2025. Management of acid sulfate rock in a Sydney road tunnel. *Australian Geomechanics March 2025.*
ITAtech Activity Group, T.M., Babendererde, T., Bonin, K., Dimmock, R., Greensted, S., Gregory, F., Haig, B., Kothe, T., Maslev, K., Reinhold, M., Saraiva, E., Tansini, G. & Wetzig, V. 2013. ITAtach Design Guidance for Spray Applied Waterproofing Membranes
Larive, C., Bouteille, S., Berthoz, N. & Zappelli, S. 2020. Fibre-reinforced sprayed concrete as permanent tunnel lining. *Structural Engineering International*.
Lemke, S. & Moran, P.S. 2015. A controversial discussion regarding the use of spray applied waterproofing for tunnel applications
Naylor, D., Salak, P. & Stephenson, S. 2011. Experiences with sprayed waterproofing, *Tunnels & Tunnelling International. GlobalData plc, London, pp. 45-48.*
Pelz, U. & Karlovšek, J. 2023. Spray-applied waterproofing membranes in tunnelling: A construction perspective. *Tunnelling and Underground Space Technology.*
Pickett, A. & Thomas, A. 2013. Where Are We Now with Sprayed Concrete Lining in Tunnels? *Tunnelling Journal Fall 2013*
Reid, S.G. & E.S. Bernard. 2019. De-bonding of shotcrete linings at the substrate boundary.
Saraiva, E., Clement, F., Mahoney, W., 2014. The Use of Sprayable Waterproofing Membranes in Underground Structures - Concept, Design Options, Benefits and Limitations, *15th Australasian Tunnelling Conference 2014, Sydney NSW.*
Su, J., Bedi, A. & Bloodworth, A. 2019. On composite action and tunnel lining design; is composite action beneficial in reducing lining thickness?, *Tunnel, 01/2018, Long-term behaviour of plastic sheet membranes*
Su, Jiang & Bloodworth, A. 2016. Interface parameters of composite sprayed concrete linings in soft ground with spray-applied waterproofing. *Tunnelling and Underground Space Technology incorporating Trenchless Technology Research 59(C):170-182.*
Verani, C.A. & Aldrian, W. 2010. Composite linings: Ground support and waterproofing through the use of a fully bonded membrane, *Shotcrete: Elements of a System - Proceedings of the 3rd International Conference on Engineering Developments in Shotcrete, pp. 269-281.*
Wille, S. & Lehr, A. 2005. Epping to Chatswood rail link waterproofing the stations, Proceedings of the *12th Australian Tunnelling Conference 2005.*

19th Australasian Tunnelling Conference – Acosta-Martínez, Stewart and Hudson-Smith (Eds.)
© 2025 Australian Tunnelling Society, ISBN 978-0-85825-002-4

Exploring innovative groundwater control methods and waterproofing techniques in Sydney tunnels (ATC2025)

A. Talos, Q. Kenny
Systra Bamser, NSW, Australia

ABSTRACT: Groundwater control is a critical aspect of all tunnelling projects, safeguarding structural integrity and providing warranty for meeting the proposed design life. Typically, in the context of Sydney mined tunnels, stringent inflow criteria are set by the Client and administered under D&C contracts through Contractor managed groundwater selection processes. This paper explores the integral role of a formal groundwater control systems process through a collaborative approach to groundwater ingress management, with a particular focus on significant changes in Client waterproofing requirements enabling innovative design and construction methods.

The intention of this paper is to highlight challenges and opportunities of an innovative tunnel groundwater management approach in the Sydney context and assess its feasibility for future projects. The viability of a collaborative groundwater control systems processes are evaluated against a challenging commercial environment along with the practicality of Client involvement in a D&C contract.

1 TUNNEL GROUNDWATER INFLOW REQUIREMENTS

1.1 Typical Sydney road tunnelling requirements

With the already stringent groundwater inflow criteria for Sydney tunnelling projects, more innovative design and construction methods have been established to minimise water ingress and maintain drier tunnel conditions. Continuous advancements in tunnel groundwater control systems have been driven by lessons learned from previous projects, as well as the increasing commercial pressure to minimise operational expenditure through improving long-term durability, operational efficiency, and safety within the underground space.

Sydney road tunnels are almost exclusively mined tunnels, excavated with a fleet of roadheaders due to the favourable geotechnical conditions of Sydney sandstone. In a challenging commercial climate with increasing cost pressures, Sydney's significant road tunnel investment is scrutinised heavily to ensure reduced whole of life costs to the taxpayer. This often leads to a reduction in tunnel scope during tender, with successful tenders typically designing thin shotcrete and rock bolt linings, with groundwater control systems typically installed within layers of shotcrete, draining into the stormwater system under the road pavement.

The Scope of Works and Technical Criteria (SWTC) within the Design and Construct contracts for Sydney road tunnelling projects typically mandate that the Contractor must ensure groundwater passes through a designated Groundwater Control System (GWCS). Water infiltration is not permitted to drip or flow onto road pavements or walkways within tunnels, nor is it allowed to run down or accumulate on the external surfaces of tunnel walls.

Despite variations in project-specific requirements, the inflow criteria for Sydney tunnelling projects have remained relatively consistent. Undrained tunnels are typically mandated in soft ground tunnels with high existing groundwater levels and are specifically designed to prevent external groundwater from infiltrating the tunnel space. This approach results in the accumula-

tion of hydrostatic pressure against the structural lining, effectively "tanking" the tunnel. The significantly higher expenses associated with constructing a fully tanked tunnel often render it a less viable option for most Sydney road projects. For these undrained tunnels, the allowable inflow is limited to: 0.2 litres per square metre of tunnel surface area per day for any 100 m length of tunnel.

Conversely, drained tunnels permit controlled groundwater ingress through the GWCS. This reduces hydrostatic pressure buildup which allows for an optimised structural lining. Most mined tunnels in Sydney are designed in this manner due to their favourable balance between quality and cost-effectiveness. Typically, Sydney drained tunnels adhere to an inflow limit of 1 litre per second per kilometre and 0.3 litres per second in any given 120 m of tunnel.

1.2 M6 requirements

The SWTC for the M6 project introduced a significant shift in Client waterproofing requirements, further improving on the standards implemented in previous Sydney tunnelling projects. Specifically, the SWTC for the M6 Project mandates that the Groundwater Control Systems (GWCS) must be installed behind the primary structural lining. This represents a departure from conventional practices, where the GWCS is typically positioned within the structural lining.

By placing the GWCS behind the structural lining the intent of this change was to:

1. Minimise operational expenditure through improving long-term durability, operational maintenance, and safety within the underground space
2. Reduce the risk of damage due to drilling of M&E anchors within the lining
3. Improved water resistance behind the structure to better direct water into the GWCS
4. Adopt a consistent amount of shotcrete applied aiming to improve the performance of the tunnel to withstand permeation, excessive cracking and drainage within the tunnel environment

Another key change within the SWTC for the M6 Project is a mandated structural connection of this structural lining to each rock reinforcement element. This was introduced to ensure a more durable structural lining, ensuring that the beneficial effects of adhesion weren't relied upon in the design space, minimising any rework to the lining in the future. This occurs by ensuring that the shotcrete structural lining is essentially hanging off the rock bolts embedded within the crown of the tunnel. The tunnel lining then acts as a single composite layer with additional redundancy to minimise the risk of shotcrete fallout. When combined, these modifications have unintendedly necessitated the adoption of an alternative construction methodology to enable installation of the revised placement of the GWCS.

2 GROUND WATER CONTROL SYSTEM (GWCS)

2.1 Components and process

Groundwater control systems in Sydney tunnels comprise of drainage elements such as strip drains, drainage mats, geotextile, sprayed / sheet membrane and are encased in shotcrete to control the impact of water on the tunnel structure and direct it into the tunnel drainage system.

There are 3 systems typically used in Sydney tunnels to direct groundwater into drainage channels:

- Groundwater Control System A (GWCS-A): Systematic use of strip drains
- Groundwater Control System B (GWCS-B): Sprayed waterproofing membrane
- Groundwater Control System C (GWCS-C): Sheet waterproofing membrane


Figure 1. Groundwater control systems GWCS-A, GWCS-B, GWCS-C

These systems can be used across both drained and tanked tunnels, but all three are more commonly applied in drained tunnel designs. Drained tunnels employ either / a combination of the GWCS types to manage and direct groundwater inflow, whereas tanked tunnels most commonly adopt sheet membrane as the primary solution due to its ability to provide a continuous and more robust barrier against water ingress.

Typically, GWCS's must be installed by the contractor at locations with significant geological structures, including faults, dykes bedding planes and joints that are, or have the potential to be water bearing during the design life of the tunnel. This includes geological structures that have or currently show evidence of water inflow/seepage, structures that are affected by seasonal change and or any ground that required grouting to restrict the water inflow. Typically GWCS-B or GWCS-C would be mandated in these areas to reduce risk of seepage through the shotcrete.

The SWTC and design drawings also stipulate specific zones which are designated as mandatory spray or sheet membrane areas to ensure the structural integrity, durability and long-term functionality of the tunnel. These mandatory membrane areas include tunnel equipment spaces such as EER's or substations, any locations that intersect major geological structures / features and areas that have been grouted for the purpose of groundwater control.

Megaflo drains have also been adopted on the M6 for all the tunnel waterproofing works instead of the typical top hat drainage system. Megaflo is a wide flat shaped HDPE system designed for effective sub-surface drainage used to capture groundwater inflow in a tunnel environment with a larger capacity compared to the top hat strip drains. Typically, on previous projects Megaflo was only used in high inflow areas and around brows or ledges of the tunnel as a collection point from multiple other drains but the M6 had adopted this solution throughout their tunnel. This system is more flexible and quicker to install system with a higher water capacity leading to it being used more and more in tunnelling projects.

2.2 GWCS selection approach

The M6 adopted a collaborative approach to the GWCS process, actively engaging all key stakeholders—including the client, independent certifier (IC) and designer—throughout every phase, from initial planning to installation and verification which is unique in the Sydney tunnelling market which is dominated by D&C Contracts.

Selection of each groundwater control system will vary between projects depending on the individual projects SWTC and design requirements / specifications. This approach was a valuable process which helped the timely alignment, approval and construction of the GWCS and was essential in achieving compliance with the stringent groundwater management requirements outlined in the M6 SWTC. A formal sign-off process was developed involving the geotechnical team, designers, contractor, IC and client in the planning, installation and verification/sign-off stages. During planning, the geotechnical team identify high-risk water-bearing zones from geological data compiling them on longitudinal maps of the tunnel. Witness points and general inspections were organized with all parties having the opportunity to assess existing site conditions and determine appropriate GWCS treatment measures based on mapping and site conditions. Following install completion, a final verification and sign off inspection was conducted allowing all parties to assess compliance and resolve issues prior to the spraying final lining over the GWCS. The involvement of the client and IC in the GWCS process enabled the

early alignment of expectations, thereby enhancing the overall project quality, ensuring more effective implementation with minimal areas of rework post.

3 CONSTRUCTION METHODOLOGY

3.1 Methodology changes

Managing groundwater ingress is a significant challenge in tunnel construction, particularly when excavating through high-risk geological zones. Uncontrolled water inflow can lead to construction delays, increased costs, and safety hazards, hence, implementing proactive measures to manage groundwater is crucial for reducing these project risks. Traditionally these risks are mitigated through an effective excavation methodology. In Sydney a sequential excavation methodology is standard with production decisions has been production driven, with groundwater control an afterthought. The process has previously consisted of:

1. Excavation
2. Rock bolting; and
3. Shotcrete

With groundwater control systems installation and final shotcrete applied months after excavation clears an area. In this method the GWCS is typically incorporated within the primary structural lining, often resulting in minimal shotcrete coverage of the GWCS which may allow greater water penetration through the lining system.

The M6 project's SWTC marks a departure from previous Sydney tunnelling standards by mandating the Groundwater Control System (GWCS) be installed behind the structural lining. This requirement necessitated the adoption of an alternative construction methodology, highlighting the need for adaptive engineering to meet evolving waterproofing requirements. Forward probing and pre-excavation grouting was heavily relied upon to mitigate water inflow ahead of the tunnel face. This also enabled the gathering of vital groundwater condition information ahead of the excavation face helping to identify high-water inflow zones and potential water-bearing structures.

To accommodate the SWTC changes, the M6 project implemented a revised construction sequence:

1. Forward probing
2. Excavation
3. Shotcrete
4. Rock bolting
5. Groundwater control
6. Final shotcrete

This methodology requires shotcreting prior to bolting which enables the bolt plates to be used as a structural connection for the additional layers of shotcrete. This allows for better integration of the bolting system with the sprayed shotcrete, enhancing overall structural performance.

3.2 Performance of the revised methodology

A notable distinction was observed in the performance of the final lining, with the revised approach yielding a perceptibly drier tunnel environment. This improved outcome could be a result from the increased thickness of shotcrete layers applied over the strip drains in the new methodology. An example of this would be the revised approach which mandates a minimum of 110 mm of shotcrete cover above GWCS-A, thickening the barrier against water ingress and promoting more effective diversion of groundwater to the nearest drain as shown in Figure 2.2 on the RHS compared to the previous typical detail in Figure 2.1 which has GWCS-A strip drains embedded within the 110mm of shotcrete.

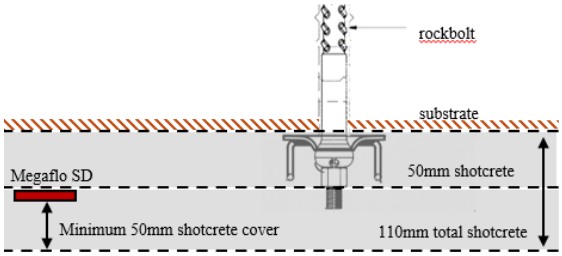


Figure 2.1. Previous GWCS-A detail.

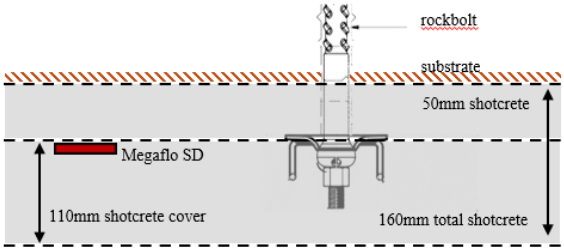


Figure 2.2. M6 adopted GWCS-A detail

Other key benefits of the revised methodology include significantly reduced damage to the Groundwater Collection System (GWCS) from mechanical and electrical penetrations, primarily due to the increased thickness of the shotcrete lining. This added layer of protection enhances the durability and resilience of the drainage infrastructure, helping to maintain its functionality throughout the tunnel's operational life. In addition, the implementation of more stringent client waterproofing requirements led to a broader application of spray-applied waterproofing membrane, which has proven effective in minimising water ingress and achieving a consistently drier tunnel environment. The methodology also introduced the use of Megaflo drainage in place of traditional top hat strip drains, offering advantages such as simplified and faster installation as well as improved flow capacity, which collectively enhance the overall efficiency of groundwater management. Additionally, the inclusion of a separate groundwater drainage line allows for more targeted and manageable system maintenance, reducing the risk of blockages or service interruptions and will ultimately contribute to lowering operational expenditure over the life of the project.

4 CHALLENGES IN WATERPROOFING & GROUND SUPPORT INTEGRATION ON M6

The revised SWTC requirements for the Groundwater Control System introduced several construction-phase challenges, resulting in the need for rework across multiple areas. In regards to spray membrane, which was used for over 30% of total lining a significant increase in duration was seen when adopting the new methodology due to the more stringent SWTC requirements. A summary of the additional works / challenges encountered with the revised sequence include:

- Shotcrete adhesion from change in construction method
- Further waterproofing detail required around rock bolt heads/handlebar plates
- Increased rework and time spent lining
- Additional works stopping leaking bolts
- Lack of sight for rock bolt operators to install spot bolts due to shotcrete being sprayed prior to bolting



Figure 3. Spray membrane install around rockbolts

4.1 Shotcrete adhesion issues

A key issue arising from the adoption of the new construction methodology was encountered during excavation, particularly in water-bearing zones where shotcrete adhesion to the crown proved problematic. Under conventional practice, rock bolts are installed immediately after excavation, providing additional anchorage points to facilitate shotcrete adherence, even in wet conditions. The modified sequence adopted for the M6 project—where shotcrete was applied prior to bolting—led to reduced adhesion and instances of shotcrete fallout in saturated ground conditions. To address this, the construction team had to revert back to the traditional "cut, bolt, then spray" sequence in affected areas. These sections were later re-bolted as initial bolts were sprayed over in SC and did not have sufficient exposure for a proper structural connection for the final lining installation.

4.2 Protrusions through membrane

The number of bolt and handlebar plate protrusions have increased significantly when compared to the traditional approach. Typically, there are two methods for the traditional approach when it comes to spray membrane areas.

1. In configurations where abutments are integrated into the excavation profile, there is no requirement for bolt tails or handlebar plate protrusions. In such cases, the shotcrete applied over the spray membrane is structurally designed to function as an arch, effectively spanning across the abutments. This eliminates the need for embedded bolts to support the final lining.
2. Alternatively, where abutments are not present, a pattern of long-tail bolts may be installed with only the threaded rod extending beyond the surface. This configuration necessitates the application of spray membrane around the protruding bolt tails prior to installing a mesh layer and applying the final shotcrete lining.

The newly adopted methodology closely aligns with the second traditional method but introduces a considerably greater number of protrusions and potential paths for water to flow through, specifically the addition of handlebar plates with all CT bolts. As a result, each of these protrusions require more focus on spray membrane application around all handlebar plates and additional coats in order to fully encapsulate and seal this system. The M6 design utilises CT bolts as a structural connection for the secondary lining to hang off hence emphasis on installing this connection correctly and sealing this system is critical.

Gaps between the handlebar plates and shotcrete are typically present as the CT bolts are not always sitting on a smooth, flush surface. The crack bridging properties of spray membrane had a minimum requirement of 2.5mm which typically was not able to bridge this gap between plates and shotcrete due to their size. This required the contractor to have crews come back before spray membrane works commenced and seal the edges of the bolts with grout. This additional works as a result of the methodology changes significantly increasing both the time, cost and amount of resources required to treat these areas.



Figure 4. Membrane gap at bolt / shotcrete interface

4.3 Construction duration and rework

Another time and resource consuming task as a result of the methodology change was the requirement to protect all CT bolts prior to smoothing and cleaning bolts in preparation for spray membrane. All handlebar plates and bolt tails needed to be free from debris/ excessive shotcrete prior to applying spray membrane hence site developed a metal cover that was screwed onto the end of the CT bolts protecting them from being covered in smoothing. This methodology worked in minimising the amount of bolt cleaning that would have been required if covers weren't used but still resulted in significant additional work in the area. After each smoothing spray site would have to remove all protective covers and in areas where smoothing was sprayed too thick would have to manually chamfer back the edges with demolition hammer which was a lengthy and costly exercise.

4.4 Leaking bolts

Leaking rock bolts were another persistent issue encountered throughout wet areas in the tunnel requiring remedial works including rebolting and resin injection prior to the application of spray membrane. The presence of wet or actively leaking bolts poses both structural and durability issues within the tunnel hence required rectification prior to subsequent works. From a construction standpoint, these conditions required substantial additional sealing efforts to establish the dry substrate conditions essential for successful spray membrane adhesion. Injection grouting—predominantly using polyurethane (PU)-based products—was frequently employed to mitigate the leakage. However, this process introduced further complications: PU injection material often migrated to nearby strip drains, resulting in unintended blockage of drainage pathways. These obstructions diminished the effectiveness of the drainage system and necessitated additional rework to restore strip drain functionality, thereby increasing labour, material costs, and construction time.

Given the critical role of rock bolts in maintaining both structural integrity and waterproofing, it is recommended that future dedicated testing regimes and durability tests for PU-injected bolts, such as prolonged water pressure testing, chemical resistance assessment or ageing simulation would be beneficial to validate the long-term effectiveness of injection materials under representative tunnel conditions. This would ensure that remedial interventions not only restore immediate function but also maintain durability throughout the assets intended design life.

5 FINDINGS / CONCLUSION: FEASIBILITY FOR FUTURE PROJECTS

The M6 was the first tunnelling project within Sydney which mandated that the Groundwater Control System (GWCS) must be installed behind the structural lining as shown in Figure 5.2, differing from the conventional practices on previous projects. The rationale behind the client implementing this change in waterproofing requirements was to achieve a drier tunnel environment and deliver a higher-quality end product.

The cut, spray, bolt approach was not the sole solution to addressing the revised tunnelling requirements; however, it was the preferred methodology selected at the time by site construction teams due to its practicality and efficiency. A potential alternative solution for drained tunnels to be investigated for future projects involves utilising longer handlebar plates for GWCS-B which protrude out further through the initial lining as shown in Figure 5.3. This approach may minimise amount of additional works around bolt tails/handlebar plates whilst potentially retaining the traditional excavation sequence where required particularly in water bearing areas. Given the significant amount of labour required for protecting the initial bolts with covers and chamfering of edges around rockbolts this proposed solution could be a viable option with less additional labour-intensive work required to achieve a similar outcome. Additionally, this would also save the need to install additional bolts in order to support the secondary lining as was done on previous projects like Rozelle and WHT enabling works as shown in Figure 5.1. Although some additional labour would still be necessary to install protection compared to the traditional method, the elimination of chamfering shotcrete, as seen on the M6 project, this system could result in a net reduction of cost and time.

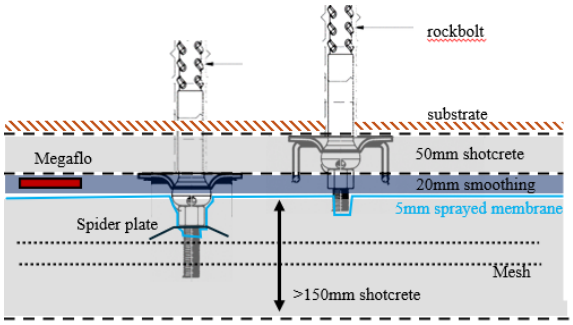


Figure 5.1. Previous GWCS-B.

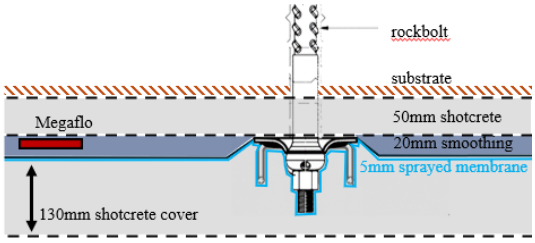


Figure 5.2. Adopted M6 GWCS-B solution.

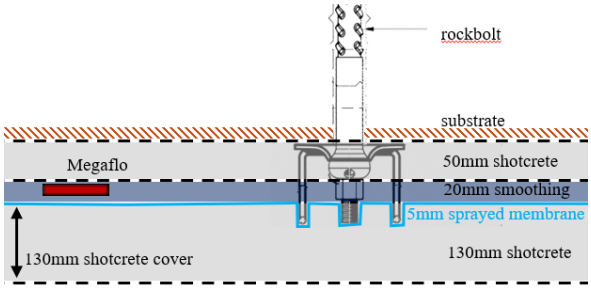


Figure 5.3. Potential solution for future projects

A key implication of this procedural change is the initial layer of shotcrete, applied immediately after excavation, serves only to provide temporary ground support for manned entry and is not considered part of the structural lining. Utilising this new methodology means that the whole tunnel is sprayed with an additional 50mm of shotcrete compared to the traditional tunnelling approach which is a costly exercise.

The below summarises the key findings arising from the implementation of the more stringent groundwater control criteria on the M6 project.

- Forward probing, combined with pre-excavation grouting is the preferred method for managing water ingress ahead of excavation.
- The involvement of the client and IC in the GWCS process was successful, enabling the early alignment of expectations, thereby enhancing the overall quality of the product. There were many areas with rework during the beginning of the process while expectations were being aligned, but following this initial phase, the contractor demonstrated improved consistency and execution.
- Innovations such as Cut-Spray-Bolt sequencing can provide benefits for groundwater control systems but do incur additional challenges and work required for spray membrane solutions. A notable distinction was observed in the performance of the final lining, with the revised approach yielding a perceptibly drier tunnel environment due to a thicker lining promoting more effective diversion of groundwater to the nearest strip drain.
- While the Cut-Spray-Bolt approach was successfully implemented for the M6, future projects may explore hybrid solutions to retain the traditional Cut-Bolt-Spray sequence with the same dry tunnel outcomes.

Though the revised waterproofing methodology introduced construction complexities, it has delivered demonstrable improvements in tunnel dryness and performance. By refining these methodologies, future Sydney tunnelling projects can achieve greater construction efficiency, cost-effectiveness, and long-term durability in groundwater management.

19th Australasian Tunnelling Conference – Acosta-Martínez, Stewart and Hudson-Smith (Eds.)
© 2025 Australian Tunnelling Society, ISBN 978-0-85825-002-4

Optimum pressure for rockmass grouting between TBM segmental linings of a twin tunnel

I. PH. Yim
Jacobs, Australia

J. H. Raymer
Jacobs, USA

ABSTRACT: Grouting pressure in the rock mass between newly installed TBM segmental linings during tunnel construction is typically limited at the point of injection to 100 kPa or less above groundwater pressure. However, because the grout pressure dissipates away from the point of injection, the grout pressure out in the rock mass may not be sufficient to overcome the hydrostatic back pressure, and the viscous resistance and cohesion of the grout, which means the grout does not adequately move out into the rock mass, displace the groundwater, and seal the rock mass. Barton and Quadros (2019) have suggested that the pressure can drop by 50 percent only 1 meter from the grout hole. This reduction is due to various factors such as applied pressure, viscosity and cohesion of the grout (Gustafson, Claesson & Fransson. 2013). This paper looks at some of the factors to consider when establishing limits on grouting pressure.

1 INTRODUCTION

Twin tunnels for highways and transit typically have cross passages between the tunnels. These cross passages are typically constructed after both the running tunnels have been excavated and lined, if lining is required. Prior to cutting through the lining and excavating the rock between the tunnels, it is common to drill through the lining and into the rock between the tunnels, and then grout that rock to control potential groundwater inflows.

In order to successfully control groundwater, the grout must be injected at a high enough pressure to displace the groundwater, not just at the point of injection, but also some distance out into the rock mass. Because the pressure dissipates with distance into the rock mass, the pressure at the point of injection must be considerably higher than the hydrostatic groundwater pressure, or the grout will not displace the water. The problem is that injection pressures are often limited to avoid damaging the lining. If the pressure limitations are too conservative, then it is quite likely that the grouting program will not successfully control groundwater. Uncontrolled inflows can cause all sorts of problems, including severe ground settlement and damage to structures.

2 GROUND CONDITIONS

The porosity and permeability characteristics of the ground are important. The most common situation for rock tunnels is for the groundwater to occur in a network of interconnected, open fractures. In most cases, the matrix of the rock between the fractures is tight or nearly tight, but in some cases the matrix can have considerable porosity and permeability itself. The goal of the grouting must be to create a thick, low-permeability halo around the excavation by filling the fractures (and matrix if necessary) with grout. The grouted halo should be a few meters thick because the grouted zone is not a membrane, but a zone of reduced-permeability rock.

The groundwater pressure around the grout zone is also important. The grout injection pressure must first overcome the hydrostatic back pressure before any grout can be injected. Furthermore, as the hydrostatic pressure increases, the grouted halo around the excavation needs to be thicker to effectively control the inflows, because it is the hydraulic gradient through the grouted zone that drives the inflows to the excavation.

3 CEMENT GROUT AS A BINGHAM FLUID

Cement grout is a slurry, not a liquid; it is a Bingham fluid, not a Newtonian fluid. As a Bingham fluid, it has both a viscosity and a cohesion, whereas a Newtonian fluid, like water or oil, has only viscosity (Figure 1). In both cases, the viscosity controls the rate at which the fluid can flow through a particular pipe or fracture. However, for grout, if the flow rate drops too low and the shear stress falls below the cohesion, the grout seizes: it stops flowing and starts behaving more like a soil. Once it seizes, continued pressure only serves to consolidate the grout through pressure filtration (which is desirable). All of this occurs well before the grout begins to take its initial set.

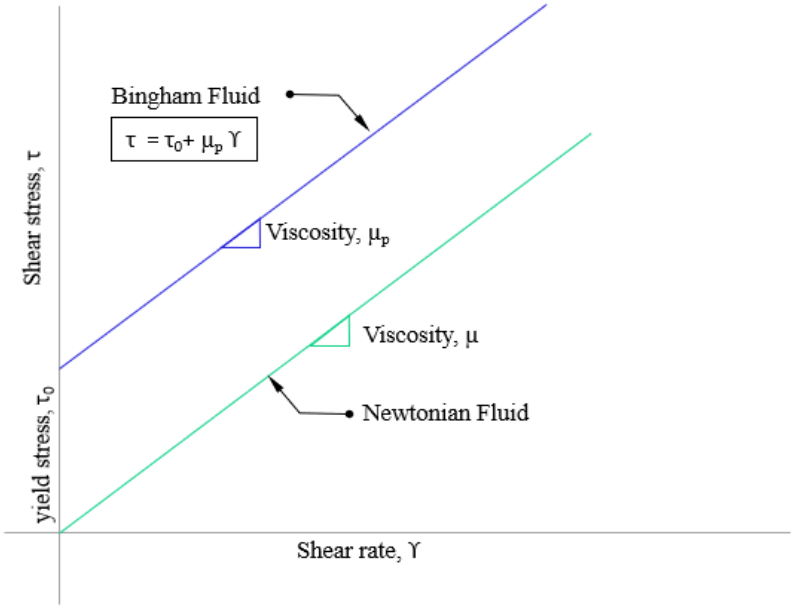


Figure 1. Bingham Fluid

4 PRESSURE ATTENUATION

Grout pressure attenuates with distance from the point of injection from three processes. The first is head loss due to viscous resistance to flow as the grout is forced through the fractures. The second is radial dissipation as the grout spreads out through the fractures from the grout hole. The third is from the grout seizing and consolidating due to cohesion. The pressure also increases or decreases as the grout is pushed lower or higher in the rock mass from the point of injection.

Head loss and radial dissipation can be modeled together using the radial form of the cubic law (derived for this paper based on Young, et al, 2011). This is a simple model based on a grout hole intercepting a single, extensive fracture at a high angle. In this model (Equation 1), Δh is the head loss along the fracture between the borehole wall at radius r_1 and some more distant point in the fracture at radial distance r_2; Q is the grout pumping rate, a is the aperture of the fracture, μ is the viscosity of the grout, and γ is the unit weight of the grout.

$$\Delta h = \frac{-Q}{2\pi a^3}\,\frac{12\mu}{\gamma}\ln\left(\frac{r_2}{r_1}\right) \tag{1}$$

For example, a typical 1 to 1 mix (by mass) of Portland cement grout might have a viscosity of 5.6 mPa·s and a unit weight of 14.3 kPa/m. If the pumping rate is 30 L/min = 0.5 L/s, and the fracture has an aperture of 0.4 mm, and the borehole has a diameter of 64 mm (r_r = 32 mm), then the head loss to a point 2.0 m away at the same level would be 24 m. Converting to pressure, where z is the elevation difference between the grout hole and the point at r_2 (z = 0 in this example):

$$\Delta p = \gamma(\Delta h - z) = 345 \text{ kPa} \tag{2}$$

If the tunnel were 30 m below the water table, then the groundwater would create a hydrostatic backpressure of about 300 kPa. Therefore, to push the grout 2 m horizontally through that fracture, the injection pressure would have to be 645 kPa, or more than twice hydrostatic pressure.

Real fracture networks are complex, unique, and difficult to model, but the simple model shown above does illustrate the nature of the problem. If a grout hole crosses more than one fracture of similar aperture, then Δh would be cumulative, but if one is much finer than the other, then the grout will probably seize in the finer one and stop flowing. The flow is typically laminar, so the roughness of the apertures is not relevant, except that, at the scale of these fractures, a little roughness can change the aperture considerably.

Figure 2 shows the excess pressure (Δp) required to push the above-described grout a certain distance through single fractures of various apertures. Obviously, finer fractures require more excess pressure. What is more interesting is that there is a pressure threshold needed to push the grout more than about 0.5 m along the fracture. For example, for a 0.2mm fracture, the excess pressure required to move grout more than 0.5m is estimated to be around 11 bar (1,100 kPa).

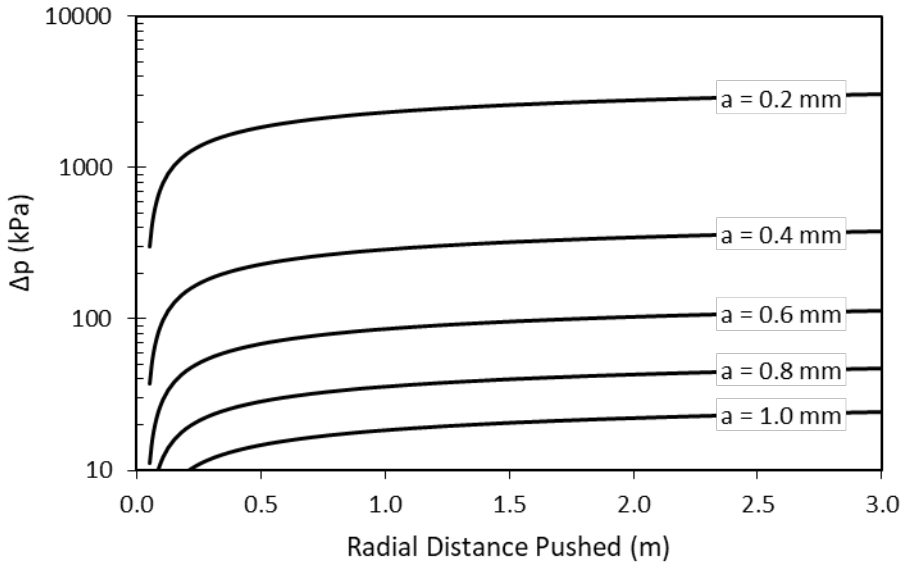


Figure 2. Excess Pressure Needed to Push Grout out into the Formation Assuming Tunnel was 30m below Water Table)

4.1 Example Projects – Waterview Auckland TBM Tunnel

Grouting in the Waterview Connection was described previously in published papers by McCarrison (2017) and Okada, Giauque & Bhargava (2017). What follows is an interpretation of what was published.

The Waterview Connection consisted of twin segmentally lined tunnels with 16 cross passages. The rock was weak siltstone and sandstone with closely spaced joints and generally low permeability. The cross passages were grouted as shown in Figure 3, prior to breaking through the lining.

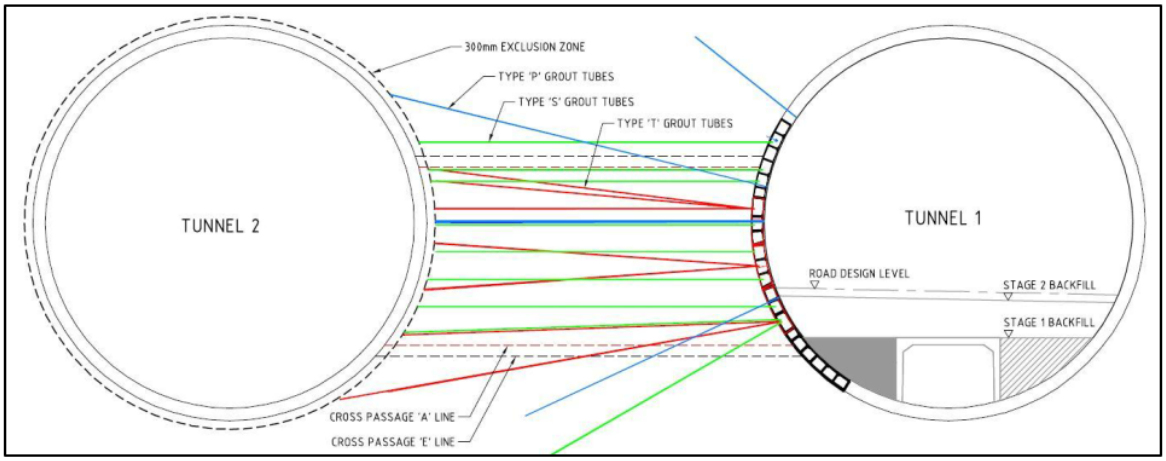


Figure 3. Typical Cross Passage Grout Holes Arrangement (Figure Extracted from the Waterview Connection Project Cross Passage Tunnels: Safety in Design and Construction (Okada, Giauque & Bhargava. 2017))

Most of the cross passages were successfully grouted and met the inflow criterion, possibly because the rock was already tight without grouting. Cross Passage 12, however, was different. It was in rock that was more fractured and under a major stream, with the hydrostatic head of about 37 m to the tunnel springline, which would have created a hydrostatic back pressure of about 3.7 bar in the grout holes.

Grout was successfully injected at pressures ranging from 5 bar up to 8.5 bar. At 8.5 bar, the injection pressure was more than twice the hydrostatic pressure. Strain gauges were applied to the lining to monitor deformation and nothing significant was observed. The designed capacity of the lining was not stated in the papers, but it was implied from the monitoring program that the pressures used significantly exceeded the design capacity with no ill effect. Why these high pressures were safe is likely to the attenuation of pressure as described above.

5 DISCUSSION

The goal of the grouting described in this paper is to consolidate the rock mass in preparation for excavating cross passages between already excavated and lined twin tunnels. Contact or tailskin grouting between the lining and the rock mass should already have been completed so, ideally, there should be no gap between the rock mass and the extrados of the lining. If, ideally, there is no gap, then the grout pressure should dissipate into the rock mass and only be weakly applied to the lining due to the elastic response of the rock mass. Also, since the grout is a Bingham fluid, it cannot hydrostatically transfer pressure like water. If the grout is flowing, it loses pressure with distance due to viscous resistance; if it stops flowing, it seizes and absorbs pressure like a consolidating soil. All of this means that there is a low probability that the injection pressure gets fully applied to the extrados of the lining.

However, in our experience, it is not uncommon for structural engineers to place severe limits on the amount of grouting pressure that can be applied to the rock mass. Sometimes the allowable pressures even account for the factor of safety in the lining design, so that the injection pressures

barely overcome the backpressure from the groundwater. The consequence of these severe limits is that there is insufficient pressure at the point of injection to adequately grout the rock mass around the area to be excavated for the cross passage.

Equation 1 models the low-probability situation where there is an extensive gap between the segments and the rock mass, presumably due to ineffective tailskin or contact grouting. Equation 1 overestimates the pressure applied to the lining if the tailskin grouting is even a little bit effective. Even so, Equation 1 and Figure 2 show that the pressure dissipates markedly over a very short distance away from the grout hole.

A good way to manage the low-probability situation is to test and improve the tailskin or contact grouting in the vicinity of the cross passage, prior to grouting the rock mass. This can be done by drilling a pattern of short injection and bleed holes through the lining and then injecting grout from the lower holes to push the water, and then grout, up and out through the upper holes. Of course, if the holes don't make any water or take any grout, then it shows that the original grouting was fully effective in that area and that the low-probably situation does not occur. If the low-probability situation does not occur or was corrected, then there is no reason to place severe restrictions on the grout pressure. This testing and improvement need to be done in both tunnels on both ends of each cross passage prior to grouting the rock mass in between.

Bleeding down groundwater pressure so that lower grout pressures can be used is not a good idea in many situations, because it can lead to consolidation of the overburden soils and structural settlement, depending on the specific geotechnical conditions along the tunnel alignment.

6 LIMITATIONS

It is difficult to accurately predict the average aperture of a rock mass; therefore, the required excess grout pressure may be either overestimated or underestimated. On site testing is essential, and as discussed in Section 5, it is important to ensure that high-quality tailskin grouting has been carried out before applying higher excess pressure for pre-excavation grouting at cross passages.

7 REFERENCES

Barton, N. & Quadros, E. 2019. Understanding the need for pre-injection from permeability measurements: What is the connection? *Journal of Rock Mechanics and Geotechnical Engineering 11: 576-597.*

Gustafson G., Claesson, J & Fransson, A. 2013. Steering parameters for rock grouting. Journal of applied mathematics 2013 (Article ID 269594): 9.

McCarrison, R. 2017. Pre excavation grouting for groundwater ingress control. *Proceeding 20th NZGS Geotechnical Symposium. Eds.*

Okada, W. Giauque, A& Bhargava, R. 2017. Waterview Connection Project Passage Tunnels: Safety in Design and Construction.

Young, D.F., Munson, B.R., Okiishi, T.H. & Huebsch, W.W. 2011. A Brief Introduction to Fluid Mechanics. John Wiley & Sons.

THIS PAGE INTENTIONALLY LEFT BLANK

19th Australasian Tunnelling Conference – Acosta-Martínez, Stewart and Hudson-Smith (Eds.)
© 2025 Australian Tunnelling Society, ISBN 978-0-85825-002-4

Water ingress into UECP-2A TBM tunnel – its mitigation and control

D.J. Lees & J.L. Sanchez
Lahmayer, Germany

C. Yi & I.Wanigasekara
China State Construction Engineering Corporation Ltd, China

S. Banda
Ministry of Mahaweli, Sri Lanka

ABSTRACT: The Upper Elehara Canal Project Contract 2A [UECP2] is part of the Mahaweli Water Security Investment Program [MWSIP]. The UECP-2A contract includes a 27 km long tunnel which is only the second tunnel to be constructed by tunnel boring machine [TBM] in Sri Lanka. The tunnel passes beneath many sensitive areas including the township of Habarana and the World Heritage area of Sigiriya, as well as many farming and forestry areas. The tunnel varies in depth typically 30-40 m below surface but is sometimes very shallow with less than 10 m of cover passing under seasonal streams and surface water storage reservoirs.

The TBM tunnel is designed as a watertight structure with a pre-cast concrete segmental lining [PCCSL] with gaskets, this annulus is filled with pea-gravel and grout. Water ingress controls included grouting from the surface, pre-excavation grouting and post grouting works.

This paper will present the details of the construction and the investigation carried out to mitigate and control the water ingress into the TBM tunnel

1 INTRODUCTION

The Mahaweli Water Security Investment Program, financed by the Asian Development Bank and the Government of Sri Lanka, aims to complete the Mahaweli Development Program, started in the 1970s to improve farmer incomes, food security, equity between different parts of the country, public health, and domestic, municipal and industrial water supplies. Up to 900 million m3 of water will be transferred annually through canals, reservoirs and tunnels from the Mahaweli River to the water-scarce north and north-west, where smallholder farmers have traditionally practiced single-season rice cultivation. The transfer will facilitate cultivation of a second, diversified, crop and must be shared with competing consumptive demands, as well as meeting daily peak energy demands through releases for hydropower (Chegwin and Kumara, 2018).

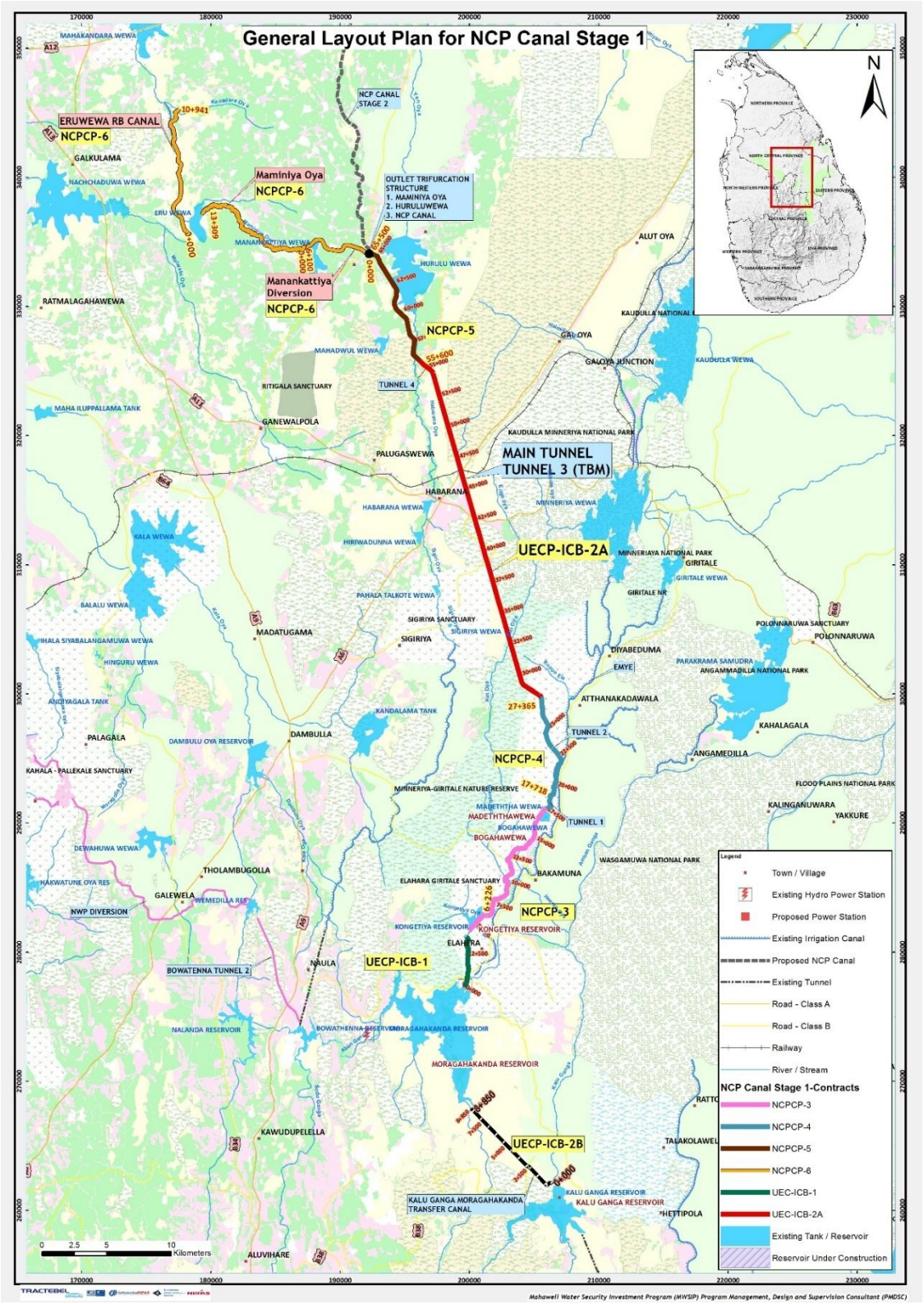


Figure 1: General Layout Plan for Northern Central Province Canal Stage 1

Phase 1 of the North Central Province Canal Project under the Mahaweli Water Security Investment Program comprises three components – namely the Minipe Left Bank Canal Rehabilitation Project (MLBCRP), the Kalu Ganga – Moragahakanda Transfer Canal (KMTC) and Upper Elahera Canal Project (UECP), and the North Western Province Canal Project (NWPCP). Funding is provided by the Asian Development Bank (ADB).

The objective of the 65.5 km long Upper Elahera Canal (UEC) is to transfer 100 MCM of Mahawelli water from the Morakahander Reservoir to the Yan Oya basin (Figure 1).

The tunnels for UECP-2A consist of a short length of drill and blast excavation to be excavated under NATM principles (Tunnel 4) and two TBM drives - one from the north and one from the southern portal (Tunnel 3) as shown in Figure 2.

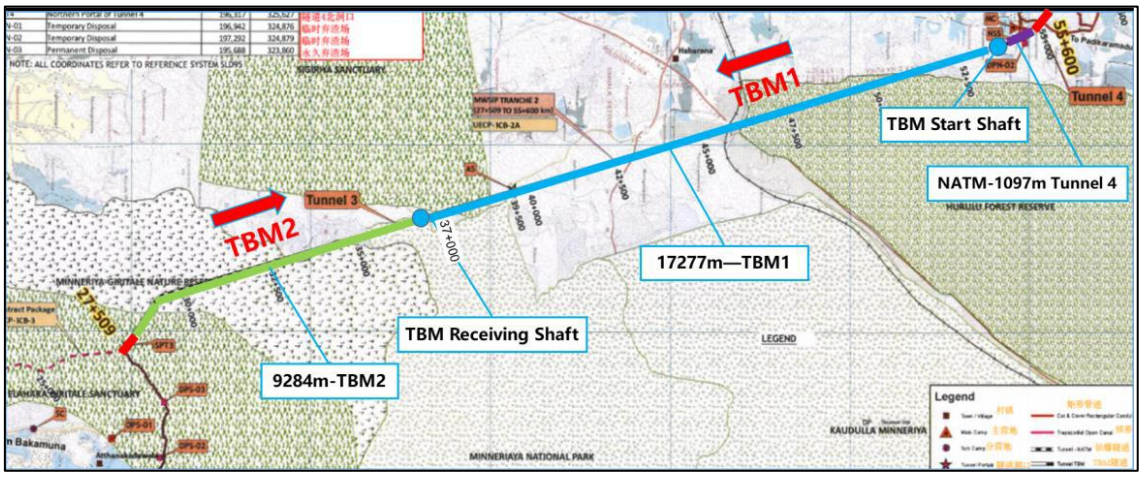


Figure 2: Project layout UECP 2A

2 GEOLOGY

The project is located in the Highland Complex (HC) area occupying them central part of Sri Lanka as shown in Figure 3.

This complex is strongly tectonized,and is characterized by the highest temperature metamorphic rocks termed generally as ‘granulites’. The rocks of the HC are Precambrian rocks formed under high grade metamorphic conditions and are composed of two main types of rocks namely metasediments and charnockitic-gneisses. The meta sediments are metamorphosed sedimentary rocks consisting of garnet sillimanite gneisses or khondalites, quartzite's, quartz feldspar granulites, garnet gneisses, and marble and impure crystalline limestone.

Deep weathering of the garnetiferrous granulitic gneiss rock produces deep rich soils. Lineaments are clearly marked by elongated valleys where deep weathering of garnetiferrous granulitic gneiss rock exist. The depth of weathering varies depending on the rock type and degree of fracturing. Along the riverbeds and creeks quite fresh rock is usually exposed while on the valley slopes decomposed and highly weathered rock can generally be found up to 8 m depth.

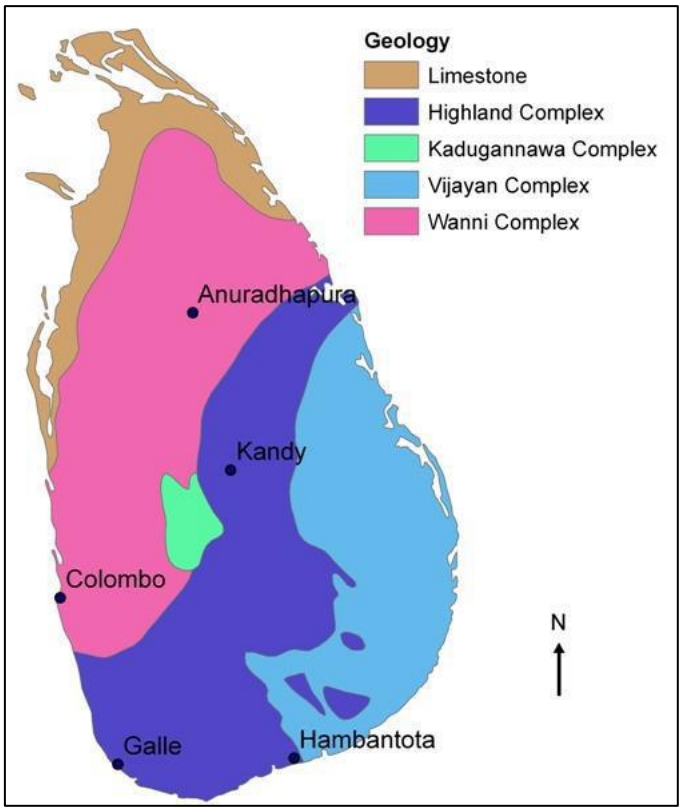


Figure 3: Geological map of Sri Lanka (Kehelpannala,1997).

3 HYDROGEOLOGY

The hydrogeology of the Highland Complex has been studied extensively (Lees and Gunatilake, 2017). There are essentially two types of aquifers occurring in this crystalline hard-rock terrain:(1) the shallow regolith (weathered zone) aquifer, and (2) the deep fracture zone aquifer (Panabokke and Perera, 2005). The thickness of the weathered zone ranges from 2 m to10 m and the deep fracture zone is located deeper than 30 to 40 m from the surface.

3.1 *Ground Water Monitoring*

Monitoring of groundwater levels was initiated in October 2017 incorporating four observation wells and five dug wells in Namalpura area. Later, the program was expanded to Habarana area by adding another seven dug wells in October 2017. To have more transparency in the monitoring program, Water Resources Board (WRB) established a groundwater monitoring network in three critical locations along the tunnel trace. With this inclusion, the groundwater monitoring program further expanded to a total number of 173 dug wells and tube wells. Apart from these wells, the contractor added new wells to the program. Additionally, the contractor established 15 new groundwater observation wells covering the entire project area. Two additional observation wells were added closer to the southern portal area in the middle of September 2022.

In 2024/25 the program has a total number of 198 wells which are monitored twice-a-month. In 2023 eleven surface water bodies were added to the monitoring program in the Sigiriya area.

4 GROUTING

4.1 *Surface Grouting*

The tunnel crosses the rivers, with shallow ground cover and possible water ingress areas. In order to ensure the safety of tunnel construction & TBM equipment, and prevent uncontrollable delays in the construction progress, pre-grouting from surface was carried out.

The perennial river Ruppe Ela is about 55 m wide, with an overburden of about 11.5 m. The excavation in this area is in Quartzo Feldspathic with an RMR value of 61-80, with some investigation holes giving RMR value of 41-60 where it was not possible to install to determine the ground water conditions, in other holes the initial water ingress volume was determined to expect between 18-200 l/s during tunnel excavation.

It was proposed to carry out grouting from either side of the riverbank with four sections of grout holes located in the right bank of the river and five sections of grout holes located in left bank of the river as shown in Figure 4.

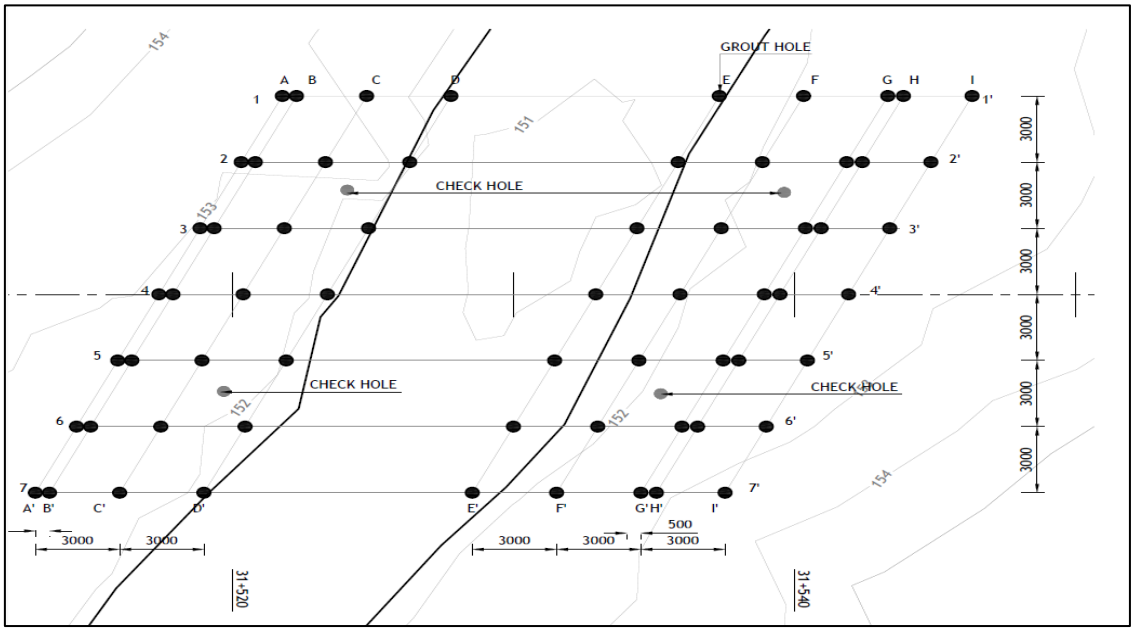


Figure 4: Plan view for primary drilling and grouting arrangement for the surface grouting at Ruppe Ela

A 3D view of the tunnel section and grout holes is shown in Figure 5.

The surface grouting was highly successful even though it had to be reduced as the tunnel excavation reached the site before the planned grouting could be completed and only 80% of the planned grouting could be carried out. No water ingress was intersected in the tunnel.

The perennial river Kiri Oya had a width of about 40 m, an overburden of about 6.5 m, with the tunnel beneath the stream in Garnet Biotite Gneiss and Quartz Feldspathic Gneiss with an RMR value of 41-60 and a high Lugeon range from 26 – 39. The RQD value in the Garnet Biotite layer was only 25 and initial water ingress was expected to be 28-100 l/s.

As this area was expected to be crossed during the dry season the layout of the surface holes was not as restricted as at Ruppe Ella as shown Figure 6. Without these limitations it was possible to complete the task with vertical holes.

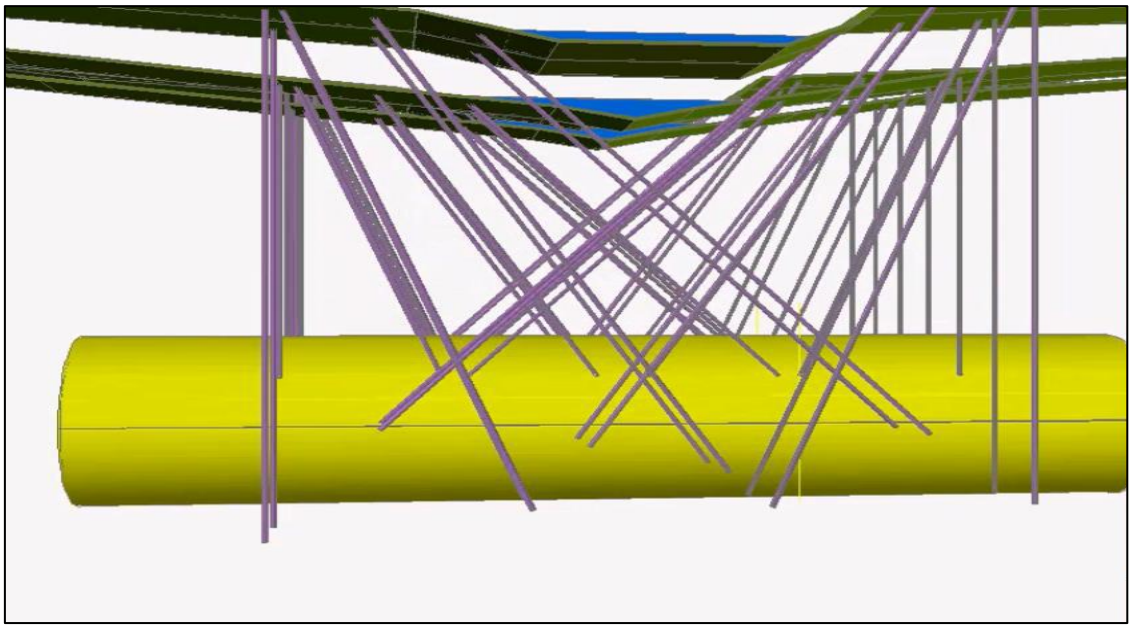


Figure 5: Longitudinal Section for drilling and grouting arrangement at Ruppe Ela

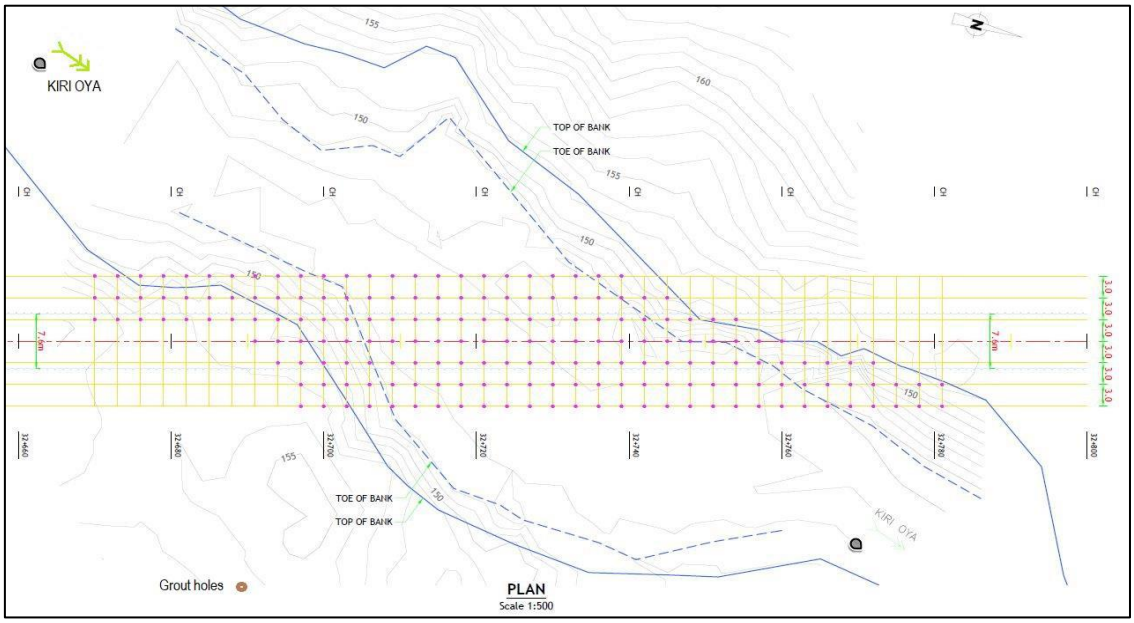


Figure 6: Plan view for primary drilling and grouting arrangement for the surface grouting at Kiri Oya

4.2 *Pre-excavation Grouting*

The identification of suitable locations for pre-excavation grouting along the T3 tunnel trace was undertaken, however, the final decision regarding the implementation of pre-excavation grouting was made depending on the actual ground conditions and results of probe drilling.

According to geological status and surface conditions. The tunnel was divided into two conditions – namely normal tunnelling and tunnelling through sensitive areas with different trigger values for the pre-excavation grouting in each area as shown in Tables 1 and 2.

Table 1. Normal excavation section (including forest, paddy field – nonurban area)

Water ingress measured in probe hole	Trigger value for pre-excavation grouting	
Ingress< 70 l/min		Continue Excavation
Ingress >70 l/min buy <120 l/min	2nd probe < 120 l/min	Continue Excavation
	2nd probe > 120 l/min	Pre excavation Grouting
Ingress > 120 l/min		Pre Excavation Grouting

Table 2. Sensitive sections (including urban areas, rivers, water tanks, geologically critical area etc.)

Water ingress measured in probe hole	Trigger value for pre-excavation grouting	
Ingress< 20 l/min		Continue Excavation
Ingress >20 l/min but <30 l/min	2nd probe < 50 l/min	Continue Excavation
	2nd probe > 50 l/min	Pre excavation Grouting
Ingress > 30 l/min		Pre Excavation Grouting

So, a single probe hole was drilled, if the water ingress in this probe hole exceeded the trigger value then a second probe hole was drilled. The combined ingress from the two probe holes determined whether pre-excavation was needed or if the excavation could continue. These trigger values were determined from experience of tunnelling in similar conditions in Sri Lanka (Lees et al, 2021). The normal tunnelling section and risky section were categorized in advance based on whether they were in urban areas, or geological critical zones, or areas with surface water bodies.

However, it was understood that the actual chainages of the postulated geological condition may differ from that expected, hence the corresponding Risk Type and water ingress/grouting trigger values to be adopted would ultimately be determined by the Geological Engineer. The target values were also considered just reference values, and the actual values would depend on the evaluation of the actual construction risks in the area based on surrounding rock conditions and environmental conditions. This was to provide a balance between risk and progress.

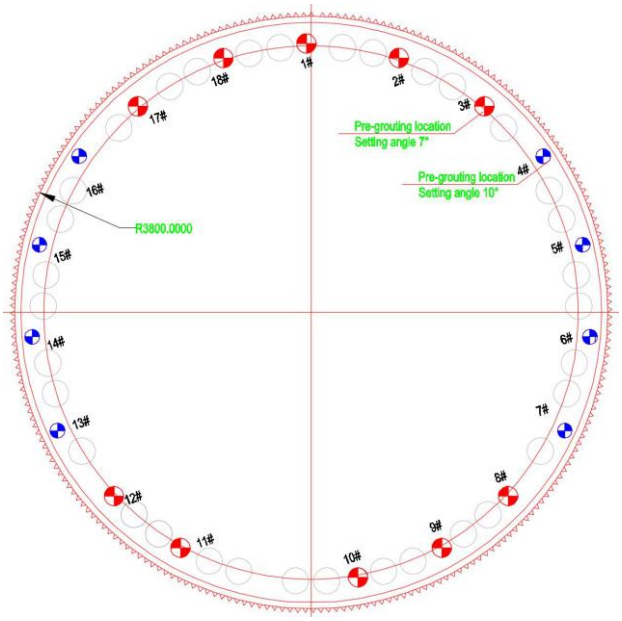


Figure 7: Pre-Excavation Grout holes Location in the Cutter Head

The TBM provided ports for 18 holes for probe drilling as shown in Figure 3 where the red and blue points indicate angles of 7°and 10°respectively.

The drilling parameters, such as the number of holes for pre-excavation grouting such as inclination, and depth, were adjusted according to the encountered conditions.

Typically, the grouting pressure was determined based on the water ingress pressure in the probe hole, adjusted to 0.5 MPa above the water pressure, however the grouting pressure may vary depending on specific conditions encountered during the grouting operation.

A normal GP cement was typically used at different water:cement ratios (1:1, 0.7:1, and 0.5:1) with injection volumes for each successive mixture limited. Initially, a 1:1 slurry was injected with 1000 l. If the termination criteria was not reached, the grout thickness was increased to 0.7:1 after an additional 1000 l, and further thickened to 0.5:1 after another 500 l. Sodium silicate grout was then added if the grout pressure failed to increase after all attempts. The termination criteria was defined as 5 l/min grout-take at the maximum allowable pressure for 10 minutes.

4.3 *Post Grouting*

The TBM tunnel is lined in some sections with a pre-cast concrete segmental lining (PCSL) and in some areas with a shotcrete lining, and in Class 1 rock conditions the tunnel is unlined. In sections of water ingress, the PCSL is installed. There are three designs of concrete lining on the project

In sections of water ingress, a compressible gasket is installed to provide a watertight lining, however this depends on the quality of the pea-gravel grouting in the annulus behind the lining.

In sections where the pre-excavation grouting was unsuccessful it was essential to seal the lining as quickly as possible. This was achieved by creating bulkheads every 10m using sodium silicate in the grout mix.

5 CONCLUSIONS

To date the excavation of the TBM tunnel has been carried out without any significant impact on the local environment or the water supply of the local community.

Surface grouting works were successful in reducing the need of pre-excavation grouting whilst crossing Ruppe Ella and Kia Ora perennial rivers.

Pre-excavation grouting has been carried out successfully and where ingress could not be halted by pre-excavation grouting this was halted by sealing the lining immediately behind the excavation.

7 REFERENCES

Chegwin, M.R. and Kumara S. 2018. “Energy, land and water nexus in Sri Lanka’s Mahaweli basin”. *Energy: Volume 171 Issue EN3*, ICE, 5th June 2018

Kehelpannala, K.V.W. 1997. Deformation of a high-grade Gondwana fragment, Sri Lanka. Gondwana Research, 4. pp 174-178.

Lees D. J. and Gunatilake J. 2017. The Hydrogeology of the Central Highlands in Sri Lanka and its effect on tunnel construction. 16th Australasian Tunnelling Conference 2017 Sydney, Australia, 30 October – 1 November 2017.

Lees D.J., Gunathilake, J., Dharmagunawardhane, H.A., and Sharp, J. 2021. Prediction and control of groundwater in TBM- excavated long hard rock tunnels. Australian Tunnelling Conference, May 2021.

Panabokke, C. R. and Perera, A.P.G.R.L. 2005. Groundwater Resources of Sri Lanka. Water Resources Board, January 2005.w

19th Australasian Tunnelling Conference – Acosta-Martínez, Stewart and Hudson-Smith (Eds.)
© 2025 Australian Tunnelling Society, ISBN 978-0-85825-002-4

Groundwater control in tunneling using injected polymer barriers

R. Colman, A. Osborne, N. Grobler & D. Van Dyk
Sovereign Hydroseal Pty Ltd, Western Australia

ABSTRACT: Cementitious grouts, such as Ordinary Portland Cement (OPC) have historically been widely used for water control in underground structures such as mines and tunnels. Although cheap and readily available, OPC exhibits performance limitations without additives. Chemical (or solution) grouts such as polyurethanes and acrylamides present with health and safety concerns during the mixing and application process. There is a third category of grouting materials, Polymer-Based Emulsion (PBE) that provide a cost-effective, non-toxic option. PBE grout was developed in the 1970s and first used to seal high pressure, high-rate water inflows into deep subsurface South African mines. Since the 1980s, PBE has also been applied in mines in Namibia, the UK, Australia, Zimbabwe, Botswana, Zambia, the United States, Canada, Poland and Russia. PBE has successfully sealed discrete inflows of 160 L/sec at pressures up to 20,000 kPa (2,900 psi), rendering it one of the few viable grout options for high-flow rate and high-pressure water leaks. In recent years, PBE has found application beyond its roots in mining. Leaking subsurface infrastructure such as subway tunnels, stations and building basements have benefited from the water-sealing properties of PBE.

1 INTRODUCTION

Uncontrolled water inflow and leak remediation into underground structures or inadequate control of the groundwater flow system impacting an open pit or underground mine, or tunnelling project, are some of the biggest challenges for engineers, owners of infrastructure, and operators of mines. Such inflows can lead to unsafe/hazardous conditions and endanger those who use and operate in them as well as impact the performance of equipment and machinery. In many cases, there is also a problem in dealing with the volume of water that needs to be managed in the dewatering process. A proactive approach to groundwater control can provide significant cost savings through reduced downtime and interruptions due to unexpected water inflows.

The success of PBE as a water-sealing grout is attributed to its unique physical properties. This paper provides an overview of the physical properties of the grout and applications. But firstly, many grouting programs designed to manage water ingress involve high pressure injection into water-bearing fractures to reduce/eliminate inflows. The optimal grout attributes for durable underground water control are considered to be:

- Exhibits low viscosity with very small particle size (suspension grouts) or no particles (solution grout) to permit deep penetration into water-bearing fractures; and
- Sets up as an insoluble, chemically inert, flexible or self-healing solid that maintains adhesion to wet rock surfaces and concrete despite recovering formation pressure and continued blasting or tunnelling, development induced subsidence and stress redistribution.

Therefore, it is considered that PBE is one of the few viable, proven grout options for successfully sealing water leaks in underground mines and tunnels, and it continues to be used to seal off high pressure/high flow rate water inflows when OPC and other specialty grouts have failed.

2 PBE PHYSICAL PROPERTIES AND BEHAVIOUR

2.1 *Introduction*

PBE is a suspension of colloidal polymer emulsoids dispersed in a solution of additives promoting flow and adhesion. PBE is injected in a fluid state and remains fluid until activated. PBE is a non-Newtonian, dilatant fluid; it sets by internal shear as the grout passes through fractures or other voids in water-bearing media. Set time may also be controlled chemically with the use of activator or inhibitor to regulate spread. Still, PBE is differentiated from solution grouts, because it is a single-part grout which does not require a chemical reaction to set.

Some PBE properties and behaviours are:

- Initial injection viscosity = 1.5 centipoise (cP)
- Specific Gravity ≈ 0.97
- Miscible in water
- Resistant to washout in high flow situations
- Will still set after dilution in formation water down to <15-25% of original concentration.
- Controlled cure rates from 2 seconds to several days
- Cures to a flexible solid with greater than 350% elasticity (elongation)
- Ultimate Tensile Strength ≈ 5 MPa
- Effective in both fresh water and water containing high Total Dissolved Solids (TDS).
- Strong adhesion to rock and concrete
- Curing is non-exothermic and non-expanding
- Non-hazardous in both liquid and solid states
- Demonstrated durability of +50 years with design life of +125 years
- Demonstrated radiation tolerance to 100 megarad (MRad)
- No adverse effects from freezing after curing
- No adverse effects from high temperature geothermal water
- NOH2O has a significantly lower carbon footprint than cementitious grouts

Because of its small particle size, low viscosity and miscibility in water, PBE can penetrate and seal water in small aperture fractures. These properties allow PBE to compete with resinous chemical or solution grouts as well as ultrafine or microfine cements for sealing water leaks in low permeability formations (Goodman et al. 2018). An advantage that PBE offers is that it can be diluted by groundwater to 15% of its original strength while passing through the formation and still set effectively. The tendency for PBE to set when agitated renders it highly useful in turbulent, high velocity flow situations where other types of grout will suffer dilution and washout.

2.2 *Differences between PBE and solution grouts*

PBE, as an emulsion, is a mixture of liquids as opposed to a cementitious, chemical or solution grout. A major difference between PBE and resinous solution grouts is in how the material sets from a fluid to a solid grout mass. Most resinous grouts require a chemical reaction between an agent and a reagent to set. Required reactions may be between a chemical solution and water, or between two to four components pre-mixed or injected simultaneously. In contrast, PBE can set solely by mechanical means; no chemical reaction is necessary. Because PBE activation can be achieved without a chemical reaction, grout set is non- exothermic.

The grouter actually has four ways to induce or influence PBE set (De Bruin et al. 1991; Gancarz et al. 2017). These are:

1. Mechanical Activation – When PBE flows through an orifice or fissure, the high shear action causes the dispersed polymer colloids to flocculate. These polymer flocs then start to adhere to the side walls of the orifice or fissure. Continued agitation causes additional flocs to form,

which, in turn, adhere to the now-rapidly-coagulating, jelly-like mass of polymers that builds up to block the orifice or fissure until flow ceases.
2. Chemical Acceleration – The grouter can use a chemical demulsifier (activator) with PBE to accelerate set when desired. The proprietary activator, Actical 500, will break the emulsion and induce the polymer colloids to coagulate into a jelly-like mass in as quickly as 2 seconds.
3. Chemical Retardation -- Conversely, if the rate of coagulation is too high (normally when injecting under high pressure in small aperture fractures or when formation water is saline) then a proprietary inhibitor, Inhibitor WP, can be used to promote greater spread of grout away from the injection point by keeping the emulsion stable in the geologic formation or behind a liner system for as long several days.
4. Exposure to Atmosphere – If PBE is exposed to atmosphere long enough for it to dehydrate, it will form a thin skin of very fine interlocking polymer laths.

A key difference in application of PBE and resinous chemical grouts is how desired set time is achieved (Gancarz et al. 2017). Set time for chemical grouts must be pre-determined and achieved by mixing a set proportion of catalyst in the resin prior to injection. Because PBE can be used as a single-component, self-activating grout, the need for a pre-determined set time is not necessary. Instead, set time is controlled based upon real-time field observations indicative of flow patterns/behaviour in a geologic formation or behind a liner system at any desired injection rate.

2.3 *Grouting equipment*

Because PBE sets when agitated, conventional high-pressure pumps cannot be used for injection. Air- powered, double-acting plunger pumps are used to inject PBE. The pumps are capable of delivery rates from about 40 to 120 liters per minute and discharge pressures up to 30MPa. Three pumps are typically mobilized to the job site: one for PBE grout, one for activator and one for inhibitor (Figure 1). High-capacity 35 MPa-rated hydraulic hoses (typically 1.27- or 0.64-cm) are used, with three separate delivery lines running from each pump to the grouting header. A valved injection manifold fitted with a pressure gauge is used, which allows for in-line mixing of PBE, Inhibitor WP and/or Actical 500, as illustrated in Figure 2.

Injection pressures can be controlled to meet site-specific criteria. For applications where injection pressure limits are critical, safety relief valves are set to the required relief pressure, together with a rupture disc which is set to relieve pressure if predetermined maximum injection pressures are exceeded.

2.4 *Other considerations*

PBE set-up is influenced by formation water chemistry (pH, total dissolved solids, major ion/geochemical facies, temperature, etc.). The PBE formulation and injection strategies can be adjusted to accommodate the specific geochemical formation conditions for each site to ensure optimal grout spread and setting. Consequently, basic water quality data or physical water samples are desirable to determine PBE behaviour in the formation water and to determine the optimal grout formulation for the project site.

Due to its tensile strength, strong bonding to rock and concrete, and its elasticity, PBE is uniquely suited for areas of high ground movement, such as nearby blasting in an active mine pit, or, in particular, where any ground movement at all may lead to migration of environmental contaminants (e.g. radionuclides, hazardous waste constituents, landfill leachate, tailings storage facility). Unlike brittle grouts (such as cements and some urethanes), PBE will not be easily ruptured during ground movements – leaving the grout seal intact. PBE-treated areas in mines and underground structures have maintained their dryness for over five decades without recurrence of leakage.

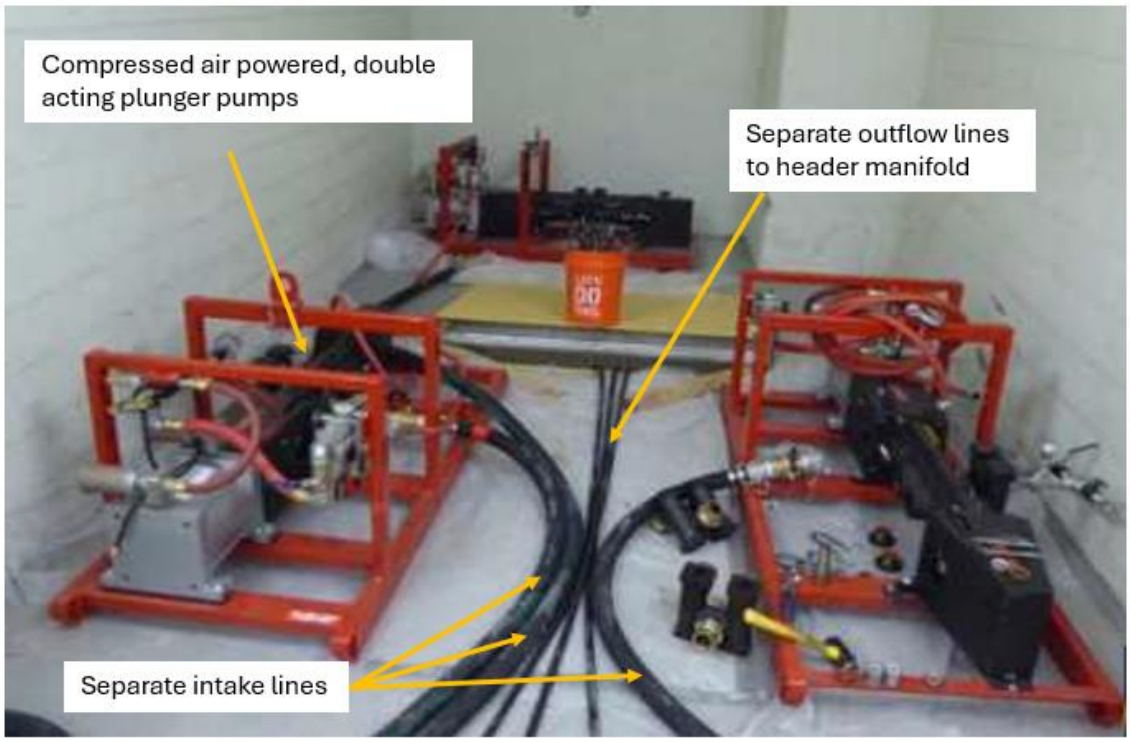


Figure 1. Separate positive displacement pumps used for PBE, activator and inhibitor.

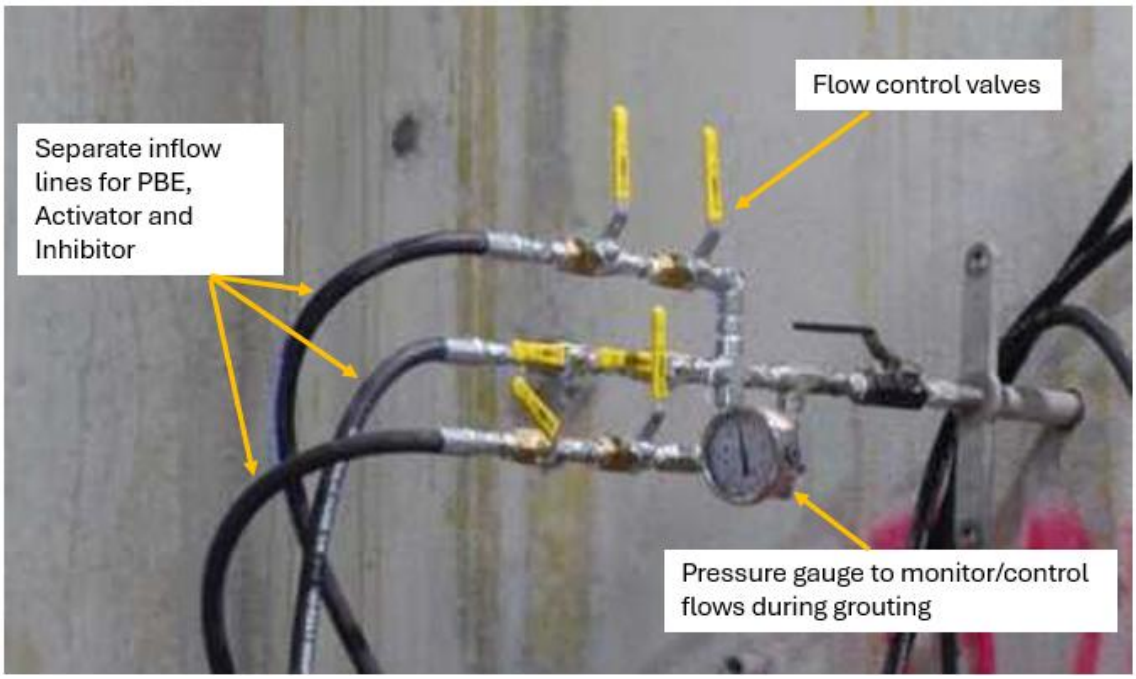


Figure 2. Grouting header manifold on injection hole to regulate mixture of PBE, activator/or inhibitor

3 MINING APPLICATIONS

3.1 *Injection strategies*

After its invention, PBE was first applied to seal leaks in deep subsurface mines. Hence, the grout had to perform well against both high pressure and high inflow rates, as well as in both fresh and saline groundwater. Sealing mine leaks is a complicated endeavor involving hydrogeological characterisation, selection of grout-hole locations and grouts to be used, and careful monitoring of mine conditions and surrounding formation pressures during and following grout injection.

Critical to success with any grout is establishing a connection between the grout injection hole and the water bearing structure contributing to the mine leak. Hence hydrogeological characterisation is a critical initial step, because even the best grouts cannot be effective if the injection holes are not drilled in positions to allow the grout to reach the leak site. The site hydrogeological characterisation is developed from project specific geology and structural information, ideally along with a geology resource model. The characterisation may also benefit from additional information gained from geophysical surveys to identify preferential groundwater flow paths.

Drilling grout holes in a radial fan around the planned opening is a standard part of shaft and initial decline excavation (Figure 3). For leaks in existing shafts, the injection holes are typically drilled beyond the liner system to avoid excessive pressure build-up on the concrete structure during grout injection. For linear structures or specific formation layers providing a conduit for flow to an open pit (Figure 4) or into an underground mine decline (Figure 5), the approach is to drill grout holes along the structure or perpendicular to the flow in the formation depending on the width of the flow line. The grout holes are typically cased (in weathered, broken rock) above the zone to be grouted and/or the grout injection interval is typically isolated using a pneumatic or mechanical packer.

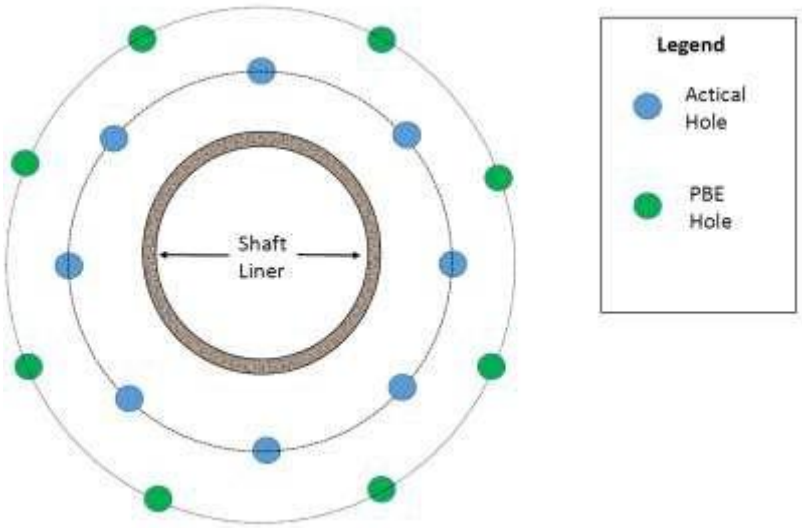


Figure 3. One of several typical ring patterns of grout holes using PBE with other products, including activator, inhibitor and/or Ordinary Portland Cement (OPC).

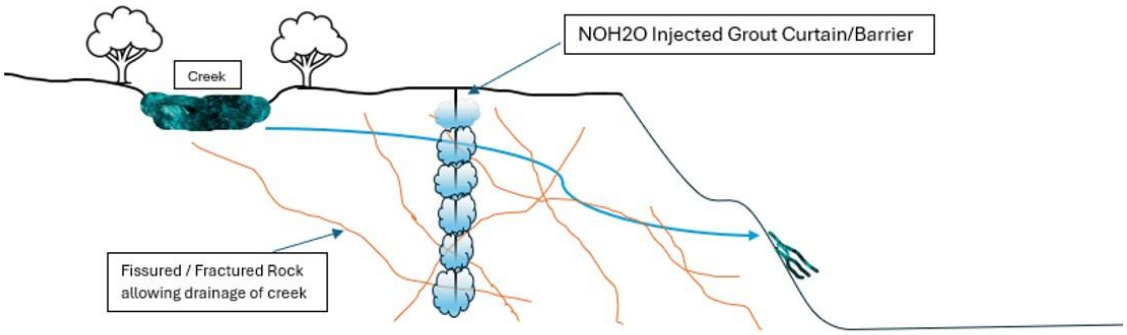


Figure 4. Installation of a PBE barrier to stop inflows to an open pit mine.

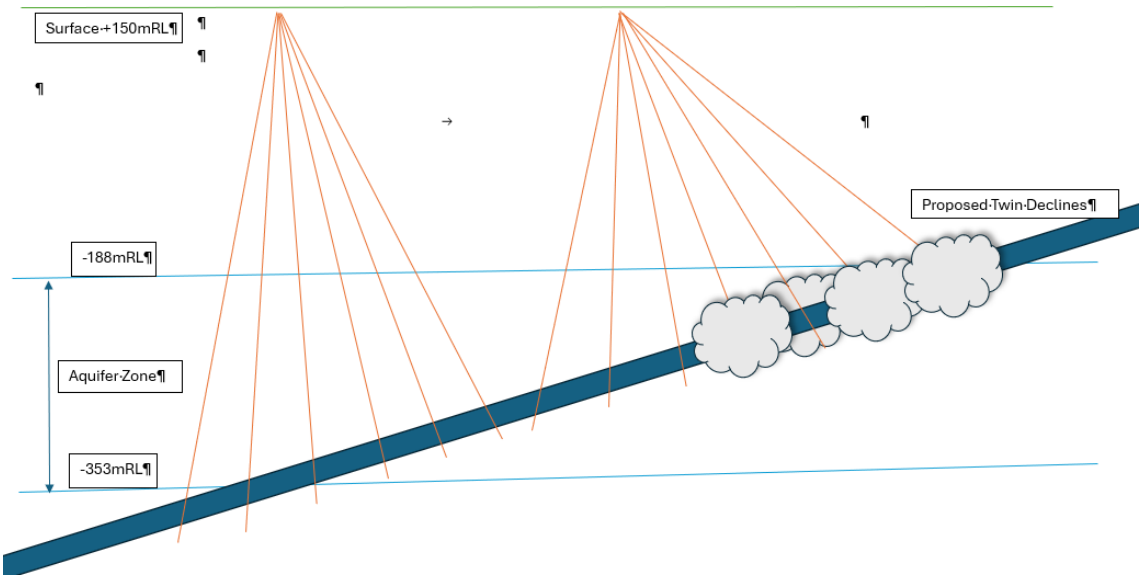


Figure 5. Pregrouting for decline development

4 TUNNELLING AND UNDERGROUND INFRASTRUCTURE APPLICATIONS

4.1 *Injection strategies: Negative side vs positive side*

The majority of PBE applications in underground infrastructure involve subway station and tunnel systems that are already constructed (Gancarz et al. 2017). If excessive leakage is discovered in a completed tunnel lining, there are two post-construction grouting methods that can be used to remedy the problem: crack-injection and curtain grouting. Crack-injection, or "negative-side grouting" is used to address individual leaks. By performing targeted drilling (usually at an angle, stopping before reaching the exterior of the lining) the individual crack is intercepted. A mechanical packer is fixed to the hole, and grout is injected directly into the plane of the crack, sealing the specific leak.

In contrast to crack-injection, which is a localised solution, curtain grouting aims to prevent all leaks in a given area. Curtain grouting aims to treat an entire area which is leaking (usually an earth-bearing wall or a roof slab in contact with the ground) by drilling a grid-like pattern of holes through the exterior of the concrete. Grout is then injected into the annular space between the tunnel's structural liner and the surrounding ground medium, creating an impermeable membrane "curtain" for that area.

4.2 *Negative side (crack) injection*

PBE is injected into the water flowing in a crack or fissure via a hole drilled to intersect the crack or fissure for this purpose. A multiport packer is inserted into the hole through which the PBE is injected. As the emulsion flows with the water along the crack or fissure it will be activated by the turbulent agitation it encounters, and a steady build-up of the coagulated rubber-like laths will occur which then form a seal. If the flow conditions dictate, then a chemical activator can be injected, either downstream from the PBE injection point, or at the same injection point through a different port in the valved manifold (see Figure 2)

4.3 *Positive side (curtain) grouting: the preferred cost-effective method*

Within a tunnel section, curtain grouting operations are sequential, one following after another in a deliberate fashion in order to push the water in one specific direction. Mini drill rigs used to create grout holes typically consist of an electric drill with a diamond core bit (usually 1.9 cm or 2.5 cm diameter) on a guided drill stand mounted to the wall. Mini drill rigs with diamond core bits have yielded the best results; they are portable, electrically powered (eliminating the need for compressed air) and can be securely mounted on a drill stand for guidance. The advantage of core drilling as compared to rotary percussive drilling is the significant reduction of lost holes due to drill cuttings obstructing the annulus.

Grout holes (typically 1.9 cm to 2.5 cm diameter) should be spaced to ensure sufficient coverage. Grid spacings of 3- to 10 m have proven adequate when using PBE for curtain grouting.

4.3.1 *Dye injection testing*

When all holes in a particular treatment area are drilled and fitted with packers, it is worthwhile to perform some preliminary injections using dye water. Since PBE has similar fluid properties to water, performing trial injections using dye water can provide insight into what to expect during grout injection. Injection parameters such as the pumping pressure required to achieve coverage, the volume of dye water injected and time it takes for dye water to communicate to cracks or nearby packers can be measured to give an estimate of what to expect while pumping PBE. It is neither necessary nor recommended to perform these measurements for every grout hole; three to four holes is more than sufficient. Most important is observing where dye water reports in the vicinity. Grout will likely report wherever dye water does, so if dye water comes out near sensitive equipment or into areas open to the public it gives advance notice of where to set up protective sheeting and what areas to section off. While usually straightforward, this task may require entry into locked rooms and gaining access to mechanical pits and overhead crawlspaces.

4.3.2 *PBE injection methods*

Treatment of a target zone means grouting each hole in that zone sequentially. In general, holes are treated in order of lower to higher elevation. Injection pressure is controlled by structural capacity of the wall or slab being treated and generally ranges from 0 to 5 MPa. Use of an activator or inhibitor may be justified if no pressure builds over time or if pressure spikes too quickly, respectively. Given the high mobility of PBE, it is prudent to periodically monitor the area for signs of discharging grout to estimate the extent of spread from a specific injection point.

5 PBE COSTS

Like any specialty grout, the unit cost of PBE is higher than the unit costs for commonly used cementitious grouts such as OPC. However, total grouting program costs compare favorably with cementitious grouting programs. The primary reasons are that PBE requires fewer labour hours, less shut-down time and less drilling than traditional grouting, and PBE exhibits long-term durability.

The penetrability of PBE contributes significantly to its cost-effectiveness for water-sealing. Because PBE is capable of spreading out over greater areas, the number of grout holes required

(and therefore the labour required to drill and repair them) is greatly reduced. Greater value is provided in the mining sector where grout-hole lengths can be significant and/or where fewer grout holes are desired because of inadvertent contamination migration concerns, and unit rates for drilling may be quite high because of stringent environmental protocols. The grout itself is only one part of the total program costs.

6 CONCLUSIONS

PBE grout is designed specifically for groundwater control in mining applications and underground structures such as tunnels. Key attributes that set it apart from cementitious and solution grouts include:

- High penetration capability due to low viscosity and ultra small particle size
- Activation without chemical additives, resistance to washout, and flexibility.
- Durability (>50 years) and environmental friendliness.
- Estimated product life of +125 years.

With a proven success record of +50 years of use, across 400 projects in more than 40 countries on 5 continents, PBE has been referred to as the water brigade of the mining and tunnelling industry, particularly when used after other grouting efforts have failed. Those projects have included sealing leaks with flow rates up to 160 L/sec, pressures of 20 MPa and to depths of 1300m bgl.

In today's cost sensitive project world, it is considered prudent to investigate pre-excavation grouting with PBE to reduce permeability ahead of any underground development, as this will result in cost savings in construction through reduced down time and expensive interruptions due to unexpected water.

7 REFERENCES

De Bruin, N. J. H., J. Grobler, and C. A. Pollard, 1991. The *SCEM 66 Water Control System.* Institute of Shaft Drilling Technology Annual Technical Conference, April 24-26, 1991, Las Vegas, Nevada

Gancarz, P., J. Minturn, N. Grobler, and D. Van Dyk. 2017. *Polymer Emulsion Grouting for Water Cutoff in Tunnel Structures.* American Society of Civil Engineers Geo-Institute, Grouting 2017: Grouting, Deep Mixing and Diaphragm Walls, July 9-12, 2017, Honolulu, Hawaii.

Goodman, W., D. Van Dyk, N. Grobler, and A. Osborne, 2018. Water Ingress Mitigation Programs for Underground Mines – Geochemical and Rock Mechanical Demands on Grout Properties. *International Mine Water Association 2018 Meeting, Pretoria, South Africa, September 10-14*.

19th Australasian Tunnelling Conference – Acosta-Martínez, Stewart and Hudson-Smith (Eds.)
© 2025 Australian Tunnelling Society, ISBN 978-0-85825-002-4

Numerical modeling of the water pressure influence on the mechanical behaviour of lining

N. Wang, X. Yang

China Railway Academy Group Co. Ltd., Chengdu, China

ABSTRACT: Groundwater exerts a continuous load on tunnel structures and has a critical impact on the mechanical behaviour of the tunnel lining. If not properly managed, this load may result in serious problems such as cracking, excessive deformation, or even collapse of the lining. Based on a review of commonly used methods for calculating water pressure in tunnels, this paper investigates the mechanical response of the tunnel lining under different water pressure scenarios using numerical modeling. The results indicate that water pressure has a significant influence on the mechanical behaviour of the lining.

1 INTRODUCTION

Water-rich zones with complex hydrogeological conditions are frequently encountered in tunneling projects.The water pressure exerted on the tunnel lining is a key factor affecting the tunnel's safety and long-term stability. Uncontrolled groundwater may cause seepage, deformation, or even structural failure of the lining, thereby compromising the tunnel's integrity and operational safety, and posing potential risks to transportation systems [1]. Therefore, effective groundwater control measures are essential throughout the entire tunnel lifecycle—not only to ensure structural safety during both construction and operation, but also to minimize adverse impacts on the surrounding hydrogeological environment [2].

The calculation of water pressure on tunnel linings is closely related to the adopted groundwater control strategy. In China, different sectors apply varying principles for groundwater management. In the highway and railway tunnel sectors [3,4], an integrated approach combining prevention, drainage, interception, and sealing is commonly adopted. This approach is tailored to site-specific geological conditions and considers factors such as the external hydrogeological environment, groundwater richness, and lining stress, aiming to develop a comprehensive waterproofing and drainage scheme. In contrast, metro tunnel projects prioritize a prevention-based groundwater control strategy to minimize impacts on urban hydrogeology [5]. These projects often utilize a combination of rigid and flexible waterproofing materials and adopt a multi-layered waterproofing design for enhanced protection. The overall waterproofing and drainage system of a tunnel typically comprises three key components: the rock mass grouting system, the waterproofing system, and the drainage system. In Europe, drainage design approaches are currently diverse and project-specific. Both drainage-dominated and full or partial waterproofing strategies are employed depending on the project requirements. For example, Germany—where the number of tunnels is relatively limited—often adopts a "fully sealed and non-drainage" design philosophy. In contrast, France generally favors drainage-based solutions [6]. In countries such as Norway, single-shell lining systems are widely used, incorporating drainage-based waterproofing systems and flexible waterproof membranes [7]. A comparative analysis of European practices reveals a general principle for tunnel groundwater control: in the absence of special environmental or structural constraints, tunnels in water-rich mountainous areas are preferably designed with drainage

systems to reduce water pressure on the lining. However, in environmentally sensitive zones or where critical infrastructure is located above the tunnel, a fully sealed design capable of withstanding full hydrostatic pressure is adopted.

This paper first reviews commonly used methods for calculating groundwater pressure on tunnel linings and then investigates the mechanical behaviour of the tunnel lining under different water pressure conditions using numerical modeling.

2 WATER PRESSURE CONSIDERATIONS IN TUNNEL LINING DESIGN

In China, a variety of methods are employed to calculate groundwater pressure in tunnel design. However, the selection of a specific method typically depends on the waterproofing and drainage strategy adopted for the project. The three commonly used approaches for water pressure calculation are as follows:

(1) No Water Pressure Considered

For certain shallow-buried mountain tunnels in China, a full-drainage approach is commonly adopted, whereby all infiltrating groundwater is effectively discharged through the drainage system. In such cases, groundwater flows unobstructed, resulting in negligible pressure on the lining. Consequently, this design approach assumes that the water pressure acting on the tunnel lining can be ignored.

(2) Reduction Coefficient Method

In water-rich zones with significant overburden and relatively stable groundwater conditions, a semi-enclosed waterproofing scheme is often adopted. Due to the effect of seepage, the water pressure acting on the lining is lower than the full hydrostatic head. The water pressure reduction coefficient is defined as the ratio of the water pressure head acting on the lining to the vertical height of the groundwater column from the water table to the tunnel crown.

This method has been extensively studied in China, with various empirical and analytical formulas proposed for determining the reduction coefficient. In this study, a method derived from hydraulic tunnel design specifications is adopted. According to these specifications, the external water pressure can be represented by the pressure head below the calculated water level. The pressure head from the calculated water level to the tunnel invert equals the product of the total water column height and the corresponding reduction coefficient. Specifically, Zhang Youtian's correction factor method is employed in this paper. The external water pressure coefficient is determined using the following formula [8]: $\beta = \beta_1 \times \beta_2 \times \beta_3$. β_1 is the correction factor for water pressure in the initial seepage field. β_2 is the correction factor for external water pressure acting on the lining after tunnel completion. β_3 is the correction factor accounting for the influence of waterproofing and drainage measures on the external water pressure of the lining.

(3) Theoretical Analytical Method[9]

For tunnels located in water-rich regions, it is essential to account for the influence of rock mass grouting on water pressure and to evaluate the associated seepage inflow. The theoretical analytical method is typically employed to calculate both the external water pressure acting on the lining and the seepage quantity. This method assumes that the surrounding rock behaves as a homogeneous, isotropic, and continuous medium. Based on Darcy's law of seepage, the method derives the distribution of pore water pressure within the grouted zone and the area adjacent to the tunnel lining. Drawing on research related to water pressure distribution in high-pressure mountain tunnels, and following the theoretical analytical framework, the external water pressure on the lining is calculated using the following formula:

$$P_l = \gamma_w H_l = \frac{\gamma_w H_0 \ln \frac{r_l}{r_1}}{\ln \frac{r_l}{r_1} + \frac{K_l}{K_g} \ln \frac{r_g}{r_l} + \frac{K_l}{K_r} \ln \frac{H_0}{r_g}} \tag{1}$$

Where: P_l—Water pressure behind the lining, γ_w—Unit weight of water, H_l—Water head behind the lining, H_0—Static water head outside the tunnel lining, r_l—External radius of the lining, r_1—Internal radius of the lining, r_g—Radius of the grouting zone, K_l—Permeability coefficient of the

lining, K_r —Permeability coefficient of the surrounding rock, K_g —Permeability coefficient of the grouting zone.

3 THE NUMERICAL MODEL

To investigate the influence of water pressure on the mechanical behaviour of tunnel linings, a case study was conducted using numerical modeling based on a single-track tunnel constructed with the New Austrian Tunneling Method (NATM). The tunnel has an overburden depth of approximately 120 meters, and the lining thickness is 0.45 meters. The groundwater table is located 70 meters above the tunnel crown, and the water pressure acting on the lining is calculated using the methodology described below.

The surrounding rock is modeled as an elastoplastic material, while the tunnel lining is represented by elastic beam elements. Geological investigations indicate that the tunnel primarily passes through Class IV surrounding rock. The lining structure is designed in accordance with relevant specifications for deep-buried tunnels in Class IV geological conditions. The reinforcement effect of grouting is simulated by increasing the deformation modulus of the surrounding rock.

The numerical modeling domain extends 40 meters radially in all directions from the tunnel periphery. The finite element model configuration and mesh discretization are shown in Figure 1, while the material properties and mechanical parameters are summarized in Tables 1 and 2.

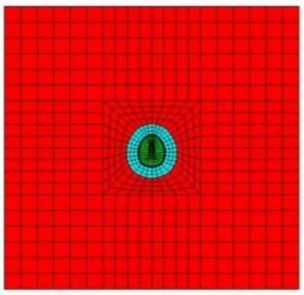


Figure 1. Computational model

Table 1 The calculating parameters of wall rock

Grade IV Rock Mass Parameters					Water Parameters		
Unit Weight (kN/m^3)	Deformation Modulus (GPa)	Poisson's Ratio	Internal Friction Angle (Degree)	Cohesion (MPa)	Unit Weight (Kg/m^3)	Tensile Strength (MPa)	Bulk Modulus (MPa)
20	3	0.3	30	0.4	1000	0	2x10^3

Table 2 The calculating parameters of concrete

Lining Concrete	Deformation Modulus GPa	Ultimate Compressive Strength Ra/MPa	Ultimate Flexural Strength Rw/MPa	Ultimate Tensile Strength R1/MPa	Poisson's Ratio	Unit Weight (kN/m3)
C35	1	26	32.5	2.45	0.2	25

Three water pressure conditions are considered in the numerical modeling: (1) no water pressure, (2) partial water pressure based on a reduction coefficient, and (3) theoretical water pressure derived from analytical methods. Following the numerical simulation, the mechanical response

at key locations of the tunnel lining is analyzed. A schematic diagram illustrating these key locations is provided in Figure 2.

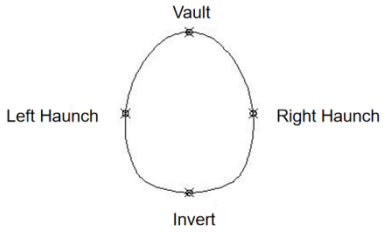


Figure 2. Location of key points on the tunnel lining

4 THE MODELING RESULTS

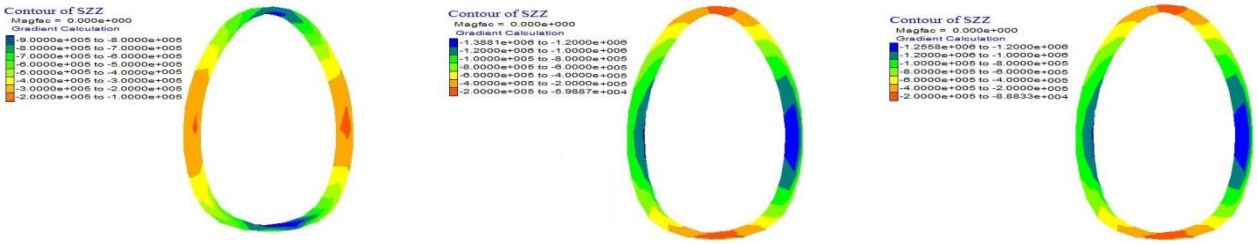
The numerical modeling results are discussed below.

(1) Stress Analysis

Stress contour plots of the tunnel lining under the three different water pressure calculation methods are shown in Figure 3. From the analysis of these plots, the following observations are made: Without considering water pressure, the maximum lining stress occurs at the tunnel crown, with a peak value of 0.9 MPa. Under the reduction coefficient method, the maximum stress shifts to the haunches on both sides of the tunnel, reaching 1.3 MPa. Using the theoretical analytical method, the maximum stress is also located at the haunches, with a value of 1.25 MPa.

Comparing the stress contours across the three scenarios reveals a distinct shift in the location of maximum stress: Without water pressure, the crown bears the maximum stress. When water pressure is considered (either via the reduction coefficient or theoretical analytical methods), stress concentration moves to the haunch regions on both sides.

This change in stress distribution is attributed to the multidirectional influence of groundwater pressure acting after tunnel excavation. Given the tunnel's relatively high flattening ratio (i.e., vertical height greater than horizontal width), the lateral sections of the lining—particularly the haunches—experience increased stress due to the greater horizontal component of the water pressure.



No Water Pressure Reduction Coefficient Theoretical Analytical

Figure 3. Lining stress of different working conditions

(2) Structural Force Analysis

Stress components in all directions were extracted at key locations on the tunnel lining to calculate the bending moments and axial forces at the crown, haunch, and invert. The results are summarized in Tables 3 and 4.

Table 3 The axial force of lining (KN)

	Vault	Left Haunch	Right Haunch	Invert
No Water Pressure	410.34	163.53	163.53	437.79
Theoretical Analytical	460.58	187.95	187.95	511.48
Reduction Coefficient	536.47	235.78	235.78	567.45

Table 4 The moment force of lining (KN·M)

	Vault	Left Haunch	Right Haunch	Invert
No Water Pressure	645.38	327.56	327.56	613.07
Theoretical Analytical	734.09	357.87	357.87	665.26
Reduction Coefficient	815.75	410.58	410.58	748.17

Analysis of Table 3 and Table 4 indicates that axial forces exhibit patterns similar to those of stresses: the No Water Pressure case yields the smallest values, followed by the Theoretical Analytical method, while the Reduction Coefficient method produces the largest axial forces. Compared to the No Water Pressure baseline, the Theoretical Analytical method shows increased axial forces at the corresponding locations: a 12.2% increase at the crown, 16.8% at the invert, and 14.9% at both haunches. Similarly, the Reduction Coefficient method demonstrates axial force increases relative to No Water Pressure of 30.7% at the crown, 29.6% at the invert, with the maximum increase of 44.2% occurring at both haunches.

Regarding bending moments, all three methods show maximum values at the invert. Both the Theoretical Analytical and Reduction Coefficient methods exhibit increased bending moments compared to No Water Pressure. At the crown, the Theoretical Analytical method increases bending moments by 13.75%, while the Reduction Coefficient method shows a 26.39% increase. At the invert, the Theoretical Analytical method shows an 8.5% increase and the Reduction Coefficient method a 22.04% increase.

(3) Displacement Analysis

Displacement data at key points of the tunnel lining were extracted, and the displacement values at each critical location are presented in Table 5 (with vertical displacement at the invert recorded as zero). Using the Reduction Coefficient method as an example, it is observed that the pattern of displacement variation differs from that of stress. The maximum displacement occurs at the crown, with a vertical settlement of 28.7 mm. At the haunches on both sides, the horizontal displacement is relatively small, measuring 13.6 mm. A comparative analysis reveals that at the haunches—where vertical stress is relatively high—the displacement is relatively low, whereas at the crown—where vertical stress is lower—the displacement is relatively higher. This phenomenon is attributed to the redistribution of internal forces caused by lining deformation, which alters the stress and displacement patterns.

The trend in displacement magnitudes across the three water pressure calculation methods aligns with that observed in the internal force analysis: The No Water Pressure case results in the smallest displacements. The Theoretical Analytical method yields moderate displacement values. The Reduction Coefficient method produces the largest displacements, indicating that this method predicts the greatest deformation of the tunnel lining. This further underscores the significant impact of water pressure assumptions on the structural response of tunnel linings.

Table 5 The displacement of lining

	Vertical Settlement at Vault	Horizontal Convergence at Haunches
No Water Pressure	18.2	8.3
Theoretical Analytical	22.1	10.3
Reduction Coefficient	28.7	13.6

Based on the characteristics of the tunnel section, burial depth, and case study calculations in this project, combined with the results from stress, structural force, and displacement analyses, a

preliminary evaluation of the three groundwater pressure calculation methods is presented. From an overall perspective, the No Water Pressure method, which neglects the influence of groundwater pressure, results in the smallest stress and displacement values. The Theoretical Analytical and Reduction Coefficient methods yield relatively close results; however, the Reduction Coefficient method tends to produce slightly higher stress and displacement values than the Theoretical Analytical method. While conceptually clear, the Theoretical Analytical method has certain limitations. It relies on Darcy's law, which may not always be applicable, and requires simplification of the tunnel cross-section into an equivalent circular shape, limiting its practical accuracy in complex geometries. On the other hand, the Reduction Coefficient method is more commonly used by design engineers due to its simplicity. However, the reduction coefficient value exhibits significant variability and depends heavily on extensive statistical analysis of engineering cases. Currently, this method remains mostly confined to academic research without widely recognized regulatory guidelines.

5 CONCLUSION

This paper, based on an actual engineering case, analyzes the impact of three groundwater pressure calculation methods on the structural behavior of tunnel linings. In summary, the No Water Pressure method yields the lowest internal forces, while the Theoretical Analytical and Reduction Coefficient methods produce overall similar results. Each method has its own advantages and disadvantages: the Reduction Coefficient method is convenient for calculation but requires large datasets to accurately determine reduction parameters; the Theoretical Analytical method possesses a solid theoretical foundation but necessitates integration of field measurements and refinement of model assumptions to enhance its applicability.

For future groundwater pressure analyses, it is recommended to adopt a comprehensive approach that integrates multiple calculation methods and validates results against actual engineering projects. Such an approach will facilitate the development of water pressure calculation guidelines that balance safety and economy, thereby providing scientific support for tunnel design under complex hydrogeological conditions.

6 REFERENCES

Jiang Hao. Experimental Study on Lining Water Pressure and Waterproof Concrete in Underground Tunnel Engineering [D]. Northeast Electric Power University, 2024.

Wu Zhonglin. Research on Limited Groundwater Discharge and Construction Control Strategies for Mountain Highway Tunnels in Water-Rich Areas [D]. Chongqing Jiaotong University, 2024.

Code for Design of Railway Tunnels: TB 10003-2016 [S]. Beijing: China Railway Publishing House, 2017.

Design Specifications for Highway Tunnels – Part 1: Civil Engineering: JTG 3370.1-2018 [S]. Beijing: China Communications Press, 2018.

Code for Design of Metro: GB 50157-2013 [S]. Beijing: China Architecture & Building Press, 2013.

Ding Xiaojun, Han Changling et al. Design Practices for Large-Span Soft Rock Highway Tunnels Under European (French) Standards [M]. Beijing: China Communications Press, 2019.

Liu Zhe, Ni Guangbin, Lin Chunnian, Huo Jianxun. Comparative Study and Revision Suggestions on Chinese-European Railway Tunnel Standards [J]. Railway Standard Design, 2023, 67 (03).

Zhang Youtian. Correction Coefficient of External Water Pressure for Hydraulic Tunnels and Pressure Pipelines [J]. Hydropower, 1996, (12): 30-35.

Tang Mingwei. Study on Lining Water Pressure of Three-Lane Mountain Highway Tunnels [D]. Southwest Jiaotong University, 2022.

Theme 10. Pipe Jacking and Trenchless Technology

THIS PAGE INTENTIONALLY LEFT BLANK

19th Australasian Tunnelling Conference – Acosta-Martínez, Stewart and Hudson-Smith (Eds.)
© 2025 Australian Tunnelling Society, ISBN 978-0-85825-002-4

XXL Pipe Jacking: Technological aspects of large-diameter and long-distance drives

B. Hayes
Herrenknecht AG, Schwanau, Germany

ABSTRACT: Pipe-jacked tunnels are considered for a large variety of applications from water and sewage, cable ducts to pipeline construction. In most cases, Slurry MTBMs are used to carry out these projects. Continuous further development of pipe jacking technology are vital to overcome feasibility limits and to meet increased project requirements.

As tightened safety regulations increasingly limit the options of segment lining in diameters below 4 m, pipe jacking has partially taken over. During the last decades, a growing number of large-diameter and long-distance pipe jacking projects has been completed. Experienced contractors successfully use the technological capacity of MTBM equipment. Continuous further development of technological features for pipe jacking is key to overcome feasibility limits and to meet increased project requirements. The overall aim is to provide clients and contractors with safe and economical solutions for successful projects. International milestone projects and latest innovations will be shared in this presentation.

1 INTRODUCTION

The main focus of contemporary underground tunnel construction is to complete tunneling structures safely and within the given time and cost frame. This is of particular interest for clients, project owners and the nominated contractors. Successfully executed projects help to gain trust and acceptance of large-scale projects among the population and to convince planning authorities of the opportunities and the benefits of mechanized tunneling.

As safety aspects in mechanized tunneling have gained more and more importance and safety standards have been consequently improved, requested space and accessibility in small-diameter segment lining projects leads to an increasing minimum diameter for such projects. As a result, pipe jacking has partly replaced small-diameter segment lining, which leads to longer drives and larger diameters in pipe jacking. Experienced contractors execute pipe jacking works with tight curves, multi-curved or inclined alignments, even under high groundwater pressures or with low overburden and related high settlement risk.

2 LONG-DISTANCE PIPE JACKING

From a technical point of view, long-distance pipe jacking can be an alternative to small diameter segment lining. Detailed investigation and project planning as well as the use of latest technological features and contractors´ experience are essential for project success. Long-distance pipe jacking usually requires accessibility for maintenance operations and disassembly measures after tunneling, even with remote-controlled equipment. As a result, long distance pipe jacks in general have a minimum inner diameter of 2,000mm. Besides the respective design of the tunneling machine and the cutting wheel according to the defined soil conditions to be expected along the

tunneling alignment, the main concern of long-distance pipe jacking is the limitation of the jacking forces.

2.1 *The role of bentonite lubrication*

In pipe jacking the control of the friction between the pipe and the surrounding ground is a key factor for project success. Besides the contractor´s experience and other important measures like the use of interjacking stations, special attention is paid to bentonite lubrication. The longer the drive or the larger the diameter, the more the focus is on lubrication. Uncontrolled distribution of bentonite along the tunnel route or tearing of the lubrication film can lead to significant increase in jacking forces. In order to ensure continuous lubrication throughout the tunnel alignment, the volume-controlled bentonite lubrication system has been developed. The automated system offers a high level of bentonite control and automation to overcome the limitations of conventional systems. Easy handling and smart, partly automated setting of the relevant parameters assist the machine operator and avoid variations caused by personnel changes or uncontrolled pumping of bentonite.

In a first step, the volume-controlled bentonite system automatically regulates the initial injection in the area close behind the machine, where the annular gap is created. The bentonite fills the annular gap, provides support and simultaneously lubricates the pipe. The subsequent injection maintains the lubricant film that has been established. Both steps are described in Figure 1. The visualization in the control container shows the volume of injected bentonite in every meter of tunnel along the alignment. The system provides unprecedented situation control, no matter if it is used in classic or volume-controlled mode. When running in volume-controlled mode the system automatically distributes the bentonite along the tunnel axis according to the needs of the prevailing project conditions.

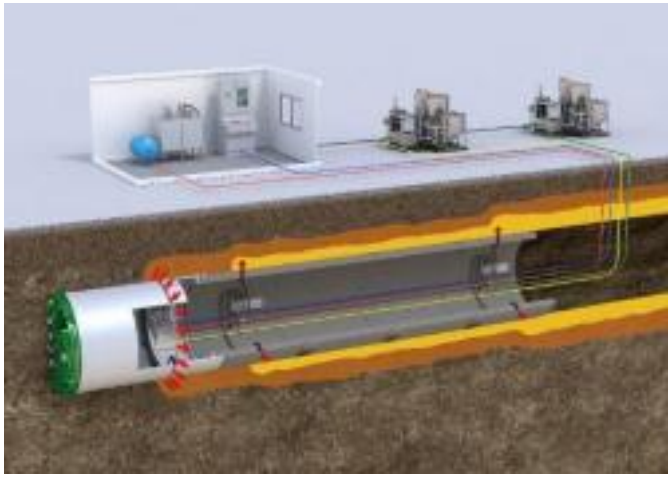


Figure 1. Overview of volume-controlled lubrication system.

In homogeneous ground, the system creates a very uniform distribution of the bentonite. This optimized continuous lubrication film can be maintained, independent from drive length, operator experience or advance rates. In changing ground conditions, the stationary sections along the tunnel are supplied with the predetermined bentonite volume by the advancing bentonite stations. An example of this is shown in Figure 2 where variable but predetermined volumes are provided throughout the tunnel drive. After selection of the prevailing ground condition in a section, the system automatically calculates the required bentonite volume, e. g. gravel needs more bentonite than sand or silt to get saturated.

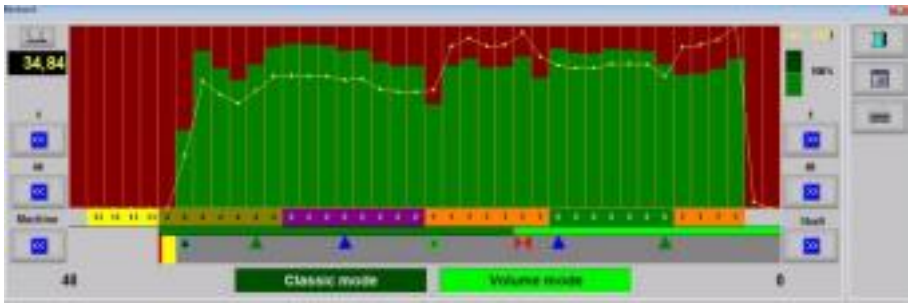


Figure 2. Exemplary visualization of the volume-controlled bentonite lubrication system with the bentonite volume injected on each tunnel meter.

The system can also be used in the conventional classic mode without volume control and parametrization. This provides maximum flexibility at all times. Monitoring, focused control and recording of relevant data (for example, lubricant volumes, pump and injection pressures, friction forces) are incorporated in the system, creating a very precise assistance system for the operator, and pushing automation and feasibility in pipe jacking further ahead.

In May 2022, two outstanding sea outfall projects with 2 kilometers (6,500 feet) length each were completed successfully. In both projects, a slurry-based MTBM, so-called AVND2000 with extension kits (for pipe ID 2,200 mm/7.2 feet and ID 2,600 mm/8.5 feet) and recovery module were deployed in different kinds of ground conditions. The volume-controlled bentonite lubrication system was used, providing efficient lubrication and reducing friction forces successfully in order to push the pipe string of 2 kilometers in both cases.

2.2 *Intermediate Jacking Stations*

Besides lubrication as described above, intermediate jacking stations are used to overcome high jacking forces in difficult ground, long-distance or large-diameter pipe jacking. They are installed in special product pipes at predetermined distances in the pipe string and serve to advance the pipe string in sections. In general, it is not foreseen to use the recoverable intermediate jacking stations continuously, but in cases when the pipe string has not been moved for a while (for example, due to maintenance reasons) it is safer to restart pushing by single sections than jacking the complete pipe string from the launch shaft. This avoids imposing extremely high jacking forces on the rear pipes. If required, the intermediate jacking stations can be used to keep sections of the tunnel moving, as shown in Figure 3, in case of downtimes of the tunneling machine.

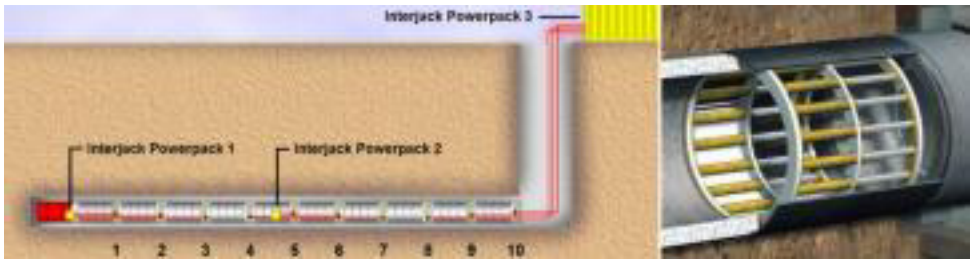


Figure 3. The use and operation of interjacking stations along the tunnel.

2.3 *Push module*

Very long pipe jacking drives, especially in challenging ground conditions, increase the risk of the pipe string getting stuck. For such demanding projects, an option is to combine pipe jacking with segment lining flexibility as a fallback option. The tunneling work can then be started in pipe jacking mode and switched over to segment lining if the tunnel stops moving. This solution requires the so-called Push Module as illustrated in Figure 4. The Push Module basically consists of an erector, push cylinders and the powerpack. In order to switch from pipe jacking to segment

lining, these components are mounted in a steel can, which is installed in the rear part of the machine right from the beginning of the project.

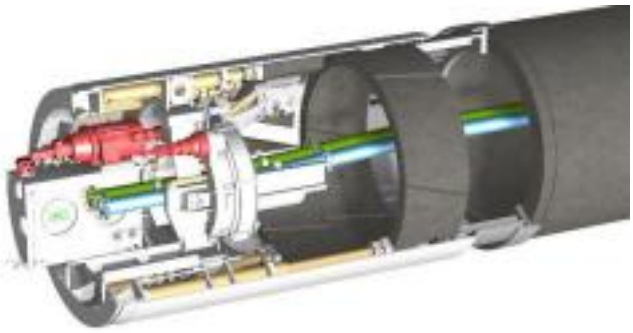


Figure 4. Example of Emergency Push Module for 2600mm (8.5 feet) inner diameter.

In the future, the use of the automated ring building system in conjunction with the Push Module will enable largely remote-controlled operation, also in segment lining mode. The vision is that man entry would only be temporarily necessary for maintenance purposes. The automated ring building system enables the segments being automatically picked up from the segment feeder and placed at the correct position within the tailskin as pre-calculated by the ring building software to follow the correct alignment of the tunnel.

2.4 *Cutting wheel design and cutting tools*

The role of the cutting wheel design with respective cutting tools is a crucial factor in pipe jacking, especially on very long drives or in hard, abrasive rock. Therefore, there is a specific focus on wear protection and prediction, monitoring techniques, and tool replacement strategies in order to facilitate the excavation process, reduce downtimes and increase productivity of the overall pipe jacking process. Very small MTBMs, like Herrenknecht´s slurry-based AVN 800 for hard rock, which are characterized by high revolution speeds, unmanned operation and no maintenance possibilities, can be equipped with special wear-resistant cutter types like Tungsten Carbide Insert (TCI) cutters to reach cutter lifetimes and drive lengths in hard and abrasive rocks which are not possible with normal disc cutters. For larger MTBM operations with the possibility of men entry for maintenance, various disc concepts, for example, monoblock versus exchangeable ring, can be considered. Hard facing solutions for wear protection and for example, the use of a camera system in the excavation chamber to control wear of the cutting tools are quite common as illustrated in Figure 5. In return, it has to be stated that wear prediction for small-diameter MTBMs is a largely undeveloped field with very little academic research and scarce information which has preciously been kept within the companies involved. Understanding the role of cutting tools and their maintenance on long-distance drives is essential for achieving safe, cost-effective, and efficient pipe jacking operation.



Figure 5. Hard facing measures and camera view into excavation chamber.

2.5 *Project references in long-distance pipe jacking*

In 1994, the current long-distance record of 2.5 kilometers (1.55 miles) in pipe jacking was set in the Europipe project in Germany with a 3,000 mm (10 feet) inner diameter Slurry TBM. In the last 10 years, a total of over 100 projects of more than 1,000 meters (3,300 feet) length have been completed worldwide using Herrenknecht equipment. In nearly all cases, AVN and AVND slurry MTBMs have been used, in the inner diameter range of 1,500 mm to 3,200 mm (5 feet to 10.5 feet). More than 40% of these long-distance projects were Sea Outfalls constructions for sewage outlets, water intakes for desalination plants or casing structures for pipeline landfalls. In coastal areas, a major focus is on the protection of the vulnerable environment. This is where trenchless technology comes in.

A new benchmark for the inner diameter of 2,600 mm (8.5 feet) was set in 2018 in Altamira, Mexico with a drive length of 2,246 meters (1.4 miles). The pipe jacked outfall casing tunnel (OD 3,200 mm / 10 feet) is one out of three landfalls for the Sur de Texas-Tuxpan gas pipeline, which connects the coasts of Texas and Mexico across the Gulf of Mexico. Trenchless Technology was chosen to cross under the environmentally sensitive areas such as the mangrove zone and coral barriers with less impact than with conventional techniques. For emergency purposes, a push module for conversion to segment lining was on standby but was not utilized.

In May 2019, the Ric-Man Construction, Inc. achieved not only the successful completion of a pipe jacking project in Painesville, Ohio, but also a new United States distance record. With a Herrenknecht AVN1500, a new casing tunnel for the 36 inches raw water intake pipeline was built under Lake Erie with a length of 1,203 meters (3,947 feet)– the longest pipe jacked drive in the US. Painesville will thereby be provided with water straight from Lake Erie in the future.



Figure 6. AVN1500 lowered into launch shaft for 1,203 meters record drive in Painesville, Ohio.

Using an AVN1800 shown in Figure 6, Ward & Burke have successfully completed a microtunnel drive of 1,132 meters (3,700 feet) in June 2020 to break the Canadian microtunnel distance record. This drive beat the previous microtunnel distance record of 950 meters (3,100) set 4 days earlier on the YDSS project in Newmarket (Ontario, Canada) into the same reception shaft.

3 LARGE-DIAMETER PIPE JACKING

The basis for decision to plan and execute a small diameter tunneling project whether with pipe jacking or segment lining strongly depends on the background of involved parties. For different reasons, planning authorities and construction companies may sometimes prefer one procedure over the other, even if there is no technical evidence of benefits or feasibility. From a planning point of view, the decision is not only driven by the specific project requirements, but also by the broad knowledge of the available technical alternatives. Ultimately, a majority of small diameter segment lining projects are executed by large construction companies acting as main contractors in the tunneling industry. Conversely, pipe jacking works are often carried out by smaller contractors that specialize in this area. Based on long traditions and know-how, they are tackling

increasingly challenging projects, comprising long drives and large diameters. Of course, the co-operation of technology suppliers and construction companies to design the best suited equipment for large diameter pipe jacking projects is indispensable for successful project completion and for a good reputation of the technology in the market.

Even if the pipe jacking procedure requires a significantly smaller jobsite footprint on the launch side compared to segment lining, the handling and storage of the jacking pipes represents a challenge that grows with the diameter. State-of-the-art on-site factories to produce large diameter jacking pipes of 3500mm outer diameter or more can solve this problem. A storage area for sufficient amount of product pipes is required for continuous tunneling advance. With rising pipe jacking diameter, the challenges faced are similar to the ones in long-distance drives with the main goal to keep the jacking forces down and to assure continuous advance with high performance at the same time. Interjacking stations and bentonite lubrication have been further developed to fulfill the requirements of increased friction forces in larger dimensions.

3.1 *Pipe brake*

The presence of groundwater also has an increased impact on the tunneling process as the tunnel cross-section increases. Even at comparatively low pressures of 1-2 bar, the use of a pipe brake may be necessary. The pipe brake is installed in the launch shaft together with the launch seal, fixed to the shaft wall by threaded rods as shown in Figure 7 or alternatively braced against the rear wall of the shaft. The pipe brake is used to secure the jacking pipes during retraction of the jacking cylinders and installation of a new pipe in the shaft jacking frame.



Figure 7. Pipe brake with launch seal installed in the launch shaft.

3.2 *Project references in large-diameter pipe jacking*

Recent milestones set by contractors in all parts of the world demonstrate the current trend towards larger diameters in pipe jacking. Similar to the evolution in drive length, the majority of about 70 projects executed with Herrenknecht equipment of 3,000 mm inner diameter and larger have been executed in the last 10 years. The main portion was for sewage and water and with rising share also for stormwater protection or storing installations. Special applications for cross passages and blind hole construction with retractable machine concept played a minor, but indispensable role in this diameter range.

Currently, a large-scale project is under way in Buraidah (Saudi Arabia), where several AVN Slurry machines are in operation to complete a total of 24km (9.5 miles) for the Main Line Stormwater project with a pipe OD of 4,200 mm (13.8 feet), in depths of up to 50 meters (164 feet).

In 2019, two large-diameter and at the same time long drives have been completed in Munich, Germany. The second construction phase of the Landsberger Strasse sewer network rehabilitation has been built to relieve the existing sewer system in the west of Munich, which dates to the middle of the 20th century. The new sewer route with an OD of 3,580 mm (11.7 feet) was constructed using an AVND slurry MTBM. For this purpose, the approximately 2.2 kilometers long route was excavated from a double launch shaft in two drives of 980 meters and 1,200 meters (3,200 feet and 3,940 feet) length in less than eight months' construction time.

The major challenge of the project was the inner-city location of the tunnel route, almost completely under the four lane, heavily frequented road Landsberger Strasse. The low overburden

between 4 and 6 meters (13 and 20 feet) required strict monitoring of the face support pressure. In addition, the logistical supply of the construction site posed a great challenge. Due to the confined space conditions of this inner-city location, pipe storage on the construction site was limited. In order to guarantee the transport of the jacking pipes around the clock, a pipe length of 3 meters (10 feet) was specified and a "just-in-time" pipe delivery was often organized. With a continuous performance of about 20 meters (65 feet) per day, more than 200 cubic meters of excavated soil had to be conveyed and removed at the same time. For this purpose, a special concept for logistics was developed to be able to transport the soil material promptly to a designated sampling area without interfering with the delivery of the pipes. Figure 8 shows Slurry MTBM, the inner-city surroundings of the jobsite installation and the considerable size of the pipe jacked tunnel.



Figure 8. Jobsite impressions Landsberger Strasse, Munich, Germany (© Wayss & Freytag Ingenieurbau AG).

During the excavation work, it was also necessary to drive through numerous unknown structural anchors that had remained in the ground from the existing development on Landsberger Strasse. This necessitated over 20 hyperbaric interventions to recover the metal objects.

The North American large-diameter record in pipe jacking has been set in December 2022 in Calgary. Ward & Burke Construction Ltd. has used an AVN2500 with extension kit, suitable for a 4056 mm OD (3,400 mm ID) pipe, on the Northwest Inner City (NWIC) – Upper Plateau Storm Separation Project. The reinforced concrete pipes of 3.3 m (11 feet) length each have been designed according to the local regulations and supplied by Langley Concrete Group. The 760 m (2,500 feet) long drive included two curves with radii of 500 m (right hand, distance 237 m) and 300 m (left hand, distance 50 m) respectively. Figure 9 shows the MTBM in the launch shaft and the jobsite team around a jacking pipe to get an impression of this extraordinarily large diameter of pipe jacking works.



Figure 9. Launch shaft and breakthrough ceremony on North America´s largest diameter pipe jacking jobsite (© Ward & Burke).

4 CONCLUSION

Technological advancements and valuable experience gained by international contractors creates

the desire to push the boundaries in terms of achievable drive length and tunnel diameter in pipe jacking, especially when using Slurry MTBMs. Current opportunities in technologies, feasibility and limitations, contractor expertise and achievements have to be taken into account when new installations are being planned, and routes are being designed. Of course, the specific project design and surrounding conditions such as diameter, tunnel length, alignment and ground conditions are crucial in selecting the most suitable and economic lining method for a tunneling project.

For Pipe Jacking, less personnel are required and due to remote-control from the surface, the level of safety is considered as a major benefit compared to segment lining. In challenging pipe jacking projects, the contractors´ experience in operating state-of-the art pipe jacking features such as volume-controlled bentonite lubrication, separation and navigation, plays a key role for production rates and final project success. In terms of tunnel diameter, the handling of the jacking pipes is considered as the most limiting factor for the feasible size in pipe jacking.

Due to the public environmental awareness and increased need for utility installations underground, advanced pipe jacking with slurry MTBMs plays a key role for fast installation, even in challenging ground like hard rock. This does not only comprise sewer and water networks but also pipelines or underground cable installations to connect and use new energy sources like offshore wind or hydropower.

5 REFERENCES

Lang, G. & Lehmann, G. 2022. Rock tunnelling in small diameters: latest trends and technologies. Proceedings of NASTT No-Dig Show 2022, Minneapolis, Minnesota, April 2022.

Schmäh, P., Lübbers, M. & Fluck, A. 2021. Progress in small-diameter tunnelling. Tunnel et Espace Souterrain 277: 16–36.

19th Australasian Tunnelling Conference – Acosta-Martínez, Stewart and Hudson-Smith (Eds.)
© 2025 Australian Tunnelling Society, ISBN 978-0-85825-002-4

Mechanized cross passage construction in tunnelling projects

M. Bischoff & P. Schmäh
Herrenknecht AG, Schwanau, Baden-Württemberg, Germany

ABSTRACT: As demand increases for safer road and rail tunnels, more cross passages are needed to connect parallel tunnel tubes or link tunnels to vertical shafts. These cross passages serve important safety functions, such as emergency escape routes and access for rescue teams. Traditionally, cross passages have been constructed using manual or semi-mechanized techniques, but in difficult ground conditions or under high groundwater pressure, these methods can be risky, slow, and expensive. Mechanized construction methods, especially pipe jacking with tunnel boring machines (TBMs), offer a more efficient and safer alternative. A key advantage of mechanized cross passage construction is that excavation and lining are done in one continuous process. The most commonly used machines are slurry-type microtunnel boring machines (MTBMs), such as AVN systems, which use a slurry circuit for the removal of the excavated soil. These machines are well-suited for water-bearing ground and can crush obstacles like rocks and boulders during excavation. Compact launch and reception designs allow TBMs to be used even in tight tunnel environments.

1 MECHANIZED CROSS PASSAGE CONSTRUCTION

With rising demand and higher safety standards, more cross passages will be required in road and rail tunnels in the future. Several approaches for rescue purpose are available. For a twin tunnel arrangement, a typical application in discussion is the provision of cross passages to link parallel tunnels, whether in new construction or in existing tunnels already in operation. Apart from the connection between two tunnels, the connection of a shaft and a tunnel is another concept for emergency exit, often used for train and metro double line tunnels or traffic tunnels. Cross passages can also play a role where sewage collectors have to be connected to extend existing schemes or to connect new interceptors to the existing system.

The general approach to connect two underground structures by a cross passage is not new. The technical approach is very similar to standard pipe jacking, where two shafts serve as launch and reception structures for the tunnelling equipment. Figure 1 gives an overview about different cross passage scenarios in tunnelling projects using the pipe jacking approach.

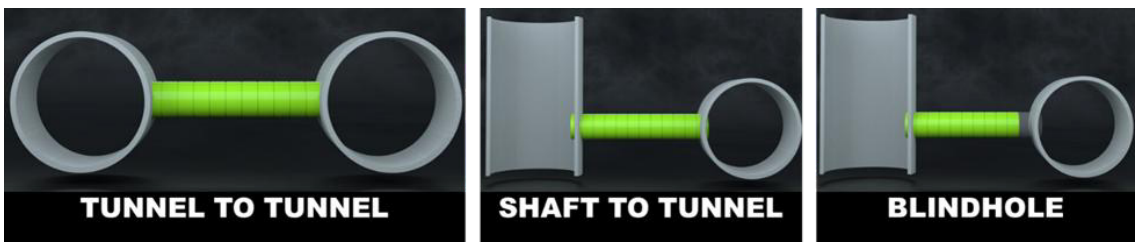


Figure 1. Different cross passage concepts

The major benefit of a completely mechanized approach for cross passage construction is the integrated concept for excavation and final lining at the same time. In the past, mechanized methods have sometimes been used for the excavation of cross passages, however the lining has been done with conventional methods.

2 TUNNELLING MACHINE CONCEPTS

In general, pipe jacking in combination with a Slurry Tunnel Boring Machine (TBM) is the most versatile solution for mechanized cross passage construction, as it is suitable for a large variety of ground conditions and can best handle high groundwater pressures. The so-called AVN machines are closed, full-face microtunnel boring machines (MTBMs) with a hydraulic slurry circuit for face support and soil disposal, which requires a separation plant on the surface. A cone-shaped crusher inside the excavation chamber can crush cobbles, boulders and other obstructions to a conveyable grain size while tunnelling and advancing. For working under water pressure, a launch seal and a pipe brake are important and need to be considered according to the available working space in the launch tunnel. A very compact equipment design for the launch and reception setup in tunnels is required. For main tunnels, which are simultaneously under construction, a minimum inner diameter of 10 m is needed to integrate the pipe jacking setup and logistics for cross passage construction additionally, as it can be seen in Figure 2.

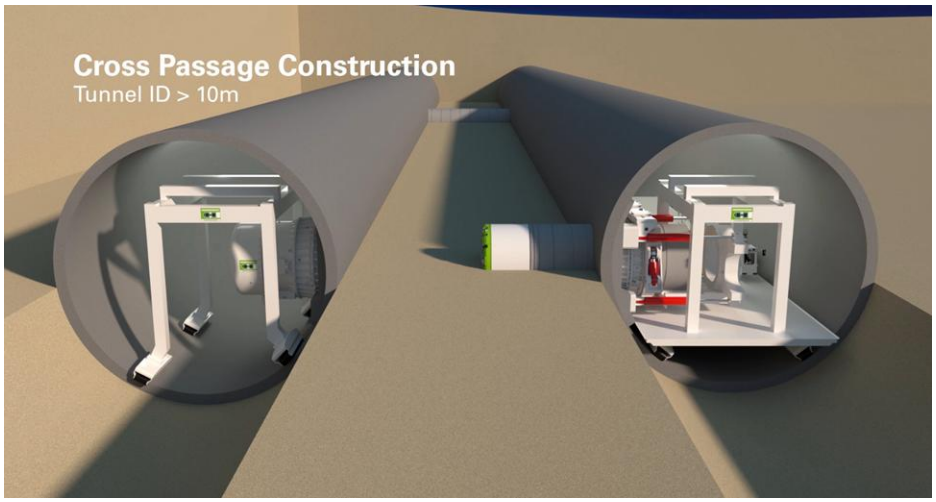


Figure 2. Exemplary equipment setup for AVN3000 MTBM cross passage construction

Nevertheless, other TBM concepts can be considered, according to the investigated ground conditions, project-specific requirements and economic considerations, as shown in Figure 3. As an example, the partial-face machine type allows the implementation of circular and non-circular cross sections. For the excavation of specific rectangular cross passages for pedestrian crossings, an adaptation of an open-face machine was designed, the so-called MH Box.

	Excavation (Excavation tools)	Face Support	Soil conveyance	
Slurry Shields AVN | AVND | Mixshields	**Full-face** (Cutting wheel design according to soil conditions)	**Cutting wheel / Slurry support** (optional air pressure)	**Slurry circuit**	
Earth Pressure Balance Shields (EPB)	**Full-face** (Cutting wheel design according to soil conditions)	**Cutting wheel / Earth pressure**	**Screw conveyor** Muck skip / tunnel belt conveyor	
Partial-face machines (MH/MHSM)	**Partial-face** (Excavator/Roadheader)	**Mechanical**	**Belt conveyor** Muck skip / tunnel belt conveyor	
Shielded Rock TBMs	**Full-face** (Hard rock cutting wheel)	**Cutting wheel / Mechanical**	**Belt conveyor** Muck skip / tunnel belt conveyor	

Figure 3. Overview of TBM types with their characteristics

3 CROSS PASSAGE DESIGN CRITERIA FOR TBM SELECTION

In order to select the most efficient TBM (Tunnel Boring Machine) concept for a mechanized approach, several key criteria must be analyzed, see overview in Table 1. A circular tunnel geometry is typically preferred for its ease of sealing and space optimization, particularly in water-bearing ground. The cross-passage equipment must be carefully positioned to avoid reducing the working space in the main tunnel. The construction process should minimize disruption to main tunnel operations, with blind or dead-end solutions with retractable TBM as the extreme case to ensure continuity. Geological and hydrogeological conditions dictate the technology and TBM concept respectively. Structural adaptations, such as reinforcement modifications and seals, are necessary to accommodate cross passage construction. Space constraints require cross passages to be as large as necessary but as small as possible, typically 2.5-4 meters in diameter. Early clarification of project-specific conditions is critical to defining the technical approach and planning for a mechanized solution.

Table 1. Cross passage design criteria for TBM selection

Geometry	• Shape (circular – rectangular) • Dimensions, cross section • Length • Position to tunnel axis	
Construction Process	Cross passage construction • During tunnel excavation • During tunnel operation • As blind hole (machine retraction)	
Geology Hydrology	• Ground stability • Ground water level	

4 REFERENCE PROJECT: TUEN MUN – CHEK LAP KOK LINK, HONG KONG

The major Tuen Mun – Chek Lap Kok Link project in Hong Kong links the airport with the Tuen Mun city district via a gigantic twin-tube road tunnel under the sea. The high safety requirements for vehicle traffic demand cross passages at regular intervals as escape and rescue tunnels between the tunnel tubes. Figure 4 shows the layout of the overall project. Building such cross passages under water pressure is very complex and expensive to realize, for example, using freezing technologies. This is why tried-and-tested AVN technology (AVN3000, OD 3605mm) was further developed for mechanized cross passage construction during the ongoing works on the main tunnels. The world´s largest TBM, a Herrenknecht Mixshield (Ø 17.6m) and two Mixshields (Ø 13.95m) have constructed the gigantic twin-tube road tunnel. With a length of around 5 kilometers each, the Tuen Mun – Chek Lap Kok Link connects the international airport and the Hong Kong-Zhuhai-Macau with the mainland to the north, crossing under a branch of the Pearl River Delta at depths of up to 50 meters. From the northern launch shaft the world record Mixshield giant first drove a 650meter long section with the larger diameter. The TBM was then scaled down to a diameter of 14 meters for the rest of the tunnelling distance towards the airport.



Figure 4. Twin-tube road tunnels and cross passage location along the tunnel route

Due to the necessity to construct 46 cross passages under extremely difficult conditions with a very tight schedule, Herrenknecht and Dragages-Bouygues Joint Venture, jointly developed a concept for the two AVN3000 specially designed cross passage TBMs. In addition, special launch and reception structures were designed. These allow for pipe jacking directly from one of the large tunnel tubes while all logistic processes for the large diameter TBMs can continue simultaneously. For the completion of the cross passages of up to 13 meters length each, two complete sets of equipment have been used to meet the tight time schedule. As logistics in both large diameter tunnels had to be considered to assure excavation of the tunnels could continue simultaneously with cross passage construction the available space for the cross-passage equipment is very restricted. Therefore, a very compact design of machine and launch structure was required. The setup of the MTBM breakthrough and recovery on target side is shown in Figure 5.



Figure 5. AVN 3000 recovery in the tunnel, after breakthrough into reception bell

On the launch side, a jacking trailer with a mobile gantry crane was used to allow quick repositioning of the equipment for the construction of the next cross passage. Due to the surrounding groundwater pressure of 5.5 bar a safe launch and breakthrough procedure was designed. While a special launch seal with emergency seal is installed on the launch side, safe breakthrough into the "target tunnel" was assured by using a reception capsule construction, which can be seen in Figure 6.

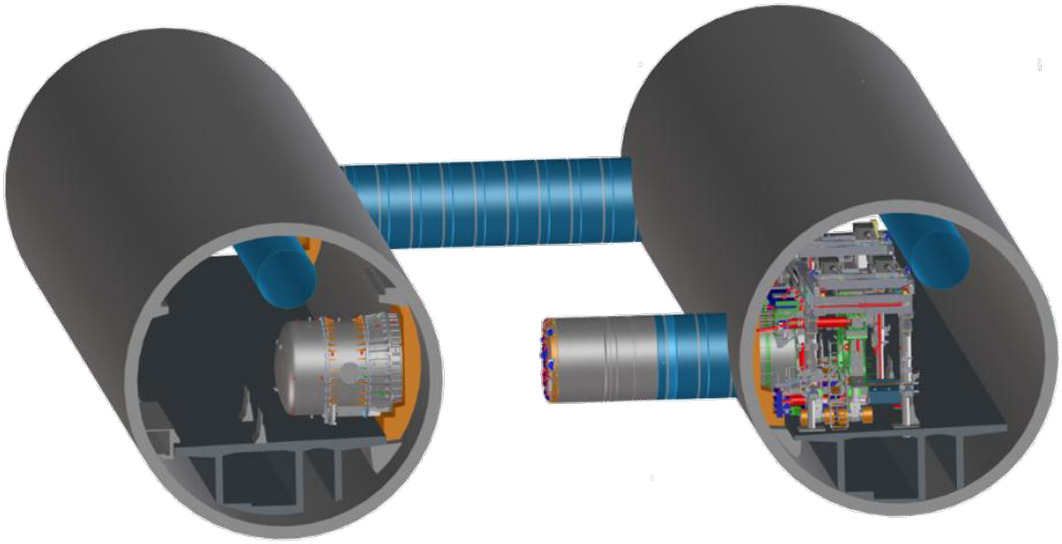


Figure 6. Cross passage installation between the two main tunnels under construction

The average performance for the construction of one cross passages on TMCLK project was 20 days, encompassing the entire advance cycle, including assembly, advancement, disassembly, and transport of the equipment within the tunnel. On a further similar cross passage project, this performance has even been significantly improved.

5 CONCLUSION

The current and worldwide trend in inner-city environment is to construct more and more infrastructure underground, which causes a growing demand for the construction of ever deeper tunnels. In challenging ground with high groundwater levels and increasing depths, conventional methods for cross passage construction reach their technical and economical limits.

The mechanized approach for cross passages is a proven technology, successfully implemented in several projects, including challenging conditions like Hong Kong's tight tunnel spaces and high groundwater pressures of up to 5.5 bar. While conventional methods like ground freezing are more complex and costly in such settings, mechanized techniques offer significant advantages in terms of safety, efficiency, and adaptability to various geological conditions. With existing expertise and practical experience, the mechanized approach ensures reduced risks, faster execution, and better cost control for future projects.

THIS PAGE INTENTIONALLY LEFT BLANK

19th Australasian Tunnelling Conference – Acosta-Martínez, Stewart and Hudson-Smith (Eds.)
© 2025 Australian Tunnelling Society, ISBN 978-0-85825-002-4

Gold Coast light rail: An example of capitalising on underground space to deliver above ground infrastructure

A. Edney & D. Keating
Systra ANZ, Brisbane, QLD, Australia

A. Browne
John Holland, Gold Coast, QLD, Australia

ABSTRACT: Gold Coast Light Rail Stage 3 (Stage 3) project involves the construction of a new light rail route that runs from Broadbeach South Station, along the Gold Coast Highway, to Burleigh Heads. The 7km extension includes new dual-track light rail, eight new light rail stations, new light rail-bus connections, and new and upgraded intersections. The project alignment is located through a high-density urban area of the Gold Coast, and is surrounded by commercial and residential properties, with the Gold Coast Highway (GC Hwy) providing a major north-south transport corridor for the city.

Extensive stakeholder constraints on the project were a key driver of the construction methodology. Trenchless technologies have been adopted for a number of service relocations and new service installations across the project to minimise impacts (and reduce risks) on stakeholders, including road users, businesses, residents, and asset owners (for numerous utilities above and below ground).

1 INTRODUCTION

John Holland Pty Ltd has been awarded the Design & Construct Contract for the Gold Coast Light Rail Stage 3A (Stage 3). This major infrastructure project involves a 7km southern extension of the Gold Coast Light Rail system from Broadbeach South station to Burleigh Heads (Figure 1). The alignment is in a high-density urban area of the Gold Coast, surrounded by commercial and residential properties, with the Gold Coast Highway providing a major north-south transport corridor for the city.



Figure 1. Artist impression of Burleigh Heads bus terminal and light rail station

Key features of the project include:
— 7km of new dual-track in the centre of the GC Hwy
— Eight new light rail stations and five additional light rail vehicles (LRV's)
— Upgrade and expansion of the existing depot and stabling facilities
— New light rail-bus connections at Burleigh Heads and Miami
— Intersection upgrades including Intelligent Transport Systems
— New signalised pedestrian crossings and upgraded pedestrian and cycle facilities

As part of the project, significant Public Utility Plant (PUP) relocations are required to accommodate the new infrastructure. A key component was the relocation of all the overhead electrical mains that crossed the GC Hwy due to their interaction with the new overhead electrical wires that supply power to the tramway.

In total there were 38 HDD crossings completed, with diameters ranging from 100mm to 700mm. Approximately 11km of electrical conduits, and 260m of gas enveloper were installed.

2 KEY CONSTRAINTS/CONSIDERATIONS

2.1 *Geology – geotechnical assessments undertaken*

Most of the excavation on the Stage 3 project was within a loose sand environment, with some pockets of weathered rock and denser clays. Due to the loose sand geology, special consideration needs to be given to hole stability during the HDD process. If the hole cannot be supported by drilling fluids during boring, the risk of settlement within the roadway increases. This was a major design factor of the bore profile when drilling in sand.

2.2 *High density urban environment*

The Stage 3 alignment runs along one of the busiest arterial roads on the Gold Coast. Located along the alignment there are businesses, schools, low rise and medium rise residential, tourist accommodation and commercial dwellings. This presented many challenges.

2.3 *Interaction with ageing infrastructure*

One of the advantages of HDD as opposed to open trench construction, is the available depth that can be achieved. This is critical in addressing the interaction of new construction with existing infrastructure. There are two main challenges encountered during the construction of Stage 3:
— Asbestos pipes
— Existing buildings/hard structures (60+ year old properties)

2.4 *Asbestos pipes interaction with ageing infrastructure*

The key risk with asbestos concrete pipes was the stability and susceptibility to cracking once the ground surrounding it is excavated.

2.5 *Existing structures*

Working alongside existing infrastructure poses challenges in any environment. This is compounded when the infrastructure is greater than 60 years old. Certain structures were built to different building codes with limited as built records. In many cases doing investigation works had the potential to damage their structural integrity.

3 OPTIONEERING/CONSTRUCTABILITY

Three main options explored for electrical relocations were:
— Open trench conduit installation

— Microtunneling
— HDD

Table 1 provides a summary, exploring the advantages and disadvantages of each option.

Table 1. Comparison of different excavation options

	Open trench	Microtunneling	HDD
Description	Conventional services installation methodology using excavators and shoring to support open trenches for placement of new service conduits	Using a suitable Microtunnel Boring Machine (MTBM) to undertake the excavation.	Using a suitable HDD rig to excavate and install conduits within drilled excavation
Advantages	- Availability of suitable contractors on Stage 3 - No settlement risk under GC Hwy - Easily scalable – can increase the number of work fronts to reduce overall programme for works if required - No enveloper requirements	- Very low settlement risk – bore is continuously supported. Ideal for GC Hwy crossings - Laser guided installation accuracy - Minimal site footprint – small entry and exit pit	- Accurate installation - Some flexibility in alignment for ensuring clearances to existing infrastructure. Ideal for below ground services found on Stage 3 - No enveloper requirements - Cost effective compared to other methods explored on Stage 3
Disadvantages	- Costly traffic management requirements for GC Hwy closures - Invasive, more disruption to stakeholders - More time consuming to complete each crossing - Increased interface with existing services - potential for service strikes. Large number of below ground services located on Stage 3 alignment	- Costly site/equipment establishment - Site footprint required for shafts at entry and exit locations - Limited scope to adjust alignment along the length of the installation - Longer mobilisation and demobilisation time compared to HDD - Jacking pipe materials more expensive compared to other methods	- Specialised equipment/contractors - Large adjacent site laydown areas required during conduit string out works - Potential settlement risks - Inclement weather runoff into entry and exit pit locations

4 OUTCOMES AND APPLICATION OF HDD ON STAGE 3

HDD was chosen for 85% of the GC Hwy electrical relocations. Open trench installation was adopted for the remaining 15% of the crossings. The driving factor in adopting HDD over other methodologies was its program and constructability benefits. For its program benefits, HDD is a much quicker alternative to other methodologies. Its constructability benefits were being able to accurately intersect tight underground working envelopes between other below ground infrastructure. Below is a summary of the numbers relating to the HDD crossings.

— 32 Energex crossings: >11Km of electrical conduit under the GC Hwy
— 6 APA crossings: 260m of gas enveloper under GC Hwy
— 18 land access agreements into private property to facilitate the HDD works

4.1 *Typical construction methodology*

A typical HDD construction methodology was adopted for use on the project. This involved a 650mm diameter tunnel bore which allowed 9 x 140mm electrical conduits to be installed. To

facilitate this an entry and exit pit were excavated. This enabled the drill rods to start boring at a location that was sub surface. This was key in managing drilling fluid levels in crossings where there were significant head level differences.

4.2 *Typical construction methodology*

During the design phase of each HDD, adjustments to the bore geometry were undertaken. This ensured the extent of the bore profile beneath the GC Hwy was always supported with drilling fluid. This included when the exit pit was required to be drained for tooling changes.

During tooling changes, the section of the bore within the existing project worksite was supported only by the drilling fluid filter cake. There was a greater risk of potential observed settlement through this zone. Where clay ground conditions are present the ground provides more short-term self-supporting properties, compared to the sandier conditions. As such, settlements are expected to be lower. It is recommended that construction traffic movements over the bore alignment are limited during these short tooling changes, when the bore beneath the service road/construction site will not be fully supported.

4.3 *Settlement monitoring*

At each location extensive monitoring was undertaken. Monitoring points were strategically placed at critical locations. These were predominantly within the GC Hwy road reserve and located where the HDD profile crosses critical infrastructure (i.e. water or sewer mains). These monitoring points were observed and monitoring reports produced from the data. Trigger levels were designed for each location. Various asset owners and stakeholders were involved in this process.

4.4 *HDD works within a dense urban environment*

A typical setup required a 10m x 2m footprint for the drill rig, along with 2m x 2m footprints for entry/exit pits. These working areas did not always fit within the available public road reserve that are typically used for construction. In certain instances, setups were required in private properties such as within front yards or schools. In some cases, emergency exits for buildings were blocked. This required adjustments to emergency plans and routes within their property.

4.5 *Mitigation of working in close proximity to structures*

4.5.1 *Working under/close to pipework*

Some of the bores went over or under existing pipework. In some cases, this required replacing the existing pipework if it was constructed out of asbestos or if the existing pipework was built out of a more durable material, supporting it during HDD construction. A complex cross section of the service crossing of the HDD alignment is shown in figure 2 & 3.

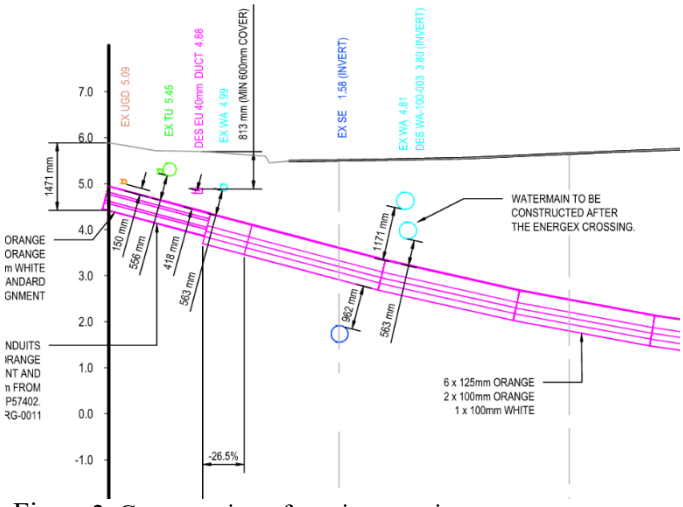
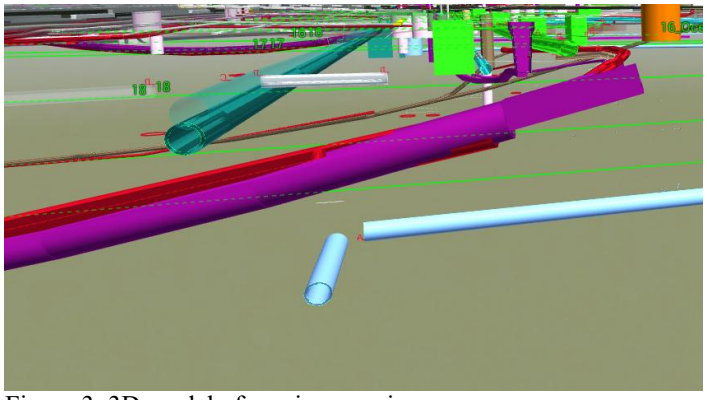


Figure 2. Cross section of service crossings


Figure 3. 3D model of service crossings

4.5.2 Working in close proximity to existing above ground infrastructure

Various construction locations required the removal or the support of existing infrastructure. These structures typically involved boundary walls, garden areas and fences. In certain cases, works involved complex temporary works, external stakeholder approvals and reinstatement works.

5 CONCLUSION

HDD was not feasible in all locations with respect to the underground electrical relocation scopes. The main reason was certain sites did not have the required space to mobilise and setup the HDD rig and associated plant. During the design and constructability process, HDD was the favoured starting point due to the benefits and advantages detailed above.

One of the key considerations going forward and applying it to future urban projects would be to explore the option of doing the HDD works as part of the project early works. This approach would minimise the interaction with adjacent project works. Another key element in the successful delivery of HDD on Stage 3 project was the use of specialised contractors and designers. They brought extensive HDD experience which was beneficial in terms of developing constructable solutions within the constraints of the project.

THIS PAGE INTENTIONALLY LEFT BLANK

Theme 11. Planning, Procurement and Risk Management

THIS PAGE INTENTIONALLY LEFT BLANK

19th Australasian Tunnelling Conference – Acosta-Martínez, Stewart and Hudson-Smith (Eds.)
© 2025 Australian Tunnelling Society, ISBN 978-0-85825-002-4

Important considerations when assessing options to manage ground risk on tunnelling and underground works

S.V.L. Barrett
PureService Pty Ltd, Melbourne, Victoria, Australia

ABSTRACT: How best to manage ground risk is one of the most important considerations when developing the procurement strategy for tunnelling and underground works. When addressing this question, how physical condition risks will be shared, evaluated and remedied under the terms of the contract needs to be carefully thought through. To assist in the decision-making process, a comprehensive assessment of potential ground risks should be completed prior to developing the procurement documentation. Careful consideration also needs to be given to how much flexibility will be given to tenderers to modify the concept design and proposed construction methodology during the tender and detailed design phases, along with how the risk sharing mechanisms will be practically administered during construction. If these items are not given sufficient consideration, the effectiveness of the adopted risk sharing mechanisms can be significantly diminished.

1 INTRODUCTION

If not managed well, the delivery of tunnelling and underground works can be confrontational, litigious and dispute driven, as opposed to collaborative and outcome driven, despite everyone's best intentions at the start. While there are many non-ground related issues that can be responsible for this, encountering unexpected ground conditions can be one of the more significant reasons. It is also important to understand and accept that uncertainty will always exist, as we can never fully eliminate it when attempting to predict the conditions which will be encountered underground. However, it is also equally important to always be asking the question what else can we readily and practically do to reduce this uncertainty when planning and executing tunnelling and underground works?

Fortunately, there are many ways to mitigate and reduce ground risks on projects, provided adequate project planning has been done beforehand. These measures include:

- Undertaking a comprehensive site investigation using a phased approach.
- Development of a well-considered, constructable concept design prior to developing the procurement strategy.
- Adopting an observational approach to excavation and support design.
- Rigorous risk management using the guidelines published by the International Tunnelling and Underground Space Association and International Association of Engineering Insurers (ITA and IMIA, 2023).
- Use of appropriate contract packaging, contractual models and risk sharing between the parties.

The remainder of this paper expands on these points, as often not enough attention is given to each, including how the assessed ground risks will be effectively managed under the contract.

2 PROJECT PLANNING

An early focus on developing the conceptual ground model and identification of the potential ground risks for a project are critical for its ultimate success, as the early planning stage is when many risks can be reduced or mitigated without significant cost. To be able to do this effectively requires an early investment in gathering quality site investigation information, as the concept design and options of how it might be constructed start to develop. It also requires early contractor involvement, so the concept design and proposed methods of construction form a robust basis on which the procurement strategy can be built, the necessary environmental approvals sought and the initial cost estimates and schedules for delivery developed.

It is also at this stage that an understanding of the required design development, environmental planning and procurement timelines for the project starts to form. These timelines need to be compared to the development time available, and if the available time is less than what is required to adequately mitigate project risk, what alternative strategies can be put in place to reduce the potential for significant cost and schedule overruns later, due to insufficient time being allowed for project planning.

2.1 *Site Investigation Planning and Execution*

Having a comprehensive understanding of the expected conditions and how they are likely to impact the design and methods of construction, are essential to effectively assess the potential ground risks and develop appropriate mitigation strategies. At the early stages of design, focusing on these items is more important for the Geotechnical Engineer, than undertaking detailed numerical analysis and calculations, given the immature state of the design's development.

As with all projects, it is important to approach the site investigations in a phased way, so the investigation scope can be optimized as the ground model develops and the ground risks become more apparent. All of this can take a significant amount of time, so the planning of the site investigation campaign should be started early and continuously progressed through the project planning phase, with the aim of having a comprehensive database of quality geotechnical, groundwater and environmental information available by the time of tender. Many projects are still planned and taken to market with inadequate site investigation, and it is not surprising that they subsequently run into difficulties, when unexpected conditions are encountered during delivery.

While the costs associated with these early site investigation phases may seem expensive relative to other early cost items, they are typically less than 0.5% of the project's final capital cost. As such, they typically pay for themselves many times over during project procurement and delivery, with the savings achieved in the form of reduced ground risk premiums needing to be added to bids to account for ground related uncertainties, as well as the potential for reduced ground-related claims and disputes.

2.2 *Design Considerations*

The level of maturity of the concept or reference design at the time of tender is another important consideration when developing the project's procurement strategy. Ideally the design should be well developed and be able to demonstrate how the Owner's project requirements can be fully achieved based on the design and construction assumptions made.

Sometimes however it is not possible to achieve this for a range of reasons. In such circumstances it is important to understand the limitations and deficiencies of the design, flag these limitations and deficiencies with tenderers as areas requiring improvement and think through how potential changes to these items might impact the assumptions on which the procurement strategy has been based.

From a ground risk management perspective, changes by the tenderers to the proposed alignment and proposed method of construction need to be carefully considered, particularly if no site investigation information is available for the proposed new alignment or insufficient or the wrong type of information is available, to allow the ground risks associated with adopting the new construction methodology to be properly assessed.

2.3 *Adopting an Observational Approach*

Given the inherent uncertainties associated with tunnelling and underground work, it is prudent to adopt an observational approach to excavation and support design, whereby a toolbox of design options is prepared to account for the range of expected conditions, with the implemented design being based on the actual conditions encountered. To be effective, the following prerequisites need to be in place:

- Sufficient geotechnical investigation and characterization of the ground have been completed to allow the majority of ground types and geohazards which may be encountered to be anticipated.
- The potential ground behaviours and failure modes associated with the proposed design and construction methodology can be predicted based on past experience in similar conditions.
- The most likely conditions, as well as the potential outliers, can be assessed with reasonable certainty for the purposes of design.
- It will be possible to adequately observe the ground conditions encountered, so an appropriate excavation and support class can be determined prior to taking the next advance, and
- It will be possible to verify the design's performance, and modify the design if necessary, through an instrumentation and monitoring program tailored to the design with alert levels and action plans specified for each of the instruments.

It also requires that these observations are practical to make, are reliable, are relevant for the assessment at hand and can be promptly reported and interpreted prior to the start of the next excavation and support cycle. It also requires that suitable contingency plans are in place if unexpected conditions are encountered and that these measures are sufficient to not allow a rapid and progressive failure to develop, before an alternate excavation and support design can be developed and implemented.

2.4 *Rigorous Risk Management*

The Code of Practice for Risk Management in Tunnel Works is a comprehensive guide jointly developed by the tunnelling and insurance industries (ITA and IMIA, 2023). It aims to reduce the frequency and severity of incidents in tunnel construction projects by promoting best practices in risk management and providing a framework for managing risks on underground works across the planning, procurement, detailed design and construction stages.

From a ground risk management perspective, the code of practice states that a project should have the following principal attributes to deliver on the code’s objectives:

- Sufficient site and ground investigation has been completed prior to project award to identify and quantity ground risks to inform design and construction risk assessments.
- The ground risk assessments and ground reference conditions against which changes will be assessed are included in the contract documents.
- Ground conditions are assessed in the temporary and permanent condition during construction, with the limitations of support designs clearly defined in the design documentation, along with the instrumentation and monitoring required to verify and validate the design’s performance.

These attributes are all closely aligned with the project planning considerations discussed earlier and a review of the guide prior to starting the procurement process for project delivery is a useful way to make sure all of these items have been suitably covered off in the tender documentation.

3 CONTRACT TYPE SELECTION

For design and construct type contracts which are common in Australia, the following contract approaches are typically taken to manage ground risk:

- All ground related risks are placed on the Contractor and none are shared with the Owner.
- The contract contains a latent conditions clause which allows a claim to be made if unexpected conditions are encountered.
- Ground risk is shared within the contract using geotechnical baselines similar to that adopted in the FIDIC Emerald Book.
- A collaborative contracting approach is taken by adopting a target price or alliance contract model and the associated open book pricing and cost sharing arrangements.

Despite its ineffectiveness at preventing ground related disputes, the first approach is commonly adopted by Owners, as it is considered that it will effectively reduce their claim exposure. This rarely proves to be the case, particularly if the unexpected conditions are significantly different from those expected, simply because of the quantum of additional costs which are difficult for one party to bear.

A summary of the alternative risk sharing approaches listed above, where a decision is made by the Owner to share some or all of the ground risk, is provided in the following sections. If there is not local experience with the more sophisticated contractual models, it may also be beneficial to consider a staged introduction, with less complex packages bid first to build up experience, before the more complex packages are procured.

3.1 *Latent Condition Clauses*

Several Australian Standard Conditions of Contract such as AS 4000 – 2025 (Construct Only) and AS 4902 – 2000 (Design and Construct) include latent conditions clauses, which are designed to allocate the risk of unforeseen physical site conditions that could not reasonably have been identified before the contract was entered into, including subsurface conditions.

These clauses typically define latent conditions as physical conditions on the site that:

- Could not have been reasonably foreseen by a competent Contractor;
- Differ materially from those that should have been anticipated based on the information provided and any site inspections completed at the time of tender.

When included, they allow the Contractor to claim time extensions and cost adjustments if latent conditions are encountered. The wording of the latent condition clauses in these standard forms of contracts however can be somewhat subjective, leading to projects still ending up in ground related disputes, given there is often some ambiguity that the unexpected conditions were truly latent and not foreseeable at the time of tender.

3.2 *Baseline approaches*

To overcome the types of difficulties described above, FIDIC in cooperation with the ITA, developed a set of Conditions of Contract specifically for Tunnelling and Underground Works (FIDIC and ITA, 2019) and elements of it have now started to be adopted on major infrastructure projects in Australia. The fundamental risk sharing principles assumed in the contract are:

- Unexpected ground conditions risk should lie with the Owner.
- Performance risk should lie with the Contractor as the party who can best handle expected conditions.

These concepts are then integrated into the contract using a Geotechnical Baseline Report (GBR) and a Baseline Schedule. The GBR sets out the contractually agreed anticipated ground types, ground behaviours, excavation methods, support types and their spatial distribution upon which the contract price is based. The baseline schedule then documents the anticipated work items, activities and production rates upon which the contractual time to completion is based. These items are all subsequently monitored and remeasured during construction to establish the final contract cost using the agreed contractual mechanisms. The contract model is therefore closely aligned with the observational approach and is ideal for the delivery of excavation and

ground support packages of work. With this form of contract, difficulties however can arise if the scope of work, design or method of construction on which the contract was based changes materially during delivery.

3.3 *Collaborative Contract Arrangements*

For projects where the Owner wishes to take a more collaborative approach to project delivery, target price contracts and alliance agreements are becoming more frequently adopted in Australia. They also provide the advantage of being more interactive during the tender period and therefore allow the Owner to gain a better understanding of how the parties are likely to work together during delivery.

3.3.1 *Target Price Contracts*

Where a project is complex and will require significant collaboration between the Owner and the Contractor to successfully deliver it, a target price contract can provide a good risk sharing model to help manage the identified risks, including ground risk. It blends elements of both fixed-price and cost-reimbursable contracts, aiming to align the interests of both parties and encourage cost efficiency. A target cost is negotiated during the tender period which includes direct costs (labour, materials) and indirect costs (overheads, profit), along with a pain/gain mechanism to share the savings or cost overruns should the actual cost be less or more than the target. The contract also specifies which party bears the risk for different types of ground conditions, with often known risks priced into the target, while unknown or latent risks are shared or retained with the client. A portion of the budget is also typically set aside to cover unexpected ground conditions, either within the target price or through a separate contingency fund.

3.3.2 *Alliance Agreements*

A project alliance is where the Owner and Non-Owner Participants (Designers, Contractors, Suppliers) work as an integrated team to deliver a project under a contractual framework where the commercial interests of all parties are aligned with the desired project outcomes. Under this model risks and opportunities are jointly shared and managed, with behavioural expectations between the parties managed through an Alliance Charter. It differs from traditional forms of contract where each party has and must fulfill its own separate obligations and risks are allocated to each party. Compensation is based on a target cost arrangement using project reimbursable costs, Non-Owner Participant fees and normal profit and a risk / reward amount using a pain / gain formula, with adjustment events used to manage variations. It is particularly useful on projects when significant value can be added by the Owner during final design and delivery and where there are:

- Complex interfaces and / or unpredictable risks
- Complex stakeholder issues and / or external threats to the project
- Very tight timeframes
- Difficult to define scope and/or likely scope change.

Because of the joint sharing and managing of risks, ground risks are not allocated to one party, but the alliance instead collectively owns them. Costs arising from ground conditions are therefore absorbed by the alliance and factored into the overall project performance. If ground conditions change, the alliance can adjust scope, budget, or schedule without formal claims or disputes, with decisions made based on a best-for-project basis.

4 DEVELOPMENT OF PROCUREMENT STRATEGY

Where a shared approach to ground risk management is adopted, a phased approach to procurement and contractor selection should also be developed, with sufficient time given to tenderers in each phase to fully develop their bids. The phased approach should be structured at high level along the following lines:

- ***Prequalification Stage:*** Establish a shortlist of qualified bidders using a pre-qualification

process. As part of the pre-qualification process, commentary should be invited on the concept or reference design, the proposed construction methodology and the Owner's assessment and proposed allocation of risk. The opportunity should also be given to provide feedback on areas for improvement and where some targeted value engineering could provide a better solution. This feedback should be used to finalise the procurement strategy and tender documents prior to progressing to the tender stage.

- ***Tender Stage:*** Based on the project complexity, the prequalified tenderers should be given sufficient time to develop a well-considered tender design, on which their commercial proposal will be based. This should include a series of interactive workshops, with some of the allocated time focused on discussing the identified ground risks and how they are proposed to be shared, so both parties have a better appreciation of each other's position. The aim of these discussions should be to make sure the material risks have been identified and fully understood, so the Owner is better informed going into the evaluation stage.
- ***Tender Evaluation and Award Stage:*** Based on the results of the tender evaluation and negotiations, the contract documentation will need to be finalised and the contract price and the Owner's contingency allowances set. If tender interactives and submission requirements have been well planned, this is the time where certain risk items can be bought back by the Contractor if they are better able to manage them or the risks further assumed by the Owner if the uncertainty is resulting in very high contingencies in the Contractor's pricing. Where a baseline approach has been taken, the baselines in the GBR can be adjusted based on the agreed outcomes of these negotiations. Depending on the complexity of the project and flexibility which has been given to change the design and construction methodology, this final stage can take some time, particularly if the preferred tender solution differs from the reference design. It is important therefore that these updates are not rushed and sufficient reviews are completed to make sure all the contract documents reflect the agreed changes and link properly prior to contract award.

5 GBR DEVELOPMENT AND ADMINISTRATION

When a baseline approach to ground risk sharing is adopted, the reference ground conditions for the shared risk model are incorporated into the contract using a GBR. The most widely recognised reference for the use of GBRs in tunnelling and underground works is the ASCE Suggested Guidelines (Essex, 2022). This originates from, and is targeted at, the North American (i.e. USA and Canadian) construction industries, but the majority of the content provides a useful set of principles and guidance for adoption in many common law jurisdictions. CIRIA Report C807 (Davis et al, 2023) is also a useful reference and documents best practice in the adoption of GBR's, based on a cross-section of industry expertise, including extensive experience from within and outside of the UK.

For the Design and Construct type of contracts which are common in Australia, the GBR needs to be prepared using the three step GBR-A, B and C process outlined in the guidelines. When preparing initial version (GBR-A), it is important for the Owner and their advisors to think through what ground risks the project faces, which of them could have a material impact on the project, which make sense for the Owner to share and how they should be baselined. When doing this both "foreseeable" systematic and non-systematic conditions should be considered (the known unknowns), as the "unforeseeable" ground risks (the unknown unknowns) should be addressed through an appropriate latent conditions clause.

For the risks which will be shared, geotechnical baselines need to be selected, which are clear, unambiguous and easily measurable. It is also advisable to include direction in the report on how the baseline is to be measured and to specify the information required to validate a claim of exceedance. If there is a need for Baseline Statements to refer to an equation, graphical plot of data and/or a geological section or plan, then these should be included in the GBR and not cross referenced to other project documents or external publications.

Baseline Statements are also commonly divided into either Material or Behavioural Baselines – a division that attempts to address either "cause" or "effect" of encountering variable ground conditions. Material Baselines usually address the extent of various geological/geotechnical strata or the engineering properties of materials. Behavioural Baselines are often easier to implement

but are usually specific to an assumed form of construction. The Behavioural Baseline Statements can address the effect of variation in some of the fundamental material properties by baselining the effect of the variability. Examples include the type of ground support class which should be installed for a given encountered condition in a mined excavation or the number of interventions which should be allowed for to deal with natural or man-made obstructions in a TBM excavation.

It is also important to focus the GBR on just the material ground risks rather than all of the assessed ground risks, otherwise the data collection and contract administration requirements can become overly complex and burdensome. Each selected baseline condition should also be reflective of the risk and the risk level the parties have agreed to share. The report should also be clear these baselines have been set for contractual purposes and are not necessarily reflective of the actual conditions expected to be encountered. If a GBR is poorly written this distinction can become blurred and lead to the baseline conditions being inappropriately used for the purposes of design.

Lastly it is important to make sure the GBR is fully integrated into the Contract and is appropriately cross referenced and linked to those clauses in the Conditions of the Contract that deal with entitlement for extensions of time and additional cost. This should happen both when preparing the tender documents and when finalising the contract documents prior to award, with both the legal and technical teams being involved in the drafting and reviews.

6 CLOSING STATEMENTS

Even with all of this planning and preparation, it is inevitable that there will still be disputes on large complex underground construction projects and the adoption of a shared ground risk model will not eliminate this from happening. However, by adopting the practices outlined in this paper the number and size of ground related disputes should be reduced, and when they do occur, it should be more efficient to assess and administer them. In this regard, consideration should also be given to including a Dispute Avoidance / Adjudication Board (DAAB) into the contract, as in the author's experience the use of a DAAB is an efficient way to reduce the number of disputes which are initially raised, as well as limit the potential for those that are raised to escalate further, once the board recommendations have been made.

7 REFERENCES

AS 4000 – 2025. General Conditions of Contract. Standards Australia. (ISBN 978 1 76139 991 6).

AS 4902 – 2000. General Conditions of Contract for Design and Construct (Incorporating Amendment No. 1). Standards Australia. (ISBN 0 7337 3524).

Davis, J. Essex, R. Farooq, I. Drake, A. 2023. Geotechnical Baseline Reports: A guide to good practice. Construction Industry Research and Information Association (CIRIA) Report C807. 74 pages. (ISBN: 978-0-86017-951-l).

Essex, R.J. 2022. Geotechnical Baseline Reports: Suggested Guidelines. Manual of Practice (MOP) 154. American Society of Civil Engineers (ASCE). 90 pages. (ISBN: 978-0-7844-1608-2)

FIDIC and ITA, 2019. Conditions of Contract for Underground Works (Emerald Book). Reprinted 2023 with amendments. International Federation of Consulting Engineers (FIDIC). 282 pages. (ISBN: 978-2-88432-087-0).

ITA and IMIA. 2023. Code of Practice for Risk Management of Tunnels Works - 3rd Edition. Jointly published by the International Tunnelling and Underground Space Association (ITA) and the International Association of Engineering Insurers (IMIA). 28 pages. (ISBN: 978-2-9701436-8-0).

THIS PAGE INTENTIONALLY LEFT BLANK

19th Australasian Tunnelling Conference – Acosta-Martínez, Stewart and Hudson-Smith (Eds.)
© 2025 Australian Tunnelling Society, ISBN 978-0-85825-002-4

Methodology for comparing dangerous goods risks in road tunnels to those on alternative routes

N. Casey
Transport for NSW, Australia

C. Stacey
Stacey Agnew Pty Ltd, Australia

G. Zaunrith & B. Kohl
ILF Risk Consultants GmbH, Austria

A. Dix
ALARP Pty Ltd., Australia

ABSTRACT: This paper describes a method for comparing the risks of routing dangerous goods (DGs) through a tunnel with the risks of routing the same DGs along an alternative route. This comparative risk assessment method has been made available to jurisdictions to inform decisions on DG carriage through tunnels. The risk assessment looks separately at different DG event scenarios related to different DG classes and subdivisions. The method also allows modifications to the assessment inputs to enable sensitivity assessments to be undertaken.

The wider decision required from a whole-of-government view also includes considerations that are not directly comparable with risks to life or to the asset. The comparative risk assessment outputs derived from this method, when considered alongside community, environmental, and economic issues, provide a standardised basis for examining DG life safety risk in support of a wider DG decision making framework.

1 INTRODUCTION

1.1 *Project deliverables*

Austroads project ART6122 has established a comparative risk assessment method for assessing whether a tunnel route is safer than a surface route for the road transit of dangerous goods materials. The resultant method has been available to jurisdictions to allow them to inform decisions on dangerous goods routes with respect to tunnel assets.

The project deliverables comprised three complementary reports produced as part of the project. Any application of this Austroads DG risk assessment method must ensure that the guidance given in all three reports is referenced and applied. The three reports are:

1 Best Practice Review (Austroads, 2023a)

This report reviews best international practice in road tunnel DG risk assessment and provides justification for the selection of the Dangerous Goods Quantified Risk Assessment Model (DG-QRAM) as the tool most appropriate for comparative DG risk assessments.

2 Case Study using DG-QRAM in the Australasian context (Austroads, 2023b)

The Case Study illustrates the stages of the comparative assessment, with incorporation of mitigation measures. It is intended that transport authorities, competent authorities and risk specialists will find the case study a useful demonstration of the intent of the method that is detailed in the Manual.

3 Manual for using DG-QRAM in the Australasian context (Austroads, 2023c)

This report provides background on the development, capabilities and limitations of the DG-QRAM tool as well as providing guidance as to how the DG-QRAM tool should be applied to road tunnels in Australia/NZ.

The resultant comparative risk assessment methodology gives guidance as to the route with the lower risk. Comparative risk is preferred to absolute risk, as it is less susceptible than absolute risk to systemic inaccuracies in either the inputs or the underlying models

1.2 *Consultation*

Extensive consultation was undertaken delivering this work. Key consultees were the National Transport Commission, the Australian Fire Authorities Council, and the Dangerous Goods Competent Authorities.

1.3 *International practice*

A review of international practice on risk assessment of dangerous goods in tunnels has produced valuable insights to be considered when developing the Australasian approach to risk-based decisions. The area of risk assessment related to road tunnels is most developed in Europe and so this project drew mostly on experience from there.

The comparative risk assessment gives guidance as to the route of lower comparative risk regardless of how small those risks are. An alternative concept that is applied in Austria, France and Germany is to accept the tunnel route, if the risks from the route fall below an acceptable expected societal risk, which is sometimes expressed in an F-N curve.

1.4 *Previous practice in Australasia*

Dangerous goods risk assessments of this type are rarely undertaken in Australia, and when they are, the documentation can be tightly held as it is deemed sensitive. The one available Australasian study which took the quantification to the required level for decision seemed unsure whether the decision acceptance criteria should be the establishment of the route of lower risk, or establishing whether all assessed routes achieved a safety level better than a certain threshold. The answer is that no such conclusion is required, with the comparative risk assessment outputs being presented as they are, to be considered alongside community, environmental and economic issues.

1.5 *Case study tunnel*

The application to a trial tunnel was used to demonstrate the suitability of DG-QRAM, and identified modifications required for Australasia. The onerous requirements for sufficient data on traffic makeup, DG movements and population density to make a detailed assessment may, in future, lead to increased importance of a screening stage, and may also require that appropriate Australasian default values are established for some inputs.

1.6 *Wider decision-making framework*

As noted above, the wider context of transport route decisions may determine the question of how to judge or act on a quantitative risk assessment. The quantitative methods that are a primary focus of this document are not an end in themselves, but a decision aid within a decision that is often more complex and judgement-based. Besides the risk to life from the QRA, a complete decision on routing might need to consider environmental risks (including to water supply catchments), community and social benefits, economic benefits, and economic risks. There is no magic formula for converting all risks to one measure (e.g. dollars, lives, or ecological cleanliness) and so judgement will still be necessary. Because the big picture cannot be entirely quantitative, the risks of both routes may be considered within the wider decision, and so perhaps it matters less whether, within the risk model, we compare risks to a benchmark, or prefer only the lowest, following a SFAIRP approach. That is: the outputs may be considered within the holistic decision without necessarily being placed into either framework.

1.7 *Limitations of quantitative risk assessment*

There are many approximations in risk assessment calculation methods. For DG risk assessment methods, the simplifications and approximations in the methodology, as well as the uncertainties in the inputs will always limit the accuracy of any risk estimate. First, the theoretically possible events and chains of events are so numerous and situation dependent, that considering them all correctly is simply not feasible. Thus, in any DG risk assessment, quantitative or qualitative,

approximations and assumptions are inevitable. Quantitative risk assessment results are a statistically-based approximation to what could most likely happen in reality. It will always be only an approximation to reality and never a foretelling of exactly what will happen in a specific event.

Second, it seems logical that the more encompassing an assessment is (e.g. by covering many scenarios), the more realistic the results will be. However, the accuracy of any risk estimation is obviously limited by the completeness and correctness of the initial information and input data processed. One must therefore be cautious to not produce tremendously detailed analyses delivering results to many decimal places and pretending a precision that is outrunning both the initial data quality and the modelling approximations. Hence, the level of detail should be truncated where the assessor's knowledge of the inputs determines that no further accuracy or certainty can be achieved.

1.8 *Focus of this paper*

The focus of this paper is on the best practice review which provided justification for the selection of DG-QRAM as the tool most appropriate for comparative DG risk assessments.

2 TYPES OF HARM

The types of harm are the same for DG-carrying vehicles as for other vehicles, perhaps with differences in the potential level of harm. In general, four different types of harm can be investigated:

– Harm to people (including injuries as well as fatalities)

This is the most important hazard type relating to the assessment of the transport of dangerous goods through tunnels. The most commonly used indicator for the quantitative assessment is statistical fatalities. The primary affected people are the tunnel users. However, people situated next to the tunnel portals and possibly also those downwind and even above the tunnel (for shallow urban tunnels) could be affected. Emergency responders may be at risk in responding to incidents. There is also a low probability that some maintenance related inspection might be underway at the time of an incident. For surface routes, the two affected groups are the road users, and the people close to the route or downwind or downstream. DG-QRAM does not include risk to emergency responders, as that risk may be completely different depending on the different approaches to emergency response that may be used. Responders will undertake risk assessments in addressing each incident and adjust their response accordingly.

– Economic losses

Two types of economic loss may be distinguished. There are the (direct) capital losses due to the damage caused by the event, and there are the (indirect) economic losses due to the tunnel closure (longer or slower travel and transport routes, higher travel and transport costs, affected business losses, possible loss of toll revenue, etc.).

– Impact on the environment

The impact on the environment may also be relevant to the transport of dangerous goods. Whilst the environmental pollution expected from an event in a tunnel is normally limited by capture of in-tunnel spillage and suppression water, the consequences of a liberation of noxious substances in the open can be significant (pollution of soil, groundwater, habitat destruction, etc.). The routes may also vary significantly in the required vehicle fuel use and resultant emissions.

– Reputational damage

Spectacular events causing higher damage (to people and/or property) attract a high media attention, causing public discussions and reactions at political level. A major road tunnel incident may result in significant damage to a tunnel operator´s reputation. In comparison to conventional tunnel risks, like collisions or vehicle fires not involving dangerous goods, incidents involving the release of dangerous substances in a tunnel are characterized by very low probabilities but very high potential consequences. Even minor spills of the material could close a tunnel for some time, generating similar media interest. The harm under this heading could include loss of trust in the asset owner or authorities (with unduly high expenditure on changes to recover trust),

reduced tolls, reduced economic use of the tunnel, or difficulty in gaining acceptance for new tunnel projects. Similar risks apply if the decision is taken to exclude DGs from a tunnel and a high consequence event occurs on the surface route.

The risks linked to these types of harm can be analysed either quantitatively or qualitatively, or both. In comparison to qualitative methods, which are mostly focussing on the interaction and the interdependence of events, quantitative methods enable the calculation of characteristic risk values. Often, due to the lack of sufficient data for complete quantitative analysis, qualitative and quantitative components might be combined in practical applications. For potential high-profile incidents, a closer look at reputational damage is required. Due to the specific influence of risk perception described above, in the process of risk evaluation, special attention is to be paid to incidents with potentially very high consequences (Kohl & Krieger, 2012).

3 RESPONSIBILITY OF THE ROAD AUTHORITY

The reader is directed to the best practice report which contains a comprehensive review of the responsibilities of the road authority. Some key points of that review are re-produced here.

It is generally accepted in all Austroads legal jurisdictions that each member of the public is entitled, as of right, to pass along a public road (whether on foot, in a vehicle or otherwise) and to drive stock or other animals along the public road. Any restriction on the passage of goods through road tunnels is a restriction of that right. Typically, such restrictions will be imposed by a road authority, dangerous goods transport regulator or a combination of statutory authorities which may have overlapping jurisdiction. The regulation of the transport of goods prescribed as dangerous, or otherwise worthy of transportation restrictions, is an exercise of power to restrict the general rights of passage of the public and must therefore be exercised in accordance with law.

Because each State in Australia is a different legal entity, and because each of the States has transferred some of its powers to the Commonwealth of Australia, and because New Zealand is a separate country, the exact identity of the authorities with power, or which claim to have power, over dangerous goods transport varies from place to place and time to time.

Tunnels are, by their nature, prone to creating hazards for users, vehicles and goods. The hazards are uniquely the responsibility of road authorities and could not reasonably be expected to be within the knowledge or control of other regulatory authorities. The unique physical properties of a tunnel when combined with a road transportation function make the regulation of dangerous goods through tunnels a responsibility of road authorities.

A decision to regulate the passage of dangerous goods through tunnels by a road authority must be both reasonable and not negligent. The requirements for a ‘reasonable’ decision for the regulation of dangerous goods and the requirement that a road authority not be ‘negligent’ are separate legal requirements. This means that a road authority must be mindful of both its statutory obligations as an authority and its civil responsibilities not to do harm. The determination of legal unreasonableness is heavily fact dependent and inherently sensitive to context. It is therefore not capable of reduction to a formula and no single legal test of unreasonableness can be stated.

A road authority that can clearly articulate its statutory powers and obligations to an identified and transparent framework for making decisions about the regulation of dangerous goods through tunnels is in an extremely strong position to demonstrate the legal reasonableness of its actions.

It is within this articulation of ‘unreasonableness’ that the methodologies for considering comparative and absolute assessment for the acceptability of risk through risk analysis techniques must be analysed. While the tools for risk analysis may be used in multiple overseas jurisdictions, it does not follow that their use by Austroads members would withstand a reasonableness test if the outcomes appear to abandon common sense. Similarly, if there are alternative tools that both meet Australasian reasonableness and common-sense requirements, road authorities could choose either according to their preference.

It must be noted that the concept of reasonableness is not within European law (the legal framework within which DG-QRAM and other models evolved). This means that the application of European methodologies in an Austroads context needs to be challenged and verified for local regulatory and factual conditions.

4 EXAMPLES OF NATIONAL STANDARDISED RISK ASSESSMENT METHODS

Typically, the risk assessment and evaluation procedure for dangerous goods transports consists of two levels:

- At the policy/overview level, there is the procedure of risk assessment and risk evaluation, including the risk acceptance approach and criteria.
- The detailed level is the choice of risk model that is applied for the quantitative investigation. In fact, there are only a limited number of models which find use in practice.

In order to evaluate the ADR category that should be assigned to a tunnel, a (quantitative) risk assessment is necessary. Note that ADR is the UN treaty concerning the International Carriage of Dangerous Goods by Road, not the Australian Design Rules. Experience has shown that submitting a tunnel to a complete examination is an extensive task and requires a large amount of data. It is time and cost expensive.

To reduce this expenditure, and in view of the large diversity of tunnels (regarding tunnel parameters, equipment and traffic parameters), some national authorities decided to divide the process into several steps. The use of quantitative models form steps or parts of steps required in their respective national risk assessment methods. The particular procedures, although similar, differ from country to country. Nevertheless, the main principle is to end the tunnel assessment as soon as it is proven that sufficient tunnel safety measures have been included such that no restriction on the transport of dangerous goods is necessary. Alternative routes are evaluated only in a last step. This is conceptually different to the proposed framework for Australasia, in which parallel assessments of the tunnel and surface route are compared.

In general, acceptance criteria are not harmonised within Europe. In fact, the definition of the acceptability limits or boundary curves for the F-N diagrams is often a complicated (national) long-term process involving multiple stakeholders. Adopting a comparative approach with F-N curves for a risk-based comparison of alternatives is useful but needs to be done carefully, as the interpretation – especially where curves intersect – is a highly sophisticated task. The complexities of all this make it attractive to apply a ‘deemed to satisfy’ approach in the US.

The use of F-N curves to judge acceptability against criteria, is also a point of difference with the ‘SFAIRP’ approach to risks that is common in Australasia. If we follow the SFAIRP approach to risk reduction, we need to see if we could reasonably reduce risk further by using the alternative route for DG, even if it has already been made ‘acceptable’ against some criterion. European approaches generally are satisfied if the tunnel route meets the criteria set, whether or not it is theoretically possible to reduce risk further. Only if the tunnel route does not meet the criteria is the comparison with alternative routes required, to decide which is preferred. Whether criteria are met or not, the French approach allows other parameters to be considered in the decision (environment, economic, non-DG incidents), alongside DG risk outcomes.

The best practice report describes and assesses the methodologies applied in France, Germany and Austria as well as reference to methodologies applied in Italy and Switzerland. It confirms that in other countries such as the USA, Great Britain and Ireland the methodology to be applied is decided on a case-by-case basis as there are not standard national approaches.

US federal regulations require a risk assessment for DG in tunnels, but specifically do not suggest a recommended risk model. This allows and forces the states to select their own model. The US lack of centralized DG regulations and therefore adoption of a preferred national risk model, is a direct result of the individual states requirements superseding federal requirements. In general, full quantitative risk assessment (QRA) for fires and dangerous goods in tunnels or surface routes is hardly used in the US. It is conventional to comply with codes and standards to fulfil the mandatory requirements, as they correspond to an assumed level of risk. These are commonly used as the benchmark for setting the initial bar.

5 DANGEROUS GOODS QUANTITATIVE RISK ASSESSMENT MODEL (DG-QRAM)

This quantitative risk assessment model (DG-QRAM) for the transport of dangerous goods was first developed in a joint project of OECD and PIARC almost 20 years ago. It is a commercial software, which is widely used and serves often as a basis for a country-specific method for the

risk-based assessment of the transport of dangerous goods through tunnels or on tunnel routes. Importantly for the present work, DG-QRAM was developed as a tool for deciding whether to forbid or authorise, partly or totally, the dangerous goods traffic through tunnels. It is intended to be used for this purpose only. The risk model is not suitable for a general risk assessment study for road tunnels. There are several reasons for this limitation such as:

- The model does not deliver a complete picture of the overall tunnel risk, as it does not include incidents (collisions / fires etc) from a range of non-DG transports (i.e. passenger cars).
- The model includes a lot of different DG-scenarios, therefore to reduce complexity the consequence sub-models in DG-QRAM for each individual scenario are rather coarse. This is particularly relevant to fire and smoke propagation modelling inside a tunnel. Other modern tunnel risk models (like TuRisMo) offer a much better and realistic representation of these effects, because they use complex combined and transient 1D/3D CFD modelling.
- There are limitations in assessing the positive effects of many quite effective tunnel safety measures – related to ventilation, evacuation, FFFS or organisational measures influencing the timeline of reactive actions in fire incidents.

The tool´s general structure allows an assessment of the tunnel alone, as well as the assessment of an open-air route in comparison with the tunnel route. This is a valuable feature, as this allows either a comparative risk assessment or an absolute risk assessment or both. Furthermore, the tool allows the user to select between the option of calculating fatalities plus injuries or fatalities only, and to select between the consideration of road users plus local populations, or road users only, or local population only. One part of the model consists of a quantitative frequency analysis. DG-QRAM encompasses an analysis of the sequence of events or occurrences that stem from an initial DG event, to a set of consequence scenarios including the respective probabilities of occurrence.

Thirteen scenarios representing the hazards most threatening to human life have been defined. Scenarios of other dangerous goods primarily affecting the environment are not considered, as the main focus is on human well-being. Within modern Australasian tunnels, the environmental impact of the release of polluting substances seems negligible, as all are equipped with sumps that capture spillage and either store it for disposal or transfer it to surface storage. For every scenario there is a probability implemented in the model, distinguishing between the different boundary conditions (tunnel or open air, urban area or rural area, etc.).

The consequences of scenarios involving those DGs not appearing in the DG-QRAM scenario list is taken as being similar, or less significant than the consequence of one already in the list. The chosen substances are representative of all other dangerous goods. The exceptions are large quantities of explosives, and radioactive materials, which are not addressed by DG-QRAM and are also regulated differently. Depending on the detonation assumption (rapid or delayed) more moderate explosive loads could be considered through BLEVEs or vapour cloud explosions of the appropriate size. It may not be appropriate to use those scenarios to model military quantities of explosives.

The general procedure to obtain a scenario´s probability of occurrence is to combine the route's HGV incident rate (or a national default value) with the traffic and the DG HGV ratio among that traffic along the (tunnel) road, as well as the conditional probability of occurrence of the scenario. Those specific probabilities are preset in the software and are a function of the dangerous goods traffic's composition. The probabilities used are based on a comprehensive (400-page) study by the University of Waterloo (Canada), which was an annex to the original work documentation. The probability can be adjusted by aggravating or diminishing factors related to the tunnel's or/and the route's characteristics, such as being an urban or rural road, the presence of exit or on-ramps, the existence of crossroads, etc. For the tunnel, it is of course important to know whether it is single tube or twin tube. A detailed description of the model is given in the DG-QRAM reference manual (PIARC 2019).

6 PREVIOUS PRACTICE IN AUSTRALASIA

We have been provided with and have reviewed risk assessments for several specific Australasian projects. We are aware of others that cannot be specifically referenced as the information is tightly

held. Of the reports that are available to the authors, we refer to one that had the depth of analysis sufficient for a comparative QRA. That report is discussed briefly here.

The transport of DG was looked at for the M5 East tunnel in 1995, as part of the planning and design. The report (Parsons Brinckerhoff Quade & Douglas, 1995) noted a lack of detail in prior work looking at DG risk in tunnels, and the paucity of data with which to make assessments. The study compared the risk in tunnels against that on alternative surface routes, and emphasised the sensitivity of the result to values and assumptions which might tend to favour the open air or the tunnel cases. The method applied was a full quantitative method, considering frequency and consequences for representative DG loads, reaching distinct conclusions on the preferred route for each DG class. The spectrum of DG loads was simplified in a manner similar to that done in DG-QRAM.

The likelihood and consequence analysis appears to have been done in some detail, although the specifics of the consequence analysis are not given. The methodology of assessing the alternative route consequences is not readily deduced.

7 CONCLUSIONS

PIARC's DG-QRAM is selected as the most appropriate quantitative tool to use within an Australasian approach, with the suggestion that a screening assessment, as is common in Europe, be applied first. The purpose of a screening assessment would be to shorten the assessment where the comparative risk result is so clear that a simple approach is sufficient, and the time and expense of a more detailed approach is unnecessary. If such an assessment is considered, it may use the same methodology, but with approximated or notional input data, appropriate to the screening function and shorter time availability.

Currently there is no standardized risk assessment approach in Australia or New Zealand. Experience shows that this lack of a uniform methodology and an associated validated assessment model has led to a certain grade of arbitrariness in the evaluation of the permissibility of the transport of dangerous goods through tunnels.

European countries have developed methodologies for assessing DG risk. While those methodologies may at first appear quite different, when reviewed in detail they have much in common:

- They all have as their basis a quantitative risk assessment;
- They are all based on the ADR;
- Most of the methods include a multi-stage approach; and
- Most rely on DG-QRAM.

This DG-QRAM (dangerous goods quantitative risk assessment model) has in fact been developed specifically for the needs of a QRA for the transport of dangerous goods. It has been developed in an international context (PIARC/EU/OECD) and encompasses the statistical background of various countries. Further, it enables "direct" comparison of the tunnel route and an alternative route. As the categorization system of dangerous goods in the ADR is the same as in Australia, a closer examination of DG-QRAM in the Australasian context seems reasonable.

Governments must consider many aspects, such as social and community benefit, risks to environment, including water supplies etc. Within that broader context, the fine details of a very detailed model may lose impact. Depending on the legal context applying to each road authority, the distinction between acceptable risk and the SFAIRP approach for model outputs may lose relevance, as the overall method outcome cannot be assessed one dimensionally.

Finally, there are differences between jurisdictions that need to be considered in the methodology. These include:

- Infrastructure differences
  - Fixed fire-fighting systems (deluge or water-mist)
  - Egress provisions (i.e. cross-passage spacing)
- Dangerous goods fleet differences
  - Bulk diesel (i.e. whether diesel is identified as a DG)
  - B-double trucks (B-doubles not permitted to carry DGs in Europe)

  - Driver training
  - Seasonal transports
- Operational differences
  - Lane use restrictions
  - Time of day

8 REFERENCES

Austroads. 2023a. *Methodology for Comparing Dangerous Goods Risks in Road Tunnels to Those on Alternative Routes – Best Practice Review.* Sydney: Austroads.

Austroads. 2023b. *Methodology for Comparing Dangerous Goods Risks in Road Tunnels to Those on Alternative Routes – Case Study Using DG-QRAM in the Australasian Context*. Sydney: Austroads.

Austroads. 2023c. *Methodology for Comparing Dangerous Goods Risks in Road Tunnels to Those on Alternative Routes – Manual for Using DG-QRAM in the Australasian Context*. Sydney: Austroads.

Kohl, B. & Krieger, J. 2012. *Current Practice for Risk Evaluation for Road Tunnels*. Paris - La Défense: PIARC World Road Association.

Parsons Brinckerhoff Quade & Douglas. 1995. *M5 Motorway East: Transport of Dangerous Goods - Supplement to M5 East Motorway Environmental Impact Statement in Working Papers Vol 2 of 3*.

PIARC. 2019. *Transport of Dangerous Goods through Road Tunnels: Quantitative Risk Assessment Model (v. 4.04) - Reference Manual.* Paris: PIARC - World Road Association.

19th Australasian Tunnelling Conference – Acosta-Martínez, Stewart and Hudson-Smith (Eds.)
© 2025 Australian Tunnelling Society, ISBN 978-0-85825-002-4

A robust approach to major tunnelling fire safety during the construction phase

A. Bruce, C. Hiscock & E. Wright
Sener, Brisbane, QLD, Australia

L. Haines
Sener, Perth, WA, Australia

T. Sandum
Sener, Melbourne, VIC, Australia

ABSTRACT: Tunnelling projects are growing in popularity and complexity, increasing exposure to various hazards. Although Fire & Life Safety (FLS) considerations are crucial in design development phase, they can be overlooked in the construction phase.

Construction of underground structures represents the most dangerous phase of projects, with heightened complexity of hazards including fire due to multiple factors. Therefore, implementing strategies to control or manage fire related hazards during construction is essential for the safety of construction personnel and to facilitate effective incident response.

Multiple tunnelling projects in Australia, including road, rail, and hydro power, have adopted more robust construction phase FLS analyses to manage fire safety hazards.

The primary objective of these FLS analysis was to reduce fire risks So Far As Is Reasonably Practicable (SFAIRP), while secondary objectives include reduced construction costs, timelines and address stakeholder concerns.

Two critical factors inform risk-based analyses, frequency and likelihood, but, the lack of historical construction incident data can complicate the frequency side of these assessments. Nonetheless, a robust risk-based assessment can provide comprehensive evaluations of fire hazards, allowing clients to demonstrate that underground fire risks have been reduced SFAIRP. Additionally, Computational Fluid Dynamics allowed optimised ventilation arrangements and construction performance.

1 INTRODUCTION

Designers and constructors must consider fire safety during tunnelling construction, especially addressing Workplace Health and Safety legislative requirements for all types of work. Before 2013, Safe Work Australia partnered with state organisations (SafeWork SA, Workplace Standards Tasmania, WorkSafe WA, Workplace Health and Safety QLD, NT WorkSafe, Work Cover NSW, Comcare, and WorkSafe ACT) to create the *'Guide for Tunnelling Work'*. Each state's Workplace Health and Safety (WHS) legislation demands safety by design, requiring designers to minimise hazards So Far As Is Reasonably Practicable (SFAIRP). WHS legislative requirements typically define workplaces as somewhere tasks occur, relevant from concept phase to decommissioning of a project. Thus, these laws require designers and constructors to manage fire safety during construction, ensuring that hazards and risks are minimised SFAIRP.

Construction fire safety guidelines developed for the building industry are not necessarily applicable to a tunnelling construction environment. Tunnel construction is more aligned to underground mining, however, differ from mining in that mining can include different risks that may not be directly attributable to tunnelling.

Therefore, considerations of fire safety hazards in tunnelling could and should be better addressed via a first principles review of the intended tunnelling methodology and in line with the operational tunnel risk assessment process.

Past projects have considered construction fire safety to varying degrees and fortunately to date, our industry has been managed such that we have not had a significant construction phase underground fire incident in Australia or New Zealand. The fire safety risks that can occur during

the construction phase vary depending on the type of construction, the tunnelling process, the method of construction and construction sequencing process. Factors influencing fire safety include but are not limited to; the presence of dead-end shafts, the provision of tunnel ventilation, the functional operation of tunnel ventilation systems, types of plant, the number of workers present, the ability to provide exits and access for emergency response crews.

The approach described in this paper has been adopted on multiple projects across Australia (road, rail and hydro). Outcomes of these studies resulted in construction phase fire risks being demonstrably reduced SFAIRP in compliance with WHS legislation.

The WorkCover NSW 2006 Guide for Tunnelling Work provides important baseline prescriptive fire safety measures for tunnelling projects under construction. However, these generic requirements are inherently limited by their one-size-fits-all prescriptive format and may not fully account for the diverse, complex, and evolving fire risks associated with modern tunnelling methods, materials, and equipment.

Therefore, a robust risk-based fire safety approach offers a more flexible and effective strategy that responds to the complex and changing nature of tunnel construction. It demonstrates that the construction phase fire risk is managed proactively and proportionately, supporting safer outcomes for workers, assets, and the public.

2 STEP ONE - SCOPING

2.1 *Considerations*

Numerous avenues need to be explored to build a comprehensive picture of the tunnelling construction approach and the environment where incidents could potentially occur.

With the primary objective being the reduction of fire safety risks to project personnel SFAIRP, considerations should include:

- Fire safety strategy for occupant egress
- The varying levels of tunnel construction completeness
- Emergency services response for varying stages of project completion
- Day-to-day fire safety measures

A comprehensive fire safety strategy can also serve to expedite construction or reduce whole of life costs if done strategically. Modern tunnel construction processes face elevated constraints, like increasing construction complexity, compressed delivery scheduling and environmental limitations. Tunnel construction methods may include Tunnel Boring Machines, Sequential Excavation, drilling and blasting, cut and cover, or trench methods for construction or combinations of these methods. Each tunnelling method carries specific hazards, often unique to the method, ground conditions, the location, and tunnel geometry at that time. Due to these factors, each project is distinct and warrants individual analysis; a copy-paste approach may prove less-than-ideal if an incident occurs.

Historical data is a valuable resource for framing scenarios and control strategies, but publicly available data for construction phase incidents is limited, necessitating alternative Risk-based Assessment (RA) approaches. Bowtie analysis has proven to be a useful tool that does not require quantitative frequency for each measure or hazard. Similarly, a Hazard Analysis and Preliminary Risk Assessment (HAPRA) has been developed to investigate hazards and control measures in more detail. Literature reviews facilitated a quantification of risks and reductions during the HAPRA process.

Assumptions made during the fire safety evaluation process require validation and consultation with the relevant parties to improve accuracy of the assessments. Existing construction policies serve as inputs to the fire safety strategy, generating awareness within the project and can highlight areas of special consideration.

2.1.1 *Fire Safety Risks During Construction*

The fire characteristics of an operational tunnel are different from those in a tunnel under construction. Similarly, evacuation, emergency response, and selecting safety equipment also differ from the completed tunnel solution. As a result, the hazards associated with fires occurring during tunnel construction can be higher than those associated with the completed operational tunnel.

Therefore, a fire safety strategy based on the final design may not be applicable until the completion of the construction phase.

The traditional understanding of fire dynamics in tunnels assumes that tunnels are complete and have two open portals, allowing airflow, access, and egress. However, this is only valid after the construction breakthrough has occurred. Each tunnel geometry and the resulting ease of egress can vary greatly by project, and the 'mainline' tunnel under construction may be the only means of access and egress.

During tunnel construction, unique measures such as special access shafts or entrance tunnels may be required to facilitate construction. These access tunnels may not be part of the final tunnel solution but can provide easier access during construction. The slope of an access shaft or tunnel typically varies with the project and depends on the geological and/or ground conditions. During certain types of tunnel construction, the access safety or tunnel provides the sole opening to the surface while both ends of the horizontal main tunnel remains closed until breakthrough. These access shafts or tunnels can be used to assist with personnel safety during an emergency

Several fires have occurred during the construction of tunnels, resulting in deaths or injuries to individuals, losses and damage to equipment, damage to tunnel structures, and delays in project delivery. Globally, fire has become a common construction accident; as there can be numerous potentially dangerous tasks being executed in parallel. The consequences of these fires depend not only on where fires occur in the tunnel, the fuel involved, the intensity and nature of the fire, the complexity of underground facilities, the response of the rescue service, and the availability of resources, including personnel and equipment. Although there is limited statistical data available, understanding the tunnel fire characteristics during construction is essential for effective fire control and evacuation management.

Previous studies showed that approximately 75%–85% of construction phase fire-related deaths arose from poisonous gas under fire conditions (Hu, Tang, Yang, Liu, & Huo, 2010). Compared to a tunnel during operation, the ventilation and smoke management systems available during tunnel construction may be considered a limiting factor, as the smoke may not be adequately discharged to provide smoke-free egress and access paths. The limited ventilation, coupled with the reduction or blocking of the tunnels' cross-sectional area or excavation faces by vehicles/equipment, can also influence the smoke spread through the construction shaft.

Fire accidents during construction of tunnels have been reported to cause smoke to quickly fill the tunnel, which can increase the difficulty for personnel to escape and for emergency responders to access. Therefore, a robust fire safety strategy developed specifically for the construction phase is paramount for personnel and responder safety in the case of an emergency.

2.1.2 *Physical Environment*

Generally, the tunnel environment during construction is rough. The tunnel construction environment is typically characterised by low illumination, wet surfaces, uneven and sometimes slippery ground, ongoing construction work with incomplete constructions, noise, and conditions that are constantly changing in appearance. These factors can impede and add complexity to the safety of personnel in the event of a fire.

Typically, tunnels are equipped with a forced ventilation system to manage air quality for the safety of workers in normal operating conditions. However, the system basis likely requires continual adjustment based on the tunnel geometry at the time or the construction method employed. Understanding the basis of the construction phase ventilation strategy and how modifications can be made to the ventilation system a key consideration of a robust fire safety strategy.

Perhaps the most crucial factor concerning evacuation is the extended travel distance from a working place (typically located in the most remote part of the tunnel) out to the tunnel entrance or a place of relative safety. This travel distance can, in some cases, be several kilometres, therefore, it's essential to have a pre-designed plan for managing an evacuation; including appropriate fire safety provisions, such as lighting, ventilation, and exits, to assist in making evacuation safe, given the conditions. A common problem for new tunnel construction projects is the lack of specific recommendations for fire safety provisions. Typically, fire safety provisions are included, but often with little understanding of the benefits of these provisions or whether they are sufficient for the specific tunnelling situation.

Whilst there are rules governing task lighting, it may not meet the egress lighting requirements away from the task location. The location and lighting levels within the tunnel's construction

environment can vary depending on the proposed excavation plan. Depending on the evacuation strategy, the height of illumination points may be as crucial as regulating the distance spacing between illumination points. Equally, it's consideration should be given to the need for these emergency lighting points to be equipped with backup power supply, to cater for potential power outages and subsequent loss of illumination.

All the factors listed above can affect the possibility of evacuating safely. A number of factors can play a critical role in the safety of site personnel. An initial site induction may not provide a comprehensive knowledge of the site and emergency procedures in place. Therefore, it is paramount to have a comprehensive strategy in place to reduce the potential for fatal emergencies to occur.

2.1.3 *Evacuation*

Evacuation conditions for construction site workers differ significantly from those expected in operational buildings or tunnels. Tunnel environments can be quite complex and are continually changing, with cognitive and physical obstacles making evacuation challenging. In addition to construction site issues, modern tunneling methods can include the use of specialised Tunnel Boring Machines (TBMs) with complex internal layouts, the presence of flammable hydraulic fluids, complex electrical systems, and extensive conveyor belt systems; introduce specific hazards where rapid fire spread can impede egress and cause access challenges during emergencies. Evacuation and the notification of an alarm could be inhibited by factors such as; competing sounds, low-light conditions, isolated locations on the equipment impairing vision of incident or alarm, or other works which reduce focus on an incident.

Much of the preventive safety work relies on traditional construction safety procedures; limited work has been published focusing on the unique problems facing construction workers during evacuation from complex tunnel environments. A key factor for a successful evacuation from tunnelling construction sites is acknowledging the importance of procedural safety aspects. A typical tunnel construction site may include workers, subcontractors, and visitors, which can result in unclear or diminished levels of safety responsibility.

One of the problems that can occur in tunnel construction environments is recognising the fire threat; fire cues must be interpreted, and a worker's decision-making processes must be initiated. There may also be extended travel distances between the location of the workers and a place of safety, or an exit may be totally cut-off, limiting the potential for escape. Thereby necessitating careful consideration of the risks and developing appropriate controls to manage it, for the safety of both site personnel and responding emergency crews.

2.1.4 *Fuel loads*

Threats on construction sites can include flammable materials and dangerous construction activities, which can lead to fire accidents. Significant fire accidents on construction sites can lead to secondary accidents, such as collapse, burial, and explosion, all of which can result in more severe damage to life and property. Introduced hazards on construction sites can include the storage of flammable materials underground and hazardous construction activities like hot works, which can cause fires. Additionally, various gases may be stored or used for construction, and these stored gases can increase the risk of fire and explosion on the construction site.

A holistic review of storing combustible materials on construction sites was determined to be essential factors in preventing or limiting the severity of fire accidents. Underground fire risks can occur wherever potential ignition sources meet a flammable or combustible fuel sources. When quantifying fire scenarios within a tunnel under construction, several parameters can influence the characteristics of the scenario including the location of the fire, tunnel ventilation conditions, influence of the fire protection system (suppression systems, smoke extraction, fire alarm, etc.) during construction, and the distribution, density, and type of combustible materials.

Vehicle fires present distinct challenge regarding their frequency and locations, as vehicles are commonly found throughout tunnel construction zones, often in substantial quantities near a work or task location. A situation involving a vehicle fire that can rapidly spread to other vehicles near zones with a high concentration of personnel or close to a main evacuation route warrants attention when planning for egress safety.

Characteristics of the most frequent fires in underground mines across Australia identified the position of vehicle fires being predominantly from within the engine area with fire caused either by fuel/oils contacting hot surfaces or electrical fault.

2.1.5 *Ventilation*

Various ventilation systems can be employed in tunnel construction to manage air quality, with ventilation arrangements depending on the tunnels length and diameter, construction method, and specific construction hazards. Numerous arrangements of ventilation are possible within a project, with each potentially being more suited to the construction method employed and the tunnel geometry at that stage of construction. Past experience has shown the value of performing CFD analysis on the ventilation system to optimize the ventilation arrangements, and the smoke management outcomes for occupants and responders in the case of an emergency.

2.1.6 *Intervention*

Fire and rescue services have limited possibilities to perform fire and rescue operations in tunnels under construction due to long response routes, complex changing environments, and sometimes the need for more information. The inability for emergency response access in an incident can leave occupants trapped in the tunnel, needing self-sufficiency for hours until the incident is suitable resolved and it is safe for emergency services to enter. Whilst self-evacuation and self-rescue are always preferred; the emergency services' potential to perform a fire and rescue operation can influence the choice of egress provisions in the tunnel, with elements such as rescue chambers sometimes necessary.

Therefore, it is essential to define the emergency response tactics, methods, and available equipment to support a fire and rescue operation in the early phase of developing the Fire Safety Strategy. Conditions that primarily influence the rescue operation's process are the fire growth, heat release rate, location of the incident and if the fire occurs before or after the breakthrough (opening both ends of the tunnel). These parameters can influence or change the tactical approach of the whole fire and rescue operation.

Fire and rescue interventions in a tunnel under construction can involve either an offensive (direct firefighting) or defensive (waiting outside for safety) response strategy. Whilst these response strategies are typically not used simultaneously, they can be switched during an incident. Typically, there are five tactical approaches to handling a fire in a tunnel; including direct firefighting, rescuing individuals, controlling airflow, fighting from a safe distance, and caring for self-evacuated people. These tactical approaches can be used individually or in combination depending on the chosen strategy and available resources.

Emergency response to an underground construction site can be highly volatile. Therefore, comprehensive measures should be in place to minimise the chances of personnel being trapped underground or if evacuation is impossible, appropriate measures should be in place for personnel to safely shelter for the required time and alert the surface of their whereabouts allowing responders to perform a headcount.

2.1.7 *Summary*

High consequence environments such as underground construction sites can place multiple personnel at risk in the event of a fire. Historical data shows that these incidents can increase in severity in a short period of time. There are a multitude of factors to consider when performing a risk-based assessment for a construction site and due to a shortage of incident data, alternative methods of risk-based analysis may need to be employed to perform a comprehensive and holistic analysis. Risk-based assessment techniques, such as bowtie analysis and/or Hazard Analysis and Preliminary Risk Assessment (HAPRA) serve as tools to evaluate construction fire safety risks comprehensively without the specific need for historical data. This methodology provides a robust approach to the construction phase fire safety of underground projects.

3 STEP TWO - ANALYSIS

3.1 *Bowtie analysis*

3.1.1 *Overview*

The Bowtie analysis is a qualitative risk assessment methodology that effectively communicates complex risk scenarios in a clear and easy-to-understand graphic format, illustrating the relationships between the causes of unwanted events and the potential for loss and damage escalation.

Whilst other risk assessment methods focus on specific aspects, like Fault Tree Analysis (FTA) identifying possible causes of an incident, Event Tree Analysis (ETA) detailing possible outcomes of an incident, or Failure Mode and Effects Analysis (FMEA) on identifying and prioritizing failure modes and its effects; the Bowtie analysis integrates these perspectives to provide a balance representation of potential threats or causes without a dependency on likelihood statistics.

Each bowtie can display preventative control measures (for each specific threat) that limit the potential for the top event to happen and show the mitigative control measures that are implemented after the event has occurred, to limit possible consequences, specific for each credible scenario evaluated.

The main advantages of the using the Bowtie approach in risk-based analysis are:

- Provides a solid technique of identifying all risk events and promotes an understanding of their reciprocal relationships.
- Uses a format that is an easy-to-understand medium to communicate the cause-and-effect relationships underlying more complex risk scenarios for a wide range of stakeholders.
- It helps to demonstrate the controls implemented to manage risks and therefore provides a way of identifying weaknesses, gaps and opportunities for a continuous risk reduction.
- Enables verification and connection to relevant sections of the construction management system that support controls, including critical security elements and critical safety activities.
- The easily communicated process increases the workforce awareness of the risks associated with their facility and how these risks are managed; and
- Uses the workforce's knowledge and expertise, which best understands the actual state of operation of existing controls and threats as inputs to the risk management process.

3.1.2 *Application of bowtie analysis*

The development of the construction phase Fire Safety Strategy is limited to considering fire safety hazards that may occur during the tunnelling construction works and demonstrating that the fire safety risks associated with these hazards have been reduced SFAIRP. Risk-based assessments can become too granular and therein lose their value in influencing fire safety outcomes. Therefore, there is no point in evaluating every single vehicle and process present during the construction process, as the granular assessment process will lose its value to the construction safety team.

To address this potential issue, and where appropriate, the assessments examined systems or subsystems, rather than individual items or topics. An example of this approach could be that the mobile plant could be classified as a system. Similarly, the TBM conveyor could be considered another type of system. For more complex plant and equipment, such as the TBM, it is considered more appropriate to focus on the TBMs subsystems, rather than the TBM itself. As an example of the TBM considerations, it may be more appropriate to focus on the hydraulic systems of the TBM, rather than the TBM itself.

This system-based approach to assessing fire safety hazards enables the Fire Safety Strategy to add value and efficiency to the fire safety risk reduction process. Developing the Bowtie analysis based on systems used in the construction process, is a foundation step to inform the HAPRA analysis which provides a deeper level of analysis.

3.2 *HAPRA analysis*

3.2.1 *Overview*

The HAPRA can employ a qualitative, semi-quantitative or quantitative risk assessment methodology that effectively communicates complex hazards as scenarios, in a more detailed manner than shown in a Bowtie analysis. When considering hazard scenarios, the HAPRA provides a

classification of preventative controls and their associated limitations. Thus, allowing a likelihood and consequence to be applied for a specific audience (for Tunnel Projects, this could be construction personnel or emergency services), resulting in a preliminary risk ranking being determined.

The HAPRA process then applies mitigative control measures, which aim to reduce either the likelihood or consequences of the event occurring, before reevaluating likelihood and consequence considering the implementation of all Risk Control Measures (RCMs). Considering the residual risk rating allows each audience to determine if the risk can be further reduced or if it is considered impractical to further reduce the risks, thereby, demonstrating that the risk has been reduced SFAIRP using the RCMs implemented. The main advantages of the approach to adopting HAPRA process are:

- Provides a solid technique for a more comprehensive identification of all fire safety hazards and events, promoting an understanding of these hazards and providing comments on their reciprocal relationships.
- It helps to demonstrate the level of control (preventative or mitigative) that has been applied to the hazards, thereby providing a way to identify weaknesses, gaps, and opportunities for reducing fire safety risks.
- Enables verification and connection to relevant sections of the construction management system that support controls, including critical security elements and critical safety activities.
- Highlights limitations of control measures that could hinder performance.
- Gives quantitative residual risk ratings once risk control measures are implemented.
- Increases the workforce awareness of the risks associated with their facility and how these risks are managed; and
- Uses the workforce's knowledge and expertise, which best understands the functional operation of the construction process, including existing controls and threats.

3.2.2 *Application of HAPRA analysis*

For a tunnel construction project fire safety strategy to be developed, the HAPRA analysis receives input from the Bowtie analysis undertaken and provides a platform for evaluating and classifying threats and controls. The risk ratings, coupled with the commentary and risk control measure classifications, can be used to substantiate decisions on which control measures are worth implementing to reduce the fire safety risks during construction.

3.3 *Worked Example – Bowtie and HAPRA analysis*

Figure 1 shows an example of Bowtie analysis for fire incident (top event) occurring in the TBM electrical system. The 'left' bow identifies the threats that can cause the event and the preventative control measures designed to stop each specific threat from leading to the TBM fire. The 'right' bow identifies the potential outcomes if a TBM fire occurs and mitigative control measures used to limit the severity of consequences of the event. Another critical aspect of Bowtie is the identification of escalation factors that can cause a barrier to fail or become less effective. The Bowtie analysis provides visual information to inform stakeholders and also to provide valuable tool for further discussion.

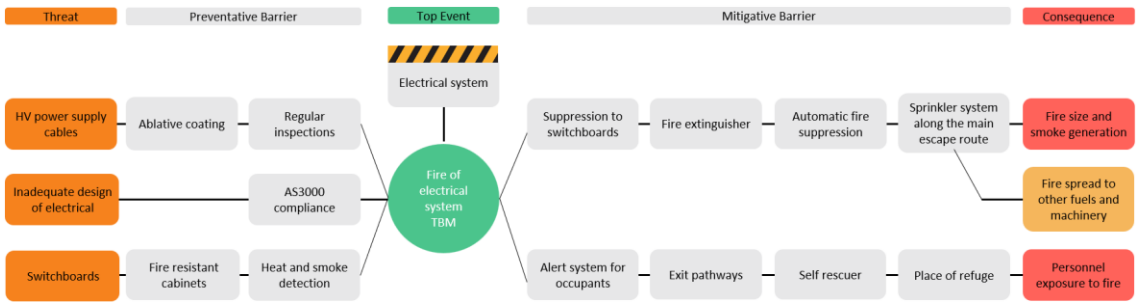


Figure 1. Sample Bowtie analysis for the electrical system in a TBM, wording has been simplified for the purposes of this paper.

Subsequently, the structured output of the Bowtie analysis directly informs and feeds into the HAPRA process, where risk ratings based on likelihood and consequences, can be calculated and actionable controls can be assigned to responsible parties.

4 STEP THREE - OUTCOMES

The documented risk-based approach to FLS in the construction phase of tunnelling projects has provided several key positive outcomes to Projects on which they have been employed. The primary positive outcome is improved levels of fire safety for the site, using controls that are reasonably practicable. The nominated risk-based assessment approach using Bowtie and HAPRA assessments, allows project hazards to be identified, understood and assessed in a systematic fashion. The HAPRA allows both a qualitative and quantitative approach to be adopted to validate the risk mitigation controls. The approach improves safety outcomes over other methods by;

- Improving stakeholders' understanding of project risks by providing simple visual explanations, e.g. Bowtie structure.
- Capturing project specific hazard details by engaging workforce/operators inputs to the HAPRA analysis process.
- Demonstrating that risks are reduced SFAIRP by assessing whether control measures that could be used to mitigate or prevent risks are reasonably practicable.

A further positive outcome of this process is projects can effectively demonstrate that their obligations to Workplace Health and Safety (WHS) legislation have been met.

5 SUMMARY

In summary, construction of tunnels are complex, unique, and can possess a relatively high fire safety risk profile due to their underground nature; which can inhibit egress and emergency response access during fire events. The underground constraints associated with tunnel construction meant that compliance-based risk assessments applicable to buildings are not suitable for these types of projects, and more suitable processes should be used instead. This paper presents a robust risk-based assessment method for assessing and addressing the fire safety risks for these projects using a combination of Bowtie and HAPRA analysis.

Using a risk-based assessment which utilises this combination of Bowtie and HAPRA analyses, allows the hazards and risks associated with construction phase works to be clearly communicated to all relevant parties. This robust process allows projects to determine which risk control measures are deemed *'reasonably practicable'* to implement. The use of the risk-based assessment methodology allows hazards and risks to be monitored during construction and satisfies the projects statutory obligations to reduce safety risks SFAIRP.

6 REFERENCES

Hu, L. H., Tang, F., Yang, D., Liu, S., & Huo, R. (2010). Longitudinal Distributions of CO concentration and difference with temperature field in a tunnel fire smoke flow. *International Journal of Heat Mass Transfer*, 2844-2855.

WorkCover NSW 2006 Guide for Tunnelling Work

19th Australasian Tunnelling Conference – Acosta-Martínez, Stewart and Hudson-Smith (Eds.)
© 2025 Australian Tunnelling Society, ISBN 978-0-85825-002-4

Selection of different arch shapes rock mass opening for underground space development – Considering rock support pressure requirements and spatial utilisation efficiency

Keith W.K. Kong
Sener Australia (formerly Tactix-Sener Group), Melbourne, Victoria, Australia

Jurij Karlovsek
School of Civil Engineering, The University of Queensland, St. Lucia, Queensland

ABSTRACT: A novel investigation has demonstrated that varying rock support pressures are required to maintain stable openings in rock masses, depending on the arch shape, specifically the roof arch rise-to-span ratio ranging from 0.1 to 0.4. Validated results indicate that optimised Q-system support pressures can be applied effectively across different arch geometries using rock reinforcement techniques. Notably, high-rise arch openings require approximately 19% less support pressure than low-rise configurations. These findings offer valuable insights for designing efficient and stable underground openings across diverse rock mass conditions. To gain deeper insight into the cost-benefit differences among various arch-shaped openings using rock reinforcement techniques, case studies were conducted comparing the number of rockbolts required and the total excavation volume generated. The results offer valuable indicators for underground space planners and constructors in selecting optimal opening geometries and support systems. This comparative analysis supports informed decision-making by balancing structural efficiency, sustainability, and economic viability in underground development projects.

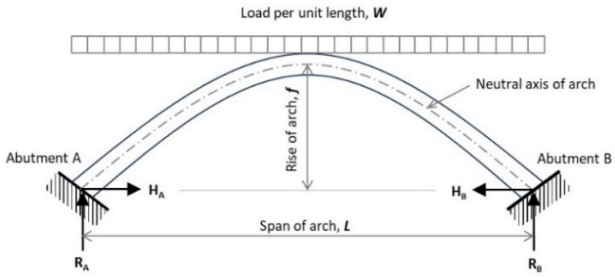
1 INTRODUCTION

Underground rock openings are typically designed with arch-shaped roofs. However, limited research has explored how different arch geometries influence the engineering behavior of rock masses stabilised with reinforcement techniques. Kong et al. (2024) investigated this by constructing various arch-shaped openings under identical ground conditions and *in-situ* stress fields. Their findings revealed that high-rise arches exhibited less deformation than low-rise arches, a result that aligns with structural arch theory.

In terms of structural arch model, the arch distributes uniformly applied loads primarily through compression, generating horizontal thrust at its supports. Mikhelson (2004) emphasised that even under purely vertical loads, arches develop horizontal reactions, termed "thrust", denoted as $H_A = H_B$, as illustrated in Figure 1. As the arch rise decreases, the outward thrust increases, necessitating internal ties or external bracing at the arch abutments to maintain stability. This behavior implies that, for a constant span and vertical load, increasing the arch rise reduces deflection and horizontal thrust. Conversely, a low-rise arch under the same conditions demands greater horizontal reaction forces at the supports. Thus, high-rise arches give an enhancement of structural efficiency, offering a more stable configuration for underground openings.

The load-carrying capacity of structural arches can be applied to underground rock openings of varying arch geometries (Kong et al., 2024). Traditionally, the design of such openings has relied on empirical methods (e.g., Terzaghi, 1946; Unal, 1983; Goel & Jethwa, 1991; Barton et al., 1974; Osgoui & Ünal, 2009) or numerical simulations to estimate support pressures, particularly at the crown. However, most empirical approaches do not account for variations in roof shape. While several studies have examined different opening geometries, such as rectangular (Abdellah et al., 2018; Park et al., 2019), circular (Abdellah et al., 2018; Taghizadeh et al., 2020; Mazraehli & Zare,

2022; Varma et al., 2022), elliptical (Shiau et al., 2022; Taghizadeh et al., 2020; Wang et al., 2023), and horseshoe-shaped (Abdellah et al., 2018; Jia & Tang, 2008; Park et al., 2019), these analyses typically assume continuum media or infinite jointed rock masses. Critically, few studies have focused on how different arch shapes influence rock loading across varied rock mass conditions.



Where:

$H_A = H_B = W \cdot L^2 / 8f$, is horizontal reaction load at bearing point of the arch.

$R_A = R_B = W \cdot L / 2$, is vertical reaction load at bearing point of the arch.

Figure 1. Simple arch beam model and equations.

Kong et al. (2025) conducted a parametric desktop study to explore the maximum stable span of arch-shaped openings across a range of rock mass conditions. Their findings indicate that openings with rise-to-span ratios between 0.1 and 0.4, when using rock reinforcement technique, exhibit structural behaviors analogous to classical arches. The study demonstrated that different arch shapes, even under identical rock mass conditions, result in varying maximum stable spans. Consequently, each arch shape supports different rock loads due to its unique span capacity.

Building on these findings, a follow-up study was conducted to quantify the load-bearing capacity of various arch shapes across different rock mass conditions. This research produced practical design charts that estimate support pressure reductions based on the Q-system (Barton et al. 1974). Four validation models were simulated to verify the results, confirming that the proposed reductions in support pressure for different arch geometries are feasible. A cost-benefit analysis was also performed for openings of equal span but differing arch shapes. The analysis offers valuable guidance for selecting optimal opening geometries and stabilisation strategies that meet functional, operational, sustainability, and spatial requirements in underground space development.

2 DETAILED INVESTIGATION

2.1 *Maximum span opening*

Kong et al. (2025) conducted a parametric study using finite element method (FEM) simulations to evaluate the maximum feasible span of rock-reinforced caverns under varying geological conditions. The study involved 180 models, incorporating three Geological Strength Index (Hoek 1994; Hoek et al. 1995; Hoek & Brown 1997; Hoek et al. 1998; Marinos & Hoek 2001; Hoek & Brown 2019) values (GSI of 35, 45, 55), three uniaxial compressive strengths (UCS of 35, 70, 100 MPa), four arch geometries (rise-to-span ratios of 0.1 to 0.4), and five *in-situ* stress ratios [3, 2, 1.5, 1.25, as $\boldsymbol{k} = 0.5 + (150 / \text{depth})$ corresponding to depths of 60–300 m, respectively]. Based on the simulation results, the authors derived an empirical equation (Equation 1) to estimate the maximum stable span for caverns constructed in these conditions.

$$span = \left(\frac{F_{arc} \cdot E_{rm} \cdot I}{P_{roof} \cdot e^{F_s \cdot k}}\right)^{\frac{1}{4}} \quad (1)$$

Where F_{arc} = Roof arch factor, refer to Table 1; F_s = Load-stress factor; refer to Table 2; E_{rm} = Rock mass deformation modulus in MPa; I = Moment of Inertia of the "effective bolt length", i.e., (Bolt length – Bolt spacing)^3 / 12; P_{roof} = Q support pressure (Barton et al. 1974) in MPa; and $\boldsymbol{k}$ = *In-situ* stress ratio, i.e., horizontal stress / vertical stress.

In the study by Kong et al. (2025), rock reinforcement techniques were evaluated without incorporating a shotcrete protection liner to isolate the effects of rock reinforcement alone. The authors noted that including a shotcrete liner would introduce structural beam effects, contributing additional support to the excavation. While the primary role of shotcrete is to retain small wedge

failures between rock bolts, its design principles are beyond the scope of this paper. The investigation focused solely on rock reinforcement performance.

Table 1. Proposed roof arch factor (F_{arc}) of different roof arch geometries for the Equation (1).

Rise-to-Span Ratio of Arch	Arch Factor, F_{arc}
0.1	19.68
0.2	34.69
0.3	41.33
0.4	43.05

Table 2. Proposed load-stress factor (F_s) for the Equation (1).

Rock mass of 35 ≤ GSI ≤ 45		Rock mass of GSI = 55	
In-situ Stress *k*-ratio (Depth)	F_s	*In-situ* Stress *k*-ratio (Depth)	F_s
1.0 (300 m)	$3711.9 \cdot E_{rm}^{-0.715}$	1.0 (300 m)	$1E7 \cdot E_{rm}^{-1.66}$
1.25 (200 m)	$790.38 \cdot E_{rm}^{-0.578}$	1.25 (200 m)	$148526 \cdot E_{rm}^{-1.24}$
1.5 (150 m)	$504.25 \cdot E_{rm}^{-0.559}$	1.5 (150 m)	$2255.5 \cdot E_{rm}^{-0.813}$
2.0 (100 m)	$208.36 \cdot E_{rm}^{-0.485}$	2.0 (100 m)	$-9E\text{-}5 \cdot E_{rm} + 1.9683$
3.0 (60 m)	$348.57 \cdot E_{rm}^{-0.584}$	3.0 (60 m)	$-0.0001 \cdot E_{rm} + 1.984$

As outlined in Eq. (1), two rock mass groups, GSI 35–45 and GSI 55, were analysed. Results showed that, under identical ground and *in-situ* stress field conditions, different roof arch shapes produced varying maximum stable spans. The probable maximum span increased exponentially with the rock mass deformation modulus. Openings in fair quality rock mass (GSI = 55) supported significantly larger spans than those in lower-quality strata (GSI 35–45), highlighting the influence of rock mass quality and arch geometry on excavation stability.

2.2 *Methodology of the current investigation*

In this study, rock support load is estimated as the product of Q-support pressure and the opening span. According to the structural arch model and Dinnik's (1946) critical load theory, an arch's load-carrying capacity is proportional to its span. Kong et al. (2025) demonstrated that, under identical rock mass conditions and *in-situ* stress fields, different roof arch geometries yield varying maximum stable spans. Among these, the high-rise arch (Arch 0.4, with a rise-to-span ratio of 0.4) achieved the largest stable span.

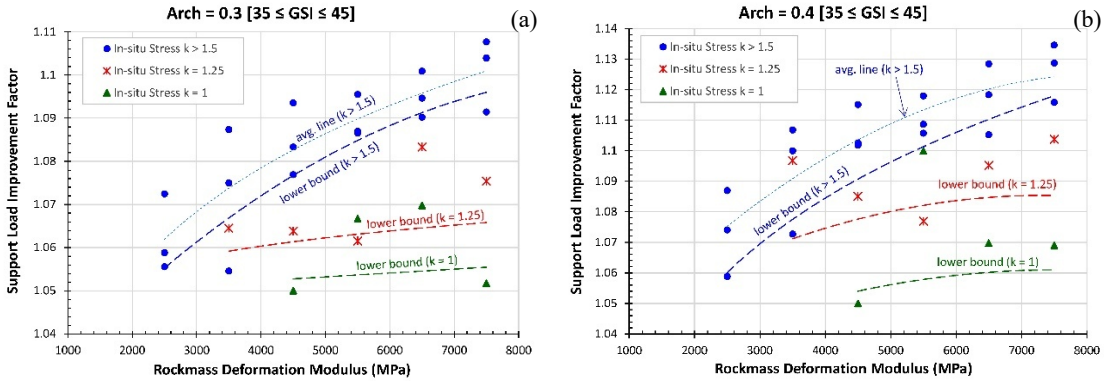


Figure 2. Recommended support load improvement factor for opening created in rock masses GSI 35–45 ground conditions. (a) Arch 0.3 opening. (b) Arch 0.4 opening.

To initiate the investigation into support pressure variations across arch shapes, a standard arch geometry with a rise equal to one-fifth of the span (Arch 0.2), as recommended by GEO (2018), was selected as the baseline for Q-support pressure. Using Eq. (1), the span differences between Arch 0.2 and Arch 0.3, and Arch 0.2 and 0.4 were expressed as fractions, representing relative load capacities. This ratio is termed the "Support Load Improvement Factor" for determining the Q-support pressure reduction. Results for Arches 0.3 and 0.4 are presented in Figure 2 (above)

and Figure 3 (below) for two rock mass groups of GSI 35–45 and GSI 55, corresponding approximately to Q-values of 0.2–1 and 4, respectively. It can be found that the Support Load Improvement Factor of Arch 0.1 is less than 1.0 because its opening span is smaller than Arch 0.2 opening (i.e. the base case) under the same rock mass conditions. These results are shown in Figure 4.

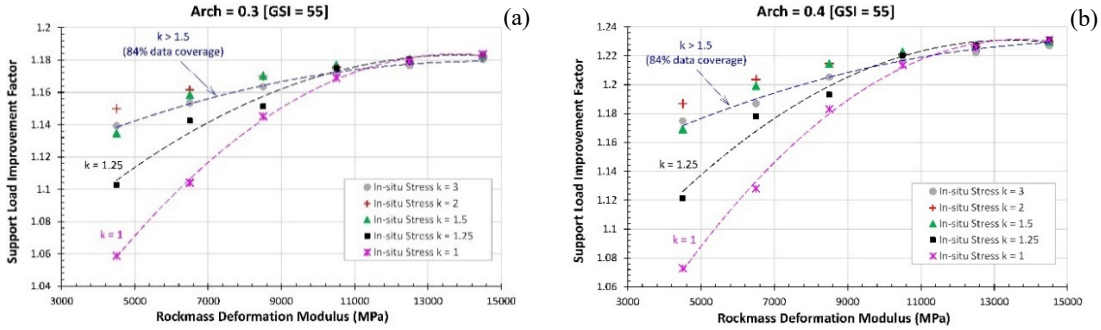


Figure 3. Recommended support load improvement factor for opening created in rock masses GSI = 55 ground conditions. (a) Arch 0.3 opening. (b) Arch 0.4 opening.

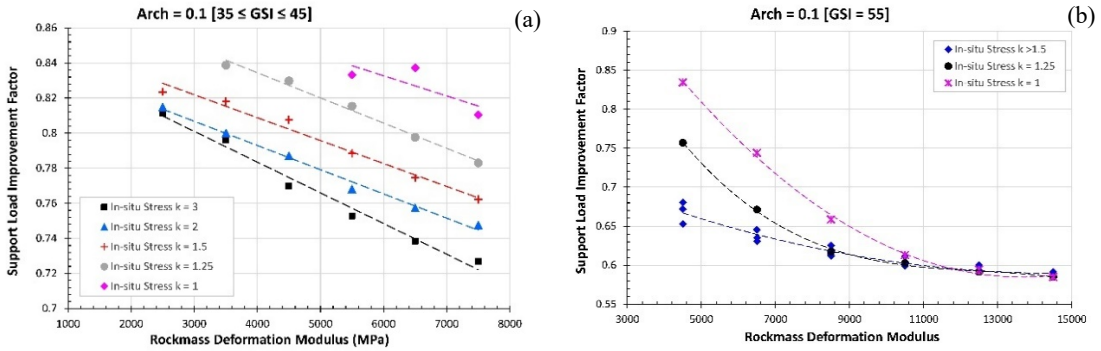


Figure 4. Support load improvement factor for Arch 0.1 opening created in a range of rock masses conditions. (a) opening created in rock masses GSI 35–45. (b) opening created in rock mass GSI = 55.

2.3 *Findings*

The investigation revealed that in poor rock mass conditions (GSI 35–45) with low rock mass deformation modulus, adopting alternative arch geometries can significantly reduce the required Q-support pressure. For example, using an Arch 0.3 shape instead of Arch 0.2 results in a support load reduction of at least 4.8%, calculated as '1 - 1/Support Load Improvement Factor'. For Arch 0.4, the reduction increases to approximately 5.7%. As the rock mass deformation modulus increases to 7.5 GPa, and under *in-situ* stress field conditions of $\boldsymbol{k} \geq 1.5$ (i.e., depths within 150 m), the required support pressure reductions rise to 9.5% and 12% for Arches 0.3 and 0.4, respectively. In media with a rock mass deformation modulus of 7.5 GPa and lower *in-situ* stress ($\boldsymbol{k}$ = 1.25 and 1.0, corresponding to depths of 200 m and 300 m), the reductions for Arch 0.3 range from 6.1% to 5.2%, and for Arch 0.4 from 7.8% to 5.7%.

In fair rock mass conditions (GSI = 55) with rock mass deformation modulus ≥ 4.5 GPa, more substantial reductions are observed. For Arch 0.3, support pressure savings range from 5.7% to 12.3% across *in-situ* stress fields from $\boldsymbol{k}$ = 1.0 to ≥ 1.5 respectively. Arch 0.4 offers even greater reductions, from 6.1% to 14.2% respectively. When the rock mass deformation modulus increases to 14.5 GPa, reductions converge to approximately 15.3% and 18.7% for Arches 0.3 and 0.4, respectively, regardless of *in-situ* stress conditions.

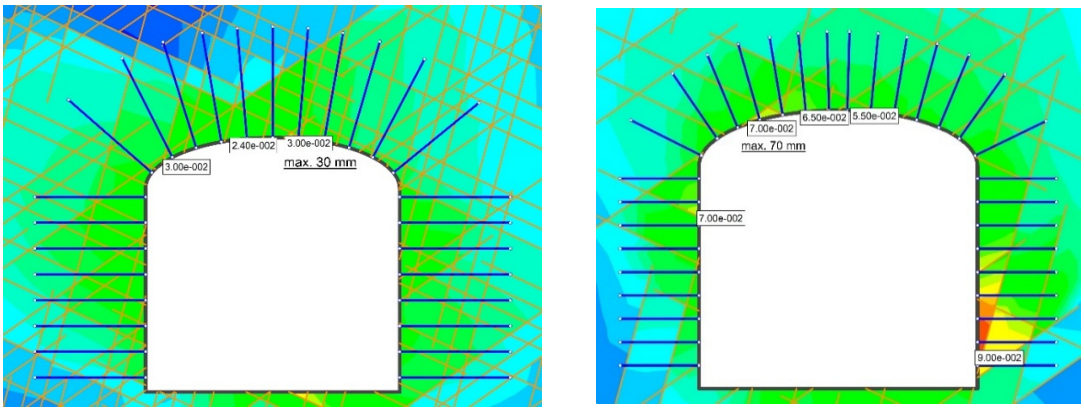
Conversely, an Arch 0.1 opening designed to match the maximum span of Arch 0.2 requires significantly more support due to its lower structural stiffness when using the same rockbolt pattern. However, if Arch 0.1 is constructed within its permissible span using reinforcement techniques, the Q-system (Barton et al. 1974) remains valid for estimating support pressure.

3 VALIDATION OF THE PROPOSED SUPPORT PRESSURE IMPROVEMENT

Original Arch 0.2 openings examined in the Kong et al. (2025) study were used as reference cases to validate the proposed Q-system support pressure reductions for Arches 0.3 and 0.4. The verification employed the RS2 (Rocscience, 2021), incorporating three main joint sets in a parallel deterministic pattern, consistent with Kong et al. (2025). Joint network configurations followed recommendations by Kong & Karlovsek (2024), yielding results closely aligned with field monitoring data. Opening stability was assessed using the Roof Sagging Ratio (RSR) criterion, where RSR > 0.50% indicates instability, as defined by Zhang & Mitri (2008), Abdellah (2015), and Abdellah et al. (2022). Input parameters for Models 1 and 2 are summarised in Table 3, with simulation outcomes illustrated in Figure 5.

Table 3. Parameters used for the original Arch 0.2 models from Kong et al. (2025).

Model	GSI	Rock Mass Deform. Mod.	Support Pressure	Bolt Spacing	Bolt Length	Depth of Opening	Opening Span
1	35	2.78 GPa	395 kPa	0.71 m	3.05 m	60 m	7 m
2	55	12.25 GPa	126 kPa	1.26 m	4.25	200 m	15 m



(a) Original Model 1 with Arch 0.2 (b) Original Model 2 with Arch 0.2

Figure 5. Simulation results for original Arch 0.2 models extracted from Kong et al. (2025).

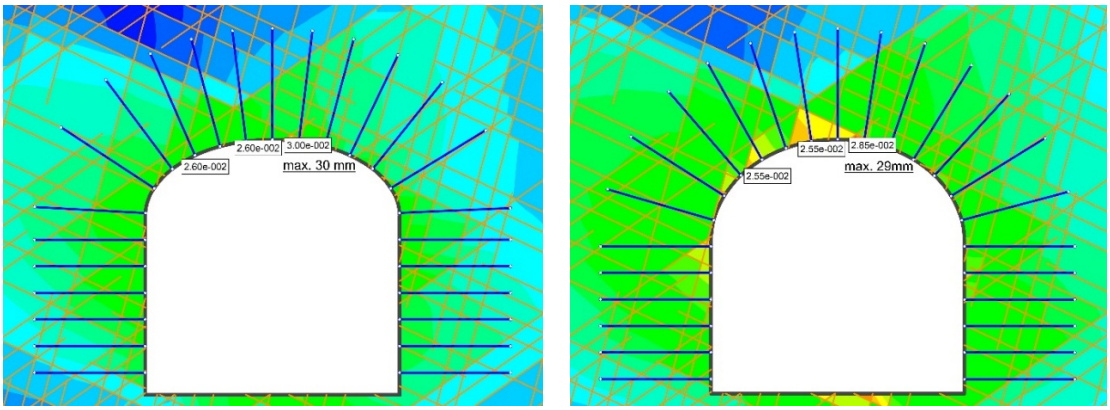
In this validation study, the support load improvement factors for Arches 0.3 and 0.4 were derived from Figures 2 and 3, corresponding to basic Models 1 and 2, respectively. Verification results for these arches, developed under the conditions of Models 1 and 2, are summarised in Table 4 and presented in Figures 6 and 7.

Table 4. Comparison of validation results for Arch 0.3 and Arch 0.4 with original Arch 0.2 models.

Model	Original Arch 0.2				Arch 0.3				Arch 0.4			
	F	P_{roof}	D	RSR%	F	P_{roof}	D	RSR%	F	P_{roof}	D	RSR%
1	1	395	30	0.429	1.055	374.3	30	0.429	1.06	372.5	29	0.414
2	1	126	70	0.467	1.11	113.5	72	0.480	1.14	110.5	72	0.480

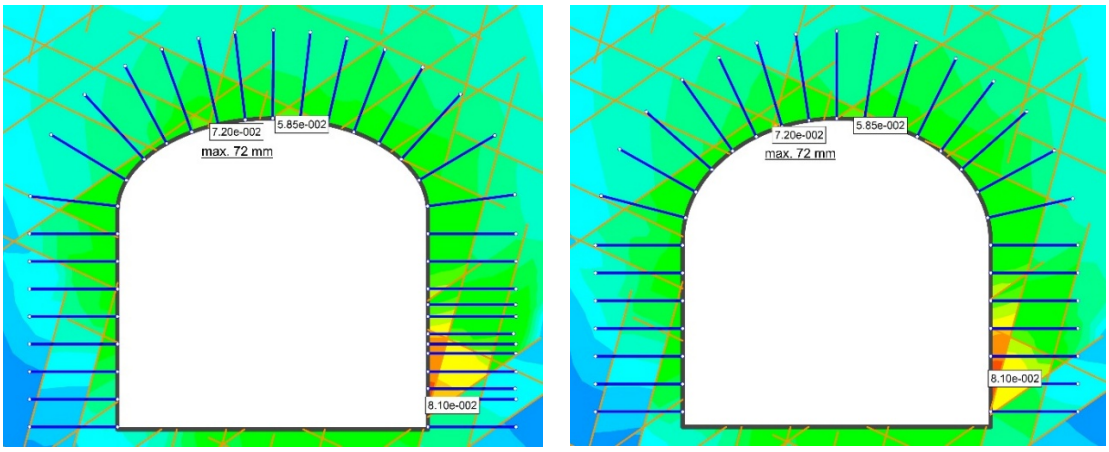
Notes: P_{roof} = Q-support pressure in kPa; D = Roof deformation at opening, in millimeters; F = Support Load Improvement Factor obtained from Figures 2 or 3; RSR% = Roof sagging ratio in percentage.

All results confirm the stability of the openings based on the RSR criterion, with less than 0.5% RSR detected. The difference in roof deformation (RSR%) between the baseline Arch 0.2 and Arches 0.3 and 0.4 remains below 3.5%. These findings validate the proposed Q-support pressure improvements for Arches 0.3 and 0.4 under the two rock mass conditions.



(a) Model 1 – Arch 0.3 (b) Model 1 – Arch 0.4

Figure 6. Validation models for Arches 0.3 and 0.4 created under identical conditions as Model 1.



(a) Model 2 – Arch 0.3 (b) Model 2 – Arch 0.4

Figure 7. Validation models for Arches 0.3 and 0.4 created under identical conditions as Model 2.

4 COST BENEFIT COMPARISON AMONG DIFFERENT ARCH SHAPES OPENING

Several countries and regions including Australia (ATS 2024), Hong Kong (GEO 2018), Scandinavia (NGI 2015), Singapore (LTA 2019), the US (NHI 2009), and the UK (BTS & ICE 2004) recognise the Q-system for estimating support in arch-shaped rock mass openings. However, the current investigation reveals that different arch geometries require varying support pressures, even under identical ground conditions and spans. Notably, high-rise arches demand less support than the baseline Arch 0.2. Consequently, rockbolt spacing must be adjusted accordingly when using bolts of equal capacity. A cost-benefit comparison, considering rockbolt usage and excavation volume, was conducted for Arches 0.2, 0.3, and 0.4, using Models 1 and 2 as baselines. Detailed results are presented in Table 5.

Table 5 presents a comparative analysis of Models 1 and 2 under two scenarios. In Case 1, where full arch void utilisation is considered, such as in multi-lane road tunnels, the high-rise Arch 0.4 opening demonstrates advantages over the baseline Arch 0.2. It requires fewer rockbolts and results in reduced excavation volume due to lower support demands and wider bolt spacing. However, in Case 2, where wall height is the primary constraint, typical of underground powerhouses, the arch void offers limited spatial benefit. Here, high-rise arch openings may lead to increased rockbolt usage and greater excavation volume compared to Arch 0.2.

This cost-benefit comparison provides practical guidance for underground space designers, emphasizing the importance of aligning opening geometry with functional, spatial utilisation, and economic considerations.

Table 5. Constructability comparison among Arches 0.2, 0.3 and 0.4 openings.

Model 1 (GSI = 35) and Cavern Span = 7 m				Model 2 (GSI = 55) and Cavern Span = 15 m			
Aspect of Interest	Arch 0.2	Arch 0.3	Arch 0.4	Aspect of Interest	Arch 0.2	Arch 0.3	Arch 0.4
Arch Rise (m)	1.4	2.1	2.8	Arch Rise (m)	3	4.5	6
Arch Void Area, m²	7.7	11.6	15.4	Arch Void Area, m²	35.3	53.0	70.7
Arch Void % Diff	-	50.0	100.0	Arch Void % Diff	-	50.0	100.0
No. of Roof Bolts	11	13	13	No. of Roof Bolts	14	15	15
Bolts Spacing (m)	0.71	0.73	0.73	Bolts Spacing (m)	1.26	1.33	1.35
Case 1				Case 1			
Clear Opening Height*	7	7	7	Clear Opening Height*	15	15	15
No. of Wall Bolts	16	12	12	No. of Wall Bolts	18	16	14
Total of Bolts	27	25	25	Total of Bolts	32	31	29
X-sect. Area of Opening, m²	46.9	45.9	44.8	X-sect. Area of Opening, m²	215.3	210.5	205.7
X-sect. Area % Diff	-	-2.2	-4.5	X-sect. Area % Diff	-	-2.2	-4.5
Case 2				Case 2			
Fixed Wall Height#	5.6	5.6	5.6	Fixed Wall Height#	12	12	12
No. of Wall Bolts	16	16	16	No. of Wall Bolts	20	18	18
Total of Bolts	27	29	29	Total of Bolts	34	33	33
X-sect. Area of Opening, (m²)	46.9	50.8	54.6	X-sect. Area of Opening, (m²)	215.3	233.0	250.7
X-sect. Area % Diff	-	8.2	16.4	X-sect. Area % Diff	-	8.2	16.4

* denotes the overall height measured from invert to crown.
# denotes the height of the wall, measured from invert to bearing point of arch, i.e. the shoulder of the opening.

5 DISCUSSIONS AND CONCLUSIONS

The findings of this study demonstrate that arch-shaped openings require varying support pressures to maintain stability, even under identical ground conditions and spans. In better-quality rock masses with greater rock mass deformation modulus, high-rise arch openings demand up to 18.7% less support pressure than the baseline Arch 0.2 configuration that is estimated using the Q-system. This reduction translates to fewer rockbolts required for stabilisation due to decreased support loads and wider bolt spacing.

For openings exceeding the permissible span limits, a hybrid support system combining patterned rockbolts with concrete or shotcrete lining, is necessary to enhance lining stiffness and ensure structural stability.

Rock reinforcement remains a cost-effective and sustainable solution for underground development. This study presents a cost-benefit comparison across different arch geometries, offering valuable insights for designers and developers. The results support the selection of opening shapes that balance sustainability, functionality, spatial utilisation, and economic viability.

It is important to note that this study focused on two rock mass groups under specific conditions. Therefore, extrapolation beyond these parameters should be approached with caution. Further research is recommended to address these limitations and expand the applicability of the findings.

6 REFERENCES

ATS. 2024. *Tunnel Design Guideline*. Australian Tunnelling Society / Engineer Australia.

Abdellah, W.R.E. 2015. Numerical Modelling Stability Analyses of Haulage Drift in Deep Underground Mines. *J. Eng. Sci.*, 43(1), 71–81. https://doi.org/10.21608/jesaun.2015.115148

Abdellah, W.R., Ali, M.A. & Yang, H. 2018. Studying the effect of some parameters on the stability of shallow tunnels. *Journal of Sustainable Mining*, 17(1), 20–33.

Abdellah, W.R., Haridy, A.K.A., Mohamed, A.K., Kim, J. & Ali, M.A.M. 2022. Behaviour of Horseshoe-Shaped Tunnel Subjected to Different in Situ Stress Fields. *Appl. Sci.,* 2022, 12, 5399.

BTS & ICE. 2004. *Tunnel Lining Design Guide*. The British Tunnelling Society and The Institution of Civil Engineers. Thomas Telford, London, UK.
Barton N., Lien R. & Lunde J. 1974. Engineering Classification of Rock Masses for Design of Tunnel Support. *Rock Mech.,* 6, 189–236.
Dinnik, A.N. 1946. *The Stability of Arches*. Gostekhizdat, Moscow-Leningrad. (in Russian)
GEO. 2018. *Guide to Cavern Engineering*. 2nd Edition. Geotechnical Engineering Office, Civil Engineering Department, the Government of Hong Kong SAR.
Goel, R.K. & Jethwa, J.L. 1991. Prediction of support pressure using RMR classification. Proc. *Indian Getech. Conf.*, Surat, India, 203–205.
Hoek, E. 1994. Strength of Rock and Rock Masses. *ISRM News Journal*, 2(2), 4-16.
Hoek, E. & Brown, E.T. 1997. Practical estimates or rock mass strength. *Int. J. Rock Mech. & Mining Sci. & Geomechanics Abstr.*, 34(8), 1165–1186.
Hoek, E. & Brown, E.T. 1988. The Hoek-Brown failure criterion – a 1988 update. *Proceedings of the 15th Canadian Rock Mechanics Symposium*, 1988, 31–38.
Hoek, E. & Brown, E.T. 2019. The Hoek-Brown Failure Criterion and GSI - 2018 Edition. *J. Rock Mech. & Geotech. Eng.*, 11-3, 445–463. https://doi.org/10.1016/j.jrmge.2018.08.001
Hoek, E., Kaiser, P.K., & Bawden, W.F. 1995. *Support of Underground Excavations in Hard Rock*. Rotterdam, Balkema.
Kong, K.W.K. & Karlovsek, J. 2024. Recommended Rock Joints Setting in 2D FEM Simulations for Engineering Design of Excavations Created in Jointed Rock mass. Australian Journal of Multi-Disciplinary Engineering, 20(1), 88–106. https://doi.org/10.1080/14488388.2024.2328454
Kong, K., Rajabi, M. & Karlovsek, J. 2024. Natural Creation of Large Rock Cavern: Can We Construct Them? Jenolan Caves as a Case Study. Appl. Sci., 2024, 14, 10983.
Kong, W.K., Rajabi, M. & Karlovsek, J. 2025. How Wide Can a Rock-Reinforced Cavern Be Opened – a Parametric Desktop Investigation. Tunnelling and Underground Space Technology. Available at SSRN: http://dx.doi.org/10.2139/ssrn.5208677
Jia, P. & Tang, C.A. 2008. Numerical study on failure mechanism of tunnel in jointed rock mass. Tunnelling and Underground Space Technology, 23 (5), 500–507.
LTA. 2019. *Engineering Group – Civil Design Criteria for Road and Rail Transit Systems*, E/GD/09/106/A2. Land Transport Authority, Singapore Government.
Marinos, P. & Hoek, E. 2001. Estimating the Geotechnical Properties of Heterogeneous Rock Masses such as Flysch. *Bull. Engg. Geol. Env.*, 60, 85–92. https://doi.org/10.1007/s100640000090
Mazraehli, M. & Zare, S. 2022. Probabilistic Estimation of Rock Load Acting on Tunnels Considering Uncertainty in Peak and Post-peak Strength Parameters. *Geotech. Geol. Eng.*, 40, 2719–2736.
Mikhelson, L. 2004. *Structural Engineering Formulas*. Mcgraw-Hill.
NHI. 2009. *Technical Manual for Design and Construction of Road Tunnels – Civil Elements*. Publication No. FHWA-NHI-10-034. National Highway Institute, U.S. Department of Transportation, Federal Highway Administration, Washington, D.C. 20590.
NGI. 2015. Handbook – Using the Q-system : Rock Mass Classification and Support Design. Norwegian Geotechnical Institute, Oslo, Norway.
Osgoui, R.R. & Ünal, E. 2009. An empirical method for design of grouted bolts in rock tunnels based on the Geological Strength Index (GSI). *Engineering Geology*, 107, Issues 3-4, 154–166.
Park, D. & Michalowski, R.L. 2019. Roof stability in deep rock tunnels. *International Journal of Rock Mechanics & Mining Sciences*, 124, Article 104139.
Rocscience. 2021. *RS2 (formerly Phase² v9) Numercial Software Package*. Rocscience Inc. Toronto. www.rocscience.com
Shiau, J., Keawsawasvong, S. & Sorawit Seehavong, S. 2022. Stability of Unlined Elliptical Tunnels in Rock Masses. *Rock Mechanics and Rock Engineering*, 55, 7307–7330
Taghizadeh, H., Zare, S. & Mazraehli, M. 2020. Analysis of Rock Load for Tunnel Lining Design. *Geotech. Geol. Eng.*, 38, 2989–3005. https://doi.org/10.1007/s10706-020-01202-y
Terzaghi, K. 1946. Rock defects and loads on tunnel support. In R. V. Proctor and T. L. White (eds), *Introduction to Rock Tunnelling with Steel Supports. Section I*. Commercial Sheering & Stamping Co, Youngstown, Ohio, USA.
Ünal, E. 1983. *Design guidelines and roof control standards for coal mine roofs*. PhD thesis, Pennsylvania State University, University Park, 355p.
Varma, M., Maji, V.B. & Boominathan, A. 2022. Seismic Assessment of Shotcrete Support in Jointed Rock Tunnels. *International Journal of Geosynthetics and Ground Engineering*, 8, Article 51.
Wang, Y., Ling, K., Yang, Y., Zhang, Z., Xing S., He, M. & Liu, D. 2023. Experimental study on rockburst of surrounding rock in an elliptical tunnel with different axial ratios. *Tunnelling and Underground Space Technology*, 140, Article 105329. https://doi.org/10.1016/j.tust.2023.105329
Zhang, Y. And Mitri, H.S. 2008. Elastoplastic Stability Analysis of Mine Haulage Drift in the Vicinity of Mined Stopes. *Int. J. Rock Mech. & Min. Sci*., 45(4), 574–593.

19th Australasian Tunnelling Conference – Acosta-Martínez, Stewart and Hudson-Smith (Eds.)
© 2025 Australian Tunnelling Society, ISBN 978-0-85825-002-4

Evaluating Progress: Trends in respirable crystalline silica exposure in tunnel construction

K. Cole & T. Driscoll
The University of Sydney, NSW, Australia

ABSTRACT: Silicosis remains the most prevalent work-related health condition reported among tunnel workers worldwide, highlighting the ongoing concern regarding respirable crystalline silica (RCS) exposure in the tunnelling industry. Advancements in engineering controls and work practices have been implemented to mitigate RCS exposure. This study analysed RCS exposure trends from 2016 to 2024 across tunnelling projects in New South Wales, Australia with the aim of evaluating the effectiveness of those measures in reducing exposure over time. Using exposure monitoring data from multiple tunnel construction projects, this analysis identifies trends in RCS levels across different workgroups, highlighting areas of progress as well as persisting challenges. The findings provide valuable insights into the effectiveness of current control strategies and pinpoints areas where additional engineering interventions are needed to further reduce exposure. Preliminary results indicate that while overall exposure levels have decreased in some tunnelling environments, certain workgroups remain at risk of high exposure to RCS. This research reinforces the need for continued innovation in engineering solutions, including improved ventilation and dust suppression technologies. By examining industry-wide exposure trends, this study aims to guide future engineering interventions, with the aim of ultimately creating a safer working environment for tunnel construction workers.

1 INTRODUCTION

Tunnel construction workers (TCWs) operate in environments that can be hazardous to their health. While various work-related diseases have been reported in TCWs globally, the literature indicates that important levels of respiratory disorders are frequently reported, silicosis being the most common. This emphasises silicosis as an on-going concern within the tunnelling sector (Cole and Driscoll 2025).

The primary risk factor for silicosis is cumulative exposure to respirable crystalline silica (RCS). Recognising the risks of RCS exposure, the Australian Tunnelling Society (ATS) established the Air Quality Working Group in 2017. The group developed standardised resources to add to the industry's body of knowledge to support the management of RCS (Cole 2019).

Several advancements in engineering controls and work practices have been implemented across various tunnelling projects to mitigate RCS exposure. These have ranged and included ventilation improvements, the increased use of enclosed heavy plant cabins, dust suppression, misting systems, mobile dust collectors for dust control, shrouds to better capture dusts at the source, improved housekeeping practices and real time monitoring (Sydney Metro 2020, Sydney Metro 2020, Sydney Metro 2020, Cole, Och et al. 2021, Fanning and Allan 2023). However, despite these advancements, challenges remain in effectively managing RCS exposure underground (Oliveira 2019).

Our research found that in the workforces that built several Queensland tunnels in the last decade, one in ten tunnel workers were estimated to develop silicosis (Cole, Carey et al. 2025), reinforcing the need to reduce exposure.

Airborne RCS measurements are routinely conducted by occupational hygienists across tunnel projects to assess workers exposure. Although this monitoring is common, researchers often have limited access to the data, making it difficult to evaluate whether exposure levels have improved, worsened, or remain unchanged over time. While tunnelling contractors retain custody of RCS monitoring reports, government agencies may also hold copies under certain circumstances. These may be obtained through contractual arrangements or as part of audit and assurance processes. In some cases, health and safety regulators request the reports to assist with compliance monitoring or enforcement.

When RCS data are held by government agencies, researchers can seek access through freedom of information (FOI) processes, with decisions based on public interest considerations. Additionally, the New South Wales Legislative Council can compel the production of documents from government agencies through an Order for Papers under Standing Order 52. Documents provided under this process are tabled in Parliament and become publicly accessible.

This study aimed to identify areas of progress and areas where additional engineering interventions may be needed to further reduce RCS exposure. It involved obtaining RCS exposure data that was collected during tunnel construction in New South Wales (NSW), Australia, between 2016 and 2024. The data was used to examine trends across multiple projects and work groups. This analysis focused on select work groups involved in three common tunnel construction methods: through tunnel boring machine (TBM), mined tunnelling, and cut and cover tunnelling.

2 METHOD

2.1 *Accessing RCS Data*

In conducting this research, applications were submitted to state and federal government agencies through their respective FOI legislative frameworks. In addition, the Australian Workers Union (AWU), which represents tunnel workers, was contacted to request voluntary access to existing datasets on air monitoring results for respirable dust and RCS in tunnelling. The AWU granted access to information they had previously obtained through their own FOI requests, which was used to support this study.

In late 2024, a request under Standing Order 52 led to the release of NSW government documents relating to RCS in air monitoring (Parliament of New South Wales 2024). These included data from multiple tunnel projects constructed since 2017, which were also accessed for this study.

2.2 *Analysing RCS Data*

The results of RCS and respirable dust exposure from personal exposure samples were reviewed and manually extracted into MS Excel. Each result was assigned a unique identifier for each tunnel project and tunnel site. The way that workers were categorised across each tunnel project was similar, but not identical. Reports containing qualitative information of worker activities performed during sample collection were used to categorise the exposure result by location, tunnelling method (e.g. TBM, mined tunnelling, cut and cover tunnelling) and work group. Duplicate records were identified and removed. Data were categorised into broad work group based on the qualitative descriptors provided.

Results were summarised by recording the number of samples (n) and geometric standard deviation (GSD). For each work group, the estimated arithmetic mean (AMest) and corresponding 90% credible interval (CI) was calculated using the Expostats toolkit, which applies Bayesian methods as described by Lavoué, Joseph et al. (2018). Censored data was processed through ND Expo.

The geological conditions in the regions where tunnels were constructed varied in their crystalline silica content of the host rock. This variability contributed to wide GSDs in RCS data. To provide a more consistent comparison, GSDs were reported using respirable dust data only. Due to this variability, it was also considered that examination of changes over time would be better undertaken using respirable dust exposures rather than RCS levels.

Where datasets contained less than three results and/or less than three days of monitoring, they were excluded from this analysis. All data presented in this analysis do not consider the use of respiratory protective equipment (RPE) where it was used. Qualitative information contained in air monitoring reports were used to identify potential factors that may have contributed to elevated or decreasing levels of respirable dust and RCS.

3 RESULTS

RCS exposure data were available from 12 tunnel projects, with data spanning an eight-year period from 2016 to 2024. The information obtained included individual and summary exposure monitoring results, qualitative descriptions of work activities and various tables. Data formats varied and included hard copy paper files, electronic PDF documents, and MS Excel spreadsheets.

Tunnel projects used various construction methods, with TBM, mined tunnelling and cut and cover tunnelling being the most common. While the complete dataset comprised approximately 3,300 individual exposure results, this study focuses on the analysis of around 2,000 results. Data are presented by tunnelling method, with each project assigned a unique identifier to preserve anonymity.

3.1 *TBM Tunnelling*

Exposure data from workers constructing tunnels using TBMs were available from six projects. Figure 1 displays the AMest and CI for both respirable dust and RCS across each project.

Hard rock TBMs were used across all projects except for one (Project 6) which employed a mixed shield slurry TBM. Worker exposures on the mixed shield TBM were significantly lower than on hard rock TBMs. Mean RCS exposures across hard rock TBM projects ranged from 0.05 to 0.1 mg/m^3 with mean respirable dust exposures ranging from 0.22 to 0.52 mg/m^3.

Data were available from four projects for trend analysis; however insufficient data were available for TBM operators and ring builders on Project 5. A general upward trend over time in respirable dust exposures for workers stationed on TBMs was identified for operators, ring builders and backend workers (Fig. 2). The most significant increases were observed among backend workers (these are the workers that extend services, manage conveyors, handle segments, and perform grouting tasks).

Several factors were identified as likely contributing to elevated levels of RCS in TBM environments. These included inadequate ventilation systems, which were observed to have air velocities below 0.5 metres per second (m/s) in areas where workers were present and therefore limiting the effective removal of airborne dust. The absence of proper sealing, filtration, and positive pressurisation in TBM operator cabins and crib rooms further reduced the effectiveness of containment controls. Instances were also reported where domestic-grade air purifiers were used to clean the air; although these units were not designed for industrial applications and provided limited benefit. In addition, housekeeping practices such as infrequent washdowns of TBMs allowed dust to accumulate and then become airborne when disturbed. Dust released from conveyor belts during operation was another common and significant source of RCS.

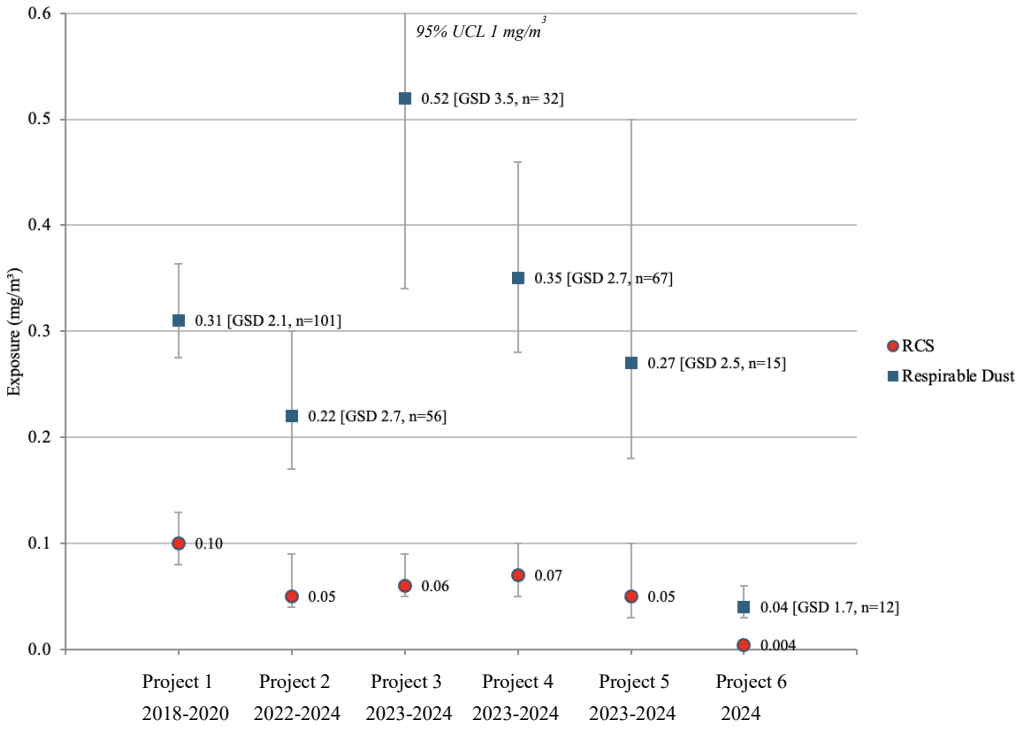


Figure 1. Respirable dust and RCS exposures to TBM workers

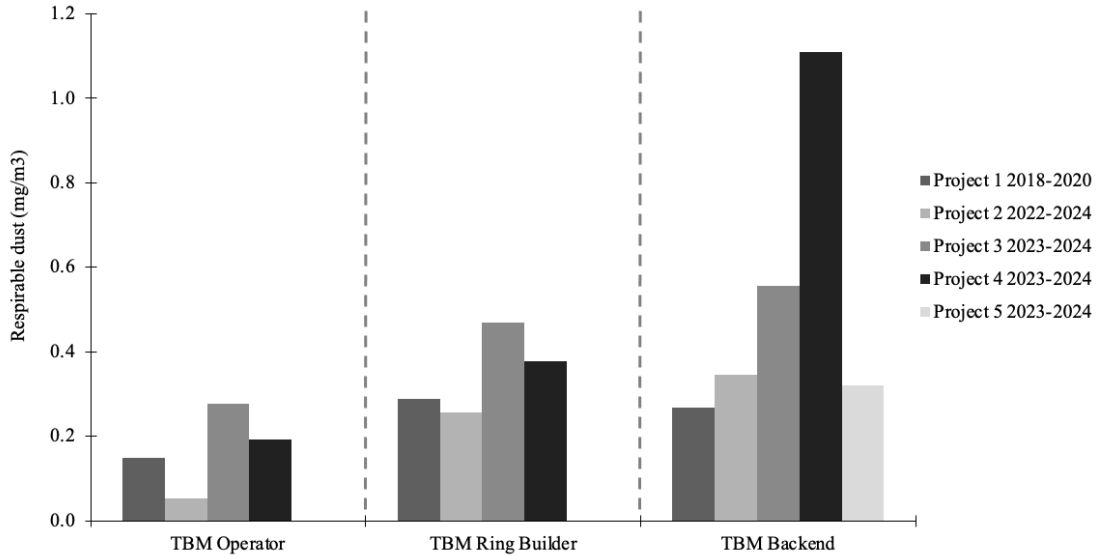


Figure 2. Mean (AMest) respirable dust exposures to workers on TBMs grouped by work group and project.

3.2 *Mined tunnelling*

Exposure data from workers constructing tunnels using mined methods were available from 12 projects. Figure 3 displays the mean (AMest) and CI for both respirable dust and RCS across each project. Mean RCS exposures ranged from 0.02 to 0.26 mg/m^3 with mean respirable dust exposures ranging from 0.22 to 0.70 mg/m^3 (Fig. 3). Note for one project (Project E) only summary exposure data by work group were provided, which prevented inclusion of the full dataset in Figure 3.

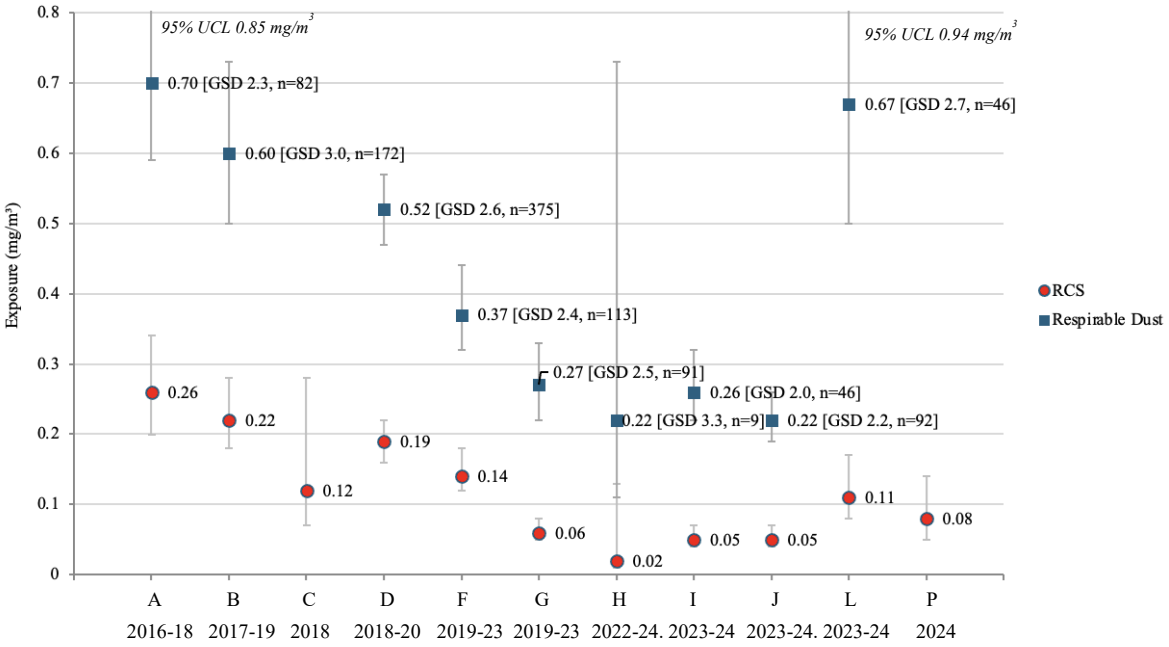


Figure 3. Respirable dust and RCS exposures to workers on mined tunnelling projects

The highest exposures to workers on mined tunnel projects were of workers who operated roadheaders without cabins. Mean (AMest) RCS exposures were 5.1 mg/m^3 (CI 2.5-19) from a project constructed between 2019-2020. While insufficient data was available to enable trending, this level of exposure demonstrates significant exposures to RCS when this machinery is employed.

Other high exposed workers included those who operated roadheaders fitted with cabins, those who operated heavy plant, and workers on foot involved in excavation of the heading. These workers were involved in ground support, waterproofing, offsiding, or were otherwise classified as 'tunnellers'.

Data were available from 12 projects to trend exposures; however, only RCS data were available from Project C so respirable dust levels were estimated based on the crystalline silica content from nearby tunnel projects under construction. Insufficient data were available for roadheader and heavy plant operators from Project H and L. A downward trend in respirable dust exposures was identified for roadheader operators, heavy plant operators and workers on foot involved in heading excavation (Fig. 4).

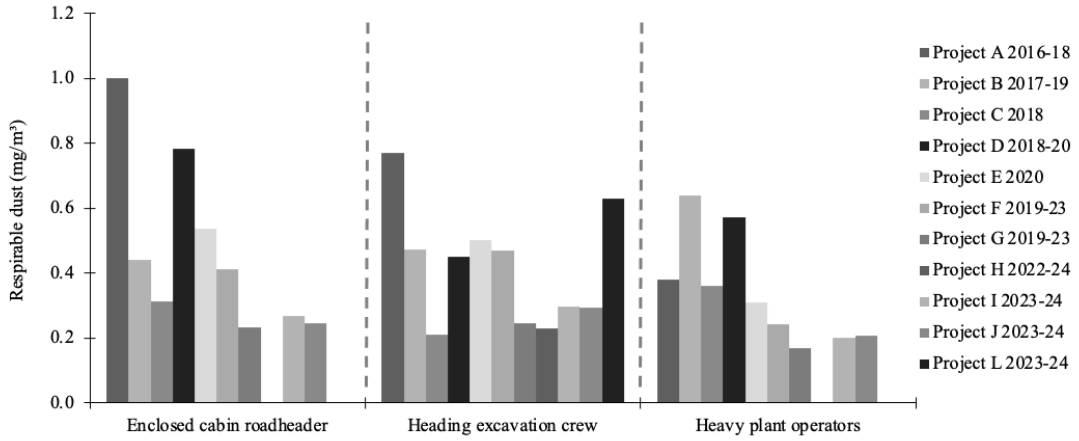


Figure 4. Mean respirable dust exposures to workers constructing mined tunnels grouped by work group and by project.

Although the data indicates a downward trend in exposures over time within mined tunnels, several challenges were evident in these environments. A common issue identified in reports was insufficient air velocity and/or extraction to effectively capture airborne dust generated during excavation. While extraction ventilation was available during roadheader operations where cabins were not used, its effectiveness was repeatedly limited. Reports also noted that extraction systems were not consistently extended following each cut or were only extended to the rear of the roadheader, allowing dust to accumulate around the machine. Elevated exposure levels were also observed during periods where multiple dust-generating activities occurred simultaneously, such as profiling in close proximity to benching operations.

Beyond roadheader operations, there was limited evidence of source-level dust extraction for heavy machinery. Water suppression systems were generally fitted to plant, though manual application by workers was also reported. Additional concerns included non-functional air-conditioning units in heavy plant, resulting in cabins being operated with doors and windows open, which compromised protection. Cabins were also reported to be affected by mud and settled dust. Over time, however, the use of sealed cabins fitted with positive pressure filtration systems became more common.

3.3 *Cut and cover tunnelling*

Exposure data from workers constructing tunnels using cut and cover methods were available from 6 projects. Figure 5 displays the mean (AMest) and CI for both respirable dust and RCS across each project. Mean RCS exposures ranged from 0.02 to 0.16 mg/m^3 with mean respirable dust exposures ranging from 0.18 to 0.25 mg/m^3 (Fig. 5).

Data were available from 6 projects for trend analysis; however, insufficient data were available for ground support workers from Project β and ε. When comparing respirable dust exposures, a downward trend was identified for ground support workers and those who operated heavy plant. However, an upward trend was identified for general labourers, who were primarily on-foot in the working area (Fig. 6).

In cut and cover tunnelling environments, fewer exposure control measures were observed compared with other tunnelling methods. Ventilation systems were rarely noted apart from the intermittent use of small air movers. While spray misters were used at times, they did not appear to effectively capture or remove airborne dust. Water suppression was applied in some instances, but its effectiveness was limited, particularly where air movement was restricted. The lack of localised dust control at the source allowed airborne dust to migrate beyond the immediate work area, exposing other workers. Similarly, water suppression systems fitted to plant equipment often did not sufficiently manage the volume of dust generated during operation. Inadequate housekeeping practices further contributed to dust accumulation in work zones.

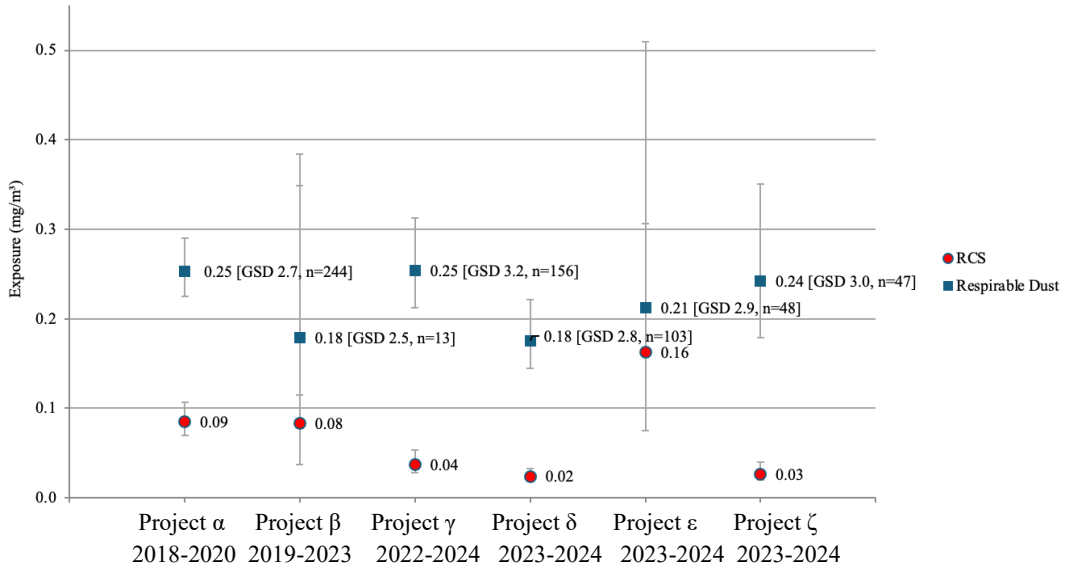


Figure 5. Respirable dust and RCS exposures to workers in tunnels built by cut and cover methods

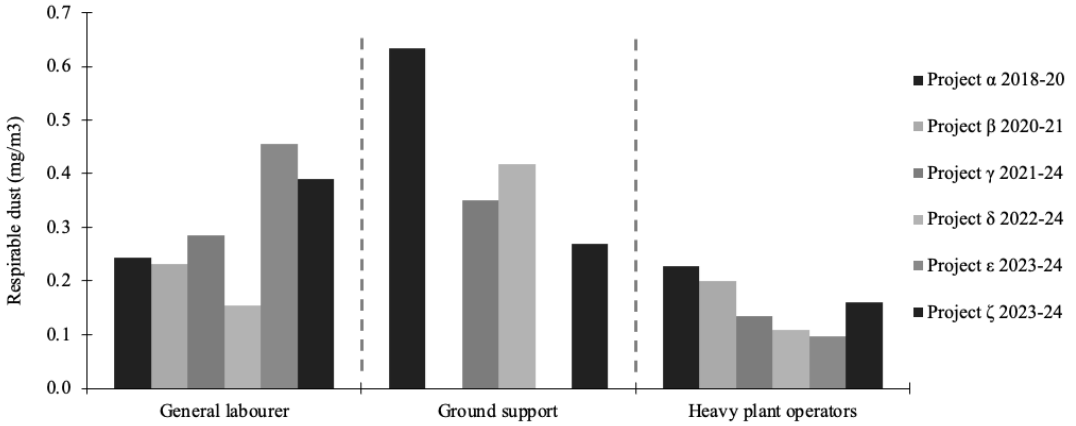


Figure 6. Mean respirable dust exposures to workers constructing cut and cover tunnels grouped by work group and by project

4 DISCUSSION

Australia has experienced a significant shift in its approach to silicosis, largely due to a rise in cases linked to the stone benchtop industry. This surge in cases has sparked broader attention to silica exposure risks across multiple sectors, including tunnelling. During the period in which this data was collected, the National Dust Disease Taskforce was established, the workplace exposure standard (WES) was halved in 2020, and in 2024, the National Silicosis Prevention Strategy was approved alongside new crystalline silica regulations. These developments reflect heightened media, political, and regulatory focus on silica-related diseases, raising expectations for enhanced risk management in high-risk industries. For the tunnelling sector, this translates into increased scrutiny and a stronger imperative to prioritise engineering controls to ensure worker protection.

The results of this study indicate both progress and ongoing challenges in reducing TCW's exposures to RCS. Decreasing exposure levels were observed over time for select work groups in mined tunnels, as well as for ground support personnel and heavy plant operators in cut-and-cover projects. However, increasing exposure levels were identified among all workers on TBMs and among general labourers in cut-and-cover tunnelling.

A review of the commentary provided in exposure monitoring reports indicated that, while some control measures were in place, there remained a heavy reliance on RPE to protect TCWs from RCS exposure. Reports included commentary on whether RPE was being used, with recommendations often focused on measures low on the hierarchy of control. In many instances, where RPE was observed and exposure levels were estimated to be below the WES, there was little emphasis in reports on improving more effective, higher order controls. However, the hierarchy of control is founded on the principle that addressing hazards at their source and modifying the work environment is more effective than relying on individual behaviour. Engineering controls offer greater effectiveness and reliability compared to ongoing reliance on personal protective equipment (Lingard and Rowlinson 2004).

There were numerous instances where RPE was not effectively used over the assessed period. This included instances where its use was not mandated, the level of protection provided was inadequate, it had not been fit-tested, workers were not clean-shaven, or it was not worn when needed. These findings highlight the importance of prioritising higher-level interventions to more effectively manage RCS exposure and reinforces the continued need for engineering controls to further improve working conditions for TCWs across multiple tunnelling methods.

Given that RCS is a confirmed human carcinogen; all measures should be taken to minimise exposure to as low as reasonably practicable, regardless of whether exposures are below the WES.

There are some limitations to consider in this study. The available exposure data covered selected periods within each tunnel project, ranging from partial to broader phases of construction. Task-specific information was sometimes limited, meaning that results were assigned based on the authors' professional judgement. While common work groups and tunnelling methods are

represented, data for all possible roles and construction approaches were not included. These limitations are considered unlikely to have introduced important bias into the study.

5 CONCLUSION

This study of exposure trends in tunnelling from 2016 to 2024 indicates both progress and ongoing challenges in improving conditions for TCWs. Decreasing exposure levels were observed over time for select work groups in mined tunnels, as well as for ground support personnel and heavy plant operators in cut-and-cover projects. However, increasing exposure levels were identified among all workers on TBMs and among general labourers in cut-and-cover tunnelling.

The data, supported by qualitative information contained in air monitoring reports, indicate that enhanced source control measures, improved ventilation and appropriate use of enclosures could provide improved protection for TBM workers. These findings also highlight the importance of integrated and fit-for-purpose dust control strategies across all aspects of TBM operations.

While exposure levels in mined tunnels showed a downward trend over time, further reductions could be achieved through more effective ventilation and dust extraction, particularly around roadheaders and during simultaneous dust-generating activities. The increased use of sealed cabins fitted with positive pressure filtration systems is a positive development in operator protection. In cut and cover tunnelling, more robust source control and ventilation measures could also reduce RCS exposure risks.

Overall, exposure levels highlight the continued need for engineering controls to further improve working conditions for TCWs across multiple tunnelling methods.

6 REFERENCES

Cole, K. (2019). "Industry bands together to address Silica Dust Exposure in the Tunnelling Industry." Journal of the Australian & New Zealand Tunnelling Societies Issue No 1: 36–38.

Cole, K., R. N. Carey and T. Driscoll (2025). "The future burden of silicosis and lung cancer among tunnel construction workers in Queensland." Annals of Work Exposures and Health.

Cole, K. and T. Driscoll (2025). A global review of work-related diseases in tunnel construction workers. World Tunnel Congress. Stockholm, ITA-AITES.

Cole, K., D. Och and L. Howard (2021). Best practice in controlling respirable crystalline silica in infrastructure. 17th Australasian Tunnelling Conference - 2020+1: 2020 Vision: Innovating the next 50 years (ATS 2020). Melbourne, Australasian Institute of Mining and Metallurgy.

Fanning, A. and C. Allan (2023). "Innovative approach for dust control in tunnel construction." Mining Engineering 75(6): 24–28.

Lavoué, J., L. Joseph, P. Knott, H. Davies, F. Labrèche, F. Clerc, G. Mater and T. Kirkham (2018). "Expostats: A Bayesian Toolkit to Aid the Interpretation of Occupational Exposure Measurements." Annals of Work Exposures and Health 63(3): 267–279.

Lingard, H. and S. Rowlinson (2004). Occupational health and safety in construction project management, Routledge.

Oliveira, D. A. F. (2019). Design and construction of large span tunnels and caverns in Sydney, Australia. Tunnels and underground cities: Engineering and innovation meet archaeology, architecture and art. V. C. E. Peila, Taylor & Francis.

Parliament of New South Wales (2024). Order for papers-Respirable crystalline silica air monitoring. Ordered 20/11/2024, Given by Banasiak, Mark.

Sydney Metro (2020). Controlling silica dust at Central Station.

Sydney Metro (2020). Real-time monitoring for silica dust.

Sydney Metro (2020). Why do we ban the broom?

19th Australasian Tunnelling Conference – Acosta-Martínez, Stewart and Hudson-Smith (Eds.)
© 2025 Australian Tunnelling Society, ISBN 978-0-85825-002-4

Importance of risk mitigation for a live tunnel refurbishment project

A. Chang, C. Biotto & R. Fernando
Aurecon, Melbourne, Australia

ABSTRACT: Working in a live tunnel presents numerous challenges, particularly when performing asset maintenance within limited shutdown periods. This paper highlights how Burnley Tunnel Low Voltage Cable Refurbishment Project succeeded through exploring the critical strategies for risk mitigation during the stages of design development, focusing on the complexities associated with live tunnel environments. With the privilege of collaborating with pre-selected contractors in the project, a proactive approach was adopted by conducting early stakeholder engagement through comprehensive workshops. These strategies facilitate effective coordination, allowing for the identification and management of potential risks before they can escalate. The collaborative efforts of the clients, contractors, and designers in early engagements ensure that maintenance activities can be executed efficiently, reducing project disruptions and enhancing overall project success.

1 INTRODUCTION

Underground structures typically comprise multiple systems and pieces of equipment, each with a designated design life. During operational construction activities, routine maintenance and repairs are often necessary to ensure the assets' longevity. However, for live tunnels, maintenance shutdowns must be limited in both frequency and duration due to the significant impact of downtime.

Given the involvement of multiple stakeholders in large construction projects, it is crucial to establish alignment with the client from the outset. This includes understanding design limitations, determining acceptable risks, and agreeing on processes such as program, design coordination, and communication methods to ensure the project's success. Poorly planned projects can lead to issues such as stakeholder misalignment, increased project risks, schedule delays, and budget overruns [1].

In Australia, several live tunnel systems are approaching the end of their design life and require critical updates and refurbishment of mechanical, electrical and ITS equipment. The Burnley Tunnel is one such example, where major Low Voltage (LV) cables, which are directly buried along the tunnel’s length, are approaching the end of their operational lifespan and require replacement to ensure continued system integrity and reliability.

Burnley Tunnel is an integral component of the CityLink Tollway managed by Transurban. The tollway tunnel facilitates eastbound traffic movement from the West Gate Freeway to the Monash Freeway. Beneath the Yarra River and traversing the inner suburbs of Richmond and Burnley, the tunnel serves as a strategic bypass, offering an alternative route that circumvents the central business district. The 3.4 km three-lane Burnley Tunnel comprises different sections, including 460m of cut and cover at the west portal, 2.84km of driven tunnel, and 180m of cut and cover at the east portal. Additionally, a 1.4km Emergency Egress Tunnel (EET) runs parallel to the eastern part of the main tunnel. The infrastructure includes eight Cross Passages (CP) linking

the Burnley Tunnel to the EET, four CPs providing an emergency exit to the Domain Tunnel and three emergency refuges located in the central section of the Burnley tunnel. The Burnley Tunnel map is shown in Figure 1.



Figure 1. Burnley Tunnel Map [2].

Burnley Tunnel LV Cable Refurbishment Project implements five essential design stages: concept design, preliminary design, detailed design, final design, and issued for construction. Risk mitigation is a critical component of construction project management. Figure 2 illustrates the correlation between risk severity and associated costs throughout the project life cycle. In the initial stages of design development, risk management is strategic, concentrating on identifying potential risks and opportunities linked to design. Although the severity of risks is higher at the initial stages of a project, the associated mitigation costs are low. However, as the project advances towards completion, the costs associated with these risks increase substantially [3]. Therefore, it is critical to implement risk mitigation strategies at the earliest possible stage to prevent cost escalation.

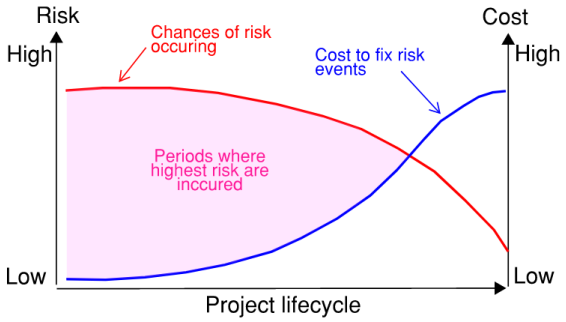


Figure 2. Project life cycle associated with risk management and project cost [3].

The main challenge of this work is the reliance on the electrical power of all the tunnel systems to sustain operations, and the maintenance planning for repair work should LV cables fail. This represents a high-risk maintenance item as replacement of the cable requires significant work that results in a major tunnel downtime. To resolve this issue, an alternative permanent and more sustainable solution is explored requiring access to the roadway tunnel areas.

With pre-established stakeholders such as clients, designers, contractors, and suppliers, the project risk is managed from the concept design by considering the whole-of-life of the asset. Given the high-risk nature of construction projects, significant emphasis has been placed on risk identification and mitigation during each design phase. This paper will explore the advantages of

early risk mitigation in Burnley Tunnel LV Cable Refurbishment Project, outlining specific processes and methodologies that can be effectively implemented to achieve successful risk management outcomes.

2 PROJECT RISKS AND CHALLENGES

Modification of existing tunnel components induces various challenges. For Burnley Tunnel, the existing cables are situated behind the concrete New Jersey Barriers (NJBs) and are encased in hardened, stabilised sand (shown in Figure 3). In addition, the cables that are the primary focus of this project are obstructed by vertically stacked conduits. Removing and replacing these conduits would require prohibitively long tunnel shutdowns. Additionally, removing existing cables can damage other services, in particular some critical control cables are also buried. Therefore, the relocation of cables is investigated.



Figure 3. Burnley Tunnel existing cable routes' location.

Due to spatial constraints and the need to accommodate existing tunnel components, the range of viable options to move a large number of cables from buried locations to open locations is limited. The confined space within the tunnel introduces feasibility and constructability challenges for the proposed new cable positioning. As the tunnel remains in operation, certain assets must be accessible during shutdowns to ensure emergency readiness, which further narrows the range of potential solutions.

Since Burnley Tunnel has been operating for many years, there are inherent risks related to discrepancies between as-built documentation and existing tunnel conditions. Such inconsistencies can affect the precision of design, and incorrect assumptions being made. Therefore, the lack of precise information may result in redundant work, threatening the project schedule and overall program integrity.

Given that the Burnley Tunnel is an operational tunnel, a contractor has been pre-selected by Transurban (the client) to facilitate early engagement, ensuring that constructability is integrated during the design phase. This proactive approach enhances coordination and minimises potential issues during construction/ installation.

Involving multiple stakeholders in a project can enhance design quality by incorporating diverse perspectives. However, collaborating with numerous stakeholders can also introduce risks such as communication challenges, decision-making delays, and conflicting interests. Therefore, effective stakeholder engagement, clear communication, and well-defined roles and responsibilities are crucial to mitigating these risks and ensuring project success.

3 RISK MITIGATION

Based on the aforementioned challenges, the following stakeholder engagement strategies are implemented in sequence throughout the design development phases to identify, assess, and agree on risk mitigation measures. These strategies ensure proactive identification, communication, and

timely escalation to the client, providing opportunities to optimise the schedule, budget, and quality of the design. The key outcome of these engagements is the selection of the cable ladder alignment and the finalisation of the overall system layout.

3.1 *Site visit*

To enhance the precision of the design, at the start of the project, the design team conducts a comprehensive site inspection and manual measurements to validate as-built structures and existing services clearance geometry. A point cloud survey is performed to refine the tunnel geometry and generate a precise Three-Dimensional (3D) model. This survey allows for the cross-verification of the 3D model's accuracy by overlaying the point cloud data, ensuring alignment and precision in the geometric representation (as shown in Figure 4). 3D models serve as a critical design reference, particularly when a plan view drawing involves multiple interfaces. The model significantly reduces the need for additional site closures for inspection or information validation.



Figure 4. Point cloud survey overlaying the 3D model.

Additionally, since Burnley Tunnel has been operating for years and cable route installation requires drilling into the tunnel lining, an Ultrasonic Pulse Echo (UPE) test is conducted during the site visit. The UPE test assures the tunnel lining thickness and concrete quality are adequate for drilling and further verifies the design's structural integrity. This approach enables accurate analysis of the existing tunnel conditions and ensures the precision of cable route design.

3.2 *Risk and Opportunity (R&O) workshop*

During the concept design phase, cable arrangement optioneering is conducted to explore potential risks and opportunities associated with identified cable routes early in the process, allowing the team to focus on the agreed-upon option moving forward. The workshop aims to rigorously assess the maintainability, constructability, and operational aspects of each design option through a collaborative exercise involving multidisciplinary stakeholders, including clients, contractors, and designers.

The workshop adopts a collaborative approach through using a common workspace for ease of collaboration, to ensure that diverse perspectives are considered, and facilitating a comprehensive risk and opportunity analysis. To support structured outcomes, a dedicated facilitator is engaged to lead the workshop objectively, promote effective team collaboration, and prevent critical aspects being missed. Additionally, to accommodate people who attend online, a secretary is in charge of transferring the physical sticky note to the Miro board to ensure everyone's voice is heard (as shown in Figure 5). Furthermore, a "parking lot" is assigned for capturing additional discussions which are to be considered outside of this workshop. This ensures all agenda items are covered, and the discussion is not being sidetracked.

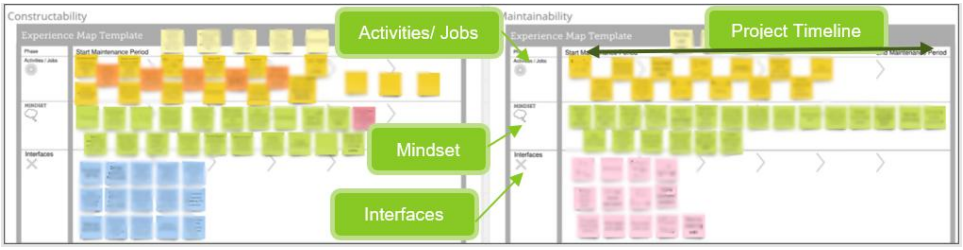


Figure 5. R&O workshop Miro board activities.

The R&O workshop ensures that all stakeholders' perspectives are heard and incorporated into design decisions, while also allows for the rapid pivoting of ideas when necessary. After the ideations and brainstorming, towards the end of the workshop, each participant has the opportunity to give scores to their preferred options. Based on the scoring and feedback that is collected during the workshop for each cable route option, a ranking table is developed to evaluate the options across key criteria: Fire Safety, Electrical Performance, Structural Integrity, Material Suitability, Constructability, Maintainability, and Business Impact. This comprehensive assessment provides a clearer direction for selecting the optimal cable route options to advance to the preliminary design phase (as indicated in Figure 6). At this stage, the focus has shifted from broad, generic design approaches applicable to all projects to project-specific criteria, including detailed consideration of cable route options.

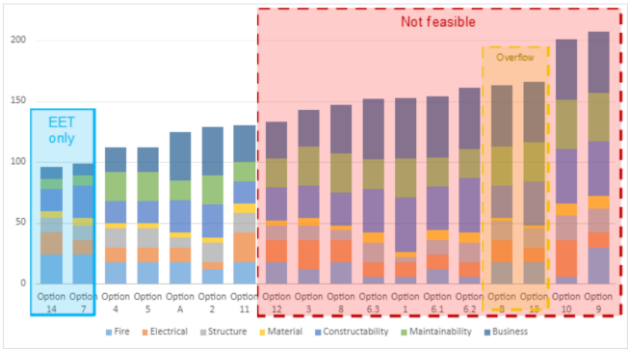


Figure 6. Ranking of options.

3.3 *Safety in Design (SiD) & Early Contractor Involvement (ECI) workshop*

A SiD workshop is an effective tool to identify potential design risks, plan mitigation strategies, and enhance stakeholder collaboration. During a SiD workshop, all relevant regulations and fire life safety aspects are considered. It focuses on risks to Health and Safety and the Environment throughout the entire lifecycle of the assets, including construction, commissioning, operations, maintenance, demolition, and disposal. Incorporating SiD workshops early in the project ensures that all risks are proactively addressed.

For the Burnley Tunnel LV Cable Refurbishment Project, it is particularly crucial to hold these SiD and ECI workshops since there are some other upgrade works happening at the same time. There are numerous interfaces that the cables traverse within the tunnel, so it is necessary to examine the associated safety risks and identify potential constructability issues. Hence, it is important to ensure the new LV cable routes do not adversely affect other concurrent work. To achieve this, the workshop involves the client and the pre-established contractors to gain a better understanding of the existing tunnel environment and minimise the number of assumptions made.

The SiD workshop encourages participants to adopt the viewpoints of various involved parties. For the Burnley Tunnel LV Cable Refurbishment Project, multiple stakeholders interface with the tunnel, such as Transurban, Fire Rescue Victoria (FRV), Department of Transport and Planning (DTP) and Tunnel users. This practice of "placing oneself in others' shoes" ensures that all potential risks are considered and addressed, for example, FRV typically focus on emergency

mitigation, which means designers must ensure that the cable route design shall not obstruct the evacuation route. DTP holds a responsibility for ensuring the safety of motorists using the tunnel and for protecting the integrity and value of this asset that they will own from the date of concession termination. This is mostly achieved by ensuring optimum application of standards, concession deeds and industry best practice, meaning that designers must achieve compliance with these requirements. The value of understanding the roles and responsibilities of each stakeholder cannot be overstated, as it fosters a holistic approach to risk management.

For information management, a risk register is used during the workshop to track information and facilitate continuous updates throughout the project. This tool not only maintains up to date records but also enables automatic risk ranking based on the likelihood and consequences of identified risks [4].

In addition, the ECI workshop focuses on assessing the constructability of design with input from all stakeholders. Contractors possess an intimate understanding of the tunnel environment, and their insights are crucial for ensuring the design can be implemented within the limited timeframe available. For instance, a deemed feasible cable arrangement is proposed during the workshop and one of the key takeaways from the contractor is that the allocated space is too tight to work effectively and can result in longer installation times. The outcomes of the workshop validate all design aspects and feasibility, allowing further refinement of the cable arrangements in the subsequent design phases to prevent impractical design.

3.4 *Failure Modes, Effects, and Criticality Analysis (FMECA) workshop*

Following the refinement of the cable arrangements and cable support systems, a FMECA workshop is conducted with the client's maintenance personnel and relevant discipline-specific owner's engineers. The workshop is led by a FMECA facilitator/ Subject Matter Expert (SME) who identifies and prioritises potential failure modes based on their likelihood and consequences in advance, allowing for effective stakeholder discussion and a more thorough assessment.

FMECA is similar to the Hazard and Operability (HAZOP) analysis which is more widely adopted in the water industry. The key difference is that FMECA focuses on assessing individual component failures and their impact on system reliability, whereas the HAZOP process evaluates process deviations, risks and their associated hazards [5].

The FMECA template is developed based on principles from the Reliability Analysis Center [6]. FMECA workshop is a systematic approach used to analyse and assess potential failure modes within a system, subsystem, or component. The following categories can be adopted in the FMECA:

- Component Identification - The analysis begins by breaking down the system or asset into its various components, identifying the lowest maintainable item within the system.
- Failure Mode Identification - Each component is evaluated to identify potential failure modes, which are events or conditions that can lead to a functional failure or loss of performance. Failure modes are described in the format of "the event" due to "a failure mechanism".
- Failure Effect Analysis - The consequences and effects of each failure mode are assessed, considering either local or higher-level impacts
- Criticality Assessment - The consequences and likelihood of each failure mode are classified. The consequences refers to the seriousness of the consequences resulting from failure, and likelihood is an estimation of how likely the failure is to happen. The Risk Priority Number (RPN) is calculated by multiplying the consequence and likelihood values.
- Prioritisation and Risk Mitigation - Based on the RPN, failure modes are prioritised, focusing on those with the highest risk levels. This allows for the identification of critical failure modes that require immediate attention and mitigation, from a reliability perspective.

By following the FMECA process, critical failure modes are identified, allowing for the development of effective maintenance strategies and allocating resources efficiently to minimise risks and increase system reliability. Additionally, it is imperative to continuously review the risk register to ensure that any newly identified risks are recorded and addressed accordingly.

4 CABLE ARRANGEMENTS PROGRESSION

Through the early stakeholder engagements outlined in Section 3, the key insights from those discussions are as follows:

- The ability to have a full tunnel closure could facilitate higher production rates by reducing operational disruptions and improving worker efficiency
- The removal of existing assets may present significant complexity, potentially leading to longer shutdown periods
- The trapeze cable ladder design has been identified as the preferred option due to its superior efficiency in terms of installation time
- The cantilever cable ladder design offers ease of anchor drilling, and simple install resulting from anchor drill holes specified perpendicular to the tunnel wall

Two cable route options were developed during preliminary design: a fully in-tunnel route and a partial in-tunnel and EET route. For the in-tunnel option, all essential and non-essential cables are installed on one side above the traffic envelope on the Equipment Room East (ERE)/escape passages side of the tunnel. Following the SiD and ECI workshop outcomes, the EET route was excluded in the post-preliminary phase. The EET route emerged as the most economically viable option, given that cable and cable ladder installation can proceed at any time, thereby avoiding the scheduling constraints and additional costs associated with night-time tunnel closures. Despite its benefits, the EET option was limited by cable volume, restricted access to overhead areas, and additional space requirements, impacting installation efficiency.

Reflecting stakeholder considerations, the in-tunnel cable route has been developed as a trapeze-supported cable ladder extending through the tunnel and to each ERE, as illustrated below.

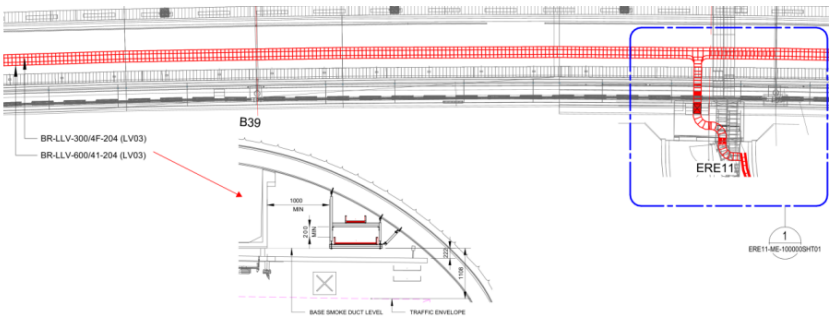


Figure 7. Final in-tunnel cable route design at a specific location for illustration.

Furthermore, at jet fan locations, there are two cable support arrangements designed to accommodate the existing tunnel geography. One of them comprises a wall mounted arrangement for essential cables and a cantilevered beam for non-essential cables (shown in Figure 8) and there is also wall mounted cable ladder arrangement for both essential and non-essential cables (shown in Figure 9).

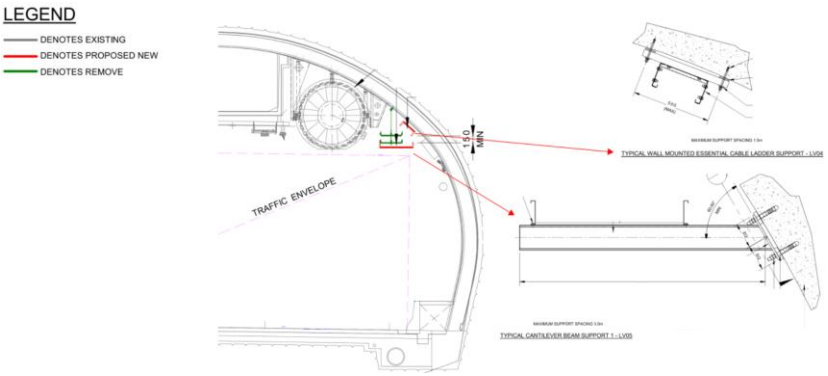


Figure 8. Cable route design near jet fans – Cantilevered & Wall mounted arrangement.

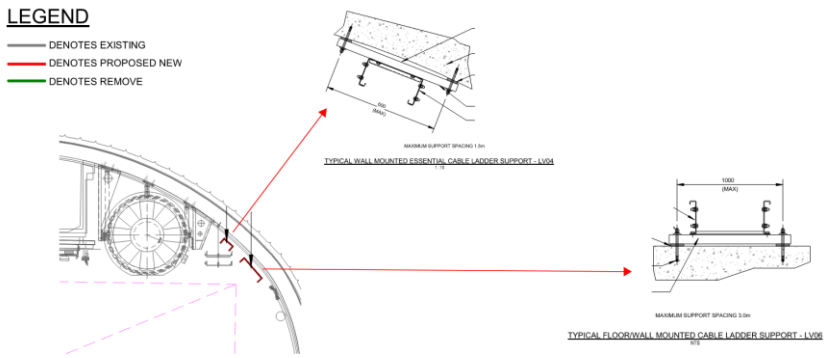


Figure 9. Cable route design near jet fans – Wall mounted arrangement.

5 CONCLUSION

The benefits of early stakeholder engagement are evident from the Burnley Tunnel LV Cable Refurbishment Project. The client recognises the process's efficiency, as it enables early identification and mitigation of risks before they escalate, which would otherwise have led to increased costs and project delays.

The engagement workshops enable the rapid iteration of ideas, ensuring that the constructability and maintainability of the cable system are shaped by the critical input and perspectives of all stakeholders, thereby embedding their concerns at the core of the design. The cables are now relocated from an area that is difficult to access to the top side of the tunnel, which can be easily accessed when needed without full tunnel closures. Additionally, there is no obstruction for future maintenance work, which is an improvement from the NJB option, where the cables are encased in hardened, stabilised sand. Moreover, through the workshops, the severity of the risks associated with the new cable arrangement is reduced, alongside the contractors' confirmation that the cable routes are simple to construct and install.

A comprehensive project plan is developed at the start of a project, incorporating a systematic risk identification and mitigation framework that is aligned and agreed upon with the client. The strategies are thoroughly reviewed and agreed upon with the client to ensure alignment with their expectations.

By leveraging workshops that prioritise and integrate stakeholder perspectives, the team achieves a deeper understanding of project requirements, resulting in more effective collaboration and improved design outcomes. Implementing the workshops demonstrates that a thorough engineering process has been adopted through the design phase and demonstrates a proactive approach to maintaining strong stakeholder relationships. Moreover, having the same designers with clear task delegation throughout the project is also an important factor in the project's success.

6 REFERENCES

Coetzer, J.D. 2023. The Power of Coordination in Construction Design: A Perspective for the Middle East.https://www.linkedin.com/pulse/power-coordination-construction-design-perspective-middle-coetzer.

Transurban Limited. 2025. Melbourne. https://www.transurban.com/roads-and-projects/melbourne.

Rad, K.M., & Yamini, O.A. 2016. The Importance and Use of Risk Management in Various Stages of Construction Projects Life Cycle (PLC). Mathematical Models and Methods in Applied Sciences, 11, 48.

Patterson, F.D., & Neailey. K. 2002. A risk register database system to aid the management of project risk. Int J Proj Manag, 20 (5).

Giardina, M. & Morale, M. 2015. Safety study of an LNG regasification plant using an FMECA and HAZOP integrated methodology. Journal of Loss Prevention in the Process Industries, 35: pp.35-45.

Reliability Analysis Center. 1993. Failure Mode, Effects and Criticality Analysis (FMECA). https://s3vi.ndc.nasa.gov/ssri-kb/static/resources/a278508.pdf

19th Australasian Tunnelling Conference – Acosta-Martínez, Stewart and Hudson-Smith (Eds.)
© 2025 Australian Tunnelling Society, ISBN 978-0-85825-002-4

Using AI Agents for research - a case study the Lane Cove Tunnel Collapse

T. Nye
E J Nye & Associates Pty Ltd, Melbourne, Australia

ABSTRACT: The Lane Cove Tunnel (LCT) Sydney collapse in 2005 was a significant failure in urban tunnelling, highlighting critical deficiencies in geotechnical risk assessment, construction methodologies, surveillance and site communication. The tunnel collapse led to costly delays, legal disputes, financial losses, personal injuries, surface building damage and community disruption, underscoring the need for more management oversight and preventative measures the tunnels construction. In addition to this author's interpretation of the available published information and using NotebookLM agent to summarise the data efficiently, this paper identifies management issues and proposes an initial check list of mitigations for future projects. Reference to the ground conditions and the use of cement grouted rock bolts as opposed to fully encapsulated resin ones, and the breakdown in communication between the contractor and the projects consultants re: related to inconsistent quality of the cement grouted rock bolt installation reporting and basic design flaws. It is vital to learn from past mistakes.

1 INTRODUCTION

The LCT collapse (on the Pacific Highway exit ramp) in 2005 was a significant failure in urban tunnelling (Figure 1). Post collapse several publicly available documents, legal proceedings and published papers were accessed and reviewed. While it was a relatively small set of documents, an example of an efficient way to research and review this information, is by using a Large Language Model (LLM). In this case study we have used NotebookLM as the AI agent reviewing documents. NotebookLM can only access and review the documents that you have uploaded to the NotebookLM website. This document summariser and research assistant is powered by a 'thinking' AI model Gemini 2.5 Pro (from Google). We have also used the agent ChatGPT, Table 1 as one means of risk mitigation brainstorming and for providing a comparison between cement and fully encapsulated resin anchored rock bolts, Table 2.

- Using the NotebookLM agent it is possible to upload 50 documents in one project session, so its capabilities have certainly have not been fully challenged here (5 documents only).
- The NotebookLM agent does not save the responses for each chat. They have to be saved manually. If you leave a session and restart, all previous chats are lost.
- To get the best out of a LLM, like the NotebookLM agent, the requests must be precise. Initially before starting a chat session, the agent must be told by you what role it is taking so that it has some context for its role.
- It is important to tell the NotebookLM agent in what format you want the response to be given in. e.g. text, table, number of words etc.
- Note that the key engineering lesson given in the conclusions section is the author's opinion and was not generated or influenced by the AI agents. It is based on the author's knowledge and experience.

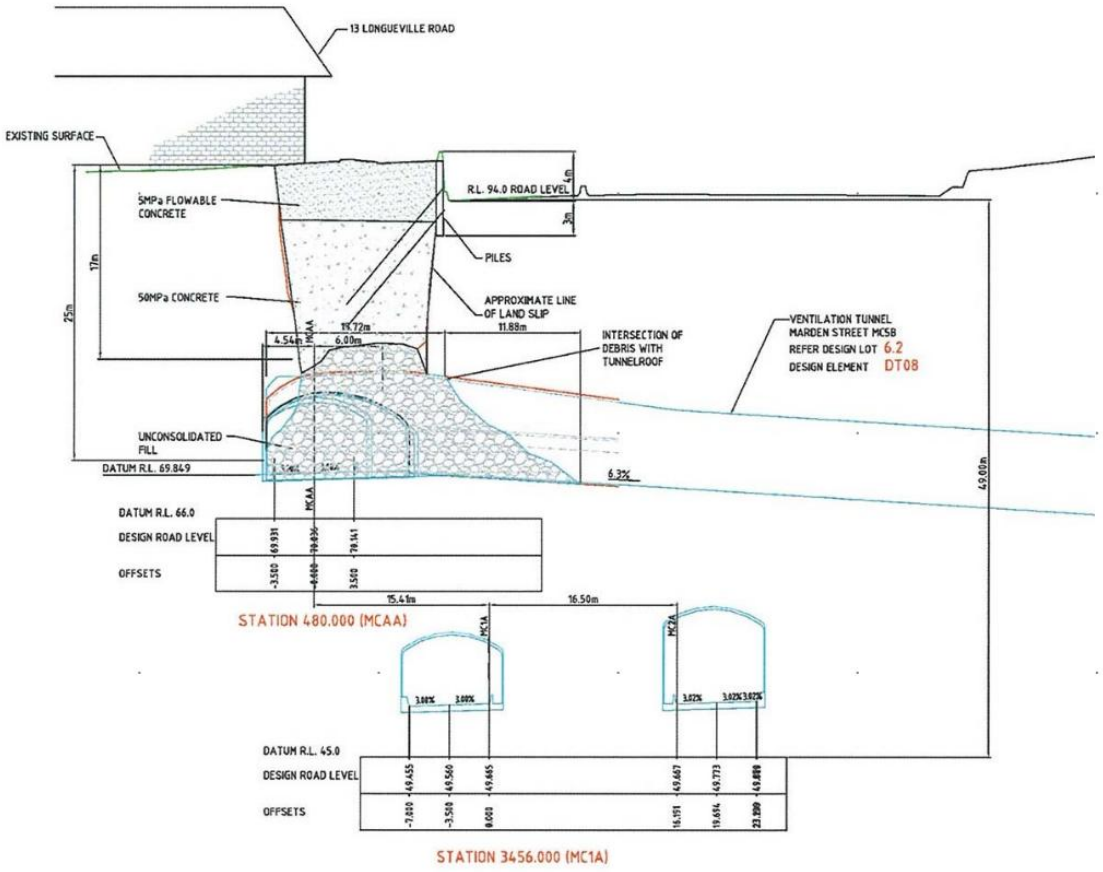


Figure 1. Vertical section through the collapse zone including post failure concrete pours (original from Brown report). Zoom into the PDF file for clearer text.

It is strongly recommended that the three companion papers referenced on the Lane Cove Tunnel Collapse are also read so that the reader can reach their own conclusion about the effectiveness of NotebookLM.

2 BRAINSTORMING USING CHATGPT AND PROMPT ENGINEERING

Table 1 has been largely generated by using the following prompt. In the first instance ChatGPT is told that it is a Project Manager on a large urban tunnelling project to give it the context of the prompt below.

"Please list the likely risk issues and mitigation methods to be managed on this project. There are 5 tunnel faces being excavated simultaneously"

Note that we did not ask ChatGPT to list the risks and mitigation in any order of priority. This was done by the author after reviewing some of the summaries produced by the NotebookLM. The summaries produced by NotebookLM also require the agent to be assigned a role so that it has framework or context around the prompts provided. Note also the process is iterative and some of the input data does not all come from the LCT references; some topics are not addressed at all. For example, the use of fully encapsulated resin rock bolts, only cement grouted rock bolts are mentioned in the LCT references.

A comparison between cement grouted and fully encapsulated rock bolts follows in Table 2.

Table 1. 95% of table content was the generated using prompt engineering in the ChatGPT Model. Priority order (1-21) modified by the author.

#	**Likely Issues**	**Mitigation Methods**
1	Tunnel Designer's over Reliance on Contractor Reporting	Ensure the tunnel designer and geotechnical engineer both regularly visit tunnel faces to assess support issues firsthand.
2	Poor Communication Between Teams	Hold daily meetings with clear agendas. Use collaborative platforms for sharing updates and decisions.
3	Inadequate Risk Assessment for the next 24 Hours	Use a risk matrix to evaluate and prioritise risks. Involve all stakeholders in the assessment process.
4	Unforeseen Ground Conditions (e.g., water ingress, weak rock)	Conduct thorough pre-excavation investigations. Have contingency plans and equipment ready for emergencies.
5	Insufficient or incorrect Ground Support Installation	Pre-plan support requirements based on geological data. Conduct regular inspections to ensure compliance with designs. Have contingency support alternatives on site.
6	Lack of Accountability for Decisions Made in Meetings	Document all decisions and assign follow-up tasks to specific individuals. Use meeting minutes for transparency.
7	Insufficient Training for New Team Members	Provide comprehensive onboarding and ongoing training. Pair new members with experienced mentors.
8	Inaccurate Face Mapping	Use advanced laser scanning and photogrammetry for precise mapping. Regularly cross-check with geologists' observations.
9	Misinterpretation of Geological Data	Ensure geologists and designers collaborate closely. Use real-time monitoring and adjust excavation plans as needed.
10	Delayed Shift Boss Reports	Implement a standardised reporting template and set strict deadlines for submission. Use digital tools for efficiency.
11	Excessive Deformation (Surface or Tunnel)	Install real-time deformation monitoring systems. Set thresholds for immediate action if limits are exceeded.
12	Over-Excavation or Under-Excavation	Train operators on precise excavation techniques. Use laser guidance systems for accuracy.
13	Delays in Approval Process	Streamline decision-making by assigning clear roles and responsibilities. Use approved protocols for common issues.
14	Fatigue or Human Error in Reporting or Decision- Making	Rotate shifts to prevent fatigue. Implement double-checking procedures for critical decisions.
15	Inconsistent Construction Summary Reports	Standardise report formats and ensure all teams are trained on how to complete them accurately.
16	Surface Settlement Affecting Nearby Structures	Monitor surface settlement continuously. Use face dowels, canopy tubes, grouting or other stabilisation techniques if necessary.
17	Lack of Alignment Between Tunnel Faces	Use precise surveying and alignment tools. Regularly verify alignment and adjust excavation paths as needed.
18	Inadequate Emergency Response Planning	Develop and regularly update emergency response plans. Conduct drills to ensure readiness.
19	Budget Overruns Due to Unplanned Work	Regularly review progress against budget. Allocate contingency funds for unforeseen issues.
20	Safety Incidents Due to Poor Ground Conditions or Equipment Failure	Enforce strict safety protocols. Conduct regular equipment inspections and maintenance.
21	Environmental Impact (e.g., noise, dust, vibrations)	Implement mitigation measures like noise barriers, dust suppression, and vibration monitoring.

The above table is a generalised list of 'Likely Issues' and 'Mitigation Methods' and has been generated without any pre-knowledge of the project management procedures adopted on the Lane Cove Tunnel project. There is also no specific reference to either cement or resin encapsulated rock bolts (see Table 2 below).

3 COMPARING CEMENT GROUT AND FULLY ENCAPSULATED RESIN ANCHORED ROCK BOLTS

Prompting NotebookLM,

"Is there any reference in the uploaded documentation to resin anchored rock bolts?"

Response: No

Using ChatGPT,

"Compare cement grouted rock bolts with fully encapsulated resin rock bolts in weak rock, no ground water present. Format output in a table."

Table 2. Comparing cement grouted and fully encapsulated resin rock bolts

#	Aspect	Cement Grouted Rock Bolts	Fully Encapsulated Resin Rock Bolts
1	Grout Material	Cementitious grout	Two-part polyester resin
2	Bond Strength	Moderate (lower than resin)	High bond strength with rock and bolt
3	Installation Time	Slower; grout needs to be pumped and allowed to set	Faster, resin sets within minutes
4	Load Transfer Mechanism	Friction and mechanical interlock along the grouted length	Strong chemical bond along the entire bolt length
5	Early Load Capacity	Delayed (requires curing time)	Immediate load-bearing possible after resin sets
6	Suitability in Weak Rock	Adequate, but may require higher quality control to ensure full encapsulation	Excellent, due to rapid setting and full encapsulation
7	Encapsulation Quality	Variable; risk of voids or incomplete grout filling	High, if installed correctly, provides continuous bond
8	Corrosion Protection	Good (alkaline environment)	Good; resin acts as a sealant
9	Sensitivity to Installation	Sensitive to hole flushing, grout mix, and timing	Sensitive to mixing and insertion speed
10	Cost	Lower material cost, higher labour cost	Higher material cost, lower labour cost
11	Inspection & Testing	Pull testing and coring may be needed to confirm grout fill	Same, but often more reliable outcomes if Quality Control is followed
12	Long-Term Performance	Good in dry conditions, but depends on grout quality	Very good; consistent encapsulation provides durability

Please note the problems associated with the installation of the cement grouted rock bolts are described in Section 4 of this paper.

Please note the first 5 items in Table 2. Given the reported problems the contractor was having installing the cement grout rock bolts the author is surprised *that using their own initiative* they could have switched over to fully encapsulated resin anchored bolts. In any case, resin anchored rock bolts should have been on site as a tunnel support contingency. The installation of the permanent support (i.e. the cement grouted rock bolts) would be carried out later, without the pressure of maintaining excavation productivity targets. There were precedents for this approach that the author is aware of. For the eastern half (the project was divided into two contracts) of the M5 (2001) road tunnel and for the treatment works chamber on the Bondi RIAMP project (2003).

We are not suggesting that the use of resin anchored rock bolts would have prevented the collapse. However, when it became obvious that the geological conditions have changed (or that there were installation issues with the cement grouted rock bolts) and that resin anchored rock bolts would have been more appropriate, it would appear that no resin anchored rock bolts were available on site for this contingency.

4 CEMENT GROUTED ROCK DESIGN INSTALLATION

Prompting NotebookLM:

"Please summarise the issues related to the installation of the cement grouted rock bolts"

NotebookLM response:

"Based on the sources, you can add a note highlighting the lack of communication regarding issues with the cement grouted rock bolts:

It is noted that the tunnel designers, PB, and the geotechnical construction team, PB and PSM, were unaware of difficulties with the installation of CT rock bolts prior to the collapse. TJH tunnelling crews reportedly had significant difficulties with tensioning and grouting the CT rock bolts in the MC5B tunnel and in the MCAA/MC5B intersection. Despite these issues, TJH did not inform PB, and PB did not enquire, whether rock bolts installed in the MC5B/MCAA intersection were properly tensioned and properly grouted. There was no documentation reporting these tensioning or grouting problems, suggesting a breakdown in the Non-Conformance Report (NCR) system. Initial inspections after the collapse revealed issues with the installation and anchoring of rock bolts in the roof of the MC5B tunnel section of the intersection, including little to no evidence of grout on the exterior of plastic sheathed bolts and overwound end anchors preventing grout penetration.

Furthermore, while rock bolt testing was required, there was no specification prescribing the locations for testing, and rock bolts were not tested in MC5B as ground conditions deteriorated. This lack of testing in the area experiencing problems meant that specific performance data in the challenging ground conditions was not available to inform the designers or geotechnical team. The effectiveness of the adopted rock bolting strategy and the stability of the rock bolted roof were therefore compromised by inadequate tunnel roof support installations, including a significant percentage of CT rock bolts that had not achieved end anchorage or a grouted bond in the roof strata".

5 WHAT WAS THE DESIGN MISSING?

NotebookLM prompt:

"Was the design approach adequate of such a large tunnel intersection"

NotebookLM response:

"A significant finding from the post-failure investigations and subsequent litigation was the apparent lack of a fully engineered design for the MC5B/MCAA intersection support. Based on the evidence, the design was not based on detailed calculations of the type undertaken post-collapse to assess its suitability. Documents presented as the support design (including reports, memoranda, specifications, Requests for Information (RFIs), emails, mapping sheets, drawings) conspicuously lacked the "Design Documentation" described in the consultancy contract, which should have included engineering calculations carried out specifically for the intersection. The trial judge later confirmed the absence of engineering calculations for the intersection design. There were no engineering calculations for any intersection in the documentary evidence, only for 2-D tunnel sections. There were also no drawings in the support toolbox for the installation of support in intersections".

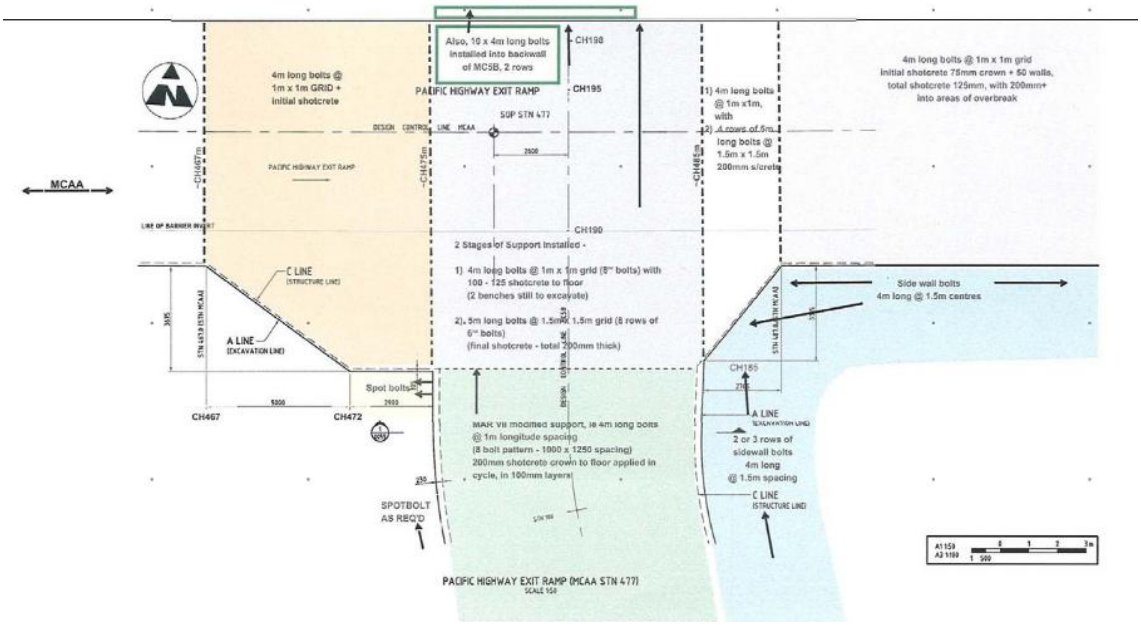


Figure 2. Schematic plan view of the tunnel intersection showing rock bolt support outline (original from Brown report). Zoom into the PDF file for clearer text.

6 WERE THE ROCK BOLTS LONG ENOUGH?

NotebookLM prompt:

"Are there any comments in the documentation related to the length of the rock bolts used? Please provide a paragraph summary".

NotebookLM response:

"Based on the sources, there are indeed comments regarding the length of the rock bolts used in the tunnel design and construction. The amount of rock bolts installed, including their length, varied depending on the Ground Support Determination (GSD) which was based on the ground classification1. Design considerations for the tunnels used precedent practice from earlier Sydney tunnels, which included information on rock bolt lengths related to tunnel spans. For specific areas like the MC5B/MCAA junction, the primary support in the transition zone consisted of 4m long bolts on a 1m by 1m spacing. Due to the increased effective span and relatively low cover at the junction, a secondary support system was augmented, which included 5m long rock bolts on 1.5m by 1.5m spacings. A chart used as a guide during design, compiling rock bolt lengths against spans in the Sydney area, suggested that 6m long bolts should be used in excavations with effective spans of 17m, and if the effective span is taken as 21m, the chart suggests bolt lengths should be at least 7m. In retrospect, it was concluded in one report that the level of support, which would include bolt length, existing in the western side of the transition was inadequate to ensure the excavation's stability given the large effective span, low rock cover, the presence of the dyke, and the poor mechanical properties of the overlying rock mass".

7 MOTIVATION FOR WRITING THIS PAPER

The motivation for this paper is both professional and personal.

During the LCT project, I was engaged by Connector Motorways to provide high-level review comments, including for the section of tunnel that ultimately collapsed. However, based on the limited documentation I received, I formally advised Connector Motorways that I could not provide a meaningful response due to insufficient information. Despite this, no further action was taken, with the assumption that responsibility lay solely with the contractor. This disconnect underscores a recurring problem in project oversight and accountability. Following the collapse, I was subsequently re-engaged to oversee the remedial design and construction methodology.

I am currently highly motivated to explore the potential of AI in engineering applications. AI has the capability to improve the speed, quality, and objectivity of technical analysis and in doing so, reduce the influence of cognitive bias that often clouds judgement on complex projects.

Finally, I am deeply concerned that despite previous lessons, another major tunnel collapse recently occurred in Sydney — the M6, approximately 18 months ago. This indicates that critical learnings from LCT collapse may not have been adequately transferred to current practice. This paper is an effort to promote ongoing vigilance, learning, and innovation through both traditional engineering scrutiny and AI-based assistance.

8 CONCLUSIONS

This case study has demonstrated the effective use of AI agents such as NotebookLM and ChatGPT in extracting and synthesising key technical and management lessons from complex engineering failures. This proved to be a significant time saver, even with a small dataset (for both researching and writing).

In the author's opinion the key engineering lesson here is the ground support strategy. Given the known limitations and difficulties in installing cement grouted rock bolts, particularly under variable ground conditions and especially production pressures the contractor should have had fully encapsulated resin anchored rock bolts available and incorporated into the tunnel support contingency plan. Resin encapsulated bolts offer clear advantages in weak ground conditions, including faster installation, superior bond strength, and reliable encapsulation, which is especially critical when construction quality control is compromised (refer to Table 2). I would classify the installation of the resin anchored rock bolts as 'temporary works' and hence the responsibility of the contractor.

While it is acknowledged that the use of fully encapsulated resin rock bolts may not have prevented the collapse, their rapid load-bearing capacity and ease of installation should have enabled a more adaptable and responsive approach to deteriorating conditions, especially at tunnel intersections. Importantly, their availability would also have eliminated any reliance on problematic cement grouted bolts until this 'permanent support' was installed in a stable environment (both geologically and production).

The broader failure also highlights the absence of a robust non-conformance reporting system, inadequate face mapping, questionable rock bolt lengths (only 4m) given the effective wide span and a lack of formal engineering calculations for a complex intersection. Together, these deficiencies reflect systemic gaps in design and construction oversight and communication, which must be urgently addressed in future tunnelling projects.

This paper is an effort to promote ongoing vigilance, learning, and innovation through both traditional engineering scrutiny and AI-based assistance. The emphasis here is 'assistance' as AI made no contribution to the scenario put forward here about the use of resin anchored rock bolts as a first pass initial tunnel support option.

As AI technologies continue to evolve and become widely adopted, their use in educating, identifying and even predicting such risks offers a powerful tool for improving both design and construction in all urban tunnelling environments.

Also please note that the three referenced papers on the Lane Cove Tunnel collapse were initially available on the AGS website and published in the Australian Geomenchanics Journal were (refer to Vol 54, No. 2 June 2019). However, copies of the three papers can still be downloaded from the internet.

9 REFERENCES

Brown, E. T. (Golder Associates Pty Ltd) (2005) *REPORT ON CAUSES OF SUBSIDENCE, 2 NOVEMBER 2005, LANE COVE TUNNEL PROJECT, SYDNEY, NSW*. Report No. 001-05632178-Rev 1, Golder Associates Pty Ltd.

Burman, B. C., Kotze, G. P. and Chan, L. (2018) *Lane Cove Tunnel collapse and sinkhole a forensic review - 1: The collapse*.

Burman, B. C., Kotze, G. P. and Chan, L. (2018) *Lane Cove Tunnel collapse and sinkhole a forensic review - 2: Post failure investigations*.

Burman, B. C., Kotze, G. P. and Chan, L. (2018) *Lane Cove Tunnel collapse and sinkhole a forensic review - 3: The legal aftermath*.

WorkCover NSW (2005) *Lane Cove Tunnel Collapse 2 November 2005*.

Theme 12. Asset Management

THIS PAGE INTENTIONALLY LEFT BLANK

19th Australasian Tunnelling Conference – Acosta-Martínez, Stewart and Hudson-Smith (Eds.)
© 2025 Australian Tunnelling Society, ISBN 978-0-85825-002-4

Durability design for tunnels and approaches

F. Papworth
Building and Construction Research and Consulting, Perth, Australia

ABSTRACT: The paper provides recommendations on assessment of tunnels exposures as a durability load, and procedures to select appropriate concrete quality and materials to resist those loads. National codes include deemed to satisfy (DtS) prescriptive requirements for limited exposure conditions. This restricts the durability designer's options. Fib Model Code 2020 (2023) discusses the application of decreasing levels of approximation (LoA) as a more expensive but more precise design approach that may lead to significant environmental and structure cost reductions. Durability is increasingly using full probabilistic analysis (FPA) for durability design as a more precise method of predicting design life. This focuses attention on establishing environmental, safety, and life cycle costs (including public and operational costs) to develop a target reliability for the structure's elements at the end of the design life and then designing to meet that reliability. Given a tunnel's life may be extended well past the original service life strategic consideration in the design is also required.

1 INTRODUCTION

The durability loading on an element depends on the exposure. Only the more common exposures are discussed here. When considering tunnel exposure, the three areas of concern are the extrados, the intrados and the approaches. While local conditions might cause a variation along the length of each the key general exposure considerations are discussed here together with factors affecting the resistance to deterioration. A key in assessing exposures for tunnels is that DtS requirements in Australian Codes frequently do not apply to tunnels and hence specific assessment is required for each project.

2 CARBONATION

Carbonation is the process of carbon dioxide ingress reacting with calcium hydroxide to form calcium carbonate. This creates a low pH in the concrete such that reinforcement in carbonated concrete can corrode. In building interiors this is not considered a major issue. In temperate external climates it is classified as only exposure class A to AS 5100.5 (2024) yet the exposure to higher carbon dioxide concentrations and moisture contents in vehicle tunnels is known. The much higher carbonation rates and corrosion risks than in normal atmospheric conditions requires specific consideration. This may be one reason why Austroads (2019) specifies B2 as a minimum exposure inside tunnels, a more severe class than B1 required internally to comply with AS 5100.5 (2024). B2 is only a minimum exposure as a specific tunnel may be determined as having a more severe exposure.

Concrete's carbonation resistance depends on the cement chemistry and penetrability. FPA using carbonation models in fib 34 (2006) can be used to predict carbonation ingress (Jong, 2023). The carbonation resistances, as given in fib Bulletin 34 (2006) are shown in Figure 1.

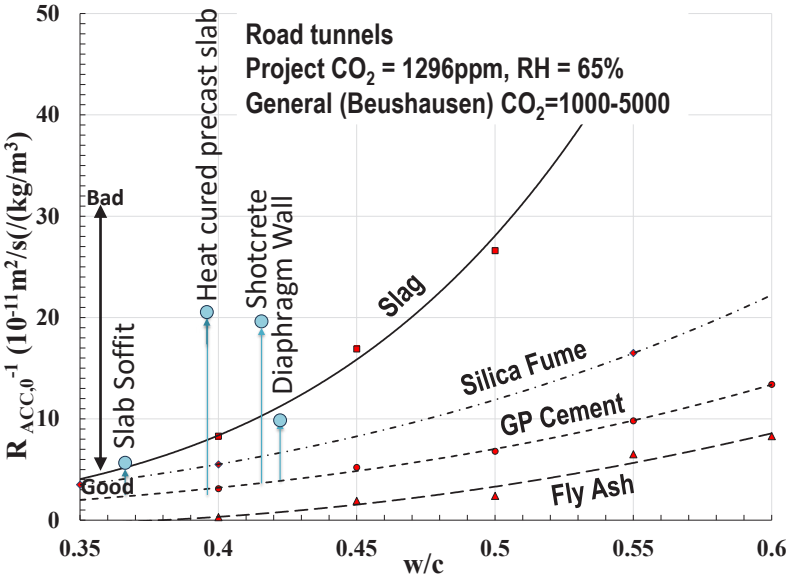


Figure 1: fib $R_{ACC,0}^{-1}$ values. A shotcrete result (from Table 1) shows effect of construction.

Table 1: Measured RACC,0-1 values for project mixes shows negative effects of curing and placing

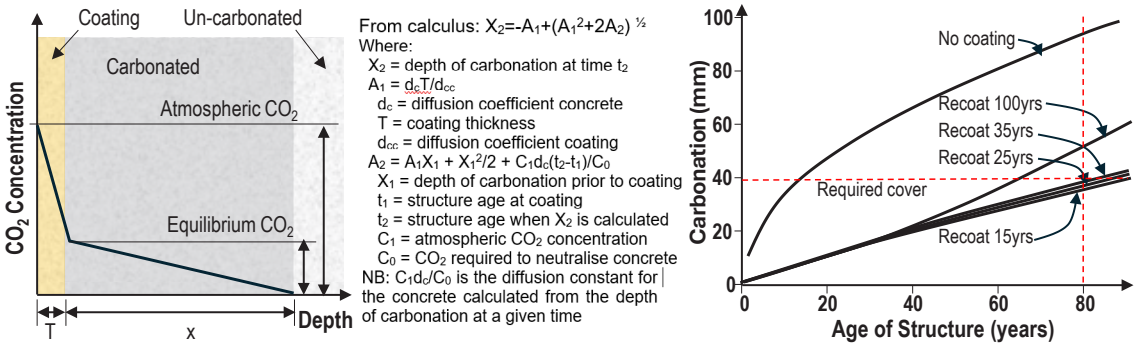
Location	Strength (MPa)	Cement (kg/m^3)	Cement Type	w/c	Curing	Mean DoC in ACC tests (mm)	$R_{ACC\cdot0}^{-1}$ (units as fig 1)	Outcome
Tunnel segments	75	420	7% FA	0.40	Steam	1.35	1.03	OK
Wall shotcrete	30	415	GP	0.42	Compound	6.00	20.4	Coat
Flat slab soffit	50	420	GP	0.37	Heat cured	2.75	4.29	Coat
Extruded planks soffit	45	445	28% FA	0.17	Heat cured	2.25	2.97	OK
Diaphragm wall	30	415	GP	0.43	None	4.25	10.2	OK
Extruded hollow core	45	445	28% FA	0.17	Heat cured	4.00	9.07	Coat
Precast flat slab	50	445	GP		Heat cured	6.00	20.4	Coat
Precast cladding	40	348	GP	0.47	Air cured	4.50	11.5	Coat
50MPa Alkali Activated Slag from a building project.						5.17	15.1	-

For vehicle tunnels Beushausen (2021) recommends a carbon dioxide loading of 1000-5000ppm. A reasonable conservative estimate should be established for the project. It should be verified in service. On one road tunnel the carbon dioxide concentrations at the tunnel exhaust was estimated as 1296 ppm average maximum over the life of the structure with a relative humidity of 65%. Caution is required in using this RH as waster penetration may cause a higher RH in the concrete. At the exhaust various material were used and the performance of each had to be assessed. An initial durability assessment was undertaken using data in Figure 1 as a guide. However, because the data was not specific to the project mixes the carbonation resistance (R_{ACC}) was measured by the ACC Test in fib Bulletin 34 (2006). Results are given for the tunnel segments and various other elements in the exhaust structure in Table 1.

The CO_2 concentration was applied to determine the cover required to achieve the required 80 years to depassivation. A propagation period of 20 years was assumed but it may not always be conservative. Where this was more than the actual cover a coating was determined to be required.

The coating effectively reduces the carbon dioxide concentration at the concrete surface as shown in Figure 2a. The reduction is a function of the relative penetrability of the coating and the concrete and the consumption of carbon dioxide in the concrete that fixes the zero for the concentration gradient.

Given the huge investment in a tunnel's construction, the high repair cost due to the public and operational cost, and the relatively low cost of improvement to durability design, the following could be mandatory design requirements for vehicle tunnels:



a) Schematic of how the CO_2 concentration reduces through the coating and carbonated concrete to provide a flux of CO_2 at the uncarbonated concrete where the carbonation reaction is taking place. Also shown is the formula for calculating the effect of the coating on the carbonation rate.

b) Example of carbonation depth with time assuming different coating re-application intervals. Carbonation depth at 80 years without coating is 86mm plus 10mm partial factor but actual cover is only 40mm. 35yr replacement interval of 450 µm thick coating gives adequate protection.

Figure 2: Carbonation With Coating

a) Prediction and monitoring of the CO_2 content of the tunnel, exhausts and approaches.
b) Test concrete for carbonation resistance where the exposure is above normal atmospheric.
c) Specific determination of reliability required for each element by the project team. For example, soffits may have a higher reliability required than walls.
d) Full probabilistic or partial factor modelling of carbonation depth with time.

3 ATMOSPHERIC TUNNELS BELOW GROUND WATER

There are two key zones for consideration, extrados and intrados tunnel exposures.

3.1 *Extrados Exposure*

The extrados exposure severity depends on the nature and pressure of the attacking water. Although there are standard classifications for different ground conditions great care is required to assess the chemical attack on concrete and corrosion resistance of the reinforcement.

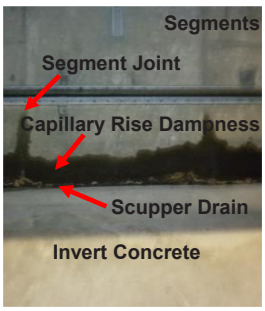
In some countries the groundwater sulphate levels can be very high. While this is very aggressive to GP cements high slag blends (>60% slag) in high performance concrete can provide excellent resistance to chemical attack, even from brines and acid sulphate soils. This is recognized in Australian standards but not in some European standards. Two key parts to design for exposures are the chemical resistance of the cement system and the penetrability of the concrete.

Reinforcement corrosion on the extrados is not a general concern as below the groundwater the pores will be saturated and hence all voids around the reinforcement, the normal location for corrosion commencement, will have a high pH from leached hydroxides (Papworth, 2018). This paper also notes that in immersed conditions localised corrosion can initiate early in a structures life and continue slowly such that loss of bar section isn't significant for up to 50 years. Such corrosion does not become visible as rust stains and spalling.

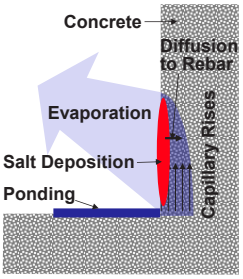
3.2 *Intrados Exposure*

Intrados exposure must consider how the durability design will cope with leaking cracks and joints. It is common that tunnels leak. Even water with low chloride levels that leaks into the tunnel and spreads over the intrados can give rise to high chloride levels on the surface due to 'evaporative concentration' of salts at the concrete surface. Chloride penetrates the concrete by a variety of mechanism involving water within the concrete pores. Mechanisms are described in Figure 2 to Figure 4.

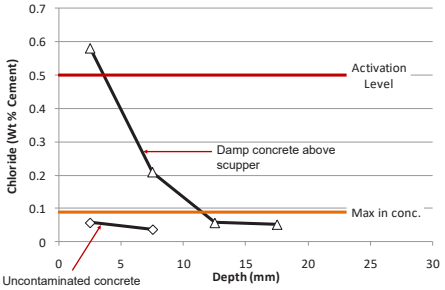
Although not developed for tunnels a chloride loading (C_s) can be used in the fib Bulletin 34 (2006) chloride ingress model to provide some guidance for ingress of chlorides. For elements in marine and coastal exposures there is guidance on C_s (Papworth, 2025/1), but there are no guides for groundwater exposure. Edvardsen (2004) found C_s of 1.5 weight percent of cement (WPC) from leakage but this isn't related to time or external chloride concentration. This is very low and based on Papworth (2025/1) is less than might be expected for coastal atmospheric exposure. It is recommended that design be based on the chloride loading expected for the extrados or the severest atmospheric chloride level of the tunnels exposed ends or intakes as shown in Table 2.



c) Scupper drains carry ground water leakage. Capillary rise can cause water to rise.



d) Evaporation off the concrete leaves behind salts. Concentrated surface chloride then diffuses back to the rebar.

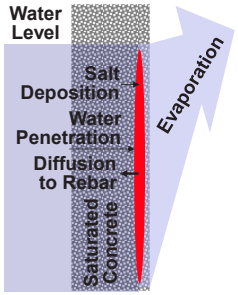


e) This shows the high chloride levels just above a scupper drain. Constant evaporation can lead to very high salt levels and can also cause salt etching and sulphate attack.

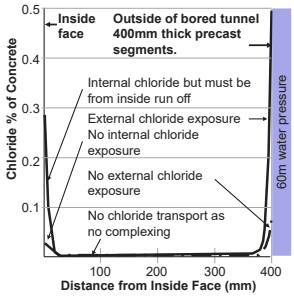
Figure 2: Capillary Rise, Evaporative Concentration and Diffusion



a) In concrete where water can penetrate the lining thickness salts will deposit at the surface leading to sulfate attack or reinforcement corrosion.



b) If evaporation is greater than flow rate no water becomes apparent but salt build up could still be occurring.

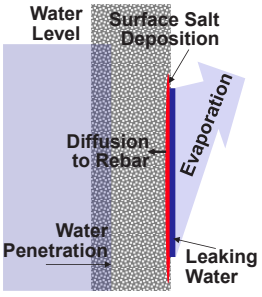


c) Edvardsen (2004) measured the chloride profile through a 400mm thick tunnel wall subject to a 60m pressure head. High chloride on the inside face occurred where there was high chloride externally even though no chloride penetrated.

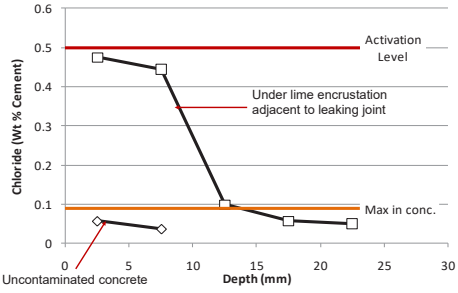
Figure 3: Water Penetration and Evaporative Concentration



a) Saline water penetrates at cracks and joints as leakage and is then swept across the concrete surface.



b) It builds up as encrustations. Evaporation concentrates the salt which then diffuse inward.



c) This shows the chloride concentration beneath a surface encrustation due to leakage after just a few years.

Figure 4: Leakage, Evaporative Concentration, and Diffusion

Modelling using C_s can determine when a critical chloride level at the reinforcement will be reached using he principal measure, i.e. chloride migration. This should be measured initially on cores from blocks cast using proposed construction practices, and subsequently on the structure. Concrete's chloride migration reduces over time. It is important to ensure the aging factors used are calibrated for the country of use. Papworth (2021) describes an approach for this.

Table 2: Exposure Classes[1] for Reinforcement Corrosion in Chloride Exposures for Tunnels and Approaches

External Exposure	Intrados Exposure Classes			Extrados Exp. Class		Approaches Exp. Class	
	AS 4312	AS 5100.5	AGRT02-19	Papworth (2025/1)[2]	Surface Cl^- WPC	Papworth (2025/1)[2]	Surface Cl^- WPC
Brine	-	U	-	XS2a (-/-/U)	N/R[3]	XS1f(-/-/U)	4.0[4]
Seawater	-	U	C	XS2a(C/-/B2)	N/R[3]	XS3b(C/-/U)	3.5[5]
Beach front	C5	B2+	B2	XS1d(B2/C5/B2)	3.0	XS1d(B2/C5/B2)	3.0
High Coastal	C4	B2	B2	XS1c(B2/C4/B2)	2.0	XS1c(B2/C4/B2)	2.0
Med. Coastal	C3	B1	B2	XS1b(B1/C3/B1)	1.0	XS1b(B2/C3/B1)	1.0

1. Environment at the concrete surface. Tunnels have different reliabilities but the same exposure class.
2. The bracketed figures are (AGRT02-19, 2019 /AS 4312, 2019/AS 5100.5,2024).
3. The mechanisms controlling reinforcement corrosion are not related to chloride level.
4. Taken as XS1f rather than XS1e as the condition is likely to be continuously wet and hence have an aging factor for wet exposure rather than a higher value typical of a coastal type exposure.
5. This value is for a typical splash zone. Papworth (2025/1) recognises higher surface chloride levels for more severe exposures and consideration should be given to those if there is evidence to support it.

The last factor in resistance to chloride induced corrosion is the chloride level at which reinforcement depassivation occurs (C_{crit}). It is known that C_{crit} varies with exposure, voids at the bar: concrete interface, metal type, cement type and many other factors. The low and broad C_{crit} distribution described for all concrete in fib Bulletins 34 (2006) and 76 (2015) resulted as the effect of other parameters could not be determined. Papworth (2025/2) describes the status of a fib Bulletin being prepared. It gives C_{crit} values for different steels, cements and exposures.

C_{crit} for black steel is often quoted as 0.4 WPC but frequently users fail to recognise this as the characteristic value for C_{crit}. The distribution expressed in Bulletin 76 is given as a mean value of 0.6 WPC with standard deviation of 0.15 as shown in Figure 5a. This is consistent with a characteristic value of 0.4 WPC.

Table 3: Recommended Lowest C_{crit} Distributions (Papworth, 2025/2)

Steel type and exposure	**Mean (μ)**	**Std Dev (σ)**	**a**	**b**	**Charact.**
Carbon steel in atmosphere	0.60	0.15	0.2	2	0.35
Carbon steel in saturated concrete	2.00	0.15	0	3	1.75
Prestressing cables, posttensioned tendons	0.40	0.15	0	0.5	0.20
Galvanised reinforcement	0.95	0.15	0	2	0.70
Stainless steel in atmospheric conditions					
304	4.00	2.00	0	5	0.70
316, 2304, 2101	7.00	2.00	0	9	3.70
Steel fibres	0.95	0.15	0	2	0.70

The broad C_{crit} distribution in Bulletin 76 (2015) is currently taken to apply to all cement types and concrete grades and qualities. However, it has also been shown that corrosion may not commence in some circumstance until much higher concentration are reached. This is clearly the case in immersed situations where Papworth (2025/2) notes theory, laboratory simulations and practice all show that in immersed situation the critical chloride content is much higher. Critical chloride levels proposed are also shown in Table 3.

Base chloride level (the chloride concentration in the as built concrete) can be critical because it determines the allowable increase in chloride before the critical chloride level is reached. On one project the contractor failed to prove that the specified base chloride level was being achieved, and it was six months before the engineer undertook their own tests and found the chloride level

was much higher than specified, even though on other projects in the area it was being achieved. The high base chloride level reduced the predicted service life considerably.

4 WATER TUNNELS

The exposure severity of the inside face of water tunnels depends on what the tunnel carries. Concrete is inherently resistant to fresh water however tunnels with running water can accelerate leaching reducing performance. The commentary to AS 3735 (2001) provides a comprehensive guide to the aggressivity of water.

Seawater intake tunnels are subject to the seawater attack and possibly low pH where dosed to reduce marine growth. CIA Z7/02 (2018) provides two exposure classes for immersed concrete, i.e. for above and below pH 6. The use of a low exposure class (e.g. AS5100.5 B2) in seawater tunnels may be inappropriate. Permanent seawater immersion will lead to high chloride penetration, but it does not lead to rebar corrosion. However, if the tunnel is closed for maintenance years after construction such that the concrete around the reinforcement becomes unsaturated widespread corrosion could commence and once started may not be easily stopped.

Precast segmental tunnels are commonly used for brine outfalls of desalination plants. The chloride and sulfate loading, particularly magnesium sulfate, can be twice that of seawater tunnels and at these levels magnesium sulfate attack has been proposed as a major issue for silica fume and slags. However close inspection of test data shows the concern arises from sample size effects and brines attack concrete at only twice the rate of seawaters very low attack rate.

5 TUNNEL APPROACHES

At some point along the atmospheric tunnel's approach the exposure changes from a tunnel to that of the surrounding atmosphere. Where the tunnel exposure is more severe than that due to the atmosphere at the approach a decision has to be made on the extent to which the tunnel exposure will be spread to the approaches. There is no data to define this but it is recommended that for tunnels where wind spreads contaminants to the approaches that a minimum of 100m be required for approaches to have the same exposure as the tunnels. In the case of carbon dioxide spread may be limited as exhaust fans remove most of the gases. The tunnel portal and all exhaust chambers should be considered part of the tunnel. Where approaches confine the dispersion of fumes the tunnel exposure might be spread to at least 50m from the portal. Data is limited in this regard, and it would be valuable to monitor carbon dioxide levels in and around vehicle tunnels.

6 CONCRETE RESISTANCE

The concrete's resistance to the exposure load is generally determined by the chemistry of the cement system, the penetrability of the concrete and the corrosion resistance of the reinforcement in its environment.

6.1 *Cement System and Exposure Type*

GP cement is the predominant cement used and is suitable for tunnels where exposure is benign, and heat of hydration is not problematic. Supplementary Cementitious Materials (SCM's), typically fly ash, slag and silica fume, provide different beneficial properties when blended with GP cement. Performance of SCM varies from country to country and hence local knowledge of materials and measurement of their performance is critical.

6.2 *Concrete Penetrability*

Three aspects determine the time to penetration of a front that will depassivate reinforcement, i.e. mix design, quality of construction and cover.

On one project the author investigated honeycombing of insitu cast tunnel concrete was a regular event throughout construction. The issue was that the high slump of the concrete mix reverted quickly leaving a thixotropic concrete difficult to place and compact. The cause was a function

of the cement system and admixtures. Modern superplasticizer, with slag and silica fume cements particularly, can be a problem if there is insufficient initial slump. Marosszeky (2023) points out how complex achieving a quality concrete is. It is concluded that concrete needs to be considered as a special process with execution plans that are thoroughly assessed.

Quality control also impacts the cover achieved. For example, spacers at the right centres and assurance the cage will not move under fresh concrete loading are key to success. However, there is also a misunderstanding on the variability of cover. AS5100.5 allows for a 5mm negative tolerance on cover. That is a 3mm standard deviation taking minimum cover as a 95% confidence level. On one project, where other concerns led to widespread cover measurements on various segment types the standard deviation was found to be consistently 9-10mm. The nominal cover of 70mm was reduced to an actual minimum cover of 52mm. Attention to achieving and verifying early cover is a lesson learned time after time. A factor to bear in mind in verification is that NDT cover often underestimates cover by 2-3mm. It can be worth calibrating the covermeter against taped cover in drill holes.

Cracks that leak with saline water are not only an issue due to evaporative concentration but also due to the risk of accelerated corrosion at cracks. Papworth (2025/3) notes that rapid corrosion at cracks can occur if cracks exceed a certain threshold width. Contributing factors are high stress in the reinforcement, lack of initial passivation, inability of diffusing hydroxyl ions to counteract acid conditions.

7 DESIGN INPUTS

7.1 *Levels of approximation*

Papworth (2021) notes that fib Model Code (2024) says the design strategy should be specified and that besides design by avoidance of degradation the LoA's can be applied for the verification of the design service life. LoA is introduced to encourage more complex design solutions where practical, in order to give more cost efficient and/or sustainable solutions. Probabilistic methods are likely to provide suitable approaches, particularly for major structures such as tunnels.

Some codes (e.g. AS 5100.5) note that the code may not always provide a safe solution. This is particularly true where the actual exposure does not closely match the code definition, a common issue with tunnels. Hence probabilistic methods which consider a broader range of variables can be used for tunnels to resolve doubt about the deemed-to-satisfy solutions and provide more economic solutions by providing a method of design for higher performance materials.

7.2 *Reliability Based Design*

A significant issue for DtS provisions is that they must be based on a certain reliability (inverse function of probability of failure) over the design life but that reliabity is not stated in the codes. Reliability for code DtS is most likely linked to Serviceability Limit State (SLS) failures, i.e. failure requiring limited cost of repair such as patching. SLS state failures are typically allowed to have a PoF of 5-10%. Reliability is a balance between the consequences of failure and the cost of improved performance. Model Code 2020 notes the validity of ISO 2394 for determination of target reliability,

A consideration for all tunnels is access for inspection and the cost of shutdowns. The project team will have to consider what reliability is required to cater for the specific situation. On one tunnel the original design had no access for inspection. This increased reliability required, and hence performance requirements, significantly as durability failure could lead to collapse without warning. Access was ultimately introduced for cost effectiveness.

Full Probabilistic Analysis (FPA) is undertaken by using distributions for all key variables in a model (equation) that is agreed to represent the actual situation. Using a Monte Carlo type analysis the reliability can be calculated. Use of small variations in distributions for variables like cover and temperature to better represent the actual tunnel gives a predicted reliability that more closely matches the real situation.

At this stage reliability requirements for Ultimate Limit State (ULS) failures, such as prestressing failure, would require much higher covers than currently used. Hence it is currently considered that ULS durability failures should be dealt with by avoidance.

7.3 *Life Cycle Cost Analysis*

The target reliability is selected by the project team for safety, budget, and life cycle cost (LCC) reasons. The durability of tunnels is often of particular importance because of safety and the cost of repair. Direct repair cost may be small compared to public and/or operational costs. The interval for maintenance type repairs comes from FPA with the cost at each interval determining the current cost.

7.4 *Specifying End of Life Requirements*

how target reliability is specified for the element at the end of its design life and for a specific limit state determined by the condition required at the end of service life. Given a tunnel's life may be extended well past the original service life this requires strategic consideration in the design. Reliability, and maintenance and repair costs, go into assessing the whole-of-life cost for different construction options.

8 CONCLUSIONS

In high value complex projects like tunnels safe DtS provisions are unlikely to provide the most economic and sustainable design. Using a higher LoA such as FPA will provide safer and more reliable structures. However, data on tunnel exposure is limited. Better understanding of the key distributions that determine deterioration rates in tunnels would enhance the modelling. It is proposed that relatively cheap monitoring systems be used to monitor new tunnels so that their performance can be assessed with time and to provide better data for new tunnel designs.

9 REFERENCES

AS 3735 Commentary (2001). Concrete structures for retaining liquids – Commentary. . Standards Australia, Sydney.

AS 4312 (2019). Atmospheric corrosivity zones in Australia. Standards Australia, Sydney.

AS 5100.5 (2024). Bridge Design Part 5: Concrete. Standards Australia, Sydney 2024

Austroads, (2019). Guide to Road Tunnels (AGRT02-19)

Beushausen. H., Ndawula. J., Helland. S., Papworth. F., Linger. L. 2021 Developments in defining exposure classes for durability design and specification. *Fib Structural Concrete,* 2021

CIA Z7/02 (2018) Durability Exposure Classifications. *Concrete Institute of Australia Concrete Durability Series* Sydney 2018

Dewah. H. (2007). Effect of sulfate concentration and associated cation type on concrete deterioration and morphological changes in cement hydrates. *Construction and Building Materials,*21, 29–39.

Edvardsen C.K.2004 Deterioration modelling – Model Verification Through In-Situ Tests – Great Belt Link (Denmark). *First International Symposium. Safe and Reliable Tunnels.* Prague 2004

Fib Model Code (2023). Model Code for Concrete Structures (2020). International Federation for Structural Concrete (fib) Switzerland. 2024

Fib Bulletin 34 (2006) Model Code for Service Life Design. Féderation internationale du béton, Lausanne, Switzerland, June 2006.

Fib Bulletin 76 (2015) Benchmarking of deemed-to-satisfy provisions in standards: Durability of reinforced concrete structures exposed to chlorides", Féderation internationale du béton, Lausanne, Switzerland, June 2006.

Jong. H., Khan. I., and Papworth. F. Comparison of Full Probabilistic Modelling and Deemed to Satisfy Requirements for Concrete Carbonation Induced Corrosion. Concrete Institute of Australia, Adelaide, *Concrete 2023*

Marosszeky, M. Papworth, F. and Munn, B. Creating Reliability in Concrete Construction—Achieving Quality Within a Complex Sociotechnical System. *Concrete 2023*, Concrete Institute of Australia Virtual Conference, Australia.

Papworth. F. 2018 Durability design for concrete immersed in seawater or brine. Australasian Corrosion Association. *Corrosion 2018*, Adelaide 2018.

Papworth. F. 2021. fib Model Code 2020 - Condition Limit States and Target Reliabilities for Durability Design. Concrete Institute of Australia, Adelaide, *Concrete 2021*

Papworth. F. 2025/1 Modelling for Improved Durability Design - Boundaries for Marine, Coastal and Inland Saline Waterways Exposure Classes. Concrete Institute of Australia, Adelaide, *Concrete 2025*.
Papworth. F., Andrade. C., Lollini. F. 2025/2 Selection of a Critical Chloride Level for Full Probabilistic Modelling. *Corrosion and Materials Degradation.* 2025
Papworth. F. 2025/3 Forensic Assessment of Cracks. Concrete Institute of Australia. Hybrid web presentation. Melbourne 2025.

THIS PAGE INTENTIONALLY LEFT BLANK

19th Australasian Tunnelling Conference – Acosta-Martínez, Stewart and Hudson-Smith (Eds.)
© 2025 Australian Tunnelling Society, ISBN 978-0-85825-002-4

Advanced engineering methods to extend and expand the use of reclaim tunnels at Pilbara mine sites

J. W. Lee
Rio Tinto, Perth, Australia

G. R. Pandey, D. Yau, P. Cutter
Rockfield Technologies Australia, Perth, Australia

ABSTRACT: Rio Tinto has operated iron ore mines in Western Australia's Pilbara region since the 1960s. Recent changes in risk management practices have driven a re-evaluation of the structural capacity of key infrastructure, particularly tunnels. These tunnels are now subject to increased external loads from heavier mobile equipment operating above them, and additional internal loads from processing equipment upgrades mounted to the tunnel directly. Subsequently, a region-wide structural assessment program has been initiated to evaluate tunnel performance under current and emerging load conditions. This paper presents a case study of an operational concrete arch tunnel, built in the late 1970s, which supports a 30 m high stockpile over a rail corridor. Initial assessments using modern design codes indicated overutilisation which resulted in stockpile height restrictions. However, by integrating tunnel monitoring data with finite element analysis, a more accurate structural rating was achieved, therefore demonstrating the importance of advanced methods in managing ageing assets.

1 INTRODUCTION AND TUNNEL BACKGROUND

Rio Tinto has been operating iron ore mines in the Pilbara region of Western Australia since the mid-1960s. To support mining activities and material processing plants, various overpass and underpass structures have been constructed. These structures provide grade separation between ore stockpiles, conveyor systems, railways, heavy mobile equipment roads, light mobile equipment roads, personnel access routes, and utility corridors that are part of the process circuit.
Across the Pilbara operations, Rio Tinto operates approximately 90 overpass and underpass structures. These structures were designed and constructed over the last 60 years, each reflecting the engineering standards, material strength and design philosophies common of their respective eras.

In recent years, evolving approaches to risk management have prompted a reassessment of the structural capacity of these tunnels. This is due to increased loading both externally (i.e., surface loading from mobile equipment above the tunnel) and internally (e.g., upgrades and/or additional mechanical equipment to ancillary systems such as instrumentation cabinets, ventilation units, and operational services) within the tunnel structure. In response, a Pilbara-wide review of the structural capacity of these tunnels has been initiated to better understand the utilization under current loading conditions. These assessments are being conducted against current design methodologies to ensure the continued safety and performance of these critical assets.

It is a general practice to use current design standards for assessing existing structures. Current assessment methodologies, which were largely developed for newer structures[1], generally yield conservative evaluations of older structures. As a result, a significant number of existing assets are identified as structurally deficient despite exhibiting no outward signs of distress. This discrepancy highlights the necessity for more sophisticated and accurate methods of structural assessment[2]. The AS ISO 13822 standard recommends that the structural assessment shall withstand a plausibility check[3].

This paper presents the reassessment of a reinforced concrete (RC) arch tunnel (Figure 1) constructed in the mid-1970s, which was designed to accommodate rail traffic beneath a large iron ore stockpile. The tunnel structure is approximately 400m long and features a roof with integrated discharge gates. These discharge gates allow for ore to be loaded into rail wagons positioned inside the tunnel. The reassessment adopts a multidisciplinary strategy, integrating a review of legacy design reports, geotechnical investigations and analysis to the current methodology, advanced nonlinear structural modelling, and targeted field instrumentation.



Figure 1. RC arch tunnel.

2 ORGINAL DESIGN

The original design of the concrete arch tunnel, developed in the mid-1970s, was driven by the intent to minimise internal bending and shear through geometry rather than material strength. A continuously curved section approximating an elliptical profile (refer to Figure 2), was adopted to promote arching action and carry loads primarily in axial compression under typical stockpile and earth pressure load combinations. While this shape was idealised for a specific vertical-to-horizontal load ratio, it remained effective across a range of load conditions, offering significantly lower internal forces than flat-sided alternatives. To accommodate the operational requirement for a flat floor, the base of the arch was concrete infilled and the final cross-section was formed from compound circular arcs.

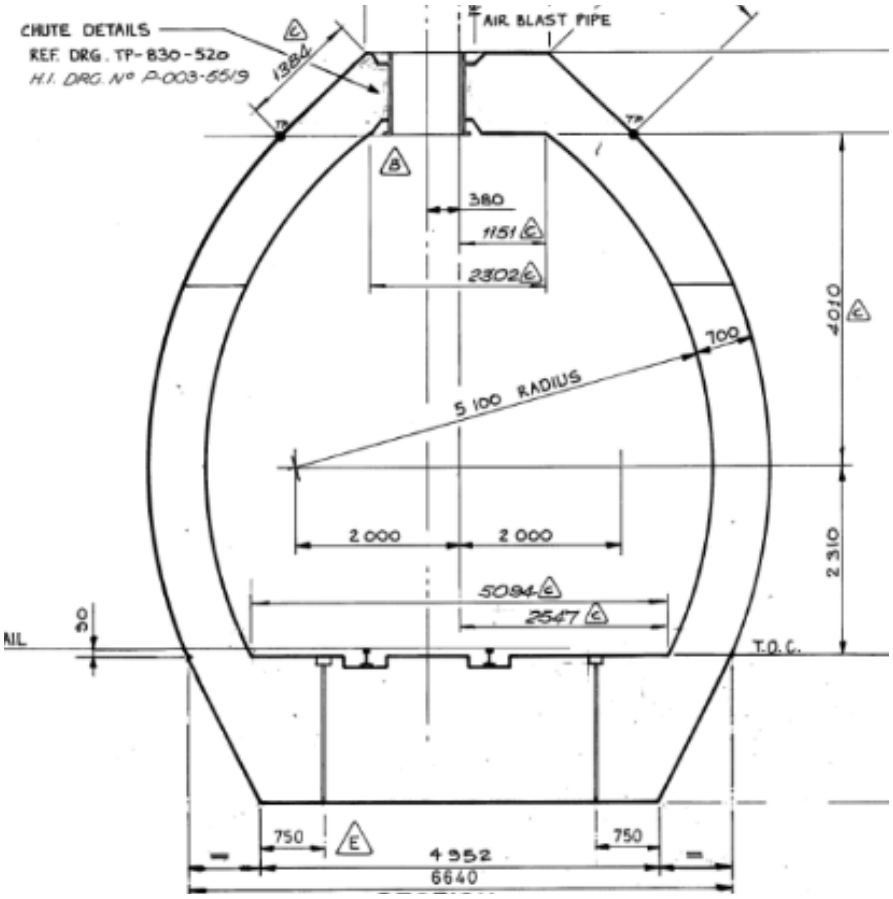


Figure 2. Original design of the arch tunnel.

Structural analysis at the time predicted minimal deformation under full loading (approximately 0.4 mm) and outward wall movement under purely vertical loads (approximately 12 mm), therefore confirming compatibility with the earth pressure assumptions. Longitudinal stresses from shrinkage and settlement were addressed through the inclusion of 12-metre construction modules with 6-metre control joints. These were aligned with discharge gate spacing, to allow the tunnel to accommodate ground movement without excessive internal stress.

3 FINITE ELEMENT MODELLING

A pseudo 3D Finite Element Analysis (FEA) model of the overall structural system was developed in ANSYS (refer to Figure 3). The model comprised of a 360 mm slice of the tunnel, the surrounding stockpile, embankment, foundation and select fill soil material.

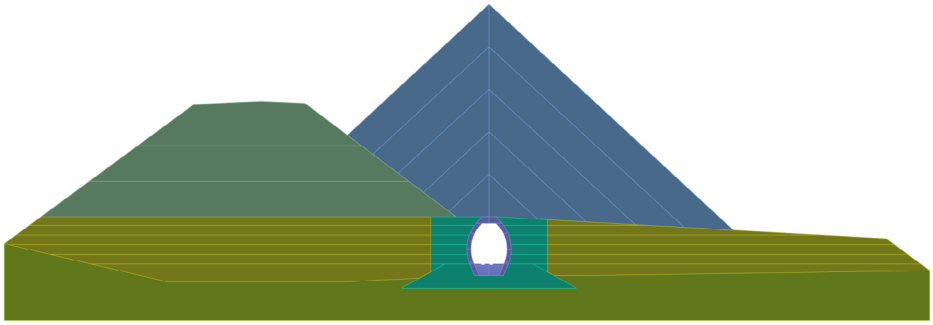


Figure 3. Pseudo 3D Finite Element Analysis (FEA) model.

The objective of the FEA assessment was to address the shortfalls of the conventional assessments which indicated significant overutilisation despite limited visible structural distress. The goals of the FEA assessment were as follows:

1. Determine realistic values for the design capacity of the tunnel by accounting for non-linear effects and non-linear material properties.
2. Determine the maximum allowable stockpile height above the tunnel.
3. Identify areas of high stress which may not have been captured in previous assessments.
4. Conduct a sensitivity analysis to understand the relationship between the tunnel's design capacity with respect to variability in the materials properties used in the FEA model.

The Menetrey-Willam model was used as an advanced constitutive model for concrete. It is based on the flow plasticity theory for modelling concrete behaviour. The baseline parameters used to define this material model were selected from FIB – Model Code[4] for Concrete Structures 2010. The parameters were then calibrated and verified by performing a simulation on a simply supported RC beam. The simulation results were compared against the expected behaviour of the RC beam to validate the use of some of the parameters. The reinforcing bars were represented with a bilinear stress-strain relationship to capture yielding and post-yield behaviour.

For the geotechnical parameters, upper and lower bound values were adopted for conducting a sensitivity analysis. Duncan & Selig's[5] method was used to interpret the soil properties including Young's Modulus, Poisson's Ratio, Cohesion, Friction Angle and Dilatancy Angle for both the upper and lower bound cases. The foundation was assumed to be a banded iron formation material (BIF). To enable comparison of our assessment with previous assessments, the same geotechnical properties were adopted for the foundation material.

4 METHODOLOGY

The state of principal stress was assessed using the FEA model. Both maximum and minimum principal stress states of the concrete, as well as the normal stress along the length of the reinforcing steel bars were investigated to understand the response of the tunnel at varying levels of stockpile load acting on top of it. The maximum principal stress results were used to understand the level of tensile stress being experienced whereas the minimum principal stress was used to understand the level of compressive stress being experienced. The principal stress results were used in conjunction with the total strain being experienced by the tunnel to get a perspective on the formation and propagation of cracks in the tunnel. A sensitivity analysis was performed and therefore the response of the tunnel in a soft and stiff select fill soil medium was investigated.

For both the upper and lower bound cases, the model was analysed with incrementally increased stockpile heights. After reaching the maximum geometrical height, the stockpile load was "virtually raised" by incrementally increasing the density of the stockpile material. The following steps were then performed:

1. The load step at which the model ceased to converge was identified.
2. The corresponding virtual stockpile density at this load step was identified.
3. The stockpile base pressure resulting from this virtual stockpile density and the maximum stockpile height was calculated.
4. An equivalent stockpile height was then determined. This is the height that would generate the same base pressure using the original (unmodified) stockpile density.
5. This equivalent height was then selected as the maximum unfactored system capacity.

The design capacity was determined by applying the system strength reduction factor in accordance with AS 5100.5:2017 into the equivalent height. FEA results indicated that at failure, the concrete at the tunnel wall reached its limit state before yielding occurred in the reinforcement steel.

Selected results at the ultimate failure point are shown in Figure 4.

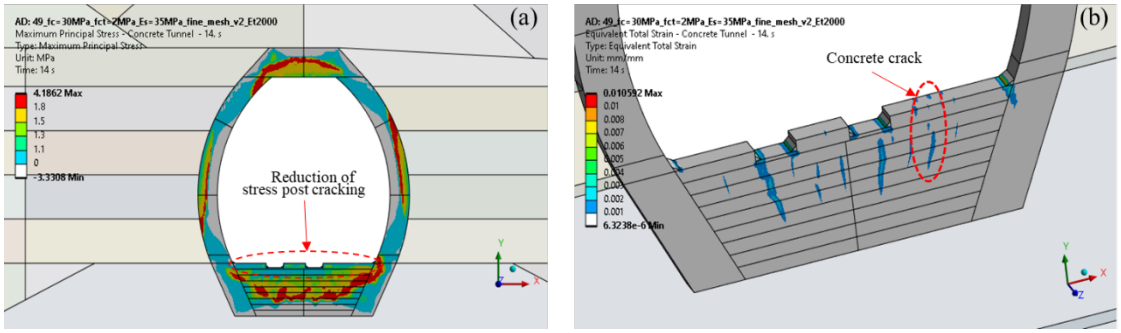


Figure 4. FEA results at the ultimate failure point.

5 INSTRUMENTATION

At the outset of the instrumentation strategy, the project team undertook a structured review of available monitoring methods and technologies to determine their suitability for assessing tunnel performance in a manner that could reliably support the verification of structural capacity. A number of technologies, including vibration-based as well as distance-based measurement systems, were explored. Strain gauges were ultimately selected as the most appropriate and accurate method for this application. These sensors can be installed on both the surface of the concrete and, where accessible, directly onto the steel reinforcement. This approach enables a direct measurement of strain, which can be confidently correlated with stress outputs from structural analysis models. As such, strain gauges provide a higher level of fidelity and reliability in understanding material behaviour and verifying structural utilisation under operational loads.

Strain gauges were installed to monitor the strain response across nine (9) cross-sections of the tunnel as shown in Figure 5. At each cross-section five (5) strain gauges were installed and the locations were selected based on the high-stress locations from the FEA results.

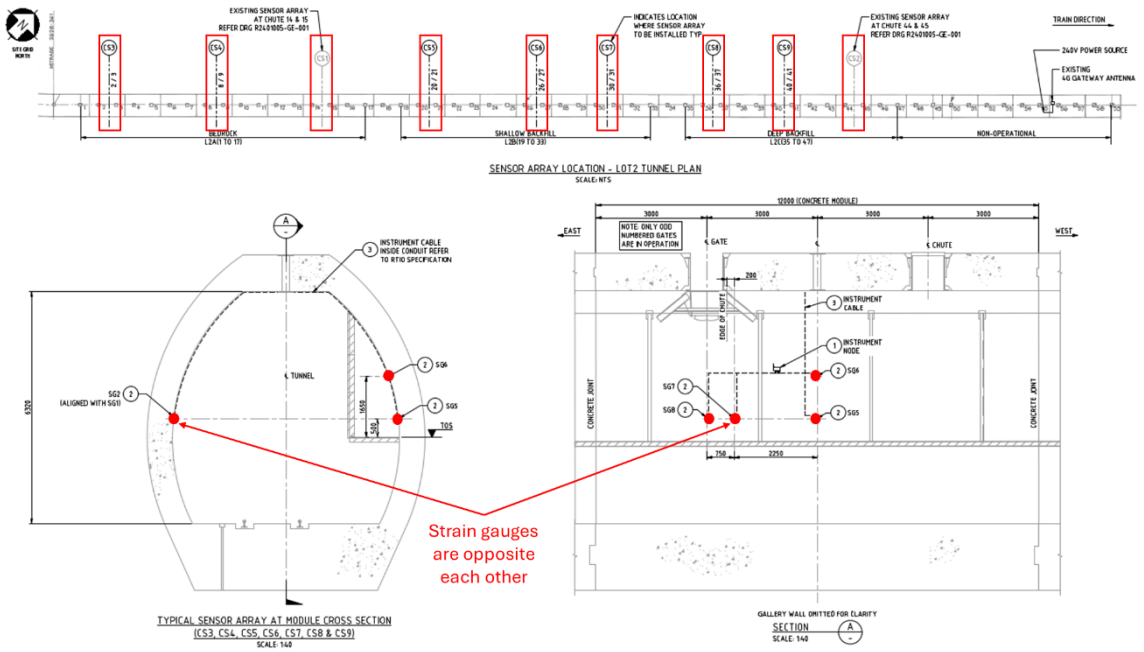


Figure 5. Strain gauge locations (red dots) repeated along 9 cross-sections (red rectangles).

Analysis of the strain data revealed clear spatial trends along the tunnel length. At the tunnel entrance, gauges consistently recorded higher compressive strain than other sections. This observation aligned with historical design documentation that indicated the presence of weaker founding material in this area, possibly associated with an infilled natural drainage line. Although recent

borehole data did not explicitly confirm this zone, the measured strain response provided empirical evidence supporting the legacy assumption of non-uniform subgrade stiffness.

Toward the tunnel midsection and exit, strain magnitudes were generally lower and more consistent with stiffer backfill and more uniform overburden geometry. Importantly, the strain trends qualitatively matched the predicted strain envelopes generated by the ANSYS nonlinear model, especially when adjusted for soil modulus and stockpile geometry variability.

Figure 6 shows the cross-sections 1 and 9 (CS1 and CS9) strain readings within a selected month in September 2024.



Figure 6. Strain gauge readings.

The field data collected from the strain gauges was compared with nonlinear FEA model predictions. Results showed a correlation match between the observed strain and local ground condition showing higher strain was detected at the tunnel entrance, in agreement with historical documentation indicating weak backfill in that area, even though recent geotechnical investigations did not explicitly identify this feature.

The strain response also aligned with predicted ground stiffness profiles along the tunnel length. However, uncertainty in the actual stockpile load, due to fluctuating ore density and a radar-based stockpile height measurement system with ±0.5 m accuracy, required careful interpretation of strain magnitudes.

Despite these limitations, the instrumentation confirmed bidirectional deformation patterns during stockpile loading/unloading, reinforcing the model's assumptions. The team verified that gauges captured the full strain range expected, and that even with imperfect loading data, relative strain behaviour provided valuable validation for the structural model.

Additionally, the use of non-linear FEA to identify critical failure points allowed a new pathway to define the failure points based on strain limit. This is a closer correlation to the actual behaviour of the tunnel, which considers the soil structure interaction. This has offered a different method to the normal load and reduction factor approach for green field design. Based on extensive ANSYS modelling and sensitivity analyses, a set of allowable strain limits were developed and provided to Site Operations to monitor the tunnel performance under varying stockpile load.

6 USING MONITORING DATA TO SUPPORT STOCKPILE HEIGHT MANAGEMENT

The strain data was post-processed to compensate the temperature effects and account for the self-weight and deadload stockpile of 2 m. The post-processed strain data of CS1 is illustrated in Figure 7. Loading and unloading events are marked on the figures as red and green dots, respectively. The negative sign convention denotes a compressive strain, where more negative values indicate higher levels of compression, corresponding to increased stockpile height.

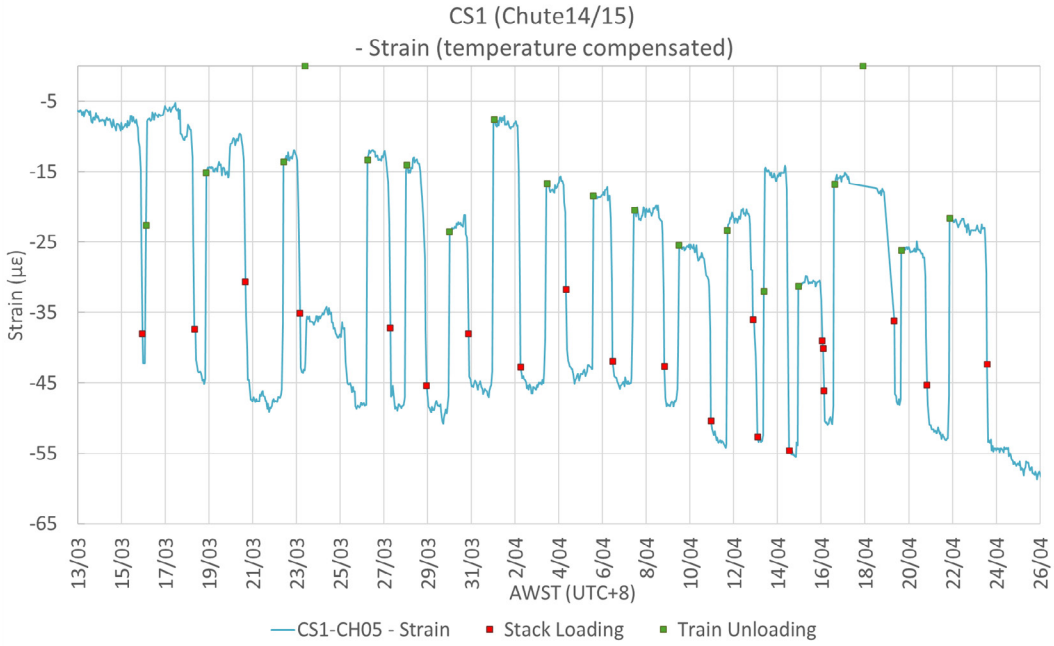


Figure 7. Stockpile loading and unloading events.

As shown in the figure above the data clearly captured the loading and unloading cycles. Utilising this information, the strain gauge monitoring has played a central role in validating the structural performance of the tunnel under operational loading and informing strategic decisions around stockpile management.

Beyond height control, the monitoring system also provided new opportunities to refine the stockpiling method employed above the tunnel. Operationally, stockpiles may be constructed using two main techniques:

- Chevron stacking, where material is deposited in longitudinal layers along the length of the tunnel until the desired height is reached; and
- Cone shell stacking, where the stacker discharges material at a fixed location to form a cone-shaped pile, then moves to the next location once the target height is achieved.

Traditionally, each of these methods require separate loading scenarios to be modelled in the design phase to confirm structural adequacy, often necessitating multiple iterations to evaluate the effects of varying load distributions. The use of strain gauge data eliminates this complexity. Because strain is a direct and reliable indicator of structural response, the effect of different stacking patterns can be assessed empirically without the need to re-analyse each case through time-consuming simulations. This approach also removes the need to explicitly model complex soil-structure interaction phenomena, such as soil arching, or account for stress-dependent backfill behaviour in the structural model.

Moreover, the strain gauge system has enabled the development of a real-time performance envelope that supports responsive stockpile management. For example, in the event of backfill saturation due to extreme weather or infrastructure leakage, the effective stiffness of the supporting ground may decrease, leading to higher strains in the tunnel structure. With continuous monitoring, excessive strain readings can serve as an early warning, prompting temporary restrictions on stockpile height while the source of the issue is investigated and addressed. This ensures that the tunnel remains within its elastic performance range and avoids the onset of damage or irreversible deformation.

The ability to monitor strain trends during both loading and unloading cycles also provides insight into the reversibility and resilience of the tunnel under varying operational conditions. No significant residual strain accumulation was observed over multiple stacking cycles, supporting the conclusion that the tunnel remains in an elastic response regime under current loading practices.

7 CONCLUSIONS

The tunnel was initially assessed as overutilised using liner-elastic based finite element models with simplified soil-structure interaction, resulting in stockpile height restrictions to manage structural risk. However, these models did not fully capture actual tunnel behaviour under operational conditions. Through the integration of advanced nonlinear finite element analysis validated with strain gauge instrumentation, it was demonstrated that the tunnel performed within acceptable limits, even under increased loads. This evidence supported the safe relaxation of stockpile restrictions.

This shift from assumption-based to performance-based management led to key outcomes:

- Justification for higher stockpile zones,
- Reduced need for multiple model scenarios,
- Early warning of structural or ground condition changes, and
- Improved coordination between engineering and operations.

The study highlights how legacy infrastructure can be safely re-rated using real-time data and advanced modelling. It provides a scalable framework for similar buried assets, demonstrating the growing importance of instrumentation-informed strategies in modern asset management.

8 REFERENCES

International Federation for Structural Concrete, “fib Model Code for Concrete Structures 2010,” 2010.

J. M. Duncan, P. Byrne, K. S. Wong, and P. Mabry, “Strength, stress-strain and bulk modulus parameters for finite element analyses of stresses and movements in soil masses UCB/GT/80-01,” 1980.

SAMCO, "Guideline for the Assessment of Existing Structures," 2006. [Online]. Available: http://www.samco.org/network/download_area/ass_guide.pdf.

Standards Australia, AS 5100:2017 Series - Bridge design, 2017.

Standards Australia, AS ISO 13822:2005 (R2016) Basis for design of structures - Assessment of existing structures, 2016.

19th Australasian Tunnelling Conference – Acosta-Martínez, Stewart and Hudson-Smith (Eds.)
© 2025 Australian Tunnelling Society, ISBN 978-0-85825-002-4

Application of geospatial data and Artificial Intelligence in underground infrastructure development near existing structures

H. Wang & A. Rawlinson
WSP Australia, Sydney, Australia

J. Sanderson
IntelliSpatial, Melbourne, Australia

W. Y. Soo
Civil Consult, Ballina, Australia (formerly WSP Australia)

ABSTRACT: As urban populations expand, especially in cities like Sydney, detailed engineering assessments are increasingly necessary to evaluate the impact of new developments near existing underground infrastructure. This is critical to ensure the structural integrity of these assets, as required by authorities. Conducting dilapidation surveys before and after construction is essential for detecting structural changes attributable to construction works. This paper discusses the application of advanced technologies, including laser scanning and 3D photorealistic imaging, to assess infrastructure conditions with millimetre precision. It also examines the integration of artificial intelligence (AI) for tunnel dilapidation surveys. These tools are pivotal in obtaining approvals from asset owners for proposed development. The case study demonstrates that 3D scanning offers greater efficiency and cost-effectiveness compared to traditional methods, while also addressing challenges related to access and operational constraints.

1 INTRODUCTION

Urban densification in cities like Sydney has increased the complexity of developments near existing underground infrastructure. These projects require detailed engineering analyses to evaluate potential structural impacts on adjacent tunnels, utilities, and subsurface structures. Dilapidation surveys are critical to documenting pre-existing infrastructure conditions to establish baselines for detecting construction-induced changes or damage. Regulatory authorities require comprehensive instrumentation and monitoring programs that compare actual construction effects with predicted impacts from engineering assessments (Pan et al., 2023). These programs should integrate with pre- and post-construction dilapidation surveys to provide complete infrastructure protection and liability management frameworks.

This study focuses on the application of advanced technologies to enhance infrastructure protection and the evaluation of new developments undertaken in an eastern suburb of Sydney, highlighting the use of high-precision geospatial data acquisition techniques, such as laser scanning and three-dimensional (3D) photorealistic imaging, to perform detailed condition assessments with millimetre-level accuracy. Additionally, AI-assisted tools such as the Dibit8 system are explored for their effectiveness in tunnel dilapidation surveys.

For rail infrastructure specifically, laser scanning facilitates precise geometry capture and lining thickness estimation, which is crucial for identifying potential conflicts and ensuring instrumentation placements do not interfere with rail or track alignment. The present case study underscores the benefits of 3D scanning technology for tunnel dilapidation surveys. Unlike traditional inspection methods, which are often constrained by limited access and operational downtime, 3D scanning offers a more efficient, comprehensive, and cost-effective alternative.

This study demonstrates how geospatial and AI-assisted technologies assist in overcoming access limitations, improve defect detection accuracy, and support structural assessment and

regulatory approvals in an underground infrastructure-adjacent development. The application of deep learning-based frameworks in tunnel condition assessment, such as those demonstrated by Jiang et al. (2023), further illustrates the potential of AI-enhanced methods to improve decision accuracy and reliability.

This paper describes the case study site conditions, engineering assessment methodology, tunnel condition survey techniques, and instrumentation strategy, illustrating the practical implementation of these technologies to address specific challenges and support project objectives.

2 OVERVIEW OF CASE STUDY

2.1 *Project Site*

An underground development undertaken in this study, adjacent to the existing rail tunnels, is shown in Figure 1. The development involved the construction of a multistorey building with two basement levels located directly above existing rail tunnels. The works required additional excavation to a maximum depth of 2 m below the existing basement level.

Records indicate that this tunnel section was excavated in 1971 using a ~5 m diameter Tunnel Boring Machine (TBM), supplemented by drill-and-blast, ripping, and roadheader excavation to achieve the final profile. (Braybrooke, 1985). The cross-section comprises twin single-tracked inverted U-shapes, each measuring 5 m in width and 6.3 m in height, as shown in Figure 2.

Between October 2004 and April 2006, a rail crossover was constructed between the two tunnels, resulting in the expansion of the Down tunnel at the case study site, which creates additional structural considerations for the overlying development.

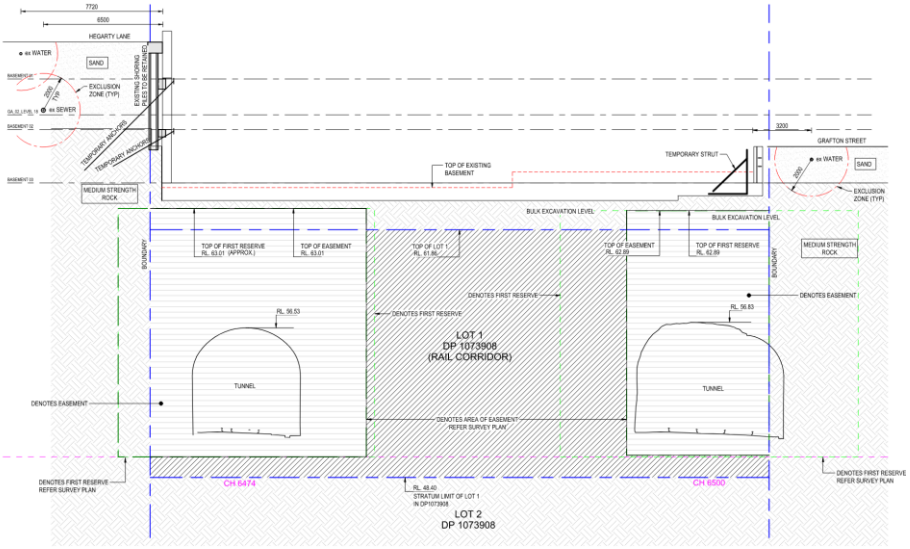
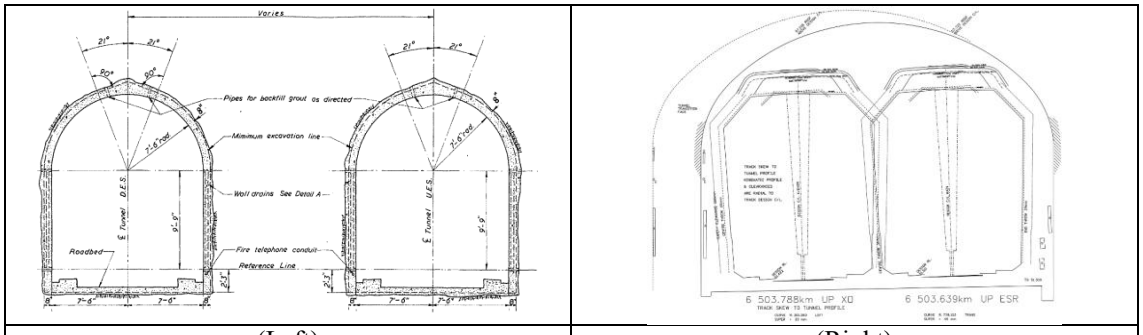


Figure 1. Development site layout showing proximity to existing underground rail tunnels and designated protection reserves.



(Left) (Right)

Figure 2. Twin single-track rail tunnels with inverted U-shaped profiles. (Left) View of tunnel cross-section. (Right) Up Track tunnel showing electrical clearance zones for pantographs and overhead wiring equipment.

2.2 *Site Geotechnical Profiles*

Site-specific geotechnical investigations, along with existing data, indicate a subsurface profile generally consisting of fill materials and residual soils overlying Hawkesbury Sandstone. The sandstone ranges from moderately to slightly weathered with medium to high strength. The Hawkesbury Sandstone typically contains two prominent sub-vertical joint sets: Set 1 trending approximately N-NE and Set 2 trending E-SE. The formation is generally thickly bedded, with east-west trending thrust faults present. Bedding planes observed in core samples are clay-coated and, above the tunnel crown, typically spaced at intervals of 1 to 2 m.

Numerical modelling was conducted to assess the impact of construction on the existing tunnels. The soil was modelled using the Mohr-Coulomb constitutive model, whereas the rock mass model utilised the Hoek-Brown failure criterion. Discontinuities were included explicitly in the analysis. Given no groundwater encountered during the investigation, the tunnels were understood to be drained, with the water table likely drawn down to the invert level. The predicted tunnel lining movement caused by the building construction and permanent conditions is less than 10 mm, which complies with the asset owner's requirement. The tunnel lining movement will be monitored with instrumentation during the building construction.

3 TUNNEL CONDITION ASSESSMENT

3.1 *General*

To establish a baseline record of tunnel conditions prior to construction, the dilapidation survey employed advanced scanning and AI-enabled tools for condition assessment. This method utilised 3D measurements and high-resolution imaging to document surface defects and structural damage, with modern scanning systems enabling 3D reconstruction, crack detection, and feature classification. Three primary approaches supported tunnel monitoring: Reality Capture, Terrestrial Laser Scanning (TLS), and 3D modelling. Reality Capture involved cameras, LiDAR, lighting systems, thermal cameras, and Unmanned Aerial Vehicles (UAVs) to gather extensive photographic and spatial data. These datasets were aligned using standard survey coordinate registration to maintain accuracy. TLS provided dense point cloud data from multiple angles, enabling the creation of precise 3D models of infrastructure, heritage sites, and complex environments.

3.2 *Tunnel Scan Data/System*

The tunnel scanning system shown in Figure 3 collected LiDAR and photogrammetry data at a spatial resolution of 1 mm × 1 mm, with colour imagery captured via digital single-lens reflex (DSLR) cameras at up to 50 megapixels. Point cloud registration to survey control utilised iterative closest point (ICP) algorithms, achieving sub-centimetre alignment accuracy. Data acquisition was completed during two tunnel access windows of approximately 2.5 hours. Raw point clouds were denoised, segmented, and meshed to create high-fidelity 3D models, consistent with methods applied in recent mobile laser scanning frameworks for tunnel environments (Liu et al., 2024). These datasets were then converted to .las, .obj, and .shp formats for integration with Computer-Aided Design (CAD) objects or Building Information Modelling (BIM) software and asset management databases. Geospatial metadata, including tunnel chainage, invert level, and station location, were tagged to each segment, enabling spatial filtering and time-based defect tracking during future inspections.



Figure 3. Vehicle-mounted tunnel scanning system equipped with laser profiler and DSLR cameras for 360° image and geometry capture.

3.3 *Data Processing and 3D Modelling*

Data is processed in phases. Initially, scans and photos are registered to survey control to produce 3D mesh models, point clouds, and high-resolution images. Defects such as cracks, spalling, delamination, water leaks, joint misalignment, and corrosion are identified through manual inspection, semi-automated tools, and machine learning techniques based on predefined defect libraries. This integrated workflow aligns with current research combining point cloud geometry and photographic imagery for accurate and automated tunnel defect classification (Huang et al., 2025).

Traditional survey methods supported and verified digital data capture. Survey control was established along the tunnel alignment using conventional total station methods, with surveyed targets positioned for accurate LiDAR and photogrammetric data georeferencing. Point cloud registration utilised iterative closest point (ICP) algorithms aligned to this established control network, ensuring spatial accuracy to sub-centimetre levels. Table 1 summarises the geospatial data workflow, digital deliverables and their source data.

Table 1. Summary of Digital Deliverables and Source Devices.

Digital Product/Deliverable	Description/Use	Primary Data Source(s)
3D Point Cloud (.las format)	High-resolution spatial dataset used for tunnel geometry modelling and measurement	LiDAR (Laser Profiler)
Textured 3D Mesh (.obj format)	Visual model of tunnel surfaces used for virtual inspection and defect review	Photogrammetry (DSLR Cameras)
High-Resolution Imagery	Still images used for manual review and input to AI-based defect detection	DSLR Cameras
Defect Mapping & Classification	Annotated records of cracks, spalling, leakage, etc., for reporting and monitoring	Combined Photogrammetry + AI Software (Dibit8)
Georeferenced CAD/BIM Layers (.shp, .dxf)	Spatially tagged infrastructure elements (e.g., lighting, services, emergency doors)	Combined LiDAR and Photogrammetry

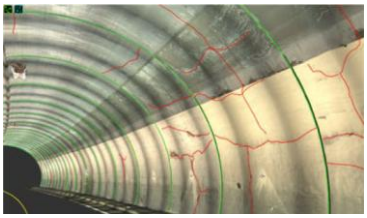
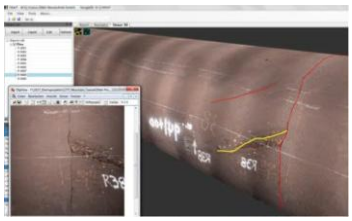
Total processing time for the tunnel scanning dataset was approximately four working days. Automated processing entailing point cloud registration, meshing, and initial AI-based defect detection required two days, while human verification, manual refinement of defect classification, and preparation of final deliverables consumed the remaining 2 days. The AI-assisted workflow significantly reduced manual interpretation time, particularly for defect identification, compared to traditional methods, typically requiring 1 to 2 weeks for comparable tunnel lengths.

3.4 *Defect Identification*

The tunnel scan system data were then analysed using dedicated software tools for defect classification and mapping. Dibit8 software enables operators to map, classify, and analyse defects through a semi-automated detection system driven by artificial intelligence and machine learning algorithms. The software employs a convolutional neural network (CNN) framework trained on a curated dataset of tunnel defect images, including cracking, corrosion, water ingress, and spalling. The trained model can detect linear and non-linear features such as cracks down to a resolution of 0.3 mm, classify them by geometry and orientation, and automatically generate geometry attributes, including crack length, width, and position. Anomaly detection using unsupervised learning identifies unfamiliar or unexpected features. AI-based techniques employed in Dibit8 and similar frameworks for real-time tunnel defect detection (Zhao et al., 2024; Fang et al., 2025) significantly reduce interpretation subjectivity and enable rapid re-analysis of updated scans, improving the accuracy and repeatability of condition assessments.

This approach significantly improves efficiency and consistency over traditional manual methods. All identified defects are stored in a database using spatial positioning and condition assessment criteria, as demonstrated in Table 2.

Table 2. Defect identification.

Data Visualisation	Defect Management	Data Management
– View and navigate large datasets – Epoch to epoch comparison – Custom visual reports	– Identify defects – Semi-automated/AI detection – Imagery overlay and digitisation	– Unique identifiers for observations – Georeferencing metadata – Open source data sharing
		

3.5 *Measuring change of condition over time*

The tunnel scanning enables side-by-side comparison of spatial data captured at different stages, facilitating detection of deformations, evolving damage patterns, crack growth, and newly formed defects. Only the pre-construction dilapidation scan has been completed at the time of writing. Planned scans during and after construction will enable direct comparisons with the baseline dataset to support comprehensive dilapidation surveys throughout construction.

3.6 Advantages of tunnel scanning and monitoring

The tunnel condition assessment demonstrated several practical benefits for infrastructure monitoring and dilapidation surveys. Approximately 190 m of rail tunnels were scanned, capturing geometric details and spatial data, as depicted in Figure 4.



(Left) (Right)

Figure 4. 3D reconstruction of tunnel lining using Dibit8 software. (Left) Colour-mapped mesh of the Down Track tunnel surface. (Right) Crown region showing darker-coloured 2004 shotcrete overlay compared to the original 1971 lining.

Photogrammetric models provided accurate visual representations of tunnel surfaces, while defect mapping for corrosion, leakage, and cracking was carried out using Dibit8 software. The software also mapped tunnel features, including emergency doors, lights, and service cables. The Down Track tunnel exhibited localised expansion and crown deformation. Figure 4 (Right) illustrates the darker coloured shotcrete applied in 2004, distinguishable from the original 1971 lining through AI-assisted 3D scanning and analysis. This diagnostic capability demonstrates enhanced accuracy compared to conventional inspection methods.

3.6.1 Technical Integration

The Dibit8 software processed the tunnel data into true-colour 3D point clouds and textured 3D mesh models exported in various data formats (e.g., .las for LiDAR point cloud, .obj for the photogrammetric model, .shp for integration with CAD and BIM software. Bentley OpenRail software was subsequently used to import point cloud files, generate a 3D track alignment model, produce 3D track alignment models and cross-sections, and export tunnel geometries for instrumentation planning (Figure 5). The tunnel dilapidation survey is shown in Figure 6, with Down Track and Up Track tunnels demonstrated in the left and right layouts.

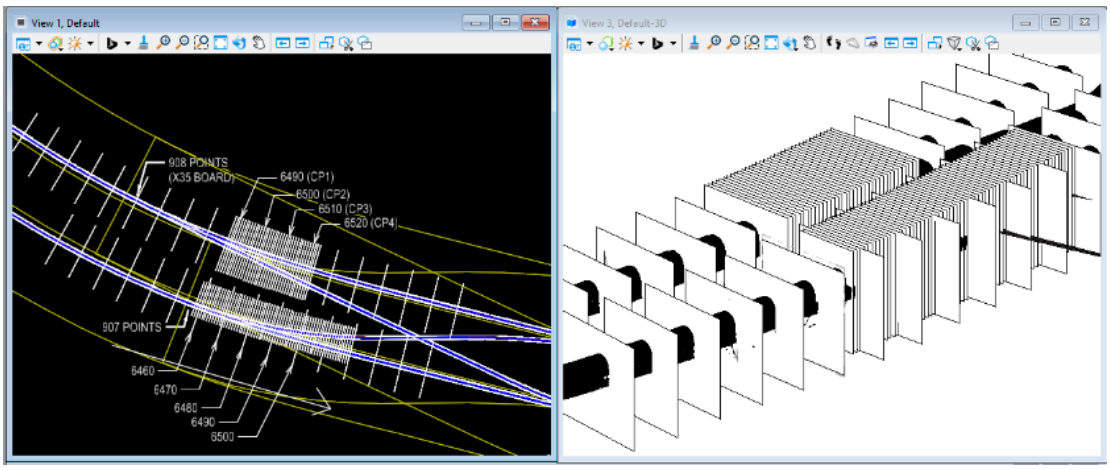
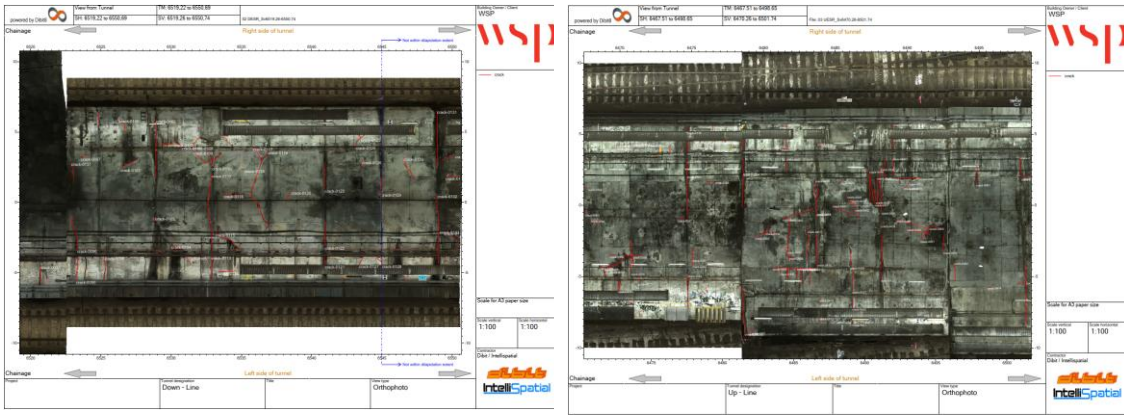


Figure 5. Bentley OpenRail software showing tunnel cross-sections, track alignments, and kinematic envelopes used for instrumentation planning.



(Left) (Right)

Figure 6. Plan layout of tunnel dilapidation survey results. (Left) Down Track tunnel. (Right) Up Track tunnel. Annotated defects mapped using AI-assisted 3D scanning.

3.6.2 Operational Advantages

The 3D scanning approach provided significant operational benefits:

- Traditional dilapidation surveys in confined tunnel environments often require multiple site visits and repeated tunnel shutdowns, typically scheduled during limited night-time access windows of approximately two hours. Conventional surveys for this project would have required eight nights of tunnel access compared to only two nights needed for 3D scanning.
- Conventional inspections struggle with crown defect identification due to obstructions and poor lighting. 3D scanning with AI-based techniques provides superior defect detection capabilities. The 1971 tunnel contained over 600 cracks, which were semi-automatically identified and classified using Dibit8 within two days, compared to the estimated two weeks required for traditional methods.

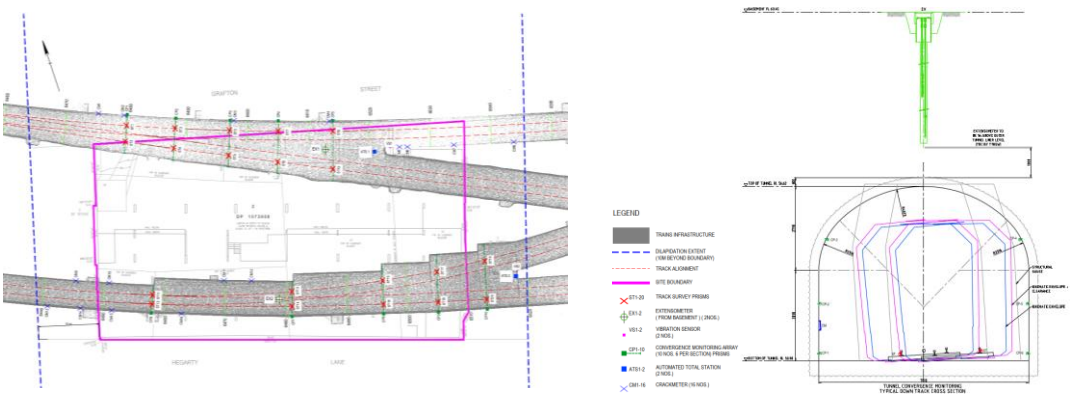
– 3D scanning enables precise kinematic assessments at any cross-section, facilitating optimal monitoring equipment placement and reducing operational risks through virtual inspection capabilities.

3.6.3 *Data Delivery and Stakeholder Engagement*

Outputs were delivered in multiple formats to accommodate varying technical expertise levels. 3D point clouds and mesh models were shared in open formats and integrated into BIM platforms. Annotated defect maps were provided as layered PDF reports and georeferenced CAD files. A web-accessible 3D viewer enabled non-technical stakeholders to visualise tunnel conditions without specialised software. Annotated PDFs and interactive 3D viewers, which provided clarity and accessibility for technical and non-technical project participants, proved most effective for stakeholder communication, enabling improved collaboration, decision-making, and alignment with asset owner requirements.

4 INSTRUMENTATION AND MONITORING

Beyond condition assessment, instrumentation and monitoring (I&M) are essential for verifying engineering predictions and ensuring infrastructure protection during construction activities near existing structures. The proposed I&M plan complies with the requirements outlined in Transport for New South Wales (TfNSW) Standard TS 01717 - Development Near Rail Tunnels (TfNSW, 2020), ensuring adequate clearances for the tunnel kinematic envelope, pantographs, and overhead wiring systems. Figure 7 illustrates the I&M implementation plan and instrumentation cross-section for this case study.



(Left) (Right)

Figure 7. (Left) I&M implementation plan. (Right) Cross section showing the instrumentation details with kinematic envelope.

4.1 *Kinematic Envelope*

Kinematic envelopes define rolling stock boundaries by incorporating static vehicle outlines, dynamic tolerances, and applied safety margins. LiDAR point clouds and alignment data were used to generate 3D kinematic envelopes at defined intervals, determining optimal instrument placement. Figure 7 (Right) illustrates the kinematic envelope (KE) and KE+200 envelope for authorised rolling stock operations. All monitoring instruments are positioned outside KE+200, with the highest prisms placed at a maximum height of 4 m from the tunnel invert level to prevent interference with overhead lines and pantographs.

5 CONCLUSION AND RECOMMENDATIONS

This study presents a methodological approach to underground development near existing infrastructure, demonstrating the application of advanced geospatial technologies and AI-assisted systems for comprehensive condition assessment in Sydney's urban environment.

The findings demonstrate that tunnel defects can be analysed in virtual 3D environments, providing high-quality data to support tunnel condition assessments. This approach delivered several tangible benefits: 3D scanning and AI-assisted detection identified and measured over 600 cracks within two days, significantly reducing time, access constraints, and resource requirements compared to traditional dilapidation surveys. High-resolution digital models facilitated coordination with rail authorities, enabling instrumentation design that complied with the kinematic envelope and clearance requirements, streamlining the approval process.

While 3D scanning and AI-assisted defect detection offer substantial advantages in efficiency, coverage, and repeatability, certain limitations warrant consideration. AI-based detection reliability depends on training dataset quality and diversity, with rare or novel defects potentially requiring manual verification. Environmental factors, including lighting conditions, surface texture, and tunnel obstructions, can affect data quality and processing accuracy, emphasising the continued importance of engineering judgment and validation alongside digital tools.

The technologies and workflows demonstrated, i.e., terrestrial laser scanning, photogrammetry, AI-based defect classification, and CAD/BIM integration, are broadly transferable across infrastructure types and operating conditions, particularly where access limitations make conventional inspections impractical. Future research should explore long-term performance implications, scalability across different infrastructure types, and effectiveness under varied site conditions.

This work contributes to the evolving field of infrastructure protection in urban development, highlighting the critical role of digital technologies in addressing complex engineering challenges. As urban densification continues, such methodologies will become increasingly critical for delivering safe, efficient, and sustainable infrastructure outcomes.

ACKNOWLEDGEMENTS

The authors acknowledge the client and asset owner for permission to publish this paper and all the construction personnel, engineers and specialists involved in the project for their dedication and professionalism, resulting in a highly successful project. Special thanks to Jiping Pan and Paul Hewitt for their guidance, project experience, and support.

The authors declare no commercial relationships or financial interests in any proprietary hardware or software referenced in this study.

6 REFERENCES

J. C. Braybrooke. 1985. Engineering geology of the Sydney Region, Australian Geomechanics Society, Chapter 18: Tunnelling in the Sydney Region.

J. Pan, A. Kuras, N. Loganathan. 2023. Development near underground rail corridors – engineering assessment with case studies. *Building Around Existing Tunnels*. p52-63.

M. Packer, K. He, B. Rouvray, A. Ambrosis. 2023. Sydney Metro Martin Place Station South Shaft – back analysis case study of ground displacements adjacent to existing railway tunnels. *Proceedings of the 14th Australia and New Zealand Conference on Geomechanics*, Cairns 2023.

L. Zhao, Y. Meng, H. Tang. 2024. Research on tunnel defect detection based on YOLOv8 model. Proc. SPIE 13421, Sixth International Conference on Photonics and Imaging in Biology and Medicine, 1342132.

Transport for NSW (TfNSW). 2020. TS 01717. Development Near Rail Tunnels. Transport for NSW, Sydney.

W. Fang, Z. Chen, H. Li. 2025. Research on real-time inspection scheme of tunnel lining surface defects based on YOLOv10. In: Proceedings of the International Conference on Artificial Intelligence for Infrastructure. Springer, pp. 21–33.

X. Liu, C. Zhang, Y. Hu, S. Li. 2024. Towards 3D reconstruction of multi-shaped tunnels utilising mobile laser scanning data. Remote Sensing, 16(22), p.4329.

Y. Jiang, Y. Qiao, W. Chen, J. Wu. 2023. A two-step deep learning-based framework for metro tunnel lining defect detection. Tunnelling and Underground Space Technology. [online] Available at: https://www.sciencedirect.com/science/article/pii/S0886779824002505

Y. Huang, R. Luo, J. Chen, Y. Xu. 2025. Automated 3D defect inspection in shield tunnel linings through integration of image and point cloud data. HKIE Transactions. [online] Available at: https://link.springer.com/article/10.1007/s43503-025-00054-w

19th Australasian Tunnelling Conference – Acosta-Martínez, Stewart and Hudson-Smith (Eds.)
© 2025 Australian Tunnelling Society, ISBN 978-0-85825-002-4

Challenges in electrical and mechanical asset renewal in established road tunnels

J. Cadena Gomez
Transurban Limited, Australia

R. Lau
RLau Services

ABSTRACT: This paper examines challenges in electrical and mechanical asset renewal in established road tunnels to address evolving risk profiles. As infrastructure ages, both technological advancements and changes in the operating context necessitate updating systems to maintain operational efficiency and mitigate emerging hazards. Changes in traffic patterns, vehicle emissions, and safety regulations have altered the risk landscape are explored, as well as their impact on existing systems, flagging where aging assets may no longer meet modern standards or operational demands. Additionally, integration of new technologies, products and materials, to enhance system reliability and ensure a safe and efficient tunnel environment are discussed. Stakeholder and client engagement is also discussed as a key to ensure technical requirements are updated for asset renewal. Proactive asset renewal and revision of original provisions are essential to manage system failure risk, improve resilience to changing conditions, and to ensure regulatory compliance.

1 INTRODUCTION

Technical specifications for the different engineering systems that make up a road tunnel are numerous, requiring a mechanism to clearly articulate what is expected from each of them. Most of these technical specifications are formulated in terms of an explicitly stated performance requirement (e.g. the tunnel drainage system shall withstand a rain event of a specified severity) or outright prescribed (e.g. the tunnel must be equipped with a linear heat detection system). These technical specifications are drafted on a case-by-case basis and reflect the available technology and current industry practice for design and construction, as reflected in publications such as AusRoads and PIARC [1-2].

Although of a technical nature, these specifications are embedded in contractual documents drafted as part of tenders for the tunnel design and construction, some of which in Australia have taken the form of Public Private Partnerships (PPP) [3]. As described by Bjelland et. al. [4] these documents constitute a Scope of Works and Technical Contract (SWTC) or PSTR (Project Scope and Technical Criteria) which are then delivered by a design and construction entity, typically a joint venture, at a significant cost. Using as reference, six established tunnels in Australia, this cost can range between 33 and 730 million dollars per km [3]. Such variability can be related to the design and construction complexities due to the scale of such projects, which in Norway (a country known for its technical proficiency and its catalogue of impressive tunnel projects) has led to a significant increase in legal disputes, the top reasons being 1. Understanding of the tender specification and contract, 2. Payment related and 3. Changes in projects [5].

The SWTC provisions, as well as any related operating license, are meant to be fulfilled by the time the tunnel is operating and few include mechanisms to update or modify the established requirements, as this could negatively impact the tunnel risk profile. As such, mechanisms for

modifying the SWTC provisions rely on an entity -typically the operator- putting forward a request for modification to the asset owner.

Despite the lack of a mechanism to review and update the technical specifications, the reality of any operating infrastructure is that it will age, deteriorate and be exposed to changes in regulation, technology advancements, and changes in operational demands. As such, Mechanical and Electrical (M&E) systems should be renewed (restored to its original condition) or modernised to ensure continued functionality and safety as these changes materialise. These drivers for renewal or modernisation of M&E assets often clash with the lack of effective mechanisms to review and update the original technical specifications, creating a risk to the end user of the roads.

This paper explores the main challenges faced in renewing M&E assets in established road tunnels and analyses the impact of aging infrastructure on operational efficiency and safety. It also outlines various influencing factors contributing to the evolving risk profile of road tunnels and addresses the complexities associated with modernising these assets in accordance with SWTC provisions and constraints. Finally, this paper considers the role of stakeholder engagement in updating technical specifications is examined, along with the need for a proactive approach to mitigate future risks.

2 CHANGES TO VEHICLE FLEET

Stricter environmental regulations have led to a decline in vehicle emissions as shown by the distribution of emissions intensity of vehicles sold between 1991 and January 2024. This indicates a drop in the national average emissions (CO_2) intensity from close to 350 to just shy of 150 g/km, constituting a change close to -60% in three decades [6]. This downward trend in vehicle emissions will continue, given the national and international commitments to lower carbon footprints and the larger proportion of electric vehicles within the total vehicle fleet. With regards to regulation, it was only in 2024 when Australia imposed CO_2 emission standards which will see a decrease from 141 g/km in 2025 to 58 g/km in 2029, targeting net zero emissions by 2050 [7]. Other vehicle emissions such as CO and NOx have been decreasing by the combined effect of regulations, vehicle engine developments and fuel improvements.

2.1 *Impact on tunnel ventilation systems*

For a road tunnel built in the late 1990s, this means its ventilation system would be overdesigned by at least 20% once the vehicle fleet in the 2020s was in operation. If said road tunnel was to be equipped with five axial fans for pollution management, this change in the operating context could translate into one of these fans going from duty to stand-by. The impact of such change would provide additional margin in the Minimum Operating Requirements and could lead to a change in the asset lifecycle model, potentially freeing up a capital expenditure allocation to enhance the ventilation system or to cover requirements from other systems.

This is a simplification where only emission rates are considered, though many other variables such as specific tunnel layout and traffic volume would also need to be considered to make an informed decision to drive a modification to the original ventilation system. Traffic volume in Australia has seen a constant growth ranging from +9% (Hobart) to +41% (Perth) and a national increase of 30% measured in vehicle-kilometre travelled (VKT) in the period of 2002 to 2020 [8]. This increase could offset the emissions reduction to date, however further decrease in emissions and the potential for a net zero future could lead to a scenario where current ventilation systems will be oversized.

As the trends above continue to develop, it is possible to contemplate changes to the original ventilation requirements, if not to reduce its capacity, to at least operate them in a more optimised fashion as demonstrated by industry case studies [9]. As most of the tunnels were designed and built in the early 2000s, the ventilation requirements were driven by CO/CO_2 emissions and visibility, with the fleet change described above shifting this towards a drive from NOx emissions.

2.2 *Changing fire risk*

As the emission profile improves with the advent of electric vehicles and alternative energy carriers, new risks also emerge which can impact the risk profile of the tunnel and both the demand and effectiveness of fire safety provisions. The increased presence of battery electric vehicles (BEVs) with lithium-ion batteries introduces different fire hazards to the tunnel environment compared to conventional internal combustion engines. This change should trigger a risk assessment process to understand the new hazard and associated scenarios under the constraints of available information and then identify the need for new or enhanced controls.

Both accidents and research campaigns have shown that BEV fires do not behave as their internal combustion engine (ICE) counterparts and can present a particularly challenging set of conditions in an enclosed space [10]. A list of non-exhaustive relevant facts about electric battery fires are presented below and their impact to the risk profile of the tunnel:

- BEV fires do not require external oxidisers to sustain a combustion reaction as its electrolyte produces them once this is broken down by excessive heating, which fundamentally alters the way in which ICE fires can be tackled such as by means of smothering the fire by applying a fire blanket over the vehicle until the oxygen is depleted.
- BEV fires occur due to a runaway exothermal chemical reaction in which the affected battery cells heat up their neighbouring cells and break down their electrolyte, anode and cathode, producing both fuel and oxidiser, which can accumulate and pressurise. Upon finding relief, the gases are expelled and can lead to jet fires or vapour cloud explosions, scenarios that are not contemplated within a tunnel design for fire safety.
- BEV fires detection is hindered due to battery location and encasing, which can limit the ability to detect such fires through existing detection technology such as CCTV cameras, automatic video detection and linear heat detection.
- BEV fires produce about 10x the amount of hydrofluoric acid (HF) than its ICE counterparts [11], posing a threat to first responders and requiring the tunnel operation to use the available ventilation system to dilute and displace such concentrations where possible.

Based on statistics from five countries with a high uptake of BEVs, the likelihood of a fire event involving the battery seems to be ~10 times less likely compared to that of ICE vehicles [12]. Although positive, such observation does not account for the aging of batteries, which as yet is not an influencing factor due to the recent uptake of the technology. Over the next five to ten years, an increase in EV fire incidents is anticipated, particularly if unauthorised repairs and batteries are utilised, as has been the case for personal mobility vehicles.

3 EMERGENCE OF NEW AND BETTER PERFORMING TECHNOLOGIES

Despite best efforts to look ahead, SWTC and designs are constrained by available technology, effectively becoming a snapshot in time of current engineering practice for ventilation, lighting, power supply and all other systems making up the M&E assets. As time goes by, research and development leads to the emergence of new technologies, while some problems are better understood and reformulated. Reassessing original designs in light of newly available pathways to address a particular tunnel need present a challenge, exemplified by the examples put forward below.

- LED lights have improved over the years and are now widely used in road and tunnel projects. These would likely replace the existing fluorescent and High Pressure Sodium lights. However, changing from florescent to LED lights would require lighting design revision as LED lights would not be linearly installed as florescent lights. This change is likely not covered in the technical specifications.
- Fire detection in tunnel mainline and ramps is quite a challenge due to the varying air flow, the presence of soot and both the relative humidity and temperature variability. This has led to the adoption in Australia of Linear Head Detection (LHD) as the go-to solution for automatic fire detection, emphasized by limitations on systems relying on field of view such as CCTV and Automatic Video Incident Detection (AVID), including their high rate of false alarms [13]. However, the issues with LHD are the significant delays due to heat transfer and airflow affecting location accuracy. Nowadays video detection technology has evolved to the point that

industry underwriters such as FM have produced standards for such products used in automatic fire alarm signalling [15]. The improvement in video software and technology makes the use of video fire and smoke detection much more reliable than the traditional LHD cable systems used in tunnels, with the acknowledgement that no instances of legitimate fire detections by LHD have been recorded in Australia [16]. The replacement of the linear heat detection system by video-based systems have the potential to improve automatic fire detection capabilities but do challenge the original provisions in SWTCs and existing Australian Standards for fire detection systems (AS1670.1).

- In fire suppression systems, almost all Australian road tunnels have fixed firefighting systems (FFFS), most of which employ deluge (water spray) and have been growing in their application across the world after their uptake in Asia and Australia [17]. Amidst this uptake, concerns about water usage (found within the range of 1-4 kL/min per suppression zone, typically of about 30 m length) and the limitations of water spray (deluge) to address concealed fires (such as in EV fire scenarios) and flammable spill fires (such as in tanker accident scenarios), have led to the introduction of water mist suppression systems. These have been widely available in other industries, through technology development had to wait several decades for readily available commercial solutions such as the one installed in the Heysen tunnel in Adelaide, South Australia [21]. Water mist systems can reduce the water usage demand compared to that from deluge systems (up to around half), with its fire suppression mechanism not relying on wetting the fuel but in effectively removing large amounts of heat generated by the fire and displacing oxygen. Although the specification of the mist parameters remains a challenge and some risks might be introduced (such as flame fanning at the initial application) [13], the technology represents a potential alternative for large, water-intensive, and expensive to maintain deluge systems.
- In tunnel ventilation, the substantial reduction in vehicle emissions presented in section 2.1 of this paper has driven air pollution control to become less of a determining parameter in ventilation system design and selection. Air flow volumes in normal operation would reduce substantially, with the system performance being driven by smoke control and fire safety. In practice, this can lead to less onerous minimum operating requirements and the potential for axial fan removal as a means to optimise long-term maintenance expenditure. Finally, reduced vehicle emissions may offer the opportunity of allowing tunnel air to be exhausted via the portals without significantly affecting ambient air quality, while providing a sustainability benefit of reduced energy use. However, would necessitate an amendment to the project specifications, as portal emissions are currently not permitted in most Australian tunnels.

4 ACCELERATED OBSOLESCENCE AND DEGRADATION

As tunnels age, plant and equipment deteriorate over time. Tunnels are usually rated as a harsh service environment for E&M equipment, especially road tunnels in the coastal states, where air salinity can lead to additional external corrosion. SWTC and O&M manuals typically prescribe the maintenance regimes, which are also based on current practice, known failure modes and on applicable maintenance standards. The provisions are tightly associated to compliance obligations within the SWTC, as well as with each technical authority such as the Electrical Safety Office associated to WorkSafe Australia, the stat based requirements such as those of the Queensland Building and Construction Commission (QBCC), as well as requirements from applicable acts and regulations. Given these compliance requirements, modifying maintenance regimes based on varying risk factors such as the external corrosion and changes in legislation can be challenging. This situation is exemplified by the following examples:

- Fire mains are typically based on galvanised steel, which can be susceptible to external corrosion, particularly if caused by ground water leaks. The normal and typically unpredictable occurrence of ground water in tunnels is not explicitly accounted for in the design of fire mains, nor in the AS1851:2012 requirements for inspection of the pipes. Based on Transurban operational experience, fire mains require condition assessments beyond the standard requirements, increasing operator costs to effectively manage the accelerated corrosion rates.
- Initially used as the go-to gas suppression agent, Halon was used between the 1970s and 1992 when it was phased out after the Montreal Protocol identified it as an ozone-depleting chemical

[18]. Similarly, the gas suppression agent FM-200 (also known as HFC-227ea) is currently undergoing phase-down despite being the main replacement for Halon. Existing gas suppression systems covering high voltage rooms in electrical substations as well as other sensitive equipment such as data rooms are then required to be upgraded, some potentially ahead of their original design life.

Though environmental and health risks associated with per- and polyfluoroalkyl substances (PFAS) was identified since the 1970s, aqueous film-forming foam (AFFF) for fire suppression has been a key fire protection element for hazardous industry as well as for road tunnel sumps, where the potential for hydrocarbon spill exists. In the 2010s, jurisdictions worldwide began efforts to replace 'long-chain' PFAS with 'short-chain' (also known as C8 and C6, respectively), with Queensland doing so through their Operational Policy for the Environmental Management of Firefighting Foam [19]. More recently, a total ban on PFAS with effect from 1 July 2025 was introduced into federal legislation in Australia by adopting the Industrial Chemicals Environmental Management Standard (IChEMS) [20]; this directly impacted all existing AFFF systems and required operators to retrospectively assess the original design requirements of their fire systems and identify viable alternatives as well as their impacts on the firefighting performance and long-term financial aspects.

5 CONCLUSIONS

This paper has presented a series of practical examples on how M&E asset renewal are driven beyond the original provisions of the applicable SWTCs. These renewals are essential to meet the performance requirements of the different mechanical, electrical and fire systems that ensure the road tunnels maintain or improve their risk profile over the decades of their expected service life. Changes in traffic patterns, vehicle emissions, and safety and environmental standards necessitate the updating of outdated systems. By integrating emerging technologies, adopting sustainable materials, and employing a proactive approach, tunnel operators can enhance safety, reliability, and efficiency.

The challenges presented in this paper have a significant impact on renewal projects and the overall asset lifecycle allocations, which in turn can inhibit or enable the adequate operation of critical life safety systems over the many decades of the tunnel design life. In this manner, this paper calls for all relevant stakeholders involved in the development of SWTC provisions to better accommodate the changing landscape and influencing factors for asset renewal.

6 REFERENCES

[1] AustRoads. 2024. Guide to Road Tunnels, *AGRT01-24 to AGRT04-24*, Sydney.
[2] PIARC. 2019. *The Road Tunnels Manual*, 2nd Edition, https://tunnelsmanual.piarc.org/en.
[3] M. Regan, J. Smith, P. Love. 2017. Financing of public private partnerships: Transaction-al evidence from Australian toll roads. *Case Studies on Transport Policy*, 5(2): 267-278.
[4] H. Bjelland, J. Gehandler, B. Meacham, R. Carvel, J. Torero, H. Ingason, O. Nja. 2024. Tunnel fire safety management and systems thinking: Adapting engineering practice through regulations and education. *Fire Safety Journal*, 146.
[5] Sabri, Omar & Lædre, Ola & Bruland, Amund. 2019. Why conflicts occur in roads and tunnels projects in Norway. *Journal of civil engineering and management*, 25:252-264.
[6] National Transport Commission. 2024. *Light vehicle emissions intensity in Australia: trends over time*.
[7] Australian Government, Department of Infrastructure, Transport, Regional Development, Communications and the Arts. 2024. *New Vehicle Efficiency Standard*. https://www.infrastructure.gov.au/infrastructure-transport-vehicles/vehicles/new-vehicle-efficiency-standard.
[8] D. Gargett, J. Gafney. 2004. *Traffic Growth in Australian Cities: Causes, Prevention and Cure*.
[9] Howden. 2023. *Tunnel ventilation efficiency optimisation*. https://files.chartindustries.com/Howden_Ventsim_Tunnels_Case_Transurban.pdf.
[10] J. Hynynen, M. Quant, R. Pramanik, A. Olofsson, Y. Zhen Li, M. Arvidson, P. Andersson.

2023. Electric Vehicle Fire Safety in Enclosed Spaces. *RISE Report 2023-42*.
[11] J. Hynynen, O. Willstrand, P. Blomqvist, P. Andersson. 2023. Analysis of combustion gases from large-scale electric vehicle fire tests. *Fire Safety Journal* 139.
[12] M. Tohir, C. Matrin-Gomez. 2023. Electric vehicle fire risk assessment framework using Fault Tree Analysis. *Open Research Europe*. https://open-research-europe.ec.europa.eu/articles/3-178/v1.
[13] Liu, Z. G.; Kashef, A.; Lougheed, G. D.; Debs, A.; Gottuk, D. T.; Almand, K. H. 2009. Fire detection systems in road tunnels - lessons learnt from the International Research Project. *Routes/Roads* 342:60-69.
[14] T.T. Aralt, A.R. Nilsen. 2009. Automatic fire detection in road traffic tunnels. *Tunnelling and Underground Space Technology* 24:75–83
[15] FM Approvals. 2023. Examination Standard for Video Image Fire Detectors for Auto-matic Fire Alarm Signaling. *Class Number 3232*. https://www.fmapprovals.com/-/media/Feature/Approval-Standards/3232-pdf.pdf
[16] N. Casey. 2020. Fire incident data for Australian road tunnels. *Fire Safety Journal* 111.
[17] K. Harris, M. Macniven. 2018. Expediting implementation of FFFS in road tunnels. *Eighth International Symposium on Tunnel Safety and Security*.
[18] FPA Australia. 2018. *Gaseous fire suppression systems in Australia, Stage 1*.
[19] Queensland Government, Department of Environment and Science. 2021. *Operational Policy Environmental Management of Firefighting Foam*.
[20] Queensland Government, Business Queensland. 2025. Per- and Polyfluoroalkyl Sub-stances (PFAS) Scheduling decisions. https://www.business.qld.gov.au/running-business/environment/ichems#per-and-polyfluoroalkyl-substances-pfas-scheduling-decisions.
[21] McConnell Dowell. 2024. Heysen Tunnel Refit and Upgrade, Improving safety and traffic management. https://www.mcconnelldowell.com/projects/heysen-tunnel-refit-and-safety-upgrade.

Theme 13. Digital Engineering

THIS PAGE INTENTIONALLY LEFT BLANK

19th Australasian Tunnelling Conference – Acosta-Martínez, Stewart and Hudson-Smith (Eds.)
© 2025 Australian Tunnelling Society, ISBN 978-0-85825-002-4

Automated extraction of geotechnical data from core photography for tunnelling projects using artificial intelligence

S. Johnson & L. D'Andrea
Datarock, Australia

ABSTRACT: Geotechnical data is critical for safe and efficient tunnelling, but manual core logging is slow, labour-intensive, and subjective. This paper presents an automated approach for extracting geotechnical parameters from core photography using computer vision. The Datarock Core platform derives datasets such as Rock Quality Designation (RQD) and dominant colour from standard drill core images. In a Sydney Metro West case study, automated RQD was compared with manually logged intervals, showing strong correlation in high-quality rock (RQD 75–100) and greater variance in lower-quality intervals, primarily due to interpretation differences. Dominant colour extraction highlighted lithological boundaries, even from legacy imagery not captured for this purpose. These results demonstrate that automated analysis can produce accurate, consistent, and high-resolution datasets, improving geotechnical confidence and enabling faster, more objective decision-making. The method supports integration into tunnelling workflows from planning to construction, offering a scalable solution to the limitations of traditional logging.

1 INTRODUCTION

Geotechnical data plays a critical role in the design, safety, and risk assessment of tunnelling projects. Accurate and detailed geotechnical information is essential for understanding the physical properties of rock masses, which influence key factors such as stability, stress conditions, and excavation strategies. Traditional methods of collecting this data, such as manual core logging and visual inspection, are often time-consuming, subjective, and prone to error. These challenges are further exacerbated by the shortage of skilled professionals in the field, making manual data collection even more inefficient (Jaeger & Cook, 1963).

The process of manually analysing core samples, such as assessing rock quality, fracture frequency, and mineral composition, requires significant expertise. However, the inherent subjectivity of human observation and the time-consuming nature of manual logging can lead to inconsistencies in the data, hindering reliable decision-making (Hancock et al., 2014). Furthermore, this traditional approach struggles to keep pace with the rapid throughput demands of modern tunnelling projects, where quick and accurate data is crucial for timely project execution.

In recent years, the integration of artificial intelligence, particularly computer vision and machine learning technologies, has emerged as a promising solution to these challenges. These technologies can automate the extraction of geotechnical data from core images, enabling the rapid and consistent identification of key parameters such as Rock Quality Designation (RQD), fracture frequency, and colour variations indicative of geological features. By processing high-resolution images of drill cores, computer vision systems can automatically detect visual patterns, such as fractures and joints, that are essential for evaluating rock mass stability and stress conditions in tunnelling environments.

Automating the extraction of geotechnical data not only improves the speed and consistency of the data collection process but also ensures a more standardised approach, reducing human error and increasing the reliability of the collected data. This advancement has the potential to significantly enhance the accuracy of geotechnical assessments, aiding in better risk management and structural modelling throughout the lifecycle of tunnelling projects. Moreover, the automated system can seamlessly integrate into various stages of tunnelling operations, from project

planning to construction, offering timely, consistent and actionable insights, ultimately allowing the engineer to make more confident decisions over the life of the tunnelling project.

This paper proposes a novel approach to automating geotechnical data extraction using the Datarock Core platform, which uses artificial intelligence (AI) to photolog. The software was then used to assess publicly available datasets from the Sydney Metro West tunnelling project for two datasets: Rock Quality Designation (RQD) because it is a very commonly logged dataset, and core dominant colour because it can often reflect key geological features that are not always logged by civil and geotechnical engineers.

Previous attempts at automated core analysis include image segmentation and edge detection for fracture mapping (Scott et al., 2014; Carlson et al., 2016), though these often required manual correction. More recent work applies convolutional neural networks for lithology classification (Kanazawa et al., 2019) and object detection for fracture identification (Ma et al., 2021). Commercial platforms such as Coreshed enable digital core storage and basic measurements but lack fully automated extraction of metrics like RQD. In contrast, this study uses deep learning models—Mask R-CNN for segmentation and RetinaNet for marker detection—to deliver high-accuracy, fully automated parameter extraction from standard core photography.

2 SYDNEY METRO WEST PROJECT

The Sydney Metro West project is delivering a new 24-kilometre underground metro line between Westmead and the Sydney CBD to double rail capacity and reduce travel times. Construction involves twin tunnels bored by large tunnel boring machines, nine new underground stations, and supporting infrastructure such as a maintenance facility at Clyde. The project traverses complex geology, requiring advanced tunnelling and ground treatment methods, with cross passages spaced every 240 metres for safety and ventilation. (Sydney Metro, 2023)

The alignment crosses Triassic Hawkesbury Sandstone, Ashfield Shale, and Mittagong Formation, as well as Quaternary alluvium in valley areas. Hawkesbury Sandstone is strong and durable but locally jointed, affecting cutter wear. Ashfield Shale is weaker and prone to slaking, requiring careful face support. The Mittagong Formation has variable strength and permeability, posing settlement risks. Alluvial deposits are soft clays and loose sands with high compressibility and groundwater inflow potential (Herbert & Helby, 1980; Sydney Metro, 2020).

Key engineering challenges include tunnelling beneath dense urban environments and protecting heritage structures, while sustainability targets are being prioritised throughout construction. Major tunnelling commenced in 2023, with system integration and station fit outs progressing towards a targeted opening by 2032.

3 METHOD

3.1 Overview

This section details the procedure for extracting two key datasets, RQD and dominant colour, from core photography. These examples demonstrate the potential of this technology for geotechnical rockmass characterisation. The necessary pre-processing steps for transforming raw images into analytics-ready data are also described.

RQD and Dominant Colour were selected to effectively illustrate how a well-structured AI workflow can derive valuable insights from core images.

Rock Quality Designation (RQD) quantifies rock mass quality based on the percentage of intact core segments exceeding 100 mm within a specified interval. It is a crucial indicator of jointing and fracturing, vital for assessing rock mass behaviour. As a widely adopted geotechnical parameter, RQD routinely informs the design of tunnels, foundations, and slopes.

Datarock's dominant colour tool identifies a single representative colour for each core image row. This generates a simplified and uniform visual output compatible with most 3D modelling platforms, improving visualisation and integration within geological models. Given that colour often correlates with significant geological attributes like lithology, oxidation, and mineralogy, dominant colour is a valuable asset for interpreting rock characteristics and stratigraphy.

3.2 *Depth registration*

Depth registration is essential for accurately assigning depths to core images. This allows for precise identification of geological structures (e.g., joints) and facilitates reliable comparison and calibration with other downhole datasets.

The process of preparing 'analytics-ready' images involves several preprocessing steps, including six chained individual Mask R-CNN (a two-stage region-based convolutional neural network) instance segmentation models which are used to identify the following features within the raw images: core trays, core tray rows, identification of coherent, broken rock, core blocks and empty tray. All of these models have been fine-tuned by Datarock on thousands of drill core images.

Using these predictions, we can quantify compaction in broken rock, core loss compensation, and optical character recognition for reading handwritten depths on the core or core blocks. In this study, the Datarock Core platform was utilised for core row image preparation and depth registration. Figure 1 provides examples of depth-registered rows and their assigned depths, including depths based on handwritten metre marks (green markers) and inferred depths (yellow markers).

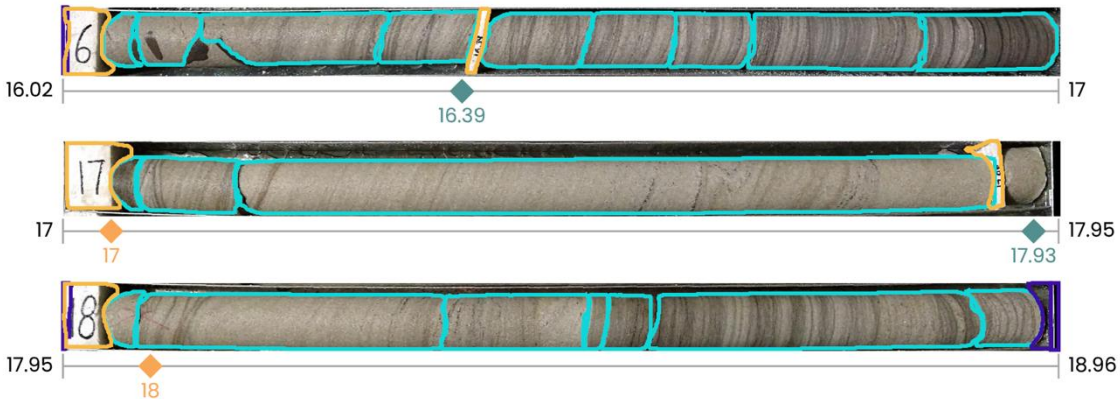


Figure 1. Example of depth-registered core rows generated by the Datarock Core platform.

3.3 *Rock Quality Designation*

The method developed involves several steps to extract RQD from core photography. As described above, RQD measures rock mass quality based on the percentage of intact core pieces >100 mm recovered from a borehole.

The first step is to take the raw image of each row and identify all the pieces of coherent, or whole, core using a segmentation model

A Mask R-CNN model is used to segment individual pieces of coherent/intact core, in the image by detecting and classifying each segment as a distinct object, generating instance-specific masks that outline the boundaries of intact core. This enables automated, pixel-level identification of core pieces, which is essential for downstream analysis. The primary metric we use for these models is lengthwise precision as understanding the length of each piece of core is important for calculating depth and RQD. The average lengthwise precision for the models on this dataset was 0.95 which is very good.

Figures 2 and 3 show the row image and identification of coherent pieces respectively.



Figure 3. Raw cropped row image



Figure 2. Coherent rock computer vision model predicts a polygon around each piece of core

Step 2: Identifying mechanical breaks

Drilling and core handling can produce artificial fractures, commonly referred to as induced, mechanical, or driller's breaks. As Huaman et al. (2018) observed, distinguishing these from natural fractures typically requires physical inspection for features such as surface profile, weathering, or staining. Image-based identification of mechanical breaks is challenging, particularly when image quality varies. In standard practice, mechanical breaks are marked manually on the core with a distinctive symbol. In our methodology, all fractures are considered natural unless explicitly marked as mechanical.

To detect these markings, we trained a RetinaNet (Lin et al., 2017) object detector to identify hand-drawn indicators adjacent to mechanical breaks in core photography. The model learns to detect and localise these distinct visual cues, outputting bounding boxes around them. This enables automated association of mechanical break markers, allowing them to be considered in downstream analysis. Figure 4 illustrates an example of successful marker detection.



Figure 4. Mechanical break model predicts a box around each mechanical break mark

Step 3: Calculate RQD

Now that all the pieces of core and mechanical breaks identified, they can utilise these to calculate RQD. Using the mechanical break marks, adjacent core pieces are "joined" to ensure only natural breaks are considered.

Since all the row images has been accurately depth registered, each piece of core is measured and classified as less than, or greater than, 100mm long and display those outcomes on the core photography.



Figure 5. Each piece of core is measured and classified as less than or greater than 100mm

Finally, the pieces greater than 100mm are utilised as per the equation below.

$$RQD = \frac{\Sigma length\ of\ core\ pieces > 100mm}{Total\ interval\ length} \times 100\%$$

Equation 1. RQD calculation as per the Deere (1964) method.

The results generated are in the form of a CSV, like standard core logging. It includes headers such as hole_id, depth_from, depth_to, rqd_m, rqd, mechanical_break_count and coherent_rock_length. This enables direct importing into any standard geotechnical analysis software package.

3.4 Dominant colour

Extracting a single colour, that is most representative of an image, involves a clustering exercise of every pixel within the image. The following steps are taken on each image, in this case each row image:

1. Taking the depth registered row image
2. Extract every pixel from the image and plot each RGB triplet onto a 3-axis plot.
3. Cluster all the RGB values into five clusters.
4. Determine the cluster with the highest number of pixels. This is the dominant cluster.
5. Find the geometric centre of the dominant cluster. The R, G and B values of this point is the Dominant Colour for the interval, in this case the row image.
6. Convert the RGB value to a hex value.

The method developed involves several steps to extract RQD from core photography. As described above, RQD measures rock mass quality based on the percentage of intact core pieces >100 mm recovered from a borehole.



Figure 6. Raw cropped row image



Figure 7. Dominant colour representation of the image in Figure 6. (R=163, G=133, B=113)

4 RESULTS AND DISCUSSION

In this section, the results are compared against a real-world project – the Sydney Metro West project, Eastern Tunnelling Package. The core photography and geotechnical logs are publicly available data on the Geological Survey of New South Wales' MinView application. The package consists of 49 drill holes for a total of approximately 2,000m of core. It should be noted that the core photography was not captured for this use.

4.1 Rock Quality Designation

RQD comparison has been completed in two ways:

1. Downhole plots; and
2. Scatter plot of Logged vs Datarock RQD.

4.1.1 *Downhole plots*

As can be seen in the figure below, there is a strong correlation between the site logging (red) and the results produced by Datarock Core (blue). A more detailed review of intervals that vary significantly is also shown below.

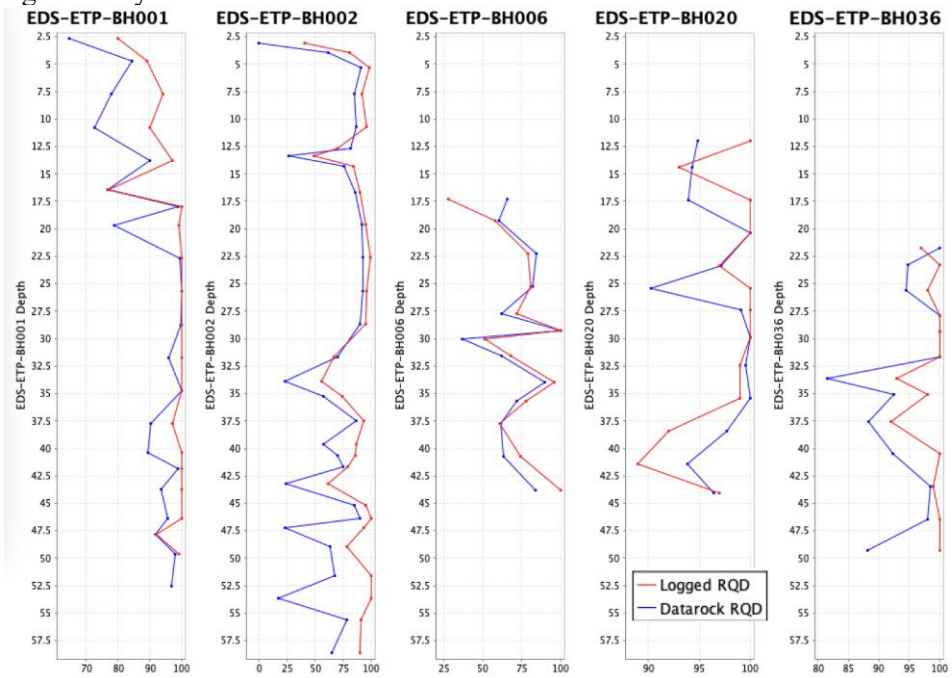
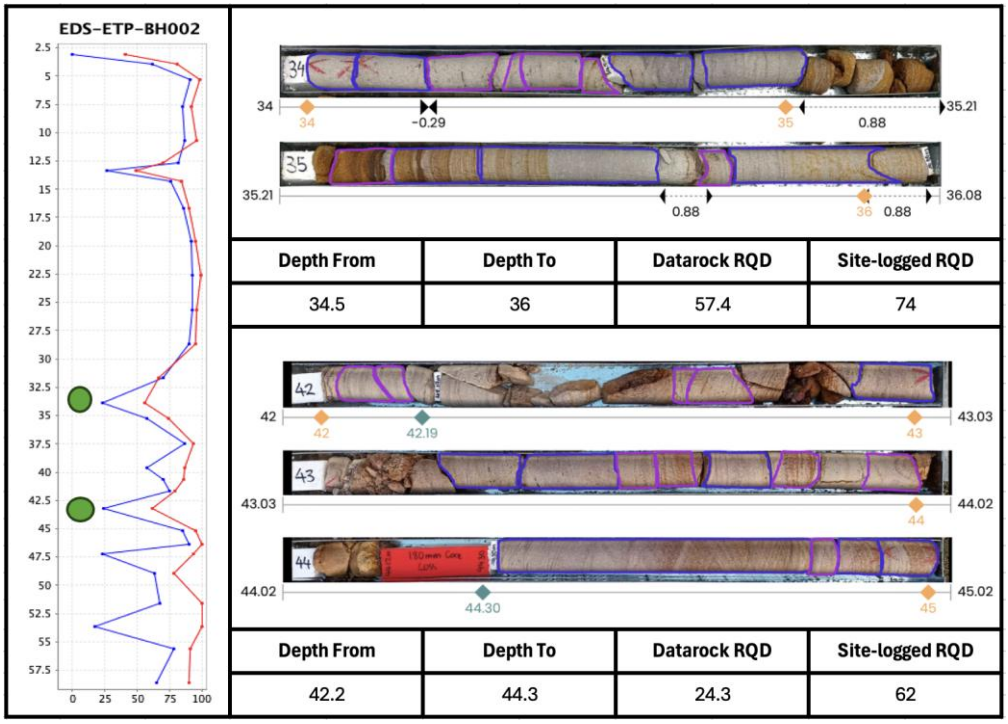


Figure 8. Example downhole plots for five of the processed holes.

Intervals within borehole EDS-EPT-BH002 that vary significantly from site logging are assessed in detail below.



Depth From	Depth To	Datarock RQD	Site-logged RQD
34.5	36	57.4	74

Depth From	Depth To	Datarock RQD	Site-logged RQD
42.2	44.3	24.3	62

Figure 9. Detailed interval comparison of logged vs Datarock RQD. Core pieces <100mm are shown in pink, >100mm shown in blue.

In reviewing the predictions on the core photography, the polygons are generally representative of the features within the image. There are some core pieces that are near the 100mm threshold and understandably loggers will make judgement calls either way. Given the predictions appear to be accurate, it is deemed that the Datarock Core results are more accurate than the logging.

4.1.2 *Scatter plot of Logged vs Datarock RQD*

In addition to reviewing downhole plots, a total of 902 intervals are compared in the figure below.

- Strong agreement is evident in the highest-density cluster of points, located in the top-right quadrant, particularly within the 75–100 RQD range. This suggests close alignment between logged and Datarock RQD values in high-quality core zones, where recovery is near complete and features are easier to interpret visually.
- Greater variance is observed at lower RQD values, where both manual logging and the automated system may under- or overestimate values. This is expected: fragmented or broken core presents challenges for automated segmentation, while human loggers may skip precise measurements of every fragment, unlike the systematic approach of the AI.
- Despite increased scatter in the lower RQD range, the overall distribution remains closely aligned with the 1:1 line, indicating strong correlation between logged and Datarock-calculated RQD, especially in the intervals of most engineering interest.

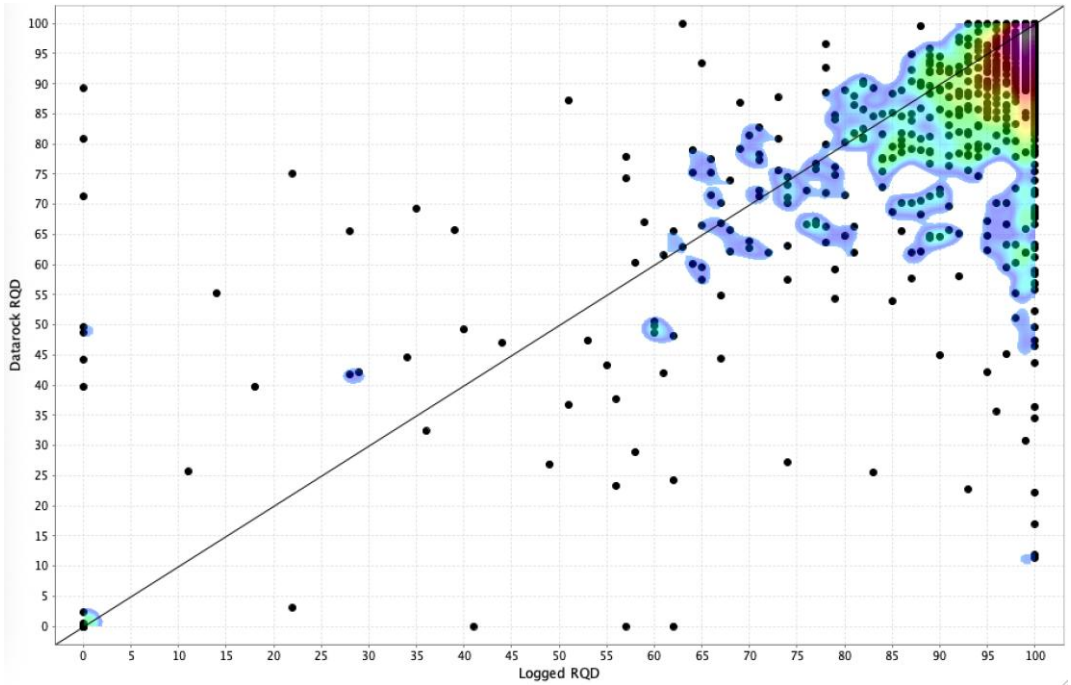
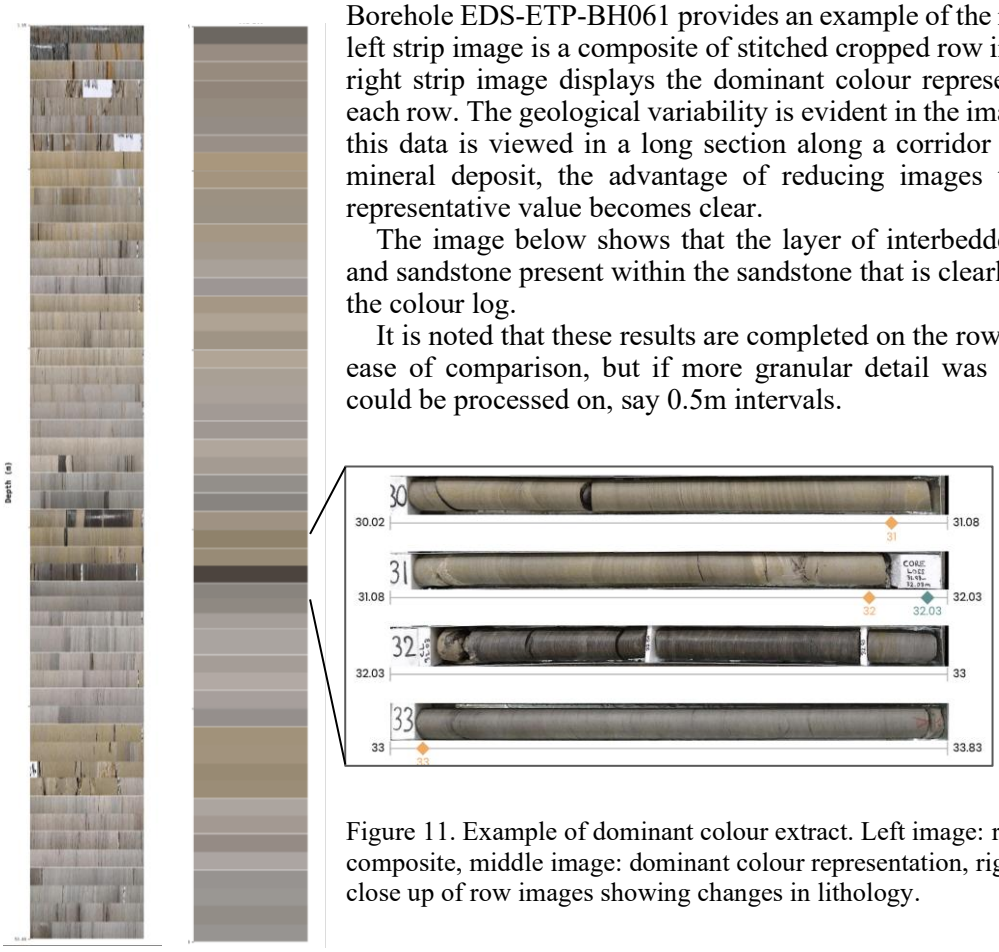


Figure 10. Comparison of manually logged RQD values and automated RQD extracted using the Datarock Core platform. Heatmap provided to indicate data point concentration.

4.2 Dominant colour



Borehole EDS-ETP-BH061 provides an example of the results. The left strip image is a composite of stitched cropped row images. The right strip image displays the dominant colour representation for each row. The geological variability is evident in the images. When this data is viewed in a long section along a corridor or across a mineral deposit, the advantage of reducing images to a single representative value becomes clear.

The image below shows that the layer of interbedded siltstone and sandstone present within the sandstone that is clearly visible in the colour log.

It is noted that these results are completed on the row images for ease of comparison, but if more granular detail was required, it could be processed on, say 0.5m intervals.

Figure 11. Example of dominant colour extract. Left image: row image composite, middle image: dominant colour representation, right image: close up of row images showing changes in lithology.

5 CONCLUSIONS

This study shows that computer vision can automate extraction of key geotechnical parameters—such as RQD and dominant colour—from standard core photography. The approach improves accuracy and consistency over manual logging while reducing subjectivity and labour.

In the Sydney Metro West case study, automated RQD closely matched manual logs in high-quality rock (RQD 75–100) and diverged more in fragmented intervals. Dominant colour analysis clearly highlighted lithological boundaries, even from legacy imagery.

Using deep learning (Mask R-CNN and RetinaNet) enables fully automated, high-precision extraction compared with earlier semi-automated methods. The structured datasets integrate directly into geotechnical models, supporting faster analysis and consistent decisions.

Future work should improve fracture detection in fragmented core and conduct controlled experiments where site logs have been reviewed for quality. Core photography should be captured specifically for computer vision processing, ensuring higher image quality and enabling more reliable comparisons with manual logging.

ACKNOWLEDGEMENTS

We would like to thank the Geological Survey of New South Wales for making the Sydney Metro West geotechnical data available on its MinView application. We would also like to acknowledge Datarock for providing analysis-ready processed photography and the compute resources required to implement the described methods.

6 REFERENCES

Carlson, J., Wilson, D., & Cundill, R., 2016, Semi-automated drill core logging using image analysis techniques, Computers & Geosciences, 89, pp. 102–114.

Deere D. U., 1964, Technical description of rock cores for engineering purposes, Rock Mechanics and Engineering Geology 1 (1), pp 16-22.

Herbert, C., & Helby, R. (Eds.)., 1980, A Guide to the Sydney Basin. Geological Survey of New South Wales, Bulletin No. 26.

Huaman A., Cabrere J., and Samaniega A., 2018, Managing and validating limited borehole geotechnical information for rock mass characterisation purposes - experience in Peruvian practice for open pit mine projects, Slope Stability 2018

Jaeger, JC & Cook, NGW 1963, 'Pinching-off and disking of rocks', Journal of Geophysical Research, vol. 68, no. 6, pp. 1759–1765.

Kanazawa, Y., Yamaguchi, T., & Sato, K., 2019, Lithology classification from drill core images using convolutional neural networks, International Journal of Rock Mechanics and Mining Sciences, 122, 104063.

LeCun Y., and Bengio Y., 1995, Convolutional networks for images, speech, and time-series, Arbib MA (ed) The handbook of brain theory and neural networks, MIT Press

Lin, T.Y., Goyal, P., Girshick, R., He, K., and Dollár, P., 2017, Focal loss for dense object detection, Proceedings of the IEEE international conference on computer vision, 2980-2988.

Ma, Z., Wang, L., & Li, X., 2021, Automated fracture detection in drill core images using deep object detection networks, Engineering Geology, 291, 106236.

Sydney Metro, 2023, Tunnelling Update, viewed 28 May 2025, https://www.sydneymetro.info/sites/default/files/2023-11/Clyde%20newsletter%20November%202023.pdf

Scott, A., Forster, A., & Berryman, K., 2014, Automated fracture logging from drill core photographs, Engineering Geology, 183, pp. 236–247.

Sydney Metro, 2020, Sydney Metro West – Project Geotechnical Baseline Report. Sydney Metro, Transport for NSW.

19th Australasian Tunnelling Conference – Acosta-Martínez, Stewart and Hudson-Smith (Eds.)
© 2025 Australian Tunnelling Society, ISBN 978-0-85825-002-4

Applying convolutional and artificial neural networks for image-based numerical modelling analysis in tunnelling

N. Mirsepassi
WSP, Sydney, Australia

A. Mastan
Sydney, Australia

ABSTRACT: Tunnel engineering relies on numerical modelling to generate complex outputs essential for design and maintenance. However, manual interpretation of these outputs can be time-consuming and inconsistent. This study presents a Convolutional Neural Network (CNN) model to automate the interpretation process by identifying the number of tunnels in an image and extracting vertical displacement values from colour contour plots. Using a dataset of 2,500 images from softwares including RS2, FLAC2D, FLAC3D, UDEC, and 3DEC, the model standardises image preprocessing and applies convolutional and pooling layers to extract spatial features. It performs two tasks: classifying tunnel count and regressing displacement values, targeting 90% accuracy for tunnel count and 85% of displacement CNN model interpretation within 5 mm of actual numerical outputs. This framework significantly reduces processing time and variability while maintaining accuracy. Initially trained on model images, it demonstrates potential for broader applications. By automating feature extraction, the CNN enhances efficiency in tunnel analysis and supports faster, more consistent decision-making in infrastructure projects.

1 INTRODUCTION

Tunnels are integral to Australian infrastructure, supporting transport corridors, mining operations, and urban underground utilities. Numerical modelling generates detailed visual outputs—ground deformation, stress and strain distributions, and imposed structural actions—that engineers rely on for tunnel ground support design. These outputs, often presented as colour-coded images, encode critical data such as deformation at the tunnel crown, sidewalls, surface movement, and displacements at utility levels, as shown in Figure 1.

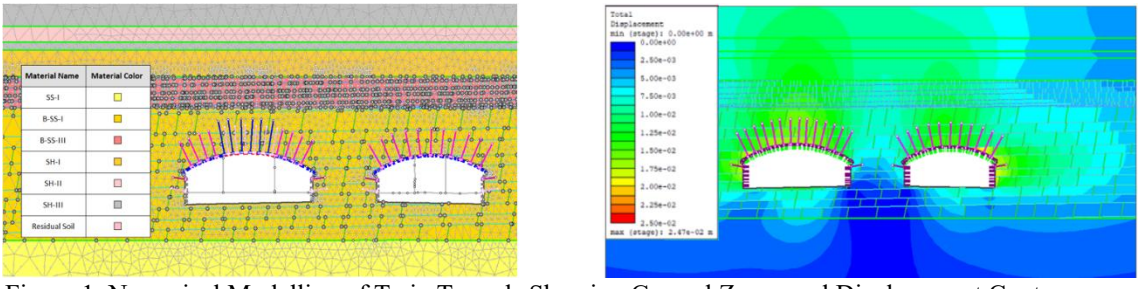


Figure 1. Numerical Modelling of Twin Tunnels Showing Ground Zones and Displacement Contours

In Figure 1 (left), the numerical model depicts subsurface geological zones and material boundaries around a twin arched-tunnel excavation, while the right-hand image shows the corresponding total displacement contours. Together, these plots highlight the spatial richness of numerical out-

puts and the challenge engineers face in interpreting them to assess tunnel stability. Manual interpretation especially 3D models can be time-consuming and subjective, introducing variability and risking delays in design delivery.

Deep learning, particularly CNNs, offers a solution. CNNs excel at image analysis by automatically detecting spatial patterns without manual feature engineering (Guo et al., 2018). While proven in fields such as medical imaging and autonomous driving, their application to tunnel engineering remains limited but promising. This study presents a CNN model designed to interpret numerical outputs, focusing on two key tasks: classifying the number of tunnels and interpreting vertical displacement at the crown. These tasks reflect broader capabilities, including stress concentration mapping and deformation detection.

The dataset comprises approximately 2,500 images from numerical models, representing varied tunnel configurations (i.e. single, twin, and multi-tunnel clusters). While vertical displacement is a key stability indicator, the model is structured to allow extension to other outputs with minimal redesign. This flexibility supports rapid interpretation across tunnelling metrics. The CNN targets 90% accuracy for tunnel count classification and 85% of displacement interpretations within 5 mm, benchmarks reflecting efficiency gains over manual analysis.

The motivation is twofold: tunnelling projects are becoming more complex, and conventional tools struggle with growing data volumes. The following sections describe the theoretical background, methodology, and future potential of CNN-driven tunnel analysis.

2 THEORITICAL BACKGROUND

2.1 *Artificial neural networks*

Artificial Neural Networks (ANNs) emulate biological systems using layers of interconnected nodes—input, hidden, and output (Goodfellow et al., 2016). Each neuron processes weighted inputs, adds a bias, and applies an activation function (e.g. Rectified Linear Unit (ReLU) to produce an output. During training, weights are adjusted via backpropagation to minimise prediction errors. While effective for simple tasks, ANNs are inefficient for images, as flattening pixel data inflates parameters and increases overfitting risk.

An ANN resembles a tunnelling design team: each engineer (neuron) evaluates multiple inputs, applies judgement (weights and biases), and passes recommendations forward. This process repeats until the final solution meets design requirements, mirroring how a network minimises prediction error.

ANNs typically follow four steps: forward propagation, output computation, error calculation, and backpropagation. In forward propagation, weighted inputs flow through hidden layers where non-linearity is introduced (Mirsepassi, 1997). Outputs are computed, compared against target values using a loss function, and errors are backpropagated using gradient descent to update weights. This iterative cycle allows the network to learn from data and refine predictions over time.

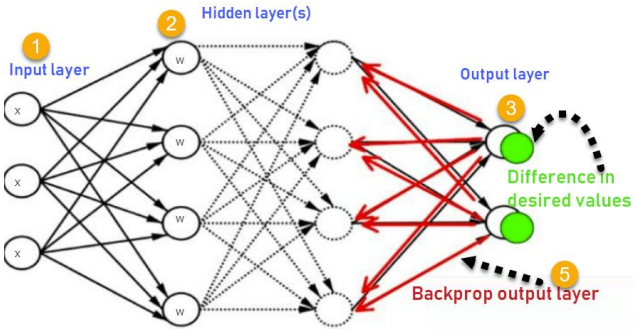


Figure 2. Schematic of an Artificial Neural Network Architecture with Forward and Backward Propagation (Ramzan et al., 2023)

2.2 *Convolutional Neural Networks*

Convolutional Neural Networks (CNNs) extend ANNs for spatial data, using convolution, pooling, and feature extraction to process images efficiently (Chollet, 2021). Convolutional layers apply filters to detect patterns like edges and textures, gradually learning more complex features. These operations produce feature maps that capture essential spatial information. Pooling layers then reduce dimensionality, typically via min/max/average-pooling while preserving critical features, improving efficiency and reducing overfitting. The resulting maps are flattened into a vector and passed to a Fully Connected Network (FCN), where hidden layers interpret higher-level patterns for classification or regression. This flow convolution → pooling → flattening → FCN → output converts raw images into meaningful predictions.

This process parallels tunnel inspections during construction: initial scans detect broad signs of movement or stress (convolutions), followed by focused investigation of critical areas (pooling), leading to detailed assessments and decisions (fully connected layers). This staged approach enables efficient interpretation without exhaustive manual review.

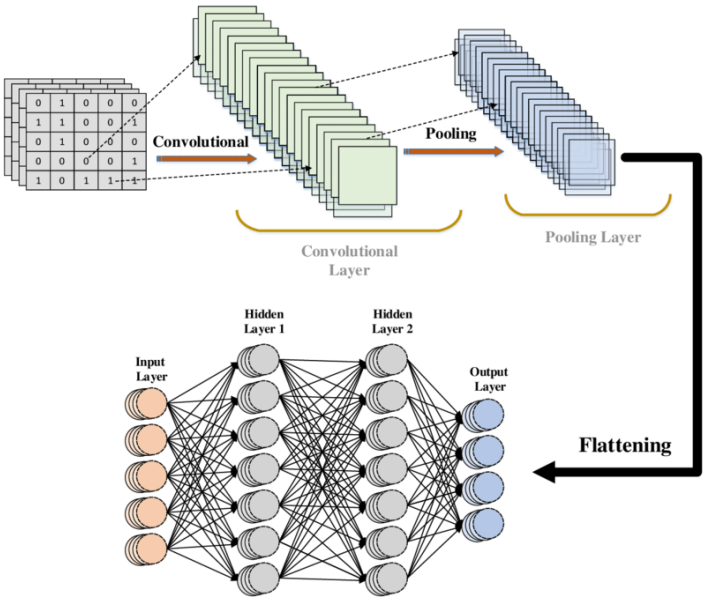


Figure 3. Overview of a Convolutional Neural Network Architecture Showing Convolution, Pooling, and Flattening Before Fully Connected Layers (Aqel and Marji, 2021)

3 METHODOLOGY

This study develops a dual-task CNN to automate the interpretation of numerical modelling outputs in tunnel engineering, focusing on tunnel count classification and CNN-based interpretation of vertical convergence at tunnel crowns. The methodology includes data collection, preprocessing, model architecture, and training.

Data Collection: The dataset comprises approximately 2,500 images generated using finite and discrete element methods from software such as RS2, UDEC, 3DEC, FLAC2D, and FLAC3D. These represent cross-sections under varied geological settings, depths, and tunnel geometries. RS2 accounts for ~1,300 images, followed by UDEC and 3DEC (~200 each), with FLAC3D contributing fewer. Tunnel counts range from 1 to 4, with a skew toward 2-tunnel images (~950). Vertical convergence is limited to images with up to two tunnels at the crown (Crown_T1 and Crown_T2), ranging from –5 mm to –55 mm. Additional parameters (e.g., stress, strain, structural actions) can be incorporated as training expands.

Preprocessing: Images are standardised to 200 by 200 pixels and normalised (0–1 range) for consistency across software outputs (Chollet, 2021). Tunnel counts are one-hot encoded; displacement values remain continuous. To address class imbalance—especially for 3- and 4-tunnel

images—oversampling is applied during training (Geron, 2022). This duplicates minority samples within batches to improve class representation and model generalisation.

The dataset is split 80/20 into training and validation subsets. Class distribution is preserved to ensure unbiased performance and reduce overfitting risk.

CNN Architecture: The architecture (Figure 4) consists of convolutional layers followed by a fully connected classifier. The tunnel classification model uses 200 × 200 × 3 inputs with filters of 32, 64, 128, and 256. The displacement model uses 256 × 256 × 3 inputs with 32, 64, and 128 filters (Guo et al., 2018). Max pooling reduces dimensionality while retaining key features.

In the regression model, features are flattened into 115,200 neurons, passed through dense layers with ~14.8M parameters, and output 2 crown values with a linear activation. The classification model flattens into 25,600 neurons, with ~3.67M parameters and a softmax output layer for 4-class classification.

Layer (type)	Output Shape	Param #
conv2d (Conv2D)	(None, 254, 254, 32)	320
max_pooling2d (MaxPooling2D)	(None, 127, 127, 32)	0
conv2d_1 (Conv2D)	(None, 125, 125, 64)	18,496
max_pooling2d_1 (MaxPooling2D)	(None, 62, 62, 64)	0
conv2d_2 (Conv2D)	(None, 60, 60, 128)	73,856
max_pooling2d_2 (MaxPooling2D)	(None, 30, 30, 128)	0
flatten (Flatten)	(None, 115200)	0
dense (Dense)	(None, 128)	14,745,728
dropout (Dropout)	(None, 128)	0
dense_1 (Dense)	(None, 64)	8,256
dense_2 (Dense)	(None, 2)	130

Total params: 14,846,788 (56.64 MB)

Layer (type)	Output Shape	Param #
conv2d (Conv2D)	(None, 198, 198, 32)	896
max_pooling2d (MaxPooling2D)	(None, 99, 99, 32)	0
conv2d_1 (Conv2D)	(None, 97, 97, 64)	18,496
max_pooling2d_1 (MaxPooling2D)	(None, 48, 48, 64)	0
conv2d_2 (Conv2D)	(None, 46, 46, 128)	73,856
max_pooling2d_2 (MaxPooling2D)	(None, 23, 23, 128)	0
conv2d_3 (Conv2D)	(None, 21, 21, 256)	295,168
max_pooling2d_3 (MaxPooling2D)	(None, 10, 10, 256)	0
flatten (Flatten)	(None, 25600)	0
dense (Dense)	(None, 128)	3,276,928
dense_1 (Dense)	(None, 4)	516

Total params: 3,665,862 (13.98 MB)

Figure 4. CNN Architecture Summaries for Image Recognition (right) and Vertical Displacement Interpretation (left), Including Layer Types, Shapes, and Parameters (TensorFlow/Keras v2.19)

The Python code used for this study includes Jupyter notebooks for model development and training, supported by custom scripts for data preparation, augmentation, and labelling. Image preprocessing and dataset handling were implemented using libraries such as NumPy, OpenCV, and Pandas. Model definition and training utilised TensorFlow/Keras frameworks, incorporating convolutional architectures tailored to classification and regression tasks. For model evaluation and presentation, Matplotlib and Seaborn were used to generate loss curves, interpretation-error plots, and confidence metrics, enabling visual interpretation of performance across tunnel types and displacement levels.

Training: The model is trained using a combined loss function: cross-entropy for tunnel count classification and mean squared error (MSE) for vertical displacement regression (Goodfellow et al., 2016). The Adaptive Moment Estimation (ADAM) optimiser (learning rate 0.001) is employed over 20 to 90 epochs with a batch size of 8 to 32, executed on a Graphical Processing Unit (GPU) in approximately 1 hour.

This methodology establishes a scalable framework for automated interpretation of the numerical outputs, with the potential to incorporate additional outputs through iterative data collection and model tuning.

4 RESULTS AND DISCUSSION

4.1 *Tunnel Count Classification*

The classification branch identifies the number of tunnels (1 to 4) by analysing spatial patterns in cross-sectional images, including boundaries, spacing, and layout. CNN convolutional layers detect tunnel outlines through edge and shape features, while max-pooling preserves spatial information, leading to a softmax layer that outputs class probabilities. Figure 5 - "Number of Tunnels

by Software" shows tunnel count distribution across various softwares, highlighting dataset diversity. The target accuracy of 90% reflects the model's ability to reliably classify tunnel groups.

Training dynamics (Figure 5 – "Model Loss and Accuracy") show training loss steadily decreases, while validation loss fluctuates slightly after 10 epochs, indicating minor overfitting. Accuracy stabilises around 0.95 for training and ~0.85 for validation by 15 epochs.

The CNN achieved 90% overall accuracy, correctly classifying 307 of 347 samples, with peak performance on 2-tunnel images (169 correct). Most misclassifications occurred between adjacent tunnel counts, particularly for 3-tunnel cases (Figure 5 – "Confusion Matrix").

Precision and recall (Figure 5 – " Precision and Recall by Class") exceed 0.9 for 1- and 2-tunnel classes but drop to 0.6–0.7 for underrepresented 3- and 4-tunnel classes. The Precision-Recall Curve (Figure 5 – "Precision and Recall Curve") shows sharper separation for dominant classes and flatter curves for minority ones, highlighting imbalance effects.

Figure 5 – "CNN Confidence" peaks near 1.0 for ~250 classifications, suggesting low uncertainty in dominant classes. The class imbalance shows two-tunnel images dominate, with few samples for 3- and 4-tunnel cases, particularly in FLAC3D and UDEC potentially affecting generalisation.

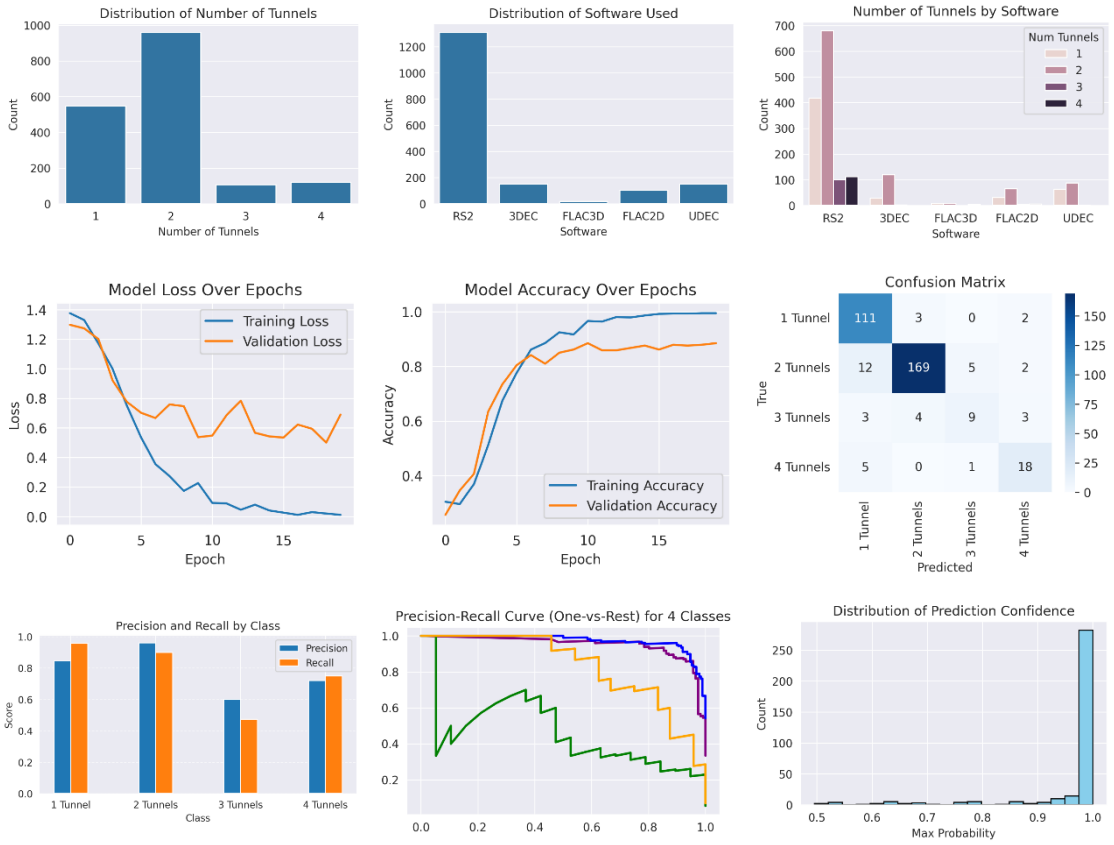


Figure 5. Model Performance Metrics for Tunnel Count Classification Including Data Distributions, Training Trends, and Evaluation Results

4.2 *Vertical Convergence Interpretation*

The regression branch interprets vertical settlement at the crown for images with a maximum of two tunnels (Crown_T1 and Crown_T2), a key indicator of tunnel stability. By analysing deformation gradients—pixel intensity shifts in displacement maps—the model aims for 85% of interpretations to be within 5 mm of the actual values, with the expectation of achieving higher accuracy and lower deviation as the dataset grows. Figure 6 – "Sample Test Interpretations" visually demonstrate the model's ability to interpret settlements (e.g., Interpreted: –0.025, –0.025 m vs.

True: –0.028, –0.025 m), with discrepancies within acceptable limits considering the data available for training. This precision supports the model's adaptability and allows retraining for other displacement metrics, such as sidewall movement or ground surface displacement.

For the vertical displacement model Figure 6 – "Loss Curve" indicates a steady decline in training loss, whereas validation loss stabilises around epoch 40, with minor fluctuations. This suggests that while the model generalises well, further regularisation techniques may improve performance. The objective is to ensure that 85% of settlement interpretations remain within 5 mm of the numerically predicted values.

The model accurately interprets settlements at Crown_T1 and Crown_T2, with 85% of absolute errors falling below 5 mm, as shown in Figure 6 – "Cumulative Distribution of Absolute Errors".

Figure 6 – "Interpreted vs Actual Vertical Settlement" demonstrates a strong linear correlation, with points closely aligned along the diagonal line, indicating that the model is effectively learning the true displacement trend.

Figure 6 – "Distribution of Interpretation Errors" shows that errors are centred around –0.001 m with a standard deviation of approximately 0.01 m, suggesting the model is relatively unbiased and its interpretations are tightly distributed around the ground truth.

Figure 6 – "Residual Plot" illustrates how interpretation errors vary across the range of interpreted settlement values. It shows the difference between interpreted and actual settlement values across the full range. Most residuals fall within ±0.02 m (±20 mm) but considering the target accuracy of ±0.005 m (5 mm), this spread suggests the model still produces a number of cases with higher-than-acceptable error, particularly for Crown_T2, which shows a slight positive bias meaning it tends to under-interpret larger (more negative) settlements. This may reflect limitations in the training data or challenges in capturing subtle deformation patterns near the crown.

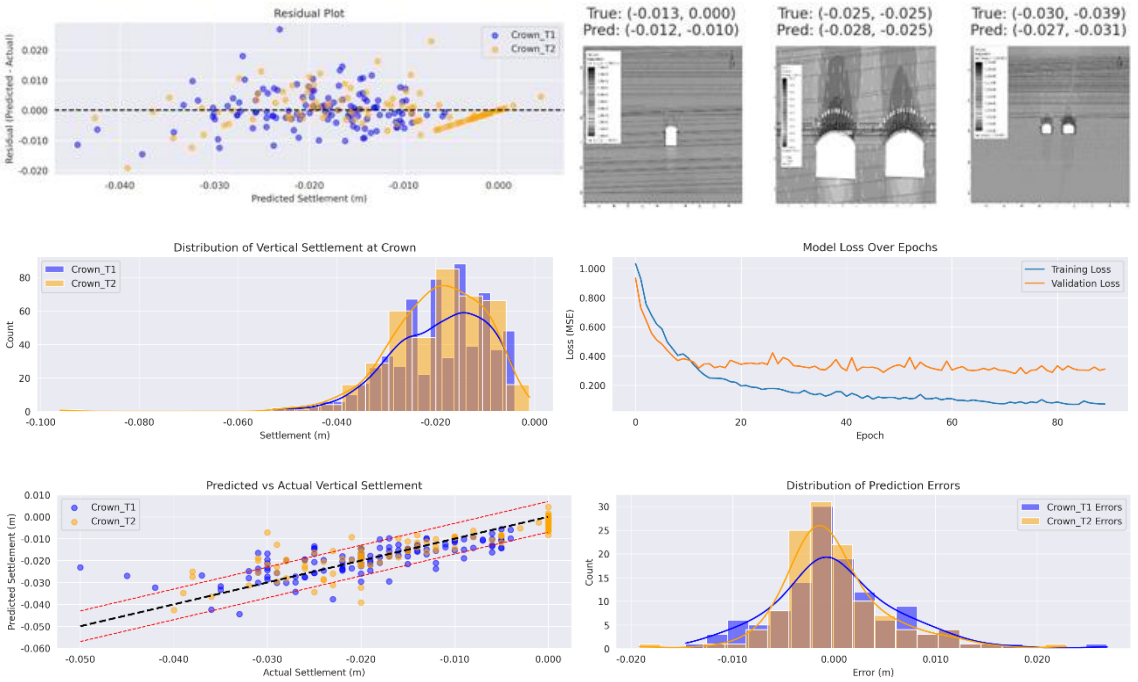


Figure 6. Model Evaluation for Vertical Settlement Interpretation Including Data Distribution, Training Curves, Error Metrics, and Sample Outputs

Sensitivity Analysis: The model's performance is influenced by data quality, class imbalance, and the diversity of geometrical scenarios. Figure 5 – " The Distribution of Number of Tunnels " highlights the significant imbalance, particularly underrepresentation of 3- and 4-tunnel cases, which correlates with the lower precision and recall observed for those classes. The Confusion Matrix reveals notable misclassifications between adjacent classes — for example, several 1-tunnel images misclassified as 2, indicating that subtle differences in geometry or colour contours may be similar without sufficient training examples.

For vertical settlement, Figure 6 – "Distribution of Vertical Settlement at Crown" shows a strong concentration around –0.025 m, but limited representation at extreme values (e.g., beyond –0.05 m). This sparsity may reduce model accuracy in regions where larger deformations occur, which are often critical for tunnel safety assessment. Such limitations suggest that current model interpretations may be less reliable under edge-case conditions.

Additionally, the model's performance may be sensitive to software-specific image styles, as the dataset is dominated by RS2 outputs, while contributions from FLAC3D, UDEC, and 3DEC remain minimal. This could introduce a form of model bias toward dominant styling or formatting, reducing generalisation to broader software ecosystems unless addressed with cross-platform augmentation.

Expanding the dataset to 5,000+ images and including greater geometric variability, different software sources, and more balanced class representation could significantly improve accuracy across both classification and regression tasks.

Comparison with Traditional Methods: Manual interpretation typically requires 5–10 minutes per image, resulting in 125–250 hours for 2,000 images, with subjective bias contributing to error rates of up to 15–20%. The CNN processes the same dataset in under one minute, producing repeatable, unbiased interpretations. Compared to traditional ML methods like Support Vector Machine (SVM), the CNN delivers a 10–15% gain in accuracy, attributed to its ability to learn complex spatial features directly from raw images.

Discussion: These results demonstrate that even with a moderately sized dataset and inherent class imbalance, a dual-task CNN can deliver reliable, automated interpretation for tunnel analysis. The model's strength lies in its ability to interpret numerical outputs rapidly and consistently, positioning it as a promising tool for design checks, model review, and quality assurance workflows.

However, limitations remain. The underperformance in 3- and 4-tunnel classification and wider interpretation error at settlement extremes indicate that data-driven blind spots exist. Performance is currently strongest in high-frequency classes, with reduced precision where data is limited or more complex. These gaps must be addressed before wider deployment.

Future Potential: Improvements could be achieved by applying synthetic oversampling or targeted data augmentation to address underrepresented classes, particularly 3- and 4-tunnel cases. Incorporating additional edge-case deformation patterns, such as soft ground behaviour or large displacement scenarios, may also improve regression performance in critical ranges. Expanding the dataset to include more complex 3D tunnel configurations, such as junctions, bifurcations, or crossover sections, would allow the model to generalise across a wider range of real-world geometries. Exploring ensemble CNN architectures could enhance interpretation stability, while the inclusion of additional outputs such as stress, strain, or plastic zone boundaries would support more comprehensive numerical output interpretation. Collectively, these improvements could raise model accuracy to 95% or higher, positioning ML-driven interpretation as a scalable, reliable tool for future tunnelling workflows.

5 CONCLUSION

This study presents a dual-task CNN for interpreting tunnel engineering numerical modelling outputs, achieving 90% accuracy in tunnel count classification (1 to 4) and interpreting vertical settlements with 85% of interpretations within 5 mm of the actual values. Trained on a dataset of 2,500 images, the model automates a time-consuming manual process, reducing processing time from minutes to seconds per image while providing consistent and repeatable outputs.

The model offers two key contributions. First, it streamlines tunnel count classification, supporting faster inventory checks and design validation. Second, it accurately derives vertical displacement values from colour contour plots, improving interpretation without manual input. The CNN's ability to extract and learn from spatial features enables detection of tunnel outlines, deformation gradients, and other key indicators, making it a practical tool for both early-stage modelling and ongoing project workflows.

Limitations include reduced performance on underrepresented classes (3- and 4-tunnel scenarios), some interpretation variability at displacement extremes, and reliance on a synthetic dataset

dominated by a single modelling platform (RS2). While generalisation was strong, model confidence was notably higher on dominant classes, and settlement interpretations, though unbiased, occasionally exceeded desired tolerances in edge cases.

Future work will focus on expanding the dataset with more diverse tunnel geometries, edge conditions, and software outputs. Additional outputs such as stress, strain, and plastic zones will be integrated, and ensemble methods will be explored to improve robustness across varying input conditions. These steps are expected to enhance interpretation accuracy and generalisation, positioning the model for broader application in digital tunnel engineering.

6 REFERENCES

Ahmed, A. et al. 2003. Neuronet prediction of tunnelling-induced settlements. Proc. 10th Int. Colloquium on Structural and Geotechnical Engineering, Ain Shams University, Cairo, Egypt, 22–24 April.

Aqel, M. & Marji, M. 2021. Convolutional neural networks for visual recognition. In: Proc. Int. Conf. on Data Science, E-learning and Information Systems 2020, 229–238. Cham: Springer.

Chollet, F. 2021. Deep learning with Python, 2nd ed. New York: Manning Publications.

Couture, H. 2023. How to design a roadmap for a machine learning project. Towards Data Science.

Géron, A. 2022. Hands-on machine learning with Scikit-Learn, Keras, and TensorFlow, 3rd ed. Sebastopol: O'Reilly Media.

Goodfellow, I., Bengio, Y. & Courville, A. 2016. Deep learning. Cambridge: MIT Press.

Guo, Y., Liu, Y., Oerlemans, A., Lao, S., Wu, S. & Lew, M.S. 2018. Deep learning for visual understanding: A review of recent advances in convolutional neural networks. Pattern Reconition 77: 701–721. https://doi.org/10.1016/j.patcog.2017.10.013

Li, G., Xie, Y. & Lin, L. 2024. A review of convolutional neural networks in computer vision. Artificial Intelligence Review. https://doi.org/10.1007/s10462-024-10721-6

Liu, X., Chen, Y. & Wang, Z. 2024. A review of deep learning applications in tunneling and underground engineering. Applied Sciences.

Mirsepassi, M.A. 1997. Application of artificial neural networks to water treatment plant operation. PhD thesis, University of Wollongong.

Mohamadnejad, M., Diederichs, M. & Carvalho, R. 2021. A convolutional neural network for predicting tunnel support and liner performance: A case study. Rock Mechanics and Rock Engineering.

Nye, T. 2023. Reinforcement learning: Tunnel design/construction – is it possible? Paper presented at the 18th Australasian Tunnelling Conference, Auckland.

Ramzan, A., Ehsan, N. & Alvi, R. 2023. Application of artificial neural network for construction and demolition waste quantification: A parametric study. Heliyon 9(7): e16148.

Zhang, Y., Wang, J. & Li, L. 2024. Deep learning–based prediction of tunnel face stability in layered soils using images of random fields. Journal of Geotechnical and Geoenvironmental Engineering.

19th Australasian Tunnelling Conference – Acosta-Martínez, Stewart and Hudson-Smith (Eds.)
© 2025 Australian Tunnelling Society, ISBN 978-0-85825-002-4

Use of photogrammetry to quantify tunnel overbreak

S. Zafari & M. Smith
Gamuda Engineering-Laing O'Rourke Consortium, Sydney, NSW, Australia

ABSTRACT: This paper presents a novel method of quantifying the overbreak or overcut experienced during tunnelling by using photogrammetry acquired during mined tunnel excavations on Sydney Metro West Western Tunnelling Package (WTP). Photographs were taken of each excavation advance and processed using photogrammetry software into as-built surface models of the rock. Models of consecutive advances were geo-located and imported into the 3D modelling software package 'Rhino 3D' using surveyed coordinates. A script to calculate overbreak was developed which would compare the model surfaces to a model of the planned excavation line (E-line). The output was a 3D colour contoured overbreak surface. The overbreak values calculated using the photogrammetry models were found to be in reasonably good agreement with excavation as-builts obtained by survey.

1 INTRODUCTION

Overbreak is the undesired fallout of material beyond the planned tunnel excavation profile (E-line) driven by an irregular breakage along defects or spalling of rock. Over cutting (for simplicity referred in this paper as overbreak), refers to excavation beyond the planned E-line of the tunnel either by accident, or through imprecise excavation methods. Excessive overbreak can increase the cost of construction and/or extend construction programs, so understanding whether the volume is within expectations can help the contractor make decisions on whether to implement additional control measures to reduce overbreak and by extension, backfilling requirements.

As-builts of the rock are obtained during the mined tunnelling process by the tunnel surveyor to inform construction whether the excavation has achieved the minimum required dimensions. Two commonly used methods to obtain rock as-builts are by total station or laser scan survey.

Total station survey involves surveying points on the rock in longitudinal arrays (typically spaced ~500mm apart), comprised of widely spaced, laterally surveyed points (200-300mm typical spacings). This method is relatively cheap, can be performed quickly, and has good accuracy; however, it provides an output of low data density.

Using the laser scanning technique, the rock is surveyed with a tripod or drone mounted laser scanner in the order of ~50,000 points per second (Wang et al., 2014), and by comparison, provides a much higher data resolution than manual total station survey. The method incurs higher labour costs, relies heavily on data, and requires expensive hardware and subscription-based software to collect and process the data. Both methods can provide a measurement of overbreak at any surveyed point.

Previous work has demonstrated that photogrammetric reconstructions of rock obtained using laser scanning, smartphone LiDAR or optical means can have applications for tunnel mapping (Torkan et al., 2023; Janiszewski et al., 2022; Garcia-Luna, 2019), tunnel monitoring (Attard et al., 2018) and rock slope stability analysis (Bonilla-Sierra et al., 2015; Kim & Gratchev, 2015). 3D photogrammetry presents a practical method for the creation of dense 3D models of tunnel

surfaces without the high equipment costs of laser scanning. The technique relies on Structure-from-Motion (SfM) algorithms to transform a series of simple photographs into a detailed point cloud. The value of this approach has been proven in recent research, which now uses photogrammetric data for demanding engineering applications (Im et al., 2025).

In this paper we explore an alternative method of quantifying the overbreak experienced during mined tunnelling by integrating optical photogrammetric model reconstructions of the excavated rock with 3D modelling and scripting tools. Our process does not need to be carried out by a surveyor; it is quick and inexpensive and uses commercially available and user-friendly software to produce. This method could be useful where laser scanning data is not being collected, and where the magnitude of overbreak is of particular concern to the contractor.

2 BACKGROUND

The data presented in this paper was captured during construction of Sydney Metro West Western Tunnelling Package (WTP) in two tunnels excavated by roadheader. The tunnels include the Clyde junction caverns, with a span ranging 10-19m and excavated to a maximum crown depth of 23m in Hawkesbury Sandstone and the Westmead stub tunnels, with a span of ~7.5m and excavated at a crown depth of 25m to 30m, within the Ashfield Shale. Automated navigation systems guided the roadheader operators in both tunnels, which unlike the drill and blast method provides a high degree of precision and a control on overbreak.

3 METHODOLOGY

3.1. Image collection

For each excavation advance three reference survey targets were placed in front of the newly excavated and washed tunnel face. Two targets were placed at ground level adjacent to the side-walls and one target was elevated and placed in the centre (Fig. 1). The targets were surveyed and their coordinates recorded.

A flood light provided consistent lighting between advances, minimising shadows and overexposure. Overlapping high-resolution images were captured of each cut using a Canon EOS 1500D DSLR camera. Multiple arrays of photographs were taken at different inclinations to ensure an abundance of overlapping points (tie points) in the data, like that shown in Figure 2.



Figure 1. Setup during photogrammetry data collection. Numbered survey targets are placed in the shot to allow orientation of the model

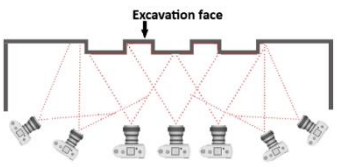


Figure 2. Geometric approach to photography used in obtaining photogrammetric data

3.2. Photogrammetry model processing

Photogrammetry software ‘3DF Zephyr’ used to create 3D as-built model of the rock surface using photographs. The 3DF Zephyr used metadata included in each image file to automatically figure out the internal camera calibration settings. This automatic calibration changed settings for our Canon EOS 1500D camera, which has a 21 mm focal length and a resolution of 6000 × 4000 pixels. This made sure that all photogrammetric models were accurate all the time. The workflow included:

3.2.1. Sparse point cloud generation

The first step was the initial processing of the raw photos. During this step, the software automatically checks each image, and identify matching points, between overlapping images. These tie points are then used to generate a sparse point cloud, which forms the foundational structure of the 3D model. To precisely scale and geo-locate the model, survey targets within the images are ‘picked’ and coordinates are assigned to each of them, ensuring accurate geo referencing of the final model. At this stage, processing was performed using the software's "high detail" reconstruction settings to maximise the accuracy and quality of the sparse point cloud, to find thousands of tie points across multiple images.

3.2.2. Dense point cloud generation

Following sparse point cloud generation, the second step involves producing a detailed, high-resolution (dense) point cloud. During this stage, the software analyses the sparse point cloud in greater depth, calculating precise spatial positions for a significantly larger number of points. This step greatly enhances the density and visual clarity of the data. In this paper, dense point cloud generation was conducted using the software's "high detail" reconstruction setting, to create a detailed depth map which contains millions of data points. This step is very important because it gives us the exact geometric model, we need to accurately recreate the tunnel surfaces. This model is then utilized to make realistic meshes and do accurate analyses of tunnel overbreak.

3.2.3 Mesh creation

The software converts the dense point cloud into a 3D mesh surface comprised of many interconnected triangles. It was found that the number of triangles comprising each photogrammetric mesh led to long processing times during overbreak calculation. To solve this problem, the number of triangles within each mesh was reduced.

To determine what reduction factor could be applied without significantly affecting the output, analysis of the output of various reduced meshes was compared to the complete mesh. These results are presented in Section 4, which found that a reduction of triangles to 25% of the original number did not make a considerable difference to the output, and this reduction factor was adopted for the models in this paper. Figure 3 shows a complete mesh alongside a 25% vertex mesh.

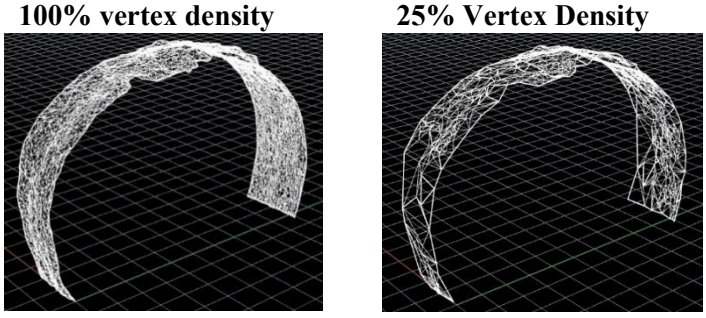


Figure 3. Comparison of meshes with different densities. Note the significant reduction of triangles in the 25% vertex density mesh

3.2.4 Textured mesh generation

A photographic image texture is then draped over the mesh to complete the model. The texture has no thickness so as not to affect the overbreak calculation and is useful in understanding if geological features contributed to the overbreak. A processed texture model is presented in Figure 4.

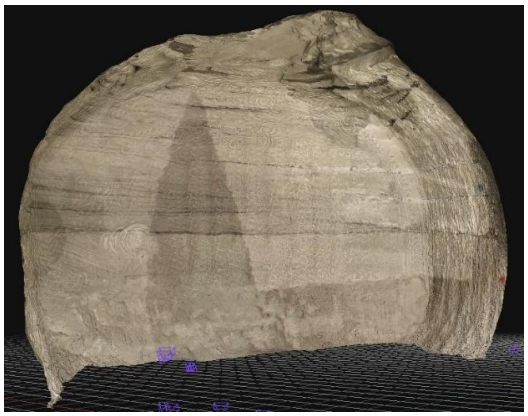


Figure 4. Shows a completed 3D textured photogrammetry model of a cut in the Clyde junction cavern

3.3 Integration with modelling software

To produce the E-line surface in which to compare the overbreak surface, a BIM of the construction line (C-line) was imported into Rhino3D and expanded outward by the sum of the various lining and convergence tolerances used during construction.

Each photogrammetry model was then imported into Rhino3D. As survey coordinates were embedded within each model, they were automatically geo-located to overlay our E-line. The face of each cut was not required in the overbreak calculation and was trimmed at the end chainages of that cut, precisely at the location where the transition from the crown to the face began. A series of four consecutive photogrammetric models representing a 12m length of tunnel is shown in Figure 5.

3.4. Overbreak analysis

A script was developed in Grasshopper (Rhino3D's scripting tool) to undertake overbreak analysis of the photogrammetry models (Fig. 6). The macro performed two main functions: Calculating and contouring the overbreak and highlighting any underbreak.

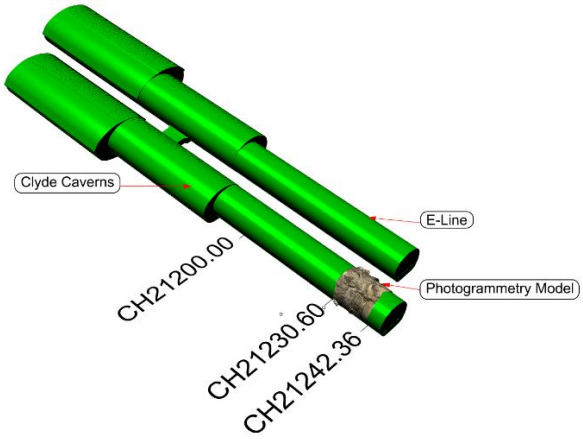


Figure 5. A series of photogrammetry models in the smaller span of a Clyde junction cavern overlay our E-Line model

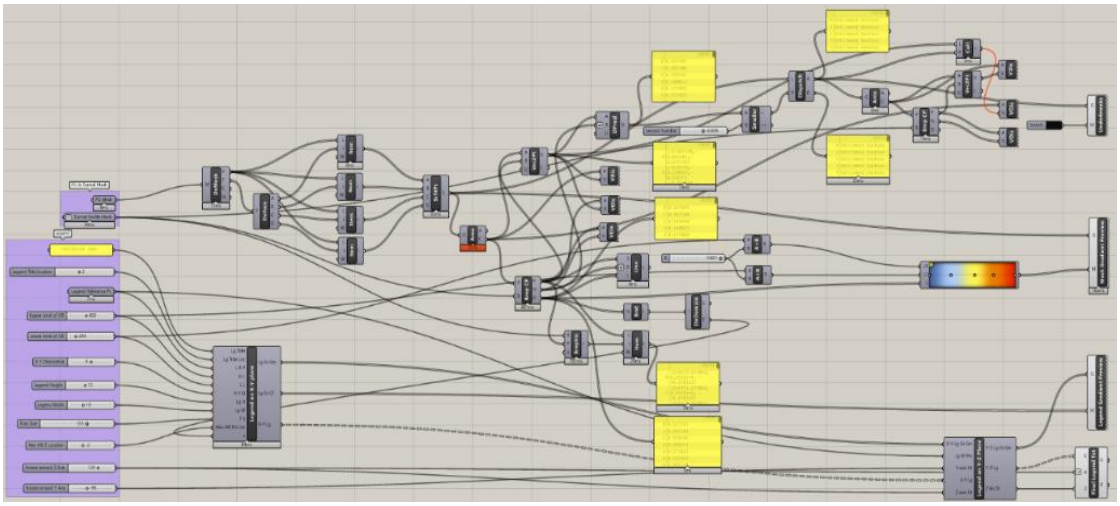


Figure 6. Grasshopper Script used to calculate the colour-contoured overbreak surface

3.4.1. Overbreak calculation

The script converts the wire mesh from each model into a poly-surface by creating small 2D interconnected surfaces between the vertices of each wire triangle. The point at the centre of each of these triangles defined the average distance of the triangle to the E-line and was measured. A colour was assigned to each triangular surface based on the magnitude of measured overbreak, with the colour range defined using the maximum and minimum overbreak magnitudes within the modelled area. The hottest colours represent areas with maximum overbreak, while the coolest colours denote minimal or zero deviation from the E-line.

3.4.2. Underbreak identification

To identify underbreak, the following vector calculation was performed for each triangle:

$$\vec{\boldsymbol{A}} \cdot \vec{\boldsymbol{B}} = |\mathrm{A}||\mathrm{B}| \cos(\theta)$$

Where:

$\vec{\boldsymbol{A}}$: The vector from the centre of the mesh triangle to the closest point on the E-line surface

$\vec{\boldsymbol{B}}$: The normal vector of the points on the E-line surface projected from centre of the triangle

θ: The angle between vector A and B

If $\vec{A} \cdot \vec{B} < 0$, then the mesh triangle lies inside of the E-line surface and was identified as under-broken. A positive dot product indicated that overbreak had occurred at the triangle. Triangles that showed underbreak were coloured black to distinguish them from the coloured over broken areas.

4 RESULTS AND VALIDATION

Both textured and overbreak contoured surfaces constructed from a series of photogrammetric models of the Westmead stub tunnels are presented in Figures 7-8 respectively.

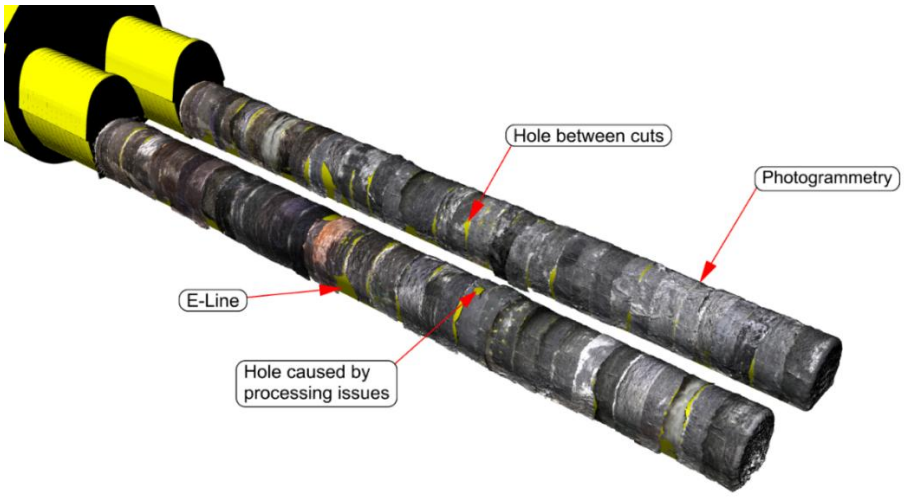


Figure 7. Complete photogrammetric model of the Westmead stub tunnels overlay the E-line used in construction

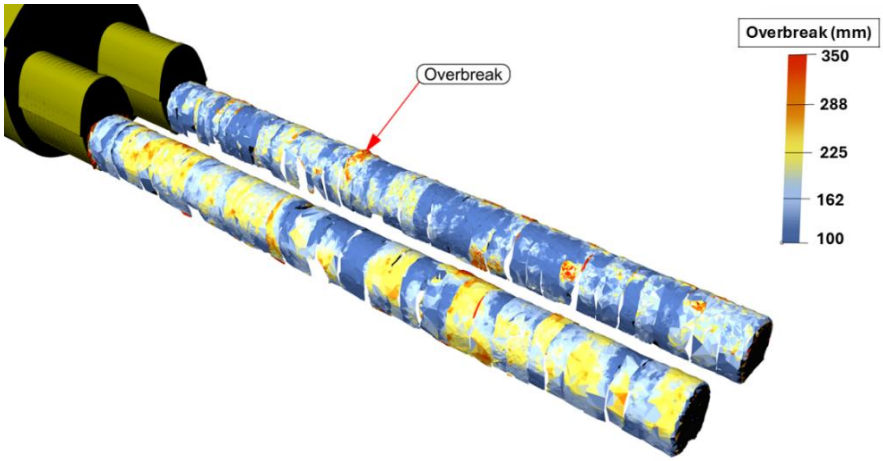


Figure 8. Output after running the Grasshopper script: A contoured plot showing overbreak along the Westmead stub tunnels

Several issues with the output were noted which may have led to some reduction in accuracy. These issues and some possible solutions are listed below:

- Holes in the photogrammetry were created when manually trimming the faces from the sidewalls/crown of each individual model. Trimming adjacent models at a specific chainage (rather than by eye) would lead to smoother transitions between cuts and reduce holes in the models.
- Further holes in the models are thought to be caused by issues processing photos within Zephyr3D. These issues are likely due to a variety of data collection issues including blurry photographs, too few photographs, insufficient tie points between photos and/or uneven lighting.
- Problems in geo-locating some of the models required them to be manually adjusted into position. We believe this issue is due to uneven lighting and too few photos/insufficient tie points between photos. A more streamlined data collection process will be trialled in future iterations.

4.1. Mesh vertex density comparison

To demonstrate how vertex density affects the overbreak magnitudes in the output, Figure 9, visualises four overbreak contour surfaces created from the same excavation advance and processed

using different vertex reduction factors. The results are summarised in Table.1, which show that reducing the mesh to 25% of its original density resulted only in a 1% reduction in accuracy, while significantly decreasing model size and improving calculation speeds.

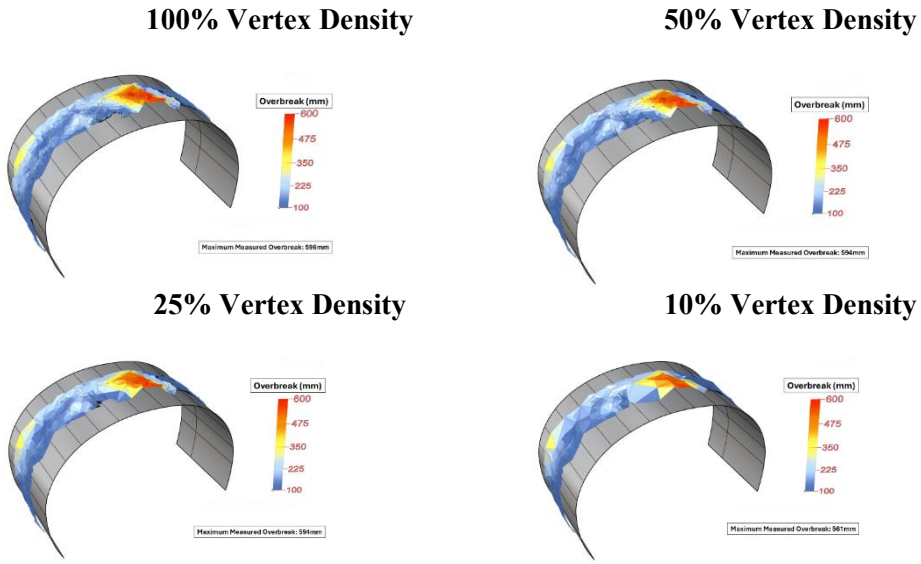


Figure 9. Comparison of overbreak contour surfaces created using various vertex reduction factors

Table 1. Comparison of overbreak magnitudes of meshes with various reduction factors applied

Mesh Density	Max Overbreak (mm)	Relative Accuracy (%)
100%	596	100
75%	594	~99
50%	594	~99
25%	594	~99
10%	561	~94

4.2. Survey validation

The accuracy of the photogrammetry-based overbreak calculation was compared to laser survey measurements taken at the same chainage. The Grasshopper script calculated a maximum overbreak of 594mm (Fig. 10a) whereas the laser survey recorded 589mm in the same cut (Fig. 10b), a difference of 5 mm. This demonstrates a close correlation between the photogrammetry and traditional methods.

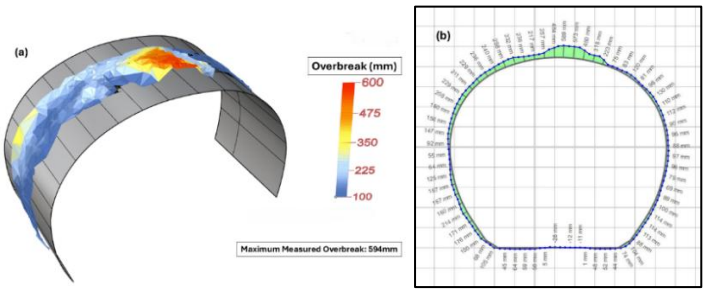


Figure 10a. Overbreak contour surface from an advance in the RT02 Clyde junction cavern. Figure 10b. The rock as-built report at a chainage through the same advance produced from laser scanning data acquired by a Leica Nova MS60. Over broken area shown in green. E-line shown in grey.

4.3. Measurement Uncertainty

There are a few things that can influence the accuracy of photogrammetric measurements. For instance, lighting conditions often change between excavation stages, and this can create shadows

or uneven contrast that affect image quality and how well tie points are detected. Moreover, the variability in the angle and distance of captured photos can affect the accuracy of the constructed model. Errors in survey data, particularly in picking up the coordinates of targets, can also affect model scaling and alignment. Furthermore, the automatic internal camera calibration which is done by the software is based on image metadata and software algorithms which can introduce small deviations if the camera settings drift. Overall, these factors can contribute to minor discrepancies in model accuracy, particularly in poorly lit regions of the tunnel.

5 DISCUSSION

This work demonstrates proof of concept, that it is possible to quantify overbreak using photogrammetry without the need for a surveyor. In this paper, the photographs were collected and processed during routine face mapping activities by the geologists and geotechnical engineers of the WTP project and as such, did not incur additional labour costs or production delays.

The results were found to be less accurate when compared to survey methods. However, we conclude that the accuracy is sufficient for the purpose of informing the decision-making process of the contractor. The accuracy of the modelling could further be improved by standardising data acquisition and data processing procedures. We acknowledge that the overbreak observed in this study was minimal and that the method would be better demonstrated when applied to excavations in poor ground or in tunnels excavated by the drill and blast method.

The use of this technique could easily extend to quantifying shotcrete thicknesses by comparing a shotcrete model surface to the rock as-built surface, or one shotcrete layer to a previous layer. This of course could not provide real-time thickness data and could not replace laser scanning at the tunnel face during the application of shotcrete.

Further to this work, an additional script could be developed to undertake volumetric calculations, which could quantify the overbreak by measuring the volume between the photogrammetry and E-line surfaces or even calculating the volume of spoil stockpiles.

6 REFERENCES

3Dflow. 2023. *3DF Zephyr* (7.531) Verona: 3Dflow srl.

Attard, L., Debono, C.J., Valentino, G. & Castro, M. 2018. Tunnel inspection using photogrammetric techniques and image processing: A review. *ISPRS Journal of Photogrammetry and Remote Sensing* 144: 180–188. https://doi.org/10.1016/j.isprsjprs.2018.07.010

Bonilla-Sierra, V. 2015. Rock slope stability analysis using photogrammetric data and DFN-DEM modelling. *Acta Geotechnica* 10: 497–511. https://doi.org/10.1007/s11440-015-0374-z

Garcia-Luna, R., Senent, S., Jurado-Pina, R. & Jimenez, R. 2019. Structure from motion photogrammetry to characterize underground rock masses: Experience from two real tunnels. *Tunnelling and Underground Space Technology* 83: 262–273. https://doi.org/10.1016/j.tust.2018.09.026

Im, H., Kurauchi, T., Sato, N., Kawamura, Y., Jang, H. & Topal, E. 2025. Tunnel overbreak prediction: An integrated approach using 3D photogrammetry and machine learning. *Mining, Metallurgy & Exploration* 42: 1441–1457. https://doi.org/10.1007/s42461-025-01278-1

Janiszewski, M., Torkan, M., Uotinen, L. & Rinne, M. 2022. Rapid photogrammetry with a 360-degree camera for tunnel mapping. *Remote Sensing* 14: Article 3791. https://doi.org/10.3390/rs14215494

Kim, D.H. & Gratchev, I. 2015. A photogrammetric approach for stability analysis of weathered rock slopes. *Geotechnical and Geological Engineering* 33: 443–454.

Robert McNeel & Associates. 2023. *Rhinoceros 3D*. Seattle: Robert McNeel & Associates.

Torkan, M., Janiszewski, M., Uotinen, L. & Rinne, M. 2023. Method to obtain 3D point clouds of tunnels using smartphone LiDAR and comparison to photogrammetry. *IOP Conference Series: Earth and Environmental Science* 1124(1): Article 012016. https://doi.org/10.1088/1755-1315/1124/1/012016

Wang, W., Zhao, W., Huang, L., Vimarlund, V. & Wang, Z. 2014. Application of terrestrial laser scanning for tunnels: A review. *Journal of Traffic and Transportation Engineering* 1(5): 325–337. https://doi.org/10.1016/S2095-7564(15)30279-8

19th Australasian Tunnelling Conference – Acosta-Martínez, Stewart and Hudson-Smith (Eds.)
© 2025 Australian Tunnelling Society, ISBN 978-0-85825-002-4

Digital engineering - lessons learnt from a major Sydney tunnel project

M. G. Sheffield, C. E. Williams & A. L. Tarua
Aurecon, Sydney, Australia

ABSTRACT: Over the last 10 years, major tunnel projects have seen a significant expansion in the requirements for digital engineering (DE). Whilst in the building industry, digital engineering requirements have become relatively well defined and developed, in underground construction, some aspects of DE are less clear. Government and industry bodies have the ongoing task of refining guidelines for underground structures by drawing on the experiences and documentation from other parts of the world where digital engineering is well established and also the lessons learnt from previous projects. For example, the unique tunnelling conditions in Sydney and bespoke ground support systems are not well considered by current DE guidelines, which has led to bespoke DE requirements for elements such as ground support. However, other elements such as civil, mechanical and electrical systems are very well defined, albeit they are potentially onerous DE requirements. As part of this paper, the authors will explore some of the challenges faced in delivering the digital engineering requirements for a recent major Sydney tunnel and offer some possible solutions.

1 BACKGROUND

Digital engineering (DE), often referred to as BIM (Building Information Management), is a very broad subject which encompasses the management and processing of digital information through the many stages of development of a project from concept through to delivery and operation. In a NSW, Australia context, one of the major infrastructure asset owners, TfNSW, describe it as "A collaborative way of working, using digital processes, to enable more productive methods of planning, designing, constructing, operating and maintaining assets." 0TfNSW (2022).

Digital information is extensive on modern major infrastructure projects. DE is not only about the storage of data, but also how data is shared and exchanged across multiple platforms and between the various parties involved in delivery of a project over its lifecycle.

For the purposes of this paper, the authors will focus on one aspect of DE; the creation, development and management of a 3D geometric model based on their views and experiences developing a complex model for a major underground infrastructure project in Sydney. They will focus on some of the detailed challenges which were faced and overcome which are not fully addressed in existing local and international guidelines which by necessity have to be broad and high level to cover a range of applications and environments.

At present, noting that the road transport industry in NSW still requires full production of comprehensive drawing sets and reports, the cumulative impact of design production including DE (both 3D modelling and asset data management) costs the industry millions of dollars. This comes at a time when there is increasing pressure on our industry to reduce escalating design and construction costs. It is recognized that many aspects of DE including clash detection and design

coordination offer significant benefits to complex projects. In the long term, there should ultimately be benefits for all parties involved in a project with a reduction of whole of life project costs.

2 APPROACH

2.1 *Current approach*

The rapid progression of technology, software and tools for data management has seen BIM/ DE change how underground infrastructure and tunnelling are designed, constructed and maintained. While the development of DE has improved the way projects are delivered it has also led to a degree of uncertainty and ambiguity regarding some of the DE concepts and their implementation. This uncertainty is also further exacerbated by differences between the expectations of the parties engaged on a project.

At present the requirements associated with the design documentation for major infrastructure projects are particularly onerous. Considerable effort is required to develop design solutions and document outcomes on thousands of drawings and in reports comprising thousands of pages to demonstrate compliance with the guidelines, project particular specifications, design standards and the opinion of the many reviewers involved in a project.

In addition, over the last decade, industry has seen an increased demand for the development of 3D models. This is generally yet to correspond with a reduction in conventional design documentation, reflecting duplication of information rather than replacement. As a result, significant associated effort and cost is added to projects to develop, review, manage and manipulate these models by all parties (Client, Contractor and Designer).

If we take the example of a major tunnel infrastructure project which brings together a diverse range of disciplines including tunnels, civil (alignment, roads, drainage, pavements), structures, mechanical and electrical (M&E), the way in which a 3D geometrical model is created is as equally diverse as the disciplines involved. For example, in the civil environment, complex 3D models have been created for a significant period of time using proprietary software packages such as 12d or OpenRoads. A similar situation exists in underground structures, where 3D models can be created using software such as Civil3D or Revit. In M&E, Revit is often the preferred modelling tool. However, for tunnel engineering design, where it is necessary to create long linear models along a control alignment, which includes complex geometry at cross passages, ventilation structures and underground traffic merge/ diverges, although there are proprietary software packages on the market, most have limitations. Further discussion on the modelling tools for tunnels is included below.

Cross discipline coordination; although an essential part of design development on large infrastructure projects; and coordination of 3D models takes considerable effort for a number of reasons:

- Package sizes and boundary limits vary between disciplines.
- The design program for each discipline are phased and sequenced slightly differently.
- There are many cross-discipline dependencies on large infrastructure projects which need to be frozen at different times to enable designs to be fixed.
- The level of design detail required for each discipline may vary.

As a result, a dedicated DE team is required to facilitate and navigate the complexities of inter-disciplinary model coordination.

2.2 *Future approach*

Ideally, as technology develops, the significant effort required to create, develop and coordinate a 3D model will be offset by a reduction in other aspects of design documentation. However, this will require a change in the approach to some aspects of design since at present this is not feasible for a number of reasons:

- On most major transport projects there is no requirement for models to be certified, which would be necessary if they are to be used as a basis for construction. For example, on recent D&C major tunnel projects the Contractor has built an independent 3D tunnel model from the 2D information provided as part of the design documentation and used the 3D model

provided by the Designer as a reference source to provide additional supplementary information in geometrically complex areas.
- Drawings associated with underground construction include a substantial number of notes which provide additional details and guidance on design boundary conditions, limitations and construction sequences. In a 3D model, where would these notes and details live?
- Can 2D drawings be created from 3D models? The answer is yes but this needs to be qualified because the intelligence of geometry (radii, angles, arcs) are often lost as geometry is converted to polylines or segmented arcs comprising a series of short straights to idealise a curve.
- How are the tunnel excavation and support sequence requirements such as maximum advance lengths for different ground conditions supposed to be captured in a model?
- Where the design includes a suite of pre-determined tunnel support types which are applied based on the exposed ground conditions, how can these be included in a 3D model?
- Do subcontractors have the capability to view manipulate and interrogate 3D models or do they require information to be distilled into a series of drawings and schedules?

3 LESSONS LEARNT ON A MAJOR TUNNELLING PROJECT

Over the last 10 years, industry has experienced progressive growth in DE requirements. A number of the authors' recent experiences are described below.

3.1 *Level of detail – How detailed is detailed enough?*

This is a complex issue because the expectations within a project team (Designer, Contractor, Owner, Operator) can vary significantly. It is therefore important to establish a clear set of guidelines and project requirements to achieve alignment.

Currently in Australia, guidelines only partially exist. There are no tunnel specific guidelines, although there are a number of standards and international guidelines which provide guidance such as 0 AS ISO 7817 (2024), 0 AIA (2024). In addition, the ITA WG22 is in the process of drafting a guideline for tunnelling 0 ITA (2022) and 0 Vojtech et al (2022) . These documents are high level and hence general in nature. At a local level clients have created a digital framework 0 Sydney Metro (2021) and 0, 0, 0 and 0 TfNSW (2022) to support projects and provide a means of connecting technologies across various disciplines. At a project level, clients create specific digital engineering technical requirements.

Whilst for disciplines such as civil, structures/ bridges, pavements and drainage, the requirements are well defined, in tunnelling the requirements are less clear. As a result, there is a need for guidelines regarding the level of detail that is necessary and achievable in 3D models. In the authors' experience there is often a tendency to over specify and request unnecessary detail.

International and local guidelines and standards often refer to this as the LOD, which is a confusing acronym as both level of development and level of detail are very different. Furthermore, the BIM Forum 0 AIA (2024) introduced the concept of Level of Information Need as described below as shown in

Figure *1*.

Level of Information Need, as defined in 0 AS ISO 7817-1:2024, is the quality, quantity, and granularity of geometric, alphanumeric, and documentation information to be included in a deliverable. While Level of Information Need requires geometry to be defined, it provides no guidance on how to do so.

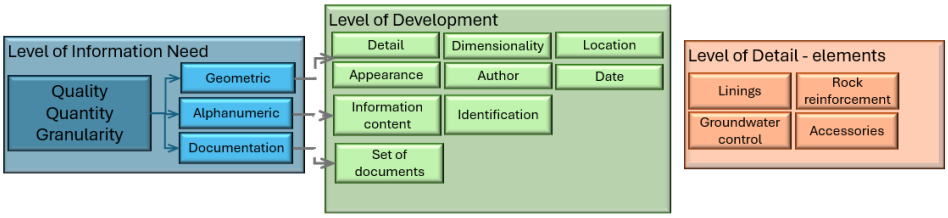


Figure 1. Relationship between Level of Detail and Level of Information Need

– Level of Development (LOD), which sits within the broader framework of Level of Information Need, defines the detail, dimensionality, location, appearance, author, and date of geometric information.

Therefore, in order to determine an appropriate level of detail for inclusion in a 3D tunnel model, it is important for the following aspects to be clearly understood:

– The specifics of the tunnelling environment
– The types of tunnels which are typically constructed and the uniqueness of the ground support systems which are employed
– The construction sequences which are adopted

For example, this is particularly important in Sydney where the underground environment is generally suited to the construction of drained tunnels and caverns which form a complex arrangement of large inter-connected spaces as shown in Figure *2*. Within these underground networks, the ground is typically supported with a combination of permanent rockbolts and permanent sprayed concrete (shotcrete) linings 0 Czegledi et al (2020) in pre-designed support types, developed to suit the different predicted ground conditions. The actual support type cannot be determined until the ground conditions are exposed and known. Therefore, inclusion of the actual ground support in a 3D model including individual rockbolts, spiles or canopy tubes is not practical. Instead, design shotcrete thicknesses can be modelled based on agreed tolerances and a surface created depicting the distal end of the element as shown in Figure *2*.

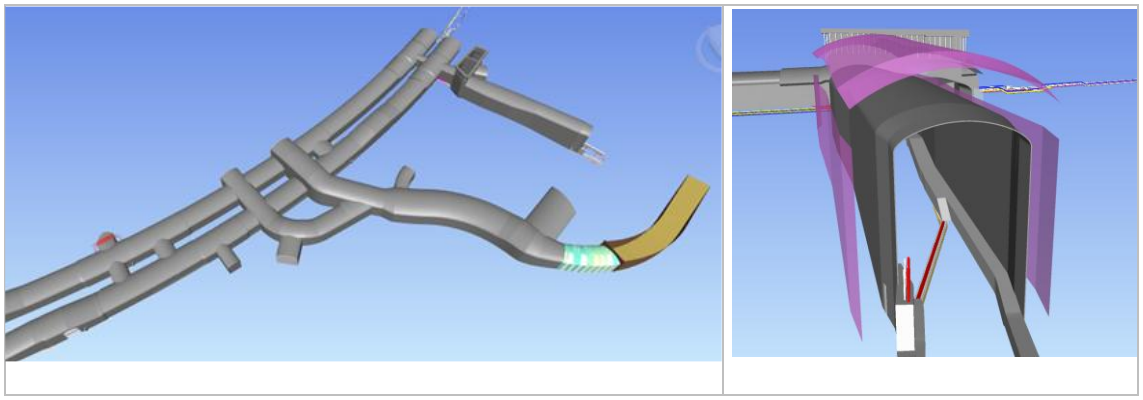


Figure 2. Approach for modelling rock reinforcement

The level of detail to be included in a model at various design gates is another area where differing expectations exist. International guidelines such as 0 DAUB (2019) and also 0 TfNSW (2022) suggests that the detail within a model is progressively developed and enhanced as designs are progressively refined through a series of design gates or stages. Whilst this approach is satisfactory in theory, a more appropriate approach would be to include more detail in the early design stages where feasible but qualify the elements in terms of their reliability, ie the level of development. The reason for this approach is because:

– The inclusion of the necessary objects, layers and thicknesses in a model in the early stages, even if there is uncertainty associated with geometry helps with interdisciplinary coordination and visualisation of complex areas.
– As shown in Figure *3*, in areas such as the cross-passage junctions in a road tunnel, where there are a significant number of services and interactions, the geometry particularly complex. Hence modelling a bank of services as a box 0 AS ISO 7817-1:2024 rather than individual conduits does not provide a realistic representation of these complex areas. It would be more valuable to make assumptions regarding the number, size, spacing which would enable coordination with other services and disciplines to commence earlier than would otherwise have been possible. Hence pinch points could be identified and additional space incorporated early in design development rather than late when the impact of design changes has increased knock-on effects.

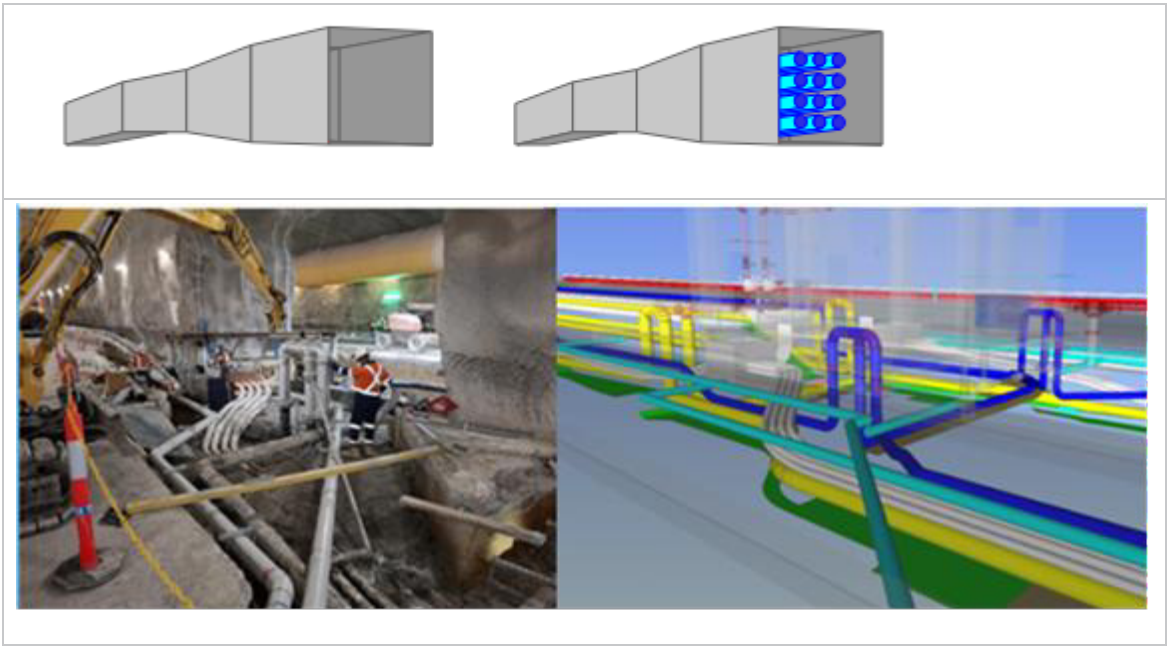


Figure 3. Example of complex services interactions

3.2 *Application of tolerances*

Construction of any form of infrastructure is not an exact science. For example, precast concrete tunnel segments incorporate very small tolerances because they have to be cast with a high degree of accuracy but the tolerances applied to the excavation of a mined tunnel have to be large, because of the accuracy of the plant which is used and because the elements which have to be included within the tunnel require different tolerances. This is why an important part of design is to consider how tolerances are applied and hence how they influence design assumptions. Hence in the old (non-DE) world, perfection was not required in design documentation provided key dimensions were defined. In the current world, where everything is modelled in a 3D environment, all too often we find ourselves chasing unnecessary high degrees of accuracy because, as an example, connections do not intersect correctly in a model which creates errors and clashes. Future projects should consider a pragmatic approach to clashes associated with tolerances, where real clashes can be differentiated from those that are the result of the cumulative effect of unlikely tolerances.

3.3 *Software and modelling challenges*

As noted above, there are many proprietary software packages on the market which can be used for design and 3D modelling of the various elements within a tunnel. These include Synergy 12D or Bentley OpenRoads for alignment, pavements, barriers and drainage design, AutoDesk Civil 3D and Revit for structural work.

3.4 *Tunnel*

The experience of the authors has highlighted that creation of a 3D model of the tunnel support system, which can comprise multilayer shotcrete lining shells, rock reinforcement, waterproofing layers and reinforced concrete linings and segments, temporary support elements is not straightforward. Whilst there are proprietary software packages on the market, such as 12D, Revit, Rhinoceros and Infraworks, they all have limitations. They may be able to accommodate uniform geometry well such as a segmentally lined bored tunnel or tunnel which incorporates a cast concrete lining but in Sydney, the prevailing ground conditions enable construction of particularly complex geometries which require complex geometrical transitions between uniform and non-uniform tunnel profiles. These complex geometries (see Figure *2*) prove challenging to model, particularly with string-based modelling programs.

In addition, as tunnellers and constructors of long linear infrastructure, we like uniformity. Uniformity means simpler design and easier construction, which also results in reduced programs and lower capital costs. However, whilst in theory it may appear that there is repetition between sections of tunnels, such as say the layout of services in cross passage apron areas, geometrically they can all be slightly different because control lines may not be perfectly parallel or at exactly the same elevations or junctions may not be precisely 90degrees. These are important factors which must be addressed if a 3D model is to be developed, which is accurate and suitable for use as a source for construction.

In the background behind any type of 3D model is a huge amount of data, which includes the following:

– Input parameters from different disciplines such as geometric profile data eg, coordinates, chainages, alignment data, space and clearances for civil and structural fitout within a tunnel, M&E equipment and systems or construction requirements and egress requirements.
– Output data such as the parameters which define a 3D shape such as the centre point of arcs, their lengths and radii together with start and end chainages for profiles.

Storage and management of all this data as well as the coordination of changes to this data as a project develops and evolves is therefore a complex process.

As a result, on recent major tunnel project, advances have been made in the storage of data, management of changes and creation/modelling of the tunnel shell and complicated geometrical transitions. This has been achieved as follows and illustrated in Figure *4*.

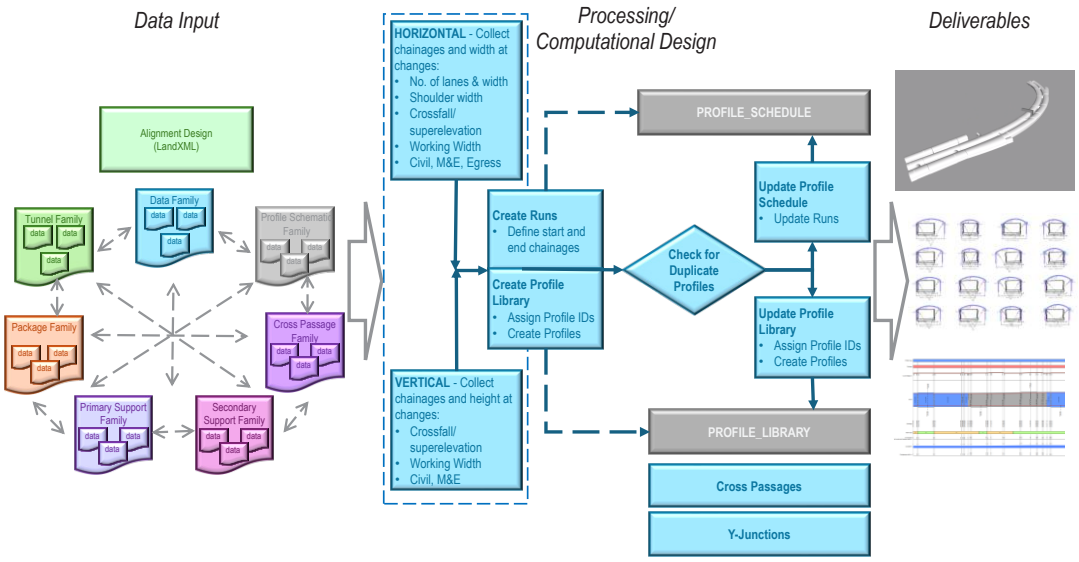


Figure 4. Process for creation of 3D Tunnel Model

– Refinement of the methodology defined in 0 Czegledi et al (2020) into a workflow which recalls geometric design parameters, runs them through in-house processing scripts which create a 3D tunnel shell and then outputs the data into a variety of formats for downstream use such as design deliverables.
– Using a database which contains a series of linked tables that use unique parameter names which creates consistency and avoids data repetition.
– Development of a series of coded scripts using C# and Grasshopper to create the tunnel shell.

3.5 *Automation*

An enormous number of parameters and variables are used in the development and definition of a 3D model. As a result, there are many opportunities for errors to occur if data is incorrect and changes are not appropriately controlled. The definition of the tunnel shell is the outcome of cross-discipline coordination and consideration of tunnel design inputs which can easily be overlooked

during the busy delivery phase of a D&C project. Automation is an important tool in reducing the workload associated with maintaining coordination between disciplines. This type of difficulty can be overcome through automated coordination of design inputs. For instance, as shown in the workflow outlined in Figure *4*, the incorporation of the road design as alignment strings is an automated process. Any changes to the road design are transferred automatically into the tunnel modelling process giving real time outputs. Previously this type of design change would have been implemented manually which takes time and risks errors. However, for the process to be automated data must be shared in a particular and consistent format to suit the code routines which have been developed.

An understanding of the input design is also required, while the layman may expect the widening of the edge of a traffic lane to be a straight edge change in direction this is in fact often represented in road modelling software as a chamfer between two straights. For identification of a change to the tunnel profile a simplification on the tunnel design side needs to be implemented as part of the automation.

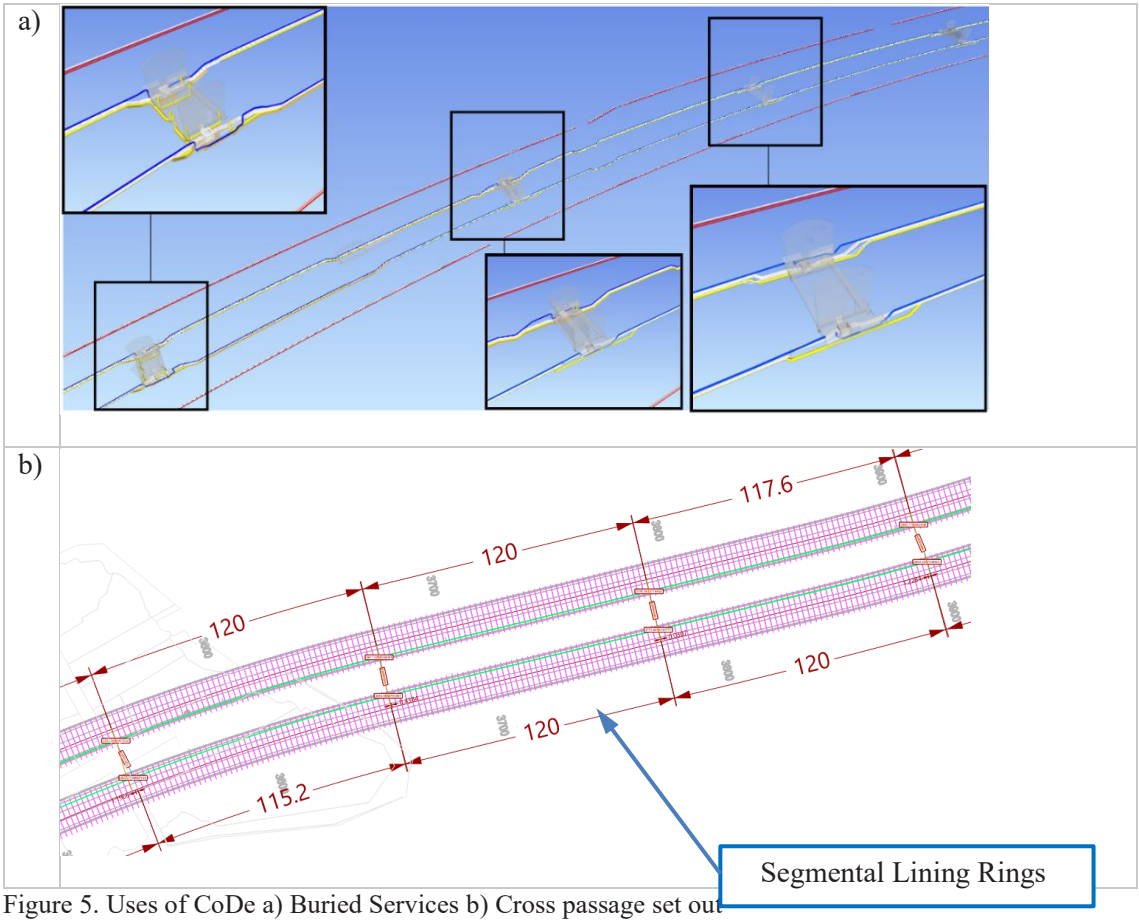


Figure 5. Uses of CoDe a) Buried Services b) Cross passage set out

In addition, the linear nature of tunnels creates opportunities for standardisation and repetition of common elements. Some elements of tunnel modelling such as creating tunnel profiles, modelling of buried services or setting out cross passages are therefore ideally suited to automation and adoption of computational design (CoDe) routines.

For example, Figure 5 illustrates how CoDe has been used to define the layout for the buried services in standard cross passages. However, whilst in the example there appears to be significant repetition, in reality, each cross passage is geometrically slightly different because they are at different locations along the alignment. Hence the tunnels at each end are at different levels, the tunnels are not perfectly parallel and the alignment geometry is different at each location. As a

result, the cross passages may not all be at exactly 90º to the mainlines. These are all important aspects to consider because the routines developed need be cognisant of the geometric variations.

Similarly, setout routines can also be developed for cross passages by checking the distances around curves such that that the maximum spacing is never exceeded as shown in Figure *5*

3.6 *Asset Referencing*

The long term usefulness of a 3D Model is its ability to be used during construction and operation / maintenance. The correct referencing of assets is integral to this and the scope for use, particularly in asset management is broad.

In the authors' experience asset referencing during the design process faces similar difficulties to that found in implementation of LoD requirements. While referencing is useful in finalised models, the effort expended to perfect and keep it updated during the stages of design development is disproportionate to value added.

Anecdotally the uptake in the use of the 3D model during construction activities is limited. This could be due to a number of factors including lack of integration into construction workflows, availability of appropriate software, limited skills in interrogating 3D models and impracticalities involved in taking screens into the tunnel.

The future use of the 3D model as an asset maintenance tool is an intended outcome of the high LoD requirements during the design phase, and further research into the successful implementation of the 3D model into asset maintenance processes is recommended.

4 CONCLUSIONS

As technology continues to advance and the benefits and capabilities of 3D modelling continue to be realized, there are significant opportunities to streamline design and construction processes. In particular, there are a number of areas for focus such as:

- Implementation of practical approaches to digital documentation requirements (LoD, tolerances and asset referencing) through the various design stages.
- Smart automation of workflows to facilitate collaboration, particularly asset referencing.
- Streamlining of design documentation and reduction of duplication.
- Improvements and changes to the ways of working on site.

5 REFERENCES

American Institute of Architects. 2024. *BIM Forum Level of Development Specification - Part 1*

Czegledi C., Sheffield M., Tarua A. 2020. Challenges of developing a digital framework for tunnel space proofing; *Proceedings Australian Tunnelling Conference 2020+1*

German Tunnelling Committee (DAUB-Working Group). 2019. *Digital Design, Building and Operation of Underground Structures - BIM in Tunnelling,*

ITA Working Group 22. 2022. *BIM in Tunnelling. Guideline for Bored Tunnels – Vol 1*

Standards Australia,. AS ISO 7817.1:2024 *Building Information Modelling – Level of Information Need*

Sydney Metro. 2021 *Sydney Metro Employers Information Requirements Part 1, Part 3, Part 3 and Part 4*

Transport for NSW. 2022. DMS-ST-208 Version 4.0 *Digital Engineering Framework*

Transport for NSW. 2022. DMS-ST-202 Version: 4.1 *Digital Engineering Standard Part 1: Concepts and Principles*

Transport for NSW. 2022. DMS-ST-207 Version: 4.1 *Digital Engineering Standard Part 2: Requirements*

Transport for NSW. 2022. DMS-SD-123 Version 4.2 *Digital Engineering Terms and Definitions*

Vojtech E. G., Angerer W., Grasmick J., Karlovsek J. 2022. *Development of the ITA "BIM in Tunnelling – Guideline for Bored Tunnels".*

19th Australasian Tunnelling Conference – Acosta-Martínez, Stewart and Hudson-Smith (Eds.)
© 2025 Australian Tunnelling Society, ISBN 978-0-85825-002-4

Advancing geotechnical construction phase workflows: leveraging digital tools for improved construction outcomes

H. Buchanan
PSM, Brisbane, Australia

R. Brehaut
PSM, Sydney, Australia

ABSTRACT: The design and construction of underground structures require robust geotechnical models and designs that can respond swiftly to geological conditions encountered during construction. This paper examines advances in geotechnical construction phase services (CPS) workflows and verification practices for Australia's major underground infrastructure projects, including tunnels and surface excavations over the past decade. Recent technological advancements, including photogrammetry, laser scanning, and cloud-based data transfer, have enhanced the precision and efficiency of geotechnical mapping by enabling real-time data collection and seamless information sharing among project stakeholders. Despite the advantages, challenges remain, including high initial investment, building team capabilities and awareness, reducing time on the critical path, and industry hesitance. Variable ground conditions and inefficient workflows have been identified as major contributors to cost overruns in tunnelling projects, underscoring the need for ongoing refinement in geotechnical data collection and design verification practices.

This paper evaluates multiple technologies for their abilities in collecting, processing, and conveying data to inform technical assessment and decision-making. Selected examples from recent Australian infrastructure projects demonstrate the practical benefits and limitations of various data collection and analysis tools, such as photogrammetry and laser scanning, in applications including digital mapping and automated structure identification. This study highlights the benefits of digital tools that provide reliable and unified datasets for multi-disciplinary use, including design analysis and optimisation, quality control, and model verification. Effective implementation of digital geotechnical workflows not only offers significant time and cost savings during construction but also simplifies future operational maintenance and design reassessment, ensuring safety and compliance across complex construction projects.

1 INTRODUCTION

Over the past two decades in Australia, ongoing investment in heavy civil infrastructure projects, including road, rail, and hydropower projects has driven the need for CPS workflows that can capture varying geological conditions as accurately as possible while minimising downtime in the construction cycle.

Cost overruns exceeding 50 percent are not uncommon in tunnelling megaprojects (Flyvbjerg, 2014) and in extreme cases have been reported at 900 percent (Paraskevopoulou & Boutsis, 2020). Multiple systematic reviews of time and cost overruns have identified variable ground conditions as a major contributor (Membah & Asa, 2015; Sharma & Gupta, 2020) and the primary contributor to cost overruns in tunnelling specific projects (Paraskevopoulou & Boutsis, 2020).

The design of excavations and underground structures relies on ground-structure interaction, support loading and stability assessments derived from geotechnical models. During the design phase, these models are informed by site investigations and, where available, previous experience

in the area or similar ground conditions. The geotechnical model is updated during construction to validate design assumptions and respond to the ground conditions encountered on site.

Rapidly developing technologies such as photogrammetry, terrestrial and airborne laser scanning, and cloud-based data transfer provide increasing efficiency in delivering high-quality data sets. While these technologies offer clear benefits, challenges remain, including increased capital costs, bulky equipment and unrefined workflows. As these elements have matured, the widespread adoption into current construction projects is beginning to accelerate.

By integrating CPS workflows with digital tools like Building Information Modelling (BIM), construction teams can create unified datasets that support stakeholder decision-making, providing benefits throughout the project lifecycle (Sanfilippo et al., 2025). This paper compares data collection and analysis tools, and presents a workflow for the integration of digital tools into CPS operations based on current capabilities.

2 GEOTECHNICAL WORKFLOW METHODOLOGIES AND DEVELOPMENTS

The primary role of the CPS representative in a Design and Construct (D&C) contract is often to compare geotechnical conditions encountered during construction against the documented design assumptions and support selection criteria. Should the encountered conditions represent a departure from the design, a notice of geological change is provided for consideration by the design team and contractor respectively. The following sections describe an evolution of CPS tunnel mapping workflows while outlining the relative benefits and compromises.

2.1 *Traditional mapping*

Traditional geotechnical mapping begins with field sketches and notes, as presented in Figure 1. This method remains widely used due to its simplicity and timely approach for on-site assessment during construction. Transferring paper maps into digital platforms for spatial referencing, as presented in Figure 2, has proven beneficial, but can be time-consuming and prone to errors. Hybrid digital mapping tools, using tablets, have streamlined the mapping process. Engineers can readily record detailed geotechnical observations directly onto digital plans and templates, allowing for quick transfer of mapping records for review while still at the excavation face. However, depending on the adopted platform and template the data is not readily exportable for use in analysis.

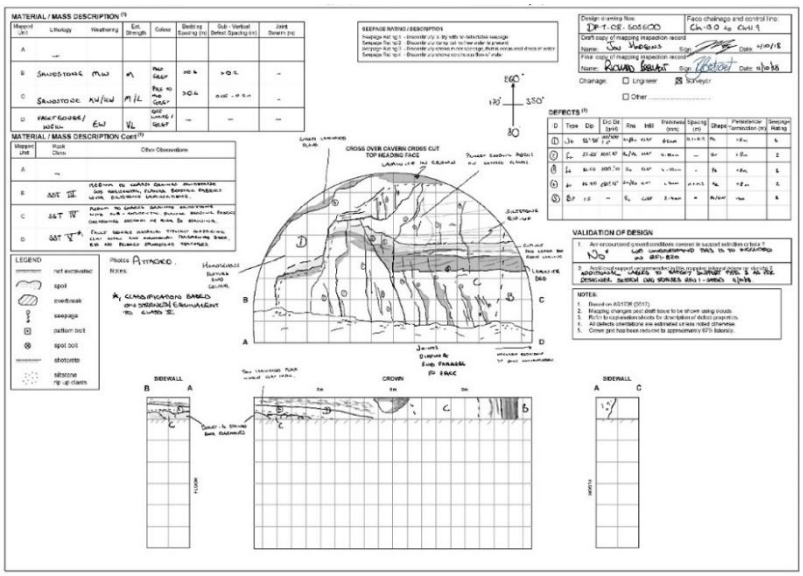


Figure 1. Example of typical geotechnical tunnel face mapping sheet digitised in the field using tablets

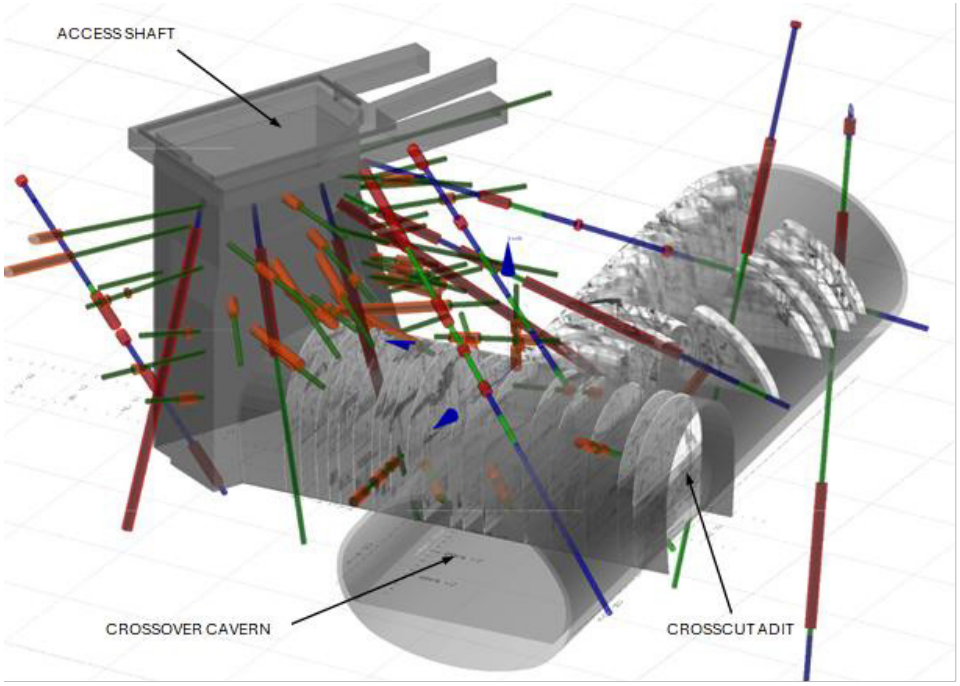


Figure 2 Example of face mapping sheets digitised in 3D space relative to design geometry and available site investigation (borehole) data from the Sydney Metro City and South-West Tunnel Station Excavation Project in 2018.

2.2 *Photogrammetry*

Stereoscopy is a technique that enables three-dimensional visualisation by combining images taken from different positions, where the displacement between images provides depth perception (Nowicki, 1942). By the early 20th century, aerial photogrammetry had become an established tool for topographic mapping, engineering surveys, and military reconnaissance (Linder, 2009). In modern CPS workflows, photogrammetry models incorporate stereoscopic imaging principles to produce high-resolution 3D point clouds, used for geotechnical assessment and design verification. Drone-based photogrammetry captures stereo images to generate digital elevation models (DEMs), allowing for volumetric calculations, slope geometry assessments, and monitoring of construction progress. Over the past 15 to 20 years photogrammetry software has evolved considerably, with improvements in user experience, processing speeds, and model accuracy making it a more practical tool in the right conditions.

Structure-from-Motion (SfM) photogrammetry provides a cost-effective solution for generating high-resolution point cloud models. Photos can be captured from handheld cameras or smartphones and SfM technology automatically solves camera pose and surface geometry using overlapping images (Wang, Zhang & Li, 2023). 3D point clouds and textured meshes are then converted from relative coordinates to project coordinates by referencing a control point. Several other studies have reported favourable outcomes adopting photogrammetry workflows underground (Duffy, Macklin, Henry and Macintosh, 2023; Garcia-Luna et al., 2019).

Over the past decade PSM has conducted several underground photogrammetry trials in numerous tunnelling environments. Challenges with data acquisition and processing reliability remain key to the successful implementation of this method:

- Accurate scaling and georeferencing of the scan depend on the surveyor supplying coordinates for the reference points captured within the image. Errors and inaccuracies introduce distortions in the 3D model.
- Poor or inconsistent lighting, dust, rain and obstructions affect feature-matching, leading to errors in camera orientation estimation.

- Image overlap and photos from different locations are needed to minimise pose errors, see Figure 3. 15 or more high-quality images were found to be sufficient to reconstruct a tunnel face of ~50 m² (Garcia-Luna, Senent, Jurado-Pina & Jimenez, 2019).
- High quality image capture in tunnel environments may require manual exposure settings and camera stabilisation, increasing the time required per photo.
- High density point clouds comparable to laser scans can take anywhere from 45 minutes (with approximately 20 photos) to greater than 4 hours (with approximately 50 photos) (Garcia-Luna et al., 2019). PSM trials indicated that 50-100 minutes was typical for a typical top heading tunnel advance.

Lighting available in a tunnel environment, such as from portable lights or a face drill rig, has been reported to be sufficient (Garcia-Luna et al., 2019), dispelling a typical criticism of this method. In addition to the practical advantages of using a camera or smartphone, SfM can better capture complex geometry that may otherwise be under sampled in laser scanning, such as shadowing behind protrusions in blocky ground (Duffy et al. 2023). Nevertheless, reliance on well-lit, low-dust environment free of obstructions such as machinery, is not always practical in a tunnelling environment.

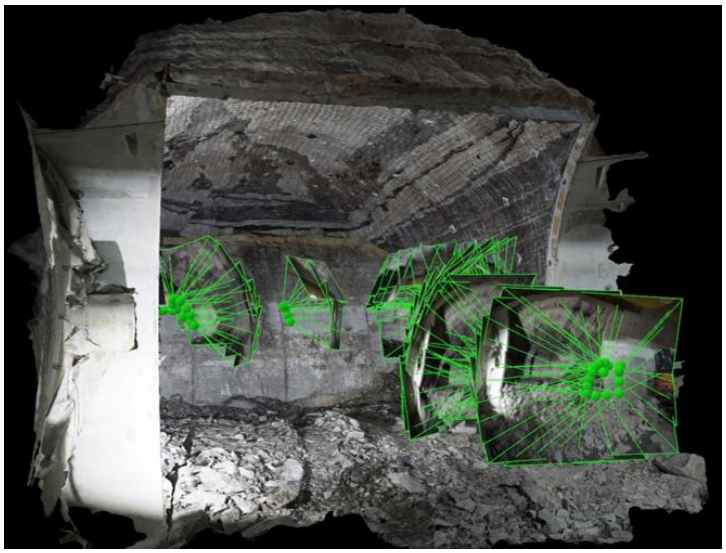


Figure 3 Photogrammetry model for TBM cross-passage during the Sydney Metro West Tunnel Station Excavation (TSE) project in 2016, including relative photo capture locations. Note, this model capture benefitted from having "supported ground" for favourable camera positioning which is not always possible during production cycles.

2.3 *Laser scanning*

2.3.1 *Professional scanners*

Terrestrial laser scanning (TLS) has been widely implemented in surveying of underground constructions (Sharma & Gupta, 2020). TLS reflects laser pulses on the rock surface to capture millions of data points, including spatial positioning, colour, and surface reflectance (only some scanners are currently capable of this) to develop a 3D point cloud surface.

Modern, lightweight portable laser scanning instruments provide high-resolution data capture (e.g. accurate to 4mm at 10m) which have proven to be successful for self-performed scanning by CPS teams. Calibrated surface reflectance value, which is independent of light conditions and range in some scanners, enables detection of humidity/water. Scans are therefore more reliable and accurate than photogrammetry in low light, low-texture and low-contrast rock environments.

In certain applications (surface excavations), integrated GPS can register scans without the need to establish reference points. However, over larger project extents such as tunnels, survey targets are required to convert GPS coordinate system readings to design coordinates (e.g. MGA). The scale factor between these systems is 0.9996 and accounts for the earth's curvature.

The Leica BLK 360 scanner was used extensively on the Lake King William Hydropower Upgrade Project in Tasmania. The use of TLS has delivered numerous project advantages:

- TLS scans provided a transparent, accurate and repeatable approach to recording as-built conditions, see Figure 4. Scans were provided to the head contractor and asset owner, which informed decision making on site and enabled proactive identification of issues such as geometry non-conformance.
- Improved safety with data capture occurring beneath "supported ground".
- Integration with survey workflows, including shotcrete scanning thickness verification.
- Georeferenced scans and automatic defect identification software supplemented traditional mapping, see
  Figure 5, reducing time required by geologists at the face, while also providing redundancy with the availability of accurate data when a geologist was not available (e.g. night shift). This was especially valuable in a drill and blast operation in blocky ground, where mapping individual defects would be otherwise very time-consuming.

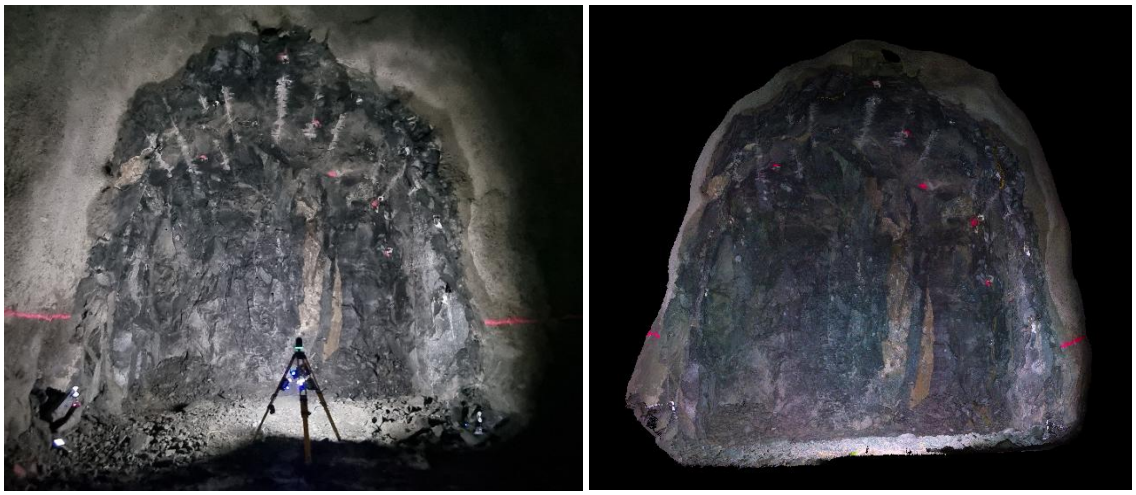


Figure 4 TLS capture of a drill and blast tunnel excavation (left) with corresponding georeferenced point cloud output (right)

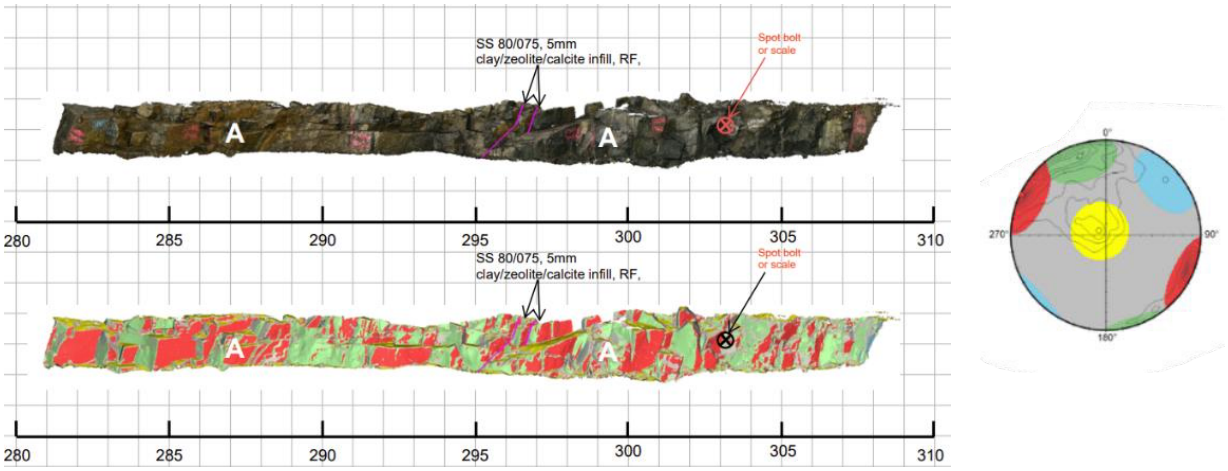


Figure 5 Mapping example using RiScan Pro LIS GeoTec: Upper plots show red, green, blue (RGB) coloured point cloud while lower plot illustrates automated defect detection with corresponding stereograph.

- 3D models enabled continuity of mapping and accurate tracking and projecting of adverse structure allowing for early identification and support selection. For example:
  - Figure 6 illustrates how scan records were used to accurately calculate the size and location of wedges requiring additional support. Scans allowed for accurate and safe defect orientation measurements when the face was inaccessible due to site safety protocols.
  - Combining field mapping observations with scanning data identified adversely dipping structures at the tunnel portal. To verify support capacity, a kinematic sliding analysis was carried out based on wedge geometries from the scans. Follow-up mapping and scanning at the portal face and within the tunnel were then used to verify design assumptions.

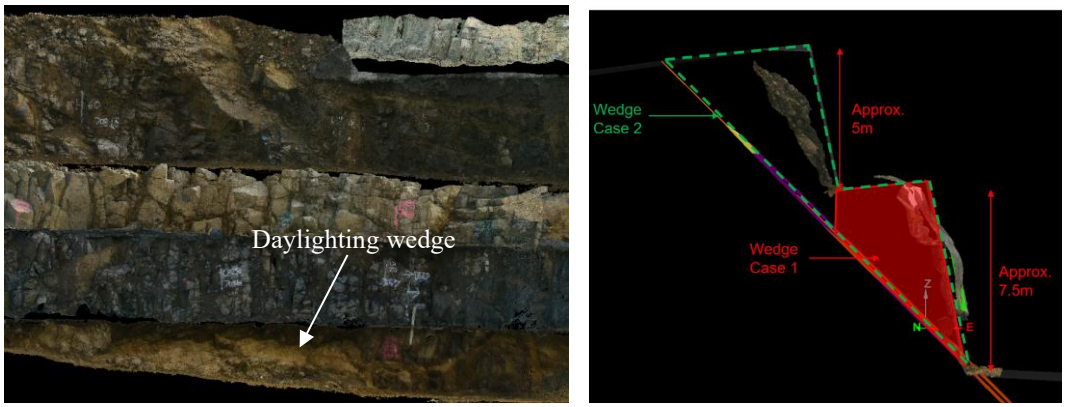


Figure 6 Visualisation of daylighting wedge using TLS data allowing for review of kinematic sliding mechanisms and potential load cases.

While TLS scanning has proven to be highly beneficial, the following limitations are noted:
- Processing and cleaning high-resolution point clouds can be a time-intensive exercise requiring high computational effort.
- Trials involving multiple underground scans did not always produce accurate true colour datasets. However, the intensity (reflectance) data provides redundancy and perspective to supplement interpretations.
- Single scans occasionally resulted in small data gaps behind protruding rock or recesses. These were considered minor and were supplemented with photos and visual mapping.

2.4 *LiDAR equipped tablets*

The use of LiDAR-equipped tablets or phones can provide a quick, cheap and accessible alternative to survey grade TLS. The simplicity of data collection means scans can be performed by CPS personnel, eliminating the need for surveyors. Data can be uploaded within minutes over Wi-Fi, enabling remote teams to commence near real time reviews, leading to rapid decision making. LiDAR-equipped iPads scans were performed by CPS on Brisbane's Cross River Rail project and integrated into a 3D model delivering the following project benefits:
- Improved continuity in mapping, especially where excavation and support occurred in small increments due to construction constraints.
- Since scans could be rapidly shared with remote design teams, potential wedge volumes and support requirements were assessed in real time, reducing construction delays.
- As an example, scans of a mined tunnel invert foundation were captured on-site and transmitted within minutes to the design office, where removal and replacement of weak material beyond the stated design tolerances could be confirmed, see Figure 7. The as-built slab treatment could also be compared against pre-treatment scans, ensuring design compliance without requiring on-site survey support. This enabled quick validation of prescribed treatments and reduced delays.

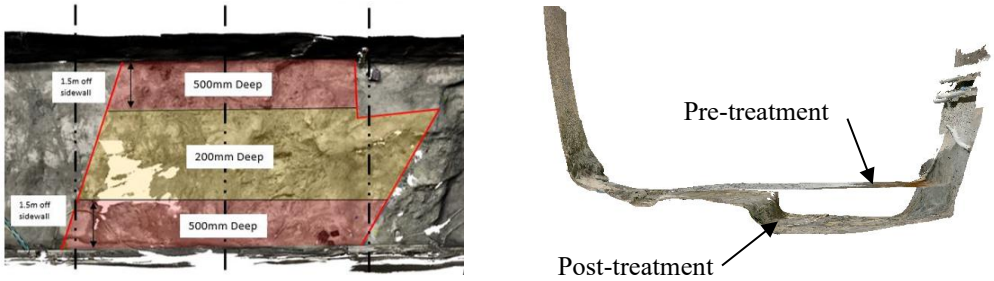


Figure 7 Example slab foundation material excavation directed from scans (left) and assessed in cross-section (right)

However, collection methods and the accuracy of this LiDAR scanning methodology have notable limitations:

- Tablet acquired scans produced lower resolution datasets compared with professional grade scanning equipment.
- The scale of the subject was limited to approximately 50m^2 per scan to minimise distortion.
- Control points were often not immediately available following excavation, aligning scan data accurately was difficult. Wall chainage and floor level are typically provided for geotechnical mapping, limiting scan alignments to approximately +/- 300mm.
- Scan acquisition requires careful planning to ensure consistent face offsets are maintained without doubling back on early captures using a sweeping type motion. This proves particularly challenging when capturing blocky rock mass in an excavated face. This is therefore impractical for tunnel headings and walls greater than 3m height while also contending with "unsupported ground".

Despite these limitations, LiDAR-based tablet scanning has proven to be a highly effective and cost-efficient solution for specific geotechnical purposes.

2.5 *Time comparison*

Time spent on the critical construction path and post-processing of scans are key considerations when considering adoption of specific methods. Table 1 compares scanning times for a typical tunnel advance and surface excavation (approximately 60m^2 area) using the respective data acquisition techniques. As technologies advance and equipment becomes lighter and more efficient, these will only continue to improve.

Table 1. Scanning and processing time comparison

	Tunnel		Surface excavation	
Method	Total scan time (minutes)	Post-processing (minutes)	Total scan time (minutes)	Post-processing (minutes)
LiDAR equipped tablet	Not applicable		5-10	10-20
Professional survey grade laser scanning	10-25	50-70	10-20	50-70
SfM photogrammetry	10-20	50-120	10-20	50-120

3 SOFTWARE DEVELOPMENT

The effective use of TLS and photogrammetry in geotechnical workflows relies on the capability of post-processing and visualisation software. Software packages vary in their ability to process point clouds, efficiently extract geotechnical features, and integrate with 3D geological modelling platforms.

3.1 *Automated and semi-automated mapping software*

Automated structure picking tools are becoming increasingly common with many CPS workflows adopting these as a means of supplementing traditional mapping data. These packages work by querying surrounding points to fit planes and generate discontinuity sets from point cloud data. This process is especially valuable in blocky rock masses or within in drill and blast excavation, where defects are typically well expressed in the excavated face and manual mapping can be time-consuming. However, users must be conscious of input assumptions used by structure picking algorithms which include:

- Algorithms favour defects with well-exposed surfaces, where a larger number of surrounding points are available to define a plane.
- True discontinuities that do not present a clear planar face in the scan, such as thin seams, tight fractures, or features sub-parallel to the scan angle, are often under sampled. Its effectiveness therefore decreases significantly in smooth excavation environments (e.g., roadheader, rotary cutter, or smooth blasting).
- The sensitivity of the defect search function (e.g., smoothing parameters and minimum point count for plane fitting) creates a trade-off between accuracy of captured planes and picking up defects that are not well expressed in the face. Smooth excavated surfaces may mistakenly be interpreted as valid discontinuities.
- Its effectiveness decreases with increasing scan area.

As with any automated process there must be QA/QC processes employed with regular review using field data to calibrate and maintain accuracy of outputs. Typical post-processing workflows included the following to mitigate these limitations:

- Filtering discontinuities based on total area to avoid over-interpretation of spurious features.
- Validating automatically identified structures against field mapping records.
- Manually querying and cross-correlating additional defects using 3D geotechnical modelling software that were not captured by the automated picking process.

While automated structure picking is not a substitute for experienced engineering judgement, it is a useful tool for supplementing face mapping in appropriate conditions. As software and processing algorithms continue to advance, the accuracy and reliability of automated defect mapping are expected to improve.

Semi-automated digital mapping tools, such as 3GSM's ShapeMetrix, are inherently integrated with engineering judgement throughout the mapping process. They can be a useful tool for faster and more accurate remote mapping while creating reliable inputs for inclusion into as-built engineering geological model and subsequent geotechnical analysis, including:

- Defect set clustering and statistical analysis.
- True defect spacing measurements on planes orthogonal to the defect orientation.
- Defect plane mesh generation to measure waviness.

3.2 *3D visualization software*

Scanned construction data forms the foundation for a digital twin of the asset, supporting project-wide collaboration, enhanced QA capabilities, and future maintenance planning and asset management. 3D geotechnical software packages (e.g Maptek Geologycore) are often used for geotechnical digital twin models where it can be integrated with site investigation and design data, see Figure 8. On some projects, digital twins may be kept on federated platforms due to the need for cross-disciplinary, real-time collaboration, and integration with BIM, structural, and operational systems. Federated platforms, for example Autodesk Navisworks, provide the advantage of readily sharing and viewing of data, and are future-proofed for file longevity to be used in operation and maintenance of the asset.

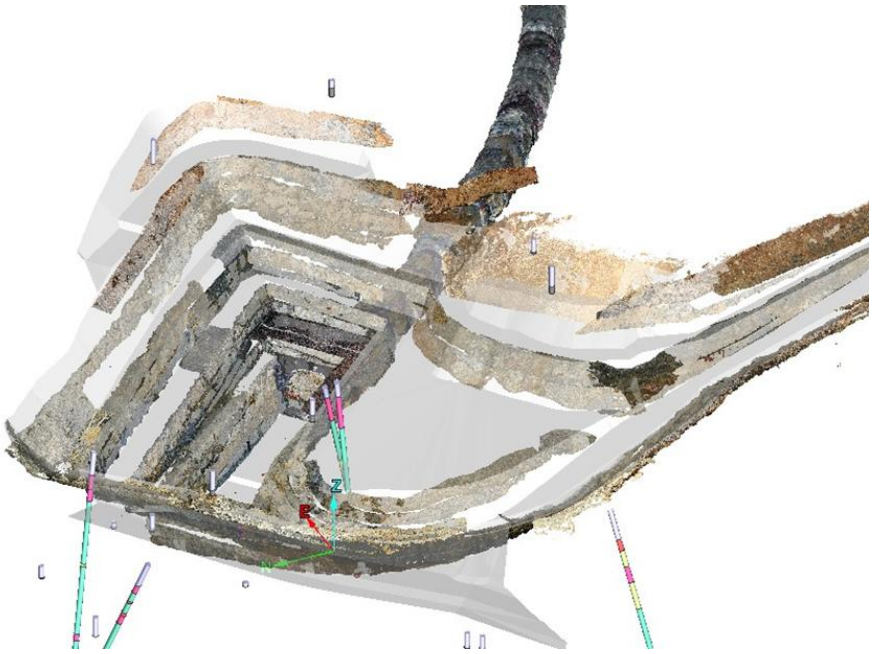


Figure 8. 3D geotechnical model including TLS rock face scans integrated with design geometry (in transparent grey) and available site investigation (borehole) data.

4 CURRENT WORKFLOW

The workflow presented in Figure 9 was developed to incorporate field inspection, TLS scanning, and 3D model refinement. It is important to note that the benefits and limitations of digital tools vary across every project, and the workflow development should be objectively driven.

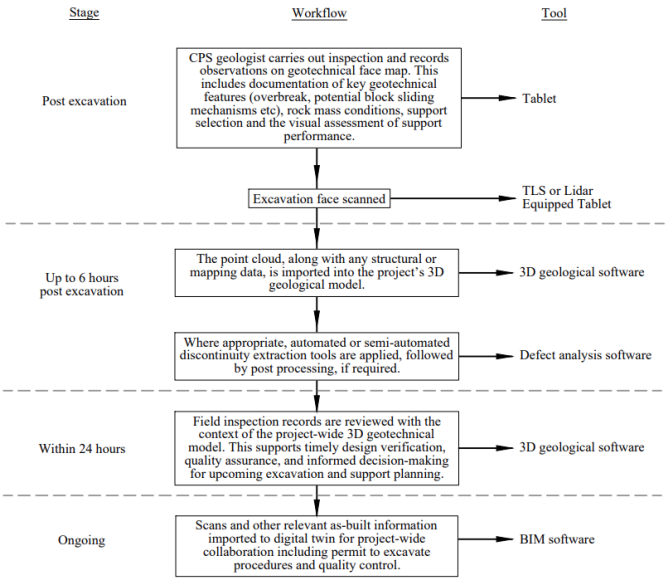


Figure 9 CPS workflow incorporating digital tools

5 CONCLUSIONS

Digital tools are transforming geotechnical construction workflows by enabling faster and more accurate visualization of ground conditions, and more collaborative decision-making during construction. When used poorly, 3D scanning can result in 'pretty pictures' without accurate data and

timely construction support. When developing a CPS workflow for a project, the benefits and limitations of each tool should be considered along with ground conditions, site conditions, project objectives and project constraints. In the opinion of the authors:

- Survey-grade TLS remains the preferred option, where budget allows, as it is more practical for use on site, can be integrated with survey workflows, and its accuracy and repeatability supports high-confidence model and design verification.
- Handheld LiDAR offers a low-cost and less resource-intense alternative to TLS in surface excavations where budgets are constrained, and a lower scan accuracy can be accepted. It can provide adequate detail for face mapping, support assessment and design validation.
- Photogrammetry offers the advantage of low setup costs and minimal hardware requirements, making it a viable option if sufficient lighting and a low dust environment can reliably be provided. However, photogrammetry outputs offer limited additional benefit compared to TLS in typical construction settings. Due to its inconsistent reliability in real-world tunnel conditions, photogrammetry is not currently considered the preferred option.
- Supplementing traditional face mapping with automated or semi-automated mapping software can provide useful outputs for geotechnical analysis and design verification, if the limitations are understood and accounted for.
- Integrating scans and other data captured on site into a 3D geological model and/or digital twin is beneficial for stakeholder decision making during construction and operation.

The broader implementation of these technologies brings demonstrated benefits to geotechnical workflows, construction outcomes and operational management. Addressing the remaining challenges requires continued software development, improved integration with design platforms, and clearer guidance for tool selection and workflow design.

6 REFERENCES

Duffy, B., Macklin, S., Henry, B. & Macintosh, K. 2023. The use of laser scanning and photogrammetry in remote mapping of rock tunnels. *Australasian Tunnelling Society Conference*. Auckland, 5-8 November.

Flyvbjerg, B. 2014. What you should know about megaprojects and why: An overview. Project Management Journal 45(2): 6–21. https://doi.org/10.1002/pmj.21409

García-Luna, R., Senent, S., Jurado-Piña, R. & Jimenez, R. 2019. Structure from Motion photogrammetry to characterize underground rock masses: Experiences from two real tunnels. Tunnelling and Underground Space Technology 83: 262–273. https://doi.org/10.1016/j.tust.2018.09.026

Linder, W. 2009. Digital photogrammetry: A practical course. Berlin: Springer Science & Business Media.

Membah, J. & Asa, E. 2015. Estimating cost for transportation tunnel projects: A systematic literature review. International Journal of Construction Management 15(3): 196–218. https://doi.org/10.1080/15623599.2015.1067345

Nowicki, A.L. 1942. Stereoscopy. Photogrammetric Engineering: 181–202.

Paraskevopoulou, C. & Boutsis, G. 2020. Cost overruns in tunnelling projects: Investigating the impact of geological and geotechnical uncertainty using case studies. Infrastructures 5(9): 73. https://doi.org/10.3390/infrastructures5090073

Potter, B., Blaise, A., Requiliani, B., Guevara, E. & Stariha, K. 2025. Case study on Snowy 2.0, Australia: Use of LiDAR and endoscopy for assessing and modelling geological features in underground caverns. In: Proceedings of the Australasian Conference on Engineering Geology (ACEG 2025), Sydney, Australia.

Sanfilippo, R., Esfandiari, M., Foria, F., Garbutt, D., Glab, K., Karlovšek, J., Menozzi, A., Paskaleva, G. & Robert, F. 2025. ITA – AITES tunnelling information modelling – A BIM approach for a sustainable life cycle management. *Tunnelling and Underground Space Technology* 165: 106711. https://doi.org/10.1016/j.tust.2025.106711

Sharma, A. & Gupta, R. 2020. Analysis of factors affecting cost and time overruns in construction projects. In: Proceedings of the International Conference on Sustainable Construction Technologies and Advancements in Civil Engineering. Singapore: Springer: 59–70. https://doi.org/10.1007/978-981-33-6969-6_6

Wang, X., Zhang, J. & Li, Q. 2023. Application of TLS in underground construction: Advances and challenges. Journal of Geotechnical and Geoenvironmental Engineering 149(3): 04023025. https://doi.org/10.1061/JGGEFK.0001675

Westoby, M.J., Brasington, J., Glasser, N.F., Hambrey, M.J. & Reynolds, J.M. 2012. Structure-from-Motion photogrammetry: A low-cost, effective tool for geoscience applications. Geomorphology 179: 300–314. https://doi.org/10.1016/j.geomorph.2012.08.021

19th Australasian Tunnelling Conference – Acosta-Martínez, Stewart and Hudson-Smith (Eds.)
© 2025 Australian Tunnelling Society, ISBN 978-0-85825-002-4

The hidden engine of project success: Best practices for managing large 3D models and 2D documentation in infrastructure projects

E. Saminfar
Delve Underground, Melbourne, Australia

C. Holt & J. Bateman
Delve Underground, Sydney, Australia

E. Westergren
Delve Underground, Cleveland, USA

ABSTRACT: Managing large 3D models and 2D documentation effectively is essential to enable efficient delivery of complex infrastructure projects. The scale and complexity of modern projects introduce challenges such as maintaining consistency, minimising errors, and supporting collaboration across multidisciplinary teams. This paper presents best practices for handling extensive digital models and the associated documentation, focusing on optimising workflows and improving outcomes. Key topics include file performance, version control, data structuring, documentation standards, cloud-based collaboration, and practical approaches to resolving interoperability issues. The role of automation in streamlining tasks and improving model reliability is also explored. In addition, the paper highlights the human factors that influence Building Information Modelling (BIM) success, such as leadership, team trust, and mindset. By implementing these strategies, organisations can achieve greater accuracy, efficiency, and coordination, leading to better project delivery and long-term value in infrastructure development.

1 INTRODUCTION

Across the globe, infrastructure projects are expanding in scale, ambition, and complexity. From underground tunnels and high-speed railways to massive bridges and utility networks, the physical assets we design and build increasingly rely on equally complex digital models. At the heart of these digital twins are 3D models and 2D documentation, which are crucial tools for design, coordination, procurement, construction, and operations. However, managing these models effectively is a daunting task that can either accelerate success or derail entire projects.

Why do some teams consistently deliver accurate, timely models while others struggle with bloated files, version conflicts, and coordination nightmares? What separates high-performing digital engineering teams from those drowning in technical debt and miscommunication? The answers lie not in software licenses or flashy presentations but in the less glamorous terrain of workflows, standards, habits, culture, and leadership.

Because "BIM" is such a broad and often misunderstood term, it's essential to clarify its meaning at the outset of any project. In this paper, BIM refers not only to the 3D model itself, but to the structured processes, data standards, and collaborative workflows that support the full lifecycle of an asset—from concept design through to construction, operation, and maintenance. This definition ensures that when we discuss BIM in the following sections, we are referring to a coordinated approach that integrates people, processes, and technology toward shared project goals.

This paper is for every engineer, modeler, BIM manager, and project leader who has opened a 2GB file only to watch it crash. For every project that's lost hours chasing missing parameters, redrawing clumsy details, or untangling corrupted links. It offers a practical, experience-based roadmap grounded in real project environments, shaped by lessons learned through both success and failure. The goal is to provide clear, actionable strategies that support more resilient and efficient digital delivery across teams and disciplines.

Managing large 3D models and 2D documentation is not just a technical issue, it's a collaborative discipline. It's about anticipating complexity, managing performance and aligning teams with the bigger picture. This paper outlines not only what can go wrong but more importantly, what to do about it. We unpack the pitfalls and bottlenecks that plague projects and provide real-world solutions that can be applied immediately.

If you're prepared to rethink your digital approach, enhance productivity, and future-proof project delivery, this paper offers a pathway forward. It's not merely about improving models—it's about achieving better outcomes, building stronger teams, and ultimately delivering superior infrastructure for the communities we serve.

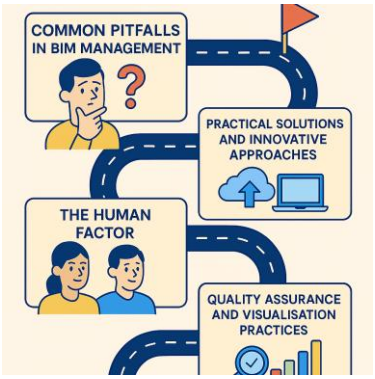


Figure 1. Visual overview of the paper's purpose.

2 COMMON PITFALLS IN BIM MANAGEMENT

While BIM offers powerful capabilities, it is not immune to pitfalls that often emerge across infrastructure projects. These challenges, if not identified and addressed early can ripple through project phases, compounding into costly delays, coordination breakdowns and missed opportunities for optimisation. Many of these pitfalls are not purely technical but rooted in implementation, communication, and human behavior.

What begins as a minor oversight, like inconsistent model structuring, unclear roles or lack of process ownership can grow into significant project risks if left unmanaged. Recognising these issues in their early stages allows teams to apply targeted solutions before they escalate. It also helps build a culture of accountability, where lessons are captured, shared, and embedded into future practice.

The sections that follow explore some of the most common pitfalls encountered across BIM-enabled projects. Alongside each challenge, practical insights are offered to demonstrate their real-world consequences and provide a foundation for more resilient, efficient digital delivery.



Figure 2. A summary of typical challenges in BIM management.

2.1 *Lack of strategy*

Many BIM initiatives falter due to the absence of a clear strategic direction. Too often, BIM is treated as a standalone technical tool or a software deployment exercise rather than a core component of the project's delivery strategy. However, BIM's true value emerges when it is directly aligned with overarching business objectives, such as cost efficiency, risk reduction, sustainability targets or improved asset performance.

A well-defined BIM strategy should begin by answering some key questions: What problems are we solving with BIM? How will success be measured? How does BIM contribute to the broader project and organisational goals? The answers to these questions should be translated into clear, measurable Key Performance Indicators (KPIs) that can be tracked over the lifecycle of a project.

Another critical step at this stage is to identify the required software, integration points, and potential limitations early in the project. Understanding how platforms will interact and resolving compatibility issues upfront helps prevent costly delays and workflow disruptions later in the lifecycle.

Without this alignment, BIM risks becoming a siloed effort, technically impressive but disconnected from the real project value. This leads to fragmented implementation, reduced team buy-in and missed opportunities for integration with procurement, construction and asset management systems.

Firms that approach BIM as a strategic enabler rather than a side initiative see markedly better outcomes. For example, organisations that connect BIM outputs to functions like cost estimation, construction phasing and risk forecasting often report stronger stakeholder confidence, improved project visibility and increased access to funding or internal investment. In these cases, BIM is no longer just a modelling exercise; it becomes a driver of performance and a tool for informed decision-making across the project's lifecycle.

2.2 *Neglecting people and change management*

BIM is 80% about people and only 20% about technology. Yet, many initiatives focus too much on tools and not enough on engaging the people using them. Resistance often arises when teams are informed, but not involved, and when changes are imposed rather than introduced through dialogue and collaboration.

Effective BIM leaders prioritise clear communication and ensure that all stakeholders understand not only what is changing but why it matters to them. Involving team members early will build ownership and reduce resistance.

Investing in internal champion team members who advocate for BIM and guide others through challenges can improve adoption significantly. Pairing this with peer mentoring and structured onboarding helps teams adapt more quickly and confidently.

Digital transformation is as much about mindset as it is about tools. Without attention to change management, even the best systems can struggle to deliver their full value.

2.3 *Overengineering processes*

Overcomplicated workflows, excessive documentation and poorly written Digital Engineering Management Plan (DEMP) hinder rather than help.

Best practices favour clarity and simplicity, designing processes that are intuitive, repeatable and scalable. Teams that document fewer but clearer protocols experience fewer coordination errors and faster onboarding.

2.4 *Failing to demonstrate ROI*

A critical oversight is the failure to link BIM efforts to tangible outcomes such as cost savings, risk reduction and productivity gains. Business leaders require a clear value proposition to support and expand BIM initiatives. Projects that align BIM reporting with project KPIs, such as earned value management or safety compliance, gain broader organisational support.

2.5 *Underestimating risk management*

Overlooking small risks, such as outdated software, duplicate elements or insufficient training, can lead to major disruptions in project timelines and budgets. To manage these risks effectively, BIM leaders should create digital risk registers, enforce strict version control and conduct regular audits of models and documentation. These practices help teams detect and resolve issues early, reducing the chance of costly rework or delays. Proactive risk management isn't just about avoiding problems, it plays a vital role in ensuring smooth, successful project delivery.

3 PRACTICAL SOLUTIONS AND INNOVATIVE APPROACHES

In response to the challenges described earlier, this section offers hands-on strategies drawn from real-world implementation across major infrastructure programs. These practices aim to empower teams with clear, scalable and efficient methodologies that foster collaboration and reduce rework. Examples and case-driven evidence accompany the approaches to provide clarity and guidance.



Figure 3. Practical solutions and innovative approaches.

3.1 *Streamlining workflows*

Efficiency comes from smart systems, not complex ones. Automation scripts, standardised templates and the intelligent use of software features can eliminate redundant tasks. For example, scripts in Revit or Dynamo can reduce modelling time by up to 80%, and templates prevent manual data entry errors. Grasshopper in Rhino enables rule-based geometry generation, making it ideal for infrastructure elements like tunnels or bridges (Saminfar 2023).

Sometimes, laziness sparks innovation. When experts look for shortcuts, they often create better templates, workflows and automation. Taking time to step back and rethink can lead to sharper insights and priorities, turning "lazy" moments into long-term efficiency.

3.2 *Embracing cloud-based collaboration*

Performance issues, such as slow Revit files, often stem from legacy server setups. Moving central files to cloud platforms like Autodesk Construction Cloud or BIM 360 can reduce syncing times, enhance cross-team collaboration and prevent costly delays. Cloud-based workflows also facilitate version control, access logging and rollback in case of corruption.

To make BIM teamwork less stressful, teams should start with purpose, clarity and passion. Purpose gives direction. Clarity ensures alignment. Passion drives innovation.

3.3 *Clarifying documentation standards*

The 2D documentation must align with the 3D models, follow clear CAD standards and support regulatory compliance. The use of view templates, sheet sets and revision tracking contributes to consistency, traceability and review readiness. Developing discipline-specific drawing lists and checklists ensures standardisation across teams and packages.

Better documentation is not just about compliance; it's also about clarity. Clarity reduces rework, speeds approvals and improves team morale.

3.4 *Overcoming IFC and interoperability challenge*

Interoperability issues are often blamed on file formats like industry foundation classes (IFC). However, the root cause is often outdated workflows and a resistance to process evolution. A mindset shift, focused on structure, clarity and discipline, is critical.
Improving user habits and investing in user training can dramatically improve outcomes.

The Architecture, Engineering, and Construction (AEC) industry has evolved from a black-and-white picture into a rich, colourful digital canvas, thanks to BIM. Today, roles like BIM coordinators, computational designers and data analysts are reshaping how we work, bringing diversity and innovation to the forefront.

4 THE HUMAN FACTOR

While tools, platforms and standards form the visible structure of digital engineering, the true engine of successful BIM implementation lies in its people. The human factor is often underestimated, but it is what transforms good systems into great outcomes. Technology alone cannot resolve communication breakdowns, unclear responsibilities, or a lack of trust. For large-scale infrastructure projects, the ability of teams to collaborate effectively, adapt to change and uphold shared values is just as critical as the models they produce.

This section explores the core human elements that underpin digital delivery: trust, mindset and leadership. High-performing BIM teams are built on open communication, mutual respect and a shared understanding of purpose. Team members are more likely to contribute their best when they feel heard, supported and empowered to grow.

Fostering the right culture takes more than motivation, it requires intention. Leaders must set the tone by aligning teams early, promoting accountability, simplifying complexity and encouraging continuous learning. When the human side of digital delivery is strong, technical challenges become easier to solve and innovation becomes a natural outcome.

In short, the strength of BIM systems will always reflect the strength of people.



Figure 4. The human factor.

4.1 *Building trust in teams*

The foundation of collaboration is trust, not tools, software, or individual skillsets. In high-performing BIM environments, trust is what allows technical systems to function effectively across disciplines. Teams thrive when members consistently deliver on their commitments, acknowledge mistakes without blame and maintain open, respectful communication. Without this foundation, even the most advanced digital platforms and workflows can fall apart under pressure.

Trust empowers individuals to speak up when something isn't working, to challenge ideas constructively and to support one another through tight deadlines and complex problems. It enables faster resolution of issues, smoother coordination across disciplines and greater innovation because people feel safe to test ideas and propose improvements.

Strong BIM teams are neither shark tanks nor petting zoos. Shark tanks breed internal competition and defensiveness, while petting zoos prioritize comfort over progress. High-functioning teams strike a balance, value clarity, welcome healthy debate and align around a common purpose. This dynamic culture is essential to turning a collection of skilled individuals into a resilient, collaborative force capable of delivering complex infrastructure with confidence and consistency.

4.2 *Cultivating the right mindset*

BIM's success doesn't hinge on high-end workstations or fancy (expensive) software platforms. It's driven by a mindset of continuous improvement. At its core, successful digital delivery is not just technical; it's cultural. It begins with how teams think, how they learn and how they adapt.

Leaders play a crucial role in shaping this mindset. They must empower their teams to ask better questions, align early in the project lifecycle and communicate clearly across disciplines, whether it's between designers, contractors, operators or clients. True digital transformation happens when people shift from reactive to proactive, from siloed thinking to collective problem-solving.

Importantly, mindset influences longevity. Projects often span years and evolve over phases. A team's ability to maintain clarity, motivation and collaboration throughout that journey hinges on its willingness to learn, reflect and reset. Creating a culture of feedback, where lessons are captured, mistakes are discussed constructively and wins are shared, ensures long-term alignment and growth.

Each new year, a project phase or challenge presents an opportunity to reset, not just workflows, but attitudes. Replacing fear with curiosity, complaints with gratitude and blame with ownership fuels both professional and personal development. The most successful BIM teams understand that every technical breakthrough is rooted in a human one. A better BIM begins with a better mindset and that mindset begins with leadership.

4.3 *Leading by example*

Leadership in BIM is not just about mastering tools or managing models. It's about shaping how teams think, work and collaborate. A great BIM manager doesn't simply oversee digital workflows; they actively remove roadblocks, simplify processes and foster an environment where digital systems feel intuitive and supportive, not overwhelming or restrictive.

While the terms "manager" and "leader" are often used interchangeably, they represent different approaches. A manager primarily focuses on planning, organising, and ensuring tasks are completed to specification and on time — maintaining systems, schedules, and compliance. A leader, on the other hand, inspires, influences, and empowers people to exceed expectations. Managers tend to direct; leaders guide. In BIM, effective delivery benefits from both: the structure and accountability of good management, and the vision, adaptability, and trust-building of strong leadership.

True leadership means leading by example. That involves staying curious and adaptable as technologies evolve but also staying grounded in the human side of delivery. Great BIM leaders champion simplicity over sophistication. They streamline instead of stacking layers of complexity. They focus not on controlling every detail, but on creating systems and habits that empower others to work confidently and independently.

Crucially, impactful BIM leaders engage across the full spectrum of project functions, from design and engineering to procurement, construction and asset management. This cross-functional visibility enables them to align digital efforts with project strategy and client goals. They become connectors who help translate technical details into business value.

Importantly, transforming a team doesn't require massive budgets or high-profile consultants. What it does require is structure: clearly defined roles, regular and honest feedback and a commitment to continuous learning. When leaders communicate clearly, set expectations and model accountability, they build trust. And when that trust is combined with vision and support, good teams evolve into great ones, capable of delivering digital outcomes that are not only efficient, but meaningful.

5 QUALITY ASSURANCE AND VISUALISATION PRACTICES

5.1 *Implementing robust QA/QC workflows*

Quality assurance (QA) and quality control (QC) in digital delivery extends far beyond simply verifying that a model looks correct on screen. They involve a comprehensive approach to ensuring that the information within the model is reliable, consistent and aligned with project requirements. This includes validating data integrity, enforcing correct naming conventions and ensuring all elements adhere to agreed protocols, such as BEP (BIM Execution Plan) standards and client-specific documentation guidelines.

Tools like Navisworks and Revizto are commonly used to support QA/QC processes. These platforms offer robust features such as visual clash detection, issue tracking and rule-based compliance checks that help identify coordination conflicts and non-compliant elements early in the workflow. Leveraging these tools enables teams to catch and resolve issues before they escalate into costly on-site problems.

Instituting a structured QA/QC cycle at defined project milestones—such as design freeze, coordination review or pre-issue submission, ensures consistency and accountability across disciplines. Peer reviews, driven by checklists tailored to each project's scope, add a valuable layer of oversight. When combined with automation tools, such as Dynamo scripts or rule-based validation engines, these practices help reduce the time and risk associated with manual checking while increasing repeatability and confidence in the output.

Ultimately, incorporating tested QA/QC measures into the digital workflow is not just about compliance, it's about ensuring the final deliverables are technically sound, contractually aligned and ready for downstream use in procurement, construction and asset management. (Saminfar 2024).

5.2 *Visualisation for decision-making*

Model-based decision-making is significantly enhanced through the use of high-quality visualisation tools. These tools transform technical models into accessible, interactive experiences that support clearer communication and faster consensus-building. Renderings, animations, real-time simulations and VR walk-throughs help stakeholders, especially non-technical ones, understand design intent, identify spatial challenges and assess safety or sequencing risks that might otherwise be overlooked in traditional documentation.

Visualisation isn't just a presentation tool; it's a powerful decision-making aid. Platforms such as Twinmotion enable teams to generate immersive, real-time outputs that convey design, construction phasing and site logistics in a way that 2D drawings or even 3D models cannot. These tools bridge the gap between disciplines, allowing designers, contractors and clients to share a common visual language.

When applied early in the design process, visualisations are particularly valuable. They allow stakeholders to explore options, raise concerns and request adjustments while changes are still relatively easy and inexpensive to make. This proactive clarity reduces the likelihood of costly rework during construction and accelerates approval cycles by increasing stakeholder confidence and engagement.

By integrating visualisation into project workflows, teams can turn models into meaningful narratives that support better decisions, faster feedback loops and more aligned project outcomes.

6 CONCLUSION

BIM is not a magic button. It is a structured, strategic framework that, when implemented thoughtfully, enhances visibility into evolving design intent, which increases predictability in construction realities. It supports collaboration and accountability for stakeholders throughout the lifecycle of complex infrastructure projects. It is not just about 3D modeling or producing drawings. Rather, BIM is about integrating information, aligning teams and delivering coordinated, data-driven decisions that reduce risk and add value at every stage of a project.

As this paper outlined, managing large 3D models and 2D documentation effectively requires more than just technical expertise. It demands a well-defined strategy, clear standards, streamlined

workflows, and most importantly a focus on people. Projects often falter not because of technical limitations, but due to fragmented communication, uncoordinated models, or resistance to change. Addressing these challenges holistically is essential to move from reactive problem-solving to proactive delivery.

The practical solutions and lessons shared, such as embracing cloud collaboration, using scripting and automation, improving documentation protocols and fostering a culture of trust, are based on real-world experiences. These aren't theoretical ideals; they are tested strategies that have helped teams deliver major infrastructure outcomes on time, within budget and to a high standard of quality.

Moreover, the influence of the human factor cannot be overstated. Projects succeed when people are empowered, respected and aligned. By investing in leadership, communication and change management, organisations can ensure that their digital tools are supported by equally strong team dynamics. Trust, clarity and collaboration are not optional extras, they are the foundation upon which successful BIM implementation is built.

Ultimately, the path to success in managing large-scale digital models and documentation is not about having the latest tools but how those tools are used, by whom and within what context. In this sense, effective model and documentation management becomes the hidden engine of project success, quietly powering coordination, reducing risk and enabling smarter decisions from design through delivery.

By aligning digital practices with business goals, simplifying complexity, leveraging automation, securing data and fostering a supportive team culture, organisations can achieve more predictable outcomes, deliver higher-value projects and build better infrastructure for the communities they serve. The opportunity lies not just in managing models, but in mastering the systems, habits and mindsets that bring them to life.

ACKNOWLEDGMENTS

This paper would not have been possible without the generous support of Delve Underground, whose dedication to innovation and collaboration has been instrumental.

I would like to thank the firm for not only encouraging this research but also for providing everything our team needed, from tools and time to trust and flexibility, to explore and improve digital engineering practices.

A special thank you to Mark Trim for his valuable insights, encouragement and guidance throughout the preparation of this paper.

7 REFERENCES

Saminfar E, Westergren E, Behrens M and Bateman J. 2023. Computational modelling in developing digital models of large-scale underground infrastructure projects with a focus on the North East Link Tunnel works packages, in *Proceedings of the Australasian Tunnelling Conference 2023,* pp 685–694, Auckland, New Zealand, 5–8 November 2023.

Saminfar E, Westergren E, Fontana J, Bateman J and Trim M. 2024. Revolutionizing Australia's large underground infrastructure projects with digital engineering, in *Proceedings of the North American Tunnelling Conference,* pp 1032-1042, Nashville, USA, 23–26 June 2024.

19th Australasian Tunnelling Conference – Acosta-Martínez, Stewart and Hudson-Smith (Eds.)
© 2025 Australian Tunnelling Society, ISBN 978-0-85825-002-4

Automation of tunnel modelling for enhanced project efficiency

P. Bueno Leal, F. Calle Lamelas & F. Ceballos Martinez
TYPSA

ABSTRACT: Cross passage (XP) modelling in tunnel infrastructure projects has unique challenges due to their complex geometry, non-standard alignment, and high volume of repetition. Manual modelling of these structures in BIM environments is time-consuming and facilitates human error. This paper presents the development and implementation of a parametric automation tool designed to model cross passages efficiently using Rhino + Grasshopper. The tool originated from practical challenges in major projects, such as Stockholm Metro or Sydney Metro, where Revit's limitations highlighted the need for a more flexible solution. Developed collaboratively by TYPSA's BIM and Geotechnical teams, the automation enables fast, accurate generation of XP geometries adaptable to various tunnel alignments. By integrating this tool into real project workflows, TYPSA improved modelling speed, reduced errors, and enhanced BIM coordination. This article outlines the conventional challenges, the development process, the tool's structure and testing, and future improvements aimed at generalizing its use.

1 INTRODUCTION

1.1 *BIM Model History*

The graphical representation of civil infrastructure designs has experienced a huge transformation in the last years. From the handmade drawings developed during the XX century, the popularization of Computer-Aided Drawing (CAD) tools during the late 90s and early 2000s revolutionized the typical workflow. Design teams were required to adapt to the technologies, adopting in a short period of time not only the typical development of CAD 2D drawings, but the implementation of 3D models.

Nowadays the design of underground structures cannot be understood without the extensive use of Building Information Modelling tools. However, the implementation of AI-powered tools and automation workflows are still under development, requiring a constant adaptation of the techniques, tools and methodologies.

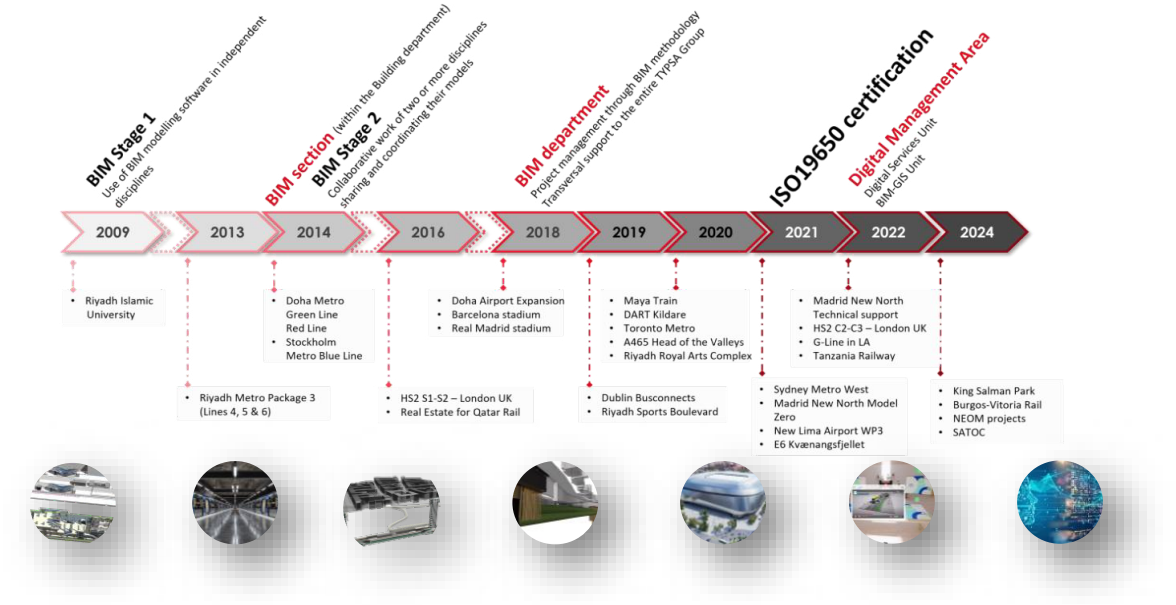


Figure 1. Evolution of BIM methodologies within the company TYPSA

1.2 BIM around the world

Despite BIM being a global methodology, its application differs across geographies. In Spain, BIM is heavily integrated with high modelling standards, and its early adoption gave rise to structured processes, specialist roles and the adoption of BIM methodology by public administrations. In North America, adoption is growing but still faces challenges related to standardization and training across project stakeholders.

Australia, on the other hand, has rapidly embraced digital processes, with demanding requirements from clients that have driven innovation and automation. The market's maturity has facilitated the adoption of advanced workflows, including data-rich models, automated validation processes, and integration with construction planning and digital twin strategies.

2 CONVENTIONAL MODELLING

2.1 *Repetitive tasks*

Modelling repetitive elements manually, especially the multiple cross passages (XP) that can exist in any linear infrastructure, involves highly repetitive workflows: copying geometries, adjusting slopes, and aligning with tunnel axes. Each cross passage is similar in function but unique in its geometry, requiring extensive manual adjustment. The workload escalates quickly, making the manual process time-consuming, inefficient and prone to fatigue-driven mistakes.

Moreover, manual modelling slows down coordination between disciplines, especially when late-stage design changes occur. Updating models one by one introduces a risk of inconsistencies, misalignments, or coordination errors with adjacent systems.

2.2 *Complex geometries*

The detail design of cross passages rarely follows a standard layout. They involve non-orthogonal geometries, varying slopes, and custom profiles. Additionally, non-standard geometries (such as elliptical surfaces) are typically used in some underground design traditions. Accurately modelling these using conventional tools like Revit is complex, as the software is designed for horizontal/vertical structures rather than linear infrastructure.

Tunnel projects often require the alignment of two or more tunnel axes at differing elevations and angles. Modelling the transition geometry between these requires spatial precision and adaptable logic—capabilities which standard BIM tools lack out-of-the-box. This leads to time-consuming workarounds that limit design agility.

2.3 *Human Errors*

Repetitive manual modelling, combined with complex geometries and coordination with multiple disciplines, often leads to human errors—misaligned components, missing elements, or naming inconsistencies. These errors introduce rework and increase review cycles.

Errors may not always be immediately visible in the model, but can propagate into documentation or clash detection, leading to on-site construction issues. Additionally, maintaining design intent across dozens of manual models becomes increasingly difficult without a controlled, automated system.

3 IMPLEMENTATION OF AUTOMATION

3.1 *Genesis*

The need for automation comes from difficulties faced during multiple projects, especially in those where Revit was preferred. Revit, being tailored to buildings, struggled to accommodate non-parallel tunnels with varying Z-coordinates. Civil 3D, with subassembly composer was considered and worked well for linear elements but not for unique features like cross passages. Bentley Suite (OpenRoads/Aecosim) proved effective for detailed geometry modelling; however, case-by-case adjustments and poor cross-discipline integration limit its practicality.

Inspired by product design workflows, the team turned to Rhino + Grasshopper. These tools allow parametric control of geometry using minimal inputs: tunnel alignments, XP types, and section templates. This provided both precision and speed. Early trials with Revit and Dynamo proved insufficient; the final setup used Rhino + Grasshopper, optionally integrated with Revit (via Rhino.Inside).

By using these tools, a cross passage could be generated automatically by simply defining connection points and a few parameters, drastically reducing modelling time and increasing flexibility. The switch from manual modelling to parametric logic marked a pivotal shift in how the team approached tunnel infrastructure.



Figure 2. Software researched

3.2 *Research and development*

Once the potential benefits of the automation tool were identified, a collaborative team was assembled, combining expertise from TYPSA's BIM and Geotechnical departments, with support from a Grasshopper specialist. Although the development was overseen by TYPSA's R&D Committee, it was primarily driven by practical project demands rather than a formal research framework. This allowed for a fast-paced and iterative process, where an agile working environment enabled rapid prototyping and continuous feedback.

Lessons from early testing cycles were quickly incorporated, creating an effective feedback loop that significantly strengthened the tool's robustness within a short timeframe. The initial draft of the Grasshopper workflow was developed in approximately two weeks. The final version was completed two weeks later, and the solution can now be integrated into new projects in just one week.

3.3 *Multidisciplinary approach*

The collaboration between tunnel engineers and digital specialists was smooth and effective. Geotechnical engineers defined the required outputs in terms of geometry, constraints and requirements, while the digital team translated these into parametric rules that allow, by means of simple tasks and logic and geometrical relationships, the definition of the solution.

Although weekly meetings and test iterations allowed the team to develop a solution naturally, the close collaboration and the continuous communication between the team members was key for the success of the initiative.

This type of integrated approach exemplifies how BIM can bridge domain expertise. Rather than separating roles, the project benefited from shared ownership, with both teams working closely to ensure the generated models met geometric, constructability, and information requirements.

4 AUTOMATION TESTING

4.1 *First tests and limitations*

Initial tests were promising. Geometry aligned correctly, and elements fit into place. However, when new alignments or sections were introduced, unexpected errors emerged—mostly due to Grasshopper's internal logic. For example, tangency or coinciding curves would cause the software to misinterpret intersections. Debugging became essential. Despite this, the tool showed the potential, being fast and improving consistency.

4.1.1 *Slope and Tunnel Geometry*

One major limitation in Revit was its inability to handle non-parallel tunnels in different Z-levels (sloped XP). Grasshopper, however, handled this seamlessly, allowing accurate interpolation between tunnel axes.

Additionally, the use of 3D curve logic enabled the tool to automatically adapt the XP orientation to the local slope and rotation of each tunnel pair, ensuring consistency with the project's geometric constraints

4.1.2 *Curve Logic and Debugging*

Many failures were due to geometric edge cases. Grasshopper treats curves with overlapping endpoints as not intersecting, which caused certain operations to fail. These were solved through careful input conditioning and script logic updates.

4.1.3 *Grasshopper Limitations*

Grasshopper still has some limitations; it is necessary to script the model in a cautious way previewing all the steps in order to make sure everything is correct.

- Grasshopper works with geometric objects but not metadata. Attributes need to be added post-modelling.
- Input order (curve direction, point index) is critical and must be controlled.
- The tool must be adapted to each project's XP types.
- Assigning BIM data requires extra steps—either via IFC scripting (e.g., Python) or through Revit integration using Rhino.Inside.

Despite these limitations, the benefits of the automation far outweigh the manual alternative. The current approach balances technical flexibility with real-world constraints, making it scalable for a wide range of projects.

4.2 *Modelling Workflow*

This workflow describes the step-by-step process followed to develop the automated system for generating 3D models of cross passages using Rhino and Grasshopper. The goal was to streamline the modelling process, ensure design compliance, and allow for rapid updates based on input changes.

4.2.1 *Input Data*

The input data are the variables that define the Cross Passage and locate it in the correct location. If any of these variables change, the Cross Passage updates automatically.

- Tunnel alignment data (main tunnel centerline) from CAD or GIS formats.
- Tunnel radius
- Cross Passages Cross-Sections, including collar (if required) and central.
- Cross Passages Chainages: The chainages of each Cross Passage
- Other geometrical data defined in the next sections.

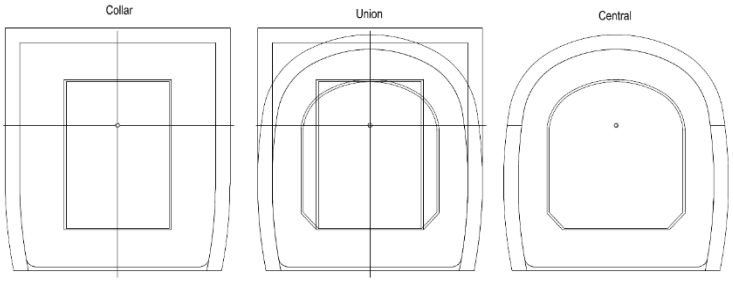


Figure 3. Collar body workflow

4.2.2 *Collar Methodology Script*

The first step in the scripting process focuses on generating the collars at both ends of the cross passage. The process begins by placing the cross-section profile at the specified chainage along the tunnel alignment. This section is then oriented vertically, ensuring correct alignment for further geometry generation.

To define the plane of the cross-section, a perpendicular vector to the tunnel alignment at the specified chainage is calculated. This vector lies in the horizontal plane (i.e., it has no Z-component), ensuring that the cross section remains upright regardless of tunnel slope.

Once the cross-section has been positioned and oriented, the next step is to generate the collar volume. This is done by:

Extruding the cross-section along the orientation vector (defined earlier) for a distance equal to the Collar Length plus the External Radius of the Tunnel. This ensures that the collar fully intersects the tunnel lining.

If the tunnel rings are not provided as input geometry, they are generated parametrically based on the tunnel alignment and known section dimensions. The extruded collar solid is then trimmed by subtracting the tunnel rings from it, using Boolean operations. This process creates a collar that precisely fits the tunnel interface, avoiding overlaps or clashes with the existing structure.

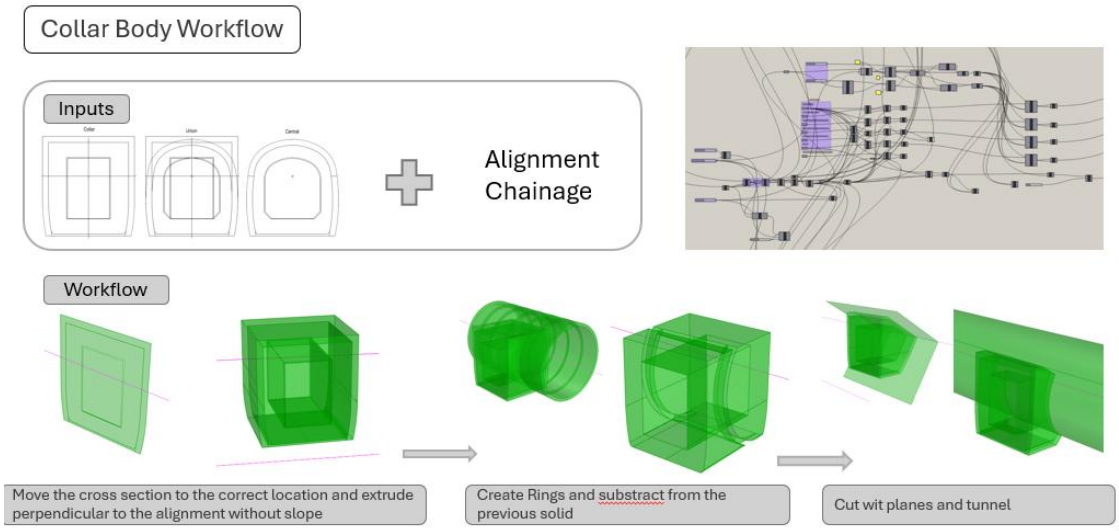


Figure 4. Collar body workflow

This collar serves as the starting point for further modelling steps, such as generating the transition geometry between both tunnel ends.

To finalize the collar geometry and ensure it integrates seamlessly with the tunnel, Cutting Planes are created at the collar's inner and outer limits, aligned with the tunnel geometry and cross passage axis. These planes define the start and end of the collar within the tunnel body.

The tunnel body (whether imported or generated) is used as a reference to trim the collar solid, ensuring it aligns correctly with the tunnel lining and does not extend beyond intended boundaries. Boolean operations are applied to perform a precise subtraction, resulting in a clean, clash-free collar that fits perfectly within the federated tunnel model.

4.2.3 *Center Body Generation Script*

With the collar geometry completed, the next step is to script the central body of the cross passage that connects both collars. This requires establishing a set of reference planes to guide the geometry generation.

Two planes are taken directly from the end faces of each collar, preserving their orientation and alignment with the main tunnel axes. A third plane is constructed perpendicular to the segment connecting the centre points of the two collar ends. These three planes serve as the control sections for interpolating the cross passage geometry, ensuring a smooth and coherent transition between both ends. They also provide a consistent framework for lofting or blending operations in the next modelling step.

To ensure that the cross passage complies with space-proofing and clearance requirements, the Minimum Clearance Outline (MCO) is modelled from the central reference plane defined earlier. This approach guarantees that the cross passage maintains the required section profile throughout the Cross Passage alignment.

The MCO is positioned at the midpoint between the two collars, using the central plane previously established and then extruded symmetrically in both directions along the axis connecting the collars. This method ensures that the section remains consistent and that the geometry is fully compliant with clearance and accessibility criteria. Once the MCO extrusion is created, it can be used to trim or guide the final solid generation of the cross passage body.

The final step involves generating the solid geometry of the cross passage body. This is achieved by lofting between cross sections, including the inner faces of both collars and any additional control sections required for curvature or clearance control.

This loft operation creates a smooth transition between both ends. The resulting solid is then validated for space-proofing using the MCO and prepared for integration into the overall 3D tunnel model.

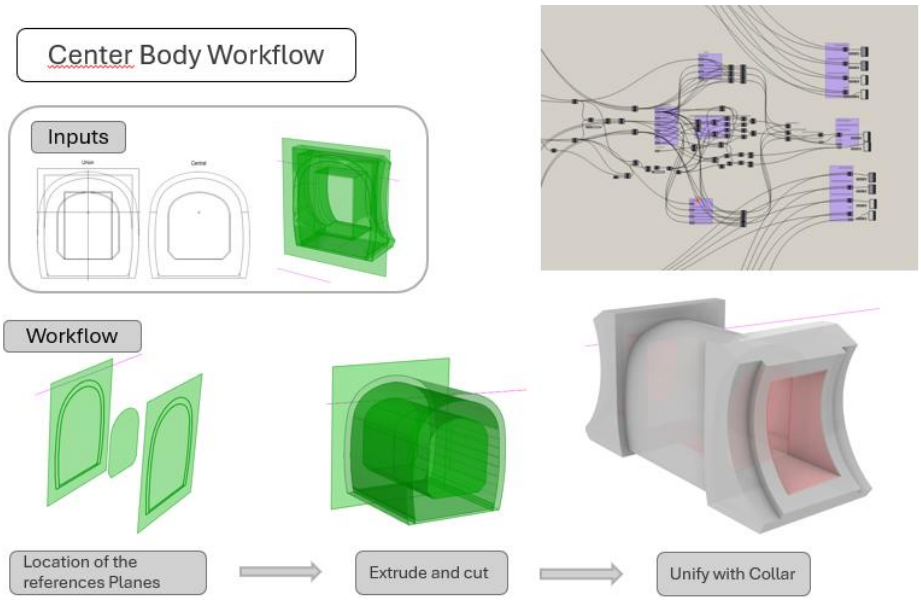
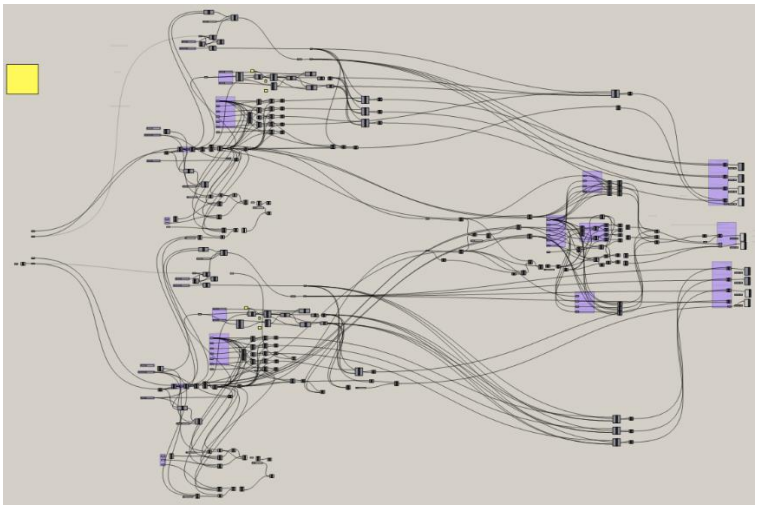


Figure 5. Center body workflow

The complete Grasshopper script developed for the cross-passage automation is shown in the following image. The script is designed to be modular and adaptable, requiring only minor adjustments to be implemented in new projects. Input parameters such as tunnel alignment, chainage, section profiles, and collar dimensions can be updated to reflect project-specific conditions, enabling rapid deployment across different design contexts.


Figure 6. Caption of Grasshopper script.

5 CURRENT SITUATION

5.1 *Workflow implementation*

The tool has been successfully used in the Sydney Metro West – Central Tunnelling Package and is being used in other roads and railways tunnel projects around the world. Its flexibility in adapting to varying geometries makes it broadly applicable. The workflow includes modelling in Grasshopper, exporting to IFC or Revit, and then assigning attributes via additional automation.

Thanks to the open-ended logic of Grasshopper, the tool supports a range of configurations, including different tunnel diameters, offsets, and orientations. This makes it easy to implement in early design stages, where changes are frequent, and standardization is still evolving.

5.2 *Integration with BIM software*

A successful integration of the Rhino-generated 3D models into other design platforms such as Revit and AECOsim has been implemented. The connection with Revit is achieved using the Rhino.Inside.Revit plugin, which enables the Rhino model to behave as if it were native to Revit, supporting parameter-driven elements and full BIM integration. For AECOsim, the models are exported in a format compatible with the platform's native environment. Additionally, the resulting models have been incorporated into the federated model using Navisworks, allowing for interdisciplinary clash detection and coordination.

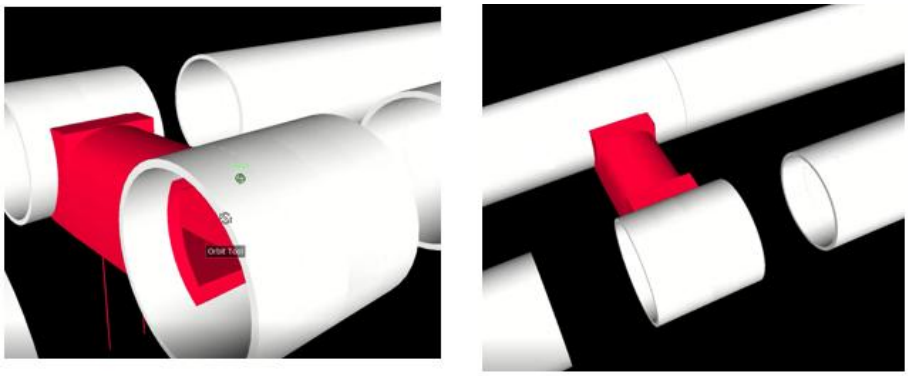


Figure 7. Integration with the Federated Model in Navisworks

5.3 *Further Developments*

The success of the R&D project and the implementation in the design methodologies of the developed tool marked an important milestone in the modelling automation. However, further enhancements of the tool are under development, including:

- Modularizing scripts for easier reuse
- Developing a user-friendly interface
- Automating property attribution to support full BIM workflows
- Creating a reusable XP section library
- Exploring AI to optimize initial configurations

These next developments aim to improve usability, reduce reliance on digital experts, and streamline integration into broader BIM workflows. Ultimately, the goal is to enable designers and engineers to generate and adapt tunnel components without needing to write or modify scripts.

With further refinement, the automation can serve as a template for similar linear infrastructure use cases beyond tunnel cross passages, opening a new frontier in digital civil engineering workflows.

6 CONCLUSIONS

The automation represents a leap forward in tunnelling and XP modelling—turning a repetitive, error-prone process into a streamlined, adaptive workflow. With parametric control, changes can be applied in minutes, and design iterations become agile and low-risk.

The ability to replicate geometries with high precision, ensure alignment, and easily incorporate design changes provides both strategic and practical advantages. It also facilitates better coordination with other disciplines by maintaining geometric consistency throughout the project.

ACKNOWLEDGEMENTS

The authors would like to acknowledge the contribution of the BIM and Geotechnical teams at TYPSA. Without their contribution and the feedback of those who tested and implemented the tool in real projects, especially in Sydney Metro West, the implementation of this tool could have not been possible.

19th Australasian Tunnelling Conference – Acosta-Martínez, Stewart and Hudson-Smith (Eds.)
© 2025 Australian Tunnelling Society, ISBN 978-0-85825-002-4

How I learned to stop worrying and manage the digital - Hard-earned lessons from a major Sydney tunnelling project

A. Monemvasioti Kappos
Jacobs Engineering Group, North Sydney, Australia

ABSTRACT: Over the past decade, Australia's digital framework and requirements for major tunnelling projects have evolved significantly, becoming core contractual components, especially since Transport for NSW's new Digital Engineering Framework was enacted in 2018. Projects awarded before these requirements relied on simpler 3D models and traditional AutoCAD drawings. The rapid transition to advanced digital deliverables has highlighted a shortage of skilled digital resources and a steep learning curve for delivering tunnel projects. Design delivery teams accustomed to traditional methods may face challenges if not supported by experienced Digital Engineers. This can lead to underestimating or misunderstanding the effort required to meet the specified digital standards. This paper shares experiences and lessons learned from overseeing the closure of a tunnelling project's digital design deliverables scope in Sydney. It provides insights for aspiring and experienced design managers of tunnelling projects, focusing on digital deliverables and their contractual implications from tender to construction.

1 INTRODUCTION

After long projects, it can be helpful to look back and consider what lessons can be extracted and applied in the next project. This is a compilation of such an endeavour. The paper presents the perspective of a design manager with moderate digital engineering experience who was entrusted with overseeing the closure of the design digital deliverables during the construction phase of a large tunnelling project in Sydney. The project was delivered under a Design and Construct (D&C) contract, where the Contractor held the primary contract with the Asset Owner, and the Contractor subcontracted the Consultant to perform the design services. The digital deliverables produced during the design and Construction Phase Support (CPS) stages were the responsibility of the Consultant, while the Contractor was accountable for the digital deliverables related to the As-Built Assets. The paper identifies critical areas for the various delivery stages that demand vigilance and awareness for effective and efficient digital delivery. Some of the lessons may appear evident to readers who are experienced with digital delivery. Nevertheless, they will be captured to benefit the wider industry.

2 GLOSSARY

BIM (Building Information Modelling) is a specialisation with its own language and terminology. For many tunnel engineers, becoming familiar with and proficient in the associated terminology can be challenging. To aid the reader in understanding digital engineering terminology, several key terms are reiterated throughout the paper and summarised in Table 1.

Table 1. Terms and Definitions

Acronym	Definition
EIR	Exchange Information Requirements. Before tender, the Asset Owner provides this document detailing all their digital requirements.
DEXP	Digital Engineering Execution Plan. In other projects, it can be referred to as the BIM Execution Plan. It is produced by the Contractor. It is a response to the EIR and lists in detail how the Contractor intends to address the EIR's requirements. Good industry practice includes producing a Pre-DEXP during the tender as a required submission of the tender document. The DEXP contains the MIDP and the MPDP.
LOI	Level of Information. The amount of non-graphical data within an information model at a given stage.
LOD	Level of Detail. The amount of graphical or 3D data within an information model at any given stage in a project. It is part of a scale ranging from the most basic at LOD100 to the most detailed at LOD500.
LOD300	This level of detail allows the element's quantity, size, shape, location, and orientation to be measured directly from the model without referring to non-modelled information such as notes or dimension call-outs (BIMForum, 2024a).
LOD*	Level of Development= LOD + LOI
MPDT	Model Production and Delivery Table. Lists the LOI and LOD requirements per model and element.
MIDP	Master Information Delivery Plan. It is used by the Asset Owner representative or project manager to validate that all suppliers are delivering what they are contractually required to do.

*Despite the counter-intuitiveness, two different definitions share the same acronym

3 TENDER PHASE

Typically, the Asset Owner provides the EIR during the tender stage. Best practice would entail the Contractor producing a Pre-DEXP detailing their plan for delivering the project in accordance with the EIR's requirements. The Pre-DEXP report can provide a basic understanding of the scope's extent and should be part of the contractual documents.

Sources of Worry: Underestimating the effort and time needed for the delivery of the digital scope, resulting in under-pricing and an unrealistic delivery program.

Lesson 1: The Pre-DEXP plan can provide a basic understanding of the digital scope during delivery. In a D&C, the Consultant needs to view this document during tendering to price and sequence design deliverables accurately.

Lesson 2: The EIR and DEXP should be contractual documents.

Lesson 3: At the tender stage, an internal strategy on how the Consultant and Contractor plan to deliver the requirements should be prepared. That would include the list of the intended models, software, LOD, and LOI.

4 DELIVERY PHASE

4.1 *Contractual Elements*

After the project award, signing the final contractual documents can take weeks to months, depending on the project.

Sources of Worry: Unclear digital delivery scope between Contractor and Consultant, especially when contractual definitions are not established early. Lack of timely agreement on digital responsibilities can cause the incorporation of digital requirements into design deliverables to be inefficient and prone to misalignment.

Lesson 4: Signing the contract can take time. The sections regarding the scope of the digital delivery should be agreed upon after the Consultants and the Contractor's delivery teams have provided input on their capabilities. That scope should be fixed during an early draft of the Professional Deed.

The DEXP is the crucial document describing the exact details of the digital delivery, and it is typically prepared by the Contractor with some input from the Consultant. The document should be provided to the consultant at an early delivery stage. The DEXP is a live document that can be updated throughout the project, but this typically refers to details such as the names of subcontractors involved, key personnel, etc. The main requirements of the MPDT should be fixed and frozen during the first stage of the delivery so that everybody is clear on the scope involved.

Lesson 5: A detailed allocation of responsibilities and tasks should be agreed upon in advance. The allocation should contain dates for providing documents (such as the DEXP, BIM Manual, MIDP, BIM Schema Specifications, etc.) and specify the documents that require joint agreement and approval between the Consultant and the Contractor before they are provided to the Asset Owner. This is essential because many of these documents define the scope of various digital deliverables, and if the Consultant is expected to deliver them, they should be aware.

Lesson 6: The DEXP's main content should be agreed on within the first delivery stage. Any changes to the DEXP need to be communicated and reviewed by the Consultant before being sent to the Asset Owner.

When the digital scope is poorly defined, its interpretation can vary between the Asset Owner, the Contractor and the Consultant. This can lead to a sudden, cascaded increase in the scope for the Consultant.

Lesson 7: The digital delivery team must work closely with the design management team to promptly identify changes in scope. These must be formally communicated, and variation proposals should be raised if required. However, to manage a scope, the scope needs to be defined (see Lessons 5 & 6).

Lesson 8: Disputes can stem from a lack of clarity, alignment and understanding regarding scope and expectations across parties. Regular, open communication between parties is crucial to prevent such misunderstandings.

Tunnels are not defined in detail in the world of BIM. For example, the BIMForum, which develops and maintains the LOD Specifications and is considered an industry-recognised source of information, does not include extensive tunnel elements in its library (Figure 1). Similarly, the MPDT template provided by most Australian government agencies includes limited or no information on tunnelling assets. As such, Consultants and contractors may have different expectations of what a tunnel with LOD300 may look like. That said, the bored tunnel-specific BIM guideline (ITA Working Group 22, 2022) published recently does offer some guidance for more recent tunnel projects.

LOD Specification 2024 Part II

Copyright © BIMForum 2024
This work is licensed under the Creative Commons Attribution-NonCommercial 4.0 International License

Breakdown Level	This project	UNIFORMAT	OMNICLASS	UNICLASS	SYSTEM/COMPONENT INFORMATION
2		G90	21-07 90		**Miscellaneous Site Construction**
3		G9010	21-07 90 10	Ss 37 50 92	**Tunnels**
4		G9010.10	21-07 90 10 10	Ss 37 50 92	Vehicular Tunnels
4		G9010.20	21-07 90 10 20	Ss 37 50 92	Pedestrian Tunnels
4		G9010.40	21-07 90 10 40	Ss 37 50 92	Service Tunnels
4		G9010.90	21-07 90 10 90	Ss 37 50 92	Tunnel Construction Related Activities

Figure 1. Extract from 2024 LOD Specification Part 2 relevant to Tunnels (BIM Forum, 2024b)

Lesson 9: An agreed-upon example of the tunnel elements that represent the required LOD should be produced, referenced, and agreed upon before signing the contract or within the first delivery stage.

Consistency is a high priority in digital delivery. To achieve this, the responsible party (agreed upon between Consultant and Contractor – though it can be a collaboration between the two) should produce a BIM manual immediately upon commencing the design phase, ensuring all modellers adhere to the same standards.

Sources of Worry: Inconsistency in digital design deliverables.

Lesson 10: Digital delivery team meetings should be organised frequently. During the sessions, the various teams coordinate and receive specific instructions regarding requirements, visualisation, elements, model structure, etc. All these requirements must be captured in the BIM manual so they can be easily referenced.

4.2 *Delivery Program and Reviews*

Typically, the Contractor's team conduct their reviews during the Cross-Disciplinary Review (CDR) period, which is facilitated by platforms such as Revu and Bluebeam, which host PDF documents and capture any comments made. The digital deliverables cannot be reviewed on such platforms. Hence, models need to be shared separately, for example, in Projectwise, to facilitate the review. Revizto, for example, can be an appropriate platform to capture and record issues on models.

Reviewing models and digital drawings for the Contractor can be a time-consuming and intensive exercise, and it requires resources to adhere to the CDR review timeline, which is often only five days. However, these reviews must be conducted before the model submissions to the Asset Owner.

Sometimes, the review conducted by the Asset Owner may focus more on design deliverables than the quality of digital deliverables, as a future Gate or review Milestones scheduled before handover will provide such an opportunity for a focused digital deliverables review.

Sources of Worry: An awkward situation where the Consultant deems their digital deliverables acceptable, considering their formal acceptance by the Asset Owner, but the Contractor disagrees.

Lesson 11: Define periods and the appropriate format of digital reviews and adhere to that agreement.

Lesson 12: Agree formally with the Contractor, in advance of the delivery, on what milestones signify that the digital deliverables are acceptable, and their scope is complete.

Design delivery programs are becoming aggressively condensed to achieve the earliest possible start of the construction phase. That can mean multiple packages planned for submission during the same week or even the same day.

Sources of Worry: The review periods are not always adequately considered in the tender high-level planning and budgeting, which sometimes results in non-compliance with digital standards not being identified before submissions.

A dedicated resource must be allocated and budgeted for, whose role as Digital Engineering Compliance Manager includes ensuring that the agreed project digital standards are appropriately communicated to the digital team and frequently reviewing the models to ensure consistency and resolve clashes. However, this resource needs sufficient time to conduct the necessary reviews, and any subsequent changes also require time to implement. If the delivery programs are too short, models are often sent for review with only hours left before their planned submission. This scenario realistically results in either a delay to the submission or a substandard submission in terms of digital quality.

Lesson 13: Allow for adequate interdisciplinary review periods for deliverables—at least five workdays and preferably ten days for internal review before submission to the Asset Owner.

Lesson 14: Stagger packages as much as physically possible so that the review periods do not coincide, allowing reviewers to focus.

Lesson 15: Do not compromise on quality and assurance to meet deadlines. Doing so will only result in resubmissions.

Lesson 16: In addition to the Digital Engineering Manager role, a Digital Engineering Compliance Manager (or a similar title) should exist. This role will exclusively involve coordinating and communicating the digital quality requirements and reviewing the quality of the digital deliverables.

4.3 *Digital and Design Learning Curve*

In the past, Revit was not preferred for linear structures and was not typically used for tunnel structures. Tunnel drafting resources and engineers might have been more familiar with AutoCAD than Revit and the production of 2D drawings instead of derived from the model. This could create a predisposition towards misunderstanding clauses that require drawings to be produced from the model, where possible.

Sources of Worry: Lack of alignment between Contractor and Consultant on the type of drawings to be extracted from models.

Nowadays, most tunnel projects will request a minimum LOD300, which requires drawings to be "cut" from the model. This also means that any dimensions, levels and coordinates portrayed on the drawings are not simply typed in as text but are accurately reflected and extracted from the model, which in turn will be reflected by the future constructed physical structure. As such, it is essential to spend time at the beginning of the design to set up the models properly before rushing to produce drawings. (That said, updating drawings after 3D models have been modified is more time-consuming than making direct changes to 2D drawings. A solution could be to limit 2D drawing only to the ones essential for conveying design information and rely more on the model.)

Lesson 17: Pre-agree with the Asset Owner and the Contractor on the type of software used for the various categories of drawings. Use a digital delivery team that is experienced in using that software and upskills those who are not during quiet times.

Lesson 18: It is better to frontload the digital resources so that the digital models are set up correctly, facilitating the smooth and easy production of drawings.

Lesson 19: Slow is smooth, and smooth is fast. Dedicating time to perform any job correctly from the outset avoids amendments later, saving time, money, and reputation.

5 CONSTRUCTION PHASE SUPPORT

In past projects, formally submitting a markup drawing to show design changes resulting from RFIs was often sufficient. All marked changes were collated, the relevant design package drawings were updated, and the drawings were formally resubmitted at the end of the construction of the relevant design package.

However, more recent projects, such as the one that inspired this paper, may require updated drawings to be issued every time a change is requested, necessitating updates to the relevant model. A seemingly simple change that may initially appear only to affect one drawing, such as increasing the thickness of a cavern headwall, can span across multiple drawings in various design packages. This is because producing drawings, especially at interfaces between design packages, often requires federating multiple models. Therefore, the impact of such changes must be accurately assessed by the CPS design team and consistently actioned to ensure uniformity across different drawings and design packages. This requires experienced CPS engineers familiar with the various design packages and a dedicated digital resource available to the Consultant throughout the CPS phase.

Sources of Worry: Risk that CPS design changes may not be reflected with consistency across all relevant design packages, leading to conflicting and inaccurate construction documentation.

Another matter that may not be widely applicable, but was relevant to the specific, unnamed project that inspired this paper, involved withdrawn RFIs. Occasionally, the Contractor would request a change in drawings through an RFI. After the update was complete and the drawings provided to the Contractor, the Contractor may reconsider the change, decide not to proceed with it and withdraw the RFI. If the withdrawal is not communicated correctly to the CPS team, it can result in inconsistencies in models. Also, the effort required to revert the digital model(s) to their previous revision must be priced and charged accordingly.

Sources of Worry: Miscommunication between the Contractor and Consultant regarding the reversion of models and drawings after RFIs are withdrawn, and a lack of allocated CPS budget for this work.

Lesson 20: The assurance process during CPS needs to be clearly articulated. A dedicated digital resource must be available during CPS and in charge of keeping the models current.

Lesson 21: After a model has been modified for an RFI change, all drawings originating from the model should be exported and checked to ascertain if the change affected them. Drawings from neighbouring design packages where the modified model is federated should also be checked. A database that lists what models are being used to create the output for each drawing could be a solution to facilitate this process.

Lesson 22: The Contractor and the CPS design coordinator must inform the digital team when CPS-issued drawings are withdrawn, and the hours needed to revert the model charged on the relevant withdrawn RFI.

6 WORTH MENTIONING

6.1 *Number of Models*

Consolidating design elements into fewer, centralised models, ideally within a Common Data Environment (CDE) like ACC, reduces the risk of inconsistencies, simplifies change management, and ensures a Single Source of Truth (SSOT) across the project.. Multiple models can lead to redundant data, increasing the likelihood of mistakes and making it more difficult to manage changes.

Sources of Worry: Too many models create complex digital interdependencies that are difficult to manage, especially for non-digital resources.

Lesson 23: The optimal number of models should be considered during the tender or early design development. Consolidation of models should be considered where possible to improve data management and consistency.

6.2 *Tool for the Designers*

BIM offers numerous valuable applications for our engineering teams, many of which remain obscure to many designers due to limited training in using the latest software and insufficient available time during delivery to teach them. Among them, clash detection is a key application of digital models as it can significantly assist in interdisciplinary delivery or even simply coordination among neighbouring design packages. For the models to be constructive, though, they should be shared frequently with the broader design team.

Source of Worry: Non-prompt sharing of models, leading to delayed identification of design development/change consequences affecting interfacing design packages.

Lesson 24: Clash detection should be used proactively as a design tool and reactively as a problem-solving measure.

Lesson 25: Timely, accurate information sharing is crucial for successful BIM implementation.

Lesson 26: Engineering teams must receive training on the full range of BIM tools that can support the design process. This training should go beyond general awareness, offering practical examples and clear steps for leveraging the 3D model effectively.

It is worth noting that the digitally modelled entities of elements represent their design (theoretically ideal) location. They do not capture the range of tolerances that can occur when the structure is built. Tolerances may be captured by a spaceproofing model, depending on the type of structure and the criticality of its interface with other structures and disciplines.

6.3 *Assurance and Collaboration Platforms*

Quality assurance is a critical component of digital delivery. The writer believes that SharePoint, which is often preferred within joint ventures due to its universal availability, should be avoided. SharePoint is a general-purpose document management and collaboration platform, and it is not ideal for workflows, document control, version management, and data exchange, particularly for digital deliverables such as Revit and AutoCAD files. Without extremely clear and strictly followed document management processes, SharePoint can lead to an unruly filing system where the latest versions of files are not easily accessible or identifiable.

Source of Worry: Difficulty in locating the latest version of design files, leading to the risk of updating a superseded file.

Bespoke platforms like ProjectWise, designed for engineering and construction delivery, offer structured storage and collaboration environments that enhance assurance processes. They simplify version control and provide clear submission workflows, reducing misinterpretation across design stages. In addition, industry-standard design tools, such as Revit and AutoCAD, can integrate with these platforms, allowing efficient data exchange and reducing the risk of errors.

Lesson 27: Software programs such as SharePoint are not designed for the complexities of delivering megaprojects. Bespoke collaboration software for engineering projects, are far better equipped and ensure consistency as single sources of truth.

6.4 *The importance of document control*

Depending on the size of the design package, document controllers may be required to review design reports that span from a few dozen pages to more than 1000 pages before each submission. A thorough review can take time if it is to be done properly. Similarly, they need to ensure that things that may not appear secondary to some, such as stamps on drawings, revision dates, etc, are correct. It is essential to allow these professionals the time they require to ensure that submissions meet quality standards and identify issues that will result in rework and resubmissions if not resolved. It is also crucial to account for this time when planning the delivery of packages.

Source of Worry: Insufficient time for document control, leading to repeated resubmissions.

Lesson 28: Document Controllers are an essential part of the digital delivery team. They are crucial for the quality of deliverables, and they need adequate time for their reviews.

7 CONCLUSION

Investing in robust planning, effective collaboration, and a deep understanding of BIM principles is critical to avoid challenges in producing and delivering digital engineering deliverables for tunnelling (and other) projects. Accelerated project timelines, increasingly prevalent in our industry, can exacerbate issues related to data management, quality assurance, and overall project efficiency, especially if combined with unclear contractual digital requirements.

A proactive approach to BIM implementation, including early planning, clear communication, and allocating sufficient resources, is essential for success. Implementing these lessons learned can improve digital engineering practices, enhance collaboration, and improve overall project outcomes for future projects.

ACKNOWLEDGEMENTS

The author thanks Pawel Kozak, Morgan Carson, Anthony Harding and the reviewer of the paper for their assistance and insightful commentary.

8 REFERENCES

BIMForum. 2024a. 2024. Level of Development (LOD) Specification Part I. Available at: https://bimforum.org/resource/lod-level-of-development-lod-specification/ (Accessed: 22 April 2025).

BIMForum. 2024b. 2024. Level of Development (LOD) Specification Part II. Available at: https://bimforum.org/resource/lod-level-of-development-lod-specification/ (Accessed: 22 April 2025).

ITA Working Group 22. 2022. BIM in Tunnelling - Guideline For Bored Tunnels - Vol 1. ITA Report No 27, July 2022. ISBN: 978-2-9701436-5-9.

19th Australasian Tunnelling Conference – Acosta-Martínez, Stewart and Hudson-Smith (Eds.)
© 2025 Australian Tunnelling Society, ISBN 978-0-85825-002-4

Enhancing tunnel design and construction through Building Information Modeling (BIM): A case study approach

A. Rajesh & M. Mohandas
PINI Australia Pty Ltd, Melbourne, Australia

ABSTRACT: Building Information Modeling (BIM) is a transformative methodology for the construction industry, yet its adoption in tunnelling has lagged behind other sectors due to unique challenges including geological complexity, stringent safety requirements, and intricate multidisciplinary coordination. This paper examines the practical application of BIM to overcome these hurdles through a case study analysis of international and Australian tunnelling projects. The analysis demonstrates that BIM implementation yields significant benefits, including enhanced clash detection, optimized construction sequencing, and improved stakeholder collaboration through a single source of truth. The study also identifies critical barriers to adoption, such as data interoperability issues and a shortage of digital skills and proposes practical strategies to address them. By synthesizing lessons from successful implementations, this research provides a valuable roadmap for advancing BIM adoption in the tunnelling industry, promising greater efficiency, cost certainty, and safety in future underground infrastructure development.

1 INTRODUCTION

Tunnel construction represents one of the most complex and high-risk domains of civil engineering, traditionally constrained by reliance on 2D drawings and fragmented communication methods. As urbanization intensifies the demand for underground transport and utility networks, these conventional approaches struggle to address the critical needs for precision, safety and interdisciplinary collaboration in geotechnically uncertain environments. Building Information Modeling (BIM) offers a transformative and alternative solution through data-rich 3D models that integrate design, construction and lifecycle management. However, despite its proven success in building construction, the adoption of BIM in tunneling remains limited due to the sector's unique challenges including the variable ground conditions, linear project nature and a lack of standardized digital workflows (Zhou et al., 2017).

This paper investigates the practical application of BIM to overcome these tunneling-specific challenges. Through a detailed case study analysis of major Australian projects alongside international benchmarks, we examine how advanced BIM processes enhance design coordination, construction sequencing and stakeholder engagement. The research aims to identify key success factors and methodologies that demonstrate BIM's value in managing complexity, ultimately providing an actionable framework for its effective implementation in future underground infrastructure projects.

2 BIM IN TUNNEL ENGINEERING: CURRENT STATE AND EVOLUTION

2.1 *Evolution of BIM in Infrastructure Projects*

The global push for infrastructure development has significantly increased the complexity and scale of tunneling projects for railways, highways and urban utilities (Lai et al., 2018). In parallel, Building Information Modeling (BIM) has evolved from a basic design tool into a comprehensive lifecycle management platform, integral to the architecture, engineering, and construction (AEC) industry (Howard & Björk, 2008; Bradley et al., 2016). This evolution is marked by the expansion from 3D modeling to multi-dimensional applications, including time (4D), cost (5D) and facility management (7D), which are critical for the long-term planning and operation of major infrastructure (Smith, 2014).

Despite its proven value in building construction, the adoption of BIM in the tunneling sector is still young. The linear nature of tunnels, coupled with unpredictable geological conditions and complex ground structure interactions presents unique challenges not adequately addressed by standard BIM tools (Zhou et al., 2017). A significant barrier is the lack of specialized component libraries because most BIM software families are designed for above-ground buildings, creating difficulties in accurately modeling tunnel-specific elements like segments, portals and lining systems (Song et al., 2019). These fundamental modeling issues are compounded by the risks of underground construction such as geological uncertainty and spatial constraints.

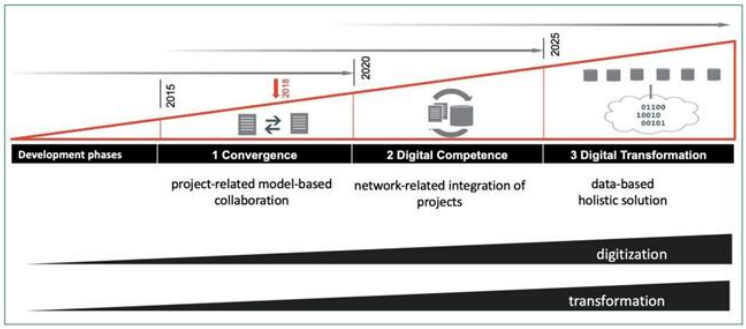


Figure 1. Development stages into the digital world (Digital Design, Building and Operation of Underground Structures-BIM in Tunnelling, DAUB

In response to these challenges, the industry is developing tailored methodologies. Researchers have proposed specialized Tunnel Information Modeling (TIM) frameworks, such as interconnected subdomain models (Koch et al., 2017) and standards for drill-and-blast tunneling (Sharafat et al., 2021). Concurrently, committees like the German Tunnelling Committee (DAUB) have published guidelines to standardize BIM application underground. These efforts collectively aim to establish consistent, effective practices for leveraging BIM in tunneling, moving the industry toward full digital integration (DAUB, 2021).

2.2 *Global Implementation Trends*

International adoption of BIM varies significantly by region. European countries particularly the UK, Germany, Norway, Switzerland and Austria lead in BIM integration due to digital transformation mandates and infrastructure modernization programs (Shivasami et al., 2019). The UK's 2016 BIM mandate for public projects catalyzed adoption in major infrastructure including crossrail and HS2. Australia's BIM adoption has progressed more slowly, with the "Australia BIM Strategic Framework" released only in 2019. Although not yet mandated, projects like Sydney Metro & Melbourne Metro have pioneered BIM use in design and delivery showcasing benefits in managing complex designs and enhancing coordination. However, challenges persist including the lack of tunnel-specific BIM libraries, inconsistent standards, limited GIS integration and the need for workforce training. Government initiatives like the Transport for NSW Digital Engineering Framework and the National Digital Engineering Policy are working to ad-

dress these issues and promote BIM across the full asset lifecycle.

3 STRATEGIC BIM WORKFLOWS IN TUNNEL PROJECTS

3.1 *Level of Development (LOD) Frameworks for Tunneling*

While conventional LOD frameworks (e.g., AIA E203-2013) define geometric and semantic granularity for building projects, tunneling demands specialized adaptations due to geological variability and linear infrastructure complexity. Sharafat et al. (2021) proposed a five-stage LOD framework tailored to tunneling:

LOD 100 (Conceptual):
Basic alignment and cross-sectional geometry and geotechnical profiles.
LOD 200 (Design Development):
Parametric lining segments, temporary support systems and probabilistic ground models.
LOD 300 (Construction-Ready):
Machine-readable TBM specifications, construction sequencing logic, and clash-resolved utility corridors.
LOD 400 (Fabrication/Assembly):
As drilled rock bolt patterns, grouting and precast segment tolerances.
LOD 500 (Operational):
Asset metadata (e.g., MEP component lifespans) linked to facility management systems.

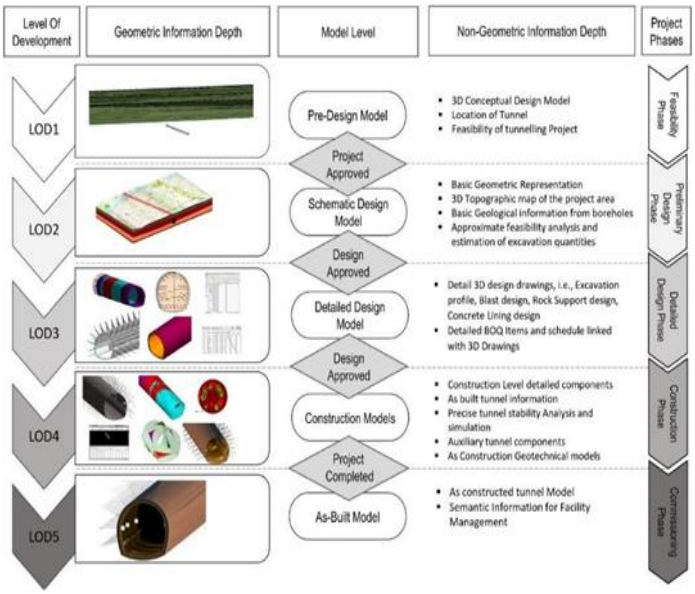


Figure 2. LOD for BIM-Based Tunnel Information Modelling *(Sharafat, A., et al. (2021). Journal of Computing in Civil Engineering, Volume 35, Issue 2)*

This framework explicitly addresses geological uncertainties through probabilistic modeling, where ground parameters are represented as distributions rather than deterministic values, enabling risk-adjusted decision-making (Zhang & Liu, 2020).

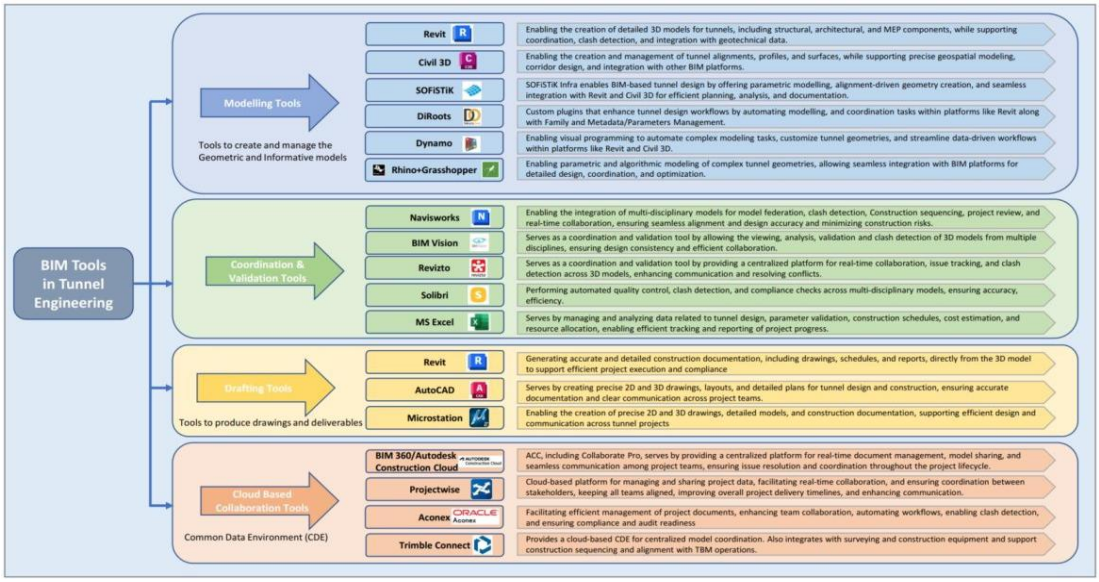


Figure 3. Tools in Tunnel BIM.

Autodesk Revit can be adapted for tunnels while Civil 3D is better for linear modeling. Bentley's suite offers integrated tools for tunnel design and structural detailing. Specialized software like Plaxis and RIB iTWO add critical geotechnical analysis and construction simulation capabilities. Together, these platforms form a robust digital toolkit, allowing engineers to manage the geometric, structural, and geotechnical complexities of tunnel projects more effectively.

3.2 *Geospatial Foundation and Coordinate Systems*

The initial and most critical step in the BIM process was the establishment of a unified geospatial framework to ensure all discipline models were aligned within a single, accurate coordinate system. This was of paramount importance for a project of this linear scale and complexity. A project wide coordinate system was defined based on the national geodetic grid (GDA2020/ MGA Zone 55 for Australia) to ensure accuracy across all software platforms (Civil3D, Revit, Navisworks, etc). This guaranteed that the tunnel alignments, surface features and subsurface models were all geospatially coherent.

3.3 *Input Data and Pre-processing*

With the coordinate system established, geological, geotechnical and structural inputs formed the basis of the models. Geological data such as rock mass rating and fault zones were processed to define the rock classes along the tunnel alignment. This data was interpolated to create 3D geological models that could be referenced within the BIM environment. Geotechnical inputs encompassed the designs for rockbolts, shotcrete, and lattice girders, while structural inputs included concrete linings and portal structures based on load assumptions. All these data are pre-processed into standardized formats (IFC for model elements, DWG for base geometry and XLSX for chainage-based data like rock class) to be efficiently consumed by BIM authoring tools for subsequent modelling and coordination activities

3.4 *Modelling Tunnels and Stations – A Multi-Model Approach*

With the geospatial framework and input data established, the modelling of primary structures commenced. This process was not monolithic but was strategically divided into distinct model types to manage complexity, enable parallel workstreams and maintain performance.

3.4.1 *Tunnel Modelling: Corridor based Parametric design*

The linear nature of the tunnel drives demanded a corridor-based modelling approach, diverging from standard building techniques. The tunnel alignment and profile defined within AutoCAD Civil 3D served as the digital “backbone”. This corridor was then leveraged to generate the primary tunnel void. Two primary methods were employed. The first one using the Civil 3D corridor was imported in Revit as a reference. Using Dynamo scripts, the tunnel’s internal lining was automatically generated by extruding a parametrically defined cross section (eg, horseshoe, circular) along the imported alignment. This created a native Revit element that could be scheduled and tagged; however, this geometric translation often introduces inaccuracies and tessellation errors. Any design change forces a slow and manual update of the entire process which may hinder performance through these heavy Revit models.

An alternative solution for this is using Sofistik, which uses a unified model environment where the tunnel is an intelligent, parametric object. The tunnel lining is defined by a parametric cross section that is associatively extruded along the alignment. If you change the alignment or lining thickness, the tunnel updates automatically throughout its length. You get a light, native and schedulable Revit model without writing a single line of Dynamo code. The link remains bidirectional which allows to update the Revit model if the Sofistik design changes.

As detailed in section 3.3, rock support classes were applied parametrically along the alignment based on chainage-specific rock class data. Dynamo scripts automated the placement of rock bolt families and defined shotcrete thickness zones, transforming geotechnical design into a constructible 3D model.

3.4.2 *Station Modelling: Building-like complexity Underground*

Stations with their large caverns, multiple levels and dense mechanical, electrical and plumbing (MEP) requirements were modelled using a more traditional building BIM approach within the established project coordinate system.These stations were developed as separate Revit models, with their locations precisely georeferenced using the project's shared coordinates to ensure alignment with the connecting tunnels. To manage complexity and enable concurrent workflows, each station model was subdivided into discipline-specific models. The Structural models defined the cavern and entrance layouts, framing, walls, and slabs, while the MEP models contained all ventilation, fire protection, cable management, and piping systems. This model separation prevented single-file overload and facilitated specialized development, with all data preprocessed into standardized formats (IFC, DWG, XLSX) to be efficiently consumed by BIM authoring tools for subsequent modeling and coordination activities.

3.5 *Federation into the Coordination Model*

The various container models (tunnels, station structures, station MEP, surface utilities) were not designed in isolation. They were periodically published to the Common Data Environment (CDE) and federated within coordination software like Navisworks Manage or BIMCollab to create an overarching Coordination Model – a single, comprehensive digital prototype of the entire project. Within this federated model, automated clash detection routines were run. The rules were sophisticated, checking not only for "hard clashes" (e.g., a pipe intersecting with a beam) but also for "soft clashes" (e.g., breaches of maintenance clearance zones around equipment). The CDE tracked identified clashes, assigned them to the relevant design team for resolution, and verified the solutions, ensuring all interdisciplinary interfaces were meticulously coordinated before construction commenced.

3.6 *Creation of the Documentation Model*

A core principle of BIM is that construction documents (drawings, schedules, quantities) are outputs or views of the model, not separate entities. The Documentation Model is the managed set of these extracted views, ensuring consistency and eliminating redundancy. Within each Revit container model (e.g., Tunnel A02, Station MEP), dedicated sheets were created for plans, sections, elevations, and details. Views on these sheets were generated directly from the 3D model. Sections and callouts were "live," meaning any change in the 3D model automatically updated all associated drawings. Annotations (dimensions, tags) were linked to model elements via shared parameters. Schedules for quantities (e.g., concrete volume, rock bolt count, rebar tonnage) were generated directly from the model database. This ensured that the Bill of Quantities was inherently tied to the design model, drastically reducing manual takeoff errors and ensuring cost certainty. The Solibri model checker was used to validate the documentation model itself, running rules to ensure that every element tagged in a drawing was present in the model, that all sheets contained the required views, and that the project's naming and numbering standards were consistently applied across all documents.

4 CASE STUDY ANALYSIS – EMERGING PATTERNS & LESSONS LEARNED

4.1 *Case Study A: Urbania Tunnel*

The complexity of the 28-kilometer Urbania Tunnel Project, with its four natural tunnels and seven bridges presented significant BIM modelling challenges particularly in accurately representing the complex, curved geometry of the tunnel bores and their interfaces with other structures. To overcome this, the team moved beyond standard modelling techniques by developing parametric Revit families with adaptive points linked directly to the Civil 3D alignment. This crucial technique ensured the tunnel lining and internal components dynamically updated with design changes. Furthermore, specific challenges like clash detection between temporary and permanent works were addressed by creating separate worksets in Navisworks, while initial inconsistencies in model detail from subcontractors were resolved by implementing a strict BIM

Execution Plan and automated validation scripts within the Common Data Environment to ensure model integrity.

This refined clash detection process resolved over 80 major interferences before construction, while the accurate 4D sequencing of activities in high risk geological and traffic sensitive areas prevented delays. The precise modelling of complex geometries combined with immersive walkthroughs for stakeholders, not only provided a superior understanding of the project but also streamlined planning approvals reducing lead times by an estimated 30%. The project establishes a benchmark for BIM implementation in complex infrastructure projects, particularly those involving multiple tunnels, bridges, and road alignments in challenging topography.

4.2 *Case Study B: A major orbital rail infrastructure in Melbourne*

The Orbital Rail Project, a metropolitan-scale underground rail system in Victoria, Australia, exemplifies the application of advanced BIM to overcome the profound complexities of building in a dense urban environment. The integration of dozens of discipline-specific models for stations which consists of complex architectural, structural, and MEP systems posed a significant coordination challenge. Instead of relying solely on post-design clash detection, the team implemented a strategy of "Federated Model Zones" within Navisworks. This involved creating rule-based filters to isolate coordination tasks by specific station areas (e.g., concourse level, platform level), significantly streamlining the clash detection process and aligning with the zone-based coordination frameworks discussed by Kassem et al. (2015) in their analysis of BIM maturity in large projects.

The project faced significant secondary challenges in data handover and logistical planning. The goal of using the digital model for future asset management was hindered by inconsistent data formats and varying Levels of Detail (LOD) from different contractors. The solution was the implementation of a Model-Based Delivery requirement, mandating COBie data drops at key milestones. This ensured that critical asset information was structured and embedded within model elements from the outset, creating a reliable digital twin for facilities management as suggested by NBS (2019). For logistical planning within a constrained right-of-way, sequencing complex construction without disrupting surface traffic required advanced analysis. The team utilized 4D BIM (Synchro 4D) to conduct "what-if" scenarios, optimizing Tunnel Boring Machine (TBM) deployment and evaluating procurement strategies. This application of 4D BIM for strategic decision-making, rather than mere visualization, is a key indicator of high BIM maturity, as noted by Heigermoser et al. (2019).

4.3 *Case Study C: Sydney Metro West – Eastern Tunneling package, Australia*

The Sydney Metro West – Eastern Tunnelling Package serves as a seminal case study on the strategic value of implementing BIM from the conceptual design phase to manage complex interfaces in dense urban area. To navigate the impossible web of existing subsurface utilities and foundations, the project established a federated model as a "single source of truth." This integrated platform consolidated geospatial, geotechnical, and existing asset data, which enabled continuous, automated clash detection and provided designers with direct feedback capabilities. This allowed for the real-time iteration and optimization of alignments and structural solutions, efficiently mitigating interface risks during design development. The benefits of this early BIM adoption extended into procurement and stakeholder engagement by providing tenderers with the comprehensive concept model, the project transformed the tender phase into a collaborative, model-based assessment. This dramatically accelerated the understanding of project constraints which prevented an estimated $15M in rework and 6 months of delays. This centralized digital environment helped facilitate consensus among diverse parties is a hallmark of mature BIM implementation, a principle strongly supported by the ISO 19650 standard on information management. The project demonstrated that embedding a digital culture from the outset creates a robust backbone for data-driven decision-making, confirming that the value of BIM in managing subsurface risks (Shivasami et al., 2019) far outweighs the initial modeling effort and secures a digital foundation for the entire project lifecycle.

4.4 *Discussions And Future Trends in Tunnel BIM*

Future advancements in BIM for tunneling are emerging through projects like Sydney Metro and Melbourne's ongoing "Mammoth Rail Project," which utilize sensor-based "live digital twins" to monitor ground movements in sensitive urban areas. These IoT-enabled BIM models integrate data from LiDAR and fiber optics to track deformation at a millimeter scale, a capability demonstrated on projects like Norway's Follo Line. Looking ahead, machine learning is poised to predict Tunnel Boring Machine (TBM) performance in varying ground conditions, thereby reducing project uncertainty. Concurrently, cross-border collaborations, such as knowledge-sharing initiatives between Australia and Singapore, aim to enhance geological models for challenging environments like tropical soils and karst. These technical efforts are supported by evolving BIM guidelines and IFC extensions, which are critical for improving software interoperability, while Augmented Reality (AR) tools are increasingly being deployed to help technicians visualize utilities and defects on-site. Ultimately, the future of BIM in tunneling will focus on the seamless integration of real-time data, AI-driven insights, and the development of global standards to de-risk megaprojects.

5 BENEFITS OF BIM IN TUNNELLING

Building Information Modeling (BIM) has revolutionized tunneling projects by enhancing precision, collaboration, and lifecycle management. BIM's 3D models surpass traditional 2D drawings by integrating geometric and non-geometric data, offering stakeholders unparalleled clarity of complex underground spaces. For instance, Sydney's West Connex project utilized BIM to detect spatial conflicts early, improving stakeholder alignment and reducing costly rework (Roads and Maritime Services, 2019). Virtual Reality (VR) further aids spatial comprehension, as seen in Crossrail's design reviews, minimizing errors in confined environments. (Dogan et al., 2022).

BIM integrates geotechnical data, enabling 3D stratigraphic models from borehole and geophysical surveys (Wang et al., 2021). This integration allows engineers to analyze how geological conditions might affect construction methods and structural designs (Hoek et al., 2019). The Melbourne Metro Tunnel project demonstrated this capability by incorporating borehole data and geotechnical surveys into the BIM environment, enabling more accurate risk assessment and construction planning (Rail Projects Victoria, 2020). Parametric modeling allows tunnel lining and reinforcement designs to be dynamically adapted to variable ground conditions. This process integrates geotechnical data directly into the structural model, embodying the "geotechnical BIM" concept where soil-structure interaction directly informs design. This is crucial for coordinating multiple systems within the confined space of underground construction.

BIM enables automated clash detection between these systems, helping to identify and resolve conflicts before construction begins. The North Connex tunnel in Sydney employed BIM-based clash detection to coordinate mechanical, electrical, and plumbing systems with the tunnel struc- ture, resulting in fewer on-site conflicts and associated delays (Transurban, 2021). As observed in the Crossrail project (Barton et al., 2016), such prioritization reduces false positives in clash detection, which are prevalent in complex infrastructure models. Federated models are systematically updated through defined cycles with version control protocols ensuring traceability - a practice shown to reduce rework by 15–20% in large-scale projects (Zou et al., 2019). BIM ex- tends beyond static 3D models to include the time dimension (4D), allowing for the simulation of construction sequences to optimize the construction schedule and identify potential logistical challenges. The Cross River Rail project in Brisbane utilized 4D BIM to plan the tunnel boring machine operations and coordinate associated activities improving resource allocation and sched- ule reliability (Cross River Rail Delivery Authority, 2021). The Sydney Metro Northwest project implemented a BIM- based asset management system that facilitated more efficient maintenance planning and reduced lifecycle costs (Sydney Metro, 2022).

6 CHALLENGES AND BARRIERS IN BIM IMPLEMENTATION FOR TUNNELING

A significant barrier to BIM implementation in tunnel engineering lies in the inherent limitations of the software and data environment. Most pre-built family components in BIM platforms are designed for general construction rather than tunnel applications, creating difficulties in foundational modeling processes (Song et al., 2015). This issue is compounded by significant software interoperability challenges, a barrier identified by Zhou et al. (2017) in the context of Chinese tunnel engineering, which reflects the broader difficulty of integrating specialized tunneling software with general BIM platforms. Furthermore, the volume, velocity, and variety of data generated throughout a tunnel's lifecycle from prospecting to structural monitoring exceed the capabilities of traditional analysis methods, necessitating advanced computational approaches like machine learning (Huang, 2019).

Beyond technical hurdles, organizational and procedural factors also impede adoption. Zhou et al. (2017) further identified disorganized management as a critical challenge, where traditional design and construction approaches often create resistance to new digital methodologies. The specialized nature of tunnel BIM also demands new skills not widely available in the existing workforce (Sulankivi et al., 2020), and the substantial investment required for hardware, software, and training can be a deterrent, especially without a clearly quantified return on investment. A root cause of many interoperability issues is the absence of standardized protocols. Current Industry Foundation Classes (IFC) standards do not fully encapsulate the unique elements of tunnel engineering. In response, researchers like Sharafat et al. (2020) have proposed an extended IFC schema to represent tunnel-specific components not yet covered by buildingSMART international definitions.

7 PROPOSED STRATEGIC FRAMEWORKS FOR BIM ENHANCEMENT

Australia requires a cohesive national BIM strategy to overcome current fragmentation across jurisdictions and sectors. Research suggests a three-tiered framework addressing critical gaps in current implementation (Succar & Sher, 2014). First, establish a federally endorsed National BIM Authority with state implementation committees to develop consistent standards while respecting regional differences (Hampson et al., 2018). Second, develop specialized technical extensions for underground infrastructure that address geological data integration challenges identified in recent studies (Newman et al., 2020). Third, implement a national BIM accreditation program addressing the skills shortage documented by Consult Australia (2021). Infrastructure Australia's research (2023) demonstrates potential productivity improvements of 15-20% through consistent BIM implementation, particularly valuable for complex underground projects. Critical to success is reforming procurement models to support collaborative digital delivery, with standardized contractual provisions addressing intellectual property and data exchange (Australian Procurement and Construction Council, 2022). This framework aligns with international best practices while addressing Australia's unique federal structure and infrastructure needs.

8 RECOMMENDATIONS

Based on the case studies and industry best practices, the following recommendations are proposed.

- Early BIM adoption: Integrate BIM from the feasibility and conceptual design stages.
- Training, Standards and Continuous feedback: Establish BIM standards and train personnel across disciplines using project lessons.
- Data Integration: Ensure interoperability with GIS, geotechnical databases and FM
- systems.
- Leadership and Governance: Assign BIM managers to lead coordination and enforce model integrity.
- Interoperability between FEM and BIM is important in civil infrastructure design, as including ground conditions and geotechnical data in the BIM model improves its quality and use-

fulness not just in design, but also during construction and lifecycle management, especially for decision-making in urban areas.

— Although BIM use in Australian tunnelling is growing, it is still inconsistent. To maximize its benefits, Australia needs to standardize practices, build skills, and support policies. Collaboration between industry and government is key to advancing digital engineering in tunnel projects.

9 CONCLUSIONS

The findings indicate that while BIM adoption in tunneling remains less advanced than in general building construction, significant progress has been made through the development of specialized Tunnel Information Modeling frameworks, adaptation of LOD concepts to tunneling contexts, and successful implementation in major infrastructure projects worldwide. Key challenges identified include the lack of specialized component libraries, integration complexities with geological data, software incompatibility issues, and the absence of standardized protocols. These challenges are being addressed through ongoing research and development efforts, including the extension of IFC schemas to incorporate tunnel-specific elements and the creation of collaborative platforms tailored to tunnel engineering requirements. Future directions for BIM implementation in tunneling include integration with emerging technologies such as digital twins, machine learning, and robotics; continued development of tunneling-specific standards; and enhanced collaborative platforms that facilitate real-time data integration and cross-disciplinary collaboration. The global implementation of BIM in tunneling represents a crucial frontier in digital transformation for underground infrastructure development.

10 REFERENCES

Australian Constructors Association. (2022). constructors.com.au/wp-content/uploads/2020/09/ACA-IA- Response-Final-Version.pdf

Australian Cyber Security Centre. (2023). Protecting critical infrastructure information systems. Canberra: Australian Government.Critical Infrastructure | Cyber.gov.au

Bradley, A., Li, H., Lark, R. and Dunn, S., 2016. BIM for infrastructure: An overall review and constructor perspective. *Automation in construction*, *71*, pp.139-152

Bui, H.G., Trung Cao, B., Ninić, J., Nösges, M. and Meschke, G., Automatic Integration of Building Data into Large-Scale Numerical Simulations. *J. and Nösges, Markus and Meschke, Günther, Automatic Inte- gration of Building Data into Large-Scale Numerical Simulations*.

BuildingSMART Australia. (2021). Interoperability challenges in Australian construction. Sydney: BSA Publications.

Chen, L., et al. (2023). Blockchain for BIM Version Control in Megaprojects. Automation in Construction, 145, 104623.

Chow, L., Kuang, Z., & Baker, M. (2019). Representing geological uncertainty in BIM for underground construction. Automation in Construction, 97, 40 -53.

Consult Australia. (2020). Digital engineering skills gap analysis. Melbourne: CA Reports. digital.tas.gov.au/data/assets/pdf_file/0019/408331/ACS-DigitalPulse-2024_digital

Cross River Rail Delivery Authority. (2023). Digital delivery strategy outcomes report. Brisbane: Queens- land Government. Home - Cross River Rail

Critical Infrastructure Centre. (2022). Security guidelines for digital infrastructure models. Canberra: Australian Government.

Deartment of Home Affairs.Cyber and Infrastructure Security CentreDigital Design, Building and Operation of Underground Structures-BIM in Tunnelling, DAUBdaub-ita.de/fileadmin/documents/daub/gtcrec5/2019-05_DAUB_BIM_im_Untertagebau_EN.pdf

Engineers Australia. (2023). Professional development framework for digital engineering in underground construction. Sydney: EA Publications.

Howard, R. and Björk, B.C., 2008. Building information modelling–Experts' views on standardisation and industry deployment. *Advanced engineering informatics*, *22*(2), pp.271-280.

Infrastructure Australia. (2024). National digital engineering policy for infrastructure. Canberra: Australian Government.

Infrastructure Australia. (2021). Data management in major infrastructure projects. Canberra: Australian Government.
Infrastructure Australia. (2023). Digital transformation of infrastructure delivery. Canberra: Australian Government.
Koch, C., Vonthron, A. and König, M., 2017. A tunnel information modelling framework to support man- agement, simulations and visualisations in mechanised tunnelling projects. *Automation in Construction*, *83*, pp.78-90.
Lee, P.C., Wang, Y., Lo, T.P. and Long, D., 2018. An integrated system framework of building information modelling and geographical information system for utility tunnel maintenance management. *Tunnelling and Underground Space Technology*, *79*, pp.263-273.
Liu, Z., Lu, Y. and Peh, L.C., 2019. A review and scientometric analysis of global building information modeling (BIM) research in the architecture, engineering, and construction (AEC) industry. *Buildings*, *9*(10), p.210.Mao, J., Wang, Q., & Li, J. (2022). Integration of geotechnical and BIM systems for tunnel projects. Journal of Computing in Civil Engineering, 36(3), 04022008.
Rail Projects Victoria. (2020). Melbourne Metro Tunnel: Geotechnical BIM integration report. Melbourne: Victorian Government.
Roads and Maritime Services. (2019). WestConnex M4 East: BIM implementation case study. Sydney: NSW Government.treasury.nsw.gov.au/sites/default/files/2020-11/0023_westconnex_summary.pdf
Royal Institution of Chartered Surveyors. (2021). Measuring the benefits of BIM in infrastructure projects. London: RICS.BIM and the power of data in construction
Sacks, R., Eastman, C., Lee, G. and Teicholz, P., 2018. *BIM handbook: A guide to building information modeling for owners, designers, engineers, contractors, and facility managers*. John Wiley & Sons.
Sharafat, A., et al. (2021). Tunnel Information Modeling (TIM) for Risk-Driven Delivery. Journal of Con- struction Engineering, 147(8).
Shivasami, A., Lai, D., Dowdell, S., Gklotsos, N., Clifton, G. and Thorin, S., 2023. Early implementation of BIM in large infrastructure projects to manage complex interfaces in a dense urban environment. In *Expanding Underground-Knowledgeand Passion to Make a Positive Impact on the World* (pp. 2893-2901). CRC Press.
Smart Cities Council Australia New Zealand. (2022). Digital twins for underground infrastructure manage- ment. Sydney: SCCANZ.Harnessing AI and Digital Twins for Transformative Urban Asset Management | Smart Cities Council
Song, Z., Shi, G., Wang, J., Wei, H., Wang, T. and Zhou, G., 2019. Research on management and applica- tion of tunnel engineering based on BIM technology. *Journal of Civil Engineering and Management* , *25*(8), pp.785-797.
Standards Australia. (2023). Framework for performance-based BIM requirements. Sydney: SA.
Wang, L., Huang, M., Zhang, X., Jin, R. and Yang, T., 2020. Review of BIM adoption in the higher education of AEC disciplines. *Journal of Civil Engineering Education* , *146*(3), p.06020001.
Victorian Auditor-General's Office. (2022). West Gate Tunnel Project: Digital delivery assessment. Melbourne: Victorian Government.bigbuild.vic.gov.au/ data/assets/pdf_file/0006/787407/Audit-report,-September-2022-to-February-2023.pdf
Zhang, Y., & Liu, X. (2020). Probabilistic Geotechnical BIM for Underground Construction. Tunneling and Underground Space Technology, 98, 103354.
Zhou, Y., Wang, C., Yuan, B., Chen, M. and Lv, J., 2021. Research on visual management technology of tunnel construction process based on bim technology. Advances in civil engineering, 2021(1), p.9738820.
https://infrastructuremagazine.com.au/tunnel-vision/
https://www.sydneymetro.info/
http://westgatetunnelproject.vic.gov.au/about/keytopics/open-space
https://crossriverrail.qld.gov.au/info/benefits-for-all-of-seq/

Theme 14. Case Histories

THIS PAGE INTENTIONALLY LEFT BLANK

19th Australasian Tunnelling Conference – Acosta-Martínez, Stewart and Hudson-Smith (Eds.)
© 2025 Australian Tunnelling Society, ISBN 978-0-85825-002-4

Design of the Sydney Metro West turnback tunnels

S.J. Clarke, A. Merritt, D. Tran, D. Wang & M. Lecina
PSM, Sydney, Australia

ABSTRACT: Sydney Metro West is a new underground metro railway connecting Westmead to the Sydney CBD. The operation of the line requires the construction of a crossover cavern and turnback tunnels just beyond Hunter Street Station in the CBD. This network of tunnels allows the trains to switch tracks and reverse direction and provides train stabling for operational purposes.

The alignment is located within a relatively narrow corridor, with several tunnel and cavern profiles required to accommodate the various track geometries. The tunnels are constructed in a highly developed area of the CBD, below existing rail tunnels and high-rise buildings. The tunnels are also required to accommodate loads from future buildings.

Due to the close spacing of the tunnels combined, construction of the turnback tunnels required complex excavation sequencing and extensive use of reinforced concrete pillars.

This paper describes the challenges for the construction of the turnback tunnels and development of the design to satisfy the various constraints and construction requirements.

1 INTRODUCTION

Sydney Metro is Australia's biggest public transport project, building, operating and maintaining a network of four metro lines, 46 stations and 113 km of new metro rail. The Sydney Metro West (SMW) project comprises a new 24 km metro line with nine new stations to be constructed at Westmead, Westmead, Sydney Olympic Park, North Strathfield, Burwood North, Five Dock, The Bays, Pyrmont, and Hunter Street in the Sydney CBD.

The SMW tunnel and excavation works is being delivered in three contracts – the Western Tunnelling Package (WTP), Central Tunnelling Package (CTP) and the Eastern Tunnelling Package (ETP).

The John Holland, CPB Contractors and Ghella Joint Venture (JCG JV) is currently constructing the ETP, whose scope of works includes:

- 3.5 km TBM twin running tunnels from The Bays Station to Hunter Street Station.
- Excavation and civil works for two new station caverns at Pyrmont and Hunter Street in the Sydney CBD and a crossover cavern at Pyrmont Station.
- Turnback tunnels to the east of Hunter Street Station, allowing trains to travel back west towards Westmead.

This paper describes the constraints related to the design of the turnback tunnels, which included both geometric limits and consideration of existing and proposed buildings directly overlying the ETP alignment. These constraints as well as the relatively poor ground conditions led to unique design solutions which comprised a complex arrangement of variable sized caverns, tunnels, and adits. A complex excavation and construction sequence allowed for early installation of permanent reinforced concrete pillars between the closely spaced tunnels.

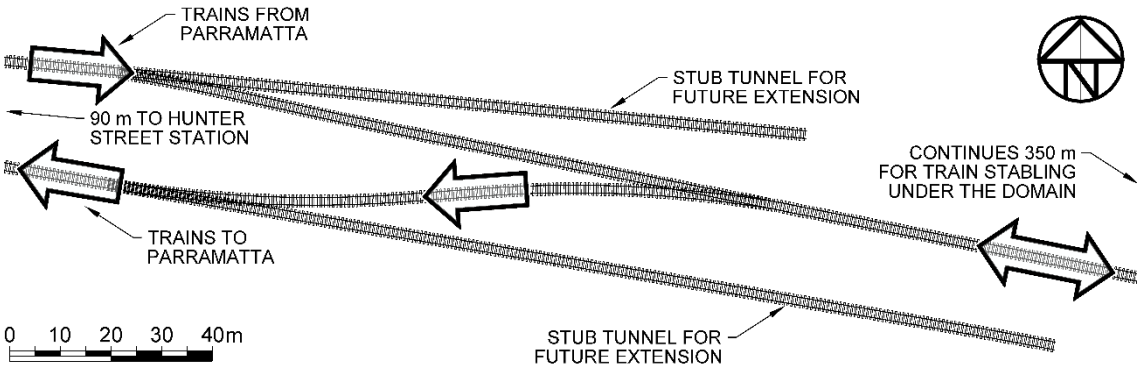


Figure 1. Schematic plan showing the functionality of the turnback tunnels, including stabling of trains and stub tunnels for future extension of the line.

2 KEY DESIGN CONSTRAINTS

2.1 *Alignment*

The required functionality of the turnback tunnels for the SMW ETP line, coupled with the location of Hunter Street Station, existing and proposed surface and underground infrastructure, and the potential future tunnel extensions, imposed significant constraints on the location, alignment and arrangement of the turnback tunnels.

Figure 1 illustrates the functionality of the turnback tunnels, allowing trains from Westmead to depart Hunter Street Station and either continue into the stabling tunnel beneath the Domain, or reverse direction back west to Hunter Street Station and on to Westmead. Two bifurcations are also included in the track alignment for trains to run through the northern and southern stub running tunnels for a future extension of the line.

To minimise the length of the turnback tunnels and the time required for trains to reverse direction during operation, the horizontal alignment of the various tracks was constrained which resulted in closely spaced tunnels of varying span. The vertical alignment of the turnback tunnels was also significantly constrained by existing and proposed infrastructure directly above and below the tunnels, together with limitations on the track grade.

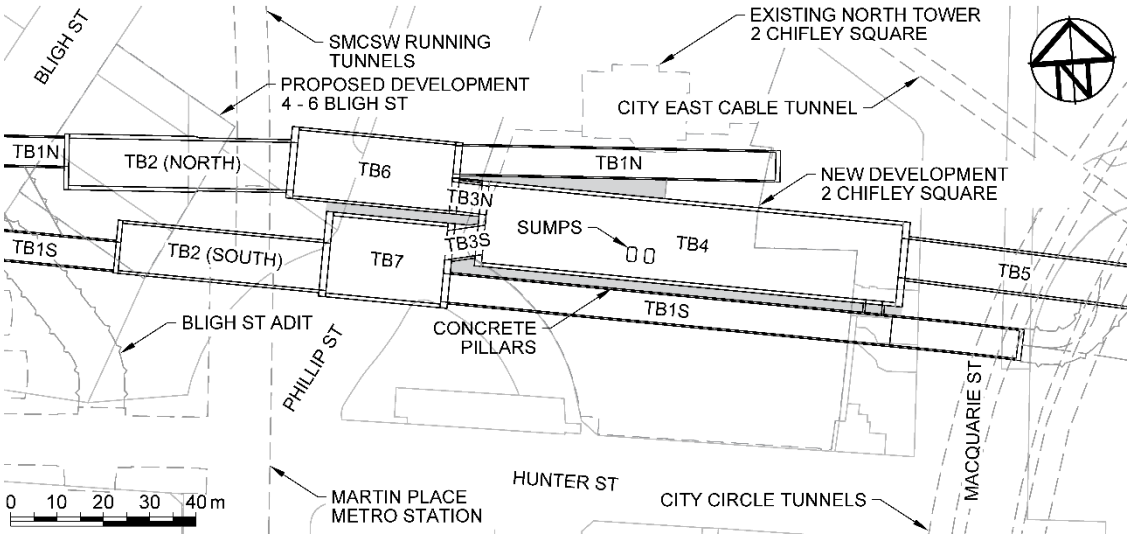
Alternative locations for the turnback tunnels west of Hunter Street Station and within the Domain were assessed during design development but the overall project requirements demanded the complex arrangement of large span tunnels be constructed in a heavily developed and highly constrained location of the CBD.

2.2 *Existing infrastructure*

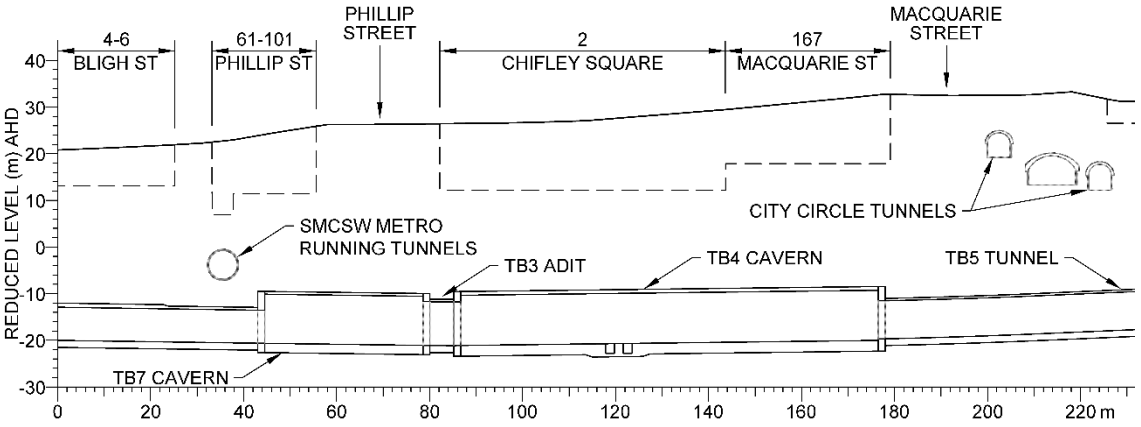
As a result of alignment and location constraints along with line-wide functionality requirements, the turnback tunnels were required to be constructed near significant and sensitive existing infrastructure including (Figure 2):

- Sydney Metro City & Southwest (SMCSW) running tunnels and Martin Place Station caverns, operational at the time of the turnback tunnel construction.
- Sydney Water heritage stormwater drainage tunnels.
- High rise buildings with deep basements and foundations directly above the tunnels, including the 53-storey North Tower at 2 Chifley Square over the TB4 cavern and TB1 North stub tunnel, noting that this was the tallest building in Sydney until 2020.
- Significant heritage buildings, including the State Library of NSW.
- City East Cable tunnel, a major power utility asset for the CBD, crossing four metres below the TB5 turnback tunnel, under the State Library building.
- Operational City Circle Line rail tunnels, and adjacent disused rail tunnels, crossing 15 m above the TB5 tunnel.

The assessment of impacts from the turnback tunnel construction on the adjacent existing infrastructure is beyond the scope of this paper, however this was a key design consideration to limit deformations and minimise effects on a wide range of sensitive infrastructure.



(a) Plan view



(b) Sectional elevation

Figure 2. Plan and sectional elevation of the western portion of the turnback tunnels.

2.3 *Future buildings*

In addition to the existing buildings and infrastructure surrounding the turnback tunnels, the design and construction was also required to accommodate development of proposed high-rise buildings above the alignment.

The new development at 2 Chifley Square involves construction of a 37-storey tower adjacent to the existing North Tower above the TB4 cavern and TB1 South stub tunnel (Figure 2). The permanent support of the turnback tunnels was designed to support loads from both Chifley Square towers. The tunnel primary support and excavation sequence was also heavily influenced by the existing and future towers, as these buildings imposed restrictions on the alignment and available substratum for ground support. The concurrent construction of the turnback tunnels and the new building necessitated detailed assessment of tunnel support design and tunnel construction effects on the buildings.

Additionally, the proposed development at 4-6 Bligh Street is located over the TB1 and TB2 turnback tunnels (Figure 2). The proposed development comprises a 59-storey building with a deep basement. Various foundation options for the new building were assessed during the design development to minimise impacts on the tunnel design. The turnback tunnel permanent linings were designed to support significant loads from the building footings, requiring modified tunnel profiles, lining thicknesses and reinforcement.

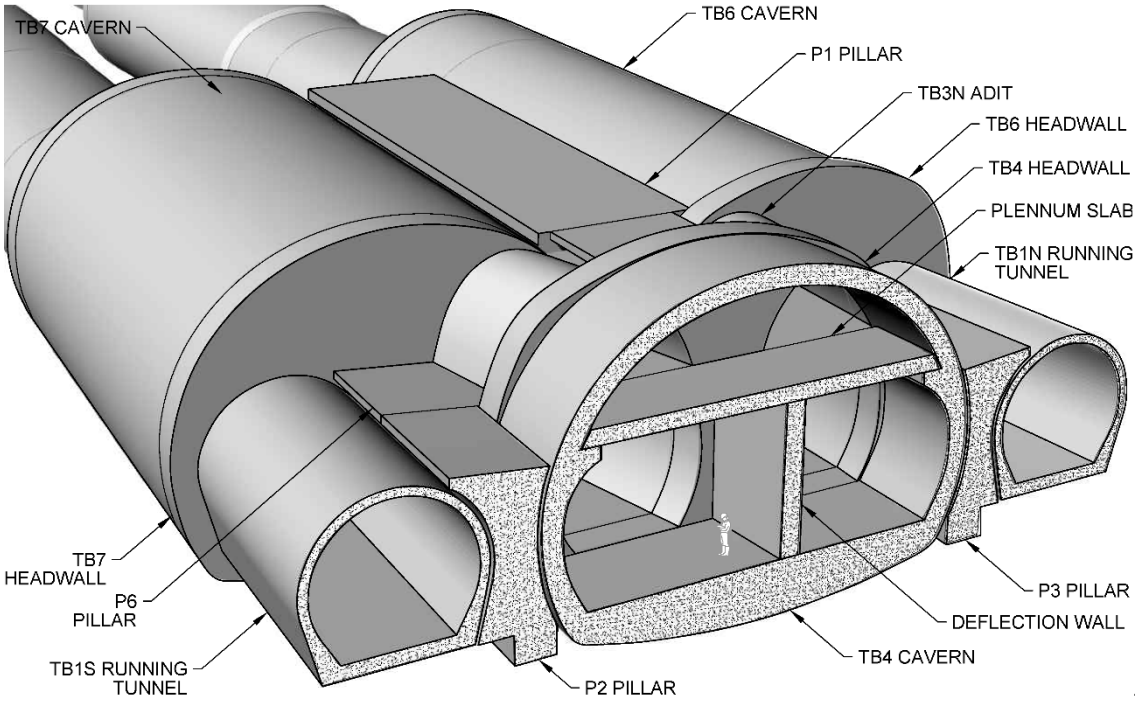


Figure 3. Perspective view of the caverns, headwalls, and adits required where the configuration changes from two adjacent caverns to a single cavern flanked by running tunnels.

2.4 *Construction methods*

The construction methods and tunnel permanent support specified for the project also constrained the design and configuration of the turnback tunnels. The use of permanent shotcrete tunnel linings was not permitted, preventing the use of tapered tunnel profiles to match the gradually diverging track alignments.

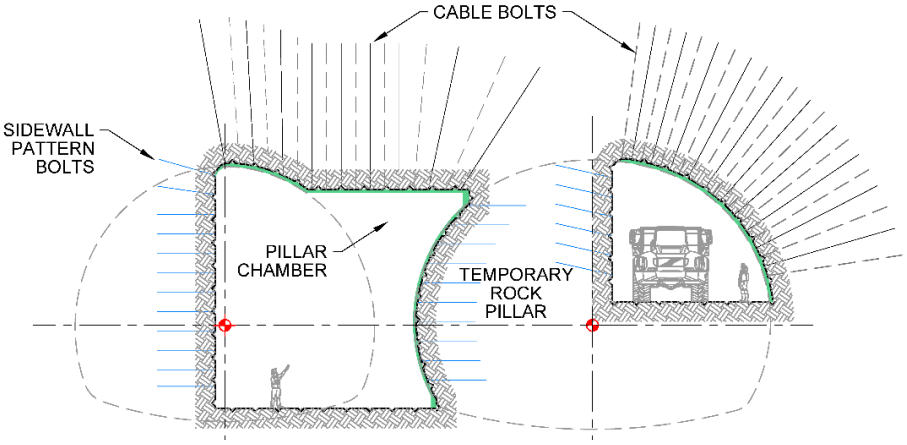
Instead, cast in situ reinforced concrete permanent linings were mandated, resulting in the complex configuration of progressively larger caverns to suit the diverging rail tracks. Six different tunnel profiles were required with multiple headwalls at profile junctions and pillar replacement between the closely spaced tunnels and caverns. The geometry and configuration resulted in complicated construction sequencing of the tunnel excavations, primary support, permanent pillars, waterproofing and permanent lining of the turnback tunnels (Figure 3).

3 GROUND CONDITIONS

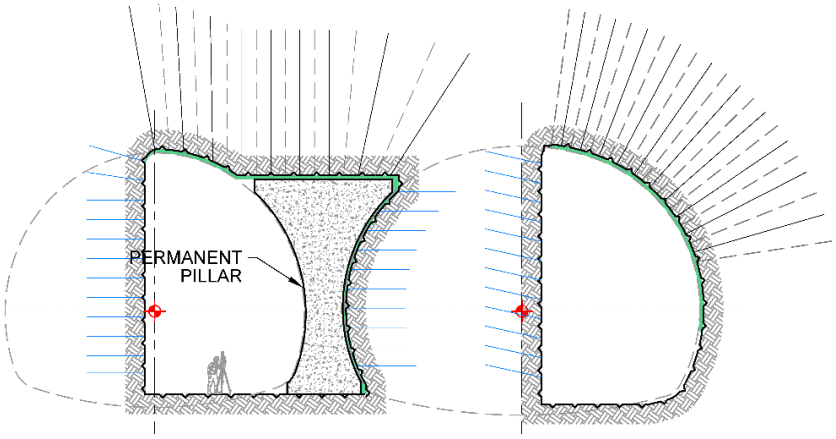
The turnback tunnels were expected to be excavated within Class I/II Hawkesbury Sandstone, classified in accordance with Pells *et al* (1998), with localised reduced rock mass class (Class III Sandstone with occasional Class IV/V) in proximity to significant geological structures. The rock cover above the crown of the tunnels ranged from 18 m to 44 m, with the minimum cover occurring beneath the existing 2 Chifley Square basement.

A significant laterally continuous, ramping, low angle fault was anticipated to be encountered by the turnback tunnels. The damage zone around the fault was inferred to extend 2 m to 4 m either side of a brecciated fault core, with the extent defined by sub-horizontal clay-infilled or extremely weathered features. Based on the expected ground conditions, relatively shallow rock cover, and site-specific stress test results, the caverns were assessed to be within the lower end of the typical in-situ stress range.

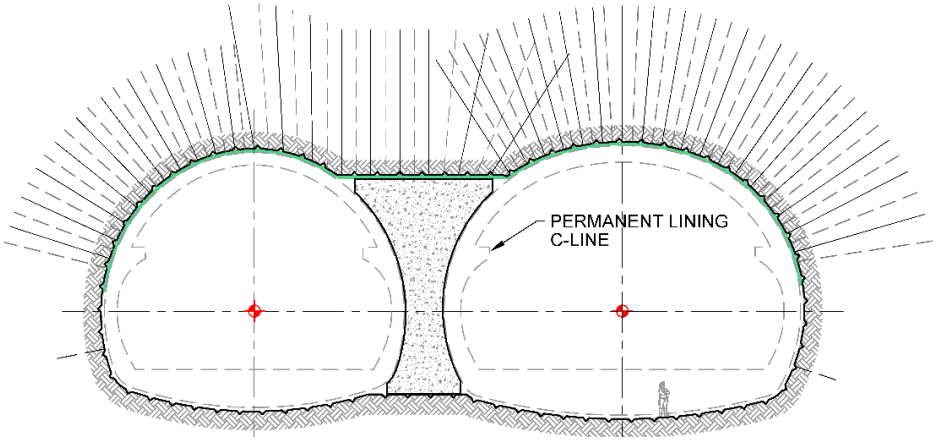
Groundwater levels prior to tunnelling were typically 12 m to 20 m above the tunnel crown level.



(a) Excavation and support of TB6 side heading, bench and invert, and pillar chamber.



(b) Construction of permanent reinforced concrete pillar and excavation of TB7 bench and invert.



(c) Excavation and support of remaining caverns.

Figure 4. Simplified sequence of the excavation and installation of primary support for the TB6 and TB7 caverns and permanent pillar P1.

4 PRIMARY SUPPORT

4.1 *Bolted support*

The majority of the turnback tunnels employed rock bolts combined with thin shotcrete for primary support. For the running tunnels and smaller tunnel profiles, the primary support comprised steel double corrosion protection (DCP) bolts with an ultimate capacity of 310 kN and

lengths of 3 m to 4.5 m, typically spaced in either a 1.25 m or 1.5 m grid pattern depending on ground conditions. DCP bolts were not required for durability but were adopted because they were easier to grout than other bolt types. Bolt lengths for the turnback cavern were also constrained by the proximity of the permanent ground anchors and substratum boundary beneath the existing 2 Chifley Square tower.

Cable anchors with an ultimate capacity of 570 kN were adopted for the larger caverns. These had lengths of 6.5 m to 7.5 m and were spaced at 1.0 m to 1.5 m centres, noting that the spacing of some profiles varied between the transverse and longitudinal directions.

Handlebar plates were adopted for both rock bolts and cable bolts to ensure an adequate structural connection between the shotcrete and the bolt heads.

Shotcrete was reinforced with synthetic fibres (SFRS) and typically sprayed to a design thickness of 100 mm to provide temporary ground support between rock bolts.

Pattern sidewall bolts were adopted in the support designs due to the known variable rock quality and likelihood of intercepted poor-quality bedrock, including faults and joint clusters. Sidewall bolts were installed for significant portions of the turnback tunnels.

Short sections of four of the turnback tunnels crossing below the operational SMCSW tunnels and Martin Place Station with low cover of 4.6 m to 5.3 m. These locations required additional support to minimise ground movements, comprising rock bolts and a 250 mm to 350 mm thick passive shotcrete arch.

4.2 *Pillar chambers*

A unique challenge of the primary support design was accommodating the unusual geometry required for the reinforced concrete pillar chambers. These included convex rather than concave sidewalls and flat crowns, all in the context of relatively poor rock conditions. The sidewall geometry restricted the installation of cable bolts across the crown of the chamber and necessitated the adoption of flatter anchor angles and use of reaming tools for the anchors located near the sidewalls.

The necessity of excavating the caverns to full height to allow construction of the pillars meant that the more conventional approach of heading, bench, then invert excavation could not be employed across the full span of the TB6 and TB7 caverns (Figure 4).

Construction of the permanent pillars part-way through excavation of the turnback tunnels also imposed additional programming and scheduling challenges.

4.3 *Monitoring*

In tunnel monitoring during construction included routine use of optical survey prisms, progressively installed with the tunnel heading excavations. Multi-point rod extensometers were installed at 10 m intervals within the larger caverns to monitor crown sag for comparison against design predictions. The highest anchor was located approximately 6.5 m above the crown. Endoscopes were used to assess ground conditions above crown level and monitor shear deformations along horizontal defects in the rock mass. These were also used for assessing ground conditions for pillars at critical locations through probe holes.

Comprehensive real-time optical survey monitoring was required for the operational SMCSW running tunnels and City Circle rail tunnels. Bi-axial tiltmeters were employed to monitor overlying sensitive buildings.

Discussion of the results of the construction monitoring are beyond the scope of this paper, though it is noted that the results fell within the range of expected movement and permitted construction to proceed without the need of having to stop work to review design assumptions or primary support details.

4.4 *Construction sequencing*

The need to complete the pillar replacements prior to opening up the caverns, combined with the unusual cavern layout involving multiple profiles of differing sizes, resulted in a complex construction sequence which was developed in conjunction with JCG to improve the construction program.

Of particular importance was gaining access to the 350 m long stabling (TB5) tunnel located at the eastern end of the project. Without timely access, tunnelling works would have been stalled due to the design constraints preventing commencement of the excavation in the other tunnels prior to the adjacent pillars' completion. This requirement was met by changes to the transition tunnels located between the two caverns to the west (i.e. TB6 and TB7) and the single cavern (TB4) to the east, as well as by excavation of a temporary access adit from the southern stub tunnel to the TB5 tunnel, allowing works within TB5 to proceed independently, thereby avoiding delays to the overall program.

5 PERMANENT CONCRETE PILLARS

5.1 *Purpose*

Owing to the closely spaced track alignments within the turnback tunnels, the minimum clearance envelope around each track, the permanent lining thickness, and construction tolerances, the remaining pillar width between most of the tunnels ranged from as little as 0.8 m to 2.7 m. These rock pillars were replaced by reinforced concrete.

Due to the overburden thickness, existing and proposed buildings, and the substantial cavern spans, the pillars were required to support substantial loads for both temporary and permanent conditions. Ground load assessments using a range of 2D and 3D numerical approaches indicated vertical working loads for the various pillars ranging from 9 MN/m run to 13 MN/m run, with mean compressive stresses at the neck (i.e. narrowest width) of the pillars ranging from approximately 3 MPa to 11 MPa.

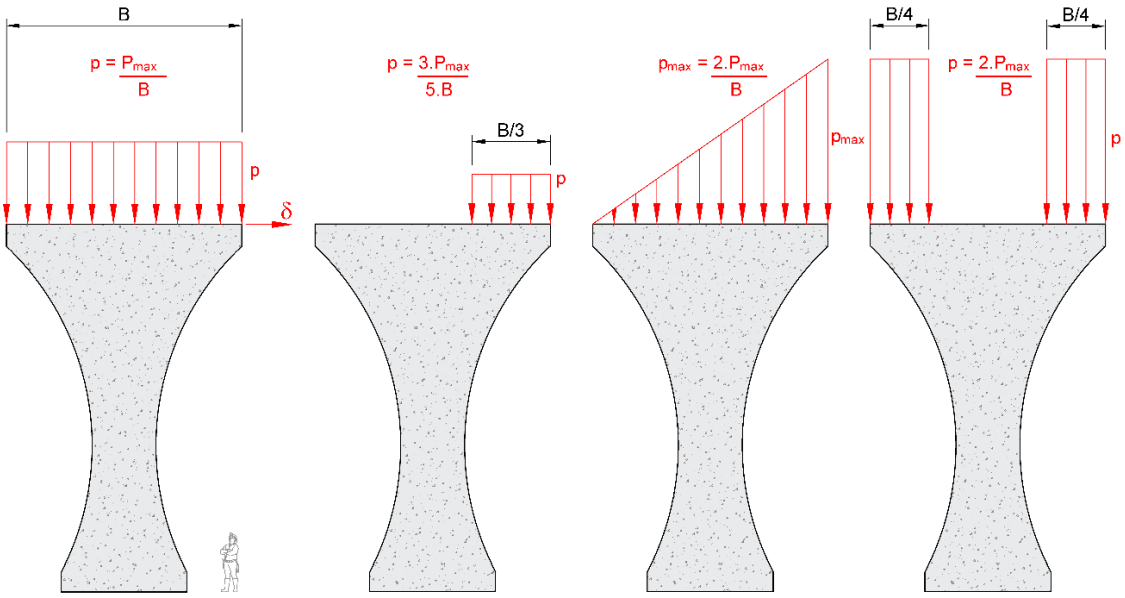
Based on the ground conditions at the pillar locations, the maximum acceptable vertical stress for retaining rock pillars (including potential treatment / reinforcement) was set at 3 MPa. This meant that virtually all the rock pillars needed to be replaced by reinforced concrete.

The use of plain concrete was not a viable option due to the pillar geometry and stress-relief deformation experienced after excavation of adjacent tunnels.

At one location the pillar width was up to 5.4 m, and upon inspection of the rock conditions during construction it was considered acceptable for this to remain as a rock pillar.

5.2 Geometry

Due to the curved sidewalls of the tunnels located either side of the pillars, each pillar comprised an hourglass shape, with a narrow neck at around mid-height, and a wider base and top (Figure 5).



(a) Uniform (b) Low axial force (c) Eccentric (d) Concentrated

Figure 5. Design loading scenarios developed for the permanent reinforced concrete pillars.

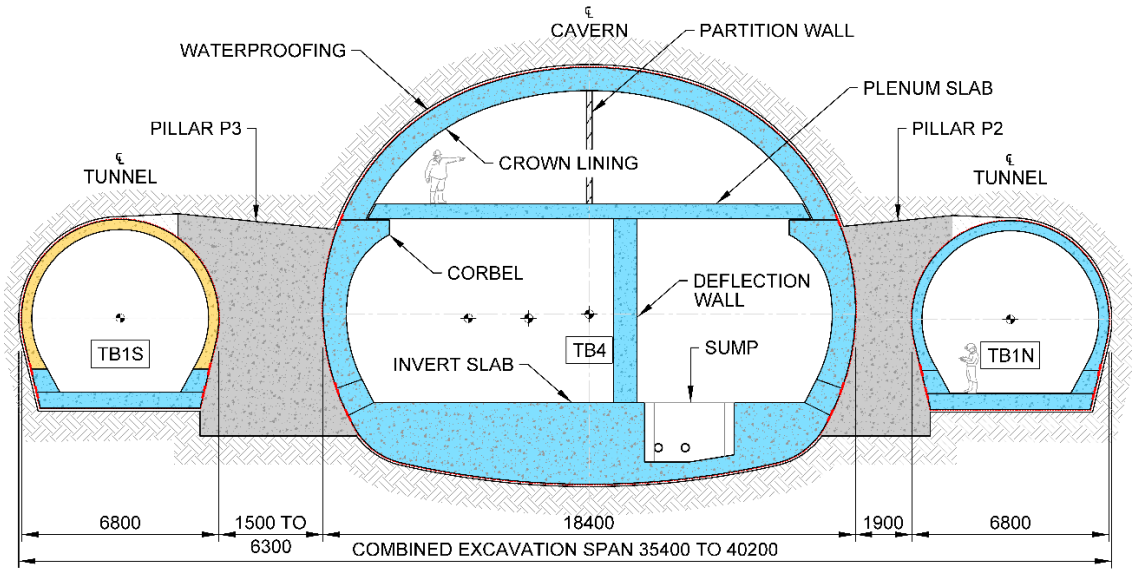


Figure 6. Section through permanent tunnel lining of TB1N running tunnel, TB4 cavern, TB1S running tunnel, and P3 and P2 pillars.

Six pillars required replacement within the turnback tunnels, with a total combined length of 175 m, and heights ranging from 6.5 m to 11.1 m (Figure 2).

The top width of the pillars ranged from 2.9 m to 7.1 m and was governed by the allowable bearing pressures applied to the poorer quality rock present in the crown. The bottom width was narrower than the top because rock quality was typically better at lower levels, although in some locations deepening of the pillar footings was required due to localised poor rock quality or to account for the lower position of the adjacent tunnel profiles.

5.3 *Design loads*

Numerical modelling of the pillars was undertaken to explore the variable loading conditions caused by the construction sequence, which initially comprised excavation of a pillar chamber, followed by construction of the pillar, then progressive enlargement of the tunnel and cavern excavations on either side (Figure 4).

The interaction between the ground and pillar structure resulted in a range of behaviours associated with the variable ground conditions, pillar and tunnel geometries, and stress-relief movements. Based on these results a series of simplified design load cases were prepared (Figure 5) to capture the different ground behaviours noting that these also included an imposed lateral deformation of up to 7 mm. The design load magnitudes, P_{max}, is described in Section 5.1.

5.4 *Design approach*

Several approaches were applied to the design of the pillars to avoid over-reliance on a single methodology and provide a basis for checking different methods. Due to the irregular and unusual shape of the pillars there was no directly applicable structural design approach, albeit there were similarities with shallow footing design approaches and reinforced concrete column design. These analogous approaches were applied to provide an initial indication of reinforcement requirements, as well as a check on the more detailed numerical modelling approach ultimately adopted.

The finite difference numerical analysis software package FLAC3D was adopted to simulate the structural response of the pillars up to and beyond the working loads. The FLAC3D models included each steel reinforcement bar with constitutive models calibrated to provide realistic material behaviours for both concrete and steel.

Validation of this analysis methodology is not given here but is documented in Tran *et al* (2025). Confirmation of the ultimate load capacity followed the requirements in Clause 2.3.6 of

AS 5100.5-2017. This clause requires the pillars to accommodate 300% of the design working load without collapse, noting that this criterion also considers the earthquake load case.

Deflection and crack width checks were also based on the FLAC3D analysis with crack widths based on correlations with the calculated tensile stresses in reinforcing bars.

The above approach resulted in reinforcement densities of 130 kg/m^3 to 185 kg/m^3, with irregular bar geometries required in some instances due to the geometric constraints imposed by the adjacent tunnel profiles.

6 PERMANENT TUNNEL LINING

6.1 *Transition structures*

A significant challenge for the turnback tunnels was the permanent lining details where the configuration changes from two adjacent caverns (i.e. TB6 and TB7) to a single cavern (i.e. TB4) flanked by running tunnels (Figure 6).

The final design involved headwalls at the ends of each cavern, with two 5 m long adits (i.e. TB3S, TB3N) conveying the track between the three caverns. The adit cross-sectional geometry was dictated by the ventilation area requirements above the continuous plenum slabs between the caverns.

The two stub running tunnels also intersect the headwalls of the two caverns. Due to the proximity of the four tunnels at the transition, permanent concrete pillars were required to be constructed prior to opening up the caverns on either side.

The geometric complexity of this configuration resulted in additional challenges for the waterproofing details and connections between the different profiles.

6.2 *Ground and groundwater loads*

Ground loads were assessed based on consideration of several methodologies, including empirical methods and those based on detailed finite element (FE) analysis. The FE analysis approach included key construction stages to simulate the load transfer mechanism from the primary support to the permanent lining:

1. Simulation of ground conditions and existing building loads prior to commencing excavation.
2. Sequential excavation capturing heading advance and excavation stages.
3. Installation of the primary support design and proposed construction sequence.
4. Installation of the waterproofing layers and permanent concrete lining.
5. Removal of temporary primary support (i.e. allowing the rock mass to relax to transfer load to the permanent lining). The concrete modulus of concrete pillars is reduced at the same stage to shed load to the permanent lining.
6. Application of future building loads.

The adopted ground loads ranged from 65 kPa to 530 kPa, with the highest loads associated with the overlying high-rise buildings.

Different groundwater levels were adopted for the serviceability (SLS) and ultimate limit state (ULS) design checks. The groundwater design levels were constrained by the requirements of the project specification. The adopted typical groundwater pressure (i.e. SLS) closely corresponded to the basement levels of the overlying buildings, while the credible worst groundwater pressure (i.e. ULS) corresponded to the ground surface level. For the larger caverns these adopted levels resulted in uplift pressures on the underside of the invert slabs of 360 kPa (SLS) to 560 kPa (ULS). Detailed 3D hydrogeological groundwater modelling predicted long-term groundwater levels substantially lower than the adopted design levels.

6.3 *Tunnel lining and waterproofing*

The tunnel linings were designed as either bar-reinforced concrete, fibre-reinforced concrete, or plain concrete, depending on the tunnel geometry and applied ground and groundwater loads.

Bar-reinforcement was required for the sidewalls of the cavern and tunnels where a corbel was required to support the internal plenum slabs. Heavy steel reinforcement was used in the crown of the tunnels for sections subject to large ground loads associated with the overlying buildings.

The headwalls, endwalls, and invert slabs comprised bar-reinforced concrete due to their unfavourable geometry and presence of large groundwater loads. Within cavern TB4 the project specification required provision of a sump for the water treatment plant. The sump geometry was optimised from the original concept to two parallel sumps to improve structural efficiency and avoid excessive deepening of the invert slab (Figure 6).

Steel fibre-reinforced concrete was adopted for the crowns of the caverns and running tunnels where ground loads were not affected by large building loads. Plain concrete was employed for the crown of the TB5 tunnel above the corbel level, given the favourable profile and ground loads.

Waterproofing for the permanent tunnel linings comprised a 2 mm thick sheet membrane, constructed from very low density polyethylene (VLDPE).

A sacrificial sump detail was designed to allow dewatering of the ground surrounding the caverns while the waterproofing membrane was being installed and concrete lining constructed. The sump was located outside the waterproofing membrane and included details to permit effective sealing of the pipework once the permanent lining was completed and able to accommodate elevated groundwater levels.

6.4 Deflection walls and plenum slabs

The turnback tunnel design scope included deflection walls and plenum slabs which extended through the majority of the caverns and tunnels.

The deflection walls are required for train impact loads and are secured to the invert slabs.

Plenum slabs in the larger caverns and TB5 tunnel were required to create a ventilation space above the tracks, with a maximum span of 14.5 m, including post tensioned sections around openings. These were designed by structural engineering firm, TTW, working alongside PSM to integrate with the tunnel lining design.

7 CONCLUSIONS

The design of the turnback tunnels currently being constructed as part of the SMW ETP project encountered numerous technical challenges associated with onerous geometric constraints, proximity to existing tunnels and high-rise buildings, together with challenging ground conditions and the need to safeguard proposed future building developments above the tunnels.

Robust and practical design solutions were developed in conjunction with JCG JV to address these challenges. This included the extensive use of permanent reinforced concrete pillars associated with a detailed construction sequence to optimise delivery of the works whilst ensuring ground stability and minimising ground movements and impacts from the works.

At the time of writing this paper the permanent pillars and tunnel excavation works had been successfully completed with the permanent tunnel linings under construction.

ACKNOWLEDGEMENTS

The authors would like to acknowledge JCG JV and Sydney Metro for granting permission to publish this paper, as well as their appreciation of the professionalism and technical expertise provided by colleagues at PSM in the development of a practical design. Also to the JCG JV design and construction teams for their collaborative input throughout the design process and their implementation of the design to a high standard.

8 REFERENCES

Pells, P.J.N., Mostyn, G. & Walker, B.F. 1998. *Foundations on sandstone and shale in the Sydney region*. Australian Geomechanics, December, pp.17–29.

Tran, D., Clarke, S.J. & Afshar, P. 2025. *Numerical analysis and design of complex bar reinforced concrete tunnel structures with FLAC3D*. In: Proceedings of the 32nd Biennial Concrete Institute of Australia National Conference. Adelaide.

19th Australasian Tunnelling Conference – Acosta-Martínez, Stewart and Hudson-Smith (Eds.)
© 2025 Australian Tunnelling Society, ISBN 978-0-85825-002-4

Tawhai tunnel lining recovery

S.F. Chau, T. Cheung
Aurecon, Auckland, New Zealand

R. Ballen
KiwiRail, Auckland, New Zealand

I. Duncan
Beca, Christchurch, New Zealand

ABSTRACT: Tawhai Tunnel, located on KiwiRail's Stillwater–Ngakawau Line (SNL) on the West Coast of New Zealand's South Island, was constructed in 1891 and is 373m long. Its tunnel lining system consists of a 250 to 400 mm thick concrete sidewall extending to the tunnel spring-line and a single-layer, 250 mm thick concrete block arch forming the tunnel crown. In mid-June 2024, the 133-year-old tunnel had three sections of tunnel lining fail. Immediately following the event, KiwiRail established a multi-disciplinary tunnel recovery team, comprising the Client (KiwiRail), Design Consultants, and Contractors. This team worked collaboratively to restore the tunnel safely, efficiently, and to a high-quality standard within a short timeframe. The recovery design and construction work were completed within 26 weeks, and the tunnel reopened for coal train operations on 12 January 2025. This paper provides a brief overview of the tunnel's construction history. Based on site observations, it also discusses the back-analysis undertaken to determine geotechnical analysis parameters plus the design and construction of the recovery and strengthening works throughout the tunnel. Special attention is given to the unique planning, design and execution challenges relating to this tunnel project.

1 INTRODUCTION

Tunnel 1, Tawhai Tunnel, on the SNL is located on the West Coast of New Zealand's South Island, near Reefton. Both tunnel portals are accessible from State Highway 7, Figure 1. The tunnel length is 373 m. State Highway 7, which connects Greymouth and Reefton, passes closely over the southeastern side of the tunnel at a location known as the 'Reefton Saddle'.



Figure 1. Location of SNL tunnel 1 and south portal.

Constructed in 1891, the existing tunnel lining system comprises lower concrete sidewall extending to the tunnel springline and a single-layer concrete block arch forming the crown. The block arch is approximately 250 mm thick, while the concrete sidewalls range from 250 to 400 mm in thickness.

In June 2024 during planned track works inside the tunnel, some issues were identified with the 133 year old tunnel lining. The tunnel was safely evacuated and drone video surveys were undertaken which identified three sections of tunnel where the lining had partially collapsed.

This paper focuses on the tunnel recovery works design and construction.

2 GEOLOGY

The regional geology is based on the GNS Science 1:250,000 geological map of the Greymouth area. The tunnel is situated within the Pliocene-aged Old Man Group, comprising weathered gravel with predominantly greywacke and schist clasts. Approximately 1 km southeast of the site, Ordovician Greenland Group basement rocks outcrop, with a thin strip of fluvial sandstone, estuarine mudstone, and minor conglomerate forming the basal unit of the Old Man Group along the unconformity. Site walkovers, test pits, drilling, and historical photos confirm the presence of Old Man Group gravels at the tunnel ends, and it is inferred the tunnel remains within these gravels along its entire length. All modelling and analysis assumes that the tunnel is entirely within the Old Man Group gravels. Figure 2 presents an interpretative ground model of the middle tunnel section.

Ground cover to tunnel crown is 20 to 56 m and at collapse locations are about 30 m. Limited piezometer monitoring data showed groundwater head is approximately 4 to 5 m above tunnel crown. Measurement of the tunnel outflow over tunnel length of approximate 200m from the northern portal has been reported as 0.2 to 0.3 L/s in dry weather conditions and 0.5 to 0.6 L/s after 100 mm of rainfall over a week, in early to mid August 2024.

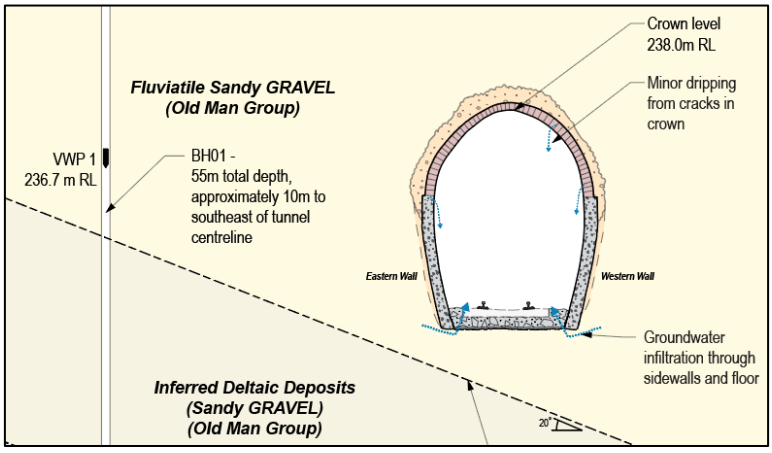


Figure 2. Interpretive geology of SNL tunnel 1.

3 TUNNEL BACKGROUND

3.1 *Tunnel construction history*

With reference to the tunnel records provided by KiwiRail, excavation and lining works for the tunnel were carried out between the late 1880s and 1891. There are no indications that suggests that temporary support was required during tunnel excavation prior to the installation of the permanent lining.

Track lowering works were undertaken in 1984 to improve train clearance. Approximately 14m from the north portal, a section of the original concrete block arch was removed and replaced with

a steel rib arch. Additionally, the concrete sidewalls were strengthened by applying an approximately 100 mm thick layer of reinforced concrete.

3.2 *Fall of grounds*

The lining failure occurred on the morning of 15 June 2024. Three separate Falls of Ground (FOGs) developed, Figure 3. After the initial failures, there were no additional ground falls observed (based on repeat drone video surveys conducted while tunnel access remained restricted). A 3D point cloud survey was undertaken to record and assess tunnel deformation and to capture detailed information related to the FOGs.

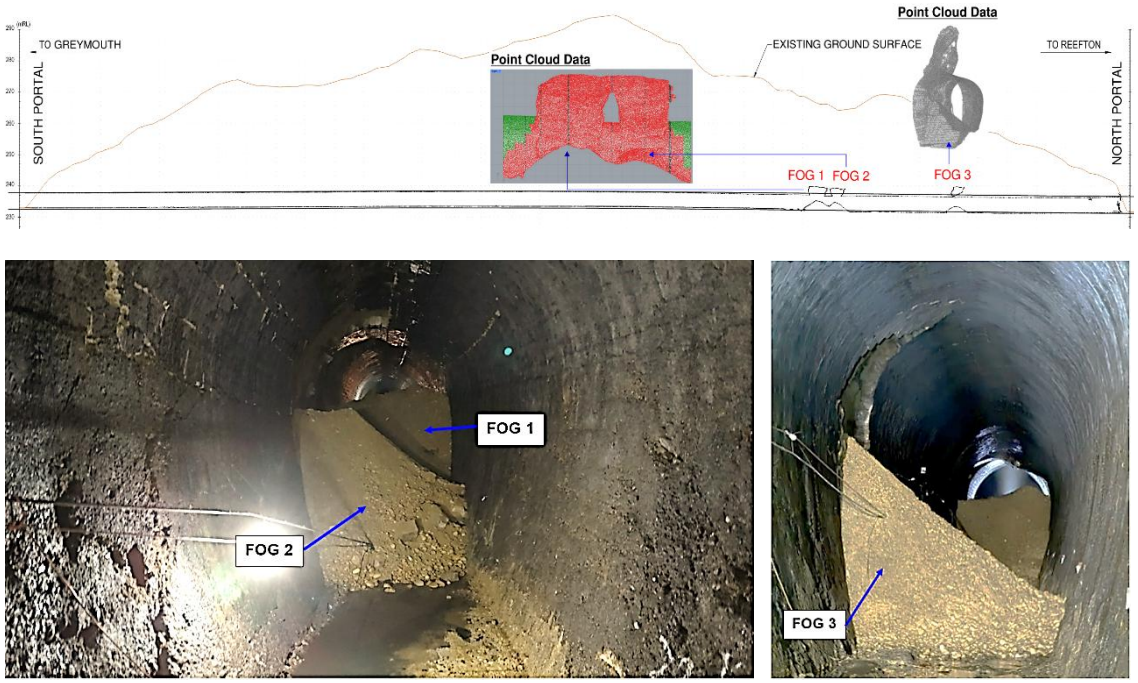


Figure 3. Tunnel long section and fogs of SNL tunnel 1

3.3 *General tunnel condition*

After the FOG event, the tunnel lining near the FOGs deformed with inward movement of 100 to 200mm at walls and shoulders. Other areas of the tunnel were observed with negligible movement by scan profile comparison before (Dec 2023) and after the event (June 2024).

The materials and construction details were consistent with a tunnel structure over 130 years old. The cored concrete test showed the concrete strength ranging 6 to 16 MPa.

To ensure a long-term resilient future for the tunnel, it was decided that the lining should be treated for the whole length of the tunnel.

4 THE TUNNEL SUPPORT SYSTEM

4.1 *General concept*

The primary focus was developing a solution which effectively treated the tunnel lining and could be executed very rapidly in order to re-open the railway line as soon as possible.

The project team considered plant and resources that were immediately available for use under emergency conditions. There were different recovery options developed considering the use of shotcrete and/or cast-in-place concrete, ground anchoring, different types of track formation plus

tunnel invert and footing treatments to achieve the required tunnel clearances, safe tunnel restoration and long-term structural resilience.

A detailed assessment was carried out to evaluate the different recovery options by comparing their advantages and disadvantages. The selected recovery solution included ground anchors, a ballast trackform over a sub-ballast concrete slab, and a new shotcrete lining as presented in Figure 4.

A clearance assessment was also conducted, which considered the independent kinematic envelopes of three different wagon and locomotive types. These represented the worst-case clearance scenarios for all rolling stock with operational access rights through the tunnel.

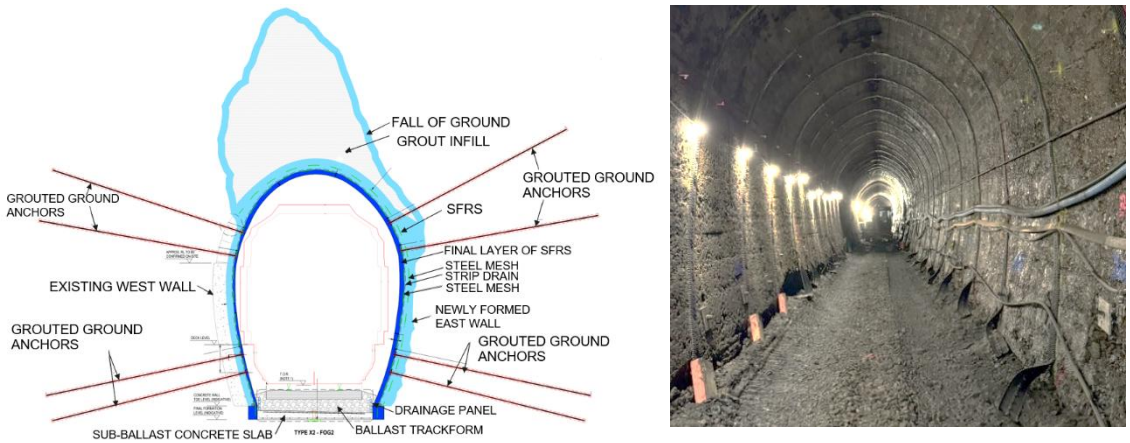


Figure 4. Typical tunnel recovery system.

4.2 *Geotechnical back analysis*

A back-analysis was conducted to determine appropriate geotechnical parameters (effective cohesion c', friction angle ϕ', and Young's modulus E) for modelling tunnel stability and observed site conditions. Using PLAXIS 2D, key parameters—particularly c' and ϕ'—were iteratively adjusted and validated against slope stability analysis results (e.g. steep and stable slopes were observed along the nearby rail corridor and State Highway 7) and 3D Point Cloud data. The modelling aligned well with the observed geometry of the FOGs.

Ground arching height was estimated using the back-calculated parameters and Terzaghi's theory. The agreement between analytical results and site observations supported the reliability of the selected parameters and confirmed the inferred ground loads.

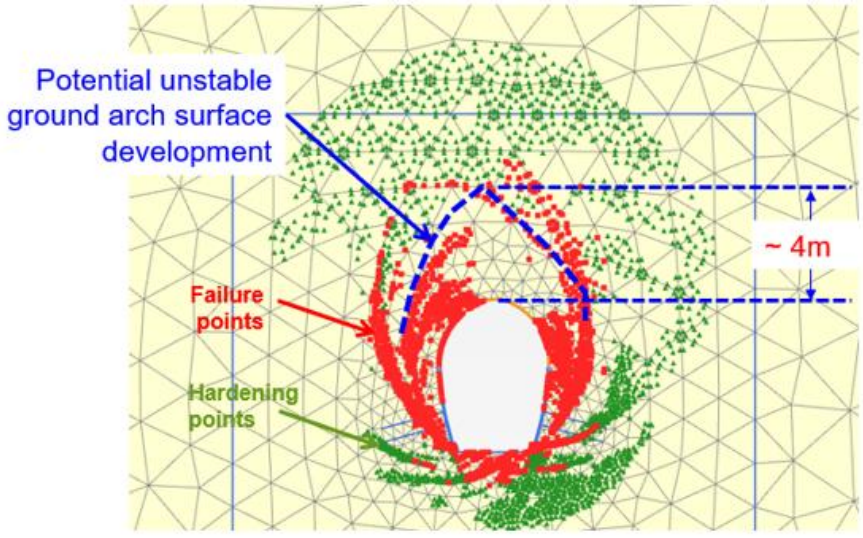


Figure 5. Ground failure development and ground arch formation, PLAXIS 2D.

4.3 *Tunnel collapse recovery and improvement works*

4.3.1 *Typical tunnel support system*

The typical tunnel support system was formed by (1) ground anchors, (2) shotcrete lining, and (3) ballast track form, and (4) sub-ballast concrete slab. This system extends to the whole tunnel with varying quantities depending on the specifics of the different tunnel sections.

1. Passive ground anchors (e.g. no pre-tensioning) were installed on the lower walls as pre-support measures to maintain lining stability for further floor lowering for track formation work and at other locations where required.
2. Steel Fibre Reinforced Shotcrete (SFRS) of 40 MPa was adopted to reinforce the existing tunnel lining. The fibres used have a maximum length of 35 mm, with a length-to-diameter ratio of 65. The minimum dosage applied was 35 kg/m³ in mixed shotcrete to achieve the required structural performance.
3. The existing tunnel is a drained tunnel, and the recovered tunnel lining remains consistent with this approach. Strip drain channels were installed at regular intervals to collect seepage and direct it to the longitudinal subsoil drain integrated within the ballast track form.
4. The reinforced sub-ballast concrete slab is designed to withstand train loading, the self-weight of overlying materials, axial loads transferred from the tunnel lining, and groundwater pressure in the event of drainage blockage. The slab is maintained in a drained condition through the installation of riser pipes with Megaflo panels, which effectively manage water beneath the slab and prevent the build-up of hydrostatic pressure.

4.3.2 *Fall of ground support*

In addition to the typical support system, reinforcement mesh was incorporated into the shotcrete lining to provide additional structural capacity at the locations of the Falls of Ground (FOGs). Furthermore, shotcrete and anchor supports were installed immediately adjacent to the FOG areas before any work commenced within these zones. The cavity was backfilled in stages using grout and lightweight expansive concrete. Any debris and damaged concrete block or wall sections were removed prior to backfilling. A 3D numerical analysis, Figure 6, was conducted in FLAC 3D to assess the effectiveness of the tunnel collapse treatment measures, specifically to evaluate the safety and feasibility of people entering and working beneath the affected areas.

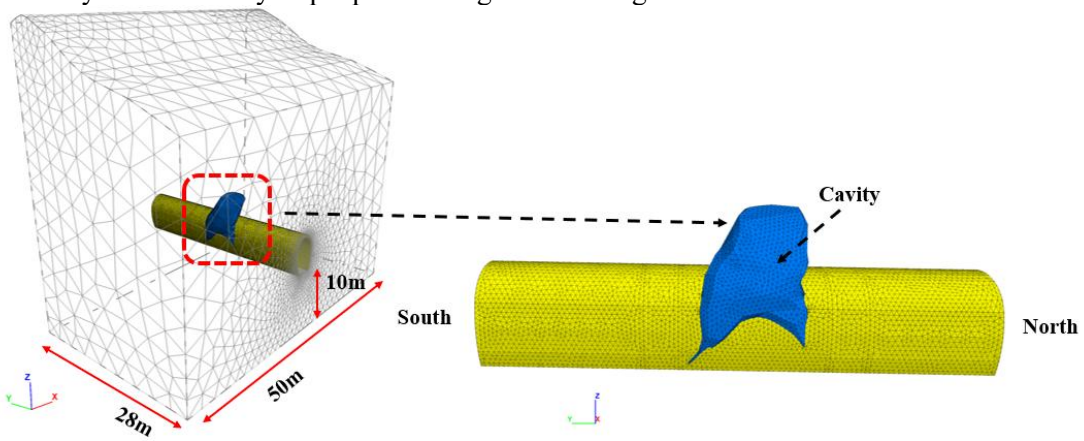


Figure 6. 3D Analysis of temporary support works, FLAC3D.

Detailed step by step support and construction sequences for FOGs crossing was developed in agreement with the client and the construction team which was then detailed in the construction drawings. The key aspects are:

- No personnel were allowed to enter the unsupported ground areas.
- Shotcrete and anchors support were completed right next to the FOGs prior to commencement of works within FOG area.

- Removal of debris and damaged concrete block/wall took place from the top in 0.5m increments.
- Sealing the exposed ground cavity with total 150mm thick SFRS in layers was undertaken.
- The damaged lining was sealed or plugged to re-form the tunnel arch using steel mesh (and prefabricated metal for FOG1 and FOG2) to receive SFRS.
- At FOG3, a full 100mm thick SFRS was applied to the entire tunnel section covering at least 2m before and after the collapse area to provide initial support.
- At FOG1 and FOG2, a construction sequence was developed for the top heading (to form a temporary working platform, seal natural the ground and re-form lining arch) and bench (to remove the remaining debris and damaged wall).
- Final structural support was constructed prior to final backfilling of the cavities.

4.3.3 *Fall of ground crossing works*

Excavation and support works were managed using a Required Excavation and Support Sheet (RESS) for each defined section, based on the design drawings. Regular Tunnel Review Meetings (TRMs) were held to assess working conditions and review the excavation and support measures outlined in the RESS. These meetings evaluated whether the current RESS remained suitable or required amendments, based on worker observations, convergence and crack monitoring, lining quality (existing and new), installed support systems, geological and hydrogeological conditions, and construction sequencing.

For the recovery of the FOG, an initial thickness of shotcrete was applied to the roof cavern to stabilise the exposed ground and restore the ground support conditions for safe entry. To rebuild the tunnel structure and re-establish ground arching, Tek mesh was installed around the new arch for the initial shotcrete application. Reinforcing bars, spaced at 1 m intervals, were bent to improve the mesh stiffness. Reinforced mesh was then bent and installed onto the bars. Tek mesh was clipped to the reinforcement mesh to ensure good adhesion of the shotcrete. The mesh was positioned above the existing tunnel profile to allow sufficient thickness for the development of a new arch, approximately 400 to 500 mm thick. The remaining void above the newly formed lining was filled with grout and low-density expansive concrete.



Figure 7. Fall of Ground (FOG) crossing works.

4.3.4 *Fall of ground crossing challenges*

The fall of ground crossings were particularly challenging (compared with the wider tunnel works) due to having to work above the spoil pile with limited visibility overhead to install roof support. The shotcrete robot had to work at the limits of its geometric range. Multiple scans were required to capture and review applied thickness and ensure adequate temporary support was installed.

Because of the fall of ground, sequential removal of spoil with immediate support installation was required to re-establish tunnel stability. The spoil pile had to be removed in small vertical increments with lower wall support installed with each cycle. Mucking out was able to be done with the use of an underground loader with long reach able to keep operators out from underneath the fall area until temporary support had been installed down to floor level.

Ensuring tunnel support at the collars of the falls of ground were also challenging to work through. To address this, where required additional anchoring was undertaken.

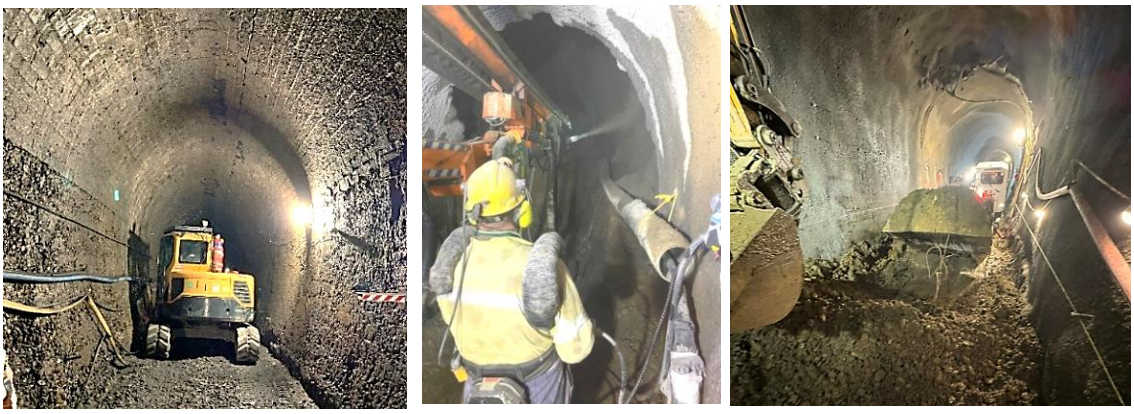


Figure 8. Machines operating in constrained work site.

5 CONSTRUCTION LOGISTIC AND CHALLENGES

The recovery works presented a range of logistical, geotechnical, and operational challenges due to Reefton's remote location in the South Island and the constrained working areas at the tunnel.

Limited local availability of materials (particularly shotcrete, steel anchors, and grout) combined with the absence of nearby suppliers and ready-mix plants, created some logistics challenges and the need for careful planning to ensure effective delivery of the recovery works. Given the remote location, turnaround times for material and quality assurance testing were longer than industry norms. These issues required special procedures to be put in place in order maintain the recovery programme.

The clearance between the finished support surface and the required design train structural gauge profile was tight, often within 10 mm. Daily scanning and depth pin control were used to manage shotcrete thickness. Depth pins could not be installed in "unsupported" sections, requiring operators to work carefully and precisely. A temporary shotcrete layer was often applied first to provide safe access for installing depth pins before the final shotcrete coat was placed with high accuracy. Ground anchor hardware had to be carefully selected to minimise anchor head protrusion and the position of every anchor had to be set out to avoid pinch points around the train structural gauge profile. Several sections of the newly sprayed shotcrete lining still fouled the train profile and required milling to achieve the required train clearances.

Site access was limited to a single-entry point with tight clearances, often preventing personnel access during machine operations. Using multiple machines introduced delays, as equipment had to be swapped in and out of the tunnel. The narrow access and profile also created safety challenges, especially for ventilation, emergency egress, and personnel movement during early recovery stages. Spatial constraints limited machine size and power, affecting excavation and support rates. The site's remoteness and tight programme further complicated the selection and transport of compliant underground machinery.

Worker safety under sections of the existing lining with varying stability was a key challenge during the recovery work. A domain map was used to communicate which areas of the tunnel were safe to work in and access. The map was kept up to date and used as a key tool communicating with the construction crews.

Given these logistical and physical challenges and programme constraints, the project team had to adopt an adaptive construction approach, with continuous re-evaluation of support designs based on observed ground behavior. Close collaboration between the Contractor, Designer, and Client representatives was essential to manage safety risks while maintaining progress. Frequent shift review and toolbox talks, revised sequencing, and temporary support modifications were employed to address emerging issues in real-time.

6 CONCLUSION

The recovery design and construction work were completed within 26 weeks, with the tunnel reopening for coal train operations on 12 January 2025. Robotic machines applied approximately 950 m³ of concrete to reinforce the tunnel lining. A total of 886 rock bolts were installed to anchor the lining to the surrounding ground. Additionally, about 373 m of modern concrete tunnel lining and a new track bed drainage system were installed.

The project was successfully delivered through a fully integrated, multidisciplinary team approach, with all parties working as one to achieve safe, efficient, and high-quality outcomes. Strong collaboration, tunnel support design re-evaluation, and shared commitment enabled the team to overcome challenges and complete the works within a short timeframe.



Figure 9. Repaired SNL tunnel 1.

7 ACKNOWLEDGEMENTS

The authors gratefully acknowledge KiwiRail Holdings Limited for granting permission to publish this paper. They also extend their appreciation to the Contractors, Geotech Limited and Joubert Pilat Limited (JPL), as well as Chris (Rick) Lee from Strata Control Technology (SCT), Active Survey Limited, Curious Engineer Limited, Gaia Engineers Limited, Holmes Group NZ Limited, NovoConsult Limited, and Aurecon as the lead designer for their invaluable contributions.

8 REFERENCES

Terzaghi, K and Peck, R. 1948. *Soil Mechanics in Engineering Practice*. John Wiley & Sons, London.

19th Australasian Tunnelling Conference – Acosta-Martínez, Stewart and Hudson-Smith (Eds.)
© 2025 Australian Tunnelling Society, ISBN 978-0-85825-002-4

Design of the Te Ara O Te Ata – Mt Messenger Bypass project tunnel

J.Q. Cooper
Mt Messenger Alliance – Tonkin + Taylor, Hamilton, New Zealand

M. Hashim
Mt Messenger Alliance – WSP, Sydney, Australia

K. Howard
Delve Underground, (formerly Mt Messenger Alliance – Tonkin + Taylor), Auckland, New Zealand

J. Lim
Mt Messenger Alliance – Tonkin + Taylor, Auckland, New Zealand

ABSTRACT: This paper discusses the design of a 235m long, single bore highway tunnel that forms a part of the upgrade of State Highway 3 in rural Taranaki, New Zealand. The tunnel is excavated within the Mt Messenger Formation, which comprises marine turbidite origin sandstones and mudstones, which are relatively soft horizontally bedded rocks. The tunnel will be excavated using the sequential excavation method with a roadheader to achieve an asymmetric horseshoe shaped tunnel with permanent shotcrete installed in each excavation advance using robotic spraying equipment. This paper describes the functional requirements and the tunnel lining design with a focus on the single pass shotcrete permanent lining. It presents lessons learned in designing this solution, being innovative for New Zealand road tunnels.

1 INTRODUCTION

The Mt Messenger Bypass project involves the construction and ongoing operation of a new section of State Highway 3 (SH3), generally between Uruti and Ahititi to the north of New Plymouth. This new section of two-lane highway will bypass the existing steep, narrow and winding section of SH3 at Mt Messenger. The primary objectives for the new section of state highway are to enhance the safety, resilience and journey time reliability of travel on SH3, and contribute to enhanced local and regional economic growth and productivity for people and freight. North of Uruti, the existing SH3 route cuts through the north Taranaki hill country, consisting of narrow ridges with steeply sloping valley sides and deeply entrenched drainage networks that typically have very small or no flood plains.

The Mt Messenger Bypass is designed and constructed by the Mt Messenger Alliance (MMA), which comprises NZ Transport Agency Waka Kotahi (NZTA), Downer Enterprises, HEB Construction, Tonkin & Taylor and WSP.

1.1 *Background*

The bypass is approximately 5.3km long, with a 235m long tunnel east of the Mt Messenger peak to cross a local ridge line and avoid an excessively deep cutting. The tunnel is bi-directional, has a slight curve with radius 1100m, 3% super elevation and a crest of radius 4200m. The tunnel is located at the highest elevation along the proposed bypass route. The finished road level at the northern portal will be at an elevation of approximately 111.3mRL. The tunnel is approximately 12m wide and 9.0m high to allow passage of over-size vehicles; equating to a cross-sectional area

of approximately 100m2. It is asymmetric in cross section due to inclusion of a longitudinal pedestrian egress passage on one side. The approaches to each portal are in cut with associated steep rock slopes.

1.2 *Functional requirements*

The overall functional requirements for the tunnel were specified in the Minimum Requirements and are summarised below at a high level:

- Enable safe and efficient movement of traffic;
- Comply with the Building Code;
- The tunnel Fire Life Safety provisions shall be acceptable to Fire and Emergency New Zealand (FENZ) based on a risk-based assessment;
- Be designed as an over-dimensioned route;
- In this rural location, accommodate cyclists and pedestrians on the shoulders;
- Permit the passage of dangerous goods.

The passage of large oversize loads with a vehicle envelope of 10m x 6m drove the selection of a single bi-directional bore for the tunnel which has the disadvantage of not having a second bore available to egress to in an emergency and increases the risk of vehicle collision.

The fire-related performance requirements proved a particular challenge. Whilst a relatively short tunnel, sufficient provision needed to be designed to maintain safety for users and asset protection in the event of a fire. Considerations include the tunnel's remote location, about 1 hour away from the nearest emergency services and isolated from water utilities, it's bidirectional traffic flow and dangerous goods are permitted.

Based on a project risk assessment and NZTA guidance codes the final solution relies on self-evacuation from portals via a dedicated longitudinal egress passage in the event of a fire. Lighting, fire hydrants, remote detection monitoring, flame traps and communications are included but no deluge system or jet fans are provided.

The tunnel portal canopies are required to protect road users from rock fall and soil slips. The tunnel is considered a significant gateway to the New Plymouth region with the constructed portals being visually dominant so that appropriate consideration was given to aesthetics and cultural representation, the final form including enhancements (textures, rebates and patterns) of the visible faces of both the portal and egress passage on their pre-cast unit panels. The tunnel electrical plant and control systems will be located in a free-standing Tunnel Control Building located on the new highway embankment approximately 150m to the south of the tunnel.

The tunnel is designed as a drained structure and the drainage system will serve to collect any water entering the tunnel from the ground, tunnel wash down water, fire-fighting water or spillage. The carriageway has a consistent 3% fall away from the egress passage. The tunnel drainage system consists of open drains along the southbound barrier face, catch pits to act as flame traps, and a main carrier pipeline. The tunnel pavement structure is designed for a minimum design life of 25 years and the asphalt surfacing has a design life of 10 years. Services are located inside the egress passage at roof level, on cable trays suspended from the tunnel roof or in ducts incorporated into the TL4 vehicle barriers.

2 GEOLOGY

The Mt Messenger Bypass tunnel is excavated within the Mount Messenger Formation (MMF), a Late Miocene sedimentary sequence comprising interbedded marine sandstones and mudstones of turbidite origin. These rocks are characteristically very weak to weak, with slightly weathered to fresh materials typically encountered within 2–3 metres of the surface, deepening to around 10 metres on exposed ridges. The formation is sub-horizontally bedded, with a gentle dip of 2–4° southwest. Bedding is typically thick to massive and often indistinct. The MMF sediments are exposed in numerous rock cuttings, short tunnels and natural outcrops along the existing State Highway 3 in the Mt Messenger area and along the 'White Cliffs' coastline to the west.

The engineering geological model identifies two broad classifications of rock mass conditions relevant to tunnel design: Rock Mass Class 1 and Rock Mass Class 2.

– Rock Mass Class 1 represents the typical ground conditions along the tunnel alignment, characterised by slightly weathered to unweathered, very weak to weak rock with relatively widely spaced defects and intact rock blocks (GSI 70 to 85+).
– Rock Mass Class 2 represents localised zones of more fractured or broken rock, associated with closely spaced joints, occasional shear zones, or fault-related disturbance (GSI 50 to 70). These zones are typically narrow (2–4 metres wide) but appear to be sub-parallel to the tunnel axis and if encountered, are expected to migrate across the tunnel from left to right (when viewed in the direction of the tunnel advance).



Figure 1. MMF rock exposures in the Taranaki area

Laboratory testing of intact rock samples indicates that the Mount Messenger Formation exhibits a typical unconfined compressive strength (UCS) ranging from approximately 2 MPa to 10 MPa, with an average UCS of around 4 MPa used for tunnel design purposes.

Hydrogeologically, the Mount Messenger Formation exhibits generally low permeability; however, perched groundwater conditions can develop along discrete sand-dominant beds and in defect networks. These factors informed the drainage strategy and support design, ensuring stability and durability during both construction and operation.

3 TUNNEL

3.1 *Tunnel cross-section*

The asymmetric tunnel cross section is shown in Figure 2.

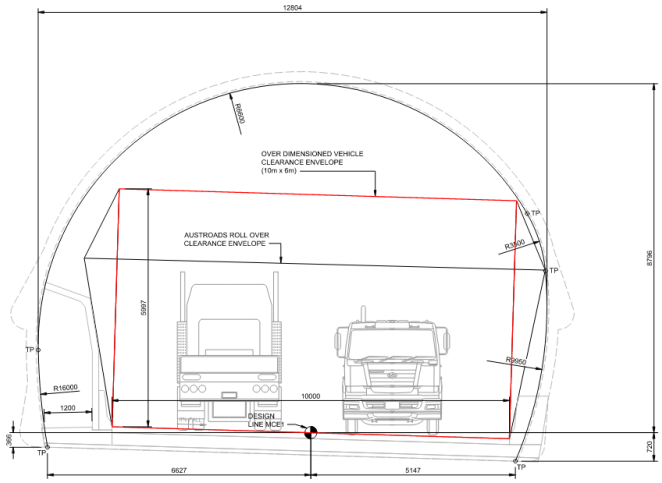


Figure 2. Tunnel cross section

The tunnel shape is space proofed to accommodate the oversize vehicle envelope (6m x 10m) and the tunnel width is then enlarged asymmetrically to provide space for an egress passage on one side of the tunnel cross-section. The passage minimum width is 1200mm. Vehicle clearances and sway allowances are made, and the shape allows room for shoulders and vehicle collision barriers. The large ceiling space that results is more than adequate for lighting and space proofed for jet fans should they be required in the future. Ancillary equipment, such as fire hydrants, fire main, drainage, mechanical, electrical and control equipment have been designed in line with standard approaches and are routed within the longitudinal egress passage.

3.2 *Tunnel excavation and support types*

The tunnel is being excavated using the Sequential Excavation Method (SEM), with a 6.5m high top heading followed by bench excavation. Mechanical excavation is undertaken using a road-header, selected for its suitability to the relatively soft, horizontally bedded rocks of the Mount Messenger Formation. Excavation is proceeding from south to north, with application of ground support following each advance to maintain stability and control deformation.

A single-pass permanent shotcrete lining was selected as the preferred option to enable a fast installation and cost-efficient lining option for this rural tunnel.

Ground support selection was based on the expected variability in ground conditions along the tunnel alignment. Six Support Types (ST1, ST1A, ST1B, ST2, ST3, and ST3A-Portal) were developed to address different rock mass conditions and geometric requirements at the portals. The following summarises the rock mass conditions applicable for each Support Type. Details of the minimum support requirements for each Support Type are presented in Section 4.3.

- Support Type ST1 is the standard design for the majority of the tunnel alignment, where the ground conditions are characterised by slightly weathered to unweathered, very weak to weak Mount Messenger Formation rocks (Rock Mass Class 1), with widely spaced defects and intact rock blocks.
- Support Types ST1A and ST1B were developed to cater for localised zones of more fractured rock (Rock Mass Class 2), typically associated with joint swarms or fault-related disturbance near the tunnel sidewalls. These types allow for enhanced support where isolated zones of reduced rock mass quality are encountered.
- Support Type ST2 was developed for conditions where extensively fractured rock (Rock Mass Class 2) is encountered across the full tunnel face. Although such ground conditions are not expected to be encountered, ST2 provides a contingency support option to ensure safe construction progress through unfavourable zones should they be encountered.
- Support Types ST3 and ST3A-Portal apply specifically to the tunnel sections near the north and south portals. These zones are associated with reduced overburden cover, greater relaxation effects, and a need to accommodate enlarged tunnel profiles for installation of precast portal canopy structures.

Support Type selection during construction is confirmed through an observational approach based on tunnel face mapping, rock bolt installation records, probe drilling results, and tunnel deformation monitoring. This adaptive methodology ensures that ground conditions are appropriately matched with support requirements, maintaining safety while optimising construction efficiency.

4 DESIGN APPROACH AND METHODOLOGY

4.1 *Design approach*

The initial design of the tunnel excavation in the relatively weak rock sought economy by moving away from a traditional primary lining and cast in situ concrete secondary lining by adopting a single pass lining with un-tensioned permanent rock bolts and thin shotcrete lining installed as the tunnel advanced. This relies critically on the strength gain from the grouted rock bolts and shotcrete to facilitate the advance rate of the tunnel and also on the quality of the shotcrete achieving permanent works standards in the challenging environment of an advancing tunnel. Durability

and watertightness of a permanent shotcrete lining is also dependent on method of the total thickness build up and workmanship of the shotcrete operators.

In the final design stage, the support system was optimised to accommodate faster advance rates driven by changed project programme demands. The permanent rock bolts were changed to temporary which provided programme and cost savings due to reduced design life requirements. The shotcrete lining build up was thickened and changed from spraying over five advances to spraying over three advances with the last layer applied at a distance from the tunnel face.

The tunnel lining was designed with adequate strength capacity under static and seismic conditions considering:

- Imposed ground and groundwater loads in temporary and permanent cases.
- General loadings (vehicular impact, self-weight and seismic) derived in accordance with the NZ Bridge Manual and NZS 1170 and on the basis of a 100-year design life and Importance Level 4 for the structure;
- Excavation methodology, advance lengths and ground stand up time; and
- Durability for a 100-year design-life

4.2 *Analysis*

4.2.1 *Fem modelling*

The tunnel shotcrete was designed as a single-pass permanent lining, requiring high early strength to allow rapid construction progress and ensure personnel safety. The specified shotcrete mix incorporates steel fibre reinforcement and targets a 28-day compressive strength of 35 MPa.

A minimum compressive strength of 1 MPa is required for safe personnel entry following application of the initial 75 mm thick safety shotcrete layer, typically achieved within a few hours of spraying. The minimum strength requirement was checked for potential failure modes including debonding, shear, and flexure using the UnWedge software, considering the anticipated joint set orientations.

The full design thickness of the lining is built up progressively over three layers, with ground–structure interaction and staged excavation analysed using the RS2 Finite Element (FE) software. The Convergence-Confinement Method [1][2] was applied to estimate the three-dimensional nature of an advancing tunnel face by developing Ground Reaction Curves (GRCs) and Longitudinal Displacement Profiles (LDPs) representative of the expected ground behaviour. LDPs were estimated using the simplifying assumption of an axisymmetric model along the axis of the tunnel (with equivalent radius) to predict the increase in ground convergence with distance from the excavation face.

Groundwater loads were incorporated into the analysis to account for the potential build-up of pore water pressures behind the lining over the tunnel's 100-year design life (the tunnel is assumed to be fully drained during construction). The design groundwater pressure distribution assumed a fully drained invert and a linearly varying hydraulic head, with a maximum pressure of 65 kPa at the tunnel crown reducing to zero at the invert level. The potential for unbalanced groundwater pressures acting asymmetrically on the tunnel lining was also considered during sensitivity analyses.

4.2.2 *Advance length*

Optimisation of the top heading advance length was a key factor in balancing construction efficiency with ground stability. For the standard tunnel section (Support Type ST1), an advance length of 1.5 metres per excavation cycle was adopted, based on numerical modelling outcomes and construction practicability. This advance length allows sufficient time for the installation and early curing of the initial shotcrete layer and temporary rock bolts without exceeding tolerable deformation limits.

A reduced top heading advance length of 1.2 metres is adopted for the portal zones (Support Types ST3 and ST3A-Portal) and where more fractured ground (Rock Mass Class 2) is encountered across a significant portion of the tunnel face (Support Type ST2). This reduction provides an additional stability margin in areas where ground conditions are less favourable.

Excavation of the bench is planned only after the full completion of the top heading and assumes that the fibre reinforced shotcrete lining of the top heading has achieved its full 28-day compressive strength. The typical bench advance length is 6 metres for ST1. In portal zones or where more fractured ground is encountered, the bench advance was limited to no more than twice the preceding top heading advance length to maintain structural stability during the staged excavation sequence.

4.2.3 *Structural fire performance*

As no restrictions were placed on the passage of Dangerous Goods Vehicles (DGVs) through the Mt Messenger Bypass Tunnel, a Rijkswaterstaat (RWS) fire curve was applied to the critical areas of the tunnel as the worst credible design fire scenario. This curve assumes that in the worst-case scenario, a 50 m3 fuel, oil, or petrol tanker fire with a fire load of 300 MW can occur, lasting up to 120 minutes. The ambient temperature within the tunnel is assumed to be 20ºC.

Two fire event scenarios, during fire and post fire, were investigated to assess the response of the tunnel structural lining. Structural analysis was carried out using the FE analysis package Strand7. Loading actions applied in the analysis included combinations of loads transmitted from the ground based on the ground conditions and thermal loads induced by the expansion of the lining. Structural analysis was performed considering the type of ground supports installed, ST1 or ST2. A rock mass modulus (Erm) of 1200 MPa was adopted for ST1 in rock mass Class 1 (SC1) and rock mass modulus of 600 MPa was adopted for ST2 in rock mass Class 2 (SC2).

During a fire in the tunnel, heat will cause thermal expansion of the lining. The induced temperature gradient exhibits high intensity temperature at the tunnel face and decreases with distance away from the face. The associated differential thermal expansion through the tunnel lining section will induce bending strain on areas exposed to the heat source. These thermal actions in combination with pre-existing loads were assessed to ensure that the structural capacity of the lining could still achieve sufficient factor of safety, even after spalling had occurred. An allowance of 40mm of spalling of the shotcrete was assumed in the design.

After the fire, these induced structural actions would cease as the lining temperature returned to normal levels. A post fire assessment was undertaken to confirm whether the reduced thickness of the lining due to the fire damage and spalling would remain stable under the pre-existing load combinations to ensure that the subsequent inspection and repair works could be carried out safely.

Calculated equivalent lining cross section dimensions and thermal inputs, applied in the Strand7 model, are summarised in Table 1.

Table 1. Equivalent section size and thermal input for beam element

Fire Type	Total Thickness (mm)	Equivalent Young's Modulus (MPa)	Equivalent Membrane Thickness (mm)	Equivalent Bending Thickness (mm)	Equivalent Temperature (°C)	Equivalent Temperature Gradient (°C/m)
RWS	250	13637	145.8	667.1	141.0	3773
RWS	300	14226	186.2	810.8	84.9	2158

The minimum tunnel lining thickness (fibre reinforced shotcrete) adopted for support types ST1 and ST2 were 250 mm and 300 mm respectively. Hence these minimum lining thicknesses were adopted in the Strand7 assessment. The minimum concrete characteristic compressive strength for the shotcrete was 35 MPa. Creep and shrinkage of the shotcrete were considered in the modelling through reducing the shotcrete modulus of elasticity (long term) from 30 GPa to 15 GPa.

Combinations of ground and fire loads were applied on all iterations of the tunnel lining fire assessment. Ground load consisted of vertical uniformly distributed loads (UDL) applied on the full tunnel lining above the tunnel spring-line and horizontal UDL applied on the full tunnel lining from crown level to the invert level. Ground wedge loads consisted of a vertical UDL applied locally on the tunnel crown centreline, a vertical UDL applied asymmetrically on the tunnel crown and a lateral UDL applied on the tunnel sidewall. Fire load consisted of temperature expansion

fire load applied at the nodal elements affected by fire and temperature gradient fire load applied on the beam elements of the lining affected by fire.

Sensitivity analysis was performed by varying the rock mass modulus (Erm) from 1200 MPa to 2400 MPa for ST1 and from 600 MPa to 2400 MPa for ST2 with all other conditions remaining unchanged. The assessment for these sensitivity checks indicated that in the event of a fire (as represented by the design fire curve) the lining had adequate capacity to perform as required both during and after the fire event.

4.3 *Tunnel support design*

The detailed design of the tunnel support types was developed to meet the functional requirements for stability, durability, and constructability under the range of ground conditions anticipated along the tunnel alignment. The requirements for each support type described in Section 3.2 were based on ground–structure interaction analyses, structural performance criteria, and practical construction considerations.

Each support type incorporates specific design features, including variations in shotcrete thickness, reinforcement detailing, rock bolt layout, and drainage provisions, tailored to match the expected ground behaviour. The design approach aimed to ensure consistent tunnel performance across both the typical and more adverse ground conditions, while maintaining flexibility to adapt to actual conditions encountered during construction.

Support Type ST1 was developed for the majority of the tunnel alignment, where slightly weathered to unweathered Mount Messenger Formation rocks (Rock Mass Class 1) are encountered. The minimum support layout for ST1 is shown in Figure 3 and comprises:

- 4 m long fully grouted temporary rock bolts installed at approximately 1.5 m spacings,
- A 250 mm thick steel fibre reinforced shotcrete lining, applied in three layers (75 mm + 100 mm + 75 mm),
- No steel reinforcing mesh under typical conditions.

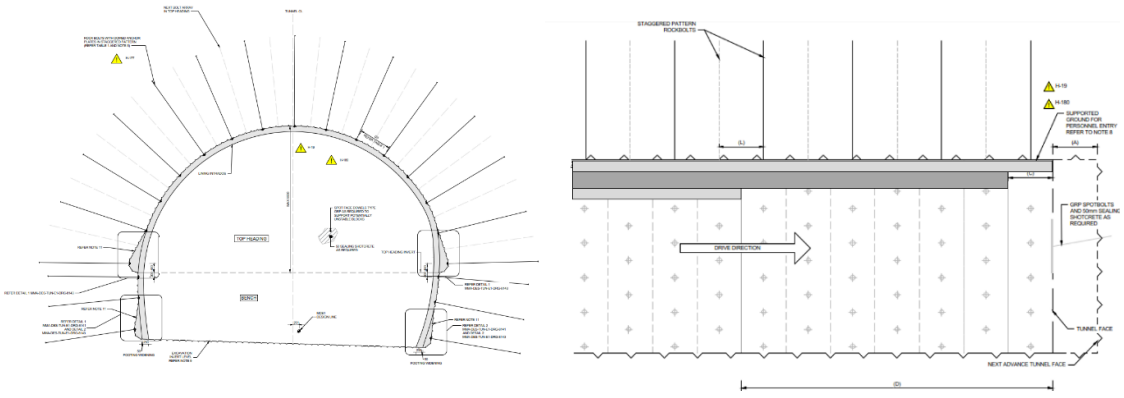


Figure 3. Tunnel support type st1. Left: cross section. Right: top heading construction sequence.

Where Rock Mass Class 2 is encountered on one side of the tunnel, Support Types ST1A and ST1B are adopted. These involve increased bolt density, a widened lining footing at the sidewall, and installation of a single layer of steel reinforcing mesh across the affected top heading sidewall. Shotcrete thickness remains at 250 mm for both support types.

In cases where Rock Mass Class 2 is encountered across the full tunnel face, Support Type ST2 is implemented. This design includes a 300 mm thick steel fibre reinforced shotcrete lining, applied in three layers (65 mm + 130 mm + 105 mm), with high-density rock bolt installation (typically at 1.2 m spacings) around the full perimeter. Two layers of steel reinforcing mesh are provided across the top heading sidewalls and shoulders.

At the portal zones, Support Types ST3 and ST3A address the combined challenges of reduced overburden, increased potential for ground relaxation, and the enlarged tunnel geometry required for the installation of precast portal canopy structures. These designs generally mirror ST1 but include a 300 mm thick shotcrete lining (applied in three layers of 75 mm + 100 mm + 125 mm) and widened lining footings at both the top heading and bench levels. In addition, a canopy of 8m long spile bars provide pre-support to the tunnel.

Minimum Requirements excluded application of waterproofing membrane with the expectation that watertightness is provided by the shotcrete lining alone. Although the Mount Messenger Formation is generally of low permeability, drainage measures were incorporated across all support types to prevent the build-up of pore water pressures behind the lining and divert groundwater to the invert. Groundwater control measures include strip drains at locations where seepage is observed during excavation, regularly spaced perimeter bored drains in the sidewalls and an invert drainage system beneath the tunnel floor. Following installation of the initial safety shotcrete layer, any minor seepage or localised dripping from the excavation surface is managed by installing strip drains prior to the placement of the full lining thickness. In cases where multiple closely spaced water-bearing defects are encountered, the excavation is locally widened to accommodate closely spaced strip drains behind the minimum design lining thickness, ensuring effective long-term drainage and preserving the integrity of the tunnel lining.

5 CONCLUSIONS

The Mt Messenger tunnel is currently under construction. The tunnel design has included a number of innovations for New Zealand encouraged by the need for cost effectiveness and close cooperation between designers and constructors facilitated by an Alliance delivery model. These are application of single pass shotcrete lining, observation-based application of drainage measures in the tunnel and an asymmetric shape around an egress passage to save excavation volume.

It is a bi-directional tunnel to allow very large, oversized loads to pass, principally because it serves New Plymouth oil and gas industries. The risk-based fire life safety provisions effectively balance the need for safety and adequate asset protection for a tunnel that includes two-way traffic and dangerous goods, including petroleum tankers, with capital and operational costs.

Tunnel design tends to focus on the civil works aspects such as ground conditions, excavation and support design noted in this paper. However, this project also demonstrates the importance of the need for appropriate functional requirements, fire life safety, durability, aesthetics and construction access which can drive many key decisions early in the design process.

6 ACKNOWLEDGMENTS

The authors would like to thank NZ transport agency Waka Kotahi and the Mt Messenger Alliance. Special thanks to Civil Quarries Ltd in Taranaki for space to carry out shotcrete trials.

7 REFERENCES

[1] AFTES (2002). Recommendations on the Convergence-Confinement Method. French Tunnelling and Underground Space Association.

[2] Carranza-Torres C. & Fairhurst C. (2000). Application of the convergence-confinement method of tunnel design to rock masses that satisfy the Hoek-Brown failure criterion. Tunneling and Underground Space Technology, 15(2).

19th Australasian Tunnelling Conference – Acosta-Martínez, Stewart and Hudson-Smith (Eds.)
© 2025 Australian Tunnelling Society, ISBN 978-0-85825-002-4

The Blue Mountains Route Clearance Project – tunnel lining modifications for the Ten Tunnels Deviation

C.K. Bodner & R.M. Gibson

Aurecon Australasia Pty Ltd, Sydney, Australia

ABSTRACT: Transport for New South Wales (TfNSW) has introduced a New Intercity Fleet (NIF) to enhance passenger comfort and accessibility, replacing aging rolling stock on the Blue Mountains and Main West railway lines. The NIF's larger kinematic envelope (KE) resulted in tunnel lining infringements at the heritage listed Ten Tunnels Deviation near Lithgow, NSW, built in 1910. To achieve the required NIF clearances, TfNSW initiated the Blue Mountains Route Clearance (BMRC) project. Within the Ten Tunnels Deviation, the scope of work involved modifications to the existing linings in eight of the ten tunnels.

This paper outlines the challenges, key learnings, and methods adopted to trim the tunnel lining within the Ten Tunnels Deviation. It presents investigations into existing lining thicknesses and the development of proposed treatment types. Key findings emphasise the importance of capturing accurate historical information and developing strategies to supplement missing data while embedding a risk-based approach to design and construction.

The knowledge gained is shared with the broader industry to benefit those rehabilitating historical tunnels in the future.

1 INTRODUCTION

The heritage listed Ten Tunnels Deviation had previously been modified in 1978 to accommodate new rolling stock. These modifications included replacing the ballasted track with a concrete track slab, lowering the track within the tunnels, and cutting chases into the tunnel walls to achieve the necessary clearances.

The ten tunnels are horseshoe-shaped and brick-lined in the crown and haunches, with the brick arch typically resting on a concrete wall below the spring line. Near the tunnel portals, the brickwork arch thickens and extends to the toe of the wall. At the portal, the brick arch is confined by brick buttresses. Tunnel 9 is unique as it is entirely brick-lined but the reasons for this are not known. The tunnels were excavated using drill and blast techniques, primarily into Banks Wall Sandstone. The lining's brick crown arch and concrete walls were constructed with timber formwork. The excavation method at the time locally resulted in significant overbreak, which was either bricked out or backfilled with tunnel spoil.

Modifying a 110-year-old heritage-listed tunnel presents significant design and construction challenges. Numerous uncertainties and constraints needed to be carefully evaluated to assess critical risks and develop safe lining treatments that allow a further reduction of the existing tunnel lining thickness. The old lining could not be expected to meet current standards because these standards did not exist at the time of construction, and its condition therefore had to be thoroughly examined. During an initial condition survey, it was found that the lime mortar had suffered substantial leaching and softening in isolated locations exposed to prolonged seepage inflow.

1.1 *The project*

The BMRC project was initiated by TfNSW to accommodate the modernised NIF along the Main Western Line through the Blue Mountains. In February 2019, construction started between Springwood and Lithgow. The Rail Corridor Modifications were to enable NIF train services all the way to Lithgow. The BMRC scope of works included providing adequate clearance for the NIF within the existing Ten Tunnels Deviation.

The BMRC project was delivered collaboratively by the Continuum Alliance which was formed between TfNSW and a joint venture between CPB and Lendlease Engineering (now Acciona). Aurecon was appointed by the Continuum Alliance to undertake the detailed design for the BMRC project. The works were undertaken in a series of allocated track possessions commencing in February 2019 through to May 2020. Site activities during track possessions ran to tight schedules and had to accommodate parallel maintenance activities scheduled by Sydney Trains within the same possessions. In addition, limited passenger and freight rail movements had to be maintained during possession windows. The Ten Tunnels Deviation is a heritage-listed 9.2 km section of the Main Western Railway Line between Newnes Junction and Zig Zag stations near the township of Clarence, New South Wales. Figure 1 shows a location map of the ten tunnels on the Main West Line in the Blue Mountains.



Figure 1. Ten Tunnel Deviation location map.



Figure 2. Tunnel 5: Country portal.

1.2 *History*

The Ten Tunnels Deviation, also known as the Zig Zag Tunnels, were commissioned to provide an alternative twin track route to the historic single track Zig Zag Railway. According to Heritage NSW (2023) the Ten Tunnels Deviation reduced journey times to Lithgow by 20 to 30 minutes. Construction of the Ten Tunnels Deviation commenced in 1908 and was completed by 1910. Fortunately, historical photographs (Figs. 3-6) were available to the project team, highlighting the tunnelling methods and technology of the time.

Tunnel excavation was undertaken using drill and blast methods. This involved the excavation of a short pilot heading followed by a heading enlargement and finally benching (Fig. 5). The photographs indicate that no temporary support was installed during these excavations. As the tunnel advanced, the rough drill and blast profiles in the heading and bench were manually scaled and smoothened to achieve the required horseshoe profile (Fig. 6). Overbreak above the springline was backfilled with tunnel spoil or bricked out during construction of the tunnel lining (Fig. 2). The treatment of overbreak was an important consideration when developing design loadings for the tunnels.

The horseshoe shaped tunnels were lined with concrete to the springline and masonry to the crown. The invert floor in each tunnel remained unlined. Each portal face was fully bricked and included an inclined buttress on both sides of the portal face (Fig. 3). The thickened brick arch lining extends approximately 7 m from the portal into the tunnel and this area was termed the "portal zone" (Fig. 4). Beyond the "portal zone" a mass concrete sidewall was placed with timber forms up to springline level (Fig. 4). Once the walls were cast, clay bricks were laid in the crown arch whilst temporarily supported by timber form and falsework. The bricks were laid in running

bond and were set in lime mortar (Fig. 4). This arrangement applied to all tunnels except for Tunnel No. 9, which was entirely brick lined.



Figure 3. Tunnel 9: Construction of brick buttress at tunnel portal.



Figure 4. Tunnel 5: Brick arch lining and concrete to brick wall interface near the portal.



Figure 5. Pilot, heading and bench excavations. Note rough tunnel profile with large over-break. Source: Lithgow History Avenue c. 2010.

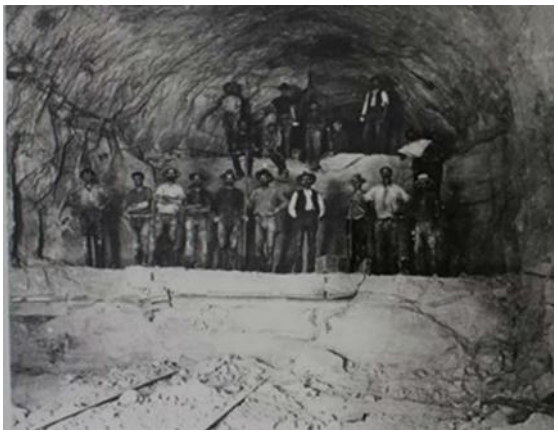


Figure 6. Heading and bench excavations. Note manual scaling of heading excavation profile.

2 THE CHALLENGE

The project objective was to provide sufficient clearance within the ten tunnels to accommodate NIF Rolling Stock (Fig. 7). To achieve this, the infringement zones for a sub-medium KE +100 mm structure clearance needed to be identified. Geometric checks confirmed two principal infringement locations within the tunnel cross section one in the tunnel haunch and at the other at the toe of the tunnel lining as depicted in Figure 8.



Figure 7. New Intercity Fleet (NIF) Rolling Stock.

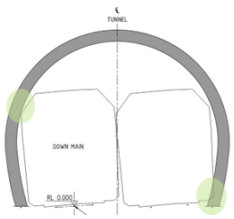


Figure 8. Infringement zones for sub-medium KE +100 mm.

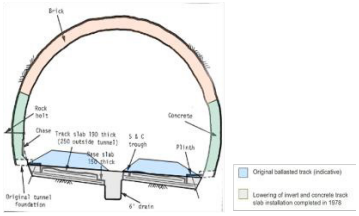


Figure 9. Typical cross section showing replacement of ballasted track in tunnels (Duncan 1980).

The initial challenge for the project team was to establish where the NIF infringements occurred within the tunnels, what trimming depths were required to remove the infringements and what remedial measures were necessary to ensure the integrity and stability of the tunnel lining. This initial investigation was further complicated because the lining was previously modified in 1978 to provide clearances for the significantly taller V-set rolling stock. This resulted in a suite of modifications including a reduced lining thickness of approximately 30% of the original lining thickness as reported by Duncan (1980).

The design objective was to develop a selection of lining treatment types for implementation during construction, whilst navigating various interrelated uncertainties such as the condition and the already locally reduced lining thickness of the existing tunnels.

3 PREVIOUS MODIFICATIONS

In the 1970s the V-set rolling stock was introduced across the Sydney Trains network. To accommodate the larger KE and increased loading, the ballasted track in all tunnels was replaced with a concrete track slab in 1978. The track slab was to also remediate drainage issues resulting in ballast fouling and formation degradation (Lord 1988). The work required major modifications to the existing tunnels including:

- Lowering of track and invert by approximately 650 mm and 400 mm respectively.
- Constructing concrete plinths with shear dowels to support the tunnel sidewall foundations.
- Cutting lining chases with a maximum design target depth of 150 mm resulting in a thickness reduction from approximately 450 mm to 300 mm (Duncan 1980).
- Installing rock bolts to horizontally confine the tunnel wall at the proposed chases.

A typical cross section of previous modifications are shown in Figure 9.

4 DESIGN APPROACH

To address the challenges and project objectives, the design team set out to investigate and identify potential remedial measures for the existing tunnel lining. A series of questions arose and had to be answered including:

- Where are the NIF infringements and what are the magnitudes?
- What is the existing lining thickness at the infringement locations?
- What is an acceptable minimum lining thickness after trimming?
- Where is underpinning of the existing lining required?
- What are suitable lining treatment types?

4.1 *NIF infringements*

The NIF infringements were located using the Amberg rail trolley (Fig. 10) which is a highly accurate laser scanning device guided by a total station. A digital version of the required KE was used by the Amberg trolley to identify and measure the NIF infringements. The infringements were recorded and could also be viewed in real time which was particularly useful during construction.

Drawings showing “heatmaps” were developed from laser scan surveys available for all ten tunnels. These drawings displayed colour contours representing the extent and depth of infringements projected onto tunnel sidewall elevations. The heatmap shown in Figure 11 presents a rather irregular infringement surface. This is attributed to the rough surface conditions resulting from the 1970s cutting campaign using jack hammers.

Infringement cross sections (Fig. 12) were developed at one metre intervals. Figure 12 shows the lining thickness reduction at the toe originating from the previous modifications referred to in §3.



Figure 10. Amberg survey trolley.

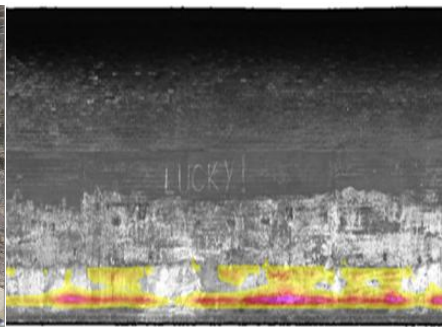


Figure 11. Infringement heat map on wall elevation.

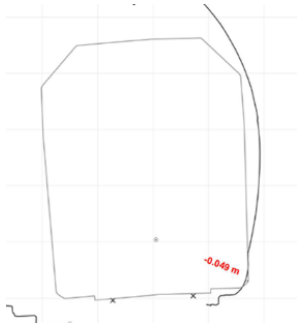


Figure 12. Example of survey infringement in cross section.

4.2 *Existing tunnel lining thickness*

Before any significant modifications could be considered, it was necessary to investigate the extent of previous lining trimming discussed in §3. Due to the lack of available construction records for the BMRC project, it was unclear how much cutting had occurred and whether the intended 300 mm residual wall thickness was consistently maintained. Therefore, early investigations for this project focused on establishing the existing wall lining thickness at the existing cut chases. Details of these investigations are set out in the following sections.

4.2.1 *Ground Penetrating Radar (GPR)*

GPR was employed by the project team to estimate the lining thickness of the tunnel concrete walls. The wall needed to be scanned approximately 1.5 m to 1.8 m above the rail to avoid adverse signal reflections from previously roughened chases. However, the point of interest for the minimum thickness was much closer to the plinth (Figs. 11-12). Consequently, the GPR data only provided an indication of the original wall thickness above the existing cut chases and further supplementary measurements were needed to obtain the minimum existing wall depths near the toe of the wall.

4.2.2 *Lining depth measurements in weep holes*

Weep holes 20 mm in diameter were drilled through the tunnel walls into rock at approximately 5 m intervals where infringements near the toe were identified. The weep holes were installed to provide drainage relief but were also utilised for endoscope measurements. The measurements involved the insertion of a small camera into a PE tube fitted with a measurement scale. The endoscope camera and tube were inserted into the weep hole until the lining extrados was observed and the corresponding depth recorded (Fig. 14). Finally, the weep holes were surveyed for inclusion in the laser scan model.

Coring through concrete and brick of the existing lining was also performed to supplement depth measurements in areas where endoscope assessments did not yield conclusive results - e.g. where vision was obstructed by murky seepage flows.

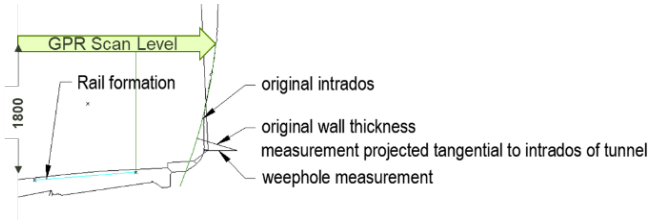


Figure 13. Measurement correlations.



Figure 14. Measurements taking place in Tunnel No. 6.

The weep hole survey and depth measurements were transferred into corresponding tunnel cross sections cut through the respective weep hole locations to infer the original tunnel wall thickness. The original tunnel lining thickness was obtained by projecting a line perpendicular to

the tangent of the extended original intrados arch through the distal end of the weep hole. The original wall thickness was then derived as the distance between the tangent point and the distal end of the weep hole as shown in Figure 13. This principle enabled the determination of the original wall thickness at 5 m intervals along each of the tunnel where toe treatments were prescribed.

Because the magnitude of the infringements was also known at the weep holes, the existing residual lining thickness, $t_{residual}$, was determined with reasonable accuracy at 5 m intervals along the tunnel.

4.3 *Acceptable lining thickness*

The lining treatments needed to consider the residual capacity of the tunnel lining after trimming. The design basis needed to consider durability allowances, design fire resistance and the interaction with new rock bolts. Material properties needed to be interpreted for the existing brick/concrete, and design loads for the arch structure had to be established for design analysis.

A critical element for the design was to determine the amount of trimming that could take place before underpinning would become necessary. The target limit, t_{min}, was established based on bedded beam and 2D finite element models superimposed with multiple load cases for service and ultimate limit states.

Apart from the thickness distribution, the other major uncertainty was the existing loading condition of the tunnels. Apart from the lining self-weight and the design fire resistance, all other load cases had to be assumed based on engineering judgement. Consequently, the true loading condition in these tunnels is unknown and can range from self-weight only to self-weight with backfill, potential seepage pressure and rock wedge loading. The design loads considered in various load case combinations included self-weight, service loads, ground loads (rock wedge loads), loads from backfilling of excessive overbreak and groundwater loads. Adopting the established potential loading conditions and considering fire resistance together with the necessary durability allowances the minimum acceptable lining thicknesses, t_{min}, in concrete and brick was determined. Thus, distributions of trimming and underpinning could be identified based on the magnitude of infringements and existing lining thickness.

5 LINING TREATMENT TYPES AND DISTRIBUTIONS

5.1 *Treatment distributions*

The treatment type distributions were based on the magnitude of infringements, existing wall thickness and the minimum structural lining design thickness. Construction tolerances to be achieved within each treatment type also needed to be considered. Figure 15 shows an example of the residual and minimum lining thickness data to highlight where underpinning would be required.

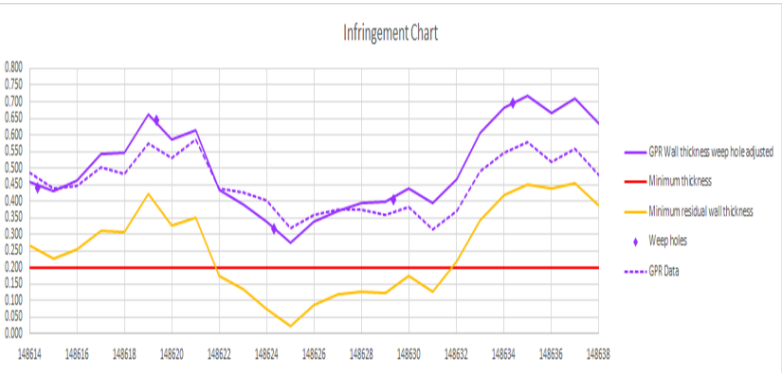


Figure 15. Infringement chart. Residual thickness distribution (yellow). Minimum required (red).

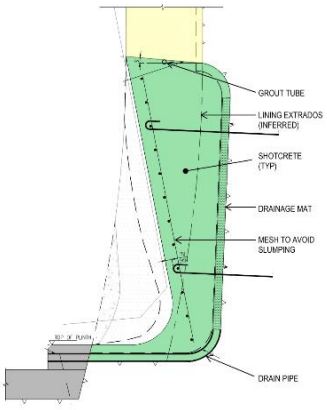


Figure 16. Underpinning typical cross section.

5.2 Treatment types

Three treatment types were designed for the BMRC project: manual trimming, mechanical trimming and underpinning. Table 2-3 summarise the key features of each treatment type in concrete and brick.

Table 2. Differences between the nominated treatment types in concrete.

Manual Trimming	Mechanical Trimming	Underpinning
		
Trimming with handheld tools/equipment for localised KE infringements up to 50 mm depth only.	Applies where $t_{residual} > t_{min.c}$ Trimming using wall shaver or rotary milling head attached to an excavator. Image shown after wall shaving.	Applies where $t_{residual} \leq t_{min.c}$ Excavation through the brick or concrete wall into rock to achieve a minimum panel thickness required for structural plinth support

Table 3. Differences between the nominated treatment types in brick.

Manual Trimming	Mechanical Trimming	Underpinning
		
Trimming with handheld tools/equipment for localised KE infringements up to 50mm only.	Where $t_{residual} > t_{min.b}$ Wall shaver or rotary milling head. Mortar repointing as required. 50 mm thick shotcrete panel.	Where $t_{residual} \leq t_{min.b}$ Hit and miss sequence. Use of temporary steel frame installed with hand tools.

Important aspects of the underpinning treatment design (Fig. 12) were to achieve the minimum section depth at the pinch point and to ensure full contact with the existing lining at the top of the panel. In addition, the toe needed to abut the existing plinth to a minimum depth of 100 mm and the rock at the back of the excavation needed to be removed to allow for a minimum lining thickness. To achieve full contact at the sprayed concrete brick/concrete interface, grout tubes were attached to the underside of the existing cut lining to enable contact grouting after concrete placement.

6 CONSTRUCTION

6.1 *Underpinning at tunnel portals*

The tunnel portals presented a unique challenge. Underpinning works at the portals was a delicate operation due to poor mortar condition, gaps at the interface between the brick lining extrados

and rock, presence of loose backfill material behind the lining and the lack of longitudinal confinement at the portal face. To mitigate these risks, special construction sequences were developed for tunnel portal zones utilising temporary steel lintel beams and frames.



Figure 17. Tunnel No. 8 temporary steel frame installation prior to stage 1 excavation.



Figure 18. Tunnel No. 8 portal underpinning after stage 2 excavation and prior to shotcreting.

The purpose of the steel frames was to temporarily confine the brick lining around the excavated panels and to maintain the integrity of the portal zone during construction. The lintels were anchored into the brick lining directly above the vertical legs. Figures 17-18 both show an image taken during stages 1 & 2 of the portal underpinning sequence. In addition, permanent rock bolts were installed above the nominated underpinning zones to stabilise the tunnel wall horizontally.

6.2 *Trimming the haunch*

Trimming the haunch (Figs. 19-20) carried greater risk and required additional controls from a safety perspective due to two main reasons. The infringement locations at the haunch are in structurally unfavourable positions and can only be reached by the workforce utilising a high rail elevated work platform and any work had to be undertaken close to the OHW system which was to be protected. Shotcreting whilst possible was not desirable in this location because it would lead to additional excavation depth at the haunch to accommodate the shotcrete thickness and the associated overspray allowance. Instead, stainless steel angles were anchored to the lining in a 'hit' and 'miss' sequence prior to the removal of a single brick course. Grouting any interface gap between the lining extrados and rock was also to take place prior to brick removal (Fig. 20).

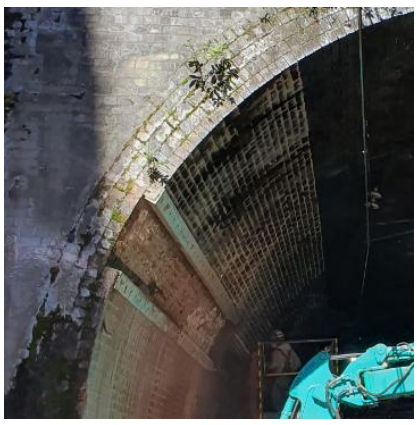


Figure 19. Completed haunch treatment between repointed mortar.

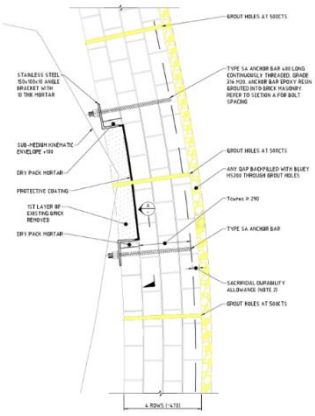


Figure 20. Haunch treatment cross section.

6.3 *Excavations in brick and concrete*

For many of the treatments involving trimming and underpinning in the walls the Continuum Alliance used a thirteen-tonne high rail excavator with a rotary milling head attachment with water spray to control dust (Fig. 21). Also in use was a trimming attachment comprising of stacked diamond discs which formed a trimming drum leaving a much smoother finish (Fig. 22).

Both methods used a machine guidance system to control trimming depths and tolerances. Controlling the profile was specifically important for trimming treatments as the design specified a minimum residual wall thickness for structural adequacy. As such, any trimming beyond the agreed construction tolerance could potentially result in the treatment type change from trimming to underpinning. Tolerances were controlled with survey set out and machine guidance.

The rotary milling head demonstrated significantly higher productivity in terms of square meters per hour compared to diamond-edged discs. It could also be positioned much closer to the toe during trimming. However, its precision was inferior due to the large cutting teeth, which often dislodged river stone aggregate from the original concrete wall. This resulted in a rougher surface profile increasing the risk of rework due to residual infringements. Notwithstanding this, the finish was no worse than the finish achieved during prior modifications.

For underpinning treatments in concrete, the rotary milling head attachment (Fig. 21) was used. Machine guidance wasn't as critical in underpinning areas as the work area was isolated and offsets to the desired depth could be set out and monitored by the operator.

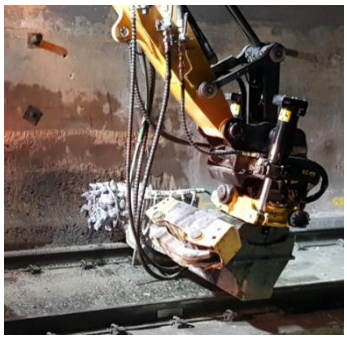


Figure 21. Rotary milling head attachment. Note size of cutting teeth and roughened wall profile.



Figure 22. Wall trimming with a diamond disc drum (light grey). Note smooth but undulating surface.

Another important element for the underpinning excavation was a 100 mm deep key to be cut behind the existing concrete plinth. The diameter of the rotary milling head could not achieve type of cut. Instead, the toe was sawn near vertically at the concrete plinth and subsequently hammered out. Underpinning in brick was also undertaken with the rotary milling head, however, to minimise vibration impacts at the portals, only handheld tools were used in these areas.

6.4 *Control of water ingress*

In Tunnels 1 and 10 significant seepage water ingress had to be managed, which posed a risk for underpinning and concreting works. Where water ponding occurred at the base of the panel (Fig. 23), a drainage relief slot was cut into the existing concrete plinth to drain the water (Fig. 24). Drainpipes connected to a drainage mat at the back of the excavation ran through this slot to permit permanent seepage water discharge into the tunnel drainage system. This was particularly important in areas of running groundwater inflow to ensure that the shotcrete was not placed against running or into ponding water, which would have likely resulted in defective concrete. The slot was finally backfilled and trowelled off during concreting of the main panels.



Figure 23. Water ponding after underpinning excavation.



Figure 24. Drainage mat and drainpipe through slot in plinth.

6.5 *Concrete placement*

Concrete placement in underpinning areas faced challenges. Both sprayed and cast in situ methods were initially trialled. The first shotcrete trial panel slumped this was caused by passing freight train movements only a couple of hours after completion. To prevent this, shotcrete panels were completed away from active rails, a steel mesh was added to stabilise the face at an early age, and the shotcrete panel curing times were increased before train operations resumed on the line.

Cast in-situ panels were also trialled but were less efficient due to the need for formwork preparation and removal. Additionally, daily survey checks were required to ensure minimum clearance between the formwork and operational rolling stock has been achieved, as the formwork protruded from the existing wall lining into the tunnel.

7 CONCLUSION

The BMRC project achieved the required NIF KE clearance in the Zig Zag tunnels, overcoming various design and construction challenges. These included identifying the location, extent, and depth of existing infringements, considering different construction methods and tolerances, assessing the condition of the existing lining, and determining its thickness. Through non-intrusive and intrusive investigations, the necessary treatment types for the infringement zones were defined. These treatments were based on the original wall thicknesses, minimum structural requirements, durability allowances and the consideration of the relevant construction tolerances.

Concrete and brick underpinning was done in a 'hit and miss' sequence to maintain tunnel stability during construction. Tailored construction sequences and temporary works ensured the integrity of brick tunnel portals and buttresses during construction.

The authors hope this paper adds valuable information to the as-built records of the Ten Tunnel Deviation. The methodologies and experiences from the BMRC project offer useful strategies for similar future projects. Publishing technical papers after modifications to historical tunnels is a long-standing tradition, providing valuable insights for future engineers involved in maintenance or rehabilitation works of the Ten Tunnels Deviation.

ACKNOWLEDGEMENTS

The authors would like to acknowledge and thank TfNSW and the Continuum Alliance for their permission to present this paper at the 2025 ATC Tunnel Conference. Special thanks to John Langford (CPB) & Martijn Tiemens (Acciona) from the Continuum Alliance for their valuable contributions throughout the project design development and during the construction phase.

8 REFERENCES

Duncan, S. D. 1980. Paved track for Australia's Blue Mountains Zig Zag tunnels, Tunnels & Tunnelling, May 1980, pp. 31-35, London, England.

Heritage NSW. 2023. Great Zig Zag Railway deviations tunnels, State Heritage Inventory, Sydney, Australia. Accessed online 23 April 2025: <https://www.hms.heritage.nsw.gov.au/App/Item/ViewItem?itemId=5012082>

Lithgow History Avenue, c. 2010. 1910 Ten Tunnels Deviation Completed, Lithgow History Avenue, Lithgow, Australia. Accessed online 23 April 2025: <https://www.lithgow.com/historyavenue/1910_tentunnels.html>

Lord, B. E. 1988. The Zig Zag Track Slabs Ten Years Later, Seventh International Rail Track Conference, pp. 18-21 October 1988, Auckland, New Zealand.

19th Australasian Tunnelling Conference – Acosta-Martínez, Stewart and Hudson-Smith (Eds.)
© 2025 Australian Tunnelling Society, ISBN 978-0-85825-002-4

Research and application of key technologies of 15m super-large diameter single shield TBM in complex geological highway tunnel

Z.G. Zhang, F. He, Y.Q. Lu, S.X Yuan, Z.F. Liu, W.H. Yin, E.J Peng & B. Zheng
China Railway Engineering Equipment Group Co., Ltd., Zhengzhou, China

H. Liu
China Railway Tunnel Co. Ltd., Zhengzhou, China

ABSTRACT: To address geological, rock breaking and tunneling efficiency challenges of super-large diameter TBM, a 15m super-large diameter single shield TBM was designed for the KK highway tunnel project in Georgia. The structure is optimized from aspects such as TBM sections, cutter head layout and main machine's anti-roll technology, solving difficult transportation, slow rock breaking and low tunneling efficiency. To tackle the adverse geological conditions such as large deformations of soft rocks, fault zones and water-rich strata encountered in this project, a number of targeted design and treatment measures are adopted to realize the smooth tunneling of the super-large diameter TBM in complex geologies. Finally, it carries out an in-depth analysis of the TBM tunneling performance. The pure tunneling time of TBM accounts for 39.7% of the whole construction period, and the equipment intact rate is 92.7 %, which demonstrates the good adaptability of super-large diameter TBM in this project.

1 INTRODUCTION

The tunnel boring machine (hereinafter referred to as TBM) is a kind of high-end tunneling equipment, which can satisfy the operation of excavation, support, muck discharge and other processes, and has advantages of high tunneling efficiency, high degree of mechanization and low safety risks (LU et al., 2021; HUANG et al., 2019; WANG et al., 2020). it has been developed rapidly in China, especially in the fields of railway (CEN et al., 2023), water conservancy (DU et al., 2021), mining (HE et al., 2023; TANG et al., 2023) and so on. With the acceleration of urbanization, the tunnels, as one of the key transportation infrastructures, are being built in increasing scales and quantities, leading to increasing demands for larger TBM excavation diameters, while the super-large excavation diameters, complex geological conditions and other factors will bring great challenges to the construction of such a TBM (GAO et al., 2021; LI et al., 2022; XIE et al., 2022).

In summary, TBM technology has developed rapidly, and prior to this study, the maximum application diameter had reached 13.91m. Many scholars have conducted in-depth studies on the structural optimization of the TBMs with medium to small diameters, as well as on the construction technologies for complex geological conditions. However, research on the design and application of 15m super-large diameter TBMs remains relatively limited, particularly regarding their systematic use in long-distance tunnels with complex and variable geological conditions. This paper is based on the Kvesheti-Kobi highway tunnel project in Georgia, which successfully applied a 15m super-large diameter TBM in practice, and conducts systematic research on structural design optimization, tunneling technology innovation and construction under complex geological conditions. Through engineering practice, the adaptability and tunneling efficiency of super-large diameter TBMs under complex geological conditions have

been verified, thereby filling a research gap in this field. This provides important theoretical and practical references for the future promotion and application of even larger diameter TBMs.

2 PROJECT OVERVIEW AND KEY DIFFICULTIES ANALYSIS

2.1 Project overview

The Kvesheti-Kobi (hereinafter referred to as KK) highway tunnel project is located between Kobi Village and Tskere Village in the Mtskheta-Mtianeti region in the northern part of Georgia. The TBM tunneling length is 8,860m, and the tunnel is designed as a two-lane super-large diameter highway tunnel with a diameter of 15.08m and a speed limit of 80km/h, which includes uphill sections with a gradient of 1.6% and downhill sections with a gradient of 2.35%. Moreover, the tunnel overburden generally exceeds 700m with a maximum overburden of 1,121m. During construction, complex geological conditions are encountered, including fault zones, high-pressure water burst, rock burst, soft rock large deformation and other adverse conditions. The strata along the tunnel are primarily composed of limestone and mudstone. The surrounding rock of the tunnel is mainly classified as Class III and Class IV, with Class IV accounting for as much as 44%. A comparison of the key parameters of the two types of surrounding rock is shown in Table 1.

Table 1. Comparison of Key Parameters between Class III and Class IV Surrounding Rock

Surrounding rock classification	Lithological characteristics	UCS/uniaxial compressive strength (MPa)	Degree of weathering	GSI/geological strength index	Q value (rock mass quality index)	RMR/rock mass rating
III	Predominantly limestone, locally containing muddy intercalation	60-130	Slightly to weakly weathered	65-80	10-40	61-80
IV	Interbedded mudstone and fractured limestone	15-60	Weakly to strongly weathered	40-65	1-10	41-60

2.2 Key difficulties for the super-large diameter TBM

As shown in Table 2, when the TBM diameter increases from 8m to 15m, the diameter only increases by 87.5%. However, the work from design and manufacturing to support, increases by a minimum of 63% and a maximum of 251%. Moreover, as the diameter of the tunnel face increases, the risks associated with surrounding rock deformation and collapse escalate significantly, and the construction difficulty rises sharply. Therefore, the work involved in the design, manufacturing and support, as well as the construction difficulty, of a 15m super-large diameter TBM are far greater than those of a medium-diameter TBM. This project is the first in both China and abroad to use a 15m super-large diameter hard rock TBM for construction, setting the record for the largest diameter hard rock TBM in the world. It faces multiple technical challenges, including transportation, tunneling efficiency, construction risks complex geological conditions and a long tunneling distance.

Table 2. Comparison of important parameters of TBMs with different diameters

Category	Item	Φ8m	Φ10m	Φ15m	Increment
TBM design	Excavation diameter/m	8	10	15	+87.5%
	Excavation area/m^3	50.2	78.5	176.6	+251%
	Installed power/kW	4,926	6,523	9,900	+101%
	Cutter qty.	49/19	62/17, 19	80/19, 20	+63%

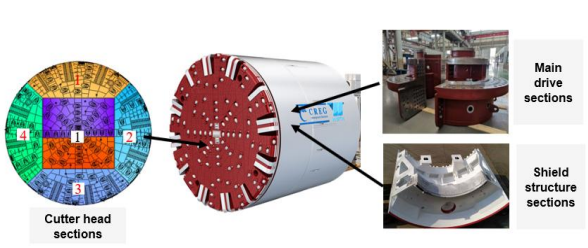
	(pieces)/diameter (inch)				
TBM manufacturing	Total weight/t	1,250	2,500	Approx. 3,400	+172%
	Transportation limit (width (m)/weight (t))	5.66/150	6.98/160	10.88/175	+92%
TBM support	Anchor bolt length per linear meter/m	29.3	47.1	74.8	+155%
	Initial shotcreting volume per linear meter/m^3	3.7	4.6	8.0	+162%
	Construction worker qty.	100	130	170	+70%

3 DESIGN OPTIMIZATION OF THE SUPER-LARGE DIAMETER TBM

To enhance the adaptability of the super-large diameter TBM during construction, targeted design optimization has been implemented, including the TBM section technology, disc cutter layout optimization and main machine's anti-roll technology. These improvements enable efficient excavation of the large cross-section tunnel.

3.1 Super-large Diameter TBM Section Technology

The super-large diameter TBM applied in this project features a cutter head weighing a total of 620t and an excavation diameter of 15.08m. It is transported from Zhengzhou, China to the Mtskheta-Mtianeti region in the northern part of Georgia via a "road-sea-road" transportation method. The road transportation route passes through restricted sections such as tunnels and bridges, which severely limit the transportation of the super-large diameter TBM cutter head and main drive system. Following the principles of modular and lightweight designs, a high-strength sectional cutter head was researched and developed. As shown in the Figure 1(a), the cutter head adopts a "4+2" section design, namely, the center section is divided into two parts, which is connected to four side sections with pins and high-strength bolts. The connection positions are designed with groove welds. The shield structure, main drive and other key parts also adopt the section design to reduce the weight and size of a single part, satisfying the transportation requirements on narrow roads.



(a) Super-large diameter TBM section technology



(b) Site assembly and launch of the super-large diameter TBM

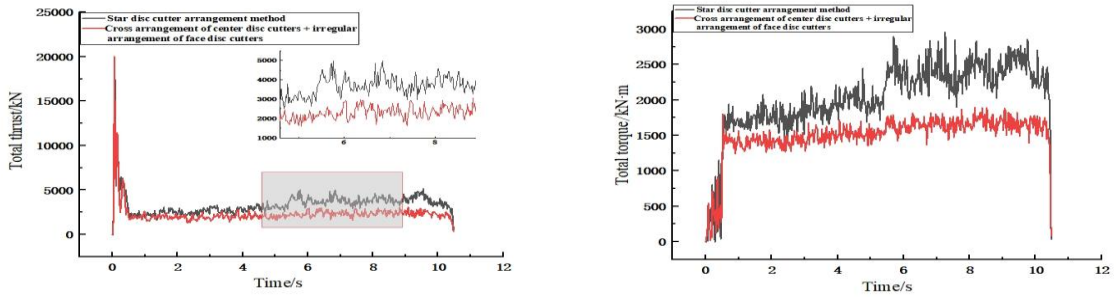
Figure 1. Application of super-large diameter TBM section technology

3.2 Disc Cutter Layout Optimization

Disc cutters are usually arranged evenly and systematically on the cutter head, and mainly have three arrangement methods (ROSTAMI et al., 2017), that is, spiral arrangement, star arrangement and asymmetrical arrangement. With the increase of the cutter head diameter, the wear of disc cutters accelerates, leading to the decrease of their service life, which greatly influences the tunneling efficiency. Thus, the super-large diameter cutter head shows relatively poor adaptability when adopting a conventional arrangement method of disc cutters. To solve the above problems, a new disc cutter arrangement method is proposed: cross arrangement of center disc cutters + irregular arrangement of face disc cutters, as shown in the Figure 2. To verify its advantages, Ansys is selected as the finite element simulation model to compare and analyze the cutter head load and torque under the star disc cutter arrangement method which is

commonly used in TBM design. The rock RHT (RockHoekT-Bimodulus) constitutive model was established (LI et al., 2017) . Taking account of the contact among rock, disc cutter and cutter head, and taking no account of gauge disc cutter impact on rock breaking, the rock's compressive strength was set to 154MPa, shear strength to 46.2MPa, and tensile strength to 9.24MPa. The static friction coefficient was set to 0.5, and the dynamic friction coefficient to 0.4. The rotation speed of the cutter head was set to 6r/min.

Through finite element analysis, the total thrust and torque of the cutter head with two different disc cutter arrangement methods are obtained, and it can be seen from Figure 3 that during the operation of the cutter head with the new disc cutter arrangement method, the total thrust and torque of the cutter head are smaller than those with the star disc cutter arrangement method. It can be concluded that for super-large diameter TBM, the cross arrangement of center disc cutters + irregular arrangement of face disc cutters can effectively reduce the load on the cutter head, avoid a stress concentration in a certain area of the cutter head, reduce the abnormal wear of the disc cutters, extend the service life of the cutter head and disc cutters, shorten the maintenance time, and improve the rock breaking efficiency in hard rock strata, which is better than the star disc cutter arrangement method. Therefore, the cross arrangement of center disc cutters + irregular arrangement of face disc cutters is selected for the TBM cutter head for the KK highway tunnel project in Georgia.



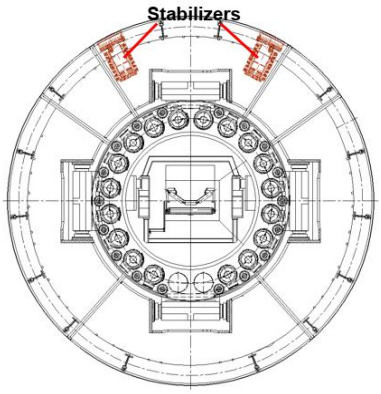
(a) Total thrust curve of cutter head

(b) Total torque curve of cutter head

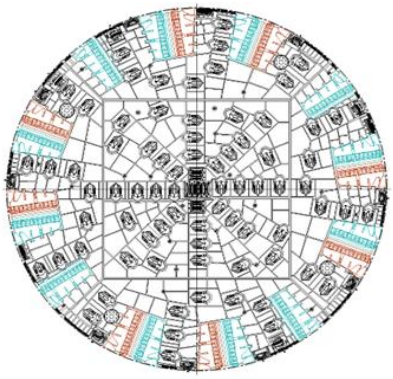
Figure 2. Finite element analysis results of cutter head

3.3 Single Shield TBM Main Machine's Anti-roll Technology

The single shield TBM mainly provides reactive torque of the cutter head through its own gravity and the friction between the shield and the surrounding rock. When the reactive torque cannot be provided sufficiently, it is very easy to cause the shield structure to roll, which brings construction risks and affects the normal tunneling of the TBM. In order to ensure the safe tunneling of the TBM in hard rock, the main machine's anti-roll technology is proposed. On the one hand, the shield structure is equipped with stabilizers. To prevent the shield structure from rolling due to the inability to stabilize itself in extremely hard rock, hydraulic stabilizers are installed on the upper part of the shield structure, as shown in Figure 4(a). During TBM tunneling, the stabilizers support on the surrounding rock to increase the friction between the shield and the surrounding rock, thereby obtaining greater reactive torque, preventing the shield structure and the segments from rolling due to insufficient reactive torque of the cutter head, and reducing the vibration of the main machine. On the other hand, bidirectional rotation technology is adopted. In addition to stabilizers, the drive is designed to be able to rotate bidirectionally, so that the cutter head can also rotate bidirectionally to break the rock and discharge the muck, as shown in Figure 4(b). When the stabilizers cannot prevent the shield structure from rolling, the attitude of the main machine can be corrected by changing the rotation direction of the cutter head. The above double preventive measures help to avoid damage to the segments caused by the rolling of the main machine, further improving the safety and efficiency of TBM construction.



(a) Layout of stabilizers



(b) Cutter head with bidirectional rotation function

Figure 3. Main machine's anti-roll technology

4 KEY TECHNOLOGIES FOR SUPER-LARGE DIAMETER TBM CONSTRUCTION UNDER COMPLEX GEOLOGICAL CONDITIONS

4.1 Large Deformation of Soft Rock

In the KK highway tunnel project in Georgia, there is limestone-dominated soft rock strata with large deformation, where the stability of the surrounding rock is poor and the risk of TBM jamming is extremely high. Furthermore, the contact surface between the super-large diameter TBM and the surrounding rock is large, resulting in greater resistance and a higher requirement for breakout ability. The breakout ability of the 15m diameter TBM shall be about three times that of the 8m diameter TBM. Therefore, in order to address the jamming problem of super-large diameter TBM in soft rock strata with large deformation, in addition to conventional anti-jamming measures, the targeted design of super-large diameter TBM is also needed. When the TBM reaches chainage 17+280m, the pressure of the gripper cylinder and the thrust cylinder increases abnormally, and the shield is locked due to the instability of the surrounding rock. It is found that there is a jamming problem (Figure 5). In response to this problem, the following four preventive measures are adopted to ensure the smooth tunneling of the TBM in the soft rock strata with large deformation.



Figure 4. TBM jamming

1) Cutter head overcut technology. The excavation radius is increased by 50mm by replacing cushion blocks of different thicknesses. On this basis, the excavation radius is increased by 50mm again by installing three 20-inch copy cutters and their inner supports. On this basis, the excavation radius is increased by 12mm again by replacing the cushion blocks of corresponding gauge disc cutters again, changing the diameter of corresponding gauge disc cutters from 19 inch into 20 inch, and replacing the inner supports of the three 20-inch copy cutters. Faced with different degrees of jamming, the above three methods are used to achieve different degrees of cutter head overcut, so as to increase the gap between the shield and the surrounding rock, and ultimately achieve the breakout of the TBM.

2) Bidirectional rotation technology. The drive is designed to be able to rotate bidirectionally and equipped with two-speed reducers, so that the main drive can switch between high-speed

gear and low-speed gear to meet the high-torque tunneling needs in the weak surrounding rock. The cutter head can also rotate bidirectionally to break the rock and discharge the muck. When the TBM is jammed, the breakout time can be greatly shortened by changing the rotation direction of the cutter head to improve the adaptability of the TBM to the surrounding rock.

3) Bentonite injection ports reserved on the shield. As shown in Figure 6, bentonite injection ports are reserved on the shield, so that when the TBM tunnels in the strata with a high jamming risk, bentonite can be injected in time to reduce the frictional resistance of the shield and also the risk of jamming.



Figure 5. Bentonite injection port on the shield

4) Deep-hole grouting technology. Soft rock strata with large deformation are prone to convergence, and the gap between the segments and the tunnel wall is filled with fractured surrounding rock, making the grout difficult to inject. Therefore, it is necessary to strictly ensure the timeliness of synchronous grouting. Furthermore, for secondary grouting, special auxiliary structures can be used to penetrate the collapsed surrounding rock for "deep-hole grouting", so as to fill the gap between the segments and the tunnel wall, and stabilize the segments.

4.2 Fault Zones

When the TBM tunnels in fault zones, it is easy to encounter problems such as collapse or spalling of the tunnel face and crown after excavation, difficulty in cutter head rotating and segment deformation, as shown in Figure 7. In order to reduce the risk of TBM construction in fault zones, targeted measures such as advanced geological prediction, changing the grout ratio and selecting reasonable tunneling parameters are taken.



Figure 6. Muck sample and segment deformation in fault zones

1) High thrust and torque design. The TBM is equipped with 57 (19×3) thrust cylinders in total. Under normal tunneling mode, a maximum total thrust of 226,255kN@350 bar can be achieved with a thrust coefficient of 130t/m^2. The TBM is also equipped with two-speed reducers, allowing the drive to have two different torque-speed curves. When tunneling in fault zones that require high torque, the two-speed reducers can be used to reduce the rotation speed of the cutter head and increase the torque, with the maximum torque reaching 1.8 times the rated torque. Through the above high thrust and torque design, difficulty in cutter head rotating and cutting in fault zones can be overcome.

2) Advanced geological prediction. When fault zones are encountered, the intensity of advanced geological prediction should be strengthened during construction, so as to accurately detect the position, scale and water distribution characteristics of the fault zones in time, and comprehensively assess the risk of instability and collapse of the fault zones, thus providing data support for the safe passage of the TBM and ensuring that appropriate countermeasures can be planned and implemented in advance during construction.

3) Changing the grout ratio. When the scale of the fault zones is small, it is necessary to erect the segments and inject grout into the gap between the segments and the surrounding rock exposed after TBM excavation in time. Therefore, it is necessary to optimize the grout ratio reasonably, so as to shorten the solidification time of the grout, and stabilize the segments in time.

4) Pre-grouting for reinforcement. As shown in Figure 8, probe drilling machines are equipped to drill holes within a 180° range at the crown, with a drilling depth of ≥40m and an inclination angle of not more than 8° . In addition, the advanced pipe shed support is also adopted to reinforce the fault zones, so that the tunneling can continue after the expected rock strength is reached.

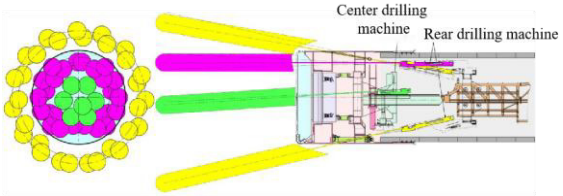


Figure 7. Pre-grouting

5 SUPER-LARGE DIAMETER TBM APPLICATION AND PERFORMANCE ANALYSIS

The TBM “Caucasus” for the KK highway tunnel project in Georgia has an excavation diameter of 15.08m, a maximum thrust of 22.6kt and a total power of 9,900kW, which is the world’s largest single shield TBM. The TBM was launched in September 2021 and realized breakthrough in April 2024 (Figure 9). With an accumulated tunneling length of 8,860m, the TBM achieved a maximum daily advance rate of 20m and a maximum monthly advance rate of 426m.

Figure 10 shows the percentage of total construction period accounted for by pure thrust time, segment erection and regripping time, normal maintenance time, downtime due to fault and problem handling time. According to the figure, the pure thrust time of the 15m super-large diameter TBM has a relatively large proportion, accounting for 39.7%. Benefiting from the optimized disc cutter layout and the applied main machine anti-roll technology, the TBM downtime, adverse geology handling time and normal maintenance time have a relatively small proportion. The application of key technologies for the super-large diameter TBM under the complex geological conditions ensures that the TBM goes through the complex ground safely and smoothly, the damage to the TBM is reduced and the performance of the TBM is generally at a high level, resulting in an equipment intact rate of 92.7%. The reason why the segment erection time has a relatively large percentage of 12.5% is that the backfill grouting is hindered and the grout fails to be solidified because of adverse geology such as fault zones and water and mud burst, requiring a lot of time to carry out secondary grouting to stabilize the segments. In summary, the 15m super-large diameter TBM performs well in its first practice, realizing safe and efficient tunneling and presenting its good adaptability in complex mountain tunnel construction.



Figure 8. TBM launch (left) and breakthrough (right)

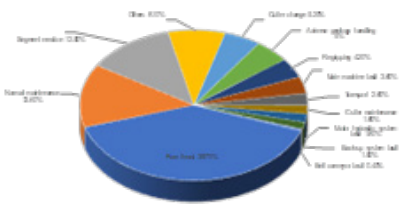


Figure 9. Construction time breakdown

6 CONCLUSION

To deal with the challenges such as long distance tunneling, large cross section and complex geology and reduce the influence of complicated construction conditions on the TBM construction safety and efficiency in the construction of KK highway tunnel in Georgia, the world's largest diameter single shield TBM (15.08m) was developed and put into use, and the conclusion includes:

1) The section design of cutter head and main drive and the optimized disc cutter layout are adopted to deal with the difficulties including inconvenient transportation, fast cutter wear and low tunneling efficiency, etc., which efficiently improves the service life and rock-breaking efficiency of the cutters; The design of shield stabilizers and main drive bidirectional rotation helps to avoid the roll of shield structure and segments caused by the insufficient anti-torque capability of cutter head; multiple targeted measures are taken to deal with such challenges as TBM jamming, segment deformation and water burst occurred in the tunneling sections with such adverse geology as large deformation of soft rock, fault zones and water-rich strata in this project, which helps to realize the successful tunneling and gain experience on the application of super-large diameter TBM in complex geology.

2) Combined with the application of 15m super-large diameter TBM in the KK highway tunnel project in Georgia, in-depth analysis on the TBM tunneling performance is carried out and the percentages of TBM tunneling time and downtime caused by some reasons in total construction time is counted up, which concludes that the pure thrust time accounts for 39.7% and the equipment intact rate after TBM breakthrough is 92.7%. This proves that the super-large diameter TBM shows good adaptability in the project. Besides, the successful breakthrough of the KK highway tunnel project is of great significance in promoting the application of the China's super-large diameter TBM, the economic development of Georgia and the rapid development of "the Belt and Road Initiatives".

7 REFERENCES

[1]CEN, D.Y. et al. 2023. Selection and Application of TBM in Super-large Diameter Tunnel Under Complicated Geology Condition. *Construction Technology* 52(5): 97-102.

[2]DU, L.J. et al. 2021. Tunnel boring machine selection and tunneling attitude control method for tunnels with small turning curves. *Tunnel Construction* 44(05): 1106-1115.

[3]GAO, S.B. et al. 2021. Rupture characteristics and seismic recurrence behaviors of Xianshuihe fault revealed by Xinyulin trenches, south of Kangding. *Advanced Engineering Sciences* 53(3):53–61.

[4]HE, F. et al. 2023 Application of TBM in coal mine adaptability type selection analysis and new technology development. *Coal Science and Technology* 51(S1):351-361.

[5]HUANG, D. et al. 2019. Development Status and Trend of Tunnel Boring Machine in Underground Metal Mine Application. *Nonferrous Metals Engineering* 9(11):108-121.

[6]LI, A. et al. 2022. Progressive collapse mechanism and safety control of deep buried tunnel vault in soft and broken surrounding rock. *Advanced Engineering Sciences* 54 (6):85–96.

[7]LI, H.C. et al. 2017. Study on Parameters Determination of Marble RHT Model. *Transactions of Beijing Institute of Technology* 37(08):801-806.

[8]LU, Z.G. et al. 2021. Design and application of a compact TBM for an ultrasmall turning radius: a case study on a drainage gallery tunnel project of Wendeng pumped storage power station in Shandong, China. *Tunnel Construction* 41(6):1047.

[9]ROSTAMI, J. & CHANG, S.H. 2017. A Closer Look at the Design of Cutterheads for Hard Rock Tunnel Boring Machines. *Engineering* 3(6):892- 904.

[10]TANG, B. et al. 2023. Full scale model tests of fabricate support structure for TBM-excavated coal mine roadways. *Advanced Engineering Sciences* 55(2):242-251.

[11]WANG, D.J. et al. 2020. Tunnel boring machine (TBM) in coal mine and its intelligent key technology. J*ournal of China Coal Society* 45(6):2031-2044.

[12]XIE, H.P. et al. 2022. Analysis and thoughts on surrounding rock mass catastrophe of deep-buried tunnels in extremely complex high mountain areas. *Advanced Engineering Sciences* 54(2):1-18.

19th Australasian Tunnelling Conference – Acosta-Martínez, Stewart and Hudson-Smith (Eds.)
© 2025 Australian Tunnelling Society, ISBN 978-0-85825-002-4

Delivering Watercare's Central Interceptor Project, Auckland New Zealand

J.B. Sickling
Watercare Services Ltd., Auckland, New Zealand

ABSTRACT: This paper explores the successful delivery of tunnelling for the Central Interceptor Project, going back to decisions made since the concept design stage (2009-2011) and more recently through construction, culminating in final tunnelling breakthrough in March 2025. The paper is written from the client's perspective, discussing the key decisions resulting in successful delivery of the project. Topics covered include contract selection and ground risk allocation, along with selection of tunnel alignment and the specification of tunnel boring machine requirements. The paper touches on some of the benefits and disadvantages of Employer's design; approach to sewer gas corrosion and durability; client-side contract delivery and administration using a blended team; and some of the outcomes recognised through collaborative working between all parties to the contract. The importance of a robust approach for budget setting and management is discussed. Perspectives are shared on some of the approaches and initiatives contributing to successful health and safety outcomes.

1 INTRODUCTION

Auckland is New Zealand's largest city, with a population of 1.7M people, located on a narrow isthmus between the Waitemata and Manukau Harbours. Central Auckland is the oldest part of the city and has a mainly combined sewer stormwater system. The area experiences significant rainfall, resulting in regular surcharging and Combined Sewer Overflow (CSO) discharges, via overflow structures located on stream banks and coastlines. In the early 2000s, Watercare recognized the need for a scheme to intercept the CSOs and convey them to the Manukau Wastewater Treatment Plant (WWTP) for treatment.

Following the detailed design phase between 2014-2018 by Watercare's consultants (a Jacobs-led team including AECOM and Delve Underground), the project was put out to international tender for construction. The appointed Contractor was Ghella-Abergeldie Joint Venture (GAJV) and construction commenced in May 2019. TBM mining of the 16.2km of main tunnel was completed in early 2025. The southern system was successfully brought into operation in early 2025.

2 PROJECT OVERVIEW

2.1 *Key requirements*

Following the concept design and consenting phases, the key requirements driving the design of the project included the following:

- Achieve 80% volumetric reduction of CSOs.
- Provide a gravity tunnel system, with a single downstream pumping station.
- Cater for the existing geology, to minimize risk to tunnelling and permanent works.
- Provide a maintenance-free underground tunnel and dropshaft system.

– Provide multiple levels of redundancy for operation of the pumping station.
– Provide a Real-Time Control (RTC) gating system, to protect the pump station from excessive inflows beyond its' pump-out capacity.

2.2 *Scheme details*

While originally designed and tendered as a 13.1km long 4.5m ID segmentally lined tunnel from MPS to Western Springs, the tunnel was subsequently extended to a 16.2km long tunnel with upstream termination in Pt Erin Park. Figures 1a and b indicate the scheme alignment, Figure 2 provides an indicative long section of the main tunnel.



Figure 1a. Scheme southern section (MPS to May Rd).



Figure 1b. Scheme northern section.

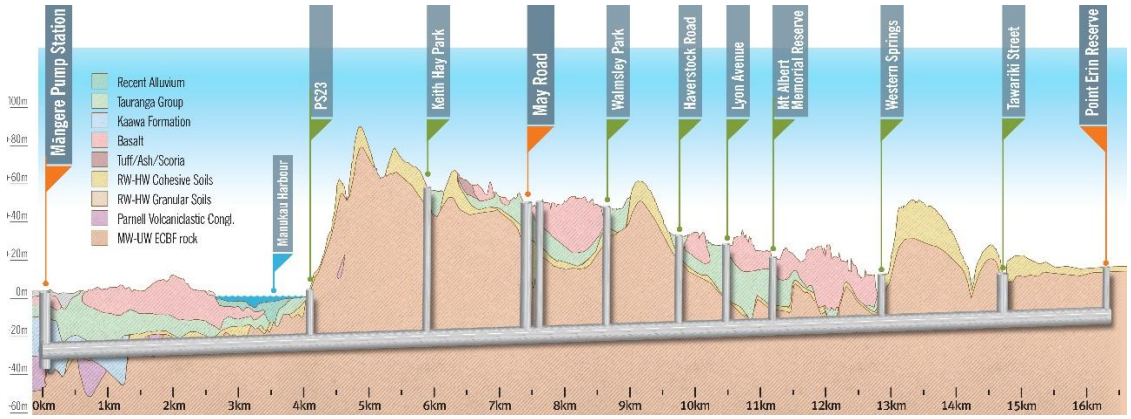


Figure 2. Indicative long section showing geology of the main tunnel alignment (exaggerated vertical scale).

The tunnel carries both dry weather flow (separate sewage) and wet weather flow (CSO), depending on the climactic conditions. The tunnel was constructed with a 1:1000 (V:H) gradient, designed to provide self-cleansing velocities. Upstream grit traps prevent larger material from entering the system. Real-Time Control (RTC) gates manage flow into the tunnel system.

The project included two pipejacked Link Sewers B and C, the purpose being to extend the reach of the scheme out to capture various CSOs that could not be intercepted directly by the main tunnel. At the downstream end, a new 7.2m^3/s max capacity pumping station (the MPS) lifts the wastewater flow from the deep gravity tunnel to the Mangere WWTP for treatment. Air Treatment Facilities (ATFs) are located at both the MPS and May Road.

The project has been future-proofed with connection points for various future upstream projects, to be delivered subsequently to the Central Interceptor. The key project statistics are summarized in Table 1 below:

Table 1. Key project details.

Main Tunnel	-	Earth Pressure Balance (EPB) TBM, precast segmental lining
	-	4.5m Internal Diameter (ID), 16.2km Length, max depth 110m
	-	11 No. shafts (7 No. cascade drops, 2 No. vortex drops, 2 No. other shafts)
Link Sewers B&C	-	EPB MTBM, jacking PE lined reinforced concrete pipe
	-	1.1km of 2.4m ID and 3.2km of 2.1m ID respectively
	-	7 No. cascade dropshafts (6 No. cascade drops, 1 No. access shaft)
MPS	-	7.2 m^3/s max capacity
	-	Peanut shaped (∞) dual diaphragm wall shaft; inlet shaft 12m ID and 33m depth; pump station shaft 26m ID and 38m depth.
	-	Trenched twin rising main, DN1400 PE pipelines, from MPS to WWTP.
Other	-	ATFs (1 x BTF and AC at May Rd; 1 x biotrickling filter at MPS)
	-	10 No. RTC gated inflow locations.

3 SCHEME DEVELOPMENT PHASE RISKS

3.1 *Ground conditions risks*

Central Auckland is underlain by East Coast Bays Formation (ECBF) weak rock, and this material is extensive throughout the project. However, the tunnel horizon was known to encounter dense Kaawa Sands and potentially touch some volcanic deposits within the downstream 3km reach of the tunnel. Previous tunnelling projects have demonstrated the ECBF to be an ideal material for Earth Pressure Balance TBM tunnelling, albeit with occasional problematic lenses of higher strength Parnell Volcaniclastic Conglomerate material.

To inform the design and manage the risk of unexpected ground conditions, several comprehensive geotechnical investigation campaigns were undertaken following the initial tunnel and route selection in 2009. These campaigns were focused on the higher risk materials that couldn't be confidently avoided, particularly aiming to provide confidence on the basal surface of volcanic deposits and characterizing the Kaawa Sands with respect to suitability for EPM TBM tunnelling.

3.2 *Contractual ground risk allocation*

Following the successful use of Geotechnical Baseline Reports (GBRs) for tunnels in Auckland dating back to the mid 2000s, Watercare and its advisors considered it necessary to implement a GBR to provide the clearest possible contractual definitions of ground risk allocation between the Employer and the Contractor. The GBR was contractually dovetailed into the modified FIDIC Red Book contract definition for 'Unforeseeable physical conditions'.

3.3 *Geotechnical Baseline Report - retrospective recommendations*

While the GBR was considered to be a useful and appropriate tool for clarifying ground conditions risk, there are a number of recommendations by Watercare's team for future GBRs and baselines:

1) Baselining groundwater infiltration inflows into shafts will tend to lead to disputes rather than avoid them. All deep shafts on a project such as this require temporary support, often of types such as secant piles, diaphragm walls or caissons, the construction of which all have a significant impact on the quantum of groundwater inflows. Groundwater infiltration into a shaft is not a fundamental property of the ground but is significantly impacted by the temporary works and construction approach. Other commercial approaches to managing the allocation of this risk may be more appropriate.

2) Site contamination was not baselined for the project, but it is recommended that clear baseline statements could and should be made in future for similar projects, depending on the knowledge of contamination and risk appetite of the Employer.
3) While ground conditions were baselined for tunnels and shafts, baselines were not provided for comparatively shallow surface sites, e.g. with permanent works up to 15m depth. This approach is considered pragmatic for the project, given the geographical spread and range of conditions which would have resulted in complex 3D models for comparatively little value.
4) Apart from one claim for Unforeseen physical conditions (UPC) relating to ground conditions for a shaft (i.e. covered under the GBR), the vast majority of UPC claims related to non-baselined items such as contaminated soils, existing assets, and utilities.

3.4 *Key tunnelling risks*

At concept design phase (2009-2011), various tunnelling related risks were identified and considered, with further assessment and mitigation during the detailed design phase (2014-2017). The key tunnelling risks and treatments recognized prior to construction are discussed below:

1) Horizontal alignment challenges
   a. Risk: Auckland has a considerable number of volcanic centres. These volcanoes present difficult ground conditions for EPB TBMs, such as high-strength basalt lava flows and 'necks', and high rockmass permeability.
   b. Treatment: it was elected to adopt a route that avoided volcanic deposits which had been identified during the previous ground investigation campaigns.
2) Vertical alignment and associated ground conditions challenges
   a. Risk: the design of a cost-effective terminal pumping station involves minimizing the pumping head required, and therefore CAPEX and OPEX. Conversely, raising the vertical alignment to the highest level would mean tunnelling through potentially unfavorable ground conditions with associated cost, delay and safety risks. The key sources of risk anticipated with tunnelling in unfavorable ground included:
      i. Abrasion and damage of the cutterhead if volcanic ground was encountered;
      ii. High hydrostatic groundwater pressures (up to 9 bar) could result in excessive groundwater inflows through the EPB screw and loss of plug;
      iii. Hyperbaric cutterhead face interventions, possibly in excess of 3 bar;
      iv. Difficulty with spoil conditioning and maintaining a screw plug when tunnelling in the Kaawa Sands;
   b. Treatment: an optimum vertical alignment was identified which achieved an acceptable trade-off between hydraulic design objectives and tunnelling risk.

3.5 *TBM Tunnelling risk mitigations*

Various tunnelling risk mitigations were included in the TBM specification and via variations:

1) TBM type: the TBM was specified as a new purpose-built EPB TBM, required to be capable of maintaining closed mode pressures for specified reaches of the tunnel in order to manage groundwater inflows and face stability, also minimising surface settlement.
2) TBM specification requirements:
   a. Given the long drive lengths envisaged (e.g. >7.5km) and the risk of encountering high strength (e.g. >200MPa) basalt, the specification included a requirement for "*chromium carbide wear protection plates and hard face welding*".
   b. Design of shield, bearings and seals for a max operating pressure of 9 bar, reflecting anticipated hydrostatic pressures under the deepest sections of the alignment.
   c. A fourth row of wire brush seals was accepted, in lieu of an inflatable safety seal when replacing/maintaining the service wire brush seals.
   d. Provision of dual screw, or substitute, for tunnelling at pressures up to 9 bar: the contractor proposed a positive displacement pump system in lieu of the second screw.
   e. Provision of double guillotine gates on the screw discharge, to manage loss of plug.
   f. Provision of airlock with operating pressure of 5 bar, for hyperbaric interventions.
3) Watercare requested a value-engineering proposal for electric locomotives, which was accepted and instructed into the works, providing benefits of air quality and sustainability.

4) Watercare instructed the Contractor to undertake fire laboratory combustion tests of the embedded PE linings on both the tunnel segments and jacking pipes. The findings indicated that misting systems would be effective at stopping fire spread, further described in reference [1].

3.6 *Pipejacking risk mitigations*

The Employer's pipejacking specifications allowed for either Earth Pressure Balance or slurry micro-tunnel boring machines to be provided. The Contractor elected to provide a refurbished Herrenknecht EPB MTBM capable of jacking pipes at 2.1m ID or 2.4m ID. The same MTBM was employed on both Link Sewers B and C, utilizing up-skinning.

Drive lengths were dictated by the location of the permanent shafts, which had access shaft and dropshaft functions. For the Link Sewer C pipejacking, the maximum drive length at tender was 966m. Post-award the Contractor offered a value-engineering proposal to delete an access-only shaft, resulting in a longest drive length of 1192m. This presented some concerns regarding personnel evacuation times under fire scenarios in the constrained conditions. Ultimately, acceptable mitigations were demonstrated by drills within the pipejack micro-tunnels.

3.7 *Employer design vs Contractor design*

At the outset of the detailed design phase, Watercare determined that it wished to substantially own the design for the scheme, rather than allocate responsibility to the Contractor. Various elements of the scheme, such as the tunnel lining, cascade shafts, and the May Road Air Treatment Facility, were delivered via Contractor's design. The perceived benefits of the Employer's design approach were considered to be:

- Maintaining control where Watercare would be operating assets day to day.
- To obtain mechanical and electrical plant and systems that were compatible with existing Watercare assets and systems, from an operations and maintenance perspective.
- To leverage lessons learned from the design, construction and operation of the 'Project Hobson Scheme' delivered between 2007-2010, considered a smaller scale prototype project.
- To facilitate better understanding of construction cost prior to tendering and budgeting.
- To allow tenderers to bid on the same basis without demanding significant energy and expenditure on tender design, given the extent and complexity of the scheme.

With the benefit of hindsight, the Employer's design approach possibly had some downside with respect to the sizing of the MPS inlet shaft, which adopted a minimum sized approach from a hydraulics, however this presented spatial (safety) and tunnel productivity issues for the Contractor's elected use of the inlet shaft as its tunnelling operation shaft.

4 PROCUREMENT PHASE RISKS

4.1 *Basis of contract, EOI and tendering*

During the detailed design phase, Watercare made the decision to procure the scheme as a single contract based on a FIDIC 1999 Red Book form of contract, modified for local conditions. As discussed in the previous sections, there was split responsibility between Employer and Contractor design elements. The design and specifications for the work were developed accordingly.

In late 2017, Watercare engaged with the international tunnel construction market for expressions of interest for the delivery of the project, ultimately shortlisting four contracting entities including constructors from New Zealand, Australia, France and Italy. The project was tendered in mid-2018, and of the four bidders the GAJV were selected.

At the time of tendering, there was a perceived risk of hyper-inflation occurring in the New Zealand economy. Watercare decided on an approach of risk-sharing, with the Contractor taking the risk of escalation up to a ceiling, beyond which the Employer would take the risk. Due to the pandemic and other Employer's risk events, the escalation ceiling war reached. The approach proved mutually fair and acceptable to both parties.

4.2 *Procurement phase – key materials and supply risks*

Prior to floating tenders, it was recognized by Watercare that the design and specification of the project included two elements which were constrained with respect to the number of suppliers that could meet the requirements. In particular, the following risks and treatments were identified:

1) Prefabricated Glass Reinforced Plastic (GRP) cascade shafts of 3m ID were to be designed by the Contractor for installation in two blind bored shafts (78m and 65m depths respectively). There was a single New Zealand based supplier deemed capable of supply, with perceived risk of pricing and obtaining conforming product. The risk was not resolved prior to floating tenders, but managed in conjunction with the following risk (ARC) post-award.
2) Elements of the works which would be exposed in-service to corrosive H_2SO_4 sewer gas were initially designed as being constructed out of Acid-Resistant Concrete (ARC), described in reference [2]. This included the main tunnel, various cascade dropshafts and the MPS inlet shaft and wet well chambers. Watercare had undertaken extensive pre-tender testing, including *in-situ* performance tests, with potential international suppliers of ARC. While the test results were encouraging, they were ultimately deemed inconclusive and presented significant procurement risk to Watercare if pursued. The following risk treatments were implemented:
    a. *Tunnel lining*: prior to floating tenders, Watercare elected to change the sewer corrosion protection approach from ARC to an embedded mechanically anchored Polyethylene (PE) lining, with additional minimum 50 year-life sacrificial concrete. A tunnel segment is shown in Figure 3, with further details in reference [3]. The concept was similar to the solution adopted on the IDRIS project, see reference [4].
    b. *Cascade Dropshafts*: the requirement for some cascade dropshafts to be constructed from ARC carried over into the contract, while others remained OPC concrete. The Contractor proposed that the GRP cascade shaft concept could be scaled up and applied in lieu of all ARC cascade dropshafts. This proposal was accepted, with GRP cascades being supplied up to 7.5m ID.
    c. *Pumping Station inlet shaft and wet well*: as part of its value engineering proposal, the Contractor successfully proposed that the cast *in-situ* secondary lining of these shafts could be protected by a combination of PE membrane and increased sacrificial ordinary Portland cement concrete, in line with the approach for the tunnel linings. Refer Figure 4 showing the MPS shafts under construction during TBM launching.



Figure 3. Tunnel PE corrosion protection liner segment in precast facility.



Figure 4. MPS shafts during TBM launch, PE corrosion protection lining is green.

4.3 *Budget and contingency management*

One of the critical success factors for Watercare has been appropriate budget management, with timely internal communication of the risks and requirements for additional budget. The development of the project as substantially Employer's design has allowed the costs to be estimated with

confidence prior to floating tenders, as compared to many projects which are delivered with a lower level of scope definition. With all four tenders below the budget threshold, Watercare were able to carry an appropriately sized risk contingency to deliver the project. The contingency was utilized for items not foreseen at the time of tender, including:

- Several projects from Watercare's Western Isthmus Water Quality Improvement Programme (WIWQIP), which directly connect into the project, were added-in as variations.
- The Employer accepted some of the Contractor's value-engineering proposals, which ultimately provided benefits to the Employer in improved health and safety outcomes, quality and design life outcomes, lower cost, and schedule certainty.
- The realization of various Employer's risks, such as UPCs, COVID-19 pandemic impacts, global supply chain disruptions due to war, extreme weather and other similar events.

5 CONSTRUCTION DELIVERY PHASE

5.1 *Governance*

Watercare developed the contract documents with the intention of achieving collaborative partnering behaviours to the extent possible within a fixed price lump sum contract. This approach included layers of governance and oversight built into the contract, as summarised below.

1) Project Governance Group (PGG): the PGG included the Engineer and senior members from all parties, including the Employer's designer. The group was set up to provide a governance function for which the main purposes were to:
   a. Pragmatically diffuse potential disputes which would otherwise be difficult for the Engineer and Contractor's Representative to resolve under the contract.
   b. Ensure collaboration between the parties focused on problem solving rather than adopting contractual positions, including initiating various working groups.
   c. Provide alternative points of view and project performance feedback from senior construction industry figures and leaders from the various company organizations.
2) Leadership Steering Group (LSG): the LSG comprised executive leaders of the Contractor participant companies, the Employer and its' designer. The purpose of this group was to regularly review the project health and culture, discuss key issues and risks, and provide direction for resolving sensitive items such as negotiations and settlement of claims.

5.2 Alignment with WorkSafe New Zealand

New Zealand's health and safety regulator is WorkSafe New Zealand (WorkSafe), and the High Hazards Unit is its' relevant division focused on work under the Mining regulations. Watercare engaged regularly with the High Hazards Unit during development of the detailed design, during tender, and alongside GAJV during construction. As at the time of writing, it is considered that proactive communications and transparency exhibited between Watercare, the GAJV and WorkSafe have contributed to good health and safety outcomes for the workers.

5.3 Construction Management

Watercare recognized during the tendering phase that there would be significant benefit to providing an appropriately sized client-side Construction Management (CM) and contract administration team, to ensure that its desired project outcomes were realized. A blended team with a 'one-team' focus were sourced from Watercare and its various consultants, including Jacobs, Rider Levett Bucknall, AECOM, and Delve Underground. The Contractor's staff, the Engineer and the Employer's CM team all adopted collaborative and 'best for project' working approaches from the outset.

In the area of health and safety, all personnel of the Contractor and Employer were chartered with a view to health and safety outcomes being everybody's responsibility, in alignment with the principles of the Health and Safety at Work Act (2015). Watercare collaboratively implemented many initiatives with the GAJV to provide enhanced outcomes. Several examples follow:

1) 'Beacon Site' programme, to award sites a special status when they achieved outstanding H&S standards;

2) Establishing a real-sized pipejacking training facility, to promote working at height and fire simulation scenario training;
3) Providing electric locomotives in the tunnels;
4) Implementing 'Heartstrong' programme (worker heart health screening and education).

6 CONCLUSIONS

Successful delivery of the Central Interceptor project has been based on a foundation of ongoing risk assessment and challenge since the initial design stages of the project. As the project has progressed through different stages, various decisions and interventions have been made to manage delivery risk to acceptable levels, as discussed in the paper.

The project is nearly complete and to date has been delivered on time, to budget and has been well received in the media.

Health and safety outcomes to date have been good, with minimal serious harm accidents and no construction-related fatalities.

Good project outcomes do not happen by accident, but rather are the result of hard work and continuous improvement, coupled with a collaborative 'best for project' partnership attitude from all parties.

ACKNOWLEDGEMENTS

The author acknowledges that this paper summarises the work and outcomes driven by many other individuals of both Watercare, GAJV and the various consultant organisations. In particular, the contributions of Shayne Cunis, Nigel Varcoe, David White, Francesco Saibene and his GAJV team are noted.

7 REFERENCES

Agnew, N., Zavlangas, D., Miles, P. 2023. Managing Fire Risk for Construction of Watercare's HDPE-Lined Central Interceptor Tunnels. *Proceedings of the 18th Australasian Tunnelling Conference 2023.* New Zealand.

Grace, S., Kay, N., Goff, S. 2019. Developing a Corrosion Strategy to Protect New Zealand's Largest Wastewater Asset. *Water New Zealand Conference & Expo 2019*. New Zealand.

Surya, P., Goff, S., Raedle, A., Suhaendi, S.L. 2023. Design of an Innovative Single-Pass Tunnel Lining for Watercare's Central Interceptor Tunnel. *Proceedings of the 18th Australasian Tunnelling Conference 2023.* New Zealand.

Najder Olliver, A.M., Lockhart, T. 2017. Innovative One-pass Lining Solution for Doha's Deep Tunnel Sewer System. *Proceedings of the World Tunnel Congress 2017 – Surface challenges – Underground solutions.* Bergen, Norway.

19th Australasian Tunnelling Conference – Acosta-Martínez, Stewart and Hudson-Smith (Eds.)
© 2025 Australian Tunnelling Society, ISBN 978-0-85825-002-4

Southern tunnel works – A case history

N Mackintosh, T Bentley & K Teruya
John Holland, Sydney, Australia

ABSTRACT: Western Harbour Tunnel (WHT) Stage 1, or Southern Tunnel Works (STW) is a complex network of road tunnels, located roughly beneath the suburb of Balmain in Sydney, NSW, Australia. The project was completed on 14 February 2025 with excavation of approximately 8.5 kilometres of mined tunnels undertaken with eight roadheaders and one surface miner. The project had a unique arrangement with all supporting site infrastructure contained underground, which is unprecedented locally. Having the project operate entirely underground reduced the impact of construction on the community and local environment. Given the unique arrangement of STW, a decision was made early in the project to focus on engineering innovative solutions, to ensure program could not only be met, but reduced beyond initial expectations. This paper aims to outline some of the unique challenges & solutions that were managed by the team and how communication and collaboration is key to a successful project delivery as logistically complex as STW.

1 GENERAL OVERVIEW – A UNIQUE TUNNEL PROJECT

STW was awarded to John Holland CPB Joint Venture (JHCPB) as a variation to the WestConnex 3B Rozelle Interchange (RIC) project. RIC required handover and opening completion more than one year before opening completion of STW. This commencement of STW during the commissioning phase of RIC provided an opportunity for a tunnel excavation project with almost nil surface footprint, reducing the impact on the community. It was during the overlap of STW and RIC that the infrastructure was established underground within STW, a process that added a significant interface coordination at a time of commissioning of one of the most complex road infrastructure projects undertaken in Australia. This setup phase would enable STW to operate independently of RIC when the time came for RIC handover.

The project itself contained 8.5km of mined tunnels, starting at WHT Cut & Cover (C&C) located adjacent to a major state road, City West Link, and extending to an underground stub, located at the northern point of Birchgrove, immediately before Sydney Harbour, (see figure 1 below for a general arrangement of STW overlaid with RIC). Excavation volumes for the project was 997,085 bank cubic meters (BCM) of Hawkesbury Sandstone, or to put this in perspective the equivalent weight of 103,697 humpback whales worth of spoil. 100 per cent of this spoil was required to be removed via underground loadout through the WHT C&C to City Westlink.

With the exception of a narrow entry/exit of the WHT C&C, the construction footprint of STW was entirely underground and unseen by the community. To add to the challenges, this approximately 1,000m2 narrow surface footprint, was on a bridge over a drainage canal, connecting the adjacent road City West Link, with the WHT Cut & Cover.

The entry itself into WHT C&C is also limited in height – to a maximum of 5.1m clear height, smaller than the machines that were required to excavate STW.

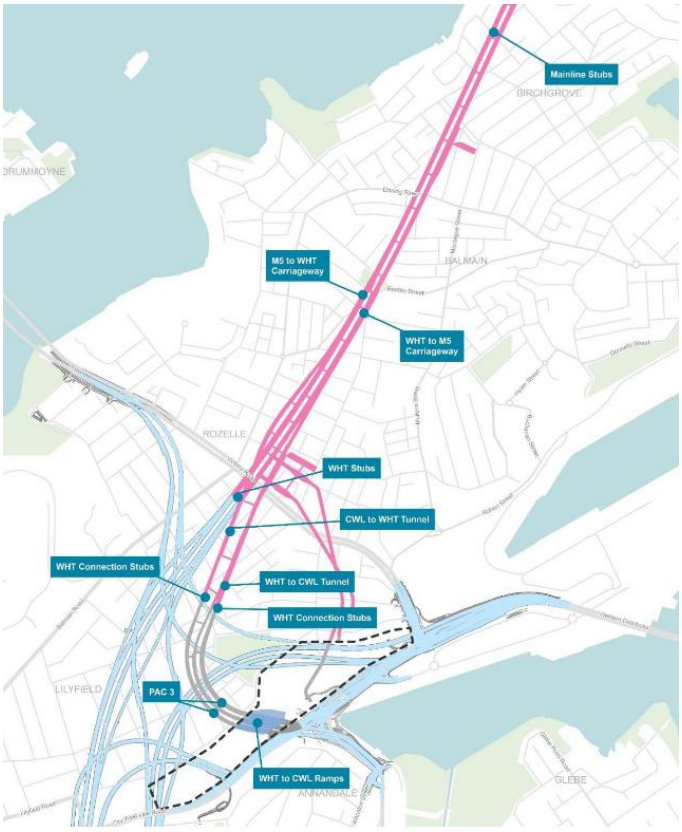


Figure 1. STW General Arrangement (shown in Pink).

2 SITE OPERATIONS & LOGISTICS - SURFACE VS UNDERGROUND

The infrastructure required to support roadheader excavation is extensive and complex. Traditionally such projects with fewer roadheaders than the eight used at STW, require a large usable surface footprint to accommodate this infrastructure. This typical infrastructure includes items such as site offices and amenities, a soundproofed spoil shed, water treatment plant, materials laydown area and plant maintenance workshops, intertwined with vehicle haul roads with sufficient swept paths for large plant.

A typical surface site of comparable scope was known as 'Tunnel Site C' at RIC. Refer to Figures 2 & 3 below, where footprints of Tunnel Site C and STW can be compared. The surface area of Tunnel Site C is approximately 20,000m^2 in area, whereas STW occupied only 1,000m^2 of surface footprint, or about 5% of the size.

Due to these limitations, and the requirement that supporting infrastructure for STW must be entirely independent from RIC - all project infrastructure was located underground, either inside the mined tunnel portals, or within the Cut & Cover. It was only the small site office with amenities which had the opportunity for taking in the view of Sydney Harbour at surface. Significant items of infrastructure that were uniquely placed underground at STW includes:

- Spoil Stockpile; a place for dump trucks to stockpile excavated material, for loadout offsite
- Truck Access Roads; for removal of tunnel spoil, to move trucks to the spoil stockpile, load, and move back offsite with material taken from the stockpile
- Water Treatment Plant (WTP); for treatment of tunnel water prior to discharge or re-use
- Sedimentation pond; to remove large solids from tunnel water prior to treatment in WTP
- Fresh air ventilation fans; to provide a safe and cool environment underground
- Bulkheads & airlocks; to ensure the fresh air fans are isolated from dirty return air
- 30,000 litre water reservoirs; to supply potable water underground and to excavation faces

- Air Compressors & Receiver Tanks; to supply high pressure and safe compressed air underground
- High and low voltage substation and switching gear to provide power to the key items of plant
- Secure communications infrastructure and network to allow efficient communication and safe work environment
- Wheel wash; to clean tires of trucks & other vehicles immediately prior to exiting the site
- Mechanical workshops; to undertake maintenance and repairs to plant
- Bulk diesel supply tanks & fuelling station; to provide plant with fuel
- Bulk accelerator tank; for dosing shotcrete so it can be sprayed effectively



Figure 2. Rozelle Interchange 'Tunnel Site C' Surface Footprint.



Figure 3. STW Surface Footprint

Spoil handling and disposal presented one of the largest challenges while establishing the tunnel project entirely underground. At peak roadheader production, approximately 36,000 tonnes of spoil was excavated from the tunnel face per week. To facilitate continuous excavation, spoil requires removal from the site at the same rate at which it is excavated, or the tunnel would have quickly become inundated, thereby stopping production and progress.

It was critical that the truck movements and spoil handling within the site is smooth and efficient. The internal footprint and alignment of a road tunnel is designed with high radius curves to facilitate safe travels of cars and trucks. This geometry is adverse for efficient spoil handling in comparison to the large open plan spoil sheds erected on the surface. With restrictions on tunnel width, height and turning radius, spoil handling locations needed to be meticulously space-proofed ahead of time. The completion of the tunnel within this footprint also had to be considered, as spoil operations would significantly hinder the ability to complete the remaining follow-on works (e.g. waterproofing, secondary lining and drainage) within the same area.

Given the above, the team elected to house the in-tunnel spoil storage within two of the three carriageway tunnels, as close to the tunnel portal as possible. Truck and dog access and turning was facilitated through an additionally constructed temporary cross passage, for loading via front end loaders. Due to the large radius required for a truck to turn around and exit the tunnel, it was necessary to provide this temporary cross passage. It would not have been possible to turn a truck around without the temporary cross passage, so this was considered a necessary addition.

A loader turning niche was also required to be excavated into the sidewall of one of the existing tunnels, to minimise the need for reversing movements. This niche eliminated the need for reversing within the path of trucks that dump spoil in the area and so was considered highly desirable as it eliminated a potential interaction between loaders and dump trucks. The addition of this cross passage and niche required further tunnel support to be installed within otherwise completed sections of the existing tunnel crown, along with an assessment on the impacts of the already completed RIC tunnels below. Refer to figure 4 below for a general arrangement of the swept paths and spoil removal system adopted.

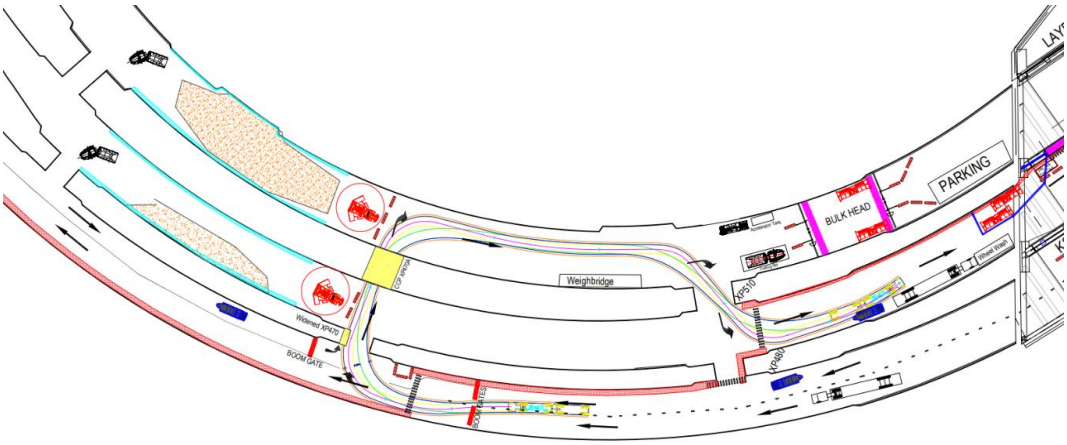


Figure 4. General Arrangement of Underground Spoil Loadout.

3 ENGINEERING INTITIATIVES – ROADHEADER RE-SEQUENCING AND ADDITIONAL CROSS PASSAGES

Upon award of STW, JHCPB began to explore various engineering and optimisation initiatives, in an attempt to shorten & de-risk the overall program beyond initial tender expectations. One of the most beneficial opportunities identified was the planned sequencing of road-header launches and excavation of ventilation tunnels and caverns early. This initiative was based on opening up work areas and getting into the complex excavation as early as possible.

Ventilation tunnels at STW comprised 1,300 linear meters of tunnelling of varying cross-sectional area. This included two tall and large span caverns, which are intended to house large axial fans mounted on a steel structure, in order to provide additional ventilation in the event of fire or poor air quality. Both ventilation caverns are 21 metres wide by 24.5 metres tall, which presents significant complexity in staging the excavation, waterproofing, and potential lateral shearing within the bolted zone.

These caverns were considered a threat to potentially delay the program if any lateral movement and subsequent shearing were to be observed. Shearing has been observed on similar projects in Sydney, as described by Bai et al (2023), and so it was considered critical to ensure this concern could be mitigated, by bringing excavation as far forward in program as possible.

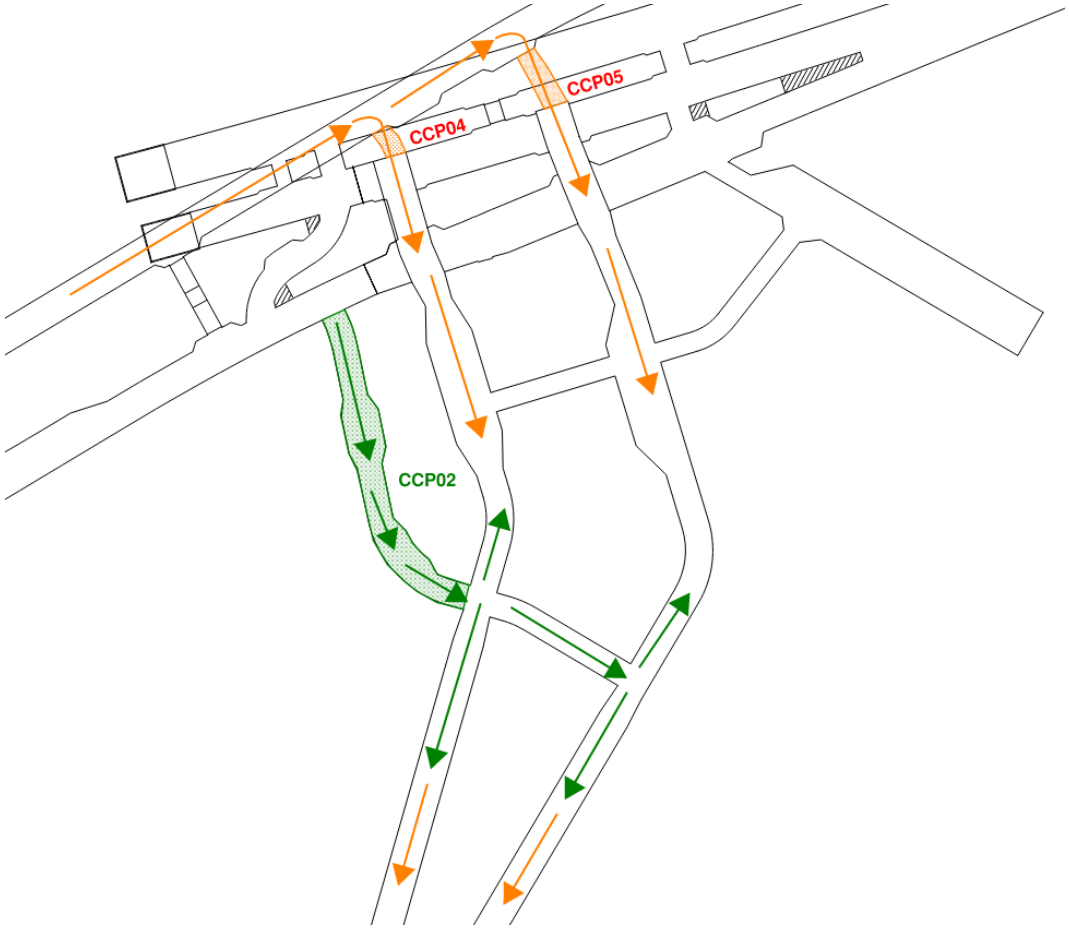


Figure 5. Concept Excavation Sequence (Orange) vs Optimized Excavation Sequence (Green)

Given the complexity involved with tall and large-span caverns and complex geology, it was critical to address program risks associated with these caverns. The concept sequence allowed for two temporary cross passages 'CCP04' and 'CCP05' connecting the main WHT on-ramp to the northern end of ventilation tunnels. In effect – this would mean the entire length of ventilation tunnels would have to be excavated from north to south via these CCPs, with room for only two roadheaders (one in each vent tunnel) to undertake the excavation. CPP04 & CCP05 would also become a bottleneck for spoil and traffic moving in and out of the ventilation tunnels and create interactions with main access ramp to the northern extents of STW.

A program impact and internal cost analysis was undertaken to assess the impact of the introduction of a new temporary cross passage 'CCP02', which would link a less critical access ramp to the ventilation tunnels at a point south of the ventilation caverns. This would result in CCP04 & CCP05 being deleted from the design, as their purpose had become redundant. This change allowed for the number of roadheaders to be doubled to four machines. Two machines to excavate

northbound, while another two can excavate southbound back towards RIC. It also allowed for multiple routes of access in and out of ventilation caverns after excavation, whilst also providing flexibility and staging options for waterproofing and secondary lining required to be completed in the ventilation caverns.

The addition of this relatively long cross passage would add additional excavation volume to the project, however the exercise determined that ventilation tunnels could be completed many months earlier through incorporation of this re-sequencing. The largest benefit realized was not only the time saving, but the reduction in overall program risk. In the STW concept program – there was minimal float between completion of ventilation tunnels and overall project critical path. This change moved vent tunnel completion forward significantly, thereby mitigating a significant risk of extending the overall project critical path.

While this exercise added some additional excavation volumes to the project, the net effect was a saving in overall effort, as excavation and tunnel finishing works within ventilation caverns could be completed much sooner, allowing resources to be focused on completing other elements within the project, and thus achieving an overall reduction in time required to project completion.

4 DESIGN MANAGEMENT - AN OBSERVATIONAL APPROACH TO TUNNEL GEOMETRY

Observational approaches to tunnel support and groundwater control systems, as decribed by Salcher et al (2023) and Brown et al (2020) respectively, are relatively common across recent mined tunnel projects in Sydney. This is an approach well defined by Nicholson et al (1999), but to be put more simply is where a 'toolbox' of options are presented within the design, and a strict system of ongoing site observations and review is undertaken, allowing for an option from the 'toolbox' to be selected and applied on site in response to observed conditions. This is a highly flexible, and generally favoured approach.

STW adopted this same approach, however expanded the observational approach to tunnel geometry & set-out in select circumstances. This was most notably implemented in a tall and wide span ventilation cavern, located adjacent to the Great Sydney Dyke (GSD) which was projected to run sub-parallel to the alignment of the ventilation cavern, somewhere within 10 metres to 30 metres of the closest sidewall. This observational approach would allow a significant improvement in overall tunnel stability and safety during construction. At the initial design phase, the confidence on the projection of the GSD was relatively low as there was limited surface site investigation data available in the area. It was identified that further in-tunnel investigation results should be incorporated as part of the tunnel selection criteria.

The ventilation cavern support nominated mandatory probing towards the GSD on the nearest sidewall (prior to benching to full height), as validation to ensure the dyke was not located within 10 metres of the sidewall. If the dyke were to be discovered – a regime of stitch bolting, with 13.5 metre long cable bolts at 1 metre centers, across the sidewall would be required as part of a special support type designed to pin the sidewall, a solution that was not pallatable.

The design proposed two options for ventilation cavern geometry to address the potential risk of the GSD. Option 1 provided the regular cavern geometry, with a 4 metre widening on both sides of the cavern. Option 2 provided an alternate geometry, with an 8 metre widening on the far side of the cavern only. Option 2 was effectively a horizontal offset of the cavern, moving the critical sidewall 4 meters away from the dyke if necessary.

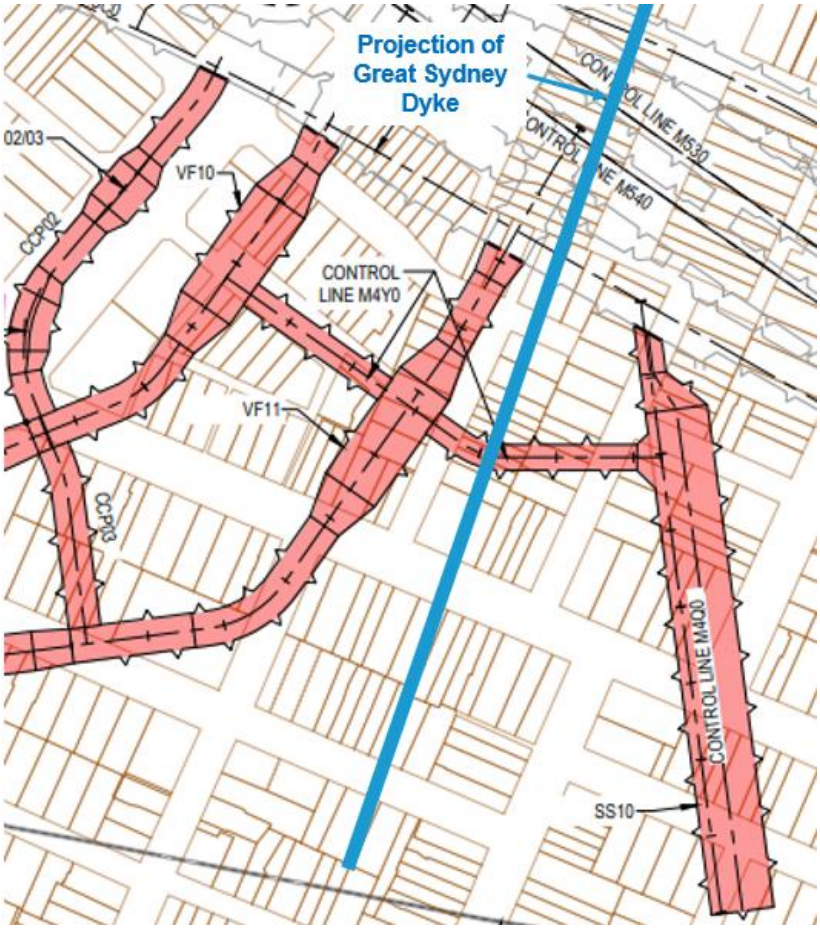


Figure 6. STW Ancillary Tunnels with projection of Great Sydney Dyke

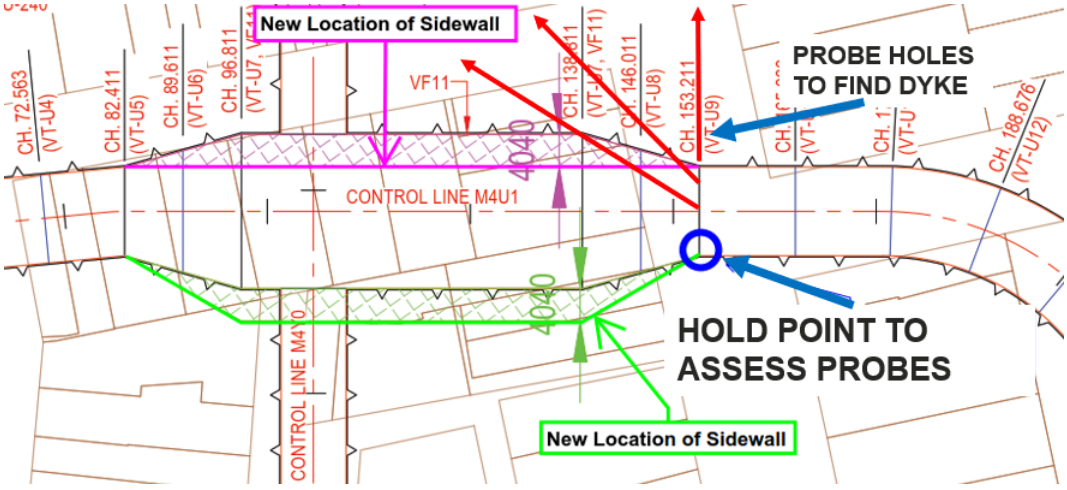


Figure 7. Probing Plan & Option for Alternative Ventilation Cavern Geometry

In order to inform, validate and ensure any impacts of this change were captured – a Hold Point was nominated in the design excavation sequence, immediately prior to entry into the cavern widening. This Hold Point nominated probing at the face and sidewall towards the GSD, in order

to find and measure the actual location of dyke relative to cavern sidewall. An informed decision on the relocation of the sidewall away from the dyke could then be made. In order to release the Hold Point – the construction team provided geological probing results, along with the nomination of which geometry was proposed, to JHCPBs Design Manager who acted as the release authority for the hold point.

The construction team undertook this probing, and elected to proceed with the alternate geometry. The approach was successful, with no stitch bolting or adverse support types required throughout the cavern.

This flexibility was made possible, as the options were carefully planned not to have any impact on tunnel space-proofing, alignment, or accessibility and maintainability requirements. This approach was only applied to ventilation tunnels and service passages, and was not permitted for road tunnels, as spaceproofing requirements are considerably more flexible when traffic and road geometry considerations are not applicable.

This concept was found to be highly effective in optimizing tunnelling activities, improving safety and overall efficiency and would be worth exploring in further detail on future projects. It is noted that strong cooperation and an open flow of dialogue between construction and design teams is key to ensuring this process operates smoothly and succesfully.

5 DISCUSSION

The delivery of STW higlights how the integration and balance between program, excavation quantities, intelligent engineering solutions and proactive design management processess are key to successful delivery of such complex infrastructure. In the authors opinion, the importance of involving staff who are both technically minded, and experts in delivery is critical, as an understanding of the reasons *why* specific design requirements exist is key, so engineering solutions can be safely, efficiently and pragmatically implemented. The benefit of having experienced and expert staff on board meant that complex time and cost judgements could be undertaken and implemented at relatively short notice, allowing for implementation of signficantly optimized and innovative engineering solutions.

6 REFERENCES

Bai, Y., Salcher, M., Fusee, R., Bentley, T., Kumar, A. and Trim, M. 2023. Rock bolt shearing during construction of multi-level tunnels in Sydney. In: *18th Australasian Tunnelling Conference 2023*.

Brown, T., Lennon, M., Nash, T. and Trim, M. 2020. Observational Approach to Water-Resistant Lining for a Major Urban Road Tunnel. In: *ITA-AITES World Tunnel Congress, WTC2020.*

Nicholson, D., Tse, C.-M. and Penny, C. 1999. The observational method in ground engineering: Principles and applications. London*: CIRIA.*

Salcher, M., Bai, Y., Trim, M., Bertuzzi, R. and Vidler, B. 2023. The Permit to Tunnel process adopted on Australian infrastructure projects. In: *18th Australasian Tunnelling Conference 2023.*

7 CONCLUSIONS

Southern Tunnel Works was considered a successful project, delivered ahead of time, with reduced disturbance to the community and local environment. This was due to excellent collaboration between Transport for NSW and contractor John Holland CPB Joint Venture.

The decision to focus on unique, innovative solutions and engineering initiatives across the project worked tremendously to minimize impacts and optimize outcomes for all stakeholders.

Transport for NSW and JHCPB have proven with this project that it is possible to shift a traditional tunnel site underground, with minimal disruption to tunnelling activities, and with less impact on the wider community.

19th Australasian Tunnelling Conference – Acosta-Martínez, Stewart and Hudson-Smith (Eds.)
© 2025 Australian Tunnelling Society, ISBN 978-0-85825-002-4

Surface settlement monitoring of the urban canyon - a case study from Brisbane metro

A.J Coulthard, L.W Walsh
Land Surveys, Brisbane, Australia

P Mathers, S. Keen
ACCIONA, Brisbane, Australia

ABSTRACT: The Adelaide Street tunnel, constructed as part of the Brisbane Metro project, delivered for Brisbane City Council and constructed by ACCIONA, involved shallow, large-diameter tunnelling beneath Adelaide Street, one of Brisbane's busiest corridors. The alignment passed through soft soils, dense underground services, heritage buildings, and mature trees, necessitating high-precision monitoring to mitigate construction risk. Automated Total Station (ATS) used to undertake both surface settlement and 3D structural monitoring. Custom installations were developed to address the challenges of the constrained urban environment, including limited sightlines, complex mounting conditions, and restricted stakeholder access.
The system successfully tracked ground and building movement, enabled early detection of trends, and informed construction decisions throughout excavation. Compared to manual methods, it delivered cost savings, enhanced safety, and more frequent data acquisition. The project highlights the value of tailored instrumentation strategies in complex city settings and provides lessons applicable to future underground infrastructure delivery.

1 INTRODUCTION

The Adelaide Street tunnel, constructed as part of the Brisbane Metro project, delivered for Brisbane City Council and constructed by ACCIONA, involved large-diameter tunnelling at shallow depth beneath Adelaide Street—one of Brisbane's most congested and infrastructure-rich corridors. The alignment passed beneath dense services, heritage buildings, and mature trees, presenting significant geotechnical and structural risks.

Land Surveys, was engaged to design and implement a high-resolution, real-time monitoring system to track both surface and 3D structural movement throughout the excavation. Automated Total Stations (ATS) were selected as the primary technology, providing the accuracy, frequency, and remote accessibility required to manage risk in this constrained city environment.

This paper outlines the design and deployment of the monitoring system, with emphasis on:

- The use of ATS to measure ground and structural movement during excavation;
- The challenges of implementing monitoring in a narrow, high-traffic CBD corridor;
- The role of remote planning tools and high-frequency data in maintaining system performance;
- Lessons learned related to sensor design, data filtering, stakeholder coordination, and system reliability.

These insights offer guidance for future tunnelling projects in similarly complex urban environments.

2 GEOTECHNICAL AND TUNNEL BACKGROUND

While a detailed discussion of the geotechnical conditions and tunnelling methodology is beyond the scope of this paper, a brief summary is essential, as these factors directly influenced the design and execution of the monitoring system.

The ground conditions beneath Adelaide Street are primarily composed of the Neranleigh-Fernvale Beds, overlain by variable layers of fill, alluvium, and residual soft soils. These alluvial deposits typically reached depths of up to 15 metres at the western end of the alignment, with thickness varying due to historical service installations and ground disturbance.

Groundwater levels were generally below the tunnel invert but rose locally—particularly near the sump—requiring active groundwater management during construction.

The tunnel was excavated using the New Austrian Tunnelling Method (NATM), with shallow cover in some locations less than 3.5 m. A split-face, four-stage excavation sequence was adopted: right and left oculars, followed by crown and bench. Temporary support was provided by canopy tubes and spile bars, with a reinforced shotcrete lining applied at 1-metre intervals to stabilise the advancing face.

3 MONITORING SYSTEM DESIGN AND IMPLEMENTATION

3.1 *ATS installation & deployment:*

Automated Total Stations (ATS) are widely recognised as a reliable and precise monitoring solution for tunnel and infrastructure projects, particularly in environments requiring high-frequency displacement tracking (Hoult & Soga, 2018). For the Brisbane Metro project, the installation of ATS was shaped by the complex spatial, structural, and stakeholder constraints of Adelaide Street's urban canyon. Unlike more uniform environments—such as open rail corridors or greenfield tunnels—this dense CBD setting presented challenges including obstructed sightlines, limited mounting surfaces, heritage-listed structures, and varied stakeholder cooperation.

ATS locations were selected through a staged process beginning at the dive structure and progressing toward City Hall. Prism arrays were mapped and the expected zone of influence (ZOI) for ground movement was modelled. Instruments were positioned outside the ZOI where feasible, with clear lines of sight to targets and stable reference points. Design iterations accounted for site constraints, excavation sequencing, and stakeholder feedback and were finalised through registered professional engineer of Queensland (REPQ) review.

A key challenge was balancing system redundancy, spatial coverage, and approval timelines. While more ATS units could reduce cycle times and improve redundancy, each added cost and complexity. Dense vegetation, narrow footpaths, and limited access often required compromises in geometry and instrument positioning.

Fixed infrastructure such as rooftops, balconies, and structural canopies were preferred due to their stability and elevation. However, elevated locations often placed instruments within or above the tree canopy, creating new obstructions. Heritage restrictions, access limitations, and mixed stakeholder responses further complicated mounting choices. Where building-mounted options were unavailable, street furniture such as bus port structures and light poles was used. These required custom brackets and careful consideration of vibration, movement, and vandalism risk.

Power and communications design was similarly constrained. In many locations, dense tree cover prevented effective solar charging. Mains power was preferred but not always available; in one case, a property owner refused access to supply, requiring a large solar panel installation despite shading risks. Temporary power disruptions during construction were mitigated using portable batteries or alternate feeds.

Despite these challenges, all five ATS units, each with bespoke mounting designs, were successfully installed without requiring post-installation relocation. The project highlighted the importance of early visibility modelling, flexible infrastructure design, and strong stakeholder engagement when deploying monitoring systems in constrained urban environments.

3.2 *Surface settlement monitoring:*

Monitoring surface settlement along Adelaide Street was a critical component of the instrumentation and monitoring strategy. Given the tunnel's shallow alignment, variable ground conditions, and constrained construction staging, accurate, high-frequency monitoring was essential to track settlement behaviour and protect overlying infrastructure. This was particularly important for validating observed movement against Gaussian-type settlement profiles, as described by Peck (1969).

The system was designed to achieve ±1 mm accuracy and repeatability. The original scope included 65 settlement markers, arranged in arrays of 5 to 10 points positioned over the tunnel crown. However, during detailed design and early construction, the need for greater spatial coverage became apparent. The final layout comprised three 17-point arrays, fourteen 13-point arrays (expanded from the original 11-point design to reach the building boundary line), and five arrays positioned directly over the tunnel headings—totalling 236 markers. This represented a 366% increase over the initial scope. A typical array cross-section is shown in Figure 1.

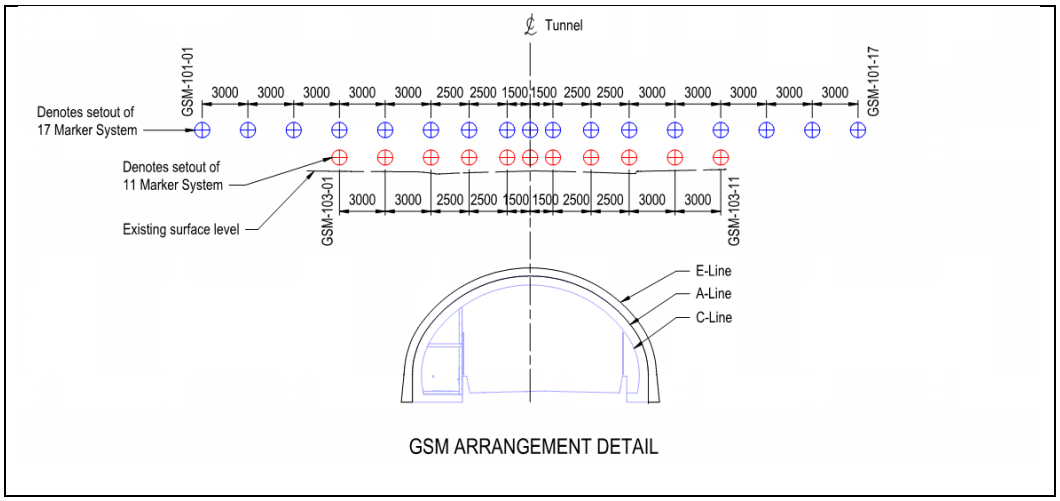


Figure 1. Typical GSM settlement array layout (from I&M Plan).

Three monitoring technologies were considered: cat's eye prisms, patch scanning, and reflectorless measurement. Each was evaluated for suitability in the live, trafficable corridor.

- Cat's eye prisms, designed for in-pavement use, offered a low-profile, durable optical target suitable for vehicle and pedestrian environments. These were installed near kerbs, bollards, and other street furniture to minimise disruption. While generally robust, they were susceptible to water ingress, vehicle wear, debris, and high-pressure street cleaning.
- Patch scanning using Leica MS60 instruments provided high-resolution surface data without fixed targets. However, the high cost and slower acquisition times (2–5 minutes per scan vs. 45 seconds per prism) made this method impractical for the required monitoring frequency and density.
- Reflectorless measurements using TM60 instruments offered quicker, contactless readings and were used as a backup when cat's eyes were damaged. However, accuracy was highly sensitive to incidence angle and surface condition. As movement occurred, the laser contact point could shift, leading to inconsistent data—particularly on cambered or irregular road surfaces.

Cat's eye prisms were selected as the preferred solution due to their accuracy, efficiency, and reliability in urban road conditions. Low traffic speeds along Adelaide Street further reduced the risk of dislodgement.

Initial installations using screw-in anchors experienced post-installation movement under traffic loads. These were replaced with embedded rods and thermal adhesive pads, a technique adapted from highway marker installation, significantly improving durability.

Other field issues included prism displacement due to road degradation near gutters, debris accumulation after rain, and water ingress. A collaborative redesign with the supplier added drainage holes and gasket seals to the prisms, improving resistance to environmental conditions. Once these improvements were implemented, performance stabilised.

In cases where prisms were temporarily unavailable, reflectorless measurements provided interim coverage. A limited number of manual levelling points were also installed along the corridor to support verification checks and confirm anomalies.

3.3 *Building movement monitoring:*

Monitoring building movement along Adelaide Street presented unique challenges, particularly due to stakeholder restrictions that prohibited the installation of physical prisms on some heritage structures. To address this, a reflectorless monitoring methodology was developed and successfully implemented.

The approach relied on capturing three independent reflectorless observations on orthogonal surfaces of each building façade. These corresponded to transverse (left/right), longitudinal (along chainage), and vertical (up/down) displacements. Suitable features—such as window ledges, sills, or frames—were selected based on their orientation relative to the Adelaide Street alignment. By isolating movement in a single plane per observation, displacement in all three directions could be derived with high repeatability.

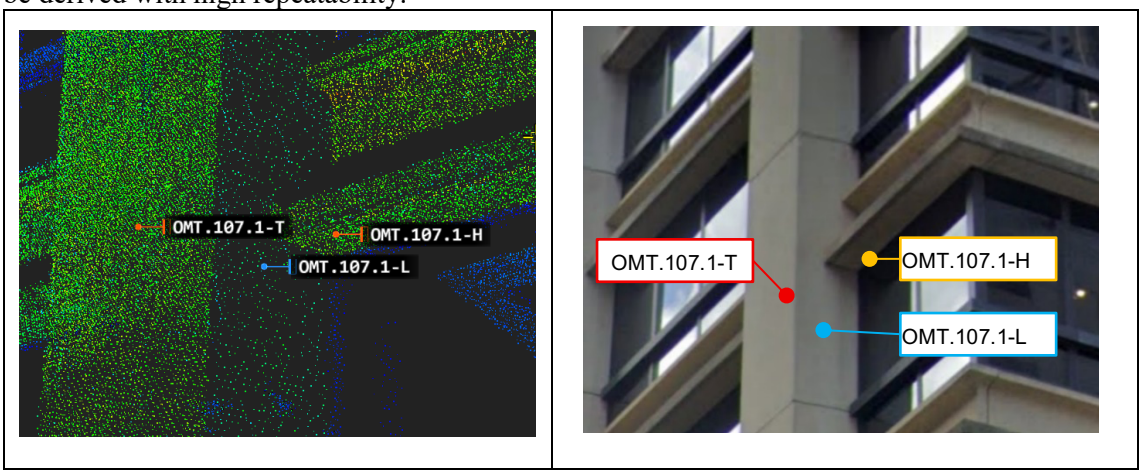


Figure 2. TLH points identified on building façade using point cloud data.

Each group of three readings was configured as a virtual monitoring point within the Leica GeoMoS platform, allowing automated monitoring without the need for physical prism installation. This method eliminated the need for patch scanning or manual measurement while maintaining consistent coverage on restricted-access buildings. Figure *2* illustrates the Transverse, Longitudinal and Height TLH points that were selected using point cloud data, monitoring points were defined in GeoMoS,

The system was validated through internal trials before field deployment, confirming its reliability for detecting structural displacement. Where unexpected readings were observed, measurement points could be quickly reviewed and adjusted in the field, preserving long-term trend integrity.

This approach enabled continuous, high-quality monitoring in locations where physical access was not possible. It provided effective risk management while respecting heritage constraints and formed a key component of the overall monitoring strategy and stakeholder engagement process.

3.4 *Use of point cloud data for planning & maintenance:*

The Brisbane Metro monitoring program commenced during the tail end of the COVID-19 pandemic, when travel and access restrictions posed challenges to traditional on-site planning. These limitations highlighted the need for remote tools to support the design, installation, and adjustment of monitoring infrastructure along the constrained Adelaide Street corridor.

Initial planning relied on publicly available tools, topographic surveys, and site inspections. However, a terrestrial laser scan (TLS) of the corridor—captured by the client's survey team during early project stages—became an invaluable resource once integrated into the monitoring workflow. Although originally acquired for general design purposes, the TLS data proved highly useful for spatial planning and coordination.

To interact with the scan, the subcontractor employed Pointerra, a browser-based 3D point cloud platform. Its intuitive interface and cloud-based delivery enabled rapid review of site conditions, visibility modelling, and clash detection from any device. Other tools, such as SketchUp and CloudCompare, were trialled but saw limited use due to workflow and accessibility constraints.

The point cloud supported several key functions throughout the monitoring lifecycle:

- ATS placement: Simulated visibility modelling from proposed instrument locations.
- Clash detection: Identification of temporary structures or vegetation affecting sight lines.
- Reflectorless targeting: Selection of viable measurement surfaces where prisms were not feasible.
- Maintenance coordination: Extraction of updated coordinates for upload to GeoMoS, enabling remote target adjustment.

Although the monitoring program could have proceeded without the point cloud, its inclusion significantly reduced the need for repeat site visits and removed ambiguity during layout and planning. It became a trusted spatial reference for both field crews and office-based stakeholders.

Looking ahead, the team recommends exploring SLAM-based mobile scanning for future projects. These solutions offer sufficient relative accuracy for monitoring applications, enable faster data acquisition, and could serve as a valuable visual archive of changes if captured at regular intervals throughout the project lifecycle.

3.5 *Data averaging and filtering strategy*

As the Brisbane Metro monitoring system matured, so too did the approach to managing high-frequency surface settlement data. Initially scoped for daily readings, the fully deployed ATS network enabled more frequent observations—progressing to 4-hourly and eventually hourly cycles during the low-traffic overnight period (12:00 am–6:00 am). This window offered optimal conditions with reduced obstruction and grazing, ensuring consistent prism acquisition.

To streamline alerts and reporting, overnight readings were averaged into a single daily value, which became the primary input for alarm logic. Both raw and averaged data were retained to support interpretation and distinguish genuine movement from environmental noise or temporary occlusions. The availability of high-frequency data also offered clearer insights into the performance of problematic prisms.

As data volumes increased, occasional outliers emerged—often linked to grazing or weather-related interference.

Two statistical smoothing options were considered:

- Option 1: 24-hour average (no filtering) – simple to implement using existing SQL logic.
- Option 2: 24-hour average with outlier filtering – excluded values outside ±3 mm of a rolling 48-hour average, but required additional logic and verification.

While Option 2 removed slightly more outliers, it did not significantly alter the interpreted movement. Given the marginal improvement and added complexity, Option 1 was adopted.

To evaluate both approaches, a representative monitoring point (GSM-103.07) was analysed, as shown in Figure *3*:

- Raw data exhibited isolated spikes caused by temporary obstructions (Figure *3* a).
- The 24-hour average reduced major noise (Figure *3* b).
- Option 1 provided a clean, stable trend suitable for alarm thresholds.

Option 1 offered a practical balance between responsiveness and simplicity. Alarms were based on this daily average, with raw data retained for engineering review.

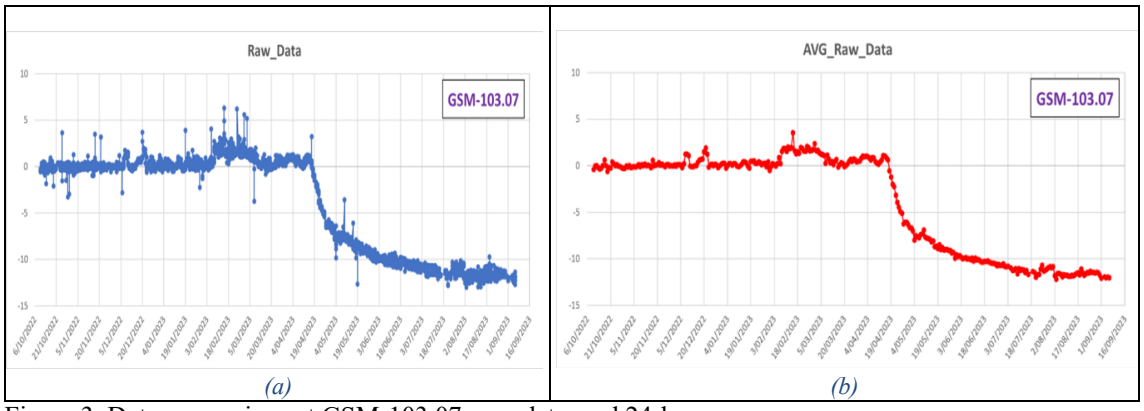


Figure 3. Data comparison at GSM-103.07: raw data, and 24-hour average.

This post-processing strategy worked alongside the built-in ATS filtering, which automatically discarded measurements considered incomplete or unreliable. While the ATS ensured data quality at a basic level, the daily averaging process helped clarify longer-term trends and reduced false alarms, particularly those triggered by weather conditions, temporary obstructions, or other short-term issues.

Clear, stable data was essential for keeping stakeholders confident, especially when unexpected ground movements occurred. By smoothing out short-term fluctuations while accurately representing genuine settlement trends, the monitoring system provided better insight and more reliable information for making construction decisions.

The success of this method also depended heavily on regular communication with site teams. Field personnel regularly checked measurements, responded quickly to unexpected data spikes, and performed targeted prism maintenance where necessary. This hands-on approach kept the monitoring system accurate and dependable over the project's duration.

In short, although more advanced filtering methods might be explored on future projects, combining built-in ATS filtering, simple averaging, and proactive field checks provided a robust, practical, and effective solution for Brisbane Metro.

3.6 *Measurement challenges in the urban canyon.*

Monitoring ground and structural movement in Brisbane's dense CBD corridor presented unique environmental and operational challenges that affected data acquisition quality and consistency. As noted by Hoult & Soga (2018), sensor accuracy and reliability are highly influenced by mounting position and surrounding environmental conditions—an issue particularly evident in constrained urban settings such as Adelaide Street. While the ATS system incorporated robust filtering and quality checks, a range of persistent urban factors required active management.

Prisms located near street gutters were particularly susceptible to visual obstructions and signal anomalies. These areas were frequently impacted by debris, mud, leaves (notably from mature leopard trees), and splashes from passing vehicles. Seasonal vegetation growth and litter buildup also contributed to temporary visibility loss and degraded signal return, especially following rainfall or during peak construction activity.

Although the ATS software performed automated quality checks—including tilt compensator validation, signal return strength analysis, and dual-face readings—subtle grazing effects could still produce measurements that mimicked true displacement. These errors were most commonly observed with cat's eye prisms mounted at pavement level. This aligns with findings by Lackner & Lienhart (2017), who demonstrated that prism orientation and non-standard geometries—such as cat's eyes—can significantly affect measurement accuracy, particularly under grazing incidence. The importance of systematic quality controls—especially dual-face observations, tilt correction, and signal strength validation—has also been widely acknowledged as critical for reliable automated monitoring (Lienhart, 2017).

When unexplained data spikes were identified, cleaning frequency was increased beyond the standard weekly or fortnightly schedule. An example of the debris as a result of rain is shown in

Figure *4*. Anomalies were reviewed alongside environmental data (e.g., rainfall or wind) and compared to adjacent monitoring points to distinguish genuine movement from noise.



(b) *(b)*

Figure 4. (a) Debris found on cats eye prism in the gutter post rain. (b) Cleaned following maintenance

Sensor placement was a key factor in measurement reliability. While low-profile prisms were chosen to reduce trip hazards, their positioning near gutters made them more vulnerable to damage and obstruction. Although smaller-diameter alternatives were considered, they posed a risk of compromised signal return due to reduced reflective surface area. Further testing would be required to evaluate their suitability in similar environments.

In contrast, cat's eye prisms installed on footpaths required minimal maintenance, while 3D monitoring prisms mounted on building façades required no maintenance at all throughout the monitoring period. Their elevated and sheltered locations protected them from environmental and mechanical effects, highlighting the advantage of locating sensors away from high-traffic, exposed zones wherever feasible.

De Rubertis (2017) notes that even well-designed monitoring systems require site-specific maintenance and validation to remain reliable - particularly in environments subject to mechanical disturbance or environmental exposure. This was especially true for Brisbane Metro, where surface-mounted sensors proved more vulnerable than elevated alternatives.

Overall, consistent field feedback, proactive maintenance, and thoughtful system design were essential to managing the challenges posed by the urban canyon environment.

4 RESULTS AND FINDINGS

The surface settlement monitoring program achieved excellent results, thanks to careful planning, accurate fieldwork, and strong collaboration between monitoring specialists and the construction team.

From the beginning, the monitoring network was tailored specifically to address the complexities along Adelaide Street. Instruments were precisely installed and regularly checked, ensuring consistently high-quality data. Field teams quickly addressed issues like prism obstructions or environmental interference, maintaining data reliability throughout the project.

Communication was a key strength of the project. Regular updates between site personnel and monitoring staff allowed rapid responses to unexpected situations, building trust in the monitoring system.

Automated monitoring also delivered practical advantages compared to traditional manual surveys. It reduced labour requirements, provided quicker access to data, and significantly improved site safety by minimising surveyors' exposure to traffic and construction hazards. These benefits align well with established monitoring practices (Dunnicliff, 1993).

Overall, the monitoring program reliably provided clear, actionable information that supported safe and efficient tunnelling operations in a challenging urban environment.

5 CONCLUSION AND IMPACT

The Brisbane Metro surface settlement monitoring program demonstrated the critical role of advanced instrumentation in managing geotechnical risk within a highly constrained urban environment. Despite spatial limitations, environmental exposure, and stakeholder-related challenges along the Adelaide Street corridor, the use of Automated Total Stations (ATS) enabled consistent, high-precision monitoring throughout the excavation period.

The integration of remote planning tools, particularly point cloud data, with automated measurement systems created a flexible and resilient monitoring framework. This enabled early trend detection, efficient maintenance scheduling, and timely construction feedback. While cat's eye prisms required occasional maintenance, the overall monitoring infrastructure proved robust and well suited to the challenges of the site.

Importantly, the system enabled safe, uninterrupted operation of one of Brisbane's busiest commuter corridors. Monitoring activities were conducted with minimal disruption to public access, and the data generated directly supported construction decision-making, stakeholder communication, and risk mitigation.

The lessons learned—particularly around early planning, stakeholder coordination, sensor placement, and adaptive maintenance—provide valuable guidance for future underground infrastructure projects in similarly complex urban settings. The success of the Brisbane Metro monitoring program highlights the importance of tailored system design, proactive planning, and close collaboration in delivering reliable, real-time instrumentation outcomes.

6 REFERENCES

Peck, R.B. 1969. Deep excavations and tunneling in soft ground. In Proceedings of the 7th International Conference on Soil Mechanics and Foundation Engineering, Mexico City.

Dunnicliff, J. 1993. Geotechnical Instrumentation for Monitoring Field Performance. New York: Wiley.

Hoult, N. & Soga, K. 2018. Sensing solutions for assessing and monitoring tunnels. In: Lynch, J.P., Sohn, H. & Wang, M.L. (eds.) *Sensor Technologies for Civil Infrastructures, Volume 2: Applications in Structural Health Monitoring*. Woodhead Publishing, pp. 105–140.

Leica Geosystems. 2012. Leica GeoMoS – Leica Geosystems TruStories
Monitoring .
https://leica-geosystems.com/-/media/files/leicageosystems/trustories/monitoring_2012_tru.ashx?sc_lang=en&hash=550F16E59EEC79A81A1EFD15A12916B9

De Rubertis, K. (ed.) 2017. Monitoring Dam Performance: Instrumentation and Measurements. New York: ASCE Press.

Lienhart, W. 2017. Geotechnical monitoring using total stations and laser scanners: critical aspects and solutions. *Journal of Civil Structural Health Monitoring*, 7(5): 573–582. https://doi.org/10.1007/s13349-017-0253-0

Authors index

Acharya, K. 433
Adcock, E. 81
Ahn, J. 375
Alaedini, H. 31
Ali, M. 791
Alvarado, F. 187
Alvarado, G. 747
Ameijde, S. 471
Asche, H. 11, 31, 811

Bai, Y. 449, 461, 653
Balakumarasingham, V. 195
Ballen, R. 1067
Banda, S. 841
Bäppler, K. 489
Barrett, S. VL. 887
Bateman, J. 1021
Baxter-Crawford, H. 773
Behrens, M. 73, 263
Bennett, A. 211
Bentley, T. 449, 461, 1109
Bernard, E. S. 289
Besharat, V. 541
Beyer, M. 669, 681
Bhatta, G. 305
Bidarmaghz, A. 645
Biotto, C. 613, 927
Bischoff, M. 873
Bodner, C. K. 1083
Bombin-Saiz, J. R. 591
Boon, C. W. 565
Booth, P. 505, 549
Booy, M. 321
Boylan, D. 23
Brehaut, R. 1011
Browne, A. 879
Bruce, A. 903
Buchanan, H. 1011
Bueno-Leal, P. 1029

Cadena-Gomez, J. 971
Cadenelli, M. 171
Calle-Lamelas, F. 1029
Cao, C. X. 153
Carnes, B. 781
Casey, N. 637, 895
Ceballos-Martinez, F. 575, 1029
Cerone, F. 397
Ceylan, O. 629
Chan, L. Y. 47
Chang, A. 927
Chang, E. 565
Chapman, B. 433
Chau, S. F. 11, 1067
Chen, A. 757
Chen, K. P. 653
Cheung, T. 1067
Ching, I. 433
Cippà, F. 171
Clark, P. 363
Clarke, S. J. 89, 375, 389, 397, 1057
Cockerall, J. 3
Cole, K. 687, 919
Colman, R. 849
Cooper, J. Q. 1075
Coulthard, A. J. 1117
Cutter, P. 955

Dai, C. 739
Dare-Bryan, P. C. 479
David, M. 3
Davidson, J. W. 645
Deng, Y. 271
Devrnja, D. 329
Diederichs, M. 433
Dix, A. 895
Dixon, E. 479
Dong, Y. 747
Driscoll, T. 919
Duncan, I. 1067
Dunleavy, A. 471
Duorina, D. 211
D'Andrea, L. 979
D'Hondt, C. 11

Edney, A. 879
Elliott, R. 255
Emadi, A. 105
Evans, D. 163
Evans, D. W. 339

Facibeni, L. 541
Faini, G. 121
Farooq, H. 801
Fernando, R. 927
Franceschi, M. 163
Francis, A. 23

Gabarron-Duran, A. 591
Gaylard, P. 497
Gelonch, L. 791
Gibson, R. M. 1083
Giordano, C. 621
Goldsmith, A. 747
Golshani, A. 113, 279
Gomes, A. RA. 105
Gourlay, T. 703, 711, 723
Gray, I. 415
Gresz, M. 329
Grobler, N. 849
Gu, T. 179
Gálffy, A. 669

Habte, M. 407
Habte, M. A. 389
Haines, L. 903
Harding, A. 3
Hashim, M. 1075
Hawkey, R. 497
Hayes, B. 865
He, F. 1093
Hiscock, C. 903
Ho, J. 39
Holt, C. 1021
Howard, K. 1075
Hughes, D. 425
Hughes-Adams, H. 781
Hui, M. C. 47
Hunt, C. 781

Jackson, N. 239
Jacob, D. 575
Jamieson, M. J. 621
Jarvis, M. 221
Jasper, C. 613
Johnson, S. 979

Kaese, E. 263
Kamal-Arifin, M. H. 23
Karlovsek, J. 791, 819, 911
Katpakanathan, K. 3
Keating, D. 255, 879
Keen, S. 1117

Kenny, Q. 827
Khoo, M. A. 565
Kobler, M. 407
Kohl, B. 895
Kong, K. WK. 911
Koul, S. 239
Kozak, P. 583
Kroon, P. 693
Kubik, D. 65, 81

Lau, R. 971
Laukner, J. 471
Lazzarin, F. 163
Lecina, M. 89, 1057
Leclere, N. 347
Lee, J. W. 955
Lees, D. J. 841
Lesmana, A. 505
Lewis, N. 113
Li, F. 203
Li, J. B. 153
Li, K. J. 653
Liebrich, P. 397
Liew, K. 723
Lim, J. 1075
Liu, H. 1093
Liu, Z. F. 1093
Loasses, S. 163
Lu, S. 179
Lu, Y. Q. 153, 1093
Luana, M. J. 321
Lyons, N. 747, 765

Macintosh, K. 497
Mackell, J. 129
Mackintosh, N. 1109
Makin, N. 211
Manoj, S. 583
Martin, J. 781
Mastan, A. 987
Mathers, P. 1117
Mattburger, N. 221
Meng, L. 179
Merritt, A. 1057
Mirsepassi, N. 987
Mirzayee, A. 113, 247
Mo, M. 557
Moghbeli, A. 55
Mohammadi, S. 575
Mohandas, M. 1045
Monemvasioti-Kappos, A. 1037
Monroe, S. 575
Moon, T. 313
Moredock, J. L. 687

Narayana, M. 441
Nash, C. 703, 711
Nash, T. 765
Nethercott, J. 113, 247
Ng, C. 39
Nimbalkar, S. 801
Ning, W. 355
Nosrati, S. 425
Nye, T. 935

Och, D. J. 645
Oguz, K. 629
Oh, J. 313
Okumusoglu, B. 583
Osborne, A. 849
O'Donovan, J. 703, 711

Palomo, A. 425
Pandey, G. R. 955
Pang, P. Y. 653
Papworth, F. 945
Patniotis, A. E. 629
Peglas, T. 31
Pelz, U. 819
Peng, E. J. 1093
Pini, G. K. 121
Poo, S. X. 747
Purwodihardjo, A. 505, 549

Quigg, G. 329

Rajesh, A. 1045
Raju-G, D. 145
Rawlinson, A. 963
Raymer, J. H. 835
Reinhold, M. 305
Requiliani, B. 187
Retsos, P. 723
Rivaz, B. De. 347
Roach, W. 513
Rogan, A. C. 375, 407
Rongguo, He. 731
Rooz, A. 531
Roper, T. P. 791

Sahayanathan, C. 613
Sainsbury, B. 531
Salari, S. 441
Salcher, M. 449, 461
Samadi, H. 55, 521
Saminfar, E. 1021
Sanchez, J. L. 841
Sancho-Perez, S. J. P. a. C. 591
Sanderson, J. 963
Sandum, T. 903
Santos, C. de. 791
Sarathchandran, A. 231
Saunsbury, D. 645
Scherwey, P. A. 659
Schmäh, P. 873
Serati, M. 239, 321
Shafee, A. 263
Shafiei, N. 39
Sheffield, M. 747, 1003
Shen, B. 255, 407
Sheng, D. 801
Shepherd, J. 11
Shi, R. 73
Shuyi, W. 355
Sia, T. 203
Sickling, J. B. 1101
Silva, H. De. 441
Sirtori, D. 121
Smith, A. G. 389
Smith, M. 995
Soni, S. 363
Soo, W. Y. 963
Sotomayor, J. 425
Sri-Sai, M. G. 145
Stacey, C. 669, 681, 895
Stariha, K. 187, 757
Stocker, R. 449, 461
Stroppa, F. 187
Subenthiran, S. 637
Suorineni, F. 55, 521
Susilo, R. A. 187
Swinn, B. 375

Talos, A. 827
Tandjiria, V. 557
Taneja, M. 137
Tarigh-Azali, S. 55
Tarrant, A. 471
Tarua, A. L. 1003
Tata, V. 129
Tepavac, D. 781
Terenzi, M. 137
Teruya, K. 1109
Thermann, K. 433
Toi, Y. H. 565
Tran, D. 1057

Trim, M. 449, 461
Tsang, C. F. 329
Tsang, C. K. 203
Tsui, W. S. 47
Turinetti, G. 541

Vallino, J. 89
Van-Dyk, D. 849
Visakan, R. 145

Walker, R. 339
Walsh, L. W. 1117
Walton, J. 497
Wang, D. 1057
Wang, H. 963
Wang, N. 857
Wang, X. 179
Wanigasekara, I. 841
Watson, A. L. 601
Wee, J. 613
Wei, Y. H. 153
Wenbo, Z. 731
Westergren, E. 1021
Whitnall, T. 703, 711
Wijk, I. v. 239
Williams, C. E. 1003
Wojtkowiak, S. 221
Wood, J. H. 415
Worrall, S. 339
Wright, E. 903
Wu, K. 179

Xiangjun, Y. 355
Xu, C. 441

Yang, L. 653
Yang, X. 857
Yao, S. 231
Yau, D. 955
Yi, C. 841
Yim, I. PH. 835
Yin, W. H. 1093
Yin, Y. F. 653
Yisan, D. 355
Yogasuthan, L. 541
Yuan, S. X. 1093

Zafari, S. 995
Zaunrith, G. 895
Zeneli, J. 65, 73
Zhang, I. 279
Zhang, Z. G. 653, 1093
Zheng, B. 1093
Zhu, X. 321
Zhu, Y. 153
Zografou, D. 557
Zoorabadi, M. 99, 757

PERTH | WESTERN AUSTRALIA | 10-14 NOVEMBER

ATC2025

UNDERGROUND SPACE: SECURING OUR FUTURE

This volume comprises the papers presented at the 19th Australasian Tunnelling Conference held in Perth, Western Australia.

The topics covered in the conference include:

- Linings and TBMs
- Temporary support
- Sprayed concrete & ground support
- Caverns
- Underground mining
- Shafts and cut & cover
- Tunnelling systems
- Geotechnics
- Groundwater control
- Pipe jacking & trenchless technology
- Planning, procurement & risk management
- Asset management
- Digital engineering
- Case histories

The conference was organised under the auspices of the Australian Tunnelling Society (ATS)

ENGINEERS AUSTRALIA

AUSTRALIAN TUNNELLING SOCIETY

ISBN 978-0-85825-002-4